

**INTERNATIONAL JOURNAL OF MODERN
ENGINEERING RESEARCH (IJMER)**

ISSN : 2249-6645



Volume 2 - Issue 3

Web : www.ijmer.com

Email : ijmer.editor@gmail.com

International Journal of Modern Engineering Research (IJMER)

Editorial Board

Executive Managing Editor

Prof. Shiv Kumar Sharma
India

Editorial Board Member

Dr. Jerry Van
Department of Mechanical, USA

Dr. George Dyrud
Research centre dy. Director of Civil Engineering, New Zealand

Dr. Masoud Esfal
R& D of Chemical Engineering, Australia

Dr. Nouby Mahdy Ghazaly
Minia University, Egypt

Dr. Stanley John
Department of Textile Engineering, United Kingdom

Dr. Valfitaf Rasoul
Professor and HOD of Electromechanical, Russian

Dr. Mohammed Ali Hussain
HOD, Sri Sai Madhavi Institute of Science & Technology, India

Dr. Manko dora
Associate professor of Computer Engineering, Poland

Dr. Ahmed Nabih Zaki Rashed
Menoufia University, Egypt

Ms. Amani Tahat
Ph.D physics Technical University of Catalonia-Spain

Associate Editor Member

Dr. Mohd Nazri Ismail
University of Kuala Lumpur (UniKL), Malaysia

Dr. Kamaljit I. Lakhtaria
Sir Padmapat Singhaniya University, Udaipur

Dr. Rajesh Shrivastava
Prof. & Head Mathematics & computer Deptt. Govt. Science & commerce College Benazir. M.P

Dr. Asoke Nath
Executive Director, St. Xavier's College, West Bengal, India

Prof. T. Venkat Narayana Rao
Head, CSE, HITAM Hyderabad

Dr. N. Balasubramanian
Ph. D (Chemical Engg), IIT Madras

Jasvinder Singh Sadana
M. TECH, USIT/GGSIPU, India

Dr. Bharat Raj Singh

Associate Director, SMS Institute of Technology, Lucknow

DR. RAVINDER RATHEE

C. R. P, Rohtak, Haryana

Dr. S. Rajendran

Research Supervisor, Corrosion Research Centre Department of Chemistry, GTN Arts College, Dindigul

Mohd Abdul Ahad

Department of Computer Science, Faculty of Management and Information Technology, Jamia Hamdad, New Delhi

Kunjai Mankad

Institute of Science & Technology for Advanced Studies & Research (ISTAR)

NILANJAN DEY

JIS College of Engineering, Kalyani, West Bengal

Dr. Hawz Nwayu

Victoria Global University, UK

Prof. Plewin Amin

Crewe and Alsager College of Higher Education, UK

Dr. (Mrs.) Annifer Zalic

London Guildhall University, London

Dr. (Mrs.) Malin Askiy

Victoria University of Manchester

Dr. ABSALOM

Sixth form College, England

Dr. Nimrod Nivek

London Guildhall University, London

On A Subclass of Harmonic Univalent Functions Defined By Generalized Derivative Operator

N. D. Sangle

Department of Mathematics, Annasaheb Dange College of Engineering, Ashta, Sangali, (M.S) India 416301.

Y. P. Yadav

Department of Mathematics, S. B. Patil Polytechnic, Indapur, Pune, (M.S) India 413106

ABSTRACT

In the present paper, a subclass of harmonic univalent functions is defined using generalized derivative operator and we have obtained among others results like, coefficient inequalities, distortion theorem and convex combination.

2000 AMS subject classification: Primary 30C45, Secondary 30C50.

Keywords: Univalent functions, Harmonic functions, Derivative operator, Convex Combinations, Distortion Bounds

1. INTRODUCTION

A continuous function $f(z)$ is said to be a complex-valued harmonic function in a simply connected domain D in complex plane C if both $\text{Re}(f)$ and $\text{Im}(f)$ are real harmonic in D . Such functions can be expressed as

$$f(z) = h(z) + \overline{g(z)} \quad (1.1)$$

where $h(z)$ and $g(z)$ are analytic in D . We call $h(z)$ as analytic part and $g(z)$ as co-analytic part of $f(z)$. A necessary and sufficient condition for $f(z)$ to be locally univalent and sense-preserving in D is that $|h'(z)| > |g'(z)|$ for all z in D . [2]

Let S_H be the family of functions of the form (1.1) that are harmonic, univalent and orientation preserving in the open unit disk $U = \{z : |z| < 1\}$, so that $f(z) = h(z) + \overline{g(z)}$ is normalized by $f(0) = h(0) = \overline{g(0)} = 1 = 0$. Further $f(z) = h(z) + \overline{g(z)}$ can be uniquely determined by the coefficients of power series expansions.

$$h(z) = z + \sum_{p=2}^{\infty} a_p z^p, \quad g(z) = \sum_{p=1}^{\infty} b_p z^p, \quad z \in U, \quad |b_1| < 1, \quad (1.2)$$

where $a_p \in C$ for $p = 2, 3, 4, \dots$ and $b_p \in C$ for $p = 1, 2, 3, \dots$

We note that this family S_H was investigated and studied by Clunie and Sheil-Small [2] and it reduces to the well-known family S the class of all normalized analytic univalent functions $h(z)$ given in (1.2), whenever the co-analytic part $g(z)$ of $f(z)$ is identically zero.

Let $\overline{S_H}$ denote the subfamily of S_H consisting of harmonic functions of the form

$$f_n(z) = h(z) + \overline{g_n(z)}$$

Where
$$h(z) = z + \sum_{p=2}^{\infty} a_p z^p, \quad g_n(z) = (-1)^n \sum_{p=1}^{\infty} b_p z^p, \quad z \in U, \quad |b_1| < 1. \quad (1.3)$$

For $f(z) = h(z) + \overline{g(z)}$ given by (1.1), we define the derivative operator introduced by Shaqsi and Darus [8] of $f(z)$ as,

$$D_{m,\lambda}^n f(z) = D_{m,\lambda}^n h(z) + (-1)^n \overline{D_{m,\lambda}^n g(z)}, \quad (1.4)$$

where

$$D_{m,\lambda}^n h(z) = z + \sum_{p=2}^{\infty} [1 + (p-1)\lambda]^n C(m,p) a_p z^p$$

$$D_{m,\lambda}^n g(z) = \sum_{p=1}^{\infty} [1 + (p-1)\lambda]^n C(m,p) b_p z^p, \quad |b_1| < 1, \quad C(m,p) = C\left(\begin{matrix} p+m-1 \\ m \end{matrix}\right).$$

Definition: The function $f(z) = h(z) + \overline{g(z)}$ defined by (1.2) is in the class $S_H(n, m, k, \lambda, \beta)$ if

$$\operatorname{Re} \left\{ \frac{D_{m,\lambda}^{n+1} f(z)}{D_{m,\lambda}^n f(z)} \right\} \geq k \left| \frac{D_{m,\lambda}^{n+1} f(z)}{D_{m,\lambda}^n f(z)} - 1 \right| + \beta \quad (1.5)$$

where $0 \leq k < \infty, 0 \leq \beta < 1$.

Also let

$$\overline{S}_H(n, m, k, \lambda, \beta) = S_H(n, m, k, \lambda, \beta) \cap \overline{S}_H \quad (1.6)$$

We note that by specializing the parameter, especially when $k = 0$, $S_H(n, m, k, \lambda, \beta)$ reduces to well-known family of starlike harmonic functions of order β . In recent years many researchers have studied various subclasses of S_H for example [1],[3],[4],[6]and [8].

In the present paper we aim at systematic study of basic properties, in particular coefficient bound, distortion theorem and extreme points of aforementioned subclass of harmonic functions.

2. MAIN RESULTS

Theorem1: Let $f(z) = h(z) + \overline{g(z)}$ be given by (1.2). If condition

$$\sum_{p=1}^{\infty} \left\{ \frac{[1+(p-1)\lambda]^n [(1+k)[1+(p-1)\lambda] - k - \beta]}{(1-\beta)} C(m,p) |a_p| + \frac{[1+(p-1)\lambda]^n [(1+k)[1+(p-1)\lambda] + k + \beta]}{(1-\beta)} C(m,p) |b_p| \right\} \leq 2 \quad \text{where} \quad (2.1)$$

$a_1 = 1, 0 \leq \beta < 1, 0 \leq k < \infty, n \in N \cup \{0\}$, then $f(z)$ is sense-preserving harmonic univalent in U and $f \in S_H(n, m, k, \lambda, \beta)$.

Proof: If the inequality (2.1) holds for coefficients of $f(z) = h(z) + \overline{g(z)}$ then by (1.2), $f(z)$ is orientation preserving and harmonic univalent in U . Now it remains to show that $f \in S_H(n, m, k, \lambda, \beta)$. According to (1.4) and (1.5) we have

$$\operatorname{Re} \left\{ \frac{D_{m,\lambda}^{n+1} f(z)}{D_{m,\lambda}^n f(z)} \right\} \geq k \left| \frac{D_{m,\lambda}^{n+1} f(z)}{D_{m,\lambda}^n f(z)} - 1 \right| + \beta$$

which is equivalent to $\operatorname{Re} \left(\frac{A(z)}{B(z)} \right) > \beta$

where $A(z) = (1+k)D_{m,\lambda}^{n+1}f(z) - kD_{m,\lambda}^n f(z)$ and $B(z) = D_{m,\lambda}^n f(z)$

Using the fact that, $\text{Re}(w) > \beta$ if $|1 - \beta + w| \geq |1 + \beta - w|$ it suffices to show that

$|A(z) + (1 - \beta)B(z)| \geq |A(z) - (1 + \beta)B(z)|$ substituting values of A(z) and B(z) with simple calculations we led to

$$\begin{aligned} &= \left| (2-\beta)z + \sum_{p=2}^{\infty} [1+(p-1)\lambda]^n [(1+k)[1+(p-1)\lambda] - k + 1 - \beta] C(m,p) a_p z^p - (-1)^n \sum_{p=1}^{\infty} [1+(p-1)\lambda]^n [(1+k)[1+(p-1)\lambda] - k - 1 + \beta] C(m,p) \bar{b}_p \bar{z}^p \right| \\ &- \left| \beta z + \sum_{p=2}^{\infty} [1+(p-1)\lambda]^n [(1+k)[1+(p-1)\lambda] - k + 1 - \beta] C(m,p) a_p z^p + (-1)^n \sum_{p=1}^{\infty} [1+(p-1)\lambda]^n [(1+k)[1+(p-1)\lambda] - k - 1 + \beta] C(m,p) \bar{b}_p \bar{z}^p \right| \\ &\geq 2(1-\beta)|z| - \sum_{p=2}^{\infty} [1+(p-1)\lambda]^n [2(1+k)[1+(p-1)\lambda] - 2k - 2\beta] C(m,p) |a_p| |z|^p \\ &- (-1)^n \sum_{p=1}^{\infty} [1+(p-1)\lambda]^n [2(1+k)[1+(p-1)\lambda] + 2k + 2\beta] C(m,p) |\bar{b}_p| |\bar{z}|^p \\ &\geq 2(1-\beta)|z| \left\{ 1 - \sum_{p=2}^{\infty} [1+(p-1)\lambda]^n \frac{[(1+k)[1+(p-1)\lambda] - k - \beta}{(1-\beta)} C(m,p) |a_p| |z|^{p-1} \right. \\ &\quad \left. - (-1)^n \sum_{p=1}^{\infty} [1+(p-1)\lambda]^n \frac{[(1+k)[1+(p-1)\lambda] + k + \beta}{(1-\beta)} C(m,p) |\bar{b}_p| |\bar{z}|^{p-1} \right\} \geq 0. \end{aligned}$$

By assumption. Hence proof is completed.

The functions

$$f(z) = z + \sum_{p=2}^{\infty} \left[\frac{(1-\beta)}{[1+(p-1)\lambda]^n [(1+k)[1+(p-1)\lambda] - k - \beta]} \right] x_p z^p + \sum_{p=1}^{\infty} \left[\frac{(1-\beta)}{[1+(p-1)\lambda]^n [(1+k)[1+(p-1)\lambda] + k + \beta]} \right] \bar{y}_p \bar{z}^p$$

where $\sum_{p=2}^{\infty} |x_p| + \sum_{p=1}^{\infty} |y_p| = 1$ (2.3)

shows that the coefficient bound given (2.1) is sharp.

Theorem 2: Let $f_n(z) = h(z) + \overline{g_n(z)}$ be so that $h(z)$ and $g_n(z)$ given by (1.6). Then $f_n \in \overline{S_H}(n, m, k, \lambda, \beta)$ if and only if

$$\sum_{p=1}^{\infty} \left\{ \frac{[1+(p-1)\lambda]^n [(1+k)[1+(p-1)\lambda] - k - \beta]}{(1-\beta)} C(m,p) |a_p| + \frac{[1+(p-1)\lambda]^n [(1+k)[1+(p-1)\lambda] + k + \beta]}{(1-\beta)} C(m,p) |\bar{b}_p| \right\} \leq 2, \tag{2.4}$$

where $a_1 = 1, 0 \leq \beta < 1, 0 \leq k < \infty$.

Proof: The if part follows from Theorem 1 with the fact that $\overline{S_H}(n, m, k, \lambda, \beta) \subset S_H(n, m, k, \lambda, \beta)$. For only if part, we show that $f_n \notin \overline{S_H}(n, m, k, \lambda, \beta)$ if the condition (2.4) is not satisfied. Note that necessary and sufficient condition for Let $f_n = h + \overline{g_n}$ given by (1.6) to be in $\overline{S_H}(n, m, k, \lambda, \beta)$ is that

$$\operatorname{Re} \left\{ \frac{D_{m,\lambda}^{n+1} f(z)}{D_{m,\lambda}^n f(z)} \right\} \geq k \left| \frac{D_{m,\lambda}^{n+1} f(z)}{D_{m,\lambda}^n f(z)} - 1 \right| + \beta$$

which is equivalent to

$$\operatorname{Re} \left\{ \frac{(1+k)D_{m,\lambda}^{n+1} f(z) + (k-\beta)D_{m,\lambda}^n f(z)}{D_{m,\lambda}^n f(z)} \right\} = \operatorname{Re} \left\{ \frac{(1-\beta)z - \sum_{p=2}^{\infty} [1+(p-1)\lambda]^n [(1+k)[1+(p-1)\lambda] - k - \beta] C(m, p) a_p z^p}{z - \sum_{p=2}^{\infty} [1+(p-1)\lambda]^n C(m, p) a_p z^p} - \frac{(-1)^{2k} \sum_{p=1}^{\infty} [1+(p-1)\lambda]^n [(1+k)[1+(p-1)\lambda] + k + \beta] C(m, p) \bar{b}_p \bar{z}^p}{+ (-1)^{2k} \sum_{p=1}^{\infty} [1+(p-1)\lambda]^n C(m, p) \bar{b}_p \bar{z}^p} \right\} > 0.$$

The above conditions must hold for all values of z , $|z| = r < 1$. Choosing z on positive axis where $0 \leq |z| = r < 1$, we have

$$\frac{(1-\beta)z - \sum_{p=2}^{\infty} [1+(p-1)\lambda]^n [(1+k)[1+(p-1)\lambda] - k - \beta] C(m, p) a_p r^{p-1} - (-1)^{2k} \sum_{p=1}^{\infty} [1+(p-1)\lambda]^n [(1+k)[1+(p-1)\lambda] + k + \beta] C(m, p) \bar{b}_p r^{p-1}}{z - \sum_{p=2}^{\infty} [1+(p-1)\lambda]^n C(m, p) a_p r^{p-1} + (-1)^{2k} \sum_{p=1}^{\infty} [1+(p-1)\lambda]^n C(m, p) \bar{b}_p r^{p-1}} \geq 0. \quad (2.5)$$

or equivalently if the condition (2.4) does not hold then the numerator in (2.5) is negative for r sufficiently close to 1.

Thus there exists $z_0 = r_0$ in $(0, 1)$ for which the quotient in (2.5) is negative. This contradicts that required condition for $f_n \in \overline{S_H}(n, m, k, \lambda, \beta)$ and hence proof is completed.

Theorem 3: Let f_n be given by (1.6). Then $f_n \in \overline{S_H}(k, \beta; n)$ if and only if

$$f_n(z) = \sum_{p=1}^{\infty} (x_p h_p(z) + y_p g_{n_p}(z))$$

where, $h_1(z) = 1$, $h_p(z) = z - \frac{(1-\beta)}{[1+(p-1)\lambda]^n [(1+k)[1+(p-1)\lambda] - k - \beta]} z^p$, $p = 2, 3, 4, \dots$

$$g_{n_p}(z) = z + (-1)^{n-1} \frac{(1-\beta)}{[1+(p-1)\lambda]^n [(1+k)[1+(p-1)\lambda] + k + \beta]} z^p, \quad p = 1, 2, 3, \dots \text{ and}$$

$$x_p \geq 0, y_p \geq 0, x_1 = 1 - \sum_{p=2}^{\infty} (x_p + y_p) \geq 0.$$

In particular, the extreme points of $\overline{S_H}(n, m, k, \lambda, \beta)$ are $\{h_n\}$ and $\{g_{n_p}\}$.

Proof: Let

$$\begin{aligned} f_n(z) &= \sum_{p=1}^{\infty} (x_p h_p(z) + y_p g_{n_p}(z)) \\ &= \sum_{p=2}^{\infty} (x_p + y_p) - \sum_{p=2}^{\infty} \frac{(1-\beta)}{[1+(p-1)\lambda]^n [(1+k)[1+(p-1)\lambda] - k - \beta]} x_p z^p \\ &\quad + (-1)^{n-1} \sum_{p=1}^{\infty} \frac{(1-\beta)}{[1+(p-1)\lambda]^n [(1+k)[1+(p-1)\lambda] + k + \beta]} y_p z^{-p} \end{aligned}$$

Then

$$\begin{aligned} &= \sum_{p=2}^{\infty} \frac{[1+(p-1)\lambda]^n [(1+k)[1+(p-1)\lambda] - k - \beta]}{(1-\beta)} |a_p| \\ &\quad + \sum_{p=1}^{\infty} \frac{[1+(p-1)\lambda]^n [(1+k)[1+(p-1)\lambda] + k + \beta]}{(1-\beta)} |b_p| \\ &= \sum_{p=2}^{\infty} x_p + \sum_{p=1}^{\infty} y_p = 1 - x_1 \leq 1 \end{aligned}$$

and so $f_n \in \overline{S_H}(n, m, k, \lambda, \beta)$.

Conversely, suppose that $f_n \in \overline{S_H}(n, m, k, \lambda, \beta)$.

Setting

$$x_p = \frac{[1+(p-1)\lambda]^n [(1+k)[1+(p-1)\lambda] - k - \beta]}{(1-\beta)} a_p, p = 2, 3, \dots$$

$$y_p = \frac{[1+(p-1)\lambda]^n [(1+k)[1+(p-1)\lambda] - k - \beta]}{(1-\beta)} b_p, p = 1, 2, 3, \dots$$

where $\sum_{p=1}^{\infty} (x_p + y_p) = 1$ we obtain $f_n(z) = \sum_{p=1}^{\infty} (x_p h_p(z) + y_p g_{n_p}(z))$ as required.

Theorem 4: Let $f_n \in \overline{S}_H(n, m, k, \lambda, \beta)$ then for $|z| = r < 1$

we have

$$|f_n(z)| \leq (1 + |b_1|)r + \frac{1}{(2\lambda)^n} \left\{ \frac{(1-\beta)}{(1+k)(1+\lambda) - k - \beta} - \frac{(1+k)(1+\lambda) + k + \beta}{(1+k)(1+\lambda) - k - \beta} |b_1| \right\} r^2$$

and

$$|f_n(z)| \geq (1 - |b_1|)r - \frac{1}{(2\lambda)^n} \left\{ \frac{(1-\beta)}{(1+k)(1+\lambda) - k - \beta} - \frac{(1+k)(1+\lambda) + k + \beta}{(1+k)(1+\lambda) - k - \beta} |b_1| \right\} r^2$$

Proof. Let $f_n \in \overline{S}_H(n, m, k, \lambda, \beta)$. Taking absolute value of f_n we obtain

$$\begin{aligned} |f_n(z)| &\leq (1 + |b_1|)r + \sum_{p=2}^{\infty} (|a_p| + |b_p|) r^p \\ &\leq (1 + |b_1|)r + \sum_{p=2}^{\infty} (|a_p| + |b_p|) r^2 \\ &\leq (1 + |b_1|)r + \frac{(1-\beta)}{(2\lambda)^n [(1+k)(1+\lambda) - k - \beta]} \left\{ \sum_{p=2}^{\infty} \frac{(2\lambda)^n [(1+k)(1+\lambda) - k - \beta]}{(1-\beta)} (|a_p| + |b_p|) \right\} r^2 \\ &\leq (1 + |b_1|)r + \frac{(1-\beta)}{(2\lambda)^n [(1+k)(1+\lambda) - k - \beta]} \sum_{p=2}^{\infty} \left(\frac{(2\lambda)^n [(1+k)(1+\lambda) - k - \beta]}{(1-\beta)} |a_p| + \frac{(2\lambda)^n [(1+k)(1+\lambda) + k + \beta]}{(1-\beta)} |b_p| \right) r^2 \\ &\leq (1 + |b_1|)r + \frac{(1-\beta)}{(2\lambda)^n [(1+k)(1+\lambda) - k - \beta]} \sum_{p=2}^{\infty} \left(1 - \frac{(2\lambda)^n [(1+k)(1+\lambda) + k + \beta]}{(1-\beta)} |b_p| \right) r^2 \\ &\leq (1 + |b_1|)r + \frac{1}{(2\lambda)^n} \left\{ \frac{(1-\beta)}{(1+k)(1+\lambda) - k - \beta} - \frac{(1+k)(1+\lambda) + k + \beta}{(1+k)(1+\lambda) - k - \beta} |b_1| \right\} r^2. \end{aligned}$$

The forthcoming result follows from left hand inequality in Theorem 2.4.

Theorem 5: The class of $\overline{S}_H(n, m, k, \lambda, \beta)$ is closed under convex combination.

Proof: For $i = 1, 2, 3, \dots$ suppose $f_{n_i}(z) \in \overline{S}_H(n, m, k, \lambda, \beta)$ where

$$f_{n_i} = z - \sum_{p=2}^{\infty} |a_{ip}| z^p + (-1)^n \sum_{p=1}^{\infty} |b_{ip}| z^{-p}$$

then by Theorem 2

$$\begin{aligned} & \sum_{p=2}^{\infty} \frac{[1+(p-1)\lambda]^n [(1+k)[1+(p-1)\lambda] - k - \beta]}{(1-\beta)} |a_{ip}| \\ & + \sum_{p=2}^{\infty} \frac{[1+(p-1)\lambda]^n [(1+k)[1+(p-1)\lambda] + k + \beta]}{(1-\beta)} |b_{ip}| \leq 1. \end{aligned} \quad (2.6)$$

For $\sum_{i=1}^{\infty} t_i = 1$, $0 \leq t_i \leq 1$, the convex combination of f_{n_i} may be written as

$$\sum_{i=1}^{\infty} t_i f_{n_i}(z) = z - \sum_{p=2}^{\infty} \left(\sum_{i=1}^{\infty} t_i |a_{ip}| \right) z^p + (-1)^n \sum_{p=1}^{\infty} \left(\sum_{i=1}^{\infty} t_i |b_{ip}| \right) z^{-p}$$

hence by (2.6)

$$\begin{aligned} & \sum_{p=2}^{\infty} \left(\frac{[1+(p-1)\lambda]^n [(1+k)[1+(p-1)\lambda] - k - \beta]}{(1-\beta)} \right) \left(\sum_{i=1}^{\infty} t_i |a_{ip}| \right) \\ & + \sum_{p=1}^{\infty} \left(\frac{[1+(p-1)\lambda]^n [(1+k)[1+(p-1)\lambda] + k + \beta]}{(1-\beta)} \right) \left(\sum_{i=1}^{\infty} t_i |b_{ip}| \right) \\ & = \sum_{i=1}^{\infty} t_i \left(\sum_{p=2}^{\infty} \frac{[1+(p-1)\lambda]^n [(1+k)[1+(p-1)\lambda] - k - \beta]}{(1-\beta)} |a_{ip}| + \sum_{p=1}^{\infty} \frac{[1+(p-1)\lambda]^n [(1+k)[1+(p-1)\lambda] + k + \beta]}{(1-\beta)} |b_{ip}| \right) \\ & \leq \sum_{i=1}^{\infty} t_i \leq 1 \end{aligned}$$

and therefore $\sum_{i=1}^{\infty} t_i f_{n_i}(z) \in \overline{S}_H(n, m, k, \lambda, \beta)$

This completes the proof.

REFERENCES

1. O. P. Ahuja, R. Aghalary and S. B. Joshi, Harmonic univalent functions associated with k- uniformly starlike functions, *Math Sci. Res. J.*, **9** (1) (2005), 9-17.
2. J. Clunie, T. Sheil-Small, Harmonic univalent functions, *Ann. Acad. Sci. Fenn. A. I. Math.*, **9** (1984), 3-25.
3. J. M. Jahangiri, Harmonic functions starlike in the unit disc, *J. Math. Anal. Appl.*, **235** (1999), 470-477.
4. J. M. Jahangiri, Y. C. Kim and H. M. Srivastava, Construction of a certain class of harmonic close-to convex functions associated with Alexander integral transform, *Integral Trans and Spec Funct.*, **14** (2003), 237-242.
5. J. M. Jahangiri, G. Murgusundarmoorthy and K. Vijay, Salagean –type harmonic univalent functions, *South J. Pure and Appl. Math.*, **2** (2002), 77-82.
6. Al-Oboudi, F. M. On univalent functions defined by generalized Salagean operator, *IJMMS*, **27**(2004), 1429-1436.
7. G. S. Salagean, Subclass of univalent functions, *Lect Notes in Math. Springer-Verlag*, **1013** (1983), 362-372.
8. K. Al-Shaqsi and M. Darus, Differential Sandwich theorems with generalized derivative oprator, *Inter. J. Comp. Math. Sci.*, **2**, (2) (2008), 75-78.
9. H. Silverman, Harmonic univalent functions with negative coefficients, *J. Math Anal Appl.*, **220**(1998), 283-289.
10. S. Yalcin, On certain harmonic univalent functions defined by Salagean derivative, *Soochow J.Math.*, **31** (3) (2005), 321-331.

Adaptive Flow Orientation Based Personal Identification Using Fingerprint Feature Extraction

¹Ms. Preeti Jain, ²H. K. Sawant

^{1,2}Department of Information Technology, Bharati Vidyapeeth Deemed University
 College Of Engineering, Pune-46

Abstract: A fingerprint is the feature pattern of one finger. It is believed with strong evidences that each fingerprint is unique. Each person has his own fingerprints with the permanent uniqueness. So fingerprints have being used for identification and forensic investigation for a long time. Two representation forms for fingerprints separate the two approaches for fingerprint recognition. The approach, which is minutia-based, represents the fingerprint by its local features, like terminations and bifurcations. This approach has been intensively studied, also is the backbone of the current available fingerprint recognition products.

1. INTRODUCTION

The fingerprint recognition problem can be grouped into two sub-domains: one is fingerprint verification and the other is fingerprint identification (Figure 1). In addition, different from the manual approach for fingerprint recognition by experts, the fingerprint recognition here is referred as AFRS (Automatic Fingerprint Recognition System), which is program-based.

1-to-1 verification case or 1-to-m identification case, is straightforward and easy.

2. SYSTEM DESIGN

To implement a minutia extractor, a three-stage approach is widely used by researchers. They are preprocessing, minutia extraction and post processing stage [Figure 2].

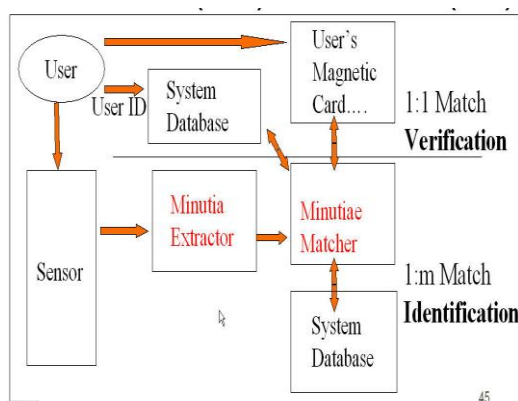


Figure 1 Verification vs. Identification

Fingerprint verification is to verify the authenticity of one person by his fingerprint. The user provides his fingerprint together with his identity information like his ID number. The fingerprint verification system retrieves the fingerprint template according to the ID number and matches the template with the real-time acquired fingerprint from the user. Usually it is the underlying design principle of AFAS (Automatic Fingerprint Authentication System).

Fingerprint identification is to specify one person's identity by his fingerprint(s). Without knowledge of the person's identity, the fingerprint identification system tries to match his fingerprint(s) with those in the whole fingerprint database. It is especially useful for criminal investigation cases. And it is the design principle of AFIS (Automatic Fingerprint Identification System).

However, all fingerprint recognition problems, either verification or identification, are ultimately based on a well-defined representation of a fingerprint. As long as the representation of fingerprints remains the uniqueness and keeps simple, the fingerprint matching, either for the

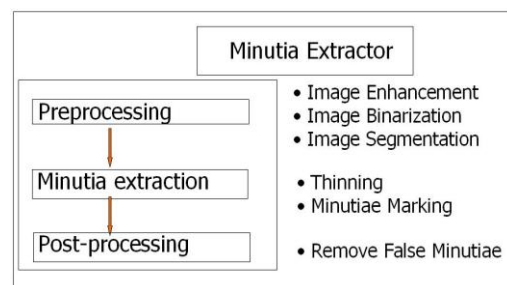


Figure 2 Minutiae Extractor

For the Image Preprocessing of Fingerprint stage, I use Histogram Equalization and Fourier Transform to do image enhancement [9]. And then the fingerprint image is binarized using the locally adaptive threshold method [12]. The image segmentation task is fulfilled by a three-step approach: block direction estimation, segmentation by direction intensity [4] and Region of Interest extraction by Morphological operations. Most methods used in the preprocessing stage are developed by other researchers but they form a brand new combination in my project through trial and error.

For minutia extraction stage, three thinning algorithms [12][2] are tested and the Morphological thinning operation is finally bid out with high efficiency and pretty good thinning quality. The minutia marking is a simple task as most literatures reported but one special case is found during my implementation and an additional check mechanism is enforced to avoid such kind of oversight.

For the postprocessing stage, a more rigorous algorithm is developed to remove false minutia based on [12][1]. Also a novel representation for bifurcations is proposed to unify terminations and bifurcations.

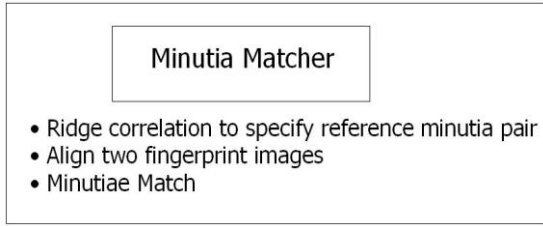


Figure3 Matching Minutiaer

The Matching Minutiaer chooses any two minutia as a reference minutia pair and then match their associated ridges first. If the ridges match well [1], two fingerprint images are aligned and matching is conducted for all remaining minutia [Figure 3].

3. IMAGE PREPROCESSING OF FINGERPRINT

A. Enhancement of Image

Enhancement of Image is to make the image clearer for easy further operations. Since the fingerprint images acquired from sensors or other medias are not assured with perfect quality, those enhancement methods, for increasing the contrast between ridges and furrows and for connecting the false broken points of ridges due to insufficient amount of ink, are very useful for keep a higher accuracy to fingerprint recognition.

B. Binarization of Image

Binarization of Image is to transform the 8-bit Gray fingerprint image to a 1-bit image with 0-value for ridges and 1-value for furrows. After the operation, ridges in the fingerprint are highlighted with black color while furrows are white.

A locally adaptive binarization method is performed to binarize the fingerprint image. Such a named method comes from the mechanism of transforming a pixel value to 1 if the value is larger than the mean intensity value of the current block (16x16) to which the pixel belongs [Figure 4].



Figure 4 the Fingerprint image after adaptive binarization, Binarized image(left), Enhanced gray image(right)

C. Segmentation of Image

In general, only a Region of Interest (ROI) is useful to be recognized for each fingerprint image. The image area without effective ridges and furrows is first

discarded since it only holds background information. Then the bound of the remaining effective area is sketched out since the minutia in the bound region are confusing with those spurious minutia that are generated when the ridges are out of the sensor.

To extract the ROI, a two-step method is used. The first step is block direction estimation and direction variety check [1], while the second is intrigued from some Morphological methods.

4. MINUTIA EXTRACTION

A. Image thinning

Ridge Thinning is to eliminate the redundant pixels of ridges till the ridges are just one pixel wide. [12] uses an iterative, parallel thinning algorithm. In each scan of the full fingerprint image, the algorithm marks down redundant pixels in each small image window (3x3). And finally removes all those marked pixels after several scans. In my testing, such an iterative, parallel thinning algorithm has bad efficiency although it can get an ideal thinned ridge map after enough scans. [2] uses a one-in-all method to extract thinned ridges from gray-level fingerprint images directly. Their method traces along the ridges having maximum gray intensity value. However, binarization is implicitly enforced since only pixels with maximum gray intensity value are remained. Also in my testing, the advancement of each trace step still has large computation complexity although it does not require the movement of pixel by pixel as in other thinning algorithms. Thus the third method is bid out which uses the built-in Morphological thinning function in MATLAB.

The thinned ridge map is then filtered

By other three Morphological operations to remove some H breaks, isolated points and spikes.

B. Minutia Marking

After the Image thinning, marking minutia points is relatively easy. But it is still not a trivial task as most literatures declared because at least one special case evokes my caution during the minutia marking stage.

In general, for each 3x3 window, if the central pixel is 1 and has exactly 3 one-value neighbors, then the central pixel is a ridge branch [Figure 5.1]. If the central pixel is 1 and has only 1 one-value neighbor, then the central pixel is a ridge ending [Figure5.2].

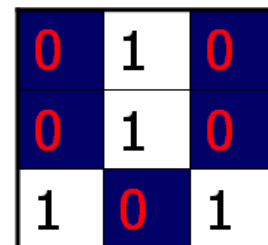


Figure 5.1 Bifurcation

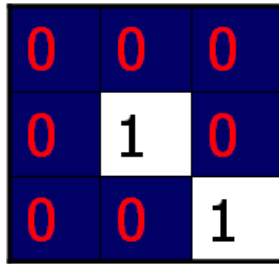


Figure 5.2 Termination

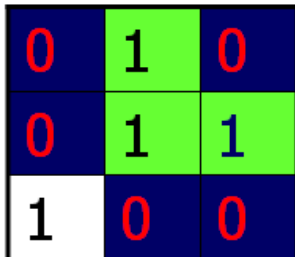


Figure 5.3 Triple counting branch

Figure 5.3 illustrates a special case that a genuine branch is triple counted. Suppose both the uppermost pixel with value 1 and the rightmost pixel with value 1 have another neighbor outside the 3x3 window, so the two pixels will be marked as branches too. But actually only one branch is located in the small region. So a check routine requiring that none of the neighbors of a branch are branches is added.

Also the average inter-ridge width D is estimated at this stage. The average inter-ridge width refers to the average distance between two neighboring ridges. The way to approximate the D value is simple. Scan a row of the thinned ridge image and sum up all pixels in the row whose value is one. Then divide the row length with the above summation to get an inter-ridge width. For more accuracy, such kind of row scan is performed upon several other rows and column scans are also conducted, finally all the inter-ridge widths are averaged to get the D .

Together with the minutia marking, all thinned ridges in the fingerprint image are labeled with a unique ID for further operation. The labeling operation is realized by using the Morphological operation: BWLABEL.

5. MINUTIA POSTPROCESSING

The preprocessing stage does not totally heal the fingerprint image. For example, false ridge breaks due to insufficient amount of ink and ridge cross-connections due to over inking are not totally eliminated. Actually all the earlier stages themselves occasionally introduce some artifacts which later lead to spurious minutia. These false minutia will significantly affect the accuracy of matching if they are simply regarded as genuine minutia. So some mechanisms of removing false minutia are essential to keep the fingerprint verification system effective.

Seven types of false minutia are specified in following diagrams:

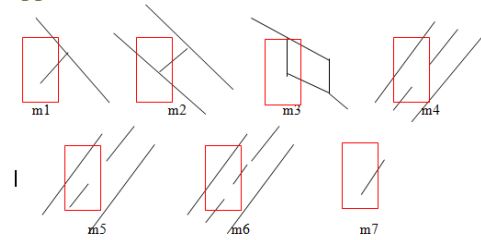


Figure 6 False Minutia Structures. m_1 is a spike piercing into a valley. In the m_2 case a spike falsely connects two ridges. m_3 has two near bifurcations located in the same ridge. The two ridge broken points in the m_4 case have nearly the same orientation and a short distance. m_5 is alike the m_4 case with the exception that one part of the broken ridge is so short that another termination is generated. m_6 extends the m_4 case but with the extra property that a third ridge is found in the middle of the two parts of the broken ridge. m_7 has only one short ridge found in the threshold window.

6. MATCHING MINUTIA

Given two set of minutia of two fingerprint images, the Matching Minutia algorithm determines whether the two minutia sets are from the same finger or not. An alignment-based match algorithm partially derived from the [1] is used in my project. It includes two consecutive stages: one is alignment stage and the second is match stage.

1. Alignment stage. Given two fingerprint images to be matched, choose any one minutia from each image, calculate the similarity of the two ridges associated with the two referenced minutia points. If the similarity is larger than a threshold, transform each set of minutia to a new coordination system whose origin is at the referenced point and whose x-axis is coincident with the direction of the referenced point.
2. Match stage: After we get two set of transformed minutia points, we use the elastic match algorithm to count the matched minutia pairs by assuming two minutia having nearly the same position and direction are identical.

7. EXPERIMENTATION RESULTS

A. Evaluation indexes for fingerprint recognition

Two indexes are well accepted to determine the performance of a fingerprint recognition system: one is FRR (false rejection rate) and the other is FAR (false acceptance rate). For an image database, each sample is matched against the remaining samples of the same finger to compute the False Rejection Rate. If the matching g against h is performed, the symmetric one (i.e., h against g) is not executed to avoid correlation. All the scores for such matches are composed into a series of Correct Score. Also the first sample of each finger in the database is matched against the first sample of the remaining fingers to compute the False Acceptance Rate. If the matching g against h is performed, the symmetric one (i.e., h against g) is not executed to avoid correlation. All the scores from such matches are composed into a series of Incorrect Score.

B. Experimentation Results

A fingerprint database from the FVC2000 (Fingerprint Verification Competition 2000) is used to test the experiment performance. My program tests all the images without any fine-tuning for the database. The experiments show my program can differentiate imposturous minutia pairs from genuine minutia pairs in a certain confidence level. Furthermore, good experiment designs can surely improve the accuracy as declared by [10]. Further studies on good designs of training and testing are expected to improve the result.

Here is the diagram for Correct Score and Incorrect Score distribution:

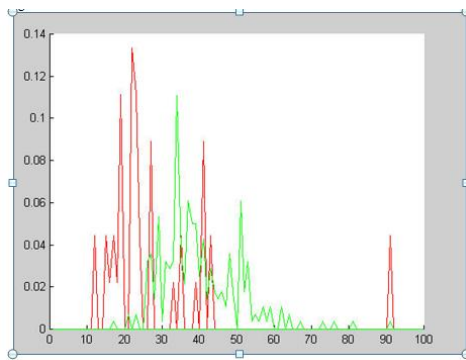


Figure 7 Distribution of Correct Scores and Incorrect Scores Red line: Incorrect Score Green line: Correct Scores

It can be seen from the above figure that there exist two partially overlapped distributions. The Red curve whose peaks are mainly located at the left part means the average incorrect match score is 25. The green curve whose peaks are mainly located on the right side of red curve means the average correct match score is 35. This indicates the algorithm is capable of differentiate fingerprints at a good correct rate by setting an appropriate threshold value.

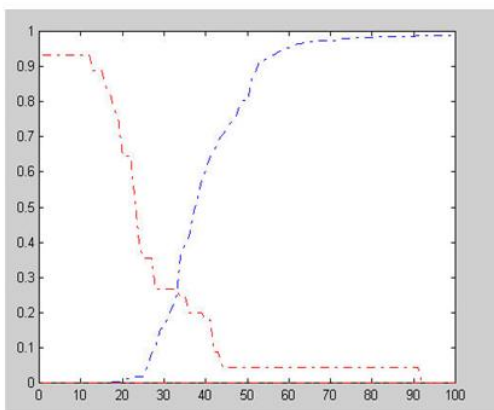


Figure 8 FAR and FRR curve -Blue dot line: FRR curve, Red dot line: FAR curve

The above diagram shows the FRR and FAR curves. At the equal error rate 25%, the separating score 33 will falsely reject 25% genuine minutia pairs and falsely accept 25% imposturous minutia pairs and has 75% verification rate.

The high incorrect acceptance and false rejection are due to some fingerprint images with bad quality and the vulnerable Matching Minutia algorithm.

8. CONCLUSION

Proposed system has combined many methods to build a minutia extractor and a Matching Minutiaer. The combination of multiple methods comes from a wide investigation into research paper. Also some novel changes like segmentation using Morphological operations, minutia marking with special considering the triple branch counting, minutia unification by decomposing a branch into three terminations, and matching in the unified x-y coordinate system after a two-step transformation are used in System. Also a program coding with MATLAB going through all the stages of the fingerprint recognition is built. It is helpful to understand the procedures of fingerprint recognition. And demonstrate the key issues of fingerprint recognition.

REFERENCES

- [1] Lin Hong. "Automatic Personal Identification Using Fingerprints", Ph.D. Thesis, 1998.
- [2] D.Maio and D. Maltoni. Direct gray-scale minutiae detection in fingerprints. IEEE Trans. Pattern Anal. And Machine Intell., 19(1):27-40, 1997.
- [3] Jain, A.K., Hong, L., and Bolle, R.(1997), "On-Line Fingerprint Verification," IEEE Trans. On Pattern Anal and Machine Intell, 19(4), pp. 302-314.
- [4] N. Ratha, S. Chen and A.K. Jain, "Adaptive Flow Orientation Based Feature Extraction in Fingerprint Images", Pattern Recognition, Vol. 28, pp. 1657-1672, November 1995.
- [5] Alessandro Farina, Zsolt M.Kovacs-Vajna, Alberto leone, Fingerprint minutiae extraction from skeletonized binary images, Pattern Recognition, Vol.32, No.4, pp877-889, 1999.
- [6] Lee, C.J., and Wang, S.D.: Fingerprint feature extration using Gabor filters, Electron. Lett., 1999, 35, (4), pp.288-290.
- [7] M. Tico, P.Kuosmanen and J.Saarinen. Wavelet domain features for fingerprint recognition, Electroni. Lett., 2001, 37, (1), pp.21-22.
- [8] L. Hong, Y. Wan and A.K. Jain, "Enhancement of Image: Algorithms and Performance Evaluation", IEEE Transactions on PAMI ,Vol. 20, No. 8, pp.777-789, August 1998.
- [9] Image Systems Engineering Program, Stanford University. Student project By Thomas Yeo, Wee Peng Tay, Ying Yu Tai. http://ise0.stanford.edu/class/ee368a_proj01/dropbox/project22/finger/
- [10] FVC2000. <http://bias.csr.unibo.it/fvc2000/>
- [11] FVC2002. <http://bias.csr.unibo.it/fvc2002/>
- [12] L.C. Jain, U.Halici, I. Hayashi, S.B. Lee and S.Tsutsui. Intelligent biometric techniques in fingerprint and face recognition. 1999, the CRC Press.
- [13] M. J. Donahue and S. I. Rokhlin, "On the Use of Level Curves in Image Analysis," Image Understanding, VOL. 57, pp 652 - 655, 1992.

A Hybrid Neural Network Approach for Face Recognition

¹Ashwini Kanade, ²Akhil Khare

^{1,2} Department Of Information Technology, Bharati Vidyapeeth Deemed University
College Of Engineering, Pune-46

ABSTRACT: *The face recognition algorithm that is presented here is a memory based face recognition system. The memory-based technique for view-based frontal face recognition can outperform more than sophisticated algorithms that use Principal Components Analysis (PCA) and neural networks. The goal of this report is to write about the most common methods that have been used till now for face recognition. Analyse these methods and give a general idea of the background of the algorithm, ARENA. The capability of the face recognition is to find the exact match of a face image from an image database System. The algorithm that is used in order to achieve that is called AREN.*

1. INTRODUCTION

The objective of our system is to recognise and identify faces, not previously presented to or in some way processed by the system. There are many datasets involved in this system. Some of them are the ORL, MIT database which consisting of a large set of images of different people. The database has many variations in pose, scale, facial expression and details. Some of the images are used for training the system and some for testing. The test set is not involved in any part of training or configuration of the system, except for the weighted committees.

The algorithm used for the face recognition, known as ARENA. Similar to several other approaches to face recognition and identification, which use Principal Component Analysis (PCA) as pre-processing, dimensionality reduction and feature extraction, of the input images. One of the main parts of the system is a neural network. The use of a neural network makes the algorithm perform better.

The purpose of face recognition algorithm is to examine a set of images and try to find the exact match of a given image. An advanced system would be a neural network face recognition algorithm. The system examines small windows of the image in order to calculate the distances of given points. That would be done from any algorithm but in a system where the system use neural networks the system arbitrates between multiple networks in order to improve performance over a single network.

The goal of the system is to formulate paradigms for detection and recognition of human faces, and especially develop an algorithm, which is going to have high performance in complex backgrounds. One of the applications would be towards adding face-oriented queries to our image database.

The fundamental principle, which we are exploiting for our face recognition algorithm, is Principal Component Analysis. Thought the algorithm is much simpler. One of the aims is to run tests in order to compare the algorithm with two PCA algorithm and also show that the calculation between two given point with the ARENA algorithm is efficient.

1.1 Face recognition

Face recognition is a part of a wide area of pattern recognition technology. Recognition and especially face recognition covers a range of activities from many walks of life. Face recognition is something that humans are

particularly good at and science and technology have brought many similar tasks to us. Face recognition in general and the recognition of moving people in natural scenes in particular, require a set of visual tasks to be performed robustly. That process includes mainly three-task acquisition, normalisation and recognition. By the term acquisition mean the detection and tracking of face-like image patches in a dynamic scene. Normalisation is the segmentation, alignment and normalisation of the face images, and finally recognition that is the representation and modelling of face images as identities, and the association of novel face images with known models.

Given the requirement for determining people's identity, the obvious question is what technology is best suited to supply this information? There are many ways that humans can identify each other, and so is for machines. There are many different identification technologies available, many of which have been in commercial use for years. The most common person verification and identification methods today are Password/PIN known as Personal Identification Number, systems. The problem with that or other similar techniques is that they are not unique, and is possible for somebody to forget loose or even have it stolen for somebody else. In order to overcome these problems there has developed considerable interest in "biometrics" identification systems, which use pattern recognition techniques to identify people using their characteristics. Some of those methods are fingerprints and retina and iris recognition. Though these techniques are not easy to use. For example in bank transactions and entry into secure areas, such technologies have the disadvantage that they are intrusive both physically and socially. The user must position the body relative to the sensor, and then pause for a second to declare himself or herself. That doesn't mean that face recognition doesn't need specific positioning.

While the pause and present interaction are useful in high-security, they are exactly the opposite of what is required when building a store that recognise its best customers, or an information kiosk that remembers you, or a house that knows the people who live there. Face recognition from video and voice recognition have a natural place in these next generation smart environments, they are unobtrusive, are usually passive, do not restrict user movement, and are now both low power and inexpensive. Perhaps most important, however, is that humans identify

other people by their face and voice, therefore are likely to be comfortable with systems that use face and voice recognition.

2. FACE RECOGNITION

There are many algorithms that can be used for face recognition. Most of them are based on the same techniques and methods. Some of the most popular are Principal component analysis and the use of eigenfaces.

2.1 Principal Component Analysis

On the field of face recognition most of the common methods employ Principal Component Analysis. Principal Component Analysis is based on the Karhunen-Loeve (K-L), or Hostelling Transform, which is the optimal linear method for reducing redundancy, in the least mean squared reconstruction error sense. 1. PCA became popular for face recognition with the success of eigenfaces. The idea of principal component analysis is based on the identification of linear transformation of the co-ordinates of a system. "The three axes of the new co-ordinate system coincide with the directions of the three largest spreads of the point distributions." In the new co-ordinate system that we have now the data is uncorrected with the data we had in the first co-ordinate system. [2] For face recognition, given dataset of N training images, we create N d -dimensional vectors, where each pixel is a unique dimension. The principal components of this set of vectors is computed in order to obtain a $d \times m$ projection matrix, W . The image of the i^{th} vector may be represented as weights:

$$\vec{\theta}_i = (\theta_1, \theta_2, \dots, \theta_m)^T \quad (1)$$

Such that

$$\vec{x}_i = \vec{\mu} + W\vec{\theta} \quad (2)$$

Approximates the original image where μ is the mean, of the χ_i and the reconstruction is perfect when $m = d$. P1

As mentioned before the ARENA algorithm is going to be tested and its performance is going to be compared with other algorithms. For the comparison we are going to use two different PCA algorithms. The first algorithm is computing and storing the weight of vectors for each person's image in the training set, so the actual training data is not necessary. In the second algorithm each weight of each image is stored individually, is a memory-based algorithm. For that we need more storing space but the performance is better.

In order to implement the Principal component analysis in MATLAB we simply have to use the command *prepca*. The syntax of the command is

$$ptrans, transMat = prepca(P, min_frac)$$

Prepca pre-processes the network input training set by applying a principal component analysis. This analysis transforms the input data so that the elements of the input vector set will be uncorrected. In addition, the size of the input vectors may be reduced by retaining only those components, which contribute more than a specified fraction (*min_frac*) of the total variation in the data set. Prepca takes these inputs the matrix of centred input (column) vectors, the minimum fraction variance

component to keep and as result returns the transformed data set and the transformation matrix.

A) Alorithm

Principal component analysis uses singular value decomposition to compute the principal components. A matrix whose rows consist of the eigenvectors of the input covariance matrix multiplies the input vectors. This produces transformed input vectors whose components are uncorrected and ordered according to the magnitude of their variance.

Those components, which contribute only a small amount to the total variance in the data set, are eliminated. It is assumed that the input data set has already been normalised so that it has a zero mean.

In our test we are going to use two different "versions" of PCA. In the first one the centroid of the weight vectors for each person's images in the training set is computed and stored. On the other hand in PCA-2 a memory based variant of PCA, each of the weight vectors is individually computed and stored.

B) Eigenfaces

Human face recognition is a very difficult and practical problem in the field of pattern recognition. On the foundation of the analysis of the present methods on human face recognition, a new technique of image feature extraction is presented. And combined with the artificial neural network, a new method on human face recognition is brought up. By extraction the sample pattern's algebraic feature, the human face image's eigenvalues, the neural network classifier is trained for recognition. The Kohonen network we adopted can adaptively modify its bottom up weights in the course of learning. Experimental results show that this method not only utilises the feature aspect of eigenvalues but also has the learning ability of neural network. It has better discriminate ability compared with the nearest classifier. The method this paper focused on has wide application area. The adaptive neural network classifier can be used in other tasks of pattern recognition.

In order to calculate the eigenfaces and eigenvalues in MATLAB we have to use the command *eig*. The syntax of the command is

$$\begin{aligned} d &= eig(A) \\ V, D &= eig(A) \\ V, D &= eig(A, 'nobalance') \\ d &= eig(A, B) \\ V, D &= eig(A, B) \end{aligned}$$

$d = eig(A)$ returns a vector of the eigenvalues of matrix A . $V, D = eig(A)$ produces matrices of eigenvalues (D) and eigenvectors (V) of matrix A , so that $A*V = V*D$. Matrix D is the canonical form of A , a diagonal matrix with A 's eigenvalues on the main diagonal. Matrix V is the modal matrix, its columns are the eigenvectors of A . The eigenvectors are scaled so that the norm of each is 1.0. Then we use $V, D = eig(A)'$; $W = W'$ in order to compute the left eigenvectors, which satisfy $W*A = D*W$.

$V, D = eig(A, 'nobalance')$ finds eigenvalues and eigenvectors without a preliminary balancing step. Ordinarily, balancing improves the conditioning of the input matrix, enabling more accurate computation of the eigenvectors and eigenvalues. However, if a matrix

contains small elements that are really due to round-off error, balancing may scale them up to make them as significant as the other elements of the original matrix, leading to incorrect eigenvectors. .

$d = eig(A,B)$ returns a vector containing the generalised eigenvalues, if A and B are square matrices. $V,D = eig(A,B)$ produces a diagonal matrix D of generalised eigenvalues and a full matrix V whose columns are the corresponding eigenvectors so that $A*V = B*V*D$.

C) Euclidean distance

One of the ideas on which face recognition is based is the distance measures, between to points. The problem of finding the distance between two or more point of a set is defined as the Euclidean distance. The Euclidean distance is usually referred to the closest distance between two or more points. So we can define the Euclidean distance d_{ij} between points x_{ik} and x_{jk} as :

$$d_{ij} = \sum_{k=1}^p (x_{ik} - x_{jk})^2 \quad (3)$$

3. ARENA ALGORITHM

As mentioned before in the introduction, the algorithm that is used in the System is called ARENA. Is a memory-based technique for view-based frontal face recognition that can outperform more sophisticated algorithms that use Principal Components Analysis and neural networks. This method does not perform any complex feature extraction, nor does it incorporate any face-specific information. The ARENA algorithm technique is closely related to correlation templates. However, the use of novel distance metrics greatly improves the performance. Augmenting the memory base with additional, synthesised face images results in further improvements in performance.

The technique is going to be tested on standard face recognition databases, and direct comparisons with other techniques will show that our algorithm achieves comparable or superior results.

Arena algorithm has also a good asymptotic computation and storage behaviour, and is ideal for incremental training. The system has been integrated with a neural-network based face detection system into a real-word visitor identification system that has been operating successfully in an outdoor environment with uncontrolled lighting for several months.

A) The algorithm

Arena is, as mentioned, a memory based algorithm that employs reduced resolution images, like in Principal Component Analysis, 16x16 and the a parameter of similarity measure L_0^* . One of the most important parts of the system is to reduce the resolution of the image. That is achieved by averaging over non-overlapping rectangular regions in the image. The aim of the system is to find the exact mach of an image from the given datasets, so the distance from the query image to each of the datasets stored images is computed and the best much is returned.

The key point of the algorithm for its good performance is the L_p^* similarity measure. The measure that is used has a better performance than the Euclidean distance. L_p^* is defined as

$$L_p(\vec{a}) \equiv (\sum |a_i|^p)^{1/p} \quad (4)$$

The Euclidean is defined for $p=2$ so that we have:

$$L_2(\vec{x} - \vec{y}). \quad (5)$$

Because we are not interested in the actual distances, but only in the ordering we can say that equation 3 becomes:

$$L_p(\vec{a}) \equiv (\sum |a_i|^p)^{1/p} \quad (6)$$

For each reduced resolution image we have is converted to a vector, \vec{x} , where each pixel in the image is represented as a component of the vector. So since the individual pixel intensities are noisy, we can define the similarity measure for $p=0$ as:

$$L_0(\vec{x} - \vec{y}) \equiv \sum_{|x_i - y_j| \geq \delta} 1 \quad (7)$$

where δ is a threshold value, such that pixels whose intensities differ by less than δ are considered equivalent.

4. COMPLEXITY

One of the most important aspects of an algorithm is the computational complexity and the storage. Testing the ARENA algorithm, and also different versions of principal component analysis, ARENA can be trained and tested faster, and also has a better storage. The advantage of ARENA compare to other algorithms can be for three main reasons.

Firstly the training time for arena scales linearly with the number of images that we use for training, in comparison with PCA methods. The training times of ARENA and two PCA methods that are used from MATLAB are as follows.

Method	Training Time (Computational Complexity)
PCA-1	$O(N^3 + N^2d)$
PCA-2	$O(N^3 + N^2d)$
ARENA	$O(Nd)$

Where N is the total number of the images that we use and d is the dimension of each image.

For the classification time of the algorithms that PCA-2 and ARENA are slower than PCA-1. But ARENA still faster than PCA-2

Method	Classification Time (Computational Complexity)
PCA-1	$O(cm + dm)$
PCA-2	$O(Nm + dm)$
ARENA	$O(Nm + d)$

Though ARENA has an advantage compare to the PCA-1 algorithm. ARENA is not computing the dimension of the reduced representation, m for each d . c is the number of people on the images.

From these two comparisons of the three algorithms but also from the tests show that ARENA requires less storage space than the other two face recognition methods. PCA-1 requires more storage because needs to store all the vectors of size d , Apart from that ARENA is performing all the computations in the reduced dimensional space. The only disadvantage of ARENA to the other algorithms is that requires more storage if the number of images that we use for training or testing is very large.

Method	Storage Space
PCA-1	$O(cm + dm)$
PCA-2	$O(Nm + dm)$
ARENA	$O(Nm)$

5. CONCLUSION

Face recognition is one of the several techniques for recognising people. There are several methods that can be used for that purpose. Some of the most common are using PCA or eigenfaces. Thought there are other new techniques more simple to understand use and implement but also with very good performance. The ARENA algorithm is one of those algorithms. As we show ARENA has very good performance and is a very accurate especially if we use a feedforward neural network.

Face recognition technology has come a long way in the last twenty years. Today, machines are able to automatically verify identity information for secure transactions, for surveillance and security tasks, and for access control to buildings. These applications usually work in controlled environments and recognition algorithms that can take advantage of the environmental constraints to obtain high recognition accuracy. However, next generation face recognition systems are going to have widespread application in smart environments, where computers and machines are more like helpful assistants. A major factor of that evolution is the use of neural networks in face recognition. A different field of science that also is very fast becoming more and more efficient, popular and helpful to other applications.

The combination of these two fields of science manage to achieve the goal of computers to be able to reliably identify nearby people in a manner that fits naturally within the pattern of normal human interactions. "They must not require special interactions and must conform to human intuitions about when recognition is likely." This implies that future smart environments should use the same modalities as humans, and have approximately the same limitations. "These goals now appear in reach however, substantial research remains to be done in making person recognition technology work reliably, in widely varying conditions using information from single or multiple modalities."

References

- 1) High Performance Memory Based Face Recognition for Visitor Identification, Terence Sim, Shumeet Baluja, Rahul Sukthankar, Mathew D. Mullin
- 2) Face Recognition: A Convolutional Neural Network Approach, Steve Lawrence, C. Lee Giles, Ah Chung Tsoi, Andrew D. Back, IEEE Transactions on Neural Networks, Volume 8, Number 1, pp. 98-113, 1997.
- 3) Face Recognition with Multi-Layer Perceptrons, Erik Hjelmås and Jørn Wroldsen, Department of Electrical Engineering and Science Gjøvik College.
- 4) Face Recognition in Dynamic Scenes, Stephen McKenna, Shaogang Gong and Yogesh Raja, Machine Vision Laboratory, Department of Computer Science Queen Mary and Westfield College.
- 5) Neural Network Based Face Recognition, Henry A. Rowley, Shumeet Baluja and Takeo Kanade, IEEE.
- 6) Face recognition: A hybrid neural network approach, S. Lawrence, C. Giles, A. Tsoi, A. Back, Technical report UMIACS-TR-96-16, University of Meriland, 1996
- 7) S. Arya and D.M. Mount. Algorithms for fast vector quantization. In J. A. Storer and M. Cohn, editors, *Proceedings of DCC 93: Data Compression Conference*, pages 381–390. IEEE Press, 1993.
- 8) Hans-Ulrich Bauer and Klaus R. Pawelzik. Quantifying the neighborhood preservation of Self-Organizing Feature Maps. *IEEE Transactions on Neural Networks*, 3(4):570–579, 1992.
- 9) Yoshua Bengio, Y. Le Cun, and D. Henderson. Globally trained handwritten word recognizer using spatial representation, space displacement neural networks and hidden Markov models. In *Advances in Neural Information Processing Systems 6*, San Mateo CA, 1994. Morgan Kaufmann.
- 10) J.L. Blue, G.T. Candela, P.J. Grother, R. Chellappa, and C.L. Wilson. Evaluation of pattern classifiers for fingerprint and OCR applications. *Pattern Recognition*, 27(4):485–501, April 1994.
- 11) L. Bottou, C. Cortes, J.S. Denker, H. Drucker, I. Guyon, L. Jackel, Y. Le Cun, U. Muller, E. Sackinger, P. Simard, and V.N. Vapnik. Comparison of classifier methods: A case study in handwritten digit recognition. In *Proceedings of the International Conference on Pattern Recognition*, Los Alamitos, CA, 1994. IEEE Computer Society Press.
- 12) R. Brunelli and T. Poggio. Face recognition: Features versus templates. *IEEE Transactions on Pattern Analysis and Machine Intelligence*, 15(10):1042–1052, October 1993.
- 13) D. K. Burton. Text-dependent speaker verification using vector quantization source coding. *IEEE Transactions on Acoustics, Speech, and Signal Processing*, 35(2):133, 1987.
- 14) R. Chellappa, C.L. Wilson, and S. Sirohey. Human and machine recognition of faces: A survey. *Proceedings of the IEEE*, 83(5):705–740, 1995.

- 15) Ingemar J. Cox, Joumana Ghosn, and Peter N. Yianilos. Feature-based face recognition using mixture-distance. In *Computer Vision and Pattern Recognition*. IEEE Press, 1996.
- 16) David DeMers and G.W. Cottrell. Non-linear dimensionality reduction. In S.J. Hanson, J.D. Cowan, and C. Lee Giles, editors, *Advances in Neural Information Processing Systems 5*, pages 580–587, San Mateo, CA, 1993. Morgan Kaufmann Publishers.
- 17) H. Drucker, C. Cortes, L. Jackel, Y. Le Cun, and V.N. Vapnik. Boosting and other ensemble methods. *Neural Computation*, 6:1289–1301, 1994.
- 18) K. Fukunaga. *Introduction to Statistical Pattern Recognition, Second Edition*. Academic Press, Boston, MA, 1990.
- 19) S. Haykin. *Neural Networks, A Comprehensive Foundation*. Macmillan, New York, NY, 1994.
- 20) S. Haykin. Personal communication, 1996.
- 21) D.H. Hubel and T.N. Wiesel. Receptive fields, binocular interaction, and functional architecture in the cat's visual cortex. *Journal of Physiology (London)*, 160:106–154, 1962.
- 22) R.A. Jacobs. Methods for combining experts' probability assessments. *Neural Computation*, 7:867–888, 1995.
- 23) T. Kanade. *Picture Processing by Computer Complex and Recognition of Human Faces*. PhD thesis, Kyoto University, 1973.
- 24) Hajime Kita and Yoshikazu Nishikawa. Neural network model of tonotopic map formation based on the temporal theory of auditory sensation. In *Proceedings of the World Congress on Neural Networks, WCNN 93*, volume II, pages 413–418, Hillsdale, NJ, 1993. Lawrence Erlbaum.
- 25) T. Kohonen. The self-organizing map. *Proceedings of the IEEE*, 78:1464–1480, 1990.
- 26) T. Kohonen. *Self-Organizing Maps*. Springer-Verlag, Berlin, Germany, 1995.
- 27) Martin Lades, Jan C. Vorbrüggen, Joachim Buhmann, Jörg Lange, Christoph von der Malsburg, Rolf P. Würtz, and Wolfgang Konen. Distortion invariant object recognition in the dynamic link architecture. *IEEE Transactions on Computers*, 42(3):300–311, 1993.

Application of Eco-Friendly Geotextiles for Landslide Mitigation in a Part of Ooty Hills, Tamil Nadu

T. SUBRAMANI

Dean & Professor, Department of Civil Engineering, V.M.K.V.Engineering college,
Vinayaka Missions University, Salem. Tamilnadu.

ABSTRACT

Landslide is one of the major natural hazards the world is facing. It happens as a result of both man-made as well as natural factors. It causes severe effects on the environment as well as for the mankind. The main triggering factors of landslide are rainfall/snowfall, tectonic activities and human activities. There are many methods adopted for controlling landslides. The study was carried out to know the application of geotextiles in slope stabilization. Ooty is one of the main areas in India which is prone to landslides. Many loose their life, property etc due to landslides every year. The present study attempted in Kattery watershed. Various thematic maps pertaining to landslide hazard studies were prepared from the toposheets and satellite imageries using GIS. Finally the landslide hazard zonation map of Kattery watershed was prepared by assigning proper weights and ranks for various themes. The north eastern and south western part of Kattery watershed is more vulnerable to landslides and the south eastern part is less vulnerable. About 200 kg of soil sample from the landslide site was collected and transported to the laboratory. Physical, chemical and engineering properties of the soil were tested in the laboratory. The laboratory results show that the soil is classified as inorganic soil of low plasticity. The optimum moisture content of the soil is 23.5% and the maximum dry density is 1.61g/cc. The result of direct shear test indicates that the angle of internal friction is 38°. The Liquid Limit of the soil is 45 % and the Plastic Limit is 31.40%. To understand the application of coir geotextile for soil erosion and slope stabilization, laboratory models were created, and the soil was tested by varying slope and moisture content. The model demonstrated that geotextiles performed better for protection of slope and soil erosion. As the coir geotextile is biodegradable and eco-friendly it will not affect the environment also.

Keywords: Eco-Friendly, Geotextiles, Landslide Mitigation, Ooty hills

1. INTRODUCTION

A landslide is a geological phenomenon which is simply defined as the mass movement of rock, debris or earth down a slope and has come to include a broad range of motions whereby falling, sliding and flowing under the influence of gravity dislodges earth material. Landslide is

Defined as the movement of a mass of rock debris, or earth down the slopes (Cruden, 1991). The term 'Landslide' encompasses events such as ground movement, rock falls, and failures of slopes, topples, slides, spreads, and flows such as debris flows, mudflows or mudslides (Varnes, 1996). They often take place in conjunction with earthquakes, floods and volcanic eruption.

TYPES OF LANDSLIDES

The various types of landslides can be differentiated by the kinds of material involved and the mode of movement. Other classification systems incorporate additional variables, such as the rate of movement and the water, air, or ice content of the landslide material.

1.1 LANDSLIDE MITIGATION

Vulnerability to landslide hazards is a function of location, type of human activity, use, and frequency of landslide events. The effects of landslides on people and structures can be lessened by total avoidance of landslide hazard areas or by restricting, prohibiting, or imposing conditions on hazard-zone activity.

1.2 LANDSLIDES AND GEOTEXTILES

Landslides are the major land disturbing activities in the Nilgiri region causing mass erosion problems leading to heavy land degradation, decline in the quality and quantity of water resources and disruption in the communication lines. Re-vegetating of these areas is the final insurance against erosion but such highly degraded lands are difficult to vegetate due to their unstable nature and poor fertility status. Jute and coir geotextile materials have been most popularly used for erosion control and slope stabilization purposes in Europe/USA and most of the geotextile material produced in India is exported to these countries. In India, however, use of these materials for erosion control is not popular. Therefore, natural geotextiles (jute and coir) were experimented to study their efficiency for providing initial mechanical protection and help in establishment of vegetation on degraded steep slopes so that the ultimate protection against erosion would be provided by the lush vegetative cover established in due course of time.

2. SCOPE OF THE STUDY

This project work is carried out in order to study the applicability of Coir Geotextiles for slope stabilization. Landslides in the hilly region causes loss of life and property, damage to natural resources and damage to roads, bridges, telephone, electric lines etc. This leads to immobility of goods and services leading to huge loss of revenue. We can recommend the use of coir geotextiles for the stabilization of the slopes in that area.

3. STUDY AREA

The area of study is Kattery Watershed, which is located in Nilgiri District, Ooty, Tamil Nadu. The study area falls between latitudes 76°41'0"E and 76°45'0"E and longitudes 11°19'0"N and 11°24'0"N. It comes under the toposheet 58 A/11 published by the Survey Of India on 1: 50,000 scale.

4. OBJECTIVES

The study has been carried out with the following objectives

- To delineate landslide hazard zones using remote sensing and GIS
- To assess the engineering properties of soil
- To create a laboratory model for understanding slope stability
- To examine the application of coir geotextiles for the control of landslides
-

5. STUDY AREA DESCRIPTION

Kattery Watershed is in the Nilgiri hills of Western Ghats mountains system. It is situated at 6 km from Ooty on the Ooty-Coimbatore Road. The watershed has a maximum elevation of 2400 m above MSL and is characterised with steep slope, lateritic soils and fairly good drainage network. The annual rainfall is about 1000 mm in two monsoons. The climate ranges from mild to very cold. It has an area of 2976 ha spread over 38 hamlets of two revenue villages with a population of 21,250. Besides forests, cultivation of potato and other vegetables on inwardly graded bench terraces was widely adopted earlier and thus problem of erosion and sedimentation down below were largely seen. However, about two decades before, with market fluctuations tea plantation has become popular. Most of the terraces were defaced to plant tea along the slope. Consequently, erosion got accelerated and silts flowing out silted up the Kattery Reservoir that caters to the needs of defence's cordite factory at Aravankadu. In 1984-85, the reservoir was desilted at a huge cost and thus this high priority watershed was taken up for treating again to arrest soil erosion, reduce sediment inflow to Kattery Reservoir and improve the Livelihood of the watershed families. The base map of the study area is given in the figure 1.

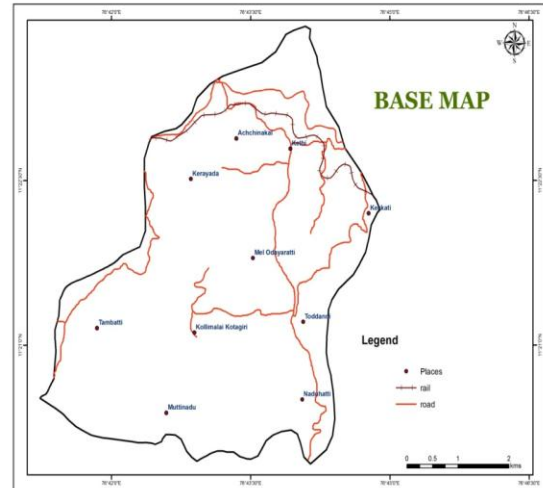


Figure.1 Base map of Kattery Watershed

6. CLIMATE AND RAINFALL

The district receives rainfall from both southwest and northeast monsoons. The southwest monsoon is more active contributing nearly 50 percent in the west and 40 percent in the east. The northeast monsoon is moderate, contributing nearly 40 percent. The precipitation of rainfall gradually decreases towards west to east. The rains during the winter and summer periods are significant. The climate of Nilgiri district is temperate and salubrious throughout the year. Mornings in general are more humid than the afternoons, with the humidity exceeding 90%.

7. GEOLOGY, GEOMORPHOLOGY, DRAINAGE & SOIL TYPE

Structurally the Kattery watershed comprise Archean metamorphic rocks made up of charnockite, biotite gneiss, quartzite & hornblende granite - along with some intrusive bodies like pegmatite dolerite and quartz veins. Apart from these small enclaves of schistose rocks like talc chlorite schist, chlorite schist are also found. The laterite found over the charnockites is hard.

The area falls in the Uthagamandalam – Kotagiri plantation surface which rises to a height of more than 2000 m above MSL. The Uthagamandalam region is more elevated containing Doddabetta peak and its eastern extension the Honnathalai RF. The elevation gradually drops from about 2500 to 1500 m which is the next plantation level referred to as Coonoor plantation surface. Much of the area forms plateau landform in this surface and the erosional action of the streams have resulted in the formation of valleys with steep to moderate slopes.

The plateau, nearly co-terminus with the Nilgiri district, is drained by hundreds of streams. The area forms part of the Moyar River drainage basin. The original consequent drainage has been superposed by a subsequent pattern as a later development, at places. The drainage is mainly dendritic in nature.

The soil of the area falls under two major types - (1) clayey soil, (2) loamy soil. The depth of the soil usually varies from one to three feet and that of the sub-soil from 10 to 14 feet. The sub-soil is invariably porous.

The soil sample was tested in the laboratory to understand its various physical and engineering properties (Figure.3).

8. METHODOLOGY

To achieve the set objectives the methodology has been divided into five major parts which is illustrated in the figure.2.

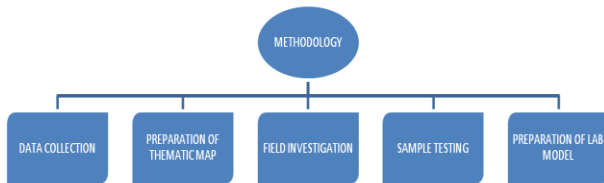


Figure.2. Flow chart of the methodology

9. DATA COLLECTION

- Various literatures related to coir geotextile and its application for slope stabilization were collected
- Toposheet of the study area and various satellite images were collected for preparation of various thematic maps pertaining to this study
- Rainfall details were collected from government departments
- The available maps such as soil and geology of the area were collected
- Coir geotextile materials were collected from a Geotextile manufacturing factory located in Alleppey

10. PREPARATION OF THEMATIC MAPS

Several thematic maps have been prepared to understand various parameters like drainage, slope, geology, geomorphology etc in order to get an idea about the study area. All the thematic maps were integrated using GIS and finally the landslide hazard zonation map of the watershed has been prepared after giving proper weightage and rank.

11. FIELD INVESTIGATION

Field work was carried out in Ooty to verify the thematic maps and also to collect soil samples for preparation of laboratory model. Recent landslides and old landslide scars were investigated in the field. About 150 kg soil sample was collected from the Kattery landslide site and transported to the laboratory for assessing engineering properties. The area of recent landslide is Achanakal which occurred in the year 2009.

12. SAMPLE TESTING

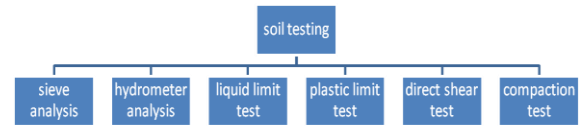


Figure.3. Soil testing

13. PREPARATION OF LAB MODEL

Since the complete study cannot be carried out in the field to understand the usage of geotextiles, a lab model was created with the samples collected from the study area. About 150 kg of soil sample was used for the construction of the model (Figure.4). A slope was decided for the model. The angle at which the slope failed (angle of repose) was measured for the two conditions namely (1) slope without geotextile (2) slope with geotextile. The experiment was also extended for the increased moisture content also.

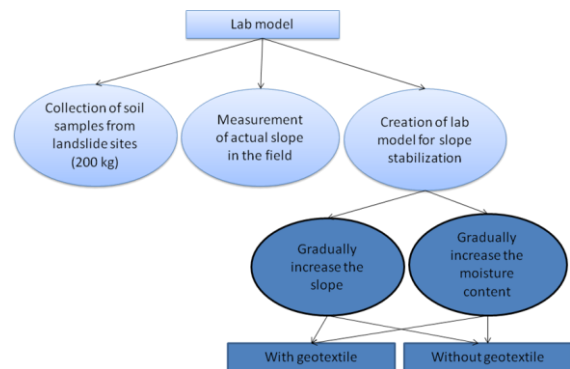


Figure.4. Flow chart of laboratory model

14. GEOTEXTILES & COIR GEOTEXTILE

Geotextiles are permeable fabrics which, when used in association with soil, have the ability to separate, filter, reinforce, protect, or drain. Typically made from polypropylene or polyester, geotextile fabrics come in three basic forms: woven (looks like mail bag sacking), needle punched (looks like felt), or heat bonded (looks like ironed felt). Coir geotextiles can be classified as woven and non-woven based on the method of manufacture. These can be further reclassified as Woven Coir Geotextiles and Non-Woven Coir Geotextiles.

15. LANDSLIDE VULNERABILITY ASSESSMENT

Several thematic maps (Figure.5.) pertaining to this study were prepared from toposheet and satellite imageries.

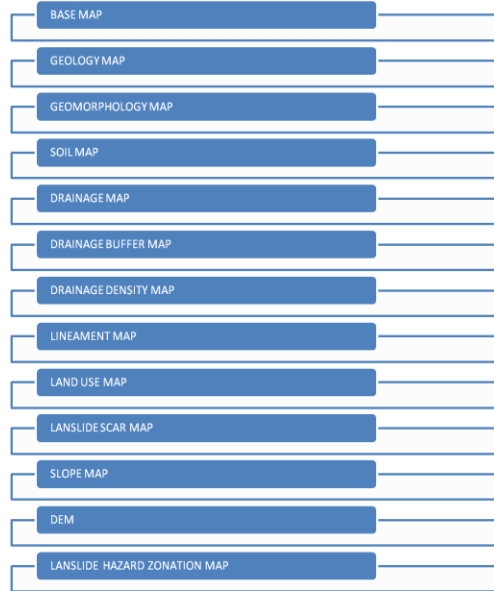


Figure.5.Several thematic maps

16. SOIL TESTING

For the implementation of geotextiles, it is necessary to determine the various physiochemical properties of the soil. Hence various tests were carried out in the laboratory.

1. Sieve Analysis 2. Hydrometer Analysis 3. Liquid Limit
4. Plastic Limit 5. Direct Shear Test 6. Compaction Test
7. Geochemical Analysis

17. GEOCHEMICAL ANALYSIS

17.1 XRF Studies

X-ray fluorescence (XRF) spectrometer is an x-ray instrument used for routine, relatively non-destructive chemical analyses of rocks, minerals, sediments and fluids. It works on wavelength-dispersive spectroscopic principles that are similar to an electron microprobe (EPMA). However, an XRF cannot generally make analyses at the small spot sizes typical of EPMA work (2-5 microns), so it is typically used for bulk analyses of larger fractions of geological materials. The relative ease and low cost of sample preparation, and the stability and ease of use of x-ray spectrometers make this one of the most widely used methods for analysis of major and trace elements in rocks, minerals, and sediment.

17. 2 XRD Studies

X-ray fluorescence (XRF) is the emission of characteristic "secondary" (or fluorescent) X-rays from a material that has been excited by bombarding with high-energy X-rays or gamma rays. The phenomenon is widely used for elemental analysis and chemical analysis, particularly in the investigation of metals, glass, ceramics and building materials, and for research in geochemistry, forensic science and archaeology.

18. PREPARATION OF LAB MODEL

First, a platform was constructed using plywood sheets covering three sides for building the landslide model ((Figure.6.)

About 150 kg of soil sample was filled in this platform in order to create a model of a hill with a slope of 36° .

The model was divided into two halves. One side was kept free without geotextile and the other side was fixed with geotextile.

Step 1:

- Slowly the slope was increased by lifting the entire model.
- The angle at which the slope failed for both the parts were noted separately.

Step 2:

- Water was added into both the parts simultaneously.
- The angles at which both the parts failed were noted separately.



Figure. 6. Landslide model constructed in the laboratory

19. RESULTS AND DISCUSSION

SIEVE AND HYDROMETER ANALYSIS:

The graph (Figure.7.) shows that the sand percentage of the soil sample of Kattery landslide is 37%; silt percentage is 50% and clay percentage is 13%. Since there are no values below D_{10} the soil can not be classified using the result of sieve hydrometer analysis.

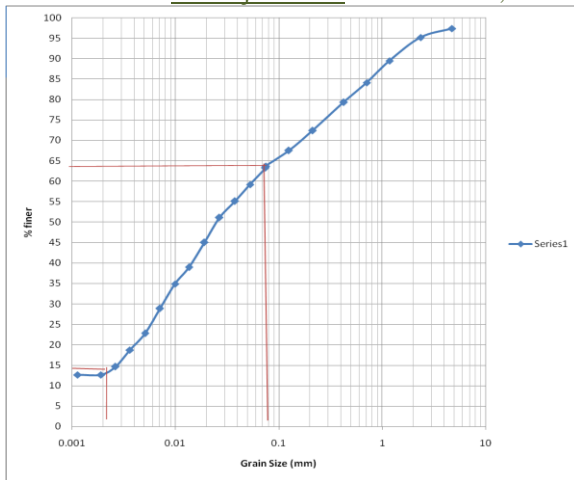


Figure.7. Graph for sieve analysis and hydrometer analysis

20. LIQUID LIMIT

Experiment result of liquid limit is presented in the graph (Figure.8) shows that the liquid limit of the sample is 45 %.

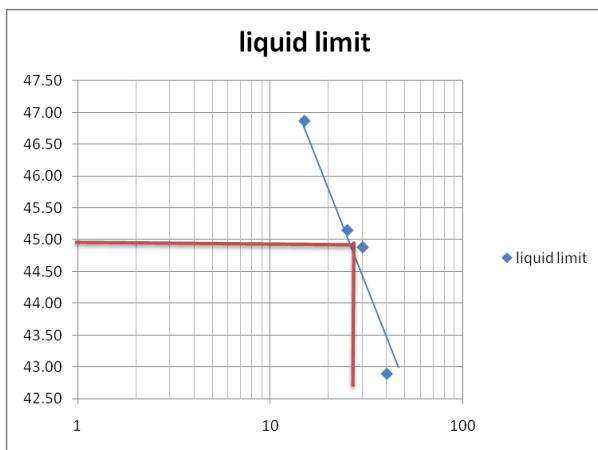


Figure.8. Plot of Liquid limit

21.PLASTIC LIMIT&PLASTICITY INDEX

Experiment result of plastic limit of the soil sample is 31.40%.

$PI = LL - PL$ where: LL = liquid limit, and PL = plastic limit.
 $PI = 45 - 32 = 13 \%$

The graph (Figure.9.) it is understood that the sample of the study area falls in the ML category, which indicate inorganic soils of low plasticity.

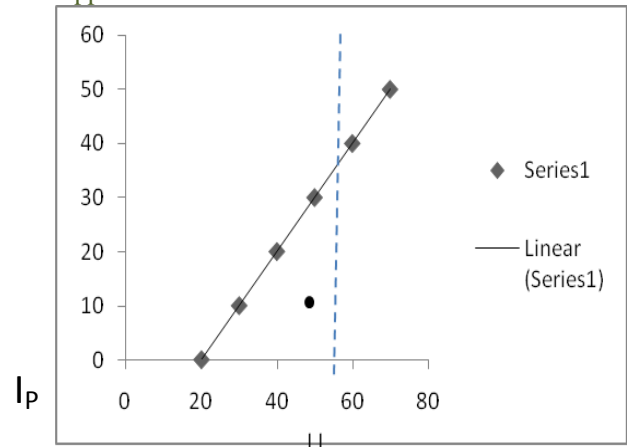


Figure.9. Plot of Plasticity Index Figure

22. DIRECT SHEAR TEST

The results of direct shear test are presented in the graph (Figure.10.), we can calculate the angle of internal friction. Beyond the angle of internal friction the failure can happen. From the graph the angle of internal friction is measured as 38° for the sample of the study area

$Slope = (1.4 - 1) / (1.5 - 1) = 0.8$ $Tan^{-1}(0.8) = 38^\circ$

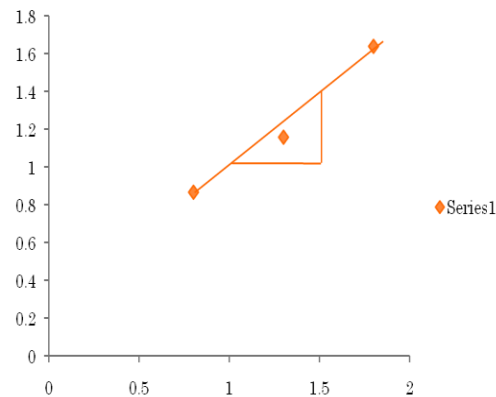


Figure.10. Plot of direct shear test

23. COMPACTION TEST

The results of compaction test are presented in the graph (Figure.11), the value for the optimum moisture content is obtained as 23.50 % and maximum dry density is obtained as 1.61 g/cc.

Table 7.8 Slope failure of soil mass

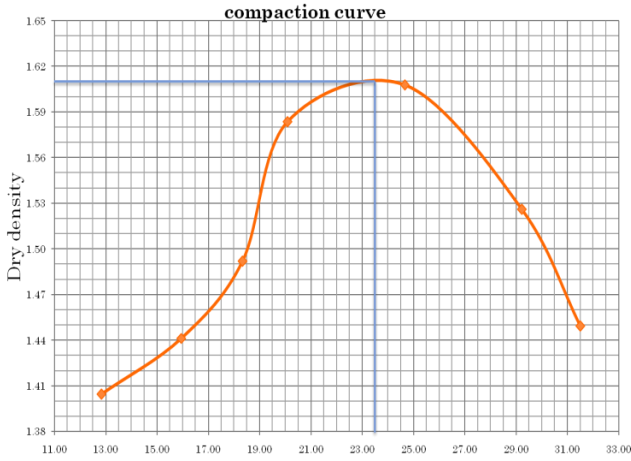


Figure.11. Compaction test curve

Initial slope	Angle of repose	
	Without geotextiles	With geotextiles
36°	56°	-

25.1 Moisture content as variable

- In both the side of the model, the moisture content is gradually increased by spraying water. (Figure.14)
- Rate of erosion was high where the geotextile was not fixed. However the rate of erosion was very less where the geotextile was fixed.

24. GEOCHEMISTRY

Chemical composition of the soil sample is determined using the handheld XRF instrument. The concentration of various elements in the soil is presented in XRD chart (Figure.12) of the soil sample shows that quartz, feldspar and pyroxenes are common

26. CONCLUSIONS

- The soil test results show that the soil is classified as inorganic soil of low plasticity and its optimum moisture content is 23.50%

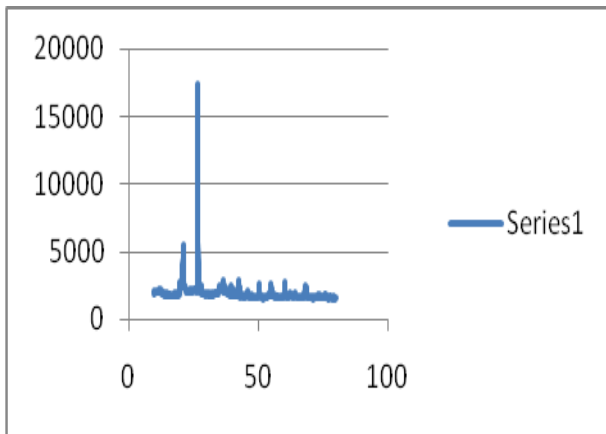


Figure.12. XRD chart of the soil sample

25. LANDSLIDE MODEL

7.7.1 Slope as variable

- ✓ The initial slope of the soil mass in the laboratory model was kept as 36° (Figure.13)
- ✓ The slope was gradually increased by lifting the entire setup
- ✓ The slope failure occurred at 56° where the geotextile is not fixed
- ✓ The slope was further increased up to 60°. However there was no failure in the soil mass where the geotextile is fixed.



Figure.13 Slope failure of soil mass in the lab model



Figure.14. Erosional behaviour of soil

- The soil of the study area contains 50% of silt and 13% of clay
- The maximum dry density of the soil is 1.61g/cc and the angle of internal friction is 38°
- The Liquid Limit of the soil sample is 45 % and the Plastic Limit is 31.40%
- The XRD results indicate that the soil contains quartz, feldspar, pyroxene and clay minerals.
- The landslide hazard zonation map shows that the north eastern and south western part of Kattery watershed is more vulnerable to landslides, whereas the south eastern part is less vulnerable.
- There are much possibilities of occurrence of landslide in the area where the landslide occurred during the year 2009 (near Achanekal)
- The laboratory model demonstrates that geotextiles can be used for slope stabilization and erosion control.
- As the coir geotextile is biodegradable and eco-friendly it will not affect the environment. Plantation can also be done over the geotextiles.

[11]. Dr B C Punmia, Ashok Kr Jain, Arun Kr Jain, Soil Mechanics and Foundations Vol I & II Laxmi Publications,

27. REFERENCES

- [1]. Balan, K, "Studies on the engineering behaviour and uses of geotextiles with natural fibres", unpublished Ph.D thesis submitted to Indian Institute of Technology Delhi, India
- [2]. Cruden, D.M., 1991. A Simple Definition of a Landslide. Bulletin of the International Association of Engineering Geology, No. 43, pp. 27-29
- [3]. Gitty, R.E and Ajitha, A.R., "Performance Studies on Coir Reinforced Pavements", M.Tech Thesis Report, College of Engineering, Trivandrum, 2008.
- [4]. Ingold, I.S. (1984), Geotextiles and Geomembranes. An International Journal, Elsevier Applied Science publishers, London, Vol. 1, 1-40
- [5]. IRC: SP: 59-2002, Rural Road Manual, Indian Road Congress (www.irc.org.in)
- [6]. Schurholz, H., "Use of woven coir geotextiles in Europe", Coir, Vol. 35, No 2, pp 18-25,1991.
- [7]. Sheeba, K.P., Sobha. S., Santha, Leah Paul and Rema Devi D. "Studies on the potential of coir reinforced structures" , Journal of Scientific and Industrial Research, Vol 59, pp 55-62,2000
- [8]. Varnes D. J.: Slope movement types and processes. In: Schuster R. L. & Krizek R. J. Ed., Landslides, analysis and control. Transportation Research Board Sp. Rep. No. 176, Nat. Acad. of Sciences, pp. 11-33, 1978.'
- [9]. Varnes, D. J.: 1984, Landslide Hazard Zonation: a review of principles and practice, Commission on landslides of the IAEG, UNESCO, Natural Hazards No. 3, 61 pp
- [10]. Venkatappa Rao, G and Dutta, R.K., "Coir products in unpaved roads—a comparative study" Proc. International Conference on Structural and Road Transportation Engineering, Kharagpur, 2005, pg 533-541.

Study of Groundwater Quality with GIS Application for Coonoor Taluk in Nilgiri District

T. Subramani¹ S. Krishnan² P. K. Kumaresan³

¹Professor & Dean, Department of Civil Engineering, VMKV Engg College, Vinayaka Missions University, Salem, India.

²Associate Professor & Head, Dept. of Mechanical Engg., Mahendra College of Engineering, Salem

³Professor & Dean, Examination, VMKV Engg. College, Vinayaka Missions University, Salem

ABSTRACT

Water is the basic element of social and economic infrastructure and is essential for healthy society and sustainable development. Due to rapid increase in density of population, fast urbanization, industrialization and agricultural, use the demand of water is increasing day by day. As a result surface water and ground water level is decreasing, pollution and increased demand have made good quality water scarcer and more expensive. Groundwater is the favourite alternative is facing threats due to anthropogenic activities in India, which has lead due to deterioration in ground water quality. The possibility of ground water contamination is due to the mixing up of toxic chemicals, fertilizers, waste disposed site and industrial sites. Hence monitoring of ground water quality has become indispensable. GIS not only facilitates data capture and processing but also serve as powerful computational tools that facilitate multimap integrations. In this project ground water quality analysis was carried out for Coonoor Taluk in Nilgiris District water samples were collected all around the taluk the strategically analysed results are presented in a GIS based water quality mapping.

KEYWORDS: Groundwater, Quality, Gis Application, Coonoor Taluk

1. INTRODUCTION

Water is the basic requirements of all life on Earth. The origin of life has been attributed is water along with other basic elements water the source of life is passionate. Too passionate to manage excess of, it leads to flood and lack of its results in drought and famine. It must be remembered that any natural or manmade activity on the surface of the earth will have its for most impact on the quality and quantity of water this will be taken into the biosphere systems and ultimately lead to hydrological extremes.

The increase in population and urbanization and urbanization necessitates growth in the agricultural and industrial sectors which demand for more fresh water. When surface water is the non-available mode the alternative is to depend on ground water.

The dependability on ground water has reached an all time high in recent decades due to reasons such as unreliable supplies from surface water due to vagaries of monsoon, increase in demand for domestic, agricultural and industrial purposes. This has resulted in over exploitation all over the country and in certain places it has reached critical levels like drying up of aquifers.

2. PROBLEMS IN STUDY AREA

There are three main sources of groundwater pollution. These includes natural sources, waste disposal activities, spills, leaks and non point source activities such as agricultural management practices. Here in Coonoor area the groundwater could be spoiled due to waste disposal and Improper Agricultural practices.

The groundwater quality in and around Coonoor is potable. All the people used the groundwater for domestic purposes. The Agricultural communities utilized the groundwater for farming in their lands. But today the scenario is completely different. In many part of Coonoor taluk, groundwater usage is obsolete. Therefore water quality monitoring is necessary in Coonoor taluk.

3. NEED FOR THE STUDY

Now a days water scarcity increases rapidly due to decrease of ground water. The ground water is also polluted due to various artificial man-made activities. Due to this, quality of the water is reduced. This will produce various adverse impacts on human beings, animals and plants. Therefore, it is necessary to monitor the water quality.

4. GEOGRAPHIC INFORMATION SYSTEM

GIS is a power tool for collecting, storing, transforming the spatial information and arriving decision from the real world for particular set of purpose in real time, where the stored information are geo-references (or) geo-coded. In this project the water quality is analyzed using GIS and mapped.

A geographic information system may be defined as an integrated system designed to collect, manage and manipulate information in a spatial context. The geographic component, the various technologies involved and the approach to information modelling set a GIS apart from other types of information systems. A geographic

information system provides an abstract model of the real world, stored and maintained in a computerized system of files and databases in such a way as to facilitate recording, management, analysis and reporting of information. It can be more broadly stated that a geographic information system consists of a set of software, hardware, processes and organization that integrates the value of spatial data.

5. OBJECTIVES

The Present study as the following objectives.

- To analysis the various ground water quality parameters using GIS.
- To interpreting various ground water quality parameter using GIS.
- To develop an integrated groundwater quality map of Coonoor Taluk using GIS.

6. GEOGRAPHICAL INFORMATION SYSTEM

Geographic Information System (GIS) is a computer based information system used to digitally represent and analyse the geographic features present on the Earth surface and the events (non-spatial attributes linked to the geography under study) that taking place on it.

7. DEFINING GIS

A GIS is an information system designed to work with data referenced by spatial / geographical coordinates. In other words, GIS is both a database system with specific capabilities for spatially referenced data as well as a set of operations for working with the data. It may also be considered as a higher order map.

GIS technology integrates common database operations such as query and statistical analysis with the unique visualization and geographic analysis benefits offered by maps. These abilities distinguish GIS from other information systems and make it valuable to a wide range of public and private enterprise for explaining events, predicting outcomes and planning strategies.

A Geographic Information System is a computer based system which is used to digitally reproduce and analyse the feature present on earth surface and the events that take place on it. In the light of the fact that almost 70% of the data has geographical reference as it's denominator, it becomes imperative to underline the importance of a system which can represent the given data geographically.

The four functions of GIS are:

1. Data acquisition and pre-processing
2. Data management, storage and retrieval
3. Manipulation and analysis
4. Product generation

The GIS has the power of organizing effective Social Information System (SIS) towards decision-making or resource management. The spatial information system comprises synthesis of spatial formation and non-spatial data within GIS framework. The GIS aims and works

at bringing together, the diverse information, which are gathered from various different sources. Hence, this is also known as integrated analysis.

8. APPLICATIONS OF GIS

GIS applicable for many fields

- Environment
- Urban planning
- Natural Hazard Management
- Archaeology
- Agriculture
- Geology

9. STUDY AREA

9.1 GENERAL

In Tamil Nadu, Nilgiris is one of the famous Tourist Destination which is well known for its Tea Cultivation. It is situated in the western part of Tamil Nadu. Out of total geographical area of 2366.89 sq.km and an elevation of 2280 to 2290 mts hectares. The entire district lies in the western Ghats. Its summer temperature is Max 25°C – Min 10°C. Winter Temperature Max 20°C – Min 0°C. The sources of irrigation are streams, tanks and wells. Ground water plays a major role for Irrigation as well as Domestic uses.

9.2 LOCATION AND EXTENT:

Nilgiri Coimbatore District is administratively divided into 4 Taluks

Block	-	4
Town Panchayat	-	13
Village Panchayat	-	25
Revenue Village No	-	54

9.3 LOCATION OF THE STUDY AREA

And our study area covers Coonoor Taluk which lies between North Latitudes 11° and 11° 55' East Longitudes 76° 13' and 77° 2'.

9.4 COONOOR TALUK

The total area of this taluk is 227.79 sq.km with a cultivatable area of 12831 Ha. Forest covers about 4107 Ha. The cultivatable area is irrigated by Local streams and also irrigated by ground water.Coonoor taluk comprises of Villages Namely Burliar, Hullical, Hubbathalai, Ketti, Yeddapalli, Mellur, Coonoor Town, Adigaratty and Coonoor Rural.

9.5 LAND UTILIZATION PATTERN

Within the Coonoor Taluk, the distribution of rainfall is uneven. The mean annual rainfall in this area is about 1920.80 mm. And a perusal of rainfall data collected over a period of ten years from 2000 reveal that the district receives major portion of its annual rainfall during the North East Monsoon.

9.6 SOIL DATA & GEOLOGY

In Coonoor Taluk, various type of soil pattern exists such as Red loams, Laterite soil, Black soil, and sandy coastal alluvium loam and clay loam

Table 3.1 Coonoor Taluk Land Utilization

Land Classification	Area in Ha.
Forest	4107
Barren and uncultivable uses	562
Non Agricultural uses	2764
Cultivable waste	28
Pasture and Grazing Ground	923
Land under Misc Tree crops	613
Current fallows	1017
Other fallow land	38
Net Area sown	12831
Geographical area according to	22884
Total cropped Area	12831

The study area is mainly covered by wide range of metamorphic rocks of unclassified Genesis. Some minor area is covered by Granite and Syenite type of rock

10. METHODS AND METHODOLOGY

10.1 CONVENTIONAL DATA BASE

1. Layout Map of Coonoor Taluk
2. Groundwater quality parameters

10.2 INSTRUMENTS USED

1. GPS – Garmin
2. Water Quality Field Kit

10.3 SOFTWARE USED

1. Surfer - 8
2. ARC GIS 9.3

10.4 CREATION OF A DATABASE

A collection of information in such a way that a computer program can quickly select desired pieces of data. Traditional database are organized by field, records and fields. A field is a single piece of information a record is one complete that of fields and a file is a collection of records. Here data base was created using ground water quality parameters.

10.5 SCANNING OF TOPOSHEETS

Scanning results in the conversion of the image into an array of pixels thereby producing an image in raster format. A raster file is an image created by a series of dots called “Pixels” that are arranged in rows and columns. A scanner captures the image by assigning a row in a column and a colour value each dot. The Coonoor Taluk Map was scanned.

10.6 DIGITIZATION

A Raster image is a type of computerized image that consists of row after row of pixels. There are many different raster image file format. Digitization is the process which converts raster to vector format. Most of the GIS technologies are vector formats are more common, so the raster format is converted into a vector format. In the vector format the position of the line is determined by the co-ordinate which are present at the starting and ending points of the line. Digitization was done by Surfer - 8.

10.7 QUERY ANALYSIS

Data query retrieves a data subset from a map by working with its attribute data. The selected data subset may be visually inspected or saved for further processing. Attribute data query requires the one of expressions which must be interpretable by a GIS. These expressions are often different from one system to another.

10.8 SPATIAL INTERPOLATION

Spatial interpolation is a process of using points with known values to estimate values at other points. Spatial Interpolation is a means of converting point data to surface data.

10.9 SUMMARY

The water quality parameters were tested in the laboratory. The Lab Test Procedure was done as per Indian standard code of Practice. The water quality parameters are given in the data base to GIS. The Coonoor map was scanned and digitized. Digitization was done by Surfer – 8. The spatial variation was done. Finally, integrated ground water quality map was created using ARC GIS 9.3.

11. ANALYSIS

11.1 GROUND WATER QUALITY PARAMETERS

The major ground water quality parameters such as,

1. pH
2. Total dissolved solids
3. Total hardness
4. Sulphate
5. Chloride
6. Calcium
7. Turbidity
8. Temperature.

have been estimated in 13 observation wells throughout the Coonoor Taluk. The ground water quality data of the study area as shown in table 5.1 and locations in study area map 5.2. Finally, integrated ground water quality map was created using ARC GIS 9.3.

11.2 ARC VIEW GIS 9.3

Using ARC VIEW 9.3 the spatial interpolation was done on the basis of attribute values. Like pH, TDS, TH, sulphate, chloride, calcium, Turbidity and Temperature, etc.

For each parameter the spatial analysis was done and map was created except for turbidity as there is less variation in turbidity values.

11.3 INTEGRATED GROUNDWATER QUALITY MAPPING

Spatial variation of ground water quality parameter map were integrated and integrated ground water quality map was created. After integration, the map shows groundwater quality in Coonoor Taluk.

12. RESULTS AND DISCUSSION

12.1 GENERAL

GROUND WATER QUALITY ANALYSIS FOR COONOOR TALUK.

Sample No	Village	Hamlet	Latitude	Longitude	Altitude	Temp (Oc)	pH value	Hardness ppm	Turbidity	TDS	Sulphate	Chlorides	Calcium
1	Ketti	Shantur	11°22' 29.72	76°43' 22.40	1852	11.6	6.51	73	3	540	250	234	62
2	Ketti	Shantur	11°22' 34.68	76°43' 23.48	1862	10.8	6.73	88	4	542	241	245	73
3	Ketti	Palada	11°21' 29.61	76°43' 56.73	1835	11.7	6.89	117	4	418	244	241	92
4	Adigaratty	Kattery Dam	11°20' 24.36	76°43' 58.58	1847	11	7.26	126	4	475	163	197	104
5	Mellur	Thaimalai	11°16' 18.22	76°43' 52.11	1596	11.3	6.78	109	3	410	213	194	98
6	Mellur	Thaimalai	11°15' 52.82	76°43' 12	1565	11.6	6.32	103	1	575	221	169	96
7	Hulical	Selas	11°19' 42	76°45' 06	1697	11.2	7.07	86	2	415	203	194	74
8	Hulical	Karrunpalam	11°20' 02	76°46' 23	1625	11.8	7.29	84	0	540	229	187	52
9	Hulical		11°19' 13	76°47' 26	1743	11.9	7.06	97	4	418	236	209	71
10	Coonoor Town	Brooklands	11°21' 11	76°48' 33	1810	11.9	7.06	127	4	572	227	228	106
11	Coonoor Town	Sims Park	11°21' 29	76°48' 08	1846	10.9	7.27	119	3	518	246	247	97
12	Yedapalli	Yedapalli	11°22' 39	76°48' 53	2026	11.7	6.83	69	2	423	213	194	48
13	Burhar	Kodamalai	11°22' 16	76°49' 37	1941	12.3	6.9	127	4	495	242	197	116

In the present study, ground water quality parameters were analyzed and integrated water quality map of Coonoor Taluk was prepared considering the ground water quality data using GIS.

12.2 RESULTS

Integrated ground water quality map of Coonoor Taluk was prepared from the ground water quality data and shown in figure The land use map of Coonoor Taluk was digitized using Surfer - 8 then exported to ARC GIS 9.3. The spatial analysis was done using ARC VIEW 9.3.

12.3 GROUND WATER QUALITY MAPPING

In order to assess the ground water quality 13 sampling points are identified throughout the Coonoor Taluk and water samples have been collected. The major water quality parameters such as pH, TDS, TH, Sulphate, Chloride, Calcium, Temperature and Turbidity have been estimated. The tested data of 13 locations for each parameters have been converted into spatial variation using GIS. (Fig.1)

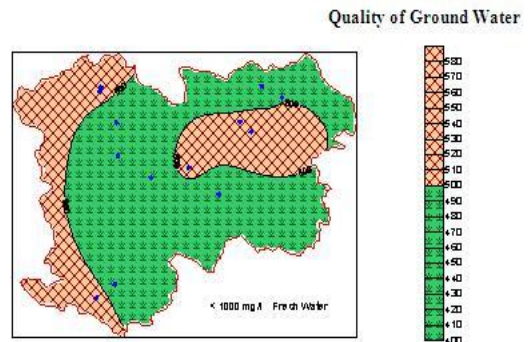


Figure.1. Ground water quality mapping

13. INTEGRATED GROUND WATER QUALITY MAP OF COONOOR TALUK

13.1 DISCUSSION

GIS is used to evaluate the quality of ground water in Coonoor Taluk. Spatial variation map of major water quality parameters like pH, TDS, TH, Sulphate, Chloride, Calcium, Temperature, were prepared for Coonoor Taluk based on these spatial variation maps of major water quality parameters and integrated ground water quality map of Coonoor Taluk was prepared using GIS. This integrated ground water quality map help us to know the existing ground water condition of the study area.

13.2 pH

The pH values of the analysed samples ranges from 6.32 to 7.29. The ranges are classified in the spatial variation map shown in figure in 2.

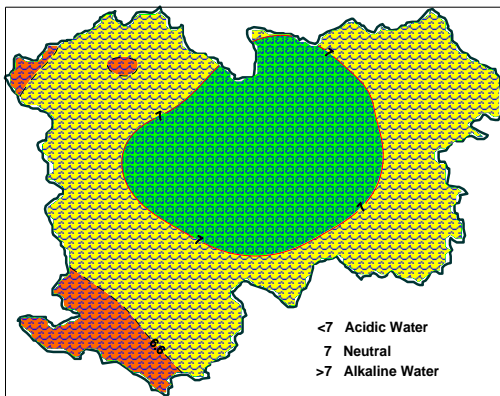


Figure.2. Spatial variation map of pH values

13.3 Total Dissolved Solids

To ascertain the suitability of ground water for any purposes, it is essential to classify the ground water depending upon their hydrochemical properties based on their TDS Values. The TDS values ranges from 410 – 540mg/l from the spatial variation map it is observed that Maximum area of the TDS Value cover <600mg/l as shown in figure.3.

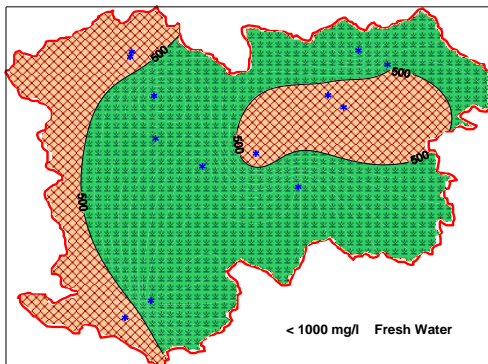


Figure.3. Spatial variation map of TDS values

13.4 Total Hardness

The classification of ground water based on total hardness (TH) shown that a majority of the most desirable limit is 100mg/l as per the sho international standard. The tested values of TH of the samples ranges from 73 to 127. From the map it is observed that most of the area cover <1000mg/l as shown in figure.4

13.5 Sulphate

Sulphate is unstable if it exceeds the maximum allowable limit of 400mg/l. The sulphate concentration varies from 163 to 250mg/l

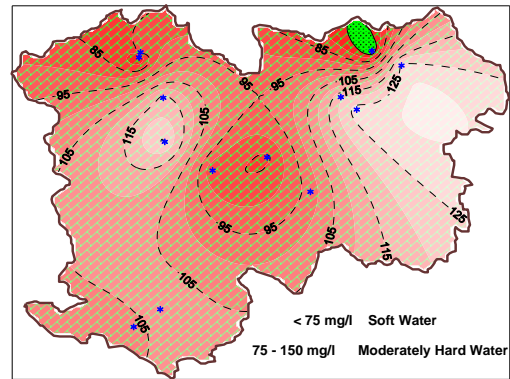


Figure.4. Spatial variation map of hardness

and illustrated in the spatial variation map shown in figure.5.

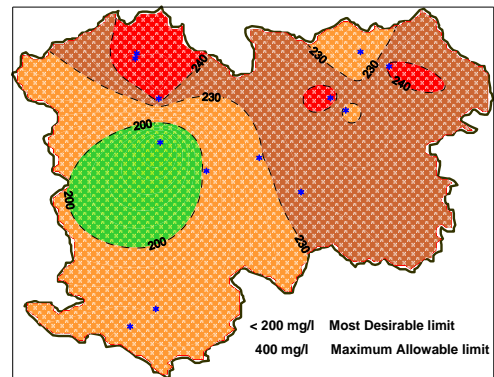


Figure.5. Spatial variation map of sulphate

13.6 Chloride

The chloride ion concentration varies between 194 to 247 mg/l. The spatial distribution of chloride concentration in ground water of the study area is illustrated in figure.6. which in <600mg/l

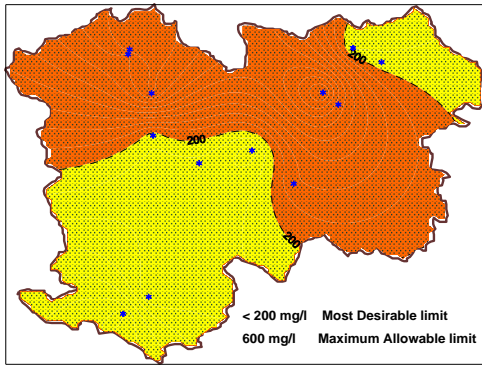


Figure.6. Spatial variation map of chloride

13.7 Calcium

Calcium the analysed samples varies from 62 to 116. Which is illustrated in the spatial variation Map shown in figure.7.

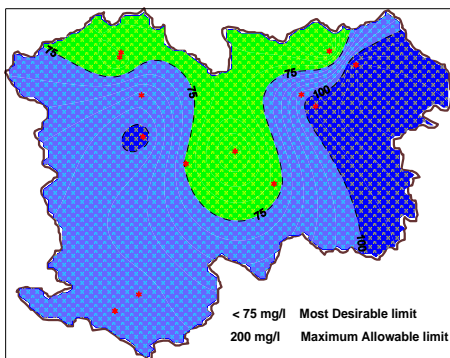


Figure.7. Spatial variation map of calcium

13.8 Temperature

Water Temperature is an important property that determines water suitability for human use, Industrial applications and aquatic ecosystem functioning. The Temperature varied from 10.80°C to 12.3°C which is also illustrated in the spatial variation Map shown in figure.8.

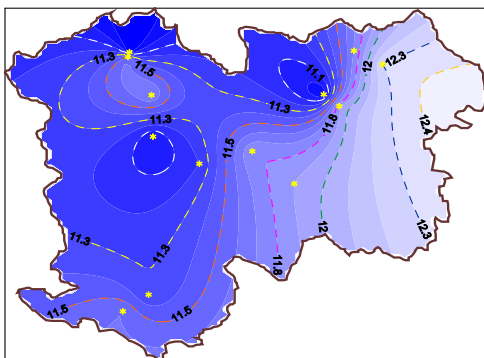


Figure.8. Spatial variation map of temperature

13.9 Turbidity

The quality of water is ascertained based on the turbidity value. The Turbidity values range from 0-4. Which is well within the permissible limit. The integrated map

illustrated the good and excellent quality of water in Coonoor Taluk.

14. CONCLUSION

Water is the prime requirement for the existence of life groundwater is a precious resource of finite extent. Over the years increasing population urbanization and expansion in agriculture has led to the scientific exploitation of ground water creating a water stress condition. Coonoor area is under threat due to the critical issues of environmental pollution and water scarcity problems. The groundwater quality in Coonoor Taluk has been reduced due to pollution. Hence monitoring the groundwater quality is indispensable. The study was carried out in entire Coonoor Taluk. GIS technologies can provide appropriate platform for convergent analysis of large volume of multi-disciplinary data and decision making for ground water studies can be effectively done. The GIS based zoning of groundwater quality map may be used as a guideline for predicting the groundwater quality to new areas. The present study provides a guideline for solving water quality problem in Coonoor Taluk.

14.1 Scope of future study

This groundwater quality analysis can be extended to ground water modeling and the present study can be kept as basic data for future investigation for analyzing various parameters of Ground water studies.

15. REFERENCES

- 1]. Arora A.N. (2002), "Use of Remote Sensing in Ground water Modelling", URL: <http://www.Gisdevelopment.Net/Application/Water resources / Ground>.
- 2]. Arun K., Saraf P, Kundu B, Sarma (1999), "Integrated Remote Sensing and GIS in Ground water Recharge Investigation and Selection of Artificial Recharge Sites in A Hard Rock terrain", URL : <http://www.Gisdevelopment.Net/Application/Water resources / Ground>.
- 3]. Choubey V.K. (1996), "Assessment of waterlogged area in IGNP Command State", Hydrology Journal, Vol.XIX (2), pp. 81-93.
- 4]. Kharad S, M, Srinivas Rao G.S. (1999), "GIS based Groundwater Assessment Model", L & T Information Technology Limited.
- 5]. Mohammed Ismal S,Pattabi S (2000), "Mapping of spatial variability of groundwater in Erode District using GIS", Proceeding of National Conference on Geoinformatics 2000, pp. 158-166.
- 6]. Raja Mohan S (2000)," GIS application in ground water quality assessment in Madurai Corporation, Proceedings of National Conference on Geoinformatics 2000, pp. 127 - 135.
- 7]. Ramalingam M, Santhakumar A.R (2000)," Case study on Artificial Recharge using Remote sensing and GIS", URL : <http://www.Gisdevelopment.Net/Application/Water resources / Ground>.

- [8]. Sharma, K.D (1996), "Remote Sensing and Watershed Modelling : Towards a Hydrological Interface Model. Indo-US Symposium Workshop on Remote Sensing and its Applications, Mumbai (India).
- [9]. Vasanthakumaran T, Shayamala R, Sridhar K, :Role of remote sensing and GIS in identifying artificial recharge zones of upper kondavanar river basin", Tamil Nadu, URL: [http://www.Gisdevelopment.Net/Application/Water resources / Ground](http://www.Gisdevelopment.Net/Application/Water%20resources%20Ground).
- [10]. Thilagavathi (1998) studied land use influence of ground water level. Using remote Sensing, GIS created a database and developed a digital model with MODFLOW software package to model the optimum utilization of land and water to increase the yield without damaging the environment.
- [11]. Christopher et al. (1996) applied GIS to ground water assessment of Northwest Florida water management district. ARC/INFO FIS and Oracle RDBMS were the primary tools used for data management and analysis. The principle purpose of the investigation is to determine whether the source of contamination lying outside the local study area.
- [12]. Choubey (1996) stated that a rapid and accurate assessment of the extent of waterlogged areas can be made using remotely sensed data. The waterlogged area was determined with the available water depth and electrical conductivity data to assess the area sensitive to waterlogging.
- [13]. Mahender et al (2000) developed an integrated remote sensing and Geographic Information Systems approach for the selection of water harvesting structures. His study is aimed at the selection of suitable sites for water harvesting structures in Dehradun and its environs using an integrated approach of Remote sensing and GIS technology Using SOI topomaps and remotely sensed data different thematic maps such as drainage, contour, geology, geomorphology, soil, and land use were prepared. The DEM was utilized for the generation of slope, aspect and soil maps. Integrating soil texture, thickness, land use, slope of the area, suitable sites were identified for Bundies, Farm Ponds, Check Dams and percolation tanks.
- [14]. Balasubramaniam (2000) applied GIS in groundwater development different parameters analysed and integrated map have been prepared.
- [15]. Swati Grover (2002) highlighted perspectives of GIS modelling at the study includes creating of various spatial analysed and preparation of digital elevation models.
- [16]. Jocab bear, (2000) Milovan S. Belijin applied GIS in groundwater issue and modelling.
- [17]. Amaresh Kr. Singh, (2003) S. Raviprakash applied GIS in groundwater quality analysis and groundwater potential modelling in Chandraprabha sub water shed in Uttar Pradesh. The Principle purpose of this study is to know the groundwater quality and groundwater potential in that areas.
- [18]. G.K. Tripathy (2002) studied, spatial modeling approach to water pollution monitoring in the sugar beet of Maharastra along the Krishna river. The objective of the study is monitoring, identification and suggesting preliminary measures of water pollution control in the Krishna basin Maharastra.
- [19]. Asok Kumar (2001) applied GIS in ground water management and planning for siwan sub-basin in Hazarbagh district, Bihar. The digital basement terrain model was prepared for that area.
- [20]. T. Subramani (April 2005) Ground Water quality and the suitability for drinking and Agricultural use in Chithar River Basin, Tamil Nadu, India.

Role of value Co-Creation Concept in e-services

Neda Ahrar¹, Azizah Abdul Rahman²

¹Department of Information System, Faculty of Computer Science and Information System,
Universiti Teknologi Malaysia, Malaysia

²Department of Information System, Faculty of Computer Science and Information System,
Universiti Teknologi Malaysia, Malaysia

Abstract

E-services are electronic ways of representing services over electronic networks such as internet. These days marketing have more attention in an electronic concepts and try to represent their services through the electronic ways. On the other hand Co-creation of value is a value creation by both customer and provider which used in marketing and without any focuses and attentions to the customer perceptions, marketing will be failed in a short period of time. The aim of this study is to identify the role, importance and applicability of value co-creation concept in e-services. The method which used in this study is assessing the documents related to this area and the technique which applied in this way is content analysis. In conclusion considering the features of value co-creation and using its concepts in e-services cause improvement of e-services and setback to its fail.

Keywords - Co-creation of value, Value co-creation, E-services, DART model, Marketing.

1. Introduction

The process of value co-creation derived innovation and evolution within the market. It also will be propelling the generation of new knowledge in business, academia, and practice. Thus, the interdisciplinary exchange of ideas and effort to increase understanding of value co-creation will not only benefit the development of service science, but also will potentially aid the advancement of all other social and economic disciplines involved. Co-creation is a form of market that emphasizes the generation and ongoing realization of mutual firm-customer value. It views markets as forums for firms and active customers to share combine and renew

each other's resources and capabilities to create value through new forms of interaction, service and learning mechanisms.

It differs from the traditional active firm - passive consumer market construct of the past. Co-created value arises in the form of personalized, unique experiences for the customer (value-in-use) and ongoing revenue, learning and enhanced market performance drivers for the firm (loyalty, relationships, customer word of mouth). Value is co-created with customers if and when a customer is able to personalize his/her experience using a firm's product-service proposition – in the lifetime of its use – to a level that is best suited to get his/her job(s) or tasks done and which allows the firm to derive greater value from its product-service investment in the form of new knowledge, higher profitability or superior brand value [9] [10].

These days services in marketing represent by electronic versions which called e-services. E-Service is providing consumers with a superior experience with respect to the interactive flow of information [1]. E-Service can be defined as the provision of service over electronic networks such as the Internet includes both pre- and post-Web site service aspects into the concept of e-service quality [2]. However, none of the authors pay attention to describing e-service content or characteristics in their definitions. The above shows that the discussion of definition, content and characteristics of e-services are really needed. Technology-based service defined as a service with both tangible and intangible elements that is performed totally or partly by the customer via a technology interface [4]. From our perspective e-service is a different concept compared to technology-based service. The concept of E-service (short for electronic

service), represents one prominent application of utilizing the use of Information and communication technologies (ICTs) in different areas [5]. During the last ten years a large amount of e-services have been launched to electronic markets and the same kind of development will certainly continue. In many cases traditional services have simply moved to electronic environment and human work is partly substituted by computers and software. This was predicted to revolutionize the way of doing marketing in a short period of time. However, the development has been slow, but the trend towards e-services is clear. Internet Revolution is still in its early stages [3]. Service system is a useful abstraction for understanding value and value co-creation, in this way Service systems are “value co-creation configurations of people, technology, value propositions connecting internal and external service systems, and shared information” [8].

In this paper, we explore the role, importance and applicability of value co-creation concept in e-services.

2. Research Objectives

Based on the research background, the work conducted aims to identify role, importance and applicability of value co-creation concept in e-services. The objectives of the work done will cover the following aspect:

- To identify role, importance and applicability of value co-creation concept in e-services.

3. Research Framework

Currently, the work is conducted in three main phases. In Phase 1, Co-creation of value, the case study of this research will be studied in-depth to elaborate the limitation and potential that can lead to research. Content analysis is the method used to gather the information.

Also in Phase 2, e-services, the case study related to this will be studied in-depth. The problem will be reviewed through potential literature such as reviews and case collections.

Finally in Phase 3, role, the study will be come up with the role, importance and applicability of value co-creation concept in e-services. The research framework derived is as in Figure 1.

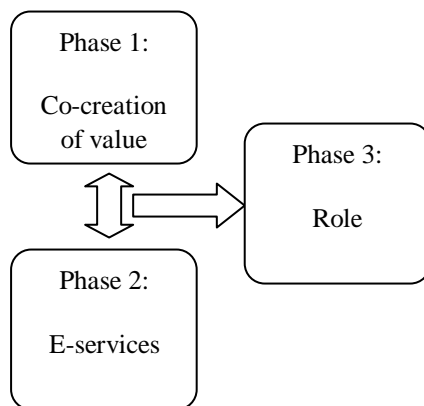


Fig. 1 Research Framework

4. Expected Finding

As mentioned earlier Co-creation of value is a value creation by both customer and provider which used in marketing, as without any focuses and attentions to the customer perceptions marketing will be failed in a short period of time. Also e-services are an electronic way of representing services over electronic networks such as internet. So for each e-service the value co-creation concept must be evaluated and the best way for that is using DART model [6] [7], which helps to built initial blocks between customer and provider. As we cannot gain and follow all expected goals of e-services just because of lack of evaluating and creating those e-services based on co-creation of value. It means that the value co-creation has an evaluating role for electronic services in all around the world.

5. Conclusion

In conclusion it is important to say that e-services are an electronic way of representing services over electronic networks such as internet. These days marketing have more attention in an electronic concepts and try to represent their services through the electronic ways. On the other hand Co-creation of value is a value creation by both customer and provider which used in marketing, as without any focuses and attentions to the customer perceptions marketing will be failed in a short period of time. Make the reliability for gain the whole objectives of using an especial e-service by elaborate that with value co-creation and using DART model is

the most important advantage of this paper. As value co-creation is a new concept in marketing, finding related research was as limitation of this study.

6. References

- [1] Roland T. Rust, P. K. Kannan, *e-service: New Directions in Theory and Practice* (Armonk, New York, 2002).
- [2] Zeithaml, V. *Services Marketing*, (3rd ed. McGraw-Hill, 2002).
- [3] Ch. Lovelock, J. Wirtz, and H. T. Keh, *Services Marketing in Asia* (Managing People, technology and Strategy, Singapore: Prentice Hall, 2002)
- [4] Heinonen, K. *Time and Location as Customer Perceived Value Drivers*, Swedish School of Economics and Business Administration, Nr 124, 2004.
- [5] J. Rowley, An analysis of the e-service literature: towards a research agenda. *Internet Research*, 16 (3), 2006, 339-359.
- [6] S. Baron, Value Co-Creation from the Consumer Perspective. *Service Science: Research and Innovations in the Service Economy*, 2011, 199-210.
- [7] Prahalad C. K, V. R. Co-Creation Experiences: The Next Practice in Value Creation. *Journal of Interactive Marketing*, 18(3), 2004, 5-14.
- [8] Maglio, P. P., J. Spohrer. Fundamentals of Service Science, *Journal of the Academy of Marketing Science*, 36(1), 2008, 18-20.
- [9] Stephen L. Vargo, Paul P. Maglio, Melissa Archpru Akaka, On value and value co-creation: A service systems and service logic perspective, *European Management Journal* 26, 2008, 145 – 152
- [10] Ahgalya Subbiah., Othman Ibrahim, Value Co-Creation Process: A Case of E-Services for G2C in Malaysia, *European Journal of Social Sciences*, 19(3), 2011, 443-449.

Traffic Study on Road Links and Estimate the Fund required for Identified Road Improvement Projects in Major Urban Centre

T. Subramani¹

¹Professor & Dean, Department of Civil Engineering, VMKV Engg College, Vinayaka Missions University, Salem, India

ABSTRACT

Salem is the fifth largest city with a population of 7.54 lakhs (2011) in Tamil Nadu. Local Authorities faced with great difficulties to identify required various road improvement projects. Repair or improvement works may have to be under taken on a basis which has to be decided based on socio-economic, administrative, technical, political factors etc., The identified road network selected for the study comprises 162 road links in Salem Corporation. Existing traffic condition, surface condition of carriageway, street lighting, footpath condition and drainage condition in the Salem Corporation area has been studied in detail. Traffic volume count survey was conducted on the identified 162 road links in Salem Corporation. Identify the type of transport facilities required for the road links. In Salem Corporation area 44 road links required removal of onstreet parking and encroachment, 52 road links required widening of carriageway, 23 road links required traffic management measures with extrawidening to carry the existing traffic flow efficiently. Total fund required for identified various road improvement projects have been calculated as Rs.100.16 Crores

Keywords – Traffic, Road links, estimate, fund

1. Introduction - Importance of Transportation in Urban Development

Transportation contributes to the economic, industrial, social and cultural development of any country. It is well recognized that transport performs a key role in achieving fast economic growth of developing countries. Export and import, industry agriculture defence, social services (health, education), general administration, maintenance of law and order, exploitation of untapped resources, mobility of persons etc., are some of the many areas of activity which are very closely linked to the availability of adequate transportation.

Growth of urban areas and nature extent of availability of various classes of labour force are influenced by the extent of development of transport facilities. This growth in term has a cause and effect impact on transport services. Since increase in urban population demands better transportation facilities and a services. It may be necessary in the case of a country of India's vastness to provide transportation facilities in anticipation of demand, so that the transportation acts as a catalytic agent in development of different sectors.

2. OBJECTIVES OF THE PRESENT STUDY

1. To examine the existing transport infrastructure facility like roads in the selected Salem urban centre.
2. To conduct Traffic volume survey on the selected 162 road links in Salem Corporation
3. To identify the required road improvement projects in the selected urban centre.
4. To identify the traffic congested road links in Salem Corporation.
5. To find the extra widening required for the different road links to carry existing traffic volume.
6. To find the roads which require Traffic management measures with widening of carriageway.
7. To find the cost required to improve each road link with respect to various items of improvement.

3. METHODOLOGY

1. Summarize the findings and recommendations of various previous studies.
2. Identify and collect an relevant information required from local agencies such as demographic trends, map showing the existing land-use and growth trends, income and expenditure, road network details – physical condition, traffic information.
3. Critically evaluate the data to understand the overall conditions of existing infrastructural facilities in the Salem urban centre.
4. Conduct traffic volume survey on identified 162 road links.
5. Analysis the data to identify the magnitude and complexity of the problems, using computer programs
6. Identify the type of road improvement projects require to meet the existing traffic.
7. Calculate the Fund required to improve each road link with respect to various items of improvement.

4. STUDY OF PAST AND PRESENT CONDITIONS IN SALEM CITY

4.1 SALEM – GENERAL

Salem is the fifth largest city in Tamil Nadu over an area of 91.34 Sq.kms. Salem city is located at distance of 350 kms from a Chennai on the west, and 160 kms from Coimbatore and it got the fifth largest population of 7.54 lakhs as per 2011 census in Tamil Nadu.. It is situated at the trijunction of Bangalore, Trichirappalli and Chennai roads. The City is located at 11 40' North and 78 10' on the East. The general topography is plain The city is surrounded by the hills viz. the shervarous and Nagarmalai

on the North, The Kanjamalai on the west, the Goodamalai on the East.

4.2 POPULATION GROWTH

The population in Salem has grown at a rate of 23 percent per decade between 1951 and 1971, the rate has been lower for the decade 1971 – 1981 at 17 percent and 14 percent per decade between 1991 and 2011. Table.1 gives the growth of population within the Salem town. Population growth of Salem City Corporation given in Table 1.

4.3. EXISTING LAND-USE STRUCTURES

The extent of Salem town is 91.34 Sq.km of this the developed area is 4648 Hectares i.e. 48.71 percent of the total area and undeveloped area is 4894 hectares i.e. 51.29 per cent of the total area. The Table 2. gives the existing land use details of Salem City Corporation area &

Table 1. Population growth of Salem City corporation

Sl. No	Use	Area in hectares	% to developed area	% to total area
	Developed area			
1	Residential	3091	66.50	32.39
2	Commercial	461	9.92	4.83
3	Industrial	465	10.00	4.88
4	Education	316	6.80	3.31
5	Public and semi-public	315	6.78	3.30
	Total developed area	4648	100	48.71
	Undeveloped area			
6	Agricultural area			
	A. Wet	1240	25.33	13.00
	B. Dry	2465	50.36	25.83
	C. Hillocks	728	14.89	7.63
7	Reserved forest	461	9.42	4.83
	Total undeveloped area	4894	100	51.29
	Net total	9542		100.00

Figure. 1. is showing the existing land use details of Salem City Corporation area.

Table 2. Existing land use details of salem city area

Year	Salem town / corporation* population	Decade variation	% of decade variation
1901	70621	-	-
1911	59153	(-) 11468	(-) 16.24
1921	52244	(-) 6909	(-) 11.68
1931	102149	(-) 49935	95.58
1941	129702	27523	26.94
1951	202335	72633	56
1961	249145	46810	23.13
1971	308716	59571	23.9
1981	361394	52678	17.06
1991*	579951	218557	60.47
2001*	672330	92379	15.92
2011*	754000	81670	12.15

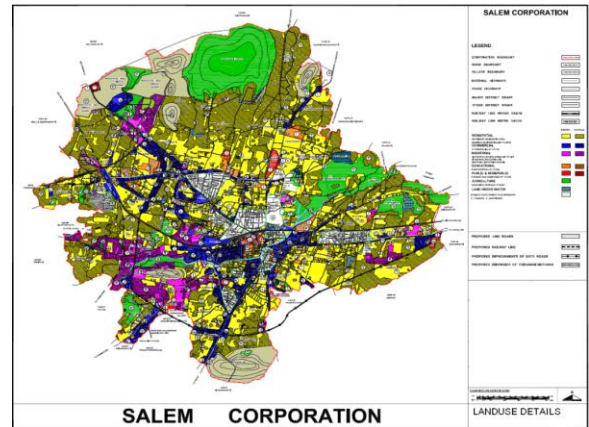


Figure.1. Existing land-use details of salem city corporation

4.4 EXISTING TRAFFIC SITUATION

The traffic in Salem town is heterogeneous in nature comprising of slow moving vehicles such as hand carts, animal drawn vehicles, bicycle and fast moving vehicles such as mini cargo vans, Passenger vans Lorries, buses etc. In the absence of separate lanes for slow moving vehicles and cyclists all the vehicles are found to use the available narrow carriageway. The pedestrian side walks have been provided only near Collectorate. In almost all the main roads vendors occupy the road margins and side walks. Hence the pedestrians are deprived of the use of road margins and side walks and use the carriage way, causing hindrance to the free vehicle movement. This may be noticed more in the central area of the old town comprising of Collectorate and Bus stand complex the main private companies.

5. IDENTIFIED ROAD NETWORK FOR THE PRESENT STUDY

Salem district as a whole has only 10,133.7 km. of road, out of which 214.6 km are cement concrete roads, 5098.1 kms. are bituminous surfaced road and the

remaining 4821 kms. are water Bound Macadam roads. The unsurfaced road of 2352.7 kms. Also exist in the district.

Salem Corporation has about 748.13kms. of surfaced roads under its control and maintenance as detailed below. The width of road ranges from 3.5 m to 14.0m in the major road network excluding the lanes and small roads. The details of the various categories of roads with their lengths in the town is show in Table. 3

Table.3 Types of roads with their length in Salem Corporation

Sl. No	Category	Road length (km)
1	Cement Concrete Super Roads	54.47
2	Black Topped Roads	628.17
3	Wbm Roads	17.04
4	Earthern Road	23.46
5	Others	24.66
	Total Length of Municipal Roads	748.13

The arterial road network of Salem Chosen for the study consists of four major radial corridors originating from the city bus stand. These roads are Attur road in the east, Trichy road and Coimbatore road in the South and Omalur road in the North west. In addition to these, there are a few secondary radial roads. One orbital corridor is identified and it consists of Shandipet road pallapatti main road and court road. Fig.2. shows the identified road network selected for the present study.

6. FIELD STUDIES TRAFFIC VOLUME SURVEY

One of the fundamental measures of traffic on a road system is the volume of traffic using the road in a given interval of time. It is also termed as flow and is expressed in vehicles per hour.

When the traffic is composed of number of types of vehicles, it is the normal practice to convert the flow into equivalent passenger car units (PCU), by using certain equivalence factors. The flow is then expressed as PCU per hour.

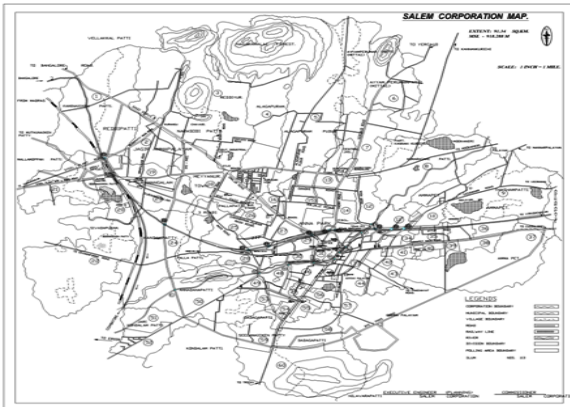


Figure.2. Identified road network of Salem city Corporation

A knowledge of the vehicular volume using a road network is important for understanding the efficiency at which the system works at present and the general quality of service offered to the road users knowing the flow characteristics, one can easily determine whether a particular section of a road is handling traffic much above or below its capacity. If the traffic is heavy, the road suffers from congestion with consequent loss in journey speeds. Lower speeds cause economic loss to the community due to time lost by the occupants of the vehicles and the higher operational cost of vehicles. Congestion also leads to traffic hazards. Volume counts are, therefore, indicators of the need to improve the transport facilities and are in an invaluable tool in the hands of transport planner.

In order to update the data base of the present existing traffic conditions, Traffic volume counts on selected road links in the urban centre were conducted. The detailed field survey programme was organized for 14 hours between 6 AM -8 PM. The block period is 15 minutes. Traffic volume count survey was conducted on the 162 road links and shown in Figure 3. With the help of these data the peak hour of traffic flow on each road link has been identified.

7. PHYSICAL CHARACTERISTICS

Physical Characteristics of road links in the network studied by field visits during the study and updated to the present existing condition. The study of physical characteristics comprises of surface condition, lighting condition footpath condition and drainage condition.

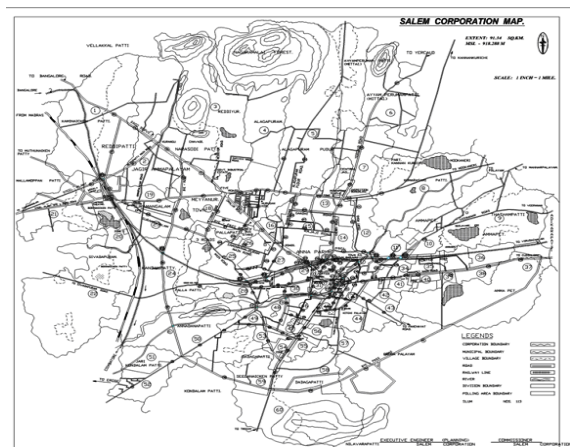


Figure 3. Traffic volume count survey points on the 162 road links

8. ROAD NETWORK DETAILS

Road network details collected from directorate of Town and Country Planning, Salem Corporation & Salem Local Planning Authority.

8.1 List of Data Collected

The following data have been collected for Salem city

i. Linkwise – road name details

The arterial road network which has been studied is broken into number of links. A link is defined as one-way part of the route between two intersections. The number of road links analyzed in the study is 162. The road links studied in the urban centres are given in Fig.3.

ii. Linkwise – Physical informations. Following Physical information are collected for 162 road links. The following details of overall road links were collected for the study

Length of road links

Carriageway width

Footpath width

Right of way

Onstreet parking and width covered

Encroached area.

iii. Linkwise Traffic Informations

Linkwise peak hour traffic flow in road links are calculated from the Traffic volume count survey

iv. Linkwise – Existing physical conditions

Linkwise existing physical conditions, surface condition, lighting condition, footpath condition and drainage condition in 162 road links are collected. Surface condition, lighting condition, drainage condition and footpath conditions are graded as very poor, poor and fair. Details of existing landuse along the roadside, type of encroachment and onstreet parking on all road links are observed.

9. PROCEDURE ADOPTED TO IDENTIFY THE CONGESTED ROAD LINKS

Table.5 The Reduction Due To Parking And Encroachment

Type of parking \ Severity of Encroachment	Reduction (m)
Parking prohibited on either side	0
Parking permitted on one side	2.5
Parking permitted on either side	5
No Encroachment	0
Marginal Encroachment	1
Substantial Encroachment	2

The extent of the traffic volume on the road links determined from the traffic volume survey conducted at different locations. The equivalent PCU value of the peak hour traffic volume on the road links has been calculated. The equivalent PCU factors adopted for various vehicles are shown in Table.4

10. ROAD LINK CAPACITY

The step by step procedure adopted for calculating road link capacity is as follows.

Table.4 The Equivalent PCU Factors Adopted For Various Vehicles

Vehicle	PCU
Bus, Lorry/Truck	3
Car / Van	1
Two wheeler	0.5
Auto rickshaw	0.6
Cycle	0.4
Cycle rickshaw	1.5
HD cart	4.5
BD cart	8

1. The absolute capacity of a road link is assumed to be between 1300 and 1500 PCU Per hour per lane. Adopting the average of 1400 PCU per land width of 3.5 m, the absolute capacity is taken as 400 PCU per hour per metre width of carriageway.
2. The absolute capacity (400 PCU per metre) multiplied by the “effective” carriageway width gives the actual capacity of the road link. The effective carriageway width has been calculated by reducing the actual width of the carriageway due to different factors affecting the capacity.
3. The factors affecting the capacity are parking, encroachment and landuse. The reduction due to parking and encroachment is shown in Table .5. Predominant land use along the road link affects the capacity and the reduction in capacity due to this factor is shown in Table.6.

Calculated the effective width of carriageway considering the above three factors (Parking, encroachment, landuse). The capacity of each road link has been calculated by using the physical information's (width of carriageway, parking space, encroachment) is follows.

Effective width of of carriageway = Actual width of carriageway x (1-landuse/ 100)) - Parking space - Encroachment.

Capacity of road link = Effective width of carriageway x 400 PCU

Table.6. Reduction in capacity due to land use

Predominant land use	Reduction (per cent)
Open space	0
Residential	5
Institutional	10
Industrial	15
Commercial	30

LEVEL OF SERVICE OF ROAD LINKS

Comparison of updated traffic volume and capacity of road link give a volume capacity ratio. According to the volume capacity ratio the level of service of the road links are identified. It led to the identification of the degree of congestion in each road link.

Table 7. Level of service adopted in this study

Volume capacity ratio	Level of service
< 0.6	A
0.6 - 0.7	B
0.7 - 0.8	C
0.8 - 0.9	D
0.9 - 1.0	E
1.0 <	F

Table.8. Shows the Level of Service adopted corresponding to the volume capacity ratio. For design purpose Level of Service "C" is suitable for urban streets (Kadiyali L.R 2007).

The road link with Volume Capacity ratio more than 0.8 are classified as congested links. The effective width of carriageway, capacity, volume capacity ratio and Level of Service of all road links in Salem City corporation area calculated

Identify the type of improvements required for road links to carry existing traffic flow

Road links which are having volume capacity ratio more than 0.8 are considered as a congested links and these road links required improvements to carry existing traffic volume. The following procedure is adopted to identify the required improvement.

Road links which are having volume capacity ratio more than 0.8 reflect that road link will have insufficient width of carriageway to carry existing traffic. Instead of providing extra widening of carriageway it has been assumed that to prohibit the existing on street parking and remove the encroachment. After removing on street parking and encroachment the effective width of carriageway, capacity and volume capacity ratio have been calculated. If the volume capacity ratio is less than 0.8 then that road link required only removal of on street parking and encroachment to carry existing traffic flow.

If the volume capacity ratio after removing the on street parking and encroachment is more than 0.8 then that road links required a widening of carriageway. For providing extra widening the available extra width has been calculated from right-of- way. If the right of way is not available to widen the carriageway then that road link required traffic management measure.

If right of way have space then widen the carriageway up to its full width leaving one metre on each side for pedestrian movements. Again the effective width of carriageway and volume capacity ratio has been calculated. If the volume capacity ratio more than 0.8 then that road link required traffic management measure with extra widening. If the volume capacity ratio less than 0.7 than it reflect that

extra widening width has been calculated by assuming average volume capacity ratio of 0.75.

12.COST ESTIMATE FOR IMPROVING VARIOUS ROAD ATTRIBUTES

Cost required for providing extra widening To improve the road surface, street lighting, footpath condition and drainage condition have been calculated

Unit cost for different type of improvements are assumed as given in the following Table.8. These are approximate unit costs of construction based on the information given by DHRW for completed projects.

Table.8. Assumption On Unit Cost Of Estimation.

S. No	Item of work	Cost
1	Resurfacing the carriage way	Rs. 160/- per sq.m.
2	Upgrading of kerb and footpaths	Rs 29.50 Lakhs / km length / 1.5M width
3	Drainage works	Rs.51 Lakhs for 2 sides / km
4	Street lighting	Rs.28.5 lakhs / Km
5	Widening of carriage way	Rs.36 lakhs / 3.5 m width / km length

The step by step procedure used for calculating the cost is follows.

1. After identifying th extrawidening width provided to carriageway for carrying existing traffic volume, the cost required for provide the extrawidening has been calculated as follows.

Cost for widening the carriageway = Length of road link (m) x Extrawidening width (m) x 36 / (3.5 x 1000) lakhs.

2. Road links having poor and very poor grades in various road attributes like drainage condition, surface condition, street lighting condition and footpath condition are required improvements .The cost required for improve various items are has been calculated as follows.

a. Cost for resurfacing the carriageway = Length of the road link (m) x carriage way width (m)x Rs.160/100000 lakhs.

b. Cost of upgrading of kerb and footpaths = Length of the footpath (m) x footpath width (m) x 29.5/(1.5 x1000) lakhs.

c. Cost for improving drainage condition = Length of the road link (m) x 51/1000 lakhs.

d. Cost for improving street ligting = Length of the road link (m) x 28.5/1000 lakhs

13. CONCLUSION

An important product of the analysis is the development of a program which outlines the improvements to be carried out. From the study made, the type of improvement

required to the road links to carry the existing traffic flow has been identified. Total number of road links requiring various types of improvements in Salem city corporation area to carry existing traffic flow is shown in Table.9.

Table.9. Types of improvements required to carry existing traffic flow

Sl. No	Type of Improvement Required	Total Number of Road links
1.	Removal of onstreet parking and encroachment	44
2.	Widening of carriageway	52
3.	Traffic Management Measure required with extrawidening of carriageway	23

Fund required to improve surface condition,of carriageway, footpath condition, street lighting, drainage condition and widening of carriageway have been calculated. Total Cost required for improving various attributes of all road links in major urban centre is 100.16 Crores and given in Table.10..

Table.10.Cost required for improving various attributes of all road links

S. No	Item of work	Cost in Crores
1	Resurfacing the carriage way	13.79
2	Upgrading of kerb and footpaths	9.9
3	Drainage works	37.37
4	Street lighting	14.2
5	Widening of carriage way	24.9

14. REFERENCES

- [1]. DTCP (1986), 'Short term improvement program ME – Traffic and Transportation study for Coimbatore, Madurai, Trichy and Salem', DTCP, Tamil Nadu
- [2]. Hanspeter Georgi (1973), 'Cost- Benefit Analysis and Public Investments in Transport: A Survey', First Edition, Butter Worths (Publishers),London.
- [3]. Kadiyali.L.R.(2007), 'Traffic Engineering and Transport Planning', 7th edition, Khanna publishers, Delhi.
- [4]. Khanna S.K – Justo C.E.G (2010), 'Highway Engineering', 9th edition, Nem Chand and Bros. publishers, Roorkee(U.P) Lindsay R. Peat (1982), 'Practical Guide to DBMS selection', Walter de Grawyter, New York.
- [5]. Meyer M.d.Miller E.J (1984), 'Urban Transportation Planning', Mcgraw – Hill series, New Delhi.
- [6]. Subramanian P. (1990) 'Capacity restrained trip assignment model for Madras City', ME Urban Engineering Thesis, Madras – 600025.
- [7]. V.N.Vazirani & S.P.Chandola, 'Transportation Engineering Vol.I', 5th edition, Khanna Publishers, New Delhi
- [8]. Dr.L.R.Kadyali & Dr.N.B.Lal, 'Principles and Practices of Highway Engineering, 5th edition, Khanna Publishers, New Delhi
- [9]. B.L.Gupta & Amit Gupta 'Highway and bridge Engineering' 3rd edition Standard Publishers Distributers, New Delhi
- [10]. C.Jotin Khisty & B.Kent Lall, 'Transportation Engineering' 3rd edition, PHI Learning Private Limited, New Delhi
- [11]. Gurcharan Singh, 'Highway Engineering' 5rd edition Standard Publishers Distributers, New Delhi
- [12]. R.K. Khitoliya, 'Principles of Highway Engineering' 1st edition, Dhanpat Rai Publishing Company, New Delhi.
- [13]. DTCP (1999), 'Comprehensive Traffic and Transportation Study for Salem', Pallavan Transport Consultancy Services Ltd., Chennai, Tamil Nadu.

Treatability Studies on Hybrid Up-Flow Anaerobic Sludge Blanket Reactor for Pulp and Paper Mill Wastewater

T. Subramani¹ S. Krishnan² P. K. Kumaresan³ P. Selvam⁴

¹Professor & Dean, Department of Civil Engineering, VMKV Engg College, Vinayaka Missions University, Salem, India,

²Associate Professor & Head, Dept. of Mechanical Engg., Mahendra College of Engineering, Salem

³Professor & Dean, Examination, VMKV Engg. College, Vinayaka Missions University, Salem

⁴Professor & Dean, Department of Computer Science & Engineering, VMKV Engg College, Salem

ABSTRACT: In India, Pulp & paper industries have been large users of potable water and consequently large generators of waste water. Anaerobic treatment of paper processing waste water has a distinct advantage of recovery of inherent energy in the form of methane gas with much less sludge production. A hybrid reactor that capitalizes on the positive features of anaerobic filter (AF) and up-flow anaerobic sludge blanket (UASB). The main objective of this thesis is to find out the start up of the hybrid up-flow anaerobic sludge blanket (HUASB) reactor for treatment of pulp & paper mill waste water. The study was conducted using Lab-scale HUASB reactor of volume 4.3 Lit at ambient temperature with packing materials in the top one third of the reactor. The reactor was made of PVC material with internal diameter of 9.5 cm and height of 61 cm. The reactor was initially filled with 2 Lit of cow dung. Remaining volume is filled with seed sludge and paper mill waste water at the ratio of 1:2, with a low organic loading rate (OLR) of 1 kg COD/m³.d and 24 hours hydraulic retention time (HRT). The initial characteristics of the paper mill waste water were studied. Reactor was designed and fabricated. Start-up was done and waiting for the steady state condition to be reached. Further study on different loading by reducing HRT will be done after obtaining the steady state.

KEYWORDS: Treatability, Pulp, Paper Mill, Wastewater

1. INTRODUCTION - GENERAL

In the rush towards industrialization, it became expedient for people to produce more products and to use more. This had resulted in large scale generation of wastes, a significant portion of which is considered to be hazardous. The wastes are disposed to the environment which poses problems to environment and also to human beings. The biological waste water treatment offers one of the major steps in eliminating biodegradable organic matter present in many industry effluent. Aerobic and anaerobic treatment systems are the major alternatives in biological treatment methods.

2. Background Of Anaerobic Treatment System

In the past, aerobic treatment system was favored as it was considered to be reliable, stable and efficient. However, aerobic treatment systems require large amounts

of power for aeration and mixing, whereas power requirement for anaerobic process is relatively low.

When compared to aerobic, anaerobic system has more potential for energy production in the form of methane gas. The energy required for the stabilization of 1 kg COD/d is 20-30 W for aerobic systems. It is known that in aerobic metabolism approximately one third of metabolized COD mass is oxidized and two third of the metabolized mass is anaerobically. In contrast, a very large fraction of digested organic material (about 97%) is transformed into methane in the anaerobic digestion. Only about 3% of metabolized mass is anaerobically resulting in very less production of sludge (Table.1-Van Haandel and Liettinga, 1994). In spite of these advantages; their utilization was limited to stabilization of the sludge and solid wastes.

Table. 1 Comparison of aerobic and anaerobic treatment systems (adopted from van haandel and liettinga, 1994)

SL. NO	Parameter	Aerobic system	Anaerobic system
1.	Energy required (W/kg COD.d)	20-30	35*
2.	Sludge production (kg VSS /kg COD)	0.2-0.3	0.05-0.15
3.	Nature of excess sludge	unstable	stable

*Anaerobic systems have potential for energy production.

The steep increase in energy prices in the 1970s reduced the attractiveness of aerobic treatment systems and intensified once again the research efforts towards the developments of systems with lower energy consumption such as modified aerobic digestion rather than aerobic metabolism the removal of organic matter from waste water.

With the development of high rate anaerobic reactors, the anaerobic waste water treatment is becoming an accepted technology for a variety of industrial waste water. High rate anaerobic digestion in recent years has been developed with a sound scientific and engineering foundation and is regarded as a mature technology (Iza et al., 1991). Thus high rate anaerobic treatment has emerged as a

viable alternative for the treatment of many industrial and municipal waste water.

During the last few years, there are number of high rate anaerobic systems such as anaerobic filter (AF), up-flow anaerobic sludge blanket (UASB) reactors and expanded /fluidized bed reactors have been developed in the last few years. All these systems are based on some kind of sludge immobilization principle in order to retain as much viable sludge as possible. One of the common threads that link these various processes is their ability to effectively separate SRT and HRT. This permits the design to be based upon the degradation capacity of anaerobes and not upon the growth rate which results in the reduction of treatment times from days to hours. Among the various high rate anaerobic reactor design, UASB (Lettinga et al., 1980; Fang et al., 1990) and AF (Suidan et al., 1983; Young and Young, 1991) have been successfully commercialized and hundreds of full scale systems have been installed worldwide.

3. HYBRID UPFLOW ANAEROBIC SLUDGE BLANKET (UASB) REACTOR

The HUASB reactor is a combination of a UASB unit at the lower part and an anaerobic fixed film unit at the upper (Lee Jr et al., 1989). This reactor enjoys the advantages of both UASB (which ensures good contact between biomass and substrate) and anaerobic filter (AFs can retain more biomass within the reactor) (Abid alikhan et al., 2003). This kind of reactor is called by various names viz., Sludge Bed Filter (SBF), Up-flow Bed Filter (UBF), Hybrid Up-flow Anaerobic Sludge Blanket (HUASB) reactor or simply "hybrid" reactor.

The standard HUASB reactor has a filter packing located in the upper third of the reactor without Gas Liquid Solid (GLS) separation device.

This kind of a design has the following advantages apart from main benefits of high rate anaerobic reactors:

- i). Biomass is free to accumulate in the unpacked zone.
- ii). For the absence of media, the concentration and level of sludge blanket is easily monitored.
- iii). The packed zone at the top acts as a GLS separator that assists in the retention of the non-attached sludge bed.
- iv). The packing provides a polishing zone of attached biomass that improves process stability under transient operating conditions.
- v). The reduced cost of the packing media.
- vi). It is a feasible alternative design also in respect of UASB reactors in many cases when the granular biomass is difficult to cultivate or to maintain and thus UASB doesn't offer warranty of stable operation.

4. OBJECTIVES OF THE PRESENT STUDY

The objectives of the present study are

- ❖ To review the existing literature pertaining to anaerobic digestion process and management of paper mill waste water.
- ❖ To study the physico – chemical characterization of paper – pulp industry waste water.

- ❖ To study the start-up time and optimum Hydraulic Retention Time for HUASB reactor under normal loading condition with same feed of Paper mill waste water.
- ❖ To study the performance of the reactor for optimum Biogas production efficiency by varying the micro organism in the HUASB reactor.

5. MATERIALS COMPOSITION OF WASTE

The effluent which is the bagasse wash water was collected from the primary clarifier in pulp and paper industry. The collected sample was kept in plastic cans in a freezer at room temperature and was studied for its characteristics.

5.1 SEEDING SLUDGE

The seed sludge was also collected from the pulp and paper industry. This was used as the inoculum because the sludge had sufficient number of acetogenic and methanogenic bacteria.

6. METHODS

The study conducted was divided into 3 aspects, they are

- i. Reactor set-up.
- ii. Process start-up.
- iii. Operation and Monitoring.

7. REACTOR SET-UP

The laboratory scale Hybrid UASB reactor (Figure.1) was fabricated using transparent flexi glass material with an internal diameter 9.5cm and overall height of 61cm. Total volume of the reactor was 4.32Lit and it working volume was 2.3lit (Table.2) A gas head space of 1Lit was provided at the top of the reactor and sampling port were located at equal intervals.

The top third of the reactor was filled with pleated PVC rings. These parking media were floating against fixed screen. The waste water entered under sludge bed through a feed distribution pipe. The effluent pipeline was connected to a water seal to prevent escape of the gas through effluent. The gas will be measured by water displacement method. Peristaltic pump was used for feeding the reactors. The reactor was supported by a frame structure made up of metal.

The following components of the HUASB reactor are,

- i. Inlet and outlet distribution system
- ii. Sampling ports
- iii. Packing media
- iv. Gas collection set up

Table 2 Construction Details of Huasb Reactor

Sl. NO.	Particulars	Specification
1.	Reactor type	Circular P.V.C. pipe
2.	Diameter	9.5cm

3.	Total height	61cm
4.	Working volume	2.3Lit
5.	Total Volume	4.32Lit
6.	Packing media depth	15cm
7.	Nos. of sampling port	5
8.	Port interval	11cm

$$= 0.18 \text{ Lit / Hr.}$$

(or)

$$Q = 4.32 \text{ L / .day}$$

7.5.3. Volumetric Hydraulic Loading

$$(\text{VHL}) = Q/V$$

$$\text{VHL} = 0.18 / 4.32$$

$$= 0.042 / \text{Hr.}$$

(or)

$$\text{VHL} = 4.32 \text{ L / L.day}$$

7.1 INLET AND OUTLET DISTRIBUTION SYSTEMS

At the bottom, the feed inlet pipe of 8mm diameter was provided which is connected to peristaltic pump, through ¼ inch check valve and silicon tubing arrangement, for pumping the feed. This 8mm diameter was enough to avoid clogging in the inlet pipe due to bio mass in the feed. The end of inlet pipe was kept open and bent towards bottom. A clearance of 5cm was provided between the feed distribution pipe and the reactor bottom. Because of this arrangement the feed splashed against the bottom and uniformly distributed while moving up. Just over the packing media a collection tube ¼ inch check valve was connected to collect the processed influent and is connected to outlet.

7.2 SAMPLING PORTS

In order to determine the sludge concentration profile over the reactor height the reactor was fixed with sampling ports made up of brass pipe ¼ inch check valve is connected below the packing.

7.2 PACKING MEDIA

Two fixed screens at a gap of 15cm and a distance of 15cm from the top of the reactor were fixed. The gap between these screens was filled with packing media such as PVC rings ID 1.1cm and OD 1.4cm in 175Nos. This was provided for better solid capture in the system and to prevent the loss of large amount of the UASB reactor solids due to process upsets or changes in the UASB sludge blanket characteristics and density.

7.4 GAS COLLECTION SET-UP

Gas is collected through the gas vent opening provided at top of the reactor. Amount of gas displaced is collected in the mad rid bottle. This collected gas will cause rise in water level in the water displacement jar.

7.5 DESIGN OF THE UASB REACTOR

7.5.1 Volume of the Reactor

$$V = \Pi r^2 h$$

$$\text{Internal Diameter of the Reactor} = 9.5 \text{ cm}$$

$$\text{Volume of the reactor} = (\Pi / 4) \times (0.095)^2 \times 0.61$$

$$= 4.32 \times 10^{-3} \text{ m}^3$$

7.5.2. Flow rate

$$Q = \frac{\text{Volume}}{\text{Time}}$$

{If the COD concentration is 750-3000 mg / lit , the Hydraulic Retention Time (HRT) is 6 – 24 Hours}

Assuming the HRT is 24 Hours (or) 1 Day

$$Q = (4.32 / 1)$$

7.5.4 Organic Loading Rate

$$(\text{OLR}) = Q \times S_0 / V$$

$$= 4.32 \times 2.8 / 4.32$$

$$= 2.8 \text{ gm of COD / Lit .Day}$$

7.5.5. Up-Flow Velocity

$$(v) = Q/A \text{ (or) } Q \times H / V$$

$$= 2.8 \times 0.61 / 0.00432$$

$$= 0.025 \text{ m / Day.}$$

$$V = 2.8 \times 10^{-7} \text{ m / sec.}$$

8 START-UP OF THE REACTOR

The reactor was inoculated with digested sludge obtained from primary clarifier. Initially the reactor was inoculated with 35% of cow dung remaining volume is filled with seed sludge.

9 OPERATION AND MONITORING

The operation and monitoring was done in order to find out the feasibility of the hybrid up-flow anaerobic sludge blanket (HUASB) reactor. In the operation phase the reactor was operated in continuous mode for different flow rate for the 4.32L /day (or) $5 \times 10^2 \text{ m}^3 / \text{sec}$

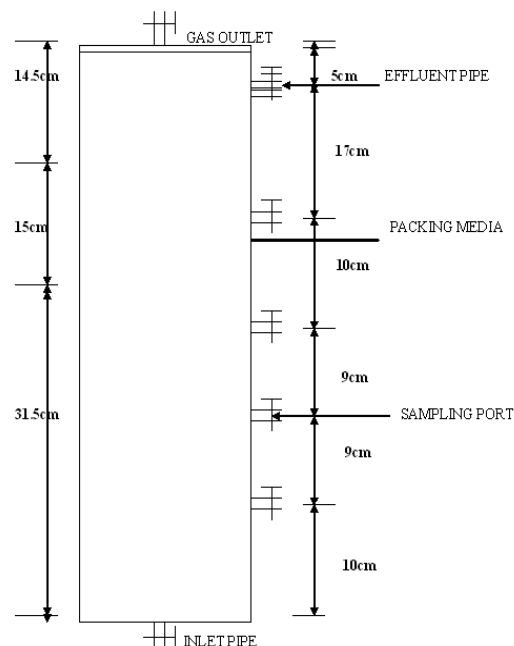


Figure 1 Hybrid Up-Flow Anaerobic Sludge Blanket Reactor

The pH of the reactor is always maintained neutral by adding necessary amount of base (or) acid solution. The outlet pH was found to be in range of 7.5 to 7.6.

10 RESULT

The waste water was collected from the pulp and paper industry. The waste water was analyzed for their characteristics.

10.1 CHARACTERISTICS OF PAPER MILL WASTEWATER

The paper mill waste water sample was carried out to determine general characteristics. The results obtained are shown in Table 3. All the values are in mg/lit except pH.

10.2 SEED SLUDGE CHARACTERISTICS

The seed sludge was obtained from secondary clarifier unit from the pulp and paper industry. The seed sludge sample was carried out to determine the following parameters are shown in Table 4.

Table. 3 Characteristics of Wastewater

Sl.no.	Parameter	Concentration (mg/l)
1.	pH	5.0
2.	Total solids	4350
3.	Total dissolved solids	3260
4.	Total suspended solids	1020
5.	Total fixed solids	3530
6.	Volatile solids	1030
7.	Alkalinity	650
8.	Chlorides	895
9.	COD	2875
10.	BOD	675
11.	Electrical Conductivity (ms/cm)	2.20
12.	Heavy metals	
	chromium	0.069
	Ni, Cd, Pb	Non-detectable

1. DISCUSSION - START-UP OF THE REACTOR

The reactor was initially filled with cow dung at 35% of working volume. The remaining volume was filled with seed sludge.

Start-up of the reactor is in initial phase, since it is an anaerobic reaction which takes long time for reacting the steady state condition and gas production.

2. OPERATION AND MONITORING

The operation and monitoring was done in order find out the following parameter such as pH, TDS, VSS, Alkalinity, COD and BOD of the treated effluent. In the phase 1 start-up was done. Only flow rate is regulated and waiting for the steady state condition to be achieved.

Table 4 Characteristics of Seed sludge

Sl.no.	Parameter	Concentration (mg/l)
1.	pH	8.0
2.	Total solids	5960
3.	Electrical Conductivity	3.33
4.	Total fixed solids	4860
5.	Volatile solids	1100
6.	Alkalinity	975
7.	Chlorides	457
8.	COD	2550
9.	BOD	473
	Heavy metals Cr, Ni, Cd, Pb	Non- detectable

All the values are in mg/lit except pH.

REFERENCES

- [1]. Lettinga, G., A.F.M. Van Velsen, S.W. Homb, and A.Klapwisk, 1980, "Use of Upflow Sludge Blanket Reactor Concept for Biological Waste water Treatment", Biotechnology and Bioengineering, No. 22, pg. 699-734.
- [2]. Coates, J and Colleran, E., (1990)., "Operational performance of Hybrid Upflow Anaerobic Reactor treating a synthetic feed." 10, 162-171.
- [3]. Yogita Chuphal, Shachi Shah and Indu Shekhar takur (2007), "Optimization of Upflow Anaerobic Sludge Blanket Reactor for treatment of Pulp and Paper mill effluent," 26(1): 49-53.

- [4]. Metcalf and Eddy (2003) "waste water Engineering treatment and Reuse". Tata McGraw - Hill Edition.
- [5]. Arun Kansal, K V Rajeshwari, Malini Balakrishnan, Kusum Lata, V V N Kishore, (1998) "Anaerobic Digestion technologies for energy recovery from industrial wastewater- a study in Indian context". TERI information Monitor on Environmental Science3(2): 67-75
- [6]. Trlche, A. and Vieira, S M.M., (1991)., "Discussion reports on reactor design of anaerobic filters and sludge bed reactors." Wat Sci Technol., 24, 193-206.
- [7]. Chawla, O.P., "Advances in Biogas technology", Indian Council of Agricultural Research, New Delhi, 1989, page-144.
- [8]. Raghu Rama Sharma, S. and Bandyopandhy Y.M. (1991) "Treatment of pulp and paper mill effluent by upflow anaerobic filter". Indian J. Environ. Hlth. Vol. 33, No.4, pg. 456-463.
- [9]. Hall ER, Cornacchio L-A - "Anaerobic Treatability of Canadian pulp and paper mill waste water". Pulp pap can 1988; 89(6): 100-4.
- [10]. Campos, C.M.M. and Anderson, S.A.- "Effect of liquid upflow velocity and substrate concentration on the start-up of UASB reactor" . Water Science and technology (1992), vol-25(7), pg-41-50.
- [11]. Muna Ali, T.R. Sreekrishnan - "Anaerobic Treatment of agricultural residue based pulp and paper mill effluents for AOX and COD reduction "- Department of Biochemical Engineering and Biotechnology, IIT, Delhi. (2000) Vol:36, pg no:25-29.
- [12]. K. Kavitha and A.G. Murugesan - "Efficiency of Upflow Anaerobic Granulated sludge blanket reactor in treating fish processing effluent " - Manonmaniam Sundaranar University, Sri Paramakalyani Centre for Environmental Sciences, Alwarkurichi, Tamilnadu, Journal of Industrial Pollution Control 23(1) (2007), pg 77-92.
- [13]. Lettinga, G. and Hulshoff Pol, L.W. 1986. "Advanced reactor design, operation and economy. Wat.Sci. Technology. 18(12): 99-108.
- [14]. Kavitha, K. and A.G. Murugesan, 2004. "Performance evaluation of paper mill effluent in a granular bed UASBR". Jr. of Indian. Environ & Ecoplanning. 8(3) :551-556.
- [15]. Chaudhry, S., Manthan.M., Saroo N., Rohella R.S., - "Anaerobic Treatment of Pulp and Paper mill effluent "- a case study Indian journal of Environmental health (1999) 41(1): 74-5.
- [16]. M.M. Ghangrekar, U.J. Kahalekar, S.V.Takalkar - "Design of Upflow Anaerobic Sludge Blanket Reactor for treatment of organic waste waters"- (2003) Indian journal of environmental health Vol-45, No:2, Pg no:121-132.
- [17]. J.R. Banu, S. Kalliappan; I.T.Yeom - "Treatment of domestic wastewater using upflow anaerobic sludge blanket reactor "- centre for environmental studies(CES) Anna university, Chennai. (2007), Institute of journal Environmental Science & Technology, 4(3): 363-370.
- [18]. K.R. Chakravarthi, M.Singan and K.Somasekhara Rao - "A correlation study on physico-chemical characteristics of paper mill effluent," Nuzvid. (1995), Indian journal of Environmental protection vol: 16 (1), pg: 46-49.
- [19]. R.F. Hickey, W.M. Wu, M.C. Veiga and R. Jones - "Start-up, operation, Monitoring and control of high rate anaerobic treatment systems" - Michigan Biotechnology Institute, Lansing, USA, & Environment Canada, Waste water technology center, Canada.—Wat. Sci. Technology, Vol. 24, No. 08, pg. 207-255, (1991).
- [20]. Dr. K.S. Jayantha, " Biogas production from high strength waste using upflow anaerobic sludge blanket (UASB) reactor "- A laboratory scale study.
- [21]. Fang, H.H.P. and Chui, H.K. 1995. "Performance and sludge characteristics of UASB process treating propionate -rich waste water" - wat. Res. 29 (3) : 895-898.
- [22]. Rajamani, S. Suthantha Rajan, R., Ravindranath, E., Muldeues, A., Vangeoneslijn, J.W. and Damgerwef, J.S. 1995—"Treatment of tannery waste water using upflow anaerobic sludge blanket (UASB) reactor, 30th leather research industry Get. Together Report, 57-60."
- [23]. Ozturk, L, V. Eroglue, G. Ubay and I. Permir, 1993, "Hybrid upflow Anerobic Sludge Blanket Reactor (HUASBR) - Treatment of Dairy Effluents " , water science and Technology, No. 23, pg.77-85.
- [24]. Guiot, S.R. and L. Van den Berg, 1984, "Performance of an Upflow Anerobic Reactor Combining a Sludge Blanket and a Filter Treating Sugar Waste", Biotechnology and Bioengineering, No-27, pg: 800-806.
- [25]. Borja, R., C.J. Banks and Z. Wang, 1995, "Performance of Hybrid anaerobic reactor, combining a sludge blanket and a filter, treating slaughter house waste water", Applied micro biology and biotechnology, No.43, pg.351-357.

Anaerobic Digestion of Aerobic Pretreated Organic Waste

T. Subramani¹

S. Ponkumar²

¹Dean & Professor, Department of Civil Engineering, V.M.K.V.Engineering College, Vinayaka Missions University, Salem, Tamilnadu.

²PGStudent of Environmental Engineering, Department of Civil Engineering, V.M.K.V.Engineering College, Vinayaka Missions University, Salem, Tamilnadu.

ABSTRACT

Anaerobic digestion is a biotechnology that can be used to convert various biodegradable organic materials into methane-rich biogas fuel. The anaerobic digestion of municipal solid waste and sewage sludge is a process that has become a promising technology in waste management throughout the world. Digestion occurs in a four-step process: hydrolysis, acidogenesis, acetogenesis and methanogenesis. Hydrolysis is the rate limiting step in the anaerobic digestion. Composting and anaerobic digestion (AD) are seen as the most favored options to deal with organic fraction of municipal solid waste (OFMSW). Both treatment options reduce the environmental burden and enable the generation of a nutrient rich fertilizer. Thus, the objective of this study is to analyze the effect of rotary drum pretreatment (pre-composting) on mesophilic anaerobic digestion of a mixture of vegetable waste and dairy sludge. Aerobic pretreatment prior to anaerobic co-digestion of fruit waste, vegetable waste, yard waste and cow dung. Aerobic pretreated organic waste was investigated using biogas plant inoculum in batch reactors at mesophilic condition. Effect of pretreatment on biogas production and TS and VS reduction was studied using batch anaerobic tests. At a F/M ratio of 1, there were a biogas production, TS and VS reduction of 465mLgVS⁻¹, 52.4% and 57.2% respectively for pretreated mixture and 340mLgVS⁻¹, 47.6% and 51.3% respectively for mixture without pretreatment. At F/M ratio of 0.5 there were a biogas production, TS and VS reduction of 325m LgVS⁻¹, 44.9% and 48.7% respectively for pretreated mixture and 275m Lg VS⁻¹, 41.1% and 46.4% respectively for mixture without pretreatment.

Keywords: Anaerobic, digestion, pretreated, organic wast

1. INTRODUCTION

Solid Waste Management (SWM) is an issue as production of Solid Waste is increasing due to the increase in population and rapid urbanization. Municipal Solid Waste Management (MSWM) is a challenging problem for developing countries. In India, the collection, transportation and disposal of solid waste is normally done in an unscientific manner. Uncontrolled dumping of wastes on outskirts of towns and cities has created serious environmental implication in terms of ground water pollution and contribution to global warming. An effective system of solid waste management is the need of the hour and should be environmentally and economically sustainable.

OFMSW of MSW is biodegradable as the moisture content present in it will be around 85-90%. Incinerating MSW generates the air pollutants such as nitrogen dioxide, sulfur dioxide and greenhouse gases and dumping it without pretreatment pollutes water by generating leachates. Also dumping of MSW causes breeding of mosquitos and rodents.

Today's waste management policies worldwide is to reduce the stream of waste going to landfills and to recycle the organic materials and the plant nutrients back to the soil. Using OFMSW for the producing of methane and energy using AD has received increasing attention in recent years. AD is nothing but decomposition of organic matter in the absence of free oxygen and involves several anaerobic microbes. Biogas production potential of AD makes it a promising solution for producing renewable energy from OFMSW. These technologies can maximize recycling and recovery of waste components. Among biological treatments, anaerobic digestion is frequently the most cost effective, due to the high energy recovery linked to the process and its limited environmental impact. The anaerobic digestion of OFMSW yields much better results in thermophilic temperature conditions than in mesophilic temperature conditions (Ivet Ferrer et al., 2008, Baoning Zhu *et al.*, 2008).

A given amount of volatile solids of a particular waste can be converted to a maximum amount of biogas at a given temperature provided optimum conditions are prevalent. Evidently, AD has a great future amongst the biological technologies of sludge treatment in view of biogas generation as well as reducing solids mass. However, the low overall biodegradation efficiency of the sludge solids and long retention times (20-30 days) result in only moderate efficiencies. In anaerobic digestion, the biological hydrolysis is identified as the rate-limiting step. Most soluble organic materials which can be converted into biogas are produced during hydrolysis process. Consequently, the biogas production depends for the most part on the biodegradability and hydrolysis rate (Zhang Hanjie *et al.*, 2010).

Pretreatment enhances sludge digestion and the rate and quantity of biogas generated, thereby reducing the retention time requirement from 15 to 25 days to approximately 7 days (Allan Elliott et al., 2007). Pretreatment methods may also be applied to increase the digestibility of the organic solids and increase the efficiencies of anaerobic digesters. Thermal, chemical, biological and mechanical processes, as well as combinations of these, have been studied as possible pretreatments cause the lysis of or disintegration of sludge cells permitting the release of intracellular matter that becomes more accessible to anaerobic microorganisms. A

pre-composting stage may be used to obtain a slight degradation of organics to prevent fast acidification during anaerobic digestion. Previous studies have also shown that a rotary drum reactor (RDR) process provided an effective means for separating the organics from MSW using a combination of mechanical forces and biological reactions AD can be carried out in mesophilic and thermophilic conditions. Thermophilic conditions have certain advantages over mesophilic conditions for digesting the organic wastes separated from MSW, such as faster degradation rate, higher biogas production rate, lower effluent viscosity, and higher pathogen destruction (Baoning Zhu *et al.*, 2008).

Capela *et al.*(1999) did a study on the anaerobic digestion of pulp mill sludge with precomposting stage as pretreatment. There were higher methane yield and higher solid reduction in the case of treated sludge than untreated sludge. Anaerobic digestion is a multistage process in which hydrolysis is the first step. During hydrolysis, complex insoluble substrate macromolecules such as polysaccharides are hydrolysed into smaller units by a large number of microbial species that act in concert synthesizing and secreting different hydrolysing enzymes (Cirne *et al.*, 2007). Ajay S Kalamdhad *et al.*(2008) designed a rotary drum composter and studied the composting process in the rotary drum composter

Engelhart *et al.* did a study on the anaerobic digestion of mechanically pretreated sewage sludge. There was a 25 % increase in volatile solids reduction.

Romero *et al.* studied the effects of biological pretreatment, on organic matter solubilization from organic fraction of municipal solid waste.

The main objective of this study is to employ aerobic pre-composting process as a pretreatment technology for enhancing the biogas production in anaerobic digestion of OFMSW and cow dung.

2. MATERIALS AND METHOD

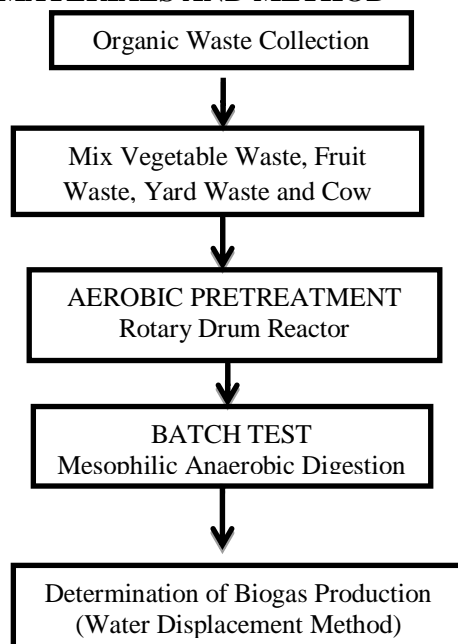


Figure 1. Flow chart shows the materials collection and method adopted in this study

2.1 Collection of Feed Stock Materials and Inoculum

Fruit waste and vegetable waste were collected from market, yard waste was collected from household garden, cow dung was collected from cattle dairy. Inoculum was collected from gobar gas plant. The wastes were tested for moisture content, total solids, volatile solids, total organic carbon and total kjeldahl nitrogen. Inoculum was tested for moisture content, total solids, volatile solids and pH.

2.2 AEROBIC PRETREATMENT

Rotary Drum Method

Aerobic pretreatment was done for one day using fabricated rotary drum reactor. Composting facilities are aerated or unaerated and covered or not covered. Composting methods include passive piles, windrow composting, static piles, and in-vessel composting. In-vessel composting refers to a diverse group of methods that confine the composting process within a container, building, or vessel and uses a combination of forced aeration and mechanical turning to speed up the composting. Compared to windrow and aerated pile methods, these systems require less labor and land area and offer potentially better odor control, faster composting (in a matter of days as opposed to weeks), and consistently good compost. The key factor of successful co-digestion is that the balance of macro and micro nutrients can be assured by the co-substrate. To perform the aerobic pre-composting pretreatment a lab scale rotary drum composter of 25L capacity was used. The dimension of drum used is 0.4m in length and 0.3m in diameter and the drum is made up of plastic. The drum is mounted on four steel bearings which revolves around two steel rods and the steel rods are mounted on wooden stand. Fruit waste, vegetable waste, yard waste and cow dung were mixed in the ratio of 1:1:1:0.5 wet mass basis. The mixture of fruit waste, vegetable waste, yard waste and cow dung was loaded up to 50% volume to give good aeration and the drum is rotated manually for 10 times at regular intervals for a day.

2.3 BATCH TEST

Raw waste sample and pre-treated waste sample was collected. Inoculum was collected from gobar gas plant. The TS, VS, VS to TS ratio (VS/TS) and pH of the inoculum is measured.

Five 500mL conical flask with rubber stopper and each with a water displacement arrangement for measuring the biogas production were used as batch reactors namely B1, B2, B3, B4, B5. Reactor B1 was used for blank. Reactor B2 was used for sample without pretreatment and for F/M ratio of 0.5. Reactor B3 was used for sample without pretreatment and for F/M ratio of 1. Reactor B4 was used for sample with pretreatment and for F/M ratio of 0.5. Reactor B5 was used for sample with pretreatment and for F/M ratio of 1. Each batch reactor was filled with 125mL inoculum and required amount of waste sample and 120mL distilled water and for blank the reactor was filled with 125mL inoculum and 125mL distilled water. 250mL of each reactor was kept as working volume. F/M was calculated by dividing feedstock VS by inoculum VS. For F/M ratio of 0.5 reactor B2 was loaded with sample without pretreatment

containing 1.05g VS and reactor B4 was loaded with pretreated sample containing 1.05gVs. For F/M ratio of 1 reactor B3 was loaded with sample without pretreatment containing 2.1gVS and reactor B5 was loaded with pretreated sample containing 2.1g VS.

2.4 ANALYTICAL METHODS

Sample Preparation

One litre of hot distilled water is added into 100 grams of each sample and shake for 24 hours in shaker. An aliquot of each is examined for total kjeldahl nitrogen (TKN), ion ammonia (NH_4^+), nitrate (NO_2^-), nitrite (NO_3^-), temperature, pH, dissolved oxygen (DO), BOD and COD. Laboratory works for all analytical measurements are in accordance with American Standard Methods (1995).

Total Solids

Twenty five grams of the sample is taken in a clean and weighed evaporating dish, dried at 103°C in a water bath and cooled in a desiccator. After cooling, the weight of the dish with the contents is noted. Calculation is done as follows.

$$\text{Total Solids (\%)} = \frac{(A - B) \times 100}{C - B}$$

Where,

A = Weight of the filter paper (g) + sample after drying (g)

B = Weight of the filter paper (g)

C = Weight of the filter paper (g) + wet sample (g)

Volatile Solids

Twenty five grams of the oven dried sample (105°C) is taken in a crucible and kept in a muffle furnace at 550°C for 1h. After cooling, the weight of the crucible is measured. Calculation is done as follows.

$$\text{Volatile Solids (\%)} = \frac{(A - D) \times 100}{C - B}$$

Where,

A = Weight of the crucible (g) + sample after drying (g)

B = Weight of the crucible (g)

C = Weight of the crucible (g) + wet sample (g)

D = Weight of the crucible (g) + dried sample (g)

Total Kjeldahl Nitrogen (TKN)

A known volume of the 35 ml is taken in a 500 mL Kjeldahl flask and 50 mL of the digestion reagent (potassium sulphate, copper sulphate and sulphuric acid) is added. The sample is digested for about two hours. After cooling, 200 mL of distilled water and 50 mL of sodium hydroxide- sodium thiosulphate solution are added and distilled. The distillate is collected in a beaker containing indicating boric acid solution and titrated against 0.2 N sulphuric acid till a pale lavender colour is produced. Calculations are done as below.

$$\text{TKN (mg/L)} = \frac{(A - B) \times 280}{35}$$

Where,

A = Volume of sulphuric acid used up for titrating sample

B = Volume of sulphuric acid used up for titrating blank

Total Organic Carbon (TOC)

Total Organic carbon is calculated by the following formula

$$\text{TOC (\%)} = \frac{\text{VS (\%)}}{1.8}$$

2. RESULTS AND DISCUSSIONS

Table. 1. Results of organic waste

Substrate	MC %	TS %	VS/T S %	C %	N %	C/N
Fruit Waste	67.52	32.48	88.3	44.4	2.09	21.24
Vegetable Waste	71.39	28.61	72.4	43	2.6	16.54
Yard Waste	10.16	89.84	67.92	61.8	0.85	72.7
Cow Dung	76.25	23.75	76.13	50.4	1.77	28.48

3.1 CHARACTERISTICS OF ORGANIC MATERIALS

The moisture content of fruit waste, vegetable waste, yard waste and cow dung were 67.52%, 71.39%, 10.16% and 76.25% respectively. Total solids of fruit waste, vegetable waste, yard waste and cow dung were 32.48%, 28.61%, 89.84% and 23.75% respectively. C/N ratio of fruit waste, vegetable waste, yard waste and cow dung were 21.24, 16.54, 72.7 and 28.48 respectively. Moisture content, total solids, volatile solids, pH of anaerobic inoculum are 95.32%, 4.68%, 2.92% and 6.91%. (Table .1)

3.2 RAW AND PRETREATED WASTE MIXTURE

Moisture content, total solids, VS/TS ratio, Carbon, Nitrogen, C/N ratio of waste mixture without pretreatment were 53.48%, 46.515%, 76.19%, 49.938%, 1.9% and 26.28 respectively. Moisture content, total solids, VS/TS ratio, Carbon, Nitrogen, C/N ratio of waste mixture with pretreatment were 52.32%, 47.68%, 72.13%, 47.92%, 1.97% and 24.28. Temperature inside the reactor increased to 47°C from 31°C.(Table.2)

Table. 2. Results of Raw waste and pretreated waste

Waste type	MC %	TS %	VS/TS %	C %	N %	C/N
Raw Waste	53.48	46.515	76.19	49.938	1.9	26.28
Pretreated Waste	52.32	47.68	72.13	47.92	1.97	24.28

3.3 ANAEROBIC BATCH TEST

Table. 3. Results of organic waste without pretreatment and with pretreatment

Parameter	Without pretreatment		With pretreatment	
	F/M = 0.5	F/M = 1	F/M = 0.5	F/M = 1
Biogas yield (mLgVS ⁻¹)	275	340	325	465
TS reduction (%)	41.1	47.6	44.9	52.4
VS reduction (%)	46.4	51.3	48.7	57.2
pH at the end of digestion	7.3	7.5	7.2	7.2

Biogas yield, TS reduction, VS reduction, pH at the end of digestion of the waste mixture without pretreatment and for F/M ratio of 0.5 were 275mLgVS⁻¹, 41.1%, 46.4% and 7.3. Biogas yield, TS reduction, VS reduction, pH at the end of digestion of the waste mixture with pretreatment and for F/M ratio of 0.5 were 325mLgVS⁻¹, 44.9%, 48.7%, 7.2. Biogas yield, TS reduction, VS reduction, pH at the end of digestion of the waste mixture without pretreatment and for F/M ratio of 1 were 340mLgVS⁻¹, 47.6%, 51.3% and 7.5. Biogas yield, TS reduction, VS reduction, pH at the end of digestion of the waste mixture with pretreatment and for F/M ratio of 1 were 465mLgVS⁻¹, 52.4%, 57.2%, 7.2.(Table.3)

For F/M ratio of 0.5, daily biogas yield reached the maximum of 80mLgVS⁻¹ in the first and second days for pretreated waste mixture while the daily biogas yield reached the maximum of 40mLgVS⁻¹ in the sixth day for

waste without pretreatment. For F/M ratio of 1, daily biogas yield reached the maximum of 95mLgVS⁻¹ in the first day for pretreated waste mixture while the daily biogas yield reached the maximum of 55mLgVS⁻¹ in the first day for waste mixture without pretreatment.

For F/M ratio of 0.5, cumulative biogas production after 20 days of study was 325mLgVS⁻¹ for pretreated waste mixture and 275mLgVS⁻¹ for waste mixture without pretreatment. For F/M ratio of 1, cumulative biogas production after 20 days of study was 465mLgVS⁻¹ for pretreated waste mixture and 340mLgVS⁻¹ for waste mixture without pretreatment.

4. CONCLUSION

Anaerobic digestion is used to convert biodegradable organic materials into methane – rich biogas. It is a renewable energy source.

Rotary drum reactor process could be used as an effective technology for pretreatment of organic materials in municipal solid waste prior to anaerobic digestion. A pre-composting stage is used to prevent fast acidification during anaerobic digestion. Pretreatment method is applied to increase the digestibility of the organic solids and increase the efficiency of anaerobic digesters.

The results of the study show that aerobic pretreated system is effective and efficient in the conversion of organic waste into biogas.

5. REFERENCES

- [1]. Allan Elliott and TalatMahmood (2007), 'Pretreatment technologies for advancing anaerobic digestion of pulp and paper biotreatment residues', *Water Research*, Volume 41, Pages 4273 – 4286.
- [2]. Baoning Zhu, Petros Gikas, Ruihong Zhang, James Lord, Bryan Jenkins, Xiujin Li (2008) 'Characteristics and biogas production potential of municipal solid wastes pretreated with a rotary drum reactor', *Bioresour. Technology*, Volume 100, Issue 3, February 2009, Pages 1122-1129.
- [3]. Bouallagui H, Ben Cheikh R, Marouani L and Hamdi M (2002) 'Mesophilic biogas production from fruit and vegetable waste in a tubular digester', *Bioresour. Technology*, Volume 86, Issue 1, January 2003, Pages 85-89.
- [4]. Braber K (2000) 'Anaerobic digestion of municipal solid waste: A modern waste disposal option on the verge of breakthrough', *Biomass and Bioenergy*, Volume 9, Issues 1-5, 1995, Pages 365-376.
- [5]. Capela I.F, Azeiteiro C, Arroja L, Duarte A.C. (1999) 'Effects of pre-treatment (composting) on the anaerobic digestion of primary sludges from a bleached kraft pulp mill'. In: Mata-Alvarez J, Tilche A, Cecchi F, (Eds), Proceedings of the Second International Symposium on Anaerobic Digestion of Solid Wastes. Barcelona, Volume 1. Grafiques 92, 15-18 June, Pages 113-120.
- [6]. Engelhart M, Kruger M, Kopp J, Dicht N, (1999) 'Effects of disintegration on anaerobic degradation of sewage excess sludge in downflow stationary fixed film digesters'. In: Mata-Alvarez J, Tilche A, Cecchi F, (Eds), Proceedings of the Second International

- Symposium on Anaerobic Digestion of Solid Wastes. Barcelono, Volume 1. Grafiques 92, 15-18 June , Pages 153-160
- [7]. Franco Cecchi, Paolo Pavan, Joan Mata Alvarez, Angelo Bassetti and CiroCozzolino (1990) 'Anaerobic digestion of municipal solid waste: Thermophilic vs. mesophilic performance at high solids', *Waste Management & Research*, Volume 9, Issue 4, August 1991, Pages 305-315.
- [8]. Lawrence K. Wang, Norman C. Periera, Yung-Tse-Hung 'Hand Book of Environmental Engineering', Volume 8, Biological Treatment Processes, Humana Press.
- [9]. Joungh-Dae Kim, Joon-Seok Park, Byung-Hoon In, Daekeun Kim, Wan Namkoong (2007) 'Evaluation of pilot-scale in-vessel composting for food waste treatment', *Journal of Hazardous Materials*, Volume 154, Issues 1-3, 15 June 2008, Pages 272-277.
- [10]. Ivet Ferrer, Sergio Ponsa, Felicitas Vazquez, Xavier Font (2008) 'Increasing Bioas Production by thermal (70°C) sludge pre-treatment prior to thermophilic anaerobic digestion', *Biochemical Engineering Journal*, Volume 42, Issue 2, 1 November 2008, Pages 186-192.
- [11]. Kalamdhad A.S. and Kazmi A.A. (2008) 'Mixed organic waste composting using rotary drum composter', *Int. J. Environment and Waste Management*, Volume 2, Nos. 1/2, Pages 24-36.
- [12]. Li Dong, Yuan Zhenhong, Sun Yongming (2010) 'Mesophilic Anaerobic Digestion of Mechanically Sorted Organic Fraction of Municipal Solid Waste', *Bioinformatics and Biomedical Engineering (iCBBE)*, 2010 4th International Conference , Pages 1-4.
- [13]. Lopez Torres M, Ma. del C, Espinosa Llorens (2007) 'Effect of alkaline pretreatment on anaerobic digestion of solid wastes', *Waste Management*, Volume 28, Issue 11, November 2008, Pages 2229-2234.
- [14]. Mata-Alvarez J, Mace S, Llabres P 'Anaerobic digestion of organic solid waste. An overview of research achievements and perspectives', *Bioresource Technology*, Volume 74, 2000, Pages 3-16
- [15]. Mudhoo A and Mohee R (2008) ' Modeling Heat Loss during Self-Heating Composting Based on Combined Fluid Film Theory and Boundary Layer Concepts', *Journal of Environmental Informatics*, Volume 11(2), Pages 74-89.
- [16]. Nengwu Zhu (2005) 'Effect of low initial C/N ratio on aerobic composting of swine manure with rice straw', *Bioresource Technology*, Volume 98, Issue 1, January 2007, Pages 9-13.
- [17]. Rao M.S, Singh S.P, Singh A.K, Sodha M.S (1999) 'Bioenergy conversion studies of the organic fraction of MSW: assessment of ultimate bioenergy production potential of municipal garbage', *Applied Energy*, Volume 66, Issue 1, May 2000, Pages 75-87.
- [18]. Sosnowski P, Wiczorek A and Ledakowicz S (2003) 'Anaerobic co-digestion of sewage sludge and organic fraction of municipal solid wastes', *Advances in Environmental Research*, Volume 7, Issue 3, May 2003, Pages 609-616.
- [19]. Yamada Y, Kawase Y (2005) 'Aerobic composting of waste activated sludge: Kinetic analysis for microbiological reaction and oxygen consumption', *Waste Management*, Volume 26, Issue 1, 2006, Pages 49-61.
- [20]. Yong Xiao, Guang-Ming Zeng, Zhao-Hui Yang, Wen-Jun Shi, Cui Huang, Chang-Zheng Fan, and Zheng-Yong Xu (2009) 'Continuous thermophilic composting (CTC) for rapid biodegradation and maturation of organic municipal solid waste', *Bioresource Technology*, Volume 100, Issue 20, October 2009, Pages 4807-4813 .

Maximizing the Lifetime of Clustered Wireless Sensor Network VIA Cooperative Communication

J. Divakaran, S. ilango sambasivan

Pg student, Sri Shakthi Institute of Engineering and Technology, Coimbatore, Tamilnadu, India
Professor, Sri Shakthi Institute of Engineering and Technology, Coimbatore, Tamilnadu, India

ABSTRACT

Wireless Sensor Networks are networks of tiny, battery powered sensor nodes with limited on-board processing, storage and radio capabilities. Sensor nodes sense and send their data toward a processing center called sink. The design of such networks has to be energy aware in order to prolong the lifetime of the network, because the replacement of the embedded batteries is a very difficult process once these nodes have been deployed. In a clustered Wireless Sensor Network the data is forwarded from non-Cluster Head sensor node to Cluster Head sensor node. The distance is large for Inter distance communication (distance between two Cluster Heads) when compare to Intra distance communication (distance between non-Cluster Head to Cluster Heads). Hence the message transfer between two Cluster Heads is via cooperative nodes. Sensors node that have highest energy will participate in cooperative communication. The cooperative communication and Cluster Head nodes are active throughout the network lifetime. Limited energy and difficulty in recharging a large number of sensor nodes, energy efficiency and maximizing network lifetime is a design issue for Wireless Sensor Networks (WSN) with battery-operated nodes: So the sensor node other than Cluster Head node and cooperative communication nodes should be switched between sleep and wakeup mode to extend the life of Wireless Sensor Network. The simulation results have confirmed that the proposed sleep and wakeup procedure scheme significantly improves the energy consumption.

KEYWORDS: lifetime maximization, sleep and wakeup procedure, Cooperative communication, Cluster, Wireless Sensor Network.

I. INTRODUCTION

Wireless Sensor Network (WSN) comprises of hundreds to thousands of small nodes employed in a wide range of data gathering applications such as military, environmental monitoring etc.

The Wireless Sensor Networks have received tremendous attention from both academic and industry. Wireless Sensor Networks are now being widely tested and deployed for different application domains [1]. The existing applications include environmental monitoring, industrial sensing and diagnostics, health care, and data collecting for battlefield awareness. Most of the applications are developed by using low-rate, short distance and low-cost wireless technologies.

A sensor network consists of sensors nodes, each of which has a limited communication range and a limited energy supply in the form of a battery. If two sensors are neighbors in the transmission range of each other can directly communicate with each other, the sensor node periodically generates a data sample to communicate with the sink. The sink may not be within direct communication range, sensor nodes data has to be forwarded to the sink through intermediate sensor nodes.

The typical model for clustered Wireless Sensor Network is depicted in Figure 1 and consists of cluster members and Cluster Heads. There are two types of transmission, namely, *Intracluster transmission*

The source node transmits the packet to the Cluster Head within the same cluster, the distance between cluster member and the Cluster Head is small.

Intercluster transmission

The Cluster Head transmits the packet to the sink node or Cluster Head via the relay transmission. In this relay transmission cooperative sending and receiving nodes are used because the distance between the Intercluster transmission is large when compared to intra cluster transmission.

A MAC protocol IEEE 802.15.4, which is designed for low-rate Wireless Personal Area Networks (WPANs), has been adopted for interconnections between Wireless Sensor Nodes [2]. IEEE 802.15.4 ensures that data packets are sent from source node, which can detect the event and generate data packets to the Sink through intermediate node i.e. Cluster Heads, Cooperative nodes.

In random sleeping mechanisms, sensor nodes enter the sleeping mode randomly and independently from each other. Energy conservation is one of the most important issues in WSNs, since sensor nodes are usually powered by batteries. The radio transceiver is the most power consuming component in a sensor node.

A typical radio transceiver consists of four possible modes with different power consumption, such as

- Transmitting
- Receiving
- Listening and
- Sleeping

The first three modes are also called active / wakeup modes, in which more energy is consumed. Observing idle listening, the status that a sensor node turns on the radio to monitor wireless medium but do not receive any packets, wastes a lot of energy, some researchers propose medium access control (MAC) protocols to turn the radio into sleeping mode as long as possible to save energy for prolonging the network lifetime. However, the radio should be scheduled to be in wakeup mode periodically to monitor, send or receive data packets.

The MAC protocols that make the radio alternate between sleeping and wakeup modes are called the SLEEP and WAKEUP schedule protocols. For example, when two neighboring nodes are exchanging data, all two-hop neighbors of the two nodes are prohibited from doing so. Those prohibited nodes stay at receiving mode until the data exchanging finished, which causes an energy-wasting status called overhearing. The RTS / CTS scheme can be used to avoid overhearing as well as to solve the hidden terminal problem. But, the scheme's overhead is relatively large for WSNs since packets in WSNs are usually very small. Hence an Asynchronous Duty Cycle is proposed in this paper.

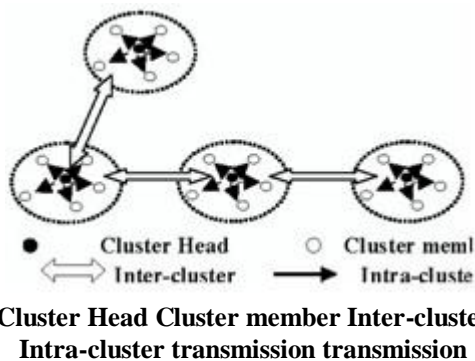


Figure 1 Typical clustered Wireless Sensor Networks

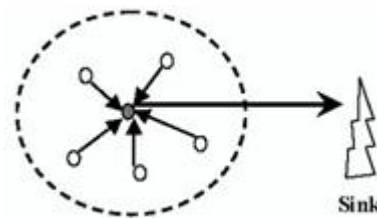
Adjustment MAC protocol provides low energy consumption, low transmission latency and high throughput in WSNs. Adjustment MAC protocol is an Asynchronous SLEEP and WAKEUP Procedure [3] which will not need to synchronize nodes timers, so the timer synchronization overhead is avoided. It also allows each node to set its own SLEEP and WAKEUP schedule independently. Simulation experiments for Asynchronous SLEEP and WAKEUP Procedure are performed and also the simulation results for both with and without Asynchronous SLEEP and WAKEUP Procedure are compared to show the advantages of Asynchronous SLEEP and WAKEUP Procedure.

II. CLUSTERING STRUCTURES IN WIRELESS SENSOR NETWORK

In a clustered Wireless Sensor Network, all members of the clusters are directly connected to the Cluster Heads (CHs). Sensor nodes in the same cluster can communicate directly with their CH. CH can transmit gathered information to the Sink as shown in Figure 2.

Each sensor node is assigned a unique ID number by the base station before it is deployed. Node ID number are saved in the Sink. A Cluster Head is a sensor node with better resources and may be used to collect and merge local traffic and send it to the base station. During the network operation, the Cluster Head is responsible for the integration of all cluster node data and transmitting the data to the sink.

The Cluster is composed of a Cluster Head and sensor node members. Each cluster has a unique cluster ID number. Cluster sensor nodes communicate with their Cluster Head directly, and there is no data exchange between sensor nodes. The Sink is typically a gateway to another network for data processing / storage center, or an access point for human interface and to collect the sensor readings.



● Cluster Head ○ Cluster

Figure 2 Clustering of Sensor Nodes

III. COOPERATIVE COMMUNICATION DESIGN

Cooperative communications is a way to select a relay node that will efficiently forward the packets in a cooperative way. Various cooperative schemes have been developed for high throughput and compared with the non cooperative scheme [4], [5], [6], [7]. The relay selective cooperative schemes have been used recently, where only higher potential nodes are chosen in the cooperative communication process.

Direct Transmission sensor nodes; transmit the data directly to the Sink / Cluster Head sensor node, as a result node that is far away from the sink would die first. Compared with the non cooperative scheme (direct transmission), the successful data transmission can be achieved by using relay cooperative transmission. However, a successful packet transmission in the relay cooperative transmission scheme involves transmitting node and the receiving node. In the energy-constrained Wireless Sensor Network, minimum energy consumption for the successful packet transmission between the source and the destination can be achieved by using proper design of cooperative transmission scheme.

IV. SYSTEM MODEL

Considering sensor networks where static sensor nodes are randomly located in a given region, the traffic in the network is light, and hence transmissions are collision free.

A sensor node is either in an active mode / asleep mode according to its sleep schedule. In the sleep mode, a node is turned off and no power is consumed. Every time, a node i goes into the sleep mode, it sleeps for a period T_{slp} of time before waking up. The sleep time of a node is fixed, but different nodes have different sleep times due to different traffic and battery distributions. A node wakes up and enters an active mode from time to time to see if it has any packets to transmit or if there are any other nodes attempting to transmit to it. An active period can be further categorized as an idle listening slot, a data transmission slot, or a data reception slot. In an idle

listening slot, if the node neither transmits nor receives data Head form cluster members and considering, the Cluster packets within this active period. In this case, the active period Head is electing the next highest energy nodes as cooperative sending and cooperative receiving nodes in the same cluster. consists of two parts,

- RF initialization
- Channel detection

An active period is said to be a data transmission slot if the node transmits a packet in this slot. Likewise, an active period is a data reception slot if the node receives a packet in this slot. A node i initializes its RF circuits immediately after it wakes up. Assuming that it takes a node T_{rf} units of time and E_{rf} amount of energy to initialize its RF circuits. If the node has data to transmit, it first listens to the channel for a period of amount of energy to initialize its RF circuits. If the node has packets to transmit, it first listens to the channel for a period of T_{lis} time to see if any of its neighbors are transmitting. Defining T_{det} as the total time from when a node wakes up to when it goes to sleep again is depicted in Equation (1).

If the channel is idle for T_{det} time, the node sends a Request to Send (RTS) preamble. If the target receiver is also in an active mode and receives the RTS preamble, it replies with a Clear to Send (CTS) packet. The transmitter will then send a data packet, which is acknowledged by an ACK packet from the receiver. Otherwise, if the receiver happens to be in a sleep mode, the transmitter will resend the RTS preamble after going to a power saving status for a short time T_{sav} . This process is repeated until the receiver wakes up and captures the RTS preamble. Throughout this paper, it is assumed that all packets, including preambles, are transmitted at a constant power level p_{tx} .

V. WORK FLOW FOR THE PROPOSED METHOD

Step 1: Initialize the Nodes

Step 2: Electing the Cluster Heads

Step 3: Transferring the message to Cluster Head from non

Cluster Head

Step 4: Cooperative node selection

Step 5: Request message send to neighbor Cluster Head to

select its cooperative its nodes

Step 6: Applying sleep and wakeup procedure to the sensor

nodes other than Cluster Head and cooperative nodes

Step 7: Transfer the message to sink via intermediate Clusters

Considering Clustered Wireless Sensor Networks where static network and sensor nodes are located in a given region.

Considering the traffic in the network to be light, transmissions are collision free. Electing highest energy node as the Cluster Head in each clusters, transferring the message to the Cluster

Head is electing the next highest energy nodes as cooperative sending and cooperative receiving nodes in the same cluster. A request is sent to next Cluster Head to select its next highest energy nodes as cooperative sending and cooperative receiving nodes. Once the Cluster Head and Cooperative nodes are selected, apply sleep and wakeup procedure for the remaining nodes, i.e. other than Cluster Heads and cooperative sending and receiving nodes. Transfer the data to the sink form source Cluster Head and the data paths is via intermediate clusters.

VI. EXAMPLE FOR THE PROPOSED METHOD

As in Figure 3, thirty seven Nodes are deployed including Sink Node. The Nodes are placed in zigzag manner form bottom left to top right, there are six rows and each row contains six Nodes; th 37 Node is the Sink Node and the Sink Node is active throughout the network lifetime. Considering Node1, Node 2, Node 3, Node 7, Node 8, Node 9, Node 13, Node 14, Node 15 as belonging to Cluster 1, and Node 4, Node 5, Node 6, Node 10, Node 11, Node 12, Node 16, Node 17, Node 18 as belonging to Cluster 2, and Node 19, Node 20, Node 21, Node 25, Node 26, Node 27, Node 31, Node 32, Node 33 as belonging to Cluster 3, and Node 22, Node 23, Node 24, Node 28, Node 29, Node 30, Node 34, Node 35, Node 36 belong to Cluster 4. The scenario used here is all-to-one environment where all Cluster periodically report data to a Sink. In this scenario, suppose Cluster 1 wants to transmit data to Sink i.e. Node 37 the possible routing is via Cluster 4; Node 8 is as Cluster Head in Cluster 1 because Node 8 holds the highest energy. Node 14 & Node 15 are selected as Cooperative sending and receiving nodes as they it hold the next highest energy. Data path from Cluster 1 to Sink is via intermediate Cluster 4, Cluster 4 chooses Cluster Head as Node 35, and Cooperative send and receiving nodes as Node 28 and Node 23. Data path for Cluster 2 is via Cluster 4 and similarly data path for Cluster 3 is via Cluster 4. Cluster 4 is at one hop distance to transmit the data packet to Sink Node, so there is no need to choose the Cooperative sending and receiving nodes.

VII. TRUETIME TOOLBOX

True Time (TT) is a MATLAB / Simulink based co simulation tool box developed by Lund University, Sweden [8]. It provides a simulation environment for network control and sensor network. The code functions for the tasks and the initialization commands may be written either as C++ functions or as Matlab M-files.

A. Installation

Add the following lines in the Matlab startup script. This will set all necessary paths to the TRUETIME kernel files.

```
setenv('TTKERNEL', 'Location')
addpath([getenv('TTKERNEL')])
addpath([getenv('TTKERNEL')
'/matlab'])
```

Starting Matlab and giving the command: **truetime**, the Matlab prompt will now open the TRUETIME block library as shown in Figure 4.

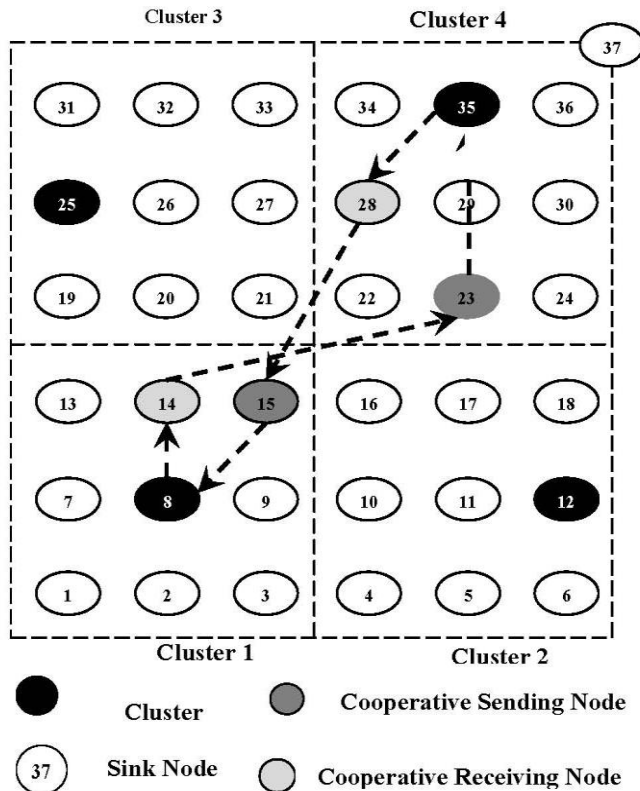


Figure 3 Example for the proposed method

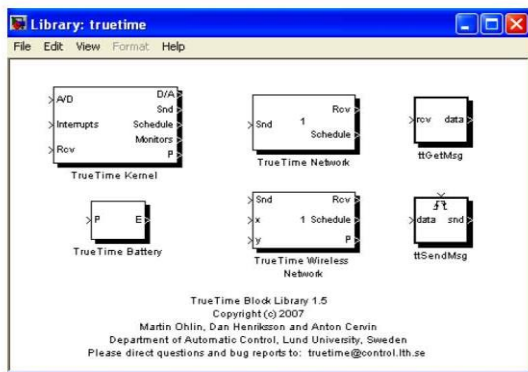


Figure 4 TRUETIME 1.5 block library

The network model uses Truetime wireless network model to realize, which is shown in Figure 6, where Rcv, x, y, and Snd, p ports are corresponding to node ports of the same label. The parameters of network are set through attribute window.

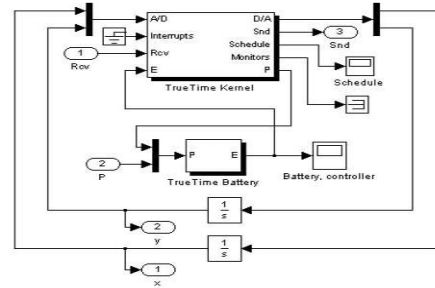


Figure 5 Individual node structure for a wireless sensor node

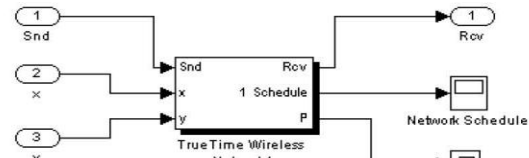
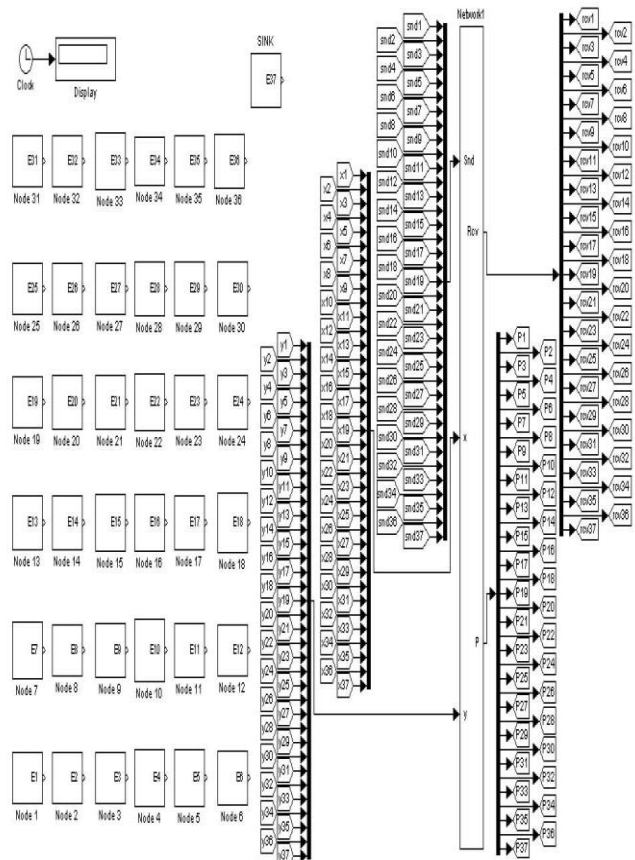


Figure 6 Internal structures for Wireless Sensor Network



The scenarios in Figure 7 are described below: simulation area is a square with 100×100 m², there is a source node to send messages to the sink stations. Simulation runs in 802.15.4 environment, and the data rate is 250 Kbits/s.

VIII. RESULTS AND DISCUSSION

In this paper the simulation is performed using MATLAB platform. Two types of Procedures have been analyzed i.e. with and without SLEEP and WAKEUP Procedure for the cooperative communication in a clustered Wireless Sensor Network. The power and energy consumption mode of Mica2mote and CC1000 transceiver, as depicted in Table have been used in simulating the wireless sensor nodes. All nodes have different battery capacity. The network life times obtained by two Procedures are compared. One scenario is all-to-one environment where all clusters transmit data to a sink.

Node 6 in Cluster 2 transmitting data to sink via intermediate Cluster 4				
Node No	Initial Energy value for Wireless Sensor Node (Joules)	Energy remaining in the Node		Energy Saved value by applying Sleep & wakeup procedure (Joules)
		By applying Sleep & wakeup procedure (Joules)	By applying Without Sleep & wakeup Procedure (Joules)	
1	4.088439	4.081798	4.04156	0.040238
2	4.905879	4.899238	4.859	0.040238
3	4.309949	4.303309	4.263	0.040309
4	0.419104	0.412464	0.37225	0.040214
5	1.688569	1.681919	1.64169	0.040229
6	1.180646	1.1687	1.1246	0.0441
7	1.589027	1.582386	1.54215	0.040236
8	4.922242	4.88709	4.88709	0
9	2.741254	2.734614	2.69438	0.040234
10	3.746256	3.700544	3.700544	0
11	4.209259	3.347038	3.347038	0
12	0.834449	0.827808	0.78757	0.040238

13	4.515488	4.508847	4.46869	0.040157
14	0.525621	0.51898	0.47871	0.04027
15	3.725465	3.718825	3.67859	0.040235
16	3.64686	3.611708	3.611708	0
17	3.587348	3.580707	3.54047	0.040237
18	0.667159	0.660518	0.620291	0.040227
19	2.228945	2.222304	2.18207	0.040234
20	2.543936	2.537295	2.49706	0.040235
21	2.652451	2.645811	2.60558	0.040231
22	4.298585	4.296466	4.296466	0
23	3.388625	3.381984	3.34175	0.040234
24	4.029191	3.982106	3.982106	0
25	2.656214	2.649574	2.60934	0.040234
26	4.779479	4.744327	4.744327	0
27	0.333385	0.326744	0.28651	0.040234
28	2.707599	2.700949	2.66072	0.040229
29	1.408302	1.401661	1.36132	0.040341
30	2.404502	2.397861	2.35762	0.040241
31	3.424319	3.417678	3.3774	0.040278
32	1.041292	1.034651	0.99442	0.040231
33	3.040805	3.034164	2.99393	0.040234
34	1.630881	1.62424	1.58401	0.04023
35	4.404236	4.366469	4.366469	0
36	0.666973	0.660332	0.6201	0.040232

IX. CONCLUSION

The flexibility, cost and rapid deployment characteristics of Wireless Sensor Networks create many new and exciting areas of application for remote sensing. In the future, these wide areas of application will make sensor networks an integral part of our lives. However, realization of energy consumption in sensor networks is essential. A Clustered

Wireless Sensor Network with Cooperative design preserves lot of energy when compared to non cooperative communication design. To improve the energy consumption further in cooperative communication design of a clustered Wireless Sensor Network, an asynchronous sleep and wakeup procedure is introduced in this project. The concept of scheduling sleep and wakeup procedure is very effective. The proposed model proves that energy consumption is reduced to a great extent by using sleep and wakeup procedure.

X. REFERENCES

- [1] Feng Liu, Chi-Ying Tsui, Member, IEEE, and Ying Jun (Angela) Zhang, Member, "Joint Routing and Sleep Scheduling for Lifetime Maximization of Wireless Sensor Networks", IEEE Transactions On Wireless Communications, pp.2258-2267, July.
- [2] G. Lu, B. Krishnamachari, and C. S. Raghavendra, "Performance evaluation of the IEEE 802.15.4 MAC for low-rate low-power wireless network", IEEE IPCC, pp. 701–706. April. 2004.
- [3] V. Rajaravivarma, Y. Yang, and T. Yang, "An overview of Wireless Sensor Network and applications", in Proc. 35th Symp. Syst. Theory, pp. 432–436, Mar. 2003
- [4] Bletsas, A. Khisti, D. P. Reed, and A. Lippman, "A simple cooperative diversity method based on network path selection", IEEE Journal on Selected Areas in Communications, vol. 24, no. 3, pp. 659–672, 2006.
- [5] Stefanov and E. Erkip, "Cooperative coding for wireless networks", IEEE Transactions on Communications, vol. 52, no. 9, pp. 1470–1476, 2004.
- [6] S. Michalopoulos and G. K. Karagiannidis, "Performance analysis of single relay selection in rayleigh fading", IEEE Transactions on Wireless Communications, vol. 7, no. 10, pp. 3718–3724, 2008.
- [7] M. M. Fareed and U. M. Murat, "On relay selection for decode-andforward relaying", IEEE Transaction on Wireless Communications, vol. 8, no. 7, pp. 3341–3346, 2009.

Automatic Segmentation of Overlapped Images

P. Nithya, M. Nirmala,

Member, IEEE

Department of Electronics and Communication Engineering
K.S.Rangasamy College of Technology, Namakkal

Abstract: Chromosomes are essential genomic information carriers. The identification of chromosome abnormalities is an essential part of diagnosis and treatment of genetic disorders such as chromosomal syndromes and many types of cancer. There are different types of chromosome aberration like mapping of the common duplications, deletions, and translocations. One of the most considerations in the field of chromosome analysis is the segmentation. Currently available cytogenetic imaging software is designed to classify only normal chromosomes [9]. The automation of chromosome analysis is involving segmentation of chromosomes and classification into 24 groups [8]. The segmentation and overlap of chromosomes are a major step toward the realization of homolog classification. Resolving chromosome overlaps is an unsolved problem in automated chromosome analysis and the analysis is complicated by the occurrence of clusters of overlapped chromosomes. Current systems for automatic chromosome classification are mostly interactive and require human intervention for correct separation between touching and overlapping chromosomes, and so are unable to segregate overlapping chromosomes. In this paper, propose an automatic procedure to obtain the separated chromosomes. The overlapped chromosomes are segmented by found the interesting (concave and convex) points with the help of chain code algorithm and the interesting points [1] are located on contour of the image and then the curvature function is found to find out concave points and the possible separation lines are plotted by using all concave points and finally construct hypotheses for possible separation lines between concave points. The segmentation is carried out by means of a curvature function scheme, which proved to be successful.

Index Terms: Diagnosis, genetic disorders, automatic chromosome classification, interesting points, hypothesis.

I. INTRODUCTION



Fig 1: Touching and overlap chromosomes

CHROMOSOMES are microscopic structures containing all of an individual's genetic information. The chromosomes are composed of DNA and various proteins. The DNA contains the actual genetic code of an individual, and the proteins protect the DNA and allow the DNA to duplicate properly when the cell divides. Chromosome analysis is performed on dividing cells in their metaphase stage. In that stage, the chromosomes may be stained in a way that creates a typical band-pattern on them. A chromosome in the metaphase stage is constructed from two identical arms (chromatides), which are joined together on a common point (centromere). The centromere actually divides each chromatide into two arms. Chromosomes are essential genomic information carriers. The chromosomes formed as 22 pairs of autosomes (1–22) and two sex chromosomes (X and Y). Thus, there are 24 classes of chromosomes.

A small proportion of the population has cells each one of which has fewer or more than 46 chromosomes, implying a substantial deficit or excess of genetic material. Others have one or more structurally abnormal chromosomes, in which a section of a chromosome has moved from its usual to another position. Chromosome analysis is performed on dividing cells in their metaphase stage [9]. The metaphase stage images are shown in fig. 1. The chromosomes in a metaphase image may be bent, their arms may be joined (along points other than the centromere), their bands may be spread, and they may touch or partially overlap each other.

Thus, all these problems should be taken into consideration when processing the metaphase image. Current systems for automatic chromosome classification are mostly interactive and require human intervention for correct separation between touching and overlapping chromosomes. The separation is performed by posing a series of hypotheses that fit certain constraints [13], [17].

II. RELATED WORKS

1) Segmentation methods try to separate between touching chromosomes by classifying the chromosome pixels and the background pixels into two different segments. Since segmentation methods are general methods that do not depend on the shape of objects, their link to the specific problem of chromosome separation is weak, and, therefore, they tend to fail in cases of incomplete information. A case of incomplete information occurs; there is no separating path between chromosomes [5], [7].

2) Heuristic search edge-linking methods try to separate between touching chromosomes by searching for a minimal-cost connected path that separates between the chromosomes. The link lost connection of such methods to the specific problem of chromosome separation leads to inferior results in cases of incomplete information, such as in the case where a separating path does not exist [19].

3) The method for separating the touching chromosomes by using shape decomposition based on fuzzy subset theory [16] is reported as giving inferior results relative to other general methods. An even greater disadvantage of this method is that it also yields erroneous decompositions of single chromosomes in cases of bent chromosomes.

III. PRELIMINARY PROCESSING

The preliminary processing of the metaphase image is performed by increasing the effective sampling resolution [14] may be achieved by sampling each metaphase image in some overlapping parts. Fig. 2 is the sample overlapped and touching image.



Fig 2: Sample overlapping and Sample touching images

A. Obtain the Chromosome Contours

The relevant information of a shape is contained in its contour, for separation purposes, only the shape contours are required. The use of shape contours actually represents a successful information compaction that reduces the amount of processed data and stresses the main features of the objects. Chromosome contour determined by using a common contour-following method to track the contours of the connected segments by row and columns [2]. Fig. 3 shows the binary approximation of the overlapped image and fig.4 shows the contour of the overlapped image.

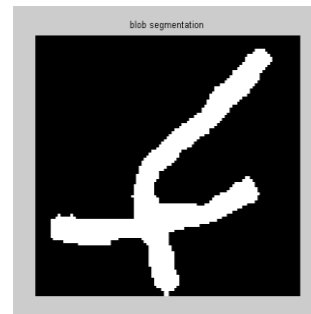


Fig 3: Binary approximation of the given overlapped image

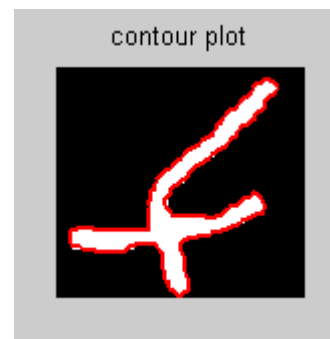


Fig 4: Contour plot of the above binary image. Contour plotted in green

B. Obtain the Discrete Curvature Function

The curvature function of a curve is defined as the rate of change of the curve slope with respect to its length. The radius of a circle is tangent to the concave side of the curve, and has the same curvature as the curve at the tangential point. The curvature function is a derivative of the contour's slope function. To reduce the computational requirements of the K-slope evaluation, an extended chain-code method is used. Using the extended chain-code, it is possible to determine the K-slope at a given pixel directly from a look-up table where the extended chain-code serves as the entry point.

This method used for detecting and locating "corners" in chain-coded curves [3]. The "corner" means that chain node with which we can associate an identifiable discontinuity in the mean curvature of the curve. The detection of a corner is a function of the magnitude of the discontinuity. The concave and convex points of the object are detected by using chain code method. Fig. 5 presents the result of interesting points detection on the curvature graph, where the interesting points are marked with triangles.

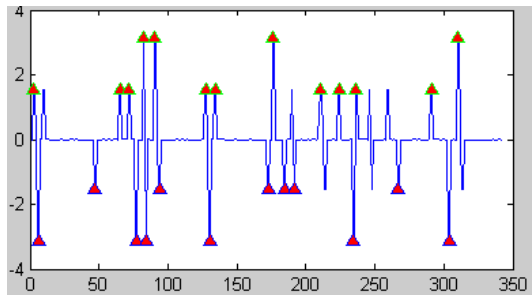


Fig 5: Interesting points on the curvature graph.

C. Obtaining the Interesting Points

The interesting points are detected as extremum points of the curvature function, or as middle points of constant curvature curve segments. The required filter should combine a low-pass filter for high frequency noise removal, and a high-pass filter for curvature peaks enhancement.

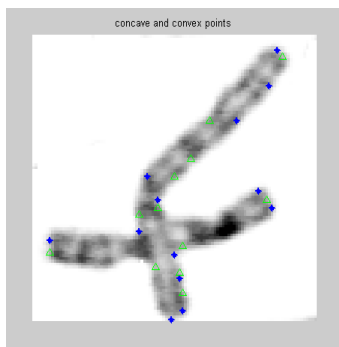


Fig 6: Interesting points on the chromosome

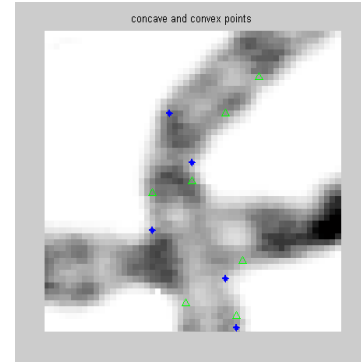


Fig 7: Extended view of the above chromosome image

Thus actually resulting in a band-pass filter. The filtered curvature function is segmented, and extremum points are detected within each segment. From that list, only concave points with a curvature measure above a certain threshold are selected. The interesting points (concave and convex points) are located on the chromosomes. Fig. 6 shows the location of interesting points on the chromosome and fig. 7 shows the extended view of fig. 6.

IV. CHROMOSOME SEPARATION

Each chromosome as a separate subset of pixels, it is possible to view the chromosome separation, the minset is obtained by taking the intersection between some subsets and the complement of the other subsets. Each minset of the chromosomes represents either a part unique to one chromosome or a part common to more than one chromosome. The minset normal form representation of the chromosomes can be constructed by a union of such parts. The required partition is obtained by splitting the object along lines that connect high concave points.

For the determination of separation lines [4], all the possible pairs of high concave points are considered. The separation lines are obtained by taking all the possible combinations of two points.

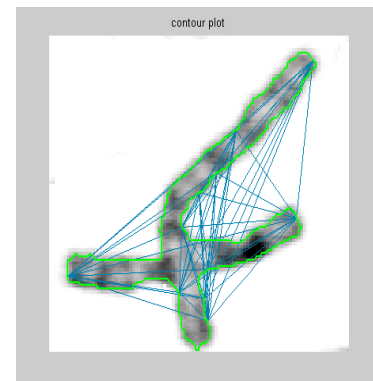


Fig 8: Possible separation lines

A. Hypotheses for Overlapping Objects

The constraint requires that the spatial distance between the vertices of a separation line of touching objects [20] should be small relative to the distance between the vertices along the shape's contour.

To construct a hypothesis for the separation of overlapping objects, an overlap minset should be located. The distance between the separation lines should be above a given threshold. Fig. 8 shows the possible separation lines between minsets.

B. Hypotheses verification

The verification of hypotheses is based on an evaluation of the fit of the obtained parts to the prototype shapes of the chromosomes [10]. In general, the shape of a chromosome is not fixed. A chromosome may have various heights and widths.

The evaluation of the fit of a chromosome to its prototype shape is done by fitting a bounding polygon to the chromosome [10], [11]. The bounding polygon is constructed by locating the shape's minimal bounding box, contracting it in the middle, and rounding its corners. In order to retain the uniqueness of the bounding polygon as a chromosome prototype, constraints are posed on possible locations of its vertices. The minimal bounding box of a shape is found by computing the principal component transformation of that shape. Fig. 9 shows the overlap region, fig. 10 shows the first chromosome segmentation from other chromosome and fig. 11 shows the second chromosome segmentation from other chromosome.

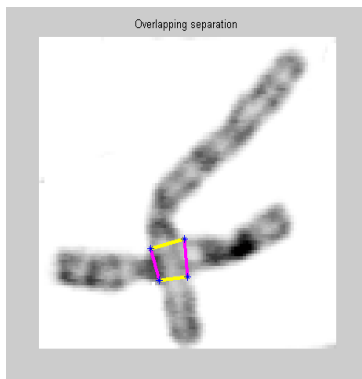


Fig 9: Region of overlapping in the chromosome

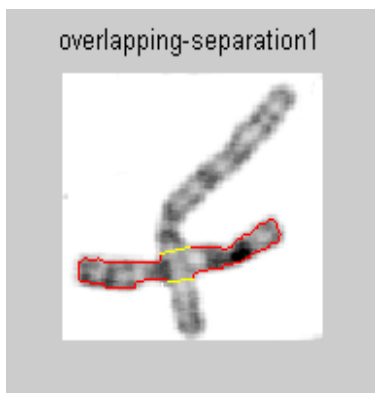


Fig 10: Separation of first Chromosome from second chromosome

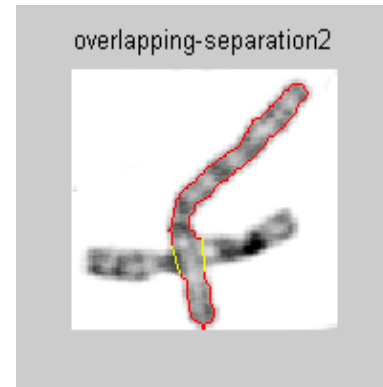


Fig 11: Separation of second Chromosome from first chromosome

V. FUTURE WORK

In the case where there are only touching objects, the problem of finding a separation hypothesis is reduced to finding the minset partition. After finding that partition, each object is composed of one minset and therefore, there is no need to find unions of minsets. Since the number of possible partitions is rather large, it is reduced by introducing an additional constraint on the possible pairs.

The constraint requires that the spatial distance between the vertices of a separation line of touching objects should be small relative to the distance between the vertices along the shape's contour.

The reduction in the number of possible partitions by using the constraint of nearly parallel separation lines. An additional reduction of the number of possible partitions is obtained by introducing a constraint on possible combinations of pairs and so possible partitions will be only part of the sets.

For example Fig. 12 shows touching region and fig. 13 and fig. 14 shows the disentangling of touching chromosomes. The experiments are going in the separation of touching chromosome with out any loss in the information [12].

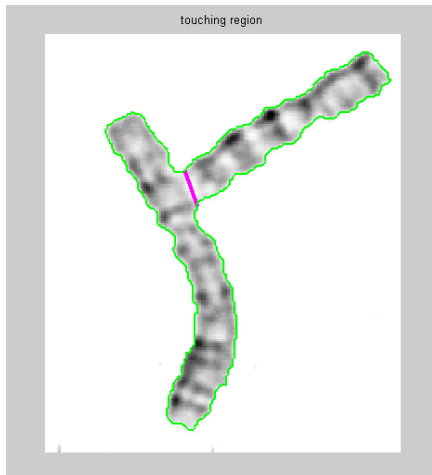
A .Sample disentangling Images

Fig 12: The region of touching chromosomes

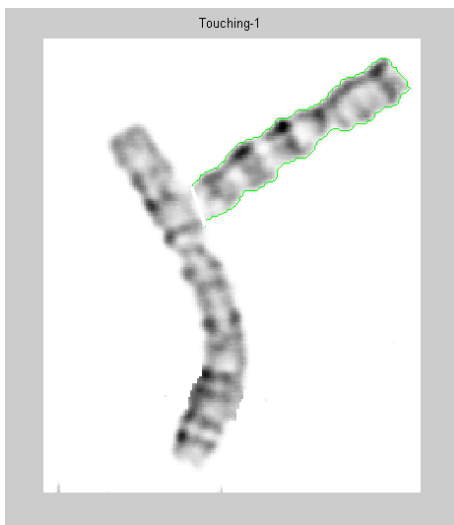


Fig 13: disentangling of first chromosome from second chromosome

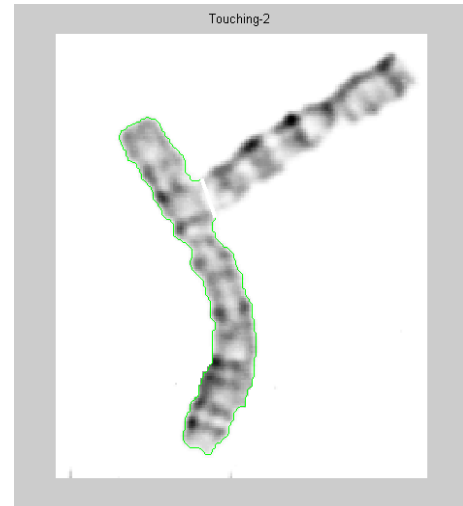


Fig 14: Disentangling of second chromosome from first chromosome

V. CONCLUSION

Karyotype analysis is a widespread procedure in cytogenetics to assess the possible presence of genetics defects. The procedure is lengthy and repetitive, so that an automatic analysis would greatly help the cytogeneticist routine work [6]. Still, automatic segmentation and full disentangling of chromosomes are open issues.

The problem of extracting individual objects from overlapping configurations is one that occurs in a number of applications in machine vision [18]. It is a difficult problem in general and can be thought of in two parts: 1) identifying overlapping objects in the first place and 2) identifying the individual components. In the case of chromosomes, it is usually fairly easy to identify an overlap on straightforward shape criteria.

This proposed method for Automatic Chromosome segmentation of touching and overlapping images are more accurate than other previous methods and this method of segmentation is applicable for large number of bents present in the chromosome structures and more number of clusters [15] by the location of each separation point is optimized, yielding the minimal possible distance between the smoothed approximation and the original curve.

The experiment proved that this algorithm can segment the overlapping chromosomes successfully.

REFERENCES

- [1] G. Agam and I. Dinstein, "Geometric separation of partially overlapping non-rigid objects applied to automatic chromosome segmentation", *IEEE Trans. Pattern Anal. Mach. Intell.*, vol. 19, no. 11, pp. 1212–1222, Nov. 1997.
- [2] E. Grisan, A. Pesce, A. Giani, M. Foracchia, and A. Ruggeri., "A new tracking system for the robust extraction of retinal vessel structure," in *Proc. 26th Annu. Int. Conf. IEEE-EMBS*. New York: IEEE Press, 2004, pp. 1620–1623.

- [3] D.L.Milgram and A.Rosenfeld, "A Corner-Finding Algorithm for Chain-Coded Curves", IEEE Trans. Pattern, 2000.
- [4] X. Bai, C. Sun, F. Zhou, Touching cells splitting by using concave points and ellipse fitting, Proceedings of Digital Image Computing: Techniques and Applications, Canberra, Australia (2008) 271–278.
- [5] K.Z. Mao, P. Zhao, P. Tan, Supervised learning-based cell image segmentation for P53 immunohistochemistry, IEEE Transactions on Biomedical Engineering 53 (6) (2006) 1153–1163.
- [6] C. Urdiales García, A. Bandera Rubio, F. Arrebola Pérez, and F. Sandoval Hernández, "A curvature-based multiresolution automatic karyotyping system," Mach. Vis. Appl., vol. 14, pp. 145–156, 2003.
- [7] M. Moradi and S. K. Staredhan, "New features for automatic classification of human chromosomes: A feasibility study," Pattern Recognit. Lett., vol. 27, pp. 19–28, 2006.
- [8] A. Carothers and J. Piper, "Computer-Aided Classification of Human Chromosomes: A Review," Statistics and Computing, vol. 4, no. 3, pp. 161–171, 1994.
- [9] M. Thompson, R. McInnes, and H. Willard, Genetics in Medicine. ON, Canada: Saunders, 1991.
- [10] Kolesnikov, A., Fränti, P.: A fast near-optimal algorithm for approximation of polygonal curves. Proc. Int. Conf. Pattern Recognition-ICPR'02. 4 (2002) 335–338.
- [11] Chen, D.Z., Daescu, O.: Space efficient algorithm for polygonal curves in two dimensional space, Proc. 4th Int. Conf. Computing and Combinatorics. (1998) 55–64.
- [12] G. C. Charters and J. Graham, "Disentangling chromosome overlaps by combining trainable shape models with classification evidence," IEEE Transactions on signal processing, vol. 50, pp. 2080–2085, August 2002.
- [13] P. Mousavi, R. K. Ward, and P. M. Lansdorp, "Feature analysis and classification of chromosome 16 homologs using fluorescence microscopy image," IEEE Can. J. Elect. Comput. Eng., vol. 23, no. 4, pp. 95–98, 1999.
- [14] K. Saracoglu, J. Brown, L. Kearney, S. Uhrig, J. Azofeifa, C. Fauth, M. Speicher, and R. Eils, "New concepts to improve resolution and sensitivity of molecular cytogenetic diagnostics by multicolor fluorescence in situ hybridization," Cytometry, vol. 44, no. 1, pp. 7 May 2001.
- [15] W. C. Schwartzkopf, A. C. Bovik, and B. L. Evans, "Maximum-likelihood techniques for joint segmentation-classification of multispectral chromosome images," IEEE Trans. Med. Imag., vol. 24, no. 12, pp. 1593–1610, Dec. 2005.
- [16] T. Law, K. Yamada, D. Shibata, T. Nakamura, L. He, and H. Itoh, "Edge extraction using fuzzy reasoning," in Soft Computing for Image Processing, S. K. Pal, Ed. New York: Physica-Verlag, 2000.
- [17] M. Moradi and S. K. Staredhan, "New features for automatic classification of human chromosomes: A feasibility study," Pattern Recognit. Lett., vol. 27, pp. 19–28, 2006.
- [18] M. Sezgin and B. Sankur, "Survey over image thresholding techniques and quantitative performance evaluation," J. Electron. Imag., vol. 13, pp. 146–168, 2004. T. Ried, "Cytogenetics—In color and digitized," New Eng. J. Med., vol. 350, no. 16, pp. 1597–1600, Apr. 2004.
- [19] Carsten Garnica, Frank Boochs, Marek Twardochlib, "A new approach to edge-preserving smoothing for edge extraction and Image segmentation", IAPRS, Vol. XXXIII, Amsterdam, 2000.
- [20] Xiangzhi Baia,, ChangmingSun, FugenZhou, "Splitting touching cells based on concave points and ellipse fitting", Pattern Recognition 42 , 2009.



Nithya. P was born in India. She received the Bachelor in Electronics and Communication degree from the Anna University and the Master in Applied electronics degree from the Anna

University. Her research interests include digital image processing in medical images.

Nirmala. M was born in India. She received the Bachelor in Electronics and Communication degree from the Anna University and the Master in Applied electronics degree from the Anna University. Her research interests include digital image processing in medical images and ultra sound images.

A Control Strategy for a Variable-Speed Wind Turbine with a Permanent-Magnet Synchronous Generator

V. Prakashkumar¹, A. Tamilselvi²,

¹ PG Scholar, Department of EEE, SNS College of Technology, Coimbatore

² Assistant Professor, Department of EEE, SNS College of Technology, Coimbatore

Abstract - This paper presents a novel control strategy for the operation of a direct-drive permanent-magnet synchronous generator-based stand-alone variable-speed wind turbine. The control strategy for the generator-side converter with maximum power extraction is presented. The stand-alone control is featured with output voltage and frequency controller that is capable of handling variable load. The potential excess of power is dissipated in the dump-load resistor with the chopper control, and the dc-link voltage is maintained. Dynamic representation of dc bus and small-signal analysis are presented. Simulation results show that the controllers can extract maximum power and regulate the voltage and frequency under varying wind and load conditions. The controller shows very good dynamic and steady-state performance.

Keywords - Maximum power extraction, permanent-magnet Synchronous generator (PMSG), switch-mode rectifier, variable-speed wind turbine, voltage and frequency control.

I. INTRODUCTION

Wind energy is clean silent and emission-free source of energy. Using small wind energy conversion system increases rapidly nowadays all over the world due to its availability, small size, high performances, low cost installation, and it has low weight compared to induction generators. PMSG is used more frequently in small wind turbine application due to its robustness, reliability and high efficiency when connected to variable speed wind turbine [1]. Most papers [2], [3], [4] are considering using PMSG and normally include controlled three phase ac to dc conversion and to extract maximum power from the fluctuating wind, variable-speed operation of the wind-turbine generator is necessary besides achieving unity power factor at the generator side. The dc/ac inverter is used to regulate the load voltage and frequency and for stand-alone systems. Additionally, a battery power flow controller is used to balance the load power as the wind power changes [3], [4]. A control strategy for the generator-side converter with output maximization of a PMSG-based small-scale wind turbine is developed. The generator-side switch-mode rectifier is controlled to achieve maximum power from the wind. The method requires only one active switching device [insulated-gate bipolar transistor (IGBT)], which is used to control the generator torque to extract maximum power. According to grid connected systems, the MPPT control is achieved using the dc/ac inverter and the controller achieve unity power factor at the grid side. The load-side pulse-width modulation (PWM) inverter is using a relatively

complex vector-control scheme to control the amplitude and frequency of the inverter output voltage. The stand-alone control is featured with output voltage and frequency controller capable of handling variable load. A dump-load-resistor controller is used to dissipate excess power during fault or over generation. The excess power is dissipated in the dump-load resistor with the chopper control, and the dc-link voltage is maintained. The Section II introduces the System overview. The Section III describes the Control of Switch-mode rectifier with maximum power extraction. The Section IV discusses on the Control of Load-Side inverter. The Section V, VI, VIII and VIII discusses on test system and waveforms/results and conclusion respectively.

II. SYSTEM OVERVIEW

The Fig. 1 shows the control structure of a PMSG-based standalone variable-speed wind turbine which include a wind turbine, PMSG, single-switch three-phase switch-mode rectifier, and a vector-controlled PWM voltage-source inverter. The output of a variable-speed PMSG is not suitable for use as it varies in amplitude and frequency due to fluctuating wind. A constant dc voltage is required for direct use, storage, or conversion to ac via an inverter. In this paper, a single-switch three-phase switch-mode rectifier is used to convert the ac output voltage of the generator to a constant dc voltage before conversion to ac voltage via an inverter. The single-switch three-phase switch-mode rectifier consists of a three-phase diode bridge rectifier and a dc to dc converter. The output of the switch-mode rectifier can be controlled by controlling the duty cycle of an active switch (such as IGBT) at any wind speed to extract maximum power from the wind turbine and to supply the loads. A vector-controlled IGBT inverter is used to regulate the output voltage and frequency during load or wind variations. Voltage drop due to sudden fall in wind speed can be compensated by the energy-storage system. During wind gust, the dump-load controller will be activated to regulate the dc-link voltage to maintain the output load voltage at the desired value.

III. CONTROL OF SWITCH-MODE RECTIFIER WITH MAXIMUM POWER EXTRACTION

This section describes the main techniques that have been reported to the control of wind turbine toward the maximization the output power. To allow the turbine to transfer a maximum fraction of available wind power for fluctuating wind velocities incident upon the turbine blades, it is desirable to maintain the tip-speed ratio at point of maximum power coefficient $c_p(\lambda)$. Based in this principle

several control techniques have been developed to optimize output power for a given wind velocity. Other techniques employed a Maximum Power Point Tracking (MPPT) algorithm with search for the turbine rotating speed, which result in the maximum power, is based on a measurement of the power generated. Therefore, since the measurement of the power generated is simpler and more accurate than the measurement of the wind velocity, the MPPT is preferred..

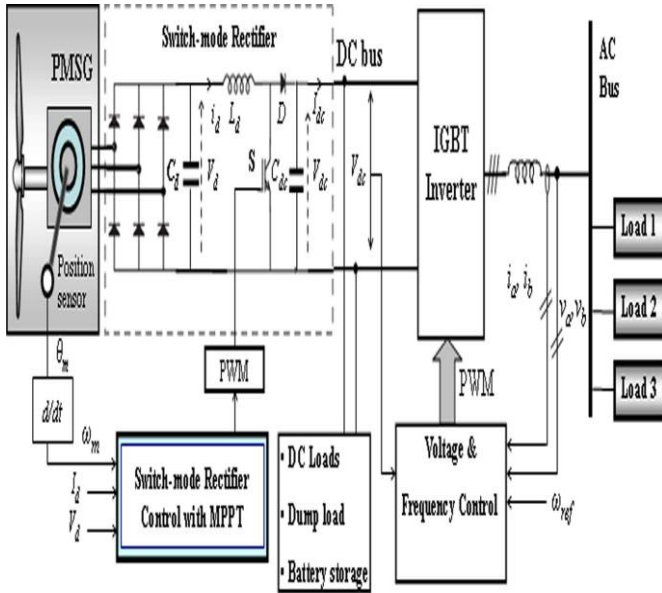


Fig 1 .Control structure of a PMSG Based Stand-alone Variable-Speed Wind turbine

The structure of the proposed control strategy of the switch-mode rectifier is shown in Fig. 2. The control objective is to control the duty cycle of the switch *S* in Fig. 2 to extract maximum power from the variable-speed wind turbine and transfer the power to the load. The control algorithm includes the following steps.

- 1) Measure generator speed ω_g .
- 2) Determine the reference torque (Fig. 4) using the following equation:

$$T_g^* = K_{opt}(\omega_g)^2 \tag{1}$$

- 3) This torque reference is then used to calculate the dc current reference by measuring the rectifier output voltage V_d as given

$$I_d^* = (T_g^* \times \omega_g) / V_d \tag{2}$$

(2)

- 4) The error between the reference dc current and measured dc current is used to vary the duty cycle of the switch to regulate the output of the switch-mode rectifier and the generator torque through a Proportional–Integral (PI) controller.

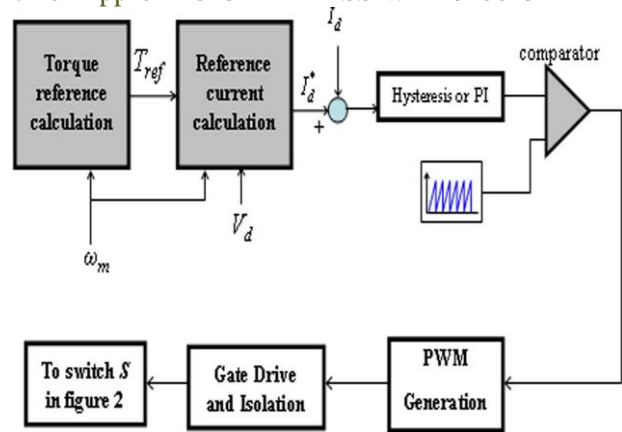


Fig. 2 Control strategy of the switch-mode rectifier.

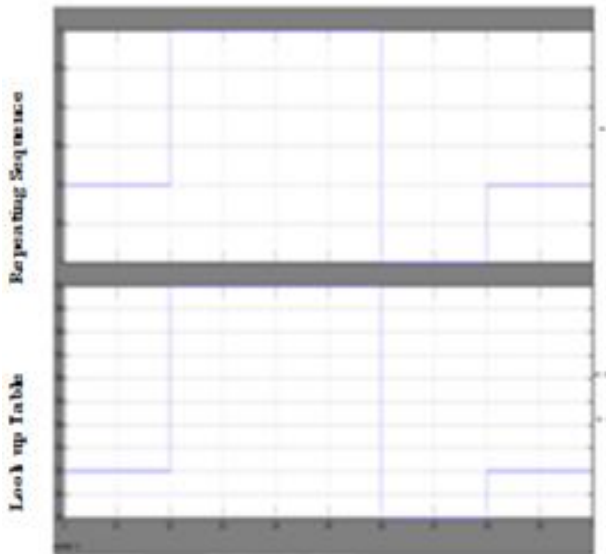
The generator torque is controlled in the optimum torque curve according to the generator speed. The acceleration or deceleration of the generator is determined by the difference of the turbine torque T_m and generator torque T_g . If the generator speed is less than the optimal speed, the turbine torque is larger than the generator torque, and the generator will be accelerated. The generator will be decelerated if the generator speed is higher than the optimal speed. Therefore, the turbine and generator torques settle down to the optimum torque point T_{m_opt} at any wind speed, and the wind turbine is operated at the maximum power point.

IV. CONTROL OF LOAD-SIDE INVERTER

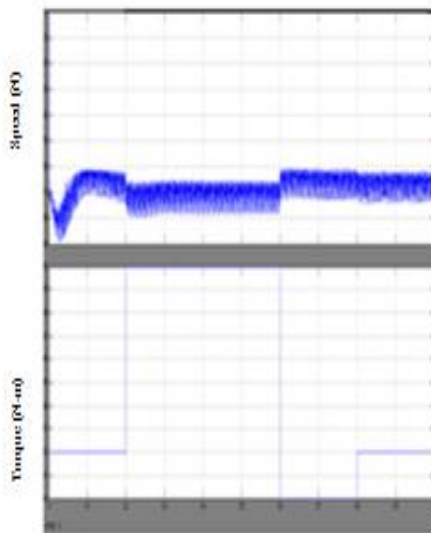
The control strategy of Vector-Control Scheme is used to perform the control of the grid side converter. They control of the DC-link voltage, active and reactive power delivered to the grid, grid synchronization and to ensure high quality of the injected power [2].The objective of the supply-side converter is to regulate the voltage and frequency. The control schemes is in the inner loops where they use different reference frames to perform the current control. In the first case, the currents are controlled in the synchronous rotating reference frame using PI controllers. The dc voltage PI controller maintains the dc voltage to the reference value. The PI controllers are used to regulate the output voltage and currents in the inner control loops and the dc voltage controller in the outer loop. This is the classical control structure, it is also known as dq-control. It transforms the grid voltages and currents from the abc to the dq reference frame. In this way the variables are transformed to DC values which can be controlled more easily. This structure uses PI controllers since they have good performance for controlling DC variable.

VIII. RESULTS FOR PROPOSED SYSTEM

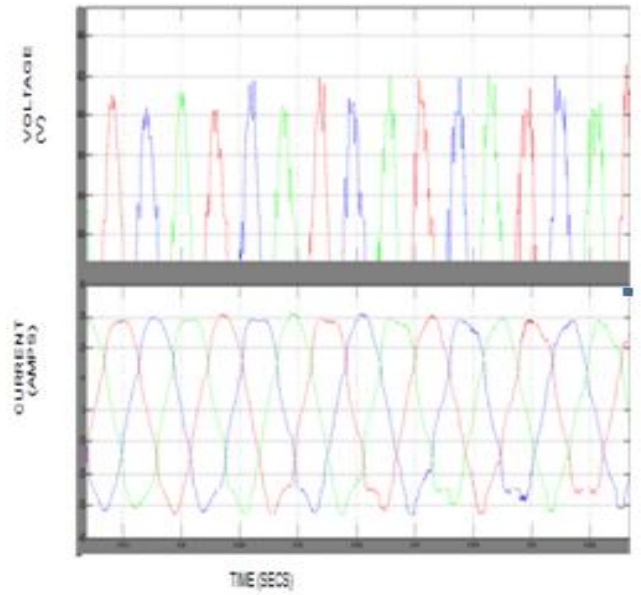
The model of the PMSG-based variable-speed wind-turbine system of Fig. 4 is built using Matlab/ Simpower dynamic system simulation software.



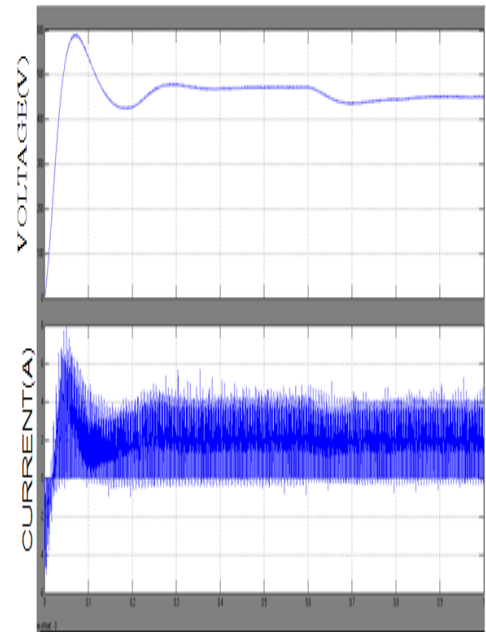
Time (secs)
(a)



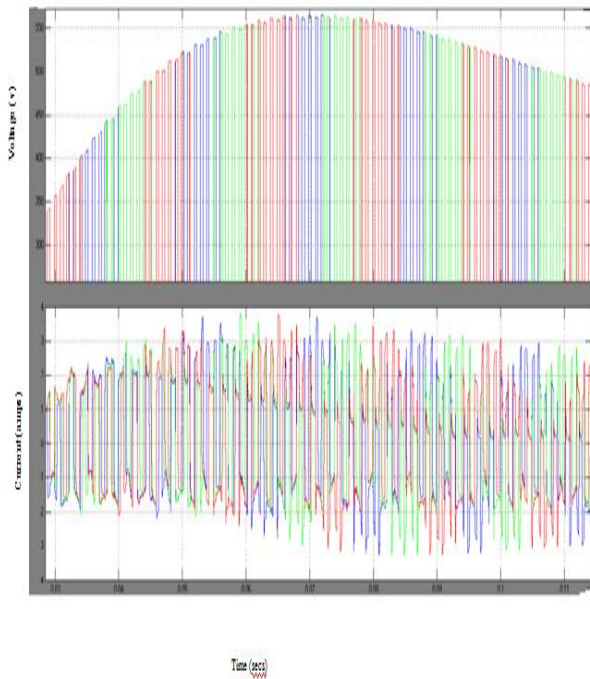
Time (secs)
(b)



(c)



(d)



(e)

Fig. 8. (a) Wind Speed (b) Torque and Speed (c) Three phase V-I Measurement (d) Inverter –side control (e) Grid-side control.

IX. CONCLUSION

A control strategy for a direct-drive stand-alone variable speed wind turbine with a PMSG has been presented in this project. A simple control strategy for the generator-side converter to extract maximum power is discussed and implemented using Simpower dynamic-system simulation software. The controller is capable of maximizing output of the variable-speed wind turbine under fluctuating wind. The generating system with the proposed control strategy is suitable for a small-scale stand-alone variable-speed wind-turbine installation for remote-area power supply. The simulation results demonstrate that the controller works very well and shows very good dynamic and steady-state performance.

REFERENCES

- [1] Munteanu, A. Bratcu, I. and Ceanga, E. (2009) "wind turbulence used as searching signal for MPPT in variable-speed wind energy conversion systems," *Renew. Energy*, Vol.34, pp.322-327.
- [2] R. Hoffmann and P. Mutschler, "The influence of control strategies on energy capture of wind turbines," in *Proc. 35th IAS Annu. Meeting World Conf. Ind. Applicat. Elect. Energy*, Piscataway, NJ, 2000, pp. 886–893..
- [3] Chan, T. F. and Lai, L. L. (2007), "Permanent-magnet machines for distributed generation: A review," in *Proc. IEEE Power Eng. Annu. Meeting*, pp. 1–6.
- [4] K. Tan and S. Islam, "Optimum control strategies in energy conversion of PMSG wind turbine system

without mechanical sensors," *IEEE Trans. on Energy Conversion*, Vol.19, No.2, pp.392-399, Jun. 2004..

- [5] C. Mademlis and N. Margaris, "Loss minimization in vector-controlled interior permanent-magnet synchronous motor drives," *IEEE Trans. On Industrial Electronics*, Vol.49, No.6, pp.1344-1347, Dec. 2002.
- [6] Z. Chen, E. Spooner, "Grid Power Quality with Variable-Speed Wind Turbines", *IEEE Trans. on Energy Conversion*, Vol. 16, No.2, June 2001, pp. 148-154..
- [7] Hui, J. and Bakhshai, A. (2008) "Adaptive algorithm for fast maximum power point tracking in wind energy systems," in *Proc. IEEE IECON 2008*, Orlando, USA, 10-13, No.1, pp. 2119-2124.
- [8] Chinchilla, M. Arnaltes, S. and Burgos, J. C. (2006) "Control of permanent magnet generators applied to variable-speed wind-energy systems connected to the grid," *IEEE Trans. Energy Convers.*, Vol. 21, No. 1, pp. 130–135.
- [9] R. S. Lai and K. D. T. Ngo, "A PWM Method for Reduction of Switching Loss in a Full-Bridge Inverter", *Proc. of 9th An. Conf. of IEEE Applied Power Electronics and Exposition*, APEC-1994. Vol.1, pp, 122 - 127, Orlando, 3-17 Feb 1994.



Prakashkuamr. V received the **B.E.** Degree in Electrical and Electronics Engineering from Sri Krishna College of Engineering and Technology in 2009, and Pursing **M.E. (POWER SYSTEM ENGINEERING)** in SNS College of technology, Coimbatore, India. His Area of interest are Wind energy, Power electronics and Power Systems.

A Empirical Framework for Facial Expression Analysis

¹Geeranjali Sharma, ² H K Sawant

^{1, 2} Department Of Information Technology, Bharati Vidyapeeth Deemed University
College Of Engineering, Pune-46

ABSTRACT

For facial expression analysis different-different approaches have been implemented. First thing preprocessing step is done and after that face detection algorithm applied for face detection. After face detection facial feature tracking or feature is extracted on the behalf of obtained feature value. Different-different classifier likes ANN, HMM, SVM is used to train the feature value obtained and then after testing is done to classify the classes to whom this feature value belongs. If high dimension feature value is obtained than PCA does work to reduce the dimension. Our approach is that apply Gabor filter on face to extract the feature. After feature extraction SVM is used to training and testing the feature value and finally similarity measure is evaluated to classify the classes to whom it belongs means it be from happy, sad, disgust, surprise, angry class. As many algorithm has been used for showing the Facial Expression of a Human. They have used different-different feature extraction method. Consideration of some similarity function has taken. Sometimes PCA, LDA was considered for dimensions reduction and for better accuracy.

Keywords - Face detection, Facial Expression analysis segmented facial region Gabor filter, Support Vector Machine.

I. INTRODUCTION

Most research in facial expression recognition is limited to six basic expression and several combination. The expression are classified into emotion categories rather than another technique. It is difficult task to show all facial expressions because in everyday life six basic expression occur so frequently. Emotion is often communicated by small changes in one or two facial features, on the other hand the same facial expression may occurred in more than one emotions. The presence or absence of one or more facial actions value may change its prediction. One man can show their facial expression in different manner than expressing the same facial expression by other person. The facial features value changes person to person for the same facial expression. The main problem in facial expression analysis is that no exact dataset is available that show 100% accuracy. The problem comes when the facial feature extraction is processed, sometimes frontal image is present and sometimes tilt in different orientation. The light condition also plays a different role so all these factors affect the preprocessing steps and the desired results are not obtained. If the main facial feature like tip of nose, eye, head, cheek is not properly extracted than no proper result comes out. During the extraction of these features value is very large so dimension reduction technique like PCA, LDA is adopted to minimize this

Problem. Different methodology is implemented to resolve the problem of emotions detection but yet not such good result has obtained because if we compare the same facial expression of two person the similarity measure threshold value does not match exactly. They show different value for the same emotions. So measure problem is in feature extraction and accurate face database.

Initially there were two methods to finding the facial expression activity.

- a) Human observer based coding system.
- b) EMG (electromyography) based system

Human observer based are basically based on manually done so it is time consuming and not fulfill the practical standards and EMG based requires the deployment of sensors on the human face which really restricts the natural observation of the facial expression analysis. So for overcome this problem computer vision based recognition system is adopted. There are two different approach used in computer vision...

- a) Facial expression recognition using 2D still image.
- b) Facial expression recognition using image sequence.

Facial expression recognition using image sequences often use optical flow analysis to the image sequence and then apply pattern recognition tools on the observing value to show particular facial expression analysis. This method has need lots of information regarding multiple frames of images to recognize the expressions and thus has limitation in real time performance and showing more accuracy with more robustness. Still images based recognition basically based on feature extraction that can play an important parameter to define some thresholding and on the basis of that the recognition rate and accuracy is evaluated and that is acceptable in real time application.

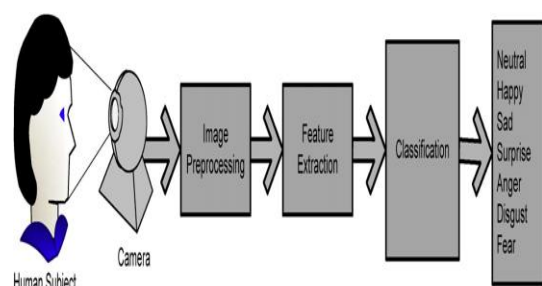


Fig1: Facial expression recognition using image

II. LITERATURE REVIEW

In this work the facial expression is based on the attributes of facial muscle that is hidden state of a HMM for individual image. Probability of the state is changed on the behalf of the feature vector obtained from image processing.[2]

Optical flow algorithm is used for the evaluation of velocity vector of two successive frames. After that FFT is applied to a velocity vector around the region of mouth and eye. The selection of feature vector is lower frequencies value and a mixture density is applied to scaled the output probability of HMM to detect the variation in human facial expression. Mixture density is very useful to enhance the accuracy as the mixture increases. Facial expression recognition is done by using the Support Vector Machine by modifying Kernels.[1] Facial expression is also recognized with the help of brain activity that is governed by the EEG signal.[3]

In this there is a proposed system that analyzes EEG system and classify them into 5 classes on the two emotional dimensions name like valance and arousal. However after using the 3-fold cross validation method the recognition rate for the valence dimension is 32% and for the 37% for the arousal and overall rate is approx 71%.

Facial expression recognition is also detected with the help Markov random Field.[4] In this the main concept is the essential factor that helpful for the expression detection is Eye and mouth expression. In this the first step is done image segmentation and skin detection for the Markov random field .second step is done for the eye and mouth feature extraction. The set of different color image is used as a training set.HLV color space that is responsible for the detection of the eyes and mouth region.3rd step module is in accordance with the detection of emotions in images with the help of edge detection and measurement of gradient of eye and mouth region.

There is also a facial expression detection is done by the using of coded form that consists of multiorientation ,multiresolution of the Gabor filters in which region of surface space and precise description of the place or region are mentions and that is aligned along the human face.[12] In this paper the similarity space is matched with the result obtained from the applying the Gabor filter and the result that is semantic value that obtained on the human observations. There is concepts that terminology is known as rank correlation which emphasize the semantic similarity and facial expression image similarity that is obtained after the applying the Gabor coding. The facial expression classification is also achieved of the frontal image by using of Eigen face [21].

In this paper whole face is not taken in consideration rather than classify the face in the regions that is beneficial for the facial expression classification and projecting that faces with the Eigen face and try to train with different types of facial expressions.Than taking the average of all different region faces showing different facial expression and after that making a mask. The important thing is that this masks fading the miss region and try to highlight the region that are changing during the different facial expression. For the recognition of the facial expression The new technique active appearance model (AAM) is used to trained the faces that is available in database that is used to represent the shape and texture variation that plays

an important role in facial expression recognition. The features are those that are extracted from the parameter obtained from the AMM and is used to discriminate among the classification of different expression. The feature extraction with the help of AMM better than a simple classifier like Euclidean distance. The AMM makes a efficient method for the texture and shape to model such that It plays an important role and it is thoughtful like (SVM) support vector machine.

Facial expression has also detected with the accuracy of 85% with the help of facial feature vectors obtained with the help of Gabor filter and that feature value is convolved with the Log Gabor filter.[1]

In this whole face is taken into consideration and than its accuracy is tested over the classification with PCA principle component analysis and LDA liner discriminate analysis and the result are quite good .The result is achieved on low resolution image without specifying the fiducially points. Facial expression recognition is also achieved with the histogram sequence of the Local Gabor binary pattern.[17] Firstly the face image is convolved with multi orientation with the help of Gabor filter than after that Gabor coefficients map are extracted. Than after local binary pattern is applied on GCM to obtain the local Gabor binary pattern. Finally the SVM is used for the classification and the result of recognition rate is quite appreciable.

III. FACIAL EMOTION RECOGNITION SYSTEM

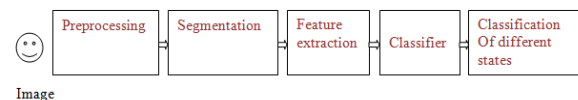


Fig 2 :block diagram

3.1 Preprocessing:--In the preprocessing step the environmental and other variations that are present in different images are minimized. The operation that is performed is contrast adjustment, image scaling, image brightness and other image enhancement method has done. Sometimes noise is associated with images with the variation in signaling and pixel variation so removal of this factor has become essential to achieving the better result.

3.2 Segmentation:--As we know that in many images processing the input is image and output is image. But for the facial expression analysis there is need of feature that is extracted from the input image. In other words we can say that input should be an image but output should be the feature value that has obtained from that input image.Segmentation plays a major role in that direction.

Segmentation basically divides an image into its regions or objects. The subdivision depends on the level of problem solving. That is the Segmentation will stop when the the objects or the regions of interest in an application has been detected. The successes or failure of the any image processing or computer vision process depends on the Segmentations accuracy. So there is proper concentration is taken place in the finding the probability of accurate Segmentation. Most of the Segmentation

algorithm basically depends on the two main properties of intensities values.

- Discontinuity
- Similarity.

The first category of Segmentation is taking place when the abrupt changes in the intensity such as Edge is found in an image. so In this case image is partitioned into regions.

In the second case of Segmentation an Image is partitioned into the regions that are similar for particular predefined criteria.

In my approach a facial image is segmented into 4 region means 2x2 grid of 128x128 size.



Fig 3 Before Segmentation



Fig 4 After Segmentation.

3.3 Feature extraction is the important method to define the any recognition System. Without extracting the key feature point it is not feasible to define the facial expression recognition System. In feature extraction method I have applied the Gabor filter on the four segmented region of the face. There is 68x68 features are coming outside from the one face region but due to application of absolute and scaling method we evaluate the major four prominent features like Gabor real part, imaginary part, magnitude and angle are evaluated. These extracted feature value is in the range of 0 and 1, so from the one face we calculates the 16 features that is defined by the Gabor filter outcome. We use the frontal face for the facial expression analysis. There is need to define such

an unique parameter that can be differentiate between different facial expression of expressers. The set of parameter that can be extracted is known as feature vector and the information achieving from the feature vector is defines an uniqueness as aspect with the extraction technique. If the feature value extracted from the one expression matches with the feature extracted with the expressions of other faces than it is not known as a good feature extraction technique and it is known as feature overlap. The feature extraction should be different in comparison with the other so there is made a correlation and on behalf of this next procedure be implemented. so there is several method adopted for feature extraction and among these the Gabor filter bank based method is good. So we can say that Gabor based feature extraction technique is excellent for facial expression analysis and avoid the feature overlap condition.

3.4 Gabor Filter

$$\psi(k, x) = \frac{k^2}{\sigma^2} \exp\left(-\frac{k^2 x^2}{2\sigma^2}\right) \left[\exp(ik \cdot x) - \exp\left(-\frac{\sigma^2}{2}\right) \right].$$

A 2-D Gabor function is a plane wave with the wave vector K and having a Gaussian envelope function that is restricted with the relative width σ . The value of σ is fixed π for the image of resolution 256x256 Like in Lyons etal (1998). In the spatial Domain 2D Gabor filter is known as the Gaussian Kernel that has produced by sinusoidal plane wave. The important property of Gabor filter is that it is self similar because all filters can be generated from the one parent wavelet with the help of rotation and multi orientation. Gabor filter impulse response is also known as the convolution of the FFT of the harmonic function and the FFT of the Gaussian.

A discrete set of Gabor kernel is used that consists of the 3 spatial frequency association with the wave number $K = \pi/4, \pi/8, \pi/16$ and with the six distinct orientation from 0 to 180 degree differing with the interval of the 30 degree that makes a filter bank of total in 18 Gabor filters.

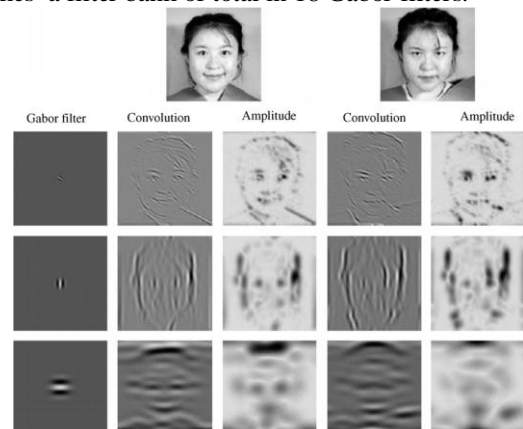


Fig 5:Gabor filter responses for the two sample images

The second term in bracket makes the Gabor wavelet kernel DC-free .as Gabor kernels is DC free than it is more robust against the variation in brightness in the image. Recognition using Gabor filter is done by the similarity function.

$$S_a(J, J') = \frac{\sum_j a_j a'_j}{\sqrt{\sum_j a_j^2 \sum_j a'_j^2}}$$

In this equation jet J has been assumed from a fixed image position and jet j'=J'(x) taken a variable position

IV. OUR APPROACH

The image is frontal and the Gaussian function is centered at the origin. we consider the value of $\sigma=\pi$ and taken the value of wave vector $\pi/4, \pi/8, \pi/16$.but in my approach we have seen there is not too much difference result comes out so mainly concentrate on the first one value. One applying the Gabor filter we see the outcomes of the result is classified into the four parts:--

- a) Gabor filter output
- b) Gabor kernel
- c) Magnitude
- d) Phase

As Gabor function is in complex form so its breaks into real and imaginary part and on the behalf of this it can be easily calculated the phase and magnitu7de that be responses of the Gabor filter on the particular facial image.

- 1) To get the real part and the imaginary part of filter output use real (gabout) and imag (gabout), respectively.
- 2) To get the magnitude and the phase of the complex filter output use abs (gabout) and angle (gabout), respectively.

As there is 68x68 real parts and imaginary parts value are coming outside on the Gabor filter output response that is also the same size of 68x68.we taken the absolute value of Gabor output response and finally consider one feature value. After evaluating the magnitude for one partition images similar we calculated the magnitude for the remaining 3 partition area. So for one face image we calculate the 4 features for magnitude only. Similarly we see the absolute value for imaginary part to calculate the Gabor kernel and evaluate one Gabor kernel among the 68x68 pixel value. the Gabor kernel value is basically in complex form but on taking absolute it just try to generate the real number. so for one facial image we calculates the 4 Gabor kernel value that value lies between the range 0 and 1.similarly the four absolute value of the real parts are evaluated and named their as Gabor filter. Similarly in the same fashion we have taken the maximum of maximum of absolute value of real parts and maximum of maximum of absolute value of imaginary parts to calculate the magnitude. So there is 4 magnitude value is evaluated from one facial image. In the similar fashion we can evaluate the phase value and finally the 4 prominent value of phase is evaluated. So there is a 16 feature value is calculated from the one facial image.16 feature value is extracted because of the segmentation of the image into the four segmented part.

SVM is a useful method for the data classification. It is easier than using the Neutral Networks.SVM provides the accuracy and fast result for the data to be classified and belongs to the particular class. In SVM the data is partitioned into the two parts that one is called Training set and other is known as the testing set and each having the instances of the attributes. Each instances having one

target means class labels and several attribute. The goal of the SVM is that to produce the model which predicts the target value of instances in the testing set which are given by only attributes value. It is based on the supervised learning methods. Support vector machine has a unique property that it creates the hyperplane or a set of hyperplane which has taken into the consideration for the classification. It defines the functional margin means a good separation is achieved by the hyperplane that has the largest distance to the nearest data points of any class. Greater the margin it is easy to find better accuracy and minimal errors has found.

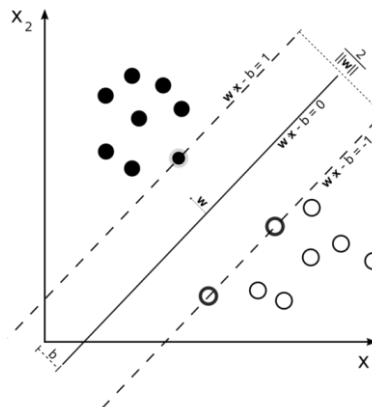


Fig 6 Hyperplane that discriminates between two classes.

Lets us assume that we have Data sets of having n features of the form

$$D = \{(x_i, c_i) \mid x_i \in \mathbb{R}^p, c_i \in \{-1, 1\}\}_{i=1}^n$$

Where C_i belongs to either -1 and +1 value indicates the which class the point X_i belongs.the equation of the hyper plane is given by in such a way

$$W \cdot X - b = 0$$

There is two cases to defining hyperplane

$$W \cdot X - b \geq 1 \text{ -----}$$

it indicates for class one

$$W \cdot X - b \leq -1 \text{ -----}$$

it indicates for the class others.

Here the training vectors X_i are projected into the higher dimensional space by the function ϕ . the main important characteristic property of SVM is that it works on the linear separable hyperplane with the minimal margin in the high dimensional space.

$C > 0$ is the main term to define the error parameter. The kernel function is defined as

$$K(x_i, x_j) \equiv \phi(x_i)^T \phi(x_j)$$

There is four basic kernels that is defined as follows:-

linear: $K(x_i, x_j) = x_i^T x_j$.

polynomial: $K(x_i, x_j) = (\gamma x_i^T x_j + r)^d, \gamma > 0$.

radial basis function (RBF): $K(x_i, x_j) = \exp(-\gamma \|x_i - x_j\|^2), \gamma > 0$.

sigmoid: $K(x_i, x_j) = \tanh(\gamma x_i^T x_j + r)$.

Where γ, r .and d are kernel parameters.

V. RESULTS

Facial Expression or Facial emotion detection through image database has been proposed: Basically Image Database is Japanese Female Faces and assumed to be frontal and preprocessed and some Indian database also has been used to evaluate the accuracy, After applying Gabor Filter on the four segmented facial region we extract the Features value that is fully defined by Gabor response,

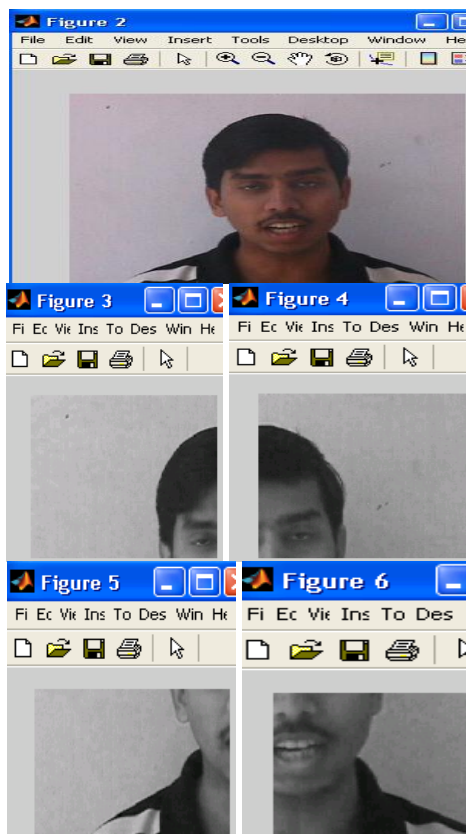


Fig 7: Input Image and Segmented Image of Surprised Class

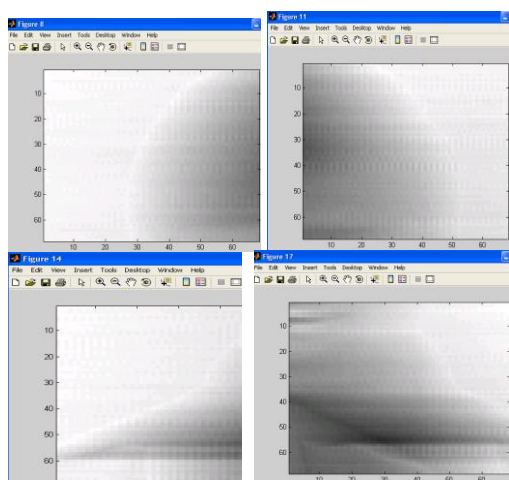


Fig 8: Gabor Filter Response

The main features that are extracted known as Gabor Real part, Imaginary part, Magnitude and lastly Phase. Basically all these features value are coming out from the segmented Face region under the response of Gabor Filter,

After the feature extraction maximum of absolute of Gabor filter responses on the faces are evaluated, After the feature extraction rescaling is done so that all features value are lie between the range of 0 and 1, When the features of all the classes are extracted than finally classifier Support Vector Machine (SVM) applied for labels classification, Extracted Features are arranged into the SVM format means all the value should be written in a single row and showing the name of their respective classes, Than features value of different classes is divided into two domain one for the Training set and the second one for the Testing And in last the accuracy is calculated, accuracy is above 80%.

VI. CONCLUSION AND FUTURE PERSPECTIVE

System that can detects the Facial Expressions like Happy, Sad, Angry, Disgust, Surprise and Fear. We have used a still images that is frontal and preprocessed. The Facial Expression analysis plays a key role in the human Machine interaction. Our approach is different to previous work done and my accuracy is above 81%. Due to segmentation and rescaling the Gabor filter output response is remarkably good. So the extracted feature detection is lie in the range of $[0,+1]$.

This range is essential when we are going to use SVM for the classification. After using the SVM the results obtained is satisfactory. In our future perspective we will try to enhance the accuracy up to 100% and try to make a robust system that can be applied to any database whatever the alignment of the Face. In future we will develop my work for the real time system that can be utilized in any sensitive area and surveillance system. Also the Facial expression analysis is useful for the security, Gaming, Intelligent tutoring system and human behavior recognition.

REFERENCES

- [1] J. Cohn, T. Kanade Cohn-Kanade AU-Coded Facial Expression Database Carnegie Mellon University
- [2] C.K. Chow, C.N. Liu. Approximating discrete probability distributions with dependence trees. *IEEE Trans. Information Theory*, 14:462–467, 1968.
- [3] I. Cohen, N. Sebe, A. Garg, L. Chen, and T.S. Huang. Facial expression recognition from video sequences: Temporal and static modeling. *Computer Vision and Image Understanding*, 91(1-2):160–187, 2003.
- [4] P. Ekman Strong evidence for universals in facial expressions. *Psychol. Bull.*, 115(2): 268–287, 1994.
- [5] J.H. Friedman On bias, variance 0/1-loss, and the curse-of-dimensionality. *Data Mining Knowledge Discovery*, 1 (1): 55–77, 1997.
- [6] N. Friedman, D. Geiger, M. Goldszmidt. Bayesian network classifiers. *Machine Learning*, 29(2):131–163, 1997. [7] A. Garg, D. Roth. Understanding probabilistic classifiers. *Proc. Eur. Conf. on Machine Learning*, 179–191, 2001.
- [8] D. Goleman. *Emotional Intelligence*. Bantam Books, New York, 1995.

- [9] Intel Research Laboratories. OpenCV: Open computer vision library. <http://sf.net/projects/opencvlibrary/>.
- [10] C.E. Izard. Innate and universal facial expressions: evidence from developmental and crosscultural research. *Psychol. Bull.*, 115(2): 288–299, 1994.
- [11] R. Lienhart, J. Maydt. An extended set of haarlike features for rapid object detection. *Proceedings of the IEEE International Conference on Image Processing*, Rochester, New York, vol. 1, pp. 900-903, 2002.
- [12] R. Lienhart, A. Kuranov, V. Pisarevsky. Empirical Analysis of Detection cascade of Boosted Classifiers for Rapid Object Detection. Intel Corporation, Technical report, 297–304, 2002.
- [13] M. Pantic, L.J.M. Rothkrantz. Automatic analysis of facial expressions: the state of the art. *IEEE Trans. PAMI*, 22(12): 1424–1445, 2000.
- [14] C. Papageorgiu, M. Oren, T. Poggio. A general framework for Object Detection. *Proceedings of the International Conference on Computer Vision*, Bombay, India, pp. 555-562, 1998.
- [15] R. Schapire, Y. Freund. Experiments with a new boosting algorithm. *Proceedings of the International Conference on Machine Learning*, Bari, Italy, Morgan Kaufmann, pp. 148-156, 1996.
- [16] R. Schapire. The strenght of weak learnability. *Machine Learning*, 5(1), 197-227, 1990.
- [17] N. Sebe, I. Cohen, A. Garg, M.S. Lew, T.S. Huang. Emotion Recognition Using a Cauchy Naive Bayes Classifier. *International Conference on Pattern Recognition (ICPR02)*, vol I, pp. 17–20, Quebec, Canada, 2002.
- [18] H. Tao, T.S. Huang. Connected vibrations: a modal analysis approach to non-rigid motion tracking. *Proc. IEEE Conf. on CVPR*, 735–740, 1998.
- [19] P. Viola, M. Jones. Rapid Object Detection Using a Boosted Cascade of Simple Features. *Proceedings of the IEEE Conference on Computer Vision and Pattern Recognition*, Kauai, Hawaii, vol. 1, pp. 511-518, 2001.

Side Lobe Suppression of Concentric Circular Arrays Using Non Conventional Beam Forming Technique

¹P. Rama Krishna, ²S. Sri Jaya Lakshmi, ³I.Sreedevi, ⁴Habibulla Khan,
⁵M.P.K.Aditya, ⁶V. Vamsi Krishna, ⁷J.Lavanya

^{1, 3, 5, 6, 7} B Tech students, Department of ECE, K L University

² Women scientist, Department of ECE, K L University

³ Professors, Department of ECE, K L University

K L University, Vaddeswaram, Guntur-522502, India.

ABSTRACT

Circular antenna array design is one of the most important electromagnetic optimization problems of current interest. The antenna must generate a pencil beam pattern in the vertical plane along with minimized side lobe level. In this paper we present non conventional method based on improved parameter of hyper beam exponent x . The circular array when implemented using hyper beam technique, there is a considerable reduction of side lobe levels and half power beam width compared to conventional beam forming. The design of circular array is with uniform inter-element spacing. Simulation results of the effect of the hyper beam exponent on the beam patterns are shown.

Keywords: Hyper beam; circular array; side lobe level; half power beam width.

1 INTRODUCTION

Circular antenna array, in which antenna elements are placed in a circular ring, is an array configuration of very practical use among all other antenna arrays present in modern day. It consists of a number of elements arranged on a circle [1] with uniform spacing between them. It possesses various applications in sonar, radar, mobile and commercial satellite communications systems [1-5]. They can be used for beam forming in the azimuth plane for example at the base stations of the mobile radio communications system [2-5]. Circular array has several advantages over other types of array antenna configurations such as all azimuth scan capability, invariant beam pattern in every ϕ -cut, i.e., ϕ symmetric pattern, flexibility in array pattern synthesis [2-5] etc. For those advantages, design of circular antennas by different methods is being encouraged in present days. There are several kinds of circular arrays. Concentric Circular Antenna Array (CCAA), one of the most important circular arrays, contains many concentric circular rings of different radii and number of elements proportional to the ring radii. The main feature of CCAA is observed in Direction of Arrival (DOA) applications providing almost invariant azimuth angle coverage.

2. METHODOLOGY

Noise reduction and improvement of detecting the target are a successful design of a high performance system. While the classic way is to increase the array's size, constraints as integration, size and cost require new technical approaches like non-classical beam forming techniques. A new beam forming technique, called hyper beam is presented. As a

result of the hyper beam offers high detection performance like beam width reduction, the target bearing estimation and reduces false alarm i.e., side lobe suppression.

1 Hyper Beam

The hyper beam formed by means of two half beams, beam one is the right half beam and the second beam is the left half beam. The process of formation of the hyper beam is illustrated by a series of directivity patterns for a linear, planar and circular transducer. Moreover the influence of isotropic noise and non- isotropic noise sources as well as the separation of multiple targets are examined. The two-dimensional Hyper beam focusing in one plane which contain the main beam direction, in order to achieve even greater reduction of beam width and the side lobes around the main beam in all directions.

The hyper beam technique yields a very narrow beam width with suppressed side lobe levels. The narrowness of beam width and side lobe suppression level depends on the variation of exponent value, which also leads to the suppression of grating lobe and also reduction of received noise level. With conventional beam forming the smallest possible beam width depends on the geometric dimensions of the receiving array. Using shading coefficients for beam forming side lobe suppression can be achieved, but at the cost of a broadened beam width.

2 Generation of Hyper Beam

In principle of hyper beam generation a simple concentric circular transducer used is shown in Fig.1. The element spacing is half the wave length ($\lambda/2$) in order to allow beam steering in that particular direction without steering, i.e. all elements have the same phase or all elements are arranged in a ring, conventionally beam forming is done by summing up all the transducer elements.

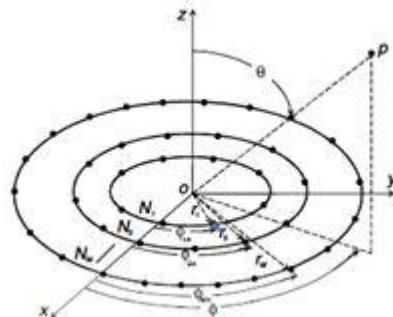


Figure 1 multiple concentric circular ring arrays of isotropic antennas in XY plane

3 Forming of hyper beam for circular array

The circular array shown in the Fig.1 is first split into two equal half parts right and left. The beams produced by each half is taken individually where beam1 is the left half beam and beam2 is the right half beam. The forming of the hyper beam, which resembles to some extent the above mentioned ideal beam, shall now be illustrated by means of the sum beam pattern which is the sum of both half beams i.e. beam1 and beam2 of Fig.2. Applicable to the proposed circular transducer in the Fig.1

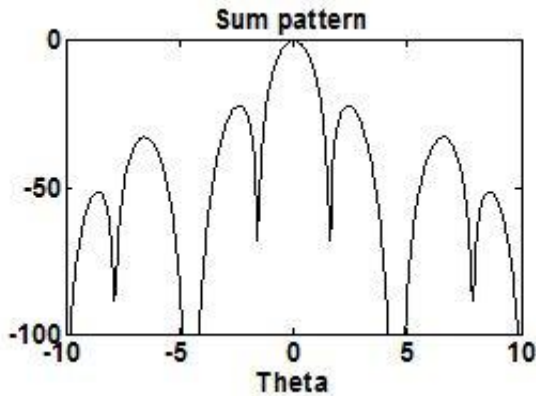


Figure 2 2D sum pattern for 10 element circular array

The sum beam pattern is now generated by the summation of beam1 and beam2 which are the left half beam and right half beam respectively. The beam magnitude is plotted in the normalized plot Fig.2. We can see that the Fig.2 beam pattern shows that the magnitude of both left and right half beams are identical.

The Difference beam generated is the magnitude of the difference of beam2 signal subtracted from the beam1 signal taking phases of the signals in to consideration.

By observing the difference beam pattern it can be easily seen that the values of the difference beam at each given direction is found to be always lower than or equal to those of the half beams. Furthermore the difference beam has a minimum point in the direction of the sum beam at 0° as shown in Fig.3.

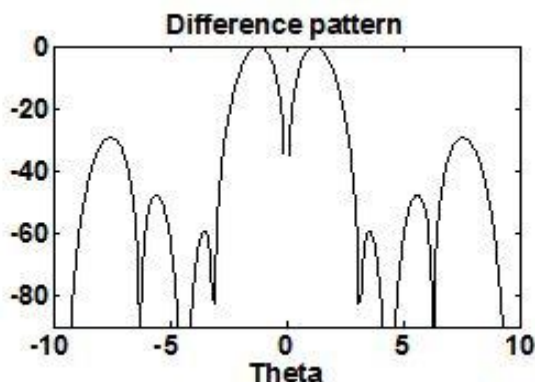


Figure 3 2D difference pattern for 10 element circular array

On proper study of both the sum and difference patterns in Fig.2 and Fig.3 we can recognize an interrelation between them. Having recognized this interrelation it is obvious to get the idea of subtracting the magnitude of the difference beam pattern from the sum beam pattern. The subtraction operation has to be performed rather on the magnitude

numbers themselves, and not on the magnitude levels. The resulted simple hyper beam in 2D simulated for a 10element circular array with exponent value x=1 is formed as shown in Fig.4.

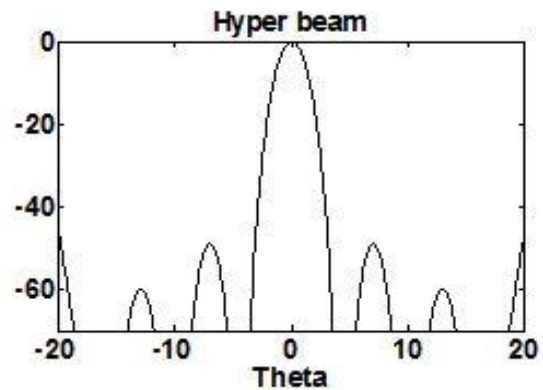


Figure 4 2D simple hyper beam pattern for 10 element circular array with x=1

3 MATHEMATICAL FORMULAS

The equations for the creation of sum, difference and simple hyper beam are as follows:

The array factor equation for simple circular array is

$$AF(\theta, \phi) = \sum_{m=1}^M \sum_{n=1}^N I_{mn} e^{j(2\pi r [\sin(\theta) \cos(\phi - \phi_n) + \alpha_n])}$$

The sum pattern is calculated from two half beams is given by

$$S(\theta, \phi) = |E_L| + |E_R|$$

The difference pattern is calculated from below equation

$$D(\theta, \phi) = |E_L - E_R|$$

Then the equation to obtain simple Hyper beam is

$$E_{hyp} = |E_L| + |E_R| - |E_L - E_R|$$

The equation of the general hyper beam is a function of the hyper beam exponent x:

$$E_{hyp} = \{ (|E_L| + |E_R|)^x - (|E_L - E_R|)^x \}^{1/x}$$

where

$$E_L = \sum_{m=1}^{M/2} \sum_{n=1}^{N/2} I_{mn} e^{j(2\pi r [\sin(\theta) \cos(\phi - \phi_n) + \alpha_n])}$$

$$E_R = \sum_{m=1}^{M/2} \sum_{n=N/2+1}^N I_{mn} e^{j(2\pi r [\sin(\theta) \cos(\phi - \phi_n) + \alpha_n])}$$

K = 2π/λ = Wave number

M = number of rings

N = number of elements present on mth ring

r = radius of the mth ring

I_{mn} = amplitude excitation of the nth element

α_n = phase excitation of the nth element

φ_n = 2π(n/N) = angular position of the nth element

To steer the main lobe in the (θ₀, φ₀) direction, the phase excitation of the nth element can be chosen to be α_n = -kr sin(θ₀) cos(φ₀ - φ_n)

And 'x' ranges from 0.1 to 1.

4 RESULTS

With the hyper beam effect, reduction of beam width and side lobe levels can be amplified and controlled by varying the exponent value u , different hyper beam patterns are obtained. As from the results the side lobe level and half power beam width is decreasing as the exponent value is decreased. For $x=1$ the half power beam width for 10 element linear array is 4 degrees where as for $x=0.1$ the half power beam width is reduced to 0.6 degrees as shown in Fig.6. The resulted simple hyper beam in 2D simulated for a 10 element circular array with exponent value $x=0.5$ is also shown in Fig.5. Where the half power beam width is observed as 2 degrees.

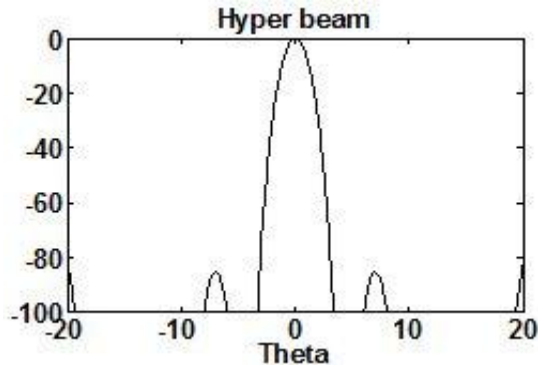


Figure 5 2D hyper beam pattern for 10 element circular array with $x=0.5$

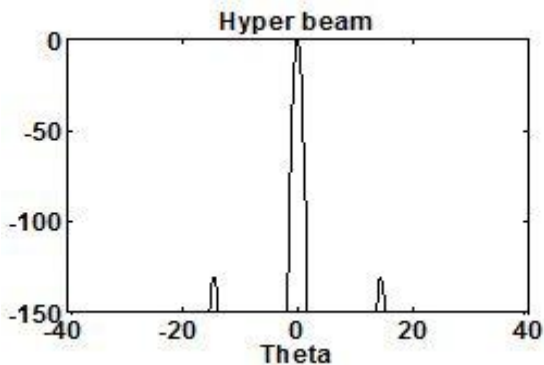


Figure 6 2D hyper beam pattern for 10 element circular array with $x=0.1$

From Fig.6 and Fig.7, for a 10 element circular array, conventional beam forming has the side lobe level and half power beam width -17dB and 10 degrees where as for Hyper beam forming technique, the side lobe level and the half power beam width is reduced to -140dB and 0.6 degrees respectively. Therefore, in comparison to conventional beam forming Hyper beam technique allows simultaneous reduction of beam width and side lobes.

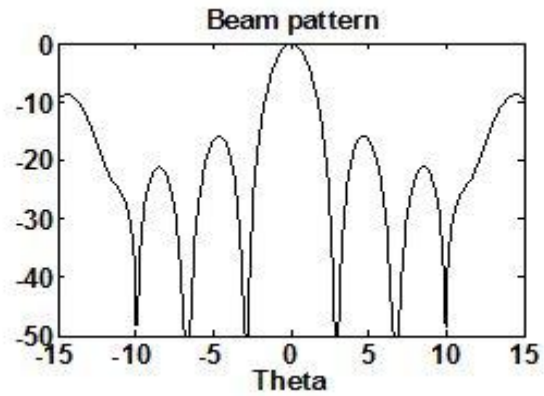


Figure 7 2D conventional beam pattern for 10 element circular array

To achieve point-to-point communication at higher frequencies, a single narrow beam of the radiation pattern is required which is usually obtained by concentric circular array, the side lobe level and half power beam width is reduced as from the results. For a 10 element circular array with exponent value $x=0.1$, the side lobe level is -140dB where as for a 15 element circular array with the same exponent value, the side lobe level is -190dB as shown in Fig.8. The resulted simple hyper beam in 2D simulated for a 20 element circular array with exponent value $x=0.1$ is also shown in Fig.9 where the side lobe level is observed as -240dB.

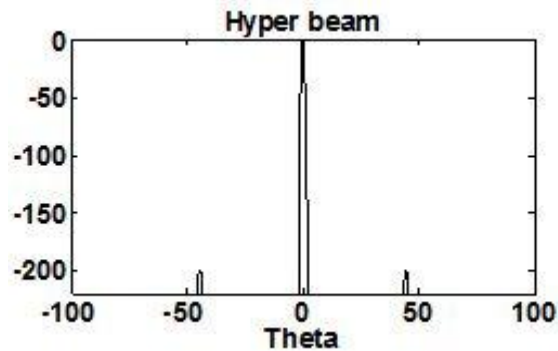


Figure 8 2D hyper beam pattern for 15 element circular array with $x=0.1$

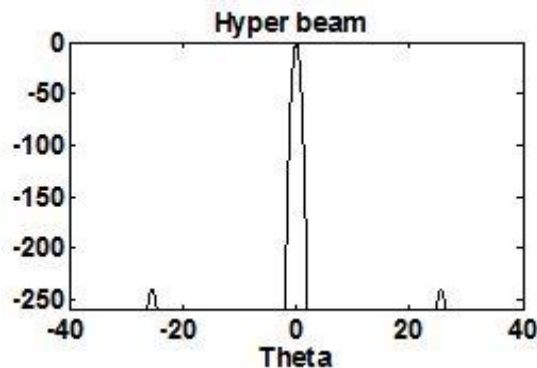


Figure 9 2D hyper beam pattern for 20 element circular array with $x=0.1$

5. CONCLUSIONS

This paper proposes a new technique for designing a concentric circular array antenna of isotropic elements to generate a pencil beam in the vertical plane with reduced side lobe level, suppression of grating lobe and also reduction of received noise level along with chance for increasing number of elements based on exponent value for certain array configurations. Results clearly show a very good resemblance between the desired and synthesized specifications for all the cases. This method is very effective and put into practice for array antennas of other shapes like planar array, liner array etc..

It has been proved that the hyper beam technique is much more effective than the conventional beam forming techniques in practice, where the high quality reception of data is allowed with an increased dynamic range and accurate target detection. This is not only applicable for high frequency surface wave radar systems but also for the other communication systems.

So our method can also be used to design antenna with any desired side lobe level while maintaining the number of elements to a reasonable value. Results for concentric circular ring antenna arrays have illustrated the performance of this proposed technique. Our further work will be focused on the design of more complex practical antenna problems.

6. ACKNOWLEDGMENT

The authors would like to thank management of KL University, Vijayawada for excellent encouragement during the tenure of work.

7. REFERENCES

- [1]. "Control of Peak Sidelobe Level in Adaptive Arrays" by Renbiao Wu, *Member, IEEE*, Zheng Bao, *Senior Member, IEEE*, and Yuanliang Ma.
- [2]. "Adaptive Array Beamforming Based on an Efficient Technique" by Shiann-Jeng Yu and Ju-Hong Lee, *Member, IEEE*.
- [3]. "Array gain/phase calibration techniques for Adaptive beamforming and direction finding" by B.P. Ng, M.H. Er, C. Kot.
- [4]. "Adaptive Beam-Space Nulling of Multipath Signals" by TITUS Lo AND JOHN LITVA, *MEMBER, IEEE*.
- [5]. Shiann-Jeng Yu and Ju-Hong Lee, "Adaptive Array Beamforming Based on an Efficient Technique".
- [6]. T.Isernia, F. J. Ares Pena, O. M. Bucci, M. D'Urso, J. F. Gomez, and J. A. Rodriguez, "A hybrid approach for the optimal synthesis of pencil beams through array antennas," *IEEE Trans. Antennas Propag.*, vol. 52, no. 11, pp. 2912–2918, Nov. 2004.
- [7]. W.P.M.N.Keizer, "Low-sidelobe pattern synthesis using iterative Fourier techniques coded inMATLAB," *IEEE Antennas Propag. Mag.*, vol. 51, no. 2, pp. 137–150, Apr. 2009.
- [8]. Gusevsky, V.I.; Lavrentiev, M.V, "Employing the aperture orthogonal polynomials method in the design of sparse unequally spaced phased arrays", Sep 2003.
- [9]. Xiang-Qian Che; Li Bian, "Low-Side-Lobe Pattern Synthesis of Array Antennas by Genetic Algorithm", Oct 2008.
- [10]. Bouyeddou, B.; Harrou, F.; Djennas, S.A.; Merad, L, "Synthesis and optimization of microstrip antennas array using minimax method", 2009.
- [11]. Junwei Dong; Cheung, R. "Optimized amplitude taper for a linear array of multiple true-time-delay beams", Oct 2010.
- [12]. Hui Huang; Hoorfar, A.; Lakhani, S., "A comparative study of evolutionary programming, genetic algorithms and particle swarm optimization in antenna design", June 2007.
- [13]. Gorobets, N.N.; Bulgakova, A.A, "Directional characteristics of rarefied antennas array with screen", Sep 2007.
- [14]. Uthansakul, M.; Bialkowski, M.E., "Wideband beam forming with a rectangular array antenna", Oct 2005.
- [15]. Elliott, R. S., *Antenna Theory and Design*, 2nd edition, John Wiley, New Jersey, 2003.
- [16]. Dessouky, M. I., H. A. Sharshar, and Y. Albagory, "Efficientsidelobe reduction technique for small-sized concentric circulararrays," *Progress In Electromagnetics Research*, Vol. 65, 187-200,2006.
- [17]. John D. Kraus, "Antennas", Mc GRAW –Hill, Newyork, 1950.
- [18]. Heiko Schliter, "Sonar Detection Improvement by Hyper Beam Technique".
- [19]. William J. Palm, "Introduction to MATLAB 6 for Engineers".
- [20]. Heiko Schliter, "Method for the formation of radiated beams in direction finder systems".

Online Image Capturing and Processing Using Vision Box Hardware: Apple Grading

C. Velappan Gnana Arivu¹, G. Prakash², A. Sada Siva Sarma³

¹PG Student, Department of Electronics and Communication Engineering, K.S.R College of Technology, Tiruchengode, Namakkal-637 215, Tamilnadu, India.

² Assistant Professor, Department of Electronics and Communication Engineering, K.S.R College of Technology, Tiruchengode, Namakkal-637 215, Tamilnadu, India.

³ Principal Scientist, CEERI- CSIR Madras Complex, Chennai-600 113, Tamilnadu, India.

Abstract - The early detection of damages in fruits is especially important in agriculture products processing because a very small number of injured fruits can cause rottenness infected by microbes and spread the infection to the whole batch and thus causing great economic loss and it also affects further storage and sale. At present manual sorting of fruits and vegetables is carried out at many places. The most important post-harvest damage in fruit picking, transport and storage is mechanical bruise caused by external forces which causes physical changes in texture. The detection accuracies are also greatly affected by many factors such as time, bruise type, bruise severity, fruit variety, and fruit pre- and post harvest conditions.

Manual sorting has many disadvantages as it requires plenty of labours to investigate it results in low productivity and grading standard is difficult to carry out. Hence the manual sorting is replaced by Machine Vision (MV) system using Vision Box hardware with the advantages of high precision and high automatization.

Key words: Machine vision (MV), Vision Box, processing, grading

I. INTRODUCTION

Inspection of fruits and vegetables is an important procedure for marketing, storing and processing as their appearance affects the consumer acceptance. Colour provides valuable information in estimating the maturity and examining the freshness of fruits and vegetables. Uniformity in size and shape of fruits and vegetables are some of the other important factors in deciding overall quality for buyer's acceptance and value addition.

The early detection of damages in fruits is especially important in agriculture products processing because a very small number of injured fruits can cause rottenness infected by microbes and spread the infection to the whole batch and thus causing great economic loss and it also affects further storage and sale. At present manual sorting of fruits and vegetables is carried out at many places. The manual sorting of fruits has the following disadvantages

- Great labour intensity
- Low productivity
- Grading standard difficult to carry out
- Grading precision instable
- Plenty of labours

The fruit quality can be improved through lots of methods, among which quality detection and sorting operations are the most important ones to increase fruit quality and the profits. Many high quality fruits intermixed with low quality ones are exported or on sale at low price due to the laggard means of quality detection and sorting operations. With the development of computer technology, machine vision grows rapidly. The manual sorting replaced by machine vision with the advantages of high precision, high automatization and belonging to non-contact detection is an inevitable trend of the development of automatic sorting.

1.1 MACHINE VISION SYSTEM

Machine vision (MV) is the application of computer vision to industry and manufacturing. Machine vision, being an engineering discipline, is interested in digital input/output devices and computer networks to control other manufacturing equipment such as robotic arms and equipment to eject defective products. Machine Vision is a subfield of engineering that is related to computer science, optics and industrial automation. One of the most common applications of Machine Vision is the inspection of manufactured goods such as semiconductor chips, automobiles, food and pharmaceuticals. Machine vision systems use digital cameras, smart cameras and image processing software to perform similar inspections.

Machine vision systems are programmed to perform narrowly defined tasks such as counting objects on a conveyor, reading serial numbers, and searching for surface defects. Manufacturers favour machine vision systems for visual inspections that require high-speed, high-magnification, 24-hour operation, and/or repeatability of measurements. Cameras are not equivalent to human optics and while people can rely on inference systems and assumptions, computing devices must 'see' by examining individual pixels of images, processing them and attempting to develop conclusions with the assistance of knowledge bases and features such as pattern recognition engines. Although some machine vision algorithms have been developed to mimic human visual perception, a number of unique processing methods have been developed to process images and identify relevant image features in an effective and consistent manner.

Machine vision and computer vision systems are capable of processing images consistently, but computer-based image processing systems are typically designed to perform single, repetitive tasks, and despite significant improvements in the field, no machine vision or computer vision system can yet match some capabilities of human vision in terms of image comprehension, tolerance to

lighting variations and image degradation, parts' variability etc.

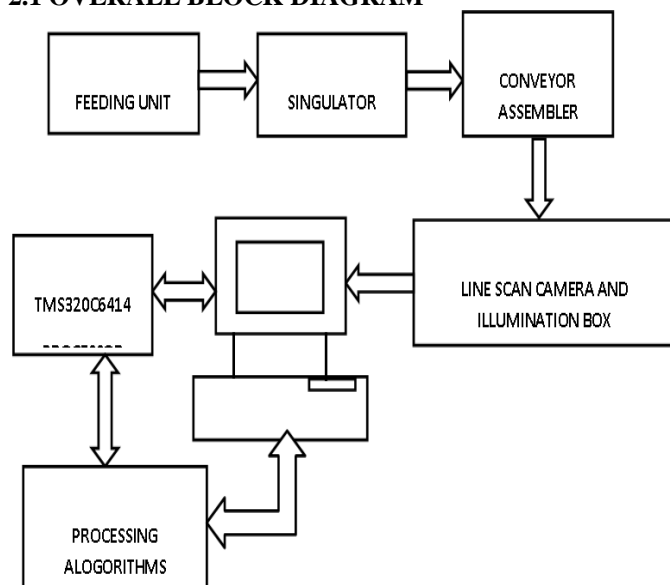
II PROPOSED METHODOLOGY

In the proposed methodology the processing of apples leading to a sorting and grading is done using machine vision system which includes the Vision Box hardware. Now using dsp processor and with image processing algorithms, the apple images can be analysed and the defects can be studied and classified according to the quality.

This method uses a machine vision technology the apples are passed in a linear fashion on a conveyer assembly and when the system is triggered the image of an apple is acquired with the aid of a line scan camera. A flash card receives the image data and then with the help of File Transfer Protocol the digital image is stored in the host computer's buffer. The image captured in the computer's buffer is fed to the TMS320C6414 DSP processor, which is a 32 bit floating point VLIW processor and algorithms for determination of size, shape and colour are applied by using appropriate machine vision techniques. These feature extraction methods are implemented using the Code Composer Studio (CCS) software that serves as an Integrated Development Environment (IDE), comprising tools for highly optimized code generation, a C compiler, an assembler and a linker.

Digital Image Processing forms the fundamental methodology adopted in this project. Digital Image Processing is defined as subjecting the numerical representation of an object to a series of image processing routines to obtain the desired results. This field combines the techniques of image processing with the power of DSP to enable the achievement of Real Time Processing, which requires the computation to be kept in pace with the reception of input signals. It is achieved with the help of highly efficient Digital Signal Processors designed specifically to cater the computationally intensive problems.

2.1 OVERALL BLOCK DIAGRAM



One of the components of the machine vision system for the apple sorting and grading system is the PC platform which acts as the host and a software which is used for inspection. The overall working of this application which would interact with the user and which has been simulated in this project is given below.

- Initially the image of the apple is captured using line scan camera
- A frame grabber (National Instruments IMAQ 1428 hardware) card or the flash card receives the digital data from the line scan camera and stores it in a buffer in the PC
- Digital data is transferred from the host computer to the DSP memory for processing through the Host Port Interface (HPI) with the help of PCI
- In the front end VC++ application interacts with the user and it does the function of grabbing the image and transferring the data to the DSP through HPI
- For accomplishing the transfer of data between the host computer and the EVM through HPI
- Certain host software components are provided along the EVM board. These host support software components consist of an operating system specific low level driver and a user mode Win32 DLL. These components are used to create and execute user mode applications for the EVM board.
- C code built with the help of CCS runs at the backend on the Digital Signal Processor to process the digital image and the result is stored in a memory location
- The result is accessed at the front end and displayed to the use.

The line scan cameras field of view covers three apples. In a real time system a total of 4 views would be captured for an apple (for each 90 degree rotation). So all 4 views are processed for a single and the final result is displayed. Given below is the sequence of steps followed for the determination of colour, size and shape for each view of the apple by using digital image processing algorithms.

2.2 PROCESSING METHODS

Commercial and open source machine vision software packages typically include a number of different image processing techniques such as the following:

- Pixel counting: counts the number of light or dark pixels
- Thresholding: converts an image with gray tones to simply black and white
- Segmentation: used to locate and/or count parts
- Edge detection: finding object edges
- Template matching: finding, matching, and/or counting specific patterns

III VISION BOX HARDWARE

The Vision Box MPS2 is equipment introduced by the STRAMPE GERMAN COMPANY. STRAMPE develops image processing and machine vision on its own line of

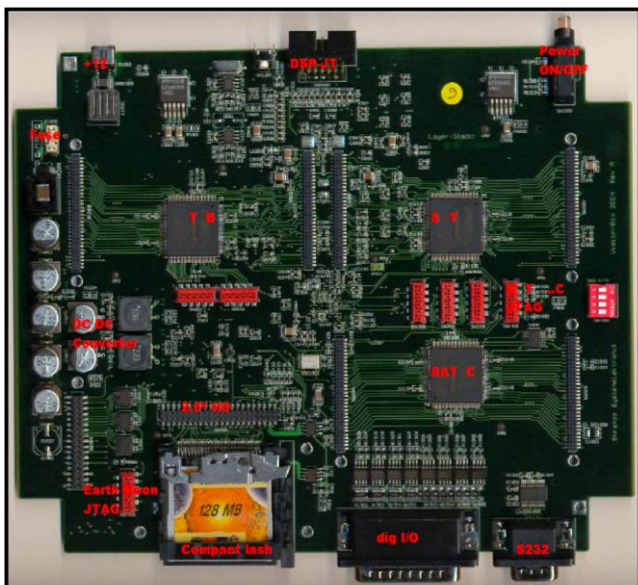
DSPC6000 Vision Box systems. Vision Box MPS2 is a stand-alone image processing computer based on Digital Signal Processing (DSP) TMS320C6414 from Texas Instrument.

3.1 VISION BOX SPECIFICATIONS:

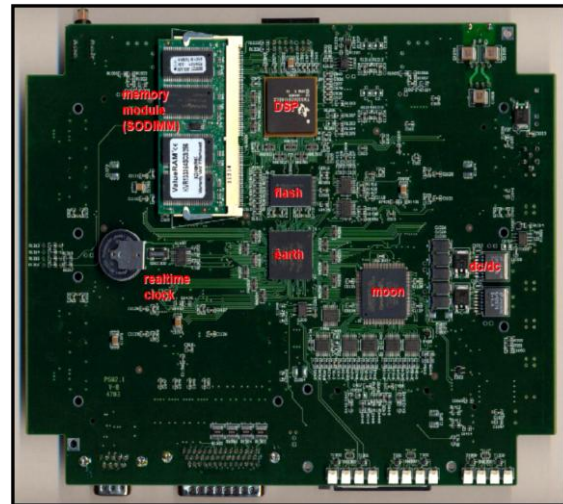
- Processor Frequency - 1000 MHz
- Calculation Power of the Processor - 8000 MIPS
- Processor Manufacture Type - Texas Instrument TMS320C6414
- SDRAM – 256 MB (option 512 MB)
- Flash EPROM – 4MB
- Compact Flash Card - >1GB
- Compact Flash Card Option – SanDisk Extreme III 4GB
- Digital I/P / O/P , optocoupled – 8/8
- Delay b/w I/p & Trigger star of camera - Typ. 20 μ s
- Ethernet, TCP/IP, FTP – 1000 [Mbits/s]
- Power consumption – 10 watts
- Ethernet, Monitor, Keyboard and mouse using a web browser - yes
- Serial Interface Max. 115 k Baud - 3
- Camera Interface Camera Link - 2
- PS/2 Keyboard input - 1
- Power Supply - 12v/ one Amp

Vision Box is equipment which hosts a DSP with 1000 MHz processor with a calculation speed of 8000 MPS, This box has a TI DSP of the family TMS320C6416 with a RAM of 256 MB and there is also a separate Flash card to hold some static images.

3.2 VISION BOXMPS2 TOP SIDE



3.3 VISION BOX MPS2 BOTTOM SIDE



IV SOFTWARE DESCRIPTION

4.1 CCS

Code Composer Studio (CCStudio) is an integrated development environment (IDE) for Texas Instruments' (TI) embedded processor families. CCStudio comprises a suite of tools used to develop and debug embedded applications. It includes compilers for each of TI's device families, source code editor, project build environment, debugger, profiler, simulators, real-time operating system and many other features. The intuitive IDE provides a single user interface taking you through each step of the application development flow. Familiar tools and interfaces allow users to get started faster than ever before and add functionality to their application thanks to sophisticated productivity tools. Here the online capturing of images is done in ccs environment.

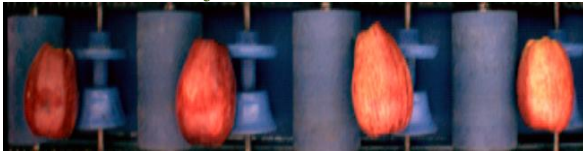
4.2 HALCON

HALCON is the comprehensive standard software library with an integrated development environment (IDE) for machine vision that is used worldwide. It leads to cost savings and improved time to market. HALCON's flexible architecture facilitates rapid development of machine vision, medical imaging, and image analysis applications. It provides an extensive library of more than 1 300 operators with outstanding performance for blob analysis, morphology, pattern matching, measuring, 3D object recognition, and binocular stereo vision. It secures your investment by supporting the operating systems Windows, Linux, and Solaris. The full library can be accessed from common programming languages like C, C++, C#.

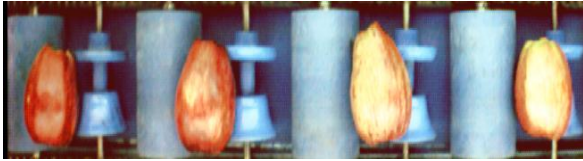
IV SIMULATION RESULTS

RESULT OF IMAGE ENHANCEMENT

Image enhancement is the process of manipulating an image so that the result is more suitable than the original image for a specific application. Histogram Equalization can be used for image enhancement.



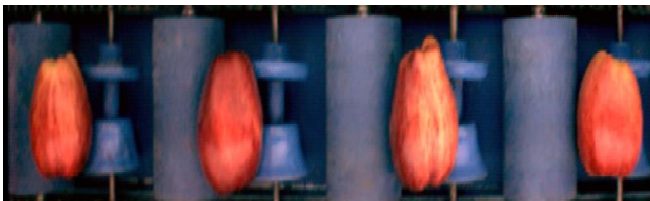
Original image



Processed image

4.1 RESULT AFTER NOISE SMOOTHING

Mean filtering is simple and easy method used for smoothing the image and hence removing the noise. Here each pixel value is replaced with average value of its neighbours. There are two main problems with mean filtering. Single pixel with a very unrepresentative value can affect the mean value of all the pixels in the neighbour. when the filter neighbourhood straddles an edge the filter will interpolate new pixels on edge and will blur that edge. Median filter overcomes the above problem.

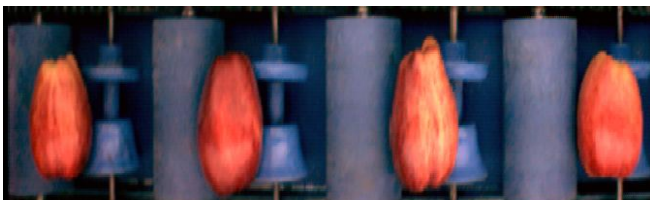


Original image

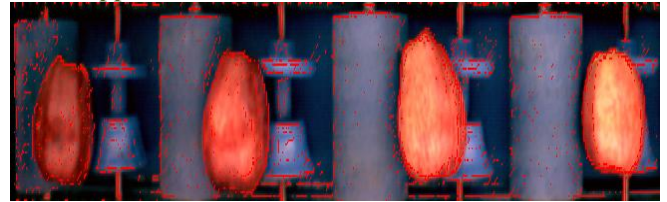


Processed image after median filtering

4.3 RESULT OF THRESHOLDING

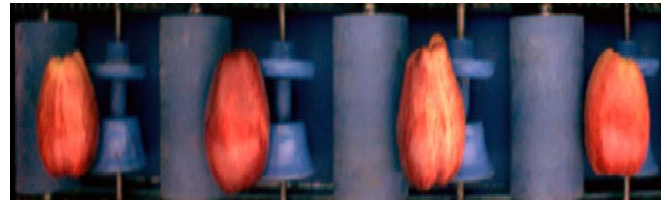


Original image

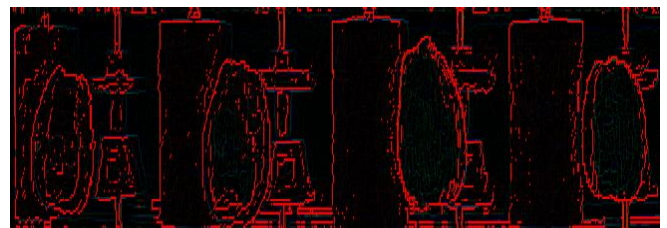


Processed image

4.4 RESULT OF EDGE DETECTION



Original image



Processed image

V. CONCLUSION

It is testified that machine vision is an alternative to unreliable manual sorting of fruits. The system can be used for fruit grading by the external qualities of size, shape, colour and surface defects. The machine vision system can be developed to quantify quality attributes of various fruits and vegetables such as mangoes, cucumbers, tomatoes, potatoes, peaches and mushrooms. The exploration and development of some fundamental theories and methods of machine vision for pear quality detection and sorting operations would accelerate the application of new techniques to the estimation of agricultural products quality.

The work in the project has resulted in a clear-cut and systematic sequence of operations to be performed in order to obtain the end result of an apple image with the defects clearly segmented followed by categorizing them as good or bad fruit. The proposed steps are based on the assumption that the images were taken under proper illumination, due to which some regions with improper illumination are considered defects. future work might include a small modification in the presented algorithm in order to adapt to this irregularity. This algorithm was tested with several images and the results were encouraging.

REFERENCES

- [1] Anil K. Jain, Robert P.W. Duin, and Jianchang Mao, "Statistical Pattern Recognition: A Review" IEEE Transactions On Pattern Analysis And Machine Intelligence, Vol. 22, No. 1, January 2010
- [2] King-Sun Fu, Azriel Rosenfeld, "Pattern Recognition and Image Processing", IEEE transactions on computers, vol. c-25, no. 12, december 1996
- [3] Mohan.V, Shanmugapriya.P, Dr.Y.Venkataramani, "Object Recognition Using Image Descriptors", Proceedings of the 2008 International Conference on Computing, Communication and Networking (ICCCN 2008)
- [4] AnangHudayaMuhamad Amin, Asad I. Khan, "A Divide-and-Distribute Approach to Single-Cycle Learning HGN Network for Pattern Recognition" Intl. Conf. Control, Automation, Robotics and Vision, Singapore, 2010
- [5] Minoru Fukumi, SigeruOmatu, Fumiaki Takeda, and ToshihisaKosaka, "Rotation-Invariant Neural Pattern Recognition System with Application to Coin Recognition", IEEE TransaciionsOn Neural Networks, Vol. 3, No. 2, March 1992
- [6] H. K. Kwan and L. Y. Cai, "Supervised Fuzzy Inference Network for Invariant Pattern Recognition", IEEE, 2010
- [7] Sung-Jung Hsiao, Shih-ChingOu, Kuo-Chin Fan, Wen-Tsai Sung, "Using the RNN to Develop a Web-Based Pattern Recognition System for the Pattern Search of Components Database" IEEE, Proceedings of the First International Symposium on Cyber Worlds (CW.02) 2007
- [8] Kuo-Chin Fan, Sung-Jung Hsiao, Wen-Tsai Sung, "Developing a Web-Based Pattern Recognition System for the Pattern Search of Components Database by a Parallel Computing"IEEE, 2008
- [9] Wang Shou-jue' Chen Xu, "Biomimetic (Topological) Pattern Recognition-A new Model of Pattern Recognition Theory and Its Application" IEEE 2003
- [10] G. Z. Gondal, "On the use of PDL, for Domain Independent", Second IEEE International Conference on Intelligent Systems, 2004

Power Flow Control Scheme for Wind Energy Conversion System using FACTS Controller

R. Vibin¹, K. Malarvizhi²

¹ PG Scholar, Department of EEE, SNS College of Technology, Coimbatore

² Professor, Department of EEE, SNS College of Technology, Coimbatore

Abstract - Injection of wind power into an electric grid affects the power quality. The performance of the wind turbine and thereby power quality are determined on the basis of measurements and the norms followed according to the guideline specified in International Electro-technical Commission standard, IEC-61400. The influence of the wind turbine in the grid system concerning the power quality measurements are the active power, reactive power, variation of voltage, flicker, harmonics, and electrical behavior of switching operation. The paper study demonstrates the power quality problem due to installation of wind turbine with the grid. In this proposed scheme STATIC COMPENSATOR (STATCOM) is connected at a point of common coupling to mitigate the power quality issues. The STATCOM control scheme for the grid connected wind energy generation system is simulated using MATLAB/SIMULINK in power system block set.

Index terms – International Electro-technical Commission (IEC), power quality, wind generating system (WGS).

I. INTRODUCTION

To have sustainable growth and social progress, it is necessary to meet the energy need by utilizing the renewable energy resources like wind, biomass, hydro, co-generation, etc. The need to integrate renewable energy like wind energy into power system is to make it possible to minimize the environmental impact on conventional plant [1]. The issue of power quality is of great importance to the wind turbine [2]. In the fixed speed wind turbine operation, all the fluctuation in the wind speed are transmitted as fluctuations in the mechanical torque, electrical power on the grid and leads to large voltage fluctuations. A STATCOM based control technology has been proposed for improving the power quality which can technically manages the power level associates with the commercial wind turbines.

The paper is organized as follows. The Section II introduces the power quality standards, issues and its consequences of wind turbine. The Section III describes the topology for power quality improvement. The Section IV, V, VI, VII, VIII and IX discusses on the control design as well as the test system waveforms/results and conclusion respectively.

II. POWER QUALITY STANDARDS, ISSUES AND ITS CONSEQUENCES

A. International Electro Technical Commission Guidelines

The guidelines are provided for measurement of power quality of wind turbine. The standard norms are specified [4].

- 1) IEC 61400-21: Wind turbine generating system, part 21. Measurement and Assessment of power quality characteristic of grid connected wind turbine.
- 2) IEC 61400-13: Wind turbine measuring procedure in determining the power behavior.
- 3) IEC 61400-3-7: Assessment of emission limit for fluctuating load.

B. Voltage Variation

The voltage variation issue results from the wind velocity and generator torque. The voltage variation is directly related to real and reactive power variations. The voltage variation is commonly classified as under:

- Voltage Sag/Voltage Dips.
- Voltage Swells.
- Short Interruptions.
- Long duration voltage variation.

The voltage flicker issue describes dynamic variations in the network caused by wind turbine or by varying loads.

C. Harmonics

The harmonic results due to the operation of power electronic converters. The harmonic voltage and current should be limited to the acceptable level at the point of wind turbine connection to the network.

D. Wind Turbine Location in Power System

The way of connecting the wind generating system into the power system highly influences the power quality. Thus the operation and its influence on power system depend on the structure of the adjoining power network.

E. Self Excitation of Wind Turbine Generating System

The self excitation of wind turbine generating system (WTGS) with an asynchronous generator takes place after disconnection of WTGS with local load. The risk of self excitation arises especially when WTGS is equipped with compensating capacitor. The capacitor connected to induction generator provides reactive power compensation. The disadvantages of self excitation are the safety aspect and balance between real and reactive power [3].

F. Consequences of the issues

The voltage variation, flicker, harmonics causes the mal-function of equipments namely microprocessor based control system, programmable logic controller. It may leads to tripping of contractors, tripping of protection devices, stoppage of sensitive equipments like personal computer, programmable logic control system and may stop the process and even can damage of sensitive equipments. Thus it degrade the power quality in the grid.

III. TOPOLOGY FOR POWER QUALITY IMPROVEMENT

The Conventional STATCOM comprises of Voltage Source Converter, DC link Capacitor and a Coupling Transformer is being connected to the Point of Common Coupling (PCC) to the grid. The STATCOM based Voltage Source Converter injects the current into the grid in such a way that the source current are harmonic free and their phase angle with respect to source voltage has a desired value [7]. The injected current will cancel out the reactive part and harmonic part of the load and induction generator current, thus it improves the power factor and the power quality [3]. The proposed grid connected system is implemented for power quality improvement at PCC as shown in Fig. 1.

A. Wind Energy Generating System

In this configuration, wind generations are based on constant speed topologies with pitch control turbine. The induction generator is used in the proposed scheme because of its simplicity, it does not require a separate field circuit, it can accept constant and variable loads, and has natural protection against short circuit.

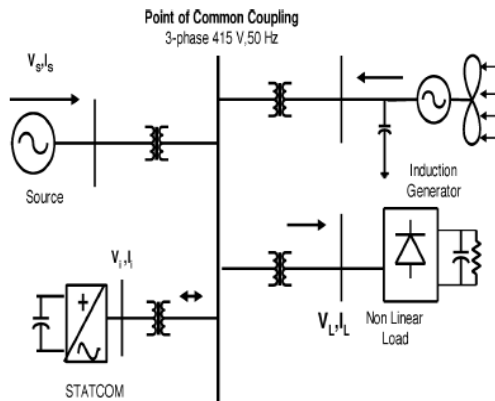


Fig.1 Grid connected system for power quality improvement

B. System Operation

The shunt connected STATCOM is connected in shunt with the induction generator and non-linear load at the PCC in the grid system [6]. The Static Synchronous compensator output is varied according to the controlled strategy, so as to maintain the power quality norms in the grid system. A single STATCOM using insulated gate bipolar transistor is proposed to have a reactive power support, to the induction generator and to the nonlinear load in the grid system. The main block diagram of the system operational scheme is shown in Fig. 2.

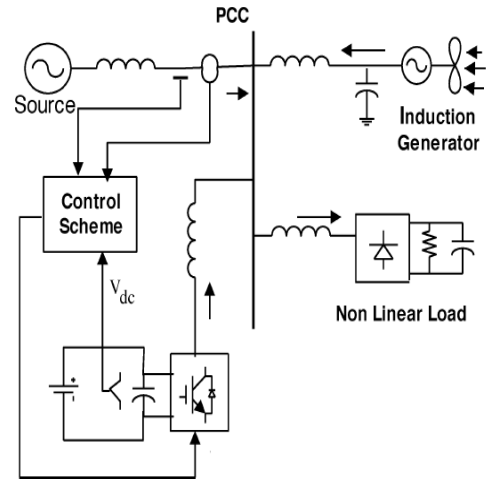


Fig.2 System operational scheme in grid system

IV.SIMULATION MODEL OF THE CONVENTIONAL SYSTEM

The conventional based STATCOM is shown in Fig 3.

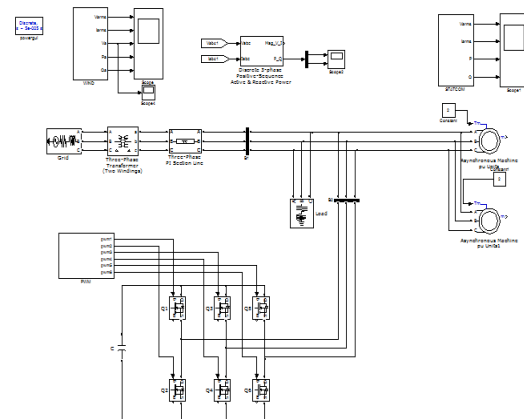


Fig.3 Simulation model of conventional system

The following parameters such as voltage, current, real power and reactive power being measured with respect to test system without induction generator, test system with induction generator and test system with both induction generator and STATCOM.

V. SIMULATION RESULTS FOR THE CONVENTIONAL SYSTEM

The Load Voltage, Load Current, Real Power and Reactive Power for the above test systems are been measured including the total harmonic distortion.

A. Load voltage

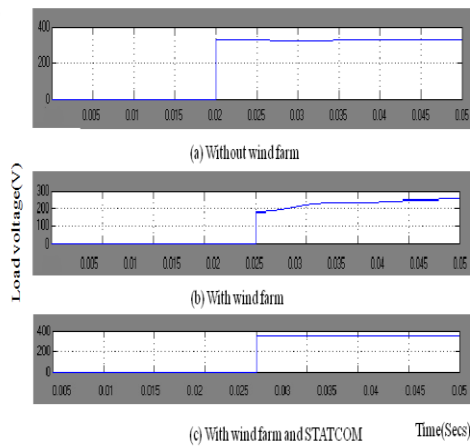


Fig.4 Load voltage

Load voltage with an induction generator connected to PCC there is a droop but with respect to STATCOM there is an improvement in the voltage profile.

B. Load Current

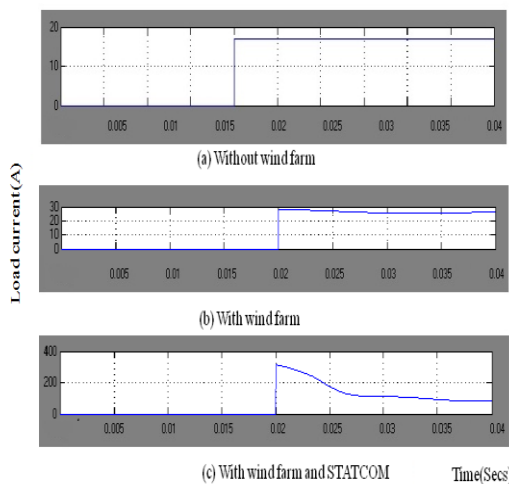


Fig.5 Load current

C. Real Power

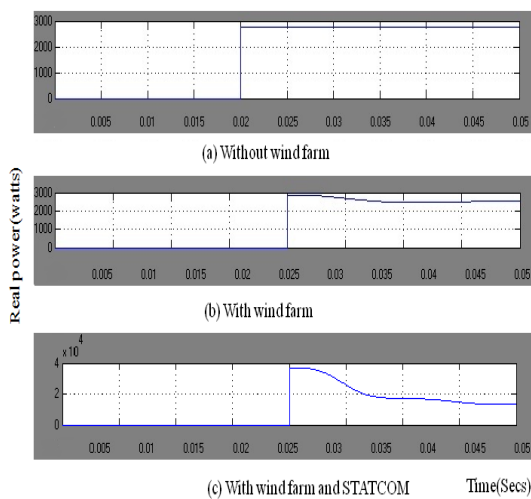


Fig.6 Real power at PCC

It has been inferred from the waveforms that there is a supply of real power to the grid from the induction generator initially but later on it decreases but after the STATCOM is been introduced into the PCC further there is an improvement in the real power flows across the load.

D. Reactive Power

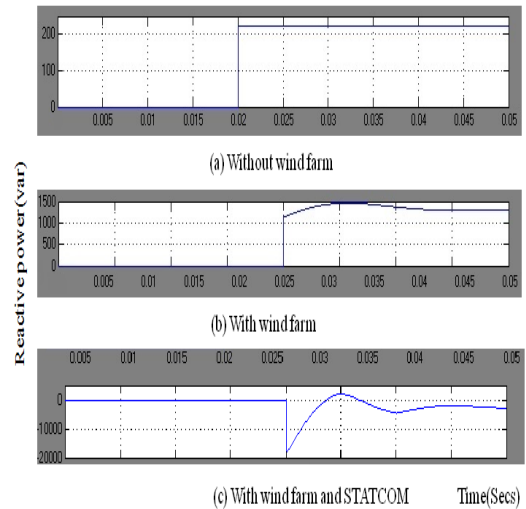


Fig.7 Reactive power at PCC

It has been inferred from the above waveforms that the reactive power is drawn from the grid by the induction generator in order to magnetize the stator and later on there is a gradual improvement in reactive power across the load from the induction generator but when the STATCOM is been connected to the grid, reactive power drawn by the induction generator is been compensated by injecting reactive power at the PCC and as a result the flow of reactive power has been controlled to a large extent and are maintained between the limits.

E. Total Harmonic Distortion

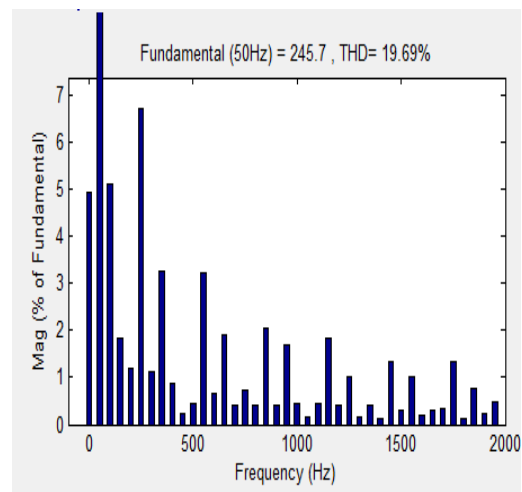


Fig.8 Total harmonic distortion for conventional STATCOM

VI. SIMULATION MODEL OF THE PROPOSED SYSTEM

The Cascaded Multilevel Converter (CMC) based STATCOM is shown in Fig 9.

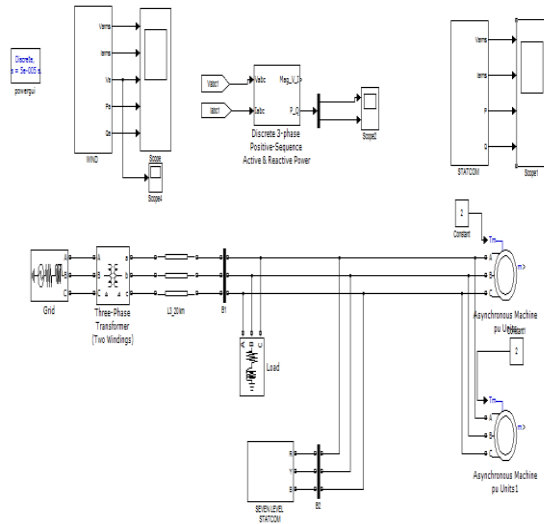


Fig.9 Simulation model of proposed system

VII. CONTROL DESIGN OF THE PROPOSED SYSTEM

The multicarrier based sinusoidal pulse width modulation control scheme has been developed in [5] with the aim of reducing the total harmonic distortion across the CMC based STATCOM output with the carrier frequency of 10kHz, modulation index of 0.9 and the corresponding simulation model is shown in Fig 10.

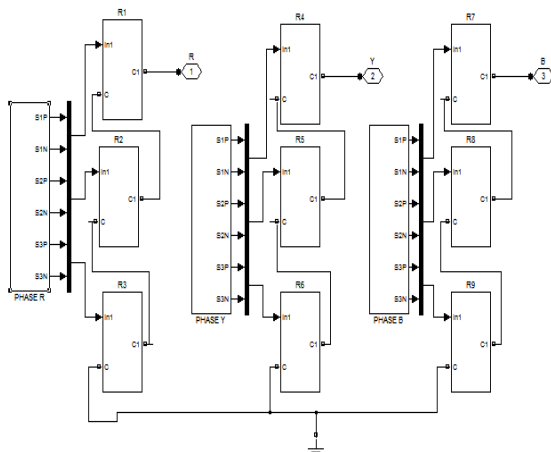


Fig.10 Multicarrier based sine PWM generation

VIII. SIMULATION RESULTS FOR THE PROPOSED SYSTEM

The parameters such as Load Voltage, Load Current, Real Power and Reactive Power for the above test system had been measured including the total harmonic distortion.

A. Load voltage

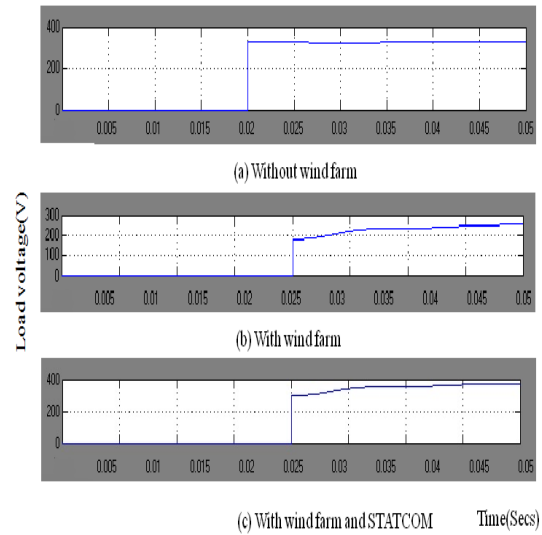


Fig.11 Load voltage

B. Load Current

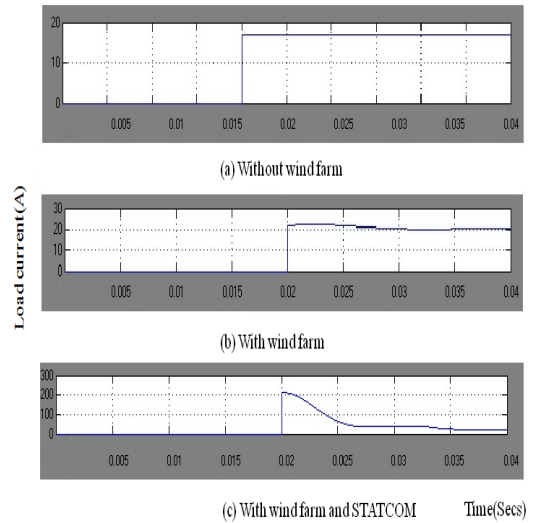


Fig.12. Load current

C. Real Power

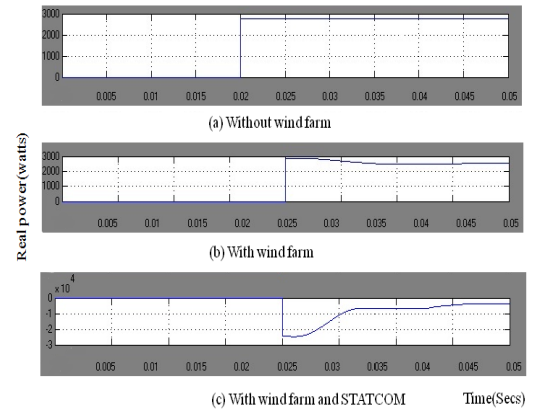


Fig.13 Real power at PCC

D. Reactive Power

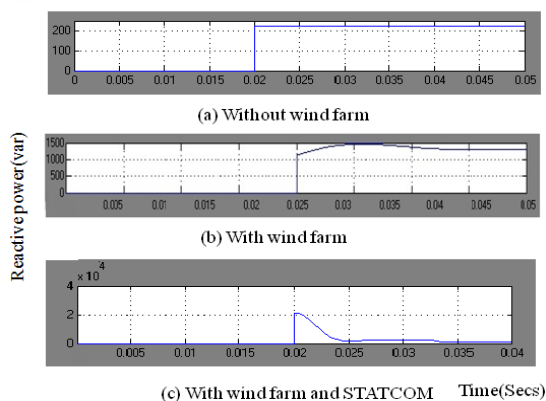


Fig.14 Reactive power at PCC

E. Total Harmonic Distortion

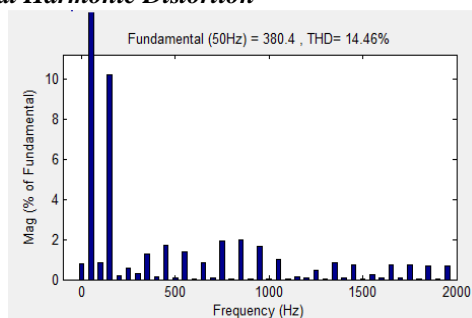


Fig.15 Total harmonic distortion for CMC based STATCOM

IX. CONCLUSION

This paper compares both conventional STATCOM and CMC based STATCOM control scheme for power quality improvement in grid connected wind generating system and with non-linear load. The power quality issues and its consequences on the consumer and electric utility are presented. The integrated wind generation along with CMC based STATCOM have shown the outstanding performance in compensating the reactive power consumed by the wind generator.

REFERENCES

- [1] A.Sannino, "Global power systems for sustainable development," in *IEEE General Meeting*, Denver, CO, Jun. 2004.
- [2] K.S. Hook, Y.Liu, and S. Atcity, "Mitigation of the wind generation integration related power quality issues by energy storage," *EPQU J.*, vol. XII, no. 2, 2006.
- [3] J.Manel, "Power electronic system for grid integration of renewable energy source: A survey," *IEEE Trans. Ind. Electron.*, vol. 53, no. 4, pp. 1002-1014, 2006, Carrasco.
- [4] M. Tsili and S. Papathanassiou, "A review of grid code technology requirements for wind turbine," *Proc. IET Renew.power gen.*, vol. 3, pp. 308-332, 2009.
- [5] V.Kumar and J.Karpagam, "Control Techniques for Multilevel Voltage Source Inverters, IPEC" vol. 5, pp.978-981, 2007.

- [6] K.Malarvizhi and K.Baskaran, "Enhancement of Voltage Stability in Fixed Speed Wind Energy Conversion Systems using FACTS Controller", *International Journal of Engineering Science and Technology*, vol. 2, No. 4, pp.1800-1810, 2010.
- [7] Fu.S Pai and S.I Hung, "Design and operation of converter for micro Turbine Powered distributed generator with capacity expansion capability", *IEEE Transactions on Energy Conversion.*, vol. 3, No. 1, pp. 110-116, 2009.
- [8] F.Zhou, G.Joos and C.Abhey, "Voltage stability in weak connection wind farm", in *IEEE PES General Meeting.*, vol. 2, No. 2, pp. 1483-1488, 2005.



R. Vibin received his B.E degree in Electrical and Electronics Engineering from V.L.B Janakiammal College of Engineering and Technology, in 2004 and pursuing M.E degree in S.N.S College of Technology, Coimbatore, India. His areas of interest include Electrical machines and Power systems.



K. Malarvizhi received her B.E degree in Electrical and Electronics Engineering from Bharathiar University, India in 1993, Master of Engineering degree in Electrical machines from Anna University - Chennai, India in 2006. She is currently pursuing Ph.D in Anna University of Technology - Coimbatore and her areas of interest include Electrical Machines, Power Systems and Power Electronics. She is a member of ISTE and SSI. She is now Professor in Electrical and Electronics Engineering, S.N.S College of Technology, Coimbatore, India.

Implementation of Selfish Overlay Network Creation and Maintenance

D. Kiran Kumar¹, Venkata Rao. J²,

Student, M.Tech (CNS), Assistant Professor,
Computer Science and Engineering Department, K L University, Vaddeswaram, Guntur (dt).

Abstract:

A foundational issue underlying many overlay network applications ranging from routing to peer-to-peer file sharing is that of the network formation, *i.e.*, folding new arrivals into an existing overlay, and rewiring to cope with changing network conditions. A typical overlay network for routing or content sharing, each node must select a fixed number of immediate overlay neighbors for routing traffic or content queries. A selfish node entering such a network would select neighbors so as to minimize the weighted sum of expected access costs to all its destinations. Connectivity management is called upon when having to wire a newcomer into the existing mesh of nodes (bootstrapping), or when having to rewire the links between overlay nodes to deal with churn and changing network conditions. Previous work on selfish neighbor selection has built intuition with simple models where edges are undirected, access costs are modeled by hop-counts, and nodes have potentially unbounded degrees. Overlay networks are substantially Different which prompts us to consider the following overlay network model. Selfish neighbor selection has considered the problem from two perspectives: devising practical heuristics for the case of cooperative peers and performing game-theoretic analysis for the case of selfish peers. In this paper, we implement by unifying the foregoing thrusts by defining and studying the selfish Neighbor selection (SNS) game and its application to overlay routing.

I. Introduction

An Overlay Network is a layer of virtually network topology on top of the physical network, which directly interfaces to User. Selfish overlay networks In selfish overlay routing end hosts are allowed to choose the route of the packets among themselves. Since the selfish overlay routing never bother about the global criteria, the performance of the network becomes worse. Earlier studies proved that by reaching Nash equilibrium in selfish overlay network latency and loss rate was decreased, link utilization and throughput was increased, giving an optimized output. In all the above studies overlay nodes are placed randomly in the network. This may cause deployment of overlay nodes even in the place where there is no link failure and it occupies more memory in Selfish Overlay Network (SON) since large number of overlay nodes is deployed. In this paper overlay nodes are deployed based on fuzzy logic and the merit of applying fuzzy logic is , the overlay nodes are deployed only where and when there is link failure. This paper is organized as

follows. Section 2 reviews the efforts made focused on flows which experience congestion and identification of packet forwarding prioritization in routers. Section 3 explains how a selfish neighbor selection can considered based on the two perspectives: Devising practical heuristics and Providing abstractions of the underlying fundamental neighbor selection problem. Section 4 deals with the contributions made to obtain pure Nash equilibrium through iterative best response walks via local search. Section 5 describes the Overlay network model and its aspects. Section 6 deals with Deriving stable wirings and Section 7 deals with Performance evolution of stable wirings.

II. Related work

To the best of our knowledge, this is the first attempt to infer router packet-forwarding priority through system-to-system measurement. Possibly the efforts most closely related to this work are those identifying shared congestion. Such efforts try to determine whether two congested flows are correlated and share a common congested queue along their paths. If we consider the flows of different packet types along a same path, our problem becomes to identify whether these flows do not share a common congested queue. While both problems are related clearly, we usually need to simultaneously consider a much larger number of packet types That the correlation based methods used for shared congestion identification requires back-to-back probing which, in our case, translates into $O(n^2)$ pairs probing for n packet types. In addition, those efforts focused on flows which experience congestion (ignoring uncongested ones), so their probe traffic rate is low and not bursty. To identify packet forwarding prioritization in routers, one must send relatively large amounts of traffic to temporarily force packet drops by saturating the link.

III. Selfish neighbor selection

In a typical overlay network, a node must select a fixed number (k) of immediate overlay neighbors for routing traffic. Previous work has considered this problem from two perspectives:

Devising practical heuristics for specific applications in real deployments, such as bootstrapping by choosing the k closest links (*e.g.*, in terms of TTL or IP prefix distance), or by choosing k random links in a P2P file-sharing system. Notice here that DHTs like Chord *solve* a different problem.

They route queries, not data traffic. The latter is left to a separate subsystem that typically opens a direct connection to the target host.

Providing abstractions of the underlying fundamental neighbor selection problem that are analytically tractable, especially via game theoretic analysis. To date, however, the bulk of the work and main results in this area have centered on strategic games where edges are undirected, access costs are based on hop-counts, and nodes have potentially unbounded degrees. While this existing body of work is extremely helpful for laying a theoretical foundation and for building intuition, it is not clear how or whether the guidance provided by this prior work generalizes to situations of practical interest, in which underlying assumptions in these prior studies are not satisfied. Another aspect not considered in previous work is the consideration of settings in which some or even most players do not play optimally a setting which we believe to be typical. Interesting questions along these lines include an assessment of the advantage to a player from employing an optimizing strategy, when most other players do not, or more broadly, whether employing an optimizing strategy by a relatively small number of players could be enough to achieve global efficiency.

IV. Contributions

A combination of modeling, analysis, and extensive simulations using synthetic and real datasets. Our starting point is the definition of a network creation game that is better suited for settings of P2P and overlay routing applications – settings that necessitate the relaxation and/or modification of some of the central modeling assumptions of prior work. In that regard, the central aspects of our model are bounded degree, directed edges, non-uniform preference vectors, and representative distance functions. Our first technical contribution within this model is to express a node's "best response" wiring strategy as a k-median problem on asymmetric distance and use this observation to obtain pure Nash equilibrium through iterative best response walks via local search.

V. Overlay network model and aspects

Overlay network creation has focused on physical telecommunication networks and primarily the Internet. Overlay networks are substantially different which prompts us to consider the following overlay network model.

We start by relaxing and modifying some of the central modeling assumptions of previous work. In that regard, the central aspects of our model are:

Bounded Degree: Most protocols used for implementing overlay routing or content sharing impose hard constraints on the maximum number of overlay neighbors. For example, in popular versions of Bit Torrent a client may select up to 35 nodes from a neighbors' list provided by the *Tracker* of a particular torrent file [4]. In overlay routing systems [8], the number of immediate nodes has to be kept small so as to reduce the monitoring and reporting overhead imposed by the link-state routing protocol implemented at the overlay layer. Motivated by these systems, we explicitly model such hard constraints on node degrees.

Directed Edges: Another important consideration in the settings we envision for our work relates to link directionality. Prior models have generally assumed bi-directional (undirected) links. This is an acceptable assumption that fits naturally with the unbounded node degree assumption for models that target physical telecommunication networks because actual wire-line communication links are almost exclusively bidirectional.

Non-uniform preference vectors: In our model, we supply each node with a vector that captures its local preference for all other destinations. In overlay routing such preference may capture the percentage of locally generated traffic that a node routes to each destination, and then the aggregation of all preference vectors would amount to a origin/destination traffic matrix. In P2P overlays such preference may amount to speculations from the local node about the quality of, or interest in, the content held by other nodes. Other considerations may also include subjective criteria such as the perceived capacity of the node, its geographic location, or its availability profile.

VI. Deriving stable wirings

Connections between the SNS game and facility location:

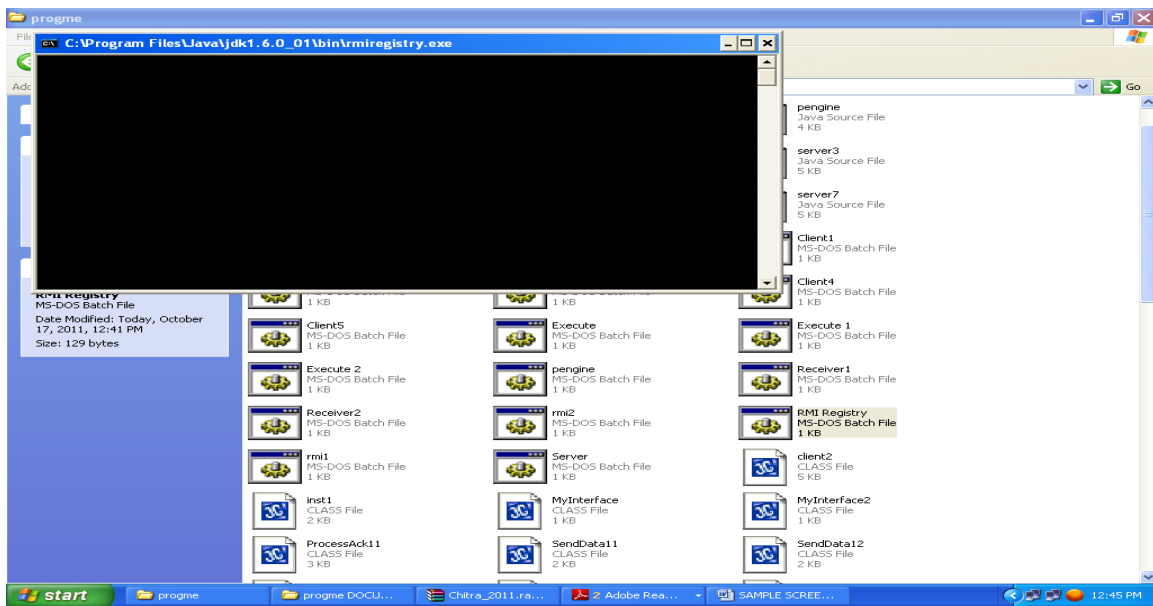
When all the wires have the same unitary weight, then the distances are essentially hop counts link cost of a node to connect to other nodes to be taken into account

Stable wirings through iterative best response:

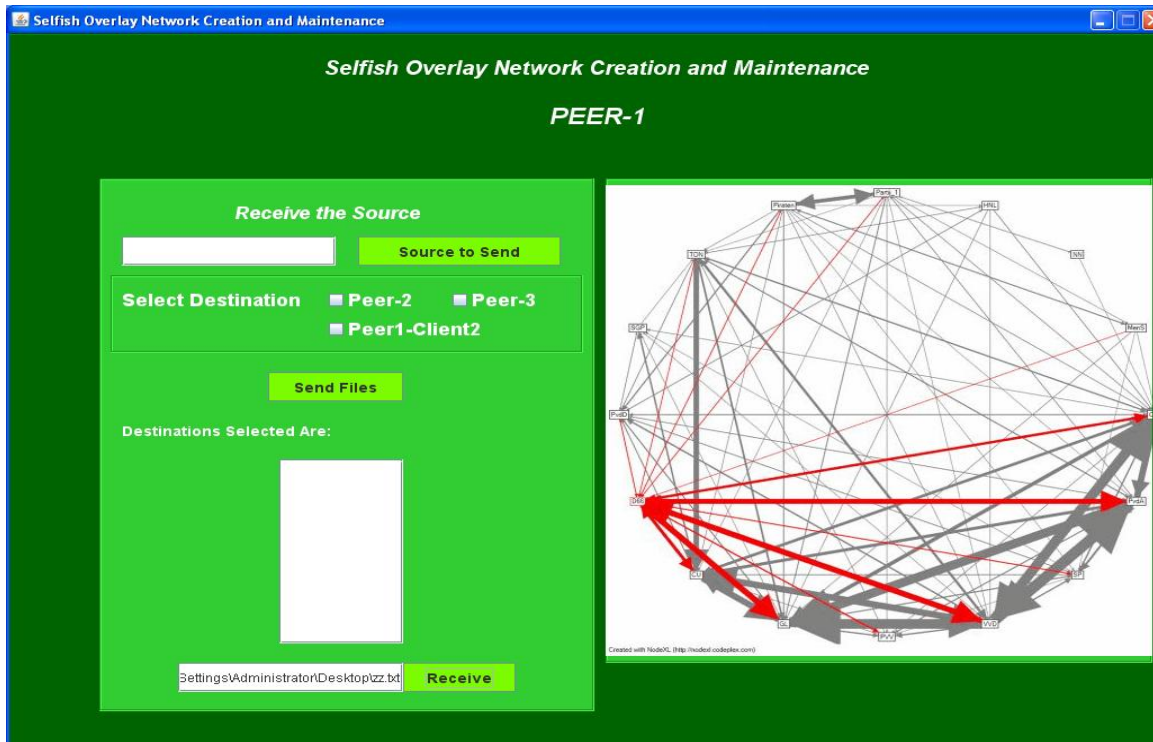
We obtain stable wirings through a simple iterative best response method in which nodes apply iteratively their best response until no unilateral improvement can be obtained based on hop-count distance best responses in several real topologies.

VII. Implementation of peer and client

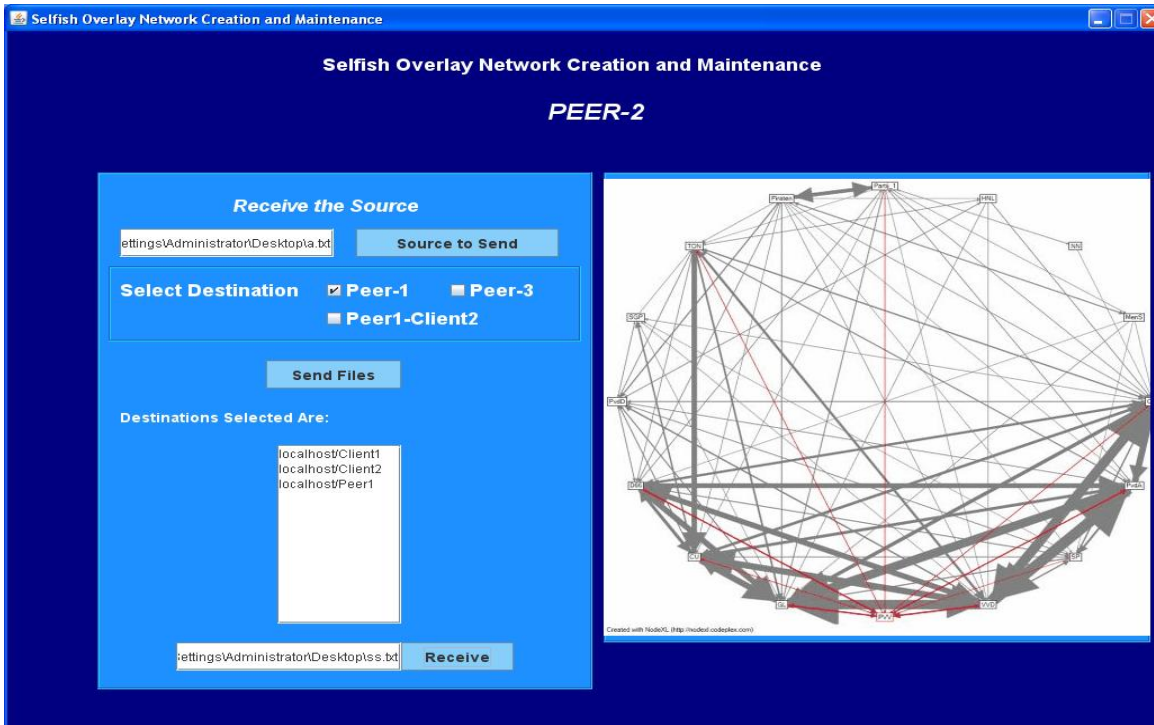
Start RMI registry



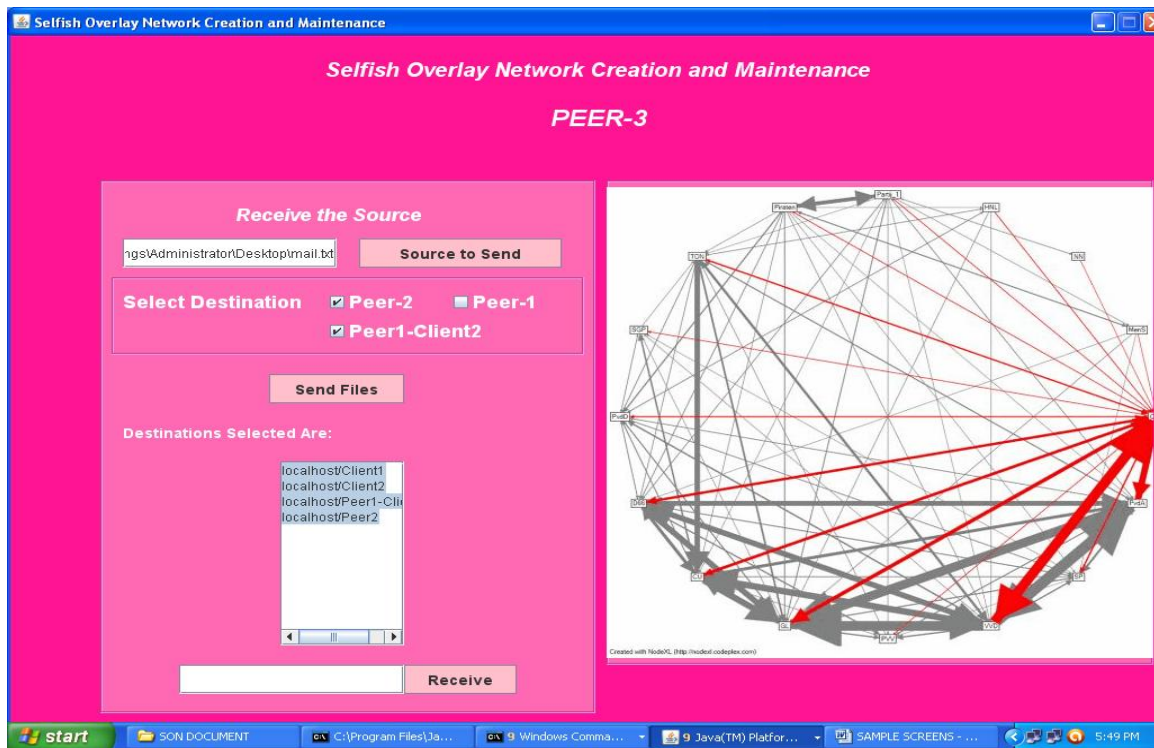
Peer-1



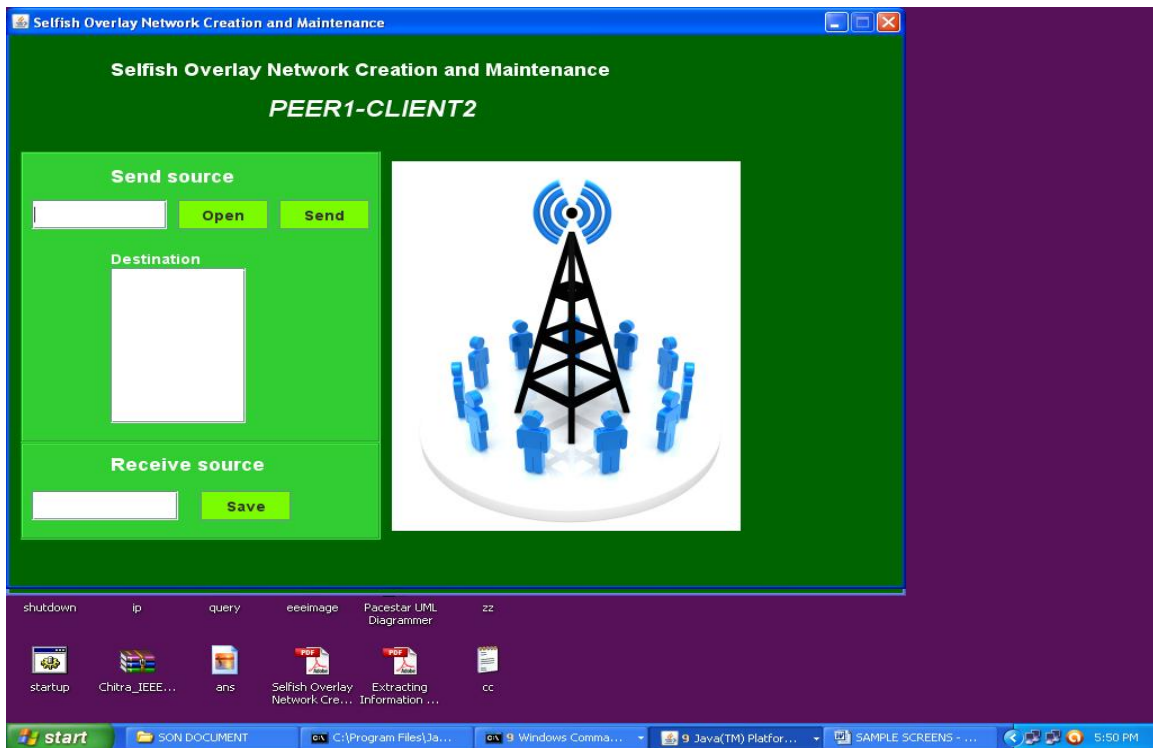
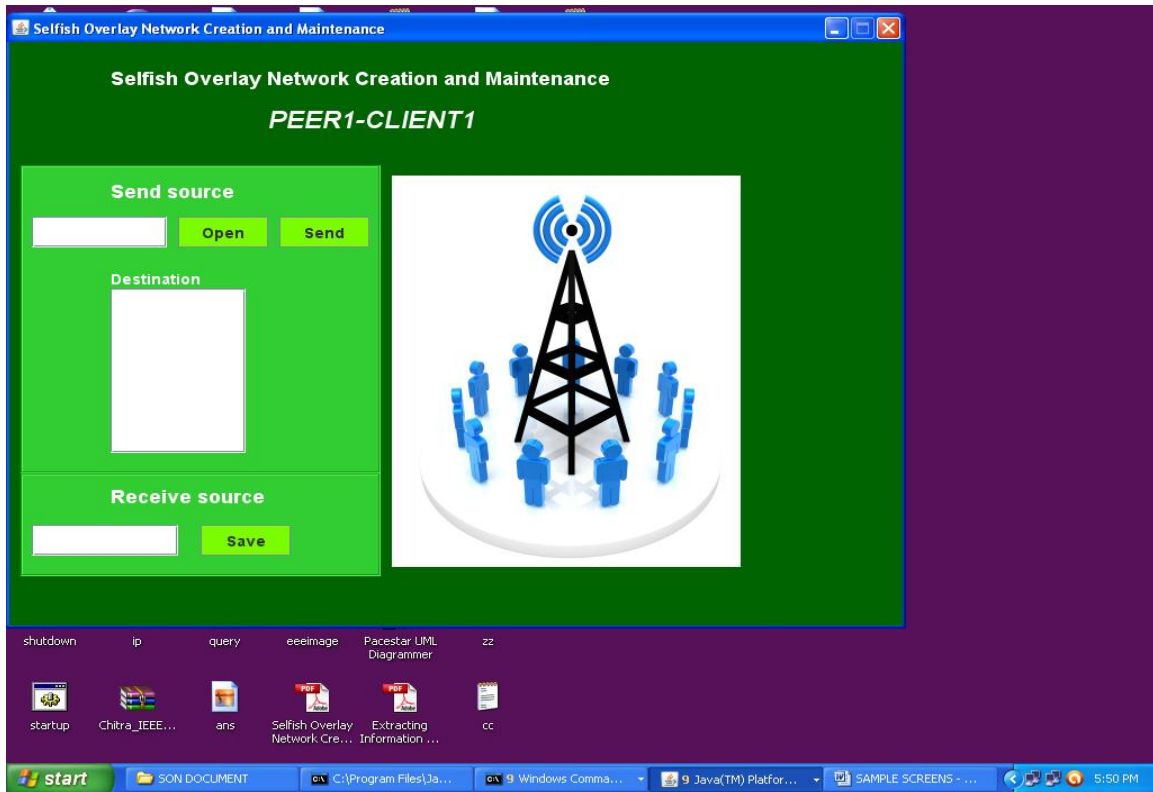
Peer-2



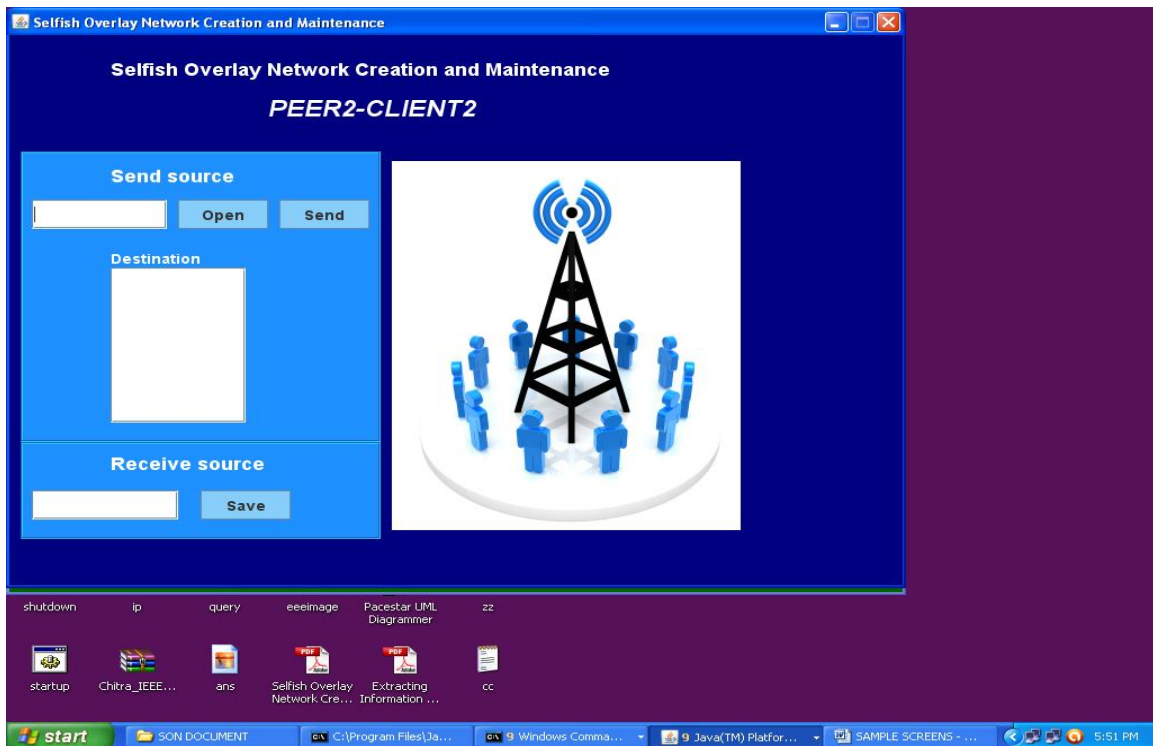
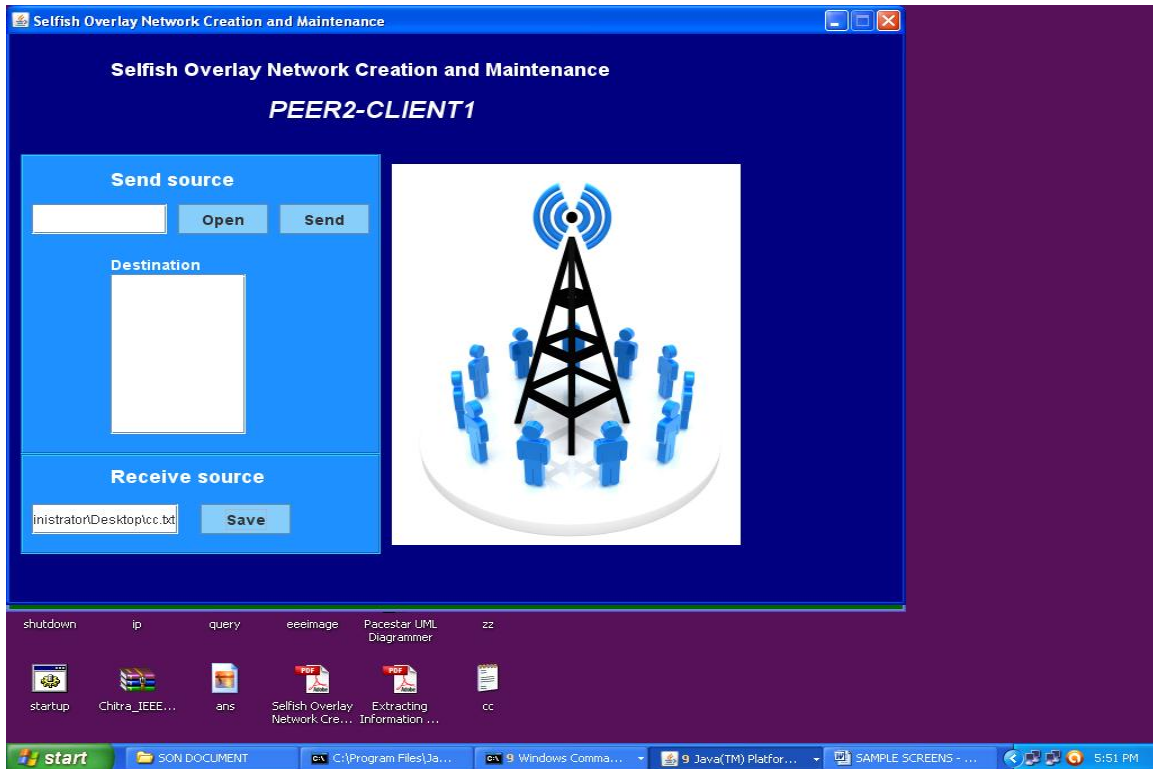
Peer-3



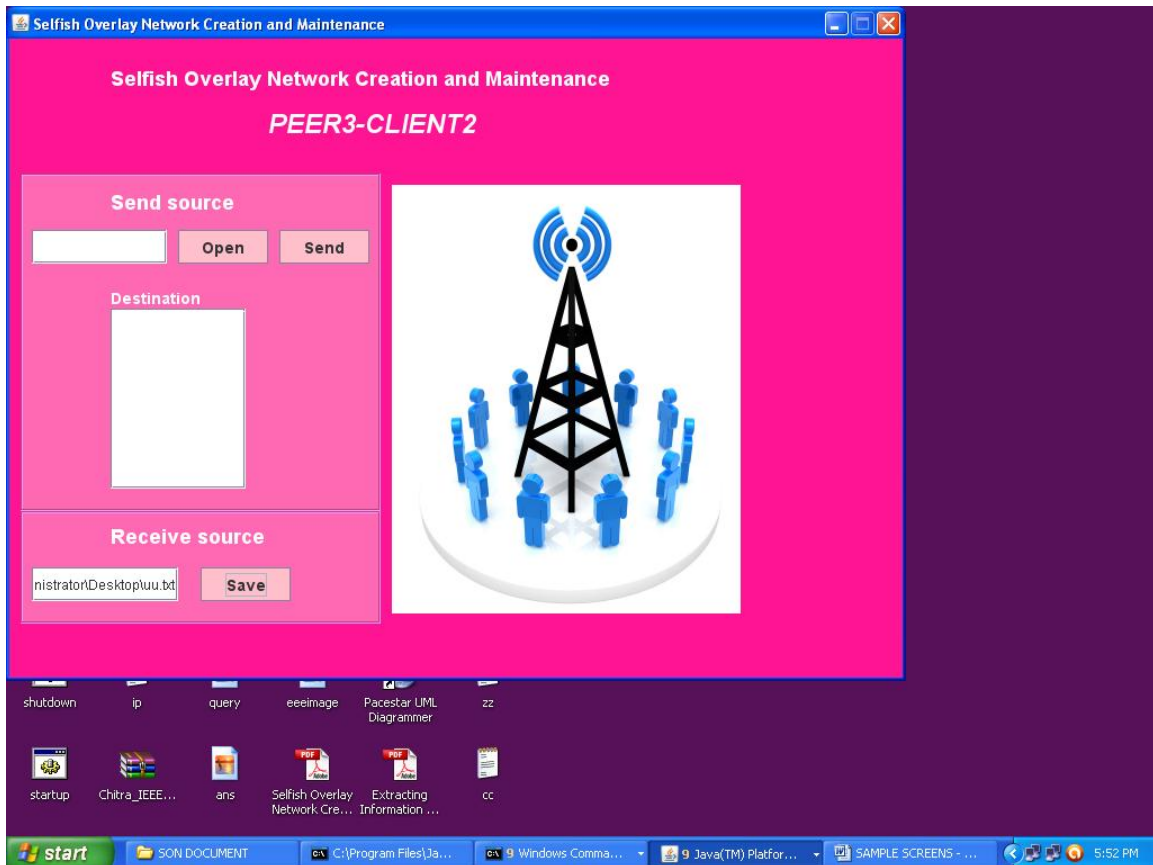
Peer1-Clients



Peer2-Clients



Peer3-clients



VIII. Conclusion

In this paper, we have shown that a best response (*i.e.*, selfish) selection of neighbors leads to the construction of overlays with much better performance than those constructed by simple random and myopic heuristics. We implemented them and evaluated their performance against heuristic wirings. In all the cases the performance of best response was way higher, especially for large values of out-degree. selfish neighbor selection under strictly enforced neighbor budgets and has come up with a series of findings with substantial practical value for real overlay networks. We have shown that a best response selfish selection of neighbors leads to the construction of overlays with much better performance than those constructed by simple random and myopic heuristics. The reason is that by being selfish, nodes embark on a distributed optimization of the overlay that turns out to be beneficial for all. Feature we have to implement reliable multicast, security provisioning, power efficiency, congestion control, scalability, and efficient membership updates. It is difficult to design a multicast routing protocol that takes all these issues into consideration, that is, a one-size-fits-all design.

Acknowledgments

We are greatly delighted to place my most profound appreciation to S.Venkateswarlu, Head of the CSE Department, under the guidance of Mr.J.Venkata Rao and Dr.K.Subramanyam in charge for M.Tech under their guidance and encouragement and kindness in giving us the opportunity to carry out the paper. Their pleasure nature, directions, concerns towards us and their readiness to share ideas enthused us and rejuvenated our efforts towards our goal. We also thank the anonymous references of this paper for their valuable comments.

REFERENCES

- [1] N. Laoutaris, G. Smaragdakis, A. Bestavros, and J. W. Byers, "Implications of Selfish Neighbor Selection in Overlay Networks," in *Proc. IEEE INFOCOM'07*.
- [2] G. Smaragdakis, V. Lekakis, N. Laoutaris, A. Bestavros, J. W. Byers, and M. Roussopoulos, "EGOIST: Overlay Routing using Selfish Neighbor Selection," in *Proc. ACM CoNEXT'08*.
- [3] D. Andersen, H. Balakrishnan, F. Kaashoek, and R. Morris, "Resilient Overlay Networks," in *Proc. ACM SOSP'01*.
- [4] Weizhao Wang; Xiang-Yang Li , "Low-cost routing in selfish and rational wireless ad hoc networks", may 2006.
- [5] Nama, H.; Mandayam, N.; Yates, R. "Network Formation Among Selfish Energy-Constrained Wireless Devices", April 2008.
- [6] Cagalj, M.; Ganeriwal, S.; Aad, I.; Hubaux, J.-P.," On selfish behavior in CSMA/CA networks ", march 2005.
- [7] Yang Jian-ren; Hu Rui-min; Chen Jun; Zhong Jian-bo,," A Service-Oriented Framework of Distributed QoS Measurement Based on Multi-Agent for Overlay Network", feb 2009.
- [8] Jin Bo; Sci. & Technol. Dept., Shunde Polytech., Foshan, China , " Heterogeneity-Aware Group-Based Semantic Overlay Network for P2P Systems",December 2009.
- [9] Kawahara, R.; Kamei, S.; Kamiyama, N.; Hasegawa, H.; Yoshino, H.; Eng Keong Lua; Nakao, A," A Method of Constructing QoS Overlay Network and Its Evaluation ", march 2010.
- [10] Tan Chen; Xin Xiong," Searching nearest neighbor in overlay network" july 2008.
- [11] Han, J.; Watson, D.; Jahanian, F.," Topology aware overlay networks ", march 2005.

Design of high speed FFT Processor Based on FPGA

G. Shafirulla*1, M. Subbareddy #2

Department of Electronics and Communication, Vaagdevi institute of Technology & Science, Proddutur, A.P.
Department of Electronics and Communication, Vaagdevi institute of Technology & Science, Proddutur, A.P

Abstract: It is important to develop a high-performance FFT processor to meet the requirements of real time and low cost in many different systems. So a radix-2 pipelined FFT processor based on Field Programmable Gate Array (FPGA) for Wireless Local Area Networks (WLAN) is Proposed. Unlike being stored in the traditional ROM, the twiddle factors in our pipelined FFT processor can be accessed directly. A novel simple address mapping scheme is also proposed. The FFT processor has two pipelines, one is in the execution of complex multiplication of the butterfly unit, and the other is between the RAM modules, which read input data, store temporary variables of butterfly unit and output the final results. Finally, the pipelined 64-point FFT processor can be completely implemented within only 67 clock cycles.

Keywords- FFT; FPGA; address mapping

I. INTRODUCTION

Fast Fourier Transform (FFT) processor is widely used in different applications, such as WLAN, image process, spectrum measurements, radar and multimedia communication services [1]. However, the FFT algorithm is a demanding task and it must be precisely designed to get an efficient implementation. If the FFT processor is made flexible and fast enough, a portable device equipped with wireless transmission system is feasible. Therefore, an efficient FFT processor is required for real-time operations [2] and designing a fast FFT processor is a matter of great significance.

In the past twenty years, FPGA has developed rapidly and gradually become universal. Compared with design flow of traditional ASIC, designs based on FPGA have the advantages of flexibility and high performance price ratio. Many researchers have studied on pipelined FFT based on FPGA [3], [4], [5]. For instance, in [3], they proposed an approach to design an FFT processor for wireless applications, but his design has too many clock cycles and isn't fast enough. In comparison to their designs, we propose a simple and feasible pipelined implementation of a 32-bit 64-point FFT processor based on FPGA for WLAN.

This paper is organized as follows. In the next section, we introduce a basic radix-2 FFT algorithm to briefly discuss which decimation is better to the system, a three-multiplication method, and a novel address mapping scheme which reduces delay and increases the speed of the system. In section III, the pipelined FFT architecture is proposed and each unit is also illustrated. Section IV is the implementation of the 64-point FFT processor based on FPGA, and

hardware resources are explicitly listed out. The last section gives the conclusion.

II. FFT ALGORITHM AND ADDRESS MAPPING SCHEME

A. Radix-2 FFT Algorithm

The FFT algorithm can compute the Discrete Fourier Transform (DFT) effectively. Given a sequence $\{x(n)\}$ of N complex numbers, we can compute its DFT, another sequence $\{X(k)\}$ of N complex numbers, according to the following formula [6]

$$X(K) = \sum_{n=0}^{N-1} x(n) W_N^{nk}, K=0,1,..N-1 \quad (1)$$

And according to the different way to decimate, it can be divided into two types, DIF (Decimation in Frequency) and DIT (Decimation in Time). The DIF algorithm is easier to design than DIT. And considering the finite word length effect, DIF has much more advantages than DIT, such as reducing the additive noise, which is introduced by the multiplication when it is implemented with the fixed point [7] and reducing the complexity of the whole system. Consequently, we use the DIF algorithm to design radix-2 FFT module and most of current FFT processors are also based on this algorithm [8].

B. Three-multiplication Method

It's undeniable that complex multiplication is the dominant factor affecting the speed and the throughput of FFT processor. Computing a complex multiplication requires four real multipliers and two real adders. As we all know, the hardware area of a real multiplier is larger than that of a real adder in FPGA. So we should do our best to convert the complex multiplication into addition and subtraction to optimize the whole performance as high as possible. Having taken into account all operands are 32-bit complex numbers, the difference of two inputs $X_m(i)$ and $X_m(j)$ can be expressed by $Z_1 = x_1 + jy_1$ and the twiddle factor $W_N^{nk} = \exp(\frac{2n}{N} \pi)$ can be expressed by $Z_2 = x_2 + jy_2$. So the product of them can be also expressed by $z = x + jy$. That's to say, the 16-bit real part x of the product is equivalent to $x_1 x_2 - y_1 y_2$ and the 16-bit imaginary part y is equivalent to $x_1 y_2 + x_2 y_1$. Therefore, we can transform the product z easily as the following equations

$$x = x_1(x_2 + y_2) - y_2(x_1 + y_1) \quad (2)$$

$$y = x_1(x_2 + y_2) + x_2(x_1 - y_1) \quad (3)$$

Obviously, using this factorization scheme, the system has some advantages [9]. The number of real multiplications

is reduced from four to three. And addition has less consumption than multiplication. So the system power consumption is also reduced. In this study, we can save sixteen embedded multiplier 9-bit elements in FPGA. As for this 64-point FFT processor, the numerical values of $x_2+y_2, x_1-y_1, x_1+y_1, x_2$ and y_2 can be gotten before they participate in the real multiplication.

C. The Novel Address Mapping Scheme

In this paper, the block size of our system is 64 points. Having considered the properties of radix-2 64-point FFT, it needs to read 8 operands from memories at a time so as to achieve a high-speed FFT. As we all know, parallel accessing data is crucial to a system [10]. Thus, these 8 operands in our design are located in different row or column of memory blocks and this arrangement ensures that 8 conflict-free memory accesses can be performed in parallel. Initially, we use 8 32-bit dual-port memories to store 64 operands in sequence. And then a new linear shift conflict-free address mapping scheme is adopted to change the addresses of operands. The primary two-dimensional addresses of operands will be mapped to new ones. For instance, we assume that the original two-dimensional coordinate is (a, b), in which a and b represent the address of the data in one memory and the number of the 8 memories, respectively. Then, we obtain a new conflict-free address

(A, B) by means of the following equations

$$A=b, \tag{4}$$

$$B=(a+b)\%8. \tag{5}$$

In our design, it can be ensured that no memory location is read from or written to at the same time, and this new mapping scheme is feasible, effective and simple.

III. THE PIPELINED FFT PROCESSOR ARCHITECTURE

For high throughput systems, pipelined architecture is a good choice, and it is also an ideal method to implement high-speed long-size FFT owing to its regular structure And simple control. The performance of pipelined FFT processor can be improved by optimizing the structure and saving hardware resources. The block diagram of our proposed FFT processor is illustrated in Fig.1. It consists of four essential units. Control unit, the kernel of the FFT processor, harmonizes the whole system. Butterfly unit (BU), which has three-stage pipelined structure, carries out the complex multiplication. Two dual-port RAMs are used to store and output data. And AGU, the abbreviation

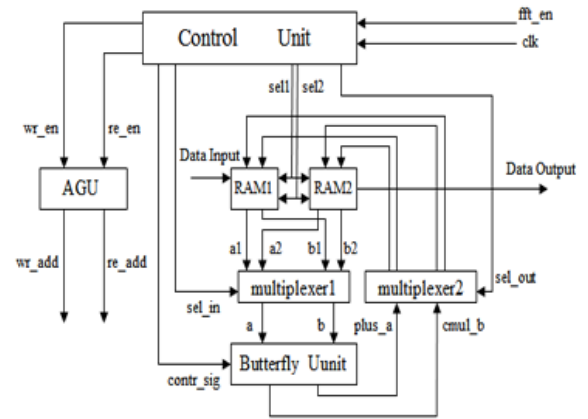


Figure 1. The pipelined FFT architecture.

of address generator unit, produces 8 3-bit read addresses and write addresses.

A. Control Unit

Control unit, which generates all control signals for the whole system, is responsible for operation control of the processor. A 48-bit signal w_con controls the whole FFT processor. And this signal w_con generates two parameters, $write_en$ and $read_en$, to control AGU. It also generates $sel1$ and $sel2$ signals to select data from two RAMs, each of which is made up of 8 32-bit registers. The BU and the remaining parts are controlled by w_con as well. This control unit harmonizes all steps of the FFT processor based on a 7-bit counter.

B. The DIF Butterfly Unit

For FFT algorithm, the central component is the BU that calculates the sum and difference of two input data, and plays an extremely important role in computing the product of the difference and twiddle factors. We only use 11 factors $w_{64}^0, w_{64}^1, w_{64}^2, w_{64}^3, w_{64}^4, w_{64}^5, w_{64}^6, w_{64}^7, w_{64}^8, w_{64}^{16}, w_{64}^{24}$ to express all 32 factors that we need in this FFT processor owing to the fact that the twiddle factor w_N^{nk} can be separated into two components. For instance, w_{64}^{28} can be derived from the product of w_{64}^4 and w_{64}^{24} . Moreover, the value of w_{64}^0 is a constant 1, and for w_{64}^6 only a negative sign is needed to add to the real part of the relevant data, and then to inverse the real part and imaginary part. So we can eliminate these two factors, that's to say, actually we just need 9 twiddle factors. In addition, we use 16-bit fixed point decimal to express these 9 twiddle factors. Although the fixed point decimal arithmetic isn't precise enough, it can satisfy the requirements of general systems.

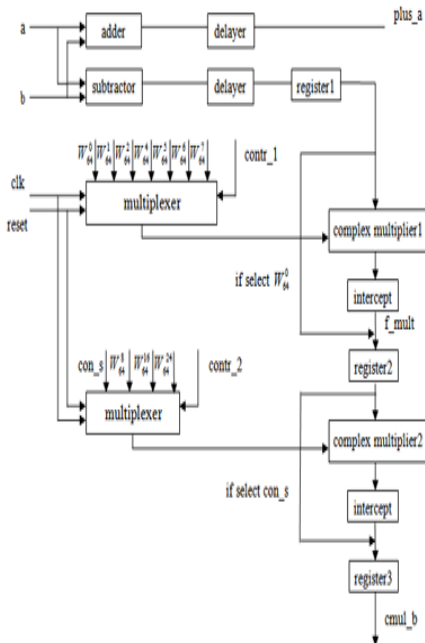


Figure 2. Block diagram of BU.

Due to the fact that the multiplication of twiddle factors and corresponding data is very important, three-stage pipeline structure is used for the complex multiplication to obtain a high speed computation. The architecture of BU is shown in Fig. 2.

In the BU, both of the complex inputs are 32 bits, including 16-bit real part and 16-bit imaginary part. The sum of them needs to be scaled down by a factor of 2 to avoid arithmetic overflow, and the same operation is applied to the difference of them. On the other hand, the factor 0 W64 and the first parameter con_s of the second Multiplexer are not involved in the complex multiplier, and they can be used as a constant 1, just as Fig.2 has depicted. Thus, the power consumption of the complex multiplier can be reduced and the hardware resources will be saved. There're some points to be emphasized. The difference and twiddle factors are both 32 bits, so the result of the first complex multiplier will be 64 bits. But because we adopt the fixed point decimal computation, we should intercept it to a 32-bit parameter f_mult as the input of the second complex multiplier.

The most remarkable advantage in this unit is that we Use 3 32-bit registers to realize the three-stage pipeline of butterfly transform, using register1 to store the difference, register2 to store the intercepted result of second stage f_mult and register3 to store the final result cmul_b.

C. The RAM Unit

The RAM1 and RAM2 are made up of 8 32-bit registers respectively. And data is always written to the outside memories from RAM2, and it is always read to RAM1 from the outside memories. Then let us introduce the key algorithm used in this unit. Considering the properties of 64-point FFT, we can use the radix-2 DIF 8-point FFT as a whole unit, so there

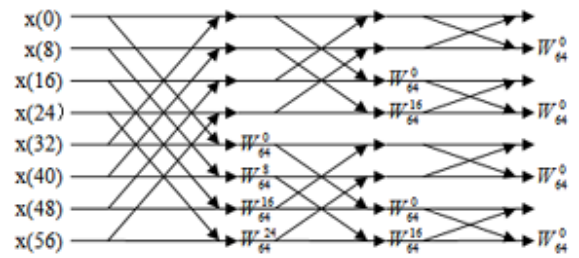


Figure 3. The example of radix-2 8-point FFT.

are only two stages to accomplish the 64-point FFT. And these two stages are identical to the six stages of the standard radix-2 DIF 64-point FFT. System parallel reads 8 32-bit operands from outer memories to RAM1 at a time, and we need only read sixteen times. An example of this Algorithm is shown in Fig.3.

The pipeline in RAM units is briefly discussed as follows. Firstly, system reads 8 operands from outer Memories and writes them to RAM1, and then the results will be stored in RAM2 after they are computed. Meanwhile, system reads the next 8 operands. Subsequently, system will access operands from RAM1 or RAM2 to compute these 16 operands. Furthermore, within a single clock four butterfly computations will be executed simultaneously. The final results of these 16 operands will be all stored in RAM2, and then they are written to outer memories. At the same time, another 8 operands will be read. Accordingly, only 76 clock cycles are needed to complete this radix-2 DIF 64-point FFT.

D. AGU

Compared with other units, AGU is also quite important. It will create 8 read and 8 write addresses, which determine the data access to outer memories.

In this FFT processor, we adopt the in-place computation method so as to make it a more simplified and faster system. That's to say, we write the results into where they are read. In contrast to the sequence of 64 input operands configured by address mapping, the final output sequence of this FFT processor are in bit-reversed order and need to be adjusted to normal order. And we can Make these appropriate adjustments before the FFT computation. So, although we adjust the sequence of inputs or outputs, the performance of our FFT processor won't be degraded.

IV. HARDWARE RESOURCES

The functional simulation and timing simulation are successfully made. The main hardware resources of this design are given as follows. The device is the EP2C70F896C6 of Cyclone II family. The total logic elements are 562/68,416 (8%), the total pins are 563/622(91%) and the total embedded multiplier 9-bit elements are 48/300(16%). Meanwhile, the clock frequency is 31.69MHz. As in [3], they proposed a fixed-point 16-bit 64-point FFT processor with 92 clock cycles in total, but our

clock cycles is 67. And our FFT processor has a higher speed and lower power consumption.

V. CONCLUSION

This paper proposes a novel radix-2 FFT processor based on FPGA for WLAN, using Verilog HDL as hardware description language and Quartus II as design and synthesis tool. To achieve high-throughput, pipelined architectures have been used in the butterfly unit and the dual-port RAM. The dedicated parallel-pipelined FFT processor architecture can process input data at high speed, and the whole system performance can be greatly improved due to adopting a novel simple address mapping scheme. For radix-two system, this mapping scheme is better and simpler than most of others. The design is implemented on a FPGA chip. And this pipelined FFT completes a complex 64-point FFT within 2.1 μ s. The hardware testing result explains that it can meet the requirements of the WLAN.

REFERENCES

- [1] J. A. C. Bingham, "Multicarrier modulation for data transmission: an idea whose time has come," *IEEE Communication Magazine*, vol. 28, no. 5, pp. 5-14, May 1990.
- [2] J. Palicot and C. Roland, "FFT: A basic function for a reconfigurable receiver," 10th International conference on Telecommunications, vol. 1, pp. 898-902, March 2003.
- [3] Min Jiang, Bing Yang, Yiling Fu, et al., "Design Of FFT processor with Low Power complex multiplier for OFDM-based high-speed wireless applications," *International Symposium on Communications and Information Technology*, vol. 2, pp. 639-641, Oct. 2004.
- [4] Kai Zhong, Hui He, and Guangxi Zhu, "An ultra-high speed FFT processor," *International Symposium on Signals, Circuits and Systems*, vol. 1, pp. 37 -40, July 2003.
- [5] Hongjiang He and Hui Guo, "The Realization of FFT Algorithm based on FPGA Co-processor," *Second International Symposium on Intelligent Information Technology Application*, vol. 3, pp. 239-243, Dec. 2008.
- [6] J. G. Proakis and D. G. Manolakis, "Introduction to Digital Signal Processing," New York: Macmillan, 1988.
- [7] R. B. Perlow and T. C. Denk, "Finite word length design for VLSI FFT processors," *Conference Record of the Thirty-Fifth Asilomar Conference on Signals, Systems and Computers*, vol. 2, pp. 1227- 1231, Nov. 2001.
- [8] J. W. Cooky and J. W. Tukey, "An algorithm for the machine calculation of complex Fourier series," *Math. of Comp.*, vol. 19, No. 90, pp. 297-301, April 1965.
- [9] S. Oraintara, Y. J. Chen, and T. Q. Nguyen, "Integer fast Fourier transform," *IEEE Trans. Acoustics, Speech, Signal Processing*, vol. 50, No. 3, pp. 607-618, March 2002.
- [10] J. H. Takala, T. S. Jarvinen, and H. T. Sorokin, "A Conflict-free parallel memory access scheme for FFT processors," *International Symposium on Circuits and Systems*, vol. 4, pp. 524-527, May 2003.

A DSTATCOM-Control Scheme for Power Quality Improvement of Grid Connected Wind Energy System for Balanced and Unbalanced Non linear Loads

Ch. Siva Koti Reddy,

M-Tech Student, Power systems,
Department of Electrical and Electronics Engineering,
KLUniversity, Guntur (A.P), India.

Dr. P.Linga Reddy,

Professor, control systems,
Department of Electrical and Electronics Engineering,
KLUniversity, Guntur (A.P), India.

Abstract: One of the main problems in wind energy generation is the connection to the grid. Injection of wind power into the grid affects the power quality resulting in poor performance of the system. The wind energy system faces frequently fluctuating voltage due to the nature of wind and introduction of harmonics into the system. The influence of the wind turbine in the grid system concerning the power quality measurements are the active power, reactive power, variation of voltage, flicker, harmonics, and electrical behavior of switching operation and these are measured according to national/international guidelines specified in International Electro-technical Commission standard, IEC-61400. The paper study demonstrates the power quality problem due to installation of wind turbine with the grid. In this proposed scheme distribution static compensator (DSTATCOM) is connected with a battery energy storage system (BESS) to mitigate the power quality issues. The battery energy storage is integrated to sustain the real power source under fluctuating wind power. The DSTATCOM control scheme for the grid connected wind energy generation system for power quality improvement is simulated using MATLAB/SIMULINK in power system block set. Finally the proposed scheme is applied for both balanced and unbalanced nonlinear loads.

Index Terms: DSTATCOM, power quality, wind generating system (WGS).

1. Introduction

One of the most common power quality problems today is voltage dips. A voltage dip is a short time (10 ms to 1 minute) event during which a reduction in r.m.s voltage magnitude occurs. It is often set only by two parameters, depth/magnitude and duration. The voltage dip magnitude is ranged from 10% to 90% of nominal voltage (which corresponds to 90% to 10% remaining voltage) and with a duration from half a cycle to 1 min. In a three-phase system a voltage dip is by nature a three-phase phenomenon, which affects both the phase-to-ground and phase-to-phase voltages. A voltage dip is caused by a fault in the utility system, a fault within the customer's facility or a large increase of the load current, like starting a motor or transformer energizing. Typical faults are single-phase or multiple-phase short circuits, which leads to high currents. The high current results in a voltage drop over the network impedance. At the fault location the voltage in the faulted

phases drops close to zero, whereas in the non-faulted phases it remains more or less unchanged [1, 2].

Voltage dips are one of the most occurring power quality problems. Of course, for an industry an outage is worse, than a voltage dip, but voltage dips occur more often and cause severe problems and economical losses. Utilities often focus on disturbances from end-user equipment as the main power quality problems. This is correct for many disturbances, flicker, harmonics, etc., but voltage dips mainly have their origin in the higher voltage levels. Faults due to lightning, is one of the most common causes to voltage dips on overhead lines. If the economical losses due to voltage dips are significant, mitigation actions can be profitable for the customer and even in some cases for the utility. Since there is no standard solution which will work for every site, each mitigation action must be carefully planned and evaluated. There are different ways to mitigate voltage dips, swell and interruptions in transmission and distribution systems. At present, a wide range of very flexible controllers, which capitalize on newly available power electronics components, are emerging for custom power applications [3, 4]. Among these, the distribution static compensator and the dynamic voltage restorer are most effective devices, both of them based on the VSC principle.

STATCOM is often used in transmission system. When it is used in distribution system, it is called D-STATCOM (STATCOM in Distribution system). D-STATCOM is a key FACTS controller and it utilizes power electronics to solve many power quality problems commonly faced by distribution systems. Potential applications of D-STATCOM include power factor correction, voltage regulation, load balancing and harmonic reduction. Comparing with the SVC, the D-STATCOM has quicker response time and compact structure. It is expected that the D-STATCOM will replace the roles of SVC in nearly future. D-STATCOM and STATCOM are different in both structure and function, while the choice of control strategy is related to the main-circuit structure and main function of compensators [3], so D-STATCOM and STATCOM adopt different control strategy. At present, the use of STATCOM is wide and its strategy is mature, while the introduction of D-STATCOM is seldom reported. Many control techniques are reported such as instantaneous

reactive power theory (Akagi et al., 1984), power balance theory, etc. In this paper, an indirect current control technique (Singh et al., 2000a, b) is employed to obtain gating signals for the Insulated Gate Bipolar Transistor (IGBT) devices used in current controlled voltage source inverter (CC-VSI) working as a DSTATCOM. A model of DSTATCOM is developed using MATLAB for investigating the transient analysis of distribution system under balanced/unbalanced linear and non-linear three-phase and single-phase loads (diode rectifier with R and R-C load). Simulation results during steady-state and transient operating conditions of the DSTATCOM are presented and discussed to demonstrate power factor correction, harmonic elimination and load balancing capabilities of the DSTATCOM system [5-10].

2. DISTRIBUTION STATIC COMPENSATOR (D-STATCOM)

2.1 Principle of DSTATCOM

A D-STATCOM (Distribution Static Compensator), which is schematically depicted in Fig.1, consists of a two-level Voltage Source Converter (VSC), a dc energy storage device, a coupling transformer connected in shunt to the distribution network through a coupling transformer. The VSC converts the dc voltage across the storage device into a set of three-phase ac output voltages. These voltages are in phase and coupled with the ac system through the reactance of the coupling transformer. Suitable adjustment of the phase and magnitude of the D-STATCOM output voltages allows effective control of active and reactive power exchanges between the DSTATCOM and the ac system. Such configuration allows the device to absorb or generate controllable active and reactive power.

The VSC connected in shunt with the ac system provides a multifunctional topology which can be used for up to three quite distinct purposes:

1. Voltage regulation and compensation of reactive power;
2. Correction of power factor; and
3. Elimination of current harmonics.

Here, such device is employed to provide continuous voltage regulation using an indirectly controlled converter.

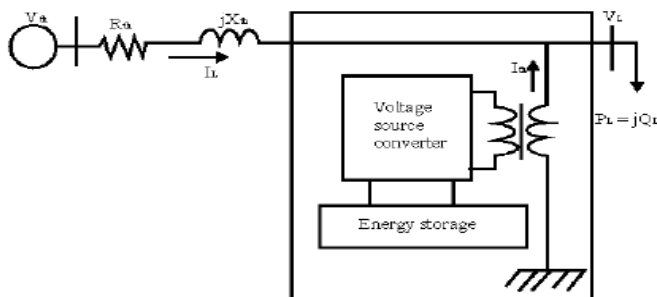


Figure. 1 DSTATCOM

Fig. 1 the shunt injected current I_{sh} corrects the voltage sag by adjusting the voltage drop across the system impedance Z_{th} . The value of I_{sh} can be controlled by adjusting the output voltage of the converter. The shunt injected current I_{sh} can be written as,

$$I_{sh} = I_L - I_S = I_L - (V_{th} - V_L) / Z_{th}$$

$$I_{sh} / \angle -\eta = I_L / \angle -\theta$$

The complex power injection of the D-STATCOM can be expressed as,

$$S_{sh} = V_L I_{sh}^*$$

It may be mentioned that the effectiveness of the DSTATCOM in correcting voltage sag depends on the value of Z_{th} or fault level of the load bus. When the shunt injected current I_{sh} is kept in quadrature with V_L , the desired voltage correction can be achieved without injecting any active power into the system. On the other hand, when the value of I_{sh} is minimized, the same voltage correction can be achieved with minimum apparent power injection into the system.

2.2 Voltage Source Converter (VSC)

A voltage-source converter is a power electronic device that connected in shunt or parallel to the system. It can generate a sinusoidal voltage with any required magnitude, frequency and phase angle. The VSC used to either completely replace the voltage or to inject the 'missing voltage'. The 'missing voltage' is the difference between the nominal voltage and the actual. It also converts the DC voltage across storage devices into a set of three phase AC output voltages [8, 9]. In addition, D-STATCOM is also capable to generate or absorbs reactive power. If the output voltage of the VSC is greater than AC bus terminal voltages, D-STATCOM is said to be in capacitive mode. So, it will compensate the reactive power through AC system and regulates missing voltages. These voltages are in phase and coupled with the AC system through the reactance of coupling transformers. Suitable adjustment of the phase and magnitude of the DSTATCOM output voltages allows effective control of active and reactive power exchanges between D-STATCOM and AC system. In addition, the converter is normally based on some kind of energy storage, which will supply the converter with a DC voltage [10].

2.3 Controller for DSTATCOM

The three-phase reference source currents are computed using three-phase AC voltages (v_{ta} , v_{tb} and v_{tc}) and DC bus voltage (V_{dc}) of DSTATCOM. These reference supply currents consist of two components, one in-phase (I_{spdr}) and another in quadrature (I_{spqr}) with the supply voltages. The control scheme is represented in Fig. 2. The basic equations of control algorithm of DSTATCOM are as follows.

2.3.1 Computation of in-phase components of reference supply current

The instantaneous values of in-phase component of reference supply currents (I_{spdr}) is computed using one PI controller over the average value of DC bus voltage of the DSTATCOM (v_{dc}) and reference DC voltage (v_{dcr}) as

$$I_{spdr(n)} = I_{spdr(n-1)} + K_{pd} \{v_{dcr(n)} - v_{dcr(n-1)}\} + K_{id} v_{dcr(n)}$$

Where $V_{de(n)} = V_{dcr} - V_{dc(n)}$ denotes the error in V_{dc} and average value of V_{dc} . K_{pd} and K_{id} are proportional and integral gains of the DC bus voltage PI controller. The output of this PI controller (I_{spdr}) is taken as amplitude of in-phase component of the reference supply currents. Three-phase in-phase components of the reference supply currents (i_{sadr} , i_{sbdr} and i_{scdr}) are computed using the in-phase unit current vectors (u_a , u_b and u_c) derived from the AC terminal voltages (v_{tan} , v_{tbn} and v_{tcn}), respectively.

$$u_a = v_{ta} / V_{tm}, \quad u_b = v_{tb} / V_{tm}, \quad u_c = v_{tc} / V_{tm}$$

Where V_{tm} is amplitude of the supply voltage and it is computed as

$$V_{tm} = \left[(2/3)(v_{tan}^2 + v_{tbn}^2 + v_{tcn}^2) \right]^{1/2}$$

The instantaneous values of in-phase component of reference supply currents (i_{sadr} , i_{sbdr} and i_{scdr}) are computed as

$$i_{sadr} = I_{spdr} u_a, \quad i_{sbdr} = I_{spdr} u_b, \quad i_{scdr} = I_{spdr} u_c$$

2.3.2 Computation of quadrature components of reference supply current

The amplitude of quadrature component of reference supply currents is computed using a second PI controller over the amplitude of supply voltage (v_{tm}) and its reference value (v_{tmr})

$$I_{spqr(n)} = I_{spqr(n-1)} + K_{pq} \{v_{tmr(n)} - v_{tmr(n-1)}\} + K_{iq} v_{tmr(n)}$$

where $V_{ac} = V_{tmr} - V_{tm(n)}$ denotes the error in V_{tm} and computed value V_{tmn} from Equation (3) and K_{pq} and K_{iq} are the proportional and integral gains of the second PI controller.

$$w_a = \{-u_b + u_c\} / \{(3)^{1/2}\}$$

$$w_b = \{u_a(3)^{1/2} + u_b - u_c\} / \{2(3)^{1/2}\}$$

$$w_c = \{-u_a(3)^{1/2} + u_b - u_c\} / \{2(3)^{1/2}\}$$

Three-phase quadrature components of the reference supply currents (i_{saqr} , i_{sbqr} and i_{scqr}) are computed using the

output of second PI controller (I_{spqr}) and quadrature unit current vectors (w_a , w_b and w_c) as

$$i_{saqr} = I_{spqr} w_a, \quad i_{sbqr} = I_{spqr} w_b, \quad i_{scqr} = I_{spqr} w_c$$

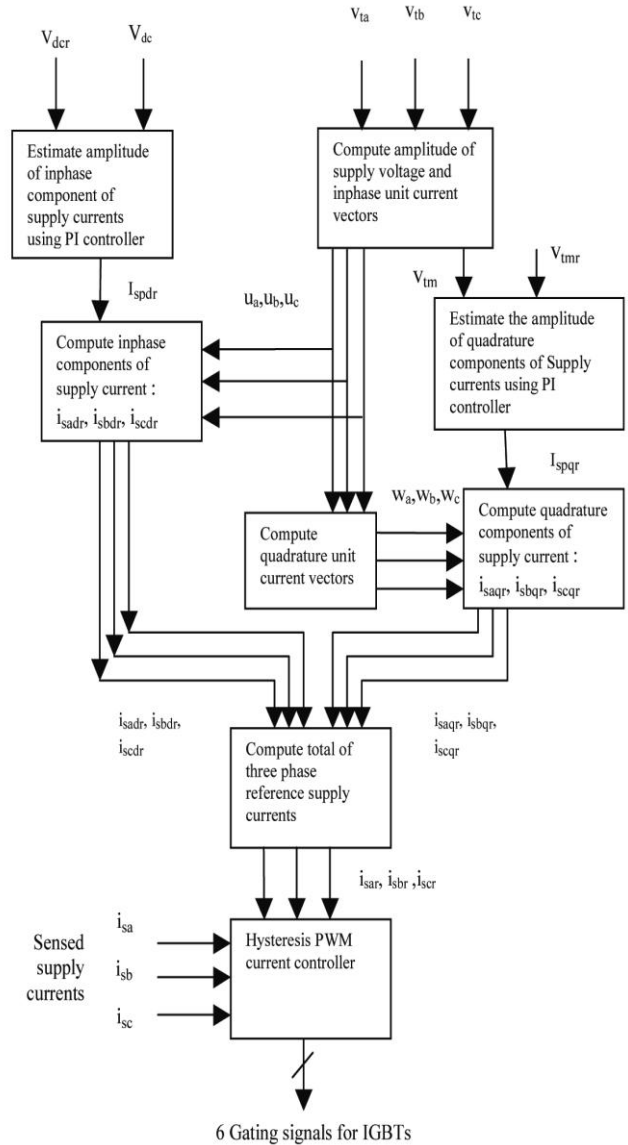


Figure. 2 Control scheme for DSTATCOM connected to grid supply

2.3.3 Computation of total reference supply currents

Three-phase instantaneous reference supply currents (i_{sar} , i_{sbr} and i_{scr}) are computed by adding in-phase (i_{sadr} , i_{sbdr} and i_{scdr}) and quadrature components of supply currents (i_{saqr} , i_{sbqr} and i_{scqr}) as

$$i_{sar} = i_{sadr} + i_{saqr}, \quad i_{sbr} = i_{sbdr} + i_{sbqr}, \quad i_{scr} = i_{scdr} + i_{scqr}$$

A hysteresis pulse width modulated (PWM) current controller is employed over the reference (i_{sar} , i_{sbr} and i_{scr}) and sensed supply currents (i_{sa} , i_{sb} and i_{sc}) to generate gating pulses for IGBTs of DSTATCOM.

3. MATLAB/SIMULINK MODELING OF DSTATCOM

3.1 Modeling of Power Circuit

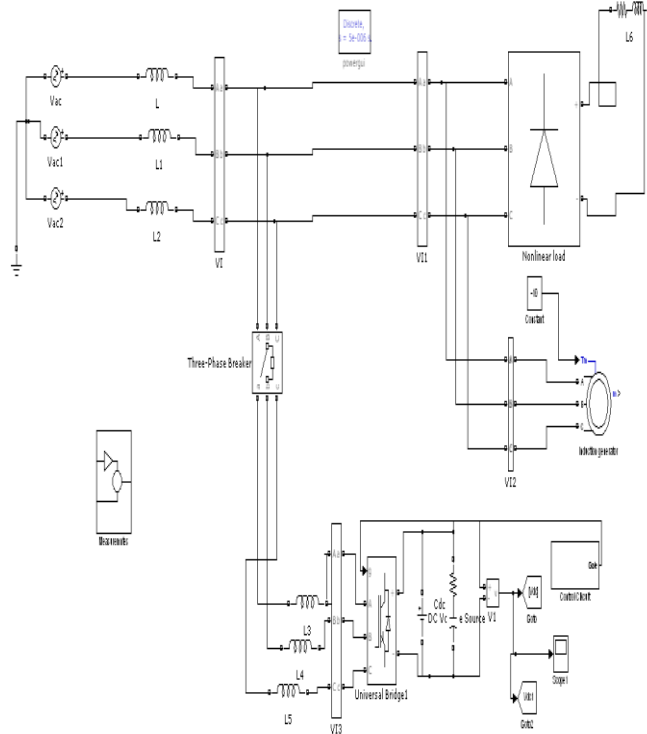


Figure. 3 Matlab/Simulink Model of DSTATCOM Power Circuit

Fig. 3 shows the complete MATLAB model of DSTATCOM along with control circuit. The power circuit as well as control system are modeled using Power System Blockset and Simulink. The grid source is represented by three-phase AC source. Three-phase AC loads are connected at the load end. DSTATCOM is connected in shunt and it consists of PWM voltage source inverter circuit and a DC capacitor connected at its DC bus. An IGBT-based PWM inverter is implemented using Universal bridge block from Power Electronics subset of PSB. Snubber circuits are connected in parallel with each IGBT for protection. Simulation of DSTATCOM system is carried out for linear and non-linear loads. The linear load on the system is modeled using the block three-phase parallel R-L load connected in delta configuration. The non-linear load on the system is modeled using R and R-C circuits connected at output of the diode rectifier. Provision is made to connect loads in parallel so that the effect of sudden load addition and removal is studied. The feeder connected from the three-phase source to load is modeled using appropriate values of resistive and inductive components.

3.2 Modeling of Control Circuit

Fig. 4 shows the control algorithm of DSTATCOM with two PI controllers. One PI controller regulates the DC link voltage while the second PI controller regulates the terminal voltage at PCC. The in-phase components of DSTATCOM reference currents are responsible for power factor correction of load and the quadrature components of supply reference currents are to regulate the AC system voltage at PCC.

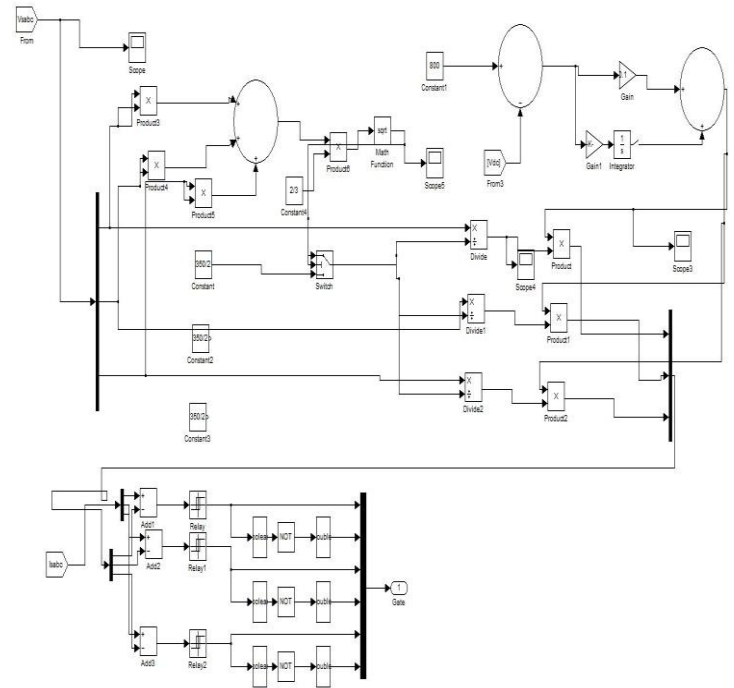


Figure. 4 Control Circuit

The output of PI controller over the DC bus voltage (I_{spdr}) is considered as the amplitude of the in-phase component of supply reference currents and the output of PI controller over AC terminal voltage (I_{spqr}) is considered as the amplitude of the quadrature component of supply reference currents. The instantaneous reference currents (i_{sar} , i_{sbr} and i_{scr}) are obtained by adding the in-phase supply reference currents (i_{sadr} , i_{sbrd} and i_{scdr}) and quadrature supply reference currents (i_{saqr} , i_{sbqr} and i_{scqr}). Once the reference supply currents are generated, a carrierless hysteresis PWM controller is employed over the sensed supply currents (i_{sa} , i_{sb} and i_{sc}) and instantaneous reference currents (i_{sar} , i_{sbr} and i_{scr}) to generate gating pulses to the IGBTs of DSTATCOM. The controller controls the DSTATCOM currents to maintain supply currents in a band around the desired reference current values. The hysteresis controller generates appropriate switching pulses for six IGBTs of the VSI working as DSTATCOM.

4.SIMULATION RESULTS

Here Simulation results are presented for two cases. In case one load is balanced non linear and in case two unbalanced non linear load is considered.

4.1 Case one

Performance of DSTATCOM connected to a weak supply system is shown in Fig.5. This figure shows variation of performance variables such as supply voltages (v_{sa} , v_{sb} and v_{sc}), terminal voltages at PCC (v_{ta} , v_{tb} and v_{tc}), supply currents (i_{sa} , i_{sb} and i_{sc}), load currents (i_{la} , i_{lb} and i_{lc}), DSTATCOM currents (i_{ca} , i_{cb} and i_{cc}) and DC link voltage (V_{dc}).

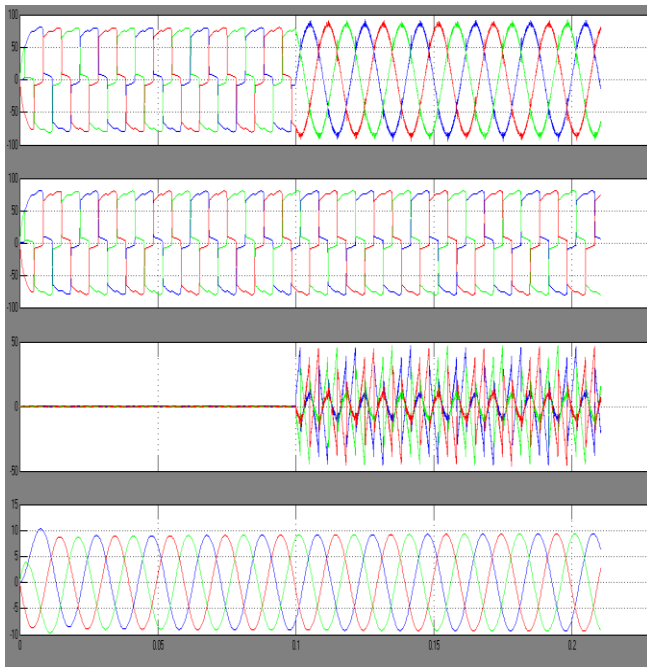


Figure. 5 Simulation results for Balanced Non Linear Load

Fig. 5 shows the source current, load current, compensator current and induction generator currents plots respectively. Here compensator is turned on at 0.1 seconds.

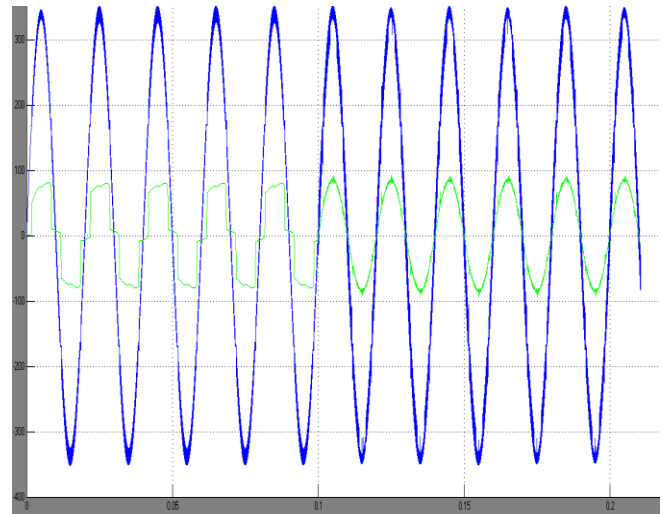


Figure. 6 Simulation results power factor for Non linear Load

Fig. 6 shows the power factor, it is clear from the figure that after compensation power factor is unity.

4.2 Case two

An Unbalanced three-phase non-linear load is represented by three-phase uncontrolled diode bridge rectifier with pure resistive load at its DC bus. Fig. 7 shows the transient responses of distribution system with DSTATCOM for supply voltages (v_{sabc}), supply currents (i_{sabc}), load currents (i_{la} , i_{lb} and i_{lc}), DSTATCOM currents (i_{ca} , i_{cb} and i_{cc}) along with DC link voltage (V_{dc}) and its reference value (V_{dcr}) at rectifier nonlinear load.

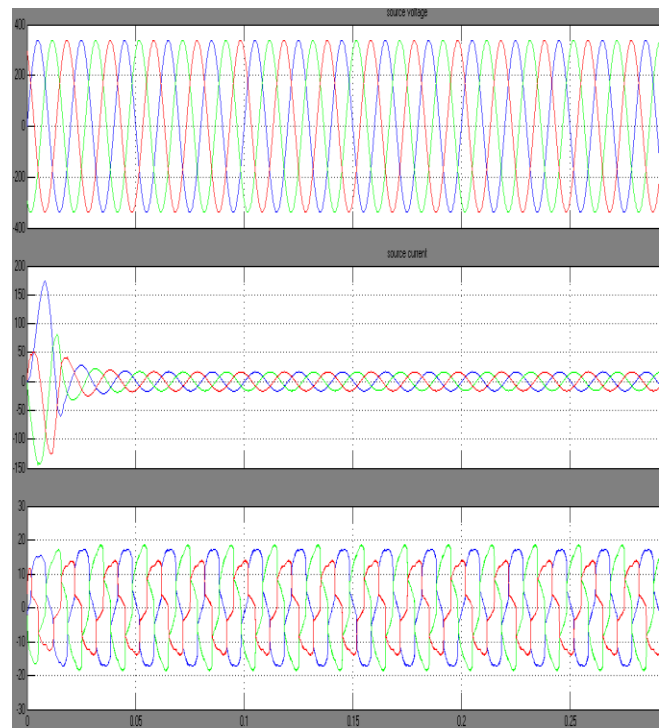


Figure. 7 Simulation results for Non- Linear Unbalanced Load

Fig.7 shows the unbalanced non linear load case. From the figure it is clear that even though load is unbalanced source currents are balanced and sinusoidal.

5. CONCLUSION

DSTATCOM system is an efficient mean for mitigation of PQ disturbances introduced to the grid by DERs. DSTATCOM compensator is a flexible device which can operate in current control mode for compensating voltage variation, unbalance and reactive power and in voltage control mode as a voltage stabilizer. The latter feature enables its application for compensation of dips coming from the supplying network. The simulation results show that the performance of DSTATCOM system has been found to be satisfactory for improving the power quality at the consumer premises. DSTATCOM control algorithm is flexible and it has been observed to be capable of correcting power factor to unity, eliminate harmonics in supply currents and provide load balancing. It is also able to regulate voltage at PCC. The control algorithm of DSTATCOM has an inherent property to provide a self-supporting DC bus of DSTATCOM. It has been found that the DSTATCOM system reduces THD in the supply currents for non-linear loads. Rectifier-based non-linear loads generated harmonics are eliminated by DSTATCOM. When single-phase rectifier loads are connected, DSTATCOM currents balance these unbalanced load currents.

REFERENCES

- [1] A.E. Hammad, Comparing the Voltage source capability of Present and future Var Compensation Techniques in Transmission System, *IEEE Trans, on Power Delivery, Volume 1, No.1* Jan 1995.
- [2] G.Yaliekaya, M.H.J Bollen, P.A. Crossley, "Characterization of Voltage Sags in Industrial Distribution System", *IEEE transactions on industry applications, volume 34, No. 4, July/August*, PP.682-688, 1999.
- [3] Haque, M.H., "Compensation of Distribution Systems Voltage sags by DVR and D-STATCOM", *Power Tech Proceedings, 2001 IEEE Porto, Volume 1*, PP.10-13, September 2001.
- [4] Anaya-Lara O, Acha E., "Modeling and Analysis Of Custom Power Systems by PSCAD/EMTDC", *IEEE Transactions on Power Delivery, Volume 17, Issue: 2002*, Pages: 266-272.
- [5] Bollen, M.H.J., "Voltage sags in Three Phase Systems", *Power Engineering Review, IEEE, Volume 21, Issue: 9*, September 2001, PP: 11-15.
- [6] M.Madrigal, E.Acha., "Modelling Of Custom Power Equipment Using Harmonics Domain Techniques", *IEEE 2000*.
- [7] R.Meinski, R.Pawelek and I.Wasiak, "Shunt Compensation for Power Quality Improvement Using a STATCOM controller Modelling and Simulation", *IEEE Proce, Volume 151, No. 2*, March 2004.
- [8] J.Nastran , R. Cajhen, M. Seliger, and P.Jereb,"Active Power Filters for Nonlinear AC loads, *IEEE Trans.on Power Electronics Volume 9, No.1*, PP: 92-96, Jan 2004.
- [9] L.A.Moran, J.W. Dixon, and R.Wallace, A Three Phase Active Power Filter with fixed Switching Frequency for Reactive Power and Current Harmonics Compensation, *IEEE Trans. On Industrial Electronics, Volume 42*, PP: 402-8, August 1995.
- [10] L.T. Moran, P.D Ziogas, and G.Joos, Analysis and Design of Three Phase Current source solid State Var Compensator, *IEEE Trans, on Industry Applications, Volume 25, No.2*, 1989, PP: 356-65.



Ch.SivaKotiReddy received B.Tech from Nalanda Institute of Engineering and Technology, India in 2010. Presently he is pursuing M.Tech in KL University. His areas of interests are power Systems, DC Machines and networks theory.



Dr.P.LingaReddy was born in 1939.He received his PhD from I.I.T (Delhi).He has a teaching experience of 42 years. Currently he is professor in school of electrical and electronic engineering K L University Guntur. He has many publications in the area of control systems. His area of interests are power systems and control systems.

An Experimental Study on the Diagnostic Capability of Vibration Analysis for Wind Turbine Planetary Gearbox

Shawki Abouel-seoud¹, Ibrahim Ahmed² and Mohamed Khalil³

**(Professor, Automotive Engineering Dept., Faculty of Engineering, Helwan University, Egypt)*

*** (Associate Professor, Automotive Technology Dept., Faculty of Industrial Education, Helwan University, Egypt)*

**** (Associate Professor, Automotive Engineering Dept., Faculty of Engineering, Helwan University, Egypt)*

ABSTRACT

Most wind turbines use planetary gearboxes to transform the relatively low rotational speed of the main shaft into higher speeds required for power generation. Because of excessive service load, inappropriate operating conditions or simply end of life time, fault can occur in wind turbine planetary gearbox components. When a fault, either distributed or localized, is incurred, the stiffness and consequently vibration characteristics of the defected component will vary. A possible non-destructive technique for fault detection and severity assessment can be derived from vibration signal analysis. This paper presents the use of vibration analysis in the detection, quantification, and advancement monitoring of fault incurred by wind turbine gearbox components. Each gearbox component fault monitoring technique has its merits and limitations. An experimental procedure is developed to assess the severity of the gearbox component fault. Gearbox components faults of planet gear tooth crack, planet gear tooth spalling, planet gear tooth breakage, planet carrier crack and main bearing inner race crack were tested under accelerated defect conditions. A conventional time and frequency domain techniques are also applied to the component vibrations to indicate the presence and progression of the fault. The experimental localized fault signals (vibration acceleration signals) were subjected to the same diagnostic techniques such as spectrum comparisons, spectral kurtosis analysis and crest factor analysis. Tests results show that RMS value is a very reliable time-domain diagnostic technique.

Keywords - Rotational vibration, Planetary gearbox, Wind turbine, Stationary signal, Defect diagnosis, Planet gear tooth crack, Planet gear tooth spalling, main bearing crack and planet gear carrier,

I. INTRODUCTION

Gears are the most important mechanisms for transmitting power or rotation, which play an important role in many sorts of machineries. Smooth operation and high efficiency of gears are necessary for the normal running of machineries. Therefore, gear damage assessment is an important topic in the field of condition monitoring and fault diagnosis. Most gear faults are due to localized gear damage, such as tooth wear, cracks, scoring, spalling,

chipping, and pitting. With such flaws existing on gears, progressive damage will occur and ultimately result in gear tooth breakage. Therefore, localized damage assessment is of great practical importance to the monitoring and diagnosis of gears [1].

Generally, in engineering applications, a large percentage of gear faults are induced by localized gear damage. Typical localized gear damage types include pits, chips, and cracks on gear tooth surface. With such damage existing on gears, the gear tooth meshing will not be as smooth as the normal gear, causing impulses to occur. Furthermore, during the running of damaged gears, impulses will be produced repetitively due to the gear rotation with the period depending on the number of damaged teeth and their distribution over the gear surface. In other word, periodic or quasi-periodic impulses characterized the vibration of damaged gears, and provide an intuitively understandable indicator of localized damage. Therefore, in this sense, the effective extraction of impulses from gear vibration signals is of gear importance for gear damage detection [2, 3].

There are essentially three mechanisms responsible for the generation of noise and vibration of gear teeth. If the transmitted force between the teeth varies in amplitude direction or position, then the gears will vibrate and generate noise. These mechanisms occur when the friction is exist between the teeth and a poor surface finish on the mating parts in addition to an imperfection in the tooth profile or a transmission error, which is the relative displacement between the gear teeth. Prediction and control of gear vibration become an important concern particularly in automotive, aerospace and power generation industries. One of the most popular applications of gear sets can be found in the vehicles gearbox. The vibration generated at the gear mesh is transmitted to the housing through shafts and bearings [4]. Acoustic emission (AE) is defined as the range of phenomena that results in the generation of structure-borne and fluid-borne (liquid, gas) that propagating waves. These waves are due to the rapid release of energy from localized sources within and/or on the surface of a material. A few investigators have assessed the application of acoustic emission technology for diagnostic and prognostic purposes for gearboxes. However; other investigators applied acoustic emission in detecting bending fatigue on spur gears and noted that acoustic emission (AE) is more sensitive to crack propagation than vibration and stiffness measurements.

Also, AE was found to be more sensitive to the scale of surface damage than vibration analysis [5].

The transmission of the helicopter has an epicyclic or planetary gear train in the final stage of the main rotor gearbox. Torque is transmitted from the central sun gear through the planets to the planet carrier and from the planet carrier to the main rotor shaft. A vibration test program on a helicopter transmission of 82mm crack was presented. It runs in a test cell at torque settings ranging from 20% to 100% of the rated torque. An exact helicopter transmission (gears, carrier, and main module case) was also installed in the ground-run at torque settings of 20% and 30% of the rated torque. Vibration data were acquired from four other undamaged transmissions: one in the test cell, and three in UH-60A helicopters. These collected data were initially analyzed using several standard diagnostic parameters that were modified for the special case of an epicyclic gearbox and applied to the time synchronous averages of the planet carrier vibration. The analysis found that two of the parameters consistently detected the presence of the fault under test-cell conditions. These were the epicyclic Sideband Index (SIe) and the epicyclic Sideband Level Factor (SLFe), which were both based on the first-order sidebands of the fundamental dominant meshing component (230 shaft-orders). However, neither of these parameters was able to detect the crack under the low-torque on-aircraft conditions [6, 7].

Rolling element bearings are the most widespread domestic and industrial applications. Proper functioning of these appliances depends, to a great extent, on the smooth and quiet running of the bearings. In industrial applications, these bearings are considered critical mechanical components. A defect in such a bearing, unless detected in time, causes malfunction and may lead to catastrophic failure of the machinery. These defects in bearings may be arising during the manufacturing process. Therefore detection of these defects is very important for condition monitoring as well as quality inspection of bearings. Different methods are used for detection and diagnosis of bearing defects; it may be broadly classified as vibration and acoustic measurements, temperature measurements and wear debris analysis. Among these, vibration measurements are the most widely used. Several techniques have been applied to measure the vibration and acoustic responses from defective bearings; i.e., vibration measurements in the time and frequency domains such as: the shock pulse method, sound pressure, pressure intensity techniques and the acoustic emission method [8-10].

The work presented here aims to use vibration analysis in the detection, quantification, and advancement monitoring of defect incurred by wind turbine gearbox component. Gearbox components faults of planet gear tooth crack, planet gear tooth spalling, planet gear tooth breakage, planet carrier crack and main bearing inner race crack were tested under accelerated fault conditions. A conventional time and

frequency domain techniques are applied to the component vibrations to indicate the presence and progression of the fault. Multi-hour tests were conducted however; data recordings were acquired using rotational vibration monitoring.

II. METHODOLOGY

There are numerous signal processing techniques for diagnostic of mechanical and electrical systems. Case-dependent knowledge and investigation are required to select appropriate signal processing tools among a number of possibilities. The most common waveform data in condition monitoring are vibration signals and acoustic emissions. However; the other waveform data including ultrasonic signals, motor current, partial discharge, etc. In the previous literature, there were two main categories of stationary waveform data analysis which are time-domain analysis and frequency-domain analysis.

II-I. TIME-DOMAIN ANALYSIS

Time-domain analysis is a method of representing a waveform by plotting amplitude over time directly that is based on the time waveform itself. It calculates characteristic features from time waveform signals as descriptive statistics such as mean, peak, peak-to-peak interval, standard deviation, crest factor, and high order statistics (HSO) that include root mean square, skewness, kurtosis, etc. A popular time-domain analysis approach is a time synchronous average (TSA), which also called time domain averaging. It is a completely different type of averaging, where the waveform itself is averaged in a buffer before the FFT is calculated. It use the ensemble average of the raw signal over a number of evolutions as an attempt to remove or reduce noise and effects from other sources, to enhance the signal components of interest.

More advanced approaches of time-domain analysis apply time series models to waveform data. The main idea of time series modeling is to fit the waveform data to a parametric time model and extract features based on this parametric model. The popular models used in the literature are the Auto Regressive (AR) model and the Auto-Regressive-Moving-Average (ARMA) model, [11]. Auto-regressive-moving-average (ARMA) models, sometimes called Box-Jenkins models after the iterative Box-Jenkins methodology usually used to estimate them, are typically applied to auto correlated time series data, [12].

Gear tooth condition indices process the vibration of the wind turbine gearbox to return a single value indicating its overall health. This signal could be either increases or decreases as the gearbox damage (crack or pit) increases. The vibration signal of a defective gearbox usually considers being amplitude modulated at characteristic defect frequency. Matching the measured vibration spectrum with the defect characteristic frequency enables the detection of the presence of a defect and determines where the defect is.

Fig. 1 shows a description of the traditional diagnostic

scheme. All of these HSO features are usually known as time-domain features [13], which include:

- a- RMS for discrete signals, is a kind of averaging the signal and if is defined as:

$$RMS = \sqrt{\frac{1}{N} \sum_{n=1}^N (x(n) - \bar{x})^2} \quad (1)$$

- b- The Crest Factor is defined as the ratio of the peak value to the RMS of a signal and in other term is equal to the peak amplitude of a waveform divided by the RMS value. The purpose of the crest factor calculation is to give an analyst a quick idea of how much impacting is occurring in a waveform.

$$Crest\ Factor = \frac{Peak}{RMS} = \frac{Crest\ Value}{RMS\ Value} \quad (2)$$

$$= \frac{Sup|x(n)|}{\sqrt{\frac{1}{N} \sum_{n=1}^N [x(n)]^2}}$$

$$Peak = Crest\ Value = \frac{1}{2} [\max(x(t)) - \min(x(t))]$$

- c- Kurtosis is a parameter that is sensitive to the shape of the signal and is well adapted to the impulse nature of the simulating forces generated by component damage. A normal distribution has a kurtosis value of 3 and it shows the good condition Its value can be given by:

$$Kurtosis(K) = \frac{1}{\sigma^4} \frac{\sum_{i=1}^N (x_i - \bar{x})^4}{N} \quad (3)$$

$$= \frac{\frac{1}{N} \sum_{n=0}^{N-1} (x(t) - \bar{x})^4}{(RMS)^4}$$

Where, $\bar{x} = \frac{1}{N} \sum_{n=1}^N x(n)$

- N The number of samples taken within the signal,
- x(n) The time domain signal,
- σ^4 The variance square,
- \bar{x} The mean value of samples,
- Xi An individual sample.



Fig. 1 Traditional gearbox diagnostics scheme

II-II. FREQUENCY-DOMAIN ANALYSIS

Frequency domain is a term used to describe the domain for analysis of mathematical functions or signals with respect to frequency, rather than time. It is able to easily identify and isolate certain frequency components of interest. The most widely used conventional analysis in the frequency domain is the spectrum analysis using Fast Fourier Transform (FFT). The term spectrum was expanded to apply to other waves, such as sound waves that could also be measured as a function of frequency. The term also applies to any signal that can be measured or decomposed along a continuous variable. The main idea of spectrum analysis is to either look at the whole spectrum or look closely at certain frequency components of interest and thus extract feature from the signal. The most commonly used tool in spectrum analysis is power spectrum which is a positive real function of a frequency variable associated with a stationary stochastic process, or a deterministic function of time, which has dimensions of power per hertz (Hz), or energy per hertz. It is often called simply the spectrum of the signal. Intuitively, the spectral density measures the frequency content of a stochastic process and helps identify periodicities. The spectrum analysis is defined as

$$E[X(f) X^*(f)], \quad (4)$$

Where

X(f) the Fourier transform of single x(t),

E denotes expectation,

'*' denotes complex conjugate.

Some useful auxiliary tools for spectrum analysis are graphical presentation of spectrum, frequency filters, envelope analysis (also called amplitude demodulation), side band structure analysis, etc. Hilbert Transform, which is a useful tool in envelope analysis, has also been used for machine fault detection and diagnostics, [14, 15].

III. EXPERIMENTAL SETUP AND PROCEDURE

The methodology of measurement used an induction motor drawing power through an electrical source and driving wind turbine gearbox. A separately-excited brake that is coupled to the output shaft of the gearbox and connected to a brake paddle to apply or release load into the the wind turbine gearbox. Wind turbine gearboxes consist mainly of three stages of planetary and parallel axis gears. The first stage is planetary however; the second and third stages are helical. Geartrain vibrations can cause premature bearing failure from elevated dynamic loads and be significant noise sources, where the generated sound propagates over long distances. Such vibrations also impact wind turbine dynamic loads, reliability, and the need for scheduled and unscheduled maintenance. Drivetrain maintenance is extremely expensive given the cost of gearbox removal, transport, and system shutdown.

In order to measure the vibration responses of the wind turbine gearbox on real condition monitoring signals, The establishment of the test rig, experimental methodology and the accelerometers positions are presented in detailed in Ref. [16], where the measuring of rotational response has been evaluated by using a pair of matched accelerometers placed at short distance apart from the gearbox's structure. The whole turbine gearbox is driven at a set input speed using an AC drive motor of 15 horsepower (hp) at a maximum speed of 1440 rev/min. The maximum speed and load used in this apparatus are 40 rpm and 40 Nm respectively. The speed variation can be accomplished by varying the frequency to the motor using an AC inverter. The mechanical and electrical losses are sustained by a small fraction of whole power. The established test rig has the capability of testing most of wind turbine gearboxes with speed ratios ranging 25 to 50. The speed ratio used in this work is about 26. The system is controlled to provide the maximum versatility to speed and load settings. The use of different speed ratios and gearboxes rather than what is listed in this study is possible if appropriate consideration to system operation is given. The test rig components are hard-mounted and aligned on a bedplate which is mounted using isolation feet to prevent vibration transmission to the floor. The shafts are connected through a flexible and rigid couplings.

Since the planetary stage has a high torque with low speed and consequently most of the failure modes occur in this stage, therefore, all the experimental work were carried out on the planetary stage rather than the helical stages. The planetary gearbox consists of three planet gears, which are sun gear, ring gear which is fixed to the gearbox frame and gear carrier. One non-destructive technique has been employed to record the gearbox vibration during operation, namely vibration acceleration generation. The sampling frequency used was 6.0 kHz and signals of 1.0 sec duration were recorded. B&K portable and multi-channel PULSE type 3560-B-X05 analyzer is used in addition to a B&K PULSE labshop, which is the measurement software type 7700 that is used to analyse the results. Recordings of results were carried out at constant speed, which is measured by a photo electric probe.

Five small faults has been made artificially on the planetary gearbox components, namely planet gear tooth, planet gear carrier and main bearing with wire electrical discharge machining to create a stress concentration which eventually led to a propagating crack. The cracks dimensions are listed on Table 1 for all the three gearbox components. For each defect, a recordings every 60 min were acquired and a total of 7 recordings (0-6 hr of test duration) were resulted until the termination of the test. This type of test was preferred in order to have the opportunity to monitor path defect modes, i.e., the natural defect propagation. Damage is assured by increasing the test period to the point of where the remaining metal in the tooth area has enough stress to be in the plastic deformation region.

Table 1 Wind turbine planetary gearbox defects dimensions

S/No.	Defect Type	Defect Dimensions
0	Healthy gearboxes	Free from defects
1	Planet gear tooth crack	Depth 1.0 mm Thickness 0.2 mm
2	Planet gear tooth Spalling	Spalling length = 0.9 mm Spalling height = 1 mm Spalling width = 4.6 mm
3	Planet gear tooth breakage	Breakage thick = 0.6 mm, Breakage width = 4.6 mm Breakage height = 1.35 mm
4	Low speed shaft (LSS) Main bearing crack	Depth 1.0 mm Thickness 0.2 mm
5	Planet gears carrier crack	Depth 1.0 mm Thickness 0.2 mm

IV. RESULTS AND DISCUSSIONS.

IV-I DIAGNOSTIC RESULTS AND DISCUSSION

IV-I-A HEALTHY GEARBOX

Figs. 2 and 3 show the rotational vibration acceleration in terms of time-domain and frequency-domain at speed of 40 rpm and torque load of 40 Nm respectively for healthy gearbox. The signal is normally dominated by tooth meshing harmonics modulation by the rotation of the gear shaft. In most cases, the modulation waveforms are also sinusoids with lower shaft orders, i.e. 1 time and/or 2 times the shaft frequency. Referring to Tables 2 and 3, the evaluation of RMS value is 12.342 rad/s², while the values of the crest factor and kurtosis are 3.5 and 3.2 respectively. On the other hand, the normal distribution has either kurtosis or crest factor value of 3 which is a good condition for the planetary gearbox components. However, the significant change around this number indicates the deterioration in condition.

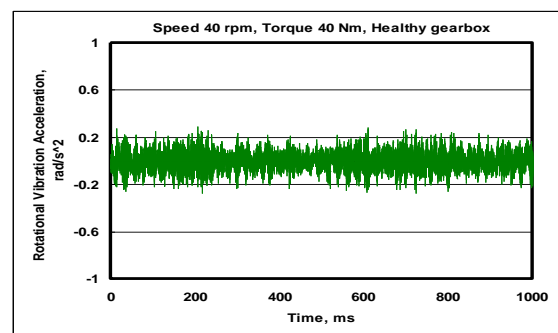


Fig. 2 Time-domain rotational vibration acceleration (40 rpm 40Nm).

Table 2 Single number of crest factor average value.

No.	Planetary Gearbox Component, Defect	Testing Time, h							
		Healthy	0.0	1.0	2.0	3.0	4.0	5.0	6.0
Speed 40 rpm-Torque Load 40 Nm - Crest Factor Average Value									
1	Planet gear crack	3.50	7.66	4.95	4.45	6.91	5.87	10.00	4.96
2	Planet gear spalling	3.50	4.25	4.84	4.53	4.11	-	-	-
3	Planet gear breakage	3.50	5.36	4.63	5.91	5.40	-	-	-
4	Planet carrier crack	3.50	4.12	4.41	4.55	5.13	4.25	4.64	5.68
5	Main bearing crack	3.50	4.35	4.32	4.03	4.32	4.38	4.02	3.98

Table 3 Single number of kurtosis average value.

No.	Planetary Gearbox Component, Defect	Testing Time, h							
		Healthy	0.0	1.0	2.0	3.0	4.0	5.0	6.0
Speed 40 rpm-Torque Load 40 Nm - Kurtosis Average Value									
1	Planet gear crack	3.20	4.94	3.49	3.30	3.75	3.72	6.71	3.43
2	Planet gear spalling	3.20	3.60	3.24	3.39	3.17	-	-	-
3	Planet gear breakage	3.20	3.44	3.37	3.62	3.44	-	-	-
4	Planet carrier crack	3.20	3.05	3.16	3.19	3.18	3.20	3.21	3.35
5	Main bearing crack	3.20	3.20	2.99	3.04	3.05	3.40	3.08	3.07

IV-I-B CRACKED PLANET GEAR

In cracked planet gear, the crack is simplified and the path of the crack considered being a straight line. The intersection angle between the crack and the centerline of the tooth is set at a constant of 45°. The crack depth is 1.0 mm and thickness is 0.2 mm at a testing time of 0.0 hr. It is considered that the gearbox signals are stationary waveform. Fig. 4 illustrates a comparison between healthy and cracked planet gear at speed of 40 rpm, and torque load of 40 Nm. In time-domain, the overall spectrum levels are higher for cracked planet gear than that of healthy condition, which indicates cracks. When a localized tooth fault occurs, such as crack, the engagement of the cracked tooth will induce an impulsive change with comparatively low energy to the gear mesh signal. This can produce some higher shaft-order modulations and may excite structure resonance.

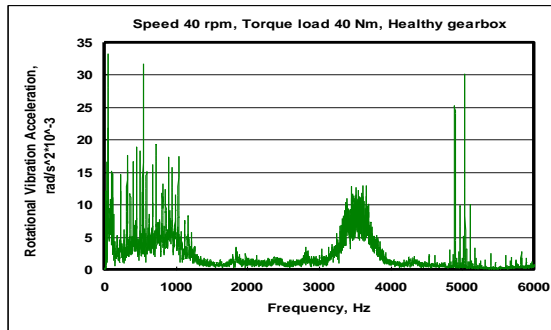


Fig. 3 Frequency-domain rotational vibration acceleration (40 rpm 40Nm).

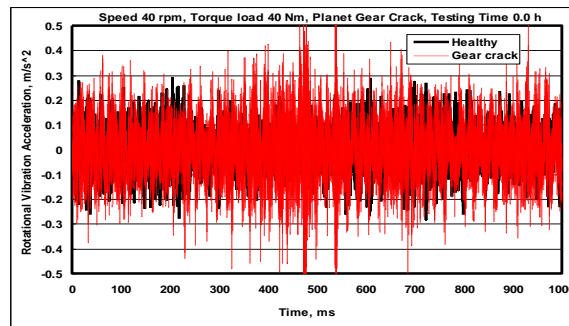


Fig. 4 Time-domain rotational vibration acceleration (40 rpm 40Nm)

Fig. 5 shows the evaluation of RMS average parameter for planet gear crack based on equation 1 at testing time ranged (0-6hr). To assist the more accurate observation of this parameter evaluation during the range of the testing time, where the RMS value is increased as the testing time is increases. A magnification is obtained and it is important and possesses diagnostic value as they can be used to define and characterize critical changes of the gears damage accumulation and evaluation. Tables 2 and 3 depict the relationship between the average crest factor and kurtosis at testing time ranged (0 to 6.0 hr) based on equations 2 and 3 respectively. It is clearly seen that the average crest factor and kurtosis values are in the ranges of 3-10 and 2-7 respectively.

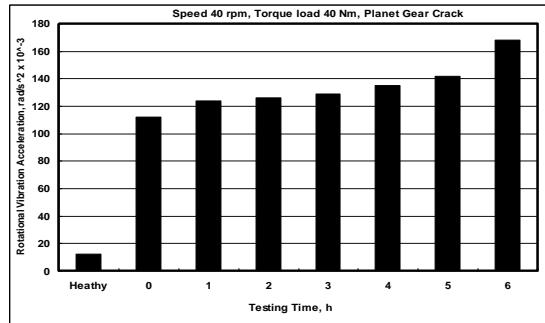


Fig. 5 RMS value rotational vibration acceleration (40 rpm 40Nm)

IV-I-C SPALLING PLANET GEAR

In spalling planet gear, the spalling dimensions are of 0.9 mm length, 1 mm height, and 4.6 mm width at a testing time of 0.0 hr. It is considered that the gearbox signals are stationary waveform. Fig. 6 shows the comparison between healthy and spalling planet gear at speed of 40 rpm, and torque load of 40 Nm. In time-domain, the overall spectrum levels are higher for spalling planet gear than that of healthy condition, which shows spalling. When a localized tooth defect occurs such as spalling, the engagement of the spalled tooth will induces an impulsive change with comparatively low energy to the gear mesh signal. This is attributed to the fact that the deviations from the ideal profile on one tooth by spalling which are not the same for each tooth-mesh and therefore gives a signal non-periodic at the tooth-meshing rate that can be ascribed to two main sources. On the one hand, there are two deflections under load, which varies as the load is not shared between different numbers of teeth during each mesh cycle.

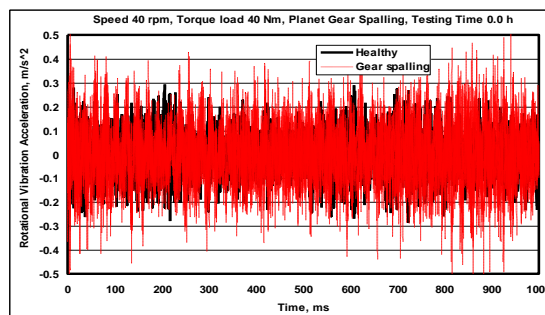


Fig. 6 Time-domain rotational vibration acceleration (40 rpm 40Nm)

Fig. 7 shows the evaluation of RMS average parameter for planet gear spalling based on equation 1 at testing time ranged (0-6hr). A magnification is obtained and it is important and possesses diagnostic value as they can be used to define and characterize critical changes of the gears damage accumulation and evaluation. Tables 2 and 3 depict the relationship between the average crest factor and kurtosis at testing time ranged (0 to 6.0 hr) relied on equations 2 and 3 respectively. It is clearly seen that the average crest factor

and kurtosis values for the planet gear spalling are in the ranges of 3-5 and 3-4 respectively.

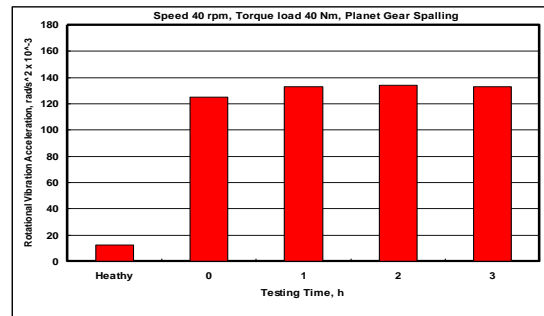


Fig. 7 RMS value rotational vibration acceleration (40 rpm 40Nm)

IV-I-D BREAKAGE PLANET GEAR

In breakage planet gear, the breakage dimensions are of 0.6 mm thickness, 4.6 mm width, and 1.35 mm height at a testing time of 0.0 hr. It is considered also that the gearbox signals are stationary waveform. Fig. 8 indicates the comparison between healthy and breakage planet gear at speed of 40 rpm, and torque load of 40 Nm. In time-domain, the overall spectrum levels are higher for breakage planet gear than that of healthy condition that indicates planet gear breakage. When a localized tooth defect occurs such as breakage, the engagement of the breakage tooth will induces an impulsive change with comparatively low energy to the gear mesh signal. This is attributed also to the fact that the deviations from the ideal profile on one tooth by breakage which is not the same for each tooth-mesh and therefore gives a signal non-periodic at the tooth-meshing rate that can be ascribed to two main sources. On the one hand, there are two deflections under load which varies as the load is not shared between different numbers of teeth during each mesh cycle.

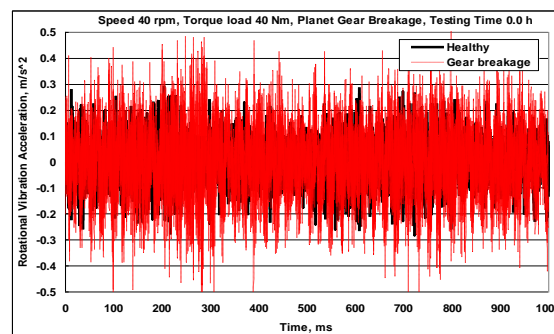


Fig. 8 Time-domain rotational vibration acceleration (40 rpm 40Nm)

Fig. 9 shows the evaluation of RMS average parameter for planet gear breakage relied on equation 1 at testing time ranged (0-6hr). A magnification is obtained and it is important and possesses diagnostic value as they can be used to define and characterize critical changes of the gears

damage accumulation and evaluation. Tables 2 and 3 describe the relationship between the average crest factor and kurtosis at testing time ranged (0 to 6.0 hr) relied on equations 2 and 3 respectively. It is clearly seen that the average crest factor and kurtosis values for the planet gear breakage are in the ranges of 3-6 and 3-4 respectively.

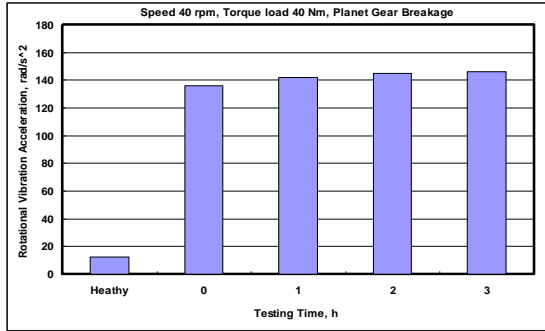


Fig. 9 RMS value rotational vibration acceleration (40 rpm 40Nm)

IV-I-E GEAR CARRIER CRACK

In planet gear carrier crack, the carrier crack depth is 1.0 mm and thickness is 0.2 mm. The testing time is taking as 0.0 hr and considering that the gearbox signals are stationary waveform. Fig. 10 illustrates the comparison between healthy and gear carrier crack also at speed of 40 rpm, and torque load of 40 Nm. In time-domain, the overall spectrum levels are higher for gear carrier crack than for healthy condition. The higher levels indicate carrier crack. When a localized planet gear carrier fault occurs, such as planet gear carrier crack, the engagement of the tooth will induces an impulsive change with comparatively low energy to the gear mesh signal. This may produce some higher shaft-order modulations and could excite structure resonance.

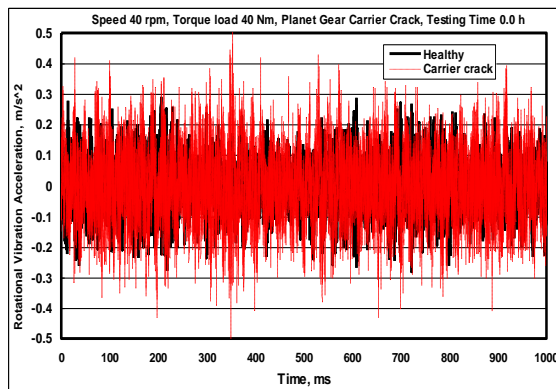


Fig. 10 Time-domain rotational vibration acceleration (40 rpm 40Nm)

Fig. 11 shows the evaluation of RMS average parameter for gear carrier crack depended on equation 1 at testing time ranged (0-6hr). A magnification is obtained and it is important and possesses diagnostic value as they can be used to define and characterize critical changes of the gear carrier

crack fault accumulation and evaluation. Tables 2 and 3 describe the relationship between the average crest factor and kurtosis at testing time ranged (0 to 6.0 hr) relied on equations 2 and 3 respectively. It is clearly seen that the average crest factor and kurtosis values for the gear carrier crack are in the ranges of 3-6 and 3-4 respectively.

IV-I-F MAIN BEARING CRACK

In the main bearing inner race crack, the main bearing inner race crack depth is 1.0 mm and thickness is 0.2 mm. The testing time is being 0.0 hr, and taking into account that the gearbox signals to be stationary waveform. Fig. 12 illustrates the comparison between healthy and cracked main bearing inner race crack at speed of 40 rpm, and torque load of 40 Nm. In time-domain, the overall spectrum levels are higher for main bearing inner race crack than for healthy condition. The higher levels indicate bearing inner race crack.

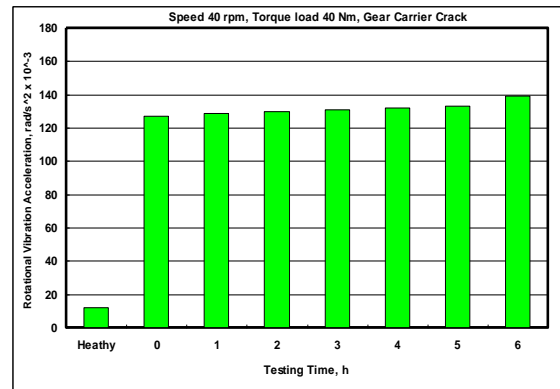


Fig. 11 RMS value rotational vibration acceleration (40 rpm 40Nm)

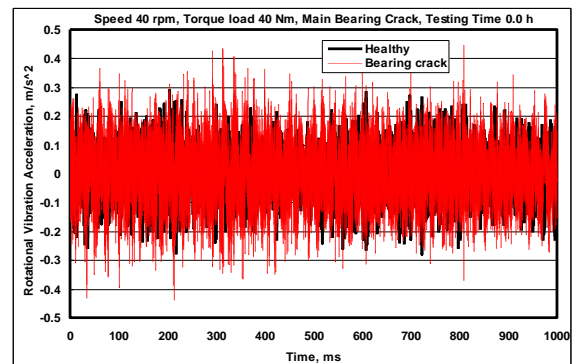


Fig. 12 Time-domain rotational vibration acceleration (40 rpm 40Nm)

Fig. 13 shows the evaluation of RMS average parameter for main bearing crack relied on equation 1 at testing time ranged (0-6hr). A magnification is obtained and it is important and possesses diagnostic value as they can be used to define and characterize critical changes of main bearing inner crack fault accumulation and evaluation. Tables 2 and 3 describe the relationship between the average crest factor and kurtosis at testing time ranged (0 to 6.0 hr) relied on

equations 2 and 3 respectively. It is clearly seen that the average crest factor and kurtosis values for the main bearing crack are in the ranges of 3-5 and 2-3 respectively.

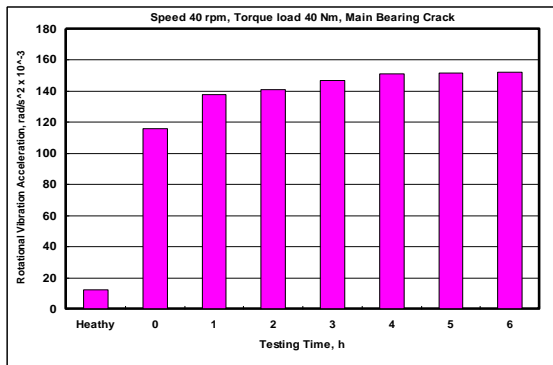


Fig. 13 RMS value rotational vibration acceleration (40 rpm 40Nm)

IV-II GEARBOX COMPONENTS DEFECTS SEVERITY ASSESSMENT

From the previous discussion, descriptive and higher order statistics (HOS) indices have been generating intensive interest. The RMS, average crest factor and kurtosis values calculated from the measured signal have nearly similar trend, where the RMS value is found to be a better indicator as compared to either average crest factor or kurtosis. However, the RMS values of rotational vibration acceleration used to evaluate the wind turbine gearbox components faults severity assessment. Fig. 14 depicts this severity assessment which has been achieved by the developed the experimental technique at speed of 40 rpm and torque load of 40 Nm and at a testing time of 0.0 hr. The figure indicates that planet gear breakage posses the highest RMS value followed by planet gear carrier crack and planet gear spalling ; and main bearing crack with planet gear crack has least RMS value. This can help to identify which type of damage can be considered first.

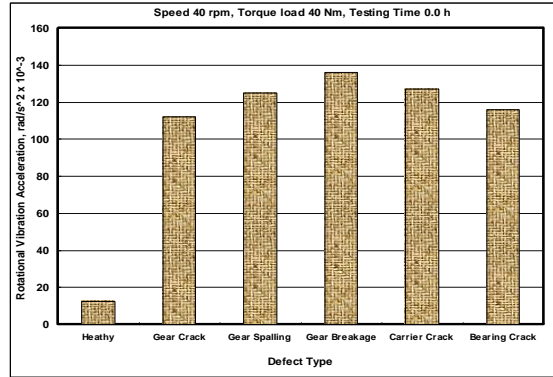


Fig. 14 RMS value for nominal vibration acceleration (40 rpm 40Nm).

On the other hand, Table 4 tabulates in percentage of the change of RMS value of rotational vibration acceleration at a testing time of 0.0 hr from that for healthy gearbox (CFHL) at speed of 40 rpm and torque load of 40 Nm based on the following equation:

$$CFHL, (\%) = \frac{(RMS)_{Healthy} - (RMS)_{Faulty}}{(RMS)_{Healthy}} \quad (5)$$

Where:

$$(RMS)_{Healthy} = \text{RMS value for healthy condition}$$

$$(RMS)_{Faulty} = \text{RMS value for faulty condition}$$

The values are 10.02% (gear breakage), 9.29% (gear carrier crack), 9.13% (gear spalling) 8.4% (main bearing crack) and 8.07% (gear crack). This information can help for diagnostic procedure. It has been shown that the fault on wind turbine planetary gear box can be detected at its early stages, and symptoms of fault on vibration is not primarily caused by the reduction components stiffness (which is the case for the detection of a localized fault), but mainly due to the deviations in component shape from the true component shape.

Table 4 Change from the healthy gearbox (%)

S/No.	Speed, rpm	Torque Load, Nm	Gear Crack	Gear Spalling	Gear Breakage	Carrier Crack	Bearing Crack
1	40	40	8.07	9.13	10.02	9.29	8.4

V. CONCLUSION

- In stationary vibration waveform feature, the periodical impulses caused by the wind turbine gearbox faults appear in both the time domain and frequency-domain signals as the fault level increases. This carries diagnostic information is of great importance for extracting features of the fault.
- In order to extract the impulse feature of damaged gearbox components, rotational vibration signals are used to analyze the vibration signals of both healthy and faulty gearbox. The wind turbine gearbox components considered are planet gear, planet gear carrier and main bearing. Furthermore, the high order statistics of RMS, crest factor and kurtosis reflect in the rotational vibration responses of the gearbox.
- The identification of gear vibration is introduced. When applied to the gearbox, the method resulted in an accurate account of the state of the gear, even, when applied to real data taken from the gearbox test. The results look promising, where the RMS value analysis could be a good indicator for early detection and characterization of faults. Moreover, Multi-hour tests were conducted and recordings and were acquired using rotational vibration monitoring.
- From this investigation, the gearbox components faults severity assessment has indicated that the values are 8.07% (planet gear crack), 9.13% (planet gear spalling), 10.02% (planet gear breakage), 9.29% (gear carrier crack) and 8.4% (main bearing crack). Moreover, the symptoms of fault on vibration is not primarily caused by the reduction components stiffness (which is the case for the detection of a localized fault), but mainly due to the deviations in component shape from the true component shape.

ACKNOWLEDGEMENTS

The authors acknowledge the support of Science and Technology Development Fund (STDF), Egypt, through the awarded grant No. ID 1484, on monitoring of wind turbine gearbox. The authors would like to thank University of Helwan, which made this study come to light.

REFERENCES

- [1] Samuel, P.D., and Pines, D.J. "A review of vibration-based techniques for helicopter transmission diagnostics" *Journal of Sound and Vibration* 282 (1- 2) pp 475–508, 2005.
- [2] Abouel-seoud, S. A., Morsy, M. S., and Rabeih, E. "Geared System Condition Diagnostics Via Torsional Vibration Measurement" *Proceeding o International Conference on Noise and Vibration Engineering ISMA* 2010, Leuven, pp. 2831-2841, 20-22 Sept 2010.
- [3] Loutas, T.H. Sotiriades, G., Kalaitzoglou, I. And Kostopoulos, V. " Condition monitoring of a single-stage gearbox with artificially induced gear cracks utilizing on- line vibration and acoustic emission measurements" *Applied Acoustics* 70, pp. 1148-1159. 20-22 Sept 2009.
- [4] Abouel-Seoud, S. A., Allam, E. and Ahmed, I. "An experimental investigation of noise Emission from a vehicle gearbox system " *Journal of Mechanical Engineering Research* Vol. 3(3), pp. 75-84, March 2011.
- [5] Abouel-Seoud, S. A., Metwalley , S. M. and Hammad, N. " Vehicle gearbox fault diagnosis using noise measurements" *International Journal of Energy and Environment*, Volume 2, Issue 2, pp.357-366, 2011.
- [6] Blunta, D. M. and Kellerb, J. A. "Detection of a fatigue crack in a UH-60A planet gear carrier using vibration analysis" *Mechanical Systems and Signal Processing* 20, pp. 2095–2111, 2006.
- [7] Walford, C. and Roberts, D. "Condition Monitoring of Wind Turbines: Technology Overview, Seeded-Fault Testing, and Cost-Benefit Analysis. EPRI, Palo Alto, CA: 1010419 Xu, R. and Kwan, C. (2003) "Robust isolation of sensor features" *Asian Journal of Control* 5, pp. 12-23, 2006.
- [8] Barszcz, T. and Randall, R. B. "Application of spectral kurtosis for detection of a tooth crack in the planetary gear of a wind turbine" *Mechanical Systems and Signal Processing* 23, pp. 1352–1365, 2009.
- [9] Jia, S. and Howard, I. "Comparison of localized spalling and crack damage from dynamic modeling of spur gear vibrations " *Mechanical Systems and Signal Processing* 20, pp. 332–349, (2006).
- [10] Tandon, N. and Choudhury A. "A review of vibration and acoustic measurement methods for the detection of defects in rolling element bearings" *Tribology International* 32, pp. 469–480, 1999.
- [11] Abouel-seoud, S. A., Hammad, N., Abd-elhalim, N., Mohamed, E. and Abdel-hady, M" *Vehicle Gearbox Condition Monitoring Using Vibration Signature Analysis" SAE, Paper No. 2008-01-1654, 2008.*
- [12] George Box, Gwilym M. Jenkins, and Gregory C. Reinsel. *Time Series Analysis: Forecasting and Control*, third edition. Prentice-Hall, 1994.
- [13] Abouel-seoud, S., Elmorsy, M. and Dyab, E. " Robust prognostics concept for gearbox with artificially induced gear crack utilizing acoustic emission" *Journal of Energy and Environment Research, Canada*, Vol. 1, No. 1, 2011.
- [14] De Almeida, R.G.T., Da Silva Vicente, S. and Padovese, L. R. " "New technique for evaluation of global vibration levels in rolling bearings" *Shock and Vibration* 9, pp. 225-234, 2002.
- [15] Abouel-seoud, S., Hammad, N., Abd-elhalim, N., Abdel-hady, M. and Mohamed, E. "Vehicle Gearbox Condition Monitoring Using Vibration Signature Analysis" *Society of Automotive Engineers (SAE), Paper No. 2008-01-2295, September 16-18, 2008.*
- [16] Abouel-seoud, S., El-morsy, M. and Saad, A."A Laboratory Apparatus for Investigation of Vibration Performance of Wind Turbine Planetary Gearbox" *Journal of Recent Research*, Vol. 3, Issue 11, 2011.

A BIST Circuit for Fault Detection Using Recursive Pseudo-Exhaustive Two Pattern Generator

K. Nivitha¹, Anita Titus²

¹ ME-VLSI Design

² Dept of ECE

Easwari Engineering College, Chennai-89

Abstract – A Built-in self-test (BIST) technique based on pseudo-exhaustive testing is proposed in this paper. Two pattern test generator is used to provide high fault coverage. Testing for delay and sequential faults requires two-pattern tests. In two-pattern testing all possible combinations of the test vectors are applied to the circuit under test. In this paper a pseudo exhaustive two-pattern generator with fewer hardware that generates two-pattern (7,k)-adjacent bit pseudo exhaustive tests for any $k < 7$ is used. Two circuits like Wallace tree multiplier and cryptographic circuit based on RSA algorithm are tested in parallel. The main advantage of this BIST is that the circuits have different cone sizes are tested at a time. This increases the speed of the BIST.

Index Terms – Built-in self-test (BIST), Pseudo-exhaustive two pattern testing, Test pattern generation.

I. INTRODUCTION

The task of testing a VLSI chip to guarantee its functionality is extremely complex and often very time consuming. A widely accepted approach to deal with the testing problem at the chip level is to incorporate built-in self-test (BIST) capability inside a chip. [1]

BIST is more suitable for periodic testing which is carried out periodically in the system itself. This can be either on-line or off-line. BIST is comprised of TPG, response analyzer and testing logic. In BIST scheme, design of TPG is very critical. Conventionally, Linear Feedback Shift Registers (LFSR) is commonly used TPG in BIST structure. Though it is suitable for BIST, it has many disadvantages. It is a random pattern generator, complex in design, it generates unwanted patterns which increases the switching activity of the CUT leads to increase in testing period. For these reasons exhaustive and pseudo exhaustive testing are preferred. In exhaustive testing number of test vector are more which is minimized in pseudo exhaustive testing [2].

BIST pattern generators are commonly discerned into one-pattern and two-pattern generators. One-pattern generators mainly detect combinational faults. It has been proved that many failure mechanisms in CMOS circuits cannot be modeled by the stuck-at faults. Furthermore, the digital circuits should operate at their highest possible speeds to increase their performance. For correct behavior of the circuits, delay faults are detected by two pattern test generators [6].

In BIST, the test pattern generation and the output response evaluation are done on chip itself so the hardware used for designing BIST should be minimized [1].

In [4] a method is proposed for generating universal pseudo-exhaustive test. Assuming n as input of TPG and m as input of the circuit it requires $7n$ registers, $8m$ counters, $3n$ multipliers and XOR gates. In [5] a method is proposed that uses Cellular Automata to generate recursive pseudo-exhaustive test patterns. The hardware requirement of the proposed scheme is 15 to 50 percent less XOR gates compared to the existing Recursive Pseudo-exhaustive Test Pattern Generation and test string length increases from 14 to 31. In [8] the hardware required to design recursive pseudo exhaustive generator is $21n$ plus $24m$ gates. Compared to all other papers, the recursive pseudo exhaustive two pattern generator (RPET) and generic pseudo exhaustive two pattern generator (GPET) in [3] requires minimum hardware utilization. RPET requires $18n$ plus $8m$ gates and GPET requires $16n$ gates. Both the TPGs are designed and GPET is used for the BIST designed in this paper. It generates all the tests for any cone size (k). By using this GPET more than a circuit is tested in parallel which increases the speed of the BIST. In this paper two circuits like 4×4 Wallace tree multiplier and 7-bit cryptographic circuit are tested in parallel. The outputs from circuits are compared with the stored values and faults are determined. The fault coverage of proposed BIST is more when compared to existing BIST.

II. TEST PATTERN GENERATOR

In this paper two pattern generators like Generic pseudo exhaustive two pattern generator (GPET) and recursive pseudo exhaustive two pattern generator (RPET) are implemented to generate two pattern tests for modules having different cone sizes.

A. GPET

The generic pseudo-exhaustive two-pattern generator is presented in Fig. 1. It consists of a generic counter, 1's complement adder, a controller and a carry generator (C_gen). The 7-bit pattern PE [7:1] is given as an input to the controller, generic counter and C_gen and the output A [7:1] is taken from the Accumulator.

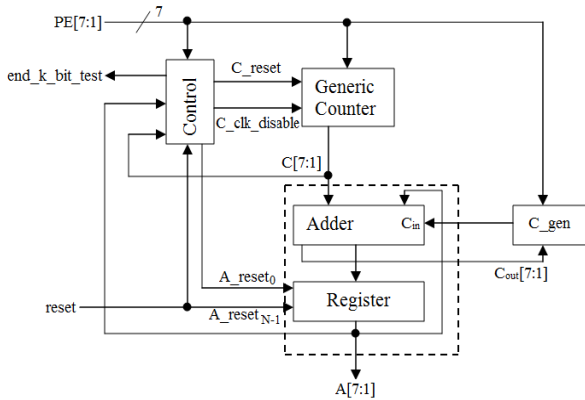


Fig.1: Generic pseudo exhaustive two pattern generator

The operation of the GPET varies based on the PE value. If the value PE[4] is enabled, a (7,3)-pseudo-exhaustive test set is generated and a 3-bit exhaustive test set is applied to the 2-bit groups A[3:1], A[6:4], and a single bit test set is generated at A[7].

1) Generic counter

The input of the 7-stage generic counter are counter reset (C_reset), 7 bit signal PE[7:1] and counter disable(C_clk_disable). If the signals PE[1] is enabled, then the generic counter operates as an 7-stage binary counter. When PE[4] is enabled, then the generic counter operates as two 3-bit subcounter and a 1-bit subcounter from LSB. Therefore, the generic counter generates all $2^{k-1} \times (2^{k-1} - 1)$ combinations to all groups of k-1 adjacent bits. When the signal C_reset is enabled, the generic counter counts from the initial value. The signal C_clk_disable is used to keep the counter idle. The operation of the generic counter is shown in the table 1.

Table 1: operation of the generic counter

PE[7:1]	Operates as...	In each clock increased by...
0000001	1x7-stage counter	0000001
0000010	7x1-stage counters	1111111
0000100	1x1-stage counter + 3x2-stage counters	1010101
0001000	1x1-stage counter + 2x3-stage counters	1001001
0010000	1x3-stage counter + 1x4-stage counter	0010001
0100000	1x2-stage counter + 1x5-stage counter	0100001
1000000	1x1-stage counter + 1x6-stage counter	1000001

2) Carry generator

The C_gen is used to give the C_in input for the adder. The inputs of C_gen module are PE[7:1] and C_out[7:1]. If the signal PE[4] is enabled, the C_out[4] is given as a C_in. Based on the signal PE[7:1] the value of C_in changes.

3) Control

The control module is used to determine that a k-stage two-pattern test is generated at the k low-order bits of the generator. The input signals of the control module are reset, ACC[7:1], C[7:1], PE[7:3], and generates the signals C_clk_disable, C_reset, A_reset0 and end_k_bit_test.

4) 1's complement adder

The inputs of adder are cin, A[7:1], C[7:1] and its outputs are C_out[7:1], A[7:1]. It consists of 7 full adders, the carry output of the full adders are propagated to the next full adders as carry input. If the value of k is considered to be 3 then the accumulator operates as two 3-stage subaccumulator and one 1-stage accumulator. The carry output of each sub accumulator is given to the carry input of next sub accumulator. If there is any carry in the 3rd bit then it is added to the lowest order bit of the adder output. The operation of adder is shown in table 2.

Table 2: operation of 1's complement adder

Previous A[7:1]	C[7:1]	Present A[7:1]	C_out[7:1]	k
1111111	1111111	1111111	1111111	1
0101010	0101010	1010101	0101010	2
1011011	0110110	0010001	1111110	3
0011001	1001100	1100110	0011000	4
0111001	0111101	1110111	0111001	5

5) TPG Algorithm

This algorithm consists of three steps which generates all 7-bit two pattern tests within $2^k \times (2^k - 1)$ clock cycles. For simplification 2^k is considered as K.

- The counter counts from 1 to K-3 and then it is reset; this is repeated until the outputs of the counter are equal to K-3 and the outputs of the accumulator are equal to K-1.
- The counter is incremented to K-2 and the accumulator repeatedly accumulates K-2 until its output is equal to K-1.
- All transitions to and from zero are generated, by resetting the accumulator and incrementing the counter every second clock cycle.

The output of the generic pseudo exhaustive two pattern generator (GPET) for PE[4] is shown in table 3.

Table 3: Output of the GPET

C	A	C	A	C	A
STEP 1					
	1111	1101	0100	0110	0010
10010	111	1001	1101	0110	1001
01	1001	001	101	110	001
00100	001	0010	1111	0110	1111
10	1011	010	111	110	111
10110	011	1011	1011	STEP 3	
11	0110	011	011	1001	0000
01001	110	0100	1111	001	000
00	1011	100	111	1001	1001
11011	011	1101	1101	001	001
01	1001	101	101	0010	0000
10010	001	1001	0110	010	000
01	0010	001	110	0010	0010
00100	010	0010	1001	010	010
10	0100	010	001	1011	0000
10110	100	1011	0100	011	000
11	1111	011	100	1011	1011
01001	111	0100	1001	011	011
00	0100	100	001	0100	0000
11011	100	1101	0110	100	000
01	0010	101	110	0100	0100
10010	010	1001	1111	100	100
01	1011	001	111	1101	0000
00100	011	0010	0010	101	000
10	1101	010	010	1101	1101
10110	101	1011	1101	101	101
11	1001	011	101	0110	0000
01001	001	0100	0010	110	000
00	1101	100	010	0110	0110
11011	101	1101	1111	110	110
01	1011	101	111	1111	0000
10010	011	STEP 2		111	000
01	0100	0110	0110	1111	1111
00100	100	110	110	111	111
10	0110	0110	1101		
10110	110	110	101		
11	0010	0110	0100		
01001	010	110	100		
00	0110	0110	1011		
	110	110	011		

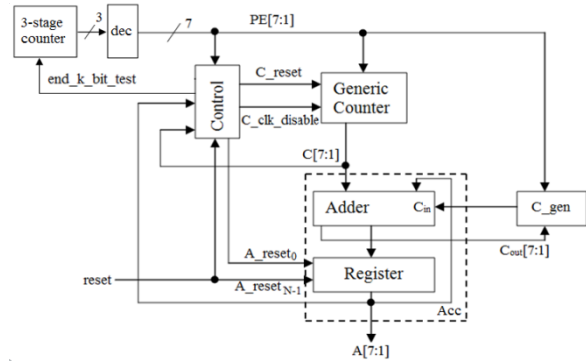


Fig2:Recursive pseudo exhaustive two pattern generator
 It recursively enable PE[k] for all values of k, $2 \leq k \leq 7$. The output of the recursive pseudo exhaustive two pattern generator (RPET) is shown in table 4.

Table 4: Output of the RPET

m[3:1]	PE[7:1]	C[7:1]	A[7:1]
011	0001000	1001001	1111111
		0010010	1001001
		1011011	0110111
		0100100	1011011
		:	:
		1111111	1111111
		1111111	1111111
100	0010000	0010001	0010001
		0100010	0110011
		0110011	1100110
		1000100	0101010
		:	:
		1111111	1111111
		1111111	1111111
101	0100000	0100001	0100001
		1000010	1100011
		1100011	1000110
		0000100	1001010
		:	:
		1111111	1111111
		1111111	1111111
110	1000000	1000001	1000001
		0000010	1000011
		1000011	0000110
		0000100	0001010
		:	:
		1111111	1111111
		1111111	1111111
111	0000001	0000001	0000001
		0000010	0000011
		0000011	0000110
		0000100	0001010
		:	:
		1111111	1111111
		1111111	1111111

B) RPET

The recursive pseudo exhaustive two pattern generator is shown in fig 2. Additionally It consists of an $m = \lceil \log_2 7 \rceil = 3$ -stage counter driving the inputs of a 3-to-7 decoder then GPET.

III. CIRCUIT UNDER TEST

The output from the two pattern test generator is applied to the CUT. In this paper two circuits, Wallace tree multiplier and cryptographic circuit are tested in parallel to increase the speed of the BIST.

A) 4 bit Wallace tree multiplier

A Wallace tree multiplier is an efficient hardware implementation of a digital circuit that multiplies two binary values. The 4 bit Wallace tree multiplier is shown in fig 3.

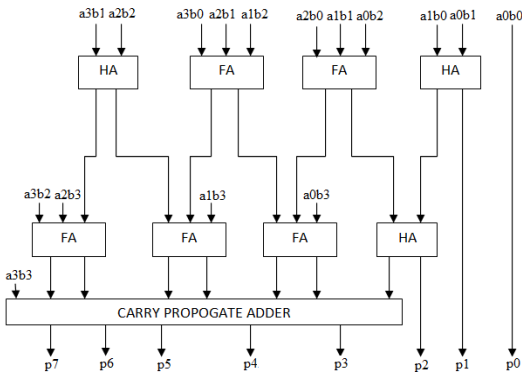


Fig 3: 4-bit Wallace tree multiplier

The Wallace tree has three steps:

- Multiply each bit of one of the arguments, by each bit of the other, yielding 16 results. Depending on position of the multiplied bits, the wires carry different weights.
- Reduce the number of partial products to two by layers of full and half adders.
- Group the wires in two numbers, and add them with a conventional adder.

B) 7-bit cryptographic circuit

It is used for secure transmission of private information over insecure channels. There are two types of cryptographic methods 1) Symmetric— same key for encryption and decryption 2) Asymmetric— Mathematically related key pairs for encryption and decryption i.e., Public and private keys.

Asymmetric circuits are more secure than symmetric circuits. In this paper RSA algorithm based cryptographic circuit is implemented. The RSA algorithm involves three steps: key generation, encryption and decryption. The public key can be known to everyone and is used for encrypting messages. Messages encrypted with the public key can only be decrypted using the private key. In run mode these circuits perform normal operation and in testing mode it performs fault detection. The block diagram of the BIST is shown in fig 4.

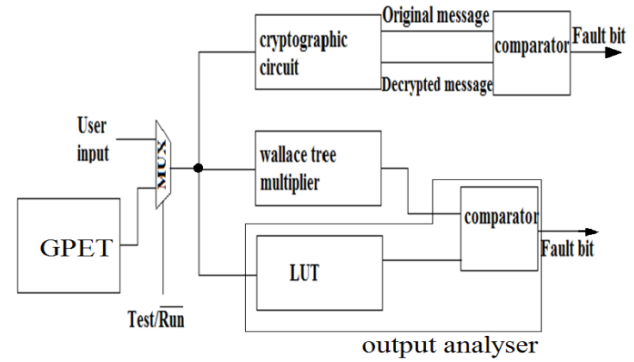


Fig: 4 Proposed Block diagram of BIST

IV. OUTPUT ANALYSER

BIST techniques usually combine a built-in binary pattern generator with circuitry for compressing the corresponding response data produced by the circuit under test. The compressed form of the response data is compared with a known fault-free response.

V. RESULTS AND DISCUSSIONS

BIST plays a vital role in modern VLSI technology. The BIST should occupy less area for compact design of digital circuit. When compared to the results of [4], [5] the test pattern generator proposed in [3] requires fewer hardware to implement. Based on the technique used in [3] a test pattern is generated. The comparison of the hardware overhead is shown in table 5.

Table 5: comparison of hardware overhead in gates

scheme	Gate equivalents	No. of gates when n=7
GPET	16×n	113
RPET	18×n + 8×m	148
[4]	7×n + XOR gates + 3×n + 8×m	202
[5]	7×n + XOR gates + 3×n + 8×m	229

The RSA based cryptographic circuit is tested with counter based one pattern BIST and proposed BIST. The fault coverage of the circuits is determined. Fault detected using Normal BIST is 25. Fault detected using Proposed BIST is 59 in the same circuit. Total number of faults in this circuit is 60. So the fault coverage of the proposed BIST is 98%. When compared to [8], [9], [10] proposed BIST detects maximum number of faults.

- [6] R. Wadsack, "Fault modeling and logic simulation of CMOS and nMOS integrated circuits," *Bell Syst. Techn. J.*, vol. 57, pp. 1449-1474, May-Jun. 1978.
- [7] C. Chen and S. Gupta, "BIST test pattern generators for two-pattern testing-theory and design algorithms," *IEEE Trans Comput.*, vol. 45, no. 3, pp. 257-269, Mar. 1996.
- [8] Chih-Ang Chen, "Efficient BIST TPG Design and Test Set Compaction via Input Reduction," *IEEE trans. on CADICS*, vol. 17, NO. 8, AUG 1998.
- [9] Dong Xiang, "A Reconfigurable Scan Architecture with Weighted Scan-Enable Signals for Deterministic BIST," *IEEE Trans. On CADICS*, Vol. 27, No. 6, Jun 2008.
- [10] K. Yang, K.T. Cheng, and L. C. Wang, "TranGen: A SAT-based ATPG for path-oriented transition faults," in *Proc. ASP-DAC*, 2004, pp. 92-97.
- [11] C. Chen and S. Gupta, "BIST test pattern generators for two-pattern testing-theory and design algorithms," *IEEE Trans. Comput.*, vol. 45, no. 3, pp. 257-269, Mar. 1996.

Power Quality Improvement of Unified Power Quality Conditioner Using Reference Signal Generation Method

C. Prakash¹, N. Suparna²

¹ PG Scholar, Department of EEE, SNS College of Technology, Coimbatore
² Assistant Professor, Department of EEE, SNS College of Technology, Coimbatore

Abstract: This project presents a power quality improvement of unified power quality conditioner (UPQC) to compensate current and voltage quality problems of sensitive loads. The UPQC consists of the series and shunt converter having a common dc link. The series converter mitigates voltage sag from the supply side and shunt converter eliminates current harmonics from the nonlinear load side. The developed controllers for series and shunt converters are based on a reference signal generation method (phase-locked loop). The dc link control strategy is based on the fuzzy-logic controllers. The conventional method using dq transformation to show the superiority of the proposed sag detection method. A fast sag detection method is also presented. The efficiency of the proposed system is tested through simulation studies using the MATLAB/SIMULINK environment.

Keywords: unified power quality conditioner (UPQC), reference signal generation, active filter, fuzzy-logic controller.

1. INTRODUCTION

Power quality is the set of limits of electrical properties that allows electrical systems to function in their intended manner without significant loss of performance or life. The term is used to describe electric power that drives an electrical load and the load's ability to function properly with that electric power. Without the proper power, an electrical device (or load) may malfunction, fail prematurely or not operate at all. There are many ways in which electric power can be of poor quality and many more causes of such poor quality power [1]. With the increasing applications of nonlinear and electronically switched devices in distribution systems and industries, Power quality (PQ) problems, such as harmonics, flicker, and imbalance have become serious concerns. In addition Lighting strikes on transmission lines, switching of capacitor banks, and various network faults can also cause PQ problems, such as transients, voltage sag and interruption [2].

Voltage-source converter (VSC)- based custom power (CP) devices are increasingly being used in custom power applications to mitigate these PQ problems in power distribution systems. A shunt converter (also known as the shunt active filter) can compensate for distortion and unbalance in a load so that a balanced sinusoidal current flows through the feeder. A series converter (also known as the dynamic voltage) can compensate for voltage sag and distortion in the supply side voltage so that the voltage across a sensitive load is perfectly regulated [3]. Control

techniques play a vital role in the overall performance of the power conditioner.

Instantaneous power theory is generally preferred to generate reference signals for the shunt converter [3]. An extended method based on instantaneous reactive power theory in a rotating reference frame is used to suppress the harmonics and to correct the power factor in [4]. Fuzzy logic is utilized to control the compensation currents of the shunt converter in [5].

There has also been interest in the circuit topologies of UPQC. UPQC is generally designed as a three-phase three-wire (3P3W) systems. The three-phase four-wire system is also realized from the system where the neutral of series transformer used in series part UPQC is considered as the fourth wire for the 3P3W system. There are also single phase UPQC system. Various topologies, such as H- bridge converters, and single-phase UPQC with three legs are examined for the UPQC applications.

This paper presents novel contributions for UPQC control and has the following functions:

- The new control approach based on enhanced phase-locked loop and a nonlinear adaptive filter for reference signals generation is derived for series and shunt converters analyzed.
- A fuzzy logic controller (FLC) in MATLAB to control dc-link voltage without any interfacing of other simulation programs.
- FLC of dc-link voltage is proposed which improves the current total harmonic distortion (THD) over the conventional PI controller.
- A fast algorithm for sag detection is also presented.

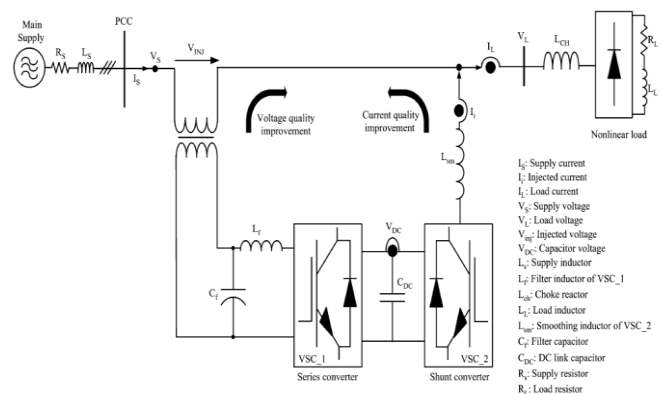


Fig. 1. Schematic diagram of UPQC.

The remainder of this paper is organized as follows. Section II of this paper presents a power circuit configuration of UPQC. Section III and IV, the controller algorithms of series and shunt converters are presented. In section V effectiveness of the proposed UPQC is tested.

II. POWER CIRCUIT CONFIGURATION OF UPQC

The UPQC shown in Fig. 1 consists of two VSCs (VSC_1 and VSC_2) that are connected back to back through common energy storage dc capacitor (C_{DC}). Series converter (VSC_1) is connected through transformers between the supply and point of common coupling (PCC). Shunt converter (VSC_2) is connected in parallel with PCC through the transformers. VSC_1 operates as a voltage source while VSC_2 operates as a current source.

The main objective of VSC_1 is to mitigate voltage sag from the supply side. The ac filter inductor L_f and capacitor C_f are connected in each phase to prevent the flow of harmonics currents generated due to switching [2]. The objective of VSC_2 are to regulate the dc link voltage between both converters and to suppress the load current harmonics [6]. The switching devices in VSC_1 and VSC_2 are insulated-gate bipolar transistors (IGBT) with anti parallel diodes. C_{dc} provides the common dc-link voltage to VSC_1 and VSC_2 . The proposed UPQC system offers two mode of operation as follows.

- VSC_1 off and VSC_2 on: When the PCC voltage is within its operation limits, VSC_1 is closed and VSC_2 works as the current source. VSC_2 suppress the load current harmonics and regulate dc-link voltage during this mode of operation.
- VSC_1 on and VSC_2 on: When the PCC voltage is outside its operating range; both VSC_1 and VSC_2 are open. VSC_1 starts to mitigate sag using energy stored in V_{DC} and VSC_2 continue to suppress the load current harmonics and to regulate dc-link voltage. Ideally once charged, the dc-link voltage V_{DC} should not fall off its charge, but due to finite switching losses of the inverter.

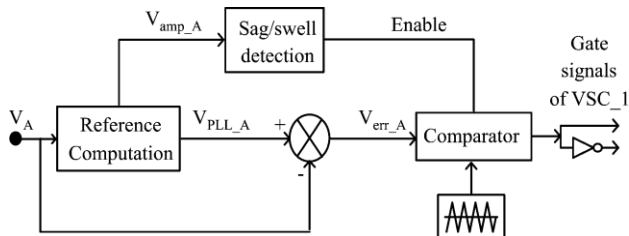


Fig. 2. Control block diagram of the series converter.

III. SERIES CONVERTER CONTROL

The series converter includes the reference voltage and sag detection method. Fig. 2 shows the control algorithm of a series converter for phase A. This control algorithm is identical for the other phases.

A. Reference Voltage Generation

A block diagram of the proposed algorithm is shown in the Fig. 3. The proposed controller algorithm is derived from the findings of both enhanced PLL and nonlinear adaptive filter. The proposed controller minimizes the mathematical operands in the system and reduces complex parameter tuning. The measurements of supply voltages are required for the control strategy of VSC_1 .

The system receives the measured input signal $A(t)$ and provides an online estimate of the following signals:

- $B(t)$, the difference of input and the synchronized Fundamental component;
- $C(t)$, the amplitude of $D(t)$;
- $D(t)$, the synchronized fundamental component;
- $E(t)$, PLL signal;
- $\Theta(t)$, the phase angle of $D(t)$.

For the series converter, $A(t)$ corresponds to the supply voltage V_A , and $E(t)$ corresponds to V_{PLL_A} as shown from the Figs. The required compensation signal V_{err_A} is obtained from $(V_{PLL_A} - V_A)$. $C(t)$ corresponds to V_{amp_a} and this signal is used to detect the voltage sag.

The supply voltage and its extracted components, such as the difference of input and the synchronized fundamental component $B(t)$, the amplitude $C(t)$, synchronized fundamental component.

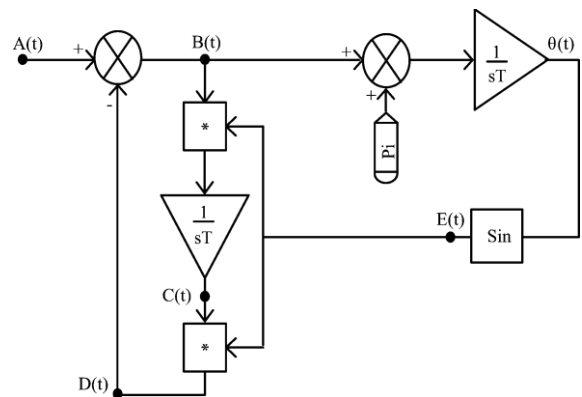


Fig. 3. Block diagram of the proposed algorithm.

B. Sag Detection Method

The proposed sag detection method is compared with the conventional method using dq transformation to show the superiority of the proposed detection method.

1. Conventional method:

The phase voltages V_a , V_b , V_c are transformed to the dq

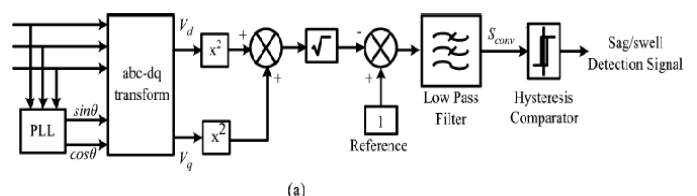


Fig. 4. (a) Conventional Method.

Plane as given with the sag is obtained in the conventional method. In fig. 4.(a), the block diagram of the dq transformation- based sag detection method is shown. After the three-phase set of voltages is transformed into d and q components, the square root of the sum of square of these components is obtained.

The obtained value is subtracted from the 1 (reference value) and then the absolute value of the resulting variable is filtered out with a 100-Hz low-pass filter to extract the positive- sequence component of voltage. If the negative sequence is generated by voltage sag or unbalance, it appears as an oscillating error in the dq- based sag detection method.

The filtered output is subjected to a hysteresis comparator, and the output of this comparator generates the sag detection signal. The signal is high when sag occurs and is low otherwise. The most important disadvantage of this method is that it uses three-phase voltage measurements for the detection.

2. Proposed Method:

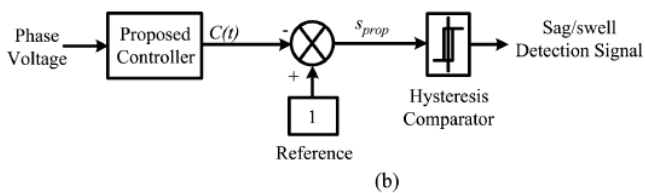


Fig. 4.(b) Proposed sag detection method.

The voltage sag detection method using PLL by subtracting the C(t) signal from the ideal voltage magnitude (1 p.u), the voltage sag depth can be detected. The comparison of this value with the limit value of 10% (0.1p.u) gives information as to whether voltage sag occurred. In fig. 4.b. the voltage sag are detected within a few milliseconds. The conventional method cannot detect the sag, but the proposed method can detect the depth with exact certainty. The single- phase voltage sag initiates at 0.3s with duration of 0.1s .The proposed method detect the voltage sag and balance without error.

IV. SHUNT CONVERTER CONTROL

The shunt converter includes the reference current computation and capacitor voltage control. Fig. 5. Shows the algorithm of the converter control.

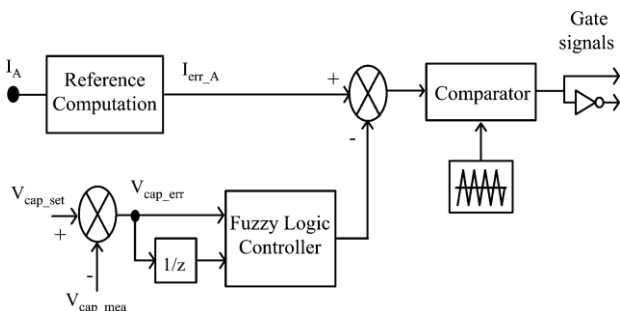


Fig. 5. Control block diagram of the shunt converter.

For the shunt converter, A(t) corresponds to I_A , and B(t) corresponds to I_{err_A} as shown from figs. 3 and 7. The measurements of load currents (I_L), injected currents (I_i), and dc capacitor voltage (V_{DC}) are required for control strategy of VSC₁.

In the proposed method, there is no need to measure supply voltages. The required compensation signal is obtained by subtracting the FLC output from I_{err_A} . the obtained signal is then compared with a carrier signal. The required compensation signal is obtained by subtracting the FLC output from I_{err_A} . The obtained signal is then compared with a carrier signal.

B. Capacitor Voltage Control

In the proposed method, V_{cap_err} is obtained from the difference of the capacitor voltage and measured capacitor voltage. V_{cap_err} and its rate off change are the inputs for the FLC. The input signal are fuzzified and represented in fuzzy set notations by the membership functions. The defined “IF.... THEN....” rules produce the linguistic variables, and these variables are defuzzified into control signals.

Membership functions and rules are obtained from the an understanding of system behavior and the application of the systematic procedure and are modified and tuned by the simulation performance. The rules table and stability of the fine- tuned controller with simulation performance are justified by using the approach evaluated in deeply discussed.

The systmatic approach evaluated in is used for the analysis and design of proposed FLC. Membership functions are preliminarily selected as a symmetrical, and the approach can be successfully applied to symmetrical membership functions.

The output of FLC is added to the current compensating signal. FLC is developed in MATLAB is applied to control the dc-link voltage for the first time without any interfecing with other simulation programs.

5. SIMULATION RESULTS AND DISCUSSION

The power quality improvement capability of the UPQC system is tested through MATLAB. A three phase diode bridge rectifier is used as a harmonic current producing load with a total harmonic distortion (THD) of 14.21% .

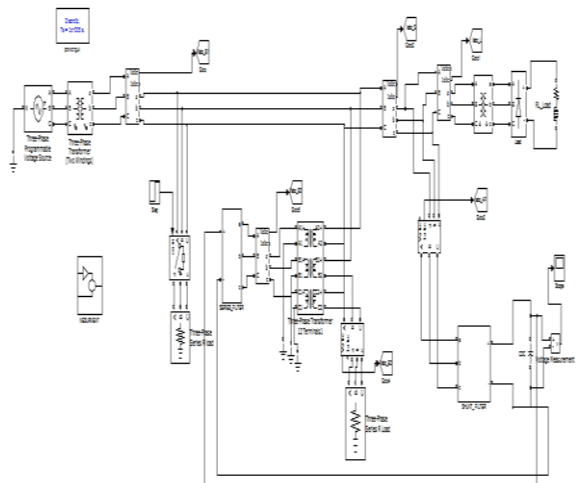


Fig. 6. Test system with UPQC.

VI. Total harmonic distortion

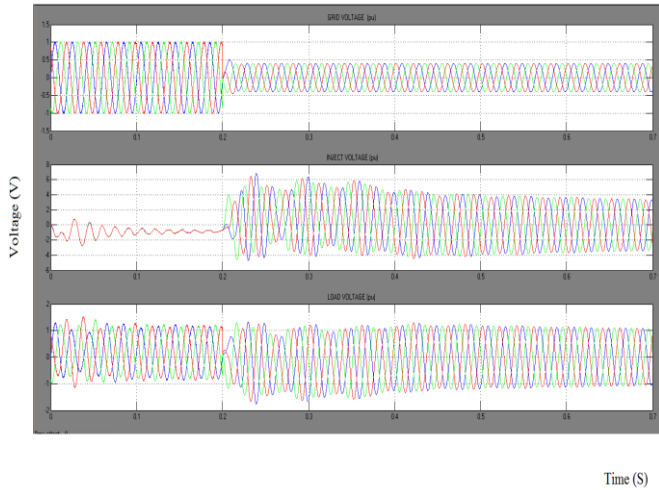


Fig. 6.a. Simulation results with series converter.

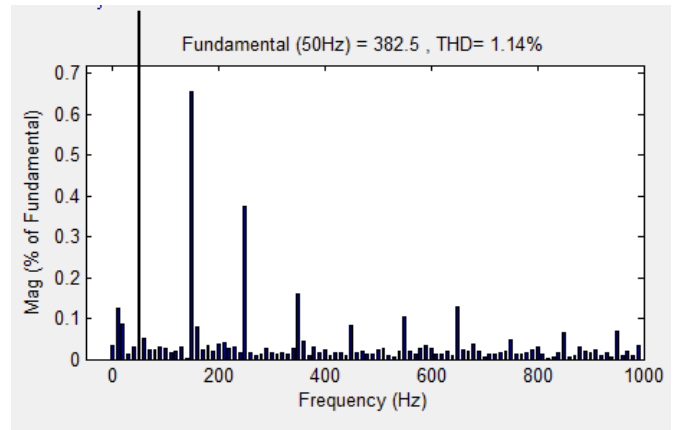


Fig. 8.a. Total harmonic distortion in source current.

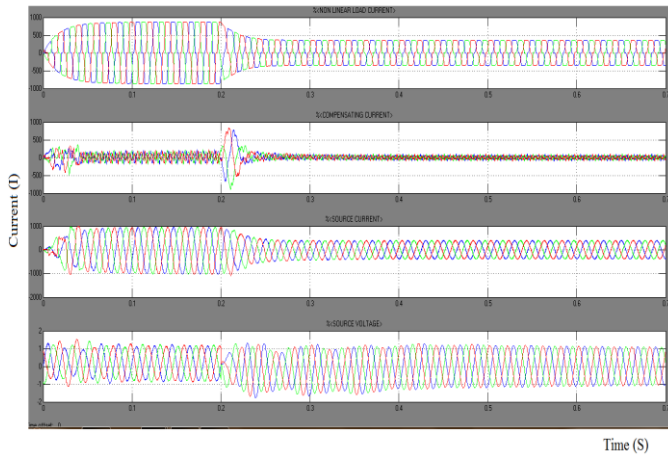


Fig. 6.b. Simulation results with shunt converter.

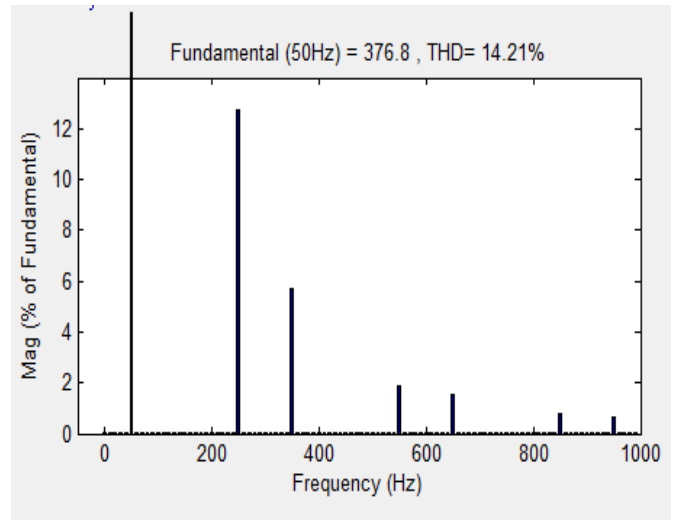


Fig. 8.b. Total harmonic distortion in nonlinear load current.

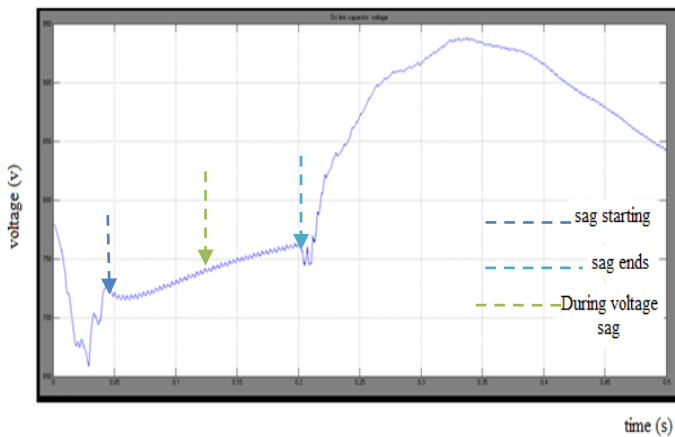


Fig. 7. Dc-link capacitor voltage.

VII. CONCLUSION

The unified power quality conditioner is introduced and analyzed by the controlling voltage source converter (VSC₁ and VSC₂) based on enhanced PLL and nonlinear adaptive filter algorithms and dc-link voltage with a fuzzy logic controller. New functionality is added to the UPQC system to quickly extract the reference signals directly for load current and supply voltage with a minimal amount of mathematical operands. The number of parameters to be tuned has also been reduced by the use of the proposed controller. The performance of the proposed UPQC and controller for the PQ improvement is tested through the simulations. The proposed UPQC system provides simultaneous mitigation of a variety of PQ problems.

REFERENCES

- [1] H. R. Mohammadi, A. Y. Varjani, and H. Mokhtari, "Multiconverter unified power quality conditioning system MC-UPQC," *IEEE Trans. Power Del.*, vol. 24, no. 3, Jul. 2009, pp. 1679–1686.
- [2] A. K. Jindal, A. Ghosh, and A. Joshi, "Interline unified power quality conditioner," *IEEE Trans. Power Del.*, vol. 22, no. 1, Jan. 2007, pp. 364–372.
- [3] H. Fujita and H. Akagi, "The unified power quality conditioner: The integration of series and shunt-active filters," *IEEE Trans. Power Electron.*, vol. 13, no. 2, Mar. 1998, pp. 315–322.
- [4] M. Brenna, R. Faranda, and E. Tironi, "A new proposal for power quality and custom power improvement OPEN UPQC," *IEEE Trans. Power Del.*, vol. 24, no. 4, Oct. 2009, pp. 2107–2116.
- [5] A. Ghosh and G. Ledwich, "A unified power quality conditioner (UPQC) for simultaneous voltage and current compensation," *Elect. Power Syst. Res.*, vol. 59, 2001, pp. 55–63.
- [6] L. Qian, D. A. Cartes, and H. Li, "An improved adaptive detection method for power quality improvement," *IEEE Trans. Ind. Appl.*, vol. 44, no. 2, Mar./Apr. 2008, pp. 525–533.
- [7] H. S. Song, H. G. Park, and K. Nam, "An instantaneous phase angle detection algorithm under unbalanced line voltage condition," in *Proc. IEEE Power Electron. Specialis. Conf.*, 1999, vol. 1, pp. 533–537.
- [8] B. Wu and M. Bodson, "A magnitude/phase-locked loop approach to parameter estimation of periodic signals," *IEEE Trans. Autom. Control*, vol. 48, no. 4, Apr. 2003, pp. 612–618.
- [9] R. Rezaeipour and A. Kazemi, "Review of novel control strategies for UPQC," *Int. J. Elect. Power Eng.*, vol. 2, 2008, pp. 241–247.

Approximation Algorithms for Minimizing Sum of Flow Time on a Single Machine with Release Dates

E. O. Oyetunji^{1*} and A. E. Oluleye^{2,b} and S.A. Akande^{2,c}

¹Academic Quality Assurance Unit University for Development Studies, Ghana

²Department of Industrial and Production Engineering University of Ibadan, Nigeria

Abstract: This paper considers the scheduling problem of minimizing the sum of flowtime on single machine with release dates. It is well known that the problem is NP-Hard, therefore in order to solve the problem, two approximation algorithms (KSA1 and KSA2) were proposed. KSA1 and KSA2 algorithms were compared with the MPSW (selected from the literature) and the Branch and Bound (BB) method. All the four solution methods were evaluated on a set of randomly generated problems. Twenty problem sizes ranging from 3 to 100 jobs and fifty problem instances under each problem size were generated. A total of 1000 (50x20) problem instances were solved. Experimental results based on effectiveness show that the MPSW algorithm performs closest to the BB method and outperformed both the KSA1 and KSA2 algorithms for all the problem sizes considered. On the other hand, based on efficiency, the KSA1 and KSA2 algorithms outperformed both MPSW and BB methods.

Keywords: Single Machine Scheduling, Sum of Flowtime, Release Dates, Effectiveness, Efficiency, Approximation Algorithm

1. INTRODUCTION

Scheduling can be defined as the allocation of a set of defined resources to a set of defined tasks subject to certain constraints, in order to satisfy a specific objective [9]. Scheduling has wide applications in computer systems, Hospital administration, Transportation management, Lecture and examination planning, Manufacturing e.t.c. Generally, scheduling problems involve jobs that must be scheduled on machines subject to certain constraints in order to optimize one or more objective function(s).

The methods for solving general scheduling problems can be classified into: exact and approximation methods. Exact method yield optimal solutions (e.g. total enumeration method, Hungarian method, Johnson's method for 2-machine sequencing, implicit enumeration method such as branch and bound or dynamic programming methods). The approximation method, on the other hand, involves the use of heuristic algorithms. Heuristic methods usually involve the use of an intuitive approach or rule of thumb. Heuristic methods are techniques for obtaining acceptable solutions to scheduling problems at reasonable computational costs. While they do not always guarantee optimal results, the techniques are relatively economical in terms of computational resources utilized. In view of the computational difficulty required by the exact methods, the benefit of lower computational costs has been an attraction to being utilized by researchers in order to solve scheduling problems [13]. This is the motivation for adopting approximation algorithms in this work.

There are several objectives (performance measures) in scheduling [12]. In systems involving queuing and networks, for example, the flow time of a job consists of both the waiting time in the queue and the job processing time on the machine so that minimizing flow time improves service quality [11]. The desire to improve service quality makes the minimization of the total flow time (or sum of flow time) an important scheduling criterion. The foregoing also motivated the selection of the sum of flow time as the criterion to be minimized. Scheduling jobs on a single machine is important because single machine environments are common and can usually be modeled as a special case of other environments. Because the assumption that all jobs are available at time zero does not always hold, we focus on problems for which jobs have distinct ready or release dates.

Therefore, the main aim of this work is to develop approximation algorithms that can be used to solve the scheduling problem of minimizing the sum of flow time on a single machine with release dates.

Three variants of the problem have been explored by researchers. These are:

(1) problems in which the release dates are zeros (i.e. $1 \mid \sum_{i=1}^n F_i$),

¹ E.O. Oyetunji holds a PhD degree in Industrial Engineering, and is currently a Senior Lecturer in the Department of Computer Science and Director, Academic Quality Assurance Unit, University for Development Studies, Ghana.

² A.E. Oluleye holds a PhD degree in Industrial Engineering, and is currently a Professor in the Department of Industrial and Production Engineering and Dean, Faculty of Technology, University of Ibadan, Nigeria.

* Corresponding author.

(2) problems in which pre-emption is allowed (i.e. $1 | pmtn, r_i | \sum_{i=1}^n F_i$), and

(3) the general non preemptive problems in which the release dates are different and distinct (i.e. $1 | r_i | \sum_{i=1}^n F_i$).

Smith [15] showed that the first variant of the problem can be solved optimally using the Shortest Processing Time (SPT) rule. The second variant of the problem (the preemptive version) can be solved optimally in polynomial time by using the Shortest Remaining Processing Time (SRPT) rule [2]. The solution of the preemptive version of the problem provides a lower bound for the third variant (the general non-preemptive version) of the problem [1]. The general non-preemptive version of the problem is known to NP-Hard [10]. We are unaware of any exact solution method for this third variant of the problem. A number of authors have developed branch-and-bound algorithms for the general non-preemptive version of the problem [3]-[6].

Guo et al. [8] noted that an optimal solution for $1 | r_i | \sum_{i=1}^n C_i$ is also an optimal solution for $1 | r_i | \sum_{i=1}^n F_i$. In view of this,

Guo et al. [8] modified the PSW algorithm (proposed for $1 | r_i | \sum_{i=1}^n C_i$ by Phillips et al., [14]) to solve the

$1 | r_i | \sum_{i=1}^n F_i$ problem. The algorithm is called MPSW.

2. PROBLEM DEFINITION

Given the general one-machine scheduling problem where a set J of n jobs has to be sequenced on a machine in order to minimize the sum of flow time (also called total flow time). We assumed that only one job can be processed at a time and that the arrival time of every job J_i at the machine is known, distinct and denoted by r_i (release date). Also, each job J_i requires p_i time units on the machine (processing time). The time the processing of job J_i starts on the machine (start time) is designated as s_i with the property:

$$s_i \geq r_i \tag{1}$$

the completion time of each job (C_i) is defined as:

$$C_i = s_i + p_i. \tag{2}$$

The flow time of each job is defined as:

$$F_i = C_i - r_i \tag{3}$$

The sum of the flow time (also called total flow time) is defined as

$$F_{tot} = F_1 + F_2 + \dots + F_n = \sum_{i=1}^n F_i \tag{4}$$

Using the notations of Graham et al. [7], the problem being explored is represented as

$$1 | r_i | (F_{tot}) \quad \text{or} \quad 1 | r_i | \sum_{i=1}^n F_i$$

It is assumed that pre-emption is not allowed and that the problem is static and deterministic i.e. number of jobs, their processing times, and ready times and due dates are all known and fixed.

3. MATERIALS AND METHODS

The methods adopted in this study are now described:

3.1. Solution Methods

In order to solve the scheduling problem of minimizing the sum of flow time on a single machine with release dates, two approximation algorithms (labeled KSA1 and KSA2) are proposed. In order to compare the performances of the proposed algorithms, the MPSW algorithm of Guo et al. [8] was selected while a branch and bound (BB) procedure was also implemented. All the four solution methods are now described.

3.1.1. Branch and Bound (BB) Method

The branch and bound (BB) procedure is an implicit enumeration scheme where certain schedules or classes of schedules are discarded by showing that the values of the objective function obtained with schedules from this class are worse than a provable lower bound. The BB procedure gives optimal results. In order to compare the performances of the proposed approximation algorithms, the branch and bound method was implemented. The Shortest Processing Time (SPT) rule was used to obtain the lower bound at each node. The SPT is optimal for the relaxed $(1 \mid \mid \sum_{i=1}^n F_i)$ problem [9]. The node that gave the best lower bound value (total flow time) determines the branch to explore. At the terminal node, when all the jobs must have been assigned, the node that gave the best solution was noted and became the solution to the considered problem.

3.1.2 MPSW ALGORITHM

The MPSW algorithm was proposed by Guo et al. [9] for the scheduling problem of minimizing total flow time criterion on a single machine with release dates (i.e. $1 \mid r_i \mid \sum_{i=1}^n F_i$ problem). The MPSW algorithm produces non-preemptive schedules from preemptive ones as follows:

- Step 1: Form a preemptive schedule using the Shortest Remaining Processing Time (SRPT) rule.
 SRPT always picks jobs with the shortest remaining processing times among those already released at the current time and processes these first. Each job i has a (preemptive) completion time C_i^p .
- Step 2: Form an ordered list L of jobs based on their preemptive completion time C_i^p using a simple sort.

A non-preemptive schedule is then obtained if we continue to assign the first job in L to the machine when it is freed and delete it from L .

3.1.3 KSA1 Algorithm

The KSA1 algorithm schedules the job that has the least value of the sum of the processing time and release date in the first position (breaking ties by selecting the job with the job that has the lowest release date among the tied jobs). The remaining jobs are scheduled in the increasing order of their waiting times. Waiting times of the remaining jobs are computed as the absolute value of the time difference between the release date of each job and the completion time of the first scheduled job. The steps of KSA1 algorithm are now described:

KSA1 Algorithm Steps

- STEP 1: Initialization
 Job_Set_A = [$J_1, J_2, J_3, \dots, J_n$], set of given jobs
 Job_Set_B = [0], set of scheduled jobs
 Job_Set_C = [$J_1', J_2', J_3', \dots, J_n'$], set of unscheduled jobs, $J_j' = J_j$
 Job_Set_D = [0]
 n = number of jobs
- STEP 2: Compute the index = $p_i + r_i$ for each of the jobs in Job_Set_A, $i = 1, \dots, n$
- STEP 3: Arrange the jobs in Job_Set_A in the order of increasing index computed in Step 2 and put the jobs in Job_Set_D. If there is a tie (i.e. two or more jobs have the same index value), select first the job that has the lowest release date among the tied jobs. If there are still ties, break ties arbitrarily.
- STEP 4: Select the job in the first position from Job_Set_D, add this job to Job_Set_B and remove same job from Job_Set_C.
- STEP 5: Compute the Completion time of the job scheduled in step 4 (C_1)
- STEP 6: Compute $\Delta W_j = |R_j - C_1|$ for all the remaining jobs in Job_Set_D. Where R_j is the release date of each of the remaining jobs in Job_Set_D and C_1 is the completion time of jobs in Job_Set_D, $j = 2, 3, \dots, n-1, i = 1, 2, 3, \dots, n$.
- STEP 7: Re-arrange the remaining jobs in Job_Set_D in the order of their increasing ΔW computed in Step 6
- STEP 8: Append Job_Set_D to Job_Set_B
- STEP 9: Stop

3.1.4 KSA2 Algorithm

The KSA2 algorithm is similar to the KSA1 algorithm. The main differences between the KSA2 and KSA1 algorithms are as follows: after obtaining the initial schedule, while the KSA1 break ties by selecting the job with the least release date, the KSA2 algorithm in addition proceeds to break ties by selecting the job with the least processing time. Also, the KSA2 algorithm computes the raw waiting time of jobs instead of the absolute values of the waiting time. The steps of KSA2 algorithm are now described:

KSA2 Algorithm Steps

STEP 1 : Initialization

Job_Set_A = [$J_1, J_2, J_3, \dots, J_n$], set of given jobs

Job_Set_B = [0], set of schedules job

Job_Set_C = [$J_1', J_2', J_3', \dots, J_n'$], set of unscheduled jobs, $J_j' = J_j$

Job_Set_D = [0]

n=number of jobs

STEP 2: Compute the index = p_i+r_i for each

of the jobs in Job_Set_A, $i= 1, 2, \dots, n$.

STEP 3: Arrange the jobs in the order of

increasing index computed in Step 2 and put the jobs in Job_Set_D. If there is a tie (i.e. two or more jobs have the same index value), select first the job that has the lowest release date among the tie jobs. Also, if there is a further tie in the release date, arrange the jobs in the order of their increasing processing time. If there are still ties, break ties arbitrarily.

STEP 4: Select the job in the first position from Job_Set_D, add this job to Job_Set_B and

remove same job from Job_Set_C.

STEP 5: Compute $\Delta W_j = (p_i+r_i) - R_j$ for all

the remaining jobs in Job_Set_D. Where R_j is the release date of each of the remaining jobs in Job_Set_D, $j=2, 3, \dots, n$; $i = 1, 2, \dots, n-1$.

STEP 6: If ΔW_j is negative or zero, set

$\Delta W_j = \Delta W_i$

STEP 7: Re -arrange the remaining jobs in

Job_Set_D in the order of increasing ΔW_j . If there is a tie in ΔW_j , arrange the tie jobs in the increasing order of their release dates. Also, if there is a further tie in the release date; arrange the tied jobs in the increasing order of their processing times. If there are still ties, break the ties arbitrarily.

STEP 8: Append Job_Set_D to Job_Set_B.

STEP 9: Stop

3.2 Data Analysis

A total of 20 problem sizes ranging from 3 to 100 jobs and 50 problem instances under each problem size were randomly generated (1000 problems in all). The processing times (p_i) of jobs were randomly generated (using random number generator in Microsoft Visual Basic 6.0) with values ranging between 1 and 100 inclusive. Also, the ready times (r_i) of jobs were randomly generated with values ranging between 0 and 49 inclusive.

Coding was carried out in Microsoft Visual Basic 6.0. The program computes the value of total flowtime (F_{tot}) obtained by each solution method and each problem instance. Also computed was the execution time taken by each solution. The Statistical Analysis System (SAS version 9.2) was used to carry out detailed statistical analysis. The hardware used for the experiment had a 1.87 GHz P6000 Intel CPU with 4 GB of main memory.

The mean value of total flowtime obtained by the various solution methods over the 50 problem instances solved under each problem size was computed using the General Linear Models (GLM) procedure in SAS. The GLM procedure was also used to carry out the test of means (t-tests). The t-test was carried out in order to determine whether or not the differences observed in the mean value of total flowtime obtained by the solution methods are statistically significant. In order to measure the tendency of the solution methods to obtain best and worse results, the percentage of time each solution method obtains best and worse results were computed using the Summary procedure in SAS. Also, the approximation ratio of each solution methods was computed. The results obtained are presented and discussed in section 4.

4. RESULTS AND DISCUSSIONS

In order to measure the effectiveness of the solution methods, the value of the total flowtime was computed for each solution method, each problem size and problem instance. The mean value of the total flowtime obtained by the various solution methods over the 50 problem instances solved under the 20 different problem sizes ranging from 3 to 100 jobs is shown in Table 1. For a minimization problem, the smaller the value of the total flowtime, the better the solution method. Based on the minimum mean value of the total flowtime, a ranking order of BB, MPSW, KSA2 and KSA1 was obtained for all the problem sizes considered ($3 \leq n \leq 100$) (Table 1).

In order to determine whether or not the differences observed in the mean value of the total flowtime obtained by the solution methods are statistically significant, the test of means (t-test) was carried out and the results obtained are

summarized in Table 2. The differences observed in the mean values of the total flowtime obtained by the four solution methods (BB, MPSW, KSA1 and KSA2) are not significant at 5% level for all the problem sizes considered (Table 2).

In order to compare the performances of MPSW, KSA1 and KSA2 algorithms with that of the BB method, approximation ratios (MPSW/BB, KSA1/BB and KSA2/BB) were computed and plotted (Figure 1). The MPSW algorithm performed closest to the BB, followed by KSA2 while the KSA1 lag behind (Figure 1). The overall approximation ratio is shown in Table 3. The MPSW, KSA2 and KSA1 algorithms when compared with the BB method have approximation ratios 1.0099 (indicating that with respect to effectiveness the MPSW algorithm is about 0.0099% worse than BB method), 1.0191 (indicating that with respect to effectiveness the KSA2 algorithm is about 0.0191% worse than BB method) and 1.0201 respectively (indicating that with respect to effectiveness the KSA1 algorithm is about 0.0201% worse than BB method) (see Table 3).

To further examine the internal performances of the MPSW, KSA1 and KSA2 solution methods, the percentage of time each solution method obtained the best and worse results was computed (see Tables 4 and 5). The MPSW gave the best results for all the considered problem sizes, indeed yielding 100% in instances involving 7, 80 and 100 jobs (Table 4). Thus, excluding the BB (which is optimal), the MPSW has the tendency to produce best results compared to KSA1 and KSA2. Generally, the KSA1 algorithm has the tendency to produce worse results compared to KSA2 and MPSW (Table 5).

In order to measure the efficiency of the solution methods, the execution time (seconds) taken by each method to obtain a solution to an instance of a problem was computed, plotted and are shown in Figures 2 and 3. As expected, the BB being an implicit enumeration method was the slowest followed by the MPSW (Figure 2). The KSA1 and KSA2 algorithms are very fast. It is observed that the BB and MPSW begin to exhibit exponential time complexity function when the number of jobs exceeds 40 and 70 respectively (Figures 2 and 3). To determine whether or not the differences observed in the mean execution time taken by the solution methods are statistically significant, the test of means (t-test) was carried out and the results obtained summarized in Tables 6 and 7.

The mean time taken by the KSA1 is not significantly different at 5% level from that of the KSA2 algorithm for all the problem sizes considered ($3 \leq n \leq 100$) (Tables 6 and 7). Also, the mean time taken by the MPSW is not significantly different at 5% level from that of the BB for $3 \leq n \leq 25$ problems (Tables 6). However, the mean time taken by the KSA1 and KSA2 algorithms are significantly different at 5% level from that of the MPSW and BB methods (indicating that both KSA1 and KSA2 algorithms are faster than both MPSW and BB) for all the problem sizes considered ($3 \leq n \leq 100$) (Tables 6 and 7). The mean time taken by the MPSW is significantly different (faster) at 5% level from that of BB for $30 \leq n \leq 100$ (Table 7).

Table 1 Mean value of total flow time by problem sizes and solution methods

Size	Mean of total flow time			
	BB	KSA1	KSA2	MPSW
3x1	253.74	256.26	256.26	254.82
4x1	427.28	442.56	441.62	432.64
5x1	554.80	577.54	577.30	565.62
6x1	797.26	820.16	818.70	808.78
7x1	1111.14	1141.80	1141.80	1127.82
8x1	1346.04	1384.12	1382.54	1362.36
9x1	1680.66	1739.62	1738.72	1719.68
10x1	1896.40	1950.98	1950.44	1923.84
11x1	2386.36	2465.50	2465.06	2438.84
15x1	4410.72	4509.24	4499.04	4469.64
20x1	7131.98	7271.92	7257.78	7211.66
25x1	11187.72	11369.34	11356.02	11287.74
30x1	16368.00	16575.20	16558.06	16443.70
40x1	28197.16	28567.22	28478.46	28351.68
50x1	43266.72	43655.86	43582.84	43416.34
65x1	72809.42	73495.42	73454.82	73034.20
70x1	84441.62	85177.96	85101.02	84700.80
80x1	111198.14	112156.78	112015.98	111490.72
90x1	141296.58	142302.42	142289.34	141617.98
100x1	172975.04	174152.22	174176.76	173297.92

Sample size=50

Table 2 Test of means (probability values) of total flow time for $3 \leq n \leq 100$ problems Solution Methods

Solution Methods	BB	KSA1	KSA2	MPSW
BB	-	>0.5x	>0.50x	>0.50x
KSA1	>0.50x	-	>0.50x	>0.50x
KSA2	>0.50x	>0.50x	-	>0.50x
MPSW	>0.50x	>0.50x	>0.50x	-

Note x indicate non significant result at 5% level; Sample size = 50
 - indicate not necessary

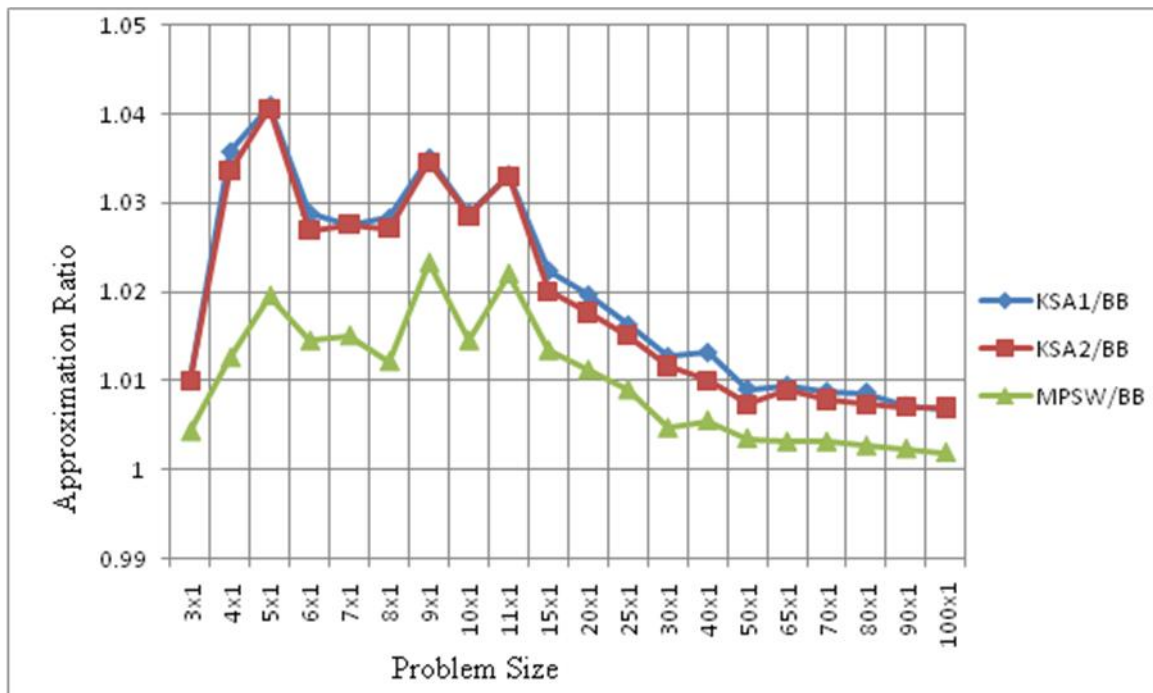


Figure 1 Approximation Ratios (KSA1/BB, KSA2/BB and MPSW/BB) by problem sizes .

Table 3 Overall approximation ratios of total flowtime by solution methods

Solution Methods	Overall approximation ratio
KSA1/BB	1.0201
KSA2/BB	1.0191
MPSW/BB	1.0099

Sample size = 1000

Table 4 Percentage of time solution methods obtain best results by problem sizes

Problem Size	Percentage (%) of time best result was obtained		
	MPSW	KSA1	KSA2
3x1	12	0	0
4x1	56	0	0
5x1	56	0	0
6x1	74	0	0
7x1	100	0	0
8x1	94	0	0
9x1	88	2	0
10x1	90	2	2
11x1	98	0	0
15x1	92	4	0
20x1	80	4	6
25x1	86	0	4
30x1	98	2	0
40x1	96	2	2
50x1	88	4	2
65x1	98	0	2
70x1	98	0	0
80x1	100	0	0
90x1	92	2	2
100x1	100	0	0

Sample size=50

Table 5 Percentage of time solution methods obtain worse results by problem sizes

Problem Size	Percentage (%) of time worse result was obtained		
	MPSW	KSA1	KSA2
3x1	0	0	0
4x1	6	0	0
5x1	4	2	0
6x1	4	4	4
7x1	4	0	0
8x1	4	6	2
9x1	8	6	4
10x1	4	10	8
11x1	2	8	6
15x1	4	14	8
20x1	8	18	12
25x1	6	14	14
30x1	0	22	20
40x1	0	50	14
50x1	8	44	16
65x1	0	40	30
70x1	2	58	20
80x1	0	66	24
90x1	4	38	40
100x1	0	46	46

Sample size=50

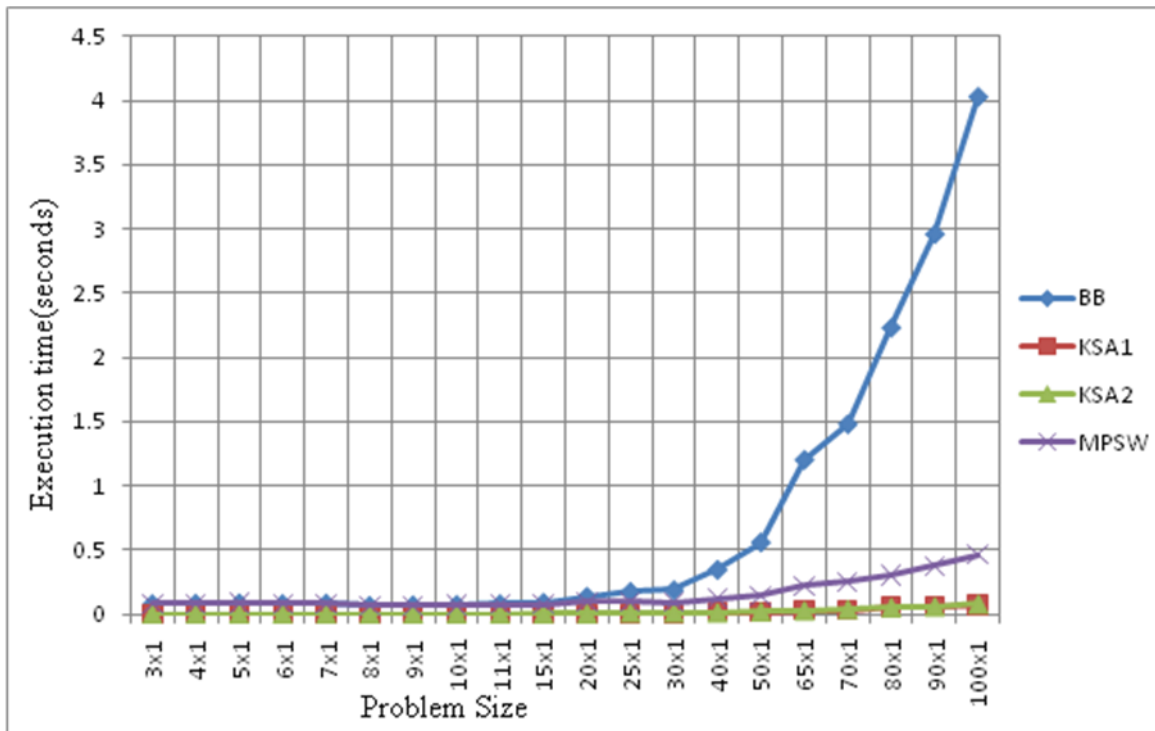


Figure 2 Comparison of the execution time (seconds) taken by four solution methods and problem sizes

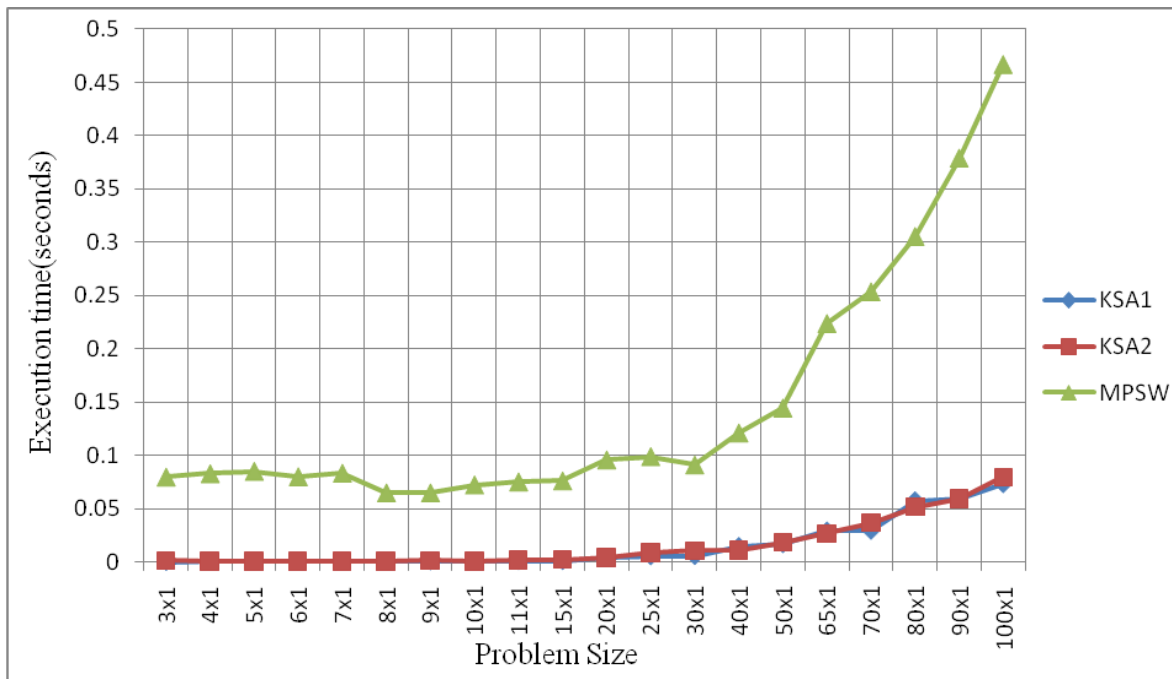


Figure 3 Comparison of the execution time (seconds) taken by three solution methods and problem sizes

Table 6 Test of means (probability values) of execution time for $3 \leq n \leq 25$ problems

		Solution Methods			
Solution Methods		BB	KSA1	KSA2	MPSW
BB		-	<0.050*	<0.050*	>0.50x
KSA1		<0.050*	-	>0.50x	>0.50x
KSA2		<0.050*	>0.50x	-	>0.50x
MPSW		>0.50x	<0.050*	<0.050*	-
Note	*	indicates significant result at 5% level;			Sample size = 50
	\bar{x}	indicates non significant result at 5% level			
	-	indicates not necessary			

Table 7 Test of means (probability values) of execution time for $30 \leq n \leq 100$ problems

		Solution Methods			
Solution Methods		BB	KSA1	KSA2	MPSW
BB		-	<0.005*	<0.005*	<0.005*
KSA1		<0.005*	-	>0.50x	>0.50x
KSA2		<0.005*	>0.50x	-	>0.50x
MPSW		<0.005*	<0.005*	<0.005*	-
Note	*	indicates significant result at 5% level;			Sample size = 50
	\bar{x}	indicates non significant result at 5% level			
	-	indicates not necessary			

5. CONCLUSIONS

We have explored the scheduling problem of minimizing the sum of flowtime (total flowtime) on a single machine with release dates. Two approximation algorithms (KSA1 and KSA2) were proposed for solving the problem. The two algorithms were compared with the MPSW algorithm selected from the literature. In order to further measure the performance of the three solution methods (KSA1, KSA2 and MPSW), they were compared with the Branch and Bound (BB) method.

Performance evaluations were based on both effectiveness (closeness of the value of the composite objective function to the optimal) and efficiency (how fast solution can be obtained i.e. a measure of execution speed). Experimental results, based on effectiveness, show that the MPSW algorithm outperformed both KSA1 and KSA2 algorithms as well as performed closest to the BB for all the problem sizes considered. Based on effectiveness, the KSA2 algorithm outperformed the KSA1 algorithm in many of the problem sizes while it performed as good as KSA1 in some of the problem sizes considered (3 and 7 jobs). However, with respect to efficiency, the KSA2 and KSA1 algorithms outperformed the MPSW algorithm for all the problem sizes considered. Also, the KSA2 was found to be as efficient as the KSA1 (i.e. none was consistently faster than the other).

Therefore, based on effectiveness, the MPSW algorithm is recommended for the scheduling problem of minimizing the total flowtime on a single machine with release dates while, based on efficiency, the KSA2 algorithm is recommended for the scheduling problem of minimizing the total flowtime on a single machine with release dates.

6. REFERENCES

- [1] Ahmadi, R. H. & Bagchi, U. 1990. Lower bounds for single-machine scheduling problems. *Naval Research Logistics*, 37, pp. 967–979.
- [2] Baker, K. R. 1974. Introduction to sequencing and scheduling. New York: Wiley.
- [3] Chandra, R. 1979. On $n|1|\overline{F}$ dynamic deterministic problems. *Naval Research Logistics*, 26, pp. 537–544.
- [4] Chu, C. 1992. A branch-and-bound algorithm to minimize total flow time with unequal release dates. *Naval Research Logistics*, 39, pp. 859–875.
- [5] Deogun, J. S. 1983. On scheduling with ready times to minimize mean flow time. *Computer Journal*, 26, pp. 320–328.
- [6] Dessouky, M. I., & Deogun, J. S. 1981. Sequencing jobs with unequal ready times to minimize mean flow time. *SIAM Journal on Computing*, 19, pp. 192–202.
- [7] Graham, R.L., Lawler, E.L., Lenstra, J.K. & Rinnooy Kan, A.H.G. 1979. Optimization and approximation in deterministic sequencing and scheduling: A survey, *Annals of Discrete Mathematics*, 5, pp. 287-326.
- [8] Guo, Y., Lim, A., Rodrigues, B. & Yu, S. 2004. Minimizing total flow time in single machine environment with release time: an experimental analysis, *Computers & Industrial Engineering*, 47, pp. 123–140.
- [9] Karger, D. Stein, C. & Wein, J. 1997. Scheduling Algorithms, A chapter written for the CRC Handbook on Algorithms (Boca Raton 1997).
- [10] Lenstra, J. K., Rinnooy Kan, A. H. G., & Brucker, P. (1977). Complexity of machine scheduling problems. *Annual Discrete Mathematics*, 1, pp. 343–362.
- [11] Leonardi, S., & Raz, D. 1997. Approximating total flow time on parallel machines, ACM Symposium on Theory of Computing.
- [12] Oyetunji, E. O. 2009. Some common performance measures in scheduling problems, *Research Journal of Applied Sciences, Engineering and Technology*, 1(2), pp. 6-9.
- [13] Oyetunji, E.O. & Oluleye, A.E. 2007. Heuristics for minimizing total completion time on single machine with release time, *Advanced Materials Research*, Trans Tech Publications Ltd., Switzerland, 18-19, pp. 347-352.
- [14] Phillips, C., Stein, C., & Wein, J. 1998. Minimizing average completion time in the presence of release dates. *Mathematical Programming B*, 82, pp. 199–224.
- [15] Smith, W. E. 1956. Various optimizers for single state production. *Naval Research Logistics Quarterly*, 3, pp.56–66.

Decoupled Logic Based Design for Implementation Low Power Memories by 8T SRAM

R. L. B. R. Prasad Reddy¹, G. Naresh²

¹Department of Electronics and Communication, Vaagdevi institute of Technology & Science, Proddutur, A.P

²Department of Electronics and Communication, Vaagdevi institute of Technology & Science, Proddutur, A.P

ABSTRACT: We present a novel half-select disturb free transistor SRAM cell. The cell is 6T based and utilizes decoupling logic. It employs gated inverter SRAM cells to decouple the column select read disturb scenario in half-selected columns which is one of the impediments to lowering cell voltage. Furthermore, “false read” before write operation, common to conventional 6T designs due to bit-select and wordline timing mismatch, is eliminated using this design. Two design styles are studied to account for the emerging needs of technology scaling as designs migrate from 90 to 65 nm PD/SOI technology nodes. Namely we focus on a 90 nm PD/SOI sense Amp based and 65 nm PD/SOI domino read based designs. For the sense Amp based design, read disturbs to the fully-selected cell can be further minimized by relying on a read-assist array architecture which enables discharging the bit-line (BL) capacitance to GND during a read operation. This together with the elimination of half-select disturbs enhance the overall array low voltage operability and hence reduce power consumption by 20%–30%. The domino read based SRAM design also exploits the proposed cell to enhance cell stability while reducing the overall power consumption more than 30% by relying on a dynamic dual supply technique in combination of cell design and peripheral circuitry. Because half-selected columns/cells are inherently protected by the proposed scheme, the dynamic supply “High” voltage is only applied to read selected columns/cells, while dynamic supply “Low” is employed in all other situations, thereby reducing the overall design power. A short bitline loading of 16 cells/BL is adopted to achieve high-performance low-power operation and lower bitline capacitance to improve stability. A newly developed fast Monte Carlo based statistical method is used to analyze such a unique cell, and 65 nm design simulations are carried out at 5 GHz. The feasibility of the cell and sensitivity to sense Amp timing has been proved by fabricating a 32 kb array in a 90-nm PD/SOI technology. Hardware experiments and simulation results show improvements of cell V_{dd} min over traditional 6T cells by more than 150 mV for 90 nm PD/SOI technology. Also experimental results based on fabricated 65 nm PD/SOI (1.6 kb/site 80 sites) hardware also asserts half-select disturb elimination and hence the ability to enable significant power savings. The

performance and speed are shown to be comparable with the conventional 6T design.

Index Terms: Column-decoupled, differential /domino read, half-select, low power 8T, SRAM, stability.

I. INTRODUCTION

Device miniaturization and the rapidly growing demand for mobile or power-aware systems have resulted in an urgent need to reduce power supply voltage (V_{dd}). However, voltage reduction along with device scaling are associated with decreasing signal charge. Furthermore, increasing intra-die process parameter variations, particularly random dopant threshold voltage variations can lead to large number of fails in extremely small channel area memory designs. Due to their small size and large numbers on chip, SRAM cells are adversely affected. This trend is expected to grow significantly as designs are scaled further with each technology generation [1]. Particularly, it conflicts with the need to maintain a high signal to noise ratio, or high noise margins, in SRAMs and is one of the

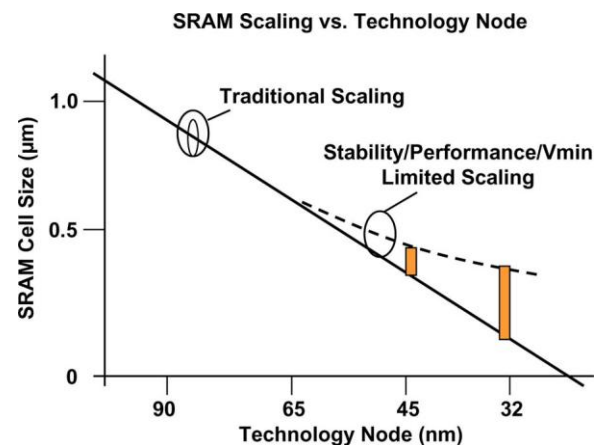


Fig. 1. SRAM cell scaling (dashed line) is limited due to process variation effect on cell yield.

Major impediments to producing a stable cell at low voltage. When combined with other effects such as narrow width effects, soft error rate (SER), temperature, and process variations and parasitic transistor resistance, the scaling of SRAMs becomes increasingly difficult due to reduced margins [2]. Fig. 1 illustrates the saturation in the

scaling trend (dashed line) of SRAM cells across technology generations. The plot indicates that the SRAM area scaling drops below 50% for 32-nm technology and beyond.

Furthermore, voltage scaling is virtually nullified. Higher fail probabilities occur due to voltage scaling, and low voltage operation is becoming problematic as higher supply voltages are required to conquer these process variations. To overcome these challenges, recent industry trends have leaned towards exploring larger cells and more exotic SRAM circuit styles in scaled technologies. Examples are the use of write-assist design [3], read-modify-write [4], read-assist designs [5], and the 8T register file cell [6], [7]. Conventional 6T used in conjunction with these techniques does not lead to power saving due to exposure to half select condition [3], [4]. Column select/half-select is very commonly used in SRAMs to provide SER protection and to enable area efficient utilization

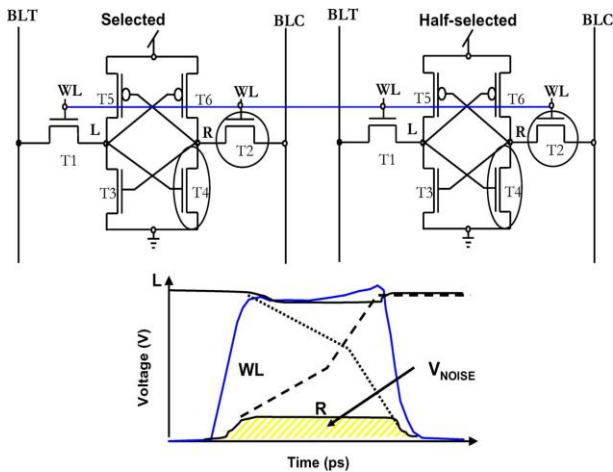


Fig. 2. SRAM half-select stability failure.

and wiring of the macro. Nevertheless, the use of column select introduces a read disturb condition for the unselected cells along a row (half-selected cells), potentially destabilizing them. In this paper we present a new column-decoupled 6T-based SRAM cell where read disturb is eliminated for column selected half selected cells [5], [8]. The decoupling logic uses two additional devices and henceforth we will refer to the cell as the 8T-column-decoupled-cell (8T-CDC). We study the cell in the presence of two design styles: namely, sense Amp-based read peripheral circuitry that was typical for the 90-nm node, and domino read peripheral circuitry [9] for 65 nm and beyond. In a sense Amp-based read design, the read disturb condition is further minimized for the selected cells by the use of a sense-amp architecture which actively discharges the selected cell(s) BL to GND, thereby eliminating the source of disturb. Through a combination of accurate simulations and hardware (HW) data acquired from a 32 kb SRAM macro, a path towards low voltage SRAM operation of the cells is shown, and the design is shown to enhance read stability and half-select stability problems thereby

enabling improved . However, process variations are increasingly affecting sense Amp designs in PD/SOI designs and it is natural to converge to domino-read designs [9]. In domino read-based designs, the column-decoupled cell still maintains guard against half-select cell disturbs. However, with the absence of read-assist feature in domino designs, we need to account for the read disturb on fully-selected cells. For this, we propose a dynamic dual supply header design that leverages the benefits of the column decoupled cell design and helps save power. As is the case with traditional dual supply techniques, the proposed header design maintains separate cell supply (Vcs) and logic supply (Vdd). However, unlike traditional techniques, the dynamic cell supply changes based on the column selection status. The new header design sets: 1) the selected cell columns at a voltage supply higher than the logic one for improved read stability and 2) maintains a low supply for half-select cells since half-select disturbs are not an issue for this design. Hence, we rely on the column-decoupled cell to enable a simplified low-power highperformance column-decoupled domino read based design. We implement the design using simplified bit-select logic and dynamic supply headers with shorter bitlines. In what follows, we provide a thorough analysis into the design modifications compared to the traditional 6T dynamic supply designs. We also highlight the advantages this methodology brings in terms of lower power and yield improvements. This paper is organized as follows. Section II provides a review of column-select disturbs. The cell is introduced in Section III. In Section IV, we study the sense amplifier based design and in Section V we study the dynamic domino based design are presented and in Section VI. Conclusions are presented.

II. BACKGROUND: COLUMN SELECT (HALF-SELECT) AND MEMORY DESIGNS

Fig. 2 shows a typical array topology which employs a two-way column select condition. In this topology, the word-line (WL) activates both the selected and half-selected cells along the decoded row. However, only the read/write data from the selected cell is allowed to pass to/from peripheral logic, while the half selected cell is isolated. When the word-line is activated during a selected read or half-select condition, the pass-gate (PG) transistor and the pulldown (PD) device (transistors T2 and T4 in Fig. 2) form a resistor- voltage divider between the BL and the storage node of the cell. This causes the “0” node of the cell (node R in Fig. 2) to bump up to some intermediate voltage which subsequently increases sub-threshold leakage (on transistor -3 in Fig. 2) and causes discharge of the “1” node in the cell thereby

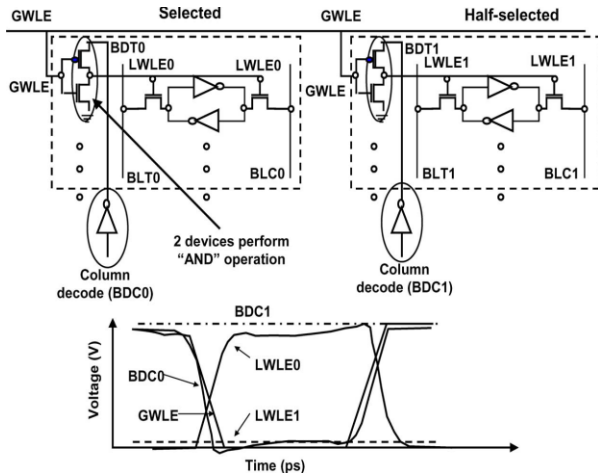


Fig. 3. Column-select decoupled 8T-CDC cell (in dashed rectangle) eliminates half-select condition. Selected column LWLE0 is high. Half-selected column LWLE1 stays low due to “ANDing” GWLE with BDC1).

destabilizing it. The read disturb to the selected cell keeps diminishing as the cell read current discharges the BL capacitance. The half-selected cell see the maximum potential in the case when the BLs are clamped to V_{dd}. This is the reason why there has been an industry wide trend towards shorter BL heights, thin cell designs and unclamping (floating) the bitlines of half-selected cells [2], [9] for 65 nm and beyond; in prior technologies, like 90 nm, the general trend was to use clamped bitlines. If the area under the curve is used as a measure of the read disturb witnessed by the cell, unclamping the BLs results in a mere 12% reduction over clamping for 128 cells/BL. While this benefit increases to 25% for 32 cells/BL, a significant area penalty is paid to achieve this. In the following section, an 8T-CDC which can result in larger area reduction of the curve for the half-selected cell is presented. This design, together with special sensing technique or special dynamic headers can lead to improved yield for both selected and half-selected cells and lower operating voltages for the overall design.

III. 8T COLUMN DECOUPLED CELL

A. Proposed 8T-CDC

Fig. 3 illustrates a new 8T-CDC SRAM cell (inside dashed rectangle) with a gated wordline which enables the decoupling of the column/half-select condition [5] hence eliminating halfselect stability fails. A localized gated inverter consisting of two additional transistors, T1 and T2, effectively perform a logical “AND” operation between the column select signal (BDT0) and the decoded row, or global wordline, GWLE. The output of the inverter is the local wordline signal (LWLE0). The local wordline is ON only when both the column and row are selected (i.e., for fully selected cells only); hence, as illustrated in the waveforms of Fig. 3, LWLE0 of the selected column turns ON while LWLE1 of the half-selected column remains low. This ensures that the local wordline for only

the selected cells is activated, thereby effectively protecting the half-selected SRAM cells from the read disturb scenario that exists in 6T cell due to wordline sharing. Alternatively, it is possible to swap the input and supply pairs of the gated inverter; however this comes at the cost of extra delay stage and power. The advantages of the 8T-CDC cell are as follows: 1) conforming with traditional 6T requirements in terms of (a) allowing the designer to integrate it in a column select fashion and (b) offering/maintaining SER protection while 2) maximizing array efficiency, 3) eliminating the read disturb to the unselected cells, and 4) reducing power with simplification in peripheral logic. Fig. 4(a) shows a layout view of the 8T-column-decoupled cell in a 90-nm PD/SOI technology. The two extra devices are integrated on top of an existing 6T cell to allow for easy cell mirroring and integration into an array topology. The addition of the two new transistors results in a cell area increase of 40% (all in -direction). Through the use of higher level metallurgy to wire in the column decode (BDC) signal, the growth to the -direction of cell was not impacted. The increase to the - mension of the cell causes a proportionate increase to the BL metal capacitance while maintaining the original diffusion capacitance contributed by the 6T cell. Column decode signal integrated with higher level metal. Area penalty can be further reduced to 30% via use of 6T thin cell integration in Fig. 4(b); further reduction can be achieved by use of non-DRC clean devices. Fig. 4(b) and (c) presents the front end of the line (FEOL) and back end of the line (BEOL) layout view of 2 2 8T-CDC thin cell. The views illustrate how the recessed oxide (ROX) and power buses are shared. The area can be reduced further to 30% by utilizing thin cells as presented in this paper without degrading the bitline capacitance.

B. Timing Advantages: Elimination of “False Read” Before Write

During the write operation in conventional 6T SRAM, when the wordline precedes ahead the column-select in timing, then the cell starts reading the data [8]. When the bitline droops, “false read” before write happens [see Fig. 5(a)]. This is a disadvantage for conventional 6T SRAM. This particular drawback is overcome by the technique that is proposed here as illustrated When the bitline droops, “false read” before write happens. (b) This particular drawback is overcome by the 8T-CDC cell; the early ordline (GWLE in dashes) will be gated by the column select and thus “false read” before write does not happen. in the Fig. 5(b); if the wordline arrives earlier than the column select it will be gated by the column select and thus “false read” before write does not ripple through the bitlines to the evaluation logic.

C. Logic and Circuit Requirements

The difference between the 8T-CDC and 6T array design can be highlighted in terms of distributed versus global wordline drivers. Hence, for the 8T-CDC cell, the wordline driver (inverting function) is eliminated as it is already accounted for inside the gated cells. This helps

reduce the area overhead and will be discussed in detail later. Fig. 6(a) and (b) illustrates the wordline logic for the 6T design and 8T-CDC design, respectively. The gated inverters

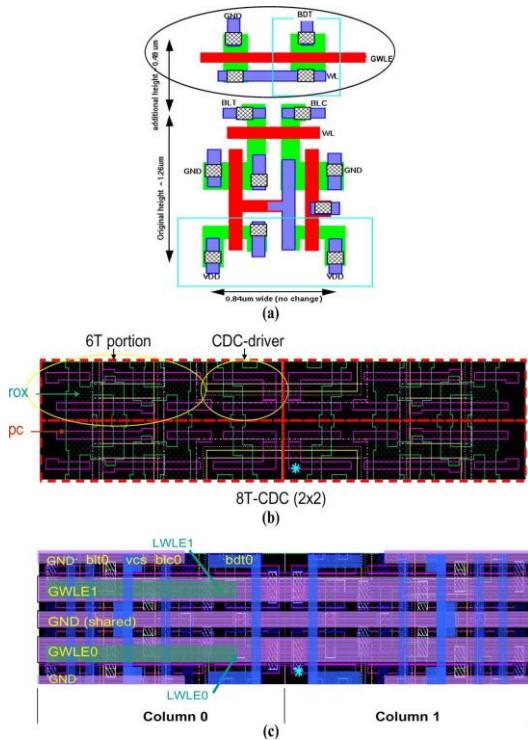


Fig. 4. Layout view of the new 8T-CDC SRAM cell for a (a) typical cell and a (b) 2x2 thin cell front end of the line layout view and (c) back end of the line layout view to show ROX and GND sharing.

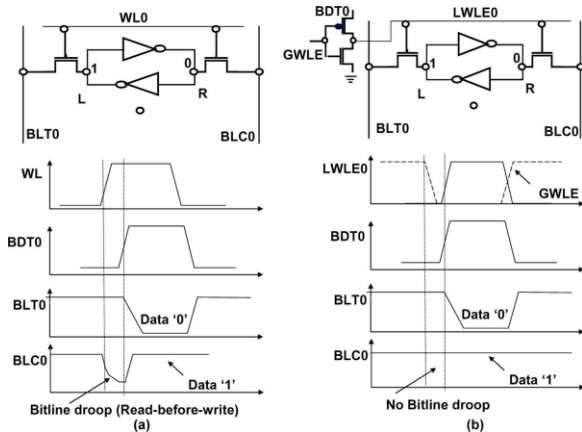


Fig. 5. (a) For conventional 6T SRAM, during write, when the wordline precedes ahead the column-select, the cell starts reading the data [8].

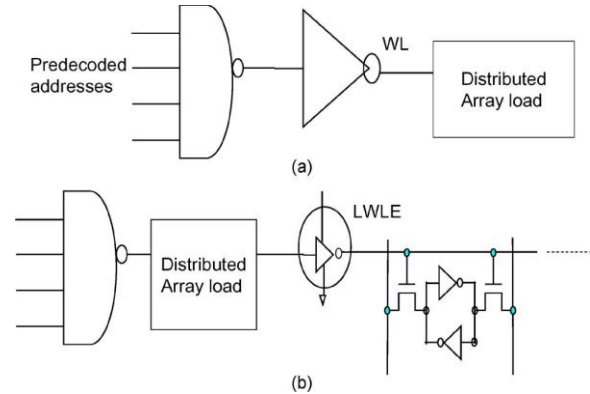


Fig. 6. Wordline logic (a) for traditional 6T cell and (b) for the 8T-CDC cell. the wordline driver (inverting function) is eliminated as it is already accounted for inside the gated cells.

transistor sizes are comparable to those of the SRAM cell. In the presence of large distributed loads, it may be desirable to optimize the NAND gate nfets further. This is feasible with minimal area penalty because the gated inverter sizes leave room for NAND gate optimization. Furthermore the gated inverters improve the local wordline slews as opposed to the case of conventional 6T wordline drivers with large pass gate loads where the slew rates are wire limited.

IV. SENSE AMP BASED DESIGN

The 8T-CDC cell together with read-assist sense amp designs [5] can mitigate the read disturb problem both for selected and half-selected designs

Read Assist Sense Amp-Based design:

Fig. 7 illustrates the 8T-CDC cell design combined with readassist sense Amp. The sense amplifier is shared among multiple columns. In a typical sense Amp scenario, the bit switch (BDC), and the WL on the selected cells columns are turned off once enough margin is developed for the sense-amplifier to accurately resolve the BL differential. This is done to save ac power (prevents discharge of BL to GND) and to speed up sense-time (smaller capacitance for sense-amplifier to discharge). For this scenario, only the PFET transistor exists (solid bit switch PFET Fig. 7) and it closes during "Sense" to save power and perform faster sense. In a read-assist scenario the bit-switch PFET is converted to a complementary (dashed line) NFET and PFET bit-switch pair. The pair is kept open during the entire WL active phase. Consequently, the sense-amp and the cell discharge the BL completely during a sense-read operation [5].

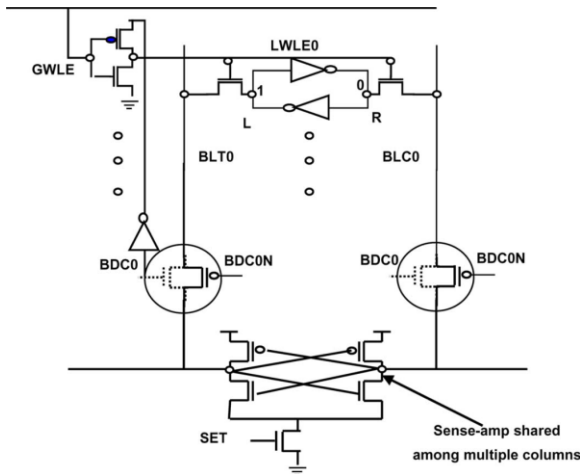


Fig. 7. Gated 8T-CDC cell design combined with read-assist sense Amp [5].

Hence the sense amplifier “sees” the full BL capacitance during a read operation; it discharges the capacitance to GND, and the cell data is “written back”. This helps minimize the amount of read disturb charge induced onto the cell from the bitlines.

V. DOMINO READ-BASED DESIGN

In the following sections, we discuss the advantages of the proposed 8T-CDC design in the presence of domino read based architectures as well as the rationale behind these architectures. As technology scales, sense-Amp devices suffer from V_t -mismatch and scaling becomes difficult particularly for PD/SOI technology designs due to hysteretic V_t variation. Thus, it is preferred to use large signal domino read circuitry [9]. During a domino read, the dual rail signals from the cell are amplified by skewed inverters to full rails. This eliminates the dependency on bitline differential which can be highly sensitive to V_t -mismatch and we refer the reader to [9] and the references within for a detailed overview of domino based read designs. However, the SRAM cell read disturbs and half-select problems are still critical in a domino read design. In what follows, we study the advantages of combining a decoupled half-select column design cell design with dynamic supply techniques for a 65-nm PD/SOI domino read-based design. Our goal is to exploit the elimination of half-select disturbs together with dynamic supply techniques for optimal yield and power. For this purpose, we propose new header designs for the dynamic supply suitable for the 8T-CDC cell. Next, we revisit traditional circuit and peripheral logic for 6T domino designs and propose simplifications/modifications as well as novel dynamic header designs suitable for low-power 8T-CDC cell design.

VI. CONCLUSION

We studied a novel 8T-CDC column-decoupled SRAM design. The half-select free design enables enhanced voltage scaling capabilities, and 30%–40% power reduction in comparison to standard 6T techniques. This study involved a 90-nm read assist-based sense Amp design, and a 65-nm domino read-based design with dynamic supply capabilities. The 8T-CDC cell enables significant power savings in terms of reduction for read-assist design, and half-select column power reduction in dynamic dual supply domino read designs with the aid of new header designs.

REFERENCES

- [1] L. Itoh, K. Osada, and T. Kawahara, “Reviews and future prospects of low voltage embedded RAMs,” in *Proc. IEEE Custom Integr. Circuits Conf.*, 2004, pp. 339–344.
- [2] C. Wann, R. Wong, D. J. Frank, R. Mann, S.-B. Ko, P. Croce, D. Lea, D. Hoyniak, Y.-M. Lee, J. Toomey, M. Weybright, and J. Sudijono, “SRAM cell design for stability methodology,” in *Proc. IEEE VLSI-TSA Int. Symp. VLSI Technol.*, 2005, pp. 21–22.
- [3] L. Chang, D. M. Fried, J. Hergenrother, J. W. Sleight, R. H. Dennard, R. K. Montoye, L. Sekaric, S. J. McNab, A. W. Topol, C. D. Adams, K. W. Guarini, and W. Haensch, “Stable SRAM cell design for the 32 nm node and beyond,” in *Proc. IEEE Symp. VLSI Technol.*, 2005, pp. 128–129.
- [4] M. Kellah, Y. Yibin, S. K. Nam, D. Somasekhar, G. Pandya, A. Farhang, K. Zhang, C. Webb, and V. De, “Wordline & bitline pulsing schemes for improving SRAM cell stability in low- V_{cc} 65 nm CMOS designs,” in *Proc. VLSI Circuits Symp.*, 2006, pp. 9–10.
- [5] V. Ramadurai, R. Joshi, and R. Kanj, “A disturb decoupled column select 8T SRAM cell,” in *Proc. CICC*, 2007, pp. 25–28.
- [6] W. Henkels, W. Hwang, R. Joshi, and A. Williams, “Provably correct storage arrays,” U.S. Patent 6 279 144, Aug. 21, 2001.

A High Sensitive and Fast Motion Estimation for One Bit Transformation Using SSD

Pratheepa.A¹, Anita Titus²

¹ ME-VLSI Design

² Dept of ECE

Easwari Engineering College, Chennai-89

Abstract: In this paper, architectures implementing fixed block size (FBS) and variable block size (VBS) for One bit transform (1-BT) using SSD (Sum of Squared Differences) to find motion between frames have been proposed. In general Motion estimation (ME) requires a huge amount of computation, and hence consumes the largest amount of power. The technique used to reduce the usage of power is 1-BT based ME algorithms. They have low computational complexity. In this less On-chip memory used than the previous 1BT based ME hardware by using a data reuse scheme and memory organization. Here the Sum of Absolute Difference (SAD) matching method is followed with the application of Diamond Search (DS). The 1-BT based ME is usually performed by applying full search (FS) algorithm. The proposed architecture reduce the power by performing the application of toroidal path in the pipelining approach on processing element with Sum Of Squared differences technique(SSD). The simulation results reveal that the application of DS on 1-BT based ME using SSD technique can significantly reduce the computational complexity and the power which is observed in SAD based 1-BT ME.

Index terms: One Bit Transformation, Motion estimation, Sum of Absolute Differences, Sum of Squared Differences, diamond search algorithm, fixed block size, variable block size.

I. INTRODUCTION

Motion estimation is the process of determining motion vectors that describe the transformation from one 2D image to another, usually from adjacent frames in a video sequence. It is an ill-posed problem as the motion is in three dimensions. The motion vectors may relate to the whole image (global motion estimation) or specific parts (local motion estimation), such as rectangular blocks, arbitrary shaped patches or even per pixel in the images. The motion vectors may represented by other models that can approximate the motion of a real video camera, such as rotation and translation in all three dimensions and zoom.

In general, motion of objects is specified in 3-D real world. In motion estimation, the 'projected motion' has been concerned with the 3-D objects onto the 2-D plane of an imaging sensor. It means the estimation of the displacement (or velocity) of image structures from one frame to another in a time sequence of 2-D images, by motion estimation. This projected motion is referred to as 'apparent motion',

'2-D image motion', or 'optical flow'. A possible first approach to **motion estimation** is to assume that the motion is locally translational, and that the image intensity is invariant to motion, i.e., it is conserved along motion trajectories. Smoothness (slow spatial variation of the displacement vector field along the motion) can be imposed either implicitly, when formulating the motion estimation algorithm, or explicitly during implementation.

Motion estimation (ME), which is the most essential part of any video coding technique, exploits and tries to minimize the temporal redundancy present between successive frames. ME, which is computationally intensive, involve about 80% of the total computational power of the encoder. So there is a **block matching** required. There are two mainstream techniques of motion estimation: pixel (pel)-recursive algorithm (PRA) and block-matching algorithm (BMA). PRAs are iterative refining of motion estimation for individual pels by gradient methods. BMAs assume that all the pels within a block has the same motion activity.

BMAs estimate motion on the basis of rectangular blocks and produce one motion vector for each block. PRAs involve more computational complexity and less regularity, so they are difficult to realize in hardware. In general, BMAs are more suitable for a simple hardware realization because of their regularity and simplicity. Here a BMA method has been taken place for the proposed technique.

Motion Estimation Algorithms vary with respect to the information, as well as the method of computation they utilize to obtain the estimate. The idea of using a block of pixels and assuming a common displacement for them in the matching process corresponds to a local smoothness (coherence). In this paper an efficient method for block matching motion estimation is considered for interframe motion compensated prediction of video signals. In contrast to other block matching methods, this approach takes into consideration the behavior of individual pels in the search to find the best match. This is achieved by classifying each pel in the block into following categories: matching pel and mismatching pel [3]. The method existing is sum of absolute difference (SAD) technique [1].

Block matching motion estimation (BMME) technique is one of the efficient methods that remove the temporal redundancy present between the successive frames. In this

method video frame is partitioned into 16×16 frames known as macro blocks.

II ONE BIT STRATEGY WITH SAD(EXISTING)

Now a transform has been constructed that maps a frame of multivalued pixels to a frame of binary value pixels. That transform is defined with respect to a convolution kernel K and the transform is denoted by Q_k . Let F denote a frame and let \hat{F} denote the filtered version of F obtained by applying the convolution kernel K to F. Let $B = Q_k(F)$ be the frame obtained by applying QK to F. The pixels of B are given by,

$$B(i, j) = \begin{cases} 1, & \text{if } F(i, j) \geq \hat{F}(i, j) \\ 0, & \text{otherwise} \end{cases}$$

Here, i and j are the spatial coordinates of the pixel. The foregoing process by which an original frame with 8 bits/pixel representation is converted into a binary frame with 1 bit/pixel representation is known as one-bit transformation.

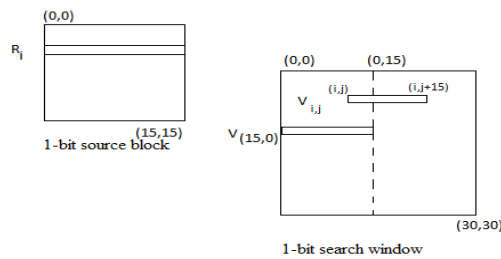


Fig.1. Pixel co-ordinates for a 16×16 source block and a one bit search window.

And for sum of absolute differences technique, the equation is

$$SAD = \sum_{(i,j) \in w} |I_1(i, j) - I_2(x + i, y + j)|$$

The similarity measure which is calculated by applying the simplest SAD method, subtracting pixels within a square neighborhood between the reference image I_1 and the target image I_2 followed by the aggregation of absolute differences within the square window, and optimized. If the left and right images are exactly matched then the resultant will be zero otherwise the window size will be increased.

else $SAD_{ij} = 1$, then threshold will be

$$V_{th} = \frac{1}{MN} \sum_{i=1}^M \sum_{j=1}^N SAD_{ij}$$

A key to accurate motion estimation is the observation on the edges of the images. A simple way to extract the edges is to carry out a high-pass thresholding, that is, compare the frame pixel by pixel to a high-pass filtered version of the frame, and threshold the pixels to zero or one, depending on the outcome of the comparison [4]. The convolution kernel

that we propose is motivated by this consideration, as well as the need to minimize the number of arithmetic operations.

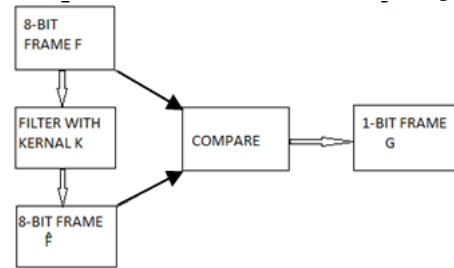


Fig.2. Operation for thresholding 8-bit frames to 1-bit frames

The operations for the one-bit transform are shown in Fig.- 2. Note that there is no global threshold for all pixels in a frame. For video coding, the one-bit motion estimation strategy consists of the following steps: 1) apply the one-bit transform Q to both the current frame and the reference frame; 2) use any motion-vector search strategy in combination with the metric defined in (fig 4).

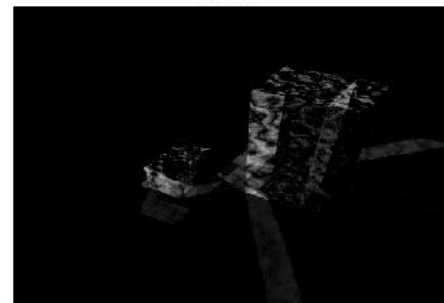
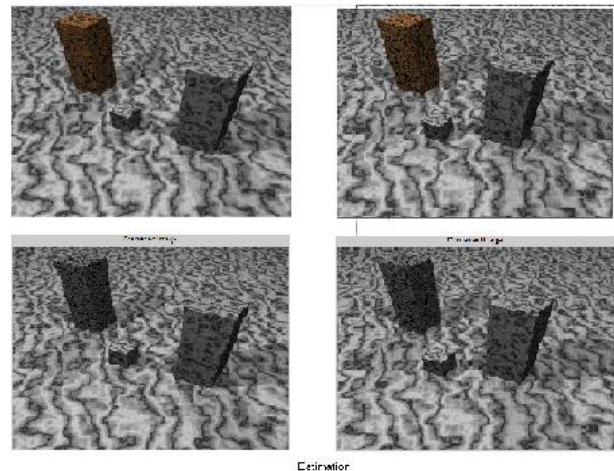


Fig.3. Flow of operations of converting to 1-b based block motion estimation.

After this operation, the number of non-matching points (NNMP) at any point (m, n) for a MB of size $N \times N$ is found as:

$$NNMP(m, n) = \sum_{i=0}^{n-1} \sum_{j=0}^{n-1} B^t(i, j) \oplus B^{t-1}(i + m, j + n)$$

Where $-S \leq (m, n) \leq S$

$$SSD = \sum_{(i,j) \in w} (I_1(i, j) - I_2(x + i, y + j))^2$$

Here, 's' is the maximum search range and \oplus denotes XOR operation. Also, B^t and B^{t-1} represent the current and the reference 1-BT frames respectively.

III THE DIAMOND SEARCH and MOTION VECTOR PREDICTION

The proposed DS algorithm employs basically for a search pattern for easy prediction of motion vector present which is originally deviated from the frames, and it is having two search patterns, the first pattern, called large diamond search pattern (LDSP), and comprises nine checking points from which eight points surround the center one to compose a diamond shape (◆). The second pattern consisting of five checking points forms a smaller diamond shape, called small diamond search pattern (SDSP). In the searching procedure of the DS algorithm, LDSP is repeatedly used until the step in which the minimum block distortion (MBD) occurs at the center point. The search pattern is then switched from LDSP to SDSP as reaching to the final search stage.

Among the five checking points in SDSP, the position yielding the MBD provides the motion vector of the best matching block. After the search pattern analyses the pattern has been given to for FBS the frame size will not be change. For example if the frame size is 4x4 means, it will be maintained the same till the last frame check. For the next search only the frame size will be changed to next criteria. And for the VBS the frame size will be changed even during the run time also. The frame size can be 2x2, 4x4, 8x8, and 16x16.

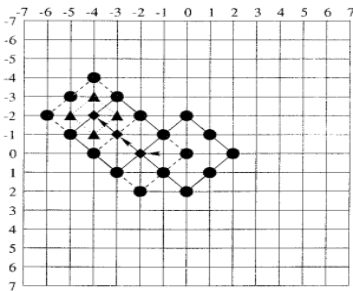


Fig. 4. Example of motion of vector

Generally, a motion estimation algorithm includes two important components for the MV search: search center and search pattern. In previous reported ME algorithms, search center is generally predicted from spatial and temporal neighbors motion vector (MV).

IV. SUM OF SQUARED DIFFERENCES

The tracking method presented as the enhancement of the base work in this paper. It is based on minimizing the sum-of-squared differences (SSD) between a selected set of pixels obtained from a previously stored image of the tracked patch (image template) and the current image of it.

In Sum of Squared Differences (SSD), the differences are squared and aggregated within a square window and later optimized by search strategy. This measure has a lower computational complexity compared to SAD algorithm as it involves less numerous multiplication operations.

Steps for SSD method:

Step 1: For the first P (previously coded) frame, FS is executed. The SSD Value (SSD_{ij}) is stored in a data table.

Step 2: According to the existing SSD value table, a threshold value V_{th} is computed and SSD table is updated: If $SSD_{ij} < V_{th}$ then $SSD_{ij} = 0$

Step 3: For the following P frames, motion estimation for the macroblock in current P frame will refer to the value in corresponding position of the obtained data in the table.

If $SSD_{ij} = 0$, a 16x16 matching search is performed.

Else, the macroblock will be split into four 8x8 blocks for further matching.

Step 4: SSD value results from the motion estimation of current P frame are stored. Go to step 2 if there is remaining P frames or terminate the loop otherwise.

V. PIPELINING ON TOROIDAL PATH AND PROCESSING ELEMENT

A. PIPELINING WITH TOROIDAL STRUCTURE

Pipelined computer architecture has received considerable attention since when the need for faster and more cost-effective systems became critical. The merit of pipelining is that it can help to match the speeds of various subsystems without duplicating the cost of the entire system involved. In this paper in pipelining a FIFO (first in first out) method is applied. In that the architecture has been changed with the application of toroidal structure. A toroidal approach to an orbit path filter was presented that provides more versatility than a simple distance function. This method uses the primary orbit to define a focus-centered elliptical ring torus with separate, user-defined, in-plane and out-of-plane bounds. Through toroidal path a data storage, retrieve, and to track the value easily from one PE to another PE with shortest minimum path calculation and this would keep the throughput at high rates also.

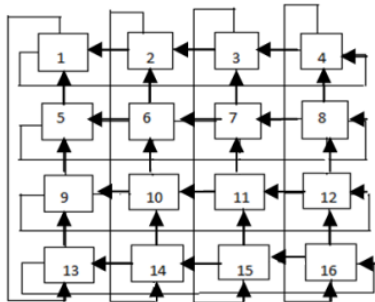


Fig.5. Toroidal Structure

B. PROCESSING ELEMENT

The architecture of the PE for both VBS and FBS is shown in Fig.7&8. The PE possesses two input ports namely, C and S for reading two 16-bit vectors from the CB and the SW respectively. There are two 8-bit XOR arrays in the PE. One of the XOR arrays operates on the eight most significant bits of the 16-bit vectors C and S, and the other operates on the remaining eight least significant bits. The number of 1^s as a result of the XOR operation is obtained by using two look-up tables (LUTs) with 2⁸ entries. The outputs of the LUTs are then applied to a 4-bit adder. The output of the adder is then applied at the input of the accumulator. The output of the accumulator provides the value of the NNMP for a particular location after 16 clock cycles for a MB of size 16x16.

VI ARCHITECTURES

The proposed architecture is,

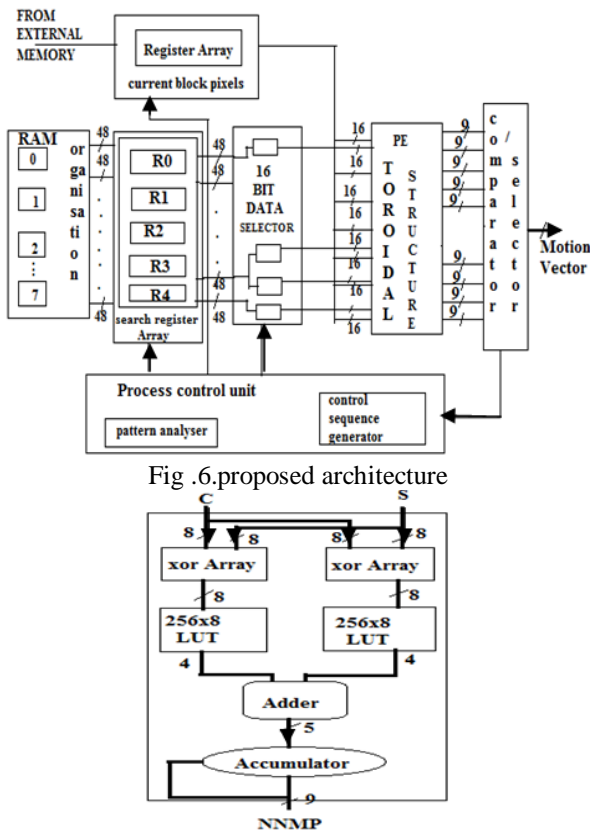


Fig .6. proposed architecture

Fig.7. PE Architecture for one bit FBS ME

In recent years, the variable block-size (VBS) motion estimation has been widely employed to improve the performance of the block matching algorithm. In this paper a comparison for both FBS and VBS is shown on power.

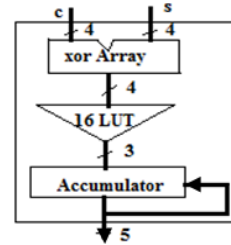


Fig.8. PE Architecture for one bit VBS ME

In the past algorithms, many fast BMAs were proposed for reducing the computational complexity for the FS, such as three-step search (TSS), four-step search (FSS), orthogonal search, and hexagon based search (HEXBS) algorithms, etc. Compared to these, diamond search algorithm on VBS and FBS reducing the computational complexity, usage of power, PSNR value compared to other algorithms. And the diamond search is applied on proposed SSD technique with toroidal pipelined architecture has reduced the power further and the speed of process is also increased.

VII IMPLEMENTATION RESULTS

A VBS motion estimation algorithm based on 16x16, 8x8, 8x4 and 4x8, for FBS 4x4,4x8 has been proposed which can efficiently reduce the computational cost while achieving similar or better visual quality as compared with other 1-BT based ME architectures, the proposed architectures involve lowest latency. The PSNR value is 30.81db, thus signal to noise ratio is increased compared to previous papers. The proposed fast binary FBS ME architecture consumes 932 slices (1533 LUTs). The on-chip memory of the proposed architecture is 2296 bits for storing the SW for a single MB.

PSNR COMPARISON:

SCHEME	PSNR
MAD	23.79db
2-BT	23.43db
MF-1-BT	23.32db
1-BT SAD	25.29db
1-BT SSD	30.81db

VIII CONCLUSION

The proposed DS based binary ME architecture for FBS and VBS are described in VHDL. The proposed architectures are implemented on ALTERA. In this paper, low power ME architectures have been developed for implementing DS on 1-BT frames with FBS and VBS support for SSD. As compared with other 1-BT based ME architectures, the proposed architectures involves the lowest latency. The clock frequency, I/O pins used, gates required for the proposed ME architectures therefore can be effectively reduced for low power designs.

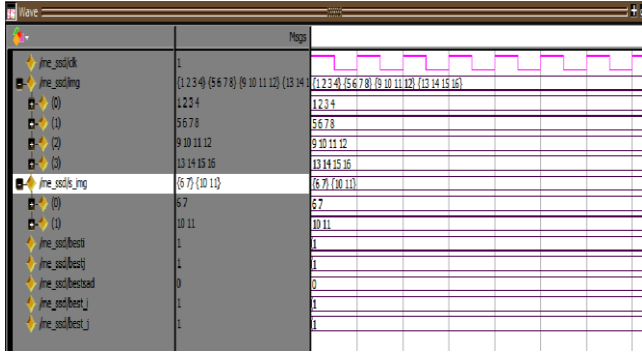


Fig.8.Example wave for ssd calculation

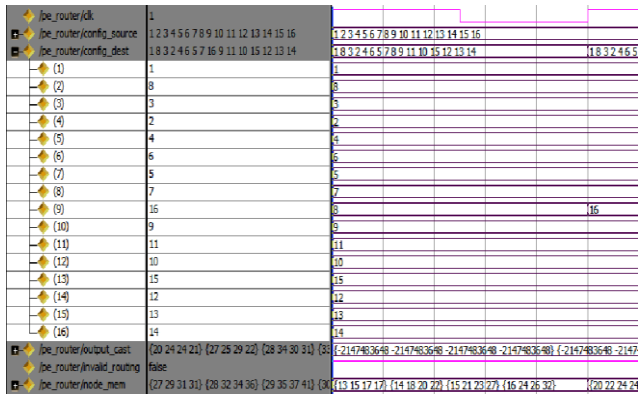


Fig.9.False invalid routing indication wave for PE

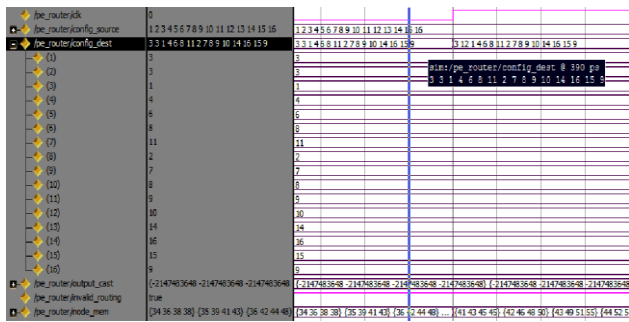
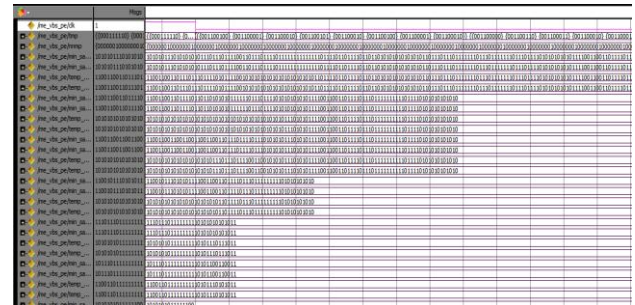


Fig.10.True invalid routing indication wave for PE



Fig.11.Output of PE for FBS (NNMP deviated data)



REFERENCES

- [1] Sumit K Chatterjee and Indrajit Chakrabarti, "Low Power VLSI Architectures for One Bit Transformation Based Fast Motion Estimation", IEEE Trans. Consumer Electronics., vol. 56, no. 4, pp. 2652-2660, November 2010.
- [2] C. H. Hsieh and T. P. Lin, "VLSI architecture for block-matching motion estimation algorithm," IEEE Trans. Circuits Syst. Video Technol., vol. 2, no. 2, pp. 169-175, June 1992.
- [3] H. Gharavi and M. Mills, "Block matching motion estimation algorithms new results," IEEE Trans. on Circuits and Systems, Vol. 37, no. 5, pp. 649-665, May 1990.
- [4] Surin Kittitornkun and Yu Hen Hu, "Frame-Level Pipelined Motion Estimation Array Processor" IEEE Transactions On Circuits And Systems For Video Technology, Vol. 11, No. 2, February 2001.
- [5] Peter H. W. Wong and Oscar C. Au, "Modified One-Bit Transform for Motion Estimation", IEEE Transactions On Circuits And Systems For Video Technology, Vol. 9, No. 7, October 1999.
- [6] A. Celebi, O. Urhan, I. Hamzaoglu, and S. Erturk, "Efficient hardware implementation of low bit depth motion estimation algorithms," IEEE Signal Processing Lett., vol. 16, no. 6, pp. 513-516, June 2009.
- [7] Rafael C Gonzalez, Richard E Woods, "Digital Image Processing", publication year 2008.

Assessment of Potential Impacts on NH7 – 4 Laning from Salem to KARUR

T. SUBRAMANI¹

¹Professor & Dean, Department of Civil Engineering, VMKV Engg College, Vinayaka Missions University, Salem, India.

ABSTRACT

For the developing countries like India, it is highly essential to concentrate on the various developmental activities which are yard sticks for the degree of heights of development in term of technology and economy. To increase our pace of achievements in various field developmental activities are planned and implemented in various fields. Any developmental activity needs prior assessment of environmental impacts before its approval to start the work. The main objective of this thesis work is to assess the potential impacts which have taken place during the 4 laning of NH7 highway from Salem to Karur. In this project area, three districts namely Salem, Namakkal and Karur are covered. Many number of small panchayats, towns are in these three districts in the National Highways. The prime aim of this work is to collect the base line environmental details of land resources, water resources, air quality, noise levels, forests and protected areas, roadside plantations, cultural and community environments, social environment etc. from the respective collectorates. This collection is done for the period prior to 2005, before the commencement of the 4 laning work. The data and figures of the various resources are tabulated and shown in figures. It could be taken as a base data prior to the study of the environmental impacts in the study area of this project. These data differed from place to place. The assessment of the impacts were made during the construction of the highways and afterwards from 2005 onwards. The potential impacts both positive and negative such as climatic condition, land resources, water resources, air quality, flora, community facilities, cultural properties and social environment were collected and analyzed. It could be seen that the impacts when compared with the base data, have created not much significant adverse impacts. However, the temporary impacts may occur and hence suitable mitigation measures should be made with periodical community consultation. It could be observed that there are reduced accidents, improved accessibility and connectivity, reduced vehicle operator and maintenance cost, facilities to road works, improved quality of life and faster travel could be carried out. To reduce the air impacts and noise impacts in future, more plantation of trees on road side and development of green belts could be carried out.

KEYWORDS: Assessment, Potential Impacts, NH7, 4 Lane, Salem To Karur

1. INTRODUCTION - GENERAL

It is common Knowledge that humans continue to have a high impact on the environment. The combination of an exponentially growing population, escalating use of the earth's resources and human desire to modify rather than adopt to our surroundings, may seriously challenge the assimilative capacity of our natural system. Upto one half of the Earth's territorial environment has already been altered from its natural state through human activity. Over the passage of time, two conflicting facts have become clear that we continue to degrade the environment that we rely on and that we disrupt the functioning of its processes for both our economic and physical survival.

2. ENVIRONMENTAL IMPACT ASSESSMENT

It is a formed process used to Predict the environmental consequence of any developments Project. It is intended by identify the environmental, social and economic impacts of a proposed development period by decision making using EIA it in Principle by assite the Suitable environments option and alterative Process at an early stage.

3. PROJECT DESCRIPTION – PROJECT BACKGROUND

The Govt. of India (GoI) through Ministry of Roads & Highways (MORT&H) has decided to enhance the traffic capacity and safety for efficient transshipment of goods as well as passenger traffic on National Highway sections with heavy vehicular traffic. It has undertaken a massive National Highway Development Program (NHDP) consisting of widening and strengthening of NH sections connecting four major metros of Delhi, Mumbai, Chennai & Kolkata, popularly known as "Golden Quadrilateral" amounting to a total length of 5846km and improvements to North-South corridors connecting Kashmir with Kanyakumari and East-West corridors connecting Silchar with Porbandar amounting to a total length of 7300km.

The project under consideration aims at developing Salem-Karur section of NH-7, located in Tamilnadu state is a part of NHDP connecting North-South corridors

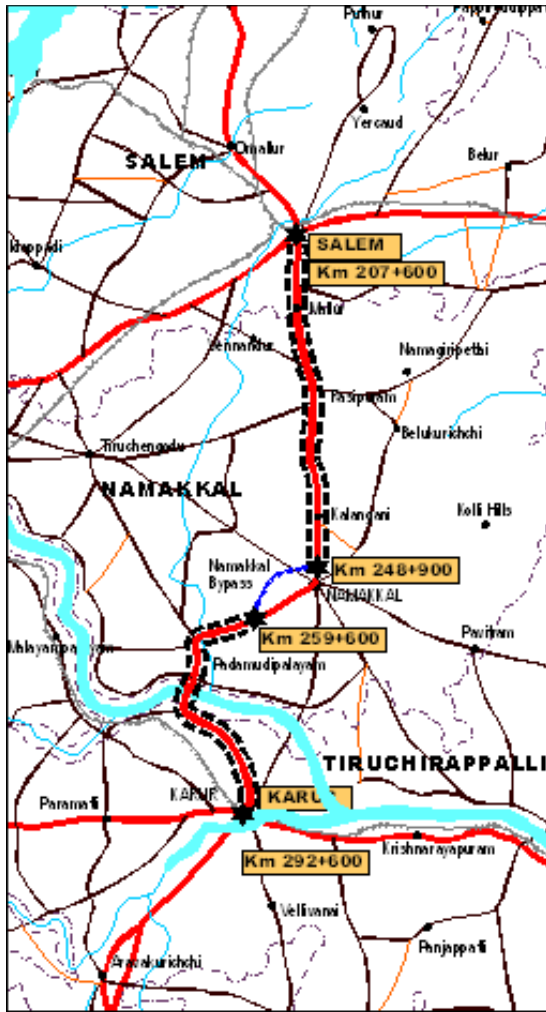


FIGURE.1 MAP OF THE PROJECT CORRIDOR

4. PROJECT CORRIDOR

The section of NH-7 under consideration takes off from a rotary intersection in the urban area of Salem. Existing four lane Salem bypass also starts at the same intersection. Chainage of the project corridor at this starting point is km 207+600, km 0+000 being at Bangalore. The project corridor travels south with an increase in the chainage towards Namakkal and Karur.

Namakkal bypass takes off from the NH-7 at km 248+900 on the outskirts of the city, and ends at chainage km 259+600. The project corridor ends at the outskirts of Karur town, where a four-lane bypass for the town is already in existence. Chainage of this intersection is km 292+600. The ToR mentions as the end point chainage to be km 301+000. However, a four-lane bypass already exists between km 292+600 and km 301. Accordingly, the end point for the present section may be considered as km 292+600 only.

The project corridor has a two lane, 6.5-7m wide carriageway with varying width of shoulders from 1-1.5m

on either side. Shoulder type varies along the corridor as some intermittent sections have paved shoulders. The project corridor generally traverses through plain terrain for most of its length except for few locations where terrain conditions are little undulating. Exposed rock has been observed at several places along the corridor. The project corridor generally has embankment height varying from 0.5-2m except at major bridge approach of Cauvery River at km 278, where an embankment height of 8-10m exists on both sides. Most of the water bodies along the project corridor are in dry state with no water. River Cauvery has a very wide course of 800m across the corridor but has narrow and shallow watercourse within.

Most of the Horizontal curves along the existing alignment fulfill the requirements of IRC standards for a design speed of 100 kmph. There are few sharp curves where it is required to improve the radius to ease out the curvature effect. Vertical geometry, in general, appears to be very smooth with flat gradients and long curves all along with few exceptions at places of rolling terrain conditions where corridor crosses small mounds. The available sight distance in both horizontal and vertical curves appears to be adequate and can still be increased with removal of bushes adjacent to the road. Combination of horizontal and vertical geometry has good pleasing aesthetics and do not have any disjointed effects along the entire corridor.

Agriculture is the predominant land use along the corridor. Several educational institutions, textile industries, hatcheries, poultry farms have also been observed along the corridor. The project corridor apart from having bypass at Namakkal also bypasses major settlements of Paramatty and Pugaloor/Veleyudampalayam.

There are as many as 146 intersections with various categories of roads along the corridor. Amongst them, nearly 16 intersections are of primary importance with SH, MDR and at existing bypass locations with old NH. In addition, there are 5 intersections of secondary importance with ODR and village roads, where good amount of motorized traffic are observed.

4. SCOPE OF WORKS

The objective of the study includes the following:

- The main objective is to establish the technical, economical, and financial viability of the project and prepare detailed project reports for rehabilitation and upgrading of the existing 2-lane National Highway (NH) sections to 4-lane divided carriageway configuration.
- The viability of the project designed as a partially access controlled facility need to be established taking into account the requirements with regard to rehabilitation, upgrading and improvement based on highway design, pavement design, provision of service roads wherever necessary, type of

intersections, underpasses / flyovers / ROB's, rehabilitation and widening of existing and/ or construction of new bridges and structures, road safety features, quantities of various items of works and cost estimates vis-à-vis the investment and financial return through toll and other revenues.

- The Detailed Project Report would inter-alia include detailed design, social and environmental action plans as appropriate and documents required for tendering the project on commercial basis for international / local competitive bidding.
- Provision of bypasses, realignments, and grade separators shall be considered where practicable and cost effective.

5. ASSESSMENT OF IMPACTS

5.1 INTRODUCTION

Road widening projects have typical potential impacts though these vary in accordance with the intensity of construction works involved, future scenario envisaged during the operation stage and the importance attached to the impacted environmental attributes. Since the project involves widening of the existing NH-7 from existing two lanes to four Lanes, the impacts will be confined to the proposed RoW. Subsequent sections detail out the likely impacts on various environmental components.

5.2 CLIMATE

By and large, there is no significant change expected in the macro-climatic setting (precipitation, temperature and wind) of the project corridor. However the microclimate is likely to be modified slightly due to removal of roadside trees and the addition of increased pavement surface. In addition, temporary loss of shade giving roadside trees will cause discomfort to the slow moving traffic and pedestrians.

5.3 LAND RESOURCES

5.3.1 Physical Settings

The project corridor traverses through plain tracts located between hillocks, especially in Salem Namakkal Stretch where rock out crops are observed. The Namakkal to Karur stretch passes through barren and also irrigated agriculture tracts of land. Since further rising of embankment height is not contemplated, fresh hindrance to the drainage pattern is not anticipated. The following impacts are likely on the physical setting along the corridor:

- Loss of productive lands along the corridor within the Corridor of Direct Impact that is presently being cultivated;

- Inappropriate disposal of wastes from the site;
- Indirect impacts at quarry and borrow locations during and after the period of construction; and
- Erosion of the murrum surface from the embankment slope to be used for casing of the underlying sand fill.

Construction of the new pavement and embankment shall require, materials in relatively large quantities, viz. Aggregates (for bituminous concrete and Wet Mix Macadam layers) from quarries; Murrum (for casing of embankment fill) from borrow pits; and Sand for (embankment fill) from borrow pits. Extraction of such materials will result in indirect impacts if the mentioned tasks are undertaken in an environmentally unsound fashion. The probable impacts in the likely quarry and borrow sites for the project is given in Table.1

Construction Material	Probable impacts
Aggregate	Formation of scars and steep slopes that are difficult to rehabilitate if full hillock is not exploited
Murrum	Disturbance to top soil Loss of vegetation (if present) Formation of steep slopes on hill bottom jeopardizing hill stability

TABLE 1: SPECIFIC IMPACTS AT PROBABLE QUARRIES AND BORROW AREAS

Other general impacts include:

- Vibrations and noise due to blasting operations on nearby habitations;
- Danger of flying debris from the blasting if quarries are close to habitations, agricultural fields or cattle grazing grounds; and
- Air, dust and noise pollution in settlements along haul roads during transportation of the quarried material to the construction site.

Processing operations like crushing of the quarried rock leads to:

- Increase in SPM levels in the surrounding areas up to 800 µg/m³; and
- High ambient noise levels during from crusher operations.

5.3.2 Soil

Soils in the Direct and the Indirect Impact Zone shall be impacted due to the proposed widening. Any impact in the direct impact zone is due to the actual construction;

where as in the indirect impact zone, impacts may be temporarily, if they serve as traffic detours, borrow areas, quarries and for construction camp.

Loss of Productive Land

The widening of road would require acquisition of agriculture lands at places where the available RoW is inadequate to accommodate the proposed improvements. The acquisition of agricultural land would cause loss of productive soil. Loss of productive land due to the road construction is a major long-term impact that results in depletion of fertile topsoil during the road construction phase. These impacts are likely to be significant along the 3 bypasses, wherein the alignment has been routed for a major length through agricultural lands to minimize resettlement impacts. The requirement for earthworks for the project has been worked out to be 6,50,000 cu.m.

Erosion Concern

Erosion of the top layer takes place as a result of construction and maintenance of the project corridor. During the construction phase, clearing of trees, construction of new fill slopes for grading bridge-end fills, possess high and pervasive potential for soil erosion. During operation or maintenance phase of highway erosion continues to occur in the areas not vegetated. Site most affected during the operational phase are generally bridge end fills and over steep banks, due to the long-term exposure to water and wind.

The project area is predominantly covered by red soil and for a significant length by sandy alluvial soil near to the Cauvery delta region. These soils are highly prone to erosion. All the bridge locations where elevated embankments are required would be more sensitive to the erosion during the construction period. 18 minor and 2 major bridges are located on the corridor. As a part of the road improvement programme, new under passes and flyovers will be provided in urban stretches. Such areas will also be vulnerable to erosion problems. However, small patches of black cotton soil are also observed in all three districts, which are more stable than the other two soil types of the project area and are highly resistant to erosion.

Construction Of New Bridges And Culverts

Two major bridges, one along the River Cauvery and the other along River Thirumanimuthar are to be constructed in the project. This involves excavation of riverbed and banks if the residual spoils are not properly disposed off, increased sedimentation downstream of the bridge may take place. During the construction phase some amount of drainage alteration and downstream erosion / siltation is also anticipated and can lead to alteration in drainage pattern and erosion / siltation; during the construction phase.

Quarries and Borrow Areas

Excavation of quarries and borrow pits used for obtaining rock, soil and aggregate material for road construction can cause major adverse environmental impacts, out of which removal of top soil is the major concern. The requirement for earthworks for the project has been worked out to be 6, 50,000 cu.m.

Compaction of Soil

Soil will be compacted during the site clearance and the construction activities due to the movement of vehicles and heavy machineries. This impact would be of short duration but adequate measures are to be undertaken to avoid the occurrence of any long-term impact.

Contamination Of Soil

Contamination of soil takes place both during construction and operation phases. The sites where in construction vehicles are parked and serviced are usually contaminating the soil because of leakage and or spillage of fuels and lubricants. Pollution of soil can also occur where Hot-Mix plants are located because of leakage or spillage of asphalt or bitumen. Refuse and solid waste from the labour camp can also contaminate the soil

5.4 WATER RESOURCES

Road construction has wide range of impact on the water resources, arising from activities such as earth moving, removal of vegetation, vehicles / machine operation and maintenance, handling and laying of asphalt, sanitation and waste disposal at labour camps. These mentioned activities lead to siltation, loss of water bodies through filling, as well as alteration of drainage, flooding, water logging and contamination of water bodies through solid and liquid waste.

Water is a limited resource in the project region. Salem and Namakkal district are notified as water scarce area. These regions are mainly dependent on ground water sources for meeting their water demand. The extraction of ground water for the construction purposes may increase the pressure on the available resources. The major adverse impacts on the water resources due to the project are discussed below:

5.4.1 LOSS OF WATER BODIES

The most significant adverse impacts to water bodies from the construction are the loss of storage capacity due to in filling by the earthmoving activities. Most of the water bodies that are likely to be impacted, are non-perennial. Therefore, conscious efforts have been made to minimize the impacts on these surface water bodies. Reduction of the area of these surface water bodies will be a moderate long-term negative impact during the construction and operation stages of the project.

There are 2 ponds located within the corridor of impact (Refer **TABLE 2: PONDS IMPACTED ALONG THE PROJECT CORRIDOR**). The existing road has been constructed along the boundary of such ponds. The proposed widening would result in cutting across the embankments and /or partial filling of such ponds thereby ultimately resulting in reduction of their storage capacities.

TABLE 2: PONDS IMPACTED ALONG THE PROJECT CORRIDOR

Chainage	Direction	Distance from Existing CL	Village Name
214.600	East	0	Ammapalayan
230.200	East	25	Kolinjipatti

These ponds were found to be dry and filled with silt. During the construction period, particularly during the summer, sourcing of the project’s water requirement would be difficult.

5.4.2 OTHER SURFACE WATER COURSES

The project corridor passes over 161 cross drainage structures, of which 141 are culverts, 18 are minor structures and 2 are major structures. The existing major structures are to be replaced with new structures, the minor structures and culvert may be retained as part of the widening option wherever the existing road cross sections are not critical.

Construction of the new structures when the channel is flowing may lead to drainage disruption through, haphazard dumping of the construction materials and wastes.

Roadside storage of construction materials too might lead to disruption in longitudinal drainage.

5.4.3 LOSS OF WELLS

A total of 161 wells are located within the proposed RoW. These wells are used for irrigation, domestic uses as well as for industrial purposes. The widening proposal of the project corridor will result in closure of 91 wells. To enhance the road safety the remaining 71 wells shall required protection measures as safety barriers.

5.4.4 LOSS OF OTHER WATER SOURCES

Widening of project entails removal and/ or shifting of water supply lines, removal of taps, wells, hand pump and tube wells within the proposed construction limits resulting in the loss of these facilities to the communities.

5.4.5 INCREASED RUN-OFF

Road construction activities will lead to an increased run-off both during the construction and operation stages. During the construction stage, removal of vegetation and compaction of soil leads to increased run-off during the

monsoon. Similarly, the area of open ground lost to built-up black top surface increases the run-off from the open ground.

The project involves creation of two lanes to the side of the existing pavement of 7m and service lanes in urban sections. There will be increase in impervious layer due to addition of median, hardening and paving of shoulders and bitumen surface. Due to the creation of impervious surfaces, there will be an increase in the run-off. The increased run-off during operation stage can be worked out using the formula:

$$\text{Increase in run-off per year (sq. m)} = \text{Increase in run-off coefficient due to construction} * \text{Annual rainfall in the area (m)} * \text{Area of the constructed surface (sq. m)}$$

The appropriate run-off coefficient for project corridor is 0.55 for black cotton soil, which is predominant in our project corridor.

5.4.6 WATER QUALITY DEGRADATION

Water quality may be degraded during construction due to the disposal of solid and liquid waste from the labour camp, fuel and lubricant spills or leaks from the construction equipments, fuel storage and distribution sites and from the bitumen and asphalt storage at hot-mix plants. Major pollutants of concern due to above mentioned activities are suspended solids, oil and grease, lead and other metals. The most susceptible locations for contamination of water resources during construction are:

- Waterlogged areas that have water in them during the period of construction;
- Surface and ground water resources close to bitumen or asphalt storages at hot-mix plants, maintenance sites of construction vehicles; and
- Surface water bodies close to labour camps. During the operation stage possible water pollution of surface and ground water bodies shall be limited to:
- Runoff and wastewater from truck parking, filling stations and automobile repair shops;
- Accidental spills from vehicles carrying hazardous chemicals; and
- Open wells adjacent to construction sites

5.4.7 GROUNDWATER RECHARGE AND FLOW MODIFICATION

Ground water recharge areas may be reduced due to an increase in impervious surface resulting from compaction. Contamination of ground water due to the runoff carrying pollutants is of major concern because most of the domestic use is from ground water. 57 wells are located within a width of 30 m on either side of the project

corridor. These wells are very large and deep and are used for irrigation, domestic uses as well as for industrial purposes. The widening proposal of the project corridor will result in closure of these wells.

The ground water levels of the wells along the project corridor were studied on a sample basis. It is observed that the depth of the ground water table varies from 3 m to 30 m below ground level. The water table goes further down in Namakkal Taluk.

5.4.8 USE OF LOCAL WATER SUPPLY FOR CONSTRUCTION

Use of water for road construction possesses large demand of water, which results in significant strain on the local water supply. During the construction phase large quantity of water is used for the compaction, suppression, concrete and formwork, causing minor and short-term impact on the local water supply. The strain on water supply ceases after the construction is completed. This shall be a significant impact given that the corridor passes through areas with scarcity of water, and the blocks being categorized either as over-exploited or dark blocks in terms of extraction and availability of ground water.

5.5 FLORA

Due to the proposed four laning and geometric improvements, trees in the RoW are likely to be removed at several locations. As a rule of thumb all trees within the proposed construction limits would be removed for reasons of safety. (Refer TABLE). As part of landscaping and mitigation for this loss, for every tree to be cut two trees would be planted.

TABLE. 3: CLASSIFICATION OF TREES TO BE REMOVED

	30-60	60-90	90-120	>120	Total
Section 1	401	601	802	201	2005
Section 2	195	292	389	98	974
Section 3	181	271	362	91	905
Section 4	67	100	133	33	333
Total					4217

5.6 AIR QUALITY

Air Quality along the project corridor will be adversely impacted both during construction and operation stages, due to increase in the volume of the traffic. Subsequent sections emphasize on various impacts during the construction and operation phases of the project.

5.6.1 IMPACT DUE TO CONSTRUCTION OF ROAD

- Generation of dust

- Due to procurement and transportation of raw material from borrow sites and quarries to the construction site.
- Due to site clearance, and use of heavy vehicles, machinery & equipments.
- Due to material transfer in stone crushing units
- Due to the handling and storage of aggregates from hot mix plant
- Generation of fine particulates during the process of mixing the aggregates and bitumen in the asphalt plant
- Generation Of Exhaust Gases
- Hot mix plant is considered to be the major contributor of exhaust gases, which includes oxides of sulphur, hydrocarbons and particulate matter.
- Bitumen production also releases volatile toxic gases through the heating process.

5.6.2 IMPACT DUE TO THE OPERATION OF HIGHWAY

During the operational phase of the highway, there is an increase in the air pollution level due to the increased traffic volume. Vehicular emission level rises either due to inadequate vehicle maintenance or due to the use of adulterated fuel in vehicles.

5.6.3 PREDICTION OF AIR IMPACTS

- the incremental pollution levels along the project corridor at various receptors are studied for the years 2003-04, 2013-14, 2023-24 and 2033-34.
- The predictions have been made for the pollutants SPM, CO and NO_x. The predicted concentration also takes into account the existing pollutant levels as established by the Ambient Air Quality Surveys.

As evident of Incremental CO Concentrations Predicted along the Project Corridor with the increase in traffic volume, the concentration of air pollutants also increases correspondingly. The increase in the CO concentration is comparatively higher than the remaining pollutants. But it is noteworthy to mention that the predicted levels of CO and NO_x are not significant even in year 2034. The predicted concentrations for CO and NO_x at all locations for all horizon years are below the National Ambient Air Quality Standards specified for rural and residential areas. For Suspended Particulate Matter exceedance of the National Ambient Air Quality Standards (as specified for rural and residential areas) is observed at some of the receptors along the project road especially in the stretch between Salem and Puduchattaram (Km 207.600 to Km 234.700). It is observed that among the 37 receptors selected for simulation of pollution levels, the limits are exceeded at 10 receptors in 2004 and at 19 receptors in

2034. The mitigation/management measures proposed as a part of the project are likely to improve the air quality scenario along the corridor during the operation stage. Tree plantation as per the proposed road landscape strategy will help to attenuate the air pollution levels. The tree species suggested include broad-leaved tree species which can help settle particulates with their higher surface areas and thick foliage and reduce the distance for which particulates are carried from the road itself. This measure is of specific importance in context of the high SPM concentrations as predicted in some of the receptor locations. Other measures such as the reduction of vehicular emissions, ensuring vehicular maintenance and up-keep, educating drivers about driving behavior / methods that will reduce emissions are beyond the scope of the project but will be far more effective in reducing the pollutant levels. Apart from provision of the mitigation measures, their effectiveness and further improvement in designs to reduce the pollutant levels with increase in traffic shall be monitored. A monitoring plan to this effect will be prepared as a part of the Environmental Management Plan (EMP).

5.7 NOISE LEVELS

Noise is perceived as one of the most undesirable consequences of road development. Though the level of discomfort caused by noise is subjective, there is a definite increase in discomfort with an increase in noise levels. The most commonly reported impacts of increased noise levels are interference in oral communication and disturbance in sleep.

Error! Reference source not found. highlights the Ambient Noise Standards according to the Noise Pollution (Control and Regulation) Rules, 2000 under the section 6 and section 25 of the Environment (Protection) Act, 1986 (29 of 1986) read with rule 5 of the Environment (Protection) Rules, 1986.

The impacts on noise quality due to the project will be of significance in both the construction as well as the operation stages.

TABLE 4 AMBIENT NOISE STANDARDS

Land use	Limits in dB(A) Leq *	
	Day Time	Night Time
Industrial area	75	70
Commercial area	65	55
Residential area	55	45
Silence Zone	50	40

*dB(A) Leq denotes the time weighted average of the level of sound in decibels on scale A which is relatable to human hearing.
 Nighttime: 10:00 pm – 6.00 am

5.7.1 CONSTRUCTION STAGE

Due to the various construction activities, there will be short-term noise impacts in the immediate vicinity of the project corridor. The construction activities include:

- Excavation for foundations with excavators;
- Grading and compaction of the site with graders and rollers; and
- Construction of cross drainage structures and other facilities.

Though the noise levels for the construction activities far exceed the permissible standards, it is important to note that the construction noise is generally intermittent and depends on the type of operation, location and function of the equipment. Proper mitigation measures like regulation of timings of construction, employing noise protection measures etc., need to be worked out.

5.7.2 OPERATION STAGE

With the increase in traffic noise levels are expected to increase along the project corridor. However, with reduced congestion levels as a result of widening of the corridor and improvement of road surface, noise levels are going to be considerably lower in the with project scenario.

5.8 COMMUNITY FACILITIES

A conscious effort is made to avoid impacts on the community facilities along the proposed alignment. However some of the properties of community facilities are being impacted upon to varying degrees. Geometric improvements to the corridor and the acquisition of a uniform RoW of 60m along the corridor necessitated encroachment onto the utilities.

5.9 CULTURAL PROPERTIES

5.9.1 ARCHAEOLOGICAL PROPERTIES AND PROTECTED MONUMENTS

As no archaeologically significant property or site or Protected monument lies within 7 km of the project corridor no impact on archaeological properties/historic sites and protected monuments are likely.

5.9.2 OTHER CULTURAL PROPERTIES

The likely impacts on cultural properties have already been discussed in the Preliminary Environmental and Social Report. These impacts are essentially subject to the location of the Cultural property in/on edge of the ROW and their extent varies and has been identified for each stage of Construction.

associated in the project are discussed in the report on Resettlement Action Plan (RAP)

TABLE ..5 DETAILS OF ACCIDENT RATES AT VARIOUS DISTRICTS

DETAILS	2005	2006	2007	2008	2009
Number of Major Accidents in the study area of Salem revenue District. (Km 207+600 to Km 216+600)	44	40	42	28	18
Number of Major Accidents in the study area of Namakkal District. (Km 216+600 to Km 275+600)	53	64	72	32	24
Number of Major Accidents in the study area of Karur District. (Km 275+600 to Km 292 + 600)	33	37	32	24	13

Direct Adverse impact on the Cultural Property will take place in case the Cultural Property is located within the Proposed Formation width and Indirect adverse impact is envisaged in case the property lies within the Proposed Embankment width of the Road. The likely impacts on each Cultural Property have been estimated on basis of the geometric section likely to be adopted at location of the Cultural Property.

5.10 SOCIAL ENVIRONMENT

The chapter on baseline environmental characteristics provides information on the nature, type and extent of impacts on private land, structures and other assets due to the proposed widening. The impacts on the communities, the loss of livelihood and other social impacts

TABLE 6 MARKET VALUE OF LAND

Location	2004 Lakhs / Acre	2006 Lakhs / Acre	2008 Lakhs / Acre	2010 Lakhs / Acre
Salem Bye pass Seelanaic kenpatty	60	150	300	400
Athanur & Cross	25	40	75	100
Rasipuram & cross	35	50	80	100
Andalur Gate	40	60	90	125
Pacchal	15	46	60	150
Pudhan chanthai	20	32	75	125
Sellappam aptti	24	36	83	200
Namakkal & cross	30	45	75	250
Velur	13	32	1,00	240
Velayutham Palayam	12	26	53	110
Karur Bye Pass	30	58	125	200

6. SUMMARY

Environmental Impact Assessment is an integral part of any developmental activity. We need to present the EIA report before commencing the development activity. Hence the need to conduct baseline study and assessment of the impacts are highly essential. The present project work is undertaken with a goal to assess the potential impacts of the project corridor from Salem to Karur NH7 4 laning of highway and to suggest the suitable mitigation measures.

After an extensive review of literature on the highway environmental impact assessment of various places, the study area Salem to Karur NH7 was selected for the study. The baseline characteristic of the study area existed before 4 laning work were collected from the collectorates of Salem, Namakkal and Karur.

The baseline environmental status such as climate, physiography and terrain, geology and soil, water resources, noise levels, forests and protected areas, plantations, cultural environments, community facilities and social environment were done. A Statistical data of the above characteristics are submitted here in this work.

The main objective of this work is to collect the assessments of impacts that have taken place during and after completion of the 4 laning of NH7 from Salem to Karur. Here also the impacts both positive and negative such as climate conditions, land resources, water resources, flora, air quality, community facilities, cultural properties, social environment were collected and analysed for making mitigation measures.

7. CONCLUSION

In this research work, the baseline environmental status and the potential environmental impacts for the study area were submitted. The positive impacts include the following.

- ❖ Reduced noise and air pollution.
- ❖ Reduced risk of accidents
- ❖ Improved accessibility and connectivity.
- ❖ Reduced vehicle operating and maintenance cost.
- ❖ Savings in fuel consumption.
- ❖ Improved Facilities to Road users.
- ❖ Improved Quality of life.
- ❖ Generation of Local employment.

Some of the direct and indirect negative impacts of the project are,

- ❖ Filling in low lying areas for embankment of the roads.
- ❖ Cutting of large number of trees.
- ❖ Increased Noise pollution in future due to vehicular movement increase.
- ❖ Impact on natural drainage area of the project corridor under study .

Anyhow, no significant adverse impacts are anticipated due to the proposed project, However, the temporary impacts on water quality, Air quality, noise levels, soil quality, flora and social economic environment of the project area are anticipated. Hence suitable mitigation measures should be made when and then with periodical community consultation. Proper implementations of traffic rules by traffic police, proper maintenance of traffic signs and implementation of accident care facilities by the project implementation agency, road side tree plantation to be restored and maintained. Development of green belt with selected species of trees for absorbing noise should be made. Use of horn should be restricted in main sensitive locations like schools and hospitals through the use of proper sign boards. The area drainage system and flood water drain should be periodically cleared. There should be periodical

monitoring of soil quality, water quality, air quality and noise levels.

8. REFERENCES

- [1]. M. L. Agrawal and A. K. Dikshit (2002), Significance of Spatial Data and GIS for Environmental Impact Assessment of Highway Projects, Indian Cartographer, MUIP – 04, PP 262-266,
- [2]. Final Feasibility Cum Preliminary Report, Section – III, Environmental Impact Assessment, Executive Summary, (2008) NHA1 PP1-13
- [3]. EA Summary Tamilnadu road Sector Project, Additional Finance
- [4]. Highways Department, Government of Tamilnadu (2003) PP1-32 Canter, L. W. (1996) Environmental Impact Assessment second Ed. Mc Graw Hill., New York.

Design of Efficient Parallel Interleaver through OPMM (Optimized Memory Address remapping)

E. Priya

ME-VLSI Design,
Dept of ECE Easwari Engineering College,
Chennai, India.

S. Sudha

Dept of ECE
Easwari Engineering College
Chennai, India.

Abstract: This work presents some mathematical models and collision free exchange rules for a parallel interleaver, using an optimized memory addresses remapping (OPMM) method that enables a classic interleaver to be exchanged for a parallel interleaver with efficiently. Both analytic and experimental results demonstrate that the rate of annealing and collision free results achieved using the OPMM approach is much faster than that achieved using the traditional Memory Address Remapping (MM) method.

Index Terms: collision-free, memory address remapping, parallel interleaver, turbo decoder .

I. INTRODUCTION

INTERLEAVING is scrambling the processing order of the data inside a block to break up neighborhood-relations. Interleaving is a process of rearranging the ordering of a symbol sequence. The interleaver in turbo decoder is used to permute the input symbols such that the constituent decoders are operating on the same set of input symbols, but in interleaved (permuted) order. It is used in many channel coding schemes and also essential for the communications performance of turbo-codes. It is an advanced technique used by high-end motherboards /chipsets to improve memory performance [1].

Interleaving is a process of rearranging the ordering of a symbol sequence. The interleavers is a one to one mapping function that maps a sequences of t bits into another sequences of t bit. Interleavers are widely used for a vast range of communications applications. In Fig.1, M SISOs in SISO1s write symbols to memory modules named MEM_1, MEM_2, ... MEM_ M ; since each memory module is written only once at a time, no collision exists. Similarly SISOs in SISO2s read symbols from memory modules MEM_1, MEM_2, ...MEM_ M ; Since memory module MEM_1 is read two times at a time, collision happens.

The problem of collision is currently being solved in several ways. Memory arbitration technique was presented in [2]-[4]. To avoid losing clock cycles using online generated parallel interleavers were proposed in [5]-[7].

These patterns is based on the parallel level M , making it particularly difficult to optimize and performance differences for the same turbo decoder but with different numbers of parallel blocks. MM is an effective way to solve the problem. This approach preserves the interleaving pattern, so

there is no performance loss both in error-correcting quality and decoding time.

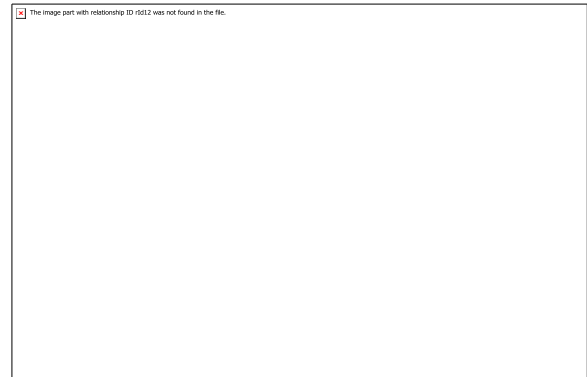


Fig. 1.Problem of collision.

The remainder of this paper is organized as follows. Section II introduces the terminologies and definitions used in this paper. Section III defines and mathematical models in parallel interleaving. Section IV explains collision-free exchange rules and the proposed OPMM method. Section V presents an example. Section VI presents experimental results. Section VII concludes the work.

II. TERMINOLOGIES AND NOTATIONS

The notations used in this papers are,

- L Length of symbol sequence.
- M Parallel level of a turbo decoder, is a divisor of L . N Word length of a memory module, $N=L/M$.
- i Matrix row index, $i \in [1,2, \dots, N]$, i_1 and i_2 are instances of i .
- j Matrix column index, $j \in [1,2, \dots, M]$, j_1 and j_2 are instances of j .
- (i,j) Matrix index with value equivalent to $(i-1)M+j$.
- g Memory module or SISO module number, $g \in [1,2, \dots, M]$, g_1 and g_2 are instances of g .
- t Memory access time, $t \in [1,2, \dots, N]$, t_1 and t_2 are instances of t .

A. Symbol Index

The symbol index of either SISO1s or SISO2s is defined as $(i-1)M+j$, where i denotes output or input time, and j is the number of the SISO module in SISO1s (or SISO2s). For instance, the symbol output from SISO1_2 at time 5 has the Symbol index $(5-1)M+2$, and symbol

input to SISO2_2 at time 5 also has the symbol index $(5 - 1)M + 2$.

B. Memory Address

The memory address of M memory modules is defined as $(i - 1)M + g$, where i denotes the position of the memory cell, g is the number of the memory module. For example, the 5's position of MEM_3 has the address $(i - 1)M + 3$.

C. Time Tile

The time tile represents a time, and defines all of the memory write/read operations of all the memory modules at that time.

D. Memory Tile

The memory tile represents a number of a memory module, and defines memory write/read operations of that memory module at all times.

E. Collision

In a time tile, if more than one attempt is made to access the memory module g , then a g -collision happens. The g -collision number equals (number of attempted-accesses -1).

F. Missing

In a time tile, if memory module g is not accessed, then a g -miss occurs.

III. PARALLEL INTERLEAVING

A Parallel Interleaver, in Fig. 2, PI plays a key role in the performance of the parallel decoder. It comprises the first interleaving stage (FIS) and the second interleaving stage (SIS). The FIS, which can hold up to $m \times d$ metrics, permutes the m metrics coming simultaneously from m SISOs (FIS depth d is termed also as FIS delay in the following).



Fig. 2.Parallel interleaver

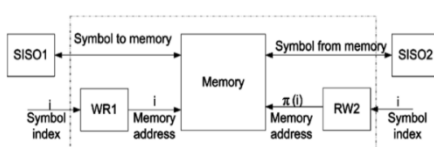


Fig.3.A Turbo decoder

A. Mathematical Model in Parallel Interleaving

The function of the interleaver defines how symbols from SISOs are written to memory modules and how symbols that are input to SISOs are read from memory modules.

1) Write Matrix: $w_{s,N \times M}^T$ describes how symbols from SISOs are stored in memory modules.

In write matrix $w_{s,N \times M}$, (i,j) represent memory address; $w_s(i,j)$ represents symbol index, $w^t(i,j)$ represents the time tile of $w_s(i,j)$.

$w^t(i,j)$ is derived from $w_s(i,j)$, $w^t(i,j)$ is the integer quotient of $(w_s(i,j) - 1)/M + 1$.

Combine $w_s(i,j)$ and $w^t(i,j)$, a matrix element called $w_{s^t}(i,j)$ can be created. w_{s^t} is represented as

In write matrix w_{s^t} , column j is memory tile j , $w^t(i,j)$.



2) Read Matrix: $R_{A,N \times M}^G$ describes how symbols are read to SISOs from memory modules.

In read matrix $R_{A,N \times M}^G$, (i,j) represents symbol index, $r_a(i,j)$ represents memory address; $r^g(i,j)$ represents the memory tile of $r_a(i,j)$, $r^g(i,j)$ is the integer remainder of $r_a(i,j)/N$. Combine $r_a(i,j)$ and $r^g(i,j)$, a matrix element called $r_{a^g}(i,j)$ can be created. Read matrix $R_{A,N \times M}^G$ is presented as

$$R_{A,N \times M}^G = \begin{matrix} \begin{matrix} r_{a^g}(1,1) & r_{a^g}(1,j) & r_{a^g}(1,M) \\ r_{a^g}(2,1) & r_{a^g}(2,j) & r_{a^g}(2,M) \\ r_{a^g}(i,1) & r_{a^g}(i,j) & r_{a^g}(i,M) \\ r_{a^g}(N,1) & r_{a^g}(N,j) & r_{a^g}(N,M) \end{matrix} \end{matrix}$$

In read matrix $R_{A,N \times M}^G$, row i is time tile i , $r^g(i,j)$ is memory tile $r^g(i,j)$.

B. Terminologies Used in OPMM Method

1) Memory Element Exchange Pair: $(g1|t1,g2|t2)$ exchange memory elements $g1$ and $g2$ between two rows (time tiles) $t1$ and $t2$ in read matrix.

2) Time Element Exchange Pair: $(t1|g1,t2|g2)$ exchange time elements $t1$ and $t2$ between two columns (memory tiles) $g1$ and $g2$ in write matrix.

3) Selected Memory Element Exchange pair: $(g1|t1,g2|t2)$ exchange memory elements and between

two rows (time tiles) $t1$ and $t2$ to reduce one or two collisions in read matrix.

4) Selected Address Exchange Pair: $(r_{-a^g}(i1,j1), r_{-a^g}(i2,j2))$ exchange two addresses in the read matrix to eliminate one or two collisions.

5) Updated Sequence Exchange Pair: $(w_{-s^t}(i1,j1), w_{-s^t}(j1,j2))$ exchanges two symbol sequences in write matrix to update the selected address exchange happened in read matrix.

6) Middle Sequence Exchange Pair: $(w_{-s^t}(i11,j11), w_{-s^t}(i22,j22))$ exchange two symbol sequences in write matrix to remove the collisions caused by the updated sequence exchange.

7) Updated Address Pair: $(r_{-a^g}(i1^a, j1^a), r_{-a^g}(i2^a, j2^a))$ exchange two addresses in read matrix to update the middle sequence exchange happened in write matrix.

IV. PROPOSED OPMM METHOD

Collision-free conditions applying to both write and read matrices can also be stated as follows: the N positions of each memory module are written and/or read at N different times.

A. Collision-Free Exchange Rules:

1) Exchange Rule 1: Each selected address exchange in read matrix must be updated in write matrix, and each middle sequence exchange in write matrix must update in read matrix. Each selected address exchange in read matrix should be updated in write matrix to ensure the interleaving pattern is maintained. An address exchange in read matrix is updated in write matrix by an updated symbol index exchange.

2) Exchange Rule 2: An updated sequence exchange in write matrix is collision-free if the two exchanged M symbol sequences are in same time tile or same column (memory tile).

In write matrix, because N symbol sequences in same time tile are written to memory modules at same time, and symbol sequences in same column (memory tile) are saved in same memory module, therefore any exchange that occurs in the same time tile or the same column (memory tile) is collision-free.

3) Exchange Rule 3: If an updated sequence exchange in write matrix is not in the same time tile or column (memory tile), then a middle sequence exchange in write matrix should be added to remove the collisions introduced by the updated sequence exchange.

4) Exchange Rule 4: An updated address exchange in read matrix is collision-free if two exchanged memory addresses are in same memory tile or row (time tile).

In read matrix, because M addresses in same row (time tile) are written to memory modules at same time, and N positions in same memory tile are saved in same memory module, therefore any exchange that occurs in the same row (time tile) or the same memory tile is collision-free.

B. OPMM Procedure

For a given interleaving pattern, the collision-free parallel interleaver with parallel level can be generated from the classic interleaver through the following steps.

1) Initialization: Generate write matrix $W_{-S_{N,M}^T}$ and read matrices $R_{-A_{N,M}^G}$, based on given interleaving pattern.

2) Check Collision: Check whether read matrix meet constraint (4). If no collision exists, then finish, otherwise go to OPMM step.

3) OPMM: If a memory element exchange pair $(g1|t1, g2|t2)$ in read matrix satisfies the conditions that row (time tile) $t1$ has $g1$ -collision, $g2$ -missing and row (time tile) $t2$ has $g1$ -collision, $g2$ -missing, then this exchange is called a type 1 selected exchange. A type 1 selected exchange can remove two collisions. If a memory element exchange pair $(g1|t1, g2|t2)$ satisfies conditions that row (time tile) $t1$ has $g1$ -collision and row (time tile) $t2$ has $g2$ -collision, $g1$ -missing, then this exchange is called type 2 selected exchange. Repeat exchange cycle: identify a selected memory element $(g1|t1, g2|t2)$ exchange pair in matrix; choose a selected address exchange pair; find its updated sequence exchange pair in the write matrix. Since the updated sequence exchange pair does not meet exchange rule 2, a middle sequence exchange pair is added to the write matrix.

4) End Condition: Repeat OPMM until read matrix is collision-free. Then new collision-free write and read matrices are acquired, based on them the content of writing and reading ROMs, e.g., input and output signals of block and $WR1_1, WR1_2, \dots, WR1_M$ and $WR2_1, WR2_2, \dots, WR2_M$ can then be easily created.

V. EXAMPLES

In this section, an example is used to demonstrate how the exchanges rules are used in the process of OPMM.

Example: an interleaving pattern with parallel level $M=3$

$$G = \begin{pmatrix} 1 & 7 & 4 \\ 3 & 5 & 6 \\ 2 & 8 & 9 \end{pmatrix}$$

In interleaving matrix G , matrix index is the sequence number of write process and matrix value is the sequence number of read process.

A. Initialization

After initialization, the original write matrix $W_{-S_{3 \times 3}^T}$ and read matrix $R_{-A_{3 \times 3}^G}$ are

$$W_{-S_{3 \times 3}^T} = \begin{pmatrix} 1^1 & 2^1 & 3^1 \\ 4^2 & 5^2 & 6^2 \\ 7^3 & 8^3 & 9^3 \end{pmatrix}$$

$$R_{-A_{3 \times 3}^G} = \begin{pmatrix} 1^1 & 7^1 & 4^1 \\ 3^3 & 5^2 & 6^3 \\ 2^2 & 8^2 & 9^3 \end{pmatrix}$$

$$W_{-S_{3 \times 3}^T} = \begin{pmatrix} 1^1 & 2^1 & ((3^1)) \\ ((4^2)) & 5^2 & 6^2 \\ 7^3 & ((8^3)) & ((9^3)) \end{pmatrix}$$

$$R_{-A_{3 \times 3}^G} = \begin{pmatrix} 1^1 & 2^2 & ((4^1)) \\ 7^1 & 5^2 & ((8^2)) \\ ((3^3)) & 6^3 & ((9^3)) \end{pmatrix}$$

B. Check Collision

Check read matrix for collision. In this example, all three rows have collisions.

C. Exchange Cycle 0

According to exchange rule 2, no collisions will be introduced. Before exchange

$$W_{-S_{3 \times 3}^T} = \begin{pmatrix} 1^1 & (2^1) & (3^1) \\ 4^2 & 5^2 & (6^2) \\ 7^3 & (8^3) & 9^3 \end{pmatrix}$$

$$R_{-A_{3 \times 3}^G} = \begin{pmatrix} 1^1 & 7^1 & 4^1 \\ ((3^3)) & 5^2 & (6^3) \\ (2^2) & (8^2) & 9^3 \end{pmatrix}$$

After exchange

$$W_{-S_{3 \times 3}^T} = \begin{pmatrix} 1^1 & 2^1 & 3^1 \\ 4^2 & 5^2 & 6^2 \\ 7^3 & 8^3 & 9^3 \end{pmatrix}$$

$$R_{-A_{3 \times 3}^G} = \begin{pmatrix} 1^1 & 7^1 & 4^1 \\ 2^2 & 5^2 & 8^2 \\ 3^3 & 6^3 & 9^3 \end{pmatrix}$$

D. Exchange Cycle 1

According to exchange rule 2, no collisions will be introduced. Before exchange

$$W_{-S_{3 \times 3}^T} = \begin{pmatrix} 1^1 & (2^1) & 3^1 \\ 4^2 & 5^2 & 6^2 \\ (7^3) & 8^3 & 9^3 \end{pmatrix}$$

$$R_{-A_{3 \times 3}^G} = \begin{pmatrix} 1^1 & (7^1) & 4^1 \\ (2^2) & 5^2 & 8^2 \\ 3^3 & 6^3 & 9^3 \end{pmatrix}$$

After exchange

$$W_{-S_{3 \times 3}^T} = \begin{pmatrix} 1^1 & 2^1 & 3^1 \\ 4^2 & 5^2 & 6^2 \\ 7^3 & 8^3 & 9^3 \end{pmatrix}$$

$$R_{-A_{3 \times 3}^G} = \begin{pmatrix} 1^1 & 2^2 & 4^1 \\ 7^1 & 5^2 & 8^2 \\ 3^3 & 6^3 & 9^3 \end{pmatrix}$$

E. Exchange Cycle 2

According to exchange rule 4, no new collisions are introduced.

After exchange

$$W_{-S_{3 \times 3}^T} = \begin{pmatrix} 1^1 & 2^1 & 3^1 \\ 4^2 & 5^2 & 6^2 \\ 7^3 & 8^3 & 9^3 \end{pmatrix}$$

$$R_{-A_{3 \times 3}^G} = \begin{pmatrix} 1^1 & 2^2 & 9^3 \\ 7^1 & 5^2 & 7^3 \\ 8^2 & 6^3 & 4^1 \end{pmatrix}$$

The interleaving pattern derived from the remapped write and read matrices are as follows:

$$G^{OPMM} = \begin{pmatrix} 1 & 7 & 4 \\ 3 & 5 & 6 \\ 2 & 8 & 9 \end{pmatrix}$$

The matrix G^{OPMM} is confirmed to maintain the original interleaving pattern.

VI. EXPERIMENTS

The OPMM scheme accelerates the remapping process in two ways: The proposed OPMM presents the collision free output

$$G = \begin{pmatrix} 5^2 & 2^2 & 9^3 \\ 7^1 & 1^1 & 8^2 \\ 3^3 & 6^3 & 4^1 \end{pmatrix}$$

With the 4 exchange cycles. These collision full read matrix is given to the MM method and got 9 exchange cycle. When compare with MM Method time period also increased from 2.627ns to 2.644ns.

1) Optimizing the selected address exchange pairs to maximize the number of OPMM steps be finished in a single remapping cycle.

2) In repeat remapping cycles, all the selected address exchange pairs are varied in two memory tiles instead M memory tiles, thus shortening the number of remapping cycles. Experimental results indicate that the OPMM method has a much shorter CPU calculation time than the traditional MM method.

VII. RESULTS

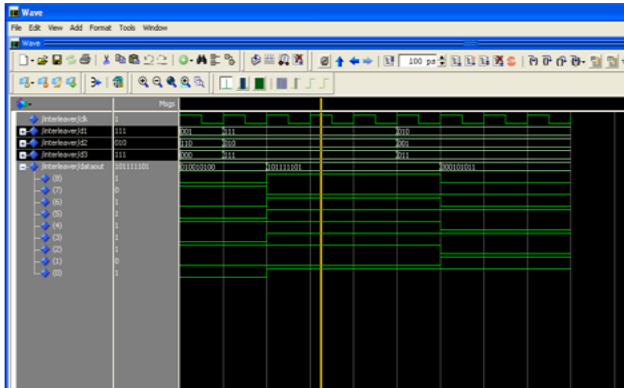


Fig 4. Interleaved Order

In Fig 4, it shows the interleaved order of the input values. MM and OPMM Method contains the Swap logic and Inter Leaving Methods used. These Modules are shown in Fig 5, 6 and Fig 7.

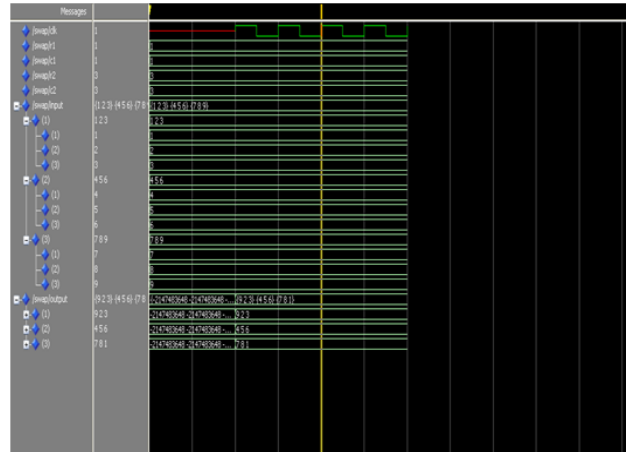


Fig 7. Swap Process

Fig 8, 9 shows MM Method and OPMM method.

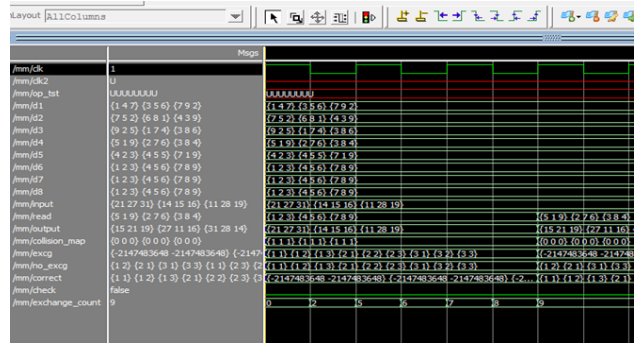


Fig 8. MM Method

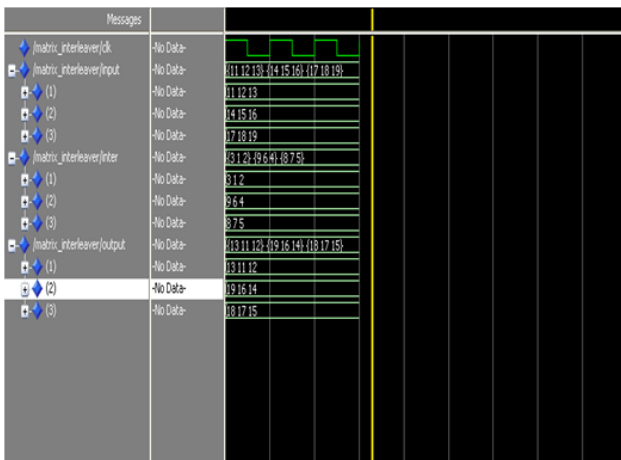


Fig 5. Interleaved Matrix

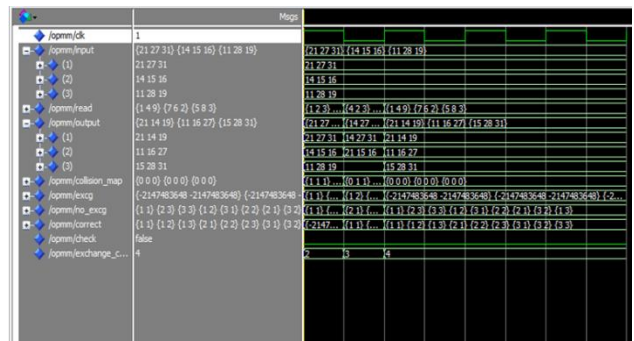


Fig 9. OPMM Method

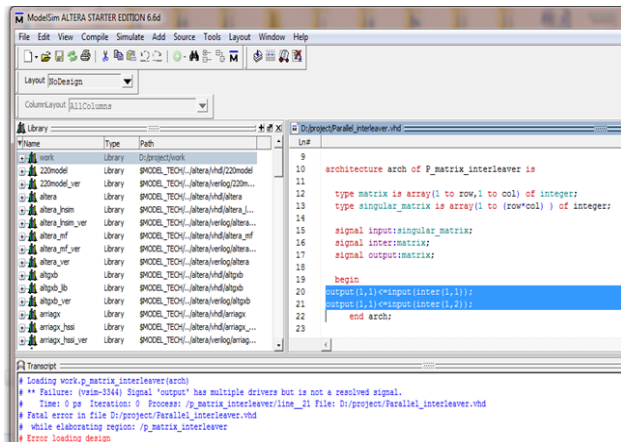


Fig 6. Memory Collision

REFERENCES

- [1] Jing-ling Yang, “ Parallel Interleavers Through Optimized Memory Address Remapping,” in *Proc. IEEE Int. Conf. VERY LARGE SCALE INTEGRATION (VLSI) SYSTEMS.*, VOL. 18, NO. 6, JUNE 2010.
- [2] M. J. Thul, F. Gibert, and N. Wehn, “Optimized current interleaving architecture for high-throughput turbo-decoding,” in *Proc. 9th Int. Conf. Electron., Circuits Syst.*, Sep. 2002, vol. 3, pp. 1099–1102.
- [3] M. J. Thul, F. Gilbert, and N. Wehn, “Concurrent interleaving architectures for high-throughput channels coding,” in *Proc. IEEE Int. Conf. Acoust., Speech, Signal Process.*, Apr. 2003, vol. 2, pp. II–613–II-616.
- [4] Z. Wang and K. Parhi, “Efficient interleaver memory architectures for serial turbo decoding,” in *Proc. IEEE Int. Conf. Acoust., Speech, Signal Process.*, Apr. 2003, vol. 2, pp. II-629–II-632.
- [5] A. Giulietti, L. v. d. Perre, and A. Strum, “Parallel turbo coding interleavers: Avoiding collisions in accesses to storage elements,” *Electron.Lett.*, vol. 38, no. 5, pp. 232–234, Feb. 2002.
- [6] R. Dobkin, M. Peleg, and R. Ginosar, “Parallel interleaver design and VLSI architecture for low-latency MAP Turbo decoders,” *IEEE Trans. Very Large Scale Integr. (VLSI) Syst.*, vol. 13, no. 4, pp. 427–437, Apr. 2005.
- [7] Z. He, P. Fortier, and S. Roy, “Highly-parallel decoding architectures for convolutional turbo codes,” *IEEE Trans. Very Large Scale Integr. (VLSI) Syst.*, vol. 14, no. 11, pp. 1147–1151, Oct. 2006.
- [8] A. Tarable and S. Benedetto, “Mapping interleaving laws to parallel turbo decoder architectures,” *IEEE Commun. Lett.*, vol. 8, no. 3, pp. 162–164, Mar. 2004.
- [9] A. Tarable and S. Benedetto, “Mapping interleaving laws to parallel turbo and LDPC decoder architectures,” *IEEE Trans. Inf. Theory*, vol. 50, no. 9, pp. 2002–2009, Sep. 2004.

Estimation of the Frequency of Artifacts Likely to Fall Down to Earth and Other Planets

A. B. BHATTACHARYA

Department of Physics, University of Kalyani, Kalyani 741235, West Bengal, India

J. PANDIT

Department of Physics, JIS School of Polytechnic, Kalyani 741235, West Bengal, India

B. RAHA

Department of Physics, University of Kalyani, Kalyani 741235, West Bengal, India

A. SARKAR

Department of Physics, University of Kalyani, Kalyani 741235, West Bengal, India

ABSTRACT

The spontaneous leakage of artifacts into the interstellar medium and the associated orbital characteristics of different planets have been considered for estimating the frequency of the artifacts likely to fall down to the Earth and the other planets. Information about the astrodynamical aspect of paleovisiting, particularly regarding the formation and extent of the artifacts in the solar planetary systems has been emphasized.

Key words – Artifacts, Interstellar medium, Planets, Solar system, Universe.

I. INTRODUCTION

Interest has developed among researchers, in recent years, to search traces of extraterrestrial intelligence within the solar system. It has already been reported that within the time of existence of our planet, about 10^4 stars capable of having inhabited planets approached the Sun to distances within 1.5 pc (1 pc = 3.09×10^{13} km) which can be covered by space probes using present day technology [1, 2]. Early works [3, 4] have attempted in a scattered way on a search for artifacts which are in orbit, on the Earth or on asteroids. It seems that this list should also include by elaborately considering orbits of different planets and their moons as well. In this paper we have considered the orbital characteristics of different planets for estimating the frequency of the artifacts likely to fall down to earth and other planets.

II. SPONTANEOUS LEAKAGE OF ARTIFACTS

Space activities largely contribute to a long duration pollution of the interstellar medium [5]. In a similar way, the interplanetary space of other inhabited planetary systems could contain artifacts. The spontaneous leakage of artifacts into the interstellar medium in absence of interstellar flights is also reasonably expected. This is mainly because of the following three reasons:

(1) A considerable portion of any large artifacts would be ejected by gravitational interaction with the planets. According to computer simulations of the asteroid and comet motion, 10-30 percent of small bodies leave the Solar system [6 - 8].

(2) Collisions between artifacts or their explosions (like spontaneous explosions of Earth satellites) in the outer parts of the planetary system could accelerate their debris up to hyperbolic velocities.

(3) Light pressure expels micron-sized debris particles (e.g. from rocket engines) out of the planetary system.

Hence, technical activities even within a planetary system lead to a diffusion of artifacts into the interstellar medium. If there are alien artifacts between the stars, some of them are likely to fall down to Earth at some time. So it is interesting to estimate the frequency of such events.

III. THEORETICAL CONSIDERATIONS

In this section we have considered some mathematical equations used for calculating the probability of the fall of artifacts on Earth and other planets of the solar system.

The velocity (v) of all artifacts relative to the Sun in interstellar medium is given by

$$v = [X^2 + Y^2 + Z^2 + (\sigma_1^2 + \sigma_2^2 + \sigma_3^2)/3]^{1/2} \quad \dots (1)$$

where, σ_1, σ_2 and σ_3 are the orthogonal dispersions in velocity of nearby stars; X, Y and Z are the components of the velocity vector of the Sun relatively to nearby stars [Allen (1973)].

Putting the widely accepted values of $\sigma_1 = 38$ km/s, $\sigma_2 = 24$ km/s, $\sigma_3 = 18$ km/s and $X = 9$ km/s, $Y = 12$ km/s, $Z = 7$ km/s, we get $v = 32.48$ km/s.

The effective radius of the Earth's orbit (A) and the effective radius of Earth (R_e) are respectively given by

$$A = a [1 + (V/v)^2]^{1/2} \quad \dots (2)$$

$$R_e \approx R [1 + u^2 / \langle v_a^2 \rangle]^{1/2} \quad \dots (3)$$

where a is the radius of the Earth's orbit which is 1.5×10^8 km (on an average); $V = 42.1$ km/s is the escape velocity at 1.5×10^8 km distance from the Sun; $R = 6371$ km is the Earth's radius; $u = 11.2$ km/s is the geocentric escape velocity of Earth and $\langle v_a^2 \rangle$ is the average square geocentric escape velocity of artifact which is given by

$$\langle v_a^2 \rangle = v^2 + 1.5V^2 \quad \dots (4)$$

The probability of the fall of an artifact on the Earth at the distance of $r \leq a$ from the Sun can be expressed as,

$$\omega = (R_e/a)^2 \quad \dots (5)$$

Again, the number density (ρ) of the artifact is given by

$$\rho = \rho_o \gamma e M C / m \quad \dots (6)$$

where, $\rho_o = 4.43 \times 10^{-42} \text{ km}^{-3}$ is the stellar density close to the Sun [9]

$\gamma = 0.3$ is the fraction of stars with planets among the nearby stars.

$M = 2.3 \times 10^{21} \text{ kg}$ is the mass of potential raw material for the artifact manufacturing in the planetary system e.g. the total mass of asteroids in the solar system [9]

$C =$ Part of raw material transformed into the interstellar artifacts

$m =$ The typical mass of artifact and

$e =$ Fraction of planetary systems generating interstellar artifacts among the nearby planetary systems.

If v_h is the heliocentric velocity of nearby stars; T , the age of the planet, v^* , the artifacts injection velocity and T_{max} the maximum duration of exposure such that $T = 1.43 \times 10^{17} \text{ sec}$, $v^* \sim 10 \text{ km/sec}$, $L = v^* \times T_{max} = 3 \times 10^{13} \text{ km}$, then maximum number of stars which could infect the planet is

$$N \sim \pi \rho_o \gamma v_h T L^2 \quad \dots (7)$$

and the frequency of *Extraterrestrial Intelligence* artifact falls is,

$$f = \pi \rho v A^2 \omega \approx 3.5 \times 10^{-11} e C / m. \text{ in } s^{-1} \quad \dots (8)$$

Taking $m = 0.1 \text{ kg}$, the upper limit of f could be calculated. In practice, e and C should be less than 1 i.e. $e \leq 1$ and $C \leq 1$. Putting the maximum value of e and C i.e. 1, we can estimate the frequency of artifact; which becomes $f = 3.5 \times 10^{-11}$ if we put $m = 1 \text{ kg}$. Then the average time between the falls of such ETI artifacts become $1/f \geq 91 \text{ yrs}$.

Again if $e = 10^{-2}$, $C = 10^{-2}$ and $m = 0.1 \text{ kg}$, then the Earth could accumulate about five thousand of 0.1kg-artifacts during 4.5×10^9 years.

The probability of survival conditions of artifact is given by

$$W = [1 - (v_h^2 + v_e^2 - 9.2/\sigma) / (2v_h v_e)] / 2 \quad \dots (9)$$

where v_h is the heliocentric velocity of artifact near the Earth and it is related by the equation

$$v_h = [u^2 + V^2 + v^2]^{1/2} \quad \dots (10)$$

Using the appropriate values of u , V and v we get $v_h = 54.33 \text{ km/s}$ and v_e , the orbital speed of the Earth 29.78 km/s .

IV. ESTIMATION OF POSSIBLE ARTIFACTS

In our estimation of the possible artifacts we have considered the planets Mercury, Venus, Earth, Mars, Jupiter and Saturn. The orbital characteristics of all these planets are given in TABLE 1.

We estimate the probability of the artifacts fall on the Earth and the other five planets due to the Sun and draw the histogram shown in Fig. 1. Fig. 2 shows the % contributions of falling artifacts.

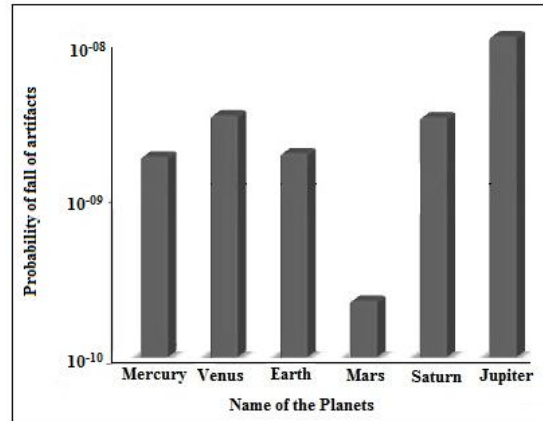


Fig.1 Probability of the fall of artifacts on Earth and other planets

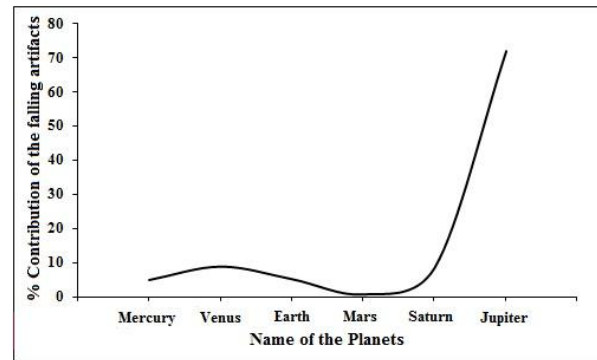


Fig.2 Percentage contribution of various Planets in the falling of artifacts

From both the figures, it is clear that contribution of artifacts to Jupiter is maximum among all the planets considered. Geocentric escape velocity (u) of the six planets of the Sun as well as, the square root of the average square geocentric velocities [$\langle v_a^2 \rangle$] have been calculated and shown in Table 2.

Table 2. The Geocentric velocity (u) and the square root of average square geocentric velocity (v_a) for various planets including Earth

Planets	u in km/s	v_a in km/s
Mercury	4.25	89.25520713
Venus	10.46	68.99337215
Earth	11.186	60.93903019
Mars	5.027	53.08133382
Jupiter	59.5	39.60909681
Saturn	35.5	36.53551423

TABLE 2 shows that the values of v_a are decreasing from the planet Mercury to the planet Saturn but it is not true for u . It is noted that the value of u is increasing from Mercury to the Earth. Then it diminishes for the planet Mars and again it increases for the other two planets considered. It appears from the table that the value of u is maximum for Jupiter and minimum for Mercury while the value of v_a is maximum for Mercury and minimum for Jupiter.

Table 1. Orbital characteristics of the different planets considered

Planet	Mercury	Venus	Earth	Mars	Jupiter	Saturn
Aphelion in km	69,816,900	108,942,109	152,098,232	249,209,300	816,520,800	1,513,325,783
Perihelion in km	46,001,200	107,476,259	147,098,290	206,669,000	740,573,600	1,353,572,956
Semi-major axis in km	57,909,100	108,208,930	149,598,261	227,939,100	778,547,200	1,433,449,370
Radius of the orbit (a) in km	5.79×10^7	1.08×10^8	1.5×10^8	2.27×10^8	7.78×10^8	1.43×10^9
Mean radius in km	2,439.7	6,051.8	6,371.0	3386.2	69,911	57,325
Mass in kg	3.3022×10^{23}	4.8685×10^{24}	5.9736×10^{24}	6.4185×10^{23}	1.8986×10^{27}	5.6846×10^{26}
Mean density in gm/cm³	5.427	5.204	5.515	3.9335	1.326	0.687
Geocentric Escape Velocity (u) in km/s	4.25	10.46	11.186	5.027	59.5	35.5
Escape Velocity at orbital distance (V) in km/s	67.88	49.70	42.1	34.28	18.51	13.66
v in km/s	32.48	32.48	32.48	32.48	32.48	32.48
$A = a[1 + (V/v)^2]^{1/2}$	1.34×10^8	1.97×10^8	2.45×10^8	3.30×10^8	8.95×10^8	15.5×10^8
Effective Radius of the Planet R_e in km	2442.464	6120.956	6477.444	3401.351	126160.7	79929.18
Average square of Geocentric Velocity $\langle v_a^2 \rangle$	7966.492	4760.085	3713.565	2817.628	1568.881	1334.844
$\omega = (R_e/a)^2$	1.780×10^{-9}	3.212×10^{-9}	1.865×10^{-9}	2.245×10^{-10}	2.630×10^{-8}	3.124×10^{-9}

The variations of u and v_a corresponding to all the six planets have taken into account and are shown in Fig. 3.

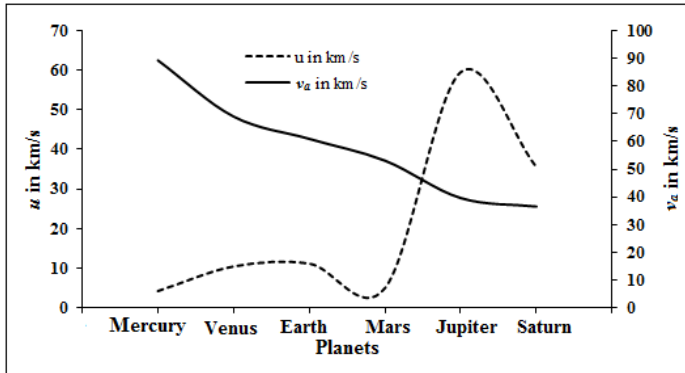


Fig.3 variations of u and v_a for various planets

A plot of u^2 in logarithmic scale vs. $\langle v_a^2 \rangle$ is made in Fig. 4 which exhibits an interesting characteristic variation. The figure clearly shows that the variation of u^2 with $\langle v_a^2 \rangle$ is non-linear in characteristic.

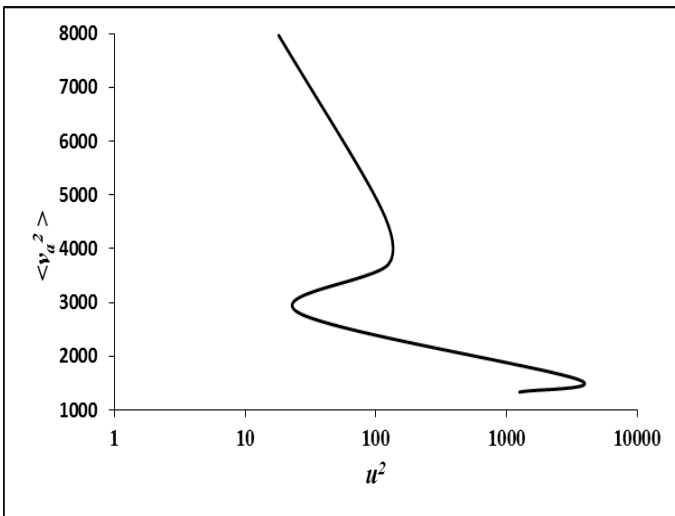


Fig.4 Plot of u^2 in log scale against $\langle v_a^2 \rangle$

The effective radius R_e as derived from equation (3), can also be obtained from
 $R_e \approx Rk$... (11)

where, $k = [1 + u^2 / \langle v_a^2 \rangle]^{1/2}$

In TABLE 3 we have shown the calculated values of k as obtained by using equation 12 and also the corresponding planet's radius R .

Table 3. Calculated values of k of the six planets and their corresponding radius in km

Planets	K	R in km
Mercury	1.001133013	2,439.70
Mars	1.004474259	3386.2
Venus	1.011427317	6,051.80
Earth	1.016707659	6,371.00
Jupiter	1.804590059	69,911
Saturn	1.394316304	57,325

The variations of the two parameters k and R have shown in Fig. 5. It appears from the figure that when we go to the higher values of the radius (R), particularly above the value of 62×10^3 km, the k values are no longer linear.

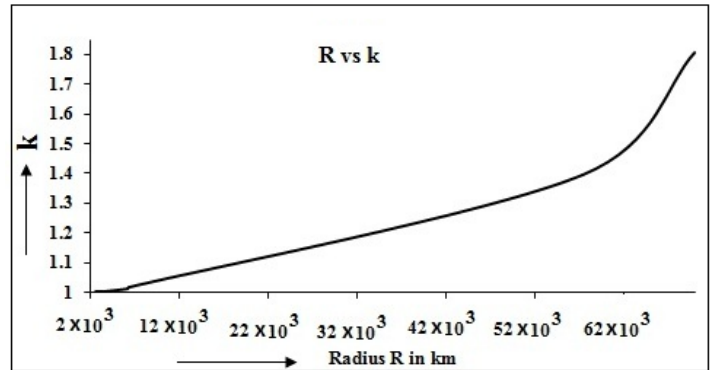
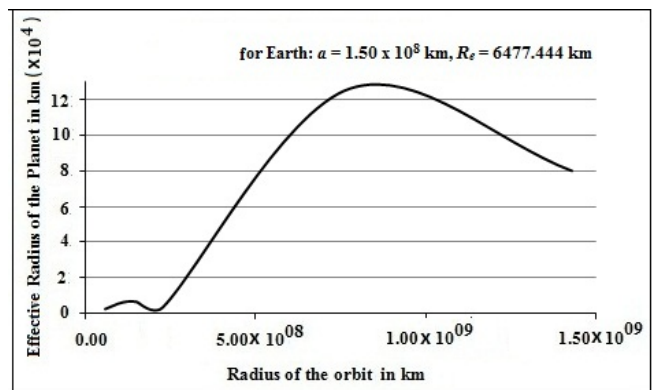
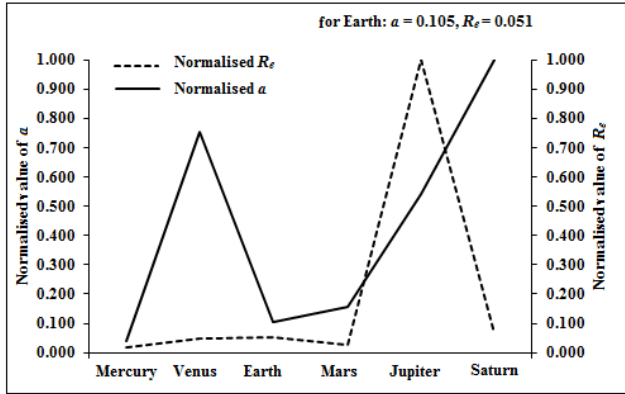


Fig.5 Plot showing the variation of R and k

This variation prompted us to re-examine the radius of the orbit (a) with the corresponding effective radius of different planets (R_e). A plot of a vs R_e is made in Fig. 6(i) and their normalized values in fig. 6(ii). From these figures we can compare the values of a and R_e of different planets with reference to Earth.



(i)



(ii)

Fig.6(i) Plot of radius of the orbit (a) vs. effective radius of the Planets (R_e),

(ii) Normalized values of a vs R_e

In TABLE 4 we have calculated the heliocentric velocity of nearby stars with the maximum number of stars which could infect the planets. The table shows that the order of the maximum number of stars for all the planets are same ($\sim 10^4$) but the heliocentric velocity varies from 50 to 75 km/s. This indicates that the heliocentric velocity (v_h) has not a major role in counting the maximum number of stars that could infect the planets.

V. DISCUSSION

The probability of the fall of the artifacts and their percentage contribution to different planets is a subject to be examined in greater details with the help of additional future information. Observational data supported by the future models developed can provide light towards falling of artifacts and eventually to the existence of extraterrestrial intelligence at our planetary systems. It has been reported that Mercury and Mars is less than 1 percent while that for the Venus and Saturn is greater than 1[10]. There is a higher chance that the artifacts on the Earth may arise from Venus or Saturn than Mercury or Mars.

Table 4. Heliocentric velocity of nearby stars and the corresponding maximum number to infect the planets

Name of the planets	Heliocentric velocity of nearby stars $v_h = [u^2 + V^2 + v^2]^{1/2}$ km/s	Maximum number of stars which could infect the planet ($N \sim \pi \rho_0 \gamma v_h T L^2$)
Mercury	75.37	4.0×10^4
Venus	60.29	3.2×10^4
Earth	54.34	2.9×10^4
Mars	47.49	2.5×10^4
Jupiter	70.27	3.7×10^4
Saturn	50.02	2.6×10^4

Some recent theories suggest that Venus and the Earth may have started out alike [11]. There might have been a lot of water on Venus and there might have been a lot of carbon dioxide on Earth. But all that was to change. On Earth, life in the oceans took in carbon dioxide and turned it into limestone. On Venus, 30% closer to the Sun, any oceans boiled away and the water vapor added to the runaway greenhouse effect. It is largely believed that microbes could survive and reproduce; floating in the thick, cloudy atmosphere and also widely protected by a sunscreen of sulfur compounds [12, 13]. "Panspermia" the theory that life on Earth came from space, comets, or other planets, has an ancient history [14-18]. There are more promising non-classical SETI possibilities than the conventional search for radio/laser signals. But these approaches conflict with the mental habits of astronomers, geologists and geochemists in studying natural formations and processes. This habit factor leads most specialists to a priori rejection of search for alien artifacts on the surfaces of the planets and their moons. Invaluable information about the astrodynamical aspect of paleovisitory, particularly regarding the formation and extent of the artifacts as well as migration of small bodies in the solar planetary systems to be considered at a greater length for evaluating ETI problems.

ACKNOWLEDGEMENTS

We are thankful to the Council of Scientific and Industrial Research for financial support in this work [Project No. 03(1153)/10/EMR-II, dated 26.04.2010]. J. Pandit expresses sincere thanks to the Director of JIS group Prof. A. Guha for constant encouragement and support. Two of us (A. Sarkar and B. Raha) are thankful to the UGC and the CSIR for awarding them Net fellowships.

REFERENCES

- [1] A. B. Bhattacharya, S. Das, A. Sarkar, M. Debnath and A. Bhoumick, A new technique for investigating extrasolar planets. *International Journal of Physics*, 4(1), 2011, 31-42.
- [2] A. B. Bhattacharya, D. K. Tripathi, A. Sarkar, A. Bhoumick, Implementation of Radio Technique in Interstellar Radiation Field for Locating Distant Stars. *International Journal of Applied Engineering Research*, Dindigul, 2(1), 2011, 63-69.
- [3] A. V. Arhipov, Astrodynamical aspect of paleovisitory. *RIAP Bulletin*, 1(1), 1994, 7-10.
- [4] A.R. Martin, Project Daedalus: bombardment by interstellar material and its effects on the vehicle. *Journal of the British Interplanetary Society, supplement*, 1978, S116-S121.
- [5] H. Heusmann, Space Debris. *Spaceflight*, 35, 1993, 182-184.
- [6] M.; Duncan, T.Quinn and S. Tremaine, The formation and extent of the solar system cloud. *Astronomical Journal*, 94, 1987, 1330-1338.

- [7] P. Farinella, Ch. Froeschlé, C.Froeschlé, R. Gonczi, G. Hahn, A.Morbidelli and G.B. Valsecchi, Asteroids failing into the Sun. *Nature*, 371, 1994, 314-317.
- [8] S. I. Ipatov, Migration of Small Bodies to the Earth. *Astron. Vestn.*, 29, 1995, 304-330.
- [9] C. W. Allen, *Astrophysical Quantities* (The Athlone Press, London 1973).
- [10] A. Tough, A critical examination of factors that might encourage secrecy. *Acta Astronautica*, 21 (2), 1990, 97-102.
- [11] M. Mark, Why SETI is science and UFOlogy is not. *Skeptical Inquirer*, 2004.
- [12] M. Chown, *The Alien Spotters* (New Scientist, 1997) 28. Venus clouds 'might harbour life'. BBC News (2004-05-25). Retrieved on 2007-12-01. (file:///G:/universe203/3746583.stm.html).
- [13] P. Curd, *Anaxagoras of Clazomenae: Fragments and Testimonia* (University of Toronto Press, Toronto 2007).
- [14] F. Hoyle and C. Wickramasinghe, *Our place in the cosmos* (J. M. Dent, London, 1993).
- [15] F. Hoyle and C. Wickramasinghe, *Astronomical origins of life, steps towards Panspermia* (Klewer Academic Publishers, 2000).
- [16] S. Arrhenius, *Worlds in the Making* (Harper & Brothers, New York 1908).
- [17] F. Crick, *Life Itself. Its Origin and Nature* (Simon & Schuster, New York 1981).

An Overview of AODV Routing Protocol

Prashant Kumar Maurya¹, Gaurav Sharma², Vaishali Sahu³, Ashish Roberts⁴,
Mahendra Srivastava⁵

^{1, 2, 4, 5} M.Tech Scholar SSET, SHIATS ALLAHABAD

³ M.Tech Scholar MNNIT ALLAHABAD

Abstract: The Ad-hoc On-Demand Distance Vector (AODV) routing protocol is designed for use in ad-hoc mobile networks. AODV is a reactive protocol: the routes are created only when they are needed. It uses traditional routing tables, one entry per destination, and sequence numbers to determine whether routing information is up-to-date and to prevent routing loops.

An important feature of AODV is the maintenance of time-based states in each node: a routing-entry not recently used is expired. In case of a route is broken the neighbors can be notified.

Route discovery is based on query and reply cycles, and route information is stored in all intermediate nodes along the route in the form of route table entries. The following control packets are used: routing request message (RREQ) is broadcasted by a node requiring a route to another node, routing reply message (RREP) is unicasted back to the source of RREQ, and route error message (RERR) is sent to notify other nodes of the loss of the link. HELLO messages are used for detecting and monitoring links to neighbors.

I. INTRODUCTION

Wireless communication technology is steadily and rapidly increasing. People wish to use their network terminals (laptops, PDAs, etc.) anywhere and anytime. Wireless connectivity gives users the freedom to move where they desire.

There exist numerous different wireless networks varying in the way the nodes interconnect. They can be classified in two main types: Networks with fixed infrastructure and Ad hoc wireless networks

Typical for networks with fixed infrastructure is using of access points. An access point (AP) can act as a router in the network, or as a bridge. Examples for this type of networks are GSM and UMTS cellular networks [1]. APs have more information about the network and are able to route the packets the best way. In contrast, ad hoc networks have no fixed infrastructure or administrative support, the topology of the network changes dynamically as mobile nodes joins or leaves the network. In ad-hoc wireless networks the nodes themselves use each other as routers, so these nodes should be more intelligent than the nodes in centralized networks with APs. There are a lot of situations where ad hoc

networks are needed: military operations, emergency services, conferencing, game parties, home networking, etc.

If the wireless nodes are within the range of each other, the routing is not necessary. If a node moves out of this range, and they are not able to communicate with each other directly, intermediate nodes are needed to organize the network which takes care of the data transmission. The purpose of a routing algorithm is to define a scheme for transferring a packet from one node to another. This algorithm should choose some criteria to make routing decisions, for instance number of hops, latency, transmission power, bandwidth, etc.

The topology of mobile ad hoc networks is time-varying, so traditional routing techniques used in fixed networks cannot be directly applied here. There are various techniques for tracking changes in the network topology and re-discovering new routes when older ones break. Since ad hoc networks have no infrastructure these operations should be performed with collective cooperation of all nodes.

Routing protocols in mobile networks are subdivided into two basic classes [12]. Proactive routing protocols (e.g. OLSR) are table-driven. They usually use link-state routing algorithms flooding the link information. Link-state algorithms maintain a full or partial copy of the network topology and costs for all known links. The reactive routing protocols (e.g. AODV) create and maintain routes only if these are needed, on demand. They usually use distance-vector routing algorithms that keep only information about next hops to adjacent neighbors and costs for paths to all known destinations. Thus, link-state routing algorithms are more reliable, less bandwidth-intensive, but also more complex and compute- and memory-intensive.

In on-demand routing protocols a fundamental requirement for connectivity is to discover routes to a node via flooding of request messages. The AODV routing protocol [2-4] is one of several published reactive routing protocols for mobile ad-hoc networks, and is currently extensively researched.

The rest of the paper is organized as follows. In the next section the AODV protocol is briefly reviewed. The properties of AODV and comparison between AODV and OLSR will be considered in Section III. Section IV will conclude this paper.

II. AD-HOC ON-DEMAND VECTOR

AODV is a relative of the Bellman-Ford distant vector algorithm, but is adapted to work in a mobile environment. AODV determines a route to a destination only when a node wants to send a packet to that destination. Routes are maintained as long as they are needed by the source. Sequence numbers ensure the freshness of routes and guarantee the loop-free routing.

Routing tables

Each routing table entry contains the following information [2] as destination, next hop, number of hops, destination sequence number, and active neighbors for this route and expiration time for this route table entry. Expiration time, also called lifetime, is reset each time the route has been used. The new expiration time is the sum of the current time and a parameter called active route timeout. This parameter, also called route caching timeout, is the time after which the route is considered as invalid, and so the nodes not lying on the route determined by RREPs delete their reverse entries. If active route timeout is big enough route repairs will maintain routes. RFC 3561 defines it to 3 seconds.

Control messages

Routing request

When a route is not available for the destination, a route request packet (RREQ) is flooded throughout the network. The RREQ contains the following fields [3]:

Source address	Request ID	Source sequence No.	Destination Address	destination sequence No.	Hop count
----------------	------------	---------------------	---------------------	--------------------------	-----------

The request ID is incremented each time the source node sends a new RREQ, so the pair (source address, request ID) identifies a RREQ uniquely. On receiving a RREQ message each node checks the source address and the request ID. If the node has already received a RREQ with the same pair of parameters the new RREQ packet will be discarded. Otherwise the RREQ will be either forwarded (broadcast) or replied (unicast) with a RREP message: if the node has no route entry for the destination, or it has one but this is no more an up-to-date route, the RREQ will be rebroadcasted with incremented hop count and if the node has a route with a sequence number greater than or equal to that of RREQ, a RREP message will be generated and sent back to the source. The number of RREQ messages that a node can send per second is limited.

There is an optimization of AODV using an expanding ring (ESR) technique when flooding RREQ messages [5, 6]. Every RREQ carries a time to live (TTL) value that specifies the number of times this message should be re-broadcasted. This value is set to a predefined value at the first transmission and increased at retransmissions. Retransmissions occur if

no replies are received. Historically such floodings used a TTL large enough - larger than the diameter of the network - to reach all nodes in the network, and so to guarantee successful route discovery in only one round of flooding. However, this low delay time approach causes high overhead and unnecessary broadcast messages. Later, it was shown [7, 8] that the minimal cost flooding search problem can be solved via a sequence of flooding with an optimally chosen set of TTLs.

Routing reply

If a node is the destination, or has a valid route to the destination, it unicasts a route reply message (RREP) back to the source. This message has the following format

Source Address	destination Address	destination sequence No.	hop count	life-Time
----------------	---------------------	--------------------------	-----------	-----------

The reason one can unicast RREP back is that every node forwarding a RREQ message caches a route back to the source node (see section 2.4.1).

Route error

All nodes monitor their own neighbourhood. When a node in an active route gets lost, a route error message (RERR) is generated to notify the other nodes on both sides of the link of the loss of this link.

HELLO messages

Each node can get to know its neighbourhood by using local broadcasts, so-called HELLO messages. Nodes neighbors are all the nodes that it can directly communicate with. Although AODV is a reactive protocol it uses these periodic HELLO messages to inform the neighbors that the link is still alive. The HELLO messages will never be forwarded because they are broadcasted with TTL = 1. When a node receives a HELLO message it refreshes the corresponding lifetime of the neighbour information in the routing table.

This local connectivity management should be distinguished from general topology management to optimize response time to local changes in the network.

Sequence numbers

Counting to infinity

The core of the problem is that when X tells Y that it has a path somewhere, Y has no way of knowing whether it itself is on the path - as Tanenbaum [9] notes. So if Y detects a link to Z is broken, but X still has a "valid" path to Z, Y assumes X in fact does have a path to Z. So X and Y will start updating each other in a loop, and the problem named "counting to infinity" arises. AODV avoids this

problem by using sequence numbers for every route, so Y can notice that X's route to Z is an old one and is therefore to be discarded.

Time stamping

The sequence numbers are the most important feature of AODV for removing the old and invaluable information from the network. They work as a sort of timestamps and prevent the AODV protocol from the loop problem (see Appendix). The destination sequence number for each destination host is stored in the routing table, and is updated in the routing table when the host receives the message with a greater sequence number. The host can change its own destination sequence number if it offers a new route to itself, or if some route expires or breaks.

Each host keeps its own sequence number, which is changed in two cases: before the node sends RREQ message, its own sequence number is incremented and when the node responds to a RREQ message by sending a RREP-message, its own sequence number becomes the maximum of the current sequence number and the node's sequence number in the received RREQ message.

The reason is that if the sequence number of already registered is greater than that in the packet, the existing route is not up-to-date. The sequence numbers are not changed by sending HELLO messages.

Route discovery

Route discovery process starts when a source node does not have routing information for a node to be communicated with. Route discovery is initiated by broadcasting a RREQ message. The route is established when a RREP message is received. A source node may receive multiple RREP messages with different routes. It then updates its routing entries if and only if the RREP has a greater sequence number, i.e. fresh information.

Reverse path setup

While transmitting RREQ messages through the network each node notes the reverse path to the source. When the destination node is found the RREP message will travel along this path, so no more broadcasts will be needed. For this purpose, the node on receiving RREQ packet from a neighbor records the address of this neighbor.

Forward path setup

When a broadcast RREQ packet arrives at a node having a route to the destination, the reverse path will be used for sending a RREP message. While transmitting this RREP message the forward path is setting up. One can say that this forward path is reverse to the reverse path. As soon as the forward path is built the data transmission can be started. Data packets waiting to be transmitted are buffered locally and transmitted in a FIFO-queue when a route is set up. After a RREP was forwarded by a node, it can receive another RREP. This new RREP

will be either discarded or forwarded, depending on its destination sequence number: if the new RREP has a greater destination sequence number, then the route should be updated, and RREP is forwarded, if the destination sequence numbers in old and new RREPs are the same, but the new RREP has a smaller hop count, this new RREP should be preferred and forwarded, and, otherwise all later arriving RREPs will be discarded.

Optimal TTL sequence

Expanding ring search strategies for AODV were recently extensively studied, and different schemes were proposed. In [8] a RREQ is initiated with a small TTL value, followed by RREQs with incremented TTL values until a certain threshold is reached. Then, if no route is found, a RREQ is flooded across the whole network.

The authors of [10] tried to find the optimal initial TTL value, TTL step, and the TTL threshold value. They found that the use of initial and step TTL values greater than 1 result in reducing overhead and delay time. They found also that initial as well as step values depend of the network topology, but the threshold value does not.

Furthermore, other strategies were proposed to make the route discovery more efficient, e.g. using the history of hop-distance to decide which initial TTL value should be chosen.

Link breakage

Because nodes can move link breakages can occur. If a node does not receive a HELLO message from one of his neighbors for specific amount of time called HELLO interval, then the entry for that neighbor in the table will be set as invalid and the RERR message will be generated to inform other nodes of this link breakage. RERR messages inform all sources using a link when a failure occurs.

Implementations of AODV

There are many AODV routing protocol implementations, including Mad-hoc, AODVUCSB, AODV-UU, Kernel-AODV, and AODV-UIUC [11]. Each implementation was developed and designed independently, but they all perform the same operations. The first publicly available implementation of AODV was Mad-hoc. The Mad-hoc implementation resides completely in user-space and uses the snooping strategy to determine AODV events. Unfortunately, it is known to have bugs that cause it to fail to perform properly. Mad-hoc is no longer actively researched.

The first release of AODV-UCSB (University of California, Santa-Barbara) used the kernel modification strategy. AODV-UU has the same design as AODV-UCSB. The main protocol logic resides in a user-space daemon; in addition, AODV-

UU (Uppsala University) includes Internet gateway support.

The AODV-UIUC implementation is similar to AODV-UCSB and AODV-UU except it explicitly separates the routing and forwarding functions. Routing protocol logic takes place in the user-space daemon, while packet forwarding is handled in the kernel. This is efficient because forwarded packets are handled immediately and fewer packets traverse the kernel to user-space boundary. All of the implementations discussed use HELLO messages to determine local connectivity and detect link breaks. In addition, all implementations (except Mad-hoc) support the expanding ring search and local repair optimizations.

III. PROPERTIES OF AODV

Merits of AODV

The AODV routing protocol does not need any central administrative system to control the routing process. Reactive protocols like AODV tend to reduce the control traffic messages overhead at the cost of increased latency in finding new routes.

AODV reacts relatively fast to the topological changes in the network and updates only the nodes affected by these changes.

The HELLO messages supporting the routes maintenance are range-limited, so they do not cause unnecessary overhead in the network.

The AODV routing protocol saves storage place as well as energy. The destination node replies only once to the first request and ignores the rest. The routing table maintains at most one entry per destination.

If a node has to choose between two routes, the up-to-date route with a greater destination sequence number is always chosen. If routing table entry is not used recently, the entry is expired. A not valid route is deleted: the error packets reach all nodes using a failed link on its route to any destination.

Drawbacks of AODV

It is possible that a valid route is expired. Determining of a reasonable expiry time is difficult, because the nodes are mobile, and sources' sending rates may differ widely and can change dynamically from node to node.

Moreover, AODV can gather only a very limited amount of routing information, route learning is limited only to the source of any routing packets being forwarded. This causes AODV to rely on a route discovery flood more often, which may carry significant network overhead. Uncontrolled flooding generates many redundant transmissions which may cause so-called broadcast storm problem.

The performance of the AODV protocol without any misbehaving nodes is poor in larger networks.

The main difference between small and large networks is the average path length. A long path is more vulnerable to link breakages and requires high control overhead for its maintenance.

Furthermore, as a size of a network grows, various performance metrics begin decreasing because of increasing administrative work, so-called administrative load.

AODV is vulnerable to various kinds of attacks, because it based on the assumption that all nodes will cooperate. Without this cooperation no route can be established and no packet can be forwarded. There are two main types of uncooperative nodes: malicious and selfish. Malicious nodes are either faulty and cannot follow the protocol, or are intentionally malicious and try to attack the network. Selfishness is noncooperation in certain network operations, f.e. dropping of packets which may affect the performance, but can save the battery power.

Comparison between AODV and OLSR

As a proactive protocol, OLSR produces large control traffic overhead on the network. This overhead consumes bandwidth. AODV surpasses OLSR in terms of storage and memory overhead because maintaining of the routing tables for the whole network requires much more communication between the nodes as well as much more storage than by using the AODV protocol. Also routes never been used are maintained.

As a reactive protocol the AODV has an evident weakness: its latency. The route discovery process can take some time. This delay can be a crucial factor in a network. Moreover, a proactive part of AODV (route maintenance, HELLO messages) increases the control messages' volume and the transmission cost. It also damages the reactive property of the AODV.

The scalability is another problem of AODV protocol: with growth of the network the average path length increases, and so does the probability that a link becomes invalid. Therefore the AODV is suited only for small and medium size networks, the scalability limit is about 1000 nodes. Simulations of Perkins' group shown that at 1000 nodes AODV performs poorly, only 25% packets are delivered. The number of RREQ messages grows fast linear with nodes population, and at 1000 nodes most packets are control messages.

So the AODV protocol can be used in networks with limited resources: bandwidth, energy, computational power, but with a limited number of nodes, too. AODV is much more adaptable to highly dynamic topologies as OLSR does.

IV. CONCLUSION

In this paper the AODV routing protocol has been reviewed. As a reactive protocol AODV transmits network information only on-demand. The limited proactive part is the route maintenance (HELLO messages). The AODV protocol is loop-free and avoids the counting to infinity problem by the use of sequence numbers. This protocol offers quick adaptation to mobile networks with low processing and low bandwidth utilization.

The weaknesses of AODV include its latency and scalability.

The main conclusion of this paper is that the choice of which protocol to use depends on the properties of the network.

References

1. Schiller J. Mobile Communications. Addison Wesley, 2nd edition, 2003.
2. Royer E.M. Perkins C.E. Ad-hoc on-demand distance vector routing. Proceedings of the 2nd IEEE Workshop on Mobile Computing Systems and Applications, p.90, 1999.
3. Das S. Perkins C.E., Belding-Royer E.M. Ad-hoc on-demand distance vector (aodv) routing. RFC 3561, IETF Network Working Group, 2003.
4. AODV homepage. <http://moment.cs.ucsb.edu/aodv/aodv.html>.
5. Pucha H. Hu Y.C. Koutsonikolas D., Das S.M. On optimal ttl sequence-based route discovery in manets. volume vol.9, p.923, 2005.
6. Schneider S. Kaddoura M., Ramanujan R. Routing optimization techniques for wireless ad hoc networks. Proceedings of the Sixth International Conference on Software Engineering, Artificial Intelligence, Networking and Parallel/Distributed Computing and First ACIS International Workshop on Self-Assembling Wireless Networks SNP/SAWN 2005, p.454, 2005.
7. Liu M. Chang N. Revisiting the ttl-based controlled flooding search: Optimality and randomization. In Proc. of ACM MobiCom, September, 2003.
8. Perkins C.E. Lee S.-J., Belding-Royer E.M. Scalability study of the ad-hoc on-demand distance vector routing protocol. Int. J. Netw. Manag., 13(2), 2003.
9. Tanenbaum A.S. Computer Networks. Prentice Hall International, 4th edition, 2003.
10. Jha S. Hassan J. On the optimization trade-offs of expanding ring search. Springer Verlag, 2004.
11. Belding-Royer E.M. Chakeres I.D. Aodv routing protocol implementation design. 2003.
12. There are also so-called hybrid protocols.

Appendix

Proof by contradiction: Let $\{K_1, \dots, K_n\}$ be a loop in a route from any source node to any destination node. That means that these nodes are chained to each other. Assume without loss of generality that

$$\text{next Hop}(K_i) = K_{i+1}, \text{ for } 1 \leq i \leq m, \text{ where } K_{m+1} \equiv K_1 \quad (\text{E.1})$$

Then, from the definition of AODV destination sequence numbers, we have

$$\text{DestSeq No}(K_i) \leq \text{DestSeq No}(K_{i+1}) \Rightarrow \text{DestSeq No}(K_i) = \text{DestSeq No}(K_j), \text{ for all } i, j \text{ belongs to } \{1, \dots, m\}$$

This means that information about the destination node was obtained from the same RREP message. Taking into account (E.1) and the definition of the hop count, we get

$$\text{hopCount}(K_i) = \text{hopCount}(K_{i+1}) + 1 \quad (\text{E.2})$$

Therefore,

$$\left. \begin{aligned} \text{hopCount}(K_1) &= \text{hopCount}(K_m) + m - 1 \\ \text{hopCount}(K_m) &= \text{hopCount}(K_1) + 1 \end{aligned} \right| \Rightarrow m = 0$$

Designing and Analysis of 8 Bit SRAM Cell with Low Subthreshold Leakage Power

Atluri.Jhansi rani*, K.Harikishore**, Fazal Noor Basha**, V.G.Santhi Swaroop*,
L. VeeraRaju*

*Assistant professor, ECE Department, K.L.University, Vijayawada, India.

*M.Tech -VLSI Students, VLSI, ECE Department, K.L.University, Vijayawada, India.

Abstract- The power consumption is major concern in Very Large Scale Integration (VLSI) circuit design and reduce the power dissipation is challenging job for low power designers. . International technology roadmap for semiconductors (ITRS) reports that “leakage power dissipation” may come to dominate total power consumption. The sub-threshold leakage power is the main reason to increase the leakage power. So there is some techniques to reduce this leakage power like sleep approach, stack & some new techniques like, sleepy-stack, leakage feedback approach and sleepy keeper techniques which reduces leakage current while saving exact logic state.

As the technology increases integration density of transistors increases, power consumption has become a major concern in today’s processors and SoC designs. Considerable attention has been paid to the design of low power and high-performance SRAMs as they are critical components in both handheld devices and high performance processors.

In this paper we design 8 bit S-RAM by using the leakage current reduction techniques. The proposed circuits were designed in 0.18 μ m CMOS/VLSI technology with-in Micro-Wind tool, and measure power consumption for design approaches, and we achieves up to nearly 50% less power consumption than existing basic SRAM.

Key-words: sub-threshold leakage power, sleep, stack, sleepy-stack keeper, Leakage Feedback.

I. INTRODUCTION

Static RAMs are used extensively in modern processors as on chip memories due to their large storage density and small access latency. Low power on-chip memories have become the topic of substantial research as they can account for almost half of total CPU dissipation, even for extremely power-efficient designs. However, static power dissipation is becoming a significant fraction of the total power. Static power is the power dissipated in a design in the absence of any switching activity and is defined as the product of supply voltage and leakage current. The absolute and the relative contribution of leakage power to the total system power is expected to further increase in future technologies because of the exponential increase in leakage currents with technology scaling. The International Technology Roadmap for Semiconductors (ITRS) predicts that leakage power would contribute to 50% of the total power in the next generation processors.

Here we present some VLSI techniques to reduce leakage power. Each technique provides an efficient way to reduce leakage power, but disadvantages of each technique limit the application of each technique. In this paper SRAM cell was designed with each technique and analyze the power consumption in each technique.

II. LEAKAGE POWER REDUCTION TECHNIQUES

Here we proposed techniques in circuit level approaches for sub-threshold leakage power reduction. The Most well-known traditional approach is the sleep approach [2][3]. In the sleep approach, both (i) an additional "sleep" PMOS transistor is placed between VDD and the pull-up network of a circuit and (ii) an additional "sleep" NMOS transistor is placed between the pull-down network and GND. These sleep transistors turn off the circuit by cutting off the power rails. Figure 1 shows its structure. The sleep transistors are turned on when the circuit is active and turned off when the circuit is idle. By cutting off the power source, this technique can reduce leakage power effectively.

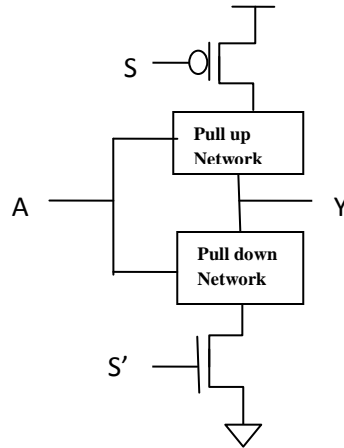


Fig.1 Sleepy approach.

Another technique for leakage power reduction is the stack approach, which forces a stack effect by breaking down an existing transistor into two half size transistors [5]. Figure 2 shows its structure. When the two transistors are turned off together, induced reverse bias between the two transistors results in subthreshold leakage current reduction. However, divided transistors increase delay significantly and could limit the usefulness of the approach.

The sleepy stack approach combines the sleep and stack approaches [6][7]. The sleepy stack technique divides existing transistors into two half size transistors like the stack approach. Then sleep transistors are added in parallel to one of the divided transistors. Figure 3 shows its structure. During sleep mode, sleep transistors are turned off and stacked transistors suppress leakage current while saving state. Each sleep transistor, placed in parallel to the one of the stacked transistors, reduces resistance of the path, so delay is decreased during active mode. However, area penalty is a significant matter for this approach since every transistor is replaced by three transistors and since additional wires are added for S and S', which are sleep signals.

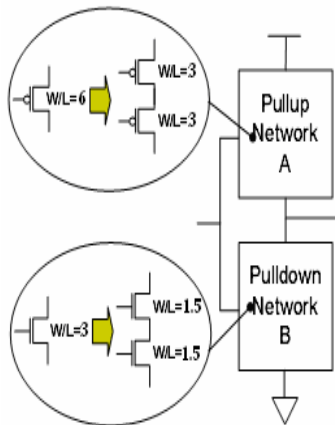


Fig.2 Stack approach

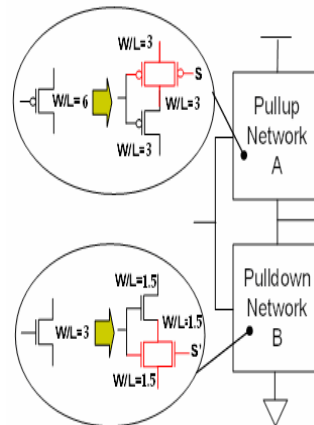


Fig.3 Sleepy Stack approach

The leakage feedback approach is based on the sleep approach. However, the leakage feedback approach uses two additional transistors to maintain logic state during sleep mode, and the two transistors are driven by the output of an inverter which is driven by output of the circuit implemented utilizing leakage feedback [17]. As shown in Figure 4, a PMOS transistor is placed in parallel to the sleep transistor (S) and a NMOS transistor is placed in parallel to the sleep transistor (S'). The two transistors are driven by the output of the inverter which is driven by the output of the circuit. During sleep mode, sleep transistors are turned off and one of the transistors in parallel to the sleep transistors keep the connection with the appropriate power rail.

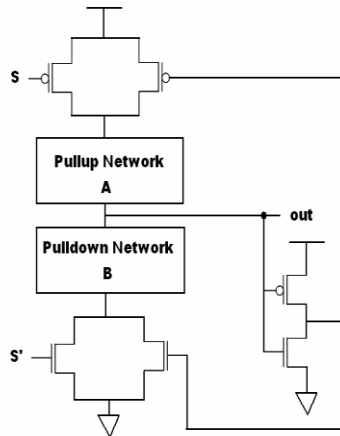


Fig.4 Leakage feedback approach.

For the sleep, zigzag, sleepy stack and leakage feedback approaches, dual V_{th} technology can be applied to obtain greater leakage power reduction. Since high- V_{th} results in less leakage but lowers performance, high- V_{th} is applied only to leakage reduction transistors, which are sleep transistors, and any transistors in parallel to the sleep transistors; on the other hand, low- V_{th} is applied to the remaining transistors to maintain logic performance [2]-[7].

III. MOTIVATION

The art of power analysis and optimization of integrated circuits used to be a specialty in analog circuit design. Power dissipation of VLSI chips is traditionally a neglected subject. In the past the device density and operating frequency were low enough that it was a constraining factor in the chips. As the technology varies, more transistors, faster and smaller than their predecessors, which leads to the growth in operating frequency and processing per capacity leads to increase in power consumption. There are two types of power dissipation in CMOS Circuits: Dynamic and Static. Dynamic power is caused by switching activities of the circuit and most significant source of dynamic power dissipation in CMOS circuits is the charging and discharging of the capacitance. Static Power dissipation is related to the logical states of the circuits rather than switching activities. In CMOS logic, leakage current is the only source of static power dissipation.

Currently, sub-threshold leakage seems to be the dominant contributor to overall leakage power. Another possible contributor to leakage power is gate-oxide leakage. A possible solution widely reported is the potential use of high k (high dielectric constant) gate insulators. In any case, this paper targets reduction of the sub-threshold leakage component of static power consumption; other approaches should be considered for reduction of gate oxide leakage. Do please note, however, that all results reported in this paper include all sources of leakage power. With application of dual threshold voltage (V_{th}) techniques, the sleep, zigzag and sleepy stack approaches result in orders of magnitude sub-threshold leakage power reduction.

IV. SRAM

Static Random Access Memory (SRAM) to be one of the most fundamental and vitally important memory technologies today. Because they are fast, robust, and easily manufactured in standard logic processes, they are nearly universally found on the same die with microcontrollers and microprocessors. Due to their higher speed SRAM based Cache memories and System-on-chips are commonly used. Due to device scaling there are several design challenges for nanometer SRAM design. Low power SRAM design is crucial since it takes a large fraction of total power and die area in high performance processors. A SRAM cell must meet the requirements for the operation in submicron/nano ranges. The scaling of CMOS technology has significant impacts on SRAM cell random fluctuation of electrical characteristics and substantial leakage current.

The schematic of SRAM cell is shown in the Fig.9. It has 2 pull up PMOS and 2 NMOS pull down transistors as two cross coupled inverters and two 2 NMOS access transistors to access the SRAM cell during Read and Write operations. Both the bit lines (BL and BLB) are used to transfer the data during the read and write operations in a differential manner. To have better noise margin, the data signal and its inverse is provided to BL and BLb respectively. The data is stored as two stable states, at storing points VR and VL, and denoted as 0 and 1.

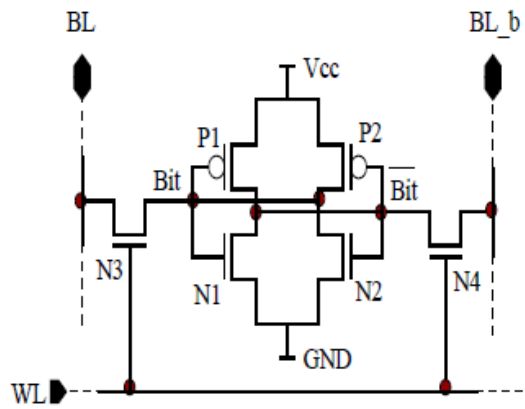


Fig.5 6T SRAM Cell

V. SIMULATION RESULTS

Here the SRAM cell is designed using all leakage power reduction techniques discussed earlier, namely stack, sleep, sleepy stack and leakage feedback approaches. Schematics and layouts are designed for all considered Techniques using Microwind.

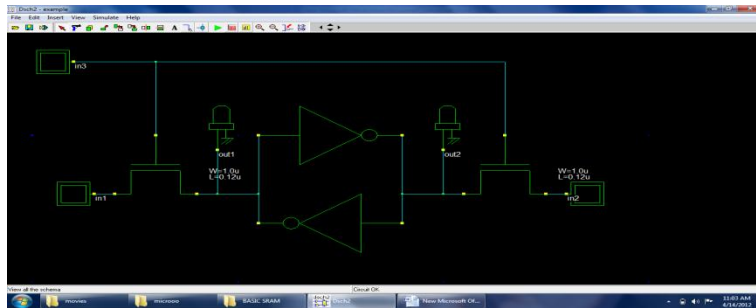


Fig 6: schematic for basic 6T SRAM cell

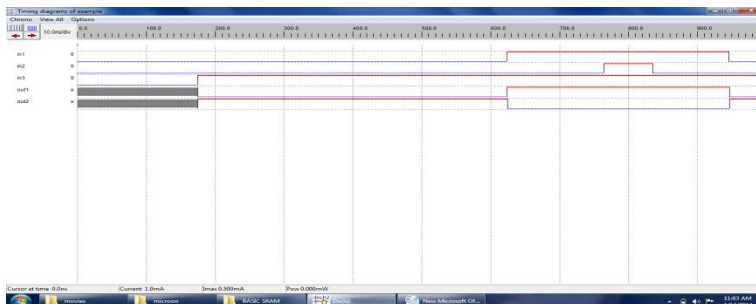


Fig 7: simulation results for basic 6T SRAM cell

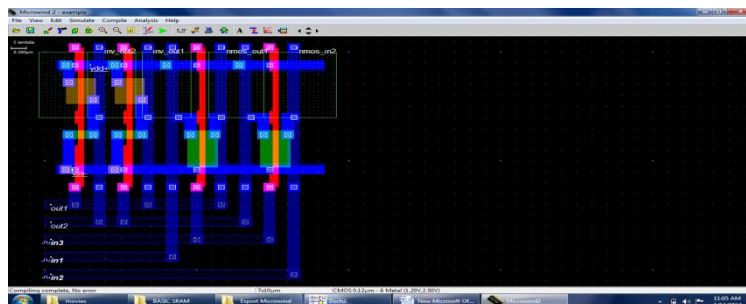


Fig 8: layout for basic 6T SRAM cell

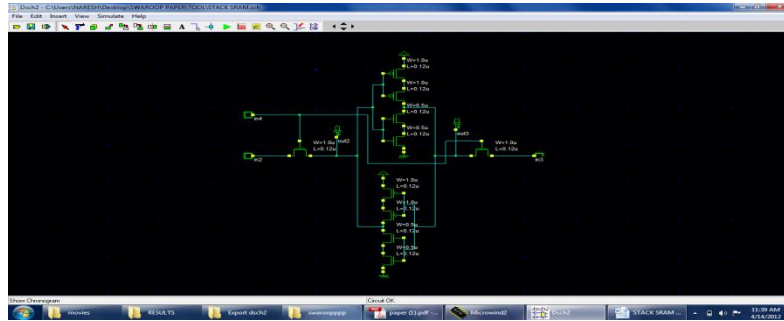


Fig 9: schematic for SRAM cell using stack approach

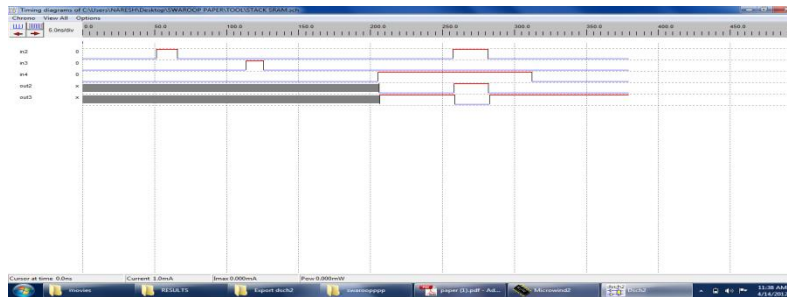


Fig 10: simulation results for SRAM cell using stack approach

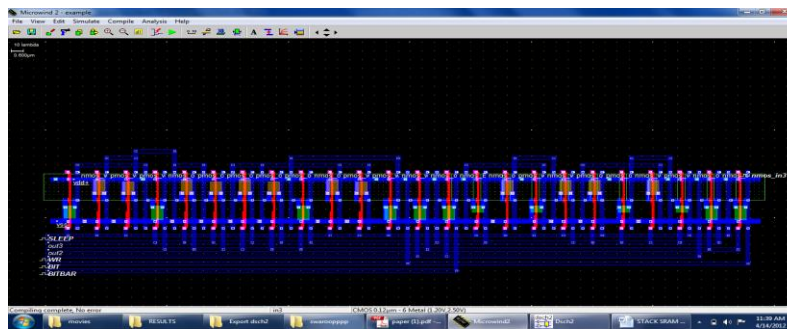


Fig 11: layout for SRAM cell using stack approach

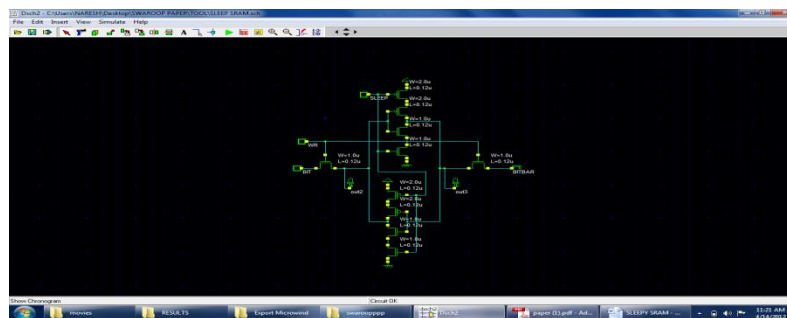


Fig 12: schematic for SRAM cell using sleep approach

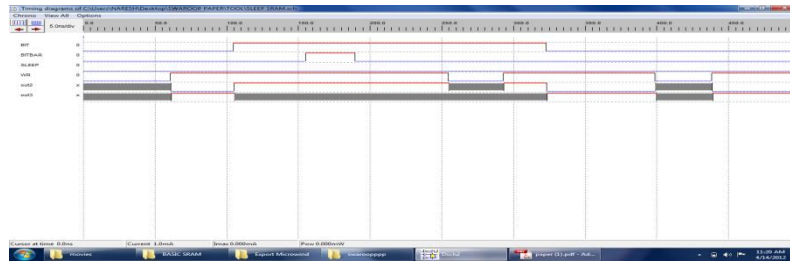


Fig 13: simulation results for SRAM cell using sleep approach



Fig 14: layout for SRAM cell using sleep approach

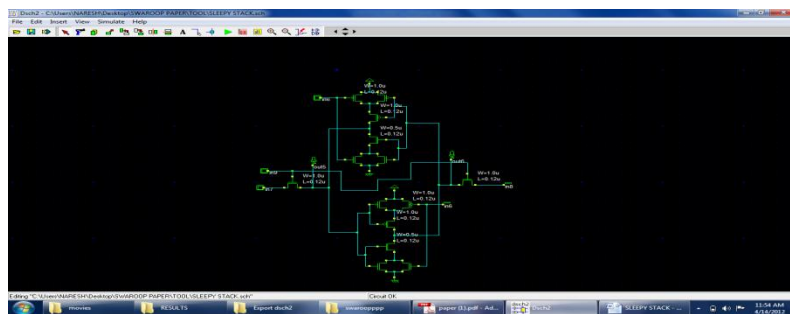


Fig 15: schematic for SRAM cell using sleep stack approach

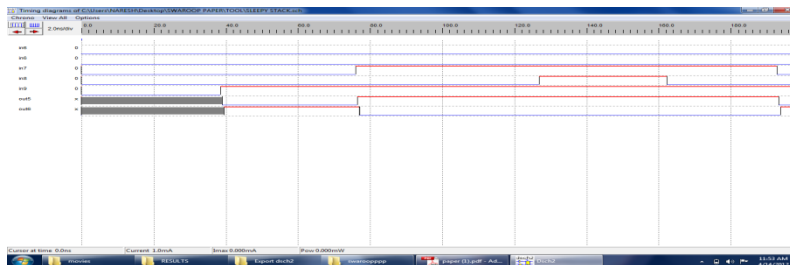


Fig 16: simulation results for SRAM cell using sleep stack approach

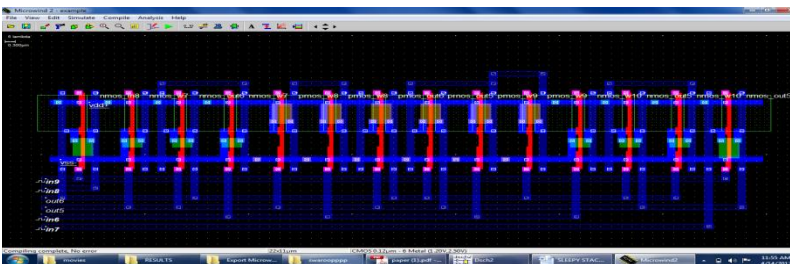


Fig 17: layout for SRAM cell using sleep stack approach

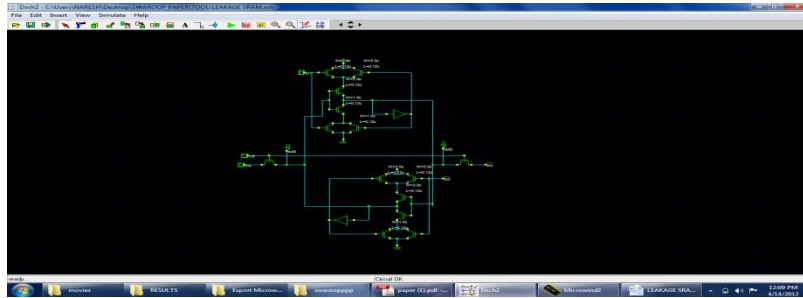


Fig 18: schematic for SRAM cell using leakage feedback approach

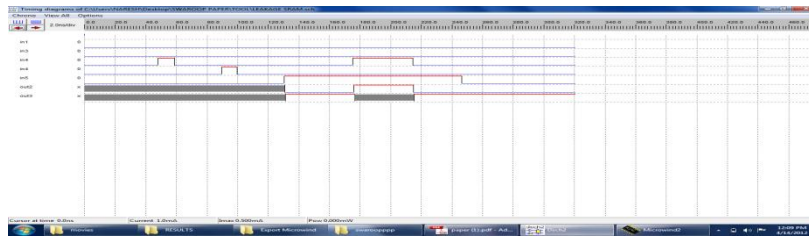


Fig 19: simulation results for SRAM cell using leakage feedback approach

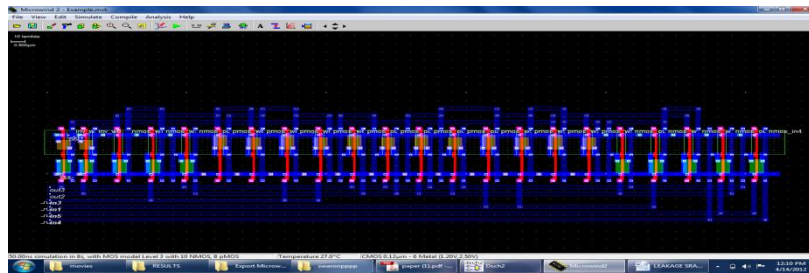


Fig 20: layout for SRAM cell using leakage feedback approach

Power dissipation analysis between Basic SRAM and SRAM using leakage power reduction technique

Topology	Basic SRAM (mw)	SRAM using STACK approach (mw)	SRAM using SLEEPY approach (mw)	SRAM using SLEEPY STACK approach (mw)	SRAM using LEAKAGE feedback approach (mw)
180nm	10.2	0.26	0.11	0.15	10.2 E-03
120nm	2.2	0.11	87.3 E-03	0.21	2.2 E-03
90nm	1.2 E-03	74.6 E-03	57.6 E-03	73.4 E-03	1.2 E-03
70nm	0.5 E-03	37.03 E-03	29.4 E-03	36.2 E-03	0.5 E-03
50nm	0.15 E-03	8.9 E-03	7.15 E-03	8.8 E-03	0.15 E-03

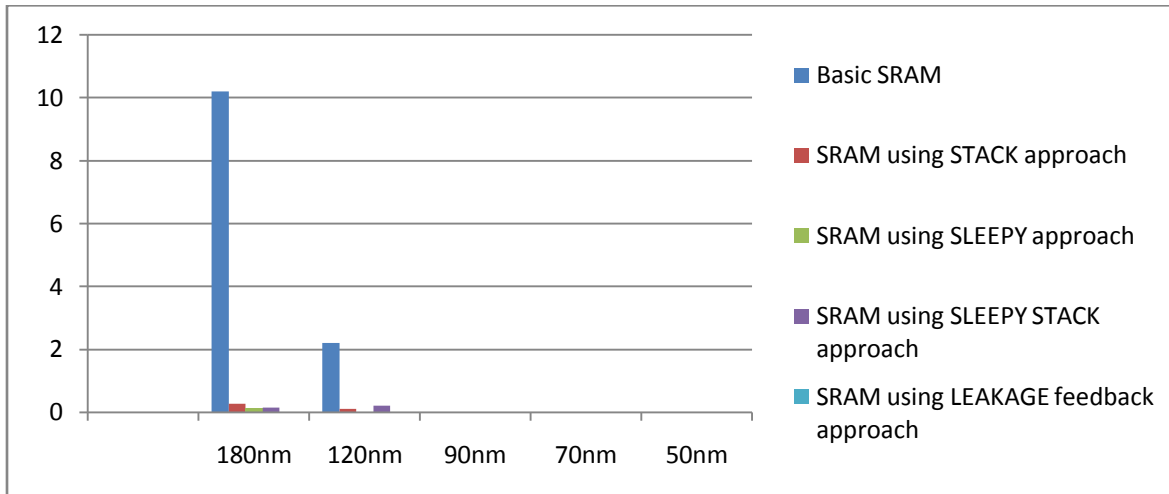


Fig 30: Power consumption graph for basic SRAM and SRAM using leakage power reduction techniques

VI. CONCLUSION

In this paper we designed SRAM cell using Leakage power reduction techniques to reduce sub-threshold leakage power. The proposed circuits were designed in 0.18 μ m technology and analyze the power dissipation between proposed techniques. Here we observed that proposed techniques have low power consumption compared to basic circuit design and having delay and area overhead.

Based on the simulation results of SRAM cell, we observed that by using these techniques we can reduce nearly 50% of power dissipation compared to general SRAM cell. Hence it is concluded that the proposed SRAM Architecture is used for low power designs and these designed techniques are used for high performance and low power applications.

VII. REFERENCES

- [1] International Technology Roadmap for Semiconductors by Semiconductor Industry Association, <http://public.itrs.net>, 2007.
- [2] S. Mutoh et al., "1-V Power Supply High-speed Digital Circuit Technology with Multi-threshold- Voltage CMOS," IEEE Journal of Solis-State Circuits, Vol. 30, No. 8, pp. 847-854, August 1995.
- [4] M. Powell, S.-H. Yang, B. Falsafi, K. Roy and T. N. Vijay Kumar, "Gated-Vdd: A Circuit Technique to Reduce Leakage in Deep submicron Cache Memories," International Symposium on Low Power Electronics and Design, pp. 90-95, July 2000.
- [5] Z. Chen, M. Johnson, L. Wei and K. Roy, "Estimation of Standby Leakage Power in CMOS Circuits Considering Accurate Modeling of Transistor Stacks," International Symposium on Low Power Electronics and Design, pp. 239- 244, August 1998.
- [6] J. Park, "Sleepy Stack: a New Approach to Low Power VLSI and Memory, " Ph.D. Dissertation, School of Electrical and Computer Engineering, Georgia Institute of Technology, 2005.
- [7] J.C. Park, V. J. Mooney III and P. Pfeiffenberger, "Sleepy Stack Reduction of Leakage Power," Proceeding of the International Workshop on Power and Timing Modeling, Optimization and Simulation, pp. 148-158, September 2004.
- [8] Jan M Rabaey, Anantha Chandrakasan and Borivoje Nikolic, Digital Integrated Circuits, A Design Perspective, Second Edition, Pearson Education, (2002).
- [9] A 2.2GHz 32 \times 4 bit 6T-SRAM Design in 45nm CMOS Xi Chen, Ting Zhu, Harun Demircioglu.
- [10] Designing an SRAM array at the 90nm CMOS tech node Shrivathsa Bhargav and Jaime Peretzman ELEN 4321 – Digital VLSI circuits Columbia University, Fall 2007.

Authors Profile

1. **Jhansirani.Atluri** was born in Narasaraopet, Guntur (Dist.), AP, India. She received B.Tech. in Electronics & Communication Engineering from St. Ann's College of Engg. ,Chirala ,prakasam (Dist.),AP, India ,M.Tech from KL University , Vijayawada, AP, India.

2. **Harikishore.Kakarla** was born in Vijayawada, Krishna (Dist.), AP, India. He received B.Tech. in Electronics & Communication Engineering from St. Johns College of Engg.,Kurnool(Dist.),AP, India, MTech from G. Pulla Reddy Engineering College, Kurnool, AP, India. He is pursuing Ph.D in the area of VLSI in KL University, Vijayawada, AP, India. He has published 01 National Conference Level.



2. **Dr. Fazal Noorbasha** was born on 29th April 1982. He received his, B.Sc. Degree in Electronics Sciences from BCAS College, Bapatla, Guntur, A.P., Affiliated to the Acharya Nagarjuna University, Guntur, Andhra Pradesh, India, in 2003, M.Sc. Degree in Electronics Sciences from the Dr. HariSingh Gour University, Sagar, Madhya Pradesh, India, in 2006, M.Tech. Degree in VLSI Technology, from the North Maharashtra University, Jalgaon, Maharashtra, INDIA in 2008, and Ph.D. Degree in VLSI from Department Of Physics and Electronics, Dr. HariSingh Gour Central University, Sagar, Madhya Pradesh, India, in 2011. Presently he is working as a Assistant Professor, Department of Electronics and Communication Engineering, KL University, Guntur, Andhra Pradesh, India, where he has been engaged in teaching, research and development of Low-power, High-speed CMOS VLSI SoC, Memory Processors LSI's, Digital Image Processing, Embedded Systems and Nanotechnology. He is a Scientific and Technical Committee & Editorial Review Board Member in Engineering and Applied Sciences of World Academy of Science Engineering and Technology (WASET), Advisory Board Member of International Journal of Advances Engineering & Technology (IJAET), Member of International Association of Engineers (IAENG) and Senior Member of International Association of Computer Science and Information Technology (IACSIT). He has published over 20 Science and Technical papers in various International and National reputed journals and conferences.



Parking Study on Main Corridors in Major Urban Centre

T. SUBRAMANI¹

¹Professor & Dean, Department of Civil Engineering, VMKV Engg College, Vinayaka Missions University, Salem, India.

ABSTRACT

Salem is the fifth largest city with a population of 7.54 lakhs (2011) in Tamil Nadu. Parking is one of the major problems that are created by the increasing vehicle traffic. It has an impact on transport development. The availability of less space in urban areas has increased demand for parking space especially in central business area. This affects the mode choice also. This has a great economical impact. Two wheeler sales at 15 million are expected to grow 14-15%, while car sales close to 8 lakhs units a year. In order to accommodate the large volume of vehicle, small cities and towns must develop the affect their infrastructures – roads, flyovers, car parks and other facilities. Otherwise their arteries are most likely to get clogged like it happens in big and mini metros. The solution for this is systemic survey and management of traffic and pedestrian, although at a nascent stage in India, it the one of the options to decongest roads and solve parking and pedestrian problems. Before taking any measures for betterment of conditioned, data regarding availability of parking space, extent of it usage and parking surveys are intended to all these information. Since the duration of parking varies with different vehicles, the data has to be analyzed to access the parking need. As the traffic on the existing road system in the cities increases, congestion becomes serious problem. Thus there could be medium and long term solution measures.

KEYWORDS: Traffic, Vehicle Parking Survey, Urban Centre, Suggestions

1. GENERAL - NEED FOR PARKING STUDY

Parking is one of the serious problems that confront the urban planner and traffic engineer. Before any measure for the betterment of the conditions can be formulated basic data pertaining to the availability of parking space, extent of its usage and parking demand are essential. If it is proposed to implement a system of parking charges it will also be necessary to know how much to charge and what will be the affect of the pricing policy on parking. Parking survey is intended to supply all these kind of information.

With the growing population of motor vehicles, the problem of parking has assumed serious proportions. A systematic study of parking characteristic and demand and regulatory measures that are possible for controlling is of great help to a traffic engineers as well as town planner.

As per as survey carried out in India it is roughly estimated that out of 8760 hours in year the car runs for an average for only 400 hours leaving 8360 hours when it is parked. Increasing concentration of human activity on limited land both in terms of residential activity and commercial activity causes the parking problem. Every car owner would wish to park the car as closely as possible to his destination so as to minimize his walking distance. This

result in great demand for parking space in central business district (CBD) and other areas where the activities are concentrated.

2. OBJECTIVES

- To study existing parking conditions
- To carry out parking studies
- To formulate strategies for better management for parking

3. LIMITATIONS

The survey has been carried out only on the working day in the middle of the week. A detailed parking study spread over longer duration of time would have yielded more reliable results. More number of parking problems is especially due to unauthorized construction of the shopping complexes in the in CBD areas; a detailed survey is not carried out.

3. SCOPE

There is need to conduct survey on the availability of all vacant spaces both public and private, to explore the possibility of converting such places in to parking areas.

4. PARKING STUDIES

Parking is an essential component of the transportation system. Vehicles must park at every destination. A typical automobile is parked 23 hours each day, and uses several parking spaces each week. Parking facilities are a major cost to society and parking conflicts are among the most common problems facing designers, operator, p[anners and other officials. Such problem can be often defined either in terms of supply (too few spaces are available, somebody must build more) or in terms of management (available facilities are used inefficiently and should be better managed). Management solutions tend to be better than expanding supply because they support more strategic planning.

5. OBJECTIVES

- Reduced development costs and increased affordability.
- Encourage use of alternative modes and reduce motor vehicle use (thereby reducing traffic congestion, accidents and pollution)
- Improved design flexibility, creating more functional and attractive communities.
- Ability to accommodate new uses and respond to new demands.
- Reduced impervious surface and related environmental and aesthetic benefits.

Parking management refers to policies and programs that results in more efficient use of parking resources. Parking management includes several specific strategies; nearly two dozen are described in this report. When appropriately applied parking management can significantly reduce the number of parking spaces required in a particular situation, providing a variety of economic, social and environmental benefits. When all impacts are considered, improved management is often the best solution to parking problems.

6. STUDY OF PAST AND PRESENT CONDITIONS IN SALEM CITY

A. Salem – General

Salem is the fifth largest city in Tamil Nadu over an area of 91.34 Sq.kms. Salem city is located at distance of 350 kms from a Chennai on the west, and 160 kms from Coimbatore and it got the fifth largest population of 7.54 lakhs as per 2011 census in Tamil Nadu.. It is situated at the trijunction of Bangalore, Trichirappalli and Chennai roads. The City is located at 11 40' North and 78 10' on the East. The general topography is plain The city is surrounded by the hills viz. the shervarous and Nagarmalai on the North, The Kanjamalai on the west, the Goodamalai on the East.

B. Population Growth

The population in Salem has grown at a rate of 23 percent per decade between 1951 and 1971, the rate has been lower for the decade 1971 – 1981 at 17 percent and 14 percent per decade between 1991 and 2011. Table.1 gives the growth of population within the Salem town. Population growth of Salem City Corporation given in Table 1.

C. Existing Land-Use Structures

The extent of Salem town is 91.34 Sq.km of this the developed area is 4648 Hectares i.e. 48.71 percent of the total area and undeveloped area is 4894 hectares i.e. 51.29 per cent of the total area. Figure. 1. is showing the existing land use details of Salem City Corporation area.

7. SALEM CITY CORPORATION ROAD NETWORK

Salem district as a whole has only 10,133.7 km. of road, out of which 214.6 km are cement concrete roads, 5098.1 kms. are bituminous surfaced road and the remaining 4821 kms. are water Bound Macadam roads. The unsurfaced road of 2352.7 kms. also exist in the district

TABLE 1. POPULATION GROWTH OF SALEM CITY CORPORATION

Year	Salem town / corporation* population	Decade variation	% of decade variation
1901	70621	-	-
1911	59153	(-) 11468	(-) 16.24
1921	52244	(-) 6909	(-) 11.68
1931	102149	(-) 49935	95.58
1941	129702	27523	26.94
1951	202335	72633	56
1961	249145	46810	23.13
1971	308716	59571	23.9
1981	361394	52678	17.06
1991*	579951	218557	60.47
2001*	672330	92379	15.92
2011*	754000	81670	12.15

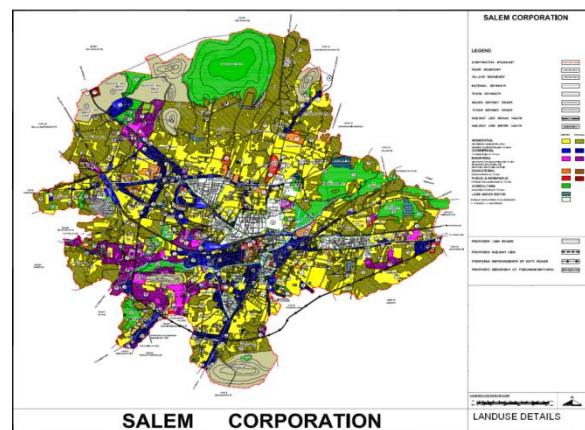


FIGURE.1. EXISTING LAND-USE DETAILS OF SALEM CITY CORPORATION

TABLE 2. EXISTING LAND USE DETAILS OF SALEM CITY AREA

Salem Corporation has about 748.13kms. of surfaced roads under its control and maintenance as detailed below. The width of road ranges from 3.5 m to 14.0m in the major road network excluding the lanes and small roads. The details of the various categories of roads with their lengths in the town is show in Table. 2

TABLE.2 TYPES OF ROADS WITH THEIR LENGTH IN SALEM CORPORATION

Sl. No	Category	Road length (km)
1	Cement Concrete Super Roads	54.47
2	Black Topped Roads	628.17
3	Wbm Roads	17.04
4	Earthern Road	23.46
5	Others	24.66
	Total Length of Municipal Roads	748.13

Fig.2. shows the identified road network of Salem city.



FIGURE.2. SALEM CITY CORPORATION ROAD NETWORK

8. PARKING STUDIES

8.1 PARKING CHARACTERISTICS

Parking accumulation:

It is defines as the number of vehicle parked at a given instant of time. Normally this is expressed by accumulation curve. Accumulation curve is a graph obtained by plotting the numbers of bays occupied with respect to time.

Parking volume:

Parking volume is the total number of vehicle parked at a given duration of time. This does not account for repetition of vehicles. The actual volume of vehicles entered in the area is recorded.

Parking load:

parking load gives the area under the accumulation curve. It can also be obtained by simply multiplying the numbers of vehicles occupying the parking area at each time interval with the time interval. It is expressed as vehicle hour.

Average parking duration:

It is the ratio of total vehicle hours to the number of vehicles parked.

$$\text{Parking duration} = \frac{\text{Parking load}}{\text{Parking volume}}$$

Parking turnover:

It is the ratio of number of vehicles parked in duration to the number of parking bays available.

$$\text{Parking duration} = \frac{\text{Parking volume}}{\text{Number of bays available}}$$

This can be expressed as number of vehicles per day per time requirement.

Parking Requirement

There is some minimum parking requirement for different types of building

- For residential plotless than 300 Sq.m. only community parking space is required.
- For residential plaut area from 500 to 1000Sq.m, minimum onefourth of the open area should be reserved for parking.
- Offices may require atleast one space for every 70Sq.m Parking area.
- One parking space is enough for 10 seats in a resturant
- where as theatres and cinema halls need to keep only one parking space for 20 seats.

Thus the parking requirement is different for different landuse zones.

8.2 TYPES OF PARKING SURVEYS

Parking surveys are conducted to collect the above said parking statistics. The most common parking surveys conducted are:

1. In-out survey:

In this survey the occupancy count in the selected parking lot is taken at the beginning. Then the number of vehicles that enter the parking lot for a particular time interval is counted. The number of vehicle that leaves the parking lot is also taken. The final occupancy in the parking lot is also taken. Here the labour required is very less. Only one person may be enough. But we won't get any data regarding the time duration for which a particular vehicle use that parking lot. Parking duration and turnover is not obtained. Hence we cannot estimate the parking fare from this survey.

2. Fixed period sampling:

this is almost similar to in-out survey. All vehicles are counted at the beginning of the survey. Han after a fixed time interval that may vary between 15 minutes to 1 hour, the count is again taken. Here there are chances of missing the number of vehicles that were parked for a short duration.

3. License plate method of survey:

this results in the most accurate and realistic data. In this case of survey, every parking stall is monitored at a continuous interval of 15 minutes or so and the license plate number is noted down. This will give the data regarding the duration for which a particular vehicle was using the parking bay. This will help in calculating the fare because fare is estimated based on the duration for which the vehicle was parked. If the time interval is shorter, than there are less chances of missing short term parkers. But this method is very labour intensive.

9. ILL EFFECTS OF PARKING

A. Congestion:

Parking takes considerable street space leading to the lowering of the road capacity.Hence, speed will be reduced,Journey time and delay will also subsequently increase. The operational cost of the vehicle increases

leading great economical loss to the community. Mixed type of parking shown in Figure.3. & Figure.4.shows that there is no proper parking bays in Salem.



FIGURE.3. MIXED TYPE PARKING (2 WHEELER & 4 WHEELER)



FIGURE.4. NO PROPER PARKING BAYS

B. Accident

Careless maneuvering of parking and un-parking leads to accidents which are referred to as accidents. Common type of parking accidents occur while driving out a car from the parked area, careless opening of doors of parked cars, (Figure.5.) and while bringing in the vehicle to the parking lot for parking.



FIGURE.5 ACCIDENT POSSIBILITY IN PARKING

C. Environment pollution

They also cause pollution to the environment because stopping and starting of vehicle while parking and un-parking results are noise and fumes(Figure.6.). They also

affect the aesthetic beauty of the building because car parked at every available space creates a feeling that building rises from plinth of cars. Sometimes they obstruct the fire fighting vehicles. Also they block access to hydrants and access to building.



FIGURE.6. ENVIRONMENTAL POLLUTION POSSIBILITY

10. PARKING STUDIES AND ANALYSIS OF DATA

Parking survey were conducted in 15 places to study the existing parking traffic condition

10.1 Five road:

It is observed that peak parking hours in between 11.3am to 1pm. Parking lot is provided on one side of the road. Parking supply for two wheeler is 30 and demand is 27, supply is meeting the demand. No parking for four wheeler. Parking accumulation graph shown in Figure.7.



FIGURE.7. PARKING ACCUMULATION GRAPH

10.2 Old bus stand:

It is observed that peak parking hour is between 10.30am to 2pm. Supply for two wheeler and three wheeler is 300 and 80 respectively. Parking demand for two wheeler and three wheeler is 280 and 60, supply is meeting the demand. Parking accumulation graph shown in Figure.8.



FIGURE.8. PARKING ACCUMULATION GRAPH

10.3 Four Road

It is observed that the peak parking hour is between 11.00am to 3.00pm. No proper parking bays are provided. The parking supply for four wheeler is 115 and the demand is 118, hence supply is not meeting the demand. Parking accumulation graph shown in Figure.9.

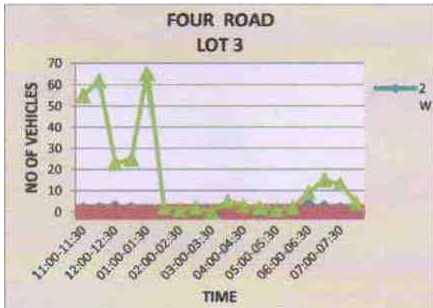


FIGURE.9. PARKING ACCUMULATION GRAPH

10.4 Saradha College Road

It is observed that the peak parking hours is between 11.00am to 2.00pm. parking is available on one side of the road. The parking supply for two wheeler is 65 and the demand is 69, hence supply is not meeting the demand. Parking accumulation graph shown in Figure.10.

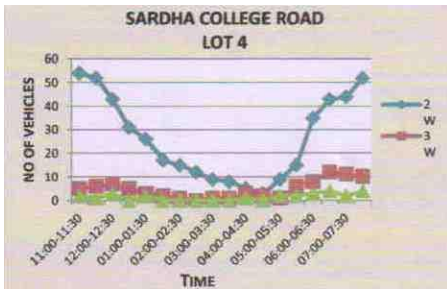


FIGURE.10. PARKING ACCUMULATION GRAPH

10.5 State Bank Colony

It is observed that peak parking hours is between 4.30pm to 7.30pm. Parking demand increases. Parking place and facility is limited. Parking accumulation graph shown in Figure.11.

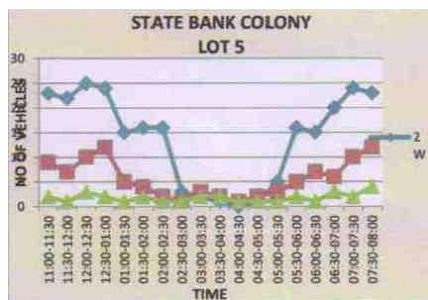


FIGURE.11. PARKING ACCUMULATION GRAPH

10.6 Cherry Road

No parking facility is available on both side of the road. Railing is provided on one side of the road. Zebra crossing is available. Parking accumulation graph shown in Figure.12.

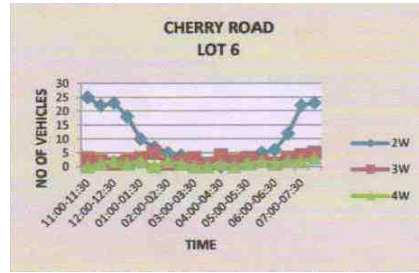


FIGURE.12. PARKING ACCUMULATION GRAPH

10.7 Permanur Road

Both side parking is available. There is no three and four wheeler parking; only two wheeler parking is available. The parking supply for two wheeler is 16 and the demand is 18, hence supply is not meeting the demand. Parking accumulation graph shown in Figure.13.



FIGURE.13. PARKING ACCUMULATION GRAPH

10.8 Sks Hospital Road

It is observed that peak parking hours is between 11.00am to 01.00pm. parking for two wheeler is available. No three and four wheeler parking. The parking supply for two wheeler is 30 and the demand is 38, hence supply is not meeting the demand. Parking accumulation graph shown in Figure.14.

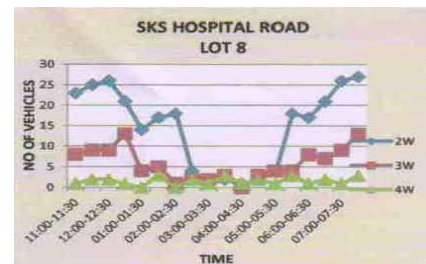


FIGURE.14. PARKING ACCUMULATION GRAPH

10.9 Bangalore Bye-Pass Road

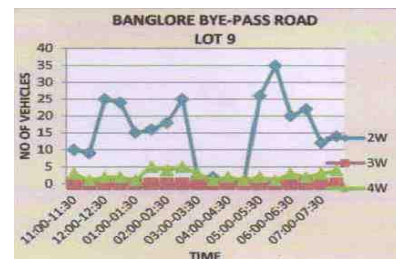


FIGURE.15. PARKING ACCUMULATION GRAPH

No proper parking bays for two and four wheeler. It is observed that peak hours is between 3.00pm to 7.00pm.

parking demand increases on Sunday due to Sunday bazaar. Parking accumulation graph shown in Figure.15.

10.10 Railway Station

Parking place is available for two, three and four wheeler. It is observed that peak parking hours is between 11.00am to 2.00pm. The parking supply for two wheeler and four wheeler are 42 and 25 respectively. The demand for two wheeler and four wheeler is found to be 37 and 21 respectively. Hence supply is meeting the demand. Parking accumulation graph shown in Figure.16.

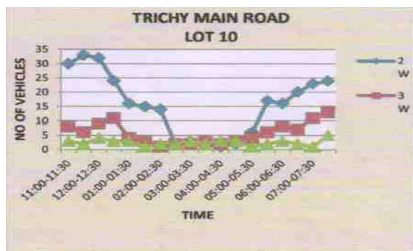


FIGURE.16. PARKING ACCUMULATION GRAPH

10.11 Bazaar Street

It is observed that peak parking hours is between 7.00pm to 07.30pm. parking for two wheeler is available. No three and four wheeler parking. The parking supply for two wheeler is 35 and the demand is 62. Hence supply is not meeting the demand. Parking accumulation graph shown in Figure.17.

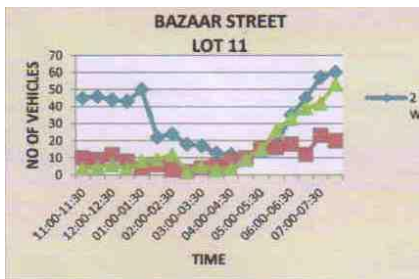


FIGURE.17. PARKING ACCUMULATION GRAPH

10.12 Railway Station

It is observed that the peak parking hours is between 11.00am to 2.00pm. parking is available on one side of the road. The parking supply for two wheeler is 40 and the demand is 44, hence supply is not meeting the demand. Parking accumulation graph shown in Figure.18.

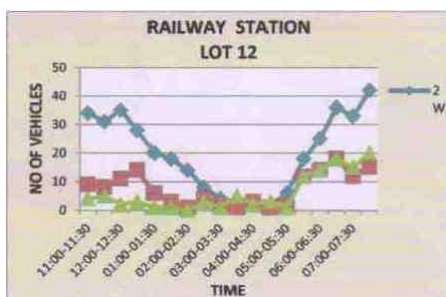


FIGURE.18. PARKING ACCUMULATION GRAPH

10.13 New Bus Stand

Parking place is available for two and four wheeler. It is observed that peak parking hours is between 05.30pm to 08.30pm. The parking bays are provided at inclined angle. The parking supply for two wheeler and four wheeler are 79 and 55 respectively. The demand for two wheeler and four wheeler is found to be 83 and 62 respectively. Hence supply is not meeting the demand. Parking accumulation graph shown in Figure.19.

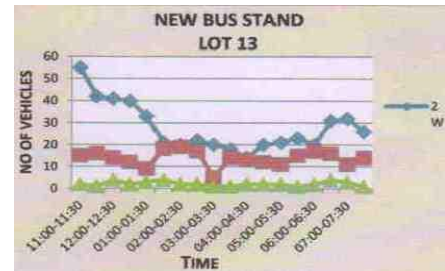


FIGURE.19. PARKING ACCUMULATION GRAPH

10.14 Meyyanur Main Road

It is observed that peak parking hours is between 11.00am to 01.00pm. parking for two wheeler is available. No three and four wheeler parking. The parking supply for two wheeler is 30 and the demand is 27, hence supply is not meeting the demand. Parking accumulation graph shown in Figure.20.

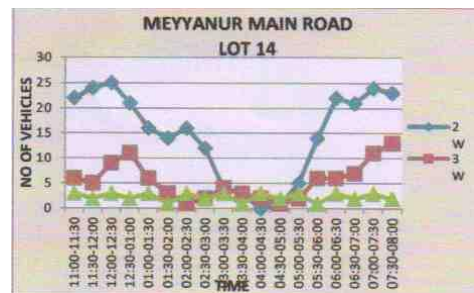


FIGURE.20. PARKING ACCUMULATION GRAPH

10.15 Kondalampatti

Both side parking is available. There is no three and four wheeler parking; only two wheeler parking is available. The parking supply for two wheeler is 25 and the demand is 27, hence supply is not meeting the demand. Parking accumulation graph shown in Figure.21.

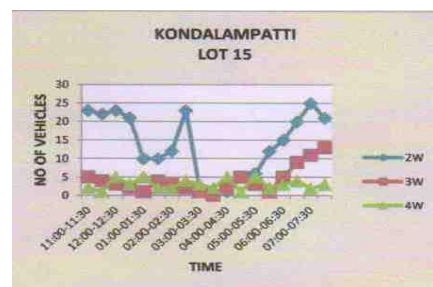


FIGURE.21. PARKING ACCUMULATION GRAPH

9. CONCLUSION

Parking takes considerable street space leading to the lowering of the road capacity. Hence, speed will be reduced, Journey time and delay will also subsequently increase. The operational cost of the vehicle increases leading great economical loss to the community. According to the parking study on existing traffic condition on the road network it is must and required to remove onstreet parking system for efficient transportation system. Careless maneuvering of parking and un-parking leads to accidents which are referred to as accidents. Common type of parking accidents occur while driving out a car from the parked area, careless opening of doors of parked cars, and while bringing in the vehicle to the parking lot for parking. They also cause pollution to the environment because stopping and starting of vehicle while parking and un-parking results are noise and fumes

To reduce the parking of vehicles we can implement the following.

- For short term measures pay and park method will be done at peak hours to control and regulate the parking.
- For long term measures Off street parking have to be provided near CBD areas, within the radius of 1 Km.

10. SUGGESTIONS FOR IMPROVEMENT

Though on street parking is an extravagant use of the precious space, it cannot be entirely prohibited. A judicious application of appropriate traffic management measures will help to mitigate some of the ill effects of on street parking. These measures should be of a comprehensive parking policy for the city. The regulatory measures range from waiting restrictions in a street to the comprehensive control over an extended area, lying down where the vehicles may or may not park, what should be the parking time and charges should be levied for parking. The measures should be periodically reviewed and altered, if necessary. The regulatory measures are generally of two types, one where the use of parking space is authorized for certain periods free or for payment and other where parking is prohibited, but which allows parking for picking up or setting down the goods and passengers. When a controlled parking scheme is planned, the zone boundaries should be delineated and suitable traffic signs are installed. While on street parking and its regulations will be an important aspect of the overall development of land use and building activities adequately take care of parking needs is to promulgate ordinance whereby all new or remodeled building will require having within their cartilage or prescribing parking space. Parking places are designed at desirable location alone, and no parking is permitted elsewhere, the measure will be successful only if the streets are probably signed and the carriageway marking are adequate.

Angle parking seems to be better than parallel parking which is usually involves a backing motion. Delay of traffic is minimized with angle parking. Regulation of parking by charging fees has the desirable effect of curbing long term parking, while encouraging short term parking. One method of collecting the charges is by installing parking meters.

11. REFERENCES

- [1]. DTCP (1986), 'Short term improvement program ME – Traffic and Transportation study for Coimbatore, Madurai, Trichy and Salem', DTCP, Tamil Nadu
- [2]. Hanspeter Georgi (1973), 'Cost- Benefit Analysis and Public Investments in Transport: A Survey', First Edition, Butter Worths (Publishers), London.
- [3]. Kadiyali.L.R.(2007), 'Traffic Engineering and Transport Planning', 7th edition, Khanna publishers, Delhi.
- [4]. Khanna S.K – Justo C.E.G (2010), 'Highway Engineering', 9th edition, Nem Chand and Bros. publishers, Roorkee(U.P)
- [5]. Lindsay R. Peat (1982), 'Practical Guide to DBMS selection', Walter de Grawyter, New York.
- [6]. Meyer M.d.Miller E.J (1984), 'Urban Transportation Planning', Mcgraw – Hill series, New Delhi.
- [7]. Subramanian P. (1990) , 'Capacity restrained trip assignment model for Madras City', ME Urban Engineering Thesis, Madras – 600025.
- [8]. V.N.Vazirani & S.P.Chandola, 'Transportation Engineering Vol.I ', 5th edition, Khanna Publishers, New Delhi
- [9]. Dr.L.R.Kadyali & Dr.N.B.Lal, 'Principles and Practices of Highway Engineering, 5th edition, Khanna Publishers, New Delhi
- [10]. B.L.Gupta & Amit Gupta 'Highway and bridge Engineering' 3rd edition Standard Publishers Distributers, New Delhi
- [11]. C.Jotin Khisty & B.Kent Lall, 'Transportation Engineering' 3rd edition, PHI Learning Private Limited, New Delhi
- [12]. Gurcharan Singh, 'Highway Engineering' 5rd edition Standard Publishers Distributers, New Delhi
- [13]. R.K. Khitoliya, 'Principles of Highway Engineering' 1st edition , Dhanpat Rai Publishing Company, New Delhi.
- [14]. DTCP (1999), 'Comprehensive Traffic and Transportation Study for Salem', Pallavan Transport Consultancy Services Ltd., Chennai, Tamil Nadu.
- [15]. Guidelines on regulation and control mixed traffic in urban areas, IRC: 70-1977.
- [16]. Guidelines for pedestrian facilities, IRC:103-1988
- [17]. ITPI Journal (Institute of town planner India) 2004, 43-46 and 2005, 62-65.

A Session Based Blind Watermarking Technique within the NROI of Retinal Fundus Images for Authentication Using DWT, Spread Spectrum and Harris Corner Detection

Nilanjan Dey¹, Moumita Pal², Achintya Das³

¹Asst. Professor Dept. of IT, JIS College of Engineering, Kalyani, WB, India.

²Asst. Professor Dept. of ECE, JIS College of Engineering, Kalyani, WB, India.

³ Professor and Head, Elec. and Telecom Engg Dept., Kalyani Govt. Engg. College, Kalyani, WB, India.

ABSTRACT

Digital Retinal Fundus Images helps to detect various ophthalmic diseases by detecting morphological changes in optical cup, optical disc and macula. Present work proposes a method for the authentication of medical images based on Discrete Wavelet Transformation (DWT) and Spread Spectrum. Proper selection of the Non Region of Interest (NROI) for watermarking is crucial, as the area under concern has to be the least required portion conveying any medical information. Proposed method discusses both the selection of least impact area and the blind watermarking technique. Watermark is embedded within the High-High (HH) sub band. During embedding, watermarked image is dispersed within the band using a pseudo random sequence and a Session key. Watermarked image is extracted using the session key and the size of the image. In this approach the generated watermarked image having an acceptable level of imperceptibility and distortion is compared to the Original retinal image based on Peak Signal to Noise Ratio (PSNR) and correlation value.

Keywords - DWT, Session Based Key, Pseudo Random Sequence, Harris Corner.

I. INTRODUCTION

Doctors and Medical practitioners often exchange medical images in various diagnostic centres for mutual availability of diagnostic and therapeutic case studies. The communication of medical data through images requires authentication and security. Embedding of watermarks in Digital images can cause distortion in the images. As the images convey information required for detection of diseases, hence any kind of distortion can result in erroneous diagnosis [1, 2, 3, 4]. Embedding of watermark in region of interest (ROI) causes compromise with the diagnosis value of medical image. To achieve medical watermarking technique, proper selection of Non region of interest selection is a crucial task.

Non region of interest is selected between optical disc and macula, at the location of less sensitive diagnostic parametric value with respect to neighboring region within ROI.

Watermarking is added "ownership" information in multimedia contents to prove the authenticity, to verify image integrity, or to achieve control over the copy process [5, 6, 7].

Blind watermarking scheme does not require the original image or any other data. Watermark insertion is done by using an embedding algorithm and a secret key.

Watermarking schemes can be classified either as Spatial Domain or Transformed Domain. Least Significant bit (LSB) [8] insertion is a very simple and common approach to embedding information in an image in special domain. The limitation of this approach is vulnerable to every slight image manipulation. Converting image from one format to another format and back could destroy information hidden in LSBs. Watermarked image can be easily detected by statistical analysis like histogram analysis. This technique involves replacing N number of least significant bit of each pixel of a container image with the data of a watermark. Watermark gets destroyed as the value of N increases. In frequency domain analysis data can be kept secret by using Discrete Cosine Transformation (DCT) [9, 10]. Main limitation of this approach is blocking artifact. DCT pixels are grouped into 8x8 blocks, and transforming the pixel blocks are transformed into 64 DCT coefficients for each block. A modification of a single DCT co-efficient will affect all 64 image pixels in that block. One of the modern techniques of watermarking is Discrete Wavelet Transformation (DWT) approach [11, 12]. In this approach the imperceptibility and distortion of the watermarked image is acceptable. Proposed method of NROI selection is based on Harris Corner Detection, and blind watermarking on retinal image is based on DWT and Spread Spectrum.

II. METHODOLOGY

A. Discrete Wavelet Transformation

The wavelet transform describes a multi-resolution decomposition process in terms of expansion of an image onto a set of wavelet basis functions. Discrete Wavelet Transformation has its own excellent space frequency localization property. Application of DWT in 2D images corresponds to 2D filter image processing in each dimension. The input image is divided into 4 non-overlapping multi-resolution sub-bands by the filters, namely LL1 (Approximation coefficients), LH1 (vertical details), HL1 (horizontal details) and HH1 (diagonal details). The sub-band (LL1) is processed further to obtain the next coarser scale of wavelet coefficients, until some final scale “N” is reached. When “N” is reached, 3N+1 sub-bands are obtained consisting of the multi-resolution sub-bands. Which are LLX and LHX, HLX and HHX where “X” ranges from 1 until “N”. Generally most of the Image energy is stored in the LLX sub-bands.

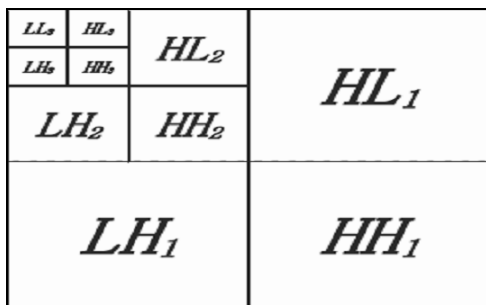


Fig 1. Three phase decomposition using DWT.

The Haar wavelet is the simplest possible wavelet. Haar wavelet is not continuous, and therefore not differentiable. This property can, however, be an advantage for the analysis of signals with sudden transitions.

B. Code division multiple access (CDMA) spread-spectrum technique

Spread-spectrum technique can be described as a method in which a signal generated in a particular bandwidth when deliberately spread in the frequency domain, results in a signal with a wider bandwidth. If distortion is introduced in this signal by some process such as noise and de-noising, when only certain bands of frequencies maybe damaged, although the message is still in a recoverable state. In spread spectrum communications, the signal energy inserted into any one frequency is too undersized to create a visible artifact and the secret image is scattered over a wide range of frequencies, so that it becomes robust against many common signal distortions. Because of its good correlation properties, noise like characteristics, are easier to generate and resistant to interference, Pseudo Noise Sequences are used for Watermarking.

C. Harris Corner Detection

Harris corner detector [13,14] is based on the local auto-correlation function of a signal which measuring the local changes of the signal with patches shifted by a small amount in different directions. Given a shift $(\Delta x, \Delta y)$ to a point (x, y) the auto-correlation function is defined as:

$$c(x, y) = \sum_w [I(x_i, y_i) - I(x_i + \Delta x, y_i + \Delta y)]^2 \dots\dots (1)$$

Where $I(x_i, y_i)$ represents the image function for (x_i, y_i) points in the window W centered around (x, y) . Here W is

$$e^{-\frac{(x+y)^2}{2\sigma^2}}$$

The Gaussian window is defined as $e^{-\frac{(x+y)^2}{2\sigma^2}}$, where σ defines the width of the window. The shifted image is approximated by a Taylor expansion truncated to the first order terms:

$$I(x_i + \Delta x, y_i + \Delta y) \approx [I(x_i, y_i) + [I_x(x_i, y_i)I_x(x_i, y_i) + I_y(x_i, y_i)I_y(x_i, y_i)]] [\Delta x \ \Delta y] \dots\dots (2)$$

Where $I_x(x_i, y_i)$ and $I_y(x_i, y_i)$ indicate the partial derivatives with respect to x_i and y_i respectively. With a filter like $[-1, 0, 1]$ and $[-1, 0, 1]^T$, the partial derivatives can be calculated from the image by substituting Eqn. (2) in Eqn. (1).

$$c(x, y) = [\Delta x \ \Delta y] \begin{bmatrix} \sum_w (I_x(x_i, y_i))^2 & \sum_w I_x(x_i, y_i) I_y(x_i, y_i) \\ \sum_w I_x(x_i, y_i) I_y(x_i, y_i) & \sum_w (I_y(x_i, y_i))^2 \end{bmatrix} \begin{bmatrix} \Delta x \\ \Delta y \end{bmatrix} = [\Delta x \ \Delta y] C(x, y) \begin{bmatrix} \Delta x \\ \Delta y \end{bmatrix}$$

$C(x, y)$ the auto-correlation matrix captures the intensity structure of the local neighborhood.

For α_1 and α_2 be Eigen values of $C(x, y)$, three cases may be considered as:

1. Both Eigen values are small signifying uniform region (constant intensity).
2. Both Eigen values are high signifying Interest point (corner)
3. One Eigen value is high signifying contour (edge)

To find out the points of interest, Characterize corner response $H(x, y)$ by Eigen values of $C(x, y)$.

- $C(x, y)$ is symmetric and positive definite that is α_1 and α_2 are >0
- $\alpha_1 \alpha_2 = \det(C(x, y)) = AC - B^2$

$$\alpha_1 + \alpha_2 = \text{trace}(C(x, y)) = A + C$$

- Harris suggested: the corner response

$$H_{\text{cornerResponse}} = \alpha_1 \alpha_2 - 0.04(\alpha_1 + \alpha_2)^2$$

Finally, it is needed to find out corner points as local maxima of the corner response.

III. PROPOSED ALGORITHM

Retinal Fundus image is collected from The Hamilton Eye Institute Macular Edema Dataset (HEI-MED) (formerly DMED) [16].

ROI Selection based on the position of the Macula with respect to the Optical Disk:

- Step 1. Colored retinal fundus image is converted into gray image from the green channel.
- Step 2. Pre-process the gray image to extract retinal blood vessel tree.
- Step 3. The image is binarized and Binary area open is applied for removing the small objects.
- Step 4. Sobel Edge detection followed by image Thinning is applied on binarized image.
- Step 5. Harris Corner Detection Algorithm is applied.
- Step 6. Based on the Harris points the best-fit ellipse center is determined (in the Least Squares sense).
- Step 7. This center point gives the position of the Macula with respect to the Optical Disk. ROI selection is done based on the presence of Macula.

Optical Disk Detection:

- Step 1. ROI containing optical disk and macula is selected from Retinal Fundus Image and converted into Gray scale image from the green channel of the RGB image for the detection of Optical Disk.
- Step 2. The Gray scale image is filtered and normalized.
- Step 3. The normalized image is converted to binary based on threshold value. Based on the threshold value selection Optical Disk is selected.
- Step 4. Sobel edge detection is applied on binarized image.
- Step 5. Harris Corner Detection Algorithm is applied.
- Step 6. Maximum Harris Diameter is calculated.
- Step 7. The center (O) and diameter (D) is computed and a circle is drawn.

- Step 8. The circle (optical disc) is overlain on the original image.

Macula and NROI Detection:

- Step 1. Minimum average intensity points from the overlain original image are detected.
- Step 2. At a distance of 1.5D from the centre of the detected optical disc, a rectangular area (search space) of length 1D and height of 0.5D is drawn parallel to X-axis. This search space contains both ROI and NROI, where the NROI is comparatively less required portion conveying any medical information.
- Step 3. The distance between center of the optical disk (o) and all average minimum intensity points are computed.
- Step 4. Considering only those minimum average intensity points within the search space, the minimum/maximum and average minimum average intensity points are detected (ROI). These are the nearby points of Macula.
- Step 5. The NROI is a square area cropped from the search space with side length of 0.5D where there is no chance of the presence of the macula.
- Step 6. Cropped NROI is the area for the image hiding process (Base Image).

Watermark Embedding:

Watermark embedding process is explained in Fig 2.

- Step 1. Base image is converted into Gray scale image from the green channel of the RGB image and decomposed into four sub bands (LL, LH, HL and HH) using DWT.
- Step 2. Watermarked image is taken and converted into 1D Vector.
- Step 3. Pseudo random 2D sequence is generated by the session based key.
- Step 4. HH sub band of the base image is modified by using PN sequence depending upon the content of the secret 1D image vector to be embedded.
- Step 5. Four sub bands including modified sub band are combined to generate the Watermarked image using IDWT.
- Step 6. Red and Blue channel is concatenated with watermarked image to get the color watermarked base image.

Step 7. Color watermarked image is overlain on the selected NROI area of original Retinal Fundus image.

Step 8. Finally, the color Retinal Fundus image is reconstructed.

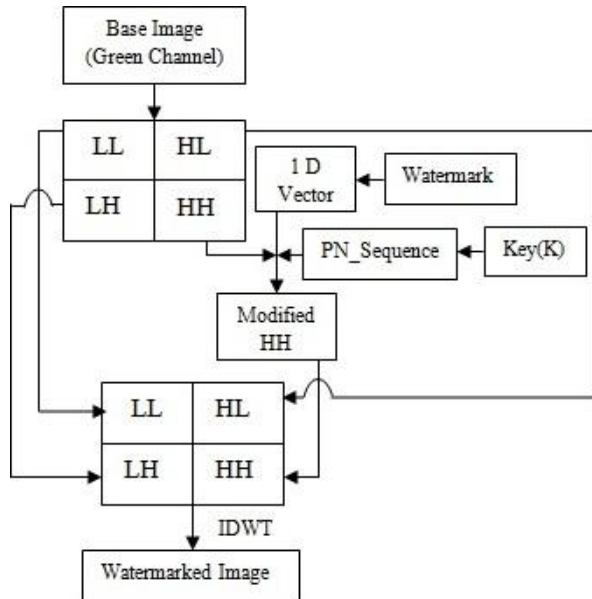


Fig 2: Watermark Embedding Process

Watermark Extraction:

Watermark extraction process is explained in Fig 3.

NROI is selected in the same way as stated earlier from the color watermarked Retinal Fundus image using Harris corner detection. NROI is converted into gray scale image from the green channel of the RGB image.

- Step 1. Session key and Sizes of the watermark image is sent to the intended receiver via a secret communication channel.
- Step 2. Watermark image can be recovered from the watermarked image using correlation function and knowing the size of the original image.
- Step 3. Extracted watermark image is filtered to remove the unwanted signal.

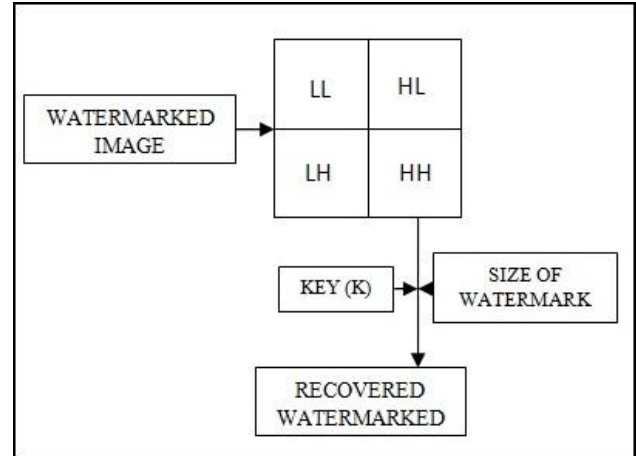


Fig 3: Watermark Extraction Process

IV. EXPLANATION OF THE ALGORITHM

Detection of the position of the Macula with respect to the Optical Disk:

The colored Retinal Fundus image is taken as an input image. The green channel exhibits the best contrast between foreground and the background in the RGB images, whereas the red and blue channels tend to be noisier. Naturally gray image from the green channel is taken into consideration for present study. The approximate background is estimated using a 7x7 Wiener filter and a 22x22 median filter on the gray image. In the pre-processing steps, extraction of the filtered image from the original filtered gray image leads to a brighter area than the background. Generated image is converted to binary data based on the threshold value. Sobel edge detection followed by image thinning is applied on binary image to obtain the retinal blood vessel tree. Harris Corners are applied on the edge detected image. Fitting an ellipse on the obtained Harris points in the plane is done by using Least-Squares Fitting [15]. The sum of the squares of the distances to the given Harris points is minimal for the ellipses, and the concerned matching is referred to as “best-fit”. The centre of the best-fit ellipse is computed. This point gives the position of the Macula with respect to the Optical Disk. ROI selection is done based on the presence of Macula in the retinal image.

Optical Cup and Macula Detection procedure:

The Retinal Fundus image is taken as an input image. The ROI is cropped from the image. The green channel exhibits the best contrast between foreground and the background in the RGB images, whereas the red and blue channels tend to be noisier. In the cases of OD detection green channel is taken into consideration for the conversion of RGB to gray. The OD area is getting darker in the gray image. The approximate background is estimated using a 7x7 Wiener filter and a 22x22 median filter on the gray image.

Complement operation is performed on the filtered image followed by normalization by extracting the complemented image from the original gray image. These lead to a brighter area than the background. The normalized image binary data based on the threshold value is converted. Sobel edge detection followed by Harris Corner detection algorithm is applied on the edge detected binarized image. Maximum Harris Diameter (HD) is calculated considering all the Harris points. Center point (o) of the HD and radius(R) is computed and finally a circle is drawn based on the R and o value. Circle is overlain on the original image.

Minimum average intensity points from the overlain original image are detected. A search space contains both ROI an NROI is cropped based on the proposed method.

Watermark Embedding procedure:

The NROI is converted into Gray scale image from the green channel. Using DWT, the gray NROI image is decomposed into four sub bands (LL, LH, HL and HH).

A binary image (watermark) is taken and converted into 2 one dimensional vectors. Pseudo random sequence is generated using a session based key and the size of HH sub band of the gray image. Each of the bits of the binary is embedded in HH sub-band depending upon the elements of the one dimensional vector and the pseudo random sequence. The general equation used to embed the secret image is:

$$IS(x, y) = I(x, y) + k \times S(x, y) \dots\dots\dots (3)$$

In which I(x, y) representing the selected DWT sub band of the gray image, IS(x, y) is the modified gray image, K denotes the amplification factor that is usually used to adjust the invisibility of the secret image in corresponding sub band. S(x, y) is the pseudo random sequence.

Taking all the sub bands including the modified HH sub-band, watermarked image is obtained applying IDWT (Inverse Discrete Wavelet Transformation). Red and Blue channel is concatenated with gray watermarked image to get the color watermarked base image and overlain on the selected NROI area of original Retinal Fundus image to get back the watermarked color Retinal Fundus image.

Watermark Extraction procedure:

NROI is selected from the color watermarked Retinal Fundus image using Harris corner detection as stated in the proposed method. NROI is converted into gray scale image from the green channel of the RGB image.

The session key and the size of the HH sub-bands of watermarked image is provided to the intended receiver through a secrete communication channel.

Select the HH sub-band of watermarked image after applying DWT. The pseudo random sequence (PN) is regenerated using the same session based key which was used in the secret image embedding procedure. The correlation between the selected watermarked sub-band and the generated pseudo random sequence is calculated. Each correlation value is compared with the mean correlation value. If the calculated value is greater than twice of the mean, then the extracted watermark bit is taken as a 0, otherwise 1. The recovery process then iterates through the entire PN sequence until all the bits of the watermark image have been recovered.

Filter is used on recovered secrete images to remove unwanted signals.

V. RESULTS AND DISCUSSION

MATLAB 7.0.1 Software is extensively used for the study of the retinal watermarking embedding and extraction process. Concerned images obtained in the result are shown in Fig. 4 through 23.

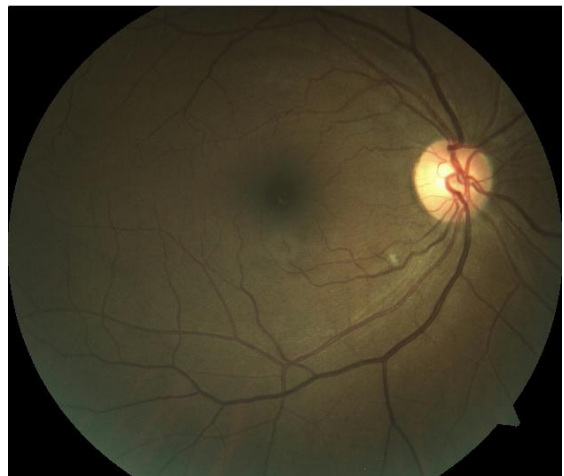


Fig. 4: Retinal Fundus Image

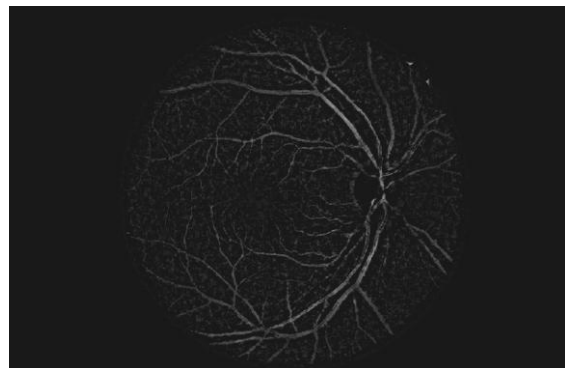


Fig 5. Pre-processed Gray Image

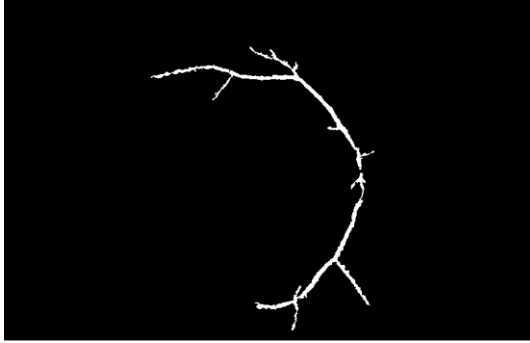


Fig 6. Extracted Retinal Blood Vessel Tree

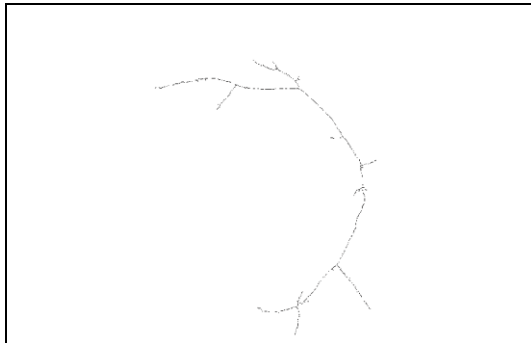


Fig 7. Vessel Tree after Thinning

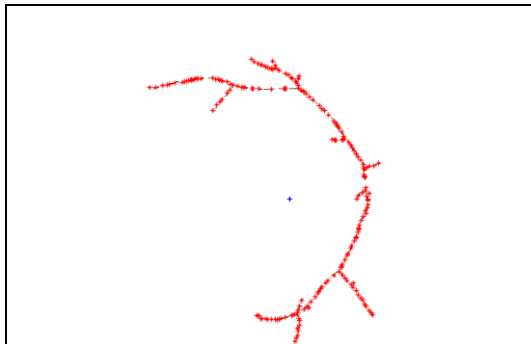


Fig 8. Harris Corner Points and Best-fit ellipse center.

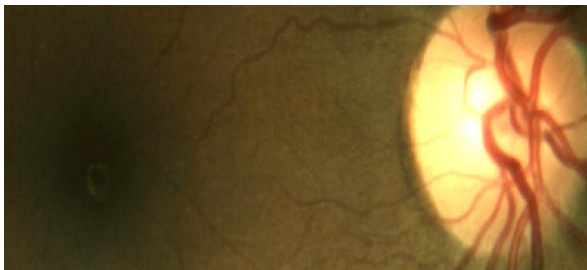


Fig 9. Cropped ROI containing Optical Disk and Macula from the Original Image to the Direction of Best-fit ellipse center.



Fig. 10. Green Channel of ROI

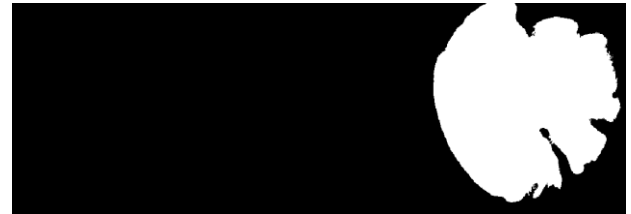


Fig 11. Filtered and normalized Image followed by Binarization.

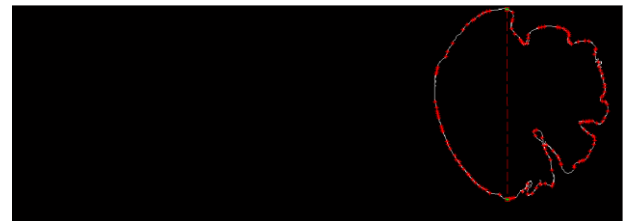


Fig 12. Maximum Harris Diameter in the Edge Detected Image.

Max Harris Point (854,7) and (752,80) Harris Dia=325.0015 Harris Radius=162.5008 Optical Disk Center (854.5000, 169.5000)

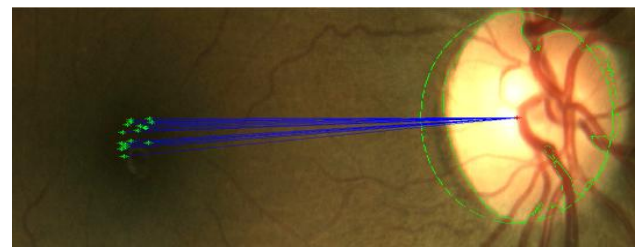


Fig. 13. Minimum Average Intensity Points in ROI

Number of minimum average intensity points in ROI is 17. Distance between all 17 points with Optical Disk Center is as follows.

670.6642,671.2544,667.8791,667.1585,664.9906,663.7985, 659.5836,653.5323,654.4635,652.5094,640.7968,637.6225, 630.6905,628.6911,624.6875,622.5018,618.5455

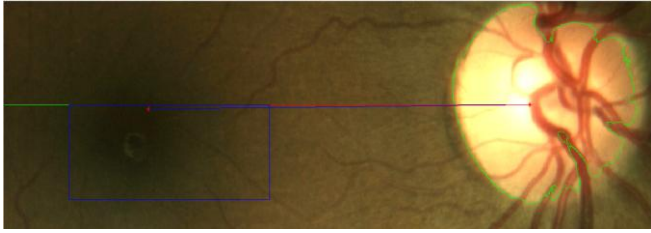


Fig. 14: Search Space

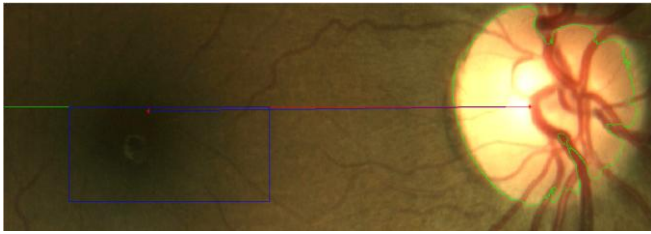


Fig. 15: Minimum Average Intensity point among all the Minimum Average Intensity Points in the Search Space.



Fig. 16: Minimum Average Intensity point among all the Minimum Average Intensity Points in the Search Space. Among all 17 points, 9 points are there within the search space.

Minimum of all Minimum Average Intensity point distances within the search area is 618.5455. Average of all Minimum Average Intensity point distances within the search space is 648.7865. Maximum of all Minimum Average Intensity point distances within the search space is 671.2544

Position of the minimum average intensity point distance within the search area is (106.9965, 431.9980)

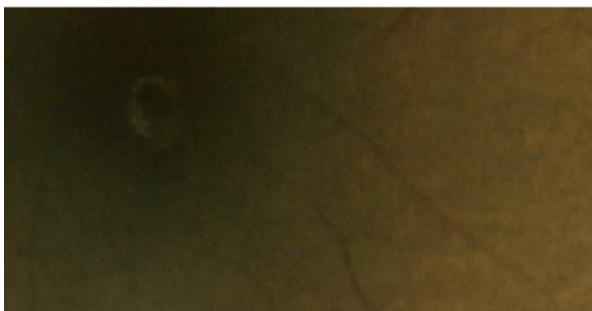


Fig. 17: Search Area (ROI+NROI) Height of Search space is 0.5D and length is 1.5D.



Fig. 18: NROI Height of NROI is 0.5D and length is 0.5D.



Fig. 19: Green Channel of NROI



Fig. 20: Watermark



Fig. 21: Watermarked Image

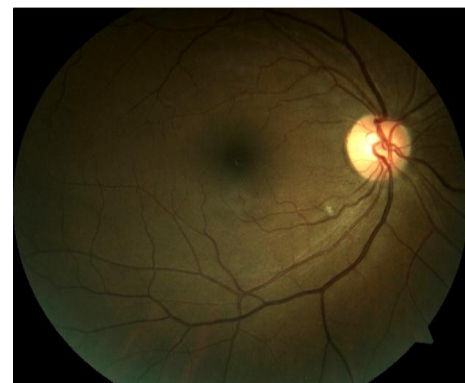


Fig. 22: Overlain Watermarked Image on Original Image (Final Watermarked Image).

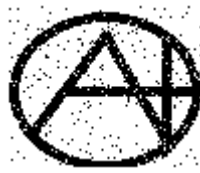


Fig. 23: Recovered Watermark

Peak Signal to Noise Ratio (PSNR)

It measures the quality of a watermarked image. This is basically a performance metric which uses to determine perceptual transparency of the watermarked image with respect to original image:

$$PSNR = \frac{MN \max_{x,y} P_{x,y}^2}{\sum_{x,y} (P_{x,y} - \bar{P}_{x,y})^2} \quad (1)$$

Where, M and N are number of rows and columns in the input image,

$P_{x,y}$ is the original image and
 $\bar{P}_{x,y}$ is the watermarked Image.

PSNR between gray NROI Image and watermarked Image is 29.7910 shown in Table1.

Table. 1

Gray NROI Image vs. Watermarked Image	PSNR
	29.7910

Correlation coefficient

After secret image embedding process, the similarity of original image x and watermarked image x' is measured by the standard correlation coefficient as follows:

$$\text{Correlation} = \frac{\sum(x-x')(y-y')}{\sqrt{(\sum(x-x')^2)\sqrt{(\sum(y-y')^2)}} \quad (2)$$

Where y and y' are the discrete wavelet transforms of x and x'.

Correlation between the watermark and recovered watermark after applying filter is 0.8894 shown in the Table2.

Table. 2

Correlation between original watermark image and recovered watermark image	Image1
	0.8894

VI. CONCLUSION

Proposed technique is useful in telemedicine applications for authentication of the source of the information. In this present work as Watermark is embedded in the HH sub band of the original image, there is a small visual change in between the original image and the watermarked image generating some imperceptibility of image data. But due to strong security aspects this small amount of imperceptibility is acceptable. As the watermark image is embedded in the NROI the diagnosis value of medical image is maintained within the tolerance level. The values of correlation and PSNR are very much encouraging regarding the faithfulness of the reconstruction of the image.

REFERENCES

- [1] C. C. Chang , Z. H. Wang , and Z. X. Yin,” An Ingenious Data Hiding Scheme for Color Retinal Image”, Proceedings of the Second Symposium International Computer Science and Computational Technology (ISCST '09)Huangshan, P. R. China, 26-28,Dec. 2009, pp. 001-006.
- [2] D. Ananad, and U.C. Niranjan, “Watermarking medical images with patient information”, In: proc. IEEE/EMBS Conference, Hong Kong, China, Oct 1998, pp. 703-706.
- [3] Salwa A.K. Mostafa, Naser El- sheimy, A.S. Tolba, F.M. Abdelkader and Hisham M. Elhindy,” Wavelet Packets-Based Blind Watermarking for Medical Image Management”, The Open Biomedical Engineering Journal, 2010,4, pp. 93-98.
- [4] Tian, "Wavelet-based reversible watermarking for authentication",Proceedings of SPIE on Security and Watermarking of Multimedia Contents IV, vol. 4675, Jan.2002, pp. 679-690.
- [5] Christian Rey, Jean-Luc Dugelay, “A Survey of Watermarking Algorithms for Image Authentication”, EURASIP Journal on Applied Signal Processing. Volume 2002 (2002), Issue 6, Pages 613-621.
- [6] G. Voyatzis, N. Nikolaidis, and I. Pitas. Digital watermarking: an overview. In S. Theodoridis et al., editors, Signal processing IX, theories and applications: proceedings of Eusipco-98, Ninth European Signal Processing Conference, Rhodes, Greece, 8–11 September 1998, pages 9–12, Patras, Greece, 1998. Typorama Editions.
- [7] Potdar, Vidysagar and Han, Song and Chang, Elizabeth, “A survey of digital image watermarking techniques”, Proceeding of 3rd IEEE-International Conference on Industrial Informatics, Frontier Technologies for the Future of Industry and Business, pp. 709-716, Perth, WA, Aug 10, 2005.
- [8] Chan, C. K. and Cheng, L. M. 2003. Hiding data in image by simple LSB substitution. Pattern Recognition, 37:469-474.

- [9] Juan R. Hernández, Martín Amado, Fernando Pérez-González, “DCT-Domain Watermarking Techniques for Still Images: Detector Performance Analysis and a New Structure”, IEEE TRANSACTIONS ON IMAGE PROCESSING, VOL. 9, NO. 1, JANUARY 2000.
- [10] B. Tao and B. Dickinson, “Adaptive watermarking in the DCT domain,” in ICCASP’97. Munich, Germany, Apr. 1997, pp. 2985–2988.
- [11] Anumol T.J, P Karthigaikumar,” DWT based Invisible Image Watermarking Algorithm for Color Images”, IJCA Special Issue on “Computational Science - New Dimensions & Perspectives” NCCSE, 2011.
- [12] Mei Jiansheng, Li Sukang. Tan Xiaomei,” A Digital Watermarking Algorithm Based On DCT and DWT”, Proceedings of the 2009 International Symposium on Web Information Systems and Applications (WISA’09) Nanchang, P. R. China, May 22-24, 2009, pp. 104-107.
- [13] Harris, C., Stephens, M., 1988, A Combined Corner and Edge Detector, Proceedings of 4th AlveyVision Conference .
- [14] KonstantinosG. Derpanis, 2004, The Harris Corner Detector.
- [15] www.emis.de/journals/BBMS/Bulletin/sup962/gander.pdf
- [16] <http://vibot.u-bourgogne.fr/luca/heimed.php>.

Study On Existing Pedestrian Traffic and Facility Study on Major Roads in Salem and Formulate Suggestions for Its Improvement

T. SUBRAMANI

*Professor & Dean, Department of Civil Engineering, VMKV Engg College,
Vinayaka Missions University, Salem, India*

ABSTRACT

Walking is an important mode of transport. In urban areas a significant proportion of trips up to 1-2Kms in length are performed on foot. Moreover every journey necessarily starts and ends as a walk trip. Since pedestrian are more vulnerable to being involved in accidents, it is imperative that adequate consideration should be given to their safety through provision of facilities like guard rails, secured crossing areas, footpath and grade separations. Pedestrian facilities should be planned in an integrated manner so as to ensure a continuous pedestrian flow. It should be useful therefore to look at pedestrian needs for an area as a whole and prepare an overall strategic plan. The basic aim should be to reduce pedestrian conflicts with vehicular traffic to the minimum. Efforts should be made to create such conditions that pedestrian are not forced to walk in unsafe circumstances and that the motorist respects the position of pedestrian. While planning the convenient of pedestrian should be paramount consideration. Otherwise the facilities provided will not be fully used. Suggestions formulated as traffic management schemes to provide safety to the pedestrians by reducing conflict in between vehicle movement and pedestrians..

KEYWORD: Pedestrian Traffic, Pedestrian Facility Survey, Major Roads, Suggestions

1. GENERAL

Pedestrian facilities should be planned in an integrated manner so as to ensure a continuous pedestrian flow. It should be useful therefore to locate pedestrian needs for an area s a whole and prepare an overall strategic plan. The basic aim should be to reduce pedestrian conflicts with vehicular traffic to the minimum efforts should be made to create such conditions that pedestrians are not forced to walk in unsafe circumstances and that the motorists respect the position of pedestrians. While planning, the convenience of pedestrians should be a paramount consideration. Otherwise the facilities provided will not be fully used.

2. OBJECTIVES

1. To carry out pedestrian studies
2. To formulate strategies for better management for pedestrian movements.

3. LIMITATIONS

The survey has been carried out only on the working day in the middle of the week. A detailed pedestrian surveys spread over longer duration of time would have yielded more reliable results. More of parking problems is especially due to unauthorized construction of the shopping complexes in the basement especially in CBD areas; a detailed survey is not carried out. During evenings, especially when pedestrian moment is too high, video shooting of the same and the count taken with on slow motion would have yielded more reliable results. In this survey the count is taken manually.

4. SCOPE

For the safer moment of pedestrian is required to carry out survey and then with decision in the CBD to locate/allot places on the roads and vendors so that the pedestrian do not keep crossing the roads and hence all the pedestrian will have safer movement. His could be a major study that can be carried out by local government.

5. STUDY OF PRESENT CONDITIONS IN SALEM CITY

5.1 Salem – General

Salem is the fifth largest city in Tamil Nadu over an area of 91.34 Sq.kms. Salem city is located at distance of 350 kms from a Chennai on the west, and 160 kms from Coimbatore and it got the fifth largest population of 7.54 lakhs as per 2011 census in Tamil Nadu.. It is situated at the trijunction of Bangalore, Trichirappalli and Chennai roads. The City is located at 11 40' North and 78 10' on the East. The general topography is plain The city is surrounded by the hills viz. the shervarous and Nagarmalai on the North, The Kanjamalai on the west, the Goodamalai on the East.

5.2 Population Growth

The population in Salem has grown at a rate of 23 percent per decade between 1951 and 1971, the rate has been lower for the decade 1971 – 1981 at 17 percent and 14 percent per decade between 1991 and 2011. Table.1 gives the growth of population within the Salem town. Population growth of Salem City Corporation given in Table 1.

TABLE 1. POPULATION GROWTH OF SALEM CITY CORPORATION

Year	Salem town / corporation* population	Decade variation	% of decade variation
1901	70621	-	-
1911	59153	(-) 11468	(-) 16.24
1921	52244	(-) 6909	(-) 11.68
1931	102149	(-) 49935	95.58
1941	129702	27523	26.94
1951	202335	72633	56
1961	249145	46810	23.13
1971	308716	59571	23.9
1981	361394	52678	17.06
1991*	579951	218557	60.47
2001*	672330	92379	15.92
2011*	754000	81670	12.15

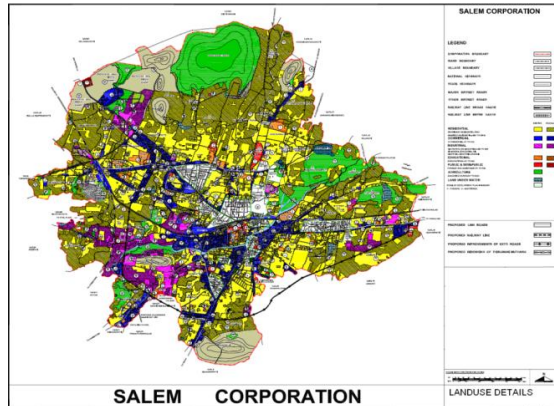


FIGURE.1. EXISTING LAND-USE DETAILS OF SALEM CITY CORPORATION

5.3 Existing Land-Use Structures

The extent of Salem town is 91.34 Sq.km of this the developed area is 4648 Hectares i.e. 48.71 percent of the total area and undeveloped area is 4894 hectares i.e. 51.29 per cent of the total area. Figure. 1. is showing the existing land use details of Salem City Corporation area.

5.4. Existing Traffic Situation

The traffic in Salem town is heterogeneous in nature comprising of slow moving vehicles such as hand carts, animal drawn vehicles, bicycle and fast moving vehicles such as mini cargo vans, Passenger vans Lorries, buses etc. In the absence of separate lanes for slow moving vehicles and cyclists all the vehicles are found to use the available narrow carriageway. The pedestrian side walks have been provided only near Collectorate. In almost all the main roads vendors occupy the road margins and side walks. Hence the pedestrians are deprived of the use of road margins and side walks and use the carriage way, causing hindrance to the free vehicle movement. This may be noticed more in the central area of the old town comprising

of Collectorate and Bus stand complex the main private companies.

6. SALEM CITY CORPORATION ROAD NETWORK

Salem district as a whole has only 10,133.7 km. of road, out of which 214.6 km are cement concrete roads, 5098.1 kms. are bituminous surfaced road and the remaining 4821 kms. are water Bound Macadam roads. The unsurfaced road of 2352.7 kms. also exist in the district.

Salem Corporation has about 748.13kms. of surfaced roads under its control and maintenance as detailed below. The width of road ranges from 3.5 m to 14.0m in the major road network excluding the lanes and small roads. The details of the various categories of roads with their lengths in the town is show in Table. 2

TABLE.2 TYPES OF ROADS WITH THEIR LENGTH IN SALEM CORPORATION

Sl. No	Category	Road length (km)
1	Cement Concrete Super Roads	54.47
2	Black Topped Roads	628.17
3	Wbm Roads	17.04
4	Earthen Road	23.46
5	Others	24.66
	Total Length of Municipal Roads	748.13

The arterial road network of Salem Chosen for the study consists of four major radial corridors originating from the city bus stand. These roads are Attur road in the east, Trichy road and Coimbatore road in the South and Omalur road in the North west. In addition to these, there are a few secondary radial roads. One orbital corridor is identified and it consists of Shandipet road pallapatti main road and court road. Fig.2. shows the identified road network selected for the present study.



FIGURE.2. SALEM CITY CORPORATION ROAD NETWORK

7. PEDESTRIAN STUDIES

Pedestrian’s accidents are common on the roads. Walking is significant mode of transport and all human beings are pedestrians. For varying time periods on roads, even though motorization is increasing at a rapid pace. Right from the early day- till the person is unable to move, walking remain an important mode of travel. Even people, who use cars and motor cycles, depending upon their needs, walk for shorter or longer distances. Walking is indeed found to be healthy as it helps in prevention and control of some non communicable diseases like diabetes, obesity, hypertension, cardiac problems and others. In a country with large populations it is common to see more people walking on roads in both cities and rural areas.

Large number of people including children, elderly, disabled, pregnant mothers and others use roads regularly. When large number of such people uses roads, the environment and operating vehicles need to be safe, so that pedestrians are not injured and killed. In recent years, pedestrian’s safety has assumed greater importance as reports indicate that pedestrians are the single largest category of those injured and killed in road crashes in India.

Walking is an important mode of transport. In urban areas, a significant proportion of trips up to 1-2Km in length are performed on foot. Moreover every journey necessarily starts and ends as walk trip. Since pedestrian are more vulnerable to being involved in accidents, it is imperative that adequate consideration should be given to the safety through provision of facilities like guard-rails, secured crossing areas, footpaths and grade separations.

8. FOOTPATH (SIDE – WALK)

In order to be effective, the side walks should be provided on both sides of the road and above the level of

the carriageway separated by non-mountable kerbs. Height of the kerb at the edge should, however, not exceed the height of non-mountable kerbs, as this might otherwise detract pedestrians from getting on to the side-walks. The width of the side-walks depends upon the expected pedestrian flows and could be fixed with the help of guidelines given in Table.3, subject to a minimum width of 1.5m Most of the footpath were occupied by the merchants (Figure.3.)



FIGURE.3. FOOTPATH & CARRIAGEWAY OCCUPIED BY THE MERCHANTS IN CBD AREA

TABLE3. CAPACITY OF SIDEWALKS

Width of side walk (meter)	Capacity in numbers of persons per hour	
	All in one direction	In both direction
1.50	1200	800
2.00	2400	1600
2.50	3600	2400
3.00	4800	3200
4.00	6000	4000

For side walks in shopping areas, the width should be increased by 1m which is treated as the “dead width”. In other situations where side-walks pass adjacent to buildings and fences the dead width can be taken as 0.5m. For areas of heavy pedestrian activity such as bus stops, railway stations and recreational area, the width of side-walk should be suitably increased to account for accumulation of pedestrian. In purely residential areas, and special cases like shopping centers and industrial office complexes, different principles will apply to side-walk design than the capacity considerations given in table 1. Enhancement of environmental values and safety are the governing criteria in pedestrian sensitive situations such as these, and layouts need to be carefully planned keeping these points in view.

9. PEDESTRIAN GUARD - RAIL

Pedestrian guard- rails are an important design element to prevent indiscriminate crossing and spilling over of pedestrians on to the carriageway. Their judicious use can help to ensure that pedestrians cross the streets at

predetermined and safe locations. As the guard rails would confine the movement of pedestrians to the footpath, it is obligatory that sufficient width of footpath be made available for the use of pedestrians

10. PEDESTRIAN CROSSINGS

Where complete segregation of pedestrians from vehicular traffic is not possible, some form of planned road sharing principle must be applied. Being the most vulnerable road user, pedestrian should increasingly be given the place and time to legally claim the right to cross the road. Pedestrian crossings are to be provided where they will be well used. Hence, it is necessary to follow certain criteria for establishing the right pedestrian crossing at a particular location.

11. PEDESTRIAN SAFETY

A large number of road accidents involve pedestrians. In Delhi, the pedestrians contribute 46 percent of the fatalities from road accidents. These figures indicate the seriousness of the pedestrian safety problem.

12. TRENDS IN PEDESTRIAN ACCIDENT PATTERN.

12.1 Age

Age has significant effect on the accident pattern involving pedestrians. Most of the research findings have concluded that children and the very old are more likely to be in a greater risk than the other age groups. This is easy to understand: the active adults are able to cross the road safely, whereas the very young and very old are not. Children are frequently involved in crossing the road on their way to or from the school. They also get involved in accidents when playing in the streets or nearby. The old people get involved in accidents due to impaired hearing and vision and decreased perception and reaction.

12.2 Sex

The influence of the sex of a person on the accident has been investigated by many. The general conclusion is that women are more careful pedestrian than men

12.3 Social conditions

Social status influences pedestrian behaviour instance, it has been noticed that under-privileged and low income groups figures prominently in pedestrian casualties. General environmental and living condition also have an influence on the accident rate.(Figure.4.)



FIGURE.4. PEDESTRIANS MOVING ACROSS AND ALONG THE ROAD WITHOUT ANY TRAFFIC AWARENESS.

13. SURVEY AND ANALYSIS OF DATA

Pedestrian survey conducted in 10 main locations of the city from morning 8.0am to night 8.0pm. From that survey we understand the existing pedestrian traffic condition in all the places and identify peak hour pedestrian strength. We have collected the existing pedestrian traffic facilities available in the locations. The details are as follows.

13.1 Four road

We observe that the peak hour pedestrian movement is 729. Footpath available on both side of the road. There is no pedestrian guard rail is provided for safety. Also zebra crossing is to be provided.

13.2 Five road

We observed that the peak hour pedestrian flow is 916, Footpath available on both side of the road. No guard rail is existed. Safety kerb guard rail is not available along both side of the road.

13.3. New bus stand

We observed that the peak hour pedestrian flow is 1493. No pedestrian guard rail is available along the road. Footpath is available on bothsides. But, it is fully occupied by the merchants.

13.4 Old bus stand

Peak pedestrian hour moment is 1422. There is no railing and zebra crossing along the road. Footpath is not available on both sides.

13.5 State bank colony

The peak hour pedestrian movement is along the road in both direction is 726. There is no guard rail available.

13.6 Bangalore bye-pass road

We observe that the peak hour pedestrian flow is 751 along one side of the road. No proper footway is available..

13.7 Saradha college road

The peak hour pedestrian movement is along the road in both direction is 728. The existing footway is of 2.8meters & no guard rail is available on both side of the road.

13.8 Railway station

It is observed that the peak hour pedestrian flow is 1171. There is no footway available on both sides of the road. No pedestrian guard rail is provided.

13.9 Cherry road

Peak pedestrian hour movement is 724. There is no footway available on both sides of the road. No pedestrian guard rail is provided.

13.10 Kondalampatti Bye-pass

The existing footway is 2.3meters each on both side of the road. Safety kerb is provided along the road. The pedestrian peak hour movement is 845.

14. CONCLUSIONS

From the pedestrian study and survey we observed that there is no proper required footpath available in most of the Salem City road links. Even if it is available, it is not maintained properly. So, the pedestrians are not properly using the available footpath because of social conditions. Even most of the available footpaths are fully occupied by the small merchants and in some places shop keepers are keeping their generators over the footpath. So, the Local body has to take necessary action over their illegal occupanancy and make clear footpath for pedestrian movements. Educate the public in the form of advertisement regarding the usage of footpath and follow necessary traffic rules and regulation to prevent road accidents.

From the pedestrian study different suggestions were formulated as follows.

- 1) According to IRC-1988 provision of safe walking places in the city with walkable footpaths must be provided. Elevated and visible designated areas for crossing of roads in all possible places.
- 2) Separation of pedestrian movement from heavy moving traffic in all possible places.
- 3) Design of safer highways with separation of pedestrians and slow moving vehicles.
- 4) Speed control by road design, traffic claiming and enforcement on highways, in residential areas and near traffic generators like educational institutions, business places, hospitals etc.
- 5) Prohibition of drinking and driving among vehicle users.

- 6) Recognizing heavy pedestrian movement areas and appropriate traffic management schemes.

15. REFERENCES

- [1]. DTCP (1986), 'Short term improvement program ME – Traffic and Transportation study for Coimbatore, Madurai, Trichy and Salem', DTCP, Tamil Nadu
- [2]. Hanspeter Georgi (1973), 'Cost- Benefit Analysis and Public Investments in Transport: A Survey', First Edition, Butter Worths (Publishers), London.
- [3]. Kadiyali.L.R.(2007), 'Traffic Engineering and Transport Planning', 7th edition, Khanna publishers, Delhi.
- [4]. Khanna S.K – Justo C.E.G (2010), 'Highway Engineering', 9th edition, Nem Chand and Bros. publishers, Roorkee(U.P)
- [5]. Lindsay R. Peat (1982), 'Practical Guide to DBMS selection', Walter de Grawyter, New York.
- [6]. Meyer M.d.Miller E.J (1984), 'Urban Transportation Planning', Mcgraw – Hill series, New Delhi.
- [7]. Subramanian P. (1990) , 'Capacity restrained trip assignment model for Madras City', ME Urban Engineering Thesis, Madras – 600025.
- [8]. V.N.Vazirani & S.P.Chandola, 'Transportation Engineering Vol.I ', 5th edition, Khanna Publishers, New Delhi
- [9]. Dr.L.R.Kadyali & Dr.N.B.Lal, 'Principles and Practices of Highway Engineering, 5th edition, Khanna Publishers, New Delhi
- [10]. B.L.Gupta & Amit Gupta 'Highway and bridge Engineering' 3rd edition Standard Publishers Distributers, New Delhi
- [11]. C.Jotin Khisty & B.Kent Lall, 'Transportation Engineering' 3rd edition, PHI Learning Private Limited, New Delhi
- [12]. Gurcharan Singh, 'Highway Engineering' 5th edition Standard Publishers Distributers, New Delhi
- [13]. R.K. Khitoliya, 'Principles of Highway Engineering' 1st edition , Dhanpat Rai Publishing Company, New Delhi.
- [14]. DTCP (1999), 'Comprehensive Traffic and Transportation Study for Salem', Pallavan Transport Consultancy Services Ltd., Chennai, Tamil Nadu.
- [15]. Guidelines on regulation and control mixed traffic in urban areas, IRC: 70-1977.
- [16]. Guidelines for pedestrian facilities, IRC:103-1988ITPI Journal (Institute of town planner India) 2004, 43-46 and 2005, 62-65.
- [17]. Sarna, A.C., et al, Road accidents on rural highways in India, International seminar on Road safety, Indian RoadCongress, New Delhi, 1986

Study of Pollution Prevention Strategies for Reclamation and Waster Management of Lake in Tourism Place

T. SUBRAMANI

*Professor & Dean, Department of Civil Engineering, VMKV Engg College,
Vinayaka Missions University, Salem, India.*

ABSTRACT

Udhagamandalam, the capital of Nigiris district in Tamil Nadu is a tourism important place. This hill station is also called as Queen of Hills and the people flow to his hill resort during the summer months and as in normal seasons is been increasing day by day. As a result of this, the pollution load on environmental components are creasing exponentially. The take, an artificial one formed by John Sullivan around 18th century is a boon to Ooty. Being the located at a low level, the entire rain water as well the sewage is flowing towards the lake and polluted year by year. In order to restore the quality of lake, several effective measures are taken by the Government including bioremediation by public works department. A study on the pollution effect to this lake been conducted as a project and the factors responsible for the pollution has been studied and present in the report. Necessary preventive measures and suggestion for the improvement of the solid and sewage management has been made.

KEYWORDS: Lake, Pollution Study, Prevention, Strategies, Waster management,

1. INTRODUCTION- GENERAL

“Nilgiris” is the name in Sanskrit means BLUE MOUNTAINS and in Tamil it means NEELAMALAI. The Nilgiris District is situated in the Western Ghat. It is surrounded by Coimbatore District, Kerala State and Karnataka State on the Eastern, Western and the Northern side respectively. The Nilgiris District is a celebrated summer resort for the tourist from all over India. Ootacamund or Udhagamandalam rightly described as “Queen of Hill Stations” is spread over an are of 36Sq.Km. it is the most popular of all the destinations of the Nilgiris. The special attraction of Ooty is its lushy vegetation, the blue screen of the mountain, blue coloured flowers and the mild climate. There are many places of tourist attraction in and around Ooty. Main attraction are the Botanical Garden, the Dhoddabetta Peak, the Udhagai Lake etc. The development of the Town started from the year 1821 and the town expands its limit year after year. Now it has 32 municipal wards and the expected population by the year 2011 is 1,50,000. The Udhagai lake was once a part of a west flowing stream. In 1824, the lower part of the stream was converted into a lake. There is a boat house where row boats and motor boats can be had on hired. The original area of the lake was 65 hectares in the year 1823 and it is shrunken to the present status of 23 hectares. The main reasons for the shrinkage of the lake is the encroachment and the silt deposition. The encroachment removal needs wide planning and the approval of the people to remove their

settlement. So, it needs political as well as social reconciliations. Hence we, in this study paper, leave a lean line covering the topic. On the other hand, the siltation and eutrophication needs deep in depth knowledge for their analysis and taking remedial measures. The siltation create the following problems.

- i. Increase the external loading into the lake
- ii. Reduces both the area and depth of the lake
- iii. Sediments becomes the Nutrients for the growth of algae.
- iv. Becomes the causes for the reduction of the spawning area of the fish.

Hence in the study paper, we give importance for the desiltation process.

The next main problem arising due to the pollutants is eutrophication. The lake is not losing materials to any other water body but they are gaining materials from the land. This may enter the stream either as organic matter such as leaf – fall or as nutrient salts from land drainage. Thus in aquatic ecosystems, the presence of inorganic and organic material and the micro organisms which are the decomposers is the result of gain of materials from the land. The most serious problems associated with eutrophication and likely to occur in sluggish water of lakes. In temperate climates with same nutrient levels, the problems are likely to be less severe. The removal of nutrients adds to the cost of treatment and sometimes leads to the withdrawal of the reservoir from service.

Although there is strong evidence to suggest that sewage effluents causes increase in growths of “Cladophora” sometimes to troublesome degrees, their effect on the growth of plants is less clear. So our aim in this study paper not only deals with the lake water but it includes the sewage system of Ooty also. The restricted sewage system is analysed by a quick review but elaborate analysis of the influent and effluent to the municipal treatment plant are attached at the end of this study paper. The remedial measures are taken as per experts’ views and we suggest some other remedial measures which are unique and if they are adopted, they may give good results. It is everyone’s duty to maintain the elegance and cleanliness of a town and tourist centre such as Ooty requires much more attention. This study paper reveals good opportunity for us to know about various aspects of pollutants and their effects. All those people who read this paper will also get the same experience what we have by this time.

2. OBJECTIVE

As discussed earlier, Ooty has too many places for its Tourist attraction. Among them, the Udhaigai Lake is an important place of attraction because of its boating activities.

The main objective of this study paper is

- i. To Study about the pollution of the Lake
- ii. To Study about the sources and causes of pollution.
- iii. To Suggest the ways for the prevention and Restoration of the Lake.

The pollution of the Lake does not need any special type of chemical testing. Instead, the growth of weeds, the greenish colour of the water, the floating impurities and like these simple things all enough for a common man to tell that the water is polluted. For an environmentalist, it is about extending that view in to numerical values of polluting parameters and presenting those values by comparing with the standard available values. The study paper consists of a part that contains the present characteristics of the Lake Water, the Characteristics of the Municipal waste entering to the treatment plant and the characteristics of the treated water let into Sandynallah Reservoir. Further to add the value, the comparison chart has been made for the lake water samples from the year 1985 to 2004. This will definitely show the degree of pollution the lake undergoes and the reclamation activities that is going on now.

The next topic "Sources and Causes of Pollution" is covered under the topic "Waste Management". The Waste management in Ooty find its own importance because, the Kodappamund Channel that runs in the heart of the city is converted into the dumping place of the different types of waters by small hotels, land encroachers, market, shop keepers etc., moreover it has been the outlet for the sewage of the unauthorized house owners and the rain water drains are utilized for this purpose. So we feel that the study is not enough if we confine the causes of pollution limit only to the lake. On the other hand, the entire waste management system both the existing and the proposal will keep checking the pollution of the lake and also improve the general appearance of the tourist town Ooty. The final one is about the suggestion. Though various experts suggest various types of treatment process to the polluted lake water and some of them are being implemented in different phases, it is on our part to suggest certain methods for both the improvement of quality and quantity to lake water.

Our suggestion recommends the usage of the treated water to improve the quantity of lake water once they meet the quality standards. For this purpose the standard quality chart is also enclosed at the latter part of the study paper. We feel that the fewer steps what we take towards the cleaner and attractive lake and even Ooty itself will definitely pay good results and serve the objectives what it intends to do.

3. MATERIALS AND METHODS

3.1 PRELIMINARY STUDY

The purpose of preliminary investigation is to find out the general trends in town development, the exposure of industries, the details about the tourist population, the waste generation and their disposal, various agricultural and recreational activities etc.

3.2 STUDY POPULATION GROWTH

Udhagamandalam, a selection grade Municipality is the Head quarter of "The Nilgiris District". The municipal area extends to 30.67sq.km. cover in 32 wards. Population of Udhagamandalam Municipality as per 1981 census in 78,277. The town has been provided with water supply scheme and the inlet water supply of the improvements scheme is also in operation. A partial sewerage scheme is also existing.

Udhagai Census 1981	:	78,277
Udhagai Census 1991	:	81,763
Udhagai Census 2001	:	1,26,904
Udhagai Census 2010	:	1,40,208

3.3 LOCATION

The Nilgiris District is situated on the Western end of Tamil Nadu state, and Udhagamandalam is the focal town of the District. Udhagamandalam Municipal town is situated in western state at 11°24' Northern latitude and 76°44' Eastern Longitude. The town is surrounded with reserved forests. Tea Estates and vegetable producing fields. The main occupation of the people is agriculture. The town is situated at the earlier altitude and the elevation of the town varies between +2220m and m.

3.4 MATHEMATICAL STUDY

The present increase of global temperature slightly alters the meteorological conditions of the district also. However the tourist visits to Ooty during the summer is to escape from the scorching sun in the plains. The climate in the district is so enthusiastic and enjoyable.

Average temperature during summer : 20°C

Average temperature during winter : 6°C

Average Annual Rainfall : 1920.80mm

3.5 TOURISM STUDY

Ooty's economy depends on the factors. The first one is the plantation and the next one is through tourism activities. The places of interest of tourists inside the Ooty municipal limit are:

- i. Botanical Garden
- ii. Boat House
- iii. Dhodabetta

During the year 2000 tourist population: 15,71,200.

During the season week day

tourist population: 4000 to 6000.

Week end tourist population: 9000 to 11000

3.6 TOURIST ACCOMMODATION STUDY

The tourist population is greatly undulating in nature. Naturally in summer, the flow of tourists to the city is more than that in the winter season. So the room rents are also fixed according to the season. All the Lodges are connected with the existing restricted sewage system and hence the wastes are treated. The very few hotel names are mentioned here for reference.

- i. Hotel Tamil Nadu
- ii. Hotel Fenhill Palace
- iii. Holiday Inn
- iv. Hotel Savoy
- v. Hotel Southern Star

The Total no's of notable hotels for providing good accommodation Facilities in and around Ooty : 51.

3.7. INDUSTRIAL ACTIVITIES STUDY

The Nilgiris District is not to famous for the industrial population. Very few industries are situated in the district. Some of the major industries in the district are:

1. Aavin, Ooty – Milk Products.
2. Hindustan Photo Films, Ooty – Xray films, Cine Positive, Cine Negative.
3. Aruvangadu Cordiate – Defence Ammunition Preparation.
4. Rallies India Ltd. – Pharmaceutical plant.
5. P.P.I.Ltd. – Children's food.
6. Pasture institute, Coonoor – Rabies Medicine.
7. Human Biological institute.

The total no. of a Tea Factories – 223

3.8.AGRICULTURAL ACTIVITIES STUDY

The Nilgiris District is situated at a high of 6500 feet above MSL. The height and the climate favors the tea plantation. However some other crops are also grown here some of them are.

- i. Tea
- ii. Cardamom
- iii. Coffee
- iv. Hill Crops like Cabbage, Carrot etc.,

The total Percentage of area sown to total geographical are : 20.90%

Agricultural workers in the district: 10.00%

3.9. STUDY OF INSTITUTIONS

The climate of the district favours the growth of institutions with hostel facilities. Such schools are generally referred with the name "Convents". Some of the famous institutions situated in and around Ooty are:

1. Good Sephered
2. Lawrence School
3. Breeks School
4. Gell Memorial Higher Secondary School
5. J.S.S. College of Pharmacy
6. Government Arts College
7. Government Polytechnic
8. C.S.I. Engineering College.

3.10. SANITARY STUDY

The success of the growth of a town depends on the sanitary conditions prevailing to that place. The sanitation includes the cleanliness of the town as well as providing treated water for consumption.

3.10.1 Sewerage System

Udhagamandalam Municipality has at present a sewage scheme. Covering an area of 12.95 sq.km. area of the existing system is situated outside the rain catchment area. Total length of the existing sewer is 31.63km. of with 20sq.km. come with in the catchment area. The sewage coming into the sewer is allocated the sewer runs parallel to the kodappamund channel children's park, and then cross the children's park from the children's park end. The trunk sewer runs along periphery of the lake to a point about 150m upstream of the treatment plant. The effluent from the aeration tank is let in to a nearby sewer which goes to a farm having area of 14 acres, maintained by the Municipality and then let into the Sandynallah reservoir, which is the surplus from the Udhagai Lake.

3.10.2. Drainage Date

1. Length of drainage main : 54.10kms
2. Extent of sewage system : 12.95sqkm.
3. Present status: The sewerage water collected through street sewers, is pumped to the treatment plant and the treated water is discharged in to Kamarajar Sagar Dam.
4. Total No. of Drainage Connections : 3960
5. No. of Connection given so for : 3901
6. Total Length of open drains : 12.33Kms
7. No. of Treatment plant : 1 no.

3.10.3. Water Supply Data

1. Daily supply of water to the town : 8.09md.
2. Per capita supply : 69.7Lpcd.
3. Water treatment plant : 1
4. Pumping station : 2
5. No. of public function : 279
6. Hours of water supply : 3to6hrs.
7. Total no. of Domestic Connection : 7642
8. Total no. of Non-Domestic Connection :448
9. Length of Mains : 32.32kms
10. Total No. of Reservoirs:
 1. Persons Valley
 2. Tiger Hill
 3. Upper Doddabetta
 4. Lower Doddabetta
 5. Marlimund
 6. Upper Kodappamund
 7. Lower Kodappamund
 8. Old Ooty
 9. Glen rock
 10. Gorishola

3.11. TOWN PLANNING STUDY

The growth of a town should coincide with the growth of population and should have enough spaces for the accommodation of floating population. The people of the town should get proper facilities for their well being. That includes good interconnection of places with roads, proper illumination of the roads, both active and passive recreational facilities, good sanitation and water facilities, hospital facilities etc. the following are the investigated data of the town planning.

3.11.1. Town Planning

- | | | |
|--|---|-------|
| i. Parks and Gardens maintained by this municipality | : | 19. |
| ii. Trees Standing and owned by the Municipality | : | 86867 |
| iii. Unauthorized Residential | : | 580 |
| iv. Commercial | : | 103 |

3.11.2. Slums

- | | | |
|------------------------------|---|-------|
| i. No. of notified slums | : | 16 |
| ii. No. of un notified slums | : | 20 |
| iii. Slum population | : | 24848 |
| iv. No. of Slum House Holds | : | 5481 |

3.11.3. Roads

- | | | |
|-------------------------|---|----------------|
| B.T. Surface | : | 142.109kms. |
| i. No. of Streets | : | 246 |
| ii. Length of Streets | : | 181.60kms. |
| iii. Maintenance Charge | : | Rs.99.58lakhs. |

3.11.4 Street lights

- | | | |
|------------------------|---|------|
| i. Sodium Vapour lamps | : | 859 |
| ii. Tube Lights | : | 2875 |
| iii. High mast lights | : | 13 |
| Total | : | 3747 |

3.12. HEALTH STUDY

The people of the town should live with good health and harmony. The healthier condition may be provided either by immunization programme or by giving enough treatment for attack of the diseases. Both these programme will be successful only if there are enough dispensaries and hospitals.

3.12.1. I. Municipal Dispensaries:

- | | | |
|----------------------------------|---|----|
| a. Medical officer | : | 2 |
| b. Pharmacist | : | 1 |
| c. Male Nursing Assistant | : | 2 |
| d. Female Nursing Assistant | : | 2 |
| II. Private Hospitals | : | 23 |
| III. Maternity and Child welfare | : | 3 |

3.13. SOLID WASTE STUDY

The generation of wastes, their collection and disposal are studied in Ooty Municipality. Though the word "Waste" includes all the wastes that are in the Solid and liquid in nature, it generally confines to the solid waste only.

3.13.1. Generation and collection of wastes

1. Average Quantity of waste per capita per day : 0.340kgs.
2. Average Quantity of waste generated each day : 30 mt
 - a. House holds shops and establishments :22.00mt
 - b. From Market :4.50mt
 - c. Meat, Fish, Slaughter House:2.00mt
 - d. Others:1.50mt
3. Hospital waste generated : 0.168mt
4. No. of Zones : 10
5. No. of Vehicles : 7
6. Staff Position:
 - a. Sanitary inspectors : 8
 - b. Sanitary Supervisors : 8
 - c. Sanitary works deployed for collection of waste : 253
 - d. Sanitary workers deployed for transporting waste : 41
7. Sweeper / Population ration in each ward: 1 sanitary worker for 324 persons.
8. Sweeper / Road length ratio in each ward: 0.72 per sanitary worker.
9. Total no. of Dust Bins : 238
10. Mild steel containers : 10
11. Masonry Bins : 72
12. Action plan for Removal of waste
 - a. Door to door collection of segregated wastes implemented in 21 wards.
 - b. Total no. of household covered in door collection: 7426
 - c. Pushcarts used for door to door collection: 24 nos.
 - d. Separate dust bins have been provided for disposing bio degradable and non degradable wastes: As per location & wards.
 - e. Awareness campaigns conducted regarding segregation of wastes:
 - f. Door to door and ward level awareness programme conducted:
 - g. Self Help Groups, Community Organizers, NGO's Ward councilors involved.

3.13.2. Disposal

- | | | |
|---|---|-------------------------|
| a. Disposal site available | : | 1 |
| b. Location | : | Theetukal |
| c. Area in Acres | : | 5acres owned by forest. |
| d. Distance from town to compost yard | : | 6 km |
| e. Method of Disposal | : | Open dumping |
| f. Cost of collection of waste per Mt per day | : | Rs.1531.00 |
| g. Cost of transport of waste per Mt per day | : | Rs.558.00 |
| h. Cost of disposal of waste per Mt per day | : | Rs.220.00 |

3.14. STUDY ON RESTRICTED SEWAGE SYSTEMS

Udhagamandalam is a selection grade Municipal town and it is the head quarters of the Nilgiris District, Tamil Nadu. It has a population of 2,60,828 as per the census 1991. It has 32 Municipal wards and the town extends to 30.67sq.km. There was one existing century old partial sewage system which has been blocked often and leaking in operation. As a result, the sewage from leaking sewers and from the un sewered area (unauthorized also) enters the Kodappamund channel, which runs in the heart of the city designed to carry the storm water from the rain catchment area of the lake, join the Udhagai lake ultimately causing comparative degree of pollution to the lake. The lake whose surplus water and the effluent of municipal waste reaches the Sandynallah reservoir which is under control of the Tamil Nadu Electricity Board (TNEB) from where the hydro electric power is generated. When the polluted effluent reaches the Sandynallah reservoir, it create lot of problems in power generation also.

As a result, a combined proposal by TNEB, the Municipality of Ooty, TWAD board requested the Tamil Nadu Government to provide the restricted sewage system to the Municipality of Ooty. Later, professional consultancy is sought for the success of the sewage system. Experts from Dutch, followed intervention by a central team of Union Commission and other Central Ministries Provided some useful methods of treatment. The following steps are to be adopted. The revised proposal contemplates the following:
 To adopt conventional activated sludge treatment process as cleared by the Technical Committee.

- a. To adopt gravity main sewer with R.C.C. pipes (instead of CI) from Kodappamund to children's Park.
- b. To adopt a pumping system consisting of a sewage pumping station at Children's Park and sewage pumping main along North lake road with C.I. main in place of gravity sewer along the periphery of Udhagai lake as cleared by the technical committee in its meeting.
- c. To provide.
 - Street Sewers in Zone I
(North of Kodappamund Channel)
 - Street Sewers in Zone II
(South of Kodappamund Channel)

Provision of House service connections.

The project was sanctioned for Rs.761.00 lakhs and Execution started:

Stage – I

Provision for treatment works.

Stage – II

Gravity mains sewer with RCC Pipes pumping main along the lake road from proposed sewage pumping station at Children's Park to treatment work at Kandhal. Proposed pumping station and Machineries purchases are made.

Stage – III

Provision of Street Sewers in Zone I

(North of Kodappamund Channel)

Stage – IV

Provision of Street Sewers in Zone II

(South of Kodappamund Channel)

Stage – V

Provision of House Service Connection.

3.14.1 Sewage Treatment Plant 5 Mld Capacity

Erected by :M/s. Enken Engineer Pvt., Limited,
 824, Poonthamalli High road,
 Keelpauk,
 Chennai – 600 010

Date of Commencement : 01.06.1992
 Date of Completion : 15.06.1995
 Estimate Amount : Rs.90.00Lakhs

Major Units:

Screen Chamber	:	1 Unit
Deteritor	:	2 Units
Aeration Tank	:	2 Units
Secondary Clarifiers	:	2 Units
Sludge Recirculation Pumps	:	2 Units

3.15. STUDY OF LAKE WATER

3.15.1. P^H Value

The acidity or alkalinity of water is measured in terms of its PH value or Hydrogen – ion concentration. Pure water (H₂O) consists of positively charges hydrogen or H – ions combined with negatively charged hydroxyl or OH – ions. But the process of dissociation taken polace in pure water and hence it contains some uncombined positively charged H – ions and some uncombined negatively charged OH – ions. The water becomes acidic when positively charged H – ions are in excess than negatively charged OH – ions and it becomes alkaline when reverse is the case. For neutral water, the concentrations of H – ions and OH – ions are equal. The P^H value should be within a range of 6.5 to 8.5.

3.15.2. Dissolved oxygen

The water contains various gases from its contact with the atmosphere and ground surfaces. The usual gases are nitrogen, methane, hydrogen sulphide, carbon dioxide and oxygen. The contents of these dissolved gases in a sample of water are suitable worked out. The oxygen in the dissolved state is obtained from atmosphere and pure natural surface water is usually saturated with it. The simple test to determine the amount of dissolved oxygen present in a sample of water is to expose water for 4 hours at a temperature of 27°C with 10% acid solution of potassium permanganate. The quantity of oxygen absorbed can then be calculated. This amount, for potable water, should be about 5 to 10 p.p.m.

3.15.2. Alkalinity

The term alkalinity with reference to the water and waste water is defined as the capacity of substances contained in the water to take up hydroxium (H₃O⁺) to reach a defined PH value (4.3 to 14). The alkalinity is due to the presence of bicarbonate (HCO₃⁻). Carbonate (CO₃⁻)

) or hydroxide (OH^-). The water having alkalinity less than 250mg/lit is desirable for domestic consumption.

3.15.3. Acidity

The term acidity with reference to the water and waste is defined as the capacity of substances contained in the water to take up hydroxyl ions (OH^-) to reach a defined P^{H} value (0 to 8.2).

The acidity is of the following two types:

- i. Carbon dioxide acidity
- ii. Mineral acidity

The water having acidity more than 50mg / Lit cannot be used.

3.15.4. Chlorides

The chloride contents, especially of sodium chloride or salt are worked out for a sample of water. The excess presence of sodium chloride in natural water indicates pollution of water due to sewage, minerals, edible oil mill operations, ice creams plant effluents, chemical industries, sea water intrusion in coastal regions, etc. the water as lower contents of salt than sewage due to the fact that salt consumed in food is excreted by body. For potable water, the highest desirable level of chloride content is 250mg/lit.

The maximum permissible level is 600mg/lit.

3.15.5 Nitrogen and its compounds

The nitrogen is present in water in the following four forms:

- Free ammonia
- Albuminoid ammonia
- Nitrites
- Nitrates

- **Free ammonia**

The amount of free ammonia in portable water should not exceed 0.15 p.p.m

- **Albuminoid ammonia**

The term albuminoid ammonia is used to represent the quantify of nitrogen present in water before the decomposition of organic matter has started. It is should not exceed 0.3p.p.m.

- **Nitrites**

The presence of niters indicates that the organic matter present in water is not fully oxidized or in other words, it indicates an intermediate oxidation stage. The amount of nitrites in potable water should be nil.

- **Nitrates**

The presence of nitrates indicates that the organic matter present in water is fully oxidized and the water is no longer harmful. For portable water, the highest desirable level of nitrates is 45mg/lit.

3.15.6. Hardness

The term hardness is defined as the ability of the water to cause precipitation of insoluble calcium and magnesium salts of higher fatty acids from soap. The

hardness or soap – destroying power of a water is of two types – temporary hardness and permanent hardness.

- **Temporary Hardness**

The temporary harness is also known as the carbonate harness and it is mainly due to the presence of bicarbonates of calcium and magnesium. It can be removed by boiling or by adding lime to the water.

- **Permanent Hardness**

The permanent hardness is also known as the non – carbonate harness and it due to the presence of sulphates, chlorides and nitrates of calcium and magnesium. It cannot be removed by simply boiling the water. It requires special treatment of water softening. The water, having hardness of about 5 degrees, is reasonably soft water and a very soft water is tasteless. Hence, for potable water, the hardness should preferably be more than 5 degree but less than 8 degrees or so.

3.15.7 Total Solids

The term solid with reference to the environmental, engineering is defined as the residue in water left after evaporation and drying in oven at 103°C to 105°C. The total solids consist of (i).Dissolved solids (ii).Suspended solids.

- **Dissolved solids**

In natural waters, the dissolved solids mainly consist of inorganic salts like carbonates, bicarbonates, chlorides, sulphates, etc. together with small amount of organic matter and dissolved gases. The permissible total dissolved solids for drinking water according to BIS is 500 mg/Lit with tolerable limit of 1500 mg/Lit.

- **Suspended Solids**

In surface water, the suspended solids consist of inorganic matter like silt or organic matter like algae. These materials are generally carried by erosive action of the flowing water over land. The ground water contains negligible quantity of suspended matter because of filtering action of soil strata through mechanical straining action. The amount of suspended solids in surface water increases with input of natural and man – made contamination. The term coefficient of fineness is sometime used to indicate the rates of weight of the suspended solids to the turbidity of water.

3.15.7 Biological Oxygen Demand

The amount of oxygen required for microbes to carry out the biological decomposition of dissolved solids or organic matter in sewage under aerobic conditions at standard temperature is known as the Biological Oxygen Demand. The organic matter in sewage can be classified in the following two groups.

- Carbonaceous matter
- Nitrogenous matter.

The test for B.O.D is very important in sewage analysis as it grants uniformity while comparing various results and tests. It is used as a measure for determining

the strength of sewage and it also helps in finding out the amount of clear water required for the successful disposal of sewage by dilution.

The B.O.D in p.p.m is then worked out by the following equation.

$$5 - \text{days B.O.D} = \text{loss of oxygen in p.p.m} \times \text{dilution ratio.}$$

3.15.8 Chemical Oxygen Demand

To measure the content of organic matter of sewage and natural waters, the chemical oxygen demand (C.O.D) test is sometimes carried out. The C.O.D can be defined as the amount of oxygen required to oxidize the organic matter by strong oxidizing agent under acid conditions. The C.O.D test can be carried out to measure organic matter present in industrial wastes having toxic compounds likely to interfere with the biological life. For many types of wastes, it is possible to establish a relation between the C.O.D and B.O.D. hence, once the correlation between the C.O.D and B.O.D has been established, it becomes easy and simple to rely on the C.O.D. test because the C.O.D can be determined in 3 hours as against 5 days for the B.O.D. For typical domestic wastes, the ratio C.O.D / B.O.D. is found to vary from 1.2 to 1.5. if it is greater than 3, the sewage is considered difficult to biodegrade and for non-biodegradable sewage, it exceeds 10.

3.15.9 Sulphates

Sulphate is naturally occurring anion (SO_4) found in all kinds of natural waters. It is found in high concentrations in some regions. Discharge of industrial waste and domestic sewage in water tends to increase sulphates consumed in drinking water, it may give offensive odour, objectionable taste and laxative effects. Sulphates also, lead to crown corrosion in sewers.

4. WASTE MANAGEMENT

As Ooty being the Head Quarter of district that consists of natural forests, picturesque tea gardens. Gardens and parks, it attracts the tourists. Hence it may be said that the whole economy of the Nilgiris depends on the arrival of the tourists and the result of the good harvesting of tea, coffee and cardamom at good prices. To keep the places clean and to maintain the street, channels, parks, garden, steps are to be taken, implementation should be made with the help of both the citizen and tourists. The following topics cover the different types of waste management. Actual these are very small ideas that are conceived at a very small level but it may fetch good results if these are implemented.

The Waste Management may be classified as follows for easier approach:

1. Solid Waste Management
2. Industrial Waste Management
3. Hospital Waste Management and
4. Plastic Waste Management

4.1 Solid Waste Management

As with other civic matters, the collection and disposal of refuse in a public utility is the primary consideration of sanitary problems in the city. For this a thorough idea of the solid wastes, their origin, their mode of transportation to the yard, the disposal into various forms, every single item plays this role here. While Ooty is the town taken for the solid waste management consideration, the following type of solid waste are created. Figure.1 shows that unauthorised sewage entering .



FIGURE1.UNAUTHORISED SEWAGE ENTERING

4.1.1 Garbage

Waste Materials mainly consists of decayed vegetables, meat diet, feather etc., Main origin of this kind of waste is Ooty market. Nearly 20 lorries of garbage are collected from the Ooty Market alone. Approximately this may go up to 10 ton /day, when this waste is not given treatment, this will be the main cause for polluting the environment. Figure.2. shows the garbage deposited in the spillway.



FIGURE.2 GARBAGE DEPOSITED BENEATH THE SPILLWAY

4.1.2 Ashes

This is a peculiar kind of waste, but its quantity is not known. However, its quantity will be more in winter while other type of wastes are reduced. So at this point of time, the present treatment (or) collection and dumping process is enough.

4.1.3 Rubbish

This is the most dangerous part of the pollutant. It contains paper, rags, packing materials, wood, crockery and metals. Plastic materials can also be included in this

type. But they are dealt in the separate topic “Plastic Management”.

4.1.4 Street Sweepings

These are made up of dust which has been worn from the road surfaces, materials, that have fallen from vehicle, sweepings from stores etc., this type of waste will give a better contribution on the waste accumulation.

The Solid Waste Management requires both skilled and unskilled labour forces, the former for the effective disposal and the later for the effective collection. However, it is the part of the general public and the visiting tourists to keep the city clean and beautiful. The collection of the garbage are done routinely and other type of solid wastes are done periodically. All the solid wastes are dumped in a place called Theettukal that is hardly 8kms away from the tourist town. Till this time, it has been dumped as it is and no recovery has been made from the dumpage. However, the following steps can be adopted for the recovery and the reusage of materials.

1. Crushing of materials.
2. By this method, the wasted electrical items, some kind of plastics can be separated.
3. ii. Selection for magnetic, non magnetic, specific gravity borne materials will be separated.
4. Thermal decomposition technique may be adopted for recovering organic substances in the form of Gas and Oil.
5. Food sources from organic wastes to meet the need for Livestock feed.
6. Composting.
7. Methane fermentation plus residual sludge may be obtained.
8. Composting.
9. Methane fermentation plus residual sludge may be obtained.
10. Some kind of solid fuel may be got.
11. Use of inceneration heat may be useful in many ways.

By using one or more ways, the dumpage load will be minimized and some kind of wealth may be obtained form this thrown away waste.

4.2. Industrial Waste Management

The picturesque Nilgiris, is the junction of eastern and western ghats is at an elevation of 6500 feet above the mean sea level. Being at a higher elevation, the district provides a good environment for the growth of tea plantation. Some extent of coffee and some extent of cardamom also cultivated here. Because of its natural altitude and the type of raw material it has, the district in general is good for agriculture and industrial population is of moderate level. The major industry that may be quoted here is the Aruvangadu Cordite Factory. The defence utilization set up produces the ammunicions like dynamite for army uses. Another industry which is sick now is Hindustan Photo Firms. They are producing Xray film, audio and video tape etc., cine positive and negative films are also manufactured under the brand name INDU. Since

only 20% of the unit is functioning how, the effluent discharge is very low.

There are some 223 tea industries that are functioning in the Nilgiris. The waste water produced by these industries are very less in quantity and they are utilized by themselves for street side plantation. Another interesting development in this sector in the hotel industry. Nearly 51 large and medium scale hotels are here and their waste have been already in connection with the municipal drainage scheme. However small scale hotels that are left either by negligence or by the lack of money for connections may be serious points of threat if their wastes are disposed in the natural drain. So it is better to announce certain schemes to regularize these kind of hotel for the sake of the town. The hospital segment is another segment whose need the careful collection and disposal and this has been discussed separately. Figure 3.shows the screening process at lake entry point



FIGURE.3 SCREENING AT ENTRY POINT

4.3. Hospital Waste Management

As discussed earlier, the hospitals are the known places for the health care products. These health care products produce the wastes of cotton, disposable syringes, bottles, bandages, gauge cloth with or without blood staining, medicines etc., unlike the municipal sewage; this type of waste requires a special care for their disposal. Hence the following steps may be adopted. There are some 23 hospitals have been identified for the waste management programme. The waste are to be carefully with a polyethene cover they have to be transported with utmost care, the waste should not spread in the streets at the time of transit. They have to be brought to the treatment place when the disinfection of the bacteria is done and deep burial should be done. The alternate for this method is to incenstrate the hospital wastes. For incenstration purpose, the combustibile solid wastes can be used. Hence it requires very less or almost negligible fuel cost.

4.4 Plastic Management

The unique feature of the nilgiris is its greenery and wildlife. The wild life includes elephant, tiger, deer, wild boar etc. The eradication of forests and the occupation of the forest land makes the life of the animals worse day by day. It is very often that we read from the newspaper

about the eminence of animals in manual habitats. All these things have happened due to the continued intrusion of man in to animal habitats. These may be in two forms one is the occupation of forest lands permanently and the other form is by tourist. The plastic management nowadays finds its own importance because, the ill effects are being identified day by day. They are not bio degradable hence they remain as they are for years. Thus may block the minute pores of the soil and affect the bacteriological growth that gives nitrate to the land. Thus the land becomes infertile in nature. The animals, if they consume the plastic accidentally, even die because it cannot be digested inside the stomach. So the plastics are to be avoided. The Nilgiris Administration had started a massive campaign for the abolition of plastics. It produced good results in the earlier days. But it seems nowadays the usage of plastic are increasing. The following measures should be compulsorily taken by the authorities.

1. A Clear Co-ordination between all the responsible authorities like HADP, Ooty Municipality, PCB, NGO's should be made. The responsibility and the information should be shared by all of them.
2. The usage of plastics should be completely avoided in the district. This could be made not only through the citizens of the district but also the tourist population also.
3. Nearly 15,71,210 people have visited the city in the year 2000 and its nos. will increase in this year. The main problem of the tourists is water. They want water is possession while they are moving around the tourists centers. For this purpose they are using plastic bottle contained with water. After the use, bottles have been thrown as and whenever and wherever they are. This could be avoided if proper assurance is made by providing safe drinking water at tourists places. This can be achieved either by the municipal authorities or by getting sponsorship programme.
4. Plastic check centers can be made at the peak tourism period to check the entry of plastic materials through tourists. Plastic containers, carry bags should be prevented into the district at the every entry point. Thus the plastic problem can be avoided.
5. Plastic crushers can be used to crush be plastic bottles efficiently.
6. A massive plastic cleaning programme may be organized by the authorities, NGO's and with the help of students, we may achieve our goal easily.
7. Introduction of new inventions – like I.B.M's Biodegradable plastics obtained from plants.

Any type of solid waste management can be successful only if the general public is participating in it. Hence the first step towards the waste management is to create the awareness among the people and the necessity of keeping the city clean not only for them but also for their successors. After all, the health is the only thing this generation can leave for the forthcoming generation. And yes, "health is wealth".

5. SUGGESTIONS

5.1 Suggestion for the reclamation of Ooty lake

The picturesque Ooty Lake can be restored for the preservation of its elegance. For this purpose the following suggestion are made under the following four main categories.

1. Restoration of water lake by increasing the water level
 - a. By removing encroachments
 - b. By providing check dams
 - c. By providing communal rain water harvesting system.
2. Restoration of the lake by improving quality of water.
3. Restoration by artificial aeration & Aquaculture.
4. By re usage of Treated Municipal waste Water.

5.2 Reclamation in increasing the quantity of water

The main source of water of Ooty Lake is the Kodappamund channel. As that channel has its origin at upper Thottabetta, a peak that has its name as the highest peak of the Nilgiris. The water flow from the channel is not perennial hence it is the first choice to store the water in lake.

There are four ways to achieve the above goal.

Clean the encroachments along the banks of the channel that are the primary source of pollution by their unauthorized entry of sewage into the channel.

- To study the feasibility of building of check dam at the upper portion of Kodappamund channel and to divert the water to the lake when there is fall in the inlet of water in lake. This may be done either by gravity or by means of pumping.

5.3. Communal Rain Harvesting System

Nowadays it finds importance to save the rain water and to harvest them whenever necessary. But the awareness among the general public is poor. It is an additional expenditure incurred by the authorities. So in order to avoid bag opinion and to get the above system works properly and efficiently, communal Rain Water harvesting systems may be utilized.

Communal Rain water harvesting system means creating a singly rain harvesting system by and for the entire community occupying the particular area.

1. Each individual has the responsibility of joining their Rain water harvesting drains to a common well situated at the end of the street. Each end are interconnected and they are brought to a same or different pumping house from where the Rain Water alone is pumped to the lake and there it is shared.
2. The usual problem of getting insect by digging of the pit for Rain water harvesting is avoided by providing at street ends.
3. Since top of the under drain is perforated, no problem of clogging is encountered here. More over by the connection made from one well to another make the uplift movement of the silt particles and

hence the cleaning work of the filter media is done continuously.

4. No mixing of sewage with the Rain water. Hence the BOD of the lake will remain under control.
5. For this purpose the middle portion of the kodappamund channel may be used.

5.4 Re Usage Of Treated Water

This way of increasing the water level is the lake in to be considered at the last moment day. Before letting it into the lake, care should be taken that all the pollutant parameter should be within control.

5.5 Reclamation Of The Lake By Improving The Quality Of Water

Improving the quality of the lake water by periodical de silting method. The solid matters try to settle to the bottom of the lake, decompose, causing odour increasing increasing the BOD load on the lake. Hence desilting process can help in reducing the BOD and helps a lot in the restoration process.

Increase the Light intensity by Vertical Circular Motion: When the depth of water is more than 1.20 m its is very difficult for the light to penetrate and hence there are chances for the anaerobic degradation. So increasing the light intensity by giving vertical circulation of the surface water up to sufficient depth, the algae would be cycled out of the euphotic zone in the dark where their basic respiratory demands would exceed the photosynthetic production, there by reducing the algal biomass.

5.6 Induce The Artificial Turbulence

For this purpose circulating rotators can be used. Two rotators are to be fixed facing each other or they may be fixed in alternative means to give powerful turbulence. The jubillance will give the movement of water particles affecting the growth of algae and reduce the BOD load.

5.7 Usage Of Chemicals

Chemicals can be used in the control of the growth of algae. Though this is an alternate method, this will seriously affect the diversity and stability of more natural aquatic ecosystems the lake. Copper sulphate is the common chemical used for this purpose.

5.8 Usage Of More Aerators

Aeration brings more oxygen for the disintegration of the BOD load. Hence aerators may be introduced at appropriate places.

5.9 Reclamation By Miscellaneous Methods

- **Increase the fishery activities**

To consider this suggestion, desilting is to be done to make the bottom of the lake clean. Then the BOD content should be reduced. For this purpose any other previously described points may be adopted. Then fish can be let into the lake for biological treatment as well as aquatic life growth. Though this may be a non profitable

one in commercial terms, but it will help to keep the lake clean.

- **Increase the recreation activities**

Already boating is the recreational activity doing its best at the Ooty Lake. Along with boating, having some kind of water fountains which will act as Aerators will enhance the tourists' joy and the Ooty Lake will increase its fame to attract more people year after year.

TABLE.1 TOLERANCE LIMITS FOR DISCHARGE OF TRADE EFFLUENT INTO INLAND SURFACE WATERS

Sl.No	Characteristics	Tolerance limits
1	P ^H Value	5.50 to 9.00
2	Suspended Solids	100mg/lit
3	Dissolved solids (inorganic)	2,100 mg/lit
4	Oil and Grease	10 mg/lit
5	Bio Chemical Oxygen demand (3 days @ 27°c)	30 mg/lit
6	Chemical Oxygen demand	250 mg/lit
7	Sulphates (as SO ₄)	1000 mg/lit
8	Dissolved PHosphatees (as P)	5.00 mg/lit
9	Chloride (as Cl)	1000 mg/lit
10	Pesticides	Absent
11	Ammoniacal Nitrogen (as N)	50 mg/lit
12	Fee Ammonia (as NH)	5.00g/lit

6. CONCLUSION

The hill station in India are a legacy of the British Rule. We have not added to the list of hill stations after independence. But the worst part is that we have allowed the existing hill stations to deteriorate. Ooty is no exception to this. The environment in this hill station repels the tourist instead of attracting them. The present condition of the lake is a mute testimony to the deterioration of the quality of the environment in this hill station.

As explained in the various chapters the Ooty channel which feeds the lake is responsible for the pollution of the lake. A stable effort should be made to keep the channel and its environs clean. A committee for the protection of the Environment with members representing the Ooty Municipality, PWD, Tourist Department etc., and prominent citizens drawn from diverse walks of life should be formed and entrusted with the responsibility of keeping the town clean with special attention being paid to the lake.

The quality of the lake water should be monitored by measuring at fortnightly intervals important parameters should be checked for the limiting values. The remedial measures consists of very common ideas and if they are implemented, they will definitely fetch good results in future. It is our duty to keep Ooty and the Nilgiris intact. Environmentalist find their increasing importance nowadays and we are proud young Engineers to take part in the preservation of the environment of the tourist town, Ooty.

7. REFERENCES

- [1]. S.K.Garg, Sewage Disposal and Air Pollution Engineering, Khanna Publishers, Delhi, 2010.
- [2]. Gurcharan Singh, Water supply and Sanitary Engineering, Standard Publishers Distributors, Delhi, 2009.
- [3]. Dr.B.C.Punmia, Ashok K.Jain & Arun K. Jain, Water Supply Engineering, Laxmi Publications (P) Ltd.,2010
- [4]. Metcalf & Eddy, Wastewater Engineering, Tata McGraw Hill Education Private Limited.2010
- [5]. Soli J Archeivala & Shyam R. Asolekar, Wastewater Treatment For Pollution control and Reuse, Tata McGraw Hill Education Private Limited.2010
- [6]. G.L.Karia & R.A.Christian, Wastewater Treatment, PHI Learning Private Limited, New Delhi, 2010.

Biodegradation of Tannery Effluent and Designing the Reactor for Clarifier and Activated Sludge Process

T. SUBRAMANI¹ D. HARIBALAJI²

¹Professor & Dean, Department of Civil Engineering, VMKV Engg College, Vinayaka Missions University, Salem, India
²Managing Director, Apollo Life Care, Salem, India

ABSTRACT

The rapid industrialization has affected the Ecosystem to a very large extent due to the pollutants discharged from their operations. Among all the industrial effluents, the effluent from the tannery industry possesses a major problem. The effluent for the present study was procured from the company which is located in Erode. This project involves the treatment of tannery effluent. In the present study, the effluents were collected from the above industry and their biodegradation studies were carried out through the microbes present in the effluent itself at varying concentration and the degrading efficiency among the various organisms were also seen. Then based on the discharge of the effluent from the industry, the reactor for the primary sedimentation (clarifier) and Activated Sludge Process were designed. A simple model has been proposed to illustrate the relationship between the basic parameters, when compared with the experimental values.

KEYWORDS: Biodegradation, Tannery Effluent, Design, Reactor, Clarifier

1. INTRODUCTION TO BIODEGRADATION STUDY

Environmental pollution has become a global concern. The toxic pollutants include acids, alkalies, oils, fats, floating organic dissolved matter and colouring agents. There are various industries such as tannery, paper and pulp, sago, sugar, distillery etc which contribute to this pollution. The disposal of waste waters is of widespread national concern. Industrial activities generate a large number and variety of waste waters which are generally discharged into water streams. The nature of industrial wastes depends upon the industrial processes in which they originate. The problem of adequately handling industrial waste water is more complex and much more difficult than sewage.

Tanning is one of the major industries in our country. There are about 3000 major tanneries in India. Approximately 314 million kilograms of skin are processed annually. The tanneries discharge 3000 litres of waste water, 100 kg-1 of processed hides and the annual discharge of 9420 kilolitres. Tannery industry is reputed globally as a major industry, which contributes to water pollution, owing to the usage of mineral tanning agents. They discharge large volumes of effluents, because except one or two process in the tannery industry, all the processes are wet processes and generate huge quantities of liquid wastes. The effluents are far from the desired level for acceptance into two ways with a heavy load

of pollutants like chromium, chlorides, sodium, dissolved solids, BOD, COD, Nitrogen and suspended solids.

Tannery effluents containing large amount of wastes especially tannins are toxic to plants, animals and soil as well as water microorganisms. In plants they cause stunting growth, chlorosis and reduction in yield. However, a few microorganisms degrade tannins and utilize their carbon source. *Chaetomium globosum*, *Chaetomium cupreum*, *Fusarium solani*, *Aspergillus niger* and *Trichoderma viridae* utilizes tannins as carbon source. Species of *Rhizobium*, *Pseudomonas putida*, *Pseudomonas solanacearum* grow luxuriantly when cultured in tannin medium. (Mahadevan and Sivaswamy, 1985).

The spent chrome liquor from tannery is one of the potential sources causing pollution. Chromium is known to be highly toxic to the aquatic organisms in the hexavalent state and somewhat less toxic in the trivalent form. Hexavalent chromium is carcinogenic, even with a little quantity, 10mg/L can cause nausea, vomiting, skin irritation and problems related to respiratory tract, can cause lung carcinoma due to chromium toxicity.

Problem of waste disposal can be greatly minimized if recovery of useful byproducts is made to the maximum extent possible. Numerous physical and chemical methods such as screening, flow equalization, primary sedimentation, chemical flocculation, aerobic activated sludge treatment, secondary sedimentation have been employed for the disposal of wastes.

The most reliable way seems to be the biological treatment in which microorganisms serves as an efficient detoxifiers of pollutants. It is cost effective and therefore highly suitable for reduction of pollutant load of an effluent as microorganisms are capable of oxidizing the organic and inorganic constituents.

In view of the above investigations, the present study is aimed to reduce pollution load of tannery effluents by using microorganisms particularly *Bacillus* species, *Pseudomonas aeruginosa* and *Aspergillus niger*.

2. INTRODUCTION TO DESIGNING OF CLARIFIER AND ASP

Mostly treatment plants use mechanically cleaned sedimentation tanks of standardized circular or rectangular design. The selection of the type of clarifier for a given application is governed by the size of the installation, by rules and regulations of local control authorities, by local site conditions and by the experience and judgement of the

engineer. Two or more tanks should be provided so that the process may remain in operation while one tank is out of service for maintenance and repair work. At large plants, the number of tanks is determined largely by size limitations. Typical design information and dimensions for the clarifier and Activated Sludge process are discussed in this chapter.

3. AIM AND OBJECTIVES OF THE STUDY

The vital objectives of the present project are to reduce the pollution from tannery industry, and to thoroughly assess and design a new treatment plant.

Following are the scope of present investigation

1. Sample collection from the tannery industry for the treatment process,
2. Analysis of samples for various physicochemical and biological characteristics,
3. Comparison between the efficiency of various microorganisms at different concentration in the degradation of tannery waste water,
4. Preliminary assessment of the possible treatment scheme(s),
5. Laboratory experimentation pertaining to the biodegradation study, and
6. Design of clarifier and Activated Sludge process to reduce the pollution from tannery industry.

4. TANNING PROCESS

In tanning industry, the animal skins and hides are treated to convert them to non-putrescible and tough leather. The processes involved in leather tanning industry are:

1. Beam House Processing
2. Tan-Yard Processing
 - a) Vegetable Tanning
 - b) Chrome Tanning

4. MATERIALS AND METHODS

5.1 COLLECTION OF SAMPLES

The effluent was collected freshly from the company which is located in Erode and it was stored in a brown bottle. Prior to the collection, the sample water bottle was rinsed with sterile water. After collecting the sample, physical, chemical and bacteriological parameters were carried out from the sample, which was collected separately. The samples were taken to the laboratory as early as possible and it has to be protected from direct sunlight during transportation. The samples were stored in refrigerator.

5.2 ISOLATION AND IDENTIFICATION OF MICROORGANISMS:

Bacteria and fungi in the effluent were isolated using pour plate technique in Nutrient Agar and Sabouraud's Dextrose Agar and the isolated organisms were subjected to staining, motility and further identification.

- Gram Staining
- Lacto phenol cotton blue staining
- Motility Test
- Catalase Test
- Oxidase Test
- Indole Test
- Methyl Red Test
- Voges proskauer Test
- Citrate utilization Test
- Urease Test
- Carbohydrate Fermentation

5.3 ESTIMATION OF PHYSICO-CHEMICAL PARAMETERS

- Estimation of pH:
- Estimation of Dissolved Oxygen:
- Estimation of Biological Oxygen Demand:
- Estimation of Chemical Oxygen Demand:
- Estimation of Total Dissolved Solids:
- Estimation of Total Suspended Solids:
- Estimation of Total Hardness:
- Estimation of Chloride:
- Estimation of Alkalinity:
- Estimation of Chromium:

5.4 BIODEGRADATION STUDY

From the sample 80ml, 70ml, 60ml, 50ml of the effluent was filtered and sterilized in separate containers. To this 80ml effluent 20ml of the respective cultures was added and incubated. Likewise for the 70ml effluent, 30ml culture was added and incubated. For the 60ml effluent, 40ml culture was added and for the 50ml effluent, 50ml culture was added and incubated. At the same time blank was also inoculated with the same cultures and incubated. After 5days incubation, the physical and chemical parameters were estimated and tabulated.

5.5 DESIGN PARAMETERS

The following factors should be analyzed for the designing of the clarifier and Activated Sludge Process

5.5.1 For The Clarifier

- Weir flow rate
- MLSS Concentration
- Volumetric Organic Loading Rate
- Hydraulic Retention Time
- Aeration time
- Oxygen requirement:
 1. Based on BOD
 2. Based on Total Nitrogen

- Surface Area:
- Length of the tank
- Scour Velocity
- Detention Time

5.5.2 For The Activated Sludge Process

- Solid Retention Time (SRT)
- Total Sludge production / day
- Observed Yield
Oxygen requirements
- Aeration Tank Volume

6. RESULTS

6.1 BIODEGRADATION STUDY

The biodegrading microorganisms like *Bacillus sps*, *Aspergillus niger* and *Pseudomonas aeruginosa* were identified and the biochemical characters of bacteria are mentioned in Table.1, and its cultural morphology is shown in Plate I, II and III.

TABLE.1 BIOCHEMICAL CHARACTERS OF THE ISOLATED BACTERIA

Name of the Bacteria	Morphology	Gram Staining	Motility	Catalase	Oxidase	Indole	MR	VP	Citrate	Urease	Glucose	Lactose	Maltose
<i>Bacillus sps</i>	Irregular, round, dull, opaque and gray/white colour colonies	+	-	+	+	-	+	-	-	-	A+	-	A+
<i>Pseudomonas aeruginosa</i>	Bluish green colour colonies	-	+	+	+	-	-	-	+	+	A+	-	-

Physico-chemical parameters of the untreated effluent was estimated and mentioned in Table.2.

TABLE. 2 PHYSICO CHEMICAL CHARACTERISTICS OF UNTREATED EFFLUENT

pH	BOD	COD	TDS	TSS	Hardness	Chloride	Alkalinity	Chromium
12	252	512	6100	7966	380	36.92	454.5	6

All the values are expressed in mg/L except pH

Biodegrading ability of *Bacillus sps* at various concentrations like 20%, 30%, 40%, 50% was determined and presented in Table.3 and Plate VI.

TABLE.3 PHYSICO CHEMICAL CHARACTERISTICS OF TREATED EFFLUENT USING BACILLUS SPS

% of inoculans	pH	BOD	COD	TDS	TSS	Hardness	Chloride	Alkalinity	Chromium
20%	8.0	70	320	5896	7660	299	35.07	428.8	6
30%	8.5	62	304	5725	7654	240	32.66	390.5	5.6
40%	9.3	59	224	4832	7506	223	26.98	390	5.6
50%	10	54	160	4761	7418	160	25.7	358	4

All the values are expressed in mg/L except pH

Biodegrading ability of *Pseudomonas aeruginosa* at various concentrations like 20%, 30%, 40%, 50% was determined and presented in Table.4 and Plate IV.

TABLE.4 PHYSICO CHEMICAL CHARACTERISTICS OF TREATED EFFLUENT USING PSEUDOMONAS AERUGINOSA

% of inoculans	pH	BOD	COD	TDS	TSS	Hardness	Chloride	Alkalinity	Chromium
20%	9.0	66	288	5902	7470	280	35.50	450	5.9
30%	9.5	55	256	5868	6872	225	32.90	438.9	5.5
40%	9.8	53	240	5460	6617	205	31.09	402.7	5.6
50%	10	47	160	5090	5213	195	27.12	387.5	4.8

All the values are expressed in mg/L except pH

Biodegrading ability of *Aspergillus niger* at various concentrations like 20%, 30%, 40%, 50% was determined and presented in Table.5 and Plate V.

TABLE.5 PHYSICO CHEMICAL CHARACTERISTICS OF TREATED EFFLUENT USING ASPERGILLUS NIGER

pH	BOD	COD	TDS	TSS	Hardness	Chloride	Alkalinity	Chromium
9.0	58	448	5721	6294	270	34.08	428.1	5
9.5	51	460	5432	5827	241	28.40	403.2	4.6
9.7	49	400	4119	5604	187	27.26	379	4.2
10	45	304	4025	5419	170	25.28	348.9	3.8

All the values are expressed in mg/L except pH

Biodegradation study details were given in Figure1. to Figure.9

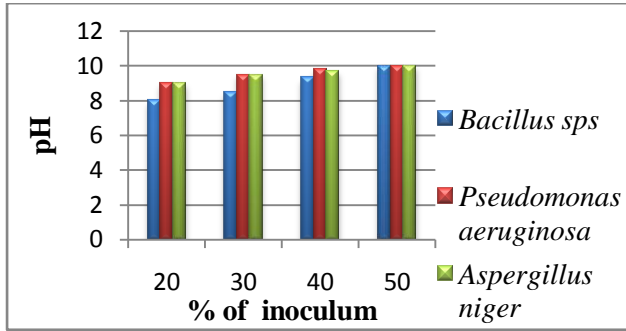


FIGURE.1 ANALYSIS OF PH AFTER DEGRADATION

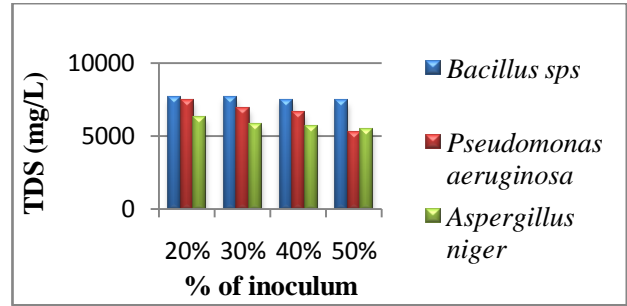


FIGURE.5 ANALYSIS OF TDS (MG/L) AFTER DEGRADATION

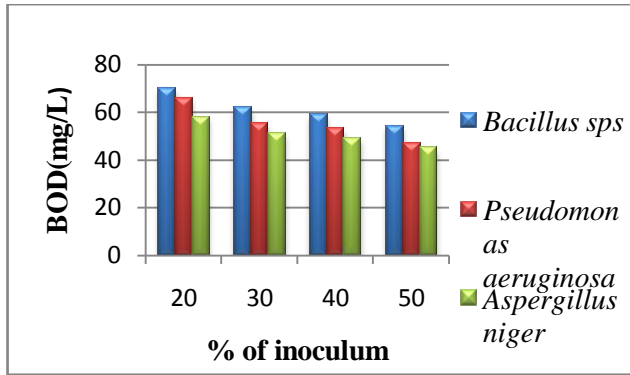


FIGURE.2 ANALYSIS OF BOD AFTER DEGRADATION

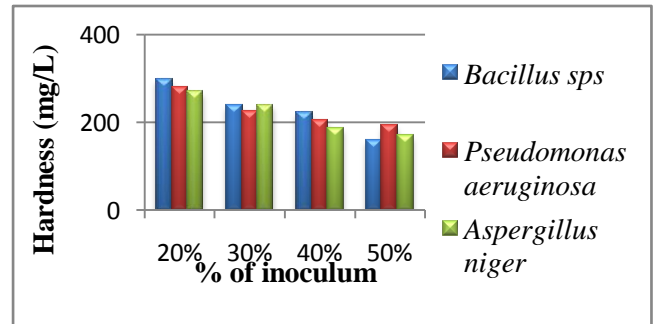


FIGURE.6 ANALYSIS OF HARDNESS AFTER DEGRADATION

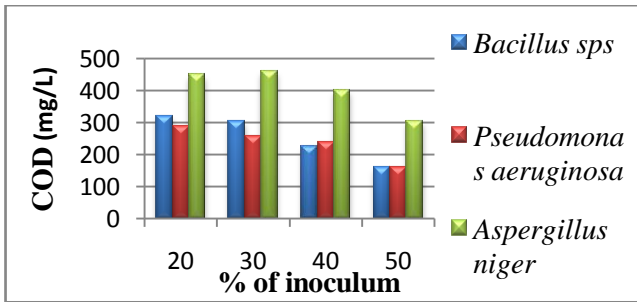


FIGURE.3 ANALYSIS OF COD AFTER DEGRADATION

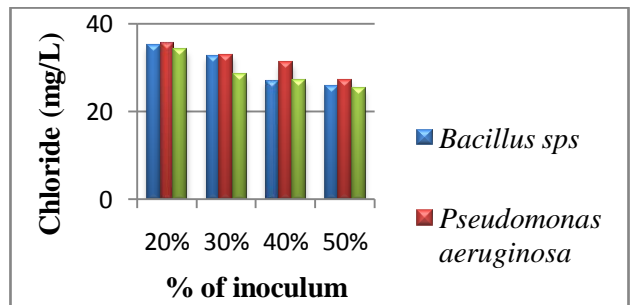


FIGURE.7 ANALYSIS OF CHLORIDE (MG/L) AFTER DEGRADATION

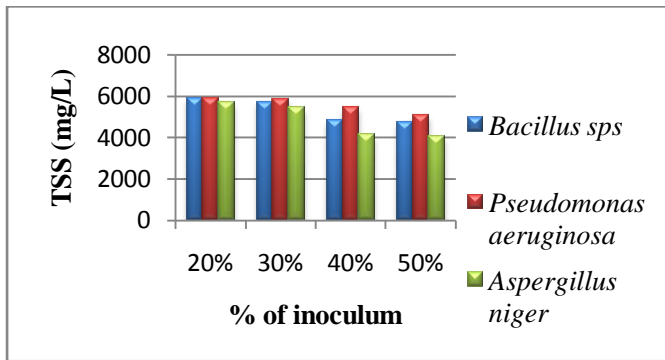


FIGURE.4 ANALYSIS OF TDS AFTER DEGRADATION

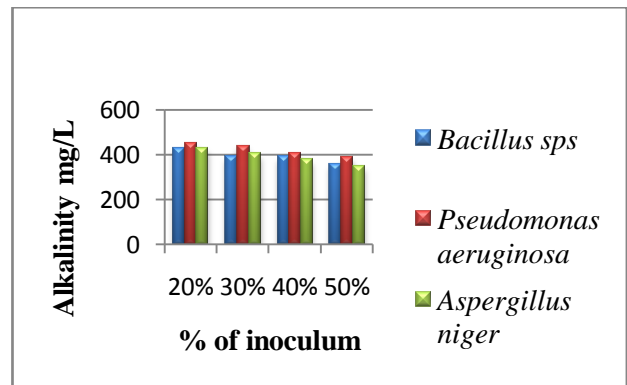


FIGURE.8 ANALYSIS OF ALKALINITY AFTER DEGRADATION

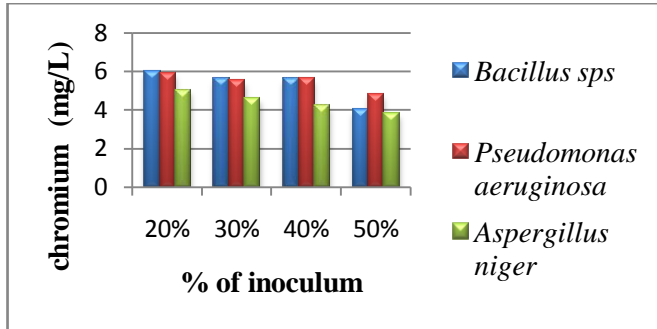


FIGURE.9 ANALYSIS OF CHROMIUM AFTER DEGRADATION

7. DESIGNING OF THE CLARIFIER AND ACTIVATED SLUDGE PROCESS

The various treatment units in different schemes were designed for a design flow of 10 Mld, in accordance with the CPHEEO Manual (1999) and/or other and appropriate criteria relevant for operation and design of appropriate units. The process design of Clarifier and activated sludge process (ASP) was done.

7.1 Design of Clarifier

The average flow rate of the industry is 10,000 m³/d and the highest observed peak daily flow rate is 25,000 m³/d. The overflow rate for the clarifier is 40 m³/m².d at average flow and the side water depth of 4m. For this industry rectangular clarifier was designed based on the following criteria.

From the data, the following parameters were identified:

7.1.1 Surface area of the clarifier

$$A = \frac{Q}{OR} = \frac{10,000 \text{ m}^3/\text{d}}{40 \text{ m}^3/\text{m}^2.\text{d}} = 250 \text{ m}^2.$$

7.1.2 Length of the Tank

$$L = \frac{A}{W} = \frac{250 \text{ m}^2}{6 \text{ m}} = 41.67 \text{ m}$$

7.1.3 Detention time and overflow rate at average flow

$$\begin{aligned} \text{Tank volume} &= \text{side water depth} \times \text{length} \times \text{width} \\ &= 4 \times 42 \text{ m} \times 6 \text{ m} \\ &= 1008 \text{ m}^3. \end{aligned}$$

$$\begin{aligned} \text{Overflow rate} &= Q = \frac{10000 \text{ m}^3/\text{d}}{250 \text{ m}^2} \\ &= 40 \text{ m}^3/\text{m}^2.\text{d} \end{aligned}$$

$$\begin{aligned} \text{Detention time} &= \frac{\text{Tank Volume}}{Q} \\ &= \frac{(1008 \text{ m}^3) (24 \text{ h/d})}{10000 \text{ m}^3/\text{d}} = 2.42 \text{ h} \end{aligned}$$

7.1.4 Detention time and overflow rate at peak flow

$$\begin{aligned} \text{a) Overflow rate} &= \frac{Q}{A} = \frac{25000 \text{ m}^3/\text{d}}{250 \text{ m}^2} \\ &= 100 \text{ m}^3/\text{m}^2.\text{d} \end{aligned}$$

$$\begin{aligned} \text{Detention time} &= \frac{\text{Tank}}{Q} \\ &= \frac{(1008 \text{ m}^3) (24 \text{ h/d})}{25000 \text{ m}^3/\text{d}} = 0.97 \text{ h} \end{aligned}$$

7.1.5 Scour Velocity:

$$\begin{aligned} V_H &= \frac{8k(s-1)gd}{f} \\ &= \left[\frac{(8)(0.05)(0.25)(9.81)(100 \times 10^{-6})}{0.025} \right]^{1/2} \\ &= 0.063 \text{ m/s.} \end{aligned}$$

7.1.6 Peak flow horizontal velocity:

$$\begin{aligned} V &= \frac{Q}{Ax} \\ &= \frac{25000 \text{ m}^3/\text{d}}{6 \text{ m} \times 4 \text{ m}} \times \frac{1}{(24 \text{ h/d})(3600 \text{ s/h})} \\ &= 0.012 \text{ m/s.} \end{aligned}$$

7.2 Design of Activated Sludge Process

The average flow rate of the industry is 10,000 m³/d and the highest observed peak daily flow rate is 25,000 m³/d. The physico-chemical parameters of the untreated primary effluents analyzed are: bsCOD = 192g/m³, nbVSS = 30g/m³, and inert organics = 10 g/m³. The aeration tank MLVSS = 2500g/m³. For this industry, Activated Sludge Process for a 6-d SRT was designed based on the following criteria.

Kinetic coefficients for the designing are:

$$\kappa = 12.5 \text{ g COD/g VSS.d}$$

$$K_s = 10 \text{ g COD/m}^3$$

$$Y = 0.40 \text{ g VSS/g COD used}$$

$$fd = 0.15 \text{ g VSS/g VSS}$$

$$kd = 0.10 \text{ g VSS/d VSS.d}$$

$$\text{Biomass VSS/TSS} = 0.85$$

From the data, the following parameters were identified:

7.2.1 Effluent bsCOD concentration

$$\text{Effluent bsCOD concentration} = \frac{K_s [1 + (kd) \text{ SRT}]}{\text{SRT} (Yk - kd) - 1}$$

$$= \frac{(10 \text{ g COD/m}^3) [1 + (0.10 \text{ g VSS/g VSS.d}) (6\text{d})]}{(6\text{d}) [(0.40 \text{ g VSS/g COD}) (12.5 \text{ g COD/g VSS.d}) - (0.10 \text{ g VSS/g VSS.d})] - 1}$$

$$= 0.56 \text{ g bs COD/m}^3.$$

7.2.2 Aeration Tank Volume

Aeration Tank Volume = $\tau(Q)$

The biomass concentration (X) = $\frac{Y(S_o-S)SRT}{[1 + (kd)SRT] \tau}$

$$= \frac{(0.40 \text{ g VSS/g COD})[(192 - 0.56) \text{ g COD/m}^3](6\text{d})}{[(1 + 0.10 \text{ g VSS/g VSS.d}) (6\text{d}) (\tau)]}$$

$$= 287.2 \text{ g/m}^3 \cdot \text{d} / \tau$$

$$X_T = \frac{Y(S_o-S)SRT}{[1 + (kd)SRT] \tau} + \frac{(fd)(kd)(X)SRT}{\tau} + \frac{(X_{o,i})SRT}{\tau}$$

$$2500 \text{ g VSS/m}^3 = \frac{(0.40 \text{ g VSS/g COD})[(192 - 0.56) \text{ g COD/m}^3](6\text{d})}{[(1 + 0.10 \text{ g VSS/g VSS.d}) (6\text{d}) (\tau)]} + \frac{(0.15 \text{ g VSS/g VSS}) (0.10 \text{ g VSS/g VSS.d})(X)(6\text{d})}{\tau} + \frac{30 \text{ g VSS/m}^3 (6\text{d})}{\tau}$$

$$2500 = \frac{287.2}{\tau} + \frac{0.09(X)}{\tau} + \frac{180}{\tau}$$

$$= \frac{287.2 + 25.8 + 180}{\tau}$$

$$\tau = 0.197\text{d}$$

Aeration Tank Volume = $\tau (Q)$
 = $0.197\text{d} (10000\text{m}^3) = 1970\text{m}^3.$

7.2.3 Total Sludge Production

a) Total sludge production based on Kg of VSS/d

Total sludge production based on Kg of VSS/d = $\frac{X_T (V)}{SRT}$

$$= \frac{(2500 \text{ g VSS/m}^3) (197\text{m}^3) (1 \text{ Kg}/10^3 \text{ g})}{6\text{d}}$$

$$= 82.1 \text{ kg VSS/d.}$$

b) Total sludge production based on Kg of TSS/d

$$P_{X,TSS} = \frac{QY(S_o-S)}{1 + (kd)SRT} \left\{ \frac{1}{0.85} \right\} + \frac{(fd)(kd)YQ(S_o-S)SRT}{1 + (kd)SRT} \left\{ \frac{1}{0.85} \right\}$$

$$+ QX_{o,i} + Q(TSS_o - VSS_o)$$

$$= \frac{(10000\text{m}^3/\text{d}) (0.40 \text{ g VSS / g COD}) [(192 - 0.56) \text{ gCOD/ m}^3]}{[1 + (0.10 \text{ g VSS / g VSS.d}) (6\text{d})] (0.85)} + (0.15)(0.10)(10000\text{m}^3/\text{d})(0.40) [(192 - 0.56) \text{ g COD/m}^3] (6\text{d})$$

$$\frac{[1 + (0.10 \text{ g VSS / g VSS.d}) (6\text{d})] (0.85)}{+ 10000\text{m}^3/\text{d} (30\text{g/m}^3) + 10000\text{m}^3/\text{d} (30\text{g/m}^3)}$$

$$= (563 + 51 + 300 + 100) (10^3 \text{ g/d}) = 1014 \times 10^3 \text{ g/d}$$

$$= 1014 \text{ Kg /d.}$$

7.2.4 Biomass Fraction

Biomass fraction = $\frac{\text{Biomass concentration (X)}}{\text{MLVSS (X}_T)}$

$$= \frac{(287.2 \text{ g/m}^3 \cdot \text{d}) (0.197)}{2500}$$

$$= 0.58$$

7.2.5 Observed Solids Yield

Y_{obs} = $\frac{\text{Solids wasted / d}}{\text{bs COD removed / d}}$

bsCOD removed / d = $Q(S_o - S)$

$$= (10000\text{m}^3/\text{d})[(192-0.56) \text{ gCOD/m}^3] (1 \text{ Kg}/10^3 \text{ g})$$

$$= 1914400 \text{ g COD/d}$$

$$= 1914.4 \text{ Kg/d}$$

Y_{obs} for VSS = $82.2 / 1914.4$

$$= 0.043 \text{ g VSS/g bsCOD}$$

Y_{obs} for TSS = $1014 / 1914.4$

$$= 0.53 \text{ g TSS/g bsCOD}$$

7.2.6 Oxygen Required

Oxygen Required (R_o) = $Q(S_o - S) - 1.42P_{X,\text{bio}}$

$$P_{X,\text{bio}} = P_{X,T,VSS} - P_{nb,VSS}$$

$$= 82.2 \text{ Kg/d} - (1000\text{m}^3)(30\text{g VSS/m}^3)(1 \text{ Kg}/103 \text{ g})$$

$$= 522 \text{ Kg/d}$$

$$R_o = (10000\text{m}^3/\text{d})[(192 - 0.56) \text{ g COD/m}^3] (1 \text{ Kg}/103 \text{ g}) - 1.42(52.2 \text{ Kg VSS/d})$$

$$= 1177 \text{ Kg O}_2/\text{d.}$$

8. DISCUSSION

Microbial analysis of tannery effluent was made and the dominating degrading organisms like Bacillus sps, Pseudomonas aeruginosa and Aspergillus niger was isolated.

Similar reports is presented in study on isolation and characterization of microflora present in the individual sectional waste water of a tannery. Despite the toxic nature the sectional

effluents exhibited microbial growth. Bacillus, Pseudomonas and micrococcus were the predominant species identified (Radha et al., 1995).

Tannery effluent used in the present study is highly alkaline and highly loaded with contaminant like BOD (252 mg/L), COD (512 mg/L), TSS (7966 mg/L), TDS (6100mg/L), Alkalinity (454.5 mg/L), Hardness (380 mg/L), Chlorides (36.92 mg/L) and Chromium (6 mg/L).

Bacillus sps was used at various concentrations to treat the effluent. Among that while at 50% inoculum was given there was a decrease in the value pH (10), BOD (54 mg/L), COD (160 mg/L), TDS (7418 mg/L), TSS (4761 mg/L), Alkalinity (358 mg/L), Hardness (160 mg/L), Chlorides (25.7 mg/L) and Chromium (4 mg/L).

Pseudomonas aeruginosa was used at various concentrations to treat the effluent. Among that while at 50% inoculum was given there was a decrease in the value pH (10), BOD (47 mg/L), COD (160 mg/L), TDS (5090 mg/L), TSS (5213 mg/L), Alkalinity (387.5 mg/L), Hardness (195 mg/L), Chlorides (27.12 mg/L) and Chromium (4.8 mg/L).

Aspergillus niger was used at various concentrations to treat the effluent. Among that while at 50% inoculum was given there was a decrease in the value pH (10), BOD (45 mg/L), COD (304 mg/L), TDS (5419 mg/L), TSS (4025mg/L), Alkalinity (348.9 mg/L), Hardness (170 mg/L), Chlorides (25.28 mg/L) and Chromium (3.8 mg/L). These three isolated organisms were used in the treatment of effluent. Since they are naturally present in the effluent, and which is a good environment for the organisms to survive. The physico-chemical parameters analyzed showed a gradual decreased values in microbially treated sample when compared to the untreated sample. It is clear from the results obtained that as the concentration of inoculum is increased the degradation of the effluent is also effective. Aerobic digesters are usually constructed as completely mixed reactors. The reactor may be fed continuously or intermittently with excess sludge. The objective of the digestion is to reduce the fraction of biodegradable organic material to such a level (in practice between 10 - 20% of the volatile solids) that the digested sludge can be disposed of without problems.

The reduction of pollution load of an effluent while using high concentration of inoculum is because of the biological respiration taking place as they oxidize organic and inorganic constituents found in the effluent (Sawyer, 1956).(Figure.10)

FIGURE.10 SCHEMATIC DIAGRAM

Where:

- Q = flowrate of influent [m³/d]
- Q_w = waste sludge flowrate [m³/d]
- Q_r = flowrate in return line from clarifier [m³/d]
- V = volume of aeration tank [m³]
- S_0 = influent soluble substrate concentration (bsCOD) [BOD g/m³] or [bsCOD g/m³]
- S = effluent soluble substrate concentration (bsCOD) [BOD g/m³] or [bsCOD g/m³]
- X_0 = concentration of biomass [g VSS/m³] in influent
- X_R = concentration of biomass [g VSS/m³] in return line from clarifier
- X_r = concentration of biomass [g VSS/m³] in sludge drain
- X_e = concentration of biomass [g SS/m³] in effluent

Even though there are numerous physical and chemical methods employed in the disposal of wastes the advantage in using bacterium is that they play a key role in the reduction of COD, BOD, total protein, total tannin and total phenol (Saravanan et al., 1998).

For the efficiency of the treatment, various design parameters were analyzed because if the solids in the effluent were discrete particles of uniform size, uniform density, uniform specific gravity and uniform shape, the removal efficiency of these solids would be dependent on the surface area of the tank and the time of detention.

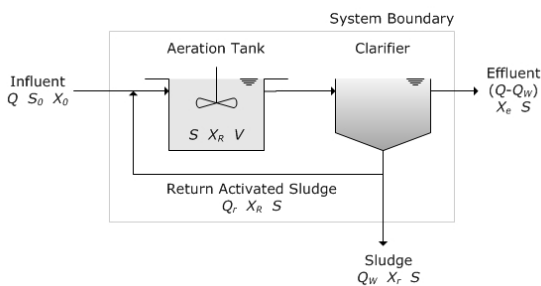
The selection of suitable loading rate depends on the type of suspension to be separated. The effect of the surface loading and detention time on suspended solids removal varies widely depending on the character of waste water, proportion of settleable solids, concentration of solids and other factors.

In the designing of the clarifier, scour velocity is very important in order to avoid the resuspension (scouring) of settled particles, horizontal velocities through the tank should be kept sufficiently low.

From the designing values identified, the horizontal velocity value even at peak flow is substantially less than the scour velocity. Therefore, settled matter should not be resuspended. All the biological treatment reactor designs are based on the mass balance. Based on this biomass mass balance the organisms load can be inoculated for the efficient treatment.

9. SUMMARY

The tannery effluent was collected from the company which is located in Erode. The effluent was subjected to microbiological and physico-chemical analysis. The microbiological analysis reveals that the effluent contains both



bacteria and fungi. Among the microorganisms two bacteria Bacillus sps and Pseudomonas aeruginosa and one fungi Aspergillus niger were found predominantly and were selected for biodegradation study. These microorganisms were cultured in large quantities and inoculated into the sterile effluent at various concentrations (20%, 30%, 40%, 50%). After incubation the physico-chemical parameters were analyzed. It clearly indicates that for the treatment processes Aspergillus niger is effective in degrading the pollutant followed by Pseudomonas aeruginosa and Bacillus sps.

From the same industry, various parameters like surface area, length of the tank, scour velocity, weir flow rate were analyzed for the designing of the clarifier and Solids Retention Time, Observed Yield, Oxygen requirements and total sludge production / day were analyzed for the Activated Sludge Process. Based on these values the designing of the clarifier and Activated Sludge Process were done.

9. REFERENCES

- [1]. APHA, AWWA, and WPCF, Standard Methods for the Examination of Water and Wastewater, 20th Ed, American Public Health Association, Washington, DC, (1998).
- [2]. Archana shukla, N.P. Shukla. 1994. Tannery and electroplating effluent treatment precipitation of chromium and Nickel. *Ind.J.Env.Prot.14: 457-461*.
- [3]. Babu R.; Bajpai, P.K.; Parwana, H.K. 1994. Characterisation and Pretreatment of Tannery Wastewater-A Case Study; Indian J. Environ. Protection, 17, 175.
- [4]. Balasubramaniam, S., V. Pugalenth. 1998. Determination of major pollutants in tannery effluents. *Ind.j.env.prot.19: 15-17*.
- [5]. Basu, S.K.; Chakraborty, S. 1989. Effluent Treatment in Leather Processing Industries; Indian J. Environ. Protection, 9, 904.
- [6]. Chakraborty, R.N. Mohinder Singh, A.Q. Khan., K.L. Sakena. 1995. An industrial waste survey report. *Env. Health, 7:235*.
- [7]. Daryapurkar, R.A., Nandy, Deshpande, Pathe and S.N. Kaul. 1989. Recovery of useful by products from Tannery wastes. *Ind.j.env.prot.9: 890 – 898*.
- [8]. Elangovan, V., Murugesan, Banuamathi Arabindoo. 1995. Evaluation of biokinetic parameters of Anaerobic activity sludge treating tannery waste. *Ind.j.env.prot.15: 580-584*.
- [9]. Mahadevan. A., S.N.Sivaswamy.1985. Tannins Microorganisms. *Frontiers in appl.micro.biol. 15: 326-330*.
- [10]. Murugesan, V.; Elangoan, R. 1994. Biokinetic Parameters for Activated Sludge Process Treating Vegetable Tannery Waste; Indian J. Environ. Protection, 14, 511.
- [11]. Pathe, P.P., T. Nandy, S.N. Kaul.1995. Properties of chromium sludge from chrome tan waste water. *Ind.j.env.prot.15: 81-87*.
- [12]. Prakash, N.B., V.Ramamoorthy, C.M. Lakshmanan. 1997. Primary Treatment of Tannery Effluent for the removal of chromium and other toxic substances. *Ind.j.env.prot.17: 561-566*.
- [13]. Radha, R., B.Prasad Rao, A.Gnanamani, R. Aarichandran, M.Mariappan, 1995. Microbes in tannery waste water. *Prot. Natl. Symp. frontiers in appl. Enn. Microbiol. 19-21*.
- [14]. Ramasami, T., Rajamani, S. Rao, J.R. 1995. Pollution Control in Leather Industry: Emerging Technological Options; CLRI: Adyar, Madras, India.
- [15]. Ryan, J.R.1998. Biological treatment of Hazardous waste. *Civil Engg. 58: 65*.
- [16]. Saravanan, G., A. Saravanan. 1998. Decolourization of tannery effluent by Flavobacterium sps. *Ind.j.env.prot.19: 19-24*.
- [17]. Sarkar, K.T. 1981. Theory and Practice of Leather Manufacture; Ajoy Sorcar: Madras, India.
- [18]. Sawyer, C.N. 1956. Biological treatment of sewage and industrial wastes : 3-17.
- [19]. Sekaran, G., K. Chitra, M. Mariappan. 1993. Removal of sulphide in tannery effluent by catalytic oxidation. *Ind.j.env.prot.13: 128-129*.
- [20]. Sastry, C.A. 1972. Pollution problems in leather industry in India. Dept.of.env.
- [21]. Thabaraj, G.J., S.M. Bose and Y. Nayudamma. 1965. Comparative studies on the treatment of tannery waste by trickling filter, activated sludge and oxidation pond. *Bull. Central leather research institute. 68: 411-430*.

Enhanced Anti-Jamming Protocol in Wireless Mesh Networks

R. Senthil kumar¹, Mahalakshmi. V. J.²

¹PG Scholar, ²Assistant Professor
SNS College of Technology, Coimbatore.

Abstract- Nowadays jamming causes the major data loss in mobile communications. During the transmission time Anti-jamming technique can be used to transmit intermittently at low power in order to conserve energy. Here we use 802.11 wireless network technology and this is to access the functions of the physical layer. There are two functions called Rate Adaptation and Power Control are used to find out whether the attackers involve over the transmission. Attackers involve and send the unwanted messages from source to the destination and use more power. During the transmission time the original messages were not sent properly and occupy more power. First, the Rate Adaptation Algorithm controls the data rate during transmission and increases the packet delivery ratio. Second, Power Control technique is used to find out who is using unwanted powers. Attackers are motivated to use a random jammer to make the jammers to sleep intermittently and increase its lifetime and decrease the probability of detection. The two types of jammers are Deceptive-random jammer and Reactive jammer model. So we primarily consider the Deceptive-random jammer model. Moreover, Reactive jammers are not easily available since they are harder to implement and require special expertise on the part of the attacker.

Keywords: IEEE 802.11, jamming, power control, rate control.

I. INTRODUCTION

Modern society has become heavily dependent on wireless networks to deliver information to diverse users. People expect to be able to access the latest data, such as stock quotes and traffic conditions, at any time, whether they are at home, at their office, or traveling. The emerging wireless infrastructure provides opportunities for new applications such as on-line banking and electronic commerce. Wireless data distribution systems also have a broad range of applications in military networks, such as transmitting up-to-date battle information to tactical commanders in the field. New applications place high demands on the quality, reliability, and security of transmissions. In order to provide a ubiquitous and powerful communication infrastructure that can satisfy security and reliability demands, sophisticated network technology, protocols and algorithms are required. Due to their open and ubiquitous nature, wireless information systems are extremely vulnerable to attack and misuse. Wireless systems can be attacked in various ways, depending on the objectives and capabilities of an adversary.

Due to high availability and relatively low cost of powerful antennas, *jamming*, i.e., the use of active signals to prevent data distribution has emerged as an attractive way of attack. As the current data communication standards such as IEEE802.11 [1] and Bluetooth [2] are not designed to resist

malicious interference, a small number of jammers with limited energy resources can disrupt operation of an entire network. Jamming is a common method of attack in military networks, where transmissions are often performed in the presence of an adversary whose goal is to disrupt the communication to a maximum degree. For example, the Global Positioning System (GPS) relies on extremely weak signals from orbiting satellites and, as a result, is very vulnerable to jamming. This constitutes a significant threat for GPS-based weapon and navigational systems. Jamming can be viewed as a form of *Denial-of-Service* (DoS) attack, whose goal is to prevent users from receiving timely and adequate information.

This makes the defense against such attacks very critical. A jammer transmits electromagnetic energy to hinder legitimate communications on the wireless medium. A jamming attack can cause the following effects in an 802.11 network: 1) due to carrier sensing, co-channel transmitters defer their packet transmissions for prolonged periods; and 2) the jamming signal collides with legitimate packets at receivers. Frequency-hopping techniques have been previously proposed for avoiding jammers [5], [6]. Such schemes, however, are not effective in scenarios with wideband jammers [7], [8]. Furthermore, given that 802.11 operates on relatively few frequency channels, multiple jamming devices operating on different channels can significantly hurt performance in spite of using frequency hopping [9]. ARES1 (Anti-jamming Reinforcement System), a novel measurement driven system, which detects the presence of jammers and invokes rate adaptation and power control strategies to alleviate jamming effects.

II. JAMMING ATTACKS

The goal of the jammer is to disrupt the normal operation of the broadcast system, which results in high waiting time and excessive power consumption of the clients. To that end, the jammer sends active signals over the channels that interfere with the signal sent by the server (see Fig. 1). The traditional defenses against jamming include *spread spectrum* techniques such as *direct sequence* and *frequency hopping*. With direct sequence, the data signal is multiplied by a pseudo-random bit sequence, referred to as *pseudo-random noise code*. As a result, the signal is spread across a very wide bandwidth such that the amount of energy present at each particular frequency band is very small. In frequency hopping systems, the signal only occupies a single channel at any given point of time. The carrier frequency is constantly changing according to a unique sequence. Both techniques spread signal over a wide frequency band, which makes it harder for an adversary to find and jam the signal.

While spread-spectrum techniques constitute an important tool for combating jamming, an additional protection is required at packet-level. First, the pseudo-random noise code or frequency hopping sequence may be

known to the adversary, as in the case of the standard wireless protocols such as IEEE802.11 and Bluetooth. Second, even if no information about the spread-spectrum protocol is available to the adversary, it can still destroy a small number of bits in each transmitted packet by sending a strong jamming signal of short duration. If no other protection mechanism is used at the packet-level, as in the case of IEEE802.11 and Bluetooth, the few destroyed bits will result in dropping of the entire packet.

Accordingly, there is a need to provide an additional packet-level protection, which has to be built on top of traditional anti-jamming techniques. Accordingly, in this paper we investigate efficient anti-jamming schedules for data broadcast. In our schedules, each packet is encoded by an error-correcting code, such as Reed-Solomon, which allows the schedule to minimize both waiting time of the clients and the staleness of the received data. As power supply is the most important constraint for practical jammers, we focus on jammers that have certain restrictions on the length of jamming pulses and the length of the intervals between subsequent jamming pulses. To the best of our knowledge, this is the first study that investigates anti-jamming schedules for wireless data distribution systems.

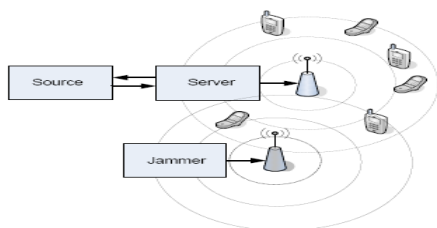


Figure.1 Jamming Attacks

A. Types of Jamming Attacks

Jammers can be distinguished in terms of their attack strategy. A detailed discussion can be found in

- 1) *Nonstop Jamming*: Constant jammers continuously emit electromagnetic energy on a channel. Nowadays, constant jammers are commercially available and easy to obtain [1], [7]. While constant jammers emit non decipherable messages, *deceptive* jammers transmit seemingly legitimate back-to-back dummy data packets. Hence, they can mislead other nodes and monitoring systems into believing that legitimate traffic is being sent.
- 2) *Intermittent Jamming*: As the name suggests, these jammers are active intermittently; the primary goal is to conserve battery life. A *random* jammer typically alternates between uniformly distributed jamming and sleeping periods. It jams for T_j s, and then it sleeps for T_s s. A *reactive* jammer starts emitting energy only if it detects traffic on the medium. This makes the jammer difficult to detect. However, implementing reactive jammers can be a challenge.

For the purposes of this paper, we primarily consider the deceptive-random jammer model. Attackers are motivated into using a random jammer because putting the jammer to sleep intermittently can increase its lifetime and decrease the probability of detection [14]. Furthermore, it is the most generalized representation of a jammer. Appropriately choosing the sleep times could turn the jammer into a constant

jammer or (with high probability) a reactive jammer. Moreover, reactive jammers are not easily available since they are harder to implement and require special expertise on the part of the attacker.

III. RELATED WORKS

Most previous studies employ frequency hopping to avoid jammers. Frequency hopping, however, cannot alleviate the influence of a wideband jammer [7], [8], which can effectively jam all the available channels. In addition, recent studies have shown that a few cleverly coordinated, narrowband jammers can practically block the whole spectrum [9]. Thus, ARES does not rely on frequency hopping.

A. Studies Based on Frequency Hopping

- 1) Navda *et al.* [5] implement a proactive frequency-hopping protocol with pseudorandom channel switching. They compute the optimal frequency-hopping parameters, assuming that the jammer is aware of the procedure followed.
- 2) Xu *et al.* [6] propose two anti-jamming techniques: reactive channel surfing and spatial retreats. However, their work is on sensor networks that only support very low data rates and transmission powers.
- 3) Gummadi *et al.* [15] find that 802.11 devices are vulnerable to specific patterns of narrowband interference related to time recovery, dynamic range selection, and PLCP-header processing. They show that due to these limitations, an intelligent jammer with a 1000 weaker signal (than that of the legitimate transceiver) can still corrupt the reception of packets. In order to alleviate these effects, they propose a rapid frequency-hopping strategy.

B. Other Relevant Work:

- 1) Xu *et al.* [14] develop efficient mechanisms for jammer detection at the PHY layer (for all the four types of jammers). However, they do not propose any jamming mitigation mechanisms. In the same authors suggest that competition strategies, where transceivers adjust their transmission powers and/or error correction codes, *might* alleviate jamming effects. However, they neither propose an anti-jamming protocol nor perform evaluations to validate their suggestions.
- 2) Lin and Noubir present an analytical evaluation of the use of cryptographic interleavers with different coding schemes to improve the robustness of wireless LANs. In the authors show that in the absence of error-correction codes (as with 802.11) the jammer can conserve battery power by destroying only a portion of a legitimate packet.
- 3) Noubir also proposes the use of a combination of directional antennas and node mobility in order to alleviate jammers. ARES can easily be used in conjunction with directional antennas or with error correction codes. We would like to refer the interested reader to our literature survey on anti-jamming systems in for more details.

C. Prior Work on Rate and Power Control:

Rate and power control techniques have been proposed in the literature as means of mitigating interference. However, they do not account for a hostile jamming environment. With these schemes, nodes cooperate in order to mitigate the impact of “legitimate” interference, thereby improving the performance. As an example, Zhai and Fang [23] consider the optimal carrier sensing range for maximum spatial reuse in MANETs. All nodes are restricted to the same maximum transmission power, and their work is purely based on analysis and simulations. In this paper, we follow a purely experimental approach, and our results indicate that ARES effectively alleviates the impact of jammers that use higher transmission powers. Our scheme is specialized toward handling malicious interference of jammers, which attempt to disrupt ongoing communications.

IV. EXPERIMENTAL SETUP

A. Test-Bed Description

Our wireless test-bed consists of 37 Soekris net4826 nodes, which mount a Debian Linux distribution with kernel v2.6, over NFS. The node layout is depicted in Fig. 2. Thirty of these nodes are each equipped with two miniPCI 802.11a/g WiFi cards, an EMP-8602 6 G with Others chipset, and an Intel-2915. The other seven nodes are equipped with one EMP-8602 6G and one RT2860 card that supports MIMO-based (802.11n) communications. We use the MadWifi driver for the EMP-8602 6 G cards. We have modified the Linux client driver of the RT2860 to enable Space Time Block Coding (STBC) support. We use a proprietary version of the ipw2200 access point (AP) and client driver/firmware of the Intel-2915 card. With this version, we are able to tune the CCA threshold parameter.

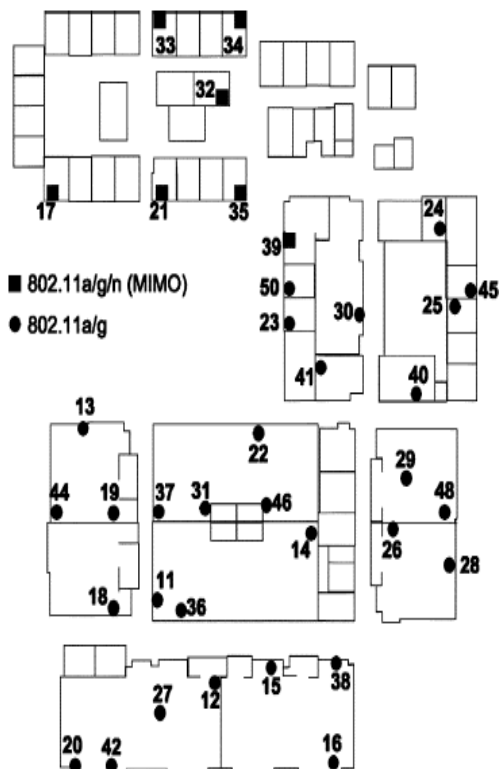


Fig.2. Deployment of our wireless test-bed.

B. Experimental Settings and Methodology

We experiment with different rate adaptation algorithms in the presence of random jammers. We also perform experiments with various transmission powers of jammers and powers/CCA thresholds of legitimate nodes. Our measurements encompass an exhaustive set of wireless links, routes of different lengths, as well as static and mobile jammers. We examine both single-input–single-output (SISO) and MIMO links. We experiment with three modes of operation: 802.11a/g/n (unless otherwise stated throughout this paper, our observations are consistent for all three modes of operation). The experiments are performed late at night in order to isolate the impact of the jammers by avoiding interference from collocated WLANs. By default, all devices (legitimate nodes and jammers) set their transmission powers to 18 dBm (for our experiments that involve only the Intel-2915 cards, the maximum power that we can use is 20 dBm).

1) *Implementing a Random Jammer:* Our implementation of a random jammer is based on a specific configuration dBm and a user space utility that sends broadcast packets as fast as possible. For the purposes of research, we have implemented our own random jammer on an 802.11 legacy device by setting the CCA threshold to 0 dBm. By setting the CCA threshold to such a high value, we force the device to ignore all legitimate 802.11 signals even after carrier sensing. Packets arrive at the jammer’s circuitry with powers less than 0 dBm (even if the distances between the jammer and the legitimate transceivers are very small). An effective random jammer should be able to transmit packets on the medium, as fast as possible, during random active time intervals.

2) *Traffic Characteristics:* We utilize the iperf measurement tool to generate UDP data traffic among legitimate nodes; the packet size is 1500 B. The duration of each experiment is 1 h. For each experiment, we first enable iperf traffic between legitimate nodes, and subsequently, we activate the jammer(s). We consider both mesh and WLAN connectivity. We experiment with different jammer distributions, namely: 1) *frequent jammers*, which are active almost all of the time; 2) *rare jammers*, which spend most of their time sleeping; and 3) *balanced jammers* that have similar average jamming and sleeping times. We have disabled RTS/CTS message exchange throughout our experiments.

V. ARES DESIGN

ARES is composed of two main modules: 1) a Rate module that chooses between fixed or adaptive-rate assignment; and 2) a Power Control module that facilitates appropriate CCA tuning on legitimate nodes.

1. Rate Control

Rate adaptation algorithms are utilized to select an appropriate transmission rate as per the current channel conditions. As interference levels increase, lower data rates are dynamically chosen. Since legitimate nodes consider jammers as interferers, rate adaptation will reduce the transmission rate on legitimate links while jammers are active. Hence, one could potentially argue that rate control on legitimate links increases reliability by reducing rate and can thus provide throughput benefits in jamming environments. To examine the validity of this argument, we experiment with three different popular rate adaptation algorithms, Sample Rate, AMRR and One . These algorithms are already

implemented on the MadWifi driver that we use. For simplicity, we first consider a balanced random jammer, which selects the sleep duration from a uniform distribution $U[1,8]$ and the jamming duration from $U[1,5]$ (in seconds).

1) *Fixed transmission rate (Rf)*: This is the nominal transmission rate configured on the wireless card.

2) *Saturated rate (Rs)*: It is the rate achieved when R_f is chosen to be the rate on the wireless card. In order to compute R_s for a given R_f , we consider links where the PDR is 100% for the particular setting of R_f . We then measure the rate achieved in practice. We notice that for lower values of R_f , the specified rate is actually achieved on such links

TABLE 1
 Saturated throughput matrix in megabits per second

Rf	6	9	12	18	24	36	48	54
Rs	6	9	12	18	24	26	27	27

However, for higher values of R_f (as an example, $R_f = 54$ Mb/s), the achieved data rate is much lower; this has been observed in other work, Table I contains a mapping, derived from measurements on our test-bed, between R_f and R_s .

Application data rate (Ra): This is the rate at which the application generates data. It is difficult (if not impossible) to *a priori* determine the *best* fixed rate on a link. Given this, and if we let R be the set of all possible fixed transmission rates, we set

$$R_f = \{\min x: x > R_a\}$$

which is the maximum rate that is required by the application (we discuss the implications of this choice later). Our key observations are summarized as follows.

- Rate adaptation algorithms perform poorly on high-quality links due to the long times that they incur for converging to the appropriate high rate.
- On *lossless* links, the fixed rate R_f is better, while rate adaptation is beneficial on *lossy* links.

We defer defining what constitute lossless or lossy links later in this section. Conceptually, we consider lossless links to be those links that can achieve higher long-term throughput using a fixed transmission rate R_f rather than by applying rate adaptation.

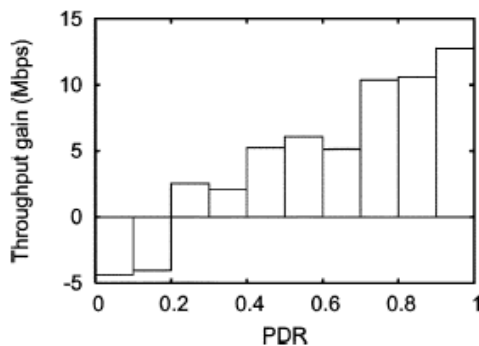


Fig.3 Throughput gain of fixed rate versus Sample Rate, for various link qualities and for application data rate of 54 Mb/s.

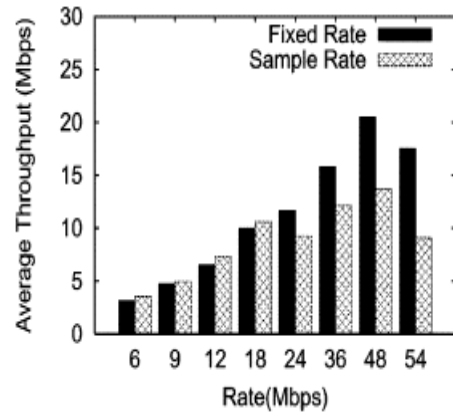


Fig.4 Performance with rare jammers is aligned with our observations for the case with balanced jammers $R_a = R_f$.

2. Power Control

Power control in 802.11 networks needs to ensure that there are no asymmetric links in the network to avoid throughput starvation of any node. To this end, two fundamental concepts are those of a contention domain and symmetry.

According to the CSMA/CA protocol of the 802.11 MAC, a node that wishes to transmit a packet needs to first measure the strength of the power received on the wireless channel, i.e. the sum of the noise and interference on its operating channel. If the received power on the channel is higher than a certain threshold referred to as the Clear Channel Assessment (CCA) threshold of node, the medium is assessed to be busy, and the transmission is deferred. Otherwise, the node transmits its packet. In this framework, we define the contention domain of a reference node as the set of nodes in the network that can generate sufficient interference to suppress the transmission of the reference node.

Power Jammers

we consider a single legitimate data link and a jammer, incrementing the transmission power on the data link should increase the signal-to-interference-plus-noise ratio (SINR) of the received data packets. Thus, one could argue that increasing the transmission power is always beneficial in jamming environments. Note here that increasing the transmission power in environments with lower power jammers can potentially increase the network-wide interference. However, as we will see in the following, ARES includes a CCA tuning mechanism that avoids starvation effects caused from legitimate interference. We vary the transmission powers of both the jammer and legitimate transceiver, as well as the CCA threshold of the latter. Note that the jammer's transmission distribution is not very relevant in this part of our study. Our expectation is that tuning the power of legitimate transceivers will provide benefits while the jammer is active. In other words, one can expect that the benefits from power control will be similar with any type of jammer.

We define the following:

- **RSSITR**: the received signal strength indicator (RSSI) of the signal of the legitimate transmitter at its receiver.
- **RSSIRT** : the RSSI of the signal in the reverse direction (the receiver is now the transmitter).
- **RSSIJT** and **RSSIJR** : the RSSI values of the jamming signal at the legitimate transmitter and receiver, respectively.
- **RSSIJ**: the minimum of{ RSSIJT , RSSIJR }
- **PL** and **CCAL**: the transmission power and the CCA threshold at legitimate transceivers.
- **PJ**: the transmission power of the jammer. Our main observations are the following.
- Mitigating jamming effects by incrementing is viable at low data rates. It is extremely difficult to overcome the jamming interference at high rates simply with power adaptation.
- Increasing CCAL restores (in most cases) the isolated throughput (the throughput achieved in the absence of jammers)

$$CCA = \min(RSSITR, RSSIRT) - \Delta$$

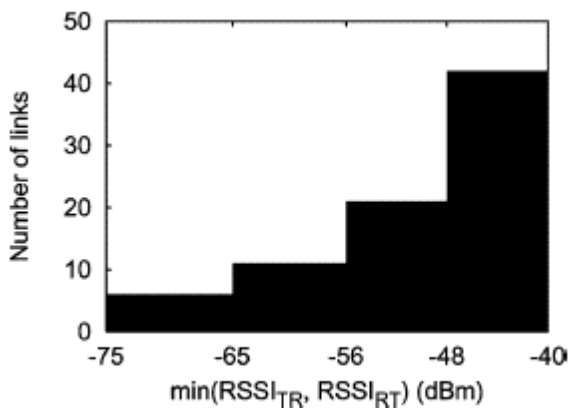


Fig. 5 Histogram with **RSSITR** and **RSSIRT** values on legitimate links.

VI. PARAMETERS AND SIMULATION RESULTS

We first evaluate ARES by examining its performance in three different networks: a MIMO-based WLAN, an 802.11 mesh network in the presence of mobile jammers, and an 802.11Awlan setting where uplink TCP traffic is considered. ARES boosts the throughput of our MIMO WLAN under jamming by as much as 100%. Our objective here is twofold. First, we seek to observe and understand the behavior of MIMO networks in the presence of jamming. Second, we wish to measure the effectiveness of ARES in such settings. Toward this, we deploy a set of seven nodes equipped with *Ralink RT2860* mini PCI cards.

TABLE 2

Simulation parameters for frequency hopping technique

Number of nodes	15
Packet size	512bytes
Terrain area	2000x1000
Number of nodes packet transmission	5

In existing method we have used the frequency hopping technique for the packet transmission for the different source to destination. Packet losses is very low in one source to one destination packet transmission time. Packet losses will be increasin for the number of source and destination increasing time.

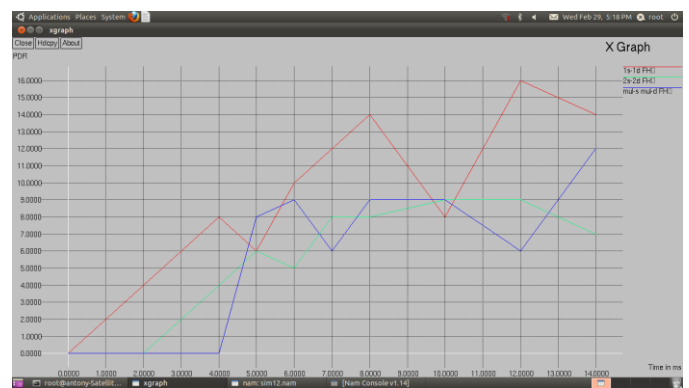


Fig. 6 Increasing the packet loss using FH method used.

TABLE 3

Simulation parameters for ARES method

Number of nodes	45
Packet size	512bytes
Terrain area	2000x1000
Number of nodes packet transmission	15

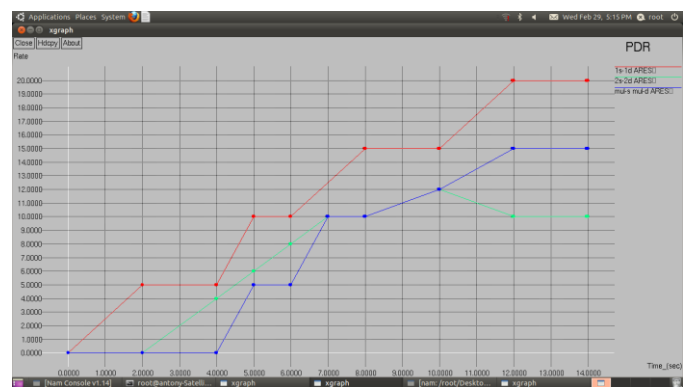


Fig.7 Reduced the packet loss when using the ARES method.

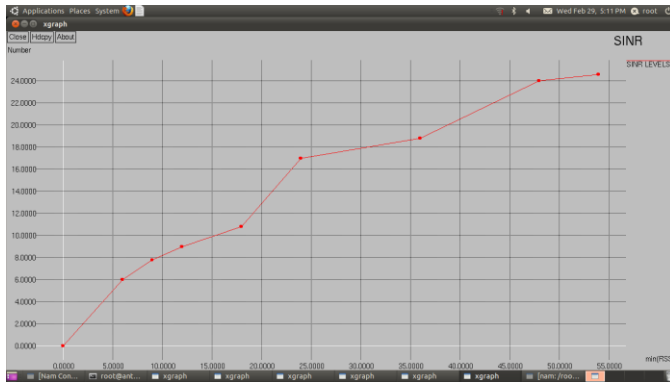


Fig.8 SINR graph for using ARES method

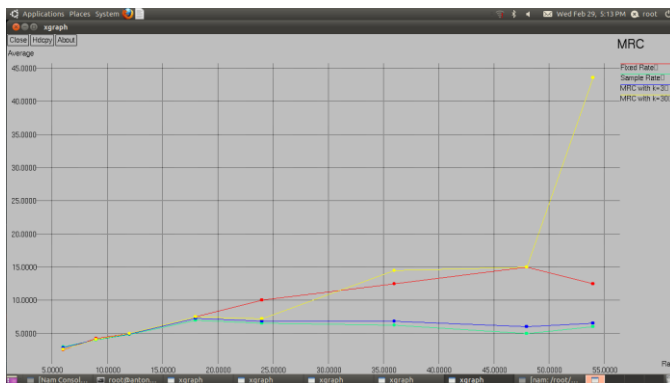


Fig.9 MRC graph for using ARES method

VII. CONCLUSION

In this paper the Evaluation and measurement driven prototype system that uses the Rate control and Power control technique which efficiently fights against the jammers. The jammers can be avoided using Frequency hopping technique. The fixed Rate assignment can be beneficial in jammed environment. Power level tuning helps only at low rates and low power jammer. Tuning the CCA threshold enables: (i) The transmitter to ignore jamming signals. (ii) The receivers capture desired packets. In our future work is to prevent the packet losses and increasing the throughput using ARES method. We will demonstrate the effectiveness of ARES in three different deployments are: (i) an 802.11n-based MIMO in WLAN; (ii) an 802.11a/g network infested with mobile jammers; (iii) an 802.11a WLAN with uplink TCP traffic. We also introduce a network security model to prevent the jammer attacks.

REFERENCES

- [1] "SESP jammers," SESP [Online]. Available: <http://www.sesp.com/>
- [2] "Wireless noise hampers DefCon; Impact of non-Wi-Fi interference surprises observers at hacker conference," *BNET.com* 2005[Online]. Available: http://findarticles.com/p/articles/mi_m0EIN/is_2005_August_2/ai_n14841565
- [3] "Techworld news," [Online]. Available: <http://www.techworld.com/mobility/news/index.cfm?newsid=10941>
- [4] "RF jamming attack," ZOH0 Corporation, Pleasanton, CA, 2010 [Online]. Available:

<http://manageengine.adventnet.com/products/wifi-manager/rfjamming-attack.html>

- [5] V. Navda, A. Bohra, S. Ganguly, and D. Rubenstein, "Using channel hopping to increase 802.11 resilience to Jamming attacks," in *Proc. IEEE INFOCOM*, 2007, pp. 2526–2530.
- [6] W. Hu, T. Wood, W. Trappe, and Y. Zhang, "Channel surfing and spatial retreats: Defenses against wireless denial of service," in *Proc. ACM WiSe*, 2004, pp. 80–89.
- [7] "ISM wide-band jammers," [Online]. Available: <http://69.6.206.229/ecommerce-solutions-catalog1.0.4.html>
- [8] D. Caro, "[ISN] Users fear wireless networks for control," 2007 [Online]. Available: <http://lists.jammed.com/ISN/2007/05/0122.html>
- [9] K. Pelechrinis, C. Koufogiannakis, and S. V. Krishnamurthy, "Gaming the jammer: Is frequency hopping effective?," in *Proc. WiOpt*, Jun. 2009, pp. 187–196.
- [10] V. Mhatre, K. Papagiannaki, and F. Baccelli, "Interference mitigation through power control in high density 802.11 WLANs," in *Proc. IEEE INFOCOM*, 2007, pp. 535–543.
- [11] J. Bicket, "Bit-rate selection in wireless networks," M.S. thesis, Dept. Elect. Eng. Comput. Sci., MIT, Cambridge, MA, 2005.
- [12] "Onoe rate control," [Online]. Available: http://madwifi.org/browser/trunk/ath_rate/onoe
- [13] S. Pal, S. R. Kundu, K. Basu, and S. K. Das, "IEEE 802.11 rate control algorithms: Experimentation and performance evaluation in infrastructure mode," in *Proc. PAM*, 2006.
- [14] W. Xu, W. Trappe, Y. Zhang, and T. Wood, "The feasibility of launching and detecting Jamming attacks in wireless networks," in *Proc. ACM MobiHoc*, 2005, pp. 46–57.
- [15] R. Gummadi, D. Wetheral, B. Greenstein, and S. Seshan, "Understanding and mitigating the impact of RF interference on 802.11 networks," in *Proc. ACM SIGCOMM*, 2007, pp. 385–396.

An Efficient Non Blocking Two Phase Commit Protocol for Distributed Transactions

V. Manikandan¹, R. Ravichandran¹, R. Suresh¹, F. Sagayaraj Francis²

^{*}(Department of Information Technology, Sri Manakula Vinayagar Engineering College, Puducherry, India

^{**}(Department of Computer Science and Engineering, Pondicherry Engineering College, Puducherry, India

ABSTRACT

The 2-phase commit protocol is a standard algorithm for safeguarding the ACID properties of transaction in the distributed system. In distributed database systems (DDBSs), transaction blocks occurs during two-phase commit (2PC) processing if the coordinator itself fails and at the same time some client has declared itself ready to commit the transaction. Thus the blocking phenomena reduce the availability of the system, since the blocked transactions keep all the resources until they receive the final command from the coordinator after its recovery. To remove the blocking problem in 2PC protocol, three phase commit (3PC) protocol was proposed. Although 3PC protocol eliminates the blocking problem, it involves extra overhead of one more cycle and in turn increases the time taken for the transaction to complete. In this paper we proposed a new architecture for 2PC by employing a Backup coordinator, which will reduce the transaction blocking considerably. However in worst case, the blocking can occur in the Backup coordinator also. In such a rare case occurs, the client has to wait until the recovery of either the coordinator or the backup coordinator. This protocol suits best for DDBS environment in which transaction fail frequently and messages take longer time to deliver.

Keywords: availability, blocking, distributed database system, two-phase commit

1. INTRODUCTION

The world of computing is moving towards a trend where tasks are performed in a distributed manner. Distributed database systems implements a transaction commit protocol to ensure transaction atomicity. From last few decades a variety of protocols has been proposed by researchers. To achieve their functionality these commit protocols typically require exchange of multiple messages, in multiple phases, between client and coordinator where distributed transaction is done. A concurrency control mechanism is also applied to ensure synchronized access to various databases by many concurrently running transactions [1]. The performance factor of concurrency control algorithms depends on system throughput and transaction response time. Four cost factors influence the performance: inter-site communication, local processing, transaction restarts, and transaction blocking [3, 14].

The two-phase commit protocol allows the management of transactions in a distributed environment. In addition to that several log record are generated, some of which has to be forced write i.e. they are flushed to disk

synchronously. Since two phase protocol suffers from a single point of failure, transaction blocking occurs. We are trying to overcome it by employing a Backup coordinator. Synchronization among the coordinator and Backup coordinator is maintained by connection manager.

In this fast world, transactions have to be committed successfully and data consistency has to be maintained. In 2PC, due to coordinator crash, the resource held locked and transactions are uncompleted till the recovery of coordinator. So resources are not able to use until it is being unlocked.

The 3PC protocol has one extra phase, called the *pre-commit phase*, compared to 2PC. It is this phase that makes this protocol non-blocking but it comes with the extra cost of message transfers [5]. Even though 3PC overcomes this problem, 2PC has its own advantages. So we are trying to resolve the problem by using Backup coordinator which performs the functions of coordinator, when it crashes and so, resources are unlocked and transactions are committed successfully.

Here we have employed EJB to create modules and implement what we have proposed in the paper. Since EJB has its own transaction API's, it's easy to implement our concept and to perform transactions in an efficient manner.

2. LITERATURE SURVEY

In this section of this paper we have discussed the earlier defined protocols like presumption protocols, single phase commit protocol, optimized commit protocol and non-blocking commit protocol. The efficiency of a commit protocol is associated with the number of communication steps, the number of log writes and its execution time at the coordinator and at each participant. The Blocking or No blocking nature and difference in recovery procedures are other important factors that have a vital impact on the overall commit protocol performance. In this paper an attempt has been made to achieve equally good performance of protocol in the presence of failure.

2.1 Variants of 2PC

Both PA(presumed commit) and PC(presumed abort) seek to reduce commit process overhead by reducing acknowledge messages and forced log writes in the decision phase, while the voting phase remains the same as for 2PC. PrA is preferable where the number of aborted transactions is more than the number of committed transaction; PrC is preferred in systems where the number of committed transactions is more than the number of

aborted transactions, a common situation considering present system reliability. A detailed comparison between PrA and PrC is given in [6].

2.2 Non-Blocking commit protocol

A number of commit protocols have been designed to attack the fundamental blocking problem. Three-phase commit (3PC) [7, 8, 9] was among the first no blocking protocols. 3PC introduces a new “buffered phase” between the voting phase and the decision phase. In the buffered phase, a preliminary decision is reached about the result of a transaction. Cohorts can reach a global decision from this preliminary decision even in face of a subsequent master failure. However, 3PC achieves the non-blocking property at the expense of increased communication overhead by an extra round of message exchanges. Moreover, both master and cohorts must perform forced writes of additional log records in the buffered phase.

2.3 Single Phase Commit

The One-Phase Commit (1PC) protocol has been first suggested in [6] and several variations have been proposed. The *Early Prepare (EP)* protocol [10] forces each cohort to enter a prepare state after the execution of each operation. It makes cohort’s vote implicitly YES and this protocol exploits the Presumed Commit as well [11]. But a coordinator may have to force multiple *membership* records, because the transaction membership may grow as transaction execution progresses. Above all, the main drawback comes from the fact that the log of each operation has to be written in the cohort’s log disk per operation, it leads to a serious disk blocking time. Only if every sever has a stable storage so that log forces are free, EP can be considered to be used.

2.4 Optimistic commit protocol

Optimistic commit protocol [15] concentrates on reducing the lock waiting time by lending the locks the committing transactions hold. Since the lock lending is done in a controlled manner, there is no possibility of cascading aborts even if the committing transaction is aborted. This protocol has a good performance due to its reduction of the blocking arising out of locks held on prepared data.

The circumstances under which distributed transactions are committed or rolled back under the 2-PC protocol are [12].

- When application instructs the transaction to rollback, then the transaction will be roll backed.
- When process failure occurs before all participant votes, then transaction will be roll backed.
- If any participant votes no, then transaction will be roll backed.
- If all participant yes, transaction will be committed.
- If Process failure occurs after all participant have voted and the transaction coordinator has received all voters as yes, then transaction will be committed but is unresolved.

2.5 Comparison of 2PC and 3PC

Comparison between 2PC and 3PC regarding message exchanges, log writes and degree of blocking where n is the number of participants [2].

In case of 2PC message exchange is $4(n-1)$, log write is $2n$ and degree of blocking is high. Whereas in 3PC message exchange is $5(n-1)$, log write is $2n$ and degree of blocking is low.

It is the extra phase in 3PC can gives the extra $n-1$ message exchanges compared to 2PC. If the distributed system has a lot of transactions to be executed, this will become a significant performance loss [16].

3. NON-BLOCKING TWO PHASE COMMIT PROTOCOL

This section is going to deals with how 2PC can be implemented as a non-blocking protocol with the help of Backup coordinator. In normal case clients request will be processed by the coordinator and the transaction will be either committed or aborted.

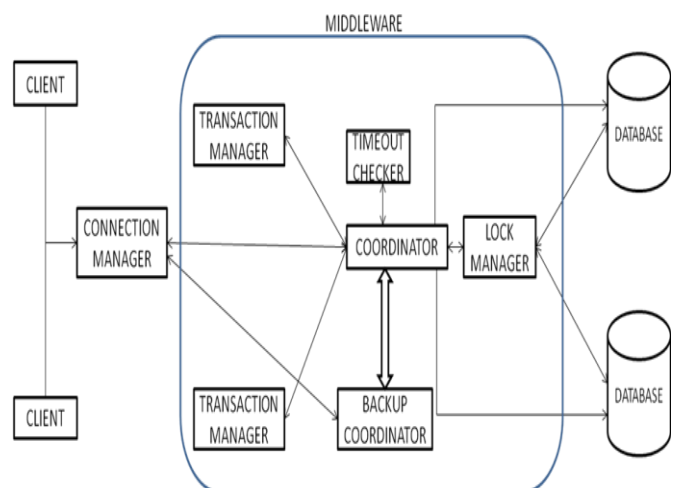


Fig 1: System Architecture with Backup coordinator

If suppose the coordinator fails means the transactions will be in a blocked state and resource is also said to be locked, clients has to wait infinite amount of time so this will affect the performance of the distributed system. In our model we included a new thing called as connection manager, will keeps on monitoring the coordinator and Backup coordinator, whenever the coordinator fails the transactions will be automatically transfer to the Backup coordinator with the help of connection manager and in vice verse. In turn connection manager will have a common log file for both coordinator and Backup coordinator. Synchronization between them will be achieved with the help of connection manager.

The components involved in the architecture are discussed below.

1. Transaction Coordinator: Coordinates and executes atomic transactions and manages data transfer between its replica and other database.

2. Transaction manager: A transaction manager provides the services and management functions required to support transaction demarcation, transactional resource management, synchronization, and transaction context propagation.

3. Database: A database consists of a resource manager provides the application access to resources. The resource manager implements a transaction resource interface that is used by the transaction coordinator to communicate transaction association, transaction completion, and recovery work.

4. Connection Manager: Connection Manager provides a fast and transparent way of making connection. Here the connection manager will keeps on monitoring the coordinator and Backup coordinator, whenever the coordinator fails the transactions will be automatically transfer to the Backup coordinator with the help of connection manager and in vice verse. Users do not have to know which connection path is chosen.

5. Timeout checker: This is a thread whose responsibility is to watch for currently active transaction that have been inactive for too long, and abort them if so. Upon request by the TM, the checker records the current clock and associated it with the specified transaction. The thread constantly checks whether any transaction's time-to-live has expired, by looking at the difference between the current clock time and the transaction's "clock stamp". If this is greater than a large, fixed value, the timeout thread itself initiates abortion of the transaction.

We have implemented this model and these will be more reliable than the previous model, and so will increase the efficiency of the transaction processing.

We created log files which are used to lists actions that have occurred. Log files in turn said to contain the complete detail of the transaction that is being taken place. In 2PC log files are categorized into two types, they are transaction manager log file and coordinator log file. These files are maintained by connection manager in order to make synchronization among coordinator & backup coordinator and to survive from transaction failure.

4. PERFORMANCE DISCUSSION

4.1 Failure probability of backup coordinator while coordinator is down

Reliability of a module is statistically quantified as mean-time-to-failure (MTTF). The service interruption of a module is statistically quantified as mean-time-to-repair (MTTR). The module availability is statistically quantified from [5, 13] as:

$$\frac{MTTF}{MTTF + MTTR}$$

Let $MTTF_c$ and $MTTR_c$ represent MTTF and MTTR of the coordinator respectively. Also, $MTTF_b$ represents

MTTF of corresponding backup coordinator. Since the backup coordinator and the coordinator are failure independent, the probability that backup coordinator fails when the corresponding coordinator is down is calculated as below.

The probability that the coordinator site is unavailable is:

$$P_c = \frac{MTTR_c}{MTTF_c + MTTR_c}$$

$$\square \frac{MTTR_c}{MTTF_c} \text{ since } MTTR_c \square MTTF_c$$

The probability that the backup coordinator fails is:

$$P_b = \frac{1}{MTTF_b}$$

The probability that backup coordinator fails and the corresponding coordinator is down is:

$$P_b \times P_c = \frac{1}{MTTF_b} \times \frac{MTTR_c}{MTTF_c} = \frac{MTTR_c}{MTTF_c \times MTTR_c}$$

From above equation, it can be observed that the probability that backup site fails while corresponding coordinator is down is reduced significantly. Thus, in case of coordinator site failure, with the introduction of the backup coordinator, blocking probability is considerably reduced as compared to 2PC protocol. Further, it can be observed that the purpose of the backup coordinator is to terminate the blocked transactions at the participant sites when the corresponding coordinator is down. After the termination of the blocked transactions, even though the backup coordinator fails, it does not affect the consistency of the database. Let `term_time` be the time duration required to terminate the blocked transactions by contacting the backup coordinator when the coordinator is down. The above equation denotes the probability that the backup coordinator fails during the entire period ($MTTR_c$) when the coordinator is down. However, in the worst case the blocked transactions are consistently terminated even if the backup coordinator is up only during `term_time` and then fails. As `term_time` (few minutes) is much less than the down time (few hours) of the coordinator, the probability that the backup coordinator fails during the `term_time` while the coordinator is down is further reduced.

5. CONCLUSION

Typically, only the coordinator node has all the information necessary to determine whether a transaction should commit or rollback. Therefore, if the coordinator node fails during a distributed transaction, all the participants in the transaction must wait for the coordinator to recover before completing the transaction. Thus,

significant delays may be caused when the coordinator fails. To minimize the delay caused by the failed coordinator, some conversional transaction systems use clustering and / or group communication protocols to provide standby coordinators. However, Clustering protocols and group communication protocols add complexity to distributed transactions, and require a change to underlying distributed transaction protocol. In this paper we proposed a new architecture for 2PC relate to distributed transactions, and more specifically to improving reliability of Distributed Transactions.

Transaction processing must ensure transaction integrity for transactions that involve databases. Transactions often involve multiple steps, all of which must be completed before a database commit can be executed. Transaction Based Middleware is critical, because without them, it would be a very difficult job to write the programs necessary to track transactions across multiple platforms and databases. Some of the services provided by Transaction Based Middleware include the following: Transaction integrity, two-phase commits, failure/recovery, and load balancing.

Load Balancing is a feature of Transaction Based Middleware in which, the server component manages the workload presented by the clients by fully utilizing the resources available. Load balancing and thread management services are important because Transaction Based Middleware need to process many transactions on many different systems in a very short time period. The Middleware can change traffic patterns, processing parameters, or increase the pool of processors. This enables the middleware to dynamically adjust to the workload [4]. Transaction Based Middleware, generally utilize transaction priorities and multiple database sessions and/or threads to optimize throughput.

ACKNOWLEDGEMENT

V Premanand, Department of Information Technology, Sri Manakula Vinayagar Engineering College, Puducherry.

REFERENCES

Journal Papers:

- [1] Toufik Taibi, Abdelouahab Abid, Wei Jiann Lim, Yeong Fei Chiam, and Chong Ting Ng, "Design and Implementation of a Two-Phase Commit Protocol Simulator", *The International Arab Journal of Information Technology*, Vol. 3, No. 1, January 2006.
- [2] Byun T, Moon S, "Nonblocking two-phase commit protocol to avoid unnecessary transaction abort for distributed systems", Cheongryang 130-012 Seoul South Korea, *Journal of Systems Architecture*. Volume 43, Issues 1-5, March 1997, Pages 245-254.
- [3] Arun Kumar Yadav and Ajay Agarwal, "A Distributed Architecture for Transactions Synchronization in Distributed Database Systems", *International Journal on Computer Science and Engineering* Vol. 02, No. 06, 2010.
- [4] Tarek Helmy and Fahd S. Al-Otaibi, "Dynamic Load-Balancing Based on a Coordinator and Backup

Automatic Election in Distributed Systems", *International Journal of Computing & Information Sciences* Vol. 9, No. 1, April 2011.

- [5] Tabassum k, Taranum F, Damodaram A "A Simulation of Performance of Commit Protocols in Distributed Environment", in *PDCTA, CCIS 203*, pp. 665-681, Springer, 2011.

Thesis:

- [6] Gray J. N, "Notes on database operating systems". *Operating Systems: an Advanced Course*, 60:397-405, 1991.
- [7] Skeen D, "Crash Recovery in a Distributed Database Systems", *PhD thesis, Department of Electrical Engineering and Computer Science, University of California at Berkeley*, 1982.

Proceedings Papers:

- [8] Skeen D, "A quorum-based commit protocol", in *Proc. Of Berkeley Workshop*, pages 69-80, 1982.
- [9] Skeen D, "Nonblocking commit protocols " in *Proceedings of the 1981 ACM SIGMOD international conference on Management of data*, Ann Arbor, Michigan, pp. 133-142 .
- [10] Stamos J.W and Cristian F, "A low-cost atomic commit protocol", in *9th IEEE Symposium on Reliable Distributed Systems (SRDS'90)*, pages 66-75, 1990.
- [11] Houmailly Y. J. Al and Chrysanthi P. K, "The Implicit-Yes Vote Commit Protocol with Delegation of Commitment," in *Proceedings of 9th International Conference on Parallel and Distributed Computing Systems*, pp. 804-810, 1996.
- [12] Boutros B. S. and Desai B. C., "A Two-Phase Commit Protocol and its Performance," in *Proceedings of the 7th International Workshop on Database and Expert Systems Applications*, pp.100-105, 1996.
- [13] Reddy K, Kitsuregawa M, "Reducing the blocking in two-phase commit protocol employing backup sites", *IFCIS Conference on Cooperative Information Systems*, 1998.
- [14] Meng Qingyuan, Wang Haiyang, Xu Chunyang, "A New Model for Maintaining Distributed Data Consistence", *International Conference on Computer Science and Software Engineering, IEEE* 2008.
- [15] Lampton B and Lomet D "A new presumed commit optimization for two phase commit", in *19th International Conference on Very Large Data Bases*, Dublin, Ireland, 1993.

Books:

- [16] Silberschatz, Korth, Sudarshan, "Database System Concepts, Fourth Edition, volume 1", (The McGraw-Hill Companies, 2001).

Noise cancellation using adaptive algorithms

Jashvir Chhikara

(M-Tech Scholar, Shobhit University)

Jagbir Singh

(Lecturer, World Institute of Technology)

Abstract: Adaptive filtering is a wide area of researcher in present decade in the field of communication. Adaptive noise cancellation is an approach used for noise reduction in speech signal. As received signal is continuously corrupted by noise where both received signal and noise signal both changes continuously, then this arise the need of adaptive filtering. This paper deals with cancellation of noise on speech signal using two adaptive algorithms least mean square (LMS) algorithm and NLMS algorithm. Choose the algorithms that provide efficient performance with less computational complexity.

Keywords: Adaptive noise cancellation (ANC), LMS Algorithm, NLMS algorithm, Adaptive filtering.

I. INTRODUCTION

Acoustic noise problems becomes more pronounce as increase in number of industrial equipment such as engines, transformers, compressors and blowers are in use. The traditional approach to acoustic noise cancellation uses passive techniques such as enclosures, barriers and silencers to remove the unwanted noise signal [1][2]. Silencers are important for noise cancellation over broad frequency range but ineffective and costly at low frequencies. Mechanical vibration is a type of noise that creates problems in all areas of communication and electronic appliances. Signals are carriers of information, both useful and unwanted. Extracting or enhancing the useful information from a mix of conflicting information is a simplest form of signal processing. Signal processing is an operation designed for extracting, enhancing, storing, and transmitting useful information. Hence signal processing tends to be application dependent. In contrast to the conventional filter design techniques, adaptive filters do not have constant filter coefficients and no priori information is known. Such a filter with adjustable parameters is called an adaptive filter. Adaptive filter adjust their coefficients to minimize an error signal and can be realized as finite impulse response (FIR), infinite impulse response (IIR), lattice and transform domain filter [4]. The most common form of adaptive filter is the transversal filter using least mean square (LMS) algorithm and NLMS algorithm.

In this paper, noise is defined as any kind of undesirable signal, whether it is borne by electrical, acoustic, vibration or any other kind of media. In this paper, adaptive algorithms are applied to different kind of noise.

The basic idea of an adaptive noise cancellation algorithm is to pass the corrupted signal through a filter that tends to

suppress the noise while leaving the signal unchanged. This is an adaptive process, which means it does not require a priori knowledge of signal or noise characteristics. Adaptive noise cancellation (ANC) efficiently attenuates low frequency noise for which passive methods are ineffective.

Although both FIR and IIR filters can be used for adaptive filtering, the FIR filter is by far the most practical and widely used. The reason being that FIR has adjustable zeros, and hence it is free of stability problems associated with adaptive IIR filters that have adjustable poles as well as zeros.

II. LEAST MEAN SQUARE ALGORITHM

To make exact measurements of the gradient vector $\nabla J(n)$ at each iteration n , and if the step-size parameter μ is suitably chosen then the tap-weight vector computed by using the steepest descent algorithm would converge to the optimum wiener solution. The exact measurements of the gradient vector are not possible and since that would require prior knowledge of both the autocorrelation matrix \mathbf{R} of the tap inputs and the cross correlation vector \mathbf{p} between the tap inputs and the desired response, the optimum wiener solution could not be reached [3]. Consequently, the gradient vector must be estimated from the available data when we operate in an unknown environment.

After estimating the gradient vector we get a relation by which we can update the tap weight vector recursively as:

$$\mathbf{w}(n+1) = \mathbf{w}(n) + \mu \mathbf{u}(n)[d^*(n) - \mathbf{u}^H(n)\mathbf{w}(n)] \quad \text{---(1)}$$

Where μ = step size parameter

$$\mathbf{u}^H(n) = \text{Hermit of a matrix } \mathbf{u}$$

$$d^*(n) = \text{Complex conjugate of } d(n)$$

We may write the result in the form of three basic relations as follows:

1. Filter output:

$$y(n) = \mathbf{w}^H(n)\mathbf{u}(n) \quad \text{---(2)}$$

2. Estimation error or error signal:

$$e(n) = d(n) - y(n) \quad \text{--- (3)}$$

3. Tap weight adaptation:

$$\mathbf{w}(n+1) = \mathbf{w}(n) + \mu \mathbf{u}(n)e^*(n) \quad \text{---(4)}$$

Equations (2) and (3) define the estimation error $e(n)$, the computation of which is based on the current estimate of the tap weight vector $w(n)$. Note that the second term, $u(n)e^*(n)$ on the right hand side of equation (4) represents the adjustments that are applied to the current estimate of the tap weight vector $w(n)$. The iterative procedure is started with an initial guess $w(0)$. The algorithm described by equations (2) and (3) is the complex form of the adaptive least mean square (LMS) algorithm. At each iteration or time update, this algorithm requires knowledge of the most recent values $u(n)$, $d(n)$ $w(n)$. The LMS algorithm is a member of the family of stochastic gradient algorithms. In particular, when the LMS algorithm operates on stochastic inputs, the allowed set of directions along which we “step” from one iteration to the next is quite random and therefore cannot be thought of as consisting of true gradient directions.

III. NOISE CANCELLATION

Fig. 1 shows the basic problem and the adaptive noise cancelling solution to it. A signal s is transmitted over a channel to a sensor that also receives a noise n_0 uncorrelated with the signal. The primary input to the canceller is combination of both signal and noise $s + n_0$. A second sensor receives a noise n_1 uncorrelated with the signal but correlated with the noise n_0 . This sensor provides the reference input to the canceller. This noise n_1 is filtered to produce an output y that is as close a replica of n_0 . This output of the adaptive filter is subtracted from the primary input $s + n_0$ to produce the system output $z = s + n_0 - y$.

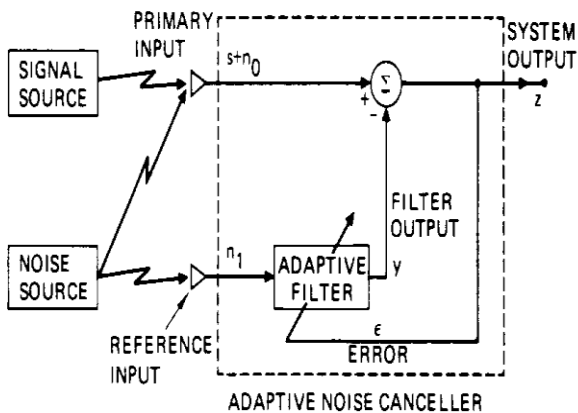


Fig 1 adaptive noise cancellation concept

If we know the characteristics of the channels over which the noise and signal was transmitted to the primary and reference sensors, it would theoretically be possible to design a fixed filter. The filter output could then be

subtracted from the primary input, and the system output would be signal alone. But the characteristics of the transmission paths are unknown and are not of a fixed nature, due to this use of a fixed filter are not feasible.

In Fig. 1 the reference input is processed by an adaptive filter. An adaptive filter is that which automatically adjusts its own impulse response. Adjustment is accomplished through an algorithm. The filter can operate under changing conditions and can readjust itself continuously to minimize the error signal.

In noise cancelling systems the practical objective is to produce a system output $z = s + n_0 - y$ that is a best fit in the least squares sense to the signal s . This objective is accomplished by feeding the system output back to the adaptive filter and adjusting the filter through an LMS adaptive algorithm to minimize total system output power. In an adaptive noise cancelling system, the system output serves as the error signal for the adaptive process.

The prior knowledge of the signal s or of the noises n_0 and n_1 would be necessary before the filter could be designed to produce the noise cancelling signal y .

Assume that s , n_0 , n_1 and y are statistically stationary and have zero means. Assume that s is uncorrelated with n_0 and n_1 , and suppose that n_1 is correlated with n_0 . The output z is

$$z = s + n_0 - y \tag{1}$$

Squaring, we obtain

$$z^2 = s^2 + (n_0 - y)^2 + 2s(n_0 - y) \tag{2}$$

Taking expectations both side of equation (2)

$$E[z^2] = E[s^2] + E[(n_0 - y)^2] + 2E[s(n_0 - y)]$$

Realizing that s is uncorrelated with n_0 that output y is

$$E[z^2] = E[s^2] + E[(n_0 - y)^2] \tag{3}$$

The signal power $E[s^2]$ will be unaffected as the filter is adjusted to minimize $E[z^2]$. Accordingly, the minimum output power is

$$\min E[z^2] = E[s^2] + \min E[(n_0 - y)^2] \tag{4}$$

When the filter is adjusted so that is $E[z^2]$ minimized, therefore $E[(n_0 - y)^2]$ is, also minimized. The filter output y is then a best least squares estimate of the primary noise n_0 . Moreover, when $E[(n_0 - y)^2]$ is minimized, $E[(z - s)^2]$ is also minimized, since, from (1),

$$\mathbf{z} - \mathbf{s} = \mathbf{n}_0 - \mathbf{y} \quad (5)$$

Adapting the filter to minimize the total output power is thus causing the output \mathbf{z} to be a best least squares estimate of the signal \mathbf{s} .

The output \mathbf{z} will contain the signal \mathbf{s} plus noise. From (1), the output noise is given by $(\mathbf{n}_0 - \mathbf{y})$. Since minimizing $E[\mathbf{z}^2]$ minimizes $E[(\mathbf{n}_0 - \mathbf{y})^2]$ minimizing the total output power minimizes the output noise power. Since the signal in the output remains constant, minimizing the total output power maximizes the output signal to noise ratio. From (3) the smallest possible output power is

$$E[\mathbf{z}^2] = E[\mathbf{s}^2]$$

When $E[(\mathbf{n}_0 - \mathbf{y})^2] = 0$

At $\mathbf{y} = \mathbf{n}_0$ and $\mathbf{z} = \mathbf{s}$.

Minimizing the output power causes the output signal to be perfectly noise free.

IV. NORMALIZED LMS (NLMS) ALGORITHM FOR ADAPTIVE FILTER

A general form of the adaptive filter is illustrated in Figure 2, where $d(n)$ is a desired response (or primary input signal), $y(n)$ is the actual output of a programmable digital filter driven by a reference input signal $x(n)$, and the error $e(n)$ is the difference between $d(n)$ and $y(n)$. The function of the adaptive algorithm is to adjust the digital filter coefficients to minimize the mean-square value of $e(n)$.

A technique to adjust the convergence speed is the Normalized LMS (NLMS) algorithm. The NLMS is shown as follows:

$$w(n+1) = w(n) + \mu(n)x(n)e(n)$$

$\mu(n)$ is adaptive step size which is computed as

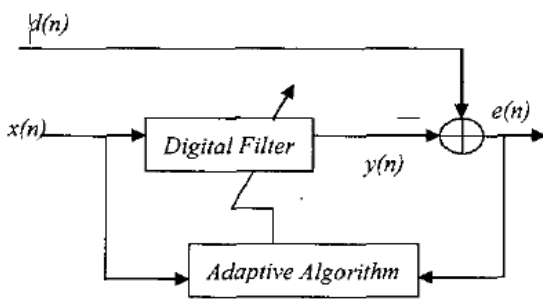


Fig:2 Basic concept of adaptive filter

$$\mu(n) = \frac{\alpha}{L \hat{P}_i(n)}, \quad 0 < \alpha < 2$$

$\hat{P}_i(n)$ is the estimated power of $x(n)$ at time n , L is order of the filter, and α is the normalized step size. An exponential window is used to estimate the power of $x(n)$

$$\hat{P}_i(n) = (1 - \beta) \hat{P}_i(n-1) + \beta x^2(n)$$

where β is a smoothing parameter, which is in terms of its equivalent (exponential) window length

$$M \equiv \frac{1}{\beta}$$

EXPERIMENTAL RESULT

In this section we compare the performance of the LMS and NLMS algorithms as noise canceller. The algorithms are implemented according to the steps. Figure 3 shows that, the input sinusoidal signal and random noise signal. Figure 4 shows that, the noise present in the sinusoidal signal and is eliminated using LMS algorithm of order 5. Figure 5 shows that, the noise present in the sinusoidal signal and is eliminated using NLMS algorithm of order 5.

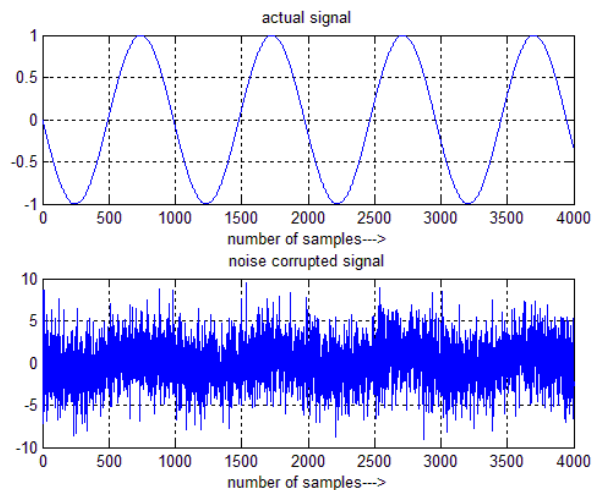


Fig:3 Input and noise signal

[5] G. Goodwin, K. Sin, Adaptive Filtering, Prediction and Control. Englewood Cliffs, Prentice-Hall, 1985.

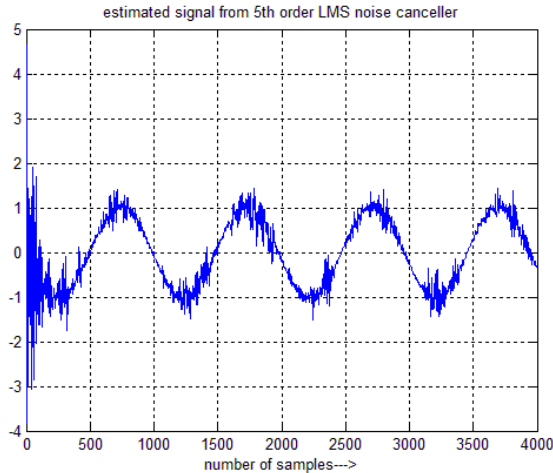


Fig: 4 LMS filter output

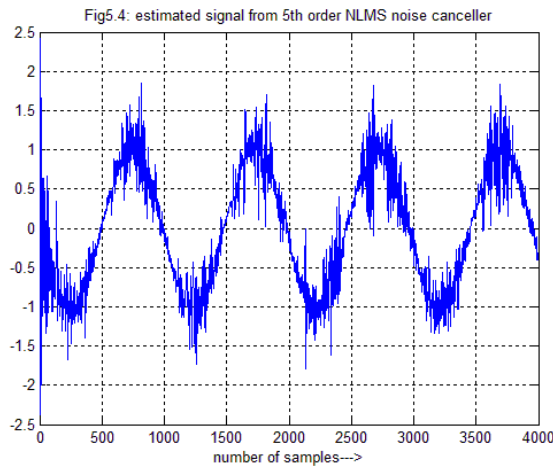


Fig: 5 NLMS filter output

CONCLUSION

This paper has described an application in which the use of an LMS and NLMS adaptive filter is particularly appropriate. The main goal of this paper is to investigate the application of an algorithm based on adaptive filtering in noise cancellation problem. The LMS algorithm has been shown to produce good results in a noise cancellation problem.

REFERENCE

- [1] Adaptive Filter Theory by Simen Haykin: 3rd edition, Pearson Education Asia.LPE.
- [2] Adaptive Signal Processing by John G Proakis, 3rd edition, Perntice Hall of India.
- [3] B. Widrow, "Adaptive noise canceling: principles and applications", Proceedings of the IEEE, vol. 63, pp. 1692-1716, 1975.
- [4] Adaptive Signal Processing by Bernard Widrow and Samuel D.Stearns; Pearson Education Asia, LPE.

Bit Error Rate (BER) Analysis of Rayleigh Fading Channels in Mobile Communication

Vinay Panwar

(M-Tech Scholar, Shobhit University)

Sanjeet Kumar

(Lecturer, World Institute of Technology)

Abstract: In a mobile communication environment the channel is not time invariant and is slowly varying. This characteristic feature of the channel leads to a phenomenon called Fading. Fading channels induce rapid amplitude fluctuations in the received signal. If they are not compensated for then this will lead to serious performance degradation. In this paper simulations have been conducted to study the Bit Error Rate (BER) performance of a Rayleigh fading channel and it is compared to the BER performance of the AWGN channel.

Keywords: Rayleigh fading channel, Bit Error Rate (BER), AWGN channel.

I. INTRODUCTION

In the study of communication systems the classical additive white Gaussian noise (AWGN) channel, with statistically independent Gaussian noise samples corrupting data samples free of intersymbol interference (ISI), is the usual starting point for understanding basic performance relationships. The primary source of performance degradation is thermal noise generated in the receiver. The external interference received by the antenna is significant than thermal noise. This external interference can sometimes be characterized as having a broadband spectrum and is quantified by a parameter called antenna temperature [1][2]. The thermal noise usually has a flat power spectral density over the signal band and a zero-mean Gaussian voltage probability density function (PDF). When modelling practical systems, the next step is the introduction of band limiting filters.

If a radio channel's propagating characteristics are not specified, one usually infers that the signal attenuation versus distance behaves as if propagation takes place over ideal free space. The model of free space treats the region between the transmit and receive antennas as being free of all objects that might absorb or reflect radio frequency (RF) energy. It also assumes that, within this region, the atmosphere behaves as a perfectly uniform and non absorbing medium. In this idealized free-space model, the attenuation of RF energy between the transmitter and receiver behaves according to an inverse-square law.

For most practical channels, where signal propagation takes place in the atmosphere and near the ground, the free space propagation model is inadequate to describe the channel and predict system performance. In a wireless mobile communication system, a signal can travel from transmitter to receiver over multiple reflective paths; this phenomenon is referred to as multipath propagation. The effect can cause fluctuations in the received signal's amplitude, phase, and angle of arrival, giving rise to the terminology multipath fading. Another name, scintillation is used to describe the multipath fading caused by physical changes in the propagating medium, such as variations in the density of ions in the ionosphere layers that reflect high-frequency (HF) radio signals. Names, fading and scintillation refer to a signal's random fluctuations or fading due to multipath propagation. The main difference is that scintillation involves mechanisms (e.g., ions) that are much smaller than a wavelength. The end-to-end modelling and design of systems that mitigate the effects of fading are usually more challenging than those whose sole source of performance degradation is AWGN[4][5].

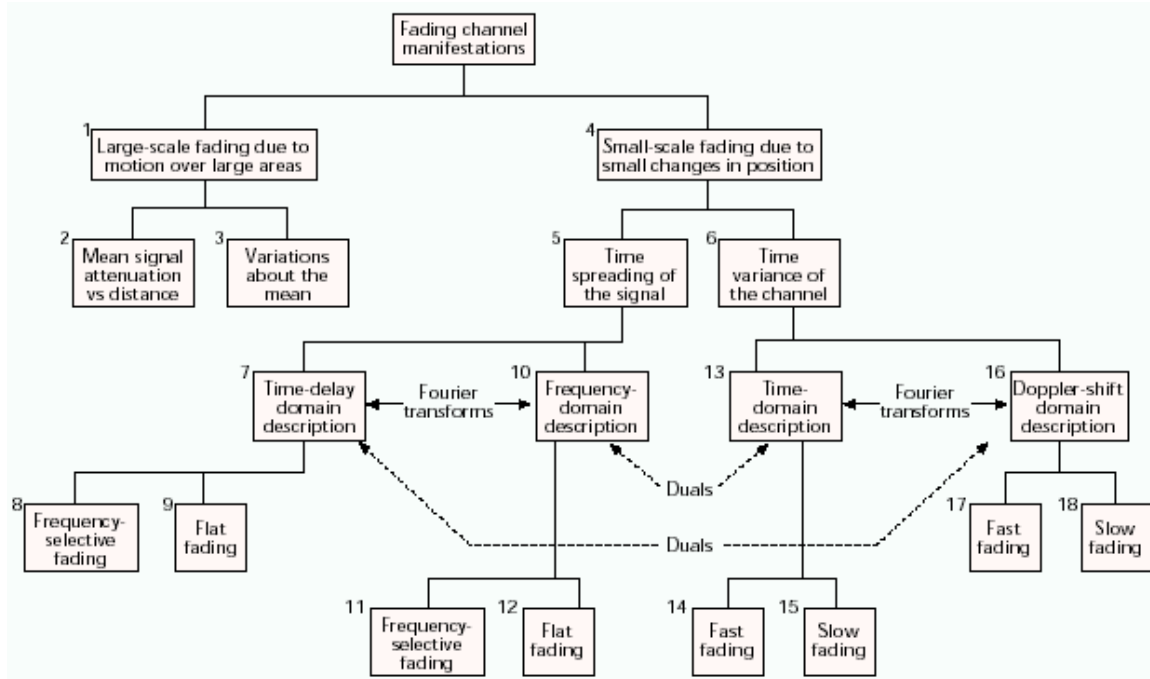


Fig: 1 Multipath fading channel

II. LARGE-SCALE FADING AND SMALL-SCALE FADING

Fig. 1 represents an overview of fading channel. It starts with two types of fading effects that characterize mobile communications: large-scale and small-scale fading. Large-scale fading represents the average signal power attenuation or path loss due to motion over large areas. In Fig. 1, the large-scale fading manifestation is shown in blocks 1, 2, and 3. This phenomenon is affected by prominent terrain contours (hills, forests, billboards, clumps of buildings, etc.) between the transmitter and receiver. The receiver is often represented as being “shadowed” by such prominences. The statistics of large-scale fading provide a way of computing an estimate of path loss as a function of distance. This is described in terms of a mean-path loss and a log-normally distributed variation about the mean. Small-scale fading refers to the dramatic changes in signal amplitude and phase that can be experienced as a result of small changes in the spatial separation between a receiver and transmitter. As indicated in Fig. 1, blocks 4, 5, and 6, small-scale fading manifests itself in two mechanisms, namely, time spreading of the signal (or signal dispersion) and time-variant behaviour of the channel. For mobile radio applications, the channel is time-variant because motion between the transmitter and receiver results in propagation path changes. The rate of change of these propagation conditions accounts for the fading rapidity (rate of change of the fading impairments). Small-scale fading is also called Rayleigh fading because if the multiple reflective paths are large in number and there is no line-of-sight signal component, the envelope of the received signal is statistically described by a Rayleigh PDF [3]. When there is a dominant non fading signal component present, such as a line-of-sight propagation path, the small scale fading envelope is described by a Rician PDF [3]. A mobile radio roaming over a large area

must process signals that experience both types of fading: small-scale fading superimposed on large-scale fading.

III. RAYLEIGH DISTRIBUTION

This is used to describe the statistical time varying nature of the envelope of an individual multipath component. The Rayleigh distribution is given by

$$P(r) = \frac{r}{\sigma^2} \exp\left(\frac{-r^2}{\sigma^2}\right) \quad 0 \leq r < \infty$$

Where, σ = rms value of the received signal
 $r^2/2$ = instantaneous power
 σ^2 = local average power of the received signal before detection

IV. BIT ERROR RATE (BER)

Bit error rate is a key parameter that is used in assessing systems that transmit digital data from one location to another. BER is applicable to radio data links, Ethernet, as well as fibre optic data systems. When data is transmitted over a data link, there is a possibility of errors being introduced into the system. If this is so, the integrity of the system may be compromised. As a result, it is necessary to assess the performance of the system, and BER provides an ideal way in which this can be achieved. BER assesses the full end to end performance of a system including the transmitter, receiver and the medium between the two.

BER is defined as the rate at which errors occur in a transmission system. In simple form,

$$BER = \frac{\text{number of bits in error}}{\text{total number of bits sent}}$$

BER expression is given by Rappaport (2002) as

$$BER = \int_0^{\infty} P_b(E/r)P(r)dr$$

Where $P_b(E/r)$ = the conditional error probability
 $P(r)$ = the pdf of the SNR

V. RESULTS

The simulation of the model under study was carried out using MATLAB application package. The simulation was carried out with BPSK modulation. The following parameters and system configurations were used:

- Modulation: BPSK
- Carrier frequency: 900 MHz
- Bandwidth of signal: 200 ns
- Noise: AWGN
- Mobile speed: 90 km/h
- Fading type: Rayleigh fading

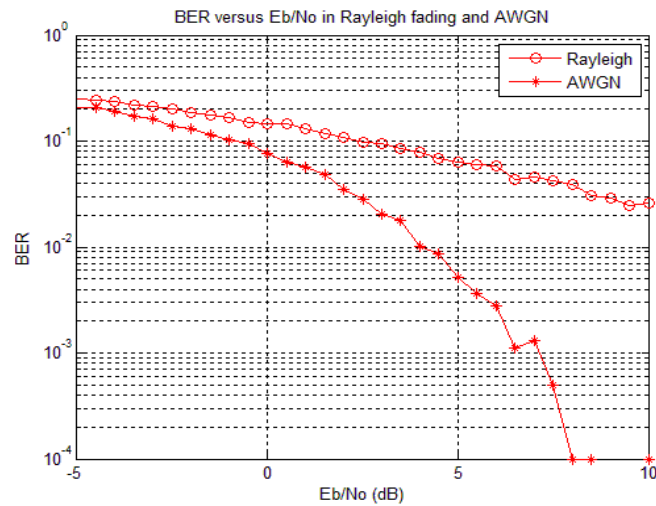


Fig:2 BER in Rayleigh fading and AWGN

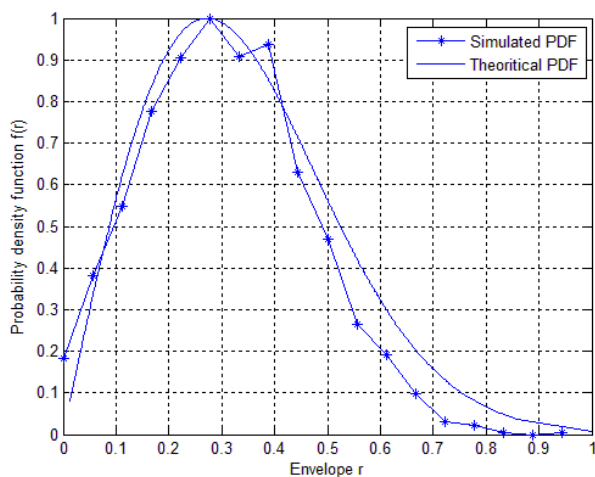


Fig: 3 Probability density function of Rayleigh fading channel

The BER performances as a function of SNR for two i.i.d paths in mobile multipath fading channel with BPSK.

Figure 2 shows the BER performance when BPSK signal was transmitted over the fast Rayleigh fading channel at a mobile speed of 90 km/h. it can be observed that at SNR of 4 dB. Figure 3 shows the probability density function of Rayleigh fading channel. Fig 4 shows the envelope of RF signal.

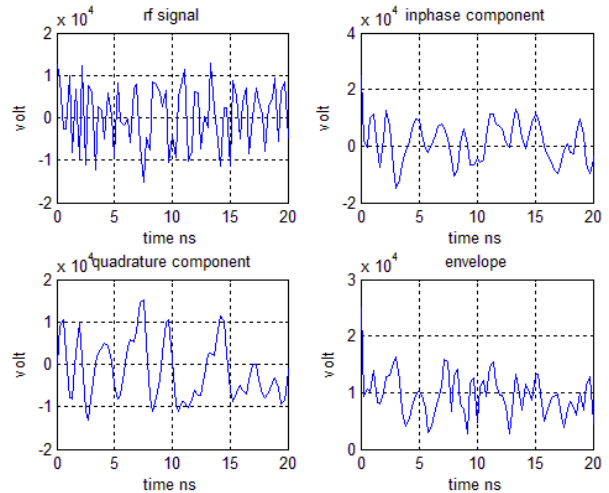


Fig:4 Envelope of RF signal

VI. Conclusion

In this paper, bit error rate performances for Mobile communication with BPSK transmission schemes have been evaluated with random data. Two types of fading, large-scale and small scale were described. Generation of Rayleigh faded envelope for varying number of paths are shown. BER Performance of a BPSK signal in presence of AWGN and Rayleigh Channel.

VII. REFERENCES

- [1] B. Sklar, Digital Communications: Fundamentals and Applications, Ch. 4, Englewood Cliffs, NJ: Prentice Hall, 1988.
- [2] H. L. Van Trees, Detection Estimation, and Modulation Theory, Part I, Ch. 4, New York: Wiley, 1968.
- [3] T. S. Rappaport, Wireless Communications, Chs. 3 and 4, Upper Saddle River, NJ: Prentice Hall, 1996.
- [4] J. G. Proakis, Digital Communications, Chapter 7, New York: McGraw-Hill, 1983.
- [5] E. Biglieri, J. Proakis and S. Shamai, "Fading channels: Information-theoretic and communications aspects," IEEE Trans. Inform. Theory, 50-th anniversary issue, Oct. 1998.
- [6] Yee, Z. and E.H. Satorius. 2003. "Channel Modelling and Simulation for Mobile User Objective System (MUOS)-part1: Flat Scintillation and Fading" in proceedings of IEEE ECC. 5(3503-3510).
- [7] Leon, W.C. 2002. Digital and Analog Communication System, 6th Ed. Pearson Education, INC, Singapore.

Application of Cyclic Shells in Architecture, Machine Design, and Bionics

Christian A. Bock Hyeng

Ph. D. (North Carolina Agricultural and Technical State University, 1601 E. Market St., Greensboro, NC 27411, USA)

Emmanuel B. Yamb,

Ph.D. (University of Bamenda, Republic of Cameroon, P.O. Box 8842 Douala)

ABSTRACT

The principal achievements of science and engineering in the sphere of static and vibrational analysis of thin-walled objects, structures, and buildings in the shape of cyclic surfaces with circular generators are used for practical needs of people. These shells are useful as fragments of pipelines, spiral chambers of refrigerating units, as well as in spiral chambers of turbines in hydroelectric power stations, in high pressure units, in public and commercial buildings such as coverings of stadiums, and more. This review paper contains 18 references, and these are practically all original sources dealing with application of thin-walled cyclic shells. The additional photos can be found on the Internet.

Keywords: architecture, bionics, canal surfaces of Joachimsthal, cyclic surfaces with circular generators, Dupin's cyclides, epitrochoidal shell, machine design, spiral chamber, tubular shell

1. Introduction

To date great progress has been achieved in the strength analysis of thin elastic shells [1]. Thin-walled shell structures combining lightness with considerable strength find widespread use in modern engineering and building. Many have noted the rapid progress of the practice and theory of the application of thin shells and thin-walled shell structures in the last 10 years. But shells used in constructions belong to a limited class of surfaces. An accurate tendency in world practice is the application of spatial structures of arbitrary form giving expressive architectural images and solving functional problems. Today we have a new generation of young architects and engineers who have shown interest in designing wide-span spatial coverings. This process amplifies occurrence of new materials, such as fibrous reinforced polymeric composites, which can be used in covers due to its ability to curve. One family of forming curves in cyclic surfaces is represented by circles of constant or variable radius that considerably reduces the cost, and simplifies the process of manufacturing thin shells in the form of these surfaces without a corresponding decrease in the operational possibilities.

2. A circular helical surface with the forming circle lying in the adjoining plane of a helical line of the centers of circles

The defining vector of a forming circle of this surface is directed along a binomial of a helical line of the centers of generatrix circles. This surface is used in the theory of screw surfaces in designing cutting tools [2].

3. Tubular surfaces

Tubular surfaces are used widely in building and machine design. One may see tubular helical surfaces in contours of cylindrical helical springs which can be classified due to given loading (Fig. 1) or design. These are conic helical springs of compression (Fig. 1a), cylindrical helical springs of compression (Fig. 1b), extension (Fig. 1c), torsion (Fig. 1d), and flat spiral springs take into account the perceived loading of springs. Due to the cross-section, cylindrical helical springs are solid [3] and hollow [4].

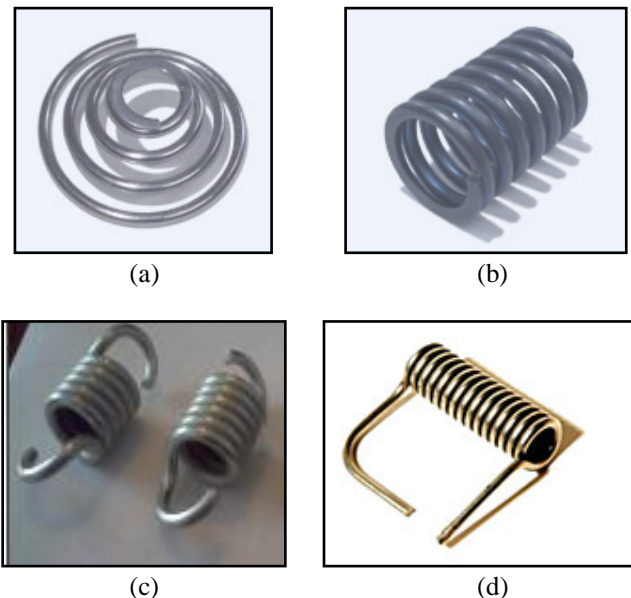


Figure 1. Classification of springs depending on a kind of perceived loading

The tubular spiral surface with a flat line center is used as a spiral heating element in electrical tiles (Fig. 2), for installation in a fan heater (Fig. 3), in drying apparatus in

the food industry, or for heating of preparations in the industry.



Figure 2. A spiral heating element in electrotile Saturn ST-EC 1165.1



Figure 3. A tubular heating element [www.scatechnology.ru]

The tubular helical surface is undertaken as a basis of designing of coils [5] of diverse function (Figs. 4-6). In particular, the cartridge of a heating element (Fig. 5) is used in the combined catching heating appliance of water for indirect heating. The heating appliance of series MORA E NTR is intended for preparation of hot water for technical and economic purposes using warmth of water heated with the help of an outside source of energy, for example, with the help of gas reactor. In addition they have an electric heating element. It allows the possibility to use a water heater as an electric boiler, for example, in the summer, when there is no necessity for use of a heating element. It is especially effective in a system with a diesel copper.



Figure 4. A heating element of the hair dryer for Lukey 852D+fan, 701,702 [www.gsm-komplekt.com.ua]

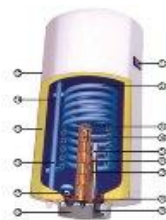


Figure 5. A cartridge of a heating element heating element [www.moramoravia.ru]



Figure 6. A coil for cooling of a liquid [clear moon.livejournal.com]

For modeling spiral tan such as Microcoil (MC) (Fig. 7), it is possible to use a tubular helical surface with a centerline of a variable step (Fig. 8). Tubular surfaces with a flat or spatial centerline are the basis for any design of pipelines [6] of constant radii. The connections of pipelines at right angles are usually taken in the form of a circular tube segment (Fig. 9a, 9b), or torus is approximated by fragments of several cylindrical surfaces (Fig. 9c, 9d). In their book, St. Polanski and L. Pianowski [7] have offered various approximations of tubular surfaces by fragments of cylindrical surfaces.



Figure 7. Spiral tan Microcoil (MC) [www.mirnagreva.ru]

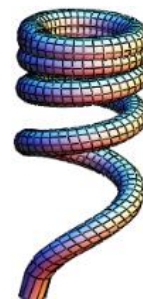


Figure 8. A tubular helical surface with a centerline of variable step

The most widespread constructive elements in power installations are pipelines with a complex outline of an axial centerline. They are applied in units of a high pressure, circular pumps, and turbine units [8].

Tubular circular helicoids and spiral surfaces are widely used in designing descents in water attractions (Fig. 10). A tubular surface on the sphere or tubular loxodrome (Fig. 11) may be recommended as a form of a trigger trench

in water attractions. Sometimes the tubular surface with any centerline is used as an exotic interior of water pool (Fig. 12) or even the whole building (Fig. 13).



(a) A tube in plastic [www.pcvexpro.ru]



(b) Gas tube [www.caspenergy.com]



(c) Connecting details of pipelines



(d) Details for connection of pipelines of identical and different diameter

Figure 9. Pipelines of diverse function



Figure 10. Water attractions

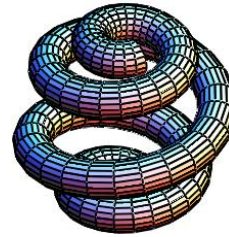


Figure 11. A tubular loxodrome



Figure 12. The Complex "Yalta," Russia [«Всеслав-Донбасс»]



Figure 13. Imaginations of the architect

4. Dupin's cyclides

Dupin's cyclides are two-canal surfaces [11]. Both families of flat lines of the principle curvatures lying in two pencils of planes are the circles. It is necessary to notice that geometrical researches on Dupin's cyclides enjoy wide popularity of geometers. However, engineers-designers and architects, until today, have not paid enough attention to these surfaces. Only two offers on the application of Dupin's cyclides in real constructions are published in the technical literature [12, 13]. For example, in a work [13], the problem of covering a building with a double shell was stated, but the lines of contours should be by lines of curvatures, and both families of lines of curvatures of the

shell surface should be by families of circles. All requirements of the problem can be executed if a compartment of Dupin's cyclide is used as a geometrical image of the shell (Fig. 14).

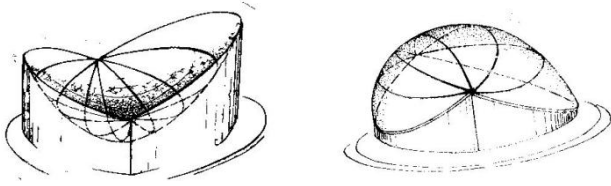


Figure 14. Offers on use of Duplin's cyclides

5. Canal surfaces of Joachimsthal

Joachimsthal's surface is a surface with a family of plane lines of curvature lying in the planes of the pencil [14]. Canal surface is called a cyclic surface with a family of circles $R(u)$ being lines of curvature of a surface. If circles of canal surfaces lay in the planes of pencil, the surface is canal surface of Joachimsthal. A centerline of canal surfaces of Joachimsthal is a flat curve $r(u)$, therefore canal surfaces of Joachimsthal are included into a group of cyclic surfaces with circles in planes of a pencil with a flat centerline. Post-graduate student of a chair of strength of materials of the Peoples Friendship University of Russia, N.J. Abbushi [15] has constructed gyps models of canal surfaces of Joachimsthal explaining three methods of their formation (Fig. 15).

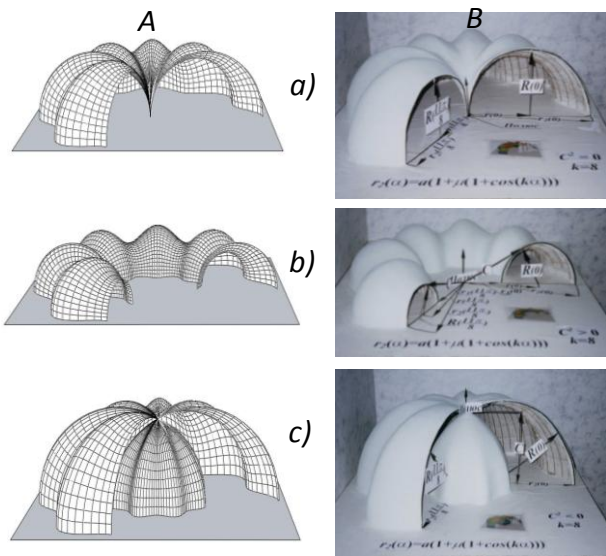


Figure 15. Mathematical and gyps models of canal surfaces of Joachimsthal [15]

6. Epitrochoidal surface

The M point located on a plane of a circle with the a radius, which rolls without sliding on other motionless circles with b radius, forms an epitrochoidal line. The planes of these two circles constitute a constant corner γ . The distance from

a point of M to the center of a mobile circle is equal to μa ($\mu = 1$, or $\mu < 1$, or $\mu > 1$). Changing parameter γ from 0 to 2π , it is possible to receive a family of epitrochoidal curves which will form epitrochoidal surfaces (Fig. 16) [16].

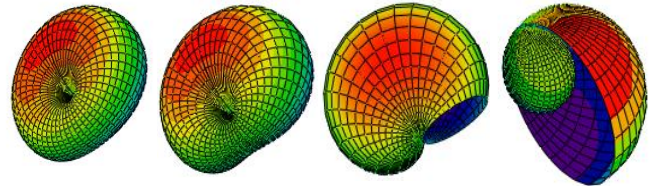


Figure 16

Now epitrochoidal surfaces draw attention to themselves only from the point of view of geometrical researches. Recommendations in the scientific and technical literature on application of these surfaces in real designs were not discovered.

7. Cyclic surfaces with circles in planes of pencil

The cyclic surface with circles in planes of the pencil is formed by circles of the constant or variable radius in which the center moves along the given centerlines of a surface, and the generatrix circles lie in planes of the pencil [11].

The cyclic surface with generatrix circles of constant or variable radius in planes of pencil and with a flat centerline in the form of a logarithmic spiral well approximates the form of spirally-curtailed ammonite bowls (Fig. 17) and bowls of the mollusks existing now [17].



Figure 17. Ammonite bowls

The spiral chamber of the waterwheel represents the cyclic surface, the cross-sections of which are circles of variable radii. This chamber winds around a cylindrical part of a rotor of the waterwheel and serves as the water admission. The diameter of the spiral chamber in each section is defined from the conditions of the best entrance of the expense of water. The function of change of the radius of the chamber has a difficult structure; however, with sufficient accuracy it may be defined by the following formula:

$$\bar{R} = \bar{R}_0 (1 + k\beta),$$

where \bar{R}_0 is the radius of the entrance aperture of the chamber, and k is the factor dependent on the expense of water. Some variants of spiral chambers of waterwheels are

presented in Figs. 18 and 19. The spiral chamber of the waterwheel provides uniform water inflow on all perimeters of the directing apparatus, i.e. an axisymmetric operating mode of all directing blades. The section of the spiral chamber of the waterwheel is in regular intervals narrowed on a stream course. On HYDROELECTRIC POWER STATIONS with pressures exceeding 50–60 m, steel spiral chambers of round sections (Fig. 18), winding the stator almost completely, are applied.

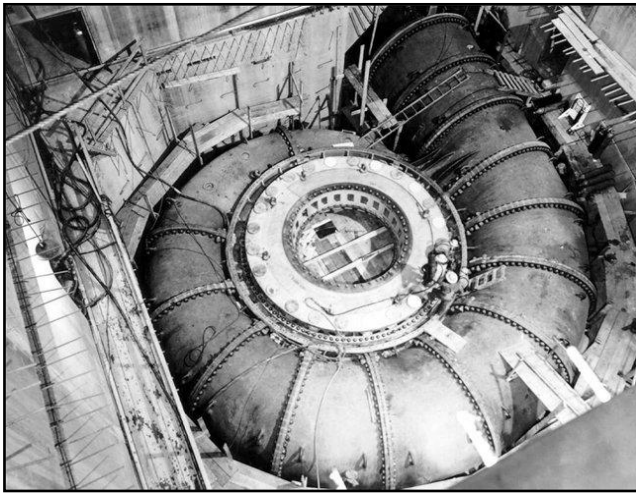


Figure 18. Process of assemblage of the spiral chamber
 [www.tvscience.ru]



Figure 19. Process of assemblage of the spiral chamber

On HYDROELECTRIC POWER STATIONS with the lesser pressure, the spiral chambers are made of reinforced concrete. Steel chambers of high-powered HYDROELECTRIC POWER STATIONS are difficult to make because of great thickness of walls. Therefore reinforced concrete chambers find more and more wide application.

Let's consider one more surface from a subclass «Cyclic surfaces with circles in planes of pencil», namely a

circular helical surface with generatrix circles in planes of pencil. This surface is used mainly in a theory of helical surfaces for design of cutting tools [2], but it can find application in architecture as well.

Due to the names of following three cyclic surfaces shown in Figs. 20–22, one may understand that they describe the form of sea or river cockle-shells.

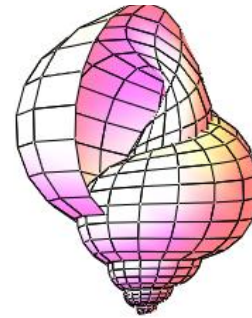


Figure 20. A spiral surface “cockle-shell without the peak”

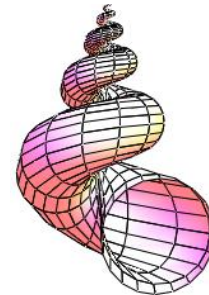


Figure 21. A spiral-type surface “cockle-shell with the peak”

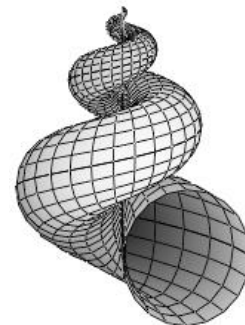


Figure 22. Seashell

8. Normal cyclic surface

A normal cyclic surface is formed by the movement of a circle of variable or constant radius along an arbitrary director curve, but the circle generatrix must lie in the normal plane of the given director curve [11].

Two types of normal cyclic surfaces with an elliptic centerline and with a generatrix circle of variable radius (Fig. 23) and the connecting channel for two cylindrical

surfaces with parallel axes (Fig. 9c; Fig. 24 [18]) are used widely as connecting parts of pipelines.

The widely-known one-sided surface «Klein's Bottle» can also be constructed in the form of a normal cyclic surface with circle generatrices of variable radius (Figure 25). Cyclic normal surfaces one may see in the forms of wind instruments (Fig. 26).

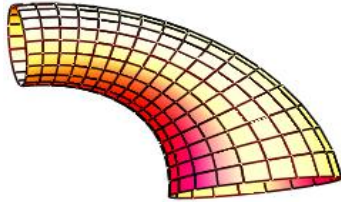


Figure 23. Normal cyclic surface with an elliptic line of the centers and with a generating circle of variable radius (type 1)

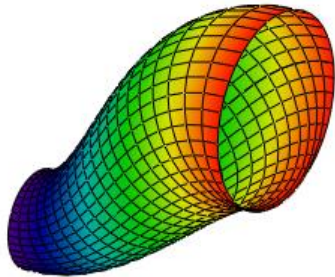


Figure 24. The connecting channel for two cylindrical surfaces with parallel axes

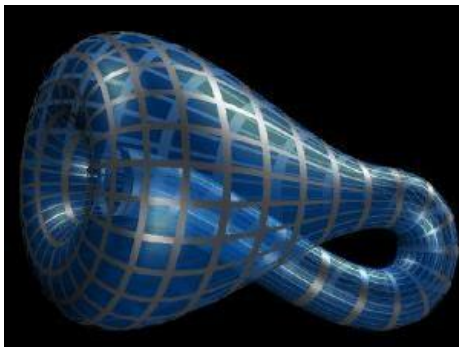


Figure 25. Klein bottle



Figure 26. Wind instrument [ru.wikipedia.org/wiki/wind]

8. Circular translational surfaces

Directing and generating curves of circular translational surface lie in mutually perpendicular planes. Surfaces of direct translation can be defined by the equation:

$$z = z(x,y) = z_1(x) + z_2(y)$$

Circular translational surfaces were taken as a basis of many erected wide-span thin-walled shells; two of them are presented in Fig. 27. The covers represented in Fig. 27 are also called a «Bohemian dome».



(a) Shopping center in Chelyabinsk (102 x 102 m), Russia



(b) The market in Chermushki, Moscow, Russia

Figure 27. Circular transition shells

9. A surface with a plane of parallelism

The shed cover erected in Bulgaria (Fig. 28) consisting of shells of conoidal type with a thickness of 3 cm, a span of 18 m, and the distance between trusses of 7 m may be considered to be a subclass of cyclic surfaces with a plane of parallelism. The form of the cover differs from the form of a conoid because their generatrices are not straight lines but flat circular curves. This form provides more favorable static conditions, and allows a smaller thickness for the cover. The cover is gathered from precast reinforced concrete fragments made in advance and its complex shape does not result in a price increase. Each shell was gathered from four elements with weight of 4.5 tons considering possibilities of elevating means.

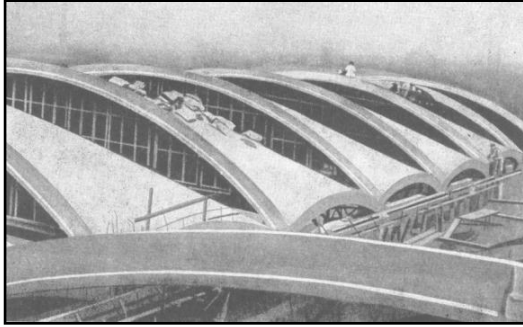


Figure 28. The shed cover

10. Surface of helical pole

Sometimes the surface of a column was taken in the form of a pole with a helical line of centers of circular generatrices of constant radius. In Fig. 29, the surface of the helical column has two generating circles, while in Fig. 30, the surface of the helical column has four generating circles.

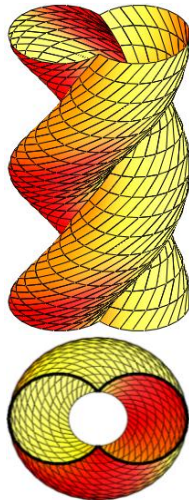


Figure 29. The surface of the helical pole with two generating circles



Figure 30. Olivenza, Spain, Church, the 16th century

11. Conclusion

The materials contained in monographs, dissertational works, scientific papers, in proceedings of conferences, and listed in the review include almost all spheres of the application of cyclic shells known in the world today.

As to the engineering possibilities of the application of cyclic shells, they have found wide application in curvilinear pipes of constant radius, basically in the form of torus, in spiral chambers of waterwheels, and in the circular translation shells used as spatial coverings of buildings. The helical cyclic surfaces help to describe the forms of some cockle-shells and to work out mathematic models of their shapes.

Cyclic surfaces with a straight center line, or shells of revolution, are widely used in architecture. Sometimes, architects especially underline the presence of generatrix circles in building design. As to cyclic structures of the general non-degenerate type, only single examples of their application are known. The author hopes that the literature resulting from the review and the analysis of tendencies of development of the application of cyclic shells will help architects, civil engineers, and mechanical engineers expand and diversify projected spatial structures using cyclic surfaces, and will help post-graduate students choose themes of scientific research.

References

- [1] *Krivoshapko S.N., Christian A. Bock Hyeng* (2012), Static and dynamic analysis of thin-walled cyclic shells,
- [2] *Lyukshin V.S.* (1968), Theory of Spiral Surfaces in Designing of Cutting Tool, Moscow, Mashinostroenie, 372 p.

- [3] Cardou A. and Jolicoeur C. (1997), Mechanical models of helical strands, *AMR*, 50(1), Jan. 1997, 1–14.
- [4] Pystogov A.S. (1978), On analysis of screw springs with tubular cross-section, *Ural. PI, Sverdlovsk, 12 p., Dep. V NIIinformtyazhmash*, 26 Apr. 1978, № 305.
- [5] Martin Ph., Dumas J.C., Girard J.P. (1986), Thermomechanical stresses in the dryout zone of slightly inclined helically coiled heat exchange tubes, *Boiler Dyn. and Contr. Nucl. Power Stat., Proc. 3rd Int. Conf., Harrogate, 21-25 Oct., 1985, London, 1986, 29–36.*
- [6] Matusok G.A., Miroshnichenko A.V., Surkova G.I. (1988), An algorithm of automatic design of tubular surfaces, *Mat. modeli i sistemy obrabotki inf. i primeneniya resheniy*, Harkov, 123–127.
- [7] Stanislaw Polanski, Leslaw Pianowski (2001), Rozwiniecia powierzchni w technice. Konstrukcje wspomaganie komputerowo, Warszawa: Wydawnictwo Naukowe PWN, 412 c.
- [8] Gulyaev V.I., Bazhenov V.A., Gozulyak E.A., Gaydaychuk V.V. (1990), An Analysis of Shells of Complex Form, Kiev, Budivelnik, 192 c.
- [9] Matveev A.S. (2004), The work out of a method of design of technological processes and machines for stamping of diverse details from tubular half-finished products, *Diss. of DSc, Rybinsk, 337 p.*
- [10] Kasarin S.K. (1982), A form for the making of tubular details, *DVD Patents of Russia, 23.07.1982, № 3, № 17844.*
- [11] Krivoshapko S.N., Ivanov V.N. (2006), Classification of cyclic surfaces, *Structural Mechanics of Engineering Constructions and Buildings*, №2, 25–34.
- [12] Yakubovskiy A.M. (1971), A research of analytical method of defining of Dupin’s cyclides with the help of congruence of circles, *Prikl. Geom.*, Moscow, UDN, № 4, 26–40.
- [13] Rekach V.G., Ryzhov N.N. (1970), Some opportunities of widening of row of problems dealing with design and strength analysis of shells, *Proc. UDN “Building”: Structural Mechanics, Moscow, UDN, Vol. XLVIII, Iss.6, 3–8.*
- [14] Frolov O.V. Конструювання каналових поверхонь Іоакимсталя виділенням з конгруенції траєкторій, ортогональних сім’ї сфер із центрами на прямій// Геометричне та комп’ютерне моделювання: Зб. наук. праць. – Вип. 9. – Харків: ХДУХТ (Ukraine), 2005. – С. 38–44.
- [15] Ivanov V.N., Nasr Yunes A. Abbushi (1997), Geometrical research of canal surfaces of Joachimsthal, *Problemi teorii i praktiki v ing. issledovaniyah: Proc. XXVIII scient. conf. of eng. faculty, Moscow: RUDN, 115–118.*
- [16] Krivoshapko S.N., Gil-oulbe Mathieu (2001), Geometrical and strength analysis of thin pseudo-spherical, epitrochoidal, catenoidal shells, and shells in the form of Dupin’s cyclides, *Shells in Architecture and Strength Analysis of Thin-Walled Civil-Engineering and Machine-Building Constructions of Complex Forms: Proc. Int. Conf., June 4-8, 2001, Moscow, M.: Izd-vo RUDN, 183–192.*
- [17] Junior Science Book of Seashells by Sam and Beryl Epstein (1963), Garrard Publishing Co., 64 p.
- [18] Krivoshapko S.N. (2005), Model surfaces of connecting fragments of two pipelines, *Montazh. i spez. raboti v stroitelstve*, № 10, 25–29.

AODV-MS: Ad-hoc on Demand Distance Vector Routing Protocol with Multipath and Selective Flooding

Manoj Kumar Singh¹, Chiranjeev Kumar² & Swati Bansal³

¹(Department of CS&IT, Moradabad Institute of Technology, Moradabad, India

²(Department of Computer Science & Engineering, Indian School Of Mines, India

³(Department of Computer Science, M.Tech Student, Banasthali University, India

ABSTRACT

Mobile ad hoc networks (MANETs) are infrastructure less networks consist of wireless mobile nodes which dynamically exchange data among themselves. Position of nodes in MANET changes frequently. Design of efficient routing protocols in such dynamic networks is a challenging issue. Many routing protocols have been proposed to improve the performance of ad-hoc networks. The on-demand protocols depend on query floods to discover routes whenever a new route is needed. Such floods results in wastage of network bandwidth. In this paper we proposed a protocol Adhoc on Demand Distance Vector Routing Protocol with Multipath and Selective Flooding (AODV-MS). In AODV-MS source node uses selective flooding during route discovery phase and stores node disjoint multiple paths to destination. Selective flooding reduces the number of packets in network and improves bandwidth utilization. Multiple paths between source and destination results in low delay, less packet drops and improves throughput.

Keywords: AODV, MANET, Multipath Routing, flooding, AODV-MS

1. INTRODUCTION

An ad hoc network is a collection of devices that change their position dynamically. The nodes in ad hoc network do not depend on any fixed infrastructure (e.g., base stations or access points) for their communication. Communication is done through wireless links among mobile hosts through their antenna. The nodes close to each other communicate directly while nodes that are not in the range of each other communicate via the intermediate nodes. The nodes that communicate directly are said to be neighbouring nodes. The intermediate nodes act as a router. Furthermore, due to the movement of nodes, the network topology changes rapidly [10]. Therefore, an efficient routing protocol is needed for better communication between the nodes. Routing

protocols in ad hoc networks are divided in to two categories: proactive (Table driven) routing protocols and reactive (On Demand) routing protocols. In proactive routing protocols [3], every node store routing information about every other node in the network. Proactive protocols lead to relatively high overhead on the network due to exchange of information periodically. On the other hand, reactive routing protocols [4][2], creates routes only when one node wants to communicate with another node which reduces routing overhead and increases bandwidth utilization. Once a route is created, it is maintained by using some route maintenance mechanism as long as the source node wants to communicate with the destination node. In Ad hoc networks link break occurs frequently due to nodes mobility, greater error rates, interference of signals, fading environment etc. But an actual route break occurs due to mobility of nodes. In AODV node that finds link break send a RERR message to the source. Source none after receiving the RERR starts a new fresh route discovery cycle if it wants further communication with the destination node.

In multipath routing [1][6][7][8][9], multiple routes from source to destination are stored during a single route discovery cycle. In case of the occurrence of link break, any of the alternative routes is selected to forward the packets. The performance of multipath routing shows better utilization of network resources but number of packet drops and delay is increased because alternative cached routes may become stale. These limitations of AODV motivated us to propose an efficient routing protocol, Adhoc on Demand Distance Vector Routing Protocol with Multipath and Selective Flooding(AODV-MS), which improves the performance of an existing on-demand routing protocols, specifically AODV.

The paper is organized as follows. The propose scheme is discussed in Section 2. The comparisons of proposed and existing schemes are presented in section 3. Finally, the conclusions of the paper are presented in Section 4.

Destination	Sequence no.	Hop count	Next Hop	Expiration Time out
-------------	--------------	-----------	----------	---------------------

Figure 1a: Structure of routing table entries for an AODV

Destination	Sequence no.	Hop count	Next Hop	Priority	Expiration Time out
-------------	--------------	-----------	----------	----------	---------------------

Figure 1b: Structure of routing table entries for an AODV-MS

2. PROPOSED SCHEME

Our proposed protocol is based on selective flooding [5] and multipath [1][6][7][8][9] routing concept.

Flooding is the root cause of routing overhead in AODV which is a consequence of broadcasting of RREQ packet during route discovery cycle. Hence, reduction of indiscriminate flooding is imperative. In a mobile adhoc network, multiple paths exist between any two nodes and particular path between a source and destination had a very little life and sub optimal paths may not really degrade the routing performance. Based on these observations, selective flooding [] is proposed in place of broadcasting. Hence we also incorporated the concept of selective flooding with slight modification in our protocol. In selective flooding first RREQ message is send to one-third neighbours randomly. If it gets reply before the request time out period it is done, otherwise, again route request message to another one-third of the neighbours and keep on doing the same operation until all the neighbours are selected or it gets an out reply. This reduces the routing packet overhead and increased throughput but increases the delay also. In our protocol AODV-MS, source node send RREQ message to one-half of neighbours instead of one-third, this results in reduction of delay that was increased in selective flooding protocol.

2.1. ROUTE DISCOVERY IN AODV-MS

In our proposed scheme, AODV-MS, source node prepares a RREQ packet and send it to one-half of its neighbors selected randomly. Source node stores multiple node-disjoint paths. If a RREQ packet is received by an intermediate node i, and it has route to destination, it sends a route reply packet, RREP, to source node S. Otherwise it broadcast the RREQ packet to its neighbors. Intermediate node i, discard duplicate RREQ packets it receives from other nodes. If RREQ is received by destination node, it sends a RREP packet to the node whom it received RREQ packet. Destination node do not discard duplicate RREQ packet, instead it sends RREP packet to all nodes from which it receives RREQ packet. When RREP packet is received by intermediate node i, it makes an entry in its routing table for that destination and forward RREP packet towards source. When a source node S received a RREP packet, it makes an entry in its routing table for that destination. Source node maintains more than one node-disjoint route for the same destination in its routing table.

The proposed scheme has introduced a new attribute priority in routing table whose value indicates the priority of route to destination D, initially when S starts route discovery for D it set the value of Priority to 0.

2.2. ROUTE DISCOVERY ALGORITHM IN AODV-MS

Suppose node S wants to communicate with Destination D.

/* Priority is a field in routing table whose value indicates number of routes to destination D exists in routing table, initially when S starts route discovery for D it set the value of Priority to 0.

n is a temporary user defined variable. It indicates maximum number of routes source S can store in its routing table for any destination D.

*/

S prepares a RREQ packet and sends it to one-half of its neighbors.

1. if (RREQ is received by an intermediate node i and it is not a duplicate packet)
2. { if node i has valid route to destination
3. { node i prepares a RREP packet and unicast towards source S
- }
- else
4. node i broadcast RREQ packet to its neighbors
- }
- }
5. if (node i receives a duplicate RREQ packet)
6. { node i discard RREQ packet
- }
7. if RREQ is received by Destination node D
8. { node D prepares a RREP packet and unicast towards source S
- }
9. if (RREP is received by an intermediate node i and it is not the duplicate packet)
10. { node i makes an entry in its routing table for that destination and forward the
11. RREP packet towards source
- } // intermediate node discard all duplicate RREP packets
12. if RREP is received by source node S
- {
- If (Priority==0)
- {
- S makes an entry in its routing table for that destination and starts sending data on that route.
- Priority++
- }
- else
13. {
- if (Priority ==1)
- {
- S makes another entry in its routing table for that destination.
- Priority++
- }
- else {
- S discards the RREP packet
- }
- }
- }
- }
14. END

2.3. ROUTE MAINTENANCE ALGORITHM IN AODV-MS

Data packets are send using the primary route unless the link breaks occurs. The operation after the intermediate node (say N2) has identified link break is presented below:

1. Node N2 prepares and sends a RERR packet to source S.
2. Source node S on receiving the RERR packet delete the entry for that destination on which it was sending data

- and search its routing table for another route to destination D.
3. If there exists another valid route to D, S starts sending data on that route having lowest value of Priority.
 4. If S did not find route to D in its routing table it starts new route discovery for D.
 5. END

Illustration of route discovery with example

Suppose node S wants to communicate with node D. Source node S sends RREQ packet to only half of its neighbors (say N2, N4, N5), Fig 2. Intermediate nodes on receiving RREQ packet broadcast it to their neighbors. RREQ packet reaches destination from node M and node T. Destination node D unicast RREP packet to node T and M. Intermediate nodes on receiving RREP packet make entry in their routing table, Table 1, for D and forward RREP packet to source node S. Intermediate nodes set the value of priority to 1 in their routing table. When source node S receives first RREP packet from one of its neighbor (say N2), it makes entry in its routing table, Table 1, for D and priority equals to 1. Now Source node S makes another entry in its routing table, Table 1, for destination D on receiving RREP from node N5 and set priority to 2.

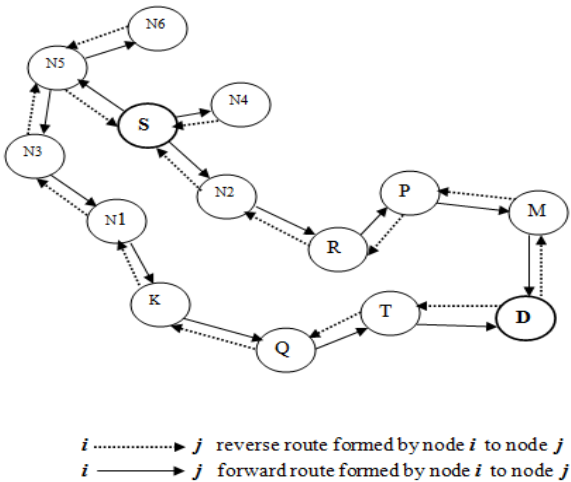


Fig. 2. Route discovery phase

Table 1. Routing table of Source node S

Destination	Sequence number	Hop count	Next Hop	Priority	Expiration Time out
D	...	5	N2	1	...
D	...	7	N5	2	...

Illustration of route maintenance with example

Suppose source node S is communicating with destination node D and link between node N2 and node R breaks. Node N2 sends RERR message to source S. Source node S upon receiving the RERR packet delete entry with next hop N2 and searches its routing table, Table 2, for another route to destination D. Source node S finds another route to node D and start sending data on this route.

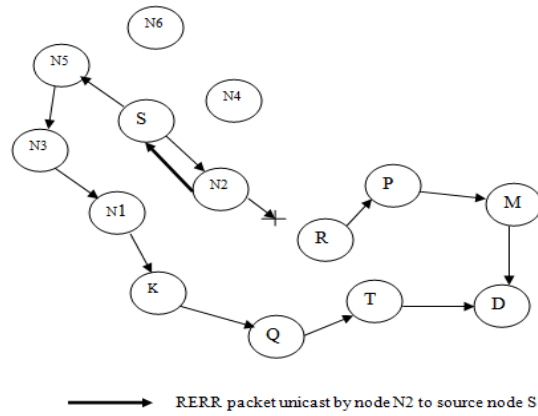


Fig. 3. Route maintenance phase

Table 2. Updated routing table of Source node S after link break

Destination	Sequence number	Hop count	Next Hop	Priority	Expiration Time out
D	...	5	N2	1	...
D	...	7	N5	2	...

3. PERFORMANCE ANALYSIS OF AODV-MS

Various cases are considered for evaluating the performance of the proposed scheme AODV-MS and it is also compared with AODV [4].

CASE 1: REDUCED ROUTING OVERHEAD

In AODV-MS source node send RREQ packet to only one-half of its neighbor which decreases routing packet overhead compare to AODV.

CASE 2: INCREASED THROUGHPUT AND BANDWIDTH UTILIZATION

As number of packets during route discovery in AODV-MS reduces, bandwidth utilization and throughput increases compare to AODV.

CASE 3: REDUCED DELAY

Since source node switch to alternate route on receiving RERR message, it reduces the delay caused due to route discovery on link break in AODV.

4. CONCLUSIONS

In this paper, AODV-MS scheme is proposed to improve an AODV routing protocol. AODV-MS uses a combined strategy of AODV, AODV with selective flooding and multipath routing protocol to improve the performance of AODV routing protocol. AODV-MS reduces the route latency time when a RERR message is generated and uses selective flooding to reduce routing overhead. Hence improves the performance of AODV. In future we implement AODV-MS on network simulator and compare its performance with other MANET protocols.

REFERENCES

[1] A.Nasipuri, R. Castaneda, and .R.Das..Performance of multipath routing for on-demand protocols in mobile ad hoc networks. *ACM/Baltzer Mobile Networks and Applications (MONET)*, 2001, *Journal-6*, 4, 339—349.
 [2] Johnson, D. B., Maltz, D. A., Hu, Y. C. and Jetcheva, J. G..The dynamic source routing protocol for mobile

ad hoc networks (DSR).*Draft-ietf-manet-dsr-07.txt.2002*

- [3] Perkins, C. E and Bhagvat , P..Highly dynamic destination-sequenced distance-vector routing (DSDV) for mobile computers.*Conference on Communications architectures, protocols and applications (SIGCOMM '94)*, 24, 4 (October 1994), 234-244.
- [4] C.E. Perkins and E.M. Royer, “Ad-Hoc On Demand Distance Vector Routing,” *Proceedings of the 2nd IEEE Workshop on Mobile Computing Systems and Applications (WMCSA)*, New Orleans, LA, February 1999, pp. 90-100.
- [5] Geetam S. Tomar, Manish Dixit & Shekhar Verma, “AODV Routing Protocol with Selective Flooding”, *published in International Conference of Soft Computing and Pattern Recognition, 2009*, pp. 682-686.
- [6] Marina, M K. and Das, S. R. 2001. On-demand multipath distance vector routing in ad hoc networks. *In Proceedings of IEEE International Conference on Network Protocols (ICNP)*, 14—23.
- [7] Raju, J. and Garcia-Luna-Aceves, J. J. 1999. A new approach to on demand loop-free multipath routing. *Published in IEEE International Conference on Computer Communications and Networks (ICCCN)*.
- [8] Ye, Z., Krishnamurthy, S. V. and Tripathi, S. K..A framework for reliable routing in mobile ad hoc networks.*In Proc. IEEE INFOCOM*, 2003.
- [9] M.T.Toussaint, “Multipath Routing in Mobile Ad Hoc Networks”, *TU-Delft/TNO Traineeship Report*.
- [10] S. Corson, J. Macker.RFC-2501- Mobile Ad hoc Networking (MANET): Routing Protocol performance *Issues and Evaluation Considerations*.(january 1999). <http://www.ietf.org/rfc/rfc2501.txt>.

Design of a frequency selective surface with multiple four legged Slots

M. Venkata Narayana¹, I. Govardhani², A. Vikranth³, Sd. Khaja Nizamuddin³,
Ch. Venkatesh³, V.V.Vamsi Siva Krishna³
K.Rajkamal⁴

1Associate professor, Department of ECE, K L University

2Women scientist, Department of ECE, K L University

3project students, Department of ECE, K L University

4. PG student

ABSTRACT

A design is presented for a triple band frequency selective surface (FSS) with triple-four-legged loaded slots elements. The resonant element considered is four legged loaded slot (FLLS). The frequency response curve of the FSS varies with respect to the scaling factors of the slots. An optimal scaling factor has been proposed for the slots such that it provides wide and multiple bands. These kinds of reflectors make structures low profile by providing the flexibility in mounting them closer to antenna without disturbing the impedance bandwidth and providing a good gain control in the main beam direction. Its frequency performance is obtained by using numerical simulation software HFSS based on finite-element method (FEM).

Keywords – Frequency selective surface (FSS), four legged loaded slot (FLLS).

I. INTRODUCTION

Frequency selective surfaces (FSSs) have been the subject of intensive investigation for their widespread applications as spatial microwave and optical filters for more than four decades. Frequency selective surfaces (FSSs) are some periodic surfaces, which are basically assembly of identical elements arranged in one- or two-dimensional infinite arrays but finite arrays in practice [1]. They have often been considered for the reflector antenna applications [2]-[4]. Typically, an FSS is employed for the subreflector and the different frequency feeds are optimized independently and placed at the real and virtual foci of the subreflector. Hence, only one single main reflector is required for the multi frequency operation. For example, the Voyager FSS was designed to diplex S and X bands [2]. In that application the S-band feed is placed at the prime focus of the main reflector, and the X-band feed is placed at the Cassegrain focal point. Note that only one main reflector is required for this two band operation. Thus, tremendous reduction in mass, volume and, most important, the cost of the antenna system are achieved with the FSS sub reflector.

FSSs have gained more and more attention in telecommunications, antenna design, and electromagnetic compatibility (EMC) recently. They are widely used as spatial filters, subreflectors for multiband frequency antennas, polarizers and as radomes for radar cross section (RCS) controlling. These surfaces provide uninhibited transmission in specific frequency bands but suppress transmission in other bands. Multiband FSSs have been investigated by many researchers. In space missions such as Voyager, Galileo, and Cassini, the use of dual-reflector antennas with a subreflector made of an FSS has made it possible to share the main reflector among different frequency bands [5]-[8].

Many configurations of the frequency selective surface are possible like layered or stacked FSS, perturbed element FSS, Dual band resonators etc. One interesting property in these structures is the self-similarity property. In plain words self-similarity can be described as the replication of the geometry of the structure at a different scale within the same structure. Self-similarity of the structure results in a multiband behavior [9]. The applications of frequency selective surfaces are many and varied, and they range over much of the electromagnetic spectrum. In the microwave region, the frequency selective properties of periodic screens are exploited, for example, to make a more efficient use of reflector antennas [10].

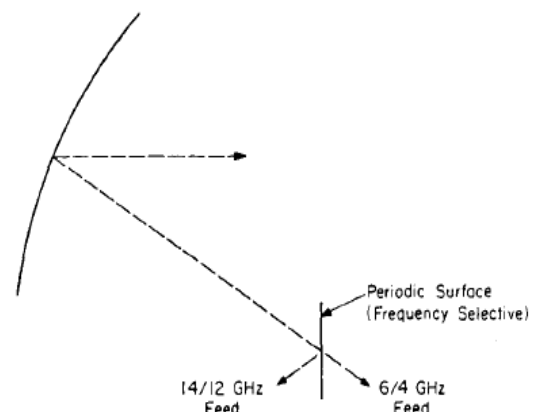


Fig 2. Reflector antenna system using frequency selective screen.

As shown in Fig. 2, a frequency selective surface is placed between two feeds, radiating at differing frequencies, and the main reflector. The screen is totally reflecting (or nearly so) over the operating band of feed one, and conversely, it is nearly totally transparent over the band of feed two. Hence, in this configuration, two independent feeds may share the same reflector antenna simultaneously, in a frequency reuse mode. The main limitation to design a truly multiband FSS is the appearance of grating lobes. To avoid grating lobes the spacing between adjacent elements has to be smaller than the free-space wavelength; however, the elements cannot be brought closer than its own length.

easier. Generally, for designing FSSs in HFSS, one can go with three options using perf E and perf H boundaries, using master/slave boundaries and PML setup and plane wave excitation or using floquet ports.

The FSS is designed first by creating a four legged loaded slot element (FLLS) with curved surface at the four corners. The measurements of the slot are specified in the table given below.

II. DESIGN PROCEDURE

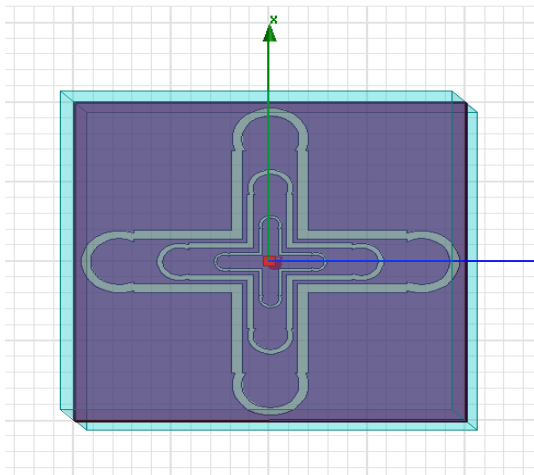


Fig 1. Proposed model of the FSS

The frequency response of an FSS is entirely described by the geometry of the structure in one period called a unit cell. Frequency selective surfaces are usually constructed from periodically arranged metallic patches of arbitrary geometries or their complimentary geometry having aperture elements similar to patches within a metallic screen. These surfaces exhibit total reflection or transmission, for the patches and apertures respectively, in the neighborhood of the element resonances. The most important step in the design process of a desired FSS is the proper choice of constituting elements for the array. The element type and geometry, the substrate parameters, the presence or absence of superstrates, and inter-element spacing generally determine the overall frequency response of the structure, such as its bandwidth, transfer function, and its dependence on the incidence angle and polarization. The resonant frequencies of a slot depend on the slots' width and length, but it is mainly controlled by the slot length. The first resonant frequency decreases with increase of a slot length and a slot width has little effect on the resonant frequency.

More recently, advanced methods based on method of moments (MoM), finite element method (FEM), and finite-difference time-domain (FDTD) with periodic boundary conditions have made the design process of FSSs substantially

dimension	Measurement (units)
Length of outer leg (l_1)	1 mm
Length of outer leg (l_2)	1.2 mm
Width of outer leg (w_1)	0.5 mm
width of outer leg (w_2)	0.4 mm
Lengths of second leg	$l_1/k_1, l_2/k_1$ mm
Lengths of third leg	$l_1/k_2, l_2/k_2$ mm
Thickness of dielectric	1.2 mm

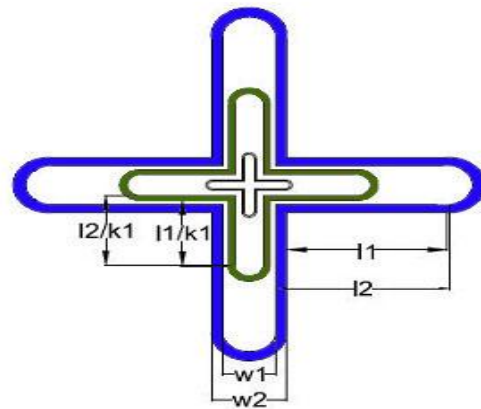


Fig2. Dimensions of the slotted element

TABLE 1
 Geometrical specifications of the FSS

The other slot elements are made by scaling the first one with two scaling factors thus creating two slot elements and hence a triple four legged loaded slot element. However, it should be kept in mind that in general, at least for mechanical reasons, all FSS eventually must be supported by a substantial assembly of dielectric slabs. A dielectric material of permittivity $\epsilon_r=2.2$ and thickness of 1.2mm is placed on either sides of the FSS. The resonance of FLLS occurs when the circumference of the four-legged element is a multiple of the wavelength. The resonant frequency can be changed by modifying the slot lengths.

However, the resonant frequency changes to somewhere between f_0 and $f_0/\sqrt{\epsilon_r}$, when a dielectric slab is added next to a periodic structure. Furthermore, the size of the outer FLLS can be obtained by multiply scale factor k and the size of inner FLLS. The scale factor used for stage 2 and stage 3 is determined by the location of the next desired resonant point in relation to the resonant frequency of the fundamental element.

III. RESULTS AND DISCUSSIONS

Transmission coefficient equals incident voltage divided by the transmitted voltage.

$$\gamma = \frac{V_{\text{transmitted}}}{V_{\text{incident}}}$$

The scattering matrix relates the outgoing waves of a port to the incoming waves that are incident on a port. The matrix elements s_{11} , s_{12} , s_{21} , s_{22} of the scattering matrix S are referred as scattering parameters. The parameters s_{11} , s_{22} have the meaning of reflection coefficients and parameters s_{21} , s_{12} the meaning of transmission coefficients. In a two port network S_{21} is described in dB as follows

$$S_{21} = 20 \log(\gamma)$$

Fig.3 shows the frequency response curve of the four legged loaded slotted FSS with scaling factors for the middle and outer slots as 1.67 and 2.6 respectively. As we can see that the bandwidth obtained for each band is narrow at these scaling factors. The resonant frequencies occur at 12GHz, 23GHz and 38GHz which represent three zeros and also represents that two poles occur at 20GHz and 33GHz.

From the frequency response it is clear that the FSS sufficiently reflects the S, K and Ku band frequencies thus making it useful in reflector applications where it reflects the S and Ku bands while transmitting X and Ka bands through it. Hence, only one single main reflector is required for the multi frequency operation. Thus the size, mass, volume and cost of the system can be greatly reduced. In the figure below the blue color graph indicates the return loss which shows a minimum value at the transmitting frequencies and the red color graph indicates the transmission coefficients S_{21} . The design is simulated for different scaling factors keeping the thickness of dielectric constant. In this case grating lobes appear at high frequencies. At low frequencies they can be neglected.

With proper values of scaling factors we can get a zero at around 25GHz also which comes in the k band of frequency range which is allocated by ITU to both near Earth and Deep Space services to enhance the downlink data rate. Given the new frequency allocation, the European Space Agency (ESA) now aims to upgrade its Deep Space Antennas (DSAs) so that this new band can be used. The DSAs are beam waveguide antennas that use frequency selective surfaces, also called dichroic mirrors, to separate the various frequency bands [14].

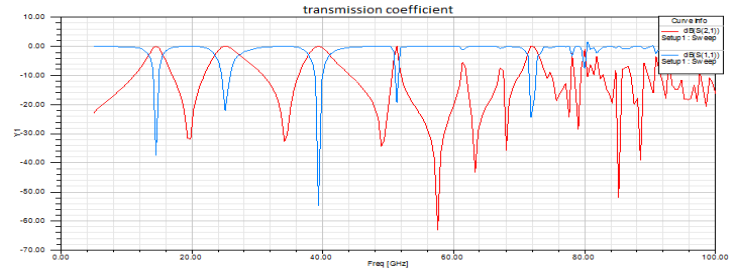


Fig 3. Frequency response curve for scaling factors of 1.67 and 2.6

Fig 4 represents frequency curve for scaling factors of 1.5 and 2.77 for the middle and outer slots respectively. As the scaling factor increases we observe that the bandwidth of the transmission band becomes wide and at the same time the number of transmission band tends to reduce.



Fig 4. Frequency response curve for scaling factors of 1.5 and 2.77

Fig 5 shows the frequency response curve for scaling factors of the outer most slot changed to 3.3 than the previous case. In this case the outer most slot dimension becomes large and thus less surface is available at the centre inside the inner slot. Therefore the curve exhibits only few transmission bands than the previous case.

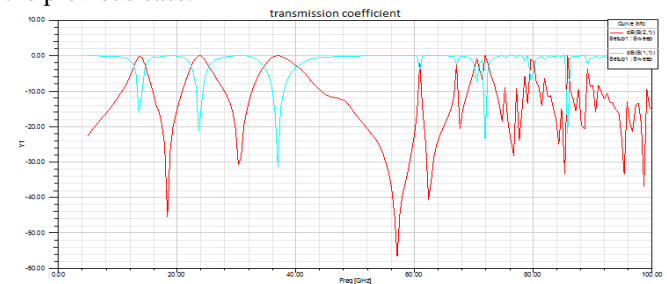


Fig 5. Frequency response curve for scaling factors of 1.67 and 3.3

Fig 6 shows the frequency response curve for scaling factors of slots as 2 and 5. Each part of the surface available on the FSS can be thought of acting at different resonant frequency. As the inner surface becomes smaller it cannot produce resonance. So only the outer slot elements can be able to produce resonance.

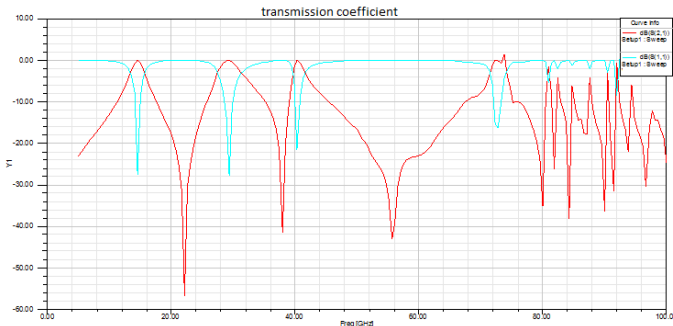


Fig 6 Frequency response curve for scaling factors of 2 and 5

Fig 7 shows the frequency response curve for a much scaled versions of the slots of 2.5 and 6.25. In this case the inner surface is very much reduced. So the bands are reduced to two. Also we can observe that the bands become more wide as the scaling factors are increased. This corresponds to the circular shapes for the four legged slots at the four corners as a result of which the circumference is increased and hence the frequency at which the resonance occurs is also increased. Hence a wide band is obtained for the same design just by changing the scaling factors for the slots.



Fig 7 Frequency response curve for scaling factors of 2.5 and 6.25

IV. CONCLUSIONS

The performance of an FSS is often attributed entirely to the elements. The elements must also be arranged in the proper grid. The proposed design of the frequency selective surface has a triple band making it useful at various reflector applications in satellite subsystems. It has been observed that by changing the scaling factors for the four legged loaded slot the frequency response varies widely as the circumference is varied with scaling factors and hence the resonant frequency also changes. From the results obtained we can conclude that to get a better frequency response the scaling factors should not be too high because high scaling factors reduces the inner surfaces area thus making it less involve in its contribution. Changing the substrate dimensions also affects the frequency response. The optimum substrate thickness can be used is 1-2 mm. Some recent applications of FSS include RFID tags, Collision avoidance, RCS augmentation, Robotic guided paths, EMI protection, Photonic band gap structures, Waveguide or cavity controlled coupling, Low-probability of intercept systems (e.g. "stealth").

ACKNOWLEDGMENT

The authors like to express their thanks to the department of ECE and the management of K L University for their support and encouragement during this work.

REFERENCES

- [1] B.A. Munk, Frequency Selective Surfaces: Theory and Design. New York: Wiley-Interscience, 2000.
- [2] G. H. Schennum, "Frequency-selective surfaces for multiple frequency antennas," *Microwave J.*, vol. 16, pp. 55-57, May 1973.
- [3] V. D. Agrawal and W. A. Imbriale, "Design of a dichroic Cassegrain subreflector," *IEEE Trans. Antennas Propag.*, vol. AP-21, pp. 466-473, July 1979.
- [4] K. Ueno, *et al.*, "Characteristics of FSS for a multiband communication satellite," in *Inr. IEEE AP-S Symp. Dig.*, Ontario, Canada, June 1991, pp. 735-738.
- [5] B. Munk, R. Kouyoumjian, and L. Peters Jr., "Reflection properties of periodic surfaces of loaded dipoles," *IEEE Trans. Antennas Propag.*, vol. AP-19, pp. 612-617, Sep. 1971.
- [6] Wu, T.K.: "Four-band frequency selective surface with double square loop patch elements", *IEEE Trans. Antennas Propag.*, 1994, 42, (12), pp. 1659-1663.
- [7] Wu, T.K., and Lee, S.W "Multiband frequency surface with multiring patch elements", *IEEE Trans. Antennas Propag.*, 1994, 42, (11), pp. 1484-1490.
- [8] Huang, J., Wu, T.K., and Lee, S.W.: "Tri-band frequency selective surface with circular ring elements", *IEEE Trans. Antennas Propag.*, 1994, 42, (2), pp. 166-175.
- [9] Jordi Romeu, Yahya Rahmat-Samii, "Fractal FSS: A Novel Dual-Band Frequency Selective Surface", *IEEE Transactions On Antennas And Propagation*, Vol. 48, No. 7, July 2000 1097.
- [10] Kamal Sarabandi, Nader Behdad, "A Frequency Selective Surface With Miniaturized Elements", *IEEE Trans. Antennas Propag.*, vol. 55, no. 5, may 2007 1239
- [11] Farhad Bayatpur and Kamal Sarabandi, "A Tunable, Band-Pass, Miniaturized-Element Frequency Selective surface: Design and Measurement", *IEEE 2007*.
- [12] Xiao- Dong Hu, Xi- Lang Zhou, Lin- Sheng Wu, Liang Zhou, and Wen-Yan Yin, "A Novel Dual-Band Frequency Selective Surface (FSS)", *IEEE 2009*.
- [13] Mudar A. Al-Joumayly, Nader Behdad. "Low-Profile, Highly-Selective, Dual-Band Frequency Selective Surfaces With Closely Spaced Bands of Peration", *IEEE Trans. Antennas Propag.*, vol. 58, no. 12, december 2010.
- [14] M. Pasian, M. Formaggi, M. Bozzi, F. Carli, L. Perregrini, G. Philippou and G. Dauron, "Multi-physics Design and Manufacturing of a Quad-band Frequency Selective Surface for Space Applications", *IEEE 2011*.

Design of Coaxial fed Spiral-Slot Microstrip Patch Antenna for DTV Reception with Shorting Plates

Govardhani.Immadi¹, M.Venkata Narayana²

M.S.R.S Tejaswi³, N.Anil Babu³, V.Vamsi Krishna³, M. Sagar Babu³, N.Ravi Teja³

1. Woman Scientist, Department of ECE, K L University, India

2. Assoc. professor, Department of ECE, K L University, India

3. Project students, Department of ECE, K L University, India

ABSTRACT

In this paper a novel design of small sized, low profile coaxial fed microstrip patch antenna is proposed for terrestrial DTV signal reception applications in the UHF band frequency range of 540-890MHz. Designed model was spiral slot microstrip patch antenna using shorting plates for size reduction. Different parameters like return loss, VSWR, gain along θ , ϕ directions, radiation pattern in 2D & 3D, axial ratio, E & H field distributions, current distributions are simulated using HFSS 13.0. The measured parameters satisfy required limits hence making the proposed antenna suitable for DTV reception applications in the UHF band.

Keywords- coaxial fed, DTV, FR4, UHF

1. INTRODUCTION

Conventionally, Yagi antenna has been used together with a TV receiver system to capture the electromagnetic wave energy broadcasted from a TV broadcasting station. This antenna has become more popular among the people living both in urban or rural. The popularity of Yagi antenna is not only due to the excellent characteristics such as gain and directivity but also other benefits like easiness in the process of design/ construction/fabrication, installation, maintenance and inexpensive [5].

Apart from these advantages and ease of practical application, this type of antenna has some limitations in terms of the flexibility of use. If there are 2 to 3 sets of TV receiver device in one house, it will take more towers to install them. The negative impact raised in the environmental issue and the crowded arrangement of the antenna installation where it occupies large space. As the position of the TV receiver changed in the building the configuration of cable connection must be reinstalled. Also the gain insufficiency for remote applications, appearance of grating lobes makes the Yagi disadvantageous.

Nowadays, there is a Yagi antenna for indoor applications widely available in the market place which can be connected to the TV receiver to replace the outdoor one. But in terms of size and model it would require the proper arrangement of the room/space so that the quality of signal reception cannot be interfered due to the mobility of moving objects/people and the influence of interference from electronic devices in the vicinity[3]. For applications in other communication systems to access various DVB services such

as from mobile phones, laptops/notebooks and PDAs the newest research and innovations concerning the construction of the internal antenna are very important to conduct. The antenna design must fits perfectly integrated inside a communication device. Some research activities to discover a new internal antenna have been published [6-10].

The results of investigations on a number of the internal antenna designed to be integrated with digital TV receiver has been proposed[4]. The choice of monopole[16],printed monopole[11-12],dipole antennas[13-14] improve the bandwidth to a greater extent. But, monopole antennas are of large size and difficult to build and integrate. Printed monopole antennas also have numerous advantages like low profile, small size, easy integration but has disadvantage of low broad impedance bandwidth and low omnidirectional radiation pattern. The dipole antennas have large input impedance. So, an impedance matching transformer or balun coil at feed point is required which increases the size of antenna[2][16-20]. Due to the numerous advantages of patch antenna[2][17-20] and in view of various techniques to improve the performance of microstrip patch antenna mentioned in [2], a C-slot to enhance the bandwidth of proposed antenna is proposed[1]. To reduce the dimensions of this antenna shorting plates are placed and slots are increased for the antenna to operate at multiple frequencies thereby receiving multiple band of channels.

In this paper, a compact size patch antenna is proposed with dielectric substrate as FR4 with $\epsilon_r=4.4$ and dimensions are base on resonant frequency. Various attempts are made to adjust the dimensions of the patch to improve the parameters like return loss, VSWR, gain along θ , ϕ directions, radiation pattern in 2-D and 3-D, axial ratio, E and H Field Distributions, Current Distributions using HFSS 13.0 which is a high performance full wave EM field simulator for arbitrary 3D volumetric passive device modelling that takes advantage of the familiar Microsoft Windows graphical user interface. It integrates simulation, visualization, solid modelling, and automation in an easy to learn environment where solutions to your 3D EM problems are quickly and accurate obtained. Ansoft HFSS employs the Finite Element Method (FEM), adaptive meshing, and brilliant graphics to give you unparalleled performance and insight to all of the 3D EM problems.

2. DESIGN CONSIDERATIONS

The proposed structure of the antenna is shown in Fig. (1). The antenna is simulated on an FR4 substrate with a dielectric constant of 4.4 and a loss tangent of 0.02. The thickness of the substrate is 1.6 cm. The size of the antenna is 11x10 cm², which is suitable for DTV reception. Rectangle shaped patch is taken with slots as shown.

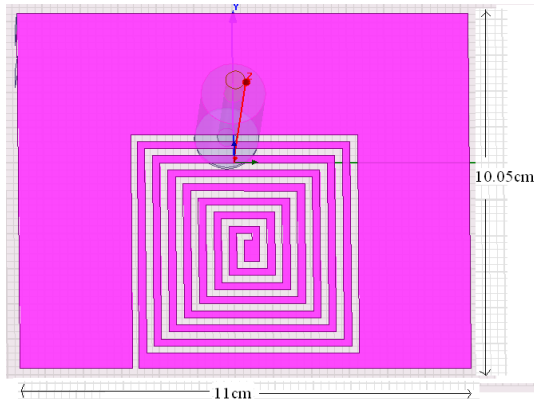


Fig. 1. Geometry of Patch antenna with Slots

The patch can be fed with a probe through ground plane. The probe position can be inset for matching the patch impedance with the input impedance. This insetting minimizes probe radiation. The ease of insetting and low radiations is advantages of probe feeding as compared to microstrip line feeding. The dimensions of rectangular shaped patch shown in Fig. (1) are L=11cm, W=10.05cm which are designed at operating frequency 1GHz. On inserting slots, shorting plates the designed antenna operates at low frequency.

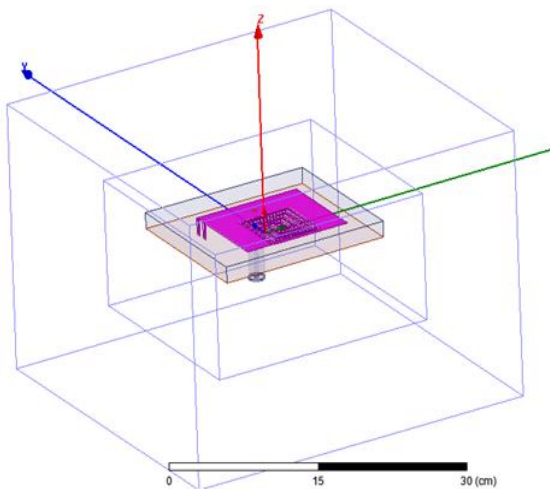


Fig. 2. Ansoft-HFSS generated antenna model

Figure (2) shows the proposed antenna on FR4 Substrate using Ansoft-HFSS.

3. SIMULATION RESULTS

3.1. Return loss

It is a measure of the reflected energy from a transmitted signal. It is commonly expressed in positive dB's. The larger the value the less energy that is reflected.

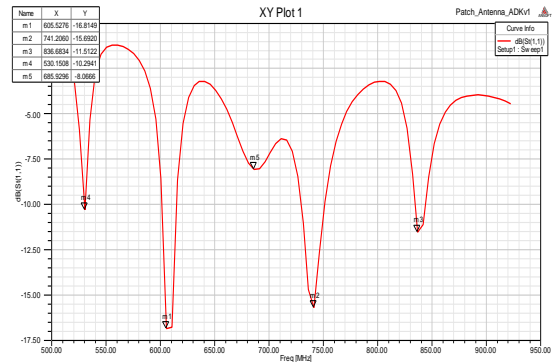


Fig 3. Return loss

Figure (3) shows the return loss Curve for the proposed antenna. Return losses of 16.82dB, 15.69dB, 11.5dB, 10.29dB is obtained at frequencies of 0.6,0.74,0.83,0.53GHz.

3.2.2D Gain & 3D gain Totals

The term Antenna Gain describes how much power is transmitted in the direction of peak radiation to that of an isotropic source.

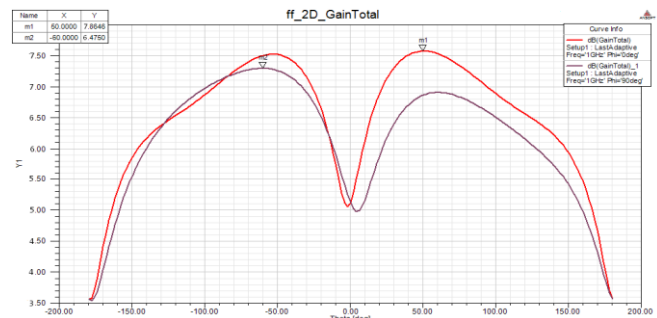


Fig 4. 2D-Gain Total

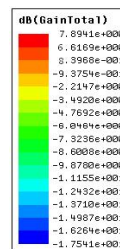


Fig 5. 3D-Gain Total

Figure (4-5) shows the antenna gain in 2D & 3D patterns. The gain of proposed antenna is obtained as 7.86dB and 6.47dB. The gain above 6dB is acceptable.

3.3. VSWR

The VSWR is a measure of the impedance mismatch between the transmitter and the antenna. The higher the VSWR, the greater is the mismatch. The minimum VSWR which corresponds to a perfect match is unity.

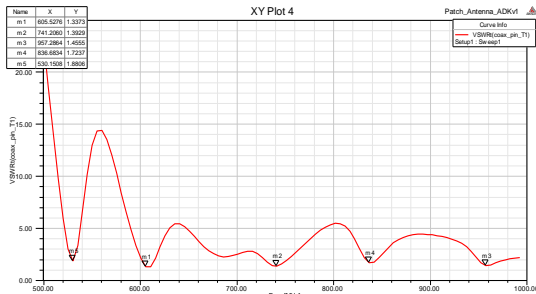


Fig.6. VSWR

The VSWR for the proposed antenna is less than the 2dB. The obtained value is 1.33,1.39,1.45,1.72,1.88 at 0.6,0.74,0.95,0.86,0.53GHz from Fig 6.

3.4. Radiation Patterns

The radiation pattern of an antenna is a plot of the far-field radiation properties of antenna as a function of the spatial co-ordinates which are specified by the elevation angle θ and the azimuth angle ϕ . It is a plot of the power radiated from an antenna per unit solid angle which is nothing but the radiation intensity.

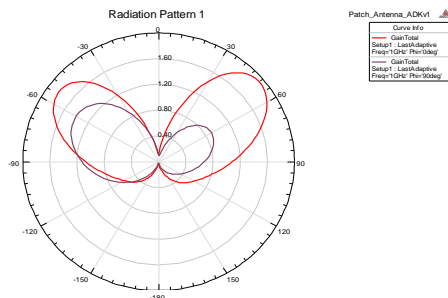


Fig. 7a. Gain in Total

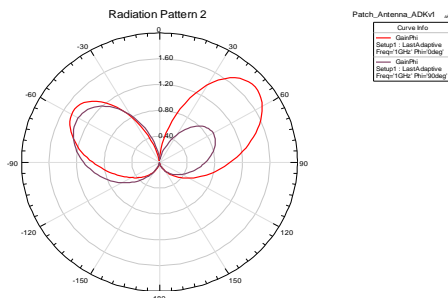


Fig. 7b. Gain along Phi

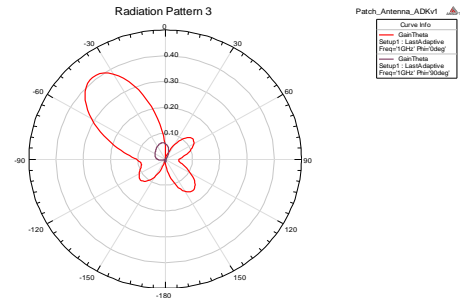


Fig. 7c. Gain along Theta

Since a Micro strip patch antenna radiates normal to its patch surface, the elevation pattern for $\phi = 0$ and $\phi = 90$ degrees would be important. The radiation pattern for proposed microstrip patch antenna for gain-Total, phi and theta at 0deg and 90deg is presented in figure 7(a),7(b), 7(c).

3.5. Axial Ratio

Axial Ratio is the ratio of peak value in the major lobe to peak value in the minor lobe direction.

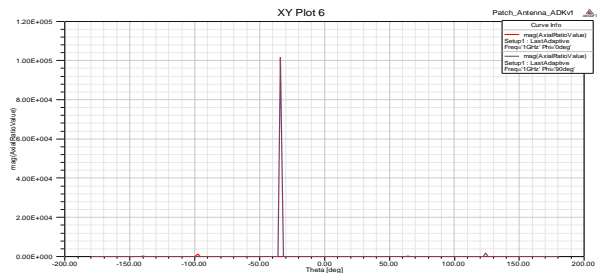


Fig. 8. Axial Ratio

Axial ratio which is the ratio of the major axis to the minor axis of the polarization ellipse where the resulting pattern is an oscillating pattern is obtained as in Fig 8

3.6. E-Field Distribution

An electric field can be visualized by drawing field lines, which indicate both magnitude and direction of the field. Field lines start on positive charge and end on negative charge. The direction of the field line at a point is the direction of the field at that point. The relative magnitude of the electric field is proportional to the density of the field lines.

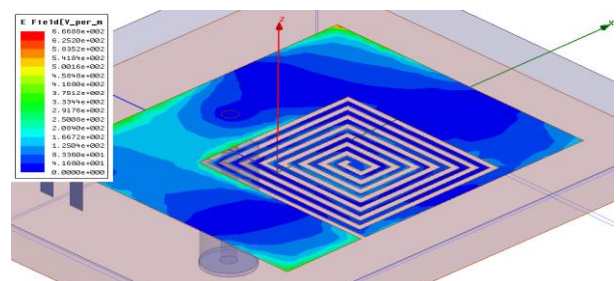


Fig.9a: E-field Distribution

The effect produced by an electric charge that exerts a force on charged objects is the E-Field and its distribution in the patch is as shown in Fig 9a.

3.7. H-field Distribution

In the case of the same linearly polarized antenna, this is the plane containing the magnetic field vector and the direction of maximum radiation. The magnetic field or "H" plane lies at a right angle to the "E" plane. For a vertically-polarized antenna, the H-plane usually coincides with the horizontal/azimuth plane. For a horizontally-polarized antenna, the H-plane usually coincides with the vertical/elevation plane.

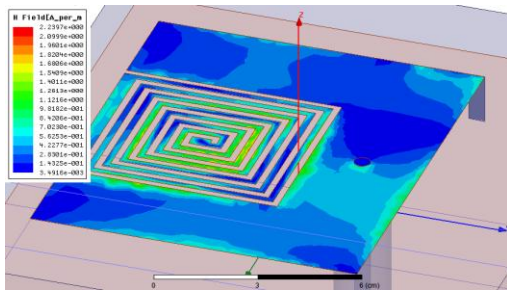


Fig.9b: H-field Distribution

The measured intensity of a magnetic field in the patch is shown in Fig 9b.

3.8. Current Distribution

Antennas are composed of conductive material on which current distribution determines antenna's defined parameters.

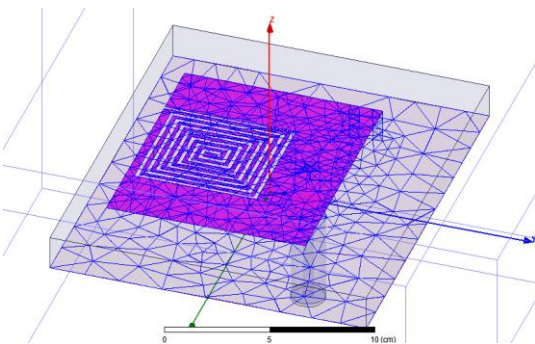


Fig.10: Mesh Pattern

The triangles show the current distribution. Here the number of triangles inside the patch are more than those on the substrate i.e., the current distribution in the patch is more when compared to that inside the substrate in Fig10.

3.9. Field Vectors

The polarization of the EM field describes the time variations of the field vectors at a given point. In other words, it describes the way the direction and magnitude the field vectors (usually E) change in time.

The electric field vector is perpendicular to both the direction of travel and the magnetic field vector. If the field travels in counter clockwise direction, and out of screen, it would be right hand elliptically polarised. If the E-field vector is rotating in opposite direction, the field would be left hand elliptically polarized.

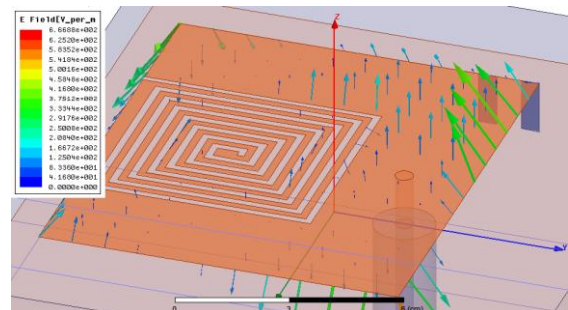


Fig 11a: E-Field Vector

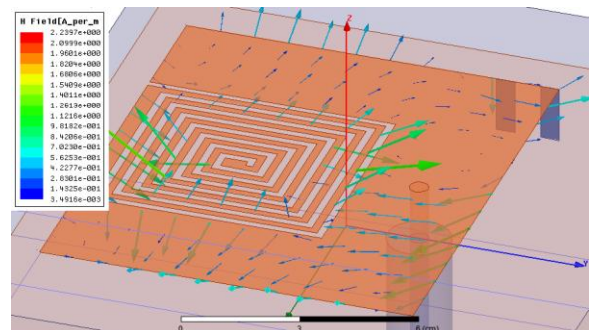


Fig 11b: H-Field Vector

The E-Field Vector and H-Field vectors of proposed patch antenna are obtained as shown in Fig 11a and 11b.

4. CONCLUSIONS

Finally, the optimum dimension of elliptically polarized patch antenna on FR4 substrate for DTV reception applications has been investigated. The performance properties are analyzed for the optimized dimensions and the proposed antenna works well at the required UHF frequency band.

ACKNOWLEDGMENTS

The authors like to express their thanks to the department of ECE and the management of K L University for their support and encouragement during this work.

REFERENCES

[1] Govardhani.Immadi 1, M.Venkata Narayana 1, M.S.R.S Tejaswi 2 N.Anil Babu 2 "Design of C-slot microstrip patch antenna for DTV reception in Advances in Computational Sciences and Technology (ACST) (communicating)
 [2] Govardhani.Immadi 1, M.S.R.S Tejaswi 2, M.Venkata Narayana 3 N.Anil Babu 4, G.Anupama 5, K.Venkata Ravi teja 6 "Design of Coaxial fed Microstrip Patch

- Antenna for 2.4GHz BLUETOOTH Applications” VOL. 2, NO. 12, December 2011 ISSN 2079-8407, Journal of Emerging Trends in Computing and Information Sciences
- [3] E. Palantei and D.V. Thiel, “Yagi-Uda Antenna Human Proximity Effects on the Link Budget at 300 MHz,” *IEEE APS Symposium Digest*, Nort Charleston, South Carolina, 1-5 June 2009.
- [4] E. Palantei, Andani A., M. Baharuddin, N.K. Nauman, S. Syarif, M. Anshar, NNRA Mokobombang, A. Suyuti, Z. Muslimin, Z. Zainuddin, Indrabayu A., F. Mayasari, A. Ejah US, S. Kanata and Z.B. Hasanuddin]”Internal Antennas for Digital TV Receiver” 978-1-4244-9561-0/11/\$26.00 ©2011 IEEE
- [5] Balanis, C.A. 2005. “Antena Theory Analysis and Design”. *Textbook* 3rd Edition. New Jersey : John Wiley and Sons.
- [6] J. Holopainen, J. Villanen, M. Kyrö, C. Icheln, and P. Vainikainen,” Antenna for Handheld DVB Terminal,” *IEEE APS Symposium Digest*, 2006.
- [7] H. Suzuki, I. Ohba, T. Minemura, and T. Amano, “Frequency Tunable Antennas for Mobile Phone for Terrestrial Digital TV Broadcasting Reception, “ *IEEE APS Symposium Digest*, 2006.
- [8] J. Kim, G. Kim, W. Seong, and J. Choi, “A Tunable Internal Antenna with An Epsilon Negative Zeroth Order Resonator for DVB-H Service,” *IEEE Transactions on Antennas and Propagation*, Vol. 57, No.12, December 2009.
- [9] J.T. Aberle, S.H. Oh, D.T. Auckland, and S. D. Rogers, “Reconfigurable Antennas for Portable Wireless Device,” *IEEE Antennas and Propagation Magazine*, Vol. 45, No.6, December 2003.
- [10] E. Palantei, D.V. Thiel, and S.G. O’Keefe, “Rectangular Patch with Parasitic Folded Dipoles: A Reconfigurable Antenna,” *Proceedings of IEEE iWAT2008 Conference*, Chiba, Japan, 4-6 March.
- [11] Shinya KASHIHARA and Futoshi KUROKI “J-Shaped Monopole Antenna Array As an Antenna for Terrestrial Digital Broadcasting at UHF Band” 978-1-4244-2804-5/09/□ 2009 IEEE, pg.292-296
- [12] Futoshi Kuroki and Hiroshi Ohta,” L-Shaped Monopole Array for Terrestrial Broadcasting Reception in the UHF Band”, *Proceedings of the 37th European Microwave Conference*,pg.1070-1074.
- [13] Chih-Yu Tsai, Oscar T.-C. Chen “CPW-Fed Wideband Printed Planar Dipole Antenna for Digital TV” 978-1-4244-4968-2
- [14] Yun-Wen Chi and Kin-Lu Wong “Wideband Printed Dipole Antenna for DTV Signal Reception” 1-4244-1272-2/07,2007 IEEE
- [15] I. Govardhani, K.Rajkamal, M.Venkata Narayana, S.Venkateswarlu published a paper on “Phased Array Antenna for Millimeter Wave Radar in W-band using Liquid Crystal Substrate” VOL. 2, NO. 12, December 2011 ISSN 2079-8407Journal of Emerging Trends in Computing and Information Sciences
- [16] M. Venkata Narayana, I.Govadhani, K.P.Sai Kumar, K. Pushpa Rupavathipublished paper on “Comparative Analysis of Exponentially Shaped Microstrip-Fed Planar Monopole Antenna With and Without Notch “VOL. 2, NO. 11, October 2011 ISSN 2079-8407 Journal of Emerging Trends in Computing and Information Sciences
- [17] M. Venkata Narayana, A.Vikranth, I. Govardhani, Sd. Khaja Nizamuddin, Ch. Venkatesh published paper on”A Novel Design of a Microstrip Patch Antenna with an EndFire Radiation for SAR Applications” Volume 2 No.1, January 2012 ISSN 2224-3577 International Journal of Science and Technology .
- [18] I. Govardhani, M.Venkata Narayana, Prof S.Venkateswarlu, K.Rajkamal Published paper in International Journal of Engineering Research and Applications (IJERA) ISSN: 2248-9622 www.ijera.com Vol. 2, Issue 1,Jan-Feb 2012, pp.764-767 on Microstrip patch antenna using holographic structure for WLAN and Ku Band application.
- [19] I. Govardhani , M.Venkata Narayana Published paper in International Journal of Computer Science & Communication Networks,Vol 2(1), 375-380, ISSN:2249-5789 on Rectangular Patch Array Antenna with Liquid Crystal Substrate for Ka and Q Band Applications
- [20] Dr.K.S.N Murthy, Venkata Raviteja.K, I.Govardhani, M.Venkata Narayana Published a paper on Multi-band Ladder-shape Microstrip Patch Antenna IJSER Volume 3, Issue 3, March 2012 Edition

Optimizing area of local routing network by reconfiguring look up tables (LUTs)

Sathyabhama.B¹ and S.Sudha²

¹ M.E-VLSI Design

² Dept of ECE

Easwari engineering college, Chennai-89

Abstract - The general way of mapping digital circuits onto field programmable gate arrays (FPGAs) usually consist of two steps. Initially the circuits are mapped into look up tables (LUTs). Then, the LUTs are mapped onto physical resources. This includes the process of reconfiguration. Reconfiguration follows three basic properties, which includes commutative property, duplicate-constant input property, and constant new input equivalence property. Logic blocks are composed of clusters with LUTs and flip flops. In particular for a logic cluster with I inputs and N K- input LUTs a set of $N \times K (I+N-K+1):1$ multiplexers can be used to connect logic cluster input to LUT input. It can increase the flexibility of FPGA routing resources. The flexibility can then be used to reduce the implementation area. This can also reduce the significant amount of fanouts for logic cluster input. Reconfiguration can also be done in correspondence with logical non-equivalency which also tender to give better area efficient result.

Index terms- Field programmable gate arrays (FPGAs), logical non-equivalency, logic cluster, reconfiguration.

I. INTRODUCTION

Look up tables (LUTs) are connected through two level routing hierarchy in FPGAs. Two level routing hierarchy includes local routing network and global routing network. LUTs are connected to logic clusters through local routing network and the logic clusters are connected to Field Programmable Gate Arrays (FPGAs) through global routing network. Routing hierarchy concentrates on flexibility and minimization of area. Logic block composed of basic logic elements (BLEs) which is connected with fast local interconnect. BLEs are generally indivisible unit with a combination of sequential and combinational logic [1]. In general BLEs consist of flip flops and LUTs. A logic block with one or more number of BLE is said to be a logic cluster. The flexibility of the routing network is increased when the logic cluster are used with logically equivalent inputs and outputs. In logical equivalency the input can enter a logic cluster through any of the input and the output can allow a signal to exit through any of the output pin. Thus, the flexibility of the routers are increased and it leads to the better utilization of routing resources. The logic cluster with logically equivalent input and output allow a signal to enter or exit in a several way. This added connectivity is used in increasing the flexibility of the routers.

This paper is organized as section II briefs about logic clusters with logic equivalency, section III explains LUT structure and properties of LUT, section IV deals with routing flexibility based on the reconfiguration of the LUT, section V comprised of sparse network with the result of the reconfiguration, section VI deals the non-equivalency of the same network which is previously implemented with logical equivalency, section VII gives all the simulation and synthesis results for both the network with logically equivalent and logically nonequivalent.

II. LOGICALLY EQUIVALENT LOGIC CLUSTERS

Logical equivalency of the network can be attained through the fully connected network [2]. Fully connected network is configured as several cluster inputs connected to the number of LUT present in the network through the multiplexers. All the input of the clusters are connected to each and every input of LUT without any merging and coincidence through the multiplexers. Since the previous work describes the fully connected network is not the most area efficient method to attain logical equivalency, the current work goes with the LUT reconfiguration. Sometimes attaining logical equivalency through the fully connected network after implementation results in less routing tracks when compared to the logically non-equivalent. There is a tool available for checking the logical equivalency named LEC (Logic Equivalence Checker). Test patterns are not required for LEC instead it will use Boolean arithmetic technique to prove the equivalency. The network for this work has a logic cluster with two LUTs and the number of cluster input is derived from 2^{k-1} , where k is the number of inputs to the LUT. The cluster size can be varied with varying the number of input to the LUT. The logic cluster input is named as I. Sometimes the output of the LUT is again given to the input of the logic cluster as feedbacks. In this network N represents the feedback given to the logic cluster. The cluster can be initiated by applying inputs, through the multiplexers the function of the network can be changed.

A fully connected local routing network is used to connect the logic cluster inputs to each LUT input in all possible ways it can. The basic fully connected local routing network taken for this work is given below

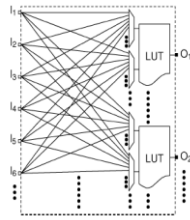


Fig.1. Fully connected local routing network.

A k-input LUT is designed to emulate the operation of a 2^k entry truth table. The LUT is constructed out of a $2^k : 1$ multiplexer and 2^k bits of configuration memory [3]. The memory is connected to the data inputs of the multiplexer and stores the truth table entries. The LUT inputs are connected to the select inputs of the multiplexer.

III. STRUCTURE AND PROPERTY OF LUT

Three properties of an LUT can be used to determine the minimum area required to implement a logic cluster containing logically equivalent input and outputs. The three main basic property [2] used for this work are

- Commutative property,
- Duplicate-constant input property,
- Constant new input equivalence property.

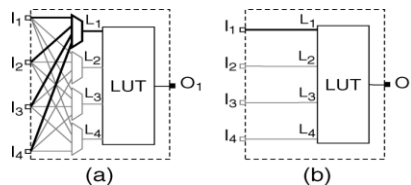


Fig.2. Fully connected network versus LUT reconfiguration.

The LUT inputs are connected to the select inputs of the multiplexer. For a four-input Boolean function such as the one shown in Table.1.1(a), a signal assigned to L_1 can be routed through cluster input I_1 . The same function, can be implemented by exchanging the signal assignment of L_1 and L_2 and by reconfiguring the LUT to implement the Boolean function shown in Table.1.1 (b). The signal originally assigned to L_2 now must enter the cluster through logic cluster input I_2 . Similarly, the same signal can be made to enter the cluster through logic cluster inputs I_3 and I_4 respectively, by using the LUT configurations shown in Table.1.1 (c) and Table.1.1 (d).

(a) LUT configuration for connection to cluster input 1
 (b) LUT configuration for connection to cluster input 2
 (c) LUT configuration for connection to cluster input 3
 (d) LUT configuration for connection to cluster input 4

L1	L2	L3	L4	O
0	0	0	0	f0
0	0	0	1	f1
0	0	1	0	f2
0	0	1	1	f3
0	1	0	0	f4
0	1	0	1	f5
0	1	1	0	f6
0	1	1	1	f7
1	0	0	0	f8
1	0	0	1	f9
1	0	1	0	f10
1	0	1	1	f11
1	1	0	0	f12
1	1	0	1	f13
1	1	1	0	f14
1	1	1	1	f15

L1	L2	L3	L4	O
0	0	0	0	f0
0	0	0	1	f1
0	0	1	0	f2
0	0	1	1	f3
0	1	0	0	f8
0	1	0	1	f9
0	1	1	0	f10
0	1	1	1	f11
1	0	0	0	f4
1	0	0	1	f5
1	0	1	0	f6
1	0	1	1	f7
1	1	0	0	f12
1	1	0	1	f13
1	1	1	0	f14
1	1	1	1	f15

L1	L2	L3	L4	O
0	0	0	0	f0
0	0	0	1	f1
0	0	1	0	f8
0	0	1	1	f9
0	1	0	0	f4
0	1	0	1	f5
0	1	1	0	f10
0	1	1	1	f11
1	0	0	0	f2
1	0	0	1	f3
1	0	1	0	f6
1	0	1	1	f7
1	1	0	0	f12
1	1	0	1	f13
1	1	1	0	f14
1	1	1	1	f15

L1	L2	L3	L4	O
0	0	0	0	f0
0	0	0	1	f8
0	0	1	0	f2
0	0	1	1	f10
0	1	0	0	f4
0	1	0	1	f12
0	1	1	0	f6
0	1	1	1	f14
1	0	0	0	f1
1	0	0	1	f9
1	0	1	0	f5
1	0	1	1	f11
1	1	0	0	f3
1	1	0	1	f13
1	1	1	0	f7
1	1	1	1	f15

Table.1. LUT configuration for LUT structure in fig.2

The k-input LUT can implement any Boolean function with less than k inputs. Implementing such a function also requires all unused LUT inputs to be connected. Three types of signals can be connected to these inputs. They are the inputs from the Boolean function that is currently being implemented, constant 1's or 0's, and an entirely new set of signals, respectively. If the logic cluster has a set of logically equivalent inputs, each input of can enter the logic cluster through any of the logic cluster inputs. If the logic cluster has a set of logically equivalent outputs, one can implement f at any logic cluster output. A feedback signal must also be able to reach f from any of the logic cluster outputs.

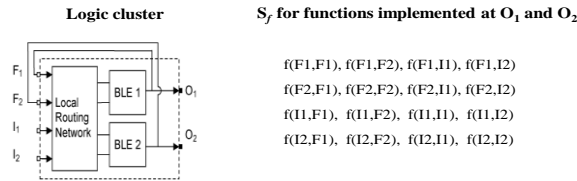


Fig.3. Logic cluster and set of functions it can be implemented.

The local routing network must be able to generate all functions in S_f for f at each logic cluster output. Conversely, if the local routing network is not flexible enough to generate all functions in S_f at a particular logic cluster output; one must avoid signal assignments that can lead to the un-implementable functions. If these un-implementable functions involve logic cluster inputs, then these inputs are no longer logically equivalent to the remaining inputs. Similarly, if the un-implementable functions involve logic cluster feedbacks, then the corresponding logic cluster outputs are no longer logically equivalent to the remaining outputs.

- (a) Three input boolean function
- (b) Duplicated input implementation
- (c) Constant input '0' implementation
- (d) New input implementation

L1	L2	L3	L4	O	L1	L2	L3	L4	O	L1	L2	L3	L4	O	L1	L2	L3	L4	O
0	0	0	0	f0	0	0	0	0	f0	0	0	0	0	f0	0	0	0	0	f0
0	0	0	1	f1	0	0	0	1	f1	0	0	0	1	f1	0	0	0	1	f1
0	0	1	0	f2	0	0	1	0	f2	0	0	1	0	f2	0	0	1	0	f2
0	0	1	1	f3	0	0	1	1	f3	0	0	1	1	f3	0	0	1	1	f3
0	1	0	0	f4	0	1	0	0	X	0	1	0	0	f4	0	1	0	0	f4
0	1	0	1	f5	0	1	0	1	X	0	1	0	1	f5	0	1	0	1	f5
0	1	1	0	f6	0	1	1	0	X	0	1	1	0	f6	0	1	1	0	f6
0	1	1	1	f7	0	1	1	1	X	0	1	1	1	f7	0	1	1	1	f7
1	0	0	0	X	1	0	0	0	X	1	0	0	0	X	1	0	0	0	X
1	0	0	1	X	1	0	0	1	X	1	0	0	1	X	1	0	0	1	X
1	0	1	0	X	1	0	1	0	X	1	0	1	0	X	1	0	1	0	X
1	0	1	1	X	1	0	1	1	X	1	0	1	1	X	1	0	1	1	X
1	1	0	0	f4	1	1	0	0	f4	1	1	0	0	f4	1	1	0	0	f4
1	1	0	1	f5	1	1	0	1	f5	1	1	0	1	f5	1	1	0	1	f5
1	1	1	0	f6	1	1	1	0	f6	1	1	1	0	f6	1	1	1	0	f6
1	1	1	1	f7	1	1	1	1	f7	1	1	1	1	f7	1	1	1	1	f7

Table.2. Table describing three properties of LUT

IV FLEXIBILITY OF ROUTING AND RECONFIGURATION

The fully connected local routing network can be configured to any network connection necessary. Hence, in this work certain connections are maintained to achieve the area efficiency. For, attaining certain necessary connection the basic network connection taken is given below.

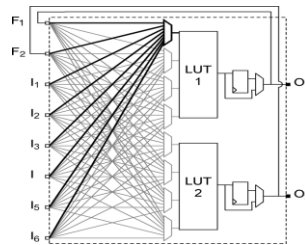


Fig.4 Logic cluster with 2 four-input LUTs, two feedbacks, six inputs, and a fully connected local routing network. The various connection of the LUT is based on reconfiguration and LUT input rearrangement. Several connection considered in this work are $\langle F_2, I_5, I_1, F_2 \rangle$ configuration, $\langle 0, I_5, I_1, F_2 \rangle$ configuration, $\langle F_2, I_1, I_5, 0 \rangle$ configuration $\langle F_2, I_1, I_5, I_6 \rangle$ configuration.

- (a) $\langle F_2, I_5, I_1, F_2 \rangle$ configuration
- (b) $\langle 0, I_5, I_1, F_2 \rangle$ configuration
- (c) $\langle F_2, I_1, I_5, 0 \rangle$ configuration
- (d) $\langle F_2, I_1, I_5, I_6 \rangle$ configuration

L1	L2	L3	L4	O	L1	L2	L3	L4	O	L1	L2	L3	L4	O	L1	L2	L3	L4	O
0	0	0	0	f0	0	0	0	0	f0	0	0	0	0	f0	0	0	0	0	f0
0	0	0	1	f1	0	0	0	1	f1	0	0	0	1	x	0	0	0	1	f1
0	0	1	0	f2	0	0	1	0	f2	0	0	1	0	f4	0	0	1	0	f4
0	0	1	1	f3	0	0	1	1	f11	0	0	1	1	x	0	0	1	1	f4
0	1	0	0	f4	0	1	0	0	f4	0	1	0	0	f2	0	1	0	0	f2
0	1	0	1	f5	0	1	0	1	f13	0	1	0	1	x	0	1	0	1	f2
0	1	1	0	f6	0	1	1	0	f6	0	1	1	0	f6	0	1	1	0	f6
0	1	1	1	f7	0	1	1	1	f15	0	1	1	1	x	0	1	1	1	f6
1	0	0	0	f8	1	0	0	0	x	1	0	0	0	f9	1	0	0	0	f9
1	0	0	1	f9	1	0	0	1	x	1	0	0	1	x	1	0	0	1	f9
1	0	1	0	f10	1	0	1	0	x	1	0	1	0	f13	1	0	1	0	f13
1	0	1	1	f11	1	0	1	1	x	1	0	1	1	x	1	0	1	1	f13
1	1	0	0	f12	1	1	0	0	x	1	1	0	0	f11	1	1	0	0	f11
1	1	0	1	f13	1	1	0	1	x	1	1	0	1	x	1	1	0	1	f11
1	1	1	0	f14	1	1	1	0	x	1	1	1	0	f15	1	1	1	0	f15
1	1	1	1	f15	1	1	1	1	x	1	1	1	1	x	1	1	1	1	f15

Table.3. Table describing several configuration of fig.4

In particular, if an LUT input is only connected to a subset of logic cluster inputs and feedbacks, a signal assigned to the LUT input can only enter the cluster through the connected inputs/feedbacks these connected inputs/feedbacks are no longer logically equivalent to the unconnected ones. The fully connected local routing network can be designed as $N \times K (I+N):1$ multiplexers where, N is the number of feedback given to the cluster, K is the number of input given to the LUT, I is the logic cluster input.

V SPARSE NETWORK AFTER RECONFIGURATION

Let A be a k -input LUT implementing a Boolean function $f(a_1, a_2, a_3, \dots, a_k)$. Let $i_1, i_2, i_3, \dots, i_n$ be the output signals from n LUTs. Let v be a k -bit wide bit vector containing a subset of k signals from $\{i_1, i_2, i_3, \dots, i_n\}$. If v is in s_i and i_x is the j th element of $n-k+j$ of, then v must be smaller than or equal to j . A local routing network can be used to connect the j th input of a k -input LUT to all signals in the set $\{i_j, i_{j+1}, \dots, i_{n-k+j}\}$ through an $(n-k+1):1$ multiplexer. Through LUT reconfiguration and function transformations, the LUT can be used to generate all functions in S_f . To generate all functions in S_f without reconfiguration, each input of the k -input LUT must be connected to all signals in $\{i_1, i_2, i_3, \dots, i_n\}$ through an $n:1$ multiplexer. For example, for the logic cluster shown in fig.2.b there are four logic cluster inputs I_1, I_2, I_3, I_4 and, and no feedbacks. The LUT input L_1 should be connected to all signals in the set $\{I_1\}$ (for $j=1, n=4$, and $k=4$), L_2 should be connected to all signals in the set $\{I_2\}$ (for $j=2, n=4$ and $k=4$), L_3 should be connected to all signals in the set $\{I_3\}$ (for $j=3, n=4$ and $k=4$, L_4 should be connected to all signals in the set $\{I_4\}$ (for $j=4, n=4$ and $k=4$). With reconfiguration, the local routing network is able to generate all functions in set S_f .

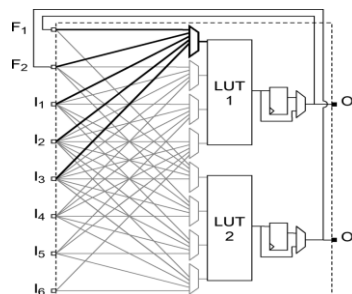


FIG.5 SPARSE LOCAL ROUTING NETWORK.

After reconfiguration the multiplexer size is reduced from 8:1 to 5:1. For N data inputs, the number of control bits should be $\text{ceil}(\log N)$ For example $N = 5, \text{ceil}(\log(5)) = 3$. Thus, there are 3 control bits. Other three inputs should be treated as don't cares.

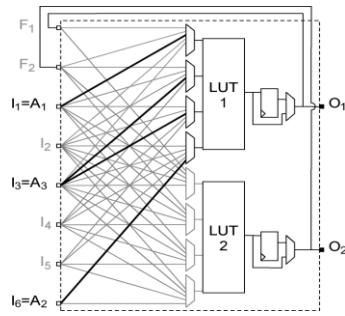


Fig.6 Implementation 1

The fanout of F_1 and I_6 is reduced from 8 to 2. The fanout of F_2 and I_5 is reduced from 8 to 4; the fanout of I_1 and I_4 is reduced from 8 to 6; and the fanout of I_2 and I_3 remains unchanged at 8. The fanouts of all logic cluster inputs and feedbacks can be reduced to 5 by rearranging the order $\{I_2, I_1, F_2, F_1, I_6, I_5, I_4, I_3\}$ of the logic cluster inputs/feedbacks to when the inputs and feedbacks are connected to LUT 2.

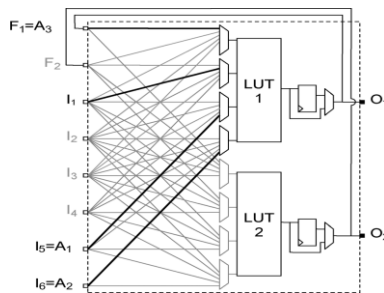


Fig.7 Implementation 2

Both logic cluster designs retain logic equivalency among logic cluster inputs and outputs. For example, consider implementing the three-input Boolean function. In the logic cluster shown in Fig. 5, there are 336 unique ways that the three inputs can enter the logic cluster. Fig.6 and 7 show two of the possibilities.

- (a) A three-input boolean function
- (b) LUT configuration for imp. 1. $I_1=a_1, I_2=a_3, I_3=a_3, I_4=a_2$
- (c) LUT configuration for imp. 2. $I_1=a_3, I_2=i_1, I_3=a_1, I_4=a_2$

A1	A2	A3	O
0	0	0	f0
0	0	1	f1
0	1	0	f2
0	1	1	f3
1	0	0	f4
1	0	1	f5
1	1	0	f6
1	1	1	f7
-	-	-	...
-	-	-	...
-	-	-	...
-	-	-	...
-	-	-	...
-	-	-	...
-	-	-	...
-	-	-	...

L1	L2	L3	L4	O
0	0	0	0	f0
0	0	0	1	f2
0	0	1	0	x
0	0	1	1	x
0	1	0	0	x
0	1	0	1	x
0	1	1	0	f1
0	1	1	1	f3
1	0	0	0	f4
1	0	0	1	f6
1	0	1	0	x
1	0	1	1	x
1	1	0	0	x
1	1	0	1	x
1	1	1	0	f5
1	1	1	1	f7

L1	L2	L3	L4	O
0	0	0	0	f0
0	0	0	1	f2
0	0	1	0	f4
0	0	1	1	f6
0	1	0	0	f0
0	1	0	1	f2
0	1	1	0	f4
0	1	1	1	f6
1	0	0	0	f1
1	0	0	1	f3
1	0	1	0	f5
1	0	1	1	f7
1	1	0	0	f1
1	1	0	1	f3
1	1	1	0	f5
1	1	1	1	f7

(a) (b) (c)

Table.4 LUT configurations for implementations 1 and 2.

$A_1, A_2,$ and A_3 are assigned to cluster inputs I_1, I_6 and I_3 respectively. A_3 is also duplicated to provide the fourth LUT input. The corresponding LUT configuration is shown in Table.4 (b) Alternatively, in fig.7 a router can assign $A_1, A_2,$ and A_3 to I_5, I_6 and F_1 respectively. Due to the sparse local routing network, none of the three inputs can be expanded into the fourth LUT input. Instead, an arbitrary cluster input I_1 is used as the fourth input. In a directional single-drive architecture, each track is driven by its own buffer. Consequently, it can be connected to any of the routing tracks since the LUT is configured to provide the same output for both and as shown in Table.4 (c). As similarly the further work goes with increasing the LUT input. For, $k=5$ all the network connections with fully connected network is implemented. The area minimization can be noted in terms of combinational ALUTs (Adaptive LUTs).

VI. LOGICAL EQUIVALENCY

Logically equivalent inputs and outputs allow a signal to enter or exit a logic cluster in several ways. This added connectivity increase the flexibility of the routers and can lead to better utilization of the routing resources. In this work a basic multiplier circuit is implemented in a fully connected network which is been created. The circuit diagram of multiplier which is implemented in this work is given below

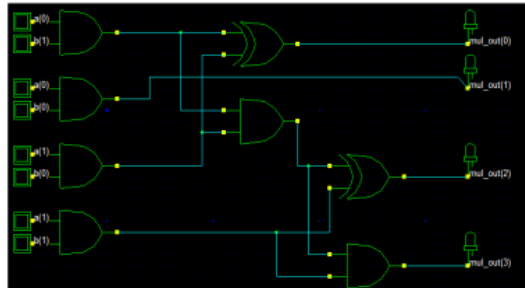


Fig.8 Multiplier circuit with logical equivalency

VII. LOGICAL NON-EQUIVALENCY

Each contains a set of non-equivalent inputs/outputs each input signal must enter the cluster through a dedicated cluster input and each output signal must exit the cluster through a dedicated cluster output [8]. This concept goes with the implementation of multiplier as the enhanced work based on the base paper. In logical equivalency the multiplier circuit is composed of combination of EXOR gate and AND gate. But, in the logical non-equivalence the multiplier circuit is composed of only universal gate. In this paper the universal gate used for multiplier circuit to attain the logical non-equivalency is NAND gate.

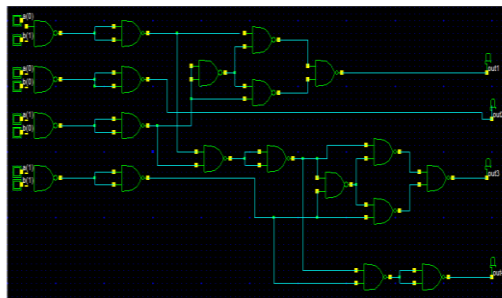


Fig.9 Multiplier circuit with logical non equivalency

VII. RESULTS AND DISCUSSION

This paper work is simulated using the tool Modelsim simulator in VHDL (Very high speed integrated circuit Hardware Descriptive Language) language. The tool used for synthesis process is Quartus. The device used while synthesing is StratixII device. The objective attained in this work is area reduction and fanout reduction. Area reduction is mentioned in terms of combinational ALUTs attained in the synthesis process. Fanout reduction can be mentioned as maximum fanout, total fanout and average fanout. The combinational ALUTs obtained

- Fully connected network is 18,
- Connection $\langle F_2, I_5, I_1, F_2 \rangle$ is 14,
- Connections for $\langle F_2, I_1, I_5, 0 \rangle$ is 11,
- Sparse local routing network is 5,
- Implementation 1 and implementation 2 is 2.

The fanout result for the synthesized networks with the LUT input of 4 can be given as

- Fully connected network average fanout is 2.21,
- Connection $\langle F_2, I_5, I_1, F_2 \rangle$ average fanout is 1.48,
- Connections for $\langle F_2, I_1, I_5, 0 \rangle$ average fanout is 1.18,
- Sparse local routing network average fanout is 0.58,
- Implementation 1 and implementation 2 average fanout is 0.31.

Similarly for 5 input LUT network all results obtained will be similar as 4 input LUT but the net result will increase because of increase in number of inputs. Such as, the whole network can be created with a collection of logic clusters with varying input of the LUT. The RTL (Register Transfer Level) for all the above mentioned network can be attained using synthesis tool Quartus. The constructed network can be implemented using VPR tool (Versatile Place and Route tool) if the implementation is based on the physical end. VPR is an industry based tool. VPR can perform placement and either global routing or combined global and detailed routing.

The implementation of multiplier with the device of stratix II results with the combinational ALUTs of 4 in logically equivalent state. Similarly, the multiplier circuit with logically non-equivalent state composed only of NAND gate also result with the same number of 4 combinational ALUTs.

Alternatively, since some of the logic clusters contain feedbacks, the 8:1 multiplexers can be used to construct logic clusters containing 4 four-input LUTs with eleven logic cluster inputs. Again, this design would require a narrower channel width in order to support the smaller four LUT clusters.

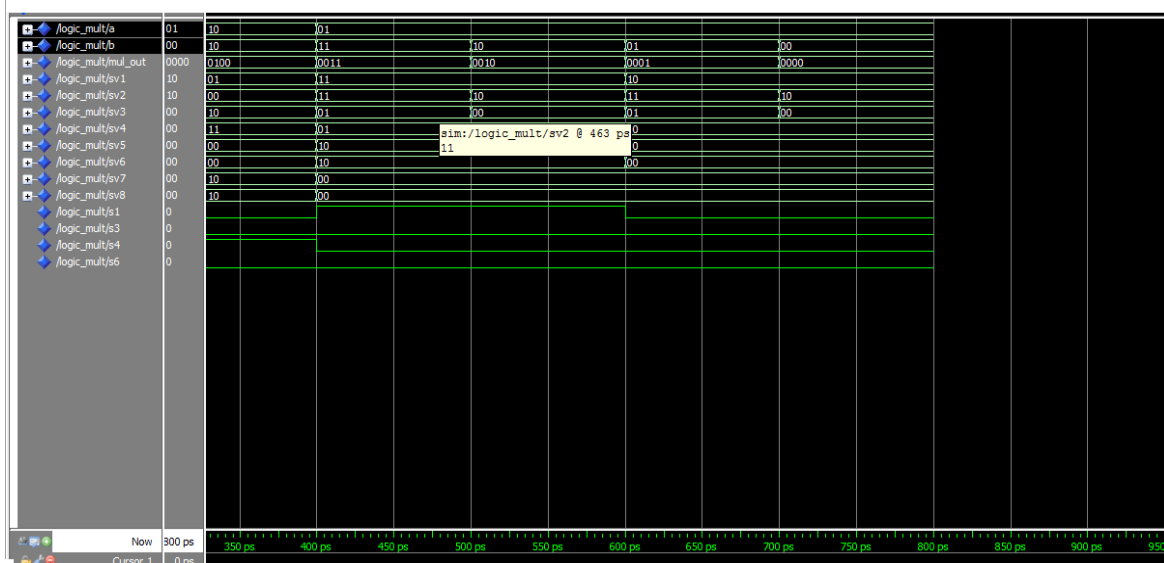


Fig.10. Simulation result of logically equivalent multiplier

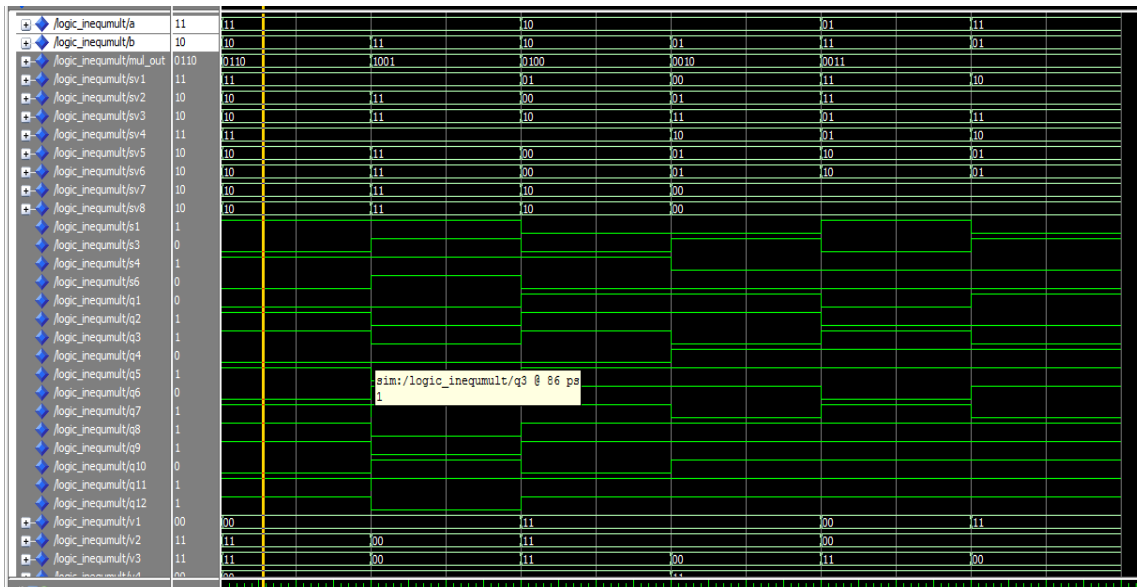


Fig.11 Simulation results of logically non-equivalent multiplier

VIII. CONCLUSION

The examination of the paper reveals the relationship between the logic equivalency of logic cluster input and outputs and LUT reconfiguration for FPGA local routing networks. Also, examined the relationship between the logical equivalency and non-equivalency of the particular network. Since the four LUT design retains logic equivalency among the logic cluster I/Os and has less logic cluster inputs per LUT. This design should also be experimentally evaluated as an extension of future work, along with an examination on the effect of the sparse local routing network design on the power efficiency of FPGAs.

REFERENCES

- [1] A. Marquardt, V. Betz, and J. Rose, "Speed and area trade-offs in cluster-based FPGA architectures," *IEEE Trans. Very Large Scale Integr.(VLSI) Syst.*, vol. 8, no. 1, pp. 84–93, Feb. 2000.
- [2] Andy Gean Ye, "Using the Minimum Set of input combinations to Minimize the Area of Local Routing Networks in Logic Clusters Containing logically Equivalent I/Os", *IEEE Trans. Very Large Scale Integr.(VLSI) Syst.*, vol. 18, no. 1, january 2010.
- [3] E. Ahmed and J. Rose, "The effect of LUT and cluster size on deepsubmicron FPGA performance and density," *IEEE Trans. Very Large Scale Integr. (VLSI) Syst.*, vol. 12, no. 3, pp. 288–298, Mar. 2004.
- [4] V. Betz and J. Rose, "How much logic should go in an FPGA logic block?," *IEEE Des. Test Comput. Mag.*, vol. 15, no. 1, pp. 10–15, Jan.-Mar. 1998.
- [5] V. Betz and J. Rose, "Effect of the prefabricated routing track distribution on FPGA area-efficiency," *IEEE Trans. Very Large Scale Integr.(VLSI) Syst.*, vol. 6, no. 3, pp. 445–456, Sep. 1998.
- [6] C. E. Shannon, "The synthesis of two-terminal switching circuits," *Bell Syst. Tech. J.*, vol. 28, no. 1, pp. 59–98, Jan. 1949.
- [7] G. Lemieux, "Directional and single-driver wires in FPGA interconnect," in *Proc. IEEE Int. Conf. Field-Programm. Technol.*, 2004, pp. 41–48.
- [8] A. Roopchansingh and J. Rose, "Nearest neighbour interconnect architecture in deep submicron FPGAs," in *Proc. IEEE Custom Integr. Circuits Conf.*, 2002, pp. 59–62.
- [9] A. Ye and J. Rose, "Using bus-based connections to improve fieldprogrammable gate array density for implementing datapath circuits," *IEEE Trans. Very Large Scale Integr. (VLSI) Syst.*, vol. 14, no. 5, pp. 462–473, May 2006.



Sathyabhama.B pursuing master's of engineering in VLSI design stream Easwari engineering college Chennai under Anna university of Chennai . This work was guided by Dr.S.Sudha, professor, Assistant HOD ECE department in Easwari engineering college Chennai. Current research interests include field-programmable gate array (FPGA) architectures, computer-aided design (CAD) tools for FPGAs, logic synthesis.

Design of dual and triple band antennas using U-slots on stacked patches

M. Siva Ganga Prasad¹, P. Poorna priya², J. Lavanya³, M. S. Rajeev Trivedi⁴,
K. Manideep⁵, V. V. Vamsi siva Krishna⁶

¹Professor, Department of ECE, K.L University

²Assistant. professor, Department of ECE, K L University

³Project student, Department of ECE, K.L University

⁴Project student, Department of ECE, K.L University

⁵Project student, Department of ECE, K.L University

⁶Project student, Department of ECE, K.L University

ABSTRACT

A different kind of approach to design dual and triple band antennas using U-slots on stacked patches is designed. Present approach is based on employing U-slots on stacked patches and the design is simulated using concerto software. It is observed that each U-slot included will include a notch in corresponding matching band. By changing certain feed position only we can achieve desired application with in single antenna. Same has been implemented by rotating planes of U-slots. This antenna can be used for several applications in X-band.

Keywords: Multiband antennas, slot antennas, stacked patches, U-slot antennas, X-band applications

1. INTRODUCTION

The rapid increase in communication standards has led to greater demands for antennas with low profile, low size, low cost of fabrication and ease of integration with feeding network. Numerous applications were developed after designing of multiband antennas with desired slots which makes antenna conformal with arrays, reduces the size of the antenna to about 37% and also avoids the usage of two or more antennas for multiband responses. In [1], a new approach to get dual band and triple band antennas is verified using U-slots and the same has been verified by various feeding technique finally results of simulated and fabricated models is compared. In [2], dual band printed microstrip antennas using single layer and multi-layer patches have been reported. Triple band performance has been reported for a square patch antenna using spurline filter and perturbation technique. In [3], Multi band 1 patch with shorting wall and slot was proposed in order to achieve different wireless applications wideband was achieved by using a slot on top patch. In [4], microstrip antennas (MSA) are loaded with monolithic stubs, shorting pins or slots, the electrical resonant length of the patch gets modified and hence tunable or multiple frequency antennas can be realized. In [5], a modified structure with a placard shaped slot having two stubs centered in the square patch is proposed to lower the frequencies of the dual band

operation. In [6], a multi band microstrip antenna operating at frequency 2.4GHz and 5.2GHz is presented. The dimensions of the single elements of the operating frequencies were calculated using the transmission line model. Two elements of inset fed microstrip antenna were used for each frequency band. In [7], microstrip line fed, printed isosceles triangular slot antennas, with a small rectangular slot for broad band operation, were proposed and experimentally investigated. Experimental result indicate that a 2:1 VSWR is achieved over a bandwidth of 2.9GHz, between 2.33 and 5.23GHz, which is nearly 4.6 times that of a conventional microstrip-line-fed, printed isosceles triangular slot.

This paper presents a multi-band antenna design approach based on inserting U-slots on rectangular stacked patches. The MSA designed is being fed by a wireedge into the substrate with input impedance of 50 Ω . This design uses two different substrates with $\epsilon_r=2.23$ and $\epsilon_r=1$ for bottom and top substrate respectively. Several results are presented and discussed to show the versatility of this antenna, developed by simple changes. The proposed antenna has many applications and can be used for any application in X-band range, by changing feed positions and by selecting slot dimensions.

2. DESIGN CONSIDERATIONS

The proposed antenna is designed using two different substrates. A substrate of $\epsilon_r=2.23$ for bottom patch and of $\epsilon_r=1$ (air). Two patches of different dimensions has been designed on two substrates. Dimensions of the patches and U-slots are mentioned in the table below. Height of substrates for both patches are mentioned in the table.

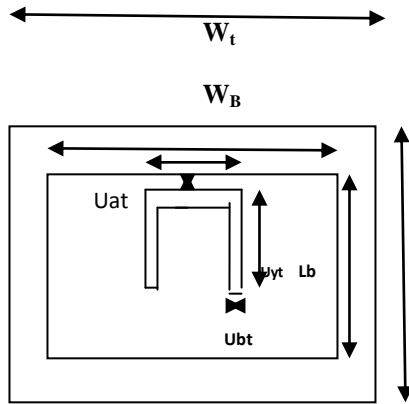


Fig1: Geometry of stacked patch antenna with U-slots

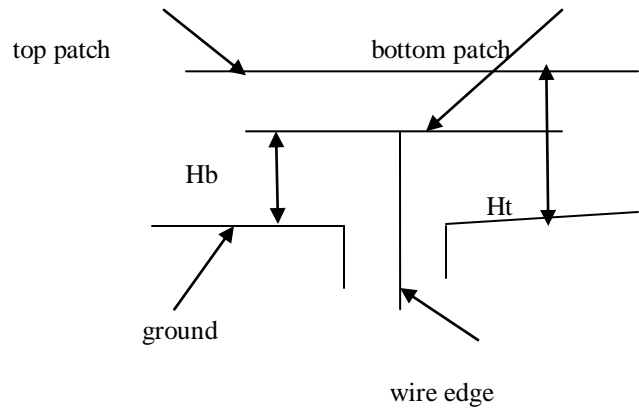


Fig2: heights of substrates from ground

Table1: dimensions of stacked patch antennas with U-slots

	W_t	L_t	W_b	L_b	U_{xt}	U_{yt}	U_{at}	U_{bt}	U_{xb}	U_{yb}	U_{ab}	U_{bb}
With no slots	16	15	12	13.5	-	-	-	-	-	-	-	-
With 1 U slot on bottom patch	16	15	12.5	13.5	-	-	-	-	6	5.5	0.5	0.5
With U-slots on both patches	16	15	12.5	13.5	6	6.5	0.25	0.5	6	5.5	0.5	0.5

DESIGN MODELS USING CONCERTO:

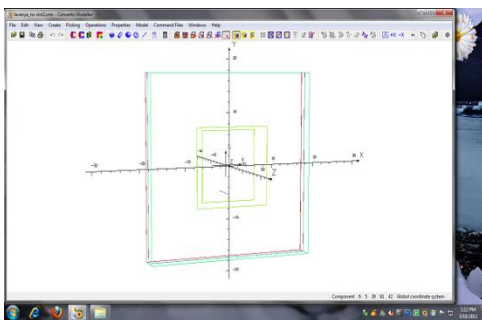


Fig1: Design with no slot on patches

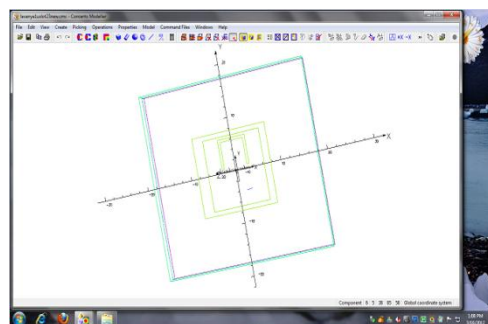


Fig2: Single U-slot on bottom patch

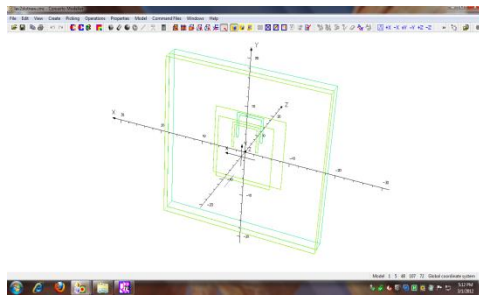


Fig3:U-slots on both patches

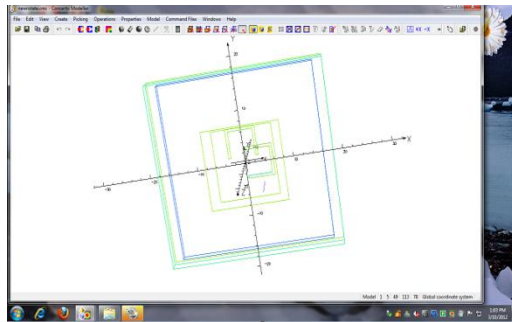


Fig4:Modified design when U-slot on top patch is rotated to 90°

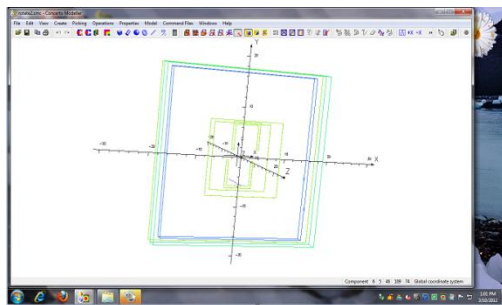


Fig5: Modified design when U-slot on top patch is rotated to 180°

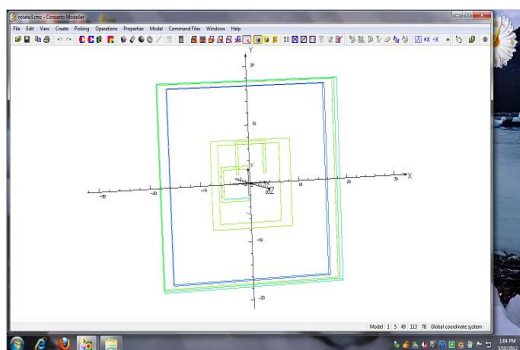


Fig6: Modifies design when U-slot on top patch is rotated to 270°

5. RESULTS & DISCUSSION

Simulation is the process to verify the performance of the device for the given specifications under the specified conditions before actual manufacture of the device. So by using Simulator tool Concerto, we can first simulate the particular design of a multi band antenna and verify required parameters. We can observe the performance of the antennas by verifying the outputs and finally fabricate the antenna following the same specifications and thus minimizing the costs. Further, a perfect optimization was done, in order to find the best feeding point of the structure. Several points were tested in order to get an overview of the defined functioning of the antenna. At first the feeding point was chosen on -ve Y-axis and is adjusted slowly to get best return losses.

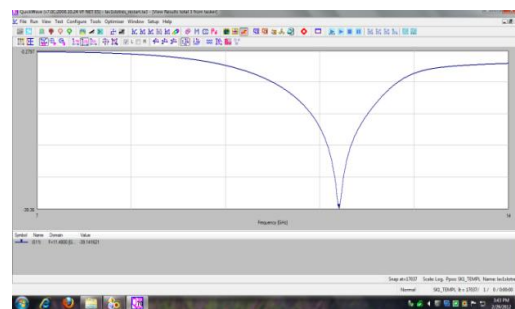


Fig 7: Return loss of design with no slots

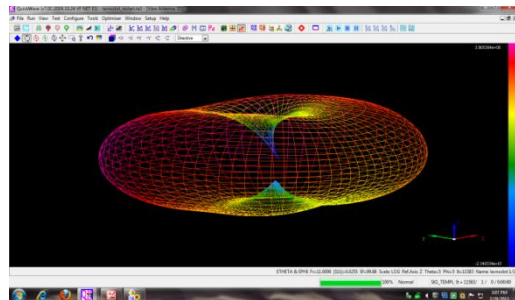


Fig 8: Simulated results for 3D gain at f=11.4GHz in concerto software



Fig9: Return loss of design with 1 U-slot

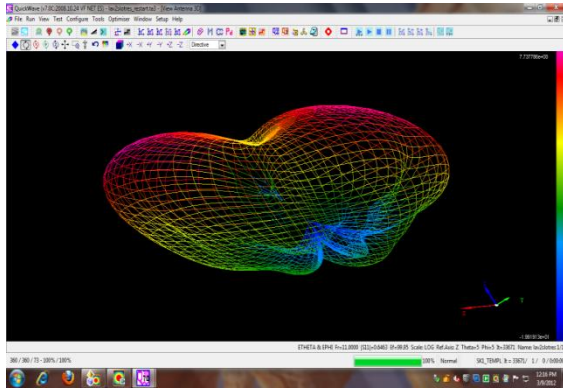


Fig 10: Simulated results for 3Dgain at f=11.42Ghz in concerto software

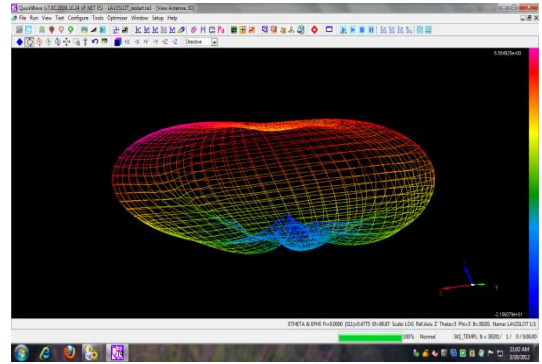


Fig 14: Simulated results for gain at f=11.6Ghz in concerto software

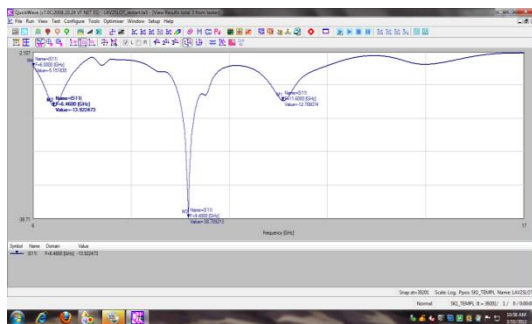


Fig11:Return loss of design with U-slots on both patches

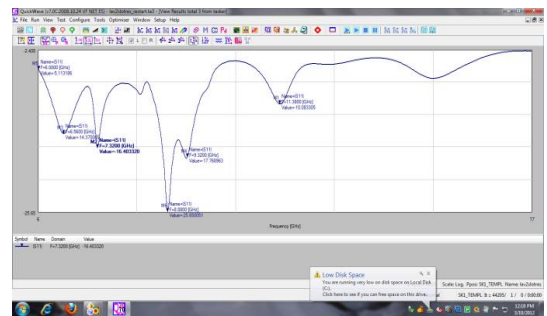


Fig15:Return loss of design with 2 U-slots and slot rotated to 90°

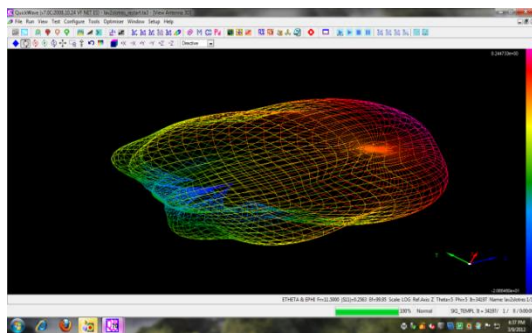


Fig 12: Simulated results for 3D gain at f=6.46Ghz in concerto software

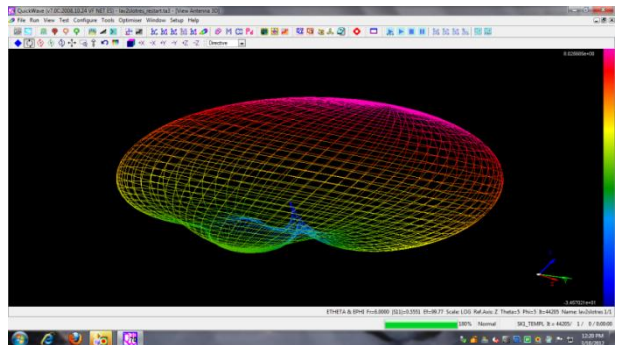


Fig 16 Simulated results for 3D gain at f=7.32Ghz in concerto software

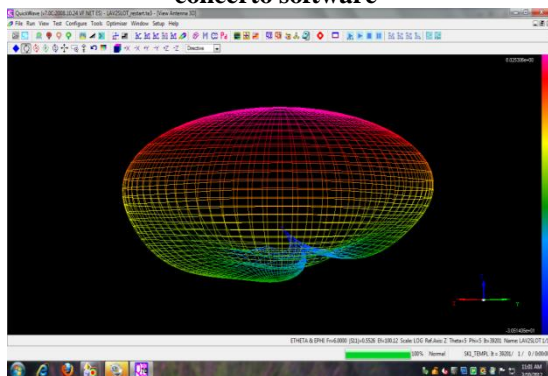


Fig 13: Simulated results for gain at f=9.48Ghz in concerto software

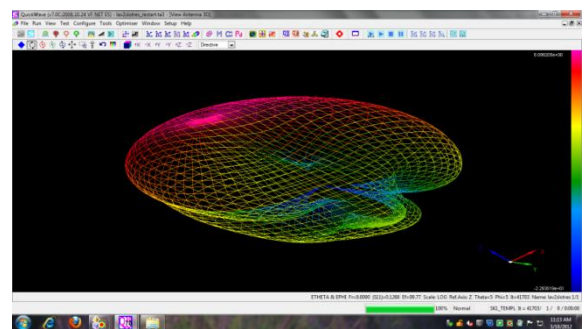


Fig 17: Simulated results for gain at f=5.8Ghz in concerto software

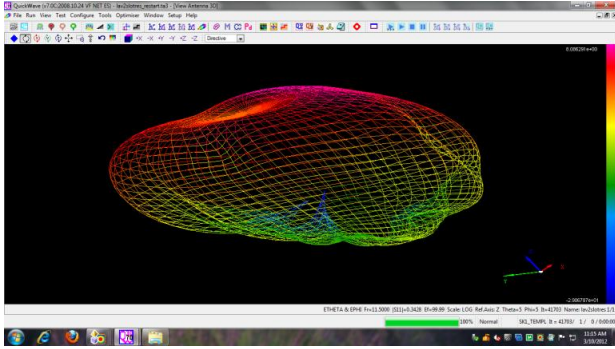


Fig 18: Simulated results for gain at $f=8.8\text{GHz}$ in concerto

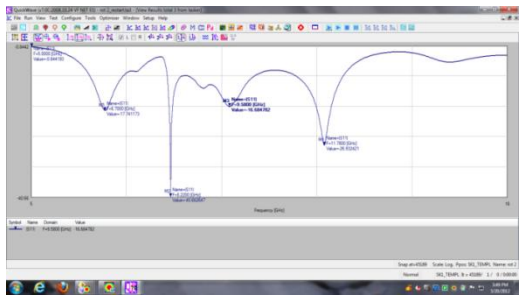


Fig19:Return loss of design with 2 U-slots and slot rotated to 180°

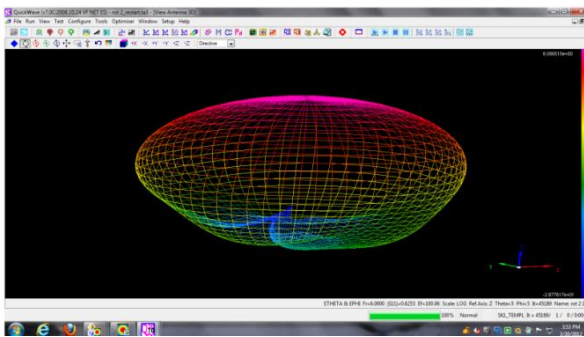


Fig 20: Simulated results for 3D gain at $f=6.7\text{GHz}$ in concerto software

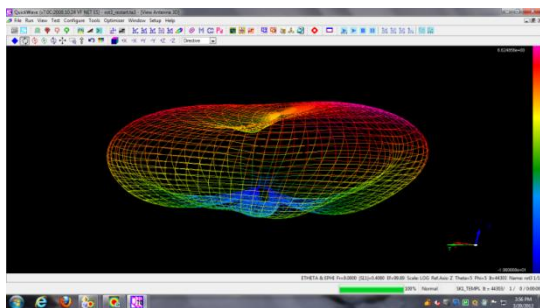


Fig 21: Simulated results for 3D gain at $f=8.22\text{GHz}$ in concerto software

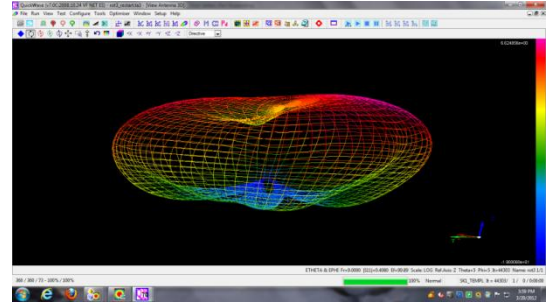


Fig 22: Simulated results for gain at $f=11.78\text{GHz}$ in concerto software



Fig23:Return loss of design with 2 U-slots and slot rotated to 270°

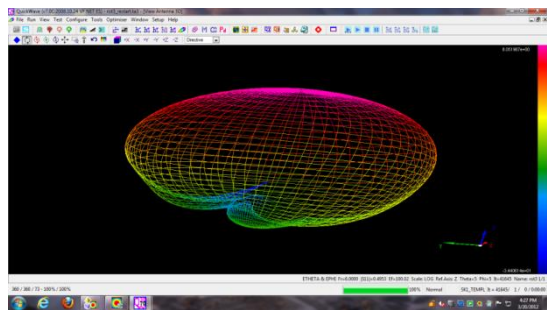


Fig 24: Simulated results for 3D gain at $f=6.32\text{GHz}$ in concerto software

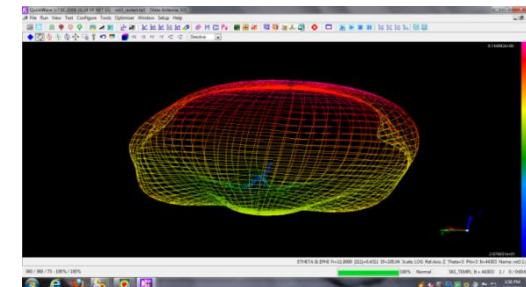


Fig 25: Simulated results for 3D gain at $f=9.38\text{GHz}$ in concerto software

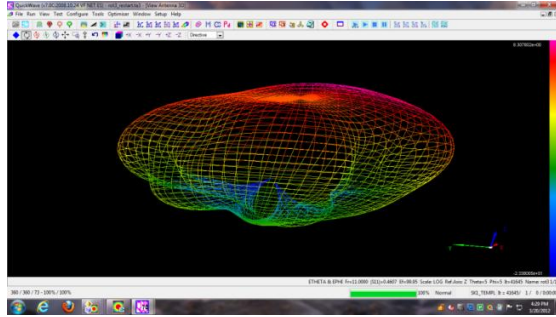


Fig 26: Simulated results for gain at $f=11.44\text{GHz}$ in concerto software

6. APPLICATIONS

Can be used for military communications satellites and various X-band applications such as radar applications including continuous-wave, pulsed, single-polarization, dual-polarization, synthetic aperture radar, and phased arrays

7. CONCLUSION

A new approach to obtain multi-band response has been presented, using U-slots to improve bandwidth (each U-slot included will introduce a notch in matching band) Same model was implemented by rotating the planes of U-slot and radiation patterns, return losses are observed and the best model is evaluated comparing various parameters. In the same model cross polarisation is reduced by designing an antenna with opposite slots. The antenna has many applications in X-band and this single antenna can be used for versatile applications in the range due to multiband response.

ACKNOWLEDGMENT

The authors like to express their thanks to the department of ECE and the management of K L University for their support and encouragement during this work

References

- [1] K.F.Lee, K.M.Luk, K.M.Mak and S.L.S.Yang "On the use of U-slots in the design of dual and triple band patch antennas", IEEE Transactions on Antennas and Propagation,
- [2] F. Yang and Y.R. Samii, "A Compact Dual Band Circularly Polarized Antenna Design For Mars Rover Mission", Antennas And Propagation Society International Symposium, IEEE Transactions on Antennas and Propagation, Vol. 3, No. 6, pp. 858-861, June 2003.
- [3] Asha E. Daniel and Girish Kumar, "tunable dual and triple frequency stub loaded rectangular microstrip antennas", IEEE transactions on Antennas and Propagation
- [4] Asha E. Daniel and R.K Shevgoankar*, "slot loaded rectangular microstrip antennas for tunable band operation"
- [5] Prapoch jirasukul porn , "Multi band cpw fed slot

antenna with L-slot Bowtie tuning stub" for WLAN and WIMAX operations, World Academy of Science, Engineering and Technology 48 2008

- [6] 1st Lieutenant Rudi Ernanto, S.T*), Dr. Achmad Munir**), Lieutenant Colonel Dr. Arwin Datumaya Wahyudi Sumari, S.T., M.T.***)" Design of 4.2GHz Collinear Antenna for CMOV/COMOB Downlink Application" Radio Telecommunication and Microwave Laboratory, STEI ITB, Bandung 40132***) Directorate of Examination, Indonesian Air Force Academy, Adisutjipto, Yogyakarta 55002
- [7] A. Asrokin, M.K.A.Rahim, and M.Z.A. Abd.Aziz, "Dual Band Microstrip Antenna For Wireless LAN Application", proceedings of the 2005 Asia Pacific Conference On applied Electromagnetics, Johor Bahru, Johor, Malaysia, December, pp.10698-10701, 2005.
- [8] W.S.Chen and F.M.Hsieh, "A Broadband Design For A Printed Isosceles Triangular Slot Antenna For Wireless Communications", Microwave Journal, Vol. 48, No. 7, pp.98-112, July 2005.
- [9] C.A. Balanis, "Antenna Theory Analysis and Design", Second Edition, New York: Wiley, 1997.
- [10] K.F.Lee, K.M.Luk, and J.S.Dahele, "Characteristics of The Equilateral Triangular Patch Antenna", IEEE Transactions On Antennas and Propagation, Vol. 36, No 10, pp. 1510-1518, November 1988.
- [11] R.F.Harrington, Time-Harmonic Electromagnetic Fields, IEEE Press, New York, 2001.
- [12] S. Jazi, A New Formulation for the Design of Chebyshev Arrays, IEEE Transactions on Antennas and Propagation, Vol. 42, No. 3, pp. 439-443, March 1994.
- [13] J. Costantine, "New Multi Wide Band Design for a Microstrip Patch Antenna" Master thesis, American University of Beirut, October 2006.

A Study of Energy Efficient Embedded Processor and its Reuse

R. KATHIRESH¹

P. KALIDASS²

M. SENTHIL KUMAR³

1. PG scholar, Department of ECE (PG), Ranganathan Engineering College, Coimbatore, India.

2. PG scholar, Department of ECE (PG), Ranganathan Engineering College, Coimbatore, India.

3. Assistant Professor, Department of ECE (PG), Ranganathan Engineering College, Coimbatore, India.

Abstract:

In Electronics Industry, designing of a processor must meet all requirements, but fails to meet one or two ones. In multi-applications like microprocessors, signal generations and testing of processors. An embedded processor must compute the necessary result when performed through instructions. The efficiency of instruction has attracted much attention since the instruction cache accesses consume a great portion of the whole processor power dissipation and finally leads to inefficient nature. We propose a memory architecture/structure cache to utilize the instructions delivery as an alternative way. The main theme is to reuse the retired instructions from the pipeline back-end of a processor and performs well and efficiency in power.

Key words: - Cache memories, Computer architecture, Energy Management, Microprocessors

I. Introduction

Improving the efficiency of instruction delivery has been an important strategy in boosting processor performance. In addition to employ cache memories, schemes for control flow also being proposed. Some of the well known research topics include branch prediction, instruction prediction and trace caches. On the other hand simply allocating more hardware to increase the size of instruction cache has become a viable option for embedded processors. To achieve better efficiency for the cache system, the filter cache scheme being developed to trade performance for better energy. However this leads to degradation in performance of increased access latency. Essentially the front end of processor improves the energy efficiency of instruction delivery. The efforts to aim to speculate the right program traces prior to the branch instructions are resolved, reduces the program execution latency or the energy consumption via the speculated trace information. Since the speculated traces given that they are correctly predicted, will ultimately be retired from pipeline and become history traces. These executed traces are potentially very useful in case of an embedded processor. For more number of instructions to execute the embedded processor will take more cycles to complete the loop due to branch prediction. Branching can be avoided, if embedded processor fetches instructions in the history trace.

II. Existing survey

To investigate the feasibility of delivering instructions from the pipeline back-end, we perform simulations using the processor model as shown in fig., The architecture consists of an embedded processor with additional D-Flip flops at each stage of the pipeline and HTB at the back end. The HTB is managed as a FIFO (first input first output) buffer to capture a fixed length of most recently retired instruction sequence. For each instruction fetched from the front-end, the HTB is searched to see if the same instruction also hits in the buffered history trace. The total instructions fetched are summed throughout the simulation to calculate the raw HTB hit rate

Due to the reduced complexity and size, the HTB is far less than power hungry than the instruction cache. If an instruction can be delivered from the HTB whenever a hit occurs, an energy saving proportional to the hit rate can be achieved. In this paper we propose a novel scheme called Trace Reuse (TR) cache to improve the energy efficiency of instruction delivery for embedded processors. These instructions are useless for program execution but are inevitable for perfect predictors.

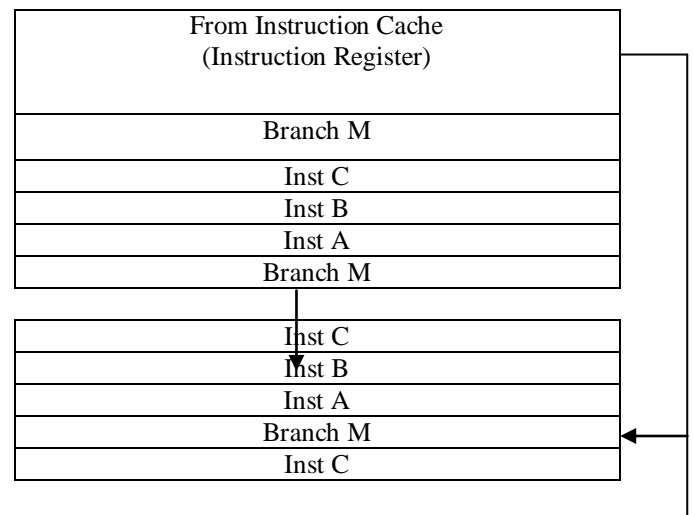


Fig. Pipeline and the history trace buffer

III. TR CACHE & design

The TR-CACHE is composed of a History Trace-Buffer (HTB), which collects the instructions retrieved from the pipeline back end of the processor, and a trace entry table. We present a TR Cache architecture that is capable of delivering instructions from HTB for embedded processors. The architecture of the TR Cache is shown as follows:

A simple multiplexer and mode switching logic are integrated into the fetch stage to select the proper instructions source. We present a TET design to index the HTB buffer for instruction source. The TET is a small memory structure used to group the instructions in the HTB buffer. The TET stores the trace-entry records each of which consists of the PC value of a control transfer instruction and the corresponding HTB entry index. The contents of HTB and TET are updated as follows: whenever an instruction is retired from the pipeline backend, it is buffered in the HTB along with its PC. Since the HTB is managed in a FIFO fashion. The oldest instruction will be discarded to make room for new one. If the discarded instruction is a marked trace entry, the corresponding record in TET will also be invalidated.

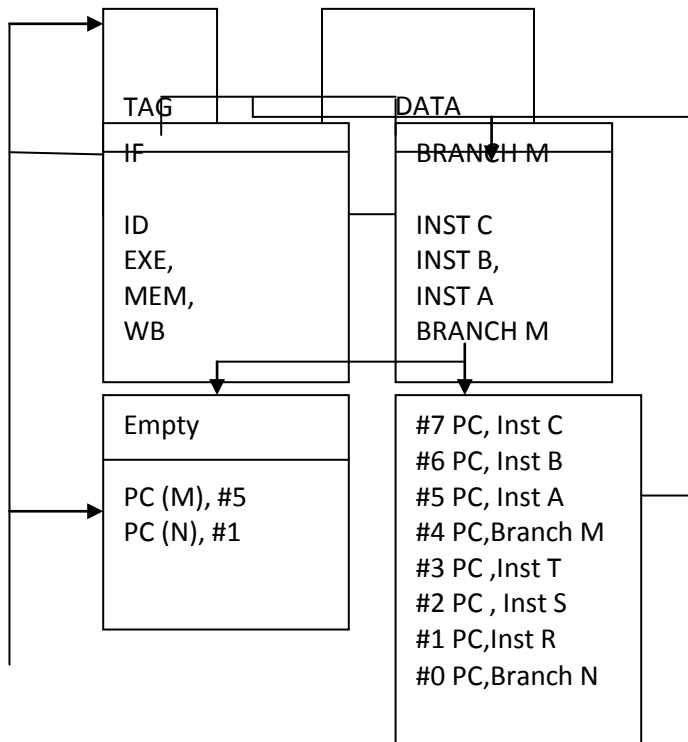


Fig: TR Cache Architecture for Embedded processor

To improve instruction buffering efficiency, a more complex basic block threading mechanism such as the design in may be used. On the other hand, the HTB is a simple FIFO without the complex logic for associative lookups. The HTB uses a simple index-based access mechanism, to be presented which brings advantages in power and area usage as compared with an associative look-up based design.

Flow method of TR Cache

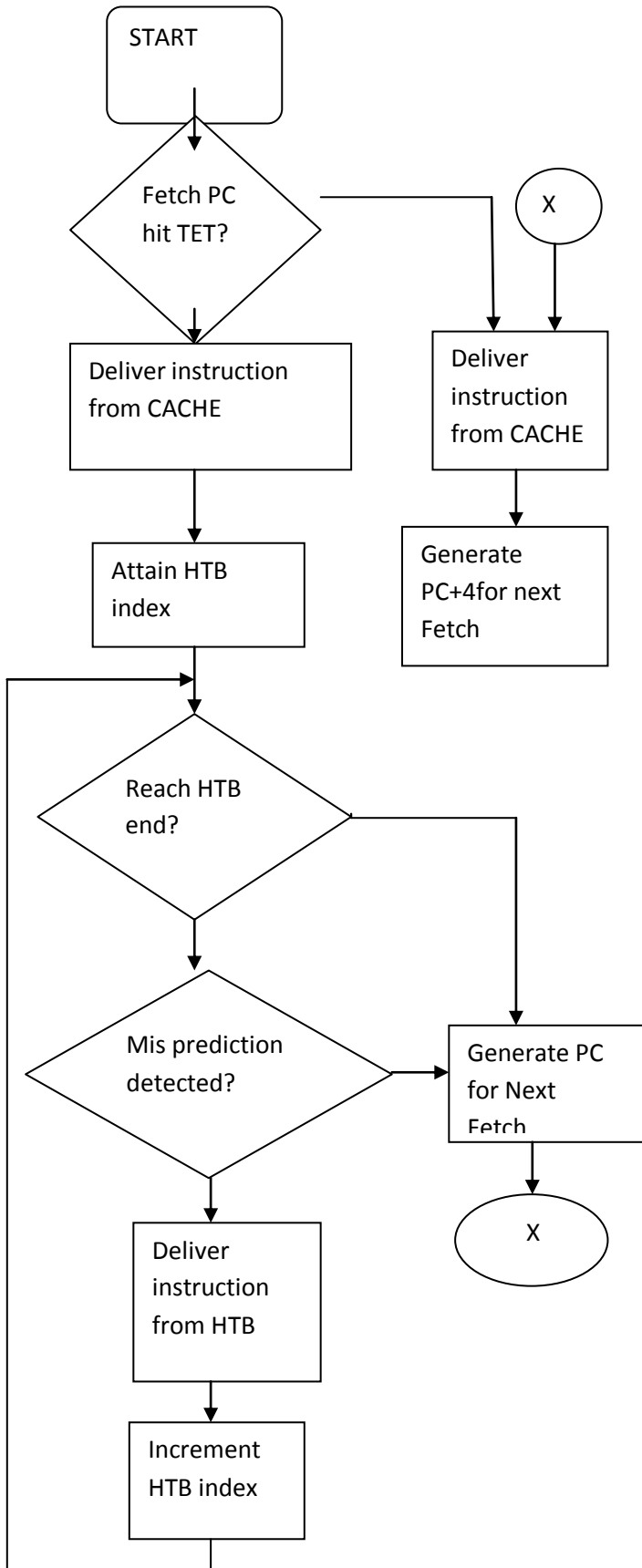
The TR Cache an alternative source for instruction delivery, a new access mode is integrated to the fetch logic. We name the original access mode as the cache mode and the new ones as the TRC Mode. By Default the processor is in cache mode cycle, the TET is searched in parallel with the cache. The processor remains in cache mode until the TET search returns a HIT.

When Hit occurs, the HTB index returned by the TET will be latched and the processor will switch to the TRC mode at the next cycle. The availability of the incoming instruction is conformed by checking the current HTB index against the HTB boundary pointers. If the index has reached the end of the HTB, the TRC-mode operation will be aborted and the next PC will be generated for the cache-mode operation.

HTB-Size (Instructions)	32	64	128	256
Max.TET record count	15	22	41	72

Table1.different HTB sizes Vs TET record count

The TET Size to be used is actually dependent on both the size of the HTB and the program behavior.The instruction delivery of TRC is as follows:



IV. RESULTS

The new RTL code of the modified processor core, which includes the register file and the completed pipelined datapath is synthesized using UMC 90-nm technology library.

A. Access time and area estimations

It is clear that the access time of the direct-mapped TETs is far less than that of the 16KB/32-Way Instruction Cache. This shows that TET search in parallel with the cache mode operation has no impact on the processor cycle time.

B. IPC Performance analysis

The average IPC is due to the large variations in the elapsed cycle counts of the programs.

$$IPC_{average} = \frac{\sum I_k}{\sum C_k}$$

The TR Cache provides significant performance improvement over the baseline processor.

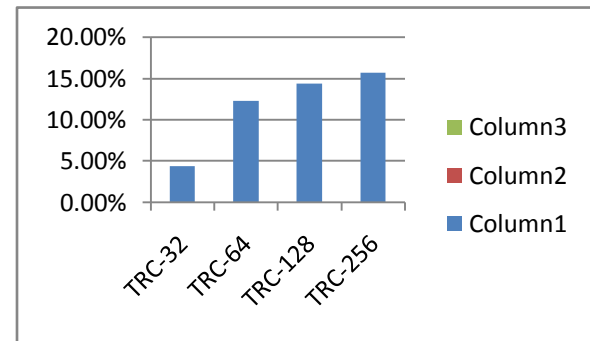


Fig. Average IPC Improvement Rate.

The basic idea behind branch prediction is to extract useful branch targets from the history trace.

C. Energy Efficiency

We present the evaluation of energy consumption and normalized energy-delay product of using the TR Cache. The Energy consumption of the fetch logic mainly comes from the power dissipation of the instruction cache and the augmented memory structures such as TET and HTB.

V. CONCLUSION

In this paper, the TR Cache architecture is proposed as an alternative source for instruction delivery of embedded processor. The processor can switch to the TR cache when a reusable trace is identified. The main difference of having TR Cache is that it can compute post-execution program information in a sequence over the conventional instruction cache.

REFERENCES

- [1] yi-yting tsai, chung-ho chen, "Efficient Embedded processors" Tech. Rep. Sep 2011
- [2] S. McFarling, "Combining Branch predictors", Digital WRL, Jun. 1993.
- [3] J.L. Hennessy and D.A. Patterson, *Computer Architecture: A Quantitative approach*, 4th ed. San Francisco, CA: Kaufman 2006.
- [4] E. Rotenberg, S. Bennett and J.E. Smith, "A trace cache microarchitecture and evaluation", *IEEE Trans. Comput.*, Vol. 48, no. 2, pp. 111-120, Feb. 1999
- [5] A. Hossain, D.J. Pease, J.S. Burns and N. Parveen, "Traces cache performance parameters", *IEEE Trans. Comput. Des.*, Feb. 2002, pp. 348-255.
- [6] J. Kin, M. Gupta and W.H. Magione-Smith, "Filter cache: An energy efficient memory structure", in *proc. 30th int. Symp./Microarch.*, Dec 1997, pp. 184-193.
- [7] T. Austin, E. Larson and D. Ernst, "Simple Scalar", "An infrastructure for computer system modeling", *IEEE Trans. Comput.*, vol. 35, no. 5, pp. 505-517, May 2007.
- [8] A. Soldani and G.S. Sohi, "Dynamic Instruction Reuse", in *Proc. 24th ANNU. Int. Symp. Comput. Arch.*, Jun. 1997, pp. 335-340.

Optimal location of STATCOM for reducing voltage fluctuations

K. Samrajyam¹, R. B. R. Prakash²

*(EEE Department, KL University, INDIA)

** (EEE Department, KL University, INDIA)

Abstract:

This paper deals with the optimal location of static synchronous compensator (STATCOM) for reducing voltage fluctuation at different buses. A 12 bus system with an actual weak power system with two near by large wind farms (WF) is introduced used as an example to illustrate the technique. The STATCOM is one of the most promising FACTS devices for solve power quality issues. In this paper the optimal location of a STATCOM is investigated based on the MATLAB/SIMULINK. The results obtained shown that optimal placement of the STATCOM varies with the change the location of the STATCOM at different buses. And the fault level characteristics at different locations also observed. Finally, a STATCOM control strategy for voltage fluctuation suppression is presented and dynamic simulations verify the performance of proposed STATCOM and its control strategy.

Keywords: optimal location, static synchronous compensator (STATCOM), wind farm (WF), Voltage fluctuations.

I. INTRODUCTION

Power systems components mainly consist of generators, transmission lines, transformers, switches, active or passive compensators and loads. Power system networks are complex systems that are nonlinear, non-stationary, and prone to disturbances and faults. Reinforcement of a power system can be accomplished by improving the voltage profile, increasing the transmission capacity and others. Nevertheless, some of these solutions may require considerable investment that could be difficult to recover. Flexible AC Transmission System (FACTS) devices are an alternate solution to address some of those problem[1]. Simple heuristic approaches are traditionally applied for determining the location of FACTS devices in a small power system. However, more scientific methods are required for placing and sizing FACTS devices in a larger power system network. FACTS sizing and allocation constitutes a milestone problem in power systems.

However, with wind being a geographically and climatically uncontrollable resource and the nature of distributed wind induction generators, the stability and power quality issues of integrating large wind farm (WF) in grid may become pronounced, particularly into a weak power system. Conventionally, the low-cost mechanical switched capacitor (MSC) banks and transformer tap changers (TCs) are used to address these issues related to stability and power quality. However, although these devices help

improve the power factor of WF and steady-state voltage regulation, the power quality issues, such as power fluctuations, voltage fluctuations, and harmonics, cannot be solved satisfactorily by them because these devices are not fast enough[3]. Moreover, the frequent switching of MSC and TC to deal with power quality issues may even cause resonance and transient overvoltage, add additional stress on wind turbine gearbox and shaft, make themselves and turbines wear out quickly and, hence, increase the maintenance and replacement cost[4]. Therefore, a fast shunt VAR compensator is needed to address these issues more effectively, as has been pointed out in many literatures [2],[4]-[7].

The static synchronous compensator (STATCOM) is considered for this application, because it provides many advantages, in particular the fast response time (1–2 cycles) and superior voltage support capability with its nature of voltage source. With the recent innovations in high-power semiconductor switch, converter topology, and digital control technology, faster STATCOM (quarter cycle) with low cost is emerging, which is promising to help integrate wind energy into the grid to achieve a more cost-effective and reliable renewable wind energy. In this paper, the effectiveness of a STATCOM in facilitating the integration of a large WF into a weak power system is presented. Firstly, an actual weak power system with two nearby large WFs is introduced. A STATCOM is proposed for dynamic voltage control, particularly to suppress the short-term (seconds to minutes) voltage fluctuations. Secondly, a model of the system, WF and STATCOM for steady state and dynamic impact study is developed in the MATLAB simulation environment. Finally, a STATCOM control strategy for voltage fluctuation suppression is presented, and the dynamic simulations are used to verify the Performance of the proposed STATCOM and its control strategy.

The main goal of this paper is to show the application of STATCOM for the optimal allocation of a Static Compensator (STATCOM), shunt FACTS device, in a power system A 12 bus system used as an example to illustrate the methodology.

Section II presents the concepts of system description. The modelling and control of the power system used in this study is presented in section III. In section IV the CMC based STATCOM described. Section V presents the Optimal location of statcom and simulation results are presented. In section VI Conclusions are given.

II.
III.

IV. SYSTEM DESCRIPTION

Fig. 1 shows the diagram of the system investigated in this paper. The two WFs, WF1 and WF2, are connected at bus 3 and 6. The system is supplied by the two main substations, which are represented by three remote boundary equivalent sources at bus 1, 2, and 12. The WF2 located at bus3 with variable-speed double fed induction generators (DFIGs). The WF1 at located at bus6 using fix-speed squirrel-cage induction generators (SCIGs). The integration of WF2 into the grid is facilitated by the power-converter-based interface as it provides VAR compensation capability and, hence, voltage control capability. On the other hand, theWF1 poses a challenge, as the SCIGs sink more VARs when they generate more real power, the generated wind power is rapidly fluctuating with uncontrollable wind speed and large surge current during frequent start ups of wind turbines. Thus, when WF1 is located at the weakest part of the loop system, these characteristics of WF1 not only increases the transmission and distribution losses, reduces the system voltage stability margin, and limits power generation, but also causes severe voltage fluctuations and irritates the customers in the system, particularly in the weak 69-kV loop, where a significant portion of the loads are induction motors, which is sensitive to voltage fluctuations.

To reduce the voltage fluctuations and improve power factor, small size MSCs (hundreds kilo var) are installed at each individual SCIG terminal and large size MSCs (1–2 Mvar) are installed at bus 6. All the main transformers T1–T4 and many customer transformers have several taps, and two additional MSCs (2.75Mvar each) are installed at bus 8. However, because of slow response time, these devices do not satisfactorily address the dynamic issues of WF1, and even exacerbate them.

WF1 produces 1–2 Mvar(capacitive) because of the shunt capacitance of the underground cables connecting individual wind turbines to the common bus6. There is also voltage fluctuation even without any WF1 generation, which means that the voltage fluctuations of local system are not only caused by generated power fluctuation of WF1, but they are also contributed by WF2 and voltage fluctuations at the remote boundary buses. Therefore, a single STATCOM using cascaded-multilevel converter (CMC) is proposed to suppress the voltage fluctuations of the weak loop system. The STATCOM is located based on different buses in the system and observing the location where voltage fluctuation reduce more.

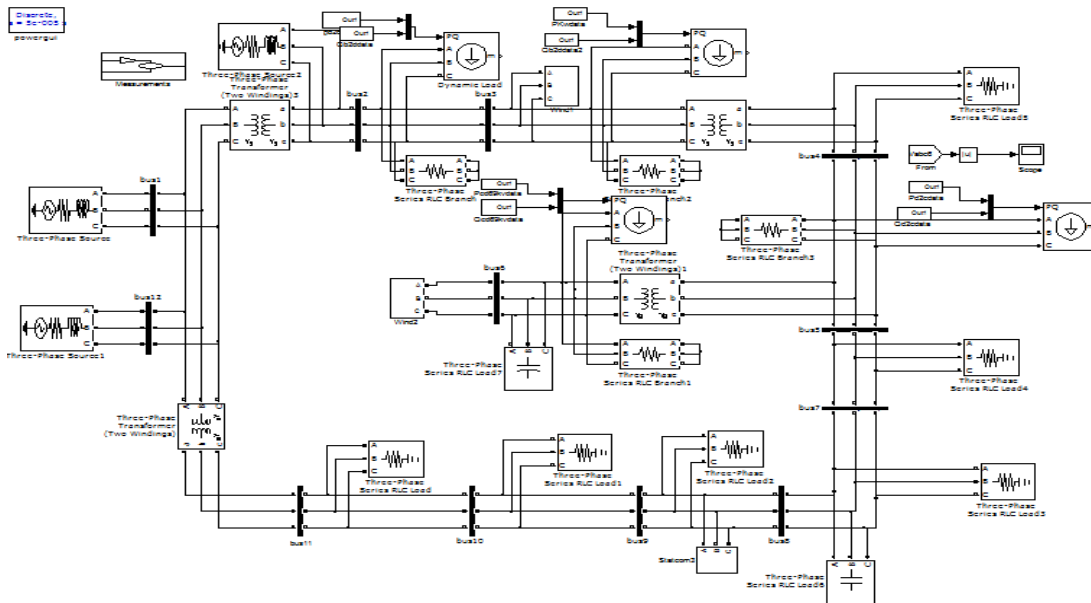


Fig1.proposed simulink model diagram

V. MODELING AND CONTROL

In this section, the modeling, MATLAB implementation and validation of the studied 12-bus power system, WF, and STATCOM are presented.

In this paper the main circuit consists of two WF. One advantage of Simulink over circuit simulators is the ease in modeling the transients of

electrical machines and drives and to include drive controls in the simulation. According to his model, the modeling equations in flux linkage form are as follows:

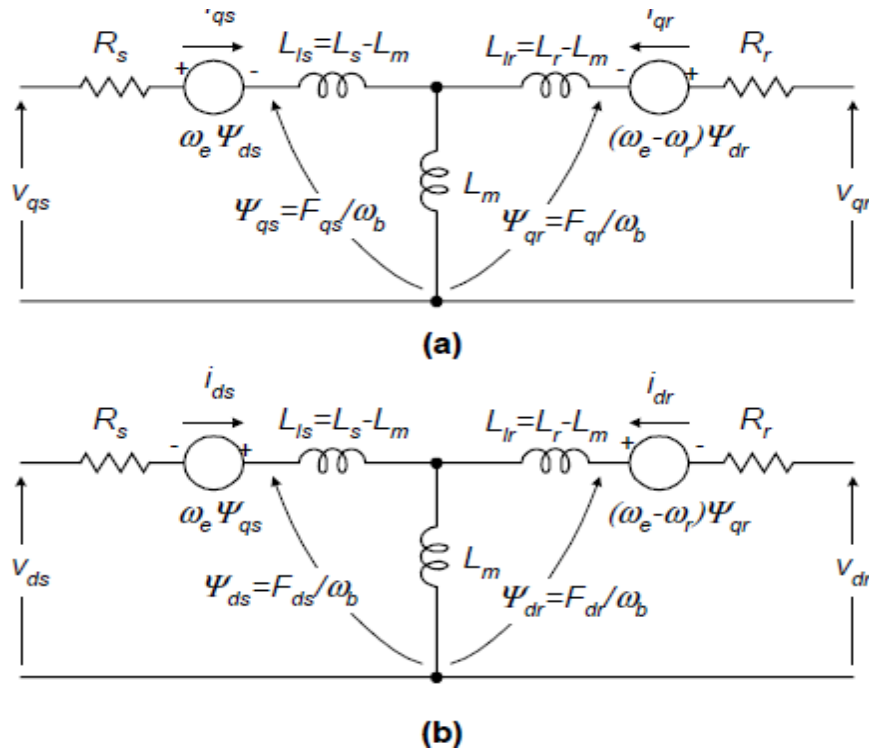


Fig. 2. Dynamic or d-q equivalent circuit of an induction machine

$$\frac{dFqs}{dt} = \omega b \left[Vqs - \frac{\omega e}{\omega b} Fds + \frac{Rs}{xls} (Fmq + Fqs) \right] \quad (1)$$

$$iqs = \frac{1}{xls} (Fqs - Fmq) \quad (7)$$

$$\frac{dFds}{dt} = \omega b \left[Vds + \frac{\omega e}{\omega b} Fqs + \frac{Rs}{xls} (Fmd + Fds) \right] \quad (2)$$

$$ids = \frac{1}{xls} (Fds - Fmd) \quad (8)$$

$$\frac{dFqr}{dt} = \omega b \left[Vqr - \frac{(\omega e - \omega r)}{\omega b} Fdr + \frac{Rr}{xlr} (Fmq - Fqr) \right] \quad (3)$$

$$iqr = \frac{1}{xlr} (Fqr - Fmq) \quad (9)$$

$$idr = \frac{1}{xlr} (Fdr - Fmd) \quad (10)$$

$$Te = \frac{3}{2} \left(\frac{p}{2} \right) \frac{1}{\omega b} (Fdsiqs - Fqsids) \quad (11)$$

$$\frac{dFdr}{dt} = \omega b \left[Vdr + \frac{(\omega e - \omega b)}{\omega b} Fqr + \frac{Rr}{xlr} (Fmd - Fdr) \right] \quad (4)$$

$$Te - Tl = J \left(\frac{2}{p} \right) \frac{d\omega r}{dt} \quad (12)$$

Where

d: direct axis,
 q:quadrature axis
 s:stator variable,
 variable,
 linkage (i=q or d and j=s or r),
 axis stator voltages,

r:rotor
 Fij is the flux
 Vqs, Vds : q and d-
 Vqr, Vdr : q and d-axis

$$Fmq = \dot{X}ml \left[\frac{Fqs}{xls} + \frac{Fqr}{xlr} \right] \quad (5)$$

$$Fmd = \dot{X}ml \left[\frac{Fds}{xls} + \frac{Fdr}{xlr} \right] \quad (6)$$

rotor voltages, F_{mq}, F_{md} : q and d axis magnetizing flux linkages, R_r : rotor resistance, R_s : stator resistance, X_{ls} : stator leakage reactance ($\omega_e L_s$), X_{lr} : rotor leakage reactance ($\omega_e L_r$), X_{ml} : $\left[\frac{1}{\frac{1}{x_{ml}} + \frac{1}{x_{ls}} + \frac{1}{x_{lr}}} \right]$, i_{qs}, i_{ds} : q and d-axis stator currents, i_{qr}, i_{dr} : q and d-axis rotor currents, P : number of poles, J : moment of inertia, T_e : electrical output torque, T_L (or T_I) : load torque, ω_e : stator angular electrical frequency, ω_b : motor angular electrical base frequency, and ω_r : rotor angular electrical speed.

For a squirrel cage induction machine as in the case of this paper, V_{qr} and V_{dr} in (3) and (4) are set to zero.

An induction machine model can be represented with five differential equations as seen above. To solve these equations, they have to be rearranged in the state-space form, $\dot{x}=Ax+b$ where $x=[F_{qs} \ F_{ds} \ F_{qr} \ \omega_r]^T$ is the state vector. Note that $F_{ij} = \psi_{ij} \cdot \omega_b$, where F_{ij} is the flux linkage ($i=q$ or d and $j=s$ or r) and ψ_{ij} is the flux.

In this case, state-space form can be achieved by inserting (5) and (6) in (1-4) and collecting the similar terms together so that each derivatives is a function of only other state variables and model inputs. Then, the modeling equations (1-4 and 12) of a squirrel cage induction motor in state-space become

$$\frac{dF_{qs}}{dt} = \omega_b \left[V_{qs} - \frac{\omega_e}{\omega_b} F_{ds} + \frac{R_s}{x_{ls}} \left(\frac{x_{ml}}{x_{lr}} F_{qr} + \left(\frac{x_{ml}}{x_{ls}} - 1 \right) F_{qs} \right) \right] \quad (13)$$

$$\frac{dF_{ds}}{dt} = \omega_b \left[V_{ds} - \frac{\omega_e}{\omega_b} F_{qs} + \frac{R_s}{x_{ls}} \left(\frac{x_{ml}}{x_{lr}} F_{dr} + \left(\frac{x_{ml}}{x_{ls}} - 1 \right) F_{ds} \right) \right] \quad (14)$$

$$\frac{dF_{qr}}{dt} = \omega_b \left[-\frac{(\omega_e - \omega_r)}{\omega_b} F_{dr} + \frac{R_r}{x_{lr}} \left(\frac{x_{ml}}{x_{ls}} F_{qs} + \frac{x_{ml} x_{lr}}{x_{ls}} - 1 F_{qr} \right) \right] \quad (15)$$

$$\frac{dF_{qs}}{dt} = \omega_b \left[\frac{(\omega_e - \omega_r)}{\omega_b} F_{dr} + \frac{R_r}{x_{lr}} \left(\frac{x_{ml}}{x_{ls}} F_{ds} + 1 F_{dr} \right) \right] \left(\frac{x_{ml}}{x_{lr}} - \right) \quad (16)$$

$$\frac{d\omega_r}{dt} = \left(\frac{p}{2J} \right) (T_e - T_L) \quad (17)$$

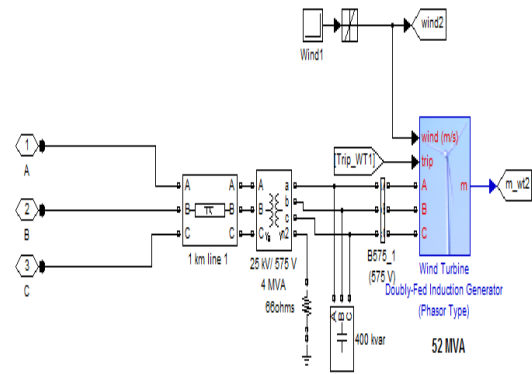


Fig.3. implementation of wind farm using MATLAB

The fig3 indicates the modeling of wind farm with doubly fed induction generator, a capacitor is connected because to improve power factor.

VI. Cascaded-Multilevel Converter-Based STATCOM

Multilevel converters are used in high power applications. These converters synthesize voltage waveform of superior harmonic spectrum and attain higher voltages with a limited maximum device rating. Several topologies with various control strategies are available in literature. These topologies are mainly classified into three types. 1) Diode clamp inverter 2) Capacitor clamp inverter 3) Cascaded inverter. In cascaded inverters, H-bridge topology is most widely used because of its modular circuit layout. In recent years cascaded two level inverter topology has become popular due to its simple power circuit configuration. The multilevel converters especially cascaded H-bridge topology are used for STATCOM application. In these converters it is difficult to control individual dc link voltages. Various control strategies are available in literature to minimize the dc voltage unbalance between converters.

The proposed STATCOM uses a CMC-based topology, as shown in Fig. 4(a). For this study, a harmonics-free dynamic model of the CMC-based STATCOM with its internal control, as shown in Fig. 4(b), is implemented on MATLAB. Fig. 4(a) responds to step change commands for increasing and decreasing its reactive power output, where the units of dc voltage, reactive current, ac voltage, ac output current, and reactive power output are kV, kA, p.u., p.u., and Mvar, respectively. As the figure illustrates, the reactive current step change response has a bandwidth as fast as a quarter cycle, and ± 10 Mvar is generated by the STATCOM, and the average dc capacitor voltage of about 1.5 kV is dynamically controlled and does not change due to the VAR command change. Therefore, the STATCOM model is validated.

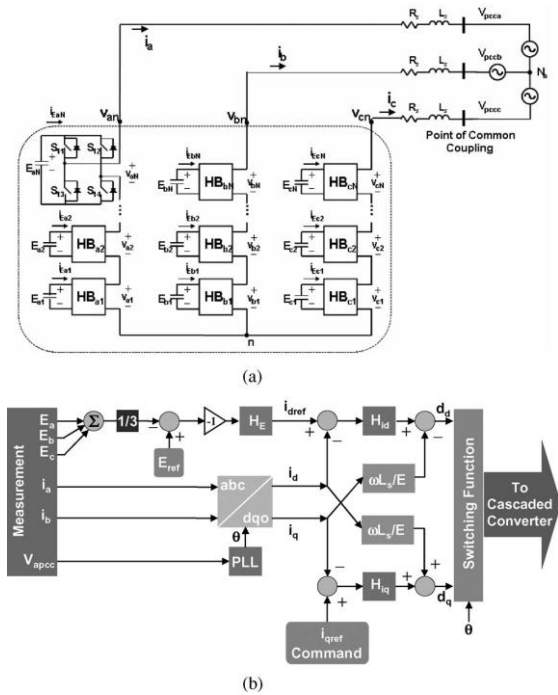


Fig. 4. Proposed STATCOM and its controller.
 a) Generalized CMC-based Y-connected STATCOM schematic. (b) Internal control strategy of CMC-based STATCOM.

To improve the performance and effectiveness of the control for the CMC-based STATCOM system, the following five contributions are proposed in this dissertation:

1. optimized design for the CMC-based STATCOM power stage and its passive components,
2. modeling of the CMC for reactive power compensation,
3. decoupling power control method,
4. DC-link balancing technique, and
5. improvement in the CMCs.

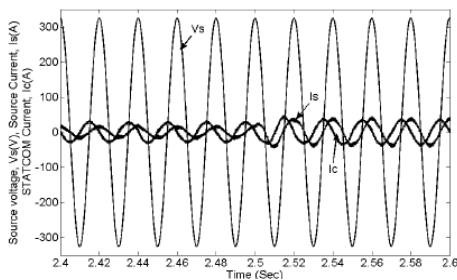


Fig.6. Source voltage, source current and STATCOM current

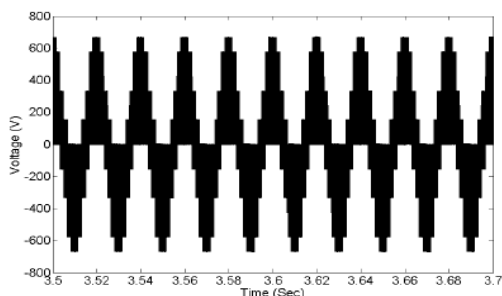
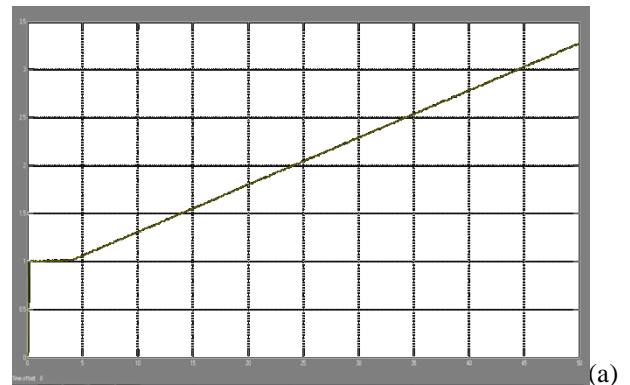


Fig.5. Cascaded converter output voltage

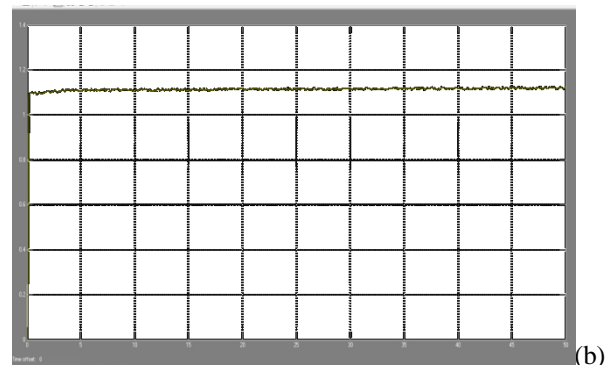
VII. Optimal location of STATCOM and simulation results

In addition, since the STATCOM suppresses the voltage fluctuation, it is apparent that, compared to the case without STATCOM, the switching times of MSCs and TCs of both main transformers and load transformers to address the voltage fluctuation issue in the system shall be significantly reduced. Therefore, the maintenance and replacement cost of MSC, TC, and wind turbines can be lowered, and the power quality issues related to the switching of MSCs and TCs can also be lessened.

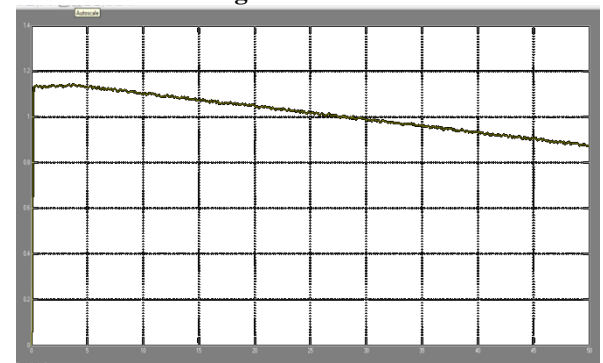
In fig the wave forms shows voltage fluctuations without and with STATCOM. In presence of STATCOM at bus8 the voltage fluctuation are completely reducing at bus5,6,8 the remaining buses are near the source so the voltage fluctuations are slightly reduced. bus 2 and 3 is almost unchanged even with STATCOM, which is obvious because they are closely connected to a very strong bus 1 with the low impedance of T1 and the short 115 kV-transmission line.



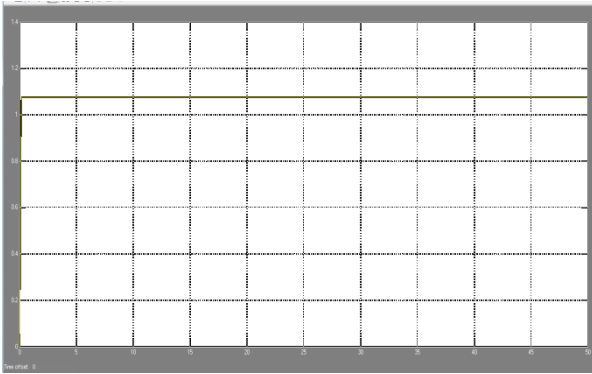
bus 5 voltage without STATCOM



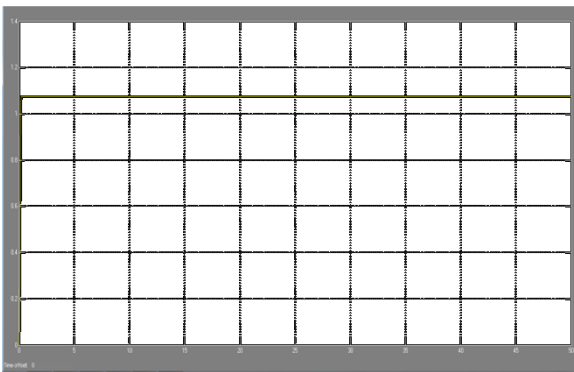
bus 6 voltage without STATCOM



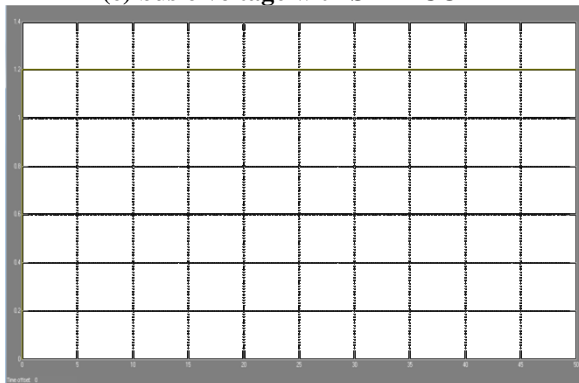
(c) bus 8 voltage without STATCOM



(d) bus 5 voltage with STATCOM



(e) bus 6 voltage with STATCOM



(f) bus 8 voltage with STATCOM

Fig.7. voltage fluctuations with and without STATCOM

If the STATCOM is connected at another bus the voltage fluctuations are reducing in that bus and remaining buses voltage fluctuations reducing depends on the distance of the STATCOM location. So from the above output waveforms we can observe in the STATCOM is connected at bus 8 the fluctuations are reducing at more number of buses. so bus 8 is the optimal location of the proposed system.

VIII. Conclusion

The optimal location of STATCOM is identifying by using matlab. This paper describes the methodology to conduct an impact study of a STATCOM on the integration of a large WF into a weak loop power system. The specific issues and solutions of the studied

WF system are illustrated. For the system study, the models for the system, WF and STATCOM are developed, and wind turbines can be reduced, and the power quality issues related to the switching of MSCs and TCs can also be lessened. For this specific application of suppressing the voltage fluctuations, the dynamic simulation results for a continuous operation period also verify the effectiveness of the proposed STATCOM and its control strategy, which can adaptively deal with voltage fluctuation, independent from system steady-state voltage regulation by operations of MSCs and TCs, and even mitigate the faster voltage fluctuations and flicker emission, possibly from WFs with well-designed fast control bandwidth. Therefore, it is concluded that the installation of a 10-Mvar STATCOM system is effective for integrating the specific WF into the weak loop power system. The fault at different location also with or without STATCOM is observed.

IX. References

1. N.G. Hingorani, and L. Gyugyi, "Understanding FACTS; Concepts and Technology of Flexible AC Transmission Systems," IEEE Press, New York, 2000.
2. T. Ackermann, *Wind Power in Power Systems*. New York:Wiley, 2005.
3. J.W. Smith and D. L. Brooks, "Voltage impacts of distributed wind generation on rural distribution feeders," in *Proc. IEEE PES Transmiss. Distrib. Conf. Exhib.*, Oct. 28–Nov. 2, 2001, vol. 1, pp. 492–497.
4. A. Kehrlri and M. Ross, "Understanding grid integration issues at wind farms and solutions using voltage source converter FACTS technology," in *Proc. IEEE PES Gen. Meeting*, Jul. 13–17, 2003, vol. 3, pp. 1822–1827.
5. Z. Saad-Saoud, M. L. Lisboa, J. B. Ekanayake, N. Jenkins, and G. Strbac, "Application of STATCOMs to wind farms," *Inst. Elect. Eng. Proc. Gener. Transmiss. Distrib.*, vol. 145, no. 5, pp. 511–516, Sep. 1998.
6. F. Zhou, G. Joos, and C. Abbey, "Voltage stability in weak connection wind farms," in *Proc. IEEE PES Gen. Meeting*, Jun. 12–16, 2005, vol. 2, pp. 1483–1488.
7. L. T. Ha and T. K. Saha, "Investigation of power loss and voltage stability limits for large wind farm connections to a subtransmission network," in *Proc. IEEE PES Gen. Meeting*, Jun. 6–10, 2004, vol. 2, pp. 2251–2256.
8. C. Han, A. Q. Huang, M. Baran, S. Bhattacharya, and W. Litzemberger, "STATCOM impact study on the integration of a large wind farm into a weak loop power system," *IEEE Trans. Energy Conv.*, vol. 23, no. 1, pp. 226–232, Mar. 2008.

Series Voltage Compensation Using UPQC For DFIG Wind Turbine Low-Voltage Ride-Through Solution

P. Ramya krishna, R. B. R. Prakash²

*(EEE Department, KL University, INDIA)

** (EEE Department, KL University, INDIA)

Abstract:

This paper describes the problem of voltage sags and swells and its severe impact on sensitive loads and introduces a new solution for doubly fed induction generators to stay connected to the grid during voltage sags. The main idea is to increase the stator voltage to a level that creates the required flux to keep the rotor side converter current below its transient rating. To accomplish this goal, a series compensator (UPQC) is added to inject voltage in series to the stator side line. The series converter monitors the grid voltage and provides compensation accordingly to accomplish this aim. To keep the current at its minimum, a control strategy has been developed to keep the injected voltage and line voltage in phase during and after the fault. Comprehensive results are presented to assess the performance of each device as a potential custom power solution.

Index terms: Doubly fed induction generator (DFIG), grid fault, low-voltage ride through, series voltage compensation, DVR, UPQC.

1. Introduction

The DFIG is an induction machine with a wound rotor where the rotor and stator are both connected to electrical sources, hence the term 'doubly fed'. The rotor has three phase windings which are energised with three-phase currents. These rotor currents establish the rotor magnetic field. The rotor magnetic field interacts with the stator magnetic field to develop torque. The magnitude of the torque depends on the strength of the two fields (the stator field and the rotor field) and the angular displacement between the two fields.

The DFIG system therefore operates in both sub- and super synchronous modes with a rotor speed range around the synchronous speed. The stator circuit is directly

connected to the grid while the rotor winding is connected via slip rings to a three-phase converter. For variable-speed systems where the speed range requirements are small, for example $\pm 30\%$ of synchronous speed, the DFIG offers adequate performance and is sufficient for the speed range required to exploit typical wind resources.

An easy way to protect the converter is to disconnect the generator during low-voltage conditions. But many regulations have been developed and are under development to support the grid during short circuits with reactive power and prevent disconnection to deliver power when the voltage is restored. Recently, many researchers

have focused on different techniques to overcome the low-voltage ride-through (LVRT) issue.

There are many different methods to mitigate voltage sags and swells, but the use of a custom Power device is considered to be the most efficient method. Switching off a large inductive load or Energizing a large capacitor bank is a typical system event that causes swells [1].

When short circuit occurs on the grid side, the rotor currents rise and if the converter is not protected against these high currents, it will be damaged. The system has two modes of operation which are: the series voltage compensation using DVR. In this mode of operation, the voltage sags are mitigated but not completely. So in this proposed solution, the system using UPQC for series voltage compensation. In this method the voltage sags are completely mitigated. The use of the Clarke transform, the real (I_d) and imaginary (I_q) currents can be identified. The Park transform can be used to realize the transformation of the I_d and the I_q currents from the stationary to the moving reference frame and control the spatial relationship between the stator vector current and rotor flux vector.

2. conventional system configuration of upqc

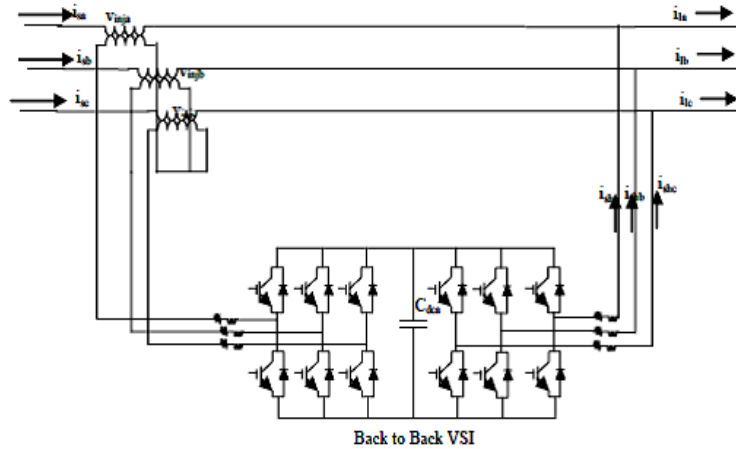


Fig.2.UPQC Block Diagram

The UPQC, realized by using two VSI is shown in Fig.2. One acting as a shunt APF, while the other as series APF. Both the APFs share a common dc link in between them. Each inverter is realized by using six IGBT (Insulated Gate Bipolar Transistor) switches. The voltage at the source side before UPQC, the load voltage at load, the voltage injected by series APF and the dc link voltage between two inverters are represented by v_s , v_L , v_{inj} and V_{dc} respectively. Whereas, the current on the source side, total current drawn by all the loads and the current injected by shunt APF are represented by i_s , i_l , and i_{sh} respectively.

DFIG during grid fault

Many references have discussed the modeling of DFIG wind turbines [8], [9]. Fig. 3 shows the block diagram of a DFIG wind turbine system. The generator has a three-phase wound rotor supplied, via slip rings, from a four-quadrant, pulse width modulation (PWM) converter with voltage of controllable amplitude and frequency [4].

A Park model in the stationary stator-orientated reference frame, developed for DFIG in [10], is used to analyze the effect of grid fault on the generator. In this model, the rotor variables are referred to the stator side for simplicity. Using motor convention, the stator and rotor voltages in *abc* frame can be expressed as

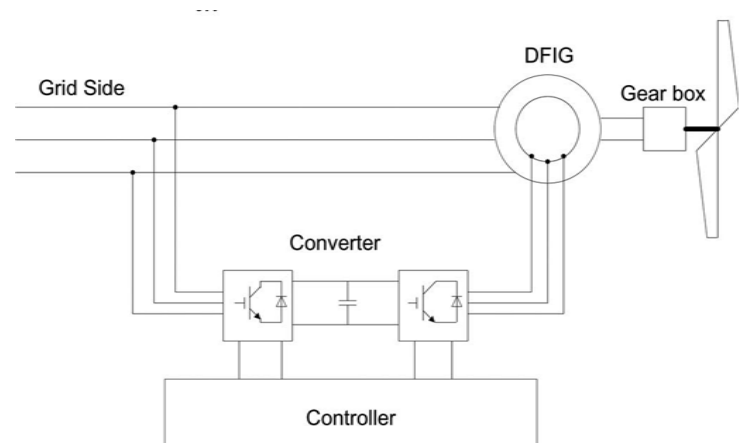


Fig. 3. Steady-state operation of the Doubly-Fed Induction Generator (DFIG)

$$\vec{V}_s = R_s \vec{i}_s + \frac{d}{dt} \vec{\Psi}_s \tag{1}$$

$$\vec{V}_r = R_r \vec{i}_r + \frac{d}{dt} \vec{\Psi}_r - j\omega_m \vec{\Psi}_r \tag{2}$$

The stator and rotor fluxes are given by

$$\vec{\Psi}_s = L_s \vec{i}_s + L_m \vec{i}_r \tag{3}$$

$$\vec{\Psi}_r = L_r \vec{i}_r + L_m \vec{i}_s \tag{4}$$

Where $L_s = (L_{ls} + L_m)$ and $L_r = (L_{lr} + L_m)$

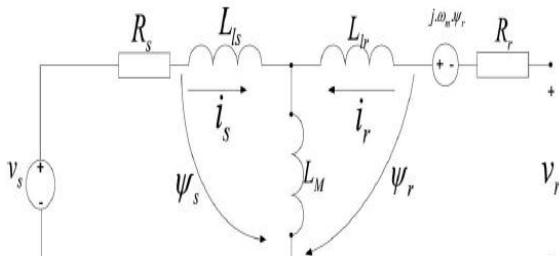


Fig.4. DFIG-equivalent circuit for short circuit analysis.

Fig. 4 shows the equivalent circuit corresponding to the aforementioned equations. For the purpose of the rotor over-current analysis during the short circuit, the rotor voltage from converter point of view is the most important variable in the analysis [10]. This voltage is induced by the variation of the stator flux, which can be calculated by deriving \vec{i}_s from (3) and substituting into (4):

$$\vec{\Psi}_r = \frac{L_m}{L_s} \vec{\Psi}_s - \sigma L_r \vec{i}_r, \quad \sigma = 1 - \frac{L_m^2}{L_s L_r} \quad (6)$$

The rotor voltage given by (6) can be divided into two terms. The first term is the open circuit voltage (\vec{V}_{r0}) and it depends on the stator flux. The second term is smaller and it is caused by the voltage drop on both the rotor resistance R_r and the rotor transient inductance σL_r . From (6), when there is no current in the rotor circuit, the rotor voltage due to the stator flux is (\vec{V}_{r0}):

$$\vec{V}_{r0} = \frac{L_m}{L_s} \left(\frac{d}{dt} - j\omega m \right) \vec{\Psi}_s \quad (7)$$

A. Analysis under normal operation

Under the normal condition, rotor current control technique is utilized to adjust the active and reactive power at the generator terminal. The rotor current phase and magnitude are controlled to regulate the reactive power at zero and keep the generator running at unity power factor. Sensed

3. proposed method

In this paper, we present a solution to use a UPQC on the stator terminal of a DFIG to mitigate the effect of the short circuit on the wind turbine. This UPQC as shown in Fig. 2, acts the same as a series active filter for voltage compensation. The UPQC internally consists of DVR and DSTATCOM which are used to mitigate the effects of unbalanced short circuit faults on the turbine. The UPQC delivers active power for a very short period. The UPQC continuously monitors the grid side voltage. When this

wind speed is used to determine the reference active power of the turbine. Under normal operation, the rotor voltage can be described as

$$\vec{V}_r = \vec{V}_s \frac{L_m}{L_s} s + \left(R_r + \sigma L_r \left(\frac{d}{dt} - j\omega m \right) \right) \vec{i}_r \quad (8)$$

Where s is the slip ($s = \frac{\omega_r}{\omega_s}$, $\omega_r = \omega_s - \omega m$).

The rotor resistance and the transient reactance are typically small. In addition, since the generator slip is limited to +30%, the rotor current frequency is $f_r < 18$ Hz [10]. As a result, the magnitude of V_{ri} in (8) is smaller than V_{r0} . The rotor voltage due to the stator flux can be written as [10]

$$\vec{V}_{r0} = j\omega_r \frac{L_m}{L_s} \vec{\Psi}_s = \frac{\omega_r L_m}{\omega_s L_s} V_s e^{j\omega m t} \quad (9)$$

The amplitude of the voltage \vec{V}_{r0} can be described as a function of the amplitude of the stator voltage as follows:

$$V_{r0} = V_s \frac{L_m}{L_s} s \quad (10)$$

During the normal operation, the rotor voltage \vec{V}_{r0} depends on the magnitude of the stator voltage and the slip.

B. Analysis During Short Circuit

At the moment of the short circuit ($t=0$), the open circuit rotor voltage due to the stator flux is given by

$$\begin{aligned} \vec{V}_{r0} &= -\frac{L_m}{L_s} \left(\frac{1}{T_s} + j\omega m \right) \cdot \vec{\Psi}_0 \cdot e^{-t/T_s}, \vec{\Psi}_0 \\ &= \frac{V_s}{j\omega_s} e^{j\omega_s t_0} \end{aligned} \quad (11)$$

where Ψ_0 is the stator flux just before the short circuit.

$$\vec{V}_{r0} = -\frac{L_m}{L_s} \left(\frac{1}{T_s} + j\omega m \right) \cdot \vec{\Psi}_0 \cdot e^{-t/T_s} e^{-j\omega_s t} \quad (12)$$

Using (12) and neglecting the term $1/\tau_s$ due to its small value ($\tau_s \approx 1s - 3s$) for a 1-MW machine and larger [7], [11], we have

$$V_{r0} = \frac{L_m}{L_s} \frac{\omega_r}{\omega_s} V_s = \frac{L_m}{L_s} (1 - s) V_s \quad (13)$$

According to (13), V_{r0} is proportional to $1 - s$.

voltage dips, the UPQC applies a voltage through series transformer to compensate for the voltage dip. The level of voltage compensation depends on the rating of the UPQC. Since the UPQC is considered to apply voltage for a very short period of time. The UPQC need to compensate for 100% of line voltage during short circuit.

voltage to produce the reference voltage for voltage regulator as shown in Fig. 11. During normal operation, the compensator is not injecting any voltage. In this case, if the

capacitor is charged at its predetermined voltage, the compensator operates at standby mode. Otherwise, it will charge the capacitor from the line.

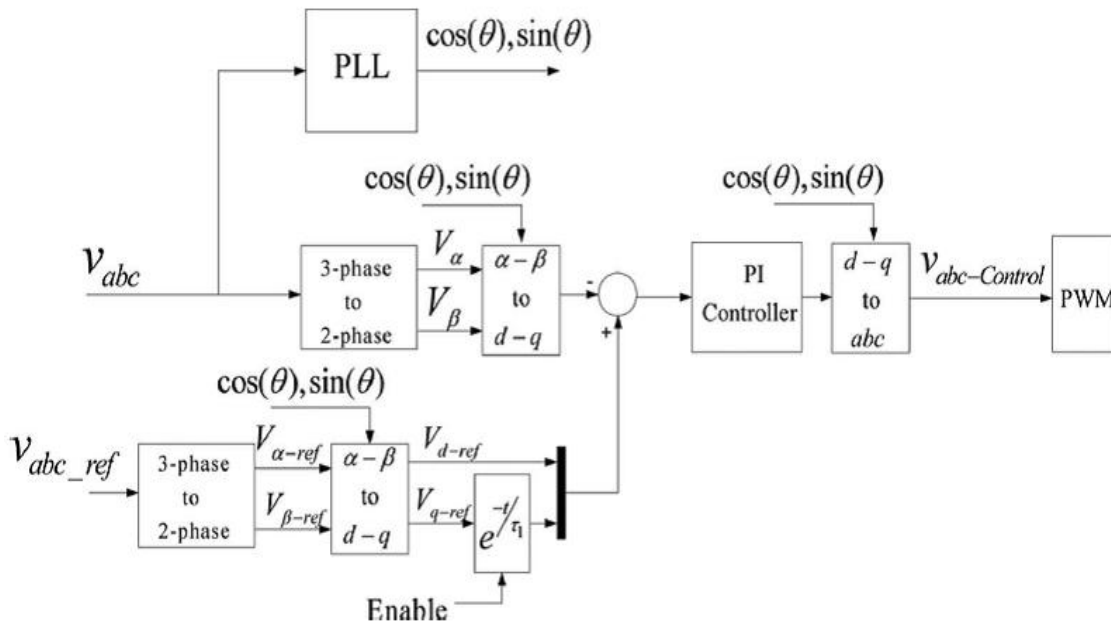
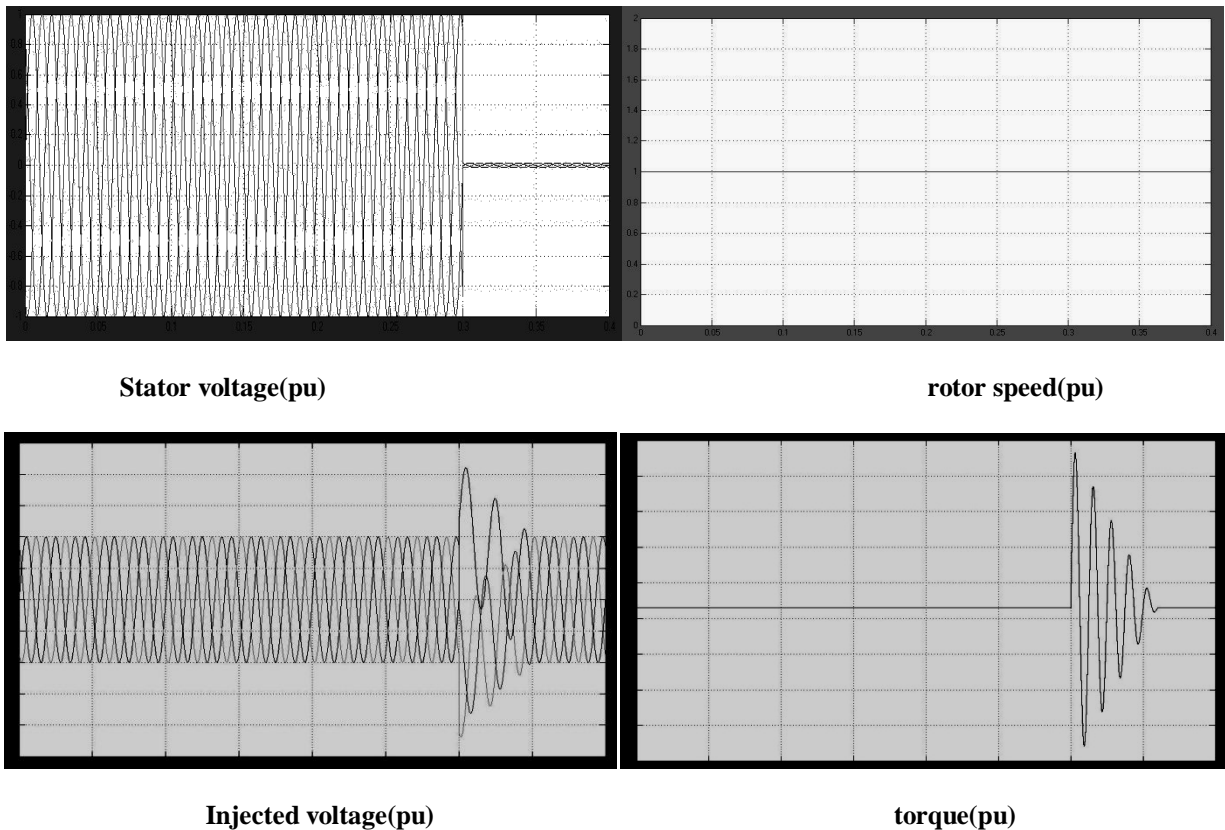


Fig. 11. Block diagram of the converter control technique.

5. simulation results:



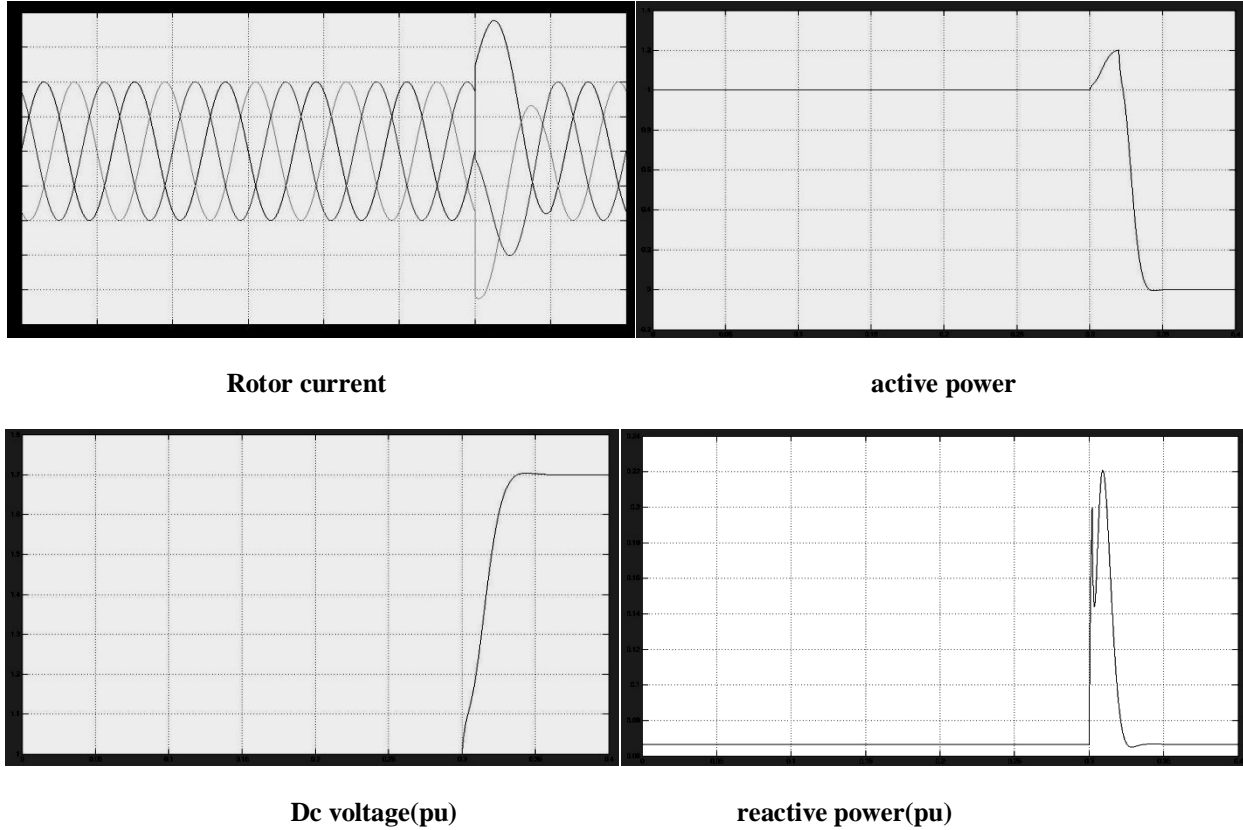
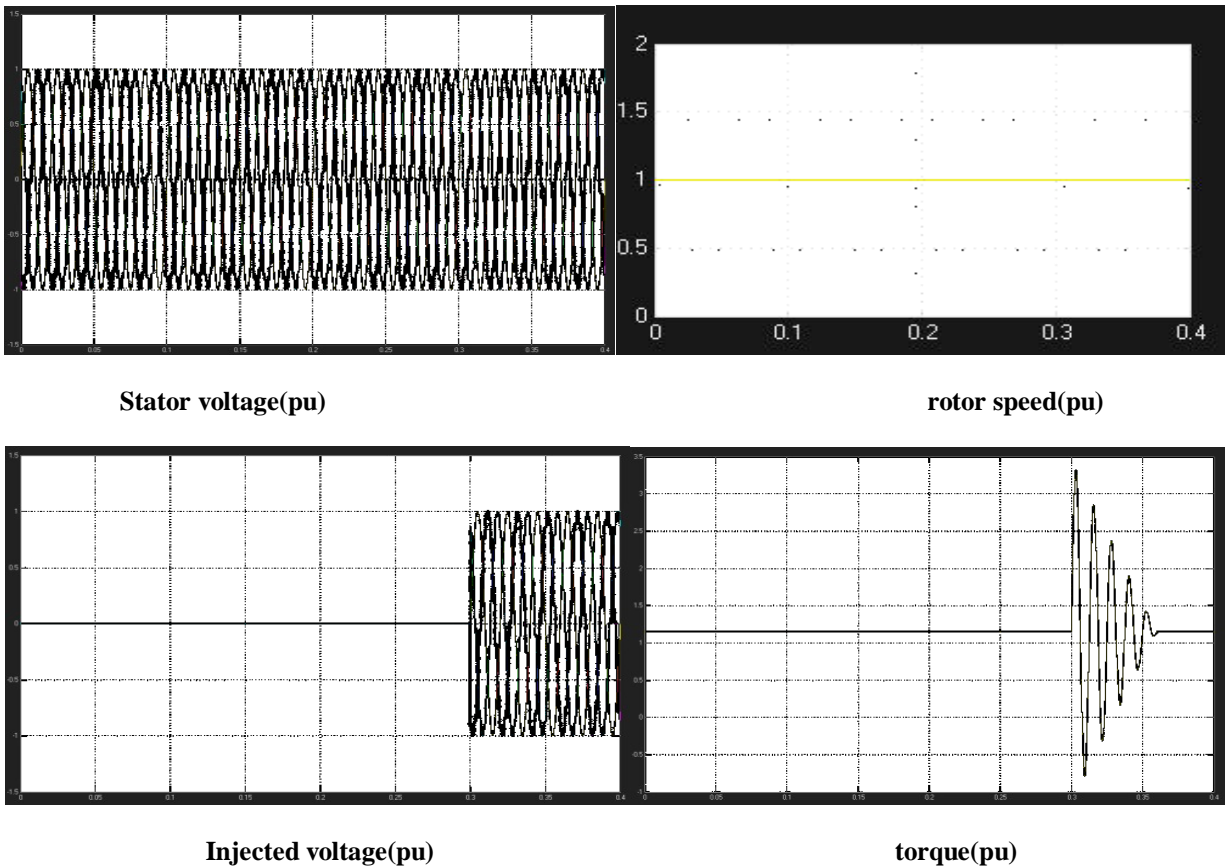


Fig.8: Simulation results for a three-phase short circuit on the terminal of a 1.5-MW DFIG wind turbine.



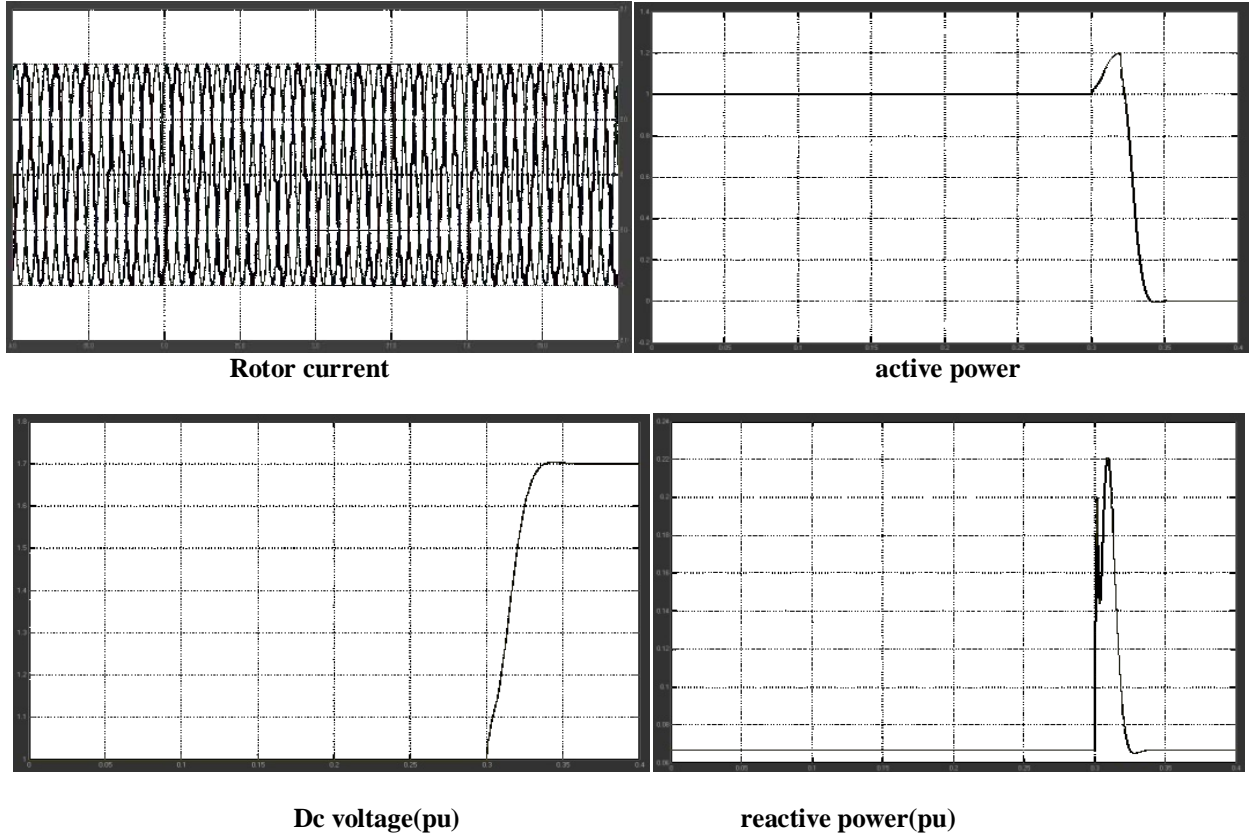
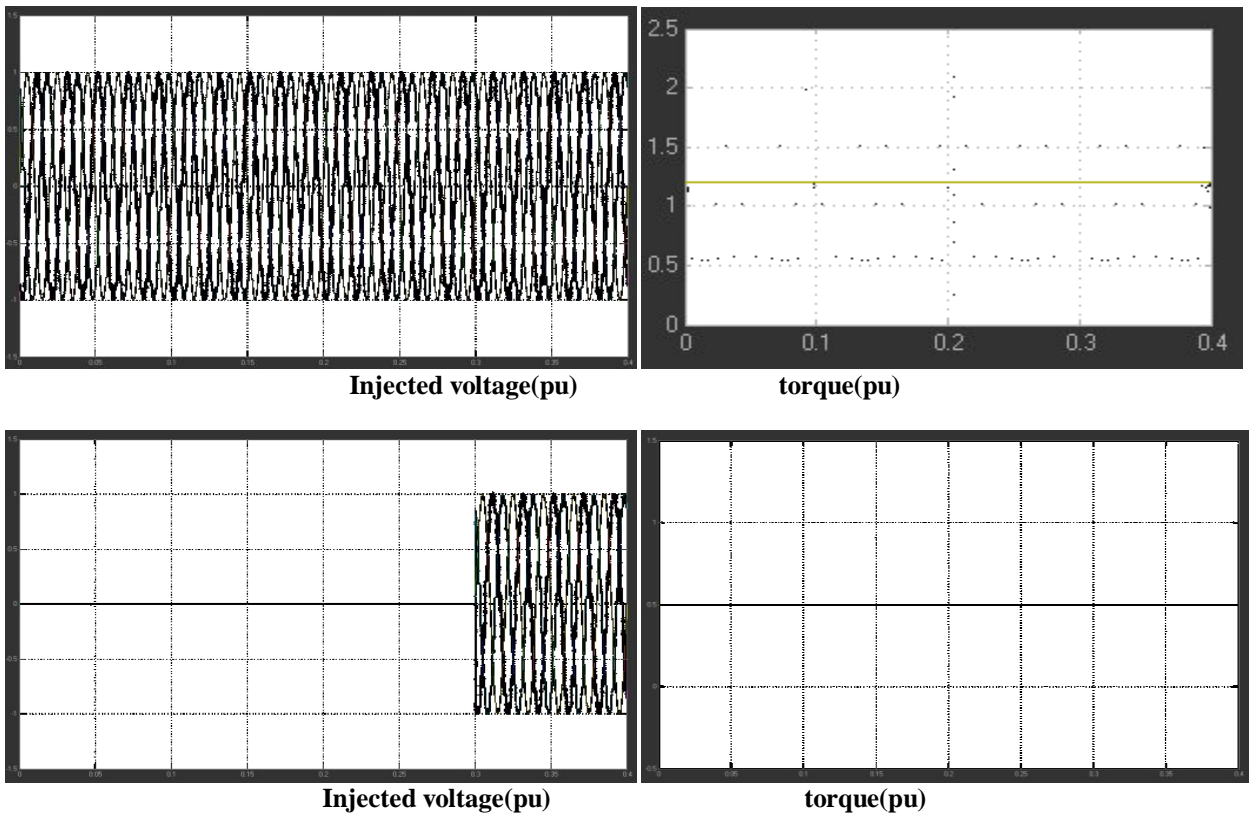


Fig.9: Simulation results for a three-phase short circuit on the terminal of a 1.5-MW DFIG wind turbine when a DVR is applied.



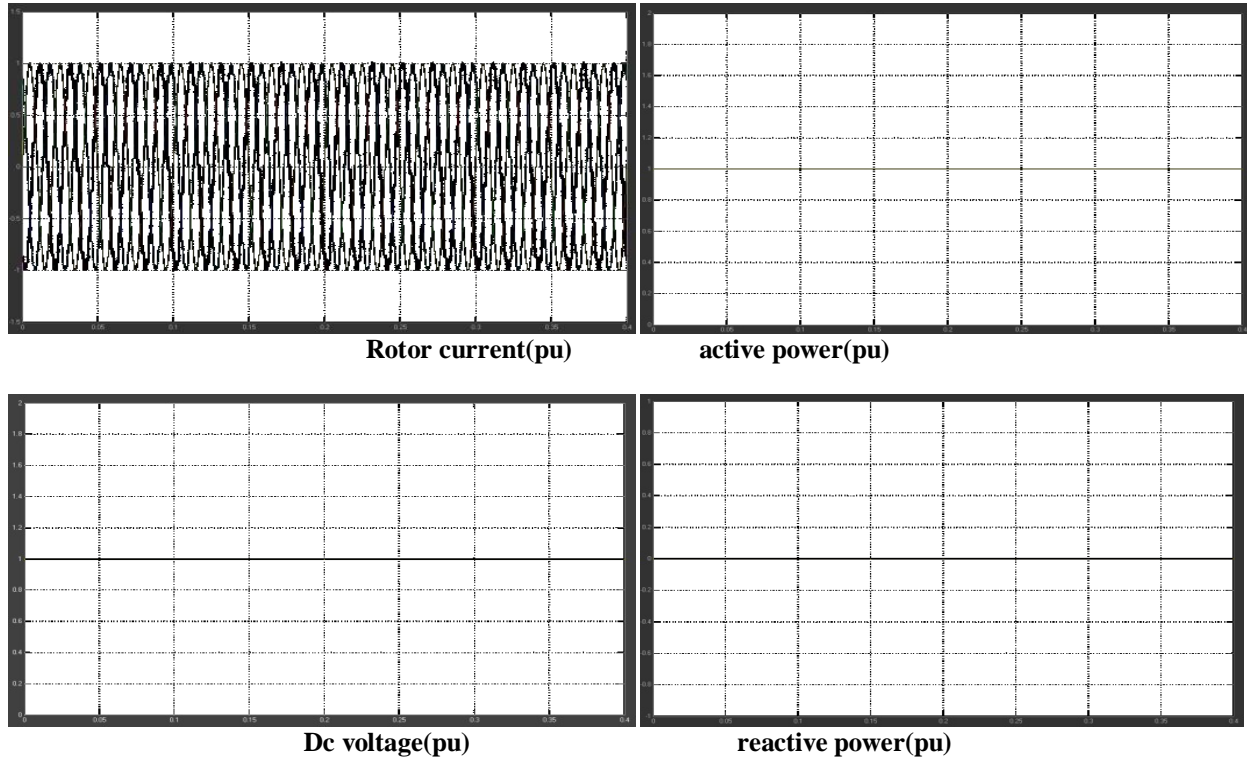


Fig.10: Simulation results for a three-phase short circuit on the terminal of a 1.5-MW DFIG wind turbine when a full compensation is applied using UPQC.

6. conclusion:

DFIG is subject to intense stress during considerable grid voltage sag. Additional measures must be taken to protect the turbine and provide LVRT even at zero grid voltage in accordance with utility requirements. Wind turbine equipped with series voltage compensator described in this paper is able to stay connected to the grid and limit the rotor currents within an acceptable range. This LVRT solution for the DFIG also allows for reactive power support to the grid during grid fault. The aim of the proposed technique is to limit the rotor side converter high currents and to provide the stator circuit with the necessary voltage via a series transformer without disconnecting the converter from the rotor or from the grid. The wind turbine can resume normal operation within a few hundred milliseconds after the fault has been cleared. For longer voltage dips, the generator can even supply reactive power to the grid. Simulation and experimental results verify the effectiveness and viability of the proposed technique. According to analyses presented, the size of the energy storage capacitor does not need to be excessively large for the system to operate.

7. Appendix

The parameters of the machine and controller that have been used for modeling and simulations are given as follows.

Simulation Parameters	Experimental Setup Parameters
Ratings: $S_n = 1.5 \text{ MW}$, $f_n = 50 \text{ Hz}$, $U_n = 690 \text{ V}$ (line-line, rms), 6 pole, PF= 0.9	Ratings: 1hp, 230V, 4 poles , 50Hz, 5A.
Stator resistance: $R_s = 0.03 \text{ Ohms}$.	Stator resistance: $R_s = 2.715 \text{ Ohms}$.
Stator leakage inductance: $L_{ls} = 59 \text{ mH}$.	Stator leakage inductance: $L_{ls} = 11.1 \text{ mH}$.
Rotor resistance (referred to the stator): $R_r' = 0.022 \text{ Ohms}$.	Rotor leakage inductance: $L_{lr} = 11.1 \text{ mH}$.
Rotor leakage inductance(referred to the stator): $L_{lr}' = 59 \text{ mH}$.	Magnetizing inductance: $L_m = 202.5 \text{ mH}$.
Magnetizing inductance: $L_m = 0.035 \text{ mH}$.	Moment of inertia is $J = 0.004 \text{ Kg-m}^2$.
Series voltage controller parameters: $K_{rp} = 20$, $K_{ri} = 5$.	$C_1 = 2.7 \mu\text{F}$.
	$L_1 = 0.5 \text{ mH}$.

8. References

1. N.G. Hingorani, "Introducing Custom Power in IEEE Spectrum," 32p, pp. 41-48, 1995.
2. IEEE Std. 1159 – 1995, "Recommended Practice for Monitoring Electric Power Quality".
3. P. Boonchiam and N. Mithulananthan, "Understanding of Dynamic Voltage Restorers through MATLAB Simulation," Thammasat Int. J. Sc. Tech., Vol. 11, No. 3, July-Sept 2006.
4. J. G. Nielsen, M. Newman, H. Nielsen, and F. Blaabjerg, "Control and testing of a dynamic voltage restorer (DVR) at medium voltage level," *IEEE Trans. Power Electron.*, vol. 19, no. 3, p.806, May 2004.

5. A. Ghosh and G. Ledwich, "Power Quality Enhancement Using Custom Power Devices," Kluwer Academic Publishers, 2002.
6. S. Chen, G. Joos, L. Lopes, and W. Guo, "A nonlinear control method of dynamic voltage restorers," in 2002 IEEE 33rd Annual Power Electronics Specialists Conference, 2002, pp. 88- 93.
7. R. Buxton, "Protection from voltage dips with the dynamic voltage restorer," in IEE Half Day Colloquium on Dynamic Voltage Restorers – Replacing Those Missing Cycles, 1998, pp. 3/1- 3/6.
8. H. Awad, J.Svensson, M. Bollen, "Mitigation of Unbalanced Voltage Dips Using Static Series Compensator", IEEE Trans. On Power Elec., Vol. 19, No. 13, May 2004
9. B. Singh, A. Adya, J. Gupta, "Power Quality Enhancement with DSTATCOM for small Isolated Alternator feeding Distribution System" Power Electronics, And Drive System 2005, (PEDS 2005), Voll., 16-18 Jan Pages: 274-279
10. C. Hochgraf, R. Lasseter, "Stacom controls for Operation with Unbalanced Voltages " IEEE Trans. On Power delivery, Vol. 13, No. 2, April 1998.

Development of an alternate Knowledge Based System for Optimization of Blanking Die Design Parameters Selection

R. S. Mohan Kumar^a, Bala Murugan .C.M^b

^aMechanical Engineering, Adithya Institute of Technology

^bMechanical Engineering, Kalaivani College of Technology

Abstract: Developing a Knowledge Based system is proposed that can elicit recommendations in selecting optimum die design parameters. Selection of optimum parameters for blanking die design is an important activity in stamping industries and mainly depends on the ability of taking decision by process planners and experienced die designers. Conventional die design method involves numerous considerations, calculations and tables. This arrangement facilitates interfacing of die design with drafting and can be loaded in a PC. The proposed system is developed using IF-THEN rule based system approach of AI. It utilizes interfacing of AutoCAD and Auto LISP for automation of selection of blanking die design parameters. The system comprises six modules. Punch and die clearances, types of die-set selection, punch and die insert material selection, hardness range selection, die-set dimensions and determination of punch holder and die holder thickness are the six parameters on which the system was build. The modules were developed based on information from manufacturing standards, industrial catalogues, brochures and best of industrial practices. Hence for the given input condition, the system generates an optimum parametric output as recommendations on the screen during its execution. The system is flexible and can be promoted depending upon both specific shop floor requirements and development of new technology solutions. The application of the proposed system is demonstrated through a sample run of all the six modules for a real time industrial component.

Index Terms: Artificial Intelligence, punch and die clearances, types of die-set selection, hardness range selection, die-set dimensions, punch holder and die holder thickness material.

I. INTRODUCTION

The main aim of Artificial intelligence is to develop technologies that allow building smart systems able to automatically adapt to changing environments and contexts, making the environment largely imperceptible to the user. One big barrier to the wide spread development of Artificial intelligence computer application lies in the increased complexity of the programming task. There is a big gap between high level applications requirements and low level complex systems organizations and operations. Artificial Intelligence (AI) system is a computer-based system with the potential to solve problems in the same way

that someone with experience would perform. An expert system can be made to support the stamping industries in die design. Proper selection of die-set of metal stamping press tool involves calculations and decisions based on experience. Therefore there exists the need to develop an intelligent system that is capable of providing expert advice to the die designers. User interface techniques help to bridge the gap supporting rapid development applications by domain experts with minimal programming expertise. Artificial intelligence may lead to greater degree of user knowledge of or control over, the surrounding environment, weather at home or in an office or car. They may also show a form of INTELLIGENCE.

II. LITERATURE SURVEY

The concept of simulating human thought through knowledge base system for designing die of sheet metal operations has attracted research interest. An intelligent system for selection of die set of metal stamping press tool can be framed in the form of modules that deals about the various key factors affecting the selection of die-set Kumar and Singh [1]. Results of this work suggest the designer to determine the appropriate die-set and its dimensions. Bor-Tseunlin and Shih-Hsinhsu [2] investigates the ability of an automated system that provides output designs of the main components of a drawing die. The system is built on top of CATIA V5 & makes use of its built-in-modules. Small & medium size enterprises appreciate the system for its low cost and flexible framework. Kumar and Singh [3] presents on a low cost expert system for progressive die design. Kumar and Singh [4] presents about an intelligent system that allows the user to model the strip layout & utilizes the model data files for automatic modeling of progressive die. The system comprises of eight modules and the system is called AUTOPROMOD. Each module suggests the progressive die components models as result. The expert system contribution and its major role towards advancing decision methods is described in detail. Sapuan [5] studies the broad area of computerized material selection system in mechanical engineering design. The system structure is built around the inter-relationships between database, inference engine, knowledge base, computer aided design (CAD) software, and user interface. A low cost modeler for strip layout was developed for checking manufacturability of the part, choice of manufacturing operations and blanking operations proposed by Singh and Sekhon [7]. The work deal more on building knowledge base system for

strip development on multi-operation dies and selection of die accessories. A low cost modeler for strip layout was developed for checking manufacturability of the part, choice of manufacturing operations, selection of press machine and die components for single stage piercing and blanking operations proposed by Singh and Sekhon [8]. This work deal more on building knowledge base system in the area of strip development for multi-operation dies and selection of die accessories. Die-set consists of a lower die shoe and an upper die shoe together with the guide posts and guide bushings. In the selection process of die-set [9] part quantity, dimensional tolerance of the component and punch and die clearance should be considered. The construction of expert system was dealt in detail with their recent advancement in technology and applications over various domains [10]. The die design fundamentals [11] deals the fourteen major steps to design die for various stamping operations, components of a die and the vital parameters to be considered during design stage. The various materials used in industrial practices in real time environment for die design [13-15] can be verified through the standard tables, industrial brochures and catalogues. The knowledge base for progressive dies was developed with production rules and the parameters influence over progressive die design was dealt in brief [16]. A step by step introduction to the design of stamping dies and new concepts of making tool and die design is appreciated with its uniqueness [17]. Various standard industrial charts, tables and proceedings help to build the knowledge base of the system [18-20]. The detailed literature survey makes to infer an overall view and knowledge about the expert systems and their applications in various domains.

III. PROBLEM DEFINITION

Selection of optimum parameters for die design is more important that determines the quality of the end product. Conventional die design system mainly depends on the ability of the die designer decision. Hence there is a need to develop an AI system that imitates the behavior of expert in the field of design. Knowledge based approach is a popular AI technique that has been used in die design process. The system supports the modifications in the knowledge base of each module depending upon the newly acquired knowledge and addition of new modules for updating the system requirements.

IV. PROPOSED METHODOLOGY

An AI system developed for stamping operation involves six modules. The basic considerations for developing the system involves identification of parameters like production quantity, stock thickness, dimensional tolerance, sheet material and punch and die clearance. The methodology for the development of knowledge base system modules is schematically shown in Fig.1. An expert system attempts to reproduce the functioning of one or more human experts, most commonly in a specific problem domain. A wide variety of methods can be used to simulate the performance of the expert however common to

most of all is the creation of "knowledge base" which uses some knowledge representation that emphasis to capture the Subject Matter Experts (SME) knowledge. These design rules are then formulated in IF-THEN variety using Auto LISP. It is intended at developing an expert system for sheet metal operations and extending the inferential capability of the system.

As the user loads the desired module in a PC with Auto CAD, the system calls the respective module when needed by the user. The input required by the system, to run the modules will be displayed on the computer screen. The system will verify the input conditions with the existing knowledge base and when the suitable conditions get satisfied, the results will be displayed as suggestions that are standard in industrial practice. In case of any wrong input given by the user the system also shows to enter the correct input range in the form of messages. The execution of each module follows the same steps as discussed above.

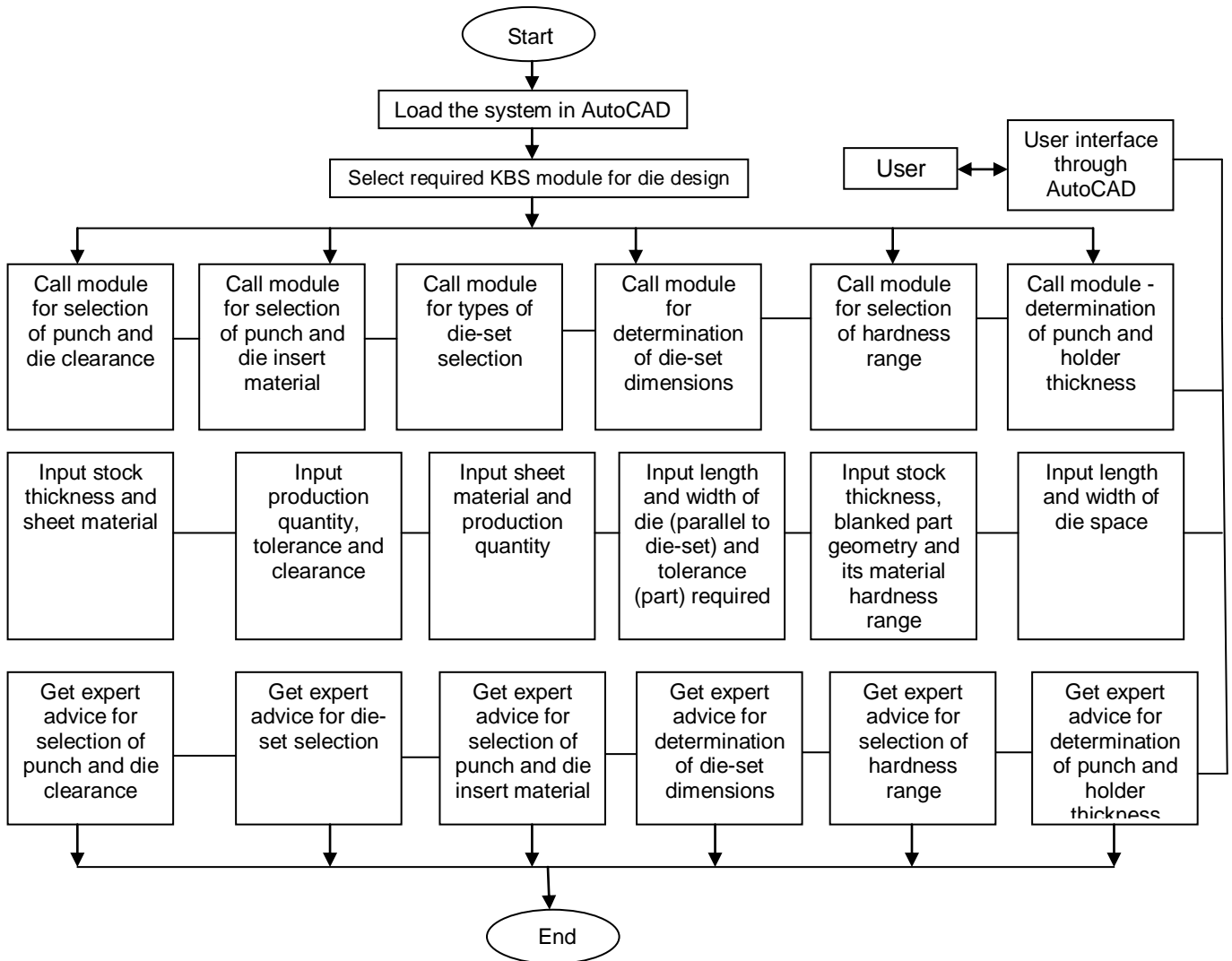


Fig.1. Methodology for the proposed system

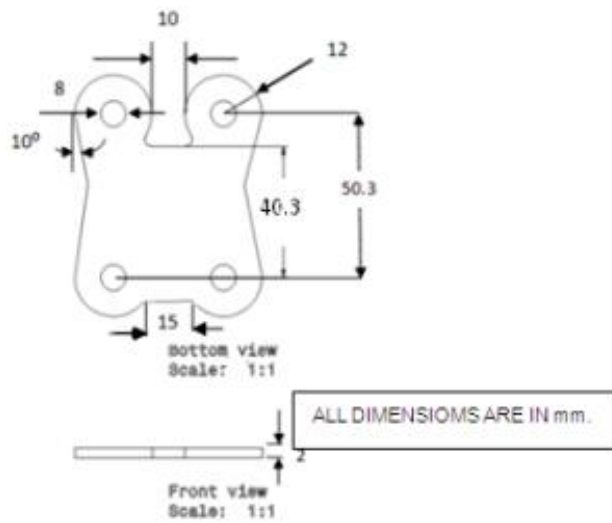


Fig.2. Footrest Bracket

V. CASE STUDY

The KBS system comprising six modules capable of assisting the user in an interactive way to solve various problems and queries. The six modules of the system were tested and demonstrated through a sample run for a real-time industrial component as shown in Fig.2.

The recommendations obtained as output of the system were listed below and found to be reasonable and very similar to those actually used in industry (M/s.KARTHEKEYA FORGINGS, TAMIL NADU, INDIA.) for the example component.

5.1. SELECTION OF PUNCH AND DIE CLEARANCE

For a blank to part cleanly from the material strip, exact punch and die clearance should be given. If too little clearance exists, excessive power consumption to operate press is required and affects productivity. Excessive clearance value will produce long and stringy burrs all around the edge.

1) Input: Enter the stock thickness in mm: 2.0 mm
Enter the material [1.softsteel, 2.mediumsteel, 3. hardsteel, 4.stainless steel, 5.phosphor bronze, 6. Brass, 7.copper, 8.aluminium]: 5

Output: Select punch and die clearances as 0.109 mm

2) Input: Enter the stock thickness in mm: 1.90 mm
Enter the material [1.softsteel, 2.mediumsteel, 3.hardsteel, 4.stainless steel, 5.phosphor bronze, 6.brass, 7.copper, 8.aluminium]: 8

Output:Select punch and die clearances as 0.109 mm

3) Input:Enter the stock thickness in mm: 1.77 mm
Enter the material [1.softsteel, 2.mediumsteel, 3.hardsteel, 4.stainless steel, 5.phosphor bronze, 6.brass, 7.copper, 8.aluminium]: 3

Output: Select punch and die clearances as 0.127 mm.

5.2 Punch and Die Insert Material Selection

Special attention is required to improve the life of active components of die (punch and die inserts). For selecting the suitable material the designer should investigate the functional requirements of that component, identify the required mechanical properties and possible causes of failure.

1) Input: Enter the sheet material [1.Al, 2.Cu, 3.Br, 4.Pb, 5. BeCu, 6.MS, 7.SS, 8.ASS, 9.HS, 10. CRCA, 11. SPRING STEEL]: 1

Enter the shear strength of sheet material in N/mm²: 135

Enter the type of operation [1.shearing, 2. forming, 3.forming and shearing both]: 1

Enter the production quantity: 100000

Output: Select material for punch and die inserts as:

EN-31(56-60HRC) (AISI52100) 'OR' UHB ARNE (54-62 HRC)(AISI O1, W-Nr.1.2510)

2) Input: Enter the sheet material [1.Al, 2.Cu, 3.Br, 4.Pb, 5. BeCu, 6.MS, 7.SS, 8.ASS, 9.HS, 10. CRCA, 11. SPRING STEEL]: 3

Enter the shear strength of sheet material in N/mm²: 125

Enter the type of operation [1.shearing, 2. forming, 3.forming and shearing both]: 1

Enter the production quantity: 100000

Output: Select material for punch and die inserts as:

EN-31(56-60HRC) (AISI 52100) 'OR' UHB-ARNE 54-2HRC)(AISIO1,WNr.1.2510)

3) Input: Enter the sheet material [1.Al, 2.Cu, 3.Br, 4.Pb, 5.BeCu, 6.MS, 7.SS, 8.ASS, 9.HS,10. CRCA, 11.SPRING STEEL]: 6

Enter the shear strength of sheet material in N/mm²: 450

Enter the type of operation [1.shearing, 2.forming, 3.forming and shearing both]: 1

Enter the production quantity: 1055250

Output: SEVERKER3 (60-64HRC) (AISI D6 (D3), W- Nr.1.2436, JIS-SKD2)'OR'UHB-VANADIS6(62-64 HRC) 'OR' UHB-VANADIS 10 (60-64 HRC).

5.3 HARDNESS RANGE SELECTION

Selection of hardness range of selected materials of die components depends upon the stock thickness and blanked part geometry.

1) Input: Enter the stock thickness in mm: 2

Enter the geometry of the blanked part

[1.simple, 2.normal, 3.complicated]:1

Enter the hardness range of selected material in HRC [1. <=4, 2. >4, 3. <=6, 4. >6, 5. >8]: 1

Output: Select upper limit of hardness range of selected material.

2) Input: Enter the stock thickness in mm: 3

Enter the geometry of the blanked part

[1.simple, 2.normal, 3.complicated]:2

Enter the hardness range of selected material in HRC [1. <=4, 2. >4, 3. <=6, 4. >6,5. >8]: 2

Output: Select lower limit of hardness = upper limit of hardness of selected material-4.0 and upper limit of hardness = upper limit of hardness of selected material.

3) Input: Enter the stock thickness in mm: 3

Enter the geometry of the blanked part

[1.simple, 2.normal, 3.complicated]:4

Enter the hardness range of selected material in HRC [1. <=4, 2. >4, 3. <=6, 4. >6,5. >8]: 2

Output: Press enter, reload the file, enter input Conditions within the range.

5.4 Determining Die-Set Dimensions

The dimensions of the die-set depend upon the length and width of the die and its placement in the die-set. If available, standard die-sets can be used or these can be custom-built.

1) Input: Enter the die length in mm: 103

Enter the die width in mm: 78

Enter the part tolerance in mm: 0.06

Output: Place die parallel to the rear pillar (19 mm diameter) with bolster dimensions in mm as: length=150, width= 145, height=39.

2) Input: Enter the die length in mm: 135

Enter the die width in mm: 95

Enter the part tolerance in mm: 0.1

Output: Place die parallel to the rear pillar (25 mm diameter) with bolster dimensions in mm as: length=200, width= 170, height=39.

3) Input: Enter the die length in mm: 140

Enter the die width in mm: 165

Enter the part tolerance in mm: 0.1

Output: Place die perpendicular to the rear pillar (25 and 32 mm diameter) with bolster dimensions in mm as: length=250, width= 200, height=49.

5.5 Determining Punch Holder and Die Holder Thickness

Die set catalogues recommend specific punch holder and die holder thickness. When die plates are too thin in relation to their length and width, they will warp, causing misalignment of punch and die members. Conversely, when plates are too thick, the overall die cost increases.

1) Input: Select the length and width of die space combination (in mm) respectively [1. 381x254, 2. 762x508, 3. 1143x508, 4. 1524x1016, 5. 1905x1270, 6. 2286x1524, 7. 2667x1778, 8. 3048x2032, 9. 3429x2286, 10. 3810x2540]: 1
Enter the force in kN [1. 0-88.9644, 2. 88.9644-266.893, 3. 266.893-444.822, 4. 444.822-622.751, 5. 622.751-800.68, 6. 800.68-978.609, 7. 978.609-1156.54, 8. 1156.54-1334.47, 9. 1334.47-1779.29, 10. 1779.29-over]: 1

Output: Select punch holder and die holder thickness in mm as 31.75x38.1 resp.

2) Input: Select the length and width of die space combination (in mm) respectively [1. 381x254, 2. 762x508, 3. 1143x508, 4. 1524x1016, 5. 1905x1270, 6. 2286x1524, 7. 2667x1778, 8. 3048x2032, 9. 3429x2286, 10. 3810x2540]: 2
Enter the force in kN [1. 0-88.9644, 2. 88.9644-266.893, 3. 266.893-444.822, 4. 444.822-622.751, 5. 622.751-800.68, 6. 800.68-978.609, 7. 978.609-1156.54, 8. 1156.54-1334.47, 9. 1334.47-1779.29, 10. 1779.29-over]: 4

Output: Select punch holder and die holder thickness in mm as 44.45x50.8 resp.

3) Input: Select the length and width of die space combination (in mm) respectively [1. 381x254, 2. 762x508, 3. 1143x508, 4. 1524x1016, 5. 1905x1270, 6. 2286x1524, 7. 2667x1778, 8. 3048x2032, 9. 3429x2286, 10. 3810x2540]: 11
Enter the force in kN [1. 0-88.9644, 2. 88.9644-266.893, 3. 266.893-444.822, 4. 444.822-622.751, 5. 622.751-800.68, 6. 800.68-978.609, 7. 978.609-1156.54, 8. 1156.54-1334.47, 9. 1334.47-1779.29, 10. 1779.29-over]: 4

Output: Please select input within the range specified From option 1 to 10.

VI. CONCLUSION

The proposed system with six modules are coded in Auto LISP language and designed to be loaded in AutoCAD. The modules of the system were tested for a real-time industrial component and are capable to impart standard industrial practice as output of the system. Development of an intelligent system for stamping operation can also be done including more parameters that can reduce the design cycle time and improve the quality of die design for stamping operations.

REFERENCES

- [1] Kumar.S and Singh.R, 2005,"An intelligent system for selection of die-set of metal stamping press tool", Materials Processing Technology, Vol.164-165, pp.1395-1401.
- [2] Bor-TseunLin and Shih-HsinHsu, 2008,"Automated design systems for drawing dies", Expert systems with applications, Vol.34, pp.1586-1598.
- [3] Kumar.S and Singh.R, 2004,"A low cost knowledge base system framework for progressive design", Material Processing Technology, Vol.153-154, pp.958-964.
- [4] Kumar.S and Singh.R, 2007,"An intelligent system for modeling of progressive die", Material Processing Technology, Vol.194, pp.176-183.
- [5] Sapuan S.M, 2001,"A Knowledge based system for material selection in mechanical engineering design", Materials and design, Vol.22, pp.687-695.
- [6] Ismail H.S., 1996,"Feature-based design of progressive tools" Int. Mach tools Manuf., pp.367-378.
- [7] Cheok b.t., 1995,"an intelligent planning aid for the design of progressive dies", Proc. Inst. Mech. Eng.210, pp.25-35.
- [8] Singh.R and Sekhon G.S., 1997,"An expert system for the sheet metal operation", International Conference on Sheet metal, pp.105-115.
- [9] Kumar.S and Singh.R, 2003,"Developmental framework of knowledge base system for engineering problems, in Proceedings of the Institution of engineers", Material Processing Technology, Vol.1, pp.290-295.
- [10] Vladimir.R,"How to build expert systems", Ann.CIRP 35(2), 1986, pp.445-450.
- [11] PaquinJ.R, VukotaBoljanovic, Die Design Fundamentals, 3rd edition, Industrial press, New York, 1963, pp.227- 230.
- [12] P.C.Sharma, 1995,"A Text book on Production Technology", S.Chand and Company Ltd., New Delhi.J. G. Kreifeldt, "An analysis of surface-detected EMG as an amplitude-modulated noise," presented at the 1989 Int. Conf. Medicine and Biological Engineering, Chicago, IL.
- [13] ASM Handbook, Material Selection and design, vol.20, ASM Handbook Committee.
- [14] ASM Handbook, Forming and Forging, vol.14, ASM Handbook Committee.
- [15] Hermann Jutz and Eduard Scharkus,"Westermann Tables for the metal trade", New Age International Ltd., New Delhi.
- [16] Vladimir.R, 1986,"How to build expert systems", Ann.CIRP 35(2), pp.445-450.
- [17] Paquin J.R., Vukota Boljanovic, 1963, Die Design Fundamentals, 3rdedition, Industrial press, New York.
- [18] Hermann Jutz and Eduard Scharkus,"Westermann Tables for the metal trade", New Age International Ltd., New Delhi.
- [19] ASM Handbook, Material Selection and design, vol.20, ASM Handbook Committee.
- [20] ASM Handbook, Forming and Forging, vol.14, ASM Handbook Committee.

Recognition of Isolated Words using Features based on LPC, MFCC, ZCR and STE, with Neural Network Classifiers

Bishnu Prasad Das¹, Ranjan Parekh²

¹ School of Education Technology, Jadavpur University, India

² School of Education Technology, Jadavpur University, India

ABSTRACT

This paper proposes an approach to recognize English words corresponding to digits Zero to Nine spoken in an isolated way by different male and female speakers. A set of features consisting of a combination of Mel Frequency Cepstral Coefficients (MFCC), Linear Predictive Coding (LPC), Zero Crossing Rate (ZCR), and Short Time Energy (STE) of the audio signal, is used to generate a 63-element feature vector, which is subsequently used for discrimination. Classification is done using artificial neural networks (ANN) with feed-forward back-propagation architectures. An accuracy of 85% is obtained by the combination of features, when the proposed approach is tested using a dataset of 280 speech samples, which is more than those obtained by using the features singly.

Keywords – isolated word recognition, linear predictive coding, mel frequency cepstral coefficients, zero crossing rate, short time energy, artificial neural networks.

I. INTRODUCTION

Speech recognition is a popular and active area of research, used to translate words spoken by humans so as to make them computer recognizable. It usually involves extraction of patterns from digitized speech samples and representing them using an appropriate data model. These patterns are subsequently compared to each other using mathematical operations to determine their contents. In this paper we focus only on recognition of words corresponding to English numerals zero to nine. Some typical applications of such numeral recognition are voice-recognized passwords, voice repertory dialers, automated call-type recognition, call distribution by voice commands, directory listing retrieval, credit card sales validation, speech to text processing, automated data entry etc. The main challenges of speech recognition involve modeling the variation of the same word as spoken by different speakers depending on speaking styles, accents, regional and social dialects, gender, voice patterns etc. In addition background noises and changing of signal properties over time, also pose major problems in speech recognition. This paper proposes an approach for identifying spoken words corresponding to English digits zero to nine using a combination of features. The paper is organized as follows: section II provides reviews of earlier work in this area, section III describes the proposed approach, section IV tabulates details of experimentations done and results obtained, section V provides an analysis of the current work vis-à-vis earlier works, section VI provides overall conclusions and outlines future scopes.

II. PREVIOUS WORKS

Over the years a number of different methodologies have been proposed for isolated word and continuous speech recognition. These can usually be grouped in two classes : speaker-dependent and speaker-independent. Speaker dependent methods usually involve training a system to recognize each of the vocabulary words uttered single or multiple times by a specific set of speakers [1, 2] while for speaker independent systems such training methods are generally not applicable and words are recognized by analyzing their inherent acoustical properties [3, 4]. Hidden Markov Models (HMM) have been proven to be highly reliable classifiers for speech recognition applications and have been extensively used with varying amounts of success [5, 6, 7]. Artificial Neural Networks (ANN) have also been demonstrated to be an acceptable classifier for speech recognition [8, 9, 10]. Support Vector Machines (SVM) classifiers have been used to classify speech patterns using linear and non-linear discrimination models [11]. Various features have been used singly or in combination with others to model the speech signals, ranging from dynamic time warping (DTW) [12], Linear Predictive Coding (LPC) [9, 13], Mel Frequency Cepstral Coefficients (MFCC) [12, 14, 15]. Often a combination of several features as mentioned above, have shown improvement in recognition accuracies as compared to single features [16], as well as using other associated features like formant frequency and Zero Crossing Rate (ZCR) [10], Discrete Wavelet Transform (DWT) [17], especially in noisy environments [7, 15]. A review of speech recognition techniques can be found in [18].

III. PROPOSED APPROACH

This paper proposes an approach to recognize automatically digits 0 to 9 from audio signals generated by different individuals in a controlled environment. It uses a combination of features based on Short Time Energy (STE), Zero Crossing Rate (ZCR), Linear Predictive Coding (LPC), Mel Frequency Cepstral Coefficient (MFCC). A neural network (multi-layer perceptron : MLP) is used to discriminate the speech data models into respective classes.

3.1 Preprocessing

An audio speech signal is represented as a collection of sample values. Each speech signal represents a spoken sample of a digit between 0 to 9, is typically of duration 0.3 seconds and is recorded using a pre-defined sampling rate Fs. The digitized audio is symbolically represented as a n -dimensional vector :

$$x = [x_1, x_2, \dots, x_n] \quad (1)$$

The pre-processing stage involves temporal domain filtering using a uniform one-dimensional filter H with an m -element coefficient vector $b = [b_1, b_2, \dots, b_m]$. The filtered output y is given by :

$$y = H(b, 1, x) \quad (2)$$

The effect of the temporal filtering is to produce an output represented as a linear combination of the input and the filter coefficients i.e. the i -th output element is given by :

$$y_i = b_1 x_i + b_2 x_{i-1} + \dots + b_m x_{i-m+1} \quad (3)$$

3.2 Short Time Energy (STE)

The energy content of a set of samples is approximated by the sum of the square of the samples. To calculate STE the filtered signal is sampled using a rectangular window function of width ω samples, where $\omega \ll n$. Within each window, energy e is computed as follows :

$$e = \sum_{i=1}^{\omega} x_i^2 \quad (4)$$

The energy for each window is collected to generate the STE feature vector having $W = \frac{n}{\omega}$ elements

$$E = \bigcup_{j=1}^W e_j \quad (5)$$

3.3 Zero Crossing Rate (ZCR)

ZCR of an audio signal is a measure of the number of times the signal crosses the zero amplitude line by transition from a positive to negative or vice versa. The audio signal is divided into temporal segments by the rectangular window function as described above and zero crossing rate for each segment is computed as below, where $sgn(x_i)$ indicates the sign of the i -th sample x_i and can have three possible values: +1, 0, -1 depending on whether the sample is positive, zero or negative.

$$z = \sum_{i=1}^{\omega} \frac{|sgn(x_i) - sgn(x_{i-1})|}{2} \quad (6)$$

The value for each window is collected to generate the ZCR feature vector having $W = \frac{n}{\omega}$ elements

$$Z = \bigcup_{j=1}^W z_j \quad (7)$$

3.4 Linear Predictive Coding (LPC)

Linear prediction is a mathematical operation which provides an estimation of the current sample of a discrete signal as a linear combination of several previous samples. The prediction error i.e. the difference between the predicted and actual value is called the residual. If the current sample x_i of the audio signal be predicted by the past p samples and x'_i be the predicted value then we have :

$$x'_i = -a_2 x_{i-1} - a_3 x_{i-2} - \dots - a_{p+1} x_{i-p} \quad (8)$$

Here $\{1, a_2, \dots, a_p, a_{p+1}\}$ are the $(p+1)$ filter coefficients. In this case the signal is passed through an LPC filter which generates a $(p+1)$ element feature vector L_A and a scalar L_G which represents the variance of the predicted signal.

3.5 Mel Frequency Cepstral Coefficients (MFCC)

The signal is divided into overlapping frames to compute MFCC coefficients. Let each frame consist of N samples and let adjacent frames be separated by M samples where $M < N$. Each frame is multiplied by a Hamming window where the Hamming window equation is given by :

$$\omega(n) = 0.54 - 0.46 \cos\left(\frac{2\pi n}{N-1}\right) \quad (9)$$

In the third step, the signal is converted from time domain to frequency domain by subjecting it to Fourier Transform. The Discrete Fourier Transform (DFT) of a signal is defined by the following :

$$X_k = \sum_{i=0}^{N-1} x_i \cdot e^{-j \frac{2\pi k i}{N}} \quad (10)$$

In the next step the frequency domain signal is converted to Mel frequency scale, which is more appropriate for human hearing and perceptions. This is done by a set of triangular filters that are used to compute a weighted sum of spectral components so that the output of the process approximates a Mel scale. Each filter's magnitude frequency response is triangular in shape and equal to unity at the centre frequency and decrease linearly to zero at centre frequency of two adjacent filters. The following equation is used to calculate the Mel for a given frequency :

$$M = 2595 \log_{10} \left(1 + \frac{f}{700}\right) \quad (11)$$

In the next step the log Mel scale spectrum is converted to time domain using Discrete Cosine Transform (DCT). DCT is defined by the following, where α is a constant dependent on N :

$$X_k = \alpha \cdot \sum_{i=0}^{N-1} x_i \cdot \cos\left\{\frac{(2i+1)\pi k}{2N}\right\} \quad (12)$$

The result of the conversion is called Mel Frequency Cepstrum Coefficient. The set of coefficients is called acoustic vectors. Therefore, each input utterance is transformed into a sequence of acoustic vectors. Out of all the coefficients usually the first q MFCC coefficients are retained, leading to a q element MFCC vector M_C

The final feature vector for modeling each speech signal consists of the collection of the $(p+1)$ element LPC vector L_A , the 1 element LPC scalar L_G , the q element MFCC vector M_C , the W element ZCR vector Z , the W element STE vector E . Hence feature vector length is : $(p+1) + 1 + q + W + W$.

$$F = \{L_A, L_G, M_C, Z, E\} \quad (13)$$

3.6 Classification Scheme

A word class i consists of set of j utterances by k speakers. For each utterance a combined feature vector is computed as per equation (13). A word class is characterized by the collection of its feature values obtained during a training phase. A test utterance with its computed feature vector is said to belong to a specific class if the probability of it being a member of that class is maximum. Class probability is determined by Artificial Neural Network (ANN) classifiers using feed-forward and back-propagation architectures.

IV. EXPERIMENTATIONS AND RESULTS

4.1 Dataset

The dataset consists of 280 speech samples recorded by 28 speakers each uttering the name of 10 digits, from 0 to 9, in English. Out of 28 speakers 14 are male and 14 female. The speech samples are recorded directly over microphone in a controlled environment. All the audio signals are stored in the WAV format with sample rate of 22050 Hz, bit rate of 16 bits and in mono (single channel) format.

4.2 Training Phase

The training set consists of 200 speech samples spoken by 20 speakers, 10 male and 10 female, each uttering the name of the 10 digits. Each speech file is subjected to a temporal domain filtering with a uniform one-dimensional filter H with a 2-element coefficient vector $[1, -0.95]$. Fig. 1 depicts pictorial representation of one of the speech files before and after temporal filtering. The filtered signal is shown in red, while the original signal in blue.

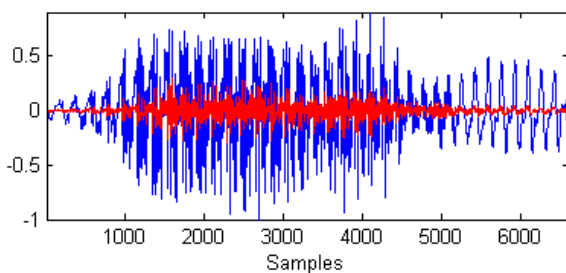


Fig. 1: Original speech signal (blue) and after temporal filtering (red)

LPC coefficients are extracted from the speech file using an LPC order of 16. This generates a 17-element vector L_A and a scalar L_G leading to an 18-element LPC vector. MFCC coefficients are then generated from the speech signal using an MFCC order of 15, which generates a 15-element MFCC vector M_C . Finally using a rectangular window of size $W = 15$, ZCR and STE vectors, each of 15 elements, are computed and added to the feature vector which becomes $(18+15+15+15) = 63$ elements in size.

Fig. 2 depicts feature plots of the 10 digits for an average of 20 speakers of the training set. The 63 elements of the feature vector are shown along the X-axis while their corresponding values are shown along the Y-axis.

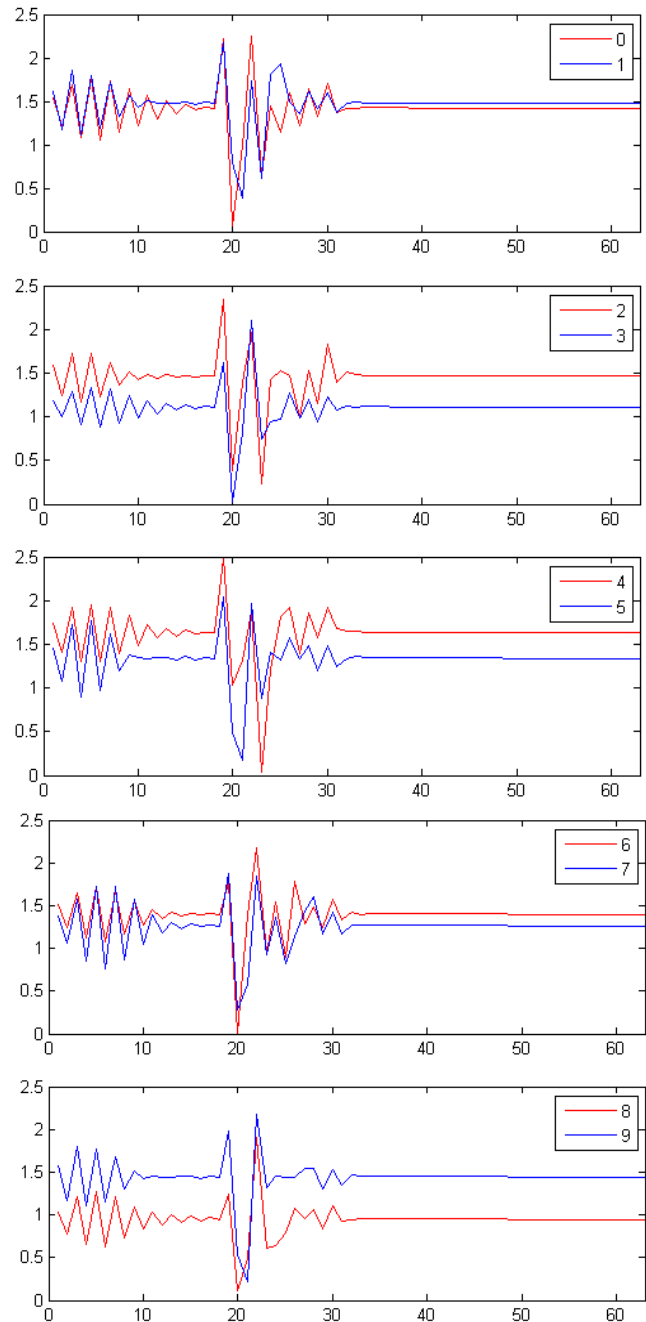


Fig. 2: Plots of the 63-element feature vector for digits 0 to 9 averaged over 20 speakers of the training set

4.3 Testing Phase

The testing set consists of 80 speech samples spoken by 8 speakers, 4 male and 4 female, each uttering the name of the 10 digits. Each speech file is subjected to the same steps of temporal filtering, followed by the extraction of the 63-element feature vector as described in the training phase. Fig. 3 depicts feature plots of the 10 digits for an average of 8 speakers of the testing set.

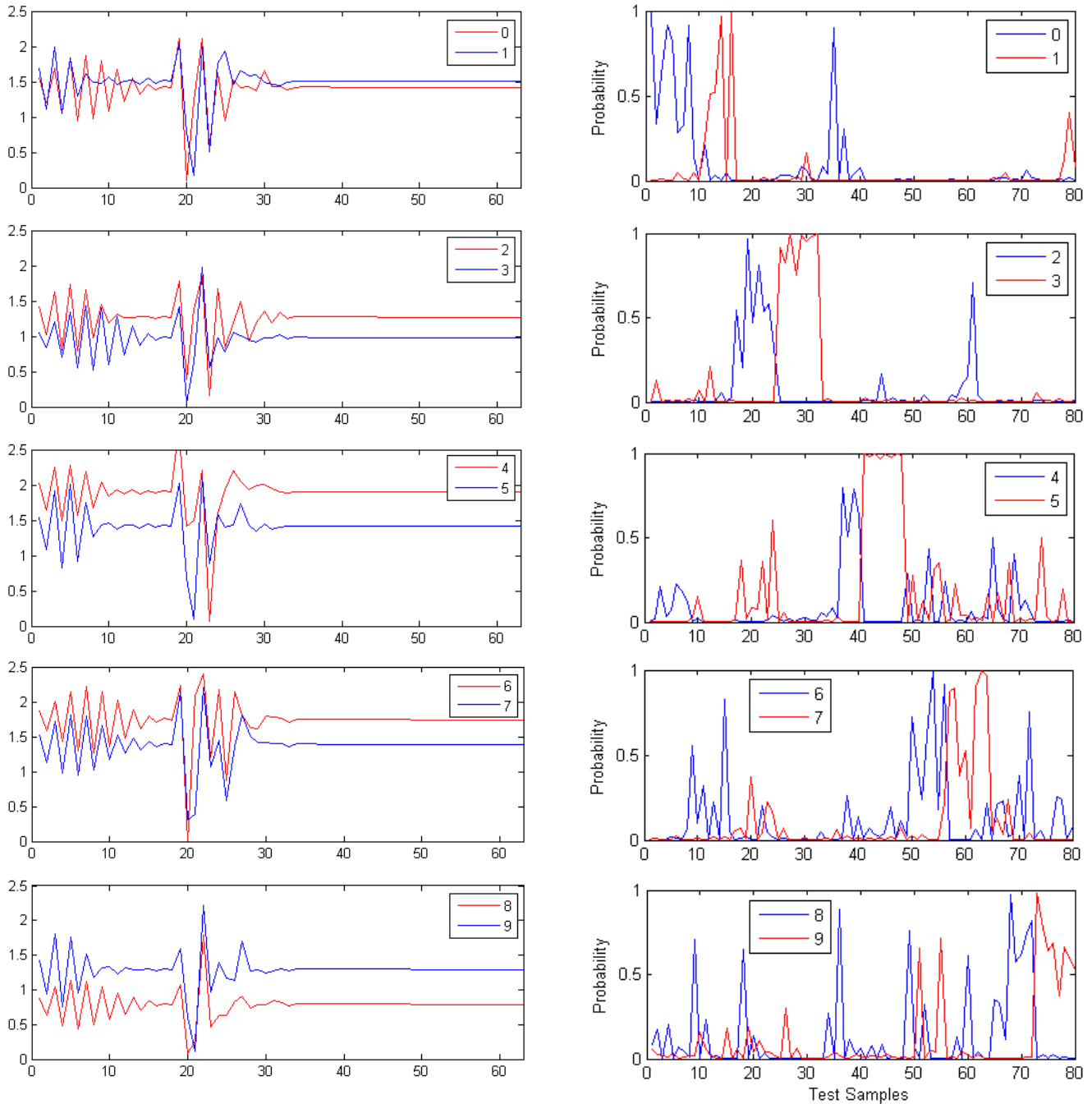


Fig. 3: Plots of the 63-element feature vector for digits 0 to 9 averaged over 8 speakers of the testing set

4.4 Classification

Classification of the speech signals is done by using a neural network (MLP : multi-layer perceptron). The MLP architecture used is 63-299-10 i.e. 63 input nodes (for the 63-element feature vector), 299 nodes in the hidden layer, and 10 output nodes (for discriminating between 10 words), log-sigmoid activation functions for both the neural layers, learning rate of 2.0 and Mean Square Error (MSE) threshold of 0.005 for convergence. The convergence plot and the MLP output are shown in Fig. 4. The accuracy obtained is 85% and requires 1097 epochs for convergence.

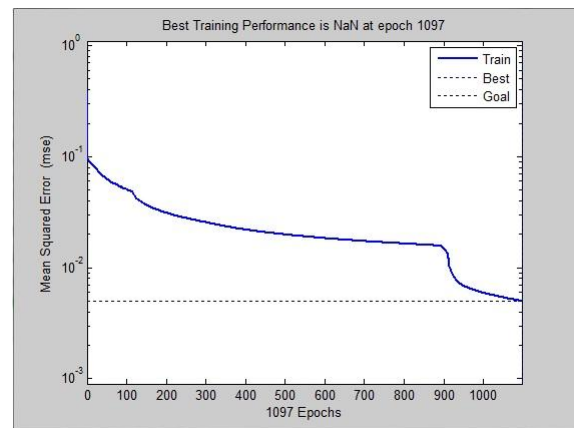


Fig. 4: NN classification of digits 0 to 9 (a) output plots (b) convergence plot

The output plots indicate the probability of the test samples as belonging to one of the 10 classes. Since the test samples are fed to ANN sequentially, samples 1-8 belong to class '0', 9-16 to class '1', 17-24 to class '2', 25-32 to class '3', 33-40 to class '4', 41-48 to class '5', 49-56 to class '6', 57-64 to class '7', 65-72 to class '8', 73-80 to class '9'. The class memberships are indicated by a peak in the probability values.

V. ANALYSIS

Table 1 indicates the accuracies obtained by implementing the proposed algorithm on a dataset consisting of speech samples by 28 different speakers (both male and female). In each of the cases, the accuracy obtained is compared with those outlined in [9] and [14] consisting of single features of LPC and MFCC, on the same data set. Classification done using ANNs are also compared with results obtained by the Euclidean metric. The time required for calculating four features of all 280 speech samples is 24 seconds on a system with 3GB RAM and Intel Core2Duo Processor. To put the results in perspective with the state of the art, the system described in [8] achieves 94% accuracy with isolated digit recognition. Error rates of 23.1% are detected if only MFCC features and PLP features are considered separately in [16]. An accuracy of 91.4% is reported in [9] and 79.5% in [14].

Table 1 Recognition Accuracies

Classifier	Only LPC	Only MFCC	LPC + MFCC + ZCR + STE
ANN	37.5%	51.25%	85%
Euclidean Distance	23.75%	30%	57.5%

VI. CONCLUSIONS AND FUTURE SCOPES

This paper outlines a system to recognize English words corresponding to digits zero to nine, spoken by a set of 28 speakers. Words are classified using a combination of features based on LPC, MFCC, ZCR and STE. The recognition accuracy is seen to be better than achieved using these features individually, as has been done in some of the previous works, and is comparable to those reported in extant literature. The overall accuracy can be enhanced by combining more features of the speech samples. Also different windows like Hamming, Hanning or Blackman windows can be considered for filtering the speech samples.

REFERENCES

[1] M. B. Herscher, R. B. Cox, An adaptive isolated word speech recognition system, *Proc. Conf. on Speech Communication and Processing*, Newton, MA, 1972, 89-92.
 [2] F. Itakura, Minimum prediction residual principle applied to speech recognition, *IEEE Transaction on Acoustics, Speech and Signal Processing*, ASSP-23, 1975, 67-72.
 [3] V. N. Gupta, J. K. Bryan, and J. N. Gowdy, A speaker-independent speech recognition system based on linear

prediction, *IEEE Transactions on Acoustics, Speech, Signal Processing*, ASSP-26, 1978, 27-33.
 [4] L. R. Rabiner, J. G. Wilpon, Speaker independent isolated word recognition for a moderate size vocabulary, *IEEE Transactions on Acoustics, Speech, Signal Processing*, ASSP-27, 1979, 583-587.
 [5] L. R. Rabiner, A tutorial on Hidden Markov Models and selected applications in speech recognition, *Proc. IEEE*, 77(2), 1989, 257-286.
 [6] A. Betkowska, K. Shinoda, S. Furui, Robust speech recognition using factorial HMMs for home environments, *EURASIP Journal on Advances in Signal Processing*, Article ID 20593, 2007, 1-10.
 [7] M. S. Rafiee, A. A. Khazaei, A novel model characteristics for noise-robust automatic speech recognition based on HMM, *Proc. IEEE Int. Conf. on Wireless Communications, Networking and Information Security (WCNIS)*, 2010, 215-218.
 [8] R. Low, R. Togneri, Speech recognition using the probabilistic neural network, *Proc. 5th Int. Conf. on Spoken Language Processing*, Australia, 1998.
 [9] Thiang, S. Wijoyo, Speech recognition using linear predictive coding and artificial neural network for controlling movement of mobile robot, *International Conference on Information and Electronics Engineering IPCSIT vol.6*, 2011, 179-183.
 [10] D. Paul, R. Parekh, Automated speech recognition of isolated words using neural networks, *International Journal of Engineering Science and Technology (IJEST)*, 3(6), 2011, 4993-5000.
 [11] J. P. Sendra, D. M. Iglesias, F. D. Maria, Support vector machines for continuous speech recognition, *Proc. 14th European Signal Processing Conference*, Italy, 2006.
 [12] L. Muda, M. Begam, I. Elamvazuthi, Voice recognition algorithms using Mel Frequency Cepstral Coefficient (MFCC) and Dynamic Time Warping (DTW) techniques, *Journal of Computing*, 2(3), 2010, 138-143.
 [13] J. L. Ostrander, T. D. Hopmann, E. J. Delp, Speech recognition using LPC analysis, *Technical Report RSD-TR-1-82*, University of Michigan, 1982.
 [14] A. A. M. Abushariah, T. S. Gunawan, O. O. Khalifa, English digits speech recognition system based on Hidden Markov Models, *Int. Conf. on Computer and Communication Engineering*, 11-13 May 2010, 1-5.
 [15] B. Kotnik, D. Vljaj, Z. Kacic, B. Horvat, Robust MFCC feature extraction algorithm using efficient additive and convolutional noise reduction procedures, *ICSLP'02 Proceedings*, 2002, 445-448.
 [16] A. Zolnay, R. Schlueter, H. Ney, Acoustic feature combination for robust speech recognition, *IEEE Transactions on Acoustics, Speech, and Signal Processing*, 2005, 457-460.
 [17] P. Ambalathody, Speech recognition using wavelet transform, unpublished (www.scribd.com/doc/36950981/Main-Project-Speech-Recognition-using-Wavelet-Transform)
 [18] W. Ghai, N. Singh, Literature review on automatic speech recognition, *International Journal of Computer Applications*, 41(8), 2012, 43-50.

PERFORMANCE ANALYSIS OF DS-CDMA RAKE RECEIVER OVER AWGN CHANNEL FOR WIRELESS COMMUNICATIONS

*¹N.Anand Ratnesh, ²K.Balaji, ¹J.V.Suresh, ¹L.Yogesh, ¹B.Anil Babu

¹M.tech Student, KL University, A.P, India

²Associate professor, Dept of ECE, KL University, A.P, India

ABSTRACT:

In this paper, a software wireless communication simulator performed which simulates a Code division Multiple Access (CDMA) as Wireless cellular telephony has been growing at a faster rate than wired-line telephone networks. This growth has also been fueled by the recent improvements in the capacity of wireless links due to the use of multiple access techniques (which allow many users to share the same channel for transmission) in association with advanced signal processing algorithms. The simulator is a tool to evaluate these design opinions and trades in different scenarios. An efficient method of system is used to speed up the simulations. The simulator can be used to study the performance of a CDMA with variation in system parameters and channel conditions. In this simulator we change the attenuation factor and simulate CDMA with RAKE receiver and without RAKE receiver. Furthermore, we will compare the BER in received data with and without RAKE receiver and also using PIC technique to eliminate further multiple access and multipath interference to improve the performance of the rake receiver.

Keywords: CDMA(code division Multiplexing), DS-SS (Direct Sequence Spread Spectrum), FDMA (Frequency division Multiplexing), Parallel interference Cancellation (PIC), BER (bit error rate), RAKE receiver.

1. INTRODUCTION:

Wireless cellular telephony has been growing at a faster rate than wired-line telephone networks. This growth has also been fueled by the recent improvements in the capacity of wireless links due to the use of multiple access techniques (which allow many users to share the same channel for transmission) in association with advanced signal processing algorithms [1]. Code division multiple access (CDMA) is becoming a popular technology for cellular communications due to its superior capacity and performance. Unlike other multiple access techniques such as Frequency Division Multiple Access (FDMA) and Time-Division Multiple Access (TDMA) which are limited in frequency band and time duration respectively, One of the main advantages of CDMA system is the capability of using signals that arrive in the receiver with different time delays this Phenomenon is called multipath. Whereas CDMA uses all of the available time-frequency space.

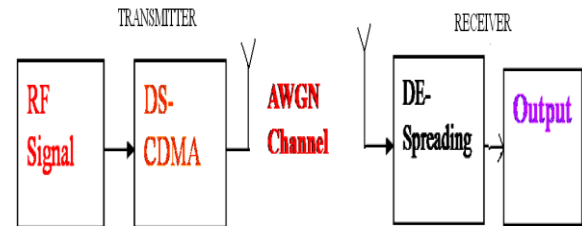


Fig 1: simple Block Diagram of DS-CDMA Transmitter and Receiver.

In CDMA spread Spectrum systems, the chip rate is typically much greater than the flat fading bandwidth of the channel. Whereas Conventional modulation techniques require an equalizer to undergo ISI between adjacent symbols, CDMA spreading codes are designed to provide very low correlation. Thus, Propagation delay spread in the radio channel merely provides multiple versions of the transmitted signal at the receiver. If these multipath components are delayed in time by more than one chip duration they appear like uncorrelated noise at a CDMA receiver, and Equalization is not required. Among Different forms of CDMA a Direct Sequence CDMA (DS-CDMA) uses a set of unique signature sequence or spreading codes to modulate the data bits of different users [2-3]. Direct Sequence (DS) Spread Spectrum is often claimed to have particular properties that makes it less vulnerable to multipath reception. Parallel interference cancellation (PIC) technique reduces the degradation effect of the user interference but with lesser implementation complexity the technique operates on the fact that parallel processing simultaneously removes from each user the total interference produced by the remaining most reliably received users accessing the channel.

2. RAKE RECEIVER:

In multipath channel, delayed reflections interference with the direct signal in a DS-CDMA can be detected by rake receiver, a RAKE receiver technique which uses several baseband correlators to individual process several signal multipath components. The correlators are combined to achieve improved communications reliability and performance [4].

RAKE receiver, used specially in CDMA cellular systems, can combine multipath components, which are time-delayed versions of the original signal transmission. Due to

reflections from obstacles a radio channel can consist of many copies of originally transmitted signals having different amplitudes, phases, and delays, a RAKE receiver can be used to resolve and combine them. This combining is done in order to improve the signal to noise ratio (SNR) at the receiver. RAKE receiver attempts to collect the time shifted versions of the original signal by providing a separate correlation receiver for each of the multipath signals. The RAKE receiver uses a multipath diversity principle. It is like a rake that rakes the energy from the multipath propagated signal components [5]. The RAKE receiver consists of multiple correlators in which received signals are multiplied by time shifted versions of a locally generated code sequence. The intention is to separate signals such that each finger only attain signals coming in over a resolvable path. The spreading code is chosen to have a very small autocorrelation value for any non-zero time offset that avoids crosstalk between fingers. It is not a full periodic autocorrelation that determines the crosstalk between signals in different fingers, but rather two partial correlations with contributions from two consecutive bits or symbols [6]. It has been attempted to find sequences that have satisfactory partial correlation values, but the cross talk due to non periodic correlations remains substantially more difficult to reduce than the effects of periodic correlations the rake receiver is designed to optimally detect as DS-CDMA signal transmitted over dispersive multipath channel.

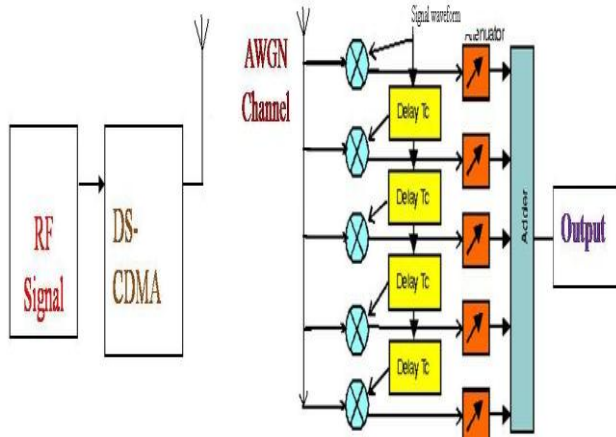


Fig 2: Simple Block Diagram of DS-CDMA with RAKE Receiver.

Like a garden rake, the rake receiver gathers the energy received over the various delayed propagation paths. According to the maximum ratio combining principle, the SNR at the output is the sum of SNR's in the individual branches, provided that, We assume that only AWGN channel is present and codes with time offset are truly orthogonal.

3. PURPOSE OF WORK:

The objective of the work is to simulate and evaluate the performance of different parameters and RAKE receiver performance for CDMA. This work will provide crucial information leading to the implementation of CDMA simulator

in the real world system. RAKE to multiply stages of interference cancellation. RAKE was used in this work along with receivers that used the information in channel. For both RAKE and without RAKE, we compare them in multipath environment. It will be shown that the use of number of bit error in the received data by the RAKE receiver is less than the received data without RAKE receiver. In order to suppress the multipath interference (MPI) and multiple access interference (MAI) in DS-CDMA system a RAKE receiver based on the parallel interference cancellation (PIC) used in this work [7]. RAKE receiver performance can be increased greatly by using PIC method with simple implementation.

The multipath link developed in the software simulation system is intended as a backbone for developing more complex systems. This exible link has a multipath interface which allows a system design to test different scenarios by changing the parameters (such as number of users, paths, channel properties and attenuation factor) [8]. The modular design of the simulation system allows easy addition of algorithms to library.

3.1 RAKE receiver based on PIC:

When the Signal through the wireless channel, it will produce multiple path fading inevitably [9]. The effects of multiple path interference to the receiver in spread spectrum communication and discussed some anti-interference techniques. The common methods Used to suppress the multiple path interference have as the back detected progression and the Rake receiver etc. In the DS CDMA systems, the time domain Rake receivers are used to distinguish, correct and combine different time delay multi-path signal so the inter-symbol interferences are overcome and the path diversity is obtained. By the signal energy of the every path, the Rake receiver obtains diversity gain and as an effective anti multi-path technique, it has become the non-absent key technique in the Third Mobile Communication. Meanwhile, because of the multi-path transmission in channels, multi-path interferences exist between different paths in the identical user [10]. Especially, when the self-correlation between spread codes is worse, the performance about conventional IC Rake receiver will degrade. Based on the research, a new parallel interference cancellation method is proposed in this paper in order to eliminate further multi-access and multi-path interference and improve the performance of the Rake receiver in CDMA systems.

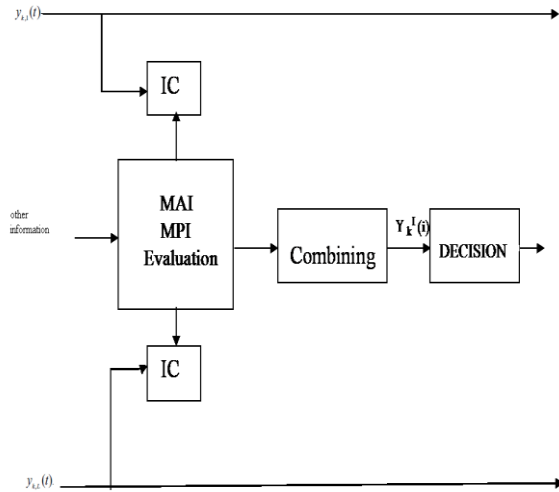


Fig 3: RAKE Receiver with PIC.

It can be proved that the interface estimators estimate MAI and MPI of each channel path according to tentative test value and other known user information (as spread codes of other users, signal amplitudes...etc) in the interference cancellation stage and subtract them then the correlated outputs after interference cancellation for each path are combined finally [11]. Some of Basic expressions used while PIC is given below,

1. The Eq (1) represents reshaping of the transmitted bits from generation of base band signal for kth user.

$$Md = reshape \left(Md, \left[nrx, ntx, \frac{N}{ntx} \right] \right); \quad \text{--- Eq (1)}$$

2. The Eq (2) represents the generation of randomly the channel co-efficients in order to transmit the data bits over a channel.

$$h = \frac{1}{\sqrt{2}} * \left[\begin{matrix} randn \left(nrx, ntx, \frac{N}{ntx} \right) + \\ j * randn \left(nrx, ntx, \frac{N}{ntx} \right) \end{matrix} \right]; \quad \text{--- Eq (2)}$$

3. The Eq (3) represents the original data transmitted over channel along with added noise signal .where, n represents the noise signal and h is the channel coefficients.

$$y = squeeze \left(sum \left(h .* Md, 2 \right) \right) + 10^{-\frac{EbN0(f)}{20}} * n \quad \text{---Eq (3)}$$

Whereas the RAKE receiver performance can be increased greatly by using PIC method with simple implementation and BER decreases compared with the Conventional IC.

4. SIMULATION RESULTS AND ANALYSIS:

In this project we will show the transmit data and received data on different attenuation factor and number of bit error also shown in GUI, this project show that the number of bit error in received data with the RAKE receiver is less than the number of bit error in the received data without RAKE, and when we increase the attenuation factor the number of bit error is decreased. The also the output without GUI for the RAKE receiver is also shown and also in order to increase the performance of the RAKE receiver a new parallel interference cancellation method utilized to eliminate MAI and MPI compare to Conventional IC and also shown PIC RAKE receiver output plot for different paths.

It is easy to explore and find your way around the system using a GUI.

4.1 GUI for DS-CDMA simulation without RAKE.

When we push the push button simulation without RAKE button with attenuation factor 7 then the transmitting data and receiving data, no. of bit error and multipath receiving data from different number of users all shown in fig 4.

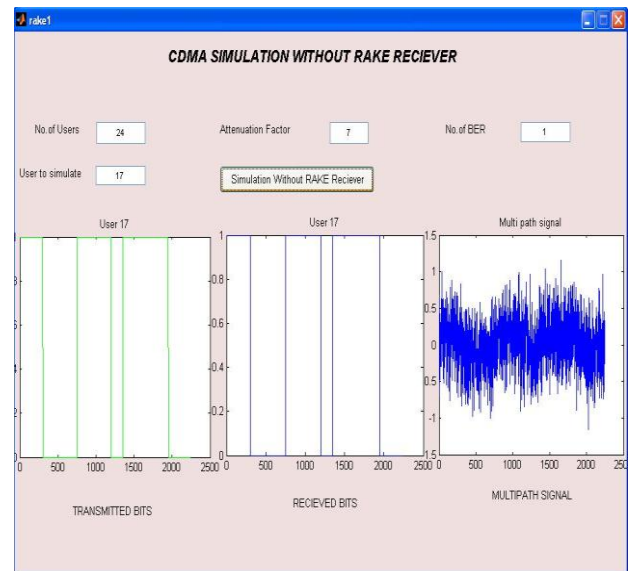


Fig 4: GUI for DS-CDMA simulation Without RAKE receiver.

4.2 GUI for DS-CDMA simulation with RAKE:

When we push the push button simulation with RAKE button with attenuation factor 7 then the transmitting data and receiving data, no. of bit error and multipath receiving data from different number of users all shown in fig 5. BER is ZERO for attenuation factor 7.

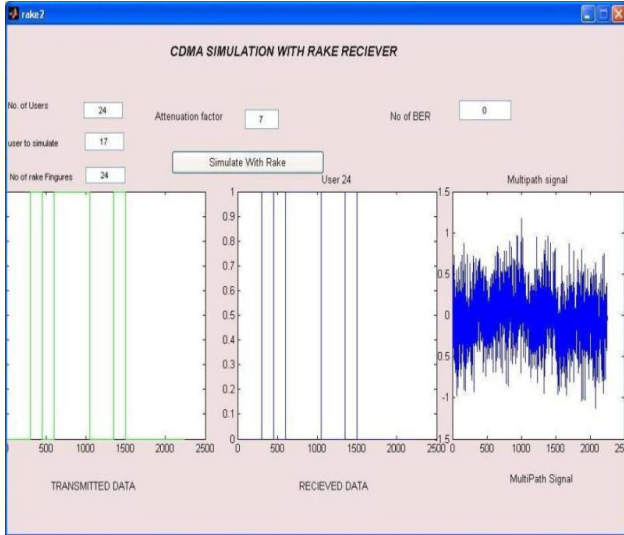


Fig 5: GUI for DS-CDMA simulation With RAKE receiver.

4.3 Output of DS-CDMA RAKE receiver:

By using RAKE receiver from the graph it is observed that as BER decreases there is an increase in SNR as shown in fig 6. This is desired for an efficient communication system.

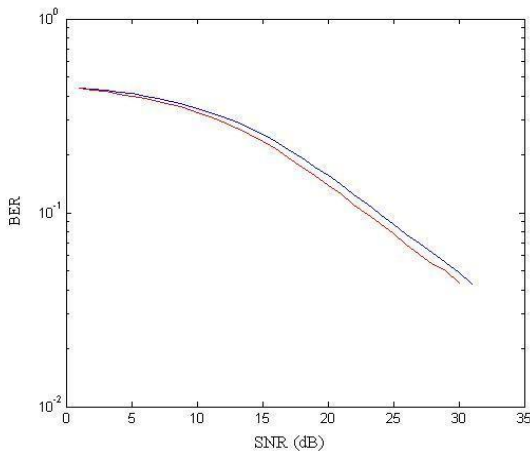


Fig 6: DS-CDMA simulation With RAKE receiver.

4.4 Conventional IC and PIC Performance Comparision using RAKE receiver:

In this section, the simulation results have been given in Fig.7 and Fig.8. The PIC shows superior performance than Conventional IC, especially, the PIC system Proposed in this paper appears the best performance.

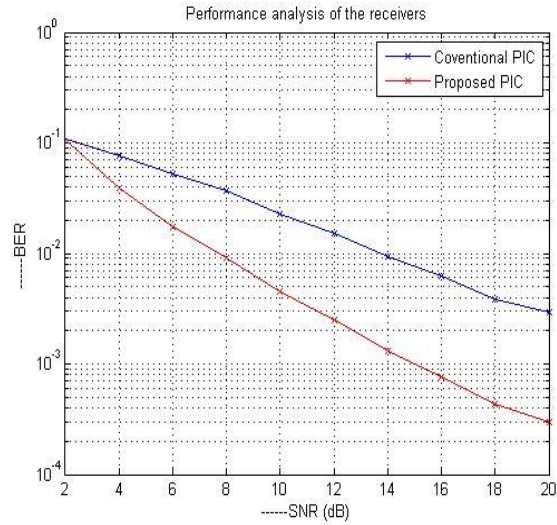


Fig 7: BER Vs SNR for performance Comparision of Conventional IC and PIC with RAKE receiver.

In Fig 8, the bit-error-ratios (BER) of the system for different path numbers are compared.

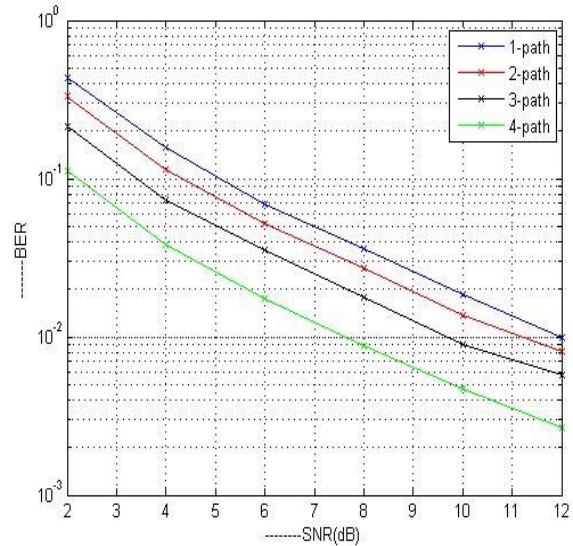


Fig 8: BER Vs SNR performance of RAKE receiver.

5. CONCLUSION:

In this paper, we have shown that how the rake receiver is used in CDMA to decrease BER due to multipath interference and also a PIC based RAKE receiver in order to suppress the multipath interference (MPI) and multiple access interference (MAI) in DS-CDMA system. In this simulator we can change the attenuation factor and simulate CDMA with RAKE and without RAKE receiver, we have compared the bit-error-ratios (BER) of the system for different path numbers over RAKE Conventional IC and RAKE PIC in order to provide best performance for communication system. It shows that RAKE based PIC is best.

6. ACKNOWLEDGEMENTS:

The authors like to express their thanks to the department of ECE and management of K L University for their continuous support and encouragement during this work.

7. REFERENCES:

- [1] Esmael H.Dinan and Bijan jabbari “*Spreading codes for Direct sequence CDMA and wideband CDMA cellular Networks*” IEEE communications magazine, Sep 1998.
- [2] Peter Flanagan, “*Personal Communications Services: The Long Road Ahead,*” Telecommunications, February 1996.
- [3] P. Jung, P. W. Baier, and A. Steil, “*Advantages of CDMA and Spread Spectrum Over FDMA and TDMA in Cellular Mobile Radio Applications,*” IEEE Transactions Vehicular Technology, Vol. 42, no. 3, pp. 357- 364, August 1993.
- [4] Tommi Heikkila, “*RAKE Receiver*”, Postgraduate Course in Radio Communications, autumn 2004.
- [5] Mohammad Farukh Hashmi and Pradeep Dhakad “*Design and Analysis of DS-CDMA RAKE Receiver Simulator for Wireless Communication*”, IEEE 2011.
- [6] <http://wireless.per.nl/reference/chaptr05/cdma/rake.htm>
- [7] Marco Michelini, Enrico Del Re, “*A Selective Parallel Interference Cancellation Receiver to mitigate Multiple Access Interference in a MC-DS/CDMA system*”, 50139 Firenze.
- [8] P. Patel and J. Holtzman. “*Performance Comparison of a DS/CDMA System using a Successive Interference Cancellation (IC) Scheme and a Parallel IC Scheme under Fading,*” IEEE Journal on Selected Areas in Communications 1, 58-67.
- [9] K. R. Shankar Kumar and A. Chockalingam “*Parallel Interference Cancellation in Multicarrier DS-CDMA Systems*“, IEEE Transactions 2004.
- [10] Zhanyun Duan, Tobias Hidalgo Stitz, “*Performance Analysis of Parallel Interference Cancellation Detector in Downlink MC-CDMA Systems*”, Proceedings of the 6th Nordic Signal Processing Symposium - NORSIG 2004.
- [11] Li-xin Song, zheng-qiang Wang, xiao-bo Li “*A New Parallel Interference Cancellation Algorithm for RAKE systems*”, IEEE transactions 2009.

8. AUTHOR’S BIBLIOGRAPHY:



Mr. N. ANAND RATNESH was born in 1988 in Guntur district, Andhra Pradesh, India. He completed his B.Tech at NIET College Affiliated to JNTUK and received his Bachelor’s degree in ECE, from JNTU Kakinada in 2010. Currently he is pursuing M.Tech in Communication and Radar Systems in the ECE department of K L University. His interested research areas are Antennas, DIP, Radars and Wireless Communications.



Mr.K. Balaji was born on 14-12-1963 in India. He did his B.Tech in 1988 from VRSEC and M.S from Bits Pilani in 1994. He is having 23 years of teaching experience and currently he is working as Associate professor in the Department of ECE, K L University. His research area includes Antennas and Communication systems.

A New Scheme for Key Exchange

Debajit Sensarma¹, Subhashis Banerjee², Krishnendu Basuli³

*(West Bengal University of Technology, West Bengal, India)

** (West Bengal University of Technology, West Bengal, India)

*** (West Bengal State University, West Bengal, India)

ABSTRACT

Key management represents a major and the most sensitive part of cryptographic systems. It includes key generation, key distribution, key storage, and key deletion. It is also considered the hardest part of cryptography. Designing secure cryptographic algorithms is hard, and keeping the keys secret is much harder. Cryptanalysts usually attack both symmetric and public key cryptosystems through their key management. We introduce a protocol to exchange keys over insecure communication channel. This protocol generates keys for symmetric encryption, especially a key exchange based on Binary Decision Diagram.

Keywords - Binary Decision Diagram, Diffie-Hellman Key exchange, Digital signature.

1. INTRODUCTION

Authenticated key exchange (AKE) is a cryptographic protocol, which enables two or more parties to establish a shared session key over an insecure channel. Later, the shared session key can be used to 'efficiently ensure data integrity and confidentiality by symmetric primitives.

It is desirable for an AKE protocol to have the following attributes:

- i) **Known-Key Security:** Client and server should generate a unique secret key in each round of key agreement protocol. Each key generated in one protocol round is independent and should not be exposed if other secret keys are compromised.
- ii) **Perfect Forward Secrecy:** If secret key is compromised, the previously established session keys are not compromised.
- iii) **No Key Control:** The key should be determined jointly by both entities. None of the entities can control the key alone.

1.1 Motivation

The goal of this process is for sender and receiver to be able to agree upon a shared secret that an eavesdropper will not be able to determine. This shared secret is used

by sender and receiver to independently generate keys for symmetric encryption algorithms that will be used to encrypt the data stream between them. The main aspect is that neither the shared secret nor the encryption key *do not ever* travel over the network. Here a special data structure called Binary Decision Diagram is used. Here also the advantage of Diffie-Hellman key exchange is taken, as well as this approach provides integrity, authenticity and non repudiation.

1.2 Binary Decision Diagram

A Binary Decision Diagram is a rooted directed acyclic graph. It has one or two terminal nodes of out-degree zero labeled 0 or 1, and a set of variable nodes also called as branch node of out-degree two. Fig 1 depicts a BDD. The root node 'a' in Fig 1. Have two successors indicated by descending lines. One of the successors is drawn as a dashed line, called '**low**' and other is drawn as a solid line, called '**high**'. These branch nodes define a path in the diagram for any values of Boolean variables. The '0' and '1' nodes also called the sink node. If low branch is being followed from the root, then that path will reach to sink node '0' and if high branch is being followed, then the path will reach to sink node '1'. The BDD obeys two important restrictions. First, it must be ordered. Second, a BDD must be reduced, in the sense that it doesn't waste space. BDD's are well-known and widely used in logic synthesis and formal verification of integrated circuits. Due to the canonical representation of Boolean functions they are very suitable for formal verification problems and used in a lot of tools to date [2].

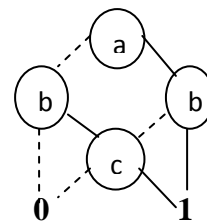


Fig 1: The Binary Decision Diagram

Diffie-Hellman Key Agreement

Public key cryptography was first publicly proposed in 1975 by Stanford University researchers Whitfield Diffie and Martin Hellman to provide a secure solution for confidentially exchanging information

online. Fig 2 shows the basic Diffie-Hellman Key Agreement process.

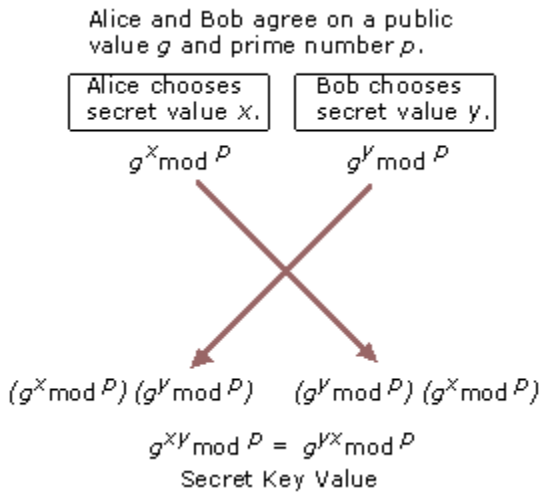


Fig 2: Diffie-Hellman Key Agreement

Diffie-Hellman key agreement is not based on encryption and decryption, but instead relies on mathematical functions that enable two parties to generate a shared secret key for exchanging information confidentially online. Essentially, each party agrees on a public value g and a large prime number p . Next, one party chooses a secret value x and the other party chooses a secret value y . Both parties use their secret values to derive public values, $g^x \text{ mod } p$ and $g^y \text{ mod } p$, and they exchange the public values. Each party then uses the other party's public value to calculate the shared secret key that is used by both parties for confidential communications. A third party cannot derive the shared secret key because they do not know either of the secret values, x or y .

For example, Alice chooses secret value x and sends the public value $g^x \text{ mod } p$ to Bob. Bob chooses secret value y and sends the public value $g^y \text{ mod } p$ to Alice. Alice uses the value $(g^y \text{ mod } p)^{(g^x \text{ mod } p)}$ as her secret key for confidential communications with Bob. Bob uses the value $(g^x \text{ mod } p)^{(g^y \text{ mod } p)}$ as his secret key. Because $(g^y \text{ mod } p)^{(g^x \text{ mod } p)}$ equals $(g^x \text{ mod } p)^{(g^y \text{ mod } p)}$, Alice and Bob can use their secret keys with a symmetric key algorithm to conduct confidential online communications. The use of the modulo function ensures that both parties can calculate the same secret key value, but an eavesdropper cannot. An eavesdropper can intercept the values of g and p , but because of the extremely difficult mathematical problem created by the use of a large prime number in $\text{mod } p$, the eavesdropper cannot feasibly calculate either secret value x or secret value y . The secret key is known only to each party and is never visible on the network.

1.3 RSA and DSS Approach

Fig 3 and Fig 4 depicts the RSA approach and DSS approaches for generating Digital signature [1]. In the proposed approach M1 and M2 are transferred to the receiver with the RSA approach and the public key is transferred with DSS approach.

2. PREVIOUS WORKS

Diffie-Hellman session key agreement is the first key exchange protocol, proposed by Diffie and Hellman [8]. Diffie-Hellman key exchange by itself achieves perfect forward secrecy because no long-term keying material exists at the end of the session to be disclosed. However, it does not provide authentication of the communicating parties; hence it is vulnerable to a man-in-the-middle attack. Next, in order to fix the security flaw in the Diffie-Hellman protocol, the **Station-To-Station (STS) protocol** was proposed in [9]. To add authentication, the STS protocol requires both the parties to have a pair of public keys for signature generation and verification, and to know a publicly released symmetric key encryption. In contrast, note that the Diffie-Hellman protocol does not have these assumptions. These assumptions can be included into the protocol by sending public key certificates if the keys are not known in advance. In the STS protocol, STS protocol uses signatures to authenticate the communicating parties. It encrypts the signatures with the session key subsequently to show the knowledge of this session key. However, signatures and certificates cause the messages to increase considerably in size. Next comes **Secure Socket Layer (SSL)** [10] involves negotiating and establishing secure connections, and securing the data transmission. SSL handshake uses certificates and PKI [13] for mutual authentication and key exchange. PKI binds public keys with particular user identities by means of a certificate authority (CA). The CA is the trusted entity that signs and issues digital certificates [11] to other parties. A digital certificate contains a public key and the identity of the owner and the validity period of the certificate. Therefore, authentication is performed through sending and verifying certificates which involve a great overhead. SSL key exchange can use an RSA algorithm, an asymmetric technique for session key exchange which encrypts the session key from the client to the server. A Diffie-Hellman key exchange can also be used which is more secure since both parties agree on the session key without having to send the key across the wire. Another protocol is **ID-based Authenticated Key Agreement**. Many protocols were proposed for ID-KEX [12]. Paterson and Price [14] noted that the aim in designing a good ID-KEX protocol is to achieve all the properties of the best usual key agreement protocols while trying to maximize efficiency. The public key can be chosen by any

client in the system as it is generated from public information (email address or network address). Each party, then contacts the trusted authority (TA) once to authenticate and get the required private key. A key agreement protocol is said to be authenticated if it offers the guarantee that only the participating parties of the protocol can compute the agreed key. Therefore, this ID-KEX protocol is authenticated because it uses public and private keys to generate a shared secret. Another protocol **SSH (Secure SHell)** is a secure network protocol used by the user to log into a remote computer running an SSH server [15]. It was designed to replace telnet which is an earlier protocol that passes username and password in plain text. However, SSH provides a secure transmission by encrypting the authentication strings and all the other data exchanged between the hosts. Ylonen and Lonvick explored three layers of the SSH protocol; the Transport Layer Protocol provides host authentication, confidentiality (encryption), and integrity; the User Authentication Protocol authenticates the client-side user to the server and provides a number of authentication methods; and the Connection Protocol [16] multiplexes the encrypted tunnel into several logical channels. SSH supports both password authentication and public key authentication. Although passwords are convenient and they require no additional configuration or setup from the users, they can be guessed, and the hacker can get into the system. Public key authentication provides better security as every machine creates a public/private key by itself. SSH clients and servers maintain and check a database containing identifications for all the hosts that have been involved in the interactions. Therefore, the first time when a user connects to a remote entity, the user has to know or trust that the key fingerprint for that entity is correct as SSH does not practice a central authority to assure access for each entity.

The Diffie-Hellman key-exchange protocol has been the subject of many works. Canetti and Krawczyk [17] analyzed key-exchange protocols (Diffie-Hellman and key-transport) authenticated via symmetric or asymmetric techniques to obtain the proof of security. In [18] they presented a security analysis of the Diffie-Hellman key exchange protocol authenticated with digital signatures used by the Internet Key Exchange (IKE) standard. Lee, Malkin, and Nahum [20] focused on the different parts of SSL such as the strength of SSL/TLS servers; Castelluccia, Mykletun, and Tsudik [19] analyzed the performance of SSL/TLS Handshakes and suggested

an improvement. Moreover, the performance of pre-shared and Public Key Exchange Mechanisms for TLS protocol has been reported by Kuo, Tschofenig, Meyer, and Fu [21].

3. PROPOSED APPROACH

Suppose 'A' wants to exchange key with 'B'.

Step 1: 'A' sends a message M1 of variable length and M2 with RSA approach (Fig: 3) to 'B'. Here M2 is a prime number. 'A' and 'B' both share the same 'secret table'.

Step 2: 'A' picks a secret number "a"; 'B' picks a secret number "b".

Step 3: 'A' picks up first 8 bit from M1, suppose the number is 'm' and computes public number

$x = m^a \text{ mod } M2$. 'B' computes public number $y = m^b \text{ mod } M2$.

Step 4: 'A' and 'B' exchange their public numbers by DSS approach (Fig: 4). 'A' knows M1, m, M2, a, x, y. 'B' knows M1, m, M2, b, x, y.

Step 5: 'A' computes $ka1 = y^a \text{ mod } M2$, $Ka2 = y^{ka1} \text{ mod } M2$.

$$\{ka1 = (m^b \text{ mod } M2)^a \text{ mod } M2$$

$$ka1 = (m^b)^a \text{ mod } M2$$

$$ka1 = m^{ba} \text{ mod } M2 \}$$

'B' computes $kb1 = x^b \text{ mod } M2$, $kb2 = x^{kb1} \text{ mod } M2$

$$\{kb1 = (m^a \text{ mod } M2)^b \text{ mod } M2$$

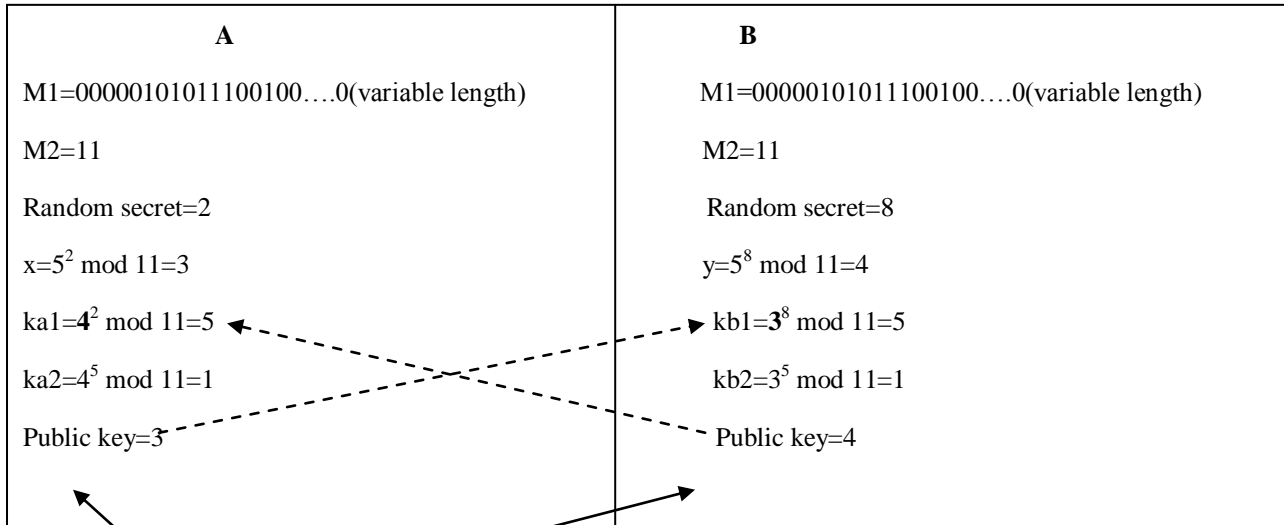
$$kb1 = (m^a)^b \text{ mod } p$$

$$kb1 = m^{ab} \text{ mod } p \}$$

Step 5: x represents the number of variables in the secret table, ka1 and kb1 represents the starting bit position in M1 which will be treated as the temporary key and lastly ka2 and kb2 represents the permutation number in the secret table.

Step 6: From the above information a Binary Decision Diagram is build with alphabetic variable ordering. Lastly from the codes of the variable in the secret table 'A' and 'B' will find their **secret key**, which is same for both 'A' and 'B'.

3.1 Example



Permutation	codes
1. a c b	a=00
2. b a c	b=100
3. c a b	c=1100
4. a b c	
5. c b a	
6. b c a	

Secret Table

a c b f

- 0 0 0 0
- 0 0 1 1
- 0 1 0 0
- 0 1 1 1
- 1 0 0 0
- 1 0 1 1
- 1 1 0 1
- 1 1 1 1

After ordering variables in alphabetical order, the truth table becomes,

a b c f

- 0 0 0 0
- 0 0 1 0
- 0 1 0 1
- 0 1 1 1
- 1 0 0 1
- 1 0 1 1
- 1 1 0 1
- 1 1 1 1

Here $m = (00000101)_2 = (5)_{10}$.

Number of variables=3

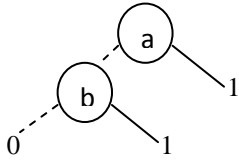
Starting bit position of temporary key=5

Permutation number=1(which is a,c,b in this case).

In this case temporary key length will be $8(2^3)$ and it will be **01010111**.

So, with this ordering and temporary key a truth table is generated,

With this variable ordering the Binary Decision diagram will be,



From the secret table,

a=00

b=100

So, **Secret Key=00100**

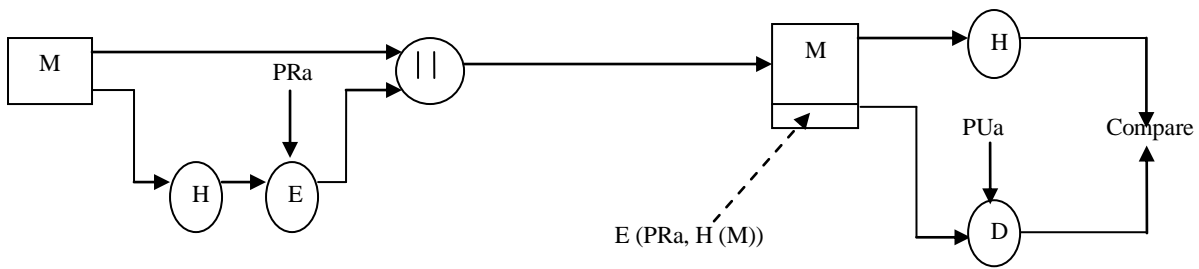


Fig 3: RSA approach

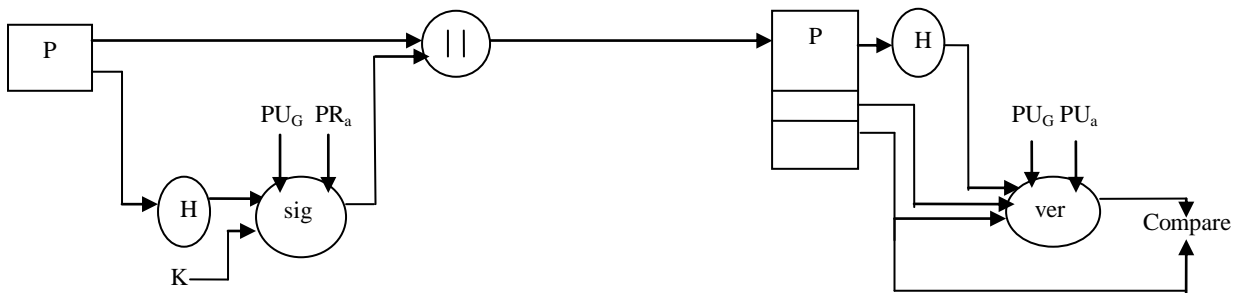


Fig 4: DSS approach

4. CONCLUSION

Designing secure cryptographic algorithms is hard, and keeping the keys secret is much harder. Cryptanalysts usually attack both symmetric and public key cryptosystems through their key management. We introduced a protocol to exchange keys over insecure communication channel. This approach takes the advantage of **Diffie-Hellman** key exchange and as well as provides integrity, authenticity and non repudiation when transferring the message and public key.

5. ACKNOWLEDGMENTS

The authors would like to thank West Bengal State University, West Bengal, India, West Bengal University of Technology, West Bengal, India. The authors also thank the reviewers for their constructive and helpful comments and specially the Computer without which no work was possible.

6. REFERENCES

- [1] Willum Stalligs, *Cryptography and Network Security principles and practice*, Fifth edition, Pearson, 2011.
- [2] Debajit Sensarma, Subhashis Banerjee, Krishnendu Basuli, Saptarshi Naskar, Samar Sen Sarma "On an optimization technique using Binary Decision Diagram", *International Journal of Computer Science, Engineering and Applications (IJCSA)*, Volume 2, Number 1, 73-86, February 2012.
- [3] Whitfield and Martin E. Hellman, "New directions in cryptography", *IEEE transactions in Information theory*, IT-22(6), pp 644-654, Nov., 1966.
- [4] Henrik Reif Andersen. "An Introduction to Binary Decision Diagrams". Lecture Notes (Technical University of Denmark, October 1997).
- [5] R.E. Bryant. "Graph-based algorithms for Boolean function manipulation". *IEEE Transactions on Computers*, C-35-8, pp.677-691, August, 1986.
- [6] RANDAL E, BRYANT. "Symbolic Boolean Manipulation with Ordered Binary-Decision Diagrams". *ACM Computing Surveys*, 1992.
- [7] Donald E. Knuth, "The Art of Computer Programming", Volume 4, Addison-Wesley.
- [8] Diffie, W., Hellman, M.E., *New directions in cryptography*, 1976.
- [9] Diffie, W., Van Oorschot, P.C., Wiener, M.J. *Authentication and authenticated key exchanges*. *Des. Codes Cryptography* 2(2), 107-125, 1992.
- [10] Frier, A., K.P., Kocher, P.. *The secure socket layer*. Technical report, Netscape Communications Corp, 1996.
- [11] Feghhi, J., Feghhi, J., Williams, P.. *Digital Certificates: Applied Internet Security*. Addison Wesley Longman, 1999.
- [12] Shim, K.. *Efficient id-based authenticated key agreement protocol based on the weil pairing*. *Electronics Letters* 39(8), 653-654, 2003.
- [13] Younglove, R.. *Public key infrastructure. how it works*. *Computing & Control Engineering Journal* 12, 99-102, 2001.
- [14] Paterson, K., Price, G.. *A comparison between traditional public key infrastructures and identity-based cryptography*. *Information Security* 8(16), 57-72, 2003.
- [15] Barrett, D., Silverman, R.. *SSH: The Secure Shell (The Definitive Guide)*. O'Reilly, 2nd edition edn, 2005.
- [16] Ylonen, T., Lonvick, C.E.. *The secure shell (ssh) connection protocol*, rfc 4254, 2006.
- [17] Canetti, R., Krawczyk, H.. *Analysis of key-exchange protocols and their use for building secure channels*. In: *EUROCRYPT '01: Proceedings of the International Conference on the Theory and Application of Cryptographic Techniques*. pp. 453-474. Springer-Verlag, London, UK, 2001.
- [18] Canetti, R., Krawczyk, H.. *Security analysis of ikes signature-based key-exchange protocol*. In: *Proc. CRYPTO02, Springer LNCS 2442*. pp. 143-161. Springer-Verlag, 2002.
- [19] Castelluccia, C., Mykletun, E., Tsudik, G.. *Improving secure server performance by re-balancing ssl/tls handshakes*. In: *in Proceedings of the 10th Annual USENIX Security Symposium*. pp. 26-34, 2005.
- [20] Lee, H.K., Malkin, T., Nahum, E.. *Cryptographic strength of ssl/tls servers: current and recent practices*. In: *IMC '07: Proceedings of the 7th ACM SIGCOMM conference on Internet measurement*. pp. 83-92. ACM, New York, NY, USA, 2007.
- [21] chun Kuo, F., Tschofenig, H., Meyer, F., Fu, X.. *Comparison studies between pre-shared and public key exchange mechanisms for transport layer security*. In: *25th IEEE International Conference on Computer Communications*. pp. 1-6, 2006.

High step up voltage gain achieved in DC-DC converters using Linear Peak Current Mode control technique

L.Malleswari*, M.Kiran Kumar**, CH.Punya Sekhar***

*(Assistant professor, Department of Electrical and Electronics Engineering, K L University, Guntur,India)

** (Assistant professor,Department of Electrical and Electronics Engineering, K L University,Guntur,India)

*** (Assistant professor,Department of Electrical and Electronics Engineering, K L University,Guntur,India)

ABSTRACT

Conventional dc-dc boost converters are unable to provide high step-up voltage gains due to the effect of power switches, rectifier diodes, and the equivalent series resistance of inductors and capacitors. In this paper a Linear Peak Current Mode Controller (LPCM) for a transformerless dc-dc converters is proposed to achieve high step-up voltage gain without an extremely high duty ratio. In the proposed converter, two inductors with same level of inductance are charged in parallel during the switch-on period and are discharged in series during the switch-off period. The structures of the proposed converter and controller are very simple. Only one power stage is used. Moreover, the steady-state analyses of voltage gains and boundary operating conditions are discussed in detail.

Index Terms—DC–DC boost converter, high step-up voltage gain, power stage.

1. INTRODUCTION

The DC-DC converter with high step up gain is used for many applications, such as high-intensity- discharge (HID) lamp ballast for automobile headlamps, fuel- cell energy conversion systems, solar-cell energy conversion systems and the battery back-up system for uninterruptible power supplies. Theoretically, the DC-DC boost converter can achieve high step-up voltage gain with an extremely high duty ratio. However, in practice, the step-up voltage gain is limited due to the effect of power switches, rectifier diodes and the equivalent series resistance (ESR) of inductors and capacitors. Also, the extremely high duty-ratio operation will result in serious reverse-recovery problem. Many topologies have been presented to provide high step-up voltage gain without an extremely high duty ratio. The DC-DC fly back converter is a very simple structure with high step-up voltage gain and electrical isolation, but the active switch of this converter will suffer high voltage stress due to the leakage inductance of the transformer. For recycling the energy of the leakage inductance and minimizing

the voltage stress on the active switch, some energy-regeneration techniques have proposed to clamp the voltage stress on the active switch and to recycle the leakage-inductance energy. The coupled-inductor techniques provide solutions to achieve high voltage gain, low voltage stress on the active switch and high efficiency without the penalty of high duty ratio. The transformer less DC-DC converters, which include the cascade boost type, the quadratic boost type, the voltage-lift type, the capacitor-diode voltage multiplier type and the boost type integrating with switched-capacitor technique. However, these types are all complex and higher cost. For getting higher step-up voltage gain, the other DC-DC converters are also presented. Compared with the converter as shown in fig.1, proposed converter has the following merits: (i) two power devices exist in the current-flow path during the switch-on period, and one power device exists in the current-flow path during the switch-off period. (ii) The voltage stresses on the active switches are less than the output voltage. (iii) Under the same operating conditions, including input voltage, output voltage, and output power, the current stress on the active switch during the switch-on period equals a half of the current stress on the active switch of the converter in fig.1. The proposed DC-DC converters fig.2 utilize the switched-inductor technique, which two inductors with same level of inductance are charged in parallel during the switch-on period and are discharged in series during the switch-off period, to achieve high step-up voltage gain without the extremely high duty ratio. The operating principles and steady-state analysis are discussed in the following sections. To analyze the steady-state characteristics of the proposed converters, some conditions are assumed as: (1) All components are ideal. The on-state resistance R_{DS} (ON) of the active switches, the forward voltage drop of the diodes and the ESRs of the inductors and capacitors are ignored. (2) All capacitors are sufficiently large and the voltages across the capacitors can be treated as constant. The modified boost type with switched-inductor technique is shown in fig.1.

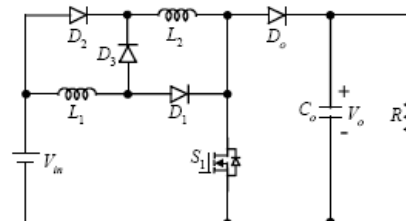


Figure 1 Transformerless DC-DC high step-up converter

The structure of this converter is very simple. Only one power stage is used in this converter. However, this converter has two issues: (i) threepower devices exist in the current-flow path during the switch-on period and two power devices exist in the current-flow path during the switch-off period. (ii) The voltage stress on the active switch equals the output voltage. When switch S_1 is ON the output voltage is zero, during this period Inductors L_1 and L_2 are charged. When switch S_1 is OFF, the output voltage is appears.

2. PROPOSED CONVERTER

A transformer less DC-DC high step-up converter is proposed as shown in figure 2. which consists of two active switches (S_1 and S_2), two inductors (L_1 and L_2) that have the same level of inductance, one output diode D_o , and one output capacitor C_o . Switches S_1 and S_2 are controlled simultaneously by using one control signal. Figure 2(d) and 2(e) shows some typical waveforms obtained during continuous conduction mode (CCM) and discontinuous conduction mode (DCM). The operating principles and steady-state analysis of CCM and DCM are presented in detail as follows.

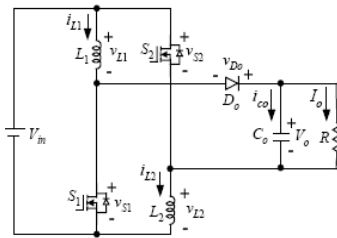


Figure 2 Proposed high step-up DC-DC converter I

2.1 CCM Operation:

The operating modes can be divided into two modes, defined as modes 1 and 2.

Mode 1 [t0, t1]:

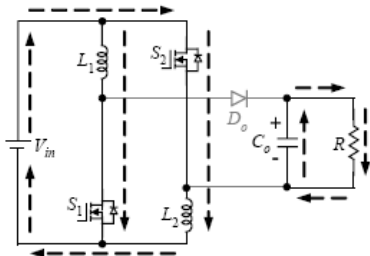


Figure 2 (a) Equivalent circuit of proposed converter I when switches ON

During this time interval, switches S_1 and S_2 are turned on. The equivalent circuit is shown in figure 2(a). Inductors L_1 and L_2 are charged in parallel from the DC Source and the energy stored in output capacitor C_0 is released to the load. Thus, the voltages

across L_1 and L_2 are given as:

$$V_{L1} = V_{L2} = V_{in} \tag{1}$$

Mode 2 [t1, t2]:

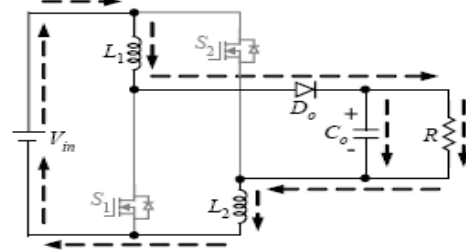


Figure 2(b) Equivalent circuit of proposed converter I when switches OFF

During this time interval, S_1 and S_2 are turned off. The equivalent circuit is shown in Fig. 2(b). The DC source, L_1 and L_2 are series-connected to transfer the energies to C_o and the load. Thus, the voltages across L_1 and L_2 are derived as

$$V_{L1} = V_{L2} = \left(\frac{V_{in} - V_o}{2} \right) \tag{2}$$

By using the volt-second balance principle on L_1 and L_2 , the following equation can be obtained:

$$\int_0^{DT_s} V_{in} dt + \int_{DT_s}^{T_s} \left(\frac{V_{in} - V_o}{2} \right) dt = 0 \tag{3}$$

Simplifying (3), the voltage gain is given by

$$M_{ccm} = \left(\frac{V_o}{V_{in}} \right) = \left(\frac{1 + D}{1 - D} \right) \tag{4}$$

From figure 2(d), the voltage stresses on S_1 , S_2 , and D_o are derived as

$$V_{s1} = V_{s2} = \left(\frac{V_o + V_{in}}{2} \right) \tag{5}$$

$$V_{D_o} = V_o + V_{in}$$

2.2 DCM Operation:

The operating modes can be divided into three modes, defined as modes 1, 2, and 3.

Mode 1 [t0, t1]: During this time interval, S_1 and S_2 are turned on. The equivalent circuit is shown in fig. 2(a). The two peak currents of L_1 and L_2 can be found as

$$I_{L1p} = I_{L2p} = \frac{V_{in} D T_s}{2} \tag{6}$$

Where L is the inductance of L_1 and L_2 .

Mode 2 [t1, t2]: During this time interval, S1 and S2 are turned off. The equivalent circuit is shown in Figure 2(b). The DC source, L1, and L2 are series-connected to transfer the energies to Co and the load. Inductor currents iL1 and iL2 are decreased to zero at t = t2. Another expression of IL1p and IL2p is given as

$$I_{L1} = I_{L2} = \left(\frac{V_o - V_{in}}{2} \right) D_2 T_s \quad (7)$$

Mode 3 [t2, t3]: During this time interval, S1 and S2 are still turned off. The equivalent circuit is shown in Fig. 2(c). The energies stored in L1 and L2 are zero. Thus, only the energy stored in Co is discharged to the load.

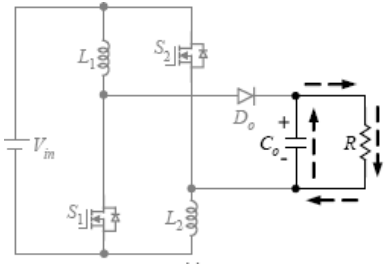


Figure 2(c) Equivalent circuit of proposed converter I when switches OFF in DCM mode

From (6) and (7), D2 is derived as follows:

$$D_2 = \left(\frac{2D V_{in}}{V_o - V_{in}} \right) \quad (8)$$

From Figure 2(e), the average value of output-capacitor current during each switching period is given by

$$I_{co} = \left(\frac{\frac{1}{2} D_2 T_2 I_{L1} - I_o T_s}{T_s} \right) = \frac{1}{2} D_2 I_{L1} - I_o \quad (9)$$

Substituting (6) and (8) into (9), Ico is derived as

$$I_{co} = \left(\frac{D^2 V_{in} T_s}{L(V_o - V_{in})} \right) - \left(\frac{V_o}{R} \right) \quad (10)$$

Since Ico equals zero under steady state, equation (10) can be rewritten as follows

$$\left(\frac{D^2 V_{in} T_s}{L(V_o - V_{in})} \right) = \left(\frac{V_o}{R} \right) \quad (11)$$

Then, the normalized inductor time constant is defined as

$$\Gamma_L = \left(\frac{L f_s}{R} \right) \quad (12) \quad \text{where } f_s \text{ is the switching frequency } (f_s = 1/T_s).$$

Substituting (12) into (11), the voltage gain is given by

$$M_{DCM} = \left(\frac{V_o}{V_{in}} \right) = \frac{1}{2} + \sqrt{\left(\frac{1}{4} + \frac{D^2}{\Gamma_L} \right)} \quad (13)$$

Typical waveforms for proposed converter I,

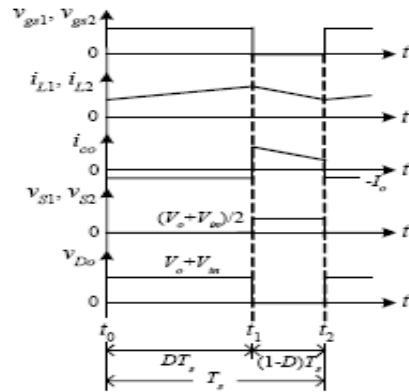


Figure 2 (d) CCM operation

2.3 Boundary Operating Condition between CCM and DCM

If proposed converter I is operated in boundary conduction mode (BCM), the voltage gain of CCM operation equals the voltage gain of DCM operation. From (4) and (13), the boundary normalized inductor time constant τ_{LB} can be derived as follows:

$$\Gamma_{LB} = \frac{D(1-D)^2}{2(1+D)} \quad (14)$$

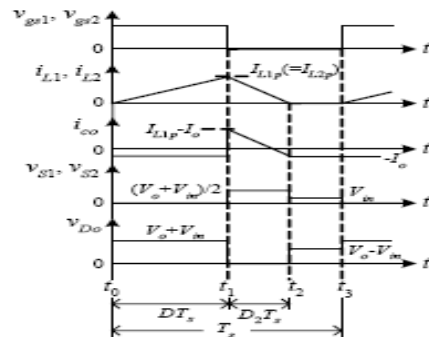


Figure 2(e) DCM operation.

The curve of τ_{LB} is plotted in Figure 2(f). If τ_L is larger than τ_{LB} , proposed converter I is operated in CCM

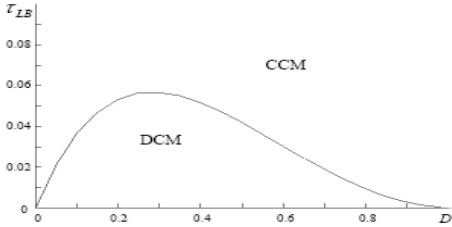


Figure 2(f) Boundary condition of proposed converter I

3. LINEAR PEAK CURRENT MODE CONTROL

Linear Peak Current Mode Control (LPCMC)-enables CCM operated rectifiers to be controlled using a much simpler controller Fig.3 (a).LPCMC offers the following advantages: Elimination of the controller multiplier and input voltages sensing circuits, unconditional stability of the current loop, and ease of implementation using low standard PWM control IC's.The control technique is based on designing a current loop whose static gain is linearly dependent upon the off-duty cycle of the switch.

Current mode control:

For current-mode control there are three things to consider:

1. Current-mode operation. An ideal current-mode converter is only dependent on the dc or average inductor current. The inner current loop turns the inductor into a voltage controlled current source, effectively removing the inductor from the outer voltage control loop at dc and low frequency.
2. Modulator gain. The modulator gain is dependent on the effective slope of the ramp presented to the modulating comparator input. Each operating mode will have a unique characteristic equation for the modulator gain.
3. Slope compensation. The requirement for slope compensation is dependent on the relationship of the average current to the value of current at the time when the sample is taken. For fixed-frequency operation, if the sampled current were equal to the average current, there would be no requirement for slope compensation.

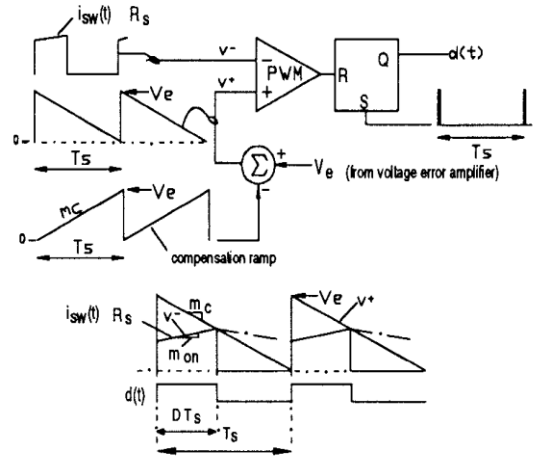


Figure 3(a) Linear Peak Current Mode Controller

The peak inductor current is expressed as

$$i_L(\text{peak}) = \frac{V_e}{R_s} \tag{15}$$

Where $I_{ref} = \frac{V_e}{T_s}$

V_e is the voltage error amplifier output signal, and R_s is the current sensing resistor, the peak inductor current becomes

$$i_L(\text{peak}) = I_{ref} - \frac{m_c T_s}{R_s} D \tag{16}$$

m_c is the slope of the compensating ramp, T_s is the switching period, and D is the duty cycle. Consider re-writing equation (16) in terms of $D'=1-D$

$$i_L(\text{peak}) = I_{ref} - \frac{m_c T_s}{R_s} D \tag{17}$$

By rearranging equation (17),we can express the static gain of current loop as

$$i_L(\text{peak}) = \left(\frac{V_e}{R_s} - \frac{m_c T_s}{R_s} \right) + \frac{m_c T_s}{R_s} D' \tag{18}$$

Equation (18) shows a positive dependence of the static current loop gain of the off-duty cycle D' .Figure 3.2 plots $i_L(\text{peak})/I_{ref}$ versus D' .

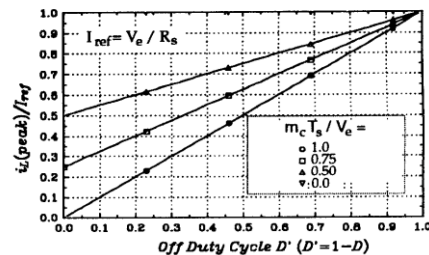


Figure 3(b) Reference current to peak current static gain

From equation (18), it is apparent that by choosing the compensation ramp appropriately, the first term will cancel, and the peak inductor current will be linearly related to D' .

$$i_L(\text{peak}) = \frac{m_c T_s}{R_s} D' \quad (19)$$

Where $\frac{m_c T_s}{v_e} = 1$, $\text{orm}_c = \frac{v_e}{T_s}$ (20), (21)

With the compensating slope defined by equation (21), equation (19) can be rewritten as

$$i_L(\text{peak}) = \frac{v_e}{R_s} D' \quad (23)$$

Equation (19) and (23) both reveal the linear relationship between the peak inductor current and the off-duty cycle D' . Hence the name Linear peak current control.

4. SIMULATION RESULTS

A Linear peak current mode control (LPCM) transformer less dc-dc converters with high step-up voltage gain has been simulated using MATLAB/Simulink. The simulation diagram of proposed controller to is shown in figure4. Simulation results are shown in fig.5 and fig.6.

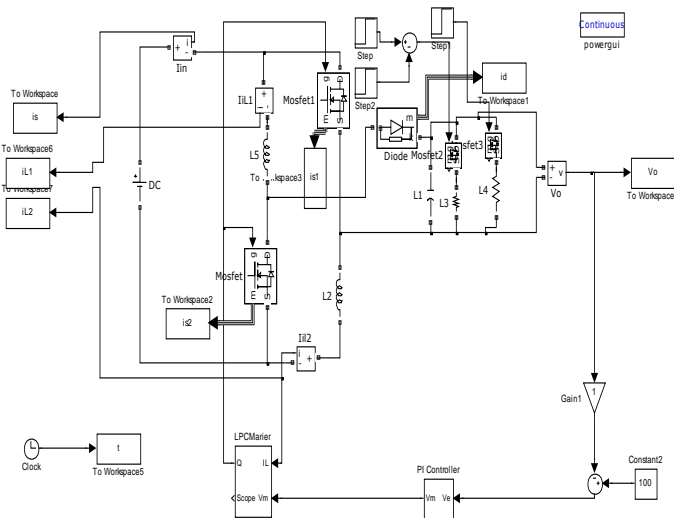


Fig4. Simulation diagram of LPCM Controller For Transformer Less Dc-Dc Converter With High Step-Up Voltage Gain

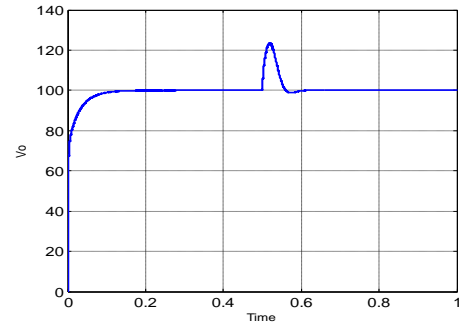


Fig5. Output voltage when load is changes from 40W to 5W at t=0.5Sec.

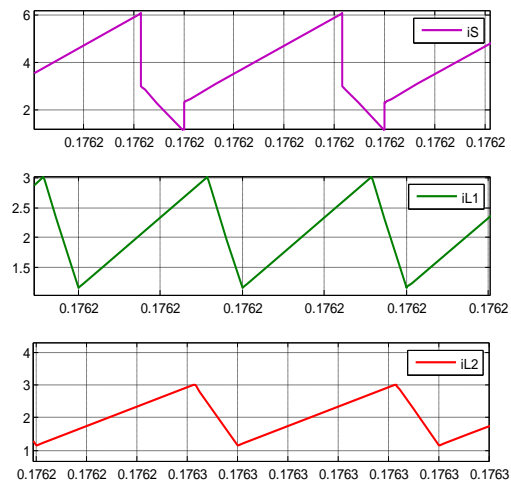


Fig6. Switch current, Inductor1 Current, Inductor2 Current waveform of Transformer Less Dc-Dc Converter With High Step-Up Voltage Gain.

5. CONCLUSION

A linear peak current mode control technique has been presented which enables simple, low cost. The technique possesses an inherently stable current loop, and the outer voltage loop is designed in a fashion similar to the other current mode control techniques. This paper has studied LPCM controller for transformerless dc-dc converter with high step-up voltage gain. Since the voltage stresses on the active switches are low, active switches with low voltage ratings and low ON-state resistance levels $R_{DS(ON)}$ can be selected. The steady-state analyses of the voltage gain and the boundary operating condition are discussed in detail. Finally the controller concept was generalized to include average current mode controller. In this case the sensed signal was a filtered version of the inductor current. In LPCM controller multiplier present in conventional current mode controller is

eliminated as a result of making profitable use of the inherent dutycycle dependent modulator gain.

6. REFERENCES

- [1.] D. C. Lu, K. W. Cheng, and Y. S. Lee, "A single-switch continuous-conduction- mode boost converter with reduced reverse-recovery and switching losses," IEEE Trans. Ind. Electron., vol. 50, no. 4, pp. 767–776, Aug. 2003.
- [2.] B. R. Lin and F. Y. Hsieh, "Soft-switching zeta-fly back converter with a buck-boost type of active clamp," IEEE Trans. Ind. Electron., vol. 54, no. 5, pp. 2813–2822, Oct. 2007.
- [3.] T. F. Wu, Y. S. Lai, J. C. Hung, and Y. M. Chen, "Boost converter with coupled inductors and buck-boost type of active clamp," IEEE Trans. Ind. Electron., vol. 55, no. 1, pp. 154–162, Jan. 2008.
- [4.] R. J. Wai and R. Y. Duan, "High-efficiency DC/DC converter with high voltage gain," Proc. Inst. Elect. Eng.—Elect. Power Appl., vol. 152, no. 4, pp. 793–802, Jul. 2005.
- [5.] B. Axelrod, Y. Berkovich, and A. Ioinovici, "Transformerless DC-DC converters with a very high DC line-to-load voltage ratio," in Proc. IEEE ISCAS, 2003, pp. III-435–III-438.
- [6.] O. Abutbul, A. Gherlitz, Y. Berkovich, and A. Ioinovici, "Step-up switching-mode converter with high voltage gain using a switched capacitor circuit," IEEE Trans. Circuits Syst. I, Fundam. Theory Appl., vol. 50, no. 8, pp. 1098–1102, Aug. 2003.



L. Malleswari received B.Tech Degree in Electrical and Electronics Engineering from R.V.R&J.C College of Engineering, Nagarjuna University, Guntur, India, in 2004. M.Tech. Degree in Electrical power Engineering from JNT University HYDERABAD, India, in 2010. Currently She Asst. Professor in Electrical and Electronics Engineering, at K L University, Guntur, India. Her research interest includes Flux reversal Machines, Power Electronics and Wind Energy Conversion Systems.



M. KIRAN KUMAR received B.Tech Degree in Electrical and Electronics Engineering from Gokula Krishna College of Engineering and Technology N T University, Hyderabad, India, in 2007. M.E. Degree in Power Electronics and Drives from SreeSastha Institute of Engineering and Technology, Anna University, Chennai, India, in 2010 and Pursuing Ph.D in Electrical Engineering at K L University, Guntur, India. Currently he Asst. Professor in Electrical and Electronics Engineering, at K L University, Guntur, India. His research interest includes Linear Switched Reluctance Machines, Power Electronics and Wind Energy Conversion Systems.



Ch. Punya Sekhar graduated in Electrical and Electronics Engineering from Chirala Engineering College, JNTU, HYD in 2008. He received M.tech degree in the stream of Power Electronics & Electrical Drives in the EEE department from Mother Teresa Institute Of Science & Technology, JNTUH, HYD in 2011. Presently he is working as Asst. Professor in EEE department in K L University, Guntur. His research interest includes Power Quality, Power Electronics and FACTS.

Fair Priority Round Robin with Dynamic Time Quantum: FPRRDQ

Asst. Proff. M. K. Srivastav¹
Sanjay Pandey², Indresh Gahoi³, Neelesh Kumar Namdev⁴
M. M. M. Engineering College Gorakhpur

Abstract—

Round Robin, considered as the most widely adopted CPU scheduling algorithm, undergoes severe problems directly related to quantum size. If time quantum chosen is too large, the response time of the processes is considered too high. On the other hand, if this quantum is too small, it increases the overhead of the CPU. Round Robin (RR) scheduling algorithm is not suitable for real time operating system because of high context switch rate, larger waiting time, and larger response time. In this paper, we have proposed an improved algorithm which is a variant of RR. Our proposed Fair Priority Round Robin with Dynamic Time Quantum (FPRRDQ) algorithm calculates optimum individual time slice for each task in each round according to the priority and the burst time of that task. Our Experimental results show that FPRRDQ algorithm performs better than Priority Based Simple Round Robin Algorithm (PBSRR) and Shortest execution First Dynamic Round Robin (SEFDRR) by decreasing the number of context switches, average waiting time, and average turnaround time .

Keywords—Operating System; Real Time System; Scheduling; Round Robin, Time slice; Priority

1.INTRODUCTION

Modern Operating Systems are moving towards multitasking environments which mainly depends on the CPU scheduling algorithm since the CPU is the most effective or essential part of the computer. Round Robin is considered the most widely used scheduling algorithm in CPU scheduling [8, 9], also used for flow passing scheduling through a network device [1].

CPU Scheduling is an essential operating system task, which is the process of allocating the CPU to a specific process for a time slice. Scheduling requires careful attention to ensure fairness and avoid process starvation in the CPU. This allocation is carried out by software known as scheduler and dispatcher [8, 9].

There are many different scheduling algorithms which varies in efficiency according to the holding environments, which means what we consider a good scheduling algorithm

in some cases which is not so in others, and vice versa. The Criteria for a good scheduling algorithm depends, among others, on the following measures [8]:

- Fairness: all processes get fair share of the CPU according to their priority and burst time,
- Efficiency: keep CPU busy 100% of time,
- Response time: minimize response time,
- Turnaround: minimize the time batch users must wait for output-
- Throughput: maximize number of jobs per hour.

Moreover, we should distinguish between the two schemes of scheduling: preemptive and non preemptive algorithms. Preemptive algorithms are those where the burst time of a process being in execution is preempted when a higher priority process arrives. Non preemptive algorithms are used where the process runs to complete its burst time even a higher priority process arrives during its execution time.

1.1 WELL KNOWN CPU SCHEDULING ALGORITHMS

First-Come-First-Served (FCFS)[8, 9] is the simplest scheduling algorithm, it simply queues processes in the order that they arrive in the ready queue. Processes are dispatched according to their arrival time on the ready queue. Being a non preemptive discipline, once a process has a CPU, it runs to completion. The FCFS scheduling is fair in the formal sense or human sense of fairness but it is unfair in the sense that long jobs make short jobs wait and unimportant jobs make important jobs wait [8, 9].

Shortest Job First (SJF) [8, 9] is the strategy of arranging processes with the least estimated processing time remaining to be next in the queue. It works under the two schemes (preemptive and non-preemptive). It's provably optimal since it minimizes the average turnaround time and the average waiting time. The main problem with this discipline is the necessity of the previous knowledge about the time required for a process to complete. Also, it undergoes a starvation issue especially in a busy system with many small processes being run[8,9].

Round Robin (RR) [8, 9] which is the main concern of this research is one of the oldest, simplest and fairest and most widely used scheduling algorithms, designed especially for

time-sharing systems. It's designed to give a better responsive but the worst turnaround and waiting time due to the fixed time quantum concept. The scheduler assigns a fixed time unit (quantum) per process usually 10-100 milliseconds, and cycles through them. RR is similar to FCFS except that preemption is added to switch between processes [2, 3, and 8].

1.2 RELATED WORK

Matarneh [2] founded that an optimal time quantum could be calculated by the median of burst times for the set of processes in ready queue, unless if this median is less than 25ms. In such case, the quantum value must be modified to 25ms to avoid the overhead of context switch time [2]. Other works [7], have also used the median approach, and have obtained good results.

Helmy et al. [3] propose a new weighting technique for Round-Robin CPU scheduling algorithm, as an attempt to combine the low scheduling overhead of round robin algorithms and favor short jobs. Higher process weights means relatively higher time quantum; shorter jobs will be given more time, so that they will be removed earlier from the ready queue [3]. Other works have used mathematical approaches, giving new procedures using mathematical theorems [4].

Mohanty and others also developed other algorithms in order to improve the scheduling algorithms performance [5], [6] and [7]. One of them is constructed as a combination of priority algorithm and RR [5] while the other algorithm is much similar to a combination between SJF and RR [6].

1.2 OUR CONTRIBUTION

In our work, we have scheduled the processes giving importance to both the user priority and shortest burst time priority rather than using single parameter. A new calculated factor based on both the user priority and the burst time priority, decides the individual time quantum for each process. We have compared the performance of our proposed Fair Priority Round Robin with Dynamic Time Quantum(FPRRDQ) algorithm with the Priority Based Static Round Robin(PBSRR) algorithm and Shortest Execution First Dynamic Round Robin(SEFDRR). Experimental results show that our proposed algorithm performs better than PBSRR and SEFDR.

1.4. ORGANIZATION OF THE PAPER

In Section II, the pseudo code and illustration of our proposed FPRRDQ algorithm is presented. Section III shows the results of experimental analysis of FPRRDQ and its comparison with PBSRR and SEFDR. Conclusion and directions for future work is given in Section IV.

2. OUR PROPOSED ALGORITHM

2.1. UNIQUENESS OF OUR APPROACH

Generally with every process two factors are associated. These factors are user priority and burst time. Above factors play an important role to decide in which sequence the processes will be executed. Sorting according to the importance of these factors, user priority comes first, and then the burst time. In FCFS, SJF and Priority algorithms, only one among these two factors are taken into consideration. If we mix up all these factors to calculate the individual time quantum of each process then average waiting time, average turnaround time and number of context switches will be decreased. But FCFS, SJF and Priority scheduling algorithms are non-preemptive in nature and they can't be used in time sharing systems. So to increase the responsiveness of the system, RR algorithm should be used. Generally in RR algorithm, processes are taken from the ready queue in FCFS manner for execution. But in our algorithm, is calculated for each process.

Since, in the previously existed algorithm like PBSRR and EFDR, they don't pay more attention regarding the user priority and burst priority (weight of the process given according to the burst time i.e. shorter burst process having more weight) of the process that the process with higher user priority and Weight (burst) should get more time quantum value for the execution of that process. That's why, we can say that the time quantum given to a process is inversely proportional to the user priority(Pr_i) and directly proportional to the weight of the process (i.e. given according to the burst time of the process W_i).

So for the time quantum calculation for process i is give as:-

$$TQ = (\sum_{i=1}^N Bt_i / N) * W_i / pr_i \dots\dots\dots(1)$$

2.2. PSEUDO CODE FOR FPRRDQ ALGORITHM

Here,

N = No. of processes

W_i = Weight of P_i based on burst time of the process. (Shorter burst processes are assigned more weight).

Input: No of processes (P_1, P_2, \dots, P_n),

Burst time of processes (Bt_1, Bt_2, \dots, Bt_n),

Priority of processes (Pr_1, Pr_2, \dots, Pr_n).

Output: T_{av} = Average turnaround time,

W_{av} = Average waiting time,

N_{cs} = Number of context switches.

Method:

1. According to the ascending order of the burst time value, the processes are sorted in the ready queue.

2. While(ready queue != null)

{

(a) calculate TQ as follows.

TQ = average (remaining burst time of all the processes) * W_i / pr_i

(b) Assign TQ to process P_i

If ($i < n$) then go to step 2(a)

}

End of while

3. Average waiting time, average turnaround time and context switch are calculated

End

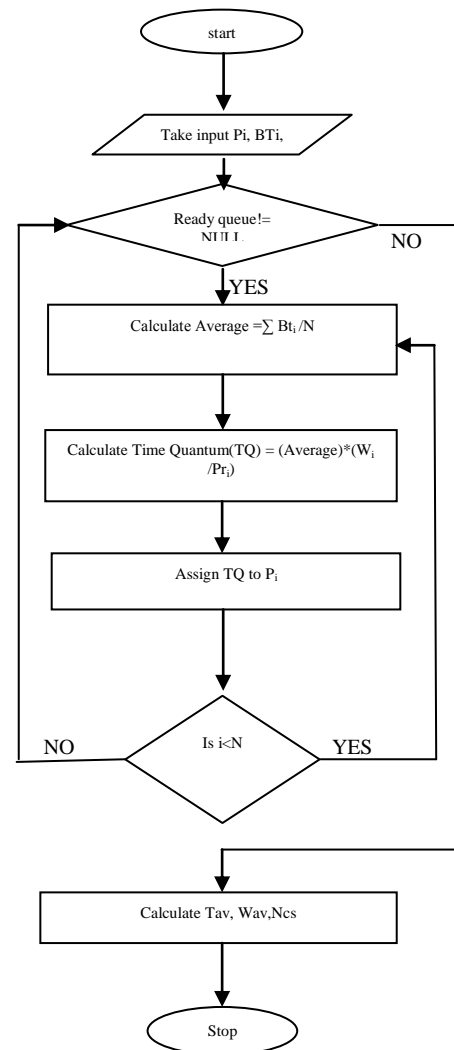


FIG 1: FLOWCHART FOR FPRRDQ ALGORITHM

3. EXPERIMENTAL RESULTS

3.1. ASSUMPTIONS

In a uni-processor environment, all the experiments are performed and all the processes are independent. Time slice is assumed to be not more than the maximum burst time. The attributes like burst time, number of processes and the user-priorities of all the processes are known before submitting the processes to the processor. All processes are CPU bound. No processes are I/O bound.

3.2 EXPERIMENTAL FRAME WORK

Taking various inputs and output parameters we have performed many experiments. The input parameters consist of the number of processes, burst time and user-priorities. The output parameters consist of average waiting

time, average turnaround time and number of context switches.

3.3. PERFORMANCE METRICS

We have used three performance metrics for our experimental analysis. Turn Around Time (TAT): For the better performance of the algorithm, average turnaround time should be less. Waiting Time (WT): For the better performance of the algorithm, average waiting time should be less. Number of Context Switches (CS): For the better performance of the algorithm, the number of context switches should be less.

3.4. EXPERIMENTS PERFORMED

To evaluate the performance of our proposed algorithm, we have taken a set of five processes in four different cases. The algorithm works effectively even if it used with a very large number of processes. In each case, we have compared the experimental results of our proposed algorithm with the priority based RR scheduling algorithm(PBSRR) and Shortest Execution First Dynamic Round Robin(SEFDRR) with dynamic time quantum Q.

CASE 1: We Assume five processes with increasing burst time (P1 = 5, P2 = 12, P3 = 16, P4 = 21, p5= 23) and priority (p1=2, p2=3, p3=1, p4=4, p5=5) as shown in Table below.

Table shows the output using PBSRR , SEFDRR algorithm and our new proposed FPRRDQ algorithm respectively.

CASE 2: We Assume five processes with decreasing burst time (P1 = 63, P2 = 54, P3 = 30, P4 = 12, p5= 5) and priority (p1=3, p2=2, p3=4, p4=1, p5=5) as shown in Table below. The Table shows the output using PBSRR, SEFDRR and our proposed FPRRDQ algorithm respectively.

Process	Burst Time	Priority
1	63	3
2	54	2

Process	Burst Time	Priority
1	5	2
2	12	3
3	16	1
4	21	4
5	23	5

3	30	4
4	12	1
5	5	5

ALGORITHM	TAV	WAV	NCS
PBSRR	109.8	77	14
SEFDRR	106.4	73.6	10
FPRRDQ	81.8	49	6

CASE 3: We Assume five processes with random burst time (P1 = 30, P2 = 8, P3 = 24, P4 = 19, p5= 46) and priority (p1=5, p2=3, p3=2, p4=1, p5=4) as shown in Table-below. The Table shows the output using PBSRR, SEFDRR algorithm and our proposed FPRRDQ algorithm respectively.

ALGORITHM	TAV	WAV	NCS
PBSRR	47.2	31.8	17
SEFDRR	42.2	26.8	11
FPRRDQ	38.2	22.8	8

Process	Burst Time	Priority
1	30	5
2	8	3
3	24	2
4	19	1
5	46	4

ALGORITHM	TAV	WAV	NCS
PBSRR	74.4	48	15
EFDRR	73.4	47	10
FPRRDQ	61.4	36	8

CASE 4: We Assume five processes with same burst time (P1 = 10, P2 = 23, P3 = 15, P4 = 34, p5= 15) and distinct priority (p1=2, p2=4, p3=1, p4=3, p5=5) as shown in Table-below. The Table shows the output using PBSRR, SEFDRR algorithm and our proposed FPRRDQ algorithm respectively .

Process	Burst Time	Priority
1	10	2
2	23	4
3	15	1
4	34	3
5	15	5

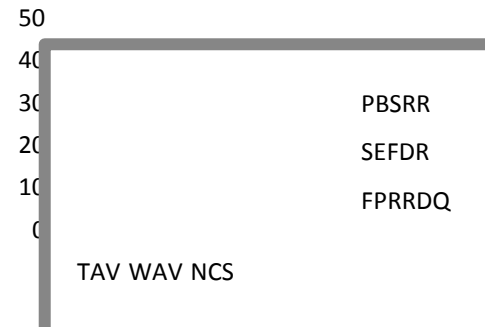


FIG. 2 : COMPARISON AMONG PBSRR , SEFDR AND FPRRDQ(CASE 1)

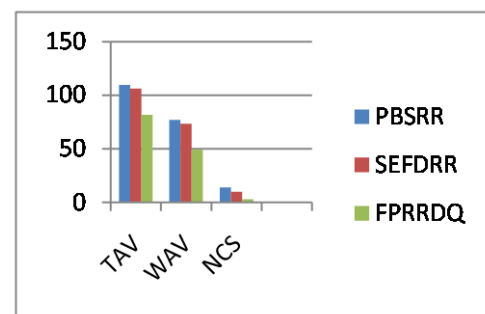


FIG. 3 : COMPARISON AMONG PBSRR , SEFDR AND FPRRDQ (CASE 2)

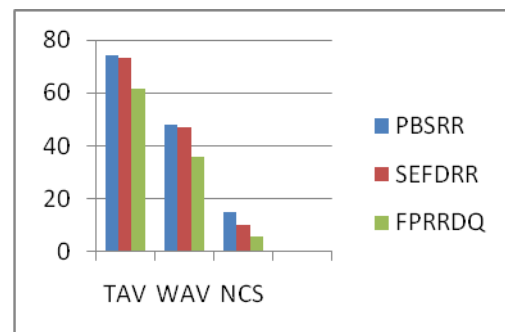


FIG. 4 : COMPARISON AMONG PBSRR , SEFDR and FPRRDQ(CASE 3)

ALGORIT HM	TAV	WAV	NCS
PBSRR	61.6	41.8	13
SEFDRR	56.8	36.8	10
FPRRDQ	52.4	33	9

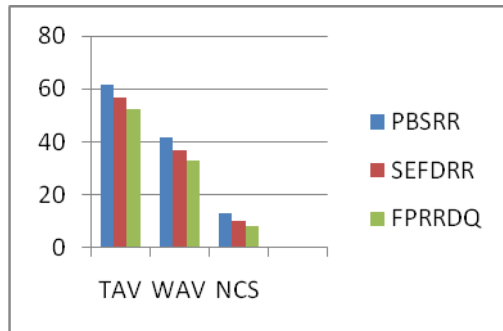


FIG. 5 : COMPARISON AMONG PBSRR , SEFDR AND FPRRDQ (CASE 4)

Where

TAV: Average Turn around time

WAV: Average Wating time

NCS: No. Of context switch

4. CONCLUSION

From the experimental results, we found that FPRRDQ performs better than the PBSRR and SEFDR in terms of decreasing the number of context switches, average waiting time and average turnaround time. The algorithm also gives a fair value of time quantum to each process according to the priority and burst time of that process.

5. REFERENCES

- [1] Weiming Tong, Jing Zhao, "Quantum Varying Deficit Round Robin Scheduling Over Priority Queues", International Conference on Computational Intelligence and Security. pp. 252- 256, China, 2007.
- [2] Rami J. Matarneh, "Self-Adjustment Time Quantum in Round Robin Algorithm Depending on Burst Time of the Now Running Processes", American Journal of Applied Sciences, Vol 6, No. 10, 2009.
- [3] Tarek Helmy, Abdelkader Dekdouk, "Burst Round Robin as a Proportional-Share Scheduling Algorithm", In Proceedings of The fourth IEEE-GCC Conference on Towards Techno-Industrial Innovations, pp. 424-428, Bahrain, 2007.
- [4] Samih M. Mostafa, S. Z. Rida, Safwat H. Hamad, "Finding Time Quantum Of Round Robin Cpu Scheduling Algorithm In General Computing Systems Using Integer Programming", International Journal of Research and Reviews in Applied Sciences (IJRRAS), Vol 5, Issue 1, 2010.
- [5] Rakesh Mohanty, H. S. Beheram Khusbu Patwarim Monisha Dash, M. Lakshmi Prasanna , "Priority Based Dynamic Round Robin (PBDRR) Algorithm with Intelligent Time Slice for Soft Real Time Systems",

(IJACSA) International Journal of Advanced Computer Science and Applications, Vol. 2, No.2, February 2011.

- [6] Rakesh Mohanty, H. S. Behera, Khusbu Patwari, Monisha Dash, "Design and Performance Evaluation of a New Proposed Shortest Remaining Burst Round Robin (SRBRR) Scheduling Algorithm", In Proceedings of International Symposium on Computer Engineering & Technology (ISCET), Vol 17, 2010.
- [7] Rakesh Mohanty, H. S. Behera, Debashree Nayak, "A New Proposed Dynamic Quantum with Re-Adjusted Round Robin Scheduling Algorithm and Its Performance Analysis", International Journal of Computer Applications (0975 – 8887), Volume 5– No.5, August 2010.
- [8] Silberschatz ,Galvin and Gagne, Operating systems concepts, 8th edition, Wiley, 2009
- [9] Lingyun Yang, Jennifer M. Schopf and Ian Foster, "Conservative Scheduling: Using predictive variance to improve scheduling decisions in Dynamic Environments", SuperComputing 2003, November 15-21, Phoenix, AZ, USA..
- [10] A.S. Tanenbaun, Modern Operating Systems.3rd Edn, Prentice Hall, ISBN:13: 9780136006633, 2008.
- [11] C. Yaashuwanth and R. Ramesh, : A New Scheduling Algorithm for Real Time System, International Journal of Computer and Electrical Engineering (IJCEE), Vol. 2, No. 6, pp 1104-1106, December, 2010.

Study & Analysis of Boom of Backhoe Loader with the Help of FE Tool

Juber Hussain Qureshi¹, Manish Sagar²

¹(Student M.E. Mechanical Engineering Department, Madhav Institute of Technology & Science
Gwalior, India

²(Assistant Professor, Mechanical Engineering Department, Madhav Institute of Technology & Science Gwalior, India

ABSTRACT

Construction industry is undoubtedly the backbone and propelling force behind our progress, in response to booming construction industry, utilization of earth moving equipment has increased considerably leading to high rate of failure. The backhoe loader mechanism must work reliably under unpredictable working conditions. Thus it is very much necessary for the designers to provide not only an equipment of maximum reliability but also of minimum weight and cost, keeping design safe under all loading conditions. It can be concluded that, force analysis and strength analysis is an important step in the design of excavator parts. FEA is the most powerful technique in strength calculations of the structures working under known load and boundary conditions. In this paper authors, describes its basic structure, stress characteristics and the engineering finite element modelling for analysing, testing and validation of backhoe loader parts under high stress zones.

Keywords: - Backhoe, FEA, Bucket

I. INTRODUCTION

Rapidly growing rate of industry of earth moving machines is assured through the high performance construction machineries with complex mechanism and automation of construction activity. Backhoe excavators are widely used for most arduous earth moving work in engineering construction to excavate below the natural surface of the ground on which the machine rests. Hydraulic system is used for operation of the machine while digging or moving the material. An excavator is comprised of three planar implements connected through revolute joints known as the boom, arm, and bucket, and one vertical revolute joint known as the swing joint. Kinematics is the science of motion which treats motion without regard to the forces that cause it. Within the science of kinematics one studies the position, velocity, acceleration, and all higher order derivatives of the position variables (with respect to time or any other variables). The excavator linkage, however, is a complex link mechanism whose motion is controlled by hydraulic cylinders and actuators. To program the bucket motion a joint-link motion, mathematical model of the link mechanism is required to refer to all geometrical and/or time-based properties of the motion. Kinematic model describes the spatial position of joints and links, and position and orientation of the bucket. The derivatives of

kinematics deal with the mechanics of motion with considering the forces that cause it.



Figure 1 The Backhoe

The basic problem in the study of mechanical link mechanism is of computing the position and orientation of Bucket of the backhoe attachment when the joint angles are known, which is referred to as forward kinematics. The inverse kinematics problem is, thus to calculate all possible sets of joint angles, which could be used to attain a given position and orientation of the bucket tip of the backhoe attachment. The problem of link mechanism control requires both the direct and inverse kinematic models of the backhoe attachment of the Excavator. The kinematic modeling helpful to follow the defined trajectory as well as digging operation can be carried out successfully at required location of the terrain using proper positioning and orientation of the bucket and ultimately digging task can be automated.

The Backhoe is essentially, soil digging machine. The working tools off the Backhoe are actuated by the Hydraulic Cylinders. The required motion for digging operation is controlled by controlling the hydraulic cylinders. Each component is actuated by a hydraulic cylinder.

A combination of extensions and retractions of the hydraulic cylinders generates the required motion of the components for digging. The hydraulic cylinder simultaneously provides the digging forces to be generated at the bucket tip. The pressure to be developed is generated by

the hydraulic pump coupled to the engine. Fig. describes the working volume of such a backhoe.



Figure 2 Working Volume of Backhoe

II. LITERATURE REVIEW

i. 3D Modelling of Boom

The Boom is the most stressed part of the backhoe loader. The boom of L&T CASE 770 is made of fabricated plates bended and welded to make one side of the boom; the two opposite parallel sub-assembly are welded with stiffener plates inside. The drawing for the Boom with sectional width is shown in the figure. All the plates welded are of 16 mm thickness, the fillet weld can be measured to be 8 to 10 mm strong.

The drawing for the Boom with sectional width is shown in the figure. All the plates welded are of 16 mm thickness, the fillet weld can be measured to be 8 to 10 mm strong.

The consideration that the weld is stronger than the base metal is kept in mind and thus the weld is not modelled in 3D software and also is not considered for any type of Finite element analysis done in the project.

ii. Kinematic Analysis

The Figure below shows the connections of Pin joint to different parts, to facilitate the motion of the system. While the linear motion of cylinders is done via use of slider mechanism constraint in the assembly mode of Pro-engineer standard module. The closed setting for cylinders is done in the mechanism to exteriorize the dependencies of motion constraint to facilitate the constraint of motions.

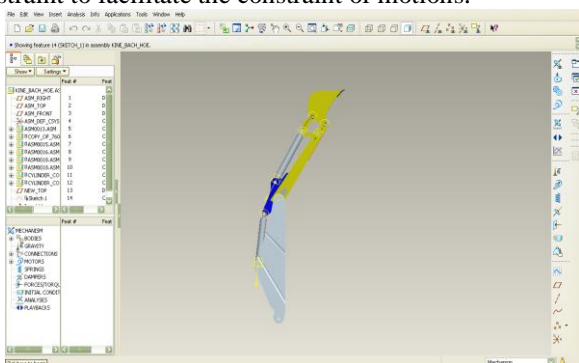


Figure 3 Connection of pin joint to different parts

iii. Dynamic Analysis

Since for dynamic analysis the mass (centre of gravity) and the time play important two inputs required to solve any dynamic analysis.

It is most difficult to predict the time of the motion. But by an average taken from viewing many cycles performed in-front of eyes by the driver driving the vehicle, we concluded the timing required to perform the operation shown in the complete video is performed in nearly 15-18 seconds of the time .

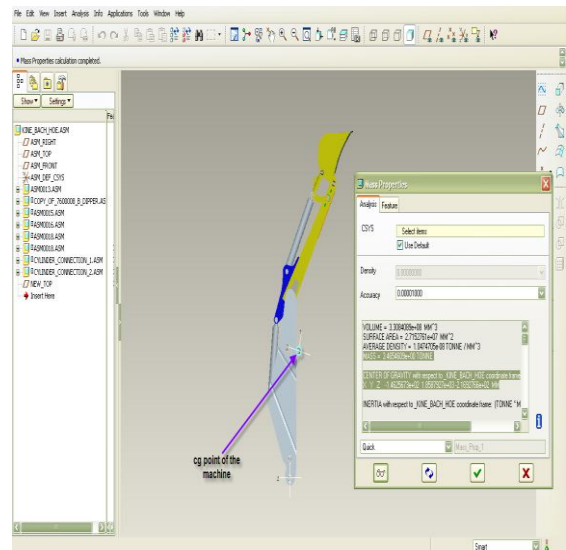


Figure 4 CG of complete machine

III. EXPERIMENTAL DATA

Finite element modelling is one of the major subjects of Computer Aided Engineering where the importance of Finite element method is sub-divided in following rules of problem solving methodologies.

- i. Pre-processing
- ii. Defining correct loads and correct Boundary conditions.
- iii. Solution and Post-processing

FEA consists of a computer model of a material or design that is stressed and analysed for specific results. It is used in new product design, and existing product refinement. A company is able to verify a proposed design will be able to perform to the client's specifications prior to manufacturing or construction. Modifying an existing product or structure is utilized to qualify the product or structure for a new service condition. In case of structural failure, FEA may be used to help determine the design modifications to meet the new condition.

FEA has become a solution to the task of predicting failure due to unknown stresses by showing problem areas in a material and allowing designers to see all of the theoretical

stresses within. This method of product design and testing is far superior to the manufacturing costs which would accrue if each sample was actually built and tested.

The use of Finite element is the second step considered in the Finite element analysis which falls after modelling of the part/assembly to be analysed. It is important to take decision before starting the Finite element modelling to ensure the results are correct and your model behaves properly as thought based on engineering principles.

The very basic decision to be taken by the FE analyst is to take the decision in the type of modelling to be done in FEA package. The Few types of modelling used are illustrated below:

- i. Shell Modelling
- ii. Solid Modelling
- iii. Beam Modelling

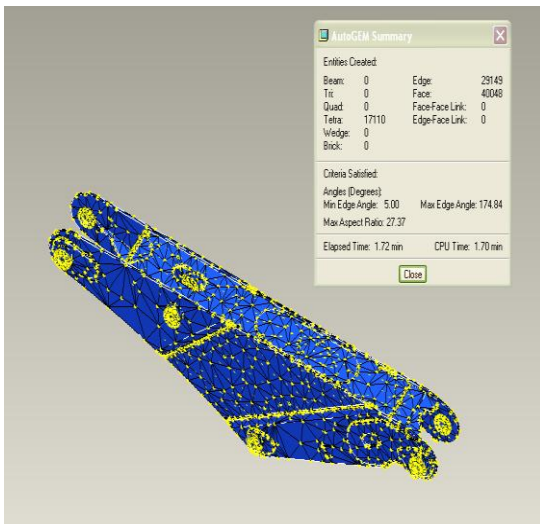


Figure 5 Showing the tetrahedral meshed model of boom

The figure above shows the no. of elements created during the analysis are 17110 in no.'s each element will create an equation to be solved for displacement which will be further used to make the assembly stiffness matrix combining the equation from all the elements. This assembly matrix will result in the values of displacements which further be solved to result in Stresses.

The different parts of the boom which are connected in assembly are also given a weld constraint in Pro-Mechanica to simulate the actual weld with 6 DOF fixed with each the two connected nodes to each other. Surface to surface weld known as perimeter weld and end weld commands are used in Pro-Mechanica.

IV. RESULT

The working operation condition will result in the machine life of 10^6 cycles with no effect and then the machine wear as said in the book of machine design by the formulation of Modified Goodman Line & Soderberg Line. The comparative chart shows the result.

V. CONCLUSION

This study tells the optimization of the Boom for including the strength of welds where welds can be modelled with shell elements along with the boom to take moments can be done to predict the failure stresses of the welds. Localization and stress linearization of the weld can be simulated for calculating the factor of safety for weld strength.

REFERENCES

- [1] P. K. Vaha, M. J. Skibniewski, "Dynamic Model of Excavator", Journal of Aerospace Engineering, Vol. 6, No. 2, April, 1993.
- [2] Sae fatigue design handbook. 400 Commonwealth Drive, 3rd ed. Warren dale (PA, USA): Society of Automotive Engineers Inc.; 1997
- [3] Bloom F, Coffin D. Handbook of thin plate buckling and post buckling. Chapman & Hall; 2001.
- [4] S. S. Rao, P.K. Bhatti, "Probabilistic approach to manipulator kinematics and dynamics", Reliability Engineering and System Safety, Elsevier Science, 2001, pp. 47-58.
- [5] Mehmet Yener, "Design of a Computer Interface for Automatic Finite Element Analysis of an Excavator Boom", M.S. Thesis, The Graduate School of natural and Applied Sciences of Middle East Technical University, May 2005, pp. 1-4, 68-69.
- [6] R. K. Mittal, I. J. Nagtath, "Robotics and Control", Ninth Reprint, Tata McGraw-Hill Publishing Company Limited, 2008, pp. 70.

BOOKS

- [1] Book "The Earthmover Encyclopedia" the complete guide to heavy equipment of the world by Keith Haddock
- [2] "Crane Handbook" Design Data and Engineering Information used in the manufacture and applications of Cranes by H.G. Greiner.

A REVIEW ON STUDY OF JAW CRUSHER

Ashish Kumar Shrivastava^{*}, Avadesh k. Sharma^{**}

^{*}Scholar M.E. Mechanical Engineering, Department, Madhav Institute of Technology & Science, Gwalior, India

^{**}Assistant Professor, Mechanical Engineering, Department, Madhav Institute of Technology & Science, Gwalior, India

ABSTRACT

Crushers are machines which use a metal surface to break or compress materials mining operations use crushers, commonly classified by the degree to which they fragment the starting material with primary and secondary crushers handling coarse materials and tertiary and quaternary crushers reducing ore particles to finer gradations. This paper focuses on review of a work carried out by researchers in the field of kinematic & dynamic analysis of the jaw crusher attachment. Kinematic & Dynamic analysis is helpful for understanding and improving the design quality of jaw crusher. There are many researcher work done by researcher in the same field but still there is a scope to develop Kinematic & dynamic analysis to jaw crusher attachment.

Keywords – Jaw crusher, Kinematic analysis, Dynamic analysis

I. INTRODUCTION

Rapidly growing rate of industry crushing machinery. A jaw or toggle crusher consists of a set of vertical jaws, one jaw being fixed and the other being moved back and forth relative to it by a cam or pitman mechanism. The jaws are farther apart at the top than at the bottom, forming a tapered chute so that the material is crushed progressively smaller and smaller as it travels downward until it is small enough to escape from the bottom opening. The movement of the jaw can be quite small, since complete crushing is not performed in one stroke. The inertia required to crush the material is provided by a weighted flywheel that moves a shaft creating an eccentric motion that causes the closing of the gap. Single and double toggle jaw crushers are constructed of heavy duty fabricated plate frames with reinforcing ribs throughout. The crusher's components are of high strength design to accept high power draw. Manganese steel is used for both fixed and movable jaw faces. Heavy flywheels allow crushing peaks on tough materials. Double Toggle jaw crushers may feature hydraulic toggle adjusting mechanisms. It is shown below Figure 1 & Figure 2.

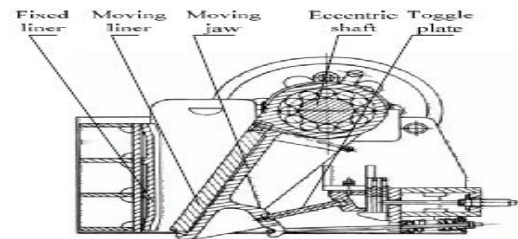


Figure 1 Single Toggle Jaw crusher

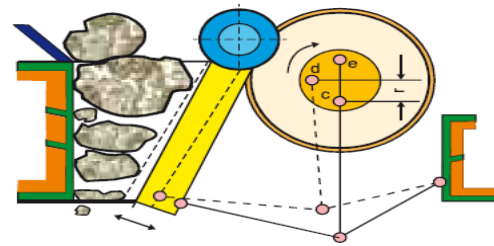


Figure 2 Double Toggle Jaw crusher

II. FORMULATION OF PROBLEM

The term size refers to the physical dimension or magnitude of an object and the reduction refers to the decrement or the process of decreasing the size thus size reduction refers to the process of converting the object from one physical dimension of higher order to another dimension of smaller order. More precisely size reduction is the operation carried out for the reducing the size of bigger particles into smaller ones of desired size and shape with the help of certain external forces. The basic problem in the study Predicts the size distribution of the product issued from crushing in function of the rotor strike radius and velocity, the material properties and size distribution of the feed well as the feed rate.

III. DYNAMIC ANALYSIS & KINEMATIC ANALYSIS

Efforts to decrease energy consumed in crushing have lead to consideration of decreasing the weight of the swing plate of jaw crushers for easily crushed material. This paper described by CHARLES H. DOWDING, in 1981, Department of Civil Engineering, Northwestern University. Evanston. IL (U.S.A.) the results of an investigation of the feasibility of using point load-deformation- failure (PDF) relationships along with interactive failure of rock particles as a model for such a weight reduction PDF relationships were determined by "Point Load-Deformation Relationships and Design of Jaw

Crusher Plates” point-loading various sizes of materials: concrete mortar. A numerical model of the swing plate ‘A’ in Figure 3 had to be developed.

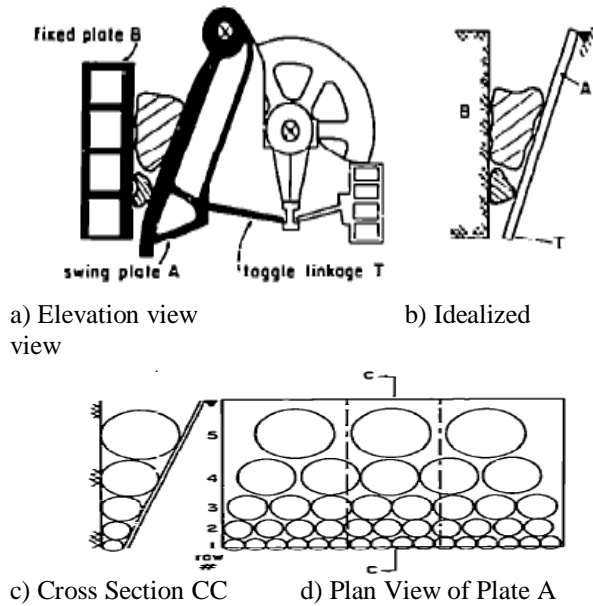


Figure 3 Idealizations of particles within jaw crusher

In this study point-loading of cylinders (or discs) was undertaken to model behavior of irregular rock particles. Modeling irregular particle behavior with that of cylinders can be appropriate by consideration of work presented by Hiramatsu and Oka. From photo elastic studies of plate-loaded spheres and point-loaded cubes, prisms and ellipsoids, they determined that the stresses produced in plate- and point-loaded spheres of identical diameter were equal. Thus, the plate idealization may be replaced by the point load shown in Figure 4. They also showed that point-load failure of a sphere was equal to that of a point-loaded ellipsoid. Therefore ultimate point loads on spheres will be approximately equal to ultimate point loads on cylinders (or discs).

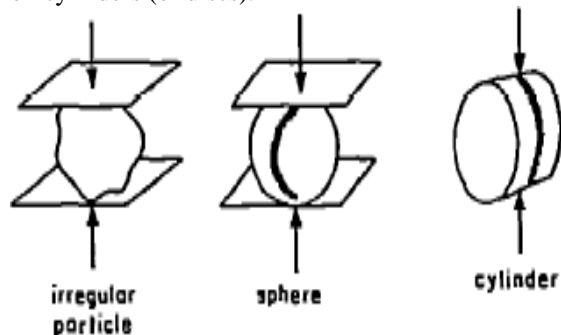


Figure 4 Comparison of plate point loaded particles

The interactive model of rock and swing-plate deformation shows a calculated reduction in both swing plate mass and maximum toggle force

compared to the no interactive assumption of simultaneous failure. These theoretical reductions indicate that design of new energy-efficient systems should include deformation properties of the crushed material. Design of crushers for specific rock types must consider the variability of point load strength and deformability implicit in any rock type name and quarry sized sampling region.

The product size distribution is obtained as function of the crusher’s rotor radius and angular velocity, the feed rate and the feed size distribution. The model is based on the standard matrix formulation that includes classification and breakage matrices. It can be applied to both hammer and vertical-axis impact crushers with the help of the corresponding estimations for the impact energy per unit mass. Here we propose classification and breakage functions for impact crushers taking into account the dynamic character of the impact breakage. The classification function has the form of a cumulative Weibull distribution incorporates a minimum breakable size of the particles depending on the impact energy and the feed rate. The breakage function is modeled as the sum of two Broadbent–Callcott distributions. It is assumed to depend on the impact energy and the feed rate through the proposed expression for the proportion of the fine fraction in the product describes “A performance model for impact crushers” by S. Nikolov 2002. The model predictions are compared with experimental data for limestone treated in a pilot-plant hammer crusher. The variations of the product size distribution resulting from changes in the rotor velocity and the feed rate are investigated.

S. Nikolov, in “Modeling and simulation of particle breakage in impact crushers” Centre Terre et Pierre, 55 Che’e d’Antoing, Tournai, in 2004 worked a phenomenological model that predicts the size distribution of the product issued from impact crushing in function of the rotor strike radius and velocity, the material properties and size distribution of the feed as well as the feed rate. The model is based on the standard matrix representation including classification and breakage matrices. It can be applied to both horizontal- and vertical-shaft impact crushers by means of the corresponding estimations for the average impact energy per unit mass presented here. We propose a new classification function for impact crushers in the form of a Weibull cumulative distribution. The minimum size of the particles that undergo breakage is assumed to be a function of the impact energy and the feed rate. The model predictions are compared with experimental data obtained for limestone treated in a pilot-plant hammer crusher. The dependence of the product size distribution on the rotor velocity is investigated. The

influence of the feed rate on the product size is also simulated. Feed rate graph is shown figure 5

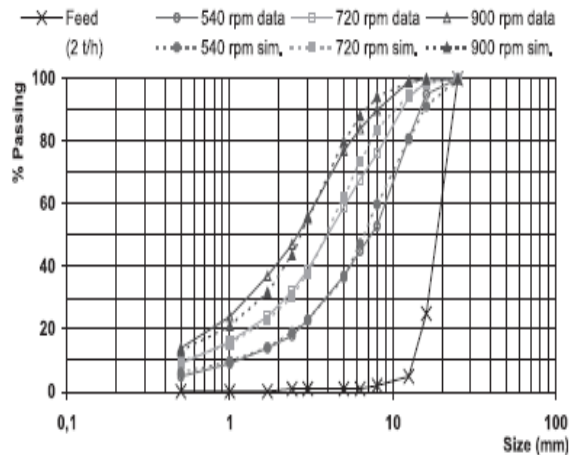


Figure 5 Experimental and simulated product size distributions at different rotor velocities for feed rate $Q=2$ t/h.

Dynamics analysis, it has been shown that the impact energy per unit mass in vertical shaft impact crushers is greater than that in horizontal shaft crushers. It is useful for prediction of the performance of both horizontal and vertical shaft impact crushers.

CAO Jinxi, RONG Xingfu, YANG Shichun, in 2006 have developed Jaw Plate Kinematical Analysis For Single toggle Jaw Crusher Design, College of Mechanical Engineering, Taiyuan University of Technology, Taiyuan, China. Jaw crusher is a kind of size reduction machine which is widely used in the mining and aggregates industry. The interaction between jaw plates and material particles brings the inevitable and serious wear to the jaw plates during the jaw crusher operation, which not only decreases the efficiency, but also increases the cost and the energy consumption of the jaw crusher. The movement of the moving jaw is described in detail. The breakage force is tested in the experiment and some information on the particles flow is gained by analyzing the force distribution. Based on the movement analysis of the moving jaw and the crushing force distribution analysis, the jaw plates wear is analyzed on a macroscopic level. The result of the wear analysis can explain some of the phenomenon in practice. With the rock material breakage character taken into consideration, the blindness brought by the traditional empirical designing can be greatly decreased. It is helpful to design the crusher for improved performance. Jaw crusher structure diagram shown in figure 6

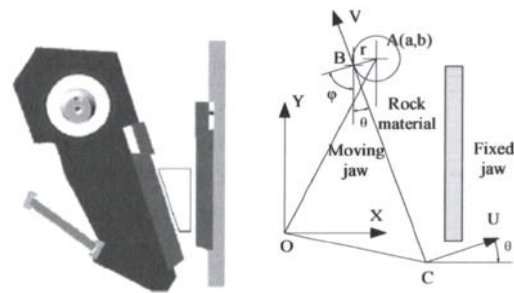


Figure 6 Single toggle jaw crusher & jaw crusher structure

The breakage force is measured in the experiment and some new information on the material flow in jaw crusher chamber is illustrated with the particle breakage character taken into consideration. Based on the movement analyses of the moving jaw and the crushing force distribution analysis, the jaw plates wear is analyzed. The relationship between the slide and the wear is reasonable and some results of the wear analysis are validated in practice. Predicting the jaw plates wear on a macroscopic level will be helpful to the jaw crusher design for better performance. Since the slide between the particles and the jaw plates is replaced by the vertical movement distance of the moving jaw plate in this paper, the further study is needed to predict the accurate wear rate.

The performance of jaw crusher is mainly determined by the kinetic characteristic of the liner during the crushing process. The practical kinetic characteristic of the liners which are located in certain domain of the coupler plane are computed and discussed in the paper titled "Investigation on Kinetic Features of Multi-Liners in Coupler Plane of Single Toggle Jaw Crusher" by Cao Jinxi, Qin Zhiyu, Wang Guopeng, Rong Xingfu, Yang Shichun 2007, IEEE, College of Mechanical Engineering, Taiyuan University of Technology, Taiyuan. Based on those computing results and analysis for the points chosen from the liners paralleling coupler plane, unique Swing features and kinematics arguments are determined in order to build the kinetic characteristic arguments. The job is helpful for a design of new prototype of this kind of machine on optimizing the frame, designing the chamber and recognizing the Crushing character. Kinetic characteristic of the crushing interface or the liner. Based on the computation and the analysis of the practical kinetic characteristic of the points in the liner domain, some traditional motion parameters and some kinetic arguments are calculated. According to the requirement for the squeezing motion of different zone in the crushing chamber, the chamber geometry can be improved.

Now use Pro/Engineer is a parametric feature-based design of 3D software, with parametric modeling functions. To reduce the development cycle and improve the design quality of jaw crusher, this paper discussed by Yuming Guan, Zhitao Zhang, Qianwei Zhang, Hebei University Of Technology Hebut Tianjin, China 2011, IEEE, "Modeling simulation and Kinematic analysis base on Pro/Engineer for Jaw Crusher mechanism" takes full advantage of the Function module of the Pro/Engineer platform to make model simulation and dynamic analysis on the actual jaw crusher mechanism, and provided the updated path for the design and manufacture of Jaw Crusher. Interference detection module is one important module of the Pro/E simulation platform, and is also one key technology of the computer graphics, and has been widely applied in the fields of virtual simulation. The appropriate level of interference detection is selected according to the need of motion simulation and collision detection of the system is carried according to the settings. The model will be shown in figure 7

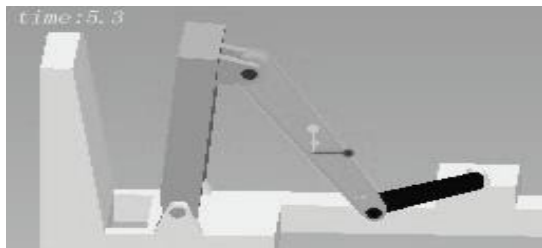


Figure 7 The complete virtual assembly chart of jaw crusher

In this module, many types, such as the reaction force, impulse, and static load of different positions can also be defined to carry out static analysis, kinematics analysis and dynamic analysis. It has very important significance for the life of the specific parts. Specific process will be no longer introduced. The dynamic analysis diagram shown in figure 8

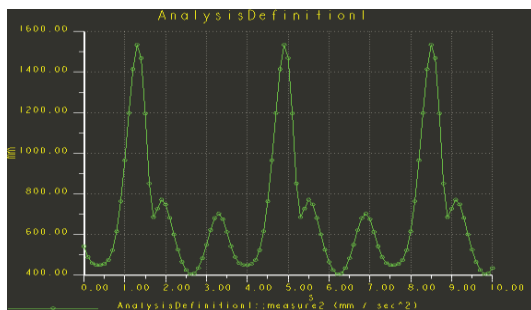


Figure 8 The output image of the acceleration

Through the application Pro/E platform on the jaw crusher, not only the result of the assembly can be expressed in the form of animation, but also can be output in the form of parameters. Thus, it is easy to know that whether to produce interference between

the parts. It makes the original motion relationships in the 2D view are difficult to be expressed become intuitive and easy to modify. At the same time, the development cycle of the jaw Crusher can be shortened and the design process of the mechanism can be simplified. And it is an important means of the modern product design.

IV. CONCLUSION

Kinematic analysis is helpful for understanding and improving the operating performance of the size reduction machine. Kinematics and dynamic analysis have very important significance for the life of the specific parts. Specific process will be no longer introduced. This concept of kinematics is followed by number of researches for their application. This review provides the background of Jaw crusher Kinematics to carried out further research work in same era.

REFERENCES

- [1] CHARLES H. DOWDING, 1981, "Point Load Deformation Relationships and Design of Jaw Crusher Plates" Department of Civil Engineering. Northwestern University. Evanston. IL (U.S.A.)
- [2] S. Nikolov, (2002), "A Performance Model For Impact Crushers" Centre Terre et Pierre, 55 Ch. d_Antoing, Tournai, Belgium, Page 715-721
- [3] S. Nikolov, (2002), "A Performance Model For Impact Crushers" Centre Terre et Pierre, 55 Ch. d_Antoing, Tournai, Belgium, Page 715-721
- [4] CAO Jinxi, RONG Xingfu, YANG Shichun, in 2006, Jaw Plate Kinematical Analysis For Single toggle Jaw Crusher Design, College of Mechanical Engineering, Taiyuan University of Technology, Taiyuan, 030024, China
- [5] Cao Jinxi, Qin Zhiyu, Wang Guopeng, Rong Xingfu, Yang Shichun (2007) "Investigation on Kinetic Features of Multi-Liners in Coupler Plane of Single Toggle Jaw Crusher" IEEE, College of Mechanical Engineering, Taiyuan University of Technology, Taiyuan, Page 1639-1641
- [6] Cap Jinxi, qin Zhiyu, Rong Xingfu, Yang Shichun, (2007), "Experimental Research on crushing Force and its Distribution Feature in jaw crusher", Page 2143-2147
- [7] Yuming Guan, Zhitao Zhang, Qianwei Zhang, (2011) IEEE, "Modeling Simulation And Kinematic Analysis Base On Pro/Engineer For Jaw Crusher Mechanism" Hebei University Of Technology Hebut Tianjin, China, Page 1407-1409.

Investigation of 24 Slots Stator Core of 0.5 HP Induction Motor and Its Performance Evaluation

I. Daut, K. Anayet, M. Asri, N. Gomesh, M. Irwan, M. A. Rashid

Electrical Energy & Industrial Electronic Systems Research Cluster

(Erstwhile Power Electronic and Electrical Machine Design)

School of Electrical Systems Engineering

Universiti Malaysia Perlis (UniMAP)

02000 Kuala Perlis, Malaysia

ABSTRACT

In this paper, we have investigated a new prototype of 24 slots stator core for 0.5hp induction motor with reduced slots to predict wherever the maximum localized flux distribution and localized power loss to be occurred. In order to evaluate the performance of this new prototype, we measured localized flux distribution in various places using search coils and also measured localized power losses using thermistor in various places of the stator core. The comparison results within 1.0T, 1.5T and 1.8T revealed that the localized flux distribution increases 39.06% from outer region to the inner region of the stator core and simultaneously power loss also increases 40% where the maximum flux distribution found compared to the outer regions of the stator core.

Keywords: Tesla (T), 24 slots stator core, non-grain materials, induction motor

I. INTRODUCTION

In this investigation, the search coil methods were used to measure flux density distribution in the stator core which is magnetised at 1.0 Tesla (low excitation), 1.5 Tesla (medium excitation) and 1.8 Tesla (over excitation). The results produced from this method are measured in terms of the magnitude of induced voltage of the stator core of induction motor. The localised flux density of stator core has been investigated under fundamental and third harmonic level. The localised flux density measurement using search coil method have been done where the magnetic cores of three phase induction machines has shown that the regions behind the teeth of stator exhibit the highest distortion of flux density [1]. The investigation of the stator cores of three-phase induction motors has shown that the regions behind the teeth of the stator cores exhibit the highest distortion of flux density distribution. Localized power losses are also seen to be highest in the teeth of the stator core, where alternating flux is forced, due to the geometry of the teeth. The observation made on the localized flux and localized loss behaviors within the three phase stator core show that a much larger flux distortion occurs within the stator teeth. The localized loss for these regions is also seen to be the highest within these regions

[1]. Localized flux density and power losses were measured in various location of the core, using small search coils and thermistors, under the core induced from 1.0T to 1.8 T, at 50 Hz.

Induction Motors (IMs) are widely used in various sectors including industrial, residential, commercial building, transport system, communication, public and household sectors. It is documented that the IMs consume about 75% of the electrical energy that consumed by all electric motors in a country, which is in fact the equivalent to about 43% of the total electrical energy consumption of a country [2]. We also noticed that one percent (1%) increase in motor electrical energy efficiency can save 20 billion kW-hrs per year or 1.4 billion dollars in electricity and 3.5 million barrels of oil in the United States. It has been then the current demand of the society to develop high efficiency low cost IMs using lower power loss stator core of induction motor. By using low cost high efficiency IMs, we can save the national revenue as well as the environment from global warming.

The stator and rotor magnetic cores are made of thin silicon steel lamination (non-grain oriented steel) to reduce hysteresis and eddy current [3]. Non grain oriented steel have magnetic properties that are as isotropic as possible. This material produced multidirectional magnetisation where useful for the rotating machines [4]. Rotating machines are considered a source of harmonics because the windings are embedded in slots which can never meet exactly sinusoidally distributed so that the mmf is distorted. Low-order harmonics have a larger impact on the three-phase induction motor than that of high-order harmonics [5-6]. The iron loss can be increased in between 15-20% under PWM excitation. Surprisingly, the increase in iron loss in a typical induction motor stator core lamination was 3% lower than that in Epstein strips of the same electrical indicating an effect of the magnetic circuit geometry and the voltage waveform [8-9].

The paper is organized as follows. The Section 2 shows the basic development process of the stator core of induction motor. The Section 3 describes the performance evaluation

of the stator core. In Section 4, we discuss the results, and some concluding remarks are drawn in the Section 5.

II. MATERIALS & METHODS

A series of steps are necessary to develop a prototype stator core of induction motor. We followed the steps as shown in Fig.1 in developing the 24 slots stator core of our developed prototype.

2.1 Development process of stator core

We followed the steps as shown in Fig.1 in developing the stator core of our developed prototype.

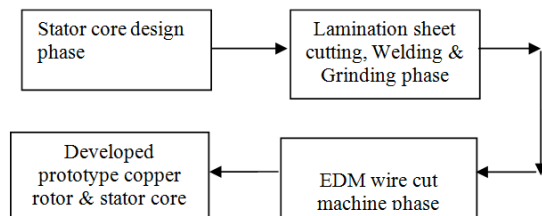


Fig. 1: Basic flow diagram of development process of stator core of IMs

Stator core design phase

This phase is the starting phase for the development process of our prototype stator core. We calculate the stator slot area for the prototype. We used AutoCAD design dxf file to perform the design work.

Lamination sheet cutting, Welding and Grinding phase

In this phase, the lamination steel sheets (grade H10 non-grain) are cut based on the specifications as obtained from design phase, which was 150mm×150mm with the thickness of 0.35mm. Then 220 pieces of single laminations sheet are divided into two lamination stacks, because the EDM wire cut machine cannot cut more than 45mm length of lamination stack. The 100 pieces of lamination steel sheets are stacked and welded together. In order to make the stacks smooth, the grinding process is done so that the stacks can be fit with EDM wire cut machine without further interruption.

EDM wire cut machine phase

The Electro discharge machine (EDM), model AQ 327L, is used to cut the lamination stacks based on the design specification as obtained from design phase. Here, we need to upload AUTOCAD dxf file in EDM machine and operate under high temperature of 11000°C to 13000°C on the conductor wire as to melt the material during the cutting process. The EDM uses 0.25 mm diameter non paraffin hard wire which is made of brass materials to cut the lamination stack.

2.2 Developed prototype of stator core of induction motor

The developed prototype of copper rotor and stator frame are shown in Fig. 2.



Fig. 2: Developed prototype of stator core of induction motor

III. PERFORMANCE EVALUATION

In this section, we evaluated the performance of our developed prototype 24 slots of stator core for 0.5hp induction motor and compared within the various tesla level. We calculated localized flux distribution and localized power loss at various places of the stator core from 1.0T to 1.8T, at 50 Hz.

3.1 Localised Flux Density of Fundamental Harmonics

Localised flux density of fundamental harmonics was shown in Fig. 4, 5 and 6 respectively, it shows the flux density distribution of the stator core magnetised at 1.0T, 1.5T and 1.8T respectively. Three factors should be considered during measurement of the localised flux density distribution throughout the stator core, e.g. (i) the effect of different positions of the lamination in the stack on the measured flux density distribution, (ii) the repeatability of the flux density measurements and (iii) the effect of the introduction of search coils on the flux density distribution in the lamination.

When the stator core were magnetised at flux density of 1.0T (low excitation), the localised flux density found increases from outer region to inner region of the stator core because the maximum induction occurred near to the slot area of the core. That is why high flux density is present in the vicinity of the slot area.

The localised flux distribution was found greater in the induction area of the core approximately 207% compared to outer core back area. The flux distribution was found at the middle of the core approximately 126.9% compared to outer core back area because in the middle area no windings i.e. it is less inductive area as shown in Fig. 4.

Fig. 3 shows the localised fundamental component of flux density at core excitation from 1.0T to 1.8 T where it shows the magnitude of the fundamental component of flux density in the tooth area gradually increases compared to outer core back area.

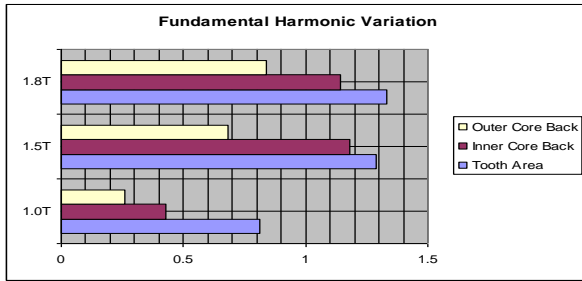


Fig. 3: Magnitude of fundamental component of flux density along the three different area of the stator core

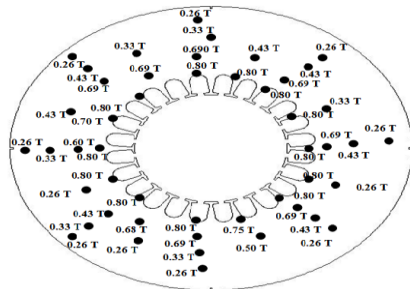


Fig. 4: Fundamental Peak Flux Density Distribution in the Stator Core Magnetised at 1.0T

When the stator core was magnetised at flux density of 1.5T (normal excitation), the localised flux density found increases from outer region to inner region of the stator core. That is why flux distribution is less uniform at the outer region and more concentrated in the inner region. The localised flux distribution was found at the inner region of the core approximately 89.7% compared to outer core back area because in stator teeth area occurred maximum induction due to its windings effect. The localised flux distribution was found at the middle of the core approximately 47.05% because this points a bit far away from the slot area.

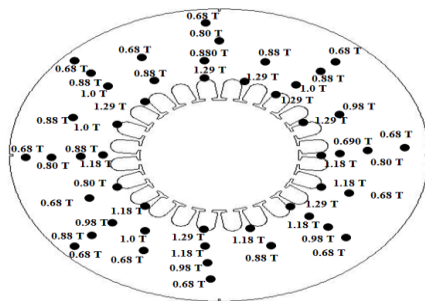


Fig. 5: Fundamental Peak Flux Density Distribution in the Stator Core Magnetised at 1.5T

While the stator core magnetised at 1.8T (high excitation), the localised flux density found still increases towards induction area tooth centre of the core and that is why it is found that localised flux density greater in the slot area instead of outer region approximately 58.21% because this area having higher induction compared to outer region of

the stator core. Localised flux distribution was found at the middle of the core approximately 35.71% because of less inductive area which is shown in Fig. 6.

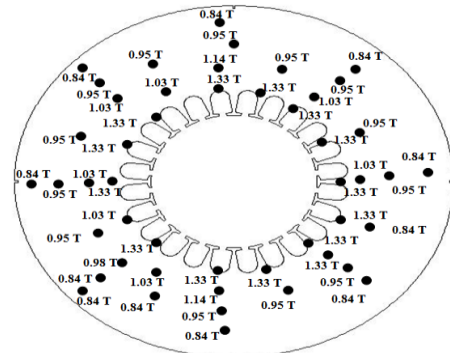


Fig. 6: Fundamental Peak Flux Density Distribution in the Stator Core Magnetised at 1.8T

3.2 Localised Flux Density of the Third Harmonics

The third harmonic components of peak flux density of the stator core shown in Fig. 8, 9 & 10 which is magnetised at 1.0T (low excitation), 1.5T (medium excitation) and 1.8T (over/high excitation) respectively.

The stator core magnetised at flux density of 1.0T as shown in Fig. 8, where the third harmonic components found increases from the outer regions to the inner regions of the stator core because in the inner region having maximum induction due to three phase windings of the core. That is why the localised flux distribution found very high in this area approximately 111.76% compared to outer core back area of the core. The localised flux distribution was found at the middle of the core approximately 47.05% compared to outer core back area because it is a bit far away from the slot area of the core.

It is therefore very important to understand the localized flux distribution within the stator core where and how much in percentage (%) occurred. It will help to design and predict of high efficiency induction motor about core losses.

Fig. 7 shows the localised third harmonic component of flux density distribution at core excitation from 1.0T to 1.8 T where it shows the magnitude of the third harmonic component of flux density in the tooth area gradually increases at 1.0T & 1.5T but at 1.8T it is going to decreased i.e. it shows during magnetization of flux density at 1.8T (high excitation) the flux distribution is maximum in the outer core back area of the stator core because of high saturation level.

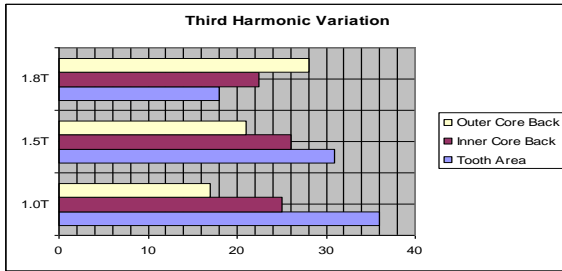


Fig. 7: Magnitude of third harmonic component of flux density distribution along the three different areas of the stator core

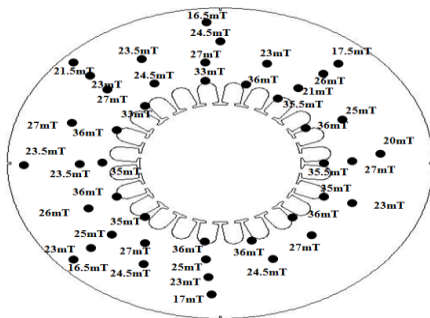


Fig. 8: Third Harmonic Component of Peak Flux Density at the Stator Core Magnetised at 1.0T

When the stator core magnetised at flux density of 1.5T (normal excitation), then the third harmonic components still found increases towards to the slot area of the stator core. The localised flux distribution was found extremely greater at the stator teeth area i.e. vicinity to the windings area of the core approximately 47.62% compared to outer core back area. Localised flux distribution was found at the middle of the core approximately 19.04% and obviously it will be less because of less induction effect of the core as shown in Fig. 9.

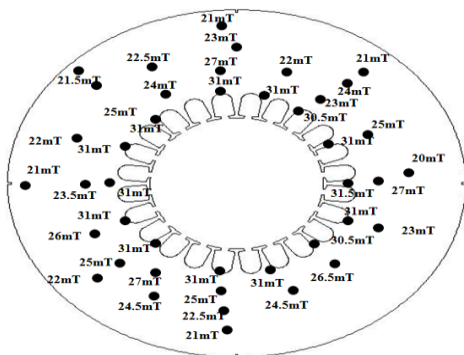


Fig. 9: Third Harmonic Component of Peak Flux Density at the Stator Core Magnetised at 1.5 T

When the stator core magnetised at flux density of 1.8T (over/high excitation) which is shown in Fig. 10, where the third harmonic components found suddenly decreases from outer regions to the inner regions of the stator core of the induction motor because of its high excitation. At this level flux density becomes saturated due to its over excitation

and as a result, it is tends to decreased. That is why localised flux distribution was found extremely greater at the outer region of the core approximately 55.55% compared to inner region of the core and at the middle of the core found approximately 22.22% compared to the slot area of the core.

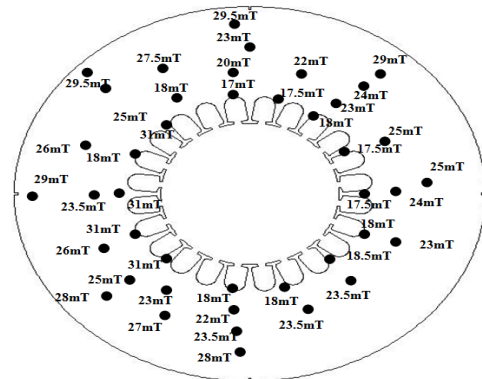


Fig. 10: Third Harmonic Component of Peak Flux Density at the Stator Core Magnetised at 1.8 T

3.3 Average Peak Flux Density Distribution In plane at Stator Core

The location of peak flux density distribution in plane in the stator core of the induction motor has shown in Fig. 11.

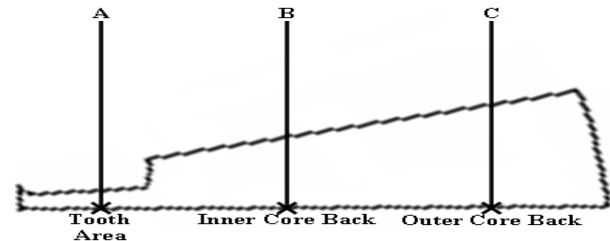


Fig. 11: Location of Peak Flux Density Distribution in Plane in the Stator Core

The overall localised flux density variation in the magnitude of the fundamental harmonic components of peak flux density magnetised at 1.0T as shown in Fig. 4, the third harmonic components of peak flux density magnetised at 1.0T in plane in the stator core shown in Fig. 8. It shows the tooth centre, inner core and outer core back area at low excitation (1.0T) data at fundamental and third harmonic level.

Table 1 shows the variation in average magnitude of fundamental and third harmonic peak flux density distribution in the stator core in different areas at flux density of 1.0T, 50 Hz. A high average of peak flux density was observed just inside the stator tooth area adjacent to the windings. In the stator core, the values of the fundamental & third harmonics found a gradual increase towards the inner region of the stator core. The highest peak values of

flux density at tooth areas found 0.78T and 35.58mT for the fundamental and third harmonic level as shown in Fig. 4 and 8 respectively.

Flux Distribution	Fundamental Harmonics (T)	Third (3 rd) Harmonics (mT)
Search Coil Location		
A- Tooth Centre	0.78	35.58
B- Inner Core Back	0.54	25.22
C- Outer Core Back	0.26	19.83

Table 1: Average Peak Flux Density Distribution of Fundamental and Third (3rd) Harmonic components in the Stator Core Magnetised at 1.0T, 50Hz

The variation in average magnitude of fundamental and third harmonic peak flux density distribution in the stator core at different areas at magnetised flux density of 1.5T as shown in Table 2. A high peak flux density was observed just inside the stator tooth area enclosed to the windings. In the stator core, only the values of fundamental peak flux density in this area show a gradual increase towards the inner region of the stator core. The highest peak value of flux density at tooth area is 1.15T for the fundamental harmonics. The magnitude of third harmonic peak flux densities found increases towards the stator tooth due to its medium excitation. The highest peak values at tooth centre are 31mT for the third harmonic level.

Flux Distribution	Fundamental Harmonics (T)	Third (3 rd) Harmonics (mT)
Search Coil Location		
A- Tooth Centre	1.15	31
B- Inner Core Back	0.94	28.38
C- Outer Core Back	0.72	21.33

Table 2: Average Peak Flux Density Distribution of Fundamental and Third (3rd) Harmonic components at the Stator Core Magnetised at 1.5T, 50Hz

The variation in average magnitude of fundamental and third harmonic peak flux density distribution in the stator core at different areas at a flux density of 1.8T as shown in Table 3. A high peak flux density was observed just inside the stator tooth area enclosed to the windings. In the stator core, only the values of fundamental peak flux density in this area show a gradual increase towards the inner region of the stator. The highest peak value of flux density at tooth area is 1.28T for the fundamental harmonic. The magnitude of third harmonic peak flux densities decreases towards the stator tooth. The highest peak values at outer core back are 28.92mT for the third harmonic.

Flux Distribution	Fundamental Harmonic (T)	Third (3 rd) Harmonic (mT)
Search Coil Location		
A- Tooth Centre	1.28	18
B- Inner Core Back	1.02	23.72
C- Outer Core Back	0.84	28.92

Table 3: Average Peak Flux Density Distribution of Fundamental and Third (3rd) Harmonic components at the Stator Magnetised at 1.8T, 50Hz

3.4 Localized Power Loss Distribution in Stator Core

The localised power loss distribution in the newly developed stator core shown in Fig. 12, 13 and 14 which is magnetised at 1.0T (low excitation), 1.5T (medium excitation) and 1.8T (over/high excitation) respectively.

The stator core magnetised at flux density of 1.0T as shown in Fig. 12, where the localised power loss found increases from outer core back area to proximity of the tooth centre of the stator core because in this area high flux density distribution are available compared to outer core area, that is why localised power loss found higher (refer to Fig. 4). The highest power loss occurred at the tooth centre around 80% compared to the outer region and at the middle power loss found around 40% compared to the outer region of the stator core.

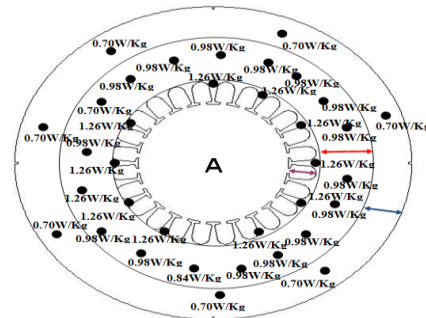


Fig. 12: Localised Power Loss in the Stator Core (A) Magnetised at 1.0T

It is very obvious because the localised flux density is higher due to its windings affect and highly inductive area, therefore, when the stator core magnetised at flux density of 1.5T as shown in Fig. 13, the localised power loss found increases from outer core back area to proximity of the tooth centre of the stator core (refer to Fig. 5). The highest power loss occurred at the tooth centre around 83.33% compared to the outer region and at the middle power loss found around 33.35% compared to the outer region of the stator core.

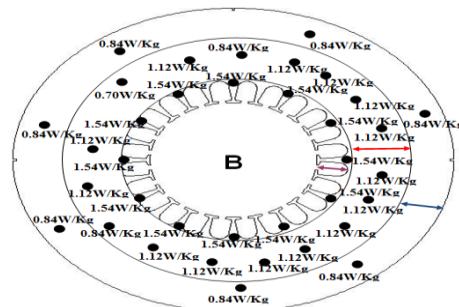


Fig. 13: Localised Power Loss in the Stator Core (B) Magnetised at 1.5T

When the stator core magnetised at flux density of 1.8T as shown in Fig. 14, where the localised power loss found still increases from outer core back area to proximity of the tooth centre of the stator core because in this area high peak localised flux density distribution are available including its high excitation and also for windings affect. Power loss varies from outer region to inner region to tooth centre of the stator core depending on that where the maximum flux distribution occurring. The highest power loss occurred at the tooth centre around 50% compared to the outer region and at the middle power loss found around 10% compared to the outer region of the stator core. Localised power loss varies from 1.40W/kg to 2.10W/Kg during high excitation in the stator core.

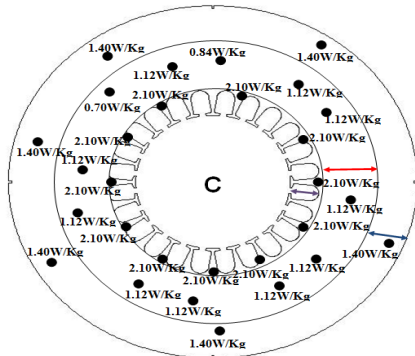


Fig. 14: Localised Power Loss in the Stator Core (C) Magnetised at 1.8T

3.5 Average Localised Power Loss Distribution In plane at Stator Core

The value of average power loss of stator core has shown in Table 4. The minimum average power loss were found when the stator core has magnetised at 1.0T refer to Fig. 12, while the maximum average power loss found magnetisation at 1.8T refer to Fig. 14.

In Table 4 also shown that the value of power loss gradually increasing from the outer core back area into the teeth area of the stator core of induction motor. The high average value of localised power loss observed very close to stator teeth area which is enclosed with the three phase windings of motor. In the stator core, all the average values of localised power loss in this area had shown a gradual increase towards the inner region of the stator because of its low excitation to high excitation. The highest average power loss found as 1.26W/kg, 1.54W/kg and 2.10W/kg in very close to tooth centre of the core, the lowest average power loss found in outer core back area as 0.70W/kg, 0.84W/kg and 1.40W/kg and the medium average power loss found in inner core back area as 0.97W/kg, 0.101W/kg and 1.06W/kg respectively.

Average Power Loss (W/kg) at Core-Flux Density (T) Measurement Area	1.0T	1.5T	1.8T
A- Teeth Area	1.26W/kg	1.54W/kg	2.10W/kg
B- Inner Core Back Area	0.97W/kg	1.01W/kg	1.06W/kg
C- Outer Core Back Area	0.70W/kg	0.84W/kg	1.40W/kg

Table 4: Average Localised Power Loss in Stator Core at Flux Density of 1.0T, 1.5T and 1.8T

IV. RESULTS AND DISCUSSIONS

Under fundamental harmonic level, the localised flux distribution (1.0T) was found greater in the induction area of the core approximately 207% compared to outer core back area and found at the middle of the core approximately 126.9% compared to outer core back area (refer to Fig. 4), the localised flux distribution (1.5T) was found at the inner region of the core approximately 89.7% compared to outer core back area and found at the middle of the core approximately 47.05% (refer to Fig. 5), the localised flux density (1.8T) greater in the slot area instead of outer region approximately 58.21% and found at the middle of the core approximately 35.71% (refer to Fig. 6).

Furthermore, under third harmonic level (1.0T, 1.5T & 1.8T) also flux distribution found increases from outer region to inner region of the stator core. From the practical observation, localised losses are also seen to be highest in the tooth regions of the stator core, where alternating flux is forced, due to the geometry of the teeth. The observations made on the localised flux and loss behaviour within the tooth tip regions of a stator core shown that a much larger flux distortion occurs within the tooth tips. The localised loss for these regions is also seen to be the highest within these regions. Localised flux and iron losses were measured in various locations of the stator core, using small search coils and thermistors, under the core overall excitations of 1.0T, 1.5 T and 1.8T at 50 Hz.

V. CONCLUSION

We developed a new prototype of stator core which is 24 slots that can be used for 0.5hp induction motor. In order to evaluate the performance of this new prototype stator core, we measured localized flux distribution and power loss in various locations to estimate the motor losses. Based on the above discussion, the following conclusions found as follows:

- The localised flux density found increases from the outer region to the inner region of the developed stator core and the distribution of localised flux density is found to be much higher density at the stator teeth i.e. induction area of the stator core.
- The localised flux density of stator teeth found increased 39.06% while the stator core magnetised from 1T to 1.8T, at 50Hz.
- The localised power loss found also increases from the outer region to the inner region in the developed stator core and the distribution of localised power loss is

found to be much higher density at the stator teeth i.e. induction area of the stator core.

- The localised power loss of stator teeth found increased 40% while the stator core magnetised from 1T to 1.8T, at 50Hz.

Acknowledgements

The author would like to thanks to School of Electrical Systems Engineering, University Malaysia Perlis (UniMAP) for the technical and financial support.

References

- [1] G Shirkoohi, and A. M. Yahya, *Localised Flux and Iron Loss in the Tooth Tip Region of a Three-Phase Induction Machine Stator Core*, *Journal of magnetism and magnetic materials*, 133 (1994) 644-646
- [2] S Nadel, M. Shepard, S. Greenberg, G. Katz, and A.T. de Almeida, *Energy-Efficient Motor System*”, by American Council for an Energy-Efficient Economy (ACEEE), Washington DC 20036, 1992, ISBN 0-918249-10-4.
- [3] Ion Boldea, S. A. N. (2001). *The Induction Machine Handbook* Retrieved 29 November 2008.
- [4] Min et al., *Effect of annealing parameter on microstructure and magnetic properties of cold rolled non-oriented electrical steel*, *Trans. Nonferrous Met. Soc. 2007, China*
- [5] R. Deshmukh, and A. Fatih, *Voltage harmonic variation in three-phase induction motors with different coil pitches*. *Journal of Magnetism and Magnetic Materials*, 2006
- [6] A G Torres et al., *Determination of the Magnetic Losses in Induction Motors based on the Generalized Epstein Test*, 2004
- [7] A G Torres, *A Generalized Epstein Test Method for the Computation of Core Losses in Induction Motors*, 2002
- [8] A J Moses, *Experimental Simulation of Magnetic Flux and Power Loss Distribution in the Stator Core of a Large Rotating Machine*, 1980
- [9] A. Moses, and N. Tutkun, *Measurement of Power Loss Distribution in Typical Stator Core under PWM voltage excitation*. *Journal of Magnetism and Magnetic Material*, 2003, 262, 230-234.

Analysis & Designing an Engineering Course Using QFD

Dr. Rupesh Gupta¹, Dr. Sheifali Gupta², Kuldeep Nagi³

**(Department of Mechanical Engineering, Chitkara University, India)*

*** (Department of Electronics & Communication Eng., Chitkara University, India)*

**** (Department of Mechanical Engineering, Chitkara University, India)*

ABSTRACT

Quality function deployment (QFD) is applied to university education system in this paper. It discusses in detail the various aspects and tools associated with QFD. Now a day's employment competition is fiercer because of global economic crisis. So how to design education program for improving undergraduate competitiveness is focused. QFD theory is applied to education program design for satisfying market requirements. Statistical Quality Control (SQC) is the course which has been analyzed and designed by using QFD. Major stakeholders of Statistical Quality Control (SQC) education were identified as students, faculty and future employers; in which future employers included enterprise, graduate institute and government department according to SQC employment situation in India. Second, a set of design requirements is developed based on the analysis of SQC education program in a University. Furthermore enterprise demands were translated into education program with the house of quality. The designed program satisfies stakeholder requirements well, so that this method can help improve the quality of SQC graduate. It is hoped that the paper can also serve the needs of researchers and practitioners for higher education institutions of QFD studies and applications, and hence promote QFD's future development.

Keywords - Engineering Institutions, house of quality, Quality Control, Quality Function Deployment, Statistical Quality Control (SQC);

I. INTRODUCTION

In QFD, the focus is on designing quality in a product or process while in quality assessment; the focus is on assuring quality in the educational process. QFD stresses knowing your customers and meeting their needs; quality assessment stresses meeting the information needs of all constituents. QFD emphasizes the enterprise functioning as a whole; quality assessment emphasizes all aspects of the educational environment. QFD requires multi-disciplinary teams; quality involves representatives from all constituents of the academic community. Both approaches stress outcomes definitions

Relevant analytical tools and techniques must be identified and incorporated into the talent training models when applied to study of higher education. Quality Function Deployment (QFD), can be modified to provide a flexible, framework for integrated training models. SQC is concerned with the design, improvement, and installation of integrated systems of people, materials, information, equipment and energy. It draws upon specialized knowledge and skill in the mathematical, physical, and social sciences

together with the principles and methods of engineering analysis and design, to specify, predict, and evaluate the results to be obtained from such systems [1].

The importance of adapting to market has been pointed out in [2]. Therefore, it is emergent to innovate the traditional education program, and design market oriented education program, especially under the new economic situation. QFD translates the customer or market requirements into design targets, which achieves market oriented principle and taking customer demands as the exclusive gist. QFD can be applied into many areas. Education is one of those, like in [3]. QFD was applied for education quality planning for SQC students. It showed the stakeholder requirements from SQC education, and then generated an education program. However, it didn't consider that different education program should be designed according to different stakeholders. Therefore, [4] QFD is applied to education program design for satisfying market and student requirements in this paper. Through the house of quality, different stakeholder requirements can be transformed to corresponding education program, which can support university to make adaptive cultivation plan.

II. QUALITY FUNCTION DEPLOYMENT

QFD is a systematic approach to design based on a close awareness of customer desires, coupled with the integration of corporate functional groups. QFD was developed by Yoji Akao in Japan in 1966. By 1972 the power of the approach had been well demonstrated at the Mitsubishi Heavy Industries Kobe Shipyard (Sullivan, 1986) and in 1978 the first book on the subject was published in Japanese and then later translated into English in 1994 (Mizuno and Akao, 1994).

In Akao's words, "QFD is a method for developing a design quality aimed at satisfying the consumer and then translating the consumer's demand into design targets and major quality assurance points to be used throughout the production phase. QFD is a way to assure the design quality while the product is still in the design stage." As a very important side benefit he points out that, when appropriately applied, QFD has demonstrated the reduction of development time by one-half to one-third. [8] The 3 main goals in implementing QFD are:

1. Prioritize spoken and unspoken customer wants and needs.
2. Translate these needs into technical characteristics and specifications.
3. Build and deliver a quality product or service by focusing everybody toward customer satisfaction

Since its introduction, Quality Function Deployment has helped to transform the way many companies:

- Plan new products

- Design product requirements
- Determine process characteristics
- Control the manufacturing process
- Document already existing product specifications

III. QUALITY FUNCTION DEPLOYMENT PHASES

QFD uses some principles from Concurrent Engineering in that cross-functional teams are involved in all phases of product development. QFD process has four different phases. Each of the four phases in a QFD process uses a matrix to translate customer requirements from initial planning stages through production control (Becker Associates Inc, 2000).

In QFD, each phase's [Ref. fig. 1] important outputs (HOWs), generated from the phase's inputs (WHATs), are converted into the next phase as its inputs (new WHATs). So each phase can be described by a matrix of "WHATs" and "HOWs", which is easy a convenient to deal with in practice.

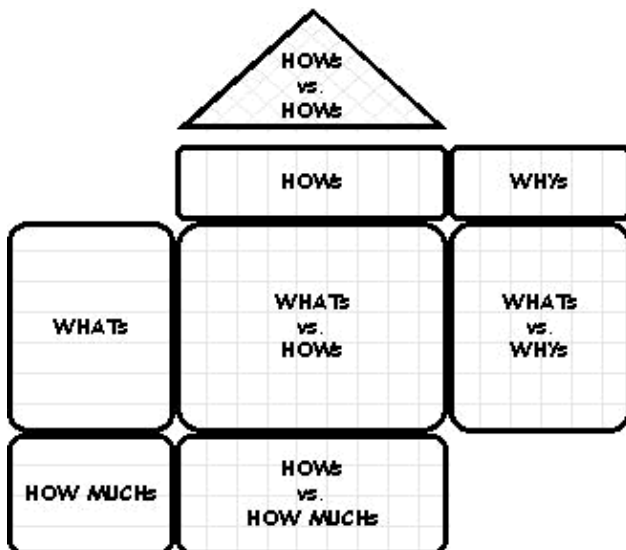


Figure.1.QFD Model

The four QFD phases include: Phase I to translate customer needs into product design attributes which we will call technical measures; Phase II to translate important technical measures into parts characteristics; Phase III to translate important parts characteristics into process operations; and Phase IV to translate key process operations into day to day production requirements[5].

Each phase, or matrix, [fig. 2] represents a more specific aspect of the product's requirements. Relationships between elements are evaluated for each phase. Only the most important aspects from each phase are deployed into the next matrix. [9]. The different four phases are explained below.

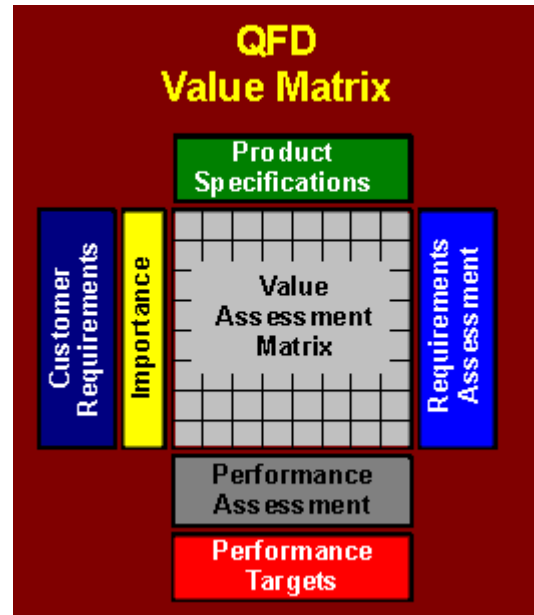


Figure.2.QFD Matrix Distribution

Phase 1, Product Planning: Building the House of Quality. Led by the marketing department, Phase 1, or product planning, is also called The House of Quality. Many organizations only get through this phase of a QFD process. Phase 1 documents customer requirements, warranty data, competitive opportunities, product measurements, competing product measures, and the technical ability of the organization to meet each customer requirement. Getting good data from the customer in Phase 1 is critical to the success of the entire QFD process.

Phase 2, Product Design: This phase 2 is led by the engineering department. Product design requires creativity and innovative team ideas. [Ref. fig. 3] Product concepts are created.

Phase 3, Process Planning: Process planning comes next and is led by manufacturing engineering. During process planning, manufacturing processes are flowcharted and process parameters (or target values) are documented. These correlation coefficients are calculated and represented in the form of symbols which are further quantified by the numbers to show the strength of association.

- = 9 (Strong association)
- = 5 (Somewhat association/ Medium Relationship)
- △ = 1 (Weak association)

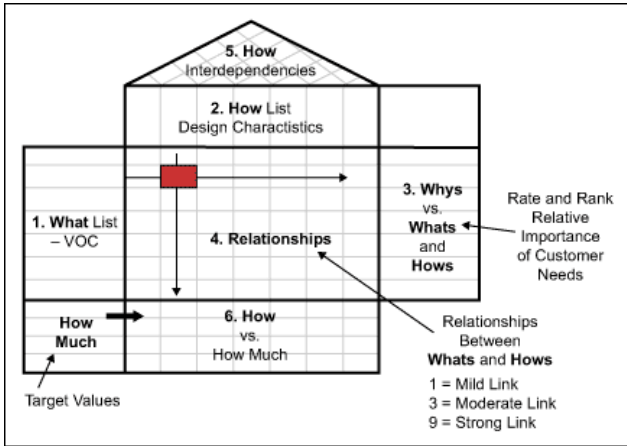


Figure.3.House of Quality to deploy QFD

Phase 4, Process Control: And finally, in production planning, performance indicators are created to monitor the production process, maintenance schedules, and skills training for operators. This phase shows inter-correlations between technical requirements provided by the Institute. The purpose of calculating inter-correlation between them is to show that whether there is association or supporting behavior or conflict between each of the technical requirements

IV. QFD APPLIED ON ENGINEERING EDUCATION

Quite a number of studies have been implemented on QFD in engineering education. In the engineering educational area, FD's applications include enrollment [6] and curriculum design [7] in colleges/institutes described the use of QFD in engineering education. Some studies have applied a QFD technical for engineering education. Study shows how QFD be used to evaluate the service quality of undergraduate nursing education. Principles of QFD in engineering education should have four aims:

- I. Training objective
- II. Training process
- III. Training system
- IV. Training evaluation

The QFD analysis in curriculum development of engineering education and the models of curriculum design and delivery will definitely help the academic administrators to implement in their curriculum development process.

A. QFD Analysis for Curriculum development

The house of quality is the first name of the QFD charts or matrices that appeared because there is a triangular shaped matrix attached to the top, sometimes called rooftop. The rooftop matrix looks just like a house, hence the name. It is a kind of conceptual map that provides the means for instructional planning and communications.

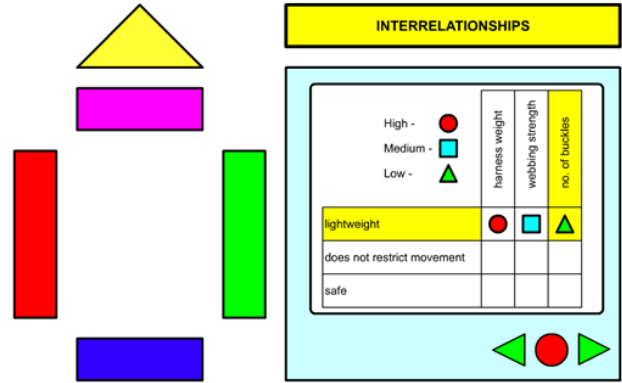


Figure.4.Matrix Relationship Model

The general model for curriculum design requires 4 matrices. The first matrix is what's matrix it is also called needs matrix. Here the customers needs for the course is developed. In order to satisfy those needs, a set of required skills should be developed and the relationships between the two sets are evaluated. Once it is validated the skills can be carried into the second matrix namely skills matrix, to match a set of primary topics. On the development of topics matrix, the primary topics are broken down into secondary topics [Ref. fig. 4] and this now creates subjects for which the instructional hours are assigned. This becomes the third matrix. The fourth matrix will be on delivery of the subjects and knowledge.

The QFD technique is used for the identification of various procedures or how's [Ref. fig. 5] for satisfying the primary requirements' of the students and the details of QFD analysis is furnished below.

Customer Reqrts	P r o d u c t D e s i g n R e q u i r e m e n t s	Bleed air ducting to interface Pt. A	Low APU weight	Low turbine wheel weight	High equivalent shaft horse power	Controlled turbine inlet temperature	Turbine easy tri-hub containment	Strong internal containment ring	Lightweight containment ring	Competitive Evaluations
		1	5							
Cust. envelope/interface	3	⊗						⊗		x o
Max.Weight 160lbs.	4	o	⊗	o			o		⊗	o x
Bleed air 75 lbs/min	4	o			⊗	⊗				o x
Turbine containment	5		o			o	⊗	⊗		ox
Elect pwr. 40KVA	3				⊗					x o
Reliable	5		o			⊗				xo
Support oil-cooled gen.	5		o							o x

Technical Evaluations	5 1	x o	o o	o o	x o	x o	o o	o o	x o	
Target Value	Target Loc.	168lb	<6 lb	350hp	1850°	2.5 lb @Pwr	3 lb @Pwr	<6 lb		Evaluations: x We o XYZ Co.
Technical Difficulty		1	4	3	5	3	4	2	4	
Importance Rating		39	35	42	35	60	62	40	20	

Figure.5.QFD Sample Matrix Solution

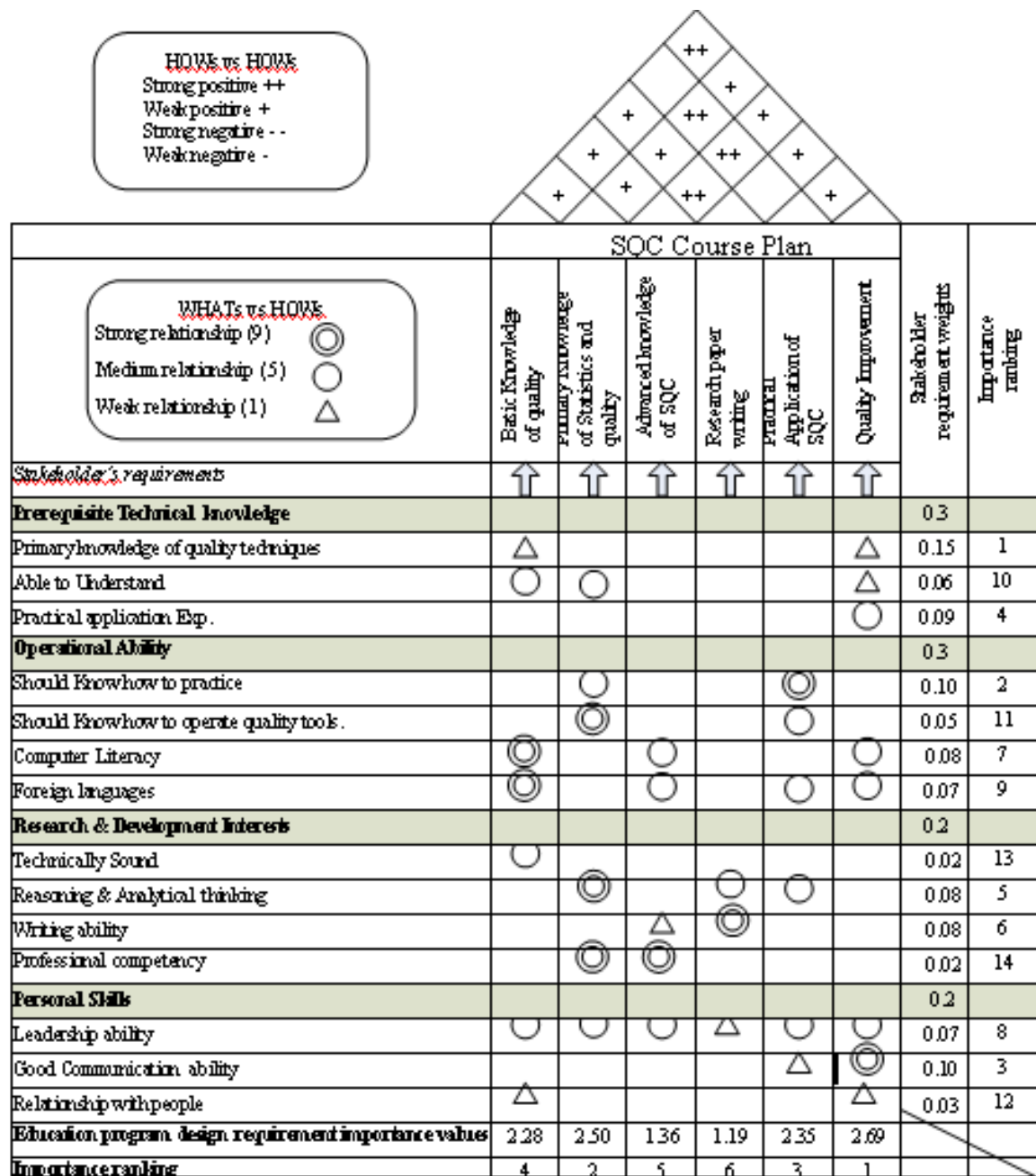


FIGURE.6.QFD MATRIX ANALYSIS FOR SQC

V. METHODOLOGY

QFD is the method proposed for the design and improvement educational program in an engineering Institute based on student requirements and benchmarks obtained from its competitor Institute B and A. The primary planning tool used in QFD is the House of Quality [10].

Step-1 This is the first step to begin the QFD process where the university seeks to capture the needs and expectations of the students. The voices of the students are taken from students . These Students requirements are verified by collecting the data through questions, in depth interviews, and focus group discussions with students who are enrolled in different engineering Institutes. Following are the student’s requirements for a particular course is

Step-2 deals with the technical requirements that are associated with the student’s needs and expectations: Basic

Knowledge of quality, Primary Knowledge of Statistics and quality, advanced knowledge of SQC, Research paper writing, Practical Application of SQC, Quality Improvement

Step-3 This step is relationship matrix showing the level of association/influence between each student needs and each technical requirement the institute is providing. These correlation coefficients are calculated and represented in the form of symbols which are further quantified by the numbers to show the strength of association.

- =9 (Strong association)
- =3 (Somewhat association)
- △=1 (Weak association)

Step-4 This step being the roof of the house of quality shows inter-correlations between technical requirements provided by the university. The purpose of calculating inter-correlation between them is to show that whether there is association or supporting behavior or conflict between each of the technical requirements. These correlation coefficients are calculated and represented in the form symbols which are further represented by the numbers to show the direction and the strength of association.

- = 9 (Strong association)
- = 3 (Somewhat association)
- △ = 1 (Weak association)
- * = -3 (Negative association)

Step-5 This step is used for developing the desires/priority based students requirements. These are categorized into columns of the house of quality i.e. importance to the customer, scale-up factor, target value, sale point and finally the absolute weight. In case of the importance to the customers for instance, the student's focus group assigns each of the student requirements by assigning a rating. These ratings are assigned 1 through 10 i.e. 1 indicating the least important to students while 10 for the very essential to students. Target values are set on the scale 1 through 5 with 1 'no change', 3 'improvement is needed' and 5 'make it better than the competitor'. The column of scale up factor is another important factor which is obtained by dividing the column of target value to the rating of Institute in the student's competitive assessment column. Lastly, the absolute values were calculated by two ways as follows:

Absolute Weight = (importance column)*(Target Value)*(Sale point) Or Absolute Weight = (Importance to customer)*(Scale up Factor)*(Sale point) [Ref. fig 3]

Step-6 This step deals with developing a prioritized technical requirements corresponding to each of the technical descriptors. This includes the technical difficulty level, relative and absolute weights. Here absolute weight is obtained for each of the technical requirements through the scalar product of the relationship matrix column and the

importance to student's column. [Ref. fig. 6]

$$T_j = \sum_{i=1}^n R_{ij} C_i$$

T_j =Absolute weight row vector for the technical requirement.

R_{ij} =Strength of association assigned to the relationships matrix (i=1...n and j=1...m)

C_i =Importance to the student's is column vector for the student requirements. (i=1...n)

m =number of technical requirement and n =number of Students requirement

The relative weights are found by calculating the sum of the products of the relationships between students and technical requirements and absolute weight of the student's requirements.

$$S_j = \sum_{i=1}^n R_{ij} d_i$$

Where S_j =Relative weights for the technical requirement row vector

d_i = Absolute weights for the student's requirements column vector.

According to the calculation results, the most important design requirement is quality development. Therefore, education program should focus on it. Besides, primary professional knowledge is the second important design requirement. In addition, as to the characteristics of SQC education, practice and application is also very important while we design an education program. In all, the outcome of the design method well satisfies enterprise's requirements. Another five stakeholders' requirements can be translated into design requirement with the same method. And the characteristics of each education program are:

- To satisfy student's requirements, Primary Knowledge of Statistics and quality, Practical application of SQC should be the most important elements in education program.
- Considering student's needs, more emphasis should be paid on advanced knowledge of SQC, practice and application.
- Primary Knowledge of Statistics and quality teaching and research paper writing are highlighted in the education program under Faculty's expectation.

VI. CONCLUSION

This study suggests that the QFD technique can be used to fulfill Student's expectations in the engineering education system. In this regard, the customer expectations mean the "voice of the customer". And the customer means the student in this study. QFD have been applied to be very powerful when designing engineering education. The universal acceptance of QFD in education after industry

highlights how important it is to raise the standards of education on universities in conformity with requirements of customers. Since the present study is concerned with exploration of the possible application of QFD to design and improve the quality of engineering course. Quality Function Deployment (QFD) theory is applied to education program design for satisfying market and student requirements. Major stakeholders of Statistical Quality Control (SQC) education are identified as graduates, undergraduates, enterprises, graduate schools, government departments and faculty. Different stakeholder does not value the same quality of SQC graduates, therefore, requirement oriented education program for SQC students are designed through QFD. Besides, it acquires design requirements of SQC engineering course based on data analysis. And it has also been observed that the designed education program well satisfy stakeholder requirements, so that the quality of SQC graduate can be improved. Moreover to find what factors the Institute should focus and to Identifying the critical factors that are needed to be enhanced in order to improve the engineering education based on the student's expectations/needs.

REFERENCES

- [1] <http://www.wiley.com/college/sc/reid/chap6.pdf>
- [2] Yang Xiaoying, Han Jianhai, and Fan Weifeng, "On orientation and talent cultivation mode of Industrial Engineering specialty," *Journal of Higher Education Management*, Vol.1 No.1 pp.90-92, January 2007.
- [3] Ayse Okur, Efendi N. Nasibov, Musa Kilic, and Murat Yavuz, "Using OWA aggregation technique in QFD: a case study in education in a textile engineering department," *Qual Quant*, Vol.43, pp.999-1009, 2009.
- [4] A.D. Che and M.S. Yang, The methods and applications of QFD. Beijing: *Publishing House Of Electronics Industry*, 2008.
- [5] L.K. Chan and M.L. Wu, A systematic approach to Quality Function deployment with a full illustrative example. *Int. J. Manage. Sci.*, vol. 33, pp. 119, 2005.
- [6] I.D. Bier and R. Cornesk, Using QFD to construct a higher education curriculum. *Qual. Progr.*, vol. 34, issu. 4, pp. 64-68, 2001.
- [7] N.A. Jnanesh and C.K. Hebbar, Use of Quality Function Deployment analysis in curriculum development fo engineering education and models for curriculum design and delivery. *Proceeding of the World congress on Engineering and computer Science*, October 22-24, 2008, San Francisco, USA.
- [8] Y. Akao, New product development and quality assurance: quality deployment system (traslated from Japanese), *Stand. Qual.Contr.*, vol. 25, issu. 4, pp. 7-14, 1972.
- [9] <http://www.ciri.org.nz/downloads/Quality%20Function%20Deployment.pdf>.
- [10] Taleeb Nadeem, Academic Management and Implementation of QFD Approach *Proceedings of ASBBS Volume 18 Number 1, ASBBS Annual Conference: Las Vegas, February 2011.*
- [11] J.J. Cristiano, J.K. Liker, and C.C. White, Customer-driven product development through quality function deployment in the U.S. and Japan. *J. Prod. Innovat. Manage.*, vol. 17, pp. 286-308, 2000.
- [12] American Supplier Institute, Quality function deployment (service QFD): 3-day workshop. Dearborn, MI: ASI Press, 1994.

Cloud Computing: In Respect to Grid and Cloud Approaches

Komal Chandra Joshi

Lecturer, Shriram Institute of Management and Technology, Kashipur

ABSTRACT

Cloud Computing, the long-held dream of computing as a utility, has the potential to transform a large part of the IT industry, making software even more attractive as a service and shaping the way IT hardware is designed and purchased. Developers with innovative ideas for new Internet services no longer require the large capital outlays in hardware to deploy their service or the human expense to operate it. They need not be concerned about over provisioning for a service whose popularity does not meet their predictions, thus wasting costly resources, or under provisioning for one that becomes wildly popular, thus missing potential customers and revenue.

Cloud computing refers to the use of Internet ("cloud") based computer technology for a variety of services. It is a computing model in which virtualized resources are provided as a service over the Internet. The concept incorporates infrastructure as a service (IaaS), platform as a service (PaaS) and software as a service (SaaS) that have the common theme for satisfying the computing needs of the users. Cloud computing services usually provide common business applications online that are accessed from a web browser. This paper pays much attention to the Grid paradigm, as it is often confused with Cloud technologies. We also describe the relationships and distinctions between the Grid and Cloud approaches.

Keywords: Incorporates infrastructure as a service (IaaS), platform as a service (PaaS) and software as a service (SaaS), Cloud Computing, Cloud Definition, Grid paradigm

1. INTRODUCTION

Cloud Computing refers to both the applications delivered as services over the Internet and the hardware and systems software in the datacenters that provide those services. The services themselves have long been referred to as Software as a Service (SaaS). The datacenter hardware and software is what we will call a Cloud. When a Cloud is made available in a pay-as-you-go manner to the general public, we call it a Public Cloud; the service being sold is Utility Computing. We use the term Private Cloud to refer to internal datacenters of a business or other organization, not made available to the general public. Thus, Cloud Computing is the sum of SaaS and Utility Computing, but does not include Private Clouds. People can be users or providers of SaaS, or users or providers of Utility Computing. We focus on SaaS providers (Cloud Users) and Cloud Providers, which have received less attention than SaaS Users.

Cloud Computing is associated with a new paradigm for the provision of computing infrastructure. This paradigm shifts the location of this infrastructure to the network to reduce the costs associated with the management of hardware and software resources [1]. The Cloud is drawing the attention from the Information and Communication Technology (ICT) community, thanks to the appearance of a set of services with

common characteristics, provided by important industry players.

2. TYPES OF CLOUD SYSTEMS AND ACTORS

This section tries to distinguish the kind of systems where Clouds are used and the actors involved in those deployments.

2.1 Actors

Many activities use software services as their business basis. These Service Providers (SPs) make services accessible to the Service Users through Internet-based interfaces. Clouds aim to outsource the provision of the computing infrastructure required to host services. This infrastructure is offered 'as a service' by Infrastructure Providers (IPs), moving computing resources from the SPs to the IPs, so the SPs can gain in flexibility and reduce costs. Depending on the type of provided capability, there are three scenarios where Clouds are used.

2.2 Infrastructure as a Service

IPs manage a large set of computing resources, such as storing and processing capacity. Through virtualization, they are able to split, assign and dynamically resize these resources to build ad-hoc systems as demanded by customers, the SPs. They deploy the software stacks that run their services. This is the Infrastructure as a Service (IaaS) scenario.

2.3 Platform as a Service

Cloud systems can offer an additional abstraction level instead of supplying a virtualized infrastructure, they can provide the software platform where systems run on. The sizing of the hardware resources demanded by the execution of the services is made in a transparent manner. This is denoted as Platform as a Service (PaaS). A well-known example is the Google Apps Engine [2].

2.4 Software as a Service

Finally, there are services of potential interest to a wide variety of users hosted in Cloud systems. This is an alternative to locally run applications. An example of this is the online alternatives of typical office applications such as word processors. This scenario is called Software as a Service (SaaS).

3. CLOUD COMPUTING IS

Cloud Computing refers to both the applications delivered as services over the Internet and the hardware and systems software in the datacenters that provide those services. The services themselves have long been referred to as Software as a Service (SaaS), so we use

that term. The datacenter hardware and software is what we will call a Cloud.

The advantages of SaaS to both end users and service providers are well understood. Service providers enjoy greatly simplified software installation and maintenance and centralized control over versioning; end users can access the service “anytime, anywhere”, share data and collaborate more easily, and keep their data stored safely in the infrastructure. Cloud Computing does not change these arguments, but it does give more application providers the choice of deploying their product as SaaS without provisioning a datacenter, Cloud Computing allows, deploying SaaS and scaling on demand without building or provisioning a datacenter.

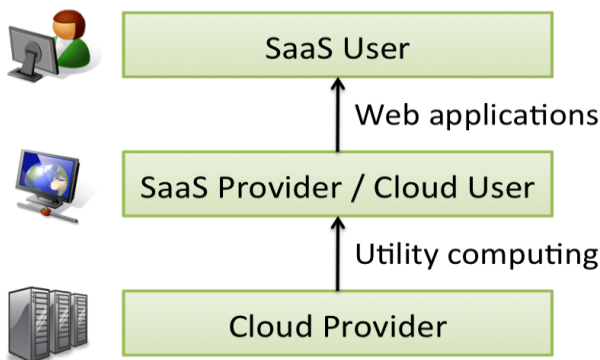


Figure 1

Figure 1: Users and Providers of Cloud Computing. The benefits of SaaS to both SaaS users and SaaS providers are well documented, so we focus on Cloud Computing effects on Cloud Providers and SaaS Providers/Cloud users. The top level can be recursive, in that SaaS providers can also be SaaS users. For example, a mash-up provider of rental maps might be a user of the Craigslist and Google maps services.

4. FACTORS TO BECOME CLOUD COMPUTING PROVIDERS:

4.1 Leverage existing investment

Adding Cloud Computing services on top of existing infrastructure provides a new revenue stream at (ideally) low incremental cost, helping to amortize the large investments of datacenters. Indeed, according to Werner Vogels, Amazon’s CTO, many Amazon Web Services technologies were initially developed for Amazon’s internal operations [3].

4.2 Defend a franchise

As conventional server and enterprise applications embrace Cloud Computing, vendors with an established franchise in those applications would be motivated to provide a cloud option of their own. For example, Microsoft Azure provides an immediate path for migrating existing customers of Microsoft enterprise applications to a cloud environment.

Technology	Cost in Medium sized DC	Cost in Very Large DC	Ratio
Network	\$95 per Mbit/sec/month	\$13 per Mbit/sec/month	7.1
Storage	\$2.20 per GByte / month	\$0.40 per GByte / month	5.7
Administration	~140 Servers / Administrator	>1000 Servers / Administrator	7.1

Table 1

Table 1: Economies of scale in 2006 for medium-sized datacenter (1000 servers) vs. very large datacenter (~50,000 servers). [4]

4.3 Attack an incumbent

A company with the requisite datacenter and software resources might want to establish a beachhead in this space before a single “800 pound gorilla” emerges. Google AppEngine provides an alternative path to cloud deployment whose appeal lies in its automation of many of the scalability and load balancing features that developers might otherwise have to build for themselves.

5. NEW APPLICATION OPPORTUNITIES

When Jim Gray examined technological trends in 2003 [5], he concluded that economic necessity mandates putting the data near the application, since the cost of wide-area networking has fallen more slowly (and remains relatively higher) than all other IT hardware costs. Although hardware costs have changed since Gray’s analysis, his idea of this “breakeven point” has not.

5.1 Mobile interactive applications.

It is believable that “the future belongs to services that respond in real time to information provided either by their users or by nonhuman sensors.” [6] Such services will be attracted to the cloud not only because they must be highly available, but also because these services generally rely on large datasets that are most conveniently hosted in large datacenters. This is especially the case for services that combine two or more data sources or other services, e.g., mash-ups. While not all mobile devices enjoy connectivity to the cloud 100% of the time, the challenge of disconnected operation has been addressed successfully in specific application domains, so we do not see this as a significant obstacle to the appeal of mobile applications.

5.2 The rise of analytics.

A special case of compute-intensive batch processing is business analytics. While the large database industry was originally dominated by transaction processing, that demand is leveling off. A growing share of computing resources is now spent on understanding customers, supply chains, buying habits, ranking, and so on. Hence, while online transaction volumes will continue to grow

slowly, decision support is growing rapidly, shifting the resource balance in database processing from transactions to business analytics.

5.3 Extension of compute-intensive desktop applications.

The latest versions of the mathematics software packages Matlab and Mathematica are capable of using Cloud Computing to perform expensive evaluations. Other desktop applications might similarly benefit from seamless extension into the cloud. Again, a reasonable test is comparing the cost of computing in the Cloud plus the cost of moving data in and out of the Cloud to the time savings from using the Cloud. Symbolic mathematics involves a great deal of computing per unit of data, making it a domain worth investigating. An interesting alternative model might be to keep the data in the cloud and rely on having sufficient bandwidth to enable suitable visualization and a responsive GUI back to the human user. Offline image rendering or 3D animation might be a similar example: given a compact description of the objects in a 3D scene and the characteristics of the lighting sources, rendering the image is an embarrassingly parallel task with a high computation-to-bytes ratio.

6. CLOUDS AND GRIDS COMPARISON

A source of confusion around the Cloud concept is its relation with Grid Computing [7]. The distinctions are not clear maybe because Clouds and grids share similar visions: reduce computing costs and increase flexibility and reliability by using third-party operated hardware.

6.1 A Grid Definition

Although the essential principles of grids have not changed much in the last decade, there are still different conceptions about what a Grid really is. In 2002, Ian Foster [8] proposed a definition of the Grid as “a system that coordinates resources which are not subject to centralized control, using standard, open, general-purpose protocols and interfaces to deliver nontrivial qualities of service”. More recent definitions emphasize the ability to combine resources from different organizations for a common goal [9]). In fact, is this divergence of conceptions about the Grid what this work aims to avoid for Clouds.

6.2 Feature Comparison:

6.2.1 Resource Sharing

Grids enhance fair share of resources across organizations, whereas Clouds provide the resources that the SP requires on demand, giving the impression of a single dedicated re-source. Hence, there is no actual sharing of resources due to the isolation provided through virtualization.

6.2.2 Heterogeneity

Both models support the aggregation of heterogeneous hardware and software resources.

6.2.3 Virtualization

Grid services are provided with interfaces that hide the heterogeneity of the underlying resources. Therefore, a Grid provides the ability to virtualizes the sum of parts into a singular wide-area resource pool. Virtualization covers both, data (flat files, databases etc.) and computing resources [10].

Cloud Computing adds the virtualization of hardware resources too.

6.2.4 Security

Virtualization is related to security since it enables the isolation of environments. While in Clouds each user has unique access to its individual virtualized environment, Grids often do not deal with end user security. Thus, some authors argue that security has not been seriously explored [11].

6.2.5 Scalability and Self-Management

Both grids and Clouds free programmers of dealing with scalability issues [8]. Grid scalability is mainly enabled by increasing the number of working nodes; Clouds offer the automatic resizing of virtualized hardware resources. Scalability requires dynamic reconfiguration as the system scales it needs to be reconfigured in an automated manner. Scalability and self-management is simpler in a single administrative domain, but many problems can be found across organizational frontiers. In grids, many difficulties lay exactly in not having a single owner of the whole system [12].

6.2.6 Usability

Clouds are easily usable, hiding the deployment details from the user [13]. This reduced entry point is a longstanding, yet unaccomplished, requirement of Grids [24]. Comparing a complex, invasive, and management-intensive vs. a simple and externally managed environment helps to explain the attention paid to Clouds.

7. CONCLUSION

Cloud Computing refers to both the applications delivered as services over the Internet and the hardware and systems software in the datacenters that provide those services. The services themselves have long been referred to as Software as a Service (SaaS). The datacenter hardware and software is what we will call a Cloud. When a Cloud is made available in a pay-as-you-go manner to the general public, we call it a Public Cloud. It is the long-held dream of computing as a utility, has the potential to transform a large part of the IT industry, making software even more attractive as a service and shaping the way IT hardware is designed and purchased. Cloud Computing refers to both the applications delivered as services over the Internet and the hardware and systems software in the datacenters that provide those services. The services themselves have long been referred to as Software as a Service (SaaS). Clouds do not have a clear and complete definition in the literature yet, which is an important task that will help to determine the areas of research and explore new application domains for the usage of the Clouds.

To tackle this problem, the main available definitions extracted from the literature have been analyzed to provide both an integrative and an essential Cloud definition. Although our encompassing definition is overlapped with many grid concepts, our common denominator definition highlights the major features of

Clouds that make them different to Grids. Virtualization is the key enabler technology of Clouds, as it is the basis for features such as, on demand sharing of resources, security by isolation, etc. Usability is also an important property of Clouds. Also, security enhancements are needed so that enterprises could rely sensitive data on the Cloud infrastructure.

REFERENCES

- [1] Brian Hayes. Cloud computing. Communications of the ACM, (7):9–11, July 2008.
- [2] Google app engine web site. Web Resource, Sept 2008.
- [3] VOGELS, W. A Head in the Clouds—The Power of Infrastructure as a Service. In First workshop on Cloud Computing and in Applications (CCA '08) (October 2008).
- [4] HAMILTON, J. Internet-Scale Service Efficiency. In Large-Scale Distributed Systems and Middleware (LADIS) Workshop (September 2008).
- [5] GRAY, J. Distributed Computing Economics. Queue 6, 3 (2008),63–68. Available from: http://portal.acm.org/ft_gateway.cfm?id=1394131&type=digital%20edition&coll=Portal&dl=GUIDE&CFID=19219697&CFTOKEN=50259492
- [6] SIEGELE, L. Let It Rise: A Special Report on Corporate IT. The Economist (October 2008).
- [7] Brian de Haaff. Cloud computing - the jargon is back! Cloud Computing Journal, August 2008. Electronic Magazine, article available at <http://cloudcomputing.sys-con.com/node/613070>.
- [8] Ian Foster. What is the grid? - a three point checklist. GRIDtoday,(6),July 2002. Available at <http://www.gridtoday.com/02/00722/100136.html>.
- [9] Miguel L. Bote-Lorenzo, Yannis A. Dimitriadis, and Eduardo Gómez-Sánchez. Grid characteristics and uses: a grid definition. pages 291–298, February 2004.
- [10] Members of EGEE-II. An egee comparative study: Grids and clouds - evolution or revolution. Technical report, Enabling Grids for E-science Project, June 2008. Electronic version available at <https://edms.cern.ch/document/925013/>.
- [11] Shantenu Jha, Andre Merzky, and Geofrey Fox. Using clouds to provide grids higher-levels of abstraction and explicit support for usage modes. Technical report, Open Grid Forum, April 2008. Available at <http://grids.ucs.indiana.edu/ptliupages/publication/cloud-grid-saga.pdf>.
- [12] Heinz Stockinger. Defining the grid: a snapshot on the current view. The Journal of Supercomputing, (1):3–17, October 2007.
- [13] Paul Watson, Phillip Lord, Frank Gibson, Panayiotis Periorellis, and Georgios Pitsilis. Cloud computing for e-science with carmen. pages 1–5, 2008.

VHDL Implementation of a Low Power Fault Tolerant System

D. Sridhar¹, K. Avinash Kumar² P. Krishna Rao³

**(Dept. of ECE, SVIET, Nandamuru, Pedana, Krishna (A.P), INDIA)*

*** (Dept. of ECE, SSCE, Chilakapalem, Srikakulam (A.P), INDIA)*

**** (Dept. of ECE, SSCE, Chilakapalem, Srikakulam (A.P), INDIA)*

ABSTRACT

Testing of digital VLSI circuits entails many challenges as a consequence of rapid growth of semiconductor manufacturing technology and the unprecedented levels of design complexity and the gigahertz range of operating frequencies. These challenges include keeping the average and peak power dissipation and test application time within acceptable limits. This dissertation proposes techniques to address these challenges during test. The first proposed technique, called bit-swapping LFSR (BS-LFSR), uses new observations concerning the output sequence of an LFSR to design a low-transition test-pattern-generator (TPG) for test-per-clock built-in self-test (BIST) to achieve reduction in the overall switching activity in the circuit-under-test (CUT). The obtained results show up to 28% power reduction for the proposed design, and up-to 63% when it is combined with another established technique. The proposed BS-LFSR is then extended for use in test-per-scan test vectors show up to 60% reduction in average power consumption.

The BS-LFSR is then extended further to act as a multi-degree smoother for test patterns generated by conventional LFSRs before applying them to the CUT. Experimental results show up to 55% reduction in average power. Another technique that aims to reduce peak power in scan-based BIST is presented. The new technique uses a two-phase scan-chain ordering algorithm to reduce average and peak power in scan and capture cycles. Experimental results show up to 65% and 55% reduction in average and peak power, respectively.

Finally, a technique that aims to significantly increase the fault coverage in test-Per scan BIST, while keeping the test-application time short, is proposed. The results obtained show a significant improvement in fault coverage and test application time compared with other techniques.

Keywords: Built-in self-test (BIST), linear feedback shift register (LFSR), low-power test, pseudorandom pattern generator, scan-chain ordering, weighted switching activity (WSA).

I. INTRODUCTION

In recent years, the design for low power has become one of the greatest challenges in high-performance very large scale integration (VLSI) design. As a consequence, many techniques have been introduced to minimize the power consumption of new VLSI systems. However, most of these methods focus on the power consumption during normal mode operation, while test mode operation has not normally been a predominant concern. However, it has been found that the power consumed during test mode operation is often much higher than during normal mode operation [1]. This is because most of the consumed power results from the switching activity in the nodes of the circuit under test (CUT), which is much higher during test mode than during normal mode operation [1]-[3]. Several techniques that have been developed to reduce the peak and average power dissipated during scan-based tests can be found in [4] and [5]. A direct technique to reduce power consumption is by running the test at a slower frequency than that in normal mode. This technique of reducing power consumption, while easy to implement, significantly increases the test application time [6]. Furthermore, it fails in reducing peak-power consumption since it is independent of clock frequency. Another category of techniques used to reduce the power consumption in scan-based built-in self-tests (BISTs) is by using scan-chain-ordering techniques [7]-[13].

These techniques aim to reduce the average-power consumption when scanning in test vectors and scanning out captured responses. Although these algorithms aim to reduce average-power consumption, they can reduce the peak power that may occur in the CUT during the scanning cycles, but not the capture power that may result during the test cycle (i.e., between launch and capture). The design of low-transition test-pattern generators (TPGs) is one of the most common and efficient techniques for low-power tests [14]-[20]. These algorithms modify the test vectors generated by the LFSR to get test vectors with a low number of transitions. The main drawback of these algorithms is that they aim only to reduce the average-power consumption while loading a new test vector, and they ignore the power consumption that results while scanning out the captured response or during the test cycle.

Furthermore, some of these techniques may result in lower fault coverage and higher test- application time. Other techniques to reduce average-power consumption during scan-based tests include scan segmentation into multiple scan chains [6], [21], test-scheduling techniques [22], [23], static-compaction techniques [24], and multiple scan chains with many scan enable inputs to activate one scan chain at a time [25]. The latter technique also reduces the peak power in the CUT. On the other hand, in addition to the techniques mentioned earlier, there are some new approaches that aim to reduce peak-power consumption during tests, particularly the capture power in the test cycle.

One of the common techniques for this purpose is to modify patterns using an X-filling technique to assign values to the

don't care bits of a deterministic set of test vectors in such a way as to reduce the peak power in the test vectors that have a peak-power violation [26]-[29]. This paper presents a new TPG, called the bit-swapping linear feedback shift register (BS-LFSR), that is based on a simple bit-swapping technique applied to the output sequence of a conventional LFSR and designed using a conventional LFSR and a 2×1 multiplexer. The proposed BS-LFSR reduces the average and instantaneous weighted switching activity (WSA) during test operation by reducing the number of transitions in the scan input of the CUT. The BS-LFSR is combined with a scan-chain-ordering algorithm that reduces the switching activity in both the test cycle (capture power) and the scanning cycles (scanning power).

II. PROPOSED APPROACH TO DESIGN THE BS-LFSR

The proposed BS-LFSR for test-per-scan BISTs is based upon some new observations concerning the number of transitions produced at the output of an LFSR. Definition: Two cells in an n-bit LFSR are considered to be adjacent if the output of one cell feeds the input of the second directly (i.e., without an intervening XOR gate). Lemma 1: Each cell in a maximal-length n-stage LFSR (internal or external) will produce a number of transitions equal to 2^{n-1} after going through a sequence of 2^n clock cycles.

Proof: The sequence of 1s and 0s that is followed by one bit position of a maximal-length LFSR is commonly referred to as an m-sequence. Each bit within the LFSR will follow the same m-sequence with a one-time-step delay. The m-sequence generated by an LFSR of length n has a periodicity of $2^n - 1$. It is a well-known standard property of an m-sequence of length n that the total number of runs of consecutive occurrences of the same binary digit is 2^{n-1} [3], [30]. The beginning of each run is marked by a transition between 0 and 1; therefore, the total number of transitions for each stage of the LFSR

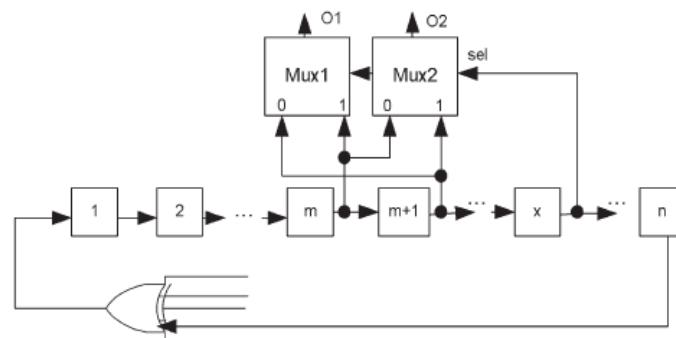


Fig. 1. Swapping arrangement for an LFSR.

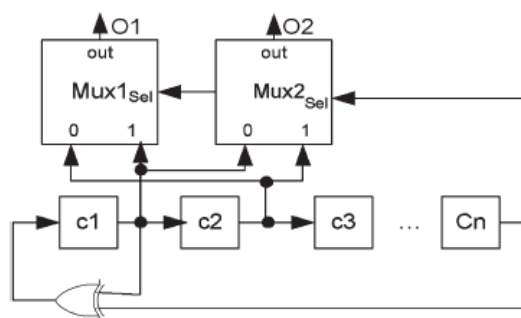


Fig. 2. External LFSR that implements the prime polynomial $x^n + x + 1$ and the proposed swapping arrangement.

2^{n-1} . This lemma can be proved by using the toggle property of the XOR gates used in the feedback of the LFSR [32]. Lemma 2: Consider a maximal-length n-stage internal or external LFSR ($n > 2$). We choose one of the cells and swap its value with its adjacent cell if the current value of a third cell in the LFSR is 0 (or 1) and leave the cells unswapped if the third cell has a value of 1 (or 0). Fig. 1 shows this arrangement for an external LFSR (the same is valid for an internal LFSR). In this arrangement, the output of the two cells will have its transition count reduced by $T_{\text{saved}} = 2^{(n-2)}$ transitions. Since the two cells originally produce $2 \times 2^{n-1}$ transitions, then the resulting percentage saving is $T_{\text{saved}\%} = 25\%$ [32]. In Lemma 2, the total percentage of transition savings after swap-ping is 25% [31]. In the case where cell x is not directly linked to cell m or cell m + 1 through an XOR gate, each of the cells has the same share of savings (i.e., 25%).

Lemmas 3-10 show the special cases where the cell that drives the selection line is linked to one of the swapped cells through an XOR gate. In these configurations, a single cell can save 50% transitions that were originally produced by an LFSR cell. Lemma 3 and its proof are given; other lemmas can be proved in the same way. Lemma 3: For an external n-bit

maximal-length LFSR that implements the prime polynomial $x^n + x + 1$ as shown in Fig. 2, if the first two cells (c_1 and c_2) have been chosen for swapping and cell n as a selection line, then o_2 (the output of MUX2) will produce a total transition savings of 2^{n-2} compared to the number of transitions produced by each LFSR cell, while o_1 has no savings (i.e., the savings in transitions is concentrated in one multiplexer output, which means that o_2 will save 50% of the original transitions produced by each LFSR cell). Proof: There are eight possible combinations for the initial state of the cells c_1 , c_2 , and c_n . If we then consider all possible values of the following state, we have two possible combinations (not eight, because the value of c_2 in the next state is determined by the value of c_1 in the present state; also, the value of c_1 in the next state is determined by " $c_1 \text{ xor } c_n$ " in the present state). Table I shows all possible and subsequent states.

TABLE I
POSSIBLE AND SUBSEQUENT STATES FOR CELLS c_1 , c_2 , AND c_n
(SEE FIG. 2)

LFSR outputs of m, m+1									Multiplexers outputs O_1, O_2						
States			Next states			transition			states		Next States		transition		
c_1	c_2	c_n	c_1	c_2	c_n	c_1	c_2	Σ	O_1	O_2	O_1	O_2	O_1	O_2	Σ
0	0	0	0	0	0	0	0	0	0	0	0	0	0	0	0
			0	0	1	0	0	0			0	0	0	0	0
0	0	1	1	0	0	1	0	1	0	0	0	1	0	1	1
			1	0	1	1	0	1			1	0	1	0	1
0	1	0	0	0	0	0	1	1	1	0	0	0	1	0	1
			0	0	1	0	1	1			0	0	1	0	1
0	1	1	1	0	0	1	1	2	0	1	0	1	0	0	0
			1	0	1	1	1	2			1	0	1	1	2
1	0	0	1	1	0	0	1	1	0	1	1	1	1	0	1
			1	1	1	0	1	1			1	1	1	0	1
1	0	1	0	1	0	1	1	2	1	0	1	0	0	0	0
			0	1	1	1	1	2			0	1	1	1	2
1	1	0	1	1	0	0	0	0	1	1	1	1	0	0	0
			1	1	1	0	0	0			1	1	0	0	0
1	1	1	0	1	0	1	0	1	1	1	1	0	0	1	1
			0	1	1	1	0	1			0	1	1	0	1
Σ Transitions									8	8	16		8	4	12

It is important to note that the overall savings of 25% is not equally distributed between the outputs of the multiplexers as in Lemma 2. This is because the value of c_1 in the present state will affect the value of c_2 and its own value in the next state ($c_{2(\text{Next})} = c_1$ and $c_{1(\text{Next})} = "c_1 \text{ xor } c_n"$). To see the effect of each cell in transition savings, Table I shows that o_1 will save one transition when moving from state (0,0,1) to (1,0,0), from (0,1,1) to (1,0,0), from (1,0,1) to (0,1,0), or from (1,1,1) to (0,1,0). In the same time, o_1 will increase one transition when moving from (0,1,0) to (0,0,0), from (0,1,0) to (0,0,1), from (1,0,0) to (1,1,0), or from (1,0,0) to (1,1,1). Since o_1 increases the transitions in four possible scenarios and save transitions in other four scenarios, then it has a neutral overall effect because all the scenarios have the same probabilities. For o_2 , one transition is saved when moving from (0,1,0) to (0,0,0), from (0,1,0) to (0,0,1), from (0,1,1) to (1,0,0), from (1,0,0) to (1,1,0), from (1,0,0) to (1,1,1), or from (1,0,1) to (0,1,0). At the same time, one additional transition is incurred when moving from state (0,0,1) to (1,0,0) or from (1,1,1) to (0,1,0). This gives o_2 an overall saving of one transition in four possible scenarios where the initial states has a probability of 1/8 and the final states of probability 1/2; hence, P_{save} is given by

$$P_{\text{save}} = 1/8 \times 1/2 + 1/8 \times 1/2 + 1/8 \times 1/2 + 1/8 \times 1/2 = 1/4. \quad (1)$$

If the LFSR is allowed to move through a complete cycle of 2^n states, then Lemma 1 shows that the number of transitions expected to occur in the cell under consideration is 2^{n-1} . Using the swapping approach, in 1/4 of the cases, a saving of one transition will occur, giving a total saving of $1/4 \times 2^n = 2^{n-2}$. Dividing one figure by the other, we see that the total number of transitions saved at o_2 is 50%. In the special configurations shown in Table II (i.e. Lemmas 3-10), if the cell that saves 50% of the transitions is connected to feed the scan-chain input, then it saves 50% of the transitions inside the scan-chain cells, which directly reduces the average power and also the peak power that may result while scanning in a new test vector. Table III shows that there are 104 LFSRs (internal and external) whose sizes lie in the range of 3-168 stages that can be configured to satisfy one or more of the special cases in Table II to concentrate the transition savings in one multiplexer output.

TABLE II
 SPECIAL CASES WHERE ONE CELL SAVES 50% OF THE TRANSITIONS

Lemmas	LFSR Polynomial	LFSR Type	Swapped cells		Selection Line	MUX Out 50% Save
			1 st	2 nd		
Lemma 3	x^n+x+1	External	C_1	C_2	C_n	O_2
Lemma 4	x^n+x+1	Internal	C_1	C_n	C_2	O_2
Lemma 5	$x^n+x^{n-1}+1$	External	C_{n-1}	C_n	C_1	O_1
Lemma 6	$x^n+x^{n-1}+1$	Internal	C_1	C_n	C_{n-1}	O_1
Lemma 7	x^n+x^2+1	External	C_1	C_2	C_n	O_1
Lemma 8	$x^n+x^{n-2}+1$	Internal	C_{n-1}	C_n	C_{n-2}	O_1
Lemma 9	$x^n+x^{n-1}+x^{ym}+ \dots+x^y2+x^y1+1$	Internal	C_1	C_n	C_{n-1}	O_1
Lemma 10	$x^n+x^{n-2}+x^{ym}+ \dots+x^y2+x^y1+1$	Internal	C_{n-1}	C_n	C_{n-2}	O_1

TABLE III
 LFSRS THAT SATISFY ONE OR MORE OF LEMMAS 3-10

# of LFSR Stages	LFSR settle one or more of Lemmas 3 to 10 in table 2
3-20	3, 4, 5, 6, 7, 8, 11, 12, 13, 14, 15, 16, 19
21-40	21, 22, 24, 26, 27, 29, 30, 32, 34, 35, 37, 38, 40
41-60	42, 43, 44, 45, 46, 48, 50, 51, 53, 54, 56, 59, 60
61-80	61, 62, 63, 64, 66, 67, 69, 70, 74, 75, 76, 77, 78, 80
81-100	83, 85, 86, 88, 90, 91, 92, 93, 96, 99
101-120	101, 102, 104, 107, 109, 110, 112, 114, 115, 116, 117
121-140	122, 123, 125, 126, 127, 128, 131, 133, 136, 138
141-160	141, 143, 144, 146, 147, 149, 152, 153, 154, 155, 156, 157, 158, 160
161-168	162, 163, 164, 165, 166, 168
Total	104

III. IMPORTANT PROPERTIES OF THE BS-LFSR

There are some important features of the proposed BS-LFSR that make it equivalent to a conventional LFSR. The most important properties of the BS-LFSR are the following.

- 1) The proposed BS-LFSR generates the same number of 1s and 0s at the output of multiplexers after swapping of two adjacent cells; hence, the probabilities of having a 0 or 1 at a certain cell of the scan chain before applying the test vectors are equal. Hence, the proposed design retains an important feature of any random TPG. Furthermore, the output of the multiplexer depends on three different cells of the LFSR, each of which contains a pseudorandom value. Hence, the expected value at the output can also be considered to be a pseudorandom value.
- 2) If the BS-LFSR is used to generate test patterns for either test-per-clock BIST or for the primary inputs of a scan-based sequential circuit (assuming that they are directly accessible) as shown in Fig. 3, then consider the case that c_1 will be swapped with c_2 and c_3 with c_4, \dots, c_{n-2} with c_{n-1} according to the value of c_n which is connected to the selection line of the multiplexers (see Fig. 3). In this case, we have the same exhaustive set of test vectors as would be generated by the conventional LFSR, but their order will be different and the overall transitions in the primary inputs of the CUT will be reduced by 25% [32].

IV. CELL REORDERING ALGORITHM

Although the proposed BS-LFSR can achieve good results in reducing the consumption of average power during test and also in minimizing the peak power that may result while scanning a new test vector, it cannot reduce the overall peak power because there are some components that occur while scanning out the captured response or while applying a test vector and capturing a response in the test cycle. To solve these problems, first, the proposed BS-LFSR has been combined with a cell-ordering algorithm presented in [11] that reduces the number of transitions in the scan chain while scanning out the captured response.

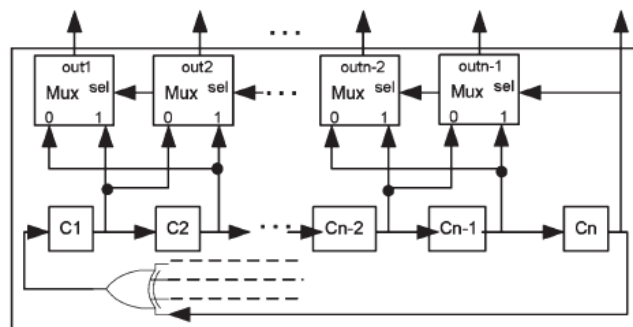


Fig. 3. BS-LFSR can be used to generate exhaustive patterns for test-per-clock BIST.

This will reduce the overall average power and also the peak power that may arise while scanning out a captured response. The problem of the capture power (peak power in the test cycle) will be solved by using a novel algorithm that will reorder some cells in the scan chain in such a way that minimizes the Hamming distance between the applied test vector and the captured response in the test cycle, hence reducing the test cycle peak power (capture power). In this scan-chain-ordering algorithm, some cells of the ordered scan chain using the algorithm in [11] will be reordered again in order to reduce the peak power which may result during the test cycle. This phase mainly depends on an important property of the BS-LFSR. This property states that, if two cells are connected with each other, then the probability that they have the same value at any clock cycle is 0.75. (In a conventional LFSR where the transition probability is 0.5, two adjacent cells will have the same value in 50% of the clocks and different values in 50% of the clocks; for a BS-LFSR that reduces the number of transition of an LFSR by 50%, the transition probability is 0.25, and hence, two adjacent cells will have the same value in 75% of the clock cycles.) Thus, for two connected cells (cells j and k), if we apply a sufficient number of test vectors to the CUT, then the values of cells j and k are similar in 75% of the applied vectors. Hence, assume that we have cell x which is a function of cells y and z.

If the value that cell x will have in the captured response is the same as its value in the applied test vector (i.e., no transition will happen for this cell in the test cycle) in the majority of cases where cells y and z have the same value, then we connect cells y and z together on the scan chain, since they will have the same value in 75% of the cases. This reduces the possibility that cell x will undergo a transition in the test cycle. The steps in this algorithm are as follows.

- 1) Simulate the CUT for the test patterns generated by the BS-LFSR.
- 2) Identify the group of vectors and responses that violate the peak power.
- 3) In these vectors, identify the cells that mostly change their values in the test cycle and cause the peak-power violation.
- 4) For each cell found in step 3), identify the cells that play the key role in the value of this cell in the test cycle.
- 5) If it is found that, when two cells have a similar value in the applied test vector, the concerned cell will most probably have no transition in the test cycle, then connect these cells together. If it is found that, when two cells have a different value, the cell under consideration will most probably have no transitions in the test cycle, then connect these cells together through an inverter. It is important to note that this phase of ordering is done when necessary only, as stated in step 2 of the algorithm description that the group of test vectors that violates the peak power should be identified first. Hence, if no vector violates the peak power, then this phase will not be done. In the worst case, this phase is performed in few subsets of the cells. This is because, if this phase of ordering is done in all cells of the scan chain, then it will destroy the effect of algorithm found in [11] and will substantially increase the computation time.

TABLE IV
 TEST LENGTH NEEDED TO GET TARGET FAULT COVERAGE FOR
 LFSR AND BS-LFSR

Circuit	n	m	PI	RF%	FC%	Test Length			
						Det.	LFSR	BS-LFSR no order	BS-LFSR with order
S641	32	19	35	0	98.0	53	5120	4910	4970
S838	32	32	35	0	86.5	90	8160	8460	7910
S1196	30	18	14	0	97.0	131	3750	3680	3370
S1238	30	18	14	5.09	91.3	141	3890	3560	3610
S5378	40	179	35	0.88	98.0	244	30110	33700	28900
S9234	40	228	19	6.52	90.0	367	397800	401930	398170
S13207	60	669	31	1.54	95.0	455	49660	47400	48110
S35932	64	1728	35	10.19	89.8	63	18700	16640	16520
S38417	64	1636	28	0.53	96.5	849	118580	125520	117080
S38584	64	1452	12	4.15	94	632	43530	39660	40090

TABLE V
 EXPERIMENTAL RESULTS OF AVERAGE- AND PEAK-POWER REDUCTION
 OBTAINED BY USING THE PROPOSED TECHNIQUES

Circuit	TL	LFSR			BS-LFSR with cell ordering			%Savings of BS-LFSR	
		FC%	WSA _{avg}	WSA _{pk}	FC%	WSA _{avg}	WSA _{pk}	WSA _{av}	WSA _{pk}
S641	3000	97.84	97.78	153	97.54	42.20	84	57	45
S838	20000	96.15	81.91	151	96.21	33.14	83	60	45
S1196	2000	95.33	53.18	74	95.51	21.52	42	60	43
S1238	3000	91.11	61.20	97	90.97	34.80	59	43	39
S5378	40000	98.42	1143.24	1639	98.40	625.28	993	45	39
S9234	100000	87.27	2817.45	3988	87.28	1108.93	2197	61	45
S13207	100000	96.45	4611.67	7108	96.39	1897.33	4172	59	41
S35932	200	87.88	7945.81	12592	87.89	2793.16	5723	65	55
S38417	100000	95.73	10965.50	16380	95.68	5022.30	10017	54	39
S38584	100000	94.46	11194.65	15974	94.48	5682.72	7851	49	51

V. EXPERIMENTAL RESULTS

A group of experiments was performed on full-scan ISCAS'89 benchmark circuits. In the first set of experiments, the BS-LFSR is evaluated regarding the length of the test sequence needed to achieve a certain fault coverage with and without the scan-chain-ordering algorithm. Table IV shows the results for a set of ten benchmark circuits. The columns labeled n, m, and PI refer to the sizes of the LFSR, the number of flip-flops in the scan chain, and the number of primary inputs of the CUT, respectively. The column labeled RF indicates the percentage of redundant faults in the CUT, and fault coverage (FC) indicates the target fault coverage where redundant faults are included. The last four columns show the test length needed by a deterministic test (i.e., the optimal test vector set is stored in a ROM), a conventional LFSR, a BS-LFSR with no scan-chain ordering, and the BS-LFSR with scan-chain ordering, respectively.

The results in Table IV show that the BS-LFSR needs a shorter test length than a conventional LFSR for many circuits even without using the scan-chain-ordering algorithm. It also shows that using the scan-chain-ordering algorithm with BS-LFSR will shorten the required test length. The second set of experiments is used to evaluate the BS-LFSR together with the proposed scan-chain-ordering algorithm in reducing average and peak power. For each benchmark circuit, the same numbers of conventional LFSR and BS-LFSR patterns are applied to the full scan configuration. Table V shows the obtained results for the same benchmark circuits as in Table IV. The column labeled test length (TL) refers to the number of test vectors applied to the CUT. The next three columns show the FC, average WSA per clock cycle

TABLE VI
COMPARISON WITH RESULTS OBTAINED IN [15]

Circuit	Results in [15]			Results of proposed method		
	TL	FC	%WSA _{av}	TL	FC	%WSA _{av}
S641	4096	97.21	38	3000	97.54	57
S838	4096	95.46	50	20000	96.21	60
S1196	4096	95.59	17	2000	95.51	60
S1238	4096	89.41	17	3000	90.97	43
S5378	65536	96.54	43	40000	98.40	45
S9234	524288	90.89	62	100000	87.28	61
S13207	132072	93.66	45	100000	96.39	59
S35932	128	87.84	56	200	87.89	65
S38417	132072	94.99	56	100000	95.68	54
S38584	132072	93.35	59	100000	94.48	49
AVG	100255	93.49	44	46820	94.04	55

TABLE VII
COMPARISON OF PEAK-POWER REDUCTIONS WITH RESULTS IN [25]

Circuit	Results in [25] WSA _{pk} Savings %	Proposed Method WSA _{pk} Savings %
S5378	36.6	39
S9234	38.9	45
S13207	46.1	41
S38417	40.1	39
S38584	35.9	51
AVG	39.5	43.0

(WSA_{avg}), and the maximum WSA in a clock cycle (WSA_{peak}) for patterns applied using the conventional LFSR. The next three columns show FC, WSA_{avg}, and WSA_{peak} for the BS-LFSR with ordered scan chain. Finally, the last two columns show the savings in average and peak power by using the BS-LFSR with the scan-chain-ordering algorithm. In order to provide a comparison with the techniques published previously by other authors, Table VI compares the results obtained by the proposed technique with those obtained in [15]. Table VI compares the TL, FC, and average-power reduction (WSA_{avg}). It is clear that the proposed method is much better for most of the circuits, not only in average-power reduction but also in the test length needed to obtain good fault coverage. Finally, Table VII compares the results obtained by the proposed technique for peak-power reduction with those obtained in [25]. It is clear from the table that the proposed method has better results for most of the benchmark circuits.

VII. SIMULATION RESULTS

Scan Cell Re ordering Algorithm : In this Fig .4, FF1 –FF3-FF2 represents the flip flops which are used to reordering itself defined in the coding by using this technique only to reduce the number of transitions (when we give four inputs to the test vector, it reduces the number of transitions by using **Scan Cell Re order** module. In this way we are reducing some amount of wastage of power.

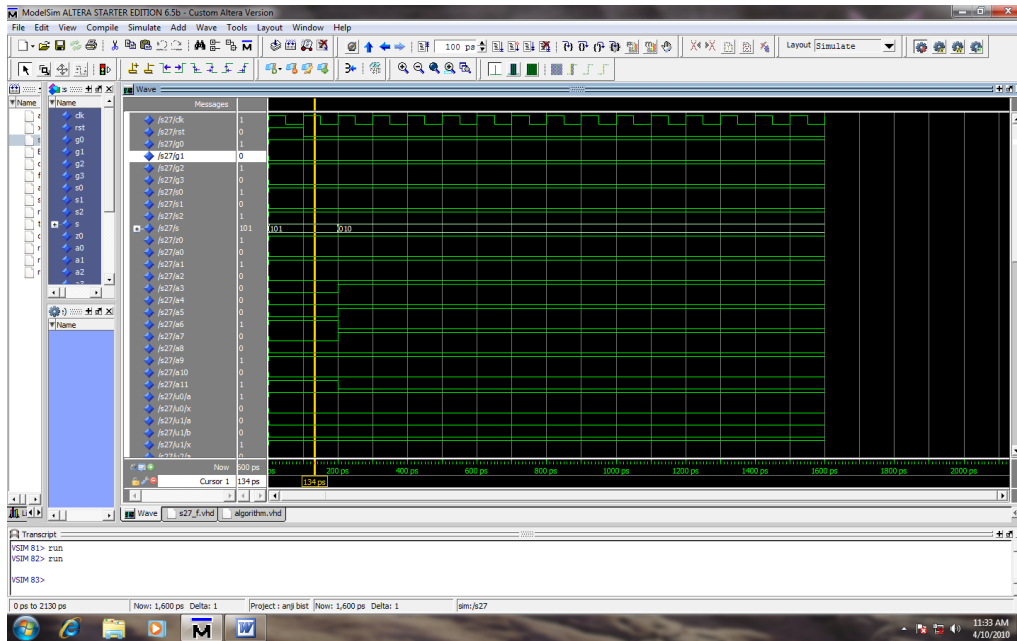


Fig.6.S27 Module

Final Module: When inputs are $clk = clk$ and $rst = 1$ initial values = 1010, then once it is run, reset value must be changed to zero. In this we insert fault in the practical circuit (`s27_f`) circuit that is $a6 = b6$ (code). Then outputs are $z = 1$ (S27 ckt) output of the sequential circuit and (`s27_f` ckt out put) $z_f = 1$ means in `s27_f` circuit fault is there that's why it represents it as =1 is shown in Fig.8. Now Fig.7. Screen shot represents fault less that is in practical circuit (`s27_f`) $a6 = a6$ (fault free) only when there is no fault we have save that and run and we get OUTPUT $z_f = 0$. It represents No fault.

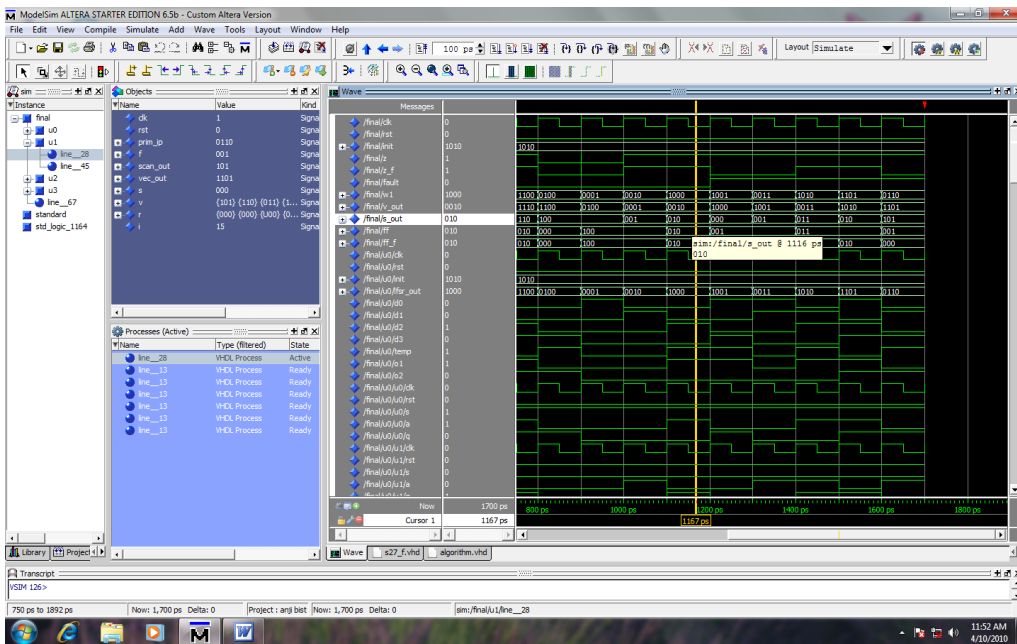


Fig.7. Fault free Final Module

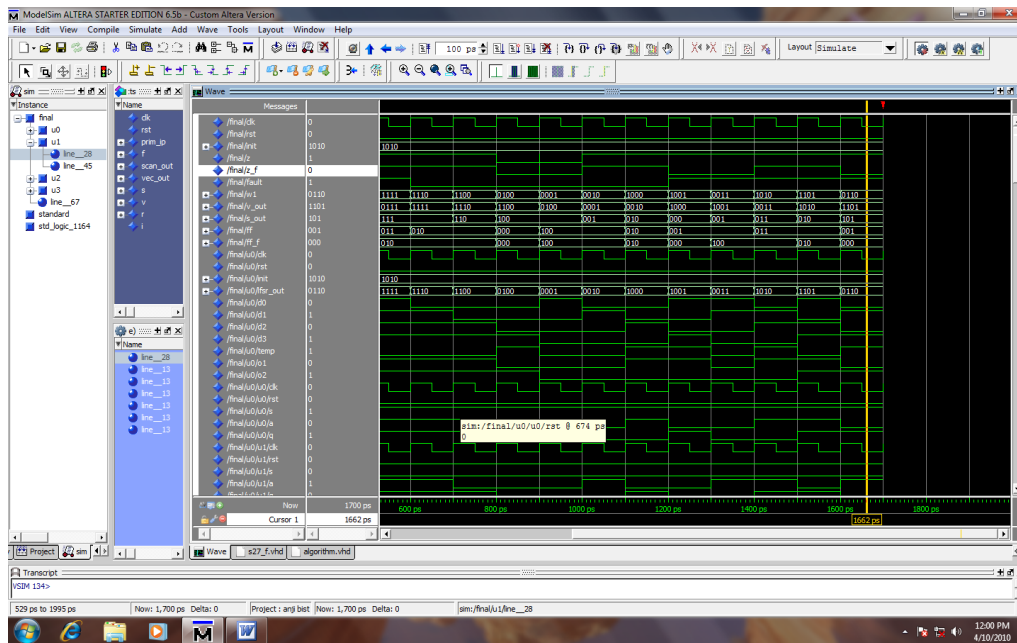


Fig.8. Faulty Final Module

VII. CONCLUSION AND FUTURE WORK

The increasing demand for portable electronic devices with long lifetime battery and reliable functionality has led to increased interest in low power design. However, many faults may arise in digital circuits either during fabrication or during operational lifetime. If these faults remain undetected, then there is no way to distinguish good chips from faulty chips. Hence, test is a necessary part of the manufacturing process. However, it is found that the power consumption during test is higher than during normal operation. Thus, it is very important to develop techniques for low power testing. On the other hand, in order for testing to be a reliable and cost-efficient process, it should detect all or most of the faults (stuck-at-faults on this thesis) that may occur in digital circuits within an acceptable test length (and, therefore, test application time) and acceptable storage space. Hence, deterministic tests (which store test vectors in memory) are not the optimal solution since they need a huge storage space for large circuits. However, random TPGs are not good since there are some faults (known as random pattern resistant faults) that need a very long sequence of test vectors (i.e. an extremely long test application time). Thus, it is very important to produce techniques that compromise between hardware overhead, test application time, and the obtained fault coverage.

1. Average Power Minimization in Test-per-Clock BIST using Low Transition LFSR

2. Average Power Minimization in Test-per-Scan BIST using Low Transition LFSR

3 Scan and Capture Peak Power Minimization in Scan-Based BIST using BS-LFSR, and 2-Phase Scan- Chain Ordering Algorithm

4. Increasing Fault Coverage in Scan-Based BIST using a Multi- Output LFSR

FUTURE WORK

1. Investigation of LFSRS' Properties
2. Random memory access test
3. System –on-a- chip (soc) memory test
4. Low power delay test

VIII. REFERENCES

- [1] Y. Zorian, "A distributed BIST control scheme for complex VLSI devices," in Proc. 11th IEEE VTS, Apr. 1993, pp. 4-9.
- [2] A. Hertwig and H. J. Wunderlich, "Low power serial built-in self-test," in Proc. IEEE Eur. Test Workshop, May 1998, pp. 49-53.
- [3] P. H. Bardell, W. H. McAnney, and J. Savir, Built-in Test for VLSI: Pseudorandom Techniques. New York: Wiley, 1997.
- [4] P. Girard, "Survey of low-power testing of VLSI circuits," IEEE Des. Test Comput., vol. 19, no. 3, pp. 80-90, May/June 2002.
- [5] K. M. Butler, J. Saxena, T. Fryars, G. Hetherington, A. Jain, and J. Lewis, "Minimizing power consumption in scan testing: Pattern generation And DFT techniques," in Proc. Int. Test Conf., 2004, pp. 355-364.
- [6] Saxena, K. Butler, and L. Whetsel, "An analysis of power reduction techniques in scan testing," in Proc. Int. Test Conf.

2001670-677.

- [7] V. Dabholkar, S. Chakravarty, I. Pomeranz, and S. M. Reddy, "Techniques for minimizing power dissipation in scan and combinational circuits during test applications," *IEEE Trans. Comput.-Aided Design Integr. Circuits Syst.*, vol. 17, no. 12, pp. 1325-1333, Dec. 1998.
- [8] Y. Bonhomme, P. Girard, L. Guiller, C. Landrault, S. Pravossoudovitch, and V. Virazel, "Design of routing-constrained low power scan chains," in *Proc. Des. Autom. Test Eur. Conf. Exhib.*, Feb. 2004, pp. 62-67.
- [9] W. Tseng, "Scan chain ordering technique for switching activity reduction during scan test," *Proc. Inst. Elect. Eng.—Comput. Digit. Tech.*, vol. 152, no. 5, pp. 609-617, Sep. 2005.
- [10] C. Giri, B. Kumar, and S. Chattopadhyay, "Scan flip-flop ordering with delay and power minimization during testing," in *Proc. Annu. IEEE INDICON*, Dec. 2005, pp. 467-471.
- [11] Y. Bonhomme, P. Girard, C. Landrault, and S. Pravossoudovitch, "Power driven chaining of flip-flops in scan architectures," in *Proc. Int. Test Conf.*, Oct. 2002, pp. 796-803.
- [12] M. Bellos, D. Bakalis, and D. Nikolos, "Scan cell ordering for low power BIST," in *Proc. IEEE Comput. Soc. Annu. Symp. VLSI*, Feb. 2004, pp. 281-284.
- [13] K. V.A. Reddy and S. Chattopadhyay, "An efficient algorithm to reduce test power consumption by scan cell and scan vector reordering," in *Proc. IEEE 1st India Annu. Conf. INDICON*, Dec. 2004, pp. 373-376.
- [14] S. Wang, "A BIST TPG for low power dissipation and high fault coverage," *IEEE Trans. Very Large Scale Integr. (VLSI) Syst.*, vol. 15, no. 7, pp. 777-789, Jul. 2007.
- [15] S. Wang and S. Gupta, "LT-RTPG: A new test-per-scan BIST TPG for low switching activity," *IEEE Trans. Comput.-Aided Design Integr. Circuits Syst.*, vol. 25, no. 8, pp. 1565-1574, Aug. 2006.
- [16] S. Wang and S. K. Gupta, "DS-LFSR: A BIST TPG for low switching activity," *IEEE Trans. Comput.-Aided Design Integr. Circuits Syst.*, vol. 21, no. 7, pp. 842-851, Jul. 2002.
- [17] H. Ronghui, L. Xiaowei, and G. Yunzhan, "A low power BIST TPG design," in *Proc. 5th Int. Conf. ASIC*, Oct. 2003, vol. 2, pp. 1136-1139.
- [18] L. Jie, Y. Jun, L. Rui, and W. Chao, "A new BIST structure for low power testing," in *Proc. 5th Int. Conf. ASIC*, Oct. 2003, vol. 2, pp. 1183-1185.
- [19] M. Tehranipoor, M. Nourani, and N. Ahmed, "Low transition LFSR for BIST-based applications," in *Proc. 14th ATS*, Dec. 2005, pp. 138-143.
- [20] I. Pomeranz and S. M. Reddy, "Scan-BIST based on transition probabilities for circuits with single and multiple scan chains," *IEEE Trans. Comput.-Aided Design Integr. Circuits Syst.*, vol. 25, no. 3, pp. 591-596, Mar. 2006.
- [21] N. Nicolici and B. Al-Hashimi, "Multiple scan chains for power minimization during test application in sequential circuits," *IEEE Trans. Comput.*, vol. 51, no. 6, pp. 721-734, Jun. 2002.
- [22] V. Iyengar and K. Chakrabarty, "Precedence-based, preemptive, and power-constrained test scheduling for system-on-a-chip," in *Proc. IEEE VLSI Test Symp.*, 2001, pp. 368-374.
- [23] R. Chou, K. Saluja, and V. Agrawal, "Power constraint scheduling of tests," in *Proc. IEEE Int. Conf. VLSI Des.*, 1994, pp. 271-274.
- [24] R. Sankaralingam, R. Oruganti, and N. Touba, "Static compaction techniques to control scan vector power dissipation," in *Proc. IEEE VLSI Test Symp.*, 2000, pp. 35-42.
- [25] S. Wang and W. Wei, "A technique to reduce peak current and average power dissipation in scan designs by limited capture," in *Proc. Asia South Pacific Des. Autom. Conf.*, Jan. 2007, pp. 810-816.
- [26] N. Badereddine, P. Girard, S. Pravossoudovitch, C. Landrault, A. Virazel, and H. Wunderlich, "Minimizing peak power consumption during scan testing: Test pattern modification with X filling heuristics," in *Proc. Des. Test Integr. Syst. Nanoscale Technol.*, 2006, pp. 359-364.
- [27] R. Sankaralingam and N. Touba, "Controlling peak power during scan testing," in *Proc. 20th IEEE VLSI Test Symp.*, 2002, pp. 153-159.
- [28] S. Remersaro, X. Lin, S. M. Reddy, I. Pomeranz, and J. Rajski, "Low shift and capture power scan tests," in *Proc. Int. Conf. VLSI Des.*, 2007, pp. 793-798.
- [29] X. Wen, Y. Yamashita, S. Kajihara, L. Wang, K. Saluja, and K. Kinoshita, "On low-capture-power test generation for scan testing," in *Proc. 23rd IEEE VLSI Test Symp.*, 2005, pp. 265-270.
- [30] R. David, *Random Testing of Digital Circuits, Theory and Applications*. New York: Marcel Dekker, 1998.
- [31] A. Abu-Issa and S. Quigley, "LT-PRPG: Power minimization technique for test-per-scan BIST," in *Proc. IEEE Int. Conf. DTIS*, Mar. 2008, pp. 1-5.
- [32] A. Abu-Issa and S. Quigley, "Bit-swapping LFSR for low-power BIST," *Electron. Lett.*, vol. 44, no. 6, pp. 401-402, Mar. 2008.

XI. ABOUT THE AUTHORS



D. Sridhar Received the **M.Tech** degree in **VLSI SYSTEM DESIGN** from Avanthi Institute of Engineering and Technology, Narsipatnam, B.Tech degree in Electronics and communication Engineering at Gudlalleru. He has total Teaching Experience (UG and PG) of 5 years. He has guided and co-guided 4 P.G and U.G students .His research areas included VLSI system Design, Digital signal processing, Embedded systems.



K.Avinash kumar pursuing the M.Tech degree in DECS from Sri sivani college of Engineering Chilakapalem, B.Tech degree in Electronics and communication Engineering from Avanthi institute of engineering and Technology. He has total Teaching Experience of 1 year. His research areas included VLSI, Digital Signal Processing.



P.Krishna Rao received the M.Tech degree in VLSI SYSTEM DESIGN from Aditya institute of Technology and Management, Tekkali B.Tech degree in Electronics and communication Engineering from Narasaraopet Engg College, Narasaraopet, Guntur. He has total Teaching Experience (UG and PG) of 6 years. He has guided and co-guided 4 P.G students .His research areas included VLSI system Design

Identifying the Different Aesthetic Quality of Building Attributes From Architects Perspective

Mohammad Ghomeshi^{1&2}, Mansour Nikpour^{1&3}
Mahmud bin Mohd Jusan¹

**(Department of Architecture, Faculty of Built Environment,
University Teknologi Malaysia, Skudai, Johor, Malaysia*

****(Islamic Azad University, Damavand Branch, Tehran, Iran*

****(Islamic Azad University, Bam Branch, Iran*

ABSTRACT

It seems that many designers do not know, from a non-designer viewpoint, what a pleasant building looks like. If designers are ever to have more pleasant buildings in the eyes of the majority of the residents who are not designers, this problem desires study and explanations which in this study the researcher tries to answer. Part of the solution lies in discovering the physical and cognitive property of the differences in aesthetic criteria in designers. The aim of the present study is to identify objective physical building cues that are connected to aesthetic quality in Architects and the designers of the buildings. The researcher used a quantitative questionnaire to find the values of each building attribute among architects. The results found that building attribute have different values among architects. Some physical cues are very important for architects and some are not so much important.

Keywords: Aesthetic Quality, Architecture Attributes, Environment Congruence, Façade design, Perception.

1. INTRODUCTION

Evaluating an environment usually involves making a judgment about whether the environment is liked or not. This type of judgment may be conscious or unconscious and the cognitive procedure normally involves perception of the visual characteristic of an environment and an emotional evaluation of the environment [1, and 2]. In environmental assessment and environmental aesthetics researches, preference is usually corresponded to by the variable like-dislike. The definition of preference for the intention of this study was the amount to which a participant liked or disliked each physical building attributes and the dependent variables linked to preference in like-dislike.

There has been a good verification relating to architects' aesthetic failures [3]. Studies have exposed difference between architects liking and what non-architects likes [4, and 5]. For example in Devlin and Nasar's [4] study which architects and other professionals evaluates 40 houses, it could be seen that architects and other professionals have different tastes of designs, architects like designs that other

professional dislike and vice versa. The difference between design experts and the lays becomes more important for projects in which the client and the user differ, and the designer has little contact with the users.

Architects distinguish physical settings in a different way than non-architects [6]. However, these differences are significant because they can frequently effect in a number of mismatches between designer and lay preferences. Knowing that part of the architect's occupation is to recognize lays perceptions, these differences are not small. Furthermore, Nasar [5] study recommended that not only do architects have different preferences than non-architects, but they do not appear to understand what non-architects likes. Nasar [7] established that when architects were asked to predict what non-architects would find pleasing, they were frequently unable to do so.

This research used questionnaire as the method to identify the differences in architects. Based on literature reviews, 36 architectural elements in nine categories (overall form, wall appearance, wall texture, wall patterns, windows, balcony, amenities, ornaments, and context) were identified. The researcher in this study identified these elements based on previous literature especially Gifford [6] which were called TACS (the architectural coding system). Since Gifford. et.al [8] used these elements to test tall office building with four surfaces, and since this research in concentrating on single surface façade designs, the researcher on this research reduce the amount of the elements from 54 to 36. One of the reasons for this reduction was because some of the physical cues did not fit into this study. For example (number of sides), since in this research the researcher was testing these elements on single surface façade design, this study did not need the answer for this cue. Another change that was made for this study was that in TASC of Gifford [6], the researcher used Stone and brick cladding as one element to be scored by architects. It could be argued that since these elements are an important physical cue in the façade designs, in this research the researcher separated this element to two separate elements to be scored by architects so the researcher could have a clearer look at the selection

of the façade material.

3. RESPONDENTS

The architect or designers (N=200) were selected from students and staff members of Universiti Teknologi Malaysia at Faculty of Built Environment that had a background of Architecture. The respondents were selected from architecture students year 4 and above at bachelor level, master students, Phd students, and lecturers in architecture.

The goals were to questionnaire designers with these architectural façade elements, and ask the responders to select their ideal single surface façade design based on the physical cues in the questionnaire. The respondents were asked to rate the cues based on a 6 figure Likert scale in format which 0 was for not relevant to 5 that was high important.

4. MEASURE

the physical features of buildings were measured as 36 separate objective elements of the building exteriors such as shape of the windows, the percentage of the façade that was window, balcony, and so on, using an instrument developed by Gifford [6] called The Architectural Coding System (TACS). This system represents an effort to expand a coding system for every distinct exterior physical feature of an architectural arrangement that may influence cognition of architecture. The goal was to ensure that the building feature in questions were a visible physical element of the façade that could be counted or perfectly estimated.

5. RESULTS

5.1. RELIABILITIES

Table 1 shows the internal consistency reliability of this study.

Table 1 Reliability Statistics

Cronbach's Alpha	Cronbach's Alpha Based on Standardized Items	N of Items
.810	.805	36

Based on George and Mallery [9] rules of thumb, since $.81 > .8$ these results are "good" for this study.

5.2 ANALYSIS

To make this research more clear and to have a better understanding of the results, the researcher divided one sample T-test results into three main categories which are: significantly high important ($P < 0.05$ and $T > 0.00$), significantly less important ($P < 0.05$ and $T < 0.00$) and not relevant ($P > 0.05$).

Table 2 demonstrates the results of one sample t-test with significantly high important values ($P < 0.00$ and $T > 0.00$). It

could be observed in table 2 that only 17 out of 36 physical cues that have been tested in this study are agreeable among designers when $T > 0.00$.

Based on table 2 which shows one sample t-test, means and standard deviations, the results indicate that these seventeen physical cues are high important for designers and they agree about the values of these cues in the ideal facade. However, for example in Shading, the significance is ($T = 21.772$) but in glass cladding the significance is ($T = 2.856$) which shows that although both attributes are significantly high important but the value for Shading is higher than glass cladding.

Table 2 One-Sample Statistics $P < 0.00$ and $T > 0.00$

	Mean	Std. D	T	Sig.
Glass cladding	2.71	1.040	2.856	.005
Brick	2.82	1.252	3.557	.000
Color uniformity	2.72	.926	3.282	.001
Articulation	2.84	.964	4.989	.000
Rectangles	2.98	1.002	6.773	.000
Square	2.96	1.029	6.255	.000
Uniformity of Smoothness	3.03	.972	7.715	.000
Material Smoothness	2.90	1.145	4.880	.000
Horizontal Lines	3.13	1.039	8.579	.000
Vertical Lines	3.01	1.063	6.717	.000
Window Size	3.12	1.005	8.722	.000
Vertical or Horizontal Window	2.93	1.209	5.029	.000
Square Window	2.72	1.175	2.588	.010
Rectangular Window	3.12	1.030	8.513	.000
Window to Wall	2.71	.922	3.221	.001
Shading	3.77	.825	21.772	.000
Vegetation	3.41	1.284	9.966	.000

Inspection of table 3 reveals the agreements in designers in disliking the physical cues in residential buildings. Based on table 3 the results reveal that in sixteen physical cues, there are agreements in designers in disliking the cues.

However to go one step further and to have a better understanding of the results, the researcher in this study compared the Means, Standard Deviation and one sample t-test to find the level of similarities between the two groups.

Table 3 One-Sample Statistics P<0.00 and T<0.00

	Mean	Std. D	T	Sig.
Metal cladding	1.68	1.247	-9.298	.000
Concrete Reflectance	2.22	1.318	-3.058	.003
Stepped stories	2.03	1.207	-5.508	.000
Triangles	2.14	1.456	-3.496	.001
Polygons	1.07	1.199	-16.924	.000
Circles or Ovals	.94	1.210	-18.235	.000
Sharp Rounded Circle	1.41	1.327	-11.673	.000
Window Abstract Shapes	2.09	1.312	-4.420	.000
Balcony Size	.66	.959	-27.144	.000
Columns	.81	1.149	-20.799	.000
Arches	2.30	1.026	-2.825	.005
Sculpture	2.04	1.316	-4.996	.000
Cylindrical Shapes	1.37	1.277	-12.573	.000
Shells	1.49	1.315	-10.864	.000
	1.31	1.099	-15.376	.000
	1.68	1.562	-7.424	.000

Based on table 3, the results indicate that although architects dislike these physical cues but there are some differences in values of disliking. For example the results show that "Circle windows" has a strongest dislike (T=-27.144) compared to other physical cues. Based on this result it could be concluded that designers prefer not to have Circle windows in their designs.

Table 4 shows the results of "not relevant" physical cues in this study. Since in this research the T test values in one sample t-test is 2.5, the analysis did not find any significance (P>0.05) for these physical cues. these results reveal the total agreement of having an average amount of the physical cues in the building is acceptable in designers.

Table 4 One-Sample Statistics P>0.00

	Mean	Std. D	T	Sig.
Stone	2.59	1.212	.991	.323
Regular stories	2.42	1.412	-.852	.395
Plainness	2.36	1.018	-1.946	.053

Table 4 reveals that only three physical cues (Stone, Regular Stories, and plainness) are not significant. Although these three physical cues are acceptable as an average amount in the building but as it could be seen in table 4, based on standard deviation, Plainness have a more concentrated agreement compared other physical cues.

6. CONCLUSION

Researchers have exposed that designers and non-designers often differ about aesthetics of modern buildings. This research demonstrates how architects react on building attributes. In addition finding of this research provides opportunity to the architects to recognize more physical elements which may have valuable involvement in designing single façade especially in the first design stages. Therefore it causes more satisfactory and pleasant facade of buildings in future.

The next step for this research should be to find the most disagreeable physical cues between designers and laypersons.

ACKNOWLEDGMENT

The work is financed by Internatinal doctoral fellowship (IDF) provided by Universiti Teknologi Malaysia and the Ministry of Higher Education of Malaysia

REFERENCES

- [1] Kaplan, S. and Kaplan, R. (1982) *Cognition and environment: functioning in an uncertain world*. New York: Praeger. Chapter 4.
- [2] Nasar, J. (2000). "The evaluative image of places." *Person-environment psychology: New directions and perspectives*: 117-168.
- [3] Balke, P. (1974). *Form follows fiasco*. Boston: Atlantic Monthly press.
- [4] Devlin, K., & Nasar, J. (1989). *The beauty and the beast: Some preliminary comparisons of "high" versus "popular" residential architecture and public versus architect judgments of same*. *Journal of Environmental Psychology*, 9,333-344.
- [5] Nasar, J. (1989). "Symbolic meanings of house styles." *Environment and Behavior* 21(3): 235.
- [6] Gifford, R., D. Hine, et al. (2000). "Decoding modern architecture: a lens model approach for understanding the aesthetic differences of architects and laypersons." *Environment and Behavior* 32(2): 163.
- [7] Nasar, J.L. (1988) *Environmental aesthetics: theory, research and applications*. Cambridge: Cambridge University Press.
- [8] Gifford, R., D. Hine, W. Muller-Clemm, and, K.T. Shaw (2002). "why architects and laypersons GE buildings differently: cognitive properties and physical bases." *Journal of Architectural and Planning Research* 19(2): 131.
- [9] George, D., & Mallery, P. (2003). *SPSS for windows step by step: A simple guide and refrence 11.0 update (4th ed.)*. Boston, MA: Allyn and Bacon.

Development of VAR / P.F Regulator for Brushless A.C Generator for Paralleling with Grid

Deepa.K. R¹, Prof. S. N. Keshavamurthy², Mr. N. Muralidhar³

¹Student of M.Tech, CAID branch, SSIT, Tumkur, ²Professor and HOD of EEE dept, ³Kirloskar Electric Company LTD, Nelamangala, Bangalore.

Abstract: The main objective is Paralleling Brushless A.C. Generator to Grid system in constant VAR or in PF mode. Presently, the trend is to feed power to Grid from different sources of potential heads. That is available in different valley regions in India for meeting the power demand. Hence, the question of feeding power to national Grid. Power generated from different mini and micro Hydel projects are fed to grid in meeting the above demand. Based on Stiff Bus concept any power feeding to Grid will not be stable. Since, the power bus from Grid is stiff in Nature. To make the Generator adoptable to parallel with Grid we need a regulator to work either in Constant VAR or Constant PF mode. So that the Generator Rotor is not over loaded under any circumstances throughout power flow pattern to Grid. To meet the above a Regulator of PF/VAR control is added to the existing AVR. So, that the excitation according to set p.f or VAR get adjustable. So, that the Generator Rotor is protected throughout.

KEY WORD: AVR, Brushless A.C Generator, Grid, VAR / p.f regulator

1. INTRODUCTION

The use of VAR/p.f. regulators and controllers has their origins in industrial applications of synchronous motors and generators, in which the synchronous machine is typically tied directly to a plant distribution bus. In many of these industrial applications, the machine voltage is expected to follow any variations in the utility-fed system voltage, in which case machine voltage regulation may not be desirable. VAR/p.f. regulators and controllers are often used in these types of industrial applications. During periods of peak system load, many areas are prone to voltage stability problems, in which voltage on the heavily loaded system can slowly decay and collapse, unless proper reactive power support is provided. Also, analysis of events leading to recent power blackouts in the western United States has shown that the system problems were at least partially related to the lack of reactive power support from a number of generators on the system. In such situations, it is important that all available generating stations provide the needed increases in excitation level that only a properly functioning voltage regulator can provide, uninhibited by any automatic VAR or p.f. controller.

Modes of Generator operation:

AC Generators are operated in following modes depending on power demand by the system.

1. Solo running (independent running)
2. Parallel running among generators
3. Parallel running with grid

1. Solo running: in solo operation the generator is feeding independent load. Hence, the load is single source dependent. Any breakdown will halt the complete system. Solo running diesel generator sets are not suitable for feeding critical loads without a stand by source as electricity board supply.

Hence the diesel generator set operation in solo mode is suitable for non critical loads only. Features available in solo running sets are self regulated voltage according to

class of voltage regulation regulated voltage variation to the extent of $\pm 5\%$ smooth voltage build up and provision for remote voltage control.

Limitations:

- Single dependent source
- Total interruption during fault
- No loads sharing since it is a single source
- Paralleling to grid is not stable because of restricted automatic voltage regulator operating zone

2. Parallel running among generators:

The necessary conditions for the parallel operation are

- Correct phase sequence.
- Voltages in phase.
- Frequencies should be equal.
- Voltage should be equal.
- Loads shared by each of the generator should be proportional to its rating.

For ensuring reliable power supply, the power demand is met by connecting multiple sources on common bus so, that the critical loads are always fed from any one source for ensuring the reliability of the power system.

Parallel running of diesel generator sets will share the loads according to power demand. For qualifying the voltage regulator suitable for paralleling, the following features are to be built in voltage regulator.

Current compensated adjustable quadrature droop compensation for equal kvar sharing.

- Voltage trimming facility to the extent of $\pm 10\%$ for initial adjustment after paralleling to ensure equal KVAR sharing among generators.
- Change over facility to change mode from solo to parallel after droop set in solo mode.

For ensuring stable parallel operation, in addition to quadrature droop compensation, engine speed droop are

current transformer in one phase as input for comparing with voltage source from two lines other than the one used for deriving current through potential transformer. The current and voltage sources are compared for phase angle and fed to comparator for deriving output proportional phase angle between voltage and current.

The output is direction sensitive for discriminating pf lead or lag for taking care of correction appropriately. For achieving the pf setting as desired between 0.8 lag to 0.8 lead, provision is made for changing the pf setting to attain pf setting as desired.

1.2 Objective of paper

The main objective of this paper is to developing a device for Paralleling A.C Generator to Grid system. When a synchronous generator is parallel operating with a stiff bus, it is bound to vary its reactive current since bus voltage is uncontrolled.

Hence any voltage variation on grid results in varying var supplied to bus in the above situation. Hence changing var on its own is cumulative unless suitable control is exercised. For achieving the same we need to add Var/p.f regulator as add on feature to the existing AVR. To have various options the regulator shall operate either in constant var or constant pf mode.

2. METHODOLOGY

Study on automatic voltage regulator control scheme for

- Stuffing printed circuit board as per the identification of components on printed circuit board (PCB).
- Static test for circuit function.
- Access control point in automatic voltage regulator for superimposing the control signal for correction.
- Implementation on automatic voltage regulator system and effect of superimposing the signal on automatic voltage regulator (AVR).

The following above steps can be explained below:

- Stuffing printed circuit board as per the identification of components on printed circuit board (PCB).
- Study the schematic and identify various components used.
- Identify the components legend wise on printed circuit board (PCB) as shown in Fig. below.
- Insert components on printed circuit board as per the legend on PCB as shown in Fig. below.
- Solder components on printed circuit board as shown in Fig. below.
- Apply protective coating on soldered area of printed circuit board.
- Static test for circuit function.

The developed device can be tested alone without using machine (by manually) is known as static test.

Wave form observed at terminal block 1(TB1).

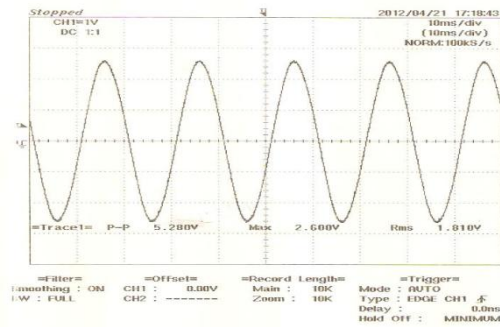


Fig.2.4

Wave form observed at terminal block 3(TB3).

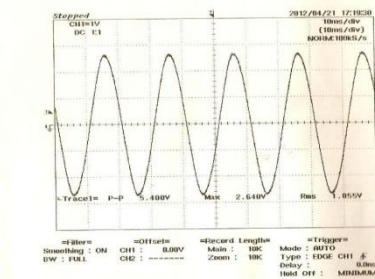


Fig.2.5

Waveform observed at pin number 8 of IC1 CD 4016.

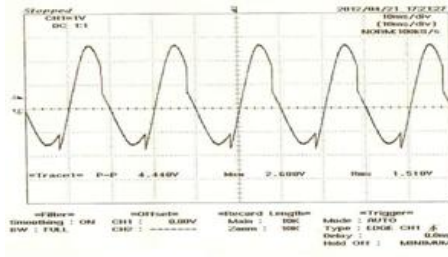


Fig.2.6

Wave form observed at test point 9, test point 10 and testing point 12:

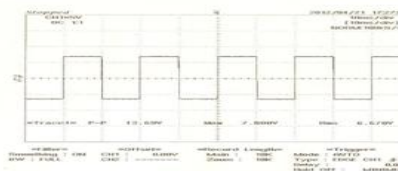


Fig.2.7

- Implementation on automatic voltage regulator system and effect of superimposing the signal on automatic voltage regulator (AVR). VAR/p.f. regulator output connected to sensing point of AVR and found voltage change in generator output. Hence results in constant p.f. Mode operation for variable load condition.

3. SYSTEM DESIGN

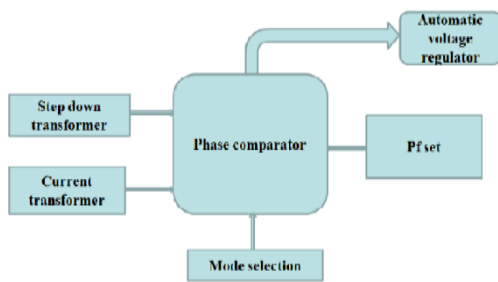


Fig. 3.1: Block diagram of VAR/p.f. regulator.

Step down transformer

A step-down transformer is one whose secondary voltage is less than its primary voltage. It is designed to reduce the voltage from the primary winding to the secondary winding. This kind of transformer “steps down” the voltage applied to it. They are commonly used to convert 220V to 110V. As a step-down unit, the transformer converts high-voltage, low-current power into low-voltage, high-current power. The larger-gauge wire used in the secondary winding is necessary due to the increase in current. The primary winding, which doesn't have to conduct as much current, may be made of smaller-gauge wire.

Current transformer

A current transformer is defined as an instrument transformer in which the secondary current is substantially proportional to the primary current (under normal conditions of operation) and differs in phase from it by an angle which is approximately zero for an appropriate direction of the connections. This highlights the accuracy requirement of the current transformer but also important is the isolating function, which means no matter what the system voltage the secondary circuit need to be insulated only for a low voltage.

The current transformer works on the principle of variable flux. In the “ideal” current transformer, secondary current would be exactly equal (when multiplied by the turns ratio) and opposite of the primary current.

A [current transformer](#) can function in:

- metering of power to track energy use
- monitoring of current flow through a circuit
- relay of power through an energy grid
- control of the state of a circuit (open or closed) in a ground fault circuit interrupter
- protection of instruments and appliances connected to [AC power supplies](#).

Phase comparator:

A phase detector or phase comparator is a frequency mixer, analog multiplier or logic circuit that generates a voltage signal which represents the difference in phase between two signal inputs.

The phase detector needs to compute the phase difference of its two input signals. Let α be the phase of the first input and β be the phase of the second. The actual input signals to the phase detector, however, are not α and β , but rather sinusoids such as $\sin(\alpha)$ and $\cos(\beta)$.

In general, computing the phase difference would involve computing the arcsine and arccosine of each normalized input (to get an ever increasing phase) and doing a subtraction. Such an analog calculation is difficult. Fortunately, the calculation can be simplified by using some approximations.

Mode selection

Select constant p.f. mode or constant VAR mode according to our use.

The complete module consists of power supply to feed op-amps and gate circuits. The module is provided with phase comparator where in the phase angle between current and voltage is compared with respect to the set power factor and the correction is applied between -5v to +5v till set power factor is attained.

The above output signal is sensed by AVR and starts correcting the excitation till the set power factor is attained. VAR/p.f. regulation is the feature built into act either mode in case of constant var mode power factor is governed to maintain the constant VAR. In case of constant p.f. mode control VAR is governed to maintain the set power factor.

This unit is switched only when generator parallel to grid to ensure this provision is made to interlock with grid circuit breaker also in independent control for switching the regulator irrespective of interlock is provided as master control. The module is fed with source voltage from u & v phases which are fed through transformer for feeding the designed voltage.

Basically in VAR/p.f. regulator circuit diagram we have two signals are voltage signal and current signal.

In voltage signal 415v is the generator voltage step-downs to 110v this 110v is again step-downs to 18v the regulated dc power supply circuit consists of full wave bridge rectifier circuit operates in pair to gives a voltage of +24v to -24v that voltage is dropped to 7.5v by the use of dropping resistor connected in series between the terminals of Test Point 3 and Test Point 5 the +7.5v and -7.5v is unregulated power supply that is given to Zener diode to provide the regulated voltage of +6.5v for the operation of op-amp circuit.

In current signal the current transformer output is dropped across capacitor for discrimination of $I_{\sin\phi}$ and $I_{\cos\phi}$. The output of the current transformer is connected with respect to ground for serving input to quad static switch the static switch is triggered with the help of level comparator driven by sine wave to get the square wave output.

The output of the quad switch under the control of zero crossing detector segregates $I_{\sin\phi}$ and $I_{\cos\phi}$ components the output so generated is fed through op-amp for avoiding loading of the switch. The output of the op-amp is fed to converter for converting the current signal in to DC varying voltage level from positive to negative with respect to ground. The output of the

converter drives transistorized switch from positive to negative with respect to ground According to the base current received by the transistor. The current drive to the transistor is totally dependent on VAR/p.f. set which the limiting point for correction is on to stop. Hence VAR/p.f. is regulated.

Advantages of VAR/p.f. regulator:

- Consistent power factor under fluctuating load conditions.
- Reduced KVA demand charges.
- This unit in association with var limiters one can ensure that the system will not demand negative excitation.

4. EXPERIMENTAL SET UP FOR VARYING THE POWER FACTOR:

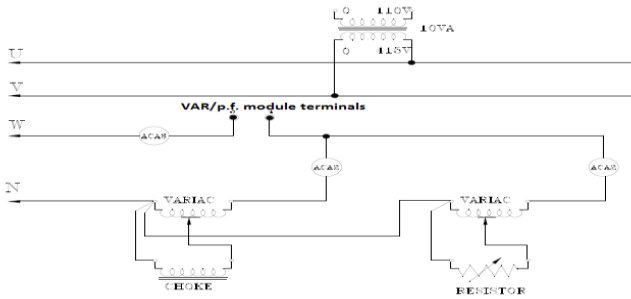


Fig.4.1

Procedure for Conducting Simulation Test:

1. Connect current transformer output to terminal block 1, terminal block 2 & terminal block 3.
2. Adjust load till current in ACA3 till 1Ampere through dimmer-1 & dimmer- 2
3. Connect voltage source of 110v through potential transformer from u & v phases.
4. Measured voltages at test points as shown in table

Sl. No.	Parameter	specification	Calculated value
1	Voltage at TP3	21.6V to 26.4V	24.26V
2	Voltage at TP4	-21.6V to -26.4V	-24.26V
3	Voltage at TP2	0	0
4	Voltage at TP5	6.75V to 8.25V	7.6V
5	Voltage at TP6	6.12V to 7.48V	6.96V
6	Voltage at TP7	-6.12V to -7.48V	-6.56V
7	Voltage at TP8	6.75V to 8.25V	-7.27V
8	Voltage at TP9	Amplitude of waveforms	
9	Voltage at TP10		

10	Voltage at TP11		
11	Voltage at TP12		

Table 4.1

Wave form observed at Test Point 9 and Test point 11:

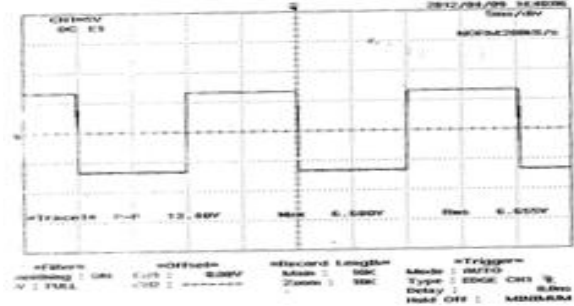


Fig 4.2

Wave form observed at Test Point 10 and Test point 12:

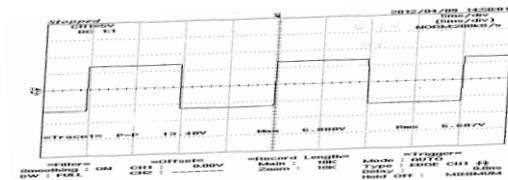


Fig 4.3

5. Connect 5kΩ VAR/p.f. pot to Terminal block 10 and terminal block 19 and Terminal block 20.
6. Observe wave form at test point 13.

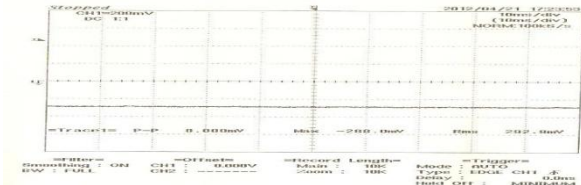


Fig.4.4

7. Observe wave form at test point 14.

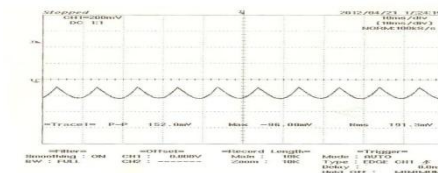


Fig.4.5

8. Vary power factor var/pf set pot and check for variation of output at TB18 and TB 19 between positive to negative.

Test of var/pf regulator module with current transformer output simulated using single phase variable voltage source.

1. Set the following current as shown below:
Initially the value of $I_{\cos\phi}$ and $I_{\sin\phi}$ has to be set by manually in ACA-1 and ACA-2.
And we can see the corresponding values of current in ACA-3.

ACA-3	ACA-1($I_{\cos\phi}$)	ACA-2($I_{\sin\phi}$)
1	0.8	0.6
0.8	0.64	0.48
0.6	0.48	0.36
0.4	0.32	0.24

Table.4.1

Calculation for 1A current:

Power factor ($\cos\phi$)=0.8, $\phi=\cos^{-1}(0.8)$, $\phi=36.86$

$\sin(36.86) = 0.6$

2. Adjust 5KΩ VAR/p.f. pot till the output at terminal block 18 and terminal block 19 is minimum (ideally signal level is zero) for the following current.

1. for 0.8 power factor

ACA-3	ACA-1($I_{\cos\phi}$)	ACA-2($I_{\sin\phi}$)
1	0.8	0.6
0.8	0.64	0.48
0.6	0.48	0.36
0.4	0.32	0.24

Table.4.2

2. for 0.85 power factor:

ACA-3	ACA-1($I_{\cos\phi}$)	ACA-2($I_{\sin\phi}$)
1	0.85	0.52
0.8	0.68	0.42
0.6	0.51	0.31
0.4	0.34	0.21

Table.4.3

3. Varying 5KΩ VAR/p.f. pot position for the above set current and check for voltage shift from negative to positive at TB18 & TB19.(change in pf setting).

4. Vary (reduce) $I_{\cos\phi}$ (ACA-1 and keeping ACA-2 constant) for the above current and check for voltage change at TB18 and TB19. (Observe voltage variation from positive to negative zone).

5. Bring back ACA-1($I_{\cos\phi}$) to initial position and vary [reduce] $I_{\sin\phi}$ for the above current and check for voltage changes at TB18 and TB19.

Advantages & Applications of VAR/p.f regulator

Advantages

- Un manned control
- Semiautomatic
- Limits the rotor current
- Easy regulation

Applications

- The major application of Var/pf regulator is used on all hydro and turbo driven
- Generators and commercial diesel generator sets.

CONCLUSIONS

To support the grid in meeting the power demand. Electricity board will buy power from different agencies. So, that the deficiency in power is compensated. Hence, power generation like co-generation, diesel power generation, and steam power generation are encouraged. During the process of power feeding to grid any change in grid will lead to change in var delivered by the generator feeding to grid. Hence, generator is operating either in varying power factor or varying Var according to mode set. Power factor/VAR regulator is excited to ensure that the generator working either in constant VAR or in constant power factor control.

REFERENCES

[1] Brushless A.C generator by Mitsuru Takahashi and Isamu Suzuki available at www.google.com

[2] J.D. Hurley, L.N. Bize and C. R.Mummert, "The Adverse Effects of Excitation, System Var and Power Factor Controllers"IEEE 1999

[3] Voltage regulator and parallel Operation by Basler Electric Company Available at www.google.com

[4]WWW.Google.com

FPGA Implementation of 64 Point FFT for Passive RADAR Applications

R. Ravindra Prasad, B.Vijaya Bhaskar

*(Department of ECE, St. Teresa college of engineering and technology/ JNTU Kakinada, India)

** (Department of ECE, St. Teresa college of engineering and technology/ JNTU Kakinada, India)

ABSTRACT

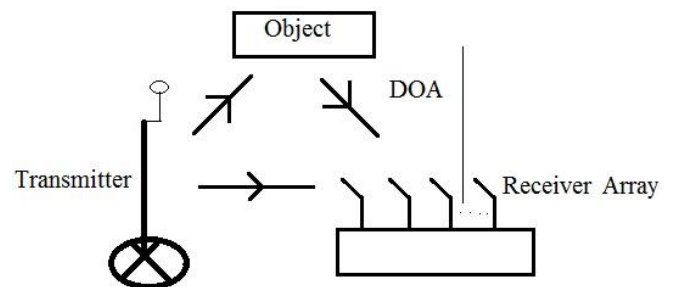
A power efficient Fast Fourier Transform (FFT) processor for use in the Direction of Arrival (DOA) estimation of a wideband waveform is presented. The target device for implementation is a Xilinx Spartan-3 Xc3s200 Field Programmable Gate Array (FPGA). The FFT processor was developed using the Xilinx ISE in Verilog code. Although the parallel and pipelined architecture uses a large portion of the available FPGA resources, the architecture does yield a high throughput.

Keywords: Direction of Arrival (DOA), Fast fourier transform (FFT), FPGA.

I. INTRODUCTION

Active and passive radar systems are two commonly used radar systems in different military and non military applications respectively. Active radar systems are commonly used in military and commercial applications for the detection and tracking of objects through a medium such as air. Most active radar systems work by transmitting a signal pulse through the medium scatters off objects in the medium. by processing the received wave field, an active radar system can determine an object's distance, velocity, and other features. The passive detection of objects has become of particular interest to the military in scenarios where the medium needs to be monitored covertly. A passive radar system can consist solely of an array of receiving antennas as opposed to an active radar system with a co-located transmitter and receiver. Without a transmitter the passive radar system relies on other sources of electromagnetic waves, such as am or fm radiowaves, tv broadcast, nearby radar, cell towers, or a wideband waveform to "illuminate" objects in the medium [1]. An active radar system has the benefit of a known transmit waveform. A passive radar system does not have knowledge of the transmitted signal and thus has to rely on digital signal processing techniques to extract information from an array of sensors over a period of time Wideband sources can have different bandwidths between 500Mhz to 5 GHz. The bandwidth of the signal in this paper is considered to be 3 GHz. The wideband passive radar system is shown below in which the object is illuminated by the wideband source while the scattered waveform along with the reference waveform is received by an array of antennas, digitized, and processed.

A well established algorithm such as the Multiple Signal Classification (MUSIC) algorithm [4] can be applied to calculate Direction of Arrival (DOA). The best method of determining the Direction of Arrival of wideband signal is to first decompose the signal into narrowband frequency components by converting the time domain signal into frequency domain through Discrete Fourier Transform, which will produce further frequency components which can be processed independently. A computationally efficient version of the DFT is known as the Fast Fourier Transform (FFT) and is commonly used increase the computational speed and reduces the computational time.



The coherent signal subspace method is the process under which the wideband DOA algorithm separated the frequency components via the Fast fourier transform. A low resolution estimate of the DOA is calculated using any beamforming algorithm. The low resolution estimate is used to identify areas where a high resolution DOA estimate is necessary. The calculation of the high resolution CCSM DOA estimate uses a set of 4096 (64^2) samples from each antenna. Each set of 4096 samples is divided into 64

segments of 64 samples and the 64-point FFT is computed for each segment. The covariance matrix for each frequency component is obtained by collecting the corresponding frequency components for each of the antennas in the array and estimating the covariance over the 64 segment record length. These covariance matrices are then combined into a single focusing matrix. After the focusing matrix is formed, a high resolution DOA can be estimated using the narrowband MUSIC algorithm. The CSSM algorithm is summarized in Figure 2 for a general array of n antennas. For this example, a phase shift and

scale block was chosen for beamforming in the frequency domain, however other beamforming methods apply.

Using the CSSM algorithm to estimate the DOA of a signal with a bandwidth of 4 GHz will require high speed digital signal processing. Per Nyquist's sampling theorem, the array's ADCs must sample at a frequency of at least 8 GHz. In order to process the data continuously, a throughput of 8 giga-samples per second must be maintained throughout the system.

In this paper the design and simulation of a 64-point FFT processor capable of 6 GS/s throughput. This FFT processor will be a building block for the CSSM wideband DOA estimation algorithm.

II. FFT DERIVATION

The DFT for N samples is defined as

$$X(K) = \sum_{n=0}^{N-1} x(n) W_N^{nK} \quad (1)$$

where $k=0,1,2...N-1$, and $X(k)$ is the frequency domain representation of $x[n]$. The twiddle factor W

N is defined as:

$$W_N = e^{-j2\pi K/N} \quad (2)$$

The FFT is a set of algorithms which are more computationally efficient than the DFT [6]. Table 1 summarizes the computational requirements of several FFT algorithms as derived in [7]. The radix-4 algorithm was selected based on the reduced number of operations compared to the radix-2 algorithm. Other algorithms such as the radix-8 and split-radix algorithms offer even more reductions; however, for a length 64 FFT these reductions are not significant. The Winograd algorithm minimizes the number of multiplications, but also adds a degree of complexity and significantly increases the total number of operations.

Table 1: Operations required for 64-point FFT

Operation	Radix-2	Radix-4	Radix-8	Split Radix	Winograd
Real Additions	1032	976	972	964	1394
Real Multiples	264	208	204	196	198
Total	1296	1174	1176	1160	1592

From [2], the expression for the radix-4 FFT is

$$X(p,q) = \sum_{l=0}^3 [W_N^{lq} F(l,q)] W_4^{lp} \quad \text{for } p = 0,1,2,3 \quad (3)$$

Where

$$F(l,q) = \sum_{m=0}^{N/4-1} x(l,m) W_{N/4}^{mq} \quad (4)$$

For $l=0,1,2,3$ and $q=0,1,...N/4-1$ and

$$x(l,m) = x(4m+l) \quad (5)$$

$$X(p,q) = X(N/4p + q) \quad (6)$$

Note that (4) is a $N/4$ length DFT. Equation (3) in matrix form, as shown in [2], is

$$\begin{matrix} X(0,q) & 1 & 1 & 1 & 1 & W_N^0 F(0,q) \\ X(1,q) & 1 & -j & -1 & j & W_N^q F(1,q) \\ X(2,q) & 1 & -1 & 1 & -1 & W_N^{2q} F(2,q) \\ X(3,q) & 1 & j & -1 & j & W_N^{3q} F(3,q) \end{matrix} \quad (7)$$

for $q=0,1,...N/4-1$.

Equation (7) can be expressed in signal flow form as shown in Figure 3. This form reveals the radix-4 butterfly which is the basic building block of the FFT processor.

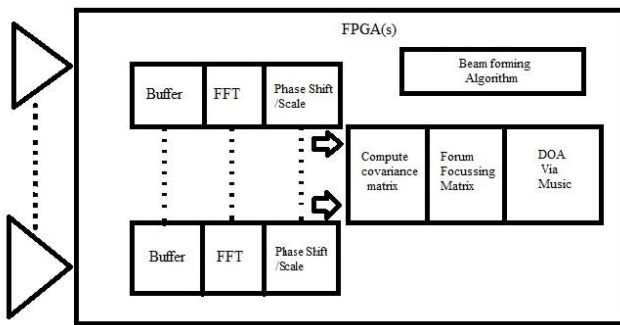


Fig 2: CSSM Algorithm.

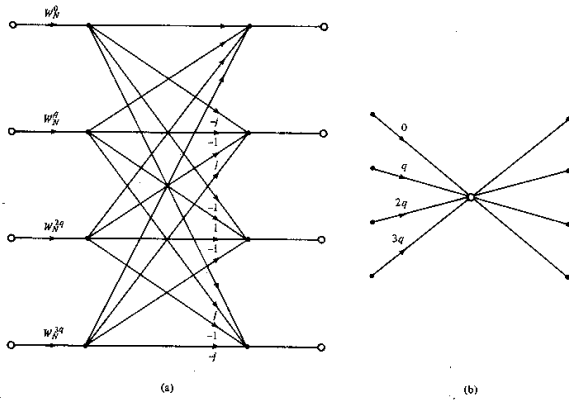


Fig 3: Radix 4 butterfly.

Equation (7) can be further decomposed by taking each of the $F(1,q)$ DFTs and applying the same process of splitting the DFT into four DFTs. The result will be a network of radix-4 butterflies.

III. FFT ARCHITECTURE

A literature survey was conducted to find a suitable architecture for implementing the radix-4 FFT algorithm. Many FFT architectures exist, ranging from power efficient architectures [9-12] to area efficient architectures [13-14]. There are also pipelined [11-12,14-16] architectures. These architectures were not optimal for a high throughput solution since they did not utilize parallel processing. In [17], a parallel FFT architecture was developed for FPGA. A quad-pipeline architecture was implemented using a front-end 4-point FFT butterfly circuit to separate the sequence into groups of four. These groups form four pipelines which are processed independently in parallel. The authors mention the possibility of extending the concept to “k” groups of parallel pipelines, but only implement the case $k=4$. In [18], a high speed FFT was implemented on a distributed array of custom designed DSPs. Each of the processors in the array was assigned a specific function, for example, in the case of a eight-processor 64-point complex FFT, three DSPs are reserved for memory operations, three are reserved for FFT butterfly operations, and two are reserved for shuffling the input and output sequences. This architecture would not be efficiently mapped to a single FPGA. Over the course of the survey, it was determined that the architecture for maximum throughput is the fully pipelined fully parallel architecture. In the literature, several authors mention this method [17] but this architecture is rarely implemented due to the large computational requirements. For the 64-point FFT, this corresponds to 3 ranks of 16 radix-4 butterfly processors in parallel. This architecture will use the maximum amount of resources, but will yield the highest throughput. Because of the parallel pipelined architecture each one of the 208 multiplications will require a dedicated multiplier circuit on the FPGA.

For the input / output (I/O) interface, multiplexers and de-multiplexers can be used to interface the FPGA with outside resources. Figure 4 shows a graphical description of an example I/O interface. The example uses two clock frequencies inside the FPGA, 500 MHz for the I/O interface, and 125 MHz for the actual FFT processor. A throughput of 8 GS/s is maintained across the entire system.

IV. IMPLEMENTATION

The FFT processor was designed in System Generator, which is a model-based design tool using the MATLAB Simulink environment. System Generator is a bit-true, cycle-true simulation and design verification program [13].

The FFT processor was implemented using the radix-4 butterfly as the basic component. After the initial radix-4 butterfly network was laid out, various hand-optimizations were made. Initially, the FFT processor used 264 multiply operations. However, certain twiddle factor multiplications resulted in simplified logic, reducing the number of multiplications to 208. This concurs with Table 1. The device for implementation was the Xilinx Spartan 3. With clock frequencies up to 550 MHz and up to 1200 I/O pins, the Spartan 3 is ideal for high-throughput applications. With regards to high speed digital signal processing, the Spartan 3 contains up to 640 dedicated arithmetic units known as DSP48E slices.

V. RESULTS

Two FFT processors were developed, one with 8-bit samples, and another with 10-bit samples from the DC. Based on ISE's timing reports, both the 8-bit and 10-bit FFT processors will meet the timing constraints and yield throughputs of 8.03 GS/S and 8.05 GS/s respectively. However, the proposed I/O interface did not meet timing. The 8-bit I/O interface achieved a throughput of 4.7 GS/s while the 10-bit I/O interface achieved a throughput of 4.1 GS/s. The slow path consists primarily of routing delays which account for 87% of the total delay. These routing delay problems may be mitigated through an intelligent selection of pins for the input and output resources, or adding delay to the input/output paths. With regards to FPGA utilization, the following table summarizes the results for the 10-bit FFT processor. The chosen Spartan 3 platform for implementation was the xc3s200-4ft256.

Table 2: Device utilization summary.

Device Utilization Summary (estimated values)			
Logic Utilization	Used	Available	Utilization
Number of Slices	2009	1920	104%

Number of Slice Flip Flops	2142	3840	55%
Number of 4 input LUTs	3071	3840	79%
Number of bonded IOBs	87	173	50%
Number of BRAMs	4	12	33%
Number of MULT18X18s	4	12	33%
Number of GCLKs	1	8	12%

VI. CONCLUSIONS

A highly parallel and pipelined architecture for a FPGA-based, high speed, FFT processor for wideband DOA applications has been presented. This 64-point FFT was simulated in System Generator and then implemented on a Spartan 3 FPGA using ISE. The FFT processor uses much of the FPGA's resources but yields a high throughput. The designed FFT processor met the throughput constraint of 8GS/s and higher throughput rates may be possible. The FPGA I/O interface could only process 4.2 GS/s due to an insufficient I/O interface. Future work would include designing an I/O interface which meets the throughput requirements for the CSSM DOA algorithm

REFERENCES

- [1] M.A. Ringer, G.J. Frazer and S.J. Anderson "Waveform Analysis of Transmitters of Opportunity for Passive Radar" DSTO Electronics and Surveillance Research Laboratory, 1999
- [2] Pollard, Robert. "How Passive Radar Sensors can Support Air Traffic Control" BAE Systems, Advanced Technology Centre, 2006
- [3] Hsio-Feng, Chiang, "Waveform Generation for Ultra-Wideband Radar System", Naval Postgraduate School, Monterey, California, 1993
- [4] R. O. Schmidt, "Multiple emitter location and signal parameter estimation" IEEE Transactions on Antennas and Propagation, vol. AP-34, No. 3, pp. 276-280, March 1986.
- [4] Hong, Wang, "Multiple-target direction finding", Graduate School of University of Minnesota, PhD Thesis, July 1985.
- [5] Proakis, J.G. "Digital Signal Processing: Principles, Algorithms, and Applications", Prentice Hall Inc., 1996.
- [6] J.W. Cooley and J.W. Tukey, "An Algorithm for the Machine Computation of the Complex Fourier Series," Math. Computation, Vol. 19, pp. 297-301, April 1965.
- [7] Chi-hau Chen, "Signal Processing Handbook", CRC Press, 1988.
- [8] Chidambaram, Ramesh. "A Scalable and High-Performance FFT Processor, Optimized for UWB-OFDM". July 2005. Technische Universiteit Delft, Department of Electrical Engineering
- [9] T. Pitkanen, T. Partanen, J. Takala. "Low-Power Twiddle Factor Unit for FFT Computation" SAMOS 2007
- [10] C. Chang, C. Wang "Efficient VLSI Architectures for Fast Computation of the Discrete Fourier Transform and Its Inverse. IEEE Transactions on Signal Processing, vol. 48 No. 11 Nov 2000
- [11] M. Hasan, T. Arslan, J.S. Thompson "A Novel Coefficient based Lower Power Pipelined Radix-4 FFT Processor for Wireless LAN Applications"
- [12] M. Hasan, T. Arslan and J.S. Thompson, "A Novel Coefficient Ordering based Low Power Pipelined Radix-4 FFT Processor for Wireless LAN Applications", IEEE Transactions on Consumer Electronics, Vol. 49, No. 1 February 2003.
- [13] www.xilinx.com
- [14] C. Wang and Y. Lin, "An Efficient FFT Processor for DAB Receiver Using Circuit-Sharing Pipeline Design", IEEE Transactions on Broadcasting, Vol. 53, No. 3, September 2007
- [15] J. J. Fuster and K. S. Gugel, "Pipelined 64-Point Fast Fourier Transform For Programmable Logic Devices", Dept. of Electrical and Computer Engineering, University of Florida, Gainesville, FL
- [16] Dillon Engineering, www.dilloneng.com.
- [17] J. Palmer and B. Nelson, "A Parallel FFT Architecture for FPGAs", Dept. of Electrical and Computer Engineering, Brigham Young University, Provo, UT 84602, FPL 2004, LNCS 3203, pp. 948-953, 2004.
- [18] Omar Sattari, "Fast Fourier Transforms on a Distributed Digital Signal Processor", University of California-Davis, 2004.
- [19] J. Takala and K. Punkka, "Scalable FFT Processors and Pipelined Butterfly Units", Tampere University of Technology, Tampere, Finland, SAMOS 2004, LNCS 3133, pp. 373-382, 2004.
- [20] W. Li and L. Wanhammar, "Efficient Radix-4 and Radix-8 Butterfly.

AUTHOR'S PROFILE:

Mr R.Ravindra prasad is pursuing his M.Tech in St. Theresa Institute of Engineering and Technology under the guidance of Mr. B.Vijaya Bhaskar, Assoc. Professor, HOD, and Department of ECE. My research interests include VLSI design and digital signal processing.

Sri. B. Vijaya Bhaskar working as Assoc. Professor and Head, Department of ECE at St. Theresa Institute of Engineering and Technology, Vizianagaram. His research interests include VLSI design and digital signal processing.

Performance Analysis of Spiral Tube Heat Exchanger used in oil extraction system

Kondhalkar G. E ^(a), Kapatkat V. N ^(b)

(a) Head of Mechanical Engineering Dept. – Dnyanganga polytechnic, Pune

(b) Professor in Mechanical Engg. Dept. – Sinhgad College of Engineering, Pune

ABSTRACT

Energy saving is major matter in our global world, and heat exchanger is very useful for energy saving. Of course heat exchanger is most significant component for chemical reaction, distillation, dissolution, crystallization, fermentation etc. So the correct selection of heat exchanger is important in these processes. Spiral tube Heat Exchangers are known as excellent heat exchanger because of far compact and high heat transfer efficiency. This paper discusses about the effective use of spiral tube heat exchanger in oil extraction process. Paper gives the performance analysis of spiral tube heat exchanger over the shell and tube type heat exchanger.

Key words: *Spiral heat exchanger, oil extraction*

INTRODUCTION

An essential oil is a concentrated, hydrophobic liquid containing volatile aroma compounds from plants. Essential oils are also known as volatile or ethereal oils, or simply as the "oil of" the plant from which they were extracted, such as oil of clove. An oil is "essential" in the sense that it carries a distinctive scent, or essence, of the plant.

Essential oils are generally extracted by distillation. Other processes include expression, or solvent extraction. They are used in perfumes, cosmetics, soap and other products, for flavoring food and drink, and for scenting incense and household cleaning products.

Various essential oils have been used medicinally at different periods in history. Interest in essential oils has revived in recent decades with the popularity of aromatherapy, a branch of alternative medicine which claims that the specific aromas carried by essential oils have curative effects. Oils are volatilized or diluted in carrier oil and used in massage, diffused in the air by a nebulizer or by heating over a candle flame, or burned as incense.

Most oils are distilled in a single process. One exception is Ylang-ylang (*Cananga odorata*), which takes 22 hours to complete through a fractional distillation.

The recondensed water is referred to as a hydrosol, hydrolat, herbal distillate or plant water essence, which may be sold as another fragrant product. Popular hydrosols include rose water, lavender water, lemon balm, clary sage and orange blossom water. The use of herbal distillates in cosmetics is increasing. Some plant hydrosols have unpleasant smells and are therefore not sold.

Table: 1 Common Essential Oils and their Uses

Sr. No.	Essential Oil	Uses
1	Basil	Perfumery, aromatherapy, sharpening concentration, headache relief and migraines
2	Bergamot	Perfumery, insect repellent, helpful to the urinary and digestive tracts, useful for skin conditions linked to stress such as cold sores and chicken pox particularly when combined with eucalyptus oil, flavouring agent
3	Black pepper	Stimulation of the circulation, Healing muscular aches, pains, and bruises.
4	Citronella oil	Insect repellent and in perfumery.
5	Tea tree, eucalyptus and sandalwood oil	Antibacterial, antifungal, antiviral, or antiparasitic and used as antiseptics and disinfectants.
6	Clove oil	Topical analgesic, especially useful in dentistry. It is also used as an antiseptic, antispasmodic, carminative, and antiemetic.
7	Lavender oil	Antiseptic

PRODUCTION OF ESSENTIAL OILS

To get essential oils the aromatic essence molecules of the plant must be captured by technical extraction methods. Essential oils are liquids stored in various places in plants that can be removed from the plant using extraction methods such as steam distillation, cold pressing, chemicals, or fat-absorption.

The most popular method for extraction is steam distillation and the majority of essential oils used in aromatherapy are distilled in this way, but as technology is advancing, more efficient and economical methods are being developed.

The extraction of an oil require large quantity of plant material and the method used to extract the oil is time

consuming, so requires a high degree of skill and care. Hence, pure essential oils are expensive, but they are also highly effective as only a few drops at a time are required to achieve the desired effect.

Essential oils are usually liquid, but can also be solid, like orris root or semi-solid according to temperature, like the rose. They dissolve in pure alcohol, fats and oils but not in water. Some of the distillation methods are as discussed below.

Distillation

In this, water is heated to produce water vapour, which carries the volatile chemical of the aromatic material with it. The water vapour is then condensed using a condenser and the resulting distillate is collected. The essential oil will normally float on top of the hydrosol (the distilled water component) and is separated out.

Various types of distillation methods are as follows,

- Water Distillation
- Steam Distillation
- Hydro Diffusion
- Fractional Distillation

a) Steam distillation method

Steam distillation was invented by the Persian chemist, Ibn Sina (known as Avicenna in the West), in the early 11th century.

Steam distillation is the most common method of extracting essential oils. Steam distillation is done in a still (The still is tall with a head and a well-insulated swan's neck proceeded by a mechanism to prevent fumes and impurities passing through). Fresh, or sometimes dried, botanical material is placed in a closed container of the still, and pressurized steam is generated which enters the container and circulates through the plant material. The heat of the steam forces the intercellular pockets that hold the essential oils to open and release them. The temperature of the steam should not be very high as it can damage the botanical material but should be high enough to open the pockets which hold the essential oil.

Tiny droplets of essential oil evaporate and attach to the steam. The steam which then contains the essential oil is passed through a cooling system to condense the steam, which form a liquid from which the essential oil and water is then separated by decantation. The oil forms a layer on the water surface as it does not dissolve in water and hence is separated easily. This method is not used for extraction of oils that are sensitive to heat.

Applications

Steam distillation is employed in the manufacture of essential oils, for instance, perfumes. In this method, steam is passed through the plant material containing the desired oils. It is also employed in the synthetic procedures of complex organic compounds. Eucalyptus oil and orange oil are obtained by this method on the industrial scale.

Steam distillation is also widely used in petroleum refineries and petrochemical plants where it is commonly referred to as "steam stripping".

The following figure provides an overview of the steam distillation process.

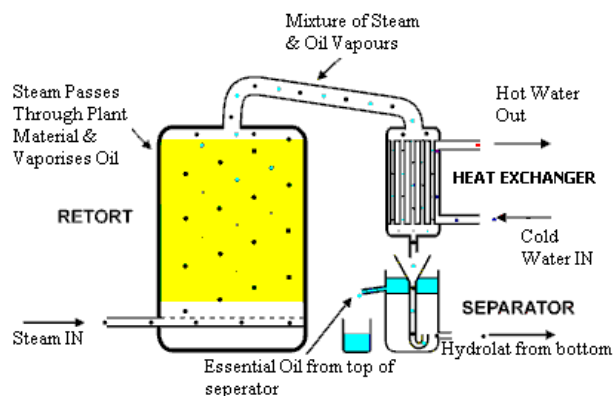


Fig. 1 Steam distillation method

PROBLEM DEFINITION AND SOLUTION

The experimentation is carried out in one of the oil extraction unit. They are dealing in extraction of herbal oils by using Field distillation unit and Steam distillation method.

The Field distillation (FDU) is used for the distillation and extraction of essential oils from herbs, shrubs, leaves, roots or whole plant by passing the saturated steam. The FDU consist of built-in-boiler tubes submerged in water for producing steam. The following oils extractions are done by company

- Lemon Grass Oil
- Sugandh Mantri Oil
- Shatavri Oil
- Manjishta Oil
- Turmeric Oil Steam Distilled
- Ashwagandha Oil

The company was using steam extraction method which is discussed earlier. Partly dry leaves of the tree are placed in a container. The steam is passed through this container, which is produced using boiler. As the steam passes through the leaves the oil is extracted and the mixture of oil and steam is passed through the condenser for condensation. After condensation it is collected in the separator vessel, where this mixture is kept to settle for some time. After settling time the oil can be separated from the water very easily.

In above mentioned equipments the company was using shell and tube type condenser. Mixture of oil vapour and steam enters in the condenser tube at high temperature and start condensing. As the tubes are straight and as condensate has to be collected, the process is very slow. Due to very low velocity the oil particles get stick up on the inner periphery of the pipe which makes the layer of oil forms at the inner periphery, which reduces the heat transfer rate and ultimately reduces the productivity.

Solution

As earlier discussed the problem of settling the oil at the inner periphery is due to the low velocity in the straight tube of shell and tube heat exchanger.

To solve this problem first the velocity of the mixture is increased but due to that the condensate collected is at higher temperature. The process at higher velocity (more

than 0.5m/s) was not suitable. So it is decided to keep the low velocity with more turbulences.

High turbulences results in increases the performance of the unit. Due to the turbulences the heat transfer rate increases as well as oil will not stick to the inner surface of the tubes.

This is achieved by using spiral tube heat exchanger instead of shell and tube type heat exchanger.

Advantages of spiral tube heat exchanger

Spiral tube heat exchanger consists of number of spirals attached to the header. One fluid flows from periphery to center of the casing while the other is moving from center to periphery, it has following advantages,

1 Because of the spiral flow paths imparted to the tube- and shell-side fluids, the effects of centrifugal force and secondary circulating flow enhance heat transfer on both sides in a counter flow arrangement.

2 The other fluid enters the unit at the periphery and moves towards the centre. The channels are curved and have a uniform cross section, which creates "spiraling" motion within the fluid.

3 The fluid is fully turbulent at a much lower velocity than in straight tube heat exchangers, and fluid travels at constant velocity throughout the whole unit, and thus the sticking of oil problem will be eliminated.

4 Spiral heat exchangers require small area for mounting resulting in lower unit installation cost compared with other.

5 Compared with other types of heat exchanger, spiral unit provides the best access to their heat transfer area with no special tools or lifting equipment required.

Literature Review

The heat transfer coefficients in a spiral plate heat exchanger are investigated by Rangasamy R. and K.Saravanan [1]. The test section consists of a plate of width 0.3150 m, thickness 0.001 m and mean hydraulic diameter of 0.01 m. The mass flow rate of hot water (hot fluid) is varying from 0.5 to 0.8 kg/s and the mass flow rate of cold water (cold fluid) varies from 0.4 to 0.7 kg/s. Heat transfer studies in two-phase flow streams are studied by S. Ramachandran, P. Kalaichelvi, [2]. The objective of the investigation was to evolve a correlation to predict two phase heat transfer coefficients with reasonable accuracy which will help to optimally design the heat exchanger. Experimental studies in laminar range were done in a spiral plate heat exchanger using the two-phase system of water- n-dodecane in different mass fractions and flow rates as the cold process fluid. The two phase heat transfer coefficients were related with Reynolds numbers and were fitted into a relation in the form $h = a Re^m$. The heat transfer coefficients were also related to the mass fraction of n-dodecane for identical Reynolds numbers. Correlations were developed between the two-phase multiplier (ratio of the heat transfer coefficient of the two phase fluid and that of the single phase fluid - Φ_L) and the Lockhart Martinelli parameter (X_{tt2}). This enables prediction of the two- phase heat transfer coefficients using single-phase data with an accuracy of $\pm 8\%$.

The heat transfer characteristics and the performance of a spiral coil heat exchanger under cooling and dehumidifying conditions are investigated by P. Naphon, S. Wongwises [3]. The heat exchanger consists of a steel shell and a spirally coiled tube unit. The spiral-coil unit consists of six layers of concentric spirally coiled tubes. Each tube is fabricated by bending a 9.27 mm diameter straight copper tube into a spiral-coil of five turns. Air and water are used as working fluids. The chilled water entering the outermost turn flows along the spirally coiled tube, and flows out at the innermost turn. The hot air enters the heat exchanger at the center of the shell and flows radially across spiral tubes to the periphery. A mathematical model based on mass and energy conservation is developed and solved by using the Newton-Raphson iterative method to determine the heat transfer characteristics. The results obtained from the model are in reasonable agreement with the present experimental data. The effects of various inlet conditions of working fluids flowing through the spiral coil heat exchanger are discussed.

Rangasamy R. and K. Saravanan [4] experimentally investigated convective heat transfer coefficient for electrolytes using spiral plate heat exchanger. The test section consists of a plate width 0.315m, thickness 0.001m and mean hydraulic diameter of 0.01m. the mass flow rate of water (hot fluid) is 0.636kg/s and the mass flow rate of electrolytes (cold fluid) varying from 0.483kg/s to 0.704 kg/s. Experiments have been conducted by varying the mass flow rate, temperature and pressure of cold fluid, keeping the mass flow rate of hot fluid constant. The effect of relevant parameters on spiral heat exchanger is investigated. The data obtained from the experimental study are compared with theoretical data. A new correlation for Nusselts number

$Nu = 0.04Re^{0.84}Pr^{0.15}$ is developed.

SPIRAL TUBE HEAT EXCHANGER

The Spiral heat exchanger was developed in Sweden by Rosenblad Patenter in the 1930s to recover waste energy from contaminated water effluents in pulp mills.

Spiral heat exchanger is self cleaning equipment with low fouling tendencies, easily accessible for inspection or mechanical cleaning with minimum space requirement.

Due to the curvature of the tube, a centrifugal force is generated as fluid flows through the curved tubes. Secondary flows induced by the centrifugal force have significant ability to enhance the heat transfer rate. [3] Helical and spiral coils are known types of curved tubes which have been used in a wide variety of applications for example, heat recovery process, air conditioning and refrigerating systems, chemical reactors, food and dairy processes.

An advantage which the spiral coil heat exchanger has over conventional heat exchanger systems is its ability to accommodate differential thermal expansion. The system is more compact. For the same heat transfer surface, the spiral coil arrangement has a volume about 15% smaller than that of cross flow shell and tube heat exchanger.

Spiral tube heat exchanger uses multiple parallel tubes connected to pipe-like manifolds to create a tube-side flow

path. Refer fig. no. 2 cross sectional view of the spiral tube heat exchanger.

The square dimensional profile of the spiral tube heat exchanger allows the unit to have a smaller footprint than the long, rectangular shell-and-tube unit. This can be observed by comparing two heat exchangers.

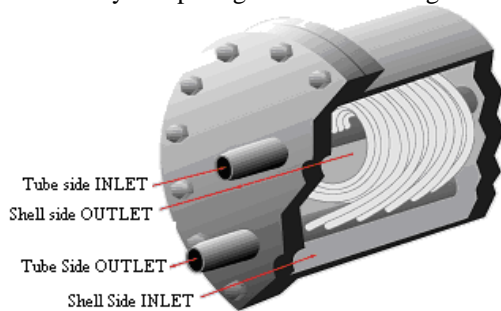


Fig. 2 Cross section of spiral tube heat exchanger

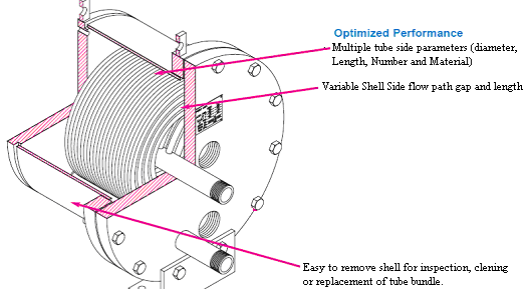


Fig. 3 Cross sectional view

A spiral tube heat exchanger is a coil assembly fitted in a spiral casing. The coil assembly is welded to a header and fitted in a compact shell. The spaces or gaps between the coils of the spiral tube bundle become the shell side flow path when the bundle is placed in the shell. Tube side and shell side connections on the bottom or top of the assembly allow for different flow path configurations. Refer fig no. 3 for the constructional details.

The spiral shape of the flow for the tube side and shell side fluids create centrifugal force and secondary circulating flow that enhances the heat transfer on both sides in a true counter flow arrangement. Advantage of spiral shape is to get tube side enhancement without the associated potential for plugging on both the shell and tube side of the heat exchanger. Since there are no baffles or dead spots to lower velocities and coefficients, heat transfer performance is optimized. Additionally, since there are a variety of multiple parallel tube configurations (diameter, number and length), efficiency is not compromised by limited shell diameter sizes as it is in shell and tube designs.

Since the tube bundle is coiled, space requirements for tube bundle removal are virtually eliminated. When exotic material is required, a spiral tube heat exchanger minimizes the material used since manifolds replace the channels, heads and tube sheets of a conventional shell and tube design. The shell side is usually smaller than a comparable shell and tube design and there are no requirements for tube supports or pass dividers.

Spiral tube heat exchanger uses single channel technology which means that both fluids occupy a single channel, which allows fully counter-current flow. One fluid enters the centre of the unit and flows towards the periphery. The other fluid enters the unit at the periphery and moves towards the centre. The channels are curved and have a uniform cross section, which creates "spiraling" motion within the fluid.

The fluid is fully turbulent at a much lower velocity than in straight tube heat exchangers, and fluid travels at constant velocity throughout the whole unit. This removes any likelihood of dead spots and stagnation. Solids are thus kept in suspension and the heat transfer surfaces are kept clean by scrubbing action of the spiraling flow.

Self-cleaning keeps cost down & the self cleaning properties of spiral heat exchangers ensure that the reliable performance of efficient heat transfer is guaranteed, within minimum down time for maintenance. Spiral heat exchangers require small area for mounting resulting in lower unit installation cost compared with other.

SPECIFICATIONS OF SPIRAL TUBE HEAT EXCHANGER

The specifications of the spiral tube heat exchanger as follows.

Surface Area: 0.45 m²

Tube Diameter:

Outer diameter = 12 mm

Inner Diameter = 10 mm

No. Spirals : 06 with pitch as 30 mm

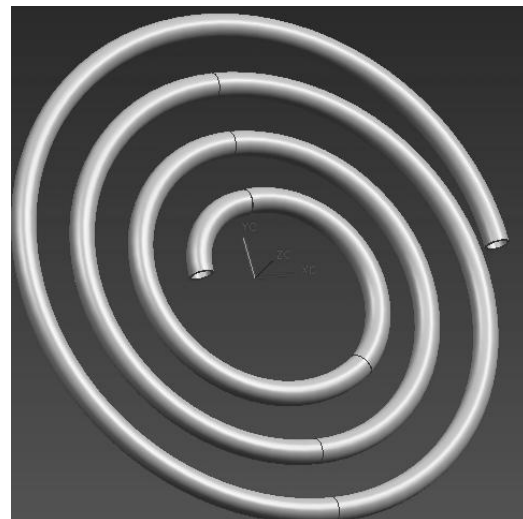


Fig. 4 Spiral Tube

Spiral of the spiral tube heat exchanger is made from copper tube with outer diameter 12mm and 10mm inner diameter, the outside diameter of the spiral is 248 mm and channel width is 30 mm, the length of the tube required is 1.88 m and the surface area available for heat transfer is 71186.83 mm² (0.071187 m²). The hot water inlet is directed from the center of the spiral where as the hot fluid outlet is taken from the periphery of the spiral, the channels for coldwater are equi-spaced with pitch of 30 mm.



Fig. 5 Spiral tube bundle

Spiral tube bundle is an assemblage of six spiral sets, the inlets are connected to a common pipe 30mm outside diameter and 21mm inner diameter, the inlet pipe is provided with an end flange that receives the inlet connector. Similarly the outlets of the spirals are connected to a common pipe 30mm outside diameter and 21mm inner diameter, the inlet pipe is provided with an end flange that receives the outlet connector.

The flanges are mounted on the casing plates. The hot water spirals offer a net heat transfer area of 0.45 m². The cold water channels are equally spaced with an overall spacing of 30mm pitch and width 80mm.



Fig. 6 Spiral Tube bundle with back plate

Casing primarily comprises of two end flanges and a circular pipe, the end flanges receive the flanges for hot water inlet and outlet as well as cold water outlet. The cold water inlet flange is welded to the periphery of the casing; overall casing is 300mm diameter and 100mm length.

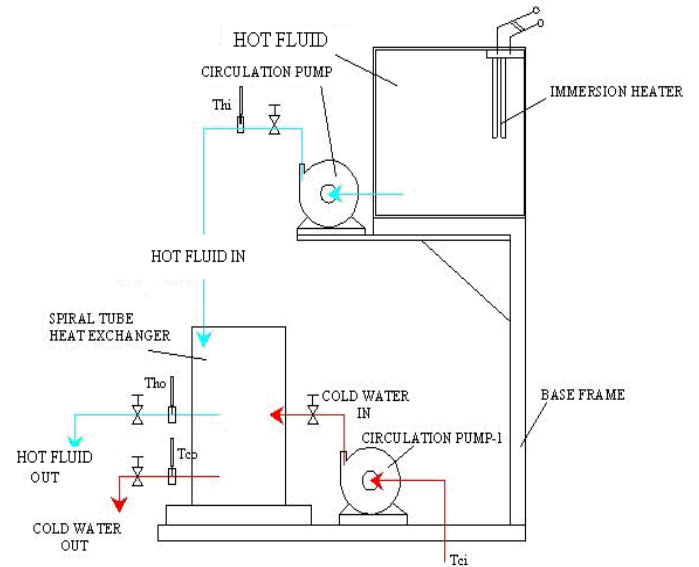


Fig. 7 Experimental set up

SUGGESTED PROCEDURE FOR EXPERIMENTATION

- Carefully check all the electrical and hydraulic connections before starting.
- Start the immersion heater supply to heat the oil in the overhead tank.
- Start the cooling water supply by opening the inlet valve to the heat exchanger
- After getting the certain temperature of the oil start the hot oil supply by opening the valve.
- Take the reading of inlet hot oil temperature, outlet hot oil temperature at steady state. Also take the cold water inlet and outlet temperature by temperature measuring instrument.
- Collect the hot oil and cooling water at the outlet of the heat exchanger in beaker. Check the time required for collection of oil and water in beaker for 1000 ml.
- Repeat the same procedure for different flow rates of the hot oil and cooling water.

Flow rate of hot oil is varied by opening the valve at different angles. The readings are taken to check the performance of the heat exchanger.

RESULTS & DISCUSSION

Following formulas are used to get the results tabulated to compare the performance of spiral tube heat exchanger with shell and tube type heat exchanger.

Reynolds Number

$$Re = \frac{\rho v d}{\mu} = \frac{VD}{\nu}$$

Prandtl Number

$$Pr = \frac{\mu c_p}{k}$$

Nusselt Number

$$Nu = 0.04 Re^{0.74} Pr^{0.4} \dots [4]$$

Effectiveness (ϵ)

$$\epsilon = \frac{(Th_i - Th_o)}{(Th_i - Tc_i)}$$

Properties of oil of lemon grass oil

$$\mu = 0.547 \times 10^{-3} \text{ Kg/ms}$$

$$\nu = 4.2 \times 10^{-6} \text{ m}^2/\text{Sec}$$

$$C_p = 4060 \text{ J/Kg K}$$

$$k = 0.505 \text{ W/m}^2\text{K}$$

Performance graphs of spiral tube heat exchanger and shell and tube heat exchanger for sugandh mantri oil emulsion.

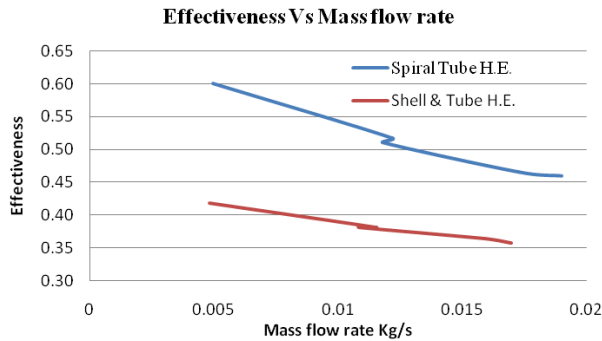


Fig. 8 Effectiveness Vs Mass Flow Rate

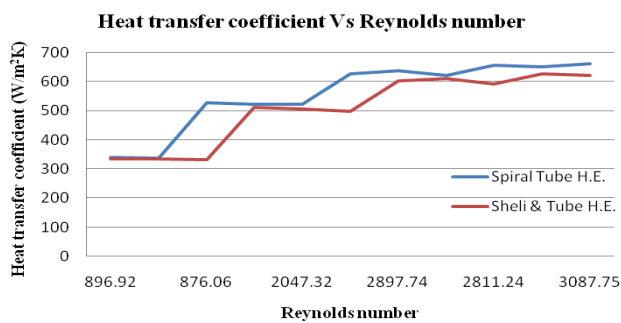


Fig. 9 Heat transfer coefficient Vs Reynolds number

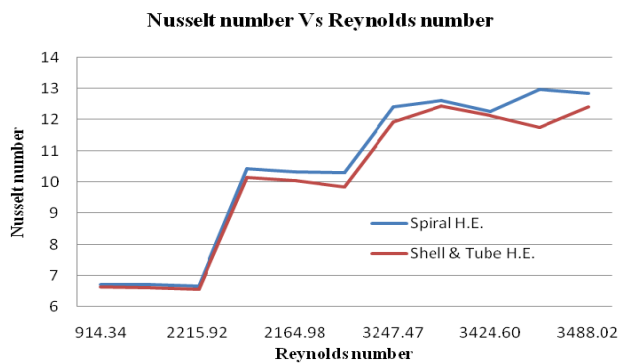


Fig. 10 Nusselt number Vs Reynolds number

Performance graphs of shell and tube heat exchanger and spiral tube heat exchanger for lemon grass oil emulsion.

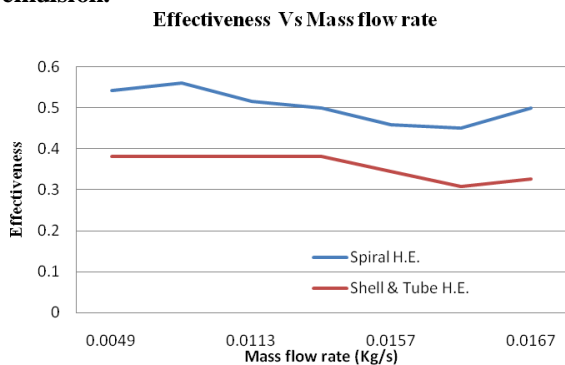


Fig. 11 Effectiveness Vs Mass Flow Rate

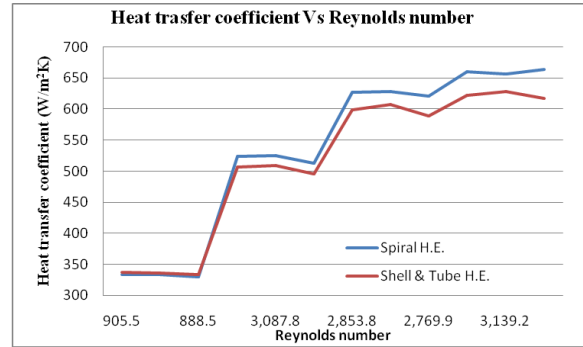


Fig. 12 Heat transfer coefficient Vs Reynolds number

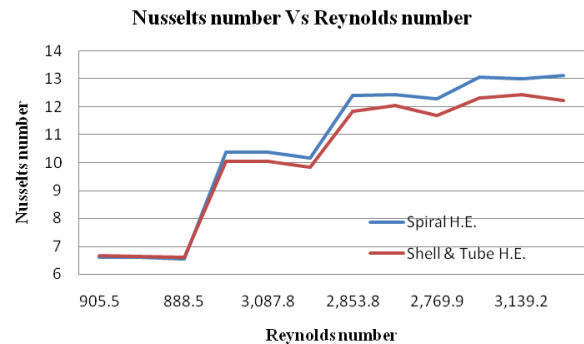


Fig. 13 Nusselt number Vs Reynolds number

- Graph 8 & 11 shows the trend for the mass flow rate and effectiveness. It is seen that as mass flow rate increases with decrease in effectiveness. It is observed that for the same mass flow rate effectiveness increases for the spiral tube heat exchanger.
- Graph 9 & 12 shows the relation between Reynolds numbers & Heat transfer coefficient. It is seen from the graph that the heat transfer coefficient increases with increase in Reynolds number. The nature of the graph is linear.
- Graph 10 & 13 shows the relation between Reynolds numbers and Nusselt number. It is seen from the graph that Nusselt number increases with increase in Reynolds number.
- From the test data available effectiveness of shell and tube heat exchanger for lemon grass oil and sugandh mantra oil is average 0.3 to 0.4 against for spiral it is 0.4 to 0.5, thus increase in the effectiveness.
- Heat transfer coefficient for shell and tube type heat exchanger is average 350 – 600 W/m²K against for spiral tube heat exchanger it's average value is 450 to 650 W/m²K, thus increase in the heat transfer rate due to use of spiral tube heat exchanger.

CONCLUSION

As prescribed in the chapter 5, for the experimental studied following can be concluded

- The continuously curved flow section contributes to improvement in overall heat transfer coefficient as compared to shell and tube type heat exchanger from 400 to 650W/m²K.
- The true concurrent flow increases the heat exchanger effectiveness from 0.3 to 0.5 for spiral heat exchanger.

- The cost saving using spiral tube heat exchanger is around 15 – 20 % as compared to shell and tube type heat exchanger apart from compactness and saving in size.
 - The scrubbing effect of the fluids in both spiral passages inhibits deposition of slug and other deposits. Fouling factors for spiral heat exchangers are commonly one third the values of conventional shell and tube heat exchanger.
 - By using spiral tube heat exchanger the oil sticking problem as in case of straight tube is reduced and total productivity is increased from 3.6 lit/day to 6.2 lit/day.
14. Yunus A. Cengel, "Heat and Mass transfer, third edition", Tata McGraw-Hill Publishing company limited, pp 285-295, 2007
 15. John E. Hesselgreaves, "Compact heat exchangers", pergamon, Second edition, pp 290-315, 2001
 16. Warren. M. R., J. P. Harthnett, "Handbook of Heat Transfer", Third Edition, McGraw-Hill, pp 1.1- 1.36, 17.1-17.100 , 1998

REFERENCES

1. R. Rajavel and K. Saravanan , "Heat transfer studies on spiral plate heat exchanger", Journal of thermal science, vol. 12(3), pp 85-90, 2008
2. S. Ramachandran, P. Kalaichlvi, S. Sundaram, "Heat transfer studies for two phase flow in spiral plate heat exchanger", Journal of the university of chemical technology and metallurgy, vol.41(4), pp 439-444, 2006
3. P. Naphon, S. Wongwises, " A study of heat transfer characteristics of a compact spiral coil heat exchanger under wet-surface conditions", Experimental thermal and fluid science, vol. 29, pp 511-521, 2005
4. R.Rajavel and K.Saravanan, " An experimental study of spiral plate heat exchanger for electrolytes", Journal of university of chemical and metallurgy, vol. 43 (2), pp 255-260, 2008
5. J.C.Ho and N.E. Wijesundera, "Performance of compact, spiral coil heat exchanger", Heat recovery system & CHP, Vol.15, pp 457-468, 1995
6. Deshpande P.M, "Spiral tube heat exchanger for heat recovery from gases", Thermal Engineering Journal, pp 80-85, 2008
7. Kanaris A.G, Mouza K.A, Paras S.V., "Designing Novel Compact Heat Exchangers For Improved Efficiency Using A CFD Code", Proceeding of 1st International Conference "From Scientific Computing to Computational Engineering, Athens, Sep. 8-10, pp 405-435, 2004
8. J.C.Ho and N.E. Wijesundera, " Study of a compact spiral coil cooling and dehumidifying heat exchanger", A T E, vol. 16(10), pp 777-790, 1996
9. Brian Allen and Rich Zoldak, "Spiral heat exchangers preheat high solids black liquor without plugging", pulp & paper, Feb. 1991
10. Olaf Strelow, "A general calculation method for plate heat exchanger", Journal of thermal science, vol.39, pp 645-658, 2000
11. Hewitt G.F., Shires G.L. and Bott T.R., "Process Heat Transfer", CRC Press, Begell House, Boca Raton, 1994.
12. G.Walker, "Industrial Heat Exchangers, a basic guide", second edition , hemisphere publishing corporation, New York, , 7-47, pp 93-119,1990
13. John E. Hesselgreaves, "Compact Heat Exchangers, Selection, Design and operation", Pergamon, First Edition, New York, 27-80, pp 275-300,2001

Robust Control of SAG/SWELL Mitigation Using Multi Converter Unified Power Quality Conditioner

K. RAMA RAJU

(M. Tech), Dept of EEE, G.Pulla Reddy Engineering College, Kurnool, Andhra pradesh, India.

ABID NAYEEMUDDIN

(Asst. profesor), Dept of EEE, G.Pulla Reddy Engineering College, Kurnool, Andhra pradesh, India.

B. RAJANI

(PhD), Dept of EEE, SV University, Tirupati, Chittoor, Andhra pradesh, India.

ABSTRACT

The paper proposes a new concept in developing outline and asses strategic business and technology aspects of cloud computing. Theoretical background and overview is presented on the basic underlying principles autonomic and utility computing, Service oriented Architecture. This configuration(MC-UPQC), capable of simultaneous compensation for voltage and current in multibus systems. In this configuration, one shunt voltage-source converter (shunt VSC) and two or more series VSCs exist. The system can be applied to adjacent feeders to compensate for supply-voltage and load current imperfections on the main feeder and full compensation of supply voltage imperfections on the other feeders. The power can be transferred from one feeder to adjacent feeders to compensate for sag/swell and interruption. The performance of the proposed configuration has been verified through simulation studies using MATLAB/SIMULATION on a two-bus/two-feeder system and results are presented. Ultimately, I conclude with an outlook and recommendations for companies and cloud providers.

Keywords: Power quality (PQ), unified power-quality conditioner (UPQC), voltage-source converter (VSC).

1. INTRODUCTION

Power quality is the quality of the electrical power supplied to electrical equipment. Poor power quality can result in mal-operation o f the equipment .The electrical utility may define power quality as reliability and state that the system is 99.5% reliable.

MCUPQC is a new connection for a unified power quality conditioner (UPQC), capable of simultaneous compensation for voltage and current in multibus/multifeeder systems. A MCUPQC consists of a one shunt voltage-source converter (shunt VSC) and two or more series VSCs, all converters are connected back to back on the dc side and share a common dc-link capacitor. Therefore, power can be transferred one feeder to adjacent feeders to compensate for sag/swell and interruption. The aims of the MCUPQC are:

- A. To regulate the load voltage (u/I) against sag/swell, interruption, and disturbances in the system to protect the Non-Linear/sensitive load L1.
- B. To regulate the load voltage (u/I) against sag/swell, interruption, and disturbances in the system to protect the sensitive/critical load L2.
- C. To compensate for the reactive and harmonic components of nonlinear load current (i/I).

As shown in this figure 1 two feeders connected to two different substations supply the loads L1 and L2. The MC-UPQC is connected to two buses BUS1 and BUS2 with voltages of u_{t1} and u_{t2} , respectively. The shunt part of the MC-UPQC is also connected to load L1 with a current of i_{l1} . Supply voltages are denoted by u_{s1} and u_{s2} while load voltages are u_{l1} and u_{l2} . Finally, feeder currents are denoted by i_{s1} and i_{s2} and load currents are i_{l1} and i_{l2} . Bus voltages u_{t1} and u_{t2} are distorted and may be subjected to sag/swell. The load L1 is a nonlinear/sensitive load which needs a pure sinusoidal voltage for proper operation while its current is non-sinusoidal and contains harmonics. The load L2 is a sensitive/critical load which needs a purely sinusoidal voltage and must be fully protected against distortion, sag/swell and interruption. These types of loads primarily include production industries and critical service providers, such as medical centers, airports, or broadcasting centers where voltage interruption can result in severe economical losses or human damages.

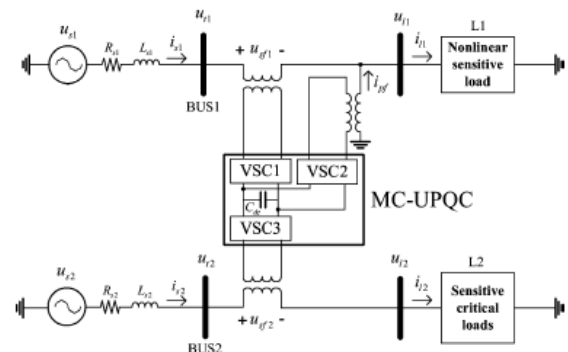


Fig.1: Typical MC-UPQC used in a distribution system.

A Unified Power Quality Conditioner (UPQC) can perform the functions of both D-STATCOM and DVR. The UPQC consists of two voltage source converters (VSCs) that are connected to a common dc bus. One of the VSCs is connected in series with a distribution feeder, while the other one is connected in shunt with the same feeder. The dc-links of both VSCs are supplied through a common dc capacitor.

It is also possible to connect two VSCs to two different feeders in a distribution system is called Interline Unified Power Quality Conditioner (IUPQC). This paper presents a new Unified Power Quality Conditioning system called Multi Converter Unified Power Quality Conditioner (MC-UPQC).

2. SAG/SWELL AND DISTORTION ON THE BUS VOLTAGE IN FEEDER-1 AND FEEDER-2

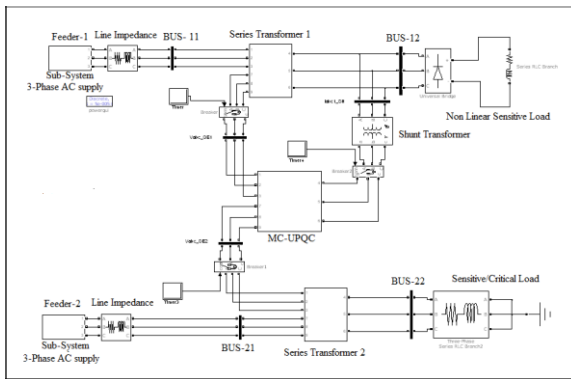


Figure 2: Simulink model of distribution system with MC-UPQC

Let us consider that the power system in Fig. 1 consists of two three-phase three-wire 380(v) (RMS, L-L), 50-Hz utilities. The BUS1 voltage (ut1) contains the seventh-order harmonic with a value of 22%, and the BUS2 voltage (ut2) contains the fifth order harmonic with a value of 35%. The BUS1 voltage contains 25% sag between 0.1s<t<0.2s and 20% swell between 0.2s<t<0.3s. The BUS2 voltage contains 35% sag between 0.15s<t<0.25s and 30% swell between 0.25s<t<0.3s. The nonlinear/sensitive load L1 is a three-phase rectifier load which supplies an RL load of 10_ and 30μH. The simulink model for distribution system with MC-UPQC is shown in figure 2.

The critical load L2 contains a balanced RL load of 10Ω and 100mH. The MC-UPQC is switched on at t=0.02s. The BUS1 voltage, the corresponding compensation voltage injected by VSC1, and finally load L1 voltage are shown in Figure 3.

Similarly, the BUS2 voltage, the corresponding compensation voltage injected by VSC3, and finally, the load L2 voltage are shown in figure 4.

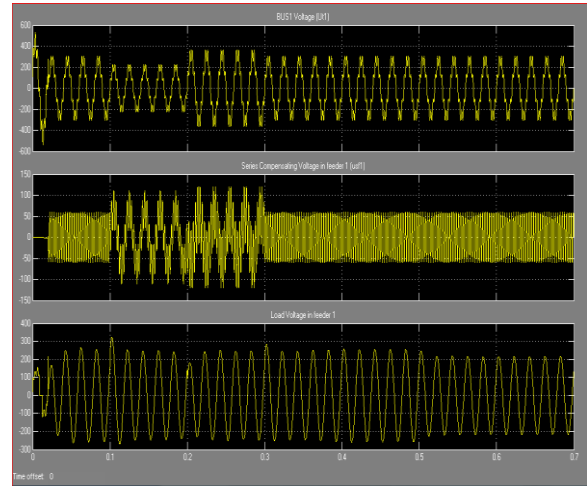


Fig 3.Simulation Result for BUS1 voltage, series compensating voltage, and load voltage in Feeder1

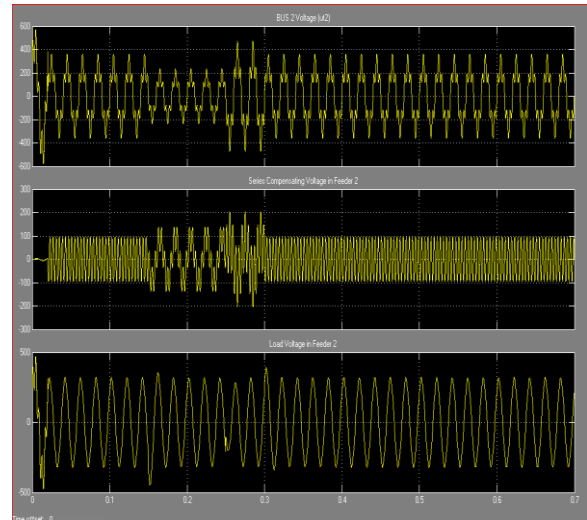


Fig 4.Simulation Result for BUS2 voltage, series compensating voltage, and load voltage in Feeder2.

As shown in these figures, distorted voltages of BUS1 and BUS2 are satisfactorily compensated for across the loads L1 and L2 with very good dynamic response.

The nonlinear load current, its corresponding compensation current injected by VSC2, compensated Feeder1 current, and, finally, the dc-link capacitor voltage are shown in Fig. 5. The distorted nonlinear load current is compensated very well, and the total harmonic distortion (THD) of the feeder current is reduced from 28.5% to less than 5%. Also, the dc voltage regulation loop has functioned properly under all disturbances, such as sag/swell in both feeders.

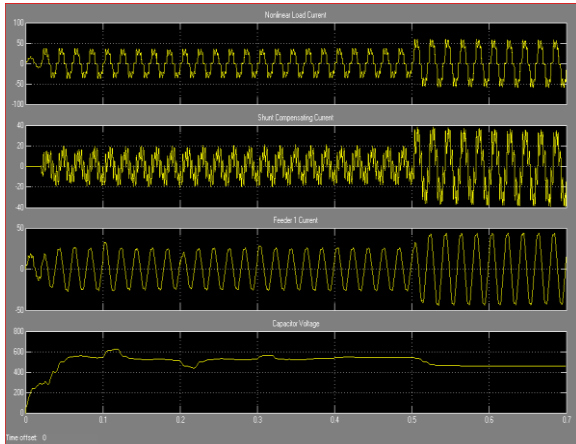


Fig 5.Simulation Result for Nonlinear load current, compensating current, Feeder1 current, and capacitor voltage.

3. UPSTREAM FAULT ON FEEDER2

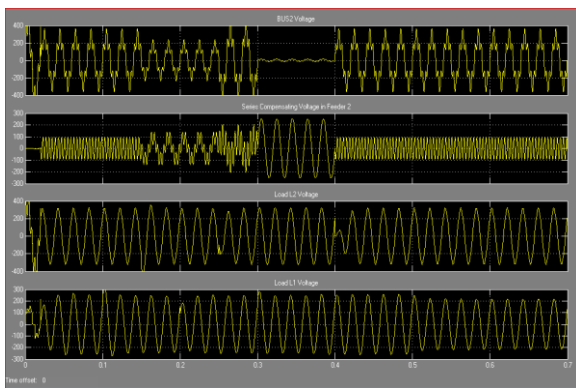


Fig 6.simulation results for an upstream fault on Feeder2: BUS2 voltage, compensating voltage, and loads L1 and L2 voltages.

When a fault occurs in Feeder2 (in any form of L-G, L-L-G, and L-L-L-G faults), the voltage across the sensitive/critical load L2 is involved in sag/swell or interruption. This voltage imperfection can be compensated for by VSC2. In this case, the power required by load L2 is supplied through VSC2 and VSC3. This implies that the power semiconductor switches of VSC2 and VSC3 must be rated such that total power transfer is possible.

The performance of the MC-UPQC under a fault condition on Feeder2 is tested by applying a three-phase fault to ground on Feeder2 between $0.3s < t < 0.4s$. Simulation results are shown in Fig.6

4. LOAD CHANGE

To evaluate the system behavior during a load change, the nonlinear load L1 is doubled by reducing its resistance to half at 0.5 s. The other load, however, is kept unchanged. In this case load current and source currents are suddenly increased to double and produce distorted load voltages (U_{l1} and U_{l2}) as shown in Fig 7.

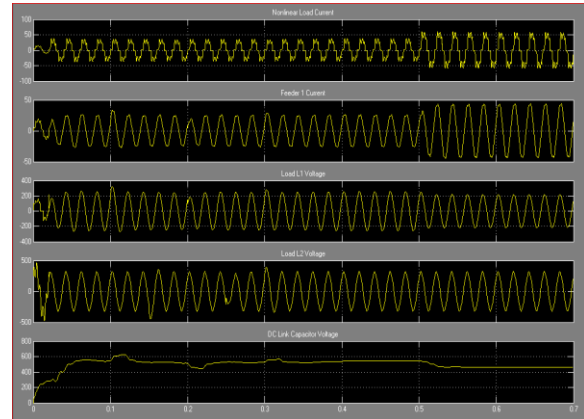


Fig 7.Simulation results for load change: nonlinear load current, Feeder1 current, load L1 voltage, load L2 voltage, and dc-link capacitor voltage.

5. SYSTEM WITH UNBALANCED SOURCE VOLTAGE IN FEEDER-1.

The performance of the MC-UPQC is tested when unbalance source voltage occurs in feeder-1 at nonlinear/sensitive load without and with MC-UPQC.

The control strategies for shunt and series VSCs, which are introduced and they are capable of compensating for the unbalanced source voltage and unbalanced load current. To evaluate the control system capability for unbalanced voltage compensation, a new simulation is performed. In this new simulation, the BUS2 voltage and the harmonic components of BUS1 voltage are similar. However, the fundamental component of the BUS1 voltage (U_{t1} fundamental) is an unbalanced three-phase voltage with an unbalance factor (U^- / U^+) of 40%.

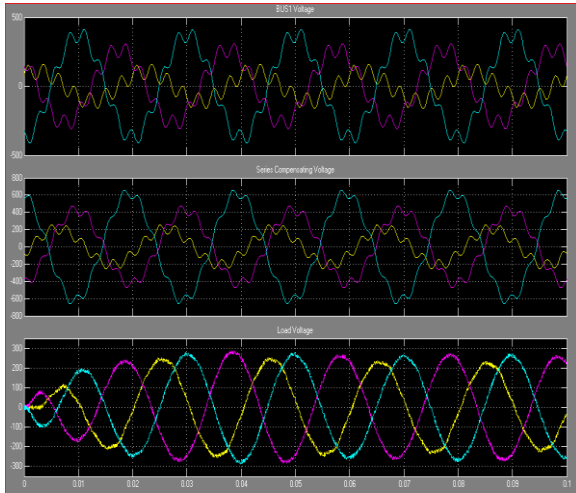


Fig 8. BUS1 voltage, series compensating voltage, and load voltage in Feeder1 under unbalanced source voltage.

The simulation results show that the harmonic components and unbalance of BUS1 voltage are compensated for by injecting the proper series voltage. In this figure, the load voltage is a three-phase sinusoidal balance voltage with regulated amplitude. The simulation results for the three-phase BUS1 voltage series compensation voltage, and load voltage in feeder 1 are shown in Fig.8.

6. CONCLUSION

The present topology illustrates the operation and control of Multi Converter Unified Power Quality Conditioner (MC-UPQC). The system is extended by adding a series VSC in an adjacent feeder. The device is connected between two or more feeders coming from different substations. A non-linear/sensitive load L-1 is supplied by Feeder-1 while a sensitive/critical load L-2 is supplied through Feeder-2. The performance of the MC-UPQC has been evaluated under various disturbance conditions such as voltage sag/swell in either feeder, fault and load change in one of the feeders. In case of voltage sag, the phase angle of the bus voltage in which the shunt VSC (VSC2) is connected plays an important role as it gives the measure of the real power required by the load. The MC-UPQC can mitigate voltage sag in Feeder-1 and in Feeder-2 for long duration. The performance of the MC-UPQC is evaluated under sag/swell conditions and it is shown that the proposed MCUPQC offers the following advantages:

1. Power transfer between two adjacent feeders for sag/swell and interruption compensation;
2. Compensation for interruptions without the need for a battery storage system and, consequently, without storage capacity limitation;
3. Sharing power compensation capabilities between two adjacent feeders which are not connected.

REFERENCES

- [1] Hamid Reza Mohammadi, Ali Yazdian Varjani, and Hossein Mokhtari, "Multiconverter Unified Power-Quality Conditioning System: MC-UPQC" IEEE TRANSACTIONS ON POWER DELIVERY, VOL. 24, NO. 3, JULY 2009.
- [2] R.Rezaeipour and A.Kazemi, "Review of Novel control strategies for UPQC" Internal Journal of Electric and power Engineering 2(4) 241-247, 2008.
- [3] S. Ravi Kumar and S.Siva Nagaraju "Simulation of DSTATCOM and DVR in power systems" Vol. 2, No. 3, June 2007 ISSN 1819-6608 ARPN Journal of Engineering and Applied Sciences.
- [4] M.V.Kasuni Perera "Control of a Dynamic Voltage Restorer to compensate single phase voltage sags" Master of Science Thesis, Stockholm, Sweden 2007.
- [5] M. Basu, S. P. Das, and G. K. Dubey, "Comparative evaluation of two models of UPQC for suitable interface to enhance power quality," *Elect.Power Syst. Res.*, pp. 821–830, 2007.
- [6] A. K. Jindal, A. Ghosh, and A. Joshi, "Interline unified power quality conditioner," *IEEE Trans. Power Del.* vol. 22, no. 1, pp. 364–372, Jan. 2007.

Synthesis and Physico-Chemical Characterisation of Polyphenylene Oxides

Susheela Bai Gajbhiye*

*Department of Engineering Chemistry, College of Engineering, Andhra University, Visakhapatnam, 530 003, India.

ABSTRACT

Homopolymers of the monomers, 2, 6-dimethyl-phenol (DMP) was synthesised by two methods involving oxidative coupling of their phenol monomer. Both the methods were found to be quite different in terms of producing polymers of different physical and mechanical properties. The first method produced polymers of low intrinsic viscosity with fairly good mechanical strength. Where as the second method produced polymers with higher intrinsic viscosity accompanied by enhanced mechanical properties. The synthesised polymers were characterised for structure-property correlations by measuring physical and mechanical properties namely, density measurements, dilute solution intrinsic viscosity measurements, tensile testing and fourier transform infra red spectroscopy (FTIR). The study reveals methodology for tailoring properties of polyphenylene oxides to suit various applications.

Keywords: Polyphenylene oxide; Oxidative coupling; Characterisation; Properties

1. INTRODUCTION

Aromatic rings attached directly to a hydroxyl group are called Phenols. The presence of polar hydroxyl groups allow phenols to make strong hydrogen bonding leading to high density, melting and boiling points [1]. However they are weakly acidic compared to alcohols due to the resonance effect of the -OH groups with the ring pi-bonds. Substitution of electron withdrawing groups makes it further weakly acidic while substitution by electron donating groups such as alkyl groups, make it strongly acidic in nature. Sterically hindered phenols have little or no acidic character. Phenols have four active centres (electron rich centres) at the ortho- and para- positions on the aromatic nucleus and also at the hydroxyl group [2]. This particular aspect provide opportunity to produce a variety of synthetic polymers from phenols by reactions at these active groups, via combination of C-C or C-O coupling reactions or oxygenation reactions where the coupling occurs fastest at the position of highest density of free electrons, except where there is steric hindrance.

Polyphenylene ether, a synthetic polymer can be formed from phenols by the reactions at the ortho- and para- and by the reactions with hydroxyl group, a powerful activating group and an ortho- para- directing group. Oxidation of phenols by using a catalyst can result in a variety of products, via proper choice of catalyst, solvent and phenol. For example (1) tetraalkyldiphenoquinones, (2) polyphenylene ethers and (3) o-benzoquinone can be prepared from catalyzed auto oxidation of phenol by using different types of copper salts and amines [3].

Discovery of oxidative polymerization of phenols to poly(phenylene oxide)s, led to the development of an entirely new family of engineering polymers [1]. They are basically polyethers having aromatic groups connected by an oxygen linkage at the backbone. Ether linkage is either at ortho- or para- position or both. When it is at para- position the polymer is called poly(1, 4-phenylene oxide) and when it is at ortho-position it is called (1, 2-phenylene oxide) and 1, 4 and 1, 2 additions may take place at the same monomeric unit. Poly(phenylene oxide)s have been synthesized in various forms since 1916 by Hunter et al. because of their mechanical, chemical and thermal properties [4]. The largest commercial usage of poly(phenylene oxide)s is in Noryl (General Electric Co.) engineering resin, which are alloys of poly(2, 6-dimethyl-1, 4-phenylene ether) [5].

In the past only low molecular weight 2, 6-di-substituted-1,4-phenylene ethers have been prepared by Dewar and James by the thermal decomposition of substituted benzene-1,4-diazooxides but only with limited success [6]. Staffin and Price have extended the work reported by Hunter, and prepared low molecular weight poly-2,6-dimethyl- 1,4-phenylene ether by oxidative displacement of the bromine in 4-bromo-2,6-dimethylphenol [7]. In 1959, A. S. Hay employed oxidative coupling method carried out at room temperature, in which a solution of 2,6-di-substituted phenol is merely passed by oxygen in an organic solvent containing an amine and a copper(I) salt as a catalyst [8]. As shown in Fig.1, when the substituent groups are small, as in 2,6-dimethylphenol, carbon-oxygen coupling occurs and linear polyphenylene ethers with intrinsic viscosities up to 3.4 dl/gm. have been obtained. With bulky groups, as in 2,6-di-tert-butylphenol, carbon-carbon coupling occurs and the diphenoquinone is the sole product. In intermediate cases such as di-isopropylphenol, carbon-carbon and carbon-oxygen coupling compete.

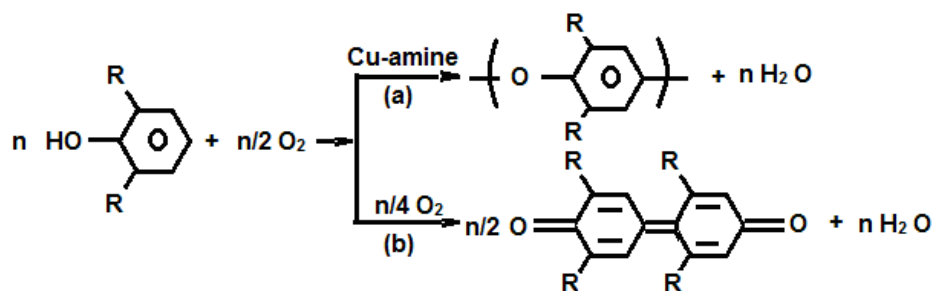


Figure 1. Oxidation products of phenols (a) polyphenylene ether and (b) diphenoquinone

Blanchard et al. studied the preparation and characterization of bis(phenolato)- bis(pyridine)-copper(II) complexes [9]. These complexes were decomposed to produce branched polymer under variety of condition. They also proposed a radical mechanism for the decomposition. In 1969, Harrod studied the thermal decomposition of copper (II) complexes containing various amine ligands [10]. They concluded that the phenoxo complexes with chelating ligands are highly resistant to thermal decomposition compared to non-chelating ligands.

Poly(2, 6-dimethyl-1,4-phenylene oxide) (PPO) is a high performance engineering plastic due to its high thermal stability (high glass transition temperature ($T_g = 210^\circ\text{C}$), high mechanical strength, and excellent hydrolytic stability. In addition, its distinctive but simple structure allows a variety of modifications in both aryl and benzyl positions: (1) electrophilic substitution on the benzene ring of PPO [11] (2) radical substitution of the hydrogen from the methyl groups of PPO [12] (3) nucleophilic substitution of the bromomethylated PPO (BPPO) [13] (4) capping and coupling of the terminal hydroxyl groups in PPO chains [14] and (5) metalation of PPO with organometallic compounds [15]. These modifications can fine tune PPO with specific properties for specific application. In this article, homopolymers of the 2, 6-Dimethyl-1, 4-Phenol monomer was synthesised using two different methods. These polymers were characterised for intrinsic viscosity, density, mechanical, thermal properties and further chemical structure confirmations were made using FTIR.

2. EXPERIMENTAL

Monomers, 2, 6-Dimethyl-phenol (DMP), Dibutyl-amine (DBA) and anhydrous hydrazine were procured from Merck Chemie, Mumbai; monomer 2, 6-Diphenyl-phenol (DPP) was obtained from Aldrich Chem Co.; Cuprous bromide catalyst from Lancaster and synthesis grade toluene and chloroform from Ranbaxy were procured. Distilled methanol was used for washing the polymer precipitate.

2.1 Synthesis

2.1.1 Synthesis of PPO by Method 1

The synthesis of polyphenylene ethers from their monomers DMP was carried out by oxidative coupling method according to the procedure given in literature [16]. DMP was purified by recrystallisation with hexane to at least 99.5%. In a three necked flask, oxygen was introduced into a vigorously stirred solution of CuBr and DBA in toluene for 10 min. Maintaining a molar ratio of CuBr: DBA: DMP equal to 1:22:77, a 25 percent solution of DMP in toluene was added over a period of 20 minutes. The temperature of solution was maintained throughout at 50°C . After 2 hrs of reaction under continuous stirring, the reaction mixture was diluted in toluene to 10 percent. Methanol (5-7 volumes) containing 0.5-1.0 percent acetic acid was added gradually with stirring, to precipitate out the PPO polymer as agglomerates which slowly turn into granular powder. The polymer obtained was filtered and washed with methanol, and dried in a vacuum oven at 60°C . Please refer Table 1.

2.1.2 Synthesis of PPO by Method 2

The synthesis of S(PPO) from its DMP monomer was carried out by oxidative coupling method according to the procedure given in literature [16]. DMP was purified by recrystallisation with hexane to at least 99.5%. In a three necked flask, oxygen was introduced into a vigorously stirred solution of CuBr and DBA in toluene for 10 min. A little excess of anhydrous magnesium sulphate (5 w/v %) was added to the solution to remove the water formed as a by-product of condensation reaction. Maintaining a molar ratio of CuBr: DBA: DMP equal to 1:22:77, a 25 percent solution of DMP in toluene was added over a period of 20 minutes. The temperature of solution was maintained throughout at 50°C . After 4 hrs of reaction under continuous stirring, a few drops (2 v/v%) of anhydrous hydrazine (10-15) were added into the reaction mixture to reduce the diphenoquinone by product formed, if any [17]. The inorganic solids were removed by filtration, and the solution was diluted in toluene to 10 percent. Then it was added dropwise to large volumes of methanol (5-7 volumes) containing 0.5-1.0 percent acetic acid, to precipitate the polymer. After stirring the solution for 2 hours, the polymer formed was collected by filtration. The polymer obtained was filtered and washed with methanol, and dried in a vacuum oven at 60°C . Please refer Table 1 for comparison of the two synthesis methods.

Table 1
Synthesis conditions for preparing polyphenylene oxide.

Method	CuBr:DBA:DMP (molar ratio)	MgSO ₄ (w/v)%	Hydrazine (v/v)%	Solvent	Temp (°C)	Time (hrs)
1	1:22:77	-	-	Hexane	50	2
2	1:22:77	5	2	Hexane	50	4

2.1.3 Purification of Polymers

All the polymers obtained were purified (reprecipitated) by redissolving in chloroform (1 volume) and precipitated in methanol (10 volumes) containing few drops of acetic acid. In the last step a final washing in methanol was carried out on all the polymers. A good yield of more than 95% was obtained. They were dried to a constant weight, in a vacuum oven at 60°C for 6 hours until constant. The measured densities, intrinsic viscosity and physical and mechanical properties of the synthesised polymers are presented in Table 2.

2.2 Polymer Characterization

The intrinsic viscosity of the dilute polymer solutions in toluene was calculated from the flow time measurements, using a Viscometer at 25°C. The required constants were taken from literature [16]. The density was measured by floatation method of the polymer films.

3. RESULTS AND DISCUSSION

The FTIR spectra of all the synthesised homopolymers and copolymers of polyphenylene oxide confirmed the presence of ether groups at 1306 cm⁻¹ and 1022 cm⁻¹, and the methyl and backbone phenyl groups at 3036 cm⁻¹ and 2954 cm⁻¹.

The measured physical properties of the polymers are presented in Table 2. We clearly observe that the measured intrinsic viscosity for PPO obtained by method 1 (hereafter called as PPO1) has a value lower than that obtained by method 2 (referred as PPO2). Lower the intrinsic viscosity, lesser is the polymer molecular weight. This implies that the PPO1 has a lower molecular weight than PPO2. This could be due to the formation of water molecules as condensation by-products which interferes with the polymerisation process by not allowing the catalyst to accelerate the reaction. On the other hand the removal of water formed as by-product in method 2, by using anhydrous salt helps in build up of molecular weight. Further, the formation of diphenoquinones if any, as explained in the introduction section, is removed by addition of small amounts of hydrazine.

The density of the polymer PPO1 is also smaller than that for PPO2. This is due to the less efficient packing of the polymer chains in polymers with low molecular weight whereas they are better packed in high molecular weight polymers. In the case of PPO2 the chain segments are more or less equally rigid as that of PPO1, as found from glass transition temperature (T_g). T_g is characteristic property of a polymer. The mechanical (tensile) properties exhibit a considerable improvement in the tensile strength and % elongation at break with increase in molecular weight, which is due to increase in chain length which builds up load bearing property and improve plastic deformations.

Thus the 2, 6-dimethyl-1, 4-phenylene oxide prepared in two different ways were found to give differing properties. This is due to the differences in reactivity of the monomer in the two cases under the conditions mentioned. Method 2 appears to be reasonably efficient in reducing the by products during the oxidative polymerisation so that the monomers are more efficiently used in polymer formation without wastage.

Table 2
Physical properties of polymers

Polymer	Intrinsic viscosity (dl/g)	T _g (°C)	Density (g/cm ³)	Tensile properties	
				Tensile strength (MPa)	Elongation at break (%)
PPO (Method 1)	0.310	212	1.05	39	16
PPO (Method2)	0.542	215	1.07	98	51

4. CONCLUSIONS

The 2,6-dimethyl-1,4-phenylene oxide prepared in two different ways were found to give differing properties. This is due to the differences in reactivity of the monomer in the two cases under the conditions mentioned. Method 2 appears to be reasonably efficient in reducing the by products during the oxidative polymerisation so that the monomers are more efficiently used in polymer formation without wastage. PPO2 was found to have higher molecular weight than PPO1. Further PPO2 has better mechanical properties than PPO1. Thus method 2 can be suggested as the best method in the preparation of polyphenylene oxide polymers. The research study reveals methodology for tailoring properties of polyphenylene oxides to suit various applications by controlling factors which critically control polymerisation, such as, the time, temperature, catalyst, use of anhydrous salts and of hydrazines.

REFERENCES

- [1] N. M. Bikales, *Concise Encyclopedia of Polymer science and Engineering*, (New York, John Wiley and Sons, 1990) 870, 1068.
- [2] F. M. Herman, G. G. Norman and M. B. Norbert, *Encyclopedia of Polymer Science and Technology*, (New York, John Wiley & Sons, 1969) 10.
- [3] R. A. Abramovitch, *Organic Preparation Proceeding International*, 23, 1991, 685.
- [4] W. H. Hunter, A. O. Olson and E. A. Daniels, *Journal of American Chemical Society*, 38, 1916, 1761.
- [5] T. W. G. Solomons, *Organic chemistry*, John Willey & Sons Inc, 6th Edition, 1996, 963, 966.
- [6] M. J. S. Dewar and A. N. James, *Journal of American Chemical Society*, 917, 1958, 20.
- [7] G. D. Staffin, C. C. Price, *Journal of American Chemical Society*, 82, 1960, 3632.
- [8] A. S. Hay, *Journal of Polymer Science*, 58, 1962, 581.
- [9] H. S. Blanchard, H. L. Finkbeiner and G. A. Russell, *Journal of Polymer Science*, 58, 1962, 469.
- [10] J. F. Harrod, *Canadian Journal of Chemistry*, 47 (4), 1969, 637.
- [11] S. Percec and G. Li, Chemical reactions on polymers, *ACS symposium series*, 364, 1988, 46.
- [12] C. Pugh and V. Percec, *Polymer Bulletin*, 16 (6), 1986, 513.
- [13] L. Wu, T. Xu, D. Wu and X. Zeng, *Journal of Membrane science*, 310 (1-2), 2008, 577.
- [14] A. Sosnik and D. Cohn, *Biomaterials*, 25 (14), 2004, 2851.
- [15] A. S. Hay, *Progress in Polymer Science*, 24 (1), 1999, 45.
- [16] J. Brandrup and E. H. Immergut, *Polymer Handbook*, 4 (New York: Wiley Interscience Publications, John Wiley and Sons, 1974) 23.
- [17] A. S. Hay, Poly (2,6-diphenyl-1,4-phenylene oxide), *Macromolecules*, 2, 1969, 107.

Index based Information Retrieval System

Ambesh Negi¹, Mayur Bhirud¹, Dr. Suresh Jain², Mr. Amit Mittal³

¹PG Scholar, IET DAVV, Indore

²Director, KCBTA, Indore

³Assistant professor, IET, Indore

Abstract: Information retrieval system based on keyword searching deals with a very large search space as documents to be searched can be of any length and thus time to search in a whole document is also proportional to length of documents i.e. number of words in all documents.

By reducing this large search space search time can also be reduced. In this paper we are proposing a method which reduces the search space with the help of indexing that uses concept of stemming and knowledge of stopwords. Indices are created for single terms and phrases both so that a single concept whether it is represented by a word or more than one word can be treated as required. Our search method uses ontology to incorporate domain knowledge while searching and thus improves the recall.

Keywords: Information Retrieval, Indexing, Keyword searching, query, search space, ontology.

I. INTRODUCTION

Information retrieval deals with the storage and representation of knowledge and the retrieval of information relevant to a specific user problem. Information retrieval systems respond to queries which are typically composed of a few words taken from a natural language. The query is compared to document representations which were extracted during the indexing phase. The most similar documents are presented to the users who can evaluate the relevance with respect to their information needs and problems.

Many previous retrieval systems based on keyword searching represent documents and queries by the words they contain and base the comparison on no. of words they have in common. The more the words the query and document have in common, the higher the document is relevant. This refers to as coordination match but there are few problems in this approach. first is that a word in a document can appear in many lexical forms for an example word information can have multiple forms as inform, informed, informing etc. in the keyword matching approach if you want to search word inform, then it should be spelled same although informed and informing could be of use. Second problem is that query words have to be matched with a bag of words* representing their respective

documents which is very cumbersome task. Another problem is that if words in the query do not appear in the documents there will be a no match situation arise so we need to somehow increase our recall**.

These problems can be solved by removing unuseful words from search space which are called stopwords. Using a proper stemming algorithm can solve multiple form problems. Also using some domain knowledge and ontology we could add recall to our system by query expansion.

With this idea in mind, we designed a system which uses a standard stemming algorithm, some ontology using domain knowledge and a proper retrieval approach that performs a ranked retrieval on documents based on user query. Also the retrieval is done term based and phrase based separately as a phrase can also be an important term consisting of multiple words.

* Bag of words contains almost each word of document except only stop words

** Recall means fraction of relevant documents that are retrieved.

The structure of this paper is as follows. A brief review of previous research is presented in Section 2, followed by Proposed method in section 3. Section 4 by a description of results. Finally, Section 5 covers conclusions and future work.

II. LITERATURE SURVEY

Many keyword based search has been performed where pros and cons of the approach and integration of it with many of the well known approaches has been carried out some of the important are discussed here.

Rajasekar Krishnamurthy Sriram Raghavan Shivakumar Vaithyanathan Huaiyu Zhu [1] address the problem of building a retrieval system that is specifically targeted to answer search tasks that fit the above description (hereafter referred to as precision-oriented search tasks).

Baid, A.; Rae, I.; AnHai Doan; Naughton, J.F.[2] gave basic idea which is to produce answers as in today's KWS systems up to the time limit, then show users these answers as well as query forms that characterize the unexplored portion of the answer space. Finally, they present some

preliminary experiments over real-world data to demonstrate the feasibility of the proposed solution approach.

In the paper Research on Ontology-Driven Information Retrieval Stein L. Tomassen Department of Computer and Information Science, Norwegian University of Technology and Science, NO-7491 Trondheim, Norway examines how ontologies can be efficiently applied to large-scale search systems for the web. We describe how these systems can be enriched with adapted ontologies to provide both an in-depth understanding of the user's needs as well as an easy integration with standard vector-space retrieval systems. The ontology concepts are adapted to the domain terminology by computing a feature vector for each concept.

Many researchers have compared the effectiveness between manual and automatic indexing techniques. Manual indices were often presumed to be better than machine generated indices. However, it has been demonstrated that both indexing techniques are equally effective for text retrieval [Salton][3]. The retrieval performance were also showed positive improvement if both techniques were combined compared to individual indexing [Rajashekar & Croft].[4]

III. PROPOSED METHOD

We proposed here the term based and phrase based text retrieval process consisting of following phases:

Indexing:

Preprocessing of document: Raw documents must be converted into bag of terms representation. These expressions are some times called document representatives. To make these representatives for each document we first collect the words and create the file containing words except the stop words, then we stem the words with in a file thus we have all the terms important to our search in their root forms.

After this we count the frequency of each word and the word having frequency above a threshold (based on a formula consisting file size) is selected as an index term. Collection of all such terms creates our index table (document representative) for that document.

Same process will be repeated for phrase based search but the difference is that all work will be done on phrases identified by a phrase identification program which identify phrases by counting their frequencies; phrase having a suitable count will be selected for processing. Thus an index table will be generated containing phrases as its indices.

Query formulation:

First step here is to expand the query based on domain knowledge (in our case computer science subjects) stored in the form of ontological structure as a tree. Query words are searched in the tree and their parent; children and siblings

words are added in the query. Now what is the significance of adding these words? Answer is that they represent similar (in case of siblings) and relative (in case of parent, child) concepts which would increase our recall while searched against documents.

Second step is to apply the Preprocessing approach described above to the query, thus we reduce our query in the form identical to our document representative.

Same process will be repeated for phrase based search as we use a separate phrasal query to search against document representatives based on phrases.

Comparison:

The system compares the user query to the stored document representatives, and makes a classification decision about which documents to retrieve and in what order. Documents or parts of documents are displayed. Before searching user can select whether he wants to expand the query using tree or not.

This comparison is carried out on the basis of matrix multiplication approach in which document representatives are converted into an id by term matrix (where no. of terms equal to all terms together in all documents and id means file id assigned initially) and a matrix is generated for query terms. Multiplication of both provides necessary result to identify which document is more relevant to the query. Mathematically it can be shown as:

Consider there are 2 documents (i and j) represented as:

$$\begin{aligned} \text{Doc (i)} &= (\text{Term (i1)}, \text{Term (i2)}, \dots, \text{Term (ik)}) \\ \text{Doc (j)} &= (\text{Term (j1)}, \text{Term (j2)}, \dots, \text{Term (jl)}) \end{aligned}$$

Where k and l are no. of terms in respective documents.

So, all terms for all documents together can be represented as =

$$\begin{aligned} &[\text{Term (i1)}, \text{Term (i2)}, \dots, \text{Term (ik)}] \cup [\text{Term (j1)}, \text{Term (j2)}, \dots, \text{Term (jl)}] \\ &- [\text{Term (i1)}, \text{Term (i2)}, \dots, \text{Term (ik)}] \cap [\text{Term (j1)}, \text{Term (j2)}, \dots, \text{Term (jl)}] \\ &= [(\text{Term (1)}, \text{Term (2)}, \dots, \text{Term (n)})] \end{aligned}$$

i.e. Term(1)...Term(n) = all distinct terms of both documents i and j.

Our comparison is based on weighted values and implication of inverted document frequency (IDF):

- Weight is how many times a term appeared in document. So weight implies how relevant the term is for that particular document
- IDF is inverse document frequency calculated for incorporating measure that favors terms which occur in fewer documents. The fewer documents a term occurs in, the higher this weight.

- Thus this weight*IDF factor together will show a greater value if terms are important to document.

Id by terms matrix generation-

- Calculate weight of each term in all term list.
- Calculate Idf factor for each term in document under processing as:
 $Idf(i) = N/n_i$; where (N = no. of documents in repository, n_i = No. of document in which term i occurred)
- Calculate $W(i) = \text{weight} * Idf(i)$ for each term in the list
 Now we will create (id X term) matrix as
- put W of term where there is match in all term list and doc id list
- put 0 where there is mismatch in all term list and doc id list

Query terms matrix generation-

- it will be a single row matrix in which we-
- When there is match in all term and query terms list
- put $10 * idf$ if tree is not selected (query is not expanded and word matched in original query).
- put $5 * idf$ if tree is selected and term matched is in the real query (query is expanded and word matched in original query).
- put $1 * idf$ if tree is selected and term matched is in the expanded query (query is expanded and word is not matched in original query).
- Finally put 0 where there is mismatch in all term list and query terms list
- This variation in first 3 weights is to incorporate the importance of a term if it is matched in a query and doesn't need to be expanded.

Result matrix and comparison-

- Multiplication of above two matrix (id by term) and (query term) matrix will give a column matrix containing 0 in its row if there is a no word match in that particular file(having id same as row no.) and an integer value showing how many word have matched.
- We can decide order of comparison by sorting results in descending order, thus file id having the most matches is at the top and lesser matches at their subsequent lower places.

IV. RESULT

We have tested our system on sample domain of computer science containing books of chapters and we are able to reduce the number of words to be searched in the file, thereby minimizing the search space. This effectively reduces the searching time as well. Reduction causes search spaces to be reduced more than 90% as our formula for selecting high frequency words finally used for index creation selects only such amount of words.

There are two type of comparisons are also performed which affects the search results. This are-

- Search using ontology or without it.
- Phrase based vs. term based search

In the first comparison using ontology recall increases more than 70% than without ontology if user enters words related to our domain in the query.

In the second comparison term based approach's results turned out be less relevant to the query in comparison to phrase based approach. For an example query operating system would fetch file system file as most relevant document while other would fetch operating system concept file as most relevant which is logically correct. This is because former approach uses both word operating and system as distinct term while later treats them as single. But recall in term based approach would be more as there are more terms to find out in the repository, also in case of single word query only term based approach would fetch a result.

Also second comparison may enjoy the benefits of using ontology in both case and hence can improve recall.

Although our searching method takes some time to index and then search the query but it reduces time of overall search in comparison to time required to search a document as a whole. By varying threshold of index creation we can vary the no. of words in document descriptive i.e. index table. We have also found that threshold value above a particular limit can eliminate some important words which is not desirable for our search. This limit depends upon the size of the documents we are using in our system.

V. CONCLUSION

In this paper we have described a technique which uses the concept of stemming so that a word can be searched using its root form and hence no need to be worried about query word's lexical forms. It also reduces search space by removing stopwords which are not helpful in search. . By varying threshold of index creation we can vary the no. of words in document descriptive i.e. index table. Our matrix multiplication approach finds out comparative results as which file are more relevant to the query and thus useful in ranked retrieval of documents. Use of ontology made a 70% recall for our system. Using phrase based approach with traditional term based approach we are able to increase relevancy between query and the result opted by user. Thus it shows an easy and fast approach to information retrieval.

VI. FUTURE WORK

We are currently in the process of attaching semantic meaning to this IR system both in query as well as documents.

We will try to have an Information retrieval system that adds word semantics to the classic word based indexing. Two of the main tasks of our system would be, the indexing and retrieval components, which will use a combined word based and sense-based approach. Main focus of our system would be a methodology for building semantic representations of open text, at word and collocation level. Also using ontology we will try to incorporate different relationships like is-a, has-a, part-of etc and make use of domain knowledge to make efficient search. Thus

incorporating semantic indexing approach with improved keyword based search approach overall efficiency of IR system can be improved.

VII. REFERENCES

- [1] Using Structured Queries for Keyword Information Retrieval; Rajasekar Krishnamurthy Sriram Raghavan Shiva Kumar Vaithyanathan Huaiyu Zhu IBM Almaden Research Center, San Jose, CA 95120
- [2] Toward industrial-strength keyword search systems over relational data; Baid, A.; Rae, I.; Anhai Doan; Naughton, J.F.; Comput. Sci. Dept., Univ. of Wisconsin, Madison, WI, USA.
- [3] Callan, J. P. and W. Bruce Croft. An Evaluation of Query Processing Strategies using TIPSTER collection. In Proceedings of ACM SIGIR International Conference on Research and Development in Information Retrieval, 347-356, 1993.
- [4] Rajashekar, T. B. and W. Bruce Croft. Combining Automatic and Manual Index Representations in Probabilistic Retrieval. Journal of the American Society for Information Science: 46(4), 272-283, 1995.
- [5] Salton, G. Automatic Text processing. Addison-Wesley Publishing Company, Reading, MA: 1989.

Heuristic Search Procedures for Cryptanalysis and Development of Enhanced Cryptographic Techniques

Rajashekarappa¹, Dr. K M S Soyjaudah²

*(Dept. of Computer Science and Engineering, JSS Academy of Technical Education Mauritius, Avenue Droopnath Ramphul, Bonne Terre, Vacoas, Mauritius)

**(Dept. of Electrical and Electronic Engineering, University of Mauritius, Reduit, Mauritius)

ABSTRACT

Cryptography is a thriving research area of great practical importance. It is a fundamental building block of communications security. Cryptographic techniques currently being utilized in the field of communication. This paper presents an approach for the heuristic search procedures for cryptanalysis and development of enhanced cryptographic techniques. To implement the proposed Tabu search, Genetic, and Simulated Annealing algorithms firstly by utilising cipher text as well as some plain text and secondly by using only the cipher text to retrieve the original data. The cryptanalysis of simplified data encryption standard can be formulated as NP-Hard combinatorial problem. The goal of this paper is to comparison between Tabu Search, Genetic Algorithm and simulated annealing were made in order to investigate the performance for the cryptanalysis on SDES. The methods were tested and extensive computational results show that Tabu Search algorithm performs better than Genetic algorithm and simulated annealing for such type of NP-Hard combinatorial problem.

Keywords: Genetic Algorithm, Key search space, Simplified data encryption standard, Simulated annealing, Tabu Search algorithm.

I. INTRODUCTION

Cryptography is the science of hiding information. It is now a part of the computer science formally, though first cryptographers appeared thousands years before the computer. The art of recovery of the hidden information, or cryptanalysis, appeared in the very beginning, and is still one of the most intriguing part of cryptography.

Cryptanalysis starts with a search for a weakness in a cryptosystem, for a flaw that was missed by its designer. An encrypted message must not reveal any information about its origin, so the cryptosystem must make it look as random as possible. Any mistake, any missed property may become a target for a cryptanalyst and a starting point for a compromise of the cryptosystem's security a break.

This survey is devoted to the cryptanalysis of symmetric primitives. Historically, by a symmetric encryption we understand that all the parties have the same information needed for encryption and decryption, with block and stream ciphers as the most famous examples. A block cipher

transforms a large block of data with an algorithm parameterized by a secret key. A stream cipher expands a secret key into arbitrarily long sequence, which is mixed with a data stream. Cryptanalysis is the art of analyzing ciphertext to extract the plaintext or the key. In other words, cryptanalysis is the opposite of cryptography. It is the breaking of ciphers. Understanding the process of code breaking is very important when designing any encryption system. The science of cryptography has kept up with the technological explosion of the last half of the 20th century. Current systems require very powerful computer systems to break the code or cryptanalyse most ciphers. While cryptanalysis has improved as well, some systems may exist that are unbreakable by today's standards.

The substitution ciphers are easy to break. Before computers were available, expert cryptanalysts would look at ciphertext and make guesses as to which letters were substituted for which other letters. Early cryptanalysis techniques included computing the frequency with which letters occur in the language that is being intercepted. For example, in the English language, the letters e, s, t, a, m, and n occur much more frequently than do q, z, x, y, and w. So, cryptanalysts look at the ciphertext for the most frequently occurring letters and assign them as candidates to be e, s, t, a, m, and n. Cryptanalysts also know that certain combinations of letters are more common in the English language than others are. For example, q and u occur together, and so do t and h. The frequency and combinations of letters help cryptanalysts build a table of possible solution letters. The more cipher text that is available, the better the chances of breaking the code.

Of the different categories of attacks such as ciphertext only attack, known plaintext, chosen plaintext, chosen ciphertext; ciphertext only attack is a harder one and thus we consider one such attack in this paper.

The objective of the study is to determine the efficiency and accuracy of Tabu Search algorithm for the cryptanalysis of SDES[6]. To compare the relative performance of Genetic algorithm, Simulated Annealing with tabu search.

The rest of the paper is organized as follows: Section 2 presents the literature review. Section 3 gives a brief overview of S-DES, Section 4 gives the overview of Tabu Search and Section 5 gives the algorithm of Simulated Annealing and Genetic Algorithm. Experimental results are

discussed in Section 6. Section 7 concludes the paper and Future works.

II. RELATED WORK

The proposed work will require an in depth understanding of the area of cryptography and enable the development of general as well as specific algorithms for cryptanalysis[1]. Moreover, the enciphering algorithms developed in this work will find many real time applications in military, banking and other sectors where secure transmission is essential. A cipher takes a message text and some secret keying data (known as the key) as its input and produces an encrypted version of the original message, (known as the cipher text). An attack on a cipher can make use of the cipher text alone or it can make use of some plaintext and its corresponding cipher text (referred to as a known plaintext attack) (Andrew John Clark, 1998).

Cryptanalysis is the process of recovering the plaintext and/or key from a cipher. Many cryptographic systems have a finite key space and, hence, are vulnerable to an exhaustive key search attack. Yet, these systems remain secure from such an attack because the size of the key space is such that the time and resources required for a search are prohibitive.

A random search through a finite but large key space is not usually an acceptable cryptanalysts tool. Massoudi et al. (2008) explored the possibility of using a random type search to break a cipher. The focus of their work was on the use of a genetic algorithm to conduct a directed random search of a key space[2]. The ability to add direction to what seems to be a random search is a feature of genetic algorithms which suggests that it may be possible to conduct an efficient search of a large key space (Ayman M. B. Albassal, Abdel-Moneim A. Wahdan, 2004). In fact, carefully tailored genetic algorithms can find efficient distinguishers for ciphers much faster than previously reported techniques (Aaron, G et.al (2007), J. C. Hernandez, J.C and Isasi, P (2004))[3][4].

An interesting survey of the application of evolutionary computation algorithms such as Genetic algorithm, simulated annealing and tabu search to provide a robust and efficient methodology for cryptanalysis, was conducted by (Garg, P. (2010))[5].

III. THE S-DES ALGORITHM

This section briefly gives the overview of S-DES Algorithm. The SDES encryption algorithm takes an 8-bit block of plaintext and a 10-bit key as input and produces an 8-bit block of ciphertext as output. The decryption algorithm takes an 8-bit block of ciphertext and the same 10-bit key used for encryption as input and produces the original 8-bit block of plaintext as output. The encryption algorithm uses five basic functions: 1. An initial permutation (IP). 2. A complex function called fK which involves both permutation and substitution operations and depends on a key input 3. A simple permutation function (SW) that

switches the two halves of the data. 4. The function fK a TS in and 5. A permutation function that is the inverse of the initial permutation (IP^{-1}). The function fK takes as input the data passing through the encryption algorithm and an 8-bit key[9].

A. Key Generation

For key generation, a 10-bit key is considered from which two 8-bit sub keys are generated. In this case, the Key is first subjected to a permutation $P_{10} = [3\ 5\ 2\ 7\ 4\ 10\ 1\ 9\ 8\ 6]$, then a shift operation is performed. The numbers in the array represent the value of that bit in the original 10-bit key. The output of the shift operation then passes through a permutation function that produces an 8-bit output $P_8 = [6\ 3\ 7\ 4\ 8\ 5\ 10\ 9]$ for the first sub key (K1). The output of the shift operation also feeds into another shift operation and another instance of P_8 to produce the second sub key K2. In all bit strings, the leftmost position corresponds to the first bit. The block schematic of the S-DES Key generation algorithm is shown in Fig. 1.

B. Encryption Algorithm

The block schematic of the SDES encryption algorithm is shown in Fig. 2. The Encryption process involves the sequential application of five functions:

1. Initial and final permutation (IP): The input to the algorithm is an 8-bit block of plaintext, which is first permuted using the IP function $IP = [2\ 6\ 3\ 1\ 4\ 8\ 5\ 7]$. This retains all 8-bits of the plaintext but mixes them up. At the end of the algorithm, the inverse permutation is applied; the inverse permutation is done by applying, $IP^{-1} = [4\ 1\ 3\ 5\ 7\ 2\ 8\ 6]$ Where, $IP^{-1}(IP(X)) = X$.

2. Function fK:

The function fK, which is the complex component of S-DES, consists of a combination of permutation and substitution functions. The functions are given as follows: $fK(L, R) = (L \text{ XOR } f(R, \text{key}), R)$ where, L, R be the left 4-bits and right 4-bits of the input, XOR is the exclusive-OR operation and key is a sub -key. Computation of $f(R, \text{key})$ is done as follows.

i. Apply expansion/permutation
 $E/P = [4\ 1\ 2\ 3\ 2\ 3\ 4\ 1]$ to input 4-bits.

ii. Add the 8-bit key (XOR).

iii. Pass the left 4-bits through S-Box S_0 and the right 4-bits through S-Box S_1 .

iv. Apply permutation $P_4 = [2\ 4\ 3\ 1]$.

The two S-boxes are defined as follows:

S_0	S_1
1032	0123
3210	2013
0213	3010
3132	2103

The S-boxes operate as follows: The first and fourth input bits are treated as 2-bit numbers that specify a row of the S-box and the second and third input bits specify a column of the S box. The entry in that row and column in base 2 is the 2-bit output.

3. The Switch Function (SW):

Since the function fK allows only the leftmost 4-bits of the input, the switch function (SW) interchanges the left and right 4-bits so that the second instance of fK operates on different 4-bits. In this second instance, the E/P, S0,S1 and P4 functions are the same as above but the key input is K2[11].

IV. TABU SEARCH

Tabu search is a widely used meta heuristic that uses some common-sense ideas to enable the search process to escape from a local optimum[8].

Any application of tabu search includes as a subroutine a local search procedure that seems appropriate for the problem being addressed. A local search procedure operates just like a local improvement procedure except that it may not require that each new trial solution must be better than the preceding trial solution. The process begins by using this procedure as a local improvement procedure in the usual way (i.e, only accepting an improved solution at each iteration) to find a local optimum. A key strategy of tabu search is that it then continues the search by allowing non-improving moves to the best solutions in the neighborhood of the local optimum[8]. Once a point is reached where better solutions can be found in the neighborhood of the current trial solution, the local improvement procedure is reapplied to find a new local optimum.

This use of memory to guide the search by using tabu lists to record some of the recent history of the search is a distinctive feature of tabu search. This feature has roots in the field of artificial intelligence[12].

Long term memory is used to help implement both concepts. However, we will focus on the basic form of tabu search summarized below without delving into these additional concepts [9].

Outline of a Basic Tabu Search Algorithm

Initialization: Start with a feasible initial trial solution.

Iteration: Use an appropriate local search procedure to define the feasible moves into the local neighborhood of the current trial solution. Eliminate from consideration any move on the current tabu list unless that move would result in a better solution than the best trial solution found so far. Determine which of the remaining moves provides the best solution. Adopt this solution as the next trial solution, regardless of whether it is better or worse than the current trial solution. Update the tabu list to forbid cycling back to what had been the current trial solution. If the tabu list already had been full, delete the oldest member of the tabu list to provide more flexibility for future moves[10].

Cost function: The ability of directing the random search process of the tabu search by selecting the fittest chromosomes among the population is the main characteristic of the algorithm. So the fitness function is the main factor of the algorithm. The choice of fitness measure depends entirely on the language characteristics must be known. The tabu search technique used to find candidate key is to compare n-gram statistics of the decrypted message with those of the language(which are assumed known). Equation 1 is a general formula used to determine the suitability of a proposed key(k), here, K is known as language Statistics i.e., for English, [A,.....,Z],D is the decrypted message statistics, and u/b/t are the unigram, bigram and trigram statistics. The values of α , β and γ allow assigning of different weights to each of the three n-gram types where $\alpha + \beta + \gamma = 1$.

$$C_k \approx \alpha \cdot \sum_{i \in A} |K^u_{(i)} - D^u_{(i)}| + \beta \cdot \sum_{i,j \in A} |K^b_{(i,j)} - D^b_{(i,j)}| + \gamma \cdot \sum_{i,j,k \in A} |K^t_{(i,j,k)} - D^t_{(i,j,k)}| - - - (1)$$

When trigram statistics are used, the complexity of equation(1) is $O(P^3)$ where P is the alphabet size. So it is an expensive task to calculate the trigram statistics. Hence we will use assessment function based on bigram statistics only. Equation 1 is used as fitness function for tabu search attack. The known language statistics are available in the literature [7].

The tabu search [7] prevents the search from returning to a previously explored region of the solution space too quickly. This is achieved by retaining a list of possible solutions that have been previously encountered. These solutions are called 'tabu'; hence the name of the technique. The size of the tabu list influences the performance of the algorithm. In each iteration, the best new key formed replaces the worst existing one in the tabu list.

The algorithm is presented as below.

1. Input: Intercepted ciphertext, the key size P, and the language statistics.

2. Initialise parameters: The size of the tabu list STABU, the size of the list of possibilities considered in each iteration SPOSS, and the maximum number of iterations MAX.

3. Initialise: The tabu list with random and distinct keys and calculate the cost for each key in the tabu list.

4. For I=1,..., MAX do:

a. Find the best key with the lowest cost in the current tabulist, KBEST.

- b. For $j=1, \dots, SPOSS$ do:
- i. apply the perturbation mechanism to produce a new key KNEW.
 - ii. Check if KNEW is already in the list of possibilities generated for this iteration or the tabu list. If so, return to step 4(b) i.
 - iii. Add KNEW to the list of possibilities for this iteration.
- c. From the list of possibilities for this iteration, find the key with the lowest cost, PBEST.
- d. From the tabu list, find the key with the highest cost, TWORST.
- e. While the cost of PBEST is less than the cost of TWORST:
- i. Replace TWORST with PBEST.
 - ii. Find the new PBEST.
 - iii. Find the new TWORST.

5. Output the best solution from the tabu list, KBEST (the one with the least cost).

An important distinction in TS arises by differentiating between short term memory and longer term memory. Each type of memory is accompanied by its own special strategies. However, the effect of both types of memory may be viewed as modifying the neighborhood $N(x)$ of the current solution x . The modified neighborhood, which we denote by $N^*(x)$, is the result of maintaining a selective history of the states encountered during the search [13].

In the TS strategies based on short term considerations, $N^*(x)$ characteristically is a subset of $N(x)$, and the tabu classification serves to identify elements of $N(x)$ excluded from $N^*(x)$. In TS strategies that include longer term considerations, $N^*(x)$ may also be expanded to include solutions not ordinarily found in $N(x)$. Characterized in this way, TS may be viewed as a dynamic neighborhood method. Characteristically, a TS process based strictly on short term strategies may allow a solution x to be visited more than once, but it is likely that the corresponding reduced neighborhood $N^*(x)$ will be different each time.

Simulated Annealing

Annealing is the process of slowly cooling a heated metal in order to attain a minimum energy state. The idea of mimicking the annealing process has been efficiently exploited by Kirkpatrick et al. [14] to solve combinatorial optimization problems. The algorithm is initialized with a random solution to the problem being solved and a starting temperature T_0 . The temperature is slowly decreased and at each temperature, a number of attempts are made to perturb the current solution. At each perturbed temperature, a change in the cost function ΔE is determined. If $\Delta E < 0$, then the proposed perturbation is accepted; otherwise it is accepted with a probability indicated by the Metropolis equation given by Probability ($E_1 \rightarrow E_2$) = $e^{(-\Delta E/T)}$, where E_1 and E_2 are the cost functions, ΔE is the change in cost function and T is the current temperature. If the proposed change is accepted, then the current solution is updated. The

temperature is reduced when a predefined number of attempts have been made to update the current solution. Possibilities of termination are when a certain minimum temperature is reached or a certain number of temperature reductions have occurred; or the current solution has not changed for a number of iterations. The Simulated Annealing algorithm is presented as below:

1. Set the initial temperature, $T^{(0)}$.
2. Generate an initial solution - arbitrarily set to the identity transformation (could be randomly generated or otherwise).
3. Evaluate the cost function for the initial solution. Call this $C^{(0)}$.
4. For temperature T do many (eg., $100 \times M$) times:

Generate a new solution by modifying the current one in some manner. Evaluate the cost function for the newly proposed solution. Consult the Metropolis function to decide whether or not the newly proposed solution will be accepted. If accepted, update the current solution and its associated cost. If the number of accepted transitions for temperature T exceeds some limit (eg. $10 \times M$) then jump to Step 5.
5. If the number of accepted transitions for temperature T was zero then stop (return the current solution as the best), otherwise reduce the temperature (eg. $T^{(i+1)} = T^i \times 0.95$) and return to step 4.

Genetic Algorithm for Cryptanalysis:

A genetic algorithm [4] is a search heuristic inspired by biological evolution. The basic GA algorithm involves the generation of a population of possible solutions, evaluation of the solutions according to a fitness function, selection of a set of fit "parent" solutions, and finally reproduction of those parents to generate a new population of possible solutions.

1. Input: Intercepted ciphertext, and the language statistics.
2. Initialise the algorithm parameters: the solution pool size M and the maximum number of iterations MAX .
3. Randomly generate an initial pool of solutions P_{CURR} , and calculate the cost of each of the solutions in the pool.
4. For $I=1 \dots MAX$ do:
 - a. Select $M/2$ pairs of keys from P_{CURR} to be the parents of the new generation.
 - b. Perform the mating operation on each of the pairs of parents to produce a new pool of solutions P_{NEW} .
 - c. For each of the M children, perform a mutation operation.
 - d. Calculate the cost associated with each of the keys in the new solution pool P_{NEW} .
 - e. Sort P_{NEW} from the most suitable (the least cost) to the least suitable (the most cost).
 - f. Merge P_{CURR} with P_{NEW} to give a list of sorted solutions (discard duplicates). Choose the best M keys to become the new current pool P_{CURR} .
5. Output the best solution from P_{CURR} .

V. EXPERIMENTAL SETUP AND RESULTS

Number of experiments is carried out to outline the effectiveness of Tabu Search. The Tabu Search algorithm is coded in MATLAB 7, and tested on more than 100 benchmark data sets adapted. Among the unigrams, bigrams and trigrams, Unigram is more useful and the benefit of trigram over digram is small.

Table. 1 shows the Comparative Results of Genetic Algorithm, Simulated Annealing and Tabu Search. In this section a number of experiments are carried out which outlines the effectiveness of all three algorithm described above. The purpose of these experiments is to compare the performance of Genetic algorithm, Simulated Annealing algorithm approach with tabu search approach for the cryptanalysis of simplified SDES algorithm. The experiments were implemented in MATLAB 7 on a Pentium IV(1.83 Ghtz). Experimental results obtained from these algorithms were generated with 200 runs per data point e.g. twenty different messages were created for all the algorithms and each algorithm was run 80 times per message. The best result for each message was averaged to produce data point.

This table 1 shows the average number of key elements (out of 10) correctly recovered versus the amount of cipher text and the computation time to recover the keys from the search space. The table shows results for amounts of cipher text ranging from 100 to 1000 character.

VI. CONCLUSION AND FUTURE WORK

Heuristic-based optimisation techniques have been finding recent application in attack of ciphers. This paper presents for the first time such a study for the attack of block ciphers. Tabu Search for the cryptanalysis of Simplified Data Encryption Standard is presented. The time complexity of the proposed approach has been reduced drastically when compared to the Genetic Algorithm, and Simulated Annealing Algorithm. Though SDES is a simple encryption algorithm, this is a promising method and can be adopted to handle other complex block ciphers like DES and AES. The cost function values used here can be applied for other block ciphers also. A simple heuristic for the attack of known ciphertext with a pair of them has been developed to retrieve the plaintext to almost 90% accuracy for a SDES 10-bit key. It is envisaged that the results reported in this paper will be useful for the attack of other stream and block ciphers; and also in solving a class of heuristic-based optimisation problems.

The second comparison was made upon the period of transposition cipher. It was found that the tabu search is most powerful to find the correct solution. Result indicates that tabu search is extremely powerful technique for attacking SDES. The future works are extending this approach for attacking DES and AES ciphers

REFERENCES

- [1] Andrew John Clark, *Optimisation Heuristics for Cryptology*, PhD thesis, Information Security Research Centre Faculty of Information Technology Queensland University of Technology, 1998.
- [2] Floreano D., Durr P., and Mattiussi C., *Neuroevolution: From architectures to learning, Evolutionary Intelligence*, 1:47–62, 2008.
- [3] Ayman M. B. Albassal, Abdel-Moneim A. Wahdan, *Genetic Algorithm Cryptanalysis of a Fiestel Type Block Cipher*, International Conference on Electrical, Electronic and Computer Engineering, Egypt, PP. 217–221, 2004.
- [4] Aaron, G., Hamilton, J and Dozier, G, *A Comparison of Genetic Algorithm Techniques for the Cryptanalysis of TEA*, International Journal of Intelligent Control and Systems, 12(4) pp. 325-330, 2007.
- [5] Garg, P, *Evolutionary Computation Algorithms for Cryptanalysis: A Study, (IJCSIS) International Journal of Computer Science and Information Security*, Vol. 7, No. 1, 2010.
- [6] Poonam Garg, Cryptanalysis of SDES via Evolutionary Computation Techniques, *Inter National Journal of Computer Science and Information Security* Vol.1, No.1, May 2009J. Clerk Maxwell, A Treatise on Electricity and Magnetism, 3rd ed., vol. 2. Oxford: Clarendon, 1892, pp.68–73.
- [7] Glover F, Tabu Search — Part I, *ORSA Journal on Computing* 2: 1, 4-32, 1990.
- [8] Frederick S. Hillier, Gerald J. Lieberman, *Introduction to Operations Research Concepts and Cases* (Eighth edition, McGraw- Hill, 2009).
- [9] William Stallings, *Cryptography and Network Security Principles and Practices* (Fourth edition, McGraw-Hill, 2003.M. Young, The Technical Writer's Handbook. Mill Valley, CA: University Science, 1989).
- [10] Behrouz A. Forouzan, *Cryptography and Network Security* (First edition, McGraw- Hill, 2006).
- [11] James Kennedy and Russell Eberhart, Particle Swarm Optimisation, *Proceedings of the IEEE International Conference on Neural Networks*, pp.1942-1948, 1995.
- [12] Laguna M. J. W. Barnes and F. Glover, Intelligent Scheduling with Tabu Search: An Application to Jobs with Linear Delay Penalties and Sequence Dependent Setup Costs and Times, *Journal of Applied Intelligence* Vol.3, pp.159-172, 1993.
- [13] Chanas S. and P. Kobylanski, A New Heuristic Algorithm Solving the Linear Ordering Problem, *Computational Optimization and Applications*, Vol. 6, pp. 191-205, 1996.
- [14] Garg Poonam, Shastri Aditya, Agarwal D. C, Genetic Algorithm, Tabu Search & Simulated annealing Attack on Transposition Cipher, *proceeding of Third AIMS International conference on management at IIMA – 2006*, pg 983-989.

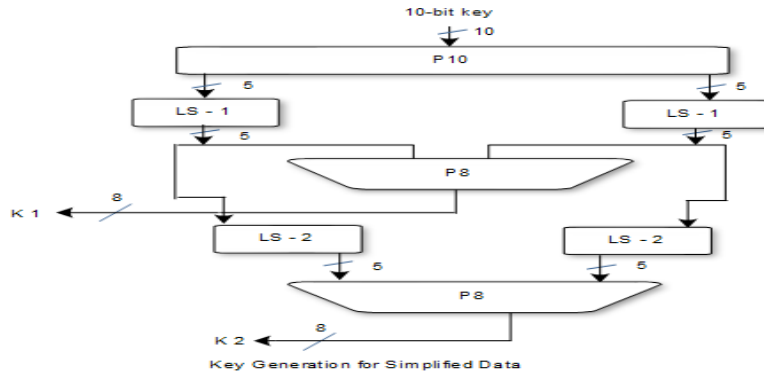


Fig. 1 Key Generation

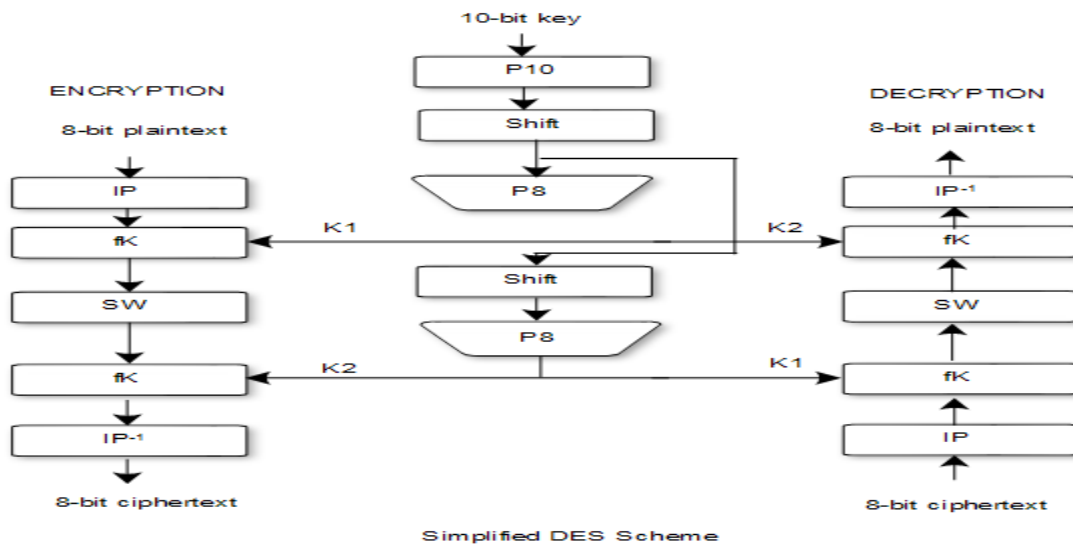


Fig. 2 S-DES Encryption.

Amount of Cipertext	Genetic Algorithm		Simulated Annealing		Tabu Search	
	Time(Minute)	Number of bits matched in the Key	Time(Minute)	Number of bits matched in the Key	Time(Minute)	Number of bits matched in the Key
100	30	3	20.9	4	7.8	6
200	44.3	1	19.7	2	6.6	5
300	22.9	4	11.1	5	8.4	7
400	28.1	3	18.6	6	8.6	7
500	34.5	4	20.3	5	11.4	8
600	65.9	5	13.7	7	10.1	8
700	12.7	2	14.5	4	7.9	7
800	11.3	1	18.9	2	4.4	5
900	70.2	7	10.4	5	8.5	7
1000	38.4	5	15.8	6	11.9	9

Table. 1 The number of bits recovered from the key as compared with Genetic Algorithm, Simulated Annealing and Tabu Search.

A Study of Binary Image Encryption Using Partial Image Encryption Technique

Parameshachari B D¹, Dr. K M S Soyjaudah²

*(Department of Electronics & Communication Engg., JSS Academy of Technical Education, Avenue Droopnath Ramphul, Bonne Terre, Vacoas, Mauritius)

** (Department of Electrical & Electronic Engineering, University of Mauritius, Reduit, Mauritius)

ABSTRACT

Chung and Chang proposed an encryption scheme for binary images based on two-dimensional run-encoding (2DRE) and scan patterns. In this paper, we indicate that their scheme is still not secure and efficient enough. Hence, an improvement scheme is proposed. There are two contributions in the proposed improvement scheme using partial image encryption techniques. One is to scrambling the pixel position and other second is by using SCAN mapping method. Hence, the improvements on encryption time, compression ratio and security are possible.

Keywords: image security, mapping, partial encryption, SCAN, scrambling,

I. INTRODUCTION

With the rapid advance of the computer network, large-sized information such as digital images can be easily transmitted. Therefore, the security of digital images has become an important issue. The traditional cryptology techniques are well defined for the security of textual data, but these techniques are not directly suitable to deal with digital media such as images, audio and video. The main reason is that the size of image data is much greater than the size of textual data. It is necessary to design a low complexity encryption/decryption method according to the properties of images. Hence, many schemes have been proposed especially for binary image encryption (Bourbakis, 1986; Bourbakis, 1992; Chang and Liu, 1994 and Chung and Chang, 1998).

In (Chung and Chang, 1998) Chung and Chang proposed an encryption scheme with higher security for binary images. In their scheme, different scan patterns are placed at the same level in the quadtree structure and then two-dimensional run-encoding (2DRE) is used to compress the encrypted images. Therefore, their scheme has higher security and a better compression ratio than previous research. However, in Chung-Chang's scheme, there are three problems worthy to discuss further.

Time-consuming

Since encryption is prior to compression, the data to be encrypted is still large. Hence, encryption is still more time-consuming. If compression is performed before encryption, the smaller size speeds up the encryption performance.

Compression ratio

When a binary image is encrypted using scan patterns, the more massed the same bits in the binary image, the better the compression ratio. If the scan patterns are uniformly random, the black bits or white bits will not mass and the result after encryption should not be suitable to be compressed. It implies that if the black bits or white bits don't mass after encrypting, the compression ratio will be decreased. Obviously, it is not a good method to encrypt before compression. On the contrary, if compression operation is prior to encryptions, it is possible to further increase compression ratio.

Security

The total number of black and white bits in the plainimage is the same as that in the cipherimage after scan patterns. This condition may disclose some important information. Especially, if a block contains all black or white bits, the result of scan patterns will also be all black or white bits in the cipherimage. This implies that if a cryptanalyst takes a cipherimage with many blocks that contain all black (white) bits, the cryptanalyst will know that those blocks are all black (white) bits in the plainimage. Hence, the cryptanalyst may infer the partial image from those redundancies and use it to break the cipherimage. Furthermore, since cryptanalysis relies on exploiting redundancies in the plainimage, compressing an image before encryption can reduce these redundancies.

In this paper, we propose an improvement scheme for Chung-Chang's scheme to address the problems mentioned above. First, exchange the sequence of compression and encryption. The data redundancy decreases after compression and encryption is then a time-saver process compared with Chung-Chang's. Simultaneously, higher compression ratio of the original image is possible because of the property of high similarity among adjacent pixels that exists in most natural images.

The remainder of the paper is organized as follows. In Section 2, we briefly introduce 2DRE and Chung-Chang's scheme. The proposed improvement scheme is illustrated in Section 3. In Section 4, the experimental results are shown. In Section 5 gives the applications. Finally conclusion is presented in section 6.

II. RELATED WORK

A. Two-Dimensional Run-Encoding (2DRE)

The main concept of 2DRE is counting how many times the same bits successively repeat according to scan order. Thus, we record the first bit of scan order and then save the successively repeated counts according to scan order. This process should be recursively and repeatedly done for the other bits until the end of the image is reached. For example, we have the following bit string:

```
0000000000000000
1111000000001111
0000011111100000
1111111111111111
```

The result of 2DRE according to the row scan order is shown as follows:

```
0 16 4 8 4 5 6 5 16
```

The first position is the initial bit and the others are the counting results. "0" and "1" are interleaving in the string; that is, we have 16 "0", 4, "1", 8, "0" and so on. We need 5 bits to represent each value, because the maximum value in the compressed string is 16. Hence, the total bits of the compressed string is 45 (9×5). Since the original size is 64 bits, the compression ratio is 1.42 (64/45).

There is no doubt that the 2DRE scheme is a good tool to compress binary data, however, a good compression ratio cannot be guaranteed simultaneously. In the following, we show the downside of the 2DRE:

```
1100011000111000
1111000011110001
0000011111000011
0000000000000000
```

The compressed result of the above example is as follows:

```
1 2 3 2 3 3 3 4 4 4 3 1 5 5 4 2 16
```

The total bits of the compressed string are then 85 (17×5), which obviously does not achieve the expectation of the compression.

Fortunately, the property of high similarity among adjacent pixels exists in most natural images, so we can directly utilize the 2DRE technique to compress the natural binary image and the compression ratio is still good.

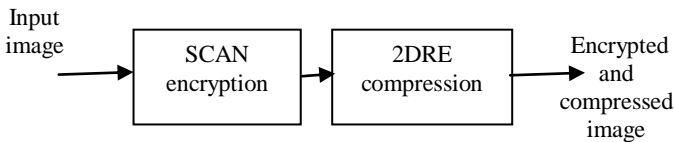
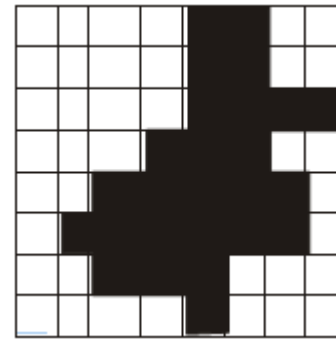


Fig 1: Chung-Chang's Encryption Scheme.



(a)



(b)

Fig 2: (a) 23x23 binary image (b) the corresponding quadtree

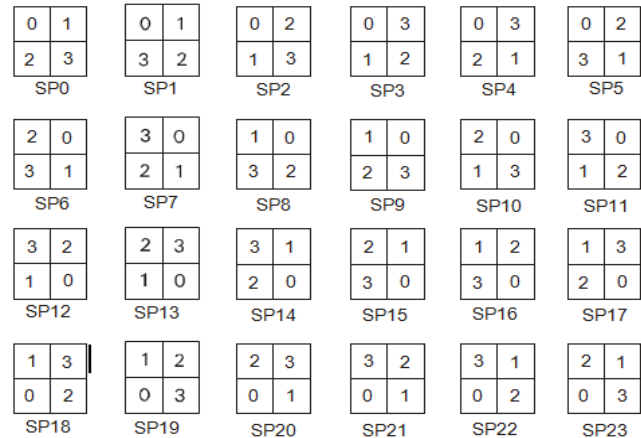


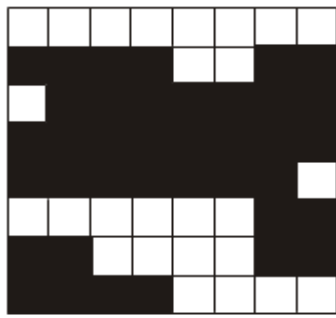
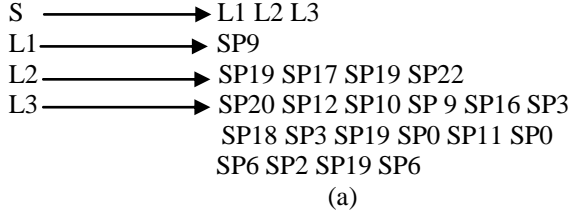
Fig 3: Scan Patterns

The main concept of Chung-Chang's scheme (Chung and Chang, 1998) is shown in Fig. 1. In their scheme, they first use a quadtree to represent a binary image and put different scan patterns at the same level in the scan quadtree structure as encryption. Fig. 2(a) presents a binary image and Fig. 2(b) illustrates the corresponding quadtree hierarchical decomposition. Each block in Fig. 2(a) is represented by one bit of a binary image. The quadtree scheme recursively divides the original image into four uniform parts. Please refer to (Chang and Liu, 1994) for details relating to the quadtree scheme.

The quadtree is then encrypted according to the 24 scan patterns originally defined in (Chung and Chang, 1998) and shown in Fig. 3. SCAN language is used to produce the scan rules shown in Fig. 4(a), where S, Li and SPi are respectively defined as the start symbol, the set of different scan patterns at

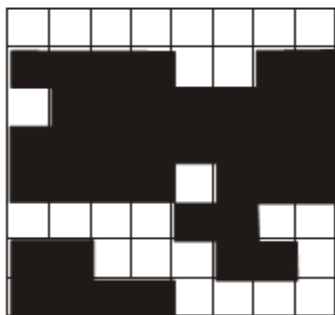
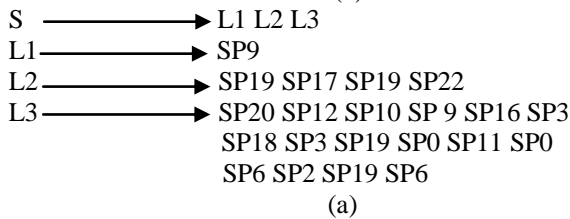
the i^{th} level in the scan quadtree and the i^{th} scan pattern. Interested readers may refer to (Bourbakis, 1986) for more details about SCAN language. Furthermore, the encrypted image can be displayed using the raster scanning method and the result is shown in Fig. 4(b).

The 2DRE technique is used to compress the result of the raster scanning. The size of the original image in Fig. 2(a) is $8 \times 8 = 64$ (bits). However, the result from 2DRE requires only 60 (bits), so the compression ratio is $64/60 = 1.067$.



(b)

Fig 4: (a) SCAN language (b) the encryption result of Fig. 2(b)



(b)

Fig. 5: (a) New SCAN language (b) the encryption result of Fig. 5(b)

Unfortunately, as in 2DRE, the compression ratio cannot be guaranteed. Because the sequence of scan patterns is randomly produced, it is reasonable to arbitrarily change the

sequence. Here we only change two scan patterns, using bold font, in Fig. 4(a) and the result is shown in Fig. 5(a). Fig. 5(b) is the result of encryption. The compression ratio then becomes 0.71 (64/90). On the other hand, if we directly utilize 2DRE for compression, it requires only 54 bits. The compression ratio is 1.185. This fact implies that the locality property of the natural image makes the direct use of 2DRE produce a compressed image with a high compression ratio.

III. THE PROPOSED IMPROVEMENT SCHEME

The 2DRE technique is directly used to compress a binary image before encryption. Because high similarity among adjacent pixels exists in most natural images, we can apply this property to preserve a good compression ratio. A smaller size can also make the encryption process easier and thus reduce the time to encrypt. Three stages are involved in our scheme: (1) employing 2DRE to compress a binary image, (2) employing scan patterns and (3) mapping the image based on SCAN pattern. The Fig.6 illustrates the main concept of the proposed scheme.

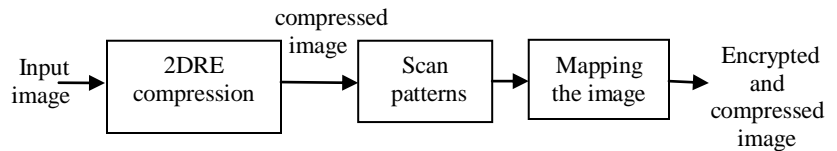


Fig 6: The proposed improvement scheme

Step 1: 2DRE

Because high similarity among adjacent pixels exists (i.e., local property) in most natural images, the compression ratio is still more effective than that after encryption. So the original image directly compressed by 2DRE in our scheme will produce a compressed image with a higher compression ratio compared to Chung-Chang’s scheme.

Step 2: Scan patterns

The compressed binary image is treated as a bit string for simplicity, then each x bits are grouped together to form a block for encryption. For each block, we randomly select one scan pattern and change position according to the selected scan pattern. We can use a pseudo random generator to generate a sequence of selected scan patterns. Hence, there are at most $x!$ kinds of scan patterns that can be selected, where the symbol “!” is defined as a factorial.

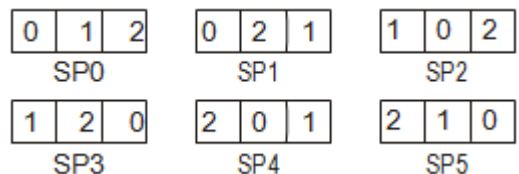


Fig 7. Scan patterns

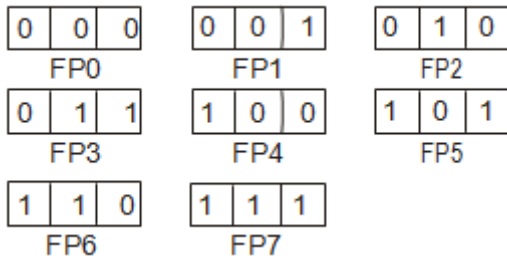


Fig 8: Scan mapping patterns

x can be flexible. Without loss of generality, the size of the compressed bit string is divisible by x.

Here we also take Fig. 2(a) according to the row scan order and use it as our example. The 2DRE compression result is as follows:

0 4 2 6 2 6 4 3 3 4 5 2 6 3 3 7 1 3

Because the maximum value is 7, 3 bits are necessary to represent each element. The following is the compressed bit string:

000 100 010 110 010 110 010 011 011 010 101 010 101 011 011 111 001 011

We can also take Fig. 3 as our scan patterns. To show our flexibility and to simplify, we use x=3 for our example. Hence, there are 3! =6 scan patterns shown in Fig. 7.

Because the size of the scan patterns is 3 bits, the above string should be grouped every

3 bits. Then for each group of 3 bits, we randomly choose a scan pattern to change bit position according to it. The scan pattern determines the substituted position. For example, for the tuple (0, 1, 2) and the selected pattern SP3 (1, 2, 0), the result is (2, 0, 1). If we take SP0 to SP5 recursively, the result of the scan patterns is as follows:

000 100 100 101 001 011 010 011 101 001 011 010 101 011 101 111 010 110

However, after the scan patterns, the total number of black and white bits in the plainimage is still the same as that in the cipherimage. This condition may disclose some important information. Just as in Chung-Chang’s encryption scheme, if a block consists of all black or white bits, the result of the scan patterns will also be all black or white bits in the block.

Step 3: Scan mapping

To solve the mentioned above problem using the mapping image based on the scan pattern. Convert every pixel of the image to be encrypted into its equivalent 8-bit binary number. The concept of combination of nibble value of a pixel is used as a mapping function. Using the scan mapping method is increase strength of encryption techniques.

IV. EXPERIMENTAL RESULTS

We use two 256X256 binary image. Table 1 shows the results of the proposed scheme. The experimental results of Chung-Chang’s scheme are shown in Table 2. In Table 2, since the compression ratio changes with the different sets of scan patterns in their scheme, the results are the average compression ratio of 5000 random sequences of scan patterns in the two original images. Comparing Table 1 and Table 2 shows that our scheme’s compression ratio for the two binary images is better than that of Chung-Chang’s scheme.

	Lena image	Step image
2DRE encrypted image	8067 bits	10345 bits
compression ratio	6.000	3.67345

Table 1: Experimental results of the proposed scheme

	Lena image	Step image
2DRE encrypted image	5000 random sequences	5000 random sequences
compression ratio	2.58318	1.742823

Table 2: chung-chang’s scheme

V. APPLICATIONS

Digital multimedia content is becoming widely used over networks and public channels (cable, satellite, wireless networks, Internet, etc.), which is unsecured transmission media. Many applications that exploit these channels (pay-TV, videoconferences, medical imaging, etc.) need to rely on access control systems to protect their content. Standard cryptographic techniques can guarantee high level of security but at the cost of expensive implementation and important transmission delays. Partial encryption comes as an alternative that aims at providing sufficient security with an important gain in computational complexity and delays. This allows a variety of possible applications for partial encryption.

VI. CONCLUSIONS

In this paper, we enhance Chung-Chang’s scheme and then a more efficient and secure encryption scheme is obtained. First, we exchange the sequence of compression and encryption to speed up encryption operation and to increase compression ratio simultaneously. Second, there are two added operations to enhance the security: Hence, the proposed scheme improves on Chung-Chang’s scheme on the part of encryption time, compression ratio and security. One is to scrambling the pixel position and other second is by using SCAN mapping method. Hence, the proposed scheme improves on Chung-Chang’s scheme on the part of encryption time, compression ratio and security. Furthermore, image size affects the speed of encryption; that is, the higher the compression, the better the efficiency. Because the property

of natural pictures preserves a good compression ratio, our scheme achieves a good efficiency.

REFERENCES

- [1] Bourbakis, N., 1986. A language for efficient accessing of a 2D array, *IEEE Workshop on LFA*, Singapore, pp: 52-58.
- [2] Bourbakis, N. and C. Alexopoulos, 1992. Picture data encryption using SCAN patterns, *Pattern Recognition*, 25: 567-581.
- [3] Chang, K.C. and J.L. Liu, 1994. An image encryption scheme based on quadtree compression scheme, *Proceedings of Internat. Comput. Symp*, Taiwan, pp: 230-237.
- [4] Chung, K.L. and L.C. Chang, 1998. Large encrypting binary images with higher security, *Pattern Recognition Letters*, 19: 461-468.
- [5] Stallings, W., 1999. *Cryptography and Network Security* (Prentice Hall International, Inc, 2nd Ed).
- [6] Wu D.C. and W.H. Tsai, 2000. Spatial-domain image hiding using image differencing, *IEE Proceedings on Vision Image and Signal Processing*, 147: 29-37.
- [7] Parameshachari B D, Chaitanyakumar M V:Image Security using SCAN Based Encryption Method, *42nd IETE Mid-term symposium on Telecom Paradigms - Indian Scenario*, April 2011, Bangalore, pp 115-118.

Clustering Technique with Potter stemmer and Hypergraph Algorithms for Multi-featured Query Processing

M. Nithya

Assistant Professor-III, Sri Sairam Engineering College

Abstract

In navigational system, it is important to provide a user with flexible and fast query processing without a search failure as well as to find optimal paths guiding the user to a destination. If a user has to repeat submitting a query several times, the user cannot be satisfied with the system. Using this new technique we can extract the correct information within less time effectively. Applications like multimedia databases or enterprise-wide information management systems have to meet the challenge of efficiently retrieving best matching objects from vast collections of data. Here a technique, "Clustering" supported by potter stemmer and hypergraph algorithm for processing multi-feature queries on diverse data sources is presented. Frequent item sets are generated from the groups of items, followed by clusters formed with a hyper graph partitioning scheme. Furthermore its performance is validated by comparing it with typical search techniques.

1. Introduction

In many emerging database applications, such as multimedia retrieval, exploratory data analysis, market basket applications, bioinformatics, and time-series matching, data are usually described by multiple features, each of which is typically high-dimensional. For example, an image may be described by a 16-dimensional color histogram, a 16-dimensional texture histogram, a 32-dimensional shape feature, and a 64-dimensional text feature. To support multifeature queries, we can build a high dimensional index on the feature space obtained from all dimensions of the multiple features. This system implements an efficient way of processing multifeature queries. In this system the indices are built based on a static combination of feature weights [1]. In multifeature query processing, the weightages of features typically are different for different queries and different weightages correspond to different results. In this process a user normally inputs a query with respect to more than one feature. A database normally is a collection of documents will be maintained separately. The user can give the query for searching the documents which are more relevant. The queries can be formulated in standard keyword form. The better solution is employed and the faster response is given for random search of the documents. From the given query the documents are extracted. By reading the full text document unwanted tags are generally eliminated from the documents and also the unwanted subjects are removed and the keywords are extracted. Initially search process is carried out based on the single feature. This could be compared with

searching the database based on multifeature query [2], [3]. The most relevant documents are fetched from the database and separately shown. Weightages are applied to the documents by receiving each keyword and finding the number of occurrences of this key word in each document. According to high preferential weightage the documents are fetched accordingly. Thus we can efficiently process the multifeatured query.

2. Existing System

Today in most of the search engines can only use queries rather than web user profiles due to the difficulty of automatically acquiring web user profiles [4]. The simplistic approach of acquiring user profiles is to describe the profiles through term vector spaces (e.g., a set of keywords) by using machine-learning techniques. The main disadvantage of the simplistic approach is the poor interpretation of user profiles to the users. To obtain an explicit specification to the users, user profiles can be represented in some predefined categories. There are two main drawbacks in using these approaches to acquire web user profiles [5]. The first one is that the effectiveness largely depends on the numbers of labeled training data. However, we may only obtain some positive documents. The second one is that it is hard to distinguish non interesting topics from interesting topics. Here, we develop an ontology mining technique to overcome the above drawbacks.

- Lacking Data Accuracy
- Computational complexity
- More Time Consumption

3. Proposed System

In the proposed system multifeature query processing, the weightages of features typically are different for different queries and different weightages correspond to differ results. In this process a user normally inputs a query with respect to more than one feature. The queries can be formulated in standard keyword form. By reading the full text document unwanted tags are generally eliminated from the documents and also the unwanted subjects are removed and the keywords are extracted. Initially search process is carried out based on the single feature. This could be compared with searching the database based on multifeature query. The most relevant documents are fetched from the database and separately shown.

- Efficient filtering of data.
- Takes less computational time.
- Data accuracy can be maintained.
- Lightweight.

4. Architecture

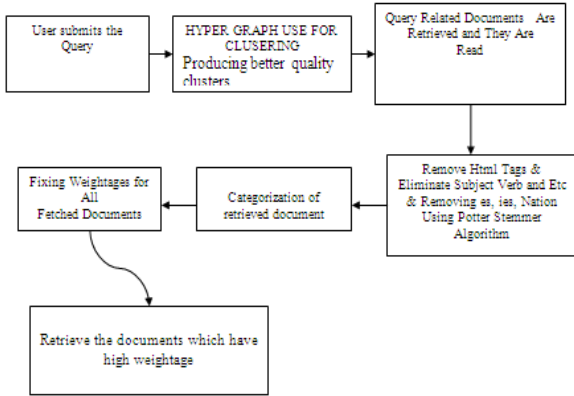


Figure.1 Architecture Design

Figure.1 states the architecture design of the proposed system. It has the following sub modules to get realized as a design.

- User Query
- Keyword Extraction
- Improving Retrieval Effectiveness
- Categorization
- Document clustering
- Mapping Documents

4.1 User Query

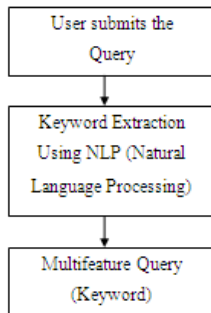


Figure.2 User Query

Figure.2 states the user query module sequence. In this module the user submits the query. The queries can be formulated in standard keyword form. Here the keywords are extracted using Natural Language Processing. Thus the search process is carried out using those keywords extracted and not with the entire standard query.

4.2 Document Clustering

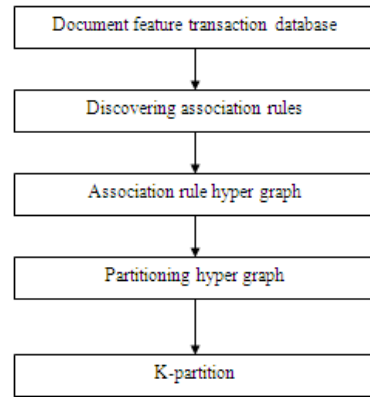


Figure.3 Document Clustering

Figure.3 states the document clustering sequence. Document clustering group all document so that the document in the same group are more similar than ones in other group. Relevant documents tend to be more closely related to each other than to non-relevant document. It founds the association between these documents and sets the partition based on their features found in the document.

- Getting keywords from database.
- Comparing these words with our document needs.
- Grouping on the basis of frequent value.

4.3 Keyword Extraction

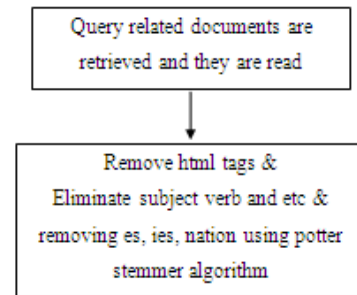


Figure.4 Keyword Extraction

Figure.3 states the keyword extraction sequence. In this module with the given query the document are extracted. By reading the full text document unwanted tags are generally eliminated from the documents and also the unwanted subjects, verb and etc, es, ies are all removed using the Potter stemmer algorithm. The keywords are extracted using Natural Language Processing and stored in the database.

4.3 Improving Retrieval Effectiveness

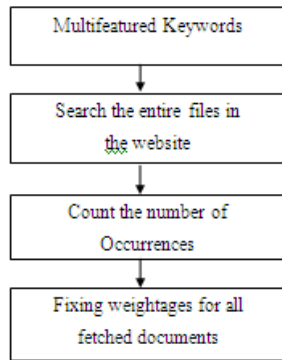


Figure.5 Retrieval Effectiveness

Figure.5 states the sequence of improving retrieval effectiveness. In this module with the extracted keywords the search process is carried out. Normally the search process is carried out by traversing the entire files in all documents. Accordingly the number of occurrences of the keywords in the database is counted. With this count weightages are fixed for all related documents fetched from the database.

4.4 Categorization

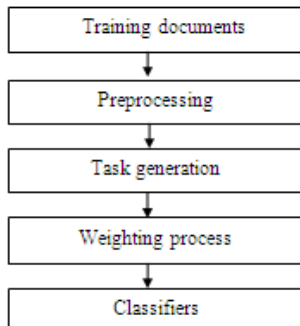


Figure.6 Categorization

Figure.6 states the sequence categorization. Here assigning one or more predefined categories (topics themes) to one document is called as categorization. It generates the task based on the topics evaluated. It consist of a set of training sets and predefined categories. It computes the similarities and assigns weightage for each category and evaluates the scores. Based on these scores it identifies the classifiers.

4.5 Mapping Documents

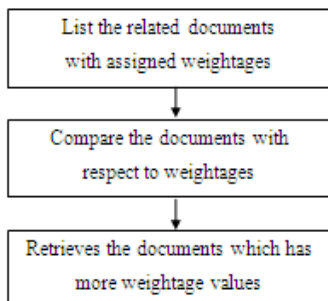


Figure.7 Mapping Documents

Figure.7 states the sequence of mapping documents. In this module all the related documents with assigned weightage values are listed after the search process gets completed. Now comparison is done with respect to the weightage values. Thus the document which has more weightage value is retrieved from the database.

5 Data Flow Diagram

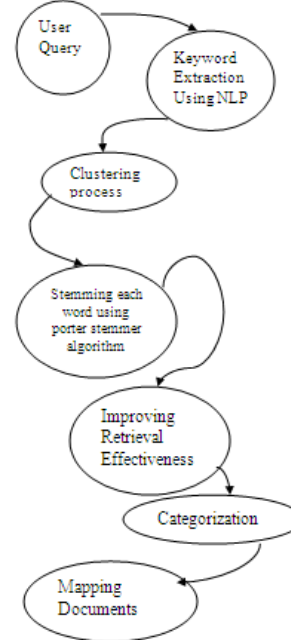


Figure.8 Data Flow Diagram

Figure.8 illustrates the data flow sequence in the proposed model. This model uses the Potter stemmer’s algorithm in Keyword extraction sub module and also uses hyper graph in document clustering sub module. Both these algorithms are presented in the subsequent section.

5.1 Potter stemmer Algorithm

Step1:

- Stop words: Words that are discarded from a document representation
 - Function words: a, an, and, as, for, in, of, the, to
 - About 400 words in English.
 - Other frequent words: “Lotus” in Lotus Support db
- Removing stop words makes some queries difficult to satisfy
 - Few queries affected, so little effect on experimental results
 - But, very annoying to people

Step2:

- Group morphological variants:
 - Plural: “streets” <=> “street”
 - Adverbs: “fully” <=> “full”
 - Other inflected word forms: “goes” <=> “go”

Grouping process is called “conflation”

- Accurate than string matching Current stemming algorithms make mistakes
 - Conflating terms manually is difficult, time-consuming.
 - Automatic conflation using rules
 - Porter Stemmer
 - Porter stemming example: “police”, “policy” => “polic”.

Step3:

- Algorithm is based on a set of condition/action rules
 - old_suffix->new_suffix
- Rules are divided into steps and are examined in sequence
 - Step 1a: sses->ss, ies->i, s->NULL
 - caresses -> caress, ponies -> poni, cats -> cat
 - Step 1b: if m>0, eed -> ee
 - Agreed -> agree
 - Many implementations available
 - Good performance

5.2 Hypergraph Definition

Hypergraph: $H = (V, E)$

V: a set of vertices, here, docs being clustered

E: a set of hyperedges which can connect more than two vertices, here, a set of related docs

A weight is assigned to each hyperedge

Each document viewed as an item

Each possible feature word as a transaction

The hypergraph representation

- Represent each document as a vertex item
- Compute all the frequent item-sets, with a given threshold support count
- Represent each frequent set as a hyperedge
- Assign the weight as the average confidence of the essential association rules of the set

6. Realization

The proposed cluster technique is integrated to a typical search engine like YAHOO and the performance of it is compared with normal search techniques.

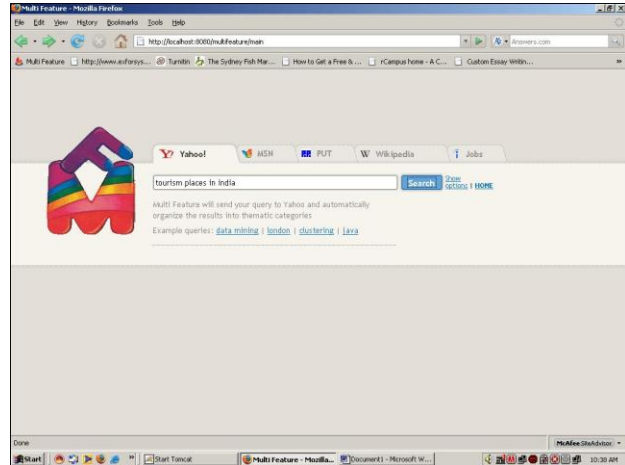


Figure.9 User placing his query

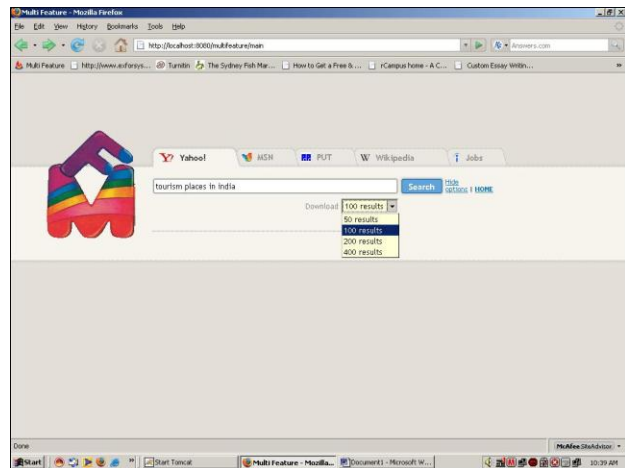


Figure.10 User selecting required search results

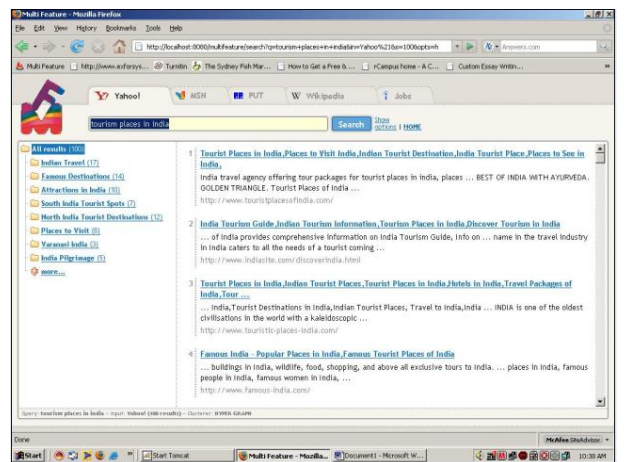


Figure.11 Results for the query

Figure 9, 10 and 11 gives the normal sequence of searching user query in the yahoo search engine with the proposed technique integrated. In figure 9 the user gives a query. And in figure 10 the user has a option to select number of search results required. Finally in figure 11, the user gets the results displayed.

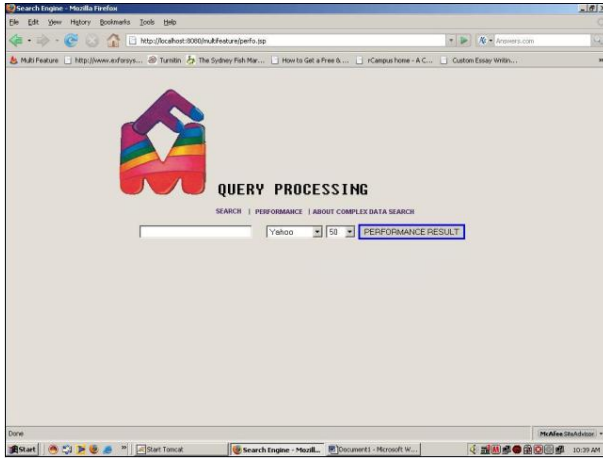


Figure.12 Comparison against typical search technique

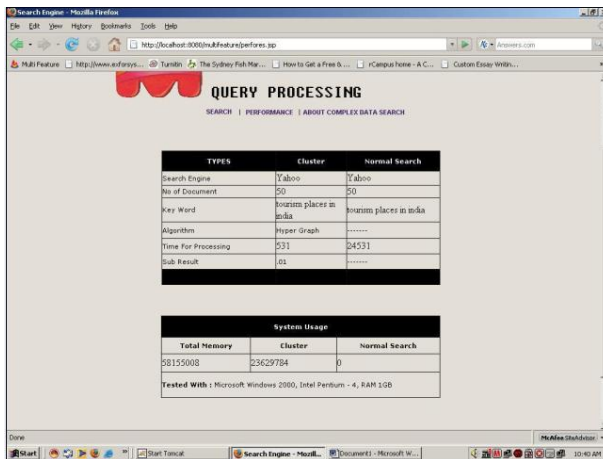


Figure.13 Comparison result

In Figure 12, an option for comparing the performance between the proposed technique and the existing search technique is carried out. Once the performance result button is clicked, the comparison results are displayed as in figure 13. From the comparison it is evident that the proposed cluster technique has superior performance in terms of time required for processing against the typical technique. For an equivalent search, the cluster technique throws result within 531 micro seconds when compared to a long time of 24531 micro seconds.

7. Conclusion

In this paper a new search technique called cluster technique which works on Potter stemmer and hypergraph algorithm is realized. The architecture and subsequently its design are realized. Its performance is compared with typical search techniques and is found that its performance is far superior to them. For an equivalent search, the time taken by this cluster technique is very less compared the existing techniques. Thus it can be concluded that the proposed design can overwhelm the existing techniques by its superior performance. Future scope of improvement will be on the system memory usage which is considerably more using this cluster technique.

8. References

- [1]. C. Bohm, S. Berchtold, and D. Keim, "Searching in High- Dimensional Spaces: Index Structures for Improving the Performance of Multimedia Databases," ACM Computing Surveys, vol. 33, no. 3, pp. 322-373, 2001.
- [2]. A. deVries, N. Mamoulis, N. Nes, and M. Kersten, "Efficient k-NN Search on Vertically Decomposed Data," Proc. SIGMOD Conf., pp. 322-333, 2002.
- [3]. N. Koudas, B. Ooi, H.T. Shen, and A. Tung, "LDC: Enabling Search by Partial Distance in a Hyper-Dimensional Space," Proc. Int'l Conf. Data Eng., 2004.
- [4]. Y. Sakurai, M. Yoshikawa, S. Uemura, and H. Kojima, "The A-Tree: An Index Structure for High-Dimensional Spaces Using Relative Approximation," Proc. Conf. Very Large Data Bases, pp. 516-526, 2000.
- [5]. R. Weber, H. Schek, and S. Blott, "A Quantitative Analysis and Performance Study for Similarity Search Methods in High Dimensional Spaces," Proc. Conf. Very Large Data Bases, pp. 194-205, 1998.

Variable Voltage, Variable Frequency Regulated High Voltage Power Supply for Coulomb crystallization Base on Microcontroller

Atul Kumar Dewangan¹, Shikha Mishra², Durga Sharma³

**Department of Electrical Engineering, Chhattisgarh Swami Vivekananda Technical University, Bhilai Chhattisgarh India*

***Department of Electrical and Electronics Engineering, Dr. C.V. Raman University, Bilaspur, India*

**** Department of Electronics and Telecommunication Engineering, Dr. C.V. Raman University, Bilaspur, India*

ABSTRACT

Coulomb crystallization in dusty plasmas is of great interest in recent years. The Control of fine particle behavior in Coulomb Crystallization Experiments requires low frequency particle driving, which involves injection of alternating voltages at low frequencies. With a repetition period shorter than the particle response time, the particles feel only time-averaged force because of large mass. Also in case of dusty plasma, one needs to excite dust acoustic wave for which low frequency perturbation of higher amplitude are required, depending upon the dust size. To perform such experiments, High Voltage power supply with variable voltage and variable frequency is required. Moreover, the power supply should be highly regulated and short circuit protected. Such low frequency, high voltage pulse generator are not commercially available and hence requires special design. To satisfy the above requirements a microcontroller based variable frequency, variable amplitude, regulated high voltage power supply is designed and developed indigenously in RF Group. The paper deals with the Design, Development and Testing of 0 to1000V (p-p), 1 to 10Hz, 10mA regulated power supply.

Keywords - About five key words in alphabetical order, separated by comma

I. INTRODUCTION

Coulomb crystallization in dusty plasmas is of great interest in recent years. The experiments generally involve a parallel plate capacitor arrangement for RF plasma generation. Plasma temperature and density is varied with the gas (typically Argon) pressure, RF frequency and power. Once the plasma is stabilized SiH4 and O2 gas are injected to generate SiO2 particles of size 2-3µm. Occasionally 10-15 µm sized quartz crystals are also formed [1]. The charged particles arrange themselves in a regular geometrical

array in the groove of the bottom plate of the capacitor. This array formation is known as **Coulomb crystallization**. The Control of fine particle behavior in Coulomb Crystallization Experiments requires low frequency particle driving, which involves injection of alternating voltages at low frequencies. With a repetition period shorter than the particle response time, the particles feel only time-averaged force because of large mass [2]. To perform such experiments, High Voltage power supply with variable voltage and variable frequency is required. Moreover, the power supply should be highly regulated and short circuit protected. Such low frequency, high voltage pulse generator are not commercially available and hence requires special design.

2. SPECIFICATIONS OF VVVF POWER SUPPLY

Specifications for VVVF power supply are given in Table 1 below.

Table 1. SPECIFICATIONS OF VVVF POWER SUPPLY

Sr.No.	Specification	Value
A	Input	
	Voltage	1-ph, 230V (+/-10 %)
	Frequency	50Hz
	Isolation	1.5kV
B	Output	
	Voltage	0 to 1000V (p-p), settable (floating)

	Current	10 mA
	Frequency	1 Hz to 10 Hz
	Regulation	< 1%
	Ripple	< 0.5% at full load
C	Protection	-Overload protection -O/P Short Circuit Protection @ 10mA
D	Control	
	Control Parameter	Output Voltage
	Voltage setting	0-5V control signal through POT
	Frequency setting	Pushbutton/ POT
E	Metering	
	O/P Voltage	1kV (p-p) Analog Voltmeter
	Frequency	20 Character LCD
F	Programmability	
	In-Circuit Reprogrammable-ICP	16-bit

	Mode of operation	Variable Voltage, Variable Frequency (VVVF)

is selected. The H-bridge topology provides the following advantages: -

- (a) It allows the current to be fed to a load in all four quadrants of voltage and current.
- (b) The frequency and amplitude can be easily controlled through control pulses from a low voltage circuit.

Also, as the frequency and time period are inversely proportional to each other, the non-linear time period generation (1sec for 1Hz and 100ms for 10Hz) introduces another issue. Based on the above requirements it is decided to go for H-bridge topology controlled by a microcontroller-based frequency controlled driver [3].

The reasons for using microcontroller are as follows:

- (a) Most of the PWM controllers available in the market generally have lower frequency range, starting from few hundreds of Hertz and hence are not fit for our requirements. Such low frequencies can be precisely generated using the inbuilt timers provided in the microcontroller.
- (b) Another important requirement of frequency driver is to generate Dead Time; time delay between the complimentary pairs Q and \bar{Q} . A precise dead time can be easily generated through a microcontroller

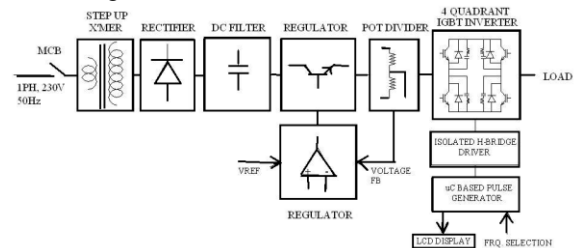


Fig.1 Block Diagram of VVVF Power Supply

Fig.1 shows the block diagram of the VVVF power supply. The voltage requirement specified for the supply is 500V peak to peak. However, the total circuit has been designed with a design value of 1000V peak to peak. The H-bridge topology has been used for switching. Consequently, in the power part the input voltage is stepped up to using a step up transformer. This obtained value of AC is converted

2. DESIGN

2.1 TOPOLOGY SELECTION

The two important requirements of the power supply are:

- (a) Variable Alternating Voltage (Square Wave shaped)
- (b) Variable Low Frequency

The transformer design becomes critical if it is to be operated at very low frequencies (1 to 10Hz) as the core gets saturated and hence a special design needs to be implemented. To avert the above problem, a low frequency, transformer-less H-bridge Topology

to an equivalent DC output using a full wave bridge rectifier using HV diodes [4]. A DC filter is designed to reduce the output ripple content. The regulated output of the filter is fed to the H-bridge circuit. The regulator is a power BJT based series pass regulator, which provides closed loop control of the total power supply. The controller is fed with a reference signal, which is compared with the feedback signal at the output, the difference of which forms the error signal for the regulator. The error signal is amplified and is fed to the base of the BJT and hence the required regulation as well as variation is achieved. The amplitude of the power supply is set using a potentiometer and its value is displayed on an analog voltmeter calibrated to show peak-peak output voltage. The H-bridge is IGBT based (Fig. 1) and its switching is controlled by a buffered isolated driver card that in turn is controlled by a micro-controller. The microcontroller adjusts the timing sequence for switching requirements of IGBT including the Dead Time. This is achieved by programming its 16bit timers, to generate pulsed waveforms of desired frequency (1-10Hz). The frequency is varied using a push button interfaced to the microcontroller. An LCD is also interfaced with the microcontroller to display the online frequency [5].

2.2 DESIGN DESCRIPTION

2.2.1 POWER CIRCUIT

The power circuit (Refer Fig.2) is divided among the following parts: -

- (a) Step up transformer
- (b) Rectifier
- (c) DC Filter
- (d) Short Circuit Protected Linear Regulator
- (e) H-bridge
- (f) Snubber design

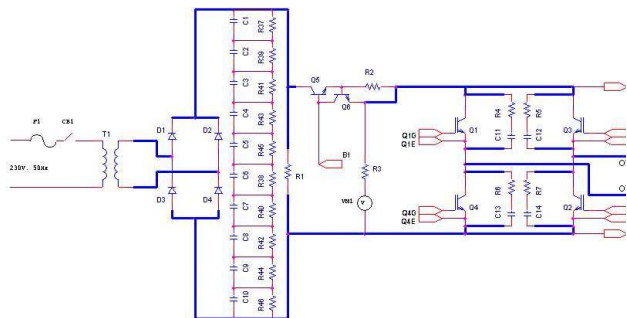


Fig. 2 Power Circuit

2.2.2 CONTROL CIRCUIT

A dedicated driver (developed for low power IGBTs used in inverter section) with inbuilt isolation (through opto-couplers) is designed and developed for the power supply. For the purpose of safety and low voltage control, the driver part is isolated from the power part. While the driver part works at a maximum voltage of 15 volts, the power part works at a maximum voltage of 1000 volts peak to peak and hence the isolation is a must. The block diagram of the driver and control card is given in Fig. 3. The basic function of the driver part is to periodically, as determined by the operator, generate triggering pulses Q and \bar{Q} through the microcontroller to govern the ON and OFF switching of the IGBT switches that constitute the H-bridge. The separate 15V power supplies needed to run the 4N35 IC's is also mounted on the driver card. The function of the driver and control is categorized into four levels as: (refer Fig.3, Fig. 4)

- (a) Buffering
- (b) Isolation
- (c) Conditioning
- (d) Level translation

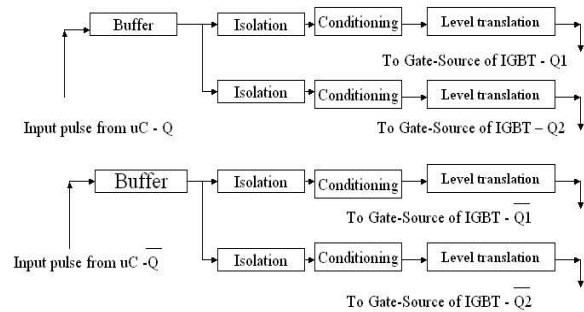


Fig. 3 Block Diagram of Driver and Isolation Card

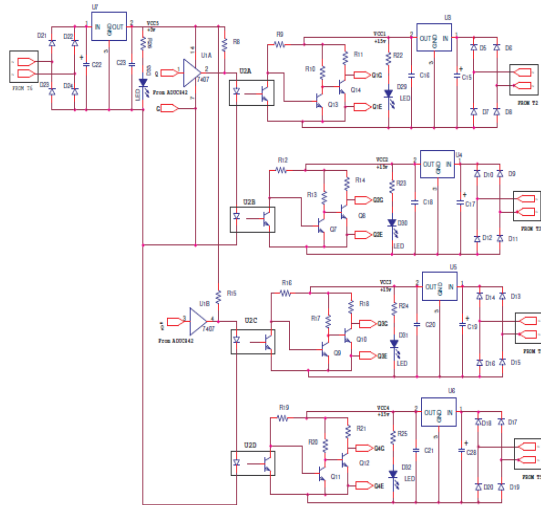


Fig. 4 Driver and Isolation Card

The buffers used in the system are two of the six in built buffers of a 7407 IC. The need for a buffer arises because during the driver operation by the microcontroller the current generated by it is not sufficient enough to feed the primary of optical isolator. The isolation function is desired to separate the L.V and the H.V circuits. In an Hbridge circuit for turning on the diagonally opposite switching devices would lead current flow through the load and lead to its reversal of direction of flow alternately. This method requires that each of the four switches receive its own control input. Since our voltage requirement at the load is high we need to provide electrical isolation and a level shifter to match the micro controllers output voltage/current requirements, as a standard practice. IC 4n35 is used for both the purposes. The SL 100 transistors provide the signal conditioning. The provision of inversion is a control measure. Inversion of the waveform is necessary because during input from the microcontroller all the pulses are high just a moment before switching starts happening, this can create a short circuit within the switching circuit. The level translation is required because up to the isolators in the driving circuit the operating voltage is 5 volts, however in order to drive the IGBT gates in hard saturation 15V supply is used. The output of 4n35 drives the Conditioning and level translation circuits, which finally drives the gates of the IGBTs.

2.2.3 MICRO-CONTROLLER BASED LOW FREQUENCY GENERATOR DESIGN

For generating programmable low frequency witching pulses, Micro-converter ADUC842 from

Analog Devices is used. This controller is a part of the Micro-controller Kit developed at RF Group (Fig. 5), and is provided with all the features to interface LCD, Keypads and external peripherals. The kit size is around 5.5” x 4” and is in-circuit programmable (ICP).

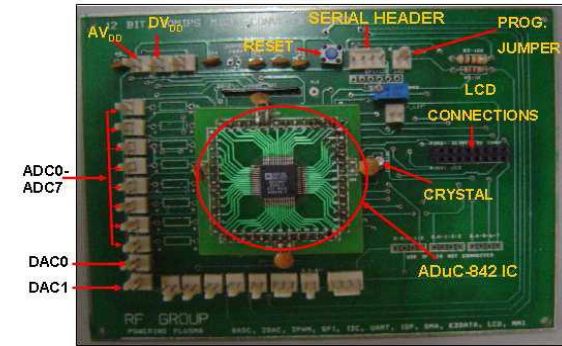


Fig. 5 Micro-Converter Kit Developed at RF Group

2.2.4 EXTERNAL DEVICE INTERFACING

A 2 line, 20Character LCD is interfaced with the ADUC842 kit using a FRC connector and cable.

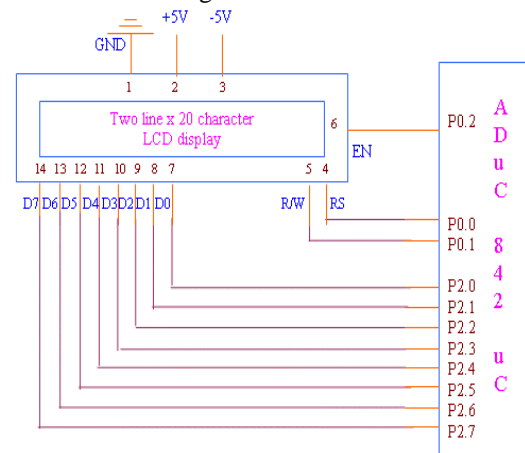


Fig. 6 Interface of LCD with Microcontroller

The connection diagram of LCD to Microcontroller is given in Fig. 6. Port 2 of the microcontroller is used as the Data Bus for the LCD. Port pins p0.1, p0.2 and p0.3 are used for controlling the data flow and Display on the LCD. The Connection between ADUC842 and LCD is through 14-wire FRC cable. The LCD is housed in a separate control box of the power supply [6]. A push button is connected to the port ‘P0.5’ and is used for frequency selection. The pin ‘P0.5’ is polled for active low (when the push button is pressed) and causes change in the output frequency with simultaneous display over the LCD.

3. FLOW CHART

The program flow is shown in Fig. 7. The default frequency of the output pulse is set to 1Hz. As soon as the system is started, the output generates 1Hz. This is simultaneously displayed over the LCD. The frequency is generated using Timer 1 in 16-bit mode. The program then waits for the push-button to be pressed (for a change in frequency). Once the push button is pressed, the program counter increments to the new value in the look up table (LUT) and collects the data and starts generating the new frequency with the simultaneous display over LCD. A circular programming loop is used for frequency increments i.e. after reaching 10Hz the frequency rolls back 1Hz.

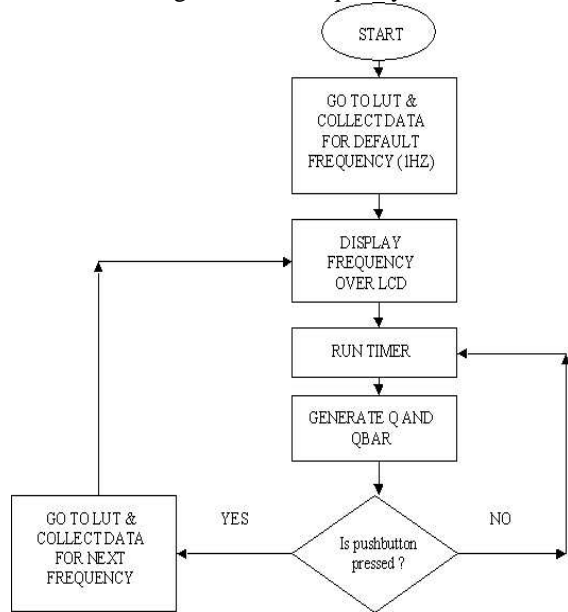


Fig. 7 Flow Chart

4. SOFTWARE

The software used is divided in three categories: -

- (a) Assembler
- (b) Simulator
- (c) Downloader

4.1 ASSEMBLER

The program is written in an ASCII text editor in assembly format. Once the code is written it is assembled using an assembler. The assembler used is 2-pass (cross) assembler from Metalink Corporation (Fig. 8). Once the code is assembled, Intel compatible hex file is generated. Fig. 9 gives a screen shot of the Intel Compatible hex file for the program used.

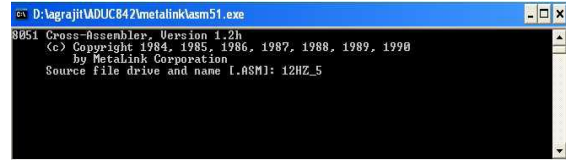


Fig. 8 Cross Assembler

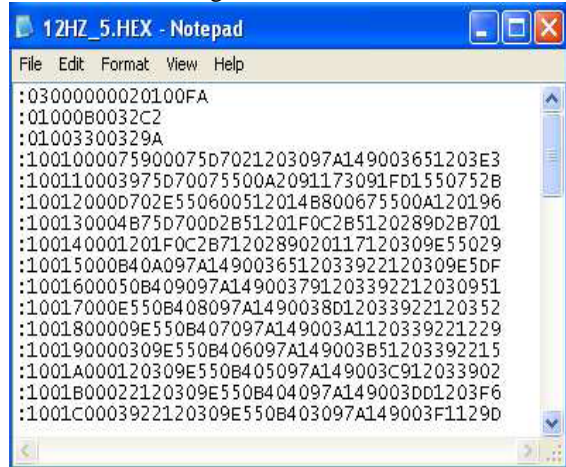


Fig. 9 Intel-Compatible Hex Code file

4.2 SIMULATOR

Before downloading the program, the hex file is loaded in a simulator. The simulator used is ADSim Simulator from Analog Devices. Fig.9 shows the screen shot of the ADSim simulator with different simulation windows like RAM Simulation, Port simulation, Timer Simulation etc. The simulator provided the facility of stepped simulation and facilities like external simulated interrupts.

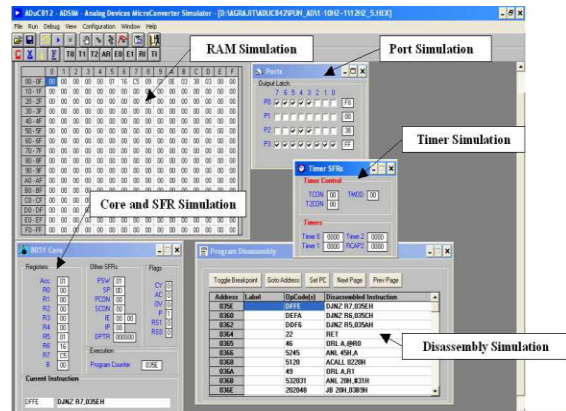


Fig. 9 AD Sim Simulator

4.3 DOWNLOADER

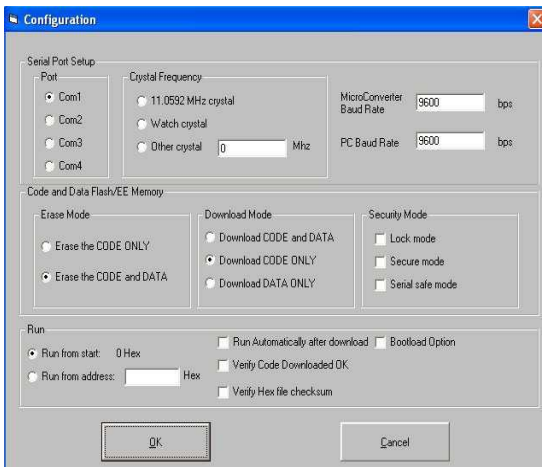


Fig. 10 Screen Shot of the Configuration Menu of Serial Downloader

For downloading the hex code into the flash of microcontroller, Serial Downloader v6.06 from Analog Devices is used. Some of the configuration capabilities (Fig. 10) of the downloaded are listed as follows: -

- (a) Downloading Port Selection facility
- (b) Crystal frequency selection
- (c) Baud rate selection for both PC and microcontroller
- (d) Erase Modes for Code and data
- (e) Download Modes for Code and data, Verification and Bootload options

5. RESULTS

5.1 TESTING OF DRIVER CARD

The IGBT driver is tested for its maximum operating frequency range. It works well up to 4 kHz, which is well above the requirement.

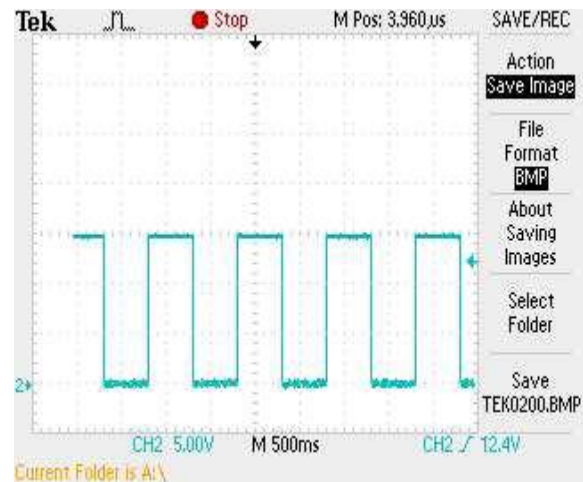


Fig. 11 Input Through Function Generator

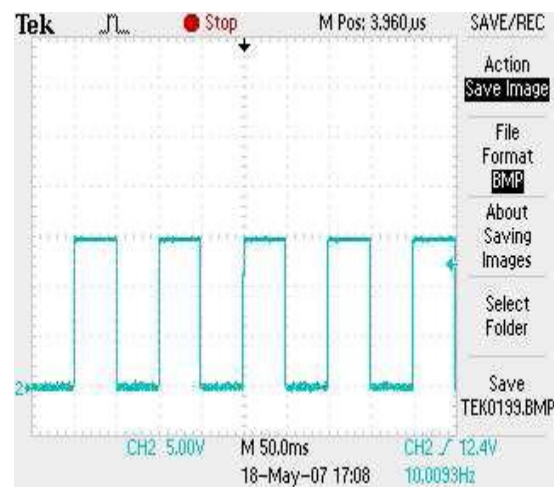


Fig. 12 Input through Function Generator

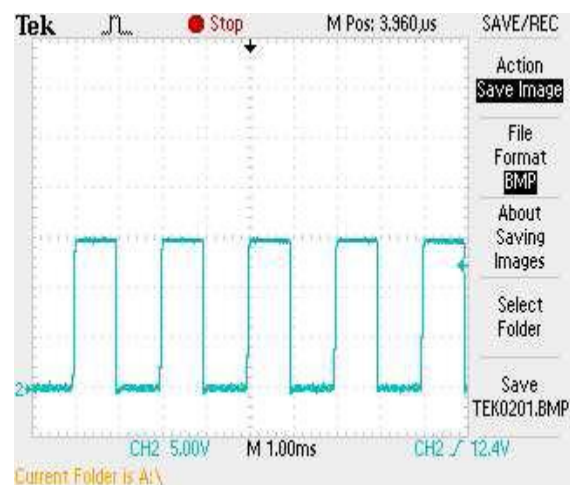


Fig. 13 Input through Function Generator

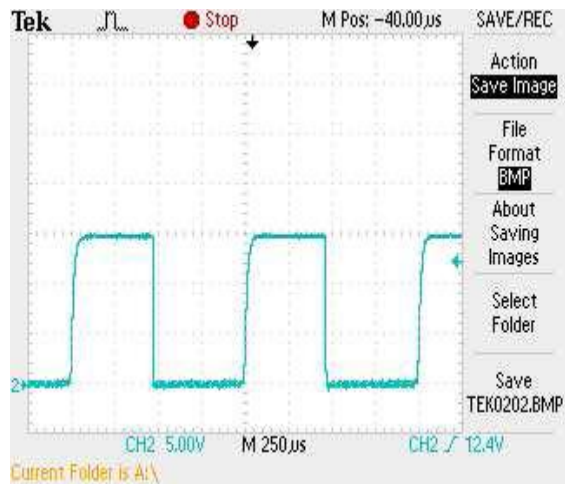


Fig. 14 Input through Function Generator

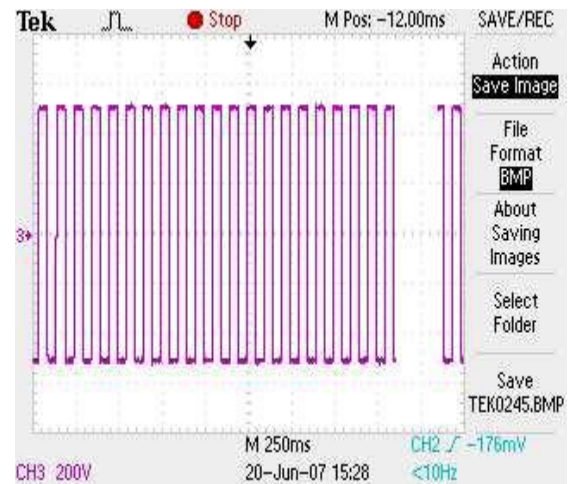


Fig 16 Voltage Output at 10Hz, 1kVp-p

5.2 TESTING OF POWER SUPPLY

The Power Supply is tested on a resistive dummy load for a load current of 10mA.

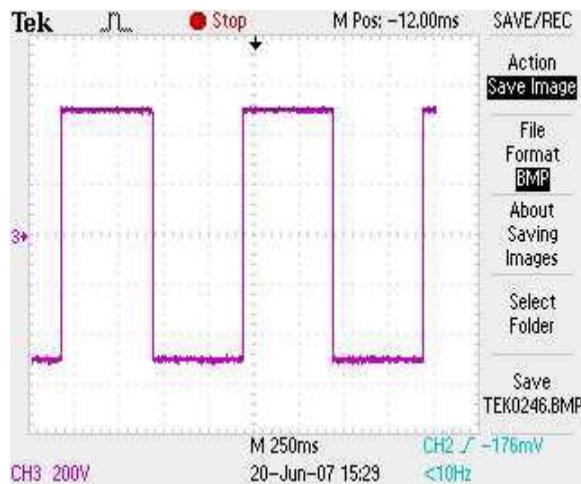


Fig 15 Voltage Output at 1Hz, 1kVp-p

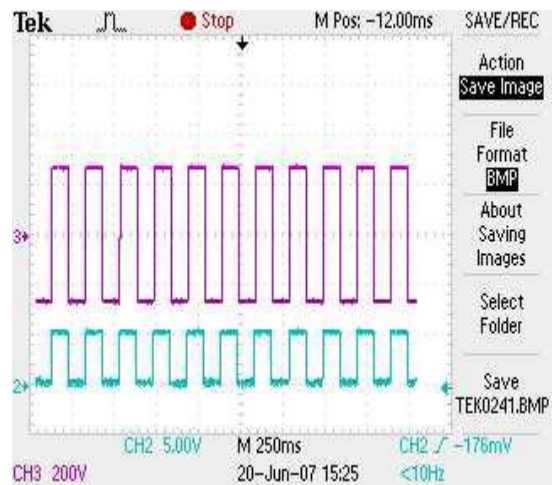


Fig 17 Voltage Output at 5Hz, 500V p-p

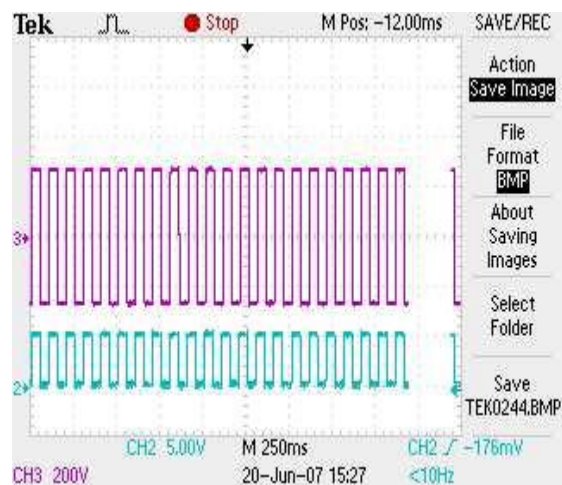


Fig 18 Voltage Output at 10Hz, 500V p-p

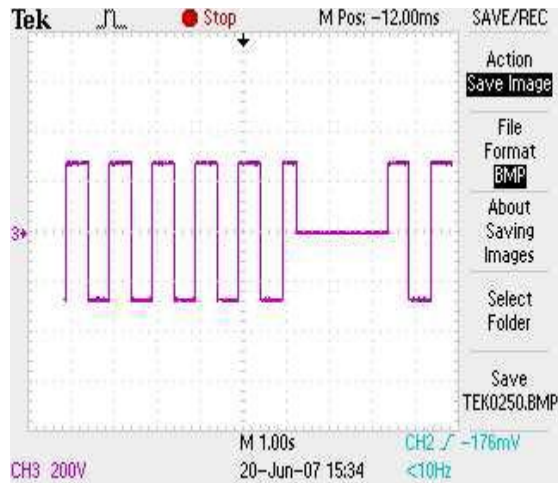


Fig 19 Voltage Output at 1Hz, 500V p-p

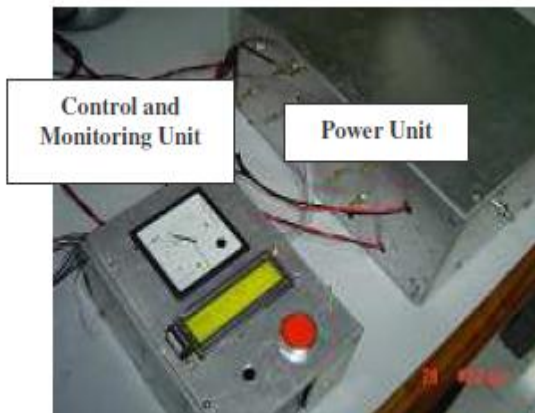


Fig. 20 Shows a view of the assembled power supply

6. CONCLUSION AND FUTURE SCOPE

- The power supply is designed and tested successfully as per the given requirements on a resistive dummy load.
- The power supply is made indigenously with the available components in a time scale of ~ 25 days
- The estimated cost of the power supply is ~ Rs10,000/-
- The power supply can be optimized for the components, size and power density as most of the components used are over rated.
- The program can be modified for higher frequency resolution.

- Features like remote programmability can be incorporated in future designs.
- Owing to the constraint of time the wiring layout can be optimized in future by designing a lanned wiring layout to avoid any interference between power and control circuits

ACKNOWLEDGEMENTS

Firstly, the authors would like to pay their respectfully thanks to God, their beloved family, teachers and their admirer supervisor. Special thanks to Mr. R. K. Patel Head of department of Kirodimal .Government Polytechnic, Raigarh for his encouragements. The authors also express their greatly thanks to all persons who had concern to support in preparing this paper.

REFERENCES

- [1] P Daki, B. Lwahori,, Application of Coulomb crystallization in parallel capacitor, *International Journal of Electrical Engineering*, 20, 2000, 98-100.
- [2] B. P. Thapar , Behavior in Coulomb Crystallization Experiments in low frequency particle driving, Brno,czech republic, 9-12, jun.1999, pp.277-282.
- [3] Mike Predko, *8051 Micro-controller programming* Prentic-Hall of India, Newdelhi, 1994.
- [4] Khoei and Hadidi, — MicroProcessor Based Closed –Loop Speed Control System for DC Motor using Power MOSFET, I Umia University ICECS 1996, pp. 2003.
- [5] Peter Spasov, —Microcontroller Technology: The68HC11, Prentice-Hall, 2002
- [6] Tavel, P. 2007 Modeling and Simulation Design. AK Peters Ltd

STUDY OF AIR POLLUTION DUE TO AUTOMOBILE EMISSION IN OOTY

T SUBRAMANI¹

S.KRISHNAN²

¹Professor & Dean, Department of Civil Engineering, VMKV Engg. College, Vinayaka Missions University, Salem, India

²Associate Professor & Head, Department of Mechanical Engineering, Mahendra College of Engineering, Salem,

ABSTRACT

Ooty the Head Quarters of Nilgiris Districts has a large Number of commercial and non-commercial vehicles, due to increasing industrialization and Tourism related activities. In this thesis a study was conducted on vehicle pollution in Ooty town to assess pollution contribution from transport sector. Pollution due to auto exhaust has assumed menacing proportion in the developing countries like India, where its contribution is nearly 45% - 75 % of the total air pollution in urban areas. The available information about mobile source emission factors has been compiled from different sector in Udhagamandalam. In this study, mobile source emission factor for carbon monoxide, hydrocarbons and smoke density for Indian vehicles have been estimated by testing different types of vehicles for their exhaust contents. It is reported from the study undertaken in this work, the emission levels of carbon Monoxide, Hydro Carbons and smoke Density of vehicle made from the year 1961 are within the permissible limits as recommended by the Environmental (Protection) Rules, 1986.

KEYWORDS: Study, Air Pollution, Automobile Emission, Ooty

1. AIR POLLUTION - INTRODUCTION

The problem air pollution has existed ever since our ancestors sat coughing around a smoky fire in a recessed cave. In fact, there probably never was an unpolluted atmosphere, since decaying vegetation and animal matter, smoke, vapours, dust soot, carbon fumes, gases, mist, odors, radioactive materials and other natural phenomena surely have emitted gaseous and particulate matter ever since world began. Starting from 14th century, when coal was introduced as a fuel, atmospheric pollution becomes social problem. Air itself is a mixture of gases containing Nitrogen (=78.09%), Oxygen (=20.95%), Argon (=0.93%) & Carbon Dioxide (=0.03%), water vapor, Traces of neon, Krypton, Helium, Hydrogen, Xenon and ozones.

In short everything that we do to become an advanced and prosperous community, puts an ever increasing amount of unwanted and harmful foreign material into the life giving atmosphere, some of them are as follows:

- 1) Burning of fuels.
- 2) Production and use of pesticides and fertilizers to increase crops.

- 3) The propulsion of trains, ships, automobiles, planes, rockets, the extensive refineries for oils and minerals.
- 4) Conversion of raw materials into finished goods.
- 5) Clearing of roads.
- 6) Conversion of roads and buildings.
- 7) Chemical and other industry exhaust.

Thus from the beginning of the world the condition and concentration of many of the components of the atmosphere has been influenced by the relative rate of these additions and removals. It seems fitting and proper to examine the problem of air pollution control from the view point of public health. An average man, breathes 22,000 times and he taken in 35 lbs of air each day. The air is main link to life. It far exceeds one's consumption of food and water. Hence there is a general interest in air pollution control.

1.1 DEFINITION

Air pollution is defined as the presence of one or more contaminants in the atmosphere such as dust, fumes gas, mist, odors, smoke or vapor in quantities, of characteristics, and of duration. Such as to be injurious to human, plant or animal life or to property or which unreasonably interfaces with the Comfortable enjoyment of life and property.

1.2 NECESSITY OF THE AIR POLLUTION STUDY

Two decades ago, most of the air pollution was due to industrial emissions and burning of fuel. But the situation has changed considerable since then. The ever increasing proliferation of automobiles would indicate that, if uncontrolled, gaseous exhaust products could increase without limit. In India, during the last four decades of progress, greater emphases has been laid on industrialization rather than motorization, yet there are strong indications that automotive vehicles are turning to be an important contributor to air pollution. Auto exhaust pollution has assumed a menacing proportion in the developing countries and its control should not be delayed any more especially in India, where its contribution is about 45% - 70% of the total air pollution in urban areas. In major Indian cities, the ambient CO levels along the roads of commercial zones have reached alarming levels indicating that though the number of vehicles in major cities is comparatively smaller, the intensity of pollutants can be compared to that of any other metropolis in the world. This

can be attributed to the age of vehicles with poor maintenance, poor road conditions and lack of traffic planning. Moreover, the automobiles leave the emission at the at the ground level resulting in greater impact on the air quality.

1.3 SOURCES OF AIR POLLUTION

Table.1 gives the picture of different pollutants and their emissions.

TABLE.1 DIFFERENT POLLUTERS AND THEIR EMISSIONS

Type	Category	Examples	Important Pollutants
1. Combustion	Fuel burning Transportation.	Domestic burning, thermal power plants, cars trucks and railways	Sulphur and Nitrogen oxide, carbon monoxide, nitrogen oxide lead smoke organic vapors, odors, etc.,
	Refuse Burning	Open burning dumps	Fly ash and particulate
2. Manufacturing Process	Chemical Plants	Petroleum refineries, Fertilizers, cement, paper mills, ceramic, and clay products.	Hydrogen sulphide, sulphur oxide, fluorides, odours, organic vapours and dusts.
	Metallurgical Plants	Aluminium Refineries, Steel Plants	Metal flumes (PH and Zn), fluoxides and particulate
	Water recovery	Scrap metal yards, rendering plants	Smoke, Soot, odours, Organic vapours, metal flumes
3. Agricultural Activities	Crop Spraying	Pest and weed control	Organic phosphates, chlorinated Hydrocarbons
	Field Burning	Burning of refuse firewood	Smoke, fly ash, soot, sulphur oxides, particulates and organic vapours.
4. Solvent Usage	Spray painting Solvent Extractions, solvent cleaning	Furniture and appliances finishing dycing painting, Dry cleaning, degreasing etc.,	Hydrocarbon and tother organic vapours.
5. Nuclear Energy Programmes	Fuel fabrication	Gaseous diffusion, crushing, grinding	Fluorides, uranium and beryllium dust and other particulates
	Nuclear device testing	Bomb explosions	Radioactive fall out, sr=90 C-14 etc.,

Table.2 gives the picture of the composition of clean, dry air, Many of the compounds which acts as pollutants are minor constituents of clean air, that is NO_2 , O_3 , SO_2 , CO and NH_3 , Though their concentrations are very low in unpolluted air, under polluted conditions they are greatly increased and Table.3 gives the estimated percentage emission of major pollutants from different sources.

1.4 MASS AND LIFETIME OF ATMOSPHERIC CONSTITUENTS

The mass and lifetime of selected atmospheric constituents such as N_2 , O_2 , CO_2 , CO , NO_3 , CH_4 particulate matter and SO_2 are tabulated in Table. 4

TABLE.2 COMPOSITIONS OF CLEAN, DRY AIR

COMPONENT	CONTENT	
	% BY VOLUME	PPM
Nitrogen	78.09	7,80,910.00
Oxygen	20.94	2,09,400.00
Argon	0.93	9,300.00
Carbon – dioxide	0.0318	318.00
Neon	0.0018	18.00
Helium	0.00052	5.20
Krypton	0.0001	1.00
Xenon	0.000008	0.08
Nitrous oxide	0.000025	0.25
Hydrogen	0.00005	0.50
Methane	0.00015	1.50
Nitrogen Oxide	0.0000001	0.001
Ozone	0.000002	0.02
Sulfur Dioxide	0.00000002	0.0002
Carbon Monoxide	0.00001	0.10
Ammonia	0.000001	0.01

TABLE.3 .ESTIMATE PERCENTAGE EMISSION (BY WEIGHT) OF MAJOR POLLUTANTS FROM DIFFERENT SOURCES

Source	Particulates	Sulphur oxides	Carbon Monoxides	Nitrogen Oxides	Hydro carbons
Transportation	4.3	2.4	63.8	39.3	51.9
Motor vehicles	2.8	0.9	59.2	34.9	48.8
Gasoline	1.8	0.6	59.0	32.0	47.5
Diesel	1.0	0.3	0.2	2.9	1.3
Aircraft	N	N	2.4	N	0.9
Railroads	0.7	0.3	0.1	1.9	0.9
Vessels	0.4	0.9	0.3	1.0	0.3
Non-highway use of Motor fuels	0.4	0.3	1.8	1.5	1.0
Coal	29.0	60.5	0.8	19.4	0.6
Fuel combustion in stationary sources	31.4	73.5	1.9	48.5	2.2
Fuel Oil	1.0	1.2	0.1	4.8	0.3
Natural Gas	0.7	11.8	N	23.3	N
Wood	0.7	N	1.0	1.0	1.3
Industries Processes	26.5	22.0	9.6	0.1	14.4
Solid Waste Disposal	3.9	0.3	7.8	2.9	5.0
Miscellaneous	33.9	1.8	16.9	8.3	26.5
Forest Fires	23.7	N	7.2	5.8	6.9
Structural Fires	0.4	N	0.2	N	0.3
Coal refuse Burning	1.4	1.8	1.2	1.0	0.6
Agricultural Burning	8.4	N	8.3	1.5	5.3
Organic Solvent evaporations	N	N	N	N	13.4
Total	100	100	100	100	100

TABLE. 4 THE MASS AND LIFETIME OF SELECTED ATMOSPHERIC CONSTITUENTS

Constituent	Lifetime	Mass (Tons X 10 ¹⁵)
N ₂	Years	4.25
O ₂	Years	1.3
CO ₂	Years	28
CO	Years	0.6
NO _x	Days	0.009
CH ₄	Years	5
Particulate matter	Days to Years	15.5
SO ₂	Days	0.25

1.5 CLASSIFICATION OF AIR POLLUTANTS

1.5.1 Aerosols

A dispersion of solid or liquid particles of microscopic size in gaseous media, such as smoke, fog or mist

1.5.2 Smog

As the word suggested, it represents the combination of smoke and fog.

Two kinds of Smog

- (1) Particularly in places where coal is the principal fuel, smog covers the areas at nights or cold days when the temperature is below about 10°C and calm meteorological condition exist. The main constituents of such a smog are sulphur compounds, smoke and fly ash, With prolonged and serious exposures it may results in high mortality rates.
- (2) The other type of smog is the photo-chemical amog which usually arises in big metropolitan cities which are highly motorized and where adverse meteorological conditions do not permit free flow of air. It is now recognized that this smog is caused by the interaction of some olefin hydrocarbons and oxidants under the influence of solar radiation, giving rise the peroxy nitrate.

The main constituent of this type of smog are nitrogen oxides, peroxy nitrates, hydrocarbons, carbon monoxide and ozone. It reduced visibility, cause eye irritation and vegetation damage.

1.5.3 Smoke

Finely divided aerosol particles from incomplete combustion, consists mainly of carbon and other combustible material. It creates odour and dirt problem. Depending on the nature of fuel and the efficiency of combustion, various volatile gases and other acids may accompany control of smoke usually finds a balance between the selection of fuel for burning qualities and improved combustion devices. Highly unsaturated hydrocarbons of the olefin and diolefin families as well as aromatics are removed from fuels by treating with sulfuric acid, clay, hydrogen, sulfur dioxide to improve burning qualities.

1.5.4 Industrials Dust

Overall, the effect of industrialization has been to increase the solid dust content of the atmosphere. Sources range from major emissions such as dust in vent gases from combustion and processing operation down to minor ones such as rubber dust and tobacco aerosols, commonly called smoke. In general, a particle 10 micron or less in diameter will be suspended in air and tend to act in accordance with gas laws. The largest sources of industrial dust are combustion process.

1.5.4 Dust

A term loosely applied to solid particles predominantly large their colloidal, and capable of temporary suspension in air or other gases. Dusts do not tend to flocculate except under electrostatic forces. They do not diffuse, but settle under the influence of gravity.

1.5.5 Droplet

A small liquid particles of such size and sensity as to fall under still conditions, but which may remain suspended under turbulent conditions.

1.5.6 Fly Ash

The finely divided particles of ash entrained in flue gases arising from the combustion of fuel. The particles of ash may contain incomplete burnt fuel.

1.5.7 Fog

A term applied to visible aerosols in which the disperses phase is liquid. Formation by condensation is usually implied.

1.5.8 Fume

Properly, the solid particles generated by condensation from the gaseous state, generally after volatilization from melted substances, and often accompanied by a chemical reaction such as oxidation.

1.5.9 Particulate Matter

Existing in the form of minute particles either solid or liquid.

1.6 POLLUTANTS OF SPARK IGNITION ENGINES AND ITS EFFECTS

Two invisible automobile emissions, hydro carbon and oxide of nitrogen reset together in the presence of sunlight to form oxidant such as ozone a principal ingredients of Loss Angles "Smog"

The pollutants now known to be caused by each type of Ignition Engines emission are listed below.

1.6.1 Hydrocarbon

The aromatics, naphthenes, olefins and parafins constitute the hydrocarbons that originate from numerous sources. The most predominant sources being the unburnt or partially burnt gasoline. Hydrocarbons are known to ne a

participant in photochemical smog and suspected as a contribute to odour. Smog has been inferred that the nature and concentration of organic vapour of an atmosphere are among the prime determinants of its sensory quality of freshness. Thus it seems that natural events contribute significantly to air quality as hydrocarbons are concerned.

Methane is the largest single source. It is evaluated primarily from bacterial decomposition which as a source seems relatively stable with time. Vegetation also contributes the hydrocarbons to the atmosphere. The automobile is the biggest single contribute to man caused hydrocarbon pollution, although the contribution of incinerators is large. Nitrogen dioxide and hydrocarbons are equally important in the photochemical formation of ozone concentrations and that the amount of ozone formed has been found to be proportionate to the product of nitrogen dioxide and hydrocarbon concentrations. Ozone may characterized photochemical smog but the eye irritation and reduced are objectionable for public health.

1.6.2 Carbon monoxide

Apart from CO₂, CO is the most abundant and widely distributed pollutant. Very little CO is due to natural events almost all is from man caused events. Approximately 90% of man caused CO is from automobiles. However, some carbon monoxide comes from natural events such as marsh gas, coal gas mines, seed germination, injured vegetation, forest etc., Carbon monoxide is odour-less and colour less gas. From health point of view CO is dangerous because it has a strong affinity for combining with the hemoglobin of the blood. Hence the hemoglobin available to carry the oxygen to body tissues is reduced. It is possible, however that the level of CO that we are reached in the streets may affect some specially susceptible persons, such as those already suffering from a disease associated with a decrease of oxygen carrying capacity of the blood or those suffering from cardio respiratory disease. Concentration in ignition is as high as 75 ppm for period of at least 5 minutes with a medium of 60 ppm are found. The California department of public health indicated that exposure of 30 ppm for 8 hours may be as serious risk to the health of sensitive people. In addition many people when smoking, voluntarily expose themselves to levels of many orders higher than those under discussion.

1.6.3 Carbon Dioxide

CO₂ is not normally considered as a pollutant. It is essential for plant life. The primary source of CO₂ from natural events is organic material, although respiration amounts are large and will increase as the population increase. Combustion is the primary source of man caused CO₂ and that the natural and man caused amounts are of the same order of magnitude. One big absorbing source is of course photosynthesis by ocean could sold some 50 times the amount of the CO₂ in the atmosphere.

1.6.4 Oxides of Nitrogen

In addition of molecular nitrogen found in the air, nitrogen is present as NO, NO₂, NO₃, N₂O₂, N₂O₄, N₂O₅ etc., However of all these compounds the only pollutants that are significantly man caused are NO and NO₂. It should be realized however, that these two oxides of nitrogen represent only a small fraction of the total circulation of Nitrogen compounds. For example, the mass rates of NH₃ circulation are some 10 times of the two oxides of nitrogen. Nitric oxide is found at high combustion temperatures with the exact amount primarily, dependent upon the temperatures, oxygen concentration and time. In the atmosphere nitric oxide reacts with oxygen and is rapidly converted to nitrogen dioxide. This reaction can be greatly accelerated by the presence of sunlight and organic materials in the air.

Most atmospheric characteristic of oxides of nitrogen dioxide and designate the combinations as NO_x. In addition to causing a reduction in atmosphere visibility nitrogen dioxide also has an affinity for hemoglobin, however because it forms acid in the lungs, it is considerably more basic than carbon monoxide for the same concentration.

1.6.5 Sulphur Dioxide

Atmospheric sulfur is primarily in these forms, SO₂, H₂S and sulphates. H₂S is evaluated primarily from natural sources. SO₂ comes primarily from man caused events, the sulphates come primarily from sea spray and from oxidation of SO₂. It is estimated that 70% of SO₂ comes from the combination of coal. It is clear that mass rates are high with respect to the mass in the atmosphere.

With regard to health, a concentration of 0.6 ppm will produce no detectable response in healthy human, most people can detect 5 ppm and find 10 ppm quite unpleasant. The situation is further complicated by the interaction and increased toxicity in so far as health is concerned when sulfur dioxide, high air temperature, high air humidity, aerosols, etc are simultaneously present.

1.6.6 Lead

Concern with atmosphere lead arises primarily from its use as a gasoline additive, test have shown fairly conclusively that lead concentration in the atmosphere below traffic density patterns. The reason shows that approximately 70% of the lead used in car is emitted from the tail pipe with 30% setting almost immediately to the ground and the 40% becoming air burns and causing deflects. The lead appears in the exhaust as PbCl. The particle size of the discharge lead compound various from those of less than 0.01 micron to those of many millimeters.

The air burns lead is small in mass in comparison with that taken in via food and water, but that a higher percentage of the airborne lead reaches the blood.

1.7 EFFECTS OF AIRPOLLUTION

Table5. Shows that health effects of airpollution, Table.6. Shows that effects of airpollution on various materials & Table.7. Shows that effects of pollutants on plants

1.8 SOURCES OF POLLTANTS FROM SPARK IGNITION ENGINES

Automobile contribute about 60% of the total mass of air pollutants. This is shown in the Table 8.

TABLE 5. HEALTH EFFECTS OF AIRPOLLUTION

POLLUTANT	SHORT TERM HEALTH EFFECTS	LONG TERM HEALTH EFFECTS
Oxidant (Ozone and other)	Difficulty in breathing, chest tightness coughing	Impaired lung function, increased susceptibility to respiratory infection.
Total suspended particulate matter	Increased susceptibility to other pollutants.	Many components of TSP are toxic and contribute to silicosis
Sulphate particles	Increased asthma attacks	Reduced lung function when oxidant is also present.
Nitrogen Dioxide	Similar to ozone but at higher concentrations.	Increased susceptibility to respiratory infection.

TABLE 6. EFFECTS OF AIRPOLLUTION ON VARIOUS MATERIALS

MATERIAL	POLLUTANT	EFFECTS
Metals	SO ₂ Acid Gases	Corrosion, spoilage of surface, loss of metal, tarnishing.
Building Material	SO ₂ acid gases, particulates	Discoloration, leaching
Paint	SO ₂ , H ₂ S, Particulates	Discoloration
Textiles and textile Dyes	SO ₂ Acid gases, NO ₂ , Ozones	Deterioration, reduced tensile strength and fading
Rubber	Oxidants, Ozone	Cracking, Weathering
Leather	SO ₂ Acid gases	Disintegration, powdered surface
Paper	SO ₂ Acid gases	Embrittlement
Ceramics	Acid Gases	Change in surface appearance

1.8.1 Sources of Hydrocarbons

There are four possible sources of pollutants in the case of automobiles. These are listed below.

1. The Engine Exhaust
2. Crank Case Vent
3. The Carburetor
4. Fuel Tank

The two latter sources can contribute only evaporated fuel and it amount 5 to only 15% of the total unburnt hydrocarbon, emission from motor vehicles. Hence the more complex and

TABLE.7. SHOWS THAT EFFECTS OF POLLUTANTS ON PLANTS

Pollutant	Dose	Effect	Special Cases
Ozone	Mild	Flecks on upper surface, premature aging, suppressed growth	0.06 ppm for 3-4 Hr damages alfalfa white pine.
	Severe	Collapse of leaf, necrosis and bleaching	
SO ₂	Mild	Intervenal chloride bleaching of leaves	1 ppm for fumigation times cause damage to alfalfa, cotton, barley.
	Severe	Necrosis in intervenial areas and skeleronized leaves	
Ethylene	Mild	Epinasty, leaf abscission	0.100 ppm for several hours affected tomatoes and pepper lants.
NO ₂	Mild	Suppressed growth leaf bleaching	0.5 ppm for 10.12 days suppressed growth on tomatoes
Fluorides	Cumulative effect	Necrosis at leaf tip	

TABLE.8 DETAILS OF AIR POLLUTANTS

Sl.No.	POLLUTANT	10 ⁶ Tones/ Years
1	Carbon Monoxide	66.0
2	Oxides of Nitrogen	6.00
3	Hydrocarbons	12.00
4	Sulfur Oxides	1.00
5	Lead Compounds	0.19
6	Particulates	1.00

more plentiful exhaust. Products of the combustion processes are potentially exhaust products of the combustion process and potentially far more harmful and easier to control than the evaporated full emission. Unburnt hydrocarbons and oxides of nitrogen in the presence of ultraviolet radiation, are mainly responsible for the irritating and damaging consequences of smog. The reactivity of hydrocarbons and their derivatives in this photosynthesized reaction is a function of their chemical structure olefinic hydrocarbons, aldehyds and other oxygenated hydrocarbons and aromatic hydrocarbons are recognized as the more reactive components of organic material. The saturated lower paraffins (i.e., methane through pentane), benzene and acetylene are practically non-harmful.

1.8.1.1 Two sources from the fuel and carburetor system

1. Evaporation losses from the carburetor itself.
2. Evaporation losses from the breather vent in the fuel tank.

In order to relieve the interval pressure within the float bowl, resulting from vaporization of gasoline as the carburetor gets heated during operation, modern carburetors are designed with the float bowl vented by either external vents to the outside or internal vents to the carburetor throat or both. The external vents are a source of hydrocarbon emission to atmosphere during engine operation. The factors responsible for evaporation losses from the carburetor are as follows:

1. The ratio of internal to external venting
2. Float bowl temperature as it affects the pressure difference between the outside and inside of the bowl.
3. Fuel volatility.

1.8.1.2 Hot Soak Losses

Another aspect of the carburetor vent loss is termed "hot soak loss" and occurs after the engine has stopped. The heat stored in the engine during operation is transferred to the carburetor causing the temperature of gasoline in the carburetor bowl to rise 60 to 70° F above ambient atmospheric temperature. The gasoline stored in the carburetor bowl is thus vaporized and is forced out of either the external or internal carburetor venting system to the atmosphere.

Hot soak losses, as the temperature of the gasoline in the carburetor bowl is rising, usually occur within the first 40 minutes after the engine is stopped. In present carburetor

design these are a function of bowl capacity. Fuel volatility and ambient temperature for the average sized carburetor using a volatile summer type fuel, the losses vary 0.004 lb at 75° F ambient temperature to 0.96 lb at 100° F ambient temperature.

1.8.1.3 Breather Vent in Fuel Tank

Losses from breather vent in the fuel tank result primarily from the slow vaporization of the gasoline in the tank, forcing the vapour through the tank breather vent to the atmosphere. These losses vary with ambient temperature, fuel volatility and car operation. For summer type fuels, with ambient temperature range of 75° to 100° F the losses result in discharge to the atmosphere of 0.008 to 0.0053 pounds per hour for a vehicle standing and 0.012 to 0.040 round per hour for a vehicle in motion.

A study of the control of hot soak and fuel tank emissions, indicates that approximately 90% of these emissions can be eliminated through changes in the fuel system of the modern car. Such modifications basically consist of insulating the fuel tank, equipping it with a pressure vacuum type pop-off valve, and providing for the automobile draining of the carburetor bowl when the engine is stopped.

1.8.1.4 Blow-by Emissions

The largest secondary source of hydrocarbon emissions associated with automobile engine operation is found in the blow by gases vented from the engine crank case. These gases consist of a mix of unburnt fuel air charge and exhaust products blown past the piston rings during the compression and power strokes of the engine cycles.

Analysis of the blow-by gases indicates that they are composed approximately 85% carbureted fuel air mixture and 15% exhaust products. Accordingly the detailed composition of the hydrocarbons emitted from the crank case reflects the composition of the injected fuel, being burnt in the engine. Concentration of the blow-by gases varies between 6,000 and 11,000 ppm of hydrocarbons.

The high concentrations of hydrocarbons and the injected fuel in the blow by gases is evident from a consideration of the engine blow-by processes. The pressure differential across the piston of the automotive four stroke engine indicates that the most of the blow-by must occur during the compression and power strokes. At piston TDC, the direction of the piston travel changes and a reversal of piston side thrust occurs. Both these factors interfere with the sealing of the piston rings near the time of maximum cylinder pressure. Owing also to the generally spherical form of the flame front the cast portion of the fuel air charge to burn is that located in the annular section at the piston top and cylinder wall. The small clearance between the cylinder wall and piston is sufficient to cause quenching of the flame.

Blow-by emissions rate for cruise, idle and acceleration are found to be generally at a fixed percentage of the rates of exhaust emissions for the given engine. For deceleration, blow-by emission rates are high. Based on an

assumed driving pattern, from 25 to 35% of the total hydrocarbon emission results from the blow-by gases.

Theoretical composition show that there is no hydrocarbons in the exhaust, if the system is in equilibrium. Thus it is believed that they are formed in quench area, that is in the cold zone immediately adjacent to the cold combustion chamber walls.

The bulk gases will be exhausted primarily during the middle portion of the exhaust period. During this time, it is experimentally observed that the hydrocarbon concentration is low. On the other hand the first and last part of the exhaust process which is primarily when the quench gases are being exhausted shows high concentration of hydrocarbons.

In looking at hydrocarbon data from real engines, however one must recognize is that oxidation does not take place in the exhaust process and exhaust system.

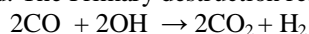
1.8.2 Carbon Monoxide:

In an attempt to reduce where and how carbon monoxide is formed the result of theoretical computations are presented in the figure. This shows CO concentration as a function of the extent of expansion of the gases for an ideal cycle for three different equivalence ratios. Experimentally measured exhaust gas concentration of CO are shown for two equivalence ratios.

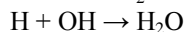
Again, the data show that the measured concentration of CO at peak cycle temperature that those existing at the end of the expansion. Thus as in the case of NO, CO is also formed in the bulk gases, and in part at least as a result of frozen products. Particularly at rich mixtures, measured concentration of CO are closer to the peak cycle concentrations than to those existing of equilibrium occurred all during the expansion process.

Interestingly enough as one approaches stoichiometric or leaner mixtures, it appears that measured concentration of CO is more nearly approach the concentration that would be expressed if equilibrium occurred during all of the expansion process.

Since there is non equilibrium in so far as the concentration of CO is concerned during the expansion process, it is necessary to look at the destruction reactions involved. The Primary destruction reaction for CO is,



When this reaction is in equilibrium, its reaction rate is relatively rapid. It appears that the CO concentrations high because the atomic hydrogen concentration are high, that is the rate of destruction of hydrogen appears to be low. The two reactions that cause hydrogen destructions are,



CO concentration follows directly the air fuel ratio and a rich mixture operation must be avoided at all times. There is a greater concentration of carbon monoxide in the exhaust than expected due to freezing.

As air fuel ratio decreased toward richer fuel mixture, the volumetric percentage of CO increases. This results in an

increase in volumetric percentage CO with decreasing cruise speed and with decreasing severity of acceleration, reaching a maximum percent of carbon monoxide deceleration. The effect of air fuel ratio on volumetric percent carbon dioxide is opposite to that for carbon monoxide. With decreasing air fuel ratio volumetric CO decreases. With increased operating temperature and oxygen concentration (ie) high air fuel ratio and high peak cycle temperature to chemical equilibrium between CO and CO₂ is shifted towards carbon for the engine operating condition of high speed cruise and acceleration.

In contrast to volumetric percent emission, weight emission of CO expressed in pound per hour in general increase with severity of engine operation varying from a maximum of rapid acceleration through cruise to a minimum at deceleration and idle. This difference results from the more rapid increase in exhaust gas flow. With severity of engine operation, overriding the decrease in volumetric percent of carbon monoxide in the exhaust.

1.8.3 Oxides of Nitrogen

Figure shows a plot of NO concentration where as the extent of expansion of the products of combustion in the cylinder. The curves show are for different equivalence ratios and shows the NO concentration that would be present if thermodynamic equilibrium were maintained during expansion. The measure levels correspond more nearly to the NO concentrations present at the beginning of expansion rather than the NO concentration at the end of expansion. Concludes from, that the NO concentration measured in the exhaust should correlate reasonable well with. The peak cycle temperature shows that the peak temperature varies with location in the combustion chamber.

The NO concentrations at approximately stoichiometric air-fuel ratios follow the same trend as the peak temperature curve and for a rich mixture, they do not follow the same trend as the peak temperature curve.

If NO is primarily related to the peak combustion temperature, it may be inferred that is formed primarily in the bulk gases as opposed to being formed in a quench zone next to the cold combustion chamber walls. This deduction is shown in figure, as a function of distance for the head manifold surface that is distance downstream from the exhaust valve. For three quarter of the cycle there is no flow in the exhaust line.

When exhaust does occur, the first gases to come out will be those adjacent to the exhaust valve which in turn will be followed by the large bulk of the gases by the quench zone gases scraped from the cylinder walls as the piston moves up on the exhaust stroke. If the deduction that the NO is formed primarily in the bulk gases is correct, the concentration of NO as a function of distance down the exhaust pipe should increase, reach a maximum and then decrease.

The amount of NO that would be present in the exhaust of an ideal, constant volume cycle were followed and if the NO concentration in the exhaust gas that formed at TDC, that is at the peak cycle temperature. It can be seen that for this

situation NO reaches a maximum of an air fuel ratio of around 18 or 19%.

Two experimental curves for spark ignition engines are shown. Both curves were taken with the spark timing adjusted as the air fuel ratio was changed so that the peak pressure always occurred at 10 degree. The reason for doing this is, that in the engine peak temperature changed with a change in the air fuel ratio for two reasons. In the first place, peak temperature will change with a change in the air fuel ratio because, of more or less excess air to be heated up, just as in a burner. However, in the engine in addition the flame speed varies with a change in air fuel ratio and as a consequence, peak pressure will occur at different cylinder volumes with a consequently change in peak temperature. One of the curve is for a premixed mixture and the other curve is for a heterogeneous mixture such as in undoubtedly present in a practical multi cylinder spark ignition engine.

The most important NO destruction reactions are,

- 1) $NO + N \rightarrow N_2 + O$
- 2) $NO + O \rightarrow N + O_2$
- 3) $NO + NO \rightarrow N_2O + O \rightarrow N_2 + O_2$

Of these reactions, number (1) is slowest while number (2) and (3) are the fastest. All of them are quite slow, thus explaining the fact that very little recombination takes place during expansion. The Table.9 explains the effect of vehicle mode on emissions.

TABLE.9 EFFECT OF VEHICLE MODE ON EMISSIONS.

Vehicle Condition	Engine	Flow	Concentration		
			HC	CO	NO _x
1. Idle	Operating	Very low	High	High	Very low
2. Cruise					
i. Low speed	Operating	Low	Low	Low	Low
ii. High Speed	Operating	High	Very low	Very low	Moderate
3. Acceleration					
i. Moderate	Operating	High	Low	Low	High
ii. Heavy	Operating	Very high	Moderate	High	Moderate
4. Deceleration	Operating	Very low	Very high	High	Very low
5. Soak					
i. Hot	Stopped	None	--	--	--

2. METHODS AND METHODOLOGY

Transport facilities is being improved every year in the town to meet the increase in demand due to the population growth and tourism growth. There are large no of commercial vehicles and non-commercial vehicle is Tourism Town. In order to access the auto emission of these vehicles. One Authorized Vehicle Emission Testing Centre is available in Udhagai Town. Survey was conducted in this emission centre through Regional Transport Office.

2.1 TESTING METHODOLOGY FOR DIESEL VEHICLES

Netel's smoke meter Model NPM-SM-111B (Figure.1) has been designed and developed to get an accurate reading of diesel engine smoke emissions, according to the specifications laid down by MINISTRY OF SURFACE TRANSPORT (MOST). Its use promotes combustion efficiency for fuel economy in diesel vehicles and stationary diesel engines.

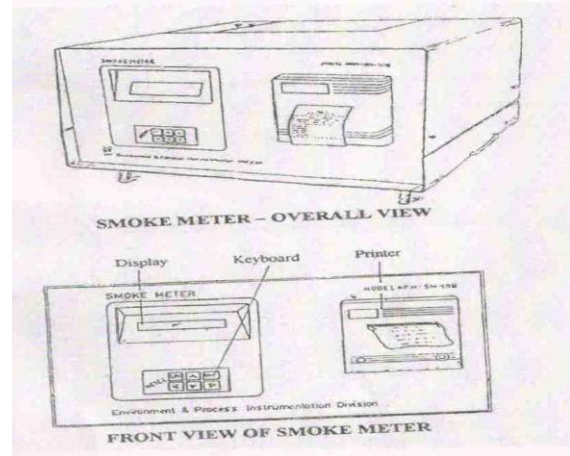


FIGURE.1 NETEL'S SMOKE METER MODEL NPM-SM-111B

The key features of smoke meter are

- Alphanumeric LCD display with back light for day & night operation.
- User friendly keyboard & display interactions.
- Built-in 24 column printer for hard copy of the report
- Autozero facility
- Easy Calibration check.

2.1.1 Technical Specifications

1. Model Number : NPM-SM-111B
2. Type of smoke : Partial Flow
3. Display Indication : Light Absorption Co-efficient (K) / percentage opacity
4. Display range : 0 to 99 / m
5. Scale Resolution : 0.1 / m
6. Linearity : 0.1 / m
7. Drift : Zero: 0.1 / m
Span: 0.1 / m
8. Repeatability : 0.1 / m
9. Light Source Details : 5 mm diameter green LED
10. Response Time : 0.3 Seconds
11. Warm-up time : 1.5 Seconds
12. Operating Temp. range : 5 to 50°C
13. Power Requirement : 260 V AC + 10 % 50 Hz
14. Weight : 24 Kgs

15. Dimensions : (W) 47.5 cm X (D) 47 cm x (H) 26 cm

2.2 TESTING METHODOLOGY FOR PETROL VEHICLES

The model NPM-CHI CO / HC analyzer (Figure.2) can be for the infrared analysis of the exhaust gases of OTTO cycle engine. A check of CO / HC exhaust values is currently essential if an engine is to be correctly set up or in order to diagnose possible operative malfunctions. Unless exhaust values are correctly adjusted. It is absolutely impossible to obtain a good engine performance of good economy of operation.

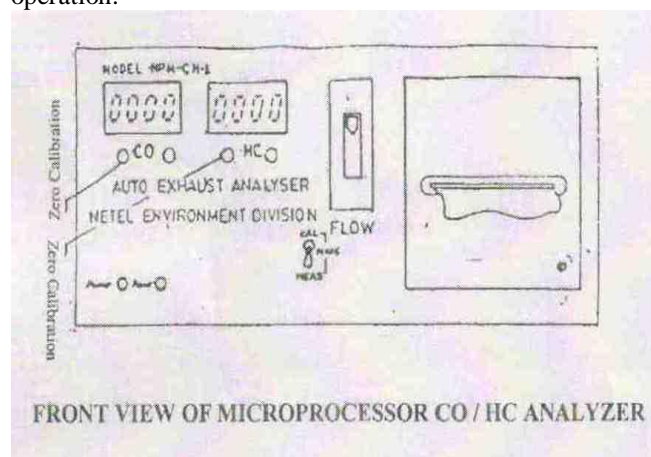


FIGURE.2 MICROPROCESSOR CO/HC ANALYZER

2.2.1 Technical Specification

Range of measurement : CO: 0 to 8.5% vol.res.0.01%
 HC: 0 to 1995 ppm, res. 5 ppm
 Operating Temperature : + 5° C to + 45° C (+2)
 Pressure variation : Max error 0.2% for variations of 50 millibars (37 mm Hg)
 Measuring gas Intake : 5 – 81 / min (approx.)
 Flow Check : Manual
 Condensate Discharge : Automatic
 Response Time : > 10 Sec.
 Warm up time : max 15 minutes
 Power supply : 230 C + 15%, 50Hz – 100 watts
 Automatic Signal with Error code
 Printout if > + 15% Zero Setting : Manual
 Calibration : Manual
 Printer : 24 Col.
 Dimensions : 400 x 200 350 mm
 Weight : 12 Kgs (approx.)

3. RESULTS AND DISCUSSION

A survey of vehicular pollution has been undertaken to access pollution contribution from transport sector. The available information are compiled from different sources and used for emission estimation from transport sector in the Ooty Town. CO, HC and smoke density for Indian vehicle and the

findings are plotted for the year of makes in the following graphs.

According to the study and the survey, it is concluded that old model vehicle are major polluters. Two wheelers emit major amount CO and HC.

Figure.1. shows that smoke density versus year of make (lorry and bus). Permissible limit of smoke density by the 4-stroke engine (lorry and bus) is 65 hatridge units. It is found from the plot that the emission of pollutant is maintained well within the permissible range. i.e., below 60 hatridge units by vehicles aged with 25 years or less. Vehicles which are put in use above 25 years normally reaches the permissible limit of smoke density

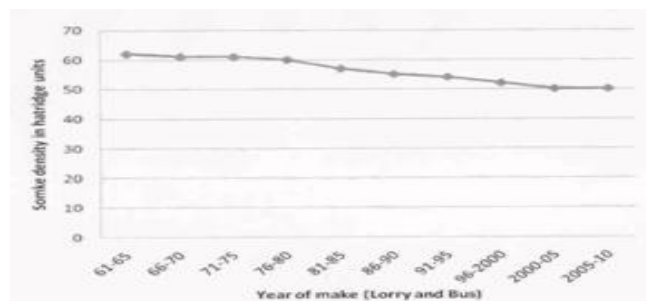


FIGURE.3. SMOKE DENSITY VERSUS YEAR OF MAKE (LORRY AND BUS)

Figure.4. shows that smoke density versus year of make of van and tempo. Vehicle aged around 40 years is about to reach the permissible limit.

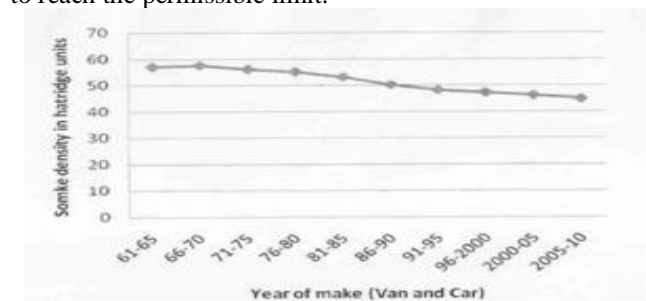


FIGURE.4 SMOKE DENSITY VERSUS YEAR OF MAKE (VAN AND TEMPO)

Figure.5. shows the emissions of CO in % of volume by 2 stroke and 4 stroke engines. It is obvious from this result that 2-stroke engines emit more CO rather than 4-stroke engines.

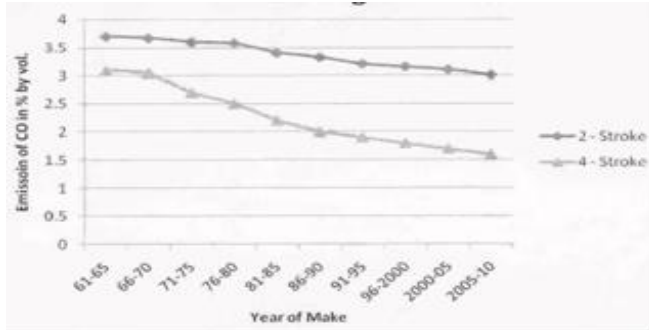


FIGURE.5 EMISSIONS OF CO IN % OF VOLUME BY 2 STROKE AND 4 STROKE ENGINES.

Figure.6 shows the emission of HC in ppm which indicates that 2-stroke engines emit more HC than 4-stroke engines.

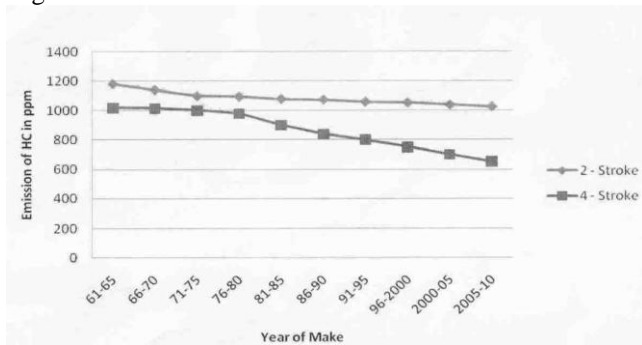


FIGURE.6 EMISSION OF HC

4. CONCLUSION

Many of the problems discussed earlier start at the local level. For quite a long time, scientists were under the impression that these problems were localized and they were trying out technologies and scientific methods to abate pollution and protect the local environment. But deep studies indicate that these problems not only affect the local environment, but the ill-effects spread to the other parts of the world as well. If this situation continues, then life on earth on become intolerable. Hence "Save our Earth" has become the slogan now. The problems and their ill-effects have to be thoroughly analyzed at the global level. But, to prevent ill-effects, suitable action has to be taken at the level. Environment is a partner to development and not an impediment. In order to maintain essential ecological process, to ensure genetic diversity, sustain species and eco-systems, prevent environment degradation, the following changes should be made in the vehicle to reduced the emission.

- **Modification in old vehicle.**

According to the study, it is often assured that gross polluters are simply old vehicles. Ashok Leyland has been able to improve its well-established range of layland

and Hino-commercial diesel engines to meet Euro I emission norms essentially by modifying the "engine heads" and by fitting slightly higher pressure injection pumps. An essential features of such modifications is that they can be retrofitted to existing engines there by providing a dramatic reduction in emissions while being relatively cheap and quick. This is obviously better than a policy of banning vehicles over certain age, because that will lead not only to a neglect of vehicle's engines over the fag end of its legal life, but also a dangerous neglect of its steering breaking and suspension systems.

- **Fuel Quality and Emissions.** No legislation or technology can bring down emission levels unless fuel quality also improves. Most Indian refineries now have Fluidized Catalytic Crackers which produce high quality petrol with little need for octane enhancing lead compounds and have operational hydro-desulphurising units which produce diesel with maximum sulphur levels of diesel with maximum sulphur levels 0.25 percent rather than the one to three percent common even last year.

- Most Automobile manufactures have launched Vehicles with a multi-point fuel injection and engine management system that uses conical injectors and is claimed to be impervious to fuel adulteration level of even 50 percent.

- The Government of Tamil Nadu Authorized the Tamil Nadu pollution Control Board to test and issue Emission Under Control Certificate (EUCC) for four wheelers.

According to the study two wheeler are gross polluters of CO and HC. Hence Government should bring legislation such a way that the Emission Under Control Certificate (EUCC) test for two wheelers also.

- Routine (and relatively cheap) maintenance and emission testing along with good quality fuel enables to control vehicular emissions.

5. REFERENCES

- [1]. Ganesan .K.Pamdit.V.I. Dixt.S.N.and Yennawar .P.K. "Flouride Industry : Air Pollution and It's Impact on the surrounding Area" IJEH. 20(1): 62 – 6 178).
- [2]. Zutshi .P.K Mahadevan T.N. Vaidyanathan .M. and Sathe.A.P. "Studies on SO2 and a Few Other Pollutants In Air and In Rainwater" IJEH, 20 (1) : 14 – 28 (1978)
- [3]. Karunanadhi .M, "Air Quality Survey of Madras City" M.E., Thesis, College of Engineering : Guindy (1979)
- [4]. Jagadeesen .D, " Pollution Survey Around Basin Bridge Power House" M.E., thesis College of Engineering Guindy (1982)
- [5]. Dharamadhikari .D.M and Yennawar .P.K, "Air Borne Manganese Level In surroundings of Ferro – Manganese factory" JIEH, 24 (1) : 36 – 43 (1982).
- [6]. Thahamjeya Veera RAj .T. "Experimental Assessment of air Quality in the Basin Bridge Power

- House Area” M.E., Thesis, College of Engineering Guindy (1985)
- [7]. Gupta .R.K., Sharma .V.P, and Arara .H.C., “A Study of Air Quality at Kanpur” IJEH, 29 (2): 180 – 182 (1987)
- [8]. Joshin .S.D, Phadke .KM. Gajrani .C.P., Kothari .J.V., Seth .A.K.Bhandari.I.M and Aggarwal .A.L., “A few measurements & Ambient Air Pollutants of Udaipur City “ IJEH, 33 (1) : 31 – 39 (1991)
- [9]. Ravindra .V, Rajeshwarker, “Evaluation of Ambient Air Quality of Gulbarga City: M.E., Thesis , Department of Environmental Engineering. H.K.E Society’s P.D.A College of Engineering Gulbarga – 2 (1993).
- [10]. Chandrasekaran .G.E., Ravichandran .C and Manibhushan Singh .K.K, “Air Borne Carbon Particulate matter with Reference to a Cement Plant at Ariyalur” IJEP, 16(5) : 356 – 358 (1996).
- [11]. Babu.R, Gopal.V, and Balasubramaniam.PR., “Assessment of Ambient Air Quality Monitoring In and Around Hindustan Photo Film Manufacturing Company (Ooty)” IJEP, 17 (7) : 511 – 512 (1997).
- [12]. Dash.T and Panda .A, “Ambient Air Quality Around Lilari Pendeast Coal Mines” IJEF, 17 (7) : 542 – 544 (1997).

Developing an Intelligent Tutoring System for Assessing Students' Cognition and Evaluating Descriptive Type Answers

Papri Chakraborty

School of Education Technology, Jadavpur University, India

ABSTRACT

An intelligent tutoring system (ITS) is a system based on artificial intelligent factor that performs some specific activities, such as, teaching the students, evaluating their performance with proper feedback, measuring their strength and weakness areas, etc. The paper presents architecture of an intelligent tutoring system which includes a metric to evaluate descriptive type answers. A system is designed to demonstrate the metric and it mainly focuses on delivering content material to the students, organizing test sessions and providing students with suggestive feedback after evaluation. The proposed metric measures the correctness of descriptive type answers with limited spelling relaxation and grammar checking under restricted conditions. The metric works moderately for simple sentence answers and can distinguish the answers as correct, error or elaboration.

Keywords - Descriptive-type Answer Evaluation in ITS, Intelligent tutoring system, Knowledge Tracing in ITS, Students' Skill Assessment

I. INTRODUCTION

The concept of using computers to assist learning process has changed the field of learning system surprisingly. At present days the systems not only deliver learning contents but also provide the learners with suggestions and feedback. Students can also ask questions and get hints to complete complex problems. With more research and developments ITS agents may model human behavior and track the students' emotional states. In commonly used Tutoring Systems the learners are generally provided with contents and the test sessions. Apart from these features it is important to determine whether the students are comfortable with the content delivery pattern or not. It is also expected that the systems will select test levels according to the capability of individual student. Moreover the evaluation process should be explicit and suggestions should be given to help the students find out their weaknesses and strengths. Another major problem area is the test sessions only allow objective type questions or MCQ type questions supported by check boxes, radio buttons or OMR sheets. The provision for descriptive type question-answer sessions is very rare. The primal objective of this paper is to deal with the above

mentioned challenges. In the paper an ITS is developed through which students can not only experience a sequential user friendly learning process but also obtain feedback through a proper evaluation technique. A metric is proposed for measuring correctness of students' descriptive type answers effectively. The paper is organized into the following sections. Section II illustrates the previous work reviews on this field, section III presents the proposed approach and metric, section IV explains the implementation details of the system, section V analyses the proposed work, and section VI briefs the conclusion, probable future scope and limitations of this paper.

II. PREVIOUS WORK

Many architectures and features have been proposed on ITS. The researches are mainly based on student's knowledge tracing, assessments and evaluation. Bayesian method is followed to identify the most important learning items which can result in the most effective tutoring strategy [2, 11]. Processes like scaffolding, prompting, self-questioning simplifies student's comprehension on subject content [4, 8]. Text-relatedness metrics are used to support the authoring in ITS [5, 7]. Natural language helps to minimize the difference between Human tutors and Computer tutors and author an ITS [9, 12]. Prediction of learning styles from an ITS mark the students as sensing or intuiting, visual or verbal, active or reflective, sequential or global learners [1, 3, 13]. Neural network based methods predict student's mood during learning and test session [10, 14].

III. PROPOSED APPROACH

The paper proposes architecture to serve some basic features of tutoring system and also evaluate the students intelligently. The system focuses on the tutor expert, domain expert and student expert. The system supports two roles: tutor and student. In this work the tutor is given the privileges to access the tutor expert and domain expert. The student has the privileges to access the student model.

3.1 Identification of Roles: Tutor and Student

The tutor and student use the system according to their assigned privileges.

3.2 Content Editing

In the system an authenticated tutor can change or edit the contents easily if required. For this no programming knowledge is required.

3.3 Delivering the Contents and Test Sessions

Content material is delivered to the students. The provided test sessions are pre-knowledge test, level-I test, level-II test, level-III test and general knowledge test. The first four test sessions are objective type test. The last one is descriptive.

3.4 Pre-knowledge Assessment Using Item Effect Model and Evaluation

The pre-knowledge assessment is mandatory for every student before learning the contents. The slip rate and guess rate is derived from this test. Pre-knowledge evaluation shows slip rate and guess rate. The general assessment follows the behavioral model and it only concentrates on the current learning. The post learning evaluation is based on the differential model and epistemic level which compares the student post learning knowledge to the pre-knowledge and determines whether student's knowledge has improved or not.

3.5 Objective Type Test Session and Evaluation

This session comes after the student has completed reading the chapters. The system selects the appropriate test level for the student. The student can also select the test level of his/her own choice. There are three test levels. The sessions are time bound. After completing the tests the students are provided with the correct answers and the score.

3.6 Descriptive Type Test Session and Evaluation

The proposed metric is included in this session. The metric is supported by two sub-modules: spell-checker and grammar-checker. The students submit their answers and go to the evaluation page. The answers are classified into three categories: error, correct, and elaboration. If the answer is completely invalid or contradictory it is an error. If the sentence is syntactically and morphologically same as the required answer it is a correct answer. If the answer is non-contradictory or reasonable with respect to the required answer it is an elaboration.

3.7 Contribution

3.7.1 Spell Checker Module

The spell checker embedded to the system is applied to the descriptive type test session. When the student input an answer the spell checker provides relaxation for minor spelling mistakes. It performs operations like addition, alteration, deletion of a single character and swapping between two consecutive characters at any position of the word. With these combinations it basically searches for all the probable correctly spelled words and forms a suggestion

list. The misspelled words are then substituted by the correct words with a priority of taking answer relevant words if found in the suggestion list.

3.7.2 Grammar Checker Module

The grammar checker is also applied to the descriptive type test session. It tags each word of the input answer with its parts of speech. It also defines the relation between different parts of speech and sets them as basic rules for grammar checking [15].

3.7.3 Steps to Evaluate Descriptive Type Answers

Step 1: Start.

Step 2: Form the correct answer and store all the words present in it in a master table.

Step 3: Identify and tag the key words and key verbs. Tag other words as the non-key terms. Put weights to all the words according to their importance in the answer. Calculate the weights for actual correct answer by adding all the assigned scores of all words present in it and store it.

Step 4: Insert all probable negative type words, such as, no, not, never, etc, to another table.

Step 5: Collect and insert all the probable synonyms and antonyms of the words of the correct answer to a synonym table and antonym table.

Step 6: If there exists any verb in the master table or synonym table or antonym table then insert their all possible tenses accordingly to the synonym table and antonym table.

Step 7: Assign a weight to each synonym considering the change of meaning of the sentence due to its presence.

Step 8: Set student's score for the answer to 0. Input student's answer. Split the input into words and store them in a temporary table.

Step 9: Check if the key words or key terms are present in the temporary table. If key words or key terms found put the weight for that word. $\text{score} = \text{score} + \text{new weight}$. Go to *Step 11*.

Step 10: If key word or key verb not found then check if any synonym word of the key terms are found. If synonyms for key terms found put the weight for that word. $\text{Score} = \text{score} + \text{new weight}$. Go to *Step 11*.

Step 11: If synonyms for key terms not found then stop further checking and consider the answer as ERROR.

Step 12: Check whether the input answer starts with any no-type word or not. If a no-type word is found at the beginning of the sentence then check whether there is any other no-type word present in the sentence. If found discard the first no-type word. If the number of other no-type words

found is n, score = score * (-1)ⁿ. Else if the no-type word at the beginning is the only no-type word in the sentence then the total score of the sentence should be multiplied by -1.

Step 13: Check if any other antonym found in the temporary table. For each antonym the net weight should be multiplied by -1. If number of antonym is n, score = score * (-1)ⁿ

Step 14: Check if any antonym is present in the temporary table. For each antonym of the key terms the net weight should be multiplied by -1. If the number of no-type words is n, then score = score * (-1)ⁿ

Step 15: Check the position vectors of the nouns and verbs combination in the input answer and compare it to that of the correct answers to verify the dependencies of the nouns and the verbs in the answer.

Step 16: Put the weights of the non-key terms accordingly. Put weight 0 for any unknown word found. Now calculate the net weight.

Step 17: Check if there exists any grammatical error in the sentence. For each grammatical error deduct 2 from the net score.

Step 18: If the net score is negative the answer is an ERROR. If the net weight is positive and in the range of 20% of original score then the answer is CORRECT. If the net weight is positive but does not fall in the range then the answer is ELABORATION.

Step 19: End.

IV. IMPLEMENTATIONS

The proposed architecture and algorithm of the metric is implemented in Microsoft Visual Basic and Oracle Database. There is option for user to select their roles for using the system. Without having a valid authentication code no user can sign in to the system as a tutor. Fig. 1 shows the authentication page.



Fig. 1: Tutor login page

The tutor home page shown in Fig. 2 has the links, such as, read chapters; edit chapters; view current question-answer sets; edit answers; discussion page; and database management pages.

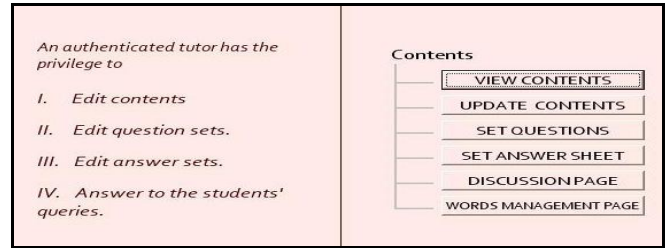


Fig. 2: Tutor home page with necessary links

The tutor can edit the chapter contents and question-answers sets as per requirement and save them accordingly. Fig. 3, 4, 5 show various pages with edit and save options.

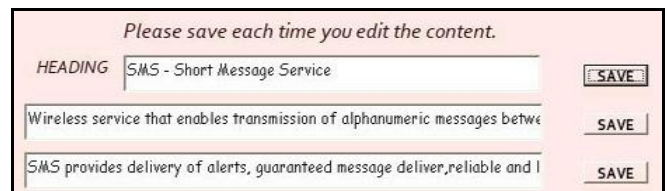


Fig. 3: Chapter contents get edited and saved

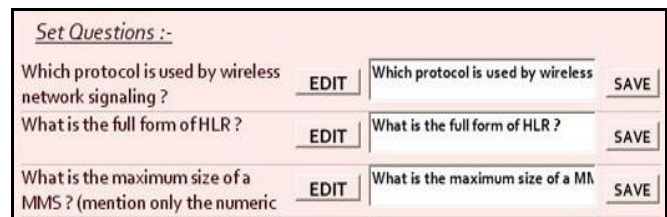


Fig. 4: Question sheet gets edited and saved

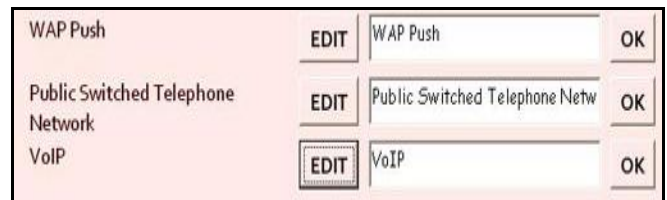


Fig. 5: Answer sheet gets edited and saved

The database management page as shown in Fig. 6 allows the tutor to enter new words, synonyms, antonyms with their weights in the tables used for the descriptive type answer evaluation.

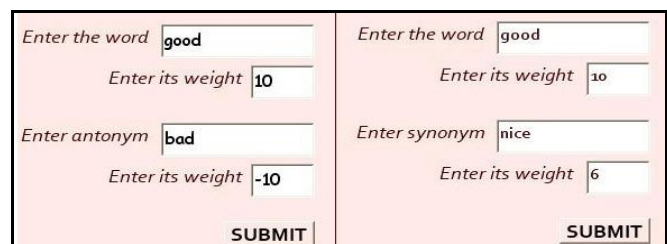


Fig. 6: Synonyms and antonyms inserted into tables

Any user who wants to login as a student will have to create a new account and sign in to the system by giving valid username and password. Fig. 7 and Fig. 8 display the login page and the registration form page respectively.

Fig. 7: Student login page

Fig. 8: New student fills up registration form

After signing in the student has to give pre knowledge test. Student has to answer each question on the basis of previous knowledge and enter the expected score for this test. The system calculates the score from the student's given answers and then calculates the slip rate and guess rate. If the student scores less than the expected score then it is depicted that he has misconception about that topic and he has considered some wrong answers as the correct answers. In this case the difference between his score and expected score in pre-knowledge test is termed as the slip rate. If the student scores more than the expected score then it is assumed that he is not confident about all the answers attempted or he has guessed some of the answers which have turned to be the right answers fortunately. In this case the difference between his score and the expected score is termed as the guess rate. Fig. 9 shows the pre knowledge test page.

Which frontnd protocol helps to store a MMS temporarily in a storage device ?	HTTP
MMSC often modifies a MMS before delivering it. What does this action known as ?	adaptation
What is the full form ofWAP ?	wireless
Name the topmost layer of the WAP protocol suite	application
WAP content is pushed to mobile handset. What does this action known as ?	WAP push
What is the full form ofPSTN ?	public switch
Name the protocol which involves signalling, media channel setup, digitization, encoding .	VoIP
Expected score	7
SUBMIT and PROCEED	

Fig. 9: Pre knowledge test session

The student enters the home page which has the links of reading page as shown in Fig. 10.

Fig. 10: Student's reading page

Fig. 11 shows that student's activities are traced and suggestions for selecting test levels are provided.

Fig. 11: Suggesting appropriate test level

The student home page has the links for three different test levels. Test sessions are time bound as shown in Fig. 12.

Fig. 12: Test session with timer activated

After submitting their answers the students get the correct answer sheets for the test levels. Fig. 13 shows the correct answer sheet.

ANSWERS TO THE TEST LEVEL-III	
Which protocol is used by wireless network signaling ?	SS7
What is the full form of HLR?	Home Location Register
What is the maximum size of a MMS ? (mention only the numeric value in kb)	100
Which frontnd protocol helps to store a MMS temporarily in a storage device ?	HTTP
MMSC often modifies a MMS before delivering it. What does this action known as ?	Content Adaptation
What is the full form of WAP ?	Wireless Application Protocol
Name the topmost layer of the WAP protocol suite .	Application
WAP content is pushed to mobile handset. What does this action known as ?	WAP Push
What is the full form of PSTN ?	Public Switched Telephone Network
Name the protocol which involves signalling, media channel setup, digitization, encoding .	VoIP

[GET DETAILED EVALUATION](#)

Fig. 13: Answer sheet provided to student after the test.

After tests detailed evaluation on previous knowledge, general overview and post learning is provided. Fig. 14 shows the screenshot of the evaluation page.

PREVIOUS KNOWLEDGE ASSESSMENT	
Your score on the basis of your previous knowledge is 6 and your slip rate is 1	
GENERAL ASSESSMENT	
Your performance on Chapter1 questions is good.	
Your performance on Chapter2 questions is good.	
Your performance on Chapter3 questions is very poor.	
Your performance on Chapter4 questions is very poor.	
POST LEARNING ASSESSMENT	
Your knowledge about Chapter 1 content has improved.	
Your knowledge about Chapter 2 content has improved.	
Read Chapter 3 content carefully. Your performance is poor.	
Read Chapter 4 content carefully. Your performance is poor.	

Fig. 14: Assessments on previous knowledge, general evaluation and post learning.

Then descriptive type general knowledge test is attended. Fig. 15 shows the work of the spell checker. Fig 16 and Fig. 17 show screenshots of different answer feedback.

The status of each answer is given with proper feedback.

Status for Answer1 Your answer is CORRECT..

Fig. 15: Spellings get corrected and answer status is shown

QUESTION 1 In which direction does the sun rise?

ANSWER SUBMIT

The status of each answer is given with proper feedback.

Status for Answer1 Your answer is an ERROR !!

Fig. 16: The wrong answer detected and tagged as an error

QUESTION 1 In which direction does the sun rise?

ANSWER SUBMIT

The status of each answer is given with proper feedback.

Status for Answer1 Your answer is an ELABORATION..

Fig. 17: The answer is an elaboration

V. ANALYSIS

Evaluating descriptive type answers is the main challenge of this paper. The evaluation process basically compares the student input to the correct answer, i.e., it checks the text relatedness between the two answers. The proposed metric minimizes the basic problems of commonly used text relatedness metric and provides moderate results. Unlike the existing intelligent tutoring systems the designed system allows both objective and descriptive type tests. Apart from generating scores the system also provides detailed evaluation based on pre knowledge of the students, general overview on answers given and comparative analysis on pre knowledge and post knowledge. Hence the system can predict how much a student has improved after going through the contents. The system if required can break the contents into sub modules guided with some templates to make the student aware of important keywords. The work has used some of feasible techniques used in previous works [5, 6, 8, 11] and has proposed more accurate assessment metric that allows a limited spelling relaxations and grammar checking under restricted condition and gives better results in evaluating the students' cognition.

VI. CONCLUSION AND FUTURE SCOPE

This paper presents an assembled approach with a number of essential features of an ITS including a metric embedded to it. The metric helps improving the evaluation of descriptive type test sessions. The system demonstrated with the proposed approach can be used as a limited content delivering tutoring system. The contents provided can be

edited by an authenticated tutor. The evaluation is done through various levels of test sessions. Feedbacks given are explicit and suggestive. The metric of evaluating the descriptive answers works best for simple sentences. The provision to enter new words in the databases makes the databases flexible. As it is dependent on spell checking and grammar checking the result may not always be satisfactory. There are definitely scopes for future research work and implementation on this algorithm and architecture. The word dictionary and databases used in the metric can be upgraded for more accurate results. Plug-ins can be used to develop well-formed spell checker and grammar checker to obtain better results. With an improved grammar checker the metric can also support compound and complex answers.

ACKNOWLEDGMENT

I express deepest thanks to my research guide, Smt. Saswati Mukherjee, Lecturer, School of Education Technology, Jadavpur University, India, for her valuable guidance during this research work. I owe a special thanks to my friend, Mr. Bishnu Prasad Das, School of Education Technology, Jadavpur University, India, for his constant support and assistance. Last but not the least I would like to express my gratitude towards my parents for encouraging me with their blessings and best wishes.

REFERENCES

- [1] Richard M. Felder, Linda K. Silverman, Learning and Teaching Styles in Engineering Education, *Engineering Education*, 78(7), California, 1988, 674-681.
- [2] Hugo Gamboa, Ana Fred, Designing Intelligent Tutoring Systems: A Bayesian Approach, *ICEIS Artificial Intelligence and Decision Support Systems*, 2001, 452-458.
- [3] Sherry Y. Chen, Robert D. Macredie, Cognitive styles and hypermedia navigation: Development of a learning model, *Journal of the American Society for Information Science and Technology*, 53(1), 2002, 3-15.
- [4] Y H Chan, Randomized Controlled Trials (RCTs) – Essentials, *Basic Statistics for Doctors*, 44(2), Singapore, 2003, 060-063.
- [5] Philip M. McCarthy, Vasile Rus, Scott A. Crossley, Arthur C. Graesser & Danielle S. McNamara, Assessing Entailer with a Corpus of Natural Language From an Intelligent Tutoring System, *Proceedings of FLAIRS Conference (2007)*, Memphis, USA, 2008, 247-252.
- [6] Heinrich Christian Dippel, Volker Neundorf, Vera Yakimchuk, WebSIS – a web based portal with an integrated e-assessment environment, *Conference ICL 2008*, Austria, September 24-26, 2008.

[7] Philip M. McCarthy, Vasile Rus, Scott A. Crossley, Arthur C. Graesser & Danielle S. McNamara, Assessing Forward-, Reverse, and Average-Entailer Indices on Natural Language Input from the Intelligent Tutoring System, iSTART, *Proceedings of the Twenty-First International FLAIRS Conference (2008)*, Memphis, USA, 2008, 165-170.

[8] Jack Mostow & Wei Chen, Generating Instruction Automatically for the Reading Strategy of Self-Questioning, *Project LISTEN*, Pittsburgh, USA, 2009.

[9] Sung-Young Jung, Using Natural Language to Represent Knowledge in an Intelligent Tutoring System, *Intelligent Systems Program*, Pittsburgh, Pennsylvania, USA, September 1-4, 2009.

[10] Christos N. Moridis, Anastasios A. Economides, Prediction of student's mood during an online test using formula-based and neural network-based method, *Computers and Education*, University of Macedonia, Greece, 2009.

[11] Zachary A. Pardos, Matthew N. Dailey, Neil T. Heffernan, Learning what works in ITS from non-traditional randomized controlled trial data, *Proceedings of the 10th International Conference on Intelligent Tutoring Systems*, Pittsburgh, 2010, 1-10.

[12] Sung-Young Jung and Kurt Van Lehn, Developing an Intelligent Tutoring System Using Natural Language for Knowledge Representation, *Intelligent Tutoring Systems. 10th International Conference*, ITS 2010, Pittsburgh, USA, June 14-18, 2010, Proceedings, Part II.

[13] Annabel Latham, Keeley Crockett, David McLean and Bruce Edmonds, Predicting Learning Styles in a conversational Intelligent Tutoring System, *Advances in Web-Based Learning - ICWL 2010, Lecture Notes in Computer Science 6483*, Manchester, 2010, 131-140.

[14] John R. Anderson, Shawn Betts, Jennifer L. Ferris, and Jon M. Fincham, Neural imaging to track mental states while using an intelligent tutoring system, *PNAS*, 107(15), Pittsburgh, USA, 25th January, 2010, 7018-7023.

[15] Debela Tesfaye, A rule-based Afan Oromo Grammar Checker, *International Journal of Advanced Computer Science and Applications (IJACSA)*, 2(8), Ethiopia, 2011, 126-130.

Design Analysis of Pressure Vessels at high stress zones using Pro/E v4.0

*Yogesh Borse ** Avadesh K. Sharma

*(M.E. Scholar, Mechanical Engineering Department, MITS, Gwalior, MP, India)

** (Asst. Prof., Mechanical Engineering Department, MITS, Gwalior, MP, India)

ABSTRACT

This paper deals with the Finite element modelling and Analysis of Pressure vessels with different end connections (i.e. Hemispherical, Ellipsoidal & Toro spherical). Considering the fact that required thickness of hemispherical head for internal pressure loading is only half of that necessary for the cylindrical shell, authors have tried to develop a finite element model taking due consideration on welding involved at the end connections of cylinder to shell end in modelling using shell elements to model cylinder. The larger the shell in diameter the more the economic benefits it achieves. In this paper authors, describes its basic structure, stress characteristics and the engineering finite element modelling for analysing, testing and validation of pressure vessels under high stress zones. The equivalent von-misses stresses for different end connections are plotted.

Keywords - High pressure vessels, reinforcing area (consideration to welding), hemispherical end, Ellipsoidal end & Toro spherical end connection

1. INTRODUCTION

Pressure vessels may theoretically be almost of any shape, but shapes made of sections of spheres, cylinders, and cones are usually employed. A common design is a cylinder with hemispherical end caps called heads. More complicated shapes have historically been much harder to analyse for safe operation and are usually far more difficult to construct. The pressure vessel of hemispherical type end connection is shown in figure 1.

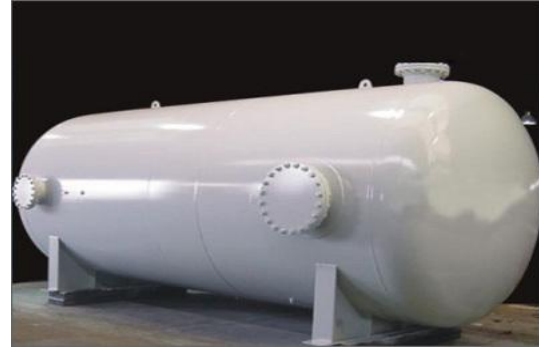


Figure 1

Many pressure vessels are made of steel. To manufacture a spherical pressure vessel, forged parts would have to be welded together. Some mechanical properties of steel are increased by forging, but welding can sometimes reduce these desirable properties. In case of welding, in order to make the pressure vessel meet international safety standards, carefully selected steel with a high impact resistance & corrosion resistant material should also be used.

2. LITERATURE REVIEW

High-pressure vessels, such as ammonia converters, urea reactors and supercritical fluid extractors, etc., are widely used in chemical, oil refining, energy industries, and so on. Such vessels are key equipments in various processes industries and have potential hazards. Much attention has been paid to using them safely and to lowering their costs, with great progress being made in the last century. For example, Analysis of Pressure Vessel junction by the Finite element Method written by Mahadeva Sivaramakrishna Iyer not only tells the use of method to solve such high tension zone problems but also gives a way to predict results for stresses and optimize the design [1], Finite element analysis of Pressure vessel by David Heckman also tells the use of computer programs instead of hand calculations for analyzing the high stress area's and different end connections [2]. The different types of stresses and modeling of pressure vessel joints are also depicted in ASME code in section "Design by analysis" [3].



Fig. 2

The use of hemispherical end in pressure vessels is the most economical and common use which can be seen in India and other developing countries. Although with the recent trends in Mechanical engineering with the use of Finite element software's the sheet thicknesses are validated for different end connections and for cylinder shell itself.

As per the conventional theory of mechanics of materials stated by S Timoshenko, the required thickness of hemispherical end is one-half the thickness of the shell to result in equivalent stresses in the cylinder.

3. RESEARCH METHODOLOGY

A pressure vessel with hemispherical end connection, up with internal pressure of 20 atm is analyzed for the study of Von-Misses Stresses at the connection using the finite element software Pro-Mechanica Integrated mode. Pro-Mechanica is a FE module integrated with CAD software Pro/E, which operates on P-element type method. A semi-mechanistic FE shell model is prepared with mean diameter of 5000 mm open at both ends and was tested in pro-mechanica for internal pressure to validate the working of thin pressure vessel theorem

$$\text{Stress } (\sigma) = Pd/2t \quad \text{--- (1)}$$

where

P: - Internal pressure

d: - Mean diameter

t: - thickness of vessel,

The pre-assumed thickness of cylindrical vessel was taken to be 50 mm for the validation problem.

Finite element software packages are more or less dependent upon the applied loads and Boundary conditions for the problem.. The theoretical result of the problem is 100 MPa while what was attained from the software lies in the range of 92-96 MPa. The results are discussed in section “**Result & Conclusion**”.

The results given by Finite element method was nearly approaching the values of theoretical results. A designer is also interested in the pattern of the stress distribution for different other decisions* to be taken while designing other related components of the vessel like baffles and stiffeners.

The same cylindrical surface model modeled in Pro/E Wildfire 4.0 with mean diameter was updated for the First case analyzed for a vessel with hemispherical end. The connection was analyzed for von-mises stresses. The polynomial was drawn with the resulted data as presented for the stress variation at the junction with different thickness of end connection.

The modeling of pressure vessel was done taking shell element for the cylinder which was also validated from the standard thin pressure vessel formula. The Hemispherical End connection was also modeled with shell element.

The difficulty of modeling the weld connection between the hemispherical end and cylindrical shell was solved by providing the alternate shell thickness greater than that of the base metal thickness, at the junction to provide it the strength of the weld. The case of similar thickness of the connecting parts is not presented here in the paper, where V or J joint type weld connection is considered to be safe taking no active participation in results of Finite element analysis. Considering the basis from J.E.Shigley Edition VII [1] that the weld joint is made stronger than the base metal thus the equations of statics are applied to base metal area of cross-section rather than the cross-section when the cantilever beam is analyzed for maximum bending.

The Hemispherical end was modeled in sub-sets of surfaces as shown in the figure given below, where different thickness of each sub-set was provided for consideration of weld strength. Here in the paper author have approached the problem with considering 3 sub-sets for the actual problem where the thickness of cylinder is 50 mm, first small surface shell element on hemispherical end is considered with thickness of 35 mm, the next element considered is of 30 mm joining the exact thickness of hemispherical end of

25 mm thickness. The solution to the approach is compared with solid element analysis considering the solid volume for the weld and analyzing the same. The comparisons of both the models are resulted. The paper was extended via analyzing the hemispherical end with different thickness to drive the polynomial for stress variation in the metal.

With the growing demand of industry to save cost, many researchers have put their efforts to optimize the shape of end connections resulting in optimization of weight. Many papers are presented on different shapes of end connections where one among the most common is ellipsoidal shape of the end-connection. Ellipsoidal end connection is shallower to that of hemispherical end connection and therefore is not able to resist the same pressure as that of hemispherical end. This is also called a 2:1 elliptical head. The shape of this head is more economical, because the height of the head is just a quarter of the diameter. Its radius varies between the major and minor axis.

The same surface model is prepared with same parameter of mean diameter and sub-sets of surfaces joining cylinder to elliptical end.

4. Experimental Work

A detailed three-dimensional (3-D) finite element (FE) computer model was constructed for Static qualification analysis of the Shell and End-Connection. The static qualification for stresses and deflection was performed using licensed FE analysis software Pro/E Wild-Fire.

The analysis was performed to determine structural integrity and performance characteristics of the components of Pressure Vessel under static loading conditions. The objective of the work performed is to quantify the part performance characteristics under the influence of static loads.

The static analysis results yield maximum stresses and maximum deflections in the structural component of the Pressure vessel. Results indicate that the components of pressure vessel will maintain its structural integrity during the specified load cases. Possible Optimization of the vessel is tried via changing the sheet thickness of the vessel.

The classical theory of thin shells of revolution is attempted here. The results from FE analysis are then be compared to the known results available in literature and also with the stresses predicted by the ASME Code. This section documents in details the technical approach, FE computer modelling,

maximum static deflections at critical locations and maximum static stresses at different locations in different components of the vessel. The general program Pro-mechanica is used for the linear static analysis of a general Vessel.

The First Model Analyzed is with internal pressure loading of 20 atm i.e. 2 MPa is made with hemispherical end connection. The FE Meshed model along with loads and boundary condition and meshing information for the same is shown in the Figure 3 given below

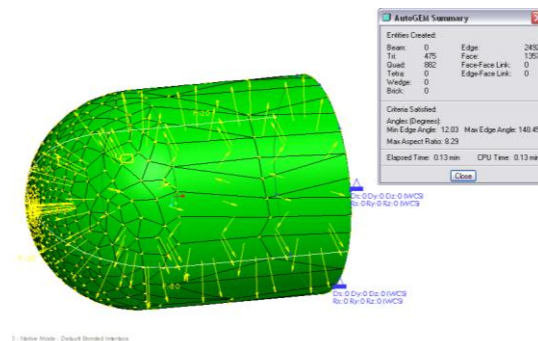


Figure 3 Sub-Structured Model for Hemispherical End Vessel

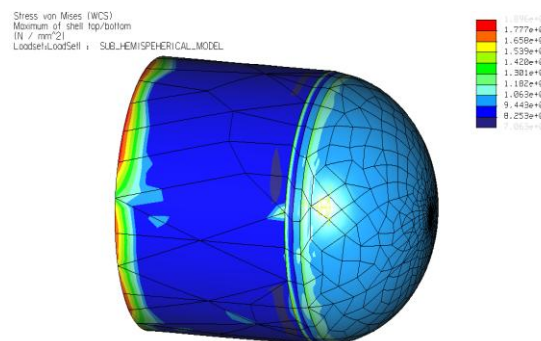


Figure 4 Von Mises Stresses with Hemispherical End Connection

Neglecting the stresses Near Constraint, we can see the value of stresses lying between the range of 106 MPa at Hemispherical end surface, while the connecting end gives the result in the range of 130 MPa.

The same analysis was performed for a Sub-structured model of the vessel with Elliptical end connection with same loads of 2 MPa and same boundary conditions at the end.

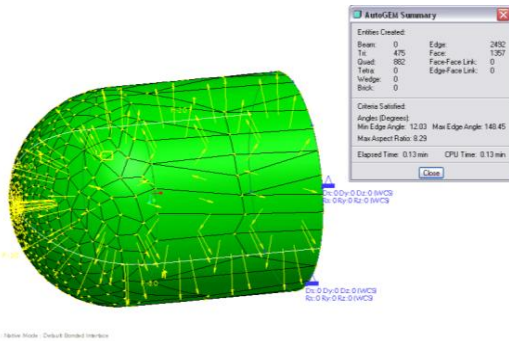


Fig.5: Meshed Model for Elliptical End

Figure 6 below shows the value of Membrane stresses for the sub-structured model with elliptical end connection which of the range of 166-195 MPa in orange to red zone.

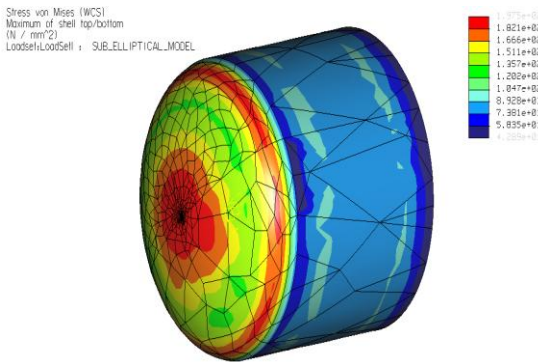


Figure 6 Membrane Stresses for Sub-Structured Model of Elliptical End Vessel

The Meshed Model for sub-model of the vessel with Toro spherical end is shown in the Figure 7, along with the details of elements used in the mesh.

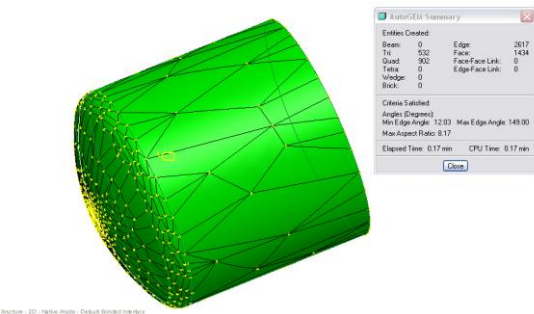


Figure 7 Meshed Model of Toro spherical End

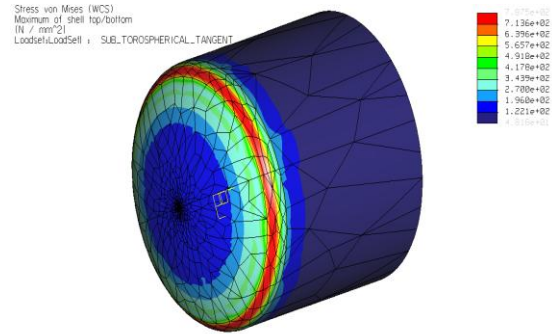


Figure 8 Von-Mises Stresses for Torospherical End

The values of stresses are found to be in range of 750-780 MPa

5. RESULT & DISCUSSION

The results with the used loads and boundary conditions which remain same for all the analysis with different end connections shows that the end connection with hemispherical shape results in the least stresses when compared to other models not only at weld zone but also at the far end of the end-connection. This can also be understood as the maximum pressure taking capacity for the hemispherical type end connection with least thickness ($t/2$ as per theory). While due to restrictions of the cost of material, and optimization in demand via industry, the use of ellipsoidal shape can be made with the increased thickness of the end connection for same level of stresses.

The results also shows that without varying the thickness of elliptical end connection i.e. with same thickness the results of stresses can be considered to lie in a safe zone and can be used for the safe working of the vessel. Third type of model analyzed was torospherical end type model where it was found the capability of undertaking pressure force is least and thus the stresses exceeds the limit of ASME standard [2] for the material under the same loads and boundary conditions, still the same can be used with a little increment in thickness as shown in the compared study chart below. The graph shown below in Figure 9 shows the results of polynomial equation developed with making number of analysis runs with varying thickness ratio which is defined via thickness of shell to shell end connection

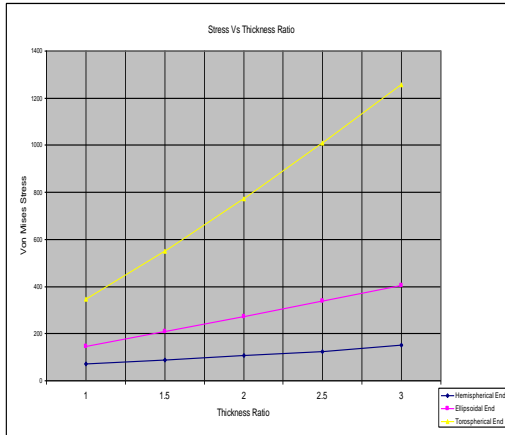


Figure 9 Stress Vs Thickness Ratio Graph
The chart in Fig 5.1 shows the Stress Vs Thickness Ratio curve for all three types of end connections analyzed.

6. CONCLUSION

A FE modeling study to analyze stresses and deformation is conducted as per the recommendation of ASME standard [2] for the comparison of three most recommended types of end connections.

With reference to literature studied [2-5]and[9], It was realized that the shell to shell end connection results best with the use of shell elements, while for nozzle to shell connections the solid to shell element connection should be used to result good quality results.

Different end connection sub-structured models were analyzed with same internal pressure of 2 MPa and the results for different end thickness were plotted with thickness ratio of 2.

Analysis results do not suggests the use of Torosphical end connection with the same thickness while the elliptical end connection can be used with FE analysis performed for the structural stability of the vessel as defined by ASME standard [2].

REFERENCES

- [1] Shigley Joseph.E Mechanical Engineering Design, 2003, Sixth Edition, Mc GrawHill, Boston, Page 133, Equation 3.52-3.53, Fig 3.28.
- [2] The American Society of Mechanical Engineers, "2007 ASME Boiler & Pressure Vessel Code" Section VIII Divisions 2, Alternative Rules for Construction of Pressure Vessels, Part-5, Design By Analysis Requirements.

- [3] Atts G.W & Lang H.A, "Stresses in Pressure Vessel with a Conical Head", ASME Transactions, 207-218, 1952.
- [4] yer Mahadevan Shrinivasan, "Analysis of Pressure Vessels Junction by the Finite Element Method", Civil Engineering Texas Tech University, PhD, 1972, 1-147.
- [5] amesh C. K., Kant Tarun & Jadhav V. B, "Elastic Analysis of Cylindrical Pressure Vessels with Various End Closures", Pressure Vessels & Piping Vol-2, 1974, 143-154.
- [6] wang D. Y. & Stallings J. M, "Finite Element Analysis of Bolted Flange Connections", Computers & Structures Vol-51, 1992, 521-533.
- [7] eib Eckart & Rudolph Jurgen, "Finite Element Analysis Concerning the Fatigue Strength of Nozzle-To-Spherical Shell Intersections", Pressure Vessels & Piping Vol 64, 1995, 101-109.
- [8] Meyer J.E., "Pressure Vessel Stress Analysis", Structural Design Notes Topic-C, C1-C10, 1996.
- [9] eckman David, "Finite Element Analysis of Pressure Vessels", Monterey Bay Aquarium Research Institute, University of California, 1998, 1-7.
- [10] Huang Fuang Yuan & Shi Gao-Liang "Finite Element Analysis of Pressure Vessel using Beam on Elastic Foundation Analysis", Finite Elements in Analysis and Design Vol-28, 1998, 293-302.
- [11] Dekker C. J. & Brink H. J, "Nozzle on Spheres with Outward Weld Area under Internal Pressure Analysed by FEM and Thin Shell Theory", Pressure Vessels & Piping Vol-77, 2000, 399-415.
- [12] Abbasi N. El, Meguid S. A. & Czekanski A, "Three-Dimensional Finite Element Analysis of Saddle Supported Pressure Vessels", Mechanical Sciences Vol-43, 2001, 1229-1242.

Optimization of In-House PCR-SSP Technique for HLA B27 detection in saurashtra patients

Dharashree Vanvi¹, Pooja Raja², Soham Trivedi³

¹*Biotechnology Engineering Department, V.V.P. Engineering college, Rajkot, India*

²*Biotechnology Engineering Department, V.V.P. Engineering college, Rajkot, India*

³*Biotechnology Engineering Department, V.V.P. Engineering college, Rajkot, India*

ABSTRACT

The HLA system is studied from various viewpoints including, organ transplantation, population genetics, disputed parentage, disease association studies and to answer basic questions of immunobiology. HLA-B27 is a MHC class I molecule that is strongly associated with the Seronegative Spondyloarthropathies (SSA). Survey suggested frequent cases of SSA in Saurashtra and many blood samples of suspected Sero-negative patients needed to be analysed on daily basis for the detection of HLA-B27. The techniques that were generally employed in routine clinical practice were based on Microlymphocytotoxicity assays. Some laboratories generally send such samples to other states that adds to the overall cost for the exact diagnosis. Moreover, there were various limitations of these serological approaches and false-negative results are a frequent problem for HLA-B27 typing. Thus there was a need to develop and encourage PCR based techniques for the detection of HLA-B27 that relies on specific DNA sequences, can be a direct determination of allelic DNA and thus serve as an ideal test for HLA-B27. PCR-SSP technique utilizes oligonucleotide primers to start the PCR that have sequences complementary to known sequences, which are characteristic to certain HLA specificities. For e.g. the primers those are specific to HLA-B27, will not be able to initiate the PCR for HLA-DR17. Using a set of different PCR's each with primers specific for different HLA antigens does typing. Thus the present studies will revolutionize the Saurashtra immuno-diagnostics and the optimized In-House PCR-SSP technique can be used in parallel with serological typing in various diagnostics laboratories across the state.

Keywords - HLA B27, PCR SSP, Serology, SSA,

I. INTRODUCTION

The HLA-B27 is a major histocompatibility complex class I molecule that is strongly associated with the disease ankylosing spondylitis (AS) and related spondyloarthritis (SpA). There is almost 90% association of HLA-B27 with ankylosing spondylitis [1]. The last two decades have seen a massive growth in the application of DNA technology in Histocompatibility and Immunogenetics [2]. DNA based HLA typing is fast replacing conventional Microlymphocytotoxicity based method, which has been regarded as the gold standard. Many laboratories in India have already switched over to molecular methods, as the results are far superior [3]. This is so as the serological methods for HLA class I detection is hindered in many cases by serological cross reactivity and decrease in expression of

HLA antigens, particularly in patients with different hematological tumors [4]. Serological typing is also difficult in those cases of poor cell viability and also in refuting phenotypic homozygosity. Sometimes due to lack of availability of reliable commercial antisera laboratories need to screen to find their own reagents and exchange these with other such-minded laboratories. This can mean difference in the quality of reagents between laboratories and thus can lead to some laboratories producing more accurate results than others. In addition these reagents could not be replenished. Whilst serology performed adequately in HLA-B27 determination can prove unsatisfactory [2]. The principle of PCR-SSP is that each individual allele (making up a serological specificity) is amplified by a primer pair exactly matched to that region. Amplification of HLA loci with PCR-SSP has thus proved to be a rapid and accurate method for genotyping HLA-A, -B and -C alleles [5,6,7,8] and indicates that HLA typing by serology may not be sufficiently reliable [9,10,11].

Currently, most HLA-B27 testing is performed with surface antigen tests that require viable cells for analysis. Two commercially available antibodies are commonly used but they cross-react with other HLA-B surface antigens, especially B7 and B40 [12]. The cross-reactivity of these antibodies can compromise the accuracy of the results generated in the antigen assays. With DNA sequence information available for alleles of the HLA system and the development of molecular biological techniques, it is possible to tissue type for allelic differences in HLA genes. The SSP based HLA typing is an economical, rapid, precise, technically simple and reproducible method. In 1994 M. Bunce described a comprehensive HLA-B PCR-SSP typing system based on available HLA nucleotide sequences which can detect all serologically defined antigens in most heterozygous combination in 48 one-step PCR reactions. Serological approach recognizes immunological relevant antigenic differences, in contrast DNA based testing may also identify differences of little biologic relevance [13]. Joannis Mytilineos in 1998 demonstrated an impressive advantage of the PCR-SSP method for HLA-A and HLA-B locus typing over serological typing in black individuals. Mehrnaz Narouei-Nejad et al in 2003 reported that there was a 31% difference in the SSP typing and serological methods. Reports suggest that HLA-DR SSP typing is far superior and almost 90% of alleles are identified as compared to 40% by serology [14]. In 2005 Michael T. Seipp reported that using DNA sequencing as standard, the sensitivity and specificity of PCR were 99.6 and 100.0, and those of the single antigen assay were 98.2 and 97.6. In the same year Derek Middleton reported that implementation of a DNA technique for HLA-

C alleles reduced the homozygosity role in stem cell donor from 50% by serology to 21%. Moreover typing of non-Caucasians by serological methods has always proved difficult when the majority of HLA sera available have been derived from Caucasian donors. Thus as the PCR-SSP technique is more strategic for HLA typing as compared to the serological approach, the present study was carried out to optimize an In-House PCR-SSP Technique for routine HLA-B27 Typing and to compare it with the traditional serological technique.

II. MATERIALS AND METHODS

DNA Extraction: Salting-out methodology was carried out for extracting the DNA. This method avoids using phenol and chloroform by using high salt concentrations to remove proteins. It is rapid, safe and inexpensive. Average yields are similar to that obtained with the phenol-chloroform extraction procedure (50- 200 ug), and the quality of DNA is excellent.

Principle: In eukaryotic cells the bulk of DNA is localized in the nucleus, which is separated from the rest of the cell sap by a complicated membrane structure. DNA Extraction by this method involves the following steps: 1). Cell Breakage: Chemical (detergents) and /or enzymatic procedures are best suited for opening cells and obtaining intact DNA. Detergent can solubilize lipids in cell membranes resulting in gentle cell lysis. In addition, detergents have an inhibitory effect on all cellular DNAses and can denature proteins, thereby aiding in the removal of proteins from the solution. Therefore lysis of cells was performed using anionic detergents such as Sodium dodecyl sulfate (SDS). Moreover buffers like Red Cell Lysis Buffer (RCLB) was employed to facilitate the extraction process. Haemoglobin (and other pigments) inhibits restriction enzymes and TAQ polymerase. Hence washing with RCLB was carried out. 2). Removal of Protein: Proteins can be removed from DNA preparations using a protease that can digest all proteins. Two such enzymes in use are proteinase k and pronase. Both enzymes are very stable, and devoid of DNase contamination, making them safe to use in the purification of nucleic acids. They can digest intact and denatured proteins and do not require any co-factors for their activities. An Special buffer Nucleas Lysis Buffer (NLB) was used to salt out proteins. NLB comprises of NaCl used to lyse all cells. High salt concentration aids the salting out of the proteins. DNA is stabilised and remains as a double helix with the utilisation of such buffers. 3). Concentration of the DNA: Ammonium acetate was utilised for the removal of heavy metals, detergents. Finally, Isopropanol and 70% ethanol (final concentration) in presence of the appropriate concentration of salts were used for DNA precipitation. Such precipitation is based on the phenomenon of decreasing the solubility of nucleic acids in water. It is also reasoned that low temperature and the presence of salts further lower the activity of water molecules thereby facilitating more efficient DNA precipitation.

Requirements: • Red Cell Lysis Buffer: Add 14.4 ml of 1 M NH₄Cl and 100µl NaHCO₃ and make up the final volume upto 100 ml with distilled water. Adjust pH upto 7.5

to 8. • Nucleas Lysis Buffer: Add 4 ml of 5 M NaCl, 200 µl 0.5 Na₂EDTA and 250 µl of 2 M Tris-HCL and make up the final volume upto 50 ml with distilled water. • 10% SDS – 10gm SDS in 100ml DW. • 20 mg/ml proteinase k. • 4 M Ammonium Acetate. • Chloroform. • Isopropanol. • Chilled absolute alcohol . • Chilled 70% ethanol

Procedure: Only fresh EDTA Samples were used for DNA Extraction.

Day 1: • 45 ml of the Red Cell Lysis Buffer (RCLB) was mixed with 5 ml of blood (EDTA) in falcon tubes that were mixed gently 2 to 3 times and left at room temperature for 10-20 minutes. • Then the mixture was centrifuged at 1800 rpm for 20 minutes. • After discarding the supernatant, the pellet was then suspended in 25 ml of RCLB and was left for 10-20 minutes at room temperature. • Again the mixture was centrifuged at 1800 rpm for 20 mins. • Now after discarding the supernatant, the pellet was suspended in 3 ml Nucleas Lysis Buffer. 200 µl of 10% SDS and 20 µl of Proteinase K Enzyme (10 mg/ml) were added respectively. • The mixture was then incubated at 37°C - 42°C for 4 hours to overnight.

Day 2: • After the incubation, 4 ml of Ammonium Acetate and 3 ml of Chloroform were added and were mixed nicely by slight vortexing. • The mixture was then centrifuged at 4000 rpm for 30 minutes. •The supernatant was then taken out carefully and mixed with Isopropanol (5-10 ml). • Now the DNA was taken out and was washed with 70% Ethanol twice. • It was then dried and dissolved in distilled water.

Determination of the purity of DNA : Ideally for samples of limited cell mass such as mononucleated bone marrow specimens The micro-sample capability of the NanoDrop provides accurate DNA quantitation with minimal consumption of sample, which is critical for HLA typing. The DNA quantification and its purity can be assessed using an NanoDrop device that employs a sample retention system requiring only 1ul of sample for DNA absorbance spectral analysis, providing a calculated DNA concentration and purity ratios. A ratio of 1.8 is generally accepted pure for DNA. If the ratio is appreciably lower it may indicate the presence of protein or other contaminants that absorb strongly at or near 280 nm. The DNA template can then be amplified using sequence specific primers for sequence specific PCR-SSP. This device can be integrated into the HLA-B27 detection workflow in the following manner: DNA extracted from the EDTA samples by the salting-out procedure, then quantified on the NanoDrop to ensure adequate template prior to amplification. However due to unavailability of the instrument in the present studies only the quality of DNA was assessed.

Checking the quality of DNA: 500ng of DNA was run on a 1 % agarose gel (low EEO) for 1hour in 0.5x TBE buffer in submerged electrophoresis chamber. A single band near the well after ethidium bromide staining and viewing on an Ultraviolet (UV) transilluminator (Biorad, Italy) indicates the presence of high molecular weight DNA. If a smear is seen, it indicates that the samples have been degraded. (2 µl DNA + 5 µl D/W + 2 µl Bromophenol dye).

Polymerase Chain Reaction with Sequence Specific Primers (PCR-SSP): Allelic variability has traditionally been determined phenotypically, but often may be more accurately investigated via molecular biology techniques either indirectly by Restriction Fragment Length Polymorphism analysis (RFLP) or directly by PCR based techniques. In the determination of allelic polymorphism by PCR amplification with sequence specific primers (PCR-SSP), Oligo-nucleotide primers are designed to obtain amplification of specific alleles. The typing method is based on the principle that a completely matched primer will be more efficiently used in the PCR reaction than a primer with one or several mismatches especially in the first critical cycles (Figure 1). Thus the specificity of the typing system is part of the PCR reaction, which reduces post-amplification processing of samples to a minimum, making the technique more attractive for tissue typing in clinical practice that includes donor-recipient matching for transplantations and HLA-B27 determination. Assignment of alleles is merely based on the presence or absence of amplified product, which can be detected by agarose gel electrophoresis. (Figure 1)

Amplification primers: Forward Primer: 5'-GCTACGTGGACGACACGCT 3', Reverse Primer 1: 5'-CTCGGTCAGTCTGTGCCTT-3', Reverse Primer 2: 5'-TCTCGGTAAGTCTGTGCCTT-3', Control primer sequences: HGH- Forward Primer - 5'-TGCCCTCCCAACCATTCCCTTA-3', HGH- Reverse Primer - 5'-CCACTCACGGATTCTGTTGTGTTTC-3'



Figure 1: Illustration of the principle for allele specific PCR Amplification - A completely matched primer will be more efficiently used in PCR Reaction than a primer with one or several mismatches allowing the discrimination of alleles differing by a single base pair mismatches, denoted by •, should be placed in the extreme 3' end of primer as the Taq Polymerase lacks 3' – 5' proof reading exonuclease activity.

Reagent Mixes: A total of 100 µl of mixes was divided into 10 PCR tubes each containing 10 µl of reagent mix. Two out of 10 tubes were of positive control and negative control.

Composition of reagent mixes for HLA-B27 typing: DDW – 62 µl, 10X PCR complete buffer – 10 µl, MgCl₂ (25mM) – 2 µl, dNTP (10mM) – 0.8 µl, Primer 1 (10 p mol/ml) – 5 µl, Primer 2 (10 p mol/ml) – 5 µl, Primer 3 (10 p mol/ml) – 5 µl, Control 1 – 5 µl, Control 2 – 5 µl, Taq – 1 µl, DNA (50-100 ng) – 1µl, Total – 100 µl.

Cycle parameters: Denaturation 94°C – 5mins 30 cycles of • 94°C for 1 min, • 65°C for 2min, • 72°C for 1min, • Final extension of 72°C for 10 min.

Visualization of amplifications by agarose gel electrophoresis: The absence or presence of PCR Products was visualized by agarose gel electrophoresis: 1) A 2 % (w/v) agarose gel in 0.5x TBE Buffer (89 mM Tris Base/89 mM Boric Acid/2 mM EDTA, pH 8) was prepared. • Agarose was dissolved by boiling, then cooled to 60°C. Ethidium Bromide (0.5 µg/ml gel solution) was then added. • A 4 mm thick gel with 3 mm wide slots was casted and was allowed to set for 10 – 20 mins. 2) The PCR Reactions were then loaded on the gel after addition of a 2.5µl loading buffer (30% v/v glycerol stained with bromophenol blue and xylene cycnol) to PCR tube. 3) The gels were run in 0.5x TBE buffer (without buffer recirculation). Minigels (8.5 × 10 cm) were allowed to run for 10 to 15 minutes and large gels (20 × 20 cm) for 20 to 30 minutes at 7 to 8 V/cm. 4) Finally the gel was examined under Ultra-Violet Illumination and the results were documented by photography.

III. RESULTS

The results of 10 samples typed by serology and PCR-SSP technique is shown in the following table. (Table 1)

Table 1: Results of Serology and PCR-SSP

	HLA B27 positive	HLA B27 negative	Total
Serology	2	8	10
PCR-SSP	3	7	10

The following table shows the comparison of the two techniques for 10 samples typed by PCR-SSP and Serology. (Table 2)

Table 2: Comparison of Serology and PCR-SSP

Serology	PCR-SSP	Results	Percentage
Positive	Positive	2/10	20% TP
Positive	Negative	1/10	10% FN
Negative	Positive	1/10	10% FP
Negative	Negative	7/10	70% TN

(TP – true positives, FN – False negatives, FP – false positives, TN –true negatives)

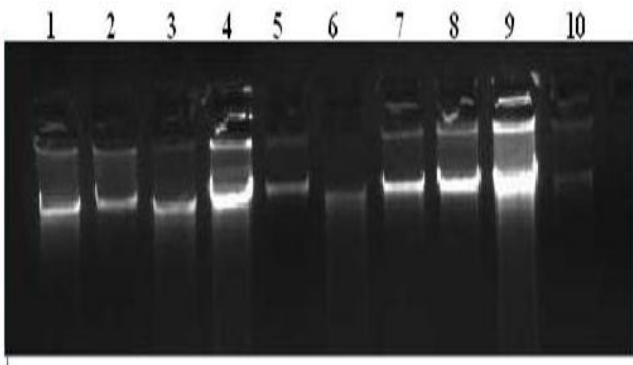
Thus it was found that 2 out of 10 (20 %) samples were HLA B27 positive by microlymphocytotoxicity and 3 out of 10 (30 %) were HLA B27 positive by PCR-SSP. The sensitivity of test was obtained as 66.66% and its specificity was 87.5%. Furthermore, the positive predictive value was found to be 66.66% and its Negative predictive value was 87.5 %. The Accuracy or efficiency of the test was calculated to be 81.81%

The false-positive rate was found to be 12.5 % and the false-negative rate was found to be 33.33 %. Based on the sensitivity and specificity of test the likelihood ratio of a positive test result (LR+) was calculated as 0.77 and the likelihood ratio of a negative test result (LR-) was 0.75. Moreover, The cost analysis of the various methods for HLA-B27 typing was carried out. The following table shows the comparison of the cost of methods (Table 3).

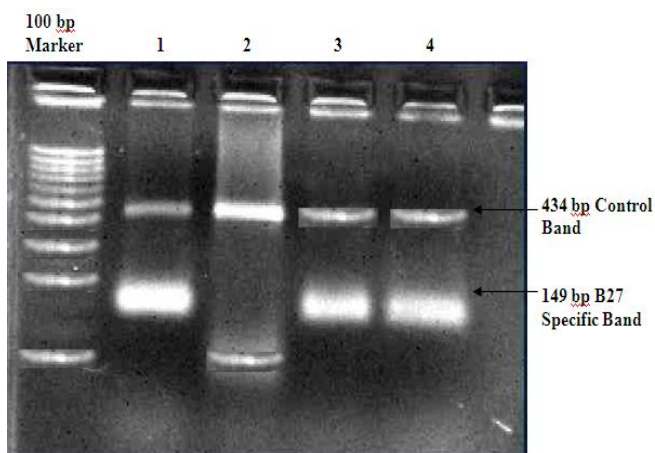
Table 3: Cost analysis of various methods for typing

Method for HLA B27 typing	Cost/test
Serology: In House tray	Rs.500/-
Serology: Commercial kit	Rs.600/-
PCR-SSP: In House (Including DNA Extraction)	Rs.150/-
PCR-SSP: Commercial kit (Excluding DNA Extraction)	Rs.600/-
Flow cytometry	Rs.1200/-
PCR-SSOP	Rs.2000/-

The sensitivity of the PCR-SSP technique was tested using B27 positive DNA samples with concentrations ranging from 0.1 to 100 ng/ μ l. It was found that the lowest DNA concentration at 1.0 ng/ μ l showed the faint positive bands of the control and B-27 specific primers. However, the bands were most clearly detected at the concentration ranging from 10 to 100 ng/ μ l. The following figure depicts the gel photograph of genomic DNA.

**Figure 2: Gel photograph showing genomic DNA**

As depicted in the Figure 2 sample 3 and sample 4 can be clearly visualized as HLA-B27 positive samples. Here the Sample 1 is a positive control for HLA-B27 and sample 2 is the negative control.

**Figure 3: Gel photograph showing B27 specific band with the control bands**

IV. DISCUSSION

Unlike recently, Serological typing had been the primary technique used for HLA Class I analysis. But due to the advent of molecular biology, the last twenty years has seen an exponential growth in the application of DNA technology to the field of Histocompatibility and Immunogenetics (H&I). DNA based typing focuses on defining differences in genes and may identify differences of little biologic relevance whereas immune based testing by serology or cellular reactions is related to known immunological differences [14]. Some limitations for serological tests include lack of availability of specific antisera for all alleles of HLA-B27 because the number of known HLA-B27 alleles has increased. Moreover, the test must be performed within 6 hours after drawing the blood, and the amount of blood used must not be less than 5 ml [15]. Serological typing can also be difficult in those cases of poor cell viability or poor expression. Moreover lots of expertise is inevitable in confirming phenotypic homozygosity. In addition when the HLA antisera available have been derived from Caucasian donors typing of non-Caucasians by serological methods can prove to be difficult [2]. Serology is also hindered in those patients owing to immunosuppression due to serological cross reactivity. In different situations, such as aplastic anemia and leukemia, when the expression of HLA antigens on the cell surface is down-regulated, it is impossible to type by serological methods [4]. Most commercial typing sera are obtained from Caucasian population and some alleles peculiar to the India population may not be identified [3]. Moreover the weak reactions may be due to Platelet contamination that can deplete antibody and complement. Also Erythrocyte contamination can make microscopic evaluation difficult because of visual confusion with negative lymphocytes. False-negative serological HLA-B27 typing results may be due to altered antigenic epitopes but it can be detected by polymerase chain reaction [16]. Thus, molecular typing techniques, which give more accurate results, have replaced or supplemented by the Microlymphocytotoxicity.

Most genotyping methods are based on the group-specific amplification of HLA-B alleles by the PCR. The PCR-SSP is more widely used to detect HLA-B27 alleles. Additionally, a real-time PCR method for the detection of HLA-B27 alleles was described [17]. Availability of SSP kits for tissue typing with advantages at a cost similar to serology based dry kits and changing donor pattern have made it imperative for most commercial labs to switch over to DNA based methods. In the present studies an In-House PCR-SSP technique was developed for confirming the results obtained by serology at our laboratory for the HLA-B27 detection. A recent study in the detection of all HLA-B27 alleles, and their methods involved an initial screening with two sequence-specific PCRs, followed by two additional PCR amplifications in order to identify a few rare subtypes of B*27, B*4202 or B*7301, which is not convenient for routine testing (Zino E, 2004).

V. CONCLUSION

In the present studies the PCR-SSP technique developed provides accurate results and can be employed for routine analysis. It is more reliable technique than the serological

approach as effective detection of HLA-B27 antigen can be visualized by the B27 bands. The HLA-B27 testing using Microlymphocytotoxicity gave a false-positive rate of 12.5% and the false-negative rate of 33.33%. The cause of false-negative results may be due to improper proportion of cells and antiserum, and possibly a weak reaction or insufficient mixing (Milken SL, 1987). Furthermore the cost of this In-house developed PCR-SSP technique as compared to other approaches is merely Rs.150 per test. This technique is about 50 times less costly than that of the imported commercial PCR-SSP test kit by few labs.

The technique is superior to serology as fresh and aged samples can be tested and only a small amount of blood is used. The results can be obtained even with a low concentration of DNA (0.1 ng/ml). Moreover the PCR-SSP technique developed in the present study is reliable, simple, convenient, and more cost effective for routine laboratories. The technique is fast and easy to perform and to handle specimens, because the viable cells necessary for serological typing are not needed. Thus such PCR-SSP techniques can be employed by the Rajkot Diagnostics laboratories as a part of routine clinical practice for exact diagnosis of Seronegative Spondyloarthritis and it can be envisaged that in the near future HLA-typing by serology will be replaced by PCR-SSP in routine clinical practice.

ACKNOWLEDGEMENTS

We would like to acknowledge the management of V.V.P. Engineering college, Principal Dr. Sachin Parikh, Head of Biotechnology Department Mr. Dharmesh Sur that gave us an opportunity to carry out the work. Our sincere thanks to entire staff members of the biotechnology department for their consistent support and encouragement throughout the present work.

REFERENCES

- [1] Michael T. Seipp, Maria PCR Melting Assay and Two Flow Cytometric Antigen Assays, *Cytometry, Part B (Clinical Cytometry)*, 63B, 10–15.
- [2] Derek Middleton (2005), "HLA Typing from Serology to Sequencing Era", *Iranian Journal of Allergy, Asthma and Immunology*, 4(2), 53-66.
- [3] M.N. Mishra, H. Mani, A.S. Narula, V.K. Saxena (2004), "HLA Typing – A Comparison of Serology and DNA Techniques", *Int J Hum Genet*, 4(2),151-153.
- [4] Mehrnaz Narouei-Nejad, Farideh Khosravi, Abdolali Danesh, Behrooz Nikbin (2003), "PCR-SSP Versus Serology in Typing of HLA-A, -B and -C in Iranian patients", *Arch Iranian Med*, 6 (1), 23 – 28.
- [5] Cadavid LF, Watkins DF (1997). "The duplicative nature of the MHC class I genes: an evolutionary perspective". *Eur J Immunogenet.*; 24: 313 – 22.
- [6] Cereb N, Maye P, Lee S 1995. Locus-specific amplification of HLA class I genes from genomic DNA: locusspecific-sequences in the first and third introns of HLA-A, -B and -C alleles. *Tissue Antigens.*; 45: 1 – 11.
- [7] Guttridge MG, Burr C, Klouda PT 1994. Identification of HLA-B35, B53, B18, B5, B78, and B17 alleles by polymerase chain reaction using sequence specific primers (PCR-SSP). *Tissue Antigens.* 44: 43 – 6.
- [8] Bidwell J.1994. Advances in DNA-based HLA typing methods. *Immunol Today.* 15: 303 – 7.
- [9] Adorno D, Canossi A, Papola F, et al 1997. Comparison between HLA class I PCR-ARMS and serologic typing in cadaveric kidney transplantation. *Transplant Proc.* 29: 1923 –5.
- [10] Bunce M, Welsh KI 1994. Rapid DNA typing for HLA-C using sequence-specific primers (PCR-SSP): identification of serological and non-serologically defined HLA-C alleles including several new alleles. *Tissue Antigens.* 43: 7 – 17.
- [11] Lo YM, Patel P, Newton CR, et al 1991. Direct haplotype determination by double ARMS: specificity, sensitivity and genetic applications. *Nucleic Acid Res.* 19: 3561 – 7.
- [12] Levering WH, Wind H, Sintnicolaas K, Hooijkaas H, Gratama JW 2003. Flow cytometric HLA-B27 screening: cross-reactivity patterns of commercially available anti-HLA-B27 monoclonal antibodies with other HLA-B antigens. *Cytometry*, 54B, 28–38.
- [13] Hurley KC, Tang T, Jennifer NG, Hartzman RJ 1997. HLA typing by molecular methods. *Manual of Laboratory and Clinical Immunology.* 5, 1098-1111.
- [14] M.N. Mishra, H. Mani, A.S. Narula, V.K. Saxena 2004, HLA Typing – A Comparison of Serology and DNA Techniques, *Int J Hum Genet*, 4(2),151-153.
- [15] O. Nathalang, S. Tantimavanich, K. Nillakupt, P. Arnutti, C. Jaruchaimontree 2006, HLA-B27 testing in thai patients using the PCR-SSP technique, *Tissue Antigens*, 67, 233-236.
- [16] Kirveskari J., Kellner H., Wourela M et al 1997. False-Negative serological HLA-B27 Typing results may be due to altered antigenic epitopes and can be detected by polymerase chain reaction. *Br. J. Rheumatol*, 36, 185-189.
- [17] Sylvain K, Aurelie H, Marc M, Christophe R, 2004. Rapid screening for HLA-B27 by a Taqman-PCR assay using sequence specific primers and a minor groove binding probe, a novel type of Taqman probe. *J Immunol Methods*, 287, 179-186.
- [18] O. Bishop, Neurophysiology of binocular vision, in J.Houseman (Ed.), *Handbook of physiology*, 4 (New York: Springer-Verlag, 1970) 342-366.

Optimization of Different Parameter of Cold Storage for Energy Conservation

Amit M Patel¹, Prof. R I Patel²

*(ME-Student, Department of Mechanical Engineering, GEC Dahod, India)

**(Asst. Professor, Department of Mechanical Engineering, GEC Dahod, India)

ABSTRACT

As the demand for refrigeration and Air conditioning has been increased during the last decade, the cold storage system can be used to the economic advantage over conventional plants. Energy conservation is required in the cold storage system so The Design of Experiment is used to Optimization of different parameters of cold storage on the bases of performance experiments. In This Experiment, three levels of Thickness, Area of wall and Compressor are kept as the control parameters, The Insulating wall material was taken as PUFF, and different energy were taken as a result in the experiment, The Objective of this paper is Optimize different parameters in the cold storage. The various tools of DOE are used for analyze the final results of the experiment with the help of Graphs. The analysis is being done with the help of Minitab-15 software. The analysis of variance ANOVA is also performed as identified the statistical significance of parameters. The result of the experiments are the optimum value of insulating thickness, energy consumption rate with the help of ANOVA, After the using Taguchi method determine the feasibility of improving cooling capacity of cold storage, establish the mathematical models relating the cold storage performance parameters & control parameters by regression analysis and obtained set of optimal cold storage parameters for better performance.

Key words: Insulation Thickness, area of wall, compressor and energy, Optimization, Cold storage,

I. INTRODUCTION

Cold Storage is a special kind of room, the temperature of, which is kept very low with the help of machines and precision instruments. India is having a unique geographical position and a wide range of soil thus producing variety of fruits and vegetables like apples, grapes, oranges, potatoes, chilies, ginger, etc. Marine products are also being produced in large quantities due to large coastal areas. The present production level of fruits and vegetables is more than 100 million MT and keeping in view the growth rate of population and demand, the production of risible commodities is increasing every year. The cold storage facilities are the prime infrastructural component for such perishable commodities. Besides the role of stabilizing market prices and evenly distributing both on demand basis and time basis, the cold storage industry renders other advantages and benefits to both the farmers and the consumers. The

farmers get opportunity of producing cash crops to get remunerative prices. The consumers get the supply of perishable commodities with lower fluctuation of prices. Commercially apples, potatoes, oranges are stored on large scale in the cold storages. Other important costly raw materials like dry fruits, chemicals, essences and processed foods like fruit juice/pulp, concentrate dairy products, frozen meat, fish and eggs are being stored in cold storages to regulate marketing channels of these products.



Fig 1.1 Cold Storage

II. LITERATURE REVIEW

M.S. Soeylemez et al (1997)[1] has suggested A thermo economic optimization analysis is presented yielding a simple algebraic formula for estimating optimum insulation thickness for refrigeration applications. The effects of design parameters on the optimum insulation thickness are investigated for three test cities using an interactive computer code written in Fortran 77. The equivalent full load hours method is used to estimate the energy requirements. Merrick Burden et al (2004)[2] has suggested Frozen storage is an integral part of effective food distribution. In general, both food quality retention and storage costs will increase as storage temperatures decrease. Mashud Ahmed et al (2009)[3] has suggested A general estimate shows that 80% of communities across the United States receive their goods exclusively by transport trucks, of which a significant number are climate-controlled because they carry perishable goods, pharmaceutical items and many other temperature-sensitive commodities. N.Yusoff et al(2010)[4] has suggested that study presents a procedure for selecting optimization variables in a Refrigerated Gas Plant(RGP) using Taguchi method with L27(3⁹) orthogonal arrays. A dynamic RGP model developed under HYSYS environment is utilized as a test bed. This model comprises 762 variables and 21 regulatory control loops. However only 9 variables or factors with three level each are studied to determine their relative significance in maximizing RGP profit.

III. EXPERIMENTAL SET UP

The experimental set up at Super Refrigeration, Near Shyamal Cross Road ,Ahmedabad on prepared model of cold storage, The compressor, condenser unit, evaporation unit, expansion valve were used and special experimental cold storage box was attached with refrigeration system , the device, Watt meter and thermo couple are to attached with this cooling unit here the design experiments is based on Taguchi Methodology A 3-Factor and 3-level,L9 Orthogonal array design is used to conduct the experiments. The levels of Thickness are 0.050, 0.075 and 0.100 meter. Area of wall are 0.96, 1.5 and 2.16 m² and Compressor 0.100, 0.125 and 0.167 HP, the inside Temperature is kept constant at 2° C through out the experimentation. Here total L9 = 9 experiments will conducted.

Experimental Constant

- Inside temperature:- 2°C
- Thermal conductivity :- 0.025 W/m k
- Material:- PUFF

Parameter and Range Selection

To select the parameters and its levels for experimentations, several exploratory experiments were conducted to determine important control factors. Out of several available controllable input parameters on the cold storage, following parameters were selected with maximum feasible range.

Sy mb ol	Control Factor	Uni t	Level 1	Level 2	Level 3
A	Thickness	Mt	0.050	0.075	0.100
B	Area of wall	Mt	0.96	1.5	2.16
C	Compressor	HP	0.100	0.125	0.167

Table 1 Parameter and Range selection

IV. INDENTATIONS AND EQUATIONS

*Calculation of Heat Transfer through wall, Ceiling & Floor

$$Q = UA(T_o - T_i)$$

Where,

A = Area of Wall, m²

U = Over all Heat Transfer Co-efficient KJ/s m² K

Ti = Internal Temperature °C

To = External Temperature °C

$$U = \frac{1}{\left(\frac{1}{H1}\right) + \left(\frac{X1}{K1}\right) + \left(\frac{X2}{K2}\right) + \left(\frac{X3}{K3}\right) + \left(\frac{1}{H2}\right)}$$

H1= Outside heat transfer Co-efficient

H2= Inside heat transfer Co-efficient

Ki= Thermal conductivity of materials

Xi= Thickness of Materials

*Calculation of Total Refrigeration required
Total refrigeration required

$$= \frac{\text{Total heat removed}}{3.5}$$

Ton of refrigeration = 3.5 KJ/s

The total amount of electrical energy consumption of a typical refrigeration system may be determined by the equivalent full loads hours energy estimation as follows[1]

$$E = Q \times \frac{\Delta t}{COP}$$

E= Annual total energy consumption of refrigeration system (kw/h)

Δt=Equivalent full load hours of operation of refrigeration system (hrs)

COP=Co-efficient of performance of refrigeration plant

V Figures and Tables

Selection of Orthogonal Array

Knowing the number of parameters and the number of levels, the proper orthogonal array can be selected. The number of process parameters in our experimental runs is three. i.e. Thickness of wall with 3 levels, Area of wall with 3 levels and Compressor with 3 levels. The numbers of levels in all control factors are equal. Therefore 3-level orthogonal is required in our experimental plan.

The L9 orthogonal array as shown in table 6 for All factor 3-levels design.

Therefore total 9 x 3 = 27 experimental runs are performed for the observations

Observation Tables

Ex p. No.	Control Parameter			Ener gy	Heat Transf er rate
	Thick ness	Area of wall	Compres sor		
1	0.050	0.96	0.100	258	14.56
2	0.050	1.5	0.125	383	23.17
3	0.050	2.16	0.167	502	32.96
4	0.075	0.96	0.125	172	10.4
5	0.075	1.5	0.167	241	15.78
6	0.075	2.16	0.100	409	22.73
7	0.100	0.96	0.167	119	7.78
8	0.100	1.5	0.100	222	12.33
9	0.100	2.16	0.125	290	17.23

Table: Observation table

In this study most important output performances in Cold Storage such as Energy consumption(E), Heat Transfer Rate(Q) are considered for optimizing Cold storage parameter. The Energy (E) value (in Watt) was obtained by using watt meter, The Heat Transfer Rate was measured by using Thermo couple The Heat Transfer Rate (HTR) is calculated as,

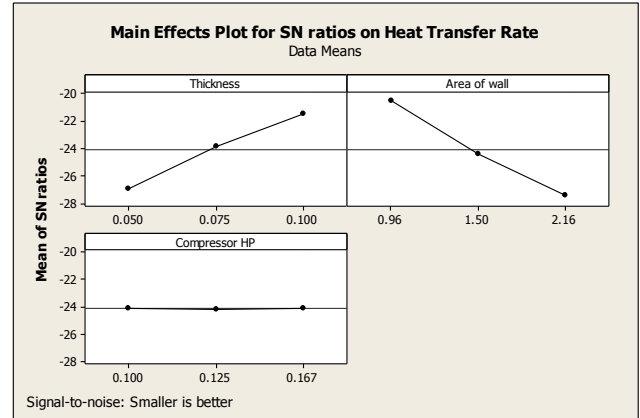
$$Q=UA\Delta T-----(1)$$

Where U = Thermal Coefficient of wall, A = Area of wall, ΔT = Temperature Difference

About Analysis software MINITAB

Minitab is a statistics package used for analysis of experimental data. It was developed at the Pennsylvania State University by researchers Barbara F. Ryan, Thomas A. Ryan, Jr., and Brian L. Joiner in 1972.

The goal of robust experimentation is to find an optimal combination of control factor settings that achieve robustness against (insensitivity to) noise factors. MINITAB calculates response tables and generates main effects and interaction plots for Signal-to-noise ratios (S/N ratios) vs. the control factors.



	C1	C2	C3	C4	C5	C6	C7	C8	C9	C10	C11	C12	C13	C14
1	0.050	0.96	0.100	258	14.56	-48.2324	-23.2632							
2	0.050	1.50	0.125	363	23.17	-51.6640	-27.2985							
3	0.050	2.16	0.167	502	32.96	-54.0141	-30.3597							
4	0.075	0.96	0.125	172	10.40	-44.7106	-20.3407							
5	0.075	1.50	0.167	241	15.78	-47.6403	-23.9621							
6	0.075	2.16	0.100	409	22.73	-52.2345	-27.1320							
7	0.100	0.96	0.167	119	7.78	-41.5109	-17.8196							
8	0.100	1.50	0.100	222	12.33	-46.9271	-21.8193							
9	0.100	2.16	0.125	290	17.23	-49.2460	-24.7257							

For the individual response maximization or minimization, chart 1 & 2 gives optimum value of each control factor. Chart interprets that Level A3,B1,C3 gives minimum result of Energy.

Analysis of Variance for Energy

Source	D F	Seq SS	Adj SS	Adj MS	F	P
Thickn ess	2	44630	44630	22315	15.12	0.062
Area of wall	2	71038	71038	35519	24.07	0.040
Compr essor	2	328	328	164	0.11	0.900
Error	2	2951	2951	1475		
Total	8	118946				

Table: Analysis of Variance for Energy
R-Sq = 97.52% R-Sq(adj) = 90.08%

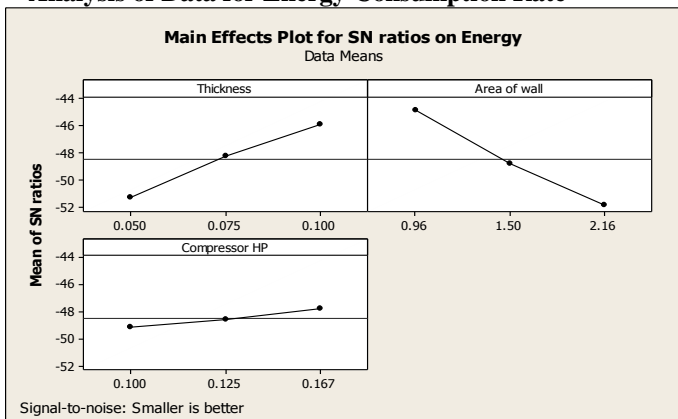
Analysis of Variance for Heat Transfer Rate

Sour ce	D F	Seq SS	Adj SS	Adj MS	F	P
Thic kne	2	191.162	191.162	95.581	16.03	0.059
Area of wall	2	269.606	269.606	134.803	22.61	0.042
Com pres	2	9.080	9.080	4.540	0.76	0.568
Error	2	11.923	11.923	5.961		
Total	8	481.771				

Table: Analysis of Variance for Heat Transfer Rate
R-Sq = 97.53% R-Sq(adj) = 90.10%

It provides standard orthogonal array for Taguchi methodology for experiment design. It also performs regression analysis to establish relation between two or more variables. It also helps in generating various types of tables and graphs.

Analysis of Data for Energy Consumption Rate



Exp No	Thickn ess	Area of Wall	Compressor	SNR_Ener gy	SNR_Heat transfer rate
1	0.050	0.96	0.100	-48.2324	-23.2632
2	0.050	1.5	0.125	-51.6640	-27.2985
3	0.050	2.16	0.167	-54.0141	-30.3597
4	0.075	0.96	0.125	-44.7106	-20.3407
5	0.075	1.5	0.167	-47.6403	-23.9621
6	0.075	2.16	0.100	-52.2345	-27.1320
7	0.100	0.96	0.167	-41.5109	-17.8196
8	0.100	1.5	0.100	-46.9271	-21.8193
9	0.100	2.16	0.125	-49.2480	-24.7257

Table: S/N Ratio for Response parameters

S/N ratio for response parameters as shown in table can be calculated using above equations. However we have obtained it using MINITAB 15 software.

Normalization of S/N Ratio for Response parameters

Step 2: In the grey relational analysis, a data pre-processing is first performed in order to normalize the raw data for analysis. Normalization is a transformation performed on a single data input to distribute the data evenly and scale it into an acceptable range for further analysis. In this study, a linear normalization of the S/N ratio is performed in the range between zero and unity. S/N ratio for response parameters as shown in table are normalized for further analysis using following equations.

Ex p No	Thickne ss	Are a of Wa ll	Compres sor	Normaliz ed SNR of Energy	Normaliz ed SNR of Heat transfer rate
1	0.050	0.96	0.100	0.4624	0.5659
2	0.050	1.5	0.125	0.1880	0.2441
3	0.050	2.16	0.167	0.0000	0.0000
4	0.075	0.96	0.125	0.7441	0.7990
5	0.075	1.5	0.167	0.5098	0.5102
6	0.075	2.16	0.100	0.1423	0.2574
7	0.100	0.96	0.167	1.0000	1.0000
8	0.100	1.5	0.100	0.5668	0.6811
9	0.100	2.16	0.125	0.3812	0.4493

Table 14 Normalization of S/N Ratio for Response parameters

Calculation of GRC and GRG for Response parameters

Ex p	Control Factor	Grey Relation	GRG
------	----------------	---------------	-----

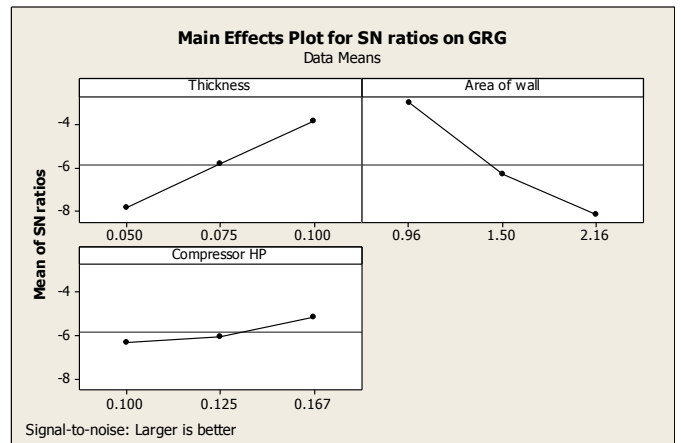
No				Coefficient		
	Thickn ess	Are a	Compres sor	GRC Ener gy	GRC HTR	
1	0.050	0.96	0.100	0.4819	0.5353	0.5086
2	0.050	1.5	0.125	0.3811	0.3981	0.3896
3	0.050	2.16	0.167	0.3334	0.3334	0.3334
4	0.075	0.96	0.125	0.6615	0.7132	0.6873
5	0.075	1.5	0.167	0.5049	0.5051	0.5050
6	0.075	2.16	0.100	0.3683	0.4024	0.3853
7	0.100	0.96	0.167	1.0000	1.0000	1.0000
8	0.100	1.5	0.100	0.5358	0.6105	0.5732
9	0.100	2.16	0.125	0.4469	0.4759	0.4614

Table Calculating GRC and GRG for Response parameters

The higher grey relational grade reveals that the corresponding experimental result is closer to the ideally normalized value. Experiment 7 has the best multiple performance characteristic among 9 experiments, because it has the highest grey relational grade shown in Table 15. The higher the value of the grey relational grade, the closer the corresponding factor combination is, to the optimal. A higher grey relational grade implies better product quality; therefore, on the basis of the grey relational grade, the factor effect can be estimated and the optimal level for each controllable factor can also be determined.

Main Effect of Factor on Grey Relation Grade

Following graph shows the grey relational grade graph. Basically, the larger the grey relational grade, the better is the multiple performance characteristic.



For the combined responses maximization or minimization, chart gives optimum value of each control factor. Chart interprets that Level A3, B1 and C3 gives optimum result. The mean of the grey relational grade for each level of the other Cold storage parameters can be computed in a similar manner. The mean of the grey relational grade for each level of the Cold storage parameters is summarized and shown in the following Table.

Symbol	Control Factor	Level-1	Level-2	Level-3
A	Thickness	0.4105	0.5259	0.6782
B	Area of wall	0.7320	0.4893	0.3933
C	Compressor HP	0.4890	0.5128	0.6128

Table 16 Main Effects of Factors on Grey Relational Grade

Mathematical Model The mathematical model for predicting the response parameters in Cold storage can be derived using methods like Regression analysis.

Regression Equation for Energy
The Regression Equation is

$$\text{Energy}(E) = 280 - 3143 \text{ Thickness} + 181 \text{ Area of wall} - 106 \text{ Compressor HP}$$

Predictor	Coefficient	SE Coef	T	P
Constant	279.54	65.56	4.26	0.008
Thickness	-3413.3	470.10	-7.26	0.001
Area of wall	181.04	19.55	9.26	0.000
Compressor HP	-106.4	347.10	-0.31	0.772

Table Regression coefficient for Energy

$$R\text{-Sq} = 96.5\%$$

In the regression analysis, the P value of factors, Thickness and Area of wall are less than 0.05, therefore these factors are significant. The co-efficient of determination (R²) indicates the goodness of fit for model. The value of R² is 96.5% which indicates that model is fit for prediction.

Regression Equation for Heat Transfer Rate

The regression equation is

$$\text{HTR}(Q) = 12.3 - 222 \text{ Thickness} + 11.2 \text{ Area of wall} + 35.5 \text{ Compressor HP}$$

Predictor	Coefficient	SE Coef	T	P
Constant	12.302	4.344	2.83	0.037
Thickness	-222.33	31.14	-7.14	0.001
Area of wall	11.153	1.295	8.61	0.000

Compressor HP	35.48	22.99	1.54	0.184
---------------	-------	-------	------	-------

Table.18 Regression coefficient for Heat Transfer Rate
R-Sq = 96.2%

The results of analysis indicate that the compressor HP is not much significant in Heat Transfer Rate. Here the value of R² is 96.2%, which is quiet high; therefore model is suitable for result prediction.

	Process Parameter	
	Orthogonal Array	Grey Relation Design
Level	A3 B1 C3	A3 B1 C3
ECR	119	119
HTR	7.78	7.78

VII. CONCLUSION

In the Present Research work there was developed cold storage model at super Refrigeration and also developed Refrigeration system, both are attached with each other for experiment. In this work our main objective is to Optimum insulation thickness, Area of wall, compressor capacity of cold storage with the help of Taguchi method, There was Three factor Thickness, Area of wall and compressor consider and take Three level each 0.050,0.075,0.100 and 0.96 1.5 2.16 and 0.100, 0.125, 0.167 in Taguchi Method. we are using L9 Orthogonal Array Design. In the research work there is using ANOVA for Develop different Graphs of S/N Ratio ,here concluded that orthogonal array and Grey relation design both are gave same result as best optimum value of Thickness 0.100 Mt, area of wall 0.96 Mt and compressor 0.167 HP and also study of Regression analysis to develop Mathematical model for calculating direct optimum value of all parameters

VII. REFERENCES

- [1] M.S.Soylmez, M.Unsal(1997) Optimum Insulation Thickness for Refrigerant applications, Energy Conservation and Management 40(1999) 13-21.
- [2] Merrick Burden, Gilbert Sylvia, Edward Kolbe(2004) Optimal storage temperature Design for Frozen Food Seafood inventories: Application to Pacific Whiting surimi, IIFET, 2004 Japan Proceeding
- [3] Mashud Ahmed, Oliver Meade, Mario A. Medina(2009) Reducing heat transfer across the insulated walls of refrigerated truck trailers by the application of phase change materials, Energy Conservation and Management 51 (2010) 383-392
- [4] N.Yusoff and M.Ramasamy(2010), Selection of RGP Optimization variables using Taguchi Method, Journal of Applied Science 10(24) 3313-3318,2010 ISSN 1812-5654
- [5] ASHRAE Hand Book of Fundamentals, New York, 1981
- [6] Duffie J A Beckman WA. Solar engineering of thermal processes. New York: Wiley,1980
- [7] Heat and Mass Transfer By Dr. D S Kumar, S.K.Kataria and Sons, New Delhi

Prediction of surface roughness for end milling process using Artificial Neural Network

Jignesh G. Parmar¹, Prof. Alpesh Makwana²

*(Department Of Mechanical Engineering, Government Engineering College/ GTU, India)

** (Department Of Mechanical Engineering, Government Engineering College/ GTU, India)

ABSTRACT

In machining, surface quality is one of the most commonly specified customer requirements in which the major indication of surface quality on machined parts is surface roughness. The aim is prediction of surface roughness by using artificial neural networks. The neural network model can be effectively find the best cutting parameters value for a specific cutting condition in milling operation and achieve minimum surface roughness. In the present work an experimental investigation of the end milling of M.S material up to 30 HRC with carbide tool by varying feed, speed and depth of cut and the surface roughness was measured using Mitutoyo Surface Roughness Tester. The neural network design and development was done using MATLAB. Neural Network Fitting Tool Graphical User Interface is used to establish the relationship between the surface roughness and the cutting input parameters (spindle speed, feed and depth of cut). The result from this research is useful to be implemented in industry to reduce time and cost in surface roughness prediction.

Keywords - End milling, Surface roughness, Neural Networks, GUI, MATLAB

1. INTRODUCTION

Among different types of milling processes, end milling is one of the most vital and common metal cutting operations used for machining parts because of its capability to remove materials at faster rate with a reasonably good surface quality. Also, it is capable of producing a variety of configurations using milling cutter. Surface roughness is a key factor in the machining process while considering machining performance and that is why in many cases, industries are looking for maintaining the good surface quality of the machined parts. Surface roughness is a measure of the technological quality of a product and a factor that greatly influences manufacturing cost and quality. It describes the geometry of the machined surface and combined with the surface texture, it can play an important role on the operational characteristics of the part. It also influences several functional attributes of a part, such as light reflection, heat transmission, coating characteristics, surface friction, fatigue resistance etc. However, the mechanism behind the formation of surface roughness is very dynamic, complicated and process

dependent; therefore it is very difficult to calculate its value through analytical formulae. Various theoretical models that have been proposed are not accurate enough and apply only to a limited range of processes and cutting conditions. Therefore, machine operators usually use ANN approaches to set-up milling machine cutting conditions in order to achieve the desired surface roughness

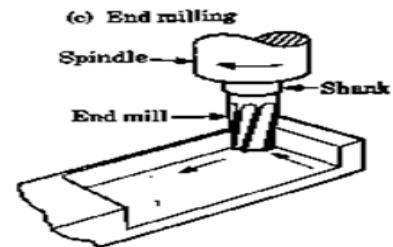


Fig.1.1 End milling operation[12]2. LITERATURE REVIEW

Chen and Savage [2001] used fuzzy net-based model to predict surface roughness under different tool and work piece combination for end milling process. Speed, feed and depth of cut, vibration, tool diameter, tool material, and work piece material are used as input variables for fuzzy system. The authors found that the predicted surface roughness is within an error of 10% [6]. Prakashvudhisarn et al. [2009] proposed an approach to determine optimal cutting condition for desired surface roughness in end milling. The approach consists of two parts: machine learning technique called support vector machine to predict surface roughness and particle swarm optimization technique for parameters optimization. The authors found that PSO shows consistent near-optimal solution with little effort [5]. Metin Kk (2010) has suggested an experimental investigation of the effects of cutting speed, size and volume fraction of particle on the surface roughness in turning of 2024Al alloy composites reinforced with Al₂O₃ particles. A plan of experiments, based on Taguchi method, was performed machining with different cutting speeds using coated carbide tools K10 and TP30. The objective was to establish a correlation between cutting speed, size and volume fraction of particle with the surface roughness in workpieces. These correlations were obtained by multiple linear regression. The analysis of variance was

also employed to carry out the effects of these parameters on the surface roughness. The test results revealed that surface roughness increased with increasing the cutting speed and decreased with increasing the size and the volume fraction of particles for both cutting tools. The average surface roughness values of TP30 cutting tools were observed to be lower than those of K10 tools. For the average surface roughness values of TP30 tool, cutting speed was found to be the most effective factor while the volume fraction of particle was the most effective factor for those of K10 tool. A good agreement between the predicted and experimental surface roughness was observed within a reasonable limit[8]. Brezocnik et al. [2004] proposed a GP approach to predict surface roughness in end milling process. The genetic programming is an evolutionary computation method that was first introduced by Koza [1992] in the year 1992. It aims to find out computer programs (called as chromosomes) whose size and structure dynamically changes during simulated evolution that best solve the problem. Cutting parameters, viz., spindle speed, feed, and depth of cut as well as vibration between tool and work piece, were used to predict the surface roughness and the authors found that the model that involves all these variables accurately predict the surface roughness[3]. Lo [2003] used ANFIS to predict the surface roughness in end milling process. Spindle speed, feed rate, and depth of cut were considered as input parameters. The ANFIS was modeled using triangular and trapezoidal membership functions. The average error of prediction of surface roughness for triangular membership function was found lower, around 4% [1]. Reddy and Rao [2005] developed an empirical surface roughness model for end milling of medium carbon steel, whose parameters were optimized using GA also Reddy and Rao used genetic algorithm to optimize tool geometry, viz., radial rake angle and nose radius and cutting conditions, viz., cutting speed and feed rate to obtain desired surface quality in dry end milling process[4]. S. Saikumar et al (2011) has reported High-speed machining centers are used for end-milling operations of a variety of parts, dies, and molds needed in power and transport industries. Different approaches are used for rough and finish end milling, since desired productivity and quality are important in the respective cases. In the present work, a feed rate adaption control system is proposed by integrating different requirements of high-speed end milling. Hardened EN 24 steel which is being widely used in the production of dies, molds, and other parts is taken as a candidate work material for implementation of the proposed control system. Based on extensive experimentation, investigations have been carried out on high speed rough and finish end-milling operations, and the details are reported by the authors (Saikumar and Shunmugam, Int J Adv Manuf Technol, under review). In this paper, relevant response surface and artificial neural network models have been used, and suitable reference parameters are obtained for the

proposed control system. In the case of rough end-milling, material removal volume is taken as the objective, and the reference values for cutting force and cutting time are used. Only a reference cutting force is used for finish end-milling in which surface roughness is considered as the objective. Implementation details of the proposed PC-based control system are presented. The results obtained for a newly devised H-A-S-H test (short run) along with those for long-run tests are presented and discussed[9]. Masoud Farahnakian (2011) has suggested polymer nanocomposites have emerged relatively as a new and rapidly developing class of composite materials and attracted considerable investment in research and development worldwide. An increase in the desire for personalized products has led to the requirement of the direct machining of polymers for personalized products. In this work, the effect of cutting parameters (spindle speed and feed rate) and nanoclay (NC) content on machinability properties of polyamide-6/nanoclay (PA-6/NC) nanocomposites was studied by using high speed steel end mill. This paper also presents a novel approach for modeling cutting forces and surface roughness in milling PA-6/NC nanocomposite materials, by using particle swarm optimization-based neural network (PSO) and the training capacity of PSO is compared to that of the conventional neural network. In this regard, advantages of the statistical experimental algorithm technique, experimental measurements artificial neural network and particle swarm optimization algorithm, are exploited in an integrated manner. The results indicate that the nanoclay content on PA-6 significantly decreases the cutting forces, but does not have a considerable effect on surface roughness. Also the obtained results for modeling cutting forces and surface roughness have shown very good training capacity of the proposed PSO algorithm in comparison to that of a conventional neural network[7]. Amir Mahyar Khorasani et al [2011] (ANN) for modeling and predicting tool life in milling parts made of Aluminum (7075) material was developed. Given the accuracy that was achieved it is safe to conclude that all the significant factors were included in the (DOE) process. extended towards three different steps. The first step is using Taguchi (DOE) and different combinations of cutting parameters for building database. The second step is modeling tool life by using (ANN). Third step is validation by carrying out the experimental tests. In generating the (ANN) model statistical (RMS) was utilized. The accuracy error was found to be insignificant (3.034%). It was found that (ANN) prediction correlates very well with the experimental results. Finally the correlation for training and test was obtained 0.96966 and 0.94966 respectively and mean square error was calculated 3.1908% for test data[10]. C. C. Tsao (2010) has discussed The grey-Taguchi method was adopted in this study to optimize the milling parameters of A6061P-T651 aluminum alloy with multiple performance characteristics. A grey relational grade obtained from the grey relational analysis is used as

the performance characteristic in the Taguchi method. Then, the optimal milling parameters are determined using the parameter design proposed by the Taguchi method. Experimental results indicate that the optimal process parameters in milling A6061P-T651 aluminum alloy can be determined effectively; the flank wear is decreased from 0.177 mm to 0.067 mm and the surface roughness is decreased from 0.44 μm to 0.24 μm , leading to a multiple performance characteristics improvement in milling qualities through the grey-Taguchi method[15].

Hasan Kurtaran et al (2005) has discussed optimum cutting parameters of Inconel 718 are determined to enable minimum surface roughness under the constraints of roughness and material removal rate. In doing this, advantages of statistical experimental design technique, experimental measurements, artificial neural network and genetic optimization method are exploited in an integrated manner. Cutting experiments are designed based on statistical three-level full factorial experimental design technique. A predictive model for surface roughness is created using a feed forward artificial neural network exploiting experimental data. Neural network model and analytical definition of material removal rate are employed in the construction of optimization problem. The optimization problem was solved by an effective genetic algorithm for variety of constraint limits. Additional experiments have been conducted to compare optimum values and their corresponding roughness and material removal rate values predicted from the genetic algorithm. Generally a good correlation is observed between the predicted optimum and the experimental measurements. The neural network model coupled with genetic algorithm can be effectively utilized to find the best or optimum cutting parameter values for a specific cutting condition in end milling Inconel 718[14].

3. Experimental study

For developing models on the basis of experimental data three main machining parameters are considered to predict surface roughness of M.S material using carbide tool. The available literature reveals that spindle speed, feed rate and axial depth of cut are primary machining parameters on which surface roughness depends. These factors are considered for experimentation study. In this study factorial method is used. DOE of all three factors and their unique factor level combinations (4Vc X 7f X 3doc) results in a total 84 observation. End mill cutter with 12 mm diameter having 4 flutes with carbide tipped is used for machining M.S material work piece. Among the range of spindle speed, feed, and depth of cut available possible in the machine the following three levels are considered as shown in table I. The machining was carried out on Vertical milling machine, The M.S material work piece is clamped on vice mounted on the table of the machine. The machining process and work tool motion of the end milling process respectively. The machining is carried out

by selecting proper spindle speed and feed rate during each experimentation. Experiment was carried out by varying the depth of cut.

Factors	Levels	Factors level values
SPEED(m/min.)	4	80,100,120,140
FEEDRATE PER TOOTH(mm/min.)	7	0.03, 0.035, 0.040, 0.045, 0.05, 0.055, 0.06, 0.065
DEPTH OF CUT(mm)	3	0.1, 0.2, 0.3

Table I Level of experiment

Surface roughness values of work pieces were measured by Mitutoyo Surface Roughness Tester by a proper procedure while measuring instrument and measurements are repeated three times.

Table II shows the experimental result.

SR. NO	FEED (mm/rev.)	CUTTING SPEED VC (m/min)	Depth of cut (mm)	Experimental ROUGHNESS VALUE Ra (μm)
1	0.03	80	0.1	0.21
2		80	0.2	0.22
3		80	0.3	0.25
4		100	0.1	0.2
5		100	0.2	0.21
6		100	0.3	0.22
7		120	0.1	0.19
8		120	0.2	0.21
9		120	0.3	0.22
10		140	0.1	0.18
11		140	0.2	0.19
12		140	0.3	0.2
13	0.035	80	0.1	0.23
14		80	0.2	0.24
15		80	0.3	0.25
16		100	0.1	0.19
17		100	0.2	0.21
18		100	0.3	0.22
19		120	0.1	0.19
20		120	0.2	0.2
21		120	0.3	0.21
22		140	0.1	0.19
23		140	0.2	0.21
24		140	0.3	0.23
25	0.04	80	0.1	0.26
26		80	0.2	0.28
27		80	0.3	0.3

28		100	0.1	0.23
29		100	0.2	0.24
30		100	0.3	0.24
31		120	0.1	0.19
32		120	0.2	0.2
33		120	0.3	0.23
34		140	0.1	0.2
35		140	0.2	0.21
36		140	0.3	0.21
37		0.045	80	0.1
38	80		0.2	0.29
39	80		0.3	0.29
40	100		0.1	0.26
41	100		0.2	0.25
42	100		0.3	0.23
43	120		0.1	0.25
44	120		0.2	0.24
45	120		0.3	0.21
46	140		0.1	0.23
47	140	0.2	0.22	
48	140	0.3	0.2	
49	0.05	80	0.1	0.29
50		80	0.2	0.3
51		80	0.3	0.3
52		100	0.1	0.28
53		100	0.2	0.3
54		100	0.3	0.31
55		120	0.1	0.27
56		120	0.2	0.29

57		120	0.3	0.29
58		140	0.1	0.25
59		140	0.2	0.27
60		140	0.3	0.28
61	0.055	80	0.1	0.3
62		80	0.2	0.31
63		80	0.3	0.31
64		100	0.1	0.29
65		100	0.2	0.3
66		100	0.3	0.3
67		120	0.1	0.28
68		120	0.2	0.29
69		120	0.3	0.31
70		140	0.1	0.27
71		140	0.2	0.28
72		140	0.3	0.28
73		0.06	80	0.1
74	80		0.2	0.35
75	80		0.3	0.33
76	100		0.1	0.31
77	100		0.2	0.3
78	100		0.3	0.32
79	120		0.1	0.29
80	120		0.2	0.3
81	120		0.3	0.31
82	140		0.1	0.27
83	140		0.2	0.29
84	140		0.3	0.31

Table II Experimental data

SR. NO	FEED PER TOOTEH	CUTTING SPEED VC (m/min)	DOC (mm)	experimental ROUGHNESS VALUE Ra (μm)	ANN ROUGHNESS VALUE Ra (μm)	Error	Error %
1	0.03	80	0.1	0.21	0.212917	-0.00292	1.38894
2	0.03	80	0.2	0.22	0.232296	-0.0123	5.58927
3	0.03	100	0.1	0.2	0.187708	0.012292	6.145831
4	0.03	100	0.2	0.21	0.220786	-0.01079	5.13629
5	0.03	120	0.1	0.19	0.185403	0.004597	2.419305
6	0.03	120	0.2	0.21	0.202975	0.007025	3.3454
7	0.035	100	0.3	0.22	0.226249	-0.00625	2.8404
8	0.045	80	0.1	0.28	0.272137	0.007863	2.808156
9	0.045	120	0.2	0.24	0.246086	-0.00609	2.53591
10	0.055	140	0.1	0.27	0.289599	-0.0196	7.25887
11	0.06	100	0.1	0.31	0.282894	0.027106	8.743766
12	0.06	120	0.2	0.3	0.304228	-0.00423	1.40927
13	0.06	120	0.3	0.31	0.314916	-0.00492	1.58579

TABLE III Comparison of ANN predictions with experimental data

4. Neural Network modeling

Neural network is a highly flexible modeling tool with the ability to learn the mapping between input and output parameters [13]. An artificial neural network (ANN) is capable of learning from an experimental data set to describe the nonlinear and interaction effects more effectively. The network consists of an input layer used to present data, output layer to produce ANN's response, and one or more hidden layers in between. The network is characterized by their topology, weight vectors, and activation function that are used in hidden and output layers of the network. Networks with biases, a sigmoid layer, and a linear output layer are capable of approximating any function with a finite number of discontinuities.

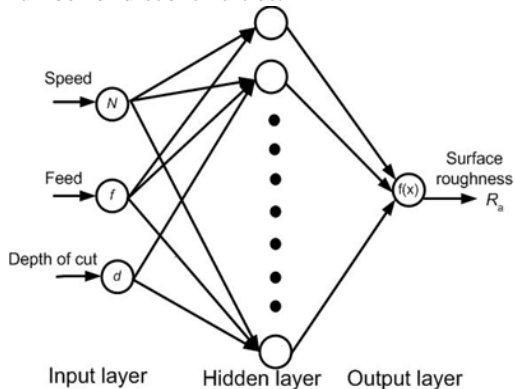


Fig.-2 Neural Network

The knowledge is presented by the interconnection weight, which is adjusted during the learning stage using the back propagation learning algorithm to minimize the mean square between the actual output of the network and the desired output pattern. Here it is used to develop surface roughness prediction model for end milling process. From 84 experiments were conducted 58 experimental datasets are used to train, 13 used for verification and 13 for testing purpose. Before applying the neural network for modeling the architecture of the network has to be decided; i.e. the number of hidden layers and the number of neurons in each layer and transfer function for each layer. As there are 3 inputs to produce one output, the number of neurons in the input and output layer has to be set to 3 and 1 respectively. Considering one hidden layer the number of neurons in the hidden layer is optimized. Table III shows the established tested experimental result and the NN model prediction. It was observed that the prediction based on an ANN model is quite close to the established observation. The average prediction error for data set is found to be 3.5% and maximum prediction error is 8.743766%. In all cases, maximum error tolerance was kept constant. It was observed that the average prediction error was minimized. The transfer functions used in this are Tan Sigmoid between input and hidden layer and pureline between hidden and output layer.

5. Conclusion

In doing this, experimental measurements, artificial neural network is exploited in an integrated manner. The goal is prediction of surface roughness in milling process by using artificial neural networks and roll of main parameters (spindle speed, feed rate and depth of cut). Generally a good correlation is observed between the predicted and the experimental measurements. This survey will help in another

important factor that greatly influences production rate and cost. So, as a whole, there is a need for allow the evaluation of the surface roughness before the machining of the part and which, at the same time, can be easily used in the production floor environment for contributing to the minimization of required time and cost and the production of desired surface quality.

- Identifies minimum surface roughness value $0.18\mu\text{m}$ was obtained at the value of 0.03 mm/tooth, 140 m/min and 0.1 for feed rate, cutting speed and depth of cut respectively.
- Identifies maximum surface roughness value $0.35\mu\text{m}$ was obtained at the value of 0.06 mm/rev, 80 m/min and 0.2 mm for feed rate, cutting speed and depth of cut respectively.
- Surface roughness increase as feed rate increase.
- These model can be used to prediction of surface roughness in end milling process.

ACKNOWLEDGEMENTS

I would like to express my deep sense of gratitude and respect to my guide Prof. A.H.Makwana sir for his excellent guidance, suggestions and constructive criticism. I consider myself extremely lucky to be able to work under the guidance of such a dynamic personality. I am also thankful to H.P.Doshi sir for his co-operation throughout the semester.

REFERENCES

- [1] Lo SP (2003) An adaptive-network based fuzzy inference system for prediction of work piece surface roughness in end milling. *J Mater Process Technol* 142:665–675. doi:10.1016/S0924-0136(03)00687-3
- [2] Saurav Datta, Asish Bandyopadhyay (2010), Parametric optimization of CNC end milling using entropy measurement technique combined with grey-Taguchi method. *International Journal of Engineering, Science and Technology* Vol. 2, No. 2, 2010, pp. 1-12
- [3] Brezocnik M, Kovacic M, Ficko M (2004) Prediction of surface roughness with genetic programming *J Mater Process Technol* 157–158:28–36. doi:10.1016/j.jmatprotec.2004.09.004
- [4] Reddy NSK, Rao PV (2005) Selection of optimum geometry and cutting conditions using surface roughness prediction model for end milling. *Int J Adv Manuf Technol* 26:1202–1210. doi:10.1007/s00170-004-2110-y
- [5] Prakashvudhisarn C, Kunnapapdeelert S, Yenradee P (2009) Optimal cutting condition determination for desired surface roughness in end milling. *Int J Adv Manuf Technol* 41:440–451. doi:10.1007/s00170-008-1491-8
- [6] Chen JC, Savage M (2001) A fuzzy-net-based multilevel inprocess surface roughness recognition system in milling operations. *Int J Adv Manuf Technol* 17:670–676. doi:10.1007/s001700170132
- [7] Masoud Farahnakian & Mohammad Reza Razfar(2011), The selection of milling parameters by the PSO-based neural network modeling method. *Int J Adv Manuf Technol* 57:49–60 DOI 10.1007/s00170-011-3262-1
- [8] Metin K k (2011) Modelling the effect of surface roughness factors in the machining of 2024Al/Al2O3 particle composites based on orthogonal arrays. *Int J Adv Manuf Technol* (2011) 55:911–920 DOI 10.1007/s00170-010-3134-0
- [9] Saikumar & M. S. Shunmugam Received: 14 February 2011 / Accepted: 1 August # Springer-Verlag London Limited 2011
- [10] Amir Mahyar Khorasani1, Mohammad Reza Soleymani Yazdi(2010) Tool Life Prediction in Face Milling Machining of 7075 Al by Using Artificial Neural Networks(ANN) and Taguchi Design of Experiment. *IACSIT International Journal of Engineering and Technology*, Vol.3, No.1, February 2011 ISSN: 1793-8236
- [11] Natarajan & PR. Periyanan & S. H. Yang[2011] *Int J Adv Manuf Technol* (2011) 56:177–185 DOI 10.1007/s00170-011-3156-2
- [12] C. C. Tsao(2009), Grey-Taguchi method to optimize the milling parameters of aluminum alloy, *Int J Adv Manuf Technol* (2009) 40:41–48 DOI 10.1007/s00170-007-1314-3.
- [13] P. Palanisamy, I. Rajendran, and S. Shanmugasundaram, “Optimization of machining parameters using genetic algorithm and experimental validation for end-milling operations”, *Int. J. Adv. Manu. Techno.*, vol. 32, pp. 644-655, 2007.
- [14] Hasan Kurtaran(2005), Optimum surface roughness in end milling Inconel 718 by coupling neural network model and genetic algorithm, DOI 10.1007/s00170-004-2175-7 *Int J Adv Manuf Technol* (2005) 27: 234–241
- [15] C. C. Tsao(2009), Grey-Taguchi method to optimize the milling parameters of aluminum alloy, *Int J Adv Manuf Technol* (2009) 40:41–48 DOI 10.1007/s00170-007-1314-3

Reducing Source Code Complexity For Software development using Code Comprehension Nurturant using Traceability

¹N. Rajasekhar Reddy

¹ Associate Professor, Department of CSE, Madanapalli Institute of Technology and Science, Madanapalli, Andhra Pradesh, India

² B. Anand kumar

² Research Scholar, Department of CSE, Madanapalli Institute of Technology and Science, Madanapalli, Andhra Pradesh, India.

Abstract- Nowadays, many papers are developing to improve the software quality control. In our paper we are going to help the developers to maintain the source code and identifiers and we will show the textual similarity between source code and related high level faults. The developers are improving the source code library. So, if the software development environment provides similarities between the source code and the high level problems then it will be quite easier for the developers to keep the software quality ahead. In our proposing system the candidate identifiers needs to implement in eclipse IDE for that we need a plug-in called **COde COMprehension Nurturant Using Traceability (COCONUT)**. This paper also reports on two controlled experiments performed with master's and bachelor's students. The quality of identifiers, comments in the produced source code with or without coconut. The approach presented in this paper relates to approaches aimed at applying IR techniques for traceability recovery and for quality improvement/assessment. So that quality of the source code lexicon will be improved. Thus the usefulness of the coconut is taken as a feature of software development environments.

Keywords: Software traceability, source code comprehensibility, source code identifier quality, information retrieval, software development environments, empirical software engineering.

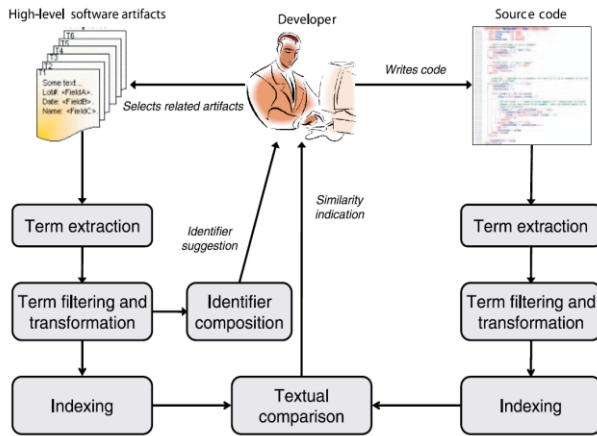
Introduction:

This paper proposes the use of traceability information combined with IR techniques from a different perspective. When a programmer writes the source code, a plug-in incorporated in the development environment shows the similarity between the source code under development and high-level artifacts on which the source code should be traced. Such a similarity provides information about the consistency between source code identifiers and high-level artifacts, suggesting the developer that the code is (or is not) properly traced to the related artifacts. In the second case, the developer can act in various ways. This chapter presents the concept of requirements tracing and discusses several aspects related to traceability. Particular importance is given to the informal aspects of requirements tracing and to the non-functional nature of requirements traceability. To give further support to the developer, the proposed approach also recommends candidate identifiers built from

high-level artifacts related to the source code. The paper also describes an Eclipse1 plug-in, named **COde COMprehension Nurturant Using Traceability (COCONUT)**, which implements the proposed approach. Its evaluation has been carried out through two controlled experiments involving master's and bachelor's students, where we asked students to perform development tasks with and without the availability of COCONUT features. The analysis of the achieved results confirms our conjecture that providing the developers with the similarity between code and high-level artifacts helps to significantly improve the quality of source code identifiers and comments, which also further increases when developers receive suggestions about candidate identifiers.

Related Work:

Recently, the artefact traceability support has been introduced in some process support systems where the traceability layer has been combined with event based notifications mainly to make users aware of artefact modifications. All these tools have a common drawback: they require a manual maintenance of the traceability layer while the system changes and evolves. The traceability recovery problem is widely tackled in the literature and several techniques are applied to support the process of traceability link recovery. Some of them deal with recovering traceability links between design and implementation. The proposed approaches represent source code and high-level models using a common language and use regular expressions, maximum match algorithm or more tolerant string matching to map source code in the high-level models. Other approaches consider text documents written in natural language, such as requirements documents. Automate the generation of traceability relations between textual requirement artefacts and object models using heuristic rules. we also evaluated the different magnitude using the Cohen d effect size. A major threat could be related to the applicability of ANOVA [2] when data deviate from normality and for crossover designs, although ANOVA is generally pretty robust to deviations from normality and the carryover effect is limited, as discussed. In addition, to confirm the results obtained by ANOVA, we performed multiple Mann-Whitney tests, with threshold p-values adjusted by means of the correction.

A novel approach of Proposed system:

The proposed approach is based on the assumption that developers are induced to make the source code identifiers more consistent with domain terms or to better comment the source code if the software development environment provides information about the textual similarity between the source code being written and the related high-level artifacts. Clearly, the proposed approach is based on the assumption that high-level documentation requirements, use cases, and module specifications is available during the development process. The flow of information between a developer and the Integrated Development Environment (IDE) in the proposed approach. The textual similarity between the source code and the related high-level artifacts is computed by using an IR-based approach. In general, an IR method compares a given query against all the documents in a collection by computing the textual similarity between these documents and the query.

1. Removing non textual tokens, e.g., numbers and punctuation for the high-level artifacts, and operators, special symbols, and programming language keywords from the source code;
2. Splitting into separate words source code identifiers composed of two or more words separated by using the underscore or camel case separators.
3. Removing stop words using a stop word removal function which removes words having a length less than a fixed threshold and also removing words belonging to a stop word list.

Hypothesis Formulation and Variable Selection:

As we wanted to investigate the usefulness of both the COCONUT similarity feature and the identifier suggestion feature, the experiments foresaw three possible treatments:

1. No plug-in (NOPL): Subjects performed their tasks without using COCONUT.

2. With simple plug-in (PL): Subjects performed their tasks with the COCONUT similarity feature available only.
3. With fully featured plug-in (PLP): Subjects performed their tasks with both features provided by COCONUT, i.e., the similarity and the identifier suggestion features.

Experimental task:

Experiment	System	Task	Description
Exp. I	ADAMS	T1	Create a module to list, insert and modify comments related to the artifacts
		T2	Create a module able to handle templates of artifacts
Exp. II	LM-06	T1	Inserting a new feature for managing book reservations
		T2	Inserting a new feature for adding a new book to the library
Exp. II	INFO-ASL	T1	Inserting a new feature for booking a visit
		T2	Inserting a new feature for adding a new patient
Exp. II	SIL-Campania	T1	Inserting a new feature to search for a new job
		T2	Inserting a new feature for adding a new company

we defined two dependent variables,

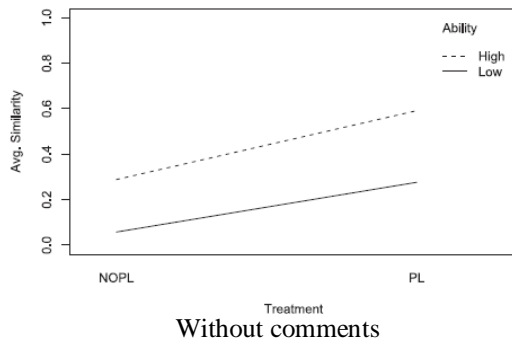
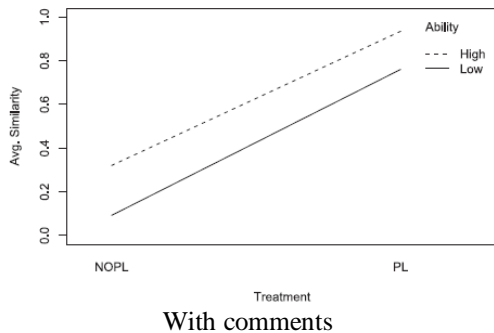
Sim with Comments and Sim no Comments, measuring the average similarity between the source code and the related high level artifact(s), including source code comments given the set of raw similarity (RSim with Comments) computed for a given combination of projects and tasks, we compute Sim with Comments as follows:

$$Sim_{withComments} = \frac{RSim_{withComments} - \min(RSim_{withComments})}{\max(RSim_{withComments}) - \min(RSim_{withComments})}$$

The first three null hypotheses the controlled experiments aimed at testing are:

1. H01 : The use of the COCONUT similarity feature does not significantly improve the similarity between the commented source code and the related high-level artifacts (compared with the use of Eclipse without the COCONUT plug-in).
2. H02 : The use of COCONUT similarity feature does not significantly improve the similarity between the uncommented source code and the related high-level artifacts (compared with the use of Eclipse without the COCONUT plug-in).
3. H03 (tested in Exp II only): The comprehensive use of COCONUT (similarity and identifier suggestion features) does not significantly improve the similarity between the uncommented source code and the related high-level artifacts (compared with the use of the COCONUT similarity feature only).

Comparison :
Effect of treatment:
Ability:



Conclusion:

The proposed approach is to intimate the developers about the current developing project with the existing one which is similar to the current project. The main terms used as identifiers or present in comments. In particular, our approach

- 1) Computes and shows to developers the textual similarity between source code and related high-level artifacts.
- 2) Recommends candidate identifiers built from high-level artifacts related to the source code under development.

References:

- [1] V.R. Basili, L.C. Briand, and W.L. Melo, "A Validation of Object- Oriented Design Metrics as Quality Indicators," IEEE Trans. Software Eng., vol. 22, no. 10, pp. 751-761, Oct. 1996.
- [2] M. Lormans, A. Deursen, and H.-G. Gross, "An Industrial Case Study in Reconstructing Requirements Views," Empirical Software Eng., vol. 13, no. 6, pp. 727-760, 2008.
- [3] T. Zimmermann, R. Premraj, and A. Zeller, "Predicting Defects for Eclipse," Proc. Third ICSE Int'l Workshop Predictor Models in Software Eng., 2007.
- [4] G. Capobianco, A. De Lucia, R. Oliveto, A. Panichella, and S. Panichella, "Traceability Recovery

Using Numerical Analysis," Proc. 16th Working Conf. Reverse Eng., 2009.

AUTHOR'S DESCRIPTION



N.Rajasekhar reddy was born in Madanapalli, February 28. He was received Bachelor's degree in Computer Science in S.V University and M.Tech degree from Satyabama University respectively. After working as a research assistant and an assistant professor in the Dept. of Computer Science and Engineering, Madanapalli Institute of Technology and Science, Andhra Pradesh, India. His research interest includes Software Engineering, Software Quality Assurance and Testing. He was published 4 international journal papers and 5 National journal papers in Software Engineering. He is a member of SCIE, ISTE, and IEEE



B.Anand kumar was born in Theni, January 05. He was received Bachelor's degree in Information technology in Anna University and M.Tech degree pursuing from J.N.T University Anapatur respectively. His research interest includes Software Engineering, Software Quality Assurance and Testing. Software methodologies. I was done my project under the esteemed guidance of Mr.N.RajaSekharReddy.

Prevention of Black Hole Attack in Mobile Ad-hoc Networks using MN-ID Broadcasting

Antony Devassy¹, K. Jayanthi²

*(PG scholar, ME communication Systems, SNS College of Technology, Coimbatore, India)

**(Associate professor, Department of ECE, SNS College of Technology, Coimbatore, India)

ABSTRACT

Black hole is a malicious node that always gives the false replay for any route request without having specified route to the destination and drops all the received packets. This can be easily employed by exploiting vulnerability of on demand routing protocol AODV. In mobile Ad hoc networks black hole attack is a severe threat which can be prevented by broadcasting the MN-ID (malicious node id) to the whole nodes in the network. The existing method identified the attacked node, retransmit the packets and again find a new route from source to destination.

Here the proposed method broadcast the MN-ID to the whole nodes in the network. This method prevents the black hole attack imposed by both single and multiple black hole nodes. The tool used to implement the proposed algorithm is NS2, which is an object oriented event drive software package. The result of the simulation study expected to get good network performance by minimizing the packet losses as well as effectively prevent the black hole attack against mobile Ad hoc networks.

Keywords- Ad-hoc, AODV, Blackhole, MN-ID

1. INTRODUCTION

A mobile ad hoc network (MANET)[5] is a collection of wireless mobile nodes which have the ability to communicate with each other without having fixed network infrastructure or any central base station. It is one of the recent active fields and has received spectacular consideration because of their self-configuration and self-maintenance. Early research assumed a friendly and cooperative environment of wireless network. As a result they focused on problems such as wireless channel access and multihop routing. Since mobile nodes are not controlled by any other controlling entity, they have unrestricted mobility and connectivity to others. Routing and network management are done cooperatively by each other nodes. Due to limited transmission power, multi hop architecture is needed for one node to communicate with another through network. In this multi hop architecture, each node works as a host and as well as a router that forwards packets for other nodes that may not be within a direct communication range. Each node participates in an ad hoc route discovery protocol which finds out multi hop routes through the mobile network between any two nodes. These infrastructure-less mobile nodes in ad hoc networks dynamically create routes among themselves to form own wireless network on the fly.

Wireless ad-hoc networks are composed of autonomous nodes that are self-managed without any infrastructure. In this way, ad-hoc networks have a dynamic topology such that nodes can easily join or leave the network at any time. Ad hoc network have many potential applications, especially, in military and rescue areas such as connecting soldiers on the battlefield or establishing a new network in place of a network which collapsed after a disaster like an earth quake. Ad-hoc networks are suitable for areas where fixed infrastructure is not possible. Since the nodes communicate with each other without an infrastructure, they provide the connectivity by forwarding packets over themselves. To support this connectivity, nodes use some routing protocols such as AODV (Ad-hoc On-Demand Distance Vector), DSR (Dynamic Source Routing) and DSDV (Destination-Sequenced Distance-Vector). Besides acting as a host, each node also acts as a router to discover a path and forward packets to the correct node in the network. In wireless ad-hoc networks lack an infrastructure and such networks are exposed to a lot of attacks. One of these attacks is the Black Hole attack.

In the Black Hole attack [2][4][7], a malicious node absorbs all data packets in itself, similar to a hole which sucks in everything in. In this way, all packets in the network are dropped. A malicious node dropping all the traffic in the network makes use of the vulnerabilities of the route discovery packets of the on demand protocols, such as AODV. Which is used for identifying a fresh route from the source to destination?

2. AD-HOC ROUTING PROTOCOLS AND BLACK HOLE ATTACK

An ad-hoc routing protocol[8] is a convention, or standard, that controls how nodes decide which way to route packets between computing devices in a mobile ad hoc network. Being one of the category of ad-hoc routing protocols, on-demand protocols such as AODV [4] (Ad-hoc On demand Distance Vector) and DSR (Dynamic Source Routing) establish routes between nodes only when they are required to route data packets. AODV is one of the most common ad-hoc routing protocols used for mobile ad-hoc networks. As its name indicates AODV is an on-demand routing protocol that discovers a route only when there is a demand from mobile nodes in the network.

In an ad-hoc network that uses AODV[4][6] as a routing protocol, a mobile node that wishes to communicate with other node first broadcasts an RREQ (Route Request) message to find a fresh route to a desired destination node. This process is called route discovery.

Every neighboring node that receives RREQ broadcast first saves the path the RREQ was transmitted along to its routing table. It subsequently checks its routing table to see if it has a fresh enough route to the destination node provided in the RREQ message. The freshness of a route is indicated by a destination sequence number that is attached to it. If a node finds a fresh enough route, it unicast an RREP (Route Reply) message back along the saved path to the source node or it re-broadcasts the RREQ message otherwise.

Route discovery is a vulnerability of on-demand ad-hoc routing protocols, especially AODV, which an adversary can exploit to perform a black hole attack on mobile ad-hoc networks. A malicious node in the network receiving an RREQ message replies to source nodes by sending a fake RREP message that contains desirable parameters to be chosen for packet delivery to destination nodes. After promising (by sending a fake RREP to confirm it has a path to a destination node) to source nodes that it will forward data, a malicious node starts to drop all the network traffic it receives from source nodes. This deliberate dropping of packets by a malicious node is what we call a black hole attack. The RREQ messages and RREP messages are shown in the figure2 and figure3.

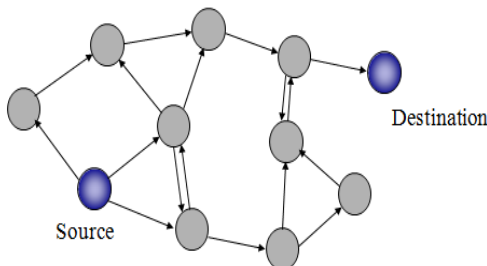


Fig 1: RREQ messages

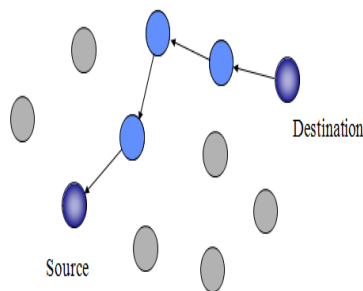


Fig 2: RREP messages

Black hole is a malicious node that falsely replies for any route requests without having active route to specified destination and drops all the receiving packets. If these malicious nodes work together as a group then the damage will be very serious. This type of attack is called cooperative black hole attack[5][9] shown in figure3.

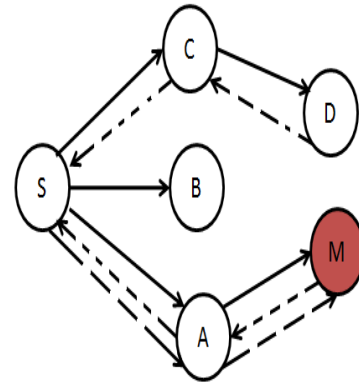


Fig 3: Blackhole

In black hole attack all network traffics are redirected to a specific node which does not exist at all. Because traffics disappear into the special node as the matter disappears into Blackhole in universe. So the specific node is named as a Blackhole. A Blackhole has two properties[5]. First, the node exploits the ad hoc routing protocol, such as AODV, to advertise itself as having a valid route to a destination node, even though the route is spurious, with the intention of intercepting packets. Second, the node consumes the intercepted packets. Blackhole attacks in AODV protocol routing level can be classified into two categories: RREQ Blackhole attack and RREP Blackhole attack.

2.1 Black Hole Attack Caused By RREQ

An attacker can send fake RREQ messages to form Black hole attack [2]. In RREQ node address. Other nodes will update their route to pass by the non-existent node to the destination node

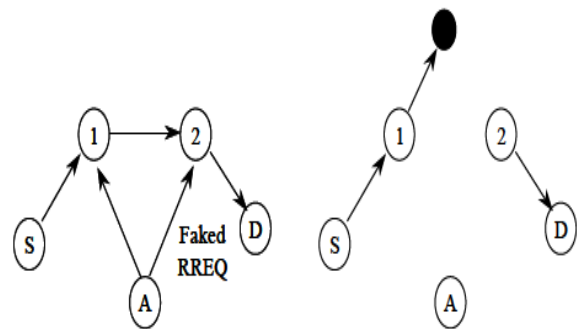


Fig 4: Blackhole Formed By Faked RREQ

As a result, the normal route will be broken down. The attacker can generate Blackhole attack by faked RREQ. The attacker forms a Blackhole attack between the source node and the destination node by faked RREQ message as it is shown in Figure 4

2.2. Blackhole Attack Caused By RREP

The attacker unicasts the faked RREP[1] message to the originating node. When originating node receives the faked RREP message

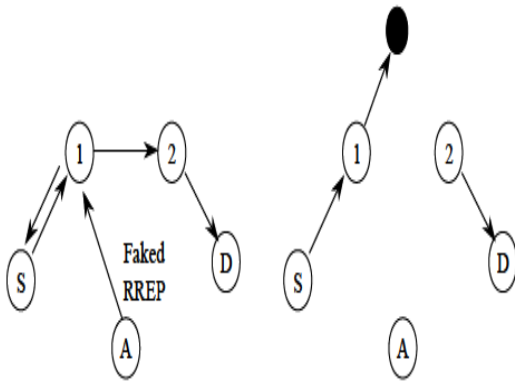


Fig 5: Blackhole Caused By Faked RREP

it will update its route to destination node through the non-existent node. Then RREP Blackhole[2] is formed as it is shown in Figure 5

3. PROTOCOL IMPLEMENTATION

Ad-hoc On-Demand Distance Vector (AODV) Routing Protocol[4] is used for finding a path to the destination in an ad-hoc network. To find the path to the destination all mobile nodes work in cooperation using the routing control messages. Thanks to these control messages, AODV Routing Protocol offers quick adaptation to dynamic network conditions, low processing and memory overhead, low network bandwidth utilization with small size control messages. The most distinguishing feature of AODV compared to the other routing protocols is that it uses a destination sequence number for each route entry. The destination sequence number is generated by the destination when a connection is requested from it. Using the destination sequence number ensures loop freedom. AODV makes sure the route to the destination does not contain a loop and is the shortest path. Here the AODV introduce data routing information table and cross checking the RREQ and RREP messages

3.1 Data Routing Information Table

Each node maintains a data routing information (DRI) table[1][2]. This table keeps track of whether or not the node did data transfers with its neighbors. This table contains one entry for each neighbor and indicates whether the node has sent data through this neighbor and whether the node has received data from this neighbor. Table entry contains *node id*, *from* and *through* as shown in Table 1. The field *from* stands for information on routing data packets from the node (in the node id field) while the field *through* stands for information on routing data packets through the node (in the node id field). Values of *from* and *through* fields will be 0 or 1 to represent false and true respectively. Table 1 shows the sample DRI table for a node. The entry 1,0 for node 3 implies that this node has routed data packets from node 3 but has not routed any data packet through node 3. The entry 1,1 for node 6 implies that this node has successfully routed data packets from and through node 6. The entry 0,0 for node 2 implies that node has not routed any data packets from or through node 2.

This DRI table is updated when any node received data packet from one of its neighbors or any

node that sent data packets through one of its neighbors. In addition, if any node finds out the reliable path to destination which it needs to send the data, DRI table is updated with entries for all intermediate nodes through the path.

Table 1. Example of DRI table

Node Id	Data Routing Information	
	From	Through
3	1	0
6	1	1
2	0	0

In this protocol, if the source node (SN) does not have the route entry to the destination, and broadcast a RREQ (Route Request) message to discover a secure route to the destination node same as in the AODV. Any node received this RREQ either replies for the request or again broadcasts it to the network depending on the availability of fresh route to the destination. If the destination replies, all intermediate nodes update or insert routing entry for that destination since the destination will be trusted. Source node also trusts on destination node and will start to send data along the path that reply comes back. Also source node will update the DRI table with all intermediate nodes between source and the destination.

If the intermediate node (IN) generates the Route Reply (RREP), it has to provide its next hop node (NHN) and its DRI entry for the next hop node. When the reply comes back, it collects the IP addresses of all nodes between source and the intermediate node but no intermediate node updates the route entry for the destination. Upon receiving RREP message from IN, the source node will check its own DRI table to see whether IN is a reliable node or not. If the source node has used IN before to route data, then IN is a reliable node and source will first send a route establishment message to IN node along the path that RREP comes according to the information contains in the RREP message. Upon receiving this message all nodes between the source and the intermediate node will update or insert route entry for the destination. Then source node starts sending data through the IN and updates the DRI table with nodes between source and IN node. If the source has not routed data through IN before, IN is not a reliable node. Then source first stores the information about IN and the nodes between the source and IN, and sends Further Request (FREQ) message to NHN of the IN to verify the reliability of the IN and ask NHN:

If the current NHN is the destination, then the next hop entry and the DRI entry for the next hop fields of FREQ contain zeros and all intermediate nodes will either update or insert route entry for the destination. When the source receives FREQ from destination, it starts routing data and updates its DRI table with all nodes

between the source and the destination. If NHN is not the destination, based on the FREP message from NHN, the source node checks whether NHN is a reliable node or not. If the source node has routed data through NHN before, NHN is reliable; otherwise NHN is unreliable.

4. PERFORMANCE METRICS

4.1 Throughput Ratio

The throughput is the number of bytes transmitted or received per second. The *throughput ratio*, denoted by *T*, is calculated as follows:

$$T = \frac{\sum_{i=1}^n T_i^r}{\sum_{i=1}^n T_i^s} \times 100\% \tag{1}$$

4.2 Average End To End Delay

Average end-to-end delay of the application data packets, denoted by *D*, is calculated as follows;

$$D = \frac{\sum_{i=1}^n d_i}{n} \tag{2}$$

Where *d_i* is the average end-to-end delay of data packets of *i*th application and *n* is the number of CBR applications.

5. COMPARISON WITH EXISTED METHOD

Researchers have proposed various techniques to prevent black hole attack in mobile ad-hoc networks. H. Weerasinghe and H. Fu[1] introduces the use of DRI (Data Routing Information) to keep track of past routing experience among mobile nodes in the network and crosschecking of RREP messages from intermediate nodes by source nodes. The main drawback of this technique is that whenever the black hole node take part in two or more transmission path, each path there is a huge packet losses due to the black hole. Therefore the delay performance is high.

5.1 MN-Id Broadcasting Method

In the proposed system, MN-ID broadcasting method is used. In this method once the malicious node is identified, the particular node id(only for simulation, real time ip address is used) is transmitted to the entire network therefore whether the malicious node take part in two or more path packets does not move towards the malicious node because whole nodes in the network should know about the malicious node. Therefore the packets transmitted through an alternative path from source to destination.

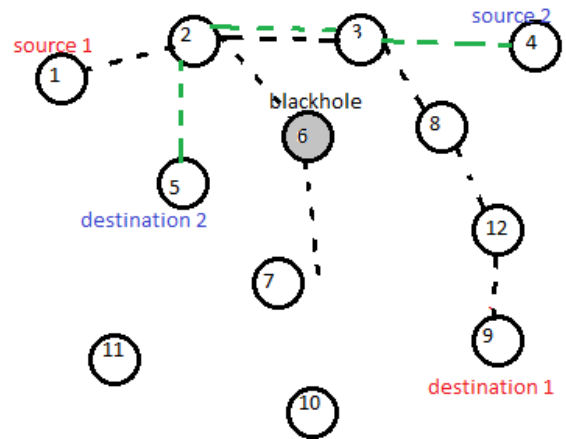


Fig.6 MN-ID broadcasting method

Figure6 shows the MN-ID broadcasting method. Here node 1 represented as source 1 and node 9 represented as destination 1and node 6 is assigned as black hole node. When the packet transmission takes place source 1 transmitted packets to destination node 9. When packet reaches on the node 6 it will drop all the received packets. Then the protocol identify an alternative path to destination and broadcasting the corresponding malicious node ID (that is node 6)to the entire nodes in the network. The actual shortest from node 4 to node 5 is 4-3-6-5. Whenever the packet transmitted from node 4, the packets are not transmitted through the correct shortest path because node 6 is a black hole and that particular node ID is broadcasted to the entire network. Hence the packet transmission takes place through the path 4-3-2-5 and reach the proper destination.

6. SIMULATION PARAMETERS AND RESULTS

The various parameters which are considered for network simulation is specified in the table2

Table 2. simulation parameters

Number of nodes	50
Packet size	512bytes
Data rate	512b/s
No. of BH nodes	2

The existing method (H. Weerasinghe and H. Fu method) simulation results throughput vs time and packet delivery ratio vs time is given below. These results are improved by MN-ID broadcasting method.

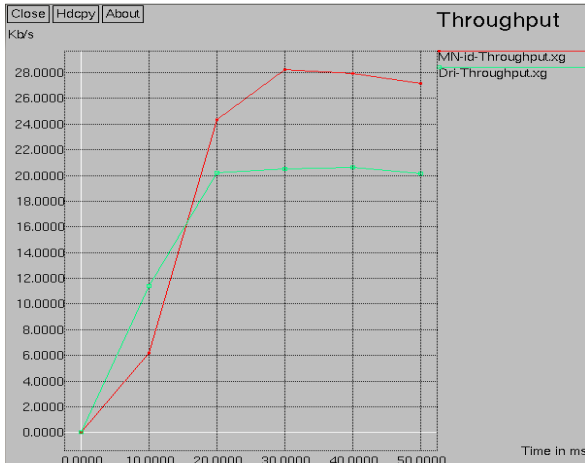


Fig6: Throughput vs time MN-ID broadcasting and DRI method(existing method)

The comparison of packet delivery ratio vs time and packet drop vs time in the MN-id method and DRI method is given in the fig7 and fig8. The graph shows that better results in MN-id method

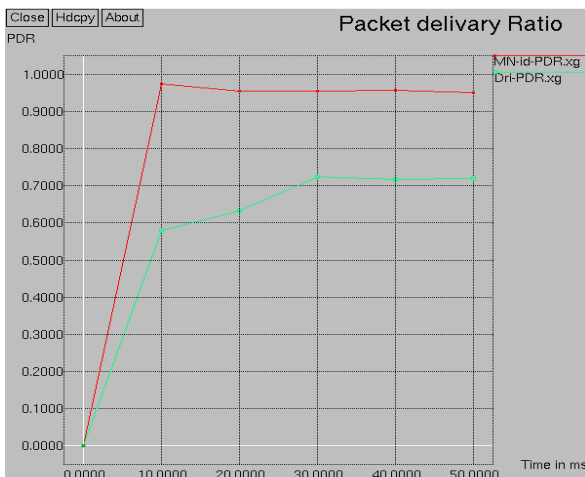


Fig7: pdr vs time in MN-ID broadcasting method and DRI(existing method) method

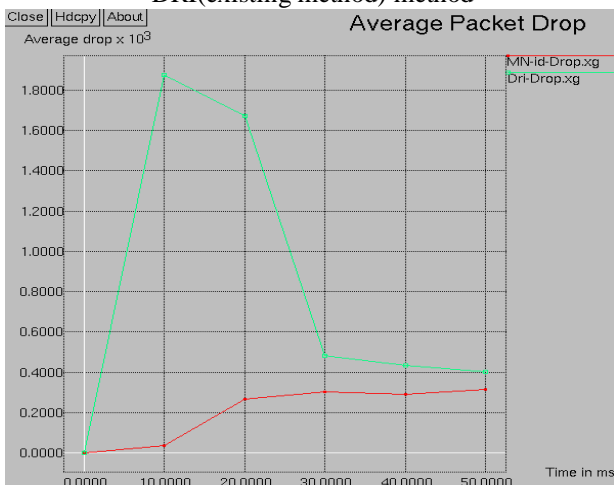


Fig 8: packet drop vs time in MN-ID broadcasting method and DRI(existing method) method

7. CONCLUSION

In this paper, we studied the problem of cooperative black hole attacks in MANET routing. The MN-ID broadcasting method provides improved performance of throughput packet delivery ratio and reduced packet loss comparing with H.Weerasinghe and H.Fu method. Therefore MN-ID broadcasting method provide improved network performance and minimum packet loss in the packet transmission.

REFERENCES

- [1] H.Weerasinghe and H.Fu(2008) "Preventing Black Hole Attack in Mobile Ad hoc Networks: simulation, implimentation and evaluation"*international journal of software engg. and its applications*,vol2,no3
- [2] Sanjay Ramaswamy, Huirong Fu, Manohar Sreekantaradhya, John Dixon, and Kendall Nygard, "Prevention of Cooperative Black Hole Attack in Wireless Ad Hoc Networks", 2003 *International Conference on Wireless Networks (ICWN'03)*, Las Vegas, Nevada, USA
- [3] Hongmei Deng, Wei Li, and Dharma P. Agarwal, (2002) "Routing Security in Wireless Ad Hoc Networks", University of Cincinnati, *IEEE Communications magazine*, Vol.40, No.10
- [4] Charles E. Perkins, and Elizabeth M. Royer, "Ad-hoc On-Demand Distance Vector (AODV) Routing," *InternetDraft*, November 2002.
- [5] S. Sharma and R. Gupta, (2009) "Simulation study of black hole attack in the mobile ad-hoc networks," *journal of engineering science and technology*, vol. 4, no. 2 pp. 243-250.
- [6] LathaTamilselvan,Dr.VSankaranarayanan "Prevention of Co-operative Black Hole Attack in MANET", *Journal Of Networks*, Vol. 3, NO. 5,2008
- [7] Jian Yin, Sanjay Madria, "A Hierarchical Secure Routing Protocol against Black Hole", *IEEE SUTC 2006 Taiwan*, 5-7 June 2006
- [8] Dokurer, S.; Ert, Y.M.; and Acar, C.E. (2007). Performance analysis of ad hoc networks under black hole attacks. SoutheastCon, 2007, *Proceedings IEEE*, 148 – 153.
- [9] Dr. Karim Konate and Abdourahime Gaye(2011)'a proposal mechanism against the attacks: cooperative black hole, blackmail, overflow and selfish in routing protocol of mobile ad hoc network',*internationaljournal of future generation communication and networking* Vol. 4, No. 2

Modeling and Analyses of Cascaded H-Bridge Multilevel Converter for Micro Grid Application

B. DEEPTHI

*M-Tech Scholar, Power systems,
Department Of Electrical And Electronics Engineering,
K L University (A.P),
India.*

CH. SUDHIR BABU

*Assistant Prof, Power systems,
Department Of Electrical & Electronics Engineering,
K L University,(A.P)
India.*

Abstract: The concept of multilevel inverters introduced about 20 years ago entails performing power conversion in multiple voltage steps to obtain improved power quality, lower switching losses, better electromagnetic compatibility, and higher voltage capability. The benefits are especially clear for medium-voltage drives in industrial applications and are being considered for future naval ship propulsion systems. Several topologies for multilevel inverters have been proposed over the years; the most popular cascaded H-bridge apart from other multilevel inverters is the capability of utilizing different dc voltages on the individual H-bridge cells which results in splitting the power conversion amongst higher-voltage lower-frequency and lower-voltage higher-frequency inverters. Considering the cascaded inverter to be one unit, it can be seen that a higher number of voltage levels are available for a given number of semiconductor devices. In this paper a 5 level Cascaded H-Bridge for micro grid application is proposed. Considering the system as separate inverters, the cascaded design can be regarded as a combination of a bulk power (higher-voltage) inverter and a conditioning (lower-power) inverter. A SIMULINK based model is developed and Simulation results are presented.

Keywords: Cas caded H-Bridge, Multilevel Converter, PWM, Micro Grid

I. INTRODUCTION

Fossil fuels are running out and current centralised power generation plants are inefficient with a significant amount of energy lost as heat to the environment, in addition to producing harmful emissions and greenhouse gases. Furthermore, current power systems, especially in developing countries, suffer from several limitations such as high cost of expansion and efficiency improvement limits within existing grid infrastructure. Renewable energy sources can help address these issues, but it can be a challenge to get stable power from these sources as they are variable in nature. Distributed generators (DG), including renewable sources, within microgrids can help overcome power system limitations, improve efficiency, reduce emissions and manage the variability of renewable sources.

A microgrid, a relatively new concept, is a zone within the main grid where a cluster of electrical loads and small micro generation systems such as solar cell, fuel cell, wind turbine and small combined heat and power (CHP) systems exist together under an embedded management and control system with the option of storage devices. Other benefits of generating power close to electrical loads include the use of waste heat locally, saving the cost of upgrading the grid to supply more power from central plants, reducing transmission losses and creating opportunities for increasing competition in the sector which can stimulate innovation and reduce consumer prices [1, 2].

Power electronic converters are used in microgrids to control the flow of power and convert it into suitable DC or AC form as required. With the advancement of power electronics and emergence of new multilevel converter topologies, it is possible to work at voltage levels beyond the classic semiconductor limits. The multilevel converters achieve high-voltage switching by means of a series of voltage steps, each of which lies within the ratings of the individual power devices. Among the multilevel Converters [1-4], the cascaded H-bridge topology (CHB) is particularly attractive in high-voltage applications, because it requires the least number of components to synthesize the same number of voltage levels.

Additionally, due to its modular structure, the hardware implementation is rather simple and the maintenance operation is easier than alternative multilevel converters. The multilevel voltage source inverter is recently applied in many industrial applications such as ac power supplies, static VAR compensators, drive systems, etc. One of the significant advantages of multilevel configuration is the harmonic reduction in the output waveform without increasing switching frequency or decreasing the inverter power output [5-10]. The output voltage waveform of a multilevel inverter is composed of the number of levels of voltages, typically obtained from capacitor voltage sources. The so-called multilevel starts from three levels. As the number of levels reach infinity, the output THD approaches zero. The number of the achievable voltage levels, however, is limited by voltage unbalance

problems voltage clamping requirement, circuit layout, and packaging constraints.

II. MODES OF OPERATION OF MICROGRID CONVERTERS

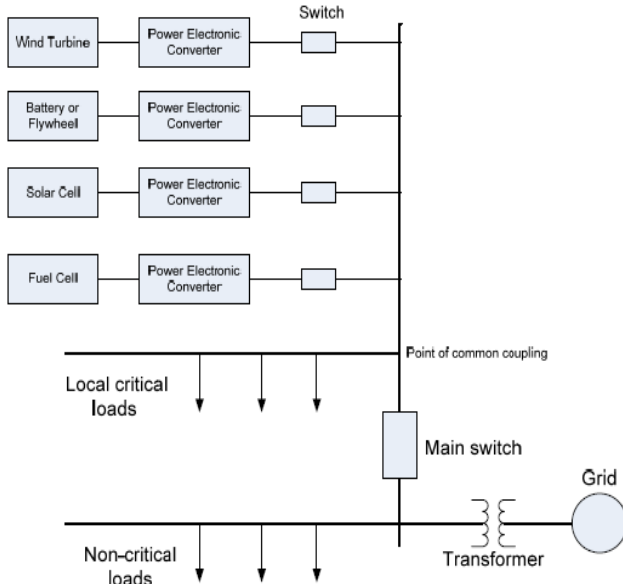


Fig. 1. A Schematic Diagram of a Microgrid

Normally, converters are used to connect DG systems in parallel with the grid or other sources, but it may be useful for the converters to continue functioning in stand-alone mode, when the other sources become unavailable to supply critical loads. Converters connected to batteries or other storage devices will also need to be bidirectional to charge and discharge these devices.

A. Grid Connection Mode:

In this mode of operation, the converter connects the power source in parallel with other sources to supply local loads and possibly feed power into the main grid. Parallel connection of embedded generators is governed by national standards [7-9]. The standards require that the embedded generator should not regulate or oppose the voltage at the common point of coupling, and that the current fed into the grid should be of high quality with upper limits on current total harmonic distortion THD levels. There is also a limit on the maximum DC component of the current injected into the grid. The power injected into the grid can be controlled by either direct control of the current fed into the grid [10], or by controlling the power angle. In the latter case, the voltage is controlled to be sinusoidal. Using power angle control however, without directly controlling the output current, may not be effective at reducing the output current THD when the grid voltage is highly distorted, but this will be an issue in the case of electric machine generators, which effectively use power angle control. This raises the question of whether it is reasonable to specify current THD limits, regardless of the quality of the utility voltage. In practice, the converter

output current or voltage needs to be synchronized with the grid, which is achieved by using a phase locked loop or grid voltage zero crossing detection. The standards also require that embedded generators, including power electronic converters, should incorporate an anti-islanding feature, so that they are disconnected from the point of common coupling when the grid power is lost. There are many anti-islanding techniques; the most common of these is the rate of change of frequency (RoCoF) technique.

B. Stand-Alone Mode

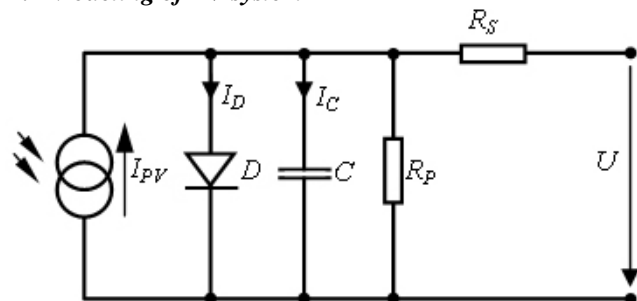
It may be desirable for the converter to continue to supply a critical local load when the main grid is disconnected, e.g. by the anti-islanding protection system. In this stand-alone mode the converter needs to maintain constant voltage and frequency regardless of load imbalance or the quality of the current, which can be highly distorted if the load is nonlinear. A situation may arise in a microgrid, disconnected from the main grid, where two or more power electronic converters switch to stand-alone mode to supply a critical load. In this case, these converters need to share the load equally. The equal sharing of load by parallel connected converter operating in stand-alone mode requires additional control. There are several methods for parallel connection, which can be broadly classified into two categories: 1) Frequency and voltage droop method, 2) Master-slave method, whereby one of the converters acts as a master setting the frequency and voltage, and communicating to the other converters their share of the power.

C. Battery Charging Mode

In a microgrid, due to the large time constants of some microsources, storage batteries should be present to handle disturbances and fast load changes. In other words, energy storage is needed to accommodate the variations of available power generation and demand. The power electronic converter could be used as a battery charger thus improving the reliability of the microgrid.

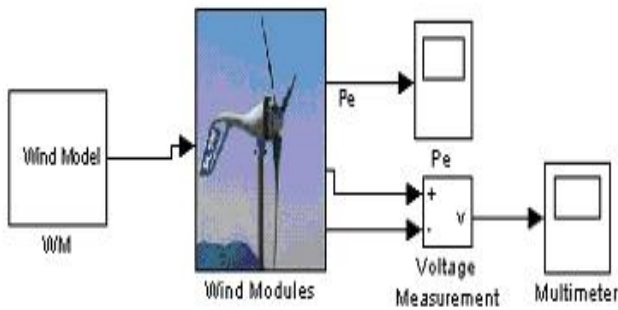
III. MODELING OF VARIOUS RENEWABLE ENERGY SOURCES

A. Modeling of PV system



The use of equivalent electric circuits makes it possible to model characteristics of a PV cell. The method used here is implemented in MATLAB programs for simulations. The same modeling technique is also applicable for modeling a PV module. There are two key parameters frequently used to characterize a PV cell. Shorting together the terminals of the cell, the photon generated current will follow out of the cell as a short-circuit current (I_{sc}). Thus, $I_{ph} = I_{sc}$, when there is no connection to the PV cell (open-circuit), the photon generated current is shunted internally by the intrinsic p-n junction diode. This gives the open circuit voltage (V_{oc}). The PV module or cell manufacturers usually provide the values of these parameters in their datasheets [14].

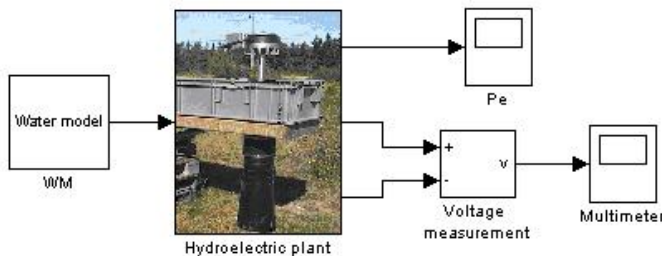
B Modeling of Wind system



The wind turbine depends on the flow of air in a rotor consisting of two or three blades mechanically coupled to an electrical generator. It is a process of power translation from wind energy to electricity. The difference between the upstream and downstream wind powers is actual power extracted by the rotor blades. It is given by the following equation in units of watts.

$$P_M = \frac{1}{2} \rho A \{V^2 - V_0^2\}$$

C Modeling of Hydro system

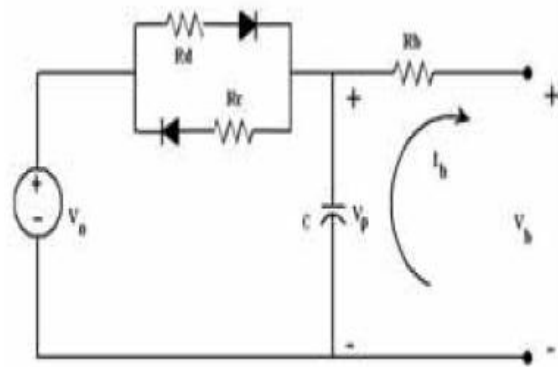


Small hydroelectric power plants harness the falling water kinetic energy to generate electricity. Turbines transform falling water kinetic energy into mechanical rotation energy and then, the alternator transforms the mechanical energy into electricity. Water flows within a river from a higher geodesic site to a lower geodesic site

due to gravitation. This is characterized by different particular kinetic and potential energy at both sites. The correct identification of the resulting energy differences of the out-flowing water can be assumed by considering a stationary and friction-free flow with incompressibility.

$$p + \rho_{water}gh + \frac{1}{2} \rho_{water}v_{water}^2 = const$$

D Modeling of Battery



The open circuit voltage, internal capacitor voltage and the terminal voltage are represented by V_0 , V_p and V_b . The charging, discharging and the internal resistance of the battery are represented by R_e , R_d and R_b and the polarization capacitance of the battery is represented by C . The current I_b is taken as positive if discharging and negative otherwise (Vairamohan, 2002).

$$\dot{V}_p = \frac{1}{C} \left(\left(\frac{V_0 - V_p}{R_d} \right) - I_b \right)$$

Switches Turn ON	Voltage Level
S2	$V_{dc}/2$
S1	$-V_{dc}/2$

IV. HIGH POWER CONVERTERS CLASSIFICATIONS

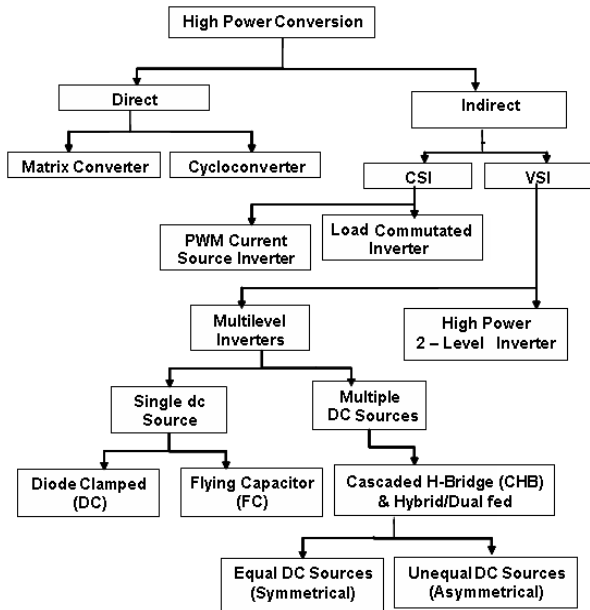


Figure 2 Classification of High power Converters

Fig.2 shows the classification of high power converters. Out of all converters Cascaded bridge configuration is more popular. Cascaded bridge configuration is again classified into 2 types 1) Cascaded Half Bridge 2) Cascaded Full Bridge or Cascaded H-Bridge. In this paper a novel cascaded hybrid H- Bridge topology is proposed for PV application.

A Half H-Bridge

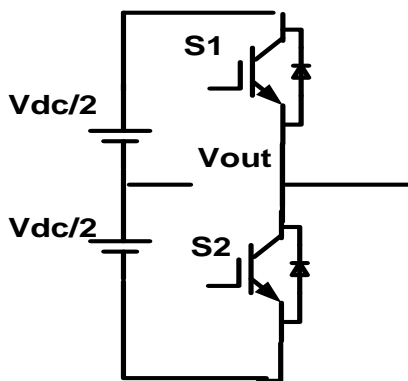


Figure 3 Half Bridge

Fig.3 shows the Half H-Bridge Configuration. By using single Half H-Bridge we can get 2 voltage levels. The switching table is given in Table 1.

B Full H-Bridge

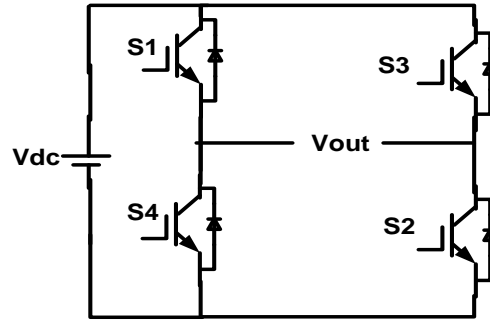


Figure 4 Full H-Bridge

Fig.3 shows the Full H-Bridge Configuration. By using single H-Bridge we can get 3 voltage levels. The number output voltage levels of cascaded Full H-Bridge are given by $2n+1$ and voltage step of each level is given by V_{dc}/n . Where n is number of H-bridges connected in cascaded. The switching table is given in Table2.

Table 1. Switching table for Full H-Bridge

Switches Turn ON	Voltage Level
S1,S2	V_{dc}
S3,S4	$-V_{dc}$
S4,D2	0

V.MATLAB/SIMULINK MODELING AND SIMULATION RESULTS

Fig. 7 and 9 shows the Matlab/Simulink model of Hybrid H-bridge and cascaded Hybrid H-bridge converters respectively.

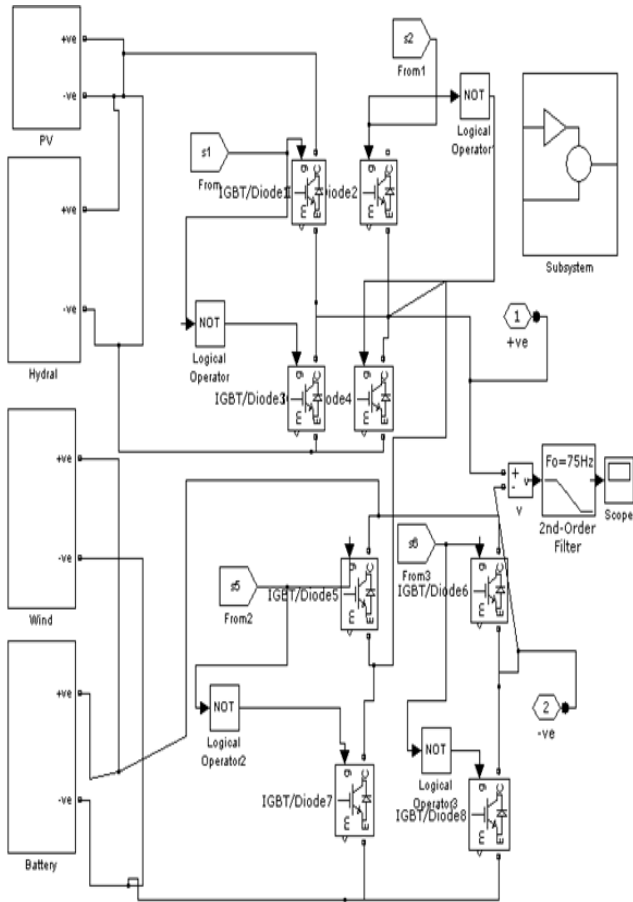


Figure. 5 Matlab/Simulink model of Micro grid

Fig. 5 shows the Matlab/Simulink model of Micro grid system. It consists of two cascaded H-Bridges. One H-brid is supplied with PV and Hydral system and second H-bridge is supplied with Wind and Battery sytem.

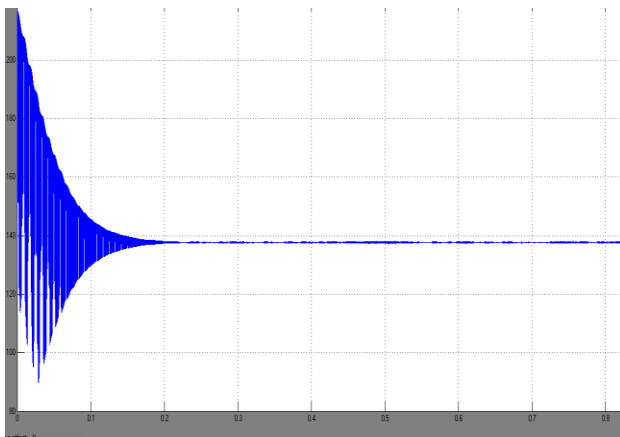


Figure. 6 Output PV and Hydral system

Fig.6 shows the combined output of PV and Hydral system. The output voltage is 130 v DC.

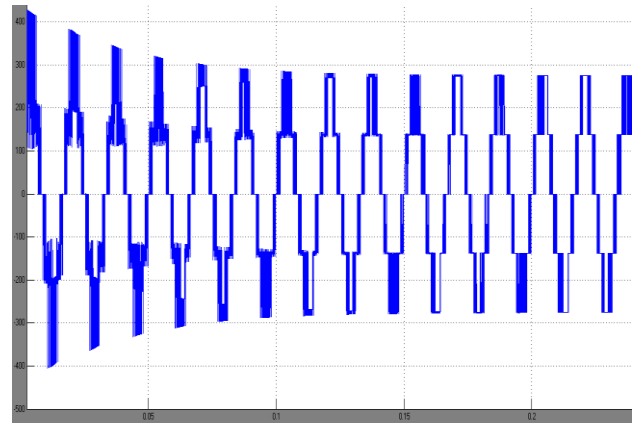


Figure. 7 Five level output Multilevel Inverter without filter

Fig. 7 shows the five level output of multilevel inverter with out filter and Fig.8 shows output voltage with filter. Peak voltage here is 280 v.



Figure. 8 Sine wave output of Multilevel Inverter with filter

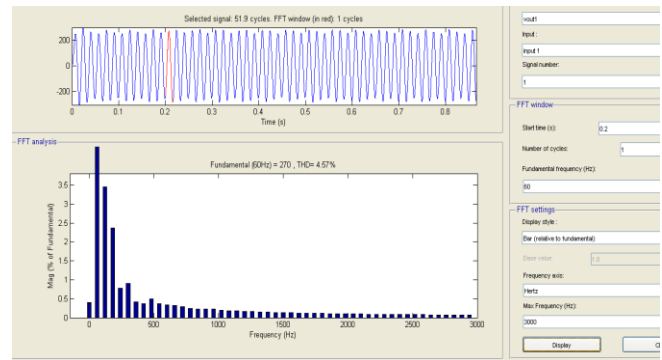


Figure. 9 THD

Fig. 9 shows output voltage THD. Form the figure it is clear that THD of output voltage is 4.1 %.

VI. CONCLUSION

A particular MG architecture has been modeled in order to analyse its behaviour during grid connected and islanding operation. The model is based on a wind turbine, a PV panels array, a backup DG and a VSI used for the

interconnection with the main grid.. A SIMULINK based model is developed and Simulation results are presented. Finally PWM based output is shown.

VII. REFERENCES

- [1] J. S. Lai and F. Z. Peng, "Multilevel converters – A new breed of power converters", IEEE Trans. Ind. Appl., V32, No. 3, pp. 509-517, May/Jun.,1996.
- [2] José Rodríguez, Jih-Sheng Lai, FangZhengPeng "Multilevel Inverters: A Survey of Topologies, Controls, and Applications "IEEE Trans. Ind. App, VOL. 49, NO. 4, August 2002.
- [3] K.A Corzine, and Y.L Familant, "A New Cascaded Multi-level H-Bridge Drive," IEEE Trans. Power.Electron., vol.17, no.1, pp.125-131. Jan 2002.
- [4] T.A.Maynard, M.Fadel and N.Aouda, "Modelling of multilevel converter," IEEE Trans. Ind.Electron., vol.44, pp.356-364. Jun.1997.
- [5] Manjrekar, M. D., Lipo, T. A. "A hybrid multilevel inverter topology for drive applications". in Proc. of APEC, 1998, p. 523–529.
- [6] R. Schnell, U. Schlapbach, "Realistic benchmarking of IGBT – modules with the help of a fast and easy to use simulation tool".
- [7] Jean-Philippe Hasler, "DC Capacitor Sizing for SVC Light Industrial Application".
- [8] G.Carrara, S.Gardella, M.Marchesoni, R.salutari,and G.sciutto, "A New Multilevel PWM Method; A theoretical analysis," IEEE Trans. Power.Electron., vol.7, no.3, pp.497-505. Jul.1992.
- [9] L.M.Tolber, T.G.Habetler, "Novel Multilevel inverter Carrier based PWM Method," IEEE Ind.Appli., vol.35. pp.1098-1107. Sep/Oct 1999.
- [10] Holmes, D. G. and Lipo, T. A., Pulse width modulation for power converters: principles and practice, IEEE.

A Series-Connected Multilevel Inverter Topology for Squirrel-Cage Induction Motor Drive

B. SUSHMITHA

*M. tech Scholar, Power Electronics & Electrical Drives
Department Of Electrical And Electronics Engineering
Koneru Lakshamiya University, Guntur (A.P),
India.*

Y. SRINIVAS RAO

*Assistant Professor,
Department Of Electrical And Electronics Engineering
Koneru Lakshamiya University, Guntur (A.P),
India.*

Abstract: The concept of multilevel inverters, introduced about 20 years ago entails performing power conversion in multiple voltage steps to obtain improved power quality, lower switching losses, better electromagnetic compatibility, and higher voltage capability. The benefits are especially clear for medium-voltage drives in industrial applications and are being considered for future naval ship propulsion systems. The application of pulsewidth-modulated (PWM) voltages using two-level high-voltage inverters to a squirrel-cage induction motor (SQIM) can cause heating of rotor shaft, voltage spike across the motor terminals, etc. The increase in the number of steps of the motor voltage and hence decreasing the dv/dt applied to the machine terminals can be a solution to this problem. The existing topologies that generate this multistep voltage include cascading of a number of single-phase inverters or use of higher order multilevel inverters. In this paper, a topology with series connection of three-phase three-level inverters is proposed, which addresses the problems of medium-voltage drives.

Keywords: Medium-voltage ac drives, multilevel converter topologies.

I. INTRODUCTION

Multilevel power conversion has been receiving increasing attention in the past few years for high power applications. Numerous topologies and modulation strategies have been introduced and studied extensively for utility and drive applications in the recent literature. These converters are suitable in high voltage and high power applications due to their ability to synthesize waveforms with better harmonic spectrum and attain higher voltages with a limited maximum device rating. In the family of multilevel inverters the three-level topology, called Neutral Point Clamped (NPC) inverter, is one of the few topologies that has received a reasonable consensus in the high power community [2]. These NPC inverters have also been implemented successfully in the industrial applications for high power drives [3]. The conventional three-level inverter comprises four switches per phase with a diode clamp connected to the mid-point of the dc link. By closing two of the four switches, the load can be either connected to the top, middle or bottom of the dc link, thereby generating a three-level voltage waveform at the phase leg output. The LC sine filter connected at the output is used to filter out the high link. By closing two of the four switches, the load can

be either connected to the top, middle or bottom of the dc link, thereby generating a three-level voltage waveform at the phase leg output. The LC sine filter connected at the output is used to filter out the high the output of the NPC inverter is directly connected through an LCL filter to the 4160V utility network. Optionally the utility side reactor can be replaced by a feeder transformer which adjusts to higher utility voltages by employing an appropriate turns-ratio. The voltages on the dc link capacitors are maintained at their nominal values by drawing necessary real power from the utility. One of the primary concerns for a successful operation is meeting the harmonic requirements given by IEEE 519-1992 even at very low short-circuit ratio. Hence, the LCL filter connected at the output of the inverter needs to be adequately sized as to meet the stringent current and voltage requirements. At multi-megawatt power levels, where inherently lower short circuit ratios are existing, the dimensioning of such filters becomes a important issue. Similar voltage profiles can also be obtained by using higher order neutral-point-clamped (NPC) multilevel inverters [8], [9] or by cascading a number of two-level inverters [6], [7]. However, the multilevel NPC inverters suffer from dc-bus imbalance [11]–[13], device underutilization problems and unequal ratings of the clamped diodes [9], [10], etc., which are not very serious problems for inverters with three levels or lower. The capacitor voltage imbalance for a five-level one is presented in [14]– [15] which suggest the need of extra hardware in the form of dc choppers or a back-to-back connection of multilevel converters. The cascaded H-bridge topology [6]–[8] suffers from the drawbacks of the usage of huge dc-bus capacitors and complex input transformers for isolated dc bus for each module. These drawbacks are addressed in the proposed topology. Furthermore, the power circuit is modular in structure, and hence, the number of modules to be connected in series depends on the power of the drive.

II. PROPOSED CONVERTER TOPOLOGY

The proposed general configuration of “ n ” number of three level inverters connected in series is shown in Fig. 1. Each inverter module is a three-phase NPC three-level inverter. At the output stage, transformers are used to have the series connection of three-level inverters, as shown in Fig. 1. If “ V_{dc} ” is the dc-bus voltage of each inverter module, then “ α ” is the turns ratio of each transformer and “ n ” is the number of inverter modules then for sine PWM (SPWM)

strategy; the motor rms phase voltage (V_{Ph_motor}) can be expressed as follows

$$\text{Rms of } V_{ph_motor} = \sqrt{3} \alpha m n \frac{V_{dc}}{2\sqrt{2}}$$

Where m is the modulation index of the inverter topology defined as follows

$$m = \frac{\text{Peak of } V_{ph_inverter}}{\frac{n V_{dc}}{2}}$$

$V_{ph_inverter}$ is the total phase voltage reference of the inverter topology. For the given peak of V_{Ph_motor} , peak of $V_{ph_inverter}$ can be computed as follows

$$\text{Peak of } V_{ph_inverter} = \frac{\text{Peak of } V_{ph_motor}}{\sqrt{3}\alpha}$$

The generation of individual reference voltage signal of each inverter is discussed as follows.

The gate pulses for each three-level inverter module can be derived using two carrier signals. Thus, “ n ” numbers of such three-level inverter modules require “ $2n$ ” number of carriers [10], [13]. The three-phase voltage reference signals are then compared with these carrier waves to produce the gate pulses for the inverters. For example, the carrier waves and the sinusoidal modulating voltage signal (SPWM technique) for R phase is shown in Fig. 2 for four series-connected three-level inverters. The carrier waves 1 and 1’ (Fig. 2) with R -phase voltage reference controls the inverter module 1. Similarly, 2 2’, 3-3’, and 4-4’ carrier waves with R -phase voltage reference generate the gate pulses for the three-level inverter modules 2, 3, and 4, respectively. Thus, each inverter module produces the voltage proportional to a part of the reference phase voltage signals. It is important to note that no two three-level inverter modules switch simultaneously (Fig. 2). Thus, the maximum dv/dt rate of the output voltage of this topology is limited to that of a single three-level inverter module (Fig. 5). The references of each inverter are shown in Fig. 3. The corresponding output line voltages of each inverter are shown in Fig. 4. The four windings, one from each transformer, are connected in series and produced the net R -phase voltage, as shown in Fig. 5 Similarly, the other two phase voltages are generated.

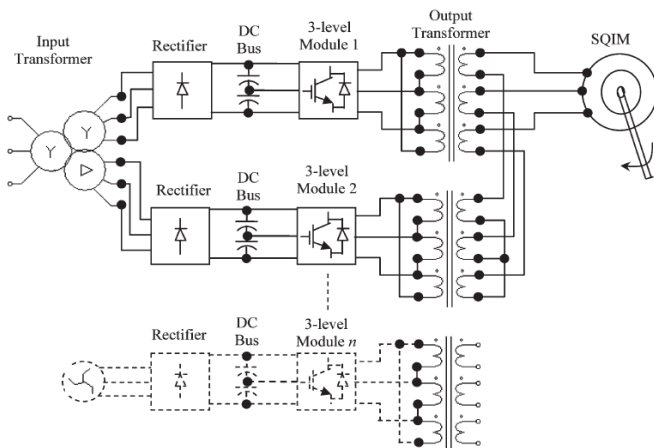


Figure.1 Block diagram of three-phase three-level inverter modules connected in series driving an SQIM.

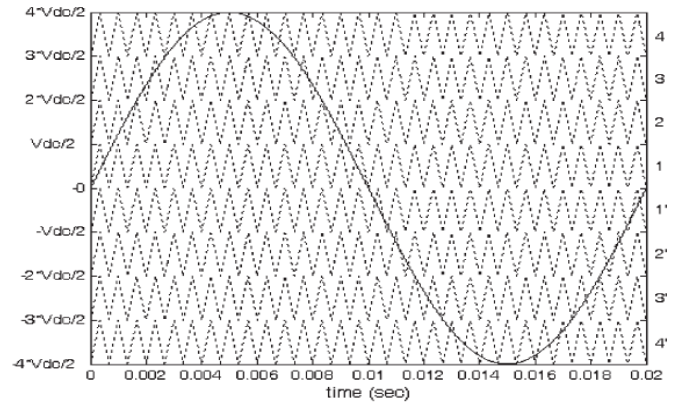


Figure.2 Carrier waves and the sinusoidal modulating voltage signal for R phase in SPWM technique

The line voltage spectra of individual inverters are shown in Fig. 4 for switching frequency of 2.5 kHz. These line voltages get added to produce the net phase voltage of the topology. The voltage spectra are expressed as a percentage of the maximum total fundamental (V_{peak}) that can be produced by the topology.

$$V_{peak} = \sqrt{2} * V_{ph_motor}$$

or $V_{peak} = 2078.5$ V for $V_{dc} = 600$ V, $n = 4$, $\alpha = 1$, and $m = 1$ using (1). Hence, the spectra show the percentage share of the fundamental of each inverter module. These spectra also suggest that the line voltages of all these inverters contain additional small amount of the 5th-, 7th-, 11th-, 13th-, and higher order harmonics besides the normal switching harmonics. However, the net phase voltage and line voltage of this topology do not contain any of these harmonics, as suggested by the spectra shown in Fig. 5. These harmonics get canceled when the line voltages of the individual inverters are added by the transformers to produce the net phase voltages. The increased number of steps in the motor terminal voltage reduces the dv/dt as that compared with a conventional two-level inverter.

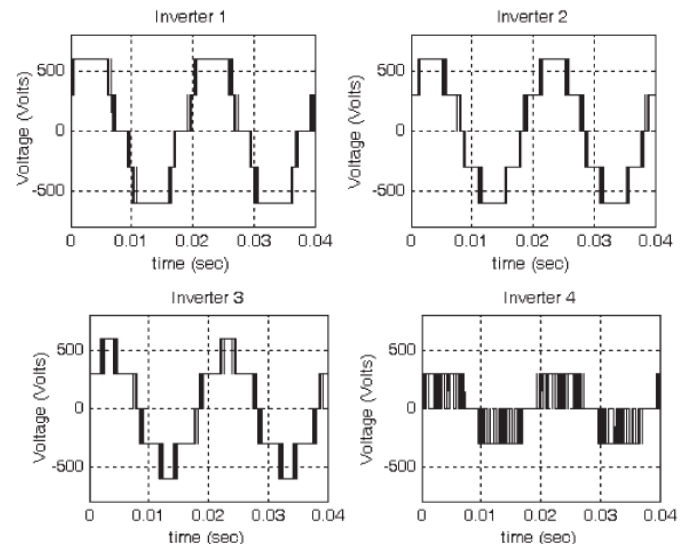


Figure.3 Four series connected Inverters Individual voltages

III. DYNAMIC MODEL OF INDUCTION MOTOR

The induction machine d-q or dynamic equivalent circuit is shown in Fig. 1 and 2. One of the most popular induction motor models derived from this equivalent circuit is Krause’s model detailed in [5]. According to his model, the modeling equations in flux linkage form are as follows:

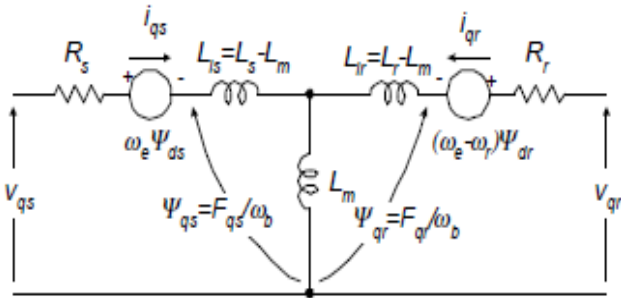


Figure. 4 Dynamic q-axis model

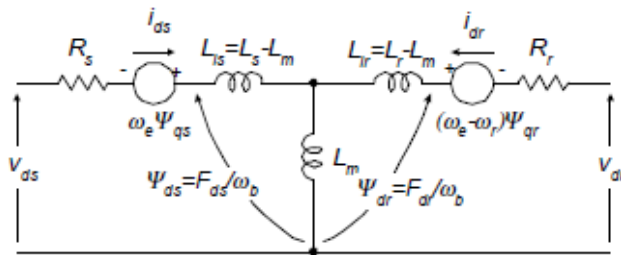


Figure. 5 Dynamic d-axis model

2.2 Voltage Source Converter (VSC)

$$i_{ds} = \frac{1}{x_{ls}} (F_{ds} - F_{md}) \tag{8}$$

$$i_{qs} = \frac{1}{x_{ls}} (F_{qs} - F_{mq}) \tag{9}$$

$$i_{dr} = \frac{1}{x_{lr}} (F_{dr} - F_{md}) \tag{10}$$

$$T_e = \frac{3}{2} \left(\frac{p}{2} \right) \frac{1}{\omega_b} (F_{ds} i_{qs} - F_{qs} i_{ds}) \tag{11}$$

$$T_e - T_L = J \left(\frac{2}{p} \right) \frac{d\omega_r}{dt} \tag{12}$$

- where
- d* : direct axis,
 - q* : quadrature axis,
 - s* : stator variable,
 - r* : rotor variable,
 - F_{ij} is the flux linkage ($i=q$ or d and $j=s$ or r),
 - v_{qs}, v_{ds} : q and d -axis stator voltages,
 - v_{qr}, v_{dr} : q and d -axis rotor voltages,
 - F_{mq}, F_{md} : q and d axis magnetizing flux linkages,
 - R_r : rotor resistance,
 - R_s : stator resistance,
 - X_{ls} : stator leakage reactance ($\omega_e L_{ls}$),
 - X_{lr} : rotor leakage reactance ($\omega_e L_{lr}$),
 - $X_{mi}^* : 1 / \left(\frac{1}{x_m} + \frac{1}{x_{ls}} + \frac{1}{x_{lr}} \right)$,
 - i_{qs}, i_{ds} : q and d -axis stator currents,
 - i_{qr}, i_{dr} : q and d -axis rotor currents,
 - p : number of poles,
 - J : moment of inertia,
 - T_e : electrical output torque,
 - T_L (or T_I) : load torque,
 - ω_e : stator angular electrical frequency,
 - ω_b : motor angular electrical base frequency,
 - ω_r : rotor angular electrical speed.

For a squirrel cage induction machine, as in the case of this paper, v_{qr} and v_{dr} in (3) and (4) are set to zero. An induction machine model can be represented with five differential equations as shown. To solve these equations, they have to be rearranged in the state-space form. In this case, state-space form can be achieved by inserting (5) and (6) in (1-4) and collecting the similar terms together so that each state derivative is a function of only other state variables and model inputs. Then, the modeling equations (1-4) of a squirrel cage induction motor in state-space become

$$\frac{dF_{qs}}{dt} = \omega_b \left[v_{qs} - \frac{\omega_e}{\omega_b} F_{ds} + \frac{R_s}{x_{ls}} (F_{mq} + F_{qs}) \right] \tag{1}$$

$$\frac{dF_{ds}}{dt} = \omega_b \left[v_{ds} + \frac{\omega_e}{\omega_b} F_{qs} + \frac{R_s}{x_{ls}} (F_{md} + F_{ds}) \right] \tag{2}$$

$$\frac{dF_{qr}}{dt} = \omega_b \left[v_{qr} - \frac{(\omega_e - \omega_r)}{\omega_b} F_{dr} + \frac{R_r}{x_{lr}} (F_{mq} - F_{qr}) \right] \tag{3}$$

$$\frac{dF_{dr}}{dt} = \omega_b \left[v_{dr} + \frac{(\omega_e - \omega_r)}{\omega_b} F_{qr} + \frac{R_r}{x_{lr}} (F_{md} - F_{dr}) \right] \tag{4}$$

$$F_{mq} = x_{mi}^* \left[\frac{F_{qs}}{x_{ls}} + \frac{F_{qr}}{x_{lr}} \right] \tag{5}$$

$$F_{md} = x_{mi}^* \left[\frac{F_{ds}}{x_{ls}} + \frac{F_{dr}}{x_{lr}} \right] \tag{6}$$

$$i_{qs} = \frac{1}{x_{ls}} (F_{qs} - F_{mq}) \tag{7}$$

$$\frac{dF_{qz}}{dt} = \omega_b \left[v_{qz} - \frac{\omega_e}{\omega_b} F_{dz} + \frac{R_s}{x_{ls}} \left(\frac{x_{mi}}{x_{lr}} F_{qr} + \left(\frac{x_{mi}}{x_{ls}} - 1 \right) F_{qz} \right) \right] \quad (13)$$

$$\frac{dF_{dz}}{dt} = \omega_b \left[v_{dz} + \frac{\omega_e}{\omega_b} F_{qz} + \frac{R_s}{x_{ls}} \left(\frac{x_{mi}}{x_{lr}} F_{dr} + \left(\frac{x_{mi}}{x_{ls}} - 1 \right) F_{dz} \right) \right] \quad (14)$$

$$\frac{dF_{qr}}{dt} = \omega_b \left[-\frac{(\omega_e - \omega_r)}{\omega_b} F_{dr} + \frac{R_r}{x_{lr}} \left(\frac{x_{mi}}{x_{ls}} F_{qz} + \left(\frac{x_{mi}}{x_{lr}} - 1 \right) F_{qr} \right) \right] \quad (15)$$

$$\frac{dF_{dr}}{dt} = \omega_b \left[\frac{(\omega_e - \omega_r)}{\omega_b} F_{qr} + \frac{R_r}{x_{lr}} \left(\frac{x_{mi}}{x_{ls}} F_{dz} + \left(\frac{x_{mi}}{x_{lr}} - 1 \right) F_{dr} \right) \right] \quad (16)$$

$$\frac{d\omega_r}{dt} = \left(\frac{p}{2J} \right) (T_e - T_L) \quad (17)$$

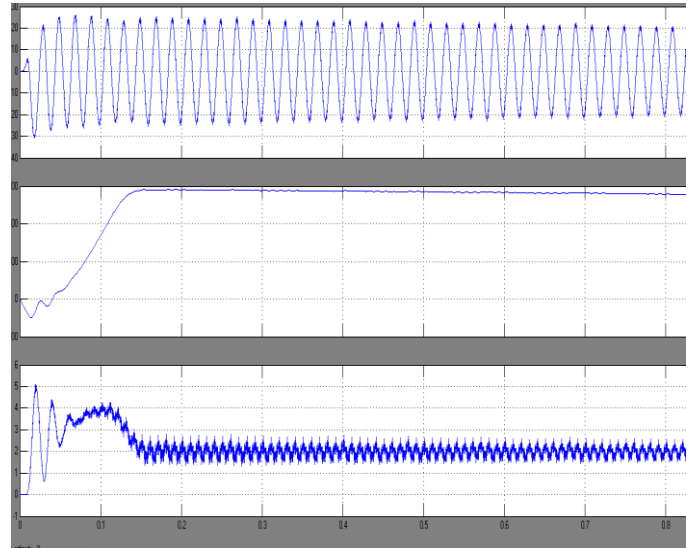


Fig.8 Stator Current, Speed and Motor Torque

IV. MATLAB/SIMULINK MODEL & SIMULATION RESULTS

Here simulation is carried out for two cases. In case I conventional three phase three level induction motor is simulated and in case II proposed multilevel drive is simulated.

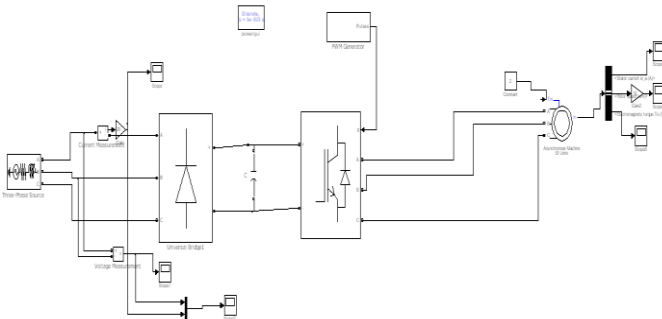


Fig. 6 Matlab/Simulink Model of Conventional IM Drive

Fig. 6 shows the Matlab/Simulink model of conventional three phase three level induction motor drive. It consists of front end rectifier followed by three phase inverter.

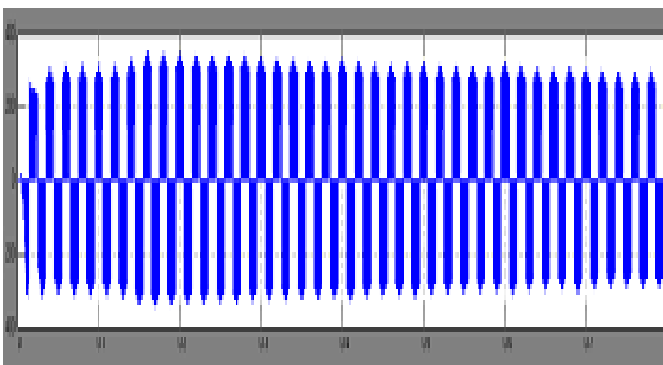


Fig. 7 Three Level output

Fig. 7 shows the three level output of the conventional inverter. Her switching frequency is taken as 1050 hz.

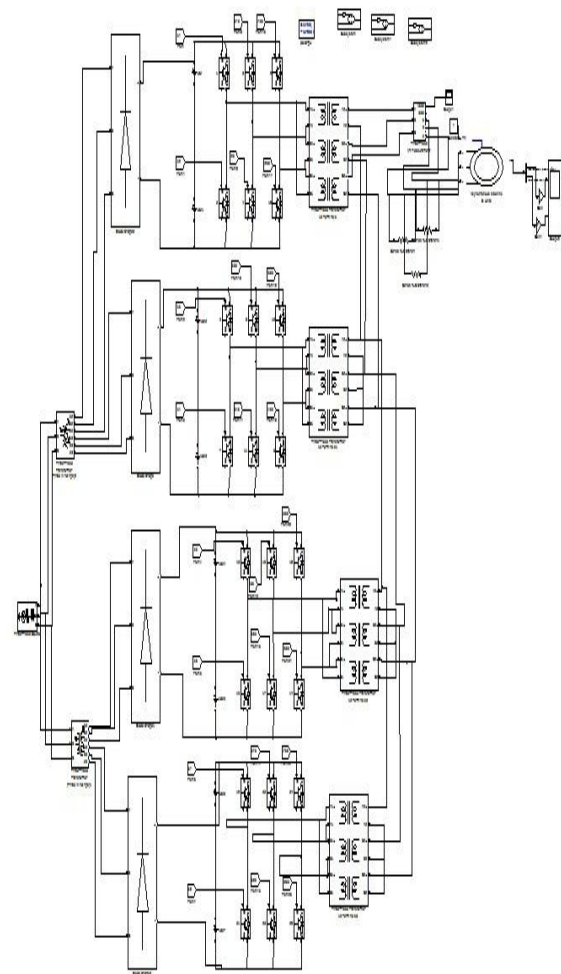


Figure.9 Block diagram of proposed circuit

Fig. 9 shows the block diagram of proposed series connected multilevel inverter fed induction motor drive. It consists of four inverters. Here we are using phase shifted carrier PWM.

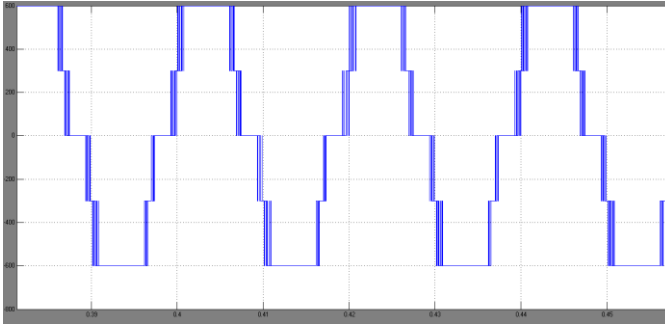


Fig. 10 Three Level output Inverter 1

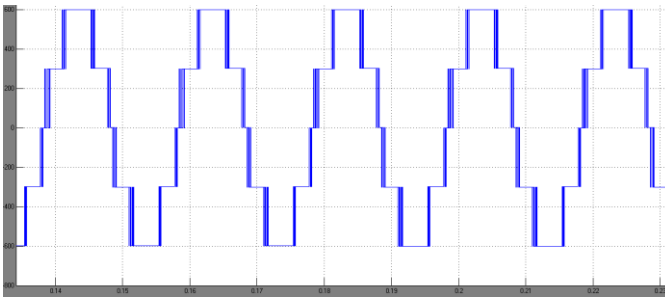


Fig. 11 Three Level output Inverter2

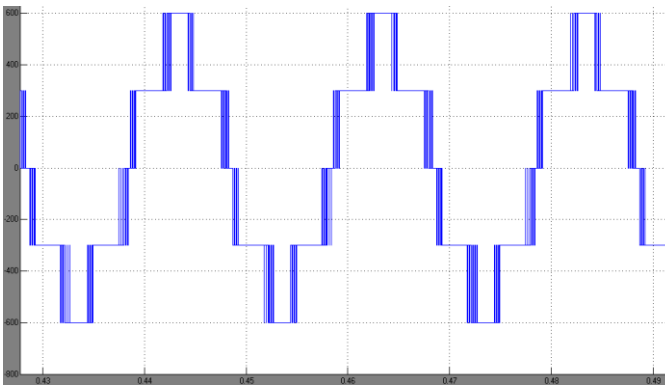


Fig. 12 Three Level output Inverter3

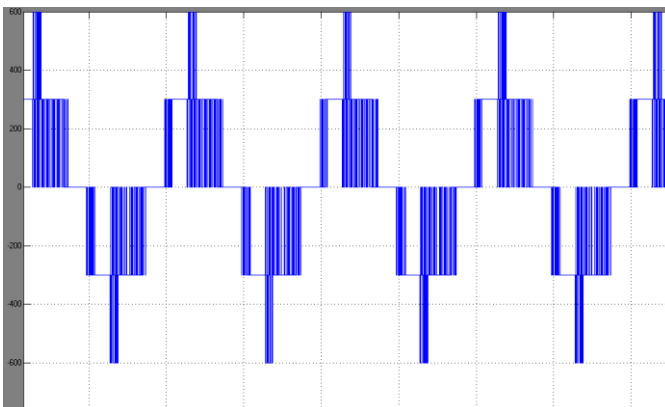


Fig. 13 Three Level output Inverter4

Fig10 to 13 shows the individual inverter outputs. From the figures it is clear that each output consists of only three levels.

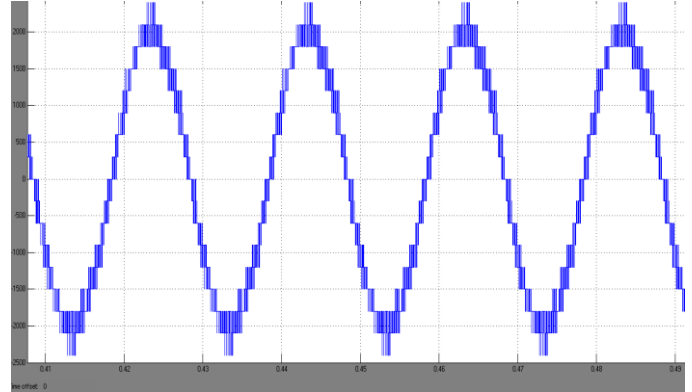


Fig. 14 Multilevel output

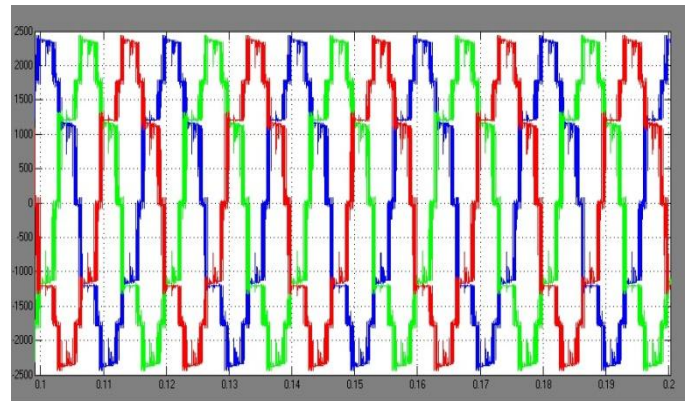


Figure.15.Multilevel output three phase

This waveform represents the output voltage of the three phase multilevel inverter.

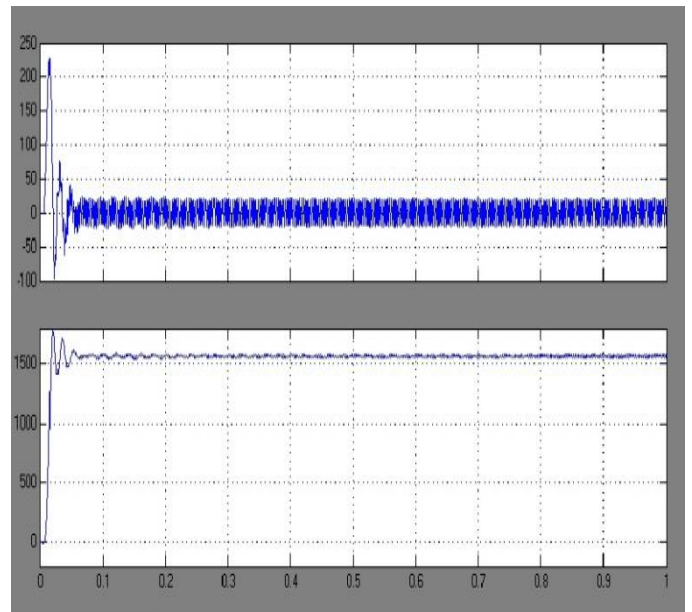


Figure.16Electromagnetic Torque and Speed curves of SQCIM

The first waveform represents the Electromagnetic Torque and rotor speed characteristics of the Squirrel cage Induction motor

V. CONCLUSION

A series connection of three-level inverters has been proposed for a medium-voltage SQIM drive with increased voltage capacity. The topology ensured high-power operations with medium-voltage output having several voltage levels. The reduction in the ratings of the dc bus capacitor and reduced imbalance problems in the dc bus are some of the advantages of the proposed topology over the existing topologies. The disadvantage of the proposed topology is that it requires additional output transformers which introduce additional cost and losses. However, these transformers do not have complex underutilized windings like that required in cascaded H-bridge topologies. Finally a Matlab/Simulink model is developed and simulation results are presented.

VI. REFERENCES

- [1] F. Wang, "Motor shaft voltages and bearing currents and their reduction in multilevel medium-voltage PWM voltage-source-inverter drive applications," *IEEE Trans. Ind. Appl.*, vol. 36, no. 5, pp. 1336–1341, Sep./Oct. 2000.
- [2] S. Chen and T. A. Lipo, "Bearing currents and shaft voltages of an induction motor under hard- and soft-switching inverter excitation," *IEEE Trans. Ind. Appl.*, vol. 34, no. 5, pp. 1042–1048, Sep./Oct. 1998.
- [3] L. M. Tolbert, F. Z. Peng, and T. G. Habetler, "Multilevel converters for large electric drives," *IEEE Trans. Ind. Appl.*, vol. 35, no. 1, pp. 36–44, Jan./Feb. 1999.
- [4] A. Muetze and A. Binder, "Calculation of circulating bearing currents in machines of inverter-based drive systems," *IEEE Trans. Ind. Electron.*, vol. 54, no. 2, pp. 932–938, Apr. 2007.
- [5] J. Rodriguez, J. S. Lai, and F. Z. Peng, "Multilevel inverters: A survey of topologies, control and applications," *IEEE Trans. Power Electron.*, vol. 49, no. 4, pp. 724–738, Aug. 2002.
- [6] P.W. Hammond, "A new approach to enhanced power quality for medium voltage drives," *IEEE Trans. Ind. Appl.*, vol. 33, no. 1, pp. 202–208, Jan./Feb. 1997.
- [7] R. Teodorescu, F. Blaabjerg, J. K. Pederson, E. Cengelci, and P. N. Enjeti, "Multilevel inverter by cascading industrial VSI," *IEEE Trans. Ind. Electron.*, vol. 49, no. 4, pp. 832–838, Aug. 2002.
- [8] A. Nabae, I. Takahashi, and H. Akagi, "A new neutral point clamped inverter," *IEEE Trans. Ind. Appl.*, vol. 17, no. 5, pp. 518–523, Sep./Oct. 1981.
- [9] J.-S. Lai and F. Z. Peng, "Multilevel converters—A new breed of power converters," *IEEE Trans. Ind. Appl.*, vol. 32, no. 3, pp. 509–517, May/Jun. 1996.
- [10] G. Cararra, S. Gardella, M. Marchesoni, R. Salutari, and G. Sciutto, "A new multilevel PWM method: A theoretical analysis," *IEEE Trans. Power Electron.*, vol. 7, no. 3, pp. 497–505, Jul. 1992.
- [11] A. M. Trzynadlowski, R. L. Kirlin, and S. Legowski, "Space vector PWM technique with minimum switching losses," *IEEE Trans. Ind. Electron.*, vol. 44, no. 2, pp. 173–181, Apr. 1997.
- [12] Y. S. Lai and S. R. Bowes, "Optimal bus-clamped PWM techniques for three-phase motor drives," in *Proc. Annu. Conf. IEEE Ind. Electron. Soc.*, Busan, Korea, Nov. 2–6, 2004, pp. 1475–1480.
- [13] Suvajit Mukherjee and Gautam Poddar "A Series-Connected Three-Level Inverter Topology for Medium-Voltage Squirrel-Cage Motor Drive Applications" *Ieee Transactions On Industry Applications*, Vol. 46, No. 1, January/February 2010

Improved Multiple File Transfer Protocol using Extended features of SCTP

Prabhanshu Jaiswal ¹, Gaurav Agrawal ², Pushendra Singh ³, Dr. A.K. Sharma ⁴
(CSED, MMMEC Gorakhpur/ GBTU, INDIA)

ABSTRACT

The Stream Control Transmission Protocol (SCTP) is a reliable transport layer protocol, standardized by Internet Engineering Task Force (IETF). Transport layer is responsible for reliable delivery of messages from one host (source) to another host (destination). We are using the key features of SCTP (multi-streaming and multi-homing) with some additional characteristics for transmission of multiple files. In current scenerio, SCTP creates streams only at the initial association establishment phase (before the transmission of files strats) and afterwards the steams are not allowed to be changed, but in this paper, we propose that these streams can be modified dynamically by using dynamic stream addition (DSA) policy of multi-streaming. And to speedup the throughput of SCTP, we use split fast retransmission (SFR) policy for the transmission of multiple files. We are also proposing a FTP architecture over this extended version of SCTP and illustrating algorithms for both ends (Server site and Client site). The peformance evaluation of our test is studied through ns-2. Our tests shows that the addition of these extended features of SCTP, significantly improve the performance of multiple file transfer.

Keywords: Dynamic stream addition, FTP protocol, multi-homing, multi-streaming, SCTP.

1. INTRODUCTION

Modern world is tightly attached with the Internet. The mainstream of communication now-a-days is via internet based applications. Internet is the worldwide, publicly accessible network of interconnected computer networks that transmit data through packet switching using the standard Internet Protocol (IP). This nature of internet demands the exchange of data be fast and reliable. Internet is an infrastructure that comprises of interconnections and by technical specifications or protocols that describe how to exchange data over the network. Technically there are 3 kinds of protocols depending at which layer they are being used:

Network layer protocols: At the lowest level is IP (Internet Protocol), which defines the datagrams or packets that carry blocks of data from one node to another.

Transport layer protocols: The protocols by which one host sends data to another. TCP and UDP are the intermediate layer protocols.

Application layer protocols: This describes the specific messages and data formats sent and understood by the applications running at each end of the communication.

In 1998, an IETF working group (SIGTRAN) was formed to design a mechanism for reliably transporting call control signaling over the Internet. SIGTRAN's goal was to create an IP complement to the telephone switching's SS7 network. SIGTRAN's work was focused to address few key problems in the use of TCP [1]:

1.1. Head of line blocking - A problem where sending independent messages over an order-preserving TCP connection causes delivery of messages sent later to be delayed within a receiver's transport layer buffers until an earlier lost message is retransmitted and arrives. These later messages often establish independent telephone calls. For call control signaling, the delay on later messages caused critical call control timers to expire, thus resulting in undesirable call setup failures.

1.2. Message Boundary— Since TCP is a byte stream oriented transfer protocol, the message boundaries are not saved multiple messages from the server to the client could be combined into one, making it difficult for the client to split the messages.

To remedy these situation, SCTP came into existence. The first key feature of SCTP is multi-streaming as describe in RFC 4960. Multi-streaming provides an aggregation mechanism to multiplex logically separate message streams to the same association. While the standard SCTP [1] creates streams only at the initial association establishment phase and afterwards the streams are not allowed to modify. When transmitting web objects concurrently with multi-streaming, it causes unnecessary waiting, as a result of large objects occupying the streams while small ones having no streams allocated.

To improve throughput of multiple file transmission, we add an extension of SCTP to reduce web response time by DSA-SCTP [3].

The second key feature of standard SCTP is multi-homing. A multi-homed SCTP host is accessible through multiple IP addresses. If one of its IP addresses fails—possibly from an interface or link failure, severe congestion, or slow route convergence around path outages—the destination host can still receive data through an alternate source interface.

We allow multiple files to transfer concurrently from multiple paths at the sender ends. To prevent the side effects as follows ,

(i) unnecessary fast retransmissions by a sender, (ii) overly conservative cwnd growth at a sender, and (iii) increased ACK traffic due to fewer delayed ACKs by a receiver, we use the three algorithms as described in [4], which facilitates

to inflate the congestion window and to retransmit the lost data packets as quickly as possible.

Finally, we propose a model for transmitting multiple files using our proposed FTP protocol. Basically, FTP is an application layer protocol, used for exchanging files over any network that supports the TCP/IP protocol. Our proposed FTP over extension of SCTP has much benefits upon FTP over standard SCTP, the performance of transmission of files through transport layer will remarkably increase. We also give the algorithms for transmission multiple files through FTP over the extended version of SCTP.

The comparison of multiple file transfer over TCP, standard SCTP and Extension of SCTP is shown in the next coming section, which clearly shows that the transmission of multiple files using extension of SCTP improve the performance.

2. EXTENSION OF SCTP

2.1. MULTI-STREAMING IN EXTENDED SCTP

SCTP multi-streaming provides an aggregation mechanism to multiplex logically separate message streams to the same association. While the current SCTP creates streams only at the establishment phase while making the initial association and afterwards the streams are not allowed to be modified. In this paper, we add an extension of the standard SCTP to support dynamic stream addition during the communication [3].

Using independent streams in a SCTP association(), SCTP decouples the reliable data transfer from the strict order-of-transmission data delivery. The messages from the application layer are assign to different streams according to the requirement of the SCTP supported client or the scheduler of the server.

In this paper, we present the necessary modification to the SCTP specification to support the function of dynamic stream addition. In the modified SCTP, both sides of an association are allowed to add new out-streams and in-streams dynamically during the communication. Dynamic stream addition scheme is able to follow the application's requirement to create new streams when it is necessary to match a bursty objects concurrent transmission. We make use of DSA-SCTP [3] to the web server to reduce its response time.

2.2. MULTI-HOMING IN EXTENDED SCTP

In the standard SCTP, multi-homed hosts are used only for the purpose of redundancy and continuous transfer of control/data chunks from the sender host to destination host. Initially one path is chosen as a primary path among the set of available paths and rest are as secondary paths.

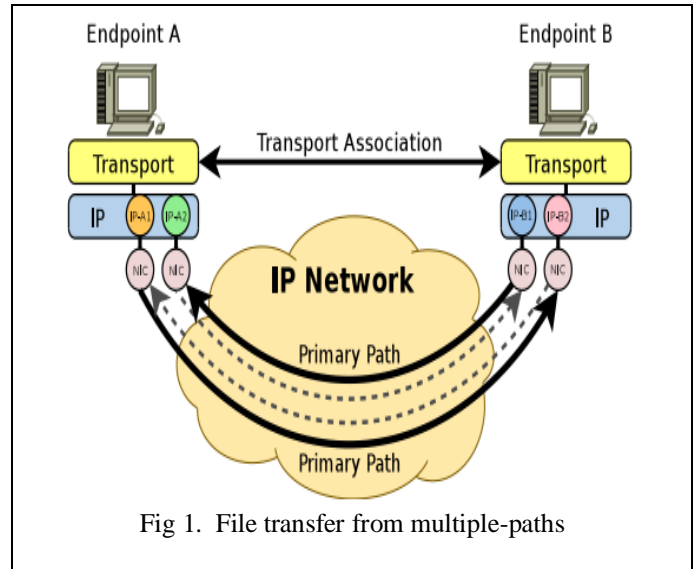


Fig 1. File transfer from multiple-paths

In the extension of SCTP, it enhance the concurrent multi-paths transfer of files in CMT-SCTP's multi-homing feature to distribute data across multiple end-to-end paths in a multi-homed SCTP association. The three negative side effects of reordering introduced by CMT are :

- (i) unnecessary fast retransmissions by a sender,
- (ii) overly conservative cwnd growth at a sender,
- and (iii) increased ACK traffic due to fewer delayed ACKs by a receiver.

These drawbacks can be removed by implementing the three algorithms as described in [4], under the strong assumption that the bottleneck queues on the end-to-end paths used in CMT are independent, which is further modified by load sharing [5].

3. PROPOSED FTP ARCHITECTURE

3.1. FTP OVER EXTENDED SCTP

FTP over Extension of SCTP is similar to that of over TCP, the major change would be the introduction of the association and usage of multi-streaming features. In this system multi-streaming combines the FTP control and data connections in a single association. So only one association is needed for one session and this eliminates the need of more than one connection for a transfer to take place. The architecture that we are proposing consists of the following steps :

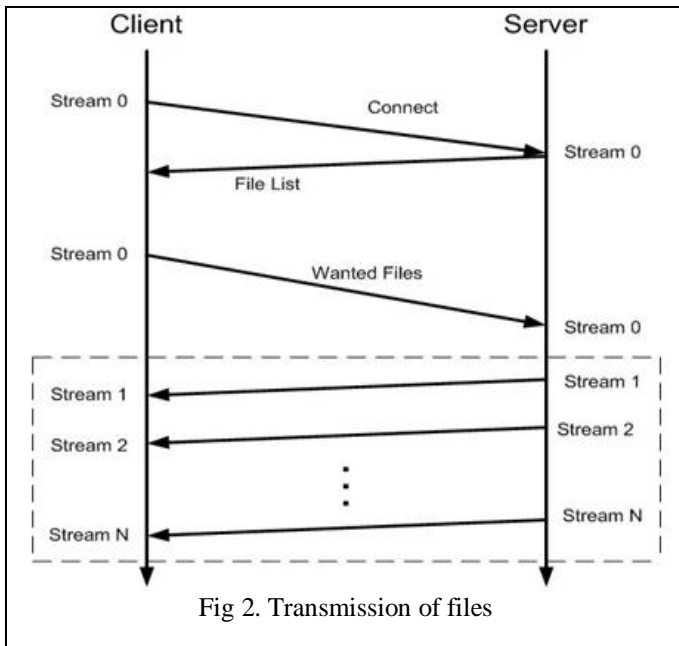
3.1.1. INITIATION PROCESS: Instead of establishing a connection with the server, now the client will request an association and during this initiation process both the hosts will open a stream which will be used for exchange of control commands and replies, say *Stream 0*. Also they agree on how many stream they will be using for the actual data transfer.

The number of streams can be dynamically increased as the need of application and the extra needed stream can be added with the help of DSA-SCTP scheme[3].

3.1.2. EXCHANGE OF CONTROL MESSAGES: Once the association is set up and the hosts have the agreed upon a control stream the exchange of the control messages take place. For instance, server sends the list of files available for download and the client sends back the list of files that it wants to upload.

3.1.3. FILE TRANSFER: After receiving the list of file(s) from the client the server opens multiple streams and then starts transferring multiple file simultaneously by using Concurrent Multipath Transfer (CMT) using SCTP Multipath Over Independent End-to-End Paths[4] and load sharing scheme [5]. On the client side, we maintain an array that has the pointers to the file streams to which the data has to be written. Depending on the stream on which the data is coming the same is written to the associated file stream.

3.1.4. TRANSFER TERMINATION: Termination of file transfer has to be considered on each stream at each path. Once the file is transferred a CLOSE command is passed on the stream, since SCTP maintains the message boundaries it is possible to send a termination message. Client upon receiving the termination message from a stream, it goes and closes the file stream as well as the path associated with that stream and then clean the array so that a new file could be sent over the same stream.



3.2 ALGORITHM USED FOR TRANSMITTING MULTIPLE FILES USING EXTENDED SCTP

These algorithms run at their respective hosts. The Server site is always in running mode and waiting for a request. Whenever a client wants to access some file from the server site, it sends a request (INIT chunk) to the server and the server responds with INIT-ACK chunk to the client. If the client is an authentic user only then it replies with a COOKIE chunk. And then server sends a COOKIE-ACK chunk to the client in the encrypted form to avoid the intrusion from attackers. In this way the connection between

user and server will be established by using four-way handshaking.

Termination of connection is done by using Full Shutdown at the both side. Hence, this procedure also provides some kind of security from the attackers because all the chunks are in encrypted form and only valid user can get access of the resources of server.

3.2.1. AT THE SERVER SITE :

```

step 1. Server waits for Clients.
step 2. Accept a request from a client and fork a child.
step 3. if PORT_NO already is in use, then
    generate an error message
    else
    {
    generate varification tag for specific Port
    and inform the client;
    }
step 4. Get list of files from Client.
step 5. Send the list to the Cllient and initializes
    stream_no .
step 6. Get requested file size information from the Client
step 7. do {
    If stream_no <objects_requested,
    {
    create extra streams dynamically and
    inform the clients;
    Add the newly created streams in the
    existing association;
    update the stream_no;
    }
    Send file object in the open streams.
}while(! SHUTDOWN);
step 8. Close all the streams.
step 9. End.
    
```

3.2.2. AT CLIENT SITE :

```

step 1. Clients request to the Server.
step 2. if "the request is not fulfilled by server", then
    terminate.
step 3. Get PORT_NO and verification tag information
    from the Server.
step 4. Get list of files from Server.
step 5. Formate and display the user.
step 6. Get wanted list of files from user.
step 7. Prepare for incoming message and create
    an array of file pointer FP and initialize to
    all by NULL .
step 8. Get the message and cache the streams, let i
step 9. If 'i' is a control stream then
    If it has terminate message, then
    {
    Close all stream;
    terminate the connection;
    }
    else
    write to FP[i].
step 10. GOTO step 9.
step 11. End.
    
```

3.3. EXPERIMENTAL RESULT AND ANALYSIS

We setup a simple network for investigating the features of the extended SCTP. In our network we use two nodes – one as Server and other as a Client. Both are running on Linux Kernel 2.4.19. We have performed various experiments on transferring multiple files, having different size, using the features of TCP, SCTP and extended SCTP as we proposed earlier. For the performance evaluation we took less than 1Mb, greater than 1Mb and less than 5Mb, and greater than 5Mb files for transmission and their respective durations were recorded. All experiments are done repeatedly and the average of that is taken and shown in the table of fig. 3.

This experiment shows that TCP and standard SCTP took much more time than the Extended SCTP for transferring multiple files between two nodes. Although Extended SCTP has some over-head of managing incoming and outgoing packets/chunks, but the overall performance of Extended SCTP much better than the standard SCTP and TCP.

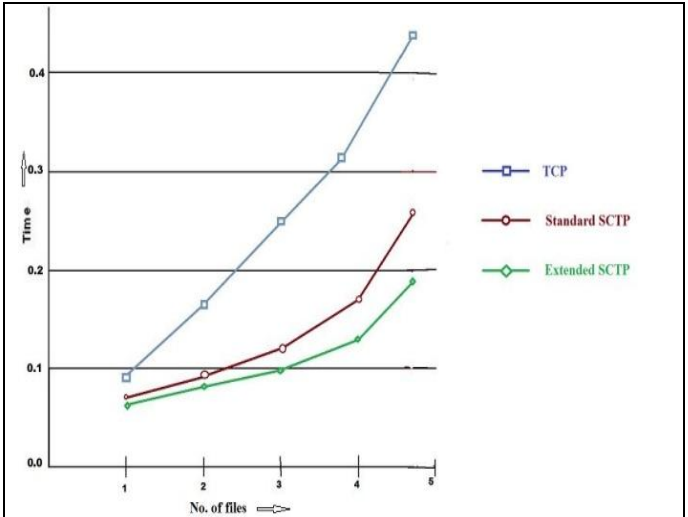


Fig 4. Comparison for files < 1Mb

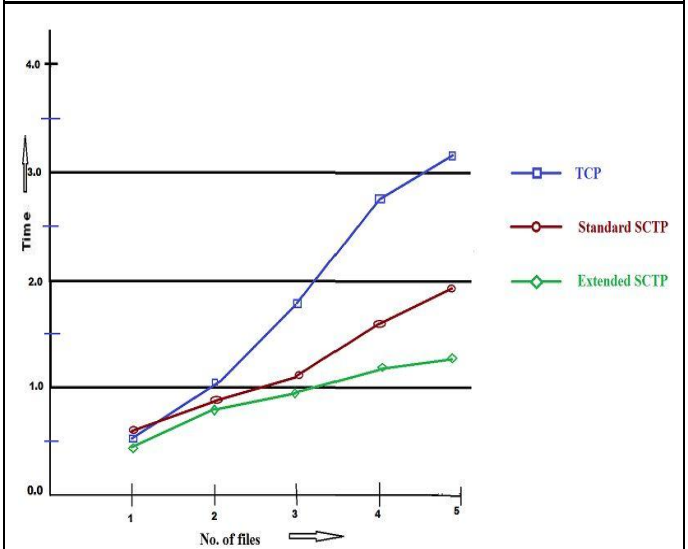


Fig 5. Greater than 1Mb and Less than 5Mb

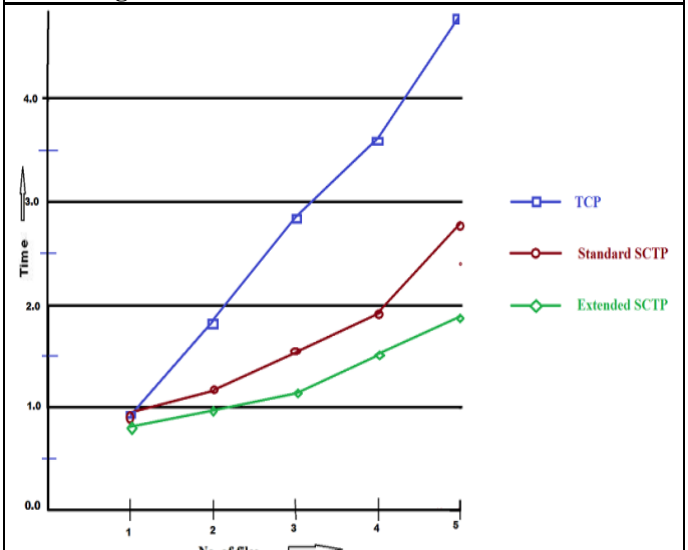


Fig 6. Greater than 5Mb

NUMBER OF FILES	Time Taken for TCP	Time Taken for SCTP	Time Taken for Extended-SCTP
File Size: less than 1Mb.			
1 File	0.085	0.070	0.067
2 Files	0.165	0.089	0.072
3 Files	0.247	0.118	0.096
4 Files	0.314	0.156	0.129
5 Files	0.435	0.246	0.184
File Size: Greater than 1 Mb and Less than 5 Mb.			
1 File	0.511	0.557	0.048
2 Files	1.035	0.864	0.792
3 Files	1.75	1.048	0.917
4 Files	2.681	1.532	1.082
5 Files	3.152	1.946	1.207
File Size: Greater than 5 Mb.			
1 File	0.942	0.950	0.839
2 Files	1.844	1.094	0.954
3 Files	2.865	1.561	1.051
4 Files	3.512	1.937	1.537
5 Files	4.836	2.720	1.964

Fig 3. Statistics of Multiple File Transfer

4. FUTURE WORKS

4.1. FTP OVER SCTP ON INTERNET: The only constraint that this project had was, the SCTP protocol was not matured enough when the work on this project began. So the availability was a problem, this protocol was only available in the CS LAN so all the modules were run on INTRANET. Now the SCTP protocol could be installed on a LINUX box that could be out of the network thus this application could be run over INTERNET and record the Performance gain.

4.2. IMPLEMENTATION OF SCTP IN MOBILE NETWORKS USING MULTI-HOMING: In the recent past, a lot of research was going on SCTP protocol and one of the areas of research is to implement Multi-Homing, a SCTP feature, in Mobile Networks and see whether this feature could do any good for the existing Mobile Networks.

4.3. HTTPS/FTPS OVER SCTP: To overcome the inefficiencies present in the standard protocols like HTTP and FTP currently enhanced and more secured protocols are being used, they are HTTPS and FTPS. An implementation of these protocols over SCTP could make the argument that SCTP could replace TCP or UDP stronger.

5. CONCLUSION

In this paper, we have evaluated the extension features of SCTP – dynamic stream addition behavior[3] in order to show the advantages of multi-streaming in multiple file transfer and by using concurrent multi-path transmission policy, we can use some of the available paths for increasing the throughput of transmission of multiple files. Then we have presented our results comparing the SCTP[1] against the TCP, assuming different scenarios such as head of line blocking problem and Denial of service attack. Furthermore, TCP use multiple connection for simultaneously transfer of multiple files when SCTP needs only one association i.e. one control stream for control connection and multiple data stream for multiple file transfer. Extension of SCTP features such as DSA[3] can also be used to find good response time in web application and multimedia application etc. We also show the comparison results of TCP, standard SCTP and Extended SCTP for multiple file transferring. We use multi-homing features for fault tolerant and load sharing in multiple file transfer.[5]

6. REFERENCES

- [1] R. Stewart, Q. Xie, “Stream Control Transmission Protocol (SCTP): A Reference Guide”, Addison Wesley, 2001, ISBN: 0-201-72186-4.
- [2] JinwookSeo, YoungjuAhn , Minki No, Hyunchel Kim, Seongjin Ahn and Jinwook Chung, “Implementof FTP application using SCTP,” *International Journal of Computer Scienceand Network Security*, VOL.6 No.12, December 2006.
- [3] MiaoXue, Haisheng Jiang, Ping Dong, Yajuan Qin,Sidong Zhang, Hongke Zhang, “DSA-SCTP: ANEXTENSION OF SCTP TOREDUCE WEBRESPONSE TIME,” in *proceedings of IEEE ICCTA,978-1-4244-4817*, Mar. 2009.
- [4] J. R. Iyengar, P. D. Amer, and R. Stewart, “Concurrent Multipath Transfer Using SCTP MultihomingOver Independent End-to-End Paths,”*IEEE/ACM Transactions on Networking*, vol. 14, no. 5, pp. 951–964,Oct. 2006, ISSN 1063-6692.
- [5] Inwhae Joe, Sijia YAN, “SCTP Throughput Improvement with Best Load Sharing based on Multi-homing,” *Fifth IEEE International Joint Conference on INC, IMS and IDC, 2009*.
- [6] P. Natarajan, N. Ekiz, E. Yilmaz, P.D. Amer,and J. Iyengar,“(NR-SACKs) Non-Renegable Selective Acknowledgments for SCTP,” in *Proceedings of the 16th IEEE International Conference on Network Protocols (ICNP), Orlando, Florida/U.S.A.*, Oct. 2008, pp. 187– 196, ISBN 978-1-4244-2506-8.
- [7] Lin Cui, SeokJooKoh, and Woo Jin Lee, “Fast Selective ACK Scheme for Throughput Enhancement of Multi-Homed SCTP Hosts,” *IEEE communications letters*, Vol. 14, No. 6, JUNE 20i0.

Study of TCP Variants Compression on Congestion Window and Algorithms in Dynamic Environment

Nishant Chaurasia

*M.Tech Scholar in CSE
Oriental institute of science and technology
Bhopal, India*

Prof. Sanjay Sharma

*Asst. Professor in CSE Department
Oriental institute of science and technology
Bhopal, India*

Abstract: The most common transport protocol is the Transmission Control Protocol. Transmission Control Protocol (TCP) is reliable, connection oriented transport protocol which provides end-to-end data delivery in networks. TCP was primarily designed for wired networks and it shows performance degradation when used in wireless networks. The main concern in wireless networks with TCP is the packet loss which is mostly considered to have occurred due to congestion. The Transmission Control Protocol comes in many variants like TCP, Tahoe, Reno, New Reno, Vegas, Sack and so on. In a Mobile Ad Hoc Network or Dynamic Environment, temporary link failures and route changes happen frequently. With the assumption that all packet losses are due to congestion, TCP performs poorly in such environment. While there has been some research on improving TCP performance over Dynamic Environment, most of them require feedback from the network or the lower layer. In this paper we constitute a realistic Dynamic Environment by considering multistage error model in the design of wireless packet losses. Mobility in structure is also conceived to estimate the actual performance of TCP. Moreover the behaviour of TCP Tahoe, Reno, New Reno, Sack, Vegas, fack, lite and westwood in Dynamic network is simulated to perceive the impact of wireless link on the behaviour of these TCP variants. Finally from the result of our simulation we conclude the best TCP variants for different circumstances and detecting or responding to out-of-order packet delivery events, which are the results of frequent route changes. In our simulation study, this approach had achieved best performance improvement, without requiring feedback from the network.

Keywords: *TCP Features, Advantages, TCP Variants, TCP algorithms and characteristics.*

I. INTRODUCTION

Transmission Control Protocol (TCP) was originally defined in RFC 793 [1]. TCP is reliable, connection oriented transport protocol which provides end-to-end data delivery in networks. TCP was primarily designed for wired networks and it shows performance degradation when used in wireless networks. TCP is a window based reliable transport layer protocol that achieves its reliability through sequence numbers and

acknowledgements [2]. TCP assumes that all the packet losses are due to congestion. When a packet is lost, TCP applies congestion avoidance mechanisms and slows its transmission rate. However, wireless networks are known to experience sporadic and usually temporary losses due to fading, shadowing, hand off that cannot be considered congestion. Packets can be lost due to hand offs as a mobile node moves out of range of a base station and into the range of another packet lost during such transitions also initiate TCPs congestion avoidance. TCP is based on the principle of “conservation of packets”, which means that in the case a connection works at the available capacity of bandwidth, the packet is not to be inserted into the network until the second packet doesn’t leave the network [3]. TCP implements the above principle by using the acknowledgements to time the outgoing packets, because the acknowledgement means that the specific packet has left the network.

TCP maintains the congestion window to represent the network capacity. The transmitter can send data up to the minimum value of congestion window and advertised window. Congestion control is the flow control imposed by the transmitter, while the advertised window is the flow control imposed by the receiver. The first control is based on the transmitter’s perception of network congestion, while the second is related to the size of available space in the buffer at the receiver for the given connection.

TCP operates in three phases:

1. Connection establishment
2. Data transfer
3. Connection termination

The basic implementations of TCP are based on Jacobson’s classical slow start algorithm for congestion avoidance and control [4- 5]. A number of solutions have been proposed to remove the problem of congestion. This paper performs analysis on the variants of TCP that have evolved for performance improvement in wireless networks.

II. TCP FEATURES AND ADVANTAGES

TCP provides a connection oriented, reliable, byte stream service. The term connection oriented means the two applications using TCP must establish a TCP connection with each other. It is a full duplex protocol, meaning that each TCP connection supports a pair of byte streams, one flowing in each direction. TCP includes a flow-control mechanism for

each of these byte streams that allow the receiver to limit how much data the sender can transmit. TCP also implements a congestion-control mechanism. TCP is a reliable connection oriented end-to-end protocol which has many mechanisms to provide reliable communication. But a small number of packets are lost due to congestion and buffer overflow. In such cases, TCP ensures reliability by using sequence numbers and time-out intervals. The packet of the particular sequence number is resent after the time-out timer runs out. TCP runs on the concept of "Conservation of Packets" [4]. The TCP provides different facilities as discussed below in the following list.

A. Stream Data Transfer

TCP transfers a continuous stream of bytes. TCP does this by grouping the bytes in TCP segments, which are passed to IP for transmission to the destination. TCP decides how to segment the data and forwards the data at its own convenience.

B. Reliability

TCP assigns a sequence number to each byte transmitted, and expects a positive acknowledgment (ACK) from the receiving TCP. If the ACK is not received within a timeout interval, the data is retransmitted. The receiving TCP uses the sequence numbers to rearrange the segments when they arrive out of order, and to eliminate duplicate segments.

C. Flow Control

The receiving TCP, when sending an ACK back to the sender, also indicates to the sender the number of bytes it can receive beyond the last received TCP segment, without causing overrun and overflow in its internal buffers. This is sent in the ACK in the form of the highest sequence number it can receive without problems.

D. Multiplexing

To allow for many processes within a single host to use TCP communication facilities simultaneously, the TCP provides a set of addresses or ports within each host. Concatenated with the network and host addresses from the internet communication layer this forms a socket. A pair of sockets uniquely identifies each connection.

E. Logical Connection

The reliability and flow control mechanisms described above require that TCP initializes and maintains certain status information for each data stream. The combination of this status, including sockets, sequence numbers and window sizes, is called a logical connection. Each connection is uniquely identified by the pair of sockets used by the sending and receiving processes.

F. Full Duplex

TCP provides for concurrent data streams in both directions.

III. TCP VARIANTS AND COMPARISON

A. TCP

TCP provides important features of flow control, reliability, congestion control and connection management. Originally, TCP designed for wired networks but it also performs well in wireless networks. In order to improve its performance TCP cuts down the size of its congestion window resulted in further performance degradation. This is a more serious problem in busy and highly mobile networks which have rapid topological changes (Henna, 2009)[9]. TCP provides division for sequenced data stream into packets, confirms the packets delivery with the possibility of losing the IP layer loses, retransmit, reorders, or packets duplication and monitoring the network band capacity to avoiding congestions. TCP protocol can provide over two end points connection, flow rate controlling with bidirectional link and data reliability.

B. TCP Tahoe

TCP Tahoe is the congestion control mechanism suggested by Van Jacobson. The actual TCP data transmission is clocked by the acknowledgements received. But at the start of the transmission, there would not be any acknowledgement. To overcome this, the Tahoe suggests a mechanism called "slow start". According to this mechanism, the congestion window size is taken as 1 at the beginning of start or a restart of data transmission. After sufficient acknowledgements are received, the congestion window size is additionally increased. After congestion is achieved, the window size is multiplicatively decreased. This is called Additive Increase Multiplicative Decrease [5]. Whenever a packet is lost, the "go back n" method is used, and the entire pipe is emptied. This results in a high bandwidth delay.

C. TCP Reno

TCP Reno has all the advantages of Tahoe like the slow start mechanism and the time-out intervals. Also, it has some intelligent mechanisms to detect the packet losses previously. After each packet loss, the entire pipe is not emptied. It uses a Fast Retransmit mechanism in which when 3 duplicate acknowledgements are received, it is understood that there is packet loss. Hence even before the actual packet loss is detected, the packet is retransmitted. It has the disadvantage of reducing the window size more than required and hence cannot afford Fast Recovery [6]. If window size is reduced very much, then the normal course grained timeout.

D. TCP New Reno

The TCP New Reno [7] is more advanced than TCP Reno. It is able to detect multiple packet losses. It also enters the fast recovery mechanism like Reno, but it does not end up reducing the congestion window size. It waits till the acknowledgements of all the congested packets are received. The actual disadvantage of the New Reno is that it takes a whole Round Trip Time to detect a single packet loss.

E. TCP Vegas

The TCP Vegas [8] is a modified version of Reno. It works on the proactive measures to control congestion rather than reactive measures. It uses an algorithm to check for timeouts. It also overcomes the problem of requiring enough duplicate acknowledgements to detect a packet loss. It also uses a slightly modified slow start mechanism. It has the mechanism to detect congestion even before packet losses occur, but it also retains the other mechanisms of Reno and Tahoe. Overall, the Vegas has a new retransmission mechanism, a modified slow start algorithm and congestion avoidance scheme.

F. TCP Sack:

TCP with selective acknowledgment (Sack) permits the receiver of data to openly acknowledge the data in out of order which arrived to data sender. If Sack is used, the TCP sender does not resend the data Sacked through the period of loss recovery. Many of research proved that Sack technique enhance TCP throughput if multiple packet loss happen during same window (Ekiz, *et al.*, 2011). Sack algorithm is a mutual between selective duplication resending strategy, has been suggested to overcoming the limits and with accumulative acknowledgment structure for TCP (Kettimuthu and All cock, 2004). TCP with Sack is behaving more easily to understand than other two algorithms, Tahoe and Reno.

TC Sack needs that packets not acknowledging accumulatively but must acknowledging in selective manner because of that every ACK includes a block that defines each segment if acknowledged. So, TCP sender has an image of the acknowledged segments and the segments that outstanding. Every time TCP sender go in fast recovery phase, it sets a mutable pipe that is determine the amount of data is still outstanding in the path of the network and fix the congestion window to half of the recent value. Whenever it accepts an acknowledgment it decreases the pipeline by one and for each it resends a segment it increases it by one. When the pipeline is going to less than congestion window size, it detects the segments which are still not received and resend them. If no segments in outstanding situation, then it will send new packets, therefore more than single segment losses can be able to send within single RTT. The major problematic with implementation of TCP Sack is that presently selective acknowledgement does not deliver via the receiver and to implementing TCP Sack it not very easy process, but it precise and complicated task.

G. TCP Fack

TCP with forward acknowledgement (Fack) is a different algorithm which works on upper options of TCP Sack. TCP Fack is use info providing via Sack to adding extra accurate control to the data injection in to the pipe of network within during recovery process. The basic concept of Fack mechanism is by considering the greatest sequence number of forward selective acknowledgement as a mark that completely previous segments which unselectively acknowledged were lost. This monitoring permits to improve the recovery process of packets losses meaningfully. Fack algorithm is taking a

more violent methodology and considering unacknowledged holes among lost packets and Sack blocks. This methodology frequently outcomes improved TCP performance than the traditional approach, it is excessively violent if packets have been rearranged in the pipeline, due to these holes between blocks of Sack does not designate packets loss in this state (Sarolahti and Kuznetsov, 2002). The congestion window of TCP Fack is illustrated in figure 6, where a different behavior of the adjusting the window size. Fack presents a good technique to halving the size of window if the congestion occurred. If cwnd is instantly halved, TCP sender breaks transferring for a while and then restarts if the sufficient amount of data leaving the network. If the congestion happens, the window size must be halved depending on the multiplicative reduction of the exact cwnd. The sender recognizes the congestion state after it happened at least single RTT and if through that RTT in slow start phase, then the recent value of cwnd will duplicated than previous value if when congestion happened. So, in this state, the congestion window is firstly halved to determine the accurate cwnd which must be further reduced. However, TCP Fack offers congestion avoidance and fast retransmit mechanisms, but it aspects a lot of circumstances in recovery processes and also is not easy to implement Fack over applications (Tayade, 2011).

H. TCP Lite

TCP Lite is a service that provides a transport method that interrupts TCP in order to reduce the overhead involved in session management in which no data is transmitted or received. TCP Lite reduces or eliminates pure TCP protocol data units used in the set up and ACK while maintaining order, integrity, reliability and security of traditional TCP. TCP lite uses big window and protection against wrapped sequence number. Lite performs over TCP same as Reno. But when window increases it have some problems to Maintain them.

I. TCP West-wood

The TCP Westwood (TCPW) is a sender-side-only modification to TCP New Reno that is intended to better handle large bandwidth-delay product paths, with potential packet loss due to transmission or other errors, and with dynamic load. TCP Westwood protocol relies on a simple modification of the TCP source protocol behaviour for a faster recovery. This is performed by setting both a slow start threshold and a congestion window values that result from the effective connection while congestion is experienced. Hence, TCPW attempts to make a more "informed" decision, in contrast with TCP Reno, which automatically halves the congestion window after three duplicate ACKs. Like TCP Reno, TCPW cannot distinguish between buffer overflow losses and random losses. However, in presence of random losses, TCP Reno overreacts and reduces the window by half. TCP West Wood cannot distinguish between buffer overflow and random losses. It does not provide fast recovery mechanism for data packet or ACK.

IV. VARIANTS SIMULATIONS

The plots of the congestion window for all TCP variants are following. The values of cwnd are taken from a simulation runtime of 200 seconds with the presence of packet error rate of 10-3. However for better understanding of the behaviour of congestion window of each TCP variants, the value of the congestion window is traced for an interval of every second.

Fig 3(a): Congestion window dynamics of TCP Tahoe

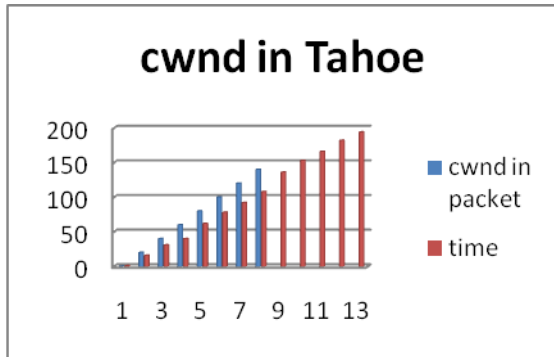


Fig 3(b): Congestion window dynamics of TCP Reno

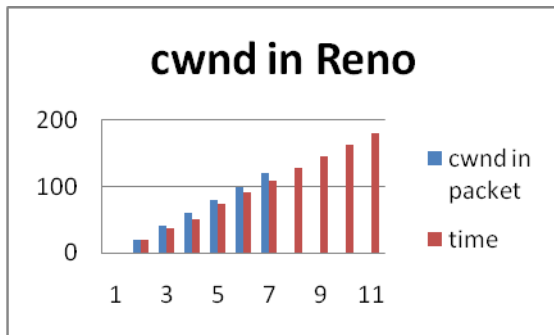


Fig 3(c): Congestion window dynamics of TCP New Reno

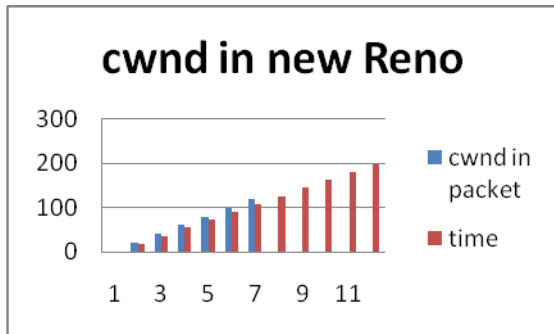


Fig 3(d): Congestion window dynamics of TCP Sack

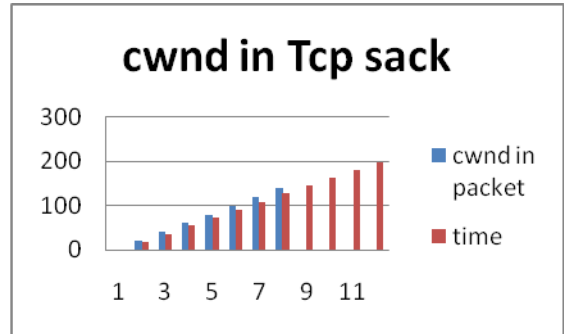


Fig 3(e): Congestion window dynamics of TCP Vegas

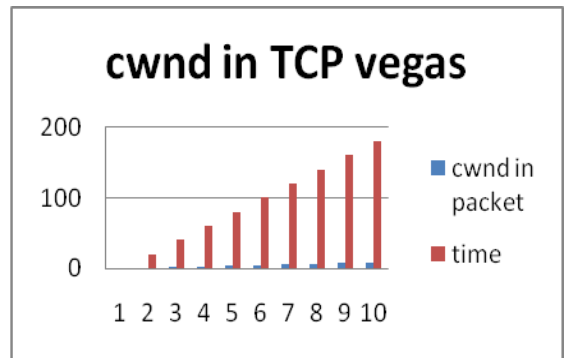


Fig 3(f): Congestion window dynamics of TCP fack

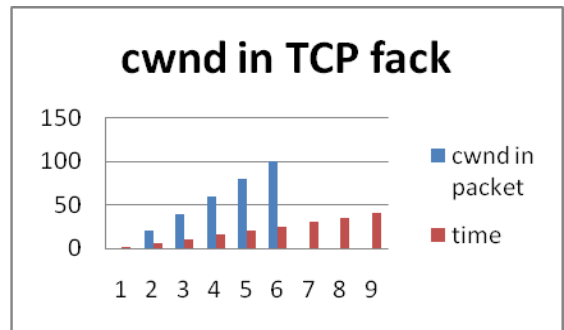


Fig 3(g): Congestion window dynamics of TCP lite

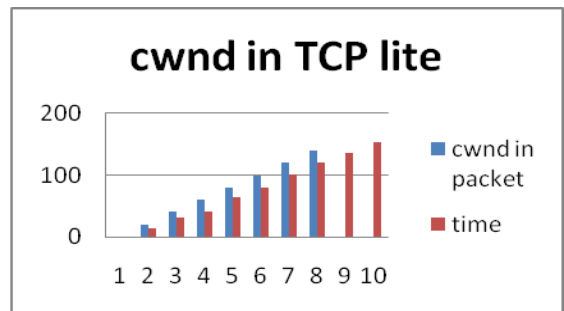
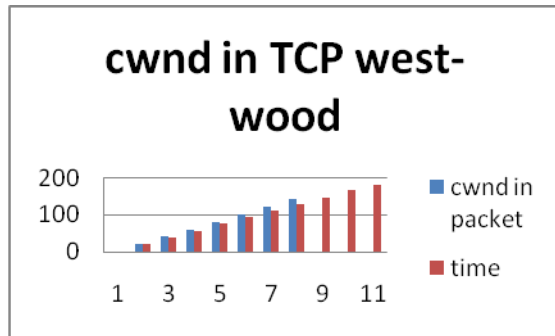


Fig 3(h): Congestion window dynamics of TCP west-wood



V. TCP ALGORITHMS AND CHARACTERISTICS

A. Slow Start

It operates by observing that the rate at which new packets should be injected into the network is the rate at which the acknowledgments are returned by the other end. Slow start adds another window to the sender's TCP: the congestion window, called "cwnd". When a new connection is established with a host on another network, the congestion window is initialized to one segment (i.e., the segment size announced by the other end, or the default, typically 536 or 512). Each time an ACK is received, the congestion window is increased by one segment. The sender can transmit up to the minimum of the congestion window and the advertised window. The congestion window is flow control imposed by the sender, while the advertised window is flow control imposed by the receiver. The former is based on the sender's assessment of perceived network congestion; the latter is related to the amount of available buffer space at the receiver for this connection. The sender starts by transmitting one segment and waiting for its ACK. When that ACK is received, the congestion window is incremented from one to two, and two segments can be sent. When each of those two segments is acknowledged, the congestion window is increased to four. This provides an exponential growth, although it is not exactly exponential because the receiver may delay its ACKs, typically sending one ACK for every two segments that it receives. At some point the capacity of the internet can be reached, and an intermediate router will start discarding packets. This tells the sender that its congestion window has gotten too large. Early implementations performed slow start only if the other end was on a different network. Current implementations always perform slow start.

B. Congestion Avoidance (Additional Increase)

If the receiver window is large enough, the slow start mechanism described in the previous routers in between the hosts will start discarding packets. As mentioned earlier TCP interprets packet loss as a sign of congestion, and when this happens TCP invokes the Congestion Avoidance mechanism [10]. Even though slow start and congestion avoidance is two different mechanisms they are more easily described together.

In the joint description below a new TCP variable is introduced. This variable, ssthresh, is the slow start threshold which TCP uses to determine if slow start or congestion avoidance is to be conducted.

1. When establishing a new connection cwnd is initialized to $0 < \text{cwnd} \leq \min(4 * \text{MSS}, \text{Max}(2 * \text{MSS}, 4380 \text{bytes}))$

2. The sender side TCP sends a maximum of $\min(\text{cwnd}, \text{rwnd})$ bytes

3. When congestion occurs $\text{Ssthresh} \leftarrow \min(\min(\text{cwnd}, \text{rwnd}) / 2, 2 * \text{MSS})$. If congestion was due to a timeout slow start is conducted.

4. When new data is acknowledged by the other end cwnd is increased. The way in which TCP increases the cwnd depends on if we are doing slow start ($\text{cwnd} < \text{ssthresh}$) or congestion avoidance. The increase of cwnd in slow start was described in the previous Section, and if we are doing congestion avoidance then $\text{cwnd} \leftarrow \text{cwnd} + (\text{cwnd} / 2)$.

C. Fast Retransmit

TCP may generate an immediate acknowledgment (a duplicate ACK) when an out-of-order segment is received. This duplicate ACK should not be delayed. The purpose of this duplicate ACK is to let the other end know that a segment was received out of order, and to tell it what sequence number is expected. Since TCP does not know whether a duplicate ACK is caused by a lost segment or just a reordering of segments, it waits for a small number of duplicate ACKs to be received. It is assumed that if there is just a reordering of the segments, there will be only one or two duplicate ACKs before the reordered segment is processed, which will then generate a new ACK. If three or more duplicate ACKs are received in a row, it is a strong indication that a segment has been lost. TCP then performs a retransmission of what appears to be the missing segment, without waiting for a retransmission timer to expire.

D. Fast Recovery

After fast retransmit sends what appears to be the missing segment, congestion avoidance, but not slow start is performed. This is the fast recovery algorithm. It is an improvement that allows high throughput under moderate congestion, especially for large windows. The reason for not performing slow start in this case is that the receipt of the duplicate ACKs tells TCP more than just a packet has been lost. Since the receiver can only generate the duplicate ACK when another segment is received, that segment has left the network and is in the receiver's buffer. That is, there is still data flowing between the two ends, and TCP does not want to reduce the flow abruptly by going into slow start. The fast retransmit and fast recovery algorithms are usually implemented together as follows.

1. When the third duplicate ACK in a row is received, set ssthresh to one-half the current congestion window, cwnd, but no less than two segments. Retransmit the missing segment. Set cwnd to ssthresh plus 3 times the segment size. This inflates the congestion window by the number of segments that have left the network and which the other end has cached.

2. Each time another duplicate ACK arrives, increment cwnd by the segment size. This inflates the congestion window for the additional segment that has left the network. Transmit a packet, if allowed by the new value of cwnd.

3. When the next ACK arrives that acknowledges new data, set cwnd to ssthresh (the value set in step).

This ACK should be the acknowledgment of the retransmission from step 1, one round-trip time after the retransmission. Additionally, this ACK should acknowledge all the intermediate segments sent between the lost packet and the receipt of the first duplicate ACK. This step is congestion avoidance, since TCP is down to one-half the rate it was at when the packet was lost.

E. Selective Acknowledgment

Multiple packet losses from a window of data can have a catastrophic effect on TCP throughput. Multiple dropped segments generally cause TCP to lose its ACK-based clock; reducing overall throughput. The Selective Acknowledgment (SACK) [11] is a strategy which corrects this behaviour in the face of multiple dropped segments. With selective acknowledgments, the data receiver can inform the sender about all segments that have arrived successfully, so the sender need retransmit only the segments that have actually been lost. It allows the receiver to acknowledge discontinuous blocks of packets that were received correctly, in addition to the sequence number of the last contiguous byte received successively. The acknowledgement can specify a number of SACK blocks, where each SACK block is conveyed by the starting and ending sequence numbers of a contiguous range that the receiver correctly received.

F. Flow Control

In computer networking, flow control is the process of managing the data rate between two nodes to prevent a fast sender from outrunning a slow receiver. It provides mechanism for the receiver to control the transmission speed, so that it is not overwhelmed. Flow Control should be distinguished from congestion control, which is used for controlling the flow of data when congestion has occurred actually. In a connection between a client and a server, the client tells the server the number of bytes it is willing to receive at one time from the server; this is the client's receive window, which becomes the server's send window. Likewise, the server tells the client how many bytes of data it is willing to take from the client at one time; this is the server's receive window and the client's send window. Since the window size can be used in this manner to manage the rate at which data flows between the devices at the ends of the connection, it is the method by which TCP implements flow control, one of the "classical" jobs of the transport layer. Flow control is vitally important to TCP, as it is the method by which devices communicate their status to each other. By reducing or increasing window size, the server and client each ensure that the other device sends data just as fast as the recipient can deal with it. Flow control is a technique whose primary purpose is to properly match the transmission rate of sender to that of the receiver and the network. It is important for the transmission to

be at a high enough rates to ensure good performance, but also to protect against overwhelming the network or receiving host. Congestion control is primarily concerned with a sustained overload of network intermediate devices such as IP routers. TCP uses the window field, briefly described previously, as the primary means for flow control. During the data transfer phase, the window field is used to adjust the rate of flow of the byte stream between communicating TCPs.

G. Retransmission Mechanism

Retransmission Mechanism [12] keeps track of when each segment was sent and it also calculates an estimate of the RTT by keeping track of how long it takes for the acknowledgment to get back. Whenever a duplicate acknowledgement is received it checks to see if the (current time segment transmission time) > RTT estimate; if it is then it immediately retransmits the segment without waiting for 3 duplicate acknowledgements or a coarse timeout [12]. Thus it gets around the problem faced by Reno of not being able to detect lost packets when it had a small window and it didn't receive enough duplicate ACK's. To catch any other segments that may have been lost prior to the retransmission, when a non duplicate acknowledgment is received, if it is the first or second one after a fresh acknowledgement then it again checks the timeout values and if the segment time since it was sent exceeds the timeout value then it re-transmits the segment without waiting for a duplicate acknowledgment [12]. Thus in this way Vegas can detect multiple packet losses.

H. Congestion Avoidance:

Congestion avoidance is the algorithm used by TCP to avoid losing packets, if packets are lost. TCP performs congestion avoidance [4,8,12] when cwnd is greater than ssthresh. In the congestion avoidance phase, the cwnd is increased by 1 full-sized segment every round-trip time (RTT). Congestion avoidance continues until congestion is detected.

Congestion can be detected in two ways:

- 1) Receipt of duplicate acknowledgment
- 2) Due to time timeout

VI. CONCLUSION

Transmission Control Protocol was designed initially for wired networks it results in performance degradation when used in wireless networks. Transmission Control Protocol is responsible for reliable transport and regulation of data flow from source to destination. The primary reasons for performance degradation are packet losses, link failures, hand offs and long round trip time.

In this research, the performance of five different clones of TCP (Tahoe, Reno, NewReno, Sack, Vegas, Fack, Lite, Westwood) have been analyzed in the presence of high bit error. We can say that as the distance between the source and destination increases the delay time also increases and hence the total throughput starts reducing so to improve the throughput we increase the window size. Therefore on the WAN when the distance increases between the source and destination the throughput starts to reduce and hence to increase and support the large number of users we increase the

window size. The effect of mobility (with incorporated Handoff) on the performance of TCP has been simulated. From the analysis, it is seen that the throughput of TCP degrades with increasing the speed of the mobile station. We have also analyzed the behaviour of these five TCP clones in the presence of both high bit error and handoff. From the analysis, it is observed that the throughput of these five TCP clones seriously degrades because of heavy packet losses due to both handoffs and high bit error.

VII. FUTURE WORK

In future, the efficiency of the TCP agents can be studied after introducing some amount of mobility to the nodes and the second is to analyze behaviour of TCP in cellular mobile environment considering coverage, battery power, and other impacts that are found in cellular mobile environment.

ACKNOWLEDGMENT

I am deeply thankful to my Guide Prof. Sanjay Sharma of Computer Science and my all friends whose help, stimulating suggestions and encouragement helped me in all the time for my review.

REFERENCES

- [1] Postel J., "Transmission Control Protocol", RFC793, Internet Request for Comments 793, Sept. 1981.
- [2] Stevens, Richard W., "TCP/IP Illustrated", 2001.
- [3] Barakat C., Altman E., Dabbous W., "On TCP performance in a heterogeneous network: a survey", 1999.
- [4] W. Richard Stevens. TCP/IP Illustrated, Volume 1: The Protocols, Addison-Wesley, 1994
- [5] K. Fall and S. Floyd, "Simulation-based comparison of Tahoe, Reno, and SACK TCP," Computer Communication Review, vol. 26, pp. 5--21, July 1996.
- [6] Jitendra Padhye , Victor Firoiu , Donald F. Towsley , James F. Kurose, "Modeling TCP Reno performance: a simple model and its empirical validation," IEEE/ACM Transactions on Networking (TON), v.8 n.2, p.133-145, April 2000
- [7] S.Floyd, T.Henderson "The New-Reno Modification to TCP's Fast Recovery Algorithm" RFC 2582, Apr 1999.
- [8] Lawrence S. Brakmo and Larry L. Peterson, "TCP Vegas: End to end congestion avoidance on a global Internet," Ekiz, N., A.H. Rahman and P.D. Amer, 2011. Misbehaviors in TCP SACK generation. ACM SIGCOMM Computer Communication Review, 41(2): 16-23.
- [9] Henna, S., 2009. A Throughput Analysis of TCP Variants in Mobile Wireless Networks, pp: 279-284.IEEE.
- [10] W. Stevens, "TCP Slow Start, Congestion Avoidance Fast Retransmit Algorithm", IETF RFC 2001, January 1997.
- [11] Lawrence, S. Brakmo, Student Member IEEE and Larry L. Peterson "TCP Vegas end congestion avoidance on a Global Internet, October 1995.
- [12] S.Floyd, T.Henderson "The New- Reno Modification to TCP's fast Recovery Algorithm" RFC 2582, Apr 1999.

AUTHORS PROFILE



Nishant Chaurasia born in 1987 in Gwalior, India. He awarded B.E in Computer Science and Engineering from the Rajiv Gandhi Technical University, Bhopal, India in 2009. From 2009-present, He has been M.Tech student in Computer Science and Engineering, at the Rajiv Gandhi Technical University, Bhopal, India.



Prof. Sanjay Sharma is an Assistant Professor of Computer Science Department in Oriental Institute of Science and Technology, Bhopal, Madhya Pradesh, India. He obtained his M.Tech degree from RGPV University. His research interest is in the field of MANETs.

Global Illumination Using Ray Tracing

K. M. Patel

(Computer Engineering, School of Engineering/RK University, India)

ABSTRACT

Hardware like rasterization provides interactive frame rates for rendering dynamic scenes, but lot of abilities of ray tracing required for efficient global illumination simulation. Existing ray tracing based methods yield high quality renderings but are far too slow for interactive use. We present a global illumination algorithm and C# OOP based programs that perfectly scales, has minimal preprocessing and communication overhead, applies highly efficient sampling techniques and benefits from shooting coherent groups of rays. Thus a performance is achieved that allows for applying arbitrary changes to the scene, while simulating global illumination including shadows from area light sources, specular effects, and caustics at interactive frame rates. Ceasing interaction rapidly provides high quality renderings.

Keywords: Illumination; Ray Tracing; Refraction; Reflection, Shadow; Texture;

I. INTRODUCTION

Overview

In computer graphics, ray tracing is a technique for generating an image by tracing the path of light through pixels in an image plane and simulating the effects of its encounters with virtual objects. The technique is capable of producing a very high degree of visual realism, usually higher than that of typical scan-line rendering methods, but at a greater computational cost. This makes ray tracing best suited for applications where the image can be rendered slowly ahead of time, such as in still images and film and television special effects, and more poorly suited for real-time applications like video games where speed is critical. Ray tracing is capable of simulating a wide variety of optical effects, such as reflection and refraction, scattering, and chromatic aberration.

An image with the following characteristics can be considered as realistic image:

- Light effects (One or more)
- Shadowing
- Refraction of lights
- Refraction
- Specular Reflection

By applying the concepts of local illumination and global illumination we can produce photo-realistic image. Illumination refers interaction of light with surface points to determine their final color and brightness

The governing principles for computing the illumination

- Light attributes (light intensity, color, position, direction, etc.)

- Object surface attributes (color, reflectivity, transparency, etc)
- Interaction among lights and objects (object orientation)

Interaction between objects and eye (viewing dir.)

Global Illumination:

It is a method (algorithm) of computation for light calculation in the scene which, takes in to account the light bounces from the neighboring surfaces, along with the normal illumination of direct lights. In Other words GI calculates the Indirect light also, thus it makes the renders more photo-realistic. Examples of GI methods are Radiosity and Ambient Occlusion in Blender and on a general scale Radiosity, Ray tracing and Caustics all use different GI algorithms.

Incorporating global illumination is important step towards realism in computer graphics. There are many areas where graphics realism is high priority. In this thesis, recursive raytracing only supports some of basic primitive objects (plane, cube and sphere).

Basics of Ray Tracing

Camera is defined by its Position in the Scene (a 3D Vector), a point to LookAt (the purple arrow) which points at the center of the Viewport, and the tilt of the Camera (the blue arrow) called Top (it usually points strait up).

- The *Light* is defined by its Position in the scene and the *Color* of the light denoted by the light bulb.

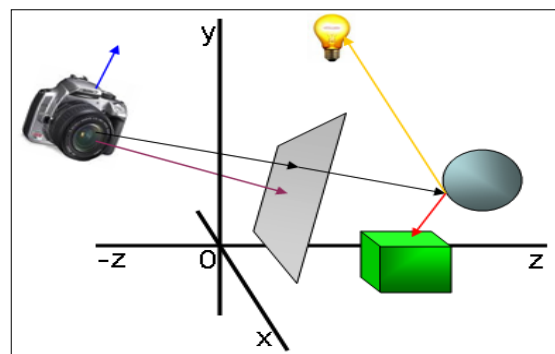


Fig-1 : Ray Tracing Example

- The Viewport is derived from the Camera settings and is defined by the LookAt point of the Camera and a fixed size of (-3,-3)-(3,3).
- A *Ray* is defined by a starting Position, and a *Direction* in which the Ray is casted.

The Background is defined by a Color that will be displayed if it is not covered by any other shape.

In a typical raytracing setting a Ray is casted through each pixel in the viewport into the scene, in this example the

black arrow. The raytracer will try and find out if the ray is intersecting with any object/shape in the scene. In this example it will intersect with the Sphere. Otherwise it will simply display the background color. To determine the color to display for the pixel, a number of techniques can be used and mixed referred as shading effects.

Shading effects and Color

Because ray tracing scenes require usually a high precision of calculations, so the R, G and B components are scaled down to a floating point number between 0 and 1. Also some of the common arithmetic operators have been overridden, so it will be easier to add, multiply and blend Colors.

The most basic technique is by simply displaying the intrinsic color of the Sphere itself. This is called Ambient lighting. Ambient light is the so called background light that will light up all objects in the scene slightly (see figure a).

The color is also influenced by the amount of light emitted by surrounding other light sources. In this case the light bulb will light up the surface of the sphere depending on how well the surface is exposed to the light. The yellow arrow shows the direction in which the light is traced back to its source. Based on this direction, and the direction the surface of the sphere is facing, the amount of light is calculated. This is called Diffuse light. It gives a nice shading effect (see figure b).

Additionally the effects can be enhanced by introducing Highlights, if the surface is somewhat reflective and the rays from the light source are reflected on the shape's surface straight into the camera, a highlight appears: usually a very shiny and bright color (see figure c).

Now for even more effects we can add Reflection and Refraction. In the case of Reflection, the Ray casted from the Camera is reflected on the surface of the sphere onto the green box denoted by the red arrow. This means the particular pixel the Ray travels through will light up with a somewhat greenish color also: the box is reflected into the sphere (see figure e).

Refraction is somewhat more complicated. Refraction is the effect of a ray bending when traveling through a different Material. This applies to transparent objects/shapes. An example of this is a glass ball, where the light rays are bent when traveling through the ball.

Another type of effect added to the scene is Shadows. Shadows do not add color to a pixel, but instead reduce the amount of Color. To find out if an intersection with an object is in a shadow of another object, simply trace the path back to the light source from intersection point (yellow arrow) and find out if any object is blocking it (does it intersect with any other object than the light source?). If it is blocked, simply reduce the amount of light by a factor.

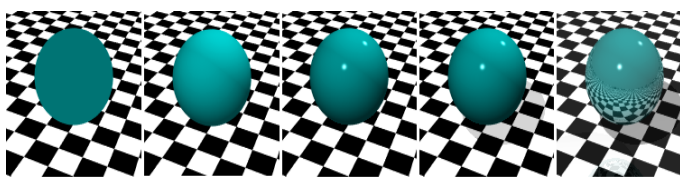


Fig-2 : Shading effects: a) Ambient, b) Diffuse, c) Highlights, d) Shadows and e) Reflection (notice the reflection on the floor also)

II. STEPS TO DETERMINE THE SHADING EFFECT:

The following steps to be used for evaluating shading effects for different cases:

- put the mathematical equation for the ray into the equation for the object and determine if there is a real solution.
- If there is a real solution then there is an intersection (hit) and we must return the closest point of intersection and the normal (**N**) at the intersection point
- For a shadow ray we must return whether any ray-object intersection is closer than the ray-light intersection
- For a ray tested against a boundary volume, we just return a simple hit or no hit
- For texture mapping we need the intersection point relative to some reference frame for the surface

Ambient Light:

- Each light source has an ambient light contribution (I_a)
- Different objects can reflect different amounts of ambient (different ambient reflection coefficient K_a , ($0 \leq K_a \leq 1$))
- So the amount of ambient light that can be seen from an object is:

$$Ambient = I_a \times K_a$$

Diffuse Light:

The illumination that a surface receives from a light source and reflects equally in all direction. It does not matter where the eye is because it distributes the light in all direction equally.

Lambert's law: the radiant energy D that a small surface patch receives from a light source is:

$$D = I \times \cos(\theta)$$

Specular:

It appears as bright spot on the object as shown in figure,

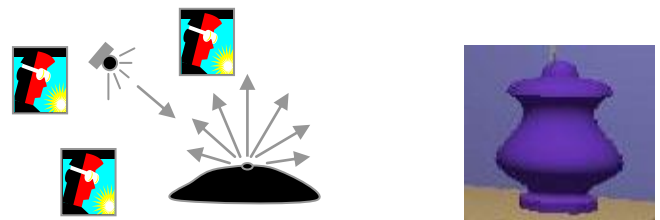


Fig-3 : Diffuse Light Effect

the result of total reflection of the incident light in a concentrate region. How much reflection you can see that depends on position of an observer.

$$specular = K_s \times I \times \cos(\theta)$$

Where,

K_s : specular reflection coefficient

N : surface normal at P

I : light intensity

θ : angle between V and R

L : Light Source

Reflection:

Mirror like reflections are made by calling both the intersection and illumination routines as part of the illumination calculation. We create a reflected ray in the correct direction and call both the intersection routine and the illumination routine for that ray. To get what can be seen

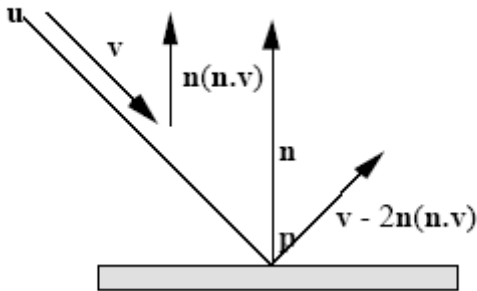


Fig-4: Reflection

in that direction from this surface. Having got back the colour of this ray, our illumination routine has to include it in the total colour calculation for the surface. We introduce another coefficient, k_s , which is multiplied by the brightness of the reflected ray and added to the total for the current surface. The original and reflected rays make equal angles with the surface normal. The direction of the reflected ray can be found easily using vectors. Assuming that the normal is represented by a unit vector, n , the component of the ray direction, v , in the direction of the normal is:

$$(v \cdot n) * n$$

Reflection has the effect of reversing this component without changing the component parallel to the surface. So the reflected ray is:

$$p + (v - 2(v \cdot n) n)t$$

Refraction

Water like transparent refraction made by calling both the intersection and illumination routines as part of the illumination calculation. We create a refracted ray in the correct direction and call both the intersection routine and the illumination routine for that ray that determine by the following equation:

$$T = [\frac{1}{\mu_2} (N \cdot I) - (1 - \frac{1}{\mu_2^2} (1 - (N \cdot I)^2))^{0.5}] \cdot N - \frac{1}{\mu_2} \cdot I$$

III..TEXTURE

One of the important factor to get more realism is texture. To make any scene look even more realistic one must be able to add textures to any shapes. Basically texture can be compared to a piece of gift wrapper, which is wrapped around the object. There are two types of texture materials: a texture material based on a colormap or image and a texture material that is calculated (e.g. the chessboard effect).

Textures are flat and therefore require two coordinates to determine the color to display: often the u and v notation is used. The (u,v) coordinates are mapped onto $(-1,-1)$ to $(1,1)$ and from there on the color is either read from the colormap, or calculated respectively. The difficulty lies in calculating

the (u,v) coordinates from an intersection point with the shape. Depending on the shape, the (u,v) coordinates need to be calculated in different ways, but this is up to that programmer to implement.

IV.ANTI-ALIASING

One other important feature to have in a Raytracer is the ability to cope with anti-aliasing. Anti-aliasing is a technique to soften huge color differences between neighbouring pixels, so it will look more soothing for the eye. Several techniques can be used to counter this aliasing effect. A quick but dirty technique is to simply apply a "mean filter". The pixel will get the mean color value of neighbouring pixels. This is implemented as the 'Quick' AntiAliasing method in this thesis.

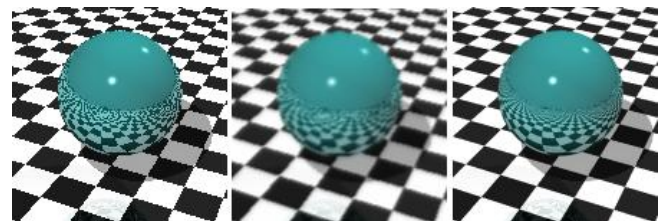


Fig-5: AntiAliasing methods: a) None, b) Mean filter, c) Monte Carlo sampling

This results is a smoothed image, however the image may also appear a bit vague/blurry. A much nicer way of anti-aliasing is using the 'Monte-carlo' method. The idea here is instead of casting a single ray into the scene through a pixel on the viewport, instead we cast multiple rays through a single pixel, scanning the neighbourhood and taking the average color of those. Although the method is slower, since we are now casting multiple rays for a single pixel, the accuracy is much better, resulting in much smoother but sharp anti-aliased images as shown in the figure below.

V. SHAPES

Have you ever wondered why in every raytraced image you always see a lot of spheres? Well apart from the nice shading effects on a sphere, more importantly, the intersection of a ray with a sphere can be calculated very fast. This is probably the most important aspect of a shape definition: how easy is it to calculate the intersection with the shape. Secondary to that, how easy is it to calculate its surface normal vector.

Calculating the intersection of a ray with arbitrary shapes turns out to be rather difficult. Instead different methods have been invented such as Voxel techniques or Marching cubes in order to determine the intersection points.

This raytracer however has not been optimized much for performance, and therefore only supports a limited set of shapes: Plane, Sphere and a Cube.

Scene contains Box (texture), Sphere (texture, reflective material) and plane (texture) with shadow and reflection effect

Ray-Sphere Intersection

A ray is defined by: $R(t) = R_0 + t * Rd$, $t > 0$

$R_0 = [X_0, Y_0, Z_0]$ = Position of ray

$Rd = [X_d, Y_d, Z_d]$ = Direction of ray

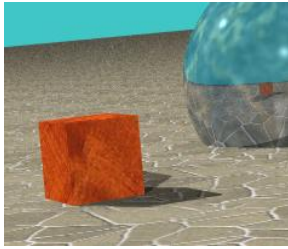


Fig-6 : Scene Example

A sphere can be defined by its center and radius with
 $S_c = [X_c, Y_c, Z_c]$

So, a sphere of radius S_r is:
 $S =$ the set of points $[X_s, Y_s, Z_s]$,
 where $(X_s - X_c)^2 + (Y_s - Y_c)^2 + (Z_s - Z_c)^2 = S_r^2$

To solve algebraically, substitute the ray equation into sphere equation and solve for t .

For a ray:
 $X = X_0 + X_d * t$
 $Y = Y_0 + Y_d * t$
 $Z = Z_0 + Z_d * t$

putting X, Y, Z into the sphere equation for X_s, Y_s, Z_s
 $(X_0 + X_d * t - X_c)^2 + (Y_0 + Y_d * t - Y_c)^2 + (Z_0 + Z_d * t - Z_c)^2 = S_r^2$

OR

$$A * t^2 + B * t + C = 0 \text{ (Quadratic Form)}$$

Where:
 $A = X_d^2 + Y_d^2 + Z_d^2$
 $B = 2 * (X_d * (X_0 - X_c) + Y_d * (Y_0 - Y_c) + Z_d * (Z_0 - Z_c))$
 $C = (X_0 - X_c)^2 + (Y_0 - Y_c)^2 + (Z_0 - Z_c)^2 - S_r^2$

Note: If $|R_d| = 1$ (normalized), then $A = 1$. So we can compute S_r^2 once.

So with $A = 1$, the solution of the quadratic equation is

$$t_0, t_1 = (-B \pm \sqrt{B^2 - 4 * C}) / 2$$

where t_0 is for (-) and t_1 is for (+)

If the discriminant is < 0.0 then there is no real root and no intersection. If there is a real root ($\text{Disc.} \geq 0.0$) then the smaller positive root is the closest intersection point. So we can just compute t_0 and if it is positive, then we are done, else compute t_1 . The intersection point is:

$$R_i = [x_i, y_i, z_i] = [x_0 + x_d * t_i, y_0 + y_d * t_i, z_0 + z_d * t_i]$$

Unit Normal at surface is
 $SN = [(x_i - x_c) / S_r, (y_i - y_c) / S_r, (z_i - z_c) / S_r]$

VI. RAY TRACING ALGORITHM

```
RAYTRACE( ray )
{
    find closest intersection
    cast shadow ray, calculate colour_local
    colour_reflect = RAYTRACE( reflected_ray )
}
```

```
colour_refract = RAYTRACE( refracted_ray )
colour = k1 * colour_local + k2 * colour_reflect
        + k3 * colour_refract
return( colour )
}
```

Limitations of ray tracing

The underlying idea of ray tracing is imitating what light rays do. But the real behaviour of light is rather complicated. We can cast a ray at a point light source to find shadows, but real light sources are not points. As a result, shadows are soft rather than sharp. There is no known cheap way to get realistic shadows from a ray tracer.

VII. IMPLEMENTATION DETAILS & RESULTS

In this work, module (Global Illumination using Ray Tracing) have been implemented as given below:

Language : C# (C-Sharp) .NET Framework v2.0

Configuration:

To run this module, there is no need to configure any additional library. But .NET 2005 must be installed on the system. Open the project in .NET, compile and run it. GUI of this module is as shown below:

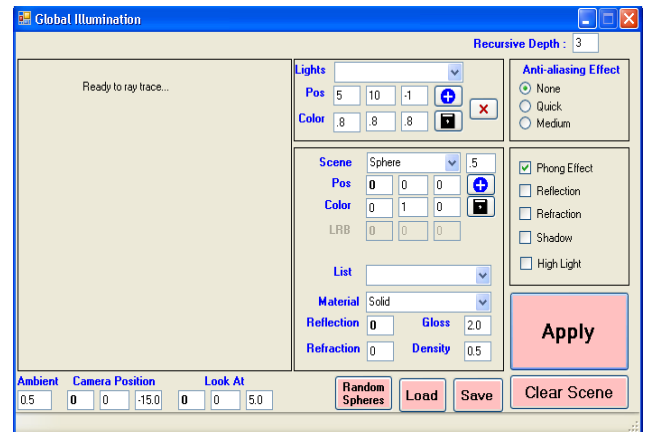
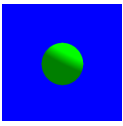
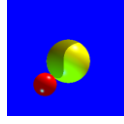


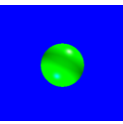
Fig-7: User Interface of Ray Tracing

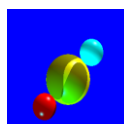
Experimental Results:

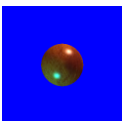
Output	Description
Light	: -Nil-
Object	: Sphere
Surface	: Solid
Type	: 0
Reflection Coefficient	: 0
Reraction Coefficient	: 0
Density :	: 0
(Highlight) Gloss :	: 0

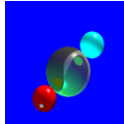
	Light	: 1 (10,5,-1)
	Object	: Sphere
	Surface	: Solid
	Type	
	Reflection Coefficient	: 0
	Reraction Coefficient	: 0
	Density :	: 0
(Highlight)	: 0	
Gloss :		

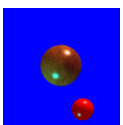
Shadow: 	Light	:1: (10,5,-1), 2: (-10,-5,-5)
	Object	: Sphere, Sphere
	Surface	: Solid, Solid
	Type	
	Reflection Const.	: 0, 0
	Reraction Const.	: 0, 0
	Density :	: 0, 0
(Highlight)	: 1.0, 1.0	
Gloss :		

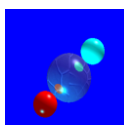
	Light	:1: (10,5,-1), 2: (-10,-5,-5)
	Object	: Sphere
	Surface	: Solid
	Type	
	Reflection Coefficient	: 0
	Reraction Coefficient	: 0
	Density :	: 0
(Highlight)	: 1.0	
Gloss :	: 2.0	

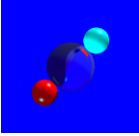
Two Shadows 	Light	:1: (10,5,-1), 2: (-10,-5,-5)
	Object	: Sphere, Sphere, Sphere
	Surface	: Solid, Solid, Solid
	Type	
	Reflection Const.	: 0, 0, 0
	Reraction Const.	: 0, 0, 0
	Density :	: 0, 0, 0
(Highlight)	: 1.0, 1.0, 1.0	
Gloss :		

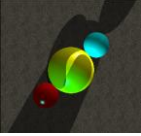
	Light	:1: (10,5,-1), 2: (-10,-5,-5)
	Object	: Sphere
	Surface	: Texture : Wooden
	Type	
	Reflection Coefficient	: 0
	Reraction Coefficient	: 0
	Density :	: 1.0
(Highlight)	: 1.0	
Gloss :	: 1.0	

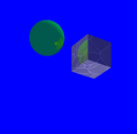
Reflection + Shadow: 	Light	:1: (10,5,-1), 2: (-10,-5,-5)
	Object	: Sphere, Sphere, Sphere
	Surface	: Solid, Solid, Solid
	Type	
	Reflection Const.	: 0.3, 0, 0
	Reraction Const.	: 0, 0, 0
	Density :	: 0, 0, 0
(Highlight)	: 1.0, 1.0, 1.0	
Gloss :		

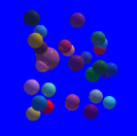
	Light	:1: (10,5,-1), 2: (-10,-5,-5)
	Object	: Sphere, Sphere
	Surface	: Texture : Wooden, Solid
	Type	
	Reflection Const.	: 0, 0
	Reraction Const.	: 0, 0
	Density :	: 0, 0
(Highlight)	: 1.0, 1.0	
Gloss :		

Relection + Texture: 	Light	:1: (10,5,-1), 2: (-10,-5,-5)
	Object	: Sphere, Sphere, Sphere
	Surface	: Texture, Solid, Solid
	Type	
	Reflection Const.	: 0.3, 0, 0
	Reraction Const.	: 0, 0, 0
	Density :	: 0, 0, 0
(Highlight)	: 1.0, 1.0, 1.0	
Gloss :		

Refraction + Shadow: 	Light	:1: (10,5,-1), 2: (-10,-5,-5)
	Object	: Sphere, Sphere, Sphere
	Surface	: Solid, Solid, Solid
	Type	
	Reflection	: 0, 0, 0
Const.		
Reraction	: 1.0, 0, 0	
Const.		
Density :	: 0, 0,0	
(Highlight)	: 1.0, 1.0, 1.0	
Gloss :		

Plane + Shadow 	Light	:1: (10,5,-1), 2: (-10,-5,-5)
	Object	: Sphere, Sphere, Sphere, Plane
	Surface	
	Type	: Solid, Solid, Solid, Texture
	Reflection	
Const.	: 0, 0, 0, 0	
Reraction	: 0, 0, 0, 0	
Const.		
Density :	: 0, 0,0, 0	
(Highlight)		
Gloss :	: 1.0, 1.0, 1.0, 0	

Cube + Sphere + Reflection: 	Light	:1: (10,5,-1), 2: (-10,-5,-5)
	Object	: Cube, Sphere
	Surface	: Texture, Solid
	Type	
	Reflection	: 0.3, 0.3
Const.		
Reraction	: 0, 0	
Const.		
Density :	: 0.5, 0	
(Highlight)	: 0, 0	
Gloss :		

Random Spheres + Reflection : 	Light	:1: (10,5,-1), 2: (-10,-5,-5)
	Object	: Thirty Spheres
	Surface	: All are Solid
	Type	
	Reflection	: 0.2 each
Const.		
Reraction	: 0 each	
Const.		
Density :	: 0 each	
(Highlight)	: 2.0 each	
Gloss :		

VIII. CONCLUSION

The most important aspects of a point based rendering system are the use of a compact and concise data representation, and a fast and efficient rendering algorithm. Reducing the workload of the renderer is important and there are several techniques for doing so. Culling is also a popular technique. If used with a tree based data representation, complete sub-trees can be culled, or pruned. Backface culling, coupled with the use of normal cones, provides an effective means of reducing the number of points to be considered. The inclusion of frustum and occlusion culling techniques may increase the overheads of the rendering algorithm, and may provide little or no benefit when the whole object is on screen, but they can speed up the rendering time for complex scene. Point hierarchies, represented as trees, are used by the point based rendering system mentioned. Although the implementation of the trees and their meanings may differ slightly, their result is the same. They provide storage solution in a manner that allow traversal quickly. The best solution would be to implement a tree based structure to store the points with octree and store information at each node.

ACKNOWLEDGMENT

Author is thankful to the Department of Computer Engineering and Information Technology of R.K.College of Engineering & Technology, Kasturbadham, Rajkot, for providing infrastructure facilities during progress of the work. Also thankful to Prof. D G Thakor & Prof. P. B. Swadas, assistant professors, BVM College of Engineering, for giving his moral and technical support to make completion of this work successfully. Authors are grateful to everyone who contributed with data to make this work successful.

REFERENCES

- [1] [1] J. Arvo and D. Kirk. Fast Ray Tracing by Ray Classification, *Computer Graphics (Proceedings of SIGGRAPH 87)*, 21(4):55–64, 1987.
- [2] M. Cohen and J. Wallace. *Radiosity and Realistic Image Synthesis*. Academic Press Professional, Cambridge, 1993.
- [3] E. Veach and L. Guibas. Metropolis Light Transport. In *Proceedings of SIGGRAPH 97*, Annual Conference Series, pages 65–76, 1997.
- [4] I. Wald, C. Benthin, and P. Slusallek. A simple and practical Method for Interactive Ray Tracing of Dynamic Scenes. Technical report, Saarland University, 2002.
- [5] I. Wald, C. Benthin, M. Wagner, and P. Slusallek. Interactive Rendering with Coherent Ray Tracing. *Computer Graphics Forum*, 20(3), 2001.
- [6] G. Ward. Adaptive Shadow Testing for Ray Tracing. In *Photorealistic Rendering in Computer Graphics (Proceedings of the 2nd Eurographics Workshop on Rendering)*, pages 11–20. Springer, 1994.
- [7] G. Ward and P. Heckbert. Irradiance Gradients. In *3rd Eurographics Workshop on Rendering*, Bristol, United Kingdom, May 1992.
- [8] T. Whitted. An improved illumination model for shaded display. *CACM*, 23(6):343–349, June 1980.
- [9] *Computer Graphics using OpenGL* by F.S. Hill, Edition-2, ISBN: 0321535863
- [10] *Procedural Elements for Computer Graphics* by David F. Rogers, Edition-3, ISBN:0070473714.

Implementation of Biometric Attendance Management System on Cloud Environment

Prassanna. J, Senthilkumar. MKS

*Department of Computer Science and Engineering
SRM University Kattankulathur, Tamilnadu, India*

Abstract

For any fast growing organization, tracking and monitoring employee time and attendance and preparing payroll are tedious, time consuming and risky as it is more prone to errors. Biometric time and attendance system is one of the most successful applications of biometric technology, serves an alternate for traditional manual signing process. The challenges in transforming towards biometric based attendance system from traditional system are, first, providing platform to store and maintain employee data, secondly the timely collection of huge amount of data from biometric machines, deployed as cluster of nodes, into a central database and finally to setting up a distributed computing environment to support the payroll process. We designed and implemented a reliable, scalable and cost effective Biometric Attendance payroll System over Cluster based Cloud technology, by which we successfully overwhelmed all these challenges. Our cloud based Biometric Attendance Manager (BAM) works with text files to collect data from different Biometric Terminals (BT) and process them to store in cloud based Enterprise Biometric Information Server (EBIS) to generate payroll.

Keyword: *Biometric Attendance, Cloud Computing, BAM, EBIS and BT.*

1. INTRODUCTION

BT is the acronym of Biometric Terminal which is used to collect the finger templates of the employees and attendance information based on the same. It interacts with the Biometric terminals to fetch the IN and OUT timings of the employees and stores in a text file. BAM is the acronym of Biometric Attendance Manager that reads the IN and out timings of the employees from text file, processes and stores the Biometric attendance data in to the Database Servers like EBIS. The profile data of employee and their attendance are very crucial which are used in the payroll process. Also, implementing Biometric Attendance is complex and expensive investment is needed. This paper tries to solve the barriers to store the huge amount of attendance data and process them for payroll using cloud technology.

2. BACKGROUND

A. Challenges in implementing Biometric Attendance

First, we need the database of the employees including important parameters like employee ID, name and department. Then, we need to collect the finger templates of each employee and store them. We need a platform to store the above information. Then the attendance of the employees like IN and OUT time which may contain thousands of records for each day should be stored in a centralized repository. We also need an application to read and process the biometric attendance data to prepare the payroll.

B. Cloud Technology

Cloud computing is the delivery of computing as a service rather than a product, whereby shared resources, software, and information are provided to computers and other devices as a utility (like the electricity grid) over a network (typically the Internet). Cloud computing provides computation, software applications, data access, data management and storage resources without requiring cloud users to know the location and other details of the computing infrastructure [1]. It uses the internet and central remote servers to store and maintain data and applications. It also allows consumers and businesses to use applications without installation and access their personal files at any computer with internet access. It increases the efficiency of computing by centralizing storage, memory, processing and bandwidth. There are three fundamental models in Cloud computing. They are SaaS (Software as a Service), PaaS (Platform as a Service) and IaaS (Infrastructure as a Service). A simple example of Cloud computing is Gmail and Yahoo as we do not need any separate software or hardware to use them.

3. SYSTEM DESIGN AND IMPLEMENTATION

In the following figure 1, we show the overview of the system. Each organization / institution has one or more Biometric Terminals (BT) to collect the finger templates and punching of IN and OUT. The number of BTs is flexible and based on the strength of the employees. This is the basic source to provide data. BAM is the Biometric Attendance Manager to read and process the data and store them. All organizations are connected with BAM under 100 Mbps network bandwidth. The EBIS is the enterprise system to hold the employee information and thousands of Biometric data.

BAM Middleware

The BAM Middleware is a system that handles the other functionalities like Leave Application Process and Data Replication Service related with BAM.

EBIS

The Enterprise Biometric Information Server is a high level database system that holds lakhs of biometric records. The data to this server is fetched from many BT (Biometric Terminals) of various locations.

B. System Workflow

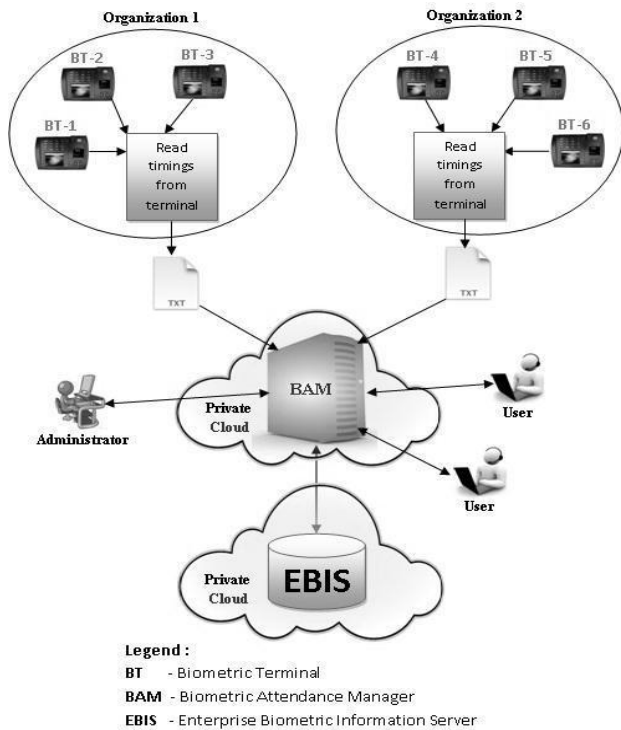


Figure – 1

A. System Architecture

BAM Server

As shown in Figure – 2, the BAM is developed in Cloud environment. The data storage is built on enterprise Microsoft SQL servers. This can be described as PaaS (Platform as a Service).

We have extended the Saas (Software as a Service) based on PaaS. The BAM system is a web based and user friendly interface. The users can easily understand and interact with the BAM system to get their attendance on various forms.

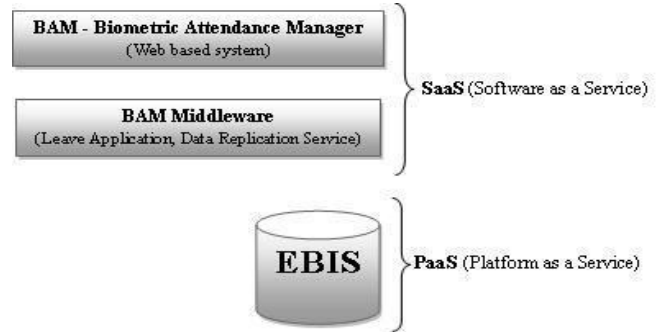


Figure - 2

The workflow of the system is shown using the figure - 3. At first, the system authenticates the users with a user friendly interface by getting user name and password. The user roles are also identified. Based on the roles, different access permissions are set on the users. Secondly, according to permissions the users can view their attendance; All Heads can view the attendance of the employees under them. The administrator can view all the records of all employees. Third, all the employees can apply for leave including CL (Casual Leave), EL (Earn Leave) and VL (Vacation Leave). Then the heads will approve the leave applications of the corresponding employees under them. It is shown in figure -4.

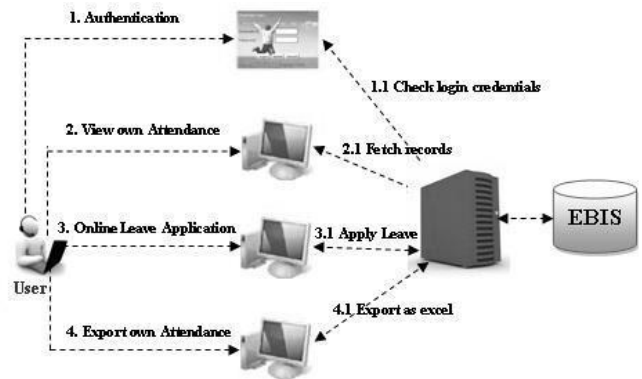


Figure – 3

The final approval is made by the attendance admin. In each stage, the employees can view the status of their leave applications in their login. All the employees can export the attendance information as excel file if required. The attendance admin can finally generate the payroll by integrating the biometric attendance with leave applications. This is shown in figure-4.

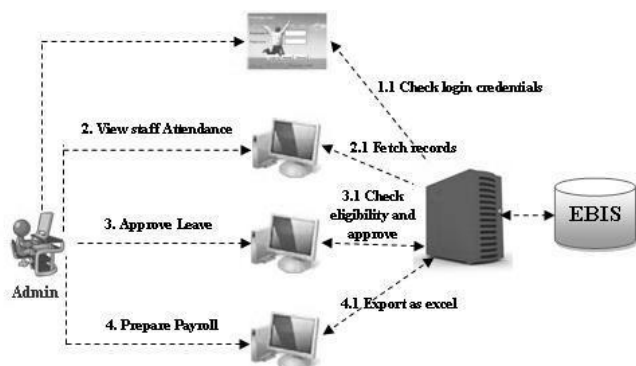


Figure – 4

4. COMPARISON WITH EXISTING SYSTEM

We have compared our system with existing one and found lot of advantages over that.

Experiment 1: Compare the cost effectiveness with the existing system. In this experiment, we compare the cost for organization with own servers and applications with organization under Cloud. It clearly shows that the organization under cloud spent less than the others since it is pay per use. Also there is no head ache over Hardware and Software maintenance as it is taken care by the Cloud provider themselves.

Cost Effectiveness comparison		
Resource	Organization with own Resource setup	Organization under Cloud
Server	400000	40000
Application	1200000	40000

The following graph clearly shows the graphical representation of the cost effectiveness.

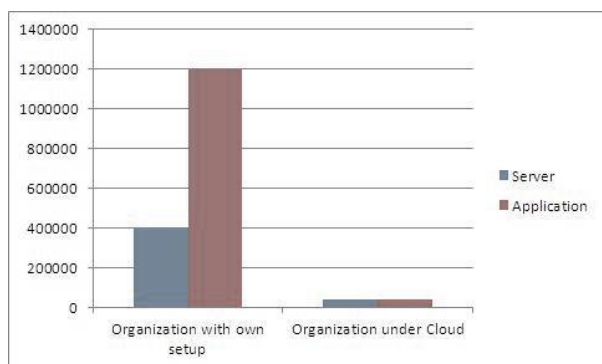


Figure – 5

Experiment 2: Then, we experiment our system with existing one in terms of process effectiveness in preparing payroll. With the current system, it is very complex to generate payroll every month since the integration of attendance data and leave applications is taking much time. Our BAM middleware system simplifies the process by integrating the both to quickly prepare the payroll. The accuracy of the data is also found improved.

Process effectiveness		
*	Manual Attendance	Biometric Attendance
Payroll process (days)	15	1
Data Accuracy	0.95	0.99

The corresponding graph in figure-6 for the above table shows it clearly that the payroll processing time is decreased and data accuracy is also improved.

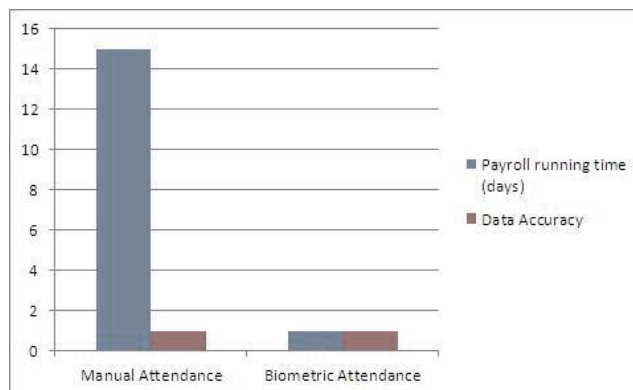


Figure - 6

5. CONCLUSION

From our experience, we conclude that the BAM is a flexible, scalable, cost effective, efficient and easily manageable system.

Scalability: We can add as many numbers of BT and users we want without doing much modification in the system.

Cost Effective: The cost effectiveness is another important factor in our system. We need not spent for dedicated servers for application and database as everything managed by the Cloud providers.

Efficient: All the users can view the attendance and the status of their leave applications. We can generate the monthly payroll in ease.

REFERENCES

- [1] Wiki electronic media record, http://en.wikipedia.org/wiki/Cloud_computing
- [2] Cloud Computing by Nick Antonopoulos
- [3] You Tube electronic media, www.youtube.com/watch?v=ae_DKNwK_ms
- [4] Advances in Biometric Person Authentication by STAN Z. LI
- [5] IBM electronic media, www.ibm.com/cloud
- [6] All is clouded by desire by Alan A Block
- [7] Online electronic media record, http://wiki.answers.com/Q/What_is_biometric_time_attendance_system
- [8] Biometric service providers, www.synel.com/
- [9] Wiki electronic media record, <http://en.wikipedia.org/wiki/Biometrics>
- [10] Biometrics: Identity Verification in a Networked World by SamirNanavati

On The Analysis of Aligned MHD Plane Flow in Porous Media in Presence of Magnetic Field

¹Naji Qatanani, ²Amjad Barham, ³Mai Musmar

¹*Department of Mathematics, An-Najah National University
Nablus-Palestine*

²*Palestine Polytechnic University, Hebron-Palestine*

³*Al-Quds Open University, Nablus-Palestine*

Abstract

An attempt is made to study the steady MHD plane aligned flow through porous media in the presence of a magnetic field. An alternative approach to the Riabouchinsky method is developed for this flow problem. The proposed method will reduce the number of arbitrary constants arising when using the Riabouchinsky method. Consequently, many of the restrictive assumptions used in assigning values to the arbitrary constants are no longer needed. The analytical solution of the compatibility equations are determined leading to the solution of the velocity components and the pressure distribution for this problem.

Keywords: Aligned flow, porous medium, Riabouchinsky flow, vorticity-stream function.

1. Introduction

In recent years, the study of flow through porous media has generated considerable interest because of its numerous applications in the basic and applied sciences, including the study of groundwater flow movements in the porous earth layer, irrigation problems, the prediction of oil reservoir behavior, and the biophysical sciences, where the human lungs, for example are modeled as porous layers [5,8].

One of the particular importance of this work is the flow through porous media in the presence of a magnetic field. This type of flow may find some industrial applications in the design of filtration systems, in addition to the study of lubrication mechanism is enhanced through the introduction of porous lining into the mechanism and the imposition of a magnetic field in a transverse direction to the flow. Other applications to this type of flow include the occurrence of this type of flow in nature. Typically, the magnetic field is available everywhere on earth, hence, the study of any natural flow phenomena mandates taking into account the magnetic effects in the flow equations. The interest in this field dates as far back as 1865 by Darcy and currently one finds various models governing different types of fluid flow in various porous structures. The main type of single-phase flow models have been developed and reviewed by [6]. A vast amounts of research has been carried out on the motion of electrically conducting fluids moving in a magnetic field. Mathematical complexity of the phenomenon induced many researches to adopt a rather useful alternative technique of investigating special classes of flows such as aligned or parallel flows, crossed or orthogonal flows, (for more details see for example [1-4]). They studied finitely conducting orthogonal MHD plane flows. In which they discussed that the velocity and magnetic field vectors are mutually orthogonal everywhere in the flow region. In this paper, we consider aligned fluid flow through porous media in the presence of a magnetic field. The aim is to analyze the nonlinear model in an attempt to find possible solutions corresponding to a particular form of the stream function. The choice of the stream function in this work is one that is linear with respect to one of the independent variables. This type of flow is referred to as the Riabouchinsky flow. In this case, the two dimensional flow equations, written as a fourth order partial differential equations in terms of stream function, may be replaced by fourth order ordinary differential equations in two unknown functions of a single variable. Solutions to the coupled set are then obtained based on the knowledge of particular integrals of one of the equations. A different type of flow may then be studied with the knowledge of one of the functions. Riabouchinsky [11] assumed one of the functions to be zero and studied the resulting flow which represents a plane flow in which the flow is separated in the two symmetrical regions by a vertical or a horizontal plane. In addition to the study of Navier-Stokes flows and their applications [12], Riabouchinsky flows have also received considerable attention in the study of non-Newtonian flows [7] and in magnetohydrodynamics [9]. The approach used to solve the resulting coupled set of order ordinary differential equations suffers from some limitations, among which is its dependence on the knowledge of the particular solutions involve a number of arbitrary constants, the determination of which usually involves making many restrictive assumptions on the flow. A major disadvantage of the previous traditional approach is its inapplicability to the analysis of the Darcy-Lapwood-Brinkman (DLB) model. In this work, a modest modifications of the previous approach is employed and a methodology that is capable of handling a plane aligned flow problem is developed. The developed methodology overcomes some of the disadvantages of the traditional approach used for the Navier-Stokes equations and the Brinkman-type flow problems in porous media [10].

2. Aligned MHD Plane Flow

2.1 Basic Equations

The steady plane flow of an incompressible electrically conducting viscous fluid of infinite electrically conductivity in the presence of a magnetic field is governed by the following system of partial differential equations:

$$\operatorname{div} \vec{V} = 0 \quad (2.1)$$

$$\rho(\vec{V} \cdot \operatorname{grad} \vec{V}) = -\operatorname{grad} p + \mu_1 \nabla^2 \vec{V} - \frac{\mu_2}{k_1} \vec{V} + k_2 (\operatorname{curl} \vec{H} \times \vec{H}) \quad (2.2)$$

$$\operatorname{curl} (\vec{V} \times \vec{H}) - \frac{1}{k_2 \sigma} \operatorname{curl} \operatorname{curl} \vec{H} = 0 \quad (2.3)$$

$$\operatorname{div} \vec{H} = 0. \quad (2.4)$$

Where \vec{V} is the velocity vector field, \vec{H} is the magnetic vector field, p is the pressure, σ is the electrical conductivity, k_1 is the medium permeability to the fluid, k_2 is the magnetic permeability, μ_1 is the fluid viscosity, μ_2 is the viscosity of fluid in the porous medium and ρ is the fluid density. It is required to solve this system for the unknowns \vec{V} , \vec{H} and p .

2.2 Simplifying the governing equations

We consider a two-dimensional aligned flow x and y with the velocity field $\vec{V} = (u, v, 0)$, a magnetic field $\vec{H} = (0, 0, H)$ and $\frac{\partial}{\partial z} = 0$.

From the definition of aligned flows \vec{H} and \vec{V} are related by

$$\vec{H}(x, y) = F(x, y) \vec{V} \quad (2.5)$$

Where

$$(\vec{V} \cdot \nabla) F = 0. \quad (2.6)$$

Setting equation (2.5) into equation (2.2) we get

$$\begin{aligned} (\nabla \times \vec{H}) \times \vec{H} = & [-F^2 v (v_x - v_y) - v^2 F F_x + uv F F_y, \\ & F^2 u (v_x - v_y) - u^2 F F_y + uv F F_x, 0] \end{aligned} \quad (2.7)$$

Substituting equation (2.5) into equation (2.3) we obtain

$$\nabla \times (\vec{V} \times \vec{H}) = 0. \quad (2.8)$$

If $\frac{1}{k_2 \sigma} \neq 0$, then

$$\nabla \times (\nabla \times \vec{H}) = \nabla^2 \vec{H} = [\nabla^2 (Fu), \nabla^2 (Fv), 0] = 0$$

or

$$\nabla^2 (Fu) = \nabla^2 (Fv) = 0. \quad (2.9)$$

Inserting equation (2.5) into equation (2.4) we have

$$u F_x + v F_y = 0. \quad (2.10)$$

Using the results (2.7)-(2.9) into equation (2.2) yields

$$\rho \left\{ \left[\frac{1}{2} q^2 \right]_x - v (v_x - u_y) \right\} = -P_x + \mu_1 \nabla^2 u - \frac{\mu_2}{k_1} u + k_2 [-F^2 v (v_x - u_y) - v^2 FF_x + uv FF_y] \quad (2.11)$$

$$\rho \left\{ \left[\frac{1}{2} q^2 \right]_y + u (v_x - u_y) \right\} = -p_y + \mu_1 \nabla^2 v - \frac{\mu_2}{k_1} v + k_2 [F^2 u (v_x - u_y) - u^2 FF_y + uv FF_x] \quad (2.12)$$

where $q^2 = u^2 + v^2$ is the square of the velocity field. Substituting equation (2.10) into equation (2.11) and (2.12) gives

$$\rho \left\{ \left[\frac{1}{2} q^2 \right]_x - v (v_x - u_y) \right\} = -p_x + \mu_1 \nabla^2 u - \frac{\mu_2}{k_1} u + k_2 [-F^2 v (v_x - u_y) - (u^2 + v^2) FF_x] \quad (2.13)$$

$$\rho \left\{ \left[\frac{1}{2} q^2 \right]_y + u (v_x - u_y) \right\} = -p_y + \mu_1 \nabla^2 v - \frac{\mu_2}{k_1} v + k_2 [F^2 u (v_x - u_y) - (v^2 + u^2) FF_y]. \quad (2.14)$$

Then equation (2.1) takes the form

$$u_x + v_y = 0, \quad (2.15)$$

Thus the system of equations (2.1) to (2.4) are the flow equations governing the motion of a steady plane aligned flow of a viscous incompressible fluid of finite electrical conductivity. Equations (2.9), (2.13), (2.14) and (2.15) are the flow equations with the presence of a magnetic field.

In case of an infinitely electrical conductivity flow ($\frac{1}{k_2 \sigma} \rightarrow 0$) the diffusion equation (2.9) is identically satisfied.

However, for finitely electrical conductivity flows, the functions F , u and v must satisfy the additional condition (2.6).

2.3 Vorticity-stream function form of equations

To derive the compatibility or integrability equations for aligned flows by employing the flow equations given in section 2.2, where the stream function is linear with respect to x and y , we introduce the vorticity function $\omega(x, y)$ and the pressure function $h(x, y)$ defined respectively by

$$\omega(x, y) = v_x - u_y \quad (2.16)$$

$$h(x, y) = p + \frac{1}{2} \rho q^2, \quad (2.17)$$

Then equations (2.13) and (2.14) take the following forms respectively:

$$h_x - \rho v \omega = \mu_1 \nabla^2 u - \frac{\mu_2}{k_1} u + k_2 [-F^2 v \omega - (u^2 + v^2) FF_x] \quad (2.18)$$

$$h_y - \rho u \omega = \mu_1 \nabla^2 v - \frac{\mu_2}{k_1} v + k_2 [-F^2 u \omega - (u^2 + v^2) F F_y] \quad (2.19)$$

With the help of equations (2.15) and (2.16), equations (2.18) and (2.19) yield respectively

$$h_x - \rho v \omega = \mu_1 \omega_y - \frac{\mu_2}{k_1} u + k_2 [-F^2 v \omega - (u^2 + v^2) F F_x] \quad (2.20)$$

$$h_y + \rho u \omega = \mu_1 \omega_x - \frac{\mu_2}{k_1} v + k_2 [-F^2 u \omega - (u^2 + v^2) F F_y] \quad (2.21)$$

Now, letting $\psi(x, y)$ be the stream function defined in terms of the components as

$$\psi_y = u \quad \text{and} \quad \psi_x = -v. \quad (2.22)$$

Then we can see clearly that the continuity equation is identically satisfied since

$$u_x + v_y = \psi_{xy} - \psi_{yx} = 0$$

And the vorticity equation (2.16) becomes

$$\omega = -\nabla^2 \psi. \quad (2.23)$$

Equations (2.20) and (2.21) are then become in terms of the stream functions as follows:

$$h_x = \rho \psi_x \nabla^2 \psi - \mu_1 (\nabla^2 \psi)_y - \frac{\mu_2}{k_1} \psi_y - k_2 [F^2 \psi_x \nabla^2 \psi - (\psi_y^2 + \psi_x^2) F F_x] \quad (2.24)$$

$$h_y = \rho \psi_y \nabla^2 \psi + \mu_1 (\nabla^2 \psi)_x - \frac{\mu_2}{k_1} \psi_x + k_2 [-F^2 \psi_y \nabla^2 \psi - (\psi_y^2 + \psi_x^2) F F_y]. \quad (2.25)$$

A compatibility equation can be derived from equations (2.24) and (2.25) by using the integrability condition

$$h_{xy} = h_{yx}.$$

Thus, if we differentiate equation (2.24) with respect to y , and equation (2.25) with respect to x and using the integrability condition we obtain the compatibility equation

$$\rho \frac{\partial(\psi, \nabla^2 \psi)}{\partial(x, y)} - k_1 F^2 \frac{\partial(\psi, \nabla^2 \psi)}{\partial(x, y)} + k_1 F \frac{\partial(|\nabla \psi|^2, F)}{\partial(x, y)} - \frac{\mu_2}{k_1} \nabla^2 \psi + \mu_1 \nabla^4 \psi = 0 \quad (2.26)$$

where $\nabla^2 = \partial_{xx} + \partial_{yy}$, $\nabla^4 = \partial_{xxxx} + 2\partial_{xxyy} + \partial_{yyyy}$.

3.Reduction of the governing partial differential equations to ordinary differential equations

Once equation (2.26) is solved for $\psi(x, y)$, the vorticity function can then be calculated from equation (2.23), the pressure function $h(x, y)$ can be obtained from equation (2.24) and (2.25) while $p(x, y)$ is obtained from equation (2.17) and the velocity components can be determined from equation (2.22). Assume that the stream function $\psi(x, y)$ is linear and has the general form

$$\psi(x, y) = y f(x) + g(x), \quad (3.1)$$

where f and g are four times differentiable arbitrary functions. Substituting equation (3.1) into equation (2.26) and equating the coefficients of similar powers of y , lead to the following coupled set of fourth ordinary differential equations

$$\mu f^{(iv)} - \frac{\mu_2}{\rho k_1} f'' + (\rho - k_1 F^2) [f' f'' - f f'''] = 0 \quad (3.2)$$

$$\mu g^{(iv)} - \frac{\mu_2}{\rho k_1} g'' + (\rho - k_1 F^2) [g' f'' - f g'''] = 0. \quad (3.3)$$

For the particular case of aligned flows $k_1 \rightarrow \infty$, we get

$$\frac{\partial(F, \psi)}{\partial(x, y)} = 0. \quad (3.4)$$

The solution of equation (3.4) is either

$$F(x, y) = c \quad \text{or} \quad F(x, y) = F(\psi),$$

where C is arbitrary constant.

If $F(x, y) = c$, then equations (2.24), (2.25), (3.2) and (3.3) take the following forms respectively:

$$h_x = \rho \psi_x \nabla^2 \psi - \mu_1 (\nabla^2 \psi)_y - k_2 [f^2 \psi_x \nabla^2 \psi] \quad (3.5)$$

$$h_y = \rho \psi_y \nabla^2 \psi + \mu_1 (\nabla^2 \psi)_x - k_2 [f^2 \psi_y \nabla^2 \psi] \quad (3.6)$$

$$\mu f^{(1v)} + (\rho - k_1 c^2) [f' f'' - f f'''] = 0 \quad (3.7)$$

$$\mu g^{(1v)} + (\rho - k_1 c^2) [g' f'' - f g'''] = 0. \quad (3.8)$$

4. An alternative approach to the Riabouchinsky method

Using alternative approach presented in [10], two choices for the function $g(x)$ can be considered.

Case 1. $g(x) = g_1(x) = \alpha x^3$, where α is constant, then we obtain the corresponding equations:

$$f(x) = \frac{6\mu_1}{(\rho - k_1 c^2)} x^{-1} \quad (4.1)$$

$$\psi(x, y) = \frac{-6\mu_1}{(\rho - k_1 c^2)} x^{-1} y + \alpha x^3 \quad (4.2)$$

$$\omega(x, y) = \frac{12\mu_1}{(\rho - k_1 c^2)} x^{-3} y - 6\alpha x \quad (4.3)$$

$$u(x, y) = \frac{-6\mu_1}{(\rho - k_1 c^2)} x^{-1} \quad (4.4)$$

$$v(x, y) = \frac{-6\mu_1}{(\rho - k_1 c^2)} x^{-2} y - 3\alpha x^2 \quad (4.5)$$

$$h(x, y) = \frac{-6\mu_1}{(\rho - k_1 c^2)} x^{-2} + \frac{18\mu_1^2}{(\rho - k_1 c^2)} x^{-4} y^2 + \frac{9}{2} (\rho - k_1 c^2) \alpha^2 x^4$$

$$+ \frac{3\mu_1}{(\rho - k_1 c^2)} x^{-2} y^2 + 3\alpha x^2 y - 36\mu_1 \alpha y + \frac{36\mu_1^2}{(\rho - k_1 c^2)} x^{-4} \quad (4.6)$$

$$p(x, y) = \frac{-6\mu_1}{(\rho - k_1 c^2)} x^{-2} + \frac{18\mu_1^2}{(\rho - k_1 c^2)} x^{-4} y^2 + \frac{9}{2} (\rho - k_1 c^2) \alpha^2 x^4$$

$$\begin{aligned}
& + \frac{3\mu_1}{(\rho - k_1 c^2)} x^{-2} y^2 + 3\alpha x^2 y - 36\mu_1 \alpha y + \frac{36\mu_1^2}{(\rho - k_1 c^2)} x^{-4} \\
& - \frac{18\rho\mu_1^2}{(\rho - k_1 c^2)} x^{-2} - \frac{18\rho\mu_1^2}{(\rho - k_1 c^2)} x^{-4} y^2 - \frac{18\rho\alpha\mu_1}{(\rho - k_1 c^2)} y - \frac{9}{2} \rho \alpha^2 x^4. \quad (4.7)
\end{aligned}$$

Case 2. $g(x) = g_2(x) = \alpha e^{\beta x}$, where α and β are constants, then similar to the previous procedures we obtain the corresponding equations

$$f(x) = c_1 e^{\beta x} + \frac{\mu_1 \beta}{(\rho - k_1 c^2)}, \quad (4.8)$$

Where C_1 is arbitrary constant that can be determined by imposing one condition on the stream function ψ or by assuming various values to produce different flow patterns:

$$\psi(x, y) = c_1 e^{\beta x} + \frac{\mu_1 \beta}{(\rho - k_1 c^2)} y + \alpha e^{\beta x} \quad (4.9)$$

$$\omega(x, y) = -\beta^2 (\alpha + c_1 y) e^{\beta x} \quad (4.10)$$

$$u(x, y) = \psi_y(x, y) = c_1 e^{\beta x} + \frac{\mu_1 \beta}{\rho - k_1 c^2} \quad (4.11)$$

$$v(x, y) = -\psi_x(x, y) = -\beta (\alpha + c_1 y) e^{\beta x} \quad (4.12)$$

$$\begin{aligned}
h(x, y) &= -c_1 \mu_1 \beta e^{\beta x} - \frac{1}{2} (\rho - k_1 c^2) \alpha^2 \beta^2 e^{2\beta x} y \\
&+ (\rho - k_1 c^2) c_1 \beta^2 e^{2\beta x} y + (\rho - k_1 c^2) c_1^2 \beta^2 e^{2\beta x} y \quad (4.13)
\end{aligned}$$

$$\begin{aligned}
p(x, y) &= -c_1 \mu_1 \beta e^{\beta x} - \frac{1}{2} (\rho - k_1 c^2) \alpha^2 \beta^2 e^{2\beta x} + (\rho - k_1 c^2) c_1 \alpha \beta^2 e^{2\beta x} y \\
&+ (\rho - k_1 c^2) c_1^2 \beta^2 e^{2\beta x} y + \frac{2c_1 \mu_1 \beta}{(\rho - k_1 c^2)} e^{\beta x} + \frac{\mu_1^2 \beta^2}{(\rho - k_1 c^2)} + c_1^2 \beta^2 e^{2\beta x} y \\
&+ 2c_1 \beta^2 \alpha e^{2\beta x} y + \alpha^2 \beta^2 e^{2\beta x}. \quad (4.14)
\end{aligned}$$

5. Conclusion

In the current work we have presented analytical solutions for aligned MHD plane flow in porous media in the presence of a magnetic field. We have addressed some modifications to the solution methodology of the Navier-Stokes equations when the stream function is linear of the form $\psi(x, y) = y f(x) + g(x)$. This approach has the following advantages:

- The number of arbitrary constants arising when using the proposed method is considerably less than that for the Riabouchinsky method. Hence, many of the restrictive assumptions used in assigning values to the arbitrary constants are no longer needed.
- This new approach extends the ability to handle other flow models through porous medium in addition to the possibility of generating more solutions due to the method flexibility in choosing $g(x)$. It should be observed that this approach is also valid when the stream function is of the form $\psi(x, y) = x f(y) + g(y)$.

References

- [1] O. Chandna and M. Garg, On steady plane MHD flows with orthogonal magnetic and velocity fields, *Int. J. Engng. Sci.* ,17, pp. 251-257, 1979.
- [2] O. Chandna, R. Barron and K. Chew, Hodograph transformations and solutions in variably inclined MHD plane flows, *J. Engg. Math.* , 16, pp. 223-243, 1982.
- [3] O. Chandna, R. Barron and K. Chew, Finitely conducting orthogonal MHD plane flows, *Can. J. phys.* , 67, pp. 56-62, 1989.
- [4] O. Chandna and P. Nguyen, Hodograph transformation method and solutions in aligned MHD plane flows, *Int. J. Engng. Sci.* , 28(10), pp. 973-987, 1992.
- [5] M. Hamdan and R. Barron, Application of Van Mises coordinates in porous media flow, *ResearchReport M/cs 89-16* , September 1989.
- [6] M. Hamdan, Single-phase flow through channels, A review : Flow models and entry conditions, *J. Appl. Math. Comput.* 62 , pp. 203-222, 1994.
- [7] P. Kaloni and K. Huschilt, Semi-inverse solution of a non-Newtonian fluid, *Inter. J.Non-Linear Mechanics* 19(4), pp. 373-381, 1984.
- [8] F. Lapropulu, Riabouchinsky flows in magnetohydrodynamics, M.sc Thesis, University of Windsor, 1987.
- [9] Kaloni, P., Huschilt, K. : Semi-inverse solution of a non-Newtonian fluid, *inter. J. Non-linear Mechanics*, 19(4), 373--381, (1984).
- [10] N. Qatanani and M. Musmar, The mathematical structure and analysis of an MHD flow in porous media, *International Journal of Mathematical Engineering and Science*, 1(2), pp. 1-12, 2012.
- [11] D. Riabouchinsky, Some considerations regarding plane irrotational motion of liquid, *C. r. heed. Séance. Acad. SCI.* , Paris 179, pp. 1133-1136, 1924.
- [12] G. Taylor, On the decay of vortices in viscous fluid, *Philosophical Magazine* 46, pp. 671-674, 1923.

Modeling and Simulation of a Solid-State Breakers in Electric Power Distribution Systems by Using GUI-Based Environment of MATLAB/SIMULINK

Atul Kumar Dewangan

Department of Electrical Engineering, Kirodimal Govt. Polytechnic Raigarh, Chhattisgarh, India

ABSTRACT

This paper proposes detail of formulating solid-state breakers (SSB) in electric power distribution systems by using GUI-based environment of MATLAB/SIMULINK. Utilization of MATLAB software simplifies problem-solving complexity and also reduces working time. In this paper, a 22-kV power distribution feeder with a load having the SSB for protection is situated. A thyristor-based circuit breaker is modeled. Detail of the power circuit and its firing control part is demonstrated in graphical diagrams using elements of the MATLAB's Power System Blockset (PSB). Test against a fault condition to verify its use is carried out. The results show that, with a moderate sensing technique to monitor voltage and current of the protected feeder, the SSB can interrupt fault instantaneously.

Keywords: Solid-state breaker, Thyristor-based switch, MATLAB/SIMULINK, Power system blockset

I. INTRODUCTION

With the growing of demand of electric power, the distribution system is expanding continuously. This results in the high level of short-circuit currents. Therefore, the electric distribution cost such as devices, installation, operation and maintenance increases gradually. Moreover, the high level of short circuit current becomes the serious problem. It may damage the electric devices or effect on machine operation. Continuity of power supply systems is very low because operations of protective devices under faulted conditions. Mechanical circuit breakers in power distribution systems give a safe handling of short-circuits under limited short-circuit power of the grid. Using delayed turn-off times, the circuit breakers can be coordinated with some other protective equipment. Hence, a high availability of the grid can be expected. However, when the short circuit event occurs in a medium-voltage distribution feeder, voltages along the feeder line are suddenly sagged. Sensitive loads such as computers or electronic-control equipment will fail even if the voltage returns within a few seconds. A solid-state circuit breaker [1-3] is able to switch at very high speed as fast as voltage or current sensing devices can response to the faulty signal. In this paper, a simple thyristor-based circuit breaker is briefly reviewed. Modeling using Power System Blockset [4] considering the requirements of a solid-state switch integrated into a 22-kV

medium voltage distribution feeder is demonstrated. Based on the thyristor characteristics, triggering signal generation for firing control is also explained. It shows that solid-state breakers offer very fast interruption and can be used in modern medium voltage power distribution systems.

II. PSB MODEL OF A SOLID-STATE BREAKER

Figure 1 shows a feeder circuit breaker of mechanical and solid-state types. Present designs of distribution feeder protection rely on expulsion fuses, which have to be reset manually. An SSB is used to protect sensitive loads by interrupting it if there exists a system fault on the supply feeder. This can be incorporated using thyristors [1].

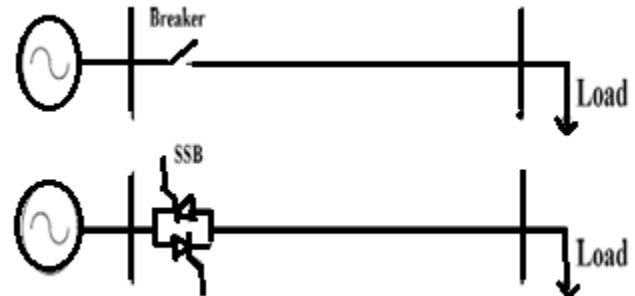


Fig.1 Feeder circuit breakers

The solid-state breaker is designed using thyristors because the switch requires a continuous current carrying and a short time over current rating equal to the feeder faults level. Thyristors have a short time rating up to 16-kA and also have low conduction losses [1]. The thyristors in the feeder are normally energized by continuous and synchronized firing control signal. On detection of voltage sags, these firing pulses are stopped to break the current. Fig. 2 explains the control structure of the SSB.

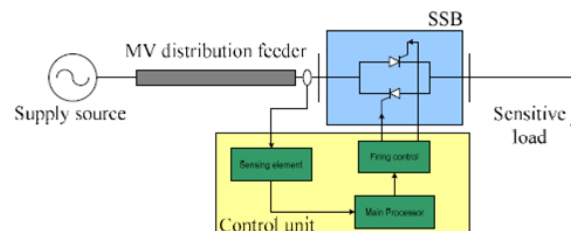


Fig.2 Control structure of the SSB

MATLAB's power system blockset (PSB) is a GUIbased tool for simulation works on power systems with power-electronic control. To create the SSB as described previously, a set of two thyristors connecting in anti-parallel fashion is required. It can be represented in a SIMULINK model using PSB as shown in Fig. 3. Line-In and Lineout are two power ports connected to the supply side and the load side, respectively. Control fw and Control bw are two signal ports that transfer the firing signals to the upper and lower thyristors, respectively. The SSB block is controlled by signals from a firing controller. Fig. 4 shows a combination of the proposed SSB with some other PSB models to simulate a medium-voltage power feeder operating under the fault condition.

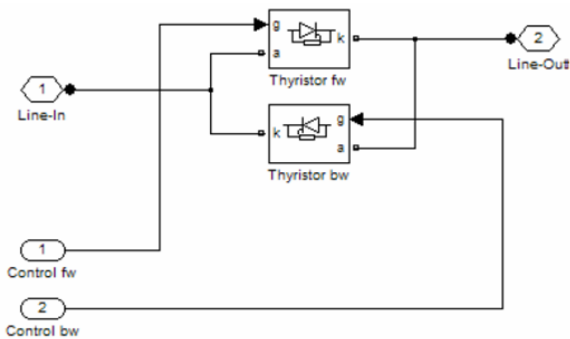


Fig.3 SIMULINK model for an SSB (SSB-1ph)

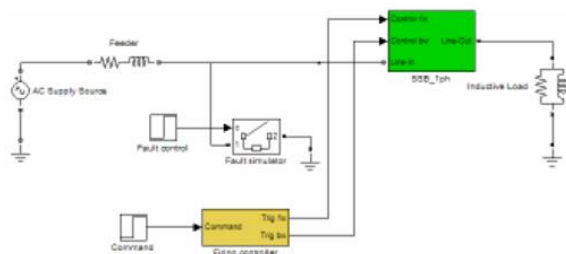


Fig.4 SIMULINK model for an MV power feeder with an SSB

II. FIRING CONTROL

To generate firing signals to turn on the thyristors, a sawtooth signal with a DC reference signal are compared. The result is the pulse signal used in the SSB block. The firing control block diagram created in SIMULINK is given in Fig. 5.

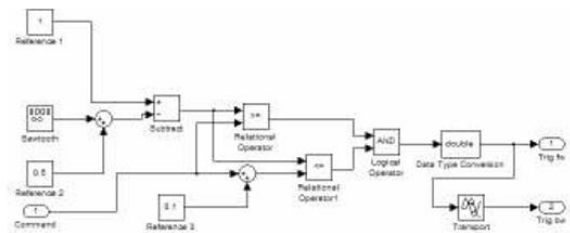


Fig. 5 SIMULINK model for a firing controller

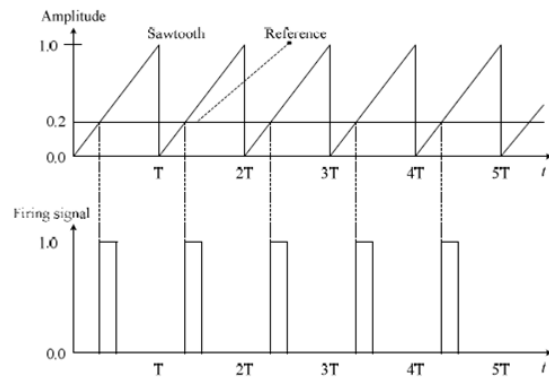


Fig. 6 Firing signal generated from the firing control

IV. VOLTAGE DETECTION SCHEME

Firing strategy to the SSB has only one objective. It is to allow full current flowing to the load. The firing angle for this case is set to zero degree. When a fault occurs, the short-circuit current must be interrupted as fast as possible. To switch off the SSB, the firing angle is set to 180 degree. To change the command to the firing control unit requires a voltage sensing device. In this work, rms voltage detection is used to monitor the voltage sag of the load. Fig. 7 shows the block diagram of rms voltage detection used for the SSB application.

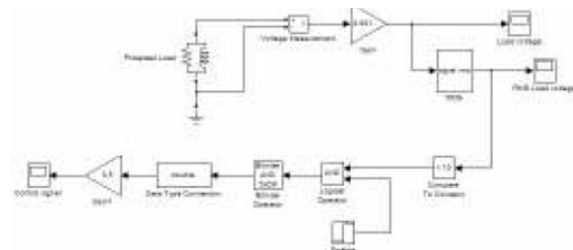
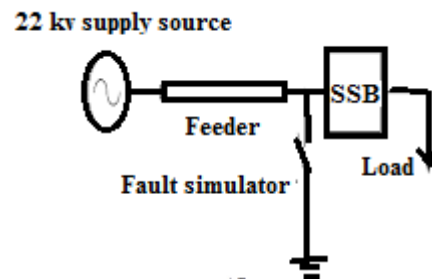


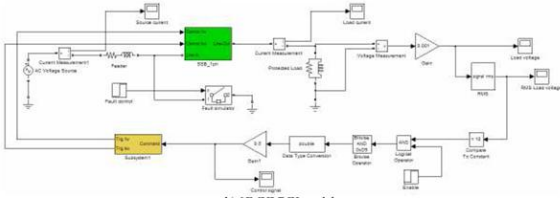
Fig.7 RMS voltage detection

V. SIMULATION RESULTS

A 22-kV distribution feeder serving the load of 200 kW, 150 kvar is created in SIMULINK as shown in Fig. 8. It assumes that a short-circuit event occurs at t = 0.16 s. The test case scenario performs with a time span of 0.2 s.



(a) Test system



(b) SIMULINK model

Fig. 8 SIMULINK model of the test feeder

It takes the first cycle for the rms value reaching its actual rms voltage. When the fault happens at $t = 0.16$ s, the load voltage drops to the value close to zero as shown in Fig. 9. The rms value for the load voltage can be presented in Fig. 10.

the fault event. Fig. 12 explains the current drawn by the load at the normal loading condition.

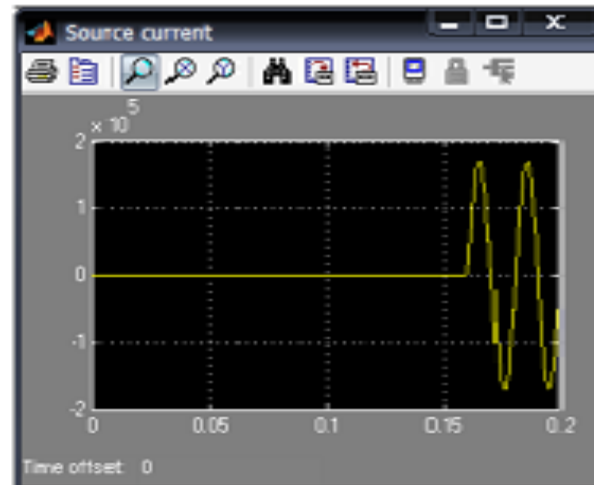


Fig. 11 Source current (A)

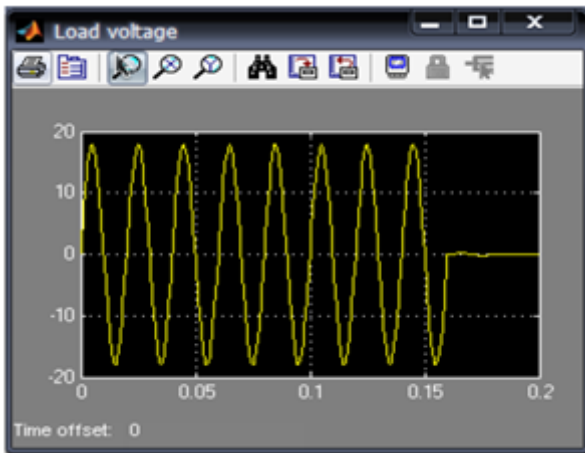


Fig. 9 Load voltage (kv)

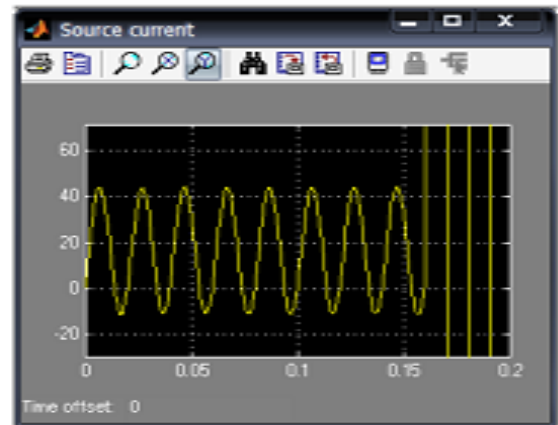


Fig.12 Source current (A) ,zoom in version

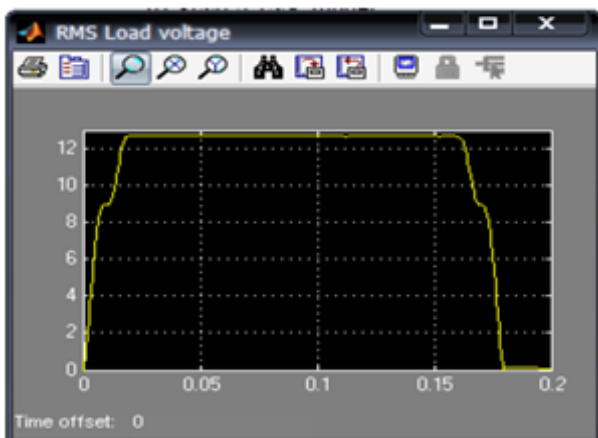


Fig. 10 RMS load voltage (kv)

To verify that the SSB can interrupt the fault current effectively, the currents supplied by the source and drawn by the load are recorded. Fig. 11 gives information of the source current. This figure intentionally indicates the current during

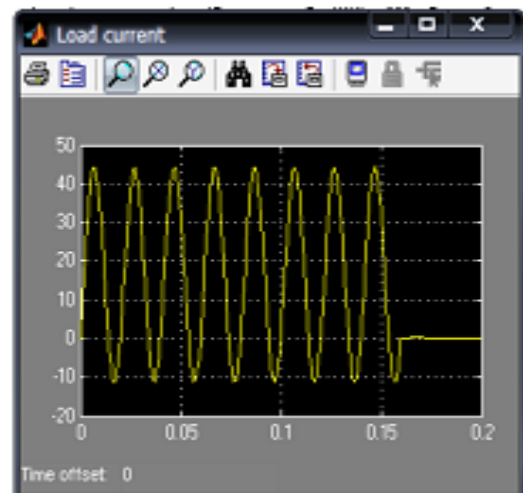


Fig 13 load current (A)

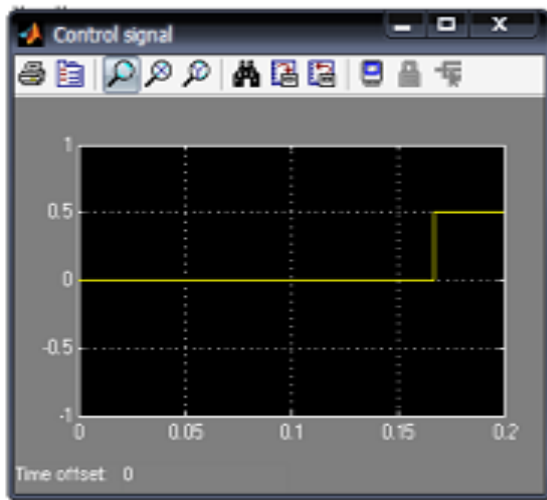


Fig. 14 Command signal

The load current responses can be shown in Fig. 13. From the figure, it can notice the DC component when operating at the normal load condition. The maximum positive peak current is just over 40 A. It can be seen that the SSB can successfully interrupt the fault current. Zeroing load current in the figure can support this reason. In addition, the firing command as shown in Fig. 14 shows the transition of the SSB status from turn on to completely turn-off for interrupting the fault current. During the fault the load current has no DC component.

VI. CONCLUSION

This paper proposes detail of formulating solid-state breakers (SSB) in electric power distribution systems by using GUI-based environment of MATLAB/SIMULINK. In this paper, a 22-kV power distribution feeder with a load having the SSB for protection is situated. Test against a fault condition to verify its use is carried out. As a result, with an appropriate sensing technique to monitor voltage and current of the protected feeder, the SSB can interrupt fault instantaneously.

ACKNOWLEDGEMENTS

Firstly, the authors would like to pay their respectfully thanks to God, their beloved family, teachers and their admirer supervisor. Special thanks to Mr. R. K. Patel Head of department of K.G. Polytechnic, Raigarh for his encouragements. The authors also express their greatly thanks to all persons who had concern to support in preparing this paper.

REFERENCES

[1] G. Dalav, and L.D Tole, *On using the solid state breaker in distribution systems*, IEEE Canadian Conference on Electrical and Computer Engineering, Volume 9, 24-28 May 1998, pp. 63 – 69.

[2] W. Bolland, Q. Takeman, T. Sakin, *Integrated 30 kV solid-state switch for pulse power applications*, Pulsed Power Plasma Science (PPPS-2001), Volume 2, 25-30 June 2001, pp. 55 – 58.

[3] P.O. Deed, E. Sakeda, *Improved power quality solutions using advanced solid state switching and static compensation technologies*, IEEE Power Engineering Society Winter Meeting 1999, Volume 1, 30 Jan-4 Feb 1998, pp. 132 – 137.

[4] The MATHWORKS Inc., *Power system blockset for use with SIMULINK*, User Guider Version 1.0, 1999.



Atul Kumar Dewangan got his bachelor degree in 2006 from Government Engennering Collage, Bilaspur, Chhattisgarh, & Masters degree in 2012 From Bhilai Instute of Technology, Durg, Chhattisgarh. Present he is Asst. Professor in EEE Department in Kirodimal Government Polytechnic Raigarh chhattisgarh. He has been writing technical books on various subjects of electrical engg for students. He has presented paper on Microcontroller Based telephone Exchange System, FM Based train Anti-collision System, Automation of Railway Gate Control before.. He is interested in power electronics, control system, Network Analysis.

Classification of Uncertain Data Using Selection Algorithm

K. Soundararajan¹, Dr. S. Suresh Kumar², C. Anusuya³

1, 3(Department of Information Technology, Vivekananda College of Engineering for Women, Nammakal, Tamilnadu, India)

2 (Department of Computer Science and Engineering, Vivekananda College of Technology for Women, Nammakal, Tamilnadu, India)

ABSTRACT

Traditional machine learning algorithms assume that data are exact or precise. However, this assumption may not hold in some situations because of data uncertainty arising from measurement errors, data staleness, and repeated measurements etc., these kinds of uncertainty have to be handled cautiously, or else the mining results could be unreliable or even wrong. In this paper, we focus on classifying uncertain data by classification and prediction algorithm called setBase. This algorithm introduces new measures for generating, pruning and optimizing. Probability distribution function and uncertain data intervals are computed by this kind of algorithm. Based on these new measures, the optimal splitting attribute and splitting value can be identified and used for classification and prediction. Uncertainty in both numerical and categorical data can be processed by this measure. Our experimental results show that setBase has excellent performance even when data is highly uncertain.

Keywords: classification, data uncertainty, prediction, setBase algorithm, traditional machines.

1. INTRODUCTION

Traditional machine learning algorithms often assume that the data values are exact or precise. In many emerging applications, however, the data is inherently uncertain. Sampling errors and instrument errors are both sources of uncertainty and data are typically represented by probability distributions rather than by deterministic values. There are many learning algorithms used in the classification of deterministic data points, but few algorithms have been proposed for classification of distribution-based uncertain data objects.

Uncertain data is ubiquitous in many real world applications, such as environmental monitoring, sensor network, market analysis and medical diagnosis [1]. A number of factors contributes to the uncertainty. It may be caused by imprecision measurements, network latencies, data staling and decision errors. Uncertainty can arise in categorical attributes and numerical attributes [1, 2]. For example, in cancer diagnosis; it is often very difficult for the doctor to exactly classify a tumour to be benign or malignant due to the experiment precision limitation. It would be better to represent by probability to be benign or malignant [2]. Since data uncertainty is ubiquitous we have to develop a data mining algorithms for uncertain datasets.

In this paper, we introduce a new selection based classification algorithm for data with uncertainty; in this process we have a number of desirable properties. Rule sets are relatively easy for people to understand [15], and rule

learning systems outperform decision tree learners on many problems [16], [17]. Rule sets have a natural and familiar first order version, namely prolong predicates, and techniques for learning propositional rule sets can often be extended to the first order case [18], [19]. However, when data contains uncertainty. For example, when some numerical data are instead of precise value, an interval with probability distribution function with that interval—these algorithms cannot process the uncertainty properly. We prove through extensive experiments that the proposed classification can be efficiently generated and it can classify uncertain data with potentially higher accuracies than the other classification algorithms. Furthermore, the proposed classifier is more suitable for mining uncertain data than the other mining algorithms.

In this paper, we propose a new selection based algorithm for classifying and predicting both certain and uncertain data. We integrate the uncertain data model into the selection based mining algorithm. For generating rules, we introduce a new measure called probabilistic information gain. The field of uncertain data management process a number of unique challenges on several methods which the uncertain data are discussed in Bayesian.

We also extend the set pruning measure for handling data uncertainty, we perform experiments on real datasets with both uniform and Gaussian distribution, and the experimental results demonstrate that setBase algorithm perform well even on highly uncertain data. There are many learning algorithms used in the classification of distribution based uncertain data objects.

In the rest of this paper, we first give some related works in section 2. Then we introduce preliminaries in section 3. Our algorithmic framework is presented in section 4. Experimental studies on accuracy and performance are presented in section 5. The paper is discussed and concluded in sections 6.

2. REVIEW OF RELATED RESEARCHES

In this section, we will introduce some related works about uncertain data mining, uncertain data classification, and more. A detailed survey of uncertain data mining techniques may be found in [5]. In the case of uncertain data mining, studies include clustering [12, 13, 14], classification [2, 3, 6, 11], frequent itemset mining [4, 7, 8, 9, 10].

At present, existing works about classification algorithms. Qin et al, proposed a rule based algorithm to cope with uncertain data [1], later, in [2], Qin et al. presented DTU, which based on decision tree algorithm, to deal with uncertain data by extending traditional measurements, such as information entropy and information gain. In [5], Tsang et al. extended classical decision tree UDT algorithm to handle uncertain data which is

represented by probability density function (pdf). In [10], Bi et al. proposed Total Support Vector Classification (TSVC), a formulation of support vector classification to handle uncertain data.

Classification is a well studied area in data mining. There may be a numerous classification algorithms have been proposed in the literature, such as decision tree classifiers [20], rule-based classifiers [21], Bayesian classifiers [22], support vector machines (SVM) [23], artificial neural networks [24], Lazy learners, and ensemble methods [25]. Decision tree induction is the learning of a decision tree from class-labeled training tuples.

A Rule based classifier is a technique for classifying records using a collection of "if...then..." rules. Bayesian classifiers are statistical classifiers and are based on Bayes theorem. SVM has its roots in statistical learning theory and has shown promising empirical results in many practical applications, from handwritten digit recognition to text categorization.

Uncertain data, also called symbolic data [36], has been studied for many years. Many works focus on clustering [37]. The key idea is that when computing the distance between two uncertain objects, the probability distributions of objects are used to calculate the expected distance. In [14], Cormode et al. show reductions to their corresponding weighted versions on data with uncertainties. In [33], Xia et al. introduce a new conceptual clustering algorithm for uncertain categorical data.

Classification is a well-studied area in data mining. Many methods have been proposed in the literature, such as decision tree [20], rule based classifications, Bayesian classifications [38] and so on. In spite of the numerous methods, building classification based on uncertain data remains a great challenge. There is early work performed on developing decision trees when data contains missing or noisy values [19]. Various strategies have been developed to predict or fill missing attribute values, for example, Dayanik presented feature interval learning algorithms which represent multi-concept descriptions in the form of disjoint feature intervals. However, the problem studied.

In this paper is different from before, instead of assuming part of the data has missing or noisy values, we allow the whole dataset to be uncertain, and the uncertainty is not shown as missing or erroneous values, but represented as uncertain intervals with probability distribution functions.

Recently, Tsang et al [6] and Qin et al [3] independently developed decision tree classifications for uncertain data. Both adopt the technique of fractional tuple for splitting tuples into subsets when the domain of its PDF spans across the cut point. Tsang et al [6] converted every numerical value into a set of sample points between the uncertain intervals $[a_j, b_j]$ with the associated value $f(x)$, effectively approximating every $f(x)$ by a discrete distribution. Qin et al. Also proposed a rule-based classification [2]. The key problem in learning rules is to efficiently identify the optimal cut points from training data. For uncertain numerical data, an optimization mechanism is proposed to merge adjacent bins which have equal classifying class distribution. In our earlier work, we proposed a Bayesian classification method for uncertain on clustering of uncertain data. In [26], [27], the K means clustering

algorithms are data. It will be compared with our new approach in this paper.

There have been studies extended so that the distance between objects are computed as the Expected Distance using a probability distribution function. For uncertain versions of k -means and k -median, Cormode et al [28] show reductions to their corresponding weighted versions on data with no uncertainties. The FDBSCAN and FOPTICS [29], [30] algorithms are based on DBSCAN and OPTICS, respectively. Instead of identifying regions with high density, these algorithms identify regions with high expected density, based on the pdfs of the objects. Aggarwal and Yu [31], [32] propose an extension of their micro-clustering technique to uncertain data. [33] Introduces a new conceptual clustering algorithm for uncertain categorical data. There is also research on identifying frequent item set and association mining [34], [35] from uncertain datasets. The support of item sets and confidence of association rules are integrated with the existential probability of transactions and items. However, none of them address the issue of developing classification and predication algorithms for uncertain datasets.

3. PRELIMINARIES

In this paper, we are mainly focus on the uncertain attributes and assume the class type is certain. In this section, we will discuss the uncertain model for both numerical and categorical attributes, which are the most common types of attributes encountered in data mining applications. Uncertain data has attracted more and more attention in the literature.

3.1. NUMERICAL DATA UNCERTAINTY

In this model, we describe numerical data uncertainty, this shows that the value of a numerical attribute is uncertain, then the attribute is said to be a uncertain numerical attribute, that must be denoted by $A_i(\text{Un})$. Further, we use $A_j(\text{Un})$ is to denote the j th instance of $A_i(\text{Un})$. The concept of this model for uncertain numerical data has been introduced in [1]. The value of $A_i(\text{Un})$ is represented as a range of interval and the probability distribution function (PDF) over this range. We notice that $A_i(\text{Un})$ is treated as a continuous random variable. This probability distribution function is denoted by $f(x)$ can be related to an attribute if all instances have the same distribution function and that are related to each instances has different distributions. For every uncertain numerical attribute instance A_i , let $\text{sum}_i = (A_{ij} \cdot \text{max} + A_{ij} \cdot \text{min})/2$ and $\text{diff}_i = (A_{ij} \cdot \text{max} - A_{ij} \cdot \text{min}) \cdot (A_{ij} \cdot \text{max} - A_{ij} \cdot \text{min})/36$.

Definition 1: An uncertain interval instance of $A_i(\text{Un})$, is denoted by $A_{ij}(\text{Un}), U$, is an interval $[A_{ij}(\text{Un}).l, A_{ij}(\text{Un}).r]$ where $A_{ij}(\text{Un}).l, A_{ij}(\text{Un}).r$ that is belongs to R , $A_{ij}(\text{Un}).r \geq A_{ij}(\text{Un}).l$. Then this realizes that this model is an application dependent.

3.2. CATEGORICAL DATA UNCERTAINTY

Under this uncertainty data model deals with categorical data, and these attributes that are allowed to take uncertain values. Then we call such attribute an uncertain categorical attributes that are denoted by $A_i(\text{Uc})$. Further, we use $A_{ij}(\text{Uc})$ to denote the j th instance of $A_i(\text{Uc})$. The notion of the uncertain categorical attributes was proposed in [2].

When dealing with uncertain categorical attribute, we utilize the same model as studies in [1, 2 and 3] to represent uncertain categorical data. Under the uncertain categorical model, a dataset can have attributes that are allowed to take uncertain values [2]. And we call these attributes Uncertain Categorical Attributes, UCA. The concept of UCA was introduced in [1]. Let's write $Auci$ for the i th uncertain categorical attribute, and $V_i = \{vi_1, vi_2, \dots, vi_{|V_i|}\}$ for its domain. As described in [2], for instance j , its attribute value of $Auci$ can be represented by the probability distribution over V_i , and formalized as $P_{ji} = \{pi_1, pi_2, \dots, pi_{|V_i|}\}$, such that $P_{ji}(Auci = vik) = pik (1 \leq k \leq |V_i|)$, and $\sum_{k=1}^{|V_i|} pik = 1.0$, which means $Auci$ takes value of vik with probability pik . Certain attribute can be viewed as a special case of uncertain attribute. In this case, the attribute value of $Auci$ for instance t_j can only take one value, vik , from domain V_i , i.e. $P_{ji}(Auci = vik) = 1.0 (1 \leq k \leq |V_i|)$, $P_{ji}(Auci = vih) = 0.0 (1 \leq h \leq |V_i|, h \neq k)$.

A_{ij} (Uc) takes values from the categorical domain Dom with cardinality $|Dom|=n$. Within a regular relation, the value of an attribute A is a single value in $Dom=1$. In this case of an uncertain relation, we record the information by a probability distribution over Dom instead of a single value domains.

4. ALGORITHMS AND APPLICATION

In this section, we deal with the algorithms and its applications. To build a set base classifier, we need to extract a set of rules that show the relationships between the attributes of a dataset and the class label. Each classification is in the form of $R \oplus (Condition) \rightarrow y$. Here the condition is called the set base antecedent, which is a conjunction of, y is called the set base consequent and it is the class label, it consists of multiple sets $Rs = \{R1, R2, \dots, Rn\}$

The **Coverage** of a rule is the number of instances that satisfy the antecedent of a rule. The **Accuracy** of a rule is the fraction of instances that satisfy both the antecedent and consequent of a rule, normalized by those satisfying the antecedent. Ideal rules should have both high coverage and high accuracy rates.

The setBase algorithm is shown in Algorithm 1. It uses the sequential covering approach to extract rules from the datasets. This algorithm extracts the rules one class at a time for a data set. Let (y_1, y_2, \dots, y_n) be the ordered classes according to their frequencies, where y_1 is the least frequent class and y_n is the most frequent class. During the i th iteration, instances that belong to y_i are labeled as positive examples, while those that belong to other classes are labeled as negative examples.

A rule is desirable if it covers most of the positive examples and none of the negative examples. Our setBase algorithm is based on the RIPPER algorithm [9], which was introduced by Cohen and considered to be one of the most commonly used rule-based algorithms in practice.

Algorithm 1: setBase (Dataset D , ClassSet C)

```

Begin
  RuleSet =  $\emptyset$ ; //initial set of rules learned is empty
  for Each Class  $ci \in C$  do
    newRuleSet = uLearnOneRule ( $D, ci$ );
    Remove tuples covered by newRuleSet from Dataset
  D;
  RuleSet += newRuleSet;

```

```

End for;
Return RuleSet;
End

```

The uLearnOneRule () procedure is shown in Algorithm 2; it is the key function of the setBase algorithm. It generates the best rule for the current class, given the current set of uncertain training tuples. The uLearnOneRule () includes two phases: growing rules and pruning rules. We will explain the first phase, growing rules, in more detail, while the other pruning rules is similar to regular rule-based classifier, thus will not be elaborated. After generating a rule, all the positive and negative examples covered by the rule are eliminated. The rule is then added into the rule set as long as it does not violate the stopping condition, which is based on the minimum description length (DL) principle. setBase also performs additional optimization steps to determine whether some of the existing rules in the rule set can be replaced by better alternative rules.

Algorithm 2 uLearnOneRule (Dataset D , Class ci)

```

Begin
  Stop = false;
  RuleSet =  $\emptyset$ ;
  Repeat
    Split  $D$  into growData and pruneData;
    Rule = uGrow (growData);
    Prune Rules based on pruneData;
    Add Rules to RuleSet;
    Remove data covered by Rule from  $D$ ;
  Until Stop Condition is true
  Return (RuleSet);
End

```

The process of growing rules, uGrow (), is shown in Algorithm 3. The basic strategy is as follows:

1. It starts with an initial rule: $\{ \} \rightarrow y$, where the left hand side is an empty set and the right hand side contains the target class. The rule has poor quality because it covers all the examples in the training set. New conjuncts will subsequently be added to improve the rule's quality.
2. The probabilistic information gain is used as a measure to identify the best conjunct to be added into the rule antecedent. This algorithm selects the attribute and split point which has the highest probabilistic information gain and adds them as follows.

Algorithm 3 uGrow (Instances growData)

```

Begin
  CoverData =  $\emptyset$ ;
  While (growData.size () > 0)  $\wedge$  (numUnusedAttributes > 0)
  do
    Find the attribute  $Ai$  and the split point  $sp$ , which has
    the highest probabilistic information gain;
    Antecedent += RuleAntecedent ( $Ai, sp$ );
    for (each instance  $Ij$ ) do
      if (covers( $Ij$ )) then
        Inst = splitUncertain ( $Ij, Ai, sp$ );
        coverData += inst;
      End if;
    End for;
    growData -= coverData;
  end while;
End

```

Function splitUncertain () is shown in Algorithm 4. As the data is uncertain, a rule can partly cover an instance.

For Example, for an instance with income [100, 110], a rule “income > 105 => default Borrower = No” only partly covers it. For an instance with tumor [Benign, 0.8Malignant, 0.2], a rule “tumor = benign => Survive = yes” also partly covers it. Function splitUncertain () computes what proportion of the instances is covered by a selection based on the uncertain attribute interval and probabilistic distribution function.

Algorithm 4 splitUncertain (Instance I_i , attribute A_i , splitPoints sp)

```

Begin
  if the rule fully covers instance  $I_i$  then
    return  $I_i$ ;
  end if;
  if ( $A_i$  is numerical or uncertain numerical) then
  if the rule partially covers instance  $I_i$  on the right side
  then
 $I_i.w = I_i.w * \int_{sp} f(x) dx / \int_{min} f(x) dx$ ;
  end if;
  if the rule partially covers instance  $I_i$  on the left side
  then
 $I_i.w = I_i.w * \int_{max} f(x) dx / \int_{min} f(x) dx$ ;
  end if;
  end if;
  if ( $A_i$  is categorical or uncertain categorical) then
 $I_i.w = I_i.w * att.value(sp).w * P(I_i, R_k)$ ;
  end if;
  return  $I_i$ ;
End

```

4.1 SPLITTING THE DATA

It is seen that when the rules are being generated from the training dataset, the goal is to determine the best split attribute and best split point. We use a measure called probabilistic information gain to identify the optimal split attribute and split point for uncertain training dataset.

4.1.1. UNCERTAIN NUMERICAL ATTRIBUTES

The value of an uncertain numeric attribute is an interval with associated PDF. Each uncertain interval has a maximal value and a minimal value, which are called critical points. For each UNA, we can order all critical points of an uncertain numeric attributes in an ascending sort with duplicate elimination. The Class Distribution of each partition is called as Class Distribution Vector (CDV). Suppose there are N critical points after eliminating duplicates, then this UNA can be divided into $N+1$ partition. Since the leftmost and rightmost partitions do not contain data instances at all, a split definitely will not occur within them. We need only consider the rest $N-1$ partitions. The Probabilistic Cardinality (PC) of the dataset over the partition $P_a = [a, b]$ is the sum of the probability of each instances whose corresponding UCA equals $P_a = [a, b]$.

4.1.2. UNCERTAIN CATEGORICAL DATA

Uncertainty in categorical data is common place in many applications, including data cleaning, database integration, and biological annotation. In such domains, the correct value of an attribute is often unknown, but may be selected from a reasonable number of alternatives. Current database management systems do not provide a convenient means for representing or manipulating this type of uncertainty.

A rule related to an uncertain categorical attribute only covers its one value, which is called split point. An uncertain categorical attribute (UCA) is characterized by probability distribution over Domain. Datasets without uncertainty can be treated as a special case of data with uncertainty. When using a matrix to represent a categorical attribute of a dataset without uncertainty, there is at most one element per row to be 1. The probabilistic cardinality (PC) of the dataset over v_k is the sum of the probability of each instances whose corresponding UCA equals v_k . Based on the Class Distribution Vector (CDV) we can compute the probabilistic information gain if the categorical attribute is selected as the antecedent of the rule.

4.1.3. PRUNING TECHNIQUES

After growing, the rule is immediately pruned by deleting any final sequence of conditions from the rule, and chooses the deletion that maximizes the function which is known as Pruning. There are two types of pruning namely Pre-Pruning and Post-Pruning. setBase employs a general-to-specific strategy to grow a rule and the probabilistic information gain measure to choose the best conjunct to be added into the rule antecedent. The new rule is then pruned based on its performance on the validation set. The following metric is used for rule pruning.

The probabilistic prune for a rule R is

$$\text{ProbPrune}(R, p, n) = \{PC(p) - PC(n)\} / \{PC(p) + PC(n)\}$$

Here $PC(p)$ and $PC(n)$ is the probabilistic cardinality of positive and negative instances covered by the rule. This metric is monotonically related to the rule's accuracy on the validation set. If the metric improves after pruning, then the conjunct is removed. Like RIPPER, setBase starts with the most recently added conjunct when considering pruning. Conjuncts are pruned one at a time as long as this results in an improvement.

4.1.4. .PREDICTION TECHNIQUES

Once the rules are learned from a dataset, they can be used for predicting class types of unseen data. Like a traditional rule classifier, each rule of setBase is in form of “IF conditions THEN Class= C_i ”. Because each instance I_i can be covered by several rules, a vector can be generated for each instance and the vector is an Class Probability Vector (CPV). As an uncertain data instance can be partly covered by a rule, we denote the degree an instance I covered by a rule R_i . An uncertain instance may be covered or partially covered by more than one rule. We allow the test instance to trigger all relevant rules. $W(I_i, R_k)$ to denote the weight of an instance I_i covered by different rules.

An uncertain instance may be covered or partially covered by more than one rule. We allow a test instance to trigger all relevant rules. We use $w(I_i, R_k)$ to denote the weight of an instance I_i covered by the k th rule R_k . The weight of an instance I_i covered by different rules is as follows $(I_i, R1) = I_i.w * P(I_i, R1) W(I_i, R2) = (I_i.w - w(I_i, R1)) * P(I_i, R2) W(I_i, Rn) = (I_i.w - \sum_{k=1}^{n-1} w(I_i, Rk)) * P(I_i, Rn)$.

After we compute the CPV for instance I_i , the instance will be predicted to be of the class C_j , which has the largest probability in the class probability vector. This prediction is different from a traditional rule based classifier. When predicting the class type for an instance, a traditional rule

based classifier such as RIPPER usually predicts with the first rule in the rule set that covers the instance. As an uncertain data instance can be fully or partially covered by the multiple rules, the first rule in the rule set may not be the rule that covers it best. setBase will use all the relevant rules to compute the probability for the instance to be in each class and predict the instance to be the class with highest probability.

5. EXPERIMENTAL RESULTS

In this section, we present the experimental results of the proposed setBase algorithm. We studied the setBase classifier accuracy and classifier construction time over multiple datasets. Probability vectors which are converted by uncertain categorical attributes. For example, a categorical attribute A_i may have k possible values v_j , $1 \leq j \leq k$.

For an instance I_j , we convert its value A_{ij} into a probability vector $\mathbf{P} = (p_{j1}, p_{j2}, \dots, p_{ji}, \dots, p_{jk})$, while p_{jl} is the probability of A_{ucij} to be equal to v_l , that is, $P(A_{ucij} = v_l) = p_{jl}$. For example, when we introduce 10% uncertainty, this attribute will take the original value with 90% probability, and 10% probability to take any of the other values. Suppose in the original accurate dataset $A_{ij} = v_1$, then we will assign $p_{j1} = 90\%$, and assign p_{jl} ($2 \leq l \leq k$) to ensure $\sum_{l=1}^k p_{jl} = 100\%$. Similarly, we denote this dataset with 10% uncertainty in categorical data by U_{10} .

To make numerical attributes uncertain, we convert each numerical value to an uncertain interval. For each numerical attribute, we scan all of its value and get this maximum X_{max} and minimum value X_{min} , respectively.

5.1. ACCURACY

In this Fig.1, we use ten-fold cross validation. Data is split into 10 approximately equal partitions; each one is used in turn for testing while the rest is used for training, that is, 9/10 of data is used for training and 1/10 for testing. The whole procedure is repeated 10 times, and the overall accuracy rate is countered as the average of accuracy rates on each partition. 2 indicate after the prediction.

Fig.1. prediction of accuracy

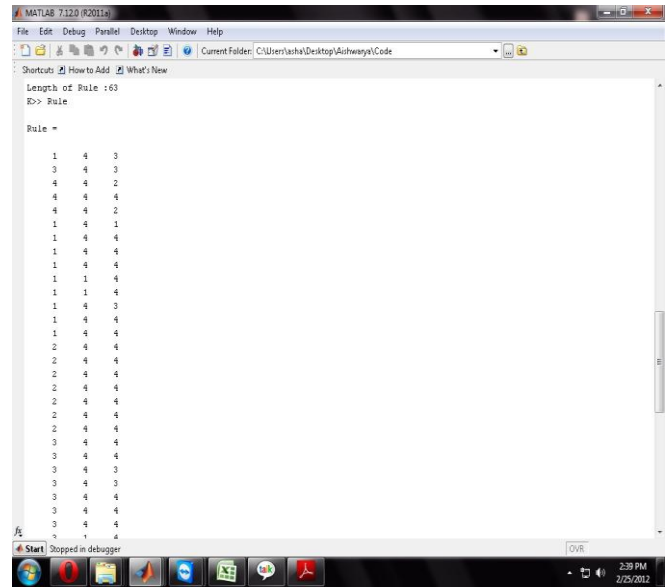
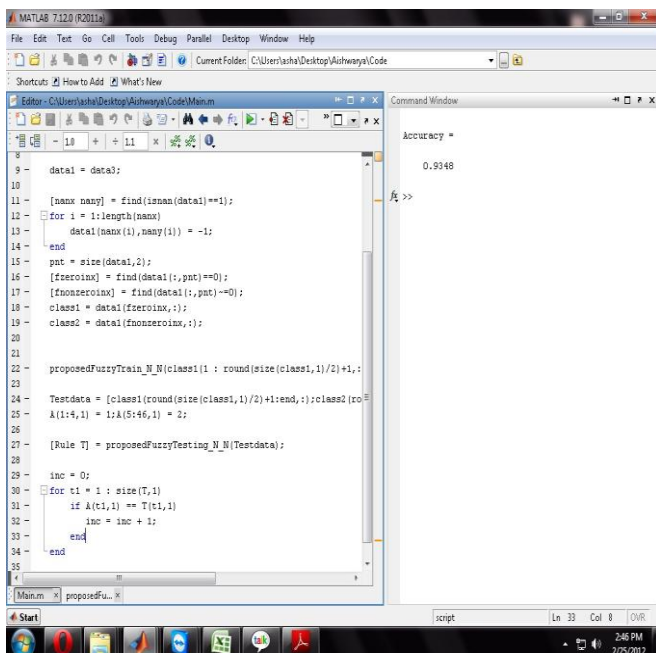


Fig.2. after prediction



5.2. COMPUTATION TIME

Table.1 depicts the absolute run time in seconds when all instances of a dataset are used to build the rule set. It is shown that it generally takes longer to construct a classifier as the uncertainty in data increases. The reason is explained in two ways of expansions. First, for uncertain data, more candidate splitting points are available and require more comparisons. Second, uncertain data can be partly covered by rules, resulting in record splitting, weight and probabilistic cardinalities computation. Furthermore, it is shown that it takes longer to generate classifier from uncertain data with Gaussian PDF than with uniform PDF.

DIST RIBU TION S	CLASSIFIER CONSTRUCTION TIME	CLASSIFIER CONSTRUCTION TIME				
		DATAS ET	U0	U5	U10	U15
Unifo rm	SONAR	0.12	0.52	0.49	0.73	0.75
	GLASS	0.1	0.12	0.18	0.13	0.16
	DIABE TES	0.13	0.47	0.49	0.58	0.59
Guas sian	SONAR	0.12	1.1	1.73	2.0	2.62
	GLASS	0.1	0.6	0.78	0.99	1.12
	DIABE TES	0.13	2.85	4.75	5.63	5.04

TABLE.1 Computation Time Calculation

6. CONCLUSION

Data Uncertainty is prevalent in many real world applications. Uncertain data often occurs in modern applications, including sensor databases, special-temporal databases, and medical or biology information systems. In this paper, we propose a new selection based algorithm for classifying and predicting uncertain datasets. We propose new approaches for deriving optimal rules out of highly uncertain data, pruning and optimizing rules, and class prediction for uncertain data. In this paper, the proposed algorithm follows new paradigm of directly mining the uncertain datasets.

Our future work include developing uncertain data mining techniques for various applications, including sequential pattern mining, association mining, spatial data mining and web mining, where data can be commonly uncertain.

REFERENCES

- [1] Singh, S., Mayfield, C., Prabhakar, S., Shah, R., Hambrusch, S.: *Indexing Uncertain Categorical Data*. In: *Proc. of ICDE 2007*, pp. 616-625 (2007)
- [2] Qin, B., Xia, Y., Prbahakar, S., Tu, Y.: *A Rule-based Classification Algorithm for Uncertain Data*. In: *The Workshop on Management and Mining of Uncertain Data, MOUND (2009)*
- [3] Qin, B., Xia, Y., Li, F.: *DTU: A Decision Tree for Uncertain Data*. In: *Theeramunkong, T., Kijisirikul, B., Cercone, N., Ho, T.-B. (eds.) PAKDD 2009. LNCS, vol. 5476, pp. 4-15. Springer, Heidelberg (2009)*
- [4] Chui, C.K., Kao, B., Hung, E.: *Mining frequent itemsets from uncertain data*. In: *Zhou, Z.-H., Li, H., Yang, Q. (eds.) PAKDD 2007. LNCS (LNAI), vol. 4426, pp. 47-58. Springer, Heidelberg (2007)*
- [5] Aggarwal, C.C., Yu, P.S.: *A survey of Uncertain Data Algorithms and Applications*. *IEEE Transactions on Knowledge and Data Engineering* 21(5), 609-623 (2009)
- [6] Tsang, S., Kao, B., Yip, K.Y., Ho, W.-S., Lee, S.D.: *Decision Trees for Uncertain Data*. In: *Proc. of ICDE 2009*, pp. 441-444 (2009)
- [7] Chui, C., Kao, B.: *A decremental approach for mining frequent itemsets from uncertain data*. In: *Washio, T., Suzuki, E., Ting, K.M., Inokuchi, A. (eds.) PAKDD 2008. LNCS (LNAI), vol. 5012, pp. 64-75. Springer, Heidelberg (2008)*
- [8] Leung, C.K.-S., Carmichael, C.L., Hao, B.: *Efficient mining of frequent patterns from uncertain data*. In: *Proc. of ICDM Workshops*, pp. 489-494 (2007)
- [9] Zhang, Q., Li, F., Yi, K.: *Finding Frequent Items in Probabilistic Data*. In: *Proc. of SIGMOD 2008*, pp. 819-832 (2008)
- [10] Bernecker, T., Kriegel, H.P., Renz, M., Verhein, F., Zuefle, A.: *Probabilistic frequent itemset mining in uncertain databases*. In: *Proc. of SIGKDD 2009*, pp. 119-128 (2009)
- [11] Bi, J., Zhang, T.: *Support Vector Classification with Input Data Uncertainty*. In: *NIPS*, pp. 161-168 (2004)
- [12] Ngai, W.K., Kao, B., Chui, C.K., Cheng, R., Chau, M., Yip, K.Y.: *Efficient clustering of uncertain data*. In: *Perner, P. (ed.) ICDM 2006. LNCS (LNAI), vol. 4065, pp. 436-445. Springer, Heidelberg (2006)*
- [13] Lee, S.D., Kao, B., Cheng, R.: *Reducing UK-means to K-means*. In: *Proc. of ICDM Work shops*, pp. 483-488 (2007)
- [14] Cormode, G., McGregor, A.: *Approximation Algorithms for Clustering Uncertain Data*. In: *PODS 2008*, pp. 191-200 (2008)
- [15] J. Catlett, "Megainduction: A test flight," in *ML*, 1991, pp. 596-599.
- [16] G. Pagallo and D. Haussler, "Boolean feature discovery in empirical learning," *Machine Learning*, vol. 5, pp. 71-99, 1990.
- [17] S. M. Weiss and N. Indurkha, "Reduced complexity rule induction," in *IJCAI*, 1991, pp. 678-684.
- [18] J. R. Quinlan, "Learning logical definitions from relations," *Machine Learning*, vol. 5, pp. 239-266, 1990.
- [19] J. R. Quinlan and R. M. Cameron-Jones, "Induction of logic programs: Foil and related systems," *New Generation Comput.*, vol. 13, no. 3&4, pp. 287-312, 1995.
- [20] J.R. Quinlan, *C4.5: Programs for Machine Learning*. Morgan Kaufman Publishers, 1993.
- [21] W. W. Cohen, "Fast effective rule induction," in *Proc. of the 12th Intl. Conf. on Machine Learning*, 1995, pp. 115-123.
- [22] P. Langley, W. Iba, and K. Thompson, "An analysis of bayesian classifiers," in *National Conf. on Artificial Intelligence*, 1992, pp. 223-228.
- [23] V. Vapnik, *The Nature of Statistical Learning Theory*. Springer Verlag, 1995.
- [24] R. Andrews, J. Diederich, and A. Tickle, "A survey and critique of techniques for extracting rules from trained artificial neural networks," *Knowledge Based Systems*, vol. 8, no. 6, pp. 373-389, 1995.
- [25] T. G. Dietterich, "Ensemble methods in machine learning," *Lecture Notes in Computer Science*, vol. 1857, pp. 1-15, 2000.
- [26] W. K. Ngai, B. Kao, C. K. Chui, R. Cheng, M. Chau, and K. Y. Yip, "Efficient clustering of uncertain data," in *IEEE International Conference on Data Mining (ICDM) 2006*, pp. 436-445.
- [27] M. Chau, R. Cheng, B. Kao, and J. Ng, "Data with uncertainty mining: An example in clustering location data," in *Proc. of the Methodologies for Knowledge Discovery and Data Mining, Pacific-Asia Conference (PAKDD 2006)*, 2006.
- [28] C. G and McGregor, "Approximation algorithms for clustering uncertain data," in *PODS*, 2008, pp. 191-199.
- [29] H. Kriegel and M. Pfeifle, "Density-based clustering of uncertain data," in *International Conference on Knowledge Discovery and Data Mining (KDD)*, 2005, pp. 672-677.
- [30] H. Kriegel and M. Pfeifle, "Hierarchical density-based clustering of uncertain data," in *IEEE International Conference on Data Mining (ICDM) 2005*, pp. 689-692.
- [31] A. C, "On density based transforms for uncertain data mining," in *Proceedings of IEEE 23rd International Conference on Data Engineering*, 2007, pp. 866-875.
- [32] A. C and Y. PS, "A framework for clustering uncertain data streams," in *Proceedings of IEEE 24th*

International Conference on Data Engineering, 2008, pp. 150–159.

- [33] Y. Xia and B. Xi, “Conceptual clustering categorical data with un-certainty,” in *IEEE International Conference on Tools with Artificial Intelligence (ICTAI), 2007*, pp. 329–336.
- [34] Z. Yu and H. Wong, “Mining uncertain data in low-dimensional sub-space,” in *International Conference on Pattern Recognition (ICPR) 2006*, 748–751.
- [35] C. Chui, B. Kao, and E. Hung, “Mining frequent itemsets from uncertain data,” in *Proc. of the Methodologies for Knowledge Discovery and Data Mining, Pacific-Asia Conference (PAKDD) 2007*, pp. 47–58.
- [36] H. H. Bock, E. D. Day, “Analysis of symbolic data. Exploratory methods for extracting statistical information from complex data”, Springer Verlag, 2000
- [37] F. Carvalho, P. Brito, H. H. Bock, *Dynamical clustering for interval data based on L2 distance*, *Computational Statistics*, 21(2)(2006) 231-250
- [38] B. Qin, Y. Xia, Li F, *A Bayesian classifier for uncertain data*, in: *Proceedings of SAC, 2010*.

Vibrational Analysis of Self Align Ball Bearing Having a Local defect through FEA and its Validation through Experiment

Prof U.A.Patel¹, Shukla Rajkamal²

¹Professor of Mechanical department, L.D. College of Engineering
Ahmedabad, Gujarat, India

²M.E. CAD/CAM, L.D.College of Engineering, Ahmedabad

Abstract: The rolling bearings dynamical behaviour analysis is a important condition to determine the machine vibration response. The rolling bearing, with outer ring fixed, is a multi body mechanical system with rolling elements that transmit motion and load from the inner raceway to the outer raceway. Modern trend of Dynamic analysis is useful in early prediction; simulation of rotor bearing system as manufacturing of prototype is time consuming, costly, and required further analysis for fatigue failure. Dynamic analysis has become a very powerful tool for the betterment of the actual performance of the system. The methodology for prediction and validation of dynamic characteristics of bearing rotor system vibration is studied. PRO-E® and ANSYS software are the promising tools for the modeling and modal analysis of the bearing rotor system. Experiment result has been taken for the analysis of the signal that has been obtained through the use of FFT analyser. Matlab® program is generated for finding the BPFO and BPF1 for bearing system; its graphical values are shown. The goal of this study is to prevent the system from the breakdown by continuous monitoring of vibration values.

Keywords: BPFO, BPF1, vibration monitoring, rollin element, frequency domain

I. INTRODUCTION

A ball bearing is a type of rolling-element bearing that uses balls to maintain the separation between the moving parts of the bearing. The purpose of a ball bearing is to reduce rotational friction and support radial and axial loads. It achieves this by using at least two races to contain the balls and transmit the loads through the balls. Usually one of the races is held fixed. As one of the bearing races rotates it causes the balls to rotate as well.

In this paper Self-aligning ball bearings is considered whose bearing number is 1205k; it is constructed with the inner ring and ball assembly contained within an outer ring that has a spherical raceway. This construction allows the bearing to tolerate a small angular misalignment resulting from deflection or improper mounting.

Experimental modal analysis, structural dynamics modification and finite element analysis were used to analyze the dynamic properties of a test structure. Most noise, vibration or failure problems in mechanical structures and systems are caused by excessive dynamic behavior. In recent years, however, the implementation of the Fast Fourier Transform (FFT) in low cost computer-based signal analyzers has provided the environmental testing laboratory

with a fast and more powerful tool for acquisition and analysis of vibration data.

The FFT spectrum analyzer samples the input signal, computes the magnitude of its sine and cosine components, and displays the spectrum of these measured frequency components. The FFT is simply a clever set of operations which implements Fourier's theorem. The resulting spectrum shows the frequency components of the input signal.

The big advantage of this technique is its speed. Because FFT spectrum analyzers measure all frequency components at the same time, the technique offers the possibility of being hundreds of times faster than traditional analogue spectrum analyzers. To measure the signal with higher resolution, the time record is increased. But again, all frequencies are examined simultaneously providing an enormous speed advantage. Today the ball bearing is used in numerous everyday applications. Ball bearings are used for dental and medical instruments. In dental and medical hand pieces, it is necessary for the pieces to withstand sterilization and corrosion. Because of this requirement, dental and medical hand pieces are made from 440C stainless steel, which allows smooth rotations at fast speeds.

II. LITERATURE SURVEY

Major contributors in the field of bearing analysis are Jones, Harris^[9] Palmgren. Firstly Lundberg and Palmgren developed a theory to predict stress distribution at point of contact for normal loading. This theory was able to predict fatigue life of bearings to some extent with inclusion of empirical proportionality constant. Then Jones developed a general method, to obtain all forces and elastic deformations analytically in a redundant system like ball and roller bearing. This theory was a successful attempt to improve precision of Lundberg and Palmgren theory.

C.Zhang, T.Kurfess^[5] did work on ball bearing which proposes a remaining life adaptation methodology based on mechanistic modeling and parameter turning through a defect propagation model and defect diagnostic model, an adaptive algorithm is developed to fine tune the parameter involved in the bearing. Antoniadis and G.Glossiotis^[3] proposes an alternative frame work for analyzing bearing vibration signal with periodically varying statics, is better able to exhibit the underlying physical concepts of the modulation mechanism present in the vibration response of bearings. Sun-Min Kim and sun-Kyu Lee^[4] investigates the effect of assembly tolerance on the spindle bearing compliance. In high speed spindle system, the bearing characteristics are significantly influenced by the initial assembly tolerance and the thermal deformation of the bearing support structure. Zeki kiral and Hira

Karagulle^[6] done Simulation and analysis of vibration signals generated by rolling element bearing with defects in 2003, in this paper dynamic loading of a rolling element bearing structure was modeled by a computer program developed in Visual Basic programming language. Peter W. Tse in 2004 has done the Machine fault diagnosis through an effective exact wavelet analysis in which to minimize the effect of overlapping and to enhance the accuracy of fault detection, a novel wavelet transform, which was named as exact wavelet analysis, had been designed for use in vibration-based machine fault diagnosis. In 2009 Abhay Utpat, R.B.Ingle and M.R.Nandgaonkar^[1] proposed a work in which vibration produced by a single point defect on various parts of the bearing under constant radial load are predicted by using a theoretical model. The model includes variation in the response due to the effect of bearing dimension, rotating frequency distribution of load. M.S.Patil, Jose Mathew, Sandeep desai in 2010^[2], they proposed an analytical model for predicting the effect of a localized defect on the ball bearing vibrations. In the analytical formulation, the contacts between the ball and the races are considered as non-linear springs. The contact force is calculated using the hertz contact deformation theory. A computer program was also developed to simulate time domain and frequency domain. The model yields both the frequency and the accelerations of vibration component of bearing.

III. MODELING OF THE SYSTEM

As a first step in investigating the vibrations characteristics of ball bearings, a model of a rotor bearing assembly can be considered as a spring-mass system, where the rotor acts as a mass and the raceways and balls act as mass less nonlinear contact springs. In the model, the outer race of the bearing is fixed in a rigid support and the inner race is fixed rigidly with the rotor. A constant radial vertical force acts on the bearing. Therefore, the system undergoes nonlinear vibrations under dynamic conditions. Elastic deformation between the race and ball gives a non-linear force deformation relation, which is obtained by using the Hertzian theory. Other sources of stiffness variation are the positive internal radial clearance, the finite number of balls whose position changes periodically and waviness at the inner and outer race. They cause periodic changes in stiffness of the bearing assembly.

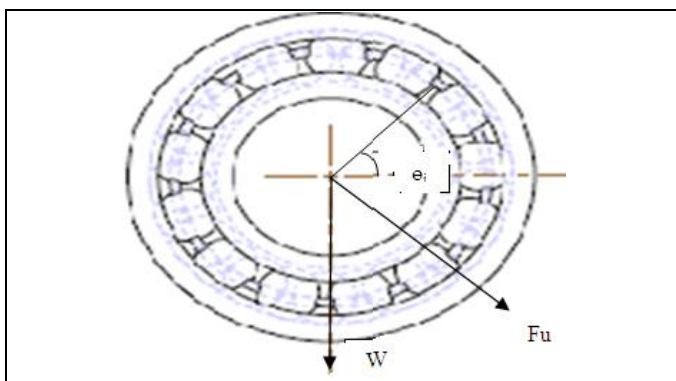


Figure 1: A schematic diagram of a rolling element bearing.

3.1 Ball passage frequency

When the shaft is rotating, applied loads are supported by a few balls restricted to a narrow load region and the radial position of the inner race with respect to the outer race depends on the elastic deflections at the ball to raceways contacts. Balls are deformed as they enter the loaded zone where the mutual convergence of the bearing races takes place and the balls rebound as they move to the unloaded region. The time taken by the shaft to regain its initial position is

$$T = \text{time for completion rotation of cage}/N_b$$

As the time needed for a complete rotation of the cage is $2\pi/\omega_c$ the shaft will be excited at the frequency of $(N_b * \omega_c)$ known as the ball passage frequency. Here ω_c is the speed of the cage.

$$\omega_c = \frac{\omega_{inner}}{2} \left(1 - \frac{d_b}{d_m}\right) + \frac{\omega_{outer}}{2} \left(1 + \frac{d_b}{d_m}\right) \quad (1)$$

Hence, ball passage frequency (ω_{bp}) is

$$\omega_{bp} = \frac{1}{2} N_b \frac{\omega_{inner}}{2} \left(1 - \frac{d_b}{d_m}\right) + \frac{1}{2} N_b \frac{\omega_{outer}}{2} \left(1 + \frac{d_b}{d_m}\right) \quad (2)$$

Since outer is assumed to be constant, the ball passage frequency is

$$\omega_{bp} = \frac{1}{2} N_b \frac{\omega_{inner}}{2} \left(1 - \frac{d_b}{d_m}\right) \quad (3)$$

III A. STRUCTURE DEFECT INDUCED VIBRATION

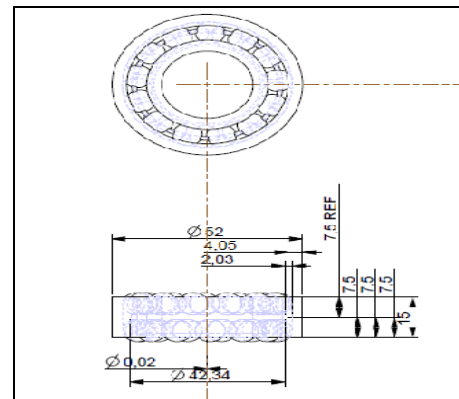


Figure 2: Geometry of self-aligning bearing 1205k

The load distribution on a rolling element bearing is given by

$$q(\theta) = q_{max} [1 - (1 - \cos \theta)^n] \quad (4)$$

Where q_{max} -Maximum load

θ -limiting angle

e - Load distribution factor

$n = 3/2$ for roller bearings

$n = 10/9$ for ball bearings

In a bearing with nominal diametral clearance, Q_{max} can be approximated as,

$$Q_{max} = \frac{Fr}{Z \sin a} \quad (5)$$

Where Fr – Applied radial Load

Z – Number of rolling elements

a - Mounted contact angle

Table I
 Parameters for the self aligning bearing

self aligning bearing 1205k	Values
Outer diameter	52mm
Inner diameter	25mm
Thickness	15mm
Mean diameter	38.5mm
Ball diameter	8.1mm
Number of balls	26

IV. EXPERIMENTAL SETUP

An experimental test rig built to predict defects in self aligning bearings is shown in Figure 3. The test rig consists of a shaft with central rotor, which is supported on two bearings. A motor coupled by a flexible coupling drives the shaft.



Figure 3: Experimental setup for bearing

Vibration characteristics are very important in the study of diagnostics for the system. In the experiment setup two bearing are considered in which one bearing was without defect and other bearing was with defect, both the bearing was attached to the system one by one for carry out the result. The dimension of the bearing are given in the Table 1. After taking the result it was seen that the values of amplitudes was more for the bearing with defect compare to bearing which has no defect. The natural frequency of the system was around the 34Hz, it was seen at the time of processing the data that for the defect bearing the values of amplitude was increasing when frequency of the was nearby natural frequency of the system. The various values of acceleration, velocity for the study of the vibration characteristics were taken and these are shown in the figure respectively.

To monitor load and vibration within the bearing structure, a sensor is embedded into a slot cut through the outer ring. The sensor has solid contact with both the top of the slot and the bearing housing. Each time a rolling element passes over the slot, the sensor generates an electrical charge output that is proportional to the load applied to the bearing F_r . Since the outer ring is structurally supported by the bearing housing, it can be assumed as rigid. The sensor is modelled as a spring with stiffness k that is related to its material composition. The section of the bearing outer ring where the slot is cut can be modelled as a

beam of varying cross-section, with a spring support at the midpoint. Since the ends of the beam are solidly connected to the surrounding bearing structure, which is directly supported by a rigid housing, clamped boundary conditions are considered appropriate.

V. DESIGN AND ANALYSIS

In this segment modelling of bearing is done with the help of PRO-E software, modelling is a complex task for designing a bearing because in the modelling of bearing various types of joints should be applied at the design stage which is very complex.

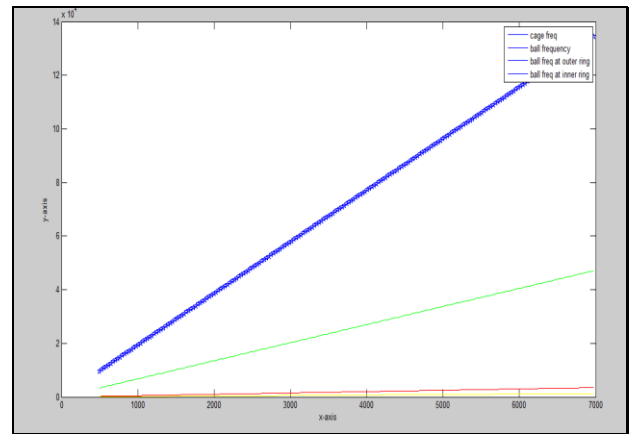


Figure 4: Bearing frequencies for shaft speed 0-7000rpm

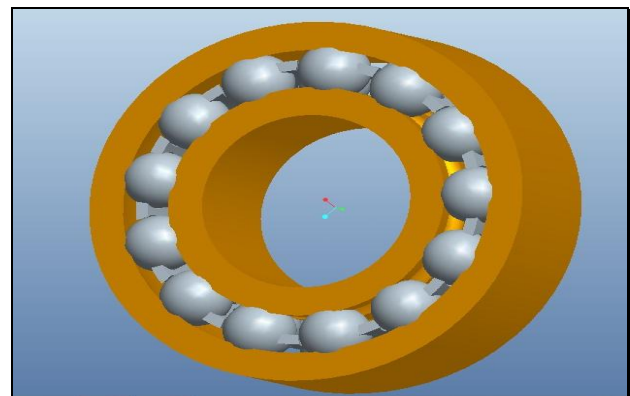


Figure 5: Self aligning bearing 1205k model with complete dimension, model in Pro-E software

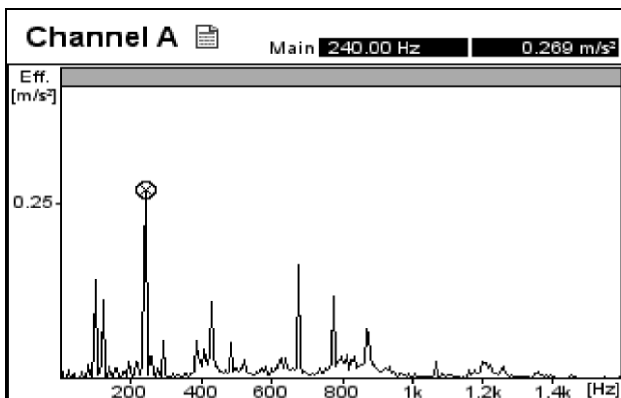
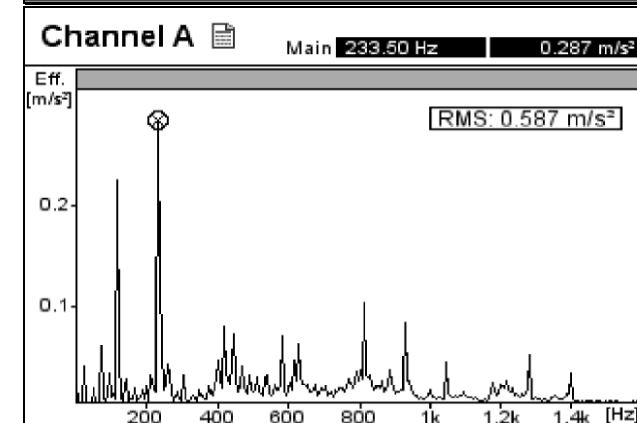
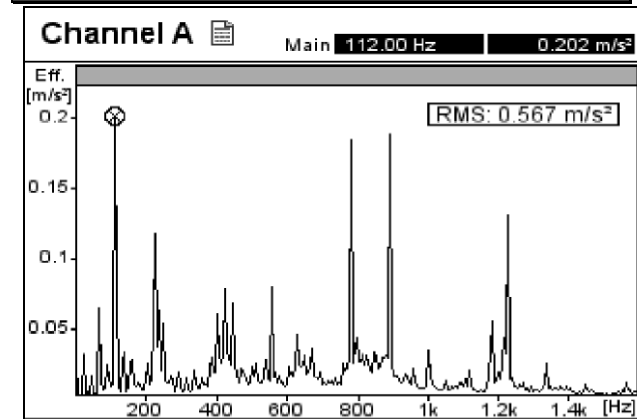
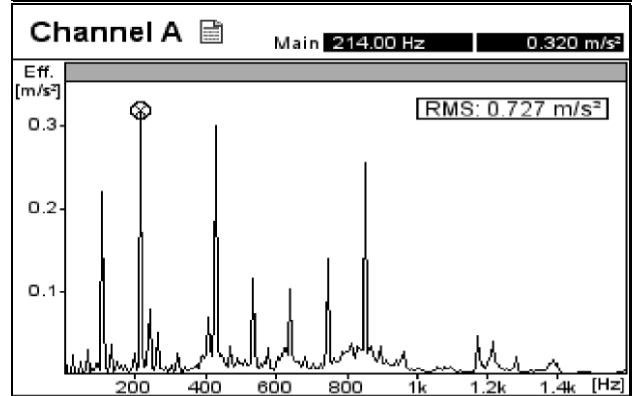
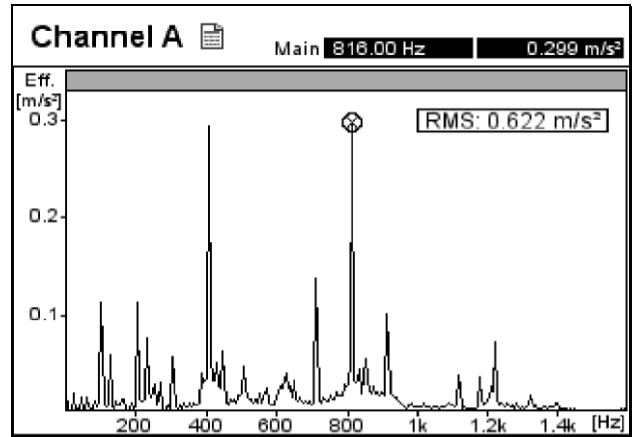
Combination of pin joint and cylindrical joint is applied in the model generation for the movement of balls with respect to inner ring, outer ring and cage part respectively. Matlab program is also prepared for finding different geometry parameters of the bearing with the help of formulae which were found from different papers and books. For finding the frequency of ball, BPFI, BPFO and cage frequency, Matlab program is prepared and their results are mentioned in the figures. Figure 5 showing the model of self align bearing which is prepared in PRO-E software whose parameter is defined in Table 1. Parameters for the bearing specifications were defined, so that they could be modified for any type of bearing that was to be analyzed. A defect in the outer ring was modelled by a cylindrical hole. Hence the parameters defined included:

outer raceway diameter, outer ring diameter, thickness of the outer ring, raceway radius, defect depth and the defect radius.

VI. RESULT AND DISCUSSION

Vibration characteristics are very important in the study of diagnostics for the system. In the experiment setup two bearing are considered in which one bearing was without defect and other bearing was with defect, both the bearing was attached to the system one by one for carry out the result. The dimension of the bearing are given in the Table 1. After taking the result it was seen that the values of amplitudes was more for the bearing with defect compare to bearing which has no defect. The natural frequency of the system was around the 34hz, it was seen at the time of processing the data that for the defect bearing the values of amplitude was increasing when frequency of the was nearby natural frequency of the system. The various values of acceleration, velocity for the study of the vibration characteristics were taken and these are shown in the figure respectively.

First setup is run for few minutes to settle down all minor vibration. After this Accelerometer along with the vibration analyzer is used to acquire the vibration signals. Vibration signals are measured at different speeds of the system for both defective and non defective bearing. Following are the few results which are taken through the help of FFT analyser. During performing the experiment shaft speed are vary from 1200 rpm to 2040 rpm, during these speed of the shaft amplitude values in terms of acceleration (m/s^2) and velocity (m/s) were taken for better understanding. For without defect and with defect bearing result were taken in time domain, correspondingly frequency domain result were also taken for defective bearing for better understanding of vibration amplitude values.



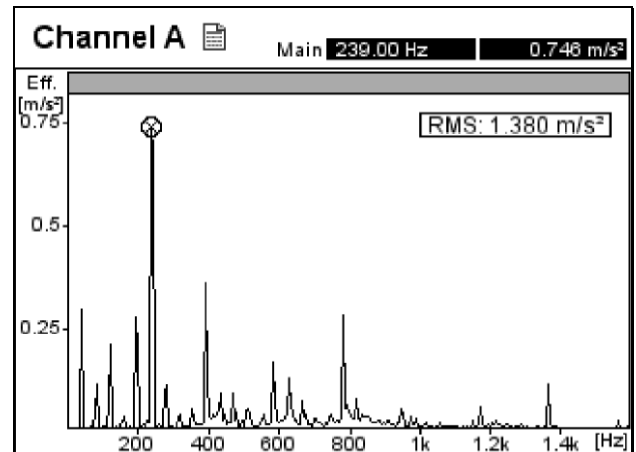
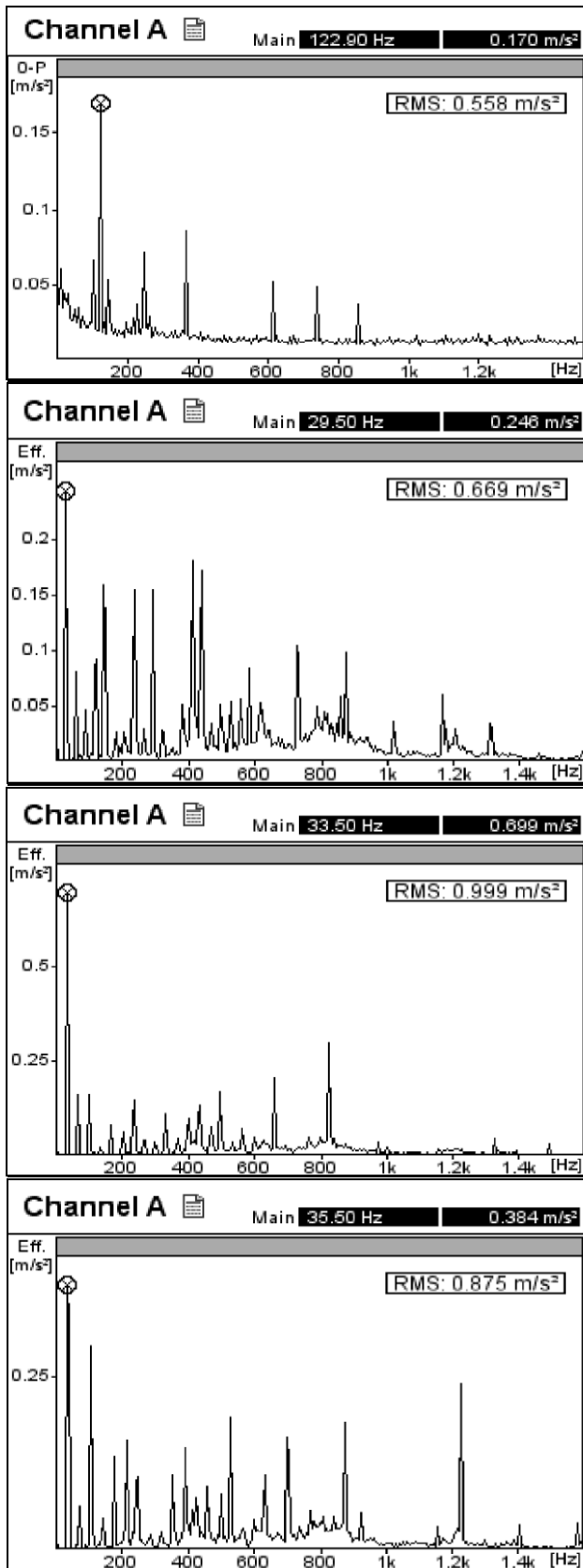
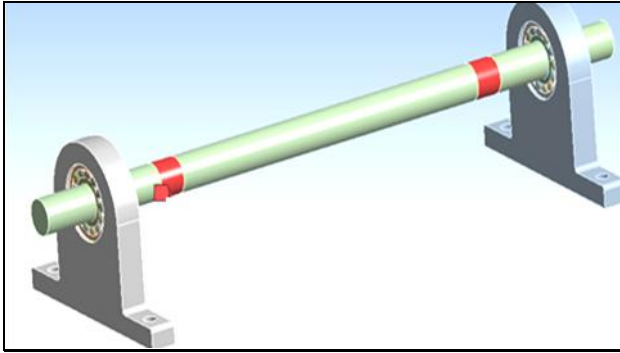


Figure 6: Acceleration plots for different speed of the shaft

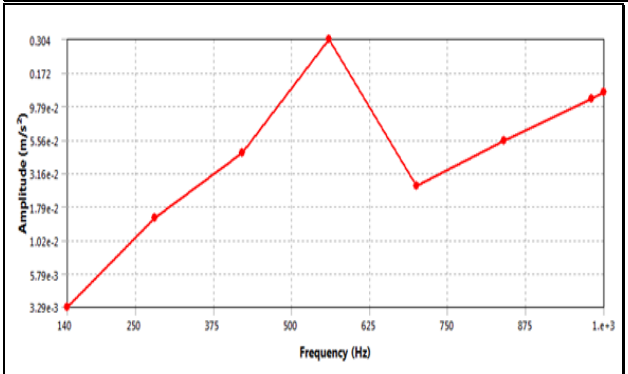
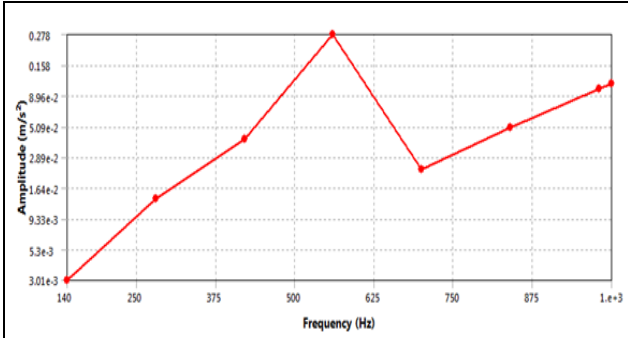
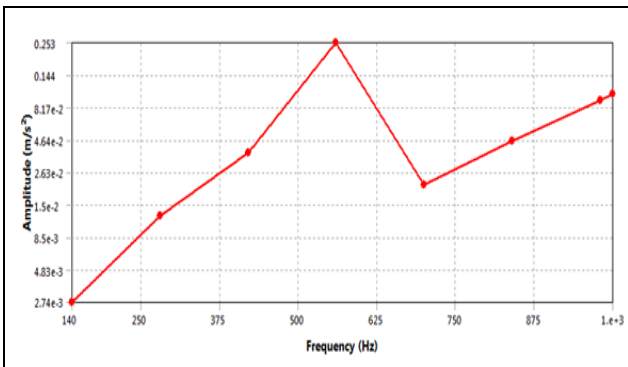
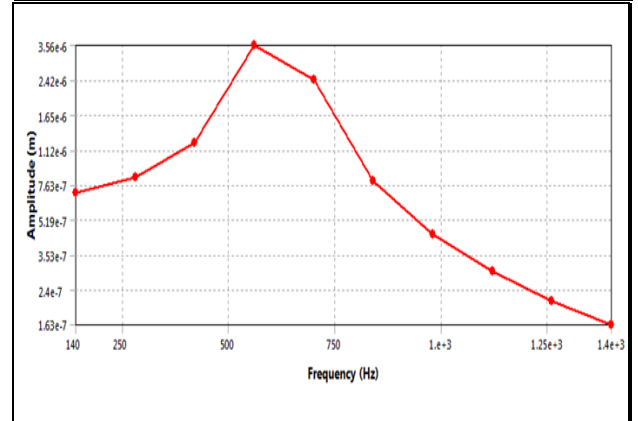
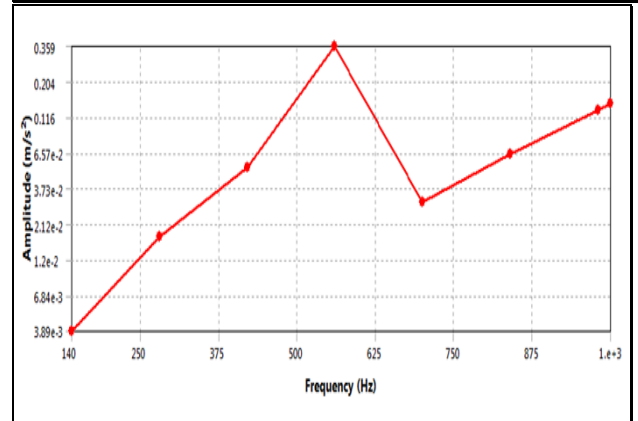
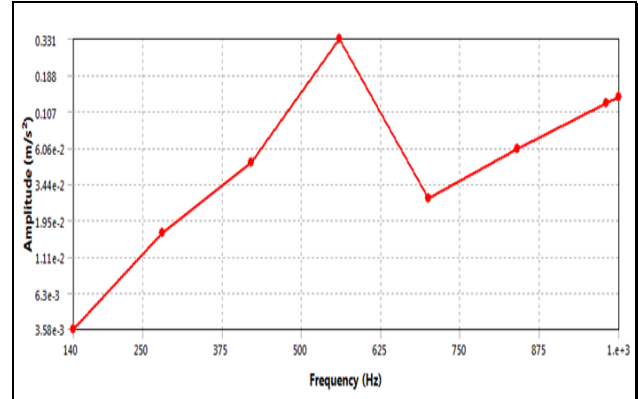
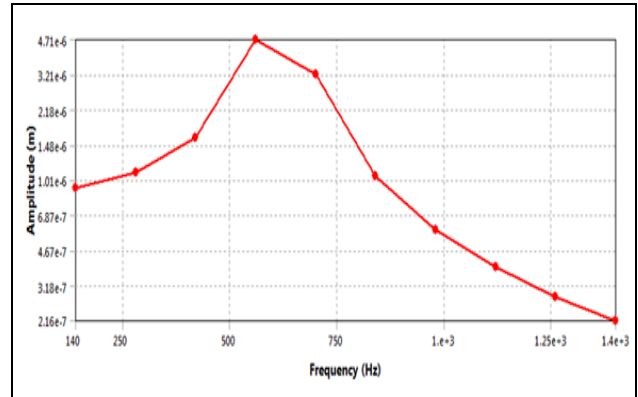
Table II
Amplitude values with respect to shaft speed

Speed of the shaft Rpm	Non-defective bearing Maximum amplitude		Defective Bearing Maximum amplitude	
	mm/s	µm	mm/s	µm
1200	1.212	29.035	2.465	46.945
1260	1.362	26.775	4.090	50.114
1320	2.267	42.570	7.954	94.750
1380	2.906	63.241	5.716	71.036
1500	3.601	44.590	3.616	44.810
Speed of the shaft Rpm	Maximum amplitude values m/s ²			RMS m/s ²
1200	0.269			0.522
1260	0.299			0.622
1320	0.727			0.727
1380	0.202			0.567
1440	0.287			0.587
1500	0.170			0.558
1800	0.246			0.669
2040	0.699			0.999
2160	0.384			0.875
2400	0.746			0.980

For the finite element analysis, ANSYS software were used for comparing the result with the experiment, at the beginning parasolid file of whole assembly was transported from the PROE software in ANSYS module, in this module firstly modal analysis was done, then the dynamic analysis was performed on the system, in the analysis two element was defined one for the bearing and another for the shaft and plumber block. These two elements were tetrahedron 4-node and tetrahedron 10-node element both are solid element. Refinement was done at ball and cage as well as at the both outer and inner ring for better result and accuracy.



After meshing properly and defining the loading condition in the system analysis were run for number of time for getting the result in FEA software ANSYS12.whose result are shown in the figure 7.these result almost matching with the maximum amplitude values of experiment result which were shown in the Table II.



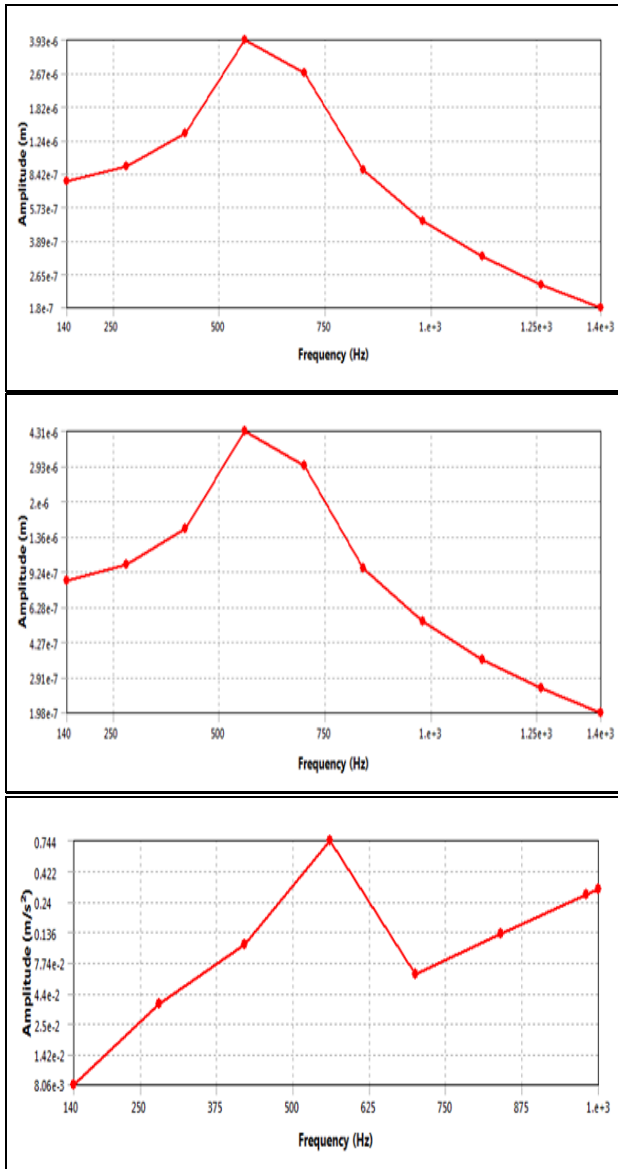


Figure 7: Amplitude values in terms of acceleration and displacement with respect to shaft speed in ANSYS 12 software.

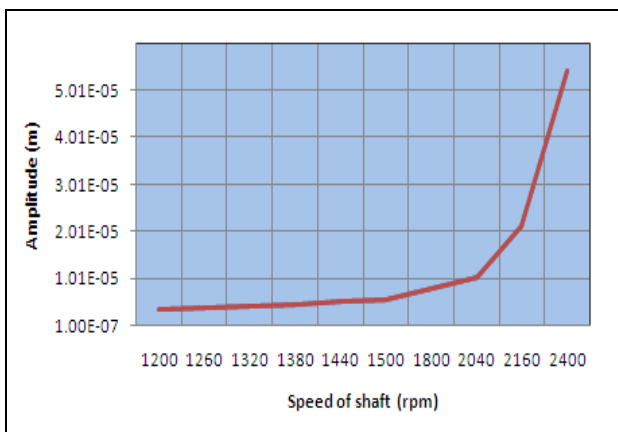


Figure 8: Amplitude values in terms of displacement wrt shaft speed.

Figure 8 is showing the amplitude values in terms of displacement with respect to the shaft speed, in the analysis the probe was set at non drive end the above result is almost same compare to the Experiment result, also for the further

analysis in finite element software different damping coefficient (Nm/s) and damping ratio was changed and correspond to that various amplitude in terms of displacement were recorded and for these values graphs were plotted by seeing these graphs, it is clear that with the increasing value of damping ratio and damping coefficient the maximum amplitude was decreasing linearly, so the fact is that if the values of vibration amplitude decrease by this approach then it is beneficial for its life of the bearing and jerks can be eliminated at a great extent. Table III is showing the all values which were obtained at the time of analysis.

Table III
 Amplitude values wrt various damping coefficient.

Damping Coefficient (Nm/s)	Amplitude at 1500 rpm	Amplitude At 1440	Amplitude At 1380
0	5.37E-06	5.13E-06	4.71E-06
50	3.32E-07	3.26E-07	2.83E-07
100	1.40E-08	1.35E-07	9.80E-08
150	3.54E-08	3.42E-08	2.99E-08
200	1.28E-08	1.19E-07	8.90E-08
250	1.76E-09	1.56E-09	1.10E-09
350	2.06E-09	1.98E-09	1.43E-09
400	3.98E-10	3.45E-10	3.02E-10
500	4.23E-11	4.12E-11	3.76E-11
600	4.35E-12	3.19E-12	2.76E-12

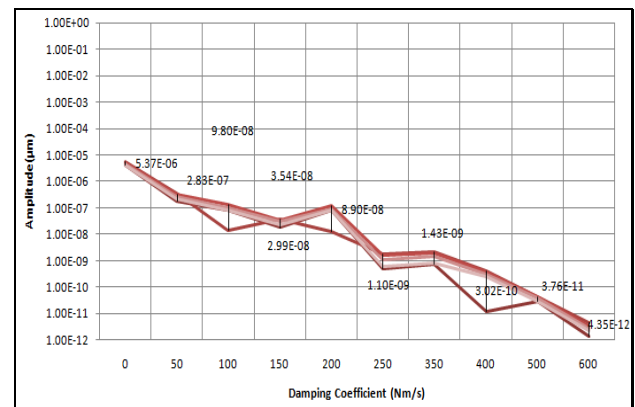
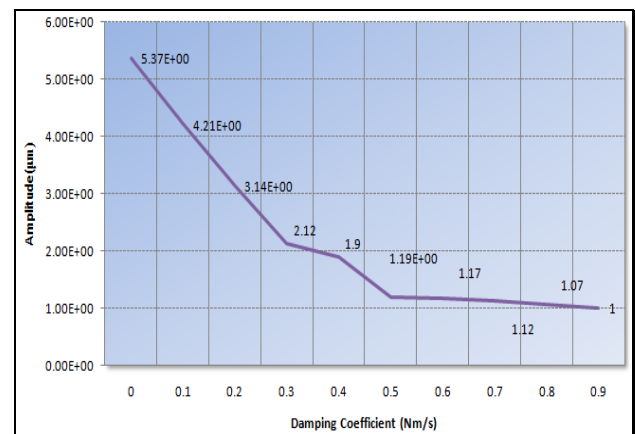


Figure 9: Comparison of maximum amplitude with respect to damping coefficient at different shaft speed.



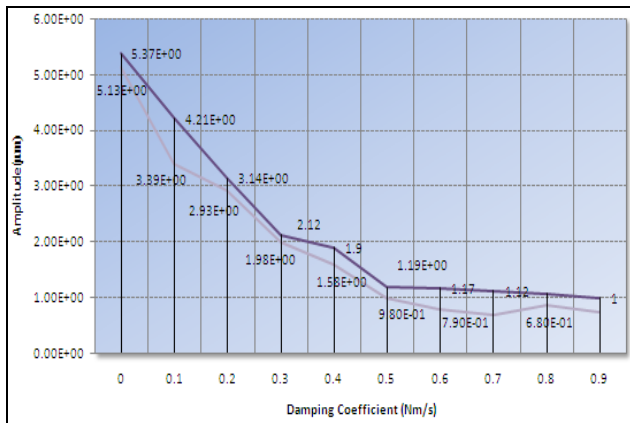


Figure 10: Comparison of maximum amplitude with respect to damping ratio at different shaft speed.

VII. CONCLUSION

It has been shown that finite element modelling can be effectively used to differentiate between vibration signatures for defects of different sizes in the bearing. Assumptions have been made for the variation of forces exerted by the rolling element on the outer ring in the vicinity of the defect. The main aim has been to understand the trend of vibration signatures for the local defect in the bearing through finite element analysis as well with the experiment that has been done with the help of FFT analyser. The natural frequency of the system was around 34Hz because for both the system the amplitude that was obtained during the study of the experimental result was maximum than any other values. Defect size was 0.02 mm^3 was studied and the different plots in terms of acceleration and displacement amplitude were generated both in the experiment and FEA software ANSYS 12. The result was almost same in both. A more detailed analysis based on this project was also done by changing the value of damping coefficient and damping ratio in the finite element analysis whose plots are shown in the paper. With the increasing damping coefficient as well as damping ratio the amplitude was constantly decreasing.

IX. FUTURE WORK

It is important to be able to precisely understand the variation of forces due to the rolling element passing over a defect in a bearing. A detailed analysis using experiments on a bearing test rig should be performed. The finite element model can then be iteratively adjusted so as to conform to the vibration signature that is arrived at by experimentation. Matlab programming and other codes would be used for better exercise to improve the accuracy of the finite element modelling results and for reducing the time consumption.

IX. ACKNOWLEDGEMENT

I owe a great many thanks to a many people who helped and supported me during mine dissertation work, from bottom of my heart I want to thank my guide Prof.U.A.patel who correct me and guided me throughout my dissertation work. I want to extent my thanks to D.N.Shah sir who is the assistance of dynamic laboratory of

L.D.College of Engineering who supported me at the time experiment a lot with its full dignity.

X. REFERENCES

1. Abhay Utpat, R.B. Ingle and M.R.Nandgaonkar, "A model for study of the defects in rolling element bearings at higher speed by vibration signature analysis," World Academy of science, Engineering and technology(56) ,2009
2. M.S Patil, Jose Mathew & P.K. Rajendrakumar, "A theoretical model to predict the effect of localized defect on vibrations associated with ball bearing," International journal of mechanical science 52,1193-1201,2010
3. I. Antoniadis and G.Glossiotis, "Cyclostationary analysis of rolling element bearing vibration signal", Journal of sound and vibration 248(5),829-845,2001
4. Sun-Min Kim, Sun-kyu lee, "Effect of bearing support structure on the high speed spindle bearing compliance," International journal of mechanical science (42), 365-373,2001
5. C.Zhang, T.Kurfess, "Adaptive prognostics for rolling element bearing condition," Mechanical systems and signal processing 13(1),103-113,1999
6. Zeki Kiral, Hira Karagulle, "Simulation and analysis of vibration signals generated by rolling element bearing with defects" Tribology International 36, 667-678,2003
7. S.P. Harsha, "Nonlinear dynamic analysis of an unbalanced rotor supported by roller bearing" World Academy of science, Engineering and technology(76),2004
8. Jang, G.H., & Jeong, S. W. (2004), "Vibration Analysis of a rotating System Due to the Effect of Ball Bearing Waviness", Journal of Sound and Vibration 269, 709-726.
9. Hoon Voon Liew,"Analysis of time varying rolling element bearing characteristics, " Journal of sound and vibration 283,1163- 1179
10. Roger boustang," A subspace method for the blind extraction of a Cyclostationary sources: application to rolling element bearing diagnostics, mechanical system and signal processing (19) 2005,1245-1259
11. Radoslav tomavic, "Calculation of the boundary values of rolling bearing deflection in relation to the number of active rolling elements," Mechanism and machine theory (21) 2011,364-368
12. Harris, T. A., Rolling Bearing Analysis, Fourth Edition New York: John Wiley & Sons Inc.1984.

Risk Assessment Methods and Application in the Construction Projects

DR. R. K. KANSAL, MANOJ SHARMA

Department of civil Engg. Madhav Institute of Technology, Gwalior

Abstract:

Risks are very common in construction sector. Risk is the Possibility of suffering loss and the impact on the involved parties. Risk is identified and then risk assessment and analysis is done. Then risk management and risk mitigation is carried out. Risk affect construction sector negatively and focusing on risk reduction measure it important. The purpose of this study is to assess the use and method of risk identification techniques in the construction industry. They are classified in specialized industrial construction, infrastructure and heavy construction. We conducted a survey research by applying a questionnaire among in the construction industry. The risk identification techniques more frequently applied in construction are checklist, flowchart, Brain storming, Delphi method etc.

Key words: Risk, Risk identification techniques,

1. Introduction

There are many risks encountered in the projects particularly construction project R Norman G (1993). The possibility of encountering loss and its impact is known as risk. Risk is a negative term referring to loss and impact of loss, but there is also positive risk involving favorable results and their impact is risk involving favorable results and their impact is known as opportunity Vaughan EJ (1986). In accordance with Ferreira (2009) the recovering of the construction area is very important to the engineering service sector. Faced with this increase of demand, we verify that it is necessary to include risk management in project planning and management so as to identify, assess, manage and control the risks that would be adverse to the project goals (Kerzner 2002). This theme is relatively new, though since this methodology was elaborated in the last decade and the companies have been adopting it in their projects in the lasting years. The risk identification phase was considered by many studies in this area as the most important phase in the risk management process. During this phase there is a lot of identification techniques that could help the identification process. The aim of this article is to assess the degree of knowledge and utilization of risk identification techniques in the construction projects.

2 Literature Review -

Hull (1990) introduces different models, based on Monte Carlo Simulation and PERT, to assess proposal risk from cost and duration point of view.

Mustafa and Al-Bahar (1991) adopt the Analytic Hierarchy Process (AHP) to assess construction project risk. It applied the concept of value and weight to assess risk probability and impact.

Dikmann (1992) discuss, from a theoretical and practical perspective, the issue of applicability and the short coming of risk analysis techniques based upon probability theory.

Paek et al.(1993) proposes a risk-pricing algorithm, using FST, to assist contractors when determining the bid price of a construction project.

A critical literature review (Williams 1995) concludes that limited research had been undertaken on quality risk and there was a lack of research into the impact of risk on different project objectives.

Williams (1996) discuss the limitations of P- I risk models, while advocating a three dimensional risk model : Probability – Impact- predictability, as recommended by Charette (1989). A stochastic model, which combines the randomness of the cost and the duration of a project activity, was developed by Tavares et al.(1998).

Hastak and Shaked (2000) deploy AHP within a framework for assessing international construction projects, with risk modeled as P-I. Using the well established Fuzzy Set Theory (FST) to assess construction risk Tah and Carr (2000) develop a qualitative risk assessment model, which incorporates linguistic variables to assess risk likelihood and impact, and the interdependencies between different risks.

A DSS for managing risk in the early stages of a construction project is proposed by Dey (2001) based on AHP and decision trees. It seeks to identify the best strategy, project scenario, for managing construction project risk through the expected monetary value (EMV) of each risk response strategy.

Baloi and price (2003) compare different theories used for dealing with uncertainty within the construction industry and recommend FST as a vital solution for assessing construction uncertainty. Shang et al. (2005) develop a DSS to facilitate construction risk assessment at design and conceptual stages.

Dikmen and Birgonul (2006) use AHP within a multi-criteria decision making (MCDM) framework for risk and opportunity assessment of international construction projects. They calculate the overall risk level of each project by multiplying the relative impact with the relative probability for each risk and then adding the score up. Hsueh et al.(2007) to develop a multi-criteria risk assessment model for construction joint-Ventures. It merely proposes that decision makers are able to make-judgements: the higher the expected utility value, the lower the overall project risk. Zayed et al. (2008) use AHP to assign weights to risks before calculating project risk level, which is defined as the sum of the weighted risk effects of risk factors.

3. Risk Identification and Risk Identification Technique -

The risk identification phase as being either one of the most important stages within the risk management process, (Martins, 2006) or even the most challenging and relevant phase in this process (Kloss-Grote and Moss, 2008) Chapman (1998) divided the risk identification phase into three categories.

1. The Risk identification conducted only by a risk analyst and based exclusively in his practice, knowledge and capacity.
2. The Risk identification was conducted through the interview of the risk analyst with one or many members of the project staff in order to analyze the reviewed data and the project life cycle based on the knowledge and expert of the people interviewed.
3. The Risk identification in which the risk analyst guides one or many work groups applying the risk identification techniques.

4. Risk Identification Techniques -

1. Brainstorming – An idea generation group technique is divided in two phases. (i) idea generation phase, in which participant generate as more ideas as possible (ii) idea selection phase, the ideas are filtered, remaining only those approved by the entire group. (Morano et al. 2006).
2. Delphi Technique – Delphi is a technique to obtain an opinion consensus about future events from a group of experts. It is supported by structured knowledge, experience and creativity from an expert panel (Wright and Giovinazzo as cited by Morano et al.,2006)
3. Interview/ Expert judgment – Unstructured, semi structured or structured interviews individually or collectively conducted with a set of experienced project members, specialist or project stakeholder (Morano et al.,2006)
4. Checklist – It consists of a list of item that are marked as yes or no , could be used by an individual project team members, a group or in an interview. (Morano et al.,2006)
5. Influence Diagram – It is a graphical representation containing nodes representing the decision variables of a problem. A traditional influence diagram is formed by three types of nodes: utility, decision and informational. The causal relationship occurs between utility and chance nodes and represents a probabilistic dependence.
6. Flowchart – Graphical tool that shows the steps of a process. This technique is applied for a better comprehension of the risks or the elements interrelation (Morano et al.,2006)
7. Cause-and-Effect Diagrams – These are also called Ishikawa diagrams or fishbone diagram, illustrate how various factor might be linked to potential problems or effects(PMBOK – PMI, 2008). The diagram is designed by listing the effect on the right sides and the causes on the left sides. There are categorized for each effect, and the main causes must be grouped according to these categories (Morano et al., 2006)

5 Methodology -

1. Data collection for risk assessment
2. Analysis of Data by – Risk Significant Index Method

The accumulated data will be grouped into categories risk and its magnitude of consequence on project objective in term of Cost, Time, Quality, Environment and Safety. The three point scales for the risk α (Highly likely, likely, less likely) and the consequence β (High magnitude, Medium magnitude, Low magnitude) will be converted into numerical scales. The numerical values and the calculation of the Risk Significance Index depending on the design of the questionnaire, different value can be assigned to α and β . A three point rating scale is chosen according to Shen et al and Zon et al.(2001) and Wang and Liu (2004), High, Highly take value of 1, Medium takes a value of 0.5 and Less or Low take a value of 0.1. The average score for each risk considering its significance an a project can be calculated by

$$r_{ij} = \alpha_{ij} \beta_{ij}$$

Where

- r_{ij}^k Significance score assessed by respondent j for the impact of risk i on project objective k
- i = ordinal number of risk
- k = ordinal number of project objective

- j = ordinal number of valid feedback to risk i
 n = total number of valid feedback to risk i ;
 α_{ij} = Likelihood occurrence of risk i , assessed by respondent j
 k
 β_{ij} = level of impact of risk i on project objective k , assessed by respondent j .

The average score for each risk considering its significance on a project objective can be calculated

$$R_i^k = \frac{1}{n} \sum_{j=1}^n \alpha_{ij} \beta_{ij}^k$$

Where R_i^k = Significance index score for risk I on project objective k .

6. Conclusions -

This paper is based on a literature review on the risk assessment methods. The risk assessments approaches are applied in various areas and the problems solve. It was found that the currently used methods for risk assessment are Brainstorming, checklist, Flowchart Delphi method, Risk significant index method. Each method of risk assessment has their limitation therefore this paper attempt to formulate integrated risk assessment tools. It was observed that currently used risk assessment methods can be integrated into new approach that can aid the decision makers applying the risk assessment effectively.

7. References -

- [1] R.C.Walke et al. "An approach to risk quantification in construction projects" International Journal of Engineering Science and Technology Vol. 3 No. 9 September 2011 .pp 6846-6855.
- [2] L. Y. Shen,1 George W. C. Wu,2 and Catherine S. K. Ng3. Risk assessment for construction joint venture in chinaJournal of construction Engineering and management Vol. 127 No. 1 January/ February 2001 pp. 76-81.
- [3] Wenzhe Tang1; Maoshan Qiang2; Colin F. Duffield3; David M. Young4; and Youmei Lu5. Risk management in the Chinese construction industry. Journal of construction Engineering and Management ASCE/ DECEMBER 2007
- [4] Dr Patrick. X.W. Zou1, Dr Guomin Zhang2 and Professor Jia-Yuan Wang3 1 and 2: Faculty of Built Environment, University of New South Wales, Sydney 2052, Australia;3: College of Architecture and Civil Engineering, Shenzhen University, Shenzhen, P.R. China. Identified Key Risks in Construction Projects: Life Cycle and Stake Holder Perspectives.
- [5] Akintoye A.S and MacLeod, M.J. (1997). Risk analysis and management in construction, International Journal of project Management. Vol 15, February 1997, pages 31-38.
- [6] Ossama A.Abdou (Asst.Prof. Dept. of Civil and Arch. Engg.Drexel University) Managing Construction Journal of Architectural Engineering, Vol 2, No.1 March 1996, pp. 3- 10.
- [7] Matins Claudia Garrido, Morano Cassia Andra Ruotolo, Fereira Miguel Luiz Riberio and Haddad Assed Naked. Risk Identification Techniques Knowledge and Application in the Brazilian Construction Vol. 2(11), pp. 242-252, November2011
- [8] Chapman R.J. (2001) The Controlling Influences on Effective Risk Identification and Assessment for Construction Design Management, International Journal of Project Management. Vol 19.Issue 3, pp. 147-160.

APPENDIX I
“Risk in construction industry” Question Survey

Type of risk		Probability level of the risk occurrence (a)						Degree of impact or the level of loss if the risk occurs (b)						Total Risk ab
		N A	Very Small	Small	Normal	Large	Very Large	N A	Very Low	Low	Medium	High	Very High	
A	Financial Risk	0	1	2	3	4	5	0	1	2	3	4	5	
1	Loss due to fluctuation of interest rate													
2	Low credibility of shareholder and lender													
3	Change in bank formalities and lenders													
4	Loss due to rise in fuel prices													
5	Insurances risk													
B	Legal Risk													
1	Breach of contract by project partner													
2	Lack of enforcement of legal judgment													
3	Improper verification of contract document													
4	Uncertainty and unfairness of court justice													
C	Management Risk													
1	Change of top management													

2	No past experience in similar project													
3	Short tender time													
4	Internal management problem													
5	Improper project feasibility study													
6	Poor relation and disputes with partner													
7	Team work													
8	Time constraint													
9	Project delay													
D	Market Risk													

The Comparative THD Analysis of Neutral Clamped Multilevel Z-Source Inverter using Novel PWM Control Techniques

S. Mohamed Yousuf¹, P. Vijayadeepan², Dr. S. Latha³

¹*Assistant Professor in EEE, Sri Subramanya College of Engg and Tech, Palani, T.N, India.*

²*Assistant Professor in EEE, Sri Subramanya College of Engg and Tech, Palani, T.N, India.*

³*Associate Professor in EEE, Thiagarajar College of Engg, Madurai, T.N, India.*

ABSTRACT

A multilevel inverter is a power electronic device made to synthesize a desired AC voltage from several levels of DC voltages. These types of inverters are suitable in various high voltage and high power application due to their ability to synthesize waveforms with better harmonic spectrum and faithful output. Multilevel inverters through a single X-shaped LC impedance network is an important development in recent years. The power quality improvement is achieved by reducing the harmonics present at the output voltage of the inverter. The total harmonics distortion (THD) values of the output voltages of the inverter are measured and compared. This paper presents the comparative analysis of several multicarrier PWM techniques, which is effectively used for harmonic mitigation in the proposed neutral clamped multilevel Z-Source inverter and this work is compared with conventional three level inverter by using MATLAB-SIMULINK.

Key words: Multi-Carrier PWM Control, Multilevel Inverter, Neutral Point Clamped (NPC) Inverter, Total Harmonic Distortion (THD), Z-Source Inverter.

I. INTRODUCTION

In the recent years, the revolution of multilevel inverters has many attractive features. In particular, high voltage capability, reduced common mode voltages near sinusoidal outputs, lower value of dv/dt , smaller or even number output filters make multilevel inverter is a suitable topology for variable frequency induction motor drives and have recently been explored for low-voltage renewable grid interfacing applications [1], [5]. Despite of their generally favorable output performance, NPC inverters are constrained by their ability to perform only voltage-buck operation if no additional dc-dc boost stages are added to their front-ends. To overcome this limitation, a buck-boost Z-source NPC inverter is proposed in [1], [2]. An additional X-shaped impedance networks are added between two isolated dc sources and a neutral clamped circuitry, as illustrated in Fig. 1. The unique structure of the multilevel Z-source inverters allows them to reach high voltage with low harmonics without the use of transformers [8].

A zero harmonic distortion of the output wave can be obtained by an infinite number of levels. To synthesize multi level output ac voltage using different levels of dc inputs, semiconductor devices must be switched ON and OFF in such a way that desired fundamental is obtained with minimum harmonic distortion. There are different types of approaches for the selection of switching techniques for the

multilevel inverters. The multilevel inverters are mainly controlled with sinusoidal PWM technique and the proposed inverter can reduce the harmonic contents by using multicarrier PWM technique arrangements [5]. The 3-level NPC inverter with Z-Source is discussed in the references [1], [2] and the same inverter along with various multicarrier PWM techniques is discussed in the references [3]-[6], [8], [10]. The 5-level NPC inverter with space vector modulation is discussed in the references [7], [11].

In this paper, various multicarrier PWM techniques like Phase disposition (PD), Phase opposition disposition (POD), Alternative phase opposition disposition (APOD), phase shifted (PS) are proposed for three phase five level neutral clamped multilevel Z-Source inverter and the total harmonic distortion (THD) analysis is done for different modulation schemes. The proposed inverter can reduce the harmonic contents in the output phase voltages significantly. The total harmonic distortion (THD) reduction performance of three phase five level neutral clamped multilevel Z-Source inverter by using multicarrier PWM techniques are presented and the proposed work is compared with conventional three level neutral clamped multilevel inverter.

II. DESIGN AND OPERATION OF NEUTRAL CLAMPED MULTILEVEL INVERTER

The neutral clamped inverter, also known as diode clamped inverter. The basic architecture of this inverter discussed in references [7], [11]. The neutral clamped inverter delivers the staircase output voltage using several levels of DC voltages developed by DC capacitors. If m is the number of level, then the number of capacitors required on the DC bus are $(m-1)$, the number of power electronic switches per phase are $2(m-1)$ and the number of diodes per phase are $2(m-2)$. This design formula is most common for all the neutral clamped multilevel inverters. The DC bus voltage is split into three levels using two capacitors C_1 and C_2 , for five levels using four capacitors C_1, C_2, C_3 and C_4 as shown in Fig .1 and Fig .2. The voltage across each capacitor is $V_{dc}/4$ and the voltage stress across each switch is limited to one capacitor voltage through clamping diodes. The switching sequences of three phase 3-level and 5-level neutral clamped multilevel inverter are shown in table. I and II. As the number of levels increase the harmonic distortion decreases and efficiency of the inverter increases because of the reduced switching losses. The number of levels in multilevel inverters is limited because of the large number of clamping diodes required. The reverse recovery of these diodes is especially with multicarrier PWM techniques in a high voltage application is a major design challenge.

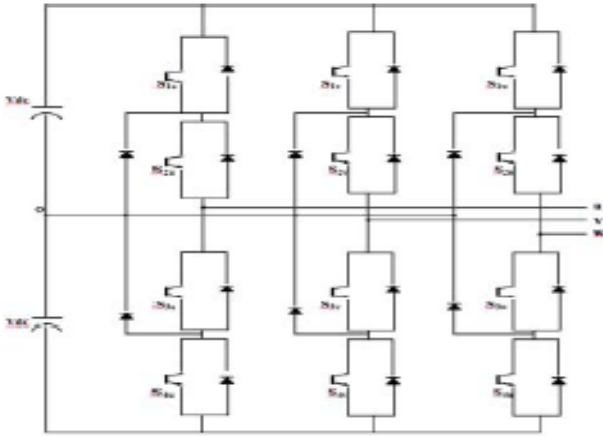


Fig .1. 3-Level Neutral Clamped Multilevel Inverter

TABLE I
THREE-LEVEL SWITCHING SEQUENCES

Terminal voltages	Switching Sequences			
	S _{a1}	S _{a2}	S _{a3}	S _{a4}
V _{DC}	on	on	off	off
0	off	on	on	off
-V _{DC}	off	off	on	on

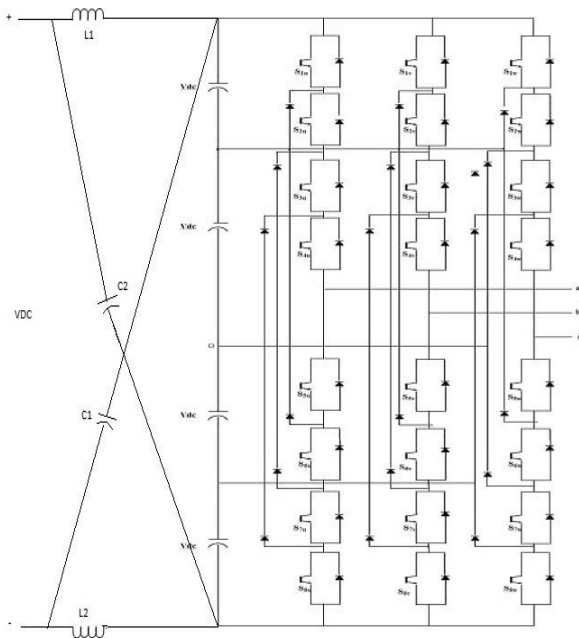


Fig .2. 5-Level Neutral Clamped Multilevel Inverter

TABLE II
FIVE-LEVEL SWITCHING SEQUENCES

Terminal voltages	Switching Sequences							
	S _{a1}	S _{a2}	S _{a3}	S _{a4}	S _{a5}	S _{a6}	S _{a7}	S _{a8}
2V _{DC}	on	on	on	on	off	off	off	off
V _{DC}	off	on	on	on	off	off	off	off
0	off	off	on	on	on	on	off	off
-V _{DC}	off	off	off	on	on	on	on	off
-2V _{DC}	off	off	off	off	on	on	on	on

III. CONTROL TECHNIQUES OF MULTILEVEL INVERTER

Multicarrier PWM Techniques involves the natural sampling of single modulating reference waveform typically being sinusoidal, through several carrier signals typically being triangular waveforms This modulation method is the logical extension of sine-triangle PWM for multilevel inverters, in which m-1 carriers are needed for m-level inverter. They are arranged in vertical shifts in continuous bands defined by the levels of the inverter. Each carrier has the same frequency and amplitude. A single voltage reference is compared to the carrier arrangement and the generated pulses are associated to each switching devices [6], [8].

A. Phase Disposition (PD)

This technique involves a number of carriers (m-1) which are all in phase accordingly. In 5 -level inverter all the four carrier waves are in phase with each other and compared with reference signal [4], [10]. According to that, the gate pulses are generated and are associated to each switching devices. The phase disposition PWM technique is illustrated in Fig. 3

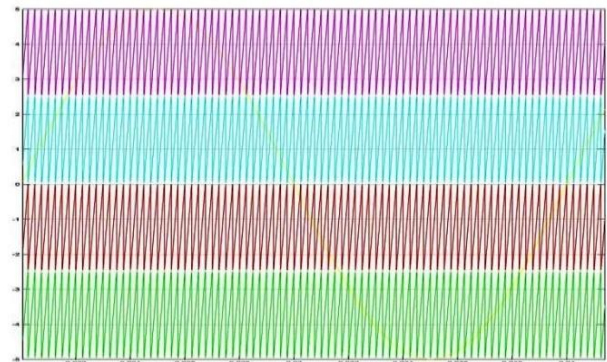


Fig .3. Phase Disposition PWM Technique

B. Phase Opposition Disposition (POD)

This technique employs a number of carriers (m-1) which are all in phase above and below the zero reference. In 5-level converters all the four carrier waves are phase shifted by 180 degrees between the ones above and below zero reference. The reference signal is compared with all four carrier waves thereby gate pulses are generated and are associated to each switching devices. The phase opposition disposition PWM technique is illustrated in Fig. 4.

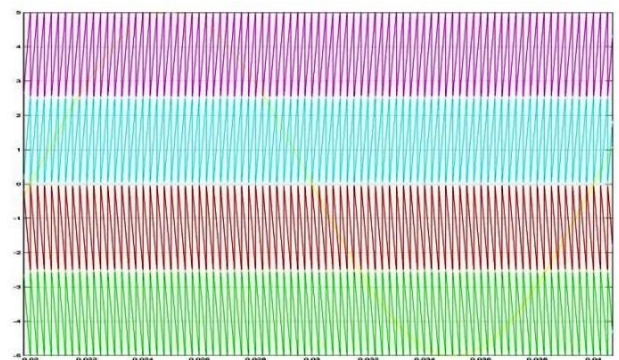


Fig .4. Phase Opposition Disposition PWM Technique

C. Alternative Phase opposition Disposition (APOD)

This technique requires number of carriers (m-1) which are all phase displaced from each other by 180 degrees alternatively. The alternative phase opposition disposition PWM technique is illustrated in Fig. 5.

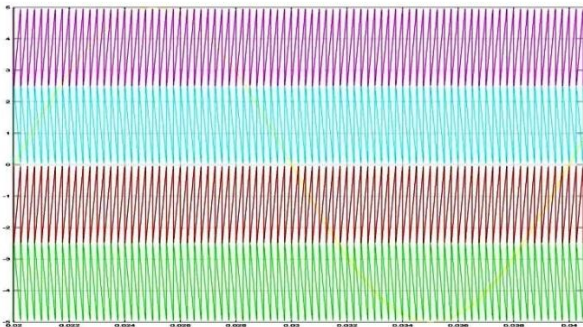


Fig .5. Alternative Phase opposition Disposition

D. Phase Shift (PS)

This technique employs a number of carriers (m-1) phase shifted by 90 degree accordingly. In 5 -level converter all the four carrier waves are phase shifted by 90 degree. The phase shifted PWM technique is illustrated in Fig. 6.



Fig .6. Phase Shifted PWM Technique

IV. SIMULATION AND EXPERIMENTAL RESULTS

The figure 7 shows the MATLAB/SIMULINK MODEL for 3-level neutral clamped multilevel inverter with PWM technique. It consists of 12 MOSFET switches, 6 clamping diodes and 2 DC link capacitors are connected with single DC source. The figure 10 shows the overall matlab/simulink model of three phase 5-Level neutral clamped multilevel Z-Source inverter. The figure 11 shows the subsystem diagram of 5-level neutral clamped multilevel inverter. This model consists of 24 MOSFET switches, 12 clamping diodes and 4 DC link capacitors with single DC source are connected in order to form 5-level neutral clamped multilevel Z-Source inverter. The figure 12 shows the multicarrier wave generation arrangement of the proposed converter. The figure 8 and 13 shows the output voltages of 3-level and 5-Level respectively. THD values of 3-level neutral clamped multilevel inverter with PWM technique as illustrated in Fig.9. THD values of different multicarrier PWM techniques are shown in figure 14 to 17. Experimental arrangement of neutral clamped multilevel z-source inverter is shown in figure 18.

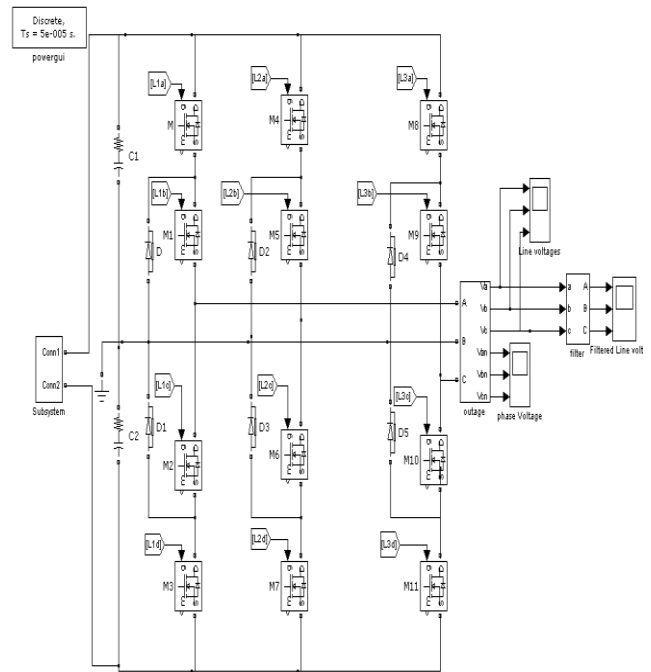


Fig .7. Three Phase 3-Level Neutral Clamped Multilevel Inverter Simulink Model

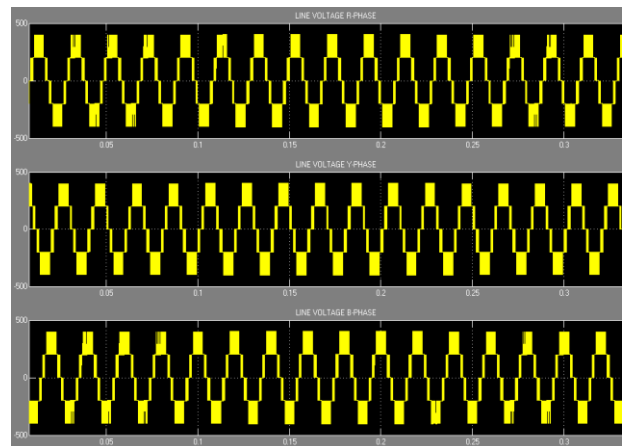


Fig. 8. Line Voltages of 3-Level Neutral Clamped Multilevel Inverter

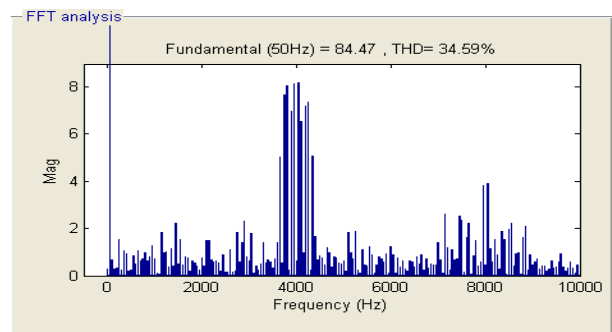


Fig .9. THD Values of 3-Level Neutral Clamped Multilevel Inverter with PWM Technique

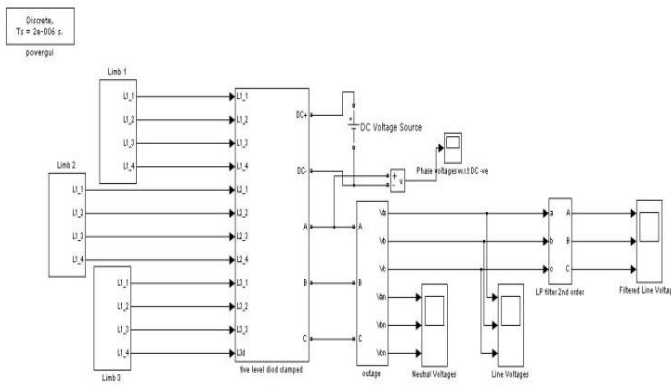


Fig .10. Three Phase 5-Level Neutral Clamped Multilevel Z-Source Inverter Simulink Model

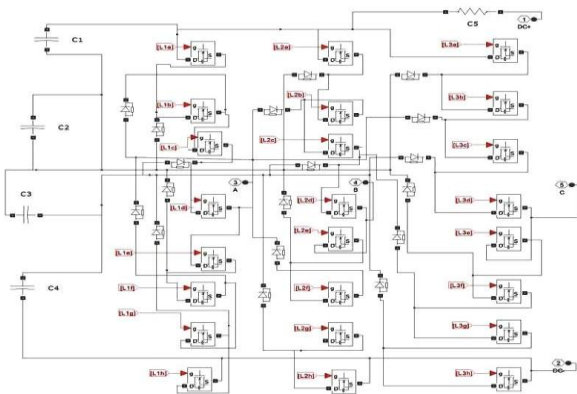


Fig .11. Subsystem Diagram of 5-Level Neutral Clamped Multilevel Inverter

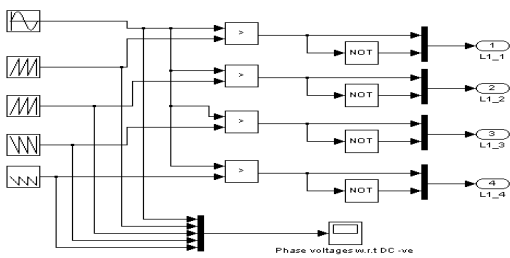


Fig. 12. Multicarrier Wave Generation

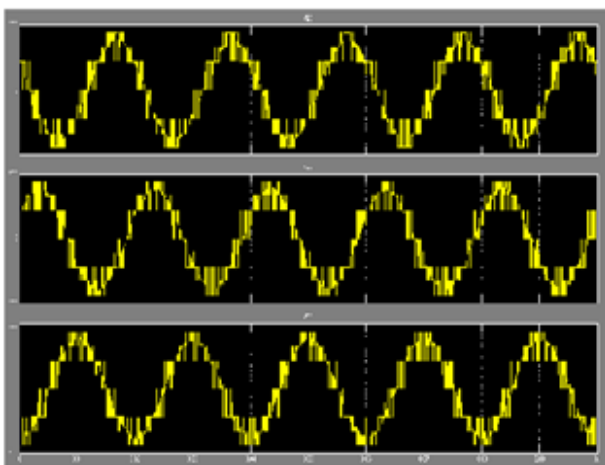


Fig.13. Line Voltages of 5-Level Neutral Clamped Multilevel Z-Source Inverter

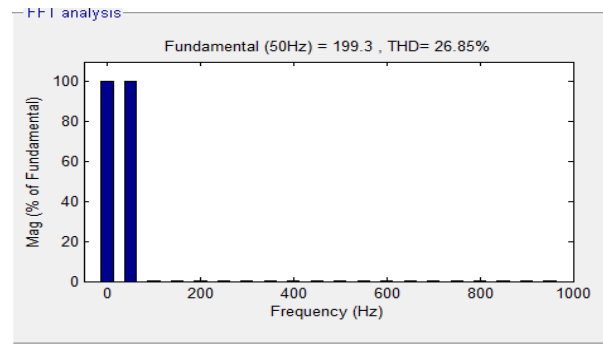


Fig .14. THD Values of Phase Disposition PWM Technique

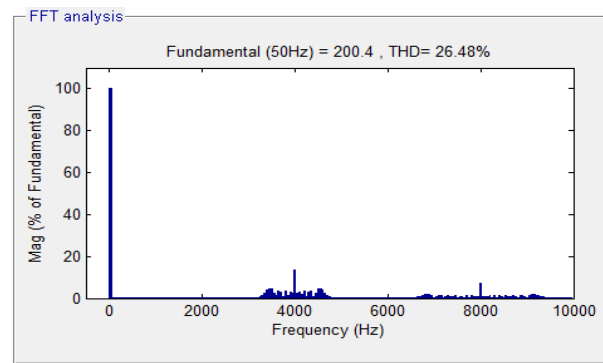


Fig .15. THD Values of Phase Opposition Disposition PWM Technique

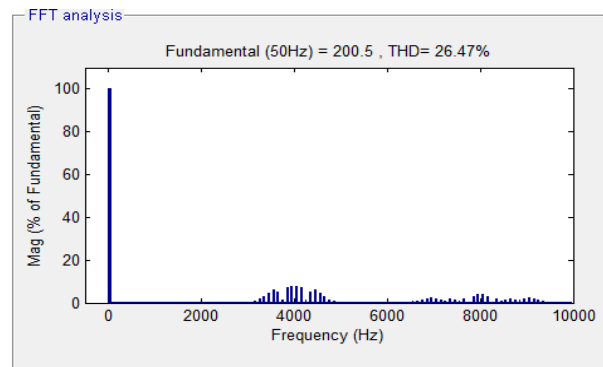


Fig .16. THD Values of Alternative Phase opposite Disposition PWM Technique

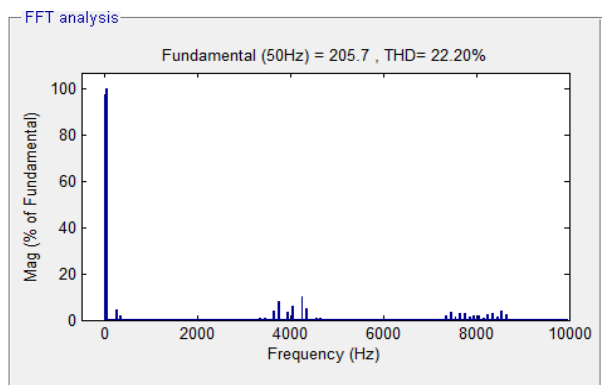


Fig .17. THD Values of Phase Shifted PWM Technique



Fig.18. Experimental Arrangement of Neutral Clamped Multilevel Z-Source Inverter

TABLE III
% OF THD VALUES

No of levels	Techniques	%THD
3-Level	PWM	34.59%
5-Level	Phase Disposition PWM	26.85%
	Phase Opposition Disposition PWM	26.48%
	Alternative Phase Opposite Disposition PWM	26.47%
	Phase Shifted PWM	22.20%

V. CONCLUSION

The comparative THD analysis of a three phase 5-level neutral clamped multilevel Z-source inverter is presented in this paper. The various multicarrier PWM technique like Phase disposition (PD), Phase opposition disposition (POD), Alternative phase opposition disposition (APOD) and Phase Shifted (PS) PWM techniques are applied to the proposed converter. The THD values of the output voltages are compared with all the above mentioned techniques. From the above discussion, it is absorbed that the phase shifted PWM technique has less harmonic content in the output phase voltage compared with other multicarrier PWM control techniques. The proposed work has compared to the conventional three level inverter with PWM technique by using MATLAB-SIMULINK.

ACKNOWLEDGEMENTS

The authors thank the Management, the Principal and EEE Department of Thiagarajar College of Engineering for providing the necessary facilities to carry out this work. Also the help and support of Management, the Principal and EEE department of Sri Subramanya College of Engg and Tech., during the course of this work is acknowledged

REFERENCES

[1] Poh Chiang Loh, Feng Gao, Frede Blaabjerg, and Sok weilim," Operational Analysis and Modulation Control of Three-Level Z-Source Inverters With Enhanced Output Waveform Quality," *IEEE Transaction On Power Electronics*, Vol.24, No.7, July 2009.

- [2] Poh Chiang Loh, Feng Gao, Pee-Chin Tan, and Frede Blaabjerg," Three-Level AC-DC-AC Z-Source Converter Using Reduced Passive Component Count," *IEEE Transactions On Power Electronics*, Vol. 24, No. 7, July 2009.
- [3] Jing Zhao, Xiangning He and Rongxiang Zhao," A Novel PWM Control Method for Hybrid-Clamped Multilevel Inverters," *IEEE Transactions On Industrial Electronics*, Vol. 57, No. 7, July 2010.
- [4] Brendan Peter Mcgrath and Donald Grahame Holmes," Multicarrier PWM Strategies for Multilevel Inverters," *IEEE Transactions on Industrial Electronics*, Vol. 49, No.4, August 2002.
- [5] Samir Kouro, Pablo Lezana, Mauricio Angulo and José Rodríguez, "Multicarrier PWM With Dc-Link Ripple Feedforward Compensation For Multilevel Inverters," *IEEE Transactions on Power Electronics*, Vol. 23, No.1, January 2008.
- [6] Leon M. Tolbert, Fang Zheng Peng and Thomas G. Habetler," Multilevel PWM Methods At Low Modulation Indices," *IEEE Transactions on Power Electronics*, Vol.15, No. 4, July 2000.
- [7] M. A. Saqib and S. A. R. Kashif," Artificial Neural Network Based Space Vector PWM for a Five-Level Diode-Clamped Inverter," *AUPEC, 2010*.
- [8] Sreenivasarao D, Pramod Agarwal and B. Das," A Carrier- Transposed Modulation Technique for Multilevel Inverters," *PEDES, 2010*.
- [9] S.Ebanazar Pravin and R.Narciss Starbell," Induction Motor Drive Using Seven Level Multilevel Inverter for Energy Saving in Variable Torque Load Application," *ICCCET March 2011*.
- [10] P.T.Josh, Jovitha Jerome and Arul Wilson," The Comparative Analysis of Multicarrier Control Techniques For SPWM Controlled Cascaded H-Bridge Multilevel Inverter," *Proceedings of ICETEECT 2011*.
- [11] G.Durgasukumar and M.K.Pathak," THD Reduction Performance of Multi-Level Inverter fed Induction Motor Drive," *IICPC, 2011*.



S. MOHAMED YOUSUF was born in Tamil Nadu, India in 1985. He received B.E Electrical and Electronics Engineering from Sri Subramanya College of Engg and Tech, Palani, Dindigul (Dt) and M.E Power Electronics and Drives branch from PSNA College of Engg and Tech, Dindigul, Dindigul Dt, India. He is pursuing Ph.D. degree at Anna University, Chennai, India. His area of interest is Power Electronics and Drives. He has published two papers in international journals, two papers in international conferences. He is currently working as a Assistant professor of Electrical and Electronics Engineering Department in Sri Subramanya College of Engg and Technology, Palani, Dindigul (Dt) Affiliated to Anna University, Chennai, Tamilnadu, India.



P. VJAYADEEPAN was born in Tamil Nadu, India, in 1983. He received B.E Electrical and Electronics Engineering from Sri Subramanya College of Engg and Technology, Palani Dindigul (Dt) and M.E Power Electronics and Drives branch from PSNA College of Engg & Technology, Dindigul, Dindigul Dt, India. He is pursuing Ph.D. degree at Anna University, Chennai, India. His area of interest is Power Electronics and Drives. He has published two papers in international conferences. He is currently working as a Assistant professor of Electrical and Electronics Engineering Department in Sri Subramanya College of Engg and Tech, Palani, Dindigul (Dt) Affiliated to Anna University, Chennai, Tamilnadu, India.



Dr. S. LATHA was born in Tamil Nadu, India, in 1965. She has completed Bachelor's degree in Electrical and Electronics Engineering on 1986 and Master's degree in Power Systems Engineering on 1987 from Thiagarajar College of Engineering, Madurai, India. She has completed Ph.D on November 2007 from Madurai Kamaraj University in the area of Flexible A.C Transmission System. She has been teaching for the past 20 years. She has secured first rank in Master's degree. She has published three papers in international journals, five papers in international conference. Her field of interest is application of Flexible AC Transmission System (FACTS) Controllers in Power System. She is currently working as a Associate professor of Electrical and Electronics Engineering Department in Thiagarajar College of Engg, Madurai, India.

X-Ray Diffraction and UV-Visible Studies of PMMA Thin Films

E. Shobhana

(Dept of Physics ,KTVR- Knowledge Park for Engineering and Technology,India)

ABSTRACT:

Thin films of Poly(methyl methacrylate) were deposited on glass micro slides using Chemical Bath Deposition Technique. The bath compositions include double distilled Toluene, double distilled Benzene which served as a complexing agent. The films were deposited at room temperature. The Structural characterizations of PMMA were carried out by XRD, which shows an amorphous nature of the material. The absorbance and transmittance of the films was measured using UV-Visible Spectroscopy which reveals that PMMA has higher transmission with very little absorption in the UV-Visible region. These films because of their high transmittance in the UV-Visible region are suitable for various optical applications, and also in non-linear optics.

Keywords: Amorphous, PMMA, UV-Visible XRD.

1.0 INTRODUCTION:

The interest in polymer material has grown continuously in the last two decades. Various methods for preparation of thin polymer films have emerged. Polymeric substances make up the most important class of organic materials, technically and economically. The familiar plastics, fibers, elastomers and biological materials that surround us attest to this importance. Such substances which are composed of great many identical groups or repeating units are known as (high polymers). Polymers composed of more than one kind of repeating units are termed copolymers. PMMA is widely used sometimes with plasticizer and or small amount of other ester as copolymers. The resins are so wide spread under the trade name of plexiglas in United States and Perspex in Europe that these words have become synonymous to transport plastic panels, windows and wind shields. The resistance of these resins to shattering and to weather has led to their large scale application in aircraft. PMMA has drawn tremendous interest due to its optical properties and its possible use in non-linear optics.

New techniques for polymer particles of controlled composition and size have been developed. Polymer thin films play an increasingly important role in technological application ranging from coatings, adhesives and lithography to organic light emitting diodes and various organic material based devices, including sensors. PMMA is one of the earliest Polymers. It is extensively used in glazing applications as a replacement for glass in various applications with good weather resistance. This polymer unlike ionic and metallic crystals and low molecular weight substances consists of long chain molecules arranged in aggregates, which assume complex shapes and structures [1]. The organic films based on poly-methyl-methacrylate (PMMA) polymer have been obtained by pulsed laser deposition (PLD) on silicon substrates [2]. The homogeneous thin films have been obtained by UV-excimer pulsed layer deposition from PMMA bulk material. The structure of films is at variance with the structure of the bulk polymer.

The microstructure of the film is found to have profound influence on the optical, electrical and mechanical properties of the film. The physical properties of thin films are known to differ widely from those of bulk materials. The techniques based on X-ray probe have dominated the field mainly because of their simplicity, more reliability, quantitative and non-destructive nature. Of these techniques, X-ray diffraction has played a leading role, as a fundamental for material characterization [3]. XRD is a powerful tool in the field of scientific research. The application of X-rays in material analysis makes it possible to determine detailed information on the state of order and disorder of the system.

In this paper, we propose a method to prepare PMMA thin films by Chemical Bath Deposition. It is a non vacuum electroless technique has many advantages such as simplicity, no requirement for sophisticated instruments, minimum material waste, economical way of large area deposition and no need of handling poisonous gases like H_2Se or Se vapour and possibility of room temperature deposition. The transmittance, absorbance and structural properties of PMMA thin films are also reported.

2.0 MATERIALS AND METHODS:

2.1 Materials:

PMMA obtained from Alfa Aesar with average molecular weight (3, 50,000), Toluene, Benzene supplied by Merck were used in this study. Benzene and Toluene solutions are distilled before mixing with PMMA to produce thin films.

2.2 Synthesis of PMMA thin film:

The Chemical Bath Deposition procedure to prepare PMMA thin films was followed which involves placing 1 to 2g of PMMA in 50ml distilled Toluene, 50 ml distilled Benzene and 100ml distilled Toluene continuous and very slow stirring for about 60 minutes by means of magnetic stirrer is carried out while adding polymer to the reacting mixture, to yield a

homogeneous mixture. Initially, Blue star special super deluxe glass micro slides with dimension 75mm x 25mm x1mm were rinsed using Extran and washed thoroughly with distilled water. Then, the glass slides were soaked in a beaker containing nitric acid for ½ an hour and washed with de-ionized water and again soaked in hydrochloric acid for the same period. Finally the substrates are dried in a hot air oven for about an hour at a temperature of 100°C. Thus, the substrate for the film deposition has been prepared. Care must be taken so that there should not be any traces of water in the slide before deposition. The deposition time range was optimized as 20 to 35 minutes to obtain films of uniform thickness. After deposition the films were taken out and dried naturally.

2.3 Instrumentation:

The X-ray diffraction patterns were recorded with the diffractometer(X-PERT-PRO) equipped with a PW 3050/60 channel control goniometer and proportional counter. Radiation was generated from a copper anode tube ($_{Cu K\alpha}$ 1.54060 Å) using a X-ray generator operated at 40 kV and 30mA. UV-Visible Spectroscopy was carried out using JASCO-UV-VIS-NIR Spectrophotometer with bare glass slide as reference.

3.0 RESULTS AND DISCUSSION:

3.1 XRD studies:

Possible directions in which the film diffracted the beam of monochromatic x-ray are determined by Bragg condition,
 $n\lambda = 2d \sin \theta$

where n is the order of diffraction, λ is the wavelength of incident x-ray, d is the distance between planes parallel to the axis of the incident beam and θ is the angle of incidence relative to the planes in question. The XRD profiles for the sample PMMA thin films prepared by Chemical Bath Deposition are shown in figure. XRD pattern was obtained in the 2θ range between 0 and 90 degree, which are similar and without any sharp diffraction peaks thereby confirm the non-crystalline nature.

Poly -Methyl Methacrylate is known to be an amorphous polymer. The shape of the first most intense peak at 2θ values of 13° and 23.7° & d spacing around 3.745, 3.742 reflects the ordered packing of polymer chains while the second peak denotes the ordering inside the main chains with their intensity decreasing systematically. This explains the homogenous nature of PMMA thin films and similar results has been reported by [4]. Table 1 shows the measured values of XRD parameters and the calculated values of the crystalline size(P), interchain distance (r). Values of P,r have been calculated using the formula as follows

$$P = K \lambda / \beta \cos \theta \quad (1)$$

$$r = 5.8 \lambda / \sin \theta \quad (2)$$

Where λ is the wavelength of X-ray radiation, K the scherrer constant taken as 0.9, β is the half-height width

TABLE 1: XRD PARAMETERS FOR PMMA FILMS:

Sample	Position (θ)	β	d-spacing	P	r
	deg	deg	(Å)	(Å)	(Å)
PMMA	11.8689	4.0000	3.74526	2.032094	4.685227

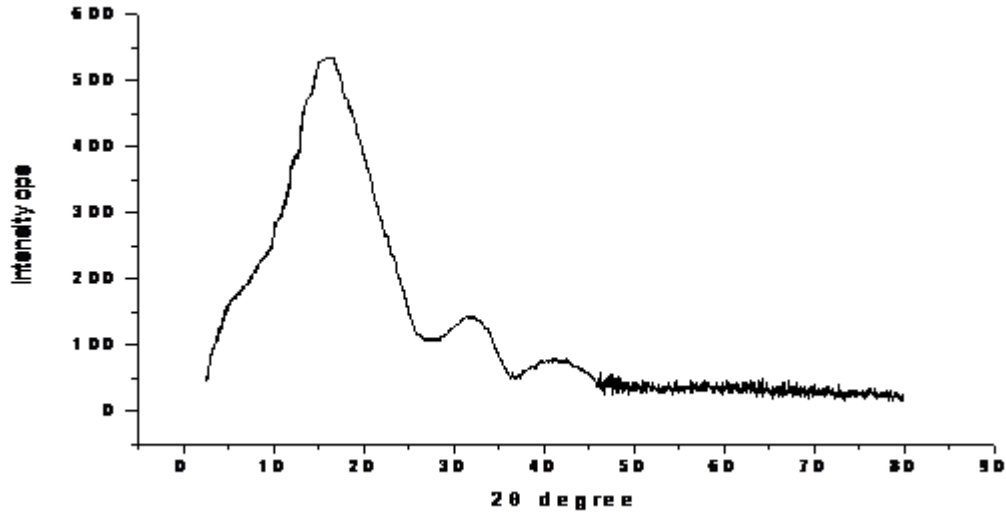


Fig. 1.XRD-Studies of PMMA

3.2UV-Visible studies:

The Transmittance and Absorbance measured for the sample is shown in figures .UV-VIS Spectra exhibited a transmittance of 50% and higher at or above 300 nm[5]. The Optical property of PMMA exhibits higher transmission through the visible wavelength range, very little UV absorption until 260 nm[6].

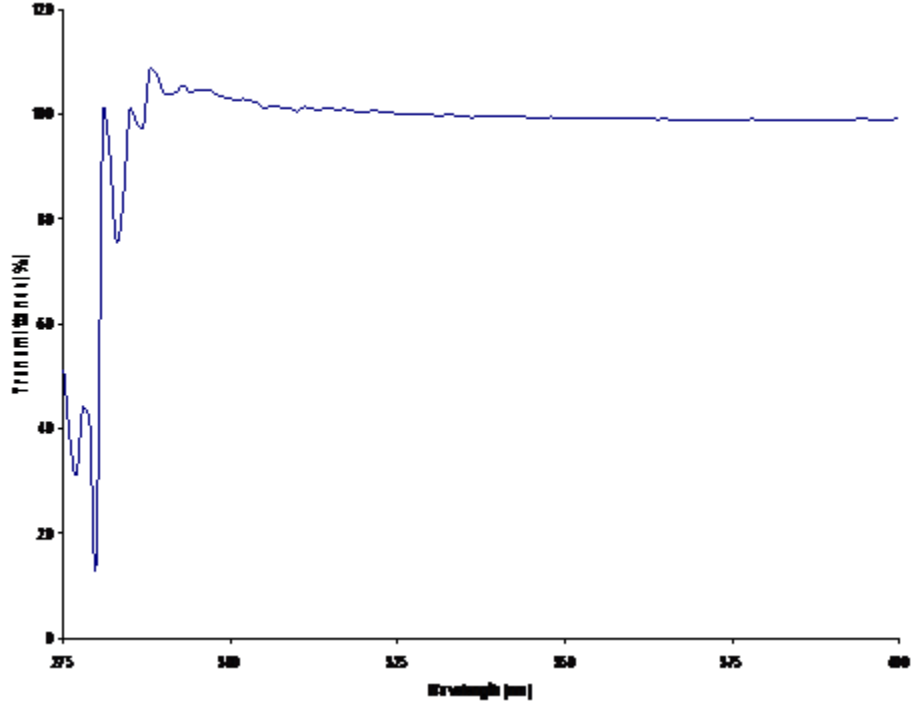


Fig. 2.Transmitivity of PMMA

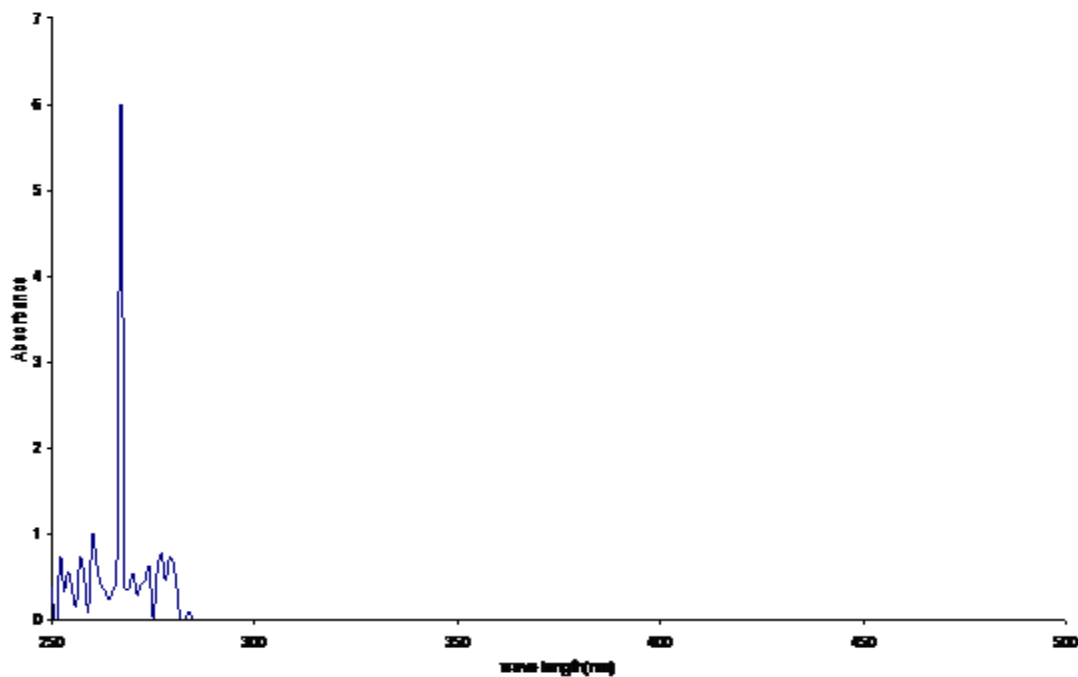


Fig. 3. Absorbance of PMMA

4.0 CONCLUSION:

Poly- Methyl Methacrylate (PMMA) thin films with thickness ranging from 0.53-0.58 microns were deposited successfully by Chemical Bath Deposition Technique. It has been attempted to understand the Structural nature of PMMA thin film samples. XRD technique indicates that the Chemical Bath Deposited film possesses the amorphous nature (i.e.) disorder in polymer chains. The behaviour of the films show higher transmission through the visible wavelength range with very little absorption.

REFERENCES:

- [1] E F. Kaelble, Hand book of X-rays for diffractions, emission, absorption and microscopy (1967), 21.
- [2] R. Cristescu, G. Socol, I. N. Mibailescu, M. Popescu, F. Sava, E. Ion, C. O. Morosanu, I. Stamatina, New results in pulsed laser deposition of poly- methyl- methacrylate thin films, Applied surface science, Vol 208-209, 2003, 645-650.
- [3] B. D. Cullity, Elements of X-ray Diffraction (Additional- Wasley Reading, USA 2001) 284.
- [4] Rizwan Hussain and Din Mohammad, X-ray diffraction study of the changes induced during the thermal degradation of poly (methyl methacrylate) and poly (methacryloyl chloride) 2004, Turk J Chem 28, 725-729.
- [5] La Netra M. Clayton, K. Arun. Sikder, Ashok Kumar, Martin Cinke, Meyya Meyyappan, G. Timofey. Gerasimov and P. Julie Harmon, (Adv. Funct. Matter, 2005) pp 15.
- [6] James E. Mark, PMMA, 1999, Polymer Data Handbook.

Impact of Population Size and Mutation Rate on Multi Clustered Parallel Genetic Algorithm

P. Vishnu Raja¹, Dr. V. Murali Bhaskaran²

¹ Assistant Professor (SrG), Dept of CSE, Kongu Engineering College, Perundurai, India

² Principal, Pavaai College of Engineering, Namakkal, India.

Abstract: Multi Clustered Parallel Genetic Algorithm using Gray value is found to be more efficient compared to Standard Genetic Algorithm. In proposed algorithm, multiple clusters are formed based on the fitness value and the reproduction operator is applied to low order clusters, so that these clusters can make active participation in GA. This paper shows the results of the algorithm based on various mutation rates applied with fixed and various population sizes. The results shows that the algorithm works well in the large population size groups.

Keywords: Genetic algorithm, Gray Encoding, Multi Clustered Parallel Genetic Algorithm.

I. INTRODUCTION

In Standard Genetic Algorithm, generally single population is used, all individuals in a single cluster. While selecting the parents for GA using selection mechanisms like Roulette Wheel Selection, Tournament Selection or Rank selection algorithms, only the high fit individuals are selected and less importance to the low valued individuals for further reproduction. To give importance to the low order individuals we proposed an algorithm, Multi Clustered Parallel Genetic Algorithm.

Multi Clustered Parallel Genetic Algorithm is a special form of GA, in which the initial population is clustered into N clusters based on fitness value. In each cluster the genetic operators are applied to produce new individuals. If the fitness value of the offspring varies in the cluster it can migrate to other cluster.

In most of the GA's, the chromosomes are represented based on the binary representation. Binary representation is the easiest way of representing the chromosome. When we have the binary value, all the genetic operators to be deployed to get the best individual in each generation. Here we represent the chromosome using gray value. Gray value encoding is done adding the adjacent gene value of a binary chromosome. Since the adjacent gene value are added it is enough to mutate a gene value in the chromosome to produce new traits.

In most of the multi population genetic algorithms the mutation is done for the best fit individual, obtained from the selection mechanism. The low fit individuals are

mutated. Here we concentrated on the low fit individuals to take part in the GA for further generations.

Since we have clustered the entire population based on the fitness value. We concentrate the cluster which has low fitness value in order to make the best outcome from the cluster to fit in high order clusters. To make experimental we had implemented the algorithm with various mutation rates applied only to low order clusters and the results are analyzed.

II. PROBLEM STATEMENT

The performance of the algorithm is analyzed with the 0/1 Knapsack problem (Martello[1990]). The problem is formulated as follows:

Given a set on N items with a capacity C. Each of N item will have a profit P_j and a weight W_j . The problem is to select a group of items such that the total weight does not exceed the maximum capacity C and the profit should be maximum.

Where x_j is the variable which has either 0 or 1 value. If it is 1 the item takes part in the knapsack and 0 otherwise.

Given a vector $(x_1, x_2, \dots, x_n) \in \{0, 1\}^n$ with the capacity constraints

$$= \sum_{j=1}^n w_{ij} \cdot x_j \leq c_i, \quad (1 < i < k)$$

Are satisfied for which $f(x)$ should be maximum.

$$f(x) = \sum_{j=1}^n p_{ij} \cdot x_j$$

Where w_{ij} is the weight of item j to the knapsack i.

P_{ij} is the profit of item j to the knapsack i.

III. METHODOLOGY

The proposed Gray coded multi clustered parallel genetic algorithm (GMCPGA) produces better profit in the knapsack compared with the binary coded algorithm. The individuals are selected at random from the initial population. Usually the initial population will be in the binary form. The fitness values for the individuals are calculated. Based on the fitness value the similar individuals are grouped into a cluster. Similarly N numbers of clusters

are formed with each Cluster having the same fitness value. The selection mechanism from any one of the selection mechanism is used to select parent in each cluster.

The selected individual is then gray coded. The mutation operator is applied to the converted parent to produce the new offspring. New offspring is converted as offspring with binary value to calculate the new fitness value and is used in the next generation. This procedure continues till the termination condition is satisfied. The best individual is obtained based on the fitness value.

The overall structure of the proposed methodology is shown in the pseudo code 1. Gray code Multi Clustered Parallel Genetic Algorithm.

- Step 1 :** Generate the initial population at random.
Step 2 : Calculate the Fitness Value for Each individual.
Step 3 : Sort the individuals based on the fitness value
Step 4 : Divide the individuals into n clusters based on the fitness value.
Step 5 : For each cluster perform the following
- Using Selection Mechanism, Select the individuals from each cluster.
 - Convert the individual to Gray code.
 - Mutate the Parent
 - Convert the offspring to Binary Value.
 - Calculate the fitness Value.
- Step 6 :** Group the clusters together
Step 7 : Allow the migration of individuals based on fitness.
Step 8 : Until Termination condition is reached repeat from step 5.
Step 9 : Select the best Individual.

Pseudocode 1 : Gray coded Multi Clustered Parallel Genetic Algorithm

IV. IMPLEMENTATION

The initial setup to analyze the performance of the genetic algorithm is done by changing the mutation rate from 0.05 to 0.5 and the other parameters remain constant.

Number of Chromosomes : 100
 Elitism % : 10 %
 Selection Mechanism : Tournament Selection
 Number of Clusters : 4 Clusters

With this setup the experiment is carried out many times with the change in the mutation rate. Figure 1 shows the

performance of the proposed algorithm with different mutation rates.

Generally mutation is applied to chromosome to have the sudden change in the value. Our concentration is focused mainly on the low fit individuals. Since the population is clustered by fitness value, the individuals with low fitness value are clustered at last. Hence the various mutation rates are applied to low order clusters and the results are shown in fig 1.

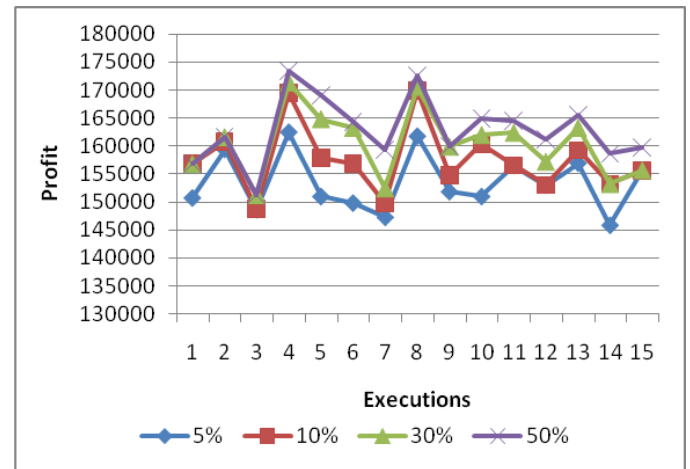


Fig 1. Impact of Various Mutation Rate.

The above figure shows the results of profits with variation in mutation rate (5%, 10%, 30% and 50%). The profit is increased when the mutation rate goes high. When the mutation rate is high, the low fit chromosome has the chance to take part in the further generations.

Impact of Population Size:

The population size is also a crucial factor to analyze the performance of the genetic algorithm. Hence, the performance of the algorithm is analyzed with various population sizes with fixed mutation rate. Here the mutation rate is fixed as 5% and the population size varies as 100, 200 and 300 respectively with number of group remains constant.

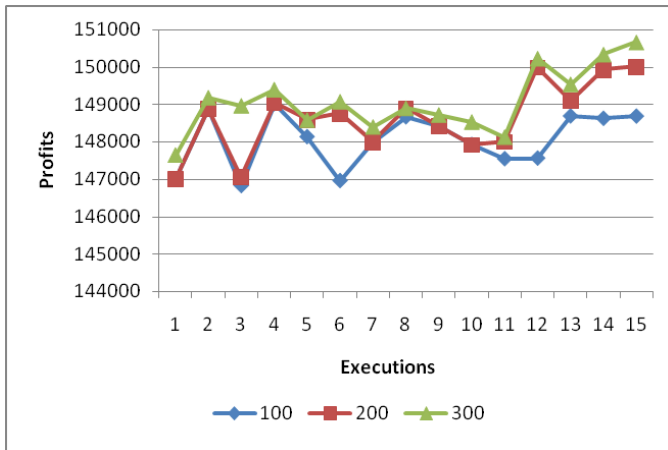


Fig 2. Impact of Population Size

Figure 2. shows that when the population is large with fixed group size the profit increases. It is also observed when the population size is high, the accuracy will be high. But when the population is high, time taken for execution is also high ie it takes more number of generations for execution.

The number of generations taken to execute the GA is measured as convergence velocity. For the above experimental setup the obtained coverage is shown in the figure 3.



From the figure 3 it is observed that if the population size is increased, time taken for execution also increases. It happens because, for larger population, the group size increases for fixed number of groups.

V. CONCLUSION

The result of the proposed methodology shows the improved performance over standard genetic algorithm. By applying the gray value it makes the algorithm much simpler and faster to execute. From the results it is identified that the algorithm is well suited for large population sized groups than small sized groups. Increased mutation rate produces

the better result in terms of profit and by execution. Hence it is concluded that the algorithm works well with gray value with increased mutation rate in fixed number of groups of large population size. The future direction is to reduce the selection pressure of the algorithm, so that the efficiency can be improved further.

VI. REFERENCES

1. Back T. 'Evolutionary Algorithms in Theory and Practice' Oxford University Press, 1996.
2. Goldberg, D.E. 'Genetic Algorithms in search, Optimization and machine Learning' Addison-wesley, 1989.
3. Martello, S, Toth, P : 'Knapsack Problems: Algorithms and Computer Implementations', J.Wiley & Sons, 1990
4. Alden H.Wright : 'Genetic Algorithms for real Optimization'
5. Davis, Lawrence: 'Adapting Operator probabilities in genetic algorithms' Proceedings of the third international conference on genetic algorithms, pg: 61-69, 1989.
6. Antonisse, Jim : 'A new interpretation of schema notation that overturns the binary encoding constraint' Proceedings of the third international conference of genetic algorithms' San mateo Pg: 86-91, 1989.
7. Schaffer, J. David, Richard A. Caruana, Larry J. Eshelman : 'A Study of control parameters affecting online performance of genetic algorithms for function optimization' Proceedings of the third international conference on genetic algorithms, pg 51-60, 1989.

Strength and Durability Properties of High Performance Concrete incorporating High Reactivity Metakaolin

B. B. Patil¹, P. D. Kumbhar²

¹Student, M.E.Civil(Structure), Department of Civil Engineering, Rajarambapu Institute of Technology, Rajaramnagar (Sangli) M.S., India.

²Associate Professor, Department of Civil Engineering, Rajarambapu Institute of Technology, Rajaramnagar (Sangli), M.S., India.

ABSTRACT

Concrete is probably the most extensively used construction material in the world. The addition of mineral admixture in cement has dramatically increased along with the development of concrete industry, due to the consideration of cost saving, energy saving, environmental protection and conservation of resources. However, environmental concerns both in terms of damage caused by the extraction of raw material and carbon dioxide emission during cement manufacture have brought pressures to reduce cement consumption by the use of supplementary materials. High Performance Concrete (HPC) is the latest development in concrete. It has become more popular these days and is being used in many prestigious projects. Mineral admixtures such as fly ash, rice husk ash, metakaolin, silica fume etc are more commonly used in the development of HPC mixes. Addition of such materials has indicated the improvements in the strength and durability properties of concrete. The utilization of calcined clay, in the form of high reactivity metakaolin (HRM) in concrete has received considerable attention in recent years.

The present paper deals with the study of properties namely workability, compressive strength and durability of M60 grade HPC mixes incorporating different percentages of high reactivity metakaolin by weight of cement along with some suitable super plasticizer. The results of the study indicate that the workability and strength properties of HPC mixes improved by incorporating HRM up to a desirable content of 7.5% by weight of cement. HPC mixes have also indicated better resistance to the attacks of chemicals such as chlorides and sulfates when the HPC mixes were exposed to these chemical for 180 days period.

Keywords: Compressive strength, Durability, High Performance Concrete, High reactivity metakaolin, Mineral Admixtures.

1. Introduction

Concrete is probably the most extensively used construction material in the world. However, when the high range water reducer or super plasticizer was invented and began to be used to decrease the water/cement (w/c) or water/binder (w/b) ratios rather than being exclusively used as fluid modifiers for normal-strength concretes, it was found that in addition to improvement in strength, concretes with very low w/c or w/b ratios also demonstrated other improved characteristics, such as higher fluidity, higher elastic modulus, higher flexural strength, lower permeability, improved abrasion resistance, and better durability. This fact led to the development of HPC. HPC is the latest development in concrete. It has become more popular these days and is being used in many prestigious projects such as Nuclear power projects, flyovers, multistoried buildings etc. [1]

Since 1990s, HPC has become very popular in construction works. At present, the use of HPC has spread throughout the world. In 1993, the American Concrete Institute (ACI) published a broad definition for HPC and is defined as the concrete which meets special performance and uniformity requirements that cannot always be achieved by using only the conventional materials and mixing, placing and curing practices. The performance requirements may involve enhancements of placement and compaction without segregation, long-term mechanical properties, early age strength, toughness, volume stability, or service life in severe environments. [2]

The addition of mineral admixture in cement has dramatically increased along with the development of concrete industry, due to the consideration of cost saving, energy saving, environmental protection and conservation of resources. However, environmental concerns both in terms of damage caused by the extraction of raw material and carbon dioxide emission during cement manufacture have brought pressures to reduce cement consumption by the use of supplementary materials. [3]

Mineral admixtures such as fly ash, rice husk ash, metakaolin, silica fume etc are more commonly used in the development of HPC mixes. They help in obtaining both higher performance and economy. These materials increase the long term performance of the HPC through reduced permeability resulting in improved durability. [4] Addition of such materials has indicated the improvements in the strength and durability properties of HPC. High reactivity metakaolin, which is a relatively newer material in the concrete industry, is effective in increasing the compressive strength, reducing the sulfate attack and improving air-void network. Unlike fly ash, slag, or silica fume, this material is not a byproduct but is manufactured from high-purity kaolin clay by calcination at temperature range of 650 to 800°C. The material, ground to an average particle size of 1.5 to 2.5 μm, is white in color. [5] However, information to understand the behavior of this mineral

additive in HPC is insufficient. Some of the recent information is discussed in this paper highlighting the role of high reactivity metakaolin in high strength high performance concrete.

Keeping all these things in view, an attempt has been made in the present paper to study various properties namely workability, compressive strength and durability of M60 grade HPC mixes incorporating different percentages of metakaolin by weight of cement along with some suitable super plasticizer. The results of the study indicate that the workability and strength properties of HPC mixes improved by incorporating HRM up to a desirable content of 7.5% by weight of cement. HPC mixes have also indicated better resistance to the attack of chemicals such as chlorides and sulfates when the HPC mixes were exposed to these chemical for 180 days period.

2. Experimental Investigations

2.1 Materials:

The materials used in making HPC mixes along with their various properties have been given in Table 1.

Table 1: Properties of Materials Used In Making HPC Mixes

Materials	Sp. Gravity	Fineness Modulus	Grade/ Type	Comp Strength	Source
Cement	3.15	-	53 OPC	54 MPa	Ultratech Cement
Fine Aggregate	2.70	3.2	Zone I	-	Krishna River, Local spot
Coarse Aggregate	2.78	7.125	60%-20mm 40%-12.5mm	22.20 %	Locally available
High reactivity metakaolin	2.50	-	-	-	20 microns India Ltd, Mumbai
Super-plasticizer	1.09	-	'GLENIUM B233' (Polycarboxylic ether polymer)	-	BASF Chemical Company Ltd., Mumbai

2.2 Mix design of HPC:

The mix design of HPC was done by using the guidelines of IS Code method (IS10262-2009). The design stipulations and the data considered for mix design HPC has been presented below. [6]

Characteristic Strength, f_{ck} (MPa): 60

Max. Size of Course Aggregate: 20mm (Crushed)

[Fraction I-60%, 20mm-12.5mm]

[Fraction II-60%, 12.5mm-10mm]

Degree of Quality Control : Good

Type of Exposure : Severe

Degree of Workability : 100mm (slump)

Target Mean Strength (f_{ck}), MPa:

$$f_{ck} + 1.65 \times S = 60 + 1.65 \times 5 = 68.25$$

Where,

f_{ck} = characteristic compressive strength at 28 days,

S = standard deviation

2.3 Mix Proportions:

Mix proportion of M60 grade HPC mix was obtained by making certain modifications in the mix proportion arrived at using the guidelines of IS Code method. The mix proportion was obtained without considering any addition or replacement of mineral admixture (i.e. high reactivity metakaolin).

After several trials, a cement content of 475 kg/m³ and water-binder ratio of 0.31 were finalized based on 28 days compressive strength gain of HPC mix and desired workability properties (slump & flow). Thus, for making HPC mixes a cement content of 475 kg/m³ and a water-binder ratio of 0.31 were used along with optimum content of high reactivity metakaolin as mineral admixture. After carrying out several preliminary mix trials, the optimum contents of high reactivity metakaolin at 7.5% and a super plasticizer dose at 0.73%, both by weight of cement, were found to give desired workability and strength properties. The water-binder ratio was calculated by dividing the weight of mixing water by combined weight of cement and high reactivity metakaolin. The final mix proportion was arrived at by altering the ratio of fine aggregate to coarse aggregate and is expressed as parts of water: cement: fine aggregate: coarse aggregate as given by 0.31: 1:1.63: 2.33.

2.4 Preparation of HPC Mix

The required quantities of all the ingredients were taken by weigh batching, with appropriate coarse aggregate fractions and mineral admixtures. Mixing of the ingredients was done in a pan mixer as per the standard procedure. A reference mix was prepared using a water-binder ratio of 0.31 and suitable super plasticizer content (by weight of cement) in order to get desired workability.

The workability of the concrete was studied by conducting slump and flow tests as per the standard procedure (IS: 1199–1959) (Figure 1 and Figure 2). Standard cube specimens of 150mm x 150mm x 150mm size were cast using the procedure described in IS Code (IS: 516–1959) and were immediately covered with plastic sheet and kept there for 24 hours and then released in water tank for 28 days curing.

All the HPC mixes were prepared using the same mix proportion, water-binder ratio and super plasticizer dose and considered for study of workability, strength and durability properties of HPC mixes. The details of workability properties of the mixes prepared with their quality are given in the Table 2.



Figure1 slump test



Figure2 flow test

2.5 Testing of specimens:

After 28 days curing period, the specimens were taken outside the curing tank and were tested under a compression testing machine of 2000KN capacity for compressive strength. For durability performance of HPC in chloride and sulfate environment after initial curing of 28 days, the specimens are kept immersed in 3.5% NaCl and 5% MgSO₄ solution for a period of 180 days.[7] The crushing loads were noted and the average compressive strength of three specimens is determined. The compressive strength values of specimens subjected to different durability conditions has been presented in Table 2.



Figure3 compression testing machine (200t capacity)



Figure4 testing of specimen

3. Results and Discussion:

Generally, high reactivity metakaolin is proven to be a reactive pozzolan. The strength enhancement is probably due to a combination of the filler effect and accelerated cement hydration. This is particularly significant in the interfacial zone regions where they produce more efficient packing at the cement paste-aggregate particle interface, reducing the amount of bleeding and produce a denser, more homogeneous, initial transition zone microstructure and also a narrower transition zone. Addition of high reactivity metakaolin results an increase in the strength of concrete possibly due to an improved transition zone. High reactivity metakaolin rapidly removes calcium hydroxide from the system and accelerates the ordinary Portland cement (OPC) hydration. It result in enhanced early strength with no detrimental effect to the long term strength and greatly improves the resistance to the transportation of water and diffusion of harmful ions. [8]

The compressive strength of all the mixes except 5%, 7.5%, 10% addition is lower than the control mix. This is generally caused by the “dilution effect”. As the addition ratios exceed 10%, the amount of high reactivity metakaolin is in excess to react with calcium hydroxide. These extra high reactivity metakaolin produce an immediate dilution effect such that the water-binder ratio is reduced. Concrete strength is reduced in approximate proportion to the degree of addition. As the results, the 15% addition endures the most critical strength loss. However, only concrete with 5%, 7.5% & 10% addition exhibits higher strength than the control mix at 28 days. The additions over 10% cause the concrete to have excess of high reactivity metakaolin to react with the hydrated calcium hydroxide and thus reduce the compressive strength of the concrete.

Compared to the findings of other studies, it appears that the results of this study do not cohere with some of the studies, although there are some studies agree the optimum high reactivity metakaolin addition is around 7.5%. These variations are not surprising as the products of hydration and pozzolanic activity depend on the Portland cement composition, the purity of the high reactivity metakaolin and the water-binder ratio. In this study, the high reactivity metakaolin samples have silica and alumina content of 81%. It is considered that the high reactivity metakaolin has a high purity and high kaolinite content. As a result, 7.5% addition is sufficient to reduce the calcium hydroxide to the minimum level and attains the highest compressive strength in 28 days.

Table 2 Details of HPC mix (M60) exposed to durability conditions

Sr. No.	% HRM addition	Slump in mm	Compressive strength in N/mm^2
I) 28 days Strength			
1	Control mix	110	63.70
2	5	115	66.96
3	7.5	60	69.04
4	10	60	65.48
5	12.5	70	63.26
6	15	40	60.74
II) Exposure to Chloride attack			
1	Control mix	160	60.59
2	5	85	64.30
3	7.5	70	66.37
4	10	65	62.96
5	12.5	45	60.89
6	15	50	59.56
III) Exposure to Sulfate attack			
1	Control mix	140	57.78
2	5	100	61.63
3	7.5	110	64.89
4	10	50	61.63
5	12.5	45	58.81
6	15	30	56.00

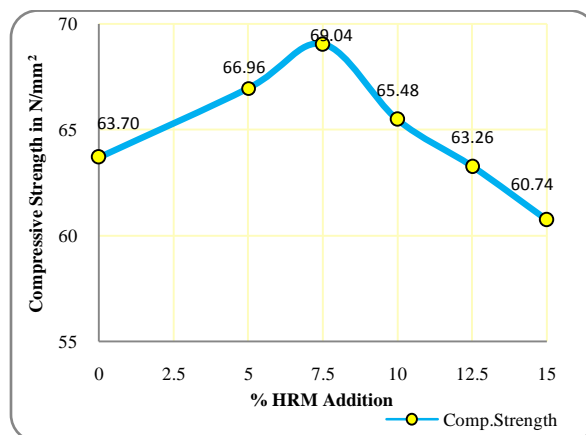


Figure5 compressive strength at 28 days

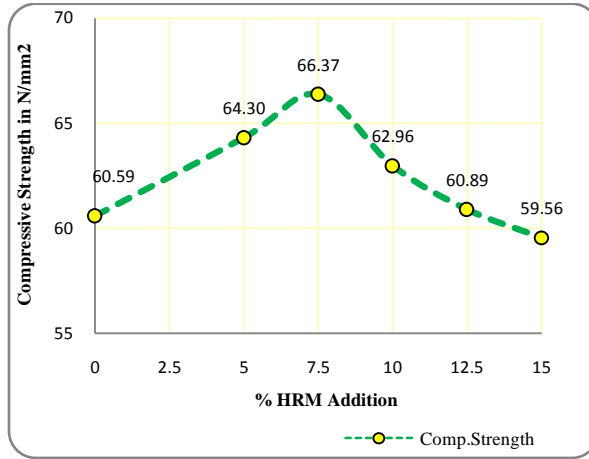


Figure6 compressive strength after chloride attack

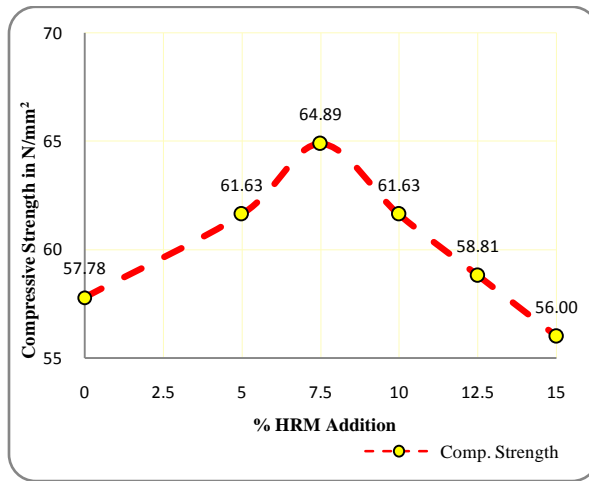


Figure7 compressive strength after sulfate attack

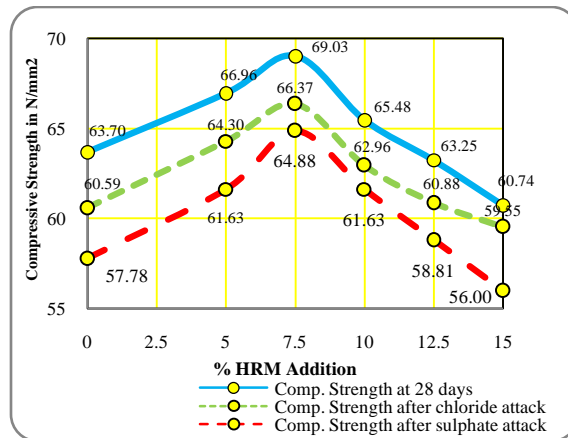


Figure 8 comparison of compressive strength

4. Conclusions:

The compressive strength of concrete increases with increase in HRM content up to 7.5%. Thereafter there is slight decline in strength for 10%, 12% and 15% due excess amount of HRM which reduces the w/b ratio and delay pozzolanic activity. The higher strength in case of 7.5% addition is due to sufficient amount of HRM available to react with calcium hydroxide which accelerates hydration of cement and forms C-S-H gel.

- The 7.5% addition of high reactivity metakaolin in cement is the optimum percentage enhancing the compressive strength at 28 days by 7.73% when compared with the control mix specimen.
- The 7.5% addition of high reactivity metakaolin in cement is enhanced the resistance to chloride attack. The compressive strength of concrete incorporated with 7.5% HRM is reduced only by 3.85% as compared with the reduction of strength of control mix specimen is by 4.88%.
- The 7.5% addition of high reactivity metakaolin in cement is also enhanced the resistance to sulfate attack. The compressive strength of concrete incorporated with 7.5% HRM is reduced only by 6.01% as compared with the reduction of strength of control mix specimen by 9.29%.

Acknowledgment

The authors thanks the management and Director of Rajarambapu Institute of Technology, Sakhrale for providing all the facilities for conducting the experimental study in material testing and P.G. laboratory.

References

1. M.B.Kumthekar, G.S.Vyas, N.T.Suryawanshi and M.B.More, *Techno-Economical Benefit of Metakaolin Over Microsilica in Developing High Performance Concrete*, CE&CR July 2007, 42-50.
2. Zongjin Li, Yunsheng Zhang, *Handbook of structural Engineering*, 15 (CRC Press, 2005) 1-58
3. Shreeti S. Mavinkurve, Prabir C. Basu and Vijay R. Kulkarni, High Performance concrete using high reactivity metakaolin, *The Indian Concrete Journal*, May 2003, 1077-1085.
4. K.A.Gruber, Terry Ramlochan, Andrea Boddy, R.D.Hooton, M.D.A.Thomas, *Increasing concrete durability with high reactivity metakaolin*, *Cement & Concrete Composites*, Vol. 23, 2001, 479-484.
5. Dinakar P. *High reactivity metakaolin for high strength and high performance concrete*, *The Indian Concrete Journal*, April 2011, 28-32.
6. IS 10262:2009, Bureau of Indian standard- Concrete Mix Proportioning-Guidelines(first revision)
7. Nabil M. Al-Akhras, *Durability of metakaolin concrete to sulfate attack*, *Cement and Concrete Research*, Vol. 36, 2010, 1727-1734.
8. C.S. Poon, S.C. Kou, L. Lam, *Compressive strength, chloride diffusivity and pore structure of high performance metakaolin and silica fume concrete*, *Construction and Building Material* Vol. 20, 2006, 858-865.
9. Andrea Boddy, R.D.Hooton, K.A.Gruber, *Long Term Testing of the chloride- penetration resistance of concrete containing high reactivity metakaolin* *Cement and Concrete Research*, Vol. 31, 2001, 759-765.
10. Sunil Mistry, *MetaCem- Metakaolin: A High Strength Creation*, *The Masterbuilder*, July 2010, 218-222.

Vector controlled PMLSM using simplified Space vector pulse width modulation

K. Divakar¹, N. Ravisankar Reddy².

¹M.tech student, G. Pulla Reddy Engineering College, Andhra Pradesh, India

²E.E.E Department, G. Pulla Reddy Engineering College, Andhra Pradesh, India

ABSTRACT

This paper aims to develop vector controlled permanent magnet linear synchronous motor (PMLSM) based on simplified space vector pulse width modulation. Mathematical models of PMLSM&SVPWM presented. The present PWM technique does not involve any sector identification and considerably reduces the computation time when compared to conventional space vector PWM technique. To validate the proposed algorithm, simulation studies have been carried out on vector controlled PMLSM drive. A comparison between Scalar control and vector control approach of PMLSM drive will be provided and verified on MATLAB.

Keywords: offset time, PMLSM, SVPWM, scalar control vector control.

I. INTRODUCTION

Permanent magnet linear synchronous motor (PMLSM) is a kind of driving equipment for converting electrical energy into linear movement directly without any in-between transferring mechanism [1]. Without the need of any mechanical transformation by using for example gears and screws, the linear drive offers high efficiency, high reliability, high performance motion control and low vibration and noise [2]. PMLSMs are increasingly used as actuators in many automation control fields, including computer controlled machining tools, X-Y driving devices, robots, semiconductor manufacturing equipment, transport propulsion and levitation[3].

The SVPWM was brought forward from 1980's, specifically used for the frequency varying and speed regulation of AC motors. It controls the motor based on the switching of space voltage vectors, by which an approximate circular rotary magnetic field is obtained. Comparing with the sine pulse width modulation (SPWM), the main SVPWM advantage is that it has e.g. a 15% higher utilization ratio of voltage [4].

The conventional SVPWM scheme requires sector identification and look up tables to determine the timings of various switching vectors of the inverter. These makes the

implementation of the SVPWM scheme is quite complicated [6-7]. A simplified method, to determine the time duration of the correct offset times duration of the middle inverter vectors in a sampling interval. Considering the voltage generation fashion of the voltage fed inverter that comprised of six power devices in parallel with a freewheeling diode, it can be found that output voltage of the inverter is determined by the different voltages between each inverter arm and the time duration in which the different voltage is maintained.

II. MATHEMATICAL MODEL OF PMLSM

The mathematical model of a permanent magnet linear synchronous motor can be described in the two axis d-q synchronously rotating frame by the following differential equations [5], as

Stator voltage balance equation is given by

$$u_d = R_s \cdot i_d + L_d \cdot \frac{di_d}{dt} - \frac{\pi}{\Gamma} \cdot L_q \cdot v i_q \quad (1)$$

$$u_q = R i_q + L_q \frac{di_q}{dt} + (L_d i_d + \Psi_f) \frac{\pi}{\Gamma} v \quad (2)$$

The electromagnetic thrust force is given by

$$F_{em} = \frac{3}{2} \frac{\pi}{\Gamma} (\Psi_f + (L_d - L_q) i_d) i_q \quad (3)$$

If $i_d=0$, electromagnetic thrust force would be expressed as

$$F_{em} = \frac{3}{2} \cdot \frac{\pi}{\Gamma} \cdot \Psi_f \cdot i_q \quad (4)$$

Therefore the thrust force of PMLSM can be controlled just through the controlling of i_q which is very like controlling a DC motor.

Considering the mechanical load, the dynamic position movement mechanical balance equation of PMLSM is given by

$$F_{em} = F_d + Bv + M \frac{dv}{dt} \quad (5)$$

Ψ_f , F_d , B , M , v , R , Γ are the flux linkage of permanent magnet, external force, viscous friction coefficient, mass of

moving part, translator velocity, phase winding resistance, pole pitch. Simulation model of PMLSM is combined with “voltage balance” subsystem and “mechanical balance subsystem”.

III. SIMPLIFIED SVPWM ALGORITHM

The standard topology of a 3-phase VSI is shown in Fig.1, and consists of three phase legs with two switches per leg, arranged so that each phase output can be connected to either the upper or the lower DC bus as desired. In Fig.2, the eight available different switching vectors of the inverter are depicted with the space vector concept. The switching state “1” means the firing for the upper device of one arm and the pole voltage (Vao, Vbo, and Vco) will have half of the DC-link voltage value.

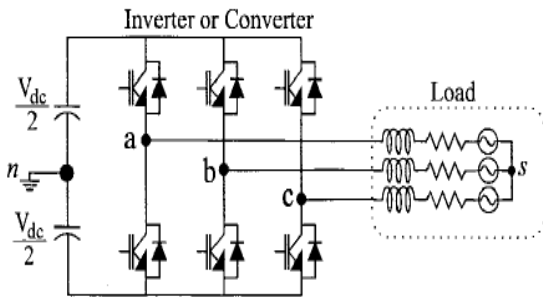


Fig 1: three phase inverter system

Note that the switching states of each arm should be combined with each other to compose the required three-phase output voltage. Because each pole voltage has only two levels according to the related switching state, the time duration in which the different voltages are maintained is definitely related to the voltage modulation task. Therefore, the modulation task can be greatly simplified by considering the relation between the time duration and the output voltage.

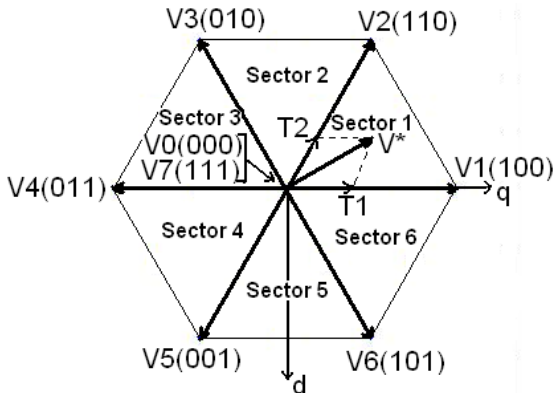


Fig 2: Space vector diagram of the available switching vectors.

The effective voltage that makes an actual power flow between inverter and load. Ts denote the sampling time and Teff denotes the time duration in which the different voltage is maintained. Teff is called the “effective time”. The imaginary time value will be the value is directly related to the phase voltage and one proportional formation can be defined [9] as

$$\begin{aligned}
 V_{as}^* : V_{dc} = T_{as} : T_s &\Rightarrow T_{as} = \frac{T_s}{V_{dc}} \cdot V_{as}^* \\
 V_{bs}^* : V_{dc} = T_{bs} : T_s &\Rightarrow T_{bs} = \frac{T_s}{V_{dc}} \cdot V_{bs}^* \\
 V_{cs}^* : V_{dc} = T_{cs} : T_s &\Rightarrow T_{cs} = \frac{T_s}{V_{dc}} \cdot V_{cs}^*
 \end{aligned} \tag{6}$$

Vas*, Vbs* and Vcs* are the A-phase, B -phase, and C-phase reference voltages, respectively. This switching time could be negative in the case where negative phase voltage is commanded. Therefore, this time is called the “imaginary switching time”. Now the effective time can be defined as the time duration between the smallest and largest of three imaginary times given by

$$T_{eff} = T_{max} - T_{min} \tag{7}$$

Where

$$T_{min} = \min(T_{as}, T_{bs}, T_{cs}), T_{max} = \max(T_{as}, T_{bs}, T_{cs})$$

When the actual gating signals for power devices are generated in the PWM algorithm, there is one degree of freedom by which the effective time can be relocated anywhere within the sampling interval. Therefore, a time-shifting operation will be applied to the imaginary switching times to generate the actual gating times (Tga, Tgb, Tgc) for each inverter arm. This task is accomplished by adding the same value to the imaginary times as [9]:

$$\begin{aligned}
 T_{ga} &= T_{as} + T_{offset} \\
 T_{gb} &= T_{bs} + T_{offset} \\
 T_{gc} &= T_{cs} + T_{offset}
 \end{aligned} \tag{8}$$

If the zero-voltage time is symmetrically distributed in one sampling period, the whole modulation task for SVPWM is easily accomplished by the proposed algorithm. To relocate the effective time at the center of the sampling interval, the time shifting value Toffset is

$$T_{offset} = \frac{1}{2} T_o - T_{min}$$

Where

$$T_o = T_s - T_{eff} \tag{9}$$

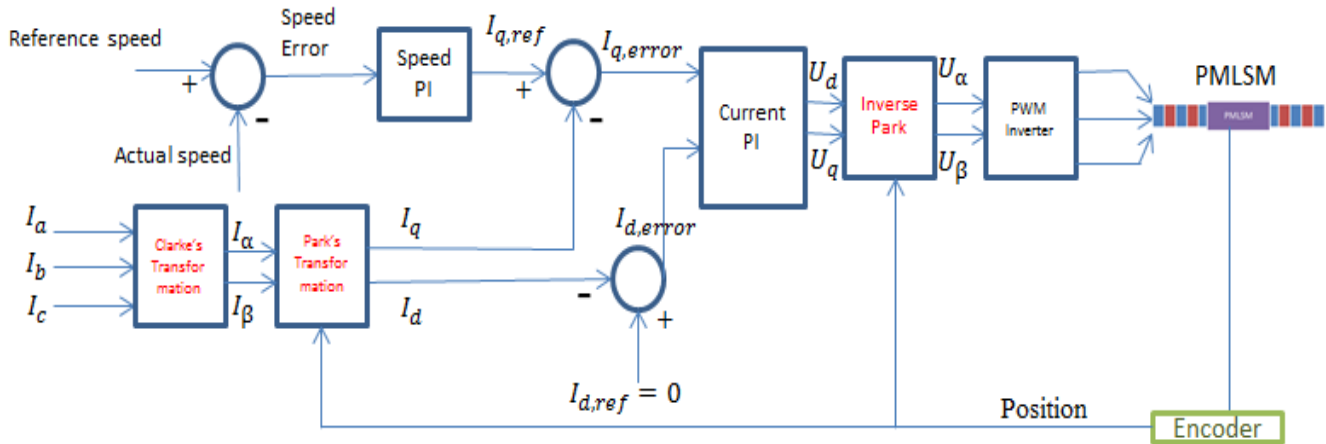


Fig 4: Block diagram of vector control

VI. SIMULATION RESULTS AND DISCUSSION

To validate the proposed method, simulation studies have been carried out by using MATLAB/SIMULINK. The motor parameters are shown in table1.

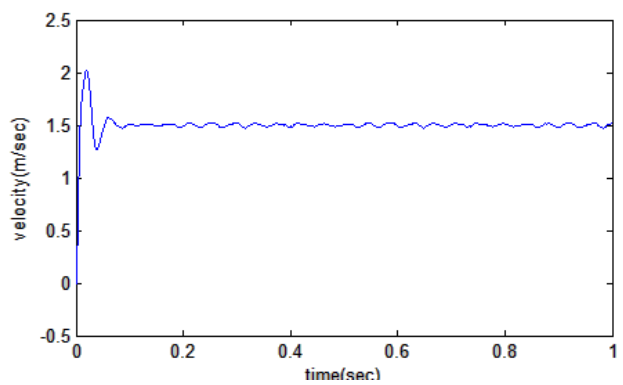
of vector control is better than the scalar control of PMLSM drive.

TABLE 1:

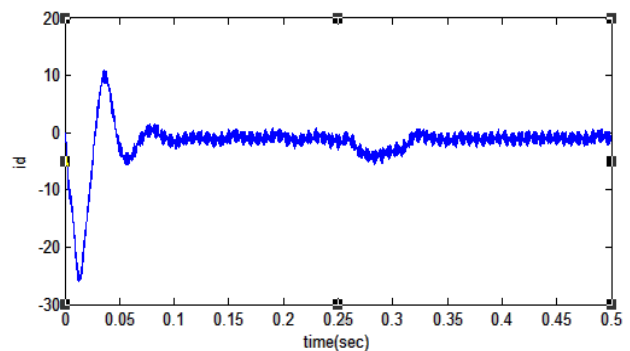
Dc bus voltage, Ud=310v,pole pairs, N=2

Stator resistance, Rs	2.04Ω
d-axis inductance ,Ld and q-axis inductance, Lq	7mH
Permanent magnet flux, ψ_f	0.085Wb
Polar pitch, Γ	33mm
Mover mass, m	3kg
Viscous friction coefficient, Bv	0.2 N.M/s

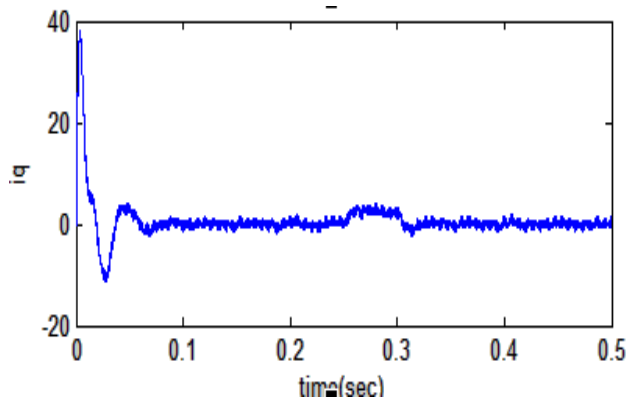
The simulation results of the proposed drive are shown in Fig. 5 and Fig.6. The scalar control plots are shown in Fig.5 and vector control plots are shown in Fig.6. Id in scalar control variable during a step load is applied but in vector control always zero shown in Fig.6. velocity provide certain overshoot during the starting condition in scalar control shown in Fig.5. in case of vector control negligible overshoot shown in Fig.5. Thrust force in scalar control provide a large ripples when compare to the vector control. From the Fig.6 velocity feedback used in vector control approach avoid overshoots during starting condition. Dynamic performance



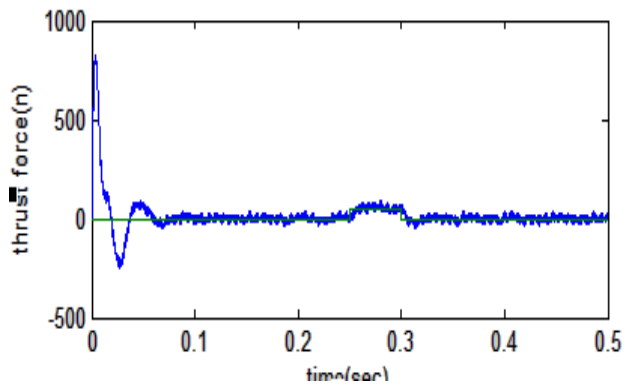
(a)



(b)

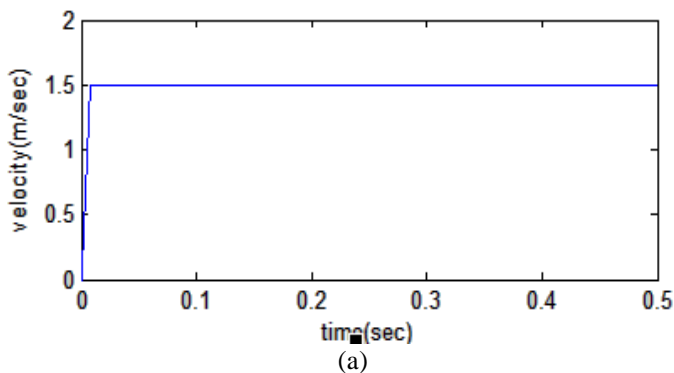


(c)

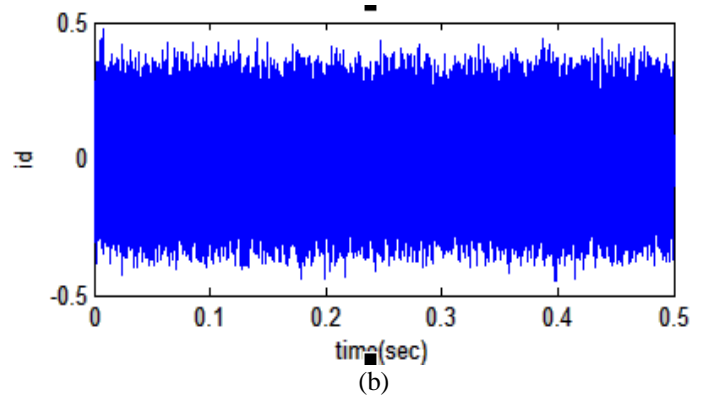


(d)

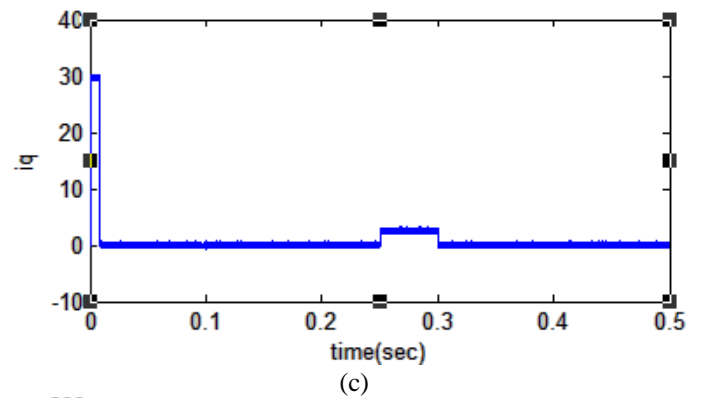
Fig: 6. Scalar control of PMLSM (a) velocity (b) id (c) iq (d) force when load of 50N applied at 0.25 sec.



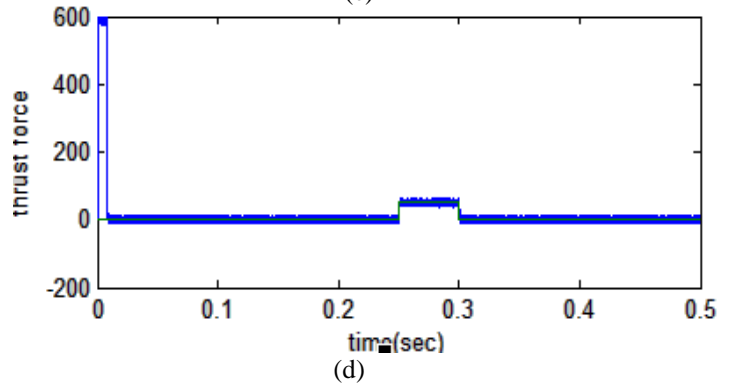
(a)



(b)



(c)



(d)

Fig: 7 vector control of PMLSM (a) velocity (b) id (c) iq (d) force when load of 50N applied at 0.25 sec.

VII. CONCLUSION

The simplified algorithm does not use sector identification and angle information. So it reduces computation time. Vector control with simplified SVPWM gives better performance than the convention current control algorithm. Vector control as the most common method of PMLSM compare than the scalar control. Vector control provides better dynamic performance than the scalar. Velocity overshoots are reduced in vector control. Magnetizing flux is kept in its nominal value during the whole operation cycle.

Using such control strategy avoids the motor to become under or over excited condition.

REFERENCES

- [1] H. B. Zhao, J. X. Jin, and J. Cheng." Virtual instrument based Fuzzy control system for PMLSM drive". Chengdu: *Proceeding of IEEE on Applied Superconductivity and Electromagnetic Devices, 2009: 299-303.*
- [2] Y. G. Guo, J. X. Jin, J. G. Zhu, and H. Y. Lu. "Design and analysis of a prototype linear motor driving system for HTS maglev transportation", *IEEE Trans. App. Super.*, 2007, 17(2), 2087-2090.
- [3] Y. S. Kung, M. H. Tsai, C. S. Chen. FPGA-based servo control IC for PMLSM drives with adaptive fuzzy control. Korea: *SICE-ICASE International joint conference 2006, 2006:1-6.*
- [4] Z. G. Wang, J. X. Jin, Y. G. Guo, and J.G. Zhu. SVPWM techniques and applications in HTS PMSM machines control, *Journal of Electronic Science and Technology of China, 2008, 6(2), 191-197.*
- [5] L. H. Zheng, and J. X. Jin. Investigation of HTS bulk magnet linear synchronous motors. *Chengdu: Proceeding of IEEE on Applied Superconductivity and Electromagnetic Devices, 2009: 17-21.*
- [6] H.W. Van der Broeck and H.C.Skudelny, "Analysis and Realization of a pulse width modulator based on voltage Space vectors," *IEEE Trans. Ind. Applicat.*, vol. 24, pp.142-150, Jan./Feb. 1988.
- [7] J.S. Kim and S.K.Sul, "A novel voltage modulation technique of the space vector PWM" in *conf.rec .IPEC'95, Yokohama, japan, 1995, pp. 742-747.*
- [8] J. X. Jin, and L. H. Zheng. "A permanent magnet linear synchronous motor control system based on space vector pulse width modulation", *CAAI Transactions on Intelligent Systems, 2009, 4(3), 251-257.*
- [9] Dae-Woong Chung," Unified voltage Modulation Technique for Real Time Three phase Power Conversion", *IEEE Transactions on industry applications*, vol.34, No.2 MARCH/APRIL 1998.
- [10] BOSE, B. K., *Power Electronics and Variable Frequency Drives* (Technology and Application Institute of Electrical and Electronics Engineers, Inc, New York, 1997).

Implementation of Cleaner Production Principles in Formaldehyde Production

¹ Jilesh M. Pandya & ² Linesh Patel

Chemical Engineering Department, V. V. P. Engineering college, Rajkot

ABSTRACT

Formaldehyde is the first of the series of aliphatic aldehydes. It is a basic chemical building block for the production of wide range of chemicals finding a wide variety of end uses. It can be manufactured by two different processes namely – dehydrogenation (Route – I) and oxidation (Route – II) process. First route being highly exothermic in nature, the removal of heat has to be done very effectively, where as the second route is endothermic in nature, addition of energy has to be done very effectively. Route – III, proposed in this paper, can be considered as more environmentally friendly route. Both the routes are carried out in a combined reactor. The total amount of energy require in this route for the production of formaldehyde is very low. Energy required from the external source for either removal or absorption of energy is ZERO. Approximately 50% of total energy and raw material requirement can be saved. Route – II is not an environmentally friendly, not a green reaction and green technology, but if it is coupled with Route – I, the scheme of reactions becomes a green reaction scheme. Thus full energy conservation is possible. Formaldehyde production by combined route is a good example in terms of energy conservation.

Keywords: Cleaner production, energy conservation, formaldehyde, green reaction.

1. INTRODUCTION:

Formaldehyde, HCHO, is the first of the series of aliphatic aldehydes. It was discovered 1859 and has been manufactured since the beginning of the twentieth century. At ordinary temperatures, pure formaldehyde is a colorless gas with a pungent, suffocating odor. Because of its relatively low cost, high purity, and variety of chemical reactions, formaldehyde has become one of the world's most important industrial and research chemicals. Formaldehyde is noted for its reactivity and its versatility as a chemical intermediate. It is used in the form of anhydrous monomer solutions, polymers, and derivatives. Formaldehyde is a basic chemical building block for the production of a wide range of chemicals finding a wide variety of end uses such as wood products, plastics, and coatings. Formaldehyde production according to use is: urea-formaldehyde resins, 24%; phenol-formaldehyde resins 16.5%; polyacetal resins, 13%; 1,4-butanediol (BDO), 11%; methylene diisocyanate (MDI), 7%; pentaerythritol, 5%; controlled release fertilizer, 3.5%; hexamethylenetetramine (HMTA), 3%; melamine-formaldehyde resins, 3%; miscellaneous, including

chelating agents, trimethylolpropane, pyridine chemicals, nitro-paraffin derivatives, textile treating and trimethylolethane, 14%;. Formaldehyde is produced and sold as water solutions containing variable amounts of formaldehyde.

2. ROUTES AVAILABLE FOR PRODUCTION OF FORMALDEHYDE:

Being an important petrochemical, formaldehyde can be manufactured by two different processes namely – dehydrogenation and oxidation. Here in this paper, the process (oxidation and dehydrogenation) for manufacturing the product is considered separately as two different routes. The detailed discussion for the production of formaldehyde via these two routes is given as under:

Route – I

- Scheme of reaction:

Unit Process – Dehydrogenation



Route – II

- Scheme of reaction:

Unit Process – Oxidation



2.1. Process Description:

Formaldehyde can be manufactured from methanol by dehydrogenation and oxidation process. In dehydrogenation process, the temperature maintained is 600°C. the reaction is carried out in presence of oxides of ferrous & chromium. The reaction is highly endothermic in nature. Conversion is 70 – 80 % and the yield of the product is 99%. (HCHO + H₂) vapors absorbed in water & H₂ gets separated, hence 37% solution of HCHO so obtained called as “Formalin”. Being highly energy intensive process, it requires large quantity of heating media. Unreacted methanol separated from formalin by distillation.

In oxidation process, here the process is maintained at a temperature of 650°C. the reaction is carried out in presence of oxides of silver & molybdenum. The reaction is highly exothermic in nature. Conversion is 80 – 90 % and the yield of the product is 90%. Being highly energy intensive process, it requires large quantity of cooling water. Non – purified air, compressed to about 0.2 atm. gauge is preheated by heat exchange with reacting gases and then it is fed to methanol evaporator, where at high temperature condition methanol is evaporated. The ratio of CH₃OH to O₂ is maintained in the range of 30 – 50%, so that the required conditions are achieved. The mixed gases from evaporator are then heated in preheater and sent to a

reactor where oxides of silver or molybdenum act as catalysts.

The activity of catalyst is controlled to maintain a balance between endothermic dehydrogenation and exothermic oxidation reactions at the reaction conditions of 450 – 650°C. Some complete combustion reaction takes place. The product gases are absorbed in a water scrubber which is cooled by external circulation and sent back to light end stripper. The bottom of stripper is then fed to alcohol fractionator where approximately 15% of unreacted methanol is recovered from top and is recycled. The bottom of fractionator contains product which is 37% solution of FORMALDEHYDE called as “Formalin”.

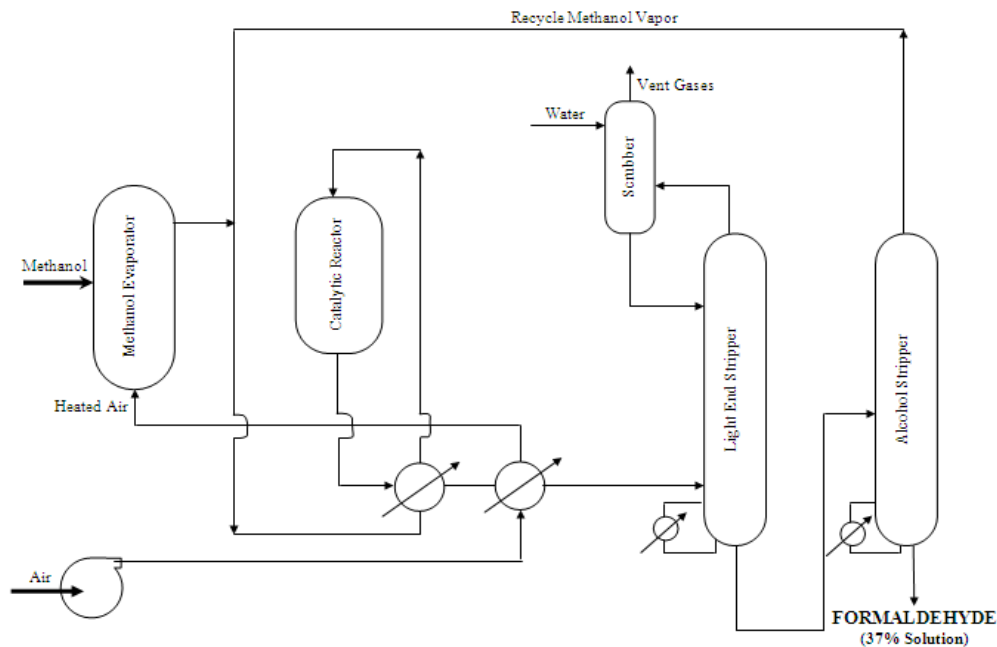


Figure: 1 Production of Formaldehyde from Methanol

3. THERMODYNAMIC CONSIDERATIONS:

Route – I

Estimation of Thermodynamic data:

Values of ΔH_R (kJ / mole), ΔG° (kJ / mole) and $\ln K$ at different temperatures in $\ln K$ are given by following equations:

$$\Delta H_R^\circ = 77910.7 + 29.47T + 0.015 * T^2 - 3.27 * 10^{-6} * T^3 + 3.3 * 10^{-9} * T^4$$

$$\Delta G^\circ = 81358 - 95T + 0.005 * T^2 - 8.1 * 10^{-7} * T^3 + 6.6 * 10^{-10} * T^4 \quad \ln k = 11.43 - \frac{9785.6}{T} + 6 * 10^{-4} * T + 9.7 * 10^{-8} * T^2 - 7.9 * 10^{-11} * T^3$$

Route – II

Estimation of Thermodynamic data:

Values of ΔH_R (kJ / mole), ΔG° (kJ / mole) and $\ln K$ at different temperatures in $\ln K$ are given by following equations:

$$\Delta H_R^\circ = -161216.5 + 20.51T - 0.0187 * T^2 + 1.833 * 10^{-6} * T^3 + 1.813 * 10^{-9} * T^4$$

$$\Delta G^\circ = -159217 - 55.17T - 0.0063 * T^2 + 4.83 * 10^{-7} * T^3 + 3.63 * 10^{-10} * T^4$$

$$\ln k = 6.63 - \frac{19150.5}{T} + 9.1 * 10^{-4} * T - 5.82 * 10^{-8} * T^2 - 4.37 * 10^{-11} * T^3$$

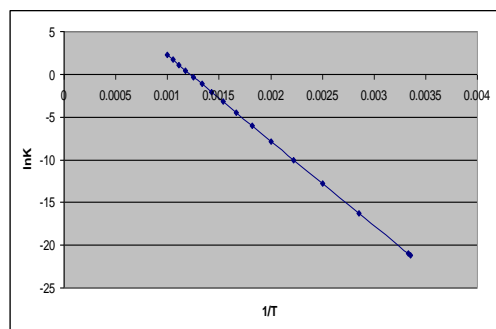
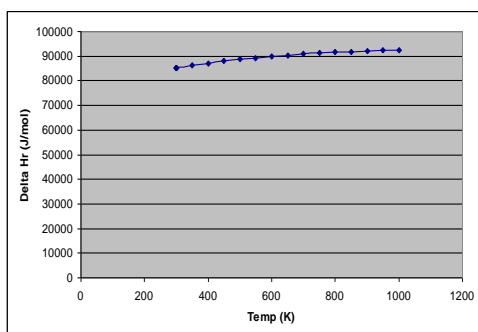
Based on the above set of equations, calculation of ΔH_R° , ΔG° and $\ln K$ is carried out for detailed thermodynamic analysis of each reaction involved in both routes in terms of feasibility of the reaction, nature of reaction. Also graphical behavior for individual reaction can also be plotted to determine the extent of reaction. From these equations the Values of ΔH_R° , ΔG° and $\ln K$ at different temperatures can be tabulated in Table: 1 as follows:

TABLE 1: Values of ΔH_R° (kJ / mole) and $\ln K$ at different temperatures for Route – I and Route – II

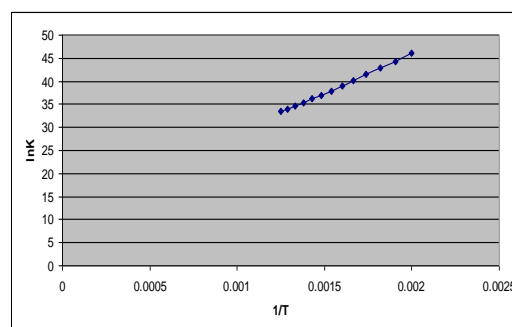
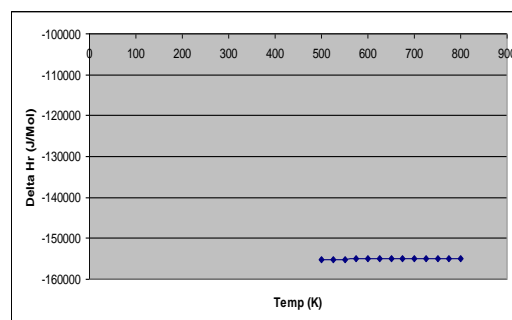
Temp (K)	Route – I (Dehydrogenation)		Temp (K)	Route – II (Oxidation)	
	ΔH_R°	$\ln K$		ΔH_R°	$\ln K$
298	85300	-21.22	298	-156700	71.2
300	85340	-21	500	-155282	46.06
350	86297	-16.31	525	-155185	44.35
400	87175	-12.78	550	-155105	42.8
450	87974	-10.03	575	-155040	41.41
500	88697	-7.827	600	-154990	40.14
550	89345	-6.016	625	-154954	38.99
600	89922	-4.501	650	-154931	37.95
650	90431	-3.215	675	-154922	37
700	90876	-2.109	700	-154924	36.14
750	91262	-1.146	725	-154938	35.36
800	91592	-0.3	750	-154964	34.64
850	91874	0.4491	775	-154999	34
900	92111	1.1181	800	-155044	33.41
950	92312	1.7192	--	--	--
1000	92482	2.2624	--	--	--

On the basis of the data tabulated in Table: 1, following are the graphs between ΔH_R° versus Temperature and $\ln K$ versus $1/T$ obtained as under:

For Route – I: Unit Process – Dehydrogenation



For Route – II: Unit Process – Oxidation



3.1. Critical Thermodynamic Analysis of FORMALDEHYDE for three routes under considerations.

For Route – I: Unit Process - Dehydrogenation

Dehydrogenation reaction is highly endothermic in nature having heat of reaction value in the range of 85 to 93 KJ /

mol of Methanol. The values of “lnK” ranges from -21.0 to 2.0. It indicates that reaction is highly reversible, so stringent control measures are required. The values of lnK are very low; practically *zero* up to 700 K. Being highly energy intensive process, it requires large quantity of heating media. Conversion is 80% and yield is above 99%. The value of conversion level can be increased at high temperature i.e. beyond 900 K. This happens to be an environmentally friendly route as O₂ (from air) is not required & has higher yield.

For Route – II: Unit Process - Oxidation

Oxidation reaction is very highly exothermic in nature having the heat of reaction value in the range of -155 to -156 KJ / mol of Methanol. The value of “lnK” ranges from 33.0 to 71.0. It indicates that reaction is highly irreversible, highly feasible and conversion level obtained can be of the order of 90%. The yield of the product is also 90%. Thus there is a full scope to increase the actual conversion levels and raw material requirements can be reduced. Stringent air pollution control measures are required. Being highly energy intensive process, large quantity of cooling media is required. The reaction is irreversible and it is a most favorable reaction for cleaner production implementation.

For Route – III: Combined Route – This route is based on the principles of carrying out dehydrogenation and oxidation reactions simultaneously using methanol as a raw material.

In this investigation, as the new technological option, Route – I being endothermic and Route – II being exothermic, combined reactor will give maximum benefits carrying both reactions (dehydrogenation and oxidation) simultaneously; the route can be converted to environmentally friendly route. Route – II is not an environmentally friendly, not a green reaction and not a green technology. However, if it couples with Route – I becomes a green reaction scheme. Conversion in dehydrogenation reaction and oxidation reaction is 80% and 90% respectively. This combined route will provide the most suitable conditions for eco – efficient environment. Route – III seems to be more environmentally friendly and more energy efficient route. Thus, it seems to be a most favorable route for cleaner production implementation.

3.2. Conclusion based on thermodynamics:

Thus, all the two reactions under considerations, first reaction being highly exothermic in nature, the removal of heat have to be done very effectively, where as the second reaction is endothermic in nature, addition of energy has to be done very effectively. The relevant material balance and energy balance flow sheet can be prepared based on actual plant capacity data.

The data tabulated in above tables is expected to be very useful while implementing energy conservation in plant manufacturing formaldehyde. Dehydrogenation being endothermic in nature, it requires large amount of energy in terms of heating media and oxidation reaction

is highly exothermic in nature, it requires large amount of energy in terms of cooling media. In other words, both the routes are highly energy intensive. If both Routes – (I) & (II) are combined i. e. oxidation process as well as dehydrogenation process occur simultaneously using shell and tube heat exchanger as a reactor, then heat evolved on tube side wherein oxidation reaction is being carried out can be utilized conveniently to heat the entire mass from shell side where dehydrogenation reaction is being carried out. Thus full energy conservation can be achieved. Energy requirements – cooling media for Route – (II) as well as heating media for Route – (I) reduces to zero. According to energy balance flow data, energy requirement from external source for this combined route is zero. Thus for the implementation of Cleaner Production principles, thermodynamics aspects are of utmost importance. Finally it can be summarized that Formaldehyde production by combined route i. e. Route – III is a good example of cleaner production principles.

4. ANALYSIS OF TECHNOLOGIES FROM CLEANER PRODUCTION POINT OF VIEW:

In Route – I, formaldehyde is produced by the dehydrogenation of methanol which would produce anhydrous or highly concentrated formaldehyde solutions. In dehydrogenation process, the temperature maintained is 600°C and the reaction is carried out in presence of oxides of ferrous & chromium. Fresh methanol with recycled quantity of methanol is fed to the reactor operated at 600°C and 1 atmospheric pressure to produce formaldehyde. The reaction is highly endothermic in nature. Conversion is 70 – 80 % and the yield of the product is 99%. (HCHO + H₂) vapors absorbed in water & H₂ gets separated, hence 37% solution of HCHO so obtained called as “Formalin”. Being highly energy intensive process, it requires large quantity of heating media. Unreacted methanol separated from formalin by distillation. Route-I happens to be environmentally friendly route as O₂ (from air) not required and has higher yield than Route-II.

In Route – II, formaldehyde is produced by the oxidation of methanol which would produce anhydrous or highly concentrated formaldehyde solutions. Methanol was oxidized over a copper catalyst, but this has been almost completely replaced with silver. The silver-catalyzed reactions occur at essentially atmospheric pressure and 600 to 650°C. The reaction is highly exothermic (-156 KJ /mol) in nature. Conversion is 80-90% and yield is 90%. The mixture passes through a super heater to a catalyst bed of silver crystals or layers of silver gauze. The product is then rapidly cooled in a steam generator and then in water cooled heat exchanger and fed to the bottom of an absorption tower. Absorber bottoms go to a distillation tower where methanol is recovered for recycle to the reactor. The base stream from distillation, an aqueous solution of formaldehyde, is usually sent to an anion exchange unit which reduces the formic acid to specification level. HCHO vapors absorbed in H₂O and one obtains 37% solution of HCHO called as Formalin. The product contains up to 55% formaldehyde

and less than 1.5% methanol. The reaction occurs at essentially adiabatic conditions. Recycled methanol required for a 50–55% product is 0.25–0.50 parts per part of fresh methanol. With increasing energy costs, maximum methanol conversion is desirable, eliminating the need for the energy-intensive distillation for methanol recovery. In another process, tail gas from the absorber is recycled to the reactor. This process can produce 50% formaldehyde with about 1.0% methanol without a distillation tower. Methanol recovery can be obviated in two-stage oxidation systems where, for example, part of the methanol is converted with a silver catalyst, the product is cooled, excess air is added, and the remaining methanol is converted over a metal oxide catalyst such as that described below. In another two-stage process, both first and second stages use silver catalysts. Formaldehyde–methanol solutions can be made directly from methanol oxidation product by absorption in methanol. Aqueous formaldehyde is corrosive to carbon steel, but formaldehyde in the vapor phase is not. All parts of the manufacturing equipment exposed to hot formaldehyde solutions must be a corrosion-resistant alloy such as type-316 stainless steel. Theoretically, equipment can be of carbon steel, but in practice alloys are required in this part of the plant to protect the sensitive silver catalyst from metal contamination. Water is also generated along with the product. Being highly energy intensive process, it requires large amount of cooling media (water). This route produces air emissions such as NO_x , CO etc. Hence stringent air pollution control measures required.

5. MATERIAL BALANCE AND ENERGY BALANCE FOR FORMALDEHYDE PRODUCTION:

5.1 Material Balance for Formaldehyde

Production for Route – I, II & III:

Basis: 50 TPD (1666.7 kgmoles/day) of Formaldehyde produced

Unit: kgmoles/day

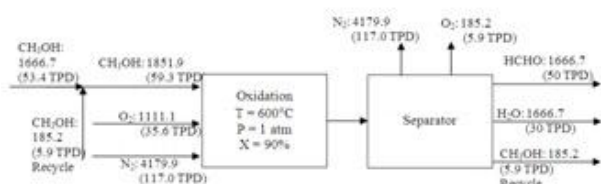


Figure: 2 Material Balance diagram for Formaldehyde Production (Route – I)

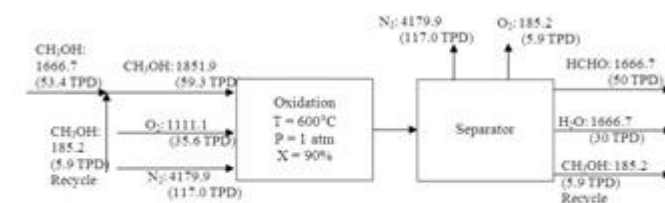


Figure: 3 Material Balance diagram for Formaldehyde Production (Route – II)

Route – III suggested in this investigation appears to be more attractive and more environmentally than Route – I and Route - II. This new technological option is considered as a combined route, in which both the reactions are carried out simultaneously. If both processes are combined i. e. oxidation reaction as well as dehydrogenation reaction occur simultaneously using shell and tube heat exchanger as a reactor, then heat evolved on tube side wherein oxidation reaction is being carried out can be utilized conveniently to heat the entire mass from shell side wherein dehydrogenation reaction is being carried out. Thus, full energy conservation can be achieved. Energy requirements in terms of heating media for route-I as well as cooling media for route-II reduces to zero. Energy evolved in oxidation process due to high exothermic reaction is fully utilized in dehydrogenation as if the reaction is highly endothermic in nature. By this option sufficient amount of energy can be saved and energy costing by thus can be reduced. Hence, this combined route can be considered to be very cost effective. Based on material balances and energy balances data, energy requirement from external source for the combined route is, thus, zero. Temperature of reaction being very high of the order of 600-650°C, some quantity of nitrogen from air is likely to get oxidized to NO_x . Thus, quantity of gaseous stream coming out of plant containing pollutants gets reduced considerably by 65%. Thus, intensity of air pollution gets reduced by a factor of three. Thus, combined route is likely to be highly energy efficient and more environmentally friendly route.

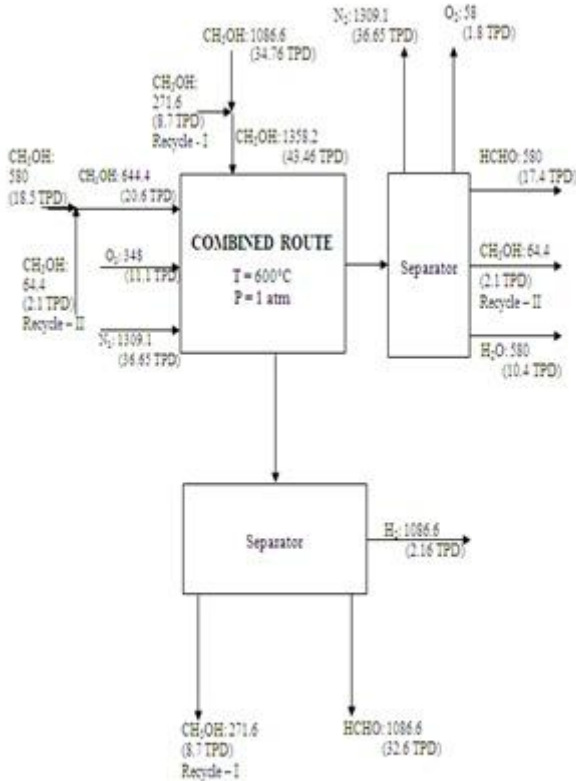


Figure: 4 Material Balance diagram for Formaldehyde Production (Route - III)

5.2 Comparison of TWO routes based on Material Balance Principles

Finally we can summarize the above two routes in common table by material balance principles for the production of 50 TPD of formaldehyde as under:

TABLE 2: Comparison of THREE routes based on Material Balance Principles

	Dehydrogenation route	Oxidation route	Combined route
CH ₃ OH required	66.66 TPD	59.3 TPD	64.06 TPD
Oxygen required	--	35.6 TPD	11.1 TPD
Air required	--	152.6 TPD	47.7 TPD

From the above table, it could be seen that formaldehyde production by combined route is a good example of in terms of waste minimization and energy Conservation and also it is taken as an eco - friendly route.

5.3 Energy Balance for Formaldehyde Production for Route - I, II & III:

Basis: 50 TPD (1666.7 kgmoles/day) of Formaldehyde produced

Unit: kJ/day

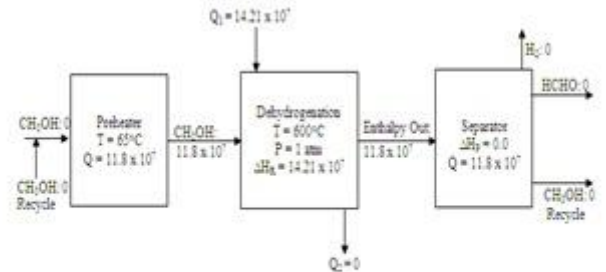


Figure: 5 Energy Balance diagram for Formaldehyde Production (Route - I)

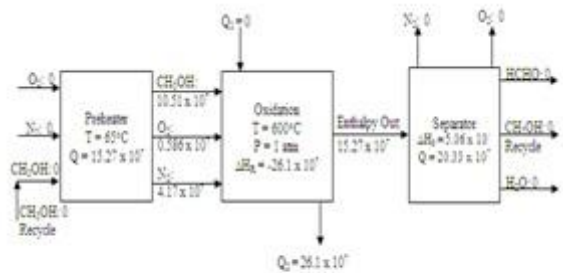


Figure: 6 Energy Balance diagram for Formaldehyde Production (Route - II)

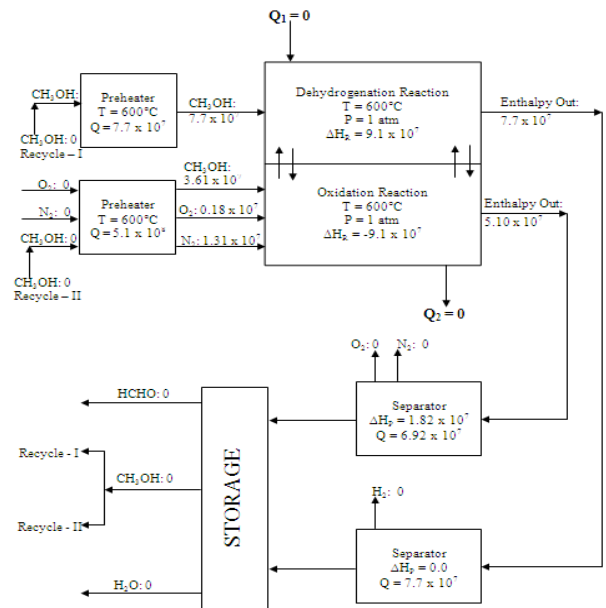


Figure: 7 Energy Balance diagram for Formaldehyde Production (Route - III)

5.4. Comparison of THREE routes based on Energy Balance Principles:

The Energy requirement for entire three routes for the production of formaldehyde can be summarized with respect to energy balance in a common table as under:

TABLE 3: Comparison of THREE routes based on Energy Balance Principles

	Preheating (kJ / day)	Heat to be absorbed / removed (kJ / day)	Separation (kJ / day)	TOTAL (kJ / day)
Route – I	11.8×10^7	14.21×10^7	11.8×10^7	37.81×10^7
Route – II	15.27×10^7	26.1×10^7	20.33×10^7	61.7×10^7
Route – III	12.8×10^7	0.0	14.62×10^7	27.42×10^7

From the above comparison, it is seen that among three routes total energy requirement (kJ / day) in terms of preheating the raw materials and separation of products from other chemical species in combined route (Route – III) is very low in comparison with the other two routes. In other words, Dehydrogenation route (since it is not so commonly used) requires total energy 37.81×10^7 kJ / day, whereas combined route requires total energy of 27.42×10^7 kJ / day. Hence in this combined route (Route – III) approximately 27 – 28% of total energy can be saved. This is the good example of energy conservation. In comparison to Route – II (most commonly used process) and Route – III, it is seen from the data tabulated above, the total energy required in Route – II is 61.7×10^7 kJ / day, whereas Route - III requires total energy of 27.42×10^7 kJ / day. Hence in this combined route (Route – III) approximately 45% of total energy can be saved. So, this combined route can also become the best example of energy conservation. As a result, this route is considered as the new technological option, in case of good energy conservation and waste minimization, for the formaldehyde production. Furthermore it requires **no (zero) energy** (as the energy evolved during oxidation

reaction is fully absorbed by dehydrogenation reaction) from external source in either terms of heating or cooling media. Thus, good energy conservation can be achieved by this option. So, combined route can be considered as most energy efficient and more eco – friendly route. “Utilizing Combined Route” for the production of Formaldehyde is a good example of “**Cleaner Production**”.

6. CONCLUSION:

From the above discussion and analysis, formaldehyde is an important and well known petrochemical manufactured by many renowned chemical industries. As discussed earlier, this petrochemical can be manufactured by two different processes namely – dehydrogenation and oxidation.

Route – I refers to dehydrogenation reaction, basically endothermic in nature. So this process requires large amount of heating media. Thus the process becomes highly intensive in nature. Critical analysis of material and energy balance states that, for the production of 50 TPD of formaldehyde, the total quantity of methanol required to feed into reactor is 66.66 TPD. Also co – product hydrogen 3.33 TPD is coming out with the main product formaldehyde. (HCHO + H₂) vapors absorbed in water & H₂ gets separated, hence 37% solution of HCHO so obtained called as “Formalin”. Route-I happens to be environmentally friendly route as it does not require O₂ (from air) and has higher yield than Route-II. The total amount of energy require in this route for the production of formaldehyde is 37.81×10^7 kJ / day. Production of formaldehyde is by the dehydrogenation of methanol which would produce anhydrous or highly concentrated formaldehyde solutions. For some formaldehyde users, minimization of the water in the feed reduces energy costs, effluent generation, and losses while providing more desirable reaction conditions.

Route – II, most of the world’s commercial formaldehyde is manufactured from methanol and air either by a process using a silver catalyst or one using a metal oxide catalyst refers to oxidation reaction, basically exothermic in nature. So this process requires large amount of cooling media. Thus the process becomes highly intensive in nature. Critical analysis of material and energy balance states that, for the production of 50 TPD of formaldehyde, the total quantity of methanol required to feed into reactor is 59.3 TPD. The quantity of air used is 152.6 TPD containing 35.6 TPD of oxygen as an oxidizing agent and nitrogen 117 TPD as an inert. The total amount of energy require in this route for the production of formaldehyde is 61.7×10^7 kJ / day. Generation of water is 30 TPD for this route. Compared this situation with Route – I more energy and raw material is required in this route. Route-II not happens to be environmentally friendly route, as it produces air emissions such as NO_x, CO etc. Hence stringent air pollution control measures required.

Route – III, in this investigation, can be considered as more environmentally friendly route. As the new technological option, both the routes are carried out in a combined reactor. The total amount of energy require in

this route for the production of formaldehyde is 27.42 x 107 kJ / day. Energy required from the external source for either removal or absorption of energy is **ZERO**. It is seen that among three routes total energy requirement in terms of preheating the raw materials and separation of products in combined route is very low in comparison with the other two routes. Hence, compared with Route – II approximately 50% of total energy can be saved. Also raw material requirement in this route can also be reduced significantly. Route – II is not an environmentally friendly, not a green reaction and not a green technology. However, if it couples with Route – I becomes a green reaction scheme. Thus full energy conservation can be achieved. Energy requirements, cooling media for Route – (I) as well as heating media for Route – (II) reduces to zero. Thus, quantity of gaseous stream coming out of plant containing pollutants gets reduced considerably by 65%. Thus, intensity of air pollution gets reduced by a factor of three. Finally it can be summarized that formaldehyde production by combined route is a good example in terms of energy conservation for the implementation of cleaner production principles.

REFERENCES:

- [1] M. Gopala Rao, Marshall Sittig; *Dryden's Outlines of Chemical Technology*; 3rd Edition, East – West Press, page: 422 – 423.
- [2] *Kirk-Othmer, Encyclopedia of Chemical Technology* (John Wiley & Sons, New York), 3rd edn, Vol. 12, 113 – 17.
- [3] L. Lefferts, J.G. Van Ommen and J.R.H. Ross, *The oxidative dehydrogenation of methanol to*
- [8] S. A. Puranik, "*Cleaner Production & Cleaner Technologies*" as remedial measures for mitigating "Climate Change", an invited lecture in a National Seminar on "Climate Changes – Corporate Opportunities", Indian Institute of Chemical Engineers, Ankleshwar Regional Centre, Bharuch, 25th July 2009.
- formaldehyde over silver catalysts in relation to the oxygen-silver interaction*, Twente University of Technology, Laboratory for Inorganic Chemistry, Material Science and Catalysis, P.O. Box 217, 75 00 AE Enschede, The Netherlands. (Received 2 December 1985, accepted 27 January 1986), *Applied Catalysis*, 23 (1986) 385-402 Elsevier Science Publishers B.V., Amsterdam - Printed in The Netherlands.
- [4] Carcia et al., Production of Formaldehyde, United State Patent; No:4,47,4996; Oct. 2, 1984, pp3.
- [5] S. A. Purnik, "*Energy Conservation in Utilities for Process Industries*", A paper presented in an India Seminar on "Energy Management in Chemical Industries", Inst. of Engineers, Andhra State Center, Hyderabad, May 1994, proceedings of Seminar, p 5 to 11, May 1994.
- [6] Jilesh. M. Pandya & S. A. Puranik, *Cleaner Production & Cleaner Technologies as remedial measures for mitigating Climate Change*, Chemical Engineering Department, L. D. College of Engineering, Ahmedabad, *International Conference on Sunrise Technologies*, 13th – 15th Jan 2011; Conference Proceeding – ME, SSVPS's B. S. Deore College of Engineering & Polytechnic, Dhule (MS) India; Page No: ME 383 – 387.
- [7] Jilesh. M. Pandya & S. A. Puranik, *Implementation of Cleaner Production principles in Petrochemical industries*, Chemical Engineering Department, L. D. College of Engineering, Ahmedabad, *Waste Minimization & Cleaner Productivity*, 28th – 29th Aug. 2010. Institution of Engineers (India), Ahmedabad.

Performance of Grid Connected DG Inverter System by Using Intelligent Controllers

K. MANOHAR^{#1}, M. VENU GOPALA RAO^{#2}

¹M.Tech Student, Department of Electrical and Electronics Engineering, KL University, Guntur (AP) India

²Professor, Department of Electrical and Electronics Engineering, KL University, Guntur (AP) India

Abstract

Recent development in the small scale power generation using distributed energy resources combined with application of power electronic systems initiated the researchers to the concepts of future power generation technologies such as microgrid.

The paper presented involves the control techniques required for microgrid operation and implementation of a simple control strategy in a microgrid model realized with MATLAB. To demonstrate the operation of a microgrid in Grid connected mode and intentional islanded mode, a simulink model has been designed with necessary parameters by connecting with the main grid allowing the sharing of different loads with reference to Grid connection and disconnection. An islanding-detection algorithm has been used to act as a switch between the two controllers and this has minimised the effect of losses in the time of transition. A reclosure algorithm has been used for the DG to resynchronize the inverter voltage with the grid.

Index Terms: Distributed Generation, Intentional Islanding, microgrid, Grid tie inverter, Algorithm, PLL, synchronization controller,

INTRODUCTION

The recent trends in small scale power generation using the with the increased concerns on environment and cost of energy, the power industry is experiencing fundamental changes with more renewable energy sources (RESs) or micro sources such as photovoltaic cells, small wind turbines, and microturbines being integrated into the power grid in the form of distributed generation (DG). These RES-based DG systems are normally interfaced to the grid through power electronics and energy storage systems[1]

One of the most critical sections of the control system for a distributed generation (DG) unit's interconnection to the utility grid lies within the grid-connected converter's control and protection system; specifically the islanding detection algorithms. Through this controller subsection, the system is able to determine whether or not it is safe to remain connected to the grid. These islanding detection algorithms, which are integrated into the control system, are mainly present to prevent the undesirable feeding of loads

during fault conditions and disconnections from the grid, whether or not the disconnection as intentional[2]

This is required by standards since the creation of such "power islands" is forbidden. Thus, in effect, standards require DG control systems to sense islanding events and disconnect themselves from the grid. This brings into question the method of how to implement such a detection scheme.[Islanding Detection Using a Coordinate Transformation Based Phase-Locked Loop]

Islanding is a condition in which a microgrid or a portion of the power grid, which contains both load and distributed generation (DG), is isolated from the remainder of the utility system and continues to operate. Some distinctions of islanding are:

non-intentional islanding occurs if after the fault it is not possible to disconnect the DG; non-intentional islands must then be detected and eliminated as fast as possible;

intentional islanding refers to the formation of islands of predetermined or variable extension; these islands have to be supplied from suitable sources able to guarantee acceptable voltage support and frequency, controllability and quality of the supply, and may play a significant role in assisting the service restoration process

microgrids, seen as particular types of intentional islands, basically operated in autonomous mode, not connected to the supply system; the whole microgrid can be seen from the distribution system as a single load and has to be designed to satisfy the local reliability requirements, in addition to other technical characteristics concerning frequency, voltage control and quality of supply.[2]

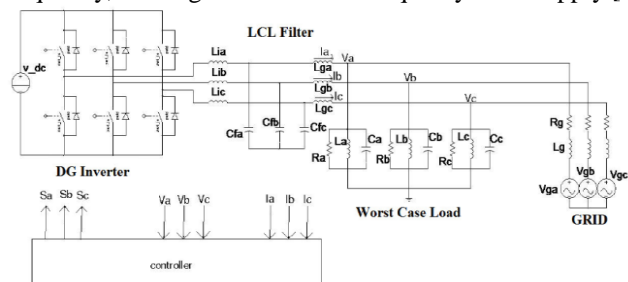


Fig 1. Schematic diagram of Grid connected Inverter

POWER MISMATCHES

The effects of power mismatches between the DG and the loads have upon the system in terms of voltage and frequency, the most rudimentary of sensed parameters, need to be known.[3]

Considering the generic system depicted in Fig. 2, and that the DG can supply anywhere from partial to the full load demand, or even an excess of power to source the grid. A parallel RLC load is used for this study's example; also that this is a local load to the DG and there will not be a large reactance between the DG and the PCC. As such, there can exist a power demand mismatch between the DG and loads[9], which the grid supplements; however when the grid is no longer supplying the remaining power demand of the loads, the system voltage and frequency at the PCC will be affected.

A. Active Power Mismatch

If the active power portion of the load demand that is calculated is coming from the DG, the following is found.

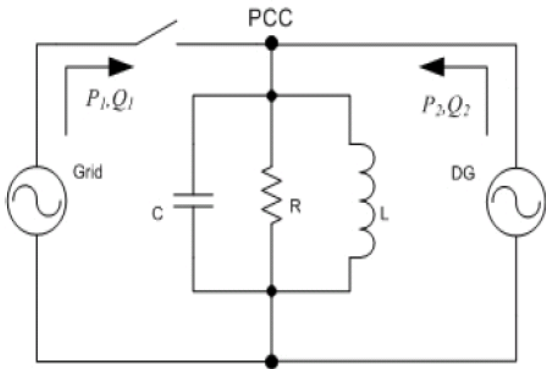


Fig. 2: Generic Interconnected System

$$P_{DG} = \frac{3V_{PCC}^2}{R_{eff}} \tag{1}$$

Where R_{eff} is the equivalent resistance seen by the DG for the amount of power it is supplying. If the grid fails and only the DG is left to supply the load at a constant active power, the voltage at the PCC would naturally change, represented in (2).

$$P_{DG} = \frac{3(V'_{PCC})^2}{R} = \frac{3(V_{PCC} + \Delta V)^2}{R} \tag{2}$$

As such, R_{eff} can be written as a function of true load resistance, the voltage and change of voltage that would occur at the PCC, seen in (3) by equating and solving (1) and (2).

$$R_{eff} = f(R, V_{PCC}, \Delta V) = R \left(\frac{V_{PCC}}{V_{PCC} + \Delta V} \right)^2 \tag{3}$$

Thus, to find the power mismatch from the load demand and DG, we can write the following:

$$\Delta P = P_{demand} - P_{DG} = 3V_{PCC}^2 \left(\frac{1}{R} - \frac{1}{R_{eff}} \right) \tag{4}$$

Plugging (3) into (4), we get the reduced equation of (5), showing that an active power mismatch between load and DG will cause voltage variations if the grid fails.

$$\Delta P = \frac{3V_{PCC}^2}{R} \left(1 - \left(\frac{V_{PCC} + \Delta V}{V_{PCC}} \right)^2 \right) \tag{5}$$

B. Reactive Power Mismatch

Now consider the reactive power mismatch between the DG and load during a grid fault. The demand required by the load is equated in (6).

$$Q = \frac{3V^2}{\omega_{line} L} (1 - \omega_{line}^2 LC) \tag{6}$$

The resonant frequency of the load is determined by the LC relationship. Therefore we can re-write (6) as (7).

$$Q = \frac{3V^2}{\omega_{line} L} \left(1 - \frac{\omega_{line}^2}{\omega_{resonant}^2} \right) \tag{7}$$

As such, if the grid stopped supplying its portion of the load's demand of reactive power, the line frequency would drift to the resonant frequency to force the mismatch to become zero.

Therefore, let us write the resonant frequency as a term of the line frequency and the frequency drift due to a mismatch.

$$\Delta Q = \frac{3V^2}{2\pi f_{line} L} \left(1 - \frac{f_{line}^2}{(f_{line} + \Delta f)^2} \right) \tag{8}$$

When the max/min values of the voltage and frequency deviations are plugged into (5) and (8), an NDZ range for power mismatch can be calculated. As such, it is seen that the standard OVP/UVP, OFP/UFP schemes are not enough to minimize the NDZs.[3]

ISLANDING DETECTION ALGORITHM

Islanding is the condition where the DG remains operating in the distribution system with the utility disconnected. In the past years, several islanding detection methods have been proposed and the detection methods can be categorized into two main groups: passive and active methods. Passive methods depend on measuring system parameters and then thresholds are set to these parameters

to differentiate between an islanding and a nonislanding condition Active methods directly interact with the power system operation by introducing perturbations in the inverter output. The most commonly used islanding detection method is the Over/Under Voltage (OVP/UVP) and Over/Under Frequency (OFP/UFP). [4],[8]

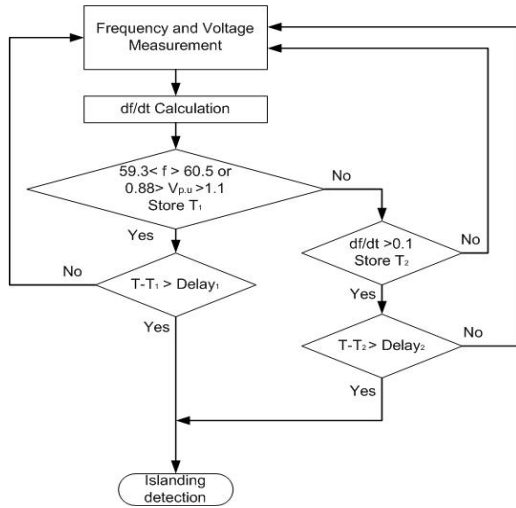


Fig 3. Intentional Islanding Algorithm

The DG interface control designed in this paper provides constant DG output and maintains the voltage at the Point of Common Coupling (PCC) at 1 p.u. Maintaining both the voltage and power constant during an islanding condition is not feasible for standalone operation of the DG since both depend on each other, and the OVP/UVP and OFP/UFP could be used to detect islanding[4]. This detection method will operate efficiently for large mismatches between load and DG capacity. Unfortunately, if the load closely matches the DG capacity, the frequency will reach the threshold value after a very long time. The DG was designed to supply 100 kW and the load connected absorbs approximately 100 kW. The grid disconnects at t = 5 seconds and the frequency at the PCC drifts away from the 60 Hz value. It can be seen that the time for the frequency to reach the 59.3 Hz threshold is greater than 5 seconds..[8]

CONTROLLERS:

The system consists of a microsource that is represented by the dc source. Under normal operation, each DG inverter system in the microgrid usually works in constant current (or constant power) control mode in order to provide a pre-set power to the main grid. When the microgrid is cut off from the main grid, each DG inverter system must detect this islanding situation and switch to a voltage control mode. In this mode, the microgrid will provide a constant voltage to the local load[2].

Condition 1: WHEN GRID IS DISCONNECTED

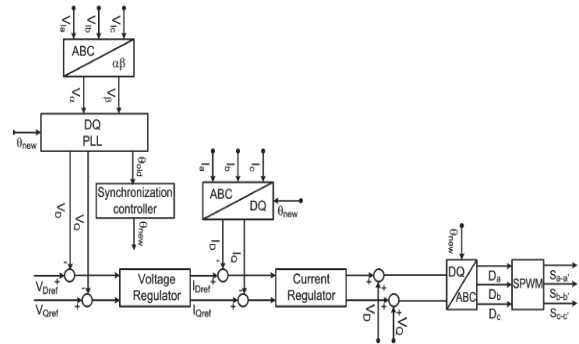


Fig: 4 Voltage-controller when the Grid is Disconnected

Condition II: WHEN GRID IS CONNECTED

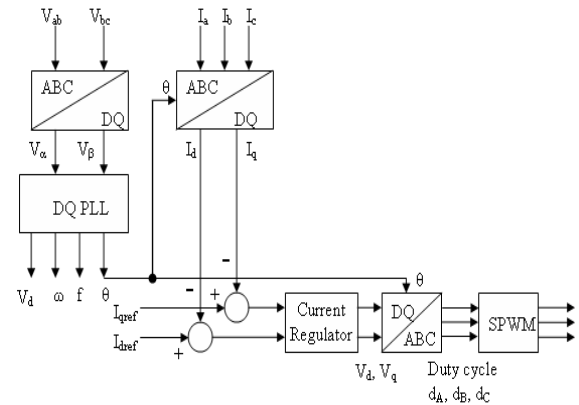


Fig 5: Current Controller when Grid is Connected

For grid-connected operation, the controller shown in Fig 5. is designed to supply constant current output. A phase locked loop is used to determine the frequency and angle reference of the Point of Common Coupling (PCC) voltage. To simplify the design and operation of the controller, the control of the system is designed in a synchronous reference frame (SRF) [5]. Fig. 6 shows this control topology employing synchronous frame current control.[6]

The inverter currents are transformed into a synchronous frame by Park's transformation and regulated in dc-quantity corresponding to the current references Idref. In the following stage, the voltage references in dc-quantities Vdq which being processed by PI controllers are transformed into a stationary frame by the inverse of Park's transformation and utilized as command voltages for generating high frequency pulse width modulated (PWM) voltage.[11]

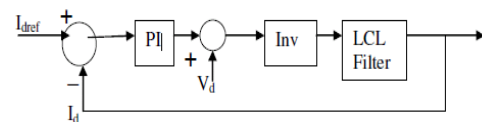


Fig 6: Block diagram of Current controlled Inverter

When using the current control, the output current from the filter is fed back and compared with reference current I_{ref} and the error is passed to the PWM to generate voltage reference for the inverter. In order to get a good dynamic response V_{dq} is fed forward. Fig. 6 shows the block diagram of the DG interface control for grid-connected operation. For unity power factor operation, i_{qref} is set to zero.[2]

A Intentional-Islanding Operation Mode

The voltage closed-loop control for intentional-islanding operation is shown. The control works as voltage regulation through current compensation. The controller uses voltage compensators to generate current references for current regulation.

As shown, the load voltages (V_d and V_q) are forced to track its reference by using a PI compensator (voltage regulator). The outputs of this compensator (I_{Dref} and I_{Qref}) are compared with the load current (I_D and I_Q), and the error is fed to a current regulator (PI controller). The output of the current compensator acts as the voltage reference signal that is fed

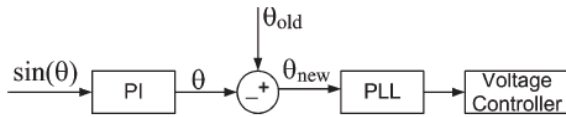


Fig 7: Synchronisation Controller

to the sinusoidal pulsewidth modulator to generate the high frequency gating signals for driving the three-phase voltage source inverter. The current loop is included to stabilize the system and to improve the system dynamic response by rapidly compensating for near-future variations in the load voltages. In order to get a good dynamic response, V_{DQ} is fed forward. This is done because the terminal voltage of the inverter is treated as a disturbance, and the feedforward is used to compensate for it .

B Synchronization for Grid Reconnection

When the grid-disconnection cause disappears, the transition from islanded to grid-connected mode can be started. To avoid hard transients in the reconnection, the DG has to be synchronized with the grid voltage . The DG is operated in the synchronous island mode until both systems are synchronized. Once the voltage in the DG is synchronized with the utility voltage, the DG is reconnected to the grid, and the controller will pass from the voltage to the current control mode. This synchronization is achieved by implementing the following algorithm.[5]

1) Assume that the phase difference between the grid and inverter voltages is given by

$$\theta = \angle V_G - \angle V_I. \tag{9}$$

2) In order to obtain the information of θ , two sets of voltage values are used

$$k = V_{Ia}V_{Ga} + V_{Ib}V_{Gb} + V_{Ic}V_{Gc} = \frac{3}{2} [\cos(\theta)]$$

$$g = V_{Ia}V_{Gb} + V_{Ib}V_{Gc} + V_{Ic}V_{Ga} = \frac{3}{4} [-\cos(\theta) + \sqrt{3} \sin(\theta)] .$$

(10)

Using the variables k and g , $\sin(\theta)$ can be found as

$$\sin(\theta) = \frac{\frac{4}{3}g + \frac{2}{3}k}{\sqrt{3}}. \tag{11}$$

Fig. Syn cotrl shows how $\sin(\theta)$ is used to obtain the new phase angle for which the grid and inverter voltages are synchronized.

MODELLING OF CIRCUIT IN MATLAB SIMULINK.

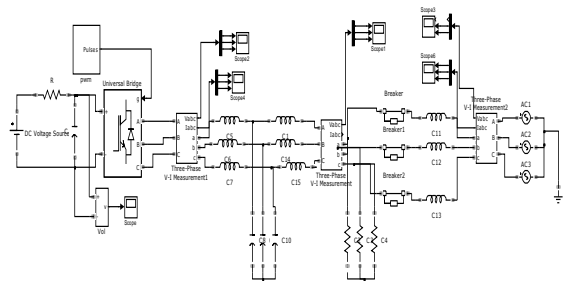


Fig.8: Without any controllers

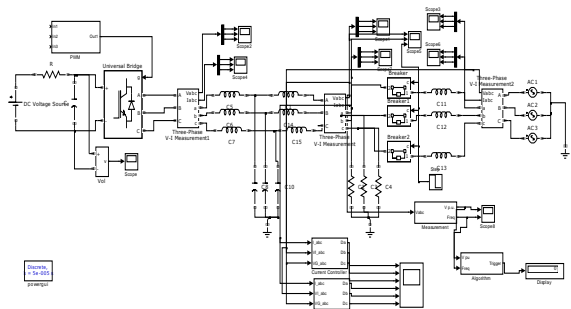


Fig 9. With controllers

SIMULATION RESULTS

The performance of the proposed control strategies was evaluated Fig. shows the simulated system. This system was tested under the following conditions:

- 1) switching frequency f_s : 10 kHz;
- 2) output frequency: 60 Hz;
- 3) filter inductor L_i : 1 mH;
- 4) filter inductor L_L : 0.5 mH;
- 5) filter capacitor C_f : 31 μ F;
- 6) dc-link voltage V_{dc} : 400 V;
- 7) output phase voltage $V_{o1\phi}$: 120 Vrms;
- 8) output capacity: 10 KW.

The RLC load was adjusted to be resonant at 60 Hz and to consume 10 KW. The DG system was designed to supply 10 KW and zero reactive power. The system was operated initially in grid-connected operation. The grid was disconnected at 0.3 s, and this event was detected at 0.30155 s. After 0.30155 s, the control mode was changed from current- to voltage controlled operation.

FFT Analysis for the Inverter.

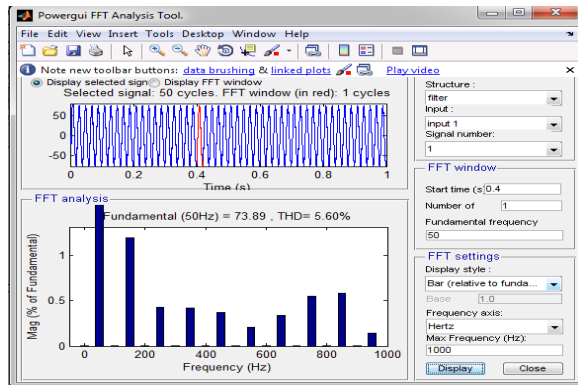


Fig 10: FFT analysis of Inverter

Using the above analysis we can observe that the inverter has operated with the THD of 5.6%



Fig 11. Inverter Voltages when connected to the Grid.

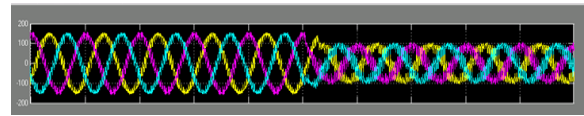


Fig:12 Voltages Without Synchronisation Algorithm

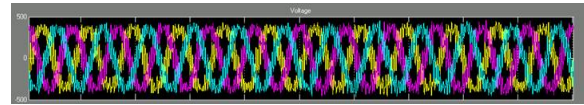


Fig 13: Voltages With Synchronisation Algorithm

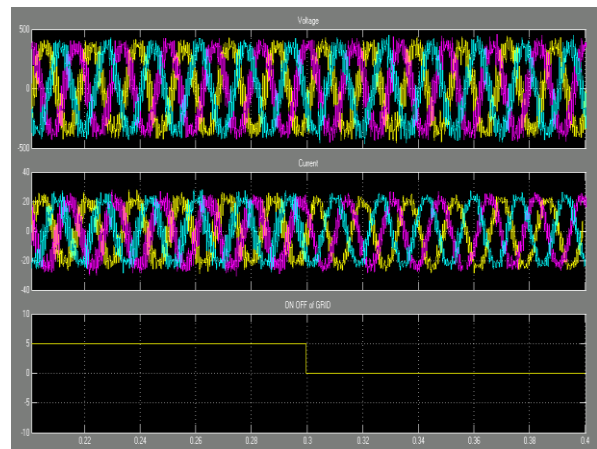


Fig 14. shows the voltages and currents at the PCC before and after grid disconnection. The grid was reconnected at 0.3 s.

The DG was operated in the synchronous island mode until both systems were resynchronized. Fig. 14 shows the synchronization of the voltages at both ends of the PCC when the synchronization algorithm starts to work in the intentional-islanding mode. As can be seen, the proposed algorithm successfully forces the voltage at the DG to track the voltage at the grid.

Once the synchronization was completed, the DG was reconnected to the grid, and the controller was switched from the voltage to the current control mode. Fig. 12,13 shows the phase voltage V_a without and with the synchronization algorithm implemented. Notice that the algorithm avoids a hard transient in the reconnection from intentional-islanding to grid-connected operation to keep the magnitude of the voltage in its normal operational range when there is a power mismatch.

CONCLUSION:

Here in this paper a controller is designed both for grid connected operation and the other for Intentional islanding operation. An algorithm for the detection of islanding is presented which was responsible for the switch

between the two controllers and also a reclosure algorithm which causes the DG to resynchronize itself with the grid is also designed.

Thus the paper summarizes the traditional independent inverter and Grid-connected inverter control strategy, combining the distributed power and microgrid inverter characteristics, a suitable microgrid inverter control strategy is put forward. Switching between Grid-connected mode and Grid-disconnected mode for microgrid inverter has been studied. On the Grid-disconnected operation microgrid inverter supplies the important loads that ensures load voltage and frequency stability. Microgrid inverter can smoothly switch between Grid-connected operation and Grid-disconnected operation, and switching operation of the system has good performance. The system controller design is simple, practical and efficient, easy to implement. The simulation results show that the proposed control method is feasible and effective.

REFERENCES

- [1] Yun Wei Li, *Member, IEEE*, and Ching-Nan Kao, "An Accurate Power Control Strategy for Power-Electronics-Interfaced Distributed Generation Units Operating in a Low-Voltage Multibus Microgrid", *IEEE transactions on power electronics*, vol. 24, no. 12, december 2009
- [2] Irvin J. Balaguer, Uthane Supatti, Qin Lei, Nam-Sup Choi, "Intelligent Control for Intentional Islanding Operation of Microgrids" ICSET 2008
- [3] Thacker, T.; Wang, F.; Burgos, R.; Boroyevich, D., "Islanding Detection Using a Coordinate Transformation Based Phase-Locked Loop," *Power Electronics Specialists Conference, 2007, PESC 2007, IEEE*, pages: 1151 – 1156, 17-21 June 2007
- [4] L. Qin, F. Z. Peng, and I. J. Balaguer, "Islanding control of DG in microgrids," in *Proc. IEEE 6th IPEMC*, 2009, pp. 450–455.
- [5] Irvin J. Balaguer, Qin Lei, Shuitao Yang, Uthane Supatti, Fang Zheng Peng, "Control for Grid-Connected and Intentional Islanding Operations of Distributed Power Generation", *IEEE transactions on industrial electronics*, vol. 58, no. 1, january 2011
- [6] Jayaweera, D.; Galloway, S.; Burt, G.; McDonald, J.R., "A Sampling Approach for Intentional Islanding of Distributed Generation," *Power Systems, IEEE Transactions on*, Volume 22, Issue 2, pages: 514 – 521, May 2007
- [7] Carpaneto, E.; Chicco, G.; Prunotto, A., "Reliability of reconfigurable distribution systems including distributed generation," *International Conference on Probabilistic Methods Applied to Power Systems*, pages: 1 – 6, 11-15 June 2006.
- [8] Zeineldin, H.; El-Saadany, E.F.; Salama, M.M.A., "Intentional islanding of distributed generation," *Power Engineering Society General Meeting, 2005. IEEE*, Vol. 2, pages: 1496 – 1502, 12-16 June 2005.
- [9] IEEE Std. 1547, "Standard for Interconnecting Distributed Resources with Electric Power Systems," 2003.
- [10] Wu Chun-Sheng; Liao Hua; Wang Yi-Bo; Peng Yan-chang; Xu Hong- Hua, "Design of intelligent utility-interactive inverter with AI detection," *Third International Conference on Electric Utility Deregulation and Restructuring and Power Technologies, DRPT 2008*, pages: 2012 – 2017, 6-9 April 2008.
- [11] T.C. Green; M. Prodanovic, "Control of inverter-based micro-grids," *Electric Power Systems Research, Distributed Generation: Volume 77, Issue 9*, pages 1204-1213, July 2007.

Error Tolerant Modified Booth Multiplier for Lossy Applications

Neethu Rose Thomas¹, V. V. Teresa²

**M.E. Student, Department of Electrical and Electronics Engineering,
Hindustan College of Engineering and Technology, Coimbatore, India*

*** Assistant Professor, Department of Electrical and Electronics Engineering,
Hindustan College of Engineering and Technology, Coimbatore, India*

ABSTRACT

Multippliers are the fundamental arithmetic unit in multimedia and digital signal processing applications. The fixed width multipliers are used in those applications where we have to maintain a fixed format and allow a little accuracy loss of output data. In this paper we have proposed a low power technique for high speed modified booth multiplication. Even though modified booth multiplier reduces truncation error it consumes more power for the purpose and reduces speed. To reduce power consumption in truncation process we introduce error tolerant adder in modified fixed width Booth multiplier. The ETA is able to ease the strict restriction on accuracy, and at the same time achieve tremendous improvements in both the power consumption and speed performance.

Keywords- Digital Signal Processing (DSP), Error tolerant adder, Fixed width multiplier, modified Booth multiplier, Signal Conditioning (SC Generator)

I. INTRODUCTION

Multiplication is an important part of real-time digital signal processing (DSP) applications ranging from digital filtering to image processing. In these systems multipliers are always the fundamental arithmetic unit and they significantly influence the system's performance and power dissipation. Many application systems based on DSP, especially the recent next-generation optical communication systems, require extremely fast processing of a huge amount of digital data. Most of DSP applications such as fast Fourier transform (FFT) require additions and multiplications. Since the multipliers have a significant impact on the performance of the entire system, many high-performance algorithms and architectures have been proposed to accelerate multiplication.

In analog computations, generation of "acceptable" results is more important than totally accurate results [8]. Hence, by using error tolerance concept in design and test, it is able to develop results. To deal with high speed and low power circuits for analog computations, different types of multipliers have been studied. Multipliers based on word length reduction for multi-precision multiplication [5] showed that power reduction of 56% can be realized in case of 16 bit Wallace tree multipliers for 8 bit truncation. However, power reduction can be achieved only at the expense of precision which exceeds tolerance for minimum bit constants. As for the "low-error area-efficient fixed-width multipliers" [6], it may have an area improvement of 46.67% but has average error reaching 12.4%.

In this paper, the design of an Error Tolerant (ET) Modified Booth Multiplier is proposed to deal with this problem. It utilizes the concept of error tolerant addition [9] for accumulation of partial products bits of modified booth multiplier. Since the system that incorporates this circuit produces acceptable results, it is said to be error tolerant. Not all digital based applications can use error tolerant concept. In digital systems such as control systems, the correctness of the output signal is extremely important, and this doesn't allow the usage of the error tolerant circuit. However, for many Digital Signal Processing (DSP) systems that process signals relating to human senses such as hearing, sight, smell and touch, e.g., the image processing and speech processing systems, the error-tolerant circuits may be applicable [7]-[9].

II. ERROR TOLERANT ADDER

2.1.ERROR TOLERANT ADDITION

The commonly used terminologies in Error Tolerant addition are overall error and accuracy. They are defined by the equations discussed below.

$$\text{Overall error (OE): } OE = |Rc - Re| \quad (1)$$

where Re is the result obtained by the Error tolerant addition technique, and Rc is the correct result (all the results are represented as decimal numbers).

Accuracy (ACC): In the case of the error tolerant design, the accuracy of an addition process is used to indicate how "correct" the output of an adder is for a particular input. Its value ranges from 0-100%.

$$\text{ACC\%} = (1 - (OE/Rc)) \times 100 \quad (2)$$

In the conventional adder circuit, the delay is mainly due to the carry propagation from the least significant bit (LSB) to the most significant bit (MSB). Glitches in the carry propagation also cause significant power dissipation. Therefore, if the carry propagation can be eliminated or curtailed, a great improvement in speed performance and power consumption [8] can be achieved. This new addition arithmetic can be illustrated via an example shown below.

In error tolerant addition technique, we first split the input operands into two parts: an accurate part that includes higher order bits and the inaccurate part that consists of lower order bits. The length of each part need not necessary be equal. The addition process starts from the middle i.e., starting point in Fig 1 towards the two opposite directions at the same time.

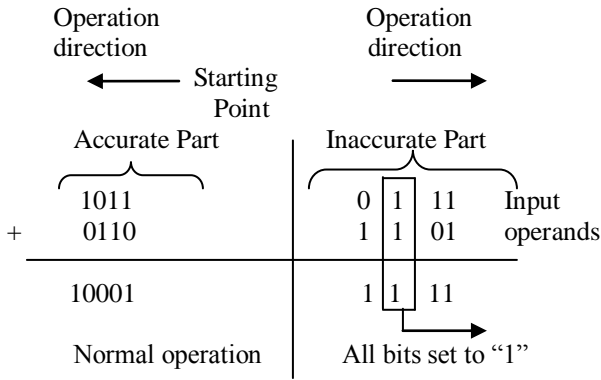


Fig 1. Arithmetic Procedure of Error Tolerant Adder

In the example of Fig. 1, the two 8-bit input operands, A="10110111" (183) and B= "01101101" (109), are divided equally into 4 bits each for the accurate and inaccurate parts. The addition of the higher order bits (accurate part) of the input operands is carried from right to left (LSB to MSB) and normal addition method is applied. This is to preserve its correctness since the higher order bits play a more important role than the lower order bits. The lower order bits of the input operands (inaccurate part) require a special addition mechanism. No carry signal will be considered at any bit position to eliminate the carry propagation path. To minimize the overall error due to the elimination of the carry chain, a special strategy is adapted, and as follows: 1) check every bit position from left to right (MSB to LSB); 2) if both input bits are "0" or different, normal one-bit addition is performed and the operation proceeds to next bit position; 3) if both input bits are "1," the checking process stopped and from this bit onward, all sum bits to the right are set to "1." The addition mechanism described can be easily understood from the example. For the addition of the MSB part in modified booth multiplication we have adopted this technique.

The block diagram of the Error Tolerant adder that adapts to our proposed addition arithmetic is shown in Fig. 2. This most straightforward structure consists of two parts: an accurate part and an inaccurate part. The accurate part is constructed using conventional adder such as the Ripple-Carry Adder (RCA). The carry-in of this accurate part adder is connected to ground. The inaccurate part constitutes two blocks: a carry-free addition block and a control block. The control block is used to generate the control signals to determine the working mode of the carry-free addition block. In addition, the Least Significant Bit (LSB) of the multiplier (bit B₀) is used as control bit for both accurate part and inaccurate part of the proposed adder. For B₀ is one, the adder cells performs normal addition operation. For B₀ equals to zero, the adder cells are brought into OFF state with NMOS and PMOS transistor brought into open state and the line from supply to ground is cut off, thus minimizing leakage power dissipation. Based on the proposed methodology, an 8-bit Error tolerant adder is designed by considering 4 bits in accurate part and 4 bits in inaccurate part.

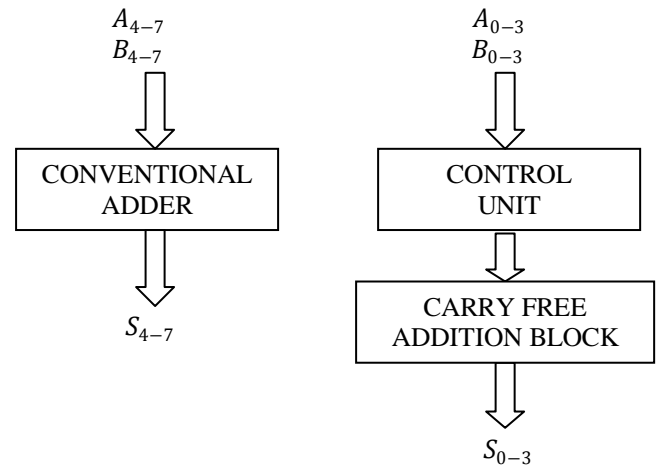


Fig 2. Block Diagram of Error Tolerant Adder

2.2. DESIGN OF THE INACCURATE PART

The inaccurate part is the most important section in the proposed ETA because it determines the accuracy, speed performance, and power consumption of the adder. The inaccurate part consists of two blocks: the carry free addition block and the control block. The carry-free addition block is designed using 4 modified XOR gates to generate a sum bit individually for LSBs. The block diagram of the carry free addition block is shown in Fig 3. In the modified XOR gate, six extra transistors are added to the conventional XOR gate. CTL is the control signal coming from the control block and is used to set the state of transistors. As the line from supply to ground is open during high impedance state, the chances of leakage power dissipation is minimized.

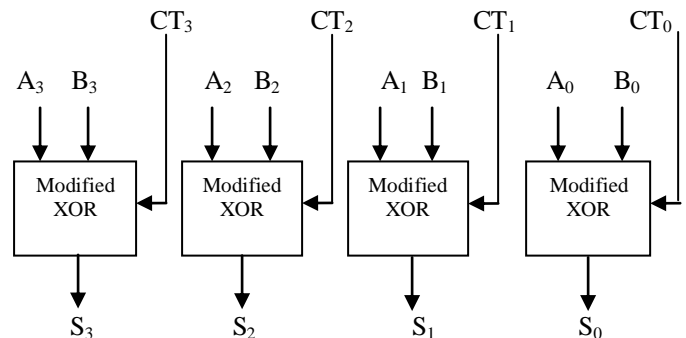


Fig 3. Architecture of Carry Free Addition Block

The function of the control block [9] is to find the first bit position when both input bits are "1," and to set the control signal CTL to high at this position as well as those to its right up to LSB. As the proposed adder has 4 bits in inaccurate part, the control block is designed with 4 control signal generating cells (CSGCs) and each cell generates a control signal for the modified XOR gate in the corresponding bit position of carry-free addition block. Two types of CSGC, labelled as type I and II are designed to develop the control signals. The control signal generated by the leftmost cell in each group is connected to the input of the leftmost cell in the adjacent group. These extra connections allow the propagated high control signal to "jump" from one group to another [8].

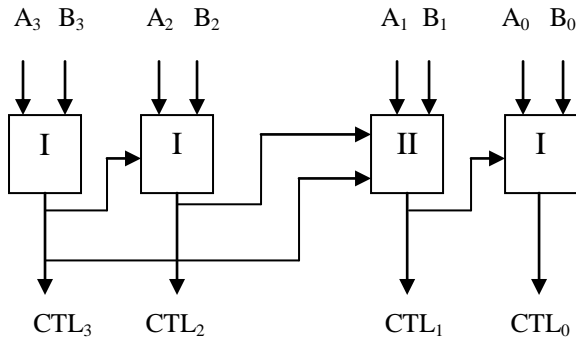


Fig 4. Overall architecture of Control Block

III. PROPOSED ERROR TOLERANT

MODIFIED BOOTH MULTIPLIER

In case of existing modified booth multiplier the partial product matrix can be segmented into MP (Major product) and LP (Lower product), where LP is further divided into LP_{major} and LP_{minor} . In the fixed-width modified Booth multiplier, only the partial product bits in LP_{minor} are removed and the carry value propagated from LP_{minor} to LP_{major} must be estimated by a simple circuit to compensate for the truncation error. The final partial product matrix developed by using existing modified fixed width booth multiplier [11] is shown in Fig 5. Even though this increases accuracy but it reduces speed of operation as well as increase power consumption.

In proposed error tolerant booth multiplier for the addition of the partial product obtained we apply the error tolerant adder. We are applying error tolerant adder in modified booth multiplier for lossy applications because we need only “good enough” results not accurate results. By applying error tolerant addition technique we divide the partial products into accurate and inaccurate part. Since it is a fixed width multiplier we append zeros to make the partial products rows of equal length. Here length is 16 bit. For the addition of the partial product bits method described in Section II is used. As Error tolerant adder used for accumulation of partial products involves carry free addition, the delay due to carry propagation can be reduced to a greater extent.

The major components of the proposed design are (i) Modified Booth Encoder (ii) SC Generator and (iii) Error tolerant adder. Fig 6.shows the block diagram for the proposed design. First the values of partial product bits are found out using modified booth encoders and carry value propagated from LP_{minor} to LP_{major} . Then the outputs of modified Booth encoders are taken as inputs and then generates the approximate carry value, is derived to reduce the truncation error and make the error distribution as symmetric and centralized as possible using SC generator [11]. For the addition of the partial product bits we use the error tolerant adder to improve power dissipation as well as speed. At this stage 16 bit output is produced. To further improve the constraints we truncate the output obtained i.e., P to 8 bits. By this technique we can improve power as well as speed.

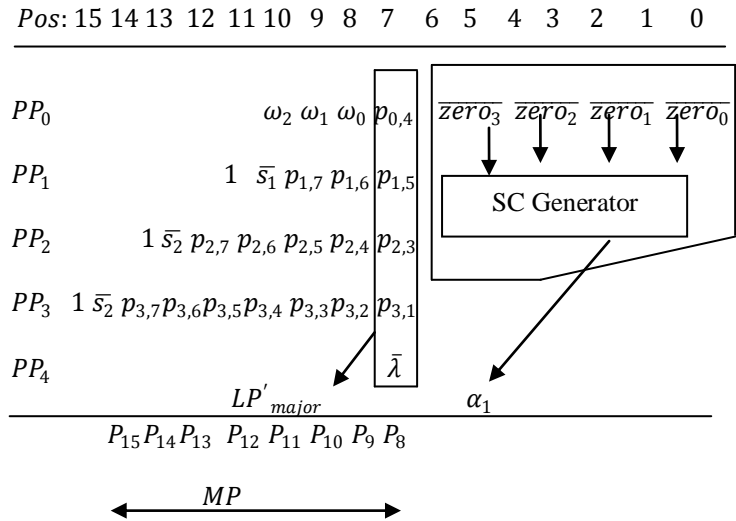


Fig. 5. Final partial product matrix of fixed-width modified Booth multiplier for n=8

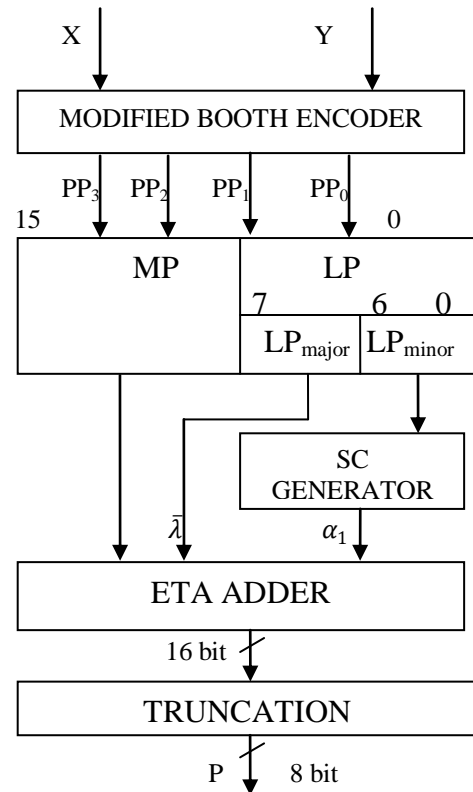


Figure 6. Generalised Architecture for ET modified booth multiplier

IV. RESULTS

The proposed Error Tolerant modified Booth multiplier is designed in XILINX 8.1 using VHDL code and simulated using Modelsim5.5.

The power dissipation and delay comparison of the booth multipliers for input data are shown in Table 1.

Reduction in power dissipation is mainly due to the reduced number of switching activities in the proposed Error Tolerant modified booth multiplier. The blocks of Error tolerant adder are brought into high impedance state during

zero bit value of multiplier, due to that a constant saving in leakage power is achieved.

Parameter	Conventional Booth Multiplier	Modified Booth Multiplier Using SC generator	Error tolerant Modified Booth Multiplier
Area (No. of gates)	2021	835	461
Delay	95ns	65ns	50ns
Power	130mW	89mW	86mW

Table 1. Comparison of (a) Power and (b) Delay of Modified booth multiplier proposed ET modified booth multipliers

Delay of proposed Error Tolerant modified multiplier decreases by 10% when compared to the Modified Booth Multiplier. The reduced delay of proposed multiplier is due to the elimination of carry propagation in inaccurate part of the Error Tolerant adder used.

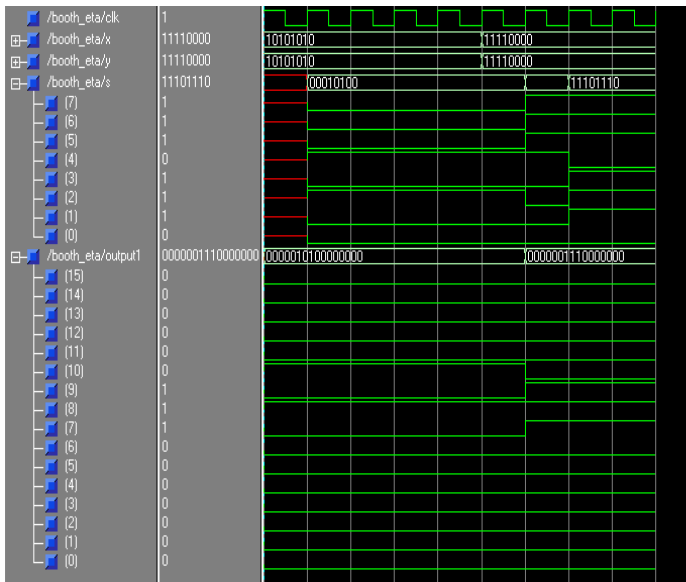


Figure 7. Output obtained for High speed error tolerant modified booth multiplier using Modelsim5.5.

V. CONCLUSION

In this paper, the error tolerance arithmetic is used in design of modified booth multiplier. The proposed multiplier reduces a certain amount of accuracy for significant power saving and performance improvement. Comparisons with conventional multipliers showed that the proposed Error tolerant modified booth multiplier reduces

area i.e., number of gate count and improves speed of performance. The applications of the Error Tolerant Multiplier are in those areas where there is no strict restriction on accuracy or when high-speed performance is more important compared to accuracy. Some applications are in Digital Image processing and DSP architectures for cell phones, laptops etc.

REFERENCES

- [1] M. A. Breuer, "Intelligible test techniques to support error-tolerance," in Proc. Asian Test Symp., Nov. 2004, pp. 386–393.
- [2] K.J. Cho, K.C. Lee, J.G. Chung, and K.K.Parhi, "Design of low- error fixed-width modified Booth multiplier," IEEE Trans. Very Large Scale Integer. Syst., vol.12, no.5, pp. 522-531, May 2004
- [3] I.S.Chong and A. Ortega, "Hardware testing for error tolerant multimedia compression based on linear transforms," in Proc. Defect and Fault Tolerance in VLSI Syst. Symp., 2005, pp. 523–531.
- [4] F.Elguibaly, "A fast papallel multiplier- accumulator using the modified Booth Algorithm," IEEE Trans. Circuits Syst.ii, Reg. Papers, vol. 47, no.9,pp.902-908, Sep. 2000
- [5] International Technology Roadmap for Semiconductors . Available: <http://public.itrs.net/>
- [6] J.M.Jou, S.R.Kuang, and R.D.Chen," Design of low-error fixed –width multipliers for DSP applications," IEEE Trans. Circuits Syst.II, Exp.Briefs, vol.46,no.6, pp.836-842, June 1999.
- [7] S.S. Kidambi, F.El-Guibaly, and A.Antoniou, " Area-efficient multipliers for digital signal processing applications," IEEE Trans. Circuits Syst.II, Exp. Briefs, vol. 43, no.2, pp. 90-94, Feb.1996
- [8] A.B.Melvin, "Let's think analog," in Proc. IEEE Comput. Soc. Annu. Symp. VLSI, 2005, pp. 2–5.
- [9] A.B.Melvin and Z. Haiyang, "Error-tolerance and multi-media," in Proc. 2006 Int. Conf. Intell. Inf. Hiding and Multimedia Signal Process., 2006, pp. 521–524.
- [10] L.D.Van and C.-C. Yang, "Generalized low-error area efficient fixed width multipliers," IEEE Trans. Circuits Syst. I, Reg. Papers, vol. 25, no. 8, pp. 1608–1619, Aug. 2005.
- [11] Jiun-Ping Wang, Shiann-Rong Kuang, and Shish-Chang Liang, "High-Accuracy Fixed Width Modified Booth Multipliers for Lossy Applications" IEEE Trans. on VLSI Systems, vol. 19, no. 1,pp 52-60, January 2011.

A Review of Energy-Aware Routing Protocols in MANETs

Shipra Gautam¹, Rakesh Kumar²

*(M.Tech Scholar, Department of Information Technology, MMU Mullana, India)

** (Department of Information Technology, MMU Mullana, India)

Abstract: Mobile Ad Hoc Networks (MANETs) is a collection of multi-hop wireless mobile nodes that communicate with each other without centralized control or established infrastructure. The energy efficient routing may be the most important design criteria for MANETs, since mobile nodes will be powered by batteries with limited capacity and the nodes in MANET are mobile. Energy efficiency doesn't mean only the less power consumption, it means increasing the time duration in which any network maintains certain performance level. So, power management becomes critical issue. The paper focuses on recent development and modifications in this widely used field and proposed energy saving algorithms, the conventional protocols and also how these are modified to make these protocols energy efficient.

Keywords: MANETs, Power Management, Energy saving algorithms.

1. Introduction: Power failure of a mobile node not only affects the node itself but also its ability to forward packets on behalf of others and thus the overall network lifetime. A mobile node consumes its battery energy not only when it actively sends or receives packets, but also when it stays idle listening to the wireless medium for any possible communication requests from other nodes. Thus, energy-efficient routing protocols minimize either the active communication energy required to transmit and receive data packets or the energy during inactive periods [1]. The transmission power control approach can be extended to determine the optimal routing path that minimizes the total transmission energy required to deliver data packets to the destination [2]. For protocols that belong to the latter category, each node can save the inactivity energy by switching its mode of operation into sleep/power-down mode or simply turns it off when there is no data to transmit or receive. This leads to considerable energy savings, especially when the network environment is characterized with low duty cycle of communication activities. However, it requires a well-designed routing protocol to guarantee data delivery even if most of the nodes sleep and do not forward packets for other nodes. Another important approach to optimizing active communication energy is load distribution approach [3]. While the primary focus of the above two approaches is to minimize energy consumption of individual nodes, the main goal of the load distribution method is to balance the energy usage among

the nodes and to maximize the network lifetime by avoiding over-utilized nodes when selecting a routing path. The paper classifies numerous energy efficient routing mechanisms proposed for MANETs. The main focus is on motivation, research challenges, recent development and modifications in this widely used field and also see how conventional routing protocols are modified to make them as energy efficient. While it is not clear whether any particular algorithm or a class of algorithms is the best for all scenarios, each protocol has definite advantages/disadvantages and is well-suited for certain situations. However, it is possible to combine and integrate the existing solutions to offer a more energy-efficient routing mechanism. Since energy efficiency is a critical issue in other network layers, considerable efforts have been devoted to developing energy-aware MAC and transport protocols.

The paper is organized as follows. In section 1 the Introduction and general discussion on energy efficiency is presented. Section 2 presents classification of routing protocols. The definition and need for energy efficiency is discussed in section 3. Section 4 provides energy efficient routing techniques and researches in energy efficient routing. Finally conclusion and future work is discussed in section 5.

2. Classification of Routing Protocols

Routing protocols can be classified according to various approaches as shown in figure 1.

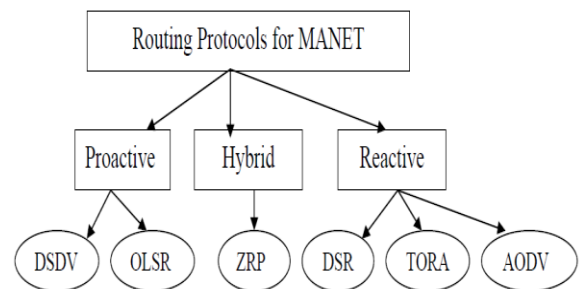


Figure 1 Classification of routing protocols for MANET

2.1 Proactive Routing: These types of protocols are called table driven protocols in which, the route to all the nodes is maintained in routing table. Packets are transferred over the predefined route specified in the routing table. In this scheme, the packet forwarding is done faster but the routing overhead is greater because all the routes have to be defined

before transferring the packets. Proactive protocols have lower latency because all the routes are maintained at all the times.. E.g. are DSDV, Wireless Routing Protocol and Optimized Link State Routing, TBRPF [4].

2.2 Reactive routing: It is also called on demand routing. It is more efficient than proactive routing and most of the current work and modifications have been done in this type of routing for making it more and more better. The main idea behind this type of routing is to find a route between a source and destination whenever that route is needed whereas in proactive protocols we were maintaining all routes without regarding its state of use. So in reactive protocols we don't need to bother about the routes which are not being used currently. This type of routing is on demand. E.g. of Ad-hoc On Demand Distance Vector (AODV), Dynamic Source Routing (DSR) [5].

2.3 Hybrid Routing: Hybrid protocols are the combinations of reactive and proactive protocols and takes advantages of these two protocols and as a result, routes are found quickly in the routing zone. E.g. ZRP (Zone Routing Protocol), Hazy Sighted Link State.

Current research challenges in ad-hoc networks are as follow:

- Energy Saving
- Limited wireless transmission range
- Broadcast nature of the wireless medium
- Packet losses due to transmission errors
- Mobility-induced route changes
- Mobility-induced packet losses
- Battery constraints
- Potentially frequent network partitions
- Ease of snooping on wireless transmissions (security hazard)
- Limited Power Supply

3. Energy Efficiency: Definition and Need

In the recent past years energy efficient routing in Ad hoc network was addressed by many research works which has produced so much innovation and novel ideas in this field. Most of the work today is based on energy efficient routing because power is main concern in ad hoc wireless networks. Each and every protocol has some advantages and shortcomings. None of them can perform better in every condition. It depends upon the network parameters which decide the protocol to be used. Several protocols have been given regarding energy efficient routing and their modifications have also been proposed for use in ad hoc networks.

Definition: For a wireless networks, the devices operating on battery try to pursue the energy efficiency heuristically by reducing the energy they consumed, while maintaining

acceptable performance of certain tasks. Using the power consumption is not only a single criterion for deciding energy efficiency. Actually, energy efficiency can be measured by the duration of the time over which the network can maintain a certain performance level, which is usually called as the network lifetime. Hence routing to maximize the lifetime of the network is different from minimum energy routing. Minimum energy routes [6] sometimes attract more flows and the nodes in these routes exhaust their energy very soon hence the whole network cannot perform any task due to the failure on these nodes [7]. In other words, the energy consumed is balanced among nodes in the networks. Routing with maximum lifetime balances all the routes and nodes globally so that the network maintains certain performance level for a longer time. It goes without saying that node failure is very possible in the wireless network. Hence saving energy at the time of broadcasting in order to recover from the node failure or to re-routing around the failed nodes is essential. By the same token, multicast has the same challenge to achieve the energy efficiency [8]. For unicast, it is highly related to the node and link status, which require a wise way to do routing as well. Sometimes, shortest path routing is possibly not the best choice from the energy efficiency point of view.

Need for Energy Efficiency: The greatest challenge in the design of wireless ad hoc networks is the limited availability of the energy resources. These resources are quite significantly limited in wireless networks than in wired networks. Energy-efficient communication is critical for increasing the life of power limited wireless ad hoc networks. Each of the mobile nodes is operated by a limited energy battery and usually it is impossible to recharge or replace the batteries during a mission. Since wireless communications consume significant amounts of battery power, therefore the limited battery lifetime imposes a severe constraint on the network performance. Energy efficient operations are critical to enhance the network lifetime. Extensive studies on energy conservation in wireless ad hoc networks have been conducted. Wireless communications consume significant amount of battery power, and therefore energy efficient operations are critical to enhance the life of such networks. Some amount of power is lost even when a node is in idle mode. A recent study shows that the power consumed in transmitting and receiving packets in standard WaveLAN cards range from 800 mW to 1200 mW. During the past few years, there has been increasing interest in the design of energy efficient protocols for wireless ad hoc networks. Most mobile nodes in a wireless ad hoc network are powered by energy limited batteries, the limited battery lifetime is a hindrance to network performance. Therefore, energy efficiency is of vital importance in the design of protocols for the applications in such networks and efficient operations are critical to enhance the network lifetime. Since the Nodes are battery-powered, thus energy is a precious resource that

has to be carefully used by the nodes in order to avoid an early network partition and hence the study and implementation of energy-efficient algorithms for wireless networks quite constitutes a vast area of research in the field of ad hoc networks.

4. Energy Efficient Routing Techniques

4.1 Lifetime Prediction Routing (LPR) [9]: This routing protocol uses battery life prediction to maximize the network lifetime by founding routing solutions. It maximizes the variance of the remaining energies of the nodes batteries in the network. Based on the past activity each node can try to estimate its battery lifetime. Simple Moving Average (SMA) predictor is used to keep track of the last N values of residual energy and the corresponding time instance for the last N packets received by each mobile node. The first drawback of this routing protocol is that it introduces additional traffic for route maintenance [10]. The second and most important is that it doesn't include the transmission power to minimize total energy consumption per packet. Large amount of energy consumption per packet may lead to die node sooner. The third is that the history may not predict accurately for high mobility of nodes in the network.

4.2 Energy Saving Dynamic Source Routing [11]: This protocol makes the DSR an energy/power aware protocol. In this protocol senders can adaptively adjust the transmission power level to suite the current need of communication rather than using fixed level. The system uses energy saving cost metrics, which selects the route with maximum "lifetime" remaining. Remaining life of a node is the remaining node energy divide by power required to transmit packet to the next node. This is known as the max-min algorithm. Energy saving dynamic source routing does not consider the energy capacity of the receiver nodes. Significant amount of energy is consumed to receive the packet. The process of receiving packets drains out the battery energy of the receiver nodes. So, energy efficient routing protocols have got to consider the receiving node battery energy capacity for route cost computation.

4.3 Energy Dependent DSR (EDDSR): DDSR is energy dependent DSR algorithm which helps node from sharp and sudden drop of battery power. EDDSR provides better power utilization compare to least energy aware routing (LEAR) [12] and minimum drain rate (MDR). EDDSR avoids node with less power supply and residual energy information of node is useful in discovery of route. Residual battery power of each node is computed by itself and if it is above the specific threshold value then node can participate in routing activities otherwise node delays the rebroadcasting of route request message by a time period which is inversely proportional to its predicted lifetime. With help of ns-2 simulator author performed simulation

which shows MDR and EDDSR is better than DSR in terms of node lifetime. EDDSR has further advantage over MDR because it can use route cache used by DSR.

4.4 Energy Efficient broadcast OLSR [13]: A new protocol EBOLSR adapts the OLSR protocol in order to maximize the network lifetime for broadcast communications. In EBOLSR energy efficient MPR [8] selection is done by the residual energy of nodes. In this protocol we consider the weighted residual energy of energy efficient MPR candidate and its one hop neighbors. The basic phenomenon about this EBOLSR protocol was to select the energy efficient multipoint relays [MPR's].

4.5 Weight Based DSR (WBDSR) [14]: Weight Based DSR is an improvement of conventional DSR. In this protocol, the weight of each route is considered as metric for route selection. Weight of each route can be calculated by computing the node weight of each node weight $i =$ battery level of this node + Stability of this node. The route-weight is the minimum of all node weights included in this route. Select the main route which has the maximum route-weight. If two or more routes have the same route-weights then choose the route which has minimum hops.

Thus WBDSR gives always the longest network life time in both high mobile networks and static networks because it timely change the used route with another one which maintains the use of the nodes which enhances the network life time.

4.6 Energy-Efficient Location Aided Routing (EELAR)[15]: Energy Efficient Location Aided Routing (EELAR) Protocol was developed on the basis of the Location Aided Routing (LAR). EELAR makes significant reduction in the energy consumption of the mobile node batteries by limiting the area of discovering a new route to a smaller zone. Thus, control packet overhead is significantly reduced. In EELAR, a reference wireless base station is used and the network's circular area centered at the base station is divided into six equal sub-areas. During route discovery, instead of flooding control packets to the whole network area, they are flooded to only the sub-area of the destination mobile node. The base station stores locations of the mobile nodes in a position table. Simulations results using NS-2 [16] showed that EELAR protocol makes an improvement in control packet overhead and delivery ratio compared to AODV, LAR, and DSR protocols.

4.7 Power-aware Routing (PAR) Protocol[17]: Power-aware routing (PAR) maximizes the network lifetime and minimizes the power consumption by selecting less congested and more stable route, during the source to destination route establishment process. PAR focuses on 3 parameters mainly Accumulated energy of a path, Status of battery lifetime and Type of data to be transferred. At the time route selection, PAR focuses on its core metrics like traffic level on the path, battery status of the path and type

of request from user side. With these factors in consideration, PAR always selects less congested and more stable routes for data delivery and can provide different routes for different type of data transfer and ultimately increases the network lifetime. Simulation results shows that PAR outperforms similar protocols such as DSR and AODV with respects to different energy-related performance metrics even in high mobility scenarios. The route that can last for a long time and encounter significant power saving has been discovered. Although, PAR can somewhat incur increased latency during data transfer.

4.8 Energy-aware Node Disjoint Multipath Routing (ENDMR)[18]: The technique of this routing is to increase the network lifetime with low overhead. It significantly reduces the total number of route request packets which results in an increased packet delivery ratio, decreasing end to end delay and decreasing power consumption. It selects optimal path using power-aware metric and optimizes the power consumption, overhead and bandwidth. The drawback is that each route request carries the cumulative cost, so very little bit overhead is increased to carry the cumulative cost but it is negligible.

4.9 Niranjana Kumar Ray et al.'s method [19] is to reduce the number of RREQ packets by putting restrictions on inter group communication. The node of one group will not forward the RREQ message to other group. Only common node will support inter-group communication to reduce the number of RREQ. In this the geographical area is partitioned on the basis of number of nodes present in it. There are two types of nodes, nodes present in the overlapping area of group are called common node and nodes belonging to particular group called active nodes. When an active node wants to send RREQ message it appends its group number in the packet and broadcast the message. Message will be forwarded by the other node if they belongs to the same group otherwise message will be dropped. When CN prepares the RREQ message it adds one group number from the group it belongs depending upon the shared index calculation.

4.10 Maximized Energy Efficient Routing Algorithm (MEER) [20]: The goal of this algorithm is the selection of routes on the remaining energy levels of the nodes of the route. In MEER, the source node 'knows' about the energy levels of the intermediate nodes and can choose the most energy efficient route. MEER differs from the conventional DSR only in the Route Discovery. The selection of the best route is based on the following algorithm: the destination node first determines the least power level in each route whose RREQ packet is received. Then it compares these least power levels and chooses the highest among them and selects the corresponding route. The destination node then transmits the RREP packet through this route. The destination copies the energy information from the RREQ packet to the RREP packet.

Thus, the destination node selects the route with the highest life time from a set of available routes.

5. Conclusion and Future Work

There is not a single protocol which can give the best performance in ad hoc network. Performance of the protocol varies according to the variation in the network parameters and ad hoc network properties continuously vary. So, the choice of the protocol is the basis to perform in a particular type of network. Apart from the availability of protocols for energy efficiency, further research is needed to identify the energy efficient routing protocols for multiple environments. These contexts can include nodes positioned in three-dimensional space and obstacles, nodes with unequal transmission powers or networks with unidirectional links. The future work can also include designing routing algorithms by adding congestion considerations.

References:

- [1] Goldsmith AJ and Wicker SB, "Design challenges for energy-constrained ad hoc wireless networks", IEEE Wireless Communications 2002, Vol. 9, Issue 4, PP. 8–27.
- [2] V. Kauadia and P.R. Kumar, "Power Control and clustering in ad hoc networks", IEEE INFOCOM 2003.
- [3] Radhika D. Joshi and Priti P. Rege, "Distributed Energy Efficient Routing in Ad-hoc Networks", in 978-1-4244-3328-5/08 in IEEE 2008.
- [4] B. Bellur, R. G. Ogier, and F.L. Templin, "Topology Dissemination Based on Reverse Path Forwarding (TBRPF)", RFC 3684, February 2004.
- [5] Benamar KADRI, Mohammed FEHAM and Abdallah M.HAMED, "Weight based DSR for Mobile Ad Hoc Networks", 3rd International Conference on Information and Communication Technologies, PP. 1-6, Vol. 7, Issue 11, April 2008.
- [6] Jangsu Lee, Seunghwan Yoo and Sungchun Kim, "Energy aware Routing in Location based Ad-hoc Networks", 4th International Symposium on Communications, Control and Signal Processing, ISCCSP 2010, PP. 3-5 March 2010.
- [7] Xiaoying Zhang, Thomas Kunz, Li Li and Oliver Yang, "An Energy-efficient Broadcast Protocol in MANETs", Communications Networks and Services Research Conference 2010, 8th Annual Communication Networks and Services Research Conference, PP. 199-206, 2010.
- [8] Tai Hieng Tie, Chong Eng Tan and Sei Ping Lau, "Alternate Link Maximum Energy Level Ad hoc Distance Vector Scheme for Energy Efficient Ad-hoc Networks Routing", International Conference on

- Computer and Communication Engineering, 11-13, Kuala Lumpur, Malaysia, May 2010.
- [9] M. Maleki, K. Dantu and M. Pedram, "Lifetime prediction routing in mobile ad hoc networks", *Wireless Communications and Networking, IEEE* Vol. 2, Issue 16-20, PP. 1185 – 1190, 2003.
- [10] O. Tariq, F. Greg, W. Murray, "Effect of Traffic Model to the Performance Evaluation of Multicast Protocols in MANET", *Canadian Conference on Electrical and Computer Engineering*, PP. 404–407, 2005.
- [11] M. Tarique, K. Tepe and M. Naserian, "Energy saving dynamic source routing for ad hoc wireless networks", *WIOPT*, 2005.
- [12] Yu Wang, Wen-Zhan Song, Weizhao Wang, Xiang-Yang Li and Teresa A. Dahlberg, "LEARN: Localized Energy Aware Restricted Neighborhood Routing for Ad-hoc Networks", 3rd Annual IEEE Communications Society Conference on Sensor, Mesh and Ad-hoc Communications, 2006.
- [13] Floriano, De Rango, Marco Fotino and Salvatore Marano, "EE-OLSR: Energy Efficient OLSR Routing Protocol For Mobile Ad-hoc Networks", *Military Communications, San Diego, CA, USA*, Issue 17-19, Nov. 2008.
- [14] Benamar KADRI, Mohammed FEHAM and Abdallah M.HAMED, "Weight based DSR for Mobile Ad Hoc Networks", 3rd International Conference on Information and Communication Technologies, PP. 1-6, Issue 7-11, April 2008.
- [15] M. Mohammed, "Energy Efficient Location Aided Routing Protocol for Wireless MANETs", *International Journal of Computer Science and Information Security*, Vol. 4, Issue 1 & 2, 2009.
- [16] The CMU Monarch Project, The CMU Monarch Extensions to the NS Simulator, Feb. 20th, 2010, URL: <http://www.monarch.cs.cmu.edu/>.
- [17] V. Rishiwal, M. Yadav, S. Verma, S. K. Bajapai, "Power Aware Routing in Ad Hoc Wireless Networks", *Journal of Computer Science and Technology*, Vol. 9, Issue. 2, PP. 101-109, Oct. 2009.
- [18] M. Bheemalingaiah, M.M. Naidu, D. Sreenivasa Rao, G. Varaprasad, "Energy Aware Node Disjoint Multipath Routing in Mobile Ad hoc Network", *Journal of Theoretical and Applied Information Technology*, PP. 1-16, 2009.
- [19] Niranjan Kumar Ray, Ashok Kumar Turuk, "Energy Efficient Technique for Wireless Ad hoc Network", 1st International Joint Conference on Information and Communication Technology, PP. 105-111, Jan. 2010.
- [20] P. Sivasankar, Dr. C. Chellappan, S. Balaji, "Performance of Energy Efficient Routing Protocol for MANET", *IJCA*, Vol. 28, Issue 8, PP. 1-6, Aug. 2011.

Singularity Spectrum Analysis of Electrical Demand Time Series

Dr. Valsamma K.M

*Associate Professor, Department of Supportive And Allied Courses, Faculty of Agricultural Engineering,
Kerala Agricultural University, KCAET, Tavanur, Kerala, INDIA.*

ABSTRACT

This study estimates systematically the dynamics of electrical power demand functions for two countries India and china using singularity spectrum analysis. In order to demonstrate the capability of fractal approach on electrical power demand, we choose Wavelet Transform Modulus maxima (WTMM) technology and results imply that this method is powerful in studying the singularities of time series signals. We show that the WTMM, the so called multi-resolution analysis, can determine the singularity spectrum of multi-fractal measures from the scaling behavior of the partition function, and account for the multi-fractal nature of the time series obtained from the chaotic phenomena. Applying the WTMM we will be able to verify that the electrical demand is a persistent series and this method can be used to compare the quality of the process in two different places. The correlation dimensions found tells us that the series obtained for china is long-range correlated than India with long term memory. This lays that China power generating system is better suited to satisfy oscillations in the demand.

Keywords – Wavelet Transform Modulus Maxima, Singularity spectrum, Lipchitz holder exponent, Developing countries, Electricity demand, Multi-fractal analysis.

I. INTRODUCTION

With an electricity demand of 322 KWh per capita per year in 2003, India's electricity demand has been growing at an average of 8.8% per year from 1986 to 2003 while the peak demand increased on average by 6.3% per annum from 540 MW to 1516 MW. The electricity demand growth, GDP growth and electricity price variation for India for the period 1986-2003, illustrates the relatively moderate Indian GDP Growth (averaging 3.5% per annum from 1986-2003), but despite this, India's per capita electricity consumption is still somewhat lower than of its neighbors China and Pakistan although both countries have experienced much lower per capita income levels. Although these economies are not directly compatible with Indian economy, they are the closest geographical neighbors to India with some cultural and trade links. Although these economies are not directly compatible with Indian economy, they are the closest geographical neighbors to India with some cultural and trade links. India consumed 439 kg of oil equivalent per person of primary energy in 2003 compared to 1090 in china, 7835 in US and the world

average of 1688. India's energy use efficiency for generating GDP in purchasing power parity terms is better than the world average. China, US, and Germany. However, it is 7% to 23% higher than Denmark, UK, and Japan and Brazil. If we look at the consumption electricity, per capita consumption in India is far below that in other countries. Moreover access to electricity is uneven. In 2003, about 68% of Indian households were connected to the electricity grid with household electricity consumption accounting for about 35% of total electricity consumption, and household and Industrial sector consumption combined accounting for 65% of the total 6.209 GWH.[1] Further, details about the institutional background of the Indian electricity supply Industry may be found in [2].

Various multi-fractal formalism have recently been developed to describe the statistical properties of the singular measure of signals in terms of their singularity spectrum $f(\alpha)$, or generalized dimension D_q . The idea of distribution of singularities all lying on interwoven sets of varying fractal dimensions called multi-fractal was introduced by Frish et al [3]. Further, Hentschel et al [4] introduced the Generalised dimension D_q , and Halsey et al [5] the $f(\alpha)$ spectrum. Wavelets are a recently developed concept and WTMM method [6] with continuous basis function, is a well known method to investigate the multi fractal scaling properties of fractal and self affine objects in the presence of non stationeries. In this paper, we intend to clarify the characteristics of electrical power demand using WTMM with continuous function.

II. WTMM METHOD

Finding the distribution of singularities in a multi-fractal signal is particularly important for detecting, identifying, and measuring the scaling behavior. It is possible to measure the singularity spectrum of multi-fractal signals from the wavelet transform local maxima using global partition function. Mallat [7] has proved that all singularities of irregular signal (multi-fractal signal) could be detected using WTMM in partition function and shown the method to measure the local singularity α . Numerical analysis performed in our work was based on WTMM method [6]. This is one of the commonly used approaches to study multi scale structures in complex time series. Using WTMM in calculating the partition function, we can avoid the deviations that are made by the oscillation of wavelet coefficients when $q < 0$. It is more accurate and efficient in detecting singularities in signal. That is, the attractiveness

of using the WTMM is associated with the possibility it provides of analyzing a wide range of scales and a broad spectrum of scaling characteristics from small fluctuations and weak singularities to large fluctuations and strong singularities. In this approach, the numerical quantification of time series is done by the so called singularity spectrum $D(h)$ characterized by the Holder exponent h .

For a continuous process with spectral density $\hat{\Gamma}_x(\theta)$, we define the wavelet transform of a function $f(x)$ as:

$$T\Psi|f(x_0,a)| = \frac{1}{a} \int_{-\infty}^{+\infty} f(x)\Psi\left(\frac{x-x_0}{a}\right) dx \quad (1)$$

Where $f(x_0)$ is a distribution at a point x_0 (location parameter), a is the scale parameter, and Ψ defines the family of wavelets. : that is, for varying values of a , wavelets of different length scales can be constructed. The wavelet transform can be seen as decomposing the function $f(x)$ in to elementary space scale contributions by combining it with a suite of localized functions, the so called wavelets, all of which are constructed by translation and dilation of a single function, the analyzing wavelet. An attractive feature of wavelets is that one could construct various analyzing patterns which satisfy the requirements for a function to be called a wavelet. A local singular behavior of $f(x)$ at the point x_0 results in an increase of $|T\Psi|f(x,a)|$ as $x \rightarrow x_0$, and can be characterized by the Hölder exponent $h(x_0)$ that quantifies the scaling of the wavelet coefficients for small a . In other words, the local singular behavior of f around x_0 is characterized by a power law behavior:

$$T\Psi|f(x_0,a)| \sim a^{-T(q)}. \quad (2)$$

Further, the statistical description of local singularities is performed using the notion of the partition function $S(q,a)$, being the sum of the q^{th} powers of the local maxima of $T\Psi|f(x,a)|$ at a scale a . For small a , the partition function $S(q,a)$ scales as:

$$S(q,a) \sim a^{-T(q)}. \quad (3)$$

with the scaling exponent $T(q)$. The singularity spectrum $D(h)$ can be estimated using the Legendre transform :

$$D(h) = q(h) - T(q), \quad (4)$$

For positive values of q , the partition function $S(q,a)$ characterize the scaling of large fluctuations in the data (strong singularities). For negative values of q , it reflects the weak singularities. Applications of the WTMM method, to time series allows us to characterize correlations of different types if $h \neq 0$ and $D(h) \neq 0$. In particular, the range $0 < h < 0.5$ implies the presence of anti-correlated behavior, while $h > 0.5$ reflects correlated dynamics.

III. APPLICATION OF WTMM METHOD TO ELECTRIC DEMAND TIME SERIES:

Application of WTMM method to an analysis of point processes extracted from the time series (Fig.1(a) & (b)) of two completely different places: India (Data of electrical power demand obtained at the website: <http://www.cea.nic.in/> statistics.) and China with 8832 points has revealed differences in the long range

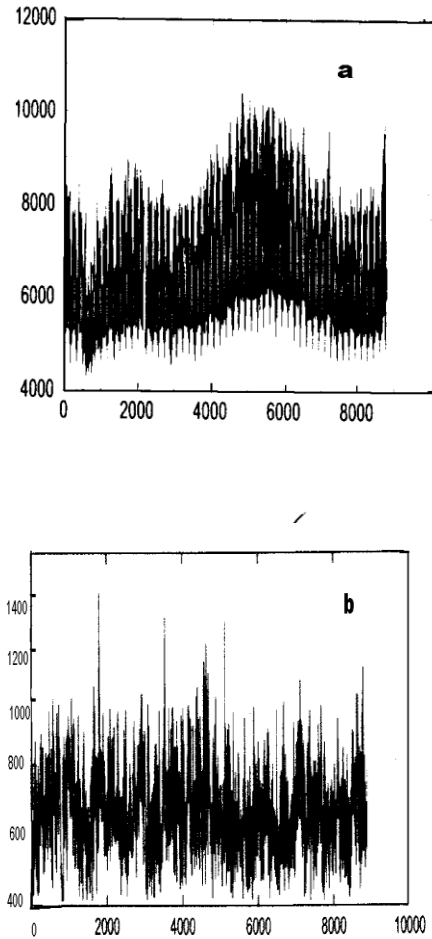


Figure.1. Electrical Power demand Time series for: (a): China (b) India.

correlations, revealing that power generating system of china is better suited to satisfy correlations in the demand. In the analysis, we use the successive derivatives of a Gaussian function (i.e., the fifth derivative of Gaussian function was chosen) as analyzing wavelet:

$$\Psi^5(t) = d^5 (e^{t^2/2}) / dt^5; \quad (5)$$

Twelve wavelet transform data files were obtained applying the wavelet transform to both electrical demand data with

Ψ^5 , ranging the scaling factor α from $\alpha_{\min} = \frac{1}{256}$ to $\alpha_{\max} = 8$ in steps of a power of two. The computed partition function for each one in the range $-20 \leq q \leq 20$ displays nonlinearity, indicating multi-fractality (Figs.2(a) & (b)).

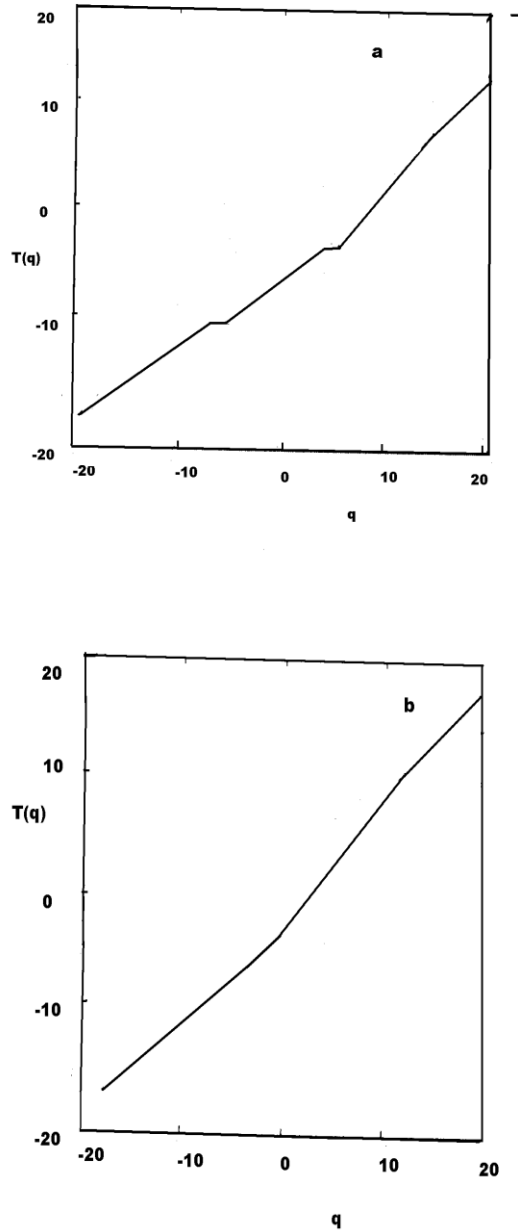
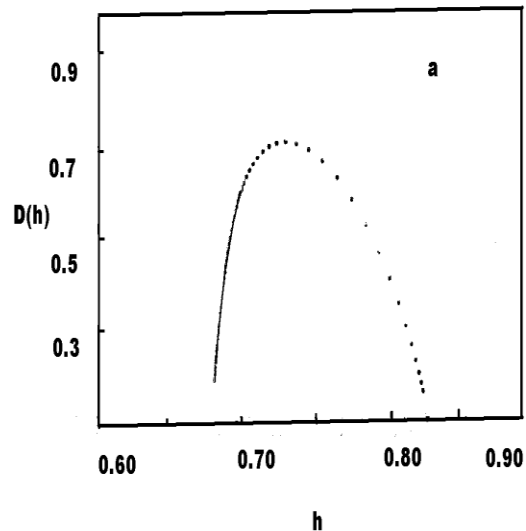


Fig.2. $\tau(q)$ for Electrical power demand of:
 (a) China & (b) India.

It is seen that $\tau(q)$ is a nonlinear convex increasing function with $\tau(0) = -0.65$ and the slopes $\alpha_{\min} = 0.66$ for $q \leq 0$ and $\alpha_{\max} = 0.84$ for china, while for India $\tau(0) = -0.54$ and $\alpha_{\min} = 0.62$ for $q \leq 0$ and $\alpha_{\max} = 0.78$. The corresponding singularity spectra $D(h)$, a single humped function with a non unique Holder exponent, are obtained by Legendre transforming $\tau(q)$ (Fig.3.(a) & (b)). As expected from $\tau(q)$,

the support of the $D(h)$ extends over a finite interval whose bounds are $\alpha_{\min} = 0.66$ and $\alpha_{\max} = 0.84$ for china, which is larger than the one for India ranging from $\alpha_{\min} = 0.62$ and $\alpha_{\max} = 0.78$. The minimum value α_{\min} , corresponds to the strongest singularity characterizing the most rarefied zones, while higher values exhibit weaker singularities until α_{\max} which corresponds to the densest zone. α_{\max} & α_{\min} both between 0.5 & 1 signifies persistent processes, (which obeys to the “Joseph’s effect” in bible of 7 years of loom, happiness & health and 7 years of hungry and illness), although a very little less persistence for the case of India than China (highly persistent) due to slight shift of the curve to the right. However, the analyzed data remain multi-fractal at all stages.

To investigate the underlying evidence for multi-scaling more carefully, it is necessary to present the statistical findings. for both countries. The support dimensions $D_0 = D_{\max} = \tau(0)$ are 0.65 & 0.54 for China & India respectively, implying capacities of the support measure fractional (i.e. ,chaotic).The numerical values of the holder exponent for the dimension supports, $\alpha(D_{\max})$, are 0.7 for China and 0.69 for India (corresponding to $D(h)_{\max}$), implying the fact that the events with $\alpha = \alpha(D_{\max})$ are the most frequent ones. A Hurst exponent of 0.7 and 0.69 describes a very persistent time series and if the distribution is homogenous, there is a unique h (or α), but if it is not,, there are several exponents h (or α), with the most frequent h will characterize the series that will play as Hurst exponent.



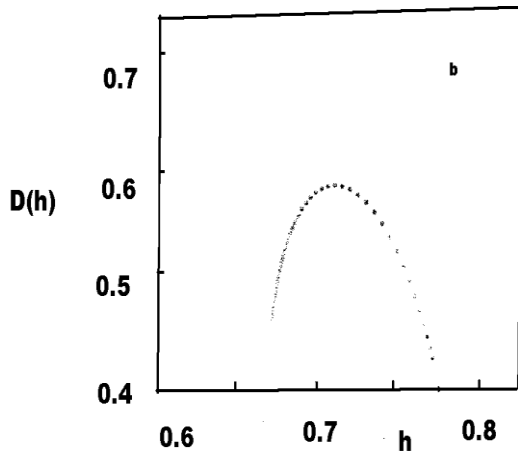


Fig.3. $D(h)$ versus h for electrical demand for:
(a) China and (b) India.

Moreover, $h^1 = (h_{\min} + h_{\max}) / 2$ is almost the same for China (0.75) and India (0.74). This implies that the curves are slightly humped to the left, an effect that is more pronounced for India than for China and a better precision is obtained for the $h > 0$ branch, where the bigger values will prevail (i.e., higher changes in demand of electricity, a rare situation). Further, the asymmetrical shape of the spectrum reveals more pronounced in homogeneities in the events associated with the $q < h < 0$ branch, associated with smaller values of the power. (Slight change in demand more common). This is indicated by $h_{\text{range}} = (h_{\max} - h_{\min})$ with the case of larger than the other one. The information dimension, on the other hand for china is $D_1 = h(q(1)) = f(0.7) = 0.7$ for which features the scaling behavior of the Information while it is $D_1 = h(q(1)) = h(0.64)$ for India. (i.e. fractional value for both countries). That is, for both china and India, the electricity demand corresponds to chaotic systems with the problems of forecasting associated with them.

The correlation dimension are $D_2 = \tau(2) = 0.79$ for India and 0.87, characterizing chaotic attractor, with $D_2 > 1/2$ indicates long range correlations, with the characteristic behavior of adaptively that plays the role of organizing principle for highly complex, non linear processes that generates fluctuations on a wide range of time scales and, in addition, the lack of characteristic scale helps in preventing excessive mode locking that would restrict the reaction of the event. In short, we can see that, there is longer range correlation for china, implying that for the case of an abrupt change of the demand china electrical system will have a better answer.

V. CONCLUSION.

We found that both the electrical demand behave, like most ones in nature, as long term memory phenomena. in both

cases the fractal dimension obtained correspond to chaotic processes. Moreover, the correlation dimension gives us an account of long range correlation, with the china long range correlated than India. This lays that china power system is better suited to satisfy oscillations in the demand. in spite of changes, of h ranges within $0.5 < h < 1$, the greater value for India indicates that the demand series varies in wider ranges, which features the variation on demography.

REFERENCES

- [1] Francois lescaurous 'Dynamics of sectoral energy demand and aggregate intensity economic studies division, October 2010.
- [2] Bureau OF energy Efficiency Book,
- [3] U. Frish and G.Parisi, in Turbulence and predictability of geophysical flows and Climate Dynamics, edited by M.Ghil,R.Benzi and G.Parisi.(North Holland, New York,1985).
- [4] H.G.E Hentechel and I Proccacia, *Physica 8D*,1983,435.
- [5] T.C.Halsey, M.H. Jensen,L.P Kadanoff, I Proccaccia , *Phys. Rev A33*,1986 ,1141.
- [6] Mallat.s.; A theory for Multi resolution signal decomposition, The wavelet representation.*IEEE TRANS ,11(7)*,1989,674-693.
- [7] Mallat.S. and W.L Hwang, *IEEE Inform theory* ,38,1992,617.

CMOS Full Adders for Energy Efficient FIR Filters

Gayathri. K. K

*ME student, Dept of EEE
Hindusthan College of Engineering and Technology
Coimbatore -641 032, India*

Suresh Babu.A

*Assistant professor, Dept of EEE
Hindusthan College of Engineering and Technology
Coimbatore-641 032,India*

Abstract: Energy-efficiency is one of the most required features for modern electronic systems designed for high-performance and/or portable applications. In one hand, the ever increasing market segment of portable electronic devices demands the availability of low-power building blocks that enable the implementation of long-lasting battery-operated systems. We present two high-speed and low-power full-adder cells designed with an alternative internal logic structure and pass-transistor logic styles that lead to have a reduced power-delay product (PDP). In this paper we are using CMOS full adders for the FIR filters. The adder element in the conventional FIR filter is replaced by the new CMOS full adder cells. So that the power consumption of the FIR filters can be reduced.

Key words: Adders, CMOS, FIR Filters, Low power, VLSI

I. INTRODUCTION

Addition is one of the fundamental arithmetic operations. It is used in extensively in many of the VLSI systems such application specific DSP architectures, microprocessors etc...Adder is the core component of an arithmetic unit. The efficiency of the adder determines the efficiency of the arithmetic unit. Various structures have been evolved trying to improve the performance of the adder in terms of area, power and speed. Full adders is the core of many arithmetic operations such as addition, subtraction, multiplication, division and address generation. The PDP exhibited by the full adders would affect the system's overall performance. There

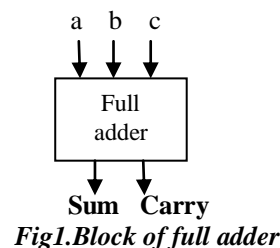
are three major components of power dissipation in complementary metal oxide(CMOS) circuits: switching power, short circuit power and static power. Reducing any of these components will end up with low power consumption of the whole system[2].

A filter is used to modify an input signal in order to facilitate further processing. FIR digital filters have many excellent features such as the stability, easiness for realization, and suitable to be used to design multi-pass band or multi-stop band digital filters. Filter consists of mainly three elements, adders, multipliers and delay elements. This paper describes the design and performance comparison of two full adder cells implemented with an alternative internal logic structure that is based on the multiplexing of the Boolean functions XOR/XNOR and AND/OR, to obtain the sum and the carry outputs respectively. These CMOS full adders are used as adder elements for the design of FIR filters. There was a pass transistor powerless/groundless logic structure to reduce the power consumption.

II. PREVIOUS WORKS

Several papers have been published regarding the power optimization of low power full adders. Even more, some works have presented intense comparisons between different full adder schemes. The different logic styles such as standard CMOS, differential cascade voltage swing restored CPL(SR-CPL) and hybrid styles are used to build the adder modules.

The internal logic structure shown in Fig. 1. has been adopted as the standard configuration in most of the enhancements developed for the 1-bit full-adder module. In this configuration, the adder module is formed by three main logical blocks: a XOR-XNOR gate to obtain A XOR B and A XNOR B and multiplexers to obtain the SUM (So) and CARRY (Co) outputs. The major problem regarding the propagation delay for a full-adder is that it is necessary to obtain an intermediate A XOR B signal and its complement, which are then used to drive other blocks to generate the final outputs. Thus, the overall propagation delay and, in most of the cases, the power consumption of the full-adder depend on the delay and voltage swing of the signal and its complement generated within the cell. So, to increase the operational speed of the full-adder, it is necessary to develop a new logic structure that does not require the generation of intermediate signals to control the selection or transmission of other signals located on the critical path.



a) Conventional CMOS Style

A basic cell in digital computing systems is the 1-bit full adder which has three 1-bit inputs (A, B, and Cin) and two 1-bit outputs (sum and carry). The relations between the inputs and the outputs are expressed as[7];

$$\text{sum} = (a \text{ XOR } b) \text{ XOR } c$$

$$\text{carry} = a \times b + c \times (a \text{ XOR } b)$$

The above Boolean expressions may be rearranged as:

$$\text{sum} = c(a + b + c) + a \times b \times c$$

$$\text{carry} = a \times b + c \times (a + b)$$

III. ALTERNATIVE LOGIC STRUCTURE FOR A FULL-ADDER

The truth table for 1 bit full adder is shown in the table1. Examining the full-adder's true-table , it can be seen that the S_0 output is equal to the A XOR B value when $C=1$ and it is equal to A XNOR B when $C=0$. Thus, a multiplexer can be used to obtain the respective value same criteria, the C_0 output is equal to the A AND B value when $C=0$, and it is equal to value when A XOR B. Again, C can be used to select the respective value for the required condition, driving a multiplexer[8]. Hence, an alternative logic scheme to design a full-adder cell can be formed by a logic block to obtain the A XOR B and A XNOR B signals, another block to obtain the A AND B and A OR B signals, and two multiplexers being driven by the C_{in} input to generate the S_0 and C_0 outputs, as shown in Fig. 1

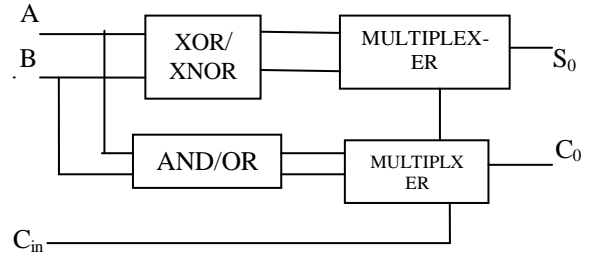


Fig 1: An alternate logic scheme for full adders[10]

A full adder consists of two XOR gates, three AND gates and one OR gate. These gates are used for obtaining the sum and carry outputs.

IV. FIR Filters

FIR means Finite Impulse Response filters. If the response of the system is of finite duration , then the system is called Finite Impulse Response systems. FIR digital filters have many excellent features such as the stability, easiness for realization, and suitable to be used to design multi-passband or multi-stopband digital filters, which makes it widely used in communication, radar, biomedical as well as automation fields. FIR filters specification include the maximum tolerable pass band ripple, maximum tolerable stop band ripple, pass band edge frequency and stop band edge frequency.

An FIR filter has a number of useful properties which sometimes make it preferable to an Infinite Impulse Response(IIR) filter. FIR filters:

- Require no feedback. This means that any rounding errors are not compounded by summed iterations. The same relative error occurs in each calculation. This also makes implementation simpler.
- Are inherently stable. This is due to the fact that, because there is no required feedback, all the poles are located at the origin and thus are located within the unit circle (the required condition for stability in a Z transformed system).
- They can easily be designed to be linear phase by making the coefficient sequence symmetric; linear phase, or phase change proportional to frequency, corresponds to equal delay at all frequencies. This property is sometimes desired for phase-sensitive applications, for example data communications.

The main disadvantage of FIR filters is that considerably more computation power in a general purpose processor is required compared to an IIR filter with similar sharpness especially when low frequency (relative to the sample rate) cutoffs are needed. However many digital signal processors provide specialized hardware features to make FIR filters approximately as efficient as IIR for many applications.

FIR filters consists of three elements; adder, multiplier and delay elements. Fig 3 shows the schematic diagram of FIR filter of order L[11]

The features and advantages of this logic structure are as follows[10].

- There are not signals generated internally that control the selection of the output multiplexers. Instead, the c input signal, exhibiting a full voltage swing and no extra delay, is used to drive the multiplexers, reducing so the overall propagation delays.
- The capacitive load for the c input has been reduced, as it is connected only to some transistor gates and no longer to some drain or source terminals, where the diffusion capacitance is becoming very large for sub-micrometer technologies. Thus, the overall delay for larger modules where the signal falls on the critical path can be reduced.
- The propagation delay for the S_0 and C_0 outputs can be tuned up individually by adjusting the XOR/XNOR and the AND/OR gates; this feature is advantageous for applications where the skew between arriving signals is critical for a proper operation (e.g., wavepipelining),and for having well balanced propagation delays at the outputs to reduce the chance of glitches in cascaded applications.
- The inclusion of buffers at the full-adder outputs can be implemented by interchanging the XOR/XNOR signals, and the AND/OR gates to NAND/NORgates at the input of the multiplexers, improving in this way the performance for load-sensitive applications.

Truth table for full adder

C	B	A	S_0	C_0
0	0	0	0	0
0	0	1	1	0
0	1	0	1	0
0	1	1	0	1
1	0	0	1	0
1	0	1	0	1
1	1	0	0	1
1	1	1	1	1

Table 1:- Truth table for full adder

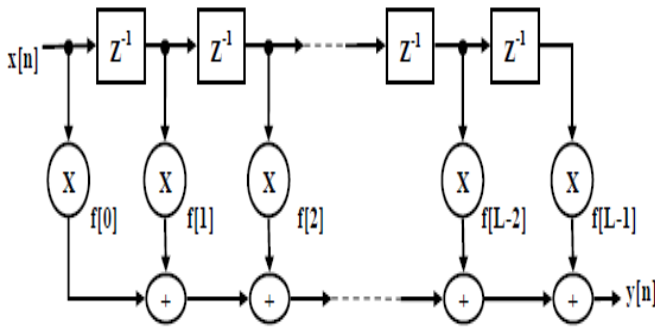


Fig 3.Schematic diagram of FIR filter of order L

V. IMPLEMENTATION

◆ /ti_new/clk	1					
◆ /ti_new/ca	0					
◆ /ti_new/n	0	1	2	3		
⇒ /ti_new/y	1001110111110010	0103111010001000	100311001010101	10000000011101		
⇒ /ti_new/a	10110101	10110101				
⇒ /ti_new/b	11011011	11011011				
⇒ /ti_new/c	00101101	00101101				
⇒ /ti_new/d	10010110	10010110				
⇒ /ti_new/x	(11000011 1010010)	(11000011 1010010 0101101 1001110 11010010 1010101 1100001)				

The adder elements in the FIR filters can be replaced by the low power CMOS full adders. So that the total power dissipation of the FIR filters is reduced. The power consumption of the filters can be find out by using the Xilinx software. The FIR filters can be simulated in the Modelsim ISE.

VI. RESULTS

The power, delay and area can be analyzed by using the Xilinx software. PDP value is the product of power and delay of the full adder cells. The comparison between the conventional full adder and the proposed full adder is shown in the table below.

Parameters	Conventional full adder	Proposed full adder
Power	123mw	67mW
Delay	7.989ns	7.476ns
No: of gates	36	12
PDP	982.65Ws	590.604Ws

Table 2: comparison between conventional and proposed full adders.

The new FIR filter will have low power consumption than the conventional FIR filters. The power consumption of the new FIR filters can be reduced up to 60% than the conventional full adders. The developed CMOS full adders can be implemented in the FIR Filters. So that the power consumption and delay can be reduced .

Thus the overall performance of the FIR filters can be increased. The comparison table of different FIR filters are shown in the table3.

FIR FILTERS	POWER CONSUMPTION	DELAY
4tapped conventional FIR Filters	154mW	3.584ns
4tapped new FIR Filters	147mW	3.014ns
8tapped conventional FIR Filters	161mW	4.587ns
8tapped new FIR Filters	152mW	3.152ns
16tapped conventional FIR Filters	175mW	4.654ns
16tapped new FIR Filters	162mW	3.225ns

Table 3: Comparison of different FIR filters.

VII. CONCLUSION

An alternative internal logic structure for designing full-adder cells was introduced. The full adder was designed using the multiplexing of XOR/XNOR gates and AND/OR gates.The full adders are designed using Xilinx software.The speed, power and area of the designed system is analysed by using the Xilinx software.

PDP is the main factor which determines the performance of the system. Power delay product is a quantitative measure of the efficiency of the trade off between power dissipation and speed, and is particularly important when low power operation is needed. The power consumption of the new full adders is reduced up to 60%. The delay of the full adder is also reduced . Thus the power delay product(PDP) of the proposed full adders have an advantage of 60%. Thus the over all performance of the full adder is improved. By using this type of full adders in the arithmetic modules of the FIR filters the power consumption can be reduced and hence the overall performance of the system can be improved.

REFERENCES

- [1] S.Agarwal,Pavankumar V.K,Yokesh R “Energy efficient high performance circuits for arithmetic units”2ndinternational conference on VLSI design Jan2008,pp371-376
- [2] M.Agure and M.Linaries,”An alternative logic approach to implement high speed low power 1-bit CMOS full adder cells”,in proc .SBCCI, Florianopolis, Brazil,Sep2005,pp.116-171
- [3] M.Aguirre Hernandez,.; Aranda, M.L.; “A low power bootstrapped cmos full adder”2nd International Conference on Electrical and Electronics Engineering, 2005 Page(s): 243 – 246

- [4] M.Ahmmmed Shams, ..; Bayoumi, M.A.; "A novel high performance CMOS 1 bit full adder cell" IEEE Transactions on Circuits and Systems
- [5] C.Chang,J.Gu,and M.Zhang "A review of 0.18 μ m full adder performances for tree structured arithmetic units" IEEE Trans. VLSI Syst., vol.13,no.6, pp.686-695,June 2005
- [6] Jin-Fa lin; Ming-Hwa Sheu; Yin-Tsung Hwang; "Low power low complexity full adder design for wireless base band application" 2006 International Conference on Communications, Circuits and Systems Proceedings, Volume: 4 ;2006 , Page(s): 2337 - 2341
- [7] D.Patel,P.G.Parate,P.S.Patil,andS.Subbaraman,"ASIC implementation of 1-bit full adder ", in proc. 1st Int. Conf. Emerging Trends Eng.Techol.,Jul.2008,pp.463-467
- [8] D.Rdha krishnan , "Low-voltage,low power CMOS full adder,"IEEE proc.circuits Devices Syst.,vol 148 no.1,pp 20-29 Feb2001
- [9] Shafiqul Khalid, A.T.M.; "A fast optimal CMOS full adder"Circuits and Systems, 1996., IEEE 39th Midwest symposium Volume: 1 ;1996 , Page(s): 91 - 93 vol.1
- [10] M. AHernandez and M. LAranda "CMOS Full-Adders for Energy-Efficient Arithmetic Applications" IEEE Transactions on VLSI Systems, Vol. 19, NO. 4, April 2011
- [11] S.Shanthala, S Y Kulkarni"High Speed and Low Power FPGA Implementation of FIR Filter for DSP Applications"
- [12] Dong Shi, and Ya Jun Yu, " Design of Linear Phase FIR Filters With High Probability of Achieving Minimum Number of Adders" IEEE Transactions on Circuits and Systems—i: regular papers, vol. 58, no. 1, January 2011 pp345-352
- [13] A.M Shams, and M.Bayoumi "Performance evaluation of 1 bit CMOS adder cells "IEEE ISCAS,Oralnado, FL, May1999, vol.1,pp.27-30

Performance and Emission Characteristics of Mahua and Linseed Biodiesel Operated at Varying Injection Pressures on CI Engine

Ashish Jawalkar¹, Kalyan Mahantesh¹, M Jagadish¹, Madhusudhan Merawade¹,
M C Navindgi²

¹UG Students, Department of Mechanical Engineering, PDA College of Engineering, Gulbarga-585102,

²Associate Professor, Department of Mechanical Engineering, PDA College of Engineering, Gulbarga-585102,

ABSTRACT

Biodiesel derived from nonedible feed stocks such as Mahua, Jatropha, Pongamia, Linseed are reported to be feasible choices for developing countries including India. This paper presents the results of investigation of performance and emissions characteristics of diesel engine using Mahua and Linseed biodiesel. In this investigation, the blends of varying proportions of Mahua biodiesel with diesel (M25, M50, M75, M100) and Linseed biodiesel with diesel (L25, L50, L75, L100) were prepared, analyzed, and compared the performance and exhaust emission with diesel using a single cylinder diesel engine. The brake thermal efficiency, brake-specific fuel consumption, CO and HC were analyzed.

In the investigation it is found that the combined increase of injection pressure increases the BTHE and reduces BSFC while having lower emissions for Mahua biodiesel as compared to Linseed biodiesel. For small sized direct injection constant speed engines used for agricultural applications (5.2 kW), the optimum combination was found at injection pressure of 160 bar with Linseed (L100), whereas the harmful pollutants such as HC, CO, are reduced in the Mahua biodiesel compared to Linseed biodiesel fuel.

Key words: Injection timing, injection pressure, Mahua biodiesel, Linseed bio diesel, performance, emission, combustion characteristics, Diesel engine

Abbreviations used:

BSFC: Brake specific fuel consumption

BTHE: Brake thermal efficiency

M25: Blend 25% Mahua Biodiesel and 75% diesel

M50: Blend of 50% Mahua Biodiesel and 50% diesel

M75: Blend of 75% Mahua Biodiesel and 25% diesel

M100: 100% Mahua Biodiesel.

L25: Blend of 25% Linseed Biodiesel and 75% diesel

L50: Blend 50% Linseed Biodiesel and 50% diesel

L75: Blend of 75% Linseed Biodiesel and 25% diesel

L100: 100% Linseed Biodiesel

INTRODUCTION

With crude oil reserves estimated to last for few decades, there has been an active search for alternate fuels. The

depletion of crude oil would cause a major impact on the transportation sector. Of the various alternate fuels under consideration, biodiesel, derived from vegetable oils, is the most promising alternative fuel to diesel due to the following reasons.

- i) Biodiesel can be used in the existing engine without any modifications.
- ii) Biodiesel is made entirely from vegetable sources; it does not contain any sulfur, aromatic hydrocarbons, metals or crude oil residues.
- iii) Biodiesel is an oxygenated fuel.
- iv) Emissions of carbon monoxide and soot tend to reduce.
- v) The use of biodiesel can extend the life of diesel engines because it is more lubricating than petroleum diesel fuel.
- vi) Biodiesel is produced from renewable vegetable oils/animal fats and hence improves the fuel or energy security and economy independence.

A lot of research work has been carried out to use vegetable oil both in its neat form and modified form. Since India is net importer of vegetable oils, edible oils cannot be used for production of biodiesel. India has the potential to be a leading world producer of biodiesel, as biodiesel can be harvested and sourced from non-edible oils like Jatropha, Curcus, Pongamia Pinnata, Neem, Mahua, Castor, Linseed, etc. Some of these oils produced even now are not being properly utilized. Out of these plants, we are focusing Mahua and Linseed which can grow in arid and wastelands. Implementation of biodiesel in India will lead to many advantages like green cover to wasteland, support to agriculture and rural economy and reduction in dependence on imported crude oil and reduction in air pollution.

In the present investigation biodiesel is prepared from Mahua oil and Linseed oil. The performance and emission characteristics were analyzed on a four stroke single cylinder direct injection diesel engine.



Figure 1. Photograph of Linseed and Mahua Seeds

BIODIESEL PRODUCTION

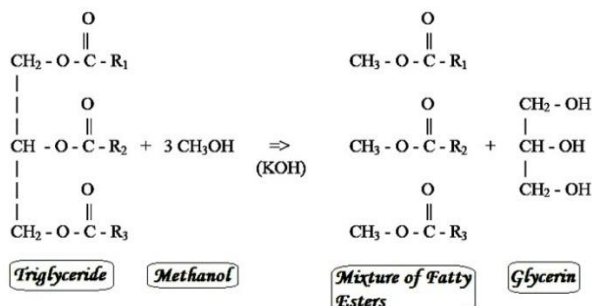
Esterification of vegetable oil comprised heating of oil, addition of sodium hydroxide and alcohol, stirring of the mixture, separation of glycerol, and biodiesel. This esterified vegetable oil is called biodiesel. Biodiesel properties are similar to diesel fuel as shown in the Table.1. After esterification of Mahua and Linseed oil their properties like density, cetane number, viscosity, and calorific value are improved. These parameters induce better combustion characteristics and performance of diesel engine. The biodiesel contain more oxygen and lower calorific value compare than diesel. As a results in lower generation of hydrocarbon and carbon monoxide in the exhaust than diesel fuel. The physical and chemical properties of Mahua biodiesel and linseed biodiesel and their blends are measured as per Indian standards (IS) methods in fuel testing laboratory and tabulated in Table 1. Calorific value and viscosity are measured by Bomb calorimeter and Redwood viscometer (Petroleum Instruments India Pvt. Ltd.), respectively. The flash point and fire point are determined by Pensky-Martin's apparatus closed-cup method.

Fuel blends	Density (Kg/m ³)	CV (KJ/Kg)	Viscosity at 40°C(cSt)	Flash point (°C)	Fire point (°C)
L25	850	41188	3.17	91	100
L50	866	39875	3.22	126	136
L75	870	38563	3.27	161	171
L100	880	37251	3.32	196	206
M25	858	41146	3.74	81	90
M50	862	40468	4.35	105	115
M75	876	39791	4.96	129	140
M100	894	38437	5.58	154	165

Table.1 Properties of Biodiesel blends compared with neat diesel

TRANSESTERIFICATION PROCESS

The most common way of producing biodiesel is the transesterification of vegetable oils and animal fats. Oil or fat reacts with alcohol (methanol or ethanol). This reaction is called transesterification. The reaction requires heat and a strong catalyst (alkalis, acids, or enzymes) to achieve complete conversion of the vegetable oil into the separated esters and glycerin. The reaction is shown in below.



EXPERIMENTAL SETUP AND PLAN

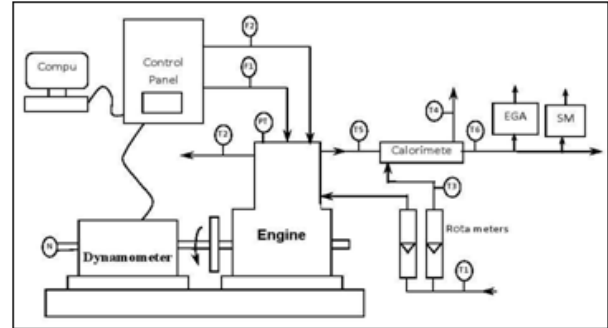


Figure 2: Schematic diagram of experimental setup

Engine specification:

Manufacturer	Kirloskar Oil Engines Ltd., India,
Model	TV-SR II, naturally aspirated
Engine	Single cylinder, DI, Four Stroke
Bore / stroke	87.5mm/110mm
Compression ratio	16.5, 17.5 and 18 (Variable)
Speed	1500 r/min, constant
Rated power	5.2 kW
Injection pressure	240 bar/23° deg BTDC
Type of sensor	Piezo electric
Response time	4 micro seconds
Crank angle sensor	1-degree crank angle

RESULT AND DISCUSSION

Experimental investigations have been carried to examine the performance and emission characteristics at different injection pressure of 160 bar, 180 bars and 200 bar. The details have been tabulated below and the graphs have been plotted. The engine was set to run at compression ratio 16.5:1, advanced injection timing 27°BTDC to arrive at the optimum for Mahua biodiesel blends (M25, M50, M75, M100) and Linseed biodiesel blends (L25, L50, L75, L100).

1. PERFORMANCE CHARACTERISTICS

1.1 Brake Thermal Efficiency

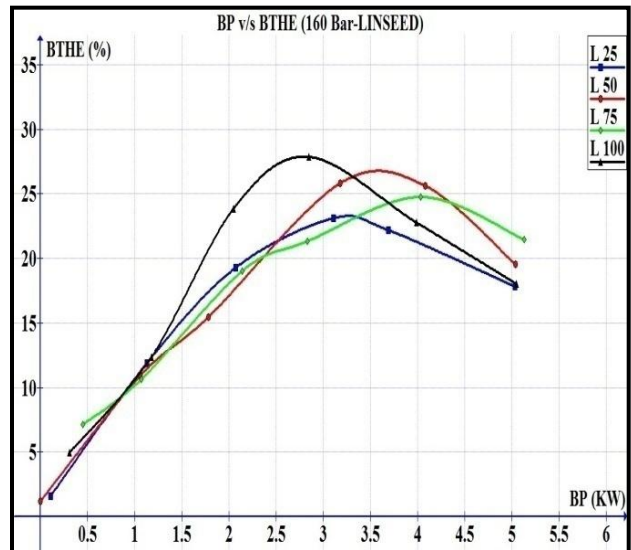
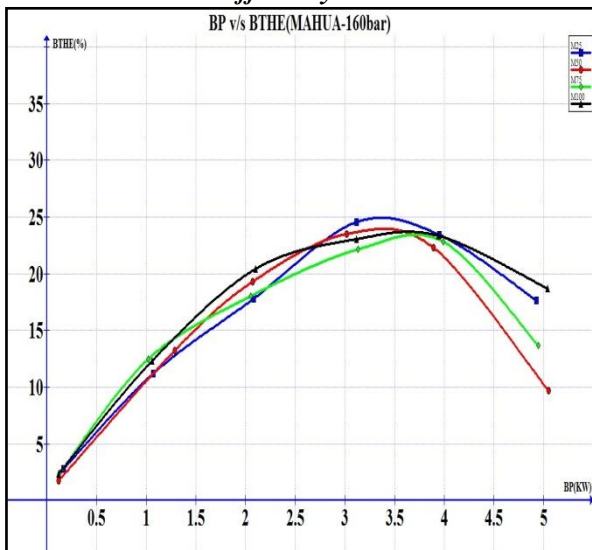


Figure 1 Comparison of BTE between Mahua biodiesel blends and Linseed biodiesel blends at 160 bar injection pressure.

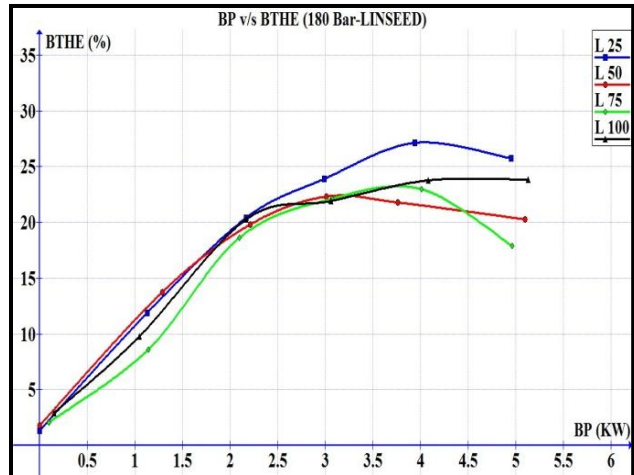
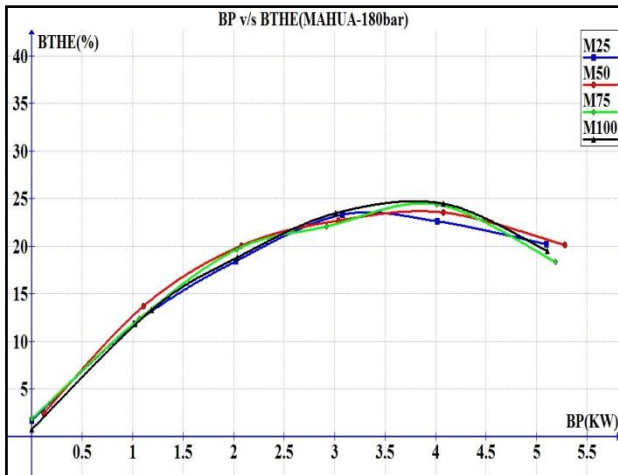


Figure 2 Comparison of BTE between Mahua biodiesel blends and Linseed biodiesel blends at 180 bar injection pressure.

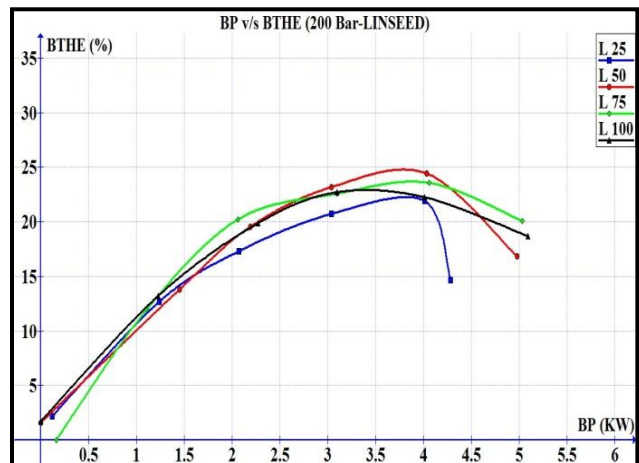
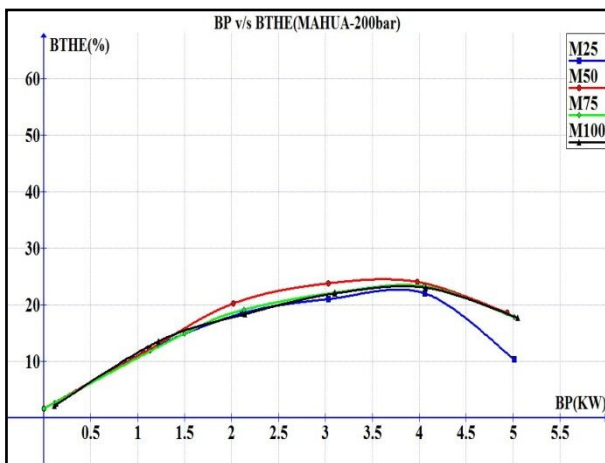


Figure 3 Comparison of BTE between Mahua biodiesel blends and Linseed biodiesel blends at 200 bar injection pressure.

It is evident from Figure 3, Figure 4 and Figure 5, that the overall trends of BTE characteristics of Mahua biodiesel, Linseed biodiesel, and their blends are almost similar in nature. It is observed that at any given load condition, the brake thermal efficiency of neat Mahua biodiesel (M100) and other blends (M25, M50, M75) is lower than that of Linseed biodiesel (L100) and its blends (L25, L50, L75) operation. It can be seen that as the percentage of Mahua biodiesel in the blend increases, there is more decrease in brake thermal efficiency as compared to Linseed biodiesel mode. This lower BTE of Mahua biodiesel operation is due to the combined effect of higher viscosity, higher density of Mahua biodiesel.

1. 2 Specific fuel consumption

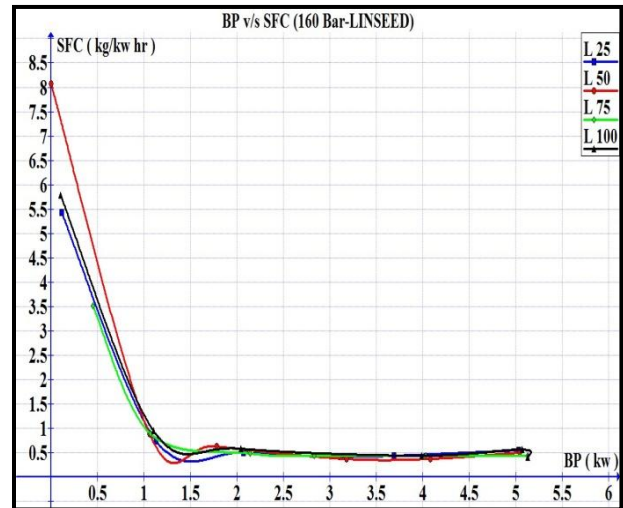
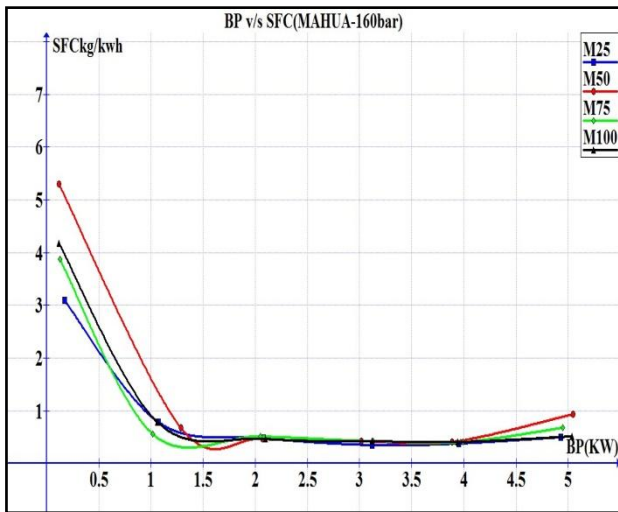


Figure 4 Comparison of SPFC between Mahua biodiesel blends and Linseed biodiesel blends at 160 bar injection pressure.

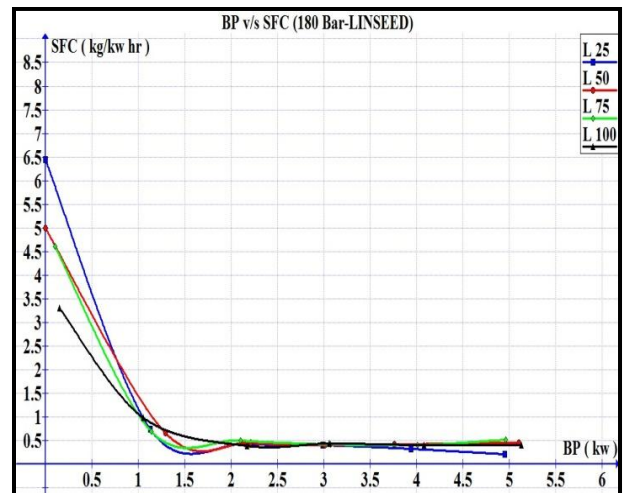
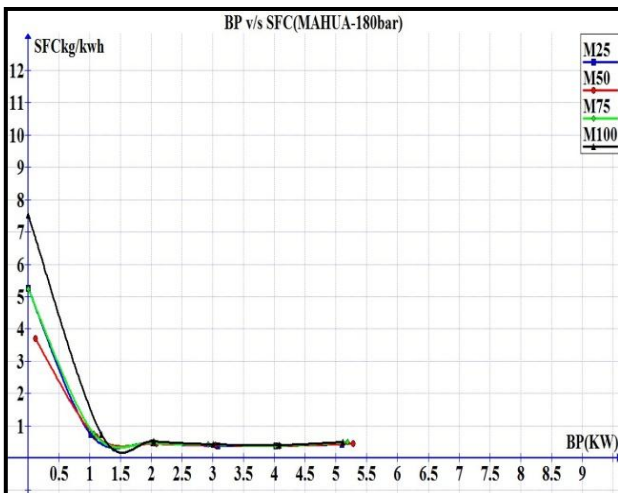


Figure 5 Comparison of SPFC between Mahua biodiesel blends and Linseed biodiesel blends at 180 bar injection pressure.

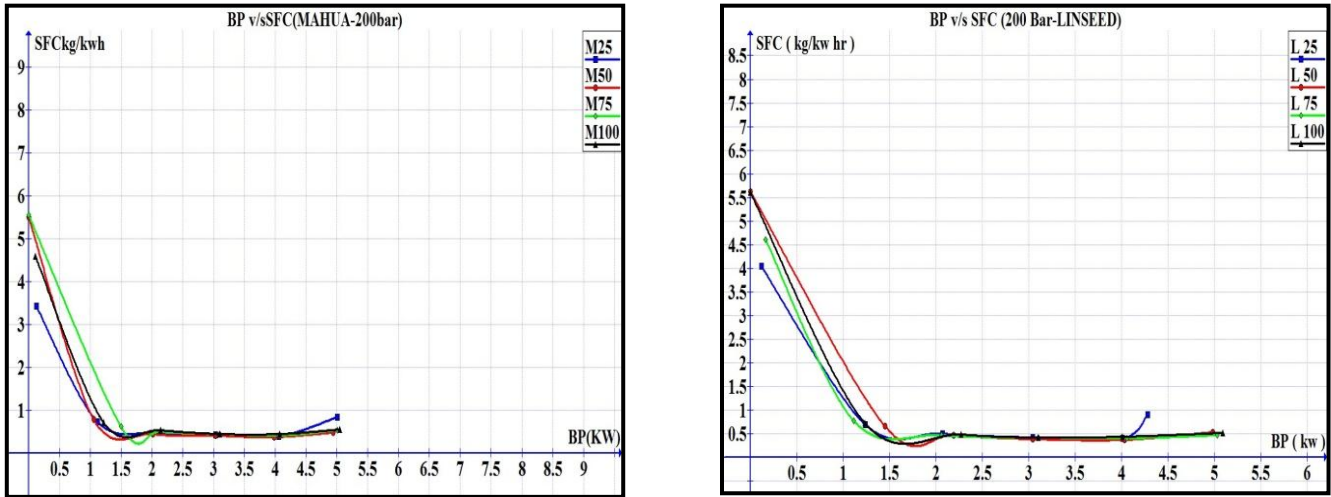


Figure 6 Comparison of SPFC between Mahua biodiesel blends and Linseed biodiesel blends at 200 bar injection pressure.

Figure 6, Figure 7 and Figure8, shows the comparison of effect of load on brake-specific fuel consumption between Mahua biodiesel and Linseed biodiesel for different blend conditions. It is seen that brake-specific fuel consumption decreases when the load is increased for all operations of Linseed biodiesel and Mahua biodiesel and their blends. However, the rate of decrease in brake specific fuel consumption is more during lower loads up to 50% than that of higher loads (50 to 100%). It can also be observed that brake-specific fuel consumption increases when Linseed

biodiesel proportion in the blend is increased for any given load, but the increase in brake-specific fuel consumption for M100 operation (neat Mahua biodiesel) is much more than that of other blends and diesel operations at higher load conditions.

2. EMISSION CHARACTERISTICS

2.1 Carbon monoxide content (%)

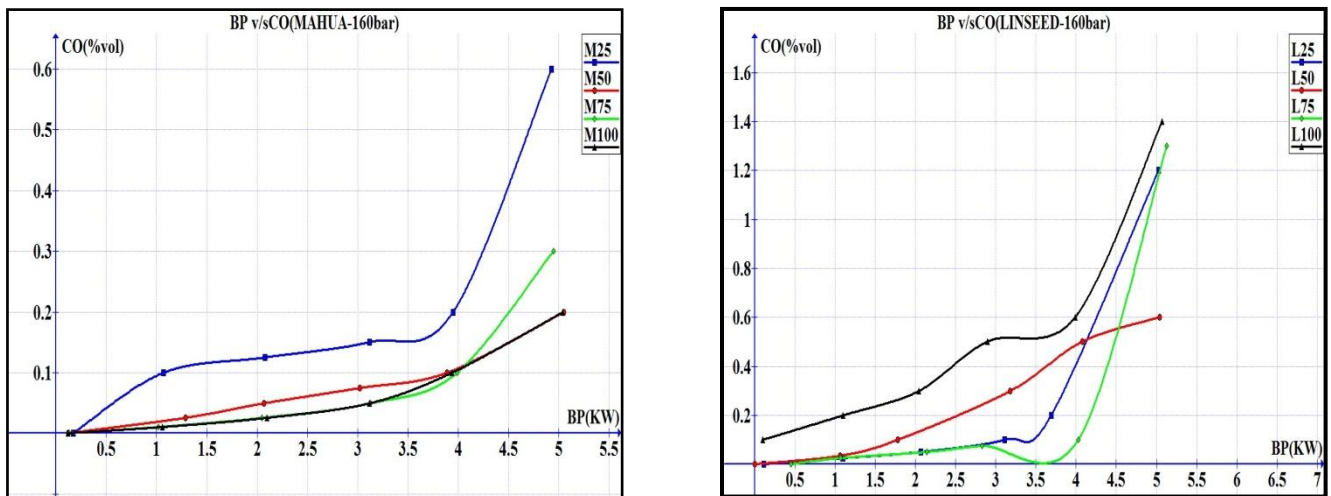


Figure 7 Comparison of CO between Mahua biodiesel blends and Linseed biodiesel blends at 160 bar injection pressure.

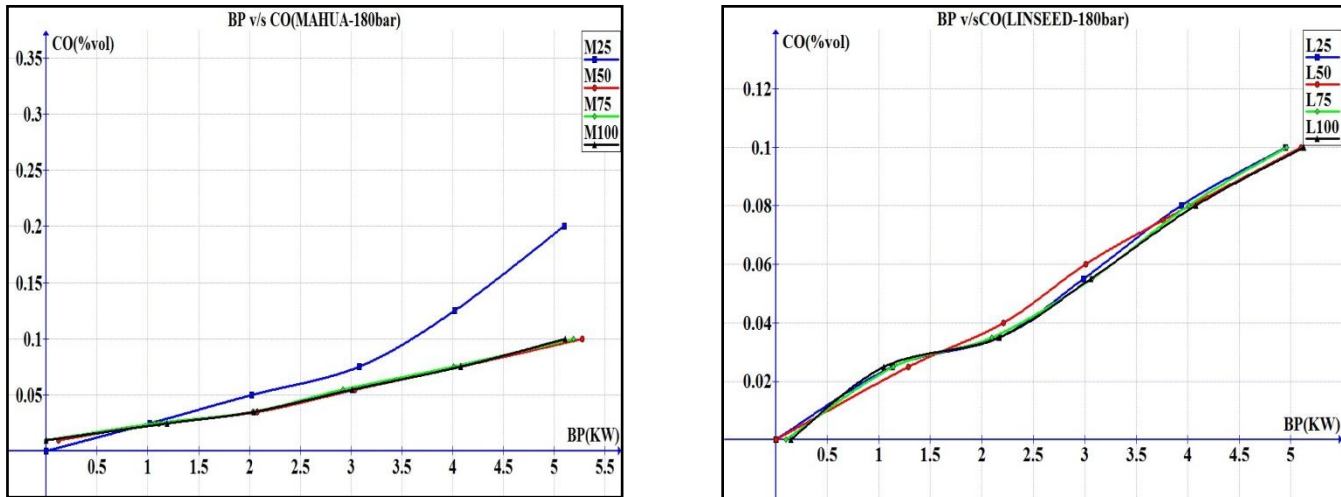


Figure 8 Comparison of CO between Mahua biodiesel blends and Linseed biodiesel blends at 180 bar injection pressure.

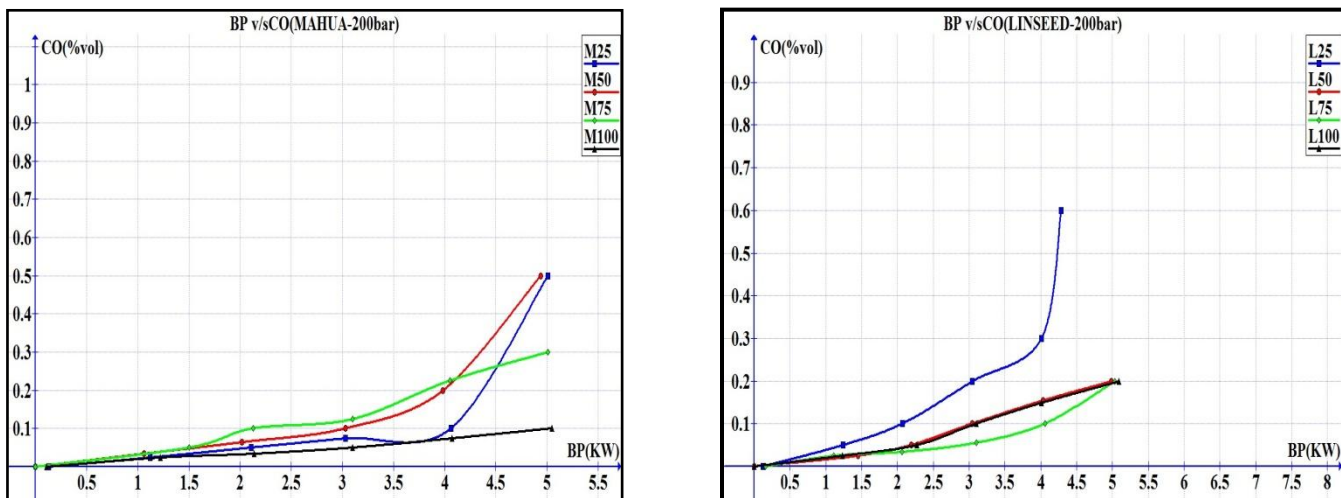


Figure 9 Comparison of CO between Mahua biodiesel blends and Linseed biodiesel blends at 200 bar injection pressure.

The effect of load on carbon monoxide (CO) emissions for diesel, Mahua biodiesel, and their blends is shown in Figure 9 Figure 10 and Figure 11. It can be seen from the figure that the higher CO emissions were obtained with Mahua biodiesel and its blends than Linseed biodiesel and its blends. The CO emission is 1.2, 0.6, 1.3 and 1.4% for Linseed biodiesel, L25, L50, L75 and L100 respectively, at 100% load and CO emissions is 0.6, 0.2, 0.3 and 0.2% for Mahua biodiesel M25, M50, M75, and M100 at 100%load. Higher CO emissions in the exhaust gas of the engine may be

attributed due to the polymerization that takes place at the core of the spray, this also caused concentration of the spray core and decreased the penetration rate. Low volatility polymers affected the atomization process and mixing of air and fuel causing locally rich mixture, which leads to difficulty in atomization and vaporization of neat Mahua biodiesel due to improper spray pattern produced. This feature increases the incomplete combustion and hence higher CO emission.

2.2 Unburnt Hydrocarbon emission

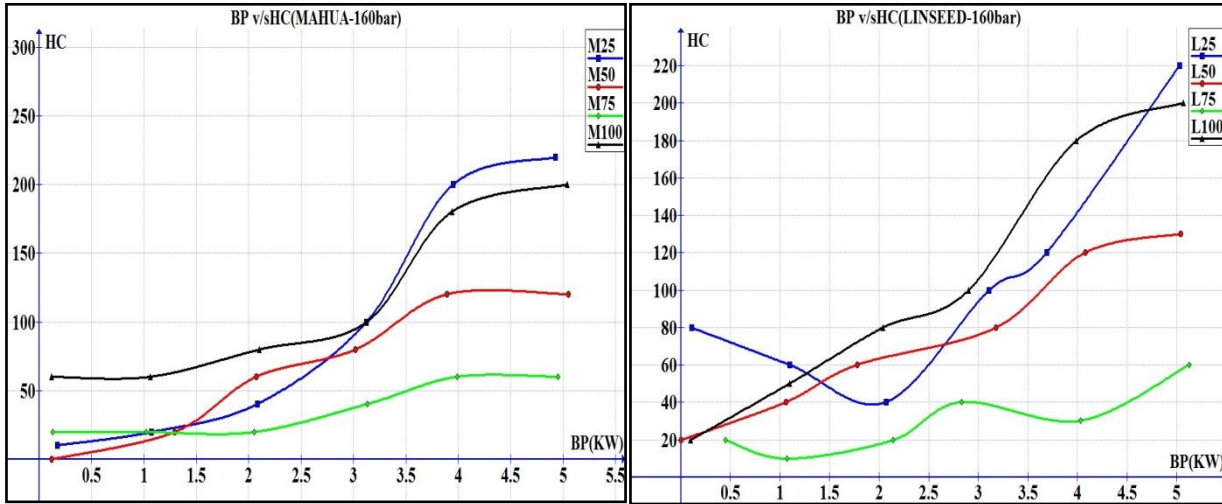


Figure 10 Comparison of HC between Mahua biodiesel blends and Linseed biodiesel blends at 160 bar injection pressure

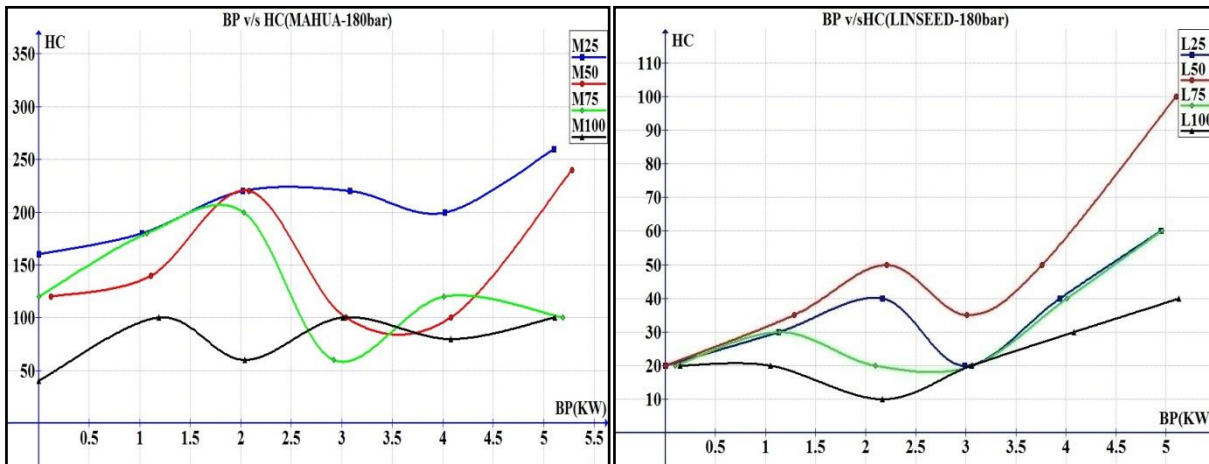


Figure 11 Comparison of HC between Mahua biodiesel blends and Linseed biodiesel blends at 180 bar injection pressure

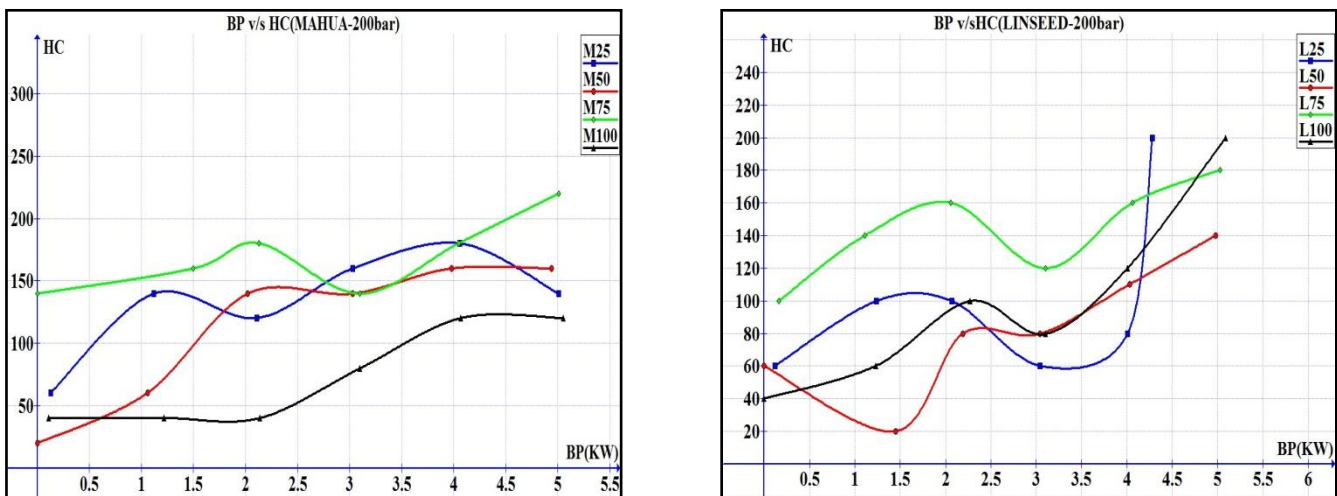


Figure 12 Comparison of HC between Mahua biodiesel blends and Linseed biodiesel blends at 200 bar injection pressure

The effect of load on unburned hydro-carbon (Hc) emissions for diesel, neat Mahua biodiesel and their blends is shown in Figure 12, Figure 13 and Figure 14. It can be seen from the figure that the lower HC emissions were obtained with blends of Mahua biodiesel-diesel and neat Mahua biodiesel mode of operation for loads above 40% compared to Linseed biodiesel and its blends. The HC emission is 40, 20, 10, 20 ppm for Linseed biodiesel, L25, L50, L75 and L100 respectively, at 100% load and Hc emissions is 10, 0, 20, 60 ppm for Mahua biodiesel M25, M50, M75, and M100 at 100% load. Lower HC emissions in the exhaust gas of the engine may be attributed to the efficient combustion of Mahua biodiesel and blends due to the presence of fuel bound oxygen and warmed-up conditions at higher loads. Whereas at lower loads (up to 40%) higher Hc emissions were observed with blends of Mahua biodiesel-diesel and neat Mahua biodiesel operations. This is due to the reason that at lower loads the lower cylinder pressure and temperatures were experienced that was caused by lower rate of burning. This feature results in higher HC emissions.

CONCLUSION

The performance characteristics, brake thermal efficiency, brake specific fuel consumption, and emission characteristics, carbon monoxide, hydro-carbon of a single cylinder vertical direct injection Kirloskar engine using Mahua and Linseed biodiesels with their blends as fuels were experimentally investigated. The following conclusions are made based on the experimental results.

1. As the proportion of Mahua biodiesel increases in the blend, the brake thermal efficiency decreases. For M50, the brake thermal efficiency was 13.49% less than that of L50 at 160 bar pressure full load.
2. More the proportion of Mahua biodiesel in the blend more is the increase in brake specific fuel consumption for any given load.
3. The carbon monoxide emissions are more with Mahua biodiesel when compared to Linseed biodiesel at full load condition.
4. At 20% load, HC emissions for Mahua biodiesel and blends are quite high. At higher loads, as the quantity of Mahua biodiesel in the blend increases HC emissions decreases.

REFERENCES:

- [1] M. Senthil Kumar, A. Ramesh, "An experimental comparison of methods to use methanol and Jatropha oil in a CI Engine". Biomass and Bioenergy, 2003; 25:309-318.
- [2] A.S.Ramadas, S.Jayraj, " Biodiesel production from high FFA rubber seed oil", Fuel 2005; 84:335-340.
- [3] O.D.Hebbal, "Performance characteristics of a diesel engine with deccan hemp oil", Fuel 2006; 85:2187-2194.
- [4] Barsic NJ, Humke AL, "Performance and emissions characteristics of a naturally aspirated diesel engine with vegetable oil fuels", SAE paper No. 810262.
- [5] Humke AL, Barsic NJ, "Performance and emissions characteristics of a naturally aspirated diesel engine with vegetable oil fuels- part(2)", SAE paper No.810955.
- [6] Vellguth G, "Performance of vegetable oils and their monoesters as fuels for diesel engines", SAE paper No. 831358.
- [7] Henham AWE, "Experience with alternate fuels for small stationary diesel engines: fuels for automotive and industrial diesel engines", I Mech E 1990:117-22.
- [8] Ramadhas AS, Jayaraj S, "Use of vegetable oils as IC Engine fuels-a review", Review energy 2004;29:727-42.
- [9] M C Navindgi, Dr.Maheswar Dutta, "Effects of preheating of honne oil (HO) on injection system, performance and emission of a diesel engine", International Journal of Mechanical Engineering Research : ISSN 2249-0019 Volume 1, Number 3 (2011), pp. 399-410
- [10] Kalam MA, Masjuki HH, " Emission and deposit characteristics of a small diesel engine when operated on preheated crude palm oil", Biomass Bioenergy 2004;27:289-97.
- [11] Rao PS, Gopalkrishnan KV, " Use of non-edible vegetable oils as diesel engine fuels", J Inst Eng India 1989;70(4).
- [12] M C Navindgi, Dr.Maheswar Dutta, "Performance and Emission Characteristics of a Diesel Engine operating on Honne oil and its blends", International Journal of Computer Applications in Engineering, Technology and Sciences :ISSN: 0974-3596|OCT 2011-MARCH 2012|Volume 4 : Issue 1
- [13] Pramanik K(2003), Properties and use of Jatropha curcus oil and diesel fuel blends in compression ignition engines. Renewable Energy, 28 239-248
- [14] Ramdas AS, Jayaraj S and Muraleedhran C (2005) Characterization and effects of using rubber seed oil as fuel in compression ignition engines. Renewable Energy, 30, 795-803
- [15] Choudhury S and Bose P K (2007) Karanja or Jatropha- a better option for an alternative fuel in CI engine. In: Intl. Conf. On IC Engines (CONICE), Hyderabad

Synthesis of Nano Titanium Dioxide Powder using MWP (microwave plasma) and its Characterization

^a P .S .RAO, ^bK. MOHANA KRISHNA CHOWDARY, ^cM.VIJAY SEKSHAR BABU, ^cP.GOVINDA RAO,
^dA. SURYA PRAKASH

^aDept. of Industrial Production Engineering, GITAM University, Visakhapatnam, India.

^bDept.of MechanicalEngineering, IIIT,Nuzivid,RGUKT,AP,India

^cDept. Of Mechanical Engineering, GMR Institute of Technology, Rajam, India

^dGMR group, Hyderabad, India

Abstract:

Titanium dioxide (titania) powders finds lot of engineering applications in many areas such as waste water detoxification, electronic circuits as mermisters, quantum dots, hydrolysis , LCD screens etc. The performance is influenced by particle size and its purity. It is preferred to have smaller particle size with high purity.

This work describes the application of microwave plasma synthesis technology to prepare a photo catalytically active TiO₂ nano powder using oxygen as plasma forming gas as well as carrier gas. The powder thus produced is characterized by means of SEM (Scanning electron microscopy), XRD , BET surface area test. The average particle size for the powder obtained is determined to be around 60-70 nm, which is quite compatible with the commercially available titania powder (P-25). The prepared powder has 67 % Anatase and 33 % Rutile phase in it with high purity and better controlled particle size .The nano titania powder obtained through MWP is tested for photo catalytically activenessTiO₂ powder is synthesized using methylene blue for decolourisation effect shown as satisfactory results..

Keywords: Photo catalysis, Microwave plasma (MWP, titania, Methylene blue, XRD (X-Ray diffraction), BET (Brunauer, Emmett and Teller).

1. Introduction

Nanopowders have a combination of small particle size, narrow size distribution and high surface area to volume ratio. The physical and chemical properties of these nano particles often deviate from their bulk materials when the particle size decreases to a specific regime. The powder shows a dramatic increase in photo catalytic action and increases strength, hardness and cutting efficiency as particles become nano sized.

Titanium dioxide occurs in nature as well as in known mineral forms such as rutile(tetragonal), anatase(tetragonal) and brookite(orthorhombic). Most common form of titania is rutile, which is also the most stable form. Anatase and brookite both convert to rutile upon heating. Rutile, anatase and brookite all contain six coordinated titanium. Titanium dioxide powder is commonly referred to as Titania.

Plasma processing of materials makes use of high energy content of 'partially ionize gas' commonly referred to as the fourth state of matter. Plasma is also encountered in our daily life such as in a lightning bolt, the conducting gas inside a fluorescent -tube and inside neon sign. Plasma consist of charged excited and neutral partial ionization of atom or molecules of a gas and therefore, is an electrical conductor, however any gas cannot be called a plasma as there is small degree of ionization in any gas .Plasma provides convenient sources of energetic ions and activated atoms which are now widely employed in densification and synthesis of ceramics, decomposition and etching of materials.

Titanium dioxide is useful in many varied applications, such as paints, pigments, films, hydrolysis, photo catalyst, water detoxification, antifouling, UV rays absorptions etc.[5]

Titanium dioxide is the most widely used white pigment because of its brightness and very high refractive index ($n = 2.7$), in which it is surpassed only by a few other materials. Approximately 4 million tons of pigmentary TiO₂ are consumed annually worldwide. When deposited as a thin film, its refractive index and colour make it an excellent reflective optical coating for dielectric mirrors and some gemstones like "mystic fire topaz". TiO₂ is also an effective opacifier in powder form, where it is employed as a pigment to provide whiteness and opacity to products such as paints, coatings, plastics, papers, inks, foods, medicines (i.e. pills and tablets) as well as most toothpastes. In paint, it is often referred to offhandedly as "the perfect white", "the whitest white", or other similar terms. Opacity is improved by optimal sizing of the titanium dioxide particles. In ceramic glazes titanium dioxide acts as an opacifier and seeds crystal formation.

Titanium dioxide is often used to whiten skimmed milk; this has been shown statistically to increase skimmed milk's palatability. Titanium dioxide, particularly in the anatase form, is a photo catalyst under ultraviolet (UV) light. Recently it

has been found that titanium dioxide, when spiked with nitrogen ions or doped with metal oxide like tungsten trioxide, is also a photo catalyst under either visible or UV light. The strong oxidative potential of the positive holes oxidizes water to create hydroxyl radicals. It can also oxidize oxygen or organic materials directly. Titanium dioxide is thus added to paints, cements, windows, tiles, or other products for its sterilizing, deodorizing and anti-fouling properties and is used as a hydrolysis catalyst. It is also used in dye-sensitized solar cells, which are a type of chemical solar cell.

The photo catalytic properties of titanium dioxide were discovered by Akira Fujishima in 1967 and published in 1972. The process on the surface of the titanium dioxide was called the *Honda-Fujishima effect* [8, 9].

Titanium dioxide has potential for use in energy production: as a photocatalyst, it can carry out hydrolysis; i.e., break water into hydrogen and oxygen. Were the hydrogen collected, it could be used as a fuel. The efficiency of this process can be greatly improved by doping the oxide with carbon. Further efficiency and durability has been obtained by introducing disorder to the lattice structure of the surface layer of titanium dioxide nanocrystals, permitting infrared absorption [10].

Titanium dioxide can also produce electricity when in nanoparticle form. Research suggests that by using these nanoparticles to form the pixels of a screen, they generate electricity when transparent and under the influence of light. If subjected to electricity on the other hand, the nanoparticles blacken, forming the basic characteristics of a LCD screen [6].

Nokia has already built functional Titanium dioxide is also used as a material in the memristor, a new electronic circuit element. It can be employed for solar energy conversion based on dye, polymer, or quantum dot sensitized nano crystalline TiO_2 solar cells using conjugated polymers as solid electrolytes.[7]

Micro Wave Plasma:

The plasma used here, falls under thermal plasma. The microwave used here is a high frequency electromagnetic wave and the generator used here is a electrode less generator.

This plasma falls under category of thermal plasma .the microwave plasma employs a high frequency electromagnetic wave and a electrode less generator. the MWP is advantages over the powder making methods such as

- Very clean plasma generated since no electrodes are used.
- Powders, liquids, vapours, and gases can be fed into the reaction chamber.
- High production rate when compared to other processes (120g/hr approx.)
- Possibilities for forming excited species of ions.

The micro wave unit is designed for production of ultra dispersed (below 100nm) powders of oxides by means of condensation from high temperature chemically reacting gaseous flow. Chemical reaction yielding the condensed product occurs in the flow of oxygen heated to 1500-3000 K due energy of micro wave irradiation.

2. Experimental setup:

The experimental set-up used in this work is represented schematically in Fig.1.



Fig. 1: Microwave plasma unit .

Microwave irradiation generated by the generator heats a stationary flow of plasma forming gas, which is delivered in plasmatron. Heated and ionized flow delivers into reactor. Chemical reagents as vapour mixed with gas carrier are delivered into the upper part of the reactor through input attachments. Dosing device ensures a uniform delivery of the reagents. In the reactor, the reagents mix with high temperature flow, and chemically react in gas phase. The chemical reaction yields highly oversaturated vapor, which yields ultra dispersed product upon condensation properties of resulting powder, can be controlled in a certain range by changing conditions like concentration, temperature and cooling rate. Gas dispersed mixture formed in the reactor delivers to heat exchanger for cooling, and then to filter, where dispersed phase is separated from gas flow. The product gets accumulated in the collector. The process duration is approximately 30 min.

2.1 Specification of MWP unit:

- Maximum output of the micro wave generator - 5kw.
- Frequency of microwave generator 2450MHz

2.2 Components of MWP

Magnetron: It is the unit that produces the micro waves that are to be introduced into the plasma. It basically contains one cathode and multiple anodes each carrying a current 1.4 Amp. The output of this unit is upto 5 kw. This system unlike others has separate cooling systems such as fans. The magnetron is followed up by a isolator which performs the function of directing waves only in one particular direction to avoid reflected waves which would otherwise generate more heat which is not desirable. Wave guides are also provided which more or less perform the same function of aligning the waves in one direction.

Plasmatron: Super high frequency plasmatron is designed for heating of stationary gas flow of oxygen to 1500-3000 k due to absorption by ionized gas of microwave irradiation delivered from magnetron via wave guides. Gas is introduced into plasmatron first passes through twisting chamber. Primary gas ionization, which is necessary for initiating stationary gas micro wave discharge, is performed by a short term insertion of stainless steel wire into the discharge zone. Plasmatron provides stable "burning" of discharge in the range of gas flow of 1.8-4.0 m³/hr, and input power of 2- 5kw. Plasmatron housing is supplied with cooling water to absorb the heat generated [5].

2.2.1 Technological Equipment

Reactor: it is a water cooled tube consisting of two separate sections .high temperature plasma jet and chemicals participating in the reaction are fed to the upper part of the reactor. They interact in the reactor and form condensed products as ultra-dispersed powder.

Injector: It is for introduction of reagents and is placed between plasmatron and the upper part of the reactor, and it is used for feeding the starting material participating in plasma chemical process. The case of the injector is supplied with water cooling.

Heat Exchanger: It is assigned for reduction of temperature of exiting dust-gas flow before it is fed into the filter. It consists of two co axially located water cooled cylinders, with axis perpendicular to the axis of running high temperature flow.

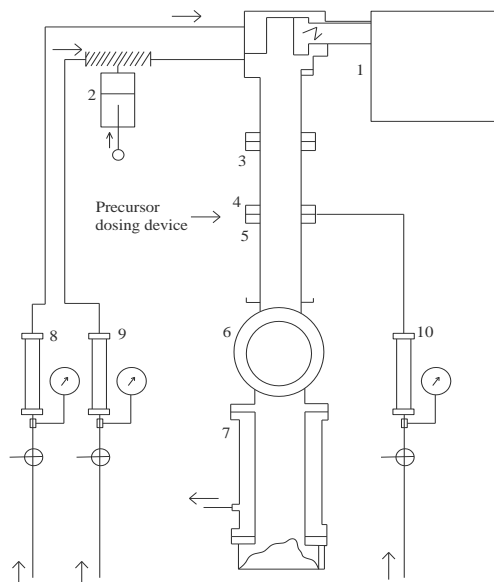


Fig 2: Schematic diagram of Microwave plasma

- (1) Microwave generator (2) Dosing device for reagents (3) Reactor zone1
 (4) Inter connector (5) Reactor zone 2 (6) Heat-exchanging device
 (7) Filter (8).(9).(10) Rota meters

Filter: It is assigned for isolation of ultra dispersed powder from cooled dust-gas flow and its accumulation during the technological process. Filtration of dust-gas flow is performed when the flow passes through a bag filter made of thermo stable phenylon tissue.

Dosing Device: This is connected to the injector for reagents and is assigned for controlled feeding of the stock into plasma chemical reactor. Performance of dosing device for a large scale production of powder is based on the entrainment of the liquid chloride vapours by carrier gas from thermostating space of the dosing device

3. Synthesis of TiO₂:

The input substance which is used to prepare the required product is called precursor. Here the precursor used is TiCl₄ which is in liquid state. It is very sensitive to moisture and has high vapour pressure. It is feed into the plasma at rate of 107 X 10⁻⁶ m³/hr. Carrier gas is used to carry the vapours of the precursor into the reaction chamber. The carrier gas used here is oxygen and is feed at rate of 0.3 m³/hr. oxygen is used as plasma forming gas here at a rate of 2.2 m³/hr.

The precursor TiCl₄ reacts with the oxygen which is sent inside as the plasma forming gas as well as the carrier gas according to the following reaction.



The powders were quenched at the wall of the heat exchanger and then separated from the gas by the filter bag via a tube. powder deposited directly in the bag provided is designated in this work as bag fraction and the residual powder stuck along the walls of the output tube is designated as tube fraction.

4. Characterization and Results:

4.1 Photocatalytic activity:

The nano titania powder obtained from tube ,bag fraction is kept in two separate beakers and mixed it with Methylene blue to form a concentrated homogenous solution, for checking the photocatalytic nature. Similarly, commercially available titania powder is mixed in a beaker containing methylene blue. The sample weighs typically for each is ,

Tube fraction	:	0.0252gm
Bag fraction	:	0.0247gm
P-25	:	0.0258gm

Some amount of pure methylene blue is taken for reference. The three beakers containing TiO₂ powder are kept in the ultrasonifier for fine dispersion of nano powder in the methylene blue solution. All the 4 beakers are introduced to direct sunlight with light intensity measuring upto 70 mW/12mm². [4]. Methylene blue is used to test for photo catalytic activity of powder manufactured. Its unique ability to remain un reacted upon action with UV rays and being a common pollutant makes it apt for this activity.

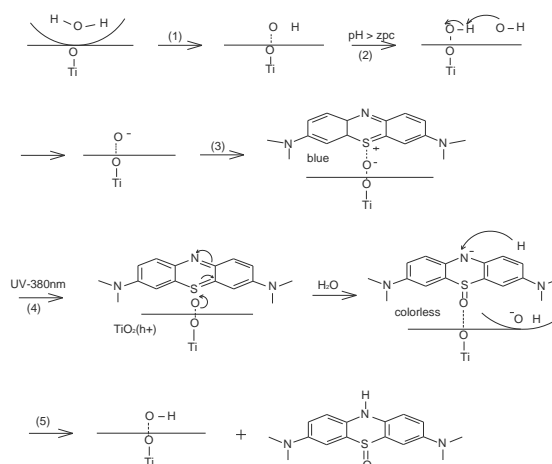


Fig 3: Reactions involved in photocatalysis

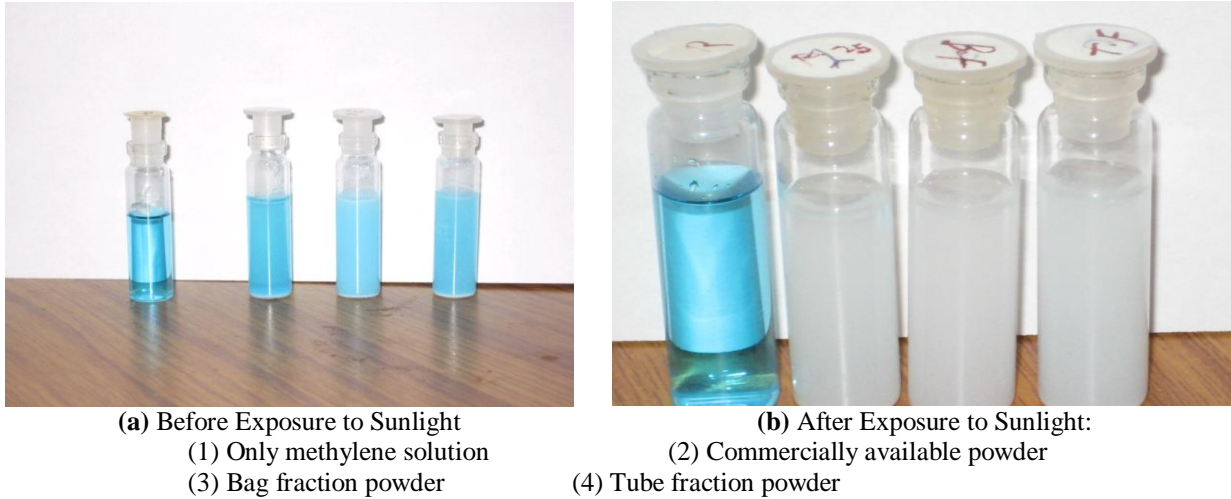


Fig 4: Bottles as they stand in order from left

- The activity was carried out for 20 min in daylight.
- The deviation in colour in the samples containing TiO_2 powder from the reference solution colour justifies the photocatalytic action of TiO_2 .
- The colour change is first observed in bag fraction.

4.2 SEM analysis

The drop of finely dispersed TiO_2 powder in distilled water is kept on a carbon tape as per standard test procedure. It is then kept under the scanning electron microscope, which has very high resolution power. Photograph of samples obtained from tube and bag fraction of nano TiO_2 atoms in nanometer dimension are shown in Fig (5)

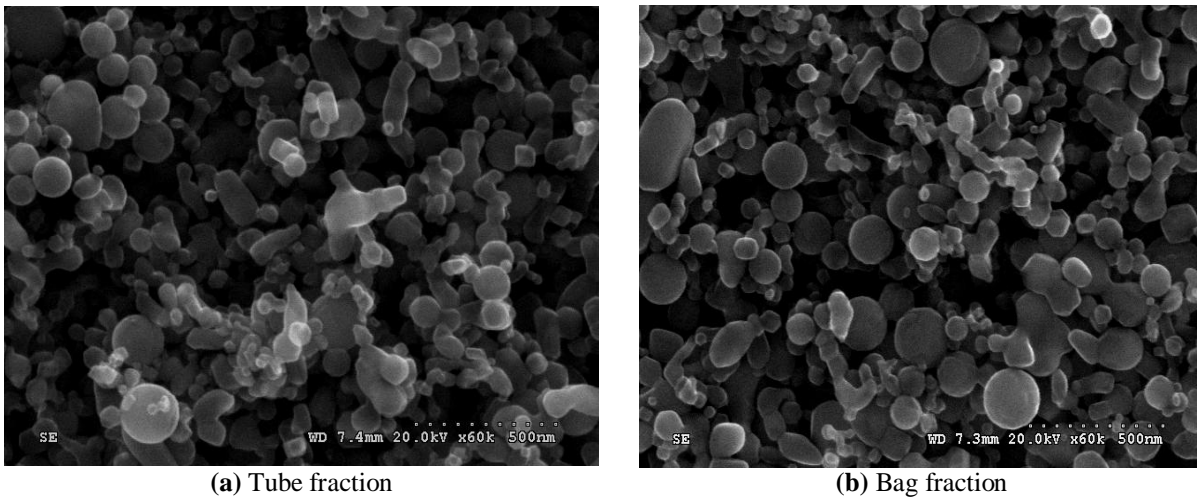


Fig 5: SEM images of TiO_2 obtained through MWP.

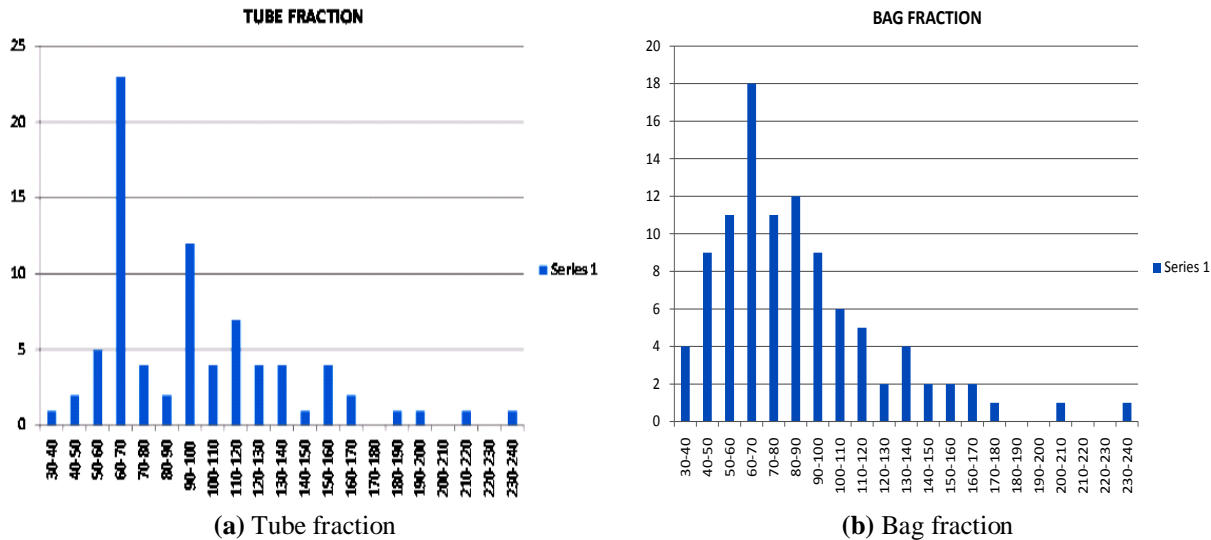


Fig 6: The average particle size of the atoms are plotted on Graphs using SEM photographs

From the SEM analysis , it is found that

- The average particle size in tube fraction is 78 nm.
- The average particle size in bag fraction is 97 nm.

4.3 XRD analysis of powder prepared through micro wave plasma:

The samples obtained from tube and bag fraction are subjected to XRD analysis. The photograph of samples obtained from tube and bag fraction of nano TiO₂ atoms in nanometer dimension are shown in Fig (5).

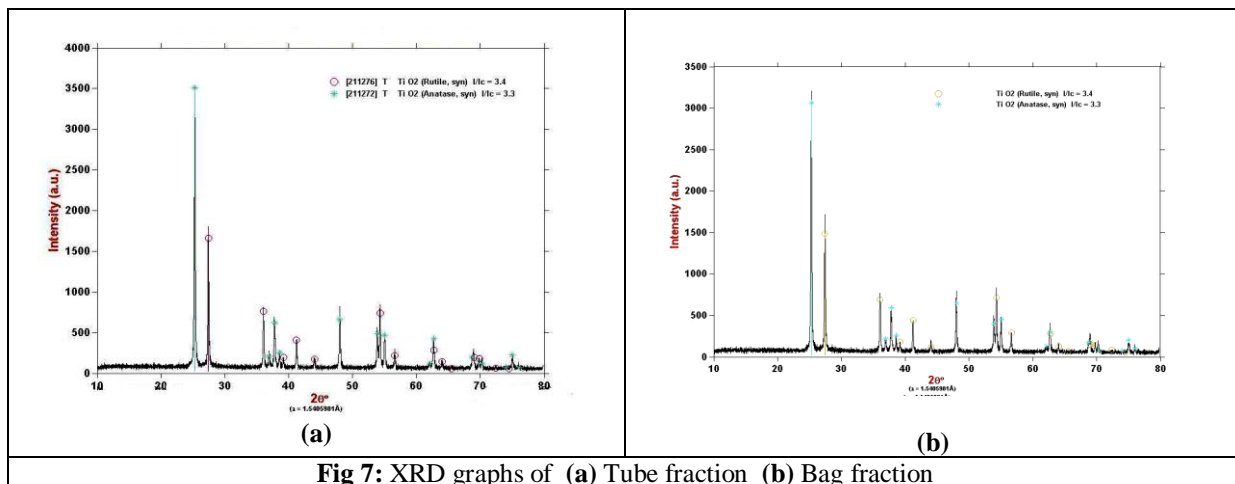


Fig 7: XRD graphs of (a) Tube fraction (b) Bag fraction

Based on the above, the XRD results obtained are as follows.

Average particle size:

Tube fraction: The average anatase crystallite size is 46.69nm. The average rutile crystallite size is 46.67 nm.

Bag fraction: The average anatase crystallite size is 59.17nm. The average rutile crystallite size is 51.11nm

%composition :

Tube fraction: Anatase is 67.77% and the Rutile is 32.23%

Bag fraction: Anatase is 67.73% and the Rutile is 32.27%

4.4 BET surface area test for the powder obtained by MWP:

BET of Make: MICROMERITICS, model ASAP 2020 V3.00 H, is employed for measuring surface area . The powder particles are then surrounded by nitrogen molecules and thus gives the empirical value of the surface area of the required nano powder. The surface area of powder in tube fraction is

20.0731 m²/gm and the surface area of the powder in the bag fraction is 18.067 m²/gm where as surface area of the sample of P-25 was found to be 15.27 m²/gm.

5. Conclusion:

Nano powder of tio₂ is successfully made using MAW plasma technique., with high percentage of antase. The powder is of nano nature as characterized by SEM, XRD. A photocatalytically active nano TiO₂ powder is successfully synthesized using micro wave oxygen plasma and its compatibility with commercially available power is checked using the photocatalytic activity and the size range is justified using the SEM analysis and slight deviation is observed in tube fraction from bag fraction. composition and phases are also analyzed using XRD analysis. The nano particles produced are of superior quality, however efforts are required to reduce manufacturing cost for large scale production..

Acknowledgements:

The authors express their gratitude to the authorities of International Advanced Research Center for Powder Metallurgy & New Materials (ARCI), India, and Department of Science and Technology (DST), India for their support.

References:

1. H.P. Klug, L.E. Alexander, X-ray Diffraction Procedures for Polycrystalline and Amorphous Materials, Wiley, New York, 1962, p. 491.
2. X.C. Ma, Y.H. Cai, X. Li, S.L. Wen, Mater. Sci. Eng., A Struct. Mater.:Prop. Microstruct. Process. 357 (2003) 308.
3. Bai Zhaohui ,Ba Xuewei ,Jia Ru ,Liu BoFrontiers of Chemistry in China, Volume 2, Number 2 / April, 2007
4. A. Fujishima, T. N. Rao, and D. A. Tryk, "Titanium dioxide photocatalysis," *Journal of Photochemistry and Photobiology C*, vol. 1, no. 1, pp. 1–21, 2000.
5. Joseph Lik Hang Chau, Ming-Kai Hsu, Ching-Chang Hsieh and Chih-Chun Kao, Microwave plasma synthesis of silver nanopowders *Materials Letters*, Volume 59, Issues 8-9, April 2005.
6. Hand book of physics and chemistry, 89 edition, 2008-2009.
7. Sax, N.I.; Richard J. Lewis, Sr. (2000). *Dangerous Properties of Industrial Materials*. (10th ed.). New York: Van Nostrand Reinhold. p. 3279.
8. Sato et al "baddeleyite type of high pressure phase of tio₂" *Science* 251 pp 786-788, 1991.
9. Greogary Mogilevsky etal "the structure of multilayred titania nanotubes based on delamiated anatase ", *chemical physics letters* , vol 460pp 517-520, 2008.
10. Hogan "carbon doped titanium di oxide is effective in photocatalyst" *Newscientist.com* 2004
11. Hogan "smog busting paint soaks up noxias gases" *Newscientist.com* 2004.

Modification in Field Measurement Applied on Exact Algorithm for Biomedical Imaging

Dr. Kabita Purkait¹, Kalyan Adhikary²

¹(Associate Professor, Department of Electronics & Communication Engineering,
Kalyani Govt. Engineering College, West Bengal, India)

²(M.Tech, Electronics & Communication Engineering, Kalyani Govt. Engineering College, West Bengal, India)

ABSTRACT

A modification has been proposed by the authors to calculate the field strength at the cells of a biological target which is illuminated by a transmitting array antenna with a beam width of 6° . The biological target is divided into large number of cells so that complex permittivity and electric fields are assumed to be constant in the small area of each cell. The electric fields are calculated at the cells which are under the illuminated zone of a transmitting beam. The electric fields are assumed to be zero in those cells which are outside the coverage zone of the said transmitting beam. Whereas in the previous cases, all the cells of the biological target are considered to be illuminated by the beam. For efficient reconstruction, narrowest possible beam is required. This modified method of field measurement when applied on a semi-human sized biological model consisting of human organs like fat, muscle, kidney and muscle type material improves the reconstructed complex permittivity value of the biological target. A comparative study of reconstructed image obtained by previous field measurement technique and improved field measurement technique are presented in this paper. Reconstruction of complex permittivity of target area is simulated using Force 209 FORTRAN and results are depicted by using colour gradation scale.

Keywords: Complex permittivity, Exact algorithm, Simultaneous iterative reconstruction technique (SIRT), Tomography

1. Introduction

The Greek word 'tomos' means parts or section and 'graph' means representation. Hence tomography is the imaging of unknown cross section of any object. Tomography of a biological body using low microwave frequency range (near about 1 GHz) will be a non invasive technique for medical diagnosis as low microwave signal has no radiation hazard like X-rays in computed tomography. Moreover, interaction of microwaves with dielectric properties of biological tissue is attractive as complex permittivity of the tissue changes with the water content in it and this water content also changes with infection of disease. The reconstruction of complex permittivity of the biological tissue discriminates the healthier tissue from the diseased one. Various iterative reconstruction algorithms based on moment method solution for randomly inhomogeneous biological model

had been developed on the assumption that change of characteristic parameter of a cell produces effects on the other and hence, results a coupled effect on the receiver point. Since exact solution of such a large number of non-linear equations containing a large number of unknown variables are impossible, the iteration methods [1]-[4] have been adopted.

Improved first order and second order algorithm [5] considering the first order and second order mutual interaction terms fails to reconstruct larger model as higher order terms greater than second order play the dominant role and perturbation equation becomes non-convergent. It also fails to detect smaller model with large perturbation by the same reason.

Considering the above facts, a new exact algorithm [6] had been developed where the difference of two electric fields which are obtained when the object medium is assumed to be a homogeneous one and when actual experimental model is used, at a particular receiver location is expressed in terms of unknown permittivity, relevant co-factors of co-efficient matrix corresponding to the homogeneous medium and perturbed internal fields.

The exact algorithm is based on the integral equation for the field of harmonic source in presence of a dielectric medium which is assumed to be divided into large number of small cells. The areas of the cells are kept very small so that electric field intensity and complex permittivity in each cell are nearly constant. According to Richmond [7] a system of linear equations are obtained by enforcing the condition that total field at the centre of each cell must be equal to the sum of the incident field and the scattered field in that cell from the neighbouring cells.

Further, the change of characteristic parameter of a cell produces effects on all other cells and hence, results a coupled effect on the receiver point. Previously, it was assumed that all the cells of the biological target are illuminated by the antenna located in each transmitter position. But, in practice each transmitting beam has a finite beam width and incident fields are calculated in those cells which are under the beam contour. Incident fields are assumed to be zero in those cells which are outside the coverage zone. Hence, cells which have incident field strength will produce a coupled effect to a particular cell for the said beam and cause no change to the other cells outside the zone. So, necessary corrections are required in the measurement technique of incident fields [8],[9],[10], perturbed fields in the target cells and finally to the received fields. In this paper, the number and location of the cells in a rectangular region of a biological

target illuminated by a transmitting antenna beam of width 6° are calculated using elemental geometrical approach.

2. Algorithm for perturbed field

As stated by Richmond [7] a system of linear equations can be obtained by equating the total field at the centre of each cell with the sum of incident and scattered fields at that centre for a sufficiently large number of cells.

The field distribution in unperturbed homogeneous medium is expressed by the equation:

$$[C]. [E_i] = [E_i^{in}] \quad (1)$$

Where E_i^{in} is the incident field at i-th cell in free space and E_i is the internal field at i-th cell when the medium is assumed to be homogeneous one having known permittivity distribution. $[C]$ is (n x n) coefficient matrix of homogeneous medium.

The permittivity values of the cells are perturbed simultaneously by small amounts of $\Delta\epsilon_i$ ($i = 1, 2, \dots, n$) when the homogeneous medium is replaced by an inhomogeneous one and the corresponding changes in the internal fields are ΔE_i 's :

$$[C'] . [E_i'] = [E_i^{in}] \quad (2)$$

where $[C']$ is the coefficient matrix corresponding to the inhomogeneous medium and $E_i' = [E_i + \Delta E_i]$ is the perturbed total field at the i-th cell.

Using necessary correction for incident field measurement, the incremental change in field at i-th cell for the k-th transmitter due to change of permittivity and fields (only illuminated cell's field will take part instead of all the cell's fields) in the other cells of the model is given by the equation as:

$$\Delta E_i(k) = -x_i E_i' + \sum_{j=1}^m x_j E_j' \frac{M_{ji}(0)}{\Delta(0)} \quad (3)$$

$\Delta(0)$ and $M_{ji}(0)$ are the determinant and cofactor of (j,i)-th element of unperturbed coefficient matrix $[C]$ respectively. x_i is the exact value of fractional changes in permittivity of the model cells with respect to saline water.

$$x_i = (\epsilon_{\text{model}} - \epsilon_{\text{homo}}) / (\epsilon_{\text{homo}} - 1)$$

where ϵ_{homo} and ϵ_{model} are the complex permittivity of i-th cell of homogeneous medium and experimental model respectively. Here m does not signify total number of cells in the target area rather number of cells illuminated by k-th transmitting beam. So, if i-th cell is outside the coverage area of k-th transmitter, at the starting of iteration in Eqn. 3, $E_i = E_i' = 0$, and then incremental field at the i-th cell will depend only upon the fields for cells, those are under the coverage area of transmitter k. This procedure is repeated for rest of the transmitter positions. For each time, iteration is performed with new value of $E_i' = (E_i + \Delta E_i)$ and continued until the difference between two successive values of incremental fields (ΔE_i) for all cells become less than 0.1% of that incremental field. Then the change of

fields at the receiver location (for transmitting beam k) is obtained by the equation:

$$\Delta E_R(k) = \sum_{j=1}^m x_j E_j' \frac{M_{j,R}(0)}{\Delta(0)} \quad (4)$$

Since $x_i = 0$ for all receiver cells as they are located in saline water region.

Therefore, measured field at the receiving point in presence of the model will be obtained after adding ΔE_R with field at the same receiver location for the same transmitting beam in absence of the model. The same procedure is repeated for 24 transmitter positions to simulate the measured data required for tomographic imaging at a frequency of 1 GHz.

The difference of homogeneous field and perturbed field is the measure of requisite reconstructed complex permittivity value. This can be written as :

$$E_{Rml}(k) - E_{Roi}(k) = \sum_{j=1}^m x_j E_j' \frac{M_{j,R}(0)}{\Delta(0)} \quad (5)$$

Where $E_{Rml}(k)$ and $E_{Roi}(k)$ denotes the scattered field intensity at the l-th receiver location for the k-th beam in the inhomogeneous and homogeneous numerical model respectively and x_j is the requisite fractional change of complex permittivity with respect to the homogeneous medium water (76-j40). If there are $k=1, 2, \dots, q$ numbers of beam passing through a particular cell, then from a set of q number of equations, the values of (x_j) can be calculated by using Eqn. (5) and SIRT technique. The same procedure is adopted for all the cells one by one in the target region.

Here it is assumed that the beam axis of the k-th beam passes through the j-th cell and all the cells contained within its beam width are equally responsible in producing some change at the l-th receiver location. All other rays passing through that cell are examined one after another and resultant correction is the average of all that obtained from different rays.

The iteration is continued until minimum rms deviation δ of the theoretical output field from the estimated one corresponding to different rays is obtained [6].

3. Comparative study between existing field measurement algorithm and its modified form

3.1. Numerical model

A semi human-sized model of 360 cells, each of 1 sq. cm. in area is chosen for verifying existing field measurement [6] and modified field measurement technique on Exact SIRT algorithm [6]. It is a complex biological model consisting of different internal structures having complex permittivity identical to those observed in different human organs viz. kidney (48-j12), muscle (50-j23), muscle type material (40-j23) and fat (25-j5). The model is surrounded by saline water region having 340 cells, each of same 1 sq. cm. area. The total area of model and saline water region is 28x25 sq. cm.

The model is illuminated by 15x15 quarter wave dipole array antenna shown in the figure 3 with a beam width of 6° operating at 1 GHz [5]. 20 half wave dipoles are used as receivers and placed at the opposite side of the transmitting antenna. To reduce the antenna length and multipath propagation exterior to the target, the transmitting antenna, receiving antenna and the biological target should be immersed in saline water. Wavelength in this medium is reduced to 3.14 cm due to large dielectric constant of value 76 in saline water. This also imposes impedance matching at the water target interface as water is the primary composition of the biological medium.

Due to large attenuation in water the target should be placed in the reactive zone of the array. As a result of which the radiation by elements of the array are not parallel to each other and hence are not in phase at a point on the axis perpendicular to array plane due the path difference. Hence amplitude and phase conjugation is highly required and this is realized by placing the array antenna in a spherical surface with focal length of 50 cm.

3.2 Figures and Tables

Numerical calculations are simulated using Force 209 FORTRAN [11] and depicted using colour gradation scale

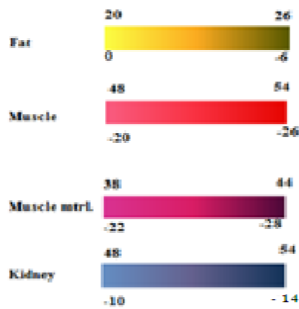


Figure 1: Gradation scale used for the imaging

I. Reconstruction of normal model

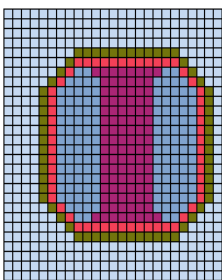


Figure 2.1

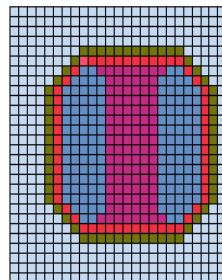


Figure 2.2

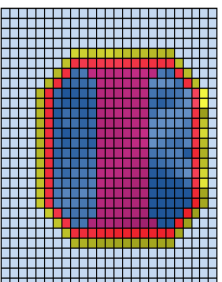


Figure 3.1

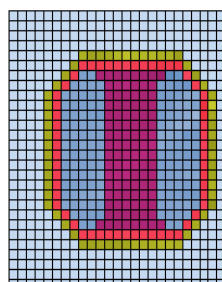


Figure 3.2

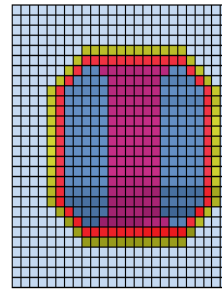


Figure 4.1

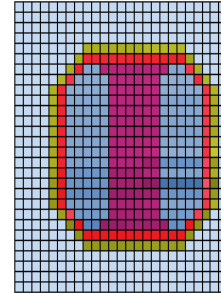


Figure 4.2

Fig. 2.1 & Fig.2.2: Real and imaginary values of complex permittivity for normal Model respectively; Fig.3.1 & Fig.3.2: reconstructed real and imaginary values of complex permittivity for normal model respectively (using previous field measurement technique); Fig.4.1 & Fig.4.2: reconstructed real and imaginary values of complex permittivity for normal model respectively (using modified field measurement technique).

II. Reconstruction of diseased model(Method –I)

The model under study is the same as that considered in earlier case, except its kidney region is affected by some disease and hence characterized by a different value of complex permittivity (52.8-j13.2) [12] where as for normal kidney it is assumed as (48-j12).

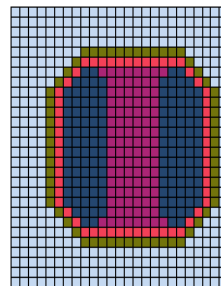


Figure 5.1

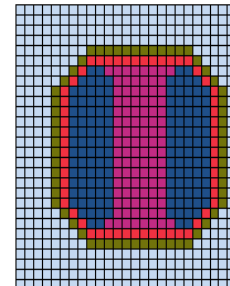


Figure 5.2

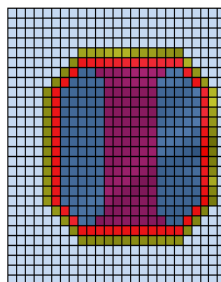


Figure 6.1

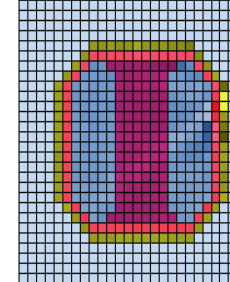


Figure 6.2

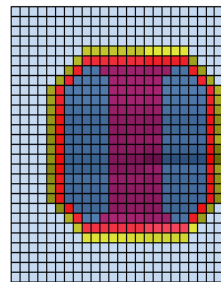


Figure 7.1

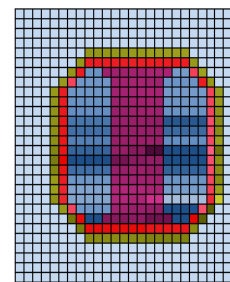


Figure 6.2 Figure 7.2

Fig.5.1 & Fig.5.2: Real and imaginary values of complex permittivity for diseased Model respectively; Fig.6.1 & Fig.6.2: reconstructed real and imaginary values of complex permittivity for diseased model respectively (using previous field measurement technique and method-I); Fig.7.1 & Fig.7.2: reconstructed real and imaginary values of complex permittivity for normal model respectively (using modified field measurement technique and method-I).

III. Reconstruction of diseased model(Method-II)

Though the reconstructed image obtained by Method-I indicates the location of a diseased organ, a more effective procedure for studying diseased organ will be to perform iteration on this suspected organ only assuming other organs are in their normal state.

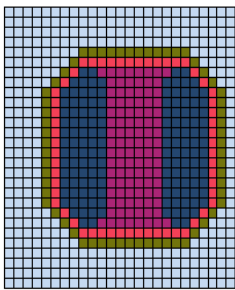


Figure 8.1

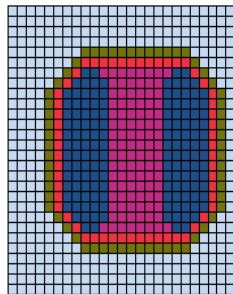


Figure 8.2

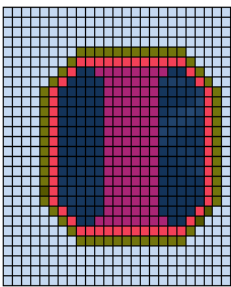


Figure 9.1

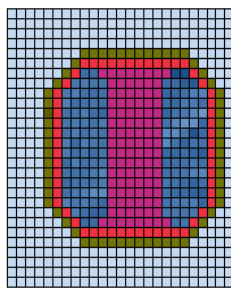


Figure 9.2

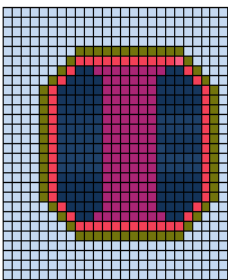


Figure 10.1

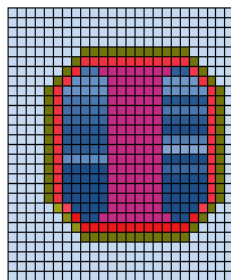


Figure 10.2

Fig.8.1 & Fig.8.2: Real and imaginary values of complex permittivity for diseased model respectively; Fig.9.1 & Fig.9.2: reconstructed real and imaginary values of complex permittivity for diseased model respectively (using previous field measurement technique and method-II); Fig.10.1 & Fig.10.2: reconstructed real and imaginary values of complex permittivity for diseased model respectively (using modified field measurement technique and method -II)

TABLE I
Average values of reconstructed complex permittivity of different organs of normal model

Different Organs of Model	Average Values of Complex Permittivity of Different Organs		
	Normal Model	Reconstructed Normal Model	
		Using Previous Field Measurement Technique	Using Modified Field Measurement Technique
Fat	25-j5	22.43-j3.00	22.57-j3.12
Muscle	50-j23	51.15-j23.82	51.28-j23.87
Muscle material	40-j23	39.60-j23.82	39.49-j23.87
Kidney	48-j12	48.77-j11.13	48.61-j11.16
Water	76-j40	76-j40	76-j40

TABLE II
Average values of reconstructed complex permittivity of different organs of diseased model (Method-I)

Different Organs of Model	Average Values of Complex Permittivity of Different Organs		
	Diseased Model	Reconstructed Diseased Model(Method-I)	
		Using Modified Field Measurement Technique	Using Modified Field Measurement Technique
Fat	25-j5	23.90-j3.49	22.72-j3.92
Muscle	50-j23	52.63-j24.24	51.90-j24.68
Muscle material	40-j23	41.29-j24.24	41.02-j24.68
Kidney	52.8-j13.2	50.49-j11.49	50.30-j11.99
Water	76-j40	76-j40	76-j40

TABLE III

Average values of reconstructed complex permittivity of different organs of diseased model (Method-II)

Different Organs of Model	Average Values of Complex Permittivity of Different Organs		
	Diseased Model	Reconstructed Diseased Model(Method-II)	
		Using Previous Field Measurement Technique	Using Modified Field Measurement Technique
Fat	25-j5	25-j5	25-j5
Muscle	50-j23	50-j23	50-j23
Muscle material	40-j23	40-j23	40-j23
Kidney	52.8-j13.2	53.98-j12.44	53.83-j12.44
Water	76-j40	76-j40	76-j40

4. Conclusion

The reconstructed image of normal model obtained by using modified field measurement technique is slightly better (average accuracy 99.89%) than that obtained by earlier field measurement technique (average accuracy 99.75%).

In case of diseased kidney model the real part of the reconstructed images obtained by using previous field measurement technique and with the proposed one show some deviations of complex permittivity from their normal values which create an erroneous suspense of being attacked by some ailment. But, now, difficult to accurately locate the region from where the disease originates. The reconstructed image for imaginary part of diseased kidney region obtained by using modified field measurement technique is able to indicate the affected portion, but not so accurate because complex permittivity of other region also deviates from their normal values due to the averaging effect of SIRT method itself.

The reconstructed image obtained by using exact algorithm method-II has been improved with modified field measurement technique showing better resemblance with the diseased model and appears to be very promising for detection of diseased portion in its early stage even in larger model with large perturbation (not more than 20%).

REFERENCES

- [1] A N Datta & B. Bondopadhyay, *Int J Electronics*, Vol. 58, No.5 ,pp.831-832, 1985.
- [2] A. N. Datta & B. Bandyopadhyay, An Improved SIRT-Style Reconstruction Algorithm for Microwave Tomography, *IEEE Transactions on Biomedical*

Engineering, Vol. BME-32, NO. 9, pp.719-723, September 1985.

- [3] A N Datta & B. Bondopadhyay, *Proc. of IEEE*, Vol. 74, pp.604-606, 1986.
- [4] A N Datta & B. Bondopadhyay, *Innov. Tech Biol. Med*, Vol. 8, pp.409-416, 1987.
- [5] K.Purkait & A.N.Datta, An Improved form of Iterative Reconstruction Algorithm for First Order and Second Order Microwave Image Reconstruction, *Indian Journal of Pure & Applied Physics*, CSIR, Vol.34, pp.420-424, June 1996.
- [6] K.Purkait & A.N.Datta, An Exact Algorithm for Microwave Tomography, presented at *symposium HOT-2003, INRAPHEL, C.U.* 3rd-5th Feb.2003.
- [7] J.H. Richmond, *IEEE Trans. Antennas Propag. Vol. AP-B*, pp 334-341, 1965.
- [8] K.D. Prasad, *Antenna & Wave propagation*(ISBN No: 81-7684-025-4, 3rd edition, 2007).
- [9] K.T. McDonald, *Radiation in the Near Zone of a Centre -Fed Linear Antenna (June 21, 2003)* (http://puhep1.princeton.edu/~mcdonald/examples/line_antenna.pdf).
- [10] K.T. McDonald, *The Fields of a Short, Linear Dipole Antenna If There Were No Displacement Current*(Joseph Henry Laboratories, Princeton University, Princeton, NJ 08544, July 5 , 2006).
- [11] Force 209 FORTRAN Compiler, www.lepsch.com.
- [12] Herman Schwan and Kenneth Foster, RF-field interaction with biological systems: Electrical properties and biophysical mechanisms, *Proc. of the IEEE*, 68(1), 1980.



Dr. Kabita Purkait has done B.Tech in Radiophysics and Electronics from Calcutta University in the year 1989 and M.Tech in Radiophysics and Electronics from Calcutta University in the year 1991. She has got CSIR fellowship as Senior Research fellow and performed

research work on Microwave Tomography. She joined as a lecturer in Electronics and Telecommunication Engineering, Jnan Ch. Ghosh polytechnic in 1999. She was awarded Ph.D (Tech) from Calcutta University in 2006. Currently she is working as Associate professor in Deptt. of Electronics and Communication in Kalyani Govt. Engineering College. Her present interest is in the development of microwave scanner and subsequent reconstruction algorithm in Microwave Tomography.



Kalyan Adhikary has done B.Tech in Electronics and Communication Engineering from West Bengal University of Technology in the year 2005 and pursuing his M.Tech in Electronics and Communication Engineering from West Bengal University of Technology. His

present interest is in efficient reconstruction algorithm for biomedical imaging system.

Comparative Analysis of Performance and Emission Characteristics of Neem Oil Using 3 And 4 Holes Injection Nozzle on DI Diesel Engine

Revansiddappa Byakod¹, Prasanna Phatate¹, Vinodkumar Kamble¹, Sharath Babu¹,
M. C Navindgi²

¹UG Students, Department of Mechanical Engineering, PDA College of Engineering, Gulbarga-585102,

²Associate Professor, Department of Mechanical Engineering, PDA College of Engineering, Gulbarga-585102,

ABSTRACT

Bio-diesel is one of the most promising alternatives for diesel needs. Use of edible oil may create shortage of oil seeds for daily food, which necessitates identification of new kinds of non-edible vegetable oil. With this objective, the present work has focused on the performance of neem non-edible vegetable oils and its blend with diesel.

In the present experimental investigation 5.2 kW diesel engine AV1 Single Cylinder water cooled, Kirloskar Make tested for blends of diesel with Castor and Neem Biodiesel. The viscosity of neem oil is reduced first by blending with diesel in 25/75%, 50/50%, 75/25%, and 100% on the volume basis, then analyzed and compared with diesel. The performance and emission characteristics of blends are evaluated at variable loads of 0, 1, 2, 3, 4, 5kw at constant rated speed of 1500rpm and results are compared with diesel. The tests were conducted for injection pressure of 160 bar with fuel injector of 3 holes and 4 holes. In this investigation it is found that the nozzle having 4 holes gives good performance results and lower rate of emissions. Thus the nozzle with 4 holes can be used preferably than the 3 holes nozzle.

Key words: Performance, emission characteristics, Neem oil, Injectors, diesel Engine

INTRODUCTION

Petroleum based fuels play a vital role in rapid depletion of conventional energy sources along ¹with increasing demand and also major contributors of air pollutants. Major portion of today's energy demand in India

Properties	Diesel	Neem oil
Calorific Value in kJ/kg	42500	37200
Density of Oil in Kg/m ³	0.8344	0.890
Kinematic Viscosity at 40°C in cSt	4.3	5.7
Flash point in °C	55	152
Fire point in °C	65	158

is being met with fossil fuels. Hence it is high time that alternate fuels for engines should be derived from indigenous sources. As India is an agricultural country, there is a wide scope for the production of vegetable oils (both edible and non-edible) from different oil seeds. The present work focused only on non-edible oils as fuel for engines, as the edible oils are in great demand and far too expensive. The past work revealed that uses of vegetable oils for engines in place of diesel were investigated. Though the concerned researchers recommended the use of vegetable oils in diesel engines, there was no evidence of any practical vegetable oil source engines.

The fuel injection performance is important for low emission combustion. During the last 20 years the maximum fuel injection pressure in the available systems has increased rapidly. Today injection pressures of about 250 bar are used and in the near future even higher pressures may be available. The development of electronic injection control has led to an increasing controllability of the injection event. Precise control of the fuel pressure, injection phasing and the use of multiple injections has increased the possibilities to influence the combustion process. This increased controllability together with the injection pressure increase is responsible for a large part of the emission reductions that have occurred in diesel engines during the past 20 years. Current combustion chambers for passenger car and truck diesel engines typically utilize direct injection system with a fairly shallow piston bowl and a central fuel injector with 5 – 8 holes. This paper outlines the main aspects of neem biodiesel as fuel in CI engine operated with fuel injector having 3 and 4 holes and injection pressure of 160 bar.

PROPERTIES OF OILS

In this project, neat vegetable oil such as neem oil is selected for experimentation. The properties of the oil are such as density, viscosity, flash point and fire point are determined using Hydrometer, Redwood Viscometer and Pensky Martin's Apparatus respectively. Table1 shows the properties of vegetable oil and diesel.

Table1: Properties of Neem and Diesel

EXPERIMENTAL SETUP

The setup consists of single cylinder, four stroke, diesel engine connected to eddy-current dynamometer for variable loading. It is provided with necessary equipment and instruments for combustion pressure, fuel injection pressure and crank-angle measurements. These signals are interfaced to computer through engine indicator for Pθ-PV diagrams and fuel injection pressure- crank angle diagram. Windows based Engine Performance Analysis software package is fully configurable. Pθ-PV diagram and performance curves are obtained at various operating points. Provision is also made for interfacing airflow, fuel flow, temperatures and load measurements with computer. The set has stand-alone type independent panel box consisting of air box, fuel tank, manometer, fuel measuring unit, differential pressure transmitters for air and fuel flow measurement, process indicator and engine indicator. The setup enables study of engine for brake power, indicated power, frictional power, BMEP, IMEP, brake thermal efficiency, indicated thermal efficiency, Mechanical efficiency, volumetric efficiency, specific fuel consumption, A/F ratio and heat balance.

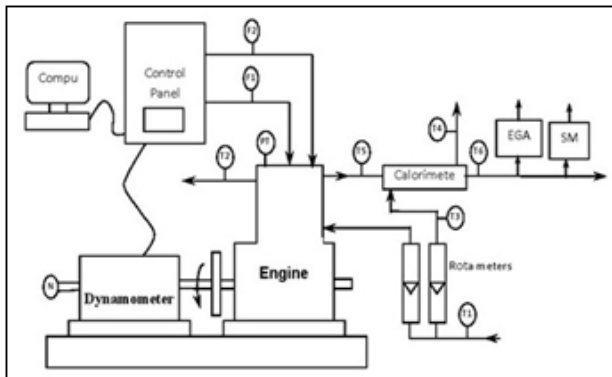


Figure1: Schematic diagram of Experimental Setup

Variable load tests are conducted for 0, 1, 2, 3, 4, and 5 KW at a constant rated speed of 1500 rpm. with fuel injection pressure of 160 bar, and cooling water exit temperature of 60°C. All observations recorded were replicated thrice to get a reasonable value.

The performance characteristics of the engine are evaluated in terms of brake thermal efficiency, brake specific fuel consumption (BSFC), brake specific energy consumption (BSFC), and exhaust temperature. Two gas exhaust gas analyse and smoke opacity meter are used to find the emission characteristics. These performance and emission characteristics are compared with the results of baseline diesel.

ENGINE SPECIFICATIONS:

Manufacturer	Kirloskar oil engines Ltd., India
Model	TV-SR, naturally aspirated
Engine	Single cylinder, DI
Bore/stroke	87.5mm/110mm

C.R.	16.5:1
Speed	1500r/min, constant
Rated power	5.2kw
Working cycle	four stroke
Injection pressure	200bar/23 def TDC
Type of sensor	Piezo electric
Response time	4 micro seconds

RESULT AND DISCUSSION

1. Brake thermal efficiency:

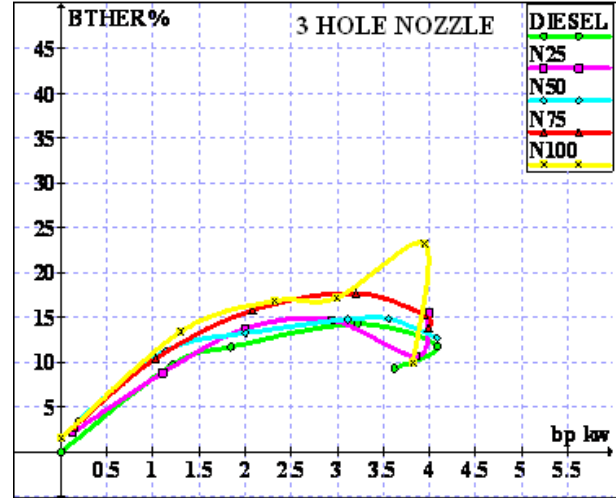


Fig.1(a) Break thermal efficiency vs bp with 3 hole nozzle

PT	Pressure transducer
N	Rotary encoder
Wt	Weight
F1	Fuel flow
F2	Air flow
F3	Jacket water flow
F4	Calorimeter water flow
T1	Jacket water inlet temperature
T2	Jacket water outlet temperature
T3	Calorimeter water inlet temperature = T1
T4	Calorimeter water outlet temperature
T5	Exhaust gas to calorimeter temperature
T6	Exhaust gas from calorimeter temperature

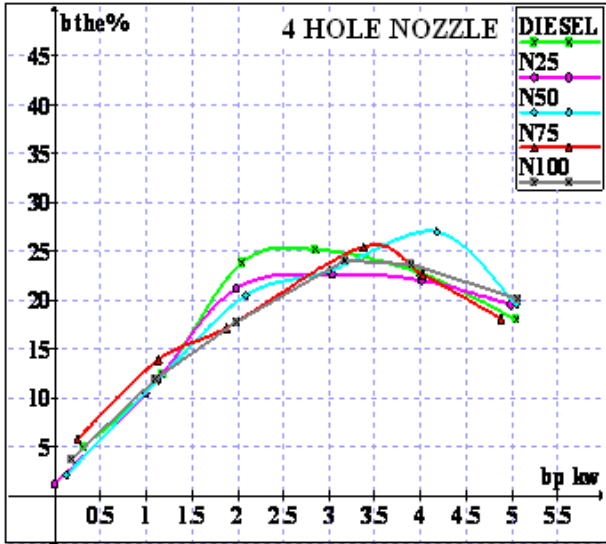


Fig.1(b) Break thermal efficiency vs bp with 4 hole nozzle

Figure 1(a) and (b) shows the comparison of break thermal efficiency with 3 hole nozzle and 4 hole nozzle for neem oil and its blends with respect to brake power. It was noticed that break thermal efficiency of 18.02% for diesel and 20.17% for N100 for 3 hole nozzle, and 14.88% for diesel and 25.08% for N25 was obtained for 4 hole nozzle. The main reason for increase in the brake thermal efficiency is due to more homogeneous mixture formation and spray characteristics.

2. Indicated thermal efficiency:

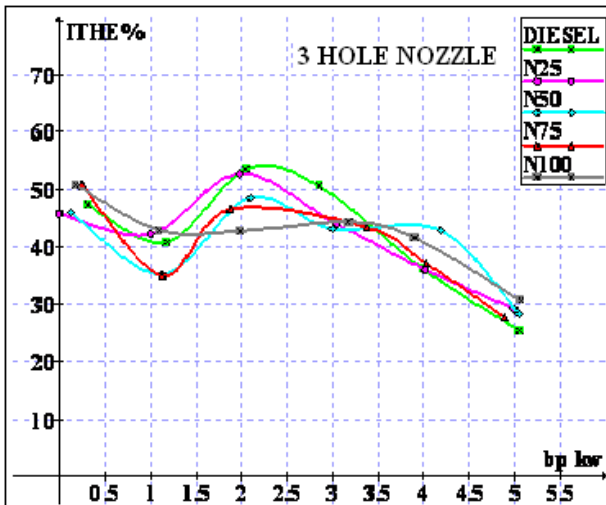


Fig.2(a) Indicated thermal efficiency v/s bp with 3 hole nozzle

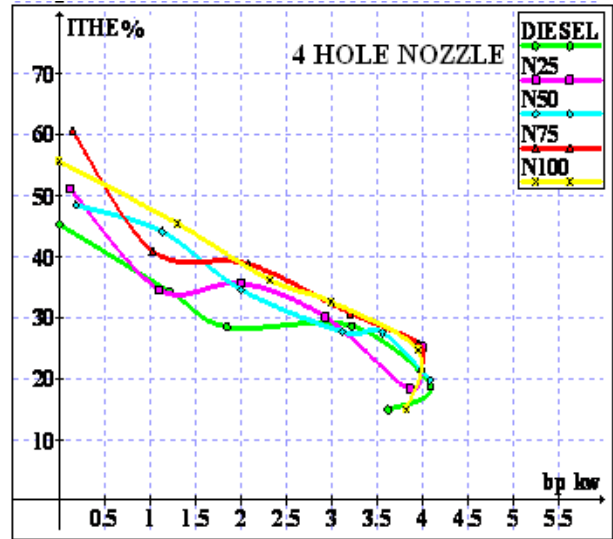


Fig.2(b) Indicated thermal efficiency v/s bp with 4 hole nozzle

Figure 2(a) and (b) shows the comparison of indicated thermal efficiency with 3 hole nozzle and 4 hole nozzle for neem oil and its blends with respect to brake power. It was noticed that indicated thermal efficiency of 25.47% for diesel and 30.62% for N100 for 3 hole nozzle, and 14.88% for diesel and 25.08% for N25 was obtained for 4 hole nozzle.

3. Specific fuel consumption:

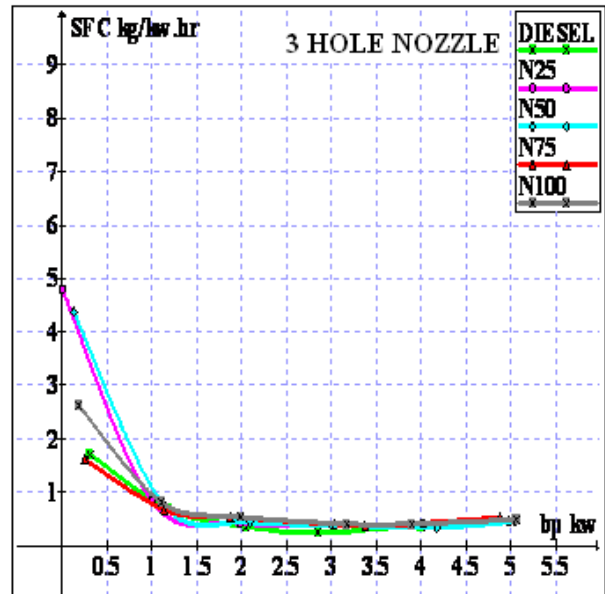


Fig.3(a) Specific fuel consumption v/s bp with 3 hole nozzle

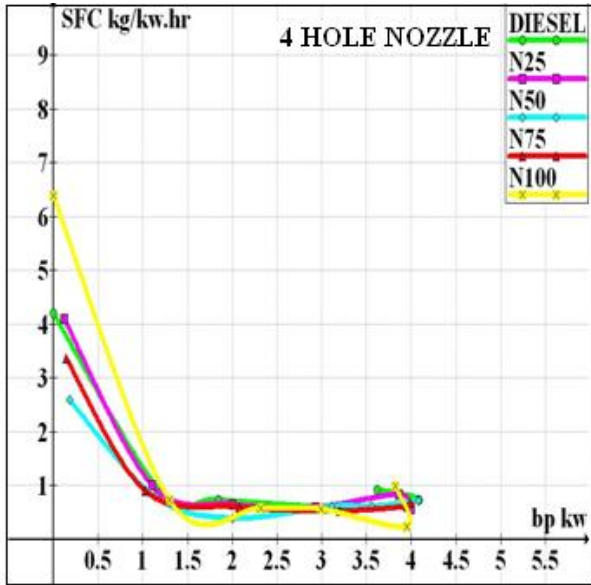


Fig.3 (b) Specific fuel consumption v/s bp with 4 hole nozzle

Figure 3(a) and (b) shows the comparison of specific fuel consumption of 3 hole nozzle and 4 hole nozzle for neem oil and its blends with respect to brake power. It was noticed that SFC of 0.47% for diesel and 0.44% for N25 for 3 hole nozzle, and 0.91% for diesel and 0.56% for N25 was obtained for 4 hole nozzle which is maintained due to presence of oxygen in the bio fuels.

4. Carbonmonoxide emission:

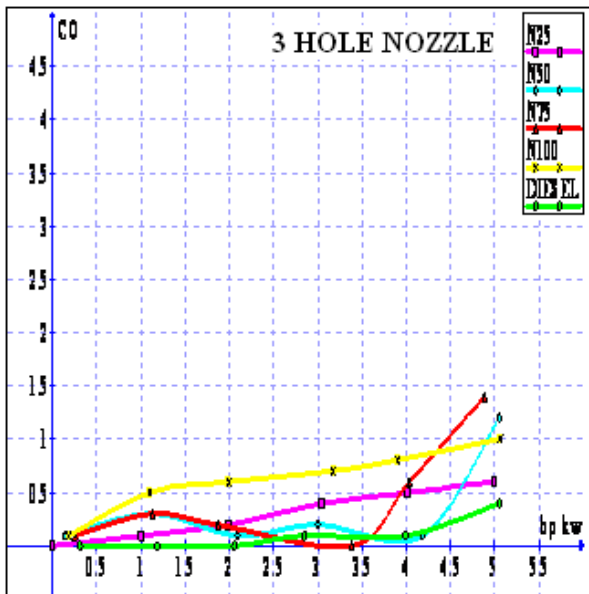


Fig.4(a) Carbon monoxide v/s bp with 3 hole nozzle

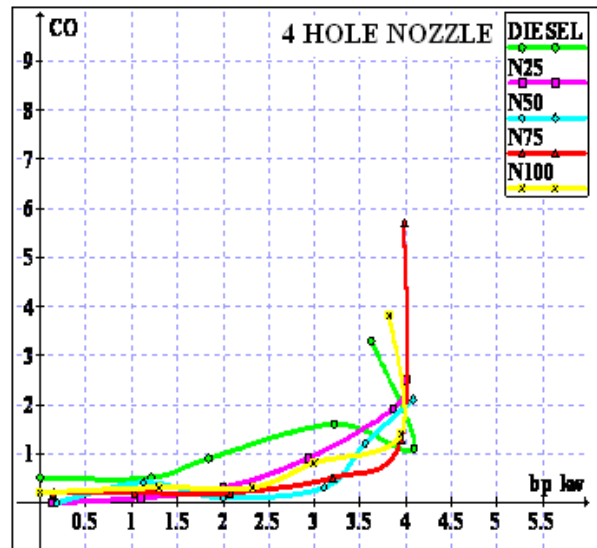


Fig. 4(b) Carbon monoxide v/s bp with 4 hole nozzle

Figure shows the comparison of carbon monoxide for 3 hole and 4 hole nozzle for neem oil and its blends with respect to brake power. It was noticed that Co emission of 0.4% volume for diesel and 0.6% volume for N25 for 3 hole and 3.3% volume for diesel and 2.1% volume for N50 for 4 holes nozzle was obtained which is maintained due to presence of oxygen in the bio fuels.

5. Hydro-carbon emission:

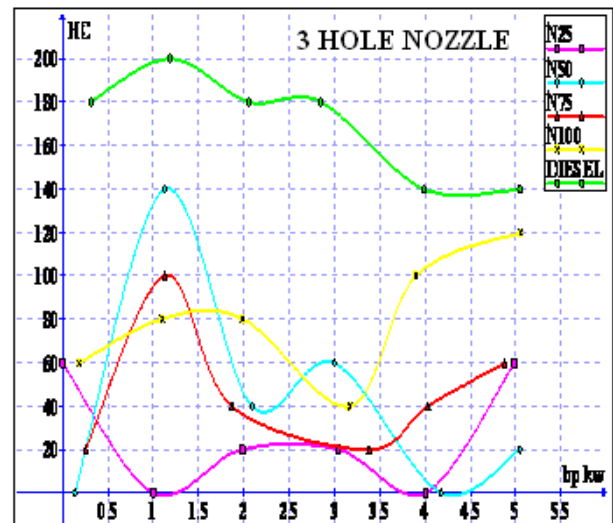


Fig 5(a) HC v/s bp with 3 hole nozzle

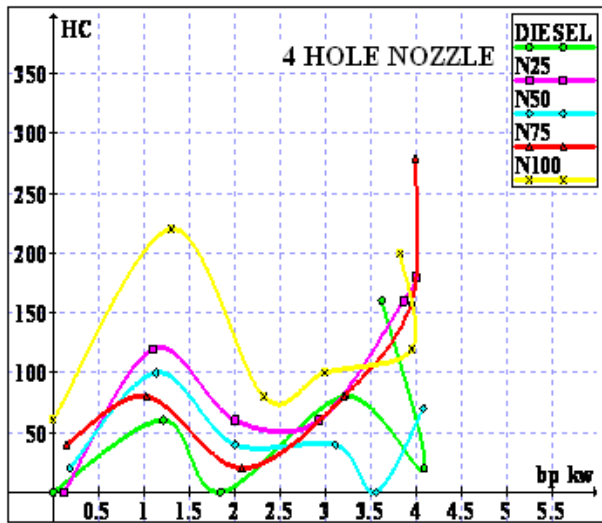


Fig 5(a) HC v/s bp with 4 hole nozzle

Figure shows the comparison of Hydrocarbon for 3 hole and 4 hole nozzle for neem oil and its blends with respect to brake power. It was observed that diesel has the maximum rate of hydrocarbon 140 ppm and hydrocarbon of 20 ppm for N50 for 3 hole nozzle among the tested fuels. It is also found that the hydrocarbon of 160 ppm for diesel and 70 ppm for N50 was obtained for 4 hole nozzle.

CONCLUSION

Experimental investigations are carried out on a single cylinder CI diesel engine to compare the performance and emission characteristics of neem oil using 3 and 4 holes nozzle. The performance characteristics of neem biodiesel and its blends are evaluated with 3 and 4 holes nozzle at 160 bars. From the above investigations, the following conclusions are drawn.

- The brake thermal efficiency for 3 hole nozzle is lower than that of 4 hole nozzle.
- The indicated thermal efficiency for 3 hole nozzle is also lower than that of 4 hole nozzle.
- The specific fuel consumption for 3 hole nozzle is slightly lower than the nozzle of having 4 holes.
- The emission of CO is more in 4 hole nozzle as compared with 3 holes nozzle.

- The amount of un-burnt hydrocarbons is more in 4 holes nozzle as compared with 3 holes nozzle.

Hence, from above investigation it is concluded that the nozzle which is having 4 holes gives good performance results but high rate of emissions. Thus the nozzle with 4 holes can be used preferably for good performance than the 3 holes nozzle.

REFERENCES

- 1]. Rao GAP, Mohan PR. Effect of supercharging on the performance of a diesel engine with neem oil. *Energy Covers Manage* 2003; 44:937-44.
- 2]. Nwafor OMI, Rice G. Performance of rapeseed oil blends in a diesel engine. *Appl Energy* 1996; 54(4):345-54.
- 3]. C.E. Goering, A.W. Schwab et al., "Fuel Properties of Eleven Vegetable Oils", *Trans. ASAE*, 25 (4-6), 1982, PP: 1472-1477.
- 4]. M. C. Navindgi, Dr. Maheswar Dutta, Dr. B. Sudheer Prem Kumar "Effect of Varying Operating Conditions on Performance of CI Engine with Different Blends of Methyl Ester of Neem Oil" National Conference on Emerging Technologies in Renewable Energy organized by GND Engineering College, Bidar
- 5]. Srinivas, R.P., and Gopalakrishnan, K.V., "Vegetable Oils and their Methyl esters as Fuels for Diesel Engines", *Indian Journal of Technology*, (29)PP: 292-297, 1991
- 6]. Nag raja. A.M, Prabhu kumar.G.P, 2005, performance of Diesel, Neat Biodiesel and 20% Biodiesel – A comparative study. *Proceedings of 19 The National Conference on I. C. engines and combustion*, Annamalai University, PP: 503-508.
- 7]. Ramdas AS, Jayaraj S, Muraleedhran C, 2004, "use of vegetable oils on IC Engines fuels – A review". *Renewable .Energy*, (29) PP: 727 -742.
- 8]. G Amba Prasad Rao and P Rama Mohan. .Effect of Supercharging on the Performance of a DI Diesel Engine with Vegetable Oils, *International Journal of Energy Conversion and Management*, vol 44, no 6, April 2003, pp 937-944.
- 9]. Ramesh and Sampathrajan, "Investigation on Performance and Emission Characteristics of Diesel Engine with Neem Biodiesel and Its Blends", *Agricultural Engineering International: the CIGR journal*. Manuscript EE 07 013 Vol X March 2008.

Processing and Characterization of Aluminium-Silver Coated MWCNT Composite Made By Vacuum Hot Pressing

UNNIKRISHNAN. R¹, RENJITH. M. S², ANEESH KUMAR. J³, T. KRISHNAKUMAR⁴

1. DEPARTMENT OF MECHANICAL ENGINEERING, GOVERNMENT ENGINEERING COLLEGE, THRISSUR, INDIA,
2. DEPARTMENT OF NANO SCIENCE AND TECHNOLOGY, ANNA UNIVERSITY, CHENNAI, INDIA.
3. DEPARTMENT OF MECHANICAL ENGINEERING, LOURDE MATHA COLLEGE OF SCIENCE AND TECHNOLOGY, TRIVANDRUM, INDIA.
4. DEPARTMENT OF MECHANICAL ENGINEERING, GOVERNMENT ENGINEERING COLLEGE, THRISSUR, INDIA.

ABSTRACT

In this research work, Al - 1wt% silver coated multi wall carbon nanotube (MWCNT) composite have been processed using powder metallurgy technique. In order to distribute CNT uniformly in the aluminum matrix high energy ball milling is required. . It was found that excessive milling can lead to carbide and alumina formation. So to reduce the milling time, the surface of CNT is modified by coating it with silver. In order to obtain surface modification of carbon nanotubes, electroless coating of silver has been given to carbon nanotubes after liquid phase oxidation, sensitization and activation. Since Al / 1wt% MWCNT could not be sintered, Silicon has been added as sintering agent. Al along with 1wt% silver coated MWCNT and 9wt% of Silicon is milled together in a planetary ball mill for 4 hour. The composite powders were compacted using Vacuum Hot Pressing (VHP). CNT dispersion, phase analysis and powder morphology of the composite is investigated using XRD, SEM and optical microscopy. Density of the composite is measured using Archimedes density principle. Hardness of the composite is measured using Brinell hardness tester.

Keywords: Activation, Carbon nanotube, Electroless coating, Sensitization, Vacuum hot pressing.

1. INTRODUCTION

Nanostructured materials have attracted many researchers due to their outstanding mechanical and physical properties. One example is Carbon Nanotube (CNT) reinforced composites. Most of the researchers have focused on using CNTs to reinforce polymeric and ceramic matrices. A single-wall carbon nanotube, i.e., a nanotube made of only one graphite sheet rolled-up in cylinder, has a young's modulus as high as 1.8TPa and a tensile strength as high as 63GPa, which is one to two orders of magnitude superior to best known steels. Multi-wall nanotubes display lower but still exceptional mechanical properties, and they are easier to synthesize. These superior mechanical properties combined with low density generate several outlets for a composite reinforced by CNTs. CNT-reinforced metallic composites are quickly emerging as attractive materials combining light weight with superior strength and stiffness. Potential application includes automobile and aerospace industry where the decrease of fuel consumption by weight reduction is a priority.

In this research work powder metallurgy techniques were employed to produce a CNT composite with unique mechanical properties. 99.7% purity Aluminium (Al) powder along with multi-wall carbon nanotube of purity greater than 90% having diameter of 5nm and length 20 – 40 microns is used. CNT have a strong tendency to form bundles and agglomerate. So the composite powder were ball milled, where particles are repeatedly fractured and welded and CNT is uniformly dispersed with in Al matrix. The excessive milling of Al / CNT composite powder can lead to oxidation of Al and formation of aluminium carbide which can hinder the mechanical properties. So to avoid this, the surface of CNT is coated with silver using electroless technique. . Since CNT is non-reactive some pre-treatments such as liquid-phase oxidation, sensitization and activation were done on the surface of CNT before coating it with silver. Since Al / 1wt% silver coated CNT milled powder could not be sintered, Silicon is added as the sintering agent. Al along with silver coated MWCNT and Si is milled together for 4hrs in a planetary ball mill. The composite powders were compacted using vacuum hot pressing.

2. EXPERIMENTAL PROCEDURE

2.1 ELECTROLESS COATING OF MWCNT WITH SILVER

For surface modification of carbon nanotubes, electroless coating of silver has been given to carbon nanotubes surface. Like graphite, the surface of carbon nanotube has low chemical reactivity and does not act as catalyst for the deposition of silver and therefore no metal coating take place. Therefore some pretreatments are required to improve chemical reactivity of CNT which includes liquid phase oxidation, sensitization and activation [1]. Liquid phase oxidation is done by immersing raw MWCNT in a mixture of H₂SO₄ and HNO₃ at 1:3 ratios. During sensitization oxidized MWCNT is immersed in a mixture of aqueous solution of 0.1M SnCl₂ and 0.1M HCl. During activation the sensitized MWCNT is immersed in a mixture of aqueous solution of

0.0014M PdCl₂ and 0.25M HCl. After each step the mixture is agitated using ultrasonic method for one hour. The agitated mixture is washed and then filtered using distilled water. The filtered MWCNT is then heated at 100^oC in an oven.

Finally, the activated carbon nanotubes were introduced in to the electroless bath kept in an alumina crucible. The electroless bath was prepared by mixing the solution I, II and III given in table I. The pH of the electroless bath is 10. The composition of the solution I, II and III and reaction condition for silver coating is given in Table 1. Nanotubes kept in the electroless bath was sonicated at room temperature for 3 hours and kept at room temperature for 30 hours. After coating treatment nanotubes were washed with distilled water and filtered and dried at 100^oC for 3 hours. All the process parameters used in this work were optimized by surface coating of graphite. During electroless plating, the Pd catalytic center would reduce silver ions present in the solution to neutral silver atoms, which get coated on the surface of CNT. The silver particles grew laterally and vertically and form a continuous layer on the surface of CNT.

Table 1 Bath composition for electroless plating

Solution	Composition	Time
Solution I	Sugar - 4-6 Gm Tartaric acid - 0.6gm C ₂ H ₅ OH-10 - 15 cc	
Solution II	AgNO ₃ - 4-6 gm NH ₄ NO ₃ - 6-8gm H ₂ O - 120cc	
Solution III	NaOH - 10-12 gm H ₂ O - 120 cc	
Electroless Ag deposition	Solution I + Solution II + Solution III.	4 -5 hrs

2.2 PREPARATION AND COMPACTION OF COMPOSITE POWDERS.

According to Esawi and Morsi [2] aluminium particles kept on welding together with time forming spherical balls. These large particles would pose processing problems during compaction and extrusion. Also CNT has a tendency to form bundles and to get agglomerated in the metal matrix. So high energy ball milling was done so that particles are repeatedly fractured and also to disperse CNT uniformly in the metal matrix. Here Al along with 1wt% silver coated MWCNT is used. 110gm of Al containing 1wt% silver coated MWCNT and 10gm of silicon (to achieve a weight fraction of 9wt%) as sintering agent is milled together using planetary ball mill at 120 rpm for 4 hours in a cylindrical vial containing tungsten carbide balls with ball-to-powder ratio 10:1. The composite powders were compacted using vacuum hot pressing. Vacuum hot pressing is done using an industrial vacuum hot press having a maximum load capacity of 250T and temperature upto 2000^oC. The powders were compacted in graphite cylindrical dies having bore diameter 30mm. The compaction was done at a load of 10T and sintering temperature of 600^oC. The entire process is done at very high vacuum of 10⁻⁵ mbar.

2.3 CHARACTERIZATION AND TESTING

In order to investigate the properties and the quality of produced sample, the physical, mechanical, and microstructural properties had to be investigated. The physical property was determined by measuring the density of the composites and comparing it with theoretical density. Hardness was used to evaluate the mechanical property. The microstructure was investigated by employing optical microscopy and XRD. XRD is done using panalytical X-Pro diffractometer. It is mainly used for phase analysis and to find out the dispersion of CNT in aluminium matrix. The optical microscope observation of compacted samples was made under Olympus microscope. Hardness of the compacted specimen was measured using universal hardness tester. The diameter of ball indenter used is 2.5mm at a load of 31.25kgf. The dwell time was 15 seconds. From each specimen five indentations are made at different sites and the average is taken as final result. The actual density of composite is measured using Archimedes density principle. It is compared with theoretical density to find out relative density of the composite.

3. RESULT AND DISCUSSION

3.1 MICROSTRUCTURE ANALYSIS

Figure 1 shows the microstructure images of Al / 1wt% silver coated MWCNT / 9wt% Si compacted using vacuum hot pressing at 600^oC. The grey phase denotes the presence of aluminium and dark phase denote the presence of CNT welded to aluminium matrix. Comparing with the microstructure of compact made using uncoated CNT, the uniform distribution of CNT is evidently

seen in compact made using silver coated CNT. It also reveals that CNT's are embedded in the aluminium particle. The microstructure reveals a typical sintered aluminium structure. From the microstructure it is evident that CNT is distributed along the grain boundaries. The microstructure also reveals that milling time can be reduced by using silver coated CNT because Silver coated CNT disperse more uniformly in less milling time which reduces alumina and carbide formation. Some porosities are also present which is clearly revealed at microstructure images taken at higher magnification.

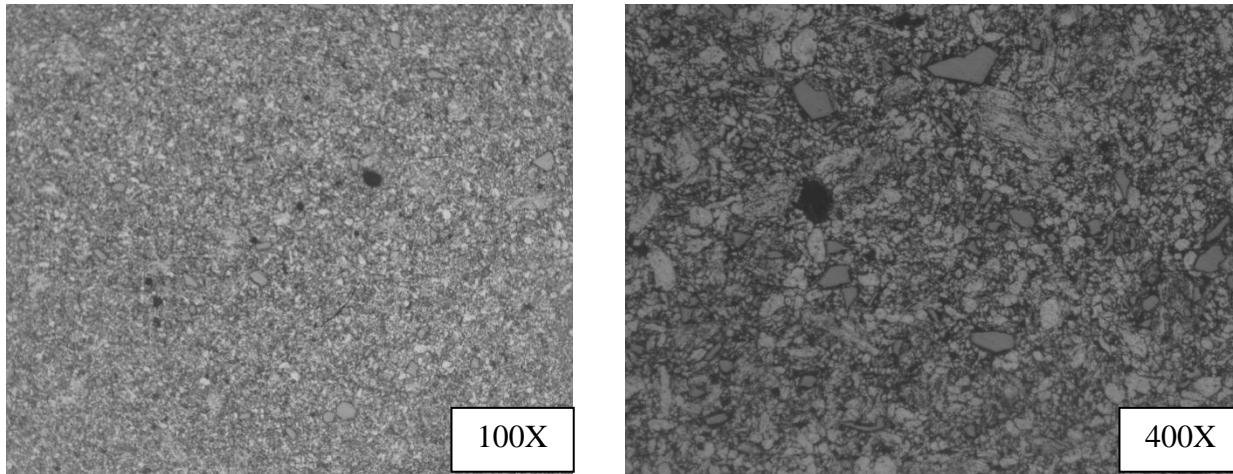


Fig.1 Microstructure images of Al / 1wt% silver coated MWCNT / 9wt% Si compact made by Vacuum hot pressing at 600°C

3.2 XRD ANALYSIS

Figure 5.25 reveals the XRD pattern for Al / 1wt% silver coated MWCNT / 9wt% Si compact. There is no characteristic peak related to CNT or silver at $2\theta = 26^\circ$. The major reason is that 4hrs milling in planetary ball mill is sufficient for uniform dispersion of silver coated CNT. The peak appears when the CNT is clustered and diminishes with dispersion of CNT. Another reason for absence of CNT peak is due to the small weight percentage of CNT used, unfavorable strain or CNT deformation and amorphization of CNT. The XRD pattern contains peak corresponding to aluminium and silicon [3].

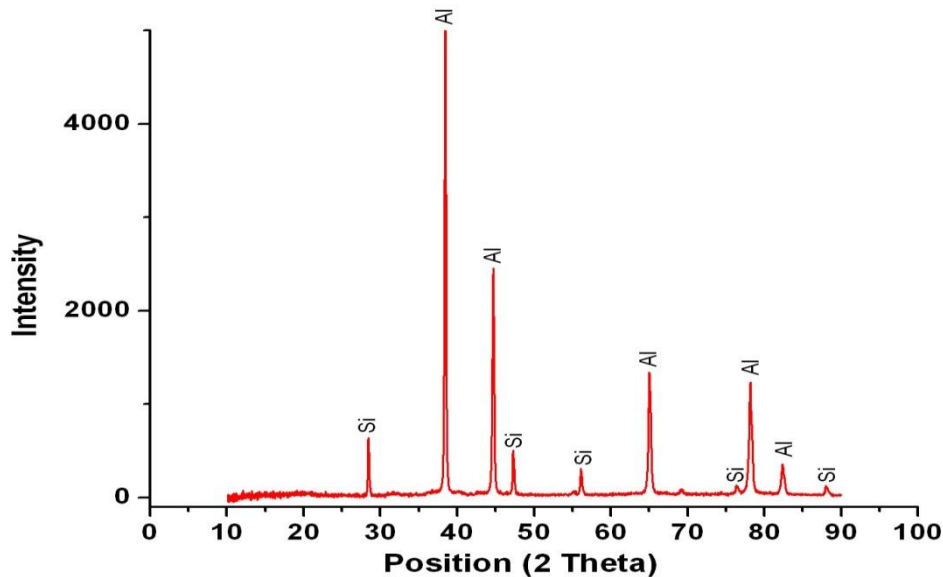


Fig.2 XRD pattern of Al / 1wt% Ag coated MWCNT / 9wt% Si compact

3.3 DENSITY AND HARDNESS MEASUREMENT

The compacted sample has a very high relative density. Sample compacted using 1wt% silver coated CNT has almost density equal to sample compacted using 4wt% CNT [4]. This reveals that silver coated CNT disperse well in aluminium matrix which reduce porosity and increases the relative density.

The compacted sample gives an hardness of 75 BHN, i.e. sample made using 1wt% of silver coated CNT gives hardness value near to sample compacted using 4wt% of uncoated CNT [4]. This shows the uniform dispersion of silver coated CNT in aluminium matrix. Silver coated CNT gives better hardness because it is distributed more uniformly in the composites leading to dispersion strengthening, and fills up the voids resulting in increase of the relative density of the composites. The uniformly dispersed CNT restrain the growth of aluminium grains during fabrication of the composites bringing on grain refinement strengthening.

4. CONCLUSION

In summary, silver coating is one of the best methods to improve the dispersion of CNT in Al matrix. Using silver coated CNT milling duration can be reduced to 1/4th of milling time taken for uncoated CNT. For silver coated CNT 4hrs of milling in planetary ball mill is sufficient for uniform distribution. Porosity is also less observed in composite made using silver coated CNT. Even small weight percentage of silver coated CNT gives better relative density and hardness value. The composite made using 1wt% of silver coated CNT gives relative density and hardness almost equal to composite made using 4wt% of uncoated CNT. This reveals the uniform distribution of silver coated CNT in aluminium matrix. Hardness of aluminium composites made using CNT is significantly higher compared to other aluminium composite compacted at similar conditions. This reveals the strengthening effect of CNT.

REFERENCE

1. Yeng, Hailong Yuan: "Electroless plating of carbon nanotube with silver", *Material Science*, 2004, Vol. 39, pp. 3241-3243.
2. R P´erez-Bustamante, I Estrada-Guel, C D G´omez-Esparza, R Mart´inez-S´anchez, M Miki-Yoshida: "Microstructural and mechanical characterization of Al – MWCNT composite produced by mechanical milling", *Material Science and Engineering*, 2009, Vol. 502(A), pp. 159-163.
3. H J Choi, G B Kwon, G Y Lee, D H Bae: "Reinforcement with carbon nanotubes in aluminium matrix composites", *Scripta Materialia*, 2009, Vol. 59, pp. 360-363.
4. C F Deng, D Z Wang, X X Zhang, A B Li: "Processing and properties of carbon nanotubes reinforced aluminium composites", *Materials Science and Engineering*, 2007, Vol. 444(A), pp. 138-145.
5. C Deng, Xue Xi Zhang, Dezun Wang, Q Lin, "Preparation and characterization of carbon nanotubes / aluminium matrix composites", *Material Letters*, 2007, Vol. 61, PP. 1725-1728.
6. A M K Esawi, K Morsi, A Sayed, A Abdel Gawad, P Borah: "Fabrication and properties of dispersed CNT – aluminium composites", *Material Science and Engineering*, 2009, Vol. 508(A), pp. 167-173.
7. S R Bakshi, Anup K Keshri, Virendra Singh, Sudipta Seal, Arvind Agrawal: "Interface in CNT reinforced aluminium silicon composites: Thermodynamic analysis and experimental verification", *Journal of Alloy and Compounds*, 2009.

Offline Signature Verification Using Neural Network

S.T. Kolhe, S. E. Pawar

(Dept. of Computer Engg, AVCOE, Sangamner, India)

(Dept. of I.T. Engg, AVCOE, Sangamner, India)

ABSTRACT

The concept of offline signature verification is challenging because of several reasons. Firstly, there exists great variation even between two signatures of the same person. They never start from the same position and neither do they terminate at the same position. Also, the angle of inclination of the signatures, the relative spacing between letters of the signatures, height of letters - all vary even for the same person. Hence it becomes a challenging task to compare between two signatures of the same person, an offline signature verification system is proposed in this paper take care of that. The proposed model has four stages: image pre-processing, feature extraction, neural network training, verification and recognition. The user introduces into the computer the scanned signature images, modifies their quality by image enhancement and noise reduction techniques, to be followed by feature extraction, training the neural network and finally verification and recognition.

Keywords- Backpropagation, Image processing, neural network, Offline signature verification.

I. INTRODUCTION

Signatures are composed of special characters and flourishes and therefore most of the time they can be unreadable. Also intrapersonal variations and interpersonal differences make it necessary to analyze them as complete images and not as letters and words put together [1]. As signatures are the primary mechanism both for authentication and authorization in legal transactions, the need for research in efficient automated solutions for signature recognition and verification has increased in recent years. Recognition is finding the identification of the signature owner. Verification is the decision about whether the signature is genuine or forgery. In this decision phase the forgery images can be classified in three groups: (i) random, (ii) simple, (iii) skilled [2]. Random forgeries are formed without any knowledge of the signer's name and signature's shape. Simple forgeries are produced knowing the name of the signer but without having an example of signer's signature. Skilled forgeries are produced by people looking at an original instance of the signature, attempting to imitate as closely as possible. The signatures can be distinguished in two different categories of verification systems depending on acquisition of signatures: online signature, for which the signature is captured during the writing process and making the dynamic information available, and offline, for which the signature is captured once

the writing process is over and, thus, only static information is available. The objective of the signature verification system is to discriminate between two signature classes: the genuine and forgery signature. A lot of work has been done in the field of off-line signature verification [4], [5]. Although a large number of works is focused on random and simple forgery detection, more efforts are still needed to address the problem of skilled forgery detection [3]. No verification algorithms are proposed which might be dealt well with skilled forgeries.

The proposed offline signature system provides automated method of verification and recognition by extracting features that characterizes the signature. The approach starts by scanning images into the computer, then modifying their quality through image enhancement and noise reduction, followed by feature extraction and neural network training, and finally verifies whether a signature is original or fake.

II. SYSTEM OVERVIEW

2.1 Preprocessing

Generally in any image processing application pre-processing is required to eliminate noise, distortions etc., from the original image. Any normal scanner with sufficient resolution can be used as an image acquisition device for offline-operation

2.1.1 Scaling

If H_I and W_I are the height and width of the image then we can make the image at uniform 100×100 pixels by the simple equations:

$$X_{\text{new}} = X_{\text{old}} * S_x \quad (1)$$

Where $S_x = 100/H_I$; X is any horizontal unit and is the horizontal scaling factor.

$$Y_{\text{new}} = Y_{\text{old}} * S_y \quad (2)$$

Where $S_y = 100/W_I$; Y is any vertical unit and is the vertical scaling factor.

2.1.2 Conversion of color image to grayscale

The luminosity method is a more sophisticated version of the average method to convert the color image to grayscale. It also averages the values, but it forms a weighted average to account for human perception. The formula for luminosity is $0.21 R + 0.71 G + 0.07 B$.

2.1.3 Thresholding

In computer vision and image processing, Otsu's method is used to automatically perform histogram shape-based image

thresholding or the reduction of a gray level image to a binary image. The algorithm assumes that the image to be threshold contains two classes of pixels (e.g. Foreground and background) then calculates the optimum threshold separating those two classes so that their combined spread (intra-class variance) is minimal. In Otsu's method we exhaustively search for the threshold that minimizes the intra-class variance, defined as a weighted sum of variances of the two classes:

$$\sigma_w^2(t) = \omega_1(t) \sigma_1^2(t) + \omega_2(t) \sigma_2^2(t) \quad (3)$$

Weights ω_i are the probabilities of the two classes separated by a threshold t and σ_i^2 variances of these classes. Otsu shows that minimizing the intra-class variance is the same as maximizing inter-class variance:

$$\sigma_b^2(t) = \sigma^2 - \sigma_w^2(t) = \omega_1(t) \omega_2(t) [\mu_1(t) - \mu_2(t)]^2 \quad (4)$$

which is expressed in terms of class probabilities ω_i and μ_i class means which in turn can be updated iteratively.

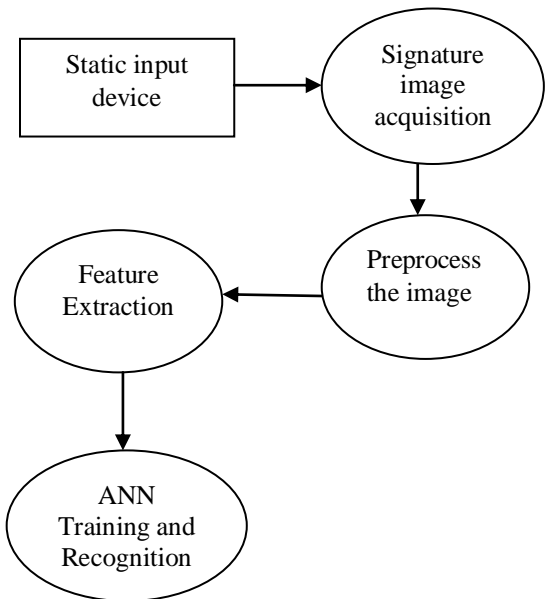


Fig 1: Flow Diagram of Offline Signature verification

2.1.4 Thinning

Thinning was introduced to describe the global properties of objects and to reduce the original image into a more compact representation. It uses a set of four templates to scan the image. Figure 2 shows these four templates.

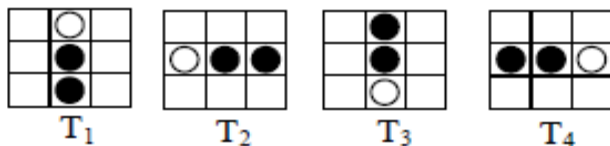


Fig 2: Templates to identify pixels to be eroded

The Stentiford Algorithm can be stated as following [6]:

1. Find a pixel location (i, j) where the pixels in the image match those in template T1. With this template all pixels along the top of the image are removed moving from left to right and from top to bottom.

2. If the central pixel is not an endpoint, and has connectivity number = 1, then mark this pixel for deletion. Endpoint pixel: A pixel is considered an endpoint if it is connected to just one other pixel. That is, if a black pixel has only one black neighbor out of the eight possible neighbors.

Connectivity number: It is a measure of how many objects are connected with a particular pixel.

$$C_n = \sum_{k \in S} N_k - (N_k \cdot N_{k+1} \cdot N_{k+2}) \quad (5)$$

where: N_k is the color of the eight neighbors of the pixel analyzed. N_0 is the center pixel. N_1 is the color value of the pixel to the right of the central pixel and the rest are numbered in counterclockwise order around the center.

$$S = \{1, 3, 5, 7\}$$

Figure 3 illustrates the connectivity number. Figure 3 a) represents connectivity number = 0. b) Represents connectivity number = 1, the central pixel might be deleted without affecting the connectivity between left and right. c) Represents connectivity number = 2, the deletion of the central pixel might disconnect both sides. d) Represents connectivity number = 3, and e) represents connectivity number = 4.

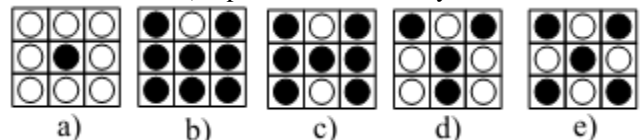


Fig 3: Connectivity Number

3. Repeat steps 1 and 2 for all pixel locations matching T1.

4. Repeat steps 1-3 for the rest of the templates: T2, T3, and T4. T2 will match pixels on the left side of the object, moving from bottom to top and from left to right. T3 will select pixels along the bottom of the image and move from right to left and from bottom to top. T4 locates pixels on the right side of the object, moving from top to bottom and right to left.

5. Set to white the pixels marked for deletion. Figure 7 shows the signature after the thinning process using the Stentiford Algorithm.



Fig 4: Original Signature image

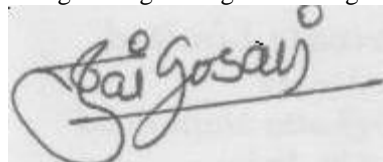


Fig 5: Grayscale signature image

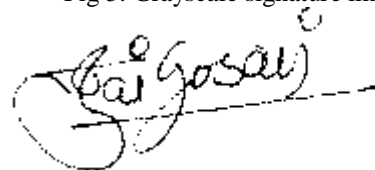


Fig 6: Signature after Thresholding

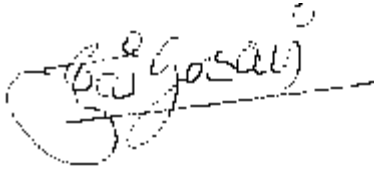


Fig 7: Signature after Thinning

III. FEATURE EXTRACTION

In Feature extraction step, the necessary features are extracted from the sample. The features to be extracted are based on the application and vary from system to system. Specific and discriminate functions or parameters are computed from the filtered data and are used to represent signature. The term feature here refers to a certain characteristic that can be measured using designed algorithms; which can then be retrieved by “extraction”.

In this system, two groups of features are categorized as global features and texture features. While global features give information about particular cases regarding the structure of the signature, texture features are projected to provide overall signature appearance information in different levels of detail.

3.1 Global features

3.1.1 Slant and Slant direction

To estimate the slant of the signature the algorithm proposed by Ammar was used. The algorithm makes use of the thinned image obtained during the pre-processing. A 3X3-sliding window is used for computation. The window is moved starting from the left-top pixel to the right-bottom pixel, one pixel at a time in a row major order.

3.1.2 Density of Thinned Image

The density of thinned image can be calculated after thinning is performed. It corresponds to the measure of density of signature traces. The density of smoothed image can be calculated by the following formula. Density of thinned image = No of non zero pixels in the thinned image / Total no of pixels in the thinned image

3.1.3 Width to Height Ratio

Finally, complete content and organizational editing before formatting. Please take note of the following items when proofreading spelling and grammar: Let \min_x and \max_x be the minimum and maximum values of x coordinates of non-zero pixels and \min_y and \max_y be the minimum and maximum values of y coordinates of non-zero pixels. Width to height ratio is the ratio of range of x coordinates to the range of y coordinates. The formula for calculating width to height ratio is given as:

$$\text{Width to Height Ratio} = (\max_x - \min_x) / (\max_y - \min_y) \quad (6)$$

3.1.4 Skewness

Skewness is a measure of symmetry or more precisely, the lack of symmetry. The measurement of skewness allows us to determine how bowed are the lines in each segment of the signature

$$\text{Skewness} = \sum (Y_i - Y')^3 / (N-1) s^3 \quad \text{for } i=1 \text{ to } N \quad (7)$$

Where Y is the mean, S is the standard deviation, and N is the number of data points. The measurement of skewness allows us to determine how bowed are the lines in each segment of the signature. The percentage of this torsion is then calculated and extracted. Furthermore, this percentage is compared to that extracted from the other image.

3.2 Texture Features

The topological features are pixel positions in the image with respect to the property of the feature. These can be processed using a matcher that uses co-occurrence matrix of the picture image. The topological features includes: End points, Branch points, crossing points.

3.2.1 Extraction of Texture Features

To extract end points, branch points, crossing points it is necessary to apply the preprocessing techniques like thresholding, smoothing and thinning on a gray scale signature image. End points are points where a signature stroke begins or ends. Branch points are points where on signature stroke bifurcates into two strokes. Crossing points are points where one signature stroke crosses another stroke

3.3 Enrollment process

During enrollment process the extracted features are stored in a reference database under a given class name, which can be used for verification process. For a given class, the enrollment process is to be done for sufficient number of samples of that class to generate the reference set.

3.3.1 Enrollment of the Global Features

1. The global features extracted (slant and slant direction, density, width to height ratio, skewness) for a signature sample are stored in a file under the given unique class name.
2. When a new sample of the same class is used for enrollment the feature values are added to the same database, otherwise they are added to a new file under its class name.

3.3.2 Enrollment of the Texture Features

1. The texture features that are extracted are the (pixel positions of) end points (E), branch points (B), crossing points (C).
2. The co occurrence matrices are obtained from the picture matrix of features extracted from signatures. The symbolic picture (picture matrix), which is obtained from

features and their locations will be used in finding the multi dimensional co-occurrence matrix.

IV. NEURAL PATTERN RECOGNITION

Back propagation neural network (BPN) with one-class one-network scheme is used. The structure of BPN used is assumed to have only one hidden layer. The numbers of units in each layer are $5 \times 3 \times 1$. (5 input unit, 3 hidden units, and 1 output unit). The 5 input units correspond to slant, slant direction, thin density, width to height ratio, and skewness. The threshold for total error rate is set appropriately. The network is trained and the weight matrices are stored separately under the given class name. So for each class that is enrolled to the system, three reference databases are created with respect to global features. The first one is to store the feature values, second is to store the normalized values, and third is to store the weight matrix of the particular class.

4.1 Algorithm Backpropagation

It is neural network learning algorithm for classification or prediction, using the back propagation algorithm. *Input:* D , a data set consisting of the training tuples and their associated target values; l , the learning rate; *Network*, a multilayer feed-forward network; *Output:* A trained neural network.

Method:

- (1) Initialize all weights and biases in *network*;
- (2) While terminating condition is not satisfied {
- (3) for each training tuple X in D {
- (4) // propagate the inputs forward:
- (5) for each input layer unit j {
- (6) $O_j = I_j$; // output of an input unit is its actual input value
- (7) for each hidden or output layer unit j {
- (8) $I_j = \sum_i w_{ij} O_i + \theta_j$; //compute the net input of unit j with respect to the previous layer, i
- (9) $O_j = 1 / (1 + e^{-I_j})$; } //compute the output of each unit j
- (10) // Backpropagate the errors:
- (11) for each unit j in the output layer
- (12) $Err_j = O_j (1 - O_j) (T_j - O_j)$; // compute the error
- (13) for each unit j in the hidden layers, from the last to the first hidden layer
- (14) $Err_j = O_j (1 - O_j) \sum_k Err_k w_{jk}$; // compute the error with respect to the next higher layer, k
- (15) for each weight w_{ij} in *network* {
- (16) $\Delta w_{ij} = l Err_j O_i$; // weight increment
- (17) $w_{ij} = w_{ij} + \Delta w_{ij}$; // weight update
- (18) for each bias θ_j in *network* {

(19) $\Delta \theta_j = l Err_j$; // bias increment

(20) $\theta_j = \theta_j + \Delta \theta_j$; } // bias update

(21) } }

V. VERIFICATION PROCESS

The verification process compares the signature that is to be tested with the reference signatures stored in the database. The comparison is based on the assumption that the values of the feature sets or structural description extracted from genuine signatures are more stable than the signatures that are forged.

That is, the intra-personal variations are smaller than inter-personal variations. So, the given test signature may be accepted or rejected based on its similarity to the reference signature set. The verification process proceeds in two levels. The final decision is based on the decisions of both stages.

5.1 Verification of Global Features

1. The first level of verification checks the global features for validity. The features extracted for test sample are normalized and these normalized values are used to test the network.
2. The weight matrix of the corresponding class is taken from the database and is assigned to the network before testing.
3. If the output of the network is less than specified threshold then the verification process marks the given sample as a genuine one.
4. Optimization can be done before testing the sample with the network. That is, the feature values (global) of the test sample are checked whether they fall within the minimum and maximum values of that feature value that is stored in the database.
5. The system sets a range of values for each feature extracted for the given class. The least value corresponds to minimum and the highest value corresponds to maximum of the feature of the given class.
6. Then, it verifies that whether all these features of the given test signature lie within the minimum and maximum of the corresponding features of the given class.
7. If they are in the range then the normalized values are tested using BPN. If not, the testing with BPN network can be skipped and report error. This is referred to as static data analysis.

5.2 Verification of Texture Features

1. The multi dimensional co-occurrence matrix is obtained for each sample that is given for training and the values are stored in the database.
2. During verification, the same has to be obtained for the test specimen. Once having obtained the multi dimensional co-occurrence matrix, each element of the multidimensional co-occurrence matrix of the test

signature is compared with the corresponding element of that in the database.

3. If the compared values in the range for a maximum number of elements then output is said to be genuine, otherwise forged.

VI. CONCLUSION

The main objective of this work is to present a robust system for off-line signature verification. The ultimate goal of signature verification is to have machines which can read any text with the same verification accuracy as humans but at a faster rate. A novel approach for off-line signature verification is proposed and implemented using a Back Propagation Neural Network algorithm. The system that is proposed based on global and texture features. Features exhibiting good performance are considered, and finally a near-optimal solution using blend of such features in terms of high verification and time efficiency is derived. Although the operations used in obtaining the features are computationally expensive, they are adopted in order to get good results

REFERENCES

- [1] Ramachandra, Jyothi Srinivasa Rao, K B Raja, K R Venugopla ,L M Patnaik, Robust Offline Signature Verification Based On Global Features, 2009 IEEE International Advance Computing Conference (IACC 2009) Patiala, India, 6-7 March 2009
- [2] Meenakshi S Arya, Vandana S Inamdar, A Preliminary Study on Various Off-line Hand Written Signature Verification Approaches 2010 International Journal of Computer Applications (0975 – 8887) Volume 1 – No. 9
- [3] V A Bharadi, H B Kekre, Off-Line Signature Recognition Systems, International Journal of Computer Applications (0975 - 8887) Volume 1 – No. 27
- [4] Alessandro Zimmer, Lee Luan Ling, “Offline Signature Verification System Based on the Online Data” EURASIP Journal on Advances in Signal Processing Volume 2008, Article ID 492910
- [5] H.N. Prakash, D. S. Guru, “Offline Signature Verification: An Approach Based on Score Level Fusion” International Journal of Computer Applications (0975 - 8887) Volume 1 – No. 18
- [6] Sonka, M., Hlavac, V., Boyle, R., “Image Processing, Analysis, and Machine Vision”, 2nd Edition, Pws. Pub. Co.

Analysis of HLFET and MCP Task Scheduling Algorithms

Samriti¹, Sandeep Gill², Ankur Bharadwaj², Navpreet Singh³,
Harsimran Singh⁴, Jashwinder Singh⁵

¹(Assistant Professor, DCSE, SSIET Patti, Punjab, India)

² (Assistant Professor Department of Computer Science, Sewa Devi SD College Tarn Taran, India)

³Technical Head, IT, MINT, Ajmer, Rajasthan

⁴ (PHP Developer, Kochhar Inoftech, Amritsar, Punjab)

⁵ (Senior Technical Assistant, Punjab Technical University, Kapurthala)

ABSTRACT

Scheduling tasks on multiprocessor system is an imperative and computationally intricate problem. Multiprocessors are used for running real-time applications that a uniprocessor system would not be competent to execute. It requires a resourceful algorithm to determine when and on which processor a given task should execute. The scheduling problem is represented by an edge-directed acyclic graph (DAG) based on homogenous processors. The objective of scheduling is to minimize the execution time, evaluate and compare the performance of the individual algorithms. Different algorithms are analyzed and classified into four groups. The algorithm in first group schedule the DAG to bounded number of processor (BNP). Algorithms in second group schedule the DAG to unbounded number of clusters (UNC). The algorithm in third group schedule the DAG to task duplication based (TDB). The algorithms in the fourth group perform allocation and mapping on arbitrary processor network topologies (APN). In this study the focus is given on two major BNP algorithm based upon homogenous environment i.e. HLFET Highest Level First with Estimated Time and Modified Critical Path commonly abbreviated as MCP.

Keywords - Parallel Environment, Directed Acyclic Graph, HLFET, MCP, Task Scheduling

I. INTRODUCTION

Parallel computing, one of the emerging concept in the field of Information Technology [4] that is used to execute number of tasks on different computers of workstations.

Parallel processing plays a significant role in solving complex and computation intensive problems in a minimum time with efficiency. The homogenous environment of parallel computing uses the similar power computers for task execution on the other hand in the heterogeneous environment of parallel computing the tasks are allocated on different capacity of computers. The major aspect of parallel environment Independent of the environment is to

improve the execution speed and to minimize the makespan [2] of task execution.

BNP uses b-level and t-level for assigning priority to different nodes for its execution. HLFET [1][2][3][4] (Highest Level First with Estimated Times) is one of the important static list scheduling algorithm that compute the sum of computation cost of call the nodes available in a DAG.

II. OBJECTIVE OF STUDY

The objective of this paper is to compare and contrast the various parallel environment metrics of HLFET and MCP task scheduling algorithms. Both HLFET and MCP are BNP Task scheduling algorithms. Here BNP stands for Bounded Number of processors. These algorithms schedule the DAG to a bounded number of processors directly. The processors are assumed to be fully connected. Most BNP scheduling algorithms are based on the list scheduling technique. List scheduling is a class of scheduling heuristics in which the nodes are assigned priorities and placed in a list arranged in a descending order of priority. The node with a higher priority will be examined for scheduling before a node with a lower priority. If more than one node has the same priority, ties are broken using some method. The Highest Level First with Estimated Time (HLFET) algorithm [4][6][7] is one of the simplest list-scheduling algorithms. It uses Static level as node priority. On the other hand the Modified Critical Path algorithm commonly abbreviated as MCP algorithm [5][6] utilizes the ALAP attribute of a node as for priority scheduling. Modified Critical Path algorithm initially calculate the value of ALAPs of all nodes and after that erects the list of nodes in increasing order of nodes ALAP. When the ALAP values of two nodes become same, the ALAPs of the children are taken into concern. It should be noted that the MCP algorithm schedules the nodes on the list taking one by one such that a node is scheduled to the processor or workstation that allows the earliest execution start time.

III. ANALYSIS

In this section the performance of two major BNP algorithms is compared by taking two different cases consisting of 5 nodes and 10 nodes.

All the tasks are allocated and executed on three processors P1, P2, P3. HLFET and MCP algorithms are used to compute various parallel environment metrics like makespan, speedup, Scheduled Length Ratio, processor utilization, complexity etc.

Case1: Consider a DAG consisting of 5 task nodes as shown in the following figure. The 5 task nodes used are T1, T2, T3, T4 and T5.

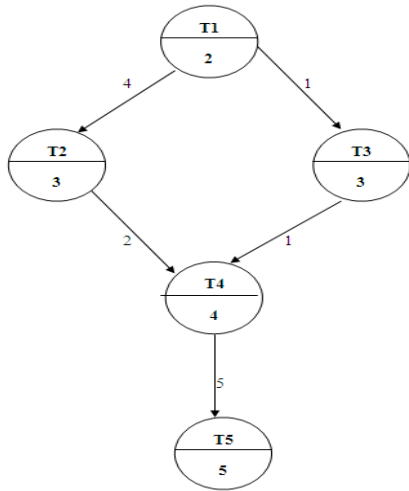


Figure1: DAG with 5 Nodes

The following table shows the various scheduling attributes used to find the performance of algorithms.

Tasks	Execution Time	Static b-level	t-level	b-level	ALAP Time	Dynamic Level
T1	2	14	0	25	0	14
T2	3	12	6	19	6	6
T3	3	12	3	18	7	9
T4	4	9	11	14	11	-2
T5	5	5	20	5	20	-15

The following chart shows the schedule generated by HLFET task scheduling algorithm, when the tasks are scheduled over three processors.

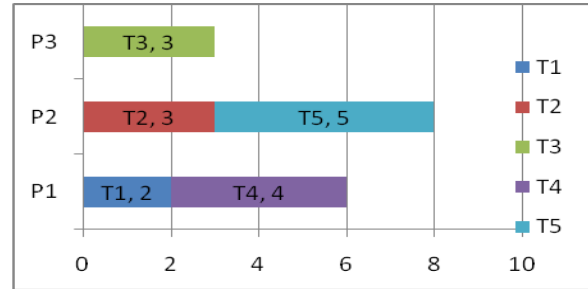


Figure 2 : HLFET Task Schedule

The following chart shows the schedule generated by MCP algorithm, when the tasks are scheduled over three processors.

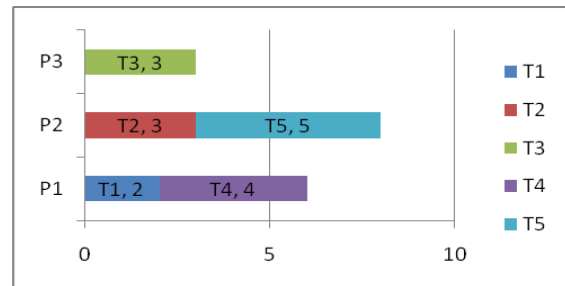


Figure 3: MCP Tasks Schedule

The following table shows how HLFET task scheduling algorithm is different from MCP task scheduling algorithm in term of various parallel environment metrics.

	HLFET	MCP
Makespan	8	7
SLR	0.32	0.28
Speed Up	2.12	2.42
Processor Utilization (P1)	75%	75%

The following table shows the nature of relation between HLFET makespan and MCP makespan for 5 nodes with their relative mathematical equations.

S.No.	Nature of Relation	Mathematical Equation
1.	Logarithmic	$y = -1.4427\ln(x) + 8$

IV.	Linear	$y = -x + 9$
V.	Exponential	$y = 9.1429e-0.1335x$

Case II: Consider a DAG consisting of 10 task nodes as shown in the following figure. The 10 task nodes used are T1, T2, T3, T4, T5, T6, T7, T8, T9 and T10. In the DAG there are two types of weight associated, one is execution time

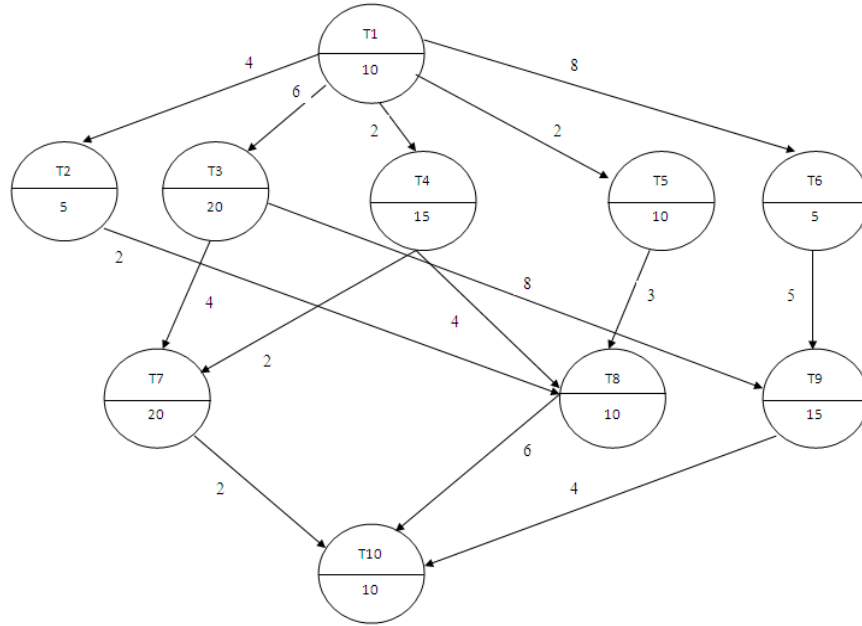


Figure1: DAG with 5 Nodes

shown in the node and other is communication cost shown by edges. By using the DAG shown in the figure, one is able to compute various parallel environment metrics like makespan, b-level, t-level, ALAP etc. By using these

parameter further performance metrics are computer as shown in the following table. The following table gives information of various computed attributes required for task scheduling.

.Tasks	Execution Time	Static level	b-	t-level	b-level	ALAP Time
T1	10	60		0	73	0
T2	5	25		14	33	4
T3	20	50		16	57	16
T4	15	45		12	49	24
T5	10	30		12	39	34
T6	5	30		18	39	34
T7	20	30		40	32	41
T8	10	20		31	26	47
T9	15	25		44	29	44
T10	10	10		63	10	63

The following chart shows how various 10 tasks are scheduled over three processor P1, P2 and P3 by using one

of the list scheduling algorithm i.e. HLFET.

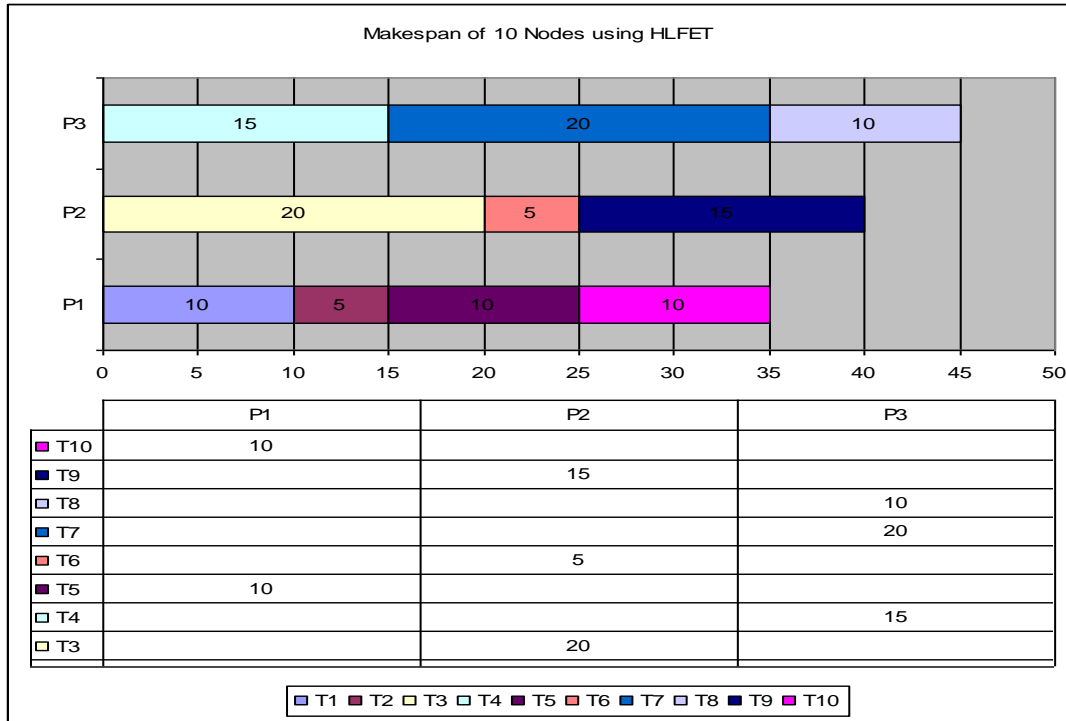
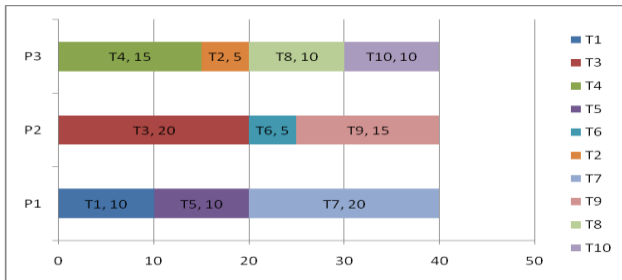


Figure: Analysis of 10 nodes DAG

The following chart shows how MCP differs in allocating above said 10 tasks to three processors.



The following table shows how HLFET task scheduling algorithm is different from MCP task scheduling algorithm in term of various parallel environment metrics.

	HLFET	MCP
Makespan	45	40
SLR	0.32	0.28
Speed Up	51.42857	62.2%
Processor Utilization (P1)	100	100%

Processor (P2)	Utilization	88.88889	100%
Processor (P1)	Utilization	77.77778	100%

IV. CONCLUSION

From the above data it is very clear that both HLFET and MCP task scheduling algorithms are used to reduce the processing time of task as compare to serial task scheduling. Further it is clear that MCP task scheduling algorithm has smaller makespan as well as SLR in both of cases as compare to HLFET task scheduling algorithm. And MCP task scheduling algorithm has high speed up as compare to HLFET task scheduling algorithm. So in regard to above said case of 5 nodes and 10 nodes one comes to conclude that MCP task scheduling algorithm is better than HLFET task scheduling algorithm. Although both are superior when compared with serial task scheduling algorithms.

V. REFERENCES

1. Yu-Kwong Kwok, Ishfaq Ahmad, "Static Scheduling Algorithm for Allocating Directed Task Graph to multiprocessors", ACM Computing Surveys, Vol. 31, no. 4, December 1999.
2. Ishfaq Ahmad, Yu-Kwong Kwok, Min-You Wu, "Analysis, Evaluation, and Comparison of Algorithms for Scheduling Task Graphs on Parallel Processors", Proceedings of the 1996 International Symposium on Parallel Architectures, Algorithms and Networks, IEEE Computer Society Washington, DC, USA.
3. T. Hagraš, J. Janecek, "Static versus Dynamic List-Scheduling Performance Comparison", Acta Polytechnica Vol. 43 No. 6/2003.
4. Manik Sharma, Smriti, "Static and Dynamic BNP Parallel Scheduling Algorithms For Distributed Database", IJCT, Vol 1, No.1, 2011.
5. Ishfaq Ahmad, Yu-Kwong Kwok, Min-You Wu, "Performance Comparison of Algorithms for Static Scheduling of DAG to Multiprocessors", ACM Computing Surveys, Vol. 31, no. 4, December 1999.
6. Yu-Kwong Kwok, Ishfaq Ahmad, "Dynamic Critical-Path Scheduling: An Effective Technique for allocating Task Graphs to Multiprocessors", IEEE Transactions on Parallel and Distributed System, Vol. 7, No. 5
7. Manik Sharma, Gurdev Singh, "A Study Of BNP Parallel Task Scheduling Algorithms Metric's For Distributed Database System", International Journal of Distributed and Parallel systems (IJDPS), 3(1), 157 - 166

PV Array Fed SEPIC and VSI Based Power Conversion System for Single Phase Induction Motor Drive

P. Sivaraman^{1*}, Dr. A. Nirmalkumar²

¹Assistant professor (Sr.G), Dept. of Electrical and Electronics Engg. Bannari Amman Institute of Technology, Sathyamangalam, India

² Professor, Dept. of Electrical and Electronics Engg.-INFO Institute of Engineering, Coimbatore, India.

ABSTRACT

This paper proposes an implementation of Single Ended Primary Inductor Converter (SEPIC) converter and Voltage Source Inverter for an Induction Motor using Photovoltaic energy as a source. Generally the larger number of drives employed for industrial and commercial applications are induction motor drives. To run such kind of motor from the PV source, it is proposed to have a DC-DC converter and an inverter circuit as interface circuits. As the PV cell posses the nonlinear behavior, a DC-DC converter with Maximum Power Point Tracker (MPPT) controller is needed to improve its utilization efficiency and for matching the load to the photovoltaic modules. In this paper SEPIC converter (DC-DC converter) with Perturb and Observe MPPT algorithm is used for matching the load and to boost the PV module output voltage. To convert the boosted DC output voltage from PV module into AC, a voltage source inverter with sinusoidal pulse width modulation is implemented on it to attain sufficient voltage to drive single phase induction motor. The simulation work of these SEPIC converter and voltage source inverter fed induction motor circuits have been done using PSIM and MATLAB software. The experimental work is carried out with the SEPIC converter and voltage source inverter to drive the single phase induction motor. A PIC microcontroller is used to generate pulses for controlling the SEPIC converter circuit.

Index Terms: Induction motor, MPPT algorithm, PV cell, SEPIC converter, Voltage source inverter,

INTRODUCTION

The photovoltaic energy system has the advantages of absence of fuel cost, no environmental impacts, low maintenance and lack of noise and also it is a kind of renewable energy system. So it is becoming popular in the recent years, as a resource of energy. Modeling and simulation of PV array based on circuit model and mathematical equations is proposed [9]. As the photovoltaic (PV) cell exhibits the nonlinear behavior, while matching the load to the photovoltaic modules, DC-DC power converters are needed. There are several converter configurations such

as Buck, Boost, Buck-Boost, SEPIC, ĆUK, Fly-back, etc. Buck and Boost configurations can decrease and increase the

output voltages respectively, while the others can do both functions. Buck, Boost, Buck Boost converters as interface circuits are proposed and analyzed in [6]. ĆUK and SEPIC converters are analyzed in [1,7].

When the solar insolation and temperature is varying, the PV module output power is also getting changed. But to obtain the maximum efficiency of PV module it must be operated at maximum power point. So it is necessary to operate the PV module at its maximum power point for all irradiance and temperature conditions. For this purpose Perturb and Observe MPPT algorithm is proposed [8]. According to this MPPT output, the duty ratio of SEPIC converter is varied, that leads to changes in output voltage.

The function of an inverter is to change a dc input voltage to a symmetric AC output voltage of desired magnitude and frequency. To drive the three phase induction motor the output dc voltage of SEPIC converter is converted into AC by means of voltage source inverter.

In this paper PV source fed induction motor drive is proposed with SEPIC converter and voltage source inverter as interface circuits. Perturb and Observe (P&O) MPPT Algorithm is used to extract the maximum power point of PV module [8]. Sinusoidal pulse width modulation technique is employed for the control of voltage source inverter. The overall block diagram is shown in fig1.

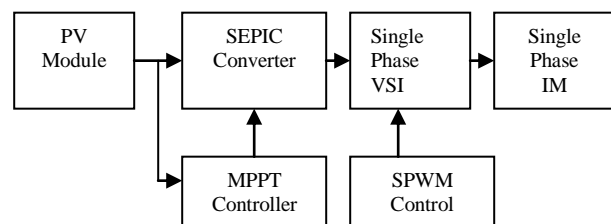


Fig. 1 Overall block diagram

The hardware prototype of SEPIC converter and VSI is constructed to run the single phase induction motor. In the literature survey an analog controller is used to generate the gate pulses and to control the inverter output voltage [3]. In this thesis to generate the gate pulses for the switches, PIC

microcontroller is used in control circuit as given in [4, 5, 14 and 15]. Along with PIC microcontroller, IR2112 driver circuit is needed to generate gate signal for SEPIC converter. The input DC voltage to the SEPIC converter is taken from the power supply unit. The two switches of VSI are gate controlled by using SG3524 PWM controller IC.

II. SEPIC CONVERTER WITH PV AND MPPT

PV system directly converts sunlight into electricity. The basic device of a PV system is the PV cell. Cells may be gathered to form modules or arrays. More sophisticated applications require DC-DC converters to process the electricity from the PV device. These converters may be used to either increase or decrease the PV system voltage at the load. The proposed SEPIC converter operates in boost mode.

A. PV Module Characteristics

The practical equivalent circuit of a PV module is shown in fig.2 [2]., while the typical output characteristics are shown in fig.3.

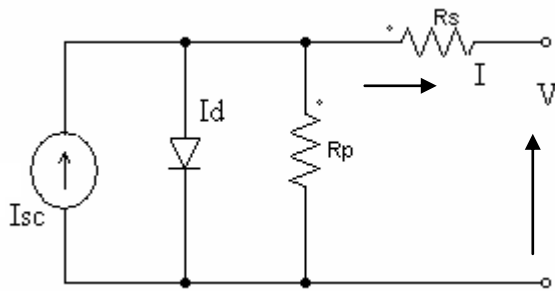


Fig. 2 Equivalent circuit of a PV module

In the equivalent circuit, the current source represents the current generated by light photons and its output is constant under constant temperature and constant irradiance. The diode shunted with the current source determines the I-V characteristics of PV module. There is a series of resistance in a current path through the semiconductor material, the metal grid, contacts, and a current collecting bus. These resistive losses are lumped together as a series resistor (R_s). Its effect becomes very noteworthy in a PV module.

The loss associated with a small leakage of current through a resistive path in parallel with the intrinsic device is represented by a parallel resistor (R_p). Its effect is much less noteworthy in a PV module compared to the series resistance, and it will only become noticeable when a number of PV modules are connected in parallel for a larger system. The characteristic equation which represents the I-V characteristic of a practical photovoltaic module is given below [9]

$$I = I_{pv} - I_o \left[\exp\left(\frac{V + IR_s}{V_t n}\right) - 1 \right] - \frac{V + IR_s}{R_p} \tag{1}$$

Where I and V are the PV cell current and voltage respectively, I_{pv} is the photovoltaic current, I_o is the reverse saturation current of diode, $V_t = N_s k T / q$ is the thermal voltage of the array with N_s cells connected in series, k is the Boltzmann constant ($1.3806 \times 10^{-23} \text{ J/K}$), T is the temperature of the p-n junction, q is the electron charge and n is the diode ideality constant. I_{pv} and I_o are given as follows [9].

$$I_{pv} = \left\{ [1 + a(T - T_{ref})] I_{sc} \right\} \left[\frac{G}{1000} \right] \tag{2}$$

$$I_o = I_o(T_{ref}) \left[\frac{T}{T_{ref}} \right]^3 \frac{q E_g}{n k} \left[\frac{1}{T_{ref}} - \frac{1}{T} \right] \tag{3}$$

Where “a” is temperature coefficient of I_{sc} , G is the given irradiance in W/m^2 and E_g is the band gap energy (1.16eV for Si). The single PV module specification is given in table I.

TABLE I PV MODULE BPSX150S SPECIFICATIONS

Electrical Characteristics	Value
Maximum Power (P_{max})	150W
Voltage at P_{max} (V_{mp})	34.5V
Current at P_{max} (I_{mp})	4.35A
Open-circuit voltage (V_{oc})	43.5V
Short-circuit current (I_{sc})	4.75A
Temperature coefficient of I_{sc}	$0.065 \pm 0.015\% / ^\circ\text{C}$
Temperature coefficient of V_{oc}	$-160 \pm 20 \text{ mV} / ^\circ\text{C}$

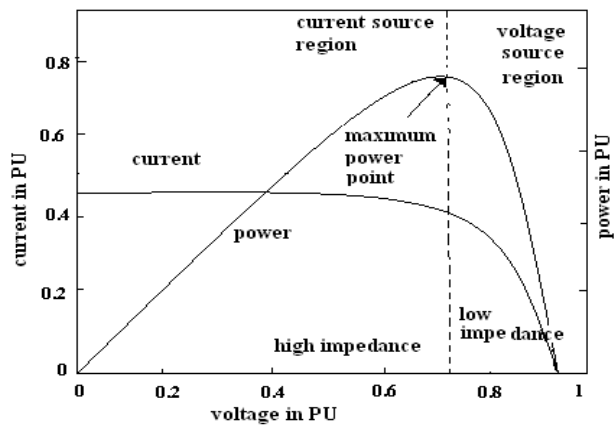


Fig. 3 PV Module IV and PV characteristics

Fig.3 illustrates the I-V and P-V characteristics of the PV array under a given insolation and temperature. As seen in the power versus voltage curve of the module there is a single maximum of power. That is there exists a peak power corresponding to a particular voltage and current. Since the module efficiency is low it is desirable to operate the module at the peak power point so that the maximum power can be delivered to the load under varying temperature and insolation conditions. Hence maximization of power improves the utilization of the solar PV module [2,6]. A maximum power point tracker (MPPT) is used for extracting the

maximum power from the solar PV module and transfers it to the load.

B. MPPT Control Algorithm

There are various types of maximum power point tracking algorithms available. Among them, P&O algorithm is used here, since it has the advantages of high tracking efficiency, low cost, easy implementation etc. In this algorithm a slight perturbation is introduced in the system voltage. Due to this perturbation, the power of the module changes [8]. If the power increases due to the perturbation then the next perturbation is continued in the same direction. After the peak power is reached the power at the next instant decreases and hence after that the direction of perturbation reverses. When the steady state is reached the algorithm oscillates around the peak point [8]. In order to keep the power variation small the perturbation size is kept very small. The algorithm is developed in such a manner that it sets a reference voltage of the module corresponding to the peak voltage of the module. Fig 4 shows the flow chart of P&O algorithm.

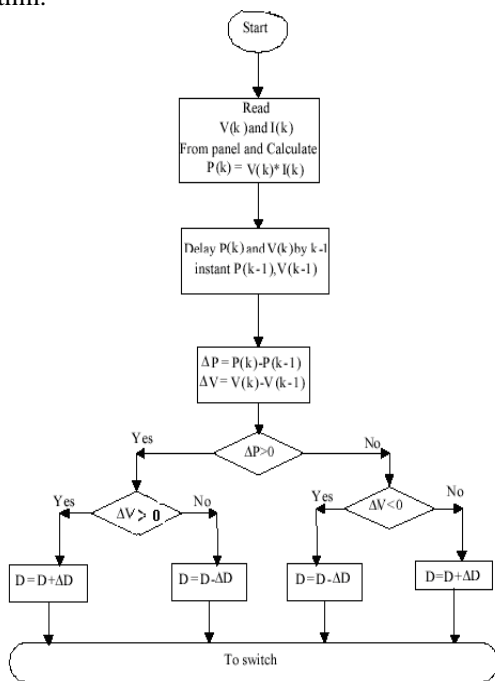


Fig.4 Flowchart of P&O MPPT algorithm

If we observe the power voltage curve of the solar PV module we see that in the right hand side curve where the voltage is almost constant the slope of power voltage is negative ($dP/dV < 0$) where as in the left hand side the slope is positive. ($dP/dV > 0$). The right side curve is for the lower duty cycle (nearer to zero) where as the left side curve is for the higher duty cycle (nearer to unity). After subtraction depending upon the sign of dP [$P(k+1) - P(k)$] and dV [$V(k+1) - V(k)$], the algorithm decides whether to increase the duty cycle or to reduce the duty cycle [8].

C. Modeling of SEPIC Converter

The important requirement of any DC–DC converter used in the MPPT scheme is that it should have a low input-current ripple. Buck converters will produce ripples on the PV module side currents and thus require a larger value of input capacitance on the module side. On the other hand, boost converters will present low ripple on the PV module side, but the load current exhibits more ripple and gives a voltage higher than the array voltage to the loads.

The buck– boost converters can be used where the requirement of load voltage, either low or higher than the array voltage. However, with this converter the input and load currents are pulsating in nature. Furthermore, the load voltage will be inverted with buck–boost or CUK converters. Under these conditions, the SEPIC converter, provide the buck–boost conversion function without polarity reversal, in addition to the low ripple current on the source and load sides.

The SEPIC (Single Ended Primary Inductor converter) topology with PV module and MPPT controller is shown in fig5 and it is proposed the converter is operated in Continuous Current Mode (CCM) [2].The inductance and capacitance values are designed from [10].This converter has two inductors and two capacitors. The capacitor C_1 provides the isolation between input and output. The SEPIC converter exchanges energy between the capacitors and inductors in order to convert the voltage from one level to another. The amount of energy exchanged is controlled by switch, which is typically a transistor such as a MOSFET.

L_1 is the input inductance, L_2 is the output inductance, C_1 is the energy transfer capacitor, C_2 is the output capacitor, V_{in} is the input voltage, V_o is the output voltage, V_{C1} is the voltage across capacitor C_1 , I_{L1} is the current though L_1 and I_{L2} is the current through L_2 .

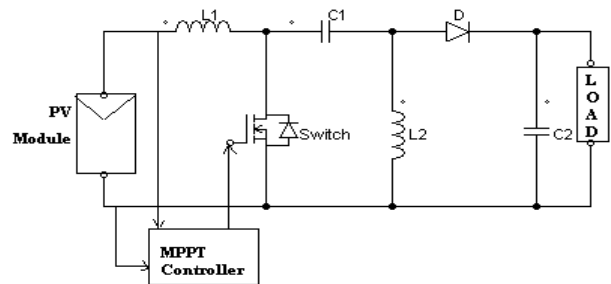


Fig. 5 SEPIC converter topology with PV and MPPT

The duty cycle D can be determined from the steady state condition and the following equation is true:

$$\frac{I_{L1}}{I_{L2}} = \frac{D}{1-D} = \frac{I_{in}}{I_o} \tag{4}$$

TABLE II SEPIC CONVERTER DESIGN SPECIFICATIONS

Parameter	Value
Input Voltage	32V
Output Voltage	220V
Output Current	1A
Duty Ratio	0.8
Switching frequency	25KHz

Assuming an ideal converter in which the input power is the same as the output power, then:

$$P_{in} = P_o \quad (5)$$

$$V_{in} I_{in} = V_o I_o \quad (6)$$

Combining equation (8) and (10), the relationship between input and output voltage is:

$$\frac{V_o}{V_{in}} = \frac{D}{1-D} \quad (7)$$

The converter design specifications are given in table II.

III. SEPIC CONVERTER AND VSI FOR INDUCTION MOTOR DRIVE APPLICATIONS

Output voltage from a voltage source inverter can be adjusted by exercising a control within the inverter itself. The most efficient method of doing this is by pulse-width modulation control (PWM)[16]. In this method, a fixed dc input voltage is given to the inverter and a controlled ac output voltage is obtained by adjusting the on and off periods of the inverter switches.

The PSIM simulation model of SEPIC converter and VSI fed induction motor is shown in fig6. The SEPIC converter output is a boosted DC voltage of PV module output. The output of the SEPIC converter is fed to the three phase voltage source inverter with the help of DC link capacitor. The aim of the DC link capacitor is to maintain the VSI input voltage as constant. The value of this capacitor is designed from the literature [13].

SPWM control is proposed in this paper in which three phase sinusoidal voltage of same magnitude and 120° phase shift is compared with the common triangle waveform. The magnitude of the output voltage of the inverter is controlled by the amplitude of the reference sine wave and hence the amplitude modulation index. The frequency of the inverter output voltage is controlled by the frequency of the reference signal. The current output of the inverter is dependent on the load impedance. The controlled magnitude and frequency of the inverter output voltage is given to the armature of the three phase induction motor. Finally the speed of the machine is measured for the given irradiance and temperature.

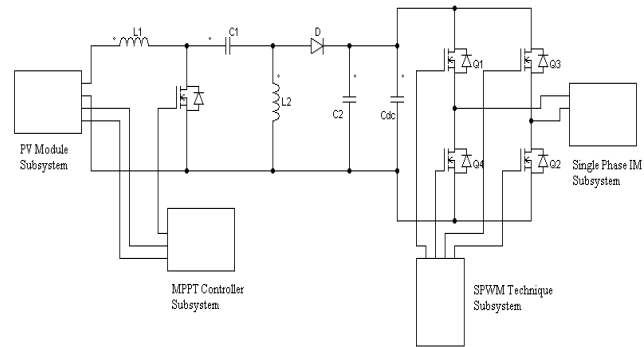


Fig. 6 Simulation model of SEPIC converter and VSI fed induction motor drive

IV. HARDWARE DESCRIPTION

The hardware prototype of SEPIC converter and voltage source inverter is constructed to run a single phase induction motor. Since the cost of the PV panel is high, dc supply for the SEPIC converter is given from the power supply unit. In both the SEPIC converter and voltage source inverter circuits the selected switch is MOSFET.

The control circuit which has the PIC microcontroller unit and driver circuit unit necessitates the power supply circuit module. The PIC microcontroller is given 5V dc as its supply and the driver circuit requires both 5V and 12V dc supply. So it is necessary to construct a power supply circuit module which produces both 5V and 12V dc output. The circuit uses two ICs 7812(IC1) and 7805 (IC2) for obtaining the required voltages.

The main device of controller circuit is a PIC 16F877A microcontroller and the coding for pulse generation is programmed and flash into the microcontroller. The microcontroller is operated at 4MHz clock frequency. The pin diagram of PIC 16F877A microcontroller and the various features of this microcontroller are referred in PIC16F87XA datasheet. Port B of this controller is assigned as output port. Pin no 13 and 14 are connected with the crystal oscillator of 4 MHz frequency. Pin 1 is connected with the reset switch through the 1K resistor. Pin 32 is given with 5V dc supply and 31 is connected with the ground. The coding for pulse generation is written in C and compiled with MPLAB IDE.

Driver circuit used to drive MOSFET switch of the SEPIC converter circuit is constructed with the IR2112 driver IC. IR2112 is a 14 pin IC. The pins 1 and 7 are the output pins and they can be given to the gate terminals of two MOSFET switches. With this IR2112 driver IC we can produce the gate voltage level up to 10-20V. The pins 10 and 12 are receiving the pulses from the microcontroller of amplitude 5V. Pin 9 is given 5V supply and pin 13 is connected with the ground. Again pin 3 is connected with the 12 V supply. Pin 5 and 2 are acting as the return paths of high and low side outputs respectively.

Power circuit of the hardware prototype consists of two circuits such as SEPIC converter and voltage source inverter. Here it is designed to boost the input dc voltage of 12-15V into 200V. The voltage source inverter converts the boosted DC voltage from the SEPIC converter into AC voltage.

The switch used in the SEPIC converter circuit is IRF840 MOSFET. The inductor L1 and L2 are having the values of 121 μ H and is constructed as coupled inductor [12]. Capacitor values are $C_1=100 \mu$ F and $C_2 = 470 \mu$ F. The boosted DC voltage of the SEPIC converter is fed to the single phase voltage source inverter through the DC link capacitor. The DC link capacitor is used to maintain the constant DC voltage in the input side of the inverter. SG3524 IC is used to produce pulses for the two switches of the half bridge inverter. The switches used in the inverter circuit are P55NF06 N channel MOSFET. An inductor is used in this inverter circuit for the voltage balancing of load. The protection circuit consists of diode, resistances and capacitors are also employed in the circuit

V. RESULTS AND DISCUSSIONS

A. Simulation Results

The simulation of SEPIC converter and VSI fed single phase induction motor is done in MATLAB/SIMULINK and PSIM software. For the purpose of the simulation, constant irradiance and temperature is considered for the PV module. Fig 8 shows the SEPIC converter output voltage from the simulation model. It is the boosted Dc voltage of PV module. Also in this fig the SPWM technique pulses are shown. When the pulses of Q1 switch are in on period (high) the pulses for lower leg switch Q4 are in the off period (low). When Q1 pulses are high we can get the output voltage in the positive half cycle and when the Q4 pulses are high the output voltage will have negative half cycle. Fig 9 shows the simulation results of SPWM technique pulses, the inverter output voltage and the output current waveforms

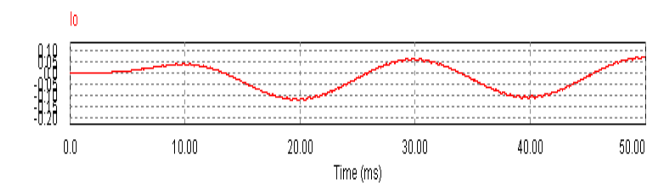
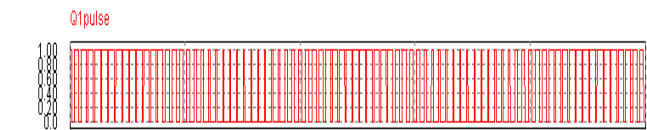
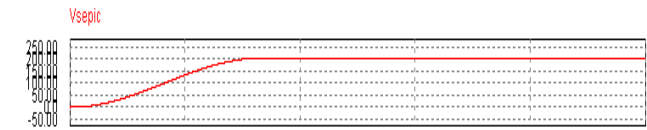
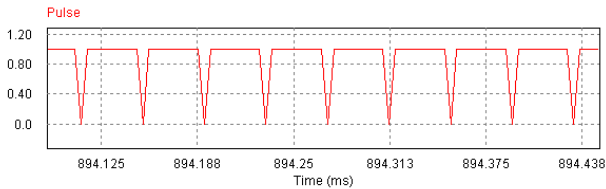




Fig. 8 The SEPIC converter output voltage and the inverted output voltage as a result of SPWM pulses

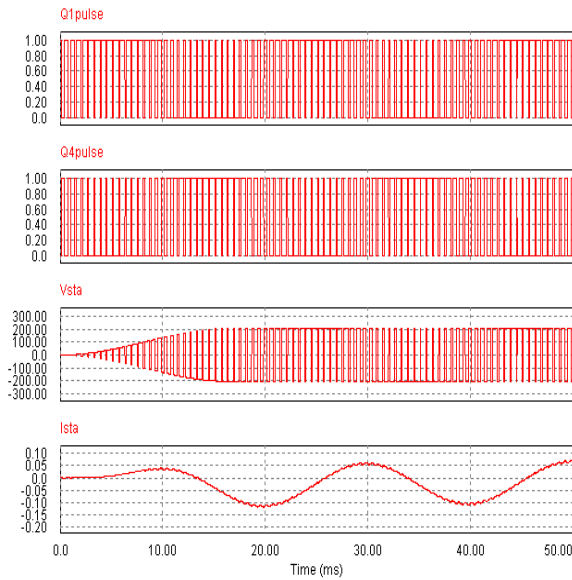


Fig 9. Upper leg switch pulse, lower leg switch pulse, output voltage and current waveforms

B. Hardware Results

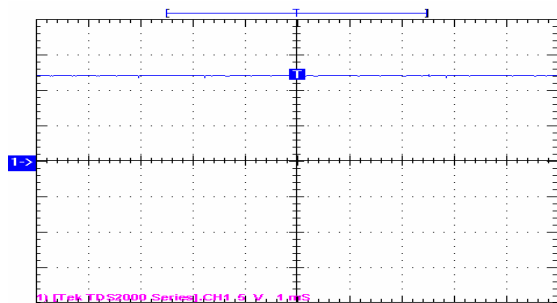


Fig.10 Input voltage waveform

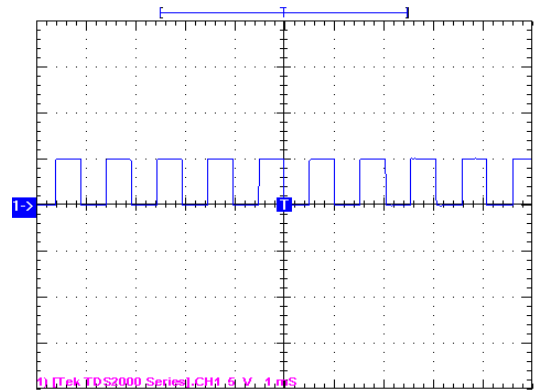


Fig.11 Pulse Output From the Controller Circuit

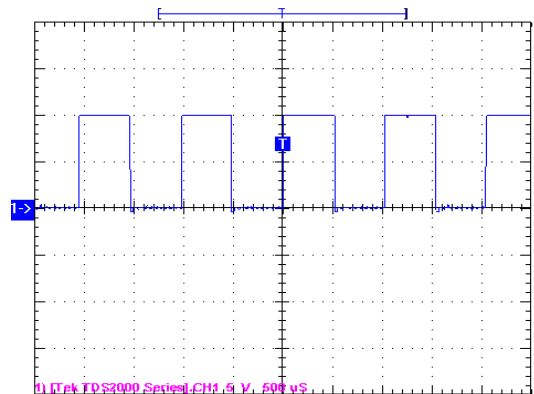


Fig.12 Driver circuit output

The input voltage of the hardware prototype is the 12V DC input of the SEPIC converter. This 12V DC input voltage is measured and shown in fig10. The controller circuit output pulse has the magnitude of 5V. This output is shown in fig11. Fig 12 shows the driver circuit output of 10V. Fig 13 shows the boosted DC voltage of 200V from the SEPIC converter circuit. Finally 180V peak to peak AC square wave, which is the output of inverter circuit, is shown in fig 14. With the implemented hardware prototype a single phase induction motor is running with the speed of 5659rpm. The rated speed of the machine is 6000rpm. The specifications of this single phase induction motor is 230V, 0.35A, 50W, 6000rpm.

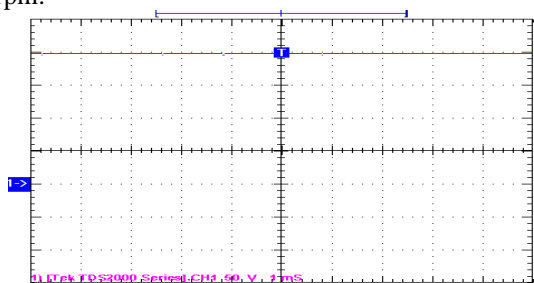


Fig.13 SEPIC converter output waveform

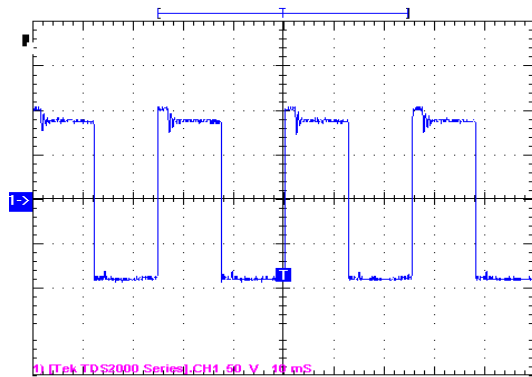


Fig.14 Inverter circuit output waveform

VI. CONCLUSION

This paper presented the simulation work of a Photovoltaic array feeding a three phase induction motor. SEPIC converter and voltage source inverter were used as interface between PV module and the induction motor. P&O MPPT Algorithm was used to obtain the maximum power point operation of PV module. The simulation works of these circuits were carried out in the MATLAB and PSIM software. The output voltage of inverter is increased and the current is reduced with the MPPT algorithm implementation. Experimental work has been done with the SEPIC converter and voltage source inverter to run the single phase induction motor using DC source. A PIC microcontroller was used to generate the pulses for driving the switch of the SEPIC converter. The boosted DC voltage of the SEPIC converter circuit output and inverted AC output waveforms were shown in the results.

VII. APPENDIX

A. Specification of BPSX150S PV Module:

Maximum Power (P _{max})	= 150W
Voltage at P _{max} (V _{mp})	= 34.5V
Current at P _{max} (I _{mp})	= 4.35A
Open-Circuit Voltage (V _{oc})	= 43.5V
Short Circuit Current (I _{sc})	= 4.75A
Temperature Coefficient of I _{sc}	= 0.065±0.015% /°C

B. Key features of PIC 16F877A Microcontroller:

Table 7.1 PIC Microcontroller Key Features

Key Features	PIC16F877A
Operating Frequency	DC - 20 MHz
FLASH Program Memory(14-bit words)	8K
Data Memory (bytes)	368
EEPROM Data Memory	256
Interrupts	15
I/O Ports	Ports A,B,C,D,E
Timers	3
Capture/Compare/PWM Modules	2
10-bit Analog-to-Digital Module	8 input channels
Instruction Set	35 instructions

REFERENCES

- [1] E. E. Jimenez-Toribio, A. A. Labour-Castro and F.M.Rodríguez, "Sensorless Control of SEPIC and Cuk Converters for DC Motors using Solar Panels" in *proceeding on Electrical Machines and Drives conference, IEMDC-09*, 2009, pp 1503-1510.
- [2] R. B. Darla, "Development of Maximum Power Point Tracker for PV Panels Using SEPIC Converter" in *proceeding on Telecommunications Energy conference, INTELEC 2007*, pp 650-655.
- [3] B. Santhosh Kumar, S. Arul Daniel, and H. Habeebullah Sait, "Analog controller for Photovoltaic array fed inverter driven Single-phase induction motor" , in *proceeding on Electrical and Electronics Engineering international conference(ELECO2009)*, pp: I-302-I-305, 2009.
- [4] B.Ismail, S.Taib, A. R Mohd Saad, M. Isa, C. M. Hadzer, "Development of a Single Phase SPWM Microcontroller-Based Inverter", in *proceedings on IEEE International Conference of Power and Energy, (PECON-06)*, pp 437-440.
- [5] S. M. Mohaiminul Islam, Gazi Mohammad Sharif, "Microcontroller Based Sinusoidal PWM Inverter for Photovoltaic Application", in *proceedings on first International Conference of Development in Renewable Energy Technology (ICDRET-2009)*, p-1.
- [6] J.G. Llorente,E.I.Ortiz-Rivera, A.S. Llinas, "Analysing the Optimal Matching of DC Motors to Photovoltaic Modules via DC-DC Converters" in *proceedings on Applied Power Electronics conference (APEC)* ,pp-1062-1068
- [7] M.Veerachary and K. S. Shinoy, "V²- Based Power Tracking for Nonlinear PV Sources", *IEE proceeding on Electrical Power Applications*, Vol. 152, No. 5, pp 1263-1270, September 2005.
- [8] M.S. Jamri and T.C.Wei, "Modeling and Control of a Photovoltaic Energy System using the State Space Average Technique" in *proceeding on American Journal of Applied Science-7*, 2010, pp 682-691.
- [9] M. G. Villalva, J.R. Gazoli, E. R. Filho, "Comprehensive Approach to Modeling and Simulation of PV Arrays", *IEEE Transactions on Power Electronics*, Vo. 24, No. 5, pp 1198-1208, May 2009.
- [10] Datasheet of "Design a SEPIC Converter" by National Semiconductor, May-2006
- [11] Datasheet of "PIC16F87X" by microchip technology, 2001.
- [12] "Transformer and inductor Design Handbook", by Colonel Wm. T. Mclyman, Third Edition, 2004
- [13] B. Wittig, W.T.Franke, F.W.Fuchs, "Design and Analysis of a DC/DC/AC Three Phase Solar Converters with Minimized DC Link Capacitance", in

proceedings on 12th European conference on Power Electronics and Applications, Aalborg, 2007

- [14] Zhou Hai-feng, Xu Zhi-long , Lin Zhong-hua, Wang Rong-jie, "Simulation Design of Inverter in Solar Photovoltaic System Based on MCU", *in proceedings on Photonics and optoelectronics conference(SOPO-2009)*,p-1.
- [15] Laurenfiu Rimifriu, Mihai Lucanu, Cristian Aghion, Ovidiu Ursaru, "Control With Microcontroller For Pwm Single-Phase Inverter", *in proceedings on international conference of Signals,Circuits and System(SCS-2003)*,pp:265-268.
- [16] Power Electronics Circuits, Devices and Applications, by M.H. Rashid, 3rd Edition, Pearson Education-2004



1 Sivaraman.P received the BE degree in electrical and electronics engineering from Bharathiar University, Coimbatore , in 2002 and the M.Tech. Degree from the School of Electrical and Electronics Engineering SASTRA University, Thanjavur, Tamilnadu, in 2004. Now he is pursuing PhD in Anna University of Technology Coimbatore. From 2004 onwards he is working with the Bannari Amman Institute of Technology, Sathyamangalam,Erode,Tamilnadu, where his current research interest include power converter for photovoltaic application and distributed power generation . He has published many papers in national and international journals and conferences to his credit.



2. Dr.A.Nirmalkumar completed his graduation and post graduation in Electrical Engg from Calicut and Kerala University in 1972 &1976 respectively. Completed his Doctorate from Bharathiar University in 1992. His area of specialization includes Power converters for renewable energy application and drives. He has more than 30 years of teaching experience. He is guiding at present 20 research scholars. He is the recipient of Institution of Engineers Gold Medal for the year 1989. He has many publications in national and international journals to his credit

Optimum Way to Increase the Fuel Efficiency of the Car Using Base Bleed

Prof. G Sivaraj^{*}, Mr. M Gokul raj^{**}

^{*}(Department of Aeronautical Engineering, Bannari Amman institute of technology, Sathyamangalam, India)

^{**}(Department of Aeronautical department, Bannari Amman Institute of technology Sathyamangalam, India)

ABSTRACT

Ever since then the invention of car have undergone several modifications in terms of speed, comfort, fuel efficiency, and other features In this paper we shall glance to reduce the drag force of car using base bleed .In this injects low velocity air into the rear side of car region. Computational analysis was carried out using Gambit and Fluent software. As per the computational analysis it's proved that, the drag coefficient of car model was reduced. In other word car spends the least power in overcoming the drag exerted by air and hence exhibits higher performance- cruises faster and longer, that too on less fuel.

Keywords: Fuel efficiency, Drag force, Computational Analysis, Base Bleed, Car Model

I. INTRODUCTION

Aerodynamic styling of a car is one of the most crucial aspects of car design-a highly complex phenomenon, encompassing the task of an artful integration of advanced engineering and stylish aesthetics. A lot of emphasize is laid on the aerodynamics in car design as an aerodynamically well designed car spends the least power in overcoming the drag exerted by air and hence exhibits higher performance- cruises faster and longer, that too on less fuel.

Apart from improved fuel economy, aerodynamically superior car offers better stability and handling at highway speeds and also minimization of harmful interactions with other vehicles on the roadway

Consequently, in the present era of enormously soaring prices of fuels with rapidly exhausting resources, and growing awareness among the consumers with regard to safety and other offered features, optimization of car aerodynamics, more precisely the reduction of associated drag coefficient (C_D), which is mainly influenced by the exterior profile of car has been one of the major issues of the automotive research centers all around the world. Average C_D values have improved impressively over the time, from 0.7 for old boxy designs of car to merely 0.3 for the recent more streamlined ones.

Aerodynamics is basically the study of how easily air glides over the surface of car. Air while moving past the car exerts two different forces on car surface,

- Tangential forces induced by shear stresses due to viscosity and velocity gradients at boundary surface, and
- Forces normal to the car surface resulting from pressure intensities varying along the surface due to dynamic effects.

Vector sum of these tangential and normal forces integrated over complete surface gives a resultant force vector. Component of this force in the direction of relative velocity past the car body is known as aerodynamic drag.

Aerodynamic drag, which compares the drag force, at any speed, with the force it would take to stop all the air in front of the car influences fuel consumption of a car, especially at higher speeds and hence is considered a crucial factor in judging its performance. An aerodynamically well designed car spends the least power in overcoming the drag and hence yields higher performance - cruises faster and longer that too on less fuel.

The forces of wind resistance against car are called drag. We measure a car's ability to slip through the wind by assigning it a drag coefficient (C_D), which is calculated through a mathematical equation. The C_D equation is

$$C_D = D / (0.5 \rho V^2 A),$$

where , D is drag,

ρ is air density,

V is velocity, and

A is the car's frontal area.

Reducing drag and lowering that C_D is one of the main goals of aerodynamic improvements, as getting a car to slice cleanly through the wind has several benefits. Probably the most important one is efficiency. Reduce the drag that is acting on a vehicle and you can reduce the power needed to push it through the air. An engine that does not have to work as hard gets better fuel economy, which is why aerodynamics are so important to the new car industry.

Over the top of the car, the air is also initially decelerated and again at the foot of the windscreen which means that pressure is tending to increase. But once over the highest point of the car, the favourable pressure gradient accelerates the air, so the pressure drops.

II. METHOD INVOLVING OF DRAG REDUCTION

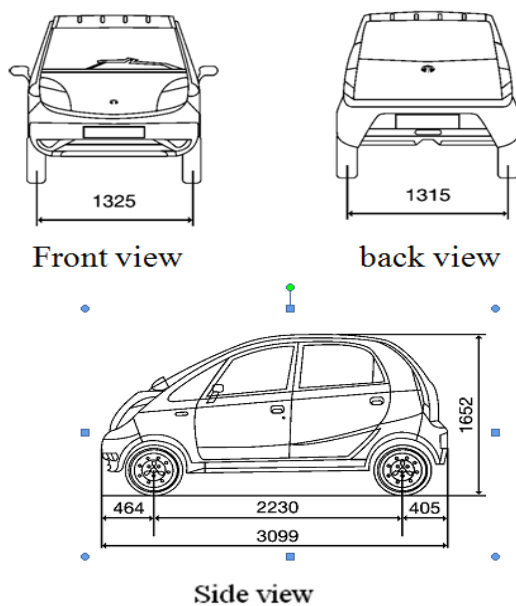
Designers have come up with all sorts of tricks to lower drag, from reducing a car's frontal area to molding

in small winglets under the trunk area to diffuse the air that comes out from underneath it.

But drag is just one aerodynamic factor that's at work on car. Two other forces we have probably heard about before are lift and down force. Look at the side view of a modern car and the shape looks something like the cross-section of an airplane wing, there could be enough lift to unload the tires and suspension, which will affect the car's traction and handling.

To investigate the aerodynamic performance of a car, computational analysis have been carried out using Gambit and fluent software.

III. DIMENSIONS OF CAR USED FOR ANALYSIS



IV. FABRICATION OF BASE BLEED AND ITS PRINCIPLE

BASE BLEED

Base bleed is two converging hollow tube which attached above the bottom of the car. Front end base bleed cross section is larger than the rear end so it injects low velocity air into the rear side of car region. This flow is known as base bleed. Which will results in reduction of the drag co-efficient.

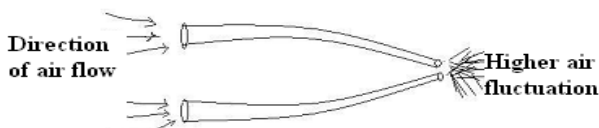


Fig. 1 Air flow of Basebleed

The main function of base bleed is

- Reduces the drag at low speed of the car itself (ie) from 50 kmph
- Increase the rear side pressure and reduce the front side pressure which intern reduces the overall drag of car.
- Reducing wake region at the rear side
- It improves the aesthetics of car as well as it improves the aerodynamics of car.

V. BASE BLEED ATTACHMENT

The nose features a single opening for the front grille and side air intakes, with aerodynamic sections and profiles designed to direct air to the coolant radiators and the new flat underbody. The nose also sports small aero elastic winglets which generate down force and, as speed rises, deform to reduce the section of the radiator intake and cut drag.

Technical development of the car's shaped started using CFD (Computational Fluid-Dynamic) techniques which helped optimize the different cross section of base bleed and interaction of the internal flows prior to wind tunnel testing.

The air intakes for engine bay cooling are situated on the aerodynamic underbody, where differences in pressure channel the air in the most efficient manner, and are positioned to increase rear downforce. Similarly air is channeled from the front air dam to the rear diffuser where the position and number of the fences has been developed to optimize the distribution of the vortex to improve rear downforce.

VI. DIFFERENT TYPES OF BASE BLEED CROSS SECTION

The base bleed has analyzed three different cross section of its. The three kinds of cross section are

- rectangle
- circle
- Ellipse

a) CIRCULAR CROSS SECTION

Frontal cross section

- circle
- radius = 4.068 mm
- area = 52mm²

Ending cross section

- circle
- radius = 1.5 mm
- area = 7.069 mm²

a) ELLIPTICAL CROSS SECTION

Frontal cross section

- ellipse
- $A = 6 \text{ mm}$
- $B = 2.75 \text{ mm}$
- $\text{area} = 52 \text{ mm}^2$

Ending cross section

- circle
- $\text{radius} = 1.5 \text{ mm}$
- $\text{area} = 7.069 \text{ mm}^2$

b) RECTANGULAR CROSS SECTION**Frontal cross section**

- rectangle
- $A = 13 \text{ mm}$
- $B = 4 \text{ mm}$
- $\text{area} = 52 \text{ mm}^2$

Ending cross section

- circle
- $\text{radius} = 1.5 \text{ mm}$
- $\text{area} = 7.069 \text{ mm}^2$

c) LOCATION OF BASE BLEED IN CAR

Figure shows base bleed is located in the car model. It made up of rubber material and it is flexible.



Fig. 2. Location of Base bleeds in car model

VII. COMPUTATIONAL APPROACH

In the computational approach, data concerning three-dimensional flow field around the body of car was visualized by simulating the flow conditions using Gambit as the preprocessing software and Fluent as the solver and post processor.

PRE PROCESSING**a). GEOMETRY CREATION**

The analysis of car aerodynamics can present a significant challenge, requiring the simulation of many different configurations and positions of both car and attachment of base bleed. Wind tunnel analysis with a rolling road is often impractical. The deployment of CFD Fluent 6.1 and Gambit within the design process, however, enables such studies to be carried out with relative ease.

When air flows over the surface of a car, a boundary layer forms where there is a large velocity gradient. In order to capture this phenomena correctly, the mesh around the surface of the body must be very fine. To perform this boundary layer study, I will be creating and solving two different meshes. All of the mesh parameters will be staying the same between the two meshes except for the boundary layers.

b) DEFINE THE GEOMETRY

When the geometry was defined in the creation of the computational mesh, all faces of the domain were assigned names. The names of the inlet and outlet planes (at $x = 0$ and $x = L$) are front face and back face of domain as velocity inlet and pressure outlet respectively. The names of the planes at $y = L$, $z=0$, and $z=L$ are outer wall as wall. The names of the model are car as a wall. And bottom face is defined as road.

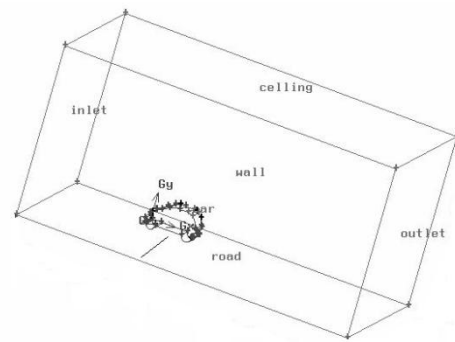


Fig. 3. Defining the geometry

Dimensions of the Domain are

Height = 20 m

Length = 35 m

Breath = 20 m

c). MESHING

An inflated boundary of prismatic elements was used near the car surface to improve spatial resolution and gain a better understanding of boundary layer phenomena. An unstructured mesh with polyhedral elements was used for volume meshing. Simulations were carried out with the turbulence model, coupled with a blend factor of 0.5 for the advection scheme.

The computational mesh was constructed automatically using polyhedral cells mesh, surrounded at solid boundaries by three prismatic extrusion layers. Because polyhedral cells fill space more efficiently than tetrahedral elements, fewer cells were required than might otherwise have been needed, significantly aiding the goal of using a small desktop machine to perform such aerodynamic analyses

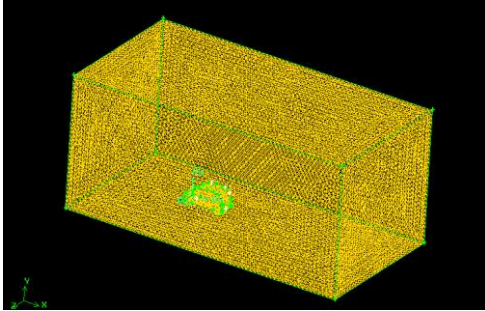


Fig. 4 .3D view of final polyhedral mesh with volume source visible around the car

A model that has already been meshed and it has only 130'000 polyhedral cells. Note that at least 5 million cells, with hexagonal in the near-wall regions, would be necessary to obtain reliable and detailed results in such a case.

The computational domain extends far upstream of the car where the boundary condition will be a velocity inlet. The top and bottom of the computational domain are "periodic" boundary conditions, which mean that whatever flows out of the top goes directly into the bottom. It is assumed that since the outer limits of the computational domain are so far apart, this car behaves as if in an infinite free stream. In order to adequately resolve the boundary layer along the car wall, grid points will be clustered near the wall. Far away from walls, where the flow does not have large velocity gradients, the grid points can be very far apart. A hybrid grid will be used in this problem. Grid adaptation within the flow solver, Fluent, will increase the grid density even more near the wall and wherever else needed.

d). IMPORTING THE MESH

Fluent reads the grid with about 130'000 cells from gambit file. Grid Check is sure there is no negative volume or face area and there is no warning of any kind.e

a. DEFINE THE PHYSICAL MODEL

Define the model of Solver is Segregated for Continuity equation is first solved for all cells, then Momentum and then turbulences. This works well for incompressible and moderate compressible flow. Applying the Implicit for each equation is solved for all cells together with actual dates. The implicit solver brings faster convergence.

Define the model as 3D and Steady. It is Absolute there is no moving mesh zone in the mesh. Define the Model is Viscous as k-epsilon for a robust and efficient turbulent model which gives good results in most cases

where turbulences have an isotropic repartition. Define the model of energy equation.

b. SPECIFY MATERIAL PROPERTIES

Define the materials is air And it is properties of

$$\text{Density} = 1.225 \text{ kg}\cdot\text{m}^{-3}$$

$$\text{Viscosity} = 1.464\text{e}^{-5} \text{ kg}\cdot\text{m}^{-1}\cdot\text{s}^{-1}$$

Those values correspond to the ICAO norm. Fluent means dynamic viscosity as we consider air as incompressible and are not looking for heat transfer problematic, we don't need to specify properties.

e). SPECIFY THE BOUNDARY CONDITIONS

OPERATING CONDITIONS

Let the 101325 Pa which corresponds to the ICAO-Norm. Fluent works with relative pressure.

VIII. BOUNDARY CONDITIONS

Car model is "wall" with "car" (in the field "Zone Name").We considers our model as a wind-tunnel model. So the car is a stationary wall, the viscosity makes the air stick at the car coachwork, so no slip the coachwork is very smooth, so a roughness of zero. Ceiling of the wind-tunnel and Side wall of the wind-tunnel are specified shear for this will allow the air to slip on the ceiling wall. This is not realistic, but so, we can use a very coarse mesh without boundary layer problems.

Road is specified as Moving Wall. As the car doesn't move, the road will have a velocity in the positive x-direction, so that the flow under the car will be correctly modeled. Velocity is $25 \text{ m}\cdot\text{s}^{-1}$ in the Speed field. Correspond to 90km/h. and 0.05m in the "Roughness Height" field.

Inlet is $25 \text{ m}\cdot\text{s}^{-1}$ in the "Velocity Magnitude" field as the car doesn't move, the air has to in the positive x-direction. Outlet is Zero Pa in the "Gauge pressure" field means we have atmospheric pressure at the outlet.

a) POST-PROCESSING

Normally we would have to enable better numerical schemes (2nd or 3rd order and run until a much better convergence of the flow solution is reached, but this would take about 3 hours with this case and about 2 weeks with an adequate mesh refinement). So we simply visualize the actual results.

IX. FLOW PARAMETERS TAKEN FOR STUDY

Five important results were obtained from the analysis.

Calculate the co-efficient of drag.

1. Drag force variation along the car model.
2. Static pressure variation along the car model.
3. Total pressure variation along the car model.
4. Path line of velocity magnitude variation along the car model.

All of the above results are analysis car with Base bleed attachment.

X. CONTOUR PLOTS (FILLED) FOR BASE BLEED

Initially three different cross section of base bleed are taken into consideration for analysis, which is circular, elliptical and rectangular.

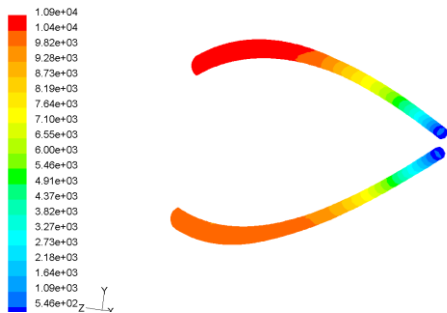


Fig. 5 Static pressure of elliptical base bleed

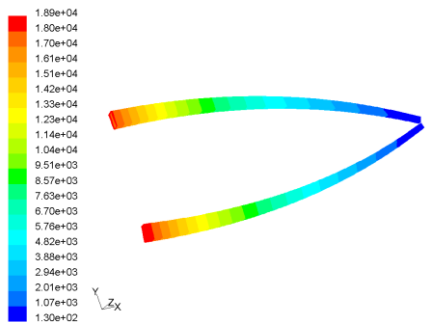


Fig. 6. Static pressure of rectangular base bleed

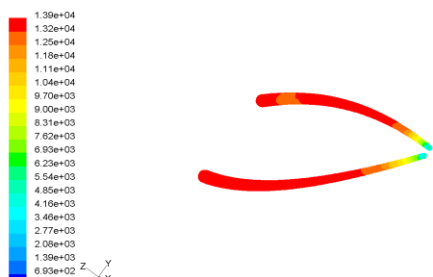


Fig. 7. Static pressure of circular base bleed

XI. STATIC PRESSURE VARIATION OF CAR AT FRONT SIDE

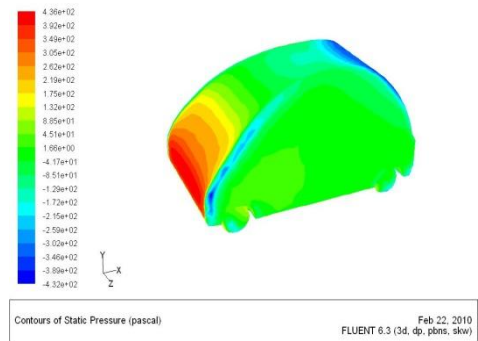


Fig. 8. Car model without base bleed

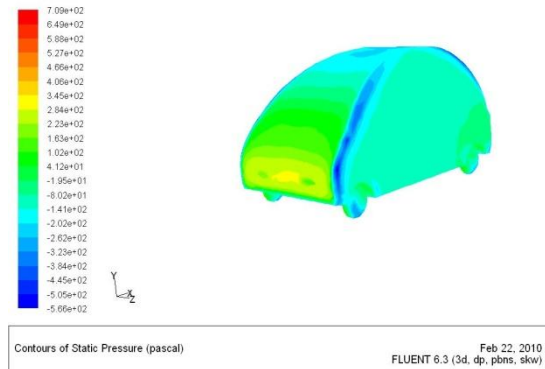


Fig. 9. Car model with base bleed

Three different cross section of base bleed are taken into consideration for analysis, which is circular, elliptical and rectangular. From analysis, it is clearly pictured that, elliptical cross section has higher fluctuation compared to that of other ones, which is clearly shown in above figures. Therefore elliptical cross section Base bleed is attached in the car model for experimental and computational work.

Three dimensional car model with and without Base bleed are taken into consideration for analysis. From analysis it is validated that, three dimensional car model with Base bleed has higher fluctuation compared to that of without Base bleed, which clearly shown in above figures.

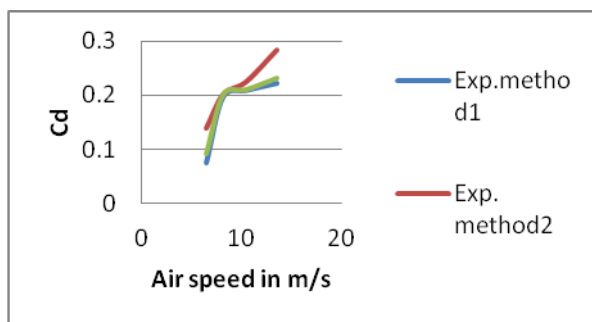
XII. RESULTS AND DISCUSSION

Pressure distribution matches with prediction that pressures would be low in the regions with streamlined profiles such as nose, base of the windshield etc. Almost identical nature of graphs of variation of pressure co efficient along car profile at different air velocities also verified that pressure co efficient is independent of speed

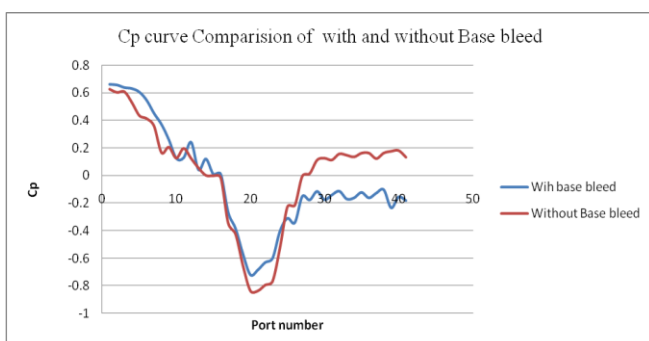
Table 1. Co efficient of drag on car model

Air speed	Computational result	
	Without Base bleed	With Base bleed
13.6m/s (1000 rpm)	0.3521	0.2321
10.52m/s (750 rpm)	0.3274	0.2109
8.23m/s (500 rpm)	0.2741	0.2013
6.52m/s (300 rpm)	0.1527	0.0927

Using this Table, variation of Co efficient of Drag C_D with air velocity (Graph. a and Graph.b) are plotted

Graph: 1 Variation of Air speed with C_D

Graph shows drag co efficient variation with air velocity of with and without base bleed. Pressure distribution matches with prediction that pressure would be low in the regions with streamlined profiles such as nose, base of the windshield etc., and almost identical nature of figs of variation of pressure co efficient along car profile at different air velocities also verified that pressure co efficient is independent of speed. Computational predictions of external aerodynamics of car showed quite a good agreement with and hence validated experimental once.



XIII. CONCLUSION

Keeping base bleed at the car model it will increase fluctuation energy of the air. As a result of verifications, it is confirmed that base bleed creates stream wise vortices. From this, we could predict that base bleed causes the pressure of the vehicle's entire rear surface to increase therefore decreasing drag.

So it is concluded that base bleed which gives very least drag and also regarding position, after front shield which has a very good effect in delaying the flow separation and also reducing wake region.

ACKNOWLEDGMENT

We first thank our 'GOD', the supreme power for giving us a good knowledge and our parents for making us study in a renowned college We owe a great many thanks to my colleagues and friends for their help and encouragement.

REFERENCES

- [1] Fukuda, H., Yanagimoto, K., China, H., Nakagawa, K., "Improvement of vehicle aerodynamics by wake control," *JSAE Review* 16:151-155, 1995.
- [2] Gaylard, A.P., "The Appropriate Use of CFD in the Automotive Design Process," *SAE Technical Paper 2009-01-1162*, 2009.
- [3] Tanner, M., "Reduction of Base Drag," *Prog. Aerospace Sci.* 16(4):369-384, 1975.
- [4] Mair, W.A., "Drag-Reducing Techniques for Axisymmetric Bluff Bodies," *AICHE Symposium Series: 161-187*, 1978.
- [5] Oertel, H., Jr., "Wakes Behind Blunt Bodies," *Annual Review of Fluid Mechanics* 22:539-564, 1990.
- [6] Viswanath, P.R., "Flow Management Techniques for Base and Afterbody Drag Reduction," *Prog. Aerospace Sci.* 32:79-129, 1996.
- [7] Morel, T., "Effect of base cavities on the aerodynamic drag of an axisymmetric cylinder," *Aeronautical Quarterly* 30:400-412, 1979.
- [8] Goodyer, M.J., "Some experimental investigations into the drag effects of modifications to the blunt base of a body of revolution," *Institute of Sound and Vibration, University of Southampton, Report No. 150*, 1966.
- [9] Nash, J.F., Quincey, V.G., Callinan, J., "Experiments on two-dimensional base flow at subsonic and transonic speeds," *Aeronautical Research Council R & M 3427*, 1966.
- [10] Khalighi, B., Zhang, S., Koromilas, C., Balkanyi, S.R., Bernal, L.P., Iaccarino, G., Moin, P., "Experimental and Computational Study of Unsteady Wake Flow Behind a Bluff Body with a Drag Reduction Device," *SAE Technical Paper 2001-01-1042*, 2001.

Biogas Scenarios

Soham M. Trivedi

Biotechnology Engineering Department, V.V.P. Engineering College, Rajkot, India

ABSTRACT

The demand of energy has been increased over the years due to increasing world population and expansion of global industries especially for food and feed. Most of the energy is consumed in transportation, industries & factories, power generation, and community sectors. Moreover, in order to fulfill our demand we are mostly dependent on energy, taken from fossil oil, gas and coal. In developing countries like India, more than 80% of the population lives in the rural areas where more than 90% of the energy being consumed comes from non-commercial sources, the major one being fuel wood. The increasing cost of conventional fuel in urban areas necessitates the exploration of other energy sources. Biogas technology provides an alternate source of energy in rural India as a substitute for fossil fuels. The generation of biogas from food waste/refuse or peelings, agricultural and animal waste produces energy. In Gujarat the fossil resources are limited, and they impose a high burden on the environment therefore looking at the ecological and economical perspectives, biogas is an important source of energy for the state. In addition to biogas generation, another important aspect of biogas compression is the scrubbing of the biogas in order to remove impurities that are generated during the digestion process such as carbon dioxide and hydrogen sulfide. Thus as effective biogas production is strategic the review highlights the various biogas scenarios that can facilitate the vision of a more cleaner environment and to effectively deal with the energy crises problems.

Keywords: - Biogas, Biomass, Energy crisis, biogas scrubbing

I. BIOGAS AND GUJARAT

The range of application of biogas technology in Gujarat is currently being limited to applications in the developing world such as India, Africa, and the Philippines for uses such as cooking fuel and heating homes [1, 2]. After independence it was realized that the country was facing severe power shortage. Therefore there was a crying need to overcome this shortage by rendering services and making the availability of Renewable Energy Sources in the most rural parts of the country. Therefore from a primitive stage long term R&D goals were set to enhance the idea of renewable energy in Gujarat state with a ultimate aim to enlighten each and every house in remote villages, facing power problems. Furthermore R&D aimed to effectively utilize eternal resources of energy like the Sun, biomass and wind to provide sophisticated services with generation of employment. Thus, biogas developments in Gujarat can facilitate the vision of a energy-independent state and ultimately can add to the country's economy.

Looking at Gujarat's ecological and economical perspectives, biogas is an important source of energy. The fossil resources are limited, and they impose a high burden on the environment. A resource-conserving alternative made from biomass poses a different scenario. The raw material is renewable, and conversion only releases as much CO₂ as was previously contained by the source material. With the technological progress made in recent years, high energy efficiency and low-maintenance operation have made investment into biogas facilities more and more attractive. Accordingly, an attractive business opportunity has been created, one that is setting new standards in matters of sustainability and efficiency. Development of Biogas technologies in the state can thus enhance the provision of electricity at guaranteed rates, a lasting heat source at constant costs. It can serve as a constant energy source for the agricultural business and has a potential to increase fertilizing efficiency of fermented liquid manure significantly reduced odor emissions of fermented liquid manure. The ease in storability of biogas allows it to be used for the lucrative peak load coverage.

Biogas is defined as the mixture of methane and carbon dioxide produced by the bacterial decomposition of sewage, manure, garbage, or plant crops [3]. In Gujarat most research in this area is currently being done to explore biogas generation through anaerobic digestion in an effort to develop inexpensive and effective methods for promoting digestion of animal and human waste. Anaerobic digestion is the breaking down of organic matter by microorganisms in an oxygen poor environment, and results in biogas [4]. There are two different types of digesters Mesophilic and Thermophilic, which refers to the temperature at which they operate and the corresponding bacteria which thrive in that environment [5]. Mesophilic digesters operate near 30°C (86°F), and in warmer climates often require no additional heating. Thermophilic digesters operate around 60°C (140°F), and thus require additional heating and are often only practical for large industrial uses.

Biogas is considered renewable because it mainly depends on the supply of grass which grows back but natural gas comes from the fossilized remains of plants and animals from thousands of years ago so it is not considered "renewable". Methane is a well known type of biomass energy. Some examples of biomass energy are wood, straw and manure. Certain seminal experiments in the state were based on the bacterial strains that are present in the intestines of many animals. When these bacterium breaks down cellulose (the main ingredient in plant fibers) it produces biogas. For this reason methane is found in many other places as well, such as bogs, swamps and landfills. It can be used as an alternative opposed to natural gas for heating and cooking.

In Gujarat, for the production of biogas generally organic material, such as animal and plant waste is placed along with water into an oxygen free tank, or in some cases plastic membrane for digestion. In a common mechanism for gas collection in a continuous digester, there is the variable volume design of a Gasometer in order to accommodate the increasing methane. In this case, the gas outlet is located at the bottom of the tank, as it is easier to install in the case of a solid walled digester and does not require elasticity in design. The organic matter is fed into the vessel and the resulting gas is outlet through a pipe that inlets above the waste liquid levels in the tank. Similar mechanisms are achieved using plastic membranes, which are contained in secure enclosures in the ground [6]. Another area of research includes attempting to simulate and model methane generation from different types of waste in different environments in order to better understand the process [7, 8].

II. SCRUBBING THE BIOGAS

In addition to biogas generation, another important aspect of biogas compression is the scrubbing of the biogas in order to remove impurities that are generated during the digestion process such as CO₂ (Carbon Dioxide) and H₂S (Hydrogen Sulfide). There are many different methods of Biogas Scrubbing, each with varying degrees of effectiveness. Many methods of Scrubbing the Biogas of single or multiple impurities are discussed in Kapdi's work [9], although few methods seem economically feasible for small scale developing world operation. The Scrubbing is viewed as very important as Hydrogen Sulfide is highly corrosive to the cooking and heating systems that would utilize the biogas, and the presence of Carbon Dioxide makes the gas more difficult to compress and store, although it does not increase the volatility [9]. A simple method for Hydrogen Sulfide utilizing steel wool in a glass bottle is modeled, and seems to be the most viable option for low cost, easy implementation Hydrogen Sulfide removal [4]. In this method of Sulfide removal, the gas reacts with the steel wool, creating black Iron Sulfide. The Iron Sulfide generation begins at the bottom of the container, and once the steel wool is 75% black (i.e. 75% of it has been turned into Iron Sulfide); the wool should be removed and replaced. The used wool can be reused after exposure to air. This oxidizes the wool to rust, which can be reused in the system, as it will react with the Hydrogen Sulfide [4]. For Carbon Dioxide removal, as well as additional Hydrogen Sulfide removal a method of water spray cross-flow can be used [4, 9]. In this method the Biogas enters one end of a tube and experiences water streams flowing in the opposite direction, effectively removing a good deal of Carbon Dioxide from the gas. This design can be varied and the wastewater can be re-used in the process [9].

Scrubbing has also been a strong area of technical development and patenting. USPN 7160456, Method and equipment for processing of organic material, outlines the use of a second chamber and ammonia in order to remove CO₂ from biogas. Complementally, USPN 6709592, Removal of Sulfur compounds from wastewater, outlines a dual chamber digester method for Sulfide removal. USPN 6221652 Process for biological removal of Sulfide outlines a method in which and aqueous washing liquid is treated with

Sulfide oxidizing bacteria. There is also a patent for a method of Wet Scrubbing for the removal of CO₂, which outlines the process and design by which this would take place. USPN 7033822, Self-contained and streamlined Methane and/or high purity Hydrogen generation system, outlines a method for hydrogen specific generation using anaerobic digestion as well as mixed gas to power a gas driven generator in order to further compress the gas for Hydrogen removal. Although this patent heavily refers to mixed gas compressors and their use, it does not discuss the method for compression in any sort of detail.

Although much work has been done in research and development of methods to produce as well as scrub Biogas, and compression is often mentioned, less work is done regarding the actual method of compression of the gas. In industrial uses, classic industrial air compression techniques are often used, however in this small scale, off the grid usage, different methods of compression and driving compression need to be determined.

III. INDIA AND ENERGY

The role of energy in India's economy has become globally relevant in recent years due to the country's high economic growth and rising concerns about the environmental impacts of energy use. Primary energy demand grew at the rate of 6 per cent a year between 1981 and 2001 (Planning Commission, 2002), and India now ranks fifth in the world in terms of primary energy consumption. It accounted for about 3.5 per cent of the world's commercial energy demand in 2003. Although there has been a gradually increasing dependency on commercial fuels, a sizeable amount of the national energy requirement, especially in the rural household sector, continues to be met by noncommercial energy sources. These include fuel wood, crop residue, and animal waste, as well as human and draught animal power. Future economic growth will lead to a rapid increase in demand for commercial energy higher levels of urbanization, and adoption of modern lifestyles.

The Renewable Energy Plan 2012 calls for achieving a 10 percent share for renewable energy in incremental power capacity by adding about 10,000 MW of new renewable energy (RE) based generation. In addition to the grid-connected RE goal, other major RE initiatives include-installment of 1 million household solar water heating systems; electrification by renewable mini-grids for 24,000 villages without electricity; deployment of 5 million solar lanterns and 2 million solar home lighting systems; (4) and establishment of an additional 3 million small biogas plants. The Electricity Act of 2003 has provided a major thrust to RE technologies via its mandate: "To promote cogeneration and generation of electricity through renewable sources of energy by providing suitable measures for connectivity with the grid and sale of electricity to any persons, and also specifying, for purchase of electricity from such sources, a percentage of the total consumption of electricity in the area of a distribution licensee." The National Electricity Policy of 2005 gives each State regulator authority to create a Renewable Energy Portfolio Standard for the transmission and distribution companies serving their jurisdictions.

The Ministry of New and Renewable Energy (MNRE) is involved in the development, demonstration and utilization

of various renewable energy-based technologies, including Solar Thermal, Solar Photovoltaics, Wind power, Biomass combustion/co-generation, Small Hydro power, Biogas, Geothermal, Waste-to-energy, and tidal power. Major MNRE activities include: (i) Project development and financing of RE-based grid power; (ii) Urban solar hot water heaters; (iii) rural biogas projects; and (iv) resource mapping.

India has the most developed and diversified renewable energy market. The annual turnover of the RE industry in India is approximately US\$500 million, with total RE investment of around US\$3 billion. Furthermore, the 3,500 MW of RE generation capacity installed so far is just a fraction of the estimated total economic potential of 100,000 MW. The Government of India has set a goal of electrifying 18,000 remote villages and meeting 10 percent of the country's power supply through RE by 2012. These targets are in addition to those fixed for other RE devices or programs, including establishing 1 million biogas plants; 1 million solar PV systems for lighting; 8,000 solar PV pumps for irrigation; 10,000 solar PV generators, stand-alone solar PV power plants, solar water heating systems, solar air heating systems, and solar cookers, including large steam cooking systems; 360 energy demonstration parks, and; more solar retail outlets and solar passive buildings.

IV. GLOBAL SCENARIO

There are currently multiple US patents for Biogas digestion technology, many dealing with Biodiesel generation, although some are Biogas specific regarding construction of digesters. USPN 7,186,339B1, Anaerobic Digester System for Animal Waste Stabilization and Biogas Recovery, addresses the design of a flexible bladder digester, as well as transmission of the Biogas from the bladder to a storage container, but it does not address any methods of compression. USPN 7,005,068, Method and Apparatus for treating animal and wastewater, addresses uses of Biogas as well as details regarding digestion methods and suggests that the Biogas can be compressed for storage, but does not specifically outline compression methods to be used. One notable patent in the area of Bio-diesel usage that should be mentioned is USPN 5501185, Biogas driven generator set, which outlines a method to use Biogas in a Bio-diesel engine, and includes a pumping process to boost the pressure of the Biogas for pumping into engine regulator.

V. CONCLUSION

Although renewable energy power generation is a genuine clean development success story, there are some problems that need to be addressed to make the industry sustainable and self-supporting. There is currently some retrenchment going on with respect to RE policy amongst the State regulators. States with strong RE policies include Andhra Pradesh, Tamil Nadu, Maharashtra, and Gujarat. A strong RE policy consists of: (i) Preferential treatment; (ii) Portfolio standards; and (iii) Standardized PPA. However, care must be taken towards over-subsidizing renewable energy development relative to other energy sources at the expense of rate payers and taxpayers. The disaggregate nature of implementing the Electricity Act's renewable energy portfolio standards has created considerable disparities and lack of analytic basis for the relative pricing

of various forms of RE within and between different States (e.g., Hydro gets a lower price than Wind or Biomass in one state, or the price is very different between two adjacent states). Because the price made available to RE project developers does not seem to be firmly grounded, transmission and distribution licensees are going to court to avoid entering into power tariffs for purchases of renewable energy. There is a need for standard methods of valuation of the relative environmental benefits accruing to different forms of RE, which could then be reflected in PPA price differentials RE resources should also play a bigger role in providing decentralized power to remote areas, in line with the goal of providing modern energy access to all by 2012. Decentralized power generation, especially in remote locations where the grid cannot be extended, should necessarily be based on RE forms to provide these regions with access to clean and reliable energy. [12]

REFERENCES

- [1] Anozie, A.N., et al. Evaluation of cooking energy cost, efficiency, impact on air pollution and policy in Nigeria. *Energy* 32 (2007) 1283-1290.
- [2] Brown, Valerie J. Biogas a Bright Idea for Africa. *Environmental Health Perspectives* 114 (2006) 300-302.
- [3] Dictionary.com Unabridged (v 1.1). <http://dictionary.reference.com/browse/biogas>. January 17, 2008.
- [4] Shannon, R. Biogas Conference Proceedings 2000. <http://www.rosneath.com.au/ipc6/ch08/shannon2/index.html>
- [5] Anaerobic Digestion. <http://www.energy.ca.gov/development/biomass/anaerobic.html>
- [6] Aguilar, Francisco. How to Install a Polyethylene Biogas Plant. Toward a better use of our natural resources.
- [7] Hill, D.T., et al. Simulation of low temperature anaerobic digestion of dairy and swine manure. *Bioresource Technology* 78 (2001) 127-131
- [8] García-Ochoa, F. et al. Kinetic model for anaerobic digestion of livestock manure. *Enzyme and Microbial Technology* 25 (1999) 55-60
- [9] Kapdi, S.S., et al. Biogas scrubbing, compression and storage: perspective and prospectus in Indian Context. *Renewable Energy* 30 (2005) 1195-1202
- [10] Regional Information Service Centre for South East Asia on Appropriate Technology (RISE-AT) (Nov 1998), Review of current status of Anaerobic Digestion Technology for treatment of MSW.
- [11] Omstead, D.R., Jeffries, T.W., Naughton, R., Harry, P.(1980) Membrane-Controlled Digestion: Anaerobic Production of Methane and Organic Acids, *Biotechnology and Bioengineering Symposium No 10*, 247-258
- [12] Annex 2, India country report from ideas to action: clean energy solutions for Asia to address climate change.

Fundamentals of Fuzzy Logic with an Easy-to-use, Interactive Fuzzy Control Application

Utku Kose¹

**Distance Education Vocational School, Afyon Kocatepe University, Turkey*

ABSTRACT

The Fuzzy Logic and the Fuzzy Control approach is an important Artificial Intelligence technique, which allows designing and developing “human-thinking” based, intelligent systems or applications that employ effective mathematical calculations to solve real-world based problems. At this point, the related technique is widely used by scientists, researchers and engineers in different disciplines and fields. In this context, this work introduces an easy-to-use, interactive Fuzzy Logic application that enables users to develop a simple “two inputs – one output” Fuzzy Control system. With its interactive using features and functions, the application also introduces fundamentals of the fuzzy logic technique.

Keywords: Artificial Intelligence, computer application, Fuzzy Control, Fuzzy Logic, Fuzzy Set Theory, visual programming

I. INTRODUCTION

In Computer Science, Artificial Intelligence field has an extremely important place with its effective approaches, methods, techniques and wide working domain. Currently, there are many different Artificial Intelligence techniques introduced to be used for providing accurate, effective and efficient solving approaches for real-world based problems. Some of these techniques are developed to be used for solving specific problems whereas other remaining ones have wide application scopes. Because of their effective and flexible mathematical foundations, some of these techniques are still used by scientists, researchers or engineers to solve real-world based problems. The Fuzzy Logic is one of these techniques, which is widely used in today’s intelligent problem solving systems or applications.

This work introduces an easy-to-use, interactive Fuzzy Logic application that enables users to develop a simple “two input – one output” Fuzzy Control system. The application is based on Adobe Flash technology and so, it uses visual, vector features of the related technology to form general using structure of the application. With its interactive using features and functions, the application also introduces fundamentals of the fuzzy logic technique. By using the application interfaces, users can easily design and test their Fuzzy Control systems. The programming infrastructure of the application has been designed and coded carefully in order to provide accurate mathematically and logically correct results for any type of “two inputs – one output” system.

The rest of the paper is structured as follows: The next section explains the fundamentals of the Fuzzy Logic; Fuzzy Set Theory, basics of the Fuzzy Logic technique and also Fuzzy Control. Next, Section 3 explains general structure and using features and functions of the developed Fuzzy Control application. Section 4 is devoted to the testing process, which were performed to evaluate effectiveness of the application. Finally, Section 5 outlines the conclusions that have been reached with the work and expresses some future works.

II. FUZZY SET THEORY, FUZZY LOGIC AND FUZZY CONTROL

Before introducing the developed application, it is better to explain its theoretical and mathematical foundations to understand the performed work better. In this sense, the related Artificial Intelligence technique: Fuzzy Logic and the Fuzzy Control concepts must be explained.

The Fuzz Logic technique is based on the Fuzzy Set Theory, which was first introduced by Lotfi A. Zadeh in a seminar organized at University of California at Berkeley, USA [1]. Following the seminar and the related ideas introduced by Zadeh, more about theoretical infrastructure of the Fuzzy Logic technique was expressed in many different sources [2, 3]. In this context, Fuzzy Logic was developed from the Fuzzy Set Theory in order to reason with uncertain and vague information and represent knowledge with an operationally powerful approach [2]. On the other hand, the Fuzzy Control term is used to define intelligent control systems designed and developed via Fuzzy Logic principles.

In addition to the related explanations, differences between the Crisp Logic and the Fuzzy Logic must also be introduced to provide more information about theoretical foundations of the Fuzzy Logic.

In the Crisp Logic, variables are provided with the value: “true” or “false”. At this point, certain classifications are made by using the Crisp Logic. So, a member can be included in only one set. For example, for the relationship with the set “S”, the characteristic function gives us “true – 1” if an element named “a” is the member of the set “S” or “false – 0” if an element named “a” is not the member of the set “S” [4]. This situation is shown in the graphic provided in Fig. 1.

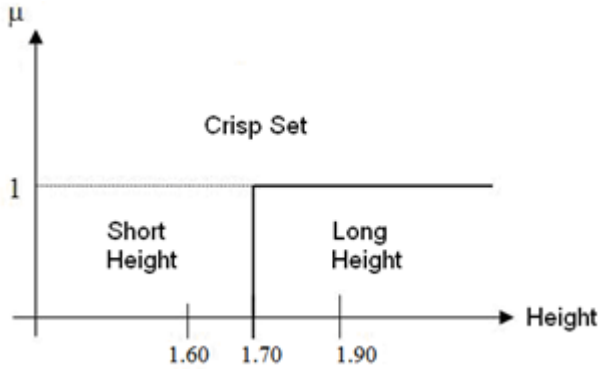


Fig. 1. A crisp set.

As different from the Crisp Logic, the related member may be in one or more sets within the Fuzzy Logic approach. In this context, it has a value defining its membership degree. The related situation is presented in the graphic within Fig. 2.

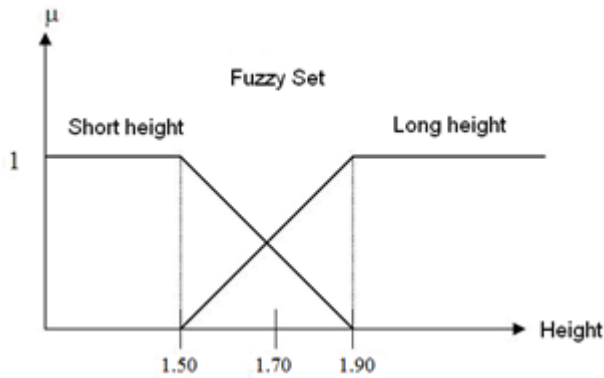


Fig. 2. A fuzzy set.

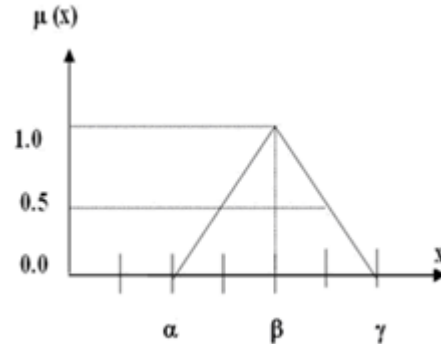
In the Fuzzy Logic, the expressed membership degree of the element is defined by using different types of functions (membership functions). In mathematical approach, the relationship between the set “S” and the element “a” can be defined as in “equation 1”.

$$\mu_S(a): F \rightarrow [0, 1]; \quad \mu_S(a): \in [0, 1] \quad (1)$$

In the “equation 1”, the set F is the fuzzy set of S(a) [4].

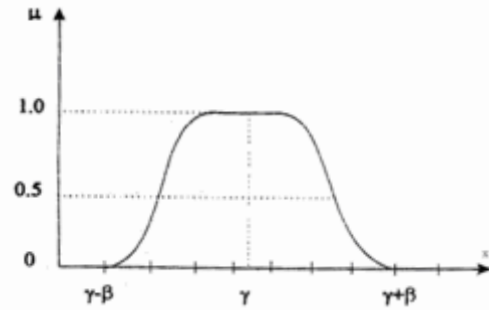
Within the Fuzzy Logic, after determining fuzzy sets that will be used, membership functions for the sets should be chosen. At this point, a membership function is some kind of curve converting the numerical value of input within a range from 0 to 1. In this sense the belongingness of the input to a fuzzy set is indicated [5]. In addition to assignment of membership functions, it also extremely important that the type of membership functions for inputs and outputs must be defined by the expert experience [2, 3, 6]. In this way, thinking structure of the person who has an expert experience about the subject the Fuzzy Logic used in is associated with the designed Fuzzy Logic based system or application.

As it was explained before, there are many different types of membership functions used within the Fuzzy Logic. Widely used ones are triangle, gaussian and trapezoid membership functions. These functions and their mathematical explanations are shown in Fig. 3.



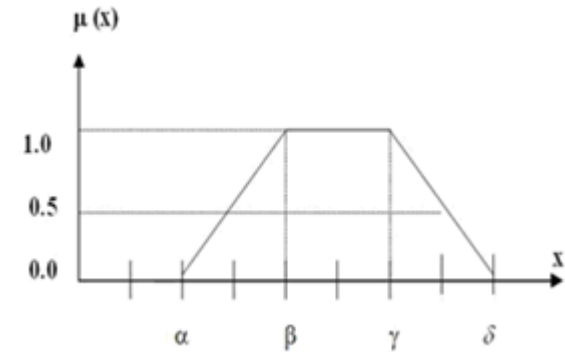
$$\Delta(x, \alpha, \beta, \gamma) = \begin{cases} 0, & x < \alpha \\ \frac{(x - \alpha)}{(\beta - \alpha)}, & \alpha \leq x \leq \beta \\ \frac{(\gamma - x)}{(\gamma - \beta)}, & \beta \leq x \leq \gamma \\ 0, & x > \gamma \end{cases}$$

a) Triangle membership function



$$\pi_s(x, \beta, \gamma) = \begin{cases} \left(x, \gamma - \beta, \gamma - \frac{\beta}{2} \right), & x \leq \gamma \\ 1 - \left(x, \gamma, \gamma + \frac{\beta}{2}, \gamma + \beta \right), & x \geq \lambda \end{cases}$$

b) Gaussian membership function



$$\mu(x, \alpha, \beta, \gamma, \delta) = \begin{cases} 0, & x < \alpha \\ \frac{(x - \alpha)}{(\beta - \alpha)}, & \alpha \leq x \leq \beta, \\ 1, & \beta \leq x \leq \gamma \\ \frac{(\delta - x)}{(\delta - \gamma)}, & \gamma \leq x \leq \delta \\ 0, & x > \delta \end{cases}$$

c) Trapezoid membership function

Fig. 3. Different types of membership functions.

After determining the related input, output fuzzy sets and so membership functions, some kind of “linguistic rules” must be determined in order to enable system to transform the input variables to the output variables during the operation. In this context, a linguistic rule is formed by writing a “if – then” rule. For example in a Fuzzy Logic system or application that uses two inputs for one output, some simple rules can be written as follows:

IF (*weight IS LOW*) AND (*height IS NORMAL*) THEN (*result IS HEALTHY*)

IF (*weight IS NORMAL*) AND (*height IS HIGH*) THEN (*result IS HEALTHY*)

IF (*weight IS VERY LOW*) AND (*height IS SHORT*) THEN (*result IS ILL*)

IF (*weight IS VERY LOW*) OR (*height IS VERY HIGH*) THEN (*result IS CRITICAL*)

In a typical Fuzzy Logic system or application, the related linguistic – “if-then” rules are combined in a table named as the “rule table”. Each output for different input variables can be observed by using this table. As it can be understood, this table is formed with the “expert knowledge”.

After the last step, the Fuzzy Logic system or application is ready to be operated. At this point, it gets the output from given input variables. However, the obtained output is also a “fuzzy set”. So, in order to use the output value in the real-world, its fuzzy value must be translated into real values.

This translation approach is named as “defuzzification” [7]. There are many methods of defuzzification such as centroid, centre of sums, mean of maxima and left-right maxima.

By combining theoretical infrastructure of the Fuzzy Logic and real-world based control problems, Fuzzy Control systems or applications are designed and developed easily. This type of intelligent control systems allows solving control problems via more accurate, effective and efficient logical and mathematical approaches. Fig. 4 shows a typical Fuzzy Control system schema [8].

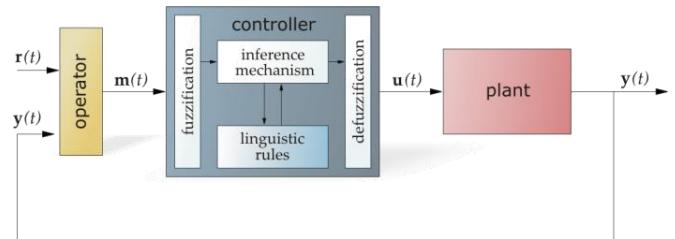


Fig. 4. A typical Fuzzy Control system schema [8].

III. AN EASY-TO-USE, INTERACTIVE FUZZY CONTROL APPLICATION

The interactive Fuzzy Control application has been designed and developed to provide a fast and easy-to-use using experience for anyone who wants to design a “two inputs – one output” system by using simple interfaces and controls provided within. The strength of the application is based on a popular, widely used animation and Web technology: Adobe Flash. With its object oriented “Action Script” coding approach and visually improved designing tools, the related technology has allowed forming such an interactive application environment. In order to improve easy using experience, colored, simple application controls and interfaces has been provided. Additionally, all working processes of a typical Fuzzy Logic and so Fuzzy Control system have been tried to be provided with visually powered tools and interfaces. In this way, users are enabled to understand performed processes better while working on a system.

In order understand the whole application, it is better to explain using features and functions of the application. For this aim, a typical working session can be explained as below:

III.I. Designing – Adjusting Inputs

As it was expressed before, the application allows user to design “two inputs – one output” systems. So, the main interface of the application was designed to fit for two different inputs and their visual presentations with membership functions. Fig. 5 presents a screenshot from the main interface of the application.

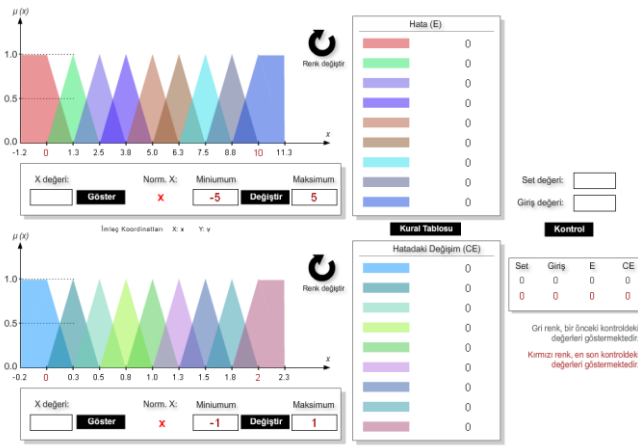


Fig. 5. A screenshot from the main interface of the application.

As shown in Fig. 5, both two inputs were formed by 9 triangular membership functions. At this point, number of membership functions, type of each membership functions and their values can be adjusted by clicking on each input graphic and so visual membership function set. After adjusting general structures of inputs, contents of each table provided on right side of inputs are also changed. These tables are used to give information about membership values for any given input.

In addition to the explained adjustments, it is also possible to change minimum and maximum values of each input. This can be done by using the provided text box objects under each input graphic. It is also important that, the application also allows users to change visual presentation of each input graphic according to determined “normalization” values. Fig 6 shows a screenshot from an input graphic (including 9 triangle membership functions) with normalization to a minimum value of 0 (according to min: 25 max: 120).

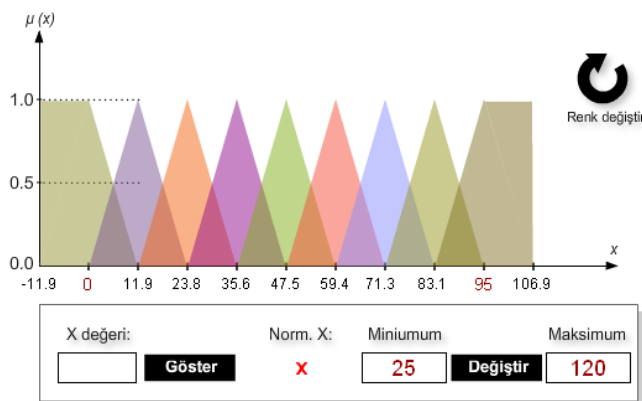


Fig. 6. A screenshot from an input with norm. min: 0.

III.II. Getting an Input Result

By using the text box located under-left side of each input graphic, it is possible to feed the related input set with a value and see the obtained results. On each input graphic, the input value is shown with a “red line indicator” over the related membership functions of the current graphic. After

feeding the input, obtained membership value results are also shown on the associated table located on right side of the graphic. Fig 7 presents a input value and obtained results on the table (In this input, min: -150 max: 150 and the normalization to min: 0)



Fig. 7. An input value and its results.

As it can be understood from the Fig. 7, the value of 23.3 has 0.379 membership value for the 5th membership function whereas it is 0.621 for the 6th membership function.

III.III. Rule Table

By clicking on the button located between two result table, users can open the rule table interface for the designed system. After opening the related interface, values each cell can be changed by clicking on them or the related button located on top side of the interface. Fig. 8 shows a screenshot from the rule table interface.

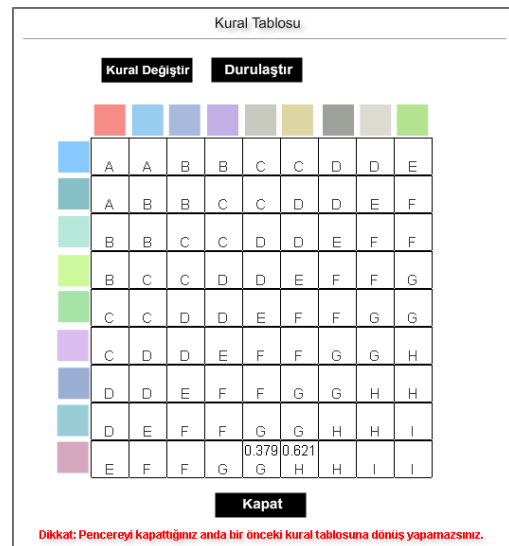


Fig. 8. A screenshot from the rule table interface.

It is also noticeable that any obtained result for input values are also shown over the rule table.

III.IV. Defuzzification

For the given input values and obtained fuzzy output, the defuzzification process can be performed by clicking on the related button located on top side of the rule table interface. After clicking on the button, the visually powered defuzzification interface is opened. Over this interface, users can see both visual presentation of the related input and output results and also “defuzzified” output value. At this

point, it is possible to change defuzzification method by clicking on the defuzzification method name on top side of the interface. Fig. 9 shows a screenshot from the defuzzification interface.

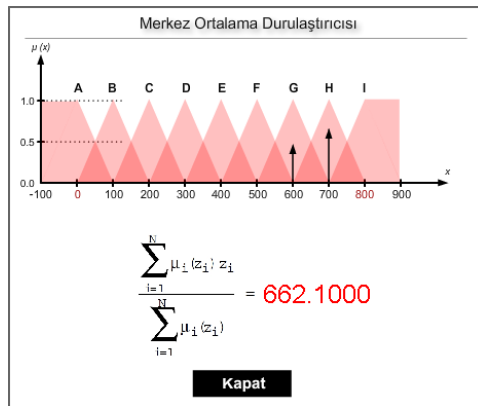


Fig. 9. A screenshot from the defuzzification interface.

III.V. Obtaining Fuzzy Control

In order to perform a Fuzzy Control, controls provided on right side of the main interface are used. In this sense, after designing the related input, output structures and any other elements, users can determine u, reference and error limit values by using the provided controls (because of the limited visual space, the related text boxes are changed during determination of the values). A screenshot from the related controls is shown in Fig. 10.



Fig. 10. A screenshot from the Fuzzy Control adjustment controls.

After determining the related values, users can start control process by clicking on the "control button". The control process is shown simultaneously by the application in order to provide better information about the process. Brief values for changes in error value, u value and the output (du) are automatically shown on the table provided within Fuzzy Control adjustment controls.

IV. EVALUATION

In order to test accurateness and effectiveness of the application, some sample inputs values and obtained output values are compared with the obtained results for same inputs provided in more advanced and popular Fuzzy Logic software systems like MATLAB Fuzzy Logic Toolbox and

Fuzzy TECH. Obtained results showed that the application provides an accurate and effective performance. At this point, one disadvantage of the application can be expressed as limitations on number of digits after the comma.

After getting accurate results against advanced software systems, same procedures are also performed to be compared with other similar academic software works. At this point, the developed system was compared with Dot Fuzzy (a C# based software) and also jFuzzy Logic (a Java based software). The developed application showed similar accurate and effective performances against these works.

The last test was performed against another academic software work, which was designed and developed by the author [3]. As similar to the developed application, this work is also based on designing and developing "two inputs – one output" Fuzzy Control systems. But its working mechanism is based on using matrix forms in the context of state-space analysis methods and controlling different systems that can be defined with A.x + B.u equation form. Additionally it also provides more advanced design, developing and testing approaches. Both environments are used to design same systems and fed with same values. Eventually, results obtained with the developed application were same with the ones via other work.

V. CONCLUSIONS AND FUTURE WORK

The application developed in this work provides an easy-to-use, interactive Fuzzy Logic environment enabling users to design and develop their own Fuzzy Control works with the support of Adobe Flash based objects. At this point, users are enabled to work on simple, fast interfaces that also allow them to understand fundamentals of the Fuzzy Logic technique. According to results obtained within evaluation process, the whole application provides accurate mathematical and logical results for any type of "two inputs – one output" Fuzzy Control system.

The application has been designed and developed with the support of Adobe Flash technology that employs effective, object oriented coding approaches and visually improved elements to provide better using experience in application projects. In this sense, the application provides an alternative, interactive way to design simple Fuzzy Control systems fast and work on them via visually improved interface tools. With its using features and functions, the developed application is also an effective, fast and simple approach for understanding fundamentals of the Fuzzy Logic technique better.

Regarding the future works for the developed system, there are some works to increase number of inputs and outputs that can be used within a Fuzzy Control system. Additionally, future versions of the application will also include templates for working on different Fuzzy Logic models like "Sugeno". The application functions will also be modified for any potential integration with other widely used Artificial Intelligence techniques like Artificial Neural Networks. In parallel with all of the future works, interfaces of the application will also be re-designed and re-adjusted in order to provide better using experiences for users.

REFERENCES

- [1] L.A. Zadeh, Fuzzy sets, *Information and Control*, 8(3), 1965, 338-353.
- [2] N. Yalcin, and U. Kose, A web based education system for teaching and learning fuzzy logic, *Proc. of ICITS 2009*, Trabzon, Turkey, 2009, 378-385.
- [3] U. Kose, and O. Deperlioglu, An educational, virtual laboratory system for fuzzy logic, *Proc. of ISCSE 2010*, Aydin, Turkey, 2010, 1335-1342.
- [4] N.K. Kasabov, *Foundations of neural networks, fuzzy systems, and knowledge* (Cambridge: MIT Press, 1998).
- [5] A. Majumdar, and A. Ghosh, Yarn strength modeling using fuzzy expert system, *Journal of Engineered Fibers and Fabrics*, 3(4), 2008, 61-68.
- [6] S. Kutuva, N.P. Reddy, Y. Xiao, X. Gao, S.I. Hariharan, and S. Kulkarni, A novel and fast virtual surgical system using fuzzy logic, *Proc. of IADIS-MCCSIS 2006*, 2006.
- [7] P. Dadone, *Design optimization of fuzzy logic systems*, doctoral diss., Virginia Polytechnic Institute and State University, Blacksburg, VA, 2001.
- [8] J. Theler, *A software-based fuzzy logic controller* (2008) Retrieved from World Wide Web: http://ib.cnea.gov.ar/~thelerg/melon/doc/html/ch03s02.html#estructura_controlador

AUTHOR

Utku Kose: Utku Kose received the B.S. degree in 2008 from computer education of Gazi University, Turkey. He received M.S. degree in 2010 from Afyon Kocatepe University, Turkey and continues Ph. D. at Selcuk University in field of computer engineering. He is currently a Lecturer in Afyon Kocatepe

University. His research interest includes artificial intelligence, the chaos theory, distance education and computer education.

Photocatalytic Degradation Study of Methylene Blue Solutions and Its Application to Dye Industry Effluent

Susheela Bai Gajbhiye*

*Department of Engineering Chemistry, College of Engineering, Andhra University, Visakhapatnam, 530 003, India.

ABSTRACT

Zinc oxide (ZnO) was used in the photocatalytic decolourisation and degradation study of a dye namely, methylene blue (MB). The effect of the various rate determining parameters like initial dye concentration, catalyst loading, pH of the medium, temperature of the dye solution on the photodegradation of MB were studied in detail. The various thermodynamic and kinetic parameters of the process were evaluated. The MB degradation and its reaction kinetics analysis was utilised in the photocatalytic treatment of an actual effluent collected from an industry manufacturing intermediates for dyes. It revealed that the effluent could be effectively decolourised and degraded by photocatalytic method, without generation of any hazardous wastes or by-products as evident from the considerable reduction in chemical oxygen demand (COD) values.

Keywords: ZnO, photocatalytic degradation, methylene blue, dye effluent

1. INTRODUCTION

Most pollutants in the waste water effluents from industrial or domestic sources comprise of organic chemicals and pathogens which must be removed or destroyed before discharge into the water bodies. Such pollutants prevailing in the ground and surface waters pose irreversible hazards to human and aquatic life. The uncontrolled and heavy discharge of chemicals from industries comprises the major source of water and air pollution. Like any other chemical industry, textile industry is the main source of coloured organic reagents which are called dyes. Dyes are extensively used in the textile industry during dyeing process and the excess dyes are released into the effluent streams as waste after colouring the fabric. The released wastes are nevertheless in highly concentrated and complex state causing difficulty in handling for further treatment. Further most modern synthetic dyes are fairly stable even to the sunlight, with some of them being carcinogenic [1, 2]. Thus the waste water from a textile industry essentially needs an efficient treatment technology which can overcome all the aforesaid challenges giving ultimately clean water for safe disposal. Various conventional methods have been pressed into practice, in the decolourisation and degradation of dyes in the waste namely - biological treatment methods, coagulation, filtration, adsorption by activated carbon, reverse osmosis [3]. Low cost methods such as adsorption by activated charcoal, amongst these have been proven to be effective but incomplete in that they produce large amounts of solid wastages for further disposal thus adding to further pollution and environmental hazards. The other methods which have been proved efficient are not cost-effective [4]. Thus these methods either fail to accomplish the complete degradation, or produce large amount of toxic sludge causing disposal problems.

Thus serious concerns for a better and sufficiently effective alternative which is environment friendly especially in treating the effluent from textile and pharmaceutical disposed waste waters have prompted the development of few advanced oxidation processes (AOP), which are currently in use. Amongst them semiconductor based photocatalytic degradation could be considered as the most efficient [5]. This particular technique involves the use of semiconductor as catalysts which act as the medium of oxidation. Currently, TiO₂ and ZnO are largely deployed as the semiconducting materials suitable in the treatment of pollutants [6]. The semiconductor having a filled valence band and an empty conduction band inherently provides a small band-gap of energy 3 - 3.5 eV. When light falls on the surface of the semiconductor, the photon of threshold energy either equal to or greater than the energy gap, excites (knocks) an electron from the occupied (filled) valence band and promotes it to the unoccupied (empty) conduction band, thus leading to excited state conduction band electrons and positive valence band holes. These charged electrons and holes constitute the charge carriers which can undergo a number of processes namely, (1) they can either recombine radiatively or non-radiatively, dissipating their input energy as heat, (2) the charge carriers can also get trapped into the surface of the catalyst, (3) recombination of the trapped charge carriers, and (4) they can also react, if not undergone recombination, with the electron donors (reducing agents) or acceptors (oxidising agents) adsorbed on the surface of the semiconductor activated under the light [7]. In a recent study it was realized that the photocatalytic behaviour of the semiconductor is mainly due to the trapped electrons and trapped holes. However a competition between all these processes determines the ultimate quantum efficiency of the photoredox reactions on the semiconductor surface. It is also important that the energy band potentials of the semiconductor be compatible with that of the redox potentials of the water/hydroxyl radical couple (2.8 eV) [8]. Several semiconductors have energies of their band gap sufficient for catalysing a wide range of redox reactions. An ideal photocatalyst should be inexpensive, non-toxic, highly photoactive and stable in the conditions in which the pollutant is present. Some examples are TiO₂, WO₃, SrTiO₃, Fe₂O₃, ZnO and ZnS. TiO₂ is the most extensively studied semiconductor found from the literature [9]. It has been found to be the

most promising for photocatalytic destruction of organic pollutants with high stability in aqueous media. The anatase phase of TiO₂ is the material with the highest photocatalytic detoxification compared to the other phase which is called the rutile phase [10].

The advantage of using semiconductor based materials as photoactive catalysts in the detoxification of pollutants is the complete mineralization into environment friendly products, without generation of waste, which is not possible in the case of any other treatment method [11]. The other advantages include easy regeneration, reusability and active under easily available UV-visible photolight. Other than TiO₂ as photocatalyst, studies have been carried out to find the efficiency of other metal oxides. Among the other semiconductors, ZnO appears to be a highly promising photocatalyst and it has a band-gap almost similar to that of the anatase phase of TiO₂ [12, 13].

The main focus of the present work is to use commercially available ZnO in the photocatalytic decolourisation and degradation study of methylene blue (MB). The effect of rate determining parameters like initial dye concentration, catalyst loading, pH of the medium, temperature of the dye solution on the photodegradation of MB were studied in detail. The thermodynamic parameters involved in the degradation process were calculated. The study of MB degradation and understanding the parameters affecting its kinetics, helped in application of the photocatalytic method to the actual effluent collected from the industry that makes intermediates for dyes. It is suggested that the photocatalytic method can be effectively applied to decolourise and degrade the effluent if repeated in multiple steps.

2. EXPERIMENTAL

2.1 Materials

ZnO was procured from Merck, Chemie, Mumbai; MB, H₂SO₄ and NaOH were purchased from Loba Chemicals, Mumbai and double deionized water was used through out the experiment.

2.2 Photocatalytic Degradation

In photocatalytic experiments, MB dye (50 ml) and the catalyst (ZnO), were taken in a beaker and exposed to UV light for up to 180 min. Dye samples of about 5 ml were taken out at a regular interval from the test solution, centrifuged for 4 min at 950–1000 rpm and their absorbance was recorded at 664 nm using a spectrophotometer (Model: Double Beam Spectrophotometer Model 2215, Elico, India). COD was estimated before and after the treatment using potassium dichromate oxidation method. The same photocatalytic experimental set up was employed in the case of effluent collected from the industry manufacturing intermediates for dyes. UV black lamp of intensity 27 W/m² was used which was procured from Sun Electricals, Hyderabad.

3. RESULTS AND DISCUSSION

3.1 Photodegradation reaction kinetics

The present photodegradation process assisted by a ZnO semiconductor was studied by varying the rate determining parameters like concentration of the dye (MB) and temperature. Photocatalytic degradation of dyes generally follows first order kinetics. The corresponding half lives and rate constants were calculated by plotting the log (C₀/C) versus time graphs, whose derived values are presented in Table 1. The kinetic investigation revealed that ZnO induced photocatalysis of MB following first order kinetics.

Table 1

Rate constants and half-lives for different concentrations of MB dye solutions at room temperature

Concentration of Dye (ppm)	Rate constant (k x 10 ⁻²) min ⁻¹	Half-life (t _{1/2}) (min)
35	1.35	51
30	1.82	38
25	2.66	26
10	3.85	18

3.2 Effect of dye concentration

Keeping the catalyst loading concentration constant at 25 mg/50 ml of the dye solution, the effect of varying amounts of the dye was studied on its rate of its degradation (from 10 ppm to 35 ppm) as given in Table 1. With increasing concentration of MB the rate of degradation was found to decrease. This is because as the number of dye molecules increase, the amount of light (quantum of photons) penetrating the dye solution to reach the catalyst surface is reduced owing to the hindrance in the

path of light. Thereby the formation of the reactive hydroxyl and superoxide radicals is also simultaneously reduced. Thus there should be an optimum value maintained for the catalyst and the dye concentration, wherein maximum efficiency of degradation can be achieved.

3.3 Effect of pH on the photodegradation reaction

The photodegradation reaction was also carried out under varying pH conditions from (2 to 11), by adjusting with HNO_3 and NaOH , with ZnO kept at constant amounts of 25mg/50 ml of dye solutions (Fig. 1). The reaction was found to have low rates at neutral ranges of pH. While at higher and lower cases it was found to increase. This implies that alkaline as well as acidic conditions are favourable towards the formation of the reactive intermediates that is hydroxyl radicals is significantly enhanced, which further help in enhancing the reaction rate. On the other hand in neutral medium conditions the formation of reactive intermediates is relatively less favourable and hence less spontaneous.

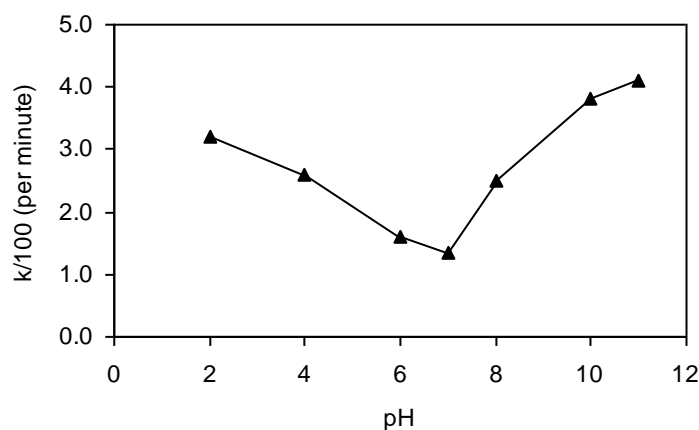


Figure 1. Effect of reaction medium pH on photodegradation of MB solution (35ppm/50 ml)

3.4 Effect of catalyst amounts on the photodegradation reaction

The amount of catalyst was varied from 10mg to 350mg per 50 ml of constant dye solution of 35 ppm concentration. The effect is graphically depicted in Fig. 2.

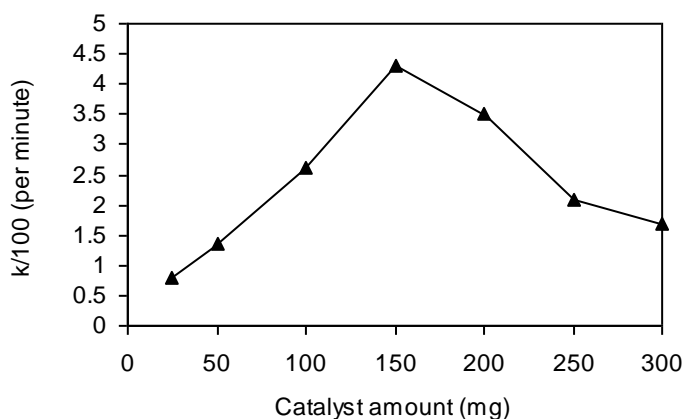


Figure 2. Effect of catalyst amount on photodegradation of dye

We observe that with increasing catalyst amounts the reaction was found to occur faster due to increase in the number of active surfaces on the catalyst. However, beyond 250 mg the reaction rate decreased, which could be due to the hindrance to the pathway of light to reach the dye molecules. Perhaps scattering of light dominates at higher catalyst loadings.

3.5 Effect of temperature on photodegradation reaction

The effect of increasing temperature was observed on the photodegradation of MB dye by varying the temperature from 298 to 328 K, keeping the dye concentration constant at 35 ppm with a catalyst concentration of 25 mg/50 ml. The results are given in Table 2 and graphically evaluated by Arrhenius based temperature dependence of the photocatalytic degradation by a plot of $\log(C_0/C)$ versus $1/T$ (as shown in Fig. 3).

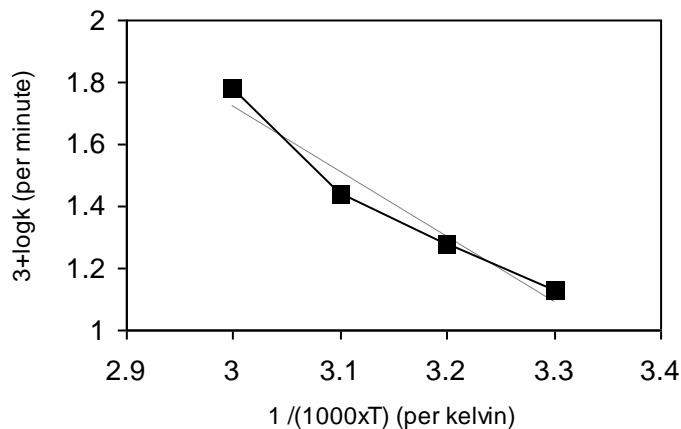
Table 2

Kinetic and thermodynamic parameters for the photocatalytic degradation of MB dye (35 ppm) and ZnO (25mg/50ml) under UV light

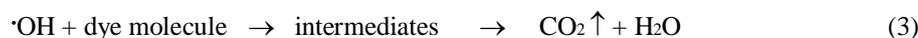
T (K)	k (min^{-1}) $\times 10^2$	E_a (kJ mol^{-1})	ΔH^\ddagger (KJ.mol^{-1})	ΔS^\ddagger ($\text{kJ.mol}^{-1}.\text{K}^{-1}$)	ΔG^\ddagger (kJmol^{-1})
298	1.35		37.97		93.79
308	1.67	40.45	37.88	-0.19	96.47
318	2.72		37.80		98.40
328	4.81		37.72		100.03

\ddagger represents activated state

The energy of activation (E_a) was calculated from the slope of the graph. Further other thermodynamic parameters enthalpy of activation, entropy and free energy of activation were also evaluated. The positive energy of activation implies that the reaction is less energy intensive and a spontaneous one. This could be because the activated state is a well solvated structure formed between the dye molecules and the reaction intermediates that is hydroxyl radicals which is also supported by positive entropy of activation.

**Figure 3. Effect of temperature on the photodegradation of methylene blue**

It can be seen that with increasing temperature, the rate of the reaction increases which is due to the reason that increase in temperature helps to speedup the velocity of both the hydroxyl radicals and the dye molecules to interact with each other thus the reaction competes more efficiently with the electron-hole recombination. The following scheme can be proposed for the degradation of the MB dye:



+ mineral salts

3.6 Photodegradation of effluent from industry manufacturing intermediates for dyes

The catalytic photodegradation was also studied for an effluent from an industry manufacturing intermediates for dyes. The results are tabulated in Table 3. The efficiency of degradation was assessed from the experimentally derived chemical

oxygen demand (COD) measured after various times of UV light exposure. It can be seen that there is considerable reduction in the COD values. The drastic lowering in the COD values after 20 hours of exposure is a significant achievement. Further, the reduction in BOD values also signifies the importance of the photocatalytic degradation treatment. The effluent could be completely decolourised and degraded by the use of semiconductor catalysts.

Table 3**Photocatalytic degradation results of effluent collected from a dye industry**

Effluent physico-chemical parameters	Pre-photocatalytic degradation	Post photocatalytic degradation after			
		1 hr	5 hrs	8hrs	20 hrs
COD (mg/L)	3885	2643	1215	665	90
BOD (mg/L)	851	536	206	117	19

4. CONCLUSION

Photodegradation of methylene dye was studied as a model system using powder ZnO catalyst, in order to assess the efficiency of such advanced oxidation technologies in the treatment of effluents from industry manufacturing intermediates for dyes. From kinetic studies it was found that the method of photodegradation is dependent on parameters such as dye concentration, catalyst loadings, temperature and other parameters. Textile effluent with very high initial COD and BOD values was effectively treated using ZnO catalyst. The significant reduction in COD, BOD and decolourization of the effluent suggests that the dye molecules could be completely mineralized with the help of ZnO which is both economically viable and environment friendly.

REFERENCES

- [1] R. H. Souther and T. A. Alspaugh, *Journal of Water Pollution Control Federation*, 29, 1957, 804
- [2] A. Hamza and M. F. Hamoda, *Proc. 35th Purdue industrial waste congress, West Lafayette*, 1980IN, USA
- [3] D. Beydoun, R. Amal, G. Low and S. McEvoy, *Journal of Nanoparticle Research* 1, 1999, 439–458,.
- [4] R. Matthews, *Photocatalysis in water purification: Possibilities, problems and prospects*. Ollis D.F. and Al-Ekabi H. eds. *Photocatalytic Purification and Treatment of Water and Air*, (New York, Elsevier Science Publishers, 1993) 121–139.
- [5] B. Ohtami, Photocatalysis- A to Z – What we know and what we do not know in a scientific sense, *J of photochemistry and photobiology C: Photochemistry Reviews*, 11(4), 2010, 157-178
- [6] V Kandavelu, H. Kastein and K. R. Thampi, *Applied catalysis B: Environment*, 48, (2), 2004, 101-111.
- [7] A. Hagfeldt and M. Gratzel, Light-induced redox reactions in nanocrystalline systems, *Chemical Reviews*, 95, 1995, 49–68.
- [8] M.R. Hoffmann, S.T. Martin, W. Choi and D.W. Bahnemann, *Chemical Review*, 95 (1995) 69.
- [9] R. F. Howe, Recent developments in photocatalysis, *Developments in Chemical Engineering and Mineral Process*, 6(1) 1998, 55–84.
- [10] D. W. Bahnemann, D. Bockelmann, R. Goslich, M. Hilgendorff & D. Weichgrebe, 1993. *Photocatalytic detoxification: Novel catalysis, mechanisms and solar applications*. In: D. F. Ollis and H. Al-Ekabi eds. In: *Photocatalytic purification and treatment of water and air*. (New York, Elsevier Science Publishers, 1993), 301–319.
- [11] U. Stanfford, K. A. Gray and D. V. Kamat, *Het. Chemical Review*, 3, 1996, 77.
- [12] A. K. Carlos, G. F. Wypych, S. G. Moraes, N. Duran, N. Nagata and P. Z. Peralta *Chemosphere*, 40, 2000, 433

The Right Projects Done with an Effective Methodology of Software Project Management

¹Dr. K. V. S. Narayana, ²Syed Khasim

¹Dr.K.V.S. Narayana, Principal, Dr. Samuel George Inst. of Engg &Tech , Markapur, A.P., India.

²Syed Khasim, Research Scholar, Dept. of Computer Science, Rayalaseema University, Kurnool, A.P, India.

Abstract: *This paper explores the idea of evaluate about the right Software Project Management. It is useful to the potential for the right project done with an effective methodology. The most discriminating characteristic of a successful software development process is the well-defined separation between “research and development activities” and “production activities”. When software projects do not succeed, the primary reason is usually a failure to crisply define and execute these two stages, with proper balance and appropriate emphasis. In this paper explain about the project management and project management activities followed by the explanation of project control variables. After that gives a note on the project management methodology. Finally presents the next generation software cost models and list on some of the project management templates.*

Keywords: *Software, Project Management, Methodology, templates,*

I. INTRODUCTION

Project Management is the discipline of defining and achieving targets while optimizing the use of resources (time, Money, people, materials, energy, space, etc) over the course of a project (a set of activities of finite duration).

Project Management is quite often the province and responsibilities of an individual project manager. This individual seldom participates directly in the activities that produce the end result, but rather strives to maintain the progress and productive mutual interaction of various parties in such a way that overall risk of failure is reduced. In contrast to on-going, functional work, a project is "a temporary endeavor undertaken to create a unique product or service." The duration of a project is the time from its start to its completion, which can take days, weeks, months or even years. Typical projects include the engineering and construction of various public or consumer products, including buildings, vehicles, electronic devices, and computer software.

In recent years, the Project Management discipline has been applied to Marketing and Advertising endeavors as they become more technologically oriented and multiple communication channels become part of the marketing mix.

II. PROJECT MANAGEMENT ACTIVITIES

Project Management is composed of several different types of activities such as:

- Planning the work
- Estimating resources
- Organizing the work
- Acquiring human and material resources
- Assigning tasks
- Directing activities
- Controlling project execution
- Report progress
- Analyzing the results based on the facts achieved

III. SOFTWARE ECONOMICS

Most software cost models can be abstracted into a function of five basic parameters. Those are size, process, personnel, environment and required quality.

The *size* of the end product (in human-generated components) which is typically quantified in terms of the number of source instructions or the number of function points required to develop the required functionality.

The *process* used to produce the end product, in particular the ability of the process to avoid non-value-adding activities (rework, bureaucratic delays, and communications overhead).

The capabilities of software engineering *personnel* and particularly their experience with the computer science issues and the applications domain issues of the project.

The *environment* is made up of the tools and techniques available to support efficient software development and to automate the process.

The required *quality* of the product is including its features, performance, reliability and adaptability.

The relationship among these parameters and the estimated cost can be written as

$$\text{Effort} = (\text{personnel}) \times (\text{environment}) \times (\text{quality}) \times (\text{size}^{\text{process}}).$$

Activity	Cost
Management	5%
Requirements	5%
Design	10%
Code and Unit testing	30%
Integration and test	40%
Deployment	5%
Environment	5%
Total	100%

Table1: Expenditures by activity for a conventional software project

IV. PROJECT CONTROL VARIABLES

Project Management tries to gain control over five variables:

Time: The amount of time required to complete the project. Typically it is broken down for analytical purposes into the time required to complete the components of the project. This is then further broken down into the time required to complete each task contributing to the completion of each component.

Cost: Calculated from the time variable Cost to develop an internal project is time multiplied by the cost of the team members involved. When hiring an independent consultant for a project, cost will typically be determined by the consultant or firm's hourly rate multiplied by an estimated time to complete.

Quality: The amount of time put into individual tasks determines the overall quality of the project. Some tasks may require a given amount of time to complete adequately, but given more time could be completed exceptionally. Over the course of a large project, quality can have a significant impact on time and cost (or vice versa).

Scope: Requirements specified for the end result. The overall definition of what the project is supposed to accomplish and a specific description of what the end result should be or accomplish.

Risk: Potential points of failure, most risks or potential failures can be overcome or resolved, given enough time and resources.

Three of these variables can be given by external or internal customers. The value(s) of the remaining variable are then set by project management, ideally based on solid estimation techniques. The final values have to be agreed upon in a negotiation process between project management and the customer. Usually, the values in terms of time, cost, quality and scope are contracted.

To keep control over the project from the beginning of the project all the way to its natural conclusion, a project manager uses a number of techniques: project planning, earned value, risk management, scheduling and process improvement.

V. PROJECT MANAGEMENT METHODOLOGY

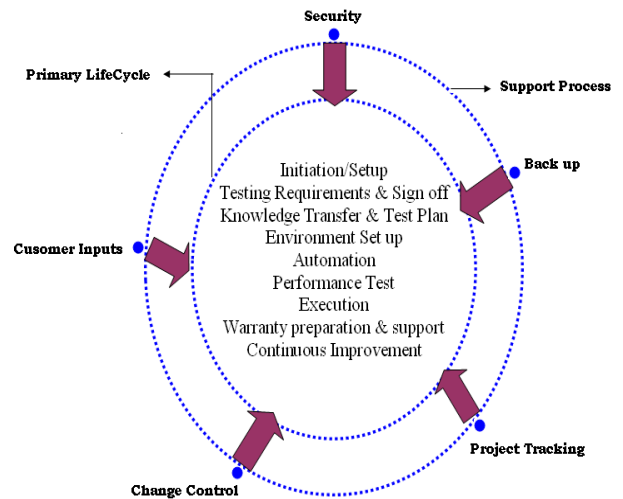


Fig.1 Project Management Methodology

The different phases are

Initiation/Setup

- Testing Strategy
- Automation Feasibility
- Manual & Automated components
- Tool selection for automation

Testing Requirements & Sign off

- Unit testing requirement
- Business Functional Requirements
- All interfaces
- Application security levels
- List of platforms for compatibility
- Critical transactions for performance testing
- Performance goals
- Globalization needs
- Effort estimates and price signoff
- Scheduling sign off
- Project Plan
- Project communication
- Workflow between Development & TS Testing teams
- Developer -Tester interaction process for UT (if required)

Knowledge Transfer & Test Plan

- Application Demo
- Domain Training
- Shadow transfer
- Study of user and operations manuals
- Globalization rules
- Test plan and Test cases

Environment Set up

- Hardware and Software resource setup
- Ghost image plan
- Test bed creation
- Special requirements for globalization testing

Automation

- Architecture
- Automation Test Flow
- Identify reusable elements
- Create and test scripts
- In-line auto test setup

Performance Test

- Critical transactions
- Scripting
- Environment setup
- Iterative test run
- Analysis

Execution

- Execute test scripts or cases
- Log, track and report defects
- Improve and increase automation
- Monitor, analyze and feedback until Q levels achieved.

Warranty preparation & support

- Allocate technical team to support warranty levels
- Optionally agree to a per/bug payment if errors are above Warranty levels
- Integrate warranty support team into maintenance team
- Live monitoring
- Warranty bug fixing

Continuous Improvement

- Increase automation levels
- Improve test scripts and cases

VI. PROJECT MANAGEMENT PHASES

The different phases are

Requirement Specification: Requirement Specification is the first and most important phase of the SDLC. During this phase our Project Manager is in constant contact with the Customer to find out requirements of the project in detail. Main tasks in this phase include Requirement Determination, Risk Analysis, Setting up Schedules, and deciding Deliverables. Communication with the Customer is carried out using any of the following means of communication, such as Instant Messenger, Email, Phone, Voice Chat or personal meeting. A System Requirement Specification Document is prepared at the end of this phase.

Requirement Analysis and Design: Project Manager and System Analyst after reviewing the Customers requirements analyze the requirement and start designing

of the project. System Architecture, Database Design, Program. Specifications and Test Scenarios are determined. A Detail Design Document is prepared at the end of analysis that can be used by the programmers to perform the coding.

Coding and Testing: Programmers begin programming in this phase using the Detail Design Document. As project progress programmer's progresses is monitored by Project Manager and Project Leader respectively. Project Manager is in constant contact with the customer and provides updates on the progress of the project using MS Project. The programmers follow coding Standards decided by the company. Project Leader helps the programmers with their coding problems and guides them to the solutions. Testing is done by the QA Team simultaneously for the finished modules and approval is given to the modules once they have passed their initial tests before integration.

Deployment and Support: This phase starts with Deployment of the project. Initial hardware and software setup necessary to run the project is a very critical phase of the project. After project is completed Project Manager contacts the customer and prepares for the set-up. Software is handed over to the customer for acceptance testing only after complete internal testing. Support to the project is provided for a limited number of days during which any minor customer changes are finished.

VII. NEXT GENERATION SOFTWARE COST MODELS

A next generation software cost model should explicitly separate architectural engineering from application production, just as an architecture-first process does. The cost of designing, producing, testing and maintaining the architecture baseline is a function of scale, quality, technology, and process and team skill. Next-generation software cost models should estimate large-scale architectures with economy of scale. This implies that the process exponent during the production stage will be less than 1.0. My reasoning is that the larger the system, the more opportunity there is exploit automation and reuse common processes, components and architecture.

VIII. PROJECT MANAGEMENT TEMPLATES

MPMM includes the complete set of project Management Templates need to manage successful projects.

This comprehensive set of templates, forms, processes and checklists will save our time and Effort when creating project deliverables.

Templates save our Time and Effort

These project management templates save our time and effort, as we never have to create project deliverables from scratch. Whether we need to create a business case, control change or manage risk, the Template Toolkit

included within MPMM will help us do it quickly and efficiently.

MPMM includes the following sets of templates, to help us manage projects:

- Project Initiation Templates
- Project Planning Templates
- Project Execution Templates
- Project Closure Templates
- Risk Management Templates
- Change Management Templates
- Quality Management Templates
- Cost Management Templates
- Issue Management Templates
- Time Management Templates
- Procurement Management Templates
- Acceptance Management Templates
- Communications Management Templates

Agile Project Management

Agile Projects Make traditional obvious.

We can't fully plan before we start, because we don't know where we're going.

--We can plan a little and continue to iterate the planning.

When we execute, things will happen

--Risk management is essential.

During the "control" phase, we need to measure what's happening, so we have a chance of guiding the project.

--What do we measure, so we know where we are and can move to where we want to be?

If we knew when we were done, we'd close

-- So if we're ready to release at a moment's notice, we can close any time

IX.CONCLUSION

As a project is a temporary effort to create a unique product or service. Projects usually include constraints and risks regarding cost, schedule or performance outcome. In order to manage these constraints and risks to achieve good output of the product or service, project management is essential. Successful software project management is hard work. Technical breakthroughs, process breakthroughs and new tools will make it easier, but management discipline will continue to be the crux of software project success. New technological advances will be accompanied by the new opportunities for software applications, new dimensions of complexity, new avenues of automations, and new customers with different priorities.

References

- [1] Chatfield, Carl. "A short course in project management".Microsoft.
<http://office.microsoft.com/en-us/project/HA102354821033.aspx>.
- [2] The Definitive Guide to project Management. Nokes, Sebastian. 2nd Ed.n. London (Financial Times / prentice Hall): 2007. ISBN 9780273 710974
- [3] Paul C. Dinsmore et al (2005) The right projects done right! John Wiley and Sons, 2005. ISBN 0787971138. p.35 and further.
- [4] Lewis R. Ireland (2006) project Management. McGraw-Hill professional, 2006. ISBN 007147t60X. p.t110.
- [5] Joseph Phillips (2003). PMP project Management Professional Study Guide. McGraw-Hill Professional, 2003. ISBN 0072230622 p.354.
- [6] Walker Royce (2010) Software Project Management, A unified framework, Pearson, 2010. ISBN 978-81-7758-378-6.

The Circuits Design using Dual-Rail Clocked Energy Efficient Adiabatic Logic

Gayatri, Manoj Kumar, Prof. B. P. Singh

*Electronics and Communication Department, FET- MITS (Deemed University)
Lakshmanagarh, Distt. - Sikar, India*

ABSTRACT

In this paper, the design of circuits using adiabatic logic and sequential circuits based on the newly proposed Energy efficient adiabatic Logic (EEAL) is presented. EEAL uses dual sinusoidal source as supply-clock. This paper proposes a positive feedback adiabatic logic (PFAL), two-phase clocked adiabatic static CMOS logic (2PASCL) and proposed adiabatic logic circuit that utilizes the principles of adiabatic switching and energy recovery compare than CMOS. 2PASCL has switching activity that is lower than dynamic logic. The power consumption of proposed adiabatic logic becomes lower compare than CMOS. Also design NAND logic gates on the basis of the 2PASCL topology and proposed NAND gate. Comparison has shown a significant power saving to the extent of 70% in case of proposed technique as compared to CMOS logic and NAND gate in 10 to 200MHz transition frequency range. The simulation results are analyzed at 180nm technology to show the technology dependence of the design. The proposed design of CMOS logic and NAND gate is better suitable for the low power VLSI applications.

Keywords: Adiabatic logic, adiabatic switching, Energy recovery, Low Power applications, Portable Applications, two phase clocked.

1. INTRODUCTION

Higher power and energy dissipation in high performance systems require more expensive packaging and cooling technologies, increase cost, and decrease system reliability. Nonetheless, the level of on-chip integration and clock frequency will continue to grow with increasing performance demands, and the power and energy dissipation of high-performance systems will be a critical design constraint [12]. The main source of power dissipation in these high performance battery-portable digital systems running on batteries such as note-book computers, cellular phones and personal digital assistants are gaining prominence. For these systems, low power consumption is a prime concern, because it directly affects the performance by having effects on battery longevity. In this situation, low power VLSI design has assumed great importance as an active and rapidly developing field.

Another major demand for low power chips and systems comes from the environmental concerns. Modern offices are now furnished with office automation equipments that consume large amount of power [13]. A study by American Council for an Energy-Efficient Economy estimated that office equipment account for 5% for the total US commercial energy usage in 1997 and could rise to 10% by the year 2004 if no actions are taken to prevent the trend [14].

The idea behind the circuit is built upon the basic diode based circuit proposed in [1] and [2]. In this paper, we propose a two-phase clocked adiabatic static CMOS logic (2PASCL) [10] circuit to achieve low power consumption; we also compare its power consumption with that of a conventional CMOS circuit. A novel method for reducing the power dissipation in a 2PASCL circuit involves the design of a charging path without diodes. In such a case, current flows only through the transistor during the charging. Thus, a 2PASCL circuit is different from other diode-based adiabatic circuits in which current flows through both the diode and transistor. By using the aforementioned 2PASCL circuit, we can achieve high output amplitudes and reduce power dissipation. In addition, in order to minimize the dynamic power consumption in this circuit, we apply a split-level sinusoidal driving voltage.

In conventional CMOS circuits, power dissipation can be minimized by reducing the supply voltage, node capacitance, and switching activity [1, 2] to a certain extent but very nascent adiabatic computing has appeared as a naturally acceptable and very practical solution in low power VLSI systems. Several adiabatic logic families based on energy recovery principle [3-5] where all charge recovered back to power supply without heat generation have been proposed & implemented earlier. The following mathematical analysis based on time period (T), Stored Charge ($C_L V_{dd}$), Load capacitance C_L and channel resistance R is sufficient to have a deeper look on it.

$$E_{diss} = (RC_L/T)C_L V_{dd}^2 \quad (1)$$

Theoretically, it is possible to reduce the power dissipation by extending the switching time.

The circuit uses a two phase clocked split-level sinusoidal power supply to reduce the voltage difference between the current-carrying electrodes to reduce the power consumption.

2. ADIABATIC SWITCHING

Adiabatic switching is commonly used to minimize energy loss during the charge/discharge cycles. During the adiabatic switching, all the nodes are charged/discharged at a constant current to minimize energy dissipation [16]. As opposed to the case of conventional charging, the rate of switching transition in adiabatic circuits is decreased because of the use of a time varying voltage source instead of a fixed voltage supply. Here, the load capacitance (C_L) is charged by a constant current source (I). In conventional CMOS logic we use constant voltage source to charge the load capacitance [2]. Here, R is the on-resistance of PMOS network. A constant charging current corresponds to a linear voltage ramp. Assume the capacitor voltage zero initially.

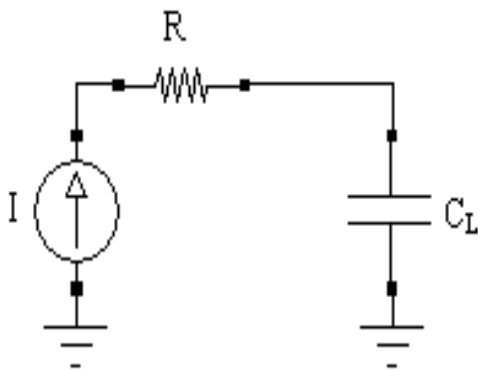


Fig1: Adiabatic logic circuit

The voltage across the switch = IR

$P(t)$ in the switch = I^2R

Energy during charge $E = (I^2R)T$

Also $Q = C_L V_{dd}$, $I = C_L V_{dd} / T$

$E = (I^2R)T = (RC_L/T)C_L V_{dd}^2$

Where, E [3] is the energy dissipated during charging time,

Q is the charge transferred to the load,

C is the value of the load capacitance,

R is the on-resistance of the PMOS switch,

V is the final value of the voltage at the load,

T is the charging time.

Theoretically, when driving voltage (V_a) switching time (T) from 0 V to V_{dd} is long, the energy dissipation is nearly zero.

When V_a changes from HIGH to LOW in the pull-down network, discharging via the NMOS transistor occurs. From equation (1), it is observed that when energy dissipation is minimized by decreasing the rate of switching transition, the system draws some of the energy that is stored in the load capacitor during the current subsequent computational steps. Systems based on above-mentioned technique for charge recovery is not necessarily reversible [8], [9].

3. CMOS INVERTER

Power dissipation in conventional CMOS circuits primarily occurs during the device switching. When the logic level in the system is "1," there is a sudden flow of current through R .

$Q = C_L V_{dd}$ is the charge supplied by the positive power supply rail for charging C_L to the level of V_{dd} . Hence, the energy drawn from the power supply is $Q \cdot V_{dd} = C_L V_{dd}^2$ [4]. By assuming that the energy drawn from the power supply is equal to that supplied to C_L , the energy stored in C_L is said to be one-half the supplied energy, i.e., $E_{\text{stored}} = (1/2)C_L V_{dd}^2$. The remaining energy is dissipated in R . The same amount of energy is dissipated during discharging in the nMOS pull-down network when the logic level in the system is "0." Therefore, the total amount of energy dissipated as heat during charging and discharging is

$$E_{\text{total}} = E_{\text{charge}} + E_{\text{discharge}} = 0.5 C_L V_{dd}^2 + 0.5 C_L V_{dd}^2 = C_L V_{dd}^2 \quad (2)$$

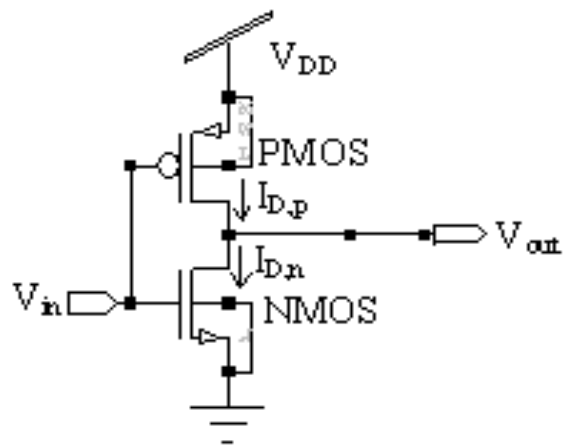


Fig2: CMOS inverter circuit

4. PFAL

The structure of PFAL logic [15], [16] is shown in figure 3. Two n-trees realize the logic functions. This logic family also generates both positive and negative outputs. The two major differences with respect to ECRL are that the latch is made by two PMOSFETs and two NMOSFETs, rather than by only two PMOSFETs as in ECRL, and that the functional blocks are in parallel with the transmission PMOSFETs. Thus the equivalent resistance is smaller when the capacitance needs to be charged. The ratio between the energy needed in a cycle and the dissipated one can be seen in figure 3. During the recovery phase, the loaded capacitance gives back energy to the power supply and the supplied energy decreases.

The partial energy recovery circuit structure so called Positive Feedback Adiabatic Logic (PFAL) [6], has good robustness against technological parameter variations [7], [8]. It is a dual rail circuit; the core of all the PFAL circuit is adiabatic amplifier, a latch made up by the two PMOS and two NMOS that avoids a logic level degradation on the output nodes. The two n-tree release the logic functions. The functional blocks are in parallel with P-MOSFETs and form a transmission gate.

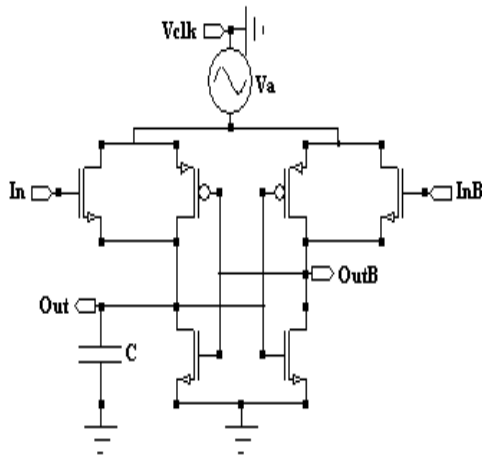


Fig3: PFAL Logic Circuit

5.2PASCL

Figure 4 shows a circuit diagram of Two-Phase Adiabatic Static Clocked Logic (2PASCL) inverter. A double diode circuit is used, where one diode is placed between the output node and power lock, and another diode is adjacent to the NMOS logic circuit and connected to the other power source [10]. Both the MOSFET diodes are used to recycle charges from the output node and to improve the discharging speed of internal signal nodes. Such a circuit design is particularly advantageous if the signal nodes are preceded by a long chain of switches.

The circuit operation is divided into two phases: evaluation and hold. In the evaluation phase, Va swing up and VaB swings down. On the other hand, in the hold phase, VaB swings up and Va swings down. Let us consider the inverter’s logical circuit demonstrated in Figure 7. The operation of the 2PASCL inverter is explained as follows.

1) Evaluation phase:

- a) When the output node Y is LOW and the PMOS tree is turned ON, CL is charged through the PMOS transistor, and hence, the output is in the HIGH state.
- b) When node Y is LOW and NMOS is ON, no transition occurs.
- c) When the output node is HIGH and the PMOS is ON, no transition occurs.
- d) When node Y is HIGH and the NMOS is ON, discharging via NMOS and D2 causes the logic state of the output to be “0” [17].

2) Hold phase:

- a) When node Y is LOW and the NMOS is ON, no transition occurs.
- b) At the point when the preliminary state of the output node is HIGH and the PMOS is ON, discharging via D1 occurs.

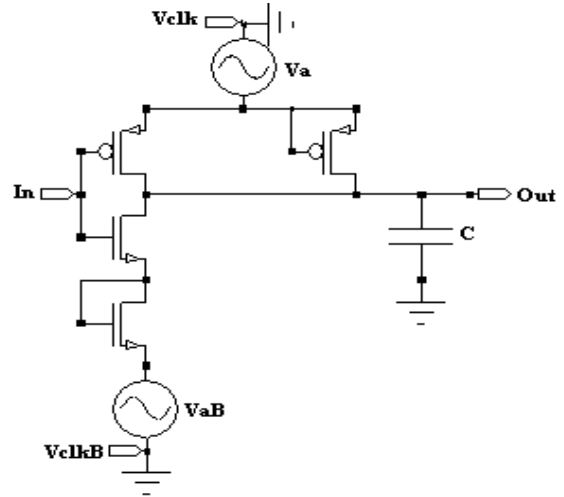


Fig4: 2PASCL Logic Circuit

6. PROPOSED ADIABTIC LOGIC INVERTER

Adiabatic switching is commonly used to minimize energy loss during the charge/discharge cycles. During the adiabatic switching, all the nodes are charged/discharged at a constant current to minimize energy dissipation. As opposed to the case of conventional charging, the rate of switching transition in adiabatic circuits is decreased because of the use of a time varying voltage source instead of a fixed voltage supply.

Hence, if I is considered as the average of the current flowing to CL, the overall energy dissipated during the transition phase can be reduced in proportion to

$$I^2 R T_p = (C_L V_{dd} / T_p)^2 R T_p = (R C_L / T_p) C_L V_{dd}^2 \quad (3)$$

Theoretically, during adiabatic charging, when Tp, the time for the driving voltage Va to change from 0 V to Vdd is long, energy dissipation is nearly zero.

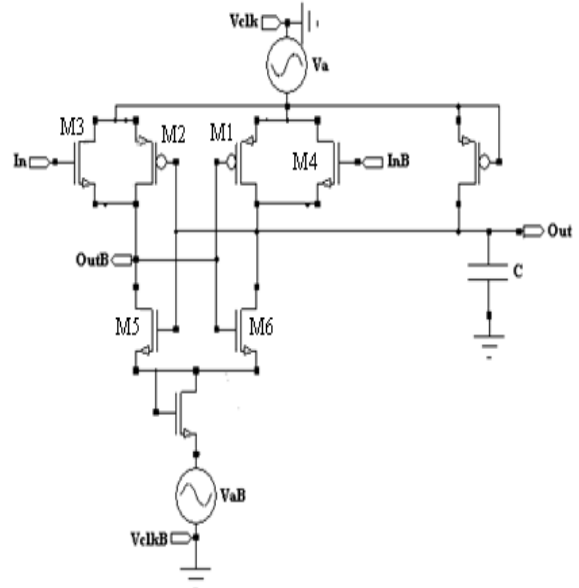


Fig5: Proposed adiabatic logic inverter circuit

The basic inverter circuit is shown in above figure of this circuit is an adiabatic amplifier, a latch made by the two PMOS M1 and M2 and two NMOS M5 and M6, that avoids the logic level degradation at Out and Out, the logic circuit M3 and M4 are in parallel with M1 and M2 and forms transmission gate [1]. This circuit uses two-phase split level sinusoidal power supplies which are denoted as Va and VaB, where Va & VaB can vary from 1.3 to 1.6V & 0.3 to 0V respectively.

The circuit operates in two phases, evaluation and hold, in evaluation phase, Va swings up and VaB swings down, and in hold phase, VaB swings up and Va swings down. Let us assume, during evaluation phase the input (In) is high and input (InB) goes low accordingly, consequently M3 is conducting and output (OutB) follows the power supply Va, and at the same time M1 gets turned ON by output (Out) and thus reduces the charging resistance. Being in parallel with M3 and during hold phase, charge stored on the load capacitance CL flows back to power supply through M1. So that power dissipation is reduced. The proposed circuit uses two MOS diodes, one is connected to Out and Va and other diode is connected between common source of M5- M6 and other power supply VaB, Both the MOS diodes are used to increase the discharging rate of internal nodes.

7. DIODE IS ADJACENT TO THE PMOS LOGIC

The proposed circuit uses one MOS diode, which is connected to Out and Va at PMOS logic, the MOS diode is used to increase the discharging rate of internal nodes.

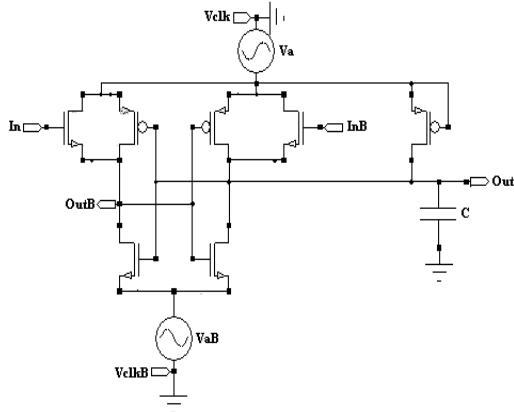


Fig6: Diode is adjacent to the PMOS logic

8. DIODE IS ADJACENT TO THE NMOS LOGIC

The proposed circuit uses one MOS diode, which is connected between common source of M5-M6 and other power supply VaB at NMOS logic, the MOS diode is used to increase the discharging rate of internal nodes.

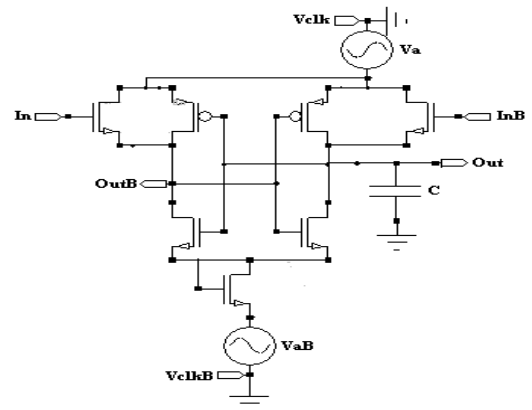


Fig7: Diode is adjacent to the NMOS logic

9. DESIGN AND SIMULATION OF A TWO-INPUT NAND GATE

(i) TWO-INPUT CMOS NAND GATE

The next basic cell to consider is the CMOS-based Two-Input NAND Gate, designed and simulated in the 180nm CMOS Technology and with a load capacitances are vary. The minimum sized NMOS and PMOS transistors have been used for the transient simulations [9].

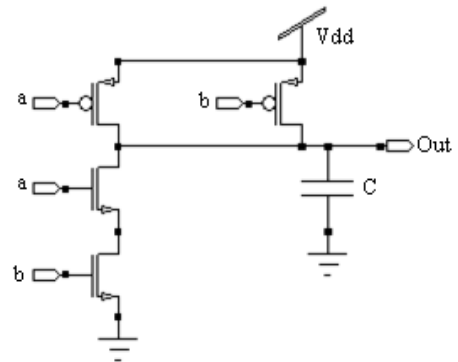


Fig8: Two-input CMOS NAND gate

(ii) TWO-INPUT CMOS NAND GATE BASED 2PASCL

Figure 9 shows a circuit diagram of Two-Phase Adiabatic Static Clocked Logic (2PASCL) inverter. A double diode logic circuit is used, where one diode is placed between the output node and power lock, and another diode is adjacent to the NMOS logic circuit and connected to the other power source [10]. Both the MOSFET diodes are used to recycle charges from the output node and to improve the discharging speed of internal signal nodes. Such a circuit design is particularly advantageous if the signal nodes are preceded by a long chain of switches.

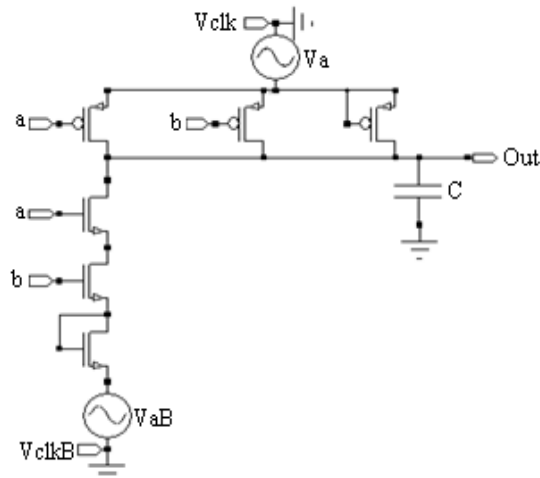


Fig9: 2PASCL NAND gate

(iii) PROPOSED ADIABATIC NAND GATE

In this circuit we use two diodes at PMOS and NMOS logic which shown in below fig10 and are used to increase the discharging rate of internal nodes. The circuit operates in two phases, evaluation and hold, in evaluation phase, Va swings up and VaB swings down, and in hold phase, VaB swings up and Va swings down [11].

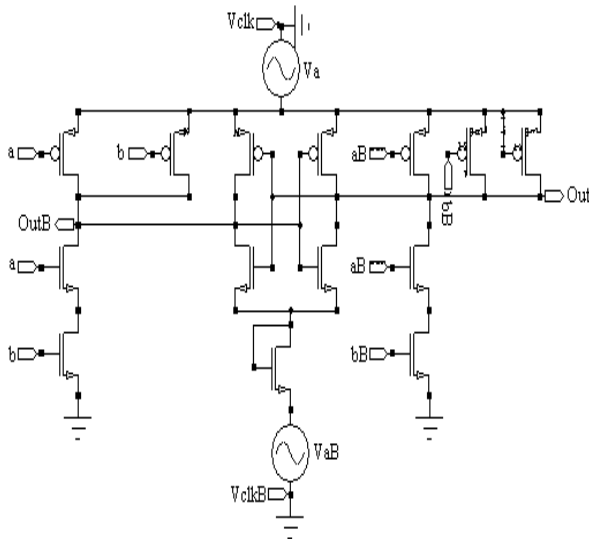


Fig10: Proposed NAND gate

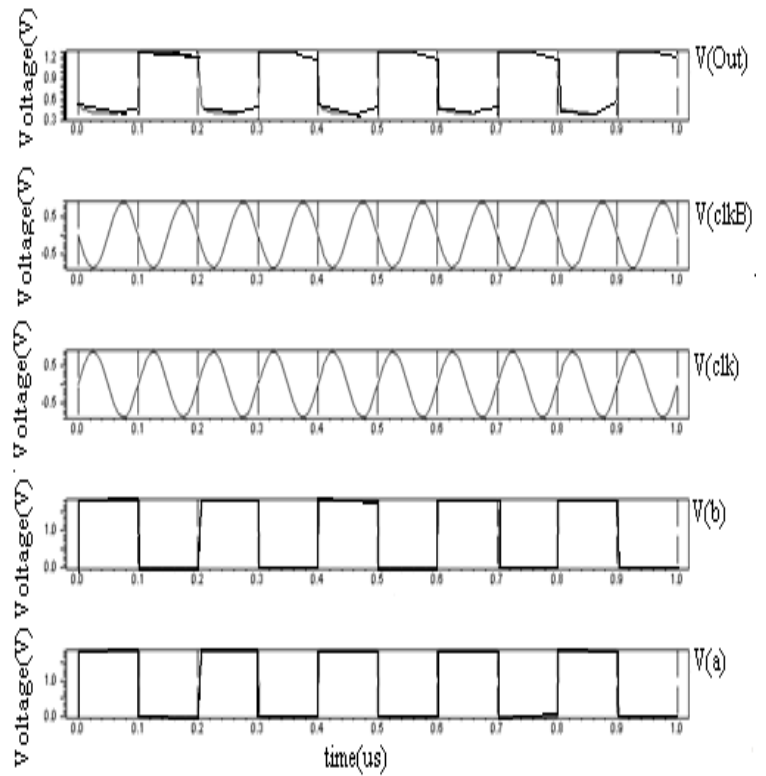


Fig11: Input and Output waveforms for 2PASCL NAND gate

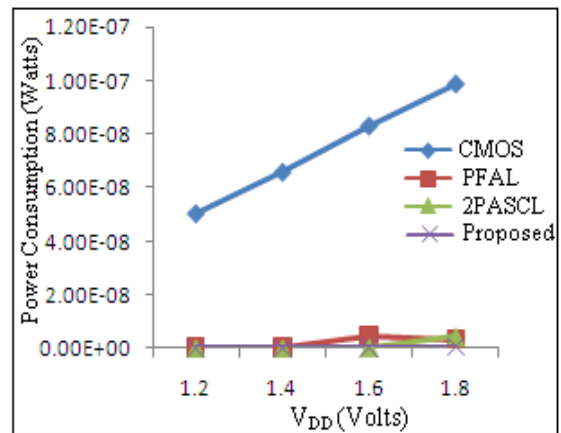


Fig12 Power Consumption comparison of proposed inverter vs CMOS at power supply

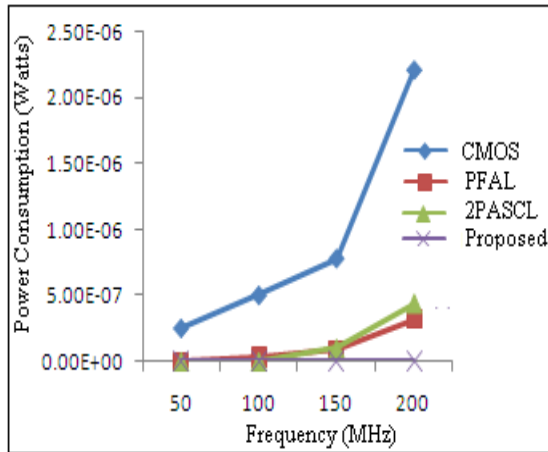


Fig13 Power Consumption comparison of proposed inverter vs CMOS at frequency

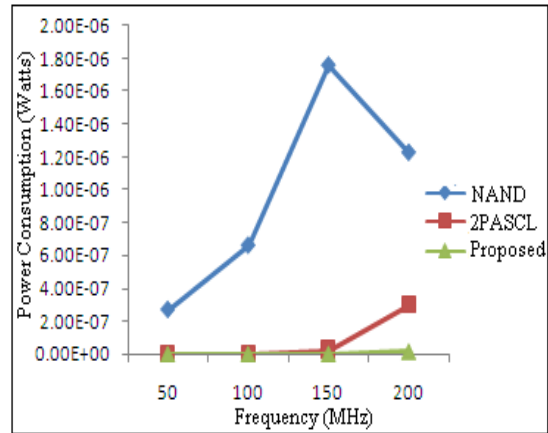


Fig 16 Power Consumption comparison of proposed NAND vs NAND at frequency

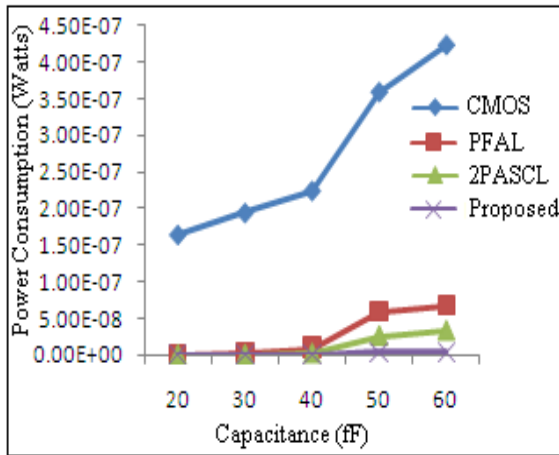


Fig14 Power Consumption comparison of proposed inverter vs CMOS at capacitance

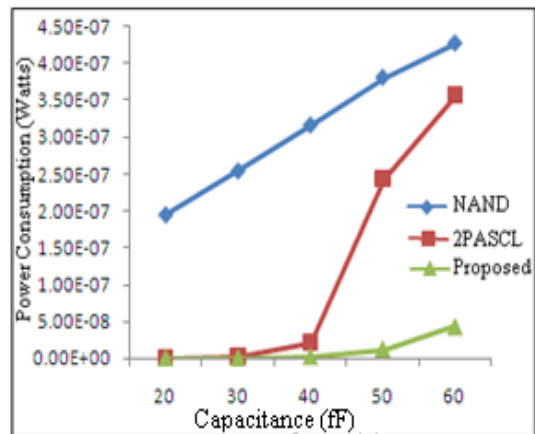


Fig17 Power Consumption comparison of proposed NAND vs NAND at capacitance

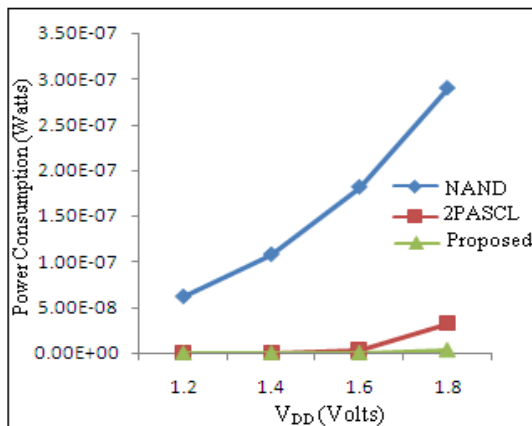


Fig15 Power Consumption comparison of proposed NAND vs NAND at power supply

In this section, we will not examine the topology and functionality of proposed inverter & 1-bit full adder. The simulation is performed using a SPICE circuit simulator at 180nm technology node & 1.8 V standard CMOS process. The Proposed circuit width W & L of the NMOS and PMOS logic gates were 600n and 180n respectively. Whereas the length and width of MOS diode D2 is 40 μm beside a load capacitance C_L of 0.05pF connected at the output node. Above figure shows the simulated waveforms of Proposed Adiabatic logic inverter, in which upper most waveform shows the input, and below two waveforms are sinusoidal power clock and compliment of that power clock, last two waveforms are output and compliment of output respectively.

10. CONCLUSION

Simulation results obtained from the proposed inverter and NAND gate has wide acceptance in low power VLSI regime at low frequency. The comparison of the proposed circuit with other traditional methodologies has proved that power consumption with the proposed logic is far less as compared to CMOS, PFAL and 2PASCL based technique. The simulation result show that power consumption of proposed

NAND is less compare than NAND, 2PASCL. The requirement for dual-rail signals and T-gates where single-rail signals and individual FET's could otherwise be used roughly doubles the area required for logic. With dual-rail signals, half of the circuit nodes will switch each cycle. From the results of simulation it has been observed that the replacement of diodes with switches controlled by power clock significantly reduces the power consumption of the adiabatic circuit.

ACKNOWLEDGMENTS

Gayatri was born in sikar 1987 received the B.E. degree in electronics & communication engineering from university of Rajasthan, jaipur in 2008.

Now doing M.Tech. in VLSI design from Mody institute of technology & science, Lakshmangarh Sikar, Rajasthan (India). She will continue on digital area of adiabatic logic circuits with emphasis on high speed and low power.

Her research interests include low power techniques for portable applications, tanner tools, and high speed Mos digital design for VLSI.

Manoj Kumar was born in uttrakhand. He received B.Tech. in U.P. Technical University (Lucknow) in July 2004 and M.Tech in VLSI technology from Mody Institute of Technology & Science, May 2011.

He served Hardware Design Engg. in duration Aug. 2004 – May 2005 Mircsocomm India Pvt. Ltd., Delhi. Lecturer in Sri Sarathi Institute of Technology, Vijayawada from 2005-2006 and in MIC College of Technology, Vijayawada from 2006-2008. Assist. Professor in Mody Institute of Technology & Science, Lakshmangarh, Jun 2008 till date.

Prof. B. P. Singh was born in a village Orro, Nawadah, Bihar, INDIA in 1947. He did B.Sc. (Engg.) and M.Sc. (Engg.) from Bihar Institute of Technology, Sindri, Dhanbad and B.I.T. Mesra Ranchi in 1967 and 1970. He did Ph.D. from Ranchi University Ranchi in 1980.

He served B.I.T. Mesra, Ranchi from 1970 to 1981, Indian School of Mines Dhanbad from 1981 to 1987 and Madan Mohan Malaviya Engg. College from 1987 to 2009. From 2009 till date he is the H.O.D. of ECE and EEE, Mody Instiute of Technology Lakshmangarh, Sikar, Rajasthan (INDIA). He has over 50 papers to his credits in International and national Journals and over 50 presentations in International and National Seminars / Symposia/ Conferences. His area of research is device modeling, low-power and high performance integrated circuit design and emerging CMOS technologies.

Prof. Singh is the senior fellow of IEEE and life member of IETE.

REFERENCES

- [1] N. Waste and K. Eshraghian, Principle of CMOS VLSI Design: A System Prospective, 2nd ed. New York: Addison – Wesley, 1993.
- [2] W. C. Athas, L. J. Svensson, J. G. Koller, et al., “Low-power digital systems based on adiabatic switching principles,” *IEEE Trans. On VLSI systems*, 2(4), Dec. 1994, pp: 398-407.
- [3] S. Samanta “Adiabatic Computing: A Contemporary Review,” International conference on computers and devices for communication, Dec. 2009, pp. 1-4.
- [4] J. Marjonen, and M. Aberg, “A single clocked adiabatic static logic – a proposal for digital low-power applications,” *J. VLSI signal processing*, vol.27, no.27, Feb.2001, pp.253-268.
- [5] M. Pedram, “Power minimization in IC design: principles of applications,” *ACM Transactions on Design automation of Electronic System*, 1(1) Jan 1996, pp 53-56.
- [6] A. Vetuli, S. Di Pascoli, and L.M. Reyneri, “Positive feedback in adiabatic logic, *Electron.Lett*” vol.32, Sept. 1996, pp.1867- 1869.
- [7] A. Blotti, M. Castellucci, and R. Saletti, “Designing carry lookahead adders with an adiabatic logic,” standard-cell library,” in proc. 12th Int. Workshop PATMOS, Seville, Spain, Sept. 2002, pp. 118-127.
- [8] E. Amirante, A. Bargagli-Stoffi, J. Fisher, G. Iannaccone, and D.Schmitt-Landsiedel, “Variations of the power dissipation in adiabatic logic gates.” In proc. 11th Int. Workshop PATMOS, Yverdon-Les_Bains, Switzerland, Sept. 2001, pp. 7 – 10.
- [9] Y. Takahashi, Y. Fukuta, T. Sekine and M. Yokoyama, “2PADCL: Two phase drive adiabatic dynamic logic CMOS logic.” *Proc. IEEE APCCAS*, Dec. 2006, pp. 1486-1489.
- [10] N. Anuar, Y. Takahashi, T. Sekine, “Two phase clocked adiabatic static CMOS logic,” *proc. IEEE SOCC 2009*, Oct. 2009, pp. 83-86.
- [11] S. Kang and Y. Leblebici, “Low Power CMOS Digital Logic Circuits”, 3rd ed., Tata McGraw Hill, 2003.
- [12] N. Anuar, Y. Takahashi, T. Sekine, “Two-Phase clocked adiabatic static CMOS logic and its logic family” *Journal of semiconductor technology and science*, vol 10, no. 1, Mar. 2010, pp. 1-10. 463.
- [13] A. P. CHANDRAKASAN, S. SHENG, AND R. W. BRODERSEN, “Low Power CMOS Digital Design,” *IEEE Journal of Solid-state Circuits*, Vol. 27, No. 04, pp. 473-484, April 1999.
- [14] J. M. RABAEY, AND M. PEDRAM, “*Low Power Design Methodologies*,” Kluwer Academic Publishers, 2002.
- [15] Vetuli, A., Di Pascoli, S., Reyneri, L.M.: Positive feedback in adiabatic logic. *Electronics Letters*, Vol. 32, No. 20, Sep. 1996, pp. 1867ff.
- [16] Atul Kumar Maurya, Ganesh Kumar, “Energy Efficient Adiabatic Logic for Low Power VLSI Applications” 2011 International Conference on Communication Systems and Network Technologies.
- [17] Blotti, A., Di Pascoli, S., Saletti, R.: Sample Model for positive feedback adiabatic logic power consumption estimation. *Electronics Letters*, Vol. 36, No. 2, Jan. 2000, pp. 116-118.
- [18] Y. Takahashi, Y. Fukuta, T. Sekine and M. Yokoyama, “2PADCL: Two phase drive adiabatic dynamic CMOS logic,” *Proc. IEEE APCCAS*, pp. 1486–1489, Dec. 2006.

Design of U Slot Patch Antenna for Wi-max and Radar Applications

¹B. Jyothi, ²V. V. S. Murthy, ³B. Pavankumar

¹Student, M.Tech (Communication and Radar), Department of ECE, K L University

²Associate Professor, Department of ECE, K L University

³Student, B.Tech (Electronics and Communications), Department of ECE, K L University

Abstract: A compact U shaped slot patch antenna is proposed and designed in this paper for Wi-max and radar applications. This antenna is designed on a Rogers RT-Duroid substrate of dielectric constant 2.2 with thickness of 0.16cm. The dimensions of the proposed antenna are 3cm X 3cm X 0.16cm. The proposed antenna resonates at three frequencies 6.05 GHz, 9.87 GHz and 10.47 GHz. The gain of the proposed model is 8.47 dBi. The proposed model is simulated using commercial antenna design software High frequency Structure Simulator(HFSS).

Keywords: Microstrip patch antenna, Return Loss, Radar, Slot, Wi-Max.

1.INTRODUCTION

The need for a low profile and compact antennas is on rise with the rapid development of the wireless communication devices. Due to low fabrication cost and compactness of the patch antennas many researchers are working in this area. Also these antennas are light weight and easy to instal[1-4]. To maintain compactness and multiple bands yet to remain high gain of the antenna is still a challenge to the antenna designers. Typically dual frequency operations can be obtained by using multilayer stack patches[5] and little attention has been paid to single layer microstrip antennas[6]. Several techniques of microstrip antennas are known, prominent among them are the use of stacked patches. The stacked patch antenna has multi layer structure consisting of several parasitic radiating elements placed one above the other and above the driven element[7]. However this approach has the inherent disadvantage of increased overall thickness and issues related to alligning various layers precisely. But slot antennas are ahead of this. The proposed antenna is of small size having the dimensions 3cmx3cmx0.16cm. The operating frequencies of the proposed model are 6.05 GHz, 9.87GHz and 10.47GHz. The 6.05 GHz frequency can be

antenna is 0.16mm. It is fed by a coaxial cable with 50Ω impedance matching. The dimensions of the substrate are 3cmx3cmx0.16cm. The dimensions of the patch are 1.2cmx1cm with slots of two different sizes. The length and width of the longer slot are 0.3cm and 0.05cm respectively. The length and width of the shorter slot are 0.1 and 0.05 respectively. The diameter of the feed is 0.05cm and the

used for wireless applications. The 9.87 GHz and 10.47 GHz band can be used for RADAR applications(I/J band). This I/J band is relatively popular RADAR band for military applications like airborne RADARs for performing the roles of interceptor, fighter and attack of enemy fighters and of ground targets. This frequency band is widely used for maritime civil and military navigation RADARs. This frequency band is also popular for space borne or airborne imaging RADARs based on Synthetic Aperture Radar(SAR) both for military electronic intelligence and civil geographic mapping.

2. ANTENNA DESIGN

The design of the proposed antenna is as shown in figure 1. The antenna is realized on Rogers RT/duroid substrate with dielectric constant 2.2 and a loss tangent of 0.0009. The thickness of the antenna

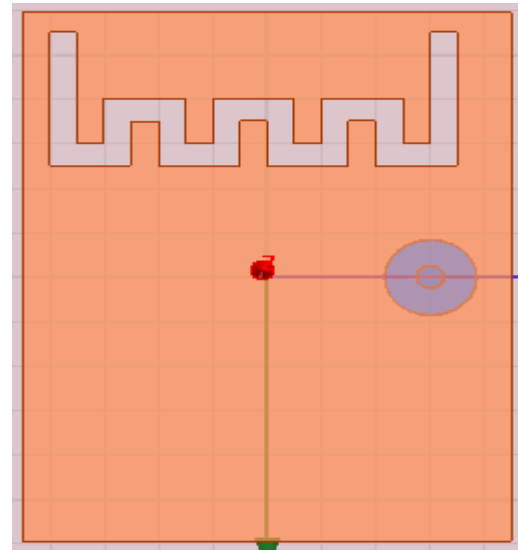


Fig 1: Proposed Model

height is 0.16cm. The proposed antenna has three resonant modes and having a maximum gain of 8.4 Dbi.

3. RESULTS AND DISCUSSIONS

The proposed antenna resonates at three frequencies 6.05 GHz, 9.87 GHz and 10.47 GHz. The First Resonant Frequency has a bandwidth from 6.01 GHz to 6.09 GHz. The other two Resonant Frequencies create a wide bandwidth ranging from 9.57 GHz to 10.77 GHz. The return loss of the proposed antenna at the three Resonant Frequencies is shown in figure 2. The return loss values are -20.5 dB, -14.42 dB and 13 dB for the frequencies 6.05 GHz, 9.87 GHz and 10.47 GHz respectively.

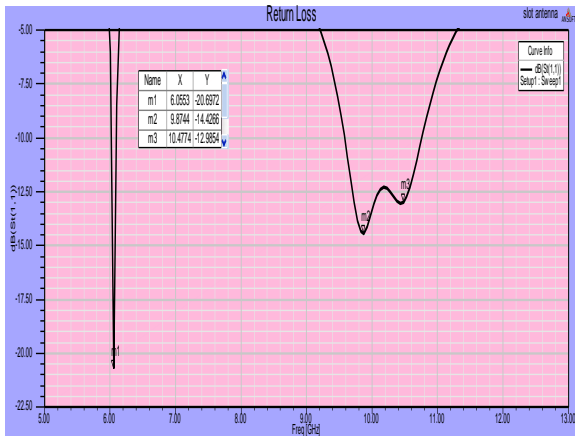


Fig 2: Return Loss vs Frequency

The Voltage Standing Wave Ratio (VSWR) describes the amount of power reflected by an antenna. In Practical, the VSWR should be between 1 and 2 for less reflection losses. The VSWR plot of the proposed antenna is shown in figure 3. The VSWR is 1.2, 1.47 and 1.57 at the three Resonating Frequencies 6.05 GHz, 9.87 GHz and 10.47 GHz respectively.

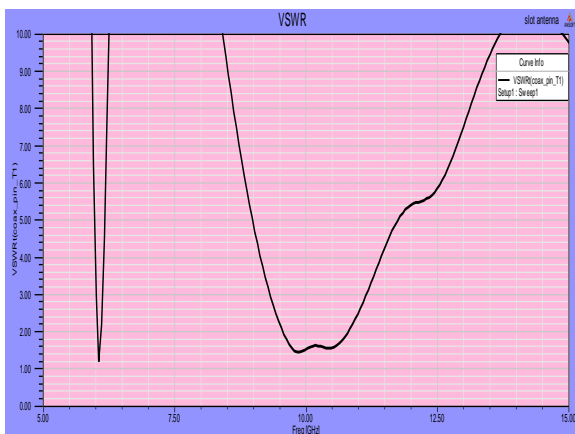


Fig 3: VSWR vs Frequency

The E-plane radiation pattern at the Resonant Frequencies is shown in figure 6. The E-plane radiation pattern is directional from the figure.

The 2-D Gain of the proposed model is shown in the figure 4. The maximum gain of the proposed antenna is 8.47dBi.

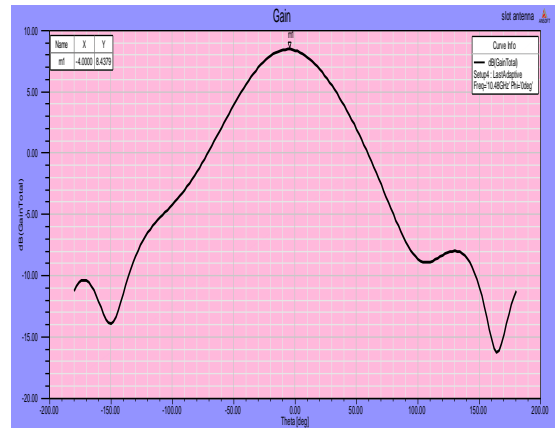


Fig 4: 2D Gain

The 3-D Gain of the proposed antenna is shown in figure 5.

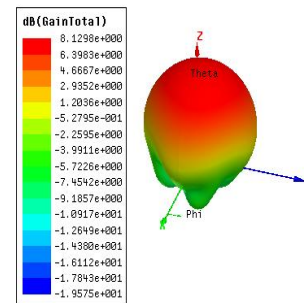


Fig 5: 3D Gain

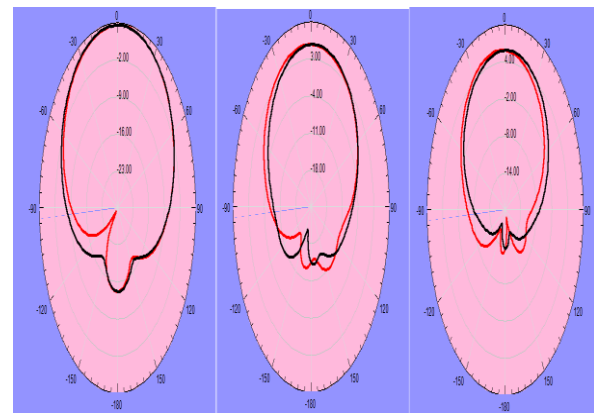


Fig 6: E-plane Radiation pattern at phi=0, 90deg.

The H-plane radiation patterns at the Resonant Frequencies are shown in figure 7.

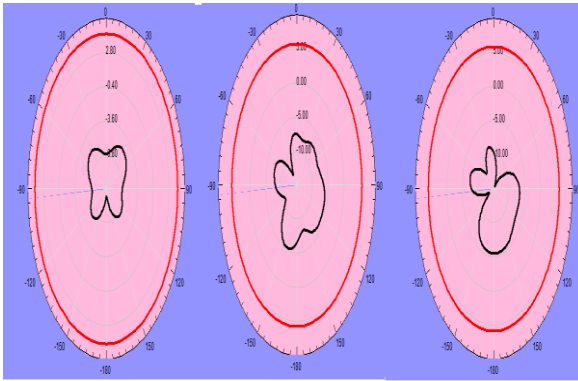


Fig 7: H-plane Radiation pattern at theta=0, 90deg

The H-plane radiation pattern is Omni directional from the figure.

The orientation of an electric field vector is known as the polarization of an electro magnetic wave of an antenna.

The E-field distribution at the three resonant Frequencies is shown in the figure 8.

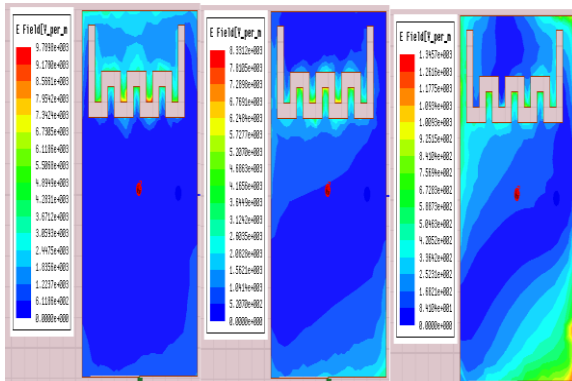


Fig 8: E-field distribution.

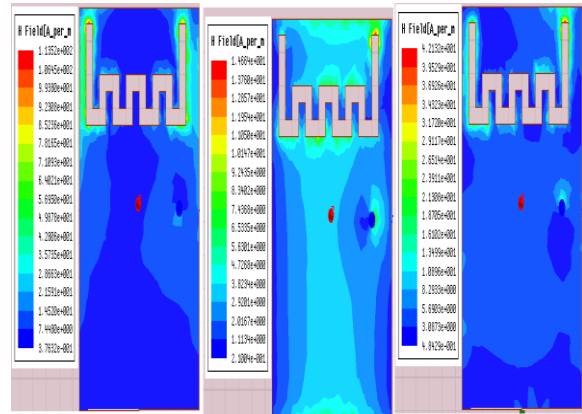


Fig 9: H-field distribution.

The mesh generation plot of the proposed antenna at the three Resonant Frequencies is shown in the figure 10.

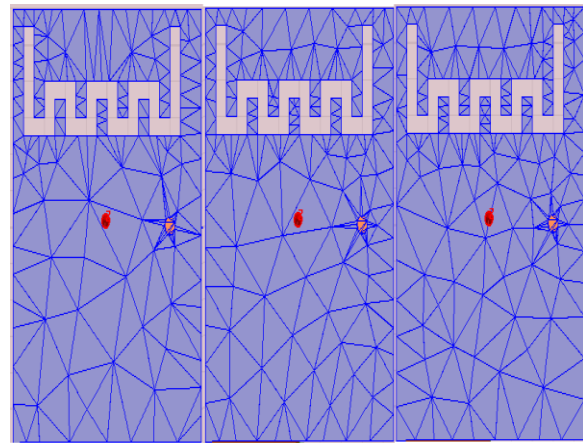


Fig 10: Mesh Plot generation

The H-field distribution is shown in the figure 9.

4. CONCLUSION

A novel compact slot antenna design and the simulations are presented in this paper. The proposed antenna has three resonant frequencies of 6.05 GHz, 9.87 GHz and 10.47 GHz. The first resonant frequency can be used for wireless applications and the remaining two frequencies can be used for Radar applications. The gain of the proposed antenna is 8.47dBi at the solution frequency. The radiation patterns are directional in E-Plane and Omni directional in H-Plane.

5. ACKNOWLEDGMENT

Authors of the paper like to express their thanks to the department of ECE and management of KLU university for their continuous support and encouragement throughout this work.

REFERENCES

- [1] C. L. Mak, R. Chair, K. F. Lee, K. M. Luk and A. A. Kishk, "Half U-slot patch antenna with shorting wall", *Electronics Letters*, vol. 39, pp. 1779-1780, 2003
- [2] H. F. AbuTarbous et al., "Bandwidth Enhancement for Microstrip Patch Antenna Using Stacked Patch and Slot", *iWAT2009 IEEE International Workshop on Antenna Technology*, 2-4 March 2009, Santa Monica, CA.
- [3] Rafi, G. and L. Shafai, "Broadband microstrip patch antenna with V-slot," *IEE Proc. Microw. Antenna Propag.*, Vol. 151, No. 5, 435-440, October 2004.
- [4] Ayoub, A. F. A., "Analysis of rectangular microstrip antennas with air substrates," *Journal of Electromagnetic Waves and Applications*, Vol. 17, No. 12, 1755-1766, 2003.

- [5] *Amit A. Deshmukh and K. P. Ray*, “**Half U-slot loaded Multi-band Rectangular Microstrip Antennas**”, International Journal of Microwave and Optical Technology, vol. 2, no. 2, July 2007, pp. 216 – 221.
- [6] *Wang, I., Pralich, R., w, c., and Lina, I.* “**Multifunctional Aperture Coupled Stack Antenna**”, Electron. Lett. 1990, 26, (25). PP.2067-2068.
- [7] *R.Q. Lee, K.F. Lee, and J. Bobinchak*, “**Characteristics of a two-layer electromagnetically coupled rectangular patch antenna,**” *Electron.Lett.*,vol. 23, no. 20, pp. 1070–1072, 1987.

AUTHORS BIOGRAPHY



B. Jyothi, was born in A.P, India in 1981. She completed her B.Tech in 2003 from CR Reddy College of Engineering affiliated to Andhra University. Presently she is pursuing her M.Tech, in Communications and Radar Systems from KLUUniversity.



V. V. S. Murthy was born on 02 January, 1981. He received his B.E. and M.Tech degrees in 2002 and 2006 respectively. He is a life member of IETE and ISTE. His research areas include Antennas and Radio wave propagation and optical image processing. Currently he is working as Associate Professor in ECE department of K.L.University, Guntur.

Dry Sliding Wear and Mechanical Behavior of Aluminium/Fly ash/Graphite Hybrid Metal Matrix Composite Using Taguchi Method

A. Anandha Moorthy¹, Dr. N. Natarajan², R. Sivakumar³, M. Manojkumar⁴, M. Suresh⁵

(Department of Mechanical Engineering, Bannari Amman Institute of Technology, India)

(Department of Mechanical Engineering, RVS Faculty of Engineering, India)

(Department of Mechanical Engineering, Bannari Amman Institute of Technology, India)

(Department of Mechanical Engineering, Bannari Amman Institute of Technology, India)

(Department of Mechanical Engineering, Bannari Amman Institute of Technology, India)

ABSTRACT

The experimental investigation of hybrid metal matrix composites with fly ash and graphite reinforced aluminium alloy (Al 6061) composites samples, processed by stir casting route are reported. The aluminium alloy was reinforced with 3 wt.%, 6 wt.%, 9 wt.% fly ash and fixed 3 wt.% of graphite to mixture the hybrid composite. Hardness of the hybrid composite were tested it was found that when the hardness of the hybrid composites can be increased when compared to (Al 6061). The parameters such as load, sliding speed, and reinforcement content were identified will affecting wear rate. The design of experiments (DOE) approach using taguchi method was employed to analyze the wear behavior of hybrid composites. Signal-to-noise ratio and analysis of variance (ANOVA) were used to investigate the influence of parameters on the wear rate.

Key words- Aluminium Alloy, ANOVA, DOE, Graphite

1. INTRODUCTION

Conventional monolithic materials have limitations in achieving good combination of Strength, stiffness, toughness and density. To overcome these shortcomings and to meet the ever Increasing demand of modern day technology, composites are most promising materials of recent interest. Metal matrix composites (MMCs) possess significantly improved properties including high specific strength; specific modulus, damping capacity and good wear resistance compared to unreinforced alloys. There has been an increasing interest in composites containing low density and low cost reinforcements. Among various discontinuous dispersoids used, fly ash is one of the most inexpensive and low density reinforcement available in large quantities as solid waste by-product during combustion of coal in thermal power plants. Hence, composites with fly ash as reinforcement are likely to overcome the cost barrier for wide spread applications in automotive and small engine applications.

Mechanical properties of composites are affected by the size, shape and volume fraction of the reinforcement, matrix material and reaction at the interface. Wear is an important property in the selection of DRAMMCs. Wear is not an intrinsic material property but characteristics of the engineering system which depend on load, speed, temperature, hardness, and the environmental conditions. Wear performances of particulate reinforced aluminium matrix composites reinforced with various reinforcements ranging from very hard ceramic particulates such as SiC and Al₂O₃ to a very soft material such as graphite have been reported to be superior when compared with unreinforced alloys. It is therefore expected that the incorporation of fly ash particles in aluminium alloy has the potential for conserving energy intensive aluminium, and thereby reducing the cost of aluminium products, and at the same time causing a reduction in the weight of the products. Researchers have also reported significant improvements in properties and higher wear resistance by the incorporation of fly ash in aluminium alloy. Graphite and graphite powders are widely used in industrial applications for their excellent dry lubricating properties. So, if a solid lubricant like graphite is contained in the aluminium alloy, it can be released automatically during the wear process and can potentially reduce wear, increase the anti-seizure effects and improve thermal stability.

2. PLAN OF EXPERIMENTS

2.1 Material Selection

(Al6061) alloy is used as the matrix material in the present investigation and has the chemical composition as shown in Table 1. The aluminium alloy was reinforced with 3 wt.%, 6 wt.%, 9 wt.% fly ash and fixed 3 wt.% graphite to synthesize the hybrid composite through liquid metallurgy route. The fly ash and graphite particles with a size range of 53 to 75 μm were used. Fly ash particles being hard in nature improve the hardness, strength and stiffness of the hybrid composite. Graphite imparts excellent self lubricating property to the hybrid composite. A small amount of Mg (0.5 wt. %) was added to ensure

good wettability of particles with molten metal. After mixing the melt was poured into a prepared mould for the preparation of specimen.

Table 1 Chemical Composition

ELEMENT	Mg	Fe	Si	Cu	Mn	V	Ti	Al
Weight %	1.08	0.17	0.63	0.32	0.52	0.01	0.02	Remainder

2.2 Preparing Specimen

Fly ash / graphite reinforced Aluminium alloy (Al6061) composites, processed by stir casting route was used in this work. Liquid metallurgy route was used to synthesize the hybrid composite specimens. The matrix alloy was first superheated above its melting temperature and then the temperature was lowered gradually until the alloy reached a semisolid state. The required quantities of fly ash (3, 6 and 9 Wt. %) and graphite (3 Wt % fixed) were taken in powder containers. Then the fly ash and graphite was heated to 450°C and maintained at that temperature for about 20 minutes. A vortex was created in the melt due to continuous stirring by a stainless steel mechanical stirrer with a rotational speed of 650 rpm.

At this stage, the blended mixture of preheated fly ash and graphite particles were introduced into the slurry and the temperature of the composite slurry was increased until it was in a fully liquid state. Small quantities of magnesium were added to the molten metal to enhance wettability of reinforcements with molten aluminium.

Stirring was continued for about 5 minutes until the interface between the particle and the matrix promoted wetting and the particles were uniformly dispersed. The melt was then superheated above the liquid us temperature and solidified in a cast iron permanent mould to obtain cylindrical samples. Sliding wear test specimens were machined from as-cast samples, to obtain cylindrical pins of diameter 10 mm and length 30 mm. The hardness tests were conducted in accordance with the ASTM E10.

2.3 Testing For Mechanical Properties

The Brinell hardness tests were conducted in accordance with the ASTM E10. Hardness of the hybrid composite was tested. It was found that when the hardness of the hybrid composites can be increased when compared to aluminium alloy (Al 6061).

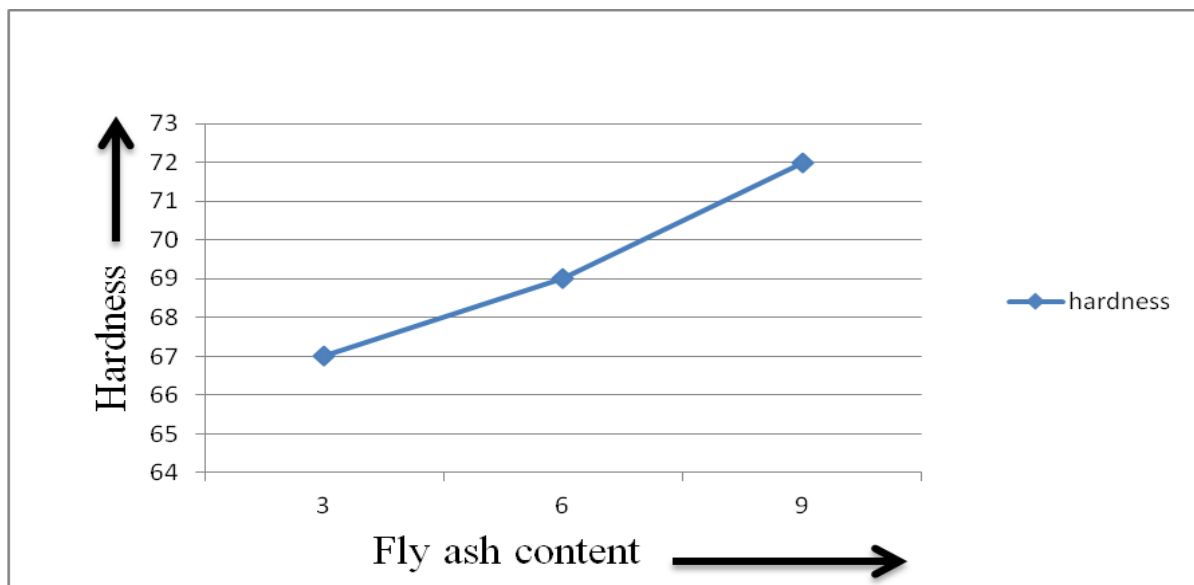


Fig .1 Hardness Level

From this figure 1, it can be clearly shown that when the fly ash content increases at the time hardness value will be increased.

2.4 Conducting Design Of Experiment Using Taguchi Method

The experimental plan was formulated considering three parameters (variables) and three levels based on the Taguchi technique. The three independent variables considered for this study were load, sliding speed and fly ash content. Of these, the first two are process parameters, and the third is a material dependent parameter. The levels of these variables chosen for experimentation are given in Table 2.

Table 2 Parameter And Their Levels

Control factors	I	II	III	Units
A. Load	9.81	19.62	29.43	N
B. Speed	2	3	4	(M/S)
C. Fly ash	3	6	9	(wt.%)

3. RESULTS AND DISCUSSIONS

In the present investigation, a L27 orthogonal array was selected and it has 27 rows and 13 columns. The selection of the orthogonal array is based on the condition that the degrees of freedom for the orthogonal array should be greater than, or equal to, the sum of the variables. Each variable and the corresponding interactions were assigned to a column defined by Taguchi method. The first column was assigned to load (L), the second column to sliding speed (S), the fifth column to fly ash content (F), and the remaining columns were assigned to their interactions. The response variable to be studied was wear rate.

Table 3 Wear Rate

Load (kg)	Speed (m/s)	Fly ash (Wt %)	Wear rate
1	2	3	0.937
1	2	6	0.7855
1	2	9	0.6322
1	3	3	0.7808
1	3	6	0.6284
1	3	9	0.4741
1	4	3	0.7808
1	4	6	0.4713
1	4	9	0.3161
2	2	3	1.561
2	2	6	1.256
2	2	9	0.9483
2	3	3	1.249
2	3	6	1.099
2	3	9	0.7903
2	4	3	0.937
2	4	6	0.6284
2	4	9	0.4741
3	2	3	2.03
3	2	6	1.571
3	2	9	0.9483
3	3	3	1.405
3	3	6	1.099
3	3	9	0.9483
3	4	3	1.249
3	4	6	0.9426
3	4	9	0.7903

3.1 S/N Ratio Analysis

The influence of control parameters such as load, sliding speed and fly ash content on wear rate has been evaluated using S/N ratio response analysis. The control parameter with the strongest influence was determined by the difference between the maximum and minimum value of the mean of S/N ratios. The S/N ratio response analysis, presented in Table 3 shows that among all the factors, load was the most influential and significant parameter followed by sliding speed and fly ash content. The figure 2 shows the mean of S/N ratios for wear rate graphically and figure 2 depicts the main effects plot for mean wear rate. From the analysis of these results, it can be inferred that parameter combination of L = 9.81 N, S = 4 m/s and F = 9% gave the minimum wear rate for the range of parameter tested.

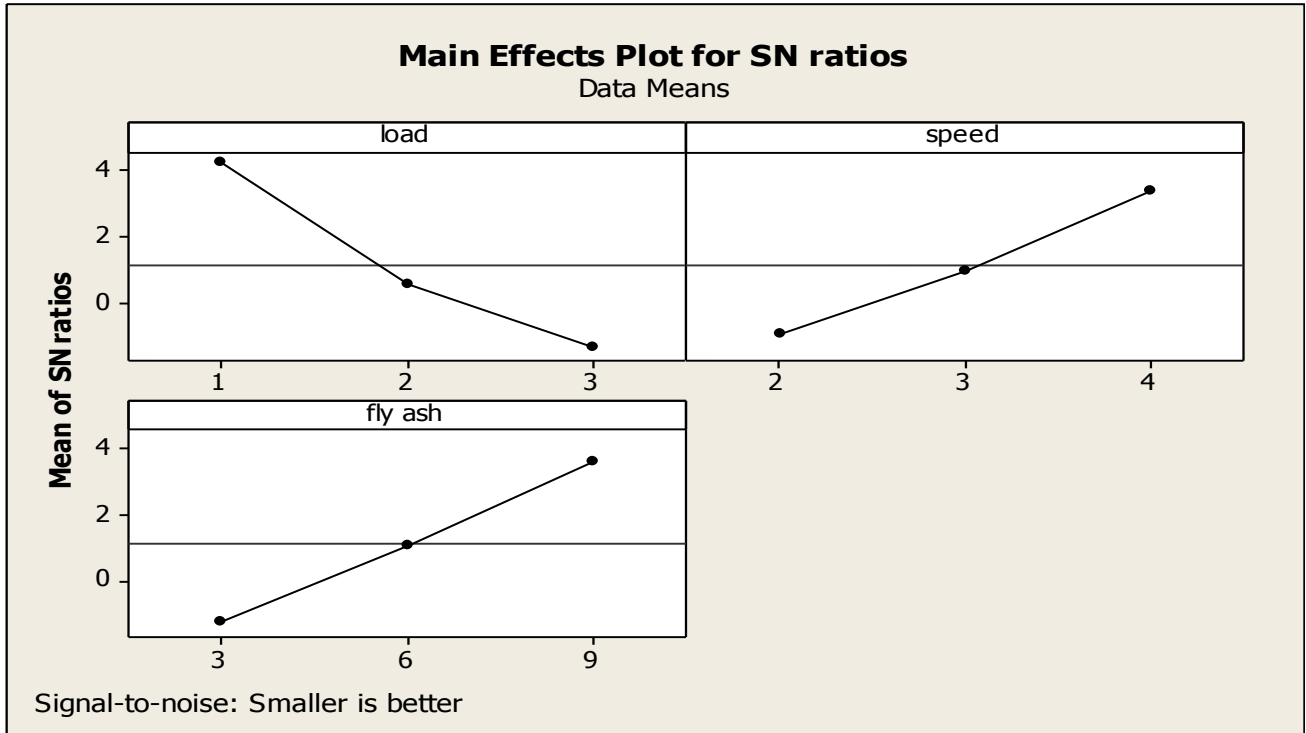


Fig.2 Mean of S/N ratios

Table 4 Response Table For S/N Ratios - Smaller Is Better (Wear Rate)

Levels	load	speed	Fly ash
1	0.6451	1.1855	1.2144
2	0.9937	0.9415	0.9424
3	1.2204	0.7322	0.7024
Delta	0.5753	0.4533	0.5120
Rank	1	3	2

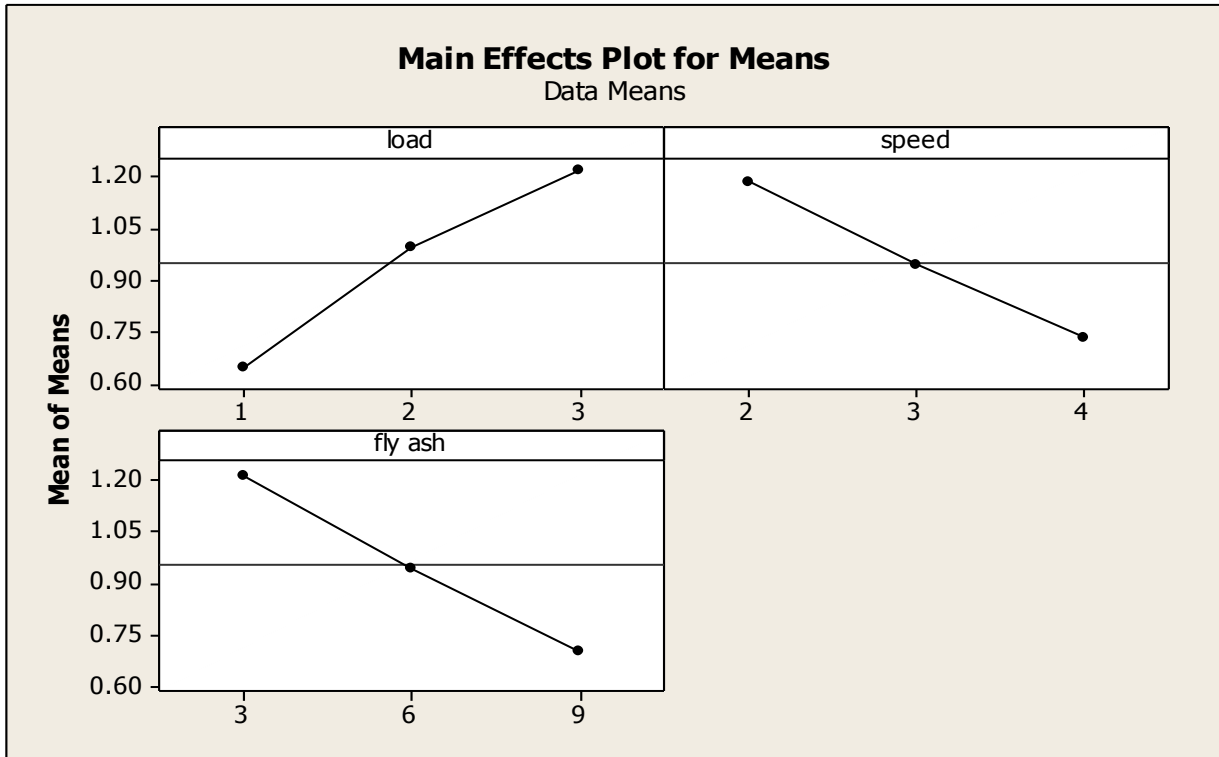


Fig. 3 Main Effects Plot For Mean Wear Rate

3.2 Analysis Of Variance

ANOVA was used to determine the design parameters significantly influencing the wear rate (response).

Table 5 shows the results of ANOVA for wear rate. The last column of Table shows the percentage of contribution (P %) of each parameter on the response, indicating the degree of influence on the result. It can be observed from the results obtained in the Table 5, that load was the most significant parameter having the highest statistical influence (37.2%) on the dry sliding wear of composites followed by fly ash content (31%) and sliding speed (25.2%).

Table 5 ANOVA

Source of variation	DF	Seq SS	Adj SS	Adj Ms	F-test	P-value	P (%)
L	2	1.51125	1.51125	0.755700	52.472	0.000	37.2
S	2	0.92212	0.92212	0.463228	32.018	0.000	25.2
F	2	1.1701	1.1701	0.590496	40.6284	0.000	30.704
L*S	4	0.11803	0.11803	0.029508	2.04913	0.1800	3.5
L*F	4	0.07157	0.07157	0.017891	1.24253	0.3665	0.0035
S*F	4	0.06783	0.06783	0.016959	1.17760	0.38957	0.0025
ERROR	8	0.1152	0.1152	0.0144			3.1
TOTAL	26	3.9761					100

3.2.1 Multiple Linear Regression Models

A multiple linear regression model is developed using statistical software “MINITAB 15”. This model gives the relationship between an independent / predictor variable and a response variable by fitting a linear equation to observed data. The regression equation for wear rate is,

$$\text{Wear Rate} = 1.57 + 0.288 \text{ load} - 0.227 \text{ speed} - 0.0853 \text{ fly ash} \quad \text{Eq (1)}$$

The above equation can be used to predict the wear rate of the hybrid composites. The constant in the equation is the residue. The regression coefficient (R^2) obtained for the model was 0.90 and this indicates that wear data was not scattered.

3.3 Confirmation Test

In order to validate the regression model, confirmation wear tests were conducted with parameter levels that were different from those used for analysis. The different parameter levels chosen for the confirmation tests are shown in Table 6.

Table 6 Confirmation Test

Experiments	Load (L)	Sliding speed (m/s)	Fly ash content (%)
1	1.5	2.5	3
2	2.25	3	6
3	2.75	3.5	9

Table 7 Wear Rate Level

Experiments	Experimental wear rate	Regression model – predicted wear rate (mm ³ /m)*10 ⁻⁶	Error (%)
1	1.142	1.1786	3.20
2	0.972	1.0192	4.85
3	0.823	0.7998	2.81

4. CONCLUSION

The results obtained from S/N ratio response analysis depict that load was the most dominant parameter influencing the dry sliding wear rate of hybrid composites. ANOVA was used to determine the design parameters significantly influencing the wear rate, and it was calculated that load was the most significant parameter having the highest statistical influence (61.12%) on the wear rate of composites, followed by sliding speed (19.6%) and fly ash content (16.03%). A multiple linear regression model was developed and it can be used to predict the wear rate of the hybrid composites.

5. REFERENCES

- [1] *The Foseco Foundryman's Handbook* (Pergamon Press, Oxford, 1965) p. 110.
- [2] Munro R. International congress and exposition. *SAE Tech Paper series* 1983;830067:789–96.
- [3] Ted Guo ML, Tsao CYA. Tribological behavior of self-lubricating aluminium/SiC/graphite hybrid composites synthesized by the semi-solid powder densification method. *Compos Sci Technol* 2000;60:65–74.
- [4] *ASM Handbook Composites* (ASM Int., 21, 2001) 3.
- [5] Stott.FH. *High temperature sliding wear of metals* (Tribol Int 2002;35) 489–95.
- [6] Krishnamurthy L. *Machinability studies on metal matrix hybrid composites*. PhD thesis, Kuvempu University, Karnataka, India; 2009.

Design of Frequency Selective Surface Radome over a Frequency Range

K. Renu¹, K.V. V. Prasad², S. Saradha Rani³, A. Gayatri⁴

^{1, 3, 4} (Department of ECE, GITAM University, India)

² (Department of EEE, MVGR College of Engineering, India)

ABSTRACT: A Frequency Selective Surface (FSS) is a metallic screen with frequency selective properties which are used as filters through which electromagnetic energy within a specific frequency range may be propagated. In Radar & Communication Systems, it is always required to filter the frequency of the plane waves. Due to its frequency selective property, Frequency Selective Surface is widely used for these applications. Frequency selective surfaces generally consist of an electrically conductive layer usually supported by a dielectric substrate. A common class of FSS can be constructed by placing periodic array of conducting elements on a dielectric substrate or slots in a conducting surface respectively. Multiple layers of such an FSS may be cascaded for greater effect. Depending upon design, it may be low-pass, high-pass, band-pass or band-stop FSS. One of the important applications is the band-pass radome antenna system. A one- or two- dimensional periodic array of resonant structures on a backing material, either apertures in a metallic sheet or metallic patches on a substrate, acts as a filter for a plane wave arriving from any angle of incidence. The primary objective of the paper is to study different approaches of the FSS radome design by using the basic concepts and the simulations. In this paper, slot element and ring element with different thickness are designed and the transmission and reflection properties of the designed elements are analyzed using the CST MICROWAVE STUDIO.

Keywords: Transmission, Reflection and Polarization

1. INTRODUCTION

Design of a band pass or band-stop FSS mostly depends on the choice of the proper element. Some elements are inherently more broad-banded or more narrow-banded than others, while some can be varied considerably by design. In this paper the typical behavior of the most common element types available to the FSS design are observed. All the curves are shown at 45° angle of incidence for orthogonal as well as parallel polarization with the resonant frequency around 10GHz. Further the FSS have 20mil $\epsilon=2.2$ dielectric slab placed on both sides. When judging an element type one might be tempted to prefer an element where the bandwidth around the first resonance varies as little as possible with polarization. However it should be kept in mind that in general at least for mechanical reasons, all FSS eventually must be supported by substantial assembly of

dielectric slabs which have a profound effect on the bandwidth variation with angle of incidence. Or more to the point, what is most stable without a substantial dielectric slab may not be the proper choice in the final FSS design. Also the bandwidth of any FSS can in general be varied significantly by variation of the interelement spacings D_x and D_z : A larger spacing will in general produce a narrower bandwidth, and vice versa.

The curves presented in the following are mostly for small inter-element spacings resulting in a rather large bandwidth and stable resonant frequency with respect to angle of incidence. The plane wave of incidence and direction of incidence are indicated in fig.1.

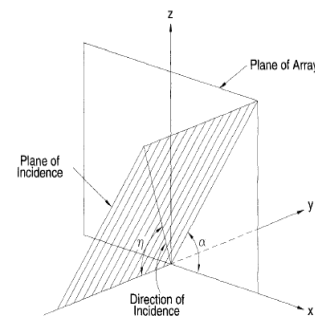


Fig. 1 The plane of incidence determined by α and the direction of incidence by η

All the cases presented in the following have been computed by using the program called "Periodic Moment Method" (PMM) [2,3]. It is considered to be one of the most reliable programs available which is being able to handle elements of arbitrary shapes, slots as well as dipole arrays mixed together in an arbitrary dielectric profile that may include loss.

2. GROUPS OF ELEMENTS

Frequency selective surfaces are used as filters through which electromagnetic energy within a specific frequency range may be propagated. Frequency selective surfaces generally consist of an electrically conductive layer usually supported by a dielectric substrate. The shapes of the apertures may include rings, crosses, slots, Jerusalem crosses. Here we use a dielectric substrate with thickness of 0.125, 0.5, 1.5, 3.2mm with a material of Rogers

RTduriod5880 (lossy metal) with dielectric constant 2.2 and the metal (copper) with 0.035mm thickness, with dielectric constant 5.8e+007.

The elements are arranged into two groups:

Group1: The center connected or N-poles, such as the simple straight element (slot), the Jerusalem crosses.

Group2: The loop types such as the four legged elements (cross), circular loops.

Group 1: The center connected or N-poles elements such as the simple straight element, three-legged element, anchor elements, Jerusalem cross and square spiral as shown in fig.2.



Fig. 2 Group I: The center connected or N-poles

Group 2: The loop types elements such as the three- and four-legged loaded elements, circular loops, square and hexagonal loops as shown in fig.3.

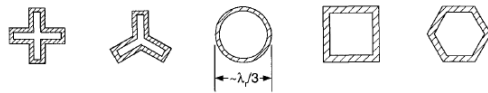


Fig.3 Group II: Loop Types

2.1 SLOT ELEMENT:

A basic slot is a radiating element which has a length of $\lambda/2$ and its width is much less than $\lambda/2$. When a high frequency field exists across a thin slot in a conducting plane, it radiates. A horizontal slot with such an excitation produces vertical polarization and vice-versa. In fact, slot radiates from both sides and it can be excited either by a coaxial cable or through waveguide.

Here $\lambda = C/F$,
Where $C = 3 \times 10^8 \text{ m/s}$, $F = 10 \text{ GHz}$.

Basically it consists of simple straight dipole arrayed in a fashion. Here we show a simple rectangular grid having a single slot. Take a dielectric slab with a material Rogers RTduriod5880 (lossy metal) with dielectric constant 2.2 and its thickness is 0.125mm. To the edge of the dielectric slab copper metal with the thickness of 0.035mm is placed. A piece of slot with length of 15mm and width of 0.3mm is cut from the copper metal. It is clear that the length of the dipole elements becomes larger; that is, the fundamental resonance becomes lower with increasing n. In the figure rectangular grid we have only one dipole for which we get broadband width. As per the waveguide the dielectric slab

length is 22.86mm and its width is 10.16mm, for metal (copper) the length and the width are same. The tangential electric and magnetic fields are matched by the boundary conditions at every boundary surface of the structure in order to obtain S-parameters.

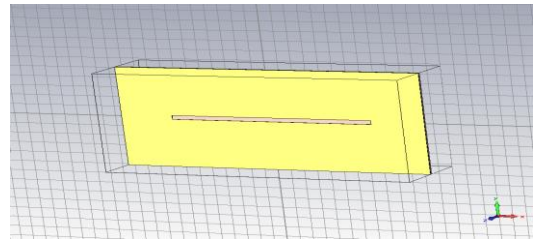


Fig.4 Single slot element with dielectric thickness of 0.125mm

As mentioned above here also same procedure is followed only by changing the dielectric substrate with a thickness of 0.5mm and a piece of slot element is cut with a length of 13mm and width of 0.4mm.

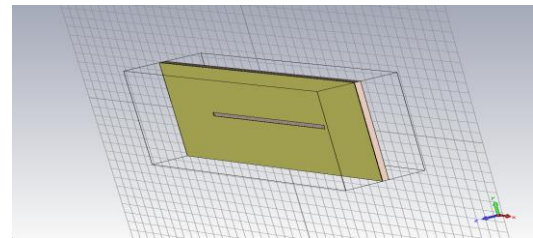


Fig.5 Single slot element with dielectric thickness of 0.5mm

2.2 RING ELEMENT:

It is only necessary to construct a single ring on its backing substrate. Construction of the geometry itself is simple: a substrate is defined using a brick primitive object, and then a hollow cylinder can be used to create the ring. The development of this element is quite instructive. Here we show a simple rectangular grid having a single ring element. Take a dielectric slab with a material Rogers RT5880 (lossy metal) with dielectric constant 2.2 and its thickness is 0.125mm. To the edge of the dielectric slab place a metal copper with the thickness of 0.035mm.

A piece of ring element is cut with outer radius of 4.6, inner radius of 4.2 and width of 0.4mm from the metal copper. As per the waveguide the dielectric slab length is 22.86mm and its width is 10.16mm, for metal (copper) the length and the width are same. Both transmission and reflection are represented in terms of S-parameters.

Development of surfaces of single ring element is shown below.

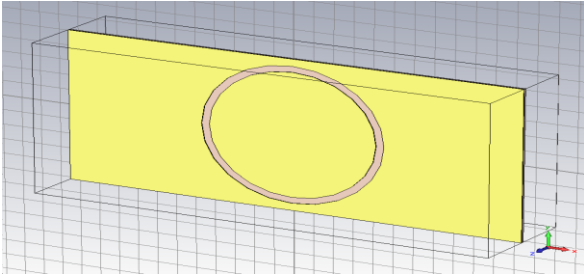


Fig.6 Single ring element with dielectric thickness of 0.125mm

As mentioned above here also same procedure is followed only by changing the dielectric substrate with a thickness of 0.5mm and a piece of ring element is cut with a outer radius of 4.6, inner radius of 4.2 and width of 0.4mm.

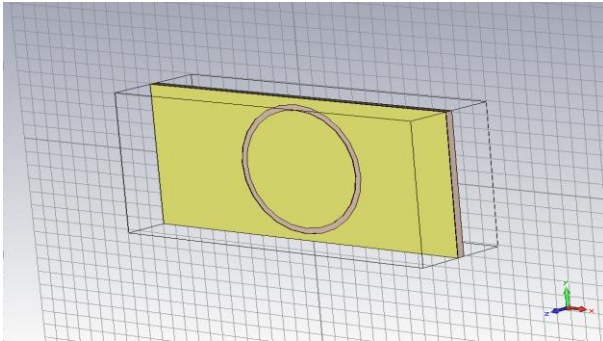


Fig.7 Single ring element with dielectric thickness of 0.5mm

3. SIMULATION

In this paper a software has been used called Computer Simulation Technology (CST) for the simulation of various elements. CST MICROWAVE STUDIO® is a fully featured software package for electromagnetic analysis and design in the high frequency range. It simplifies the process of inputting the structure by providing a powerful solid modeling front end which is based on the ACIS modeling kernel. Strong graphic feedback simplifies the definition of your device even further. After the component has been modeled, a fully automatic meshing procedure is applied before a simulation engine is started. A key feature of CST MICROWAVE STUDIO® is the *Method on Demand* approach which allows using the simulator or mesh type that is best suited to a particular problem.

All simulators support hexahedral grids in combination with the Perfect Boundary Approximation (PBA method). Some solvers also feature the Thin Sheet Technique (TST) extension. Applying these highly advanced techniques normally increases the accuracy of the simulation substantially in comparison to conventional simulators. Since no method works equally well in all application

domains, the software contains four different simulation techniques they are transient solver, frequency domain solver, integral equation solver, Eigen mode solver to best fit for their particular applications. The frequency domain solver also contains specialized methods for analyzing highly resonant structures such as filters. Furthermore, the frequency domain solver supports both hexahedral and tetrahedral mesh types. The most flexible tool is the transient solver, which can obtain the entire broadband frequency behavior of the simulated device from only one calculation run in contrast to the frequency step approach of many other simulators. This solver is remarkably efficient for most kinds of high frequency applications such as connectors, transmission lines, filters, antenna etc.

The transient solver is less efficient for electrically small structures that are much smaller than the shortest wavelength. In these cases it is advantageous to solve the problem by using the frequency domain solver. The frequency domain solver may also be the method of choice for narrow band problems such as filters or when the usage of tetrahedral grids is advantageous. Besides the general purpose solver that supports hexahedral and tetrahedral grids, the frequency domain solver also contains fast alternatives for the calculation of S-parameters for strongly resonating structures. These solvers are currently available for hexahedral grids only.

Important features of Frequency domain solver are:

- a) Efficient calculation for loss-free and lossy structures
Including lossy waveguide Ports
- b) General purpose solver supports both hexahedral and tetrahedral meshes.
- c) High performance radiating/absorbing boundary conditions.
- d) Continuation of the solver run with additional frequency samples
- e) Conducting wall boundary conditions (tetrahedral mesh only)
- f) Automatic fast broadband adaptive frequency sweep
- g) User defined frequency sweeps
- h) Adaptive mesh refinement in 3D
- i) Antenna far field calculation (including gain, beam direction, side lobe suppression, etc.) with and without far field approximation
- j) Calculation of various electromagnetic quantities such as electric, magnetic fields, surface currents, power flows, current densities, power loss densities, Electric energy densities, magnetic energy densities.
- k) Plane wave excitation with linear, circular or elliptical polarization (tetrahedral mesh only)
- l) High performance radiating/absorbing boundary conditions.

- m) Network distributed computing for optimizations and parameter sweeps
- n) Antenna array far field calculation
- o) RCS calculation (tetrahedral mesh only)
- p) Besides the general purpose solver, the frequency domain solver also contains two solvers specialized on strongly resonant structures (hexahedral meshes only). The first of these solvers calculates S-parameters only whereas the second also calculates fields with some additional calculation time, of course.

Important features of transient simulators are:

- a) Efficient calculation for loss-free and lossy structures
- b) Broadband calculation of S-parameters from one single calculation run by applying DFTs to time signals
- c) Calculation of field distributions as a function of time or at multiple selected frequencies from one simulation runs.
- d) Frequency dependent material properties
- e) Surface impedance model for good conductors
- f) Automatic waveguide port mesh adaptation
- g) User defined excitation signals and signal database.
- h) Automatic parameter studies using built-in parameter sweep tool.
- i) Frequency dependent material properties with arbitrary order for permittivity.
- j) Multipin ports for TEM mode ports with multiple conductors
- k) Plane wave excitation (linear, circular or elliptical polarization)
- l) S-parameter symmetry option to decrease solve time for many structures
- m) Auto-regressive filtering for efficient treatment of strongly resonating structures
- n) Re-normalization of S-parameters for specified port impedances
- o) Phase de-embedding of S-parameters
- p) Full de-embedding feature for highly accurate S-parameter results
- q) Single-ended S-parameter calculation
- r) Excitation of external field sources imported from CST MICROWAVE STUDIO or Sigrity.
- s) High performance radiating/absorbing boundary conditions
- t) Calculation of various electromagnetic quantities such as electric fields, magnetic fields, surface currents, power flows, current densities, power loss densities, electric energy densities, magnetic energy densities, voltages in time frequency domain.

4. RESULTS

Using CST MICROWAVE STUDIO® software, different elements such as single ring element, single slot element, single Tripole element are simulated. Transmission and reflection curves of single slot element are presented with different element thickness. It is observed that beam width and frequency of the transmission and reflection curves are changing with thickness of the element.

Fig.8 represents the transmission and reflection curves of single slot element with thickness of 0.125mm.

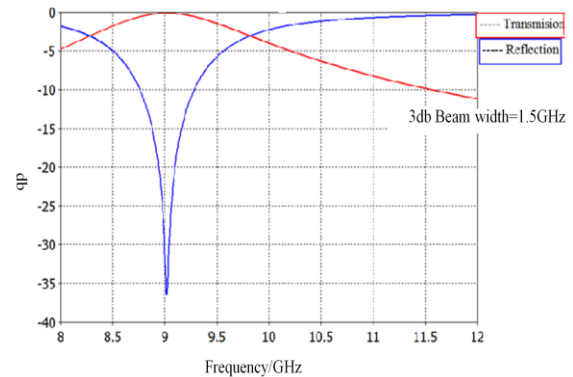


Fig. 8 transmission and reflection curves of single slot element with thickness of 0.125mm

From Fig.8 it is observed that the 3db beam width of the single slot element of thickness 0.125 mm is 1.5GHz and the centre frequency is 9.024GHz.

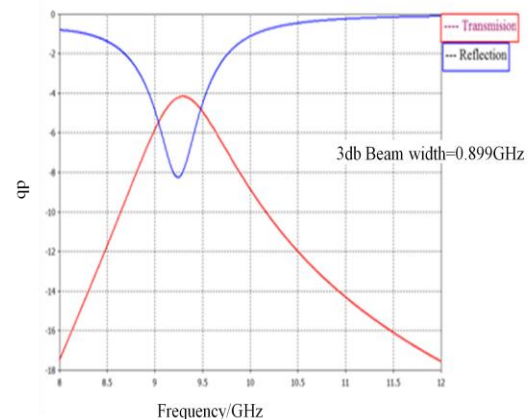


Fig. 9 transmission and reflection curves of single ring element with thickness of 0.125mm

From Fig.9 it is observed that the 3db beam width of the single ring element of thickness 0.125 mm is 0.899 GHz and the centre frequency is 9.29GHz

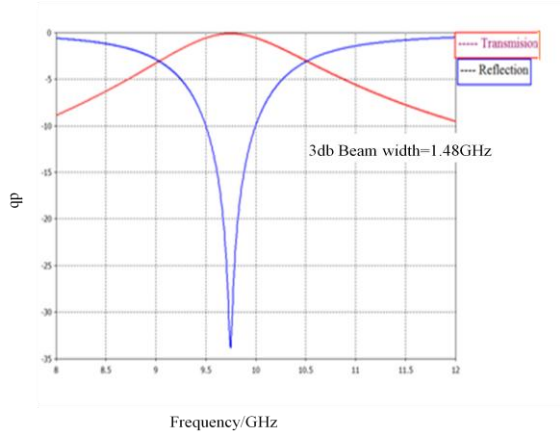


Fig.10 transmission and reflection curves of single slot element with thickness of 0.5mm

Fig.10 shows the transmission and reflection curves of single slot element with thickness of 0.5mm

From Fig.10, the 3db beam width of the single ring element of thickness 0.5 mm is 1.48 GHz and the centre frequency is 9.75GHz.

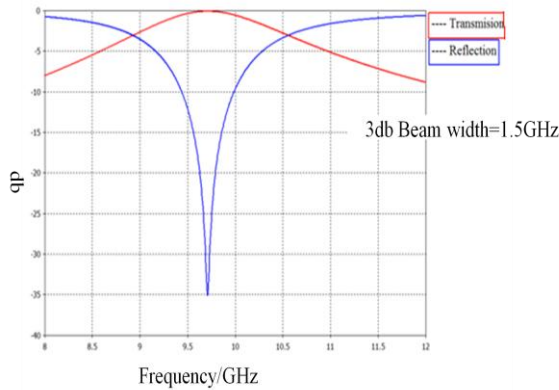
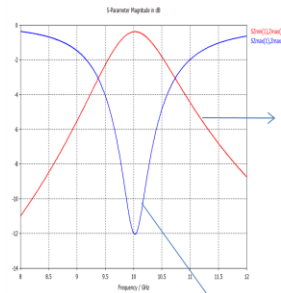


Fig.11 transmission and reflection curves of single ring element with thickness of 0.5mm

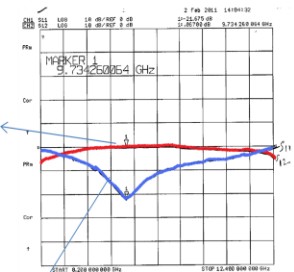
From Fig.11, the 3db beam width of the single ring element of thickness 0.5 mm is 1.5GHz and the centre frequency is 9.71GHz

All the results are calibrated using network analyzer. As an illustration Fig.12 and Fig.13 shows the comparison of simulated results with calibrated results for single slot of thickness 1.5mm and also single ring of thickness 1.5mm. Also the simulated and calibrated results are compared for single ring elements for thickness of 3.2 mm. The results are comparable and are encouraging.

Simulated results



Calibrated results



Transmission

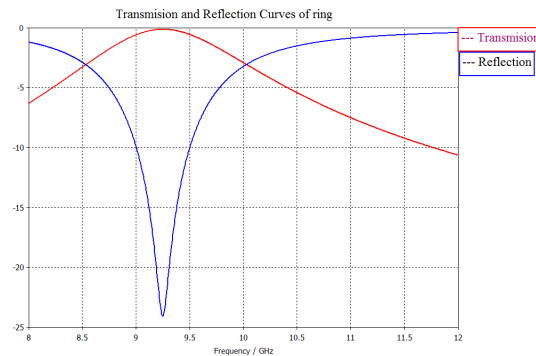
Reflection

Fig.12 comparison of transmission and reflection curves of single slot element with thickness of 1.5mm

With the calibration of single slot element using network analyser, the transmission and reflection curves resonate at 9.73 GHz where as the simulation result is at 10 GHz. The phase shift observed is due to the manual cutting of slot element.

Below the results of single ring element with a thickness of 1.5mm is compared.

Simulated results



Calibrated results

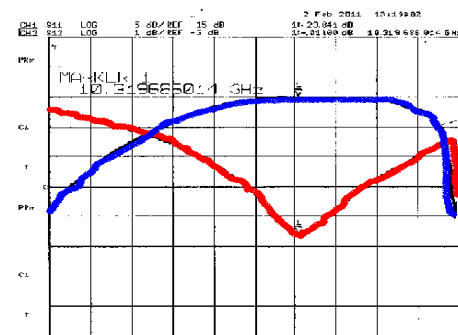


Fig.13 comparison of transmission and reflection curves of single ring element with thickness of 1.5mm

From the above figure it is observed that transmission and reflection curves resonate at 9.3GHz with simulation where as the calibrated value is resonating at 10.32GHz which is comparable.

Below the results of single ring element with a thickness of 3.2mm is compared.

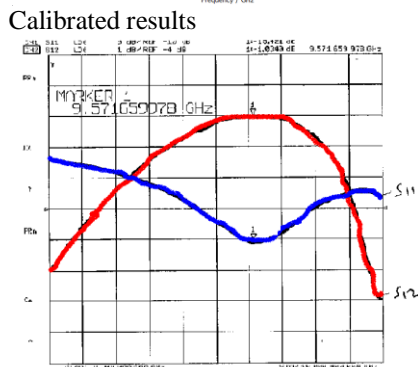
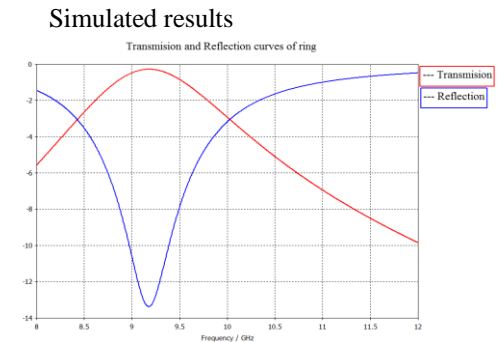


Fig.14 comparison of transmission and reflection curves of single slot element with thickness of 1.5mm

By using ring element of thickness it is observed that transmission and reflection curves resonate at 9.178GHz with simulation where as the calibrated value is resonating at 9.57 GHz which is comparable. The difference in resonating frequency between simulated results and calibrated results are mainly due to the manual cutting of the ring elements.

5. CONCLUSION

Using CST microwave studio, the transmission and reflection properties of a slot element(single) and ring element (single) designed for a frequency of 10GHz, with thickness of 0.125mm and 0.5 mm are analysed. Using the Network Analyzer, the transmission and reflection properties of a slot element(single) and ring element (single) are calibrated. The simulated results obtained using CST microwave studio are compared with the calibrated values and minimum deviation(0.27GHz) is observed. This work can be further extended to analyse transmission and reflection properties of different elements like cross and tripole elements, which are also used in designing of a Radome. As these elements are having the

property to allow the particular frequency(10GHz) and attenuates the other frequencies, detection of the signals by the enemy is difficult.

6. REFERENCES

- [1] B. A. Munk and R. D. Fulton, "Transmission through a Bi-Planar Slot Array Sandwiched Between Three Dielectric Layers, March 1973-Nov. 1975," Tech. Rept. 3622-7, Ohio State Univ. ElectroScience Lab., Dept. of Electrical Eng., Columbus, Feb. 1976.
- [2] L. W. Henderson, "The Scattering of Planar Arrays of Arbitrary Shaped Slot and/or Wire Elements in a Stratified Dielectric Medium," Ph.D. Dissertation, Ohio State Univ., Dept. of Electrical Eng., Columbus, 1983.
- [3] L. W. Henderson, "Introduction to PMM," Tech. Rept. 715582-5, Ohio State Univ.
- [4] B. A. Munk and G. A. Burrell, "Plane Wave Expansion for Arrays of Arbitrarily Oriented Piecewise Linear Elements and Its Application in Determining the Impedance of a Single Linear Antenna in a Lossy Half-Space," *IEEE Trans. on Antennas and Propagation*, **AP- 34(3)**, 331-343, May 1979.
- [5] B. A. Munk, G. A. Burrell, and T. W. Kornbau, "A General Theory of Periodic Surfaces in Stratified Media," Tech. Rept. 784346-1, Ohio State Univ. ElectroScience Lab., Dept. of Electrical Eng., prepared under contract AFAL-TR-77-2 19, Nov. 1977.
- [6] T. W. Kornbau, "Analysis of Periodic Arrays of Rotated Linear Dipoles, Rotated Crossed Dipoles, and of Biplanar Dipole Arrays in Dielectric," Ph.D. Dissertation, Ohio State Univ., Dept. of Electrical Eng., Columbus, 1984.
- [7] S. W. Schneider, "On the Scattering Properties of Super Dense Periodic Surfaces," Ph.D. Dissertation, Ohio State Univ., Dept. of Electrical Eng., Columbus, 1992.
- [8] B. A. Munk, United States Patent 3,789,404, Periodic surface for large scan angles, Jan. 29, 1974.
- [9] E. L. Pelton and B. A. Munk, United States Patent 3,975,738, Periodic antenna surface of tripole slot elements, Aug. 17, 1976.

Fuzzy Inference System Based Reputation Model for Grid Computing

Biswajit Sinha, P. Sateesh Kumar

*Information Technology Electronics & Computer Engg. Dept. Indian Institute of Technology, Roorkee
Roorkee, Haridwar, Uttarakhand-247667, India*

Abstract: Development of grid computing enforces the implementations of economic and efficient models, though the assumptions are there that both transaction parties are honest and trustworthy. In reality there is serious information asymmetry between transacting entities. Introducing trust and reputation can solve this problem to a great extent though the issue which is related with reputation and trust is its imprecise nature which makes it difficult to be determined by precise conventional mathematics. In this paper we focus on a Fuzzy Inference System based Reputation model that will provide an previous experience based custom rule-setting to determine reputation for a transacting party. Malicious recommendations in indirect trust transmission has been also removed and punished in this model. The design and simulation of the controller is done using GRIDSIM and the simulation results are presented to demonstrate the efficiency of the Fuzzy Inference System Based Reputation Model (FISRM). The experimental results on different type of fraudulent users shows its stability and steady performance over the conventional Reputation Based Allocation Model (RBAM).

Keywords: *Fuzzy Inference System; Mamdani Type Fuzzy inference; Global Information Service*

I. INTRODUCTION

A grid computing system is an open, dynamic and competitive service oriented field. Due to its openness, resource management and their safety is one of the prime concern in grid. There are good number of service providers present in grid network which offers various competitive services and there are plenty of buyers to pay for that. But resource which are offered by several resource providers are not always trustworthy, and may be a huge number of them providing non-efficient and non-authorized resources with a huge amount of cost to make profit. And situation becomes more grave when the consumer deal with the transacting party who is entirely unknown to it.

Openness, dynamic nature and easy to get high computing services in less cost features of Grid computing comes under the cost of its serious information asymmetry. The primitive unit in Grid is a node or a system capable of computation along with some computer resources like memory (main and auxiliary), CPU units, printer etc. connected to each other by LAN or MAN or wireless network. Therefore, a Grid node or system can play at a time dual nature like resource provider and resource consumer. A grid network consists of grid nodes could be huge and overlaid over several states as well as several countries. So it's difficult for each resource provider and consumer to know each other at the first hand, resource node completely masters their own information. The available

information is only a description of the resource node. Due to the serious information asymmetry, resource nodes may carry out dishonest transaction and in order to pursue maximum benefit and attract more customer to buy their merchandise. Since it is unrealistic to expect that all transacting parties are honest to behave proper measurements should be taken to stop fraudulent practice.

Introduction of trust and reputation model solves the issues of security in resource transactions in Grid network up to a great extent. The trust and reputation mentioned here is about the behavioral trust. Trust is often classified two categories: Identity trust and Behavioral trust. Identity trust is static. Once the identity is identified, the behaviors of the entities are not getting monitored any more even though they might do something harmful, whereas behavior trust is dynamic trustworthiness. Behavior trust is based on transactions between entities in the past time. If the entities do something wrong or harmful, its behavioral trust value will get dropped and it'll help the other resources to decide that whether they still want to do any more transaction with the same entity or not.

Many trust models based on behavior trust had been proposed already. In the trust model proposed by Alfarez Abdur Raheman and Stephen Hailers, trust is divided into Direct Trust and Recommend Trust [1]. Literature [2] proposed a trust and reputation-based resource selection in grid computing, amended the reputation of resource provider based on trust factors to select the trustworthy transaction participators. Literature [3] examined the role of reputation in grid environments, introducing reputation and trust avoided the potential risk of opportunistic behavior of service providers or users who opportunistically exploit the information gap between providers and consumers on the quality of services. Therefore reputation mechanism can provide reference for resource node selecting transaction participators and resource node transact with trust. But trust is a subjective and inaccurate value which is decided by the Grid entity, it is difficult to describe with accurate probability distribution. Few behavior trust models based on fuzzy logic in Grid are proposed [4] [5] [6]. But the fixed weighted fuzzy comprehensive evaluation in [4] is not suited;

For these reasons, combining the grid resource oversupply situation and subjective and imprecise nature of Behavioral Trust, this paper proposes a Fuzzy Inference System based Reputation model (FISRM) for resource allocation in grid computing. This model based on user defined fuzzy inference rules enables grid node to decide a resource provider's trust and reputation value and secure a transaction between two unknown participator. After transaction a entity is asked to provide feedback on a resource provider for future reference and false recommendations are removed and punished in this model. Trust is an entity's belief in another entity's

capabilities, honesty and reliability based on its own direct experiences within a specific context at a given time; Reputation can be obtained by fuzzy derivation and combination of recommendation trust.

II. FUZZY LOGIC IN TRUST DOMAIN

With fuzzy logic trust can partially belong to a set and this is represented by the set membership [7].

Let $X=\{x_0,x_1,\dots,x_{n-1}\}$ be the problem domain that trust manage will be researched in $x_i (i=1,\dots,n)$ denote the entity in Grid. The definition of fuzzy set is :

A fuzzy set is any set that allows its members to have different grade of membership (membership function) in the interval between [0,1].

Definition: Let X be the domain, and let x be the element of the set $X, \forall x \in X$ and the mapping is as :

$$X \rightarrow [0,1], x \rightarrow \mu_A(x) \in [0,1]$$

The fuzzy set A in X is expressed as a set of ordered pair

$$A = \{(x|\mu_A(x)), \forall x \in X$$

$\mu_A(x)$ is the membership function of fuzzy set A , which describes the membership of the element x of the base set X in the fuzzy set A . The grade of membership $\mu_A(x_0)$ of a membership function $\mu_A(x)$ describes for the special element $x=x_0$, to which grade it belongs to the fuzzy set A . This value is in the unit interval [0, 1].

In Grid, the grade of trust can be described by membership degree of different fuzzy sets in X which denote different trust levels. M different fuzzy sets $T_i (i = 1, 2, \dots, M)$, which are in the set of all fuzzy sets in X can be used to denote M different trust levels. For example, when $M=6$, seven fuzzy sets $T_i (i = 1, 2, \dots, 7)$, can be used to denote ix different trust levels in Grid. The trust level of $T_i (i = 1, 2, \dots, 7)$, is defined as follows:

- T_1 denotes the "very low" fuzzy set;
- T_2 denotes the "low" fuzzy set;
- T_3 denotes the "mid low" fuzzy set;
- T_4 denotes the "mid " fuzzy set;
- T_5 denotes the "mid high" fuzzy set;
- T_6 denotes the "high" fuzzy set;
- T_7 denotes the "very high" fuzzy set;

The membership function of x to fuzzy set T_i denoted as $T_i(x)$. To a concrete x_i , the membership degree is $T_j(x_i)$, which can be marked as T_{ij} . Trust vector of x_i is :

denoted as $T_i(x)$. To a concrete x_i , the membership degree is $T_i(x_i)$, which can be marked as T_{ij} . Trust vector of x_i is :

$V = \{v_1, v_2, \dots, v_7\}, v_i (i = 1, \dots, 7), v_i$ denotes the membership degree of x_i to T_i . But x_i can simultaneously belong to another fuzzy set T_k , such that $T_k(x_i)$ characterizes the grade of membership of x_i to T_k .

III. THE OVERVIEW OF FISRM

Introduction of trust and reputation mechanism into grid network protects the resource consumer by saving them the fraudulent resource providers . Trust and reputation reflects a grid node's past behavior as well as its future expected performance . A task node periodically collects the information about all registered resource nodes and their reputation information from concerned Grid Information Service (GIS). When a resource register itself for the first time the local GIS assigns it a neutral trust value which just above from the par.

Later according to its performance, efficiency and consistency increase its own trust and reputation value which make it more acceptable than other nodes. In this model Grid Information Service plays a very important role, the dependency of resources on the Local GIS make the entire network more scalable compared to earlier models because the complexity of the computation of trust and reputation reduced to $O(n)$ from $O(n^2)$. In this paper, we pay more attention to the task and reputation of resources node, because the task node has less information but takes larger risk at the same time in transaction process and its trust and reputation have a comparatively small impact to results of the transaction, contrary to the resource node.

A. Logical Structure Of FISRM

The Logical structure of FISRM is shown in Figure 1. The module definition of FISRM is introduced in section B. Grid resource allocation workflow based FISRM has been in section D.

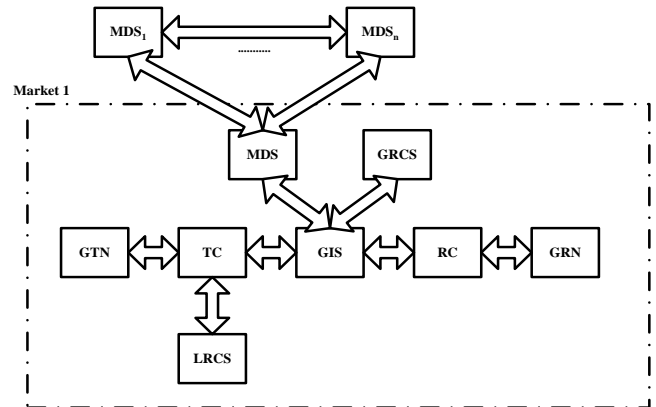


Fig. 1. Logical Structure Of FISRM

B. Related Definitions

Market in grid network is a platform for transaction between a resource and a task. Without existence of market a task cannot assign it's tasks to a proper resource. Transaction manager is significantly responsible for maintaining the benefits of transaction participators, making market resources to achieve balance of supply and demand, contacting with other grid resource markets and sharing grid resources.

But in this paper our motive is not to describe the role of transaction manager, it's beyond the scope of this paper. We mainly focused on the behavior of the following components of market in grid network including GIS(Global Information Service), TCS(Trust Computation Server), RCS or CCS(Reputation Computation Server or Credibility Computation Server).Apart from them, other components are as follows:

Grid Resource Nodes(GRN): grid node gains benefit through selling resource and permitting others to use its resource, which is recorded as resource node.

Grid Task Nodes(GTN): grid node gets the service through paying for the resource, which is recorded as task node. It also keeps its own record of the ratio of successful and failed transactions for each resource node.

Task collector(TC): collect the request information of grid task nodes and submit it to the GIS.

Resource collector(RC): collect the request information of grid resource provider and submit it to the GIS.

Grid Information Servers(GIS): The primary task of GIS is to keep records of all available resource nodes and task nodes in a single market in a grid network. Task nodes which are interested to consume a resource should register itself with GIS and wait for the periodic updates of the resource nodes with their reputation values, then a task node decide whether it will perform transaction with the resource node or not. Along with that GIS is also responsible for to assign reputation values for newly registered resource and to keep track of the information about ratio of total transaction a resource node participated and the number of successful transaction irrespective of any task node. After the completion of each transaction task node calculate the trust value of the resource node and send it as a feedback to the GIS for future reference.

Market Directory Servers(MDS): Record the grid resource market directory information. It can map to other resource market information servers through the directory, query the information of other resource market members, including the registration information, the transaction record, reputation information and so on.

Trust Computation Server(TCS): Compute the trust value of the resource node after the completion of a transaction on behalf of a task node and after defuzzification send it to task node.

Reputation Computation Server(RCS): Check the credibility of the node giving feedback on different node and punish it if any discrepancy happened and reward the node which is performing consistently in a honest and efficient approach.

Reputation: Grid node's reputation is the expectation of future transaction behavior which is based on the observation of transaction behavior from other resource nodes during a given period.

Local Reputation Value: Grid node j's local reputation value LR_{ji} is the expectation of i to j's future transaction behavior based on the transaction history and the evaluation of transaction history by i .

Global Reputation Value: Resource node j's global reputation value R_j is the credibility which is got by integrating the evaluation given by other resource nodes which have transactions with node j.

C. Reputation Value Computation

This procedure starts from the time a node in grid network register itself for the first time in GIS. In this paper we have assumed that initially GIS assign every node a initial reputation value of 0.6. If it seems to naive to assign a value in such manner , GIS can conduct some initial test procedure to decide appropriate reputation value what should be suited it better.

Reputation value of a node in grid network get decided through a two-fold system. First after completion of a transaction consumer decide the reputation of the provider and later in GIS based on the feedback submitted by the consumer, reputation of both consumer and provider got affected globally.

Local reputation computation depends on the following three metrics,

Capability: Capability of a grid node indicates the capability of this node to accomplish a task submitted by a task node successfully. The ratio of total transactions it has participated to the number of transactions it had accomplished successfully has been taken here as a node's capability.

$$C_j = \frac{n_{tj}}{n_{sj}} \tag{1}$$

For a node j, (j = 1,...,n) it's capability C_j is the ratio of total transactions it participated n_{tj} to the number of successful transaction n_{sj} .

Reliability: Reliability feature of a grid node prevent a fraudulent node to practice slow poisoning or frog-boiling frauds. It reflect that how spontaneous a node is by measuring it's activity coefficient. Here is an empirical formula to measure it

$$R_i = e^{\left(\frac{n_{tj}}{n_t} - 0.8\right)} \tag{2}$$

Here n_t is the total number of system transactions between all nodes in a grid market. 0.8 is a upper threshold value which indicates that for a node, it's not possible to participate in more than 80% transactions.

User-Satisfaction: User satisfaction is the measurement of the satisfaction of a node with another node based on the status of the transaction as well as the previous transactions happened between them.

$$U_{ji} = \frac{n_{sji}}{n_{tji}} \tag{3}$$

For a node j, (j = 1,...,n) n_{sji} is the number of successful transaction between node i and node j and n_{tji} is the number of total transaction between them.

Now using the above mentioned metrics as input parameters for fuzzy inference system, Trust Computation Server calculates the trust value of the grid node which has provided the resource.

Initially the reputation value of a newly registered resource node, a node receive from GIS is 0.6 which just above the bottom watermark 0.5 for a node to decide to take part in a transaction. Later the value get changed based on its consistency and honesty in feedback to other resources. Values of capability, reliability and user-satisfaction are though in the interval between [0,1], to decide that which trust level they come under fuzzification is required using different membership functions, one for each of capability, reliability and user-satisfaction. The range of values for different trust levels for the membership functions are shown in Table 1. Users can set their customized value range based on their past experience and expert knowledge.

Trust-level	Very Low	Low	Mid - low	Mid	Mid-high	High	Very High
Capability	(0.0, 0.1)	(0.0, 0.15, 0.2)	(0.1 5.0, 3, 0.4)	(0.3 , 0.4 5, 0.6)	(0.4, 0.55, 0.7)	(0.6 , 0.8, 0.9)	(0.85, 1.0)
Reliability	(0.0, 0.2)	(0.1, 0.25 ,0.4)	(0.3, 0.4, 0.5)	(.45 , 0. 5, 0.6)	(0.55 , 0.65, 0.8)	(0.7 , 0.8, 1.0)	(0.95, 1.0)

User-satisf action	(0.0, 0.1)	(0.0, 0.15, 0.2)	(0.1, 5, 0.4)	(0.3, 0.4, 0.5, 0.6)	(0.4, 0.55, 0.7)	(0.6, 0.8, 0.9)	(0.85, 1.0)
--------------------	------------	------------------	---------------	----------------------	------------------	-----------------	-------------

Table 1. Range Of Different Trust Levels

The fuzzy inference system we have used here is Mamdani type. The Mamdani-type fuzzy inference process [8] is performed in four steps:

1. Fuzzification of the input variables
2. Rule evaluation (inference)
3. Aggregation of the rule outputs (composition)
4. Defuzzification

We examine a simple two-input one-output problem that includes three rules:

- Rule: 1 IF x is A₁ OR y is B₁ THEN z is C₁
- Rule: 2 IF x is A₂ AND y is B₂ THEN z is C₂
- Rule: 3 IF x is A₃ THEN z is C₃

The behavior of fuzzy system is studied through the rule viewer and surface viewer which are simulated in Matlab. Figure 2 shows the trust model, having three input parameters and one output. The fuzzy inference used is depicted in Figure 3. shows the rule viewer of various rules taken into the consideration. The rule viewer gives the graphical representation of rule base designed.

Once the trust evaluation is accomplished by Trust computation server, it defuzzify back it in the range [0,1]. Defuzzification is the reverse process of fuzzification. Trust and reputation calculated by TCS is a "fuzzy" result, described

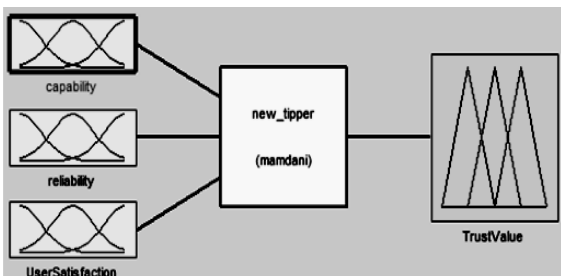


Fig. 2 Trust Model based on Mamdani-type Fuzzy Inference

in terms of fuzzy member sets. Defuzzification would transform this result into a single number indicating the trust level of an entity. This may be necessary if we wish to output a real number to the user. An average of maxima method or a centroid method [8] can be used to do this work. We have used centroid method in our work.

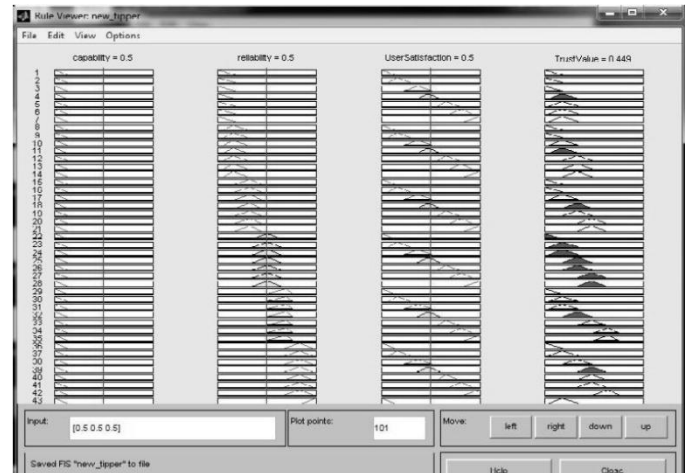


Fig. 3 A sketch map of Mamdani-type Fuzzy Inference

After the computation of local reputation, task node sends the reputation information to GIS for future reference. In GIS for security purpose and to prevent foul practice the reputation value sent by has been checked using some firsthand rules.

Because of the self-interest of the many and varied organizations in the Grid, there will be some unfair ratings for strategic lying and collusion amongst agents in the all ratings from entities in the Grid. To remove false reputation recommendation, local reputation value checked against the node's global reputation value. If the deviation is more than some user defined value $\pm\sigma$ then it will be discarded and the reputation value of the feed backing resource will be defamed by the given empirical formula:

$$R_i = R_j(1 - e^{-0.5}) \quad j = 1, 2, \dots, n \quad (4)$$

Global reputation value of a grid node is the mean value of the feedback received for that node. A node constantly performing with a steady efficiency is rewarded by this model after a short interval of 5 to 10 feedbacks by the following empirical formula:

$$R_j = R_j(1 + e^{-0.3}) \quad j = 1, 2, \dots, n \quad (5)$$

D. ResourceAllocation Based On FISRM

Resource allocation based on FISRM has been shown using a flowchart in Figure 4.

In the flow chart terms are used like n(F) means no. of feedbacks and LR means local reputation and GR means global reputation.

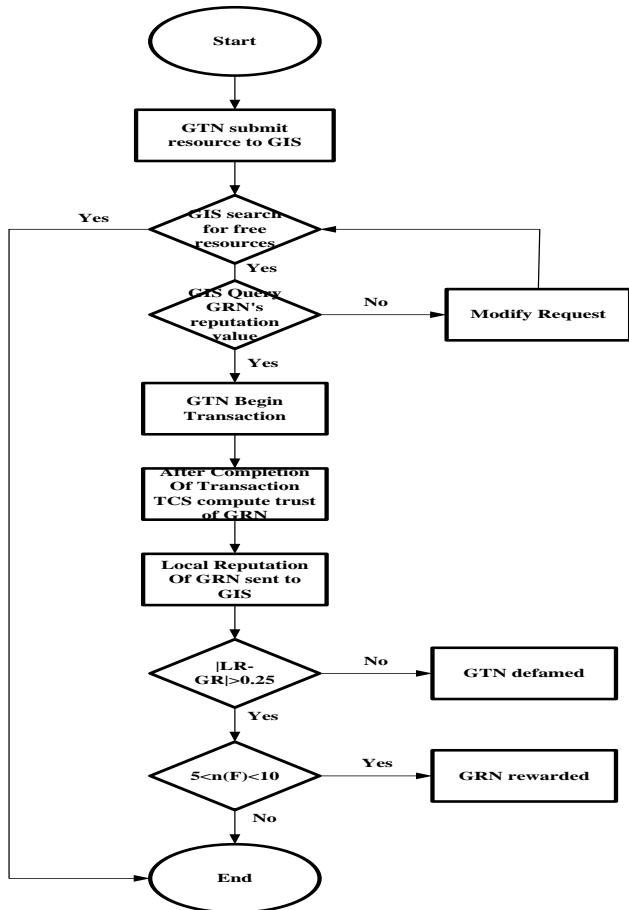


Fig. 4 Resource Allocation Based On FISRM

IV. EXPERIMENTS AND SIMULATION RESULTS

To check that the model we have implemented is working efficiently or not we carry out a number of experiments. Before stating about them, to check the trend of trust transfer between Capability, Reliability and User-satisfaction, we have simulated the corresponding surface viewer of these parameters in Matlab and depicted here in Figure 5.

Experiment environment is set in GridSim by doing a series of changes to make suitable for FISRM model. GridSim is a discrete event simulation toolkit based on java and its main object is to study effective methods of resource allocation based on computational economy model by simulating the grid environment.

In our experiment we have set a grid network of 30 grid nodes and each node has their own tasks and resource. The constraint is no node can submit their task to their own resource and has to register their resources in GIS. By this constraint each node is able to play the roles of both resource provider and task node. In grid market resource nodes can be divided in two categories:

Good Node: Nodes which performs with consistency and honesty.

Malicious Node: Nodes which are notorious to do foul practice.

But the malicious node definition is really broad category to realize. Literature [9] describe a more specific sub category of them.

Slander nodes: These malicious nodes of this type provide unauthentic resource and false negative evaluation when

resource node is asked to feedback other nodes transaction evaluation.

Collusive fraud nodes: These malicious nodes of this type collude with each other and provide authentic resources and good feedbacks for inside members, but provide unauthentic resources and incorrect evaluation for external nodes.

A. Experiment 1: Growth of reputation values of resource nodes with the increase of transaction

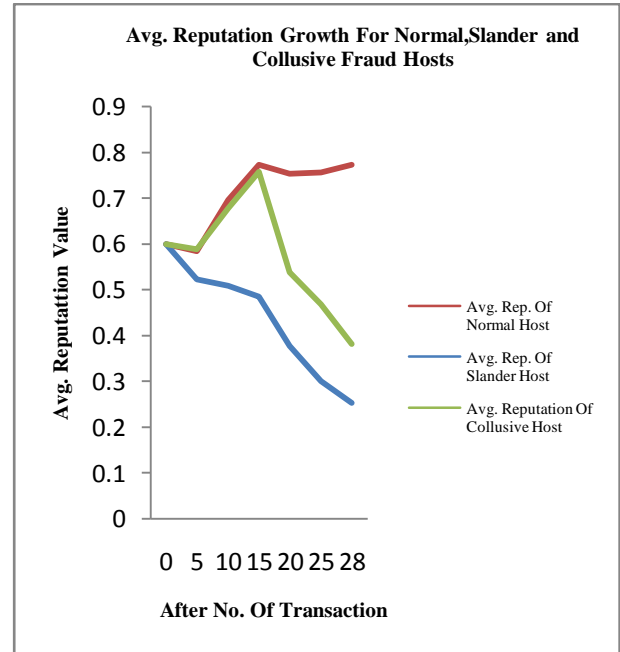


Fig. 6 Avg. Reputation Growth For Normal, Slander and Collusive Fraud Hosts

Figure 6 shows that growth of reputation values of normal nodes or good nodes are steady after the first transactions. The dip in first five transaction is due to the initial assignment of reputation value of 0.5. After 5 to 7 transactions it adjusts it's reputation value to it's true reputation value what it deserves. Slander hosts are started to dip from very beginning itself due to their malicious activity, results shows that it can detect the maliciousness efficiently and in a short frame of time window. Collusive nodes are hide themselves in a crafty manner but still in this model they are getting detected after a short interval with respect to other models.

B. Experiment 2: Trend of average successful transactions with the increase of transaction

Figure 7 shows that the average number of successful transactions are steadily increasing from the very beginning as expected. The curves for the successful transactions for slander and collusive nodes are expected as well and they are consistent to their characteristics.

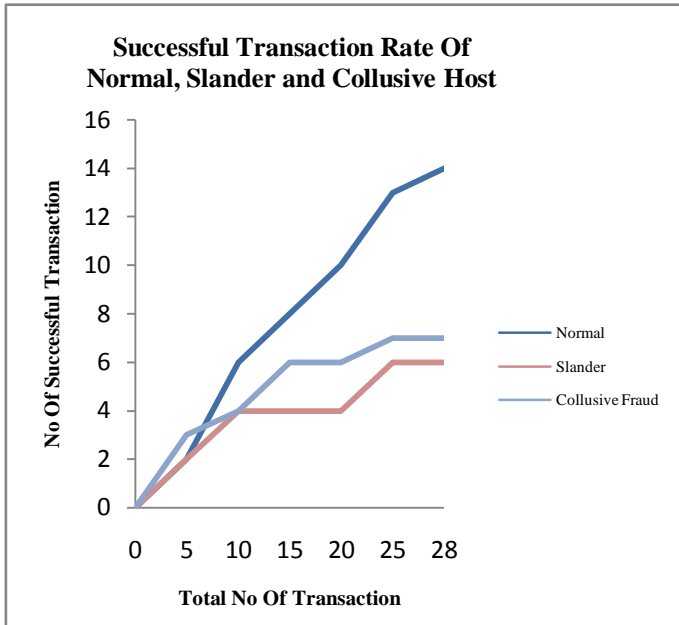


Fig. 7 Avg. Successful transactions For Normal, Slander and Collusive Fraud Hosts

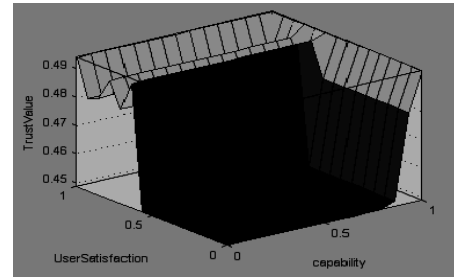


Fig. 5 A three dimensional simulative sketch map of capability, reliability, user satisfaction and Trust Value

C. Experiment 3: Growth of Successful transaction ratio with the increase of percentage of malicious nodes

Figure 8 shows that with the increase of malicious nodes this model still provide a good performance. With the increment of collusive fraud nodes up to 50 still it gives a high successful transaction ratio around 78% which is comparatively very with respect to other models. With the presence of slander nodes also these shows a great stability with respect to earlier models. With the increment of slander nodes up to 50% still this model ensures the average amount of successful transaction ratio up to 75%.

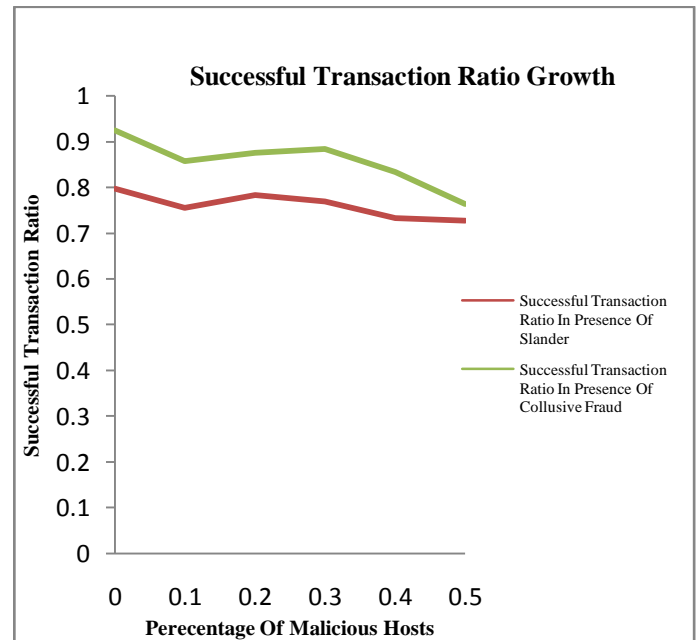
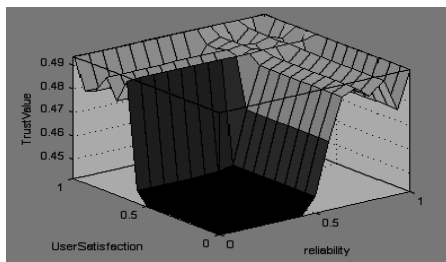
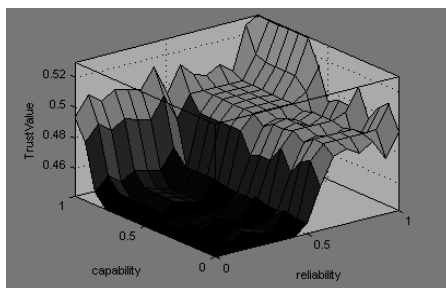


Fig. 8 Successful transactions with the increase of Malicious Hosts



V. CONCLUSIONS

This paper has implemented a reputation model based on fuzzy inference system that gives simple and but quite efficient way of ensuring security in grid network among various grid nodes. It also provides a scalable solution for the computation of reputation. After that number of inputs are three, required number of rules (7^3) are very high and it demands a high performance processor and large computation time. To avoid these problem, in future we can enhance our work in some information infusion techniques to reduce this overhead. Also in future we will try to explore Data Mining techniques of rule based classification and other artificial intelligence techniques in this field to make it more scalable and more stable with huge loads of data. Though the dependency of grid nodes on Global Information Services to get reputation information of other nodes makes it more scalable but at the same time the entire system turned into more vulnerable to system faults. We will also try to sketch new parameters to build the reputation model for intra market or grid network level to build cross platform between different security systems deployed in different grid networks.

ACKNOWLEDGMENT

This work is supported by the Indian Institute of Technology-Roorkee (Roorkee-247667, India).

REFERENCES

- [1] Alfarez Abdul-Rahman and Stephen Hailes, "Supporting Trust in Virtual Communities," *33rd Hawaii International Conference on System Sciences* -Volume 6, 2000 IEEE Press, pp. 6007, Dec. 2007
- [2] V. Vijayakumar and R.S.D.W. Banu, "Security for resource selection in grid computing based on trust and reputation responsiveness," *International Journal of Computer Science and Network Security*, Volume 8, No. 11, pp 107-115, November 2008
- [3] Torstenn Eymann, Stefan Konig, Raimund Matros, "A framework for trust and reputation in grid environment," *Journal Of Grid Computing*, Volume 6, No. 3, pp.225-237, 2008
- [4] Tang W, Chen Z, "Research of subjective trust management model based on the fuzzy set theory," *Journal Of Software*, Volume 14, No. 8, pp.1401 – 1408, 2003
- [5] Tang W, Hu JB, Chen Z, "Research on a Fuzzy Logic-Based Subjective Trust Management Model," *Journal of Computer Research and Development*, Volume 42, No. 10, pp. 1654-1659, 2005.
- [6] Shanshan Song, Kai Hwang and Mikin Macwan "Fuzzy Trust Integration for Security Enforcement in Grid Computing," *International Conference On Network and Parallel Computing*, LNCS 3222, pp 09-21, 2004
- [7] H. Liao, Q. Wang, and Guoxin Li, "A Fuzzy Logic-Based Trust Model in Grid," *9th International Conference On Network Security, Wireless Communication and Trusted Computing*, Volume 1, pp. 608-614, April 2009.
- [8] Timothy J. Ross, "Fuzzy Logic With Engineering Application," *Second edition - Wiley India*, pp.283, 509, 514
- [9] J. Tian, P. Yuan, Yuzhen Lu, "Security for Resource Allocation Based on Trust and Reputation in Computational Economy Model for Grid," *4th International Conference on Frontier of Computer science and Technology*, pp.339-345, December 2009

Interaction of Non-Chloride Hardening Accelerator with Type of Cement and Method of Curing in the Strength Development of Pavement Concrete

Mushtaq Ahmed Bhavikatti¹, Vilas V. Karjinni²

⁽¹⁾Department of Civil Engineering, Anjuman Engineering College, Bhatkal, Karnataka - 581 320. India)

⁽²⁾Sanjay Ghodawat group of institutions, Atigeri, Kolhapur, Maharashtra- 416 118. India)

ABSTRACT

This paper explains the interaction of commercial non-chloride hardening accelerator with type of cement and method of curing in the strength development of pavement concrete. Ordinary Portland Cement (OPC) and Portland Pozzolana Cement (PPC) were the two cements used to produce concrete mixtures. Concrete mixtures were designed as per the new guidelines of IS 10262:2009. Accelerator dosage was varied from 2 liters to 5 liters per cubic meter of concrete in seven equal intervals. Compressive strength of standard cube specimens (150 mm) at early and later age cured with water and alternatively with commercial wax based membrane forming curing compound, was studied. Performance of accelerator at a given age of concrete was assessed based on the maximum percentage increase in the compressive strength, measured with reference to the strength of control mixture (without accelerator), at the corresponding age. Average efficiency of the curing compound at a given age, calculated as the ratio of average compressive strength of concrete cured with it to that cured with water, was also studied. The test results revealed that the type of curing affected the optimum performance of accelerator in OPC mixtures but not in PPC mixtures. Curing compound was more effective in PPC mixtures.

Keywords - Accelerator, Blended cements, Compressive strength, Curing, Fast-track

1. INTRODUCTION

Capacity enhancement of National Highways qualitatively and quantitatively initiated by National Highway Development Project (NHDP) under the aegis National Highway Authority of India (NHAI) is an ambitious plan which involves design and construction of high speed corridors including concrete roads. With continuous increase in the traffic of heavy vehicles, repair and rehabilitation of these roads is imminent due to the fact that most of our infrastructure deteriorates at unacceptable rates. New vistas need to be explored to extend the needful life of distressed structures cost-effectively, especially in developing countries like India. Traditional methods of rehabilitation of rigid pavements are time consuming and cause several days of traffic interruption, more so in heavy-traffic areas. Further,

these methods incur high replacement cost. Emergence of fast-track pavement technology particularly for concrete roads has overcome this problem [1]. Fast-track paving typically does not require any special equipment or newly developed technique [2]. Design of suitable concrete mixtures is the most important aspect in the fast-track pavement technology and with conventional ingredients it is possible to design reasonably good fast-track concrete mixtures by incorporating mineral and chemical admixtures. Concrete roads are typically built and rehabilitated with Ordinary Portland Cement (OPC). But due to acute shortage of OPC, all government construction projects in India are made to suffer from the non-availability of cement [3]. Hence need for supplementary cementitious materials, which can replace OPC partially or completely has increased substantially [4]. Two industrial by products, namely Fly Ash and Blast Furnace Slag if used appropriately in cement concrete as supplementary cementitious materials, can enhance the durability of concrete. [5].

Research on the use of these supplementary cementitious materials in cement concrete hints at the limitation of their blending with cement at site due to lack of testing facility to check their pozzolanic characteristics and due to other practical reasons [3]. Hence blending of cementitious materials during the production of cement under strict quality control is prudent to reap the benefits. Fly ash based Portland Pozzolana Cement (PPC) is one such blended cement used widely in various construction works but has very limited application in pavement construction in India. One of the nagging problems associated with concrete pavements in the tropical regions is the evolution of heat of hydration and its undesirable effects on their performance. Heat of hydration is seen as an aging parameter in concrete [6]. The objective of reducing heat of hydration can be achieved by using mineral admixtures and blended cements [3]. Further, concrete containing Fly Ash has shown improved workability, less segregation and bleeding, increased water tightness and reduced tendency of time to leach out [5]. For same water to cementitious materials ratio and cementitious materials content, the plain cement concrete has found to exhibit more chloride permeability than blended cement concrete. [7]. It is further investigated that resistance of concrete against long-term environmental conditions such as chloride attacks and freeze-thaw cycles can be improved with the use of blended cements.

Many state departments of transportation (DOTs) are allowing the use of blended cements as the construction material in transportation structures instead of typically disposing them off to landfills [8]. In India, IS 456:2000, Code of Practice for Plain and Reinforced Concrete permits use of PPC but Ministry of Road Transport and Highway (MORT&H) specification clause 602 and 1000 do not permit its use. Further, IS 15:2002, Code of Practice for Construction of Concrete Roads allows PPC conforming to IS 1489. Other organizations like Central Public Works Department (CPWD), Military Engineering Services (MES) and Indian Railways permit the use of PPC in the construction works.

There are many methods that can be used in the production of concrete to accelerate rate of hydration. Accelerators, especially hardening accelerators are desirable admixtures in the fast-track paving mixtures. They increase the rate of hydration, thereby giving high early- strength for concrete. They primarily target aluminate phase resulting in rapid workability loss [9]. Study on accelerators suggests that they help in improving the resistance to wear, depending on the curing age [2]. They also play a vital role in reducing chloride attack on concrete [10]. Limited application of accelerator is seen in fast-track construction and generally only calcium chloride is tried as accelerator [2]. Non-chloride accelerators are now being tried in place of calcium chloride in order to minimize potential of steel corrosion [11]. Production of concrete should be followed by effective curing to get the desired strength and durability. There are various methods of curing; each one has its own merits and demerits. In the recent times, curing compounds and high early-strength concrete have become the key features of the fast-track construction for rigid pavements, especially in the regions that suffer from the scarcity of water [1, 2]. Heat treatment is one of the methods employed to get early strength in concrete but there is a possibility of decline in strength at full maturity [12]. Curing compounds namely, acrylic and water based are effective in decreasing plastic and drying shrinkage strain for both ordinary and blended cements. [13].

Experimental findings in the past have modeled concrete by varying admixtures, cement and curing method qualitatively and quantitatively. Zhang and Zhang [14] demonstrated effect of moist curing in tropical regions at different temperatures on the strength and other properties of concrete produced with Portland Cement (ASTM Type I) and found strength of concrete cured at higher temperature to be higher. Buch et al. [15] in their work on high early- strength of plain cement concrete mixtures concluded that these mixtures could be prepared but interactions between various constituents could result in durability problems, moreover their work did not take into account the method of curing. Khokhar et al. [16] have used high content of mineral additions to improve early age strength of concrete without chemical admixture. Al-Gahatani [13] has studied properties of concrete with blended cement and acrylic based curing compound and experimentally found the curing efficiency of

such compounds with respect to compressive strength to be typically in the range of 84 to 96 percent. In their study on the impact of admixture on the hydration kinetics of Portland cement concrete, Cheung et al. [9] have concluded that a number of specific requirements like type of cement, type of aggregate, climatic conditions, type of curing etc. were needed to model the behavior of accelerators. Yilmaz and Turken [17] have studied the effect of various curing materials on the compressive strength of concrete produced with multiple chemical admixtures excluding accelerators and concluded that laboratory preliminary tests were required to check the compatibility of curing material and chemical admixture to get favorable results for concrete.

Going through the literature in the form of experimental findings and reviews, the authors are of the opinion that independent effects of type accelerator, type of cement and method of curing on the property of concrete are assessed but interaction of a non-chloride hardening accelerator with type of cement and method of curing in the strength properties of concrete at early and later age is hitherto not assessed in the tropical environments like India, particularly with the revised guidelines for mix proportioning as given by IS 10262:2009 [18]. The present experimental task is an effort in this direction.

The objective of the present experimental program is to give initial guidelines based on the compressive strength of concrete towards accelerated construction and rehabilitation of concrete roads in India, particularly by exploring the feasibility of PPC and membrane curing as possible alternatives to OPC and conventional water curing respectively.

2. MATERIALS AND METHODS

2.1 Materials

Two types of cements manufactured in India, namely Ordinary Portland Cement (OPC), conforming to IS 8112-1989 and fly ash based Portland Pozzolana Cement (PPC), conforming to IS 1489-1991 (Part 1) were used to prepare concrete mixtures, whose physical and chemical characteristics are given in Tables 1 and 2 respectively. Oven dried river sand conforming to grading zone IV of IS 383:1970 [19] was used as fine aggregate. Saturated surface dry angular aggregates (Crushed Granite) of size 20 mm and 10 mm, mixed in the ratio of 60:40 were used as coarse aggregates such that the combined gradation conformed to IS 383:1970 [19] grading limits for graded coarse aggregates. Table 3 shows the physical properties of aggregates. Ordinary tap water was used for mixing the concrete mixtures of the experimental study. Commercial non-chloride hardening accelerator conforming to ASTM C-494 Type C and IS 9103:1999 standards, in the form of colorless free flowing liquid having relative density 1.2 ± 0.02 at 25°C , $\text{pH} \geq 6$ and chloride ion content $< 0.2\%$, manufactured by BASF Construction Chemicals (India) Private Limited with brand name Pozzoloth 100 HE, was used to accelerate hardening process of the concrete mixtures.

Table 1. Physical characteristics of OPC and PPC

Cement	Fineness (m ² /kg)	Soundness Autoclave (%)	Setting Time (Min.)		Compressive Strength-28 Day (MPa)	Specific Gravity
			Initial	Final		
OPC	230	0.8	95	230	45.2	3.15
PPC	305	0.7	105	240	37.50	2.90

Table 2. Chemical characteristics of OPC and PPC

Cement	Lime Saturation Factor (%)	MgO (%)	Ignition Loss
OPC	0.80	1.20	1.45
PPC	0.85	1.30	1.40

Table 3. Test results on aggregates

Aggregate	Specific Gravity	Bulk unit weight (kN/m ³)
Fine	2.60	15.77
Coarse	2.71	15.49

2.2. Concrete Mix Proportioning

Concrete mixtures of grade M 40 were designed for pavement concrete using revised guidelines of

IS 10262:2009[19]. Table 4 shows ingredients of control mixtures (without accelerators), produced with OPC and PPC.

Table 4. Ingredients per cubic meter of concrete (Control mixtures)

Mixture	Cement (kg)	Fine Aggregate (kg)	Coarse Aggregate (kg)	Water (liters)
OPC0	432.56	609.03	1199.87	186
PPC0	442.85	591.20	1175.10	186

The control mixtures were modified with accelerator dosage from 2 liters to 5 liters per cubic meter of concrete as per the instructions of the manufacturer, i.e. 0.583 to 1.456 and 0.569 to 1.422 percent by weight of cement, in seven equal intervals for OPC and PPC mixtures respectively. Laboratory Drum-type, electrically operated mixer was used for mixing the ingredients and table vibrator was used for the purpose of compaction.

2.3 Curing

Cast concrete cube specimens (150 mm) were cured with water by immersing specimens in water tank at room temperature and alternatively with wax based membrane forming curing compound (Compliance-ASTM C309 Type II Class A, BS 7542: 1992) of brand name Mastercure, manufactured by BASF Construction Chemicals (India) Private Limited. Curing compound was applied after six hours of casting to all the surfaces of specimen by ordinary paint brush.

2.4. Tests

Workability tests were conducted on the mixtures by slump test. 288 cube specimens of 16 different mixtures(8 each with OPC and PPC) were tested (Figure.1) at different age of curing by compressive strength test in accordance with IS 516:1959 [20] to evaluate the interaction of accelerator with type of cement and method of curing in the compressive strength development of concrete, as often compressive strength of concrete is deemed as the sole criterion to approve any concrete mixture and moreover it is possible to relate compressive strength to other strength and durability parameters using customary empirical equations.



Fig 1. Section of tested cube specimens in Compression Testing Machine

3. RESULTS AND DISCUSSION

The range of slump values for all the mixtures was 5 to 10 mm. The mixtures with higher dosage of accelerator recorded lower slump as the increased dosage of accelerator targeted aluminate phase resulting in rapid workability loss hence all the mixtures were insensitive to the Slump test [9]. Increase in compressive strength of a given concrete mixture at a given curing age in presence of accelerator, assessed with respect to the compressive strength of control mix at the corresponding curing age, was taken as the performance indicator of accelerator. With a view of early strength requirement in fast-track construction and rehabilitation , compressive strength of all the sixteen mixtures was tested at one, two, three, five, seven and twenty-eight day of curing. The strength results are tabulated in tables 5 to 8. Figures 2 to 5 show the percentage gain in compressive strength of the mixtures, measured with reference to compressive strength of control mixtures for different periods of curing, different accelerator dosage, type of cement and method of curing. Efficiency of curing compound at a given age of concrete and for a given dosage of accelerator, defined as the ratio of compressive strength of the given mixture, cured with it to the compressive strength of the mixture cured with water, expressed as percentage was assessed for all the mixtures. Average efficiency of curing compound for OPC and PPC mixtures (for varied dosage of accelerator) for different periods of curing is as shown in figures 6 and 7 respectively.

Table 5. Compressive strength of OPC mixtures (Cured with water)

Mixture	% Accelerator	Compressive strength (MPa)					
		1 day	2 day	3 day	5 day	7 day	28 day
OPC0	0	24.67	26.50	28.40	30.20	37.20	49.96
OPC1	0.583	26.36	28.40	30.40	32.99	38.20	50.45
OPC2	0.728	26.77	30.50	34.37	36.55	38.38	51.85
OPC3	0.874	26.80	31.20	35.20	38.56	39.16	52.30
OPC4	1.019	27.20	31.67	35.80	39.53	40.10	53.40
OPC5	1.165	29.96	31.90	36.10	40.20	43.74	53.40
OPC6	1.31	30.20	31.50	37.20	41.56	42.96	52.96
OPC7	1.456	30.40	31.50	39.56	42.20	43.10	53.10

Table 6. Compressive strength of OPC mixtures (Cured with curing compound)

Mixture	% accelerator	Compressive strength (MPa)					
		1 day	2 day	3 day	5 day	7 day	28 day
OPC0	0	17.95	26.45	27.22	28.24	30.37	37.92
OPC1	0.583	18.20	27.32	27.92	30.16	33.86	38.46
OPC2	0.728	19.50	28.15	28.16	31.45	33.92	38.46
OPC3	0.874	20.45	28.20	28.27	31.82	34.29	38.67
OPC4	1.019	22.36	28.20	28.98	32.45	34.86	38.12
OPC5	1.165	22.10	28.92	29.12	32.38	34.92	38.93
OPC6	1.31	23.32	28.92	29.45	32.96	34.76	38.67
OPC7	1.456	23.80	29.12	30.16	33.12	34.92	39.12

Table 7. Compressive strength of PPC mixtures (Cured with water)

Mixture	% accelerator	Compressive strength (MPa)					
		1 day	2 day	3 day	5 day	7 day	28 day
PPC0	0	17.49	19.62	24.852	30.084	33.572	48.652
PPC1	0.5690	19.184	24.852	28.34	31.828	34.444	48.652
PPC2	0.7213	20.056	25.288	29.12	32.264	35.28	49.289
PPC3	0.8535	21.215	28.34	30.084	33.185	36.124	51.012
PPC4	0.9950	22.316	29.324	31.125	34.285	36.85	51.012
PPC5	1.1380	23.428	30.212	32.43	35.18	37.125	51.448
PPC6	1.2800	24.852	31.645	33.185	35.28	38.28	50.704
PPC7	1.4220	25.12	31.645	34.285	36.78	38.98	50.928

Table 8. Compressive strength of PPC mixtures (Cured with curing compound)

Mixture	% accelerator	Compressive strength (MPa)					
		1 day	2 day	3 day	5 day	7 day	28 day
PPC0	0	14.75	17.51	23.78	24.82	25.30	35.46
PPC1	0.5690	15.62	19.91	26.38	27.38	27.58	36.42
PPC2	0.7213	16.20	24.56	27.83	29.96	30.31	36.92
PPC3	0.8535	16.80	25.00	27.83	30.31	31.16	37.12
PPC4	0.9950	18.16	25.62	28.21	31.46	32.45	37.12
PPC5	1.1380	19.24	26.12	28.25	32.12	32.28	38.20
PPC6	1.2800	19.96	26.76	28.45	32.12	32.92	38.46
PPC7	1.4220	18.78	26.76	28.96	32.72	33.42	38.92

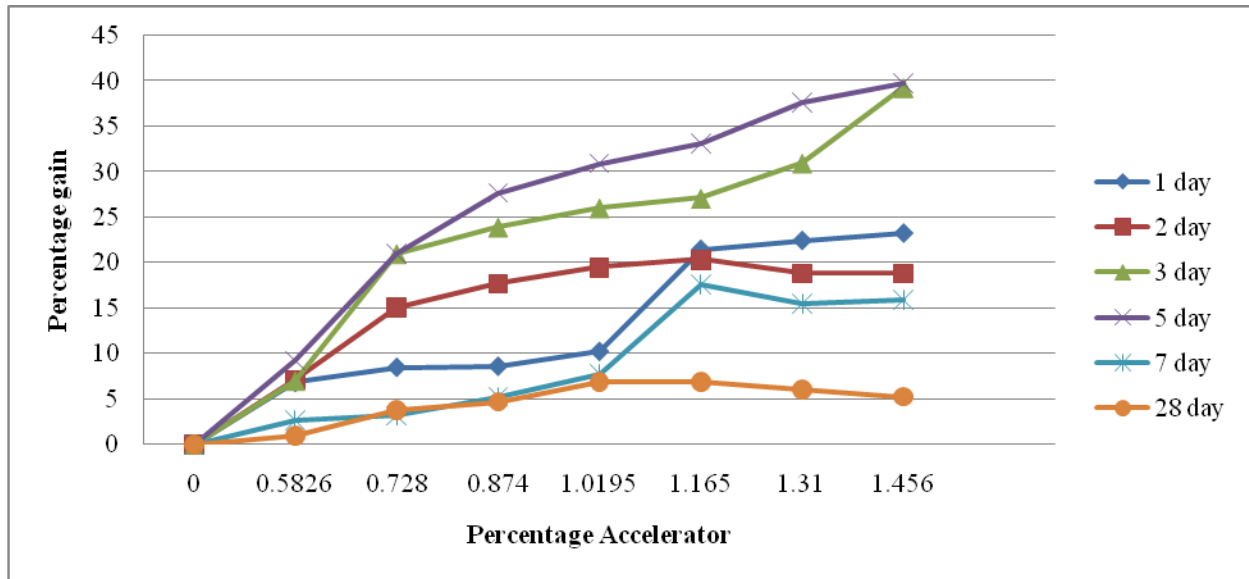


Fig 2. Percentage gain in compressive strength of OPC mixtures cured with water for varied dosage of accelerator

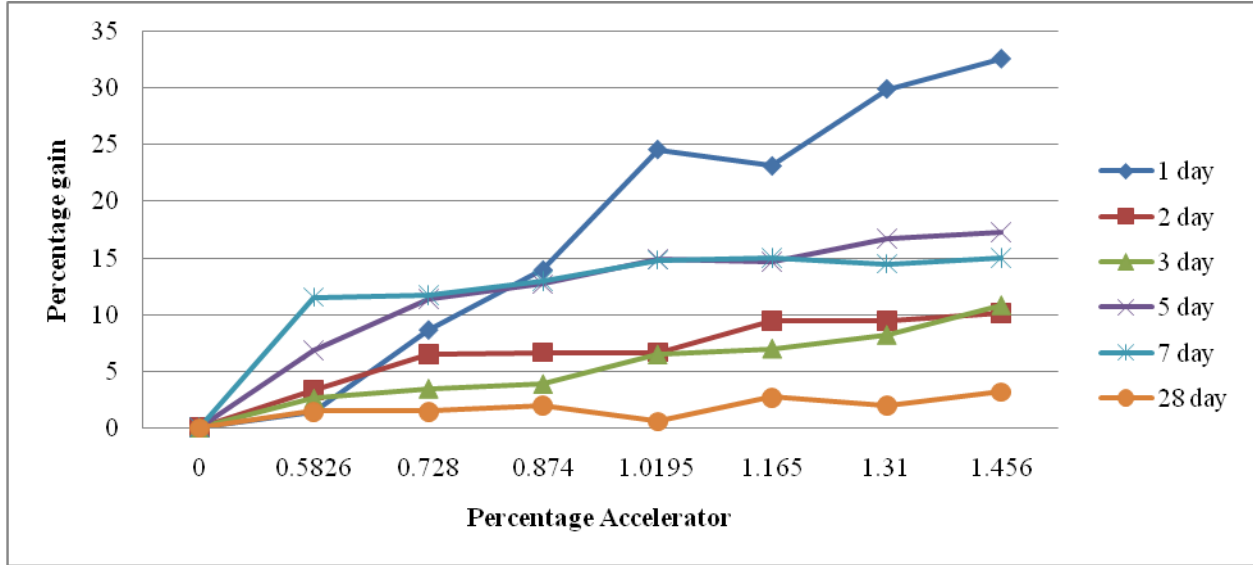


Fig 3. Percentage gain in compressive strength of OPC mixtures, cured with curing compound for varied dosage of accelerator

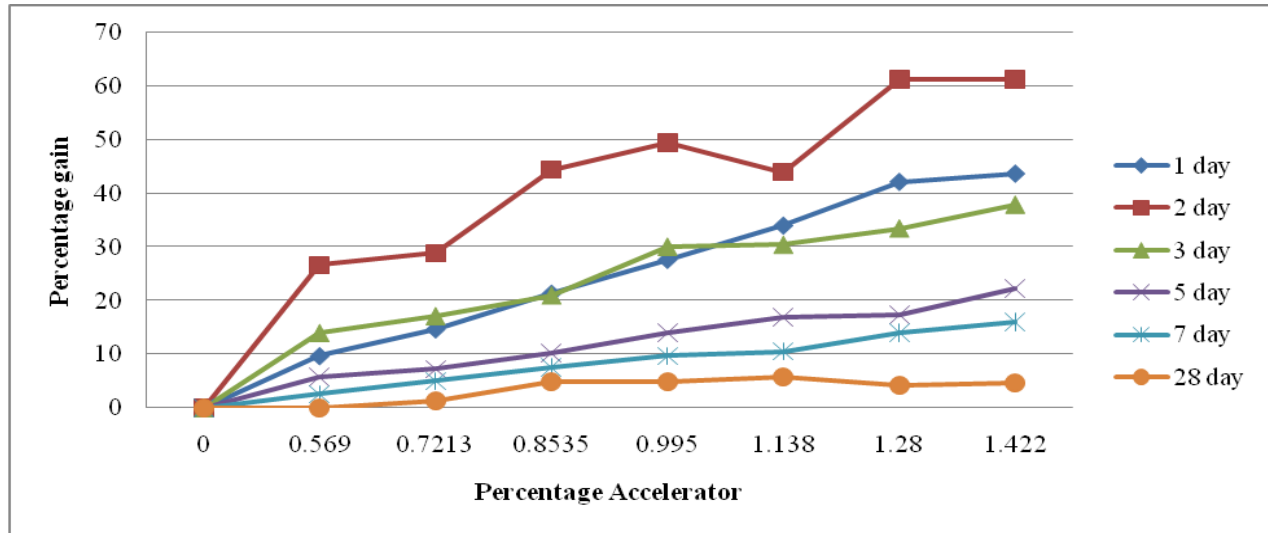


Fig 4. Percentage gain in compressive strength of PPC mixtures cured with water for varied dosage of accelerator

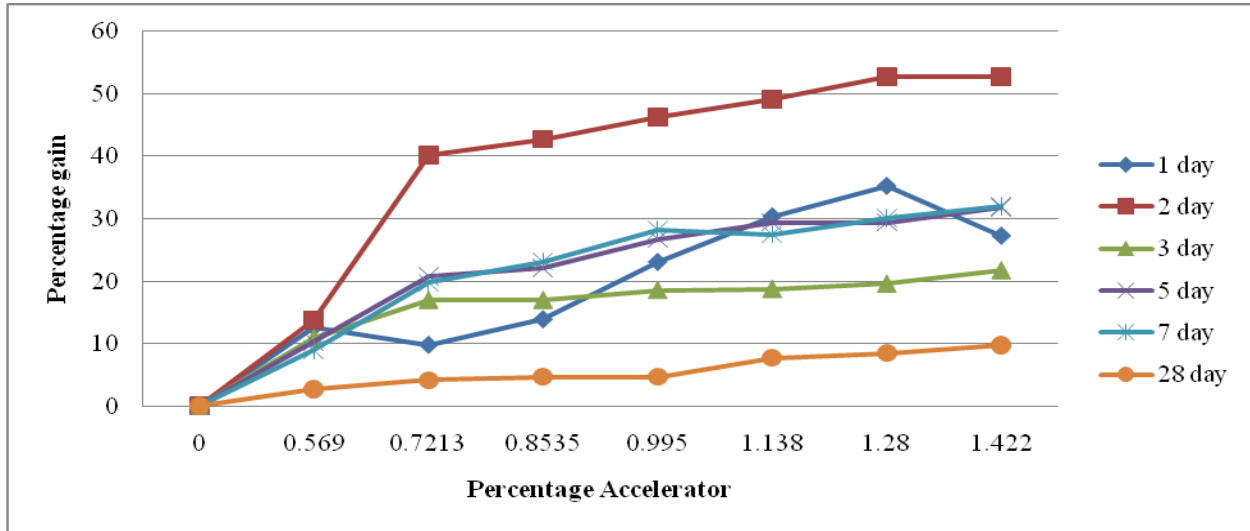


Fig 5. Percentage gain in compressive strength of PPC mixtures, cured with curing compound for varied dosage of accelerator

For a given dosage of accelerator and for a given period and type of curing, the compressive strength of OPC mixtures was more than that of PPC mixtures and the mixtures cured with curing compound failed to attain the stipulated design strength. The rate of strength gain in PPC mixtures, cured with water and with curing compound was slow at early age as hydration process of these mixtures was slow due to presence fly ash which is known to be less pozzolanic but the strength at twenty-eight day of all the PPC mixtures was on par with that of OPC mixtures for a given dosage of accelerator. Accelerator could not influence greatly to the twenty-eight day strength of all the mixtures. All the mixtures of OPC and PPC responded well to the addition of accelerator and there was gradual increase in the strength at early age.

In case of water-cured OPC mixtures, the uppermost maximum percentage gain in strength was 39.73, recorded at five day, by the mixture with maximum dosage (1.456 percent) of accelerator. The maximum percentage gain in strength at three day was close to that of five day with a value of 39.29, observed by the mixture with maximum dosage of accelerator. The maximum percentage gain in strength at one day was moderate with a value of 23.23, recorded by the mixture with maximum dosage of accelerator. With increase in the dosage of accelerator, the percentage gain in strength at two day increased gradually with a maximum value of 20.38 for the mixture with 1.165 percent accelerator and then attained a constant value of 18.87 for the mixtures with further dosages of accelerator. The seven day strength too increased gradually with the addition of accelerator and attained a maximum percentage hike of 17.58 for the mixture with 1.165 percent accelerator before attaining a percentage gain of 15.86 for the mixture with maximum dosage of accelerator. There was marginal hike of 5 to 6 percent in twenty-eight day strength recorded

by the mixtures with greater dosage (above 1 percent) of accelerator.

The OPC mixtures cured with curing compound had moderate to low percentage gain in strength. The maximum percentage gain in strength observed at one day was 32.59. The maximum percentage hike was low with the values of 10.09 and 10.8 respectively at two and three day, moderate with the values of 17.28 and 14.98 respectively at five and seven day and negligible with a value of 3.16 at twenty-eight day. The maximum percentage gain in strength for all the days of curing was recorded by the mixtures with maximum dosage of accelerator.

In case of PPC mixtures cured with water, the uppermost maximum percentage gain in strength was 61.28 percent, recorded at two day by the mixture with maximum dosage (1.422 percent) of accelerator. The mixtures showed reasonably good gain in strength at one and three day of curing. The maximum percentage hike was 43.625 and 37.956 percent at one and three day respectively, again recorded by the mixtures with maximum dosage of accelerator. The maximum percentage gain in strength at five and seven day was marginal with the values of 22.26 and 16.109, recorded with maximum dosage of accelerator. The percentage gain in twenty-eight day strength was low with a maximum increase of 4.678 percent, observed by the mixture with maximum dosage of accelerator.

The PPC mixtures cured with curing compound recorded lesser strength in comparison to that cured with water, but performed better in recording maximum percentage gain in strength. The uppermost maximum percentage gain in strength in these mixtures was observed at two day with a value of 52.83 percent in the mixture with maximum dosage of accelerator. The one day strength also gradually peaked with increase in the dosage of accelerator with maximum percentage hike of 35.32, recorded for the mixture with 1.28 percent of accelerator and then slipped to a lower value of 27.32, observed for the mixture with

maximum dosage of accelerator. After peaking to a percentage increase of 17.03 for the mixture with accelerator dosage of 0.721 percent, the percentage gain in three day strength had a narrow range with further increase in the dosage of accelerator. The trend in percentage hike for five and seven day was almost similar to that of three day, with maximum percentage increase of 31.83 and 32.09, respectively recorded by the mixtures with maximum dosage of accelerator. The peaking of twenty-eight day strength was marginal with increase in the dosage of accelerator; a maximum of 9.76 percentage gain was recorded by the mixture with maximum dosage of accelerator.

Interaction of accelerator was better at three and five day of curing in the OPC mixtures cured with water and at one day in the same mixtures cured with curing compound. This could be attributed to the fact that OPC mixtures due

to type of cement and accelerator, though generated more heat of hydration (in OPC half of the total heat of hydration is liberated within three day of curing), moist curing kept the heat under control and prevented drying of the surfaces of the specimens which resulted in effective hydration and high increase in strength at early age. With absence of this condition in membrane curing, rapid drying of the surfaces of the specimens, coupled with more heat of hydration, resulting in lessee gain in strength after one day. In case of PPC mixtures the optimum performance of accelerator was recorded at two day irrespective of type of curing. Lesser heat of hydration due to presence of fly ash could be the reason for such consistent performance of accelerator at early age. The optimum performance of accelerator in OPC mixtures was affected by type of curing.

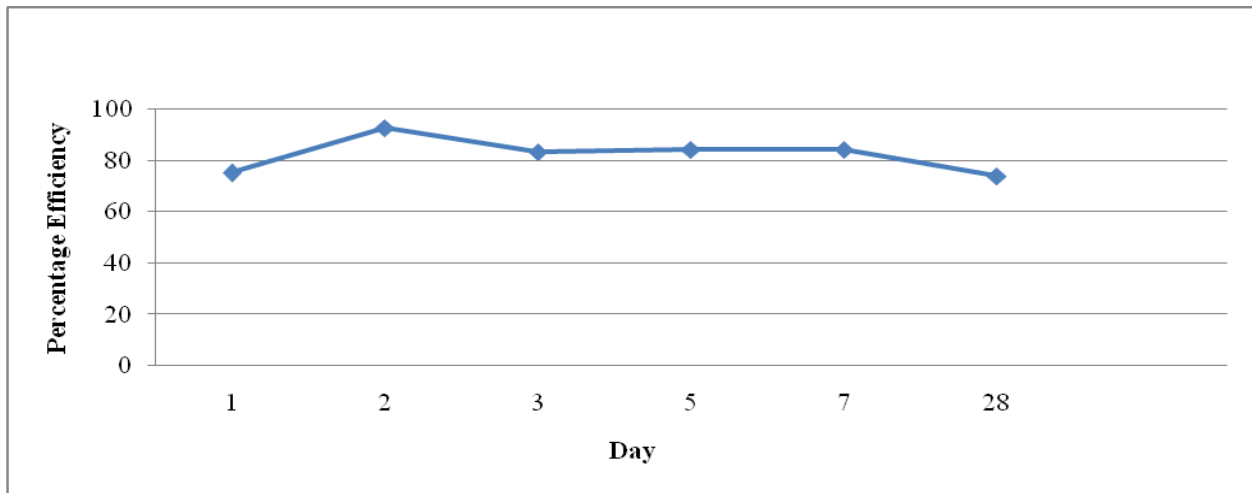


Fig. 6. Average efficiency of curing compound for OPC mixtures at different days of curing

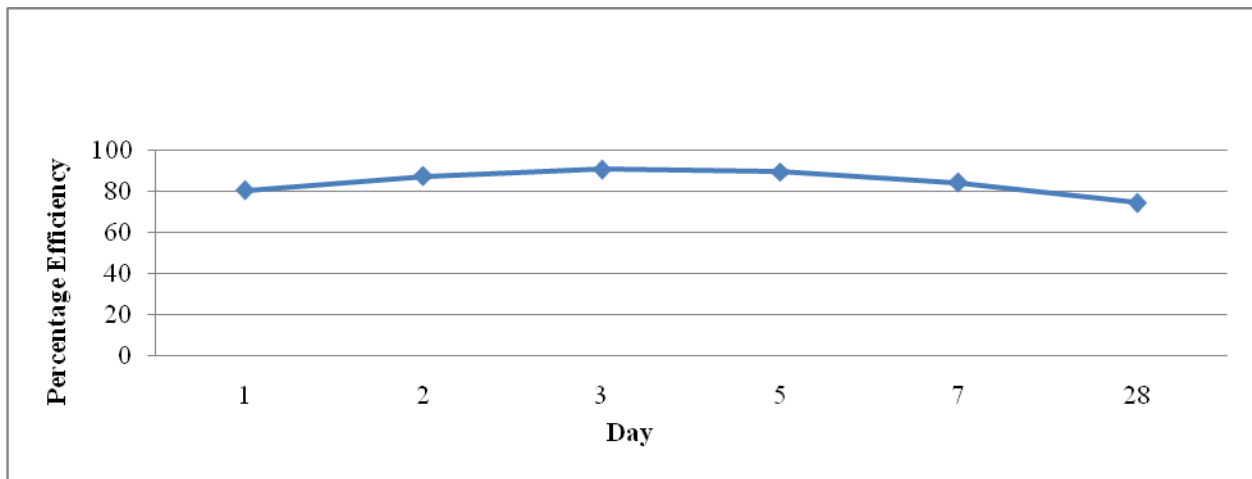


Fig.7. Average efficiency of curing compound for PPC mixtures at different days of curing

Average efficiency of curing compound for OPC mixtures attained a moderate value of 75.27 at one day of curing, peaked to 92.83 at two day and gradually decreased for subsequent days of curing before settling for a lowest value of 73.9 at twenty-eight day. For PPC mixtures it increased gradually from 80.488 percent at one day, peaked to 90.59 percent for three day and then decreased gradually at five and seven day before attaining a lowest value of 74.36 at twenty-eight day. Average efficiency of the curing compound at a given age, was found to be more for PPC mixtures than for OPC mixtures. Further, Efficiency was found to be more at early age for both OPC and PPC mixtures, as decline in the quality of protective curing membrane due to variation in day and night room temperature could be the reason for the lower efficiency at later age.

4. CONCLUSIONS

Following are the conclusions from the outcome of the experimental program. Accelerator was effective in increasing the compressive strength of all the concrete mixtures. Performance of accelerator at a given age of concrete was assessed based on the maximum percentage increase in the compressive strength, measured with reference to the strength of the control mixture (without accelerator) at the corresponding age. Interaction of accelerator was better at three and five day in the OPC mixtures cured with water and at one day in the same mixtures cured with curing compound. In the PPC mixtures the optimum performance of accelerator, recorded at two day was not affected by type of curing. Average efficiency of the curing compound at a given age, calculated as the ratio of average compressive strength of concrete cured with it to that cured with the water was found to be more for PPC mixtures than for OPC mixtures. Efficiency was found to be more at early age for both OPC and PPC mixtures.

The present findings can serve as initial guidelines towards accelerated construction and rehabilitation of concrete roads in India, especially by exploring the feasibility of PPC and membrane curing as possible alternatives to OPC and conventional water curing respectively.

REFERENCES

1. Buch N., Fast track concrete paving- an emerging technology, *Journal of Indian Road Congress*, 32(2), 1997, 253-69.
2. Ghafoori N., and Tays M.W., Resistance to wear of fast-track portland cement concrete, *Construction and Building Materials*, 24(8), 2010, 1421-31.
3. Chahal H.S. et al., Use of Portland Pozzolana Cement (PPC) in civil works, *Journal of Indian Highways*, 35(6), 2007, 27-32.
4. Ravishankar A.U. et al., Fly ash and rice husk ash concrete for rigid pavement, *Journal of Indian Highways*, 35(8), 2007, 33-47.
5. Pathak P.P., Inclusion of Portland pozzolana (fly ash based) in specifications, *Journal of Indian Highways*, 37(4), 2009, 23-29.
6. Pane Ivindra, Hansen Will, Investigation on key properties controlling early- age stress development of blended cement concrete, *Cement and Concrete Research* 2008; 38(11), 1225- 35.
7. Al-Amoudi O.S.B. et al., Correlation between compressive strength and certain durability indices of plain and blended cement concretes, *Cement & Concrete Composites*, 31 (9), 2009, 672-76.
8. Hale W.M. et al., Properties of concrete mixtures containing slag cement and fly ash for use in transportation structures, *Construction and Building Materials*, 22(9), 2008, 1990-00.
9. Cheung J. et al., Impact of admixtures on the hydration kinetics of Portland cement, *Cement and Concrete Research*, 41(12), 2011, 1289-09.
10. Prakash K.B. and Kulkarni D. K., Reinforced Concrete with different combinations of Admixtures for the Construction of Pavements, *Journal of Indian Highways*, 36(2), 2008, 29-40.
11. Riad M.Y. et al., Concrete mix pouring sequence for uniform setting and curing of bridge decks, *Construction and Building Materials*, 25(4), 2011, 1653-62.
12. Topcu I.B. and Toprak M.U., Fine aggregate and curing temperature effect on concrete maturity, *Cement and Concrete Research*, 35(4), 2005, 758-62.
13. Al-Gahtani A.S., Effect of curing methods on the properties of plain and blended cement concretes, *Construction and Building Materials*, 24(3), 2010, 308-14.
14. Zhang S. and Zhang M., Hydration of cement and pore structure of concrete cured in tropical environment, *Cement and Concrete Research*, 36(10), 2006, 1947-1953.
15. Buch N., Evaluation of high-early strength PCC mixtures used in full depth repairs, *Construction and Building Materials*, 22(3), 2008, 168-174.
16. Khokhar M.I.A. et al., Mix design of concrete with high content of mineral additions: Optimisation to improve early age strength. *Cement and Concrete Composites*, 32(5), 2010, 377-385.
17. Yilmaz U. S. and Turken H., The effects of various curing materials on the compressive strength characteristic of the concretes produced with multiple chemical admixtures, *Scientia Iranica*, 19(1), 2012, 77-83.
18. IS 10262:2009, Indian Standards guidelines for concrete mix design, *Bureau of Indian Standards*, New Delhi.
19. IS 383:1970, Indian Standards Specification for coarse and fine aggregates from natural sources for concrete, *Bureau of Indian Standards*, New Delhi.
20. IS 516: 1959, Indian Standards Method of test for strength of concrete, *Bureau of Indian Standards*, New Delhi.

Drag Optimization on Rear Box of a Simplified Car Model by Robust Parameter Design

Sajjad Beigmoradi¹, Asghar Ramezani²

*(Automotive Engineering Department, Iran University of Science and Technology, Iran)

** (Automotive Engineering Department, Iran University of Science and Technology, Iran)

ABSTRACT

Reducing fuel consumption of cars is one of the main targets of the automotive manufacturers. Optimum design of car from the aerodynamic viewpoint to reduce drag coefficient is one of the efficient methods toward this aim. In this paper, optimum geometrical parameters of rear box in a simplified car model are obtained to minimize aerodynamic drag. For this purpose, the powerful method of robust parameter design (RPD) along with computational fluid dynamics is used. Optimum values of the parameters obtained by the RPD method is compared with the results of numerical simulations. The comparisons show good agreement between the results.

Keywords: Vehicle Aerodynamic, Drag Coefficient, Robust Parameter Design, CFD

1. INTRODUCTION

Different models are used in the literature to study aerodynamics of vehicles [1]. One of the standard models to study air flow over the vehicle rear end is the Ahmed model [2], which is used in many experimental [3-7] and numerical [8-13] investigations. In sedan cars, besides the slant angle considered in the standard Ahmed model, there are other geometric parameters like rear box length, rear box angle, and boat tail angle, which have considerable effect on the aerodynamic drag coefficient of the vehicle [14].

Conventional methods fail in finding optimal values of aerodynamic parameters of the vehicle rear end due to large number of parameters and time-consumption and expense of conducting experimental and numerical procedures for different levels of parameters. Therefore, Taguchi and response surface methods of design of experiments approach are used in these studies. These methods are applied not only in experimental and industrial works [15-18] but also in expensive and time-consuming numerical studies such as CFD and crash simulations [19-24].

In this paper, a simplified vehicle model with four parameters, namely slant angle, rear box length, rear box angle, and tail boat angle is studied. Each of the parameters are considered in five levels. For reducing computational cost, Taguchi method based on the robust parameter design is used in the study and the optimal levels of parameters for drag reduction are determined. The process of optimization using Taguchi method is shown in Fig. (1).

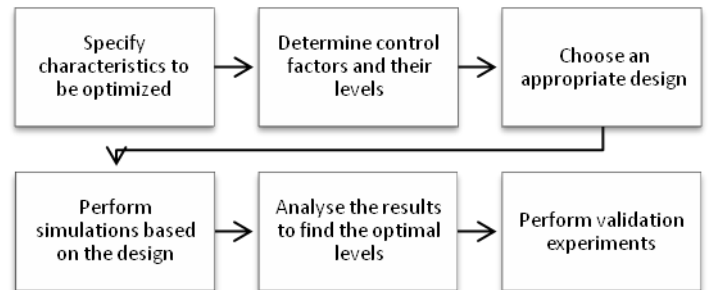


Fig. (1) Aerodynamic optimization using Taguchi method

2. VEHICLE MODEL

The vehicle model used in this research is an extended version of Ahmed model [2] which is proposed for studying drag coefficient variation due to slant angle.

In sedan cars, geometric parameters of rear box has considerable effect on the aerodynamics of the vehicle. These parameters are rear box length, rear box angle, and boat tail angle. In this study, as well as slant angle (ϕ) which was considered by Ahmed, rear box angle α , boat tail angle β , and rear box length l , which are effective parameters on drag coefficient [14] are considered. The parameters and dimensions of the model are shown in Fig. (2).

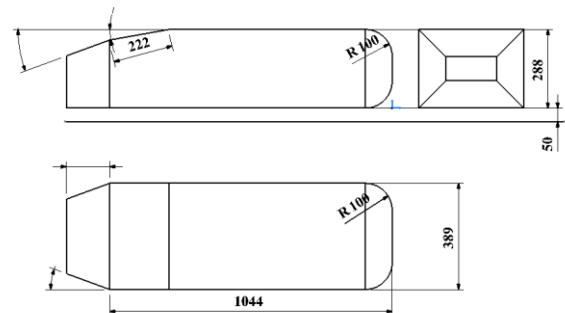


Fig. (2) Extended Ahmed model (dimensions are in mm)

The range of parameter values are assumed to be $5 \leq \varphi \leq 25$ for slant angle, $0 \leq \alpha \leq 20$ for rear box angle, $0 \leq \beta \leq 20$ for boat tail angle, and $80 \leq L \leq 400$ for rear box length

3. TAGUCHI METHOD

Robust parameter design (RPD) is an approach to obtain the levels of controllable parameters in a process to set the output mean at a desired target and to minimize the variability around this target value. Taguchi formulated the general RPD problem and proposed an approach to solving it based on designed experiments. He also presented some novel methods for analysis of the results [25].

Taguchi’s methodology provides some rules, which simplify and standardize design of experiments. The key tool in Taguchi’s method of parameter design is designed experiments by statistical methods. The experiments are designed using a set of orthogonal arrays and conducted in-parallel. Utilizing orthogonal arrays in design of experiments, considerably decreases the number of required experiments.

In Taguchi’s method, results of experiments are analyzed for:

Determining Optimal operation conditions

Investigating the influence of each of the factors on the response

Estimating the response in optimal conditions

The tool used in Taguchi’s method for analyzing results of experiments is signal to noise ratio (SN). SN is the ratio of signal variables to noise variables, which are uncontrollable. The aim of SN analysis is determining the best combination of variables to obtain optimal response. SN parameter is obtained by minimization of loss function, which is defined as

$$SN = -10 \log MSD \tag{1}$$

MSD stands for Mean Squared Deviations. Definition of MSD depends on the desired conditions, i.e.,

When smaller is more desirable

$$MSD = \frac{\sum_{i=1}^r Y_i^2}{r} \tag{2}$$

When bigger is more desirable

$$MSD = \frac{\sum_{i=1}^r \left(\frac{1}{Y_i^2} \right)}{r} \tag{3}$$

When closer is more desirable

$$MSD = \frac{\sum_{i=1}^r (Y_i - M)^2}{r} \tag{4}$$

Where Y_i is response value, M is mean value, and r is number of repetition of each experiment. Using this method ensures that the effects of noise variables are less than the signal variables, i.e., the final response has the minimum sensitivity with respect to noise variables. The attractiveness of Taguchi method is that instead of controlling noise variables, by reducing their effects minimizes deviation in the quality characteristic. This is cost effective since controlling noise variables in the production process is very expensive.

In this study, since the target is to obtain minimum drag coefficient, the SN definition in (1) is used with MSD in the case of smaller is more desirable, i.e. (2). Considering the number of parameters and levels assumed for each parameter, L25 design is used in this study, which reduces number of simulations from 625 cases to 25 cases.

Table (1) Parameter values at each level

Parameter levels	$\varphi (^{\circ})$	L(mm)	$\alpha (^{\circ})$	$\beta (^{\circ})$
1	5	80	0	0
2	10	160	5	5
3	15	240	10	10
4	20	320	15	15
5	25	400	20	20

The studied parameters and their levels are given in Table (1). The configuration of Taguchi L25 design for the problem with 4 variables, each of which are in 5 levels, are shown in Table (2). After performing 25 simulations of the designs given in Table (2), equations (1) and (2) are used to calculate signal to noise ratio. It should be noted that since the number of repetition of each experiment is 1, the value of r is set to 1 in (2). Therefore,

$$SN = -10 \log (Y^2) \tag{5}$$

Table (2) Taguchi L25 design for aerodynamic optimization problem with 4 variables and 5 levels

Simulation No.	$\varphi (^{\circ})$	L(mm)	$\alpha (^{\circ})$	$\beta (^{\circ})$
1	1	1	1	1

2	1	2	2	2
3	1	3	3	3
4	1	4	4	4
5	1	5	5	5
6	2	1	2	3
7	2	2	3	4
8	2	3	4	5
9	2	4	5	1
10	2	5	1	2
11	3	1	3	5
12	3	2	4	1
13	3	3	5	2
14	3	4	1	3
15	3	5	2	4
16	4	1	4	2
17	4	2	5	3
18	4	3	1	4
19	4	4	2	5
20	4	5	3	1
21	5	1	5	4
22	5	2	1	5
23	5	3	2	1
24	5	4	3	2
25	5	5	4	3

Taguchi analysis results are given in Figs. (3) and (4) as signal to noise ratios and mean value of drag coefficient for different levels of parameters, respectively. The mean value of drag coefficient reported for each level of parameters is summation of drag coefficients at that level divided by 5, e.g., The mean value of drag coefficient at the first level of the parameter β is the average of drag coefficients in the simulation number 1, 9, 12, 20, and 23.

Considering the signal to noise ratio graphs for different levels of parameters, the optimum value of parameters are obtained. Reminding the definition of signal to noise ratio in (5), it is obvious that maxima of these graphs are the optimal levels of parameters for minimum drag coefficient.

Table (3) Simulation results and signal to noise ratios

Simulation No.	φ (°)	L(mm)	α (°)	β (°)	Drag Coef.	SN ratio
1	5	80	0	0	0.253	11.948
2	5	160	5	5	0.207	13.666
3	5	240	10	10	0.169	15.422
4	5	320	15	15	0.138	17.188
5	5	400	20	20	0.130	17.688
6	10	80	5	10	0.203	13.830
7	10	160	10	15	0.176	15.077
8	10	240	15	20	0.146	16.701
9	10	320	20	0	0.231	12.728
10	10	400	0	5	0.207	13.696
11	15	80	10	20	0.196	14.158
12	15	160	15	0	0.232	12.687
13	15	240	20	5	0.188	14.530
14	15	320	0	10	0.206	13.710
15	15	400	5	15	0.149	16.527
16	20	80	15	5	0.222	13.058
17	20	160	20	10	0.187	14.569
18	20	240	0	15	0.195	14.195
19	20	320	5	20	0.166	15.592

4. RESULTS AND DISCUSSION

4.1. Taguchi Results Analysis

After performing 25 simulations based on the Taguchi L25 design and using orthogonal arrays algorithm, the response can be predicted in the other levels of variables. The simulation results for each design are shown in Table (3). Using equation (5), the signal to noise ratio is computed for each drag coefficient obtained by simulations.

20	20	400	10	0	0.207	13.686
21	25	80	5	15	0.213	13.435
22	25	160	0	20	0.208	13.656
23	25	240	5	0	0.234	12.616
24	25	320	10	5	0.189	14.479
25	25	400	15	10	0.167	15.566

As can be seen in Fig. (3), slant angle $\varphi = 5^\circ$, length $L = 400\text{mm}$, rear box angle $\alpha = 15^\circ$, and boat tail angle $\beta = 20^\circ$ are the optimum values of parameters, which are verified by mean value of drag coefficient graphs in Fig. (4).

Fig. (4) shows that increasing slant angle has direct effect while increasing the rear box length and boat tail angle has inverse effect on increasing drag. Increasing rear box angle up to $\alpha = 15^\circ$ decreases the drag coefficient and beyond this value increases the drag coefficient.

The parameter range is defined as

$$R_p = \frac{\max(SNR_{i|L=1,2,3,4,5}) - \min(SNR_{i|L=1,2,3,4,5})}{R} \quad (6)$$

Where p can be replaced by φ , L , α , and β . The contribution ratio of parameters to drag coefficient is estimated by

$$c = \frac{R_p}{R} \quad (7)$$

Where R is

$$R = \sum R_p \quad (8)$$

The pie chart obtained by equation (13) is shown in Fig. (5). It is observed that contribution of parameters to drag coefficient reduction is in the order of boat tail angle, rear box length, and slant angle.

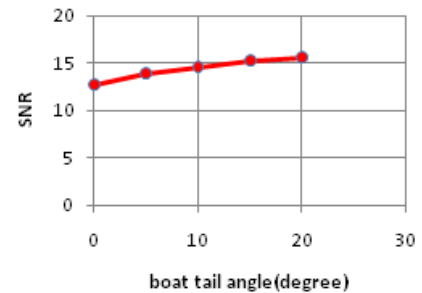
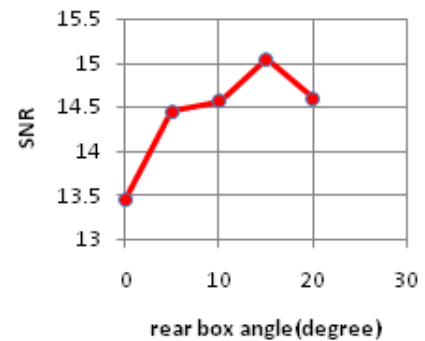
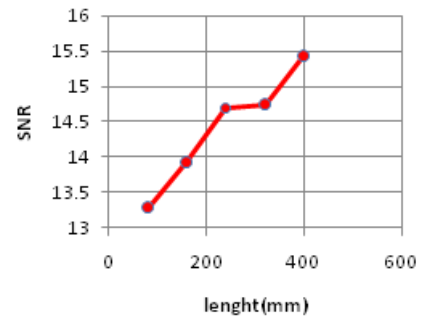
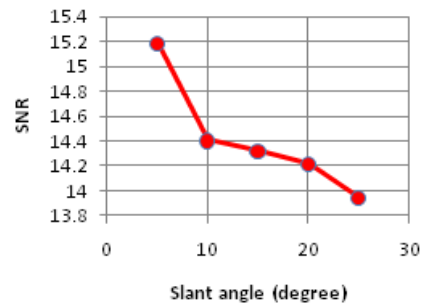


Fig. (3) Signal to noise ratios for different levels of parameters

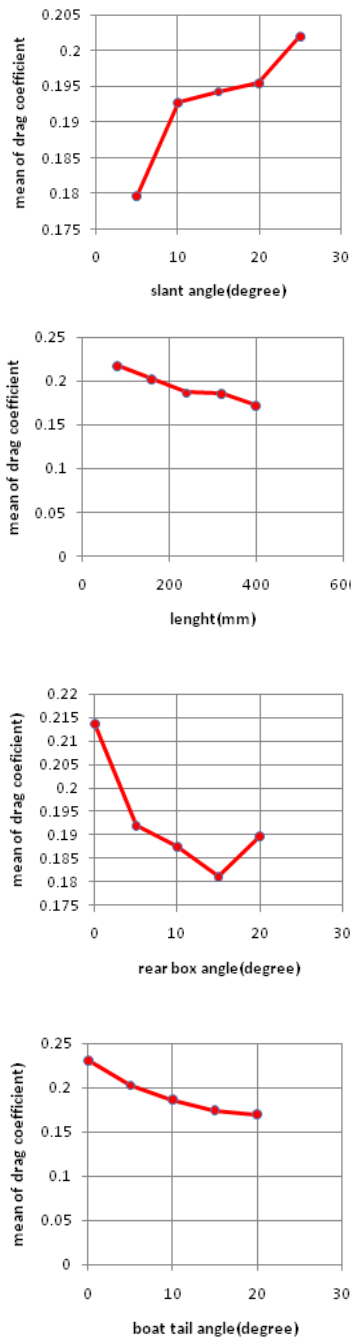


Fig. (4) Mean value of drag coefficient for different levels of parameters

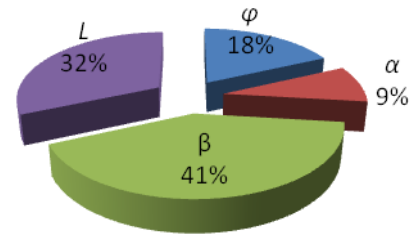


Fig. (5) Contribution ratios of parameters to drag coefficient

4.2. Validation of Taguchi Results

In the previous section, the optimum values of parameters for obtaining minimum drag coefficient is computed by Taguchi method. The optimal drag coefficient predicted by Taguchi method is $CD = 0.124$. Now Taguchi prediction is validated by simulation.

Table (4) Optimum values of parameters and drag coefficient

Parameter	Optimum Value
Slant angle (degree)	5
Rear box length(mm)	400
Rear box angle (degree)	15
Boat tail angle (degree)	20
Drag coefficient by Taguchi	0.124
Drag coefficient by simulation	0.132
Difference between Taguchi & simulation	6%

As can be seen in Table (4), Taguchi results are in good agreement with the simulation results. Therefore, the parameter values obtained by Taguchi method can be accepted as optimum values.

4.3. Investigation of Flow Around Optimal Model

Figures (6) and (7) show that similar to the Ahmed model, 2 D and 3 D vortices are formed at the rear end of the optimal model.

In contrast to the Ahmed model, due to the configuration of optimal model, the size of vortices is decreased considerably and the existence of rear box makes delay in separation of flow. Despite this fact, formation of four 3 D vortices on side edges of the rear box slipping downward is clearly observed. The other important issue to be noted is formation of vortices due to

boat tail angle comparable to vortices on rear box due to slant angle and rear box angle.

As can be seen in Fig. (8), the variation of pressure coefficient distribution on the optimal model is reduced. The friction drag is increased due to generation of boundary layer on the rear box. Therefore, the contribution of the pressure drag is reduced and the contribution of the friction drag is increased to overall drag.

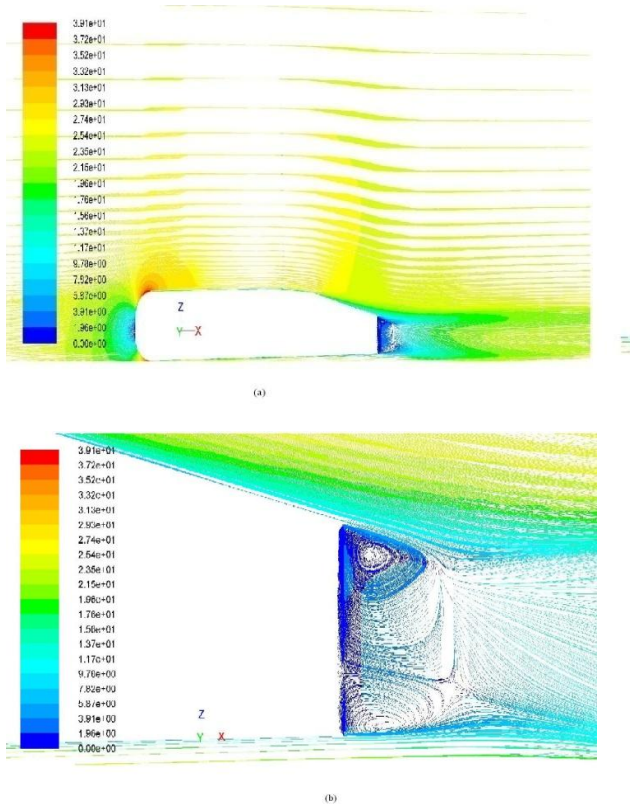


Fig. (6) (a) Streamlines based on velocity field on symmetry plane, (b) 2 D vortices formed at the rear end of the optimal model

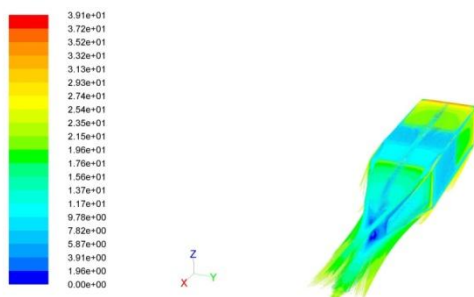


Fig. (7) Formation of 3 D vortices at rear end of the optimal model

In optimal model 51% and 49% of overall drag is due to friction drag and pressure drag, respectively. In contrary to Ahmed model with 80% and 20% of overall drag is due to pressure drag and friction drag, respectively. This discrepancy between the optimal and Ahmed models can be justified by streamlining of the optimal model.

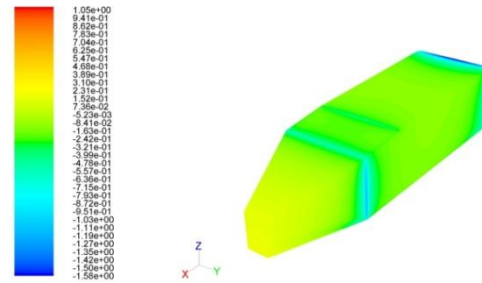


Fig. (8) Pressure coefficient distribution on the optimal model

5. CONCLUSION

In this paper, Taguchi method is used for optimal aerodynamic design of a simple vehicle model. The optimum values of parameters are obtained and the contribution of parameters to aerodynamic drag are determined. Using Taguchi method has considerable effect on reducing computational cost of the CFD simulations in design process. Comparing simulation results of optimal model with the Ahmed model reveals that the contribution of friction drag increases and the contribution of pressure drag decreases to overall drag.

REFERENCES

- [1] G. M. Le Good, K. P. Garry, " On the Use of Reference Models in Automotive Aerodynamics" ,SAE TECHNICAL PAPER SERIES, 2004-01-1308.
- [2] S.R.Ahmed, G.Ramm, Salient Features of the Time-Averaged Ground Vehicle Wake,SAE-Paper 840300, 1984.
- [3] P.Gilliéron, A.Leroy, S.Aubrun,P.Audier, Influence of the Slant Angle of 3D Bluff Bodies on Longitudinal Vortex Formation" *Journal of Fluids Engineering* , Vol. 132 / 051104-1, MAY 2010.
- [4] J. Aider,J.Franc ,o.Beaudoin ,J.E.Wesfreid, Drag and lift reduction of a 3D bluff-body using active vortex generators, *Exp Fluids* (2010) 48:771–789.
- [5] G. goire Fourrie´ , L. Keirsbulck ,L. Labraga , P. Gillie´ron, Bluff-body drag reduction using a deflector, *Exp Fluids* (2010), DOI 10.1007/s00348-010-0937-6.
- [6] R. K. Strachan , K. Knowles , N. J. Lawson, The vortex structure behind an Ahmed reference model in the presence of a moving ground plane, *Exp Fluids* (2007) 42:659–669.
- [7] P. Gillie´ron , A.Kourta, Aerodynamic drag reduction by vertical splitter plates, *Exp Fluids* (2010) 48:1–16.
- [8] E. Fares, Unsteady flow simulation of the Ahmed reference body using a lattice Boltzmann approach, *Computers & Fluids* 35 (2006) 940–950.

- [9] S. Kapadia and S. Roy, K.Wurtzler, Detached Eddy Simulation Over a Reference Ahmed Car Model, *AIAA-2003-0857*.
- [10] J. Frohlich, D. von Terzi, Hybrid LES/RANS methods for the simulation of turbulent flows, *Progress in Aerospace Sciences 44 (2008)*, 349–377.
- [11] W.Rodi, DNS and LES of some engineering flows, *Fluid Dynamics Research 38 (2006)* 145–173.
- [12] M. Minguez, R. Pasquetti, and E. Serre, High-order large-eddy simulation of flow over the “Ahmed body” car model, *PHYSICS OF FLUIDS 20, 095101_2008*.
- [13] E.Guilmineau, Computational study of flow around a simplified car body, *Journal of Wind Engineering and Industrial Aerodynamics 96 (2008)* 1207–1217.
- [14] W-H. Hucho, Aerodynamics of Road Vehicles, Edition: 4, (SAE International, Published: February 1998).
- [15] L.A.Dobrzański, J.Domaga, J.F.Silva, Application of Taguchi method in the optimisation of filament winding of thermoplastic composites, *International Scientific Journal, March 2007, Pages 133-140*.
- [16] A.M. Omekanda, T. Geib, D.Buehler, K.wan and L. G.Lvan, Acoustic Noise Assessment of Gasoline Direct Injection (GDi) Components Using Taguchi Methods- Application to GDi High-Pressure Pumps, *SAE, 2010, 2010-01-0586*.
- [17] F.Ryoichi, Application of Taguchi's Methods to Aero-Engine Engineering Development, *IHI Engineering Review, Vol. 36 No. 3 October 2003*.
- [18] V. N. Gaitonde, S. R. Karnik, B. T. Achyutha, B. Siddeswarappa, Methodology of Taguchi optimization for multi-objective drilling problem to minimize burr size, *Int J Adv Manuf Technol, 2007, DOI 10.1007/s00170-006-0571-x*.
- [19] Sh. Obayashi, Sh. Jeong, K. Chiba, Multi-Objective Design Exploration for Aerodynamic Configurations” *AIAA-2005-4666, Revised Aug. 22, 2007*.
- [20] F. Duddeck, Multidisciplinary optimization of car bodies, *Struct Multidisc Optim (2008) 35:375–389, DOI 10.1007/s00158-007-0130-6*.
- [21] S. Krajinović, Optimization of Aerodynamic Properties of High-Speed Trains with CFD and Response Surface Models, *Lecture Notes in Applied and Computational Mechanics, 2009, Volume 41/2009, 197-211*.
- [22] A. Jafari, T. Tynjala, S.M. Mousavi, P. Sarkomaa, CFD simulation and evaluation of controllable parameters effect on thermomagnetic convection in ferrofluids using Taguchi technique, *Computers & Fluids 37 (2008)* 1344–1353.
- [23] A. R. Yıldız, N. Öztürk, N. Kaya, F. Öztürk, Hybrid multi-objective shape design optimization using Taguchi's method and genetic algorithm, *Struct Multidisc Optim (2006), DOI 10.1007/s00158-006-0079-x*.
- [24] Q. Wang, Q. Chen, M. Zeng, A CFD-Taguchi Combined Method for Numerical Investigation of Natural Convection Cooling Performance of Air-Core Reactor with Noise Reducing Cover, *Numerical Heat Transfer, 2009, Part A, 55: 1116–1130*.
- [25] D.C. Montgomery, Design and Analysis of Experiments”, 7th Edition, (Wiley, 2008).

Optimum Performance of Heat Pipes in Mould Cooling

Sulas G.Borkar^{*}, R.S.Shelke^{**}

^{*}(PG Student, Department of Mechanical Engineering, G. H. Raisoni College of Engineering Nagpur, MS (India))

^{**}(Assistant Professor, Department of Mechanical Engineering, G. H. Raisoni College of Engineering Nagpur, MS (India))

ABSTRACT

Conventional water jacket method is used to cool the various products manufactured by molding processes. Injection moulding and die casting moulds are the basic casting methods which are cooled with conventional water jacket method. Cooling of mould is essential in order to obtain the good quality of moulded part. Further the factor which is also absolutely essential is the rate of production. Conventional water jacket method is not suitable to obtain the good results and possess many disadvantages. Hence heat pipes are used in conventional water jacket method to cool the molding processes. In this paper, the experiment is performed and observations are taken with conventional water jacket method and heat pipe system and results are shown. It is observed that the liquid cooling with heat pipe system is more effective than liquid cooling with conventional water jacket method.

Keywords: Conventional water jacket, heat pipe, moulds cooling.

1. Introduction

Plastics are available in two types i.e. thermosetting plastics and thermoplastic materials. Thermosetting plastics are also known as heat setting materials and are formed in to shape under heat and pressure and results in a permanently hard product. Thermoplastic materials are also known as cold setting materials and they do not become hard with the application of heat and pressure and no chemical change occurs. They remain soft at elevated temperature and become hard on cooling. Both types of plastics moulded with the various moulding processes. Moulding is most common method employed for the fabrication of plastics. Plastics are moulded into any desired shape with the application of heat and pressure [3].

Injection moulding and die casting moulds are basic methods of casting. These processes are cooled by conventional water jacket method to obtain the good quality of moulded part. But this system is not suitable to obtain the good results and having many disadvantages. Hence the cooling with conventional water jacket is not optimum. Hence to obtain the good results and optimum performance, application of heat pipes are done in conventional water jacket method. Heat pipes transfer heat faster and hence the cycle time is reduced and the production rate is increased. Thus with the application of heat pipes in conventional water jacket method, the various disadvantages associated

with conventional water jacket method are eliminated and the moulding processes become optimum. Hence by utilization of heat pipes in conventional water jacket method, the optimum performance of heat pipes is achieved. In plastic injection moulding the function of the cooling system is to provide thermal regulation in the injection molding process. When the hot plastic melt enters into the mould impression, it cools down and solidifies by dissipating heat through the cooling system [4]. Injection mould cooling influences both technology and economy of production cycle. Main requirement given on to cooling system of injection moulds is quick and homogenous heat removal from injection part [5].

2. Experimental Set-Up

2.1 Components of Experimental Set-up

It consists of

- Heat Pipe
- Ceramic Band Heater
- Cooling water jackets
- Thermometers
- Mould cavity

2.1.1 Heat Pipe

Heat pipe is a heat transfer device with an extremely high effective thermal conductivity. Heat pipes are evacuated vessels which are partially back filled with a small quantity of working fluid. They are used to transfer heat from a heat source to a heat sink with minimal temperature gradient. As heat is input at the evaporator; fluid is vaporized creating a pressure gradient in the pipe. This pressure gradient forces the vapour to flow along the pipe to the cooler section where it condenses giving up its latent heat of vaporization. The working fluid is then returned to the evaporator by capillary forces developed in the porous wick structure. Heat pipe working fluids range from helium and nitrogen for cryogenic temperatures and to liquid metals like sodium and potassium for high temperature applications. Some of the, more common heat pipe fluids used for electronic cooling applications are ammonia, water, acetone and methanol. Heat pipe is a very good thermal conductor [6]. Among the various cooling techniques, heat pipe technology is emerging as a cost effective thermal design solution due to its excellent heat transport efficiency and capability [7]. Cooling of electronics is one of the major

fields of application for the heat pipes, especially in notebook computers and telecommunications applications [8].

2.1.2 Ceramic Band Heater

To maintain the good quality, the temperature of the moulding must be appropriately set and precisely controlled [9].

2.1.3 Mould cavity

Various products are moulded in mould cavity.

2.1.4 Water Jacket Set-up

The cooling system is one of the most important systems in a plastic injection mould to affect the quality and productivity of the molded part [10].

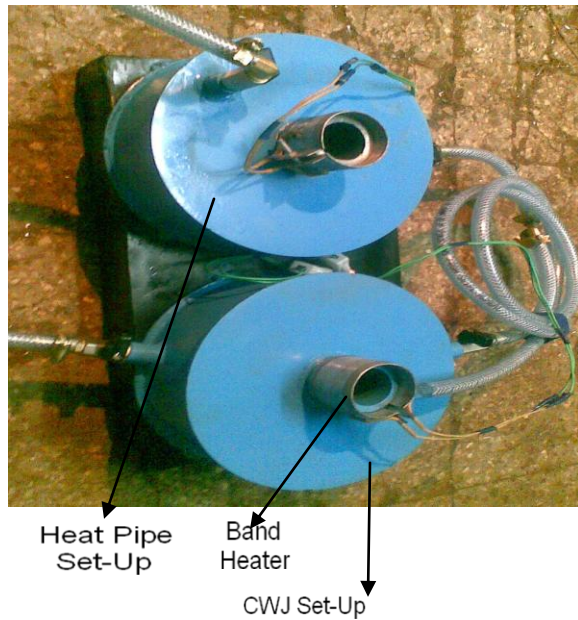


Fig 1: Experimental set-up

2.1.5 Heat Pipe Set-up

The performance of heat pipe depends upon various factors such as its diameter, length; application (how and where the heat pipe is used) and its orientation [11]. The various orientations performed for heat pipe are as follows

1. Horizontal orientation
2. Inclined orientation
3. Vertical orientation

Out of these orientations heat pipe gives better thermal performance in horizontal orientation.

3. Experimental Results

We have taken various readings for both the set-up as follows.

Table 1: Observation table for cold water jacket set-up

Sr. no.	Volume in Beaker (ml)	Time (sec)	Mass flow rate kg/sec	T1 (°C)	T2 (°C)	ΔT (°C)
1.	100	266	0.0036	24	34	10
2.	100	240	0.0040	24	33.2	9.2
3.	100	190	0.0051	24	32.3	8.3

Total Heat Transfer= $Q = U \cdot A \cdot \Delta T$

Where U= Overall heat transfer coefficient

= 340 to 455 w/m²k

A = Heat Transfer Area

= $\pi \cdot D \cdot L$

= $\pi \cdot 0.048 \cdot 0.075$

= 0.011m²

$Q = 340 \cdot 0.011 \cdot 10$

$Q_{cwj} = 37.4 \text{ Watt}$

Table 2: Observation table for heat pipe set-up

Sr. no.	Volume in Beaker (ml)	Time (sec)	Mass flow rate kg/sec	T1 (°C)	T2 (°C)	ΔT (°C)
1.	100	266	0.0036	24	44	20
2.	100	240	0.0040	24	43.2	19.2
3.	100	190	0.0051	24	42	18

Total Heat Transfer= $Q = U \cdot A \cdot \Delta T$

Where U= Overall heat transfer coefficient

= 340 to 455 w/m²k

A1= Heat transfer area

= $(\pi \cdot D \cdot L) - 2(\pi/4) \cdot d^2$

= $(\pi \cdot 0.048 \cdot 0.075) - 2(\pi/4) \cdot (0.022)^2$

$A1 = 0.0105 \text{ m}^2$

$Q1 = 340 \cdot 0.010 \cdot 20$

= 71.4 watt

A_2 = Heat transfer area for evaporator of Heat pipe

$$= 2(\pi * D * L_{\text{evap}})$$

$$= 2(\pi * 0.012 * 0.025)$$

$$A_2 = 0.001884 \text{ m}^2$$

$$Q_2 = 340 * 0.001884 * 20$$

$$= 12.81 \text{ watt}$$

Total heat transfer through heat pipe system

$$Q_{\text{hp}} = Q_1 + Q_2$$

$$Q_{\text{hp}} = 71.4 + 12.81 = 84.21 \text{ watt}$$

3.1 Effectiveness of heat pipe system over cooling water jacket system

$$\varepsilon = \frac{mcp\Delta T \text{ with Heat pipe}}{mcp\Delta T \text{ with CWJ}}$$

$$\varepsilon = Q_{\text{hp}} / Q_{\text{cwj}}$$

$$\varepsilon = 84.21 / 37.40$$

$$\varepsilon = 2.25$$

Thus liquid cooling with heat pipe system is 2.25 times effective than liquid cooling with water jacket method.

4. Conclusion

With the application of heat pipes in conventional water jacket methods in mould cooling, it is observed and can be stated that the liquid cooling with heat pipe system is more efficient and effective than liquid cooling with water jacket cooling method. Thus heat pipes are proved to be the basic need in conventional water jacket methods in mould cooling processes for optimum performance.

References

[1] A Faghri, *Heat pipe Science and Technology*, Taylor and Francis, Washington D C, 1995.

[2] P D Dunn and D A Reay, *Heat Pipes* 4th Edition (Oxford publication, 1994).

[3] R. S. Khurmi, J. K. Gupta, *A Textbook of Workshop Technology* (Manufacturing Process).

[4] C. L. Li, C. G. Li, A. C. K. MoK Automatic layout design of plastic injection mould cooling system, *Computer-Aided Design* 37(2005) 645-662.

[5] Lubos Behalek, Jozef Dobransky, *Process of cooling injection mould and quality of injection parts* ACTA Technica Corviniensis Bulletin of Engineering.

[6] Jaroslaw Legierski and Boguslaw Wiecek "Steady State Analysis of cooling Electronic Circuits Using Heat Pipes". *IEEE Transactions on components and packaging technologies*, VOL. 24, no. 4, December 2011.

[7] H. Xie and M. Aghazadeh, J. Toth *the Use of heat pipes in the cooling of portables with High Power Packages- A Case Study with the Pentium Processor Based Notebooks and Sub -Notebooks*.

[8] Ioan Sauciuc, Masataka Mochizuki, Kouichi Mashiko, Yuji Saito, Thang Nguyen, The Design and Testing of the Super Fiber Heat Pipes for Electronics Cooling Applications *Sixteenth IEEE SEMI – THREM Symposium*.

[9] Wu-Chung Su, Ching-Chih Tsai Discrete-Time VSS Temperature Control for a Plastic Extrusion Process with Water Cooling Systems. *IEEE Transactions on control systems technology*, vol. 9, no. 4, July 2001.

[10] C. G. Li, Yuguang Wu, Evolutionary optimization of plastic injection mould cooling system layout design. *2010 International Conference on Intelligent system Design and Engineering Applications*.

[11] C K Loh, Enisa Harris and DJ Chou, Comparative Study of Heat Pipes Performances in Different Orientations *21st IEEE SEMITHERM Symposium*.

Experimental Investigation and Failure Analysis of helical pinion shaft in WAG-9 Locomotive

C.B. Chaudhari¹, Dr. R. N. Baxi²

¹(Research scholar, Department of Mechanical Engg. G.H. Raisoni College of Engg. Nagpur University, India)

²(Professor, Department of Mechanical Engg, G.H.Raisoni College of Engg. Nagpur, Nagpur University India)

ABSTRACT

Railway transport is an important aspect in the transportation system of our country. For timely service in passenger as well as goods transport, the efficiency and long service life of the systems components are important factors. The component for the study has been obtained from the Central Railway, Electric Loco Shed Ajani Nagpur M. S. India. In the present study the premature failure of one of the component of traction motor assembly (Helical pinion shaft) is carefully investigated. Different analytical tools such as Non Destructive Test for identification of the crack and for measuring the depth of the crack are used for experimentation. The cause of the identified failure is systematically analyzed by performing chemical test, hardness measurement and metallographic examination of the failed component. The results of all the analysis is correlated in the present study.

Keywords: Failure Analysis, Hardness Measurement, Microstructure.

1. INTRODUCTION

WAG9 is an electric locomotive engine of Indian railways used to haul specially goods train. The locomotive has six axles in two sets of three frontal and rear wheels, shown in figure 1. The traction motor of WAG9 is a main power transmission part of locomotive. It runs at 850 kW at 100 rpm. The traction motor is an assembly used in Indian railway locomotive as the main power transmitting unit as shown in fig 2. The whole assembly consists of an arrangement transmitting the torque generated by the traction motor through helical pinion to main gear and through main gear to wheel assembly. The traction motor is mounted on the chesis of the bogie. The tractive effort required to run the locomotive is transmitted by traction motor through helical pinion and main gear. As this assembly is main power transmitting unit, numerous types of forces acts on the assembly which may be static or dynamic. A Helical pinion is a very common part in many machine assemblies. In helical gears, the contact between meshing teeth begins with a point on the leading edge of the tooth and gradually extends along the diagonal line across the tooth. [1] There is a gradual pick up of load by the tooth, resulting in smooth engagement and quiet operation even at high speed. Helical gears are used in automobiles, turbines and high speed application even up to 3000 m/min.

The material of the helical pinion shaft in the proposed study is forged steel.

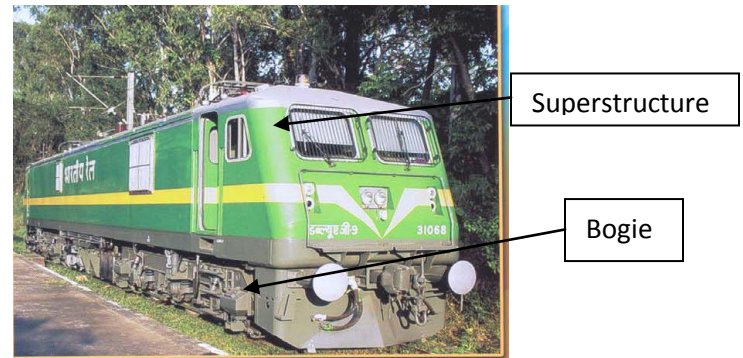


Figure: 1 WAG9- Locomotive

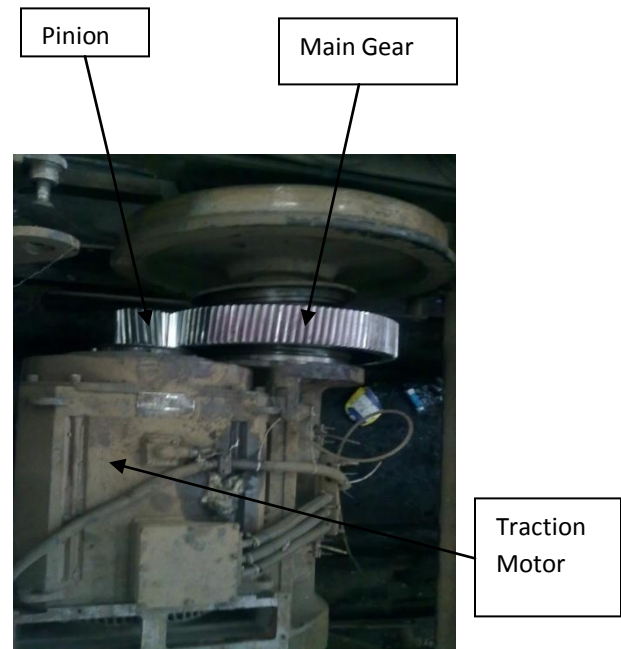


Figure 2 Traction motor assembly



Figure3: Helical pinion of traction motor

Dimensional details of helical pinion are as follows which are mentioned in the input data [2].

Table 1 Dimensional details of helical pinion shaft.

Outside diameter (mm)	Inside diameter (mm)	Weight (kg)
110	25	41

The helical pinion shaft material is made up of forged steel (DIN 17182 -17CrNiMo4) [2]. In this proposed study the failure investigation of the crack formed at notch region (figure4) and premature failure of the shaft of the helical pinion is discussed in details.

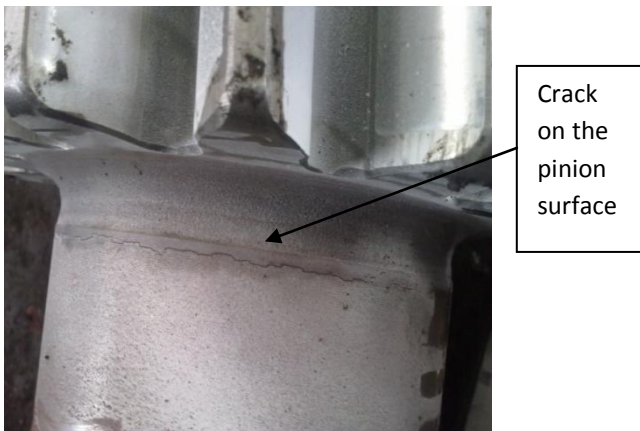


Figure 4 Failure Component Helical pinion with crack on the surface

2. Experimentation and Methodology

Experimental testing that has been carried out to investigate the failure of the helical pinion shaft.

- Non-destructive test for crack detection:

a) Magnetic particle test : as per ASTM SE-709 ARTICLE-7

Fluorescent powder with ultraviolet Light.

MODEL:MG-410 Make MAGNAFLUX

b) Ultrasonic flaw detection as per ASTM-A-388 Back wall Reflection.

- Chemical Test: Wet quantitative analysis of the helical pinion as per the standard procedure.
- Mechanical Test: hardness testing using standard Rockwell hardness tester (B scale).
- Microstructure: Metallographic examination using standard procedural steps for sample preparation. This is followed by optical microscopic examination using inverted binocular (Censico make) microscope installed with image analysis software.

3. RESULT AND DISCUSSION

A] Non Destructive Testing

Non-destructive testing is the use of physical methods which will test materials, components and assemblies for flaws in their structure without damaging their future usefulness. NDT is concerned with revealing flaws in the structure of a product.

a) MAGNETIC PARTICAL TEST:-

The magnetic particle (magna flux) inspection method is used to detect cracks, laps, seams, inclusions and other types surface of near surface discontinues in ferromagnetic materials. Typically, we used magnetic particle inspections to find fatigue induced surface and near surface cracks in helical pinion parts. For carrying out the test the fluorescent powder mixed in liquid is spread on the pinion surface. At the same time pinion is magnetized with instrument and ultraviolet light is focused on it. The image below shows the typical crack lining along circumference of pinion shaft.



Crack detected on the surface by Magnetic particle test

Fig 5 Helical pinion

b) Ultrasonic Test

It uses high frequency sound energy to conduct examinations and make measurements. Ultrasonic inspection can be used for flaw detection/evaluation, dimensional measurements, material characterization, and more. Ultrasonic sound waves are much higher than the audible range are produced and made to pass through the pinion. The time interval between the transmitted ray and reflected ray is recorded by a cathode ray oscilloscope. The depth of the crack from the surface of the helical pinion can be easily calculated by ultrasonic testing.[3] In this inspection the ultrasonic graph or signals shows discontinuities near notch region as well as at the end of shaft.



Fig 6 Ultrasonic test

With the ultrasonic test a crack is detected on the surface of the pinion shaft at a depth of 25-30mm

B) Chemical Analysis Test

Quantitative chemical analysis of the helical pinion shaft is carried out as per the standard procedure to validate the input data. The results are shown in table no.2.

Table2: Chemical analysis of helical pinion shaft.

Sample	%C	%Si	%Mn	%S	%P	%Cr	%Ni	%Mo
As per drawing	0.15 to 0.20	0.4 Max	0.4 to 0.6	0.035 max	0.035 max	1.5 to 1.8	1.4 to 1.7	0.25 to 0.35
As per experimentation	0.24	0.13	0.78	0.025	0.031	0.98	1.64	0.31

It is observed that carbon content of the helical pinion is quite higher (0.04%) than the specified value. Similarly lower Chromium content (0.82%) is observed after investigation in the report as against specified value of 1.8%. In order to cross check this observed value, further investigations such as hardness measurement and metallographic examination were carried out.

C) Mechanical testing: (Hardness measurement)

Standard Rockwell Hardness Tester is used to measure the hardness value at the failure section. Table 3 shows the results of hardness measurement. Wide variation in the hardness value is observed.

The observed range of hardness is 34 -28 BHN, where as the required hardness value as per the drawing is 52 BHN. Absence of alloyed carbide (chromium carbide) might be responsible for lowering of the hardness. (52 BHN specified in the drawing). Possibility of non homogeneity in the chemical composition is also evident from this wide variation of hardness value.

Table3: Hardness Measurement at various locations of the failure surface.

Sr No	Rockwell Hardness B SCALE (100kg load)	Corresponding BHN Using standard conversion chart. (3000kg load)
1	34HRB	49

2	30HRB	47
3	28 HRB	42
4	27HRB	41
5	29 HRB	44
6	33 HRB	48

D] Metallographic analysis (Micro structural examination)

Variation in the chemistry of the helical pinion shaft and measured hardness value of the helical pinion shaft is correlated with the metallographic examination of the failed component. Standard procedure of polishing the samples using Emery papers Grade 0/1, 0/2, 0/3, 0/4 was followed before micro examination.

Before etching the sample, velvet cloth polishing was done using alumina abrasive paste [4, 5]. The observed microstructure is shown in figure7.

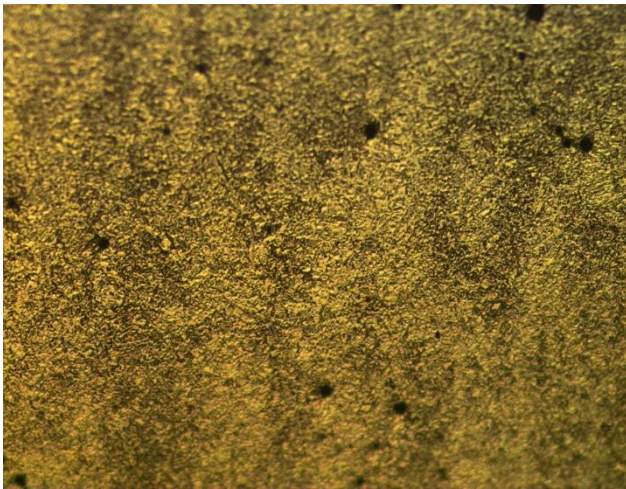


Figure:7 Metallograph of the failure component of the Helical pinion shaft. X100.

From the figure7, following observations are made:

1. Almost 30 % region in the microstructure shows Carbide phase (Fe_3C) with ferrite background.
2. The metallographic analysis can be very well correlated with the chemistry of the component. The observation as per the microscopic examination gives clear-cut indication of higher carbon content in the material, although specified value of the carbon is 0.20%.

4. Conclusion and further suggestions

Based on experimental investigation of helical pinion shaft in WAG-9 Locomotive following conclusions are drawn:

1. Validation of entire input data has shown some discrepancy as in the quantitative chemical analysis and hardness measurement.

2. This variation is reconfirmed by micro examination of the helical pinion shaft.

Also for further analysis to confirm failure causes it is recommended,

- 1) To conduct stress analysis of the helical pinion
- 2) The design aspects such as sudden change in design (notch region in this case) also should be taken in to consideration for analysis.

5. ACKNOWLEDGEMENT

The authors gratefully acknowledge Central Railway Electric Loco Shed Ajani, Nagpur (M.S) India, for providing necessary support in order to conduct the failure analysis.

6. REFERENCES

- [1] V. B. Bhandari, *Design of Machine Elements* 18 (Tata McGraw-Hill 2008)694-695
- [2] INDIAN RAILWAYS WAG-9 *Maintenance and Repair Manual*
- [3] P.P.NANEKAR and B.K. SHAH 'Characterization Of Material Properties By Ultrasonic's Atomic Fuels Division, Bhabha Atomic Research Centre, 2003 Pp.25-38.
- [4] M. R. LOUTHAN, 'Optical Metallography'1986, Jr., Department of Materials Engineering, Virginia Polytechnic Institute and State University" *ASM Handbook, Volume 10: Materials Characterizations R.E. Whan, editor, pp.299- 308.*
- [5] VIRENDRA K. BAFNA and PARESH U. HARIBHAKTI TCR Engineering Services Pvt. Ltd. Mumbai India. 'In Situ Metallographic for the Plant Health Assessment Study and Failure Investigation' 2007, Pp.1-19.

Optimization of media composition for the production of gentamycin by *Micromonospora echinospora* MTCC 708 using Response Surface Methodology

Ch. A. I. Raju, Ch. V. Satya, C. Chaman Mehta,
N. M. Yugandhar, S. Subba Rao

Center for Biotechnology, Department of Chemical Engineering, Andhra University, Visakhapatnam-530003, India

ABSTRACT

Response surface methodology (RSM) was applied to determine optimal medium composition for gentamycin production by an indigenous *Micromonospora echinospora* MTCC 708 with a view to reduce the number of experiments and obtaining the mutual interactions between the variables. A 2^4 full factorial central composite design was employed for experimental design and analysis of the results. Four independent variables, viz: concentrations of starch, soya bean meal, zinc sulfate and ammonium phosphate in the production media were tested. The optimum values of the four variables were starch 12.7252g/l, soya bean meal 10.593g/l, zinc sulfate 0.2714g/l and ammonium phosphate 5.4032g/l. The corresponding maximum concentration of gentamycin produced was 408.8844 μ g/ml. The goodness of the fitness of the model was checked by the determination coefficient R^2 which is 0.94421 and which indicates that 94.421% of the variability in the response could be explained by the model.

Keywords: Optimization, gentamycin, Response Surface methodology, *Micromonospora echinospora*, Central Composite Design

I. INTRODUCTION

Gentamycin is a new broad spectrum, basic, water soluble antibiotic produced by *M.echinospora*, *M.purpurea* and *M.rosarea* (K.S.Kim et.al 1990, A.AAbou-Zeid et.al 2002, Juchu etal 2004). It has a wide variety of uses: in the treatment of infections of blood, kidney and lungs (Sarre S.G and Mohn FE.N.Y 1967, Milanesi G. and Ciferri.O1996). The importance of gentamycin is mainly due to its action on pathogenic microorganisms like *Pseudomonas aeruginosa* which is resistant to other antibiotics. It is frequently used in burns, pneumonias, urinary, respiratory and gastrointestinal tract infections. It can also be used in bone, skin, tissues and joint infections caused by susceptible gram positive as well as to prevent fouling of soft contact lenses. The present work deals with the media optimization for the production of gentamycin by *M.echinospora* MTCC 708 using RSM.

RSM is a sequential procedure with an initial objective to lead the experiments rapidly and efficiently along a path of

improvement towards the general vicinity of the optimum. It is appropriate when the optimal region for running the process has been identified. This method has been successfully applied to optimize alcoholic fermentation (Bandaru etal 2006), optimize vegetable oil bioconversion (Cheyner.V et.al 1983), biomass production (Moresi M. et.al 1980), α -amylase production (M .Saban et. al 2005) and neomycin production (K.Adinarayana et.al 2003). A detailed account of this technique has been outlined (Cochran.N.G and Cox.G.M 1968). Basically, this optimization process involves three major steps: performing the statistically designed experiments, estimating the coefficients in a mathematical model and predicting the response and checking the adequacy of the model.

Hence the authors report the application of the RSM using the Box-Wilson design (Box.,G.E.P and Wilson, K.B 1951) of experiments to develop a mathematical correlation among the starch, soya bean meal, zinc sulfate, ammonium phosphate and yield of gentamycin.

II. MATERIALS AND METHODS

Microorganism and cultivation:

M.echinospora MTCC 708 supplied by IMTECH Chandigarh, India was used through out the study for the production of gentamycin.

Growth media:

The above organism is maintained on the following ingredients (g/l): glucose 10; soluble starch 20; yeast extract 5; tryptone 5; CaCO_3 1; agar agar 15 and distilled water 1000 ml, maintained at a pH of 7.6 and temperature 28°C.

Inoculum and production media:

The production of gentamycin was carried out using inoculum media and production media. The ingredients of the inoculum media were (g/l): beef extract 3; tryptone 5; glucose 1; soluble starch 24; yeast extract 5; CaCO_3 4 and distilled water 1000ml, maintained at a pH of 7.6 and temperature 30°C. The production medium consists of dextrose 5g/l, soya bean meal 10g/l, corn steep liquor 5g/l, CaCO_3 7g/l and distilled water 1000ml, maintained at a pH of 7.0 and temperature 30°C.

Assay of gentamycin

At the end of the incubation period, the amount of gentamycins produced by *M.echinospora* 708 were biologically determined by *E.coli* as the assaying organism (Indian Pharmacopia 1996).

III. EXPERIMENTAL DESIGN AND OPTIMIZATION

Central composite experimental design (CCD) (Box., G.E.P and Wilson, K.B 1951) was used in the optimization of gentamycin production. Starch(g/l), soya bean meal(g/l), zinc sulfate (g/l), ammonium phosphate(g/l) were chosen as the independent variables. Yield of gentamycin (Y, µg/ml) was used as the dependent variable. For statistical calculations the variables X_i were coded as x_i according to Eq. (1)

$$x_i = (X_i - \bar{x}_i) / (\Delta x_j) \quad (i = 1, 2, 3, \dots, k) \quad \dots \dots \dots (1)$$

where x_i is dimensionless value of an independent variable, X_i is real value of an independent variable, \bar{x}_i is real value of the independent variable at the center point and Δx_j is step change.

RSM includes full factorial CCD and regression analysis. Also this method evaluates the effective factors and building models to study interaction and selects optimum conditions of variables for a desirable response. The full CCD, based on three basic principles of an ideal experimental design, primarily consists of (1) a complete 2^n factorial design, where n is the number of test variables, (2) n_0 center points ($n_0 \geq 1$) and (3) two axial points on the axis of each design variable at a distance of $2^{n/4} = 2$ for $n = 4$ from the design center. Hence, the total number of design points (30) is $N = 2^n + 2n + n_0$. Using CCD, a total number of 30 experiments with different combinations of starch, soyabean meal, zinc sulfate and ammonium phosphate were performed (Table 2 and 3). The response was taken as the maximum citric acid production which was observed at fourth day.

A 24 – factorial central composite experimental design, with eight axial points ($\alpha = \sqrt{3}$) and six replications at the center points ($n_0 = 6$) leading to a total number of thirty experiments was employed (Table 2) for the optimization of the parameters. The second degree polynomials (Eq. (2)) were calculated with the statistical package (Stat-Ease Inc, Minneapolis, MN, USA) to estimate the response of the dependent variable.

$$Y = b_0 + b_1X_1 + b_2X_2 + b_3X_3 + b_4X_4 + b_{11}X_1^2 + b_{22}X_2^2 + b_{33}X_3^2 + b_{44}X_4^2 + b_{12}X_1X_2 + b_{13}X_1X_3 + b_{14}X_1X_4 + b_{23}X_2X_3 + b_{24}X_2X_4 + b_{34}X_3X_4 \quad \dots \dots \dots (2)$$

where Y is predicted response, X_1, X_2, X_3, X_4 are independent variables, b_0 is offset term, b_1, b_2, b_3, b_4 are

linear effects, $b_{11}, b_{22}, b_{33}, b_{44}$ are squared effects and $b_{12}, b_{13}, b_{14}, b_{23}, b_{24}, b_{34}$ are interaction terms.

IV. RESULTS AND DISCUSSION

The four factors which highly influence the fermentative production of gentamycin are starch, soyabeanmeal, zincsulfate, ammonium phosphate. Hence these four factors are considered as major constituents of the medium.

The experimental design matrix was given in Tables 1 and 2. Thirty experiments were performed using different combinations of the variables as per the CCD. Using the results of the experiments the following second order polynomial equation giving the amount of gentamycin as a function of starch ($X_1, g/l$), soyabeanmeal ($X_2, g/l$), zinc sulfate ($X_3, g/l$) and ammonium phosphate ($X_4, g/l$) was obtained:

$$Y_i = -631.47 + 9.68X_1 - 3.53X_2 + 156.35X_3 - 11.03X_4 - 753.21X_{12} - 1487.18X_{22} + 93.59X_{32} - 8.53X_{42} + 5X_1X_2 + 50X_1X_3 + 2.5X_1X_4 + 100X_2X_3 - 2.5X_2X_4 - 25X_3X_4 \quad \dots \dots \dots (3)$$

The predicted levels of gentamycin using the above equation were given along with experimental values in Table 3. The coefficients of the regression model (Eq.(3)) calculated are listed in Table 4, in which they contain four linear, four quadratic and six interaction terms and one block term. The effects of all four parameters i.e. starch, soya bean meal, zinc sulfate, ammonium phosphate and their interactions with each other on gentamycin concentration were found to be significant ($p \leq 0.05$). The parity plot showed a satisfactory correlation between the values of experimental values and predicted values (Fig. 1), wherein, the points cluster around the diagonal line which indicates the good fit of the model, since the deviation between the experimental and predicted values was less. And also the goodness of the model could be checked by different criteria. The coefficient of determination, R^2 is 0.94421 which implies that 94.42% of the variability in the response could be explained by the model. The corresponding analysis of variance (ANOVA) was presented in Table 5. The predicted optimum levels of starch, soyabeanmeal, zinc sulfate, ammonium phosphate were obtained by applying the regression analysis to the Eq. (3). The predicted and experimental gentamycin concentration at the optimum levels were also determined by using Eq. (3). Fig 2-7 represent the response surface and contour plots for the optimization of medium constituents of gentamycin production. The optimum medium constituents for higher metabolic production can be attained at the concentration of 12.72516(g/l) of starch, 10.59384(g/l) of soyabeanmeal, 0.27144(g/l) of zinc sulfate and 5.40323 (g/l) of ammonium phosphate. At these optimum medium concentrations maximum gentamycin production of 408.8844µg/ml was obtained.

V. FIGURES AND TABLES

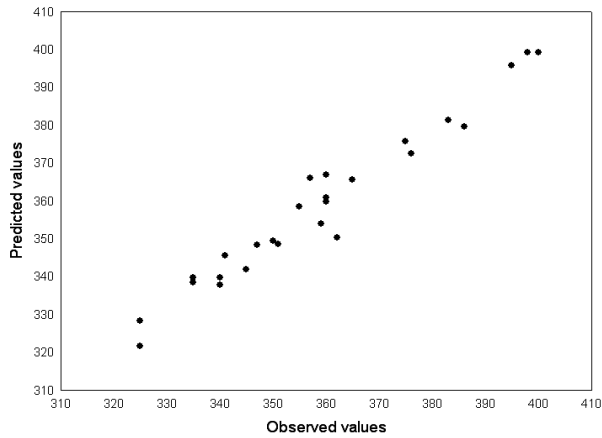


Figure 1. parity plot

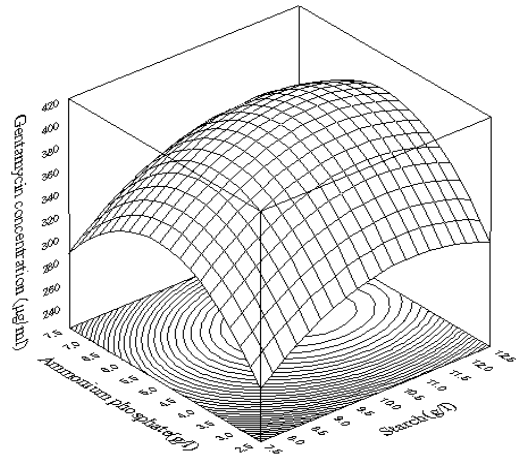


Figure 4. Response Surface and Contour plots for the production of Gentamycin using Starch and Ammonium Phosphate

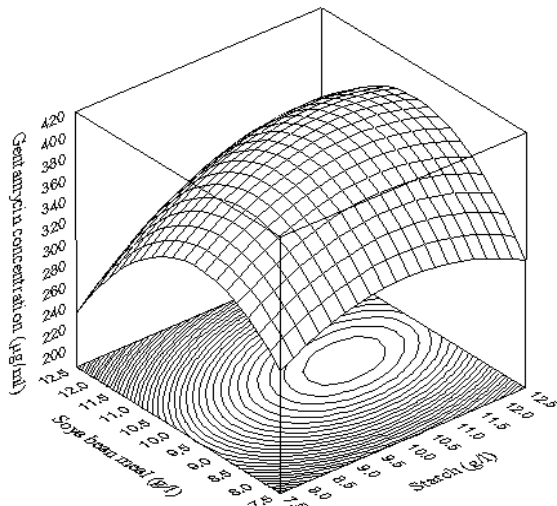


Figure 2. Response Surface and Contour plots for the production of Gentamycin using Starch and Soya bean meal

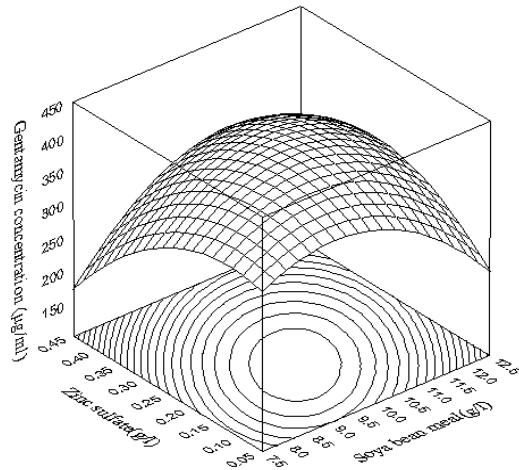


Figure 5. Response Surface and Contour plots for the production of Gentamycin using Soya bean meal and zinc sulfate

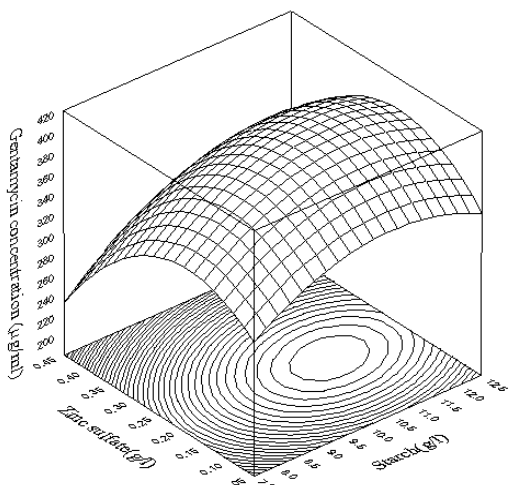


Figure 3. Response Surface and Contour plots for the production of Gentamycin using Starch and zinc sulfate

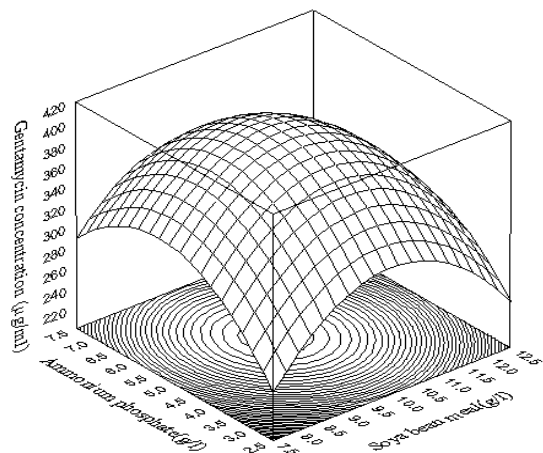


Figure 6. Response Surface and Contour plots for the production of Gentamycin using Soya bean meal and Ammonium Phosphate

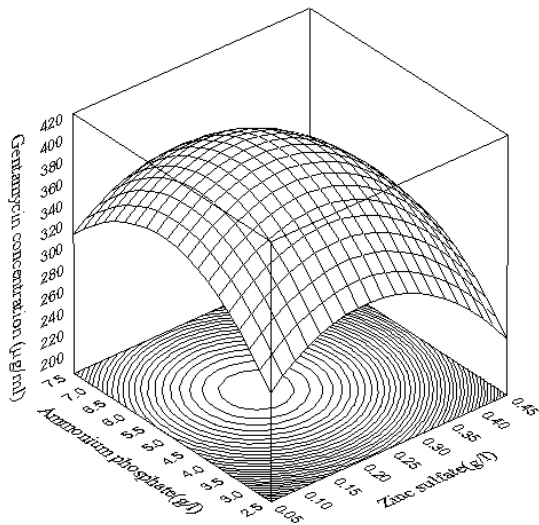


Figure 7. Response Surface and Contour plots for the production of Gentamycin using Zinc sulfate and Ammonium phosphate

11	1	-1	1	-1
12	1	-1	1	1
13	1	1	-1	-1
14	1	1	-1	1
15	1	1	1	-1
16	1	1	1	1
17	-2	0	0	0
18	2	0	0	0
19	0	-2	0	0
20	0	2	0	0
21	0	0	-2	0
22	0	0	2	0
23	0	0	0	-2
24	0	0	0	2
25	0	0	0	0
26	0	0	0	0
27	0	0	0	0
28	0	0	0	0
29	0	0	0	0
30	0	0	0	0

Variables	Coded levels				
	-2	-1	0	1	2
Starch (g/l)	8	9	10	11	12
Soya bean meal (g/l)	8	9	10	11	12
Zinc sulphate (g/l)	0	0.1	0.2	0.3	0.4
Ammonium phosphate (g/l)	3	4	5	6	7

Starck	Soya bean meal	Zinc sulfate	Ammonium phosphate	Production of Gentamycin (µg/ml)	
				Experimental	Predicted
9	9	0.1	4	360	359.8590
9	9	0.1	6	376	372.5256
9	9	0.3	4	340	337.7436
9	9	0.3	6	347	348.4103
9	11	0.1	4	325	321.6923
9	11	0.1	6	325	328.3590
9	11	0.3	4	341	345.5769
9	11	0.3	6	362	350.2436
11	9	0.1	4	357	366.0256
11	9	0.1	6	386	379.6923
11	9	0.3	4	359	353.9103
11	9	0.3	6	365	365.5769
11	11	0.1	4	345	341.8590

Table 2 The central composite design matrix employed for four independent variables (actual values given in Table 1)

Run No.	Starch	Soya bean meal	Zinc sulfate	Ammonium phosphate
1	-1	-1	-1	-1
2	-1	-1	-1	1
3	-1	-1	1	-1
4	-1	-1	1	1
5	-1	1	-1	-1
6	-1	1	-1	1
7	-1	1	1	-1
8	-1	1	1	1
9	1	-1	-1	-1
10	1	-1	-1	1

11	11	0.1	6	350	349.525 6	m phosphate		9	07	9	77
11	11	0.3	4	375	375.743 6	Starch x starch	b_{11}	-5.53	1.074 1	- 5.144 3	0.0001 20
11	11	0.3	6	383	381.410 3	Soya bean meal x soya bean meal	b_{22}	- 12.40	1.074 1	- 11.54 4	0.0000 00
12	10	0.2	5	395	395.897 4	Zinc sulfate x zinc sulfate	b_{33}	- 1612. 1	120.6 12	- 13.36 6	0.0000 00
10	12	0.2	5	335	338.564 1	Ammonium phosphate x ammonium phosphate	b_{44}	- 10.40	1.074 1	- 9.682 9	0.0000 00
10	10	0.4	5	335	339.730 8	Starch x soya bean meal	b_{12}	3.50	1.398 7	2.502 3	0.0243 94
10	10	0.2	3	351	348.564 1	Starch x zinc sulfate	b_{13}	25.00	13.98 70	1.787 4	0.0940 95
10	10	0.2	5	398	399.333 3	Starch x ammonium phosphate	b_{14}	0.25	1.398 7	0.178 7	0.8605 35
10	10	0.2	5	400	399.333 3	Soya bean meal x zinc sulfate	b_{23}	115.0 0	13.98 70	8.221 9	0.0000 01
10	10	0.2	5	400	399.333 3	Soya bean meal x ammonium phosphate	b_{24}	-1.50	1.398 7	- 1.072 4	0.3004 80
10	10	0.2	5	400	399.333 3	Zinc sulfate x ammonium phosphate	b_{34}	-5.00	13.98 70	- 0.357 5	0.7257 16

Table 4 Coefficients, *t*-statistics and significance probability of the model

Term	Coef	Value	Standard error of coefficient	t-value	P-Value
Constant	B_0	- 1220. 6	244.8 63	- 4.984 8	0.0001 63
Starch	B_1	78.60	26.74 27	2.939 0	0.0101 59
Soya bean meal	B_2	191.9 3	26.74 27	7.176 9	0.0000 03
Zinc sulfate	B_3	- 705.7 1	217.0 90	- 3.250 7	0.0053 75
Ammonium	B_4	122.0	22.71	5.375	0.0000

Table 5 Analysis of variance (ANOVA) for the entire quadratic model

Source of variation	Sum of squares (SS)	d.f	Mean squares (MS)	F-value	Probe >F
Model	16725.1 7	14	1194.65 5	38.1 6	0.000

Error	469.53	15	31.302
Total	17194.7		0

$$R=0.98625; R^2=0.97269; \text{Adjusted } R^2=0.94720759$$

$$F_{0.01(14,15)} = S^2_r/S^2_e = 38.16582 > F_{0.01(14,15)Tabular} = 3.56$$

$$P_{\text{model}} > F = 0.000000$$

VI. CONCLUSION

The one factor at a time operation used in optimization process which involves changing one parameter at a time, while keeping the others at fixed levels is laborious and time consuming. This method requires a complete series of experiments for every factor of interest. Moreover, such a method does not provide means of observing possible factors interactions. In contrast, CCD offers a number of important advantages. For instance, the researchers could easily determine factor effects with considerable less experimental effort, identify factors, find optima, offer greater precision and facilitate system modeling.

Thus, the present study using the RSM with CCD enables to find the importance of factors at different levels. Thus the optimum values of medium constituents found are starch 12.7252(g/l), soya bean meal 10.5938(g/l), zinc sulfate 0.2714(g/l) and ammonium phosphate 5.4032(g/l) and the gentamycin production obtained with the above optimum values are 408.8844µg/ml. A high similarity was observed between the predicted and experimental results, which reflected the accuracy and applicability of RSM to optimize the process for gentamycin production. The results of this study have clearly indicated RSM is an effective method for maximum production of gentamycin using *Micromonospora echinospora* MTCC 708.

REFERENCES

- [1] A. A. Abou-Zeid, A.I. Eissa and H. M. Salem. The fermentative production of gentamycin by *Micromonospora purpurea*. J. Appl. Chem. Biotechnol. 24(655-661),1974.
- [2] K.S.Kim. Effect of intercalating dyes on the production of antibiotics by *M.purpurea* and *M.rosarea*. Enzyme and Microbial technology.22(564-570),1990.
- [3] Juchu, Wenze Niu, Siliang Zhang, Huita Yingping Zhuang and Yourong Li.Effect of metal ions on the binding of gentamycin to the peptidoglycon of *M.echinospora* Process Biochemistry.39(1145-1150),2004.
- [4] Sarre, S.G.; Mohn,F.E.N.Y. Acad. Sci.1967, 29(5),575.
- [5] Milanese. G.; Ciferri, O. Biochemistry 1996,5(12),3926.
- [6] Veera Venkata Ratnam Bandaru, Subba Rao Somalanka, Damodara Rao Mendu, Narasimha Rao Madicherla, Ayyanna Chityala. Optimization of fermentation conditions for the production of ethanol from sago starch by co-immobilized amyloglucosidase and cells of *Zymomonas mobilis* using response surface methodology.Enzyme and Microbial Technology.38(209-214)2006.

- [7] Cheynier, V., Feinberg, M., Chararas, C. & Ducauze, C. 1983 Application of response surface methodology to evaluation of bioconversion experimental conditions. Applied and Environmental Microbiology 45, 634–639.
- [8] Moresi, M., Colicchio, A. & Sansovini, F. 1980 Optimization of whey fermentation in a jar fermenter. European Journal of Applied Microbiology and Biotechnology 9, 173–183.
- [9] M.Saban Tanyildizi, Dursun Ozer and Murat Elibol. Optimization of α -amylase production by bacillus species using response surface methodology. Process Biochemistry. 40(2291-2296), 2005.
- [10] K.Adinarayana, P.Ellaiah, B.Srinivasulu, J.Lakshminarayana and KVVS.N.Bapiraju. Optimization of media and culture conditions for neomycin production using response surface methodology. Ind. J.of Biotechnol.2(564-570), 2003.
- [11] Cochran, N.G. & Cox, G.M. 1968 Experimental Designs. John Wiley and Sons Inc., p. 611.
- [12] Box, G.E.P. & Wilson, K.B. 1951 On the experimental attainment of optimum conditions. Journal of the Royal Statistical Society (Series B) 13, 1–45.
- [13] Indian Pharmacopia.1996.Gentamycin injection. Microbial assay of antibiotics.Method A, appendix 9.1, 230-231. vol 2.

Investigations on Three Phase Five Level Diode Clamped Multilevel Inverter

C. R. Balamurugan¹, S. P. Natarajan², R. Bensraj³

¹Department of EEE, Arunai Engineering College, Tiruvannamalai, Tamilnadu, India

²Department of EIE, Annamalai University, Chidambaram, Tamilnadu, India

³Department of EEE, Annamalai University, Chidambaram, Tamilnadu, India

ABSTRACT

Multilevel inverters have become more popular over the years in high power electric applications without use of a transformer and with promise of less disturbance and reduced harmonic distortion. This work proposes three phase five level Diode Clamped Multilevel Inverter (DCMLI) to simulate various modulating techniques for induction motor load. These Pulse Width Modulation (PWM) techniques include Carrier Overlapping (CO) strategy, Variable Frequency (VF) strategy, Phase Shift (PSPWM) strategy and Sub-Harmonic Pulse Width Modulation (SHPWM) i.e. Phase Disposition (PD) strategy, Phase Opposition Disposition (POD) strategy and Alternate Phase Opposition Disposition (APOD) strategy. The Total Harmonic Distortion (THD), V_{RMS} (fundamental), crest factor, form factor and distortion factor are evaluated for various modulation indices. Simulation is performed using MATLAB-SIMULINK. It is observed that PODPWM method provides output with relatively low distortion and COPWM is found to perform better since it provides relatively higher fundamental RMS output voltage for Induction Motor (IM) load.

Keywords: CF, DCMLI, FF, PWM, THD, V_{rms}

I. INTRODUCTION

In recent years, industry has begun to demand higher power equipment, which now reaches the megawatt level. Controlled AC drives in the megawatt range are usually connected to the medium-voltage network. Today, it is hard to connect a single power semiconductor switch directly to medium voltage grids. For these reasons, a new family of multilevel inverters has emerged as the solution for working with higher voltage levels. Depending on voltage levels of the output voltage, the inverters can be classified as two-level inverters and multi level inverters. The inverters with voltage level 3 or more are referred as multi level inverters. Multilevel inverters have become attractive recently particularly because of the increased power ratings, improved harmonic performance and reduced EMI emission that can be achieved with the multiple DC levels that are available for synthesis of the output voltage. Xiaoming Yuan and Ivo Barbi [1] proposed fundamentals of a new diode clamping multilevel inverter. Bouhali et al [2] developed DC link capacitor voltage balancing in a three phase diode clamped inverter controlled by a direct space vector of line to line voltages. Anshuman Shukla et al [3] introduced control schemes for DC capacitor voltages equalization in diode clamped multilevel inverter based

DSTATCOM. Monge et al [4] proposed multilevel diode clamped converter for photovoltaic generators with independent voltage control of each solar array. Renge and Suryawanshi [5] developed five level diode clamped inverter to eliminate common mode voltage and reduce dv/dt in medium voltage rating induction motor drives. Hideaki Fujita and Naoya Yamashita [6] discussed performance of a diode clamped linear amplifier. Hatti et al [7] proposed a 6.6-KV transformer less motor drive using a five level diode clamped PWM inverter for energy savings of pumps and blowers. Srinivas in [8] discussed uniform overlapped multi carrier PWM for a six level diode clamped inverter. Engin Ozdemir et al [9] introduced fundamental frequency modulated six level diode clamped multilevel inverter for three phase stand alone photovoltaic system. Berrezzek Farid and Berrezzek Farid [10] made a study on new techniques of controlled PWM inverters. Anshuman shukla et al [11] proposed flying capacitor based chopper circuit for DC capacitor voltage balancing in diode clamped multilevel inverter. This literature survey reveals few papers only on various PWM techniques and hence this work presents a novel approach for controlling the harmonics of output voltage of chosen MLI fed IM employing sinusoidal switching strategies. Simulations are performed using MATLAB-SIMULINK. Harmonics analysis and evaluation of performance measures for various modulation indices have been carried out and presented.

II. MULTILEVEL INVERTER

The general structure of the multilevel inverter is to synthesize a sinusoidal voltage from several levels of voltages typically obtained from capacitor voltage sources. The so-called "multilevel" starts from three levels. A three-level inverter, also known as a "neutral-clamped" inverter, consists of two capacitor voltages in series and uses the center tap as the neutral. Each phase leg of the three-level inverter has two pairs of switching devices in series. The center of each device pair is clamped to the neutral through clamping diodes. The output obtained from a three-level inverter is a quasi-square wave output if fundamental frequency switching is used. Multilevel inverters are being considered for an increasing number of applications due to their high power capability associated with lower output harmonics and lower commutation losses. Multilevel inverters have become an effective and practical solution for increasing power and reducing harmonics of AC load. The main multilevel topologies are classified into three categories: diode clamped inverters, flying capacitor inverters, and cascaded inverters. In a three-phase inverter

system, the number of main switches of each topology is equal. Comparing with the number of other components, for example, clamping diodes and dc-link capacitors having the same capacity per unit, diode clamped inverters have the least number of capacitors among the three types but require additional clamping diodes. Flying capacitor inverters need the most number of capacitors. But cascaded inverters are considered as having the simplest structure.

The diode clamped inverter, particularly the three-level one, has drawn much interest in motor drive applications because it needs only one common voltage source. Also, simple and efficient PWM algorithms have been developed for it, even if it has inherent unbalanced dc-link capacitor voltage problem. However, it would be a limitation to applications beyond four-level diode clamped inverters for the reason of reliability and complexity considering dc-link balancing and the prohibitively high number of clamping diodes. Multilevel PWM has lower dv/dt than that experienced in some two-level PWM drives because switching is between several smaller voltage levels. Diode clamped multilevel inverter is a very general and widely used topology. DCMLI works on the concept of using diodes to limit voltage stress on power devices. A DCMLI typically consists of $(m-1)$ capacitors on the DC bus where m is the total number of positive, negative and zero levels in the output voltage. Figure1 shows a three phase half-bridge five level diode clamped inverter. The order of numbering of the switches for phase a is $S_{a1}, S_{a2}, S_{a3}, S_{a4}, S_{a1}', S_{a2}', S_{a3}'$ and S_{a4}' and like wise for other two phases. The DC bus consists of four capacitors C_1, C_2, C_3 and C_4 acting as voltage divider. For a DC bus voltage V_{dc} , the voltage across each capacitor is $V_{dc}/4$ and voltage stress on each device is limited to $V_{dc}/4$ through clamping diode. The middle point of the four capacitors 'n' can be defined as the neutral point. The principle of diode clamping to DC-link voltages can be extended to any number of voltage levels. Since the voltages across the semiconductor switches are limited by conduction of the diodes connected to the various DC levels, this class of multilevel inverter is termed diode clamped MLI. Table 1 shows the output voltage levels and the corresponding switch states for one phase of the chosen five level DCMLI. The switches are arranged into 4 pairs $(S_{a1}, S_{a1}'), (S_{a2}, S_{a2}'), (S_{a3}, S_{a3}'), (S_{a4}, S_{a4}')$. If one switch of the pair is turned on, the complementary switch of the same pair must be off. Four switches are triggered at any point of time to select the desired level in the five level DCMLI.

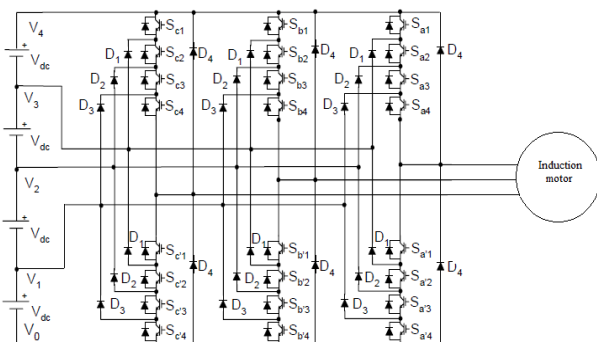


Figure 1 A three phase five level DCMLI

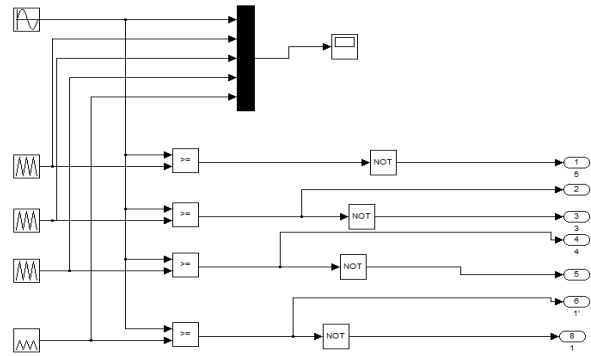


Figure 2 Sample PWM generation logic using SIMULINK developed for PDPWM technique

The steps to synthesis the five level phase a output voltage in this work are as follows:

1. For phase a output voltage of $V_{an}=0$, two upper switches S_{a3}, S_{a4} and two lower switches S_{a1}' and S_{a2}' are turned on.
2. For an output voltage of $V_{an}=V_{dc}/4$, three upper switches S_{a2}, S_{a3}, S_{a4} and one lower switch S_{a1}' are turned on.
3. For an output voltage of $V_{an}=V_{dc}/2$, all upper switches S_{a1} through S_{a4} are turned on.
4. To obtain the output voltage of $V_{an}= -V_{dc}/4$, upper switch S_{a4} and three lower switches S_{a1}', S_{a2}' and S_{a3}' are turned on.
5. For an output voltage of $V_{an}= -V_{dc}/2$, all lower switches S_{a1}' through S_{a4}' are turned on.

The phase a output voltage V_{an} has five states: $V_{dc}/2, V_{dc}/4, 0, -V_{dc}/4$ and $-V_{dc}/2$. The gate signals for the chosen five level DCMLI are developed using MATLAB-SIMULINK. The gate signal generator model developed is tested for various values of modulation index. The results of the simulation study are presented in this work in the form of the PWM outputs of the chosen multilevel inverter.

TABLE 1 Switching Scheme for one phase of three phase five Level DCMLI

S_{a1}	S_{a2}	S_{a3}	S_{a4}	S_{a1}'	S_{a2}'	S_{a3}'	S_{a4}'	V_{an}
1	1	1	1	0	0	0	0	$V_{dc}/2$
0	1	1	1	1	0	0	0	$V_{dc}/4$
0	0	1	1	1	1	0	0	0
0	0	0	1	1	1	1	0	$-V_{dc}/4$
0	0	0	0	1	1	1	1	$-V_{dc}/2$

III. MULTI CARRIER BASED PWM METHODS

This work used the intersection of a sine wave with a triangular wave to generate firing pulses. There are many alternative strategies to implement this. They are as given below.

- 1) Phase disposition PWM strategy.
- 2) Phase opposition disposition PWM strategy.
- 3) Alternate phase opposition disposition PWM strategy.
- 4) Carrier overlapping PWM strategy.

- 5) Variable frequency PWM strategy.
- 6) Phase shift PWM strategy.

III.1. Phase Disposition PWM Strategy

The rules for phase disposition method Fig.3 for a multilevel inverter are

- 1) 4 carrier waveforms in phase are arranged.
- 2) The converter is switched to + Vdc/2 when the sine wave is greater than both upper carrier.
- 3) The converter is switched to + Vdc/4 when the sine wave is greater than first upper carrier.
- 4) The converter is switched to zero when sine wave is lower than upper carrier but higher than the lower carrier.
- 5) The converter is switched to - Vdc/4 when the sine wave is less than first lower carrier.
- 6) The converter is switched to - Vdc/2 when the sine wave is less than both lower carrier.

The following formula is applicable to sub harmonic PWM strategy i.e. PD, POD and APOD

The frequency modulation index

$$m_f = f_c / f_m$$

The Amplitude modulation index

$$m_a = 2A_m / (m-1) A_c$$

where

- f_c – Frequency of the carrier signal
- f_m – Frequency of the reference signal
- A_m – Amplitude of the reference signal
- A_c – Amplitude of the carrier signal
- m – number of levels.

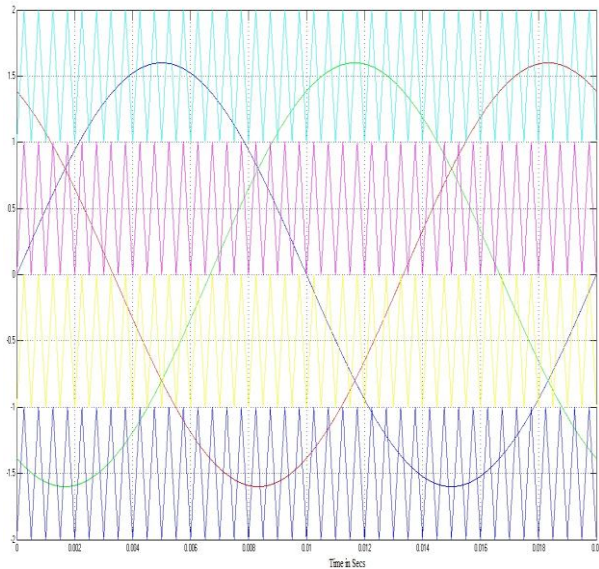


Figure 3 Carrier arrangement for PDPWM strategy ($m_a=0.8$ and $m_f=40$)

III.2. Phase Opposition Disposition Strategy

Four carrier waveforms are arranged so that all carrier waveforms above zero are in phase and they are 180 degrees out of phase with those below zero (Fig.4)

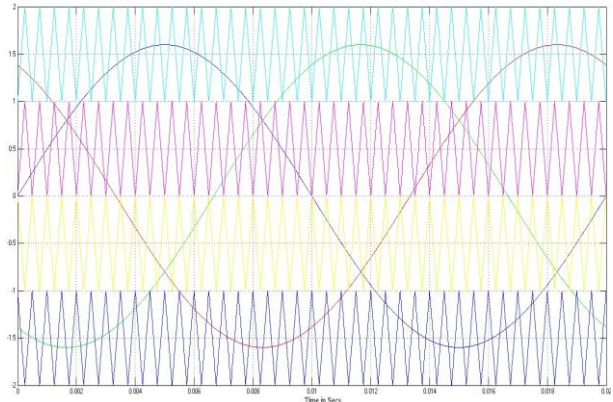


Figure 4 Carrier arrangement for PODPWM strategy ($m_a=0.8$ and $m_f=40$)

III.3. Alternative Phase Opposition and Disposition Strategy

Carriers are arranged in such a manner that each carrier is out of phase with its neighbor by 180 degrees (Fig.5).

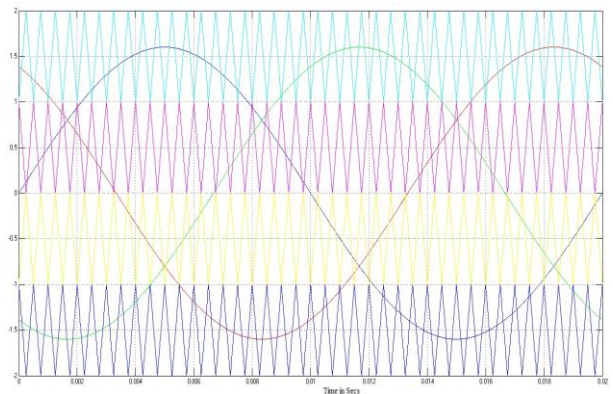


Figure 5 Carrier arrangement for APOD PWM strategy ($m_a=0.8$ and $m_f=40$)

III.4. Phase Shift PWM (PSPWM) Strategy

The phase shift multicarrier PWM technique (Fig.6) uses four carrier signals of the same amplitude and frequency which are shifted by 90 degrees to one another to generate the five level inverter output voltages. The gate signals for the chosen inverter can be derived directly from the PWM signals (comparison of the carrier with the sinusoidal reference).

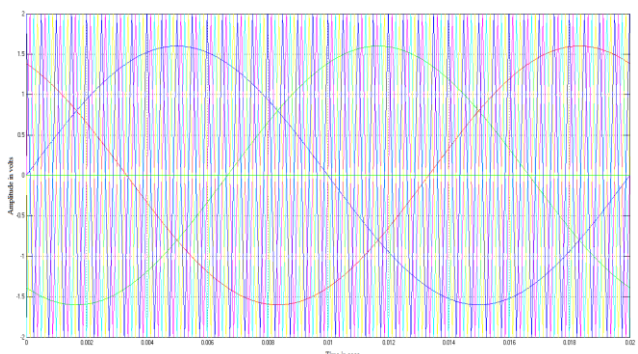


Figure 6 Carrier arrangement for PSPWM strategy ($m_a=0.8$ and $m_f=40$)

III.5. Carrier Overlapping PWM (COPWM) Strategy

For an m-level inverter using carrier overlapping technique, m-1 carriers with the same frequency f_c and same peak-to-peak amplitude A_c are disposed such that the bands they occupy overlap each other; the overlapping vertical distance between each carrier is $A_c/2$. The reference waveform has amplitude of A_m and frequency of f_m and it is centred in the middle of the carrier signals. The reference wave is continuously compared with each of the carrier signals. If the reference wave is more than a carrier signal, then the active devices corresponding to that carrier are switched on. Otherwise, the devices switch off. The amplitude modulation index m_a and the frequency ratio m_f are defined in the carrier overlapping method (Fig.7) as follows:

$$m_a = A_m / (m / 4) * A_c$$

$$m_f = f_c / f_m$$

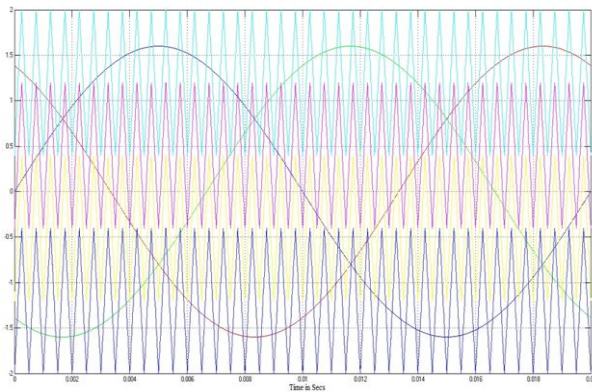


Figure 7 Carrier arrangement for COPWM strategy ($m_a=0.8$ and $m_f=40$)

III.6. Variable Frequency PWM (VFPWM) Strategy

The number of switchings for upper and lower devices of chosen MLI is much more than that of intermediate switches in SHPWM using constant frequency carriers. In order to equalize the number of switchings for all the switches, variable frequency PWM strategy is used as illustrated in which the carrier frequency of the intermediate switches is properly increased to balance the numbers of switching for all the switches (Fig.8).

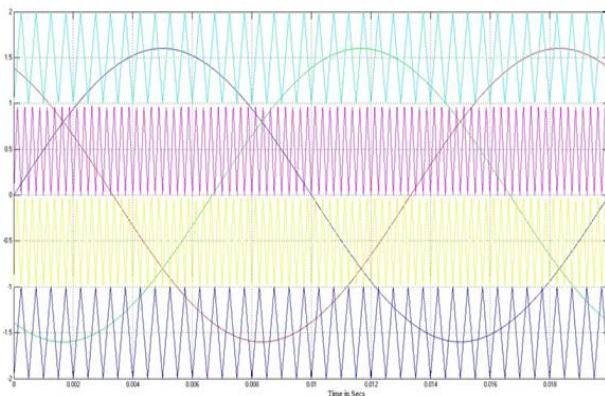


Figure 8 Carrier arrangement for VFPWM strategy ($m_a=0.8$ and $m_f=40$)

IV. SIMULATION RESULTS

The three phase diode clamped five level inverter is modeled in SIMULINK using power system block set. Simulations are performed for different values of m_a ranging from 0.6 to 1 and the corresponding %THD are measured using the FFT block and their values are shown in Table 2. Figs.9 – 23 show the simulated output voltage of DCMLI fed IM and their harmonic spectrum, speed and torque characteristics of Induction Motor (IM) with above strategies but for only one sample value of $m_a = 0.8$. Fig. 10 shows the five level output voltage generated by PDPWM strategy and its FFT plot is shown in Fig. 11. From Fig. 11, it is observed that the PDPWM strategy produces significant 30th, 32nd, 36th and 38th harmonic energy. Fig 13 shows the five level output voltage generated by PODPWM strategy and its FFT plot is shown in Fig. 14. From Fig. 14 it is observed that the PODPWM strategy produces significant 33rd and 35th harmonic energy. Fig 16 shows the five level output voltage generated by APODPWM strategy and its FFT plot is shown in Fig. 17. From Fig. 17 it is observed that the APODPWM strategy produces significant 33rd, 35th and 37th harmonic energy. Fig 19 shows the five level output voltage generated by COPWM strategy and its FFT plot is shown in Fig. 20. From Fig. 20 it is observed that the COPWM strategy produces significant 38th harmonic energy. Fig 22 shows the five level output voltage generated by VFPWM strategy and its FFT plot is shown in Fig. 23. From Fig. 23 it is observed that the VFPWM strategy produces significant 34th and 38th harmonic energy. The following parameter values are used for simulation : $V_{dc} = 440V$, induction motor load – 50HP(37 KW), 400V, 50Hz, 1480rpm, $T_m = 4Nm$, $f_c = 2000Hz$, $f_m = 50Hz$. Figs. 9, 12, 15, 18, 21 show speed torque characteristics of IM fed by chosen MLI for PD, POD, APOD, CO, VF PWM strategies.

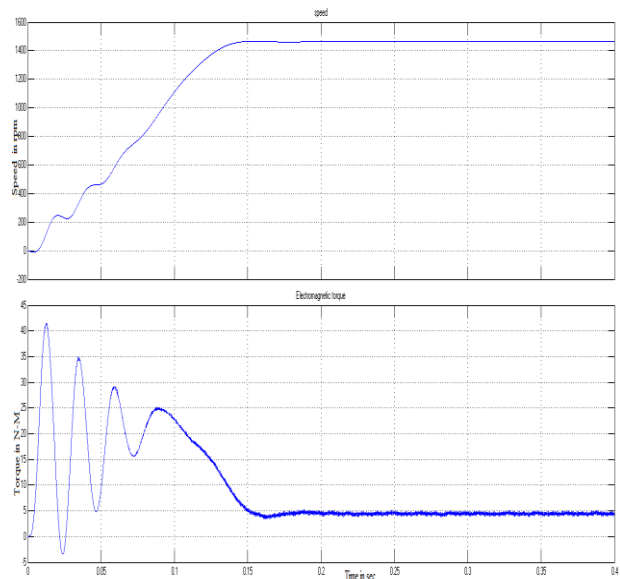


Figure 9 Speed and torque characteristics of IM for PDPWM strategy

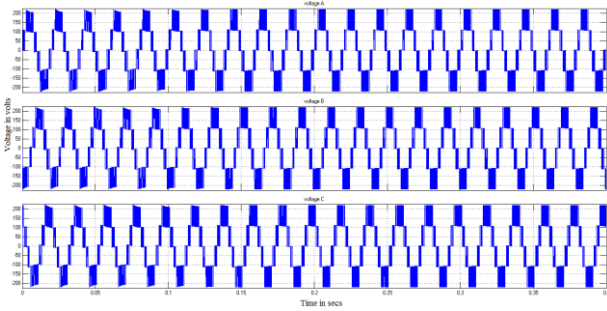


Figure 10 Output voltage generated by PDPWM strategy for IM load

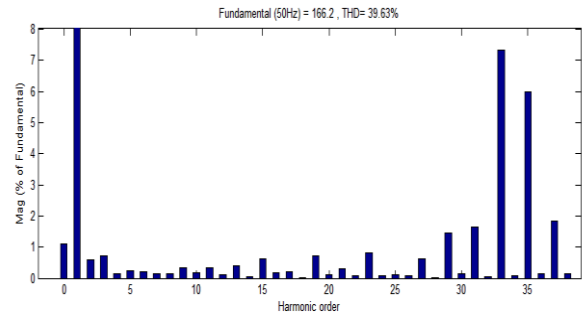


Figure 14 FFT plot for output voltage of PODPWM strategy for IM load

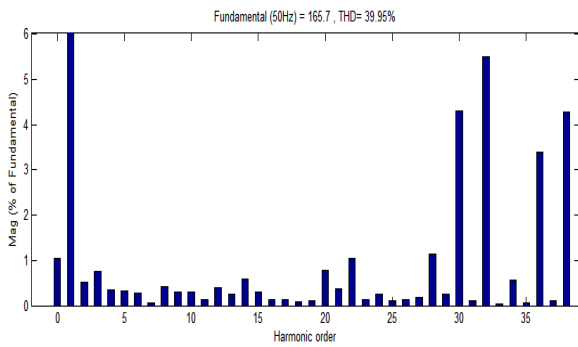


Figure 11 FFT plot for output voltage of PDPWM strategy for IM load

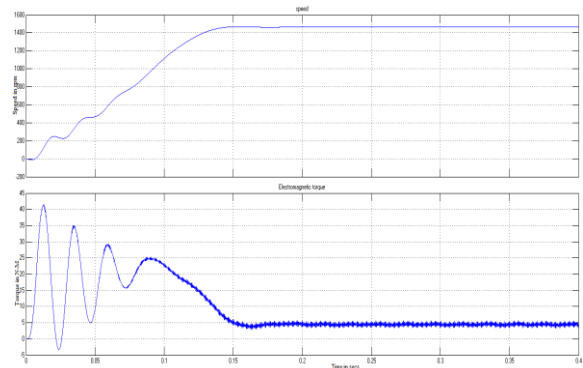


Figure 15 Speed and torque characteristics of IM for APODPWM strategy

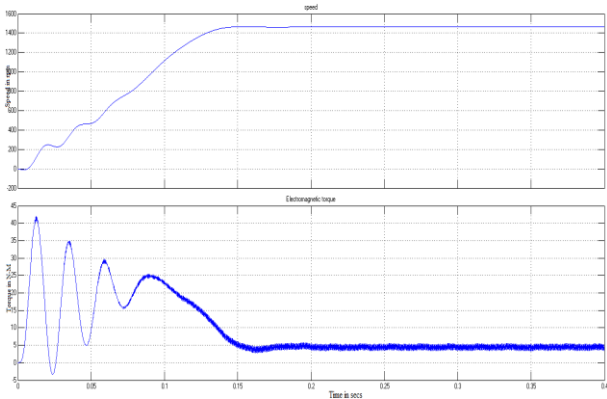


Figure 12 Speed and torque characteristics of IM for PODPWM strategy

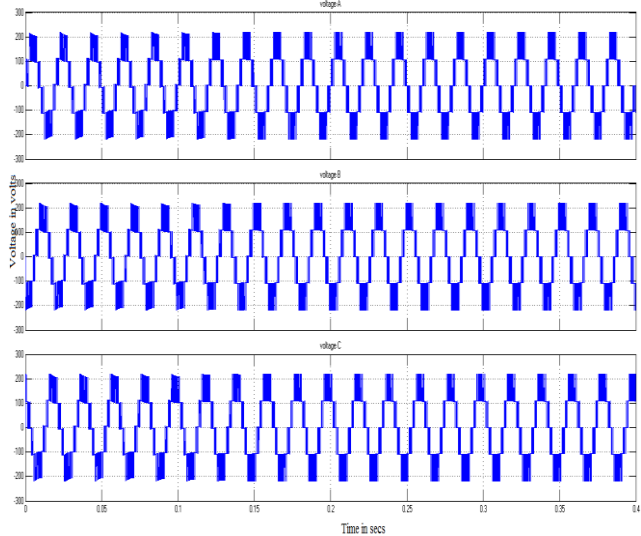


Figure 16 Output voltage generated by APODPWM strategy for IM load

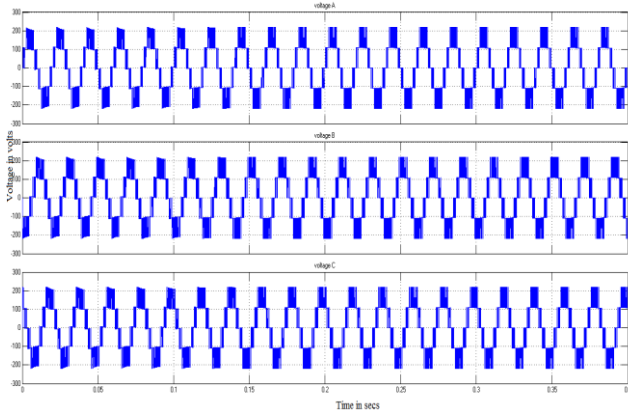


Figure 13 Output voltage generated by PODPWM strategy for IM load

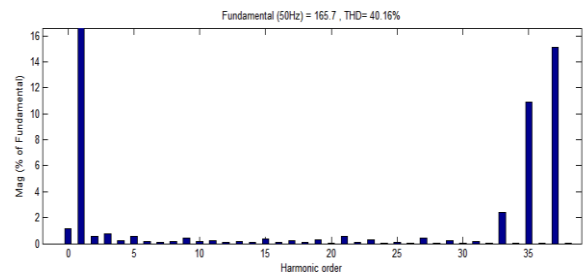


Figure 17 FFT plot for output voltage of APODPWM strategy for IM load

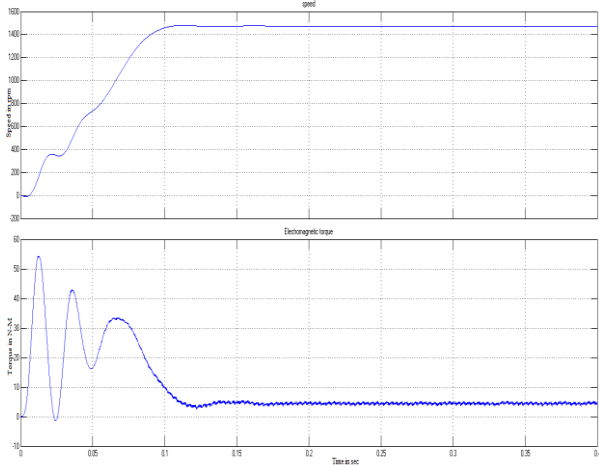


Figure 18 Speed and torque characteristics of IM for COPWM strategy

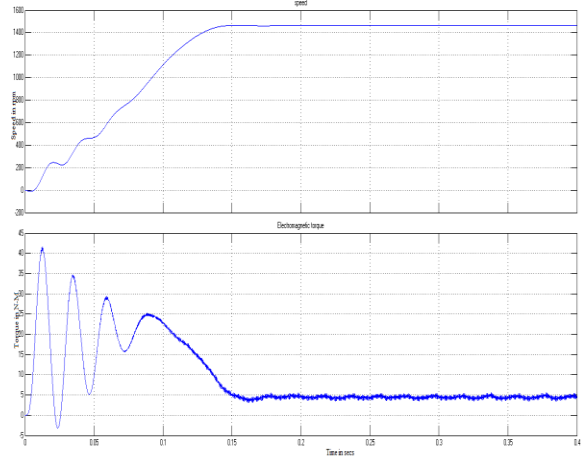


Figure 21 Speed and torque characteristics of IM for VFPWM strategy

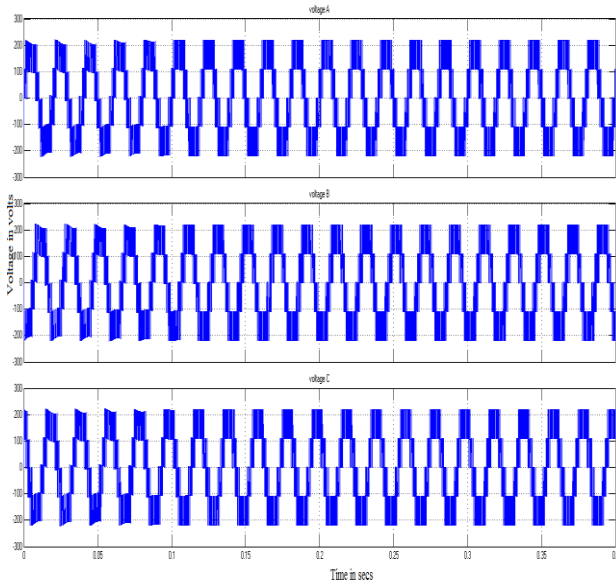


Figure 19 Output voltage generated by COPWM strategy for IM load

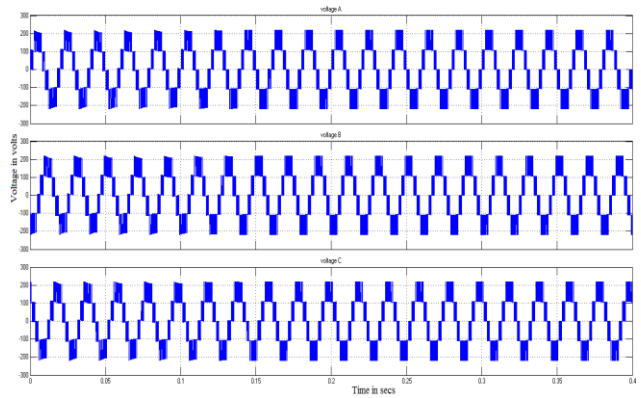


Figure 22 Output voltage generated by VFPWM strategy for IM load

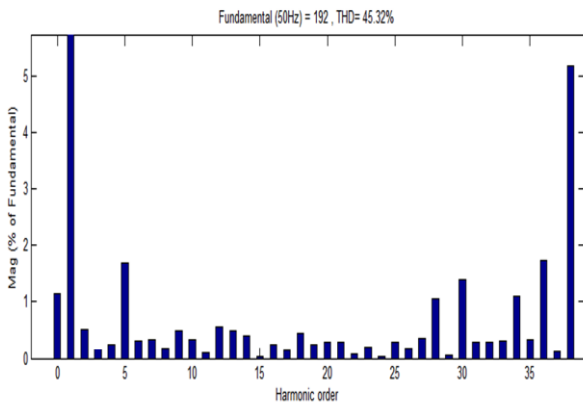


Figure 20 FFT plot for output voltage of COPWM strategy for IM load

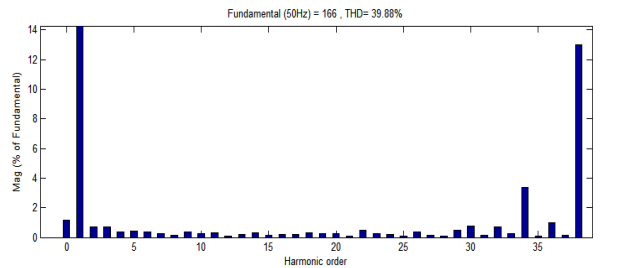


Figure 23 FFT plot for output voltage of VFPWM strategy for IM load

TABLE 2 % THD comparison for different modulation indices for IM load

m_a	PD	POD	APOD	CO	VF
1	27.99	27.78	28.43	34.72	28.05
0.9	34.9	34.89	35.32	34.72	34.89
0.8	39.95	39.63	40.16	45.32	39.88
0.7	43.67	43.53	43.77	52.09	44.14
0.6	46.22	46.48	46.26	60.68	46.33

TABLE 3 V_{RMS} (fundamental) for different modulation indices for IM load

m_a	PD	POD	APOD	CO	VF
1	146.1	146.3	146.2	156.5	146.1
0.9	131.8	131.5	131.6	146.5	131.6
0.8	117.2	117.5	117.2	135.8	117.3
0.7	102.6	102.5	102.7	123.4	102.4
0.6	88.08	87.68	88.06	110.6	88.3

TABLE 4 Form factor for different modulation indices for IM load

m_a	PD	POD	APOD	CO	VF
1	120.74	125.04	121.83	126.20	137.83
0.9	104.60	112.39	110.58	135.64	112.47
0.8	111.61	107.79	104.6	119.12	102.89
0.7	77.14	101.48	96.88	113.2	83.93
0.6	74.01	81.19	84.67	97.87	80.27

TABLE 5 Crest factor for different modulation indices for IM load

m_a	PD	POD	APOD	CO	VF
1	1.414	1.4156	1.414	1.4144	1.4142
0.9	1.4139	1.4143	1.4145	1.414	1.4142
0.8	1.414	1.414	1.4142	1.414	1.4143
0.7	1.414	1.4137	1.414	1.414	1.4140
0.6	1.4141	1.4146	1.4144	1.4139	1.4140

TABLE 6 Distortion factor for different modulation indices for IM load

m_a	PD	POD	APOD	CO	VF
1	0.1494	0.1306	0.1444	0.856	0.0955
0.9	0.1588	0.1543	0.1597	0.7711	0.1407
0.8	0.1611	0.1694	0.1682	0.5953	0.2
0.7	0.1811	0.16	0.1533	0.2876	0.1759
0.6	0.1796	0.226	0.1949	0.1485	0.1841

V. CONCLUSION

In this work the simulation results of three phase five level diode clamped multilevel inverter fed Induction Motor load with various modulating strategies are obtained through MATLAB/SIMULINK. The output quantities like phase voltage, THD spectrum for phase voltage, and torque-speed characteristics of induction motor are obtained. It is observed from Table 2 that PODPWM method provides output with relatively low distortion. COPWM is found to perform better since it provides relatively higher fundamental RMS output voltage. Table 3, 4 and 5 show the crest factor, form factor and distortion factor.

REFERENCES

[1] Xiaoming Yuan and Ivo Barbi "Fundamentals of a New Diode Clamping Multilevel Inverter", *IEEE*

Trans. on Power Electronics, Vol.15, No.4, 2000, pp.711-718.

- [2] O. Bouhali, B. Francois, E. M. Berkouk, and C. Saudemont, "DC Link Capacitor Voltage Balancing in a Three-Phase Diode Clamped Inverter Controlled by a Direct Space Vector of Line-to-Line Voltages", *IEEE Trans. on Power Electronics, Vol.22, No.5, 2007, pp.1636-1648.*
- [3] Anshuman Shukla, Arindam Ghosh and Avinash Joshi, "Control Schemes for DC Capacitor Voltages Equalization in Diode-Clamped Multilevel Inverter Based DSTATCOM", *IEEE Trans. on Power Delivery, Vol.23, No.2, 2008, pp.1139-1149.*
- [4] Sergio Busquets Monge, Joan Rocabert Pedro Rodriguez, Salvador Alepuz and Josep Bordonau, "Multilevel Diode Clamped Converter for Photovoltaic Generators With Independent Voltage Control of Each Solar Array", *IEEE Trans. on Industrial Electronics, Vol.55, No.7, 2008, pp.2713-2723.*
- [5] Mohan M. Renge and Hiralal M. Suryawanshi, "Five-Level Diode Clamped Inverter to Eliminate Common Mode Voltage and Reduce dv/dt in Medium Voltage Rating Induction Motor Drives", *IEEE Trans. on Power Electronics, Vol.23, No.4, 2008, pp.1598-1607.*
- [6] Hideaki Fujita, and Naoya Yamashita, "Performance of a Diode-Clamped Linear Amplifier", *IEEE Trans. on Power Electronics, Vol.23, No.2, 2008, pp.824-831.*
- [7] Natchpong Hatti, Kazunori Hasegawa and Hirofumi Akagi, "A 6.6-KV Transformer less Motor Drive Using a Five-Level Diode-Clamped PWM Inverter For Energy Savings of Pumps and Blowers", *IEEE Trans. on Power Electronics, Vol.24, No.3, 2009, pp.796-803.*
- [8] S.Srinivas, "Uniform Overlapped Multi-Carrier PWM for a Six-Level Diode Clamped Inverter", *International Journal of Electrical and Electronics Engineering*, 2009, pp.763-768.
- [9] Engin Ozdemir, Sule Ozdemir and Leon M. Tolbert, "Fundamental-Frequency-Modulated Six-Level Diode-Clamped Multilevel Inverter for Three-Phase Stand-Alone Photovoltaic System", *IEEE Trans. on Power Electronics, Vol.56, No.11, 2009, pp.4407-4415.*
- [10] Berrezzek Farid and Berrezzek Farid, "A Study of New Techniques of Controlled PWM Inverters", *European Journal of Scientific Research, ISSN 1450-216X, Vol.32, No.1, 2009, pp.77-87.*
- [11] Anshuman shukla, Arindam Ghosh and Avinash Joshi, "Flying-Capacitor-Based Chopper Circuit for DC Capacitor Voltage Balancing in Diode-Clamped Multilevel Inverter", *IEEE Trans. on Industrial Electronics, Vol.57, 2010, pp 2249-2261.*

Evaluation of Students' Answer scripts Using Soft Computing Techniques

Vaishali Malpe¹, Shalini Bhatia²

^{1,2} Computer Department, TSEC, Mumbai University, India

ABSTRACT

By introducing a new fuzzy evaluation sheet, we believe it portrays additional information on students' performances in answering each question in a test or examination compared to conventional marking method. Moreover, this approach can be used to compare students' performances which have the same final linguistic terms by looking into each question and each criterion. This paper presents a new method for students' learning achievement evaluation by automatically generating the weights of the attributes "accuracy rate", "time rate", "difficulty", "complexity", "answer-cost" and "importance", respectively, with the fuzzy reasoning capability. The proposed method normalizes the adjustment quantity to insure the fairness of the adjustment in each inference result. It can provide us much fairer and more reasonable inference results for students' learning achievement evaluation. It can evaluate students' answerscripts in a more flexible and more intelligent manner.

Keywords: Degrees Of Confidence, Index of Optimism (λ), Interval-valued fuzzy sets, Fuzzy Evaluation Marksheet, Fuzzy reasoning, Fuzzy rules, Grade Membership Functions, Result Transformer, Satisfaction Levels, Student Answer-script.

I. INTRODUCTION

Evaluation of students' answerscripts normally done by the two popular existing systems: grading system and traditional marking system. Types of questions are assumed to be such that answers are of subjective types only. In traditional system of evaluation, "marking" i.e. awarding of marks is done, whereas in the Grading system of evaluation, "grading" i.e. awarding of grades is done. Evaluation of students' learning achievement is the process of determining the performance levels of individual students in relation to educational objectives.

1.1 Theoretical Issues

At present, students' answerscripts have subjective evaluation by evaluator in many universities/ institutions. In current scenario, the evaluation done by evaluators has some limitations as follows:

1. Single vs. Multiple evaluator

Single evaluator evaluates all the answerscripts as per his own judgement so there is no unfairness to those students. But if some papers are evaluated by one evaluator while others are by different evaluator, then depending on the nature of assessment (i.e. strict, normal, lenient) of

evaluator there is a chance that some students get good marks as compared to others because of diversity in subjective assessment level of different evaluators.

2. Level of satisfaction

In subjective evaluation there is no flexibility to consider the evaluator's different levels of satisfaction so as to accurately assess the answerscripts.

3. Degree of confidence

In current situation, evaluator's degree of confidence in awarding a particular grade/mark is not considered which reflects in less accurate evaluation.

4. Lack of details in result

Student is provided only with the final marks of subject and not the detailed additional information in assessment like how marks are awarded based on accuracy, coverage, difficulty, complexity, etc. in answering each question in a test/examination.

5. Assurance for similar scoring criteria

Assessing a particular student's answerscript by an evaluator can be problematic because this makes it hard to ensure that the scoring criteria are applied to one student is also applied in the same way to other students.

6. Increasing number of evaluators and answerscripts

As the number of evaluators and the number of papers to be evaluated increases, there is less and less likelihood of applying the scoring criteria the same way every time.

7. Personal factors

Personal factors like fatigue and myriad may affect consistency in the evaluation process.

II. RELATED WORK

Until now, some methods have been presented for dealing with students' evaluation:

In [1], Bai and Chen presented a method for automatically constructing grade membership functions of lenient-type grades, strict-type grades, and normal-type grades given by teachers. Based on the constructed grade membership functions, system can perform fuzzy reasoning to infer the scores of students. It provides a useful way to evaluate students' answerscripts in a smarter and fairer manner.

In [2], Biswas presented Fuzzy Evaluation Method (fem) and a Generalized Fuzzy Evaluation Method (gfem) for applying fuzzy sets in students' answerscripts evaluation is

developed. These methods have the drawbacks. (1) Because a matching function is used to measure the degrees of similarity between the standard fuzzy sets and the fuzzy marks of the questions, it will take a large amount of time to perform the matching operations. (2) Two different fuzzy marks may be translated into the same awarded grade and it is unfair for students' evaluation.

Chen and Lee [3] presented two methods for applying fuzzy sets in students' answerscripts evaluation to overcome these drawbacks. The methods presented in [3] are much faster in execution and fairer in the task of student evaluation. The method has the drawback. It cannot deal with the situation where the evaluating values are represented by fuzzy numbers associated with degrees of confidence between zero and one and they do not consider the degree of optimism of the evaluator in evaluating students' answerscripts. If these factors are considered, there is room for flexibility.

In [4], Chen and Wang presented new methods for evaluating students' answerscripts based on interval-valued fuzzy grade sheets. Marks awarded to the answers in the students' answerscripts are represented by interval-valued fuzzy sets. The degree of similarity between an interval-valued fuzzy mark and a standard interval-valued fuzzy set is calculated by a similarity function. An index of optimism k determined by the evaluator is used to indicate the degree of optimism of the evaluator.

In [5] Hui-Yu Wang and Shyi-Ming Chen presents a new approach for evaluating students' answerscripts using fuzzy numbers associated with degrees of confidence of the evaluator. The satisfaction levels awarded to the questions of students' answerscripts are represented by fuzzy numbers associated with degrees of confidence between zero and one.

In [6], Saleh and Kim proposed a method for evaluation of students' answerscripts using fuzzy system. This method applies a fuzzification, fuzzy inference, and defuzzification considering the difficulty, the importance and the complexity of questions. This method has an advantage. The transparency, objectivity, and easy implementation provide a useful way to automatically evaluate students' achievement in more reasonable and fairer manner. It persuades students who are skeptical and not satisfied with the evaluation results. This system has a drawback. It requires the domain experts to decide the values of complexity and importance. Experts' decision is the challenging task.

In [7], Li and Chen proposed the method for answerscripts' evaluation in which the weights of the attributes accuracy rate, time rate, difficulty, and importance are generated automatically with the fuzzy reasoning capability. This method normalizes the quantity to insure the fairness of adjustment in each inference results for student's learning achievement evaluation.

Nolan has discussed the design and development of an expert system fuzzy classification scoring system [8]. The

main function of the expert fuzzy classification scoring system is to support teachers in the evaluation by providing them with uniform framework for generating ratings based on the consistent application of scoring rubrics. An experiment demonstrated that teachers using expert fuzzy classification scoring system can make assessments in less time and with a level of accuracy.

In [9], Wang and Chen presented a new method for evaluation using vague values. The vague mark awarded to each question can be regarded as a vague set, where each element in the universe of discourse belonging to the vague set is represented by the vague values. Methods presented in [2] have used the fuzzy sets. In a fuzzy set, the grade of membership of an element is represented by a real value between zero and one. Single value between zero and one tells nothing about the accuracy of a number. So if the number is presented as a vague set, then there is a room for more flexibility.

In [10], Bardul proposed a method to evaluate the students' performances as individual and as a group. The main objective of this study is to improvise the existing fuzzy approach in assessing students' performance. This study focuses on two types of assessments namely students' answer scripts assessment and students' group assessment. In the students' answer scripts assessment the trapezoidal fuzzy number is used to represent the standard satisfaction level for the grading scales and the students' fuzzy scores. The center points of both standard satisfaction levels and the fuzzy score is calculated using the center of gravity method. In the students' group assessment instructors as well as students are involved in selecting and determining the assessment criteria. The pair-wise comparison technique based on fuzzy scales is used to find the relative strength between each criterion. The weights of selected criteria are represented by the normalized fuzzy eigenvectors. The fuzzy relation composition method is employed in order to combine the instructor and students' evaluation, which finally gives the overall students' group performance. Both the answer scripts assessment and group assessment processes can be easily performed with the aid of fuzzy assessment sheet. This integrated fuzzy approach provides additional information on students' performance and can be used as an option for instructors to assess students' performance.

Wang and Chen presented new methods for evaluating the answerscripts of students [11], where the evaluating values are represented by fuzzy numbers, and an optimism index λ determined by the evaluator is used to indicate the degree of optimism of the evaluator for evaluating the answerscripts of students, where the value of λ is between zero and one. The universe of discourse is formed by a set of satisfaction levels. The fuzzy mark awarded to the answer of each question of the answerscript of a student is represented by a type-2 fuzzy set. The proposed methods can overcome the drawbacks of the methods presented in [2] and [3]. It can evaluate the answerscripts of students in a more flexible and more intelligent manner.

In [12], the analysis of students' evaluation, especially in the case of the students' answerscripts under the evaluation grade of linguistic data is discussed. Chih-Hsun Hsieh transfer mostly linguistic data, subjective message into triangular fuzzy numbers, and use the function principle instead of the extension principle to calculate the students' score. The principle does not change the type of membership function and will reduce the trouble and tediousness of operations. In addition, the degree of similarity between two fuzzy numbers is defined with the utility value of fuzzy number to transfer the students' score into letter-grade score.

In [13], Bardul and Mohamad presented a method that uses normalized values to represent some of extreme cases of satisfaction levels and utilize fuzzy numbers to generate more consistent fuzzy marks. After the instructors mark the scripts by using the traditional method, the satisfaction levels of each question will be identified by using fuzzy numbers. Then, the degree of satisfactions of each question will be calculated. The fuzzy marks will be generated to produce the total score. Finally, the fuzzy grade will be obtained. The result that based on the fuzzy sets approach could provide more and better information which portrays the student performance of each question. Thus, this paper attempts to overcome the drawbacks identified in technique carried out by Chen and Lee [3].

The drawbacks and the alternative ways suggested to overcome them are explained as follows:

1. Chen and Lee [3] have a fixed value for each satisfaction level. However, in [12], researchers used normalized values to represent the degree of satisfaction for lower extreme cases (i.e. grade E) and for upper extreme cases (i.e. grade A) while keeping the degree of satisfaction of A-, B+, B, B-, C+, C, C-, D+, and D.
2. Chen and Lee [3] did not utilize the advantage of using fuzzy numbers in their evaluation method. In [12], fuzzy numbers are used as this technique can provide equations for each grade and finally produce a consistent result.
3. Chen and Lee [3] also mentioned that the higher the degree of satisfaction the more the fuzzy mark satisfies the instructor's opinion. The drawback is that the fuzzy marks given are merely based on the instructor's opinion. In [12], the authors used fuzzy numbers to generate a more consistent fuzzy mark.

III. WORKFLOW OF PROPOSED FUZZY EVALUATION SYSTEM

In the proposed project, a new method for evaluating students' answerscripts is presented where evaluating marks awarded to the questions in answerscripts are represented by vague values. An index of optimism λ is determined using common answerscript assessed by each evaluator. This indicates the degree of optimism of the evaluator, where $\lambda \in [0, 1]$. The evaluation satisfaction levels awarded

to each questions are obtained by using the expected truth values of each vague satisfaction values. Degree of confidence associated with satisfaction level is used to calculate α -cut which in turn is used to calculate the total mark of each student. A method is presented to automatically construct the grade membership functions of lenient-type grades, strict-type grades and normal-type grades, given by teachers, respectively. Based on the constructed grade membership functions, the system performs fuzzy reasoning to infer the scores of students. Automatic generation of weights of attributes "accuracy rate", "coverage rate", "difficulty", "complexity", "answer-cost" and "importance" is done with the fuzzy reasoning capability. It is used to normalize the adjustment quantity with which the result is adjusted to insure fairness. It provides a useful way to evaluate students' answerscripts in a smarter and intelligent manner.

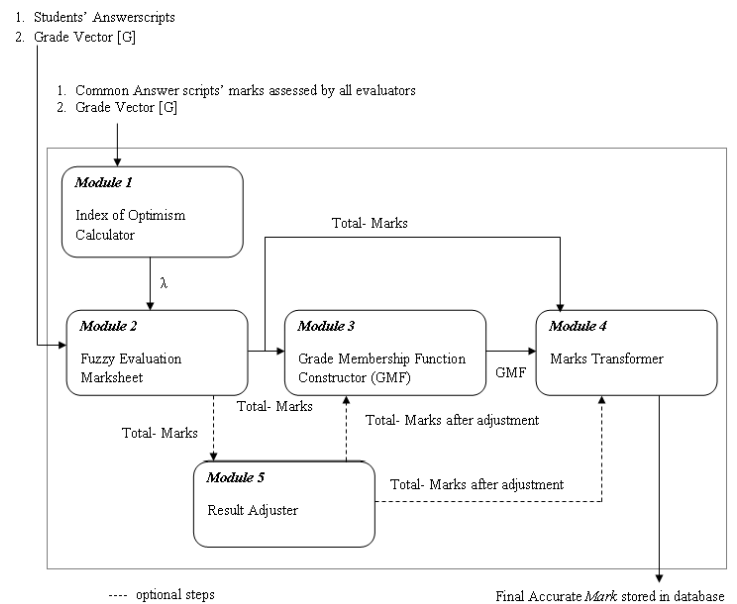


Fig. 1 Workflow of proposed Fuzzy Evaluation System

Modules:

1. Index of Optimism Calculator of a Teacher
2. Fuzzy Evaluation Marksheet
3. Grade Membership Function Constructor
4. Marks Transformer
5. Result Adjuster

The formulation for this proposed system done as follows:

Module 1: The Evaluators' index of optimism λ is calculated, where $\lambda \in [0, 1]$. A common answerscript is shared with all the evaluators to assess by traditional marking method. All these marks are collected to identify the diversity of range in awarding marks to students. Minimum & Maximum numbers are identified from these numbers to set the evaluators index of optimism λ .

Module 2: Evaluator uses vague grade sheet as shown in Table 2 to award his/her satisfaction level of answer to each question rather than marks. The system converts vague marksheet into fuzzy marksheet as shown in Table 3 from

fuzzy marksheet, total mark of each student is calculated which is a crisp number.

Module 3: This optional module is considered when results obtained by module 2 are adjusted three node fuzzy evaluation system. The three node fuzzy evaluation system is shown in figure 6. The adjustment is done by considering the factors like complexity, difficulty of question paper which is decided by domain expert. This step gives adjusted mark that is scaling up or down the total marks.

Module 4: Using the marks obtained by module 2 / module 3, the grade membership functions are constructed for mapping strict / lenient mark to normal mark. The grade membership functions are formed using interpolation technique.

Module 5: Marks obtained by module 2 / module 3 are transformed to normal type using grade membership functions and detailed evaluation report is generated for each student.

IV. DESIGN CONSIDERATION

Module 1: Index of Optimism Calculator of a Teacher Marks of single shared common answerscript assessed by all evaluators are input to this module. The aim of this module is to calculate the index of optimism of a teacher. This module is shown in figure 2.

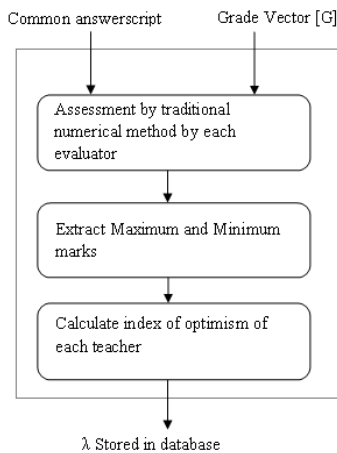


Fig 2 Calculation of index of optimism

Input:

1. Common subjective answerscript,
2. Grade vector [G] denoting assigned maximum mark of each question

Output:

1. Index of optimism of each evaluator

Algorithm:

- Step 1: Common subjective answerscript is given to all evaluators to assess it by traditional method.
- Step 2: The evaluated marks are stored in database.
- Step 3: Maximum (Max) & Minimum (Min) marks are extracted.
- Step 4: Index of optimism of Evaluator is then calculated

as,

$$\lambda = \frac{\text{Evaluator's_score} - \text{Min}}{\text{Max} - \text{Min}} \tag{1}$$

Step 5: Index of optimism is stored in database.

Module 2: Fuzzy Evaluation Marksheet

Evaluator's degree of confidence is taken into account to generate the fuzzy interval of marks [x,y]. Question level degree of satisfaction is judged by evaluator with the help of satisfaction level rubric. Then defuzzify the question level interval marks to calculate total marks of each student. This module is shown in figure 3.

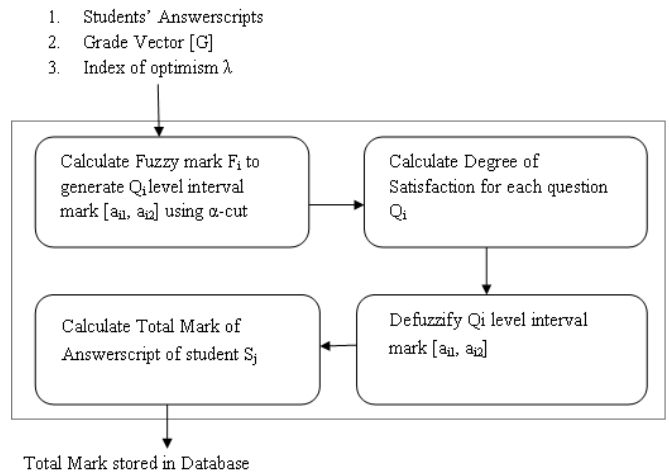


Fig 3 Fuzzy evaluation of student's answerscripts

Input:

1. Subjective answerscript of each student Sj,
2. Grade vector [G] denoting assigned maximum mark of each question,
3. Satisfaction level Table 1,
4. Evaluators' index of optimism λ, where λ ∈ [0,1]

Output:

1. Total marks stored in database

Algorithm:

Step 1: Calculate the expected truth value E(Xi) (Table 3) of each vague truth value Xi in the vague grade sheet shown in Table 2, where E(Xi) ∈ [0,1] and 1 ≤ i ≤ 11.

$$E(X) = (1 - \lambda) \times t_x + \lambda \times (1 - f_x) \tag{2}$$

Step 2: Calculate the corresponding expected truth value E(Y) of each satisfaction level Y in the vague grade sheet shown in Table 2, where Y ∈ {EG, VVG, VG, G, MG, F, MB, B, VB, VVB, EB} and E(Y) ∈ [0,1].

The degree of satisfaction D(Q.i) of the question Q.i of the student's answerscript can be evaluated by the function D,

$$D(Q_i) = [E(X_{i1}) \times E(EG) + E(X_{i2}) \times E(VVG) + \dots + E(X_{i11}) \times E(EB)] / [E(X_{i1}) + E(X_{i2}) + \dots + E(X_{i11})] \quad (3)$$

$E(X_i)$ is expected satisfaction value of vague satisfaction value X_i , $1 \leq i \leq 11$, and $0 \leq D(Q_i) \leq 1$. The larger the value of $D(Q_i)$, the higher the degree of satisfaction that the answer of question Q_i satisfies the evaluator's opinion.

Step 3: Based on Step 2 output, find the matching satisfaction level. Input that in fuzzy grade sheet as shown Table 4.

Step 4: Calculate α -cut of each fuzzy mark F_i , based on degree of confidence of evaluator

$$(F_i)_\alpha = [a_{i1}, a_{i2}], \text{ where } \alpha \in [0,1] \quad (4)$$

Step 5: Calculate interval-valued mark $[m_{i1}, m_{i2}]$ of each question Q_i , where

$$[m_{i1}, m_{i2}] = \left[\frac{s_i}{s_1 + s_2 + \dots + s_n} * [a_{i1}, a_{i2}] \right] \quad (5)$$

Step 6: Calculate defuzzified crisp mark of each question Q_i using optimism index λ .

$$Q_{i_mark} = (1 - \lambda) * m_{i1} + \lambda * m_{i2} \quad (6)$$

$$\text{Total_Mark_of_Student_} S_j = \sum_{i=1}^n Q_{i_mark} \quad (7)$$

Step 7: Store these Total_Mark_of_Student in Mark database along with the corresponding evaluators' index of optimism λ .

Marks are of three categories depending upon λ value,

If $\lambda < 0.5$, Evaluator and the marks are strict (g_L),

If $\lambda = 0.5$, Evaluator and the marks are normal (g_N),

If $\lambda > 0.5$, Evaluator and the marks are lenient (g_H)

Module 3: Grade Membership Function Constructor

Index of optimism is used to extract strict / normal / lenient type marks using which the grade membership functions are constructed. This module is shown in figure 4.

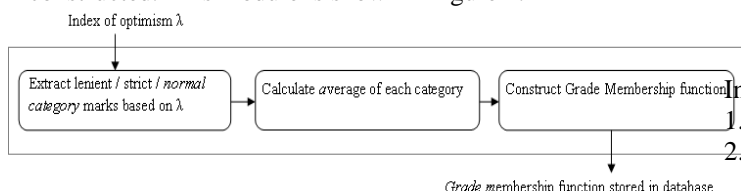


Fig 4 Mapping grade membership function generator

Input:

1. Evaluators' index of optimism λ , where $\lambda \in [0, 1]$,
2. Total marks

Output:

Grade membership functions (Strict / Lenient to Normal)

Algorithm:

Step 1: Calculate the total average strict-type grade

$$\text{Avg}G_{L\text{ of } g_{Li}}, \quad \text{Avg}G_L = \frac{\sum_{i=1}^{m1} g_{Li}}{m} \quad (8)$$

Calculate the total average normal-type grade $\text{Avg}G_N$ of g_{Ni}

$$\text{Avg}G_N = \frac{\sum_{i=1}^{m2} g_{Ni}}{m} \quad (9)$$

Calculate the total average lenient-type grade $\text{Avg}G_H$ of g_{Hi}

$$\text{Avg}G_H = \frac{\sum_{i=1}^{m3} g_{Hi}}{m} \quad (10)$$

where $m1, m2, m3$ are number of students of strict/normal/lenient type categories respectively, and m is total number of students ($m=m1+m2+m3$)

Step 2: Use parabolic curve interpolation techniques to get the most appropriate relational function between

(g_{Li} and g_{Ni}) and between (g_{Hi} and g_{Ni}) respectively.

Module 4: Marks Transformer

Final evaluation mark sheet is generated after marks are transformed to normal type. This marksheet shows the detailed information. This module is shown in figure 5.

1. Mapping Grade Membership function from Module 3
2. Students' marks from Module 2 or 4

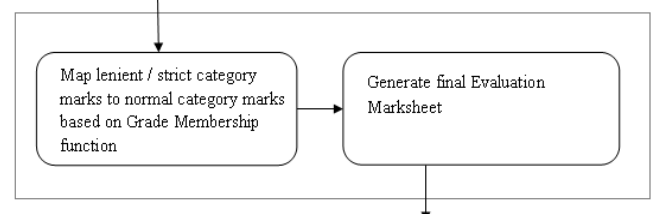


Fig 5 Marks transformer

Input:

1. Grade membership functions
2. Total marks obtained from Module 2 or module 4

Output:

Transformed normal type marks stored in database

Step 2: Produce final student evaluation mark sheet showing detail information.

Algorithm:

Step 1: Convert (Strict type / Lenient type) marks obtained in Step 6 of module 2 to normal marks using grade membership function obtained in Step 2 of Module 3 and store final result in database.

Module 5: Result Adjuster

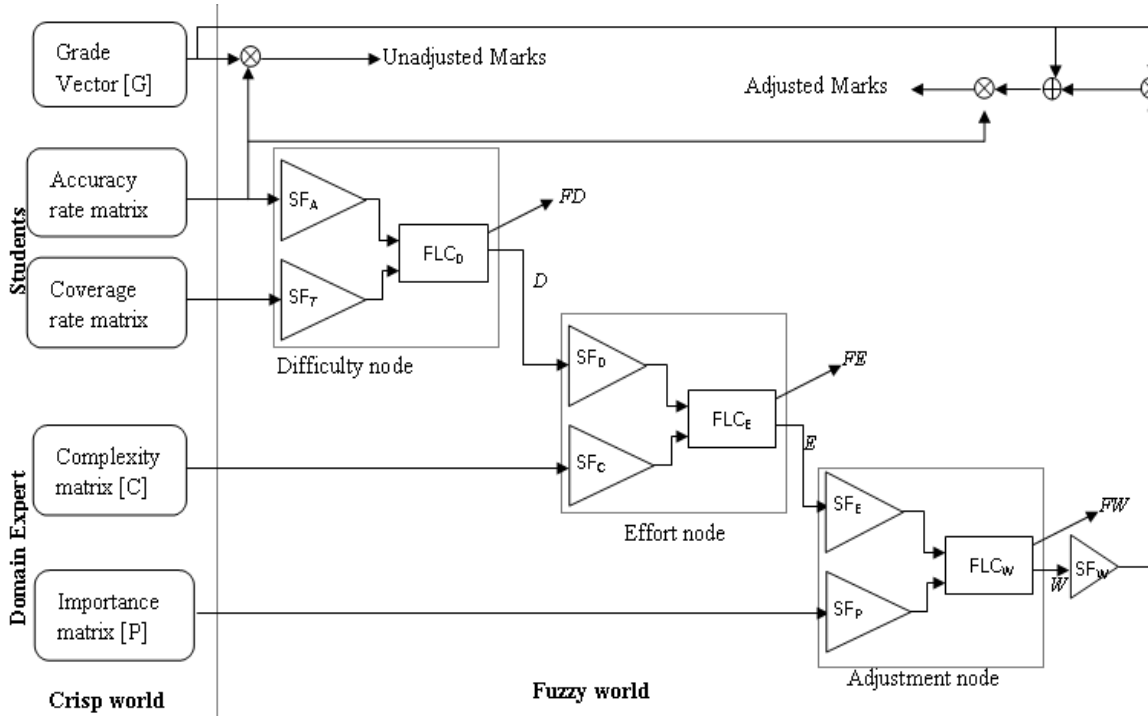


Fig 6(a): Result adjuster

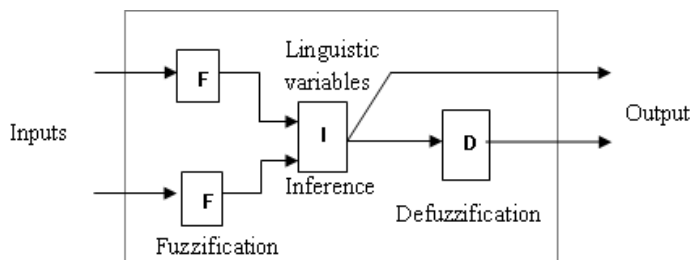


Fig 6(b): Representation of node process as a fuzzy logic controller

Difficulty and Complexity level of each question in the question paper are taken from domain expert. Accuracy & Coverage rate of each answer is generated using marks and coverage level obtained from Module 2 respectively. Result obtained by Module 2 is adjusted with respect to complexity and difficulty of question paper. This module is shown in figure 6(a) [6]. Fuzzy logic controller is shown in 6(b) [6].

Input:

1. Each Question level marks & coverage level obtained from module 2,
2. Grade Vector [G] denoting the assigned maximum score of each question,
3. Complexity & Importance matrices given by Domain Expert

Output:

1. Adjusted total marks stored in database

Algorithm:

Step 1: Generate the Accuracy matrix $A[a_{ij}]_{m \times n}$,

$$a_{ij} = \frac{Q_i_mark}{Weightage_Mark_of_Question_Q_i} \quad (11)$$

Where, m is the total number of questions in question paper and n is the total number of students. Generate the coverage matrix $T[c_{ij}]_{m \times n}$, where c_{ij} is (coverage level / total number of coverage points) of each question Q_i . Coverage level is obtained from Step 1 of Module 1.

Step 2: Based on the accuracy rate matrix A and the coverage matrix T, calculate the average accuracy rate

$AvgA_i$ and the average coverage rate $AvgT_i$ for each question Q_i , as:

$$AvgA = \frac{\sum_{j=1}^n a_{ij}}{n} \quad (12)$$

$$AvgT_i = \frac{\sum_{j=1}^n t_{ij}}{n} \quad (13)$$

Where n is total number of students.

Based on fuzzy sets “low”, “more or less low”, “medium”, “more or less high” and “high” shown in figure7, fuzzy the average accuracy rate $AvgA_i$ and average coverage rate $AvgT_i$ for each Q_i and calculate their membership grades belonging to each fuzzy set, respectively. Then, we can get the fuzzy score matrix F_A for the average accuracy and can get the fuzzy score matrix F_T for the average answer-coverage rate, shown as follows:

$$F_A = [f_{a_{ij}}]_{m \times 5} \quad (14)$$

$$F_T = [f_{t_{ij}}]_{m \times 5} \quad (15)$$

where $f_{a_{ij}} \in (0,1)$ and $f_{t_{ij}} \in (0,1)$ denotes the membership value of the score and coverage of ith question Q_i belonging to the jth fuzzy set shown in Figure 7.

Step 3:

3.1 Obtain the weights of accuracy rate W_A and coverage rate W_T to perform fuzzy reasoning. These weights are decided by domain experts ($W_A + W_T = 1$).

Based on fuzzy accuracy rate matrix F_A , fuzzy coverage rate matrix F_T and fuzzy rules R_D given in the form of IF-THEN rules, the fuzzy difficulty matrix is derived as $D = [d_{ik}]_{m \times 1}$ where m is total number of questions and 1 is total number of levels as per the fuzzy sets in figure 7. $d_{ik} \in (0,1)$ denotes the membership value of the difficulty of question i belonging to level k.

The value of d_{ik} is obtained as:

$$d_{ik} = \max_{((A,T) \in R_D, (A,T)=k)} \{WA * f_{a_{i,A}} + WT * f_{t_{i,T}}\} \quad (16)$$

Weight of the difficulty D & complexity C matrix WD & WC can be determined by domain expert such that ($WD + WC = 1$).

3.2 Based on the fuzzy difficulty matrix D, and the fuzzy complexity matrix C, given the fuzzy rules RE, we obtain the effort (i.e., answer cost) matrix of dimension $m \times 1$, in the same manner as we obtained the difficulty matrix

above,

$$E = [e_{ik}]_{m \times 1} \quad (17)$$

Where $e_{ik} \in [0, 1]$ denotes the membership value of the effort to answer question i belonging to level k, which is a measure of effort required by students to answer question i.

3.3 Weight of the effort E & importance P matrices, W_E & W_P can be determined by a domain expert such that ($W_E + W_P = 1$)

3.4 Based on the fuzzy effort matrix E, and fuzzy importance matrix P with their weight W_E, W_P , we obtain the adjustment matrix of dimension $m \times 1$

$$W = [W_{ik}]_{m \times 1} \quad (18)$$

Where $w_{ik} \in [0, 1]$ denotes the membership value of the adjustment to answer question i belonging to level k.

We use the following formula to obtain the adjustment vector,

$$\bar{W} = [w_{i\bullet}]_{m \times 1} \quad (19)$$

Where $w_{i\bullet} \in [0,1]$ denotes the final adjustment value required by question i obtained by

$$w_{i\bullet} = \frac{0.1 * w_{i1} + 0.3 * w_{i2} + 0.5 * w_{i3} + 0.7 * w_{i4} + 0.9 * w_{i5}}{0.1 + 0.3 + 0.5 + 0.7 + 0.9} \quad (20)$$

Where 0.1, 0.3, 0.5, 0.7 and 0.9 are the centres of fuzzy membership functions shown in Figure 7.

Step 4:

We calculate the bias B as follows, here AV is nothing but W

$$(g_1 * AV_1) * B + (g_1 * AV_1) * B + \dots (g_m * AV_m) * B = 100 \quad (21)$$

$$B = \frac{\sum_{i=1}^m g_i}{\sum_{i=1}^m g_i * AV_i} \quad (22)$$

Step 5: Calculate the assigned score AS_i after the adjustment of the ith question Q_i , shown as:

$$AS_i = g_i * W_i * B \quad (23)$$

Finally, we can obtain the adjusted total score ATS_j of the student S_j , where

$$ATS_j = a_{ij} * AS_i \quad (24)$$

V. RESULTS

We are still in progress for implementation of module 3, 4, and 5. Following are results of MATLAB implemented module 1, and 2 of proposed fuzzy evaluation system

Module 1: Index of Optimism Calculator

[0.57, 0.64, 0.21, 0.28, 0, 0.71, 1, 0.14, 0.07, 0.35];

Total Evaluators = 10,

Students' marks assessed by different teachers,

Module 2: Fuzzy Evaluation Marksheet

T = [69, 70, 64, 65, 61, 71, 75, 63, 62, 66];

Assume Index of optimism (λ) = 0.60

Index of Optimism $\lambda =$

TABLE 1: SATISFACTION LEVELS AND THEIR CORRESPONDING VAGUE SATISFACTION VALUES

Satisfaction levels	Vague satisfaction values
Extremely Good (EG)	[1,1]
Very Very Good (VVG)	[0.90,0.99]
Very Good (VG)	[0.80,0.89]
Good (G)	[0.70,0.79]
More or less Good (MG)	[0.60,0.69]
Fair (F)	[0.50,0.59]
More or less Bad (MB)	[0.40,0.49]
Bad (B)	[0.25,0.39]
Very Bad (VB)	[0.10,0.24]
Very Very Bad (VVB)	[0.01,0.09]
Extremely Bad (EB)	[0,0]

TABLE 2: VAGUE MARK REPRESENTED BY VAGUE VALUES OF THE QUESTION Q. I IN A VAGUE GRADE SHEET

Question No.	Points covered (pc)	Satisfaction levels											Degree of satisfaction	
		EG	VVG	VG	G	MG	F	MB	B	VB	VVB	EB		
.
Q. i	pci	X1	X2	X3	X4	X5	X6	X7	X8	X9	X10	X11		
.	
.	

TABLE 3: EXPECTED TRUTH VALUES OF VAGUE TRUTH VALUES OF THE QUESTION Q.I OF TABLE 3.2

Question No.	Points covered (pc)	Satisfaction levels											Degree of satisfaction
		EG	VVG	VG	G	MG	F	MB	B	VB	VVB	EB	
.
Q. i	pci	E(X1)	E(X2)	E(X3)	E(X4)	E(X5)	E(X6)	E(X7)	E(X8)	E(X9)	E(X10)	E(X11)	
.
.

TABLE 4: FUZZY GRADE SHEET WITH SATISFACTION LEVELS ASSOCIATED WITH DEGREE OF CONFIDENCE

Question No.	Satisfaction levels	Degree of confidence of satisfaction levels
Q.1	F1	α
Q.2	F2	β
Q.3	F3	γ
.	.	.
Q.n	Fn	δ
		Total Mark=Degree of Confidence of Total Mark

TABLE 3.5: FUZZY RULE BASES TO INFER DIFFICULTY AND EFFORT

(a) Fuzzy Rule base RD for obtaining Difficulty (b) Fuzzy Rule base for RE obtaining Effort

Accuracy	Coverage rate				
	1	2	3	4	5
1	5	5	4	4	3
2	5	4	4	3	2
3	4	4	3	2	2
4	4	3	2	2	1
5	3	2	2	1	1

Difficulty	Complexity				
	1	2	3	4	5
1	1	1	2	2	3
2	1	2	2	3	4
3	2	2	3	4	4
4	2	3	4	4	5
5	3	4	4	5	5

1: "Low", 2: "more or less low", 3: "medium", 4: "more or less high", 5: "high"

TABLE 5: SATISFACTION LEVELS, CORRESPONDING VAGUE SATISFACTION VALUES, EXPECTED VAGUE TRUTH VALUES

Satisfaction levels	Vague satisfaction values (Y)	E(Y)
Extremely Good (EG)	[1,1]	1.0
Very Very Good (VVG)	[0.90,0.99]	0.954
Very Good (VG)	[0.80,0.89]	0.854
Good (G)	[0.70,0.79]	0.754
More or less Good (MG)	[0.60,0.69]	0.654
Fair (F)	[0.50,0.59]	0.554
More or less Bad (MB)	[0.40,0.49]	0.454
Bad (B)	[0.25,0.39]	0.334
Very Bad (VB)	[0.10,0.24]	0.184
Very Very Bad (VVB)	[0.01,0.09]	0.058
Extremely Bad (EB)	[0,0]	0

TABLE 6: VAGUE MARK REPRESENTED BY VAGUE VALUES OF THE QUESTION Q. I IN A VAGUE GRADE SHEET

Question No.	Degree of Confidence	Satisfaction levels										Degree of satisfaction	
		EG	VVG	VG	G	MG	F	MB	B	VB	VVB		EB
Q.1	0.75	[0.8,0.9]	[0.9,0.95]	[0,0]	[0,0]	[0,0]	[0,0]	[0,0]	[0,0]	[0,0]	[0,0]	[0,0]	[0,0]
Q.2	1.0	[0,0]	[0,0]	[0,0]	[0.6,0.7]	[0.9,0.95]	[0.55,0.6]	[0,0]	[0,0]	[0,0]	[0,0]	[0,0]	[0,0]
Q.3	0.75	[0,0]	[0,0]	[0.85,0.9]	[0.75,0.8]	[0.5,0.6]	[0,0]	[0,0]	[0,0]	[0,0]	[0,0]	[0,0]	[0,0]
Q.4	0.95	[0,0]	[0,0]	[0,0]	[0,0]	[0,0]	[0,0]	[0,0]	[0.5,0.6]	[0.9,0.95]	[0.2,0.4]	[0,0]	[0,0]

TABLE 7: EXPECTED TRUTH VALUES OF VAGUE TRUTH VALUES OF THE QUESTION Q.I OF TABLE 4.10

Question No.	Degree of Confidence	Satisfaction levels											Degree of satisfaction
		EG	VVG	VG	G	MG	F	MB	B	VB	VVB	EB	
Q.1	0.75	0.86	0.93	0	0	0	0	0	0	0	0	0	0.976
Q.2	1.0	0	0	0	0.66	0.93	0.58	0	0	0	0	0	0.658
Q.3	0.75	0	0	0.88	0.78	0.56	0	0	0	0	0	0	0.768
Q.4	0.95	0	0	0	0	0	0	0	0.56	0.93	0.32	0	0.208

Calculate α -cut of each fuzzy mark F_i , based on degree of confidence of evaluator

(Very Very Good) 0.75 = [94, 96]

(More or Less good) 1.0 = [65, 65]

(Good) 0.75 = [74, 76]

(Very Bad) 0.95 = [17, 17]

TABLE 8: FUZZY GRADE SHEET WITH SATISFACTION LEVELS ASSOCIATED WITH DEGREE OF CONFIDENCE

Question No.	Satisfaction levels	Degree of confidence of satisfaction levels
Q. 1	Very Very Good	0.75
Q.2	More or Less good	1.0
Q. 3	Good	0.75
Q. 4	Very Bad	0.95
Total Mark obtained by Module 2 =		59

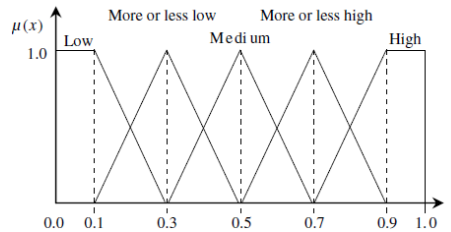


Fig. 7: Fuzzy membership functions of five levels

VI. CONCLUSION

By introducing a new fuzzy evaluation sheet, we believe it portrays additional information on students' performances in answering each question in a test or examination compared to conventional marking method. Moreover, this approach can be used to compare students' performances which have the same final linguistic terms by looking into each question and each criterion. This information can be very useful and beneficial for students, instructors, and other authorized or related bodies to have overall picture of students' performances.

Time reduction is yet another goal. The task of grading students' answerscripts is very repetitive and labour intensive. Faithful application of scoring rubric takes considerable amount of time. The proposed system leads to quicker and valid evaluation as it maintains the consistency while evaluating the answerscripts.

REFERENCES

- [1] S. M. Bai and S. M. Chen, "Automatically constructing grade membership functions for students' evaluation for fuzzy grading systems," In proceeding *World Automation Congress (WAC)*, Budapest, Hungary, 2006.
- [2] R. Biswas, "An application of fuzzy sets in students' evaluation," *Fuzzy Sets System*, vol. 74, 1995.
- [3] S. M. Chen and C. H. Lee, "New methods for students' evaluating using fuzzy set," Proceedings of *International Conference on Artificial Intelligence*, 1996.
- [4] Shyi-Ming Chen, Hui-Yu Wang "Evaluating students' answerscript based on interval-valued fuzzy grade sheets", *ELSEVIER Journal of Expert System with Application*, Vol 36, 2009.
- [5] Hui-Yu Wang and Shyi-Ming Chen, "Evaluating Students' Answerscripts Using Fuzzy Numbers Associated With Degrees of Confidence", *IEEE Transactions on Fuzzy Systems*, Vol. 16, No. 2, April 2008.
- [6] Ibrahim Saleh, Seong-in Kim, "A fuzzy system for evaluating students' learning achievement", *Expert Systems with Applications*, Vol. 36, 2009.
- [7] Ting-Kueili, Shyi-Ming Chen, "A new method for students' learning achievement evaluation by automatically generating the weights of attributes with fuzzy reasoning capability", Proceedings of *the Eighth International Conference on Machine Learning and Cybernetics, Baoding, IEEE* 2009.
- [8] James R. Nolan, "An expert fuzzy classification system for supporting the grading of student writing samples", *Expert Systems With Applications*, Vol. 15, 1998.
- [9] Hui-Yu Wang · Shyi-Ming Chen, "Evaluating students' answerscripts using vague values", *Appl Intell*, Vol. 28, 2008.
- [10] Bardul and Mohamad, "A Fuzzy Approach on Students' Answer Scripts Criteria Based Evaluation".
- [11] Hui-Yu Wang and Shyi-Ming Chen, "New Methods for Evaluating the Answerscripts of Students Using Fuzzy Sets", *IEA/AIE 2006, LNAI 4031*, 2006.
- [12] Chih-Hsun Hsies, "Evaluating students' answerscripts with fuzzy arithmetic", *Tamsui Oxford Journal of Management Sciences*, Vol 12, 1996.
- [13] Bardul and Mohamad, "A fuzzy set approach on students' answerscripts evaluation".

Flexible Tasks Scheduling Problem using A Genetic Algorithm-based Approach

D. R. Raut^{*}, S. M. Patil^{**}, T. M. T. Khan^{***}

^{*} WIEECT/Computer Engineering, Mumbai, India

^{**} BVCOE/Information Technology, Navi Mumbai, India

^{***} AIKTC/Computer Engineering, New Panvel, India

Abstract: Flexible Task Scheduling in a multiprocessor environment is NP complete problem. In literature, several heuristic methods have been developed that obtain suboptimal solutions in less than the polynomial time. Recently, Genetic algorithms have received much awareness as they are robust and guarantee for an effective solution. Genetic algorithm is widely used to solve Flexible Task Scheduling Problem. The genetic algorithm we proposed uses many different strategies to get a better result. During the phase of create initial population, the genetic algorithm takes into account the number of operations in each job. And the intelligent mutation strategy is used which makes every individual and gene have different probability to mutate. In this paper, the object of scheduling algorithm is to get a sequence of the operations on machines to minimize the make span. During the experiments the performance of the genetic algorithm is compared with other heuristic algorithm. In our project we comprises of three parts: Quality of solutions, robustness of genetic algorithm, and effect of mutation probability on performance of genetic algorithm.

I. INTRODUCTION

The general problem of multiprocessor scheduling can be stated as scheduling a task graph onto a multiprocessor system so that schedule length can be optimized. Task scheduling in multiprocessor system is a NP-complete problem. Task scheduling algorithms can be broadly classified into two main groups: heuristic based [5] and guided random search based algorithm [5]. Heuristic based algorithm searches a path in the solution space based on the heuristic used while ignoring other possible paths. Due to this reason, they give good results for some inputs while bad for others. List scheduling algorithms [5], clustering [5] and duplication based algorithms [2] fall under this category. Guided random search techniques use random choices to guide them selves through the problem space. Genetic algorithms [1, 3 and 8] are the most popular random search techniques for different kind of task scheduling problems.

In the Multitasking environment considered here, an application task can be decomposed into subtasks, where each subtask is computationally homogeneous well suited to a single machine and different subtasks may have different machine architectural requirements. These subtasks can have data dependences among them. Once the application task is decomposed into subtasks, the following decisions have to be made: matching, i.e., assigning subtasks to machines, and scheduling, i.e., ordering subtask execution for each machine and ordering inter machine data transfers. In this context, the goal of Heterogeneous Computing is to achieve the minimal completion time, i.e., the minimal overall execution time of the application task in the machine suite.

In general genetic algorithm, works on three operators natural selection, crossover and mutation [3, 6]. A genetic algorithm continuously tries to improve the average fitness of a population by construction of new populations. Quality of solution depends heavily on the selection of some key parameters like fitness function, population size, crossover probability and mutation probability. In this paper, we first introduce task scheduling problem having some specified characteristics, after that genetic approach is discussed in detail and the last section presents experiments and results.

Many parallel applications consist of multiple functional units. While the execution of some of the tasks depends on the output of the other tasks, others can be executed independently at the same time, which increases parallelism of the problem. The task scheduling problem is the problem of assigning the tasks in the multiprocessor system in a manner that will optimize the overall performance of the application, while guarantee the correctness of the result. Multiprocessor scheduling problems can be classified into many different categories based on characteristics of the program and tasks to be scheduled, the multiprocessor system, and the availability of information. Multiprocessor scheduling problems may be divided in two categories: Static and dynamic task scheduling. A static or deterministic task scheduling is one in which precedence constraints and the relationships among the task are known well in advance while non-deterministic or dynamic scheduling is one in which these information is not known in advance or not known till run time.

II. PROBLEM DESCRIPTION

A static scheduling problem consists of three main components: A multiprocessor system, an application and an objective for scheduling. The multiprocessor system consists of a limited number of fully connected processors (P1, P2... Pm). All the processors are heterogeneous meaning thereby a task may take different execution time on each processor. An application comprises tasks and their dependencies on each other. It can be represented as a directed acyclic graph (DAG) [7, 9], $G = (V, E, W)$, where the vertices set V consists of v non preemptive tasks, and v_i denotes the i th task. The edge set E represents the precedence relationships among tasks. A directed edge e_{ij} in E indicated that v_j can not begin its execution before receiving data from v_i . W is a matrix of $v \times m$, and w_{ij} in W represents the estimated execution time of v_i on j th processor. Here we assume that communication costs do not exist. The main objective of the task scheduling is to determine the assignment of tasks of a given application to a given parallel system such that the execution time (or schedule length) of this application is minimized satisfying all precedence constraints.

III. GENETIC BASED APPROACH

Genetic Algorithms or evolutionary algorithms are developed by John Holland in 60s. They are random search based algorithm premised on the evolutionary ideas of natural selection and genetic. The basic concept of GA is designed to simulate processes in natural system necessary for evolution. They use three operators known as natural selection, crossover and mutation. Natural Selection [3] process forms a new population of strings by selecting strings in the old population based on their fitness values. Crossover [3] produces new chromosomes that have some parts of both parent's genetic material. Mutation [3] is a genetic operator that alters one or more gene values in a chromosome from its initial state to produce new chromosomes.

A. Structure of Genetic Algorithm

Typically, a genetic algorithm consists of the following steps:

GA1: Initialization – initialize the population.

GA2: Evaluation – evaluate each chromosome using fitness function.

GA3: Genetic operations – Select the parent and apply genetic operators on them to produce new chromosomes.

GA4: Repeat steps GA2 and GA3 until termination condition reached.

From the above steps, we can see that genetic algorithms utilize the concept of survival of the fittest; passing “good” chromosomes to the next generation, and combining different strings to explore new search points.

B. Initial population (Structure of the chromosome)

Designing of chromosome structure is crucial for devising GA. We define our chromosome structure as a combination of two strings SQ and SP, whose length equal to the number of tasks. SQ (scheduling queue) maintains precedence constraints between tasks, and an entry in SQ represents a task to be scheduled. An entry in SP (scheduling processor) represents the processor the corresponding task is scheduled onto.

The details to generate a chromosome can be seen in following steps:

IP1: Select randomly a task from the entire entry tasks. Set this task as the first task in SQ.

IP2: Repeat step IP3 for $(v-1)$ times.

IP3: Randomly select a task who is not in SQ and whose predecessors all have been in SQ, and add this task to SQ.

IP4: For SP part, randomly generate an integer number between 1 and m for each task in SQ and add it to SP.

C. Evaluation and Selection:

Roulette Wheel Mechanism In order to select good chromosomes, we define the fitness function as: $F(i) = \frac{1}{\max FT - FT(i) + 1}$ (1) Where: $\max FT$ and $\min FT$ is the maximum and minimum finishing time of chromosomes in current generation, respectively. $FT(i)$ is the finishing time of the i th chromosome. Once the fitness values of all the chromosomes have been evaluated, we can select the higher fitness value chromosomes using the roulette wheel mechanism.

D. Reproduction: Crossover and Mutation

Crossover As our chromosome comprises two separate parts SP and SQ having different characteristics, for each part we employ different crossover policies. We randomly select one or the second part and apply two different crossover operators for these two parts. Details about crossover are given in following steps: CR1: Input the Crossover probability P_c .

CR2: Randomly select pairs of chromosomes and generate a float number (FLC) between 0 and 1 for each pair.

CR3: If $FLC \leq P_c$, then repeat step CR4 to step CR5 Else directly reproduce those two chromosomes to the next generation.

CR4: Randomly generate two crossover points, p and q , between 1 and v and crossover flag CF between 0 and 1.

CR5: If $CF=0$ then rearrange the order of tasks in SQ between p and q of one chromosome according to the order of tasks of another chromosome, the rest of the two chromosomes are remained. Else exchange the part in SP between p and q of two chromosomes and the rest of the two chromosomes are remained.

Mutation

Mutation can be considered as a random alternation of the individual. We employ two policies to mute the chromosome as given in following steps:

MT1: Input the Mutation probability P_m .

MT2: For each chromosome, generate a float number (FLM) between 0 and 1.

MT3: If $FLM \leq P_m$, then repeat step MT4 to step MT5 Else directly reproduce this chromosome to the next generation.

MT4: Randomly generate a mutation point p between 1 and v and mutation flag MF between 0 and 1.

MT5: If $MF=0$ then select randomly a location between location of the nearest immediate predecessor and that of successor of s_{qp} . Then move s_{qp} to this location. Else change randomly the processor of s_{qp} between 1 and m as s_{pp} .

IV. EXPERIMENTS AND RESULTS

In our work, we implemented Genetic algorithm for solution of multiprocessor flexible task scheduling problem. Detail block diagram(Fig.1) represents the sequence of operations to get the desired results. We have compared our results with heuristic algorithm. For performance evaluation of our algorithm we generated some problems of varying sizes and solved them by both the algorithms. We assume that size of problem ranges from 10 to 50 with an interval of 5, there is no limit on the number of successors of each task except the exit task which does not have any successor, the execution time for each task is a random number between 5 and 25 and number of processors varies from 4 to 8 according to the size of problems. As we did not put any restriction over the number of successor a task may have, task graph may be much complicated. So, the problems we have chosen may be considered difficult in comparison to the kind of problems we normally see in literature, where a restriction on maximum number of successor tasks has been put.

The proposed genetic algorithm discussed in previous sections was implemented and evaluated on an application of college campus. In college campus application we considered various tasks relates to entities like Student, Teacher, Employee, Books etc. Results obtained are re shown in Table I. We set parameters for our Genetic Algorithm as: Population Size=25, Maximum Generations=5000, Crossover Probability=.6 and Mutation Probability=.2.

Comparison of GA and Heuristic Algorithm.

Results obtained from our experiments are analyzed for following factors:

1)Quality of solution: Results of average schedule length of the GA is given in Table I. Results demonstrate that our proposed Genetic Algorithm is able to compete with heuristic based algorithms as far as quality of solution is concerned. As heuristics are biased towards certain characteristics of solution so they tend to search solution

only in a small part of whole search space. It is also possible that they never explore a particular region of search space. Thus for some problems heuristics may give bad results also if they are not chosen carefully. On the other hand GA is a more powerful method as it searches simultaneously in many parts of search space. Because of mutation operator, change in region being searched, gives potential to GA to search in any part of the search space. Thus it is more likely to find a better or best solution.

2)Robustness and guarantee for good solution: During our experiments on GA we noted Average schedule lengths of populations emerging generations after generation. Though we have shown results for problem size 10 to 50 in Table. 1, for each problem irrespective of its size we observe that average schedule length is continuously decreasing as more and more generations are evolving. This shows that Genetic Algorithm is robust and ultimately it will give us a good quality solution as quality of solution set is continuously improved. It also reveals that more generations we evolve; it is likely to have better quality in solution.

3)Effect of mutation probability on the performance of GA: As mutation is the key to change the region of search space, mutation probability may have dominating role in finding solutions of good quality. Thus, we repeated our experiments by fixing crossover probability and changing mutation probabilities from 0.05 to .40 and noted average schedule lengths. We done our experiments on the problem having size 25. we can observe the similar trend in the problems of all sizes. Table. 1 shows the further average of results, mixing the effect of all crossover probabilities which clearly shows that up till mutation probability is .20, increase in mutation probability leading to better results. After .20 results are fluctuating in a small range but normally are not better than that we obtained for .20. So, we have found best mutation probability for our set of problems as .20. So, we have found best mutation probability for our set of problems as .20. During the experiments, we have seen that for 28.8% problems GA gives lower schedule length, for 4.44% problems GA gives slightly higher schedule length while for 66.67% problems GA gives equal schedule length in comparison with HEFT. On an average, we analyzed that GA gives better results than the heuristic based algorithm and it is robust also as the average schedule length is continuously decreases as more and more generations evolve.

IV. CONCLUSION

A genetic algorithm based on principles of evolution found in nature for finding an optimal solution. Genetic Algorithm use random choices to guide themselves to the problem space and they are used for different kind of task scheduling problems. It continuously tries to improve the average fitness of a population by construction of new population .Quality of solution depends heavily on the selection of some key parameters like fitness function ,population size , crossover probability and mutation probability.

Task scheduling in multiprocessor system using genetic algorithm is an efficient way due to the characteristics of Genetic Algorithm as : quality of solution ,robustness and guarantee for good solution effect of mutation probability on the performance on Genetic Algorithm.

REFERENCES

[1] A.Chipperfield and P. Flemming. Parallel Genetic Algorithms. Parallel and Distributed Computing Handbook ,first ed.A.Y Zomaya.ed.,1,118-1,143. Mcgraw-Hill,New York,1996.

[2] B. Kruatrachue and T.G. Lewis. Duplication Scheduling Heuristic, a New Precedence Task Scheduler for Parallel Systems. Technical Report 87-60-3, Oregon State Univ., 1987.

[3] D.C. Goldberg. Genetic Algorithms in Search, Optimization and Machine Learning. Add.Wesley publishing,1989.

[4] H. EL-Rewini, T.G. Lewis, and H.H. Ali. *Task Scheduling in Parallel and Distributed Systems*. Prentice Hall . 1994.

[5] H. Topcuoglu, M.Y. Wu. Performance-effective and low-complexity task scheduling for heterogeneous computing. IEEE Transactions on parallel and distributed System, Vol. 13, pp.260-274, 3, 2002.

[6] J.H. Holland. Adaptation in Natural and Artificial Systems. MIT Press, 1975.

[7] Jonathan I. Gross, Jay Yellen. *Handbook of Graph Theory*. CRC Press.

[8] M. Srinivas and L.M. Patnaik. Genetic Algorithms: A Survey. Computer vol. 27, pp. 1726, 1994.

[9] Martin Charles Golumbic. *Algorithmic Graph Theory and Perfect Graphs*. Second Edition, Elsevier, 2004.\

[10] M. R. Garey and D. S. Johnson. *Computers and Intractability: A Guide to the Theory of NP Completeness*, San Francisco, CA, W. H.Freeman, 1979.

TABLE I
RESULTS OF GENETIC ALGORITHM

Problem size	PIN(0-4)					Average Schedule Length
	0	1	2	3	4	
10	80	90	107	101	93	94.2
15	111	96	98	107	104	103.2
20	130	132	118	115	117	122.4
25	116	118	135	145	167	136.2
30	165	145	187	125	160	156.4
35	172	190	165	169	180	175.2
40	190	187	175	169	180	180.2
45	225	230	190	185	199	205.8
50	222	220	232	218	217	221.8

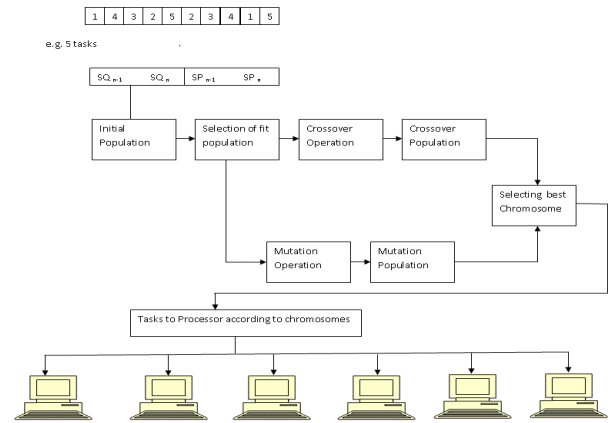


FIGURE I
BLOCK DIAGRAM OF PROPOSED SYSTEM

Design and Implementation of SIP based VoIP Application for Mobile Devices using J2ME

T. M. T. Khan^{*}, S. M. Patil^{**}, D. R. Raut^{***}

^{*} AIKTC/Computer Engineering, New Panvel, India

^{**} BVCOE/Information Technology, Khargar, India

^{***} WIEECT/Computer Engineering, Mumbai, India

Abstract: Voice over Internet Protocol (VoIP) is a way to carry out a telephonic conversation over a data network. VoIP applications, with SIP and RTP, promise converged telecommunications and data services that are cheaper, more versatile and provide good voice quality as compared to traditional offerings. Although VoIP is widely used, VoIP on mobile devices is still in its infancy. Currently, there are number of VoIP solutions for mobile phones, however VoIP solutions developed using Java 2 Platform Micro Edition (J2ME) are not available. Java based solutions are widely compatible with many devices. In this paper strong focus has been given to cross-device compatibility through the use of the widely supported J2ME framework. The design and implementation details of VoIP client using J2ME are illustrated.

Keywords: VoIP, RTP, SIP, J2ME.

I. INTRODUCTION

To date, the Public Switched Telephone Network (PSTN) has been used to conduct telephone calls over a wired network. With the development of computing technology, Voice over Internet Protocol (VoIP) has been established as an alternative to traditional telephony networks. VoIP allows telephone conversation to take place over a data packet switched networks like the Internet. VoIP products promise converged telecommunications and data services that are cheaper, more versatile and provide improved voice quality as compared to traditional offerings. Although VoIP is widely used, VoIP on mobile devices is still an area of research.

II. TECHNOLOGICAL OVERVIEW

VoIP is the digitalizing of voice using an analog to digital converter (ADC), sending this data through a data network and the reassembling of this data to form the original analog format using a digital to analog converter (DAC). VoIP is made of two parts, signaling and data transport. The VoIP signaling function can be performed using protocols such as Session Initiation Protocol (SIP), H.323 and Media Gateway Control Protocol (MGCP). Data transport can be performed by The Real time Transport Protocol (RTP). This protocol is used to deliver voice data during conversation.

A. Session Initiation Protocol (SIP)

The Session Initiation Protocol (SIP) [1] is an application-layer control and signaling protocol. SIP is used to create, modify, and terminate multimedia sessions or conferences such as Internet Telephone calls. The SIP message format is similar to the Hyper Text Transfer Protocol (HTTP) message format. Two main components in

SIP are user agent (UA) and servers. UAs are regarded as a client that can send the request and response together. This includes a user agent client and a user agent server. Servers are used to receive requests from clients for servicing and sending responses back to the clients. The servers are typed as redirect server, proxy server and registrar.

B. Real-time Transport Protocol (RTP)

Once signaling functions are implemented, voice data needs to be transmitted between clients. Real-time Transport Protocol (RTP) [2] is viewed as the most powerful protocol to deliver multimedia packets in a session. RTP is defined by Internet Engineering Task Force (IETF). It consists of two parts:

RTP: is used to carry voice data.

RTCP: is used to monitor the quality of services and information about the participants who are in a sessions.

C. Voice Codecs

In VoIP, there are many different audio codecs. The bandwidth required during a VoIP conversation naturally depends on the codec. The G.711 codec is used on most telephony systems all over the world. The G.729 codec provides the best voice quality. However, due to the native support of G.711 by mobile devices, it is more suitable to use G.711.

III. MOBILE APPLICATION DEVELOPMENT ENVIRONMENT

There are number of integrated development environments, languages, frameworks and libraries that can be used to develop the solution proposed in this paper. J2ME is chosen as the development tool in this paper, since most of the mobile phones has support for Java. Although

RTP is not supported on J2ME, implementation of RTP on J2ME framework is one of key features of this paper.

A. PROPOSED ARCHITECTURAL FRAMEWORK

Depending upon the required functionality of SIP client under constraint specific mobile platforms, the system design is divided into two major proposed frameworks.

a. Proposed SIP Framework

SIP performs signaling functions in a session. In this paper, SIP functions are implemented based on the specifications of SIP Protocol, as shown below.

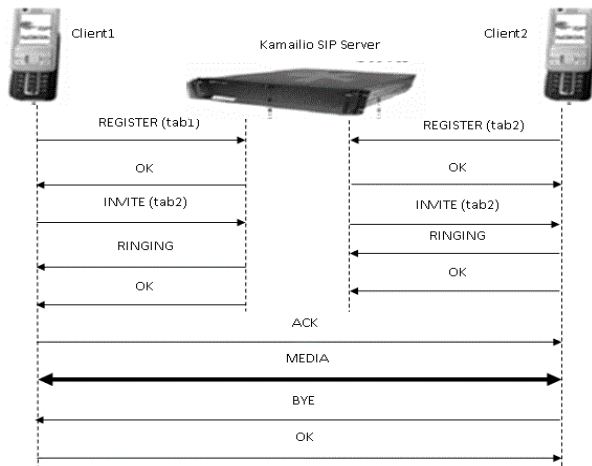


Figure. 1 SIP sequence diagram.

As signaling functions are provided, SDP is used to negotiate media session description between clients. The media session description includes encoding format, payload type and sampling rate of voice packets. Also, IP address and port number for receiving voice packets is included.

b. Proposed RTP Framework

After both parties reach the same media session description, the RTP protocol is used to deliver voice data. Figure 2 shows the details of RTP Framework that is used as a basis for the implementation. The implementation carries out the functions illustrated in Fig. 2.

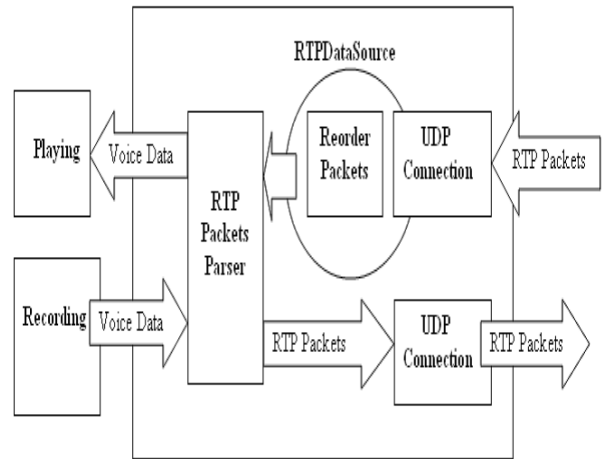


Fig. 2. RTP Framework.

B. IMPLEMENTATION OF PROPOSED FRAMEWORK

In this section, the implementation of the proposed architecture is going to be discussed. Requirements for setting up development environment is presented. SIP for J2ME is implemented to initiate VoIP calls on mobile emulator. Moreover, Session Description Protocol (SDP) is used for negotiating media session description. RTP is used to deliver voice data in this implementation.

Requirements of Proposed Architectural Framework

A number of additional softwares and tools are required for implementation and evaluation. They performs different functions during the implementation process. They are outlined as follows:

- a) Kamailio is a free and open source SIP proxy server..
- b) Sun Java Wireless Toolkit is a mobile phone emulator.
- c) Ethereal is a network protocol analyzer that is used to capture network packets during transmission.
- d) J2ME is used to develop the VoIP application.

SIP for J2ME

JSR 180 is an optional package that supports basic SIP API on J2ME [7]. It can run on devices with limited memory. There are six SIP request methods are explained as following in SIP specification: REGISTER, INVITE, ACK, CANCEL, BYE, OPTIONS. Two main requests are introduced in the following:

- **REGISTRATION:** registration is the first essential part for starting a session. A SIP registration message is generated and sent to Kamailio server. According to SIP specification, the transactions between clients can only be done if they are registered to the SIP registrar server. In this implementation, kamailio acts as registrar server.
- **INVITATION:** The invitation is the second step that a VoIP call needs to do after registration. According to

SIP API, SIP Invitation Message is generated as follows:

```
INVITE sip:tab2@192.168.1.3
To: tab2<sip:tab2@192.168.1.3>
From: tab1 <sip:tab1@192.168.1.2>
tag=1928301774
Call-ID: a84b4c76e66710
CSeq: 314159 INVITE
Contact: <sip:tab1@192.168.1.2>
Content-Type: application/sdp
Content-Length: 142
```

SDP for J2ME

When a client wants to communicate with another client, the session description details must be received by both parties. Then, the callee and caller will negotiate to choose a common media for voice packets. Session Description Protocol(SDP) [5] is used to describe the media details for clients. The functions of SDP are to define where the voice data should be sent such as the port number and IP address and define the codec to be used by other party and also identify the channel and sample rate of voice data. The following is one of the SDP message example according to SDP specification.

```
String SDP = " " +
"v=0\n"+
"o=tab1 0 0 IN IP4 192.168.1.2 \n" +
"s=-\n"
"c=IN IP4 192.168.1.2 \n" +
"t=0 0\n" +
"m=audio 10086 RTP/AVP 8\n" +
"a=rtpmap:0 PCMU/8000\r\n";
```

RTP on J2ME

As J2ME does not RTP, it is necessary to implement the RTP features. It is widely known that RTP packets house in UDP packets. Experiments shows that audio recording of 1 second generates around 8000 bytes of data. The RTP header size is 32 bytes but in implementation, only 12 bytes for header is used for shortening the total packet size and thereby improving voice quality. The recommended audio recording of 20 milli seconds generates about 160 bytes of data to which RTP header is added resulting into packet of size 172 bytes. Then this data is encapsulated into UDP packet and sent to the destination.

According to RTP specification, the following features are required:

- Constructing/Extracting RTP packets from UDP packets.
- Receiving/Sending UDP packets.
- Streaming and playing voice data.

IV. CONCLUSION

In this paper, the background and related work of VoIP on mobile devices were discussed. The proposed design and implementation were also detailed. This paper proves that a VoIP client can be developed using J2ME followed the standard and deployed on a mobile phone with the necessary features. The features of the implemented client are suitable for mobile devices. Although the implemented client is compatible with the VoIP standard, the client is not implemented for all the existing Mobile Operating systems.

REFERENCES

- [1] J. Rosenberg, H. Schulzrinne, G. Camarilla, A. Johnston, R. Sparks, M. Handley, E.Schooler. "SIP: Session Initiation Protocol.". The Internet Engineering Task Force, June 2002.
- [2] H. Schulzrinne, S. Casner, R. Frederick, V. Jacobson. "RTP: A Transport Protocol for Real-Time Application". Network Working Group, July 2003.
- [3] W. Muller, H. Glasmann, J. Kellerer. "Service Development and Deployment in H.323 and SIP". IEEE, 2001.
- [4] E Andreasen, B. Foster. "Media Gateway Control Protocol (MGCP)" Version 1.0, pages 5-33. Network Working Group, January 2003.
- [5] M. Handley, V. Jacobson. "SDP: Session Description Protocol", Network Working Group, 1998.
- [6] L. Burdet, P.Stuedi, A. Frei and G. Alonso. "Symphone: Design and implementation of a VoIP peer for Symbian Mobile phones using bluetooth and SIP", The ACM Ditial Library, 2006.
- [7] Inc Sun Microsystem. Porting Guide Java 2 Platform, MicroEdition. "Technical Report: Mobile Media API", June 2002.

Biosorption performance of *Albizia lebbek* pods powder for the removal of lead: Application of statistical method

Ch. A. I. Raju*, R. Sarala Kumari, Ch. V. Satya, P. J. Rao and M. Tukaram Bai

Department of Chemical Engineering, Andhra University, Visakhapatnam – 530 003

ABSTRACT

The impact of industries on ground water resources is immense and only through good pollution prevention practices the contamination and deterioration of ground water sources will decrease. Biosorption a promising method for removal of metal ions from aqueous solution is under taken for the present experimentation. This paper determines the thermodynamics, isotherms and kinetic studies on biosorption of lead ions from an aqueous solution onto low cost biosorbent from waste plant namely *Albizia lebbek* pods powder. The biosorption was carried out in a batch process varying six parameters. Results have shown that the biosorption of lead increases with an increase in biosorbent dosage and decreases with increase in biosorbent size. A significant increase in percentage removal of lead is observed as pH is increased from 1 to 6 and the percentage removal is maximum at pH = 6. Freundlich, Temkin and Langmuir models are applied to describe the equilibrium isotherms. The kinetic study showed that biosorption of lead followed pseudo second order kinetics. Various thermodynamic parameters such as change in enthalpy, entropy and gibb's free energy are also determined. The Box-Behnken Design (BBD) was used for optimization using Response Surface methodology. The ANOVA of the regression model demonstrated that the model is highly significant which is evident from Fisher test.

Keywords: Biosorption, optimization, *Albizia lebbek* pods powder, Box-Behnken Design, Isotherms, Kinetics

1. INTRODUCTION

Water resources are of critical importance to both natural ecosystem and human development but enhanced industrial activity after the industrial revolution has led to the discharge of chemicals, which caused environmental and public health problems. The presence of heavy metals in the environment is of major concern because of their extreme toxicity and tendency for bioaccumulation in the food chain even in relatively low concentrations [1, 2]. The studies made on investigation of economic and effective methods for the removal of heavy metals have resulted in the development of new separation technologies. Biological treatment, ion exchange, coagulation, electrochemical operation and filtration are commonly applied to the treatment of industrial effluents [3, 4]. Recent research on biosorption has shown that biomaterials containing acidic

groups such as hydroxyls and carboxyls were effective in binding metal cations [6]. Other biomaterials containing weak basic groups such as amides and amines are efficient for adsorbing metal anions [7]. There are three major factors affecting metal biosorption behavior [8]. Recently efforts are being made to harness this phenomenon into a technique for the detoxification of metal bearing industrial effluents by removing or eventually also recovering the metals [9]. Biosorption removal of toxic heavy metals is especially suited as a 'polishing' waste water treatment step because it can produce close to drinking water quality from initial metal concentrations of 1-100 mg/L to final concentrations < 0.01-0.1 mg/L [10,11]. Alternatively due to its low cost even the unprocessed, once through used up metal laden biosorbent can be disposed of by either incineration or it could be landfilled, having a rather small volume when compared to the wastewater – the biosorption process serves to reduce the overall waste volume [12-21]. . A multitude of biomass types comprising fungal biomass, bacterial biomass, algae, peat etc., have been studied for their biosorption of metals [16, 18, 19, 20]. Agricultural wastes such as tree bark, peanut skin, hull, tobacco, tomato root tissues and plants waste have been used to remove heavy metals from water [22-24].

2. EXPERIMENTAL PROCEDURE

2.1 Biosorbent

Albizia lebbek pods were obtained from A.U. Engg college premises in Visakhapatnam. The A.L. pods was washed thrice with tap water and once with distilled water in order to remove adhering mud, impurities etc. It was dried in sunlight for one week until all the moisture was evaporated. The crispy A.L. pods were then crushed and grinded to powder, separated using British Standard Sieves (BSS) and stored in dry vacuum packs to prevent moisture content and readily used as biosorbent.

2.2 Batch Sorption studies

Preliminary experiments were conducted in 250 ml Erlenmeyer flasks containing 50 ml of 20 mg/L metal solution using single step optimization procedure. The flasks were agitated on an orbital shaker at 180 rpm and samples were taken at predetermined time intervals (1, 3, 5, 10, 15, 20, 25, 30, 40, 50, 60, 90, 120, 150 & 180 min) & centrifuged at 14000 rpm and the supernatant liquid was analysed in Atomic Absorption Spectrophotometer (AAS) for final concentrations. Similarly the other variables were

varied in a wide range: Biosorbent Size (53, 75, 104, 125 & 152 μm), pH of the aqueous solution (2, 3, 4, 5, 6, 7 and 8), Initial concentration of lead solution (25, 40, 80, 120 & 160 mg/L), Biosorbent Dosage (10, 20, 30, 40, & 50 g/L) and Temperature (283, 293, 303, 313 & 323 K).

2.3 Process Optimization

Final experimental runs for optimization were obtained through Response Surface Methodology from Design of Experiments (DoE) using STATISTICA software. The extent of biosorption of lead calculated at the preliminary optimum conditions is verified with the final runs for the optimum conditions.

3. RESULTS AND DISCUSSION

In the present investigation, the potential of dry *Albizia Lebbeck* pods powder as a biosorbent for removal of lead present in an aqueous solution is investigated. The effects of various parameters are:

3.1 Effect of agitation time

The equilibrium agitation time is determined by plotting the % biosorption of lead against agitation time as shown fig. 1 for the interaction time intervals between 1 to 180 min. For 53 μm size of 10 g/L biosorbent dosage, 64.45 % of lead is biosorbed in the first 5 min. The % biosorption is increased briskly up to 50 min reaching 78.3 %. Beyond 50 min, the % biosorption is constant indicating the attainment of equilibrium conditions. The maximum biosorption of 78.3 % is attained for 50 min of agitation time with 10 g/L of 53 μm size biosorbent mixed in 50 mL of aqueous solution ($C_0 = 20$ mg/L) [25,26].

3.2 Effect of biosorbent size

The variations in % biosorption of lead from the aqueous solution with biosorbent size are obtained. The results are drawn in fig. 2 with percentage biosorption of lead as a function of biosorbent size. The percentage biosorption is increased from 72.36% to 78.34 % as the biosorbent size decreases from 152 to 53 μm . This phenomenon is expected, as the size of the particle decreases, surface area of the biosorbent increases; thereby the number of active sites on the biosorbent also increases.

3.3 Effect of pH

In the present investigation, lead biosorption data are obtained in the pH range of 2 to 8 of the aqueous solution ($C_0 = 20$ mg/L) using 10 g/L of 53 μm size biosorbent. The effect of pH of aqueous solution on % biosorption of lead is shown in fig. 3. The % biosorption of lead is increased from 55.22 % to 76.16% as pH is increased from 2 to 6 and decreased beyond the pH value of 6 [27]. % biosorption is decreased from pH 7 to 8 reaching 68.18 % from 74.38 %. Low pH depresses biosorption due to competition with H^+ ions for appropriate sites on the biosorbent surface. However, with increasing pH, this competition weakens

and Lead ions replace H^+ ions bound to the biosorbent [28, 29].

3.4 Effect of initial concentration of lead

The effect of initial concentration of lead in the aqueous solution on the percentage biosorption of lead is shown in fig. 4. The percentage biosorption of lead is decreased from 76.14 % to 61.32 % with an increase [30] in C_0 from 20 mg/L to 160 mg/L. Such behavior can be attributed to the increase in the amount of concentration of the aqueous solution to the unchanging number of available active sites on the biosorbent.

3.5 Effect of biosorbent dosage

The biosorption of lead increased from 76.14 % to 82.98 % with an increase in biosorbent dosage from 10 to 40 g/L is shown in fig. 5. Such behavior is obvious because with an increase in biosorbent dosage, the number of active sites available for lead biosorption would be more. The change in percentage biosorption of lead is marginal from 82.98 % to 83.68 % when 'w' is increased from 40 to 60 g/L. Hence all other experiments are conducted at 40 g/L dosage.

3.6 Effect of Temperature

When temperature was lower than 303 K, lead uptake increased with increasing temperature, but when temperature was over 303 K, the lead uptake increased very marginally (fig. 6). This response suggested a different interaction between the ligands on the cell wall and the metal. Below 303 K, chemical biosorption mechanisms played a dominant role in the whole biosorption process, biosorption was expected to increase by increase in the temperature [31] while at higher temperature, the plant powder were in a nonliving state, and physical biosorption became the main process. Physical biosorption reactions were normally exothermic, thus the extent of biosorption generally is constant with further increasing temperature.

3.7 Isotherms

3.7.1 Langmuir Isotherm

Irving Langmuir [32, 33] developed an isotherm named Langmuir isotherm. It is the most widely used simple two-parameter equation. Langmuir isotherm is drawn for the present data and shown in fig. 7. The equation obtained is $C_e/q_e = 0.0565 C_e + 2.871$ with a good linearity (correlation coefficient, $R^2 \sim 0.9976$) indicating strong binding of lead ions to the surface of *Albizia Lebbeck* pods powder.

3.7.2 Freundlich Isotherm

Freundlich [34] presented an empirical biosorption isotherm equation that can be applied in case of low and intermediate concentration ranges. The Freundlich isotherm is given by $q_e = K_f C_e^n$ where K_f (mg) represents the biosorption capacity when metal equilibrium concentration and 'n' represents the degree of dependence of biosorption with equilibrium concentration. It is easier to handle

mathematically in more complex calculations. Freundlich isotherm is drawn between $\log C_e$ and $\log q_e$ in fig. 8 for the present data. The resulting equation $\log q_e = 0.7246 \log C_e - 0.2798$; has a correlation coefficient of 0.9924.

3.7.3 Temkin Isotherm

Temkin and Pyzhev [35] isotherm equation describes the behavior of many biosorption systems on the heterogeneous surface and it is based on the following equation $q_e = RT \ln(A_T C_e) / b_T$. The equation obtained for lead biosorption is: $q_e = 3.2144 \ln C_e - 4.0314$ with a correlation coefficient 0.9758. The best fit model is determined based on the linear regression correlation coefficient (R^2). From the figs 7, 8 & 9, it is found that biosorption data are well represented by Langmuir isotherm with higher correlation coefficient of 0.9976, followed by Freundlich and Temkin isotherms with correlation coefficients of 0.9924 and 0.9758 respectively.

3.8 Kinetics of biosorption

The order of biosorbate – biosorbent interactions have been described using kinetic model. Traditionally, the first order model of Lagergren [36] finds wide application. In the case of biosorption preceded by diffusion through a boundary, the kinetics in most cases follows the first order rate equation of Lagergren: $(dq_t/dt) = K_{ad} (q_e - q_t)$ where q_e and q_t are the amounts adsorbed at t , min and equilibrium time and K_{ad} is the rate constant of the first order biosorption.

$$\log (q_e - q_t) = -0.3828 - 0.0279t$$

Plot of $\log (q_e - q_t)$ versus ' t ' gives a straight line for first order kinetics, facilitating the computation of adsorption rate constant (K_{ad}). If the experimental results do not follow the above equation, they differ in two important aspects: $K_{ad} (q_e - q_t)$ does not represent the number of available biosorption sites and $\log q_e$ is not equal to the intercept. In such cases, pseudo second order kinetic equation [37]:

$$(dq_t/dt) = K (q_e - q_t)^2 \text{ is applicable,}$$

where 'K' is the second order rate constant.

Rearranging the terms, we get the linear form as:

$$(t/q_t) = (1/Kq_e^2) + (1/q_e) t.$$

$$(t/q_t) = 0.6431 t + 0.7029.$$

The pseudo second order model [38] based on above equation, considers the rate-limiting step as the formation of chemisorptive bond involving sharing or exchange of electrons between the biosorbate and biosorbent. If the pseudo second order kinetics is applicable, the plot of (t/q_t) versus ' t ' gives a linear relationship that allows computation of q_e and K.

In the present study, the kinetics are investigated with 50 mL of aqueous solution ($C_0 = 20$ mg/L) at 303 K with the interaction time intervals of 1 min to 180 min. Lagergren plots of $\log (q_e - q_t)$ versus agitation time (t) for biosorption of lead the biosorbent size (53 μm) of *Albizia Lebbeck* pods powder in the interaction time intervals of 1 to 180 min are drawn in figs. 10 & 11.

3.9 Thermodynamics of biosorption

Biosorption is temperature dependant. In general, the temperature dependence is associated with three thermodynamic parameters namely change in enthalpy of biosorption (ΔH), change in entropy of biosorption (ΔS) and change in Gibbs free energy (ΔG).

The ΔH is related to ΔG and ΔS as $\Delta G = \Delta H - T \Delta S$

The Vant Hoff's equation is

$$\log (q_e / C_e) = \Delta H / (2.303 RT) + (\Delta S / 2.303 R)$$

$$\log (q_e / C_e) = -0.4783 (1 / T) + 0.77525$$

Experiments are conducted to understand the biosorption behavior varying the temperature from 283 to 323 K. The Vant Hoff's plot for the biosorption data obtained is shown in fig. 12. The corresponding values are $\Delta G = -4488.519382$, $\Delta H = 9.158078$ and $\Delta S = 14.84382$.

3.10 Optimization using Box Behnken Design (BBD)

The experiments conducted with different pH values ranging from 5–7, different biosorption dosages of 30–50 g/L and different lead concentrations of 10–30 mg/L and varied simultaneously to cover the combination of parameters in BBD. The levels and ranges of the chosen independent parameters are given in Table-5.1. Table-5.2 is employed for the optimization of the parameters. The regression equation for the optimization of the biosorption of lead: % biosorption of lead (Y) is function of the biosorption dosage, w (X_1), initial lead concentration, C_0 (X_2) and pH (X_3). Multiple regression analysis of the experimental data has resulted in the following equation for the biosorption of lead:

$$Y = 48.89 + 8.23 X_1 + 0.417 X_2 + 0.0755 X_3 - 0.675 X_1^2 - 0.00495 X_2^2 - 0.00175 X_3^2 \text{ ----- (1)}$$

The result of above regression model in the form of analysis of variance (ANOVA) for Eq. (1) is given in Table-5.3. In general, the Fischer's 'F-statistics' value ($F = MS_{\text{model}} / MS_{\text{error}}$), where MS (mean square) with a low probability 'P' value indicates high significance of the regression model.

The ANOVA of the regression model demonstrates that the model is highly significant, as is evident from the Fisher's F-test ($F_{\text{model}} = 2188.8093$) and a very low probability value ($P_{\text{model}} > F = 0.000000$). More ever, the computed F-value ($F_{0.05} (14.15) = MS_{\text{model}} / MS_{\text{error}} = 0.4924821 / 0.000225$) is

greater than the tabular F-value ($F_{0.05}$ (14.15) tabulars = 3.56) at the 5% level, indicating that the treatment differences are significant. From the Table-5.4, we can observe that, the larger the value of t and smaller the value of P, more significant is the corresponding coefficient term. By analyzing the 't' values and 'P' values from Table-5.4, it is found that the X_1 , X_2 , X_3 , X_1^2 , X_2^2 , and X_3^2 have high significance to explain the individual and interaction effect of biosorption variables on the biosorption of lead to predict the response. The optimal set of conditions for maximum percentage biosorption of lead is pH = 6.09630, biosorption dosage (w) = 42.12121 g/L and initial lead concentration (C_0) = 21.57143 mg/L. The extent of biosorption of lead calculated at these optimum conditions is 83.57285 %. Fig. 13 shows the comparison between the % biosorption obtained through experiments, which are in good agreement with predicted values. In fig. 14 pareto chart depicts the variables which have significance at 95 % conf level. Fig. 15 (a, b, c) shows the response surface contour plots for different variables effects. The experimental optimum values are compared with those predicted by BBD in table-5 and are in close agreement.

4. FIGURES AND TABLES

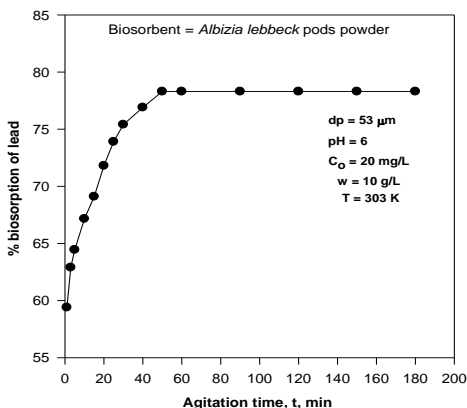


Fig. 1 Effect of agitation time on % biosorption of lead

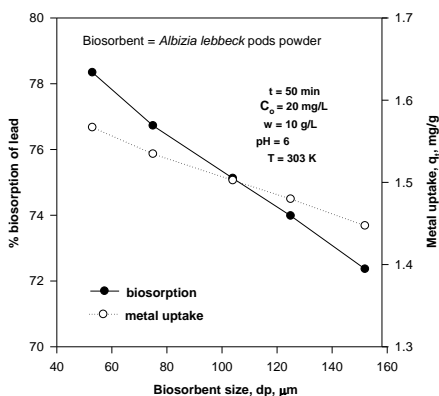


Fig. 2 % Biosorption of lead as a function of biosorbent size

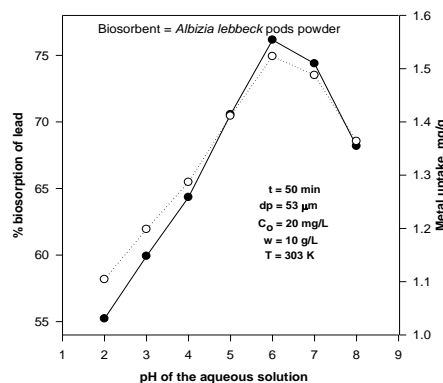


Fig. 3 Observation of pH along with % biosorption of lead

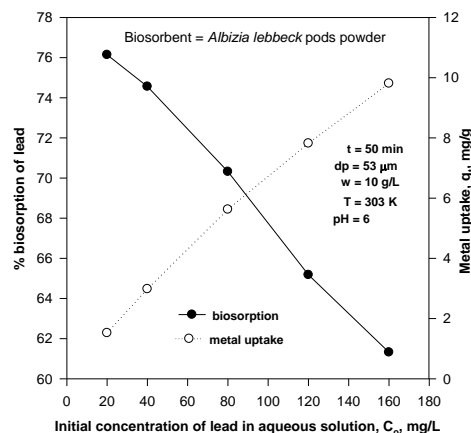


Fig. 4 Variation of initial concentration with % biosorption of lead

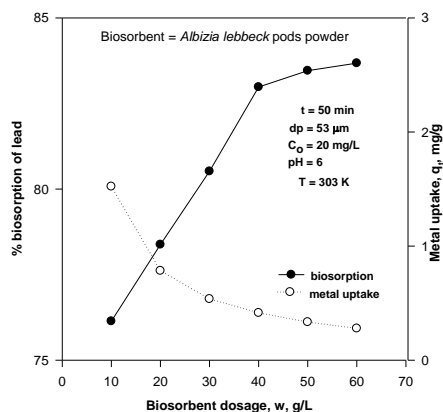


Fig. 5 Dependency of % biosorption of lead on biosorbent dosage

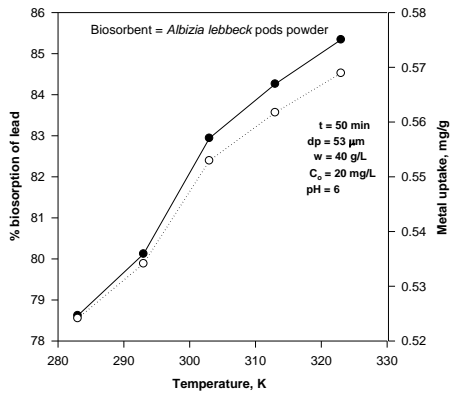


Fig. 6 Effect of temperature on % biosorption of lead

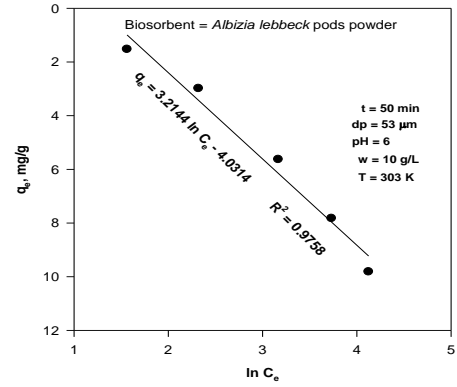


Fig. 9 Temkin isotherm for % biosorption of lead

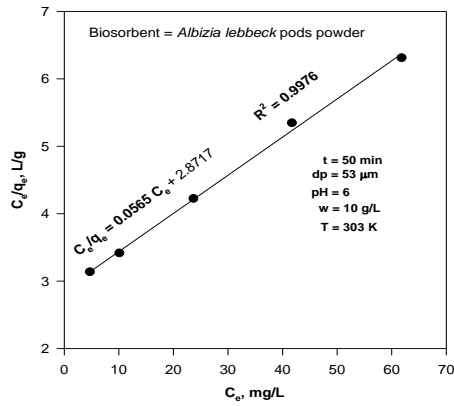


Fig. 7 Langmuir isotherm for % biosorption of lead

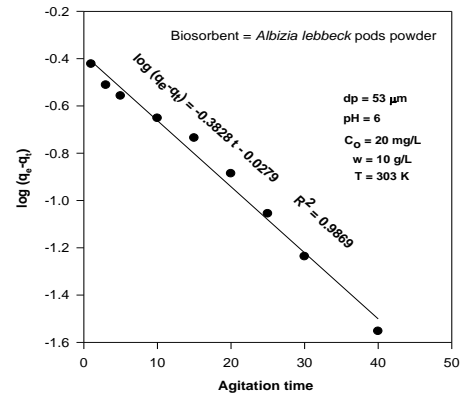


Fig. 10 First order kinetics for % biosorption of lead

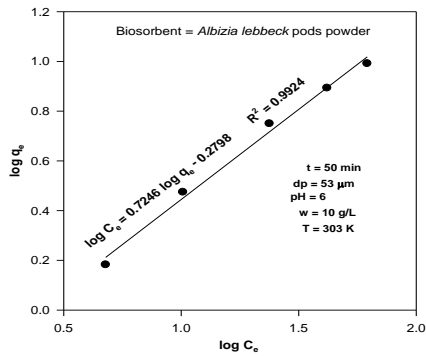


Fig. 8 Freundlich isotherm for % biosorption lead

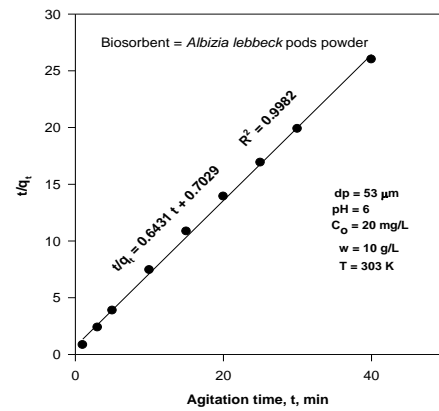


Fig. 11. Second order kinetics for % biosorption of lead

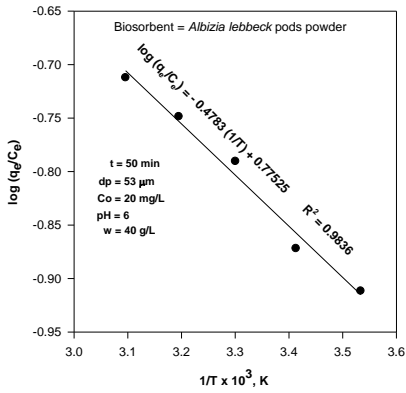


Fig. 12 Vantoff's plot for % biosorption of Lead

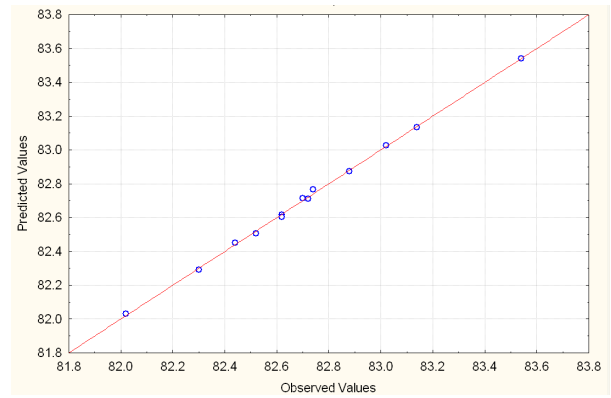


Fig. 14 Observed Vs Predicted Values

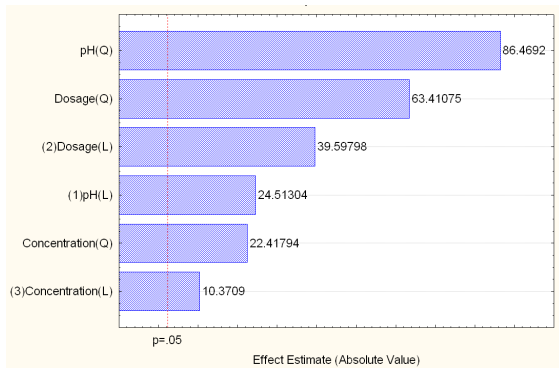


Fig. 13 Pareto Chart

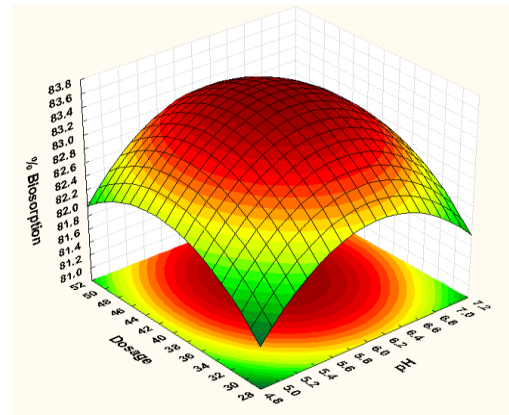


Fig. 5.15 (a) Surface contour plot for the effects of dosage and pH of lead on % biosorption

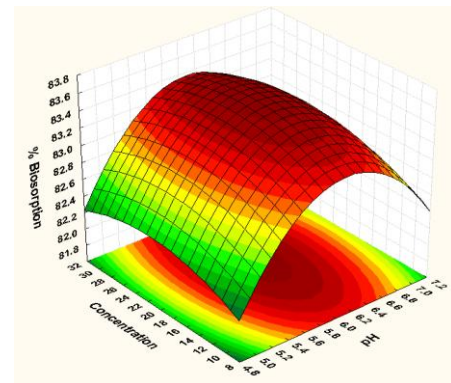


Fig. 5.15 (b) Surface contour plot for the effects of pH and initial concentration of lead on % biosorption

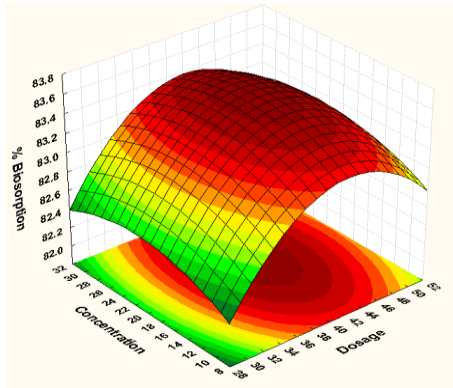


Fig. 5.15 (c) Surface contour plot for the effects of dosage and initial concentration of lead on % biosorption

14	0	0	0	83.54000	83.54000
15	0	0	0	83.54000	83.54000

Table-3 Analysis of variance (ANOVA) for the entire quadratic model

Source of variation	Sum of squares (SS)	d.f	Mean squares (MS)	F-value	Probe >F
Model	2.954893	6	0.492482	2188	0.0000
Error	0.001800	8	0.000225		
Total	2.956693				

Table-1 Levels of different process variables in coded and un-coded form for % biosorption of lead using <i>Albizia lebbek</i> pods powder			
Variables	Coded levels		
	-1	0	1
Biosorbent dosage, w, g/L	30	40	50
Initial concentration, Co, mg/L	10	20	30
pH of aqueous solution	5	6	7

Table -4 Coefficients, t-statistics and significance probability of the model

Term	Reg Coeff	Standar error of coefficient	t-value	P-Value
Mean/Interc.	48.8900	0.31678	154.333	0.0000
(1)Dosage, w, g/L(L)	8.23000	0.09382	87.7165	0.0000
Dosage, w, g/L(Q)	-0.6750	0.00780	-86.469	0.0000
(2)Concentration, Co, mg/L(L)	0.41700	0.00626	66.5340	0.0000
Concentration, Co, mg/L(Q)	-0.0049	0.00007	-63.410	0.0000
(3)pH (L)	0.07550	0.00316	23.8380	0.0000
pH (Q)	-0.0017	0.00007	-22.417	0.0000

Table-2 Results from BBD for biosorption of lead using *Albizia lebbek* pods powder

Run No.	X ₁	X ₂	X ₃	% biosorption of lead	
				Experimental	Predicted
1	-1	-1	0	82.02000	82.03000
2	1	-1	0	82.30000	82.29000
3	-1	1	0	82.44000	82.45000
4	1	1	0	82.72000	82.71000
5	-1	0	-1	82.52000	82.50500
6	1	0	-1	82.74000	82.76500
7	-1	0	1	82.62000	82.61500
8	1	0	1	82.88000	82.87500
9	0	-1	-1	82.62000	82.60500
10	0	1	-1	83.02000	83.02500
11	0	-1	1	82.70000	82.71500
12	0	1	1	83.14000	83.13500
13	0	0	0	83.54000	83.54000

Table-5 Comparison between optimum values from experimentation and BBD		
Variable	Experimental	BBD
Biosorbent dosage, w, g/L	40	42.12121
Initial lead concentration, mg/L	20	21.57143
pH of aqueous solution	6	6.09630
% biosorption	82.94	83.57285

5. CONCLUSION

The equilibrium, kinetic and thermodynamic studies are carried out for biosorption of lead experimentally and the analysis of the experimental data resulted in the following conclusions. The equilibrium agitation time for lead biosorption is 50 minutes. The percentage biosorption of lead decreased with the increase in biosorbent size from 53 μm (78.34 %) to 152 μm (72.36 %). Percentage biosorption of lead from the aqueous solution increased significantly with the increase in pH from 2 (55.22 %) to 6 (76.16 %). The optimum dosage for biosorption is 40 g/L. The maximum uptake capacity of 17.1526 mg/g is obtained at 303 K. The maximum biosorption of lead (83.57285 %) onto *Albizia Lebbeck* pods powder is observed when the processing parameters are set as pH = 6.0963, w = 42.12121 g/L and $C_0 = 21.57143$ mg/L using BBD. This investigation also revealed the endothermic nature of biosorption as ΔH (9.158078) is positive, irreversible nature of biosorption as ΔS (14.84382) is positive and spontaneity of biosorption as indicated by negative ΔG ($\Delta G = -4488.519382$ J/mole). Hence the above said *albezia lebbeck* pods powder is effective and efficient biosorbent and is capable of removing lead.

References

- [1] P. Malakul, K.R. Srinivasan, H.Y.Wang, Metal biosorption and desorption characteristics of surfactant modified clay complexes, *Ind.Eng.Chem.Res.* 37 (1998) 4296-4301.
- [2] D. Mohan, K.P. Singh, Single and multi-component biosorption of cadmium and zinc using activated carbon derived from bagasse -an agricultural waste, *Water Res.*, 36 (2002) 2304-2318.
- [3] A.Sari, M. Tuzen, M. Soylak, Biosorption Of Pb(II) and Cr(II) from aqueous solution on Celtek clay, *J. hazard. Mater. B*, 141 (2007) 258-263.
- [4] P.Xiangliang, W. Jianlong, Z.Daoyong, Biosorption of Pb(II) by pleurotus ostreatus immobilized in calcium alginate gel, *Process Biochem.*, 40 (2005) 2799-2803.
- [5] Kratochvil D., volesky, B, Advances in biosorption of heavy metals, *Trends Biotechnol.* 16 (1998) 291-300.
- [6] Volesky, B., *Biosorption of Heavy Metals*, (CRC Press, Boca Raton, FL 1990a)
- [7] Niu, H., Volesky, B., 2003a, Biosorption mechanism for anionic metal species with waste crab shells. *Hydrometallurgy* 71 (1-2), 209-215.
- [8] Schiewer S., *Multi-metal ion Exchange in Biosorption* Ph. D. Thesis, McGill University, Montreal, Canada 1996.
- [9] W.A.P. Black and R.L. Mitchell, Trace elements in the common brown algae and in sea water, *J. Marine Biol. Assoc.* 30 (3), 575-584 (1952).
- [10] N. Kuyucak, Feasibility of biosorbents application, *Biosorption of heavy metals, B. Volesky*, (CRC Press, Boca Raton, FL, 1990), 371-378.
- [11] UNEP, Environmental aspects of the metal finishing industry: A technical guide, United Nations Environment Programme, Industry and Environment Office, Paris, 1989, 19-39 and 53-57.
- [12] B. Volesky, *Sorption and biosorption*, (BV Sorbex, Inc., Montreal, Canada, 2003) 316.
- [13] B. Volesky and Z.R. Holan, biosorption of heavy metals, *Biotechnol. Prog.* 11(3), 235-250 (1995).
- [14] Kapoor, A. and Viraraghavan, T. Fungal biosorption- An alternative treatment option for heavy metal bearing waste water: a review, *Bioresource Technology*, May 1995, vol. 53, no. 3, p. 195-206. (1995).
- [15] H.Mann, Biosorption of heavy metals by bacterial biomass, *Biosorption of heavy metals B. Volesky*, (CRC Press, Boca Raton, FL, 1990), 93-137.
- [16] N. Kuyucak and B. Volesky, Biosorption by algal biomass, *Biosorption of heavy metals B. Volesky*, (CRC Press, Boca Raton, FL, 1990), 173-198.
- [17] Holan, Z.R. and Volesky, Biosorption of lead and nickel by biomass of marine algae, *Biotechnology and Bioengineering*, 1994, vol. 43 (1994) 1001-1009.
- [18] Ferguson, J. and Bubela, B, The concentration of Cu (II), Pb (II), and Zn (II) from aqueous solutions by particulate algae matter, *Chem. Geol.*, 13 (1974) 163-186.
- [19] Ho, Y.S., Wase, D.A.J. and Forster, C.F., Batch nickel removal from aqueous solution by sphagnum moss peat, *Water Research*, 29 (5) (1995) 1327-1332.
- [20] X.H. Chen, T. Gosset and D.R. Thevenot, Batch copper ion binding and exchange properties of peat. *Water Res.*, 24 (1990) 1463-1471.
- [21] Pethkar AV, Kulkarni SK and Paknikar KM, Comparative studies on metal biosorption by two strains of *Cladosporium cladosporioides*, *Bioresour Technol* 80 (2011) 211-215.
- [22] Randall, J. M. and Hantala, E. Removing heavy metal ions from water. *U.S. Patent 3925192* (1975).
- [23] Scott, C. D., Removal of dissolved metals by plant tissue, *Biotechnology and Bioengineering* 39 (1992) 1064-1068.

- [24] Lujan, J. R., Darnal, D. W., Stark, P. C., Rayson, G. D. and Gardea_Torresdey, L. G., Metal ion binding by algae and higher plant tissues. *Solvent Extr. Ion Exch.*, 12, (4) (1994) 803-816.
- [25] Chandrasekhar K, Subramanian S, Modak JM, Natarajan KA, Removal of metals using an industrial biomass with reference to environmental control, *Int J Miner Process* 53 (1998), 107–120.
- [26] K. Parvathi, R. Nareshkumar R. Nagendran, Biosorption of lead by *Aspergillus niger* and *Saccharomyces cerevisiae*, *World J Microbiol Biotechnol* 23 (2007), 671–676.
- [27] R.N. Sylva, The environmental chemistry of copper (II) in aquatic systems, *Water Res.* 10 (1976), 789–792.
- [28] O. Masala, E.J.L. McInnes, P. O'Brien, Modelling the formation of granules: the influence of lead ions on calcium pyrophosphate precipitates, *Inorg. Chim. Acta* 339 (2002), 366–372.
- [29] Goyal N, Jain SC, Banerjee, Comparative studies on the microbial adsorption of heavy metals, *Adv Environ Res* 7 (2003), 311–319.
- [30] Sag, Y., D. Ozer and T. Kutsal, A comparative study of the biosorption of lead(II) ions to *Z. ramigera* and *R. arrhizus*, *Process Biochem.*, 30, (2) (1995), 169-174.
- [31] R.H.S.F. Vieira, B. Volesky, Biosorption: a solution to pollution, *Int. Microbiol.* 3 (2000) 17–24.
- [32] I. Langmuir, The constitution and fundamental properties of solids and liquids. Part 1: Solids, *J. Am. Chem. Soc.*, 38 (1916) 2221–2295
- [33] I. Langmuir, The adsorption of gases on plane surface of glass, mica and platinum, *J. Am. Chem. Soc.*, 40 (1918) 1361–1403.
- [34] H. Freundlich, Uber die adsorption in losungen (Adsorption in solution), *Z. Phys. Chemie.*, 57 (1906) 384-470.
- [35] M.J Temkin and V Pyzhay, Recent modifications to Langmuir isotherms, *Acta Physiochim.*, 12 (1940) 217–222
- [36] S. Lagergren, On the theory of so called adsorption of dissolved substances, *Handlingar*, 24 (1898) 1–39
- [37] Y.S. Ho and G McKay, A Comparison of Chemisorption Kinetic Models Applied to Pollutant Removal on Various Sorbents, *Process Safety and Environmental Protection*, 6B, (1998) 332-340.
- [38] Y.S. Ho and G. McKay, Pseudo-second order model for sorption processes, *Process Biochemistry*, 34 (1999) 451–465.

Implementation of Cluster based Adaptive Fuzzy Switching Median Filter for Impulse Noise Removal

Isaivani Perumal.P

ME -VLSI Design, Dept of ECE
Easwari engineering college
Chennai-89, India

Murugappriya.S

Dept of ECE
Easwari engineering college
Chennai-89, India

Abstract: A new framework for suppression of impulse noise from corrupted digital images is presented in this paper. A Filter called Cluster based Adaptive Fuzzy Switching Median Filter(CAFSM) for window size 5x5 is designed for noise removal. The filter consists of a impulse noise detector and a detail preserving noise filter. The noise detector has been used to discriminate the uncorrupted pixels from the corrupted pixels. These corrupted pixels are then subjected to the second phase of filtering action where the noise free pixels are retained and left unprocessed. The filtering mechanism also employs fuzzy reasoning to handle the uncertainties present in the local information. A window of size 5x5 is used in this paper for more accuracy. Many existing filters focus only on a particular impulse noise whereas CAFSM filter is capable of filtering all kinds of impulse noise – the random valued and/or fixed valued impulse noise models. In this paper, we also describe the design and implementation of the proposed filter in VLSI. Simulation experiments shows that the proposed filter can efficiently remove impulse noise from digital images without distorting the useful information in the image.

Index terms: Impulse noise; image denoising; switching median filter; fuzzy filtering.

I. INTRODUCTION

The visual information from high quality digital images plays a major role in many daily life applications and thus image processing has become an ordinary component in modern science. Unfortunately, during image acquisition, transmission and storage many types of distortions contaminate the image. In digital image processing, denoising is one of the important and active research area. Reduction of noise without producing distortion in the image is very difficult and challenging task.

Three main types of noise existing are impulse noise, additive noise and multiplicative noise. In this paper, we focus only on impulsive noise. Malfunctioning of pixels in camera sensors, faulty memory locations in hardware, transmission of the image in noisy channel, electromagnetic interferences and timing errors in analog-to-digital conversion are some of the common causes for impulse noise. Impulse noise is an instantaneous sharp noise where the amplitude of corruption is relatively very large compared to the strength of the original signal. As a consequence, when the signal is quantized into L intensity

levels, the corrupted pixels are generally digitized into either of the two extreme values which are minimum or maximum values in the dynamic range (i.e., 0 or L-1). Thus the impulse noise normally appears as white or black dots in the image. Large number of sensors are packed on a chip per unit area and

hence image capturing devices are more exposed to impulse noise. Thus to improve the quality of the image, digital camera manufacturers depend on image denoising algorithms. As a result, for the removal of impulse noise large numbers of techniques have been proposed.

Normally, non linear filters are used for the removal of impulse noise. Standard Median Filter(SM) [2] is one of the popular non linear filters. Median Filter is an order statistics filter where image blurring occurs since it replaces the median value for all the noise and noise free pixels. But due to its simplicity, various modifications are done in SM filter such as Weighted Median Filter (WM)[3], Centre Weighted Median Filter(CWM) and Directional Weighted Median Filter (DWM)[4]. Then Simple Adaptive Median Filter (SAM) [5] was introduced which adaptively changes the size of the median filter based on the number of noise free pixels in the neighbourhood.

Median filtering applies the filtering operation to all the pixels without considering the uncorrupted pixels which leads to serious image blurring. To overcome this problem, Switching Median Filters [7] are developed where only noisy pixels are considered and noise free pixels are left unchanged. Image degradation occurs in all the above filters. To avoid this, we go for fuzzy filters [8] [9] [10]. Then to attain more efficient result, Noise Adaptive Fuzzy Switching Median Filter [11] is introduced.

This paper explains a robust filter called Cluster Based Adaptive Fuzzy Switching Median Filter (CAFSM) [12] for detail preserving restoration. None of the above mentioned filters touched on the heavily corrupted images and they all focus on only particular impulse noise model. This filter overcomes that problem and can remove noise effectively for higher noise densities also that is it can operate on wide range of noise densities.

In this paper, we use 25 pixels as sample size that is a window size of 5x5. Always sample size should be greater than or equal to 8 pixels. If sample size is small, it is not good enough to present the local information of the image properly. The local information cannot be presented even if the sample size is very large since the samples come from many objects in the image. Large sample size

also requires more computational time and introduces distortions. Thus 25 pixels are used.

The outline of this paper is as follows. Section II elaborates the algorithm and flow chart. Section III describes the impulse noise models. The CAFSM filter design is explained in the Section IV and V. VLSI implementation and simulation results are explained in VI and VII. Finally, conclusion and future work is explained in section VIII.

II. ALGORITHM AND FLOW CHART

A. Flowchart

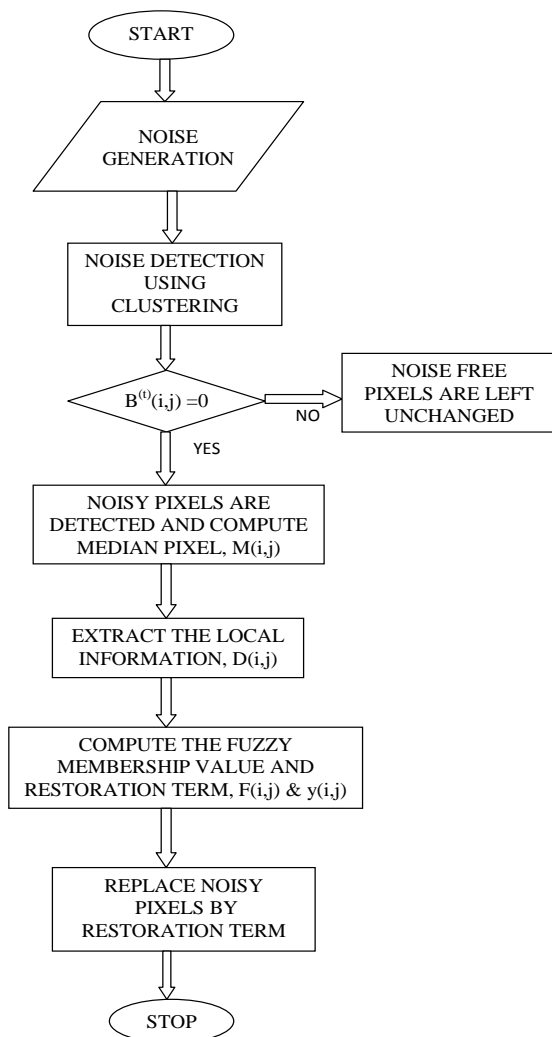


Fig 1. Flow chart for the CAFSM filter

The flow chart for converting a noisy image into a noise free image is given in fig.1. It describes steps to be followed while denoising. The generation of the noise is the first step where the original image is converted into a noisy image. The noise generation is done by multiplying a magnitude of noise density with the original image. Thus the noisy image has been obtained. Then a robust impulse noise detector is used for detecting the noisy pixels where clustering algorithm is applied. In clustering a 5x5 window size is used. The clustering algorithm distinguishes the

noisy and noise free pixels and then the filtering operation is performed. During filtering as we see in switching median filters only noisy pixels are considered and noise free pixels are left unchanged. For filtering, many computations are to be done. The fuzzy membership value and the restoration term are to be calculated. Then the noisy pixels are to be replaced with the restoration term. Finally, comparison is done by calculating PSNR and MSE values.

B. Algorithm

1. The process starts with reading the original image.
2. Convert the original image into a noisy image by adding some noise with a particular density.
3. Calculate the PSNR value for the noisy image.
4. The pixels in the noisy image are converted to window of sample size 5x5.
5. Detect whether each pixel is noisy or not using clustering procedure.
6. Then the noisy pixels and noise free pixels are separated.
7. Compute fuzzy membership value for the noisy pixels.
8. For each and every noisy pixel, compute the median value of the neighboring pixels.
9. Compute the restoration term.
10. Replace all the noisy pixels with the corresponding restoration term.
11. The above steps are to be followed iteratively for each and every pixel in the noisy image with the window size of 5x5.
12. A noise free image is obtained. Now calculate the PSNR value for the noise free image.

III. IMPULSE NOISE MODELS

In this section, we describe about the types of impulse noise. For an image of size $M \times N$, the pixel intensities lies in the range $[L_{min}$ and $L_{max}]$, where L_{min} is the lowest intensity and L_{max} is the highest intensity.

The model for impulse noise with probability ρ is defined as follows:

$$x(i, j) = \begin{cases} 0(i, j) & : \text{with probability } 1 - \rho \\ f(i, j) & : \text{with probability } \rho \end{cases}$$

where $x(i, j)$ represents the pixel in the location (i, j) and $o(i, j)$ and $f(i, j)$ represents the original and noisy image respectively.

There are two types of impulse noise in the image processing: the fixed valued impulse noise, also called as Salt and Pepper(SNP) impulse noise and the random valued impulse noise, also known as Uniform noise(UNIF). The salt and pepper impulse noise takes the value of minimal and maximal intensities, i.e., $f_{snp}(i, j) \in (L_{min}, L_{max})$. Whereas, the uniform impulse noise takes any value within the dynamic range, i.e., $f_{unif} \in [L_{min}, L_{max}]$. The impulsive noises have random amplitudes which results from interference of noise signals. Consequently, the amplitude of the impulse noise could lie within the image dynamic range or out of it. When the amplitude of impulse noise lies within the dynamic range it appears as salt and pepper noise and when it lies out of the dynamic range it is said to be uniform noise.

The general impulse noise model can be defined as:

$$x(i, j) = \begin{cases} o(i, j) & : \text{with probability } 1 - \rho \\ \text{funif}(i, j) & : \text{with probability } \rho/2 \\ \text{fsnp}(i, j) & : \text{with probability } \rho/2 \end{cases}$$

IV. CLUSTER BASED IMPULSE NOISE DETECTOR

The impulse detection is carried out by analyzing the local image statistics within a window patch whose size is bounded by the filter. A local window $W_d(i, j)$ with odd $(2L_d+1) \times (2L_d+1)$ is defined as:

$$W_d(i, j) = x(i+k, j+l) \quad \forall k, l \in \{-L_d, L_d\}$$



Sorted first order absolute differences, $D_s(m)$ and the indexed pixels, $x^l(m)$
 $D_s(m) = \{0, 1, 1, 4, 4, 37, 42, 101\}$
 $x^l(m) = \{127, 126, 126, 123, 123, 90, 169, 228\}$

No. of cluster, n , based on the Second-order absolute differences, $D^2(m)$

$$D^2(m) = \left\{ \begin{array}{l} n=1 \\ \{1, 0, 3, 0\} \\ n=2 \\ \{33, 5\} \\ n=3 \\ \{59\} \end{array} \right\}$$

$$D^2(m) < T_d(t)$$

Cluster elements, $C(n)$

$$C(1) = \{127, 126, 126, 123, 123\}$$

$$C(2) = \{90, 169\}$$

$$C(3) = \{228\}$$

Largest Cluster, $C_L(n) = C(1)$ with mean $\mu_c(1) = 125$ and standard deviation $\sigma_c(1) = 1$

Local noise free pixels boundaries(LB and HB)
 $C_L(n) = \{123, 126, 126, 127, 127\}$

$$LI = 123$$

$$HI = 127$$

$$LB = LI - \sigma_c(1) = 123$$

$$HB = HI + \sigma_c(1) = 128$$

$[LB < x(i, j) = 127 < HB]$ AND $[x(i, j) \neq L_{salt}$ AND $L_{pepper}]$
 Thus the centre pixel is a NOISE - FREE pixel

Fig 2. Clustering algorithm for noise detection

If we define LB and HB as the lower and higher boundaries for the set of noise-free pixels in $C_L(n)$, LB and HB are:

$$LB = LI - \sigma_{C(n)} \text{ and } HB = HI + \sigma_{C(n)}$$

At the end of the detection stage, a two-dimensional binary decision map $b^{(t)}(i, j)$ is formed based on

$$b(t)(i, j) = \begin{cases} 1 & : [LB \leq x(i, j) \leq HB] \\ & \cap [x(i, j) \neq L_{salt} \cap L_{pepper}] \\ 0 & : \text{otherwise} \end{cases}$$

where logic '1s' indicate the positions of noise-free pixels and logic '0s' for those noisy ones.

V. ADAPTIVE FUZZY SWITCHING MEDIAN FILTER

1. Determine the number of noise-free pixels $G(i, j)$ by computing the number of '1s' in $B(t)(i, j)$:

$$G(i, j) = \sum_{p, q \in \{-L_f, L_f\}} B^{(t)}(i+p, j+q)$$

2. Expand $W_f(i, j)$ by one pixel at each of its four sides (i.e., $L_f \leftarrow L_f + 1$) if $G(i, j) < 1$. Repeat Steps 1 and 2 until the criterion $G(i, j) \leq 1$ is satisfied.

3. Compute the median pixel $M(i, j)$ using all noise-free pixels in the current $W_f(i, j)$. The median pixel $M(i, j)$ is given as:

$$M(i, j) = \text{median} \{ x(i+p, j+q) \} \quad \forall p, q \text{ with } B^{(t)}(i+p, j+q) = 1$$

4. Extract the local information $D_f(i, j)$ from $W_f(i, j)$ according to:

$$D_f(i, j) = \max \{ D^l(m) \} = D_s((2L_d+1)^2 - 1)$$

5. Compute the fuzzy membership value $F(i, j)$ based on the local information $DI(i, j)$:

$$F(i, j) = \begin{cases} 0 & : DI(i, j) < T1 \\ \frac{DI(i, j) - T1}{T2 - T1} & : T1 \leq DI(i, j) < T2 \\ 1 & : DI(i, j) \geq T2 \end{cases}$$

Where $T1$ and $T2$ are two predefined thresholds.

6. Compute the restoration term $y(i, j)$ as follows:

$$y(i, j) = F(i, j).M(i, j) + [1 - F(i, j)].x(i, j)$$

VI. VLSI IMPLEMENTATION

For real-time embedded applications, the VLSI implementation of switching median filter for impulse noise removal is necessary and should be considered. For customers, cost is usually the most important issue while choosing consumer electronic products. We hope to focus on low-cost denoising implementation in this paper. The cost of VLSI implementation depends mainly on the required memory and computational complexity. Hence, less memory and few operations are necessary for a low-cost denoising implementation. Based on these two factors, we propose a CAFSM filter and its VLSI implementation for removing fixed-value impulse noise. Compared with previous VLSI implementations in image processing, our design achieves better image quality and also less area is occupied. This architecture work can also

be extended to RGB colour images from monochrome image.

VII. SIMULATION RESULTS

Simulation results for the noisy cameraman image using various filters is given below.

Noise Densities

Methods	0.1	0.2	0.3	0.4	0.5
Corrupted	15.07	12.08	10.29	9.024	8.088
Sam Filter	26.02	23.73	20.52	17.32	14.26
FuzzyFilter	34.27	30.69	27.96	25.91	24.13
NAFSM Filter	34.26	30.67	28.18	26.25	24.44
CAFSM Filter	40	33.98	30.46	27.96	26.02



a) original cameraman image, b) noisy cameraman image with 50% noise, simulation results using c) weighted median filter, d) partition filter, e) SAM filter, f) NAFSM filter, g) CAFSM filter.

VIII. CONCLUSION AND FUTURE WORK

In this paper, a CAFSM filter for effective removal of impulse noise is presented. This filter is able to suppress high density of impulse noise, at the same time preserving fine details, textures and edges. Further, it does not require any training or tuning of parameters once optimized. Future work, in authors opinion could be removal of impulse noise from colour images using the same algorithm.

REFERENCES

- [1] R. C. Gonzalez and R. E. Woods, Digital Image Processing, 2nd ed., Englewood Cliffs, NJ: Prentice Hall, 2002.
- [2] I. Pitas and A. N. Venetsanopoulos, "Order statistics in digital image processing," Proc. IEEE, vol. 80, no. 12, pp. 1893-1921, Dec. 1992.
- [3] D. R. K. Brownrigg, "The weighted median filter," Commun. ACM, vol.27, no. 8, pp. 807-818, Aug. 1984.
- [4] Y. Dong and S. Xu, "A new directional weighted median filter for removal of random-valued impulse noise," IEEE Signal Process. Lett., vol. 14, no.3, pp. 193-196, Mar. 2007.
- [5] H. Ibrahim, N. S. P. Kong, and T. F. Ng, "Simple adaptive median filter for the removal of impulse noise from highly corrupted images," IEEE Tr.
- [6] Y. Dong, R. H. Chan, and S. Xu, "A detection statistic for random-valued impulse noise," IEEE Trans. Image Process., vol. 16, no. 4, pp. 1112-1120, Apr. 2007.
- [7] P. E. Ng and K. K. Ma, "A switching median filter with boundary discriminative noise detection for extremely corrupted images," IEEE Trans. Image Process., vol. 15, no. 6, pp. 1506-1516, June 2006.ans. Consumer Electron., vol. 54, no. 4, pp. 1920-1927, Nov. 2008.
- [8] W. Luo, "Efficient removal of impulse noise from digital images," IEEE Trans. Consumer Electron., vol.52, no. 2, pp. 523-527, May 2006.
- [9] P. Civicioglu, "Using uncorrupted neighborhoods of pixels for impulsive noise suppression with ANFIS," IEEE Trans. Image Process., vol. 16, no.3, pp. 759-773, Mar. 2007.
- [10] F. Russo and G. Ramponi, "A fuzzy filter for images corrupted by impulse noise," IEEE Signal Process. Lett., vol. 3, no. 6, pp. 168-170, June 1996.
- [11] K. K. V. Toh and N. A. Mat Isa, "Noise adaptive fuzzy switching median filter for salt-and-pepper noise reduction," IEEE Signal Process. Lett., vol.17, no. 3, pp. 281-284, Mar. 2010.
- [12] Kenny Kal Vin Toh, and Nor Ashidi Mat Isa, "Cluster-Based Adaptive Fuzzy Switching Median Filter for Universal Impulse Noise Reduction," IEEE Transactions on Consumer Electronics, Vol. 56, No. 4, November 2010.

Functionalization and Fabrication of MWCNT on Screen Printed Carbon Electrode

A. RUHAL¹, J. S. RANA^{2*}, S. KUMAR¹, A. KUMAR³

¹Department of Bio and Nanotechnology, G. J. University of Science and Technology, Hisar-125001, India

²Department Biotechnology D.C.R University of Science & Technology Murthal, Sonipat 131039, India

³Institute of Genomics and Integrative Biology, Mall Road, Delhi-11007, India

Abstract

Carbon nanotubes (CNT) are one of the most widely used nonmaterials. It is applied in various fields due to its special physical characteristics, excellent electronic performance and stable chemical activity. There are two types of CNT occur (a) Single walled carbon nanotube (b) Multiwalled carbon nanotube. As their names shows, SWNTs consist of a single, cylindrical graphene layer, where as MWNTs consist of multiple graphene layers. CNT facilitate electron-transfer between electro-active species and electrode when it used as electrode material. To obtain quick and specific response of electrode, a functional group is attached to the nanotube. Functionalization shows the presence of C-O groups at the open end of nanotubes. Chemical changes were monitored by FTIR. Carboxylated Multi walled CNT treated with mixture of DMF and water to overcome its solubility problem. Now this homogenized mixture was used for fabrication of Screen printed carbon electrode for further use in formation of biosensor.

Keywords: c-MWCNT, CNT, DMF, Screen printed carbon electrode (SPCE) and Ultrasonication.

1. Introduction

Carbon is the basic element of life. It exhibits a richness of allotropes with different carbon-carbon bonds and different physical and chemical properties. In the history of carbon, discovery of CNT is an important milestone (1). Sumio Iijima in 1991 discovered CNT which is the allotrope of carbon with cylindrical nanostructure. CNT resemble graphite rolled up to a tube. Rolling of a single layer of graphite into a seamless cylinder composed single walled carbon nanotube (SWCNT) with diameter 1-2 nm (2). Assembly of cylinder of SWCNT one within another formed MWCNT. The three main methods for the production of CNT are (a) arc discharge method (b) laser vaporization and (c) chemical vapor deposition (CVD) (3). Due to their unique structural, physical, chemical and electronic properties many researchers are involved in CNT study. These properties provide a wide range of applications such as DNA biosensor, field emission devices, scanning probe microscopy tips, gas sensors, chemical sensors, potential hydrogen storage material, batteries, nanoelectronic devices etc (4). CNT properties and their applications has been the subject of many studies. It depends on structure, diameter and helicity of carbon nanotube whether it will act as semiconductors or show metallic behaviour. Open end of CNTs originate electro- catalytic properties (5). In recent past CNTs have been used for production of electrodes to improve electron transfer kinetics. So CNTs have acquired broad consideration as an electrode material. In comparison to SWCNT electrode, MWCNT electrode is easy to develop which shows promising electrochemical properties. CNT facilitate electron-transfer between electro-active species and electrode when it is used as electrode material (6). Functionalization of CNTs improve their solubility in physiological solutions and selective binding to biotarget (7).

The walls of CNTs are hexagonal carbon rings and are generally formed in large bundles. The ends of CNTs are domed structures of six membered rings capped by five membered rings (8). But when CNTs are functionalized by different acids, cap and sidewall break in different sites, producing defects on the CNT walls by introducing functional groups. Two types of acid treatments used for CNT are reflex with solution of nitric acid and exposing sample to mixture of HNO₃/H₂SO₄ (1:3) under ultrasonication for 6 h (9). Kyotani *et al.* (10) used nitric acid for oxidation treatment of inner wall of multiwalled carbon nanotubes and claimed that during their experimental conditions no damage to the MWCNTs occurred. A layer of Sp²-bonded carbon atoms form the basic structure of CNT in which each atom in x-y plane is connected to three other carbon atoms and in z-axis by a weakly delocalized- electron cloud. This composition of CNT is responsible for the buildup of strong van der waal's forces that notably obstruct dispersion and solubility of carbon nanoparticles (11). Main disadvantage of CNT is their crucial solubilization. To overcome this problem organic solvent like DMF or DMSO and aqueous solution of nafion are being used. Even highly carboxylated CNTs(c-CNTs) are dissolve in aqueous solutions without using surfactants. Carboxylic groups of c-CNT admit covalent bonding with biomolecules or solid surfaces (12). Three types of SPE are commercially available. SPE have working disk electrode of different nature: carbon, gold/ink high temperature and gold/ink low temperature. The auxiliary electrode imprint on each strip is made up of same ink as working electrode and a silver pseudo-reference electrode was always used (13). To alter the surface of commercially available screen-printed electrode carboxylated multiwall carbon nanotube dissolved in a mixture of DMF & water. Modification begins with dissolving CNT in solution and after that CNT fabricate on

SPE. The morphology of MWCNT-COOH and modified SPE are characterized by scanning electron microscopy SEM (14). Such screen printed CNT electrodes offer large scale mass production of highly reproducible low-cost electrochemical biosensors (15). In this study functionalization of CNT and then fabrication on Screen printed carbon electrode which is further used for biosensor preparation have been elucidated.

2. Materials and Method

2.1 Materials and instruments

Multiwalled carbon nanotube (MWCNT) was purchased from Nanostructured and Amorphous Materials, Inc. Houston, USA. DMF was procured from Sisco Research Laboratory, India. Other chemicals were of Analytical Reagent (AR) grade. Commercially available screen printed carbon electrode (SPCE) was obtained from Dropsens, Spain. Screen printed electrode include three-electrode configuration in which carbon (working), platinum (counter) and silver (reference) electrodes are printed in close proximity. Ultrasonicator (SCIENTZ Biotechnology Co. Ltd.) used for sonication. Fourier transformed infrared spectroscopy (Model: IRAffinity -1 Shimadzu) was conducted at Guru Jambheshwar University of Science & Technology, Hissar. Scanning electron microscopy (Model: JEOL JSM-6510) was conducted at IIT Delhi.

2.2 Functionalization of multiwalled carbon nanotubes

This experiment was conducted with a mixture of nitric acid and sulfuric acid. 10mg Multiwalled carbon nanotube was suspended into 13 ml mixture of concentrated H_2SO_4 and HNO_3 in 3:1 ratio and ultrasonicated them at 34°C for 8 h to obtain a homogeneous mixture (Fig.1). After sonication MWCNT dispersion was filtered through milipore nylon filter membrane. Now the supernatant of MWCNT was washed thoroughly with distilled water until the pH of the washing discard was 7 and then dried overnight in a vacuum oven at 120°C . Functionalized MWCNT was characterized by FTIR.

2.3 Fabrication of functionalized CNT on SPCE

Carboxylated multiwalled carbon nanotubes (6.0 mg) were dispersed in 10 ml solution of Dimethylformamide (DMF) & Water(1:1) and ultrasonicated at room temperature for 6 h to obtain a completely homogenized solution. $5\ \mu\text{l}$ of the c-MWCNT solution was coated on the surface of working electrode (carbon) of SPCE and kept for 12 h at room temperature (Fig.2). The excess unbound c-MWCNTs were removed by 2-3 washing with water. Then, c-MWCNT/SPCE was dried completely at room temperature. The fabricated electrode was characterized by scanning electron micrograph (SEM).

3. Results and Discussions

3.1 FTIR Spectra

FTIR samples prepared by grinding multiwalled carbon nanotube into potassium bromide powder. Low concentration of MWCNT is necessary due to high absorption of the nanotubes. Spectra performed at 120°C in absorption mode. Fig.3 shows the FTIR spectra of carboxylated MWCNTs. Peak at $1570\ \text{cm}^{-1}$ can be associated with the stretching of carbon nanotubes backbone. Chemical treatment with the acid mixture introduces additional peaks in the spectra. Peak obtained at $1635\ \text{cm}^{-1}$ is associated with the stretching of CNT backbone. Peak at $3022\ \text{cm}^{-1}$ shows the O-H stretching. One small peak appearing at $1404\ \text{cm}^{-1}$ is possibly associated with O-H bending deformation in carboxylic acid groups whilst increased strength of the signal at $1226\ \text{cm}^{-1}$ may be associated with C-O stretching in the same functionalities. In addition, a small peak appears at $945\ \text{cm}^{-1}$, which can be associated with ether R-O-R functionalities, for H_2SO_4 & HNO_3 treatment. The FTIR spectrum of c-MWCNT shows a peak at $2360\ \text{cm}^{-1}$ associated with O-H stretch from strongly hydrogen bonded -COOH.

3.2 SEM studies

The morphology of fabricated c-MWCNT/SPC electrode was characterized by SEM studies Fig.4 shows the presence of c-MWCNT on SPCE.

4. Conclusion

Treatment with mixture of nitric acid & sulphuric acid (1:3) for 8 h show relevant effect on side walls of multiwalled carbon nanotubes. Results show the presence of C-O groups at the open end of nanotubes. Modification of electrodes with CNT is used to increase the rate constant for electron transfer and electro active area. Fabrication of functionalized MWCNT on screen printed carbon electrode results in a mesoporous coating where original electrode surface become an electrical contact.

Acknowledgement

Anita Ruhai is grateful to State Government of Haryana for providing Sir C.V Raman fellowship to carry out this work.

References

- [1] W. Kangbing, J. Xiaobo, F. Junjie and H. Shengshui, The fabrication of a carbon nanotube film on a glassy carbon electrode and its application to determining thyroxine, *Nanotechnology*, 15, 2004, 287–291.
- [2] A. M. Pulickel and Z. Z. Otto, Applications of Carbon Nanotubes, *Topics Applied Physics*, 80, 2001, 391–425.
- [3] C. H. Hung, U. Y. Wu, K. T. Chien, L. M. Shan, Y. N. Tsun, L. Y. Zhen and C. C. Chin, Selective growth of well-aligned carbon nanotubes by APCVD, *Journal of Material Science: Material Electronics*, 20, 2009, 407–411.
- [4] P. S. Germaire and C. R. Carlos, Vertical attachment of DNA–CNT hybrids on gold, *Journal of Electroanalytical Chemistry*, 606, 2007, 47–54.
- [5] S. Laschi, E. Bulukin, I. Palchetti, C. Cristea and M. Mascini, Disposable electrodes modified with multi-wall carbon nanotubes for biosensor applications, *ITBM-RBM*, 29, 2008, 202–207.
- [6] T. G. Nikos and R. Uwe, Synthesis and electrochemistry of multiwalled carbon nanotube films directly attached on silica substrate, *Journal of Solid State Electrochemistry*, 4, 2010, 1101–1107.
- [7] R. B. Jahan, O. Reza and C. Fereshteh, Fabrication of functionalized carbon nanotube modified glassy carbon electrode and its application for selective oxidation and voltammetric determination of cysteamine, *Journal of Electroanalytical Chemistry*, 633, 2009, 187–192.
- [8] S., Iijima, Helical microtubules of graphitic carbon, *Nature*, 354, 1991, 56–58.
- [9] S. Goyanes, R. G. Rubiolo, A. Salazar, A. Jimeno, A. M. Corcuera and I. Mondragon, Carboxylation treatment of multiwalled carbon nanotubes monitored by infrared and ultraviolet spectroscopies and scanning probe microscopy, *Diamond & Related Materials*, 16, 2007, 412–417.
- [10] T. Kyotani, L. Tsai and A. Tomita, Formation of platinum nanorods and nanoparticles in uniform carbon nanotubes prepared by a template carbonization method, *J. Chem. Soc. Chem. Commun.*, 1997, 701–702.
- [11] S. Karen, S. W. Patricia, H. Gabrielle, M. A. Germán and G. D. Carlos, Recent applications of carbon-based nanomaterials in analytical chemistry: Critical review, *Analytica Chimica Acta*, 691, 2011, 6–17.
- [12] A. M. Abdul and Y. Haesik, Electrochemical immunosensor using the modification of an amine-functionalized indium tin oxide electrode with carboxylated single-walled carbon nanotubes, *Bull. Korean Chem. Soc.*, 28, 2007, 7.
- [13] L. A. P. Jose, Q. Paula, F. B. Pablo and C. G. Agustin, Multiwalled carbon nanotube modified screen-printed electrodes for the detection of *p*-aminophenol: Optimisation and application in alkaline phosphatase-based assays, *Analytica Chimica Acta*, 615, 2008, 30–38.
- [14] F. B. Pablo, Q. Paula, L. A. P. Jose and C. G. Agustin, Manufacture and evaluation of carbon nanotube modified screen-printed electrodes as electrochemical tools, *Talanta*, 74, 2007, 427–433.
- [15] S. Sanchez, M. Pumera, E. Cabruja and E. Fabregas, Carbon nanotube/polysulfone composite screen-printed electrochemical enzyme biosensors, *Analyst*, 132, 2007, 142–147.

Legends

Fig 1. Image of a stable solution of carboxylated multiwalled CNT after sonication.

Fig 2. Fabricated Screen Printed Carbon Electrode with carboxylated multiwalled CNT.

Fig 3. FTIR Spectrum obtained for c-MWCNT

Fig 4. SEM Images of c-MWCNT/SPC electrode



Fig 1.



Fig 2.

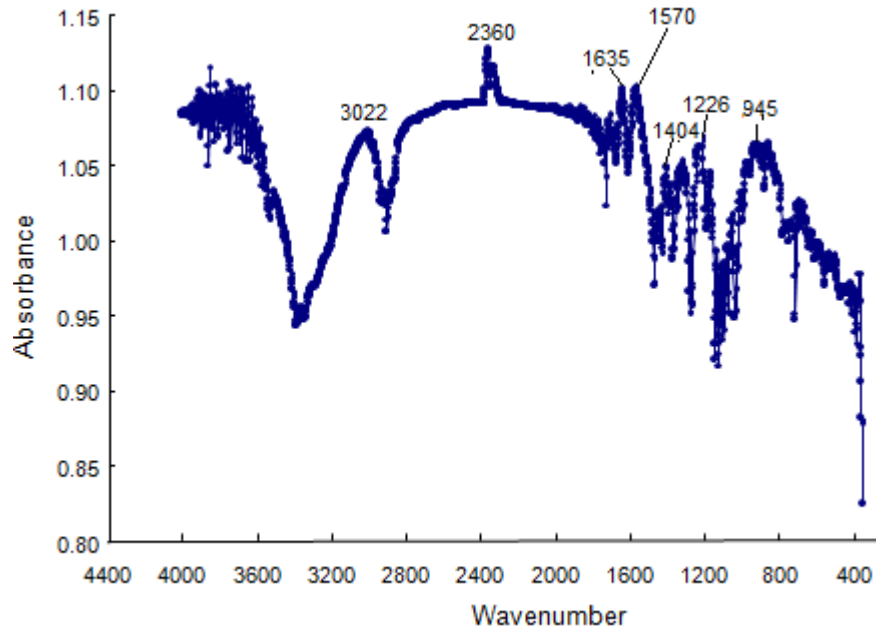


Fig 3.

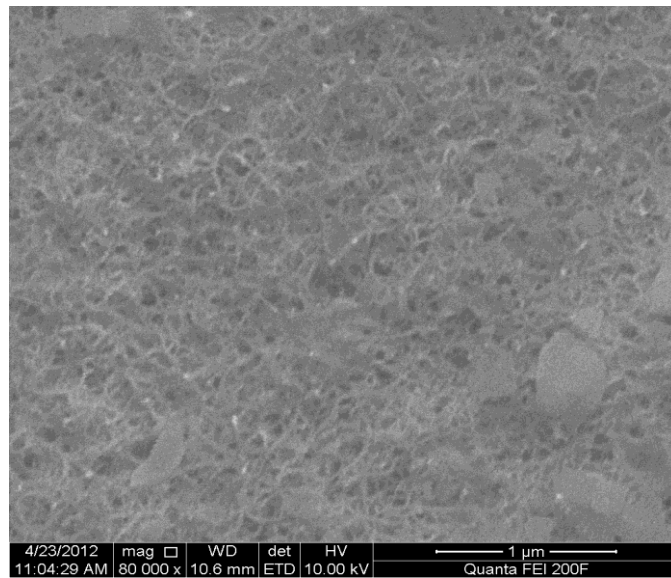


Fig 4.

Design and Implementation of Data Rate Controller Using Micro blaze Processor

B. Murali Krishna¹, B. Raghu kanth², G. Phani Kumar³, K. Gnanadeepika²,
S. R. Sastry kalavakolanu²

¹ Assistant Professor, ECE Department, K.L. University, Vijayawada, Andhra Pradesh, India.

² P.G students, ECE Department, K.L. University, Vijayawada, Andhra Pradesh, India.

³ Assistant Professor, ECE Department, S.V. Engineering College, Bobbili, Andhra Pradesh, India

Abstract: - *FPGA-based solutions become more common in embedded systems these days. These systems need to communicate with external world. Considering high-speed and popularity of Ethernet communication, developing a reliable real-time Ethernet component inside FPGA is of special value. The Ethernet Mac (Media access control), sub level with in data link layer of the OSI reference model. Ethernet performance has increased from megabits per second (M bits/s) to gigabits per second (G bits/s) and its popularity reflects not only its status as an IEEE standard, but because the Ethernet protocol has a number of features and benefits that have proved attractive to designers and engineers. The Mac is the portion of the Ethernet core that handles transmitting and reception of the frames. It performs the frames data encapsulation and de-capsulation, frame transmission and frame reception. In this paper the authors presented up to the data rate transmission from a PC to FPGA board and the work is carried out in XILINX10.1 EDK tool in C language.*

Keywords – EDK, FPGA, MAC, OSI, Microblaze processor.

I. INTRODUCTION

FPGAs are increasingly being used for many systems and efficient SoC (System-on-a-Chip) designs. Competitive market environment and high security areas such as military systems are among the factors that make protecting designs implemented in FPGAs more important. Without proper safeguards, design information and proprietary intellectual properties face major security risks and attackers will be able to steal the design contained in the bit stream of

FPGAs. In common with earlier IEEE 802.3 standards, 10 Gigabit Ethernet will ultimately define a standard which ensures interoperability between products from different vendors. The standard primarily specifies the physical layers and only a small change will be made to the media access control (MAC). [1][3]The adoption of cost effective, robust technologies largely enabled Ethernet to dominate the LAN market; the same approach is being used in the development of the 10 Gigabit Ethernet (10GbE). A significant difference however is that 10GbE represents the merging of data communications and telecommunications. In the International Standards Organization's Open Systems Interconnection (OSI) model, Ethernet is fundamentally a Layer 2 protocol. 10 Gigabit Ethernet uses the IEEE 802.3 Ethernet Media Access Control (MAC) protocol, the IEEE 802.3 Ethernet frame format, and the minimum and maximum IEEE 802.3 frame size. Just as Gigabit Ethernet remained true to the Ethernet model, 10 Gigabit Ethernet continues the natural evolution of Ethernet in speed and distance. Since it is a full-duplex only and fiber-only technology, it does not need the carrier-sensing, multiple-access with collision detection, (CSMA/CD) protocol that defines slower, half-duplex Ethernet technologies. In every other respect, 10 Gigabit Ethernet remains true to the original Ethernet model.

An Ethernet PHYSical layer device (PHY), which corresponds to Layer 1 of the OSI model, connects the media to the MAC layer, which corresponds to OSI Layer 2. Ethernet architecture further divides the PHY (Layer 1) into a Physical Media Dependent (PMD) and a Physical Coding Sublayer (PCS). Optical transceivers, for example, are PMDs. The PCS is made up of coding (e.g., 64/66b) and a serialize or multiplexing functions. the following figure shows the architecture of the data flow from physical layer to the data link layer.[5]

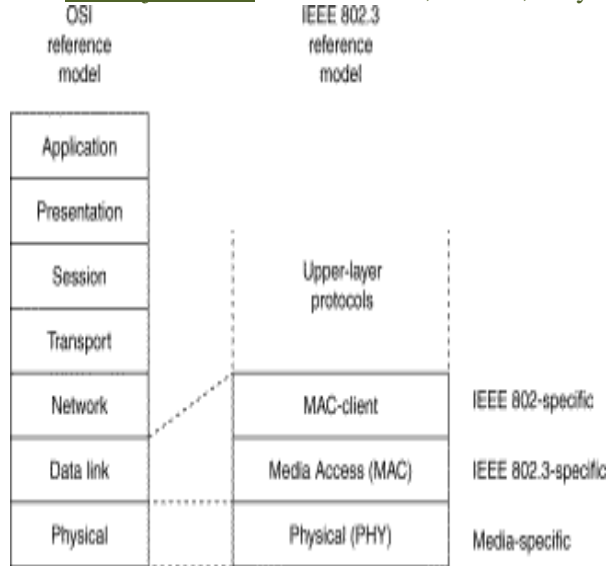


Fig 1. Layer representation of LAN Model with respective to OSI reference model.

The combination of the physical coding sub layer (PCS), the physical medium attachment (PMA), and the physical medium dependent (PMD) sub layers consists the physical layer protocol.

II. ABOUT LAN

Ethernet is the most widely-installed local area network (LAN) technology. Specified in a standard, IEEE 802.3, Ethernet was originally developed by Xerox from an earlier specification called *Alohanet* (for the Palo Alto Research Center Aloha network) and then developed further by Xerox, DEC, and Intel. An Ethernet LAN typically uses coaxial cable or special grades of twisted pair wires. Ethernet is also used in wireless LANs. The most commonly installed Ethernet systems are called 10BASE-T and provide transmission speeds up to 10 Mbps. Devices are connected to the cable and compete for access using a Carrier Sense Multiple Access with Collision Detection (CSMA/CD) protocol. Fast Ethernet or 100BASE-T provides transmission speeds up to 100 megabits per second and is typically used for LAN backbone systems, supporting workstations with 10BASE-T cards. Gigabit Ethernet provides an even higher level of backbone support at 1000 megabits per second (1 gigabit or 1 billion bits per

second). 10-Gigabit Ethernet provides up to 10 billion bits per second.[5]. The frame format for the Ethernet is given below in which the data is transmitted in between the physical medium and the data link layer medium.

PRE	SOF	DA	SA	Type	Data	FCS
7	1	6	6	2	1500	4

Fig 2: Ethernet frame structure.

The following gives the detailed description of the parameter used in the Ethernet frame structure.

PRE(Preamble) : it is of 7byte and is an alternating patterns of 1`s and 0`s that tells receiver stations that a frame is coming and that provides a means to synchronize the frame reception portions physical layer with incoming bit stream.

SOF(Start of frame delimiter) : it is of 1 byte, and an alternating patterns of 1`s and 0`s ending with two consecutive 1-bits indicating that the next bit is the left most bit in the left most byte of destination address.

DA(destination Address) : it is of 6 bytes indicating the which station should receive the frame.

SA(sending Address) : it is of 6 bytes indicating the which station should sends the frame.

LENGTH/TYPE: it is of 2 bytes, this field indicates either the number of the MAC client data bytes that are contained in the data filed of the frame of the frame type ID if the frame is assembled using an optional format.

DATA : it is a sequence of ‘n’ bytes ($46 \leq n \leq 1500$) of any value of total frame with 64 bytes.

FCS(Frame check sequence) : it is of 4bytes contains 32-bit crc value which is creates by the sender MAC and is re-calculated by the recovering MAC to the check for damage format.

III. CYCLIC REDUNDANCY CHECK

The cyclic redundancy check is a technique for detecting errors in digital data, but not for making corrections when the error are detected. It is used primarily in data transmission. In CRC a certain number of check bits, often called check sum are appended to the message being transmitted. The receiver can determine whether or not the check bits agree with the data to ascertain with a certain degree of probability whether or not an error occurred in transmission. If an error occurred the receiver sends a –ve acknowledgement back to the sender, requesting that the message be re transmitted. The technique is also some times applied to the data storage devices, such as disk drives. In this situation each block on the disk would have check bits and the hardware might automatically initiate a re-thread of the block when the error is detected , or it might report the error to software . the material that follows speaks in terms of a ‘sender’ and a ‘receiver’ of a message but it should be under stood that it applies to storage writing and reading. Theory of CRC is straight forwarded, the data is treated by the CRC algorithm as a binary number[8]. This number is divided by another binary number called the polynomial. The rest of the division is the CRC check sum which is appended to the transmitted message . the receiver divides the message by the same polynomial the transmitted used. If the result of this addition is zero then the transmission was successful. However if the result is not equal an error occurs during transmission. CRC is a common method for detecting errors in transmitted messages or stored data. The CRC is a very powerful but easily implemented technique to obtain data reliability.

IV. MICROBLAZE ARCHITECTURE

Micro blaze is a 32-bit RISC Harvard soft core processor that can be embedded in the re-configurable logic of an fpga.The fixed feature set of the processor includes:

- 32-bit general purpose registers
- 32-bit instruction word with three operands and two addressing modes
- 32-bit address bus
- Single issue pipeline
- Having up to 14 special purpose registers.

The micro blaze core is parameterized to allow enabling of a set of configurable features. The micro blaze is having an extensive instruction set with many of a operations having large number of variants for registers, immediate, const, signed and unsigned[6][5]. The basic design can be configured with advances features such as barrel shifter, memory management unit, floating point, caches, exception handling and debug logic. In addition some of the logics such as floating point multiplication and division are optional in various hardware configurations. Micro blaze soft core processor is a major component of XILINX EDK. The EDK also includes the XPS(Xilinx Platform Studio) and a library of peripheral Ip soft cores. The Micro blaze architecture is shown below. Designing a microblaze embedded processor with multiple peripherals using both vendor supplied and the user created custom IP's each of which has a different level of priority.

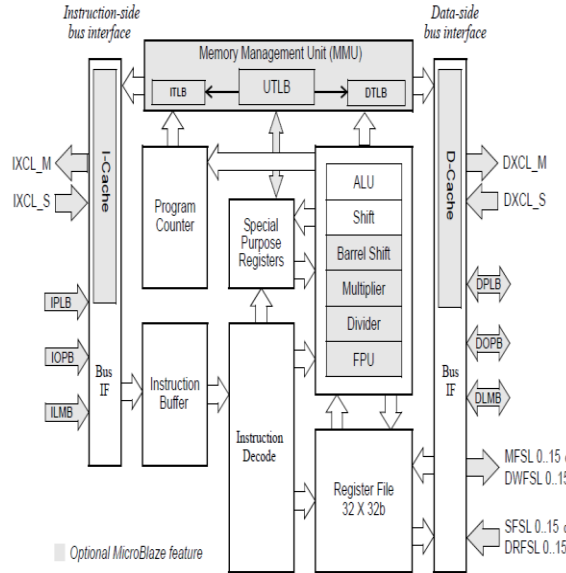


Fig3. Micro blaze Architecture.

V.EXPERIMENTALSETUP AND RESULTS

The main aim of this paper is to show that even we can create a web server application basing on the SPARTAN xc3s500e FPGA. There are certain adjustments that should be done in the XILINX10.1 EDK tool to get the data rate controlling in between the PC and the FPGA Board. This paper only provides up to some extend where the data is transferred and received by the board i.e., through physical medium and data link layer using MAC's sub portion layers and establishing a connection between FPGA and regular PC. There are two more libraries that to be included in the XILINX EDK project they are XILMFS [XILINX MEMORY FILE SYSTEM] and LWIP [Light weight IP]. The LWIP is again having 5 more sub libraries to modify as they are

- TFTP server.
- ECHO server.
- WEB server.
- TCP Rx through put test.
- TCP Tx through put test.

After initializing the above mentioned libraries which are available in 'software' and 'software setting libraries as shown in the below two figures.

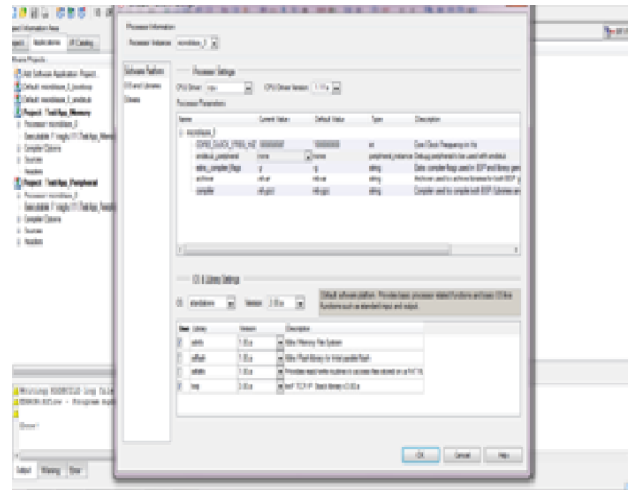


Fig 4 Adding XILMFS to the existing EDK project.

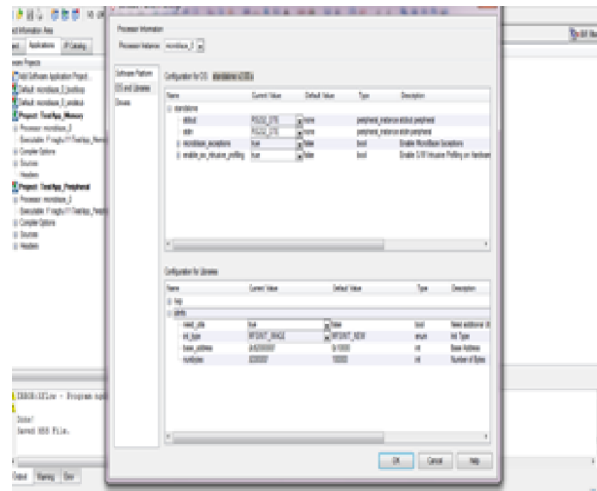


Fig 5 Adding LWIP to the existing EDK Project.

The code is written in C language for the web server application and we check for the details of the MAC and then we go for the output results. The experimental set up for this paper is shown in the below figure.

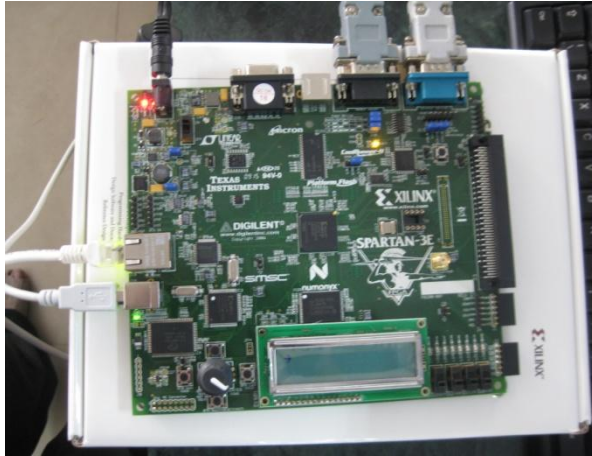


Fig6 Experimental set up SPARTAN 3E board.

First we verify the MAC layers which is a sub portion of the physical layer and data link layer.

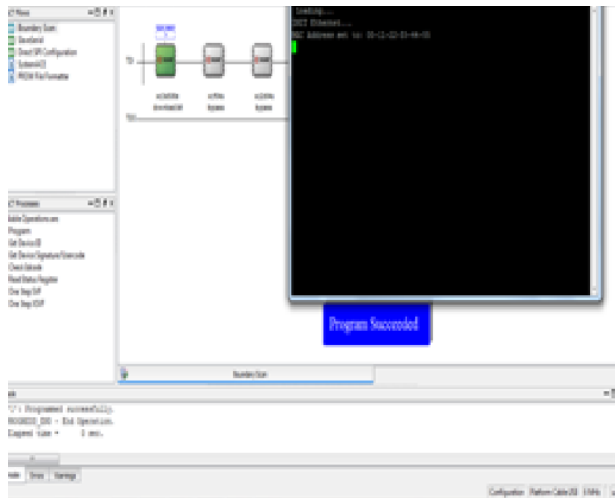


Fig 7 testing MAC layers.

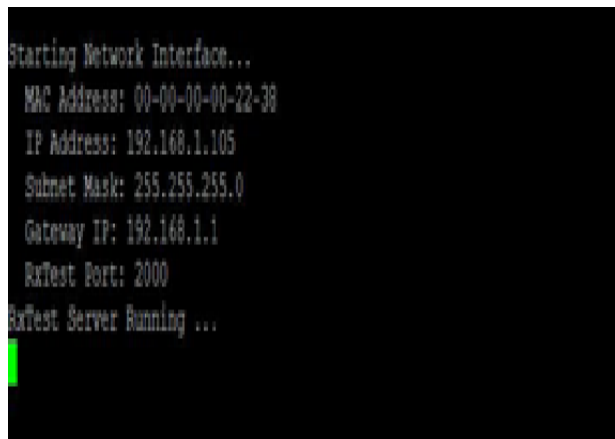


Fig8 PC and FPGA board are pinged with each other.

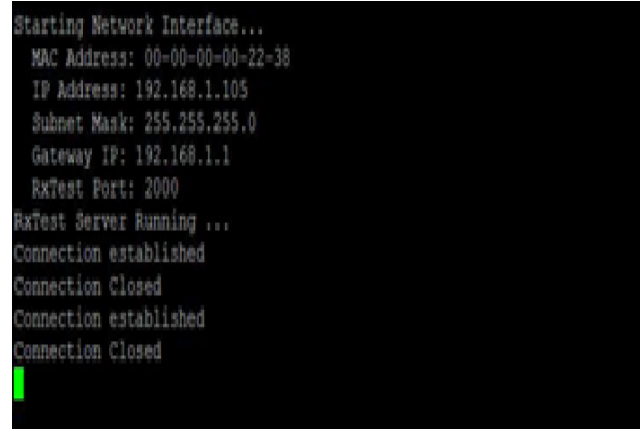


Fig9 connection established and closed.

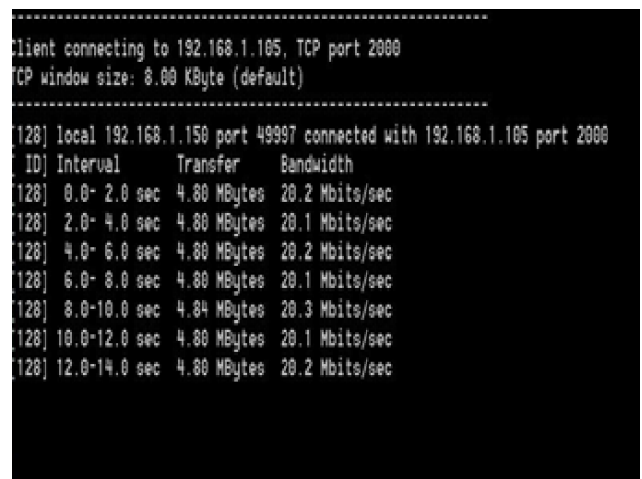


Fig 10 data rate transmission between FPGA board and PC.

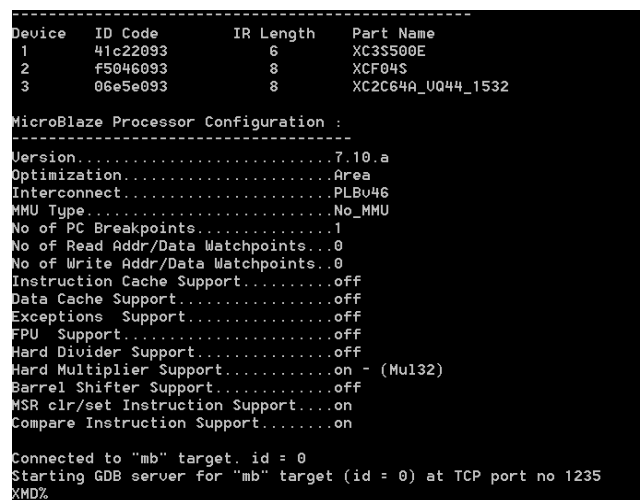


Fig11. TCP/IP connected with the local host or the targeted device

The above results all are verified in the putty terminal using the cross over Ethernet cable. Hence we can say that by using a microblaze processor we can access the data flow between two peripherals.

VI. CONCLUSION

The Ethernet is intended primarily for use in such areas as office automation, distributed data processing, terminal access, and other situations requiring economical connection to a local communication medium carrying bursty traffic at high peak data rates. Hence we can conclude that the web server application can be possible by using SPARTAN 3E fpga and we can monitor the other peripherals which are presented on the FPGA board but require time to initialize that application.

REFERENCES

- [1] Design and Optimization of Medium Access Control Protocol of IEEE 802.3 Transmitter with VHDL by Puran Gour Ravi Shankar Mishra Saima Khan Rajesh Nema in IJCA in JAN 2011.
- [2] www.Xilinx.com
- [3] www.Picocomputing.org.
- [4] FPGA implementation of Real-time Ethernet communication using RMII Interface by Nima Moghaddami Khalilzad and Sheida Pourshakour.
- [5] www.wikipedia.org
- [6] Spartan 3e fpga user guide
- [7] Getting Started with the MicroBlaze Development Kit - Spartan-3E 1600E Edition by diligent systems
- [8] computer networks by William stallings.

Authors profile:-



B. Raghu Kanth was born on 28th June at Vijayawada. He obtained his Bachelor's degree from JNTU, HYD in ECE Department in 2007. He is pursuing M.Tech in VLSI from K.L.University at Vijayawada. He has more than two and half years of teaching experience and having four International Journal publishing. His area of interest are analog vlsi and testing and FPGA.

B.Muralikrishna was born in AP, India. He received his, Diploma degree in Electronics & Communication Engineering from SIR C.R.Reddy Polytechnic, Eluru, A.P., B.Tech degree in Electronics & Communications Engineering from Nimra College of Engineering & Technology, Vijayawada, A.P., India, Affiliated to the JNTU Hyderabad in 2007, M.Tech degree in VLSI Design from GITAM University Vishakhapatnam, A.P India, in 2010. Presently he is working as Assistant Professor, Department of ECE in K.L.University, Guntur, AP, India. He had one year experience in Viraj IT solutions PVT Ltd. as Software Engineer during 2007-2008. His area of interest are Low-Power VLSI, Design for Testability, CPLD's & FPGA Architectures, Embedded Systems and Fault Tolerance.



G. Phani Kumar was born on 26th October at Kakinada. He obtained his Bachelor's degree from JNTU, HYD in ECE Department in 2007. He obtained his M.Tech from SATYABHAMA University, Chennai in 2009. He is currently working as an assistant professor in S.V. Engineering College at Bobbili from 2009. He is having two and half years of teaching experience. His area of interest is in Analog VLSI, FPGA, and testing.

Performance of a Low Cost Tabletop Die Sinker Electric Discharge Machining [EDM] Unit

¹P. S. Rao, ²B. Surendrababu, ³M. Rambabu,

¹ Professor, GIT, GITAM UNIVERSITY, Visakhapatnam A.P., India

² Professor, GIT, GITAM UNIVERSITY, Visakhapatnam A.P., India

³ Asst. Professor, GMR Institute of Technology, Rajam-532127, A.P., India

Abstract: New developments in the field of material science have led to new engineering metallic materials, composite materials, and high tech ceramics, having good mechanical properties and thermal characteristics as well as sufficient electrical conductivity so that they can readily be machined by spark erosion. The recent development of new materials that are hard and difficult-to-machine such as tool steels, composites, ceramics, super alloys, hast alloy, nitralloy, waspalloy, nemonics, carbides, stainless steels, heat resistant steel, etc. being widely used in die and mould making industries, aerospace, aeronautics, and nuclear industries. Many of these materials also find applications in other industries owing to their high strength to weight ratio, hardness and heat resisting qualities. EDM has also made its presence felt in the new fields such as sports, medical and surgical instruments, optical, dental including automotive R&D areas. EDM technology is increasingly being used in tool, die and mould making industries, for machining of heat treated tool steels and advanced materials (super alloys, ceramics, and metal matrix composites) requiring high precision, complex shapes and high surface finish. Heat treated tool steels have proved to be extremely difficult-to-machine using traditional processes, due to rapid tool wear, low machining rates, inability to generate complex shapes and imparting better surface finish. EDM provides a easy solution. This ,present work provides an approach to make an EDM unit at reasonably low cost, and its performance.

Keywords: Sinker EDM, Die-electric media, Spark erosion.

THE SETUP:

The present paper deals with making a low cost setup of Sinker type EDM for general machining of hard materials like machining steels, ceramics, etc., using RC circuit with copper and graphite as tool material and kerosene as dielectric medium as shown in the Fig. 1. The performance and process capabilities of the developed setup are here under.

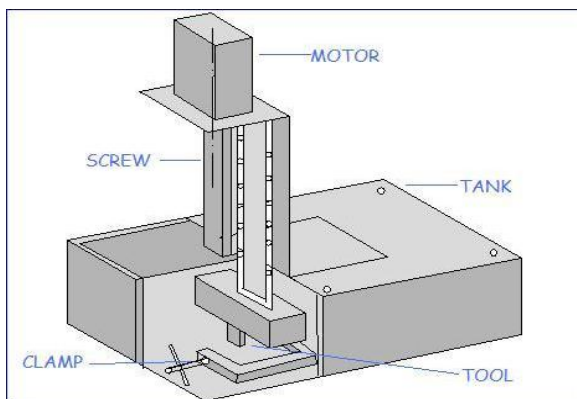


Fig. 1: Low Cost EDM Setup



Fig. 2: Low cost Sinker EDM

Part List:

Stepper Motor, Controller, Pulse Generator Circuit, Power Supply, Basic Electrical Components(Wires, Capacitors Etc), Graphite Electrode/Copper Electrode, Electrolyte-Kerosene, Plastic Tank, Fuel Filter, Etc. With Cost Of Re 7,000/-.[\$300]

The power supply must provide enough spark to the sparking gap for material removal. It must also monitor the electrical conditions at the sparking gap and direct the machine servo in advancing, retracting, or maintaining the position of the electrode, in reference to the work piece. The dielectric unit must provide the dielectric fluid to the machine submersing the work piece. In addition, the dielectric unit must send fluid to the dielectric gap for cooling purposes and to remove the EDM chip. The

dielectric unit includes a filtration system for cleaning the dielectric fluid. The machine tool is the focal point of the die-sinker.

DEVELOPMENT OF POWER SUPPLY:

A relaxation generator (R-C type) used as as power supply unit. The power supply unit used is quite simple. A VARIAC (Variable Auto Transformer) is used to adjust output voltage. In the power supply unit, rectification is normally achieved using a solid state diode. Diode has the property that will let the electron flow easily at one direction at proper biasing condition. Bridge rectifiers of 4 diodes are used to achieve full wave rectification. Two diodes will conduct during the negative cycle and the other two will conduct during the positive half cycle. Therefore bridge rectifier is used to convert AC to DC. This DC power supply is used to charge the capacitor connected in series to resistor. A filter capacitor provides smoothing of the DC voltage produced. A resistor allows the electrode to short to the work without blowing fuses, and also moderates the flow of current from the raw DC supply to the EDM capacitor and electrode.

The required circuit is connected and simulated by using the PSPICE software. The following is one such circuit.

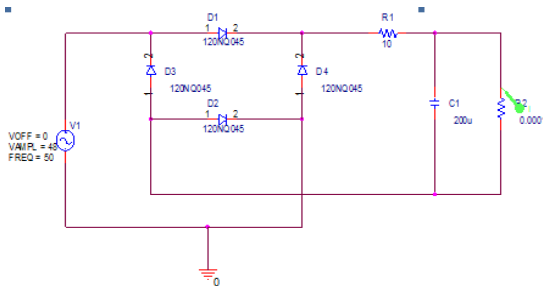


Fig.3 : Circuit of Power System

The current of 4.5amps was obtained in the simulation result. This circuit was then tested on the mild steel plate and the metal removal was observed on the work-piece surface. Thus this circuit was adopted.

SIMULATION RESULT:

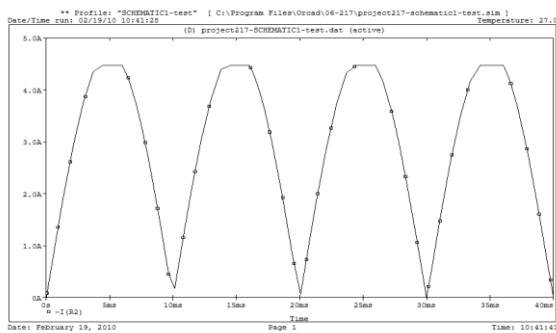


Fig.4: Charging and discharging with respect to time – for power circuit employed

RAM :

The Electrode used in the EDM machine should follow the predictable linear path free from the errors like back lash.

The machine Ram designed by us consists of the following parts: 1. Drawer slide, 2. Lead Screw (1/4 -20”), 3. Coupling, 4. Stepper motor , 5. Aluminium column, 6. Electrode (Graphite and Copper)

The slide is actuated by the lead screw driven by the DC Stepper motor which is controlled by the 100:1 reduction gear box. The Lead Screw is UNC (Unified Coarse thread) 1/4 -20 in dimension. An appropriate nut of 3/8” dimension was made. This screw of longer length helps in reducing the back-lash.

The diagram shows the schematic of the RAM build. (From Bottom to Top)The insulated wooden block is used as an electrode holder. A metallic clamp is placed on the wooden block to hold the electrode firmly. The clamp can be connected to the power source. This block is mounted on the lower side of the slide. The next component is the mild steel block which carries the lead-screw nut. This block is mounted on the slide by Gas welding. Through this nut passes the lead screw, the other end of the screw is coupled to the motor shaft by a coupling made to size using mild steel cylindrical block. This coupling holds the screw and the shaft together without causing any relative motion between them.

This whole system is mounted on the aluminium “S” shaped frame as shown in the diagram and the picture. A (Dimension) plate is mounted on the Tub to carry the RAM. Two firm aluminium strips are used to support frame and stop the longitudinal motion caused by the motor vibration.

The whole system can be mounted on the milling machine table so that the machine remains flat and can be free from any other vibrations.

The followings are the different electrode materials which are used commonly in the industry: Graphite, Electrolytic oxygen free copper , Tellurium copper – 99% Cu + 0.5% tellurium, Brass.

For the present case copper and graphite electrodes are employed and their performance is observed for same workpiece.The properties of copper and graphite are presented below [6]

S.No	Property	Copper	Graphite
1	Density	8960 KG/M ³	(1.3-1.95) ³ G/CM ³
2	Specificheat(293 K)	0.383 KJ/KG.K	(710-830) J/KG.K
3	Thermal conductivity	394 W/M.K	(25-470) W/M.K
4	Electrical conductivity	100%	(90-100)%
5	Cross Sectional Area	82.7267mm ² (d=10.217mm)	132.1049mm ² (d=12.911mm)

PERFORMANCE WITH RESPECT TO POLARITY:

COPPER AS ELECTRODE: Here we conducted the experiment by connecting both the polarities to the work piece (MS) and the copper electrode of 10.217mm diameter. The picture shows the effect of the experiment on the work piece and electrode. Silver colored portion on the work piece shows the material removal. Darker portion on the electrode is carbon deposit.

S. No	Electrode	Polarity	Dielectric	Time in min	Current in A	Voltage in V	Surface Roughness
1.	Copper	-ve	Kerosene	15	4	48	0.03 mm
2.	Copper	+ve	Kerosene	15	6	48	0.07 mm

OBSERVATIONS:

By connecting the straight polarity in the circuit we got the following observations.

1. Temperature change was almost negligible.
2. Lower value of current is observed.
3. Metal removal was even.

By connecting the negative polarity to the work piece and the positive to the Tool in the circuit we got the following observations: The temperature change was around 2⁰c, Observable carbon deposit was seen on crater, Color the kerosene changed drastically, Higher value of current was observed, Metal removal was uneven, Observable roughness was high.

GRAPHITE AS ELECTRODE: Here we conducted the experiment by connecting both the polarities to the work piece (MS) and the graphite electrode of 12.911mm diameter. The picture shows the effect of the experiment on the work piece and electrode. Silver colored portion on the work piece shows the material removal. Darker portion on the electrode is carbon deposit.

S. No	Electrode	Polarity	Time	Current(A)	Voltage(V)	Surface Roughness
1.	Graphite	-ve	15 min	5A	48V	0.05mm
2.	Graphite	+ve	15 min	6A	48V	0.09mm

OBSERVATIONS:

The following observations made ,by connecting the straight polarity in the circuit .

1. Temperature change was around 1⁰C negligible,
- 2.Higher Metal removal rate was observed.

By connecting the negative polarity to the work piece and the positive to the Electrode in the circuit we got the following observations:

The temperature change was around 2⁰c, Observable carbon deposit was seen on crater, Color the kerosene changed drastically, Higher value of current was observed, Metal removal was lesser, higher surface roughness .

TESTS BY VARYING VOLTAGE:

This test was conducted to show that effect of the change in applied voltage on the cutting of the Electrical Discharge Voltage. The Experiment was conducted by varying the voltage applied to the EDM.

TEST WITH COPPER TOOL:

The electrolytic copper electrode was used as tool for conducting the experiment.

S. No	Voltage	Breakdown voltage	Cu Current	Time In Min	Average Current	Surface Roughness	Depth of Cut
1.	40V	28V	4A	10	0.8 A	0.03 mm	0.31 mm
2.	45V	29V	5A	10	1A	0.07 mm	0.53 mm
3.	50V	38V	6A	10	1.6 A	0.1 mm	0.68 mm
4.	55V	40V	6.4 A	10	2A	0.13 mm	0.84 mm
5.	60V	44V	7A	10	3A	0.15 mm	1.01 mm



The table shows the increase in the Roughness with increase in breakdown voltage.

TESTING WITH GRAPHITE TOOL :

The graphite Electrode was used as tool for this experiment:

S. No	Vol tage	Bre ak down volt age	Cu rre nt	Ti me in mi n	Ave rage Cur rent	Surfa ce Roug hnes s	Dep th Of Cut in mm
1.	40V	32V	5A	10	1.0 A	0.04 mm	0.79
2.	45V	36V	5.6 A	10	1.6 A	0.09 mm	0.94
3.	50V	40V	6A	10	1.8 A	0.13 mm	1.09
4.	55V	42V	6.4 A	10	2.3 A	0.15 mm	1.37
5.	60V	44V	7A	10	3.0 A	0.18 mm	1.89



The table shows the increase in the roughness value with increase in the breakdown voltage.

The depth of cut values increases like the trend shown with copper tool with increase in the voltage values. The results of work-piece surface roughness for copper and graphite tools at negative and positive polarity can be seen respectively in graphs. It is observed that negative graphite tool electrodes promoted higher roughness than copper tools for all the Discharge voltage values (40, 45, 50, 55 and 60).

TESTS BY VARYING CURRENT:

This experiment is conducted to evaluate the effect of the current on the cutting of the Electrical Discharge Machine.

TEST WITH COPPER TOOL(VARYING CURRENT):

S. No	Vol tag e	Re sist anc e	Brea k down volta	Cu rre nt	Ti me in mi n	Surf ace roug hnes s	Dep th Of Cut in
-------	-----------	---------------	-------------------	-----------	---------------	----------------------	------------------

			ge			in mm	mm
1.	60 V	3	32V	10 A	10	0.2	1.97
2.	60 V	3.5	34V	9A	10	0.18	1.73
3.	60 V	4	40V	8A	10	0.15	1.55
4.	60 V	4.5	44V	7A	10	0.14	1.04
5.	60 V	5	47V	6A	10	0.12	0.98

It has been observed that the roughness value increases with increase in the current value. The variation in the current is brought by varying the resistance value from 3 ohms to 5 ohms.

The Depth of cut shows a gradual increase in the trend with the increase in the current values.

TEST WITH GRAPHITE TOOL (VARYING CURRENT):

S. No	Vo lta ge	Re sist anc e	Brea k down volt age	Cu rre nt	Ti me in mi n	Surf ace roug hnes s in mm	Dept h of cut In mm
1.	60 V	3	32V	10 A	10	0.22	2.2
2.	60 V	3.5	34V	9A	10	0.2	1.98
3.	60 V	4	40V	8A	10	0.17	1.76
4.	60 V	4.5	44V	7A	10	0.15	1.34
5.	60 V	5	47V	6A	10	0.13	1.03



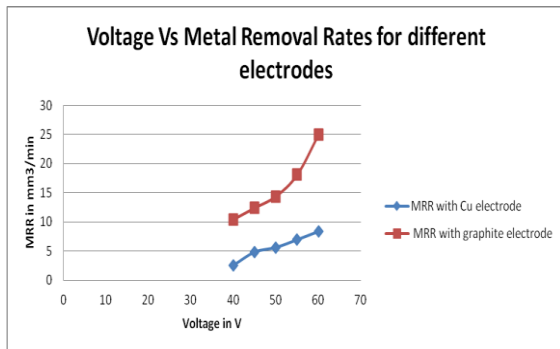
The roughness value increases gradually with increase in the current value by using graphite electrode tool.

The Depth of cut increases with increase in the current value for the graphite tool.

MATERIAL REMOVAL RATE:

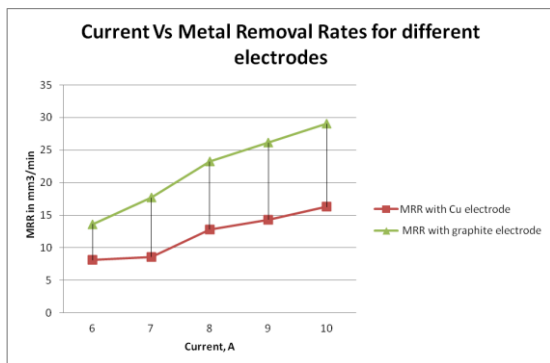
VARYING VOLTAGE:

S.No	Voltage	Copper Tool mm ³ /min	Graphite Tool mm ³ /min
1	40	2.5645	10.4362
2	45	4.8454	12.4178
3	50	5.6254	14.3994
4	55	6.9490	18.0983
5	60	8.3553	24.9678



VARYING CURRENT:

S.No	Current	Copper Tool mm ³ /min	Graphite Tool mm ³ /min
1	6	8.1072	13.6068
2	7	8.6035	17.7020
3	8	12.8226	23.2504
4	9	14.3117	26.1567
5	10	16.2971	29.0630



RESULTS & DISCUSSIONS:

ROUGHNESS:

Varying Voltage: Roughness increases with increase in the voltage for both copper and graphite tool, the possible reason for this can be increase in the power supplied per spark. Due to increase in spark power there is considerable increase in crater size which results in greater roughness.

Varying Current: Roughness values increases with increase in the current density. The increase in the current causes more sparks to generate causing increase in total roughness

values. The same trend is observed in both the tool materials (Copper & Graphite).

DEPTH OF CUT:

Varying Voltage: There is significant increase in the depth of cut value with increase in voltage with both the tool materials. The increase in voltage causes more discharge through the dielectric which causes the increase in material removal rate.

The material removed by the graphite tool is more compared to the Copper tool; this is the result of good electrical and thermal conductivity of the graphite tool compared to copper tool.

Varying Current: With the increase in operating current there is increase in the depth of cut of the work-piece. This is the result of increased current density causing more material removal from work surface.

MATERIAL REMOVAL RATE:

Varying Voltage: It's been observed that the Material removal is more with increase in the operating voltage, this thing is verified by the increasing DOC.

Varying Current: The Material removal increases with the increase in the current value. The increase in the sparking is the reason for the increase in the material removal rate.

CONTROLLING OF DOC:

The Observed Values of MRR and Roughness suggests that controlling of Depth Of Cut can be effectively done by the controlling of the current, as the better surface finish is obtained in this case.

CONCLUSION:

The carried out experiments show that the time for machining and surface generated are almost equal to commercially available sinker machines. The performance of the Table Top Electric Discharge Machine using Copper and Graphite tools on the Mild Steel, HSS work-pieces has been investigated by varying important EDM variables such as Discharge Current, Discharge Voltage and Tool-Work-piece polarity. From the results of this work the following conclusions can be drawn:

- The machine was tested with change in the polarities of tool and work-piece and was concluded that the straight polarity gives better value of MRR and surface roughness.
- Copper tool with straight polarity gives better surface finish than the Graphite tool.
- The machine was tested with change in operating voltage and was found out that with the similar average current utilization; Copper tool gave better surface finish than the Graphite tool.
- Depth of cut for the Graphite tool was found to be more than Copper tool.
- The machine was tested with change in current density and was found that the roughness increases with the increase in the current density.

- Copper was proved to be better material as tool because of the good surface finish compared to graphite tool.
- Depth of cut was more for graphite tool with increase in the current density.
- The Material removal rate for the Graphite tool is more than the Copper tool in any operating conditions.
- The Current variation is better parameter for controlling Depth of Cut.

The present unit can be further improved by having PLC control for work fixtures, , flushing systems,

REFERENCES

1. Fleming, B: *The EDM How-To Book*, Fleming Publishing, USA, 2005, ISBN-0-9767596-08.
2. Rawlinson, P: *Mk.3. Wire Eroder (I)*, Model Engineers' Workshop, Issue #95, Dec 2003/Jan 2004, Highbury House Publishing Ltd, England, p38.
3. Oakes, G: *A Simplified Spark Erosion Machine*, Model Engineers' Workshop, Issue #104, Feb/Mar 2005, Highbury House Publishing Ltd, England, p43.
4. Rumbo, E: *A Simple Spark Erosion Machine*, Model Engineers' Workshop, Issue #117, Highbury House Publishing Ltd, July, 2006, England, p51.
5. K.H. Ho, S.T. Newman, State of the art electrical discharge machining (EDM), *International Journal of Machine Tools & Manufacture* 43 (2003) 1287–1300.
6. S. Singh, S. Maheshwari, P.C. Pandey, Some investigations into the electric discharge machining of hardened tool steel using different electrode materials, *Journal of Materials Processing Technology* 149 (2004) 272–277.
7. C.J. Luis, I. Puertas, G. Villa, Material removal rate and electrode wear study on the EDM of silicon carbide, *Journal of Materials Processing Technology* 164–165 (2005) 889–896

Optimization of Phytase Production by *Pseudomonas* sp. Isolated from Poultry Faces

T. Selvamohan*, V. Ramadas*, M. Rejibeula**

(*Research Centre & P.G Department of Zoology, Raja Dooraisingam Govt. Arts College, Sivagangai, Tamil Nadu, India,

(**Department of Microbiology Sivanthi Aditanar College, Pillayarapuram - 629 501, Nagercoil, Tamilnadu, India)

ABSTRACT

Phytase production in *Pseudomonas* sp isolated from poultry faces was investigated and optimized. in the present investigation. Effect of different agricultural substrates on phytase production by the *Pseudomonas* sp revealed that the maximum amount of phytase was produced with ragi bran as a substrate than other substrates used in the study. All the kinds substrates used in the study for phytase production were observed at 72 hours of fermentation and pH 5 and 37 °C were observed as the optimum pH and temperature for maximum phytase production at 72 h. Ammonium sulphate and sucrose were observed as the best nitrogen and carbon sources for higher rate phytase production. Similarly Tricalcium phosphate was identified as suitable phosphate source for maximum phytase production by the *Pseudomonas* sp..

Keywords: Poultry faces, *Pseudomonas* sp, agricultural substrates, effect of pH, temperature, carbon, nitrogen and phosphate sources – optimization of phytase production.

1. INTRODUCTION

Phytase *myo*-inositol hexaphosphate phosphohydrolase is an enzyme that hydrolyses phytin which comprises 50% to 80% of the total phosphorus in most foods of plant origin. It is a type of anti-nutritional factor commonly present in edible legumes, cereals, and seeds [1]. While preparing animal feeds using these plant materials, phytic acid make unavailability of essential nutrients in the feed hence, phytases have been mainly, used as animal feed supplement in diets mainly for swine and poultry and also for fish. The first commercial phytase products were launched into the market in 1991, and now the market volume is increased to 150 million euro dolar [2].

Phytases have a wide distribution in plants, microorganisms, and in some animal tissues. Several strains of bacteria, yeasts and fungi have been used for production of phytase in large scale for commercial purpose. Many bacterial strain have been studied for the phytase production such as *Pseudomonas* sp., *Bacillus* sp., *Raoultella* sp., *Escherichia coli*, *Citrobacter braakii*, and *Enterobacter*, and including anaerobic rumen bacterial species like *Selenomonas ruminantium*, *Megasphaera elsdenii*, *Prevotella* sp., *Mitsuokella multiacidus*, and *Mitsuokella jalaludinii* [3].

Phytases are mainly applied to reduce phytate content in feed and food stuffs, they are mainly used in bread making; corn wet milling and for production of plant proteins [3]. Supplementing phytases in the feed have been significantly improving phosphorus utilization from phytate to commercially important animals under various dietary conditions. Phytase production is greatly affected by medium composition used for bacterial culture and the phytase production is mainly induced by nutrient and physical conditions. Hence, the present study was carried out to optimize the phytase production by *Pseudomonas* sp. using different nutritional and physical conditions.

2. MATERIAL AND METHODS

2.1. Microorganism and phytase production

The microorganism used in this study was isolated from the poultry faeces from Pillyarpuram poultry farm. The bacterial isolate was identified as *Pseudomonas* sp. by its morphological, physiological and biochemical characteristics according to Bergey's Manual of Determinative Bacteriology. To begin the phytase production, overnight seed culture was prepared by cultivating the strain in nutrient agar, afterwards, 10% of the seed culture was inoculated into 50 ml of production medium containing K_2HPO_4 (0.1%), NaCl (1%), $MgSO_4 \cdot 7H_2O$ (0.01%) and peptone (0.5%) using fermentor. Fermentation was carried out at 32°C for 72 h with 150 rpm. All the experiments were done in triplicate and average values were recorded. After 72 hours of incubation the cells were harvested by centrifugation at 10,000 rpm for 15 minutes and the supernatant was used as a enzyme source for estimation of phytase activity.

2.2. Assay of Phytase production.

Phytase production was analysed using the method suggested by [4]. To the 0.2 ml of enzyme sample, 2.4 ml phytic acid solution (0.32gm Sodium phytate, dissolved in 50ml of 0.2 m sodium acetatic acid buffer with pH 5.5) was added. To this mixture 1ml of 0.1 molar $Mg SO_4 \cdot 6 H_2O$ and 0.4ml of distilled water were added. The content was incubated at room temperature for 15 minutes and the reaction arrested with the addition of 0.5ml Trichloro acetic acid (10%) and after that 1 ml of distilled water and 2.5ml of Taussky-schoor reagent (freshly prepared) were to

this mixture, the absorbance was measured at 660nm using spectrophotometer. Phytase activity was calculated using phosphorus standard; 1U phytase activity is equivalent to 1 µg phosphorus released under assay conditions.

2.3. Parameters controlling phytase production

2.3.1. Effect of different agricultural substrates

Phytase production with agricultural substrates was studied by using different substrates such as rice bran, ragi bran, green gram, wheat bran and corn bran at 1% level. This was studied with different time intervals such as 24, 48, 72 and 96 hours..

2.3.2. Effect of different initial pH on phytase production

The effect of incubation pH on phytase production was determined by varying the pH values such as 5, 7 and 9, their influence on phytase production was determined at different time intervals (24, 48, and 72 hours).

2.3.3. Effect of different incubation temperature on phytase production

The organisms inoculated in the production media were incubated at different temperatures such as 27°C, 37°C and 47°C and their influence was noticed at different time intervals (24, 48, 72 and 96 hours).

2.3.4. Effect of different nitrogen sources on phytase production.

The effect of nitrogen sources on phytase production was determined using different organic (malt-extract, yeast extract) and inorganic nitrogen sources (ammonium nitrate, ammonium sulphate (0.5%)) and their influence of nitrogen sources was observed at different time intervals (24, 48, 72 and 96 hours).

2.3.5. Effect of different carbon source

Suitability of different carbon sources such as glucose, lactose, maltose and sucrose were studied at 0.5% level. The influence of carbon sources on phytase production was noticed at different time intervals (24, 48, 72 and 96 hours).

2.3.6. Effect of phosphate on phytase production

The effect of phosphates on phytase production was also studied using Tricalcium phosphate and sodium dihydrogen ortho phosphate at 0.1% level at different time intervals such as 24, 48, 72 and 96 hours.

3. RESULTS AND DISCUSSION

The effect of different agricultural substrates on phytase productions at different time intervals were represented in Table-1 & Fig.1. The results indicated that among the tested substrates ragi bran showed maximum phytase production when compared to other substrates used in the study.

Table-1. Effect of different agricultural substrates on phytase production at different time intervals

Agricultural substrates	Time Intervals			
	24	48	72	96
	Phytase Activity (U/ml)			
Ragi Bran	0.669	0.88	0.891	0.81
Rice Bran	0.105	0.61	0.551	0.598
Green gram	0.575	0.633	0.468	0.399
Corn bran	0.434	0.234	0.639	0.493
Wheat bran	0.305	0.223	0.61	0.315

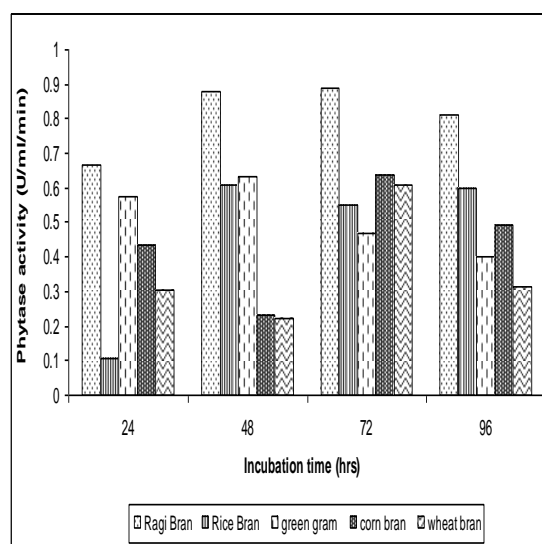


Fig.1. Effect of different agricultural substrates on phytase production at different time intervals

Among the tested different time intervals it was observed that phytase production was maximum in 72 hours of fermentation. Next to ragi bran, green gram and corn bran showed good results with *Pseudomonas* sp. Production of phytase using agricultural wastes provides many advantages especially reduce the production cost. Many authors have reported the compatible use of agricultural wastes for phytase production by different bacterial strains. It is reported that the phytase production using sesame oil cake by *Sporotrichum thermophile* [5]. Similarly, high level of phytase production was observed with the wheat bran and oil cakes in *Mucor racemosus* [6]. Likewise the level of phytase production in soybean meal by *Aspergillus oryzae* AK9 [7] these results were corroborated with the present investigation.

Effect of pH on phytase production with different time intervals resulted that pH 5 and 72 hours of incubation period were suitable for maximum phytase production (Table.2 & Fig. 2).

Table-2. Effect of pH on phytase production with different time intervals

pH	Time Intervals			
	24	48	72	96
	Phytase Activity (U/ml)			
5	0.434	0.516	0.657	0.399
7	0.399	0.41	0.633	0.575
9	0.399	0.14	0.61	0.223

This incubation period was observed in all set of experiments with different substrates. These results showed that the phytase produced by this strain was with acidic enzyme synthesized by the organism. Supporting the present study *Saccharomyces cerevisiae* CY are reported to produced phytase in acidic pH and has an optimum pH of 5.5 [8]. Similarly, it was also reported that, phytate degradation by *S. cerevisiae* YS18 in the cultivation medium was high at initial pH 6.0 [9]. Likewise, the maximum phytase production reported in *Mucor indicus* MTCC 6333 at pH 5.0 [10].

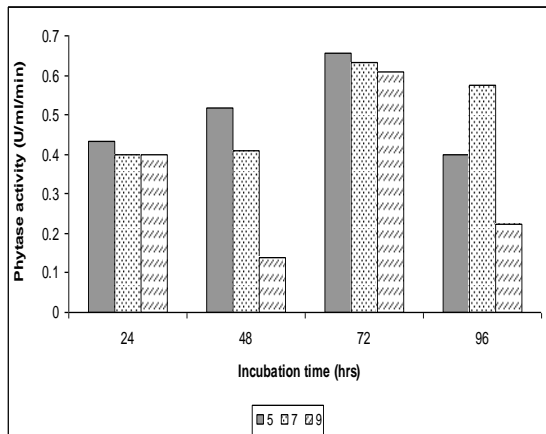


Fig. 2. Effect of pH on phytase production with different time intervals

Effect of different incubation temperature on phytase production with different time intervals showed that 37°C at 72h was the optimum temperature for optimum phytase production (Table.3 & Fig.3).

Table-3 Effect of different incubation temperature on phytase production with different time intervals

Temperature	Time Intervals			
	24	48	72	96
	Phytase Activity (U/ml)			
27°C	0.434	0.399	0.575	0.422
37°C	0.434	0.422	0.657	0.551
47°C	0.422	0.44	0.442	0.316

This is the mesophilic temperature and above this temperature the phytase production was decreased which may probably be due to cell death. Supporting the present study, It was reported that, the phytase production by *Rhizopus oligosporus* was maximum at 30°C [11]. Similar results on phytase production by *Aspergillus ficuum* TUB F-1165 was observed as maximum at 30°C [12].

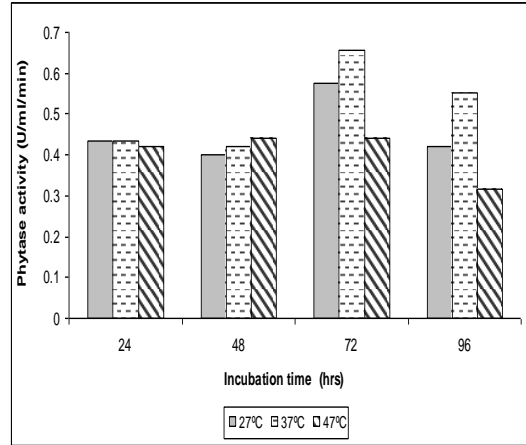


Fig.3. Effect of different incubation temperature on phytase production with different time intervals

Effect of different carbon sources on phytase production at different time intervals resulted that all the carbon sources produced considerable amount of phytase and it was specifically high at sucrose. For all the carbon sources used in the study phytase production was maximum at 72 hours of incubation (Table.4 & Fig. 4). Sucrose is a disaccharide it evident as a good energy source for phytase production by the organism. This was supported by the studies in *A.niger*, where the phytase production was heavily induced by sucrose in *A. niger* [13].

Table. 4. Effect of different carbon sources on phytase production at different time intervals

Carbon sources	Time Intervals			
	24	48	72	96
	Phytase Activity (U/ml)			
Maltose	0.493	0.516	0.704	0.496
Lactose	0.457	0.692	0.724	0.469
Sucrose	0.457	0.516	0.739	0.410
Glucose	0.481	0.522	0.727	0.469

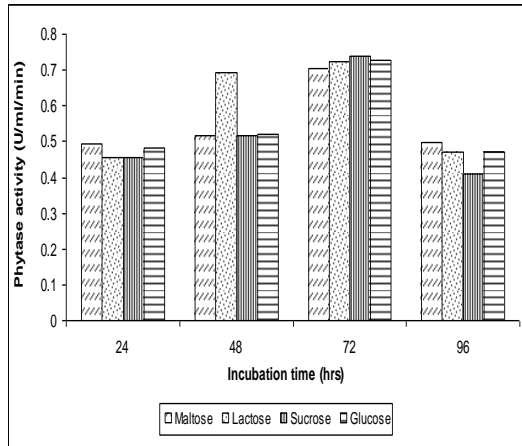


Fig. 4. Effect of different carbon sources on phytase production at different time intervals

Nitrogen sources are important nutrients for phytase production and the effect of different nitrogen sources at different time intervals resulted in higher rate of phytase production with ammonium sulphate as a nitrogen source at 72 hours of incubation (Table.5 & Fig 5).

Table.5. Effect of different nitrogen sources on phytase production at different time intervals

Nitrogen Sources	Time Intervals			
	24	48	72	96
Ammonium nitrate	0.551	0.469	0.692	0.516
Ammonium sulphate	0.457	0.516	0.751	0.540
Malt extract	0.516	0.540	0.633	0.493
Yeast extract	0.469	0.540	0.739	0.457

Next to ammonium sulphate yeast extract was also produced considerable amount of phytase. Supporting the present study *Saccharomyces cerevisiae* CY are reported to produce maximum phytase in ammonium sulphate [8]. Similarly, it was also reported that the ammonium sulphate was a significant nutrient for maximum phytase production by

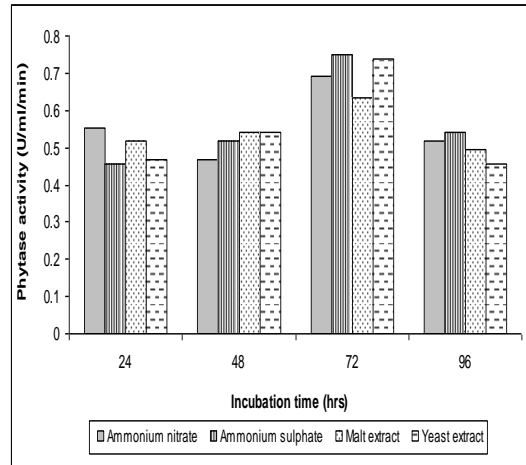


Fig.5. Effect of different nitrogen sources on phytase production at different time intervals

Aspergillus ficuum NRRL3135 [14]. Likewise, the phytase production by *Mucor indicus* MTCC 6333 was reported as maximum in the presence of ammonium phosphate as a nitrogen source [10].

Phosphates have been reported to be either a repressor or an inducer of phytase production in different microorganisms. Two different inorganic phosphates namely Tricalcium phosphate and Sodium dihydrogen ortho phosphate were screened for phytase production. The results showed that, the phytase production was maximum in Tricalcium phosphate at 72 hours of incubation (Table-6 & Fig. 6).

Table. 6. Effect of inorganic phosphates as phosphate source on phytase production at different time intervals.

Phosphate Sources	Time Intervals			
	24	48	72	96
Tricalcium phosphate	0.457	0.516	0.751	0.422
Sodium phosphate	0.493	0.54	0.727	0.446

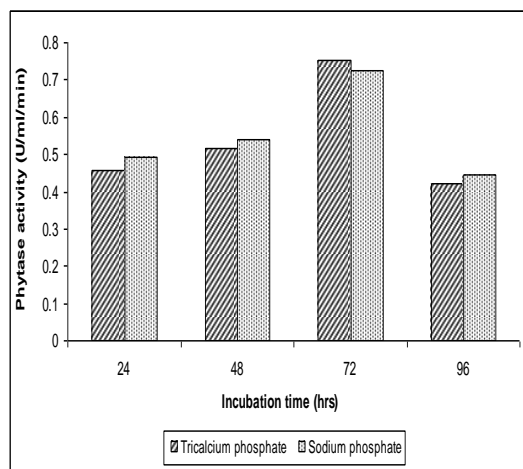


Fig.6. Effect of inorganic phosphates as phosphate source on phytase production at different time intervals.

In agreement with the present study phytase production by *Aspergillus niger* NCIM 1207 increased by supplementary phosphates [15]. Similarly, it was reported that the phytase production by *Thermoascus aurantiacus* was increased with increase in concentration of potassium dihydrogen orthophosphate [16].

REFERENCES

- Kim Y, Kim HK, Baeks, Yu JH, Oh TK (1998). Purification and properties of a thermostable phytase from *Bacillus* sp. DSII. *Enzyme Microbial Technology*.22:2-7.
- Haefner S, Knietzsch A, Scholten E, Braun J, Lohscheidt M, Zelder O (2005) Biotechnological production and applications of phytases, *Appl. Microbiol. Biotechnol.* 68;588–597.
Konietzny U and Greiner R (2004) Bacterial phytase: potential application, *in vivo* function and regulation of its synthesis. *Brazilian Journal of Microbiology* 35:11-18
- Chunshan, Q, Linghua Z, Yunji W and Yoshiyuki O, (2001). Production of phytase in slow phosphate medium by a novel yeast *Candida krusei*. *J. of Biosci. and Bioeng.*, **92**:154-160.
- Singh B and Satyanarayana T (2008) Phytase production by a thermophilic mould *Sporotrichum thermophile* in solid state fermentation and its potential applications *Bioresource Technology* 99:2824–2830.
- Roopesh K, Ramachandran S, Madhavan Nampoothiri K, Szakacs G and Pandey A (2006) Comparison of phytase production on wheat bran and oilcakes in solid-state fermentation by *Mucor racemosus*. *Bioresource Technology* 97:506–511.
- Chantasartrasamee K, Na Ayuthaya DI, Intarareugsorn S and Dharmstithi S (2005). Phytase activity from *Aspergillus oryzae* AK9 cultivated on solid state soybean meal medium. *Process Biochemistry*, 40:2285–2289.
- Jin In M, Seo SW and Oh NS (2008) Fermentative production and application of acid phytase by *Saccharomyces cerevisiae* CY strain. *African Journal of Biotechnology* 7(17): 3115-3120,
- Andlid TA, Veide J and Sandberg AS, (2004). Metabolism of extracellular inositol hexaphosphate (phytate) by *Saccharomyces cerevisiae*. *Int. J. Food Microbiol.* 97: 157-169.
- Gulati HK, Chadha BS and Saini HS (2007) Production of feed enzymes (phytase and plant cell wall hydrolyzing enzymes) by *Mucor indicus* MTCC 6333: purification and characterization of phytase. *Folia Microbiologica* 52 (5) 491-497.
- Sabu A, Sarita S, Pandey A, Bogar B, Szakacs G, and Soccol CR (2002) Solid-State Fermentation for Production of Phytase by *Rhizopus oligosporus* *Applied Biochemistry and Biotechnology*. 102–103: 251-260.
- Gautam P, Sabu A, Pandeya A, Szakacs G, Soccol CR (2002) Microbial production of extra-cellular phytase using polystyrene as inert solid support. *Bioresource Technology* 83 229–233.
- Gunashree BS and Venkateswaran G (2008) Effect of different cultural conditions for phytase production by *Aspergillus niger* CFR 335 in submerged and solid-state fermentations *J. Ind Microbiol Biotechnology* 135:1587–1596.
- Bogar B, Szakacs G, Linden JC, Pandey A and Tenderdy RP (2003). Optimization of phytase production by solid substrate fermentation. *J Ind Microbiol Biotechnol.* 30: 183–189.
Soni SK and Khire JM (2007) Production and partial characterization of two types of phytase from *Aspergillus niger* NCIM 563 under submerged fermentation conditions. *World J Microbiology and Biotechnology*. 23:1585–1593.
- Nampoothiri KM, Tomes GJ, Krishnan R, Szakacs G, Nagy V, Soccol CR and Pandey A (2004). Thermostable phytase production by *Thermoascus aurantiacus* in Submerged Fermentation. *Applied Biochemistry and Biotechnology*. 118:205-214

Optimal Design of CMOS OP-AMP VIA Geometric Programming

Vikas Upadhyaya

Electronics & Communication Department
NIIT University, Neemrana, Rajasthan, India

Abstract: In this paper a new method for determining the component values and transistor dimensions for CMOS operational amplifiers (Op-Amps) is presented. As a wide variety of design objectives and constraints are Posynomial function of the design variables, the Optimization is done by Geometric Programming. As a consequence we can efficiently determine globally optimal trade-offs among competing performance measures such as power, open-loop gain and bandwidth. In this paper I applied this method to a Folded Cascode operational amplifier. The paper shows how the method can be used to synthesize robust design, i.e., design guaranteed to meet the specifications for a verity of process condition and parameters. The synthesis method is fast and determines the globally optimal design.

Keywords: Op-amp, Geometric Programming

I. INTRODUCTION

In response to the ever increasing demands of mixed mode integrated circuits, a variety of techniques have been developed for the efficient sizing of the CMOS op-amp circuits. One possible solution for this is to use Geometric Programming in convex form with which the globally optimal solution can be computed with great efficiency [2]. The performance measures such as input-referred noise, output voltage swing, unity-gain bandwidth, open-loop voltage gain common-mode rejection ratio, slew rate and so on are determined by the design parameters, e.g., transistor dimension, bias current and other component values. By Geometric Programming we can determine values of the design parameters that optimize an objective measure while satisfying specification or constraint on the performance measures [3]. There are other approaches also for the designing of op-amp e.g., classical optimization methods, knowledge-based methods, or global optimization methods. Classical Optimization methods such as steepest descent, sequential quadratic programming and lagrange multiplier methods have been widely used in analog circuit CAD. The main disadvantage of the classical optimization methods is that they only find locally optimal design and also can fail to find a feasible design. Classical methods tend to slow down if complex models are used [5]. On the other hand knowledge-based methods find locally optimal design instead of globally optimal design and the final design depends on the initial chosen parameters also the substantial human intervention is required during the design or training process. Global optimization methods such as branch and bound and simulated annealing are widely used in analog circuit design that guaranteed to find the globally optimal design. As with the other approaches both branch and bound and simulated annealing suffers from the slow speed and

cannot guarantee a global optimal solution. In the comparison of other approaches the most important feature of geometric programming is that the globally optimal solution can be computed with great efficiency, even for the problems with hundreds of variables and thousands of constraints, using recently developed interior-point algorithms. By means of geometric programming infeasible specifications are unambiguously recognized i.e. the algorithm either produce a feasible point or a proof that the optimization procedure is completely irrelevant. The method can be used to simultaneously optimize the design of a large number of op-amps in a single large mixed mode integrated circuit. Another application is to use the efficiency to obtain robust design. In particular since the global optimum is found, the op-amps designed are not just the best this method can design, but the best any method can design [1].

In this novel work folded-cascode op-amp is designed with the help of Geometric Programming. The simulation results obtained from the MATLAB i.e., the width and the length of all transistors, are used for the spice verification.

II. FOLDED-CASCODE OP-AMP DESIGN

The designing of the folded cascode op-amp shown in Fig.1 is done using ggplab toolbox in the MATLAB [4]. The performance specifications and constraints like symmetry and matching, device sizing, area, bias conditions, common mode input range, output voltage swing, gate overdrive, quiescent power, open loop gain, slew rate and gain bandwidth are expressed as posynomial functions and posynomial constrained so automated design is done with sensitivity analysis via geometric programming [6]. The simulation results obtained from the MATLAB i.e., the width and the length of all transistors, are used for the spice verification.

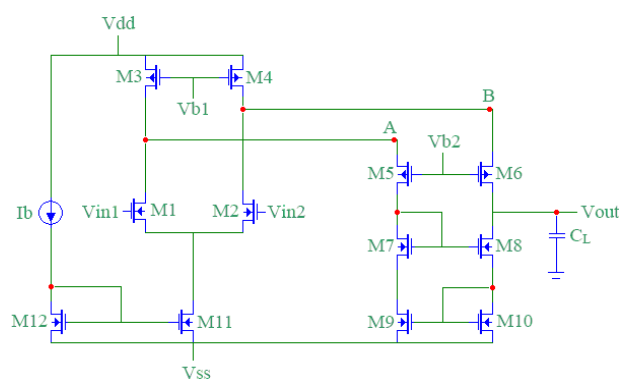


Fig. 1. Folded-Cascode op-amp

On the basis of simulation results, the optimised parameters for the designed circuit are given in table.1:

Variable	Value	Unit
Ib	24.6	μA
W ₁ / L ₁	40 / 1	μ / μ
W ₂ / L ₂	40 / 1	μ / μ
W ₃ / L ₃	80 / 1	μ / μ
W ₄ / L ₄	80 / 1	μ / μ
W ₅ / L ₅	80 / 1	μ / μ
W ₆ / L ₆	80 / 1	μ / μ
W ₇ / L ₇	40 / 1	μ / μ
W ₈ / L ₈	40 / 1	μ / μ
W ₉ / L ₉	40 / 1	μ / μ
W ₁₀ / L ₁₀	40 / 1	μ / μ
W ₁₁ / L ₁₁	80 / 1	μ / μ
W ₁₂ / L ₁₂	20 / 1	μ / μ

Table. 1. Optimal design points for the folded cascode op-amp

III. RESULTS AND DISCUSSION

Simulation results obtained from the MATLAB i.e. Width and Length of all transistors are used for the spice verification. The proposed design has been simulated and verified using spice. Spice simulation results using optimal design point variables against various given specifications are shown in Table.2. Spice simulation graphs are also shown for low frequency gain Fig.2, slew rate Fig.3, phase margin Fig.4, output swing Fig.5 and common mode gain Fig.6.

Performance measure	Specification	Spice simulation
Gain (dB)	≥ 60	76
Unity-gain BW (MHz)	≥ 5	55
Phase margin ($^{\circ}$)	≥ 60	89
Power (mW)	≤ 5	1.6
Output swing (V)	-3, 3	-2.2, 2.4
Slew rate (V/ μs)	≥ 10	63
CMRR (dB)	≥ 60	95
BW (KHz)	-	8.5

Table. 2. Spice simulated results for folded cascode op-amp

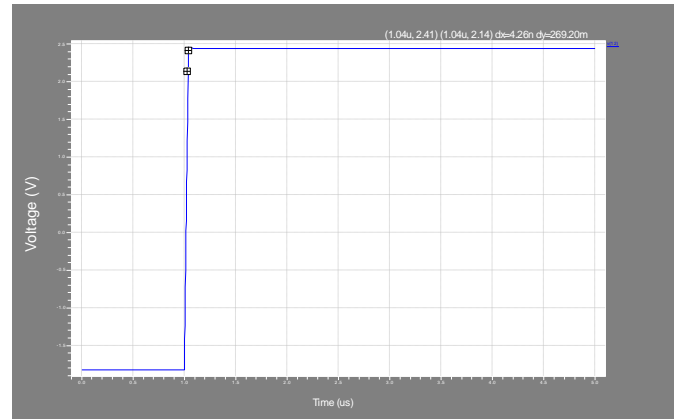


Fig. 3. Slew rate

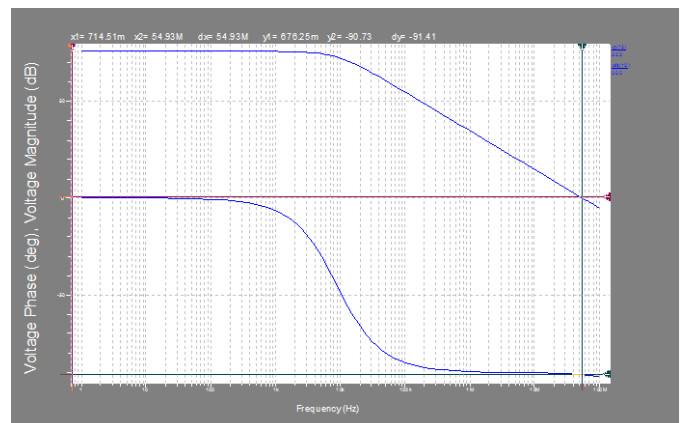


Fig. 4. Phase margin

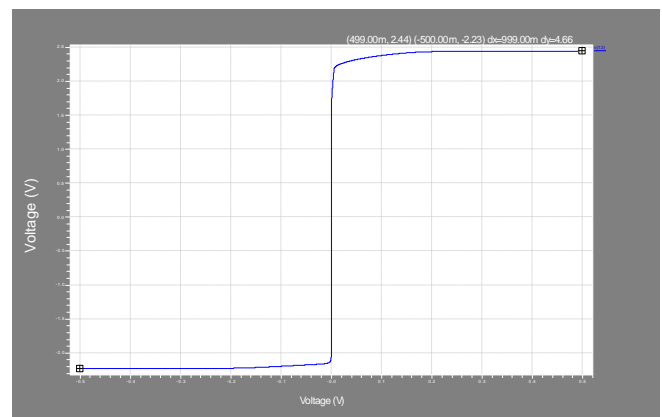


Fig. 5. Output swing

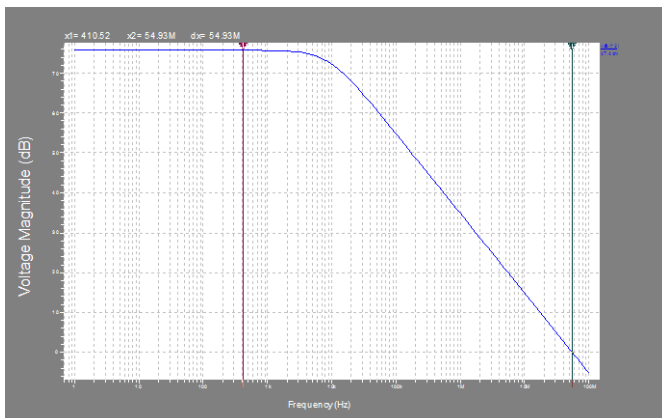


Fig. 2. Low Frequency Gain

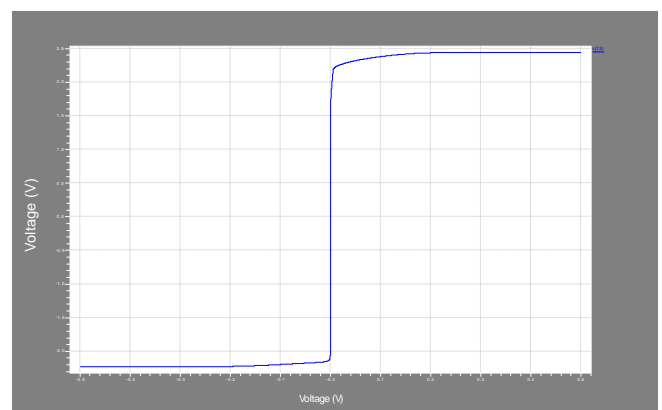


Fig. 6. Common mode Gain

IV. CONCLUSIONS

The method yields globally optimal design, is extremely efficient and handles a wide variety of practical constraints. The method could be used to do full custom design for each op-amp in complex mixed signal integrated circuit. The method unambiguously determines feasibility of a set of specifications, or it provides a proof that the specification cannot be achieved. The main disadvantage of the method is that it handles only certain types of constraints and specifications, i.e., monomial equality constraints and posynomial inequality constraints, despite this apparently restricted form, we can handle a very wide variety of practical amplifier specifications.

REFERENCES

- [1] Maria del Mar Hershenson, Stephen P. Boyd, Thomas H. Lee, "Optimal Design of a CMOS Op-amp via Geometric Programming." Submitted to Transactions on Computer-Aided Design, November 1997
- [2] P. Mandal and V. Visvanathan, "A new approach for CMOS Op-amp Synthesis," in Proc. 12th Int. Conf. VLSI Design, 1999, pp. 189–194.
- [3] Pradip Mandal and V. Visvanathan, "CMOS Op-Amp Sizing Using a Geometric Programming Formulation," IEEE Transactions on Computer- Aided Design of Integrated Circuits and Systems, Vol. 20, No. 1, January 2001.
- [4] M. M. Hershenson, S. P. Boyd, and T. H. Lee, "GPCAD: A tool for CMOS op-amp synthesis," in Proc. Int. Conf. Computer-Aided Design, 1998, pp. 296–303.
- [5] G W.Roberts & Adel S. Sedra,"SPICE second edition," Oxford University Press, 1959.
- [6] Maria del Mar Hershenson, Stephen P. Boyd, Thomas H. Lee, "Automated Design of Folded-Cascode Op-amps with Sensitivity Analysis." Center for Integrated Systems, Stanford University, Stanford, CA 94305.

Design and Implementation of speed control Induction Machine by Using Interface programming

Hussein TH. Khamees

University of Al-Nahrain College of Engineering Department of Laser and Optoelectronic Engineering

Abstract

This article describes the Systematic development of the analysis design and testing by simulation the closed-loop speed control of separately excited dc motor drive system. The motor controlled armature voltage is supplied from a three-phase controlled bridge converter. Closed-loop control is analyzed by using transfer function technique and the necessity of an inner current control loop is demonstrated. Design of both a proportional and proportional- integral controllers are outlined by using transfer function technique. The feed forward loop is also presented for load case. The simulation speed and current responses are presented in this project for speed proportional-current proportional controllers and speed proportional plus integral -current proportional controllers. The system responses in load case are presented and the sudden drop in the speed response is accessed by using feed forward-loop to reduce the load disturbances.

Keyword: speed control, simulation, Interface programming, thyristor, motor

1. Introduction

D.C motors have been used in variable-speed drives for along time. The versatile control characteristics of a dc motor have contributed to their extensive use in industry [1]. Control over a large speed range for both below and above the rated speed can be easily achieved. The speed of the dc motor is relatively easy to control by either its armature voltage; it's field voltage or both, depending upon the desired performance characteristics of the drive. The methods

of control in a dc-drive are simpler and less expensive than those of alternating current motors.

In the late 1950s solid-state devices, silicon diodes, and silicon-controlled rectifiers (SCR) became available in the market at economic prices. The classical M-G set (electromechanical control) has been replaced by thyristorized power converter (electronic control) [1].

2. PIP Controllers

- The industrial controllers may be classified according to their control action as[2]:
- Two position or on-off controllers
- Proportional controllers
- Integral controllers
- Derivative controllers
- Proportional-plus-integral controllers
- Proportional-plus-derivative controllers
- Proportional-plus-integral-plus-derivative controllers

4. System Analysis and Design

In this section presents a systematic development, using transfer function techniques of a closed loop speed control scheme and an outline of the control design. Each block in the Fig.(1) is discussed in this chapter and described by a mathematical model to enable us to analyze, design and frequently testing the system. The speed controller is chose proportional controller and proportional plus integral controller in other times. The values of speed controller are designed for both types of controller (proportional controller and proportional-integral controller). The current controller is designed as proportional controller. The necessity of the current control loop and current controller is shown in this figure (1).

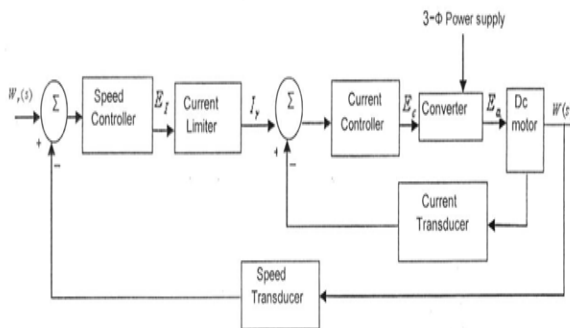


Fig.(1) : A basic block diagram of a speed control system of a dc motor

4. 1Microprocessor Based DC Motor Control

A conventional analog control scheme implemented in dc drives consists of an outer-control loop and an inner-current control loop. The analog control method has several disadvantages such as; difficulty in accurately transmitting the analog signal, errors due to temperature component aging, drift and offset of the analog components, extraneous disturbances, and soon. A digital control system, on the other hand, is free from this disadvantage. The microprocessor, as the brain of a system, can digitally control the angular velocity of the motor. In addition it can perform other tasks that may be needed in the application. In other words the microprocessor controllers are generally carry out in a supervisory role, acting as an intelligent link between the plant

and the conventional thyristor phase controlled converter and supplying to them latter the appropriate control signals advantages of replacing hardware circuits by microprocessor controllers for a variable speed drive are reducing the size and cost of the hardwired electronics, and having more precise, stable and easy to maintain dc- motor drives [3]

4.2 D.C Motor Transfer Function

Separate excitation of a separately excited dc motor makes the speed control of the motor relatively easy. Consider the separately excited dc motor with armature voltage control shown in Fig. (5). the voltage loop equation is. These relationships are shown in a block diagram form in Fig. (2). note that the feedback loop present in the form of the back EMF. This provides the moderate speed regulation inherent in the separately excited dc motor. [4]

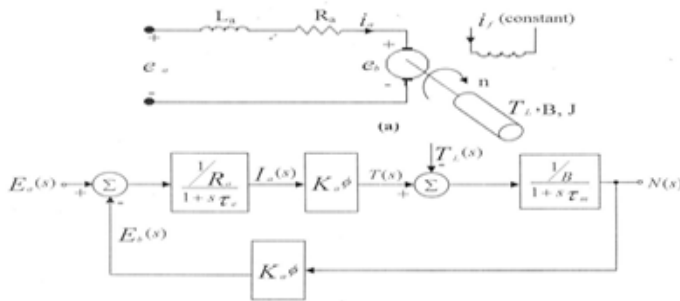


Fig. (2) Development of motor transfer function, (a) Separately excited dc motor model, (b) Functional block diagram

4.3 Closed-Loop Control

DC motors are widely used in many speed-control drives. Open-loop control is sending a signal to the motor, but not sensing the operation of the motor, hence, the control system cannot verify the exact operation of the motor (i.e. make it move at a certain speed or to a certain location). A closed-loop control system senses the rotation

of the motor shaft, and/or the voltage and current delivered to the motor.

This information can allow the speed, location of the motor to be easily found. Open-loop operation of dc motors may not be satisfactory in many applications. If the drive requires constant speed operation the firing angle has to be changed to maintain a constant speed. This can be achieved in a closed-loop control system. A closed-loop system generally has the advantages of greater accuracy, improved dynamic response,, and reduced effects of disturbances such as loading. When the drive requirements include rapid acceleration and deceleration, closed-loop control is necessary. In a closed-loop control system even the drive characteristics can be modified. Thus, the system can be made to operate at constant torque or constant horsepower over a certain speed range, a requirement in traction systems. In fact, most industrial drive systems operate as closed-loop feedback systems. The block diagram of a microcontroller based closed-loop speed control system of a separately excited dc motor fed from three-phase fully controlled bridge converter is shown in Fig. (3). If the motor speed decreases due to application of additional load torque, the speed error ϵ increases, which increase the control signal J_7 . This in turn changes the firing angle of the converter, and thus increases the, motor armature voltage. An increase in the motor voltage develops more torque to restore the speed of the drive system. The system thus passes through a transient period until the developed torque matches the applied torque at the reference speed. In this project the closed-loop system is used instead of the open-loop control system. In the following sections, a controller parameter design is presented for both speed and current control loops. [4]

4.4Current-Controlloop

A change in the reference speed may result in a large sudden change in current .This transient over current is undesirable from the viewpoint of converter rating and protection. This is particularly the case of starting or other large changes. Therefore the current must be limited to some maximum allowable value. The current limiting is an integral part of a variable speed drive and suitably designed so that its maximum value corresponds to the maximum permissible current of the thyristors-motor setup. The current limiting cannot be done on the speed error signal because the motor voltage (armature voltage) is controlled by the speed error signal, therefore, any attempt to clamp this speed error will limit the motor voltage. However, a current limiting can be implemented if we first construct an inner current control loop using the clamped speed error as the current reference. The current control loop provides fast response and overcome the adverse effects of supply disturbances. The electrical time constant of the armature is small compared with the mechanical time constant and therefore the armature current rather than the speed is subject to almost instantaneous variations due to occurring disturbances. As a consequence, with the current loop

present, the corrective action will be faster and the speed regulation will be improved. Fig. (3) represents the current control loop, the nonlinearity of the system due to converter can be overcome by using a proper firing control scheme to fire the SCR_s, a linear relationship between the control voltage (Ec) and the armature voltage) can be obtained. For current controller operation the back emf (Eb) can be assumed-constant because the latter depends on the speed (N), and since the mechanical time constant is greater than the electrical time constant, then the speed can be considered constant. Hence the current control loop can be reduced to the system shown in Fig. (6). The parameters of the test motor are given in Appendix-A with the controller parameters, which are determined by the design. The current sampling period (Ti)

4.5 Speed Control Loop:

From this Fig. (6.a) shows the digital speed control loop. If an actual speed of a separately excited dc motor can be measured and a speed signal can be fed back, the speed error signal (n) can be calculated by comparing the reference speed with the measured speed (actual speed) in the microcontroller. This error signal represents the input signal to the speed controller to adjust the reference the current control loop, consequently to control the armature voltage. In designing the speed controller, three assumptions have been made:

The current control loop can be considered to be a first order system with new electrical time constant. This time constant is very small when compared with the mechanical time constant, so it can be neglected for simplicity.

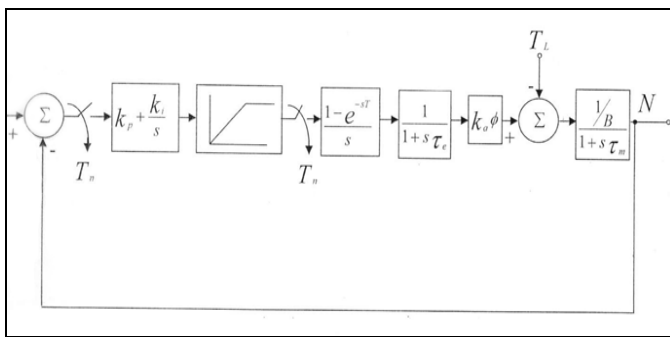


Fig.(3) Discreet speed control loop

5. Result

5-1 No Load Results

5.1.1 Proportional Speed -Proportional Current Controllers

The speed and current responses for step change in speed reference for $K_p = 14.169$, $K_i = 19.407$ Shown in Fig.(4a,b). The current and speed controller are operational type controller, with reference speed equal to 120 rad/s. The limit value of current limiter is 3A. It's clear

from Fig.(7a,b) the current is limited at 3 A, where the limiter prevent the suddenly.
mp of current response at the starting

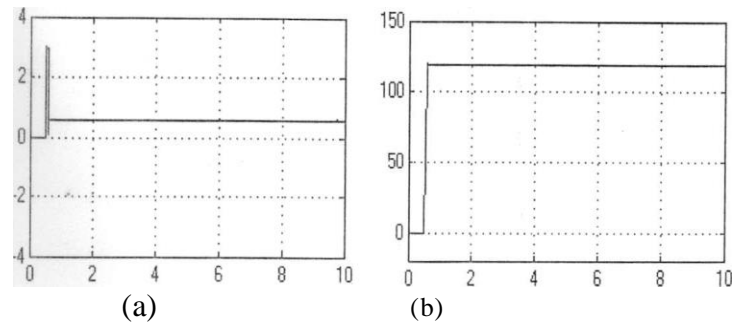


Fig.(4) a ,b Response of proportional control to step change in speed reference (a)current response (b) speed response

5.2 Proportional Integral Speed -Proportional Current Controllers

From the speed response, the rise time is equal to 0.067s, while the peak time s 0.592s. The overshoot of the speed response is 0.467% and the steady state error equal to 0.370.

5.3 Proportional Integral Speed -Proportional Current Controllers

To reduce the steady state error and the peak time, the speed controller is designed as Pi-controller with transfer function, Where the $r_2 = 0.0707$, $r = 0.1414$. The current controller is proportional type controller with constant value 14.169, Fig.(5) shows the speed and current response of speed control system for tip change in the response speed.

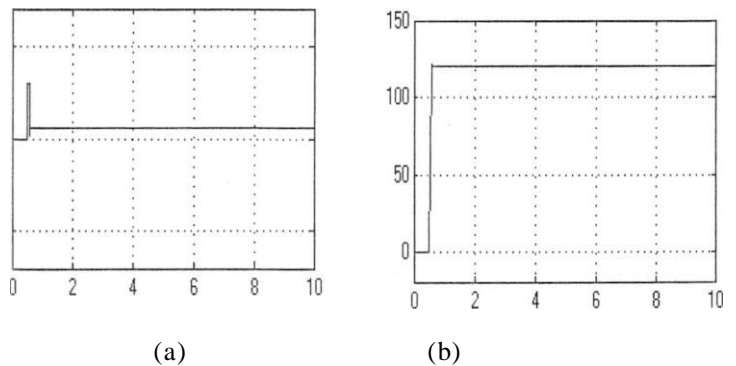


Fig. (5) Response of PI-control to step change in speed reference (a) current response, (b) speed response

From the speed response the rise time is equal to 0.067s, while the peak time is 0.25 Is. The overshoot of the speed response is 1.5% and the steady state error equal to zero.

5.4 Step Increasing and Decreasing of Reference Speed

If the motor reference speed increase, the speed errors increases. This in turn changes the firing angle of the converter, and thus increases the motor armature voltage .An increase in the motor voltage develops more torque to increase the motor speed to reach approximately to the reference speed .Fig (5) shows the speed and current responses for step increasing in the reference speed, while Fig.(6) shows the system response for decreasing case. When the speed and current controllers are proportional type controllers with value $k_s = 14.169, k_r = 19.407$.

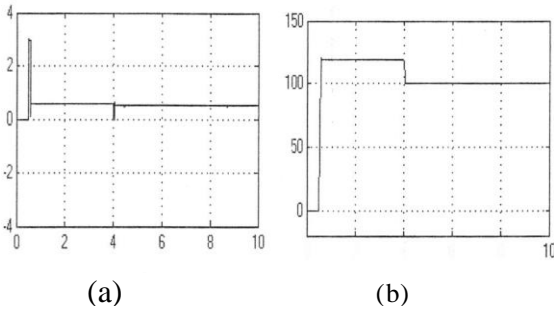


Fig.(6) Response of P-control to step increasing in speed reference (a) current response (b) speed response

From the fig.(6) and Fig(10) are show the current and speed response for step increase and step decrease in reference speed respectively. Where the speed controller is proportional plus integral type controller with the transfer function

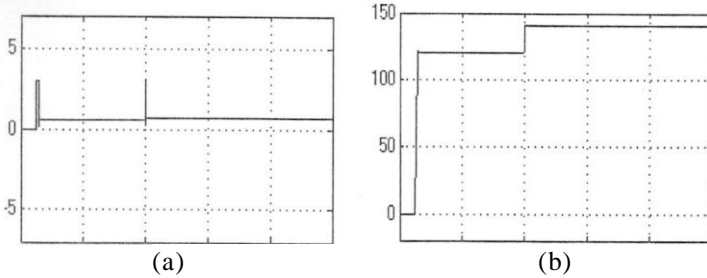


Fig.(7)Response of PI- control to step increasing in speed reference (a) current response (b) speed response

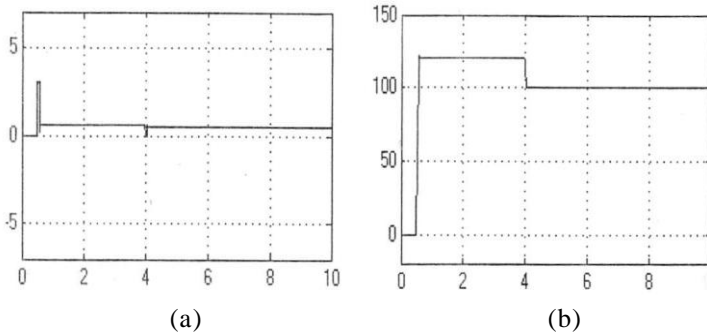


Fig. (7) Response of PI control to step decreasing in speed reference (a) current response (b) speed response

6.1 Proportional Speed Controller

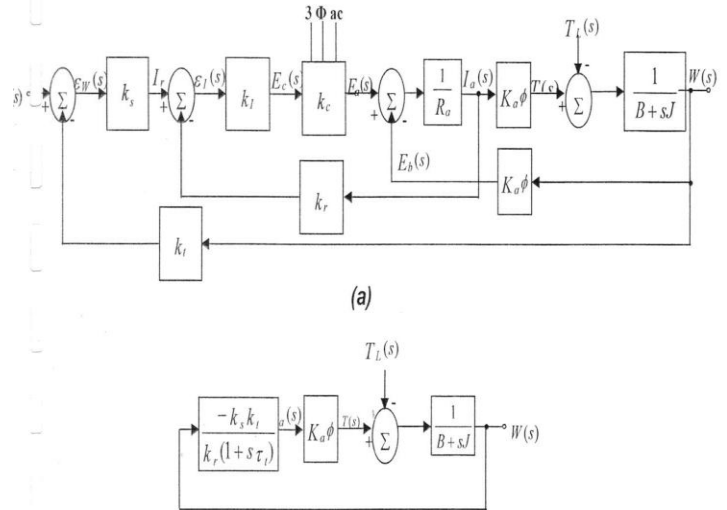


Fig.(8) Effect of load torque disturbances, (a) Functional block diagram, (b) Simplified Functional block diagram

Fig.(8a) shows the complete block diagram for the speed loop with proportional speed and current controllers. If changes in the reference speed W_r are neglected, Fig.(8b).

7. Load-Results

7.1 Proportional Speed -Proportional Current Controllers:

We saw the Fig.(9) shows the current and speed responses for speed control system with load torque applied at $t = 4$ sec. The system is tested with speed and current controllers are proportional type controller where $k_s = 14.169$ and $k_r = 19.407$. From the speed response, the steady state error defer applied the torque is very small, but is increased to become (8.1) after applied a load to the dc-motor. The steady state error of the speed response in speed control dc motor system is reduce by replacing the proportional speed controller by proportional-plus-integral speed controller , However, the steady state error is reduced from 8.1 to 0.31 as show in Fig.(9).

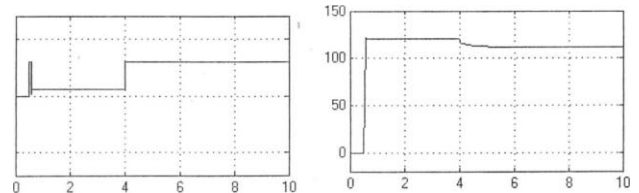


Fig.(9) Response to step increase in load torque with PI-controller (a) current response,(b)speed response

7.2 Feed Forward Loop

To reduce the dynamic speed variations of dc motor due to the step change in load torque, a feed forward scheme is presented as shown in Fig.(10). In this scheme.

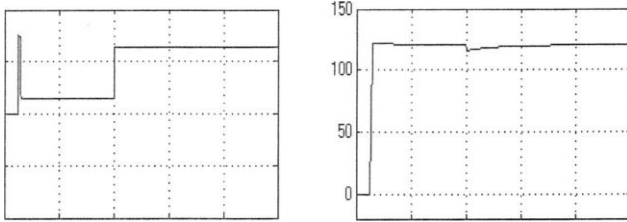


Fig. (10): Speed control of dc motor with feed forward loop.

8. Conclusion

In the present work a closed-loop analog speed control of dc-motor has been described. The closed-loop control technique is used instead of open-loop technique to increasing the accuracy, improved the dynamic response, and reduction of the effects of disturbances such as sudden loading. A transfer function technique is used to design the controller parameters. The current limiter is used to limit the armature current to some maximum allowable value (3A). The simulation response of the system is found for P and PI controllers. The steady-state error is reduced by using Pi-speed controller. The response of the system for step increasing and decreasing of reference speed is getting and found that the output of the system $w(s)$ is tracked the reference speed w_r . Table (1) shows the characteristics of speed response of proportional and proportional integral controllers. An improved response is achieved by using a feed forward loop with load torque case. The theoretical responses (simulation results) are not the same of practical responses, because some time constants are neglected in the system analysis, but the results are approximately closed to the practical results. The analog speed control of dc-motor is very easily in the analysis phase and in the simulation phase. But very complex experimentally, sometime need to change or replace some elements of the circuit to get the system response and specification, therefore we conclude that the digital speed control system is better than analog scheme.

Table (1)

Controller Type		Rise time	Peak time	overshoot	Steady state error	Not
Current	Speed	0.067	0.592	0.467%	0.370	NO Load
P	P					
P	PI	0.067	0.0251	1.5%	0	NO Load

References

1. Sen P.C., "Thyristor DC Drives", John Wiley and Sons, 1981.
2. Paresh C. Sen and Murray L. Macdonald, "Thyristorized DC Drives with Regenerative Braking and. Speed Reversal" IEEE, Transactions on Industrial Electronics and Control Instrumentation, Vol. IECI-25, No. 4, Nov. 1978, pp. 347-354.
- 3- Hamed Shakir Hassan, "Microprocessor-Controlled Four Quadrant Single Phase Thyristor DC Drive", M.Sc. Thesis, College of Engineering, University of Baghdad, 1985.
- 4- J.L. Duarte, J.F. Aubry and C. lung, " Current and Speed Digital Control of Commutation less dc Drives" IEEE, Transactions on Industrial Electronics, Vol. IE-36, No. 4, Nov. 1989, pp. 480-484.

Mobility and Reputation consideration in Manets

Rajesh. Attaluri¹, CH. Radhikarani², S. Venkateswarlu³

¹Student M.Tech CNS, K.L. University, Greenfields, Guntur.

²Asst. prof., Dept of CSE, KL University, Guntur

³H.O.D, Dept of CSE, KL University, Guntur

Abstract: Mobility is main problem in manets. Node movement increases the chance for potential contactors to gather more trust information and evidence, thus enlarging the scope of reputation qualified candidate nodes popularly. Micro Mobility and macro mobility are two movements we have to consider. So checking mobility is main important. Existing system uncertainty deeply impacts a node's anticipation of others' behavior and decisions during interaction, After defining a way to reveal and compute the uncertainty in trust opinions we consider mobility, one of the important characteristics of MANETs, to efficiently reduce uncertainty and to speed up trust convergence. In existing System, Two different categories of mobility-assisted uncertainty reduction schemes are provided: the proactive schemes exploit mobile nodes to collect and broadcast trust information to achieve trust convergence; the reactive schemes provide the mobile nodes methods to get authenticated and bring their reputation in the original region to the destination region. In this paper, we consider mobility to support our reputation system. Two types of mobility are included based on distance.

Keyterms: mobility, trust information, manets

Introduction: Mobility is main feature in Manets. In Manets node to node connectivity is checked. If mobiles are moving then handover increases based on distance. MOBILE ad hoc networks (MANETs) aim to provide wireless network services without relying on any infrastructure. The main challenge in MANETs comes from their self-organized and distributed nature. There is an inherent reliance on collaboration between the participants of a MANET in order to achieve the aimed functionalities.

Collaboration is productive only if all participants operate in an honest manner. Therefore, establishing and quantifying trust, which is the driving force for collaboration, is important for securing MANETs. Trust can be defined as the firm belief in the competence of an entity to act dependably, securely, and reliably within specified context. It represents a MANET participant's anticipation of other nodes' behavior when assessing the risk involved in future interactions. Here, the participant is usually called the trustor, and other nodes are called the trustee. The trust relationship usually builds on the basis of the trustor's past direct interaction experiences and others' recommendations related to the trustee. The abstracted value from past experiences and recommendations is defined as the

trustee's reputation. Many reputation systems have been proposed in literature. Most of them sharply divide the recorded behavioral information into right or wrong. For example, in the EigenTrust model [1], behavioral information is obtained by counting the number of "satisfactory" and "unsatisfactory" interactions, and the difference between these two values is stored as reputation. Besides lacking a precise semantic, this information has abstracted away any notion of time. In EigenTrust, value 0 may represent both "no past interaction" and "many unsatisfactory past interactions." Consequently, one cannot verify exact properties of past behavior based on this information alone.

Two types of mobility schemes are to be considered. One is micro mobility which stands for minimum distance. Another stands for macro mobility which is long distance.

Previous Works: In existing System, a one-dimensional representation of belief, disbelief, and uncertainty is extended from the subjective logic [2]. Each node keeps a belief and disbelief value toward other nodes as a prediction of their future behavior. As these two values are only predictions, uncertainty always exists. We use a triplet to represent a node's opinion (b,d, u) b,d,u are designate belief, disbelief, and uncertainty, respectively.

Our approach: When the requirement is a short convergence time to quickly start a trust-based application, or a controllable cost, the above two mobility models will offer extreme options. However, these two methods are not flexible enough and we lack a way to find a trade-off between convergence time and cost to satisfy different application objectives. Here, we present a two-level controlled mobility model, which is called hierarchical scheme. In hierarchical scheme, we divide the whole network into several regions, allowing each region to contain a specified number of grids, and choose mobility models for inter- and intraregion movement. Hierarchical scheme combines the advantages of the above two models and offers more options for MANET implementation. Various kinds of clustering mechanisms have been proposed in the MANETs [8], [9]. After using one of the existing clustering mechanisms, this hierarchical scheme can be applied on top of the clusters.

Algorithm 1. VoteForMove

```

1: while t<Tlimit
2: if m<mthreshold
3: get opinion(node)
4:else if m>=mthreshold
5: Get opinion(node,Supervisor)
4: end while
5: Compute(b; d; u) for each node;
6: if the largest b in all the opinions satisfy b >= Bmin then
7: Vote the node with the largest b;
8: Wait (elected moving node)
9: else
10: Continue();
11: end if;

```

In this algorithm, movement is calculated based on distance. If m is within threshold then it is called micro mobility. Micro mobility doesn't require confirmation from supervisor. Because movement is within distance. But Macro mobility requires confirmation from nearest supervisor. This supervisor acts as Foreign agent from one place to another place. All nodes will store mobile behavior but supervisor will store particular opinion only.

Algorithm 2. Vote Gathering

```

1:Counter++;
2: if counter>=threshold then
Start move();
Broadcast();
4: end if;

```

This algorithm shows counter increment. If counter meets threshold then node broadcasts information to all nodes including supervisor. And it starts moving. The moving nodes repeat the local contact process after they arrive in the capital. The pause time period in the capital allows them to build trust between each other and the local nodes of the capital. One node, which is commonly trusted by all moving nodes, will be elected to be the keeper of that region through a process similar to Algorithms 1 and 2. The keeper selects several nodes it trusts as supervisors, which will travel between regions to collect information and feed it back to the keeper.

Conclusion:

We study the impact of nodes' behavior inconsistency on our reputation system. Our approach finds well in all types of mobility schemes like micro and macro mobility. This approach well says about moving mobility. Uncertainty is one important metric in MANETs. Certainty-oriented reputation systems can achieve good detection rates while keeping the false positive rate at a low level. With proactive or reactive schemes, we can efficiently disseminate trust and reduce uncertainty by exploiting nodes' movement. All the schemes illustrate the uncertainty reduction effect with the assistance of mobility. Different mobility schemes provide different tradeoffs between delay, cost, and uncertainty. The controlled mobility-based

schemes appear to offer better performance in terms of uncertainty reduction.

References:

- [1] P. Michiardi, R. Molva. Simulation-based Analysis of Security Exposures in Mobile Ad Hoc Networks. European Wireless Conference, 2002.
- [2] S. Marti, T. Giuli, K. Lai, and M. Baker. Mitigating routing misbehavior in mobile ad hoc networks. In Proceedings of MOBICOM, 2000.
- [3] The Terminodes Project. www.terminodes.org.
- [4] L. Blazevic, L. Buttyan, S. Capkun, S. Giordano, J-P. Hubaux, and J-Y. Le Boudec. Selforganization in mobile ad hoc networks: The approach of Terminodes. IEEE Communications Magazine, June 2001.
- [5] L. Buttyan and J-P. Hubaux. Enforcing service availability in mobile ad hoc networks. In proceedings of MobiHOC, 2000.
- [6] J.-P. Hubaux, T. Gross, J.-Y. Le Boudec, and M. Vetterli. Toward self-organized mobile ad hoc networks: The Terminodes Project. IEEE Communications Magazine, January 2001.
- [7] L. Buttyan and J-P. Hubaux. Nuglets: a virtual currency to stimulate cooperation in selforganized ad hoc networks. Technical Report DSC/2001/001, Swiss Federal Institute of Technology -- Lausanne, 2001.
- [8] L. Zhou and Z. Haas. Securing ad hoc networks. IEEE Network, 13(6):24--30, November/December 1999.
- [9] G. Zacharia. Collaborative Reputation Mechanisms for online communities. Master's thesis, MIT, September 1999.
- [10] D. Zhou and J. Wu, "Survivable Multi-Level Ad-Hoc Group Operations," Proc. Int'l Workshop Mobile and Wireless Networks, 2003.
- [11] J. Yu and P. Chong, "A Survey of Clustering Schemes for Mobile Ad Hoc Networks," IEEE Comm. Surveys and Tutorials, vol. 7, no. 1, pp. 32-48, 2005.



Reputation Analysis and Impact of Node Mobility on Manets for Wireless Networks

Rajesh.Attaluri *, CH. Radhikarani **, S. Venkateswarlu***

* *M.Tech CNS Student, K.L. University, Greenfields, Guntur*

** *Asst. prof., Dept of CSE, KL University, Guntur.*

*** *H.O.D, Dept of CSE, KL University, Guntur.*

ABSTRACT

A wireless network is formed without any pre existing infrastructure , in which every layer act as a router is called a mobile ad hoc network (MANET). Ad hoc networks is one of the subset of wireless network that dynamically forming a temporary network without using any existing network infrastructure or centralized administration. Mobility is the main problem in Manets. The movement of the mobile node is one of the important characteristics because it can effects the performance of the ad hoc network protocol. Node movement increases the chance for potential contactors to gather more trust information and evidence.

Checking mobility is the main aspect in every Manet, Micro Mobility and macro mobility are two movements we have to consider for this mobility checking. Mobility is one of the important characteristic of Manet, to efficiently reduce uncertainty and to speed up trust convergence.

In this paper we analyze the impact of mobility on Manets. we consider mobility to support our reputation to analyze the performance of Manets and two types of mobility's are consider based on distance.

Keywords - mobile ad hoc network (MANET), mobility.

I. INTRODUCTION

Mobile ad hoc networks (MANETs) are self-organizing networks that do not require a fixed infrastructure. Two nodes communicate directly if they are in the transmission range of each other. Otherwise, they reach via a multi-hop route. Each MANET node must therefore be able to function as a router to forward data packets on behalf of other nodes . Because of their unique benefits and versatilities, MANETs have a wide range of applications such as collaborative, distributed mobile computing (e.g., sensors, conferences), disaster relief (e.g., flood, earthquake), war front activities and communication between automobiles on highways.

Most of these applications demand multicast or group communication. In manets mobility is the main considerable character, In Manets node to node connectivity is checked. If mobiles are moving then handover increases based on distance. MOBILE ad hoc networks (MANETs) aim to provide wireless network services without relying on any infrastructure. The main challenge in MANETs comes from their self-organized and distributed nature. There is an inherent reliance on collaboration between the participants of a MANET in order to achieve the aimed functionalities. Collaboration is productive only if all participants operate in

an honest manner. Therefore, establishing and quantifying trust, which is the driving force for collaboration, is important for securing MANETs. Trust can be defined as the firm belief in the competence of an entity to act dependably, securely, and reliably within specified context. It represents a MANET participant's anticipation of other nodes' behavior when assessing the risk involved in future interactions. Here, the participant is usually called the trustor, and other nodes are called the trustee. The trust relationship usually builds on the basis of the trustor's past direct interaction experiences and others' recommendations related to the trustee. The abstracted value from past experiences and recommendations is defined as the trustee's reputation. Many reputation systems have been proposed in literature. Most of them sharply divide the recorded behavioral information into right or wrong. For example, in the EigenTrust model [1], behavioral information is obtained by counting the number of "satisfactory" and "unsatisfactory" interactions, and the difference between these two values is stored as reputation. Besides lacking a precise semantic, this information has abstracted away any notion of time. In EigenTrust, value 0 may represent both "no past interaction" and "many unsatisfactory past interactions." Consequently, one cannot verify exact properties of past behavior based on this information alone.

Two types of mobility schemes are to be considered. One is micro mobility which stands for minimum distance. Another stands for macro mobility which is long distance.

II. MOTIVATION

A MANET has got some of the important properties like self organized and rapid deployable capability; which makes it widely used in various applications like emergency operations, battlefield communications, relief scenarios, law enforcement, public meeting, virtual class rooms and other security-sensitive computing environments.

MANETs have a wide range of applications, Each of these applications can potentially involve in different scenarios with different mobility patterns, traffic rates dependent on the environment and the nature of the interactions among the participants. In order to thoroughly study the protocols for these applications, it is imperative to use the mobility models that accurately represent the mobile nodes which utilize the protocols. So This paper gives analysis of mobility in Manets to increase the performance in different applications.

III. PREVIOUS WORK

In existing System ,one-dimensional representation of belief, disbelief, and uncertainty is extended from the subjective logic [2]. Each node keeps a belief and disbelief value toward other nodes as a prediction of their future behavior. As these two values are only predictions, uncertainty always exists. We use a triplet to represent a node's opinion (b,d,u) b,d,u are designate belief, disbelief, and uncertainty, respectively.

IV. OUR APPROACH

When the requirement is a short convergence time to quickly start a trust-based application, or a controllable cost, the above two mobility models will offer extreme options. However, these two methods are not flexible enough and we lack a way to find a trade-off between convergence time and cost to satisfy different application objectives. Here, we present a two-level controlled mobility model, which is called hierarchical scheme. In hierarchical scheme, we divide the whole network into several regions, allowing each region to contain a specified number of grids, and choose mobility models for inter- and intraregion movement. Hierarchical scheme combines the advantages of the above two models and offers more options for MANET implementation. Various kinds of clustering mechanisms have been proposed in the MANETs [8], [9]. After using one of the existing clustering mechanisms, this hierarchical scheme can be applied on top of the clusters.

Algorithm 1

VoteForMove

```

1: while t<Tlimit
2: if m<mthreshold
3: get opinion(node)
4:else if m>=mthreshold
5:Get opnion(node,Supervisor)
4: end while
5: Compute(b; d; u) for each node;
6: if the largest b in all the opinions satisfy b >= Bmin then
7: Vote the node with the largest b;
8: Wait (elected moving node)
9: else
10: Continue();
11: end if;

```

In this algorithm, movement is calculated based on distance. If m is within threshold then it is called micro mobility. Micro mobility doesn't require confirmation from supervisor. Because movement is within distance. But Macro mobility requires confirmation from nearest supervisor. This supervisor acts as Foreign agent from one place to another place. All nodes will store mobile behavior but supervisor will store particular opinion only.

Algorithm 2

Vote Gathering

```

1: Counter++;
2: if counter>=threshold then
Start move ();
Broadcast ();
4: end if;

```

This algorithm shows counter increment. If counter meets threshold then node broadcasts information to all nodes

including supervisor. And it starts moving. The moving nodes repeat the local contact process after they arrive in the capital. The pause time period in the capital allows them to build trust between each other and the local nodes of the capital. One node, which is commonly trusted by all moving nodes, will be elected to be the keeper of that region through a process similar to Algorithms 1 and 2. The keeper selects several nodes it trusts as supervisors, which will travel between regions to collect information and feed it back to the keeper.

V. CONCLUSION

In this paper, we analyzed the impact of mobility pattern on performance of mobile ad hoc networks. Here our approach gets a good performance in all types of mobility schemes like micro and macro mobility. We find out that Certainty-oriented reputation systems can achieve good detection rates while keeping the false positive rate at a low level. All the schemes illustrate the uncertainty reduction effect with the assistance of mobility. We observed that different mobility schemes provide different tradeoffs in delay, cost and uncertainty and controlled mobility-based schemes have a better performance in terms of uncertainty reduction.

This work can be further explored to study the impact of mobility on the performance in Manets. Several other parameters such as traffic patterns, node density and initial placement pattern of nodes may affect the performance and hence this work can be extended to investigate them further.

REFERENCES

- [1] C. E. Perkins, "Mobile Ad Hoc Networking Terminology," *draft-ietf-manet-term-00.txt*, October 1997.
- [2] P. Michiardi, R. Molva. Simulation-based Analysis of Security Exposures in Mobile Ad Hoc Networks. European Wireless Conference, 2002.
- [3] S. Marti, T. Giuli, K. Lai, and M. Baker. Mitigating routing misbehavior in mobile ad hoc networks. In Proceedings of MOBICOM, 2000.
- [4] The Terminodes Project. www.terminodes.org.
- [5] L. Blazevic, L. Buttyan, S. Capkun, S. Giordano, J-P. Hubaux, and J-Y. Le Boudec. Selforganization in mobile ad hoc networks: The approach of Terminodes. IEEE Communications Magazine, June 2001.
- [6] L. Buttyan and J-P. Hubaux. Enforcing service availability in mobile ad hoc networks. In proceedings of MobiHOC, 2000.
- [7] J.-P. Hubaux, T. Gross, J.-Y. Le Boudec, and M. Vetterli. Toward self-organized mobile ad hoc networks: The Terminodes Project. IEEE Communications Magazine, January 2001.
- [8] L. Buttyan and J.-P. Hubaux. Nuglets: a virtual currency to stimulate cooperation in selforganized ad hoc networks. Technical Report DSC/2001/001, Swiss Federal Institute of Technology -- Lausanne, 2001.
- [9] L. Zhou and Z. Haas. Securing ad hoc networks. IEEE Network, 13(6):24--30, November/December 1999.
- [10] G. Zacharia. Collaborative Reputation Mechanisms for online communities. Master's thesis, MIT, September 1999.
- [11] D. Zhou and J. Wu, "Survivable Multi-Level Ad-Hoc Group Operations," Proc. Int'l Workshop Mobile and Wireless Networks, 2003.
- [12] J. Yu and P. Chong, "A Survey of Clustering Schemes for Mobile Ad Hoc Networks," IEEE Comm. Surveys and Tutorials, vol. 7, no. 1, pp. 32-48, 2005.

Ontology based Secured Data Migration

SureshKumar R¹, Vijayakaran V², SampathKumar TT³

*(Department of Information Technology, Sri Manakula Vinayagar Engineering College, India)

**(Department of Computer Science, Sri Manakula Vinayagar Engineering College, India)

***(Department of Computer Science, Sri Manakula Vinayagar Engineering College, India)

ABSTRACT

This work proposes an ontology based data migration for large database. Our approach provides a reduction and integration of the ontology from the diverse databases. The ontology is classified into two major categories: global ontology and local ontology. During the data migration process all the local data, relationships among the local data is represented into ontology tree and this local ontology tree is mapped with the global ontology tree. This mapping process involves ontology disintegration, merging of sub-tree and validation of the ontology mapping process. Once the ontology tree has been created and mapped to the global tree, the process of data migration starts on its way. During the migration process there is a possibility of the attackers in the network from whom the data has to be protected. Since we also propose a secured way of data migration process in which there is a least possibility of the data theft.

Keywords: "Data migration, Ontology Mapping, XML, Schema Mapping".

I. INTRODUCTION

According to Moore's law, the number of transistors that can be placed inexpensively on an integrated circuit doubles approximately every two years. This creates a technological shift from the legacy system to the current supercomputing systems. The data persisted in every organisation also been increasing in the past decade due to the cheap availability of several Databases. This creates the need to migrate the data from the existing databases to new database. Data migration is the process of transferring data between storage types, formats, or computer systems. Many cloud applications [4] [5] [6] [7] [8] requires migration process where the data is the very important entity.

Data migration [1] [2] [3] [9] is usually performed programmatically to achieve an automated migration, freeing up human resources from tedious tasks. It is required when organizations or individuals change computer systems or upgrade to new systems, or when systems merge (such as when the organizations that use them undergo a merger or takeover). During this process of migration there cannot be a direct migration from older databases to new databases. There arises variation in the storage level, access level, meta-data[10], schema, relationships among the data which differs from database to database. In such process of migration one has to be keen in the integrity and the consistency of the data during migration. Hence there is a need of the data to be transformed into a flexible model such that the migration process is flexible to apply.

This work describes about the data migration for large database using ontology mapping and schema mapping technique. Since ontology is proven technique in today's world for web data migration and to represent the data/relationship among data. Several tools such as ETL tools available for the data migration process but those ETL cannot be applied for the data migration when there are different types of databases and has many relations among the data. In present decade the amount of data to be stored and retrieved is increasing exponentially due to the increasing business process and to capture the customer's data. Several methods of construction of ontology are proposed to assist in the creation of ontologies but most of them are not interested in how to acquire the relevant information in the domain of discourse.

II. Data Migration process

In the migration process the data and the relationships of the data have to be converted into suitable ontological structure, hence we use XML to represent the meta-data of the database. In this representation the XML is ontological tree which is generated locally and it has to be checked with the global ontology. Sometimes the entire data has a complex relationship; hence we can construct the ontological tree from the Entity relationship diagram as explained in [ref]. In the process of capturing the meta-data the prior information about the database has to be tabled since each database has its own representation to represent the data and the relationship.

2.1 Data Type Mapping

The data-type also differs from the versions of the same database due to the technological advancement. In recent days there has been a wider support for the xml data types and the query to retrieve the xml data is increasing due to the interoperability of the XML.

In migrating the multi-media contents there is a extensive variations in the storage level of the contents, due to the difference in the data types of the database. This difference may not arise due to the specifications of the database, it also arises due to the difference in creation of the attributes (ex: to represent employee id, both integer and String can be chosen as in figure 1). In such scenario the local ontology tree has to be matched with the global ontology tree.



Figure 1. Data type mapping

This issue can be resolved by

- Change the data type in either side which suits the change
- Xml representation

2.3 Normalization in Attribute Mapping

In the normalization process the attributes of the database is converted into the local ontology tree (XML format). During this process the attributes which are named specifically are generalized with the attribute names of the global ontological tree. The global ontological has the set of rule base for attribute generalization process.

- FNAME <=> FIRSTNAME
- ENO <=> EMPLOYEEENUMBER
- STDID <=> STUDENTID
- MGRID <=> MANAGERID

2.4 Attribute Level Mapping

The attribute level mapping describes about the representation of the attributes. In Figure 2, Name can be represented as a combination of FName, MName, LName and the same Name can be represented only by FName and LName. In such scenario FName and MName has be combined or the LName has to be splitted into MName and FName. Hence we provide a merge () and split () algorithm to handle this situation in the ontology tree mapping.

- Merge()
- Split()

III. ONTOLOGY BASED DATA MIGRATION

Ontology technologies have recently been introduced in the field of semantic web to organize data and knowledge of a domain in order to share, disseminate and update them. These technologies seem to provide a solid methodological framework, both relevant and innovative, to deal with document images. In figure 4, the ontological tree creation and ontology comparison is explained. Initially after the normalization process, ontology Tree is created with the meta-data and relationship between the data. After local ontology creation both in source and destination databases the comparison of the ontology tree has be performed with the size level mapping process and attribute level mapping.

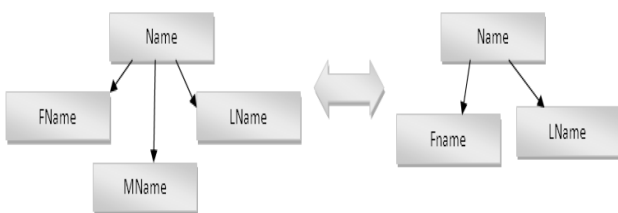


Figure 2.Attribute Level Mapping

2.4 Size Level Mapping

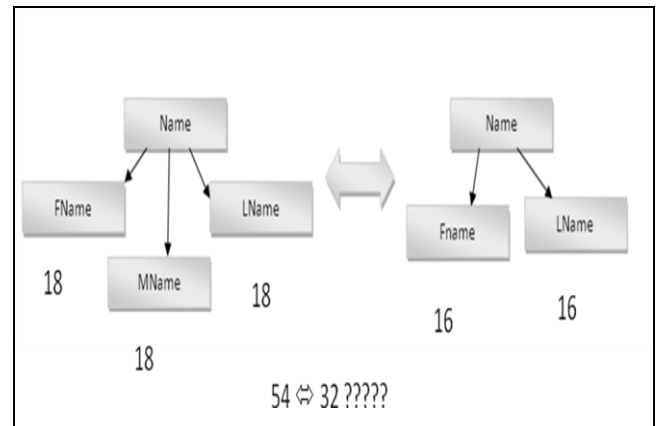


Figure 3. Size Level Mapping

3.1 Ontology and Sub-Ontology Matching Algorithm

- Step 1. CreateOntologyTree()
- Step 2. Verification and Validation()
- Step 3. Normalization
- Step 4. Attribute-Level-Mapping()
- Step 5. Size-Level-Mapping()
- Step 6. Data-type-Maping()
Samedatatype()

Differentdatatype()

- Step 7. Data_Migrate()

3.2 Ontology Tree Creation Algorithm

- Step 1. Create_ontology_tree()
- Step 2. {
- Step 3. Fetch_table_structure()
- Step 4. Map_attributes;
- Step 5. Map_relations;
- Step 6. Represent_ontology;

3.3 Verification Process Algorithm

- Step 1. validation()
- Step 2. {
- Step 3. errors=verification();
- Step 4. If(errors) then
- Step 5. Alter_ontology()
- Step 6. Else
- Step 7. No Action;
- Step 8. }

3.4 Validation Process Algorithm

- Step 1. verification()

```

Step 2.    {
Step 3.    Fetch_table_structure;
Step 4.    Fetch_ontology_structure;
Step 5.    Fetch_relations;
Step 6.    Compare_table_ontology;
Step 7.    Return errors;
Step 8.    }
    
```

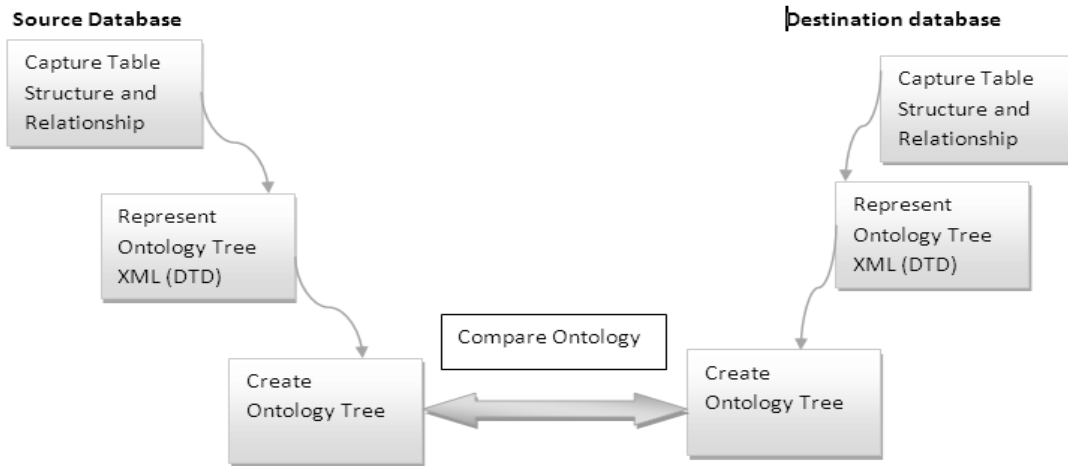


Figure 4. Ontology tree creation and comparison

IV. Secured Data Migration Architecture

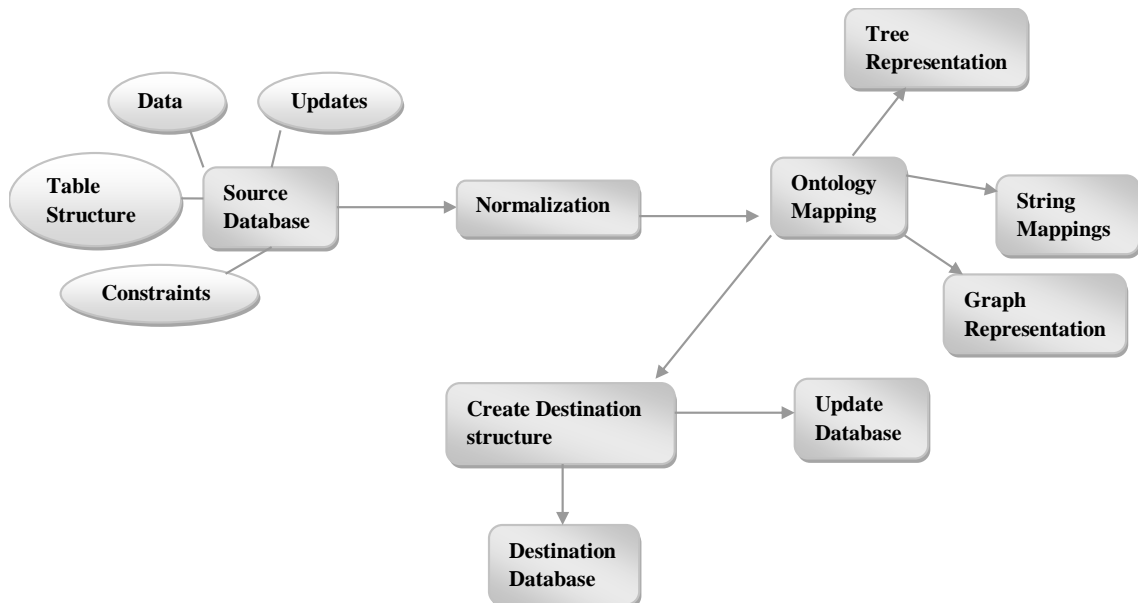


Figure 5. Ontology Based Secured Data Migration Architecture

In figure 5 the secured data migration architecture is described. In this process source data is encrypted before the data migration process. The ontology tree is created and the source and destination ontology is matched and the migration process is initiated once the ontology tree matching is successful.

V. IMPLEMENTATION DETAILS

In our approach we have taken the university database. The migration process can be taken in two processes.

1. Periodical migration
2. Complete Migration

Periodical Migration

In our institution there has been a heavy traffic and queue attendance enrolment of the staffs. This traffic is due to all the staffs of various departments and administration staffs have to enroll in the finger print scanner. The database is updated severely during the entry process.

We proposed and implemented a migration process where the queue is reduced to very least amount. We created a department wise database and updated the attendance records by 9 O clock. This update is taken place in the local database of the departments. Our algorithm will update the periodically according to the departments.

Hence there is a great reduction in the

1. Waiting time of the staffs
2. Server's congestion as the data is migrated periodically
3. Data loss is reduced as the congestion is reduced to a greater extend

Fig 6 shows that the migration using the ontology mapping consumes lesser time when compared to the schema mapping. Fig 7 shows the comparison between the average waiting times of the staffs in the queue. Our proposed migration process drastically reduces the waiting time and also it reduces the server overload by creating lesser congestion for the server to update the data. Due to the lesser overload of the server there is very least amount of data lost during the updates. During the migration process from local server to centralized server the data are encrypted to avoid the intruders to see the important data.

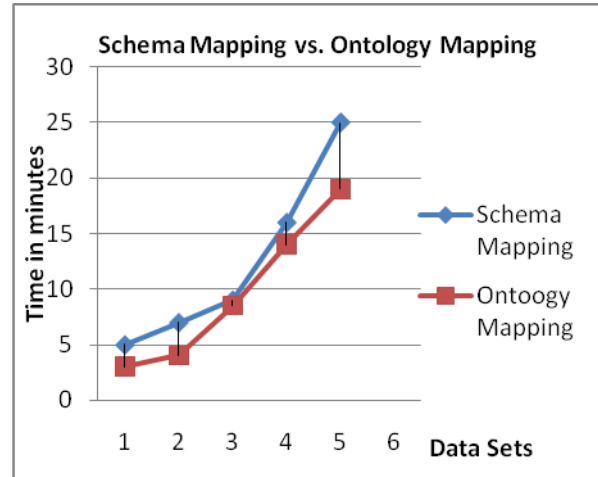


Figure 6. Comparison of Ontology Mapping and Schema Mapping Migration

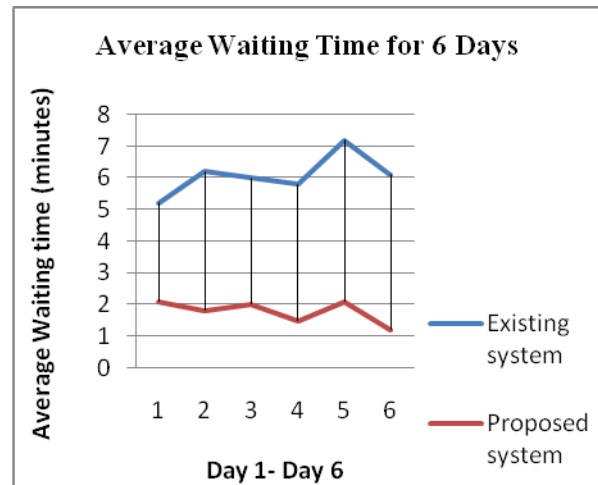


Figure 7. Average waiting time of the Staffs

VI. Conclusions

The Ontology based data migration process is explained with the initial data pre-processing technique. The ontology tree creation with the XML and ontology matching is also discussed with the algorithm in our work. We also proposed an algorithm for the university record updation and migration which reduces the queue, waiting time, server's overload. The secured migration is proposed for the data security but the time is utilized during the encryption and decryption process that we will cover up in our future work.

ACKNOWLEDGEMENTS

We would like to thank the institution for providing us the greater support in our research.

REFERENCES

- [1] Xiaonan Zhao, Zhanhuai Li, Xiao Zhang and Leijie Zeng "Block-Level Data Migration in Tiered Storage System", Second International Conference on Computer and Network Technology, pp.181-185, 2010
- [2] Jonghyun Lee, Marianne Winslett, "Enhancing Data Migration Performance via Parallel Data Compression" in proc. International Parallel and Distributed Processing Symposium (2002)
- [3] F.H.Chanchary and S.Islam, "E-government Based on Cloud Computing with Rational Inference Agent," HONET, KSA, December 2011.
- [4] Hakan Hacigümüs, Sharad Mehrotra, Bala Iyer, "Providing Database as a Service," icde, pp.0029, 18th International Conference on Data Engineering (ICDE'02), 2002
- [5] Oracle Enterprise Manager Cloud Administration Guide 12c Release 1 (12.1.0.1), Part Number E25179-01, available at http://docs.oracle.com/cd/E24628_01/doc.121/e25179/cloud_db_overview.htm
- [6] Jonathan Strickland, "How Cloud Storage Works," available at <http://computer.howstuffworks.com/cloud-computing/cloud-storage1.htm>
- [7] C. Curino, E. P. C. Jones, R. A. Popa, N. Malviya, E. Wu, S. Madden, H. Balakrishnan, N. Zeldovich, "RelationalCloud: a Database Service for the cloud," CIDR 2011, 14th February 2011.
- [8] C. Curino, E. P. C. Jones, R. A. Popa, N. Malviya, E. Wu, S. Madden, H. Balakrishnan, N. Zeldovich, "RelationalCloud: a Database Service for the cloud," Computer Science and Artificial Intelligence Laboratory Technical Report, MIT-CSAIL-TR-2010-014, March 2010.
- [9] Data migration management, a methodology: Sustaining data integrity after the go live and beyond, UTOPIA Inc., 2009
- [10] William H. Inmon, Bonnie O'Neil, Lowell Fryman, "Business Metadata: Capturing Enterprise Knowledge"; Morgan Kaufmann, 1st edition 2007, ISBN-10: 0123737265.

Removal of Cu & Zn from industrial wastewater by using steel industry waste (Slag) as an adsorbent

Animesh Agarwal¹, Megha Agarwal² and Manish Saxena³

*Department of Applied Sciences & Humanities,
Moradabad Institute of Technology, Ram Ganga Vihar Phase – 2, Moradabad-244001*

Abstract

The removal of two heavy metals Cu and Zn from their aqueous solution, using steel industry slag as an adsorbent was studied as slag consist of calcium oxide, aluminum oxide, magnesium oxide etc. The research is a bench scale experimental type and analysis have performed by using different amount of adsorbent in solution with five different concentration of both metals and also in mixed combination. About 93.6% and 100% Cu removal was achieved by using 1 and 3g adsorbent for solution having concentration of 5 and 10 mg/L Cu. It was also found that adsorption efficiency depend on the amount of adsorbent as adsorption efficiency of Zn was increased from 82% to 100% in the same solution(5 mg/L).It was also observed that adsorption efficiency was decreased about 2% and 4% of Cu and Zn in Mixed metal solution.

Key words: Adsorption, Contact time, Heavy metals, Industrial wastewater, Steel Industry Slag

1. Introduction

Water is a vital resource for agriculture, manufacturing and other human activities. In urban areas, the careless disposal of industrial effluents and other wastes in rivers & lacks may contribute greatly to the poor quality of river water [1-4]. Most of the rivers in the urban areas of the developing countries are the ends of effluents discharged from the industries. African countries and Asian countries experiencing rapid industrial growth and this are making environmental conservation a difficult task [5].

Toxic heavy metals are constantly released into the environment. They are dangerous environmental pollutants due to their toxicity and strong tendency to concentrate in environment and in food chains, [6-7].The source of environmental pollution with heavy metals is mainly industry, i.e. metallurgical, electroplating, metal finishing industries, tanneries, chemical manufacturing, mine drainage and battery manufacturing [8].

Removal of metals from wastewater is achieved principally by the application of several processes such as adsorption [6,10], sedimentation [11], electrochemical processes [12], ion exchange [13], cementation [14], coagulation/flocculation [15], filtration and membrane processes [16],Chemical precipitation and solvent extraction [17-18].Adsorption is the one of the important procedure for the removal of heavy metals from the environment because of strong affinity and high loading capacity [6].

Moradabad also known as brass city of India, having urban population more than 3.7 million and has seen rapid industrialization during last few decades. The city is full of brass, steel & glass cottage industries. The annual turn over of the city is nearly rupees 10,000 million. All these industries are in unorganized sector and thus have unplanned growth leaving to high degree of air, water and soil pollution [19-20]. The most of the industries are dumping their effluents in Gagan River pass from the heart of the city. A large number of small-scale manufacturing units of Steel have been also situated in the heart of the city. During manufacturing process, high temperature coal based furnaces used to melt the metal. After the completion of the process, large amount of slag is produced as a waste. This Slag consists of calcium oxide, magnesium oxide, and other metal oxides and can be used as an adsorbent for the removal of heavy metals in the environmental field. For sorption properties of slag, several researchers reported the removal of heavy metals from wastewaters using slag [21-25]. This give us imputes to extends our work on steel industry slag which is used as an adsorbent for the removal of Cu and Zn from industrial wastewater.

2. Material and Method

2.1 Adsorbent

The steel industry waste (Slag) was collected from the bank of river Gagan River where local small industries generally dump their waste and were sieved to less than 2mm size and its composition was as follows:

CaO – 60.5%

SiO₂ – 20.3%

Al₂O₃– 8%

MgO – 6%

2.2 Adsorbate Solution

Stock solution of Copper was prepared (1000mg/L) by dissolving the desired quantity of $\text{CuSO}_4 \cdot 5\text{H}_2\text{O}$ (Analytical grades), Stock solution of Zinc was prepared (1000mg/L) by dissolving its Chlorides.

2.3 Adsorption Studies

Individual and mixed solutions of Cu and Zn with different concentrations of 5, 10, 20, 40, 100 mg/L were prepared, the experiment were performed using three different amount of adsorbent 1,2,3gm in single solution. 1 gm adsorbent was placed in a conical flask in which 100 ml of solution with known concentration of Cu was added and the mixture was shaken in shaker. The mixture was than filtered after 3 hours contact time and final concentration of metal ion was determined in filtrate by atomic adsorption spectrophotometer (GBC 902). All the Experiments were carried out in triplet and mean concentration was calculated by averaging them. The procedure was repeated by varying the adsorbent dose and concentration of Cu and Zn solution both individual and in mixed solution and the results are summarized in Tables (1-3). On the basis of residual concentrations, the adsorption efficiency of slag is calculated and summarized in Table (4-6).

Table-1: Mean concentration of Residual Cu after Adsorption by Slag (3 hour contact time)

SNo.	Quantity of Slag(gm)	Initial Concentration of Cu (mg/L)				
		5	10	20	40	100
1.	1	0.32	0.9	2.2	6.6	22
2.	2	0.05	0.1	0.9	1.5	3.3
3.	3	0	0	0.4	1	2.8

Table-2: Mean concentration of Residual Zn after Adsorption by Slag (3 hour contact time)

SNo.	Quantity of Slag(gm)	Initial Concentration of Zn(mg/L)				
		5	10	20	40	100
1.	1	0.9	1.9	4.2	8.6	36.4
2.	2	0.1	0.7	1.9	3.8	19.2
3.	3	0	0	1	2	10.8

Table-3: Mean concentration of Residual Metal in mixed metal solution using 1 g Slag after adsorption (3 hour contact time)

SNo.	Metal Solution	Initial Concentration (mg/L)				
		5	10	20	40	100
1.	Cu	0.42	1.7	3.4	6.9	24
2.	Zn	1.1	2.2	5.1	10.2	39.2

Table-4: Slag Adsorption Efficiency for Cu at various Concentrations (3 hour contact time)

SNo.	Quantity of Slag(gm)	Initial Concentration of Cu (mg/L)				
		5	10	20	40	100
Adsorption Efficiency (%)						

1.	1	93.6	91	89	83.5	78
2.	2	99	99	95.5	96.25	96.7
3.	3	100	100	98	97.5	97.2

Table-5: Slag Adsorption Efficiency for Zn at various Concentrations
(3 hour contact time)

SNo.	Quantity of Slag(gm)	Initial Concentration of Zn (mg/L)				
		5	10	20	40	100
		Adsorption Efficiency (%)				
1.	1	82	81	79	78.5	63.6
2.	2	98	93	90.5	90.5	80.8
3.	3	100	100	95	95	89.2

Table-6: Slag Adsorption Efficiency for Cu and Zn in Mixed Metal solution using 1g Slag
(3 hour contact time)

SNo.	Metal Solution	Initial Concentration (mg/L)				
		5	10	20	40	100
		Adsorption Efficiency (%)				
1.	Cu	91.6	83	83	82.75	76
2.	Zn	78	78	74.5	74.5	60.8

3. Result and Discussions

The data obtain from above analysis indicate that the adsorption efficiency is maximum for Cu (Table- 1and 2). Table-1 shows the residual concentration of Cu in solution after 3 hours contact time and Fig -1 shows the adsorption efficiency for various concentrations of Cu and Zn by 1g slag. It is clear that slag is a good adsorbent for removal of Cu from wastewater. The adsorption rate is dependent on adsorbent amount and initial concentration of metal in synthetic solution. 93.6% removal of Cu from a 5 mg/L solution was possible by applying 1 g slag where as the similar amount of adsorbent was not enough to treat 100mg/L Cu solution to above 78% but by increasing the amount of slag to 3 g it was possible to increase the efficiency of adsorption to about 97.2% for the same solution (100mg/L Cu). It shows that we would have better treatment by using excess slag. As this adsorbent is cheap and available in brass industry waste, there would be no problem to increase its consumption.

Table- 4 & 5 indicate that adsorption efficiency is dependent on the type of metal too , as for Zn we have not more than 82% removal in same condition (1 gm adsorbent in solutions 5,10,20,40,100, mg/L) but for Cu the efficiency is reported to be 93.6%.Table-3 represent the results of adsorption experiments conducted on the mixture of metal solution as mentioned before , the maximum and minimum removal efficiency in the first stage experiments with 1 g of adsorbent was 93.6% and 82% for Cu and Zn . But for the mixture of these metals a decrease of 2% has been observed for Cu whereas Zn adsorption has decreased about 4%. The efficiency of Cu and Zn adsorption by various amounts of slag shown in fig-1 to 3 for individual solution and for mixed solution of Cu and Zn (fig-4) and in comparison to individual solution in fig-5.

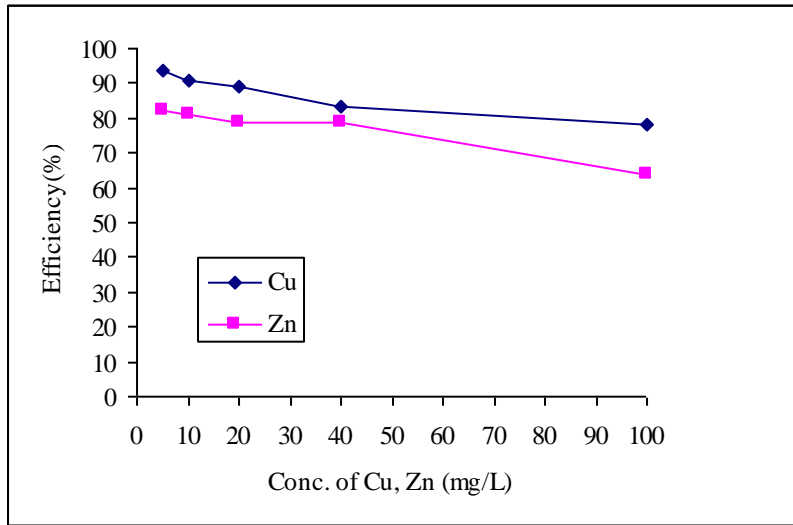


Fig. 1: % Adsorption of Cu and Zn by 1 g Slag

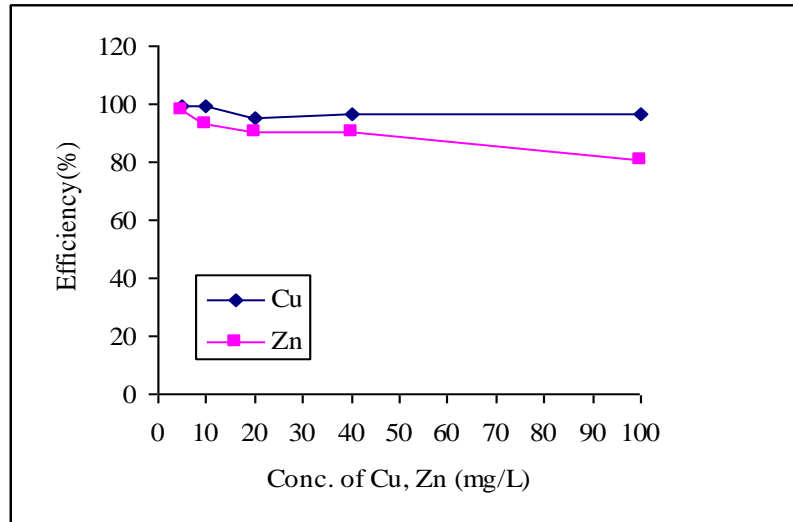


Fig. 2: % Adsorption of Cu and Zn by 2 g Slag

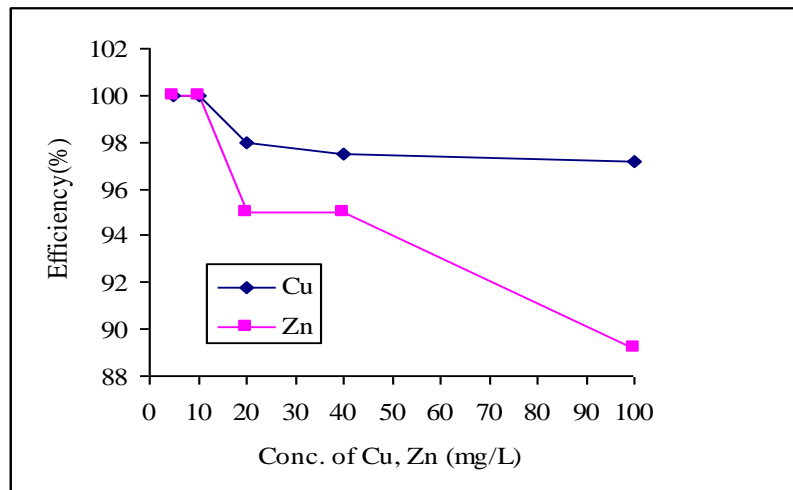


Fig. 3: % Adsorption of Cu and Zn by 3 g Slag

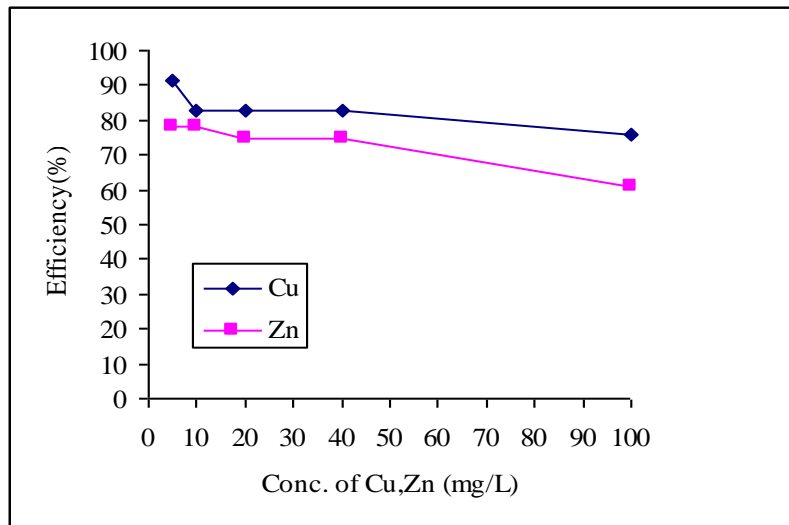


Fig. 4: % Adsorption of Cu and Zn in Mixed Metal Solution by using 1 g Slag

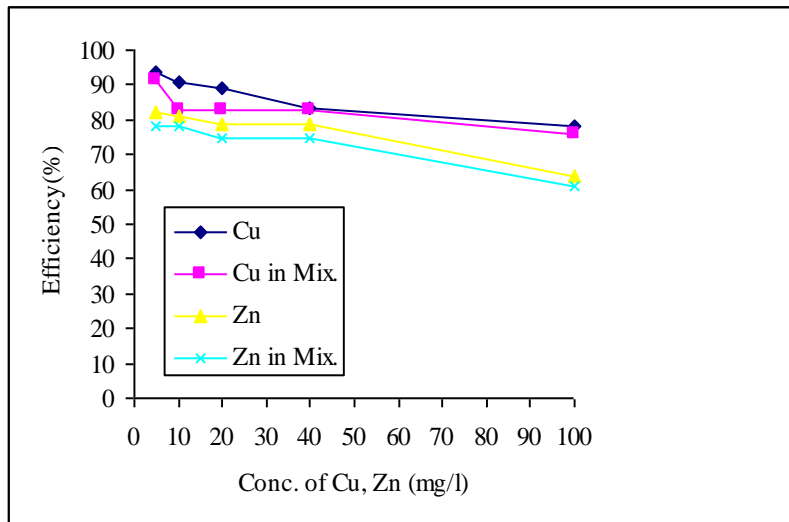


Fig.5: A Comparison Between % Adsorption of Cu and Zn in individual and Mixed Metal Solution by 1 g Slag

4. Conclusions

The above results shows that steel industry slag like the most other natural adsorbents can be used in the treatment process of heavy metals and the treatment efficiency may be as high as 100% by precise choosing of adsorbent amount. It was also found that the concentration of heavy metals has an important effect on the result of this treatment. Slag is a waste material and can be conveniently used for the treatment of industrial wastewater, it is like the industrial waste is utilizing for the treatment of industrial wastewater. Further it is recommended that the industries should developed pretreatment process by using slag as an adsorbent before mixing the industrial wastewater into the river.

References

- [1] Chindah A C, Braide A S and Sibeudu O C, 2004. Distribution of hydrocarbons and heavy metals in sediment and a crustacean from the bonny/new calabar river estuary, Niger Delta, *Ajeam-Ragee*, **9** 1-14.
- [2] Emongor V, Kealotswe E, Koorapetse I, Sankwasa S and Keikanetswe S, 2005. Pollution indicators in Gaberone effluent, *J. Appl. Sci.*, **5** 147-150.
- [3] Furtado A A L, Albuquerque R.T, Leite S G F and Pecanha R P, 1998. Effects of hydraulic retention time on nitrification in an airlift biological reactor, *Brazilian Journal of Chemical Engineering*, **15** 1-7.
- [4] Ugochukwu C N C, 2004. Effluent monitoring of oil servicing company and its impact on the environment, *Ajeam-Ragee*, **8** 27-30.

- [5] Waziri M and Ogugbuaja V O, 2010. Interrelationships between physicochemical water pollution indicators, *Am. J. Sci. Ind. Res.*, **1**, 76-80.
- [6] Sari A, Tuzen M and Soylak M, 2007. Adsorption of Pb(II) and Cr(III) from aqueous solution on Celtic clay, *J. Hazard. Mater.*, **144** 41- 46.
- [7] Bulut Y and Baysal Z, 2006. Removal of Pb(II) from wastewater using wheat Bran, *J. Environ. Manage.*, **78** 107-113.
- [8] Matheickal J T and Yu Q, 1997. Biosorption of lead (II) from aqueous solutions by *Phellinus badius*, *Miner Eng.* **10** 947-957.
- [9] Carvalho de R P, Freitas J R, de Sousa M G, Moreira R L, Pinheiro M V B, Krambrock K, 2003. Biosorption of copper ions by dried leaves: chemical bonds and site Symmetry, *Hydrometallurgy*, **71** 277-283.
- [10] Valdman E, Leite S G F, 2000. Biosorption of Cd, Zn and Cu by *Sargassum* sp. waste biomass, *Bioprocess Engineering*, **22** 171-173
- [11] Song Z, Williams C J, Edyvean R G J, 2004. Treatment of tannery wastewater by chemical coagulation, *Desalination*, **164**, 249-259.
- [12] Fahim N F, Barsoum B N and Eid A E, 2006. Removal of Chromium (III) from tannery wastewater using activated carbon from sugar industrial waste, *J. Hazard. Mat.*, **136**, 303-337.
- [13] Tiravanti G, Petruzzelli D and Passino R, 1997. Pretreatment of tannery wastewaters by an ion exchange process for Cr (III) removal and recovery, *Water Sci. Technol.*, **36** 197-207.
- [14] Filibeli A, Buyukkamaci N and Senol H, 2000. Solidification of tannery wastes, *Resour. Conserv. Recy.*, **29** 251- 261.
- [15] Song Z, Williams C J and Edyvean R G J, 2000. Sedimentation of tannery wastewater, *Water Res.*, **34**, 2171-2176.
- [16] Fabianil C, Rusciol F, Spadonil M and Pizzichini M, 1996. Chromium (III) salts recovery process from tannery wastewaters, *Desalination*, **108** 183.
- [17] Brooks C S, 1991. Metal recovery from industrial waste, *Lewis Publisher*, USA,
- [18] Macchi G, Pagano M, Pettine M, Santrori Mand Tiravanti G, 1991. A bench study on Chromium recovery from tannery sludge, *Water Res.*, **25** 1019-1026.
- [19] Agarwal A and Saxena M, 2011. Assessment of toxic effect of Brass and Steel industries waste on lake Rohita in nearby river, *International Journal of Environmental Engineering and Management*, **2(1)** 107-110.
- [20] Agarwal A and Saxena M, 2011. Correlation between physicochemical water parameters using regression analysis, *Asian J. of Water, Environment and Pollution*, **8** 97-100.
- [21] Jha V K, Kameshima Y, Nakajima A and Okada K, 2004. Hazardous ions uptake behavior of thermally activated steel-making slag, *J. Hazard. Mater.*, **B114** 139-144.
- [22] Cha W, Kim J and Choi H, 2006. Evaluation of steel slag for organic and inorganic removals in soil aquifer treatment, *Water Res.*, **40** 1034-1042.
- [23] Penpolcharoen M, 2005. Utilization of secondary lead slag as construction material, *Cem. Concr. Res.*, **35** 1050-1055.
- [24] Bijen J, 1996. Benefits of slag and fly ash, *Constr. Build. Mater.*, **10** 309-314.
- [25] Dimitrova S V and Mehandgiev D R, 1998. Lead removal from aqueous solutions by granulated blast-furnace slag, *Water Res.*, **32** 3289-3292.

Encryption and Decryption of Data by Using Geffe Algorithm

Hussein Th. Khamees, Jalal A. Kahlf and Ali A. Al-sajee

University of Al-Nahrain College of Engineering Department of Laser and Optoelectronic Engineering

Abstract

In this modern world of communications, cryptography has an important role in the security of data transmission and is the best method of data protection against passive and active fraud. In this paper, we used the stream cipher which is the best way with the algorithm Geffe generator with a specific length to Encryption the information from plain text in the first compute. This has been sent via the cable which called RS-232 standard interface, which connected between the two computers, and receiving the cipher text in the second computer, and then it will be Decryption by added the same algorithm to the cipher text to return to the plain text.,we satisfy the random statistical tests of the sequence generation from the Geffe algorithm .

1. Introduction

Before the modern era, cryptography was concerned solely with message confidentiality (*i.e.*, encryption)—conversion of messages from a comprehensible form into an incomprehensible one and back again at the other end, rendering it unreadable by interceptors or eavesdroppers without secret knowledge (namely the key needed for decryption of that message)[1].Encryption was used to (attempt to) ensure secrecy in communications, such as those of spies, military leaders, and diplomats. In recent decades, the field has expanded beyond confidentiality concerns to include techniques for message integrity checking, sender/receiver identity authentication, digital signatures, interactive proofs and secure computation, among others ,the earliest forms of secret writing required little more than local pen and paper analogs, as most people could not read. More literacy, or literate opponents, required actual cryptography. The main classical cipher types are transposition ciphers, which rearrange the order of letters in a message (*e.g.*, 'hello world' becomes 'ehlol owrdl' in a trivially simple rearrangement scheme)[2], and substitution ciphers, which systematically replace letters or groups of letters with other letters or groups of letters (*e.g.*, 'fly at once' becomes 'gmz bu podf' by replacing each letter with the one following it in the Latin alphabet). Simple versions of either offered little confidentiality from enterprising opponents, and still do. An early substitution cipher was the Caesar cipher, in which each letter in the plaintext was replaced by a letter some fixed number of positions further down the alphabet [2, 3].

It was named after Julius Caesar who is reported to have used it, with a shift of 3, to communicate with his generals during his military campaigns, just like EXCESS-3 code in Boolean algebra. There is record of several early Hebrew ciphers as well. The earliest known use of cryptography is some carved ciphertext on stone in Egypt (ca 1900 BC), but this may have been done for the amusement of literate observers. The next oldest is bakery recipes from Mesopotamia .A stream cipher may be regarded as one of the many modern cipher system, which uses as one secret key in encryption process.As Now days, It is one of the most encryption system, because of its extremely important properties such as error elimination, high reliability and ease of use in practical application, as well as high speed of execution, it's used in voice encryption as well as in text encryption [4].

Stream cipher operates on stream of plain text and cipher text on one bit or byte as a time

A stream cipher consists of two basic parts:

- 1- Pseudo random sequence algorithm.
- 2- Mixer

When we use a binary representation for XOR relation, Figure (1) illustrates the operation of a stream cipher [5].

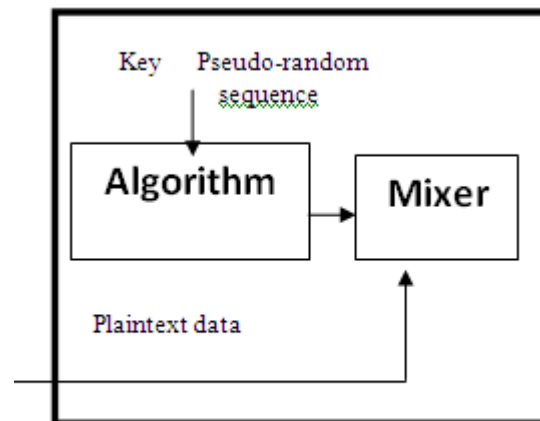


Figure (1): A Stream Cipher.

Many considerations must be taken into account in designing the algorithm in the stream cipher systems are divided into [6]:

- 1- Speed of key generation.
- 2- Security degree of the designed system.
- 3- The time required to decrypt the cipher text.

There are many essential requirements which must be providing by the key stream [7]:

- 1- Key stream must have a long period.
- 2- Key stream must have a good statistical property.
- 3- It must have a large linear complexity.

The security of the stream cipher is depending on the security of key and not on algorithm. So the generation key operation is so important and should be random

2. Statistical test

The statistical Test for Randomness divided as shown below [8]:

2.1 frequency test:-

This is applied on sample of (n) bit s of our sequence to ensure that there is roughly the same number of 0s (n0) and 1s (n1) .for this we merely compute.

$$St=(n0-n1)^2/n \dots\dots (1)$$

To decide if the value (St) obtained is good enough for the sequence to pass, we have merely to compare our value with a table of the x2 distribution, for one degree of freedom. From this table we find that the value of x2 for a 5% significance level is 3.84 the sequence passes. Otherwise we must reject it. (See appendix).

2.2 serial tests:-

The serial test is used to ensure that the transition probability are reasonable; i.e. that the probability of consecutive entries begin equal or different is about the same. Suppose 01 occur n01 times, 10 occur n10 times, 00 occur n00 times and 11 occur n11 times. Thus for this test we compute

$$St=4/(n-1) \sum_{i=0}^1 \sum_{j=0}^1 (nij)^2 - 2/n \sum_{i=0}^1 (ni)^2 + 1 \dots(2)$$

This test is successful if $St \leq 5.99$ because to two freedom degree, the value of x^2 corresponding to a 5% significant level is 5.99 .

2.3 poker test:-

For any integer (m) there are 2^m different possibilities for a section of length (m) of a binary sequence . In this test we partition our sequence in to blocks of size (m) and then we count the frequency of each type of section of length (m) in our sequence.

If $F=n/m$, then, we evaluate

$$St=2^m/F \sum_{i=0}^m \frac{(xi)^2}{i^m} - F \dots\dots\dots (3)$$

Where $i^m = (m! / (m - i)!) * i!$

Where Xi is the number of m-bit blocks having (i) ones and (m-i) zeros. Finally we compare our value with the table for x^2 having $2m - 1$ degrees of freedom to see if we have a 5% significance level.

2.4 runs test:-

For the runs test we divide the sequence in to blocks and gaps. We let r_{0i} be the number of gaps of length i and r_{10} be the number of blocks of length i, if r_0 and r_1 are the number of gaps and blocks respectively then

$$r_0 = \sum_{j=0}^n r_{0j} \dots\dots\dots (4)$$

$$r_1 = \sum_{j=1}^n r_{1j} \dots\dots\dots (5)$$

$$n_{01} = r_0 - 1 \text{ or } r_0, n_{10} = r_1 - 1 \text{ or } r_1, n_{00} = n_0 - r_0, n_{11} = n_1 - r_1$$

The equation is used in this test is:-

$$t_0 = [\sum_{i=0}^{r_0} (r_{0i} - \frac{n}{2^{2+i}})^2 * 2^{2+i}] / n \dots\dots\dots (6)$$

$$t_1 = [\sum_{i=1}^{r_1} (r_{1i} - \frac{n}{2^{2+i}})^2 * 2^{2+i}] / n \dots\dots\dots (7)$$

number of freedom degree used with t_0 and t_1 equal to the value of the length of large gap and length of the large r block respectively .

2.5 auto correlation test:-

Suppose the sequence of (n) bits which we wish to test for randomness properties is $a_1, a_2, a_3, \dots, a_n$. Then set:

$$A(d) = \sum_{i=1}^{n-d} a_i(a_i + d), \quad 0 \leq d \leq n-1 \dots\dots\dots (8)$$

Clearly $A(d) = \sum_{i=1}^n a_i = n1$

If the sequence has n_0 zeros and n_1 ones, the expected value of $A(d)$, ($d \neq 0$), is

$$\mu = n_1^2(n-d)/n^2 \dots\dots(9)$$

This test is successful if $St \leq 3,841$ to all value of d

Where

$$St = (A(d) - \mu)^2 / \mu \dots\dots\dots(10)$$

3. Experimental work and results

The description of the hardware and software design will be presented in this paper, the system consist of many parts as shown in figure (2).

By using the matlab program the key stream is represented by Geffe algorithm figure (3), to encrypt the plaintext and decrypt the cipher text. The cable RS_232 serial port is connected between two computers ,the sender and receiver programs between two computers are done by visual basic program. Decryption .Geffe algorithm is used linear shift register with different length such as $m=5$, $n=7$, and $o=11$. and the length of the key is d

Where: $d = (2^5 - 1) (2^7 - 1) (2^{11} - 1)$

The 1'st shift register consists of 5 stages with an initial state 10101, the 2'nd consists of 7 stage with an initial state 1010111 and the 3'rd stage of 11 with an initial state 11011101011.

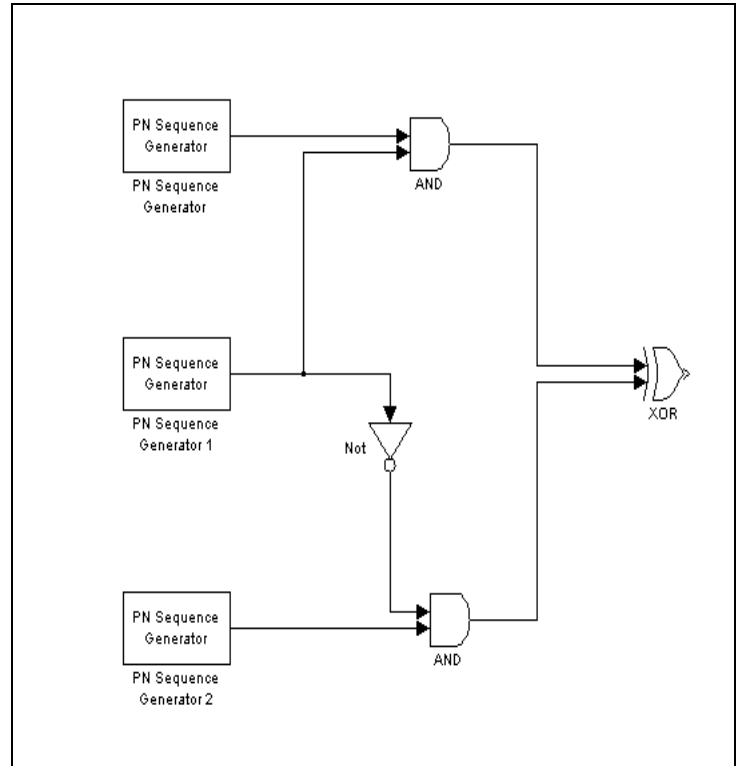


Figure (3): the sequence generation from Geffe algorithm.

It is important to apply statistical test of the generated sequence and to check the key; they also appear to be pseudo random. So that, It was decided whether a sequence has successful or failed in the test. It was took a three different lengths of this sequence which were generated from Geffe algorithm such as (1000, 500 and 300), table (1) shows the results of the statistical testes of the Geffe algorithm.

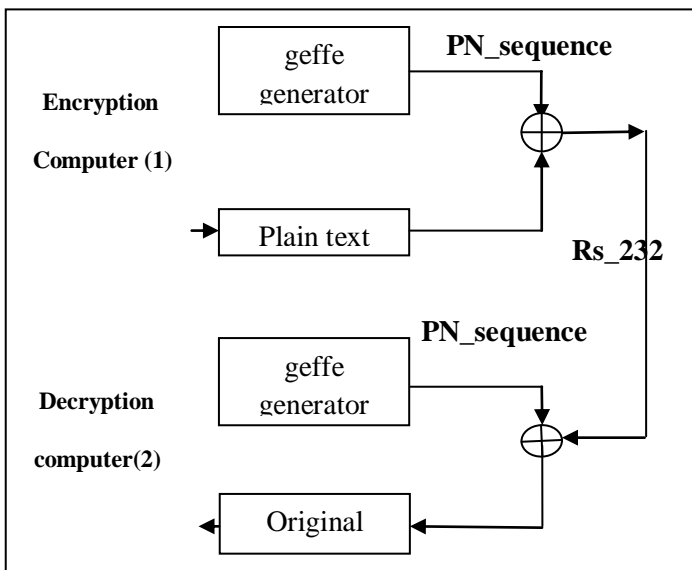


Figure (2): the block diagram of the encryption and decryption.

Table (1): The results of the statistical testes of the Geffe algorithm.

Length of Pseudo	Statistical test	Value of statistical test	Degree of freedom	Value of X ²	
1000	Frequency test	0.2560	1	3.841	
	Serial test	2.0030	2	5.99	
	Poker test	1.0920	7	14.1	
	Run test	0.5080	7	14.1	
		0.4920	5	11.100	
	Autocorrelation test	0.2421	1	3.841	
	500	Frequency test	0.2000	1	3.841
		Serial test	1.0040	2	5.99
		Poker test	1.7970	7	14.1
Run test		0.4900	7	14.1	
		0.5100	5	11.100	
Autocorrelation test		2.1048	1	3.841	
300		Frequency test	0.1200	1	3,841
		Serial test	0.0083	2	5.99
		Poker test	0.6820	7	14.1
	Run test	0.4900	7	14.1	
		0.5100	4	9.49	
	Autocorrelation test	2.1048	1	3.841	

Figure (4) show the block diagram of the encryption and decryption by the simulink_matlab.

The RS232 is the communication line which enables the data transmission by only using three wire links. The three links provides 'transmit', 'receive' and common ground, the 'transmit' and 'receive' line on this connecter send and receive data between the computers. As the name indicates, the data is transmitted serially the next flowchart described the main program of RS_232 transmitter serial port as shown in figure (5).

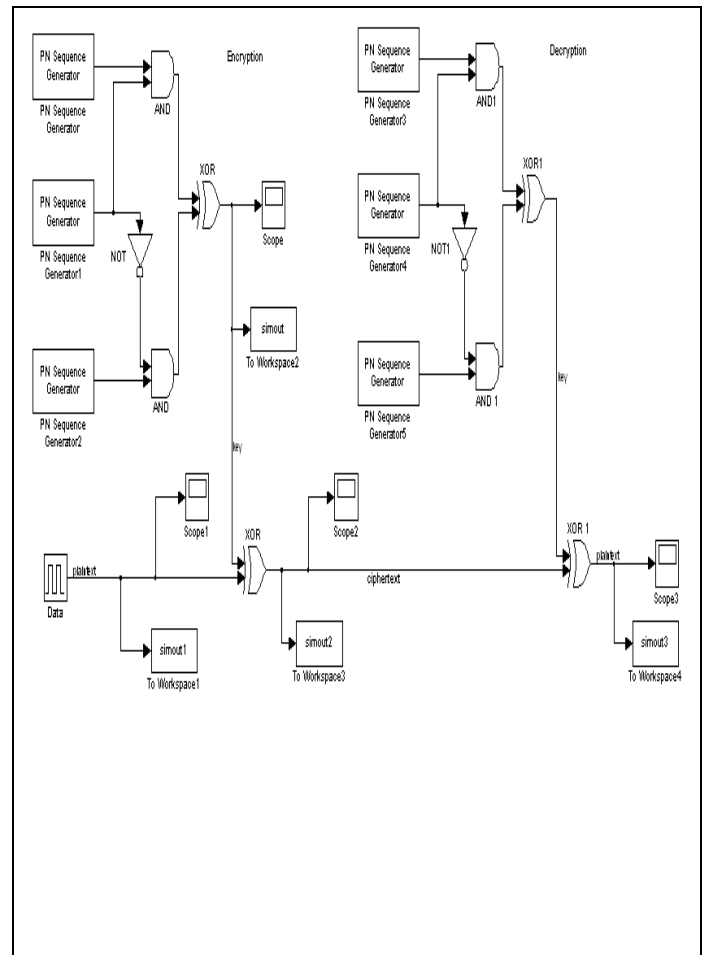


Figure (4): the block diagram of the encryption and decryption by the simulink_matlab.

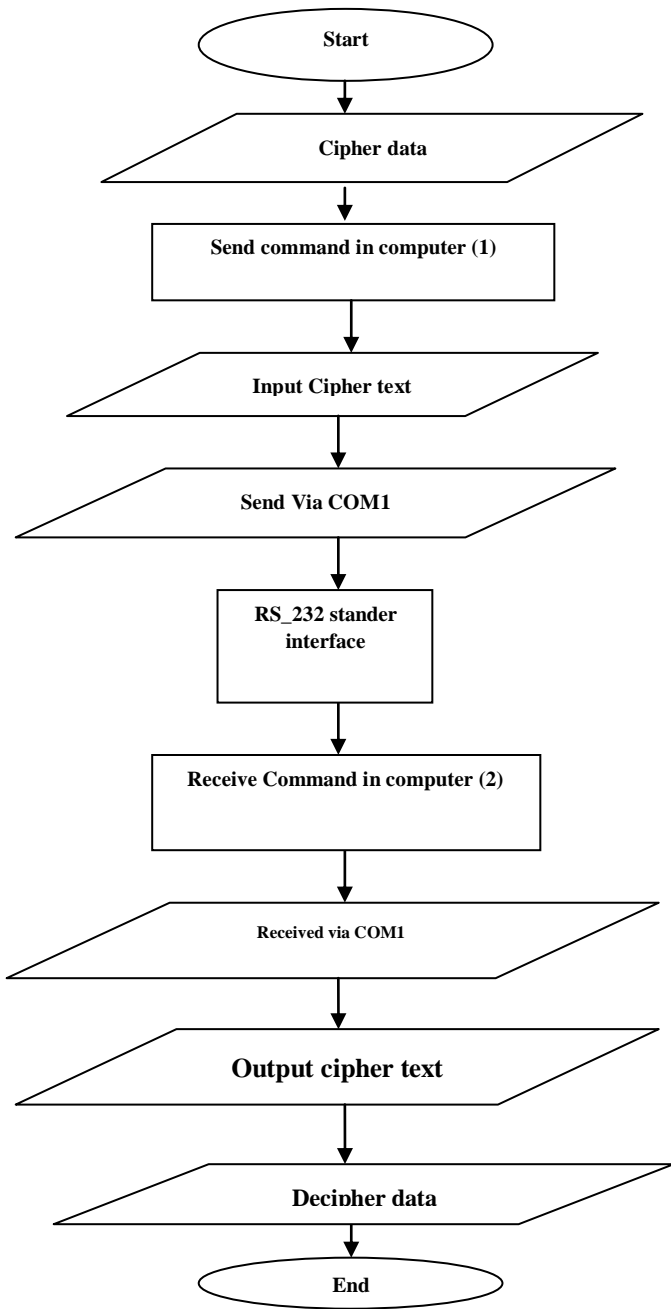


Figure (5): The Flowchart of Main Program of Rs_232 Transmitter link.

The Geffe algorithm was used linear shift register with different length such as $m=5$, $n=7$, and $o=11$.

$$d=(2^5-1)(2^7-1)(2^{11}-1)=(31)(127)(1047)=4122039 \text{ bit}$$

The Geffe algorithm will repeat itself after 4122039 bit

The bits are: 1 1 1 1 1 0 0 1 0 1 1 1 0 0 1 0 1 1 0 0 0 1 0 0 0 1 0 0 0 1 0 As shown in figure (6)

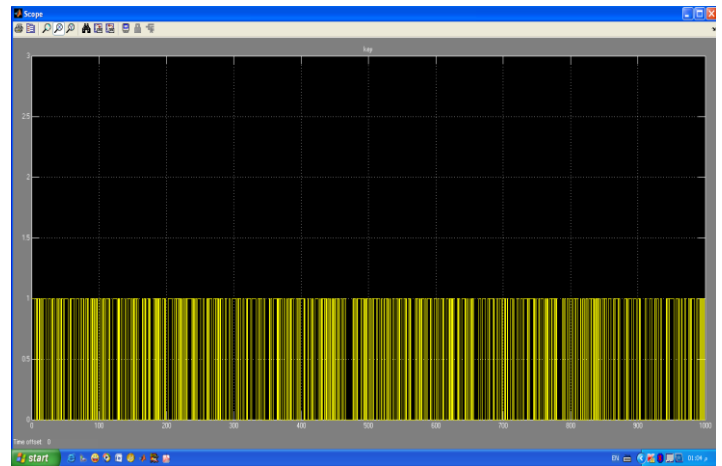


Figure (6): the key generation (Geffe algorithm)

The transmitted data between transmitter and receiver represented the plaintext or original message by a binary system. the input data bits (plaintext) are: 1 1 1 1 1 1 1 1 1 1 1 1 1 0 0 0 0 0 0 0 0 0 as shown in figure (7)

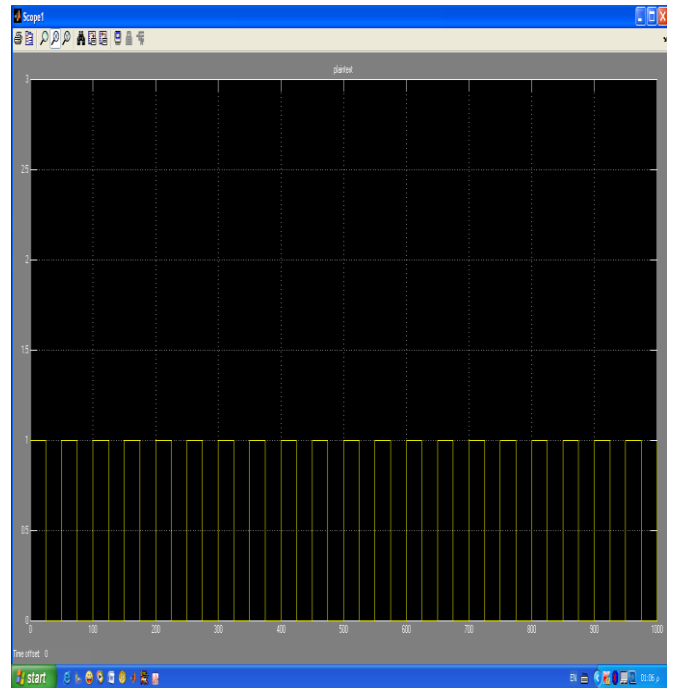


Figure (7): the plaintext (original data).

using XOR boolean function to make a bit wise operation between the plaintext or original data with a binary sequence generation from geffe algorithm to the encryption bits (ciphertext) are: 0 0 0 0 0 1 1 0 1 0 0 1 0 1 0 as shown in figure (8)

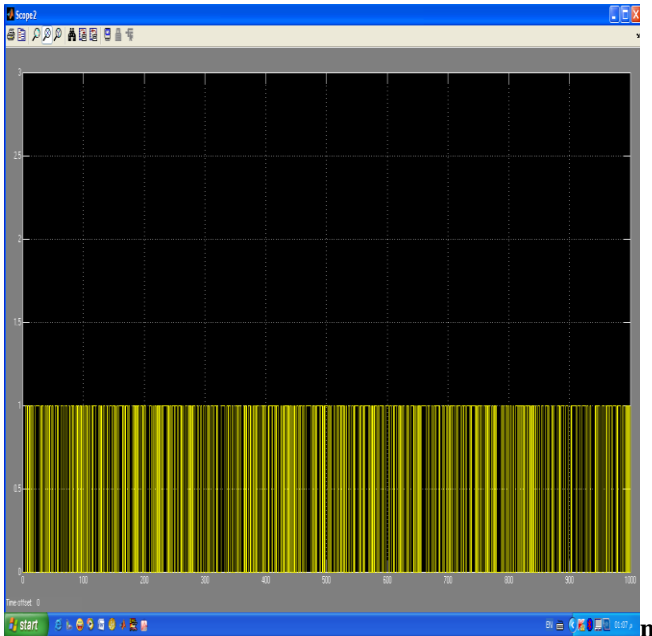


Figure (8): the encrypted data (after encryption)

The original data will back after the decryption process as shown in figure (9)

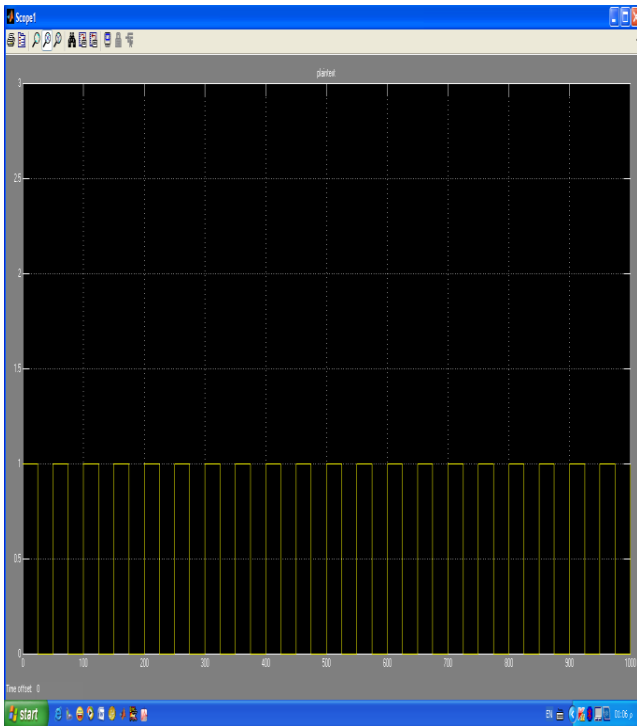


Figure (9): the plaintext (after decryption).

Conclusions

1. The stream ciphering technique is a highly secure and has a high speed to generate the keys.
2. The generator sequence from the nonlinear stream cipher (Geffe algorithm) has a high linear complexity therefore; the nonlinear sequence has a good degree of security.
3. The maximum period length to the generator binary sequence from any generator is much better, which have maximum period length 4122039.

REFERENCES

- 1- Merriam-Webster's Collegiate Dictionary "Cryptology (Definition)" (11th Editioned.). Merriam-Webster.Retrieved 2008-02-01.
- 2- Alfred J. Menezes Paul C. Van Oorschot Scott A. Vanstone "Handbook Of Applied Cryptography", 1996.
- 3- An Introduction To Cryptography Copyright © 1990-1999 Network Associates, Inc. And Its Affiliated Companies. Printed In The United States Of America.
- 4- Tom Davis" Cryptography" February 7, 2000
- 5- David R. Kohel , ' Cryptography' July 11, 2008.
- 6- Rsa Laboratories Technical Report Tr-701 , M.J.B. Robshaw 'Stream Ciphers' Version 2.0|July 25, 1995
- 7- Tin Lai Win, And Nant Christina Kyaw 'Speech Encryption And Decryption Using Linear Feedback Shift Register (Lfsr) '
- 8- Tsang-Yean Lee, Huey-Ming Lee, Homer Wu, Jin-Shieh Su 'Data Transmission Encryption and Decryption Algorithm in Network Security Department Of Information Management, September 22-24, 2006

Critical J-Integral of Thin Aluminium Sheets Employing a Modified Single Edge Plate Specimen

P. S. Shinde¹, K. K. Singh², V. K. Tripathi¹, P. K. Sarkar², P. Kumar¹

1(Department of Mechanical Engg., College of Engineering Pune, India)

2 (Department of ME & MME, Indian School of Mines, Dhanbad, India)

ABSTRACT

A new kind of specimen geometry, modified single-edge crack specimen - is designed to determine fracture toughness (critical J-Integral) of a crack in thin plates of aluminum alloy 6061-T6, such that the line joining the centers of the load-points passes through the crack-tip. In this specimen geometry, high stress concentration at the crack-tip is generated with minimum chances of buckling of any part of the specimen. An experimental-cum-numerical methodology is developed in which the critical load is obtained from an experiment, and the stress field is determined in the specimen, through a finite element analysis. The stress field yields the critical J- Integral (J_c). The fracture toughness of thin aluminum 6061-T6 sheets is found to be much higher than the plane strain toughness.

Keywords - Fracture toughness, J- Integral, modified single edge crack specimen, thin plates.

I. INTRODUCTION

Thin sheets of metals have wide applications such as in aircrafts, pressure vessels, ship building, bridges, ground vehicles, etc. The fracture toughness of thin sheets in Mode I is known to be substantially higher than the plane strain toughness of thick sheets and, therefore, its value is more relevant for many applications. In thick plates of ductile materials, where there is a large plastic zone near the crack tip, their fracture toughness is often characterized with the critical J-integral (J_c). However, it is difficult to determine the fracture toughness of thin sheets as their specimen tends to buckle during testing.

There are several techniques available in the literature to determine fracture toughness (i.e. J_c) of thin plates. Several studies have been made on double edge notched tensile (DENT) specimen to determine fracture toughness of thin plates.

Investigations have been developed for both sub critical crack extension and final fracture of thin walled geometries. In [1,2] experiments are conducted to study the effect of thickness on the critical values of J integral and CTOD (J_c and δ_c) of aluminum thin plates of 1-6 mm thickness using double edge notched tension (DENT) specimens. The work required to fracture the ligament of DENT specimen is partitioned in two components, the first component is called the essential work of fracture and

second component as non-essential work of fracture caused due to necking. Their research showed that with increase in thickness J_c and δ_c increases linearly for thinner specimens and nonlinearly for larger thicknesses. They attended almost same results by testing sixteen different alloys of aluminum, brass, stainless steel, bronze, Zinc and lead [3]. Investigations are done on the fracture toughness of thin DENT specimens made up of copper foils with thickness ranging from 0.02 to 1 mm using an improved digital speckle correlation method (DSCM). The results showed that J_c increases with increasing thickness upto 0.3 mm and there after it decreases for both specimens, prepared in rolling and transverse directions [4]. A brief overview of the existing methods for simulating stable crack extension and failure, including the research in fatigue and fracture of thin-walled structures over the past decades [5].

In a DENT specimens used by several investigators, the tensile load in the un-cracked ligament is high and it tends to make the specimen fail in localised yielding and thus stress concentration due to the crack tip is subdued which leads to necking formation at crack tip and, thereby, it suppresses the crack propagation. Consequently, it becomes difficult to isolate the fracture toughness from such a test.

Over the years, J integral is determined using a single edge notched compact tension (CT) specimen applying combined bending and tension load [6-8]. In [6], the J-Integral is evaluated for single edge notched (SEN) specimen under bending and tension, both in terms of loads and displacements and as the original path independent integral. An expression for determining J-Integral from the load displacement record of SEN specimen is given and the result is compared with other analytical expressions and with FE calculations [7]. In the middle-cracked tension specimens of different geometry, experimental data on steady state tearing (SST) are examined with the use of global parameters characterizing the mechanical behavior of a moving crack tip embedded into a fully developed moving neck [8]. If a compact tension specimen is employed, guide plates, one on the side of each face of the specimen, are required to avoid buckling of the thin specimen [9]. This makes the technique cumbersome and there is always a doubt on the role of friction between guides and the specimen.

The aim of the present study is to develop a simple and effective specimen geometry to determine the fracture toughness (i.e critical J-Integral (J_c)) of thin sheets of aluminum 6061-T6. A single-edge crack specimen is modified in such a way that the line joining the centers of the loading points passes through the crack-tip. This maintains high stress concentration at the crack-tip with reduced chances of buckling along the crack front. In this experimental-cum-numerical technique, the critical load was obtained from experiment. The numerical analysis determined the stress field in the specimen by employing the nonlinear stress-strain behavior of monotonic loading of the specimen material. This stress field is used to determine critical J-Integral.

II. SPECIMEN

Thin sheet of thickness ranging from 0.7 to 2.0 mm is the prevalent and extensively used vehicle construction material. This investigation is focused on evaluating critical J-Integral (J_c) of thin plates of aluminum alloy 6061-T6. As per the availability of material in the market, the specimen thicknesses were chosen as 1.0 mm and 1.6 mm.

Tensile test of these materials were conducted to determine elastic-plastic properties as per ASTM-E8 [10]. The specimens were tested under plane stress conditions using a 100 KN Universal Testing Machine. The cross-head speed was chosen to be very slow, 0.1 mm/min. Fig. 1 shows the stress-strain behavior of 1.6 mm thick sheet of aluminum alloy 6061-T6. The stress-strain behavior of 1.0 mm thick sheet of aluminum alloy 6061-T6 was similar.

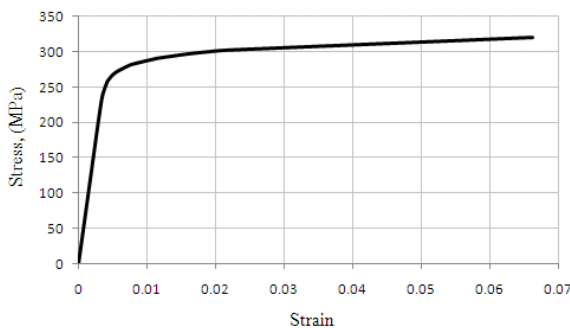


Figure 1: Stress-strain curve of aluminum 6061-T6 with thickness of 1.6 mm

The material behavior was found to follow Ramberg-Osgood relation, as given in equation (1):

$$\frac{\epsilon}{\epsilon_0} = \frac{\sigma}{\sigma_0} + \alpha \left(\frac{\sigma}{\sigma_0} \right)^n \quad (1)$$

where α is a coefficient and n is an exponent of the power hardening material, σ_0 and ϵ_0 are the flow stress and flow strain, respectively. α and n are found by fitting the curve of the Ramberg-Osgood equation on the original stress-strain

curve [11] and they are listed in Table 1 along with other experimentally obtained material properties.

While designing the specimen of the thin aluminum alloy sheets, a very approximate estimation was made. The plastic zone size (r_p) was estimated using the following Irwin's formula [12] for plane stress (2):

$$r_p = \frac{1}{\pi} \left(\frac{K_{Ic}^2}{\sigma_{ys}^2} \right) \quad (2)$$

where K_{Ic} is the critical stress intensity factor and σ_{ys} is the yield stress. When available value of toughness of aluminum alloy is used for plane stress as $K_{Ic} = 25 \text{ Mpa}\sqrt{\text{m}}$, r_p was found to be 2.6 mm. The actual plastic zone size is much larger as the toughness of the thin sheets, determined through this investigation, was found to be much greater than plane strain toughness. Thus the specimens of this study were definitely loaded in plane stress.

Table 1: Mechanical properties of aluminum alloy 6061-T6 specimens tested as per ASTM-E8

Sheet thickness	Young's modulus (GPa)	Yield stress (MPa)	Ultimate strength (MPa)	n	α
1.6 mm thick	69.8 ± 1.5	277.6 ± 8.3	319.8 ± 16.2	22	67.73x10 ⁻⁶
1.0 mm thick	70.4 ± 1.5	267 ± 5.3	294.9 ± 2	32.19	52.39x10 ⁻³

Preliminary experiments were conducted on symmetric DENT specimens made from the aluminum alloy 6061-T6. It was found that the tensile load in the un-cracked ligament was high and the specimen failed predominantly in yielding. In fact, the necking was found to form on the entire length of the un-cracked ligament of the specimen. The stress concentration due to the crack tip was not high enough for the crack to grow before the material yielded. Consequently, it became difficult to isolate the fracture toughness from such a test. Thus DENT specimen geometry was found to be inappropriate for fracture toughness testing of thin sheet aluminum alloy 6061-T6.

A new single edge crack specimen geometry was developed to suppress yielding of un-cracked ligament and enhance the chances of failure through fracture growth. In a DENT specimen, the un-cracked ligament is primarily subjected to tensile stresses caused by the external load. On the other hand, in a single-notch specimen, there is a superposition of two loads, bending moment because the specimen is not symmetric and tensile due to external pulling load. The bending moment develops high stress concentration at the crack tip but at the same time high compressive stresses are usually generated in the region far away from the crack tip. These compressive stresses may

cause the buckling of the thin specimen which should not be allowed so as to facilitate two dimensional analysis of the specimen. However, the tensile load suppresses the compressive stresses. In a conventional single-edge specimen, load P is applied at the mid-thickness; $d = W/2$, as shown in Fig. 2.

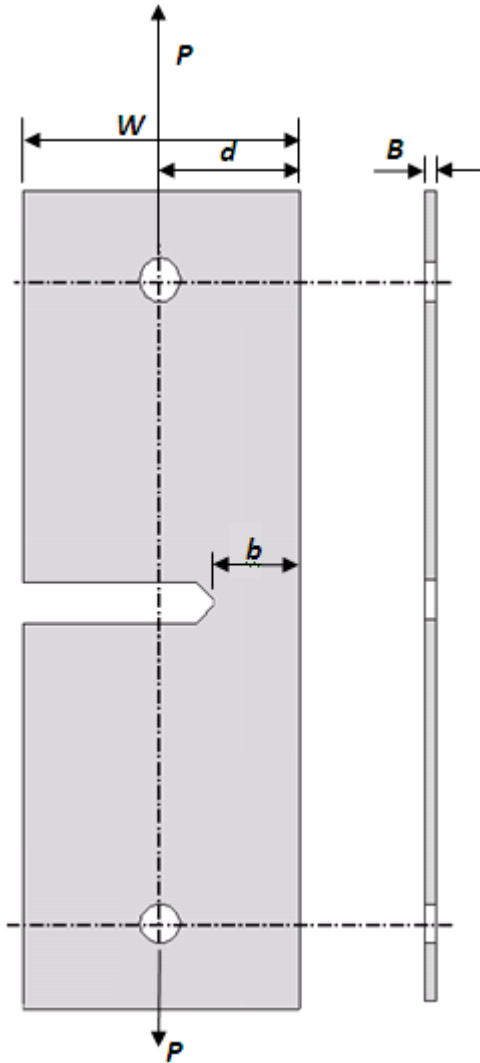


Figure 2: Modified single-edge crack specimen

However, it was felt that the conventional single-edge specimen might not be appropriate specimen configuration. The load distance, d , should be chosen appropriately. Thus, preliminary numerical simulations were carried out to determine distance d of the load point: The case $d = b$ was chosen because, high compressive stresses were not generated in the specimen and the specimen was unlikely to buckle. However, during experiment, close attention was paid to assure that buckling was not taking place.

Fig. 3 presents the geometry of the specimen. The specimens of size $190 \text{ mm} \times 60 \text{ mm}$, were cut on a conventional milling machine.

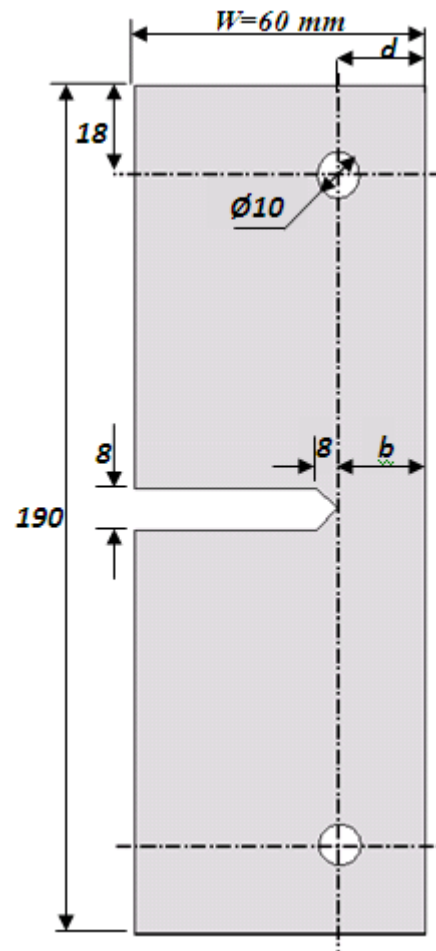


Figure 3: Geometry of Modified Single-edge crack specimen.

To minimize the distortion of the specimen plate while preparing the dimensions, five specimen plates were bonded together using double stick tapes, to make a reasonable thick stack. The crack dimensions (Figure 3) of the specimens are achieved by cutting a slot from the milled stack of specimens, with the help of a wire-EDM machine. The tip of the crack, prepared through a wire-EDM machine, was not sharp enough. It was required to be extended to obtain a sharp initial pre-crack. A suitable fixture was developed to hold a fresh razor blade and apply a reasonable large force to make crack tip very sharp. The crack was extended by about 2 mm. The radius of curvature at crack tip was monitored through a shadow-graph (LEICA) and was found to be of the order of $12 \mu\text{m}$. Pardoen T et al. (1999) also used the similar technique to sharpen a crack. The single-edge crack, cut in the specimens were such that the propagation of the crack was perpendicular to the rolling direction; that is, the tensile load was applied along the rolling direction during testing. Experimental tests were performed by varying the uncracked ligament length, b , for both kinds of the aluminum alloy sheets.

III. EXPERIMENTAL-CUM NUMERICAL TECHNIQUE

Experimental tests were performed on the modified single-edge crack specimens, by pulling the specimen in a 10-ton Universal Testing Machine at the very slow speed of 0.1 mm/min as shown in Fig. 4. The detection of crack initiation was done by closely monitoring the crack-tip with the help of magnifying glass and simultaneously observing the run-time load-displacement curve. It was found that the crack grew suddenly and the load started dropping at the same time. Thus, the load-displacement curve yields the critical load. The critical load obtained from experiments was used as loading boundary conditions in a nonlinear numerical analysis to obtain stress-strain fields.

In this study, a two-dimensional, plane stress, numerical analysis of the modified single-edge crack specimen was done using software package ANSYS 10.0. PLANE82 element was used for this fracture mechanics analysis. PLANE82 is an 8-noded element and is able to account for plasticity, creep, swelling, stress stiffening, large deflection and large strain. Because of the symmetry of the specimen with respect to the crack plane, only half specimen was modeled for the analysis.

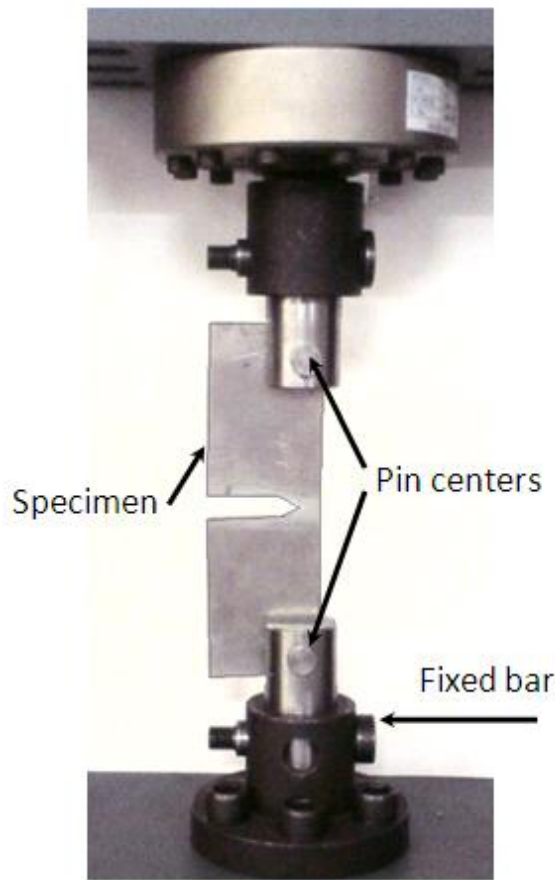


Figure 4: A Photograph of the Experimental set-up with a specimen loaded in a UTM.

The crack-tip was modeled by converting the quadrilateral iso-parametric element (PLANE82) in to a special element with mid-side nodes moved to the quarter points, called quarter-point element[13]. The load on the specimen was applied on a mass-less element at the pin center of the hole which gets equally distributed on all the nodes along the circumference of the hole by defining a rigid-region.

In the numerical analysis, the material non-linearity was accounted for by inputting the experimental stress-strain data of the material, presented in section 2. However, only monotonically increasing loading was considered to determine J-Integral. The results obtained from the converged nonlinear analysis were used to calculate the fracture parameter, J-Integral, by a subroutine written in ANSYS's scripting language.

IV. RESULTS AND DISCUSSION

Five specimens were tested for each thickness 'B' (1.0 mm and 1.6 mm) and the un-cracked ligament length 'b' (10 mm, 16 mm & 20 mm). It was found that in the thin plate of aluminum alloy 6061-T6, significant plastic deformation took place prior the crack growth at the region close to the crack-tip. A dimple was formed prior to the crack growth on each face of the specimen as shown in Fig. 5 (a). The 'V' formed by the tangents to the upper and lower edges of the dimple at the crack-tip had an included angle of $64^\circ \pm 7^\circ$. At the critical load the crack grew suddenly along one of the two edges of the dimple as shown in Fig. 5 (b), and the load on the specimen started dropping. If the crack initiated along the upper edge of the dimple on the front surface, the crack moved inside the material at an angle in such a way that it comes out along the lower edge of the dimple on the rear surface.

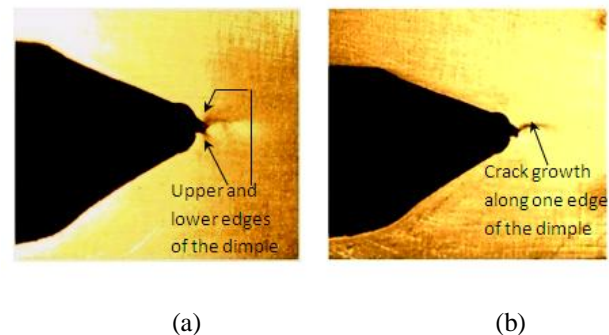


Figure 5: A Photograph of the specimen just before crack initiation (a); and after crack initiation (b).

Table 2 shows the average critical load obtained from the experiments on all five specimens of each size. Fig. 6 shows a typical experimental load vs. load-point displacement plots for a 1.6 mm thick specimen with un-cracked ligament length $b = 16$ mm.

Table 2: Experimental observations of the critical load of all specimen geometries

Specimen thickness B (mm)	Un-cracked ligament length b (mm)	Critical load for five samples of each specimen (N)				
1.6	10	3001	2799	2947	2900	2893
1.6	16	3912	4010	3925	3921	3607
1.6	20	4733	4655	4475	4669	4620
1.0	10	1748	1780	1862	1693	1862
1.0	16	2300	2336	2374	2186	2155
1.0	20	2727	2773	3006	2763	2716

The J-Integral, computed by the sub-routine was found to be independent of the paths except when the path chosen was close to crack tip or the free surface of the specimen.

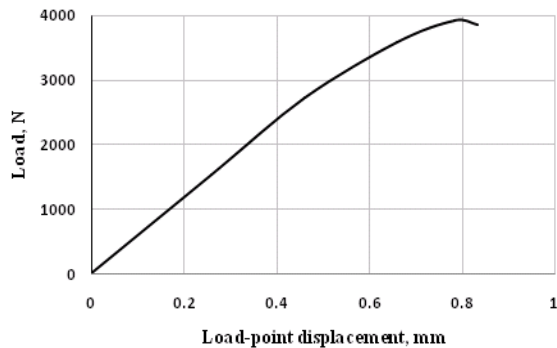


Figure 6: Load versus the load-point deflection curve for specimen with B = 1.6 mm and b = 16 mm.

Fig. 7 presents the critical J-Integral for 1.6 mm and 1.0 mm thick sheets of aluminum alloy 6061-T6 with varying un-cracked ligament. The J_c values obtained for thickness of 1.6 mm with varying un-cracked ligament length b were found to be consistent with b as 10, 16 and 20 mm. Pardoen T. et al. (1999) have observed that the fracture toughness does not depend much on the ligament length for DENT geometry. The average value of J_c obtained for B = 1.6 mm was 121 kJ/m^2 .

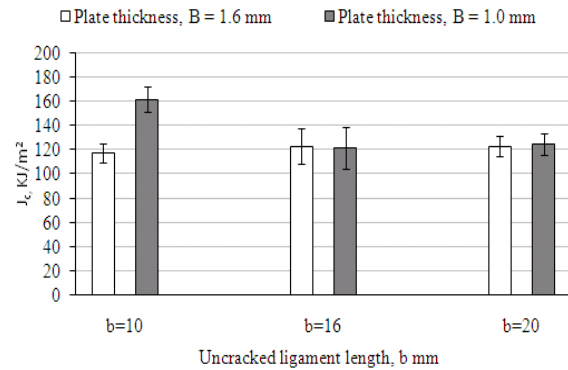


Figure 7: Variation of J_c with varying b for B = 1.6 mm and B = 1.0 mm.

In case of the thinner aluminum alloy 6061-T6 sheets of 1.0 mm thickness, J_c ($\approx 120 \text{ kJ/m}^2$) determined for the specimen of higher un-cracked ligament b (16 mm and 20 mm) was same as J_c of thicker specimen of 1.6 mm thickness. However, the J_c of smallest b = 10 mm, was found to be 160 KJ/m^2 which is significantly higher. The reason for this difference is still not understood. The experiment was carefully monitored to check whether buckling close to the free edge was taking place. No visible sign of buckling was observed. It needs further exploration to identify the reasons for higher value of J_c for b=10 mm cases of 1.0 mm thick aluminum sheet.

The investigators of this study are not aware of any study that has obtained J_c of thin sheets of aluminum alloy 6061-T6. However, data on aluminum alloy 7075-T6 is available (Zerbst U. et al. 2009).

Fig. 8 shows the J_c obtained in this study on the results of aluminum alloy 7075-T6. The higher value of J_c for B= 1.0 mm and b= 10 mm is not included in J_c of thin sheets. It is worth noting here that J_{Ic} of plane strain specimens of aluminum alloy 6061-T6 is much smaller, about 12 KJ/m^2 only. It is thus important to develop a technique to determine toughness of thin sheets.

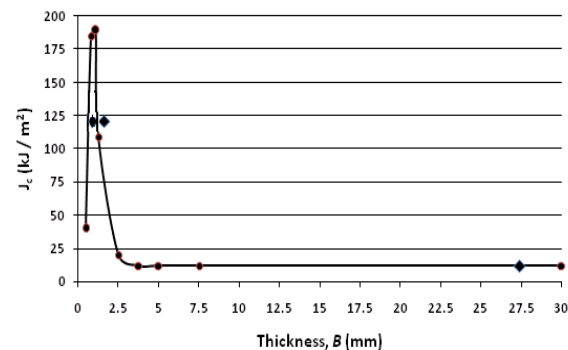


Figure 8: Variation of fracture toughness with respect to thickness as observed by Zerbst U. et al. for aluminum 7075-T6 and by this study for aluminum 6061-T6.

V. CONCLUSIONS

A modified single-edge crack specimen was designed to evaluate the fracture toughness (J_c) of crack thin sheets made of aluminium alloy: 6061-T6 with thicknesses 'B' of 1.6 mm and 1.0 mm. The geometry developed in this study is such that the line joining the centers of the loading points passes through the crack-tip (i.e $d=b$). This maintains high stress concentration at the crack-tip with reduced buckling along the crack front. The crack-tip was sharpened by applying controlled force on the fresh razor blade. The stress-strain curves of the specimen material aluminium 6061-T6 showed power hardening material behavior with strain hardening. An experimental-cum-numerical technique was used in which data (critical loads) was extracted from experiments and then the data was used to perform numerical analysis which was post-processed to evaluate the fracture toughness (J_c). Experiments were performed by pulling the specimens in a 10-ton Universal Testing Machine at a speed of 0.1 mm/min. The detection of crack initiation was done by closely monitoring the growth of the crack-tip and the run-time load-displacement curve. In this study, it was found that the crack-tip grows suddenly and the load on the specimen starts dropping. The critical load thus obtained from the experiments was used as loading boundary conditions in numerical analysis to obtain stress-strain field in the specimen by employing the nonlinear stress-strain behavior of monotonic loading of the specimen material. This field is further used to determine critical J-Integral (J_c) with the help of a ANSYS.

The average value of critical J-Integral (J_c) obtained from the experimental-cum-numerical technique for thickness 'B' of 1.6 mm was 121kJ/m². The values are found to be consistent for un-cracked ligament lengths 'b' of 10, 16 and 20 mm for the modified single-edge crack specimen used in this study. The fracture toughness values were found to be less consistent with respect to varying 'b' for thickness of 1.0 mm, as compared to 1.6 mm. The average value of J_c was found to be 135.9 kJ/m² for 1.0 mm thick plate.

REFERENCES

Journal Papers:

- [1] T Pardoen, et. al., Thickness dependence of cracking resistance in thin aluminium plate, *Journal of the Mechanics and Physics of Solids*, 47(10), 1999, 2093-2123.
- [2] T Pardoen, et. al., Essential work of fracture compared to fracture mechanics—towards a thickness independent plane stress toughness, *Engineering Fracture Mechanics*, 69(5), 2002, 617-631.
- [3] T Pardoen, et. al., Mode I fracture of sheet metal, *Journal of the Mechanics and Physics of Solids*, 52(2), 2004, 423-452
- [4] H Wang, et. al., Size effect on the fracture toughness of metallic foil, *International Journal of Fracture*, 123(3-4), 2003, 177-185.
- [5] U. Zerbst, et. al, Fracture and damage mechanics modelling of thin-walled structures – An overview, *Engineering Fracture Mechanics*,76(1), 2009, 5-43.
- [6] S Henrik and S Kaiser, The J-Integral for a SEN specimen under Non proportionally applied bending and tension, *Engineering Fracture Mechanics*, 24(5), 1985, 637–646.
- [7] Sten Kaiser, The J-Integral and tearing modulus for a SEN specimen under bending and tension, *Engineering Fracture Mechanics*, 22(5), 1985, 737–749.
- [8] A.R Shahani, et. al, Experimental and numerical investigation of thickness effect on ductile fracture toughness of steel alloy sheets, *Engineering Fracture Mechanics*, 77(4), 2010, 646–659.
- [9] R Barsoum, Triangular quarter-point elements as elastic and perfectly-plastic crack tip elements, *International Journal for Numerical Methods in Engineering*, 11(1), 1977, 85-98.

Books:

- [10] ASTM code E8. *Standard Test Methods for Tension Testing of Metallic Materials*.
- [11] M Pendola, et. al, Combination of finite element and reliability methods in nonlinear fracture mechanics, *Reliability Engineering & System Safety*,70(1), 2000, 15-27.
- [12] P Kumar, *Elements of Fracture Mechanics*, 5, 6, 8 (Tata McGraw-Hill, New Delhi, 2009).

Proceedings Papers:

- [13] V.P Naumenko and Y Skrypyuk, Steady state tearing in thin Aluminium sheets under Uniaxial Tension, *ECF15 proceedings, The 15th European Conference of Fracture*, Stockholm, Sweden, 2004.

Face Recognition Using PCA-BPNN Algorithm

*Prof.Ujval Chaudhary, ** Chakoli Mateen Mubarak, ** Abdul Rehman,
** Ansari Riyaz, ** Shaikh Mazhar

*HOD department of electronics engineering, MHSS College of engineering, Byculla, Mumbai

**Student of MHSS College of engineering, Electronics branch, Byculla, Mumbai

Abstract

In this paper we will explore the concept of facial recognition using back propagating neural networks. Eigenfaces are produced by transforming the pixels in an image to (x; y) coordinates and forming a matrix with the coordinates. The eigenfaces or the principal components of the faces are the eigenvectors of the matrix and it is the eigenvectors. These eigen vectors are given as input to the neural networks which performs the recognition process.

Keywords: Back-propagation Neural Network, Biometric Identification, Eigen faces, Eigen vectors, Principal components analyses.

I. INTRODUCTION

Information and Communication Technologies are increasingly entering in all aspects of our life and in all sectors, opening a world of unprecedented scenarios where people interact with electronic devices embedded in environments that are sensitive and responsive to the presence of users. Indeed, since the first examples of “intelligent” buildings featuring computer aided security and fire safety systems, the request for more sophisticated services, provided according to each user’s specific needs has characterized the new tendencies within domestic research. The result of the evolution of the original concept of home automation is known as Ambient Intelligence (Aarts & Marzano, 2003), referring to an environment viewed as a “community” of smart objects powered by computational capability and high user-friendliness, capable of recognizing and responding to the presence of different individuals in a seamless, not-intrusive and often invisible way. As adaptivity here is the key for providing customized services, the role of person sensing and recognition become of fundamental importance[8][9][10]. This scenario offers the opportunity to exploit the potential of face as a not intrusive biometric identifier to not just regulate access to the controlled environment but to adapt the provided services to the preferences of the recognized user. Biometric refers to the use of distinctive physiological (e.g., fingerprints, face, retina, iris) and behavioural (e.g., gait, signature) characteristics, called biometric identifiers, for automatically recognizing individuals. Because biometric identifiers cannot be easily misplaced, forged, or shared, they are considered more reliable for person recognition than or knowledge-based methods. Others typical

objectives of biometric recognition are user convenience (e.g., service access without a Personal Identification Number), better security (e.g., difficult to forge access). All these reasons make biometrics very suited for Ambient Intelligence applications, and this is specially true for a biometric identifier such as face which is one of the most common methods of recognition that humans use in their visual interactions, and allows to recognize the user in a not intrusive way without any physical contact with the sensor. We present a face recognition system based on pca features extraction and neural networks to recognize the identity of subjects accessing the controlled Ambient Intelligence Environment and to customize all the services accordingly.[2]

II. WORKING PRINCIPLE

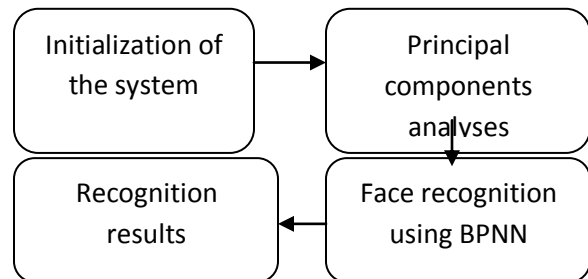


Fig 1: Generic block diagram

2.1. Initialization of the system

The Algorithm for Face recognition using neural classifier is as follows:

- a) Pre-processing stage –Images are made zero-mean and unit-variance.
- b) Dimensionality Reduction stage: PCA - Input data is reduced to a lower dimension to facilitate classification.
- c) Classification stage - The reduced vectors from PCA are applied to train BPNN classifier to obtain the recognized image.

2.2 Principal Component Analyses:

Principal component analysis (PCA) [2] involves a mathematical procedure that transforms a number of possibly correlated variables into a smaller number of uncorrelated variables called principal

components. PCA is a popular technique, to derive a set of features for both face recognition.

Any particular face can be

- (i) Economically represented along the eigen pictures coordinate space, and
- (ii) Approximately reconstructed using a small collection of Eigen pictures

To do this, a face image is projected to several face templates called eigenfaces which can be considered as a set of features that characterize the variation between face images. Once a set of eigenfaces is computed, a face image can be approximately reconstructed using a weighted combination of the eigenfaces. The projection weights form a feature vector for face representation and recognition. When a new test image is given, the weights are computed by projecting the image onto the eigen-face vectors. The classification is then carried out by comparing the distances between the weight vectors of the test image and the images from the database. Conversely, using all of the eigenfaces extracted from the original images, one can reconstruct the original image from the eigenfaces so that it matches the original image exactly.[5]

2.2.1 PCA algorithm:

The algorithm used for principal component analysis is as follows.[4]

- (i) Acquire an initial set of M face images (the training set) & Calculate the eigen-faces from the training set, keeping only M' eigenfaces that correspond to the highest eigenvalue.
- (ii) Calculate the corresponding distribution in M' -dimensional weight space for each known individual, and calculate a set of weights based on the input image.
- (iii) Classify the weight pattern as either a known person or as unknown, according to its distance to the closest weight vector of a known person.[5]

Let the training set of images be G_1, G_2, \dots, G_M . The average face of the set is defined by[5]

$$\Psi = \frac{1}{M} \sum_{i=1}^M \Gamma_i \quad (1)$$

Each face differs from the average by vector

$$\Phi_i = \Gamma_i - \Psi \quad (i = 1, \dots, M) \quad (2)$$

The co- variance matrix is formed by

$$C = A \cdot A^T \quad (3)$$

where the matrix A is given by

$$A = [\Phi_1 \ \Phi_2 \ \dots \ \Phi_M] \quad (4)$$

This set of large vectors is then subject to principal component analysis, which seeks a set of M orthonormal vectors u_1, \dots, u_M . To obtain a weight vector W of contributions of individual eigen-faces to a facial image $_$, the face image is transformed into its eigen-face components projected onto the face space by a simple operation.[6]

$$W_k = u_k^T \Phi \quad (5)$$

For $k=1, \dots, M'$, where $M' \leq M$ is the number of eigen-faces used for the recognition. The weights form vector $W = [w_1, w_2, \dots, w_m]$ that describes the contribution of each Eigen-face in representing the face image $_$, treating the eigen-faces as a basis set for face images. The simplest method for determining which face provides the best description of an unknown input facial image is to find the image k that minimizes the Euclidean distance e_k

$$e_k = \|(\Omega - \Omega_k)\|^2 \quad (6)$$

Where W_k is a weight vector describing the k th face from the training set. It is this Euclidean distance that is given as an input to the neural networks.

2.3. Neural Network:

A successful face recognition methodology depends heavily on the particular choice of the features used by the pattern classifier. The Back-Propagation is the best known and widely used learning algorithm in training multilayer perceptrons (MLP). The MLP refer to the network consisting of a set of sensory units (source nodes) that constitute the input layer, one or more hidden layers of computation nodes, and an output layer of computation nodes. The input signal propagates through the network in a forward direction, from left to right and on a layer-by-layer basis. Back propagation is a multi-layer feed forward, supervised learning network based on gradient descent learning rule. This BPNN provides a computationally efficient method for changing the weights in feed forward network, with differentiable activation function units, to learn a training set of input-output data. Being a gradient descent method it minimizes the total squared error of the output computed by the net. The aim is to train the network to achieve a balance between the ability to respond correctly to the input patterns that are used for training and the ability to provide good response to the input that are similar.[1]

2.3.1 Back Propagation Algorithm:

A typical back propagation network with Multi-layer, feed-forward supervised learning is as shown in the figure. 2. Here learning process in Back propagation requires pairs of input and target vectors. The output vector 'o' is compared with target vector't'. In case of difference of 'o'

and 't' vectors, the weights are adjusted to minimize the difference. Initially random weights and thresholds are assigned to the network. These weights are updated every iteration in order to minimize the mean square error between the output vector and the target vector.

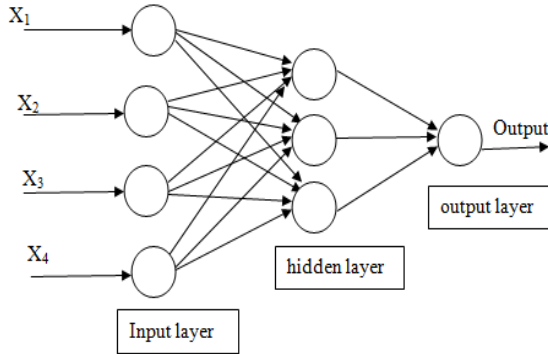


Fig 2: Multilayered neural network. [1]

In formula Pk output signals of BPNN are determined as[7]:

$$P_k = f_k \left(\sum_{j=1}^{h2} v_{jk} \cdot f_j \left(\sum_{i=1}^{h1} u_{ij} \cdot f_i \left(\sum_{l=1}^m w_{li} \cdot x_l \right) \right) \right) \quad (7)$$

$$P_k = 1 / (1 + e^{-\sum_{j=1}^{h2} v_{jk} \cdot y_j}) \quad (8)$$

2.3.1 Parameters Learning:

At the beginning, the parameters of BPNN are generated randomly. The parameters v_{jk}, u_{ij}, and w_{li} of BPNN are weight coefficients of second, third and last layers, respectively. Here k=1,...,n, j=1,...,h2, i=1,...,h1, l=1,...,m. To generate BPNN recognition model, the training of the weight coefficients of v_{jk}, u_{ij}, and w_{li} has been carried out. During training the value of the following cost function is calculated

$$E = 1/2 \sum_{k=1}^n (P_k^d - P_k)^2 \quad (9)$$

Here n is the number of output signals of the network and P_k^d and P_k are the desired and the current output values of the network, respectively. The parameters v_{jk}, u_{ij}, and w_{li} of neural network are self adjusted. The adaptive learning rate is applied in order to increase learning speed and guarantee convergence. The following strategy is applied for every given number of epochs.

2.3.2 Selection of training parameters:

For the efficient operation of the back propagation network it is necessary for the appropriate selection of the parameters used for training. Initial Weights This initial weight will influence whether the net reaches a global or local minima of the error and if so how rapidly it converges. To get the best result the initial weights are set to random numbers between -1 and 1.

2.3.2.1 Training a Net :

The motivation for applying back propagation net is to achieve a balance between memorization and generalization; it is not necessarily advantageous to continue training until the error reaches a minimum value. The weight adjustments are based on the training patterns. As long as error the for validation decreases training continues. Whenever the error begins to increase, the net is starting to memorize the training patterns. At this point training is terminated.

Number of Hidden Units If the activation function can vary with the function, then it can be seen that a n-input, m output function requires at most 2n+1 hidden units. If more number of hidden layers are present, then the calculation for the 's are repeated for each additional hidden layer present, summing all the 's for units present in the previous layer that is fed into the current layer for which is being calculated.

2.3.2.2 Learning rate :

In BPN, the weight change is in a direction that is a combination of current gradient and the previous gradient. A small learning rate is used to avoid major disruption of the direction of learning when very unusual pair of training patterns is presented. Various parameters assumed for this algorithm are as follows.

- No.of Input unit = 1 feature matrix
- Accuracy = 0.001
- learning rate = 0.4
- No.of epochs = 400
- No. of hidden neurons = 70
- No.of output unit = 1

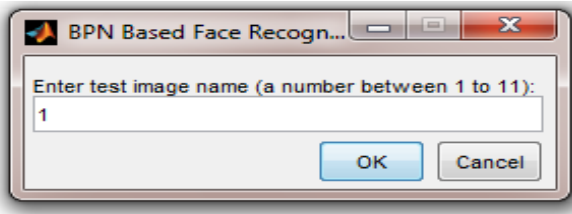
III. CONCLUSION

The neural networks aimed at providing artificial intelligence to the system. Neural networks using back propagation is presented in this paper for face recognition The recognition rate of BPNN system was found to be 99.25%.The identification result obtained using the neural network approach illustrates the success of its efficient use in face recognition. The BPNN algorithm is preferred over other neural network algorithms because of its unique ability to minimize errors. BPNN is found to be very accurate where recognition is required over other neural networks. Main advantage of this back propagation algorithm is that it can identify the given image as a face image or non face image and then recognizes the given

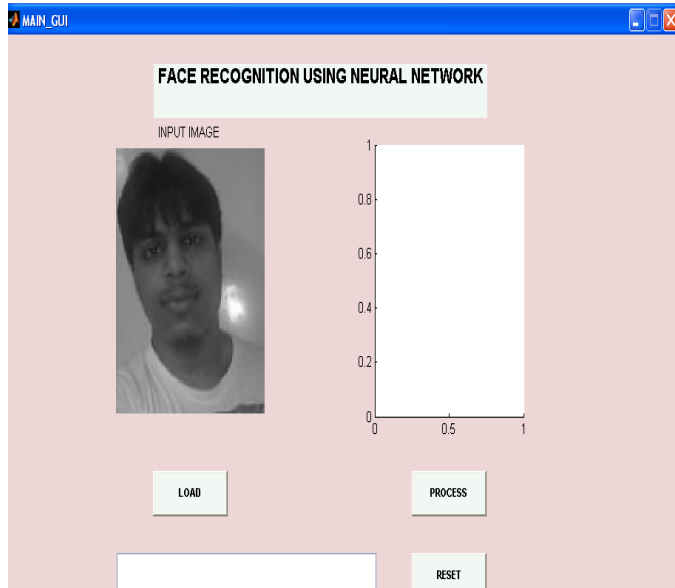
input image .Thus the back propagation neural network classifies the input image as recognized image.

IV. RESULTS AND DISCUSSION

Step1: Testing of image



Step2: Selected image is displayed



Step3: Recognized Image

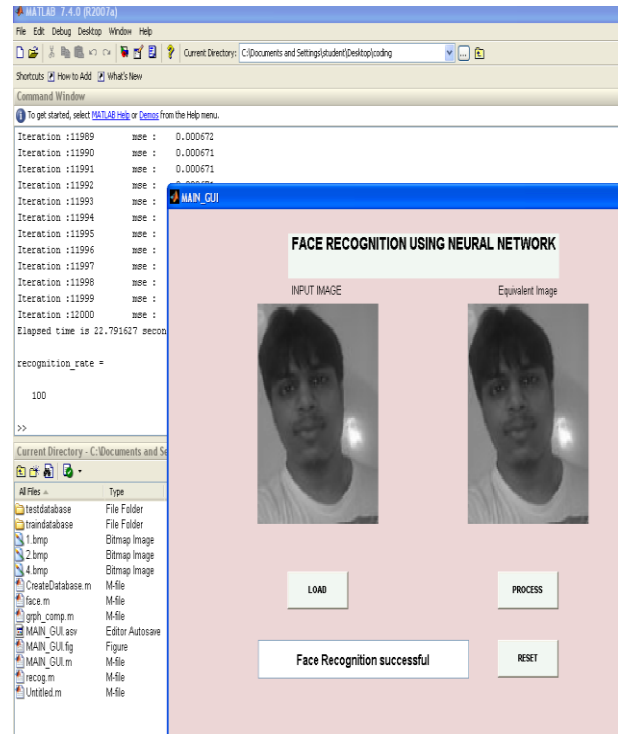


Fig 3: The obtained result on MATLAB

The first step consists of a basic input step where we need to give the input image to be recognized. This is done by pressing the push button "load". This is shown in the step 1 in the above figure. The second step shows the image selected for recognition in the left hand side box. After this we start the recognition process by pressing on the push button "process".

The final step shows the recognized image in the right hand side box. In workspace of the MATLAB we even got the elapse time needed in the entire recognition process. For the above example the elapse time was 22.9secs.

Performance Comparisons: In this section we found that as we increase the number of subjects in the recognition process, the execution time goes on increasing and the efficiency of recognition also decreases. Also graphical results shows that the BPNN algorithm with PCA is more accurate and quick than PCA alone.

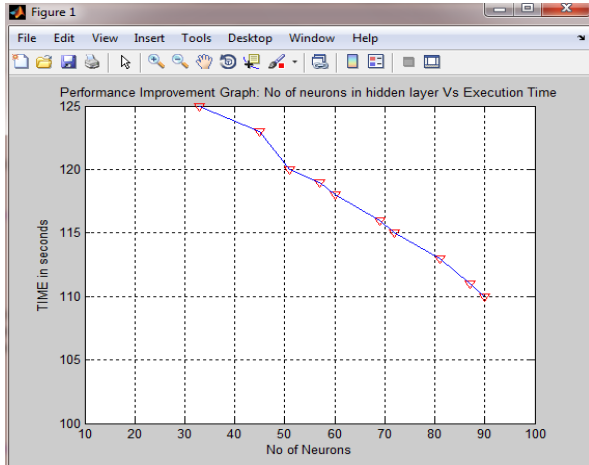


Fig 4:Graph of execution time versus no. of neurons

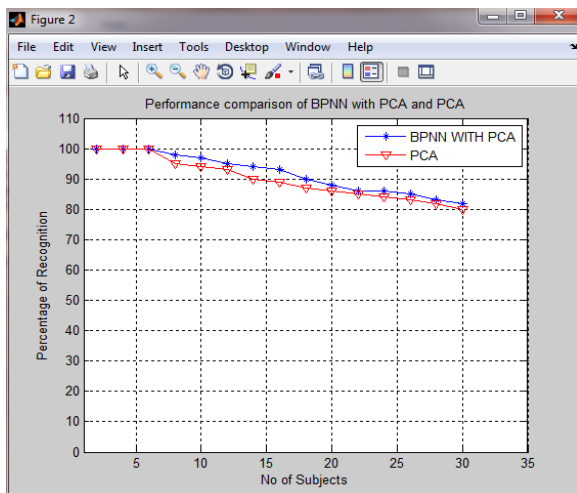


Fig 5 :Graphical comparison between BPNN with PCA and PCA in terms of recognition rate

- [6] Xiaofei He, Shuicheng Yan, Yuxiao Hu, Partha Niyogi, and Hong-Jiang Zhang, "Face Recognition Using Laplacianfaces" IEEE TRANSACTIONS ON PATTERN ANALYSIS AND MACHINE INTELLIGENCE, VOL. 27, NO. 3, MARCH 2005
- [7] Igor Aizenberg, Naum Aizenberg, Constantine Butakov, Elya Farberov, "Image Recognition on the Neural Network based on Multi-Valued Neurons" Neural Networks Technologies Ltd., Hashmonaim str., 3, Bnei-Brak, 51264, Israel
- [8] Henry A. Rowley, Shumeet Baluja, and Takeo Kanade "Neural Network-Based Face Detection"(PAMI, January 1998) pp 4-20
- [9] Santaji Ghorpade, Jayshree Ghorpade, Shamla Mantri, Dhanaji Ghorpade "NEURAL NETWORKS FOR FACE RECOGNITION USING SOM", Dept. of Information Technology Engineering, Pune University, India, IJCST Vol. 1, Iss ue 2, December 2010
- [10] Kailash J. Karande Sanjay N. Talbar "Independent Component Analysis of Edge Information for Face Recognition" International Journal of Image Processing Volume (3) :Issue (3) pp: 120 -131.
- [11] Jawad Nagi, Syed Khaleel Ahmed, Farrukh Nagi "A MATLAB based Face Recognition System using Image Processing and Neural Networks" Department of Electrical , Electronics and Mechanical Engineering Universiti Tenaga Nasional, Malaysia, 4th International Colloquium on Signal Processing and its Applications, March 7-9, 2008,.

VI. REFERENCES

BOOKS:

- [1] S.N.Sivanandam Introduction To Neural Network Using Matlab 6.0 -, 2nd edition Tata McGraw Hill publications.
- [2] Rafael C. Gonzalez, Richard E. Woods Digital Image Processing, 2nd edition — PHI publication.
- [3] Simon Haykin Introduction to Neural Network -, 2nd edition, McGraw Hill Publication.

JOURNAL PAPERS:

- [4] R. Rojas(1996), Neural Network An Introductions, Springer-Verlag, Berlin, "IEEE Transactions of Neural Networks. vol.8, no.1,pp158-200
- [5] 'Pattern Recognition and Neural Networks'by B.D. Ripley Cambridge University Press, 1996, ISBN 0-521-46086-7

Stability analysis and solution of head lice growth model

Tailor Ravi M.¹, Bhatwala P.H.²

¹(Head Department of Mathematics, Vidhyadeep Institute of Management and Technology, Anita, Kim, Gujarat, India)

²(Principal of Maniba Institute of Management, Sabargam, Gujarat, India)

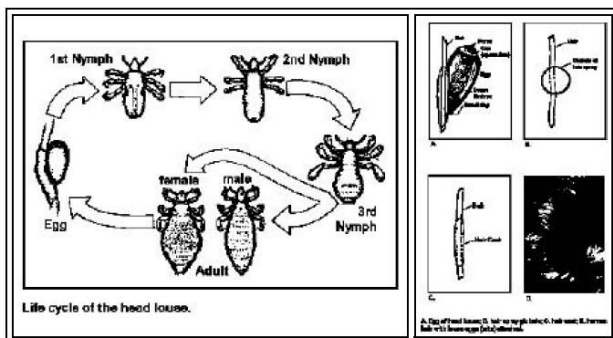
ABSTRACT

In this paper, we discuss the basic introduction on head lice problem and find the differential equations related to our assumption. Solve the differential equation by using equilibrium points and checked the stability of differential system. Finally, we will find the solution of differential system.

Keywords: equilibrium points, eigenvalues, lice model, stability.

I. INTRODUCTION

Head lice are small wingless worm, which are ectoparasites specific to humans. They nourish on human blood 3-4 times a day and cannot survive for more than 2 days away from the host. They lay eggs close to the scalp on hair shafts where the temperature is Standard for incubation. Usually temperatures between 75 and 98.6°F are optimum for lice. The eggs are glued to the hair shaft and it is difficult to dislodge them. Lice insert their mouthparts into human skin to draw blood and inject their mucus that prevents blood from clotting and also causes irritation and subsequent causes itching. Excessive scratching can lead to secondary infections and Burning. Head louse can spend its whole life on human head. The details of life cycle of lice are as follows



Highly magnified

Front view of an actual louse on a hair shaft (highly magnified)



Stage 1 – Eggs

The head louse begins life as an egg, commonly referred to as a nit. Nits are laid by the adult female. The nits are attached to the hair shaft by a glue-like substance produced by the louse. Nits range in color from white to yellow to tan to grayish in color, depending upon the stage

of development and whether or not they have hatched or been killed by treatment. Nits are oval or tear-drop shaped, smooth and very small (0.5-0.8 mm). Nits are hard to see and often are confused for dandruff, hair spray droplets or other debris.

Stage 2 –Nymphs

The nits incubate for about seven to 14 days, then they hatch to release a nymph. The nit shell that remains after hatching then becomes a dull yellow or translucent white and may have a wrinkled look. The nymph looks like an adult louse, but is only about the size of a pinhead. The nymph begins eating within one hour of hatching. During the next seven to 10 days, the nymph continues to grow and mature, going through three molts, until it becomes a full adult louse.

Stage 3 –Adults

The adult louse is about the size of a sesame seed. The life span of an adult louse is about 30 days. The female is usually larger than the male and can lay three to five nits per day, or up to 150 nits during her life span (only nits that are fertilized will develop and hatch). The live, adult louse needs to feed on blood every three to six hours. Without blood meals, or once away from the human host, the adult louse can usually survive for no longer than 24 to 36 hours.

II. PROBLEM DESCRIPTIONS

Lice can spend their whole lifetime as ectoparasites feeding on an infested person's blood. They suck blood from skin capillaries painlessly. Usually people get it treated because of itching, secondary infections and inflammation. But the amount of itching caused varies from person to person depending on their sensitivity. A person might have been infested with lice months before any itching is noticed. In cases where no itching is observed it is left untreated. In India in many rural areas people don't get any treatment done for lice infestation. The children in such families may also be malnourished and on the borderline of becoming anemic.

III. ASSUMPTIONS

- Male and Female is only die by natural death and transmission and fall off.
- I am assuming natural death only after the completion of life cycle.
- The rate of transmission and fall off depends on two factors:
- The total number of lice per unit area at a particular point of time.

- Density and length of hair. People with long and dense hair can support more lice and therefore transmission rate is low in such cases.
- Based on the above considerations I tried to calculate the number of lice with time for about 120 days. To start with I assumed that one adult female louse which is ready to lay eggs (on its 19th day) infects the person on the first day. Initially the data was generated considering only natural death and neglecting the effect of transmission to other persons or rate at which the lice fall off while grooming hair etc. and also the unproductiveness of the eggs i.e. it was assumed that all eggs will hatch to produce nymphs.

IV. DIFFERENTIAL EQUATIONS

$$\frac{dF}{dt} = h_e(1 - m_p)E - n_d F - t_f F^2$$

$$\frac{dM}{dt} = h_e m_p E - n_d M - t_f M^2$$

$$\frac{dE}{dt} = g_e F - e_m E - h_e E \dots\dots\dots (1)$$

Where F, M and E are the number of female, male and eggs respectively.

The model $\frac{dF}{dt} = h_e(1 - m_p)E - n_d F - t_f F^2$

- $\frac{dF}{dt}$, the growth rate of female population defined by three different terms.
- It is positively influenced by current female population size, as shown by the term $h_e(1 - m_p)E$.
- It is negatively influenced by natural death rate of female, as shown by the term $-n_d F$.
- It is negatively influenced by death rate of female due to transmission and fall off, as shown by the term $-t_f F^2$.

The model $\frac{dM}{dt} = h_e m_p E - n_d M - t_f M^2$

- $\frac{dM}{dt}$, the growth rate of male population defined by three different terms.
- It is positively influenced by current male population size, as shown by the term $h_e m_p E$.
- It is negatively influenced by natural death rate of male, as shown by the term $-n_d M$.
- It is negatively influenced by death rate of male due to transmission and fall off, as shown by the term $-t_f M^2$.

The model $\frac{dE}{dt} = g_e F - e_m E - h_e E$

- It is positively influenced by eggs population size, as shown by the term g_e .

- It is negatively influenced by death rate of eggs, as shown by the term $-e_m E$.
- It is negatively influenced by death rate of hatching of eggs, as shown by the term $-h_e E$.

V. ESTIMATION OF PARAMETER

The parameters are determined assuming equal distribution of the lice and egg population over various phases and ages through the life cycle.

- The rate constant for hatching of eggs is given by $h_e + e_m = \frac{1}{8}$ in an equal distribution as it takes 8 days for an egg to hatch. It has been found that 88% is the maximum hatch rate i.e. 12% of the eggs turn out to be unproductive. So the rate of egg mortality is 88% of the rate of generation of eggs.
- ∴ $h_e = 0.88 \times \frac{1}{8} = 0.11$ and $e_m = 0.12 \times \frac{1}{8} = 0.015$.
- A female in its lifetime of 27 days (excluding 8 days of egg stage) lays eggs for the last 17days. So the ratio of number of egg laying female to the total number of females is $\frac{17}{27}$.

$g_e * N = \text{rate of generation of eggs} = 6 * f \text{ per day}$

$$\therefore g_e = \frac{6 * f}{N} = \frac{102}{27} = 3.778.$$

- Since the population is distributed equally over different ages the death rate constant n_d is given by $\frac{1}{27} = 0.037$.
- The fraction of male population is found to be 0.4 and hence $m_p = 0.4$.
- The rate constant for transmission and fall off varies from person to person depending on the length and density of hair, surface area as it determines the number of lice per unit area. Depending on t_f the severity of the infestation also varies. So different values of t_f were tried out to find the t_f for the case of severe infestation where the total number of lice usually saturates at about 100.

Therefore, the differential system (1) is,

$$\frac{dF}{dt} = 0.66E - 0.037F - t_f F^2,$$

$$\frac{dM}{dt} = 0.044E - 0.037M - t_f M^2,$$

$$\frac{dE}{dt} = 3.778F - 0.125E$$

VI. EQUILIBRIUM POINTS

These are showed by the following computation. Let

$$X = \frac{dF}{dt} = 0.66E - 0.037F - t_f F^2,$$

$$Y = \frac{dM}{dt} = 0.044E - 0.037M - t_f M^2,$$

$$Z = \frac{dE}{dt} = 3.778F - 0.125E.$$

To compute the equilibrium points we solve $X = 0, Y = 0$ and $Z = 0$.

Here, the equilibrium point is $(0, 0, 0)$. i.e. $F = 0, M = 0$ and $E = 0$.

Now, to study the stability of the equilibrium points we first need to find the Jacobian matrix which is:

$$J(F, M, E) = \begin{bmatrix} \frac{\partial X}{\partial F} & \frac{\partial X}{\partial M} & \frac{\partial X}{\partial E} \\ \frac{\partial y}{\partial F} & \frac{\partial y}{\partial M} & \frac{\partial y}{\partial E} \\ \frac{\partial Z}{\partial F} & \frac{\partial Z}{\partial M} & \frac{\partial Z}{\partial E} \end{bmatrix} = \begin{bmatrix} -0.037 - 2Ft_f & 0 & 0.66 \\ 0 & -0.037 - 2Mt_f & 0.044 \\ 3.778 & 0 & -0.125 \end{bmatrix}$$

To study the stability of $(0, 0, 0)$

$$\therefore J(0, 0, 0) = \begin{bmatrix} -0.037 - \lambda & 0 & 0.66 \\ 0 & -0.037 - \lambda & 0.044 \\ 3.778 & 0 & -0.125 - \lambda \end{bmatrix}$$

The characteristic polynomial is,

$$\lambda^3 + 0.19900000000000007\lambda^2 - 2.4828609999999993\lambda - 0.09208763499999956$$

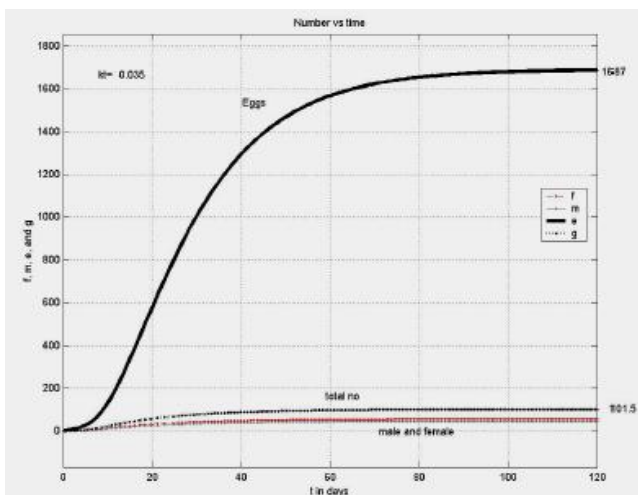
And the eigenvalues of the equation is

$$\{-1.6606885769036883, -0.036999999999999985, 1.4986885769036882\}$$

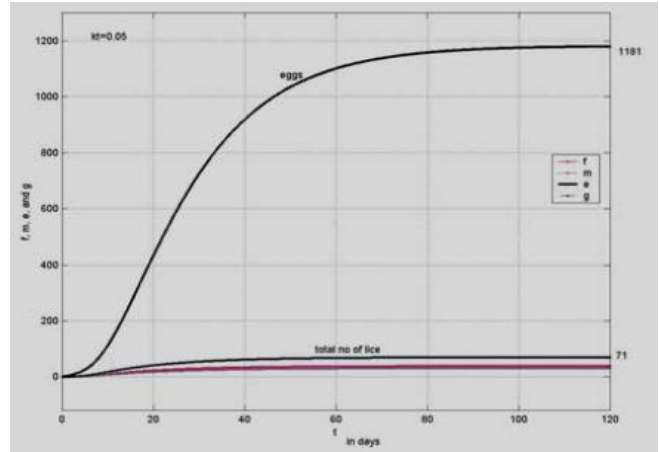
Here two eigenvalues negative and one eigenvalues positive.

Hence, the system is unstable.

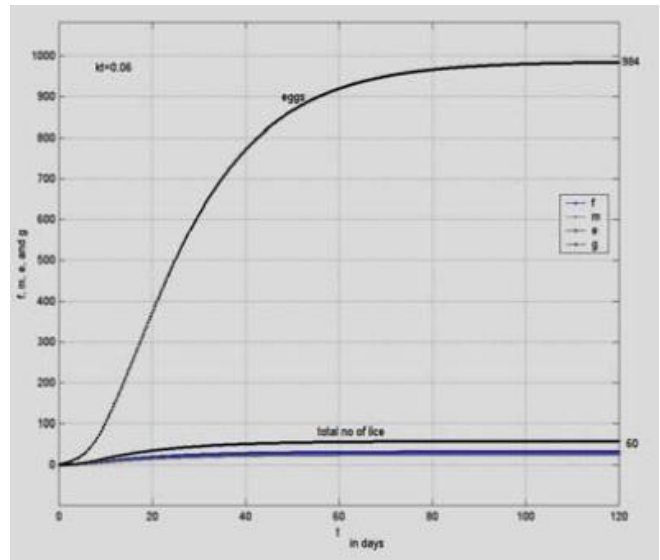
VII. SOLUTION OF DIFFERENTIAL EQUATIONS USING MATLAB



The above graph for $t_f = 0.035$ gives the total no of lice that saturates at about 100 which is the real situation in cases of severe infestation. The following graphs show the variation of total no of lice and eggs with respect to time for different values of t_f (varying levels of infestation). A saturation of value of number of lice at about 20 is considered to be moderate infestation.



$t_f = 0.05, E = 1181, L = 71$



$t_f = 0.06, E = 984, L = 60$

VIII. CONCLUSION

By the above discussion we say that lice do not increase in number indefinitely but are limited due to crowding effects and lack of area. So the rate of transmission or fall off is significant. Here, we find that the louse is unstable in human heads by eigenvalues of system. The claim of antilice treatment to ensure freedom from lice in 4 weeks is quite authentic.

Acknowledgements

I thank P.H.Bhathawala for helpful comments concerning the role of regularity in this work.

Nomenclature:

- h_e : Hatching of eggs
- n_d : Natural death

t_f	:	Transmission and fall off
g_e	:	Egg generation or laying of eggs
e_m	:	Egg mortality
m_p	:	Fraction of male population
E	:	number of eggs
F	:	female lice
M	:	male lice
G	:	total number of live lice

References

- [1] Craig G Burkhart et al. 2006, Safety and Efficacy of Pediculicides for Head Lice.
- [2] Z Vermaak, Model for the control of pediculus human capitis, Public health(1996)110, 283-288
- [3] Michigan Head Lice Manual, July 2004 – Version 1.0
- [4] Controlling Head Lice, Revised - September 2010
- [5] Preventing The Spread of Infection and Infestations, Niagara Region Public Health January 2012
- [6] [http://www.stephentvedten.com/16_Lice_%26_Scabie s.pdf](http://www.stephentvedten.com/16_Lice_%26_Scabie%20s.pdf)
- [7] http://samples.jbpub.com/9780763766221/66221_CH01_5398.pdf
- [8] Felso B et al. 2006. Reduced taxonomic richness of lice (Insecta: Phthiraptera) in divining birds.
- [9] Clayton DH 1990. Mate choice in experimentally parasitized rock doves: Jousy males lose. *American Zoologist*, **30**, 251–262.
- [10] Goates, Brad M.; Atkin, Joseph S; Wilding, Kevin G; Birch, Kurtis G; Cottam, Michael R; Bush, Sarah E. and Clayton, Dale H. (5 November 2006). An effective nonchemical treatment for head lice: A lot of hot air. *American academy of pediatrics*. **118** (5): 1962–1970.

Experimental Investigation on the Performance & Emission Characteristics of non edible oil (Jatropha Curcus & Honge) as an alternate fuel in variable compression ignition engine

C.V. Mahesh¹, E.T. Puttaiah² and Praveen R³

¹ Research Scholar, Dept. of P.G. Studies & Research Center in Environmental Science, Kuvempu University, Shimoga, Karnataka, India.

² Professor, Dept. of P.G. Studies & Research Center in Environmental Science, Kuvempu University, Shimoga, Karnataka, India.

³ P.G. Student, Thermal Power Engg, Dept. of Mech. Engg, Sri Siddhartha Institute of Technology, Tumkur, Karnataka, India.

ABSTRACT

Due to increase in the demand and scarcity in the availability of the fossil fuel, there is a need of alternate fuel in order to overcome the present crisis. The properties of the alternate fuel should be sustain the technology and have less detrimental effect on the environment in the light of the above properties, the researchers are attempting to develop the alternate fuel in the aspect of economic, environment and to continue the technology without the modification. Among all the available alternate fuel like hydrogen, methanol, etc., Biodiesel is considered as promising alternative fuel for the future. The present work aims to investigate the performance and emission characteristics of the Biodiesel like Honge and Jatropha for the CI engines. Engine test was performed at different loads and different compression ratio for constant engine speed. The emission characteristics are analyzed for different loads, compression ratio and for different blends. The experimental results showed J10 and H10 has less emission characteristic and have agreeable performance in compared with the diesel.

Keywords: Biodiesel, Honge, Jatropha, Emission, Methyl Ester

I. INTRODUCTION

Indeed, we are really experiencing the warmth of the global warming, where the climatic condition has changed, the level of sea has increased global temperature is increasing at an alarming rate as a result we had global meet and Kyoto protocol has drafted rules to minimize the global warming, where as automobile also have there contribution in global warming. It is a pure indication that to think of the Alternate fuels where the existing vehicles can use and reduce the pollution along with less dependable on the fossil fuel.

The economic situation of India which is mainly depending on the rural agriculture the use of Jatropha and Honge can increase the employment factor of rural India along with the increase in their income, which indirectly helps to increase the GDP growth of India. In the future scope the use of Biodiesel from blends to the 100% (cent percent) pure Biodiesel will remove the dependability on fossil fuel completely.

The processes of Biodiesel includes from the collection of dry seeds to the esterification of the oil, Esterification is the process where the methyl ester & glycerol are formed and glycerol being heavier settles down and methyl ester can be used as Biodiesel. Advantages of Biodiesel is

- It is renewable
- It is carbon neutral
- Blends up to 20% Biodiesel with 80% petroleum diesel can be used in unmodified diesel engines.

Banapurmath *et al.*, [1] have reported tests on a single cylinder C.I. engine with 3 different biodiesels viz methyl esters of honge, jatropha and sesam. All the fuels gave slightly lower efficiency. HC and CO emissions were slightly higher and NOx emission decreased by about 10%. Recep Altin *et al.*, [2] have studied the potential of using vegetable oils and their methyl esters in a single cylinder diesel engine. They have used raw sunflower, cottonseed, soyabean oils and their methyl esters. Their results indicate a reduction in NOx emission and methyl esters are better than raw oils due to their inherent property of high density, higher viscosity, gumming and lower cetane number.

B. Baiju *et al.*, [3] used methyl and ethyl ester from karanja oil to run C.I engine. They observed good engine performance with reduced emissions of HC and smoke. Deepak Agarwal *et al.*, [4] conducted experiments with esters of linseed, mahua, rice bran and Lome. They observed that the performance and the emission parameters were very close to diesel. They even observed that a diesel engine can perform satisfactorily by esterified biodiesel blends without any hardware modifications. Suresh Kumar *et al.*, [5] have investigated the performance and emission characteristics on a single cylinder diesel engine and reported decrease in NOx and HC emissions.

Nagarahalli. M.V *et al.*, [6] conducted experiments on Karanja biodiesel and its blends in a C.I. engine. Concluded that tests for emission and performance were conducted on 4 stroke, constant speed diesel engine said that the results are in line with that reported in literature by different literature and recommended 40% biodiesel 60% diesel (B40). Shivkumar *et al.*, [7] conducted experiments on honge methyl ester using artificial neural network and

concluded Break thermal efficiency of honge biodiesel with 20% diesel are very close for biodiesel operation for all compression ratios. Increase in NO_x emission was observed for biodiesel blends compared to that of diesel for all compression ratios.

P.Selva Havarasi et al. [8]. The main objective of this work is to optimize the transesterification process for methyl ester production and testing its performance in diesel engine. Used cooking oil is used as feedstock for the production of methyl esters in this work as they provide a viable alternative to diesel, due to its availability. The effect of excess methanol, catalyst amount, temperature, time of reaction was studied to optimize the transesterification process. All the reactions were carried out under the same experimental conditions. The performance and emission characteristics of used cooking oil methyl esters and its blend with diesel oil were analyzed in a diesel engine. The minor decrease in thermal efficiency with significant improvement in the reduction of particulates, carbon monoxide, and unburnt hydrocarbon was observed compared to diesel. **GVNSR Ratnakara Rao et al. [9]** Experimental investigations were carried out on a single cylinder variable compression ratio C.I engine using neat mahua oil as the fuel. Both the performance and exhaust analysis were carried out to find the best suited compression ratio. Tests have been carried out at 7 different compression ratios. All the experiments were carried out at standard test conditions like 70°C cooling water temperature and at constant speed of 1500rpm. The result shows that 15.7 is the best compression ratio with mahua oil.

Sukumar Puhan, N et al. [10] in this study, mahua oil was transesterified with methanol using sodium hydroxide as catalyst to obtain mahua oil methyl ester. This biodiesel was tested in a single cylinder, four stroke, direct injection, constant speed, compression ignition diesel engine to evaluate the performance and emissions. **Hidekki Fukuda et. al. [11]** enzymatic transesterification using lipase has become more attractive for biodiesel fuel production, since the glycerol produced as a byproduct can easily be recovered and purification of fatty methyl ester is simple to accomplish. **Mustafa Canakci [12]** free fatty acids and moisture reduce the efficiency of transesterification in converting these feed stocks into biodiesel. Hence, this study was conducted to determine the level of these contaminants in feedstock samples from a rendering plant. Levels of free fatty acids varied from 0.7% to 41.8%, and moisture from 0.01% to 55.38%. These wide ranges indicate that an efficient process for converting waste grease and animal fats must tolerate a wide range of feedstock properties. **Purnananda Vishwanatha Rao Bhale et al. [13]** this paper is aimed to investigate the cold flow properties of 100% biodiesel fuel obtained from mahua oil, one of the important species in the Indian context. The performance and emissions with ethanol blended mahua biodiesel fuel and ethanol diesel blended mahua biodiesel fuel have also been studied.

II EXPERIMENTAL SETUP

2.1 Equipment Introduction:

First standard engine is fully instrumented and connected to the dynamometer. The experiments are conducted at constant speed and at four different loads levels viz., 20%, 40%, 60% and 80% of full load. The required engine load percentage is adjusted by using the eddy current dynamometer.

Fig.5.2 shows the schematic diagram of the complete experimental setup for determining the effects of TBC on the performance parameters of compression ignition engine. It consists of a single cylinder four stroke water cooled compression ignition engine connected to an eddy current dynamometer. It is provided with temperature sensors for the measurement of jacket water, calorimeter water, and calorimeter exhaust gas inlet and outlet temperature. It is also provided with pressure sensors for the measurement of combustion gas pressure and fuel injection pressure. An encoder is fixed for crank angle record. The signals from these sensors are interfaced with a computer to an engine indicator to display P- θ , P-V and fuel injection pressure versus crank angle plots. The provision is also made for the measurement of volumetric fuel flow. The built-in program in the system calculates indicated power, brake power, thermal efficiency, volumetric efficiency and heat balance. The software package is fully configurable and averaged P- θ diagram, P-V plot and liquid fuel injection pressure diagram can be obtained for various operating conditions.

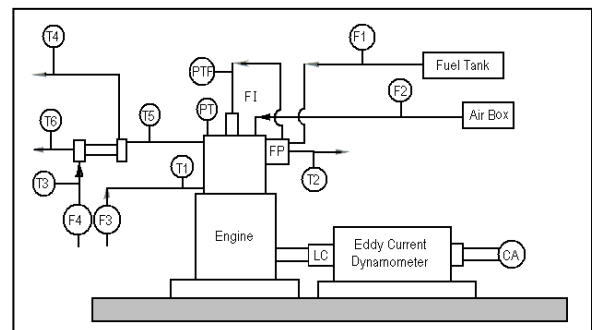


Fig. 5.2: Schematic Diagram of the Experimental Set-up.

PT	Combustion Chamber Pressure Sensor
F1	Liquid fuel flow rate
PTF	Fuel Injection Pressure Sensor
F2	Air Flow Rate
FI	Fuel Injector
F3	Jacket water flow rate
FP	Fuel Pump
F4	Calorimeter water flow rate
T1	Jacket Water Inlet Temperature
LC	Load Cell
T2	Jacket Water Outlet Temperature
CA	Crank Angle Encoder
T3	Inlet Water Temperature at Calorimeter
EGC	Exhaust Gas Calorimeter

T4	Outlet Water Temperature at Calorimeter
T5	Exhaust Gas Temperature before Calorimeter
T6	Exhaust Gas Temperature after Calorimeter

2.2 Measurement System:

The test bed is fully instrumented to measure the various parameters such as flow measurement, load measurement, pressure measurement, etc during the experiments on the engine.

2.2.1 Flow Measurement:

Air flow measurement is done by the flow sensors, a conventional U- tube manometer as well as air intake differential pressure transducers unit present in the control panel. There are two parallel air suction arrangements, one for U- tube manometer having arranged of 100-0- 100 mm and another for pressure differential unit, which senses the difference in pressure between suction and atmospheric pressure. This difference in pressure will be sent to transducer which will give the DC volt analog signal as output which in turn will be converted into digital signal by analog to digital converter and fed to the engine software.

For liquid fuel flow rate measurement, the fuel tank in the control panel is connected to the burette for manual measurement and to a fuel flow differential pressure unit for measurement through computer.

Cooling water flow to the engine and calorimeter is measured by means of a calibrated Rota-meter with stainless steel float.

2.2.2 Load Measurement:

The eddy current dynamometer is provided to test the engine at different loading conditions. A strain gauge type load cell mounted beneath the dynamometer measures the load. The signals from the load cell are interfaced with analog to digital converter to give torque in N-m. The dynamometer is loaded by the loading unit situated in the control panel.

2.2.3 Pressure Measurement:

A water cooled piezo sensor mounted on the cylinder head measures the cylinder dynamic pressure and a piezo sensor mounted on the fuel line near the injector measures the fuel injection pressure.

2.2.4 Engine Speed Measurement:

Engine speed is sensed and is indicated by an inductive pickup sensor in conjunction with a digital RPM indicator, which is a part of the eddy current dynamometer control unit. The dynamometer shaft rotating close to inductive pickup rotary encoder sends voltage pulses whose frequency is converted to RPM and displayed by digital indicator in the control panel, which is calibrated to indicate the speed directly in number of revolutions per minute.

2.2.5 Temperature Measurement:

Chromium-aluminum thermocouples connected to digital panel meter are positioned at different locations to measure the following temperatures:

- Jacket water inlet temperatures (T1)
- Jacket water outlet temperatures (T2)
- Calorimeter inlet water temperature (T3)
- Calorimeter inlet water temperature (T4)
- Exhaust gas temperature before calorimeter (T5)
- Exhaust gas temperature after calorimeter (T6)

All the sensors which sense the temperature of respective locations are connected to the control panel, which gives the digital reading of the respective temperatures.

2.3 Working Procedure:

- 1) Switch on the mains of the control panel and set the supply voltage from servo stabilizer to 220volts.
- 2) The main gate valve is opened and the pump is switched ON and the water flow to the engine cylinder jacket (300 liters/hour), calorimeter (50 liters/hour), dynamometer and sensors are set.
- 3) Engine is started by hand cranking and allowed to run for a 20 minutes to reach steady state condition.
- 4) The engine soft version 3.0 is run to go on ONLINE mode.

The engine has a compression ratio of 17.5 and a normal speed of 1500 rpm controlled by the governor. An injection pressure of 190 bar is used for the best performance as specified by the manufacturer. The engine is first run with neat diesel at loading conditions such as no load, 20%, 40%, 60% and 80%. Between two load trials the engine is allowed to become stable by running it for 3 minutes before taking the readings. At each loading conditions, performance parameters namely speed, exhaust gas temperature, brake power, peak pressure are measured under steady state conditions along with the emission parameters of CO, CO₂, HC and NO_x. The experiments are repeated for various combinations of diesel and honge biodiesel blends and also diesel with jatropha oil blends. With the above experimental results, the parameters such as total fuel consumption, brake specific fuel consumption, brake mean effective pressure; brake specific energy consumption, brake thermal efficiencies are calculated. And finally break power with respect to percentages of CO, CO₂ and PPM's of HC, NO_x are plotted with respect to loading conditions for diesel and each diesel oxygenate blend. From these plots, emission characteristics of the engine are determined.

III. RESULTS AND DISCUSSIONS

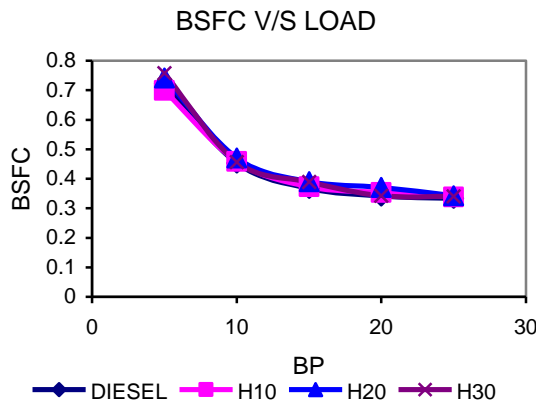


FIG.1

In the above fig.1 one cannot find much difference between the biodiesel of honge H10, H20, H30 along with the pure diesel the graph won't show much variation between the diesel and biodiesel

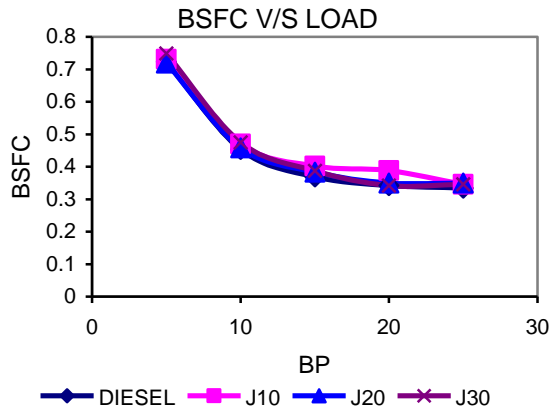


FIG.2

Similarly in the fig.2 graph of BSFC Vs BP we don't find much difference only slight variation in J10 otherwise it is equivalent to the pure diesel so the total conclusion from the above two graphs that we can use the biodiesel either jatropa or honge without the modification of the engine which gives similar result as of diesel.

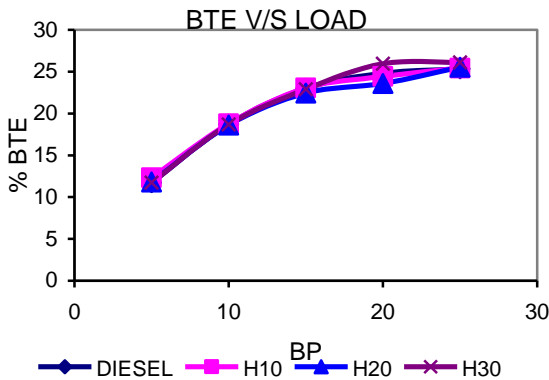


FIG.3

The Brake thermal efficiency for the pure diesel along with the blends of honge biodiesel is plotted in fig.3 and we find similar path followed by the diesel and biodiesel but little variation in load 20 for which H20 shows little less efficiency where as H30 is little bit more.

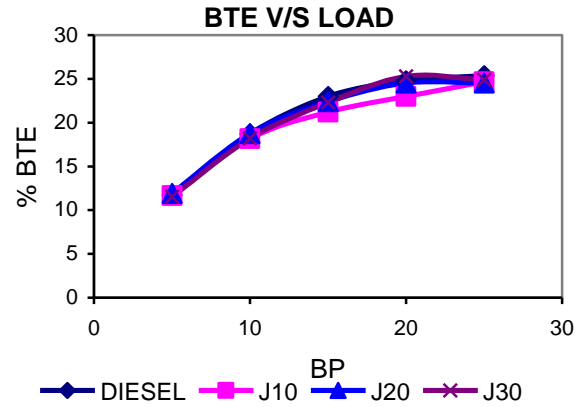


FIG.4

In case Jatropa biodiesel similar graph is obtained as in case of honge biodiesel but here J10 is showing bit less efficiency and remaining is almost equivalent to that of pure diesel as shown in fig.4. Hence we get similar efficiency as in case of pure diesel.

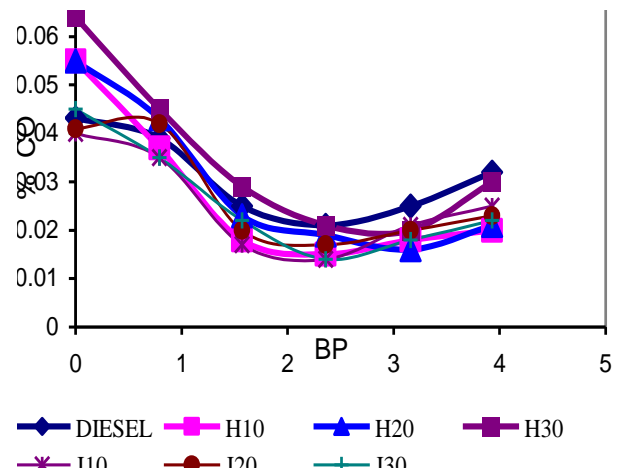


FIG.5

For the compression ratio 17.5 from figure5 it can be concluded that the percentage of carbon monoxide is higher at the beginning and keeps on decreasing as the load rate increases for BP 2.36 kw Honge10 gives the lower result compare to diesel H20 & H30 blends later there will be slight increase in the percentage of CO. emission of CO is higher at low load and again increases at high load due to the fact that incomplete combustion occurs at this loads (rich mixture).

Similarly for the same compression ratio the percentage of carbon monoxide is higher at the beginning and the blend of J10 has given the optimal result lower in the percentage of carbon monoxide for the similar BP 2.36 kw as shown in figure 5 comparatively the emission percentage of carbon monoxide for the pure diesel is more with respect to the Biodiesel of different blends but it can be concluded that the H10 and J10 is emitting lower percentage of

carbon monoxide. Emission of CO is higher at low load and again increases at high load due to the fact that incomplete combustion occurs at these loads (rich mixture).

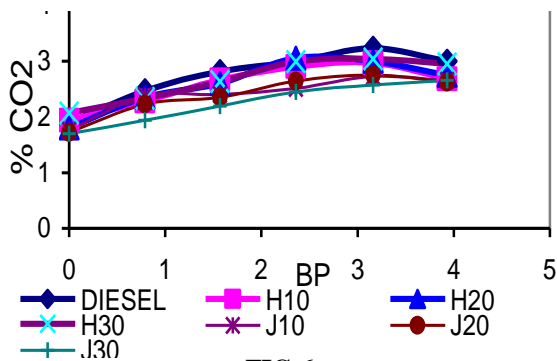


FIG.6

Where as in figure 6 the percentage of carbon di oxide keeps increasing as the Brake power increases and at the end there is a little decrease in the percentage of carbon di oxide even with the different blends of Honge along with pure diesel gives almost similar percentage of carbon di oxide emission of carbon di oxide is lower at less loads and increases at the higher loads, due to incomplete combustion.

For the blends of Jatropha along with the pure diesel the percentage of carbon di oxide is drawn for the emission result from figure 6 it can be concluded that the percentage of carbon di oxide for the blend J30 is much lower than the other blends of Jatropha and with pure diesel which is much higher than biodiesels.

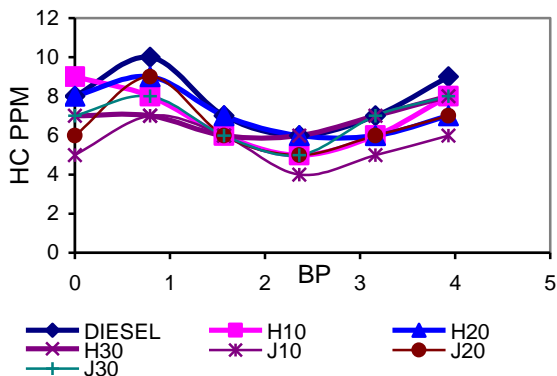


FIG.7

Graph is drawn for the hydrocarbon emission with respect to Brake power as shown in figure 7 for pure diesel and H20 blend the hydrocarbon emission increases slightly at the beginning and there is steep decrease in the hydrocarbon emission but for the blend H10 which varies moderately with the increase in Brake power and finally there is increase in the emission ppm for all the Honge blends with respect to pure diesel. In hydrocarbon emission can be observed at 50% loading.

In case of Jatropha Biodiesel blends with respect to the pure diesel as shown in figure 7 the emission of hydrocarbon varies with the increase in Brake power but

we can conclude that the optimum results between 10 & 20 blends.

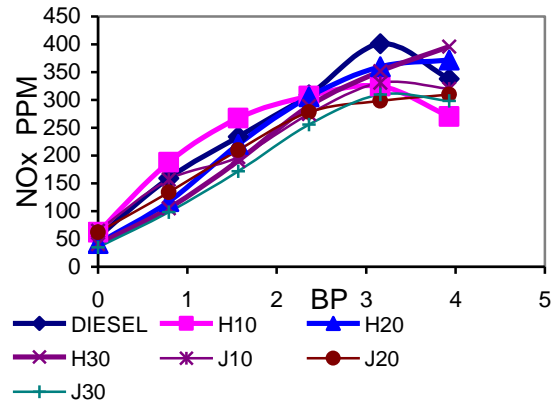


FIG.8

For NOx it increases as the load increases as at higher loads, higher combustion temperature causing more NOx formation refer figure 8.

IV CONCLUSION

Tests for emission and performance characteristics were conducted on a single cylinder, 4 stroke, constant speed diesel engine. From the above we can conclude that

- The engine can run without the manufacturer's modification for 20% blends with pure diesel either for jatropha or honge biodiesels.
- Emission for honge and jatropha with respect to pure diesel is lesser but for jatropha it is still lesser.
- Brake thermal efficiency for both honge and jatropha is similar and it walks along the path of pure diesel.
- The results are in line with that reported in literature by different researchers using various biodiesel fuels and their blends.

V. ACKNOWLEDGEMENT

The authors would like to thank the management of Sri Siddhartha Institute of Technology, Tumkur for their kind co-operation, principal for providing the lab facility to conduct the experiments and valuable support from the staff members of the mechanical department for their support during the course of this work.

VI. REFERENCES

- [1] N.R. Banapurmath *et al.*, 2008. Performance and emission characteristics of compression ignition engine operated on Honge, Jatropha and sesame oil methyl esters. *Renewable energy*, 33:1982-1988.
- [2] Recep Altin *et al.*, 2001. The potential of using vegetable oil fuel as fuel for diesel engine. *Energy conversion and management*. 42:529-538.
- [3] B. Baiju M.K naik, L.M.Das. 2009. A comparative evaluation of compression ignition characteristics using methyl and ethyl esters of karanja oil. *Renewable energy*. 34:1616-1621.

- [4] Deepak Agarwal, Lokesh kumar, Avinash kumar agarwal. 2008. Performance Evaluation of a vegetable oil fuelled compression ignition engine. *Renewable energy*, 33:1147-1156.
- [5] K. Suresh Kumar *et al.*, 2008. Performance and exhaust emission characteristics of a C.I engine fuelled with pongmia pinnata methyl ester (PPME) and its blends with diesel. *Renewable Energy*. 33:2294-2302.
- [6] Nagarahalli. M.V. Nandedkar. V.M and Mohite. K.C. 2010 Emission and performance characteristics of Karanja biodiesel and its blends in a C.I. Engine and its Economics. ISSN 1819-6608. arpnjournals.com
- [7] Shivakumar, Srinivas Pai. P, Srinivasa Rao B.R. and Samaga B.S..2010, Performance and emission characteristics of a 4 stroke C.I.engine operated on honge methyl ester using artificial neural network ISSN 1819-6608. arpnjournals.com
- [8] P.Selva Havarasi, G.Lakshmi Narayana Rao, G.Devasagayam, T.V.Balasubramaniam, P.V.R.Iyer "Production and Testing Of Methyl Esters of Used Coking Oil", *ICONICE 2007*.
- [9] GVNSR Ratnakara Rao, V. Ramachanra Raju and M. Muralidara Rao, "Optimizing the Compression Ratio for a Mahua Fuelled C.I. Engine", *ARPJN Journal of engineering and applied sciences*, volume4, NO: 3 MAY 2009.
- [10] Sukumar Puhan, N.Vedaraman, Boppana V.B. Ram, G.Sankaranarayanan, kJayachanderan, "*Mahua Oil Methyl Ester as Biodiesel Preparation and Emission Characteristics*", *Biomass&Bioenergy* 28(2005)87-93.
- [11] Hidekki Fukuda, Akihiko Kondo, Hideo Noda, "*Biodiesel Production by Transesterification of Oils*" *Journal of Bio science and Bioengineering*, volume92, NO. 5, 405-416.2001.
- [12] Mustafa Canakci, "The Potential of Restaurant Waste Lipids as Biodiesel Feedstock", *Bio resource Technology* 98(2007)183-190.
- [13] Purnananda Vishwanatha Rao Bhale, Nishikant V. Deshpande, Shasikant b. Thombre, "Improving The Low Temperature Properties Of Biodiesel Fuel", *Renewable Energy* 34(2009)794-800.

High solar energy concentration with a Fresnel lens: A Review

Gaurav A. Madhugiri

M. Tech. IV Semester Heat Power Engineering-Student, Mechanical Engineering Department, G. H. Raison College of Engineering, Digdoh hills, Nagpur-440016, Maharashtra State, India.

S. R. Karale

Assistant Professor, Mechanical Engineering Department, G. H. Raison College of Engineering, Digdoh hills, Nagpur-440016, Maharashtra State, India.

ABSTRACT

Solar technology offers great potential in terms of supplying the world's energy needs. The effective way of utilizing sunlight with solar energy concentration technology and recent developments of its applications using Fresnel lens is reviewed in this paper. The present status of application, the ongoing research and development works suggest that Fresnel lens solar concentrators will bring a breakthrough of commercial solar energy concentration application technology in the near future. The paper was focused on the Solar Energy high temperatures using parabolic solar concentrator, Fresnel lens, Reflecting materials and solar tracking. It identified their level of performance. This paper will provide an up-to-date review of solar concentrators and their benefits to make solar technology affordable. It will also analyze on some of the existing solar concentrators used in the solar technology for the past four decades and performance of each concentrator will be explained and compared.

Keywords: *Parabolic solar concentrator, Fresnel lens, Reflecting materials, Solar tracking.*

Introduction

The continuous increase in the level of green house gas emissions and the increase in fuel prices are the main driving forces behind efforts to more effectively utilize various sources of renewable energy. In many parts of the world, direct solar radiation is considered to be one of the most prospective sources of energy. Among the different energy end uses, energy for cooking is one of the basic and dominant end uses in developing countries. Solar energy, which is an abundant, clean and safe source of energy, is an attractive to substitute for the conventional fossil fuels. In concentrated solar system, concentration by reflection or refraction through mirrors. The mirrors can be plane or parabolic.

The reflectivity of the surface materials is an important factor in the optical efficiency. Mirror precision is important and conventional methods to fabricate precision parabolic mirrors are complex and costly. In solar energy applications, back silvered glass plates, anodized aluminum sheets serve as reflectors. They are widely commercially available. Thus improved solar reflectors play an important role in achieving the required cost reductions in solar collectors.

Parabolic dish type concentrators become bulky and transportability is a problem and the rising of temperature is slow.

To overcome this, the change in materials for concentrators and use of Fresnel lenses will raise more temperature than conventional one and can be used in furnace heating. The review was divided in two parts.

First one is selection of solar concentrator with tracking and another one is Fresnel lenses.

Selection of solar concentrator

Various designs of the solar concentrator were studied in order to optimize their performance and the variation was depending upon the geometrical form as well as the place of the pot. For the past four decades, there have been a lot of development involving the designs of solar concentrator. Some of distinguish designs which have shown significant contribution to the solar technology are as shown in table 1 and table 2;

Table 1: Types of solar concentrators

Type	Description
Reflect or	Upon hitting the concentrator, the sun rays will be reflected to the PV cell. Example: <i>Parabolic Trough, Parabolic Dish, CPC Trough, Hyperboloid Concentrator.</i>
Refract or	Upon hitting the concentrator, the sun rays will be refracted to the PV cell. Example: <i>Fresnel Lens Concentrator.</i>
Hybrid	Upon hitting the concentrator, the sun rays can experience both reflection and refraction before hitting to the PV cell. Example: <i>DTIRC, Flat High Concentration Devices.</i>

Luminescent	The photons will experience total internal reflection and guided to the PV cell. Example: <i>QDC</i> .
-------------	---

(F. Muhammad-Sukki et al, "Design of Solar Concentrators," International Journal of Applied Sciences (IJAS), Volume (1): Issue (1))

Table 2: Summary of the Advantage and Disadvantage of the Concentrators

Type of Concentrator	Advantage	Disadvantage
Parabolic Concentrator	<ul style="list-style-type: none"> • High concentration 	<ul style="list-style-type: none"> • Requires larger field of view. • Need a good tracking system.
Hyperboloid Concentrator	<ul style="list-style-type: none"> • Compact 	<ul style="list-style-type: none"> • Need to introduce lens at the entrance aperture to work effectively.
Fresnel Concentrator lens	<ul style="list-style-type: none"> • Thinner than conventional lens. • Requires less material than conventional lens. • Able to separate the direct and diffuse light - suitable to control the illumination and temperature of a building interior. 	<ul style="list-style-type: none"> • Imperfection on the edges of the facets, causing the rays improperly focused at the receiver.
Compound Parabolic Concentrator	<ul style="list-style-type: none"> • Higher gain when its field of view is narrow. 	<ul style="list-style-type: none"> • Need a good tracking system.
Dielectric Totally Internally Reflecting Concentrator	<ul style="list-style-type: none"> • Higher gain than CPC. • Smaller sizes than CPC. 	<ul style="list-style-type: none"> • Cannot efficiently transfer all of the solar energy that it collects into a lower index media.

Flat High Concentration Devices (RR, XX, XR, RX, and RXI)	<ul style="list-style-type: none"> • Compact. • Very high concentration 	<ul style="list-style-type: none"> • Difficulty to create electrical connection and heat sinking due to the position of the cell. • The cell dimension must be designed to a minimum to reduce shadowing effect.
Quantum Dot Concentrator	<ul style="list-style-type: none"> • No tracking needed. • Fully utilize both direct and diffuse solar radiation 	<ul style="list-style-type: none"> • Restricted in terms of Development due to the requirements on the luminescent dyes.

(F. Muhammad-Sukki et al, "Design of Solar Concentrators," International Journal of Applied Sciences (IJAS), Volume (1): Issue (1))

A.R. El Ouederni et. al. (2008) in this paper a parabolic solar concentrator has been experimentally studied. The experimental device consists of a dish of 2.2 m opening diameter. Its interior surface is covered with a reflecting layer and equipped with a disc receiver in its focal position. The orientation of the parabola is assured by two semi-automatic jacks. Experimental measurements of solar flux and temperature distribution on the receiver have been carried out. These experimental results describe correctly the awaited physical phenomena.

M. Ouannene et. al. (2009) designed, built and studied a parabolic solar concentrator. The characteristic equations and the experimental results showed that the favorable conditions of getting better solar concentrations are; first is the best hour of getting maximum solar energy is 13h: 30 to 14h: 30 and second is the concentrator is more effective if the solar tracking is perfect.

Pelemo et al. (2002) have noted the importance of materials used as shells for solar cooker. For their concentrators, the shell of the cooker were developed using various combinations of paper pulp with starch, sawdust and resins, and concrete cement. They considered cement mixed with sawdust and reinforced with palm fibers as a better alternative and more suitable for their environment. In their work, two types of materials were considered for use as the reflective material. These are aluminum sheet and glass mirrors. They concluded that both materials are suitable as

reflective materials in Ile-Ife environment even though they have different years of effective service durations.

Ajiya et al. (1995) designed and constructed a parabolic solar cooker at University of Maiduguri, Nigeria. The design was based on point focus using small square glass mirrors fixed on abricated parabolic dish as the reflecting surface. The parabolic is then placed on a mounting with some kind of steering arrangement that can be used to track the sun manually as it transverses its path from east to west. Blackened flat plate placed at the focal point serves as the absorber on which cooking pot is placed. Locally sourced materials were used for fabrication of the various parts. Testing revealed that the parabolic solar cooker performed at about 30% efficiency in Maiduguri environment.

Mshelbwala et al. (1996) carried out modification on Ajayi work in order to improve its efficiency. He introduced "L" shaped flat bars to replaced the blackened flat plate for the support of the cooking pot, and painted the bottom of cooking pot black. This modification made the bottom of the cooking pot to be the receiver thereby causing direct heating of the pot without any intermediary as was in the original design. Heat loss due to conduction between the flat-plate and cooking pot was eliminated by the new modification. Analysis of the data collected from the experimental tests carried out on the modified cooker revealed an efficiency of 46.6% which is an improvement on the earlier design.

Asere et al. (2003) carried out the design, construction and testing of a compound parabolic solar cooker (CPC). The temperature of up to 90°C was obtained while highest instantaneous efficiency of the cooker for the clear day was 44%. The effect of spherical scatters on the thermal performance of the CPC was found to be quite high even when the particles are assumed to be non-absorbing. And in order to boost the energy available for cooking, the need of energy storage in the CPC system has been suggested.

Hasan et.al. (2003) simply designed and the low-cost parabolic-type solar cooker (SPC) was made and tested. The energy end energy efficiencies of the cooker were experimentally evaluated. The experimental time period was from 10:00 to 14:00 solar time. During this period, it was found that the daily average temperature of water in the SPC was 333 K and the daily average difference between the temperature of water in the cooking pot and the ambient air temperature was 31.6 K. The energy output of the SPC varied between 20.9 and 78.1 W, whereas its energy output was in the range 2.9–6.6 W. The energy and energy efficiencies of the SPC were in the range, respectively, 2.8–15.7% and 0.4–1.25%.

Lifang Li et.al. (2011) parabolic concentrator mirrors are an important component of many solar energy systems, particularly solar mirror collectors. Precision

parabolic mirrors are expensive to fabricate and to transport. Here, a new concept for designing and fabricating precision parabolic mirrors is presented. Mirror precision is important and conventional methods to fabricate precision parabolic mirrors are complex and costly. The reflectivity of the surface materials is an important factor in the optical efficiency. In solar energy applications, back silvered glass plates, anodized aluminum sheets and aluminized plastic films serve as reflectors. They are widely commercially available. Films are usually adhered to a supporting material such as aluminum. However, the supporting material must be held with a precision parabolic shape by some supporting structures.

C. E. Kennedy at.al. (2005) Concentrating solar power (CSP) technologies use large mirrors to collect sunlight to convert thermal energy to electricity. The viability of CSP systems requires the development of advanced reflector materials that are low in cost and maintain high specular reflectance for extended lifetimes under severe outdoor environments. Durability testing of a variety of candidate solar reflector materials at outdoor test sites and in laboratory accelerated weathering chambers is the main activity within the Advanced Materials task of the CSP Program at the National Renewable Energy Laboratory (NREL) in Golden, Colorado. Test results to date for several candidate solar reflector materials will be presented. These include the optical durability of thin glass, thick glass, aluminized reflectors, front-surface mirrors, and silvered polymer mirrors.

The development, performance, and durability of these materials will be discussed. Based on accelerated exposure testing the glass, silvered polymer, and front-surface mirrors may meet the 10 year lifetime goals, but at this time because of significant process changes none of the commercially available solar reflectors and advanced solar reflectors have demonstrated the 10 year or more aggressive 20 year lifetime goal. CSP technologies are capital intensive and, for the first truly commercial systems, about half of the total capital cost of a power plant will be invested in the solar collectors. This makes reducing the cost of solar collectors critical to achieving energy cost targets compatible with economic viability, depending on the technology.

Dr. Steven F. Jones et.al. (2001) FSEC comments that aluminized Mylar was used in the development of the solar funnel. He reported that aluminized Mylar was a good reflective material but was relatively expensive and rather hard to come by in large sheets.

Mohammed S. Al-Soud et. al. (2010) a parabolic solar cooker with automatic two axes sun tracking system was designed, constructed, operated and tested to overcome the need for frequent tracking and standing in the sun, facing all concentrating solar cookers with manual tracking, and a programmable logic controller was used to control the motion of the solar cooker. The results of the continuous test – performed for three days

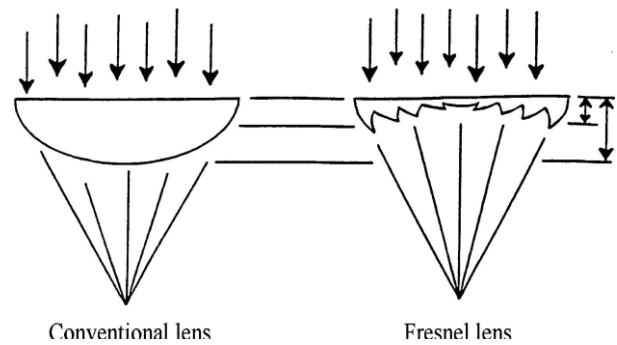
from 8:30 h to 16:30 h in the year 2008 – showed that the water temperature inside the cooker's tube reached 90°C in typical summer days, when the maximum registered ambient temperature was 36 °C. It was also noticed that the water temperature increases when the ambient temperature gets higher or when the solar intensity is abundant. This is in favor of utilizing this cooker in many developing countries, which are characterized by high solar insulations and high temperatures. Besides cooking, the proposed cooker could be utilized for warming food, drinks as well as to pasteurize water or milk.

A.K.Agrawal et.al. (1991) a two axis tracking system is described for the focusing of sunlight in parabolic type reflector used in solar thermal devices like solar cooker. This system consists of worm gear drives and four bar type kinematic linkage and accurate focusing of reflectors at low cost

C.Saravanan et. al. (2011) paper presents the hardware design and implementation of a system that ensures a perpendicular profile of the solar panel with the sun in order to extract maximum energy falling on it. Renewable energy is rapidly gaining importance as an energy resource as fossil fuel prices fluctuate. The unique feature of the proposed system is that instead of taking the earth as its reference, it takes the sun as a guiding source. Its active sensors constantly monitor the sunlight and rotate the panel towards the direction where the intensity of sunlight is maximum. The light dependent resistor's do the job of sensing the change in the position of the sun which is dealt by the respective change in the solar panel's position by switching on and off the geared motor. The control circuit does the job of fetching the input from the sensor and gives command to the motor to run in order to tackle the change in the position of the sun. With the implementation of the proposed system the additional energy generated is around 25% to 30% with very less consumption by the system itself. In this paper, an improvement in the hardware design of the existing solar energy collector system has been implemented in order to provide higher efficiency at lower cost.

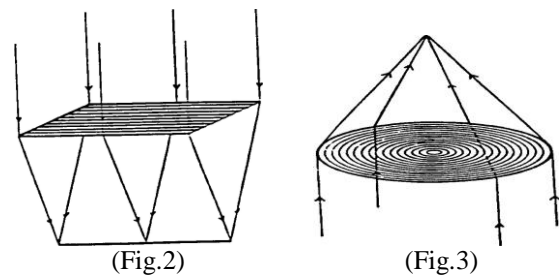
Selection of Fresnel lenses

Solar radiation is concentrated by reflection or refraction through mirrors or lenses. The mirrors can be plane, called heliostats, or parabolic; the lenses can be simple lenses or Fresnel lenses (FL). Concentrators are used to improve the solar energy caption in specific applications. In a lens, the refraction phenomenon is produced in the surface, while the bulk material between the two surfaces doesn't have any influence in the refraction. In 1748 Georges- Louis Leclerc had the idea of reducing lens weight and size acting on the lens surface, but it was a French mathematician and physicist, Augustin-Jean Fresnel, who built, in 1820 the first lighthouse using Leclerc's design. The FL is a flat optical component where the bulk material is eliminated because the surface is made up of many small concentric grooves (Fig. 1).



Each groove is approximated by a flat surface that reflects the curvature at that position of the conventional lens, so each groove behaves like an individual prism. There are two basic FL configurations: linear (Fig. 2) and circular (Fig. 3).

A linear FL has linear parallel grooves and the focus is a line. A circular FL has circular concentric grooves and the focus is a small circle. FL manufacture processes have developed. First designs were cut and polished in glass. In 1950 they started to be made by pressing hot glass in metal molds, and since the eighties they are made of plastics. Modern plastic FL, cheaper and lighter than a conventional lens of the same size, has high optical quality and no spherical aberration.



(Cristina Sierra, Alfonso J. Va' Zquez," High solar energy concentration with a Fresnel Lens," Journal of Materials Science (40), (2005), pp.1339 – 1343).

Cristina Sierra et. al. (2004) the high solar energy density achieved in our simple and cheap Fresnel installation has been used for several surface modifications of metallic materials. This equipment is a very useful tool to apply concentrated solar energy in the field of high and very high temperatures. These temperatures are achieved in a few seconds and usually the materials treatments are completed in minutes. Fresnel lens installation is a serious alternative to the conventional equipment for material treatment and even to the large solar installations. In this work we review the surface modifications produced by concentration of solar energy with a Fresnel lens.

Musa et al. (1992) carried out the design, construction and performance test of a parabolic Fresnel concentrator cooker using locally available materials. The design of the concentrator cooker was based on the Fresnel principle which consists of concentric parabolic

rings – frustums of cones. These components were arranged on a flat structure having the same focus and properties for light perpendicular to their axis or revolution. Glass mirrors were used as the reflective material. The pot was placed on a grill fixed at the focal point of the concentration which is suspended such that it rotates freely about the focal axis. In this way, the pot remains stationary irrespective of tracking angle setting. The concentrator presents a smaller amount of area to the wind compared to a parabolic dish concentrator, thereby promising greater stability and pot accessibility. Tracking the sun with the concentrator is by manual adjustment at 20 minutes time interval for altitudinal change in the sun's position. Series of water boiling and controlled cooking tests carried out with the concentrator under various levels of atmospheric turbidity yielded very encouraging and satisfactory results. Though the Fresnel concentrator performed satisfactorily despite a 34.3% reduction in reflective area compared to a parabolic of the same diameter, the 20 minutes ritual needed for manual adjustment in order to track the sun proved to be a major disadvantage with this device.

Conclusion

The paper was focused on the Solar Energy high temperatures using parabolic solar concentrator, Fresnel lens, Reflecting materials and solar tracking. It identified their level of performance. Earlier studies have shown that use of parabolic solar concentrator gives high concentration requires larger field of view and need a good tracking system. The use of reflective material plays an important role. Parabolic dish type concentrators become bulky and transportability.

To overcome this, there is change in material like anodized aluminum sheets, aluminized plastic films for concentrators. The use of Fresnel lenses will raise more temperature than conventional one and can be used in furnace heating. Solar energy concentrated by Fresnel lenses is a cheap and environmentally friendly energy source suitable for surface materials treatments. The current investigation introduced that with two axes sun tracking to resolve the problem of frequent tracking and standing in the sun, which are the main drawbacks of most concentrating solar cookers with manual tracking. The provision of two way tracking mechanism for a parabolic type solar concentrator permits accurate and effortless focusing of solar radiation on the receiving surface of the utensil placed at the focus of the reflector.

Acknowledgment

The author would like to acknowledge the Professor S. R. Karale for great support to this project.

References

1. F. Muhammad-Sukki et al,"Design of Solar Concentrators," International Journal of Applied Sciences (IJAS), Volume (1): Issue (1).
2. A.R. El Ouederni, A.W. Dahmani, F. Askri, M. Ben Salah and S. Ben Nasrallah," Experimental study of a parabolic solar concentrator," Revue des Energies Renouvelables CICME'08 Sousse (2008) 193 – 199.
3. M. Ouannene, B. Chaouachi, S. Gabsi,"Design and Realisation of a Parabolic Solar Cooker," Int. Symp. On Convective Heat and Mass Transfer in Sustainable Energy, April 26- May 1, 2009, Tunisia.
4. Pelemo D.A., Fasasi M.K., Owolabi S.A. and Shaniyi J.A. (2002b). Effective Utilization of Solar Energy for Cooking. Nig. J. of Eng. Mgt. (NJEM), 3 (1): 13 – 18.
5. Ajiya M. (1995),"Design and Construction of a Parabolic Solar Cooker," "Unpublished B.Eng. Project, Mechanical Engineering Department, University of Maiduguri.
6. Mshelbwala S. A. (1996). Experimental Evaluation of a Parabolic Solar Cooking Device. Unpublished B.Eng. Project, Mechanical Engineering Department, University of Maiduguri.
7. Asere A. A., Habou D. and Sambo A. S. (2003). Performance of a Compound Parabolic Solar Cooker. NJERD, 2 (1) 30 - 37.
8. Hasan,Huseyn,Ozturk,"Experimental determination of energy and exergy efficiency of the solar parabolic-cooker", Solar energy 77(2004) 67-71.
9. Lifang Li, Andres Kecskemethy, A. F. M. Arif, Steven Dubowsky,"Optimized Bands: A New Design Concept for Concentrating Solar Parabolic Mirrors", Journal of Solar Energy Engineering (2011) by ASME.
10. C. E. Kennedy, K. Terwilliger," Optical Durability of Candidate Solar Reflectors,"(2005) by ASME.
11. John Harrison ,"Investigation of Reflective Materials for the Solar Cooker," Florida Solar Energy Center(2001).
12. Mohammed S. Al-Soud, Essam Abdallah, Ali Akayleh, Salah Abdallah, Eyad S. Hrayshat," A parabolic solar cooker with automatic two axes sun tracking system," Applied Energy 87 (2010) ,pp.463–470.
13. A.K.Agrawal,"Two axix tracking system for solar concentrator,"Renewable Energy vol.2,No.2, pp.181-182,1992.
14. C.Saravanan, Dr.M.A.Panneerselvam, I.William Christopher,"A Novel Low Cost Automatic Solar Tracking System," International Journal of Computer Applications (0975 – 8887) Volume 31– No.9, October 2011.
15. Cristina Sierra, Alfonso J. Va' Zquez," High solar energy concentration with a Fresnel Lens," Journal of Materials Science (40), (2005), pp.1339 – 1343.
16. Musa U.,Sambo A.S. and Bala E.J. (1992)."Design construction and performance test of Parabolic Concentrator Cooker," "National Solar Energy Forum,Sokoto.

Effect of wood material and pyrolytic conditions on biocarbon production

Sherif S. Z. Hindi

(Department of Arid Land Agriculture, Faculty of Meteorology, Environment and Arid Land Agriculture, King Abdul-Aziz University, Saudi Arabia)

Abstract

Outer and inner-zone wood of characterized eucalypt (*Eucalyptus camaldulensis*), casuarina (*casuarinas glauca*), tamarisk (*Tamarix aphylla*) and acacia (*Acacia saligna*) were pyrolyzed in a flowing nitrogen atmosphere at conditions of maximum final temperature (MFT) of 450° and 600°C and heating rates (HR) of 10° and 25°C/min. for a residence time (RT) of 90 and 120 min. Yield and the proximate analysis of biocarbon differed significantly according to species and pyrolysis conditions. Tamarisk and eucalypt gave the highest yields. Further, the yield decreased significantly with the increasing of the MFT and HR decreased. Apparent density (AD) of biocarbon was affected inversely only by the pyrolysis conditions, especially HR. The volumetric shrinkage (VS) of biocarbon is dependent on species, wood zone and pyrolysis conditions. The VS, ash (AC) and fixed carbon (AC) of biocarbon were affected directly only by the MFT. The gross heat of combustion (GHC) of biocarbon was affected by wood zone and pyrolysis conditions. For all species, the GHC As well as volatiles of biocarbon obtained at 450°C were lower than those at 600°C.

Keywords: Biocarbon, Apparent density, Gross heat of combustion, Proximate analysis, Shrinkage, Wood, Yield.

1. Introduction

Each year, more than 40 million tonnes of inedible plant material, including wheat stems, corn stover (the stalks and leaves) and wood shavings from logging, are produced-much of which is thrown away [1]. The increasing environment protection requirements for waste timber materials attract interest regarding the use of traditional slow pyrolysis equipment, which is employed to produce charcoal, for their utilization, since the raw material is lump wood [2]. It was concluded that their species studied were the most suitable species for short rotation fuel wood forestry programmes because of their high wood density, biomass yield, low ash and moisture content, and good heat of combustion at the juvenile stage [3]. In both Egypt and Saudi Arabia, each of wood, biocarbon made by earthen pits and their briquettes were used as sources of energy by direct burning especially in desert and villages for domestic purposes. Biocarbon is being used in Egypt in combination with sulfur and cellulosic pulp in synthetic silk production. Further, it is used frequently to manufacture special sizes of electrodes for electric analysis of copper in some factories.

The characteristics of the wood charcoals depend not only on the wood used, but also the carbonization system. In particular, the eucalyptus charcoal produced in continuous furnace has interesting characteristics: the lowest ash content ($\sim 2\%$), the highest fixed carbon content ($\sim 90\%$) and the highest total pore volume ($\sim 1 \text{ cm}^3 \text{ g}^{-1}$) [4].

Increasing reaction temperatures decreased charcoal yield, increased its carbon-to-oxygen ratio, and promoted cellulose carbonization [5]. The char yield in pyrolysis decreased rapidly with an increase in temperature until 400 °C, after which there was a gradual decrease in the yield to ca. 40% at 750 [6]. The char yield decreases and the char structure becomes more deranged with increasing temperature [7].

Empirical models of shrinkage as a function of conversion are presented. The volume shrinkage of birch was found to be 45–70% and the shrinkage in the different directions 5–25, 25–40 and 15–40% for longitudinal, tangential and radial directions, respectively. Longitudinal shrinkage commenced after about 60% mass loss and is not strongly dependent on heating rate or on cellulose chain scission. A maximum shrinkage was found for tangential and radial directions at 400 and 500–700°C, respectively, and above these temperatures the shrinkage decreases [7]. It was found that under high heating rates the char particles underwent plastic deformation (i.e. melted) developing a structure different to that of the virgin biomass [8].

It was concluded that both the temperature and heating rate had a significant effect on both yield of pyro-oil and bio-char resulting from pyrolysis of beech trunkbark. The yield of bio-char decreases from 59 to 42% for 2 K/s run and it decreases from 43 to 29% for 100 K/s run as the final temperature was raised from 550 to 800 K [9]. When the pyrolysis temperature is increased, the bio-char yield decreases. The bio-char yield increased with increasing particle size of the sample. A high temperature and smaller particles increase the heating rate resulting in a decreased bio-char yield. The higher lignin content in olive husk results in a higher bio-char yield comparison with corncob. Bio-char from olive husk was more reactive in gasification than bio-char from corncob because of the higher ash content [10].

The higher heating values of oven dry poplar were from 15,787 to 24,275 kJ/kg. The average calorific values of willow wood (whole tree with bark) were from 16,169 to 22,572 kJ/kg [11]. It was showed that there was no significant difference in calorific values between the three eucalypt species studied when considering a similar age category. Similarly, there was no significant difference in calorific values between disc positions and wood types (heartwood versus sapwood) within species. However, calorific values tend to increase along the tree stem towards the tree top for each of the three species [12].

It was showed that high temperature carbonized coconut shell char and activated carbon samples derived from high temperature carbonized coconut shell chars had higher BET surface area, total volume, micropore volume and yield as compared to those of low temperature carbonized coconut shell char and activated carbon derived from low temperature carbonized coconut shell char [13]. The pyrolysis temperature has an important impact on the yield and composition of bio-oil, char, and gases [14].

It was found high negative correlations of the wood heat value with holocellulose and ash, and high positive correlations with wood density, lignin, and alcohol-benzene and hot-water solubles. The exotic species studied gave equal or better charcoal, in terms of yield and quality, compared with the traditionally preferred talh [15].

Very good charcoal yields (35% for karkadeh and 38% for usher) with high energy transformation (58% and 62%, respectively) was obtained. The karkadeh charcoal, except for a somewhat high ash content, was good for domestic uses (79% fixed carbon and 30.3 MJ kg⁻¹ heat value). The usher charcoal was better with respect to fixed carbon (86.5%) and gross heat value (32.4 MJ kg⁻¹). Both charcoals were of low density (140–160 kg m⁻³) [16]. The effects of final carbonisation temperature on the yield, heating value and proximate analysis of charcoal from the tree species were determined. *Gliricidia sepium* gave the highest charcoal yield of 51.6% with a gross heating value of 31.45 MJ/kg at 300°C final carbonisation temperature. There was no significant difference in the charcoal yield of *Gmelina arborea* and *Leucaena leucocephala* at 5% level of testing. The charcoal yield decreased with an increase in carbonisation temperature. The percentage volatiles in charcoal decreased with an increase in temperature, while there was an increase in the percentage fixed carbon [17].

Virtually, nothing has been carried out in Saudi Arabia and Egypt relevant to pyrolyze woods from eucalypt, casuarina, tamarisk and acacia at the selected pyrolysis conditions. Therefore, this study was conducted to evaluate the physico-chemical characterization of biocarbon and the parent wood from each of the four species.

2. Materials and Methods

Four hardwood species were used in the present investigation for biocarbon production, namely eucalypt (*Eucalyptus camaldulensis* Dehn.), Casuarina (*Casuarina glauca* Sieb.), tamarisk (*Tamarix aphylla* (L.) Karst.) and acacia (*Acacia saligna* (Labill.) H. Wendl.). These species are promising fast-growing timber trees for new reclaimed lands, deserts and sand dune fixation. Due to the different physical, chemical and anatomical characteristics of wood between and within species, study of outer-and inner-zone wood was additionally considered in the study. Four trees were selected from each species from different locations near Alexandria, Egypt. The age of the selected trees was about 30 years except for acacia whereby its age was 5 years. The diameters outside bark of the trees varied from 15-40 cm.

2.1. Samples preparation

After the selected trees were felled, one bolt, 0.5 m long each was cut from each stem at a height of 0.5 m above ground level. One diametric strip of 1.5 cm tangentially and 0.5 m longitudinally was removed from each bolt. Selected sticks from each of outer- and inner-zone woods were isolated and subsequently cross cut into cubic samples free of visible defects. Each twenty subsequent samples were specified for each pyrolysis run to determine the different properties of biocarbon as well as the volume of the wood samples assigned for volumetric shrinkage of biocarbon.

2.2. Pyrolysis process

The pyrolysis runs were carried out with a bench scale reactor (Fig. 1) which consists of an electric tube furnace (carbolite furnace modle MTF 12/338) controlled by a microprocessor temperature programmer with an error of ±5°C with an accuracy of 1°C and heating rate of 0.01°C/min., digital thermometer with a chromel alumel thermocouple (type K with an error of ±1°C), nitrogen regulator system consisted of a regulator and a flowmeter with an accuracy of ±2% of the full scale and the reactor body made up of Pyrex glass that consists of the samples tube (with outer diameter of 2.8 cm) and the train of traps. This train is consisted of two connected traps: The first one is immersed in covered Dewar flask filled with liquid nitrogen and the second one is simply a water scrubber, held at room temperature.

Before starting a pyrolysis run, nitrogen flow was introduced at 354 ml/minute until a steady gas flow was obtained, increased to 825 ml/minutes for 10 minutes and re-adjusted at 354 ml/minute for the duration of the pyrolysis run. The cover of the Dewar flask was raised only while the liquid nitrogen was being poured. Then, after ten minutes of pouring, the liquid nitrogen trap was connected to the water scrubber trap. However, this period is long enough for the nitrogen gas inside the reaction body to approach, relatively, its original state after addition of N₂-liquid to prevent a back suction that force water to move inversely from the water scrubber toward the pipe attached to N₂-liquid trap where the water freezes and plug it. This can prevent the nitrogen gas to pass through it increasing the pressure inside it and explores the glassy reactor. At the beginning of the run, the furnace was switched on and the temperature program was set on the desired maximum final temperature (MFT) of 450°C with a heating rate (HR) of 2.5°C/min., starting from a room temperature. After the MFT was reached, the heating system was shut off and the samples were allowed to cool to 100°C with maintenance of nitrogen flow at 354 ml/minute.

2.3. Determination of wood and biocarbon properties

Wood properties, namely extractives (EC), lignin (LC) and ash (AC) contents were determined according to the ASTM standard methods [19], [20] and [21], respectively. The volumes of wood samples assigned for specific gravity (SG) and volumetric shrinkage (VS) of biocarbon were determined using mercury displacement using Amsler volume meter. The SG of biocarbon was determined based on the oven-dry weight and volume, whereas the VS was based on the oven dry volume of the parent wood. Gross heat of combustion of biocarbon was determined using an adiabatic oxygen bomb calorimeter, Parr 1341, according to the procedures recommended by Parr instruction manual and in accordance with ASTM [22].

The biocarbon yield was calculated based on the oven-dry weight of wood. The moisture, volatile matter, ash, and fixed carbon contents were determined according to the ASTM [23] for proximate analysis of wood charcoal.

Split-split plot design in three replicates was applied and the statistical analysis of the recorded data was done according to Steel and Torrie [24] using the analysis of variance procedure and least significant difference test (LSD) at $P \leq 0.05$.

3. Results and Discussion

Mean values of extractives content (EC), lignin content (LC) and ash content (AC) of wood were presented at Table 1. It can be seen that the three properties was affected significantly by species. The eucalypt wood had the highest EC and LC while acacia was the lowest. Further, tamarisk wood contained the highest ash among the four species while eucalypt wood had the lowest one.

Biocarbon properties, namely yield, volumetric shrinkage, ash, volatiles and fixed carbon contents of biocarbon made under the controlled pyrolysis conditions of maximum final temperature (MFT) of 450° and 600°C, heating rate (HR) of 10° and 25 °C/min. and residence time (RT) of 90 and 120 min.

Yield of biocarbon differed significantly according to species and pyrolysis conditions. The yields from tamarisk and eucalypt (33.45% and 32.86%, respectively) were higher than those from casuarina and acacia (27.62% and 27.58%, respectively) as shown in Fig. 2. Further, the yield decreased significantly with the increasing of the MFT and HR decreased without any effect due to RT (Fig. 3). There is no clear effect due to wood zone on biocarbon yield. The differences between species in their productivity of biocarbon may be attributed to their differences in extractives, lignin and ash contents of the parent wood. Eucalypt and tamarisk woods with the greatest extractives content (Table 1.) produced more biocarbon comparing with casuarinas and acacia with the lowest extractives content (Fig. 2). This is supported by the finding of Kryla [25] who stated that removing extractives from wood caused greater mass loss and therefore lower yield at carbonization temperatures of 350°C and higher. He attributed this behavior to the fact that extractive remaining in the unextracted samples are degrading at a slower rate than the corresponding wood substance. Furthermore, lignin content of wood is the most important factor influencing the productivity of biocarbon. It has been stated that species with higher contents of lignin give higher yields than those with lower contents of lignin [25] and [26]. This is can be attributed to that lignin generally leaves a larger residue, due to its thermal stability, than do the polysaccharide at the end of carbonization process [10]. Accordingly, eucalypt and tamarisk with the greatest lignin content of wood produce more biocarbon than casuarinas and acacia with the lowest lignin content (Table 1. and Fig. 2.). In addition, ash content of wood may affect the biocarbon yield. This is obvious in the case of tamarisk which contained the highest ash content of wood (5.4 %) and reasonably the highest biocarbon yield (Fig. 1.). However, other researchers did not find a species effect on biocarbon yield [10].

The slight differences in the apparent density (AD) of biocarbon made from the four hardwood species are presented at Fig. 4 with the highest value for casuarinas and the lowest one for acacia. Actually, the AD of biocarbon was affected only by the pyrolysis conditions, especially HR. The AD decreased as HR increased from 10° to 25°C/min. (Fig. 5), whereas neither the MFT nor RT had a significant effect on it. This is adapted to that concluded for the much greater effect of heating rate on the pyrolysis of biomass and the quick devolatilization of the biomass rapid pyrolysis that favors the formation of char with high porosity [10] and accordingly lower apparent density. In addition, the AD of biocarbon was directly related to the specific gravity of the parent wood.

The volumetric shrinkage (VS) of biocarbon is dependent on species, wood zone and pyrolysis conditions. The VS of biocarbon made from inner-zone wood of eucalypt was much lower than that from outer-zone (Table. 2). This effect was not evident in the case of the other species. For the pyrolysis conditions, the VS of biocarbon was affected only by the MFT, whereby it increased as the MFT increased (Fig. 3). Examining Fig. 3 revealed that most of the VS took place up to 450°C, thereafter, the increase in shrinkage was small due to most of thermal degradation of the polysaccharides takes place below 450°C [25], [26] and [10].

Gross heat of combustion (GHC) of biocarbon was affected by wood zone and pyrolysis conditions. The GHC of tamarix biocarbon made from outer-zone wood was greater than that from innerzone wood (Table 2). However, this behavior is not evident for the other species. Generally, at all pyrolysis conditions, the GHC of biocarbon for tamarisk biocarbon was lower than those for the other species (Fig. 6). For all species, the GHC of biocarbon obtained at 450°C were lower than that at 600°C. There were no evident effects on the GHC of biocarbon due to HR and RT (Fig. 7). The differences in the GHC of biocarbon between species at different pyrolysis conditions may be related to their fixed carbon (FC) and ash (AC) contents [27], [28] and [29]. Accordingly, the highest GHC values of eucalypt, casuarinas and acacia biocarbons can be attributed to their higher FC and lower AC values (Fig. 3). On the other hand, tamarisk biocarbon with the lowest FC and highest AC contents gave the lowest GHC value.

The ash content (AC) of biocarbon varied according to species and pyrolysis conditions. Tamarisk biocarbon had generally much higher content of ash than the other species (Fig. 2). However, this content was increased only with

increasing of MFT (Fig. 3). The volatiles of biocarbon made from different species was affected by pyrolysis conditions. At the same conditions of MFT of 450°C, HR of 10° or 25°C/min. and RT of 90 or 120 min., the volatiles of biocarbon was generally higher than that at 600°C, HR of 10 or 25°C/min. and RT of 90 or 120 min. (Fig. 3). Up to 450°C, the volatiles of acacia and casuarina biocarbon were lower than those for eucalypt and tamarisk. However, up to 600°C, tamarisk biocarbon contained higher volatiles than the other species. In addition, Fixed carbon (FC) of biocarbon was affected by species and pyrolysis conditions as single variables. At pyrolysis conditions of MFT of 450°C, HR of 10° or 25°C/min. and RT of 90 or 120 minutes, the FC of biocarbon was generally lower than that at 600°C, HR of 10° or 25°C/min. and RT of 90 or 120 min. Up to 450°C, the FC of acacia and casuarina biocarbon were lower than those for eucalypt and tamarisk. However, up to 450° or 600°C, the FC content of tamarisk biocarbon was lower than the other species (Fig. 3).

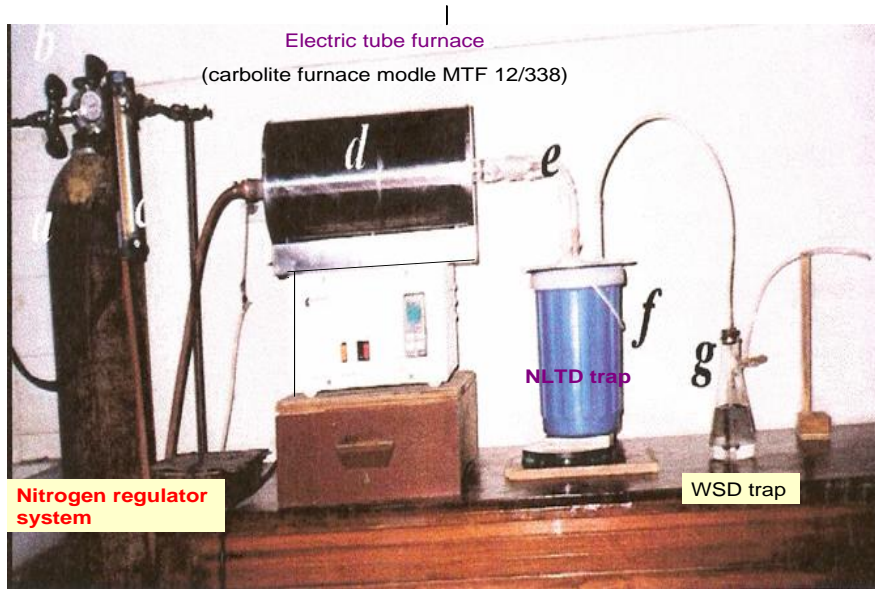


Fig. 1. Pyrolytic apparatus used for the wood pyrolysis.

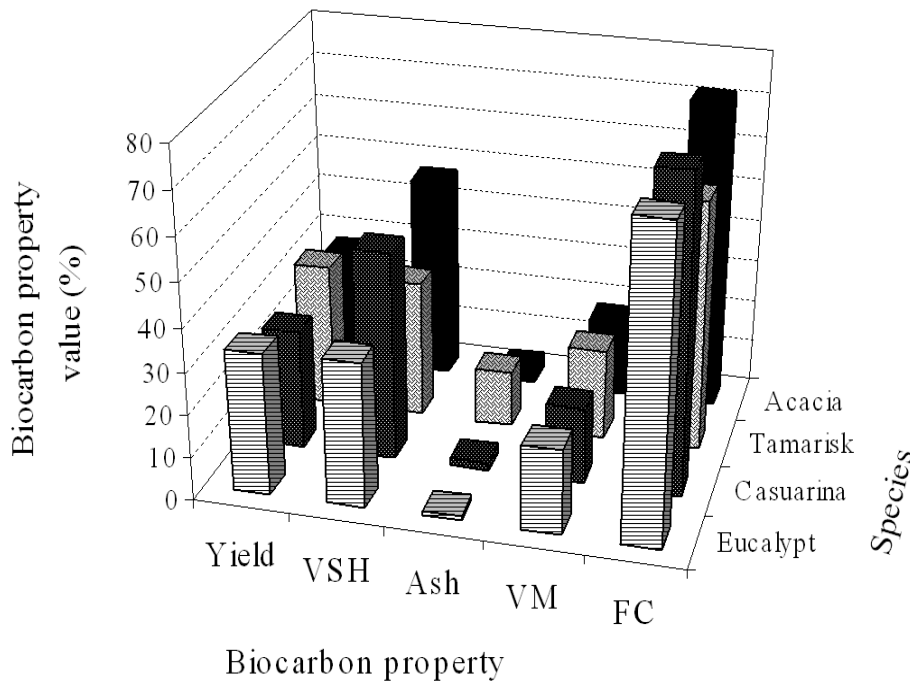


Fig. 2. Yield, shrinkage, ash, volatiles and fixed carbon contents of biocarbon made from the four wood species.

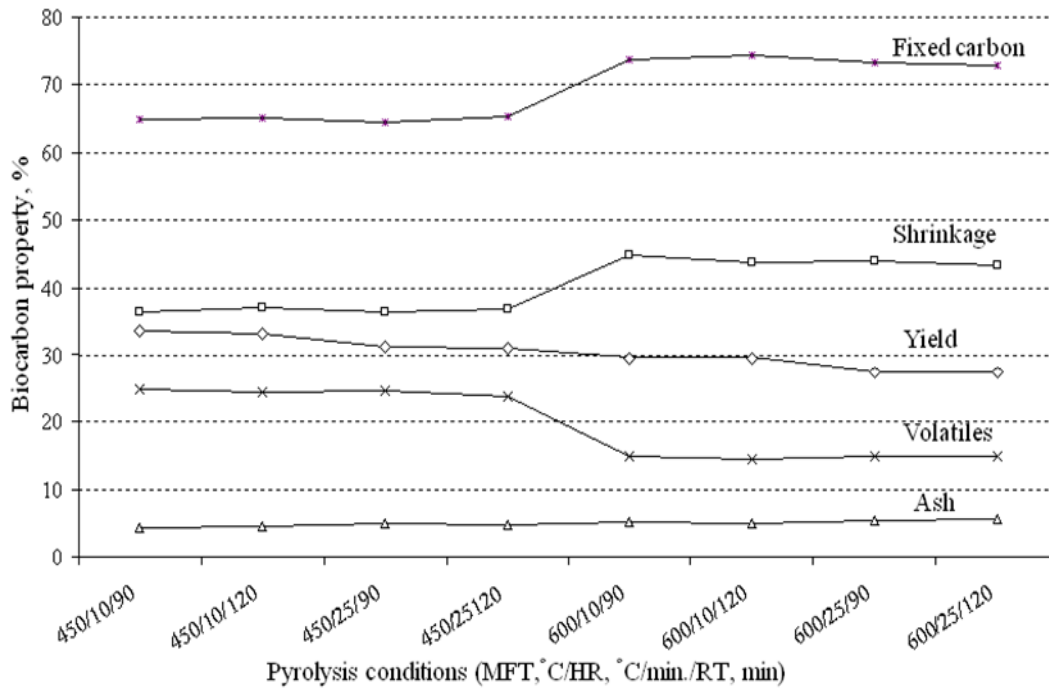


Fig 3. Yield, shrinkage, ash, volatiles and fixed carbon contents of biocarbon made under controlled pyrolytic conditions of maximum final temperature (MFT) of 450° and 600°C, heating rate (HR) of 10° and 25 °C/min. and residence time (RT) of 90 and 120 min.

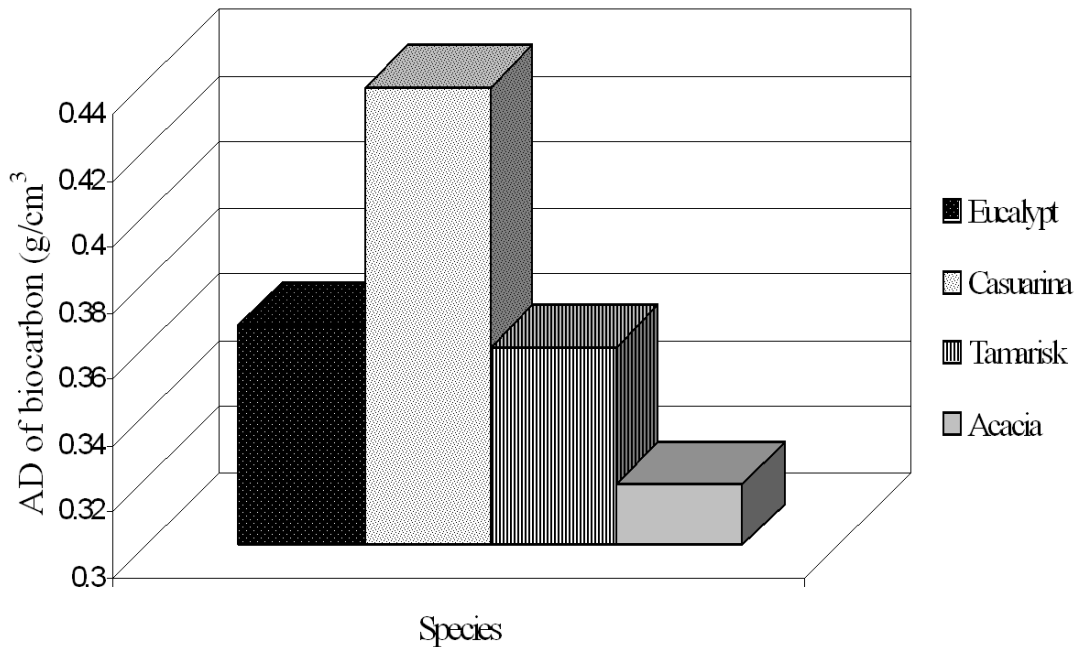


Fig. 4. Apparent density (AD) of biocarbon made from the four wood species.

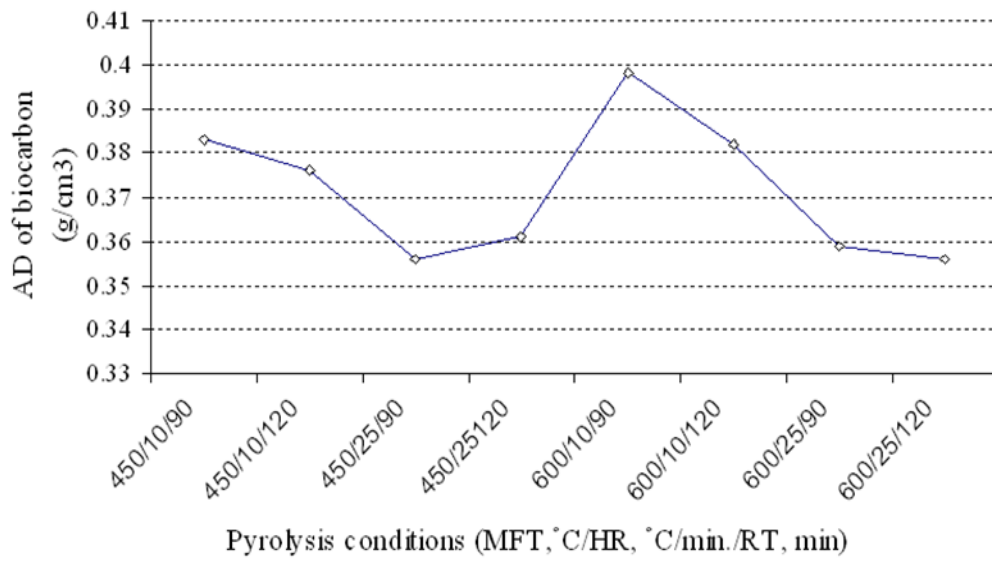


Fig. 5 Apparent density (AD) of biocarbon made under controlled pyrolytic conditions of maximum final temperature (MFT) of 450° and 600°C, heating rate (HR) of 10° and 25 °C/min. and residence time (RT) of 90 and 120 min.

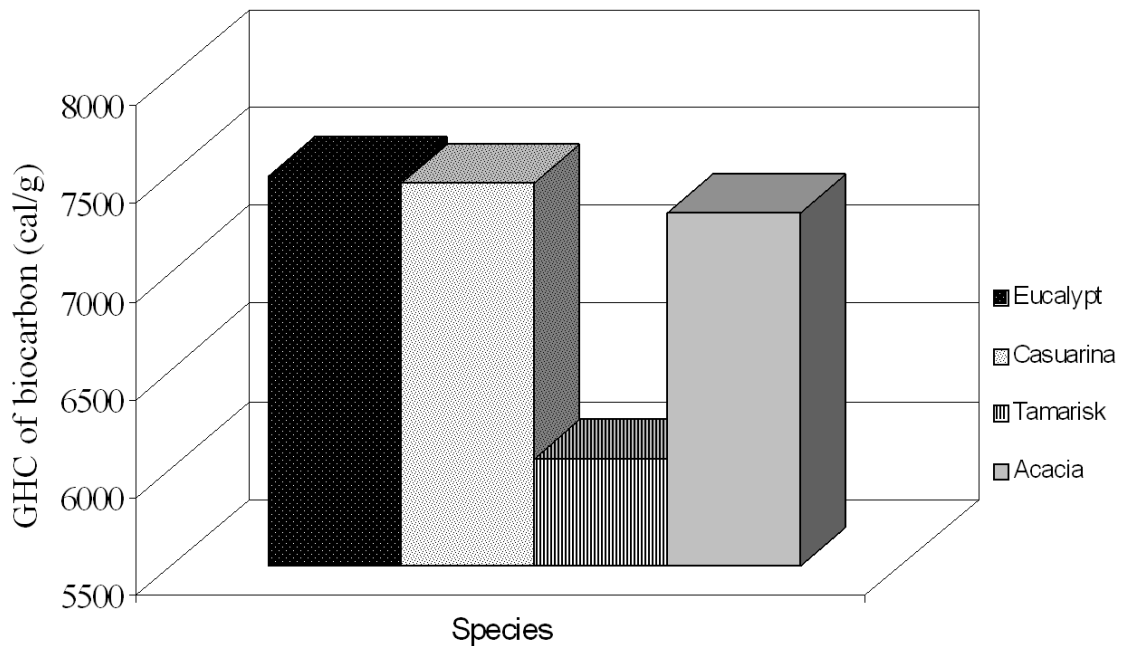


Fig.6. Gross heat of combustion (GHC) of biocarbon made from the four wood species.

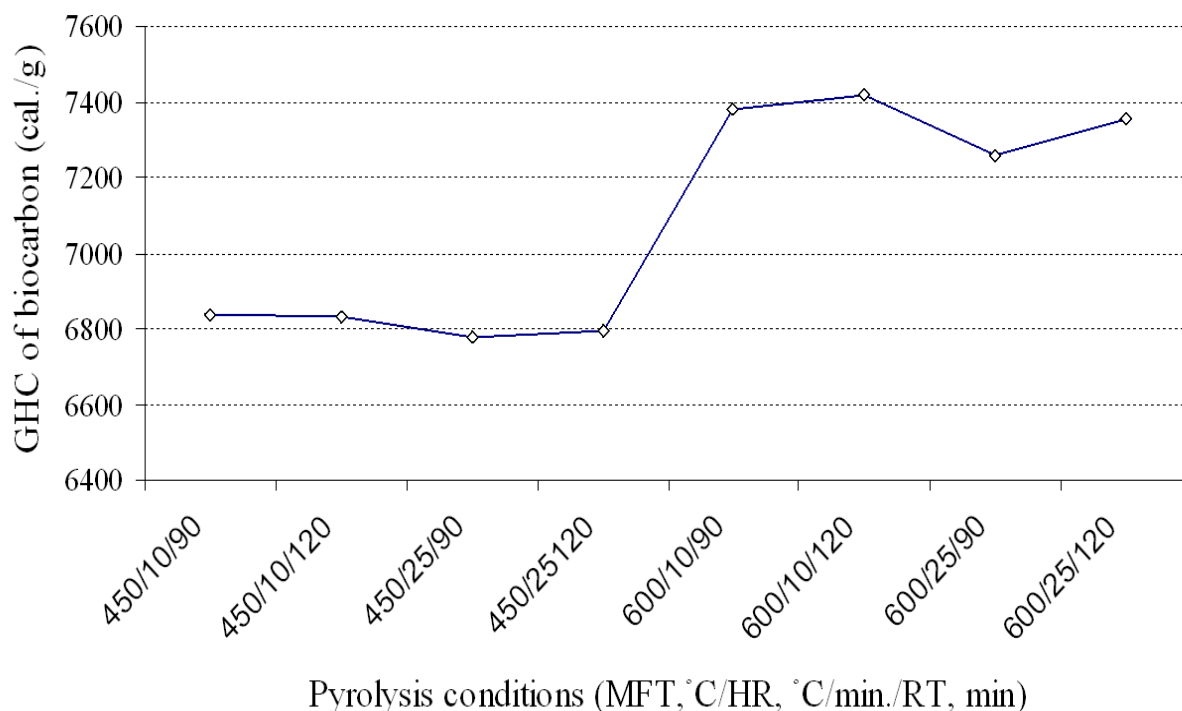


Fig. 7. Gross heat of combustion (GHC) of biocarbon made under controlled pyrolytic conditions of maximum final temperature (MFT) of 450° and 600°C, heating rate (HR) of 10° and 25 °C/min. and residence time (RT) of 90 and 120 min.

Table 1. Mean values* of extractives content (EC), lignin content (LC) and ash content (AC) of wood.

Species	EC (%)	LC (%)	AC (%)
<i>Eucalyptus camaldulensis</i>	19.62 ^a	31.65 ^a	0.169 ^c
<i>Casuarina glauca</i>	5.38 ^c	28.37 ^b	0.922 ^{bc}
<i>Tamarix aphylla</i>	15.77 ^b	27.92 ^b	5.429 ^a
<i>Acacia saligna</i>	2.78 ^d	19.88 ^c	1.308 ^b

*Means with the same letter are not significant.

Table 2. Mean values* for volumetric shrinkage (VS) and gross heat of Combustion (GHC) of biocarbon made of the four wood species from each of the outer-and inner- zone woods.

Species	VS (%)	GHC (cal/g)
<i>Eucalyptus camaldulensis</i>		
a-outer-zone wood	40.74	7517
b-inner-zone wood	26.52	7488
<i>Casuarina glauca</i>		
a-outer-zone wood	51.56	4749
b-inner-zone wood	45.90	7472
<i>Tamarix aphylla</i>		
a-outer-zone wood	29.94	6250
b-inner-zone wood	33.97	5852

<i>Acacia saligna</i>		
a-outer-zone wood	46.75	7372
b-inner-zone wood	47.43	7252
LSD ¹ _{0.05}	7.56	89
LSD ² _{0.05}	11.26	97

*Each value is an average of 32 specimens.

¹LSD_{0.05} = Least significant difference at 95% level of confidence, to test the difference between two wood-zone means at the same level of species.

²LSD_{0.05} = to test the difference between two species means at the same or different levels of wood zone.

4. Conclusion

Biocarbon produced from tamarisk, irrespective of the yield, was generally lower in its quality than other species at the same pyrolysis conditions. This is due to its higher contents of ash and volatiles as well as its lower GHC and FC. *Acacia* biocarbon is generally of better quality compared to that of tamarisk but is lower in some quality parameters due to its lower AD and relatively higher ash content than the biocarbons made from casuarinas and eucalypt. Accordingly, *Acacia saligna* biocarbon is of better industrial quality subsequent by *Casuarina glauca*. They are suitable as reductants in metallurgy as well as for production of CS₂ required for silk synthesis, internal and external fuels and sorbents.

5. References

1. K. Sanderson. Lignocellulose: A chewy problem. *Nature*, 474(24), 2011, 512–514.
2. A. Zhurinsk, J. Zandersons and G. Dobeles. Slow pyrolysis studies for utilization of impregnated waste timber materials. *Journal of Analytical and Applied Pyrolysis*, 74(1-2), 2005, 439-444.
3. V. L. Goel and H. M. Behl. Fuelwood quality of promising tree species for alkaline soil sites in relation to tree age. *Biomass and Bioenergy*, 10(1), 1996, 57-61.
4. J. Pastor-Villegas, J. F. Pastor-Valle, J. M. M. Rodríguez and M. G. García. Study of commercial wood charcoals for the preparation of carbon adsorbents. *Journal of Analytical and Applied Pyrolysis*, 76(1-2), 2006, 103-108.
5. I. Seichi, S. Uno. and T. Minowa. Carbonization of Cellulose Using the Hydrothermal Method. *Journal of Chemical Engineering of Japan*, 41(3), 2008, 210-215.
6. R. K. Sharma, J. B. Wooten, V. L. Baliga, X. Lin, W. G. Chan and M. R. Hajaligol. Characterization of chars from pyrolysis of lignin. *Fuel*, 83(11-12), 2004, 1469-1482.
7. K. O. Davidsson and J. B. C. Pettersson. 2002. Birch wood particle shrinkage during rapid pyrolysis. *Fuel*, 81(3), 2002, 263-270.
8. E. Cetin, B. Moghtaderi, R. Gupta and T. F. Wall. Influence of pyrolysis conditions on the structure and gasification reactivity of biomass chars. *Fuel*, 83(16), 2004, 2139-2150.
9. A. Demirbas. Determination of calorific values of bio-chars and pyro-oils from pyrolysis of beech trunk-barks. *Journal of Analytical and Applied Pyrolysis*, 72(2), 2004^a, 215-219.
10. A. Demirbas. Effects of temperature and particle size on bio-char yield from pyrolysis of agricultural residues. *J. of Analytical and Applied Pyrolysis*. 72(2), 2004^b, 243-248.
11. B. Klasnja, S. Kopitovic and S. Orlovic. Wood and bark of some poplar and willow clones as fuelwood. *Biomass and Bioenergy*, 23(6), 2002, 427-432.
12. M. Lemenih and T. Bekele. Effect of age on calorific value and some mechanical properties of three Eucalyptus species grown in Ethiopia. *Biomass and Bioenergy*, 27(3), 2004, 223-232.
13. W. Li, J. Yang, J. Peng, L. Zhan, S. Guo. and H. Xia. 2008. Effects of carbonization temperatures on characteristics of porosity in coconut shell chars and activated carbons derived from carbonized coconut shell chars. *Industrial Crops and Products*, 28(2), 2008, 190-198.
14. M. Garcia-Perez, W. Xiao Shan, J. Shen, M. J. Rhodes, F. Tian, L. Woo-Jin, W. Hongwei, and L. Chun-Zhu. Fast Pyrolysis of Oil Mallee Woody Biomass: Effect of Temperature on the Yield and Quality of Pyrolysis Products. *Ind. Eng. Chem. Res.*, 47(6), 2008, 1846–1854.
15. P. Khristova and A. W. Khalifa. Carbonization of some fast-growing species in Sudan. *Applied Energy*, 45(4), 1993, 347-354.
16. P. Khristova. and L. Vergnet. Evaluation of usher wood and karkadeh stem for charcoal in Sudan. *Biomass and Bioenergy* 4(6), 1993, 455-459.
17. J. A. Fuwape. A. Effects of carbonisation temperature on charcoal from some tropical trees. *Bioresource Technology*, 57(1), 1996, 91-94.

18. S. Z. Hindi. 2011. Evaluation of Guaiacol and syringol emission upon wood pyrolysis for some fast growing species. *Proc. of ICEBESE conf. on Environmental, Biological, and Ecological Sciences, and Engineering, Paris, France*, 583-587.
19. ASTM. D 1105-84. 1989. Standard method for preparation of extractive-free wood. Philadelphia, Pa. U.S.A.
20. ASTM. D 1106-84. 1989. Standard test method for acid-insoluble lignin in wood. Philadelphia, Pa. U.S.A.
21. ASTM, D 1102-84. 1989. Standard test method for ash in wood. Philadelphia, Pa. U.S.A.
22. ASTM. D 2015-85.1987. Standard test method for gross calorific value of coal and coke by the adiabatic bomb calorimeter. Philadelphia, Pa. U.S.A.
23. ASTM, D 1762-84. 1989. Standard method for chemical analysis of wood charcoal. Philadelphia, Pa. U.S.A.
24. R. G. D. Steel and T. H. Torrie. *Principles and procedures of statistics* (N. Y., U. S. A. 1980).
25. J. M. Kryla. Characteristics of carbonized wood affected by extraction. *Wood Science*. 13 (1), 1981, 18-25.
26. D. H. Slocum, E. A. McGinnes and F. C. Beall. Charcoal yield, shrinkage and density change during carbonization of oak and hickory woods. *Wood Sci*. 11 (1), 1978, 42-47.
27. G. L. Stimely. and P. R. Blankenhorn. Effects of species, specimen size and heating rate on char yield and fuel properties. *Wood and Fiber Sci*. 17 (4), 1985, 477-489.
28. S. S. Z. Hindi. *Pyrolytic products properties as affected by raw material*. doctoral diss., Faculty of Agriculture, Alexandria University, Egypt, 2001.
29. V. Sayakoummane and Ussawarужи, A. Comparison of the Physical and Chemical Properties of Briquette and Wood Charcoal in Khammouane Province, Lao PDR. *Environment and Natural Resources Journal*, 7 (1), 2009, 12-24.

Gated Driver Tree Based Low Power Delay Buffer Architecture

¹Manjusha. P, ²Gopinath. B

¹PG Scholar, ²Associate Professor

^{1,2} SNS College of Technology, Coimbatore-35.

Abstract: This paper presents circuit design of a low-power delay buffer. The proposed delay buffer uses several new techniques to reduce its power consumption. Since delay buffers are accessed sequentially, it adopts a ring-counter addressing scheme. In the ring counter, double-edge-triggered (DET) flip-flops are utilized to reduce the operating frequency by half and the C-element gated-clock strategy is proposed. A novel gated-clock-driver tree is then applied to further reduce the activity along the clock distribution network. Moreover, the gated-driver-tree idea is also employed in the input and output ports of the memory block to decrease their loading, thus saving even more power. Both simulation results and experimental results show great improvement in power consumption

Index Terms: C-element, delay buffer, first-in-first-out, gated-clock, ring counter.

I. INTRODUCTION

Portable multimedia and communication devices have experienced explosive growth recently. Longer battery life is one of the crucial factors in the wide spread success of these products. As such, low-power circuit design for multimedia and wireless communication applications has become very important. In many such products, delay buffers (line buffers, delay lines) make up a significant portion of their circuits. Such serial access memory is needed in temporary storage of signals that are being processed, e.g., delay of one line of video signals, delay of signals within a fast Fourier transform (FFT) architectures and delay of signals in a delay correlator. Currently, most circuits adopt static random access memory (SRAM) plus some control/addressing logic to implement delay buffers. For smaller-length delay buffers, shift register can be used instead. The former approach is convenient since SRAM compilers are readily available and they are optimized to generate memory modules with low power consumption and high operation speed with a compact cell size. The latter approach is also convenient since shift register can be easily synthesized, though it may consume much power due to unnecessary data movement. Previously, a simplified and thus lower-power sequential addressing scheme for SRAM application in delay buffers is proposed. A ring counter is used to point to the target words. Since the ring counter is made up of an array of D-type flip-flops (DFFs) triggered by a global clock signal. In this paper, we propose to use double-edge-triggered (DET) flip-flops instead of traditional DFFs in

the ring counter to halve the operating clock frequency. A novel approach using the C-elements instead of the R-S flip-flops in the control logic for generating the clock-gating signals is adopted to avoid increasing the loading of the global clock signal. In addition to gating the clock signal going to the DET flip-flops in the ring counter, we also proposed to gate the drivers in the clock tree. The technique will greatly decrease the loading on distribution network of the clock signal for the ring counter and thus the overall power consumption. The same technique is applied to the input driver and output driver of the memory part in the delay buffer. In a delay buffer based on the SRAM cell array such as the one in, the read/write circuitry is through the bit lines that work as data buses. In the proposed new delay buffer, we use a tree hierarchy for the read/write circuitry of the memory module. For the write circuitry, in each level of the driver tree, only one driver along the path leading to the addressed memory word is activated. Similarly, a tree of multiplexers and gated drivers comprise the read circuitry for the proposed delay buffer. Simulation results show the effectiveness of the above techniques in power reduction.

II. CONVENTIONAL DELAY BUFFERS

The simplest way to implement a delay buffer is to use shift registers as shown in Fig. 1. If the buffer length is n and the word-length is m , then a total of $n \times m$ DFFs are required, and it can be quite large if a standard cell for DFF is used. In addition, this approach can consume huge amount of power since on the average binary signals make transitions in every clock cycle. As a result, this implementation is usually used in short delay buffers, where area and power are of less concern.

SRAM-based delay buffers are more popular in long delay buffers because of the compact SRAM cell size and small total area. Also, the power consumption is much less than shift registers because only two words are accessed in each clock cycle: one for write-in and the other for read-out. A binary counter can be used for address generation since the memory words are accessed sequentially. The SRAM-based delay buffers do away with many data transitions, there still can be considerable power consumption. In the SRAM address decoder and the read/write circuits. In fact, since the memory words are accessed sequentially, we can use a ring counter with only one rotating active cell to point to the words for write-in and read-out. This method, known as the pointer-based scheme. This type flip-flops is initialized with only one "1" (the active cell) and all the other DFFs are kept at "0." When a clock edge triggers the DFFs, this "1" signal is propagated forward. Consequently, the traditional binary

distribution network for the global clock and activate only those drivers.

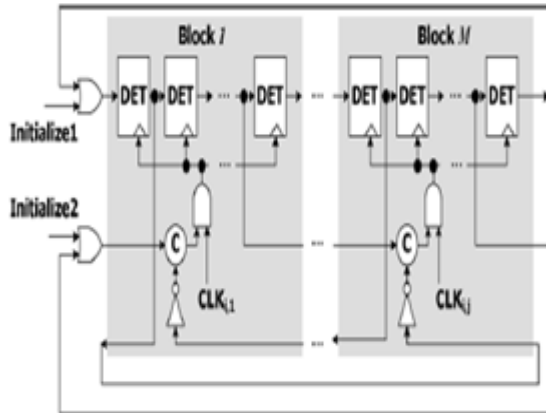


Fig.5 ring counter with clock gated by C-elements,

B. Advantages

1. For low power operations Special read/write circuitry, such as a sense amplifier, is needed.
2. The logarithmical decrease in loading can dramatically reduce the power consumption
3. .the memory module of a delay buffer is often in the form of an SRAM array with input/output data bus inorder to reduce area

IV. ANALYSIS AND DESIGN OF GATED DRIVER TREE USING D FLIP FLOP

A. Simulation methodology

The MICROWIND program allows the student to design and simulate an integrated circuit. The package itself contains a library of common logic and analog ICs to view and simulate. MICROWIND includes all the commands for a mask editor as well as new original tools never gathered before in a single module. Circuit Simulation can be achieved by pressing one single key. The electric extraction of circuit is automatically performed and the analog simulator produces voltage and current curves immediately.

DSCH is digital schematic editor and simulator. The DSCH software, which is a user-friendly schematic editor and a logic simulator presented in a companion manual, is used to generate Verilog description. The cell is created in compliance with the environment, design rules and fabrication specifications. The Logic Cell Compiler is a particularly sophisticated tool enabling the automatic design of a CMOS circuit corresponding to logic description in VERILOG. A set of CMOS processes ranging from 1.2µm down to state-of-the-art 0.25µm are proposed.

B.Simulation result

The simulation results are given below.

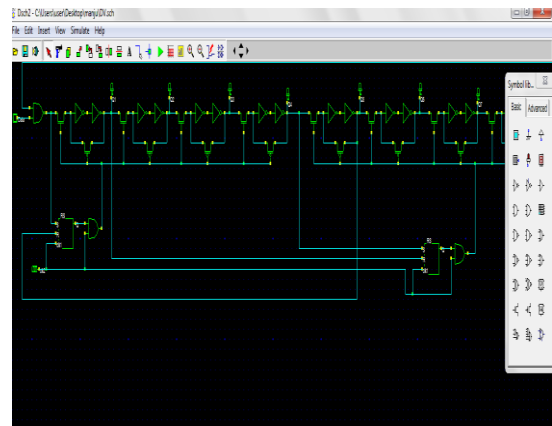


Fig.6. gated driver tree using D flip flop.

It shows the schematic is drawn in DSCH. Then the verilog module of this is generated The verilog file is compiled in microwind to generate the layout of the gated driver tree this is shown in the figure 8.

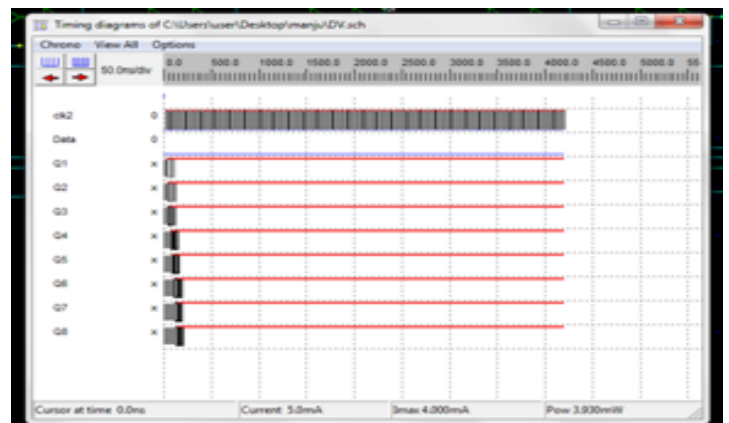


Fig.7.Timing analysis of gated driver tree, data is shifted using D flip flop.

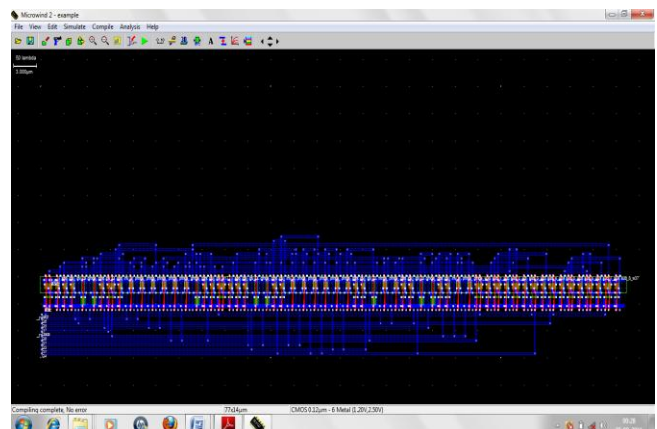


Fig.8.Layout of gated driver tree using d flip flop

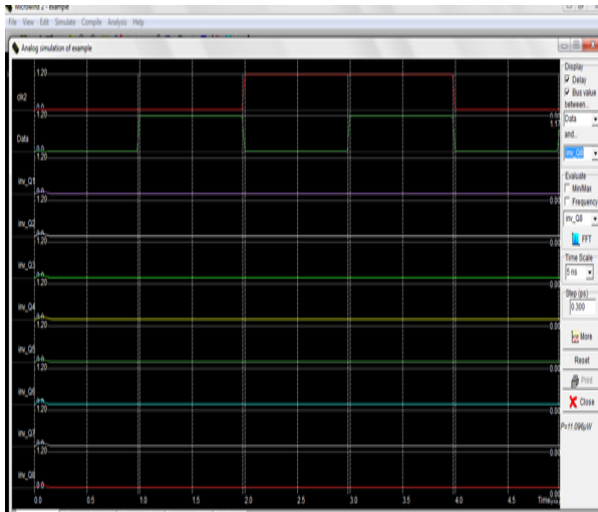


Fig.9. simulation result of gated driver tree using D Flip flop

After simulating this layout simulation result is appeared in a new window. This is the voltage Vs time graph. This will shows the input and output responses. This also shows the amount of power consumption.

The power consumed by this gated driver tree can be measured by simulating this layout.the simulation result is shown in figure 9 shows the consumed power is 11.09mw.

V. ANALYSIS OF GATED DRIVER TREE USING D FLIP FLOP AND DET FLIP FLOP.

TABLE I
POWER CONSUMPTION OF THREE RING COUNTERS

Ring Counter Structure (N=1024, M=128, D=8)	Simulated Power @ 1.8V, 50 MHz, 0.18µm	Estimated Loading Ratio by Eqs. (3)-(5)
Traditional Ring Counter	2127 µW	2048
Gated Clock Ringer Counter [6]	433 µW	400
The Proposed Ring Counter	20 µW	21

The loading of the clock signal in the proposed scheme can be analyzed as follows. Assume that a quad tree is used for clock drivers, then for a length-N ring counter constituted by a total of flip-flops N partitioned in M blocks.

VI. CONCLUSION

In this paper, we presented a low-power delay buffer architecture which adopts several novel techniques to reduce power consumption. The ring counter with clock gated by the C-elements can effectively eliminate the excessive data transition without increasing loading on the global clock signal.

The gated-driver tree technique used for the clock distribution networks can eliminate the power wasted on drivers that need not be activated. Another gated-demultiplexer tree and a gated-multiplexer tree are used for the input and output driving circuitry to decrease the loading of the input and output data bus. All gating signals are easily generated by a C-element taking inputs from some DET flip-flop outputs of the ring counter.

Further simulations also demonstrate its advantages in nanometer CMOS technology. With more experienced layout techniques the cell size of the proposed delay buffer can be further reduced, making it very useful in all kinds of multimedia/communication signal processing ICs.

REFERENCES

- 1) Eberle.W et al 2001 80-Mb/s QPSK and 72-Mb/s 64-QAM flexible and scalable digital OFDM transceiver ASICs for wireless local area networks in the 5-GHz band IEEE J. Solid-State Circuits, vol. 36, no. 11, pp. 1829–1838.
- 2) Hosain.R, L. D. Wronshi, and albicki.A, 1994. Low power design using double edge triggered flip-flop,” IEEE Trans. Very Large Scale Integr. (VLSI) Syst., vol. 2, no. 2, pp. 261–265.
- 3) Li.W and Wanhammar.L, 1999 A pipeline FFT processor in Proc. Workshop Signal Process. Syst. Design Implement pp. 654–662.
- 4) Liou.M.L, P. H. Lin, C. J. Jan, S. C. Lin, and T. D. Chiueh, 2006. Design of an OFDM baseband receiver with space diversity IEEE Proc. Commun., vol. 153, no. 6, pp. 894–900.
- 5) Pastuszak.G, 2005 A high-performance architecture for embedded block coding in JPEG 2000,” IEEE Trans. Circuits Syst. Video Technol., vol. 15, no. 9, pp. 1182–1191
- 6) Shibata.N, Watanabe.M, and Tanabe.Y, 2002 A current-sensed high-speed and low-power first-in-first-out memory using a wordline/bitline-swapped dual-port SRAM cell,” IEEE J. Solid-State circuits, vol. 37, no. 6, pp. 735–750.
- 7) Sutherland.E 1989 Micropipelines Commun. ACM, vol. 32, no. 6, pp.720–738
- 8) Tsern.E.K and Meng.T.H 1996 A low-power video-rate pyramid VQ decoder IEEE J. Solid-State Circuits, vol. 31, no. 11, pp. 1789–1794.

Advanced Remote With HAPTIC

Dr. K. rameshbabu¹, Ch. Vekatramreddy², Ch. Rohit³, K. S. Chary⁴

1(professor, ECE dept, hitam, JNTUH, INDIA)

2, 3, 4(student, ECE HITAM JNTUH, INDIA)

ABSTRACT

We introduce a new universal remote control that gives easy-to-control interface for home devices such as TV, video/audio player, room lighting and temperature control. In order to use conventional remote controls, people need to understand complex instruction manuals and remember functions assigned to buttons. In addition, the button-based control does not provide an intuitive interface so the user presses a button several times to browse information and has difficulty in searching the right button among many buttons. Our universal remote control addresses these limitations by using a touch screen, a force-feedback dialknob, and two buttons instead of many buttons. We suggest an example scenario to interact with a conventional TV set, oomlighting, and air conditioner using our universal remote control. The result of a user study to evaluate the usability of the device shows that the universal remote control is very efficient and intuitive interface to control customer electronicsdevices1.

Key words: Universal Remote Control, Haptic Interface, Home device.

I. INTRODUCTION

Usually home appliances such as TV, radio, video/audio players, home theater, air conditioner, and room lighting come with remote controls that are used to select items and change status. As a result, people keep many remote controls to interact with their home devices. In addition, each control has different look and feel and functions assigned to buttons. This configuration gives the user difficulty in browsing information and finding a correct button. Sometimes the user needs to press a button repeatedly to set the volume and TV channel.

In order to address theses limitations, we developed a universal remote control that provides easy-to-use control and simple interface to control home appliances (see Fig. 1). The remote control we have developed consists of a touch screen, a force-feedback dial knob, and two buttons instead of many buttons.

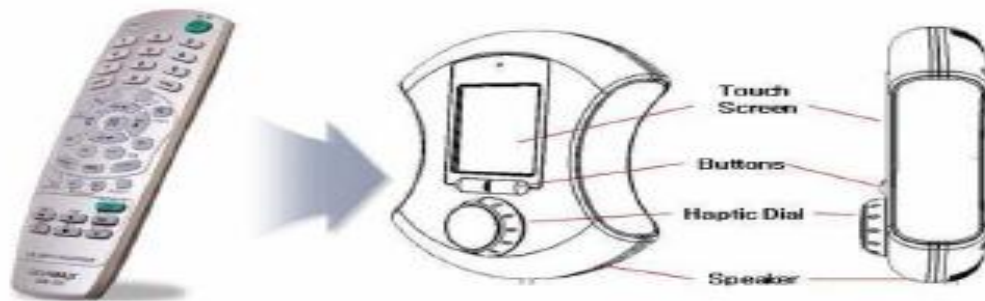


Fig. 1. Concept of the universal remote control. It consists of a LCD touch screen, two buttons, and a haptic dial.

II. PREVIOUS WORK

Recently haptic interfaces have been developed that allow users to interact with digital information via the sense of touch. Haptic technology has various customer electronics such as mobile phones, touch screen, automobiles, and games.

Over the past several years, there have been a number of studies of haptic feedback controls. Karon E. MacLean et al. introduced a variety of haptic devices and design parameters [1-3]. They considered characteristics of the touch sense and designed various tactile signals on their experimental devices. El Saddik A. suggested an identity authentication method using a haptic device [4]. He extracted behavioral features when users controlled the device and used the features to identify them.

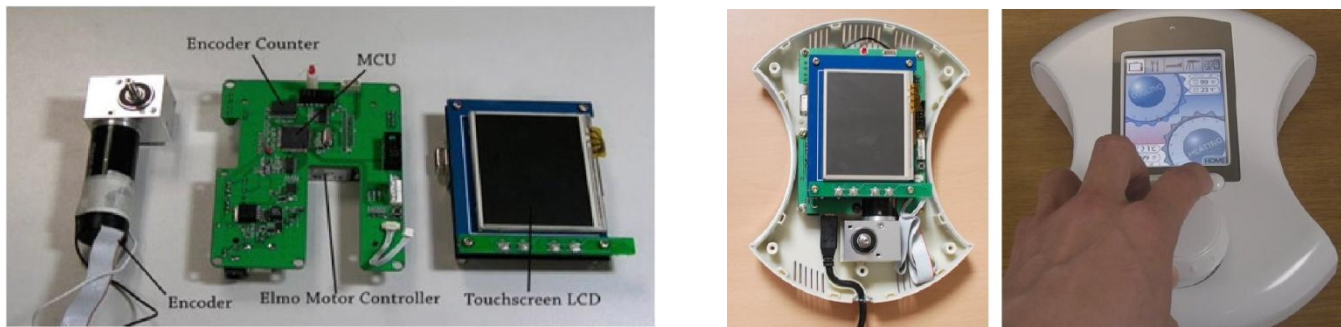
Several studies have been conducted of the 1 DOF (Degree of Freedom) dial knob. Scott S. Snibbe et al. suggested several haptic techniques for manipulating digital media based on intuitive physical metaphors [5]. Mircea Badescu et al. developed a single force feedback knob to imitate the senses of various conventional control knobs in motor vehicles [6]. Laehyun Kim et al.

used a haptic dial system for multimodal prototyping in the early phase of product development [7]. They applied the haptic technology to prototype the dial module of a washing machine. There are several works to apply the haptic interface to games. Yuichiro Sekiguchi applied the haptic effect to a game, proposing a device that gives a user the illusion of a virtual object inside the device when shaking it using accelerators and actuators [8]. Wanjoon Park et al. proposed a breakout game using a haptic dial interface and some haptic effects for the game [9].

Recently a remote control manufacture announced a universal remote control with tactile feedback and touch screen. When the user touches the button, the remote generate simple vibration.

III. IMPLEMENTATION OF THE CONTROL

In this section, we explain in detail the hardware configuration of the haptic dial knob. A block diagram of the system is shown in Fig. 2.



(a) Motor, Control unit PCB and Touch screen module

(b) Haptic remote control

Fig. 2. Implementation of the universal haptic remote control

MCU (Micro Controller Unit) computes the torque amount at a given angular position and sends the command to a DC motor via a DAC (Digital to Analog Converter). The DC motor executes the command and generates various haptic patterns. We use a gear box of 5:1 ratio to change the angle of rotation axis. The dial knob is installed on the motor gear box, allowing the user to rotate the knob and to feel various haptic effects which are programmed along the angular position. An encoder measures the angular position with 1000 pulse per turn and an encoder counter has a 24-bits quadrature counter and 25MHz count frequency. A Touch LCD Module is used to display visual information and to allow touch input.

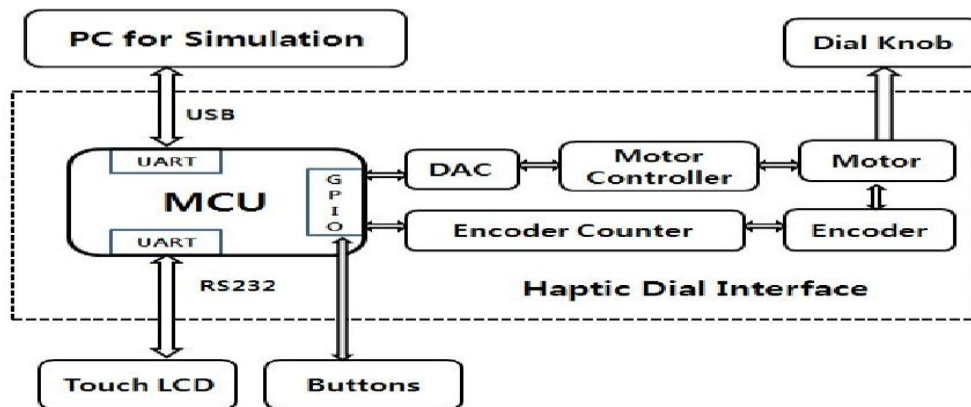


Fig. 3. System architecture of the haptic dial interface.

IV. GRAPHICAL USER INTERFACE (GUI)

GUI for the universal remote control consists of main (home) menu, TV channels, room temperature, and room lighting. The main menu has three icons that represent three sub menus to control home appliances. The user can select one of them by touching an icon. He/she can go back to the main menu by pressing the right button (we called it 'home button') anytime and select other home devices (Fig. 4(a)).

TV channel menu shows the channel list and information about current selected channel. The channel numbers are displayed on the rounded band to go well with rotational action of the dial knob. Some numbers has the heart mark that indicates popular channels or favorite channels programmed by the user. When the user selects the channel with the heart mark, he/she feels different tactile feedback. It helps the user to find intuitively the channel that he/she may want to see (Fig. 4(b)).

In room temperature menu, the user can select cooling or heating function by touching the screen and control the room temperature by spinning the dial knob. Yellow point indicates the current temperature the user select. The user spins the dial easily in the proper temperature range. But he/she feels strong tactile feedback out of the range (Fig. 4(c)).

Room lighting menu shows a light bulb to visualize room lighting. As the user rotates the dial knob, the brightness of the bulb is changed to indicate the room lighting level. The user feels the increasing/decreasing friction when he/she spins the dial clockwise/counterclockwise. It gives very institutive interface visually and haptically (Fig. 4(d)). The red point indicates the current brightness level on the bulb.

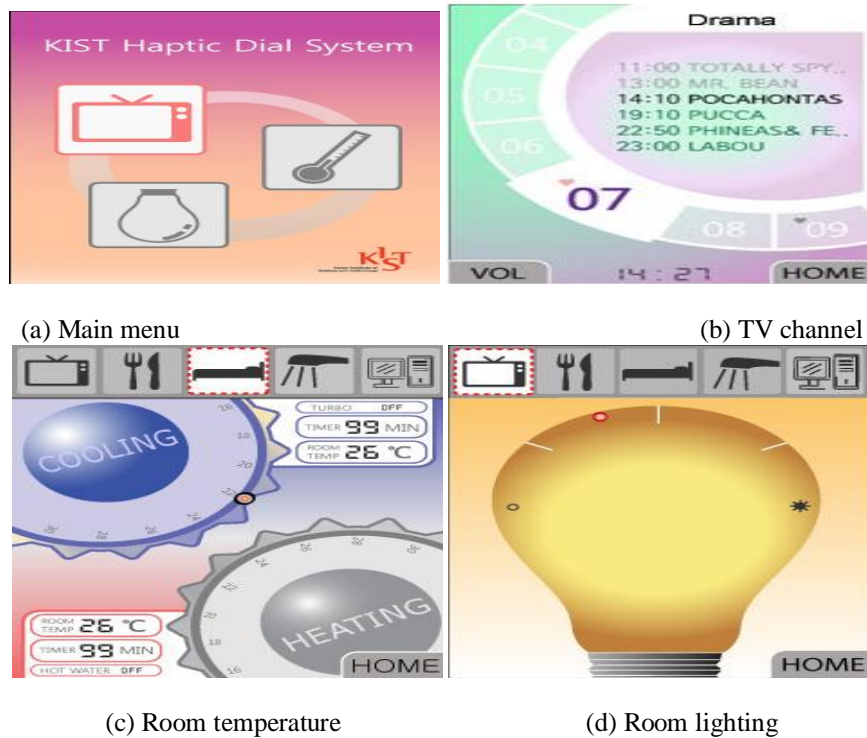


Fig. 4. Graphical user interface for the universal remote control. Main menu (a), TV channel (b), room temperature (c) and room lighting (d)

V. HAPTIC EFFECTS

In this section, we describe how to implement various haptic effects for the universal remote control. We designed various haptic effects which are defined by adjusting torque profiles along the angular position and time. Haptic effects include detent, friction, hard stop, and a combination of these effects. These haptic effects help the user to browse and find information easily and intuitively.

A. TV channel control

In order to give a feeling to select a channel to the user, we use the detent effect. The detent effect simulates notches with different height along the angular position using sine functions. Feeling a notch confirms each channel selection. Eq.

(1) shows the detent effect which is defined by a sine function.

$$f_a(\theta) = A \sin(b \theta) \quad \text{-----} \quad (1)$$

where, A_φ is the amplitude, b is the number of notch per turn, φ is the rotation angle of the dial knob.

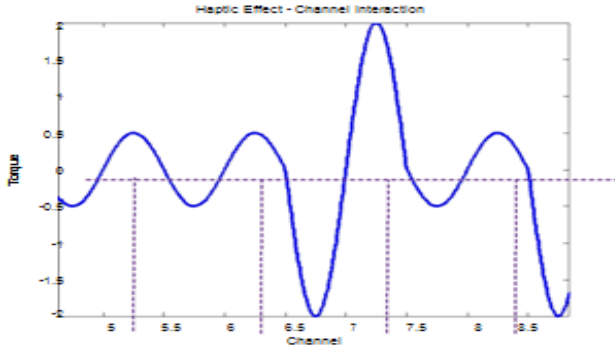


Fig. 5 Haptic profile by channel changing

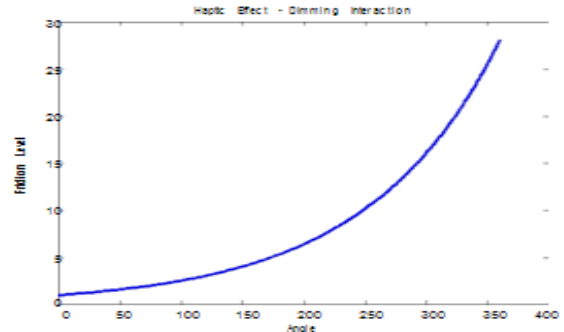


Fig. 6 Friction level by angle position

The torque profile for the detent effect is shown in Fig. 5. By modulating A_φ and b , the amount and frequency of torque can be changed. We set A_φ to a bigger value for the popular or favorite channels having a heart mark in Fig. 4(b) so that the user can identify the channels intuitively. For instance, channel 7 is a favorite channel and channel 5, 6, and 8 are non popular channels (Fig. 5).

B. Room lighting control

Friction haptic effect is used to adjust the room brightness level by rotating the dial knob. The friction effects generate resistant torque opposite to the direction of movement as a movement-based effect. This is implemented based on the friction con model [10]. The friction torque can be calculated by eq. (2).

$$\begin{aligned}
 L_f &= \exp(P_{now}(n) / S_{f1}) \\
 P_{curr_f}(n) &= P_{prev}(n-1) + (P_{now}(n) - P_{pre}(n-1)) \cdot S_{f2} \\
 P_{diff}(n) &= (P_{now}(n) - P_{curr_f}(n)) \cdot L_f \\
 P_{prev}(n) &= P_{curr_f}(n) \\
 \text{if } P_{diff}(n) > T_{f_max} & \text{ then } T_f(n) = T_{f_max} \\
 \text{elseif } P_{diff}(n) < T_{f_min} & \text{ then } T_f(n) = T_{f_min} \\
 \text{else } T_f(n) &= P_{diff}(n)
 \end{aligned}
 \tag{2}$$

where P_{curr_f} is the current position, P_{now} is the angular position of the dial knob, P_{pre} is the previous position, S_{f1} and S_{f2} are the scaling factors, P_{diff} is the difference of position, L_f is the friction level, T_f is the friction torque. L_f (friction level) increases exponentially as the brightness level increases since the exponential increasing make much better feeling than the linear motion (Fig. 6). We designed the friction profile depending on the dial knob’s movement. When On the other hand, when the user spins the dial fast, he/she feels more string friction. Fig. 7 shows the profile of the friction according to the knob movement. the dial knob is rotated slowly, the rotational friction is low.

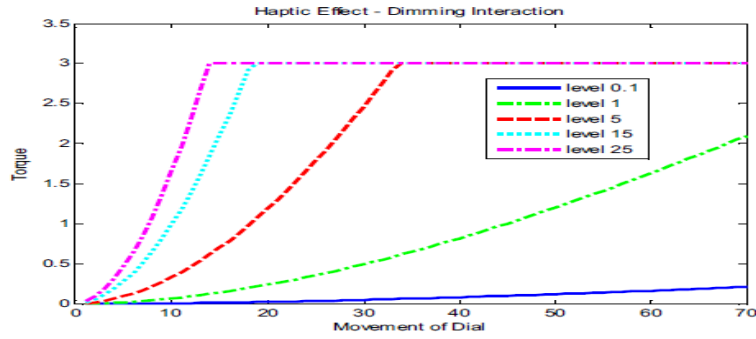


Fig. 7 Torque profile comparison of levels

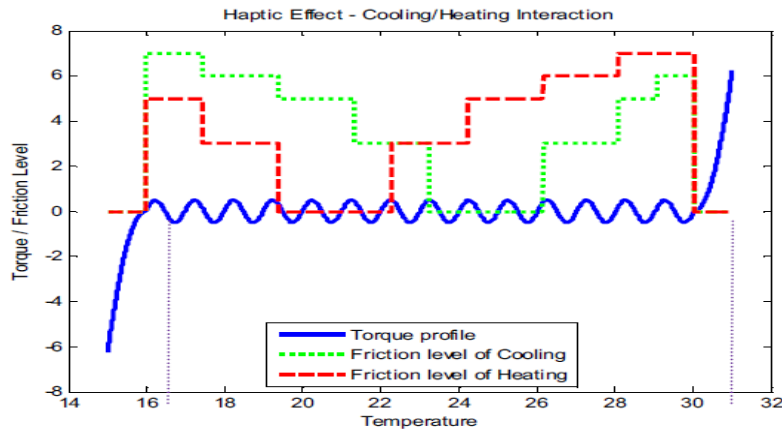


Fig. 8 Haptic profile and friction level by temperature

where, T is temperature, Sb is scaling factor, AT is the amplitude, b is the number of notch per turn, \square is the rotation angle of the dial knob.

VI. APPLY TO GAME CONTROLLER

We applied the universal remote controller to a game controller that gives the user haptic feedback during the game. For this, we developed a new brickout game in which conventional bricks are replaced by banana bricks, a game ball is replaced by a monkey, and a paddle is replaced by people holding up boards. In addition, a new item is added, a cloth wrapper. The banana bricks work the same as general bricks and the cloth wrapper contains haptic items. The game ball bounces off the top or side of the wall depending on the collision conditions between the ball and the paddle. When the ball hits a cloth wrapper, the haptic item falls down. If the user catches the item by moving the paddle, a predefined haptic effect is felt that lasts a few seconds. This haptic feedback can make the game easier or more difficult.

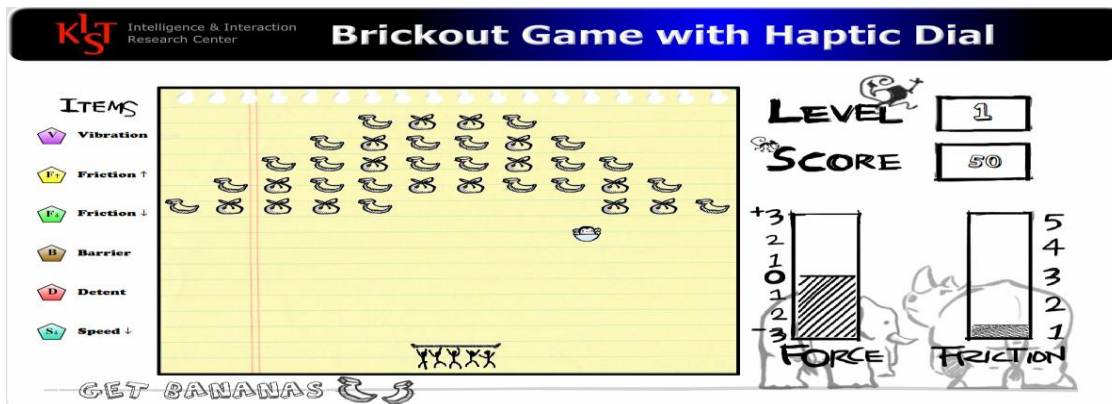


Fig. 9 Development of a new brick out game

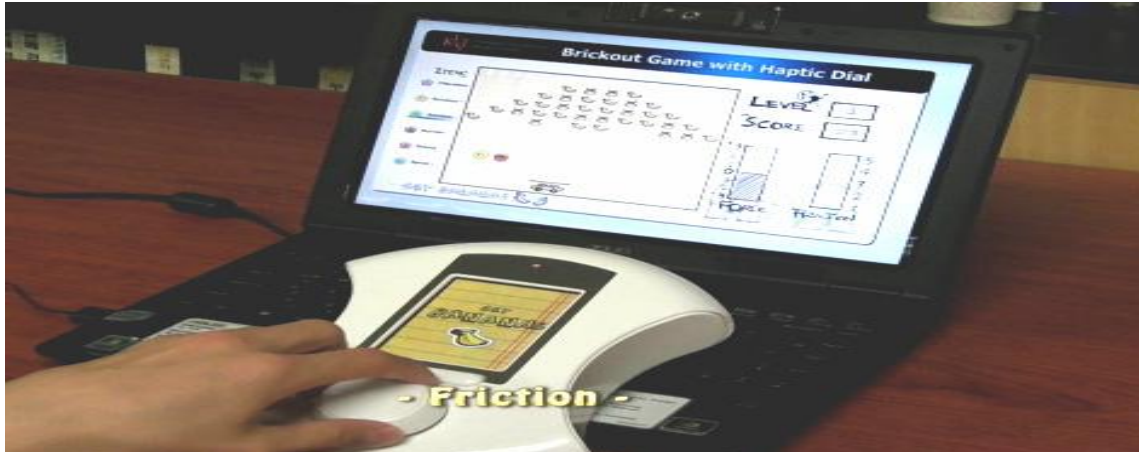


Fig. 10 Playing a brickout game using the universal remote control

VII. USER STUDY

We performed a user study to evaluate usability of the universal remote control.

A. Usability factors

For the user study, we followed a guideline suggested by Jinwoo Kim [11] who defined usability factors with a hierarchical structure. We choose appropriate factors to measure the usability of the universal remote control (Fig. 11).

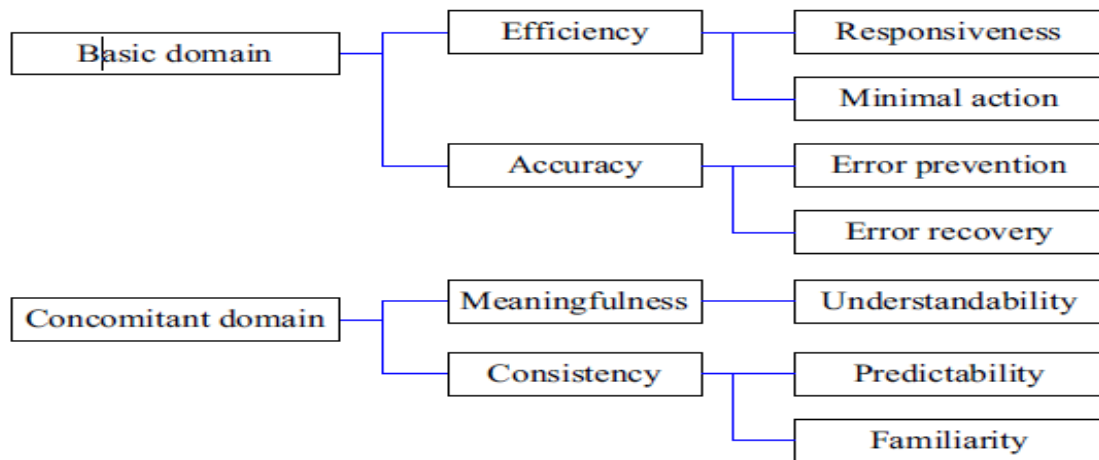


Fig. 11 Evaluation factors of usability suggested by Jinwoo Kim.

Evaluation factors in the first level consist of basic and concomitant domains. In the second level, the basic domain has two factors; efficiency and accuracy factor. Efficiency factor is about how effectively users can achieve given tasks in terms of responsiveness and minimal action. Responsiveness is a factor to measure the response time and minimal action is about how simply users can deal with given tasks. Accuracy factor is about user's mistakes while using the control and has error prevention and error recovery. Error prevention is about how well the remote control prevent user's mistake and error recovery is about how easily users can correct the mistakes.

Similarly, the concomitant domain has meaningfulness and consistency factors. Meaningfulness is a factor to measure how well the remote control provides information and functions which users want to use. Meaningfulness has understandability that is about how well users can understand system status via given information. Consistency is to measure how similar a function of the remote control is to other conventional ones. Consistency has predictability and familiarity as detailed factors. Predictability is about how well users can predict instructions of the remote control through experience of using other similar ones. Familiarity is about how easily users can know instructions of a system through experience of real world.

B. Method

Subjects are 20-30's thirty people who are familiar with the conventional remote controls. Before starting the survey, we gave information about the universal remote control and allow subjects to use it freely for 5 minutes. Subjects did not know the task scenario and are asked to do tasks one by one using the universal remote control. These tasks are below:

1. Temperature control: You came back home and it is too cold, -5 °C outside. You are sitting down a sofa and control indoor temperature to 28°C.
2. TV Channel control: Now, you want to watch TV. The default channel is number 2 and it is boring to you so you change the TV channel to your favorite channel, number 11.
3. Temperature control: you feel it is too warm. You control indoor temperature to proper temperature in winter season, 24°C.
4. TV Channel control: Now, TV shows some advertises. You change the TV channel to number 17 for searching another program.

After completing the tasks, subjects were asked to answer a questionnaire. The questionnaire for the user study is divided into three sections such as general control (touch screen), TV channel control and temperature control. The light control section is excluded because it is not popular way to control by a remote control. There are five questions excepting sponsiveness and recovery factor in general section. For channel and temperature section, there are eleven and ten questions each section with seven factors. Questions on the questionnaire were 7-point (-3 to 3) Likert scales.

C. Result

Fig. 12 shows results for each factor. For 'Efficiency' dimension, both of 'Responsiveness' and 'Minimal Action' got the high scores (2.50 and 2.08 respectively). It means that the user can use the universal remote control effectively. The subjects said that the haptic dial knob is very intuitive interface to control TV channel and temperature. The touchscreen also provides easy-to-use interface to select menus. For 'Accuracy' factor, both of 'Error prevention' and 'Error recovery' got the medium scores. 'Error prevention' factor got medium score (1.39). The score for 'Error prevention' of General (main screen) was not high (0.86) because if it is not correct position on touch screen, the system operates another program. In the case of 'Error Recovery' factor, temperature control got high score (2.27). As the results of interview, subjects recognized it is useful that friction is increased as deviate degree from proper temperature.

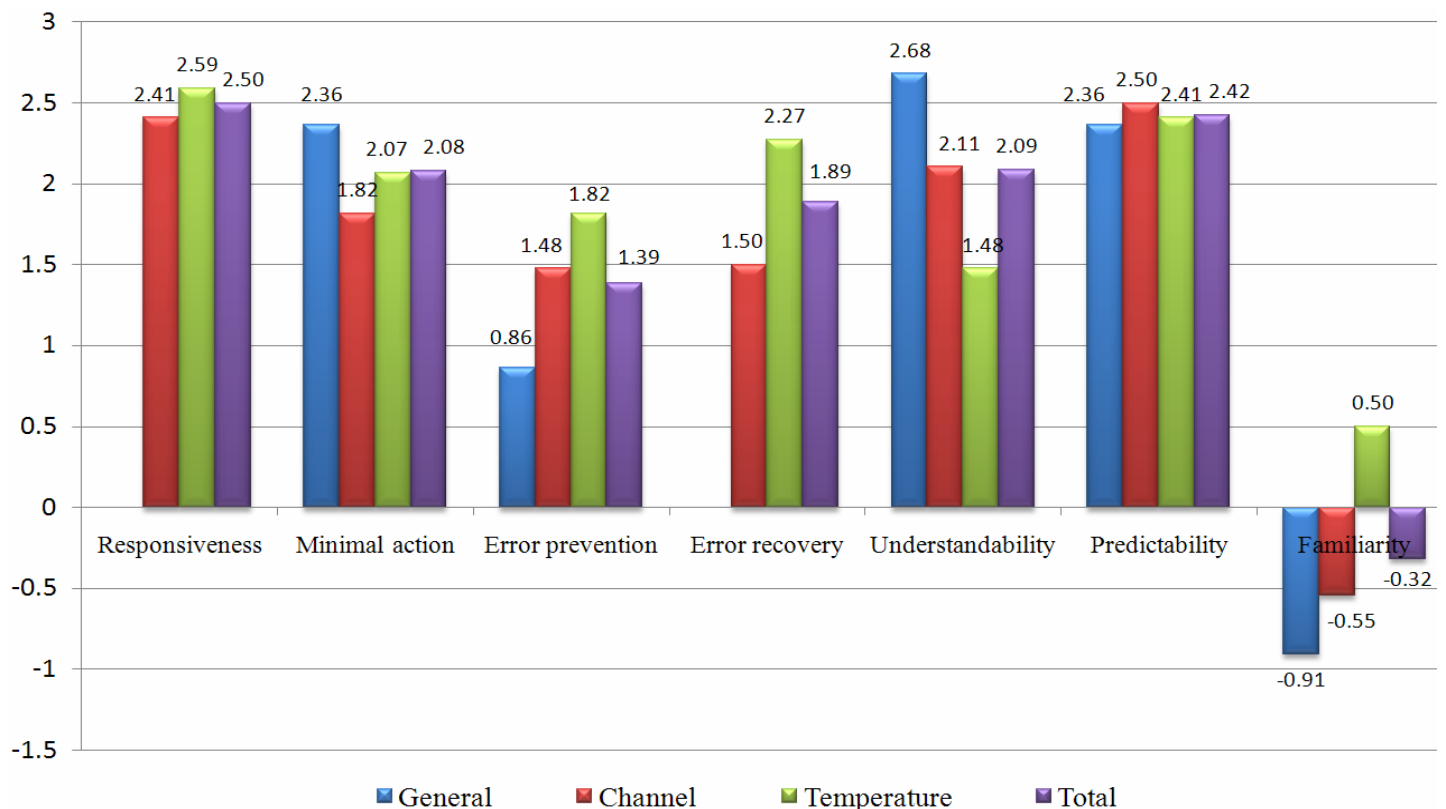


Fig. 12 The results of user-study

For 'Meaningfulness' factor, 'Understandability' got highscore (2.09) and especially for the general section got the highest score (2.68) because touch screen display shows various information according to context such as current temperature and channel information. In case of 'Consistency' factor, 'Predictability' got highscore (2.42). It means the universal remote control has very simple and stable interface. However 'Familiarity' has very low score (-0.32) because our universal remote control has a dial knob with haptic feedback and a touch screen unlike conventional remote controls.

VIII. CONCLUSION

Today people need to keep several remote controls to control home appliances in their living room. Universal remote control allows people to control multiple devices using a single remote control. However conventional universal remote controls still have problems. Many buttons make the user spend time to browse and find the right one. In many cases, people need to press a button several times, for instance volume control and TV channel selection. In addition, the user needs to read and remember the manual before he/she uses it.

In this paper, we introduce a new universal remote control to address these limitations. It has a simple interface which consists of a touch screen, two buttons, and a dial knob with haptic feedback. Touch screen can display various information and be used as an input device to select home device the user wants to control. Two buttons are used for the power on/off and returning to the home menu. Haptic dial knob provides a very intuitive input and output interface. The user can change the status by rotating the dial knob and at the same time, he/she receives tactile feedbacks depending on the situation.

Our universal remote control allows the user to control TV channel, room temperature, and room light brightness. In addition, we applied the device to a game controller for a brickout game. It makes the game more fun and more immersive. The result of a user study to evaluate the usability shows that our universal remote control is very efficient and intuitive device to control home appliances.

In the future we will design new haptic effects to control other devices and make the universal remote control smaller and lighter for better usability.

REFERENCES

- [1] Karon E. MacLean, "Designing with Haptic Feedback" *Symposium on Haptic Feedback in the Proc. of IEEE Robotics and Automation (ICRA 2000)*, pp.22-28, 2000
- [2] Vincent Hayward and Karon E. Maclean, "Do It Yourself Haptics: Part1", *IEEE Robotics & Automation Magazine December 2007*, pp. 88-104, 2007
- [3] Karon E. MacLean, "Foundations of Transparency in Tactile Information Design", *IEEE Transaction on Haptics, Vol. 1, No. 2*, pp.84-95, 2008
- [4] El Saddik A., et al., "A Novel Biometric System for Identification and Verification of Haptic Users", *IEEE Transactions On Instrumentation and Measurement, Vol. 56, No. 3*, pp.895-906
- [5] Scott S. Snibbe, et al., "Haptic Techniques for Media Control", *Proceedings of the 14th Annual ACM Symposium on User Interface Software and Technology (UIST 2001)*, pp.199-208, 2001
- [6] Mircea Badescu, Charles Wampler and Constantinos Mavroidis, "Rotary Haptic Knob for Vehicular Instrument Controls", *Haptics'02, Haptic Interfaces For Virtual Envir & Teleoperator Sys*, pp. 342-343, 2002
- [7] Laehyun Kim, Manchul Han, Sang Kyun Shin, Se Hyung Park, "A Haptic Dial System for Multimodal Prototyping", *18th International Conference on Artificial Reality and Telexistence (ICAT 2008)*, 2008
- [8] Yuichiro Sekiguchi, Koichi Hirota and Michitaka Hirose, "The Design and Implementation of Ubiquitous Haptic Device", *Eurohaptics Conference, 2005 and Symposium on Haptic Interfaces for Virtual Environment and Teleoperator Systems, 2005. World Haptics 2005. First Joint*, pp. 527 – 528, 2005
- [9] Wanjoon Park, Laehyun Kim, Hyunchul Cho and Sehung Park, "Design of Haptic Interface for Brickout Game", *IEEE International Workshop on Haptic Audio Visual Environments and Games (HAVE 2009)*, pp. 64-68, 2009
- [10] N. Melder and W. S. Harwin, "Extending the Friction Cone Algorithm for Arbitrary Polygon Based Haptic Objects", *Proceedings of the 12th International Symposium on Haptic Interfaces for Virtual Environment and Teleoperator Systems (HAPTICS'04)*, pp 234 – 241, 2004
- [11] Jinwoo Kim, et al, *Introduce to Human Computer Interaction*, AhnGraphics Press: 2005, pp. 195-235

Author's profile



¹Dr K.RameshBabu professor ECE Hyderabad Institute of Technology and Management, Hyderabad, holding B.E (ece), M.E PhD, India. He has 16 years of experience in electronics and communication Engineering. He has published papers in National level international level journals. He has guided 60 +students of B.Tech degree in Electronics and Communication Engineering in their mini & major projects and has guided 20 projects for M.Tech. He is a member of IETE, IEEE. He is active member in all directions like, Research, admin, teaching activities.



²Ch.venkatramreddy,



³Ch. Rohith



⁴K. S. Chari

These are the students of IV B.Tech ECE, Hitam, Hyderabad bearing roll no's 08E51A0415, 416, 9014349071 respectively. it is their main project in B.Tech ece, hitam, Hyderabad.

Charting of a Strategy for the Application of Aluminium Metal Matrix Composites for Different Engineering Service Requirements

Dr. J. Fazlur Rahman¹, Mr. Mohammed Yunus², Mr. T. M. Tajuddin Yezdani³

**(Professor Emeritus, Department of Mechanical Engineering, H.K.B.K.C.E., Bangalore, India)*

*** (Professor, Department of Mechanical Engineering, H.K.B.K.C.E., Bangalore, India)*

**** (Professor, Department of Mechanical Engineering, H.K.B.K.C.E., Bangalore, India)*

ABSTRACT

The necessity for the design of efficient load bearing materials together with superior functional properties, high strength and stiffness that can be tailored for specific applications where monolithic materials and conventional alloys that cannot be used, has given impetus to the development of modern composites. The development of composite technology spanning several decades has given rise to an exotic class of materials whose characteristics could be tailored for specific applications to enhance mechanical and other properties besides, incorporating easy machinability by conventional machining methods using conventional tools. This paper deals with the charting of a strategy for the application of aluminium metal matrix composites citing the specific reasons for selecting the particular material system to its functionality as a worthy candidate meriting its applications. A brief review of the modern composites is followed by a general discussion and logical choice of a particular material system that has gained wide acceptance. With this knowledge as the basis, the materials engineer is well placed to create innovative designs that are having vast improvement over its predecessor designs and achieve not only fast effective gains, but also material enhanced properties.

Keywords: Fabrication Route, Field of Applications, Matrix, MMC, Selection Strategy Reinforcement.

1. INTRODUCTION

Composites may be broadly classified as Metal Matrix Composites (MMC), Polymer Matrix Composites (PMC) and Ceramic Matrix Composites (CMC), all the matrices are formed by combining two or more materials to achieve enhanced and superior properties compared to their component parts. There are quite a few properties that are relevant to all the three categories. They are low density, enhanced strength and stiffness, weight optimized performance and in the case of aerospace structures fuel efficient design and high temperature resistance. While these properties are more or less general requirements for all the three types of composites, they may however be imparted additional properties enhancement in certain critical areas of applications, notably in the aerospace sector. In the applications area, Aluminium Matrix

Composites have taken a lead, the thrust being a legion. The selection of a particular system require tailored depends on the host of conflicting requirements, which a system has to satisfy. It is important to know that the production and properties of several AMC's either for continuous fiber, discontinuous fiber or particulate reinforced is profoundly affected by the reinforcements. These property enhancements due to the reinforcement are compared to the matrix composites. The introduction of the paper should explain the nature of the problem, previous work, purpose, and the contribution of the paper. The contents of each section may be provided to understand easily about the paper.

1.1 The Road Map for the Selection of Composites

The selection of the materials comprising the composites is by no means a random process. The systematic selection apart from the composition of the components comprising the MMC also takes into account the optimization factor, where the so called merit parameters play a significant role in analyzing the competitiveness between the materials that are functionally related to materials properties, such as density, resistance to temperature, resistance to corrosion besides, cost and value of weight savings. This approach is conducive is to the evaluation of AMC's in specific realm of application, whether aerospace, military, automotive or sport. This analysis will lead to the conclusion that continuous fiber reinforced AMC's have low density, are stiff and strong, are known to have a weight optimized performance and are fuel-efficient design. In the aerospace sector, cost is not necessarily the governing factor because of the low production volume and the profit realized by weight savings. Perhaps, another reason is that aerospace sector defense overtone outweighs cost factors. Be this as it may today's sophisticated defence industries of advanced nations develops aerospace products and systems that are market specific and performance oriented. This has led to a situation in which aerospace technologies have become highly competitive design for excellence and optimum performance. As far as the automotive sector is concerned, cost plays a vital role (since large volumes prevails and as such material cost will significantly affect the competitiveness of the component produced).

1.2 Application Potential

There are three different types of Aluminium Metal Matrix Composites depending on the specific field of application. They can be reinforced with

- Particulates
- Whiskers - Mono crystalline or Discontinuous fiber that are poly crystalline.
- Continuous fibers.

Common reinforcements are silicon carbide (SiC), Alumina (Al₂O₃) also Titanium Carbide (TiC), Barium Carbide (B₄C), Barium (B), Graphite, etc.

1.3 Selection of Matrix

Matrix is selected on the basis of oxidation, corrosion resistance and other properties [1, 2]. Commonly used matrix materials are Aluminium, Titanium, Magnesium, Nickel, Copper, Lead, Iron, Silver, Zinc Tin and Silicon.

The most widely used matrix materials are Aluminium, Titanium and Magnesium. Our main focus as a matrix is on Aluminium [3], because it has good corrosion resistance, low electrical resistance and excellent mechanical properties. This is one reason for the use of Aluminium Metal Matrix as an aerospace material. Titanium Metal matrixes are mainly used in aero-engines [4], Compressor blades and discs, because they offer very high resistance at elevated temperatures. Magnesium Matrix materials are used in reciprocating parts, piston, gudgeon pins and springs cap in automotive engines [5]. Also in aerospace sector to limited extent where low coefficient of expansion, high stiffness and low density are required. Reinforcement characteristics will depend on chemistry, morphology, and microstructure, mechanical and physical properties subject to cost consideration. The matrix characteristics factors are density, strength potential and strength retention at high temperature, ductility, toughness are also important.

For example, 7xxx Aluminium alloy has the best combination of strength and toughness in aerospace applications rather than 2xxx alloy. But this does not preclude the selection of 2xxx for aerospace applications since one has to select depending on what final properties to bestow on the composites. The reason for the above is that if 7xxx Al alloy composites are used, an interface is developed between 7xxx Al alloy and reinforcement which degrades the strength of composites [6].

2xxx, 6xxx, 7xxx Al alloys are widely used as matrix materials for making composites. Aluminium Lithium Alloy 8xxx engaged the attention of researchers, because of its good wettability characteristics. For good bonding and high strength in the composites, metal alloys are used as the matrix element instead of monolithic metals (Pure metals).

All alloys containing reactive elements such as Mg, Li, etc. normally aid interfacial bonding with dispersoids as they will be ideal matrix materials. Generally, Al-Cu-Mg (2xxx) Matrix systems have excellent combination of strength and

damage tolerance. However, Al-Zn-Mg-Cu (7xxx) matrix systems offer higher potential. Al-Mg- Si-Cu (6xxx) systems provide improved resistance to corrosion in severe environment and give improved product fabricability. Al-Fe-Li (8xxx) systems provide the opportunity for high temperature applications [7].

1.4 Reinforcements

Reinforcement increases strength, stiffness, temperature resistance capability, but generally lowers the density of MMC's.

1.4.1 Role of fibers

The prime role of reinforcement is to carry the load that of the matrix to transfer the load to the fibers with maximum efficiency. Reinforcements are of two types.

1. Continuous reinforcements
2. Discontinuous reinforcements
3. Continuous reinforcements are associated with MMC's which are produced by using continuous fibers and discontinuous reinforcements are associated with MMC's produced with discontinuous fibers. These two types of reinforcements can be divided into five major categories.
 - a. Continuous fibers
 - b. Short fibers (chopped fibers, not necessarily of the same length)
 - c. Whiskers.
 - d. Particulate or Platelets, generally ceramics which are oxides, carbides, nitrides and carbonates. They are used because of high strength, stiffness at room at elevated temperatures. The common reinforcing elements are SiC, Al₂O₃, TiB₂, B and Graphite.

1.4.1.1 Continuous fiber reinforcement

The main Continuous fibers usually called filaments include Boron, Graphite, Al and SiC fibers which are unique for unidirectional load when oriented in same direction as the load. The strength perpendicular to the fiber orientation is low.

1.4.1.2 Characteristics of the fibers

Multi filament family of C-C, SiC, and Aluminium fibers are available in the form of single yarns or three dimensional waves. The mono filaments family is based on Boron only.

1.4.1.3. Boron Fiber

Boron fiber shows the greatest strength in comparison with other fibers and MMC's are relatively easy to make with these fibers. However, high cost of these fibers prevents widespread use. It is made by chemical Vapor Deposition (CVD) on a tungsten core. To retard reaction between

Boron and metal at high temperatures, fibers coatings of SiC or Boron carbide are used.

1.4.1.4. Carbon Fiber

It is unsuitable to form Al based MMC's because of fiber degradation during processing but T300 is used successfully to form the cheapest Mg composites [8]. Sometimes CVD coatings of carbon fiber using Ni and Si has been used to improve the wettability of carbon fiber MMC's to improve tensile properties.

Silicon carbide monofilament is made by the CVD process utilizes tungsten or a carbon core. There are SiC fibers sold under the brand name Nicalan and Tyranno containing additives of Titanium which possess enhanced strength and stiffness characteristics. MMC materials reinforced with Tyranno possess high transverse strength and are used in the aerospace industry.

Boron fiber possesses the greatest strength in compression with other fibers with additional advantage that it is easy to make MMC's with this fiber. However, their high cost restricted used in aerospace structure. SiC and Al_2O_3 are very popular in high temperature applications and consequently they figure prominently in the aerospace industry. MMC's with Al, Ti, Ni alloys as one of the matrix materials with Al_2O_3 , B, C, SiC and SiO_2 as reinforcements are attractive propositions for the use in the aerospace industry Al alloys with Al_2O_3 , SiC etc. are effectively used in areas where turbine entry temperature of 600^0 K are encountered.

1.4.1.5. Short Fibers

Short fibers exceeds the critical length $l_c = d (S_r / S_m)$, where d = fiber diameter, S_r is the reinforcement strength S_m is the matrix strength and hence show a high strength in composites considering aligned fibers. Mis-oriented (randomized) short fibers (used with AMC) have been used with some success as AMC. Certain oxide fibers mainly saffile and Kaowool find applications as reinforcements in the manufacture of automobile engine components. Zirconia fibers are not compatible with AMC's but short fibers of Zirconia are widely used for refractory insulation purposes. Their main stay is in the refractory industry due to their low cost.

1.4.1.6 Whiskers

They are fibrous, single crystal structure with no crystalline defects. A whisker has a single dislocation, which runs along its central axis. This factor renders it immune from dislocation which is the reason for its high yield strength close to the theoretical strength of the materials [18]. The method of Vapor deposition is widely used in the whisker preparation. It has been established that its response to elevated temperature is better when compared to any other fiber [18]. So outstanding have been the specific mechanical properties of whiskers that they have become the focus of many researchers, in this area of fabricating

MMC's using whiskers [19-25]. Another attractive feature is the smaller diameter of the whiskers ($d = 0.1$ to $2\mu m$) and hence the small length ($l/d = 50$ to 100) facilitates the efficient transfer of the load [9].

SiC whisker reinforcements are produced from rice husk (a low cost material). SiC whisker reinforced Al has been widely used in aerospace vehicles. It must be remembered that the physical characteristics of whiskers play a role for different chemical activity with the matrix alloy [9]. For e.g. high strength C fibers exhibit a much higher chemical reactivity towards liquid Al than to high modulus Carbon fiber because of their different states of crystallization.

1.4.1.7. Particulate

They are the cheapest and widely used reinforced material used in MMC's as reinforcement. They produce isotropic properties and hence are popular in structural application. Some research has been reported in producing reinforced Al alloy with graphite powder [13, 14] with low volume reinforcement ($<10\%$). Currently success with higher volume fractions of reinforcements for various kinds of ceramics particles (oxide, Carbide and Nitride) has been reported [9]. The emphasis is now shifted to the use of SiC short fiber, whiskers and particulate in Al alloy matrix. The reason for the shift is due to the fact that SiC imparts inadequate thermal stability with Al alloys during synthesis and application in the aerospace sector. Another feature is that SiC has good wettability with Al alloys. The density of SiC and Al alloy are pretty close (2.8 and 3.3 gm cm^{-3}) and reinforcements imparts substantial increase in the modulus and Ultimate tensile strength. If soft particulates (Graphite, Mica, etc) are dispersed in the Al alloys they do not contribute to the strength. Indeed they lower the mechanical properties, but other special properties such as adhesion wear resistance are enhanced. In an identical situation the dispersion of Zircon particulates in Al alloys improves abrasion resistance properties to the composites, provided the amount of dispersion in 5% weight. Higher amounts deteriorate mechanical properties [15].

The USA leads in the field of particulate research followed closely by Japan. Current research has reached such an advanced stage that 20% SiC in particulate form has shown improvement in yield strength and tensile strength of an equal percentage . while there is no change in density, stiffness it seems has improved by 50% [4], which contradicts the "rule", that the specific thickness of all engineering metals, regardless of density is roughly the same [16]. Research in the field of SiC_p - Al and SiC_w - Al composite materials has shown that the SiC particulate reinforced Al matrix composites are not strong as the SiC whisker reinforced composites. But this as it may, SiC particulate reinforced Al matrix composites are good candidates in wear-resistant materials. Their potential is further enhanced by the fact that the particulates have a favorable effect on other mechanical properties such as hardness, wear resistance and compressive strength.

In industrial applications particulates have demonstrated their potential as the most favored candidates in a number of particulates reinforced system, such as cermets in electric industry for the tracks of precision variable resistors and high speed cutting tool tips.

1.4.1.8. Wire

Essentially they are metallic filaments having high elastic modulus, some of them are molybdenum and tungsten. Current research has also shown some promise in using a steel wire. Their obvious disadvantage is the high density they possess when compared to ceramic whisker. However, they have good ductility and are therefore used to fabricate composites where high tensile loads are to be hauled with toughness [17]. Honda Japan is credited for using 45% by volume of stainless steel fiber in Al alloy for the fabrication of connecting rods using squeeze-casting method. These rods seem to have demonstrated 40% reduction in weight than the equivalent forged design while simultaneously contributing to substantial improvement in engine power and fuel economy. This is just one indication of the fact how versatile and fascinating composites are wherein unfavorable situations can be reversed by ingenuity to yield the most favorable solution in the frontier areas of this technology. There is another disadvantage associated with this at high temperature there is a high possibility of metal to metal reaction, thus creating fabrication problem [18]. Thus, a rapid survey of the part played made by the reinforcement in AMC's citing in general the area of application, has been made. It is continued to proceed along with the road map keeping in focus the application potential of AMC's and how profoundly the fabrication route affect them.

The application potential of Al matrix materials will also depend on

1. The Production process involved in tailoring of the specific properties.
2. It will depend on the type of the reinforcement, namely, Particulate, Whiskers and Continuous fibers.

2. PRODUCTION PROCESS VIA THE FABRICATION ROUTE

There are different fabrication techniques that are currently being used in the manufacture of MMC materials. However they need not be unique as the designer evolve his own methodology to either modify or even completely replace the existing technique by using his knowledge expertise at his command. This is so, because the choice of the matrix and reinforcing material and of the types of reinforcement and the fabrication techniques vary considerably.

2.1.1. Types of Fabrication Methods

1. The solid phase fabrication method. This method includes diffusion bonding, hot rolling, extrusion,

drawing, explosive welding, powder metallurgy route, pneumatic impaction etc.

Liquid fabrication methods: these methods involve liquid metal infiltration, squeeze casting, compo-casting, pressure casting, spray co-deposition which come under liquid metallurgy. Generally liquid phase fabrication is regarded as more efficient because the matrix material is used varies with different fabrication methods. As an example powder is used in the powder matrix impaction and powder metallurgy techniques and obviously liquid matrix material is used in liquid metal infiltration, plasma spray, squeeze casting, pressure casting, gravity casting, compo-casting and investment casting etc. but in today's industry diffusion bonding, powder metallurgy route, liquid metal infiltration, squeeze casting, spray co-deposition and compo-casting [19] are sufficiently advanced to merit their industrial status. There is a keen competition between these methods, the focus being on producing the lowest cost material with the best mechanical properties. Without going into the specifics of each of these methods, a brief comparison of different techniques refers to above are given below. A detailed appraisal is given in the appendix 1.

3. MECHANICAL PROPERTIES

The tensile strength, stiffness and elongation of different AMC's in respect of Al6061-T6, SiC_w - Al6061-T6 shows significant increase in modulus yield strength and ultimate tensile strength due to the addition of reinforcements SiC [21]. Whisker additions are seen to be more effective in strengthening than with particulate addition. Particulate reinforcement composites are the more isotropic material which is a desirable characteristic for use in structural unit, aerospace, automobile, etc [21]. Among the casting routes, sand casting results shows slightly higher tensile strength but generally in all casting techniques, the mechanical properties are considerably high if heat treatment is applied to both particulate and whisker reinforce composites, the particulate reinforce composites give higher strength than that of whisker reinforced composites.

It has been found out that the strength of both matrix and composite drops down remarkably at high temperature. At about 200 - 250°C the strength of particulate reinforced composite shows better performance at high temperature [7], so that at elevated temperature SiC_p / x8019 composites can be used successfully.

It has been indicated that like the tensile strength and stiffness, the hardness also increases if heat treatment is used as a secondary operation [20].

The fracture toughness of composites increase if heat treatment is applied [21]. The fracture toughness decreases with increase of reinforcement as ductility decreases.

Aluminium alloys are widely used in aerospace and most recently in automobile industry and in architectural applications. The demand for improved attention on a

number of new materials including Aluminium Metal Matrix Composites. Aluminium is susceptible to localized corrosion such as pitting and crevices corrossions.

3.2 Corrosion and Oxidation

Galvanic corrosion is a major concern between the reinforcement constitutes and metal matrix, which governs the corrosion behavior of any MMC. In an Aluminium Metal Matrix Composites, Al which is an active metal is coupled to reinforcement constituents such as graphite and silicon carbide. There is a tendency for galvanic couple to form between Al and the reinforcement constituents. This galvanic corrosion is responsible for the higher corrosion rates observed in Metal Matrix Composites [18].

The corrosion damage in Al/SiC_p composites is generally caused by pitting attack and by the nucleation growth of Al₂O₃ on the metal surface. The corrosion protection of Al alloys and Al based MMC can be effected by chemical passivation like by immersion of Al alloys and Al MMCs in serium chloride solution for a known period of time, which produces a corrosion resistance surface. Besides, a pitting corrosion can also be protected by this treatment [20].

Another method of preventing corrosion is by giving an epoxy coating and a combination of chemical passiveness in metal chlorides with the polymer coating, gives an excellent corrosion resistance.

3.3 High temperature Applications

With regards to the usage of components made of Aluminium Metal Matrix composites at high temperatures like aerospace and automobile applications, a thermal barrier coating of PSZ, Super-Z alloy, Zirconia Toughened Alumina (ZTA) Alumina-Titania (Al₂O₃ + TiO₂) and Alumina could be plasma sprayed to impart maximum thermal resistance and thermal fatigue resistance to the components[22-23].

4. CONCLUSIONS

The following inferences are made with the charting of strategy for the application of Aluminium metal matrix composites

1. 8xxx alloys can be used as a matrix material for the use of composite at high temperature.
2. For making the composite with high strength, hardness and fracture toughness x6061 matrix is the best.
3. As reinforcement material SiC can be used for making AMC.
4. For the manufacturing route, Powder Metallurgy with extrusion and heat treatment can be used for making AMC with good mechanical properties.
5. The surfaces of Al MMCs can be protected from pitting corrosion and oxidation by a special surface treatment like dipping the components in a solution of serium chloride for a known period of time and also by anodizing of Al alloy components.

6. High temperature resistance quality on the components of Al MMCs can be provided by giving a proper Plasma sprayed ceramic oxide coatings.

REFERENCES

- [1] J. eliasson and R. Sandstrom, Application of Aluminium Matrix Composites, key engineering materials, Vol. 104-107, pp.3-36, 1995, Trans Tech Publications, Switzerland.
- [2] M. Taya, & R.J. Arsenault, Metal Matrix Composites-thermo mechanical behavior, porgamon press, 1989.
- [3] R.L. Trumper, Metal & Materials, 3, pp. 662, 1987.
- [4] J. Lock, Professional Engineering, 21, April 1990.
- [5] K.U. Kainer, PD-VOL, Composite Material Technology, 37, 191 (1991)
- [6] R.G. Gilliland, Symposium on future industrial technology, Kobe, Japan, March 23, 1998.
- [7] W.H. Hunt, T.J. Rodjom, Proceedings of the Powder Metallurgy World Congress (Eds J.M. Capus and R.M. German) June 21-26, 1992, sanfrancisco, California, USA, Vol.9, pp.21.
- [8] E. A. feest, M.J.Ball, A.R.Begg, D. Biggs, Report on OSTEM visit to Japan October1986.
- [9] F.A.Girot, J.M.Quenisset and R.Naslain, Composites Science and Technology, 30,155, 1987.
- [10] R.A. Higgins, properties of Engineering Materials, Hodder & Stoughton, 1986.
- [11] B.S. Majumder, A.H. Yegneswaran and P.K. Rohatgi, Mat. Sci, Eng, 68,85 (1984).
- [12] M.A. El. Baradie, Journal of Material Processing Technology, 24, 261, 1990.
- [13] F.A.Badia, D.F. Macdonald & J.R. Pearson, AFS Transaction, 265, 1971.
- [14] P.R.Gibson, A.J. Clegg & A.A. Das, Journal of Foundry Trade, 253, 1982.
- [15] K.G.Satyanarayana, R.M.Pillai and B.C. Pai, Handbook of ceramics and composites, vol.1, pp.495.
- [16] S.Kohara, Materials and Manufacturing Process, 5(1), 51 (1990).
- [17] J.R. Vinson & T.W. Chou, Composite Materials & their use in structures, Applied science publishers Ltd. London, 1975.
- [18] M.M. Schwartz, Composite Materials Handbook, Mc Graw hill book company, 1984.
- [19] D. Huda, M.A. El Baradie and M.S.J.Hashmi, Journal Material Process Technology, 37, pp5-13, 1993.
- [20] C. Milliere, M.Surey, Materials Science and Technology, 4, pp.41, Jan.1998.
- [21] C.R.Crowe, R.A. Gray and D.F.HASSON, Proc. ICCM 5 (eds. W.C. Harrigan), 29-30 July, 1 August, 1985, pp.843.
- [22] Mohammed Yunus and Fazlur Rahman, J., Study on the influence of spray parameters of Ar- N2 plasma spray process using CFD analysis, International Journal of Advanced Engineering Sciences And Technologies, Vol. 10 (2), pp.275 – 284, 2011

[23] Mohammed Yunus, Fazlur Rahman J., Optimization of usage parameters of ceramic coatings in high temperature applications using Taguchi design,

International Journal of Engineering science and Technology, Vol.3(8), pp.193- 198, 2011.

Appendix 1.

Fabrication Route	Cost effectiveness	Field of application	comments
Diffusion bonding	High to very high	Suited for making sheets, rotor blades, vane and shaft structural components.	Capable of handling foils or sheets of matrix and filaments of reinforcing elements.
Powder metallurgy technique	Medium to high	Suitable for the production of small items that are round in shape, bolts, pistons, valve and generally high strength and high resistance materials.	The matrix as well as the reinforcements is used in powder form particularly suitable for using particulate reinforcement. There is no existence of so-called reaction zone.
Liquid metal infiltration fabrication	Low to medium	Particularly suitable for the production of structural shape such as tubes, beams, rods with excellent properties in the uni-axial direction.	The reinforcement is in the form of filament.
Squeeze casting	Medium	Has matured to achieve and in dispute industrial status in the automotive industry for providing automotive components such as pistons, connecting rods, rocker arm, cylinder head of various geometry.	It is very versatile and as such applicable to any type of reinforcement. Its application can be widened to cater for large scale manufacturing.
Spray co-deposition	Medium	Particularly suitable to produce friction materials such as brake lining, cutting and grinding tools etc.,	Reinforcements is in particulate form. Maximum density materials can be produced.
Compo casting	Low	Has wide usage in automotive, aerospace, industrial equipment and sporting goods industry. Also used to manufacture bearing materials.	Suitable for discontinuous fiber especially particulate reinforcement.

Scatter correction improvement based on the Convolution Subtraction Technique in SPECT imaging

Mohsen Zand¹

¹(Department of Computer, Islamic Azad University, Doroud, Iran)

ABSTRACT

SPECT is a tomography technique that can greatly show information about the metabolic activity in the body and improve the clinical diagnosis.

In this paper, a convolution subtraction technique is proposed for scatter compensation in SPECT imaging.

In simulation with Gate, 128 projections were simulated evenly spaced over 360° by a circular orbit, each with 128 bins. Simulation results show that this method is effective in SPECT imaging.

Keywords – Convolution, Scatter, Simulation, SPECT

I. INTRODUCTION

Since the early days of the last century, ionizing radiation in particular gamma-rays, thanks to their penetrating property, are used to image the interior of objects. This is done with an external source of radiation, which illuminates an object and projects the shadows of its internal structure on a detecting surface. Later on, it was shown that a true three-dimensional image can be reconstructed if there is a sufficient number of such two dimensional projections generated by the displacement of the source/detector assembly on a specific space curve. In essence, this reconstruction procedure relies on the inversion of the so-called x-ray transform, which is known since many decades [1], [2].

It should be noted that one can also turn passive objects into radiating ones. For example, in nuclear medicine, this is achieved by injecting a radiotracer such as ^{99m}Tc to produce a nonuniform distribution of the tracer within the patient's body. An image (or projection) can be produced by a parallel-hole collimated gamma camera, set to register 140 keV photons emitted by ^{99m}Tc. If the gamma camera is made to rotate around the patient's body, so as to generate a series of images from distinct view angles, then the tracer distribution hidden inside of the body can be reconstructed. This imaging modality is known as single-photon emission computed tomography (SPECT) [3].

In SPECT 2D projections are acquired with a gamma camera at different angles around the patient. The projections are used for reconstruction of a 3D image volume, which ideally should correspond to the activity distribution in the patient. A continuous acquisition of data is possible but requires complicated data management, and in most cases a "step and shoot" technique is used instead, with no data collected during the detector movements. The 2D projections are acquired in a circular or elliptical orbit around the patient, and the number of projections usually varies between 64 and 128, equally distributed in space. A complete acquisition measures projections over a 360°

rotation but a restricted acquisition of 180° is sometimes used. A multiple head system is advantageous for SPECT since it is a relatively time-consuming procedure.

In SPECT, because of photoelectric absorption and Compton scattering, the emitted gamma photons are attenuated inside the body before arriving at the detector. Thus the photon is not necessarily completely stopped but may be scattered. Scattered photons are diverted from their original path with some loss in energy.

In practice some of the scattered photons are still detected within the photo-peak energy window and are physically deflected, so as to be mis-positioned. Although scatter and attenuation are closely linked, when correction is applied the two effects are considered separately; attenuation involves loss of counts whereas scatter involves the detection of additional misplaced counts (see Fig. 1).

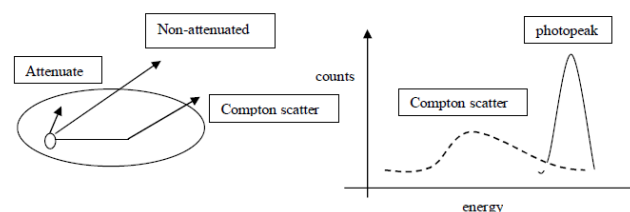


Figure 1: Compton scatter photons lose energy as a result of the deflection but, due to the limited energy resolution of the gamma camera the scattered photons may still be detected in the photo-peak.

The extent of attenuation can be quantified mathematically by the transmitted fraction (TF (t' , s' , θ)), which is the fraction of the photons from location (t' , s') that will be transmitted through a potentially non-uniform attenuator at angle θ . The transmitted fraction is given by (1):

$$1: TF(t', s', \theta) = \exp(-\int \mu(t', s') ds)$$

where $\mu(t', s')$ is the distribution of linear attenuation coefficients as a function of location.

To account for the presence of scatter, this Equation can be modified by multiplying the exponential term by a buildup factor (B) [4]. The buildup factor is the ratio of the total number of counts detected within the energy window (primary plus scatter) to the number of primary counts detected within the window. In the "good geometry" case there is no scatter detected, so the buildup factor is 1.0.

Thus one can use energy windowing to reduce the amount of scattered photons imaged, but not eliminate scatter, due to the presence of classically scattered photons and the finite energy resolution of current imaging systems. In fact, the ratio of scattered to primary photons in the photo-peak energy window (scatter fraction) is typically 0.34 for Tc-99m [5] and 0.95 for Tl-201 [6]. When scatter is neither removed from the emission profiles prior to reconstruction nor incorporated into the reconstruction process, it can lead to over-correction for attenuation because the detected scattered photons violate the “good geometry” assumption of (1).

Several methods for the effects of scattered events have been proposed. The difference between methods is the way of estimating the scatter contribution. For example some methods involve events collection in one or more energy windows lower than the photo-peak one, and these data can be subtracted from the true data, before or after reconstruction. Other methods try to estimate the shape of the scatter component within the photo-peak window as a convolution of the photo-peak projection with the scatter distribution function.

The proposed method in this paper is based on convolution subtraction but uses wavelet to create matrix of scatter fractions instead of a global scatter fraction. In these techniques scatter correction in the projection relies on filter functions, evaluated by wavelet.

The aim of this work is try to estimate the shape of scatter within photo-peak window as a convolution of the lower energy projection (86-100keV) with the wavelet transform. The scatter projection was calculated from measurements of a 99mTc line source in a water cylindrical phantom within both photo-peak and lower energy windows. Then the term of calculated scatter was subtracted from photo-peak window (scatter plus primary). Gate software package was used for simulation and MATLAB software was used to design a 2D wavelet filter for estimating scatter in photo-peak. Finally their results were used to correct scatter for a more realistic phantom such as NCAT.

II. METHODS AND MATERIALS

Scatter corrections based on convolution or deconvolution were introduced by Axelsson et al [7] as a 1D method which was further developed to 2D by Msaki et al [8]. These methods take the spatial distribution of the scattered photons into account instead of the energy spectra. The methods operate on geometrically mean valued images to decrease the depth dependence. A scatter kernel describes the spatial distribution of the scattered photons, which in most cases, but not always [9], is assumed to have mono-exponential form. The exponential describing the fall-off of the scatter kernel is called “slope” in this work. Methods based on deconvolution use a one-step operation to calculate the scatter corrected image [8, 10] whereas methods based on convolution can be seen as two-step operations [6]. For the 2D two-step operation, convolution scatter subtraction, the geometric mean valued image of primary registrations $g(x,y)$ can ideally be calculated as (2) [11]:

$$2: g(x, y) = g_{\text{obs}}(x, y) - k_p(g(x, y) \otimes s)$$

where g_{obs} is the observed, non-corrected geometrically mean valued projection image, k_p is the scatter-to-primary ratio and s is the stationary scatter kernel. In this equation the image of primary registrations appear on both sides, and an approximation is therefore used where the original image is convolved with the scatter kernel (3):

$$3: g(x, y) = g_{\text{obs}}(x, y) - k_T(g_{\text{obs}}(x, y) \otimes s)$$

k_T in this equation is the scatter-to-total ratio. The method is based on the approximation that both the scatter-to-total ratio and the slope of the scatter kernel are constant. For a uniform object such as a cylindrical water phantom with uniform activity, this approximation is not too serious, but the severity of the approximation will increase for more inhomogeneous source distributions and density variations [12]. Instead of using a global scatter fraction as for convolution scatter subtraction, a scatter fraction is calculated for each pixel in the image to be corrected. In this way one of the stationary factors in convolution scatter subtraction is removed. The scatter fractions can be calculated from transmission measurements but they can also be calculated from ray sums through an attenuation map obtained by some other method, for example from CT images. This scatter correction technique can therefore easily be implemented if a non-uniform attenuation correction is utilized.

TDCS has been shown to give quantitative results with an accuracy better than 95% in the heart and lung region in a thorax phantom [13]. Quantitative results that are more accurate than results obtained using the TEW scatter correction technique and with a higher signal to noise ratio have also been demonstrated for simulations and measurements of a chest phantom. The primary source of weakness lies in the fact that it is a 2D method with a scatter kernel that is independent on object thickness and source distribution. The composition and shape of the object can however be taken into account to some degree because of the spatially varying scatter-to-total ratio.

We have investigated the impact of scatter on “cold” and “hot” tumor detection for Tc-99m -labeled antibody fragments used for hepatic imaging.

The Gate program was used to create 128 SPECT projections of the abdominal region as defined by the Zubal phantom.

The primary and scattered photons were stored in separate data files. Similarly, high-count projections of a 2.5-cm diameter spherical “tumor” in each of 3 locations within the liver were also created via Gate. These projections were scaled and added to (“hot” tumors) or subtracted from (“cold” tumors) the background distribution.

Projections were made with solely the primary photons present. These were used to assess the impact of perfect scatter rejection as might be approximated by imaging with a detector with extremely good energy resolution.

Projections were also made with both the primary and scattered photons present (standard imaging of Tc-99m), and with 2.5 times the scattered Tc-99m photons present.

To get a set of complete data needed for three-dimensional reconstruction, it is necessary to move the detector in space around the object, so as to get all the lines traversing the object in all directions (spaced over 360° by a circular orbit). Hence for a given single linear projection, only voxels lying on a straight line are concerned. Because of photon attenuation and the presence of a physical collimator, few from these primary photons (actually one out of 10⁴) would actually reach the detector [14].

To provide more convincing arguments regarding the viability of this idea, we use Gate software with the following working conditions:

- the used gamma detector is a conventional SPECT camera. It has discretized dimensions N length units × N length units. We have chosen N = 16 to keep the calculations required at a reasonable level.
- the scattering medium is represented by a cube of dimensions N × N × N,
- the electron density in biological medium is $n_e = 3.5 \times 10^{23}$ electrons/cm³,
- the radionuclide employed is Tc-99 with an activity concentration corresponding to 4.84×10^{10} counts per minutes per cm³,
- the acquisition time per projection is set to 0.1 sec,
- the 3D original object (cylinder of height 6 arbitrary units) is placed at the center of the scattering medium (cube),
- the distance from the camera to the upper face of the scattering medium cube is $l = 200$ arbitrary units.

A 256 × 256 pixels detector is placed on the xy plane. The pixel size is 0.4 × 0.4 mm². The scattering medium is a rectangular box of dimensions 30 cm by 30 cm by 15 cm, which is at a distance of 1 cm above the planar detector. The electronic density inside the scattering medium is $n_e = 3.341023$ electrons/cm³ since most biological tissues have an electronic structure close to that of water. The radionuclide used in this simulation is ^{99m}Tc, which emits photons at an energy of 140.1 keV. The scattering medium is discretized with 13 voxels in x and y axis directions and with 9 voxels in z axis direction. The detector is reduced to 13×13 pixels. We construct the weight matrix of the medium by calculating from our previous models, for each point of the mesh, the PSF of the detector at the different scattering angles. The reconstruction is carried out using the conjugated gradient method with positivity constraint.

The wavelet transform used in the present study is realized through an iterative decomposition algorithm known as the dyadic discrete wavelet transform (dyadic DWT).

Photoelectric absorption is most likely to occur for low photon energies (hv) and high atomic numbers (Z) of the absorbers, according to the following relation (4):

$$4: \sigma = Z^n / (hv)^{7/2}$$

where σ is the atomic cross section for the interaction, which is a measure of its probability. n is between 4 and 5, depending on both hv and Z. The photoelectric absorption involves complete absorption of the gamma photon and ejection of a bound electron.

The non-corrected geometrically mean valued projection image is re-normalized by σ according to the following relation (5):

$$5: \beta_\sigma(h, t) = \beta(h, t) \sigma(t)$$

respect to the (x, y) coordinate system then h and t can be written in terms of x and y (6,7), and the rotation angle θ as [15]:

$$6: t = x \cos \theta + y \sin \theta$$

$$7: h = -x \sin \theta + y \cos \theta$$

where h denotes the height and t denotes the time variable.

Our studies show that a simple estimate of a pixel-wise scatter threshold is given by (8):

$$8: eC = 1 + 3\sqrt{2}$$

Based on eC a simple indicator function can be introduced (9):

$$9: I(h, t) = \int \chi \{ \beta_\sigma(\xi, t) > eC \} (\xi, t) d\xi$$

where χ is the characteristic function with $\chi(\xi, t) = 1$ for $\beta_\sigma(\xi, t) > eC$ and $\chi(\xi, t) = 0$ elsewhere. Therefore, at locations (h, t) where $I(h, t) = 0$ we may assume that no scatter are present.

Hence, we may define corrected geometrically mean valued projection image data f (scatter- free) by (10):

$$10: f(h, t) = \beta(h, t) \chi \{ I(h, t) = 0 \} (h, t)$$

with $\chi(h, t) = 1$ for $I(h, t) = 0$ and zero elsewhere.

For temporal averaging, every k profiles are summed (thus reducing the number of profiles to Nt/k). Spatial smoothing is accomplished with a sliding-average length of l height bins (for ceilometer data with a bin width of 15 m, l = 20 is typical). The averaged data, F(h, t), are then used for the wavelet analysis.

The final step of the this procedure is the gradient analysis of F(h, t) of each individual spatial measurement, i.e. for each individual t. We define the wavelet transform as (11):

$$11: W_\psi F(h, a; t) = 1/\sqrt{c_\psi} \int F(\gamma, t) 1/\sqrt{a} \psi((\gamma-h)/a) d\gamma$$

Where the normalization constant c_ψ , given by (12):

$$12: 0 < c\psi = 2\pi \int |\psi(\omega)|^2 / |\omega| d\omega < \infty$$

reflects the constraint on the analyzing wavelets to produce an invertible and isometric transform. The isometric property is relevant since it ensures norm equality between the signal F and its wavelet transform (allowing a physical interpretation of the wavelet-transformed signal). ψ^\wedge denotes the Fourier transform of the analyzing wavelet.

which allows one to analyze also the behavior of derivatives of F of higher order, and this can give a hint at where the gradient growth (or decay) becomes maximum or minimum (C is a constant).

Our algorithm uses the Daubechies wavelet family (1st, 2nd, 3rd order) [15], thus yielding more structural information on the signals to be analyzed. In order to detect scatter, we evaluate the wavelet spectrum at all scales simultaneously.

This can be easily done by temporal spectrograms (13),

$$13: S(h, t) = \int |W\psi F(a, h; t)|^p da$$

With $p > 0$, which can alternatively be replaced by (14):

$$14: S(h, t) = (\int |W\psi F(a, h; t)|^p \text{sing}[W\psi F(a, h; t)] da$$

This equation additionally takes into account the sign of the gradient information (which is, for our purpose, rather important).

In general, the evaluation of S(h, t) will not yield a single, unique scatter function but a set of scatter candidates.

III. RESULTS

Two simulations of the Zubal phantom with an activity distribution were then performed one allowing scatter, and one without scatter. The images without scatter can be seen as the ideal images. The images including scatter were scatter corrected using parameters for the geometries, and for each geometry a range of different scatter kernel slopes were applied (Fig.2). The images compared with the reconstructed ideal image volume by means of the normalized mean square error (NMSE) [16]. NMSE quantifies the difference between the corrected images and the ideal images.

This simulated study showed that the method improves the image quality and quantitative accuracy up to 1.5 dB in comparison to scatter reduction in the convolution-based method (Fig.3).

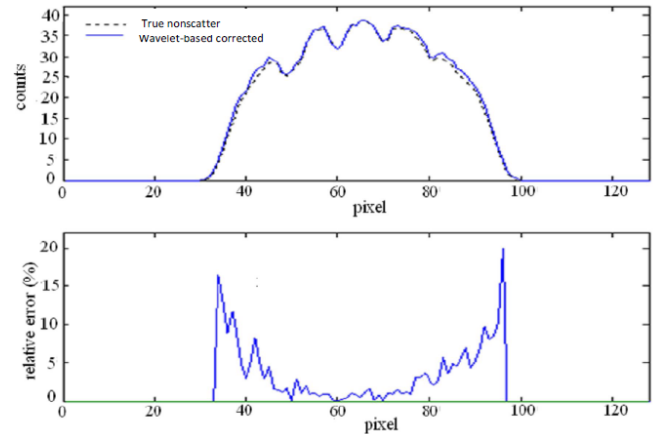


Figure2: Profile image including scatter that were scatter corrected and relative error.

For both simulations, primary images gave a statistically significant increase in detection accuracy in comparison to the images with an artificially elevated amount of scatter. Here the difference in areas was larger (0.88 versus 0.81 for cold tumors, and 0.84 versus 0.74 for hot tumors). In no case did scatter compensation result in a statistically significant increase in detection accuracy over any compensation. However, with the artificially elevated amount of scatter the areas did increase with scatter compensation (0.81 with no compensation versus 0.83 with scatter compensation for the cold tumors, and 0.74 with no compensation versus 0.78 with scatter compensation for the hot tumors).

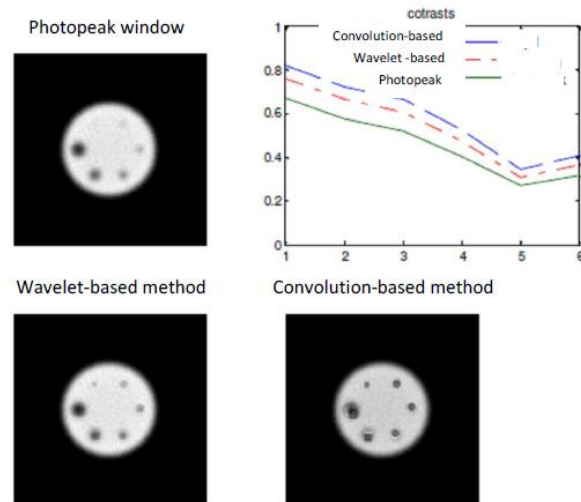


Figure3: comparison between scatter reduction in the convolution-based method and wavelet-based method

IV. CONCLUSION

The reconstruction results from computer simulations show that the wavelet-based SPECT reconstruction algorithm is accurate.

In summary, the results obtained with our algorithm are promising, but the quality of the retrieval has to be assessed in future studies. Questions that have to be addressed in this context evolve around the definition of scatter in general, and the threshold and parameter values used in the retrieval algorithm.

To evaluate accurately the spatial resolution, it is necessary to use real data and to compare it with conventional methods which do not make use of scattered radiation. At the present time, it is too early to use our preliminary simulation results for this purpose. This work is ongoing using realistic experimental conditions.

ACKNOWLEDGEMENTS

My friend and coworker Mohammad Seifabadi for support, encouragement and for sharing your inspiring ideas with me.

REFERENCES

- [1] H Tuy, An inversion formula for cone-beam reconstruction, *SIAM J. Appl. Math.*, vol. 43, pp. 546-552, 1983.
- [2] S Zhao, H Yu and G Wang, A unified framework for exact cone-beam reconstruction formulas, *Med. Phys.*, vol. 32, pp. 1712-1721, 2005.
- [3] Wernick M, Aarsvold J. Emission Tomography: *The Fundamentals of PET and SPECT* (San Diego, Academic Press, 2004).
- [4] Attix FH. *Introduction to Radiological Physics and Radiation Dosimetry* (John Wiley & Sons, New York, 1983).
- [5] de Vries DJ, King MA. Window selection for dual photo-peak window scatter correction in Tc-99m imaging. *IEEE Trans Nucl Sci* 41:2771-2778, 1994.
- [6] Hademenous GJ, King MA, Ljungberg M, Zubal G, Harrell CR. A scatter correction method for Tl-201 images: a Monte Carlo investigation. *IEEE Trans Nucl Sci* 30:1179-1186, 1993.
- [7] Axelsson B, Msaki P, Israelsson A. Subtraction of compton-scattered photons in singlephoton emission computed tomography. *J Nucl Med* 1984 25: 490-494
- [8] Msaki P, Axelsson B, Dahl CM, Larsson SA. A generalized scatter correction method in SPECT using point scatter distribution functions. *J Nucl Med* 1987 28: 1861-1869
- [9] Narita Y, Eberl S, Iida H, Hutton BF, Braun M, Nakamura T, Bautovich G. Monte Carlo and experimental evaluation of accuracy and noise properties of two scatter correction methods for SPECT. *Phys Med Biol* 1996 41: 2481-2496
- [10] Floyd CE, Jaszczak RJ, Greer KL, Coleman RE. Deconvolution of Compton scatter in SPECT. *J Nucl Med* 1985 26: 403-408
- [11] Msaki P, Erlandsson K, Svensson L, Nolstedt L. The convolution scatter subtraction hypothesis and its validity domain in radioisotope imaging. *Phys Med Biol* 1993 38: 1359-1370
- [12] Msaki P. Position-dependent scatter response function: will they make a difference in SPECT conducted with homogeneous cylindrical phantoms, *Phys Med Biol* 1994 39: 2319-2329
- [13] Meikle SR, Hutton BF, Bailey DL, Fulton RR, Schindhelm K. SPECT scatter correction in non-homogeneous media. In: Colchester A C F and Hawkes D J, eds. *Information processing in medical imaging, 12th international conference*. Berlin: Springer-Verlag 1991 34-44
- [14] Brooks, I.M. 2003: Finding boundary layer top: application of a wavelet covariance transform to lidar backscatter profiles. *J. Atmos. Ocean. Technol.*, 20, pp. 1092-1105.
- [15] Daubechies, I. *Ten Lectures on Wavelets* (SIAM, Philadelphia, U.S.A., 1992).
- [16] King MA, Schwinger RB, Penney BC. Variation of the count-dependent Metz-filter with imaging system modulation transfer function. *J Med Phys* 1986 13: 139-149.

An Efficient Method for Monitoring, Management and Treatment of Diabetes

M. Gautham¹, Devi. B.²

*1PG Scholar, 2Professor
SNS College of Technology, Coimbatore*

Abstract: SMARTDIAB is a platform designed to support the monitoring, management, and treatment of patients with diabetes. Here we are creating a platform that mainly consists of two units Patient Unit (PU) and Patient Management Unit (PMU). The PU consists of patient personal details and glucose level. These values are stored in the central data base that can be accessed by both the Patient and the Physician. The PMU consists of a diabetes data management system (DDMS) that provides risk assessment for long-term diabetes complications. The aim is to facilitate the patient information in a distributed manner; the details include all the medical records and daily intake of food and glucose level and visit entry. Effective information sharing through web services and mobile services is the aim of the proposed system SMARTDIAB.

Keywords: diabetes management, home care, information and communication technologies

I. INTRODUCTION

To a large extent computer based monitoring and intensive care unit systems have become cheap enough to be deployed on a large scale in many intensive diabetic care units around the world. The bedside has become an important point of displaying data. Bedside monitors have capabilities of intelligent monitoring, intelligent alarming, plug and play modules, TCP/IP and Ethernet networking and many other features provide easy, integrated monitoring in any facility. The systems often provide database and analysis functions that previously only was available on large systems. Most bedside monitors sold today can incorporate data from clinical laboratories, bedside laboratories devices.

In order to improve the monitoring and glycaemic control of patients with diabetes mellitus both academic and diabetes technology industry research is focused on the design and development of personal details as well as patient medical report. It is likely that the doctors and nurses would want to be mobile. When they visit a patient they could have a tablet PC with all the current charts and data for that particular patient ready. The architecture for supporting this could be designed in different ways, but the main parts that have to be realized would be:

- □An infrastructure for the monitoring devices to push their data into, for example a server with a database.
- □An infrastructure for the mobile devices to get the data.
- □It could also be realized in such way that the monitoring device stores all the data and applications needing data connected directly to the monitoring device.

Diabetes mellitus, previously known as insulin dependent diabetes mellitus, is a chronic metabolic disease characterized by absence of insulin secretion due to destruction of pancreatic beta-cells. Inadequate treatment leads to short-term (hypoglycaemia and hyperglycaemia) and long-term (e.g., neuropathies, nephropathy, retinopathy, heart disease, and stroke) complications, whereas intensive glycaemic control has been shown to reduce the risk to develop such complications [1]. In Diabetes, intensive glycaemic control is achieved by means of: 1) insulin therapy either through administration of multiple daily injections (MDI), known also as intensive conventional therapy, or through continuous subcutaneous insulin infusion (CSII) via insulin-pumps; and 2) regular self-monitoring of glucose levels by using either conventional finger-stick glucose meters (three to four times daily), or continuous glucose monitors (CGMs) that provide high frequency (e.g., every 5 min) measurements of glucose levels. In order to improve the monitoring and glycaemic control of patients with diabetes mellitus both academic and diabetes technology industry research is focused on the design and development of personal sensors for CGM multisensor device SMARTDIAB: A COMMUNICATION AND INFORMATION TECHNOLOGY APPROACH for physical activity monitoring, novel instruments for delivery of insulin, computational algorithms for insulin treatment optimization[13], data mining and visualization tools for better management of diabetes data, and intelligent decision support systems (DSS) to be used for patients health status assessment and prediction of diabetes-related complications.

Furthermore, advances in Information and Communication Technology have accelerated the design and implementation of telemedicine platforms, [11] for various diagnosis and treatment applications. Several telemedicine platforms have been proposed for diabetes

monitoring and management [10]. Systems using Internet and Public Switched Telephone Network (PSTN), allows a diabetes patient to send glucose measurements to a hospital, where a physician with a set of tools for data visualization, analysis, and decision support can analyze them and advise the patient on appropriate treatment adjustments. In the IDEATel project, Web-based computing and telecommunication networks have been established in both urban and rural economically disadvantaged areas within New York State. The project has involved 1500 diabetes patients. Another EU funded research project, entitled multiaccess services for managing diabetes mellitus (M2DM), has proposed a high-performance Web and a computer telephony integration server that can be accessed using different communication links, such as standard telephone lines, mobile phones, and Internet. Users (physicians and all types of diabetes patients) can access information using customized applications, general applications and terminals. Core of the platform is the multiaccess organizer, which is responsible for the coordination of a series of software agents.

This paper refers to the design and development of a pilot platform named SMARTDIAB, which is based on the combined use of information and communication technologies for the intelligent monitoring, management and followup of individuals with T1DM [11]. The platform integrates mobile infrastructure, Internet technology, novel, and commercially available continuous glucose measurement devices and insulin pumps, advanced modeling techniques, control methods, and tools for the intelligent processing of diabetes patients information. The platform allows 1) intensive monitoring of glucose levels; 2) diabetes treatment optimization; 3) continuous medical care; and 4) improvement of quality of life of individuals with T1DM.

The rest of the paper is organized as follows, The specifications and overall architecture of the SMARTDIAB platform. Design and implementation issues of the basic platform's units, the patient unit (PU) and the patient management unit (PMU), are presented. Functional issues emphasizing on security aspects and service usage scenarios. The strategy toward SMARTDIAB evaluation is described. While future research directions and conclusions are presented.

II. SMARTDIAB CONCEPT AND ARCHITECTURE

The SMARTDIAB platform consists of two units: 1) the PU; and 2) the PMU. In the PU, patient's related information, e.g., glucose levels, insulin intake, diet, and physical activity is acquired and transmitted, through telecommunication networks, using cellular phones or PC/laptops to the PMU. The PMU can be accessed from both medical personnel and patients, with appropriate security access rights. In the PMU, advanced tools for the intelligent processing of the patient's data are provided to the physician, who is able to monitor the health evolution

of the subject patient and make recommendation about his/her treatment.

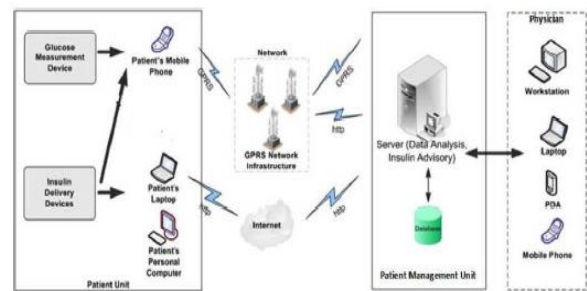


Fig.1. General architecture of SMARTDIAB

Furthermore, advanced computational tools permit the estimation of optimum insulin infusion rate in case the individual is under insulin pump treatment. Moreover, the T1DM individual can have a clear picture of his/her health status and how his/her habits influence the glucose profile. The major specifications of the PU are summarized in the following: 1) accurate, portable, lightweight devices for glucose measurement and insulin delivery; 2) visualization abilities; 3) wired and wireless communication capabilities; and 4) user-friendly interfaces. The specifications of the PMU comprise: 1) connectivity to the Internet and GPRS; 2) user-friendly interfaces; 3) ability to retrieve and manage patient information and data; and 4) advanced tools for data analysis, processing, modeling, decision support, and visualization.

III. EXPERIMENTAL SETUP

The experimental setup includes the following units namely Patient Management, Patient unit Management, Diabetic Management system, Policy analysis.

A. Patient Management:

The patient module contains all details about patients such as name, age, gender, date of birth, blood group and address. Rather than this the system maintains sugar level, glucose levels, insulin intake, diet and physical activity is acquired and transmitted, through telecommunication networks, using cellular phones or mail to the Patient Management Unit.

- personal data, such as height, weight, etc.;
- his/her personal logbook, consisting of important data, such as daily glucose level measurement, insulin intake, meal intake, and time of the action;
- medical record, such as medical exams, illness, etc.;
- Lifestyle and daily habits, such as exercise, etc.

B. Patient Unit management

This module can be accessed by the Patient Unit through the internet or using devices, such as mobile. The

Patient Management Unit consists of a diabetes data management system, a decision support system that provides risk assessment for long-term diabetes complications, and an insulin infusion advisory system, which reside on a Web server. Here the decision support has been developed with some flexibility, which can be used by patient as well as personnel with appropriate security access rights.

C. Diabetic Management system

This module maintains all the details about the patients and as well as the status in the web server. So that the data can be viewed by anyone with security access. This helps to know physicians to evaluate a patient's clinical state through the web application. For secured data processing the system implements secured TCP/IP connection by using 3 DES algorithms, which encrypts all sensitive data before transmission. The overall diabetic information management shared through mobile or PC with consistence security. The central DB is designed on the basis of the Health Level. Standard enabling communication with the hospital information system, where the patient management unit will be deployed. In the DB, information related to patient's data, records regarding laboratory examination results, Meta analysis results, and comments about the patient health state are stored.

D. Policy analysis.

This policy module defined to maintain the data's in a secured manner. For privacy and security this module has been proposed. This module establishing security policies, guidelines, and procedures is a critical step toward securing an infrastructure and its information. Policies set the overall tone and define how security is perceived. In the current information and communication technologies platform, appropriate security policies have been designed and applied in such a way that they will protect confidential, proprietary and sensitive information from unauthorized disclosure, modification, theft or destruction.

IV. FUNCTIONAL ISSUES

Treatment based on Patient's Profile: The fig 2 shows the process of the treatment of a T1DM patient and how the physician can be supported by SMARTDIAB in order to decide the necessary treatment alterations. More specifically, the T1DM patient uses the system's front-end interface to enter particular information concerning:

- personal data, such as height, weight, etc.;
- his/her personal logbook, consisting of important data, such as daily glucose level measurement, insulin intake, meal intake, and time of the action;
- medical record, such as medical exams, illness, etc.;
- lifestyle and daily habits, such as exercise, etc.

All the aforementioned information is stored in the central DB and is online available to the physician. Based on this information, the physician can use the platform to recommend alterations in patient's treatment, such as changes in the predefined glucose or insulin limits that can be tolerated by the patient, changes in insulin bolus dosage, in the nutrition program, or the exercise or even the pharmaceutical treatment, if considered necessary. These changes are stored in the central DB and are available online on patient's front-end application.

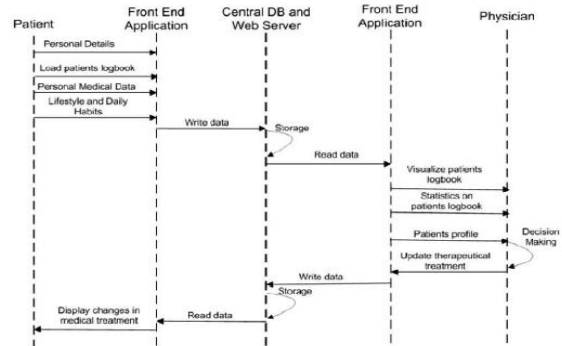


Fig.2. Treatment based on Patient's Profile
V. SECURITY FRAMEWORK

The used security framework is based on a component design approach [15], [16], which is comprised of the following four main components.

1) Platform Component:

Role-based access control (RBAC) was used to grant permissions to certain functionalities of the system for the three main categories of the users. RBAC was implemented using the object-oriented paradigm by authenticating the user to a role object in the DB. Thereafter, the role object loaded is passed as a parameter to the tasks that compose the overall functionality of the system and permission to invoke the task is granted to the initiating user according to her role.

Furthermore, several different GUI views have been implemented and the final front-end is constructed after role assignment achieving an extra layer of transparency for the separate roles. Three basic role groups were defined in the system.

The *patient role* that allows the patient to remotely access information concerning his/her current treatment status as well as any information stored in the DDMS.

- The *healthcare professional role* that gives access to the patient information in the DDMS. Each healthcare professional is tightly coupled with certain patients and can only view and alter their clinical information. An auditing mechanism ensures recording of every change made. This poses a strong security mechanism for intentional or nonintentional malalteration of information. Furthermore, the healthcare professional is

provided with a smart interface to interact with the IIAS. He has the ability to enable reporting for all or part of the decision made by the system.

- The *administrator role* that allows knowledge administrators to import new knowledge entities in the system. New medications and diseases can be imported to the system for future use by healthcare professionals. Furthermore, new users and their roles can be defined. User authentication is achieved at a DB scope through the usual username–password scheme. Hashing algorithms are implemented for secure transmission of user data. User-oriented data
- views provide further security by restricting access to specific medical data only to relevant users. On hardware level, a high level of redundancy is achieved using technologies, such as redundant array of inexpensive disk (RAID) with hard disk (HD) mirror imaging. Online transaction processing (OLTP) and online analytical processing (OLAP) algorithms that are implemented in the proposed system reside on different server machines to avoid interference between usual transactions on the patient object and decision support algorithms.

2) Network Component:

This research resulted in the implementation of a system with increased extranet traffic consisting of critical data. IPSec on the network layer, secure socket layer (SSL) on the transport layer are used to ensure secured communication between the remote servers. SSL over GPRS ensures secure transmission from the mobile phone. Hypertext Transfer Protocol Secure (HTTPS) is the protocol relied on to deliver secure transmission via the DDMS component. The central DB is protected using a router with specific access lists as well as an application layer firewall–intrusion detection system (IDS) that continuously monitors network traffic.

3) Physical Component–Securing Access:

The physical security component’s main role is to prevent unauthorized users to physically contact the SMARTDIAB’s devices. Furthermore, this subcomponent has to deal with the possibility of a natural disaster or possible lack of energy resources. Critical systems of the proposed project will operate in controlled environments, safe from intrusion.

4) Policy Component–Designing Guidelines:

Establishing security policies, guidelines, and procedures is a critical step toward securing an infrastructure and its information. Policies set the overall tone and define how security is perceived. In the current information and communication technologies (ICT) platform, appropriate security policies have been designed and applied in such a way that they will protect

confidential, proprietary, and sensitive information from unauthorized disclosure, modification, theft, or destruction.

VI. SIMULATION RESULTS

The design are done with the help of dot net. The patient details along with their continuous glucose measurements are designed by using dot net and patient registration , patient lifestyle and patient reports are given below.

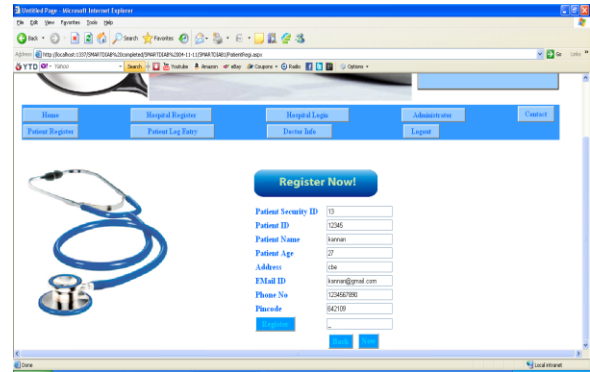


Fig.3.Patient Registration

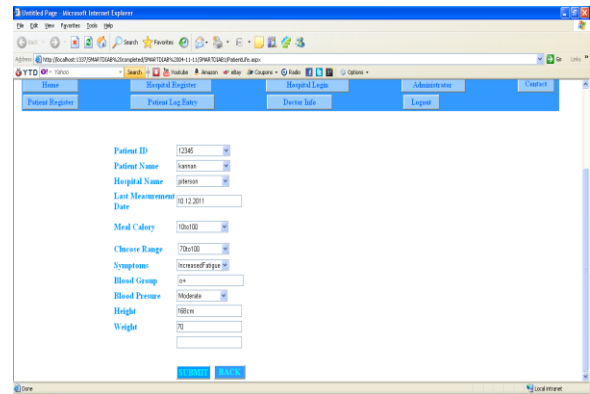


Fig.4. Patient Lifestyle

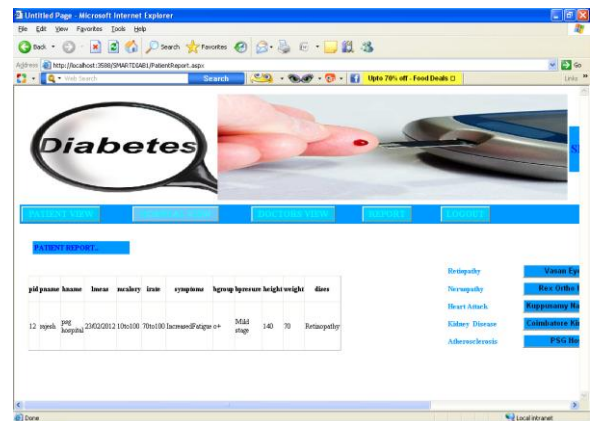


Fig.5. Patient Report

VII. CONCLUSION

In this paper, SMARTDIAB platform has been designed by using Information and Communication Technology for the monitoring, management and treatment of diabetes. The platform permits the continuous monitoring and the continuous provision of healthcare to diabetes patients using telemedicine, through the Internet. User-friendly Web and mobile phone interfaces along with advanced data processing functionalities allow for the optimization of diabetes mellitus treatment. Additionally, a central DB, containing patients related data, clinical and laboratory exams, along with appropriate tools for data storage, management, mining and visualization allow healthcare professionals to assess the health status of their patients and update/modify the applied treatment.

REFERENCES

- [1] The Diabetes Control and Complications Trial Research Group, "The effect of intensive treatment of diabetes on the development and progression of long-term complications in insulin-dependent diabetes mellitus," *New Engl. J. Med.*, vol. 329, no. 14, pp. 977–986, 1993.
- [2] C.M. Girardin, C. Huot, M. Gonthier, and E. Delvin, "Continuous glucose monitoring: A review of biochemical perspectives and clinical use in type 1 diabetes," *Clin. Biochem.*, vol. 42, pp. 136–142, 2009.
- [3] C. Dalla Man, R. A. Rizza, and C. Cobelli, "Meal simulation model of the glucose-insulin system," *IEEE Trans. Biomed. Eng.*, vol. 54, no. 10, pp. 1740–1749, Oct. 2007.
- [4] R. Bellazzi, C. Larizza, A. Riva, A. Mira, S. Fiocchi, and M. Stefanelli, "Distributed intelligent data analysis in diabetic patient management," in *Proc. 1996 AMIA Annu. Fall Symp.*, pp. 194–198.
- [5] E. Ruiz-Velázquez, R. Femat, and D.U. Campos-Delgado, "Blood glucose control for type I diabetes mellitus: A robust tracking H_∞ problem," *Control Eng. Pract.*, vol. 12, pp. 1179–1195, 2004.
- [6] R. Bellazzi, "Telemedicine and diabetes management: Current challenges and future research directions," *J. Diabetes Sci. Technol.*, vol. 2, no. 1, pp. 98–104, 2008.
- [7] R. Bellazzi, C. Larizza, S. Montani, A. Riva, M. Stefanelli, G. d'Annunzio, R. Lorini, E. J. Gomez, E. Hernando, E. Bruges, J. Cermeño, R. Corcoy, A. de Leiva, C. Cobelli, G. Nucci, S. Del Prato, A. Maran, E. Kilkki, and J. Tuominen, "A telemedicine support for diabetes management: The T-IDDM project," *Comput. Methods Programs Biomed.*, vol. 69, pp. 147–161, 2002.
- [8] E. J. Gómez, M. E. Hernando, A. García, F. Del Pozo, J. Cermeño, R. Corcoy, E. Bruges, and A. De Leiva, "Telemedicine as a tool for intensive management of diabetes: The DIABTel experience," *Comput. Methods Programs Biomed.*, vol. 69, pp. 163–177, 2002.
- [9] Y.-T. Liao, S.-T. Tang, T.-C. Chen, C.-H. Tsao, T.-C. Lee, Y.-F. Huang, and S.-T. Young, "A communication platform for diabetes surveillance," presented at the 26th Annu. Int. Conf. IEEE EMBS, San Francisco, CA, Sep. 1–5, 2004.
- [10] S. G. Mougiakakou, J. Stoitsis, D. Iliopoulou, A. Prentza, K. S. Nikita, and D. Koutsouris, "A communication platform for tele-monitoring and tele-management of type 1 diabetes," in *Proc. 27th Annu. Int. Conf. Eng. Med. Biol. Soc. (IEEEEMBS 2005)*, pp. 2207–2210.
- [11] M. Skevofilakas, S. G. Mougiakakou, K. Zarkogianni, E. Aslanoglou, S. A. Pavlopoulos, A. Vazeou, C. S. Bartsocas, and K. S. Nikita, "A communication and information technology infrastructure for real time monitoring and management of type 1 diabetes patients," in *Proc. 29th Annu. Int. Conf. IEEE Eng. Med. Biol. Soc. (EMBS 2007)*, pp. 3685–3688.
- [12] S. G. Mougiakakou, K. Proutzou, and K. S. Nikita, "A real time simulation model of glucose–insulin metabolism for type 1 diabetes patients," presented at the IEEE Eng. Med. Biol., 27th Annu. Conf., Shanghai, China, 2005.
- [13] R. Williams and D. Zipser, "Gradient based algorithms for recurrent NN and their computational complexity," in *Back-propagation: Theory Architectures and Applications*. Hillsdale, NJ: Erlbaum, 1995.
- [14] K. Zarkogianni, S. G. Mougiakakou, A. Proutzou, K. S. Nikita, A. Vazeou, and C. S. Bartsocas, "An insulin infusion advisory system for type 1 diabetes patients based on non-linear model predictive control methods," presented at the IEEE Eng. Med. Biol. Conf. 2007 (EMBC 2006), Lyon, France, Aug.
- [15] R. Orfali, D. Harkey, and J. Edwards, *The Essential Client Server Survival Guide*. New York, Wiley, 1999.
- [16] J. Mundy, W. Thornthwaite, and R. Kimball, *The Microsoft Data Warehouse Toolkit: With SQL Server 2005 and the Microsoft Business Intelligence Studio*. New York: Wiley, 2006.
- [17] "SMARTDIAB: A Communication and Information Technology Approach for the Intelligent Monitoring, Management and Followup of Type 1 Diabetes Patients," *IEEE Transactions on Information Technology in Biomedicine*, Vol. 14, No.3, pp 62–633, May 2010.

Banked Approach of Low Power Design of Pre-Computation Based Content Addressable Memory

Rafeekha M. J ¹, V. Lakshmi Narasimhan²

¹PG Scholar, Department of Electrical and Electronics Engineering, Hindusthan College of Engineering and Technology, Coimbatore 641032, Tamilnadu, India

²Assistant Professor, Department of Electrical and Electronics Engineering, Hindusthan College of Engineering and Technology, Coimbatore 641032, Tamilnadu, India

ABSTRACT

Content-addressable memory (CAM) or associative memory is used in applications that require large amount of data transfer in less time. It is a storage device that is addressed by its contents. It is able to perform look-up table function in a single clock-cycle. They are mainly used in network routers for packet forwarding and packet classification. But the parallel comparison technique used in CAM reduces search time, but it increases power consumption. The main challenge in the design of CAM is the reduction in power consumption. This paper presents a banked approach to improve the efficiency of low power precomputation-based CAM (PB-CAM). It is simulated using modelsim. The experimental results show that the Banked PB-CAM system can achieve greater power reduction without the need for a special CAM cell design. This implies that approach is more flexible and adaptive for general designs.

Keywords: Associative memory, Content-addressable memory (CAM), low-power, PB-CAM, precomputation.

1. Introduction

Content-addressable memory (CAM) is a special type of computer Memory used in certain very high speed searching applications. It is also known as associative memory, associative storage, or associative array. Fig 1 shows the comparison between a traditional memory and a content addressable memory. In a traditional memory input is the address of the memory location that we are interested and output will be the content of that address. In CAM it is the reverse. A content-addressable memory is a critical device used for applications involving asynchronous transfer mode (ATM), communication networks, LAN bridges/switches, databases, lookup tables, and tag directories, due to its high-speed data search capability. A CAM is a functional memory with a large amount of stored data that simultaneously compares the input search data with the stored data. The vast number of comparison operations required by CAMs consumes a large amount of power [1].

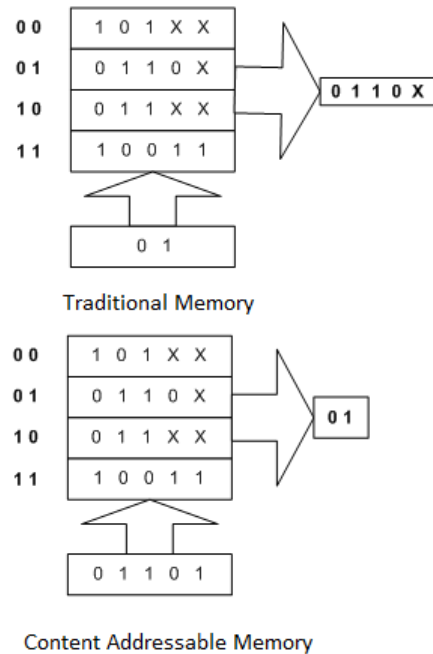


Fig 1: Comparison between traditional memory and content addressable memory.

Since CAM is an outgrowth of Random Access Memory (RAM) technology, in order to understand CAM, it helps to contrast it with RAM. A RAM is an integrated circuit that stores data temporarily. Data is stored in a RAM at a particular location, called an address. In a RAM, the user supplies the address, and gets back the data. The number of address line limits the depth of a memory using RAM, but the width of the memory can be extended as far as desired. With CAM, the user supplies the data and gets back the address. The CAM searches through the memory in one clock cycle and returns the address where the data is found. The CAM can be preloaded at device startup and also be rewritten during device operation. Because the CAM does not need address lines to find data, the depth of a memory system using CAM can be extended as far as desired, but the width is limited by the physical size of the memory.

CAM can be used to accelerate any application requiring fast searches of data-base, lists, or patterns, such as in image or voice recognition, or computer and communication designs. For this reason, CAM is used in applications where search time is very critical and must be very short. For example, the search key could be the IP

address of a network user, and the associated information could be user's access privileges and his location on the network. If the search key presented to the CAM is present in the CAM's table, the CAM indicates a 'match' and returns the associated information, which is the user's privilege. A CAM can thus operate as a data parallel or Single Instruction/Multiple Data (SIMD) processor [2].

Content Addressable Memory (CAM) or associative memory, is a storage device, which can be addressed by its own contents. Each bit of CAM storage includes comparison logic. A data value input to the CAM is simultaneously compared with all the stored data. The match result is the corresponding address. A CAM operates as a data parallel processor. CAMs can be used to design Asynchronous Transfer Mode (ATM) switches. Implementing CAM in ATM applications are specifically described in this application note. As a reference, the application note XAPP201 "An Overview of Multiple CAM Designs in Virtex™ Devices" presents diverse approaches to implement CAM in other designs.

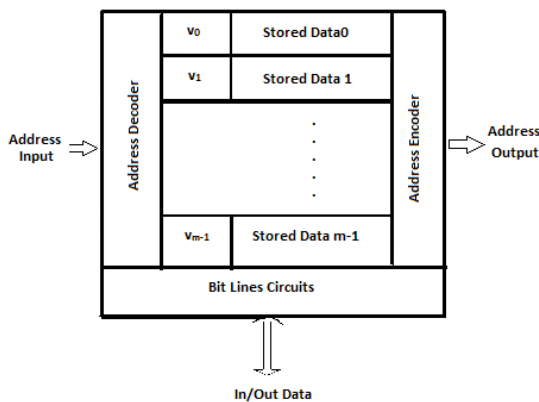


Fig 2: General CAM Architecture

Fig 2 shows the general CAM architecture. It consists of data memory with valid bit field, address decoder, and address priority encoder. The valid bit field indicates the availability of stored data. In the data searching operation, the input data is sent into CAM to compare with all valid data stored in CAM simultaneously, and an address from among those matches of comparison is sent to the output. In this architecture, the CAM circuit performs large amount of comparison operations to identify all valid data stored in CAM during each data searching operation. This comparison consumes most of the total CAM power. In the past decade, much research on energy reduction has focused on the circuit and technology domains provide a comprehensive survey on CAM designs from circuit to architectural levels. Several works on reducing CAM power consumption have focused on reducing match-line power [3].

Although there has been progress in this area in recent years, the power consumption of CAMs is still high compared with RAMs of similar size. At the same time, research in associative cache system design for power efficiency at the architectural level continues to increase. The

filter cache and location cache techniques can effectively reduce the power dissipation by adding a very small cache. However, the use of these caches requires major modifications to the memory structure and hierarchy to fit the design.

Pagiartzis *et al.* proposed a cache-CAM (C-CAM) that reduces power consumption relative to the cache hit rate. Lin *et al.* presented a ones-count pre computation-based CAM (PB-CAM) that achieves low-power, low cost, low-voltage, and high-reliability features. Although Cheng further improved the efficiency of PB-CAMs, the approach proposed requires considerable modification to the memory architecture to achieve high performance [8]. Therefore, it is beyond the scope of the general CAM design. Moreover, the disadvantage of the ones count PB-CAM system is that it adopts a special memory cell design for reducing power consumption, which is only applicable to the ones count parameter extractor.

This paper deals with banked approach for reducing comparison operations in the second part for the PB-CAM. This approach employs a brand new parameter extractor, which can better reduce the comparison operations required than the ones-count approach. Hence this reduces the power consumption by reducing comparison operations. The BANKED APPROACH that has been presented is suitable for applications demanding a large size of the storage device while the performance is still required. Architecture employs the precomputed parameter to perform a power-aware ordering of the data.

2. System Architecture

The memory organization of the PB-CAM architecture proposed by Lin *et al.*, which consists of data memory, parameter memory, and parameter extractor, where $k \ll n$. To reduce massive comparison operations for data searches, the operation is divided into two parts. In the first part, the parameter extractor extracts a parameter from the input data, which is then compared to parameters stored in parallel in the parameter memory. If no match is returned in the first part, it means that the input data mismatch the data related to the stored parameter. Otherwise, the data related to those stored parameters have to be compared in the second part [10].

It should be noted that although the first part must access the entire parameter memory, the parameter memory is far smaller than that of the CAM (data memory). Moreover, since comparisons made in the first part have already filtered out the unmatched data, the second part only needs to compare the data that match from the first part. The PB-CAM exploits this characteristic to reduce the comparison operations, thereby saving power. Therefore, the parameter extractor of the PB-CAM is critical, because it determines the number of comparison operations in the second part [12].

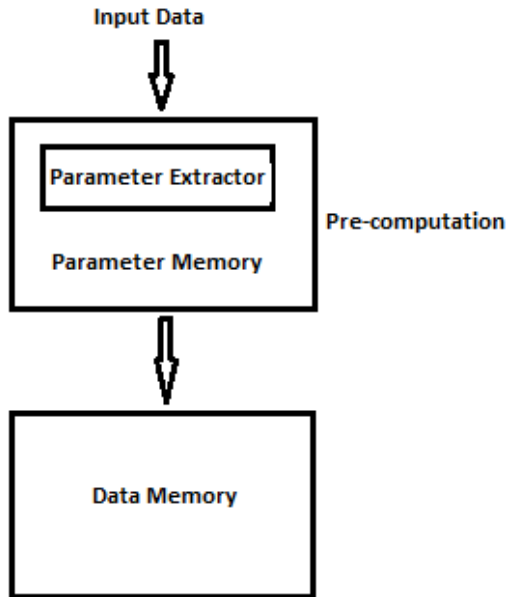


Fig. 3: Basic PB-CAM architecture

2.1. 1's count PB- CAM

Recently pre-computation technique has received as one of the most effective approaches for low-power designs. Pre-computation –based CAM (PB-CAM) stores extra information along with data used in the data searching operation to eliminate most of the unnecessary comparison operation, thereby saving power [14].

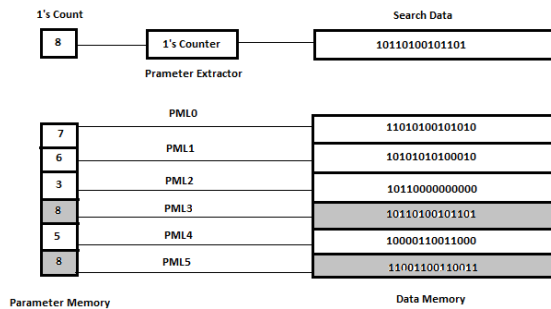


Fig 4: 1's Count Parameter Extraction for a 14 Bit Data

The total number of CAM cell comparisons in 1's count approach is equal to $m \times \log(n+2) + (m \times n) / (n+1)$, where m is the number of words and n is the number of bits in the word. The traditional CAM architecture has $(m \times n)$ CAM cell comparisons and it is known that $m \times (\log(n+2) + 1) \leq (m \times n)$ for $n > 4$ therefore the PB CAM architecture consumes less comparison power than traditional CAM architecture. The ones count parameter extractor is implemented with many full adders, so it consumes huge power and hardware consumption which not only wastes area but increases delay. And also the cost is high. To overcome this Block-XOR circuit is designed.

3. Block- XOR Approach

3.1. Block-XOR PB-CAM Structure

In this approach, the input data bit is first partitioned into several blocks, from which an output bit is computed using XOR logic operation for each of these blocks. The output bits are then combined to become the input parameter for the second part of the comparison process. To compare with the ones-count approach, then set the bit length of the parameter to $d \log(n+2)^e$, where n is the bit length of the input data. Therefore, the number of blocks is $dn = \log(n+2)^e$ in this approach. Taking the 14-bit input length as an example, the bit length of the parameter is

$$\log(14 + 2) = 4\text{-bit, and the number of blocks is } d14 = \log(14 + 2)^e = 4.$$

The selected signal is defined as $S = P3P2P1P0$:
 (2) According to (2), if the parameter is "0000_1110" ($S = \setminus 0$), the multiplexer will transmit the $i0$ data as the output. In other words, the parameter does not change. Otherwise, ($P3P2P1P0 = \setminus 1111$, $S = \setminus 1$), the first block of the input data becomes the new parameter, and "1111" can then be used as the valid bit. Note that the case where the first block is "1111" was not considered, because the "1111" block is the parameter.

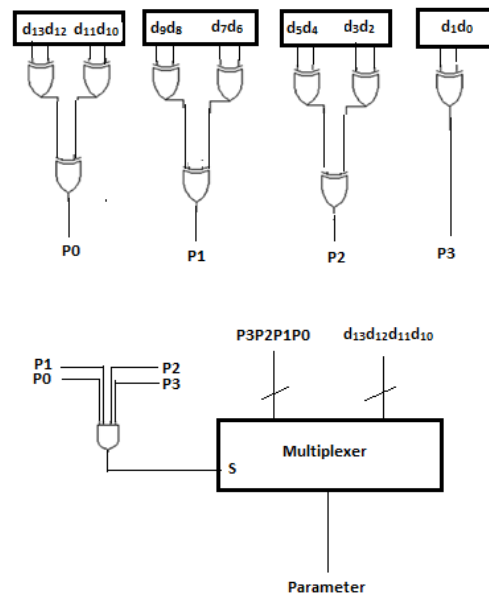


Fig. 5: Structure of Block-XOR approach with valid bit.

3.2. Mathematical Analysis

The concept of Block-XOR approach is to uniformly distribute the parameter over the input data. By the rule of product, the number of input data that results in the same parameter (without valid bit) is $8 \times 8 \times 8 \times 2 = 1024$. Consequently, the average probability can be determined as $1024 = (1024 \times 16) \times 100\% = 6:25\%$. Accordingly, the maximum number of comparison operations is 1024 for each parameter in the second part. Obviously, the concept of Block-XOR approach can reduce the comparison operations, hence minimize power consumption (i.e., with valid bit).

Table1. Comparison between block-XOR approach and banked approach

	Banked Approach		Block- XOR Approach	
	Used	available	used	Available
IOS utilization	14	232	64	232
Utilisation %	6		27	

The power comparison table of the three approaches is shown in table2. The conventional PB-CAM has an average power consumption of 266.84mW, the Block-XOR PB-CAM has 146.48 mW and the BANKED PB-CAM has 26.79 mW.

Table 2. Power comparison between three approaches.

	PB-CAM	BLOCK XOR PB-CAM	BANKED PB-CAM
Technology	0.35µm	0.35µm	0.35µm
Configuration	2048×32	2048×32	2048×32
Search delay	25ns	15ns	7.5ns
Average power	266.84mW	146.48mW	26.79mW
Average power reduction (%)		45	81.7

References

- [1] K. Pagiamtzis and A. Sheikholeslami, "Content-addressable memory (CAM) circuits and architectures: A tutorial and survey," *IEEE J. Solid-State Circuits*, vol. 41, no. 3, pp. 712–727, Mar. 2006.
- [2] M. Tanaka, H. Miyatake, and Y. Mori, "A design for high-speed-low power CMOS fully parallel content-addressable memory macros," *IEEE J. Solid-State Circuits*, vol. 36, no. 6, pp. 956–968, Jun. 2001.
- [3] I. Arsovski, T. Chandler, and A. Sheikholeslami, "A ternary content-addressable memory (TCAM) based on 4T static storage and including a current-race sensing scheme," *IEEE J. Solid-State Circuits*, vol. 38, no. 1, pp. 155–158, Jan. 2003.
- [4] I. Arsovski and A. Sheikholeslami, "A mismatch-dependent power allocation technique for match-line sensing in content-addressable memories," *IEEE J. Solid State Circuits*, vol. 38, no. 11, pp. 1958–1966, Nov. 2003.
- [5] Y. J. Chang, F. Lai, and S. J. Ruan, "Design and analysis of low power cache using two-level filter scheme," *IEEE Trans. Very Large Scale Integr. (VLSI) Syst.*, vol. 11, no. 4, pp. 568–580, Aug. 2003.
- [6] S. Bhattacharyya, T. Srikanthan, and Vivekanandarajah, "Dynamic filter cache for low power instruction memory hierarchy," in *Proc. Euromicro Symp. Digit. Syst. Des.*, Sep. 2004, pp. 607–610.
- [7] Y. Hu, W. B. Jone, and R. Min, "Location cache: A low-power L2 cache system," in *Proc. Int. Symp. Low Power Electron. Des.*, Apr. 2004, pp. 120–125.
- [8] K. Pagiamtzis and A. Sheikholeslami, "Using cache to reduce power in content-addressable memories (CAMs)," in *Proc. IEEE Custom Circuits Conf.*, Sep. 2005, pp. 369–372.
- [9] J. C. Chang, B. D. Liu, and C. S. Liu, "A low-power precomputation-based fully parallel content-addressable memory," *IEEE J. Solid-State Circuits*, vol. 38, no. 4, pp. 622–654, Apr. 2003.
- [10] K. H. Cheng, S. Y. Jiang, and C. H. Wei, "Static divided word matching line for low-power content addressable memory design," in *Proc. IEEE Int. Symp. Circuits Syst.*, May 2004, vol. 2, pp. 23–26.
- [11] Anh Tuan Do, Shoushan Chen, Zhi-Hui Kong, and Kiat Seng Yeo, "A Low power CAM with Efficient Power and Delay Trade-off," *Circuits and Systems, 2011 IEEE International Symposium*, pp. 2573–2576, 2011.
- [12] Echeverria, P.; Ayala, J. L.; Lopez-Vallejo, M.; "Leakage Energy Reduction in Banked Content Addressable Memories", *Electronics, Circuits and Systems, 2006. ICECS '06. 13th IEEE International Conference*, pp. 1196–1199, Dec. 2006.
- [13] Echeverria, P.; Ayala, J. L.; Lopez-Vallejo, M.; "A banked precomputation-based CAM architecture for low-power storage-demanding applications," *hi Electrotechnical Conference, 2006. MELECON 2006. IEEE Mediterranean*, pp. 57–60, May 2006.
- [14] Eshraghian, Kyoung Rok Cho, Soon Ku Kang, Abbott D., "Mermistor MOS content Addressable Memory: Hybrid architecture for future High Performance Search Engines"; *VLSI Systems IEEE Transactions*, pp. 1407–1417, 2011.
- [15] Jianping Hu, Jinghong Fu, Xiaoyan Luo; "A Single Phase Adiabatic CAM Using Adiabatic CAL Circuits," *Circuits, Communications and Systems 2009 Pacific Asia Conference*, pp. 338–341, 2009.
- [16] Jui-Yuan Hsieh; Shanq-Jang Ruan; "Synthesis and design of parameter extractors for low-power pre-computation-based content-addressable memory using gate-block selection algorithm," *Design Automation Conference, 2008. ASPDAC 2008. Asia and South Pacific*, pp. 316–321, March 2008.
- [17] Kavitha, V.; Jeeva, S.; "Low power design of pre-computation based content-addressable memory," *Communication and*

- Computational Intelligence(INCOCCI), 2010 International Conference*, pp. 223-228, Dec.2010.
- [18] Mahini Alireza, Bergani, Reza, Fatemah, Seyedah,," "low power TCAM forwarding engine for IP packets" *2007 Military Communications Conference*, pp 1-7,2007.
- [19] Rueichi Shen; Chinhung Peng; Feipei Lai,;" An early design estimation approach to synthesize the low-power pre-computation-based content addressable memory ". *Open Systems (ICOS), 2011 IEEE Conference*, pp 21 – 25, Sept. 2011.
- [20] Tsung-ShengLai; Chin-HungPeng;FeipeiLai,;" Data driven approach for low power precomputation based content Addressable memory" *Computers & Informatics (ISCI), 2011 IEEE Symposium*, pp328-333, March2011 .
- [21] Yu-Ting Pai; Chia-Han Lee; Shanq-Jang Ruan; Naroska,E; "An improved comparison circuit for low power pre-computation- based content-addressable memory designs",*Electronics, Circuits, and Systems, 2009. ICECS 2009. 16th IEEE International Conference*, pp.663-666. Dec.2009.

Selection of spiral capillary tube for refrigeration appliances

Nishant P. Tekade

M. Tech. IV Semester Heat Power Engineering, Mechanical Engineering Department, G. H. Raison College of Engineering, Digdoh hills, Nagpur-440016, Maharashtra State, India.

Dr. U. S. Wankhede

Professor, Mechanical Engineering Department, G. H. Raison College of Engineering, and Digdoh hills, Nagpur-440016, Maharashtra State, India.

Abstract:

Selection of spiral capillary tube for refrigeration appliances and the effect of changes in the parameters such as capillary tube dimensions i.e. capillary tube diameter, coil pitch, capillary tube length and inlet conditions of refrigerant to the capillary tube i.e. degree of subcooling, inlet pressure on the mass flow rate of the refrigerant, also investigation about the coiling effect of spiral capillary tube on mass flow rate of refrigerant for same cooling load is reviewed in this paper. The characteristics coiling parameter for a spiral capillary tube is the coil pitch; hence, the effect of the coil pitch on the mass flow rate of refrigerant for several spiral capillary tube test sections plays vital role in investigation of the performance.

The review is focused on the influence of tube diameter, tube length, coil pitch, and inlet condition on mass flow rate of refrigerant through spiral capillary tube, and also on investigation about the Coefficient of Performance (COP) of the system due to coiling effect of capillary tube. The use of spiral capillary tube reduces the space for the refrigeration system which is the need for more compact refrigeration system in the current trend. As the spiral capillary tube can be efficient in refrigeration appliances, it can also be employed in the air conditioning appliances.

Keywords: Spiral capillary tube, mass flow rate, coiling effect.

Introduction:

Capillary tubes are used to expand the refrigerant from the condenser pressure to the evaporator pressure in low capacity refrigerating machines such as domestic refrigerators and window type room air conditioners. It also controls the refrigerant mass flow rate and balances the system pressure in the refrigeration cycle. However, it has no provision to adjust the mass flow rate when load conditions changes. In spite of this fact, capillary tubes are preferred in small capacity refrigerating machines, where the load is fairly constant due to its several advantages such as simplicity, low cost, zero maintenance, and requirement of a low starting torque motor to run the compressor.

To overcome Ozone depletion and global warming problems, replacement of chlorofluorocarbon refrigerant like R 22 is required. The search for eco-friendly alternative of R-22 has brought out R-407C as the best promising ozone-safe substitute of R-22. If the refrigerants are changed in the existing VCRS system, the COP of the system will be affected thereby either reducing cooling effect or increasing the amount of compressor work. The review is divided in two parts. First one is selection of refrigerant and another one is select proper size of capillary tube.

A) Selection of refrigerant:

There is no general rule governing the selection of refrigerants. It depends upon thermo physical properties, technological and economic aspects, safety and environmental factor, the capacity required for household refrigerators, which have refrigerating capacities of 400-500 W and electrical power input within 100-150 W range. The energy efficiency is far from that achieved using vapour-compression systems.

After many years of testing and investigation, R407C is recognized as a suitable alternative refrigerant for R22 in medium and high temperature applications such as residential and light commercial air conditioning. R407C is a ternary blend of hydro fluorocarbon or HFC compounds, comprising 23% of R32 (Di-fluoro-methane, CF_2H_2), 25% of R125 (Penta-fluoro-ethane, CF_3CHF_2) and 52% of R134a (Penta-fluoro-ethane, $\text{CF}_3\text{CH}_2\text{F}$). It has no chlorine content, no ozone depletion potential, and only a modest direct global warming potential. $\text{ODP} = 0$, $\text{GWP} = 1610$.

B. G. Lee et al. (2005) concluded that ternary mixtures composed of HFCs and HCs can be used to develop the HCFC-22 alternative refrigerant mixtures. They selected HFC-32, HFC-125, HFC-134a, HFC-143a, HFC-152a, HFC-227ea, and HFC-236ea as HFCs, and propane and iso-butane as HCs. The simulator which could predict theoretically the performance of given refrigerant mixtures was developed and tested for various refrigerant systems. Nineteen different kinds of ternary mixtures were chosen for thermodynamic simulation. Among nineteen mixtures, six ternary refrigerant mixtures were selected as candidates for HCFC-22 alternatives. They were R-32/143a/600, R-32/152a/227ea, R-32/134a/236ea, R-

2/143a/236ea, R-32/152a/236ea, and R-32/134a/600a. Performance of these mixtures was obtained experimentally by the thermodynamic calorimeter and was compared with that of HCFC-22, R-407C and R-410A.

L. B. Ortiz et al. (2001) investigated theoretically and experimentally, for an adiabatic flow in capillary tube covering R-22 and three substitutes; two binary mixtures, R-32/ R-134a (30/70% by weight) and R-32/R-125(60/40%), and R-407c{R-32/R-125/ R-134a (23/25/52%)}. A comparison was carried out between experimental results and model predictions for one single length and two diameters. Result had showed similar performances for R-22 and R-407c. For particular geometry with large degrees of subcooling (above 12⁰C), refrigerant mass flow rates were very similar. As the subcooling decreases, refrigerant R-407c mass flow rate becomes a fraction larger for different operating conditions (condensing temperature and degree of subcooling).

S. M. Sami et al. (2003) experimentally investigated the performance of new alternative refrigerant mixtures such as R-410A, R-507, R-407C, and R-404A under various conditions of magnetic field. The test results were obtained using an air-source heat pump set-up with enhanced surface tubing under various magnetic field conditions. Performance tests were conducted according to the ARI/ASHRAE Standards. The test results demonstrated that as magnetic field force increases, compressor head pressure and discharge temperature slightly increase as well as less liquid refrigerant is boiling in the compressor shell. This has a positive effect in protecting the compressor. The effect of magnetic field on mixture behavior varies from one mixture to another depending upon the mixture's composition and its boiling point. Furthermore, the use of magnetic field appears to have a positive influence on the system COP as well as thermal capacities of condenser and evaporator.

Hira Lal Sachdev et al. (2004) carried out experimental analysis along with energy analysis of vapour compression refrigeration cycle for R-22 and its alternate refrigerant R407C, R410A and R417A has been carried out by varying evaporator temperature between -38 °C to 7°C and condenser temperature between 35 °C to 60°C, with the help of Engineering Equation Solver (EES). The parametric investigation such as coefficient of performance, volumetric cooling capacity, pressure ratio, exergy destruction ratio, exergetic efficiency, and efficiency defect in individual components for R-22, R-407C, R-410A and R-417A have been carried out theoretically and have been compared with the experimental available data. The results indicate that evaporating and condensing temperatures have pronounced effect on exergy destruction in the air-conditioner components such as compressor, condenser, and throttle valve where as in the evaporator it is negligible. The exergetic efficiency and COP of the cycle change to large extent with the variation in evaporator and condenser temperatures. The computational analysis has allowed the determination of the best energetic and exergetic performances of R-22 and its substitute refrigerant R-407C, R410A and R417A.

B) Selection of capillary tube:

Several combinations of length and bore are available for the same mass flow rate and pressure drop. However, once a capillary tube of some diameter and length has been installed in a refrigeration system, the mass flow rate through it will vary in such a manner that the total pressure drop through it matches with the pressure difference between condenser and the evaporator. Its mass flow rate is totally dependent upon the pressure difference across it; it cannot adjust itself to variation of load effectively. Most of the studies in coiled capillary tubes have been performed with helically coiled capillary tubes, as the helically coiled capillary tubes can be accommodated in a small space. Hence relatively little information in open literature is available on the flow characteristics of refrigerants in a spiral capillary tube.

M. K. Mittal et al. (2009) investigated the effect of coiling on the flow characteristics of R-407C in an adiabatic spiral capillary tube. The characteristic coiling parameter for a spiral capillary tube is the coil pitch. The effect of the coil pitch on the mass flow rate of R-407C was studied on several capillary tube test sections. They observed that the coiling of the capillary tube significantly reduced the mass flow rate of R-407C in the adiabatic spiral capillary tube. In order to quantify the effect of coiling, they conducted experiments for straight capillary tube and observed that the coiling of the capillary tube reduced the mass flow rate in the spiral tube in the range of 9–18% as compared with that in the straight capillary tube. A generalized non dimensional correlation for the prediction of the mass flow rates of various refrigerants was developed for the straight capillary tube on the basis of the experimental data of R-407C, 134a, R-22, and R-410A measured by other researchers. Additionally, a refrigerant-specific correlation for the spiral capillary was also proposed on the basis of the experimental data of R-407C.

M.K. Khan et al. (2008) experimentally investigated the flow of R-134a inside an adiabatic spirally coiled capillary tube. The effect of various geometric parameters like capillary tube diameter, length and coil pitch for different capillary tube inlet subcooling on the mass flow rate of R-134a through the spiral capillary tube geometry has been investigated. It has been established that the coil pitch significantly influences the mass flow rate of R-134a through the adiabatic spiral capillary tube. The effect of providing pressure taps on the capillary tube surface has a negligible effect on the mass flow rate through the capillary tube. It has been concluded that the effect of coiling of capillary tube reduces the mass flow rate by 5–15% as compared to those of the straight capillary tube operating under similar conditions. The data obtained from the experiments are analyzed and a semi-empirical correlation has been developed. The proposed correlation predicts more than 91% of the mass flow rate which is in agreement with measured data in an error band of ±10%.

P.K. Bansal et al. (1998) worked for homogeneous two-phase flow model, CAPIL, which was designed to study the performance of adiabatic capillary tubes in small, vapour compression refrigeration systems, in particular household refrigerators and freezers. The model was based on the fundamental equations of conservation of mass, energy and momentum that are solved simultaneously through iterative procedure and Simpson's rule. The model uses empirical correlations for single-phase and two-phase friction factors and also accounts for the entrance effects. The model uses the REFPROP data base where the Carnahan-Starling-De-Santis equation of state is used to calculate the refrigerant properties. The model includes the effect of various design parameters, namely the tube diameter, tube relative roughness, tube length, level of subcooling and the refrigerant flow rate. The model is validated with earlier models over a range of operating conditions and is found to agree reasonably well with the available experimental data for HFC-134a.

Jongmin Choi et al. (2003) developed a generalized correlation for refrigerant flow rate in adiabatic capillary tubes by implementing dimensionless parameters based on extensive experimental data for R-22, R-290, and R-407C. Dimensionless parameters are derived from the Buckingham- π theorem, considering the effects of tube inlet conditions, capillary tube geometry, and refrigerant properties on mass flow rate. The generalized correlation yields good agreement with the present data for R-22, R-290, and R-407C with average and standard deviations of 0.9 and 5.0%, respectively. Approximately 97% of the present data are correlated within a relative deviation of $\pm 10\%$. Further assessments of the correlation are made by comparing the predictions with measured data for R-12, R-134a, R-152a, R-410A, and R-600a in the open literature. The correlation predicts the data for those five refrigerants with average and standard deviations of ± 0.73 and 6.16%, respectively.

P.K. Bansal et al. (1996) provided new selection charts for selecting the capillary tube size from the refrigerant mass flow rate and flow condition or for predicting the refrigerant mass flow rate through adiabatic capillary tubes from a given capillary tube size and flow condition. The mathematical model is developed from the homogeneous flow model and the governing equations are based on the basis of conservation of mass, energy, and momentum. The selection charts and flow correction factors are proposed for practical use. The developed selection charts are verified by comparing them with the limited available experimental data.

Chang Nyeun Kim et al. (2000) experimentally investigated the capillary tube performance for R-407. The experimental setup is a real vapor compression refrigerating system. Mass flow rate is measured for various diameters and lengths while inlet pressure and degree of sub cooling are changed. These data are compared with the results of numerical model. The mass flow rate of the numerical model is about 14% less than the measured mass flow rate. They found that mass flow rate and length for R-407C are less than those for R-22 under same conditions. They used the numerical method for finding the diameter and length by using the continuity equation, momentum equation and energy equation.

Dongsoo Jung et al. (2006) modeled pressure drop through a capillary tube in an attempt to predict the size of capillary tubes used in residential air conditioners. They provided simple correlating equations for practicing engineers. Stoecker's basic model was studied with the consideration of various effects due to subcooling, area contraction, and different equations for viscosity and friction factor, and finally mixture effect. McAdams' equation for the two-phase viscosity and Stoecker's equation for the friction factor yielded the best results among various equations. With these equations, the modified model yielded the performance data that are comparable to those in the ASHRAE handbook. After the model was validated with experimental data for CFC12, HFC134a, HCFC22, and R407C, performance data were generated for HCFC22 and its alternatives such as HFC134a, R407C and R410A under operating conditions such as condensing temperature (40, 45, 50, 55 °C), subcooling (0, 2.5, 5 °C), capillary tube diameter (1.2±2.4 mm), and mass flow rate (5±50 g/s). These data showed that the capillary tube length varies uniformly with the changes in condensing temperature and subcooling. Finally, a regression analysis was performed to determine the dependence of mass flow rate on the length and diameter of a capillary tube, condensing temperature, and subcooling. Simple practical equations yielded a mean deviation of 2.4% for 1488 data obtained for two pure and two mixed refrigerants.

S. G. Kim et al. (2002) developed a dimensionless correlation on the basis of the experimental data of adiabatic capillary tubes for R22 and its alternatives, R407C (R32/125/134a, 23/25/52 wt. %) and R410A (R32/125, 50/50 wt.%). Several capillary tubes with different length and inner diameter were selected as test sections. Mass flow rate through the capillary tube was measured for several condensing temperatures and various degrees of subcooling at the inlet of each capillary tube. Experimental conditions for the condensing temperatures were selected as 40, 45 and 50 °C, and the degrees of subcooling were adjusted to 1.5, 5 and 10 °C. Mass flow rates of R407C and R410A were compared with those of R22 for the same test conditions. The results for straight capillary tubes were also compared with those of coiled capillary tubes. A new correlation based on Buckingham- π theorem to predict the mass flow rate through the capillary tubes was presented based on extensive experimental data for R22, R407C and R410A. Dimensionless parameters were chosen considering the effects of tube geometry, capillary tube inlet conditions, and refrigerant properties. Dimensionless correlation predicted experimental data within relative deviations ranging from -12% to +12% for every test condition for R22, R407C and R410A. The predictions by the developed correlation were in good agreement with the results in the open literature.

M. A. Akintunde et al. (2008) investigated the effects of various geometries of capillary tubes based on the coil diameters and lengths alone, with no particular attention placed on the effect of coil pitch. This paper examined the effects of pitches of both helical and serpentine coiled capillary tubes on the performance of a vapor compression refrigeration system. Several capillary tubes of equal lengths (2.03 m) and varying pitches, coiled diameters and serpentine heights were used. Both inlet and outlet pressure and temperature of the test section (capillary tube) were measured and used to estimate the COP of the system. In the case of helical coiled geometries, the pitch has no significant effect on the system performance. In the case of serpentine geometries, both pitch and height affects the system performance. Performance improves with both increase in the pitch and the height. Correlations were proposed to describe relationships between straight and coiled capillary tube and between helical coiled and serpentine coiled capillary tubes. The COP obtained was 0.9841 for mass flow rates of helical and serpentine with straight tubes, 0.9864 and 0.9996 for mass flow rates of serpentine and helical coiled tube respectively. This study investigated the performance of capillary tube geometries having R-134a as the working fluid.

M.A. Akintunde et al. (2007) concluded that some parameters such as friction factor, dryness fraction and Reynolds number affect the required length and diameter of a capillary tube for a given refrigeration capacity. The friction factors were based on the dryness fraction ranges between 0.05 - 0.85% and 0.5 - 1.9% above that of ASHRAE under the same conditions. Furthermore, both McAdams' and Duckler's equations for two-phase viscosity were employed so that the deviation in the estimated lengths could be compared. The tube lengths generated by combining various friction factor models with McAdams' equation are much closer to that of ASHRAE standard than those of Duckler's equation. The estimated lengths using McAdams' and Duckler's equations exceeded ASHRAE standard by 1.65% and 4.13% respectively. The required capillary tube length for a specified condenser condition depends on both Reynolds number and dryness fraction and not on either alone and these two factors should not be in exponential form. The generated lengths approach the ASHRAE requirement as the degree of sub cooling is increased.

Chun-Lu Zhang et al. (2004) had done parameter analysis, an insight into the flow characteristics of capillary tubes. Based on the approximate analytic solutions, influences of geometrical parameters (inner diameter and length) and inlet operating parameters (pressure, subcooling or quality) on the mass flow rate through an adiabatic capillary tube have been intensively studied in this work. Some simple theoretical relations were developed. The relations show that the mass flow rate is the power function of the geometries. Experimental data was supplemented by numerical data for R22, R410A and R407C.

Worachest et al. (2006) provided new selection charts for the sizing of adiabatic capillary tubes operating with alternative refrigerants. The mathematical model is based on conservation of mass, energy, and momentum of fluids in the capillary tube. After the developed model is validated by comparison with the experimental data reported in literature, selection charts that contain the relevant parameters are proposed for sizing adiabatic capillary tubes. The selection charts are presented for some alternative refrigerants and a wide range of operations. These newly developed selection charts can be practically used to select capillary tube size from the flow rate and flow condition or to determine mass flow rate directly from a given capillary tube size and flow condition.

M.K. Khan et al. (2008) developed a mathematical model to predict the performance of a helical capillary tube under adiabatic flow conditions. The proposed model can predict the length of the adiabatic helical capillary tube for a given mass flow rate or the mass flow rate through a given length of capillary tube. The effect of parameters like condensing pressure, degree of subcooling, pitch of helix and the coil diameter has been studied for the flow of refrigerant R-134a through the adiabatic helical capillary tube. A capillary tube selection chart has been developed, using the proposed model, to predict the mass flow rate of refrigerant R-134a through a capillary of size 1.07 mm diameter and 2 m length.

S. M. Sami et al. (2001) experimentally investigated the capillary tube behavior, using various new alternatives under different geometrical parameters. Capillary geometrical parameters include length, diameter, as well as entrance conditions. The results clearly showed that the pressure drop across the capillary tube is significantly influenced by the diameter of the capillary tube, inlet conditions to the capillary and refrigerant type. The data demonstrated that the capillary pressure drop decreases with the increase of the capillary diameter and the alternatives of R-22 had higher pressure drop than that of R-22.

C. Melo et al. (1999) discussed the effect of capillary length, capillary diameter, refrigerant subcooling, condensing pressure and type of refrigerant on the mass flow-rates through the capillaries. The experiments were performed with three refrigerants such as CFC-12, HFC-134a and HC-600a, and at different condensing pressures and levels of subcooling under choked flow conditions. Eight capillaries with different combinations of lengths, diameters and tube roughness's were used, and extensive data was collected. A conventional, dimensional analysis was performed to derive correlations to predict the mass flow rates for different refrigerants.

Conclusions

Earlier studies have shown that use of alternative refrigerants play an important role in forming problems such as global warming and ozone depletion. The coefficient of performance of refrigeration appliances improves in case of retrofitting with the spiral capillary tube. It is possible to obtain the effective size (diameter, length & coil pitch) of capillary tube by using of experimental techniques and by maintaining proper pressure equalization between condenser and evaporator. It is possible to predict about mass flow rate of refrigerant in spiral capillary tube. The influence of degree of subcooling, pressure and geometric parameters such as diameter, length, and coil pitch on the performance i.e. COP of the system and mass flow rate of refrigerant through capillary tube was reviewed in this paper.

References

1. B. G. Lee, J. Y. Park, J. D. Kim, and J. S. Lim, "A study on the performance of alternative refrigerant mixtures for HCFC-22/CFC," Alternatives research center, Korea Institute of Science and Technology (KIST), Cheongryang, Seoul, South Korea, (2005), pp. 130-150.
2. L. B. Ortiz, S. Y. Motta, S. L. Braga, 2001 "Experimental analysis of adiabatic flow of non- azeotropic mixture R-407c through a capillary tube" Engenharia Termica, No. 1, pp. 41-46.
3. S. M. Sami, Shawn Aucoin, "Effect of magnetic field on the performance of new refrigerant mixtures," Int. J. Energy Res. 2003, 27, pp. 203-214.
4. Hira lal Sachdev, Akhilesh Arora, B.B.Arora, 2004, "Performance analysis of R-22 and its alternate refrigerants," M. Tech Thesis, Department of Mechanical Engineering, Delhi College of Engineering, University of Delhi.
5. M. K. Mittal, R. Kumar, A. Gupta, "An Experimental Study of the Flow of R-407C in an Adiabatic Spiral Capillary Tube," Journal of Thermal Science and Engineering Applications, Vol. 1, DECEMBER (2009), pp. 041003-041011.
6. Mohd Kaleem Khan, Ravi Kumar, Pradeep K. Sahoo, "An experimental study of the flow of R-134a inside an adiabatic spirally coiled capillary tube," International Journal of Refrigeration 31(2008), pp.970-978.
7. P. K. Bansal, A. S. Rupasinghe, "An Homogeneous Model for Adiabatic Capillary Tubes," Applied Thermal Engineering Vol. 18, No's 3-4(1998), pp. 207-219.
8. Jongmin Choi, Yongchan Kim, Ho Young Kim, 2003, "A generalized correlation for refrigerant mass flow rate through adiabatic capillary tubes," Int. J. Refrig., 26, pp. 881-888.
9. P. K. Bansal, A. S. Rupasinghe, "An empirical model for sizing capillary tubes," International Journal of Refrigeration, Volume 19, Issue 8, November (1996), pp. 497-505.
10. Chang Nyeun Kim & Young Moo Park, " Investigation on the Selection of Capillary Tube for the Alternative Refrigerant R-407C," International Journal of Air-Conditioning and Refrigeration Volume 8, May (2000), pp.40-49.
11. Dongsoo Jung, Chunkun Park, Byungjin Park, "Capillary tube selection for HCFC22 alternatives," International Journal of Refrigeration 22, (2006), pp. 604-614.
12. Kim, S. G., Ro. S. T., and Kim, M. S., 2002, "Experimental Investigation of the Performance of R22, R407C and R410A in Several Capillary Tubes for Air-Conditioners," Int. J. Refrig., 25, pp. 521-531.
13. M.A. Akintunde, Ph. D., "Effect of Coiled Capillary Tube Pitch on Vapor Compression Refrigeration System Performance," The Pacific Journal of Science and Technology Volume 9. Number 2. November (2008), pp. 284-294.
14. M.A. Akintunde, Ph. D., "The Effects of Friction Factors on Capillary Tube Length," The Pacific Journal of Science and Technology, Volume 8, Number 2, November (2007), pp. 273-281.
15. Chun-lu Zhang, Guoliang Ding, 2004, "Approximate analytic solutions of adiabatic capillary tube," Int. J. Refrig., 27, pp.17-24.
16. Worachest, Pirompugd, Wongwises, Somchai, 2006, "Capillary tube sizing charts for fluorine-based refrigerants," ASHRAE Transactions.
17. Khan. M.K., R. Kumar, and P.K. Sahoo. 2008, "A homogeneous flow model for adiabatic helical capillary tube," ASHRAE Transactions 114(1), pp.239-49.
18. S. M. Sami, P.E., H. Maltais and D. E. Desjardins, "Influence of Geometrical Parameters on Capillary Behavior with New Alternative Refrigerants," M.Tech Thesis, Department of Mechanical Engineering, School of Engineering University of Moncton, Moncton, NB, E1A 3E9.
19. Melo, C., Ferreira, R. T. S., Neto, C. B., Goncalves, J. M., and Mezavila. M.M., 1999, "An Experimental Analysis of Adiabatic Capillary Tubes," Appl. Therm. Eng., 19(6), pp. 669-684.

Field Modeling of Meander Energy Conservation, Case Study Meander of Karon River in Shoushtar

Hadi Molaei Tavani

Department of Physics, Shoushtar Branch, Islamic Azad University, Shoushtar, Iran

ABSTRACT

A river current energy conversion system could be defined as an electromechanical energy converter that employs a RCT to harness the kinetic energy of river water. The growing demand for electrical energy is one of the most important subjects today. Renewable energies give a good perspective to be an alternative to fossil and nuclear-fueled power plants, in order to meet growing demand for electrical energy. In this research, investigated the use of computational fluid dynamics in predicting the formation, development of meander current and with field studying and daily-monthly measurement of effective parameters present a field modeling of river's meander in Karoon River in Shoushtar city domain to generate hydro electrical energy. The survey shows that in this case study can generate justifiable energy in meander and it show that can use the meander of rivers are one of the renewable source.

Keywords: renewable energy, river meander, hydro electrical energy, field modeling, energy conservation

I. INTRODUCTION

A river current energy conversion system (RCECS) could be defined as an electromechanical energy converter that employs a RCT to harness the kinetic energy of river water. In the field of hydrokinetic energy extraction, i.e. converting energy from water currents such as tides or in rivers, several models have been developed to study and understand the resource. One-dimensional analytical models have been used to study the effects on water level and velocity [1&3] whereas more advanced 2D and 3D models have been used to calculate the potential of tidal energy [4&6]. Some attempts have also combined analytical models with numerical ones to estimate the potential [4]. A large number of simulation models have been proposed in the past two decades to reproduce their planform dynamics (Ikeda et al., 1981; Blondeaux and Seminara, 1985; Crosato, 1989; Howard, 1996; Seminara et al., 2001; Luchi et al., 2007; Frascati and Lanzoni, 2009). In almost all these models the changes in planform of meandering rivers have been quantified through the spatial distribution of channel curvature. As a long-term requirement, these models assume that the river width remains constant in space and in time. River current energy conversion systems are electromechanical energy converters that convert kinetic energy of river water into other usable forms of energy. However, the potentials of this technology as

an effective and renewable source of alternative energy have not yet been explored to a great extent. In this research, investigated the use of computational fluid dynamics (CFD) in predicting the formation, development of meander current and with field studying and daily-monthly measurement of effective parameters present a field modeling of river's meander in Karoon River in Shoushtar city domain to generate hydro electrical energy. The survey shows that in this case study can generate justifiable energy in meander and it show that can use the meander of rivers are one of the renewable source. However, some limitations and uncertainties exist that have to be clarified in future investigations.

II. NUMERICAL METHODS

2.1 Flow and turbulence simulation

The numerical model used in the present study was developed by [9]. The flow field for the 3D geometry was determined by solving the continuity equation and the Reynolds-averaged Navier–Stokes equations:

$$\frac{\partial U_i}{\partial x_i} = 0 \quad \text{with } i = 1,2,3 \quad (1)$$

$$\frac{\partial U_i}{\partial t} + U_j \frac{\partial U_i}{\partial x_j} = \frac{1}{\rho} \frac{\partial}{\partial x_i} (-P \delta_{ij} - \rho \overline{u_i u_j}) \quad (2)$$

Where U is the velocity averaged over time t , x is the spatial geometrical scale, ρ is the water density, P is the pressure, δ is the Kronecker delta, and u is the velocity fluctuation over time during one time step Δt . The control volume method was used as the discretisation method [7], and the convective terms in the Navier–Stokes equations were solved by the second-order upwind scheme. The Reynolds stress term was modelled by the k - ϵ turbulence model (Rodi, 1980). This two-equation turbulence model computed the turbulent stresses $u_i u_j$ using the eddy viscosity relation:

$$-\overline{u_i u_j} = \nu_t \left(\frac{\partial U_i}{\partial x_j} + \frac{\partial U_j}{\partial x_i} \right) - \frac{2}{3} k \delta_{ij} \quad (3)$$

with $\nu_t = \frac{C_\mu k^2}{\epsilon}$

where the turbulent kinetic energy k and its dissipation rate ϵ determining the eddy viscosity ν_t were obtained from the following equations:

$$\frac{Dk}{Dt} = \frac{\partial k}{\partial t} + U_j \frac{\partial k}{\partial x_j} = \frac{\partial}{\partial x_j} \left[\left(v + \frac{v_t}{\sigma_k} \right) \frac{\partial k}{\partial x_j} \right] + P_k - \varepsilon \quad (4)$$

$$\begin{aligned} \frac{D\varepsilon}{Dt} &= \frac{\partial \varepsilon}{\partial t} + U_j \frac{\partial \varepsilon}{\partial x_j} \\ &= \frac{\partial}{\partial x_j} \left[\left(v + \frac{v_t}{\sigma_\varepsilon} \right) \frac{\partial \varepsilon}{\partial x_j} \right] + C_{\varepsilon^1} \frac{\varepsilon}{k} P_k \\ &\quad - C_{\varepsilon^1} \frac{\varepsilon^2}{k} \quad (5) \end{aligned}$$

The production of turbulent kinetic energy P_k was defined as:

$$P_k = v_t \frac{\partial U_i}{\partial x_j} \left(\frac{\partial U_j}{\partial x_i} + \frac{\partial U_i}{\partial x_j} \right) \quad (6)$$

An implicit method was used to solve transient terms, and the pressure field was computed with the SIMPLE method [9]. The Rhie and Chow (1983) interpolation was applied to compute the velocities and the fluxes at the cell surfaces. Zero gradient boundary conditions were used for all variables at the outflow boundary. The upstream velocities were defined by a Dirichlet boundary condition.

2.2 Energy Calculations

The transfer of kinetic energy from the eddies to the mean flow can be expressed as:

$$E = \overline{\rho u'v'} \frac{\partial \bar{v}}{\partial x} \quad (7)$$

Where a bar represents a time average of a quantity, a prime represents a deviation from the time average, u and v are the velocity components in the cross-stream (x) and downstream (y) direction, and ρ is the density of the water. For case study, the data were divided into 4 zones across the current, each zone being 30 meters wide. The eddy momentum transfer $\overline{u'v'}$ was calculated by applying Simpson's rule to the value of $u'v'$, over the total time of observation, for each of the 4 zones. The value of $\frac{\partial \bar{v}}{\partial x}$ was calculated for each zone from the profile of average velocity \bar{v} . Table I show for each zone: $\overline{u'v'}$ the average transport of eddy momentum; $\frac{\partial \bar{v}}{\partial x}$ the shear of the average velocity; and the term (7) representing the production of mean kinetic energy by meanders. (ρ was assumed constant, and equal to one gram per cubic centimeter.)

The standard error of the means, \bar{u} , \bar{v} , and $\overline{u'v'}$ are given for each value in Table I. The standard error of a mean is defined, for large N , as σ/\sqrt{N} , where σ is the standard deviation of the sample from which the mean is calculated, and N is the number of individual observations.

2.3 Kinetic Energy Equation for the Mean Flow

The following model is a simple version of the Reynolds model, intended to provide an orientation. Better models may follow later. Let us consider an ocean current, with a mean

flow in the y -direction, having velocity components u , v , and w in the x , y , and z directions, x being directed to the right of y , and z being directed downward

The momentum equations are

$$\rho \frac{\partial u}{\partial t} + \rho v \cdot \nabla u = \rho f v - \frac{\partial P}{\partial x} - X \quad (8)$$

$$\rho \frac{\partial u}{\partial t} + \rho v \cdot \nabla u = \rho f u - \frac{\partial P}{\partial y} - Y \quad (9)$$

Where ρ is the density of the water, f is the acceleration parameter, p is the pressure, and X and Y are components of a dissipative force. With the aid of the continuity equation, $\frac{\partial \rho}{\partial t} + \nabla \cdot \rho v = 0$ we may write:

$$\frac{\partial \rho u}{\partial t} + \nabla \cdot \rho u v = \rho f v - \frac{\partial P}{\partial x} - X \quad (10)$$

$$\frac{\partial \rho u}{\partial t} + \nabla \cdot \rho v v = -\rho f u - \frac{\partial P}{\partial y} - Y \quad (11)$$

The quantities u , v , and w can be separated into mean motion and deviations as:

$$\begin{aligned} u &= \bar{u} + u' \\ v &= \bar{v} + v' \\ w &= \bar{w} + w' \end{aligned}$$

With solve this equation and is integrated over a cross-section of the current in the x - z plane, the result gives the balance of horizontal kinetic energy of the mean flow in a unit cross-section of the current:

$$\begin{aligned} 0 &= \iint V \cdot \nabla \bar{k} dx dz - \iint \bar{u} \nabla \cdot \overline{\rho u'v'} dx dz \\ &\quad - \iint \bar{v} \nabla \cdot \overline{\rho u'v'} dx dz - \iint \left(\bar{u} \frac{\partial P}{\partial x} \right. \\ &\quad \left. + \bar{v} \frac{\partial P}{\partial y} \right) dx dz - \iint d dx dz \quad (12) \end{aligned}$$

With the limited amount of information available now, it is not possible to evaluate each term in equation (12) for the river current. However, an estimate of the role of some of the terms can be made.

First, consider terms 2 and 3 of above integral:

$$\begin{aligned} &\bar{u} \nabla \cdot \overline{\rho u'v'} + \bar{v} \nabla \cdot \overline{\rho v'v'} \\ &= \bar{u} \frac{\partial}{\partial x} \overline{\rho u'u'} + \bar{u} \frac{\partial}{\partial x} \overline{\rho u'v'} + \bar{v} \frac{\partial}{\partial y} \overline{\rho u'u'} \\ &\quad + \bar{v} \frac{\partial}{\partial y} \overline{\rho v'v'} + \bar{u} \frac{\partial}{\partial z} \overline{\rho v'w'} + \bar{u} \frac{\partial}{\partial z} \overline{\rho u'w'} \end{aligned}$$

The axes were chosen so that the mean current is in the y-direction, so that $\bar{v} \gg \bar{u}$. In addition, the perturbations travel in the y-direction, so that for the time averaged velocity perturbation terms $\frac{\partial}{\partial y} \cong 0$. Hence, terms 2 and 3 become:

$$\begin{aligned} & \bar{u}\nabla \cdot \overline{\rho u'V'} + \bar{u}\nabla \cdot \overline{\rho v'V'} \\ &= \bar{u} \frac{\partial}{\partial x} \overline{\rho u'u'} + \bar{v} \frac{\partial}{\partial x} \overline{\rho u'v'} + \bar{u} \frac{\partial}{\partial z} \overline{\rho v'w'} \\ &+ \bar{v} \frac{\partial}{\partial z} \overline{\rho u'w'} \end{aligned}$$

The terms in $\overline{u'w'}$ and $\overline{v'w'}$ represent contributions of kinetic energy to the mean flow by vertical perturbations. Since observations of vertical motions are not available, this term has not been calculated. It might represent an important contribution to the mean downstream kinetic energy.

The term $\bar{v} \frac{\partial}{\partial x} \overline{\rho u'v'}$ includes the expression used in the surface calculation of this study. It may be re-written as

$$\frac{\partial}{\partial x} (\rho \bar{v} \cdot \overline{u'v'}) - \overline{\rho u'v'} \frac{\partial \bar{v}}{\partial x}$$

The term $\frac{\partial}{\partial x} (\rho \bar{v} \cdot \overline{u'v'})$ represents an eddy advection across the boundaries of mean kinetic energy and can be integrated easily across a stream to become:

$$[\rho \bar{v} \cdot \overline{u'v'}]_A - [\rho \bar{v} \cdot \overline{u'v'}]_B$$

If the stream is bounded by walls, u' will be zero at the walls, or if the mean stream velocity drops to zero at each side of the current, \bar{v} will be zero, and the term (a) is zero. River, where the current is not bounded by walls, and the observations did not cover the whole width of the current, calculation of the term (a) has revealed that its integral across the width of observations is zero. Hence the cross-stream integral of the term:

$$\overline{\rho u'v'} \frac{\partial \bar{v}}{\partial x}$$

is a measure of the increase of mean kinetic energy at the expense of kinetic energy of horizontal eddy motion.

Maximum values of $\frac{\partial}{\partial x} \overline{\rho u'u'}$ at the surface JX were observed to be almost as large as average values of $\frac{\partial}{\partial x} \overline{\rho u'v'}$. However, since $\bar{v} \gg \bar{u}$, the term $\bar{u} \frac{\partial}{\partial x} \overline{\rho u'u'}$ is negligible in comparison $\bar{v} \frac{\partial}{\partial x} \overline{\rho u'u'}$.

Term 1 of above integral represents the advection across the boundaries of the region under consideration of mean horizontal kinetic energy. Equation (12) states that this boundary advection 1 must be balanced by the generation of

mean kinetic energy by meanders, 2 and 3, pressure forces, 4, and by the frictional dissipation, 5.

Assuming only partial correlation, or more characteristic values of wind stress and meander velocity, the energy contributed to the meanders by the wind is about 1×10^{-4} ergs/cm²/s.

In comparison with the transfer of energy between meanders and mean flow of 80×10^{-4} ergs/cm²/s, the wind would appear to be eliminated as a significant source of kinetic energy for the meanders.

III. AREA AND MEASUREMENT DESCRIPTION

The data used to calculate eddy momentum fluxes were obtained from Karoon river in Shoushtar domain. The big and important Karoon River in Iran, Shushtar, is divided to two branches Shotait and Gargar, and Shushtar city as an island between these two branches. Shotait and Gargar rivers reach together in a place named Bandeghir. Figure 1 shows the location of these sections and their meander.

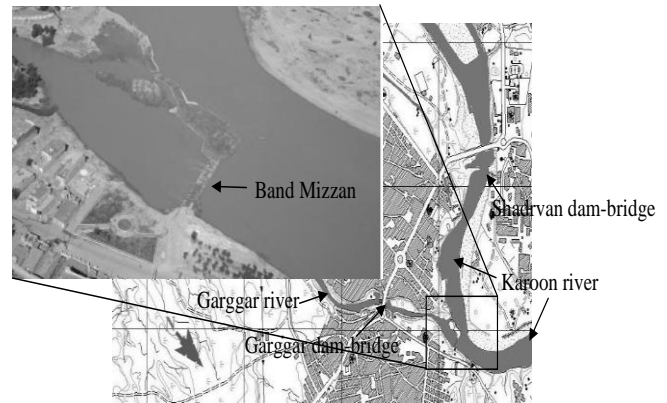


Figure 1. Meander of river in this place that divided to two branches Shotait and Gargar

The optimum design of a RCECS is a significant technical challenge. From cost and performance point of view, simple design using off-the-shelf materials is desirable. train with suitable gearing and bearing mechanism is also of due interest. Since these turbines are exposed to water and run on lower speed, selection of an electrical generator from asynchronous, synchronous, dc and brushless dc categories requires in-depth understanding of cost and performance indices of electric machines. Integrating these parts with the flotation/augmentation mechanism and designing a complete system requires structural and reliability analyses.

IV. SIMULATION RESULTS

In different months of year in two season of winter and summer of deby in Karun River, in the two places before and after balance band, Shoushtar basin by Flow meter contain

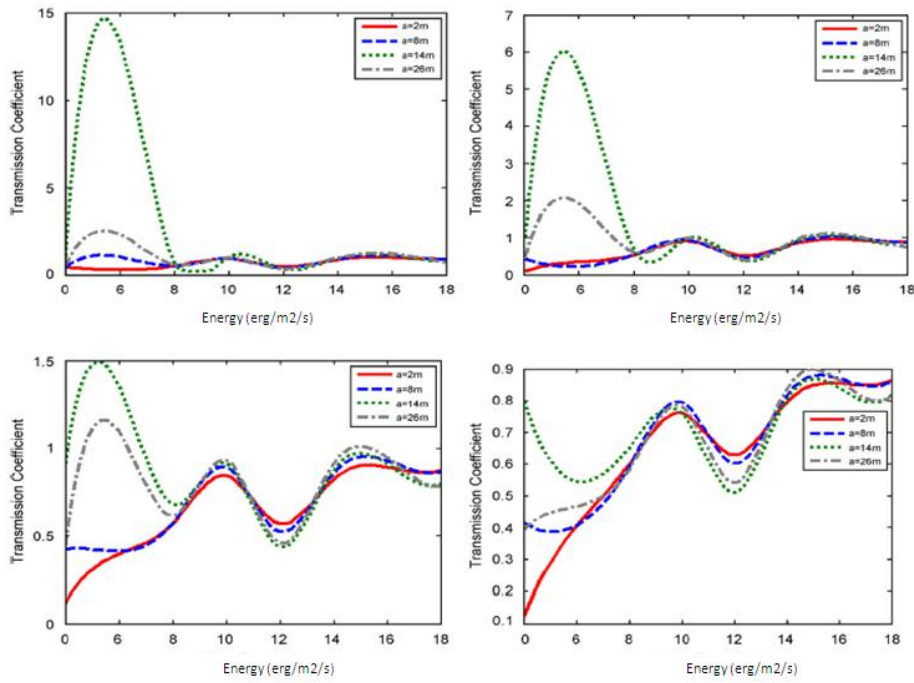


Fig. 2. Effect of channel width on the energy in four seasons (2011)

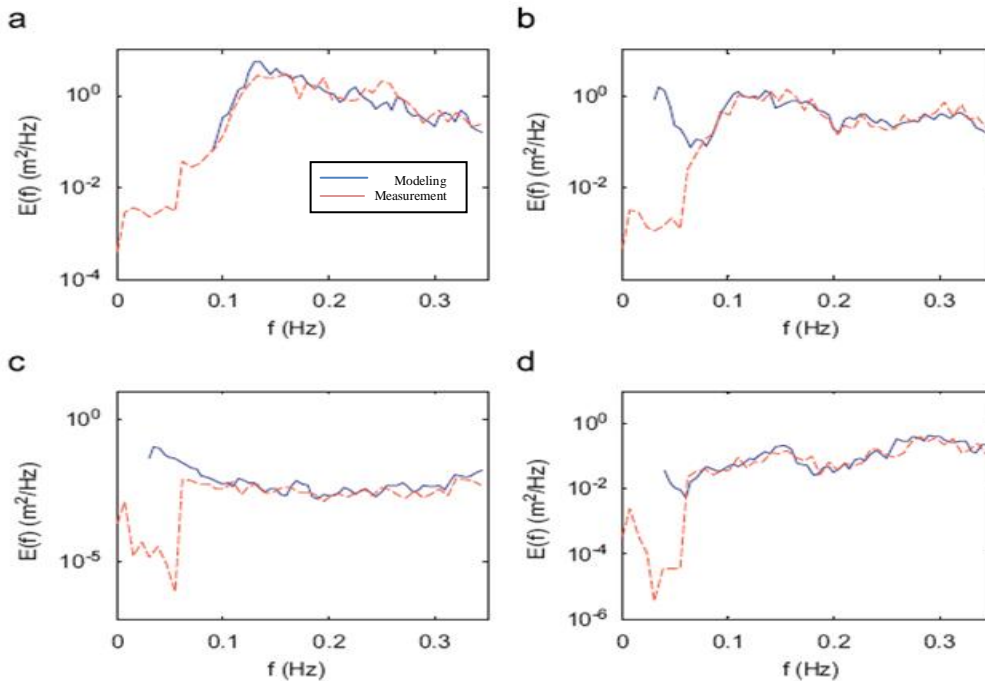


Fig. 3. Energy generation due to channel of the meander in four seasons (2011)

The effects of a power extraction device on the water level in a river site are studied here. As described in Section 2, the height drop along the channel is increased when energy is extracted. Main focus of this section is to study the magnitude of these effects and how they are altered when the water level at the

downstream side of the channel varies. The turbine function which is inbuilt in MIKE was evaluated. In the numerical program, the turbines are described in a sub grid scale so that the turbines should be much smaller than the cell size. The turbines are assumed to exert a force on the flow which can be

expressed using a drag coefficient according to Eq. (5). Since the turbines are modeled in a sub-grid scale, the cell size will affect the force calculations. For the considered channel, this meant that the force changed when the grid cell was altered, even maintaining the CD-value constant. Force and velocity through the turbine are the two output parameters for each turbine in MIKE. To calculate turbine power, Eq. (6) can then be used. However, the equation assumes the turbines are ideal and internal losses are not included. The actual energy capture would have to be multiplied with efficiency constant.

V. CONCLUSION

In this paper, we use data from Karoon River and simulation to further explore the concept of optimality in energy expenditure in meander of rivers to generate renewable energy. In this work the effects upstream on the water level has been studied. A special focus on river sites has been applied although the results are equally valid on any channel. Two main conclusions can be drawn from this work. The first is that a kinetic energy extractor causes a head loss upstream at an upstream power plant. This is important since it shows that a converter that is able to convert the total head loss would be much more efficient than an in-stream converter. The second conclusion was that the turbine function in the numerical program MIKE did not account for the power loss connected with in-stream energy converters. The river current energy conversion system technology is probably at its infancy. A set of more recent reports indicate that such devices are slowly entering into the implementation phase, graduating from the laboratory environment. This work shows that the meanders of river are one of the suitable renewable resources to generate energy.

ACKNOWLEDGMENT

The author would like to thank the Islamic Azad University Shoushtar Branch for their support.

REFERENCES

- [1] J. Hooke, "River meander behavior and instability: a framework for analysis," *Institute of British Geographers Transactions* 28, 238–253, 2003.
- [2] A.D. Howard, "Modeling channel evolution and floodplain morphology," In: Anderson, M.G., Walling, D.E., Bates, P.D. (Eds.), *Floodplain Processes*, Wiley, Chichester, UK, pp. 15–62, 1996.
- [3] H. Johannes son, G. Parker, "Linear theory of river Meanders," In: Ikeda, S., Parker, G. (Eds.), *River Meandering*. Water Resources Monograph 12, American Geophysical Union, Washington, DC, pp. 181–212 (Chapter 7), 1989.
- [4] S.T. Lancaster, "A nonlinear river meander model and its incorporation in a landscape evolution model," Ph.D. Dissertation, Massachusetts Institute of Technology, Cambridge, MA, 177pp, 1998.
- [5] H.-H. Stlum, P.F. "Friend, Percolation theory applied to simulated meander belt bodies," *Earth and Planetary Science Letters* 153, 265–277, 1997.
- [6] T. Sun, P. Meakin, T. Jossang, K. Schwarz, "A simulation model for meandering rivers," *Water Resources Research* 32 (9), 2937–2954, 1996.
- [7] P. Garman, "Water current turbines: a fieldworker's guide," UK: Intermediate Technology Publishing; ISBN: 0946688273, 1986.
- [8] S, Kihon, M. Shiono "Electric power generations from tidal currents by darrieus turbine at kurushima straits," *Trans IEE Japan*; 112-D (6):530–8, 1992.
- [9] K, Nilsson, E. Segergren, M. Leijon, "Simulation of direct drive generators designed for underwater vertical axis turbines," In: *Proceedings of the fifth European wave energy conference*, Cork, Ireland; 2003.
- [10] J.M. Hooke, "River channel adjustment to meander cutoffs on the River Bollin and River Dane," *Northwest England. Geomorphology*, vol. 14, 1995, pp. 235–253.
- [11] S. Ikeda, G. Parker, K. Sawai, "Bend theory of river meanders. Part 1 - Linear development," *Journal of Fluid Mechanics* 112, 1981, pp.363–377.
- [12] C. Garrett, P. Cummins, "The power potential of tidal currents in channels," *Proceedings of the Royal Society A* 2005;461:2563e72.
- [13] M. Khan, M. Iqbal, E. Quaiocoe, "River current energy conversion system: progress, prospects and challenges," *Renewable and Sustainable Energy Reviews* 2008;12:2177e93.
- [14] J.S.G. Ehnberg, M.H.J. Bollen, "Generation reliability for small isolated power systems entirely based on renewable sources," *Proc. IEEE Symp. Power Engineering Society General Meeting*, 2004. IEEE, IEEE Press, June 2004, pp. 2322 - 2327 Vol.2, 10.1109/PES.2004.1373300.

Wind Turbine Planetary Gearbox Health Diagnostic Using Varying –Time Meshing Stiffness Variation

Prof. Shawki A. Abouel-seoud, Dr. Eid S. Mohamed

*Faculty of Engineering, Helwan University,
Cairo, Egypt*

ABSTRACT

In wind turbine planetary gearbox, the ability to identify ring-planet-sun gears meshing stiffness from the real data of vibration responses makes it possible to determine the physical existed planet gear defects which used for severity assessments. There are limitations for vibration based gear diagnostic methods. Vibrations are secondary effects in the sense that they are dynamic responses of a gearbox excited by meshing stiffness and other excitations. The aim of this work is to diagnosis the level of defects (gear tooth crack, gear tooth spalling and gear tooth breakage) in wind turbine gearbox using gears meshing stiffness. Varying-time meshing stiffness is used, where, a technique consists of a nonlinear numerical optimization is applied. The optimization uses a dynamic model of the gears mesh and forms an estimate of both time-varying and frequency-varying mesh stiffness that best corresponds to the given set of vibration data. Multi-hour tests were conducted and recordings were acquired using rotational vibration monitoring, where the optimum meshing stiffness was computed. The optimum meshing stiffness with the recording time were highlighted suggesting critical changes in the operation of the gearbox. The results indicate that if one tooth is defected due to cracks, spalling and breakage to reach the setting maximum level, the maintenance regime will be called despite a new damage is prone in the adjacent tooth to save time and cost.

KEYWORDS: Optimum meshing stiffness, spalling, breakage, crack, optimization, vibration responses, planetary gearbox

NOMENCLATURE

m_e	Equivalent mass of the pinion (sum gear)
$K_{me}(t)$	Equivalent gears time-varying meshing stiffness
$C_{me}(t)$	Equivalent gears time-varying meshing damping
$h[k]$	The filter coefficient.
$Y[n]$	The filter output.
$X[n - k]$	Input data

1- INTRODUCTION

Over the last two decades, problems arising from excessive wear, crack and gear tooth surface pitting in gear transmission systems have been of increasing concern for a variety of gear users. At increased power and high loads,

gear wear and fatigue failures are major concerns in wind turbine applications. While regular visual inspections and preventive maintenance can help to reduce the failure rate of gear systems, the cost and downtime required make such programs inefficient and uneconomical. On the other hand, vibration signature analysis methodologies are being developed to examine non-intensively the health and wear of gear transmission systems. Using spectra analysis, the amplitude of the frequency spectrum of the measured vibration signal is obtained and displayed in a continuous manner. However, the spectral analysis technique is difficult to apply in a highly complex system where the large number of spectral lines often makes it difficult to detect significant changes in the spectrum [1].

Several methods have been recently developed to tray to produce an index that, when tracked over time, gives some indication of the health of a gearbox. One of these indices is the time-varying meshing stiffness which can be extracted from the vibration of a gearbox (either calculated or measured). In turn, it gives an accurate account of the state of gears. Gear tooth damage and other defects reduce time-varying meshing stiffness and therefore produce changes (or "modulations" in the amplitude envelope and phase of the tooth mesh vibration [2].

A technique for processing vibration data to quantify the level of damage (crack only) in gear system is shown. The technique consists of a nonlinear numerical optimization. The optimization uses a dynamic model of the gear mesh used in vehicle gearbox and forms an estimate of both time-varying and frequency-varying mesh stiffness that best corresponds to the given set of vibration data [3, 4]. The procedure developed in these studies can be applied as a part of either an onboard machine health monitoring system or a health diagnostic system used in the regular maintenance. As the developed methodology is based on the analysis of gearbox vibration under normal operating conditions, no shutdown or special modification of the operating parameter is required during the diagnosis process.

The detection and quantification (which is based on the reduction in tooth stiffness) of damage incurred by spur gear teeth were presented using vibration analysis. Gear tooth damage can be caused by a variety of factors including inadequate lubrication, inappropriate operating conditions or specifications, material insufficiencies, and manufacturing or installation problems. Effective lubrication of gear systems is of critical importance because it prevents direct tooth contact, reduces friction

and vibration levels, removes heat generated in the mesh, and protects the gears from corrosion. When the tooth surfaces are subjected to excessive stress conditions, tooth surface failure may occur. This can cause removal and/or plastic deformation of the contacting tooth surfaces [5, 6]. In some cases, surface fatigue cracks occur in plastically deformed regions under excessive contact stress, and these can also be caused by scuffing or wear failure. Once initiated, crack propagation is accelerated by the hydrolic effect of gear lubricant and tangential tractive force. If surface deterioration is not corrected in the early stages of development, catastrophic tooth failure may result. In general, tooth damage causes a reduction in gear tooth stiffness, and severity of tooth damage can be assessed by considering the reduction in its stiffness. Tooth stiffness is a key parameter in gear dynamics in determination of factors such as load-carrying capacity of gears, dynamic tooth loads, vibration characteristics of geared system, and many works have been carried out to calculate the tooth stiffness and its effects upon those factors for many years [7].

However, the aim of this work is to diagnosis the level of defects (gear tooth crack, gear tooth spalling and gear tooth breakage) in wind turbine gearbox using gears meshing stiffness. Varying-time meshing stiffness is used, where, a technique consists of a nonlinear numerical optimization is applied. The optimization uses a dynamic model of the sun-planet-ring gears mesh and forms an estimate of both time-varying and frequency-varying mesh stiffness that best corresponds to the given set of vibration data.

2- GEAR TOOTH DAMAGE DETERMINATION

2.1 Background

A damage changes stiffness of the tooth, which, in turn, has an effect on the gear meshing dynamics and actual dynamic load. Therefore, it is necessary to compute the dynamic load after each damage increment on order to obtain an accurate prediction of the residual life. As it is, it is assumed that good gears can only be simulated because all the teeth on the same gear have the same meshing stiffness which is not the case in the presence of a cracked tooth.

2.2 Single-Degree-of-Freedom Model

Figure 1 shows a simple single degree-of-freedom model that will account for residual vibration as well as quantification of element damage in a contact force-closed gear teeth system. The system considered in this task consisted of a small pinion (sun gear) in mesh with a larger gear combination (planet and ring), where the ring gear is fixed to the gearbox structure. The two gear masses connected by a spring and a damper. The larger gear combination (planet and ring) is much heavier than the small pinion; hence, it is assumed to be rigid, so that all relative motion between the two is attributed to the motion of the pinion (sun gear). Then, the equation of motion of the pinion (sun gear) takes the form.

$$\sum F = m \ddot{X} \quad (1)$$

$$m_e \ddot{X} + C_{me}(t) \dot{X} + K_{me}(t) * X = 0 \quad (2)$$

$$C_{me}(t) = \mu K_{me}(t) \quad (3)$$

$$m_e * \ddot{X} + \mu K_{me}(t) * \dot{X} + K_{me}(t) * X = 0 \quad (4)$$

$$m_e * \ddot{X} + K_{me}(t) * (\mu \dot{X} + X) = 0 \quad (5)$$

Where:

m_e = Equivalent mass of the pinion (sum gear)

$$= [(m_s * 3m_p) / (m_s + 3m_p)]$$

$K_{me}(t)$ = Equivalent gears time-varying meshing stiffness

$C_{me}(t)$ = Equivalent gears time-varying meshing damping

$$\mu = 3.99 * 10^{-3} (s) \quad [8].$$

2.3 Optimization Technique

The unknown time-varying meshing stiffness is assumed to be periodic and therefore can be represented by a truncated Fourier series, which is then embedded into the lumped parameter model. For a healthy gear that has regularly spaced identical teeth, the time-varying meshing stiffness is largely repeated from one tooth to the next with the fundamental frequency of tooth meshing. On the other hand, a faulty gear tooth gives a meshing pattern that is repeated largely once a revolution. The optimization technique is used to process vibration data to quantify the level of damage in a gear transmission system. The optimization uses a dynamic model of the gear mesh and forms an estimate of the time-varying mesh stiffness that best correspond to the given set of vibration data. An analysis of this relationship demonstrates that the perturbation of the stiffness function from the nominal profile can be used to quantify the level of crack damage. Referring to equation (5), the meshing stiffness is not constant but is nominally a periodic function of the time, with each period corresponding to one tooth pass. It has been found in experiments on gearbox vibrations that the gear meshing stiffness changes with the damages of the gear teeth. Such changes in the gear meshing stiffness inevitably lead to changes in the vibration signatures of the mechanical system. The objective of the optimization technique developed in this task is to reconstruct the true stiffness profile for a damaged gear tooth from the measured vibration. That is, the objective is to determine the function $K_{me}(t)$ that would result in the measured vibration according to the system model in Fig. 1.

2.4 The Optimization Algorithm

A) Background

Basically, digital filters are used to modify the characteristic of signals in time and frequency domain and have been recognized as primary digital signal processing (DSP). In DSP, the design methods were mainly focused in multiplier-based architectures to implement the multiply-and-accumulate (MAC) blocks that constitute the central piece in finite impulse response (FIR) filters and several functions. Several multiplier-less schemes had been proposed. These methods can be classified in two categories according to how they manipulate the filter coefficients for the multiply operation. The first type of multiplier-less technique is the conversion-based approach, in which the coefficients are transformed to other numeric representations whose hardware implementation or manipulation is more efficient than the traditional binary representation. Example of such techniques are the Canonic Sign Digit (CSD) method, in which coefficients are represented by a combination of powers of two in such a way that multiplication can be simply implemented with adder/subtractors and shifters, and the Dempster-Mcleod method, which similarly involves the representation of filter coefficients with powers of two but in this case arranging partial results in cascade to introduce further savings in the usage of adders. The second type of multiplier-less method involves use of memories (RAMs, ROMs) or Look-Up Tables (LUTs) to store pre-computed values of coefficient operations. These memory-based methods involve Constant Coefficient Multiplier method and the very-well known Distributed Arithmetic method as examples. Distributed Arithmetic (DA) algorithm appeared as a very efficient solution especially suited for LUT-based FPGA architectures. For this reason, the FIR filter is used in this task to optimize the predicted time and frequency-domain meshing stiffness, where the multiplier-less method is used. The multiplier-less method contains look-up tables (LUTs) to store pre-computed values of coefficient operations. These memory-based methods involve constant coefficient multiplier method and the very-well known distributed arithmetic algorithm (DA) [9, 10].

B) Finite impulse response (FIR) filter

Digital finite impulse response (FIR) filters have been used in signal processing as ghost cancellation and channel equalization. FIR filtering of which the output is described in Equation (6) is realized by a large number of adders, multipliers and delay elements.

$$Y[n] = \sum_{k=0}^{N-1} h[k] \cdot X[n-k] \quad (6)$$

Where $Y[n]$ is the filter output, $X[n-k]$ is input data, and $h[k]$ is the filter coefficient. Direct form of a finite word truncating is the optimum infinite precision coefficients determined by McClellan and Parks algorithm [11]. Due to the enormous occupied area of FIR filters with a large number of taps, hardware-reusing architectures such as time-multiplexing architectures and a distributed arithmetic (DA) approach based on bit-serial access, have

been widely adopted for implementation. Canonical Signed-Digit (CSD) coefficient representation has also been used by many researchers for designing multiplier-less high speed FIR filters. Canonical Signed Digit encoding is used for coefficients to minimize the number of additions. In many signal processing and communication applications such as FIR filters, video and image processing, a multiplication with constants e.g. filter coefficients have to be performed. Therefore, the use of multiplier-less techniques is inspired to avoid the need of establishing an expensive general purpose multiplier e.g. on the FPGA and instead computing constant multiplications using table lookups and additions.

C) Distributed arithmetic (DA)

An alternative approach is the DA technique which is well known method to save resources. However, using this approach, the filter can be implemented in bit serial or parallel mode to trade bandwidth for area utilization. The input variable in equation (6) can be represented in its weighted format as in equation (7).

$$x_k = -x_{n,k-1} + \sum_{m=0}^{k-1} x_{n,k-1-m} 2^{-m} \quad (7)$$

Using equation (7) in (6) and after some mathematical manipulations the filter output given in equation (6) can be written as in equation (8).

$$Y = \sum_{m=0}^{k-1} \sum_{k=0}^{k-1} Z_{k-1-m}^{2^{-m}} \quad (8)$$

Implementing equation (8) in bit serial DA basic structure [12] will result in constructing lookup table (LUT) of size 2^m (m is the number of input variables, e.g. filter coefficients). This is the major drawback of the basic DA architecture which made it sometimes impractical for designing high order FIR digital filters. In this problem has been overcome by proposing a new architecture for the DALUT so that its size is independent of the number of input variables or filter coefficient.

D) Pulse shaping

In any transmission system, where pulses are transmitted and ultimately detected by the receiver, the goal is to sample the received signal at optimal points in the pulse interval so that the probability of an accurate binary decision is maximized. This implies that the fundamental shapes of the pulses be such that they do not interfere with one another at the optimal point i.e. have zero value at sampling points. In addition, the pulse amplitude must decay rapidly outside the pulse interval. In real systems, it is proved that the quicker a pulse decays outside its interval, the less likely it allow timing jitter to introduce errors when sampling adjacent pulse [13].

E) Algorithm analysis

The algorithm analysis starts with obtaining the filter coefficients based on desired specifications. Using the round function in MATLAB these coefficients are rounded to the nearest integer after being multiplied with a constant

integer value. Finally, a block diagram for the DA implementation of a FIR filter is shown in **Fig. 2 [14]**.

3. EXPERIMENTAL METHODOLOGY

The establishment of the experimental methodology and the accelerometers positions are presented in detailed in **Ref. [15]**, where the measuring of rotational response has been evaluated by using a pair of matched accelerometers placed a short distance apart on the gearbox's structure. Tests were conducted in order to calibrate the sensor configuration and insure the reaptability of the recordings and the proper operation with minimum noise of the system as well as the various cables and connections. **Fig. 3** shows photograph of test layout, while **Fig. 4** shows the accelerometers positions. Defects with their dimensions have been artificial made in the wind turbine gearbox planet tooth (crack, spalling and breakage) are presented in **Fig. 5**. In terms of various parameters evolution during the test; from a representative test on the planetary gearbox system with different damages will be presented. The defects were made artificially with wire electrical discharge machining (EDM) and chemical electrode on the gearbox to create a stress concentration which eventually led to a propagating fault. This type of test was preferred in order to have the opportunity to monitor bath defects modes, i.e., the natural fault propagation.

Two Bruel & Kjaer accelerometers were used for the rotational vibration monitoring both mounted upon the gearbox case, one in each side-axis. The signal was lowpass filtered at 6.0 kHz through a filter, in order to aliasing distortion and retain waveform integrity as much as possible. A number of 2048 samples have been acquired in the experiments corresponding to a time history length of 1.0 s. B&K portable multi-channel PULSE type 3560-B-X05 analyser is used. The B&K PULSE labshop with the measurement software type 7700 is used to analyse the results, while the speed is measured by photo electric probe. Recordings were carried out at constant speed conditions and closed windows. The output speed range is 40 rpm and the torque load is 40 Nm. For each defect, recordings every 60.0 min were acquired and a total of 7 recordings (~ 6.0 h of test duration) were resulted until the termination of the test.

4. RESULTS AND DISCUSSION

4.1 Diagnostic Results and Discussion

a) Healthy gearbox

In healthy gearbox, **Fig. 6** shows the time-domain of mean vibration displacement, velocity and acceleration responses for speed 40 rpm and 40 Nm. **Fig. 7** shows the comparison between the computed time-varying nominal meshing stiffness based on equation (5) and optimum meshing stiffness based on equation (8) at speed 40 rpm. Note that the frequency range is up to 6000 Hz (**Fig. 7- b**), where the highest stiffness levels are observed to be up to 1000 Hz (**Fig. 7-c**), while the levels of the remaining frequency are lower and almost constant. However, the

frequency's range up to 1000 Hz which shown in **Fig. 7-c** is used for the diagnostic purpose.

b) Cracked planet gear

Figure 8 shows the comparison between optimum meshing stiffness in healthy gearbox and cracked planet gear at speed 40 rpm and 40 Nm in terms of frequency-domain (1000Hz). The effect of irregular optimum meshing stiffness associated with a cracked planet gear tooth is filtered by the gearbox dynamics and contaminated by other vibrations. It is clearly seen from the figure that the optimal meshing stiffness for the cracked planet gear is lower than that for the healthy gearbox particularly at low frequency up to 500 Hz. This is important information for fault detection and severity assessment. Samples for the RMS averages of optimum meshing stiffness at different testing time up to 6.0 h is shown in **Fig. 9**. To assist the more accurate observation of this parameter evaluation during the range of testing time possess diagnostic value as they can be used to define and characterize critical changes of the gears faults accumulation and evaluation. On the other hand, it can be observed that the RMS value decreases as the testing time is increased, where the planet gear tooth crack can make the tooth lose instantaneous loading capacity and consequently work and torque transfer ability. This can be an effective way to carry out the predictive maintenance regime and consequently to save money and look promising.

c) Spalling planet gear

Figure 10 shows the comparison between optimum meshing stiffness in healthy gearbox and spalling planet gear at speed 40 rpm and 40 Nm in terms of frequency-domain (1000Hz). The effect of irregular optimum meshing stiffness associated with a spalling planet gear tooth is filtered by the gearbox dynamics and contaminated by other vibrations. It is clearly seen from the figures that the optimal meshing stiffness for the spalling planet gear is lower than that for the healthy gearbox particularly at low frequency up to 500 Hz. This is important information for fault detection and severity assessment. Samples for the RMS averages of optimum meshing stiffness at different testing time up to 6.0 h is shown in **Fig. 11**. To assist the more accurate observation of this parameter evaluation during the range of testing time possess diagnostic value as they can be used to define and characterize critical changes of the gears damage accumulation and evaluation. The correct detection and diagnosis of a tooth spalling is very important in practical diagnosis because spalling may just result in some noise and extraneous dynamic response. On the other hand, it can be observed that the RMS value decreases as the testing time is increased. This can be an effective way to carry out the predictive maintenance regime and consequently to save money and look promising.

d) Breakage planet gear

Figure 12 shows the comparison between optimum meshing stiffness in healthy gearbox and breakage planet gear at speed 40 rpm and 40 in terms of frequency-domain

(1000Hz). The effect of irregular optimum meshing stiffness associated with a breakage planet gear tooth is filtered by the gearbox dynamics and contaminated by other vibrations. It is clearly seen from the figures that the optimal meshing stiffness for the breakage planet gear is lower than that for the healthy gearbox particularly at low frequency up to 500Hz. This is important information for fault detection and assessment. Samples for the RMS averages of optimum meshing stiffness at different testing time up to 6.0 h are shown in **Fig. 13**. To assist the more accurate observation of this parameter evaluation during the range of testing time possess diagnostic value as they can be used to define and characterize critical changes of the gears damage accumulation and evaluation. The correct detection and diagnosis of a tooth breakage is very important in practical diagnosis because breakage may just result in some noise and extraneous dynamic response. On the other hand, a reduction in the optimum meshing stiffness is observed. This reduction is more accentuated when the testing time increases. This is explained by the fact that when the breakage affects the whole height of the tooth. This can be an effective way to carry out the predictive maintenance regime and consequently to save money and look promising.

4.2 Planet gear damages severity assessment

In terms of RMS optimum meshing stiffness, **Fig. 14** depicts planet gear tooth faults (crack, spalling and breakage) severity assessment which has been achieved by the developed the experimental technique at speed 40 rpm and 40 Nm. The testing time is being 0.0 h. The figure indicates that gear breakage posses the highest RMS value followed by gear spalling with gear crack has least RMS. This can help to identify which type of faults can be detected. On the other hand, **Table 1** tabulates in percentage of the change of RMS optimum meshing stiffness at testing time of 0.0 h from that for healthy gearbox (*CFHL*) at speed 40 rpm and 40 Nm based on the following equation:

$$CFHL, (\%) = \frac{(RMS)_{Healthy} - (RMS)_{Faulty}}{(RMS)_{Healthy}} \quad (9)$$

Where

$(RMS)_{Healthy}$ = RMS value for healthy condition

$(RMS)_{Faulty}$ = RMS value for faulty condition

The values are 47.15% (gear breakage), 40.26% (gear spalling) and 30.46% (gear crack). This information can help for diagnostic regime. It has been shown that the fault on gear teeth can be detected at its early stages, and symptoms of defect on vibration is not primarily caused by the reduction in tooth stiffness (which is the case for the detection of a localized tooth defect), but mainly due to the deviations in tooth shape from the true involute profile. The results have revealed that tooth surface fault causes an approximately linear reduction in gear tooth stiffness with time.

5. CONCLUSIONS

1- The ability to identify ring-planet-sun gears meshing stiffness from the real data of vibration responses makes it possible to determine the physical existed planet gear damages which used for severity assessments. By using the proposed technique in the real time applications, if one tooth is damaged due to cracks, spalling and breakage to reach the setting maximum level, the maintenance regime will be called despite a new fault is prone in the adjacent tooth to save time and cost.

2- The optimization technique developed in this work provides a very reasonable estimate of the meshing stiffness change due to planet gear fault, which can be related to the state of the gear. Moreover, for more accurate evaluation of the system mesh stiffness, the optimization technique presented needs to be developed.

3- Multi-hour tests were conducted and recordings were acquired using translational vibration monitoring, where the optimum meshing stiffness was computed, where the optimum meshing stiffness with the recording testing time were highlighted suggesting critical changes in the operation of the gearbox.

4- From this investigation, the gearbox components faults severity assessment has indicated that the values are 30.46% (planet gear crack), 40.26% (planet gear spalling) and 47.15% (planet gear breakage). Moreover, the symptoms of fault on vibration is not primarily caused by the reduction components stiffness (which is the case for the detection of a localized fault), but mainly due to the deviations in component shape from the true component shape.

6. ACKNOWLEDGEMENTS

The authors acknowledge the support of Science and Technology Development Fund (STDF), Egypt, through the awarded grant No. ID 1484, on monitoring of wind turbine gearbox. The authors would like to thank University of Helwan, which made this study possible.

REFERENCES

- 1 Choy, F. K., Polyshchuk, V., Zakrajsek, J. J., Handschuh, R. F. and Townsendi, D. P. " Analysis of the effects of surface pitting and wear on the vibration of a gear transmission system "Tribology International Vol. 29, No. 1, pp. 71-83, 1996.
- 2 Cai, Y. "Simulation on the rotational vibration of helical gears in consideration of tooth separation phenomenon (A new stiffness function of helical involutes tooth pair)" ASME, Journal of Mechanical Design, Vol. 177, pp. 460-469, 1995.
- 3 Choy, F. K., Vilette, R. J., Polyshchuk, V. and braun, M. J. " Quantification of gear tooth damage by optimal tracking of vibration signatures" Sixth International Symposium on Transport Phenomena and Dynamics of Rotation Machinery, NASA Technical Memorandum 107100, Feb. 25-29, 1996.

- 4 Abouel-seoud, S. A., Hmmmad, N., Abdel-halim, N. Abdel-hady, M. amd Mohamed, E. S. " The importance of vehicle gear tooth meshing stiffness in gear tooth Damage quantification" SAE Paper No. 2008-01-2631, 2008.
- 5 Lin, J. and Parker, R. G. "Planetary gear parametric instability caused by mesh stiffness variation" Journal of Sound and Vibration (2002) 249(1), 129}145, 2002.
- 6 Stewart RM. "Through-life monitoring of transmission system" Proceedings of the First International Conference on Gearbox Noise, Vibration, and Diagnostics, London: Institute of Mechanical Engineers, pp. 135–40, 1990.
- 7 Yesilyurta, I., Gub, F. and Ballc,A. D. "Gear tooth stiffness reduction measurement using modal analysis and its use in wear fault severity assessment of spur gears" NDT&E International 36, pp. 357–372, 2003.
- 8 Bartelmus, W. "Mathematical modelling and computer simulations as an aid to gearbox diagnostics" Mechanical Systems and Signal Processing 15 (5), pp. 855–871, 2001.
- 9 Eshtawie, M. A. and Othman, M. B. "An Algorithm Proposed for FIR Filter Coefficients Representation" World Academy of Science, Engineering and Technology 26, 2007.
- 10 Vigneswarn, T. and Reddy, P. S." Design of Digital FIR Filter Based on DDA algorithm" Journal of Applied Science, 2007.
- 11 Pal, N. S., Singh, H. P., Sarin, R.K. and Singh, S. "Implementation of High Speed FIR Filter using Serial and Parallel Distributed Arithmetic Algorithm" International Journal of Computer Applications (0975 – 8887), Volume 25– No.7, July, 2011.
- 12 Eshtawie M. A. and Othman, M. B. " On-Line DA-LUT Architecture for High- Speed High-Order Digital FIR Filters," paper status is published in the tenth IEEE international conference on communication systems (IEEE ICCS 2006), 30-1 Nov 2006.
- 13 Eshtawie, M. A. and Othman, M. B."An Algorithm Proposed For FIR Filter Coefficients Representation" International Journal of Mathematics and computer Sciences, pp24-30, 2008.
- 14 Proakis, J. G., Salehi, M. and Bauch, G. "Contemporary Communication Systems using MATLAB. Brooks/Cole, 2004.
- 15 Abouel-seoud, S., El-morsy, M. and Saad, A."A Laboratory Apparatus for Investigation of Vibration Performance of Wind Turbine Planetary Gearbox" Journal of Recent Research, Vol. 3, Issue 11, 2011.

S/No.	Speed, rpm	Torque, Nm	Gear crack	Gear Spalling	Gear Breakage
1	40	40	30.46	40.26	47.15

Table 1 Change from the healthy gearbox (%)

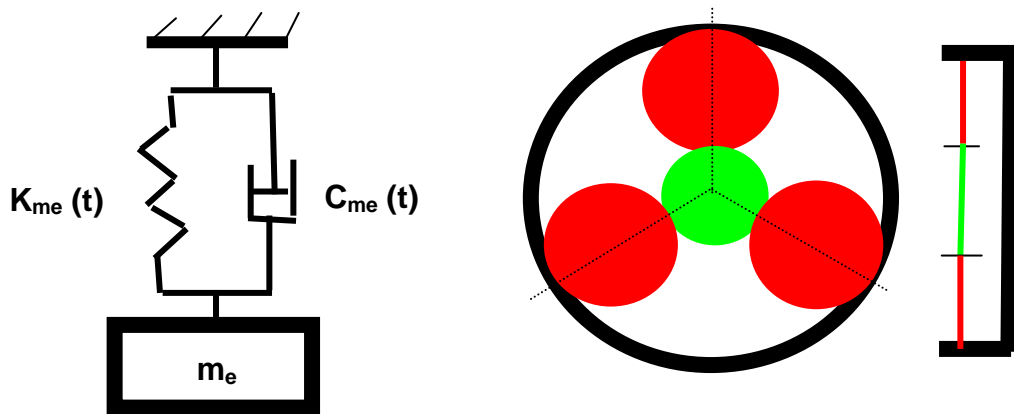


Fig. 1 Single-degree-of-freedom model

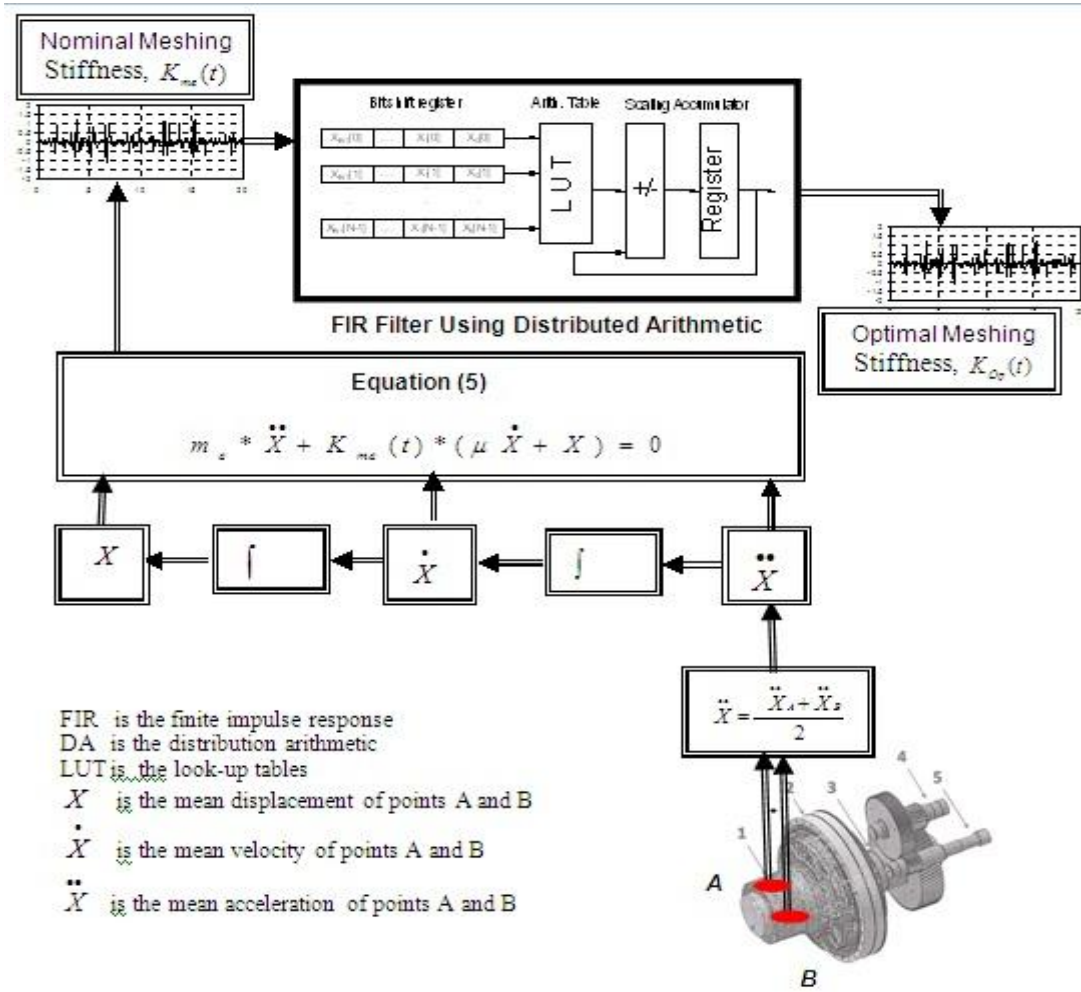


Fig. 2 Block Diagram for the sequence of optimum meshing stiffness estimation



Fig. 3 Photograph of the layout of the test rig



Fig. 4 Accelerometers positions

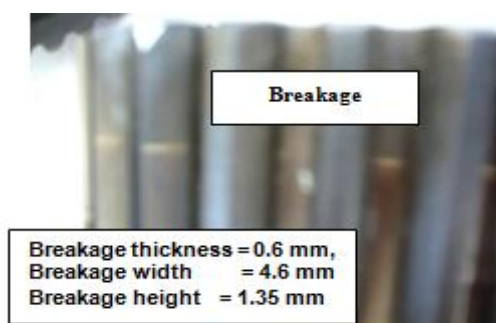
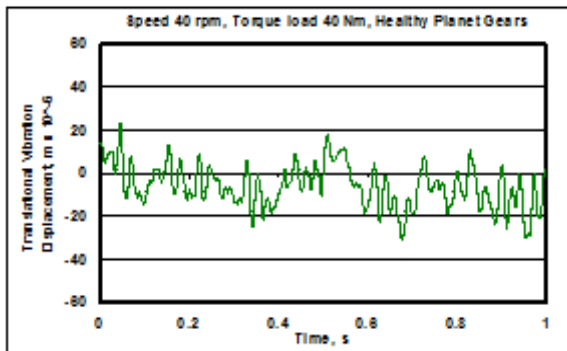
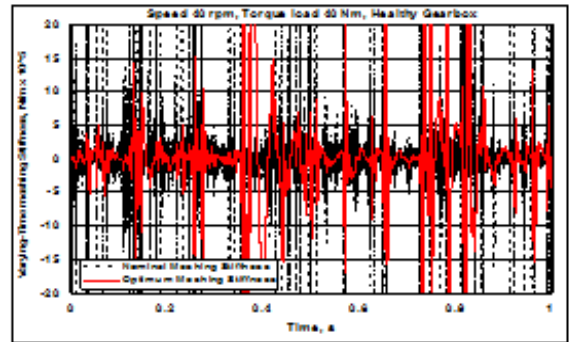




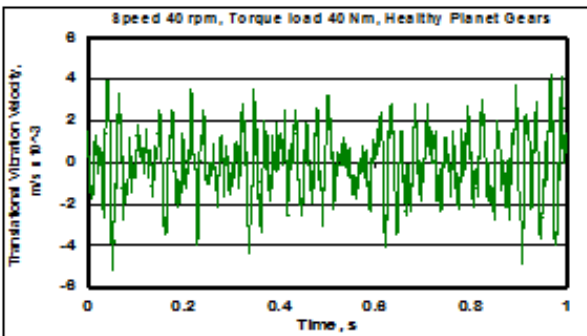
Fig. 5 Wind turbine planetary gearbox planet gear tooth faults



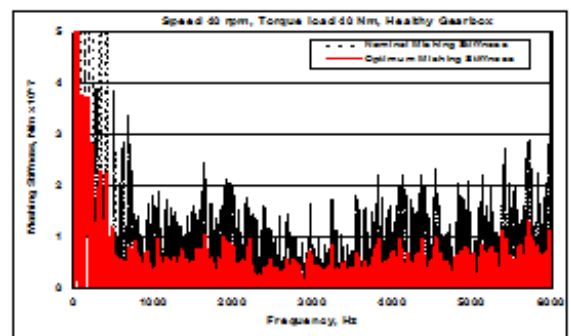
a) Mean vibration displacement



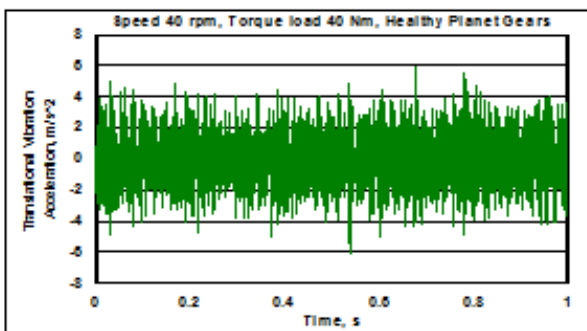
a) Time domain signals



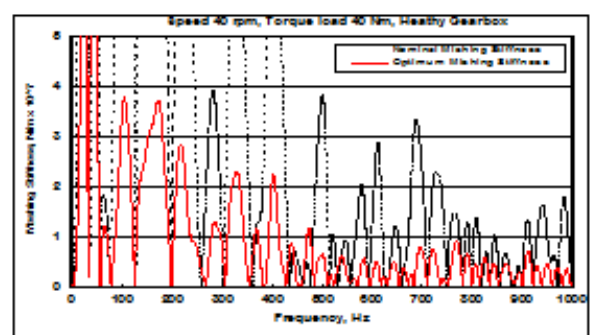
b) Mean vibration velocity



b) Frequency-domain (6000 Hz)



c) Mean vibration acceleration



c) Frequency-domain (1000 Hz)

Fig. 6 Vibration responses at 40 rpm, 40 Nm (Healthy gearbox)

Fig. 7 Meshing stiffness at 40 rpm, torque 40 Nm (Healthy gearbox)

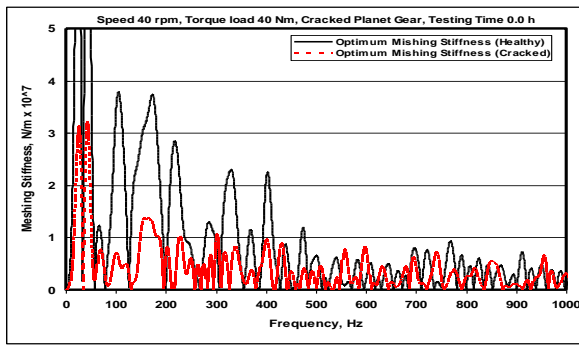


Fig. 8 Optimum meshing stiffness at 40 rpm, 40 Nm (Cracked Planet Gear)

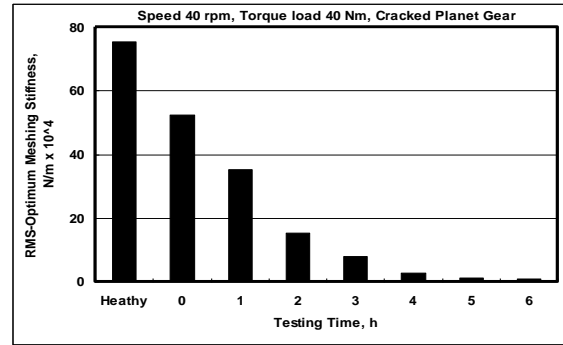


Fig. 9 RMS-optimum meshing stiffness at 40 rpm 40 Nm (Cracked Planet Gear)

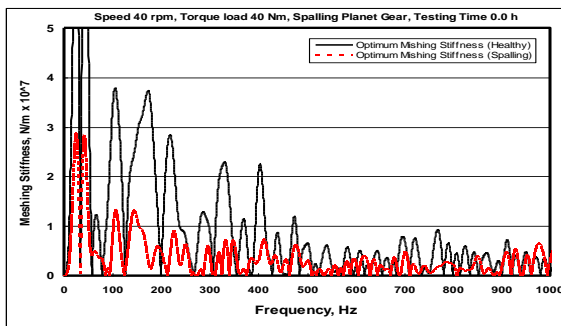


Fig. 10 Optimum meshing stiffness at 40 rpm, 40 Nm (Spalling Planet Gear)

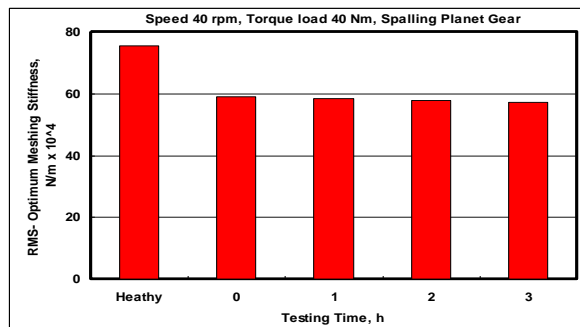


Fig. 11 RMS-optimum meshing stiffness at 40 rpm 40 Nm (Spalling Planet Gear)

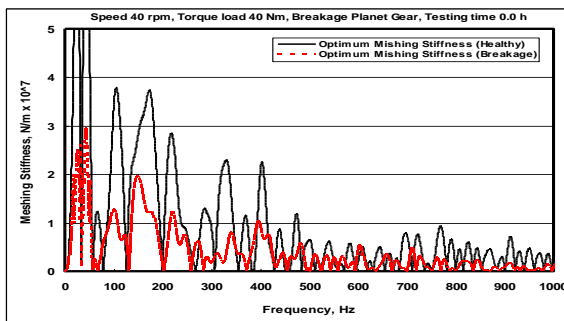


Fig. 12 Optimum meshing stiffness at 40 rpm, 40 Nm (Breakage Planet Gear)

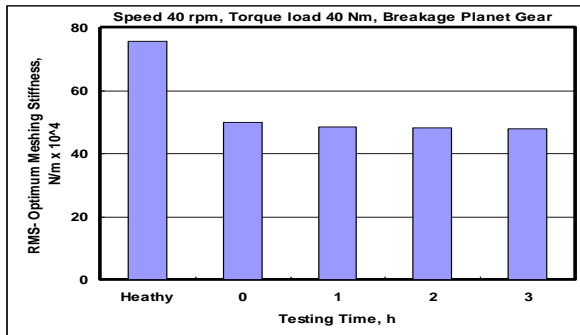


Fig. 13 RMS-optimum meshing stiffness at 40 rpm 40 Nm (Breakage Planet Gear)

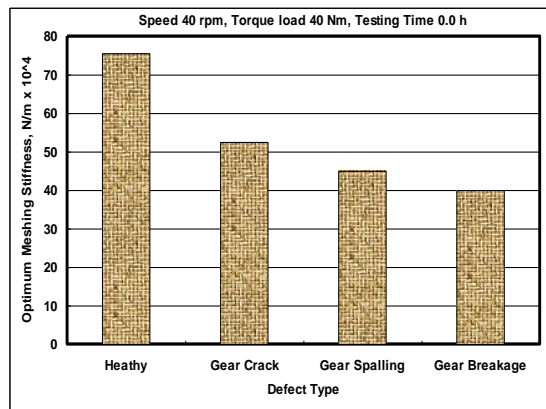


Fig. 14 RMS-optimum meshing stiffness at 40 rpm 40 Nm